

GEOPHYSICAL FLUID MECHANICS

VOLUME I: MATHEMATICS, KINEMATICS, THERMODYNAMICS, DYNAMICS

VOLUME II: SHALLOW WATER FLOW, VORTICITY, BALANCED FLOW, WAVES, INSTABILITIES

VOLUME III: VERTICAL COORDINATES, SCALAR MECHANICS, SOLUTIONS TO EXERCISES

Stephen M. Griffies
Princeton University
Atmospheric and Oceanic Sciences Program
SMG@princeton.edu
Draft from July 30, 2023



COPYRIGHT ©2023 BY STEPHEN M. GRIFFIES
ALL RIGHTS RESERVED

GRIFFIES, STEPHEN M., 1962-

ELEMENTARY GEOPHYSICAL FLUID MECHANICS

THIS BOOK WAS TYPESET USING L^AT_EX.

CONTENTS

	Page
PREFACE	iii
A GUIDE TO THIS BOOK	xi
PRINCETON UNIVERSITY AOS 571 AND 572	xvii
LIST OF SYMBOLS	xxxiii
Part I. Mathematical methods	1
1 CARTESIAN TENSOR ALGEBRA	5
2 CARTESIAN TENSOR CALCULUS	23
3 PARTIAL DIFFERENTIAL EQUATIONS	49
4 GREEN'S FUNCTION METHODS	71
5 FOURIER ANALYSIS	117
6 CURVES AND SURFACES	137
7 GENERAL TENSORS IN BRIEF	149
8 GENERAL TENSOR ANALYSIS	159
9 ORTHOGONAL COORDINATES	181
Part II. Particle mechanics	195
10 NEWTONIAN PARTICLE MECHANICS	197
11 PARTICLE MECHANICS ON A ROTATING SPHERE	211
12 SYMMETRY AND CONSERVATION	241
Part III. Fluid kinematics	265
13 CONTINUUM APPROXIMATION	269
14 FUNDAMENTALS OF FLUID KINEMATICS	279
15 MATERIAL FLUID OBJECTS	309
16 MASS CONSERVATION	337
17 TRACER CONSERVATION	361
18 NON-DIVERGENT FLOWS	385

Part IV. Equilibrium thermodynamics	405
19 EQUILIBRIUM THERMODYNAMICS	407
20 EQUILIBRIUM THERMODYNAMICS WITH A GEOPOTENTIAL	437
Part V. Dynamics of geophysical flows	457
21 MOMENTUM DYNAMICS	461
22 STRESS IN FLUIDS	479
23 THERMODYNAMICS AND ENERGETICS	517
24 APPROXIMATE HYDROSTATIC FLOW	561
25 PRESSURE FORM STRESS	581
26 THE BOUSSINESQ OCEAN	605
27 BUOYANCY	653
28 ROTATING FLUID FLOW	683
29 TANGENT PLANE FLOW BALANCES	707
30 EKMAN MECHANICS	723
31 SPACE AND TIME DEPENDENT GRAVITY	747
Part VI. Shallow water mechanics	759
32 FORMULATING SHALLOW WATER MODELS	761
33 SHALLOW WATER DYNAMICS	789
Part VII. Vorticity mechanics	837
34 VORTICITY AND CIRCULATION	839
35 NON-DIVERGENT BAROTROPIC FLOW	863
36 SHALLOW WATER VORTICITY AND POTENTIAL VORTICITY	889
37 VORTICITY AND CIRCULATION MECHANICS	931
38 POTENTIAL VORTICITY MECHANICS	979
39 POTENTIAL VORTICITY BUDGETS	1001
Part VIII. Mechanics of nearly geostrophic flows	1021
40 SHALLOW WATER PLANETARY AND QUASI-GEOSTROPHY	1023
41 CONTINUOUSLY STRATIFIED PLANETARY GEOSTROPHY	1045
42 CONTINUOUSLY STRATIFIED QUASI-GEOSTROPHY	1075
Part IX. Wave mechanics	1099
43 WAVE KINEMATICS	1103
44 ACOUSTIC WAVES	1131
45 SURFACE WAVES	1161
46 INERTIAL WAVES	1197

CONTENTS

47 BAROTROPIC VORTICITY WAVES	1209
48 SHALLOW WATER WAVES	1233
49 INTERNAL GRAVITY WAVES	1275
Part X. Mechanics of unstable flows	1315
50 STABILITY OF SYMMETRIC FLOWS	1317
51 STABILITY OF FLUID INTERFACES	1355
52 STABILITY OF SHEARED BAROTROPIC FLOW	1367
53 STABILITY OF STRATIFIED SHEAR FLOW	1375
54 INSTABILITIES LEADING TO CONVECTION	1377
55 STABILITY OF QUASI-GEOSTROPHIC FLOWS	1379
Part XI. Mechanics with generalized vertical coordinates	1397
56 MATHEMATICAL BASICS	1401
57 KINEMATIC EQUATIONS	1421
58 DYNAMICAL EQUATIONS	1445
59 ISOPYCNAL PRIMITIVE EQUATIONS	1455
60 SHALLOW WATER THICKNESS WEIGHTED AVERAGING	1469
Part XII. Mechanics of scalar fields	1491
61 TRACER ADVECTION AND DIFFUSION	1493
62 EDDY AND MEAN TRACER KINEMATICS	1545
63 MATHEMATICS OF PARAMETERIZED TRACER TRANSPORT	1573
64 OCEAN DENSITY AND SEA LEVEL	1603
65 WATER MASS TRANSFORMATION ANALYSIS	1627
Part XIII. Bibliography and Index	1667
BIBLIOGRAPHY	1669
INDEX	1695

CONTENTS

CONTENTS

CONTENTS

PREFACE

Geophysical fluid mechanics (GFM) is the study of natural fluid motion on a rotating and gravitating planet using concepts and methods from classical continuum mechanics and thermodynamics. In this book, our primary inspiration comes from the motion of terrestrial fluids in the atmosphere and ocean, though the discipline is applicable to extra-terrestrial planetary flows. Geophysical fluids are in near solid-body motion with the rotating planet, thus prompting a description from the rotating (non-inertial) planetary reference frame. Body forces from both rotation (Coriolis) and gravitation (buoyancy) are fundamental features of the motion, as are contact forces from stresses (pressure and friction). We limit attention to the motion of a single phase of matter (gas or liquid), with the study of multiphase geophysical fluid mechanics (highly relevant to a moist atmosphere) outside our scope.

Fluid motion is complex and multiscaled, with geophysical flows expressing a huge range of space and time scales. Insights into such flows typically results from considering a hierarchy of conceptual models. Some models are formulated within the context of a *perfect fluid* comprising a single material constituent with fundamental processes limited to the reversible and mechanical. Others are posed within *real fluids* comprised of multiple matter constituents exposed to *irreversible processes* such as friction, mixing, and heating. Some models ignore rotation, and thus tacitly apply to flows with length scales too short to feel the Coriolis acceleration, whereas others ignore stratification, and thus allow one to focus on the dynamics of a homogeneous rotating fluid.

We develop geophysical fluid mechanics from a mathematical physics perspective. Those with little prior exposure are supported by development of the salient physics and maths in the process of building understanding. Hence, with proper study, the book should be accessible to the advanced undergraduate student or entering graduate student in fields such as physics, atmospheric sciences, oceanography, geophysics, astrophysics, engineering, and applied mathematics. We are guided by the perspective that fundamental physical concepts are more readily understood than special cases, and that a grounding in fundamentals offers a robust and versatile framework for exploring the gamut of special cases encountered in applications. Hence, subjects are approached by establishing general principles and mathematical methods that then guide an examination of case studies.

Though motivated by natural phenomena, our treatment is centered on the mechanics of geophysical fluid motion. That focus supports exploration that often extends beyond that required for phenomenological purposes. Correspondingly, we welcome the opportunity to examine physics through multiple lenses that render a variety of perspectives and complementary insights. In a nutshell, if a physical problem can be formulated and analyzed in more than one way, then we do so if it enhances pedagogy and exposes layers of understanding. As a result, brevity is generally sacrificed to support exposition and exploration.

The presentation is based on the premise that skills in theoretical physics are optimally taught by nurturing physical reasoning, with physical reasoning supported by mathematical precision

coupled to the elucidation of concepts using words and pictures. Hence, the presentation is both deductive and descriptive. The deductive approach supports understanding through the use of elementary physical notions that are expressed mathematically. The descriptive approach serves to build skills in reasoning along with the ability to articulate physical ideas using words and pictures to offer substance to the maths.

We cultivate the deductive and descriptive approaches by embracing the synergism between physics and maths, whereby physics informs the maths and maths reveals the physics. This synergism is facilitated by a writing style inspired by [Mermin \(1989\)](#), who identified the following characteristics for the clear articulation of mathematical physics.

- RULE 1: All displayed equations are given numbers to facilitate cross-referencing. Any equation supporting another equation or a discussion is itself displayed with an equation number.
- RULE 2: Equations are referenced both by their number as well as descriptive phrases or names. Coupling maths to english supports learning, and reduces the need to flip pages to view the cited equation.
- RULE 3: Equations are part of the prose and thus subject to punctuation.

Following this style, we generally offer extensive details to mathematical derivations. Doing so nurtures technical skills required for the practicing theorist, and allows those with less well developed mathematical training to refine their skills and remain an active participant in the exploration. Exposing details also helps to unpack many of the physical concepts encapsulated by mathematical equations. As we are studying classical physics, concepts generally accord with common experience, thus affording a check on the validity of the maths by checking whether an equation agrees with common experience. Furthermore, as we are studying physics, mathematical equations must satisfy dimensional consistency, with this constraint offering the practicing physicist a powerful tool for exposing spurious mathematical statements.

Concerning the book's title

The study of rotating and stratified geophysical fluid motion largely started in the first half of the 20th century, and has evolved much over its history. During recent decades the study has seen particular evolution through deepening physical foundations, refining mathematical formulations, increasing the intellectual and predictive value of numerical simulations, extending applications across terrestrial and planetary systems, and expanding observational and laboratory measurements and techniques. What has emerged is a recognition that a fruitful study of rotating and stratified fluid flows makes use of ideas that go beyond the traditional notions of *geophysical fluid dynamics* (GFD). A contemporary practitioner develops insights by weaving together concepts and tools from mathematics, classical mechanics, fluid mechanics, thermodynamics, scalar mechanics, numerical simulations, laboratory experiments, field measurements, and data science. Acknowledging this broadening of the practice motivates the term *mechanics* in this book's title, rather than the more focused *dynamics*. It is a minor change in verbiage that reflects a broadening of the perspective pursued here.

Two pillars of theoretical geophysical fluid mechanics

We conceive of two pillars to theoretical geophysical fluid mechanics that are synergistic, thus offering lessons, guidance, and feedback to the other. The *elements* pillar comprises the physical and mathematical formulation of conceptual models used to garner insight into rotating and

stratified fluid motion. This pillar is concerned with setting the stage by deductively and descriptively exposing how physical concepts are mathematically expressed in a mechanical description of geophysical flows. The complement *emergent pillar* studies solutions to equations, such as waves, instabilities, turbulence, and general circulation, all of which emerge from the equations. This book is more heavily weighted on the elements pillar. Even so, we do study waves and instabilities, which are the canonical examples of emergent phenomena in geophysical fluid flows. Part of the reason for the enhanced treatment of the elements pillar concerns its relatively brief treatment commonly afforded in current literature, with the present book an attempt to slightly remedy this bias.

Some themes found in this book

This book covers an extensive number of topics in theoretical geophysical fluid mechanics. Throughout, we encounter a number of themes that appear in various guises, with the following offering a brief survey.

Causation

We develop equations describing the evolution of fluid properties, with such equations derived from physical principles such as Newton's laws of motion, thermodynamic relations, mass conservation, and vorticity mechanics. As part of this development we often seek information about what *causes* fluid motion. The question of causality is posed when studying Newton's equation of motion, which says that acceleration (motion) arises from a net force (the cause of the motion). Even though seemingly a clear decomposition of cause and effect, this fundamental statement of Newtonian mechanics offers little more than the definition of a force. We break the self-referential loop, and thus make physical progress, after specifying the nature of the force, for example gravitational, electromagnetic, as well as by offering properties of these forces as per Newton's third law (the action/reaction law).¹

In geophysical fluid mechanics, we refer to equations that determine time changes as *evolution equations* or, more commonly, *prognostic equations*, with terms in the prognostic equation referred to as *time tendencies*. For prognostic equations, knowledge of the processes contributing to the net time tendency enables a prediction of flow properties. The question arises how to practically determine the tendencies acting in the fluid, particularly when tendencies are generally dependent on the flow itself. This question is not always simple to answer. Such is the complexity and beauty inherent in nonlinear field theories, such as fluid mechanics, where cause and effect are intrinsically coupled.

We can sometimes make progress by turning the problem around, whereby kinematic knowledge of the motion offers inferential knowledge of the processes contributing to time tendencies. This situation is exemplified by pressure forces acting within a non-divergent flow whereby pressure provides the force that acts, instantaneously and globally, to maintain the constraint that the velocity is non-divergent.² We may also make use of constraints that restrict the flow properties in manners that assist in prediction and understanding.

¹For more on this perspective of Newton's laws, see Chapter 1 of [Symon \(1971\)](#) or Chapter 2 of [Marion and Thornton \(1988\)](#).

²For non-divergent flow, pressure acts as the *Lagrange multiplier* enforcing flow non-divergence.

Constraints

Determining the forces, either directly or indirectly, provides physical insight into the cause of fluid flow and its changes. This approach is sometimes referred to a *momentum-based viewpoint* since it is based on working directly with the momentum equation (i.e., Newton's second law of motion). However, we are commonly unable to deduce the forces due to complexities inherent in nonlinear field theories. Furthermore, there are many occasions when we are simply uninterested in the forces. In these cases, we are motivated to use constraints that can allow us to sidestep forces but still garner insights into the motion.

One example of a constraint concerns the inability of fluid to flow through a solid static material boundary. To understand how this constraint impacts on the fluid, we do not need to understand details of the electromagnetic forces that underlie the resistance to this motion. Instead, we simply impose the kinematic boundary condition whereby the component of the velocity that is normal to the boundary vanishes at the boundary. The forces active within the fluid, no matter what flavor they may take, are constrained to respect the kinematic boundary condition. Another example concerns our study of vorticity developed in Part VII of this book. A variety of vorticity constraints offer the means to deduce flow properties without determining forces. Indeed, *vorticity-based viewpoint* often provides a practical framework that is superior than the momentum-based view, thus prompting the importance of vortex mechanics in our study of geophysical fluid mechanics.

Associations and balances

Besides seeking causal relations pointing toward the future, many basic questions of fluid mechanics arise either instantaneously, as in the constraints maintaining non-divergent flows, or when the flow is steady, in which case properties at each point in space have no time dependence. In steady flows, the net acceleration, and hence the net force, vanish at each point within the fluid, although the fluid itself can still be moving (steady flows are not necessarily static). For steady flows we are unconcerned with causality since time changes have been removed. In this manner, the steady state equations are *diagnostic* rather than prognostic. Diagnostic relations thus provide mechanical statements about *associations* between physical processes that manifest as *balances*. The *geostrophic balance* is the canonical association in geophysical fluid mechanics, where the horizontal Coriolis force is balanced by the horizontal pressure force. Another balance concerns the vertical pressure gradient and its near balance with the weight of fluid above a point in the fluid, with this *hydrostatic balance* approximately maintained at the large scale even for moving geophysical fluids. Further associations arise when studying steady vorticity balances, with the *Sverdrup balance* a key example that is commonly used in physical oceanography.

We summarize the above by saying that diagnostic equations are concerned with the way things are, whereas prognostic equations point to how things will be. So although a predictive theory requires prognostic equations that manifest causal relations, an understanding of how fluid motion appears, and in particular how it is constrained, is revealed by studying diagnostic relations that expose associations through balances.

Transformations between kinematic perspectives

Geophysical fluid flows are complex. Hence, it proves useful to avail ourselves of a variety of methods and perspectives that support a mechanistic description of the fluid motion. These methods are typically associated with distinct kinematic perspectives that reveal facets of the flow that are less readily revealed through alternative lenses. Examples include the Eulerian and Lagrangian kinematics used throughout fluid mechanics; the position space and wavevector spaces

used for wave mechanics; the variety of vertical coordinates used to describe vertically stratified flows; and the analysis of motion in property spaces such as exemplified by watermass analysis. We make use of these perspectives throughout this book, and offer the mathematical skills needed to transform between them.

Geophysical Fluid Mechanics and Climate Science 2.0

Fluid mechanics has a history of applications that span science and engineering, from blood flow to the stability of stars and the evolution of galaxies. A key 21st century application of geophysical fluid mechanics concerns the questions of climate science associated with the uncontrolled greenhouse gas experiment pursued by industrialized civilization's carbon centered energy use. Leading order questions about climate warming have been sufficiently addressed to recognize that the planet has reached a crisis point threatening the viability of the biosphere. Even so, mechanistic answers to a number of questions remain at the cutting edge of climate science research. What will happen to the atmospheric jet stream and storm tracks in a world without summer Arctic sea ice? Will tropical storms be more powerful in a warmer world? What are the patterns for coastal sea level rise and their connections to large-scale ocean circulation? What are the key processes acting to bring relatively warm ocean waters to the base of high latitude ice shelves? How stable are the ocean and atmosphere's large-scale overturning circulations and their associated heat transport? Are there feasible and sustainable climate intervention options that equitably reduce the negative impacts of climate warming without introducing new problems? These questions, and countless others, constitute the scientific challenges of *Climate Science 2.0*.

Numerical circulation models, a core tool for Climate Science 2.0, have reached a level of maturity allowing them to vividly reveal details of the complex and multi-scaled nature of planetary fluid flow. Geophysical fluid mechanics is essential for the development of robust numerical methods used by such models, as well as subgrid scale parameterizations that capture a sensible approximate description of scales unresolved by the model. Geophysical fluid mechanics also provides the intellectual framework for developing mechanistic analyses and robust interpretations of simulated data. In this way, geophysical fluid mechanics furthers predictive capability for weather and climate forecast systems and enhances confidence in projections for future climate. Absent creative inspiration and motivation based on foundational physical sciences, such as geophysical fluid mechanics, the analysis of numerical model output can be driven more by the needs of data science than the questions of atmospheric, oceanic, or climate science. Indeed, in a world of increasingly large volumes of data, we conjecture that it is only via the marriage of fundamental physical theory to statistical tools that real progress will be made in addressing the key questions of climate science.

Moving from the numerical world to the natural world, we find that the many elements of geophysical fluid mechanics are key to the design of observational field campaigns and novel laboratory experiments, as well as for the analysis of their measurements. Such field campaigns and laboratory experiments probe process-oriented questions through the use of technologies that facilitate increasingly ambitious investigations of environmental fluid flows.

We thus conclude that the principles and methods of geophysical fluid mechanics provide the means to conceptually digest and rationalize the underlying physics probed by both natural and simulated experiments. It also provides a mechanistic language to communicate the findings to the broader scientific community. In turn, geophysical fluid mechanics, as part of the scientific investigation of the earth's climate and the role of humans in affecting that climate, serves an essential role in humanity's quest for sustainability, equity, and justice.

About the cover

The cover photo of an iceberg, ocean, clouds, and sea bird (can you find the bird?) was taken in the Orkney Passage region of the Southern Ocean during a research cruise from March-May 2017 aboard the British ship James Clark Ross. I am grateful to Alberto Naveira Garabato, the chief scientist on this cruise, for taking me to this amazing part of the planet. Although I largely pursue theoretical research, my experiences with seagoing field research have greatly enhanced my scientific viewpoint and profoundly deepened a connection to the natural forces and phenomena that are in part described by geophysical fluid mechanics.

Gratitudes

This book greatly benefited from interactions with students taking part in the Princeton University Program in Atmospheric and Oceanic Sciences, particularly the two-semester graduate course, AOS 571 and AOS 572, that formed the initial motivation for writing this book. Further inspiration was offered by students, postdocs, and fellow scientists and scholars encountered on my path. I also thank those who offered specific suggestions, corrections, and comments on various drafts of this book, whose names are too many to list.

I remain humbled and grateful for being part of the unique research environment cultivated at NOAA's Geophysical Fluid Dynamics Laboratory (GFDL) as well as Princeton University's Atmospheric and Oceanic Sciences program. The focus of my research concerns physical oceanography and the ocean's role in climate. Even so, the community of scientists at GFDL and Princeton University provide an ideal setting for those interested in both broadening scientific perspectives while diving deep into particular research areas. Furthermore, as part of my research and mentoring in this community, I have encountered thinkers whose style, questions, and insights have taken root in my work. This work has also afforded me the opportunity to travel the world to interact with colleagues whose wisdom and love of the scientific endeavor are infectious and inspiring. Throughout these interactions, I have entered into trusting and non-judgmental spaces where deep learning and understanding arise. Partaking in these spaces, where heart and mind meld, has been among the most satisfying experiences of my life. Safe spaces for honest, diverse, non-judgemental, and inclusive learning are precious, and I am grateful to those who nurture such spaces.

A book of this nature is not a simple endeavor. It starts modestly, grows over time, and eventually becomes a passion if not an obsession. I was particularly drawn to writing during the COVID-19 pandemic that kept me sequestered at home far more than during non-pandemic times. Writing this book has been an exercise in rational thought fed by spiritual food from meditation, yoga, family, and community. In particular, each step of this project was supported by my wife, Adi, and our son, Francisco. I am deeply grateful for their patience and trust as I satisfied the goal of writing this book through countless nights, weekends, and holidays. I treasure being part of this family and I dedicate this work to you two amazing human beings.

Caveats and limitations

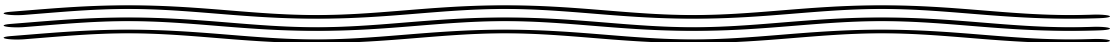
Although reaching some level of maturity, this book remains a work in progress not yet ready for publication. Here are just a few of the items required before it is ready for its next stage in life.

- A number of further topics will fill these pages. In particular, waves and instabilities remain a work in progress.

- More effort is needed to unify notation, develop further exercises, enhance figures, improve discussions, and correct errors.
- Many sections and chapters have yet to be scrutinized by readers. I hope to garner help from those interested in providing candid feedback to improve presentation and correct mistakes. Feedback is solicited particularly where the reader identifies poor or confused writing, incorrect concepts, or math errors. Nothing is too trivial for comment.

Disclaimer

Facets of this book originate from research papers published while I was a US Government federal employee. Reference to these papers is provided at the appropriate place in the text. However, no sentence in this book was taken verbatim from published papers. Rather, the material has been extensively reworked and refined to enhance pedagogical value for the book reader, thus going well beyond that appropriate for research papers or reports. Additionally, this book's writing occupied personal time and was not part of any official assigned government duty, and I made use of personal equipment for typesetting and producing figures.



A GUIDE TO THIS BOOK AND ITS STUDY

No book is an island, with this book generously making use of other books, review articles, research papers, and online tutorials. Many readers find value in studying a subject from a variety of perspectives, thus justifying the proliferation of books with overlapping subject matter. In an attempt to support this form of study, we commonly provide pointers to written and/or video presentations. Many more resources are available through a quick internet search.

There is no pretense that any reader will penetrate all topics in this book, nor read this book cover-to-cover. This recognition is particularly keen in a world where research and educational agendas often spread rather than focus our attention. Hence, an attempt has been made to facilitate picking up the book at a variety of starting points. For this purpose, each chapter and/or part is written in a reasonably self-contained manner even at the cost of modest redundancy. When redundancy becomes onerous, cross-referencing identifies allied material treated elsewhere in the book. Here we summarize the book's organization and offer some pointers on how to pursue its study.

Organization

This book is organized into parts according to their particular focus, with each chapter starting with a brief guide to the material and pointing to dependencies to other chapters. Some chapters focus on topics required for a basic understanding of the subject and offer exercises to test that understanding. Other chapters offer monograph style topics that further the foundations and exemplify applications largely taken from a selection of the author's research interests. Although this book is sizable, there are many topics omitted. These omissions reflect on the author's limited energy as well as the desire to keep the book from growing even larger.

MATHEMATICAL METHODS AND CONCEPTS

Part 1 presents a suite of mathematical topics that are of use for studying geophysical fluid mechanics. Some chapters concern topics readily found in applied mathematics or mathematical physics texts, though offered here with a distinctively geophysical perspective. Other chapters provide a grounding in mathematics rarely seen outside of geophysical fluid mechanics, in particular the maths of generalized vertical coordinates. The casual reader can skim these chapters without sacrificing too much from later chapters, assuming a working knowledge of Cartesian tensors (Chapter 1) as well as vector differential and integral calculus (Chapter 2). Where more unfamiliar math topics arise in later chapters, the reader is encouraged to return to these maths chapters to develop skills and to firm understanding. A variety of avenues for physical insights should be embraced by the practitioner of geophysical fluid mechanics, with mathematical acuity offering great rewards to the physicist.

GEOPHYSICAL PARTICLE MECHANICS

Part II provides a summary of Newtonian particle mechanics with particular emphasis on particles moving around a rotating sphere. This study exposes the physics of motion when viewed from the non-inertial reference frame of a terrestrial observer. By doing so, we encounter such topics as the Coriolis and centrifugal accelerations as well as spherical coordinates, all within the relatively simple context of point particle mechanics.

KINEMATICS OF FLUID FLOW

Mechanics is comprised of kinematics (the study of intrinsic properties of motion) and dynamics (the study of forces causing motion). In Part III we initiate a study of fluid mechanics by focusing on the kinematics of fluid flow and matter transport within that flow. Our treatment exposes both the Eulerian and Lagrangian viewpoints and emphasizes the variety of kinematic notions and tools key to describing fluid motion. We also encounter facets of material transport as described by the tracer equation, thus laying the foundation for *tracer mechanics*. Fluid flow, and the transport of matter within that flow, have many features fundamentally distinct from point particle and rigid body motion. We thus cultivate distinct tools and concepts that can take much practice to intellectually digest.

Quite often a course in fluid mechanics skims over fluid kinematics, preferring instead to focus mostly on dynamics. Indeed, some kinematic topics can seem a bit esoteric on first encounter, particularly the study of Lagrangian kinematics. However, an incomplete understanding of fluid kinematics can lead to many difficulties appreciating facets of fluid dynamics. The reader is thus encouraged to study the chapters here in detail, and to revisit the material as the need arises during later chapters. Doing so will nurture the brain-muscle and conceptual tools needed to deductively describe fluid motion.

THERMODYNAMICS

Part IV provides a relatively thorough introduction to equilibrium thermodynamics commonly found in undergraduate physics courses. We pay particular attention to the role of gravity in modifying the treatment of thermodynamic equilibrium states, with gravity an essential facet of geophysical fluids. In teaching this course, one may choose to skip this part of the book with minimal disruption to the logical flow. Even so, the subject matter is incredibly rich and central to understanding the fundamental nature of geophysical flows, thus forming a central pillar in our treatment of geophysical fluid mechanics. So the student is strongly encouraged to dive into these chapters.

DYNAMICS OF GEOPHYSICAL FLUID FLOW

Part V presents the core chapters of geophysical fluid dynamics as studied in this book. Within these chapters we study how Newton's laws of mechanics and the principles of thermodynamics are used to describe fluid motion on a rotating and gravitating sphere. We approach the subject by focusing on how forces that act on fluid elements lead to accelerations and thus to motion. These forces act both throughout the volume of a fluid element (*body forces* from gravity, Coriolis, and centrifugal) as well as on the boundary of a fluid element (*contact forces* from pressure and friction).

SHALLOW WATER MECHANICS

In Part VI we study the mechanics of a shallow water fluid, with a shallow water fluid comprised of hydrostatically balanced homogeneous fluid layers. The layers are also typically assumed to be immiscible, so that interactions between layers occur only via mechanical forces from pressure acting at the layer interfaces. The shallow water fluid allows us to focus on rotation and stratification without the complexities of vertically continuous stratification and thermodynamics. Many physical insights garnered by studying shallow water fluids extend to more realistic fluids, thus making the shallow water model very popular among theorists.

VORTICITY AND POTENTIAL VORTICITY

Part VII dives into the subject of vorticity and potential vorticity. This subject is rich and elegant, though it requires perhaps the most work for the student to penetrate given the heavy reliance on vector and integral calculus. Vorticity plays a role in the motion of all geophysical fluids since motion on a rotating planet provides a nonzero *planetary vorticity* even to fluids at rest on the planet. This feature of geophysical fluids contrasts to many other areas of fluid mechanics, where irrotational flows are commonly encountered. Potential vorticity is a strategically chosen component of the vorticity vector that marries mechanics (vorticity) to thermodynamics (stratification). Material conservation properties of potential vorticity are striking and render important constraints on fluid motion. Indeed, perhaps the most practical reason to study vorticity concerns the various constraints imposed on the flow moving on a rotating and gravitating sphere. These constraints provide conceptual insights and predictive power.

NEARLY GEOSTROPHIC BALANCED FLOWS

Part VIII introduces the topic of balanced models, with our attention limited to the shallow water and continuously stratified versions of quasi-geostrophy and planetary geostrophy. Balanced models generally remove the divergent motions associated with gravity waves, thus allowing a focus on the large-scale vortical motions. Balanced models have a rich history among theoretical geophysical fluid studies, providing insights into both laminar flows through planetary geostrophy, and turbulent flows through quasi-geostrophy.

WAVE MECHANICS

Part IX provides survey of geophysical waves and the various methods used to characterize these waves. We include waves not commonly included in a book on geophysical fluids, such as sound and capillary waves. We do so given their ubiquity in our everyday experience of the environment.

MECHANICS OF FLOW INSTABILITIES

Part

ELEMENTS OF GENERALIZED VERTICAL COORDINATES

Part XI brings together the various elements of a generalized vertical coordinate description of geophysical fluid mechanics. The chapters offer details of the maths, kinematics, dynamics, and applications. This material is central to many current research activities, including subgrid scale parameterizations and the design of numerical atmosphere and ocean models.

MECHANICS OF OCEAN SCALARS

Part XII dives into the mechanics of scalar fields as realized in the ocean, with our focus on active tracers (temperature and salinity), passive tracers, and buoyancy. Much of this study forms the basis of *tracer mechanics*, which has proven very important for the ocean since it is generally very difficult to measure vector fields such as velocity and vorticity, whereas tracer distributions are far more readily measured.

Written and spoken communication

To succeed in research and teaching requires one to master elements of both written and spoken communication. Here we offer a few pointers about the two.

CLEAR THINKING LEADS TO CLEAR COMMUNICATION

Clear communication is the sign of clear thinking. Some people communicate better in writing, where one has the opportunity to carefully organize thoughts and refine the writing style. Others are better at speaking, where spontaneous and interactive reflections and experience can bolster the clarity of a presentation. Both modes of communication are important in science and engineering.

As inspiration, for both clear and obscure, pick up one of your textbooks or class lecture notes and analyze the presentation for clarity. Where are you confused? Where is the material crystal clear? Then pick up a journal article and perform the same analysis. What do you like? What do you dislike? Then go to the internet and find a science or engineering lecture, old or new. What makes the speaker engaging and clear, or boring and obscure?

EMPATHY IS KEY

Empathy is a basic facet of effective communication and teaching. Place your mind inside that of an interested and smart reader or listener. Identify with their quest to understand what you wish to communicate. What assumptions are you making? Are the assumptions justified based on the audience? How compelling is your scientific story?

CLARITY HELPS, BUT SOME MATERIAL IS JUST TOUGH

Although poor communication hinders our ability to digest new ideas and concepts, it is also important to appreciate that some material is tough no matter how well it is communicated. We should aim to make a subject matter as simple as possible, but not simpler (paraphrasing Einstein). Furthermore, it sometimes takes one or two generations of teaching before some scientific material can be sufficiently digested to allow for the core conceptual nuggets to be revealed. As an example, try reading Newton or Maxwell's original works as compared to a modern presentation of Classical Mechanics or Electromagnetism. So we do strive for clear communication, but we cannot presume that clarity is sufficient to remove the struggles we all experience when learning.

Pointers on physics problem solving

Most people are not born with *a priori* physics problem solving skills. Rather, it takes extensive practice to develop the necessary brain muscle. Here are some general pointers to keep in mind when diving into a physics problem, whether it is for a class or the basis of a broader research question.

CHECK FOR DIMENSIONAL CONSISTENCY

The symbols we use in mathematical physics correspond to geometrical objects (e.g., points, vectors, tensors) describing a physical concept (e.g., position in space, velocity, temperature, angular momentum, stress). Hence, the symbols generally carry physical dimensions. The physical dimensions we are concerned with in this book are length (L), time (T), mass (M), and temperature. Physical dimensions of the equations must be self-consistent. For example, if one writes an equation

$$A = B, \quad (1)$$

where A and B have different physical dimensions, then the equation makes no sense physically. Something is wrong. Although not always sufficient to uncover errors, dimensional analysis is an incredibly powerful means to debug the maths.

CHECK FOR TENSORIAL CONSISTENCY

In the same way that mathematical equations in physics need to maintain dimensional consistency, they must also respect tensor rules. For example, the equation

$$A = B, \quad (2)$$

makes mathematical sense if A and B are both scalars. Likewise,

$$\mathbf{A} = \mathbf{B} \quad (3)$$

makes sense if \mathbf{A} and \mathbf{B} are both vectors. However, if both \mathbf{A} and \mathbf{B} are vectors, then the equation

$$\mathbf{A} = \nabla \cdot \mathbf{B} \quad (4)$$

does not make sense because the left hand side is a vector and the right hand side is a scalar. A more subtle example is when \mathbf{A} is a vector yet \mathbf{B} is an axial vector. In this case \mathbf{A} remains invariant under a change from right hand to left hand coordinates whereas \mathbf{B} flips sign. Maintaining basic tensorial rules can be considered the next level of sophistication beyond dimensional analysis.

USE WORDS AND PICTURES

It is important to explain the problem and solution using words and pictures. Hence, it is good practice to liberally sprinkle sentences in between the key equations for the purpose of explaining what the maths means using clear English. Here are some practical payoffs for this style of presentation.

- The process of explaining the maths using words and pictures requires one to dive deeper into the logic of the problem. Doing so often reveals weak points, incomplete or unmentioned assumptions, and errors. This process is a very important learning stage in preparing to stand in front of an audience to present results and to answer questions. It is a key facet of research and teaching.
- Physics teachers are often more forgiving of math errors if you convince the teacher that you have a sensible physical understanding of the problem. Plain English and pictures are very useful means for this purpose.

THERE IS OFTEN MORE THAN ONE PATH TO A SOLUTION

In physics, there is often more than one path to a solution. Pursuing distinct paths offers added physical and mathematical insight, exposes assumptions, and allows one to double-check a solution. Some of the most profound findings in physics came from pursuing distinct formulations. One example concerns the distinct formulation of mechanics offered by Newton (1642-1746), and then later by Lagrange (1736-1813) and then Hamilton (1805-1865). Had Lagrange or Hamilton rested on the merits of Newton's formulation, we may well have had a very different intellectual evolution of 19th and 20th century physics.



PRINCETON UNIVERSITY AOS 571 AND AOS 572

Princeton University's AOS 571 and AOS 572 are two courses that focus on geophysical fluid mechanics. The first semester, AOS 571, is concerned with developing conceptual and mathematical foundations of the subject by studying elemental features of planetary fluid motion, and by providing a mathematical physics basis for understanding these patterns. The second semester, AOS 572, makes use of the foundations from AOS 571 to study emergent phenomena arising from linear waves, linear instabilities, and turbulence.

DETAILS OF YOUR TEACHER AND THE COURSE

Dr. Stephen M. Griffies

SMG@princeton.edu

<https://stephengriffies.github.io/>

Classes are held in Guyot Hall on Monday and Wednesday (times TBD).

Q & A following the lecture on Wednesday

Zoom Q & A by appointment

Worked homeworks to be uploaded onto Canvas before class on the due-day.

Class materials and communication are enabled via Canvas.

Recorded class lectures are available via Canvas for AOS 571 from 2020.

Class structure and expectations

Our goal for this two-semester sequence of courses is develop an understanding of the basic physical theory, and in so doing to learn how to formulate and to solve problems. To help reach these goals, I have prepared extensive notes (now a book in progress) and we will work through selected chapters in class. You will be expected to read far more material than covered in class.

As with any other topic in physics, garnering an understanding and appreciation of geophysical fluid mechanics can require effort and practice. To help that process, you are expected to read the assigned material, work through the derivations, and hand-in homework exercises. You will have many opportunities to develop the necessary brain muscle assuming you maintain the discipline to keep up with the material. Please ask questions, preferably in class, when you are unsure of anything. Also, please strive to solve all of the assigned exercises, either alone or collaboratively with other students.

CULTIVATING A SAFE SPACE FOR HEALTHY LEARNING

A fundamental feature of any class concerns the atmosphere developed for learning. My aim as class teacher is to foster an inclusive, friendly, generous, patient, and non-judgmental space for

learning. Key principles that support this space include equity, diversity and inclusion, each of which are intrinsically valuable and an essential feature of ethical research and education. We also acknowledge and honor past generations whose efforts, some of which were garnered through force and oppression, have led to the rewarding environment that we now study and conduct research. It is our sincere hope that practicing the above principles will support present and future generations in a way that helps to heal past injustices. Cultivating this safe and grateful space supports deep learning while genuinely appreciating contributions from individuals without regard to race, ethnicity, culture, religion, sexual orientation, gender identity and expression, physical ability, age, socioeconomic status or nationality. As a participant in this space, we each celebrate diversity and nurture an inclusive and friendly community that is optimized for shared learning and mutual understanding.

For many, this class will require a tremendous amount of effort. It will require much focus and energy to master the material even for those with an established background. Regardless your background, talents, or interests, I am here to help. So please reach out if you are struggling. I also encourage you to develop working relations with your classmates. Homework exercises can be done collaboratively, and working with others offers great opportunities for learning.

Even if you prefer to work alone, I ask that you develop some form of a relation with one or more of your classmates. Part of this recommendation is based on the need to informally monitor our mutual health, particularly given that graduate school can be very stressful. Even so, it can be a time for building deep friendships and community as we share in the process of learning how to thrive as budding researchers and scholars.

CLASS LECTURES AND CLASS BOOK

The class lectures (with the exception of turbulence in AOS 572) closely follow selected material from [Griffies \(2023\)](#) available online. Prior to each class, you are expected to read through the assigned sections and view the assigned videos. During class we will discuss salient points from the readings and videos. To allow sufficient time for interactive discussion and questions, not all of the assigned reading material will be directly covered in class. Hence, you are expected to read and to understand more material than is covered on the chalkboard. Correspondingly, you are welcome to bring any questions related to the reading to the class, even if the material was not covered in class.

The pace of the lectures will be gauged by questions during the class and my sense for how well you are grokking the material. You are encouraged to follow lectures by having a copy of the class book on-hand, preferably electronically to conserve paper.

PLEASE DISCONNECT ELECTRONICS FROM INTERNET DURING CLASS

To support your learning and teaching experience, and those of your classmates, please ensure that you turn all electronic devices into "airplane mode" so that you are not tempted to divert attention to non-class issues. To get the most from the lectures and class time requires focused attention and active participation.

Some pointers for the problem sets

Here we consider some context for the class problem sets, which are an important part of learning the material.

AIM FOR A BALANCE BETWEEN BEING THOROUGH AND BRIEF

There is often a conflict between showing full mastery of a problem and keeping the solution write-up brief. In general, there is no need to re-derive equations already presented in the class lecture notes. Proper referencing of the equation is all that you need; i.e., tell me something like “starting from equation (X.YY) from the class notes.” Additionally, when presenting a derivation, you may choose to show just the key steps rather than all intermediate steps. Determining what is a “key” step is largely up to you, but it should be something you learn to do in time. Nonetheless, as per the previous pointer, you are encouraged to show more than one approach to a solution.

QUESTIONS FOR POINTS OF CLARIFICATION

Questions for points of clarification will be entertained if you feel the problem is ill-posed or if you are totally lost. Email is the most efficient means to communicate to me. Responses will generally be sent through Canvas so that all students can see the response, thus keeping everyone with the same information. Correspondingly, questions within 24 hours of the deadline are generally not entertained so to ensure that all students have time to see the response.

MISTAKES OFFER IMPORTANT OPPORTUNITIES FOR LEARNING

Everyone makes mistakes, some more than others. The toughest part is the self-imposed shame or embarrassment. Please try to keep a positive mind about your mistakes. As you will discover, mistakes offer significant opportunities for learning. I am a poster-child for this process!

So do not be overly anxious if you find many marks on your homeworks and exams. Rather, aim to use mistakes as learning opportunities. That is how life in academics (life in general!) works. Furthermore, be completely honest with yourself to candidly identify weaknesses. I will do my best to work personally with you if something remains uncertain or you feel there is a weakness in your skills that needs some extra help. Please seek help should you wish it. And finally, please do question my marks should you feel they are unfair or incorrect. I am prone to mistakes in my grading.

PRESENTATION OF THE SOLUTION: PLEASE USE LATEX

Please write clearly and legibly. I strongly encourage you to learn and use LATEX as this mark-up language is an indispensable tool for writing documents with or without mathematics. Indeed, LATEX is required for all AOS 572 assignments, so it is wise to start learning early in AOS 571. If you choose to hand-write your solutions, then please ensure that the equations and words are clearly written. In my experience, sloppy hand-writing generally leads to graders who are less forgiving of errors. You must convince the grader that you understand the solution and present the maths in a legible manner. Sound communication skills are key to being a good scientist or engineer.

DEADLINES ARE STRICT IN ORDER TO BE FAIR TO EVERYONE

Please do your best to be on time with handing in homeworks and exams, with disasters, personal tragedy, and significant accidents the only excuses for late assignments. Fairness to those meeting the deadlines is the fundamental reason to insist on this rule. Additionally, I generally aim to grade the homework soon after everyone hands it in, and then to provide solutions for quick feedback. Doing so helps to identify issues and obstacles sooner rather than later. If someone is given extra time, then that delays the feedback time, thus eating into the learning experience for everyone else.

In brief: a homework problem will receive zero credit if handed in late, with rare exceptions.

GENERAL RUBRIC FOR MARKING YOUR WORK

Problem sets are marked using the following general rules, with grading less forgiving as the class progresses through the semester. The following mistakes are marked by an increasing amount moving through the list.

POINTS ABOUT GRADING YOUR WORK

1. SIGN ERRORS: Sign errors are a nuisance. We all must spend time to uncover them. One means of detecting errors is to try explaining the maths to yourself or someone else. Does the result make sense? If not, then perhaps there is a sign error. I am generally not too upset with sign errors if they have minimal physical relevance. But when they indicate a physical misconception then I will mark it more harshly.
2. MATH ERRORS: Math errors, such as those associated with basic calculus mistakes, are generally marked.
3. DIMENSIONAL AND TENSORIAL ERRORS: I am relatively unforgiving of dimensional mistakes and tensorial inconsistencies.
4. PHYSICALLY MISSING THE POINT: Evidence of physically missing the point will generally invoke the most negative marks depending on the depth of the misconception. The best way to convince me you grasp the basic physics is to use words and pictures. If the maths is missing or totally wrong, but you present some sensible words and pictures, then that will help earn some credit.

Grades for AOS 571

AOS 571 CLASS GRADE = PROBLEM SETS (75%) + FINAL EXAM (25%)

For AOS 571, there are two areas where grades are earned: problem sets and take-home final exam. Additionally, I ask that everyone aim to attend all classes and participate by asking questions or sharing your insights during discussions.

Worked problem sets are due on Canvas prior to the start of class when they are due. Each problem set normally is allocated one week for completion, unless otherwise noted. Students can make use of any resources for solving problem sets, including other people. Clarification of questions can also be obtained via email to me. If you find a solution from a source other than your own head, then be sure that you fully understand both the essence and the detail of the solution. Although you are encouraged to discuss the problems with other students, you are cheating yourself if you merely parrot another person's answer without fully grokking it yourself.

There is no pretense that the exercises offered in class are clearly formulated. Indeed, a certain degree of ambiguity reflects the *status quo* in research, where formulating a novel and insightful question is generally the most difficult part of the research process. Additionally, the solutions may not be 100% correct or ideal from a pedagogical perspective. Rather, they represent a work in progress. If mistakes or ambiguities are found, then please share your questions and concerns.

There is a takehome final exam during exam period. You are asked to do the work as a solo student, with no help or consultation from another human. However, you can make use of

books, notes, online resources, etc. The questions are generally taken from published papers with relevant references provided to the student.

Grades for AOS 572

AOS 572 CLASS GRADE = PROBLEM SETS (60%) + FINAL REPORT/PRESENTATION (40%)

The style of the problem sets is just as in AOS 571, but with one important addition (except for very special cases):

ALL PROBLEM SETS MUST BE PREPARED USING L^AT_EX.

This requirement supports your skills in preparing scientific documents using L^AT_EX, preferably making use of your Princeton Overleaf account. It will also prepare you for the written report.

Rather than a final exam, you will prepare a final project for AOS 572. The project consists of a written report and a tutorial presentation. The topic of the final project will be mutually agreed upon and directly related to waves, instabilities, and/or turbulence, with topic chosen no later than mid-term. The topic either is one that is *not* covered in the class, or one that you pursue in much more depth than covered in class. You will be graded on your mastery of the subject, your skills at pedagogically communicating the subject using written and oral methods, and your ability to answer fair questions from anyone in the audience.

Here are further details for the project.

- WRITTEN REPORT = 25% OF CLASS GRADE

1. The report surveys the physics and maths of the chosen topic in a manner allowing you to teach it to AOS 572 students. There should be deductive/pedagogical math derivations along with physical principles and connections to topics in other AOS classes. Citations should be given for all sources.
2. The report is *not* original research. Rather, it represents an intellectually digested view of a topic from the literature that is pedagogically connected to material covered in the class.
3. The report must be typeset in L^AT_EX using Overleaf and using the provided L^AT_EX template.
4. The report should be no less than 20 pages (excluding references), and no more than 30 pages total.
5. A thorough report draft (via Overleaf) is due no later than one week prior to the oral presentation. I will give brief feedback on your progress that you should address for the final draft.
6. Focus on the report writing starting soon after the middle of the semester. Homework assignments will lighten then (though not vanish) to allow time for writing.
7. Feel free to discuss with others the content of the report. However, 100% of the writing and presentation must originate from you. Do not use any artificial intelligence for generating your report.
8. Refer to [Mermin 1989](#) and [Griffies et al \(2013\)](#) for specific pointers on writing styles for science.
9. Grading rubric
 - (a) intro/background (20)

- (b) concepts/methods (60)
- (c) pedagogy/clarity/style (20)

- ORAL PRESENTATION = 15% OF CLASS GRADE

1. The presentation is to the full class (and any interested visitors) using a chalkboard with zero electronic media (i.e., no slides or videos). Eliminating all electronic media encourages you to focus your time preparing the intellectual content of the report and the presentation rather than tweaking the presentation aesthetics. It also gives you experience working on the chalkboard rather than “hiding” behind electronic slides.
2. The presentation should be designed to last 15 minutes without interruptions. It is not simple to stand in front of a class and convey information. So please practice the presentation beforehand to optimize your time and clarity.
3. Your aim is to teach the class one or two items from your report. Teaching requires a tremendous amount of study and practice. Be humble at what you can reasonably cover in 15 minutes. Practice your oral presentation either alone or with others.
4. After your presentation, 15 minutes will be devoted to questions from students, visitors, and teacher.
5. All students must be present for all presentations.

- GRADING RUBRIC

1. intro/background (20)
2. concepts/methods (20)
3. pedagogy/speaking skills (20)
4. understanding: presentation (20)
5. understanding: questions (20)

Course material and strategies for thriving

The course material consists of a class book plus a selection of online videos. Ideally, the book material is to be read and the videos viewed **prior to each class**. Salient points related to the material will be presented during class on the chalkboard, along with further discussion and questions. We will *not* cover all the material in class that is expected to be learned as part of the reading assignments and problem sets. Since there is no laboratory portion of this class, it is very important to view the various videos linked to each lecture. More generally, you are strongly encouraged to peruse [this library of classic videos](#) that have stood the test of time for their pedagogy on various topics in fluid mechanics. Additionally, [the Homsky Multi-media Fluid Mechanics](#) lectures is an incredibly valuable tool for basic fluid mechanics concepts. The full content of Homsky is available online through the Princeton University library.

STRATEGIES FOR THRIVING IN THIS COURSE

- ESSENTIALS FROM PROF. BAZETT FOR THE START OF THE SEMESTER
 - View [this 12-minute lecture](#) on study tips.
 - View [this 12-minute lecture](#) on how to learn effectively.
 - View [this 19-minute lecture](#) on how to write L^AT_EX documents using Overleaf.
- PRIOR TO EACH CLASS
 - Review material from previous lecture (5 to 10 minutes).
 - View assigned videos (5 to 45 minutes).
 - Read assigned class book sections (30-120 minutes).
- AFTER EACH CLASS
 - Reread class book material and review assigned videos.
 - Identify questions for class discussion or during Q & A session.
 - As needed, view recorded class lecture from 2020 to fill in gaps.
 - Work assigned exercises alone and then gather with classmates to discuss and complete.
- QUESTIONS: Address questions by reaching out during class, after class, during office hours, during group gatherings, or via Ed Discussion. There are no silly questions!

AOS 571 course outline

Here we offer specifics of the course material covered during AOS 571. There are 24 class lecture periods. Most of the following topics take a full class, though some are shorter so that there are a total of 25 listed topics.

0. Lecture-0 consists of pre-class study of the course introduction and mathematics refresher. This material will be assumed when starting the first lecture, so please be prepared. However, if there is a general consensus, we can have extra sessions on this material during the in-person Q & A.
 - Watch this [9-minute video](#) from Prof. N. Hall introducing some basic images from terrestrial fluid flows.
 - Watch this [16-minute video](#) from 3Blue1Brown on the divergence and curl operations with examples taken from fluid mechanics.
 - Read the preface to this book.
 - Read Chapter 1 on cartesian tensors.
 - Read Chapter 2 on vector calculus.
 - Read Chapter 10 on Newtonian particle mechanics.
 - Read Chapter 13 on the continuum hypothesis used for describing fluids as a continuous media.
1. Geophysical particle mechanics

- Chapter 11: kinematics of a particle moving around a rotating sphere, including position, velocity, acceleration, Cartesian and spherical coordinates, rotating reference frame, Coriolis acceleration, planetary centrifugal acceleration
 - Chapter 11: dynamics of a particle moving around a rotating sphere using Newton's equation of motion, rotating reference frames, gravitational geopotential
 - [Watch the first 5-minutes from this UCLA Spin Lab video](#) on Coriolis effect.
 - Exercises 11.1, 11.3, 11.4, 11.6.
2. Symmetries, conservation laws, and constrained motion
- Chapter 12: mechanical energy, potential momentum, inertial oscillations, axial angular momentum
 - Exercise 12.1
3. Fluid kinematics
- Chapter 14: Fluid kinematics, Eulerian and Lagrangian descriptions, Galilean invariance, material time derivative, flow lines
 - [4-minute video on Eulerian and Lagrangian descriptions](#) from Prof. Hogg
 - [27-minute video on Eulerian and Lagrangian descriptions](#) from Prof. Lumley.
 - Exercises 14.1, 14.2
4. Mass conservation
- Chapter 16: continuity equation, mass budget for fluid elements and finite regions, kinematic boundary conditions
 - [5-minute video on mass conservation](#) from Prof. Hogg.
 - Exercises 16.1, 16.2, 16.4
5. Tracer conservation
- Chapter 17: barycentric velocity, tracer equation, budgets for infinitesimal fluid elements, budgets for finite fluid regions, Leibniz-Reynolds transport theorem, boundary conditions
 - Exercise 17.1
6. Kinematics of non-divergent flows
- Chapter 18: scalar streamfunction, vector streamfunction, area and volume conservation, meridional-depth overturning circulation
 - [4-minute video on streamlines](#) from Prof. Hogg.
 - Exercises 18.2, 18.3, 18.4, 18.7
7. Momentum dynamics
- Chapter 21: momentum dynamics, accelerations, contact forces, body forces, special forms of the momentum equation, axial angular momentum, acoustic waves
 - [6-minute video on momentum](#) from Prof. Hogg.
 - Exercises 21.2 and 21.6

8. Stress in fluids

- Chapter 22: stresses and the stress tensor, linear momentum budget, relating stress to strain, form stress, boundary conditions
- [2.5-minute video on stress and strain](#) from Prof. Hogg.
- [8-minute video on stress](#) from Prof. Hogg.
- Exercise 22.1

9. Energy dynamics and filtered equations

- Chapter 23: kinetic energy, gravitational potential energy
- [8-minute video on hydrostatic pressure](#) from Prof. Hogg.
- Exercises 23.2, 23.3

10. Pressure in fluids

- Chapter 24: primitive equations, hydrostatic approximation, hydrostatic pressure
- Chapter 25: pressure form stress
- Exercises 24.1, 24.2

11. Mechanics of the Boussinesq ocean

- Chapter 26: oceanic Boussinesq approximation, hydrostatic scaling, pressure and non-divergent velocity
- Exercises 26.4, 26.5

12. Buoyancy

- Chapter 27: Archimedes' principle, buoyancy, stratification, gravitational stability, mass density for perfect and realistic fluids
- [49-minute video from Prof. Lewin](#) for an overview of buoyancy as well as other features of fluid mechanics.
- Exercises 27.1, 27.4

13. Geostrophic mechanics

- Chapter 28: Rossby number, geostrophy, planetary geostrophy, Taylor-Proudman, thermal wind, isopycnal form stress
- [30-minute video from Prof. Fultz](#) for an overview of rotating fluids.
- [4-minute video from the UCLA SpinLab](#) for examples of Taylor columns.
- Exercises 28.1, 28.2

14. Horizontal flow using natural coordinates

- Chapter 29: natural coordinates; centripetal, centrifugal, and Coriolis accelerations; exact geostrophic flow; inertial motion of fluid particles; cyclostrophic balance; gradient wind balance

15. Ekman mechanics

- Chapter 30 on Ekman mechanics: natural coordinates, spiral motion across isobars, non-dimensionalization and the Ekman number, net mass transport
 - Start around the 23-minute mark [of this video from Prof. Fultz](#) for his discussion of Ekman layers.
 - Exercises 30.1, 30.2
16. Formulation of shallow water models
- Chapter 32: thickness equation, momentum equation, reduced gravity model, stacked shallow water layers, shallow water layer in a rotating tank
 - [30-minute video](#) on shallow water model from Prof. Hall.
 - Exercises 32.1, 32.5
17. Shallow water dynamics
- Chapter 33: geostrophy, thermal wind, form stress, mechanical energy including available potential energy
 - Exercises 33.2, 33.7, 33.8
18. Vorticity and circulation
- Chapter 34: vorticity and circulation
 - [23-minute video on vorticity](#) from Prof. Shapiro
 - Exercises 34.1, 34.2, 34.3, 34.4, 34.5.
19. Two-dimensional non-divergent barotropic vorticity model
- Chapter 35: two-dimensional barotropic vorticity model; properties of this model.
 - Exercises 35.2, 35.3
20. Shallow water vorticity and potential vorticity
- Chapter 36: shallow water vorticity and potential vorticity
 - Exercises 36.3, 36.4
21. Vorticity mechanics
- Chapter 37: vortex lines and tubes, Kelvin's circulation theorem, mechanics of baroclinicity, stretching and twisting of vortex lines, β -effect
 - [21-minute video on vorticity](#) from Prof. Shapiro.
 - [5-minute video on vortex rings and Helmholtz's theorems](#) from the Physics Girl.
 - Exercises 37.3, 37.4, 37.5, 37.8
22. Potential vorticity mechanics
- Chapter 38: Ertel potential vorticity, PV evolution with friction and other irreversible processes.
 - Exercise 38.1
23. Balanced models I (single layer)

- Chapter 40: Buckingham's II theorem, asymptotic expansion in terms of small Rossby number, shallow water planetary geostrophy and quasi-geostrophy

24. Balanced models II (continuous stratification)

- Chapter 41: asymptotic derivation of continuously stratified planetary geostrophy and properties of these equations.
- Chapter 42: asymptotic derivation of continuously stratified quas-geostrophy and properties of these equations.

25. Advection and diffusion

- Chapter 61: advection maths and physics; diffusion maths and physics

AOS 572 course outline

Here we offer specifics of the course material covered during AOS 572, which is roughly organized as 1/2-waves, 1/3-instabilities, and 1/6-turbulence.

1. Fourier analysis

- Chapter 5: Fourier analysis
- [This video, also from 3Blue1Brown](#) provides a visual introduction to Fourier transforms.
- [This video from 3Blue1Brown](#) provides a visual introduction to Fourier series.
- Exercise 5.1

2. Wave kinematics

- Chapter 43: wave kinematics
- Sections 6.1 and 6.2 of [Vallis \(2017\)](#)
- Appendix B of [Cushman-Roisin and Beckers \(2011\)](#)
- Exercises 43.1, 43.2

3. Acoustic waves

- Chapter 44
- [The second half of this video](#) offers an introduction to acoustic waves.
- Exercises 44.1, 44.2

4. Surface gravity and capillary waves

- Chapter 45
- Section 7.1 of [Vallis \(2017\)](#)
- Exercises 45.1, 45.2, 45.4, 45.6

5. Inertial waves and intro to Rossby waves

- Chapter 46
- Chapter 47
- Section 6.4 of [Vallis \(2017\)](#)
- Exercise 47.1

6. Rossby waves I (horizontally non-divergent barotropic model)

- Chapter 47
- Section 6.4 of [Vallis \(2017\)](#)

7. Rossby waves II (horizontally non-divergent barotropic model)

- Chapter 47
- Section 6.4 of [Vallis \(2017\)](#)

8. Shallow water waves I

- Chapter 48

- [The first half of this video](#) offers an introduction to shallow water waves.
- Exercises [48.1](#), [48.3](#), [48.4](#), [48.5](#).

9. Shallow water waves II

- Chapter [48](#)
- [14-minute video on gravity waves](#) from Prof. N. Hall.
- Exercise [48.6](#)

10. Internal gravity waves I

- Chapter [49](#)
- Lectures 7 and 8 of [Pedlosky \(2003\)](#)
- Chapter 13 of [Cushman-Roisin and Beckers \(2011\)](#)
- Chapter 7 of [Vallis \(2017\)](#)
- [Tank experiment](#) from Prof. Peter Rhines' lab
- [Simulations](#) from Prof. Dale Durran
- Exercise [49.1](#)

11. Internal gravity waves II

- Chapter [49](#)
- Lecture 10 of [Pedlosky \(2003\)](#)
- Chapter 13 of [Cushman-Roisin and Beckers \(2011\)](#)
- Chapter 7 of [Vallis \(2017\)](#)

12. Internal gravity waves III

- Chapter [49](#)
- Lecture 9 of [Pedlosky \(2003\)](#)
- Chapter 7 of [Vallis \(2017\)](#)

13. Internal inertia-gravity waves

- Chapter [49](#)
- Lecture 11 of [Pedlosky \(2003\)](#)
- Chapter 7 of [Vallis \(2017\)](#)
- Exercises [49.2](#) and [49.3](#)

14. Centrifugal and inertial instabilities

- Chapter [50](#)
- Sections 17.1 and 17.2 of [Cushman-Roisin and Beckers \(2011\)](#)
- Exercise [50.1](#)

15. Symmetric instability

- Chapter [50](#)
- Section 17.2 of [Cushman-Roisin and Beckers \(2011\)](#)

- Exercise 50.2 and 50.3
16. Rayleigh-Taylor and Kelvin-Helmholtz instability
- Chapter 51
 - Sections 9.1 of *Vallis* (2017)
 - Wikipedia for Rayleigh-Taylor
 - Wikipedia for Kelvin-Helmholz
17. Horizontal shear instability I
- Section 47.5
 - Chapter 52
 - Section 3.12 of *Smythe and Carpenter* (2019)
 - Sections 9.2-9.3 of *Vallis* (2017)
 - Chapter 10 of *Cushman-Roisin and Beckers* (2011)
18. Horizontal shear instability II
- Chapter 52
 - Section 3.12 of *Smythe and Carpenter* (2019)
 - Sections 9.2-9.3 of *Vallis* (2017)
 - Chapter 10 of *Cushman-Roisin and Beckers* (2011)
 - Exercise 52.1
19. Stratified shear instability
- Chapter 52
 - Section 11.7 of *Kundu et al.* (2016)
 - Sections 14.1 and 14.3 of *Cushman-Roisin and Beckers* (2011)
 - Chapter 4 of *Smythe and Carpenter* (2019)
20. Baroclinic instability I
- Chapter 8 of *Smythe and Carpenter* (2019)
 - Sections 9.4-9.8 of *Vallis* (2017)
 - Sections 17.3-17.6 of *Cushman-Roisin and Beckers* (2011)
 - Rotating tank experiment from Prof. Wing
 - Rotating tank experiment from MIT
21. Baroclinic instability II
- Chapter 8 of *Smythe and Carpenter* (2019)
 - Sections 9.4-9.8 of *Vallis* (2017)
 - Sections 17.3-17.6 of *Cushman-Roisin and Beckers* (2011)
22. Incompressible turbulence I
- Chapters 1 and 3 of *Davidson* (2015)

- Section 11.1 and 11.2 of *Vallis* (2017)
- Chapter 12 of *Smythe and Carpenter* (2019)
- Turbulence and the 5/3 spectrum from 3Blue1Brown
- Rayleigh-Bernard convection generated turbulence as simulated using Dedelas
- 3d turbulence video from Prof. Stewart
- MicroHH simulations

23. Incompressible turbulence II

- Sections 5.1 and 5.2 of *Cushman-Roisin and Beckers* (2011)
- Sections 11.1 and 11.2 of *Vallis* (2017)
- Section 12.5 of *Kundu et al.* (2016)

24. Two-dimensional turbulence

- Section 11.3 of *Vallis* (2017)
- Chapter 10 of *Davidson* (2015)
- Decaying two dimensional turbulence
- Forced two dimensional turbulence from Prof. Ed Zaron
- Two dimensional turbulence and cascade from Prof. Ryan Abernathey
- Shallow water turbulence from Prof. Ed Zaron

25. Geostrophic turbulence

- Chapter 12 of *Vallis* (2017)
- Geostrophic turbulence from Prof. Bill Young
- CM2.6 surface temperature simulation
- Neverworld2 shallow water simulations



LIST OF SYMBOLS

Many symbols encountered in this book are defined local to their usage and are not found far outside of that location. Many other symbols appear in a variety of places and are included in the following list that offers a quick reminder of their meaning. Symbols are here categorized according to whether they are English (Latin-based), Greek, or mathematical operators.

NON-DIMENSIONAL NUMBERS

SYMBOL	MEANING
Bu	Burger number: $Bu = (\text{deformation radius}/\text{horizontal length scale of flow})^2 = (L_d/L)^2$
Ek	Ekman number: $Ek = \text{friction acceleration from vertical shears divided by coriolis acceleration}$
Fr	Froude number: $Fr = \text{fluid particle speed divided by wave speed}$
Ge	Geostrophic number: $Ge = \text{Coriolis acceleration divided by pressure gradient acceleration}$
Kn	Knudsen number: $Kn = \text{molecular mean free path divided by macroscopic length scale}$
Ma	Mach number: $Ma = \text{fluid particle speed divided by sound speed}$
Re	Reynolds number: $Re = \text{inertial acceleration divided by frictional acceleration} = U L/\nu$
Ri	Richardson number: $Ri = \text{squared buoyancy frequency divided by squared vertical shear}$
Ro	Rossby number: $Ro = \text{inertial acceleration divided by Coriolis acceleration} = U/(f L)$

LATIN SYMBOLS: PART I

SYMBOL	MEANING
\mathbb{A}	skew diffusion tensor: $\mathbb{A}_{mn} = -\mathbb{A}_{nm}$
A^v	Avogadro's number: $A^v = 6.0222 \times 10^{23} \text{ mole}^{-1}$
b	Archimidean buoyancy with $b > 0$ for relatively light fluid: $b = -g(\rho - \rho_0)/\rho_0$
c_s	sound speed: $c_s^{-2} = [\partial\rho/\partial p]_{\Theta,S}$
c_p	heat capacity at constant pressure: $c_p = [\partial\mathcal{H}/\partial T]_{p,C}$
C_p	wave phase speed
\mathbf{c}_p	wave phase velocity: $\mathbf{c}_p = C_p \hat{\mathbf{k}}$
\mathbf{c}_g	wave group velocity: $\mathbf{c}_g = \nabla_{\mathbf{k}}\varpi(\mathbf{k})$
C	tracer concentration = mass of tracer per mass of fluid = tracer mass fraction
C_D	dimensionless bottom drag coefficient: $C_D > 0$
\mathcal{C}	circulation of velocity around the boundary of a surface $\mathcal{C} \equiv \oint_{\partial\mathcal{S}} \mathbf{v} \cdot d\mathbf{r}$
\mathcal{E}	total energy per mass of a fluid element = sum of internal plus mechanical energies
$\hat{\mathbf{e}}_a$	basis vectors for a chosen coordinate system, with index $a = 1, 2, 3$ for 3-dimensional space.
f	Coriolis parameter, also the planetary vorticity: $f = 2\Omega \sin\phi$
f_0	Coriolis parameter at a particular latitude: $f_0 = 2\Omega \sin\phi_0$
F	frictional acceleration
F_i^m	deformation tensor; also transformation matrix between material and position coordinates
$G = G^{\text{grav}}$	Newton's gravitational constant: $G = 6.674 \times 10^{-11} \text{ N m}^2 \text{ kg}^{-2} = 6.674 \times 10^{-11} \text{ m}^3 \text{ kg}^{-1} \text{ s}^{-2}$
$G(\mathbf{x} \mathbf{x}_0)$	Green's function with \mathbf{x} the observation point (or field point) and \mathbf{x}_0 the source point
$\mathcal{G}(\mathbf{x} \mathbf{x}_0)$	Free space Green's function; i.e., the Green's function without boundaries
g	metric tensor
\mathcal{G}	Gibbs potential per mass of a fluid element
g	effective gravitational acceleration from central gravity + planetary centrifugal: $g \approx 9.8 \text{ m s}^{-2}$
g^r	reduced gravity defined between two shallow water layers: $g_{k+1/2}^r = g(\rho_{k+1} - \rho_k)/\rho_{\text{ref}} \ll g$
h_k	layer thickness for a shallow water fluid: $h_k = \eta_{k-1/2} - \eta_{k+1/2} = \delta_k \eta_{k-1/2}$
h	layer thickness for a continuously stratified fluid: $h = \bar{h} \delta\sigma$
h	specific thickness for a generalized vertical coordinate: $h = \partial z/\partial\sigma = 1/(\partial\sigma/\partial z)$
$\mathcal{H}(x)$	Heaviside step function: $\mathcal{H}(x) = 0$ for $x < 0$ whereas $\mathcal{H}(x) = 1$ for $x > 0$
H	vertical length scale of the flow under consideration
H	sometimes used as depth of the ocean bottom: $z = -H(x, y) = \eta_b(x, y)$
\mathcal{H}	enthalpy per mass of a fluid element
\mathcal{I}	internal energy per mass of a fluid element
i	$i = \sqrt{-1}$ used for imaginary numbers
$\text{Im}[\cdot]$	imaginary part of a complex number; e.g., $\text{Im}[e^{-i\omega t}] = -\sin(\omega t)$
J	tracer flux; for material tracers the dimensions are mass per time per area
\mathbf{k}	wavevector (dimensions inverse length) for a wave of wavelength $\Lambda = 2\pi/ \mathbf{k} $
$\hat{\mathbf{k}}$	unit vector in the direction of a wave: $\mathbf{k} = \hat{\mathbf{k}} \mathbf{k} $ (as distinct from the vertical unit vector, $\hat{\mathbf{z}}$)
$ \mathbf{k} $	wavenumber: $ \mathbf{k} = 2\pi/\Lambda$
K	kinetic energy for a point particle of mass m : $K = m \mathbf{V} \cdot \mathbf{V}/2$
\mathcal{K}	kinetic energy per mass of a fluid element arising from macroscopic motion: $\mathcal{K} = \mathbf{v} \cdot \mathbf{v}/2$
\mathcal{K}^{hyd}	kinetic energy per mass for an approximate hydrostatic flow: $\mathcal{K}^{\text{hyd}} = \mathbf{u} \cdot \mathbf{u}/2$
\mathcal{K}^{sw}	kinetic energy per horizontal area for a shallow water layer: $\mathcal{K}^{\text{sw}} = \rho h \mathbf{u} \cdot \mathbf{u}/2$
\mathbb{K}	diffusivity tensor: positive and symmetric second order tensor parameterizing diffusive mixing
k	integer index to label a layer in a shallow water model with $k = 1, N$ layers ($k = 1$ is top layer)
k_B	Boltzmann constant: $k_B = 1.3806 \times 10^{-23} \text{ m}^2 \text{ kg s}^{-2} \text{ K}^{-1}$
L	horizontal length scale of the flow under consideration
L_d	deformation radius: (a) shallow water $L_d = \sqrt{g H}/f$; (b) continuous internal $L_d = H N/f$
m	mechanical energy per mass of a fluid element arising from macroscopic motion
m^{sw}	mechanical energy per area of a shallow water fluid column: $m^{\text{sw}} = \mathcal{K}^{\text{sw}} + \mathcal{P}^{\text{sw}}$
M^{air}	mass per mole of air: $M^{\text{air}} = 28.8 \times 10^{-3} \text{ kg mole}^{-1}$
M_k^{dyn}	Montgomery potential for a shallow water layer: $M_k^{\text{dyn}} = \sum_{j=0}^{k-1} g_{j+1/2}^r \eta_{j+1/2}$
N	buoyancy frequency
\mathcal{O}	order of magnitude

LATIN SYMBOLS: PART II

SYMBOL	MEANING
p	pressure at a point in the fluid
p_a	pressure applied to the ocean surface from the atmosphere or cryosphere
p_b	pressure at the bottom of a fluid column, at the fluid-solid earth interface
p_{slp}	sea level pressure with an area average, $\langle p_{slp} \rangle = 101.325 \times 10^3 \text{ N m}^{-2}$
$p_{k-1/2}$	hydrostatic pressure at the layer interface with vertical position $z = \eta_{k-1/2}$
p_k^{dyn}	dynamic pressure in a shallow water layer: $p_k^{dyn} = \rho_{ref} \sum_{j=0}^{k-1} g_j^f \eta_{j+1/2}$
P_k	pressure integrated over a shallow water layer: $P_k \equiv \int_{\eta_{k+1/2}}^{\eta_{k-1/2}} p_k(z) dz = h_k (g \rho_k h_k / 2 + p_{k-1/2})$
\mathcal{P}_k^{sw}	potential energy per horizontal area for a shallow water fluid: $\mathcal{P}_k^{sw} = g \rho_k \int_{\eta_{k+1/2}}^{\eta_{k-1/2}} z dz$
\mathcal{P}	phase of a wave
Q	potential vorticity for continuously stratified (Ertel PV) or shallow water (Rossby PV)
q	quasi-geostrophic potential vorticity either for a continuous fluid or shallow water fluid
Q_m	mass flux (mass per horizontal area per time) across ocean surface: $Q_m > 0$ enters ocean
\mathcal{Q}_m	mass flux (mass per surface area per time) across ocean surface: $\mathcal{Q}_m dS = Q_m dA$
Q_C	turbulent tracer flux (tracer per horiz area per time) across ocean surface: $Q_C > 0$ enters ocean
\mathcal{Q}_C	turbulent tracer flux (tracer per surface area per time) across ocean surface: $\mathcal{Q}_C dS = Q_C dA$
r	radial distance of a point relative to an origin
\mathbb{R}	rotation tensor: $2 \mathbb{R}_{mn} = \partial_n v_m - \partial_m v_n = -2 \mathbb{R}_{nm}$
\mathbb{R}^1	real number line
\mathbb{R}^2	two-dimensional space of real numbers
\mathbb{R}^3	three-dimensional space of real numbers
R	radius of a sphere
R_e	radius of sphere whose volume approximates that of the earth: $R_e = 6.371 \times 10^6 \text{ m}$
R^g	universal gas constant: $R^g = 8.314 \text{ J mole}^{-1} \text{ K}^{-1} = 8.314 \text{ kg m}^2 \text{ s}^{-2} \text{ mole}^{-1} \text{ K}^{-1}$
R^{air}	specific gas constant for air: $R^{\text{air}} = R^g / M^{\text{air}} = 2.938 \times 10^2 \text{ m}^2 \text{ s}^{-2} \text{ K}^{-1}$
\mathcal{R}	arbitrary region or manifold
$\text{Re}[\cdot]$	real part of a complex number; e.g., $\text{Re}[e^{-i\omega t}] = \cos(\omega t)$
S	entropy per mass of a fluid element
\mathbb{S}	rate of strain tensor: $2 \mathbb{S}_{mn} = \partial_n v_m + \partial_m v_n$
\mathbb{S}^{dev}	deviatoric rate of strain tensor: $\mathbb{S}_{mn}^{\text{dev}} = \mathbb{S}_{mn} - \delta_{mn} \mathbb{S}_{qq} / 3$
S	salt concentration = mass of salt in a fluid element per mass of seawater
S	Absolute Salinity, generically referred to as salinity: $S = 1000 \mathbb{S}$
s	expression for a generic surface: $s = s(x, y, z, t)$.
s	arc-length along a curve $\mathbf{x}(s)$ with infinitesimal increment $ds = \sqrt{d\mathbf{x} \cdot d\mathbf{x}}$
\hat{s}	unit tangent vector to a curve, also written as $\hat{s} = \hat{\mathbf{t}}$ (see below)
sgn	sign function related to Heaviside step function via $\text{sgn}(x) = 2 \mathcal{H}(x) - 1$
T	absolute thermodynamic <i>in situ</i> temperature (Kelvin if in a thermodynamic equation)
\mathbb{T}	stress tensor
$\mathbb{T}^{\text{kinetic}}$	kinetic stress tensor: $\mathbb{T}^{\text{kinetic}} = -\rho \mathbf{v} \otimes \mathbf{v}$
$\mathbb{T}^{\text{sw kinetic}}$	kinetic stress tensor for shallow water fluid: $\mathbb{T}^{\text{sw kinetic}} = -\rho \mathbf{u} \otimes \mathbf{u}$
t	time (universal Newtonian time)
\hat{t}	unit tangent vector to a curve: $\hat{t} = d\mathbf{x}/ds$, where s is the arc-length so that $ds = \sqrt{d\mathbf{x} \cdot d\mathbf{x}}$
\mathbf{u}	horizontal velocity of a fluid element: $\mathbf{u} = \hat{\mathbf{x}} u + \hat{\mathbf{y}} v$
U	horizontal velocity scale of the flow under consideration
\mathbf{U}	depth integrated horizontal velocity: $\mathbf{U} = \int_{\eta_b}^{\eta} \mathbf{u} dz$
\mathbf{v}	velocity of a fluid element: $\mathbf{v} = D\mathbf{x}/Dt$ with Cartesian component $\mathbf{v} = \hat{\mathbf{x}} u + \hat{\mathbf{y}} v + \hat{\mathbf{z}} w$
\mathbf{v}_a	velocity of a fluid element measured in the inertial or absolute reference frame: $\mathbf{v}_a = \mathbf{v} + \boldsymbol{\Omega} \times \mathbf{x}$
W	vertical velocity scale of the flow under consideration
w	vertical component to the velocity: $w = Dz/Dt$
w^{dia}	dia-surface flux = volume per <i>horizontal area</i> per time across a σ -surface: $w^{\text{dia}} = (1/ \nabla \sigma) \dot{\sigma}$
$w^{(\dot{\sigma})}$	dia-surface velocity = volume per <i>horizontal area</i> per time across a σ surface: $w^{(\dot{\sigma})} = (\partial z/\partial \sigma) \dot{\sigma}$
(x, y, z)	triplet of Cartesian coordinates
\mathbf{x}	spatial position using a Cartesian representation: $\mathbf{x} = \hat{\mathbf{x}} x + \hat{\mathbf{y}} y + \hat{\mathbf{z}} z$
$(\hat{\mathbf{x}}, \hat{\mathbf{y}}, \hat{\mathbf{z}})$	triplet of Cartesian unit vectors oriented in a righthand sense
z_σ	specific thickness for a generalized vertical coordinate: $z_\sigma = \partial z / \partial \sigma = \kappa$

GREEK SYMBOLS

SYMBOL	MEANING
α	thermal expansion: $\alpha = -\rho^{-1} \partial \rho / \partial \theta$ or $\alpha = -\rho^{-1} \partial \rho / \partial \Theta$ or $\alpha = -\rho^{-1} \partial \rho / \partial T$
α_T	thermal expansion in terms of <i>in situ</i> temp: $\alpha = -\rho^{-1} \partial \rho / \partial T$
$\alpha^{(\Theta)}$	thermal expansion in terms of Conservative Temperature: $\alpha^{(\Theta)} = -\rho^{-1} \partial \rho / \partial \Theta$
α_{aspect}	aspect ratio; ratio of vertical to horizontal scales of the flow: $\alpha_{\text{aspect}} = H/L$
$\beta, \beta^{(S)}$	saline contraction coefficient: $\beta = \beta^{(S)} = \rho^{-1} \partial \rho / \partial S$
β	meridional derivative of planetary vorticity: $\beta = \partial_y f$
$\hat{\gamma}$	dianeutral unit vector pointing perpendicular to the neutral tangent plane
δ^{ab}	components to the Kronecker tensor in Cartesian coordinates
δ^a_b	components to the Kronecker tensor in general coordinates
ϵ	kinetic energy dissipation from viscosity (energy per time per mass)
ϵ_{ab}	components to the permutation symbol in two space dimensions
ϵ_{abc}	components to the permutation symbol in three space dimensions
ε_{abc}	components to the Levi-Civita symbol in three space dimensions: $\varepsilon_{abc} = \sqrt{\det(Q)} \epsilon_{abc}$
η	vertical position of the free upper surface of a fluid domain: $z = \eta(x, y, t)$
$\eta_{k-1/2}$	vertical position of the top interface of the shallow water layer k
$\eta_{k+1/2}$	vertical position of the lower interface of the shallow water layer k
$\eta_b = -H$	vertical position of static solid-earth boundary: $z = \eta_b(x, y) = -H(x, y)$
Λ	wavelength of a wave: $\Lambda = 2\pi/ \mathbf{k} $, where \mathbf{k} is the wavevector and $ \mathbf{k} $ the wavenumber.
λ	reduced wavelength of a wave: $\lambda = \Lambda/(2\pi) = 1/ \mathbf{k} $.
(λ, ϕ)	(longitude, latitude) on the sphere: $0 \leq \lambda \leq 2\pi$ and $-\pi/2 \leq \phi \leq \phi/2$
κ	molecular kinematic diffusivity
κ_T	molecular diffusivity for <i>in situ</i> temperature in water: $\kappa_T = 1.4 \times 10^{-7} \text{ m}^2 \text{ s}^{-1}$
κ_S	molecular diffusivity for salt in water: $\kappa_S = 1.5 \times 10^{-9} \text{ m}^2 \text{ s}^{-1}$
κ_{eddy}	kinematic eddy diffusivity: $\kappa_{\text{eddy}} \gg \kappa$
μ_n	chemical potential for constituent n within a fluid (energy per mass)
$\tilde{\mu}_n$	chemical potential for constituent n within a fluid (energy per mole number)
μ	relative chemical potential for a binary fluid
μ	chemical potential for seawater: $\mu = \mu_{\text{salt}} - \mu_{\text{water}}$
μ_{vsc}	dynamic viscosity = $\rho \nu$
ν_s	specific volume: $\nu_s = \rho^{-1}$
ν	molecular kinematic viscosity
ν_{air}	molecular kinematic viscosity of air: $\nu_{\text{air}} \approx 1.3 \times 10^{-5} \text{ m}^2 \text{ s}^{-1}$
ν_{water}	molecular kinematic viscosity of fresh water: $\nu_{\text{water}} \approx 10^{-6} \text{ m}^2 \text{ s}^{-1}$
ν_{eddy}	eddy viscosity: $\nu_{\text{eddy}} \gg \nu$
ω	the relative vorticity axial vector: $\omega = \nabla \times \mathbf{v}$
ω	angular frequency for a wave so that the wave period is $2\pi/ \omega $
ϖ	dispersion relation for linear waves, relating angular frequency to the wavevector: $\omega = \varpi(\mathbf{k})$
Ω	earth's angular frequency vector oriented through the north pole: $\Omega = 7.2921 \times 10^{-5} \text{ s}^{-1}$
Φ	geopotential from central gravity plus planetary centrifugal; also, potential energy per mass
Π	Exner function
ψ	streamfunction for two-dimensional non-divergent flow: $\mathbf{u} = \hat{\mathbf{z}} \times \nabla \psi$
Ψ	vector streamfunction for three-dimensional non-divergent flow: $\mathbf{v} = \nabla \times \Psi$
ρ	<i>in situ</i> density (mass per volume) of a fluid element
ϱ	potential density referenced to a specified pressure
ρ_0	constant reference density used for the oceanic Boussinesq fluid
ρ_{ref}	constant reference density used for the shallow water fluid
σ	generalized vertical coordinate surface with $\sigma(x, y, z, t) = \text{constant}$
τ	stress vector
θ	potential temperature
Θ	Conservative Temperature
ζ	vertical component to the relative vorticity; e.g., $\zeta = \partial_x v - \partial_y u$
ζ_a	vertical component to the absolute vorticity; e.g., $\zeta_a = f + \zeta = f + \partial_x v - \partial_y u$

MATHEMATICAL OPERATIONS AND SYMBOLS

SYMBOL	MEANING
$[\equiv]$	“has dimensions” and used when referring to the physical dimensions
\times	vector cross product of vector calculus
∇	gradient operator
∇_z	horizontal gradient operator: $\nabla_z = \hat{\mathbf{x}}(\partial/\partial x) + \hat{\mathbf{y}}(\partial/\partial y) = \hat{\mathbf{x}}\partial_x + \hat{\mathbf{y}}\partial_y$
$\nabla \cdot$	divergence operator that acts on a vector to produce a scalar
$\nabla \times$	curl operator
∇_σ	horizontal gradient on constant σ -surface: $\nabla_\sigma = \hat{\mathbf{x}}(\partial/\partial x)_\sigma + \hat{\mathbf{y}}(\partial/\partial y)_\sigma$
∂_σ	vertical partial derivative with general vertical coordinate: $\partial_\sigma = \partial/\partial\sigma = (\partial z/\partial\sigma)\partial/\partial z$
$\partial/\partial t$	Eulerian time derivative acting at a fixed spatial position, \mathbf{x}
$[\partial/\partial t]_\sigma$	time derivative computed on constant σ -surface
D/Dt	material, Lagrangian, or substantial time derivative following a fluid particle
D^g/Dt	time derivative following a ray (integral lines of the group velocity): $D^g/Dt = \partial/\partial t + \mathbf{c}_g \cdot \nabla$
\mathfrak{d}	inexact differential operator commonly found in thermodynamics
δ	differential increment that is often written when following the fluid flow
$\delta(x)$	one-dimensional Dirac delta with dimensions of inverse length
$\delta^{(2)}(\mathbf{x})$	two-dimensional Dirac delta with dimensions of inverse area
$\delta(\mathbf{x})$	three-dimensional Dirac delta with dimensions of inverse volume
$\delta(t)$	temporal Dirac delta with dimensions of inverse time
Δ	finite difference increment in space: $\Delta_x, \Delta_y, \Delta_z, \Delta_\sigma$
dA	infinitesimal horizontal area element: $dA = dx dy$
$d\mathcal{S}$	infinitesimal area element on a surface
dV	infinitesimal volume element, sometimes written $dV = d\mathbf{x}$
$d\mathbf{x}$	infinitesimal volume element, with Cartesian expression $d\mathbf{x} = dV = dx dy dz$
δV	infinitesimal volume for a region moving with the fluid (Lagrangian region)
$\int_{\mathcal{R}} dV$	volume integral over an arbitrary region, \mathcal{R}
$\int_{\mathcal{R}(v)} dV$	volume integral over a region following the fluid flow (Lagrangian integral)
$\int_{\mathcal{S}} d\mathcal{S}$	surface integral over an arbitrary surface \mathcal{S}
$\oint_{\partial\mathcal{R}} d\mathcal{S}$	surface integral over a closed surface $\partial\mathcal{R}$ that bounds the volume \mathcal{R}
$\oint d\ell$	closed line integral over a periodic domain
$\oint_{\partial\mathcal{S}} d\ell$	counter-clockwise closed line integral over the boundary of a surface, $\partial\mathcal{S}$
\sim	“similar to” or “scales as”
\approx	approximately equal to
$\dot{\Psi}$	time derivative following a particle trajectory; for fluid particle trajectories, $\dot{\Psi} = D\Psi/Dt$

Part I

Mathematical methods

Fluid mechanics is a classical field theory based on Newton's laws of mechanics and quasi-equilibrium thermodynamics as applied to a continuous fluid media. Geophysical fluid mechanics is concerned with gravitationally stratified fluids with multiple matter constituents moving on a rotating sphere. The speed for all motion is small relative to the speed of light so that relativistic effects are negligible, thus enabling the use of universal Newtonian time for all observers. Our goal for this part of the book is to review mathematical topics for use in our study of geophysical fluid mechanics. Depending on the reader's background and interests, this material can be readily skipped on first reading and/or accessed later to fill gaps.

PHYSICS PROVIDES RELATIONS BETWEEN GEOMETRIC OBJECTS

Mathematical objects of use for the study of fluid mechanics include scalar fields (e.g., temperature, mass density, specific entropy), vector fields (e.g., velocity, vorticity), and second order tensor fields (e.g., diffusion tensor, stress tensor, moment of inertia tensor). These and other fields have an existence independent of the arbitrary coordinate choices used for their description. Thinking abstractly, these physical fields are geometric objects such as points, vectors, surfaces, volumes, etc. In the study of geophysical fluid mechanics, we use physical principles to develop differential equations relating geometric objects. Mathematical tools are used to compute numbers as required to compare with experiments and field measurements, and to formulate discrete equations for numerical simulations.

Our perspective can be summarized by “physics as geometry”, which forms a foundation to theoretical physics such as that detailed in [Thorne and Blandford \(2017\)](#). It has both conceptual and practical use for our study. It furthermore provides the framework for this part of the book, in which we develop mathematical tools that are later used to formulate a variety of theoretical geophysical fluid models. Our overall aim is to develop mathematical tools to help unpack the physics encapsulated by equations. This aim extends to those cases where analytical solutions are unavailable, which is the norm for nonlinear field theories such as fluid mechanics or even in many cases when the equations are linearized. Such qualitative and conceptual tools are of great value for the analysis of numerical simulations and field measurements.

TENSOR ANALYSIS AND GEOPHYSICAL FLUID MECHANICS

There are many occasions where a geophysical fluid system is more physically transparent when using a particular coordinate description or reference frame. However, there is no *a priori* choice that fits all systems. Thus, being adept at transforming from one description to another eases the study. Tensor analysis is the proven means for systematically performing such transformations thus motivating its use throughout fluid mechanics. In its more abstract realization via differential (or exterior) forms (not pursued in this book), tensor analysis provides the means to mathematically express physical ideas without any display of coordinate artefacts, thus exposing the underlying physical and mathematical essence.

The following offers an incomplete list of geophysical fluid systems where various coordinate descriptions or reference frames are encountered, and thus where tensor analysis can be put to use. Granted, each system listed here can be studied without the formalism of tensor analysis. However, by doing so one often encounters clumsy manipulations that can obfuscate the underlying physical concepts. Indeed, imagine the tedium required to write continuous field equations in multiple dimensions prior to vector analysis! That situation is akin to the tedium and awkward nature required to work across multiple coordinate systems and reference frames absent the formalism of tensor analysis. Hence, an adept use of vector analysis and its generalization to tensor analysis reveals how maths can inform the physics and how physics can be transparently embodied by the maths.

- RELATING EULERIAN AND LAGRANGIAN KINEMATICS: There is a duality in fluid kinematics between Eulerian and Lagrangian descriptions of fluid motion. To develop an understanding of this duality we make use of tensor analysis to facilitate the transformation between the two kinematic descriptions.
- SPHERICAL PLANET: Geophysical fluids move on an approximately spherical planet, making spherical coordinates the preferred choice for studying planetary flows. We make use of tensor methods to transform between planetary Cartesian coordinates (origin at the center of the planet) and spherical coordinates.
- CYLINDRICAL ROTATING TANK: Rotating laboratory fluids move in a circular tank, with cylindrical polar coordinates of use to respect symmetry of the domain. We make use of tensor methods to transform between Cartesian and cylindrical polar coordinates when considering rotating tank systems.
- ROTATING REFERENCE FRAME: Geophysical fluids move around a rotating earth and the fluid maintains a close to solid-body motion. Terrestrial observers also move in near solid-body motion. We are thus motivated to study geophysical fluids from a rotating reference frame. We use rudimentary tensor methods to transform between a fixed inertial frame and the non-inertial rotating reference frame, with this transformation revealing non-inertial accelerations (Coriolis and centrifugal) that impact on the observed fluid flow.
- STRATIFIED FLUIDS AND GENERALIZED VERTICAL COORDINATES: Geophysical fluids move in a gravitational field that acts to stratify the fluid according to its local buoyancy. For many purposes it can be useful to describe the vertical position of a fluid element according to its buoyancy rather than its height. This “isopycnal” vertical coordinate choice leads to a non-orthogonal coordinate description of the fluid motion. There are other vertical coordinates that can be of use for other situations, such as the terrain following coordinates commonly used for atmospheric simulations and coastal ocean models. Transforming between Cartesian coordinates and such *generalized vertical coordinates* requires the mathematical precision of general tensors.

SUMMARY OF THE MATH CHAPTERS

Some of the chapters in this part of the book are essential for nearly all subsequent chapters (e.g., Chapters 1 and 2), with the bulk of this book accessible to those with a solid undergraduate training in multi-variate calculus and the rudiments of analytic geometry. Other chapters target those interested in penetrating various special topics presented in this book. Readers are encouraged to take a close look at each chapter if only to know where to find topics of use later in the book or later in one’s career.

- CARTESIAN TENSOR ALGEBRA: Chapter 1 is a synopsis of Cartesian tensor analysis. This topic provides a systematization of ideas from Cartesian geometry and linear algebra. Material in this chapter is essential for nearly every topic in this book.
- CARTESIAN TENSOR CALCULUS: Chapter 2 extends the algebraic ideas from Chapter 1 to differential and integral calculus. This chapter provides a resume of multivariate or vector calculus of use for fluid mechanics. Material in this chapter is essential for nearly every topic in this book.
- PARTIAL DIFFERENTIAL EQUATIONS: Chapter 3 provides a summary of linear partial differential equations (PDEs) commonly encountered in mathematical physics. Even though

the equations of fluid mechanics are nonlinear PDEs, their linear counterparts offer much insight into fluid behavior.

- GREEN’S FUNCTIONS: Chapter 4 provides a survey of Green’s function methods used to solve linear partial differential equations of mathematical physics. Although this book is less concerned with specific solutions to these equations, we study the Green’s function method since it facilitates rather general insights into both the mathematical and physical content of fluid equations. Furthermore, Green’s function methods are commonly used across various areas of the geophysical sciences, thus making it quite useful to be familiar with the method.
- FOURIER ANALYSIS: Chapter 5 summarizes salient points about Fourier series and Fourier transforms. We make particular use of Fourier transforms in the study of wave mechanics in Part IX of this book.
- GEOMETRY OF CURVES AND SURFACES: Chapter 6 introduces rudimentary differential geometry used to characterize curves (such as fluid particle trajectories) and surfaces (such as isopycnals) embedded in a background Euclidean space. Here we encounter such notions as normal and tangent directions and curvature.
- GENERAL TENSOR INTRODUCTION: Chapter 7 provides an introduction to general tensor analysis and its applications to geophysical fluids. The discussion is accessible to anyone who has read Chapter 1, and is recommended for all readers of this book, even for those who do not wish to study the details of general tensors in Chapter 8.
- GENERAL TENSOR ANALYSIS: Chapter 8 extends the Cartesian tensor algebra and calculus to allow for the use of arbitrary, or general, coordinates. This chapter is essential to understand the mathematics underlying non-Cartesian coordinates, such as spherical coordinates and generalized vertical coordinates.
- ORTHOGONAL COORDINATES: Chapter 9 offers a reference for the three locally orthogonal coordinate systems (Cartesian, spherical, cylindrical) used in this book and how various mathematical objects appear when written in these coordinates.

Chapter 1

CARTESIAN TENSOR ALGEBRA

An isomorphism from Euclidean space to the space of three-dimensional real numbers, \mathbb{R}^3 , associates to each point of Euclidean space the *Cartesian coordinates* of that point. In this chapter we introduce the formalism of Cartesian tensor analysis with a focus on linear algebraic relations. The study of Cartesian tensors restricts attention to geometric objects described by Cartesian coordinates on a flat Euclidean space. Furthermore, all Cartesian reference frames (of equivalent handedness) are related by rotations as realized by orthogonal transformations.¹

CHAPTER GUIDE

We follow standard treatments of Cartesian tensors such as that in Chapter 2 of [Aris \(1962\)](#), Chapter 1 of [Segel \(1987\)](#), and Chapter 2 of [Lovelock and Rund \(1989\)](#) (where they use the term *affine tensors* rather than *Cartesian tensors*). The discussion should be accessible to those having studied undergraduate calculus and linear algebra. For geophysical fluid mechanics, mastery of Cartesian tensors is nearly sufficient for mastery of general tensors. This chapter is basic to all of the maths in this book.

1.1	Introduction to tensors and tensor fields	6
1.2	Points and vectors	6
1.3	Distance and the scalar product	8
1.3.1	Distance between points	8
1.3.2	Magnitude of a vector and the scalar product	9
1.4	Vector product	9
1.4.1	Basis vector orientation and the Levi-Civita tensor	9
1.4.2	Axial (or pseudo) vector	10
1.4.3	Orthogonality relations between cross products	11
1.4.4	Vector product of arbitrary vectors	11
1.4.5	Geometric interpretation of the vector product	12
1.4.6	Generalization to arbitrary vectors	13
1.5	Measuring volume	13
1.5.1	Volume defined by three vectors	13
1.5.2	Cartesian volume element for integration	14
1.5.3	n -space volumes and the Levi-Civita tensor	15
1.6	Example vector identities using the Levi-Civita tensor	15
1.6.1	Double vector product	15
1.6.2	Scalar product of two vector products	16
1.7	Transforming the coordinate representations	16
1.7.1	Inverse transformation	16

¹Such orientation preserving transformations are all that we consider in this book.

1.7.2	Orthogonal transformation	17
1.7.3	Geometric interpretation of orthogonal transformations	17
1.7.4	Transforming the coordinate representation of a vector	18
1.7.5	Invariance of the scalar product	18
1.7.6	Transforming the coordinate representation of a second order tensor	19
1.7.7	Distinguishing between tensors and matrices	19
1.8	Homogeneity and isotropy	20
1.8.1	Homogeneous tensor	20
1.8.2	Isotropic and anisotropic tensors	20
1.9	Exercises	21

1.1 Introduction to tensors and tensor fields

Fluid mechanics involves fields of scalars, vectors, and higher order tensors. We generically refer to all of these geometric objects as *tensors*, with a scalar a zero order tensor and a vector a first order tensor. A scalar field provides a single number at each point in space-time. Example scalar fields include temperature, mass density, entropy, salinity, humidity, and mechanical energy. On a flat manifold, such as the Euclidean space considered in this chapter, a vector connects two points on the manifold and is specified by a direction and a magnitude. Correspondingly, a vector field provides a time dependent vector at each point in space. Example vector fields include the fluid velocity, acceleration, and forces acting on fluid elements. A second order tensor can be represented by a matrix, with a tensor field providing a matrix at each point in space.² The stress tensor and the diffusion tensor are example second order tensors encountered in this book.

Geophysical fluids make use of *Newtonian universal time* and are embedded in flat *Euclidean space*. This space and time structure induces the familiar Euclidean norm or *metric* when measuring the spatial distance between two points, whether the points are on a plane, a sphere, or an arbitrary surface within the fluid such as a surface of constant Archimedean buoyancy. We can thus make use of Cartesian coordinates as the starting point for a mathematical formulation of geophysical fluid mechanics. Transformations to alternative coordinates are made when they lend insight to the symmetry of the flow and/or the geometry of the space on which the flow occurs. It is for this reason that we devote this chapter to developing the formalism of Cartesian tensor analysis. Furthermore, it is for this reason that Cartesian tensors gives us nearly all of the formalism necessary to employ general tensors in geophysical fluid mechanics.

1.2 Points and vectors

Consider a point, $\mathcal{P} \in \mathbb{R}^3$, as represented by its Cartesian coordinates relative to an arbitrary origin. As such, the position is a vector whose tail is at the origin and head at the point as shown in Figure 1.1. We write this coordinate representation as

$$\mathcal{P} \mapsto \vec{P} = \hat{x} P_1 + \hat{y} P_2 + \hat{z} P_3, \quad (1.1)$$

with the arrow over a symbol commonly used for vectors. The right hand side of equation (1.1) provides the *coordinate representation* of the position vector through the triplet of numbers, (P_1, P_2, P_3) , that measure the coordinate distance along their corresponding Cartesian unit vectors, $(\hat{x}, \hat{y}, \hat{z})$. The Cartesian unit vectors form a right-handed basis for three dimensional

²We comment on the distinction between a matrix and tensor in Section 1.7.7.

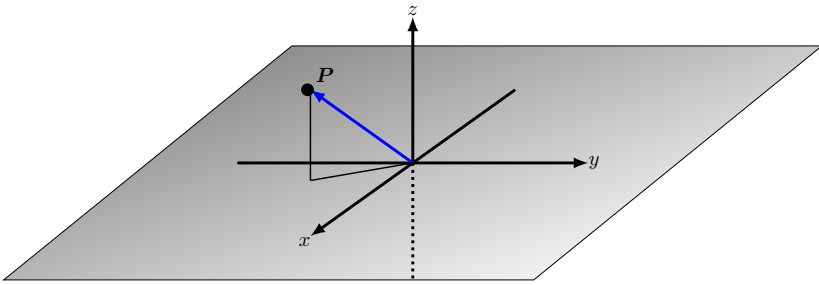


FIGURE 1.1: An arbitrary point in space, \mathcal{P} , has an objective existence independent of our subjective choice of coordinate system used to describe its position. We here represent its position with respect to the origin of a right-handed Cartesian coordinate system. The Cartesian representation of the position vector is $\mathcal{P} \mapsto \vec{P} = \mathbf{P} = \hat{\mathbf{x}} P_1 + \hat{\mathbf{y}} P_2 + \hat{\mathbf{z}} P_3$, with the Cartesian basis vectors the normalized triplet of unit vectors $(\hat{\mathbf{x}}, \hat{\mathbf{y}}, \hat{\mathbf{z}})$ and the triplet of Cartesian coordinates given by (P_1, P_2, P_3) . There is a continuous infinity of possible Cartesian coordinate systems that are rotated and/or translated with respect to the one shown here.

Euclidean space.³ Hence, the position vector for any point in Euclidean space can be represented in terms of these three basis vectors.

At times we find it useful to make use of alternative notations in which the position vector is written

$$\vec{P} = \mathbf{P} \quad (1.2a)$$

$$= \hat{\mathbf{x}} P_1 + \hat{\mathbf{y}} P_2 + \hat{\mathbf{z}} P_3 \quad (1.2b)$$

$$= \sum_{a=1}^3 \vec{e}_a P_a \quad (1.2c)$$

$$= \vec{e}_a P_a. \quad (1.2d)$$

The first equality introduced the boldface notation, which we commonly use for the representation of vectors in Cartesian coordinates. Indeed, although less convenient when moving to the general tensors of Chapter 7, we still maintain the boldface in this book given its common usage in the literature and since much of this book makes use of Cartesian tensors. Equation (1.2d) introduced the Einstein summation convention in which repeated indices are summed over their range, thus allowing us to drop the summation symbol. Equation (1.2c) introduced a generic notation for the basis vectors

$$\vec{e}_1 = \hat{\mathbf{x}} \quad \text{and} \quad \vec{e}_2 = \hat{\mathbf{y}} \quad \text{and} \quad \vec{e}_3 = \hat{\mathbf{z}}. \quad (1.3)$$

The Cartesian basis vectors each have unit magnitude (normalized), meaning that their scalar products yield⁴

$$\hat{\mathbf{x}} \cdot \hat{\mathbf{x}} = \hat{\mathbf{y}} \cdot \hat{\mathbf{y}} = \hat{\mathbf{z}} \cdot \hat{\mathbf{z}} = 1. \quad (1.4)$$

Use of a hat or carot symbol over a vector signifies that the vector is normalized to unity. For Cartesian coordinates we generally work with the normalized basis vectors (1.3). Furthermore, a normalized vector can change only through rotation since by definition it remains of unit norm and so cannot change its magnitude (see Section 2.1.4). For the general tensors of Chapters 7, 9 and 56, we sometimes find it more convenient to work with unnormalized basis vectors. Hence, the basis vectors, \vec{e}_a , retain the arrow symbol rather than the carot since they are not always

³The unit vectors are sometimes denoted $(\hat{i}, \hat{j}, \hat{k})$ in the literature. We generally avoid that notation in this book.

⁴The Cartesian scalar (or dot or inner) product is discussed more formally in Section 1.3.

normalized.

We emphasize that the tensor labels denote components of a specific coordinate representation, P_a , as well as members from the set of basis vectors, \vec{e}_a . These labels are not to be confused with partial derivative operations.⁵ Finally, we sometimes write the vector components and basis vectors in the form of a list or triplet

$$P_a = (P_1, P_2, P_3) \quad \text{and} \quad \vec{e}_a = (\vec{e}_1, \vec{e}_2, \vec{e}_3) = (\hat{x}, \hat{y}, \hat{z}). \quad (1.5)$$

1.3 Distance and the scalar product

In defining a vector to have unit magnitude, we are assuming we know how to measure the magnitude of a vector. We here make this notion precise.

1.3.1 Distance between points

Consider two points in Euclidean space, \mathcal{P} and $\mathcal{P} + d\mathcal{P}$, separated by a small distance and specified by their respective position vectors

$$\mathcal{P} \mapsto \vec{P} = \vec{e}_a P_a \quad (1.6a)$$

$$\mathcal{P} + d\mathcal{P} \mapsto \vec{P} + d\vec{x} = \vec{e}_a (P_a + dx_a). \quad (1.6b)$$

Euclidean space is afforded a metric whereby the squared distance between two points is measured via *Pythagoras' theorem*

$$[\text{distance}(\mathcal{P}, \mathcal{P} + d\mathcal{P})]^2 = (\vec{P} + d\vec{x} - \vec{P}) \cdot (\vec{P} + d\vec{x} - \vec{P}) \quad \text{definition of distance} \quad (1.7a)$$

$$= (\boldsymbol{P} + d\boldsymbol{x} - \boldsymbol{P}) \cdot (\boldsymbol{P} + d\boldsymbol{x} - \boldsymbol{P}) \quad \text{boldface notation} \quad (1.7b)$$

$$= dx_a dx_b (\vec{e}_a \cdot \vec{e}_b) \quad \text{expose tensor indices} \quad (1.7c)$$

$$= dx_a dx_b \delta_{ab} \quad \text{basis vector orthonormality} \quad (1.7d)$$

$$= dx_a dx_a \quad \text{contraction of tensor indices} \quad (1.7e)$$

$$= (dx_1)^2 + (dx_2)^2 + (dx_3)^2 \quad \text{expanding the sum.} \quad (1.7f)$$

To reach this result we introduced the components to the Kronecker delta tensor, which can be represented by the 3×3 identity matrix

$$\vec{e}_a \cdot \vec{e}_b = \delta_{ab} = \begin{bmatrix} \delta_{11} & \delta_{12} & \delta_{13} \\ \delta_{21} & \delta_{22} & \delta_{23} \\ \delta_{31} & \delta_{32} & \delta_{33} \end{bmatrix} = \begin{bmatrix} 1 & 0 & 0 \\ 0 & 1 & 0 \\ 0 & 0 & 1 \end{bmatrix}. \quad (1.8)$$

The Kronecker tensor provides the Cartesian coordinate representation of the *metric tensor* for Euclidean space. The metric provides the means to measure the distance between points in space, and thus how to measure the length of a vector. It thus allows us to *normalize* a vector to have unit magnitude, motivating the often used term *norm* rather than metric. In Section 8.1 we introduce alternative representations for the metric based on the use of non-Cartesian coordinates and non-Euclidean manifolds.

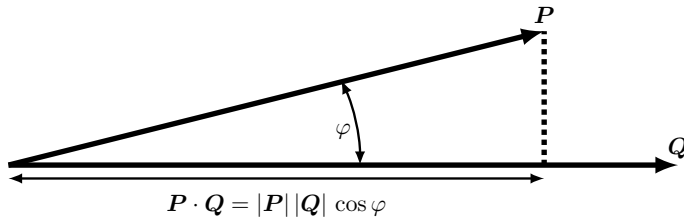


FIGURE 1.2: Illustrating the geometry of the scalar product (also known as the dot product or inner product) between two vectors, $\mathbf{P} \cdot \mathbf{Q} = |\mathbf{P}| |\mathbf{Q}| \cos \vartheta$.

1.3.2 Magnitude of a vector and the scalar product

By defining the distance between two points, we in turn have a prescription for defining the squared magnitude of a vector

$$|\mathbf{P}|^2 = \mathbf{P} \cdot \mathbf{P} = P_a P_b (\vec{e}_a \cdot \vec{e}_b) = P_a P_a = (P_1)^2 + (P_2)^2 + (P_3)^2. \quad (1.9)$$

Correspondingly, we have the *scalar product* between two arbitrary vectors

$$\mathbf{P} \cdot \mathbf{Q} = P_a Q_b (\vec{e}_a \cdot \vec{e}_b) = P_a Q_a, \quad (1.10)$$

which also goes by the name *dot product* or *inner product*. Given our expression for the scalar product and the magnitude of vectors, we can introduce a geometrical interpretation by defining the angle between the vectors according to

$$\cos \vartheta \equiv \frac{\mathbf{P} \cdot \mathbf{Q}}{|\mathbf{P}| |\mathbf{Q}|} = \frac{P_a Q_a}{\sqrt{P_b P_b} \sqrt{Q_c Q_c}}. \quad (1.11)$$

We illustrate this equation in Figure 1.2. It is useful to convince oneself that this definition is consistent with $-1 \leq \cos \vartheta \leq 1$. Furthermore, note that this definition of an angle between two vectors makes use of the metric tensor, so that angles on a manifold, just as distance, require a metric.⁶

1.4 Vector product

The scalar product provides a means to measure the magnitude of a vector and the distance between two points. We here introduce the vector (or cross) product, which provides a means to measure area associated with two vectors and to specify the *orientation* of that area.

1.4.1 Basis vector orientation and the Levi-Civita tensor

Consider a flat plane defined by any two of the Cartesian basis vectors, \vec{e}_a and \vec{e}_b . We seek a means to specify what side of the plane is up and what side is down. Doing so allows us to orient

⁵In this book we generally eschew the notation where partial derivatives are denoted by a subscript. One exception occurs in our discussion of the density evolution in Sections 64.2 and 64.3.

⁶This point about the need for a metric tensor might seem pedantic to those having only worked with Euclidean space, where the formalism of linear algebra and calculus generally builds in the Kronecker metric from the start. However, the study of calculus can be generalized to differential manifolds that have no metric, with [Nurser et al. \(2022\)](#) offering an example use of this formalism for studies of fluid motion in continuous property spaces rather than Euclidean space.

objects within space.⁷ Notably, there is no objective means for this specification, since “up” and “down” are subject to our chosen orientation. Therefore, we must choose a convention. For that purpose, we follow the *right hand rule*, in which the out-stretched thumb, index, and middle fingers of the right hand orient the three Cartesian basis vectors.

We algebraically specify the right hand rule for the basis vectors through the relation

$$\vec{e}_a \times \vec{e}_b = \epsilon_{abc} \vec{e}_c. \quad (1.12)$$

The left hand side introduces the *vector (or cross) product* of two basis vectors. The right hand side algebraically defines the vector product as the *contraction* of the Levi-Civita tensor with another basis vector. Here, the term contraction can be considered a generalization of the inner product. The Cartesian components of the Levi-Civita tensor are given by the totally anti-symmetric permutation symbol or ϵ -tensor

$$\epsilon_{123} = 1 \quad (1.13a)$$

$$\epsilon_{abc} = \begin{cases} 1, & \text{even permutation of } abc \text{ (123, 312, 231)} \\ -1, & \text{odd permutation of } abc \text{ (321, 132, 213)} \\ 0, & \text{all other } abc. \end{cases} \quad (1.13b)$$

Exchanging indices (an odd permutation) flips the sign of the permutation symbol

$$\epsilon_{abc} = -\epsilon_{bac} = -\epsilon_{acb} \implies \epsilon_{123} = -\epsilon_{213}, \quad (1.14)$$

whereas cycling indices (an even permutation) preserves the sign

$$\epsilon_{abc} = \epsilon_{cab} = \epsilon_{bca} \implies \epsilon_{123} = \epsilon_{312} = \epsilon_{231}. \quad (1.15)$$

Correspondingly, the vector cross product changes sign when its elements are commuted

$$\vec{e}_a \times \vec{e}_b = \epsilon_{abc} \vec{e}_c = -\vec{e}_b \times \vec{e}_a. \quad (1.16)$$

1.4.2 Axial (or pseudo) vector

The vector cross product defines a vector whose properties are dependent on the orientation of the space. That is, the vector cross product changes its sign upon changing from a right handed to left handed orientation of the coordinate system. Such vectors are known as *axial vectors* or *pseudo vectors*. Example axial vectors that we encounter in this book include the angular velocity for the planet as well as the vorticity vector of fluid motion.

⁷There are surfaces, such as the Möbius strip, that are not orientable. We only consider orientable surfaces in this book.

1.4.3 Orthogonality relations between cross products

As defined, the permutation symbol ensures that $\vec{e}_a \times \vec{e}_b$ is orthogonal to both \vec{e}_a and \vec{e}_b

$$\vec{e}_a \cdot (\vec{e}_a \times \vec{e}_b) = \vec{e}_a \cdot \epsilon_{abc} \vec{e}_c \quad \text{definition} \quad (1.17a)$$

$$= \epsilon_{abc} \vec{e}_a \cdot \vec{e}_c \quad \text{rearrangement} \quad (1.17b)$$

$$= \epsilon_{cba} \vec{e}_c \cdot \vec{e}_a \quad \text{relabel } a \text{ to } c \text{ and } c \text{ to } a \quad (1.17c)$$

$$= -\epsilon_{abc} \vec{e}_c \cdot \vec{e}_a \quad \text{cba is an odd permutation of abc} \quad (1.17d)$$

$$= -\epsilon_{abc} \vec{e}_a \cdot \vec{e}_c \quad \text{scalar product commutes} \quad (1.17e)$$

$$\Rightarrow \vec{e}_a \cdot (\vec{e}_a \times \vec{e}_b) = 0. \quad (1.17f)$$

We made the final conclusion since equation (1.17b) has the opposite sign to equation (1.17e), which can only be satisfied by zero. To fully digest step (1.17c), it can be useful to reintroduce the summation symbol

$$\epsilon_{abc} \vec{e}_a \cdot \vec{e}_c = \sum_{a=1}^3 \sum_{c=1}^3 \epsilon_{abc} \vec{e}_a \cdot \vec{e}_c \quad \text{summation symbols reintroduced} \quad (1.18a)$$

$$= \sum_{c=1}^3 \sum_{a=1}^3 \epsilon_{cba} \vec{e}_c \cdot \vec{e}_a \quad \text{swap } a \text{ and } c \quad (1.18b)$$

$$= \epsilon_{cba} \vec{e}_c \cdot \vec{e}_a \quad \text{reintroduce summation convention} \quad (1.18c)$$

Additionally, to digest step (1.17d) we step through the permutations

$$\epsilon_{cba} = -\epsilon_{bca} \quad \text{swap } c \text{ with } b \text{ to pick up a minus sign} \quad (1.19a)$$

$$= \epsilon_{bac} \quad \text{swap } c \text{ with } a \text{ to pick up a minus sign} \quad (1.19b)$$

$$= -\epsilon_{abc} \quad \text{swap } b \text{ with } a \text{ to pick up a minus sign.} \quad (1.19c)$$

The same procedure shows that $\vec{e}_b \cdot (\vec{e}_a \times \vec{e}_b) = 0$. Hence, the vector product is orthogonal to the plane specified by any two of the basis vectors. That is, the vector product points orthogonal to that plane and in a direction determined by the right hand rule. We note that this proof reveals a general property. Namely, the contraction of a symmetric tensor (e.g., the scalar product $\vec{e}_c \cdot \vec{e}_a = \vec{e}_a \cdot \vec{e}_c$) with an anti-symmetric tensor results in zero. We further illustrate this property in Exercise 1.2.

1.4.4 Vector product of arbitrary vectors

The expression (1.12) for the vector product of two basis vectors renders the vector product of arbitrary vectors.

$$\mathbf{P} \times \mathbf{Q} = P_a \vec{e}_a \times Q_b \vec{e}_b \quad (1.20a)$$

$$= P_a Q_b \vec{e}_a \times \vec{e}_b \quad (1.20b)$$

$$= P_a Q_b \epsilon_{abc} \vec{e}_c \quad (1.20c)$$

$$= (P_2 Q_3 - P_3 Q_2) \vec{e}_1 + (P_3 Q_1 - P_1 Q_3) \vec{e}_2 + (P_1 Q_2 - P_2 Q_1) \vec{e}_3. \quad (1.20d)$$

We can write the vector product as a determinant

$$\mathbf{P} \times \mathbf{Q} = \det \begin{bmatrix} \vec{e}_1 & \vec{e}_2 & \vec{e}_3 \\ p_1 & p_2 & p_3 \\ q_1 & q_2 & q_3 \end{bmatrix}. \quad (1.21)$$

As with the basis vectors, the vector product is orthogonal to both of the individual vectors, such as

$$\mathbf{P} \cdot (\mathbf{P} \times \mathbf{Q}) = (P_d \vec{e}_d) \cdot (P_a Q_b \epsilon_{abc} \vec{e}_c) \quad (1.22a)$$

$$= P_c P_a Q_b \epsilon_{abc} \quad (1.22b)$$

$$= 0, \quad (1.22c)$$

where the final equality follows since the product $P_c P_a$ is symmetric on the labels ac ($P_c P_a = P_a P_c$), whereas ϵ_{abc} is anti-symmetric.

1.4.5 Geometric interpretation of the vector product

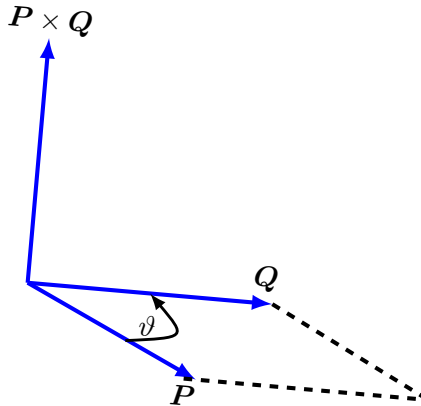


FIGURE 1.3: The magnitude of the vector product between two vectors is given by the product of their magnitudes and the sine of the angle between them, $|\mathbf{P} \times \mathbf{Q}| = |\mathbf{P}| |\mathbf{Q}| \sin \vartheta$. This magnitude equals to the area of the parallelogram formed by the two vectors. The vector product is directed perpendicular to the plane determined by the two vectors and oriented according to the right hand rule. The right hand rule is followed by placing the fingers of the right hand along the first vector, \mathbf{P} . Closing the fingers in the direction of the second vector, \mathbf{Q} (as here depicted by the arrow on the arc for the angle ϑ), then ensures that the thumb orients the vector product, $\mathbf{P} \times \mathbf{Q}$.

The expression (1.20d) leads to the identity

$$|\mathbf{P} \times \mathbf{Q}|^2 = |\mathbf{P}|^2 |\mathbf{Q}|^2 - (\mathbf{P} \cdot \mathbf{Q})^2 \quad (1.23a)$$

$$= |\mathbf{P}|^2 |\mathbf{Q}|^2 (1 - \cos^2 \vartheta) \quad (1.23b)$$

$$= |\mathbf{P}|^2 |\mathbf{Q}|^2 \sin^2 \vartheta, \quad (1.23c)$$

where we used the scalar product expression (1.11) to introduce the angle subtended by the two vectors. Trigonometry indicates that the area of the parallelogram defined by \mathbf{P} and \mathbf{Q} is given by $|\mathbf{P}| |\mathbf{Q}| \sin \vartheta$. Hence, the vector product has a magnitude given by this area

$$\text{area}(\mathbf{P}, \mathbf{Q}) = |\mathbf{P}| |\mathbf{Q}| \sin \vartheta = |\mathbf{P} \times \mathbf{Q}|. \quad (1.24)$$

Since $\mathbf{P} \times \mathbf{Q}$ is orthogonal to the plane defined by \mathbf{P} and \mathbf{Q} , we can write the vector product in

the purely geometric manner

$$\mathbf{P} \times \mathbf{Q} = \hat{\mathbf{n}} \operatorname{area}(\mathbf{P}, \mathbf{Q}) = \hat{\mathbf{n}} |\mathbf{P}| |\mathbf{Q}| \sin \vartheta, \quad (1.25)$$

where $\hat{\mathbf{n}}$ is a unit vector pointing normal to the area and in a direction given by the right hand rule. This formula is illustrated in Figure 1.3.

To further emphasize the geometric interpretation, let \mathbf{P} equal to the vertical direction, $\mathbf{P} = \hat{\mathbf{z}}$. The vector cross product then defines a vector,

$$\mathbf{Q}^{\hat{\mathbf{z}}\perp} = \hat{\mathbf{z}} \times \mathbf{Q} \quad (1.26a)$$

$$= \hat{\mathbf{z}} \times [\mathbf{Q} - (\hat{\mathbf{z}} \cdot \mathbf{Q}) \hat{\mathbf{z}}] \quad (1.26b)$$

$$= (\hat{\mathbf{z}} \times \hat{\mathbf{x}})(\hat{\mathbf{x}} \cdot \mathbf{Q}) + (\hat{\mathbf{z}} \times \hat{\mathbf{y}})(\hat{\mathbf{y}} \cdot \mathbf{Q}) \quad (1.26c)$$

$$= \hat{\mathbf{y}}(\hat{\mathbf{x}} \cdot \mathbf{Q}) - \hat{\mathbf{x}}(\hat{\mathbf{y}} \cdot \mathbf{Q}). \quad (1.26d)$$

By construction, $\mathbf{Q}^{\hat{\mathbf{z}}\perp}$ is in the horizontal plane and it is perpendicular to the horizontal projection of \mathbf{Q}

$$\mathbf{Q}^{\hat{\mathbf{z}}\perp} \cdot \hat{\mathbf{z}} = 0 \quad \text{and} \quad \mathbf{Q}^{\hat{\mathbf{z}}\perp} \cdot \mathbf{Q} = 0 \implies \mathbf{Q}^{\hat{\mathbf{z}}\perp} \cdot [\mathbf{Q} - (\hat{\mathbf{z}} \cdot \mathbf{Q}) \hat{\mathbf{z}}] = 0. \quad (1.27)$$

Hence, the vector $\mathbf{Q}^{\hat{\mathbf{z}}\perp}$ is geometrically computed by rotating the horizontal component of \mathbf{Q} by $\pi/2$ radians counter-clockwise about the $\hat{\mathbf{z}}$ axis. That interpretation holds for all coordinate directions so that

$$\hat{\mathbf{x}} \times \mathbf{Q} = \hat{\mathbf{z}}(\hat{\mathbf{y}} \cdot \mathbf{Q}) - \hat{\mathbf{y}}(\hat{\mathbf{z}} \cdot \mathbf{Q}) = \text{project } \mathbf{Q} \text{ to y-z plane} + \text{rotate } \pi/2 \text{ CCW around } \hat{\mathbf{x}} \quad (1.28a)$$

$$\hat{\mathbf{y}} \times \mathbf{Q} = \hat{\mathbf{x}}(\hat{\mathbf{z}} \cdot \mathbf{Q}) - \hat{\mathbf{z}}(\hat{\mathbf{x}} \cdot \mathbf{Q}) = \text{project } \mathbf{Q} \text{ to z-x plane} + \text{rotate } \pi/2 \text{ CCW around } \hat{\mathbf{y}} \quad (1.28b)$$

$$\hat{\mathbf{z}} \times \mathbf{Q} = \hat{\mathbf{y}}(\hat{\mathbf{x}} \cdot \mathbf{Q}) - \hat{\mathbf{x}}(\hat{\mathbf{y}} \cdot \mathbf{Q}) = \text{project } \mathbf{Q} \text{ to x-y plane} + \text{rotate } \pi/2 \text{ CCW around } \hat{\mathbf{z}}. \quad (1.28c)$$

1.4.6 Generalization to arbitrary vectors

Thus far the discussion has considered vectors to represent the position of a point in space. As such, the vectors have the physical dimensions of length and $\operatorname{area}(\mathbf{P}, \mathbf{Q})$ has dimensions of squared length. However, the vector analysis is general, so that the above notions extend to vectors of arbitrary physical dimensions, such as velocity. In these more general cases the physical dimensions are adjusted accordingly.

1.5 Measuring volume

The vector product offers a means to measure area defined by two vectors. We now extend that result to measure the volume determined by three non-parallel vectors. This result has particular relevance to the volume element used for integration over space.

1.5.1 Volume defined by three vectors

Consider the scalar product of an arbitrary vector with the vector product, $(\mathbf{P} \times \mathbf{Q}) \cdot \mathbf{R}$. This scalar product projects that portion of the vector, \mathbf{R} , onto the direction parallel to the normal to the plane defined by $\mathbf{P} \times \mathbf{Q}$. Given that $|(\mathbf{P} \times \mathbf{Q})|$ is the area of the parallelogram defined by \mathbf{P} and \mathbf{Q} , we conclude that $(\mathbf{P} \times \mathbf{Q}) \cdot \mathbf{R}$ is the volume of the parallelepiped defined by the three vectors. However, note that this volume is not guaranteed to be positive definite since the sign depends on the relative orientation of $\mathbf{P} \times \mathbf{Q}$ and \mathbf{R} . So more precisely, we need to apply an absolute value around the triple product to get a positive volume.

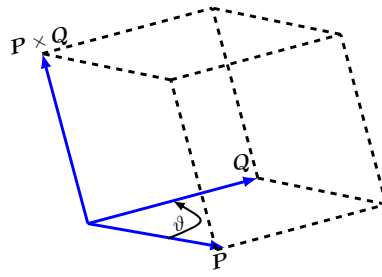


FIGURE 1.4: Three linearly independent position vectors determine a volume given by $|(\mathbf{P} \times \mathbf{Q}) \cdot \mathbf{R}| = |(\mathbf{R} \times \mathbf{P}) \cdot \mathbf{Q}| = |(\mathbf{Q} \times \mathbf{R}) \cdot \mathbf{P}|$

We can prove cyclic symmetry of $(\mathbf{P} \times \mathbf{Q}) \cdot \mathbf{R}$ through the following manipulations

$$(\mathbf{P} \times \mathbf{Q}) \cdot \mathbf{R} = (P_a \vec{e}_a \times Q_b \vec{e}_b) \cdot R_d \vec{e}_d \quad \text{expose coordinates and basis vectors} \quad (1.29a)$$

$$= P_a Q_b (\vec{e}_a \times \vec{e}_b) \cdot R_d \vec{e}_d \quad \text{rearrange} \quad (1.29b)$$

$$= P_a Q_b (\epsilon_{abc} \vec{e}_c) \cdot \vec{e}_d R_d \quad \text{vector product as per equation (1.12)} \quad (1.29c)$$

$$= P_a Q_b \epsilon_{abc} (\vec{e}_c \cdot \vec{e}_d) R_d \quad \text{rearrange} \quad (1.29d)$$

$$= P_a Q_b \epsilon_{abc} \delta_{cd} R_d \quad \text{orthonormality: } \vec{e}_c \cdot \vec{e}_d = \delta_{cd} \quad (1.29e)$$

$$= P_a Q_b \epsilon_{abc} R_c \quad \text{perform contraction on index } d: \delta_{cd} R_d = R_c \quad (1.29f)$$

$$= R_c P_a Q_b \epsilon_{abc} \quad \text{rearrange} \quad (1.29g)$$

$$= R_a P_b Q_c \epsilon_{bca} \quad \text{relabel: } a \rightarrow b \text{ and } b \rightarrow c \text{ and } c \rightarrow a \quad (1.29h)$$

$$= R_a P_b Q_c \epsilon_{abc} \quad \text{even permutation: } \epsilon_{bca} = \epsilon_{abc} \quad (1.29i)$$

$$= (\mathbf{R} \times \mathbf{P}) \cdot \mathbf{Q} \quad \text{redintroduce boldface notation.} \quad (1.29j)$$

This identity yields the geometric result illustrated in Figure 1.4

$$\text{volume}(\mathbf{P}, \mathbf{Q}, \mathbf{R}) = |(\mathbf{P} \times \mathbf{Q}) \cdot \mathbf{R}| = |(\mathbf{R} \times \mathbf{P}) \cdot \mathbf{Q}| = |(\mathbf{Q} \times \mathbf{R}) \cdot \mathbf{P}|. \quad (1.30)$$

1.5.2 Cartesian volume element for integration

We need the volume of an infinitesimal region when performing an integration over space. When making use of Cartesian coordinates we need the volume of a rectangular prism defined by infinitesimal distances along each of the axes. We thus set

$$\mathbf{P} = \hat{x} dx \quad \text{and} \quad \mathbf{Q} = \hat{y} dy \quad \text{and} \quad \mathbf{R} = \hat{z} dz, \quad (1.31)$$

in which case the volume element is

$$dV = (\mathbf{P} \times \mathbf{Q}) \cdot \mathbf{R} = dx dy dz (\hat{x} \times \hat{y}) \cdot \hat{z} = dx dy dz. \quad (1.32)$$

This expression for the volume element could have been written down without the formalism of a vector triple product. However, in Chapter 7 we find the general relation $(\mathbf{P} \times \mathbf{Q}) \cdot \mathbf{R}$ provides a useful starting point for deriving the volume element with arbitrary coordinates.

1.5.3 n -space volumes and the Levi-Civita tensor

We combine the geometric specification of the vector product as a means to measure area, (1.25), with the algebraic specification (1.20d) by writing

$$\text{2-volume} = \epsilon(\mathbf{P}, \mathbf{Q}) = \epsilon_{ab} P_a Q_b = \det \begin{bmatrix} P_1 & Q_1 \\ P_2 & Q_2 \end{bmatrix}. \quad (1.33)$$

In this equation, ϵ_{ab} is the totally anti-symmetric 2×2 tensor. It has Cartesian components that can be organized as a matrix according to

$$\begin{bmatrix} \epsilon_{11} & \epsilon_{12} \\ \epsilon_{21} & \epsilon_{22} \end{bmatrix} = \begin{bmatrix} 0 & 1 \\ -1 & 0 \end{bmatrix}. \quad (1.34)$$

In words, the first equality in equation (1.33) states that the ϵ -tensor in two dimensions takes two vectors as its argument and produces a 2-volume (i.e., an area). The three dimensional generalization yields

$$\text{3-volume} = \epsilon(\mathbf{P}, \mathbf{Q}, \mathbf{R}) = \epsilon_{abc} P_a Q_b R_c = \det \begin{bmatrix} P_1 & Q_1 & R_1 \\ P_2 & Q_2 & R_2 \\ P_3 & Q_3 & R_3 \end{bmatrix}. \quad (1.35)$$

Suppressing the first vector argument in the 3-volume produces a vectorial surface area defined by the other two vectors

$$\text{surface area} = \epsilon(\ , \mathbf{Q}, \mathbf{R}). \quad (1.36)$$

By construction, the vectorial surface area is orthogonal to both \mathbf{Q} and \mathbf{R} .

1.6 Example vector identities using the Levi-Civita tensor

The Levi-Civita tensor is a versatile tool for deriving vector identities. We illustrated some of these features in the previous discussion and here illustrate two more. These examples, and others in this chapter, generally expose many of the *index gymnastics* involved with tensor manipulations. A bit of practice readily allows one to skip many of the steps exposed in the following.

1.6.1 Double vector product

Consider the double vector product

$$\mathbf{P} \times (\mathbf{Q} \times \mathbf{R}) = P_a Q_b R_c \vec{e}_a \times (\vec{e}_b \times \vec{e}_c) \quad \text{expose coordinates and basis vectors} \quad (1.37a)$$

$$= P_a Q_b R_c \vec{e}_a \times (\epsilon_{bcd} \vec{e}_d) \quad \text{vector product as per equation (1.12)} \quad (1.37b)$$

$$= P_a Q_b R_c \epsilon_{bcd} \epsilon_{ade} \vec{e}_e \quad \text{again, vector product as per equation (1.12)} \quad (1.37c)$$

$$= -P_a Q_b R_c \epsilon_{bcd} \epsilon_{aed} \vec{e}_e \quad \text{permute } a, d \text{ and pick up a minus sign.} \quad (1.37d)$$

Explicit substitution verifies that the contraction $\epsilon_{bcd} \epsilon_{aed}$ equals to

$$\epsilon_{bcd} \epsilon_{aed} = \delta_{ba} \delta_{ce} - \delta_{be} \delta_{ca}, \quad (1.38)$$

which is a very useful identity for Cartesian tensor analysis. It then leads to

$$\epsilon_{bcd} \epsilon_{aed} \vec{e}_e = \delta_{ba} \vec{e}_c - \delta_{ca} \vec{e}_b \quad (1.39)$$

so that

$$\mathbf{P} \times (\mathbf{Q} \times \mathbf{R}) = -P_a Q_b R_c (\delta_{ba} \vec{e}_c - \delta_{ca} \vec{e}_b) \quad (1.40a)$$

$$= -(\mathbf{P} \cdot \mathbf{Q}) \mathbf{R} + (\mathbf{P} \cdot \mathbf{R}) \mathbf{Q}. \quad (1.40b)$$

1.6.2 Scalar product of two vector products

We make further use of the Levi-Civita identity (1.38) to write

$$(\mathbf{P} \times \mathbf{Q}) \cdot (\mathbf{R} \times \mathbf{S}) = (\epsilon_{abc} p_a q_b) (\epsilon_{dec} R_d s_e) \quad \text{expand two vector products} \quad (1.41a)$$

$$= p_a q_b R_d s_e \epsilon_{abc} \epsilon_{dec} \quad \text{rearrange} \quad (1.41b)$$

$$= p_a q_b R_d s_e (\delta_{ad} \delta_{be} - \delta_{ae} \delta_{bd}) \quad \epsilon\text{-tensor identity (1.38)} \quad (1.41c)$$

$$= (\mathbf{P} \cdot \mathbf{R}) (\mathbf{Q} \cdot \mathbf{S}) - (\mathbf{P} \cdot \mathbf{S}) (\mathbf{Q} \cdot \mathbf{R}) \quad \text{reintroduce boldface notation.} \quad (1.41d)$$

1.7 Transforming the coordinate representations

The Cartesian basis vectors are mutually orthogonal and fixed in space. However, the orientation of the basis vectors is arbitrary. We thus consider an alternative specification to the basis vectors by performing a linear transformation

$$\vec{e}_{\bar{a}} = \mathcal{R}_{\bar{a}b} \vec{e}_b. \quad (1.42)$$

This expression introduced components to the transformation matrix moving between the unbarred and the barred Cartesian coordinates

$$\mathcal{R}_{\bar{a}b} = \begin{bmatrix} \mathcal{R}_{\bar{1}1} & \mathcal{R}_{\bar{1}2} & \mathcal{R}_{\bar{1}3} \\ \mathcal{R}_{\bar{2}1} & \mathcal{R}_{\bar{2}2} & \mathcal{R}_{\bar{2}3} \\ \mathcal{R}_{\bar{3}1} & \mathcal{R}_{\bar{3}2} & \mathcal{R}_{\bar{3}3} \end{bmatrix}. \quad (1.43)$$

In Cartesian tensor analysis studied in this chapter, the transformation matrix is assumed to be independent of space.⁸ Although the transformation matrix carries two indices, it is not a tensor. Instead, it is a matrix operator used to transform from one set of basis vectors to another.⁹ We now deduce some constraints on this transformation matrix.

1.7.1 Inverse transformation

Assuming the transformation is invertible leads to the inverse transformation

$$\vec{e}_a = (\mathcal{R}^{-1})_{a\bar{b}} \vec{e}_{\bar{b}}. \quad (1.44)$$

As a self-consistency check we combine this relation with equation (1.42) thus rendering

$$\vec{e}_a = (\mathcal{R}^{-1})_{a\bar{b}} \vec{e}_{\bar{b}} = (\mathcal{R}^{-1})_{a\bar{b}} (\mathcal{R}_{\bar{b}c} \vec{e}_c). \quad (1.45)$$

This relation holds since

$$(\mathcal{R}^{-1})_{a\bar{b}} \mathcal{R}_{\bar{b}c} = \delta_{ac}, \quad (1.46)$$

or as a matrix identity

$$\mathcal{R}^{-1} \mathcal{R} = I. \quad (1.47)$$

⁸The transformation matrix is a function of space and time for the general tensors considered in Chapter 8.

⁹We have more to say about the distinction between a matrix and tensor in Section 1.7.7.

1.7.2 Orthogonal transformation

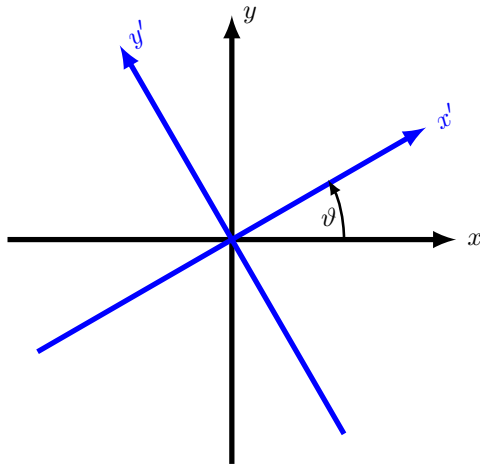


FIGURE 1.5: Counter-clockwise rotation through an angle ϑ of a right-handed horizontal Cartesian axes.

We now assume that the two sets of Cartesian basis vectors are orthonormal. That assumption leads to the following constraint on the transformation matrix

$$\delta_{\bar{a}\bar{b}} = \vec{e}_{\bar{a}} \cdot \vec{e}_{\bar{b}} \quad (1.48a)$$

$$= \mathcal{R}_{\bar{a}a} \vec{e}_a \cdot \mathcal{R}_{\bar{b}b} \vec{e}_b \quad \text{relate barred to unbarred basis vectors} \quad (1.48b)$$

$$= \mathcal{R}_{\bar{a}a} \mathcal{R}_{\bar{b}b} \vec{e}_a \cdot \vec{e}_b \quad \text{rearrange} \quad (1.48c)$$

$$= \mathcal{R}_{\bar{a}a} \mathcal{R}_{\bar{b}b} \delta_{ab} \quad \text{orthonormality of basis vectors} \quad (1.48d)$$

$$= \mathcal{R}_{\bar{a}a} \mathcal{R}_{\bar{b}a} \quad \text{perform contraction } \mathcal{R}_{\bar{b}b} \delta_{ab} = \mathcal{R}_{\bar{b}a} \quad (1.48e)$$

$$= \mathcal{R}_{\bar{a}a} (\mathcal{R}^T)_{a\bar{b}} \quad \text{introduce transpose matrix,} \quad (1.48f)$$

where \mathcal{R}^T is the transpose of the rotation matrix whose components are

$$(\mathcal{R}^T)_{a\bar{b}} = \mathcal{R}_{\bar{b}a}. \quad (1.49)$$

Written as a matrix equation we see that

$$\mathcal{R} \mathcal{R}^T = I. \quad (1.50)$$

This relation defines an *orthogonal transformation*, whereby the inverse matrix equals to the matrix transpose

$$\mathcal{R}^{-1} = \mathcal{R}^T. \quad (1.51)$$

1.7.3 Geometric interpretation of orthogonal transformations

Orthogonal transformations convert one set of Cartesian coordinates to another. Geometrically, an orthogonal transformation corresponds to a rotation so long as the determinant of the transformation is +1, with Figure 1.5 illustrating this axis rotation in two dimensions.¹⁰ For this two

¹⁰If the determinant of the transformation is -1, then the transformation involves a reflection in addition to a rotation, with the reflection changing the handedness of the basis vectors.

dimensional example, the rotation matrix can be written in terms of the cosine of the angles between the unit vectors; i.e., the *direction cosines*

$$\mathcal{R}_{\bar{a}a} = \begin{bmatrix} \cos \vartheta & \sin \vartheta \\ -\sin \vartheta & \cos \vartheta \end{bmatrix} = \begin{bmatrix} \cos \vartheta & \cos(\pi/2 - \vartheta) \\ \cos(\pi/2 + \vartheta) & \cos \vartheta \end{bmatrix} = \begin{bmatrix} \vec{e}_1 \cdot \vec{e}_1 & \vec{e}_1 \cdot \vec{e}_2 \\ \vec{e}_2 \cdot \vec{e}_1 & \vec{e}_2 \cdot \vec{e}_2 \end{bmatrix}. \quad (1.52)$$

The final form of the rotation matrix reveals that it is built from the projection of the rotated basis vectors onto the original basis vectors. This result holds for rotations in three dimensions as well, thus leading to

$$\mathcal{R}_{\bar{a}a} = \begin{bmatrix} \vec{e}_1 \cdot \vec{e}_1 & \vec{e}_1 \cdot \vec{e}_2 & \vec{e}_1 \cdot \vec{e}_3 \\ \vec{e}_2 \cdot \vec{e}_1 & \vec{e}_2 \cdot \vec{e}_2 & \vec{e}_2 \cdot \vec{e}_3 \\ \vec{e}_3 \cdot \vec{e}_1 & \vec{e}_3 \cdot \vec{e}_2 & \vec{e}_3 \cdot \vec{e}_3 \end{bmatrix}. \quad (1.53)$$

With the basis vectors all normalized, elements of the rotation matrix have magnitude less than or equal to unity and are given by the cosine of the angle between the respective basis vectors. As such, one sometimes refers to this rotation matrix as the *direction cosines* matrix.

1.7.4 Transforming the coordinate representation of a vector

We introduced the transformation (1.44) according to how it acts on the basis vectors. Now consider how it acts on the coordinate representation of an arbitrary vector by moving brackets

$$\mathbf{P} = P_a \vec{e}_a = P_a (\mathcal{R}^T)_{a\bar{a}} \vec{e}_{\bar{a}} \equiv P_{\bar{a}} \vec{e}_{\bar{a}}, \quad (1.54)$$

where we defined the transformation of the vector components

$$P_{\bar{a}} = P_a (\mathcal{R}^T)_{a\bar{a}} = \mathcal{R}_{\bar{a}a} P_a. \quad (1.55)$$

1.7.5 Invariance of the scalar product

The above properties of an orthogonal transformation ensure that the scalar product

$$\mathbf{P} \cdot \mathbf{Q} = P_a Q_a \quad (1.56)$$

is the same regardless the choice of Cartesian coordinates

$$\mathbf{P} \cdot \mathbf{Q} = P_a Q_a \quad \text{expose tensor indices} \quad (1.57a)$$

$$= P_a \vec{e}_a \cdot Q_b \vec{e}_b \quad \text{orthonormal basis vectors: } \vec{e}_a \cdot \vec{e}_b = \delta_{ab} \quad (1.57b)$$

$$= P_a Q_b \vec{e}_a \cdot \vec{e}_b \quad \text{rearrange} \quad (1.57c)$$

$$= P_a Q_b (\mathcal{R}^T)_{a\bar{a}} \vec{e}_{\bar{a}} \cdot (\mathcal{R}^T)_{b\bar{b}} \vec{e}_{\bar{b}} \quad \text{rotate basis vectors to barred frame} \quad (1.57d)$$

$$= P_a Q_b (\mathcal{R}^T)_{a\bar{a}} (\mathcal{R}^T)_{b\bar{b}} \vec{e}_{\bar{a}} \cdot \vec{e}_{\bar{b}} \quad \text{rearrange} \quad (1.57e)$$

$$= P_a Q_b (\mathcal{R}^T)_{a\bar{a}} (\mathcal{R}^T)_{b\bar{b}} \delta_{\bar{a}\bar{b}} \quad \text{orthonormality: } \vec{e}_{\bar{a}} \cdot \vec{e}_{\bar{b}} = \delta_{\bar{a}\bar{b}} \quad (1.57f)$$

$$= P_a Q_b (\mathcal{R}^T)_{a\bar{a}} (\mathcal{R}^T)_{b\bar{a}} \quad \text{contraction: } (\mathcal{R}^T)_{b\bar{b}} \delta_{\bar{a}\bar{b}} = (\mathcal{R}^T)_{b\bar{a}} \quad (1.57g)$$

$$= P_a Q_b (\mathcal{R}^T)_{a\bar{a}} (\mathcal{R})_{\bar{a}\bar{b}} \quad \text{transpose: } (\mathcal{R}^T)_{b\bar{a}} = (\mathcal{R})_{\bar{a}\bar{b}} \quad (1.57h)$$

$$= P_a Q_b \delta_{ab} \quad \text{orthogonal rotation: } (\mathcal{R}^T)_{a\bar{a}} (\mathcal{R})_{\bar{a}\bar{b}} = \delta_{ab} \quad (1.57i)$$

$$= P_{\bar{a}} Q_{\bar{a}} \quad \text{perform contraction: } Q_b \delta_{ab} = Q_a. \quad (1.57j)$$

1.7.6 Transforming the coordinate representation of a second order tensor

The stress tensor in Chapter 21; the moment of inertia tensor in Section 34.8.4; and the diffusion tensor in Chapter 61 are examples of second order tensors. Second order tensors have a coordinate representation given by

$$\mathbb{T} = T_{ab} \vec{e}_a \otimes \vec{e}_b, \quad (1.58)$$

with T_{ab} the Cartesian coordinates that can be organized as a matrix. Notably, there is not a scalar product between the basis vectors in equation (1.58). Instead, the \otimes symbol represents the *outer product* of the two basis vectors. For our purposes the outer product simply provides a formal means for two vectors to be positioned next to one another. For many purposes we drop the \otimes symbol for brevity.

We determine how the Cartesian coordinate components T_{ab} transform by following the now familiar procedure for transforming the basis vectors. The key new facet is that now we have two basis vectors to carry around

$$\mathbb{T} = T_{ab} \vec{e}_a \vec{e}_b \quad \text{expose indices and basis vectors} \quad (1.59a)$$

$$= T_{ab} (\mathcal{R}^T)_{a\bar{a}} \vec{e}_{\bar{a}} (\mathcal{R}^T)_{b\bar{b}} \vec{e}_{\bar{b}} \quad \text{rotate basis vectors to barred frame} \quad (1.59b)$$

$$= T_{ab} (\mathcal{R}^T)_{a\bar{a}} (\mathcal{R}^T)_{b\bar{b}} \vec{e}_{\bar{a}} \vec{e}_{\bar{b}} \quad \text{rarrange} \quad (1.59c)$$

$$\equiv T_{\bar{a}\bar{b}} \vec{e}_{\bar{a}} \vec{e}_{\bar{b}} \quad \text{define transformed tensor components.} \quad (1.59d)$$

The final equality introduced the transformed components to the second order tensor

$$T_{\bar{a}\bar{b}} = T_{ab} (\mathcal{R}^T)_{a\bar{a}} (\mathcal{R}^T)_{b\bar{b}} = T_{ab} \mathcal{R}_{\bar{a}a} \mathcal{R}_{\bar{b}b}. \quad (1.60)$$

The transformation of the components to higher order tensors follows analogously simply by carrying around further basis vectors.

1.7.7 Distinguishing between tensors and matrices

Matrices are useful for organizing the coordinate components to a tensor. For example, the coordinate components to a first-order tensor (a vector)

$$\mathbf{P} = P_1 \vec{e}_1 + P_2 \vec{e}_2 + P_3 \vec{e}_3, \quad (1.61)$$

can be organized into a *row vector*

$$\mathbf{P} = (P_1, P_2, P_3). \quad (1.62)$$

We are justified in assigning the name “vector” in this context since we know that the array elements comprise the coordinate representation of the vector, \mathbf{P} . However, if we just see an array of numbers, say (Q_1, Q_2, Q_3) , on its own, then we generally have no idea whether the elements of that array are related to each other, or if the list is just an ordering of numbers. If the array is merely a list of numbers, then in general nothing changes when we alter coordinates. But if the array is the coordinate representation of a vector (e.g., a row vector), then we know that the elements of the row vector are related, and we know how they are changed when the coordinates are changed.

We now consider two examples of objects that are not tensors. First, consider the rotation matrix, $\mathcal{R}_{\bar{a}a}$, whose elements are built from the direction cosines according to equation (1.53). Although carrying two indices, this matrix is not the coordinate representation of a second order tensor. Rather, it is the matrix used to transform the components of tensors from one coordinate system to another. That is, the rotation matrix is not a geometric object like a vector or tensor,

but it is an ordered array containing information for how a coordinate transformation alters the representation of geometric objects.

Although jumping ahead somewhat, we mention one further example encountered when studying general tensors in Chapter 8. Namely, the *Christoffel symbols* in Section 8.11.1 are built from the spatial derivatives of the basis vectors. Although carrying three indices, the Christoffel symbols are not elements of a third order tensor since they do not transform as elements to a tensor. One way to understand this point is to note that a tensor that vanishes in one coordinate system is zero for all coordinate systems. However, all of the Christoffel symbols vanish for Euclidean space using Cartesian coordinates, because the Cartesian basis vectors are spatially constant. However, there are some nonzero Christoffel symbols when representing Euclidean space with spherical coordinates. We conclude that the Christoffel symbols cannot be components of a tensor.

The key point we re-emphasize is that a tensor is a geometric object (Section 1.1) that can be represented using any arbitrary set of coordinates. Since the tensor has an objective existence independent of coordinates, its coordinate components are constrained to transform in a precise manner when changing coordinates. These properties of tensors are generally not shared with arbitrary matrices, hence the importance of making the distinction between tensors and matrices.

1.8 Homogeneity and isotropy

We have many occasions to consider basic symmetry properties of tensor fields, with homogeneity and isotropy two rather basic symmetry properties.

1.8.1 Homogeneous tensor

A tensor field is *homogeneous* if it possesses the same value at each point in space. For example, a uniform temperature field is homogeneous, as is a uniform velocity field. As defined, a homogeneous tensor field has no spatial dependence and thus it does not provide any means to distinguish points in space. Likewise, a time independent tensor is said to be homogeneous in time.

1.8.2 Isotropic and anisotropic tensors

A tensor field is *isotropic* if its representation remains independent of coordinate basis. A scalar tensor is, by definition, isotropic since it has no information about spatial directions. A nonzero vector field cannot be isotropic since it points in a particular direction and so its representation is dependent on the orientation of the basis vectors.

A second order isotropic tensor, J , has components that are unchanged when undergoing rotation, so that

$$J_{\bar{a}\bar{b}} = J_{ab} \mathcal{R}_{\bar{a}a} \mathcal{R}_{\bar{b}b} \equiv J_{ab} \quad (1.63)$$

where we used the identity (1.60) for the component transformation. For nonzero tensors, this equation is satisfied by

$$J_{ab} = \lambda \delta_{ab}, \quad (1.64)$$

with λ an arbitrary scalar. Hence, the most general second order isotropic tensor is proportional to the Kronecker (identity) tensor.

We often find it useful to decompose an arbitrary second order tensor into its anisotropic and isotropic components according to

$$T_{ab} = T_{ab} - \underbrace{\frac{T_{pp}}{\delta_{pp}} \delta_{ab}}_{\text{anisotropic}} + \underbrace{\frac{T_{pp}}{\delta_{pp}} \delta_{ab}}_{\text{isotropic}}, \quad (1.65)$$

where

$$T_{pp} = \sum_{p=1}^N T_{pp} = \text{trace of } T_{ab} \quad \text{and} \quad \delta_{pp} = \sum_{p=1}^N \delta_{pp} = N \quad (1.66)$$

with N the number of space dimensions. We know that $T_{ab} - (T_{pp}/\delta_{pp}) \delta_{ab}$ is the anisotropic portion of T_{ab} simply because $(T_{pp}/\delta_{pp}) \delta_{ab}$ is isotropic.



1.9 Exercises

EXERCISE 1.1: PRODUCT OF SYMMETRIC MATRICES

Let $A = A^T$ and $B = B^T$ be two symmetric matrices. Under what condition is their product also symmetric: $AB = (AB)^T$?

EXERCISE 1.2: PRODUCT OF SYMMETRIC AND ANTI-SYMMETRIC MATRICES AND TENSORS

Let $A = -A^T$ be an anti-symmetric matrix, and $S = S^T$ be a symmetric matrix. Show that the trace of their product vanishes: $\text{Tr}(AS) = 0$. Alternatively, in terms of tensors, show that the full contraction of an anti-symmetric tensor with a symmetric tensor vanishes: $A_{mn} S_{mn} = 0$.

EXERCISE 1.3: PROJECTION OPERATOR

Consider an arbitrary direction in space specified by the unit vector $\hat{\mathbf{n}}$ with components \hat{n}_a . Define the projection operator

$$P_{ab} = \delta_{ab} - \hat{n}_a \hat{n}_b, \quad (1.67)$$

and show that

$$P_{ab} T_{bc} \hat{n}_a = 0. \quad (1.68)$$

Hence,

$$S_{ac} = P_{ab} T_{bc} = (\delta_{ab} - \hat{n}_a \hat{n}_b) T_{bc} = T_{ac} - \hat{n}_a (\hat{n}_b T_{bc}) \quad (1.69)$$

is the projection of T_{bc} onto the plane perpendicular to the direction $\hat{\mathbf{n}}$.



Chapter 2

CARTESIAN TENSOR CALCULUS

This chapter presents elements of differential and integral calculus that we later use for our study of geophysical fluid mechanics. We build from the Cartesian tensor algebra of Chapter 1 to develop elements of Cartesian tensor calculus, which is the basis for vector calculus. The material is extensively used throughout this book.

CHAPTER GUIDE

The material in this chapter can be found in various forms in nearly all books on calculus with analytic geometry. Particular treatments, with applications to physics, are given in the following.

- FEYNMAN LECTURES: Chapters 2 and 3 in Volume II of the [Feynman Lectures](#) offers insightful discussions of vector differential calculus. Although written for students of electrodynamics, many of the examples are drawn from fluid mechanics.
- DIV, GRAD, CURL AND ALL THAT ([Schey, 2004](#)): This text presents the methods and theorems of vector calculus in a manner that greatly assists the development of intuition.
- Chapter 2 in [Segel \(1987\)](#) provides a lucid review of vector calculus using Cartesian tensors.
- THEORY AND PROBLEMS OF VECTOR ANALYSIS ([Spiegel, 1974a](#)): This “Schaum’s Outline Series” book has nearly 500 worked exercises and provides a useful resource to develop problem solving in vector calculus. Some of the exercises in Section 2.9 at the end of this chapter are drawn from [Spiegel \(1974a\)](#).
- [This video from 3Blue1Brown](#) provides some compelling graphics to support intuition for the divergence and curl operators.
- [This Youtube channel from Steve Brunton](#) offers some pedagogical lectures on vector calculus.

2.1	Gradient of a scalar field	24
2.1.1	Direction of steepest ascent	25
2.1.2	Tangent to an isosurface	26
2.1.3	Normal to an isosurface	26
2.1.4	Unit vectors change only by rotation	26
2.1.5	Showing that $\delta\hat{\mathbf{n}} \cdot \hat{\mathbf{n}} = 0$	27

2.2	Divergence of a vector field	28
2.2.1	Divergence of a scalar field times a vector field	28
2.2.2	Laplacian of a scalar field	29
2.3	Curl of a vector field	29
2.3.1	Computing the curl	29
2.3.2	Curl-free vector fields	30
2.3.3	Curl-free and divergence-free fields	31
2.3.4	Identities involving the curl	31
2.4	Path integral of a scalar function	33
2.4.1	Cartesian coordinates	33
2.4.2	Arc length parameterization	34
2.4.3	Linear path example	34
2.5	Path integral of a vector function	35
2.5.1	Circulation	35
2.5.2	Circulation example	36
2.5.3	Fundamental theorem of calculus	36
2.6	Stokes' curl theorem	36
2.6.1	Statement of Stokes' theorem	36
2.6.2	Stokes' theorem for a rectangular region	37
2.7	Gauss's divergence theorem	38
2.7.1	An example rectangular volume	39
2.7.2	Divergence theorem for scalar fields	39
2.7.3	Surface integral of the outward unit normal	39
2.7.4	First and second form of Green's identities	40
2.7.5	Integral of a curl over a closed surface	40
2.7.6	The domain integral of a non-divergent field	41
2.8	Exact and inexact differentials	42
2.8.1	Exact differentials	42
2.8.2	Inexact differentials	42
2.8.3	Integrating factors	43
2.8.4	An example using the velocity field	43
2.8.5	Heuristic physics of exact and inexact differential operations	43
2.9	Exercises	44

2.1 Gradient of a scalar field

Consider a real valued scalar field, $\psi(\mathbf{x})$, defined on Euclidean space. The argument to his field is the position in space that has a Cartesian coordinate representation

$$\mathbf{x} = \sum_{a=1}^3 x_a \vec{e}_a = x_a \vec{e}_a, \quad (2.1)$$

where the second equation made use of the Einstein summation convention introduced in Chapter 1. In our applications, we encounter scalar fields such as the temperature, the mass density, and the specific entropy. We can estimate the value of the field at an adjacent point an infinitesimal distance away, $\mathbf{x} + d\mathbf{x}$, through use of a truncated Taylor series

$$\psi(\mathbf{x} + d\mathbf{x}) = \psi(\mathbf{x}) + \frac{\partial \psi}{\partial x_1} dx_1 + \frac{\partial \psi}{\partial x_2} dx_2 + \frac{\partial \psi}{\partial x_3} dx_3 + \mathcal{O}(d\mathbf{x} \cdot d\mathbf{x}) \quad (2.2a)$$

$$\approx [1 + dx_a \partial_a] \psi(\mathbf{x}), \quad (2.2b)$$

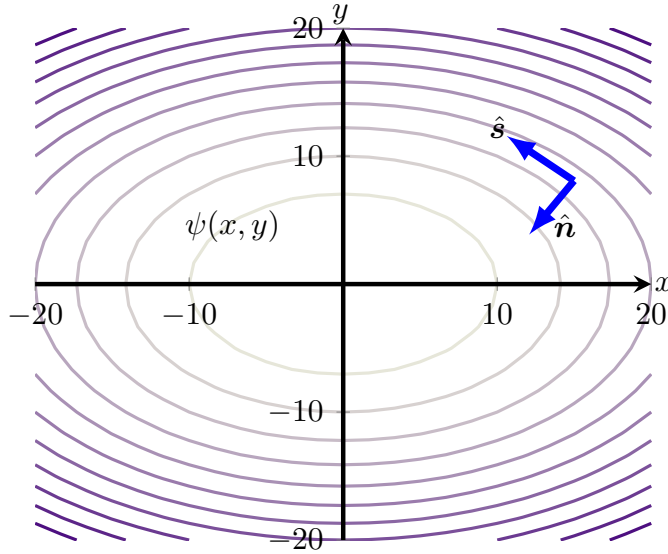


FIGURE 2.1: Contours of a scalar field $\psi(x, y) = -x^2/2 - y^2$. At any point in space, the gradient, $\nabla\psi = -(x \hat{\mathbf{x}} + 2y \hat{\mathbf{y}})$, points in the direction of steepest increase (ascent) and orients the unit normal vector $\hat{\mathbf{n}} = |\nabla\psi|^{-1} \nabla\psi$. The unit tangent vector, $\hat{\mathbf{s}}$, points in a direction tangent to a ψ isosurface so that it is everywhere orthogonal to the direction of steepest ascent: $\hat{\mathbf{n}} \cdot \hat{\mathbf{s}} = 0$. We follow the convention in which the unit normal is oriented to the left of the tangent when facing in the tangent direction.

where we dropped higher order terms to reach the final approximate expression. We also introduced the shorthand notation for the partial derivative operator

$$\partial_a = \frac{\partial}{\partial x_a}, \quad (2.3)$$

which is a notation used throughout this book. We can introduce the Cartesian gradient operator according to

$$\nabla = \vec{e}_a \partial_a = \hat{\mathbf{x}} \partial_x + \hat{\mathbf{y}} \partial_y + \hat{\mathbf{z}} \partial_z \quad (2.4)$$

in which case

$$\psi(\mathbf{x} + d\mathbf{x}) \approx (1 + d\mathbf{x} \cdot \nabla) \psi(\mathbf{x}). \quad (2.5)$$

Note that in some treatments, ∇ is referred to as *Hamilton's operator*.

2.1.1 Direction of steepest ascent

Using the approximate relation (2.5), and the geometric expression (1.11) for the scalar product, renders

$$\psi(\mathbf{x} + d\mathbf{x}) - \psi(\mathbf{x}) \approx |d\mathbf{x}| |\nabla\psi| \cos \vartheta, \quad (2.6)$$

where ϑ is the angle between the differential increment, $d\mathbf{x}$, and the gradient, $\nabla\psi$. Orienting the increment $d\mathbf{x}$ so that $\vartheta = 0$ ensures that $\psi(\mathbf{x} + d\mathbf{x}) - \psi(\mathbf{x})$ is maximal. Consequently, $\nabla\psi$ points in the direction of *steepest ascent* across constant ψ isosurfaces (Figure 2.1). The opposite direction is that of *steepest descent*, where $\vartheta = \pi$.

2.1.2 Tangent to an isosurface

Consider a family of isosurfaces defined by points satisfying

$$\psi(\mathbf{x}) = \text{constant}. \quad (2.7)$$

Figure 2.1 shows a two dimensional example where the isosurfaces are lines where ψ is a constant. As another example, consider $\psi(\mathbf{x}) = \psi(r)$, where $r^2 = \mathbf{x} \cdot \mathbf{x}$ is the squared radius of a sphere. Isosurfaces for this spherically symmetric function are spherical surfaces of radius r .

In general, moving along an isosurface keeps the scalar field unchanged. Let $\hat{\mathbf{t}}$ be a unit vector that points in the direction tangent to the isosurface at any point \mathbf{x} . By construction

$$\psi(\mathbf{x} + \hat{\mathbf{t}} ds) - \psi(\mathbf{x}) = 0, \quad (2.8)$$

where ds is an infinitesimal arc length along the tangent direction. In words, this identity says that if we move an infinitesimal distance in the direction tangent to the isosurface, then the function ψ does not change its value. Now expanding this identity in a Taylor series leads to the vanishing of the tangential partial derivative

$$\hat{\mathbf{t}} \cdot \nabla \psi = \frac{\partial \psi}{\partial s} = 0. \quad (2.9)$$

That is, isosurfaces of a function ψ are defined by directions along which the partial derivative of the function vanishes. For the spherically symmetric function, $\psi(\mathbf{x}) = \psi(r)$, the tangent vector points in either of the two angular directions along the spherical surface.

2.1.3 Normal to an isosurface

We may normalize the direction of maximal ascent, in which case we define the unit normal direction

$$\hat{\mathbf{n}} = |\nabla \psi|^{-1} \nabla \psi. \quad (2.10)$$

By construction, the gradient computed in the $\hat{\mathbf{n}}$ direction yields the maximum change for the function so that the *normal derivative* is given by

$$\hat{\mathbf{n}} \cdot \nabla \psi = \frac{\partial \psi}{\partial n} = |\nabla \psi|. \quad (2.11)$$

For the spherically symmetric example,

$$\hat{\mathbf{n}} = \frac{\mathbf{x}}{|\mathbf{x}|} = \hat{\mathbf{r}}, \quad (2.12)$$

where $\hat{\mathbf{r}}$ is the unit vector pointing radially outward from the origin. In this case the normal derivative is equal to the radial derivative

$$\hat{\mathbf{n}} \cdot \nabla \psi = \frac{\partial \psi}{\partial r} \quad \text{spherically symmetric } \psi. \quad (2.13)$$

2.1.4 Unit vectors change only by rotation

Consider an arbitrary unit vector, $\hat{\mathbf{m}}$. The defining feature of a unit vector is that it has unit magnitude

$$\hat{\mathbf{m}} \cdot \hat{\mathbf{m}} = 1. \quad (2.14)$$

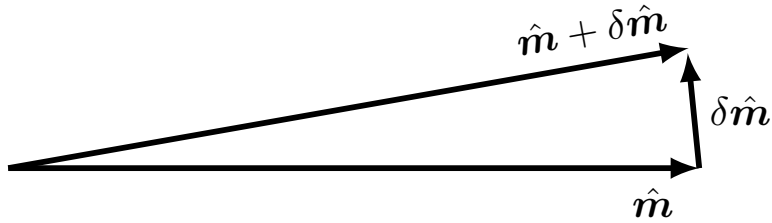


FIGURE 2.2: The infinitesimal change to a unit vector is itself perpendicular to the unit vector: $\delta\hat{m} \cdot \hat{m} = 0$. The reason is that the unit vector is constrained to retain its unit length, so that the only way that it can change is to change its direction. So in this image we have $|\hat{m} + \delta\hat{m}| = |\hat{m}| = 1$, which requires $\delta\hat{m} \cdot \hat{m} = 0$.

Unit vectors can only be modified through changes in their direction since their magnitude is fixed at unity. Hence, they are only modified by rotations. An important consequence of this constraint is that the infinitesimal change to a unit vector is perpendicular to the unit vector itself (see Figure 2.2). We see this property through considering an arbitrary infinitesimal change, symbolized by δ , in which

$$0 = \delta(1) = \delta(\hat{m} \cdot \hat{m}) = 2\hat{m} \cdot \delta\hat{m}. \quad (2.15)$$

In Section 11.3, we formally show that the constraint

$$\delta\hat{m} \cdot \hat{m} = 0 \quad (2.16)$$

means that unit vector changes can only arise from rotations. Even so, the above assertion should make intuitive sense.

2.1.5 Showing that $\delta\hat{n} \cdot \hat{n} = 0$

As an illustration of the constraint (2.16), let us verify that it holds for the special case of a unit normal vector (2.10) defined according to surfaces of constant scalar field

$$\hat{n} = |\nabla\psi|^{-1} \nabla\psi. \quad (2.17)$$

The proof follows first by writing

$$\delta\hat{n} = |\nabla\psi|^{-1} [\delta(\nabla\psi) - \hat{n} \delta|\nabla\psi|], \quad (2.18)$$

so that

$$|\nabla\psi| \hat{n} \cdot \delta\hat{n} = \hat{n} \cdot \delta(\nabla\psi) - \delta|\nabla\psi| = \frac{\nabla\psi \cdot \delta(\nabla\psi)}{|\nabla\psi|} - \delta|\nabla\psi| = 0. \quad (2.19)$$

The last equality made use of the identity

$$\delta(|\nabla\psi|) = \delta(\sqrt{\nabla\psi \cdot \nabla\psi}) = \frac{1}{2\sqrt{\nabla\psi \cdot \nabla\psi}} \delta(\nabla\psi \cdot \nabla\psi) = \frac{\nabla\psi \cdot \delta(\nabla\psi)}{|\nabla\psi|}. \quad (2.20)$$

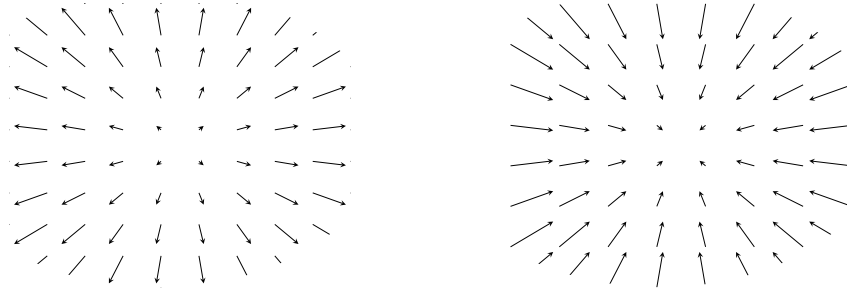


FIGURE 2.3: Two vector fields with a non-zero horizontal divergence. Left panel: The vector field $\mathbf{F} = x \hat{x} + y \hat{y}$ has a spatially constant positive divergence at each point with $\nabla \cdot \mathbf{F} = 2$. We thus say that the vector field is “diverging from each point.” Right panel: with the opposite sign, the vector field $\mathbf{G} = -\mathbf{F} = -x \hat{x} - y \hat{y}$ has a spatially constant negative divergence at each point with $\nabla \cdot \mathbf{G} = -2$. We thus say that the vector field is “converging to each point.” Note that these two vector fields have zero curl, $\nabla \times \mathbf{F} = \nabla \times \mathbf{G} = 0$.

2.2 Divergence of a vector field

The divergence of a vector field, \mathbf{F} , is the scalar product of the divergence operator with the vector

$$\text{div}(\mathbf{F}) = \nabla \cdot \mathbf{F} = \partial_a F_a \begin{cases} > 0 \Rightarrow \text{diverging vector field,} \\ < 0 \Rightarrow \text{converging vector field} \\ = 0 \Rightarrow \text{divergence-free vector field.} \end{cases} \quad (2.21)$$

If the vector field in the surrounding neighborhood of a point is directed away from that point, then the vector field is diverging as if there is a source at the point (Figure 2.3). In this case the divergence of the vector field is positive. The converse occurs for a vector field converging to a point as if there is a sink.

If the vector field under consideration is the velocity field of a moving fluid, then these considerations are directly related to the conservation of matter that we study in Chapter 16. That discussion motivates us to consider a positive divergence for a vector field as representing the creation of “stuff” at a point where there is a positive divergence. Again for the case of a fluid velocity, there is a net divergence if more fluid leaves a point than enters, and the converse holds if the velocity field is converging. We further discuss these ideas as part of our study of Gauss’s divergence theorem in Section 2.7.

2.2.1 Divergence of a scalar field times a vector field

We have many opportunities to make use of properties of the divergence operator following from application of the chain rule. For example, use of the chain rule indicates that the divergence of a scalar field times a vector field is given by

$$\nabla \cdot (\phi \mathbf{F}) = \partial_a (\phi F_a) \quad (2.22a)$$

$$= F_a \partial_a \phi + \phi \partial_a F_a \quad (2.22b)$$

$$= \mathbf{F} \cdot \nabla \phi + \phi \nabla \cdot \mathbf{F}. \quad (2.22c)$$

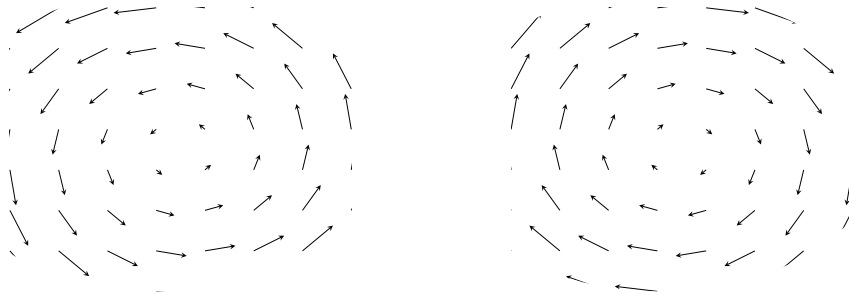


FIGURE 2.4: A horizontal vector field with a constant curl and zero divergence. Left panel: $\mathbf{F} = -y \hat{x} + x \hat{y}$, $\Rightarrow \nabla \times \mathbf{F} = 2 \hat{z}$ and $\nabla \cdot \mathbf{F} = 0$. Right panel: $\mathbf{G} = -\mathbf{F}$ so that $\nabla \times \mathbf{G} = -2 \hat{z}$.

2.2.2 Laplacian of a scalar field

The Laplacian of a scalar field is the divergence of the gradient

$$\nabla^2 \psi = \nabla \cdot \nabla \psi. \quad (2.23)$$

Scalar fields that have a vanishing Laplacian are said to be *harmonic*

$$\nabla^2 \psi = 0 \quad \text{harmonic function.} \quad (2.24)$$

Familiar examples of harmonic functions are the sines and cosines used for Fourier analysis in Euclidean space, and the spherical harmonics used for Fourier analysis on the sphere. The name *harmonic* originates from the relation of harmonic functions to characteristic vibrational modes of a taut string such as those found on musical instruments (when played with skill). Furthermore, harmonic functions play a central role in complex analysis.

2.3 Curl of a vector field

The curl characterizes how a vector field spins around each point in space. In fluid mechanics we make great use of the vorticity field, which is the curl of the velocity (Chapter 37).

2.3.1 Computing the curl

We measure the curl of a vector by computing the cross product of the divergence operator with the vector field. Hence, just like the cross product from Section 1.4, the curl is specified by both a magnitude and a direction

$$\text{curl}(\mathbf{F}) = \nabla \times \mathbf{F} \quad (2.25a)$$

$$= \vec{e}_a \partial_a \times \vec{e}_b F_b \quad \text{coordinate representation and basis} \quad (2.25b)$$

$$= \vec{e}_a \times \partial_a (\vec{e}_b F_b) \quad \text{move derivative operator onto } \mathbf{F} = \vec{e}_b F_b \quad (2.25c)$$

$$= (\vec{e}_a \times \vec{e}_b) \partial_a F_b + F_b (\vec{e}_a \times \partial_a \vec{e}_b) \quad \text{perform product rule} \quad (2.25d)$$

$$= \epsilon_{abc} \vec{e}_c \partial_a F_b \quad \partial_a \vec{e}_b = 0 \text{ for Cartesian coordinates.} \quad (2.25e)$$

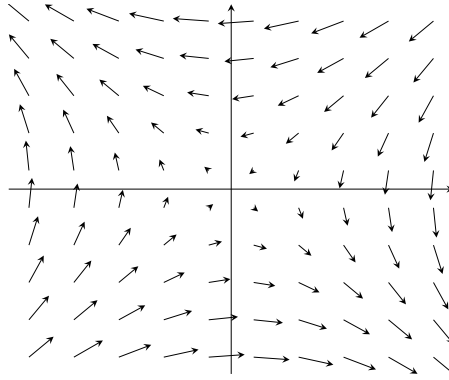


FIGURE 2.5: A horizontal vector field with a zero curl, where $\mathbf{F} = -\nabla\psi$ with the scalar potential given by $\psi = \sin(x/10) \sin(y/10)$.

To reach this result we set $\partial_a \vec{e}_b = 0$ since the Cartesian basis vectors are fixed in space.¹ We also made use of the relation (1.12) for the cross product of basis vectors. Expanding the final expression leads to the familiar expression

$$\text{curl}(\mathbf{F}) = \nabla \times \mathbf{F} = \left[\frac{\partial F_3}{\partial x_2} - \frac{\partial F_2}{\partial x_3} \right] \hat{x} + \left[\frac{\partial F_1}{\partial x_3} - \frac{\partial F_3}{\partial x_1} \right] \hat{y} + \left[\frac{\partial F_2}{\partial x_1} - \frac{\partial F_1}{\partial x_2} \right] \hat{z}, \quad (2.26)$$

which can also be written as a determinant

$$\nabla \times \mathbf{F} = \det \begin{bmatrix} \vec{e}_1 & \vec{e}_2 & \vec{e}_3 \\ \partial_1 & \partial_2 & \partial_3 \\ F_1 & F_2 & F_3 \end{bmatrix}. \quad (2.27)$$

The horizontal vector field $\mathbf{F} = x \hat{x} + y \hat{y}$ shown in Figure 2.3 has zero curl yet non-zero divergence. Figure 2.4 shows another vector field, $\mathbf{F} = -y \hat{x} + x \hat{y}$, with zero divergence yet nonzero curl $\nabla \times \mathbf{F} = 2 \hat{z}$. We encounter this vector again in Section 34.5, where we see that it corresponds to the velocity due to solid-body motion on a rotating planet, and with its curl measuring the planetary vorticity.

2.3.2 Curl-free vector fields

There are some cases of physically relevant vector fields that have a vanishing curl

$$\nabla \times \mathbf{F} = 0. \quad (2.28)$$

We sometimes refer to such curl-free vectors as *irrotational*. In fluid mechanics a curl-free velocity field has zero vorticity², which is a property maintained by linear gravity waves in the absence of rotation (Section 48.5). We illustrate a curl-free vector field in Figure 2.5.

The curl of a gradient vanishes, which follows from

$$\nabla \times \nabla \psi = \vec{e}_a \partial_a \times \vec{e}_b \partial_b \psi = (\vec{e}_a \times \vec{e}_b) \partial_a \partial_b \psi = 0, \quad (2.29)$$

¹Basis vectors corresponding to non-Cartesian coordinates are spatially dependent (see Chapters 7 and 8), thus making this step invalid for general tensors. We will find a “fix” for this step in Section 8.17, thus leading to the *covariant curl operator*.

²We study vorticity in Part VII of this book.

where the final equality follows since $\vec{e}_a \times \vec{e}_b$ is anti-symmetric on the labels ab (i.e., $\vec{e}_a \times \vec{e}_b = -\vec{e}_b \times \vec{e}_a$) whereas $\partial_a \partial_b$ is symmetric (i.e., $\partial_a \partial_b = \partial_b \partial_a$). This property allows us to introduce a scalar field whose gradient equals to the curl-free vector field

$$\mathbf{F} = -\nabla\psi \quad \text{scalar potential.} \quad (2.30)$$

The scalar ψ is known as the *scalar potential*. In the specific case of \mathbf{F} representing the gravitational force, then ψ is called the gravitational potential (see Section 11.11 and Chapter 31).

2.3.3 Curl-free and divergence-free fields

Consider a vector field that has zero curl *and* zero divergence. The curl-free property means that

$$\nabla \times \mathbf{F} = 0 \implies \mathbf{F} = -\nabla\psi. \quad (2.31)$$

The divergence-free property means that ψ is a harmonic function (Section 2.2.2)

$$\nabla \cdot \nabla\psi = \nabla^2\psi = 0. \quad (2.32)$$

The velocity field arising from a linear non-rotating gravity wave (Section 48.5) in a Boussinesq fluid (Section 26.1) maintains zero vorticity and zero divergence. Furthermore, curl-free and divergence-free velocity fields are commonly encountered in engineering applications such as aerodynamics (e.g., see [Acheson \(1990\)](#) for many elementary examples).

2.3.4 Identities involving the curl

We close this section by deriving a suite of identities involving the curl operator. These identities are especially useful when developing dynamical equations for vorticity. Furthermore, by making use of the rules for general tensor analysis developed in Chapters 7 and 8, these identities take on the same form regardless the coordinate choice.

Divergence of the curl vanishes

The divergence of the curl vanishes, as seen through the following

$$\nabla \cdot (\nabla \times \mathbf{F}) = \partial_a(\epsilon_{abc} \partial_b F_c) = \epsilon_{abc} \partial_a \partial_b F_c = 0. \quad (2.33)$$

The final equality holds since $\partial_a \partial_b$ is symmetric on ab whereas ϵ_{abc} is anti-symmetric.

Divergence of a cross product

We now derive an expression for the divergence of a cross product through the following manipulations

$$\nabla \cdot (\mathbf{F} \times \mathbf{E}) = \vec{e}_a \cdot \partial_a (F_b \vec{e}_b \times E_c \vec{e}_c) \quad (2.34a)$$

$$= \vec{e}_a \cdot (\vec{e}_b \times \vec{e}_c) \partial_a (F_b E_c) \quad (2.34b)$$

$$= \epsilon_{abc} \partial_a (F_b E_c) \quad (2.34c)$$

$$= F_b \epsilon_{abc} \partial_a E_c + E_c \epsilon_{abc} \partial_a F_b \quad (2.34d)$$

$$= -\mathbf{F} \cdot (\nabla \times \mathbf{E}) + \mathbf{E} \cdot (\nabla \times \mathbf{F}). \quad (2.34e)$$

Curl of a scalar times a vector

We can compute the curl of a scalar field $\psi \mathbf{F}$ through the following steps

$$\nabla \times (\psi \mathbf{F}) = \vec{e}_a \partial_a \times \psi \vec{e}_b F_b \quad (2.35a)$$

$$= (\vec{e}_a \times \vec{e}_b) \partial_a (\psi F_b) \quad (2.35b)$$

$$= \epsilon_{abc} \vec{e}_c (\psi \partial_a F_b + F_b \partial_a \psi) \quad (2.35c)$$

$$= \psi \nabla \times \mathbf{F} + \nabla \psi \times \mathbf{F}. \quad (2.35d)$$

Curl of a cross product

The curl of a cross product of two vectors is given by

$$\nabla \times (\mathbf{F} \times \mathbf{E}) = \vec{e}_a \partial_a \times (\vec{e}_b F_b \times \vec{e}_c E_c) \quad (2.36a)$$

$$= \vec{e}_a \times (\vec{e}_b \times \vec{e}_c) \partial_a (F_b E_c) \quad (2.36b)$$

$$= \vec{e}_a \times (\epsilon_{bcd} \vec{e}_d) \partial_a (F_b E_c) \quad (2.36c)$$

$$= \epsilon_{ade} \epsilon_{bcd} \vec{e}_e \partial_a (F_b E_c) \quad (2.36d)$$

$$= -\epsilon_{aed} \epsilon_{bcd} \vec{e}_e \partial_a (F_b E_c) \quad (2.36e)$$

$$= -(\delta_{ab} \delta_{ec} - \delta_{ac} \delta_{eb}) \vec{e}_e \partial_a (F_b E_c) \quad (2.36f)$$

$$= (-\delta_{ba} \vec{e}_c + \delta_{ca} \vec{e}_b) \partial_a (F_b E_c) \quad (2.36g)$$

$$= \mathbf{F} (\nabla \cdot \mathbf{E}) + (\mathbf{E} \cdot \nabla) \mathbf{F} - \mathbf{E} (\nabla \cdot \mathbf{F}) - (\mathbf{F} \cdot \nabla) \mathbf{E}. \quad (2.36h)$$

Curl of a curl

A special case of the identity (2.36h) allows us to write the curl of a curl as

$$\nabla \times (\nabla \times \mathbf{F}) = \vec{e}_a \times (\vec{e}_b \times \vec{e}_c) \partial_a \partial_b F_c \quad (2.37a)$$

$$= (-\delta_{ba} \vec{e}_c + \delta_{ca} \vec{e}_b) \partial_a \partial_b F_c \quad (2.37b)$$

$$= \nabla (\nabla \cdot \mathbf{F}) - \nabla^2 \mathbf{F}. \quad (2.37c)$$

Relating advection, curl, and kinetic energy

We now apply some of the previous manipulations to derive a relation required to derive the vorticity equation (Section 37.3.1). Here, we aim to show that

$$(\mathbf{v} \cdot \nabla) \mathbf{v} = \boldsymbol{\omega} \times \mathbf{v} + \nabla (\mathbf{v} \cdot \mathbf{v})/2, \quad (2.38)$$

where

$$\boldsymbol{\omega} = \nabla \times \mathbf{v} \quad (2.39)$$

is the vorticity, $\boldsymbol{\omega} \cdot \boldsymbol{v}/2$ is the kinetic energy per mass, and \boldsymbol{v} is the fluid velocity field. We here show all the steps along with their justification

$$\begin{aligned}
\boldsymbol{\omega} \times \boldsymbol{v} &= (\nabla \times \boldsymbol{v}) \times \boldsymbol{v} && \text{insert } \boldsymbol{\omega} = \nabla \times \boldsymbol{v} && (2.40a) \\
&= (\vec{e}_a \partial_a \times \vec{e}_b v_b) \times \vec{e}_c v_c && \text{Cartesian representation of } \boldsymbol{v} \text{ and } \nabla && (2.40b) \\
&= (\vec{e}_a \times \vec{e}_b) \times \vec{e}_c (\partial_a v_b) v_c && \text{rearrange} && (2.40c) \\
&= \epsilon_{abd} (\vec{e}_d \times \vec{e}_c) (\partial_a v_b) v_c && \text{first cross product expanded} && (2.40d) \\
&= \epsilon_{abd} \epsilon_{dce} \vec{e}_e (\partial_a v_b) v_c && \text{second cross product expanded} && (2.40e) \\
&= \epsilon_{abd} \epsilon_{ced} \vec{e}_e (\partial_a v_b) v_c && \text{arrange indices to prepare for next step} && (2.40f) \\
&= (\delta_{ac} \delta_{be} - \delta_{ae} \delta_{bc}) \vec{e}_e (\partial_a v_b) v_c && \text{use identity (1.38)} && (2.40g) \\
&= \vec{e}_a v_c \partial_c v_a - \vec{e}_a v_c \partial_a v_c && \text{contract the Kronecker deltas} && (2.40h) \\
&= \vec{e}_a [(\boldsymbol{v} \cdot \nabla) v_a - \partial_a \boldsymbol{v}^2 / 2] && \text{re-express as Cartesian tensor} && (2.40i) \\
&= (\boldsymbol{v} \cdot \nabla) \boldsymbol{v} - \nabla[\boldsymbol{v} \cdot \boldsymbol{v} / 2] && \text{rearrange.} && (2.40j)
\end{aligned}$$

Note that Section 4.4.4 of [Griffies \(2004\)](#) exhibits these steps making use of general coordinates rather than Cartesian.

2.4 Path integral of a scalar function

Consider the integral of a scalar function, ψ , over an arbitrary one-dimensional path in space, C

$$\mathcal{I} = \int_{\varphi_A}^{\varphi_B} \psi(\varphi) d\varphi. \quad (2.41)$$

Since any path is a one-dimensional curve, a point along the path can be specified by a single parameter, denoted here by φ with endpoints φ_A and φ_B .³ We now consider some explicit examples of how to parameterize a curve to thus enable an explicit evaluation of the integral.⁴

2.4.1 Cartesian coordinates

Lay down a Cartesian coordinate system with an arbitrary origin, in which case the Cartesian coordinate representation of a point along the path is written

$$\boldsymbol{x}(\varphi) = \hat{\boldsymbol{x}} x(\varphi) + \hat{\boldsymbol{y}} y(\varphi) + \hat{\boldsymbol{z}} z(\varphi), \quad (2.42)$$

along with the endpoints along the path

$$\boldsymbol{x}(\varphi_A) = \boldsymbol{x}_A \quad \text{and} \quad \boldsymbol{x}(\varphi_B) = \boldsymbol{x}_B. \quad (2.43)$$

In this way the path integral is written

$$\mathcal{I} = \int_{\varphi_A}^{\varphi_B} \psi(\varphi) d\varphi = \int_{\varphi_A}^{\varphi_B} \psi[\boldsymbol{x}(\varphi)] d\varphi. \quad (2.44)$$

To bring the integral (2.44) fully into a Cartesian parameterized form requires us to perform

³We have more to say about the geometry of paths in paths in Sections 6.1 and 6.2.

⁴In the more general language of differential forms, the evaluation of a path integral requires one to parameterize points along the path so to then write the path integral as a Riemann integral. This process is known as *pulling back* the path integral to a Riemann integral.

a coordinate transformation from φ to \mathbf{x} along the curve. For this purpose, consider two points on the path that are separated by an infinitesimal parameter difference, in which the difference in their Cartesian coordinates is given by

$$d\mathbf{x} = \mathbf{x}(\varphi + d\varphi) - \mathbf{x}(\varphi) = \frac{d\mathbf{x}}{d\varphi} d\varphi. \quad (2.45)$$

We thus have

$$(d\varphi)^2 = \frac{d\mathbf{x} \cdot d\mathbf{x}}{d\mathbf{x}/d\varphi \cdot d\mathbf{x}/d\varphi}. \quad (2.46)$$

Assuming $d\varphi > 0$ then leads to the integral (2.44) taking on the rather clumsy, but nonetheless general, form

$$\mathcal{I} = \int_{\varphi_A}^{\varphi_B} \psi(\varphi) d\varphi = \int_{\varphi_A}^{\varphi_B} \psi[\mathbf{x}(\varphi)] d\varphi = \int_{\mathbf{x}_A}^{\mathbf{x}_B} \psi[\mathbf{x}(\varphi)] \sqrt{\frac{d\mathbf{x} \cdot d\mathbf{x}}{d\mathbf{x}/d\varphi \cdot d\mathbf{x}/d\varphi}}. \quad (2.47)$$

2.4.2 Arc length parameterization

We now consider a common special case for path parameterization where $\varphi = s$ is the arc length along the path⁵

$$\mathcal{I} = \int_{\varphi_A}^{\varphi_B} \psi(\varphi) d\varphi = \int_{s_A}^{s_B} \psi[\mathbf{x}(s)] ds. \quad (2.48)$$

For Euclidean space using Cartesian coordinates, the differential increment of arc length is given by

$$ds = \sqrt{d\mathbf{x} \cdot d\mathbf{x}}. \quad (2.49)$$

Inserting $\mathbf{x}(s)$ into this expression renders

$$ds = \sqrt{d\mathbf{x} \cdot d\mathbf{x}} = ds \sqrt{\frac{d\mathbf{x}}{ds} \cdot \frac{d\mathbf{x}}{ds}}. \quad (2.50)$$

This expression is self-consistent if

$$\sqrt{\frac{d\mathbf{x}}{ds} \cdot \frac{d\mathbf{x}}{ds}} = 1, \quad (2.51)$$

which is merely a rewrite of the defining expression (2.49). Note that the derivative of the curve with respect to the arc-length, $d\mathbf{x}/ds$, defines a unit tangent vector to the curve

$$\hat{\mathbf{t}} = \frac{d\mathbf{x}}{ds} \implies \hat{\mathbf{t}} \cdot \hat{\mathbf{t}} = 1. \quad (2.52)$$

2.4.3 Linear path example

As a specific example, consider a line between two points, \mathbf{x}_A and \mathbf{x}_B , as in Figure 2.6. We can parameterize the line using a dimensionless parameter φ according to

$$\mathbf{x}(\varphi) = \mathbf{x}_A + (\mathbf{x}_B - \mathbf{x}_A) \varphi \quad \varphi \in [0, 1]. \quad (2.53)$$

Alternatively, we can parameterize using the arc length

$$\mathbf{x}(s) = \mathbf{x}_A + \hat{\mathbf{t}} s \quad s \in [0, L], \quad (2.54)$$

⁵We offer a more focused discussion of curves and tangents in Section 6.2.1 (see in particular equation (6.9)).

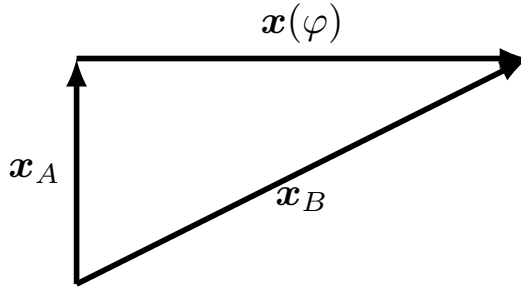


FIGURE 2.6: A linear path, $\mathbf{x}(\varphi)$ extending from \mathbf{x}_A to \mathbf{x}_B can be parameterized by a non-dimensional parameter $\varphi \in [0, 1]$ via $\mathbf{x}(\varphi) = \mathbf{x}_A + (\mathbf{x}_B - \mathbf{x}_A)\varphi$. Alternatively, it can be parameterized by the arc-length along the path via $\mathbf{x}(s) = \mathbf{x}_A + \hat{\mathbf{t}} s$ with $s \in [0, L]$, $L = |\mathbf{x}_B - \mathbf{x}_A|$, and $\hat{\mathbf{t}}$ the unit tangent vector pointing from \mathbf{x}_A to \mathbf{x}_B .

where $L = \int_A^B ds = |\mathbf{x}_B - \mathbf{x}_A|$ is the total arc length of the line, and where $\hat{\mathbf{t}}$ is the unit tangent vector pointing along the path from \mathbf{x}_A to \mathbf{x}_B

$$\hat{\mathbf{t}} = \frac{\mathbf{x}'(s)}{|\mathbf{x}'(s)|} = \frac{\mathbf{x}_B - \mathbf{x}_A}{|\mathbf{x}_B - \mathbf{x}_A|}. \quad (2.55)$$

As defined we have $|\mathbf{x}'(s)| = |\hat{\mathbf{t}}| = 1$, so that the path integral is given by

$$\mathcal{I} = \int_C \psi(\varphi) d\varphi = \int_0^L \psi[\mathbf{x}(s)] ds. \quad (2.56)$$

2.5 Path integral of a vector function

Generalizing to a vector field, $\mathbf{F}(\mathbf{x})$, we could conceivably integrate each component of the vector along the curve independently, making use of the approach for scalar fields in Section 2.4. In practice, however, that quantity rarely appears in physics. Instead, we more commonly wish to integrate that component of $\mathbf{F}(\mathbf{x})$ that projects onto a curve

$$\int_C \mathbf{F} \cdot d\mathbf{x} = \int_C \mathbf{F} \cdot \frac{d\mathbf{x}}{ds} ds = \int_C \mathbf{F} \cdot \hat{\mathbf{t}} ds, \quad (2.57)$$

where $\hat{\mathbf{t}} = d\mathbf{x}/ds$ is tangent to the curve given by equation (2.52). A common physics example for the path integral of a vector concerns the work performed by a force field applied to a physical system that is moving along a path (this example is studied in Section 10.1.5).

2.5.1 Circulation

For the case of a closed curve or a circuit (see Section 6.1), we refer to the path integral as the *circulation* and use the convention of putting an arrowed circle on the integral sign

$$\text{circulation of vector field} = \oint_C \mathbf{F} \cdot d\mathbf{x}. \quad (2.58)$$

The arrow indicates that we conventionally traverse the closed path in a counter-clockwise (right hand) manner when looking down on the path from above.⁶

2.5.2 Circulation example

Consider the vector field $\mathbf{F} = -y \hat{\mathbf{x}} + x \hat{\mathbf{y}}$ shown in Figure 2.4. What is the circulation for this field computed around a circle of radius r whose center is the origin? To compute this circulation we make use of plane polar coordinates, in which $x = r \cos \varphi$ and $y = r \sin \varphi$, with $\varphi \in [0, 2\pi]$ the polar angle measured from the positive x -axis. The position of a point on the circle is thus written $\mathbf{x}(\varphi) = r(\hat{\mathbf{x}} \cos \varphi + \hat{\mathbf{y}} \sin \varphi)$, and the tangent to the circle is $d\mathbf{x}(\varphi)/d\varphi = r(-\hat{\mathbf{x}} \sin \varphi + \hat{\mathbf{y}} \cos \varphi)$. The integrand to the circulation (2.57) thus takes the form

$$\mathbf{F} \cdot \frac{d\mathbf{x}(\varphi)}{d\varphi} = r(y \sin \varphi + x \cos \varphi) = r^2. \quad (2.59)$$

Hence, the circulation around the constant radius circle is given by twice the area of the circle

$$\oint_C \mathbf{F} \cdot d\mathbf{x} = 2\pi r^2. \quad (2.60)$$

We apply this result in Section 37.6.2 to geophysical fluids when computing the vorticity induced by the rotating planet.

2.5.3 Fundamental theorem of calculus

The special case of $\mathbf{F} = -\nabla\psi$ for a scalar field ψ recovers the fundamental theorem of calculus

$$\psi(\mathbf{x}_B) - \psi(\mathbf{x}_A) = \int_{\mathbf{x}_A}^{\mathbf{x}_B} d\psi = \int_{\mathbf{x}_A}^{\mathbf{x}_B} \nabla\psi \cdot d\mathbf{x}. \quad (2.61)$$

It follows that for any closed curve with $\mathbf{x}_A = \mathbf{x}_B$, the circulation of $\nabla\psi$ vanishes

$$\oint_C d\psi = \oint_C \nabla\psi \cdot d\mathbf{x} = 0. \quad (2.62)$$

2.6 Stokes' curl theorem

Stokes' theorem relates the integral of a vector field projected onto the tangent of a boundary around surface to the integral of the unit normal component of the vector field's curl over the area of the surface. This theorem is used extensively in our study of circulation and vorticity in Part VII of this book. The geometry of Stokes' theorem is illustrated in Figure 2.7.

2.6.1 Statement of Stokes' theorem

For an oriented⁷ two-dimensional surface, \mathcal{S} , with a closed boundary, $\partial\mathcal{S}$, Stokes' theorem says that the circulation around the boundary equals to the area integrated curl projected onto the

⁶By choosing a viewpoint as “above”, we necessarily allow for an unambiguous definition of “counter-clockwise”, thus providing chosen *orientation*.

⁷For a surface to be orientable means that we can unambiguously describe its two sides, thus allowing us to determine a positive (top) side and negative (bottom) side. We are here only concerned with surfaces that are orientable, thus precluding surfaces such as the Möbius strip that are not orientable.

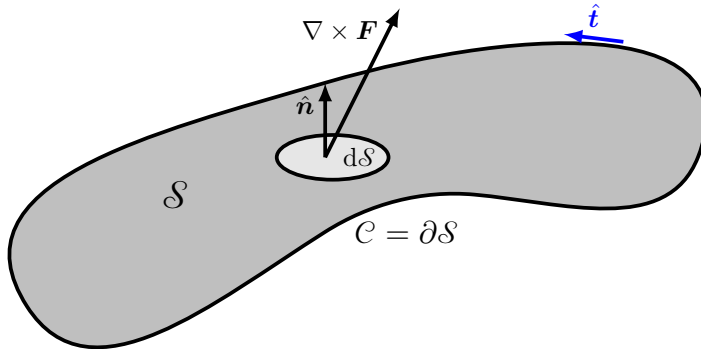


FIGURE 2.7: Illustrating the geometry of Stokes' theorem (2.63). The unit normal vector, $\hat{\mathbf{n}}$, points outward from the surface, \mathcal{S} , thus defining the positive or up direction. The integrand $(\nabla \times \mathbf{F}) \cdot \hat{\mathbf{n}}$ is the projection of the curl of a vector field onto the surface outward normal. The boundary of the area, $\mathcal{C} = \partial\mathcal{S}$, is traversed counterclockwise following the unit tangent vector, $\hat{\mathbf{t}}$, when computing the circulation. Counter-clockwise is oriented relative to the positive side of the surface as defined by the outward normal.

surface outward unit normal

$$\oint_{\partial\mathcal{S}} \mathbf{F} \cdot d\mathbf{x} = \int_{\mathcal{S}} (\nabla \times \mathbf{F}) \cdot \hat{\mathbf{n}} dS. \quad (2.63)$$

In this equation,

$$d\mathbf{x} = \frac{d\mathbf{x}}{ds} ds = \hat{\mathbf{t}} ds \quad (2.64)$$

is the vector line element along the closed path (circuit), $\hat{\mathbf{t}}$ is the unit tangent vector along the path, and s is the arc-distance along the path. For the surface integral we have the outward unit normal vector, $\hat{\mathbf{n}}$, and dS is the infinitesimal surface area element. The orientation of the outward normal determines, through the right hand rule, the counter-clockwise circulation direction.

2.6.2 Stokes' theorem for a rectangular region

To build experience with Stokes' theorem, consider the case of a rectangle in the x - y plane with dimensions L_x and L_y . In this case $\hat{\mathbf{n}} = \hat{\mathbf{z}}$, so that

$$(\nabla \times \mathbf{F}) \cdot \hat{\mathbf{z}} = \frac{\partial F_2}{\partial x} - \frac{\partial F_1}{\partial y}, \quad (2.65)$$

in which case the right hand side of Stokes' theorem reduces to

$$\int_{\mathcal{S}} (\nabla \times \mathbf{F}) \cdot \hat{\mathbf{n}} dS = \int_0^{L_x} \int_0^{L_y} \left(\frac{\partial F_2}{\partial x} - \frac{\partial F_1}{\partial y} \right) dx dy. \quad (2.66)$$

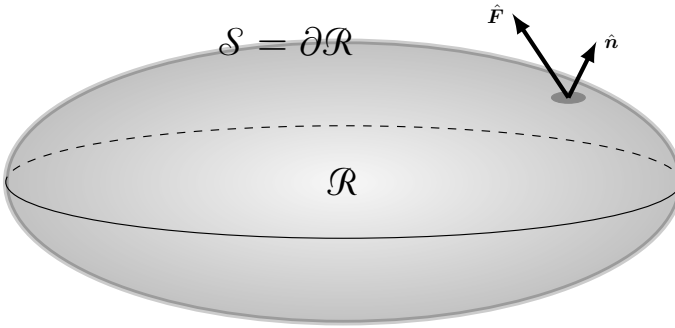


FIGURE 2.8: Illustrating the geometry of Gauss's divergence theorem for an ellipsoidal volume, \mathcal{R} , with closed boundary surface, $\mathcal{S} = \partial\mathcal{R}$. The outward unit normal along the boundary, $\hat{\mathbf{n}}$, is projected onto the vector field, \mathbf{F} , via the scalar product, $\mathbf{F} \cdot \hat{\mathbf{n}}$. Gauss's divergence theorem says that integrating this scalar product over the closed boundary surface, \mathcal{S} , yields the same result as computing the volume integral of the divergence, $\nabla \cdot \mathbf{F}$, over the closed region, \mathcal{R} , bounded by the closed surface \mathcal{S} .

Integration around the rectangle then leads to a direct verification of Stokes' theorem

$$\int_0^{L_x} \int_0^{L_y} \left(\frac{\partial F_2}{\partial x} - \frac{\partial F_1}{\partial y} \right) dx dy = \int_0^{L_y} F_2(x, y) \Big|_{x=0}^{x=L_x} dy - \int_0^{L_x} F_1(x, y) \Big|_{y=0}^{y=L_y} dx \quad (2.67a)$$

$$= \int_0^{L_x} F_1(x, 0) dx + \int_0^{L_y} F_2(L_x, y) dy + \int_{L_x}^0 F_1(x, L_y) dx + \int_{L_y}^0 F_2(0, y) dy \quad (2.67b)$$

$$= \oint_{\partial\mathcal{S}} \mathbf{F} \cdot d\mathbf{x}. \quad (2.67c)$$

We can generalize this result to verify Stokes' theorem for an arbitrary surface. We do so by breaking the surface into a lattice of tiny rectangles. Integrating around the tiny rectangles and summing their contributions leads to a cancellation of the line integrals over all interior boundaries. The cancellation occurs since an internal edge of a rectangle is integrated once in each direction thus cancelling its contribution. The only nonzero contribution comes from integration over the boundary.

2.7 Gauss's divergence theorem

For a vector field \mathbf{F} , Gauss's divergence theorem states that

$$\int_{\mathcal{R}} \nabla \cdot \mathbf{F} dV = \oint_{\partial\mathcal{R}} \mathbf{F} \cdot \hat{\mathbf{n}} d\mathcal{S}, \quad (2.68)$$

where $\hat{\mathbf{n}}$ is the outward unit normal to the boundary surface and $d\mathcal{S}$ is the surface area element. In words, Gauss's divergence theorem says that the divergence of a vector field integrated over a volume equals to the area integrated unit normal projection of the vector field through the closed surface bounding the volume. We follow the convention that $\oint_{\partial\mathcal{R}}$ refers to a surface integral over a closed surface that bounds a volume. This notation is used to contrast with the surface integral, $\int_{\mathcal{S}}$, that generally does not enclose a volume. Figure 2.8 illustrates the geometry of Gauss's divergence theorem. In physics jargon, we say that the divergence of a vector field, $\nabla \cdot \mathbf{F}$, integrated over a volume equals to the flux of that vector field, $\mathbf{F} \cdot \hat{\mathbf{n}}$, integrated over the area bounding the volume.

2.7.1 An example rectangular volume

To build intuition for Gauss's divergence theorem, consider a rectangular volume with dimensions L_x , and L_y and L_z . The volume integral on the left hand side of equation (2.68) gives

$$\int_{\mathcal{R}} \left[\frac{\partial F_1}{\partial x} + \frac{\partial F_2}{\partial y} + \frac{\partial F_3}{\partial z} \right] dx dy dz. \quad (2.69)$$

Focusing on just the leftmost term, integration in x gives

$$\int_{\mathcal{R}} \frac{\partial F_1}{\partial x} dx dy dz = \int_{y=0}^{y=L_y} \int_{z=0}^{z=L_z} [F_1(L_x, y, z) - F_1(0, y, z)] dy dz \quad (2.70a)$$

$$= \int_{\mathcal{S}_1 + \mathcal{S}_2} \mathbf{F} \cdot \hat{\mathbf{n}} d\mathcal{S}, \quad (2.70b)$$

where \mathcal{S}_1 is the rectangle's face with outward unit normal $\hat{\mathbf{n}} = \hat{\mathbf{x}}$ and \mathcal{S}_2 is the rectangle's face with unit normal $\hat{\mathbf{n}} = -\hat{\mathbf{x}}$. Repeating this procedure on the other terms in equation (2.69) gives the area integrated flux through the full boundary. To verify the theorem for a general volume V , we take the approach used to prove Stokes' theorem. First, divide the volume into many rectangular sub-volumes. Then apply the above result to each sub-volume and sum up the result. The area integrated fluxes through internal rectangular faces cancel exactly. Therefore, the sum of all the area integrate fluxes equals just the flux integrated over the external boundary, thus yielding the divergence theorem.

2.7.2 Divergence theorem for scalar fields

We consider two corollaries of the divergence theorem, the first of which arises from the special case of a vector field $\mathbf{F} = \phi \mathbf{c}$ with \mathbf{c} an arbitrary *constant* vector. Substitution into the divergence theorem (2.68) yields

$$\oint_{\partial\mathcal{R}} \phi \mathbf{c} \cdot \hat{\mathbf{n}} d\mathcal{S} = \int_{\mathcal{R}} \nabla \cdot (\phi \mathbf{c}) dV. \quad (2.71)$$

Pulling the constant vector out of the integrals and rearrangement leads to

$$\mathbf{c} \cdot \left[\oint_{\partial\mathcal{R}} \phi \hat{\mathbf{n}} d\mathcal{S} - \int_{\mathcal{R}} \nabla \phi dV \right] = 0. \quad (2.72)$$

Since \mathbf{c} is an arbitrary vector, this equality is generally true in only if,s

$$\oint_{\partial\mathcal{R}} \phi \hat{\mathbf{n}} d\mathcal{S} = \int_{\mathcal{R}} \nabla \phi dV. \quad (2.73)$$

In words, this result says that the integral of a scalar field over the boundary of a closed surface, when weighted by the outward unit normal to the surface, equals to the volume integral of the gradient of the scalar field integrated over the region bounded by the closed surface. We make use of this result in Section 21.2.3 when formulating the contribution of stresses to the motion of a fluid element, in particular when considering how pressure affects motion.

2.7.3 Surface integral of the outward unit normal

A corollary of equation (2.73) can be found by setting the scalar field, ϕ , to a constant so that $\nabla \phi = 0$. We thus find that the area integral of the outward unit normal vector vanishes when

integrated over the surface of a closed volume

$$\oint_{\partial\mathcal{R}} \hat{\mathbf{n}} dS = 0. \quad (2.74)$$

An example of this result can be seen by integrating over a closed rectangular volume, whereby the area integrals cancel component-wise. Another example is the sphere, where $\hat{\mathbf{n}} = \hat{\mathbf{r}}$ is the radial outward unit vector, so that integration of the radial unit vector over the spherical surface identically vanishes. For some purposes we can take equation (2.74) as the definition of a simply closed volume.

2.7.4 First and second form of Green's identities

The further corollary to the divergence theorem arises from considering another special vector field

$$\mathbf{F} = \psi \nabla \phi, \quad (2.75)$$

with ψ and ϕ scalar fields. Substitution into the divergence theorem (2.68) leads to

$$\oint_{\partial\mathcal{R}} \psi \frac{\partial \phi}{\partial n} dS = \int_{\mathcal{R}} [\nabla \psi \cdot \nabla \phi + \psi \nabla^2 \phi] dV \quad \text{Green's first integral identity.} \quad (2.76)$$

We can make this result more symmetric by swapping ψ and ϕ and then subtracting, thus yielding

$$\oint_{\partial\mathcal{R}} \left[\psi \frac{\partial \phi}{\partial n} - \phi \frac{\partial \psi}{\partial n} \right] dS = \int_{\mathcal{R}} [\psi \nabla^2 \phi - \phi \nabla^2 \psi] dV \quad \text{Green's second integral identity.} \quad (2.77)$$

Finally, setting $\phi = 1$ renders

$$\oint_{\partial\mathcal{R}} \frac{\partial \psi}{\partial n} dS = \int_{\mathcal{R}} \nabla^2 \psi dV \iff \oint_{\partial\mathcal{R}} \nabla \psi \cdot \hat{\mathbf{n}} dS = \int_{\mathcal{R}} \nabla \cdot \nabla \psi dV. \quad (2.78)$$

We make use of these identities in Chapter 4 when studying the Green's function method for solving linear partial differential equations.

2.7.5 Integral of a curl over a closed surface

Application of Gauss's divergence theorem leads us to conclude that the following integral vanishes

$$\oint_{\partial\mathcal{R}} (\nabla \times \Psi) \cdot \hat{\mathbf{n}} dS = \int_{\mathcal{R}} \nabla \cdot (\nabla \times \Psi) dV = 0, \quad (2.79)$$

where the final equality follows since the divergence of a curl vanishes. Hence, the integral of the unit normal projection of the curl of a function over an oriented closed surface vanishes. We can understand this result geometrically by splitting the closed volume into two regions and then applying Stokes' theorem separately to the two regions (see Figure 2.9)

$$\oint_{\partial\mathcal{R}} (\nabla \times \Psi) \cdot \hat{\mathbf{n}} dS = \int_{\mathcal{S}_1} (\nabla \times \Psi) \cdot \hat{\mathbf{n}} dS_1 + \int_{\mathcal{S}_2} (\nabla \times \Psi) \cdot \hat{\mathbf{n}} dS_2 \quad (2.80a)$$

$$= \oint_{\partial\mathcal{S}_1} \Psi \cdot d\mathbf{x} - \oint_{\partial\mathcal{S}_2} \Psi \cdot d\mathbf{x} \quad (2.80b)$$

$$= 0. \quad (2.80c)$$

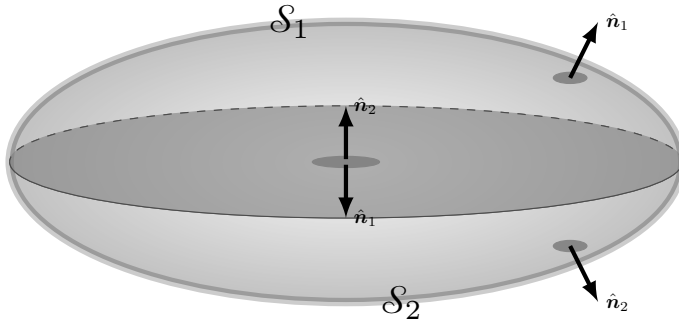


FIGURE 2.9: The integral of the unit normal component of the curl of a function vanishes when integrated over an oriented closed surface, $\partial\mathcal{R}$, which forms the boundary to a closed volume, \mathcal{R} . This result follows from both Gauss's divergence theorem as well as Stokes' curl theorem. For Gauss's theorem we find $\oint_{\partial\mathcal{R}} (\nabla \times \Psi) \cdot \hat{\mathbf{n}} dS = \int_{\mathcal{R}} \nabla \cdot (\nabla \times \Psi) dV = 0$, which follows since the divergence of the curl vanishes. For Stokes' theorem we split the closed volume into two so that its boundary surface has also been split into two, $\partial\mathcal{R} = \mathcal{S}_1 + \mathcal{S}_2$. Separately applying Stokes' theorem to \mathcal{S}_1 and \mathcal{S}_2 leads to the calculation of the circulation around the common boundary along the equatorial plane. Since orientation of the outward unit normal along the equatorial plane is opposite for the two regions, the two circulations exactly cancel since they are computed in opposite directions.

The minus sign appearing in front of $\oint_{\partial\mathcal{S}_2} \omega \cdot \hat{\mathbf{n}} dS$ occurs since the orientation of the circulation integral is opposite that for $\oint_{\partial\mathcal{S}_1}$. We are thus left with a cancellation of the circulations. When applied to the vorticity of a fluid (Chapter 34), we see that

$$\oint_{\partial\mathcal{R}} \omega \cdot \hat{\mathbf{n}} dS = \int_{\mathcal{R}} \nabla \cdot \omega dV = 0, \quad (2.81)$$

where $\omega = \nabla \times \mathbf{v}$ is the vorticity and \mathbf{v} is the fluid velocity.

2.7.6 The domain integral of a non-divergent field

Consider a vector field that has zero divergence everywhere within a domain, \mathcal{R} . Consequently, $\int_{\mathcal{R}} \nabla \cdot \mathbf{F} dV = \oint_{\partial\mathcal{R}} \mathbf{F} \cdot \hat{\mathbf{n}} dS = 0$. Now what can we say about $\int_{\mathcal{R}} \mathbf{F} dV$? One might be tempted to say that it vanishes. But that is generally an incorrect statement as we now show.⁸

Since $\nabla \cdot \mathbf{F} = 0$ we know that

$$0 = \int_{\mathcal{R}} x_i \nabla \cdot \mathbf{F} dV = \int_{\mathcal{R}} [\nabla \cdot (x_i \mathbf{F}) - F_i] dV, \quad (2.82)$$

where we used $\partial_j x_i = \delta_{ij}$. Use of the divergence theorem leads to

$$\int_{\mathcal{R}} F_i dV = \int_{\mathcal{R}} \nabla \cdot (x_i \mathbf{F}) dV = \oint_{\partial\mathcal{R}} x_i (\hat{\mathbf{n}} \cdot \mathbf{F}) dS. \quad (2.83)$$

The right hand side does not generally vanish since $\hat{\mathbf{n}} \cdot \mathbf{F}$ does not generally vanish at each point along $\partial\mathcal{R}$. Hence, we find that $\int_{\mathcal{R}} \mathbf{F} dV = 0$ only for those domains where $\hat{\mathbf{n}} \cdot \mathbf{F} = 0$ at each point along $\partial\mathcal{R}$.

⁸As a technical note, we observe that the integral of a vector field is generally only well defined in Euclidean space. A general manifold requires us to add extra formalism for the purpose of comparing vectors at two different points.

2.8 Exact and inexact differentials

Thus far in this chapter all differentials have been exact. However, the thermodynamics discussed in Chapter 19 makes use of both exact and inexact differentials. We here introduce the mathematics of such differentials. Our focus concerns differentials taken between space points, though we note that in some applications it may be appropriate to consider space-time displacements.

2.8.1 Exact differentials

As in Section 2.1, consider an arbitrary function of space, $\Phi(\mathbf{x})$. A differential increment for that function, computed between two close points \mathbf{x} and $\mathbf{x} + d\mathbf{x}$, is given by

$$d\Phi(\mathbf{x}) = \Phi(\mathbf{x} + d\mathbf{x}) - \Phi(\mathbf{x}) \quad (2.84a)$$

$$= d\mathbf{x} \cdot \nabla \Phi, \quad (2.84b)$$

where we dropped higher order terms due to the infinitesimal nature of the increments. It follows that we can determine the finite increment between two points through integration

$$\Phi(\mathbf{x}_B) - \Phi(\mathbf{x}_A) = \int_{\mathbf{x}_A}^{\mathbf{x}_B} d\Phi(\mathbf{x}) = \int_{\mathbf{x}_A}^{\mathbf{x}_B} d\mathbf{x} \cdot \nabla \Phi. \quad (2.85)$$

These results are familiar from elementary calculus, with the increment $d\Phi$ given by equation (2.84b) termed an *exact* differential. Importantly, the finite increment, $\Phi(\mathbf{x}_B) - \Phi(\mathbf{x}_A)$, depends only on the endpoint values of Φ . It does not depend on the path taken to go from \mathbf{x}_A to \mathbf{x}_B . Correspondingly, the integral of an exact differential vanishes when computed around a closed loop

$$\oint d\Phi = 0. \quad (2.86)$$

2.8.2 Inexact differentials

Consider now a general differential expression written as

$$\mathbf{A} \cdot d\mathbf{x} = A dx + B dy + C dz, \quad (2.87)$$

where $\mathbf{A} = A \hat{\mathbf{x}} + B \hat{\mathbf{y}} + C \hat{\mathbf{z}}$ is an arbitrary vector function. If $\nabla \times \mathbf{A} = 0$, then \mathbf{A} can be written as the gradient of a scalar

$$\nabla \times \mathbf{A} = 0 \implies \mathbf{A} = \nabla \Psi, \quad (2.88)$$

in which case we have an exact differential expression

$$\mathbf{A} \cdot d\mathbf{x} = \nabla \Psi \cdot d\mathbf{x} = d\Psi. \quad (2.89)$$

That is, the differential $\mathbf{A} \cdot d\mathbf{x}$ is exact if

$$\nabla \times \mathbf{A} = 0 \implies \mathbf{A} \cdot d\mathbf{x} \text{ exact differential}. \quad (2.90)$$

In the more general case where $\nabla \times \mathbf{A} \neq 0$, then $\mathbf{A} \cdot d\mathbf{x}$ is termed an *inexact differential*. We make use of the following notation for inexact differentials

$$d\Psi = \mathbf{A} \cdot d\mathbf{x}. \quad (2.91)$$

Notably, the path integral of an inexact differential depends on the path taken between the

endpoints. Correspondingly, the integral of an inexact differential around a closed loop does not generally vanish

$$\oint d\Psi \neq 0. \quad (2.92)$$

2.8.3 Integrating factors

Consider again the inexact differential $d\Psi = \mathbf{A} \cdot d\mathbf{x}$. Let us presume there exists a function τ so that the product $\tau^{-1} d\Psi$ is an exact differential. For τ to exist it must be such that

$$\nabla \times (\mathbf{A} \tau^{-1}) = 0. \quad (2.93)$$

Consequently, we can write

$$\mathbf{A} = \tau \nabla \Phi, \quad (2.94)$$

so that

$$d\Psi = \mathbf{A} \cdot d\mathbf{x} = \tau \nabla \Phi \cdot d\mathbf{x} = \tau d\Phi. \quad (2.95)$$

The function τ is known as an *integrating factor*. As seen in Section 19.2.3, pressure is the integrating factor for mechanical work, temperature is the integrating factor for heating, and the chemical potential is the integrating factor for chemical work.

2.8.4 An example using the velocity field

Consider the scalar product, $\mathbf{v} \cdot d\mathbf{x}$, where \mathbf{v} is the velocity field for a fluid and $d\mathbf{x}$ is a differential increment in space directed along a path. Furthermore, introduce the curl of the velocity, which defines the vorticity (Section 34.1) $\boldsymbol{\omega} = \nabla \times \mathbf{v}$. For cases where the vorticity vanishes, $\boldsymbol{\omega} = 0$, then $d\Psi = \mathbf{v} \cdot d\mathbf{x}$ is an exact differential. Consequently, Stokes' theorem means that the circulation vanishes for an irrotational velocity field computed around an arbitrary closed loop (Section 34.3)

$$C \equiv \oint_{\partial S} \mathbf{v} \cdot d\mathbf{x} = \int_S \boldsymbol{\omega} \cdot \hat{\mathbf{n}} dS = 0. \quad (2.96)$$

Another way to see this result is to note that a vanishing curl means that the velocity field can be expressed as the gradient of a scalar, $\mathbf{v} = \nabla \psi$, so that $d\Psi = \nabla \psi \cdot d\mathbf{x}$, which is manifestly exact.

2.8.5 Heuristic physics of exact and inexact differential operations

Consider a hiker climbing a mountain. The mechanical work, which is force applied over a distance, is a function of the path taken. Some paths are smooth and well marked, whereas others are rough and poorly marked. Likewise, the frictional heating (of the hiker's feet, for example) depend on details of the path (and the shoes!). So although the start and finish points are fixed, the work exerted and heat generated in going between these points is a function of the path.

In contrast, the change in gravitational potential energy between the start and finish points is a function only of the elevation difference between the start and finish points. It does not depend on the path between the points. So the gravitational potential energy increment between the two points is an exact differential, with the potential energy for each point a function of the elevation at the point.

The First Law of thermodynamics says that the sum of path-dependent processes (work and heat) used in going from one thermodynamic state to another equals to the difference in the internal energy between the two states. That is, the sum of the inexact differentials for heat and work equal to the exact differential for internal energy.



2.9 Exercises

Throughout these exercises we consider a point whose Cartesian position vector, relative to an arbitrary origin, is written

$$\mathbf{x} = x \hat{\mathbf{x}} + y \hat{\mathbf{y}} + z \hat{\mathbf{z}} \quad (2.97)$$

and whose squared distance from the origin is

$$r^2 = \mathbf{x} \cdot \mathbf{x} = x^2 + y^2 + z^2. \quad (2.98)$$

EXERCISE 2.1: PRACTICE WITH THE GRADIENT OPERATOR

Prove the following identities:

- (a) $\nabla(|\mathbf{x}|) = \mathbf{x} |\mathbf{x}|^{-1} \equiv \hat{\mathbf{r}}$
- (b) $\nabla \ln |\mathbf{x}| = \mathbf{x} |\mathbf{x}|^{-2} = \hat{\mathbf{r}} |\mathbf{x}|^{-1}$
- (c) $\nabla |\mathbf{x}|^{-1} = -\mathbf{x} |\mathbf{x}|^{-3} = -\hat{\mathbf{r}} |\mathbf{x}|^{-2}$.

EXERCISE 2.2: PRACTICE WITH THE LAPLACIAN OPERATOR

Show that the Laplacian of the function

$$\psi = \frac{z x^2}{r^2} \quad (2.99)$$

is given by

$$\nabla^2 \psi = \frac{2 z (r^2 - 5 x^2)}{r^4}. \quad (2.100)$$

Perform the proof using both Cartesian coordinates as well as spherical coordinates (see Figure 9.1), making use of the following expressions for Laplacian operator acting on a scalar field

$$\nabla^2 \psi(x, y, z) = \frac{\partial^2 \psi}{\partial x^2} + \frac{\partial^2 \psi}{\partial y^2} + \frac{\partial^2 \psi}{\partial z^2} \quad (2.101a)$$

$$\nabla^2 \psi(\lambda, \phi, r) = \frac{1}{r^2 \cos \phi} \left[\frac{1}{\cos \phi} \frac{\partial^2 \psi}{\partial \lambda^2} + \frac{\partial}{\partial \phi} \left(\cos \phi \frac{\partial \psi}{\partial \phi} \right) + \cos \phi \frac{\partial}{\partial r} \left(r^2 \frac{\partial \psi}{\partial r} \right) \right]. \quad (2.101b)$$

EXERCISE 2.3: MORE PRACTICE WITH OPERATORS

Prove the following identities with $r \neq 0$:

- (a) $\nabla^2 r^{-1} = 0$
- (b) $\nabla \cdot (\mathbf{x}/r^3) = 0$
- (c) $\nabla \cdot (\mathbf{A} \times \mathbf{x}) = \mathbf{x} \cdot (\nabla \times \mathbf{A})$ for an arbitrary vector field $A(\mathbf{x})$.
- (d) $\nabla \times [\mathbf{x} f(r)] = 0$ for an arbitrary function $f(r) = f(|\mathbf{x}|)$.

EXERCISE 2.4: SOLID-BODY ROTATION

Define a velocity field according to

$$\mathbf{v} = \boldsymbol{\Omega} \times \mathbf{x} \quad (2.102)$$

with $\boldsymbol{\Omega}$ a spatially constant angular rotation velocity (e.g., rotation of the earth). This velocity field describes solid-body rotation as discussed in Section 34.5. Show that $2\boldsymbol{\Omega} = \nabla \times \mathbf{v}$. See also Exercise 34.1.

EXERCISE 2.5: DIVERGENCE-FREE AND IRROTATIONAL VECTOR

Let Φ be a harmonic function so that $\nabla^2 \Phi = 0$. Show that $\mathbf{v} = -\nabla \Phi$ satisfies

$$(a) \quad \nabla \cdot \mathbf{v} = 0$$

$$(b) \quad \nabla \times \mathbf{v} = 0.$$

In this way we prove that all harmonic scalar fields correspond to a divergence-free and curl-free vector field.

EXERCISE 2.6: CONSERVATIVE VECTOR FIELD AND SCALAR POTENTIAL

Show that the curl, $\nabla \times \mathbf{F}$, of the following vector field vanishes

$$\mathbf{F} = 2xz\hat{x} + 2yz^2\hat{y} + (x^2 + 2y^2z - 1)\hat{z}. \quad (2.103)$$

Hence, deduce that \mathbf{F} is a *conservative vector field*, meaning that it can be written as the gradient of a scalar potential ψ according to $\mathbf{F} = -\nabla\psi$, where (to within an arbitrary constant)

$$\psi = -[x^2z + (yz)^2 - z]. \quad (2.104)$$

EXERCISE 2.7: PRODUCT RULE IDENTITIES

Prove the following identities for vectors in \mathbb{R}^3 :

$$(a) \quad \mathbf{F} = \partial_n(F_n \mathbf{x}) - \mathbf{x} \nabla \cdot \mathbf{F}$$

$$(b) \quad 2F_m = [\mathbf{x} \times (\nabla \times \mathbf{F})]_m - \partial_m(\mathbf{x} \cdot \mathbf{F}) + \nabla \cdot (\mathbf{x} F_m).$$

Make use of Cartesian tensors and show all relevant steps, including use of the Levi-Civita tensor from Section 1.4.1 for the cross-product.

As discussed in Section 12.4.1 of [Bühler \(2014a\)](#), these product rule identities have use for the study of impulses imparted by a body force per volume, \mathbf{F} , to a fluid on an unbounded domain where the force has compact support (i.e., the force vanishes outside a finite domain). In that case the above product rule identities allow us to make use of the corresponding integral identities

$$\int \mathbf{F} dV = - \int \mathbf{x} \nabla \cdot \mathbf{F} dV = \frac{1}{2} \int \mathbf{x} \times (\nabla \times \mathbf{F}) dV. \quad (2.105)$$

EXERCISE 2.8: BELTRAMI FLOW

Beltrami flow is defined by velocity and vorticity fields satisfying

$$\nabla \cdot \mathbf{v} = 0 \quad (2.106a)$$

$$\boldsymbol{\omega} = \nabla \times \mathbf{v} = \lambda \mathbf{v} \quad (2.106b)$$

where λ is a constant. Show that the following velocity field is a Beltrami flow

$$\mathbf{v} = (A \sin z + C \cos y) \hat{x} + (B \sin x + A \cos z) \hat{y} + (C \sin y + B \cos x) \hat{z}, \quad (2.107)$$

where A, B, C are constants. Hint: the solution follows directly from computing

$$u = \frac{\partial w}{\partial y} - \frac{\partial v}{\partial z} \quad v = \frac{\partial u}{\partial z} - \frac{\partial w}{\partial x} \quad w = \frac{\partial v}{\partial x} - \frac{\partial u}{\partial y}. \quad (2.108)$$

EXERCISE 2.9: PRACTICE WITH PATH INTEGRALS

Consider the vector field

$$\mathbf{F} = x y^2 \hat{\mathbf{x}} + 2 \hat{\mathbf{y}} + x \hat{\mathbf{z}}. \quad (2.109)$$

Let \mathcal{L} be a path parameterized by

$$x = c t \quad y = c/t \quad z = d \quad t \in [1, 2], \quad (2.110)$$

where c and d are constants. Show that the following identities hold

$$\int_{\mathcal{L}} \mathbf{F} dt = c^3 \ln 2 \hat{\mathbf{x}} + 2 \hat{\mathbf{y}} + \frac{3c}{2} \hat{\mathbf{z}} \quad (2.111a)$$

$$\int_{\mathcal{L}} \mathbf{F} dy = -\frac{3c^4}{8} \hat{\mathbf{x}} - c \hat{\mathbf{y}} - c^2 \ln 2 \hat{\mathbf{z}} \quad (2.111b)$$

$$\int_{\mathcal{L}} \mathbf{F} \cdot d\mathbf{x} = c^4 \ln 2 - c, \quad (2.111c)$$

where $d\mathbf{x} = \hat{\mathbf{x}} dx + \hat{\mathbf{y}} dy + \hat{\mathbf{z}} dz$. Although all three integrals are computed along the same path, they are not necessarily of the same type. In particular, the first two integrals are vector fields, whereas the third integral is a scalar.

EXERCISE 2.10: STOKES' THEOREM ON A PLANE

Show that

$$\mathcal{I} = \oint_{\partial\mathcal{S}} [y(4x^2 + y^2) dx + x(2x^2 + 3y^2) dy] = \frac{\pi}{2} b a^3 \quad (2.112)$$

when integrating around the boundary of an ellipse \mathcal{S} defined by

$$\frac{x^2}{a^2} + \frac{y^2}{b^2} = 1, \quad (2.113)$$

where a, b are constants. Hint: make use of Stokes' theorem on a plane, otherwise known as Green's Theorem. Also make use of the substitution $x = a \cos \phi$ and the identity

$$\int_{\pi}^0 \sin^2(2\phi) d\phi = -\frac{\pi}{2}. \quad (2.114)$$

EXERCISE 2.11: PRACTICE WITH GAUSS'S DIVERGENCE THEOREM

We here demonstrate the validity of Gauss's divergence theorem for a particular vector field

$$\mathbf{F} = \frac{\alpha \mathbf{x}}{(r^2 + a^2)^{3/2}}, \quad (2.115)$$

where α and a are constants and $r^2 = \mathbf{x} \cdot \mathbf{x}$ is the squared radial distance to a point. Using fluid mechanics jargon, we think of \mathbf{F} as a matter flux with physical dimensions of $M L^{-2} T^{-1}$ (mass length $^{-2}$ time $^{-1}$). Now compute the transport of \mathbf{F} through a spherical surface, \mathcal{S} , of radius $|\mathbf{x}| = a\sqrt{3}$

$$\Phi = \oint_{|\mathbf{x}|=a\sqrt{3}} \mathbf{F} \cdot \hat{\mathbf{n}} d\mathcal{S} = \frac{3\pi\alpha\sqrt{3}}{2}. \quad (2.116)$$

With \mathbf{F} a matter flux then Φ has physical dimensions of $M T^{-1}$, so that it is the *mass transport* through the spherical surface. Next, show that this transport is equal to the integral of the

divergence over the volume of the sphere

$$\Phi = \int_{|\mathbf{x}|=a\sqrt{3}} \nabla \cdot \mathbf{F} dV. \quad (2.117)$$

We thus verify, for this particular vector field, the divergence theorem

$$\int_{\mathcal{R}} \nabla \cdot \mathbf{F} dV = \oint_{\partial\mathcal{R}} \mathbf{F} \cdot \hat{\mathbf{n}} dS, \quad (2.118)$$

where $\hat{\mathbf{n}}$ is the outward unit normal on the bounding surface \mathcal{S} .

EXERCISE 2.12: MORE PRACTICE WITH GAUSS'S DIVERGENCE THEOREM

Prove the following identities, which are readily shown using Gauss's divergence theorem.

- (a) $\oint_{\partial\mathcal{R}} \mathbf{x} \cdot \hat{\mathbf{n}} dS = 3 \int_{\mathcal{R}} dV = 3V$, where \mathcal{R} is a closed region bounded by $\partial\mathcal{R}$ and with volume $\int_{\mathcal{R}} dV = V$.
- (b) $\oint_{\partial\mathcal{R}} (\hat{\mathbf{n}} \times \mathbf{F}) dS = \int_{\mathcal{R}} \nabla \times \mathbf{F} dV$, for an arbitrary vector field \mathbf{F} and with $\hat{\mathbf{n}}$ the outward unit normal on the bounding surface $\partial\mathcal{R}$. Hint: in a manner similar to the result shown in Section 2.7.2, make use of Gauss's theorem with $\mathbf{A} = \mathbf{F} \times \mathbf{C}$ where \mathbf{C} is a constant vector.
- (c) Let $\partial\mathcal{R}$ be a closed surface bounding a volume \mathcal{R} , and let \mathbf{x} denote the position vector of a point measured from an arbitrary origin. Prove the following

$$\oint_{\partial\mathcal{R}} \frac{\hat{\mathbf{n}} \cdot \mathbf{x}}{r^3} dS = \begin{cases} 0 & \text{if the origin lies outside of } \partial\mathcal{R} \\ 4\pi & \text{if the origin lies inside of } \partial\mathcal{R}. \end{cases} \quad (2.119)$$

EXERCISE 2.13: HELMHOLTZ DECOMPOSITION FOR CORIOLIS ACCELERATION

Consider a vector field

$$\mathbf{F} = 2\boldsymbol{\Omega} \times \mathbf{v}, \quad (2.120)$$

where $\boldsymbol{\Omega}$ is a spatial constant and $\nabla \cdot \mathbf{v} = 0$. As seen in Part V of this book, the vector \mathbf{F} is minus the Coriolis acceleration in the presence of an incompressible velocity. Since \mathbf{v} is non-divergent, there exists a vector potential so that

$$\mathbf{v} = \nabla \times \mathbf{B}. \quad (2.121)$$

Show that we can perform a Helmholtz decomposition

$$\mathbf{F} = 2\boldsymbol{\Omega} \times \mathbf{v} = -\nabla\Psi + \nabla \times \mathbf{A}, \quad (2.122)$$

where

$$-\nabla^2\Psi = -2\boldsymbol{\Omega} \cdot (\nabla \times \mathbf{v}) \quad (2.123a)$$

$$\nabla \times \mathbf{A} = (\boldsymbol{\Omega} \cdot \nabla) \mathbf{B} + \nabla\lambda, \quad (2.123b)$$

with λ an arbitrary gauge function.



Chapter 3

PARTIAL DIFFERENTIAL EQUATIONS

Fluid mechanics is a classical field theory whose mathematical description involves partial differential equations (PDEs). Although most of these partial differential equations are nonlinear, some are linear. Regardless, an understanding of linear partial differential equations provides useful insights into the physics and maths of geophysical fluids. For this purpose, we here explore the rudiments of linear partial differential equations.

CHAPTER GUIDE

One can penetrate much of this book without reading this chapter. What this chapter adds, however, is an appreciation for the mathematical structure and physical behavior of the equations describing geophysical fluid mechanics. Indeed, it is remarkable how useful it is, both mathematically and physically, to develop a basic understanding of linear partial differential equations. Furthermore, those aiming to develop solution methods, either analytical or numerical, should have a working knowledge of this chapter. Additionally, the Green's function method detailed in Chapter 4 assumes a firm understanding of the material in this chapter.

There are many resources devoted to the theory and application of partial differential equations throughout physics, engineering, and applied mathematics. Chapter 8 of [Hildebrand \(1976\)](#) offers a pedagogical starting point whereas [Stakgold \(2000a,b\)](#) thoroughly develops the theory and methods available for boundary value problems encountered in physics. [Duchateau and Zachmann \(1986\)](#) concisely summarize partial differential equations and provide nearly 300 worked exercises, with much of the presentation in this chapter following their treatment.

3.1	Loose threads	50
3.2	The advection equation	50
3.2.1	Constant advection velocity	50
3.2.2	Arbitrary functions resulting from PDEs	51
3.2.3	Further study	52
3.3	Characteristic curves for first order PDEs	52
3.3.1	General formulation	52
3.3.2	Examples	53
3.4	Classifying second order partial differential equations	54
3.5	Elliptic partial differential equations	55
3.5.1	Some general properties of Laplace's equation	55
3.5.2	Mean-value property of harmonic functions	55
3.5.3	Laplace's boundary value problem	56
3.5.4	Poisson's equation	57

3.5.5	Extended max-min principle for Poisson's equation	57
3.5.6	Poisson's boundary value problem	58
3.6	Parabolic partial differential equations	59
3.6.1	Initial and initial-boundary value problems	59
3.6.2	Smoothing property	59
3.6.3	Duhamel's superposition integral for the heat equation	60
3.6.4	Further study	61
3.7	Hyperbolic partial differential equations	61
3.7.1	Initial value problem for the infinite-domain wave equation	62
3.7.2	Domain of influence for wave signals	64
3.7.3	Helmholtz equation	64
3.7.4	Duhamel's superposition integral for the wave equation	65
3.7.5	Further study	66
3.8	Evolution of time averages	66
3.8.1	Time averages	67
3.8.2	Massaging the double time integrals	68
3.8.3	Making use of a double integral identity	68

3.1 Loose threads

- Nothing ATT.

3.2 The advection equation

Consider a tracer concentration, C , which for present purposes is a scalar field that is a function of space and time. As derived in Section 61.5, the tracer concentration in the absence of diffusion satisfies the advection equation

$$\frac{\partial C}{\partial t} + \mathbf{v} \cdot \nabla C = 0. \quad (3.1)$$

The space and time derivatives acting on C are both first order, indicating that the advection equation is a first order partial differential equation. It is a nonlinear partial differential equation for those *active* tracers such as temperature, where active tracers affect the velocity through changes to density and hence to pressure. In contrast, the advection equation is linear for *passive* tracers (e.g., colored dye, dust), which are tracers whose effects on velocity are negligible (Section 17.2). We limit the present discussion to passive tracers so that the advection equation is linear.

3.2.1 Constant advection velocity

To expose the gist of the advection equation, consider one space dimension and let the advection velocity be constant in space and time,

$$\frac{\partial C}{\partial t} + U \frac{\partial C}{\partial x} = 0 \quad (3.2)$$

where U is a constant velocity in the \hat{x} direction. An inspired guess reveals that

$$C(x, t) = \Gamma(\alpha) = \Gamma(x - Ut) \quad (3.3)$$

is a general solution to equation (3.2). Here, Γ is an arbitrary differentiable function that is determined by the initial conditions of the tracer field. Furthermore, there is only one argument

to Γ , here written as $\alpha = x - Ut$. As discussed in Section 3.3, $\alpha = x - Ut$ is referred to as a *characteristic curve* for the constant speed one-dimensional advection equation.

Verification of the solution (3.3) is readily found by noting

$$\frac{\partial C}{\partial x} = \frac{d\Gamma(\alpha)}{d\alpha} \frac{\partial \alpha}{\partial x} = \Gamma'(\alpha) \frac{\partial(x - Ut)}{\partial x} = \Gamma' \quad (3.4a)$$

$$\frac{\partial C}{\partial t} = \frac{d\Gamma(\alpha)}{d\alpha} \frac{\partial \alpha}{\partial t} = \Gamma'(\alpha) \frac{\partial(x - Ut)}{\partial t} = -\Gamma' U. \quad (3.4b)$$

We have thus verified that

$$\frac{\partial C}{\partial t} + \mathbf{v} \cdot \nabla C = -\Gamma' U + U \Gamma' = 0. \quad (3.5)$$

The functional dependence,

$$C(x, t) = \Gamma(\alpha) = \Gamma(x - Ut), \quad (3.6)$$

reveals that as time progresses with $U > 0$, an observer that moves in the positive \hat{x} direction with a speed U maintains a constant value for the tracer concentration. This behavior means that the tracer concentration is transported by advection with a speed U without changing its structure. We illustrate this behavior in Figure 3.1.

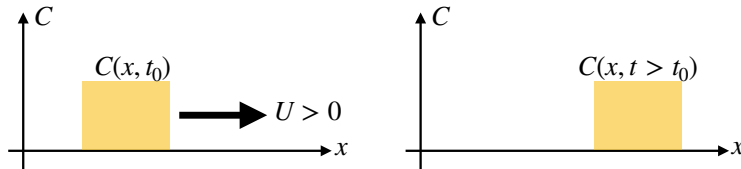


FIGURE 3.1: Illustrating the advection of a scalar field resulting from a constant advection velocity $\mathbf{v} = U\hat{x}$ with $U > 0$. The initially square pulse of tracer concentration is translated, unchanged, by the constant advection velocity.

3.2.2 Arbitrary functions resulting from PDEs

As revealed from the above example, the solution to a partial differential equation is typically given in terms of an arbitrary function with a specified dependence on the independent variables. The function itself is unspecified without additional information from initial and/or boundary conditions. For example, consider an initial tracer concentration in the form of a sine-wave

$$C(x, t = 0) = C_0 \sin(k x), \quad (3.7)$$

with k a wavenumber (dimensions of inverse length), and allow the domain to be infinite in extent (no boundaries). When advected by a constant advection velocity, the solution to the advection equation is a tracer concentration in the form of a sine-wave moving in the positive \hat{x} direction with speed U

$$C(x, t) = C_0 \sin[k(x - Ut)]. \quad (3.8)$$

The arbitrary functional degree of freedom is a generalization of the case with ordinary differential equations, whose solutions are specified up to unknown constants with values set by initial and/or boundary conditions.

3.2.3 Further study

Advection plays a fundamental role in the transport of matter, energy, and momentum within fluids. As seen in our discussion of fluid kinematics in Chapter 14, advection appears in the fluid mechanical equations when viewing the fluid from the fixed laboratory or *Eulerian* reference frame. We thus encounter advection throughout this book, with further development of the mathematics and physics provided in Sections 61.5 and 61.6.

3.3 Characteristic curves for first order PDEs

The advection equation is the canonical first order partial differential equation commonly found in fluid mechanics. A more general form for a first order partial differential equation in one space dimension is given by¹

$$P(x, t, \psi) \frac{\partial \psi}{\partial x} + Q(x, t, \psi) \frac{\partial \psi}{\partial t} = R(x, t, \psi), \quad (3.9)$$

where P , Q , and R are arbitrary smooth functions. This partial differential equation is linear if P , Q , and R are independent of ψ , and quasi-linear if P and Q are independent of ψ and R is at most a linear function of ψ . In this section we develop a formalism that determines the functional dependence of solutions to these partial differential equations. This *method of characteristics* is quite useful for exposing general properties of the solutions, even for those cases where the solution is not analytically available.

3.3.1 General formulation

In the first order partial differential equation given by equation (3.9), assume there is a functional relation

$$\Upsilon(x, t, \psi) = \text{constant} \quad (3.10)$$

that determines ψ consistent with the PDE (3.9). We refer to Υ as an *integral surface* that specifies a solution to the partial differential equation. For Υ to specify an integral surface it must satisfy

$$d\Upsilon = 0, \quad (3.11)$$

since the differential of a constant vanishes. This condition then leads to the differential constraints

$$\frac{d\Upsilon}{dt} = 0 = \frac{\partial \Upsilon}{\partial \psi} \frac{\partial \psi}{\partial t} + \frac{\partial \Upsilon}{\partial t} \quad (3.12a)$$

$$\frac{d\Upsilon}{dx} = 0 = \frac{\partial \Upsilon}{\partial \psi} \frac{\partial \psi}{\partial x} + \frac{\partial \Upsilon}{\partial x}. \quad (3.12b)$$

Assuming $\partial\Upsilon/\partial\psi \neq 0$ allows us to write

$$\frac{\partial \psi}{\partial t} = -\frac{\partial \Upsilon / \partial t}{\partial \Upsilon / \partial \psi} \quad \text{and} \quad \frac{\partial \psi}{\partial x} = -\frac{\partial \Upsilon / \partial x}{\partial \Upsilon / \partial \psi} \quad (3.13)$$

so that the first order partial differential equation (3.9) takes on the equivalent form

$$P \frac{\partial \Upsilon}{\partial x} + Q \frac{\partial \Upsilon}{\partial t} + R \frac{\partial \Upsilon}{\partial \psi} = 0. \quad (3.14)$$

¹Much from this section is taken from Section 8.2 of [Hildebrand \(1976\)](#).

Through this construct we have brought the functions P, Q, R into a symmetric form. Consistency of equation (3.14) with

$$d\Upsilon = \frac{\partial \Upsilon}{\partial x} dx + \frac{\partial \Upsilon}{\partial t} dt + \frac{\partial \Upsilon}{\partial \psi} d\psi = 0, \quad (3.15)$$

requires

$$P = \mu dx \quad \text{and} \quad Q = \mu dt \quad \text{and} \quad R = \mu d\psi, \quad (3.16)$$

for some non-dimensional function $\mu(x, t, \psi)$. Eliminating the unknown function μ renders the ordinary differential equations

$$\frac{dx}{P} = \frac{dt}{Q} = \frac{d\psi}{R}. \quad (3.17)$$

Paths in (x, t, ψ) space that satisfy these differential equations are known as *characteristic curves*. Note that if any one of the functions P, Q , or R vanish, then we merely remove that term from these relations.

3.3.2 Examples

We now determine characteristic curves for some specific examples. First consider the linear homogeneous advection equation with constant advection speed

$$U \frac{\partial \psi}{\partial x} + \frac{\partial \psi}{\partial t} = 0, \quad (3.18)$$

in which we identify $P = U$, $Q = 1$, and $R = 0$. The single ordinary differential equation defining the characteristic curve is given by

$$\frac{dx}{U} = \frac{dt}{1}, \quad (3.19)$$

so that characteristics are given by the family of space-time lines

$$x - U t = \alpha \quad (3.20)$$

with α an arbitrary constant. These lines determine the paths in space-time along which advective signals are transmitted.

Now add a constant source to the linear advection equation

$$U \frac{\partial \psi}{\partial x} + \frac{\partial \psi}{\partial t} = R. \quad (3.21)$$

The two ordinary differential equations defining the characteristic curve are

$$\frac{dx}{U} = \frac{dt}{1} = \frac{d\psi}{R}. \quad (3.22)$$

In addition to the relation $x - U t = \alpha_1$ determined from the homogeneous case, we also have $\psi - R t = \alpha_2$ for α_2 an arbitrary constant. Hence, the characteristic equations render the general solution of the form

$$\Gamma[x - U t, \psi - R t] = \text{constant}, \quad (3.23)$$

for Γ an arbitrary function. One example solution is given by

$$\psi = f(x - U t) + R t o \quad (3.24)$$

for an arbitrary smooth function, f . This solution has the form of a traveling signal, $f(x - U t)$,

plus a growing source, Rt .

For the final example, consider the linear advection equation with non-constant coefficients and non-constant source

$$x \frac{\partial \psi}{\partial x} + t \frac{\partial \psi}{\partial t} = \psi, \quad (3.25)$$

in which the ordinary differential equations determining the characteristics are given by

$$\frac{dx}{x} = \frac{dt}{t} = \frac{d\psi}{\psi}. \quad (3.26)$$

We are thus led to the relations

$$\frac{t}{x} = \alpha_1 \quad \frac{\psi}{x} = \alpha_2. \quad (3.27)$$

Hence, the general solution of the partial differential equation (3.25) is given by

$$\Gamma(t/x, \psi/x) = 0 \Rightarrow \psi = x F(t/x) \quad (3.28)$$

for an arbitrary smooth function F .

3.4 Classifying second order partial differential equations

There are many second order partial differential equations appearing in fluid mechanics, a general form of which in one space dimension is given by

$$A \frac{\partial^2 \psi}{\partial x^2} + B \frac{\partial^2 \psi}{\partial x \partial t} + C \frac{\partial^2 \psi}{\partial t^2} = \Lambda. \quad (3.29)$$

For linear partial differential equations, A, B, C are arbitrary functions of space and time that are independent of ψ . Furthermore, Λ is a function of space and time and at most a linear function of ψ and its derivatives. The most general solution to a linear partial differential equation consists of the sum of any *particular solution* and a solution to the homogeneous problem (where $\Lambda = 0$).

The terms involving second derivatives in equation (3.29) are of principle importance for determining the character of the solutions, with importance placed on the sign of the discriminant $B^2 - 4AC$. By analogy with conic sections we classify 2nd order partial differential equations as follows

$$\text{PDE form} = \begin{cases} \text{hyperbolic} & B^2 - 4AC > 0 \\ \text{elliptic} & B^2 - 4AC < 0 \\ \text{parabolic} & B^2 - 4AC = 0. \end{cases} \quad (3.30)$$

We can further motivate this terminology by considering the case of a homogeneous constant coefficient partial differential equation and an assumed solution of the form

$$\psi(x, t) = f(mx + t). \quad (3.31)$$

Plugging into the 2nd order partial differential equation (3.29) with $\Lambda = 0$ leads to

$$Am^2 + Bm + C = 0. \quad (3.32)$$

The two solutions m_1 and m_2 are both real for the hyperbolic case, conjugate complex for the elliptic case, and a perfect square for the parabolic case.

3.5 Elliptic partial differential equations

The elliptic case from Section 3.4 has discriminant $B^2 - 4AC < 0$, in which case there are two imaginary characteristics. The canonical example elliptic equation is *Laplace's equation*

$$\frac{\partial^2 \psi}{\partial x^2} + \frac{\partial^2 \psi}{\partial y^2} = 0, \quad (3.33)$$

where we converted from t as an independent variable to the space coordinate y . Formally, this transition is realized by setting $t = iy$, where $i = \sqrt{-1}$. Laplace's equation is satisfied by time-independent (i.e., *steady state*) solutions to the heat/diffusion equation (Section 3.6). Another common elliptic equation is *Poisson's equation*, which results from adding a source to Laplace's equation

$$\frac{\partial^2 \psi}{\partial x^2} + \frac{\partial^2 \psi}{\partial y^2} = \Lambda. \quad (3.34)$$

As there is no time present in the Laplace and Poisson equations, information is transmitted instantaneously so that the structure of the solution is determined by boundary conditions or boundary *data*. Strictly speaking, instantaneous information transfer is not physical since all physical signals have a finite propagation speed no greater than the speed of light. However, an infinite speed can be a useful mathematical construct. For example, acoustic signals in fluids propagate much faster than other waves and particle speeds, and they carry a very small energy.² For many purposes it is thus suitable to assume acoustic speeds are infinite, and in so doing we *filter* or remove acoustic modes from of the dynamical equations. In the process, the hyperbolic equation describing acoustic signals is converted into an elliptic equation. We consider acoustic signals in Chapter 44.

3.5.1 Some general properties of Laplace's equation

Solutions to Laplace's equation, $\nabla^2 \psi = 0$, are known as *harmonic functions*. Here are some example harmonic functions for two space dimensions:

$$\psi = x^3 - 3xy^2 \quad \psi = \ln(x^2 + y^2) \quad \psi = e^{\gamma x} \cos(\gamma y) \quad \psi = ax + by, \quad (3.35)$$

for arbitrary constants a, b, γ . Furthermore, with

$$\nabla^2(\psi\phi) = \psi\nabla^2\phi + 2\nabla\phi \cdot \nabla\psi + \phi\nabla^2\psi, \quad (3.36)$$

we see that the product of two harmonic functions ($\nabla^2\psi = \nabla^2\phi = 0$) is itself harmonic if and only if their gradients are orthogonal, $\nabla\psi \cdot \nabla\phi = 0$. In the remainder of this section we present, without proof, some general properties of harmonic functions and develop self-consistency for the boundary data appearing in the Laplacian boundary value problem defined by equations (3.39a)-(3.39b) stated below.

3.5.2 Mean-value property of harmonic functions

Harmonic functions possess a remarkable *mean-value* property. This property says that the value of a harmonic function, ψ , at a point \mathbf{x}_o within an open region of \mathcal{R} equals to the average of ψ

²A scuba diver feeling the beat of a ship underwater, or an audience member at a rock concert may question this statement. However, acoustic energy is in fact tiny relative to planetary waves and gravity waves, and utterly negligible for studies of large scale geophysical fluid motions.

taken over the surface of a sphere within \mathcal{R} that is centered at \mathbf{x}_o . In equations this property states that

$$\psi(\mathbf{x}_o) = \frac{\oint_{\mathcal{S}_R} \psi(\mathbf{x}) d\mathcal{S}}{\oint_{\mathcal{S}_R} d\mathcal{S}}, \quad (3.37)$$

where \mathcal{S}_R is a sphere with radius R centered at \mathbf{x}_o with “area” given by

$$\oint_{\mathcal{S}_R} d\mathcal{S} = \begin{cases} 2\pi R & n = 2 \text{ space dimensions} \\ 4\pi R^2 & n = 3 \text{ space dimensions.} \end{cases} \quad (3.38)$$

We illustrate this property in Figure 3.2.

The mean-value property of harmonic functions holds anywhere within the domain where $\nabla^2\psi = 0$, so long as the sphere is fully contained within that domain. It implies that there can be no extrema of ψ within the domain, since if there was an extrema then it could not satisfy the mean-value property. Hence, all extrema of harmonic functions must exist on the domain boundary. These properties lend mathematical support for considering harmonic functions to be solutions to continuous physical systems that are in equilibrium or a steady state. As a physical example, consider a temperature field, $T(\mathbf{x})$, in a region with zero heat sources and zero fluid flow. As shown in Section 61.3.4, the steady state temperature satisfies $\nabla^2T = 0$, and as such it is harmonic and hence has no extrema within the domain.

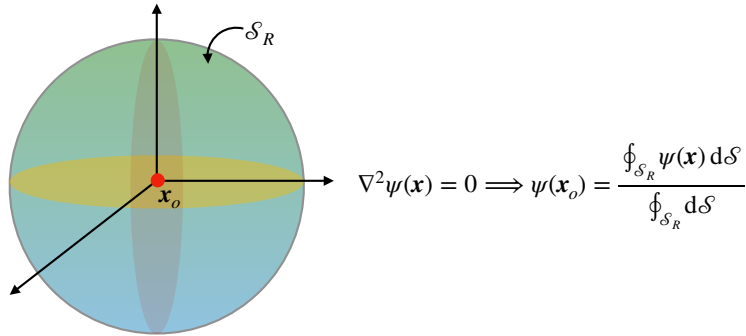


FIGURE 3.2: The value of a harmonic function at a point \mathbf{x}_o equals to the area average of the function over a sphere centered at \mathbf{x}_o . We here illustrate this property for 3-dimensions, but it holds for arbitrary space dimensions.

3.5.3 Laplace’s boundary value problem

Laplace’s equation requires boundary conditions to fully specify the harmonic function. We here consider the Laplacian *boundary value problem* in the form

$$\nabla^2\psi = 0 \quad \mathbf{x} \in \mathcal{R} \quad (3.39a)$$

$$\alpha\psi + \beta\hat{\mathbf{n}} \cdot \nabla\psi = \sigma \quad \mathbf{x} \in \partial\mathcal{R}, \quad (3.39b)$$

where \mathcal{R} is a smooth and simply connected volume, $\partial\mathcal{R}$ is the boundary surface enclosing \mathcal{R} with outward unit normal, $\hat{\mathbf{n}}$, and with α , β , and σ given boundary data functions.

We can establish constraints on the boundary conditions that lead to a self-consistent Laplacian boundary value problem (3.39a)-(3.39b). We do so through the use of Gauss’s divergence theorem (Section 2.7) in which integration over the full domain leads to

$$0 = \int_{\mathcal{R}} \nabla^2\psi dV = \oint_{\partial\mathcal{R}} \hat{\mathbf{n}} \cdot \nabla\psi d\mathcal{S}. \quad (3.40)$$

In physical applications the boundary condition (3.39b) usually appears with either $\alpha = 0$ or $\beta = 0$, and these two cases are associated with distinct self-consistency constraints.

Dirichlet boundary condition

The case with $\beta = 0$ is referred to as a *Dirichlet boundary condition* whereby

$$\psi = \sigma \quad \mathbf{x} \in \partial\mathcal{R}, \quad (3.41)$$

where we set $\alpha = 1$ without loss of generality. In this case all boundary data result in a self-consistent Laplacian boundary value problem so there is no constraint on σ . Thinking again about temperature, this boundary condition specifies the temperature on the domain boundary to equal $T = \sigma$, with all boundary functions σ consistent with a harmonic temperature distribution within the domain interior.

Neumann boundary condition

The case with $\alpha = 0$ results in a *Neumann boundary condition*. Without loss of generality we set $\beta = 1$ and reach the following self-consistency condition

$$\oint_{\partial\mathcal{R}} \sigma \, dS = 0. \quad (3.42)$$

A self-consistent boundary condition for Laplace's equation with the Neumann boundary condition must satisfy this surface integral constraint. For the temperature example, this boundary condition says that to realize a steady state harmonic temperature distribution within a region, we can at most apply a zero area averaged boundary heating. If the boundary constraint (3.42) is not satisfied, then the interior temperature field cannot be harmonic so that it will not be in a steady state.

3.5.4 Poisson's equation

The generic boundary value problem for Poisson's equation takes on the form

$$\nabla^2 \psi = \Lambda \quad \mathbf{x} \in \mathcal{R} \quad (3.43a)$$

$$\alpha \psi + \beta \hat{\mathbf{n}} \cdot \nabla \psi = \sigma \quad \mathbf{x} \in \partial\mathcal{R}, \quad (3.43b)$$

where $\Lambda(\mathbf{x})$ is a specified source function. We here present, without proof, some general properties of solutions to Poisson's equation and develop self-consistency conditions for the boundary data appearing in equation (3.43b).

3.5.5 Extended max-min principle for Poisson's equation

A subharmonic function is one where

$$\nabla^2 \psi = \Lambda \geq 0 \quad \mathbf{x} \in \mathcal{R}. \quad (3.44)$$

Here, the source function makes the curvature of a subharmonic function positive. Correspondingly, every point within \mathcal{R} satisfies the minimum principle

$$\psi(\mathbf{x}_o) \leq \frac{\oint_{\partial\mathcal{R}} \psi(\mathbf{x}) \, dS}{\oint_{\partial\mathcal{R}} dS}, \quad (3.45)$$

for spheres, \mathcal{S}_R , that are fully within \mathcal{R} . The signs switch for superharmonic functions whereby $\nabla^2\psi \leq 0$ for $\mathbf{x} \in \mathcal{R}$

Returning to the temperature example, consider a temperature field in a region with a positive heat source, $\Lambda > 0$. The steady state temperature in the presence of zero fluid flow satisfies Poisson's equation $\nabla^2 T = \Lambda \geq 0$ for regions with the heat source. The minimum principle (3.45) means that the temperature at any point within the heating region is less than the temperature averaged over a sphere centered on the point, so long as the sphere remains within the region of heating. It is only in the absence of a heat source or sink, where $\nabla^2 T = 0$, that we recover the mean-value property of harmonic functions given by equation (3.37).

3.5.6 Poisson's boundary value problem

We follow the method in Section 3.5.3 to develop constraints on the boundary conditions applied as part of the Poisson boundary value problem (3.43a)-(3.43b). Use of Gauss's divergence theorem leads to the constraint

$$\oint_{\partial\mathcal{R}} \hat{\mathbf{n}} \cdot \nabla \psi \, d\mathcal{S} = \int_{\mathcal{R}} \Lambda \, dV. \quad (3.46)$$

We separately consider the Dirichlet and Neumann cases.

Dirichlet boundary condition

The Dirichlet condition with $\beta = 0$ leads to

$$\psi = \sigma \quad \mathbf{x} \in \partial\mathcal{R}. \quad (3.47)$$

Just as for Laplace's boundary value problem, all boundary data result in a self-consistent Poisson boundary value problem so there is no constraint on σ . Thinking again about temperature, this boundary condition specifies the temperature on the domain boundary to equal $T = \sigma$, with all boundary functions σ consistent with the interior heating Λ and a temperature field satisfying $\nabla^2 T = \Lambda$ within the interior.

Self-consistent Neumann boundary condition

The *Neumann* boundary condition leads to the following self-consistency condition

$$\oint_{\partial\mathcal{R}} \sigma \, d\mathcal{S} = \int_{\mathcal{R}} \Lambda \, dV. \quad (3.48)$$

A self-consistent boundary condition for Poisson's equation with a Neumann boundary condition must satisfy this surface integral constraint. For the temperature example, this boundary condition says that the area integrated boundary data must be consistent with the volume integrated source function in order for the temperature to satisfy Poisson's equation. Otherwise, the temperature field will evolve in time and thus not be in a steady state. Compatibility of the boundary conditions ensures the existence of a solution to the Poisson equation that is unique up to an arbitrary constant.

3.6 Parabolic partial differential equations

The parabolic case from Section 3.4, $B^2 - 4AC = 0$, contains a single real characteristic. The canonical example is the *heat equation*, which is also known as the *diffusion equation*

$$\frac{\partial \psi}{\partial t} = \kappa \frac{\partial^2 \psi}{\partial x^2}, \quad (3.49)$$

where $\kappa > 0$ is the kinematic diffusivity with dimensions of squared length per time.

3.6.1 Initial and initial-boundary value problems

The *Cauchy Problem* is the name given to the initial value problem for the heat equation over all space, here given by Euclidean space

$$\frac{\partial \psi}{\partial t} = \kappa \nabla^2 \psi \quad \mathbf{x} \in \mathbb{R}^n, t > 0 \quad (3.50a)$$

$$\psi(\mathbf{x}, t=0) = \sigma(\mathbf{x}) \quad \mathbf{x} \in \mathbb{R}^n \quad (3.50b)$$

$$|\psi(\mathbf{x}, t)| < \infty \quad \mathbf{x} \in \mathbb{R}^n, t > 0. \quad (3.50c)$$

The general initial-boundary value problem over a finite domain \mathcal{R} takes the form

$$\frac{\partial \psi}{\partial t} = \kappa \nabla^2 \psi \quad \mathbf{x} \in \mathcal{R}, t > 0 \quad (3.51a)$$

$$\psi(\mathbf{x}, t=0) = \sigma(\mathbf{x}) \quad \mathbf{x} \in \mathcal{R} \quad (3.51b)$$

$$\alpha(\mathbf{x}) \psi(\mathbf{x}, t) + \beta(\mathbf{x}) \hat{\mathbf{n}} \cdot \nabla \psi(\mathbf{x}, t) = g(\mathbf{x}, t) \quad \mathbf{x} \in \partial \mathcal{R}, t > 0, \alpha \beta \geq 0. \quad (3.51c)$$

Following from the discussion of Laplace's and Poisson's boundary value problems, choices for the boundary functions α and β impact on the character of the boundary conditions. The Neumann condition is most commonly applied to set the flux of a tracer or temperature at the boundaries. The alternative use of the Dirichlet condition is commonly applied for idealized "diagnostic" tracers in geophysical fluid applications (see [Haine et al. \(2022\)](#) for a review of such idealized ocean tracers).

3.6.2 Smoothing property

The extended max-min principle from Section 3.5.5 holds also for the heat equation, which is consistent with solutions to the heat equation generally decaying their initial condition towards zero by reducing the amplitude of all extrema. Hence, no extrema are introduced in the interior of the domain by the heat equation; extrema only arise via boundary and/or initial conditions. Furthermore, the steady state limit of the heat equation is a harmonic function, and so solves Laplace's equation whereby the mean-value property holds (Section 3.5.2). These characteristics of the heat equation are generally shared by all linear parabolic partial differential equations.

Illustrating the smoothing property in a finite domain

We illustrate the smoothing property for the specific case of the one-dimensional initial-boundary value problem with homogeneous Dirichlet boundary conditions

$$\frac{\partial \psi}{\partial t} = \kappa \frac{\partial^2 \psi}{\partial x^2} \quad 0 < x < L, t > 0 \quad (3.52a)$$

$$\psi(x, t) = I(x) \quad 0 < x < L, t = 0 \quad (3.52b)$$

$$\psi(0, t) = \psi(L, t) = 0 \quad t > 0. \quad (3.52c)$$

A variety of methods, such as separation of variables, can be used to derive the following Fourier series solution

$$\psi(x, t) = \sum_{n=1}^{\infty} I_n e^{-\kappa t (n\pi/L)^2} \sin(n\pi x/L) \quad \text{with} \quad I_n = \frac{2}{L} \int_0^L I(x) \sin(n\pi x/L) dx. \quad (3.53)$$

As per the smoothing property of diffusion, note how the amplitude of each Fourier mode decays exponentially in time.

Smoothing property for an initial value problem on the real line

Now consider the one-dimensional heat equation on the real line, with the only boundary conditions being regularity at infinity

$$\frac{\partial \psi}{\partial t} = \kappa \frac{\partial^2 \psi}{\partial x^2} \quad -\infty < x < \infty, t > 0 \quad (3.54a)$$

$$\psi(x, t) = I(x) \quad -\infty < x < \infty, t = 0. \quad (3.54b)$$

One can show by direct differentiation that the following Gaussian is a solution

$$\psi(x, t) = \frac{1}{\sqrt{4\pi\kappa t}} \int_{-\infty}^{\infty} I(\xi) \exp\left[-\frac{(x-\xi)^2}{4\kappa t}\right] d\xi. \quad (3.55)$$

Again, this function smooths/damps the initial condition function $I(x)$ as time increases.

3.6.3 Duhamel's superposition integral for the heat equation

Consider a scalar field that starts from zero initial conditions and evolves according to the heat equation in the presence of a source

$$\frac{\partial \Psi}{\partial t} = \kappa \nabla^2 \Psi + f(\mathbf{x}) \quad \mathbf{x} \in \mathbb{R}^n, t > 0 \quad (3.56a)$$

$$\Psi(\mathbf{x}, t) = 0 \quad \mathbf{x} \in \mathbb{R}^n, t = 0. \quad (3.56b)$$

Now consider the converse, in which another scalar field evolves without a source and yet is initialized according to the source

$$\frac{\partial \psi}{\partial t} = \kappa \nabla^2 \psi \quad \mathbf{x} \in \mathbb{R}^n, t > 0 \quad (3.57a)$$

$$\psi(\mathbf{x}, t) = f(\mathbf{x}) \quad \mathbf{x} \in \mathbb{R}^n, t = 0. \quad (3.57b)$$

Remarkably, these two scalar fields are related by *Duhamel's superposition integral*

$$\Psi(\mathbf{x}, t) = \int_0^t \psi(\mathbf{x}, t - \tau) d\tau. \quad (3.58)$$

We verify the connection by direct differentiation

$$\frac{\partial \Psi(\mathbf{x}, t)}{\partial t} = \psi(\mathbf{x}, 0) + \int_0^t \frac{\partial \psi(\mathbf{x}, t - \tau)}{\partial t} d\tau = f(\mathbf{x}) + \kappa \nabla^2 \Psi(\mathbf{x}, t). \quad (3.59)$$

Duhamel's superposition integral allows us to move the source between the partial differential operator and the initial conditions. It says that the forced solution, $\Psi(\mathbf{x}, t)$, is built by time integrating the “retarded” values of the unforced solution, ψ , from the initial time, $t = 0$, to the current time, t . Note that a more general presentation allows for the source function to be a function of time, $f(\mathbf{x}, t)$, in which case we must develop a family of solutions, $\psi_f(\mathbf{x}, t; \tau)$, generated by reinitializing $\psi_f(\mathbf{x}, t = \tau; \tau) = f(\mathbf{x}, \tau)$ and then superposing the members of this family to generate $\Psi(\mathbf{x}, t)$.

As an example, consider the initial value problem for the heat equation on a line as given by equations (3.54a)-(3.54b)

$$\frac{\partial \psi}{\partial t} = \kappa \frac{\partial^2 \psi}{\partial x^2} \quad -\infty < x < \infty, t > 0 \quad (3.60a)$$

$$\psi(x, t) = f(x) \quad -\infty < x < \infty, t = 0, \quad (3.60b)$$

whose solution is given by the Gaussian function in equation (3.55). Duhamel's superposition integral (3.58) says that

$$\Psi(x, t) = \int_0^t \psi(x, t - \tau) d\tau = \int_0^t \frac{1}{\sqrt{4\pi\kappa(t-\tau)}} \int_{-\infty}^{\infty} f(\xi) \exp\left[-\frac{(x-\xi)^2}{4\kappa(t-\tau)}\right] d\xi d\tau \quad (3.61)$$

satisfies the forced (inhomogeneous) initial value problem with zero initial condition

$$\frac{\partial \Psi}{\partial t} = \kappa \frac{\partial^2 \Psi}{\partial x^2} + f(x) \quad -\infty < x < \infty, t > 0 \quad (3.62a)$$

$$\Psi(x, t) = 0 \quad -\infty < x < \infty, t = 0. \quad (3.62b)$$

We make use of this result in our discussion of Green's functions in Chapter 4.

3.6.4 Further study

We examine physical and mathematical properties of the heat/diffusion equation in Sections 61.3 and 61.4. Section 9.11 of [Hildebrand \(1976\)](#) offers a lucid discussion of Duhamel's superposition integral.

3.7 Hyperbolic partial differential equations

The hyperbolic case from Section 3.4 has $B^2 - 4AC > 0$ and thus contains two real characteristics. The canonical example of a hyperbolic partial differential equation is the linear homogeneous wave equation

$$(\partial_{tt} - U^2 \partial_{xx})\psi = 0. \quad (3.63)$$

Solutions have the form of a moving wave in both directions (the two wave characteristics)

$$\psi(x, t) = \mathcal{F}(x - Ut) + \mathcal{G}(x + Ut), \quad (3.64)$$

where \mathcal{F} and \mathcal{G} are differentiable functions whose form is determined by the initial conditions. Note that we can factor the differential operator into the form

$$(\partial_t - U \partial_x)(\partial_t + U \partial_x)\psi = 0. \quad (3.65)$$

Consequently, if either one of the linear first-order partial differential equations are satisfied

$$(\partial_t - U \partial_x)\psi = 0 \quad (3.66a)$$

$$(\partial_t + U \partial_x)\psi = 0 \quad (3.66b)$$

then ψ will satisfy the full wave equation. These first-order partial differential equations are the one-dimensional advection equations considered in Section 3.3 with opposite advection direction, and each of which has a single characteristic. In this manner, we can think of advection by constant velocity as the square root of the wave equation. Similarly, some disciplines refer to the linear advection equation (3.2), with constant advection speed, as the *one-way wave equation*. It represents the simplest of the hyperbolic partial differential equations.

3.7.1 Initial value problem for the infinite-domain wave equation

Since there are two time derivatives, specification of a solution requires initial conditions for the field and its first time derivative. To illustrate the structure of a solution to the wave equation, we develop a solution to the *Cauchy problem*, which is the initial value problem for the one-dimensional wave equation on the real line (infinite spatial domain so no boundary conditions)

$$\partial_{tt}\psi = c^2 \partial_{xx}\psi \quad -\infty < x < \infty, t > 0 \quad \text{wave equation on a line} \quad (3.67a)$$

$$\psi = F(x) \quad -\infty < x < \infty, t = 0 \quad \text{initial condition} \quad (3.67b)$$

$$\partial_t\psi = G(x) \quad -\infty < x < \infty, t = 0 \quad \text{initial tendency,} \quad (3.67c)$$

where the initial condition data, F, G , are arbitrary functions of space and c is a constant wave speed. Following from the discussion of characteristics in Section 3.3, we are motivated to transform the wave equation into wave characteristic coordinates

$$\xi = x + ct \quad \text{and} \quad \eta = x - ct \implies (\xi + \eta)/2 = x \quad \text{and} \quad (\xi - \eta)/(2c) = t. \quad (3.68)$$

Wave signals propagate in directions defined by constant ξ and η , so that these coordinates isolate the signal transmission. Furthermore, as we will see, this coordinate transformation facilitates a direct integration of the wave equation.

Transformation to characteristic coordinates

To help organize the transformation to characteristic coordinates, we write equation (3.68) as a matrix-vector equation

$$\begin{bmatrix} \xi \\ \eta \end{bmatrix} = \begin{bmatrix} c & 1 \\ -c & 1 \end{bmatrix} \begin{bmatrix} t \\ x \end{bmatrix} \iff \begin{bmatrix} t \\ x \end{bmatrix} = \frac{1}{2} \begin{bmatrix} c^{-1} & -c^{-1} \\ 1 & 1 \end{bmatrix} \begin{bmatrix} \xi \\ \eta \end{bmatrix}. \quad (3.69)$$

Furthermore, define

$$x^n = (x^0, x^1) = (x, t) \quad \text{and} \quad x^{\bar{n}} = (x^{\bar{0}}, x^{\bar{1}}) = (\xi, \eta) \quad (3.70)$$

and use index notation from Chapter 1 so that the transformation (3.69) takes the tidy form

$$x^{\bar{n}} = \Lambda^{\bar{n}}_m x^m \iff x^n = \Lambda^n_{\bar{m}} x^{\bar{m}}, \quad (3.71)$$

where the transformation matrices are given by

$$\Lambda^{\bar{n}}_m = \begin{bmatrix} c & 1 \\ -c & 1 \end{bmatrix} \quad \text{and} \quad \Lambda^n_{\bar{m}} = \frac{1}{2} \begin{bmatrix} c^{-1} & -c^{-1} \\ 1 & 1 \end{bmatrix}. \quad (3.72)$$

Note the use of an upstairs position for the row index on the transformation matrix, which conforms to the use with general tensors from Chapter 7. For present purposes there is no significance to this position placement; it is only used here to anticipate the general tensor machinery. The coordinate transformation (3.71) and the transformation matrices (3.72) then lead to the partial derivative relationship

$$\partial_{\bar{n}} = \Lambda^{\bar{m}}_{\bar{n}} \partial_m \iff \partial_n = \Lambda^{\bar{m}}_n x^{\bar{m}}, \quad (3.73)$$

so that

$$\frac{\partial^2}{\partial x^2} = \left[\frac{\partial}{\partial \xi} + \frac{\partial}{\partial \eta} \right]^2 = \frac{\partial^2}{\partial \xi^2} + 2 \frac{\partial}{\partial \xi} \frac{\partial}{\partial \eta} + \frac{\partial^2}{\partial \eta^2} \quad (3.74a)$$

$$c^{-2} \frac{\partial^2}{\partial t^2} = \left[\frac{\partial}{\partial \xi} - \frac{\partial}{\partial \eta} \right]^2 = \frac{\partial^2}{\partial \xi^2} - 2 \frac{\partial}{\partial \xi} \frac{\partial}{\partial \eta} + \frac{\partial^2}{\partial \eta^2}. \quad (3.74b)$$

General solution for the initial value problem

The operator transformations (3.74a) and (3.74b) bring the initial value problem (3.67a)-(3.67c) into

$$\frac{\partial^2 \psi}{\partial \xi \partial \eta} = 0 \quad -\infty < \eta < \xi < \infty \quad (3.75a)$$

$$\psi(\xi, \eta) = F(\xi) \quad -\infty < \xi < \infty, \xi = \eta \quad (3.75b)$$

$$\frac{\partial \psi}{\partial \xi} - \frac{\partial \psi}{\partial \eta} = c^{-1} G(\xi) \quad -\infty < \xi < \infty, \xi = \eta. \quad (3.75c)$$

Integrating equation (3.75a) in two steps leads to $\partial_\xi \psi = \theta(\xi)$ so that

$$\psi(\xi, \eta) = \Phi(\eta) + \int^\xi \theta(s) ds \equiv \Phi(\eta) + \Theta(\xi), \quad (3.76)$$

for two functions $\Phi(\eta)$ and $\Theta(\xi)$. The initial conditions (3.75b) and (3.75c) determine relations between $\Phi(\eta)$ and $\Theta(\xi)$ and the initial data

$$\Theta(\xi) = \frac{1}{2} \left[F(\xi) + \frac{1}{c} \int^\xi G(s) ds \right] \quad (3.77a)$$

$$\Phi(\eta) = \frac{1}{2} \left[F(\eta) - \frac{1}{c} \int^\eta G(s) ds \right], \quad (3.77b)$$

in which case the general solution to the initial value problem (3.67a)-(3.67c) takes the form

$$\psi(x, t) = \frac{1}{2} [F(x + ct) + F(x - ct)] + \frac{1}{2c} \int_{x-ct}^{x+ct} G(s) ds, \quad (3.78)$$

where we reintroduced the variables (x, t) . This solution is known as the *D'Alembert formula* for the wave equation. Note how the initial profile, $F(x)$, is propagated along the two characteristics, $\xi = x + ct$ and $\eta = x - ct$, without any change. In contrast, the initial tendency, $\partial_t \psi(x, t = 0) = G(x)$, is smoothed through the time integration. This behavior contrasts to the heat equation in Section 3.6, with its single time derivative resulting in a smoothing of the full solution.

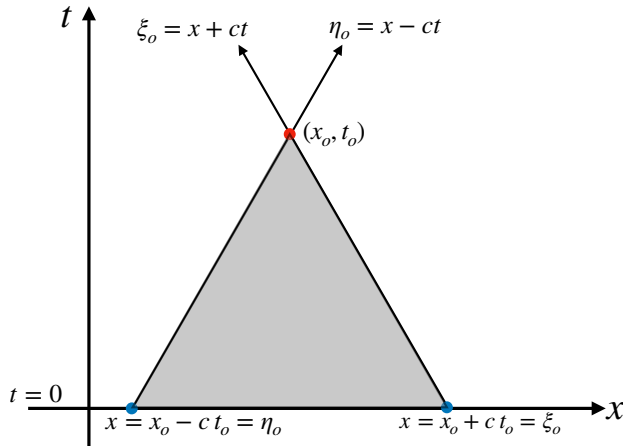


FIGURE 3.3: According to the wave solution (3.78) to the initial value problem on a line, an arbitrary space-time point, (x_o, t_o) , is causally connected via wave signals to all space-time points within the blue region. This *domain of influence* is bounded by the two wave characteristics, $\xi_o = x_o + ct_o$ and $\eta_o = x_o - ct_o$, with these characteristics the pathway for propagating information about the initial wave profile, $\psi(x, t = 0) = F(x)$. Points in between the characteristics are causally connected via the initial time tendency, $\partial_t \psi(x, t = 0) = G(x)$, which is integrated over the region $x_o - ct_o \leq x \leq x_o + ct_o$. Points outside the domain of influence are causally disconnected from the point (x_o, t_o) .

3.7.2 Domain of influence for wave signals

The wave solution (3.78) at a point in space time, (x_o, t_o) , depends on data to its past within a causality triangle, or *domain of influence*, as shown in Figure 3.3. The domain of influence is bounded by the two wave characteristics, $\xi_o = x_o + ct_o$ and $\eta_o = x_o - ct_o$. These characteristics are the pathways for propagating information about the initial wave profile, $\psi(x, t = 0) = F(x)$. Points in between the characteristics are causally connected via the initial time tendency, $\partial_t \psi(x, t = 0) = G(x)$, which is integrated over the region $x_o - ct_o \leq x \leq x_o + ct_o$. Points outside the domain of influence are causally disconnected from the point (x_o, t_o) .

3.7.3 Helmholtz equation

Consider the wave equation with a constant wave speed

$$\partial_{tt} \psi - c^2 \nabla^2 \psi = 0. \quad (3.79)$$

Assuming a monochromatic periodic time dependence ansatz³ of the form

$$\psi(\mathbf{x}, t) = e^{-i\omega t} \Psi(\mathbf{x}) \quad (3.80)$$

results in the *Helmholtz equation* for the amplitude function

$$[\nabla^2 + (\omega/c)^2] \Psi = 0. \quad (3.81)$$

The Helmholtz equation thus plays a central role in wave theory. In Exercise 44.1, we encounter this equation when deriving the standing acoustic modes in a rectangular cavity.

3.7.4 Duhamel's superposition integral for the wave equation

We here present Duhamel's superposition integral for the wave equation, following from the similar discussion for the heat equation in Section 3.6.3. For this purpose, consider the forced wave equation with time independent forcing

$$\frac{\partial^2 \Psi}{\partial t^2} = c^2 \nabla^2 \Psi + G(\mathbf{x}) \quad \mathbf{x} \in \mathbb{R}^n, t > 0 \quad (3.82a)$$

$$\Psi(\mathbf{x}, t) = 0 \quad \mathbf{x} \in \mathbb{R}^n, t = 0, \quad (3.82b)$$

and the corresponding unforced wave equation with inhomogenous initial time tendency

$$\frac{\partial^2 \psi}{\partial t^2} = c^2 \nabla^2 \psi \quad \mathbf{x} \in \mathbb{R}^n, t > 0 \quad (3.83a)$$

$$\psi(\mathbf{x}, t) = 0 \quad \mathbf{x} \in \mathbb{R}^n, t = 0. \quad (3.83b)$$

$$\frac{\partial \psi(\mathbf{x}, t)}{\partial t} = G(\mathbf{x}) \quad \mathbf{x} \in \mathbb{R}^n, t = 0. \quad (3.83c)$$

The two scalar fields are related by Duhamel's superposition integral

$$\Psi(\mathbf{x}, t) = \int_0^t \psi(\mathbf{x}, t - \tau) d\tau. \quad (3.84)$$

We can verify this formula through direct differentiation

$$\frac{\partial \Psi(\mathbf{x}, t)}{\partial t} = \int_0^t \frac{\partial \psi(\mathbf{x}, t - \tau)}{\partial t} d\tau \quad (3.85a)$$

$$\frac{\partial^2 \Psi(\mathbf{x}, t)}{\partial t^2} = \frac{\partial \psi(\mathbf{x}, 0)}{\partial t} + \int_0^t \frac{\partial^2 \psi(\mathbf{x}, t - \tau)}{\partial t^2} d\tau = G(\mathbf{x}) + c^2 \nabla^2 \Psi(\mathbf{x}, t). \quad (3.85b)$$

As an example, consider the initial value problem for wave equation on a line with time independent forcing

$$\frac{\partial^2 \Psi}{\partial t^2} = c^2 \frac{\partial^2 \Psi}{\partial x^2} + G(x) \quad -\infty < x < \infty, t > 0 \quad (3.86a)$$

$$\Psi(x, t) = 0 \quad -\infty < x < \infty, t = 0 \quad (3.86b)$$

$$\frac{\partial \Psi(x, t)}{\partial t} = 0 \quad -\infty < x < \infty, t = 0. \quad (3.86c)$$

³*Ansatz* is a German word meaning an educated guess for the form of the solution. Monochromatic refers to the refers to the time dependence where each portion of the wave oscillates with the same angular frequency, ω . We study wave kinematics in Chapter 43.

Duhamel's superposition integral says that Ψ is related to the solution of the unforced wave equation with initial time tendency given by the forcing

$$\frac{\partial^2 \psi}{\partial t^2} = c^2 \frac{\partial^2 \psi}{\partial x^2} \quad -\infty < x < \infty, t > 0 \quad (3.87a)$$

$$\psi(x, t) = 0 \quad -\infty < x < \infty, t = \tau \quad (3.87b)$$

$$\frac{\partial \psi(x, t)}{\partial t} = G(x) \quad -\infty < x < \infty, t = \tau > 0. \quad (3.87c)$$

We know from Section 3.7.1 that the solution ψ is given by the D'Alembert formula in equation (3.78), only here with the initial condition function set to zero

$$\psi(x, t) = \frac{1}{2c} \int_{x-ct}^{x+ct} G(s) ds. \quad (3.88)$$

Hence, D'Alembert's formula says that the solution to the forced wave equation (3.86a)-(3.86c) is given by the superposition integral

$$\Psi(x, t) = \frac{1}{2c} \int_0^t \int_{x-c(t-\tau)}^{x+c(t-\tau)} G(s) ds. \quad (3.89)$$

Introducing the *antiderivative* function via

$$\mathcal{G}(s) = \int^s G(s') ds' \iff \frac{\partial \mathcal{G}(s)}{\partial s} = G(s) \quad (3.90)$$

allows us to interpret the solution (3.89) as the superposition of two oppositely traveling waves

$$\Psi(x, t) = \frac{1}{2c} \int_0^t [\mathcal{G}[x + c(t - \tau)] - \mathcal{G}[x - c(t - \tau)]] d\tau. \quad (3.91)$$

3.7.5 Further study

[Stakgold \(2000a,b\)](#) provides a thorough discussion of the wave equation and the related Helmholtz equation. We further our understanding of wave maths and physics in Part IX of this book, where we refer to the hyperbolic waves of this section as *non-dispersive waves*. For non-dispersive waves, the linear superposition of many waves retains its integrity since each wave travels with the same speed. However, most waves of interest for geophysical fluid mechanics are *dispersive*, so that waves mix among themselves; i.e., they change wavelengths as they interact. Dispersive waves are described by partial differential equations that are not necessarily hyperbolic. For example, surface gravity waves of Chapter 45 satisfy an elliptic equation, with time dependence arising from boundary conditions. The dispersion of surface gravity waves leads to the familiar spreading of waves on the surface of a pond whereby longer waves travel faster than shorter waves.

3.8 Evolution of time averages

In geophysical fluid mechanics, we generically refer to an equation with a time derivative, such as a parabolic or hyperbolic equation, as a *prognostic equation* or an *evolution equation*. In the analysis of such equations, for example when analyzing simulation output or time series data, it is common to take the time average in order to focus on lower frequency behavior. This section provides a technical discussion concerning this time averaging operation, with the material here

following [Bladwell et al. \(2022\)](#).

For this purpose, ignore all space coordinates and write a generic prognostic equation in the form

$$\frac{dA}{dt} = \mathcal{B}. \quad (3.92)$$

For example, the quantity A might be the velocity or temperature at a point in space, and \mathcal{B} might be the acceleration due to pressure or the heating due to temperature diffusion. We term dA/dt the *time tendency* of the quantity A whereas \mathcal{B} is the “forcing” that gives rise to the time tendency. In the analysis of fluid flows, we commonly wish to diagnose terms appearing in the evolution equations for the purpose of ascribing physical understanding to the flow regime; e.g., what forces are more active in certain regions. Although sitting a bit outside the scope of a chapter on partial differential equations, the material in this section exposes some common questions that arise when time averaging terms appearing in the prognostic equations of geophysical fluid mechanics.

Time integration of equation (3.92) leads to

$$A(t) = A(t_0) + \int_{t_0}^t \mathcal{B}(s) ds, \quad (3.93)$$

thus providing an expression for the instantaneous value of A at an arbitrary time t , assuming knowledge of the initial value, $A(t_0)$, as well as the time integral of \mathcal{B} . In practice, particularly when working with numerical models, we typically have access to time averages over some time interval (e.g., days, months, years, decades) rather than instantaneous (snapshot) values of A . Furthermore, instantaneous snapshots can be prone to relatively large fluctuations that expose the diagnostic calculations to numerical precision errors (e.g., small differences between relatively large fluctuating values). We are thus interested in relating time averages of A to time averages of \mathcal{B} .

3.8.1 Time averages

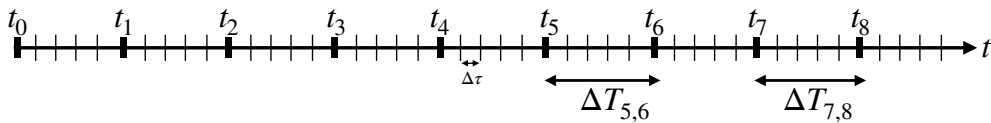


FIGURE 3.4: Example time axis for the discussion of time averaging. The labeled times, t_n , can represent, for example, days, months or years with the time interval, $\Delta T_{n,n+1} = t_{n+1} - t_n$, not necessarily the same (e.g., different number of days in a month or a leap year versus non-leap year). The smaller unlabeled time steps represent the time steps for the model’s prognostic equations (e.g., days, hours, seconds, etc.), with fixed time step $\Delta\tau$.

Introduce a discrete partitioning of the time axis as in Figure 3.4 and define an unweighted time average over a chosen time interval $\Delta T_{n,n+1} = t_{n+1} - t_n > 0$

$$\bar{A}_{n,n+1} = \frac{1}{\Delta T_{n,n+1}} \int_{t_n}^{t_{n+1}} A(t) dt \quad (3.94a)$$

$$\bar{\mathcal{B}}_{n,n+1} = \frac{1}{\Delta T_{n,n+1}} \int_{t_n}^{t_{n+1}} \mathcal{B}(t) dt. \quad (3.94b)$$

These integrals are realized in practice as a discrete sum over the model time steps, with only the lower limit inclusive so as to not double-count endpoints; i.e., $[t_n, t_{n+1})$. We allow for non-constant time intervals, $\Delta T_{n,n+1}$, as arises in monthly and yearly (with leap-years) time averages.

Substituting expression (3.93) into the time mean (3.94a) renders

$$\bar{A}_{n,n+1} - A(t_0) = \frac{1}{\Delta T_{n,n+1}} \int_{t_n}^{t_{n+1}} \left[\int_{t_0}^t \mathcal{B}(s) ds \right] dt, \quad (3.95)$$

and a similar expression over a later time interval $[t_p, t_{p+1}]$ with $p \geq n + 1$ leads to the difference between time averages

$$\bar{A}_{p,p+1} - \bar{A}_{n,n+1} = \frac{1}{\Delta T_{p,p+1}} \int_{t_p}^{t_{p+1}} \left[\int_{t_0}^t \mathcal{B}(s) ds \right] dt - \frac{1}{\Delta T_{n,n+1}} \int_{t_n}^{t_{n+1}} \left[\int_{t_0}^t \mathcal{B}(s) ds \right] dt. \quad (3.96)$$

The formalism allows us to take differences between time averages over intervals that are separated, such as might be of interest in taking decadal means between the beginning and end of a century, for example. Importantly, the initial value, $A(t_0)$, is absent from the difference in time means so that there are only time integrated quantities appearing in equation (3.96).

3.8.2 Massaging the double time integrals

The double time integrals in equation (3.96) can be massaged into a simpler form. We start by making the following decomposition and noting that $t_n \leq t \leq t_{n+1}$

$$\int_{t_n}^{t_{n+1}} \left[\int_{t_0}^t \mathcal{B}(s) ds \right] dt = \int_{t_n}^{t_{n+1}} \left[\int_{t_0}^{t_n} \mathcal{B}(s) ds + \int_{t_n}^t \mathcal{B}(s) ds \right] dt \quad (3.97a)$$

$$= \Delta T_{n,n+1} \int_{t_0}^{t_n} \mathcal{B}(s) ds + \int_{t_n}^{t_{n+1}} \left[\int_{t_n}^t \mathcal{B}(s) ds \right] dt. \quad (3.97b)$$

We are thus led to the difference

$$\begin{aligned} \bar{A}_{p,p+1} - \bar{A}_{n,n+1} &= \left[\int_{t_0}^{t_p} \mathcal{B}(s) ds - \int_{t_0}^{t_n} \mathcal{B}(s) ds \right] \\ &+ \frac{1}{\Delta T_{p,p+1}} \int_{t_p}^{t_{p+1}} \left[\int_{t_p}^t \mathcal{B}(s) ds \right] dt - \frac{1}{\Delta T_{n,n+1}} \int_{t_n}^{t_{n+1}} \left[\int_{t_n}^t \mathcal{B}(s) ds \right] dt \\ &= \int_{t_n}^{t_p} \mathcal{B}(t) dt + \frac{1}{\Delta T_{p,p+1}} \int_{t_p}^{t_{p+1}} \left[\int_{t_p}^t \mathcal{B}(s) ds \right] dt - \frac{1}{\Delta T_{n,n+1}} \int_{t_n}^{t_{n+1}} \left[\int_{t_n}^t \mathcal{B}(s) ds \right] dt. \end{aligned} \quad (3.98)$$

The double integrals in equation (3.98) take place over triangular time domains, such as shown in Figure 3.5.

3.8.3 Making use of a double integral identity

We here derive an identity (originally due to *Cauchy* (1823)) that reduces the double integral in equation (3.98) to a single integral to expose the underlying geometry of the time windowing. For this purpose we make use of the following identity

$$\int_{t_n}^{t_{n+1}} \left[\int_{t_n}^t \mathcal{B}(s) ds \right] dt = \int_{t_n}^{t_{n+1}} (t_{n+1} - t) \mathcal{B}(t) dt. \quad (3.99)$$

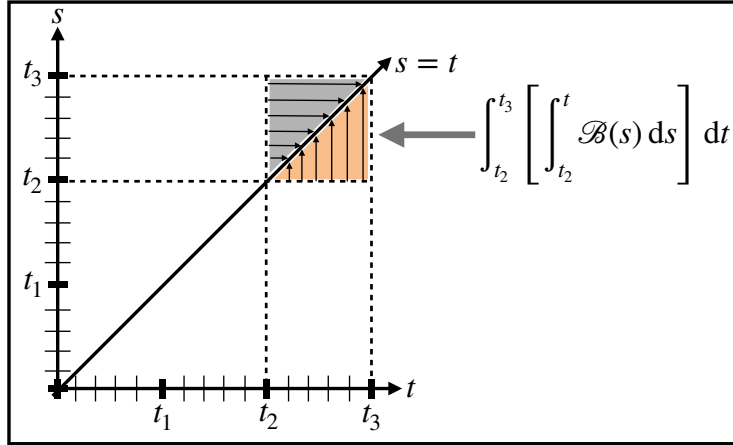


FIGURE 3.5: Gold region depicts the time integration domain used in one of the double integrals from equation (3.98) for the special case of $n = 2$. Note that the gray triangular region generally leads to a distinct integral.

To prove this identity we make the substitution $\mathcal{B}(s) = dA/ds$ from equation (3.92) and then show that both sides to equation (3.99) yield the same result. For the left hand side we have

$$\int_{t_n}^{t_{n+1}} \left[\int_{t_n}^t \mathcal{B}(s) ds \right] dt = \int_{t_n}^{t_{n+1}} \left[\int_{t_n}^t \frac{dA(s)}{ds} ds \right] dt \quad (3.100a)$$

$$= \int_{t_n}^{t_{n+1}} \left[\int_{t_n}^t dA(s) \right] dt \quad (3.100b)$$

$$= \int_{t_n}^{t_{n+1}} [A(t) - A(t_n)] dt \quad (3.100c)$$

$$= \int_{t_n}^{t_{n+1}} A(t) dt - (t_{n+1} - t_n) A(t_n), \quad (3.100d)$$

whereas the right hand side is

$$\int_{t_n}^{t_{n+1}} (t_{n+1} - t) \mathcal{B}(t) dt = \int_{t_n}^{t_{n+1}} (t_{n+1} - t) \frac{dA(t)}{dt} dt \quad (3.101a)$$

$$= \int_{t_n}^{t_{n+1}} (t_{n+1} - t) dA(t) \quad (3.101b)$$

$$= \int_{t_n}^{t_{n+1}} d[A(t)(t_{n+1} - t)] + A(t) dt \quad (3.101c)$$

$$= -A(t_n)(t_{n+1} - t_n) + \int_{t_n}^{t_{n+1}} A(t) dt, \quad (3.101d)$$

which is identical to the left hand side given by equation (3.100d). We have thus proven the double integral formula (3.99).

The right hand side of the double integral formula (3.99) can be written

$$\int_{t_n}^{t_{n+1}} (t_{n+1} - t) \mathcal{B}(t) dt = t_{n+1} \Delta T_{n,n+1} \bar{\mathcal{B}}_{n,n+1} - \int_{t_n}^{t_{n+1}} t \mathcal{B}(t) dt, \quad (3.102)$$

which might be useful in some contexts. However, it is awkward for our purposes since it exposes the absolute time, t_{n+1} , in the first term on the right hand side and the time, t , within the integral.

Since we generally do not hold any initial time as special (i.e., the initial time, t_0 , is arbitrary), it is preferable to retain the time differences throughout the formulation. Hence, when making use of the double integral identity (3.99) we bring equation (3.98) into the form

$$\bar{A}_{p,p+1} - \bar{A}_{n,n+1} = \int_{t_n}^{t_p} \mathcal{B}(t) dt + \int_{t_p}^{t_{p+1}} \frac{(t_{p+1} - t) \mathcal{B}(t)}{t_{p+1} - t_p} dt - \int_{t_n}^{t_{n+1}} \frac{(t_{n+1} - t) \mathcal{B}(t)}{t_{n+1} - t_n} dt \quad (3.103a)$$

$$= \int_{t_n}^{t_{n+1}} \frac{(t - t_n) \mathcal{B}(t)}{t_{n+1} - t_n} dt + \int_{t_{n+1}}^{t_p} \mathcal{B}(t) dt + \int_{t_p}^{t_{p+1}} \frac{(t_{p+1} - t) \mathcal{B}(t)}{t_{p+1} - t_p} dt. \quad (3.103b)$$

The first right hand side term is a weighted integral with a linearly increasing weight from zero to unity, whereas the final right hand side term has a linearly decreasing weight from unity to zero. The middle term has a unity weight throughout and it vanishes if $p = n + 1$, as when the averaging regions are adjacent. Figure 3.6. illustrates the time windowing used for equation (3.103b).

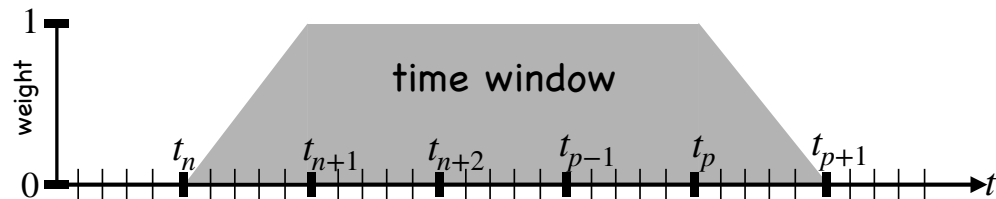


FIGURE 3.6: Illustrating the time window weighting used in computing the right hand side of equation (3.103b). Note that if $p = n + 1$, then the middle term in equation (3.103b) and there is no plateau region of unit weight, in which case the window region becomes two adjacent triangles.

As a final means to write equation (3.103b), extend the middle term to the end of the time period and then subtract the extra piece and recombine to render

$$\bar{A}_{p,p+1} - \bar{A}_{n,n+1} = \int_{t_{n+1}}^{t_{p+1}} \mathcal{B}(t) dt + \int_{t_n}^{t_{n+1}} \frac{(t - t_n) \mathcal{B}(t)}{t_{n+1} - t_n} dt - \int_{t_p}^{t_{p+1}} \frac{(t - t_p) \mathcal{B}(t)}{t_{p+1} - t_p} dt. \quad (3.104)$$

The first term on the right hand side is an unweighted integral from the end of the first interval to the end of the final interval, whereas the other two terms both have increasing weights over their respective integration intervals. This form allows for some advantages diagnostically since we only need to save unweighted integrals plus linearly increasing weighted integrals; there is no need to save decreasing weighted integrals.



Chapter 4

GREEN'S FUNCTION METHODS

There are many methods to solve linear partial differential equations (PDEs). Some methods, such as the separation of variables, Fourier transforms, and Laplace transforms, are suited to idealized domains with relatively simple geometries that enable closed form analytic solutions. However, for many physical applications we encounter domains and boundary conditions where analytical methods are unavailable. It is thus often useful to have a general closed-form solution to study properties of the solution either analytically or numerically. The Green's function method provides this solution.

In this chapter we develop the Green's function method for the elliptic and parabolic linear partial differential equations of mathematical physics introduced in Chapter 3. We are most interested in the Green's function method as a conceptual framework and as such we are relatively unconcerned with how to determine the Green's function for any particular problem. Even without an explicit form of the Green's function, an appreciation of Green's function methods deepens both physical and mathematical understanding of the various linear partial differential equations encountered in this book, such as the Poisson equation in Newtonian gravity (Section 11.11), and quasi-geostrophic theory (Chapter 42), as well as the diffusion equation and the advection-diffusion equation of Chapter 61.

In this chapter, our treatment of the *Dirac delta* and Green's functions is *physically formal*, meaning that it offers a deductive formulation that is motivated predominantly from a physical perspective rather than serving the needs for a *mathematically rigorous* presentation.¹ The physically formal treatment presented here is supported by *heuristic* arguments taken from Newtonian gravity (see Section 11.11); electrostatics (e.g., Jackson (1975)); and the diffusion of temperature or matter within a continuous media.² The tracer and temperature examples are directly relevant to geophysical fluid mechanics and will be developed in this book, whereas the electrostatic and gravity examples provided motivation for development of Green's function methods in the 19th and 20th centuries.

READER'S GUIDE TO THIS CHAPTER

We encounter a variety of Green's functions that differ according to the differential operator and boundary conditions. Use of the common symbol, G , minimizes the adornments otherwise needed to distinguish Green's functions. Confusion is avoided by noting that properties of any

¹The term *physically formal* is often used in the mathematical physics and applied mathematics literature as a complement to *mathematically rigorous*. A mathematically rigorous treatment for the topics of this chapter require an array of mathematical apparatus outside our scope.

²A heuristic technique or argument employs a practical method not guaranteed to be fully rational or deductive from all perspectives, but is sufficient for establishing a self-consistent formalism. The study of the Dirac delta and Green's functions are examples where physical heuristics established a formalism whose mathematical rigor followed later.

particular Green's function are specific to the section where the function is discussed. Much in this chapter is based on the treatments found in Chapter 7 of *Morse and Feshbach* (1953) as well as *Stakgold* (2000a,b). Both of these books are classics whose presentations have stood the test of time.

4.1	Loose threads	73
4.2	Conceptual foundations	73
4.3	Dirac delta	74
4.3.1	A point mass source	74
4.3.2	Sifting property	75
4.3.3	Cartesian and spherical coordinates	75
4.3.4	Example $\delta^{(e)}(x)$ functions	75
4.3.5	Connection to the Heaviside step function	77
4.3.6	Sifting property for the Dirac dipole	77
4.3.7	Temporal Dirac delta and impulses	78
4.3.8	Shifting the space-time position of the source	78
4.3.9	Dirac delta carries physical dimensions	79
4.4	Laplace's free space Green's function	79
4.4.1	Gravitational potential from a point mass source	79
4.4.2	Free space Green's function for Laplace's equation	80
4.4.3	Details of the three-dimensional free space Green's function	81
4.5	One-dimensional Poisson's equation	81
4.5.1	Integral expression for ψ in terms of G	82
4.5.2	Preliminary steps for obtaining the Green's function	82
4.5.3	Green's function satisfying Dirichlet boundary conditions	83
4.5.4	Green's function satisfying Neumann boundary conditions	84
4.5.5	Uniqueness of the solution to the Dirichlet problem	85
4.6	Poisson's equation with Dirichlet boundaries	85
4.6.1	Constraints on the source and boundary normal derivative	86
4.6.2	Uniqueness of the solution	86
4.6.3	The Green's function problem	87
4.6.4	Reciprocity of the Green's function	88
4.6.5	The integral solution	89
4.6.6	Properties of the solution	90
4.6.7	Boundary Green's function	92
4.7	Poisson's equation with Neumann boundaries	93
4.7.1	Constraints on the source and boundary data	93
4.7.2	Uniqueness of the solution up to a constant	94
4.7.3	The Green's function problem	94
4.7.4	Properties of the solution	94
4.7.5	Verifying the solution	96
4.8	The diffusion equation	97
4.8.1	Causal free space Green's function	97
4.8.2	Causal Green's function	97
4.8.3	Adjoint causal Green's function	98
4.8.4	Reciprocity of the Green's function and its adjoint	99
4.8.5	Composition property of the Green's function	101
4.8.6	Integral solution	103
4.8.7	Properties of the solution	106
4.8.8	Boundary propagator	107
4.9	Initial value problems and response functions	109
4.9.1	Impulse response function	110
4.9.2	Step response function	111

4.9.3	Reciprocity relation	112
4.9.4	Response function for general forcing	113
4.9.5	Connection to the boundary propagator	114
4.9.6	Comments and further study	114

4.1 Loose threads

- Biot-Savart expression for the free space vorticity as per the magnetic field. Discuss on in the context of 2d turbulence and connect to the inverse cascade arguments given in Section 11.3.1 of [Vallis \(2017\)](#). Need to understand the two-dimensional Green's function (4.38b). Note that as written, equation (4.38b) is dimensionally problematic since the \ln function must be dimensionless.

4.2 Conceptual foundations

The basic mathematical problem of classical continuum field theory concerns an arbitrary field, $\psi(\mathbf{x}, t)$, that represents a physical property such as material tracer concentration, velocity stream-function, temperature in a continuous media, Newtonian gravitational potential, or classical electrostatic potential. The space-time structure of the field is the result of a space-time distributed source (e.g., tracer source, potential vorticity distribution, mass distribution, or electric charge distribution) along with differential operators (e.g., time derivative, Laplacian, diffusion operator, wave operator) that connect the field across points in space-time as well as initial and boundary conditions that fix the behavior of ψ in selected space-time regions.³

For our studies, the differential equations describing ψ are generally nonlinear. However, in some important cases it is possible to linearize the governing equations and learn much about the underlying mathematical and physical properties of the system. Furthermore, the advection-diffusion equation describing a passive tracer (Chapter 61) is linear even when the dynamical flow field is nonlinear. The conceptual foundation of the Green's function method is based on observing that if the field equations are linear, then ψ can be constructed by accumulating contributions from point-sized portions of the distributed source, including sources on the region boundaries. Let us write $G(\mathbf{x}, t | \mathbf{x}_0, t_0)$ for the field at an observation space-time point (\mathbf{x}, t) (the *field point*) caused by a point source at (\mathbf{x}_0, t_0) (the *source point*). We then observe that $\psi(\mathbf{x}, t)$ caused by a source that is distributed through space and time is the product of G multiplied by the source and integrated over the space-time domain. Similar superpositions are made for the initial and boundary conditions. The function, G , is referred to as the *Green's function* in honor of the 19th century mathematician who first developed the method for studies of electrostatics.

The above arguments rely on the *superposition principle* of linear systems. It does so by finding a particular solution (the Green's function) to a linear initial-boundary value problem with a singular point source (Dirac delta) and homogeneous boundary conditions. The solution to the original problem is found by integrating (convolving) the Green's function with the boundary conditions, initial conditions, and distributed sources. The Green's function is generally simpler to determine than the solution to the original initial-boundary value problem, thus providing a key practical reason to pursue the method. Furthermore, the Green's function provides a formal inverse to the linear partial differential operator in a manner reminiscent of matrix inversion used to solve a matrix-vector problem. Just as for the matrix-vector problem, once we have the Green's function we can write the solution to any of the associated initial-boundary value problems regardless the details of the distributed source, initial data, or boundary data. Herein

³In some cases, sources are present only along spatial boundaries.

lies the power of the Green's function method and why it has found much use across mathematical physics.

4.3 Dirac delta

The *Dirac delta* provides an idealization of a point source and it serves a core role in the study of Green's functions. In mathematics, the Dirac delta is known as a *generalized function* (e.g., chapter 5 of [Stakgold \(2000b\)](#)). We use the terse nomenclature *Dirac delta*, rather than the commonly used “delta function”, to emphasize its special nature as a generalized function.

4.3.1 A point mass source

In Newtonian gravity we encounter the Poisson equation for the gravitational potential, Φ , arising from an arbitrary mass density, ρ

$$\nabla^2 \Phi = 4\pi G^{\text{grv}} \rho, \quad (4.1)$$

with G^{grv} Newton's gravitational constant (see Section 11.11.1).⁴ The gravitational potential for an arbitrary spherically symmetric mass, when sampled at a point outside the mass, equals to the potential of a point mass located at the origin. Making precise the notion of a “point mass” provides a venue to introduce the Dirac delta.

For that purpose, consider a mass, M , distributed uniformly within a sphere of radius ϵ and volume

$$V_\epsilon = \frac{4}{3}\pi\epsilon^3, \quad (4.2)$$

and let the sphere be centered at the origin of a coordinate system. The mass distribution thus has a density

$$\rho(\mathbf{x}) = M \delta^{(\epsilon)}(\mathbf{x}), \quad (4.3)$$

where we introduced the ϵ -distribution

$$\delta^{(\epsilon)}(\mathbf{x}) \equiv \begin{cases} V_\epsilon^{-1} & \text{if } |\mathbf{x}| \leq \epsilon \\ 0 & \text{if } |\mathbf{x}| > \epsilon. \end{cases} \quad (4.4)$$

By construction, an integral over a domain fully encompassing the sphere yields the mass

$$\int_{\mathcal{R}} \rho dV = M \int_{\mathcal{R}} \delta^{(\epsilon)}(\mathbf{x}) dV = M, \quad (4.5)$$

with this result holding even as the radius of the sphere becomes arbitrarily small, $\epsilon \rightarrow 0$. We define the Dirac delta as the limiting ϵ -distribution

$$\delta(\mathbf{x}) \equiv \lim_{\epsilon \rightarrow 0} \delta^{(\epsilon)}(\mathbf{x}). \quad (4.6)$$

By construction, the Dirac delta arises from taking the limit of a mass source that is zero everywhere in space except at a single point, at which point the Dirac delta is formally infinite. Concerns with how to interpret the infinite value of $\delta(\mathbf{x})$ at the origin are ameliorated by recognizing that $\delta(\mathbf{x})$ is evaluated only within an integral, with these integral properties described in the remainder of this section. Connecting to the other physical analogs, the Dirac delta corresponds to a point charge in electrostatics or to a point source of trace matter within a fluid.

⁴Elsewhere in this book we write $G^{\text{grv}} = G$. We add the “grv” label in this chapter and reserve G for the Green's function.

4.3.2 Sifting property

Now consider multiplying an ϵ -distribution by an arbitrary smooth function, $\psi(\mathbf{x})$. Since the ϵ -distribution has support only within the ϵ -sphere surrounding the origin, an integral of $\delta^{(\epsilon)}(\mathbf{x}) \psi(\mathbf{x})$ over the sphere, in the limit that $\epsilon \rightarrow 0$, leads to the *sifting property*

$$\lim_{\epsilon \rightarrow 0} \int_{\mathcal{R}} \delta^{(\epsilon)}(\mathbf{x}) \psi(\mathbf{x}) dV = \int_{\mathcal{R}} \delta(\mathbf{x}) \psi(\mathbf{x}) dV = \psi(\mathbf{x} = 0). \quad (4.7)$$

Hence, the Dirac delta acts to “sift” out the value of the function at the location of the Dirac delta source. For our purposes, the sifting property is the key defining feature of the Dirac delta.

4.3.3 Cartesian and spherical coordinates

The definition (4.6) was constructed in three space dimensions, with the Dirac delta having dimensions of inverse volume. We can consider the same procedure for a single space dimension, with the one-dimensional Dirac delta having dimension of inverse length and thus satisfying the normalization condition

$$\int_{\mathcal{R}} \delta(x) dx = 1, \quad (4.8)$$

where the integration domain, \mathcal{R} , includes the origin. Correspondingly, we can decompose the three-dimensional Dirac delta according to

$$\delta(\mathbf{x}) = \delta(x) \delta(y) \delta(z), \quad (4.9)$$

so that, with the domain \mathcal{R} containing the origin, we have

$$\int_{\mathcal{R}} \delta(\mathbf{x}) dV = \int_{\mathcal{R}} \delta(x) \delta(y) \delta(z) dx dy dz = 1. \quad (4.10)$$

Rather than Cartesian coordinates, we sometimes find it useful to make use of the spherical coordinates⁵ to render

$$\delta(\mathbf{x}) = \frac{1}{r^2 \cos \phi} \delta(r) \delta(\phi) \delta(\lambda), \quad (4.11)$$

so that

$$\int_{\mathcal{R}} \delta(\mathbf{x}) dx dy dz = \int_{\mathcal{R}} \delta(\mathbf{x}) r^2 \cos \phi dr d\phi d\lambda = \int_{\mathcal{R}} \delta(r) \delta(\phi) \delta(\lambda) dr d\phi d\lambda = 1. \quad (4.12)$$

Notice how the dimensions of a particular Dirac delta equals to the inverse dimensions of its argument, so that both $\delta(\phi)$ and $\delta(\lambda)$ are dimensionless whereas $\delta(r)$ has dimensions of inverse length. Similar treatments hold for other coordinates.

4.3.4 Example $\delta^{(\epsilon)}(x)$ functions

The particular construction of the Dirac delta given by equation (4.6) is not unique. That is, there are many other suitable ϵ -distributions whose limiting behavior also result in a Dirac delta as defined by the unit normalization and sifting properties. We here list a few that appear in

⁵We discuss spherical coordinates in Section 9.2.

applications

$$\delta^{(\epsilon)}(x) = \epsilon^{-1} \text{ for } |x| < \epsilon/2 \text{ and } 0 \text{ for } |x| > \epsilon/2 \quad (4.13a)$$

$$\delta^{(\epsilon)}(x) = \frac{e^{-|x|/\epsilon}}{2\epsilon} \quad (4.13b)$$

$$\delta^{(\epsilon)}(x) = \frac{\epsilon}{\pi(x^2 + \epsilon^2)} \quad (4.13c)$$

$$\delta^{(\epsilon)}(x) = \frac{e^{-x^2/\epsilon^2}}{\epsilon\pi} \quad (4.13d)$$

$$\delta^{(\epsilon)}(x) = \frac{\sin(x/\epsilon)}{x\epsilon} \quad (4.13e)$$

$$\delta^{(\epsilon)}(x) = \frac{\epsilon \sin^2(x/\epsilon)}{\pi x^2}. \quad (4.13f)$$

With x corresponding to a spatial position, note how each of these one-dimensional functions has dimensions of inverse length. Figure 4.1 depicts the rectangular function (4.13a) as a canonical example.

Consider the multiplication of each of the above functions $\delta^{(\epsilon)}(x)$, by a non-dimensional, continuous and bounded function, $F(x)$, that is unity at the origin, $F(0) = 1$. In this case, $F(x)\delta^{(\epsilon)}(x)$ still satisfies the normalization and sifting properties required of a Dirac delta

$$\lim_{\epsilon \rightarrow 0} \int_{\mathcal{R}} F(x) \delta^{(\epsilon)}(x) dx = F(0) = 1 \quad (4.14a)$$

$$\lim_{\epsilon \rightarrow 0} \int_{\mathcal{R}} \psi(x) F(x) \delta^{(\epsilon)}(x) dx = \psi(0) F(0) = \psi(0), \quad (4.14b)$$

so that

$$\lim_{\epsilon \rightarrow 0} F(x) \delta^{(\epsilon)}(x) = \delta(x). \quad (4.15)$$

Correspondingly, whenever working with a Dirac delta, if it is multiplied by a non-dimensional function $F(x)$ with $F(0) = 1$, then we can disregard this function since it does not modify the Dirac source.

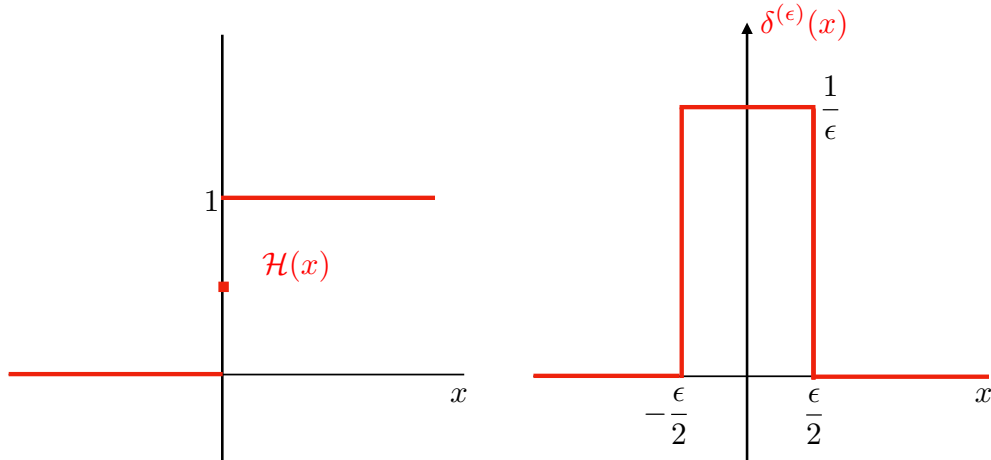


FIGURE 4.1: Left panel: Heaviside step function, $\mathcal{H}(x)$, as given by equation (4.16). Right panel: the square pulse function $\delta^{(\epsilon)}(x)$ given by equation (4.13a), with $\lim_{\epsilon \rightarrow 0} \delta^{(\epsilon)}(x) = \delta(x) = d\mathcal{H}(x)/dx$.

4.3.5 Connection to the Heaviside step function

The Heaviside step function (Figure 4.1) is given by⁶

$$\mathcal{H}(x) = \begin{cases} 0 & \text{if } x < 0 \\ 1/2 & \text{if } x = 0 \\ 1 & \text{if } x > 0, \end{cases} \quad (4.16)$$

and it is related to the sgn function

$$\operatorname{sgn}(x) = \begin{cases} -1 & \text{if } x < 0 \\ 0 & \text{if } x = 0 \\ 1 & \text{if } x > 0, \end{cases} \quad (4.17)$$

according to

$$\operatorname{sgn}(x) = 2\mathcal{H}(x) - 1. \quad (4.18)$$

Both the Heaviside and sgn functions are piecewise continuous and have infinite derivatives at $x = 0$. In particular, the derivative of the Heaviside step function equals to the Dirac delta

$$\frac{d\mathcal{H}(x)}{dx} = \delta(x). \quad (4.19)$$

This identity is most apparent by considering the square pulse approximation to the Dirac delta given by equation (4.13a), which can be written

$$\delta(x) = \lim_{\epsilon \rightarrow 0} \delta^{(\epsilon)}(x) = \lim_{\epsilon \rightarrow 0} \frac{\mathcal{H}(x + \epsilon/2) - \mathcal{H}(x - \epsilon/2)}{\epsilon} = \frac{d\mathcal{H}(x)}{dx}. \quad (4.20)$$

Equivalently, we see that the Heaviside step function is the cumulative distribution of the Dirac delta

$$\int_{-\infty}^x \delta(x') dx' = \int_{-\infty}^x \frac{d\mathcal{H}(x')}{dx'} dx' = \mathcal{H}(x) - \mathcal{H}(-\infty) = \mathcal{H}(x). \quad (4.21)$$

Connecting to the language of probability theory, the Dirac delta corresponds to a probability density function peaked over an infinitesimal region, whereas the Heaviside step function is the corresponding probability distribution function.

4.3.6 Sifting property for the Dirac dipole

The derivative of a Dirac delta represents an idealization of a dipole (e.g., see exercise 1.14 of *Stakgold (2000a)*). There are occasions when it is useful to know how a dipole acts on a function inside of an integral. For this purpose we make use of the identity

$$\int_{-\epsilon}^{\epsilon} \frac{d[\psi(x) \delta(x)]}{dx} dx = \psi(\epsilon) \delta(\epsilon) - \psi(-\epsilon) \delta(-\epsilon). \quad (4.22)$$

Each term on the right hand side vanishes when $\epsilon > 0$ since the Dirac delta never fires. Applying the product rule inside of the integral renders the identity

$$\int_{-\epsilon}^{\epsilon} \frac{d[\psi(x) \delta(x)]}{dx} dx = \int_{-\epsilon}^{\epsilon} \left[\psi(x) \frac{d\delta(x)}{dx} + \delta(x) \frac{d\psi(x)}{dx} \right] dx = 0, \quad (4.23)$$

⁶In some treatments, $\mathcal{H}(x)$ is undefined at $x = 0$. For our purposes, the properties of the Heaviside step function remain unchanged whether it is defined at $x = 0$ or not. See footnote on page 20 of *Stakgold (2000a)* for more details.

so that

$$\int_{-\epsilon}^{\epsilon} \psi(x) \frac{d\delta(x)}{dx} dx = - \left[\frac{d\psi(x)}{dx} \right]_{x=0}. \quad (4.24)$$

For example, let $\psi(x) = x$, in which case

$$\int_{-\epsilon}^{\epsilon} x \frac{d\delta(x)}{dx} dx = -1, \quad (4.25)$$

which can be formally written

$$x (d\delta(x)/dx) = -\delta(x). \quad (4.26)$$

4.3.7 Temporal Dirac delta and impulses

Poisson's equation for the gravitational potential is an elliptic partial differential equation (see Section 3.5), in which there is no time derivative. We now introduce the temporal Dirac delta to build towards our study of evolution equations, such as the diffusion equation of Section 4.8 and the advection-diffusion equation of Section 61.10. The temporal Dirac delta is a point source that is turned on just at one time instance and it is normalized according to

$$\int_{\mathcal{T}} \delta(t) dt = 1, \quad (4.27)$$

where \mathcal{T} is a time interval containing the source time, $t = 0$. This normalization means that $\delta(t)$ has dimensions of inverse time. The temporal Dirac delta also possesses the sifting property from Section 4.3.2, in which

$$\int_{\mathcal{T}} \delta(t) \psi(t) dt = \psi(t = 0). \quad (4.28)$$

In the study of transient behavior of dynamical systems, it is often of interest to examine the response of the system to an idealized force, $\mathcal{F}(t)$, where the force occurs over a small time increment. The time integral of this force is referred to as the *impulse*

$$I(\tau) = \int_{-\tau}^{\tau} \mathcal{F}(t) dt. \quad (4.29)$$

If the force is further idealized to occur just at a single moment in time, and it is normalized to unity, then we have the *unit impulse*, which is just the integral of the Dirac delta

$$I(\tau) = 1 = \int_{-\tau}^{\tau} \delta(t) dt. \quad (4.30)$$

The corresponding response of the dynamical system is referred to as the *impulse response function*. If the dynamical system is linear, then the impulse response function equals to the Green's function for the initial value problem. We further discuss the response function in Section 4.9.

4.3.8 Shifting the space-time position of the source

Thus far we have assumed the point source is located at the origin in space and time. But there is nothing special about that point. Correspondingly, we can arbitrarily place the source at (\mathbf{x}_0, t_0) , in which case the Dirac delta is written

$$\delta(\mathbf{x} - \mathbf{x}_0) \delta(t - t_0) = \delta(x - x_0) \delta(y - y_0) \delta(z - z_0) \delta(t - t_0). \quad (4.31)$$

Defining the region, \mathcal{R} , to now encompass the source point in space, $\mathbf{x} = \mathbf{x}_0$, and the time increment \mathcal{T} to encompasses the source time, $t = t_0$, we have the normalization condition

$$\int_{\mathcal{R}} \int_{\mathcal{T}} \delta(\mathbf{x} - \mathbf{x}_0) \delta(t - t_0) dV dt = 1, \quad (4.32)$$

as well as the sifting property

$$\int_{\mathcal{R}} \int_{\mathcal{T}} \psi(\mathbf{x}, t) \delta(\mathbf{x} - \mathbf{x}_0) \delta(t - t_0) dV dt = \psi(\mathbf{x}_0, t_0). \quad (4.33)$$

4.3.9 Dirac delta carries physical dimensions

In this book, the Dirac delta carries physical dimensions given by the inverse dimension of its arguments. For example, $\delta(z)$ has dimensions inverse length (here, z is a Cartesian space coordinate), $\delta(t)$ has dimensions inverse time (t is time), and $\delta(\phi)$ is non-dimensional (ϕ is latitude in radians). The dimensional properties of a Dirac delta are manifest from its corresponding sifting property.

It is notable that many treatments, particularly in the maths literature, ignore physical dimensions. Hence, it is important to exercise care when transferring Dirac delta identities from a maths text to a physics problem.

4.4 Laplace's free space Green's function

We introduced the Dirac delta in Section 4.3 by considering the Newtonian gravitational potential in the presence of a point mass source. This physical example also serves to introduce the notion of a Green's function, in this case a particularly simple Green's function known as a *free space Green's function* for Laplace's equation. The free space Green's function serves an important role in the analytical theory of Green's functions, and it offers us a pedagogical introduction to Green's functions.

4.4.1 Gravitational potential from a point mass source

Consider the gravitational potential, Φ , in the presence of a point mass source at $\mathbf{x} = \mathbf{x}_0$ in the absence of boundaries (i.e., in *free space*), and with an assumed decay of the potential when moving away from the source. In the study of Green's functions this potential is referred to as the *fundamental solution* to Laplace's equation. In other contexts it is referred to as the *free space Green's function*, which is the terminology we choose, where “free space” refers to the absence of any spatial boundaries. From our discussion of Newtonian gravity in Section 4.3.1, the free space Green's function for Newtonian gravity satisfies the Poisson equation with a point mass source

$$\nabla_{\mathbf{x}}^2 \Phi(\mathbf{x}|\mathbf{x}_0) = 4\pi G^{\text{grav}} M \delta(\mathbf{x} - \mathbf{x}_0) \quad \text{and} \quad \Phi(\mathbf{x}|\mathbf{x}_0) \rightarrow 0 \text{ as } |\mathbf{x}| \rightarrow \infty, \quad (4.34)$$

where we wrote the point mass density in terms of the Dirac delta

$$\rho(\mathbf{x}|\mathbf{x}_0) = M \delta(\mathbf{x} - \mathbf{x}_0). \quad (4.35)$$

We write the gravitational potential with two arguments, $\Phi(\mathbf{x}|\mathbf{x}_0)$. The first argument, \mathbf{x} , is the point where the field is sampled and is referred to as the *field point* or sometimes the *observation point*. The second argument, \mathbf{x}_0 , is where the source is located and is thus referred to as the *source point*. Figure 4.2 summarizes the notation. The Laplacian operator acts on the field

point and is written as $\nabla_{\mathbf{x}}^2$ for clarity. The dimensional multiplier, $4\pi G^{\text{grav}} M$, acting on the Dirac delta in equation (4.34) is specific to the physical problem, here being for Newtonian gravity. In this case the Green's function has dimensions of $L^2 T^{-2}$ since it is a gravitational potential. In other cases, the Green's function will have distinct dimensions, whereas the Dirac delta remains with the same dimensions.⁷

The gravitational potential for a point mass source, in the absence of any boundaries, is the free space Green's function for Newtonian gravity. Anticipating our study in Section 11.11.2, we write this free space Green's function in the form

$$\Phi(\mathbf{x}|\mathbf{x}_0) = -\frac{M G^{\text{grav}}}{|\mathbf{x} - \mathbf{x}_0|}. \quad (4.36)$$

This function is singular when sampling the field at the source location, $\mathbf{x} = \mathbf{x}_0$, and it decreases according to the inverse distance when moving away from the source.

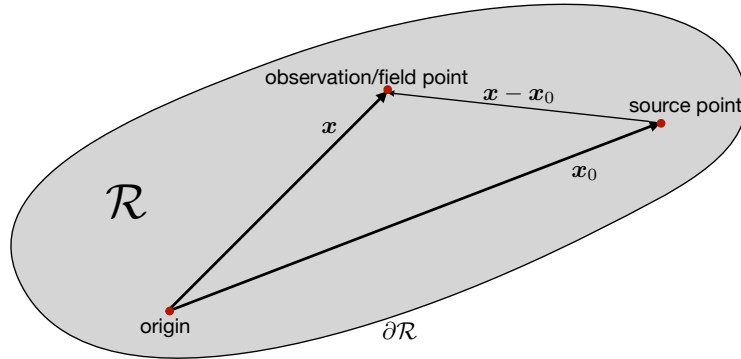


FIGURE 4.2: Depicting the geometry of a typical Green's function problem in space, shown here for a finite domain whereas the free-space Green's function has no boundaries. The field or observation point, \mathbf{x} , is where the Green's function is sampled, whereas the source point, \mathbf{x}_0 , is where the Dirac delta source is located. The origin is at an arbitrary position within the domain, \mathcal{R} , whose boundary is written $\partial\mathcal{R}$.

4.4.2 Free space Green's function for Laplace's equation

Abstracting the previous discussion motivates us to define the free space Green's function, $\mathcal{G}(\mathbf{x}|\mathbf{x}_0)$, for the Laplace operator as the solution to the singular Poisson equation

$$-\nabla_{\mathbf{x}}^2 \mathcal{G}(\mathbf{x}|\mathbf{x}_0) = \delta(\mathbf{x} - \mathbf{x}_0) \quad \text{and} \quad \mathcal{G}(\mathbf{x}|\mathbf{x}_0) \rightarrow 0 \text{ as } |\mathbf{x}| \rightarrow \infty. \quad (4.37)$$

It is conventional in many treatments to place a minus sign on the Laplacian operator to correspond to how it appears in the diffusion equation of Section 4.8. In one, two and three space dimensions the free space Green's function is given by

$$\mathcal{G}(\mathbf{x}|\mathbf{x}_0) = -|\mathbf{x} - \mathbf{x}_0|/2 \quad \text{for } \mathbf{x}, \mathbf{x}_0 \in \mathbb{R}^1 \quad (4.38a)$$

$$\mathcal{G}(\mathbf{x}|\mathbf{x}_0) = -(2\pi)^{-1} \ln |\mathbf{x} - \mathbf{x}_0| \quad \text{for } \mathbf{x}, \mathbf{x}_0 \in \mathbb{R}^2 \quad (4.38b)$$

$$\mathcal{G}(\mathbf{x}|\mathbf{x}_0) = (4\pi |\mathbf{x} - \mathbf{x}_0|)^{-1} \quad \text{for } \mathbf{x}, \mathbf{x}_0 \in \mathbb{R}^3. \quad (4.38c)$$

We study the three-dimensional Green's function in Section 4.4.3 and encounter the one-dimensional Green's function in Section 4.5.

⁷As emphasized throughout this book, checking for physical dimensional consistency offers a powerful means to ensure that a mathematical expression makes physical sense. If the equation is not dimensionally consistent, then something is wrong either with the maths or the physics.

4.4.3 Details of the three-dimensional free space Green's function

We here verify that the expression (4.38c) is indeed the free space Green's function for \mathbb{R}^3 . This exercise provides some exposure to some of the formal manipulations encountered with Dirac deltas and Green's functions.

To simplify notation, place the Dirac delta at $\mathbf{x}_0 = 0$ so that

$$G(\mathbf{x}|0) = \frac{1}{4\pi r}, \quad (4.39)$$

where $|\mathbf{x}| = r$ is the radial distance from the origin. Introduce the continuous and non-singular function

$$G^{(\epsilon)}(\mathbf{x}) = \frac{1}{4\pi} \begin{cases} r^{-1} & \text{for } r > \epsilon \\ \epsilon^{-1} & \text{for } r \leq \epsilon, \end{cases} \quad (4.40)$$

with $\epsilon > 0$, in which case $G^{(\epsilon)}(\mathbf{x})$ has removed the singularity at $r = 0$. Now consider the integral

$$\mathcal{I}(\epsilon) = \int_{r \leq \epsilon} \psi(\mathbf{x}) \nabla^2 G^{(\epsilon)}(\mathbf{x}) dV, \quad (4.41)$$

for an arbitrary smooth function ψ and for a spherical region of radius $r = \epsilon$ centered on the origin. Since ψ is a smooth function, taking the limit as $\epsilon \rightarrow 0$ allows us to remove ψ from the integral

$$\lim_{\epsilon \rightarrow 0} \mathcal{I}(\epsilon) = \psi(r=0) \lim_{\epsilon \rightarrow 0} \left[\int_{r \leq \epsilon} \nabla^2 G^{(\epsilon)}(\mathbf{x}) dV \right]. \quad (4.42)$$

Making use of the divergence theorem brings the volume integral to a surface integral over the ϵ -sphere

$$\lim_{\epsilon \rightarrow 0} \mathcal{I}(\epsilon) = \psi(r=0) \lim_{\epsilon \rightarrow 0} \left[4\pi \int_{r=\epsilon} \hat{\mathbf{r}} \cdot \nabla (1/r) r^2 dr \right] = -4\pi \psi(r=0), \quad (4.43)$$

where we introduced spherical coordinates from Section 9.2. This result establishes the sifting property for $\nabla^2 |\mathbf{x}|^{-1}$. The sifting property is the key property of a Dirac delta required for our purposes, in which case we write

$$-\nabla^2 \frac{1}{4\pi |\mathbf{x}|} = \delta(\mathbf{x}). \quad (4.44)$$

4.5 One-dimensional Poisson's equation

To illustrate the Green's function method for solving differential equations, consider the one-dimensional Poisson equation on a finite domain

$$-\frac{d^2\psi}{dx^2} = \Lambda \quad \text{for } -L \leq x \leq L. \quad (4.45)$$

The corresponding Green's function satisfies

$$-\frac{d^2G(x|x_0)}{dx^2} = \delta(x - x_0) \quad \text{for } -L \leq x, x_0 \leq L, \quad (4.46)$$

with boundary conditions taken as the homogeneous form of whatever boundary conditions are satisfied by ψ . For the Green's function problem, the source, $\Lambda(x)$, appearing in the ψ equation has been replaced by the Dirac delta, $\delta(x - x_0)$. Since the Dirac delta has dimensions of inverse length, equation (4.46) implies that the Green's function has dimensions of length. Keeping

track of physical dimensions offers an essential means to check the integrity of the mathematical manipulations.

4.5.1 Integral expression for ψ in terms of G

Multiplying the differential equation (4.45) with G and the Green's function equation (4.46) with ψ , and then subtracting, yields

$$-G(x|x_0) \frac{d^2\psi(x)}{dx^2} + \psi(x) \frac{d^2G(x|x_0)}{dx^2} = G(x|x_0) \Lambda(x) - \psi(x) \delta(x - x_0). \quad (4.47)$$

Integrating this equation over the domain, and use of the sifting property (4.7), yields

$$\psi(x_0) = \int_{-L}^L G(x|x_0) \Lambda(x) dx + \int_{-L}^L \left[G(x|x_0) \frac{d^2\psi(x)}{dx^2} - \psi(x) \frac{d^2G(x|x_0)}{dx^2} \right] dx \quad (4.48a)$$

$$= \int_{-L}^L G(x|x_0) \Lambda(x) dx + \int_{-L}^L \frac{d}{dx} \left[G(x|x_0) \frac{d\psi}{dx} - \psi(x) \frac{dG(x|x_0)}{dx} \right] dx \quad (4.48b)$$

$$= \int_{-L}^L G(x|x_0) \Lambda(x) dx + \left[G(x|x_0) \frac{d\psi}{dx} \right]_{x=-L}^{x=L} - \left[\psi(x) \frac{dG(x|x_0)}{dx} \right]_{x=-L}^{x=L}, \quad (4.48c)$$

where the final expression exposed the boundary contributions. Specializing to *Dirichlet boundary conditions*, with $G(x = \pm L|x_0) = 0$, renders

$$\psi^{\text{Dirichlet}}(x_0) = \int_{-L}^L G(x|x_0) \Lambda(x) dx - \left[\psi(x) \frac{dG(x|x_0)}{dx} \right]_{x=L} + \left[\psi(x) \frac{dG(x|x_0)}{dx} \right]_{x=-L}, \quad (4.49)$$

whereas the solution with *Neumann boundary conditions*, where $dG(x = \pm L|x_0)/dx = 0$, is

$$\psi^{\text{Neumann}}(x_0) = \int_{-L}^L G(x|x_0) \Lambda(x) dx + \left[G(x|x_0) \frac{d\psi(x)}{dx} \right]_{x=L} - \left[G(x|x_0) \frac{d\psi(x)}{dx} \right]_{x=-L}. \quad (4.50)$$

4.5.2 Preliminary steps for obtaining the Green's function

The solution to the Green's function equation (4.46) is given by the linear functions

$$G(x|x_0) = \begin{cases} Ax + B & \text{for } -L \leq x \leq x_0 \\ Cx + D & \text{for } x_0 \leq x \leq L. \end{cases} \quad (4.51)$$

The constants A, B, C, D are determined by the following conditions: (i) jump condition for $dG(x|x_0)/dx$ at $x = x_0$, (ii) continuity of $G(x|x_0)$ at $x = x_0$, and (iii) homogeneous boundary conditions at $x = \pm L$.

Jump condition for the Green's function derivative at $x = x_0$

The Green's function differential equation (4.46) shows that the second derivative to the Green's function equals to a Dirac delta. Integrating this equation over an arbitrary region straddling $x = x_0$ yields the finite jump condition for the first derivative of the Green's function

$$\lim_{\epsilon \rightarrow 0} \left[\frac{dG(x|x_0)}{dx} \right]_{x=x_0+\epsilon} - \lim_{\epsilon \rightarrow 0} \left[\frac{dG(x|x_0)}{dx} \right]_{x=x_0-\epsilon} = -1. \quad (4.52)$$

That is, the derivative of the Green's function is not continuous across the point $x = x_0$. Instead, it has a finite jump.⁸ Making use of this condition in equation (4.51) leads to $C = A - 1$ so that

$$G(x|x_0) = \begin{cases} Ax + B & \text{for } -L \leq x \leq x_0 \\ (A-1)x + D & \text{for } x_0 \leq x \leq L. \end{cases} \quad (4.53)$$

Continuity of the Green's function at $x = x_0$

A finite jump in the derivative at $x = x_0$ means that the Green's function is continuous at this point

$$\lim_{\epsilon \rightarrow 0} G(x = x_0 + \epsilon|x_0) = \lim_{\epsilon \rightarrow 0} G(x = x_0 - \epsilon|x_0). \quad (4.54)$$

Making use of this condition in equation (4.53) yields

$$G(x|x_0) = \begin{cases} Ax - x_0 + D & \text{for } -L \leq x \leq x_0 \\ (A-1)x + D & \text{for } x_0 \leq x \leq L. \end{cases} \quad (4.55)$$

4.5.3 Green's function satisfying Dirichlet boundary conditions

The two constants A and D in equation (4.55) are determined by specifying the boundary conditions. With Dirichlet conditions we set $G(x = \pm L|x_0) = 0$, which then leads to

$$G(x|x_0) = \frac{1}{2L} \begin{cases} (L - x_0)(L + x) & \text{for } -L \leq x \leq x_0 \\ (L - x)(L + x_0) & \text{for } x_0 \leq x \leq L, \end{cases} \quad (4.56)$$

which is depicted in Figure 4.3. The structure of this function motivates the name *impulse response function* or *influence function*. We identify the following properties of this Green's function, with these properties also appearing in the higher dimension elliptical problems discussed in Sections 4.6 and 4.7.

Reciprocity condition

The Green's function (4.56) satisfies the symmetry condition

$$G(x|x_0) = G(x_0|x), \quad (4.57)$$

so that the Green's function is invariant under interchange of the source point, x_0 , and field point, x . In Section 4.6.4, we show how this *reciprocity condition* generally holds for all Green's functions of the Poisson equation.

Sum of free-space Green's function plus harmonic function

We can write the Green's function (4.56) as the sum of the free space Green's function (4.38a) plus a harmonic function

$$G(x|x_0) = -|x - x_0|/2 + \frac{L^2 - x x_0}{2L} = \mathcal{G}(x|x_0) + H(x|x_0), \quad (4.58)$$

⁸The jump condition on the derivative of the Green's function is related to the jump found in the Heaviside step function discussed in Section 4.3.5. Namely, both the derivative of the Heaviside and the second derivative of the Green's function render a Dirac delta.

where

$$-\frac{d^2 H(x|x_0)}{dx^2} = 0 \quad \text{and} \quad H(x = \pm L|x_0) = -G(x = \pm L|x_0). \quad (4.59)$$

As shown in Section 4.6.3, the Green's function for an elliptic partial differential equation generally takes on this form.

Boundary condition satisfied by Green's function derivative

The Green's function is itself independent of the Dirichlet boundary conditions placed on the function ψ , as well as the source function Λ . Hence, we can establish general properties of the Green's function by considering special cases for the boundary conditions and source function. For this purpose, set $\Lambda = 0$ and $\psi(x = -L) = \psi(x = L)$, in which case ψ is itself a constant throughout the domain. The Dirichlet solution (4.49) then leads to the condition placed on the Green's function derivatives at the boundaries

$$\left[\frac{dG(x|x_0)}{dx} \right]_{x=L} - \left[\frac{dG(x|x_0)}{dx} \right]_{x=-L} = -1. \quad (4.60)$$

Interpreting G as a tracer concentration, this result means that the positive tracer input by the Dirac delta source is exactly balanced by a negative tracer departing the region through its boundaries. It is by this balance that the Green's function is able to maintain its homogeneous Dirichlet boundary condition, $G(x = \pm L|x_0) = 0$. A similar interpretation holds when G is the gravitational potential induced by the Dirac source in the region interior. In this case, for the gravitational potential to vanish on the boundaries, the positive gravitational acceleration induced by the Dirac delta source at $x = x_0$ must be compensated by an opposing gravitational acceleration along the boundaries.

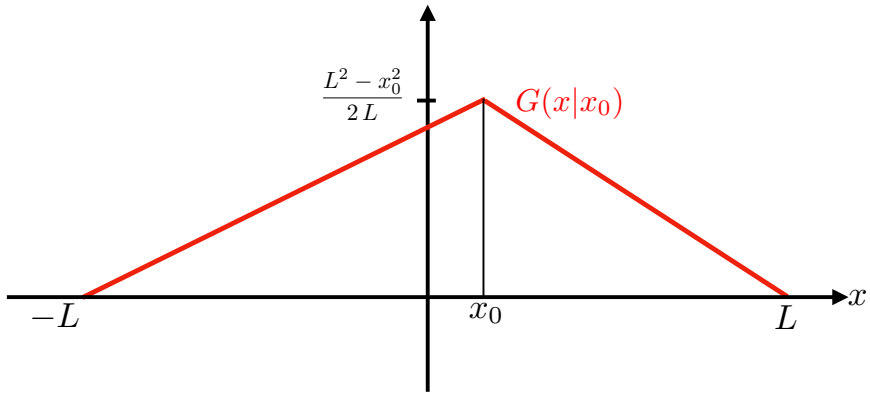


FIGURE 4.3: The Green's function (4.56) for the one-dimensional Poisson equation satisfying Dirichlet boundary conditions at $x = \pm L$. The Dirac delta source is located at $x = x_0$, which is the point where the Green's function has its maximum displacement of $(L^2 - x_0^2)/(2L)$.

4.5.4 Green's function satisfying Neumann boundary conditions

A constant is the only solution to $-d^2G/dx^2 = 0$ with homogeneous Neumann boundary conditions, $dG/dx = 0$ at $x = \pm L$. However, a constant cannot satisfy the derivative jump condition at $x = x_0$, and thus cannot satisfy the differential equation $-d^2G/dx^2 = \delta(x - x_0)$. Hence, there is no Green's function satisfying Neumann boundary conditions for a one-dimensional bounded domain. As we will see, in higher space dimensions there are nontrivial Green's functions for the Neumann boundary case. Even so, this result identifies a key condition required for a Green's

function to exist. Namely, if the completely homogeneous problem ($\Lambda = 0$ with homogeneous boundary conditions) only has the trivial solution, then the Green's function exists and is unique. For the case of Dirichlet boundary conditions

$$-\frac{d^2\psi}{dx^2} = 0 \quad \text{and} \quad \psi(x = \pm L) = 0 \implies \psi = 0, \quad (4.61)$$

whereas for Neumann boundary conditions

$$-\frac{d^2\psi}{dx^2} = 0 \quad \text{and} \quad \left[\frac{d\psi}{dx} \right]_{x=\pm L} = 0 \implies \psi = \text{constant}. \quad (4.62)$$

The existence of a nontrivial (an arbitrary constant) solution to the one-dimensional homogeneous Neumann boundary value problem signals the absence of a corresponding Green's function.

4.5.5 Uniqueness of the solution to the Dirichlet problem

Consider again the Dirichlet problem

$$-\frac{d^2\psi}{dx^2} = \Lambda \quad \text{for } -L \leq x \leq L \quad \text{with} \quad \psi(x = \pm L) = \text{prescribed constants}. \quad (4.63)$$

To prove that the solution to this problem is unique, assume there are two distinct solution, ψ_A and ψ_B , and define $\Psi = \psi_A - \psi_B$. By construction, Ψ satisfies Laplace's equation with homogeneous Dirichlet boundaries

$$-\frac{d^2\Psi}{dx^2} = 0 \quad \text{for } -L \leq x \leq L, \quad \Psi(x = \pm L) = 0. \quad (4.64)$$

As discussed above, the only solution to this problem is $\Psi = 0$, which means that $\psi_A = \psi_B$, hence proving that the solution to equation (4.63) is unique. Uniqueness holds regardless the source function, so that the Green's function from Section 4.5.3 is also unique.

4.6 Poisson's equation with Dirichlet boundaries

In this section we develop the Green's function method for Poisson's equation in three-dimensions with a *Dirichlet boundary condition*

$$-\nabla^2\psi = \Lambda, \quad \text{for } \mathbf{x} \in \mathcal{R} \quad \text{and} \quad \psi = \sigma, \quad \text{for } \mathbf{x} \in \partial\mathcal{R}. \quad (4.65)$$

We separately consider the Neumann boundary condition in Section 4.7, whereby $\hat{\mathbf{n}} \cdot \nabla\psi$ is specified on the boundary rather than ψ itself. Although the Dirichlet and Neumann problems share many features, there are sufficient distinctions to warrant a separate treatment.

In the following, our mathematical goal is to determine an integral expression for ψ in terms of the distributed source, $\Lambda(\mathbf{x})$, and boundary data, $\sigma(\mathbf{x})$. Before doing so, we highlight the two elements determining the solution to any boundary value problem. The first element concerns the region interior, $\mathbf{x} \in \mathcal{R}$, whereby we have the partial differential operator (here the Laplacian) and the distributed source, Λ . The second element concerns the boundary data that prescribes the solution (either its value or its boundary normal derivative) for points on the boundary, $\mathbf{x} \in \partial\mathcal{R}$. The distributed source can be defined everywhere, including the boundary. However, it only affects the solution for points within the region interior since the boundary conditions determine the solution structure on the boundary. Conversely, the boundary conditions are only prescribed

along the boundary, and yet they affect the solution throughout the interior. A key feature of the Green's function method is that it clearly delineates these aspects of the solution, and in so doing it provides both a useful conceptual and computational framework.

4.6.1 Constraints on the source and boundary normal derivative

Assuming there exists a solution to the boundary value problem (4.65), we can derive a constraint on the normal derivative of ψ along the domain boundary.⁹ This constraint is revealed by integrating the Poisson equation (4.65) over the spatial domain, with the left hand side yielding

$$-\int_{\mathcal{R}} \nabla^2 \psi \, dV = -\oint_{\partial\mathcal{R}} \nabla \psi \cdot \hat{\mathbf{n}} \, dS, \quad (4.66)$$

where we made use of the divergence theorem and with $\partial\mathcal{R}$ the closed boundary of the domain \mathcal{R} . Equating this result to the integral of the source, Λ , leads to the constraint

$$\oint_{\partial\mathcal{R}} \nabla \psi \cdot \hat{\mathbf{n}} \, dS = -\int_{\mathcal{R}} \Lambda \, dV. \quad (4.67)$$

We can physically understand this constraint by invoking the steady state tracer diffusion interpretation of the Poisson equation. For a steady state solution to exist in the presence of specified boundary tracer concentration along with interior sources, there must be a balance between the normal gradient of the tracer concentration, as integrated over the boundary, plus the volume integrated source in the interior. This balance is required to maintain the specified Dirichlet boundary values in the presence of the interior source. Absent this balance, there will be depletion or accumulation of ψ that leads to a transient adjustment, thus breaking the steady state assumption. Notably, the constraint (4.67) can be realized for arbitrary Dirichlet boundary data, σ . An analogous interpretation holds when ψ is the gravitational potential resulting from the mass source, Λ . For ψ to be a specified value along the domain boundary requires the volume integrated mass source to balance a gravitational acceleration integrated along the boundary.

4.6.2 Uniqueness of the solution

Just like the one-dimensional case in Section 4.5.5, we can readily establish uniqueness of the solution to the Dirichlet problem by considering two functions, ψ_A and ψ_B , each satisfying the boundary value problem (4.65). In turn, their difference, $\Psi = \psi_A - \psi_B$, satisfies the homogeneous problem

$$-\nabla^2 \Psi = 0, \quad \text{for } \mathbf{x} \in \mathcal{R} \quad \text{and} \quad \Psi = 0, \quad \text{for } \mathbf{x} \in \partial\mathcal{R}. \quad (4.68)$$

The solution to this Laplace equation is $\Psi = 0$, which then means that $\psi_A = \psi_B$ so that the solution to equation (4.65) is unique. This result also means that the Green's function considered in Section 4.6.3 is unique.

We provide a formal proof that the solution to equation (4.68) is indeed zero. To do so, assume it is not zero and see what happens. First consider the case where Ψ is a constant, so that $\psi_A - \psi_B = \text{constant}$. But zero is the only constant that can satisfy the Dirichlet boundary condition, $\Psi = 0$. Next, assume Ψ has spatial dependence so that $\nabla \Psi \neq 0$ and consider the non-negative integral over the domain

$$\mathcal{G} = \int_{\mathcal{R}} \nabla \Psi \cdot \nabla \Psi \, dV. \quad (4.69)$$

⁹To be self-contained, we here repeat the discussion of the constraint (4.67) that is also provided in Section 3.5.6.

Since $\nabla^2 \Psi = 0$ we have $\nabla \cdot (\Psi \nabla \Psi) = \nabla \Psi \cdot \nabla \Psi$ so that

$$\mathcal{I} = \int_{\mathcal{R}} \nabla \cdot (\Psi \nabla \Psi) dV = \oint_{\partial\mathcal{R}} \Psi \nabla \Psi \cdot \hat{\mathbf{n}} d\mathcal{S}, \quad (4.70)$$

where we used the divergence theorem. But since $\Psi = 0$ on $\partial\mathcal{R}$ we find that $\mathcal{I} = 0$, in which case $\nabla \Psi = 0$ everywhere. We are thus led to $\Psi = 0$ throughout the domain, thus allowing us to conclude that the solution to the boundary value problem (4.65) is indeed unique.

4.6.3 The Green's function problem

The Green's function corresponding to the boundary value problem (4.65) is the solution to the Poisson equation with a Dirac delta source (rather than Λ) and a homogeneous Dirichlet boundary condition (rather than σ)

$$-\nabla_{\mathbf{x}}^2 G(\mathbf{x}|\mathbf{x}_0) = \delta(\mathbf{x} - \mathbf{x}_0) \quad \text{for } \mathbf{x}, \mathbf{x}_0 \in \mathcal{R} \quad \text{and} \quad G(\mathbf{x}|\mathbf{x}_0) = 0 \quad \text{for } \mathbf{x} \in \partial\mathcal{R}. \quad (4.71)$$

For this three-dimensional problem, we see that the Green's function has dimensions of inverse length since the Dirac delta has dimensions of inverse volume. By construction, the Green's function, $G(\mathbf{x}|\mathbf{x}_0)$, is harmonic everywhere except at the location of the singular Dirac delta source, $\mathbf{x} = \mathbf{x}_0$, at which point the Green's function equals to minus the inverse Laplacian of the Dirac delta. Furthermore, the Green's function satisfies a homogenous Dirichlet boundary condition whenever the field point, \mathbf{x} , is on the boundary and for an arbitrary source position, \mathbf{x}_0 .

Connection to the free space Green's function

Since $G(\mathbf{x}|\mathbf{x}_0)$ satisfies a boundary condition, it is distinct from the free space Green's function, $\mathcal{G}(\mathbf{x}|\mathbf{x}_0)$, which has no concern for boundaries. Even so, linearity enables us to write the Green's function as the sum of the free space Green's function plus a harmonic function

$$G(\mathbf{x}|\mathbf{x}_0) = \mathcal{G}(\mathbf{x}|\mathbf{x}_0) + H(\mathbf{x}|\mathbf{x}_0), \quad (4.72)$$

where the free space Green's function and harmonic function satisfy

$$-\nabla_{\mathbf{x}}^2 \mathcal{G}(\mathbf{x}|\mathbf{x}_0) = \delta(\mathbf{x} - \mathbf{x}_0) \quad \text{for } \mathbf{x}, \mathbf{x}_0 \in \mathbb{R}^3 \quad (4.73a)$$

$$-\nabla_{\mathbf{x}}^2 H(\mathbf{x}|\mathbf{x}_0) = 0 \quad \text{for } \mathbf{x}, \mathbf{x}_0 \in \mathcal{R} \quad (4.73b)$$

$$-H(\mathbf{x}|\mathbf{x}_0) = \mathcal{G}(\mathbf{x}|\mathbf{x}_0) \quad \text{for } \mathbf{x} \in \partial\mathcal{R}. \quad (4.73c)$$

Assuming we know the free space Green's function from equation (4.38c), the mathematical problem of finding $G(\mathbf{x}|\mathbf{x}_0)$ reduces to finding the harmonic function, $H(\mathbf{x}|\mathbf{x}_0)$, satisfying the inhomogeneous Dirichlet boundary condition (4.73c).

Although the Green's function, G , cares about the existence of spatial boundaries, it is independent of the boundary data, σ , and the distributed source, Λ , that appear in the boundary value problem (4.65) for ψ . In that manner, the Green's function is connected to the original boundary value problem only through the differential operator (here the Laplacian) and the type of boundary condition (here the Dirichlet condition).

Jump condition induced by the Dirac source

Integrating the Green's function partial differential equation (4.71) over a volume, \mathcal{R}_0 , that encloses the Dirac delta source point at $\mathbf{x}_0 \in \mathcal{R}_0$ leads to

$$\int_{\mathcal{R}_0} \nabla_{\mathbf{x}} \cdot \nabla_{\mathbf{x}} G(\mathbf{x}|\mathbf{x}_0) dV = \oint_{\partial\mathcal{R}_0} \hat{\mathbf{n}} \cdot \nabla_{\mathbf{x}} G(\mathbf{x}|\mathbf{x}_0) dS = -1, \quad (4.74)$$

where we used the divergence theorem for the first equality. This result means that for any domain enclosing the Dirac source point, the normal derivative of the Green's function has a jump condition across the boundary of this region. We encountered this property in Section 4.5.2 for the one-dimensional Green's function, and will see it again when discussing the boundary Green's function in Section 4.6.6.

4.6.4 Reciprocity of the Green's function

The Green's function satisfies reciprocity

$$G(\mathbf{x}|\mathbf{x}_0) = G(\mathbf{x}_0|\mathbf{x}), \quad (4.75)$$

with this property holding for both Dirichlet and Neumann boundary conditions. As introduced in Section 4.5.3 for the one-dimensional Poisson equation, reciprocity says that the Green's function at the field point, \mathbf{x} , arising from a Dirac delta source at the source point, \mathbf{x}_0 is identical to the Green's function at the field point, \mathbf{x}_0 , arising from a Dirac delta source at point, \mathbf{x} . By inspection, the free space Green's functions (4.38a)-(4.38c) satisfy reciprocity. Hence, by implication the harmonic function, $H(\mathbf{x}|\mathbf{x}_0)$, also satisfies reciprocity. Even so, we find it pedagogically useful to offer a direct derivation of reciprocity by using steps similar to those used for establishing the second form of Green's integral identity (2.77). These steps are utilized for many purposes when working with Green's functions.

Derivation of reciprocity

Consider the two Green's functions, $G(\mathbf{x}|\mathbf{a})$ and $G(\mathbf{x}|\mathbf{b})$, arising from Dirac delta sources at source points $\mathbf{a} \in \mathcal{R}$ and $\mathbf{b} \in \mathcal{R}$

$$-\nabla_{\mathbf{x}}^2 G(\mathbf{x}|\mathbf{a}) = \delta(\mathbf{x} - \mathbf{a}) \quad (4.76a)$$

$$-\nabla_{\mathbf{x}}^2 G(\mathbf{x}|\mathbf{b}) = \delta(\mathbf{x} - \mathbf{b}). \quad (4.76b)$$

Multiplying the first equation by $G(\mathbf{x}, \mathbf{b})$ and the second by $G(\mathbf{x}, \mathbf{a})$, and subtracting leads to

$$-G(\mathbf{x}|\mathbf{b}) \nabla_{\mathbf{x}}^2 G(\mathbf{x}|\mathbf{a}) + G(\mathbf{x}|\mathbf{a}) \nabla_{\mathbf{x}}^2 G(\mathbf{x}|\mathbf{b}) = G(\mathbf{x}|\mathbf{b}) \delta(\mathbf{x} - \mathbf{a}) - G(\mathbf{x}|\mathbf{a}) \delta(\mathbf{x} - \mathbf{b}). \quad (4.77)$$

Now integrate this equation over the region \mathcal{R} , with the right hand side rendering

$$\int_{\mathcal{R}} [G(\mathbf{x}|\mathbf{b}) \delta(\mathbf{x} - \mathbf{a}) - G(\mathbf{x}|\mathbf{a}) \delta(\mathbf{x} - \mathbf{b})] dV = G(\mathbf{a}, \mathbf{b}) - G(\mathbf{b}, \mathbf{a}), \quad (4.78)$$

where we made use of the sifting property (4.7). Integrating the left hand side of equation (4.77) leads to

$$\int_{\mathcal{R}} [-G(\mathbf{x}|\mathbf{b}) \nabla_{\mathbf{x}}^2 G(\mathbf{x}|\mathbf{a}) + G(\mathbf{x}|\mathbf{a}) \nabla_{\mathbf{x}}^2 G(\mathbf{x}|\mathbf{b})] dV \quad (4.79a)$$

$$= \int_{\mathcal{R}} [-\nabla_{\mathbf{x}} \cdot [G(\mathbf{x}|\mathbf{b}) \nabla_{\mathbf{x}} G(\mathbf{x}|\mathbf{a})] + \nabla_{\mathbf{x}} \cdot [G(\mathbf{x}|\mathbf{a}) \nabla_{\mathbf{x}} G(\mathbf{x}|\mathbf{b})]] dV \quad (4.79b)$$

$$= \oint_{\partial\mathcal{R}} [-G(\mathbf{x}|\mathbf{b}) \nabla_{\mathbf{x}} G(\mathbf{x}|\mathbf{a}) + G(\mathbf{x}|\mathbf{a}) \nabla_{\mathbf{x}} G(\mathbf{x}|\mathbf{b})] \cdot \hat{\mathbf{n}} d\mathcal{S}, \quad (4.79c)$$

where we made use of the divergence theorem for the second equality. The final result vanishes when making use of either the homogeneous Dirichlet boundary condition (4.71) or the homogeneous Neumann boundary condition (4.102) considered in Section 4.7. We are thus led to the reciprocity relation (4.75).

Comments on self-adjoint operators

Reciprocity in the relatively simple form of equation (4.75) is a signature of *self-adjoint* differential operators. Self-adjointness reflects properties of both the differential operator and the boundary conditions, with the discussion in this section revealing that the Laplacian operator is self-adjoint with either Dirichlet or Neumann boundary conditions. Operators that are not self-adjoint, such as the diffusion operator in Section 4.8, satisfy a slightly more general reciprocity relation (see Section 4.8.4).

The absence of self-adjointness reflects some form of symmetry breaking either through the operator itself or through the boundary and/or initial conditions. The diffusion operator has a single time derivative, ∂_t , which breaks symmetry between past and future thus leading to the absence of self-adjointness. Furthermore, self-adjointness is a property that depends on the nature of the chosen inner product, with the inner product in the present discussion defined by integration over the domain \mathcal{R} . See [Stakgold \(2000a,b\)](#) for a thorough discussion accessible to physicists.

4.6.5 The integral solution

We have the elements in place to determine ψ as an integral expression involving $G(\mathbf{x}|\mathbf{x}_0)$ along with the prescribed source, Λ , and boundary data, σ . To do so we follow steps similar to those used to establish reciprocity. Recall the Poisson boundary value problem for ψ and the associated Green's function problem, here exposing arguments for clarity

$$-\nabla_{\mathbf{x}}^2 \psi(\mathbf{x}) = \Lambda(\mathbf{x}) \quad (4.80a)$$

$$-\nabla_{\mathbf{x}}^2 G(\mathbf{x}|\mathbf{x}_0) = \delta(\mathbf{x} - \mathbf{x}_0). \quad (4.80b)$$

Multiply the $\psi(\mathbf{x})$ equation by $G(\mathbf{x}|\mathbf{x}_0)$ and the $G(\mathbf{x}|\mathbf{x}_0)$ equation by $\psi(\mathbf{x})$ to find

$$-G(\mathbf{x}|\mathbf{x}_0) \nabla_{\mathbf{x}}^2 \psi(\mathbf{x}) = G(\mathbf{x}|\mathbf{x}_0) \Lambda(\mathbf{x}) \quad (4.81a)$$

$$-\psi(\mathbf{x}) \nabla_{\mathbf{x}}^2 G(\mathbf{x}|\mathbf{x}_0) = \psi(\mathbf{x}) \delta(\mathbf{x} - \mathbf{x}_0), \quad (4.81b)$$

and then subtract these two equations

$$-G(\mathbf{x}|\mathbf{x}_0) \nabla_{\mathbf{x}}^2 \psi(\mathbf{x}) + \psi(\mathbf{x}) \nabla_{\mathbf{x}}^2 G(\mathbf{x}|\mathbf{x}_0) = G(\mathbf{x}|\mathbf{x}_0) \Lambda(\mathbf{x}) - \psi(\mathbf{x}) \delta(\mathbf{x} - \mathbf{x}_0). \quad (4.82)$$

Now integrate over observational points, \mathbf{x} , sampled over the region \mathcal{R} , in which case the right hand side becomes

$$\int_{\mathcal{R}} [G(\mathbf{x}|\mathbf{x}_0) \Lambda(\mathbf{x}) - \psi(\mathbf{x}) \delta(\mathbf{x} - \mathbf{x}_0)] dV = -\psi(\mathbf{x}_0) + \int_{\mathcal{R}} G(\mathbf{x}|\mathbf{x}_0) \Lambda(\mathbf{x}) dV, \quad (4.83)$$

where we made use of the sifting property (4.7) to expose the function, ψ , at the location of the Dirac source, \mathbf{x}_0 . Integrating the left hand side of equation (4.82) yields

$$\int_{\mathcal{R}} [-G(\mathbf{x}|\mathbf{x}_0) \nabla_{\mathbf{x}}^2 \psi(\mathbf{x}) + \psi(\mathbf{x}) \nabla_{\mathbf{x}}^2 G(\mathbf{x}|\mathbf{x}_0)] dV \quad (4.84a)$$

$$= \int_{\mathcal{R}} \nabla_{\mathbf{x}} \cdot [-G(\mathbf{x}|\mathbf{x}_0) \nabla_{\mathbf{x}} \psi(\mathbf{x}) + \psi(\mathbf{x}) \nabla_{\mathbf{x}} G(\mathbf{x}|\mathbf{x}_0)] dV \quad (4.84b)$$

$$= \oint_{\partial\mathcal{R}} [-G(\mathbf{x}|\mathbf{x}_0) \nabla_{\mathbf{x}} \psi(\mathbf{x}) + \psi(\mathbf{x}) \nabla_{\mathbf{x}} G(\mathbf{x}|\mathbf{x}_0)] \cdot \hat{\mathbf{n}}_{\mathbf{x}} d\mathcal{S}. \quad (4.84c)$$

Bringing the two sides to equation (4.82) together leads to

$$\psi(\mathbf{x}_0) = \int_{\mathcal{R}} \Lambda(\mathbf{x}) G(\mathbf{x}|\mathbf{x}_0) dV + \oint_{\partial\mathcal{R}} [G(\mathbf{x}|\mathbf{x}_0) \nabla_{\mathbf{x}} \psi(\mathbf{x}) - \psi(\mathbf{x}) \nabla_{\mathbf{x}} G(\mathbf{x}|\mathbf{x}_0)] \cdot \hat{\mathbf{n}}_{\mathbf{x}} d\mathcal{S}. \quad (4.85)$$

As a final step, it is convenient to relabel $\mathbf{x}_0 \leftrightarrow \mathbf{x}$ and make use of reciprocity, $G(\mathbf{x}|\mathbf{x}_0) = G(\mathbf{x}_0|\mathbf{x})$, so that

$$\psi(\mathbf{x}) = \underbrace{\int_{\mathcal{R}} \Lambda(\mathbf{x}_0) G(\mathbf{x}|\mathbf{x}_0) dV_0}_{\text{volume integral over } \mathcal{R}} + \underbrace{\oint_{\partial\mathcal{R}} [G(\mathbf{x}|\mathbf{x}_0) \nabla_{\mathbf{x}_0} \psi(\mathbf{x}_0) - \psi(\mathbf{x}_0) \nabla_{\mathbf{x}_0} G(\mathbf{x}|\mathbf{x}_0)] \cdot \hat{\mathbf{n}}_{\mathbf{x}_0} d\mathcal{S}_0}_{\text{boundary area integral over } \partial\mathcal{R}}. \quad (4.86)$$

We have thus established ψ as a volume integral of the Green's function with the source, Λ , plus a boundary integral of the Green's function with the boundary data. This expression holds for either the Dirichlet condition or Neumann condition, whereby the distinction occurs only for the boundary integral. Furthermore, note that the Green's function is independent of the source, Λ , and the boundary data, so that $G(\mathbf{x}|\mathbf{x}_0)$ can be used to express ψ for arbitrary source functions and boundary data.

4.6.6 Properties of the solution

Specializing the general solution (4.86) to Dirichlet boundary conditions results in

$$\psi(\mathbf{x}) = \int_{\mathcal{R}} \Lambda(\mathbf{x}_0) G(\mathbf{x}|\mathbf{x}_0) dV_0 - \oint_{\partial\mathcal{R}} \sigma(\mathbf{x}_0) \nabla_{\mathbf{x}_0} G(\mathbf{x}|\mathbf{x}_0) \cdot \hat{\mathbf{n}}_{\mathbf{x}_0} d\mathcal{S}_0. \quad (4.87)$$

Notice how the boundary integral involves the normal gradient of the Green's function, which is consistent with the one-dimensional case (4.49) derived in Section 4.5.1. We refer to the inward normal gradient of the Green's function as the *boundary Green's function*

$$G^{\text{bd}}(\mathbf{x}|\mathbf{x}_0) \equiv -\nabla_{\mathbf{x}_0} G(\mathbf{x}|\mathbf{x}_0) \cdot \hat{\mathbf{n}}_{\mathbf{x}_0} = -\frac{\partial G(\mathbf{x}|\mathbf{x}_0)}{\partial \hat{\mathbf{n}}_{\mathbf{x}_0}}, \quad (4.88)$$

in which case the Dirichlet solution takes the form

$$\psi(\mathbf{x}) = \int_{\mathcal{R}} \Lambda(\mathbf{x}_0) G(\mathbf{x}|\mathbf{x}_0) dV_0 + \oint_{\partial\mathcal{R}} \sigma(\mathbf{x}_0) G^{\text{bd}}(\mathbf{x}|\mathbf{x}_0) d\mathcal{S}_0. \quad (4.89)$$

This form for the solution emphasizes the role of the Green's function as the mediator between the distributed source, Λ , and all surrounding points $\mathbf{x} \in \mathcal{R}$, whereas the boundary Green's function mediates between information prescribed along the boundary, $\mathbf{x} \in \partial\mathcal{R}$, and interior points. In this subsection we summarize certain properties of the solution (4.87) and (4.89), and infer (through insisting on self-consistency) corresponding properties of the Green's function and boundary Green's function.

Linear superposition

The Dirichlet solution (4.87) manifests the linear superposition principle by writing $\psi = \psi_1 + \psi_2$ as given by Table 4.1. By construction, ψ_1 satisfies Poisson's equation with homogeneous Dirichlet boundary conditions, whereas ψ_2 satisfies Laplace's equation with inhomogeneous Dirichlet boundary conditions.

PDE: $\mathbf{x} \in \mathcal{R}$	BC: $\mathbf{x} \in \partial\mathcal{R}$	SOLUTION $\psi = \psi_1 + \psi_2$
$-\nabla^2\psi_1 = \Lambda$	$\psi_1 = 0$	$\psi_1(\mathbf{x}) = \int_{\mathcal{R}} G(\mathbf{x} \mathbf{x}_0) \Lambda(\mathbf{x}_0) dV_0$
$-\nabla^2\psi_2 = 0$	$\psi_2 = \sigma$	$\psi_2(\mathbf{x}) = \oint_{\partial\mathcal{R}} G^{\text{bd}}(\mathbf{x} \mathbf{x}_0) \sigma(\mathbf{x}_0) d\mathcal{S}_0$

TABLE 4.1: Decomposing the Dirichlet solution (4.87) into $\psi = \psi_1 + \psi_2$, with ψ_1 and ψ_2 satisfying the properties shown in this table. For the boundary contribution we made use of the boundary Green's function, $G^{\text{bd}}(\mathbf{x}|\mathbf{x}_0) = -\nabla_{\mathbf{x}_0} G(\mathbf{x}|\mathbf{x}_0) \cdot \hat{\mathbf{n}}_{\mathbf{x}_0}$, as given by equation (4.88).

Verifying the partial differential equation for $\mathbf{x} \in \mathcal{R}$

We derived the Dirichlet solution (4.87) with manipulations that are reversible; i.e., equal signs were used at every step. Hence, we know that the expression (4.87) indeed satisfies the Dirichlet boundary value problem (4.65). Even so, the exercise of verifying the solution reveals valuable insights into the Green's function.

To verify that the partial differential equation is satisfied for points within the interior of the region, $\mathbf{x} \in \mathcal{R}$, operate with $-\nabla_{\mathbf{x}}^2$ on equation (4.89) to find

$$-\nabla_{\mathbf{x}}^2 \psi(\mathbf{x}) = \int_{\mathcal{R}} \Lambda(\mathbf{x}_0) [-\nabla_{\mathbf{x}}^2 G(\mathbf{x}|\mathbf{x}_0)] dV_0 + \oint_{\partial\mathcal{R}} \sigma(\mathbf{x}_0) [-\nabla_{\mathbf{x}}^2 G^{\text{bd}}(\mathbf{x}|\mathbf{x}_0)] d\mathcal{S}_0. \quad (4.90)$$

For the first term on the right hand side, make use of the Green's function identity $-\nabla_{\mathbf{x}}^2 G(\mathbf{x}|\mathbf{x}_0) = \delta(\mathbf{x} - \mathbf{x}_0)$ and then use the sifting property of the Dirac delta, $\int_{\mathcal{R}} \Lambda(\mathbf{x}_0) \delta(\mathbf{x} - \mathbf{x}_0) dV_0 = \Lambda(\mathbf{x})$. To show that the boundary contribution vanishes, make use of the following

$$\nabla_{\mathbf{x}}^2 G^{\text{bd}}(\mathbf{x}|\mathbf{x}_0) = \nabla_{\mathbf{x}}^2 [-\nabla_{\mathbf{x}_0} G(\mathbf{x}|\mathbf{x}_0) \cdot \hat{\mathbf{n}}_{\mathbf{x}_0}] \quad (4.91a)$$

$$= \hat{\mathbf{n}}_{\mathbf{x}_0} \cdot \nabla_{\mathbf{x}_0} [-\nabla_{\mathbf{x}}^2 G(\mathbf{x}|\mathbf{x}_0)] \quad (4.91b)$$

$$= \hat{\mathbf{n}}_{\mathbf{x}_0} \cdot \nabla_{\mathbf{x}_0} \delta(\mathbf{x} - \mathbf{x}_0), \quad (4.91c)$$

and, without loss of generality, let the unit normal direction be parallel to the vertical, $\hat{\mathbf{n}}_{\mathbf{x}_0} = \hat{\mathbf{z}}$, so that

$$\hat{\mathbf{n}}_{\mathbf{x}_0} \cdot \nabla_{\mathbf{x}_0} \delta(\mathbf{x} - \mathbf{x}_0) = \partial_{z_0} [\delta(x - x_0) \delta(y - y_0) \delta(z - z_0)] = \delta(x - x_0) \delta(y - y_0) \frac{d[\delta(z - z_0)]}{dz_0}. \quad (4.92)$$

With $\mathbf{x}_0 \in \partial\mathcal{R}$ yet $\mathbf{x} \notin \partial\mathcal{R}$, the Dirac delta never fires, thus eliminating the boundary contribution. We have thus verified that $-\nabla_{\mathbf{x}}^2 \psi = \Lambda$ for points $\mathbf{x} \in \mathcal{R}$.

Verifying the Dirichlet boundary condition for $\mathbf{x} \in \partial\mathcal{R}$

To verify that the boundary conditions are satisfied by the Dirichlet solution (4.87), bring the field point, \mathbf{x} , onto the boundary

$$\mathbf{x} \rightarrow \mathbf{x}_{\partial\mathcal{R}} \in \partial\mathcal{R}. \quad (4.93)$$

For such boundary points, the volume integral in the solution (4.87) vanishes since the Dirichlet Green's function vanishes on the boundary, $G(\mathbf{x}_{\partial\mathcal{R}}|\mathbf{x}_0) = 0$. Self-consistency with the Dirichlet boundary data, $\psi(\mathbf{x}_{\partial\mathcal{R}}) = \sigma(\mathbf{x}_{\partial\mathcal{R}})$, leads to

$$\sigma(\mathbf{x}) = \oint_{\partial\mathcal{R}} \sigma(\mathbf{x}_0) G^{\text{bd}}(\mathbf{x}|\mathbf{x}_0) d\mathcal{S}_0 = - \oint_{\partial\mathcal{R}} \sigma(\mathbf{x}_0) \nabla_{\mathbf{x}_0} G(\mathbf{x}_{\partial\mathcal{R}}|\mathbf{x}_0) \cdot \hat{\mathbf{n}}_{\mathbf{x}_0} d\mathcal{S}_0 \quad \text{for } \mathbf{x} \in \partial\mathcal{R}. \quad (4.94)$$

This integral equation is consistent so long as the boundary Green's function satisfies the boundary condition

$$G^{\text{bd}}(\mathbf{x}|\mathbf{x}_0) = -\nabla_{\mathbf{x}_0} G(\mathbf{x}|\mathbf{x}_0) \cdot \hat{\mathbf{n}}_{\mathbf{x}_0} = \delta^{(2)}(\mathbf{x} - \mathbf{x}_0) \quad \text{for } \mathbf{x}, \mathbf{x}_0 \in \partial\mathcal{R}, \quad (4.95)$$

where $\delta^{(2)}(\mathbf{x} - \mathbf{x}_0)$ is the surface Dirac delta with physical dimensions of inverse area. This property of the boundary Green's function is consistent with the jump condition (4.98) found for the one-dimensional Poisson equation. It furthermore leads to the corresponding integral identity

$$\oint_{\partial\mathcal{R}} G^{\text{bd}}(\mathbf{x}|\mathbf{x}_0) d\mathcal{S}_0 = \oint_{\partial\mathcal{R}} \delta^{(2)}(\mathbf{x} - \mathbf{x}_0) d\mathcal{S}_0 = 1 \quad \text{for } \mathbf{x}, \mathbf{x}_0 \in \partial\mathcal{R}. \quad (4.96)$$

We emphasize¹⁰ that the expressions (4.95) and (4.96) are found by first placing the source point, \mathbf{x}_0 , on the boundary and thereafter moving the field point to the boundary, $\mathbf{x} \rightarrow \mathbf{x}_{\partial\mathcal{R}} \in \partial\mathcal{R}$.

4.6.7 Boundary Green's function

Boundary value problem for the boundary Green's function

As part of the development in Section 4.6.6, we revealed that the boundary Green's function satisfies the following boundary value problem

$$-\nabla_{\mathbf{x}}^2 G^{\text{bd}}(\mathbf{x}|\mathbf{x}_0) = 0 \quad \text{for } \mathbf{x} \in \mathcal{R} \quad \text{and} \quad G^{\text{bd}}(\mathbf{x}|\mathbf{x}_0) = \delta^{(2)}(\mathbf{x} - \mathbf{x}_0) \quad \text{for } \mathbf{x}, \mathbf{x}_0 \in \partial\mathcal{R}. \quad (4.97)$$

As seen by equation (4.71), the Dirichlet Green's function, $G(\mathbf{x}|\mathbf{x}_0)$, feels the Dirac source in the interior of the domain, $\mathbf{x} \in \mathcal{R}$, and satisfies homogeneous Dirichlet boundary conditions for $\mathbf{x} \in \partial\mathcal{R}$. As a complement, the boundary Green's function, $G^{\text{bd}}(\mathbf{x}|\mathbf{x}_0)$, is harmonic everywhere in the domain interior and yet equals to the Dirac source along the boundary. By construction, the boundary Green's function incorporates boundary information into the region as part of the Dirichlet solution (4.89). We make further use of the boundary Green's function when studying the diffusion equation in Section 4.8 and the advection-diffusion equation in Section 61.10, at which point the boundary Green's function is referred to as the *boundary propagator*.

Normalization of the boundary Green's function

Consider the special case of constant boundary data, $\sigma = \sigma_{\text{const}}$, in which case the harmonic function in Table 4.1 is itself a constant, $\psi_B(\mathbf{x}) = \sigma_{\text{const}}$. Consequently, the boundary Green's

¹⁰As per page 801 of *Morse and Feshbach* (1953).

function satisfies

$$-\oint_{\partial\mathcal{R}} \nabla_{\mathbf{x}_0} G(\mathbf{x}|\mathbf{x}_0) \cdot \hat{\mathbf{n}}_{\mathbf{x}_0} d\mathcal{S}_0 = \oint_{\partial\mathcal{R}} G^{\text{bd}}(\mathbf{x}|\mathbf{x}_0) d\mathcal{S}_0 = 1. \quad (4.98)$$

This relation is built by placing Dirac delta sources along the boundary, $\mathbf{x}_0 \in \partial\mathcal{R}$, and then area integrating over the boundary area. It holds for any field point, $\mathbf{x} \in \mathcal{R}$. Although derived by considering the special case of constant boundary data, equation (4.98) holds in general since the Green's function is independent of the boundary data.

To help understand the identity (4.98), consider the Green's function to be the steady state temperature or tracer concentration resulting from a Dirac delta source placed within the domain interior. The area integrated condition (4.98) acts to maintain the homogeneous Dirichlet boundary condition, $G(\mathbf{x}_{\partial\mathcal{R}}|\mathbf{x}_0) = 0$, for every point $\mathbf{x}_{\partial\mathcal{R}} \in \partial\mathcal{R}$. It does so by providing a boundary flux, via the normal gradient, whose area integral precisely cancels the unit positive source from the Dirac delta. We encountered this property for the one-dimensional equation studied in Section 4.5.3 and the three-dimensional Poisson equation with Dirichlet boundaries in Section 4.6.1.

Equation (4.98) represents a normalization of the boundary Green's function at each point within the region interior, and it is consistent with the boundary condition given in equation (4.97). If we place Dirac delta sources along the boundary and integrate over the boundary, then every point within the domain feels a net unit source from these boundary sources, which is reflected by the normalization of the boundary Green's function. We return to this normalization when considering the boundary propagator for the diffusion equation in Section 4.8.8.

4.7 Poisson's equation with Neumann boundaries

We now switch from the Dirichlet boundary conditions in Section 4.6 to the Poisson equation with *Neumann boundary conditions*

$$-\nabla^2\psi = \Lambda, \quad \text{for } \mathbf{x} \in \mathcal{R} \quad \text{and} \quad \hat{\mathbf{n}} \cdot \nabla\psi = \Sigma, \quad \text{for } \mathbf{x} \in \partial\mathcal{R}. \quad (4.99)$$

Rather than specifying the value of ψ along the boundary, the Neumann condition specifies the normal derivative. Although much is shared between the Dirichlet and Neumann problems, there are distinctions that arise in the present section.

4.7.1 Constraints on the source and boundary data

As in our discussion of Dirichlet boundary conditions in Section 4.6.1, we can realize a solution to the boundary value problem (4.99) only so long as the constraint (4.67) is satisfied. For Neumann boundary conditions, we specify the normal derivative along the boundary so that the constraint (4.67) is now imposed on the volume source and boundary data¹¹

$$\oint_{\partial\mathcal{R}} \Sigma dS = - \int_{\mathcal{R}} \Lambda dV. \quad (4.100)$$

If the source and boundary data do not satisfy this constraint, then there is no solution to the Poisson problem (4.99). If the Poisson problem arises physically from steady state tracer diffusion, then the constraint (4.100) imposes a balance between the diffusive flux integrated around the boundary (left hand side) with the volume integrated tracer source (right hand side). In the absence of this balance, there is no solution to the Poisson problem thus indicating the presence

¹¹To be self-contained, we here repeat the discussion of the constraint (4.100) that is also provided in Section 3.5.6.

of transients (i.e., time dependent diffusion). If the Poisson problem arises from Newtonian gravity, then the condition (4.100) means that the area integrated gravitational acceleration specified on the boundary must be consistent with the volume integrated mass source distributed within the domain.

4.7.2 Uniqueness of the solution up to a constant

As in Section 4.6.2, we consider the uniqueness of the solution to the boundary value problem (4.99). We do so, again, by considering two functions, ψ_A and ψ_B , each satisfying the boundary value problem (4.99) and noting that their difference, $\Psi = \psi_A - \psi_B$, satisfies the homogeneous problem

$$-\nabla^2\Psi = 0, \quad \text{for } \mathbf{x} \in \mathcal{R} \quad \text{and} \quad \hat{\mathbf{n}} \cdot \nabla\Psi = 0, \quad \text{for } \mathbf{x} \in \partial\mathcal{R}. \quad (4.101)$$

The same arguments we used in Section 4.6.2 lead us to conclude that $\nabla\Psi = 0$, but for the Neumann problem this result is consistent with Ψ being an arbitrary spatial constant. We can understand this arbitrariness since the Neumann boundary condition involves a derivative, with the derivative of a constant vanishing. We thus conclude that the solution to the boundary value problem (4.99) is unique up to an arbitrary constant.

4.7.3 The Green's function problem

The Green's function corresponding to the Poisson boundary value problem (4.99) is the solution to the Poisson equation with a Dirac delta source and a homogeneous Neumann boundary condition

$$-\nabla_{\mathbf{x}}^2 G(\mathbf{x}|\mathbf{x}_0) = \delta(\mathbf{x} - \mathbf{x}_0) \quad \text{for } \mathbf{x}, \mathbf{x}_0 \in \mathcal{R} \quad \text{and} \quad \hat{\mathbf{n}} \cdot \nabla_{\mathbf{x}} G(\mathbf{x}|\mathbf{x}_0) = 0, \quad \text{for } \mathbf{x} \in \partial\mathcal{R}. \quad (4.102)$$

Linearity enables us to write the Green's function as the sum of the free space Green's function plus a harmonic function

$$G(\mathbf{x}|\mathbf{x}_0) = \mathcal{G}(\mathbf{x}|\mathbf{x}_0) + H(\mathbf{x}|\mathbf{x}_0), \quad (4.103)$$

where

$$-\nabla_{\mathbf{x}}^2 \mathcal{G}(\mathbf{x}|\mathbf{x}_0) = \delta(\mathbf{x} - \mathbf{x}_0) \quad \text{for } \mathbf{x}, \mathbf{x}_0 \in \mathbb{R}^3 \quad (4.104a)$$

$$-\nabla_{\mathbf{x}}^2 H(\mathbf{x}|\mathbf{x}_0) = 0 \quad \text{for } \mathbf{x}, \mathbf{x}_0 \in \mathcal{R} \quad (4.104b)$$

$$-\hat{\mathbf{n}} \cdot \nabla_{\mathbf{x}} H(\mathbf{x}|\mathbf{x}_0) = \hat{\mathbf{n}} \cdot \nabla_{\mathbf{x}} \mathcal{G}(\mathbf{x}|\mathbf{x}_0) \quad \text{for } \mathbf{x} \in \partial\mathcal{R}. \quad (4.104c)$$

4.7.4 Properties of the solution

Specializing the general solution (4.86) to Neumann boundary conditions results in

$$\psi(\mathbf{x}) = \int_{\mathcal{R}} \Lambda(\mathbf{x}_0) G(\mathbf{x}|\mathbf{x}_0) dV_0 + \oint_{\partial\mathcal{R}} \Sigma(\mathbf{x}_0) G(\mathbf{x}|\mathbf{x}_0) d\mathcal{S}_0. \quad (4.105)$$

In this section we summarize certain properties of the solution (4.105) along with properties of the Green's function that are inferred (through insisting on self-consistency) from the solution.

Linear superposition

This Green's function solution (4.105) manifests the linear superposition principle by writing $\psi = \psi_1 + \psi_2$ as given by Table 4.2. By construction, ψ_1 satisfies Poisson's equation with homoge-

neous Neumann boundary conditions, whereas ψ_2 satisfies Laplace's equation with inhomogeneous Neumann boundary conditions.

PDE: $\mathbf{x} \in \mathcal{R}$	BC: $\mathbf{x} \in \partial\mathcal{R}$	SOLUTION $\psi = \psi_1 + \psi_2$
$-\nabla^2\psi_1 = \Lambda$	$\psi_1 = 0$	$\psi_1(\mathbf{x}) = \int_{\mathcal{R}} G(\mathbf{x} \mathbf{x}_0) \Lambda(\mathbf{x}_0) dV_0$
$-\nabla^2\psi_2 = 0$	$\hat{\mathbf{n}} \cdot \nabla\psi_2 = \Sigma$	$\psi_2(\mathbf{x}) = \oint_{\partial\mathcal{R}} \Sigma(\mathbf{x}_0) G(\mathbf{x} \mathbf{x}_0) dS_0$

TABLE 4.2: Decomposing the Neumann solution (4.105) into $\psi = \psi_1 + \psi_2$, with ψ_1 and ψ_2 satisfying the properties shown here. The function ψ_1 is identical to ψ_1 appearing for the Dirichlet problem (see Table 4.1), whereas the function ψ_2 is distinct since it is determined by the respective boundary conditions.

Transforming the boundary data to the interior

The Neumann solution (4.105) allows for a dual formulation of the boundary data. To motivate this formulation, assume the only nontrivial Neumann boundary data appears along the constant geopotential surface $z = z_b$, with all other boundaries maintaining the homogeneous boundary condition, $\hat{\mathbf{n}} \cdot \nabla\psi = 0$. In this special case the Neumann solution (4.105) takes the form

$$\psi(\mathbf{x}) = \int_{\mathcal{R}} \Lambda(\mathbf{x}_0) G(\mathbf{x}|\mathbf{x}_0) dV_0 + \int_{z=z_b} \Sigma(x_0, y_0) G(\mathbf{x}|\mathbf{x}_0) dx_0 dy_0 \quad (4.106a)$$

$$= \int_{\mathcal{R}} [\Lambda(\mathbf{x}_0) + \Sigma(x_0, y_0) \delta(z_0 - z_b)] G(\mathbf{x}|\mathbf{x}_0) dV_0 \quad (4.106b)$$

$$= \int_{\mathcal{R}} \Lambda^*(\mathbf{x}_0) G(\mathbf{x}|\mathbf{x}_0) dV_0. \quad (4.106c)$$

These manipulations have absorbed the non-homogeneous Neumann boundary condition into a modified source, $\Lambda^*(\mathbf{x})$. We are thus led to two equivalent formulations for the Poisson boundary value problem with Neumann conditions. The first is given by equation (4.99), whereby ψ is the solution to the Poisson equation with source, Λ , and with inhomogeneous Neumann boundary data, Σ . The second formulation considers ψ to be the solution to Poisson's equation with homogeneous Neumann boundary conditions yet with a modified source function

$$\Lambda^*(\mathbf{x}) = \Lambda(\mathbf{x}) + \Sigma(x, y) \delta(z - z_b) = \Lambda(\mathbf{x}) + \partial_z \psi(\mathbf{x}) \delta(z - z_b). \quad (4.107)$$

As a check, note that the physical dimensionality of $\Lambda^*(\mathbf{x})$ is indeed correct since the Dirac delta, $\delta(z - z_b)$, has dimensions of inverse length. We interpret the term $\Sigma(x, y) \delta(z - z_b)$ as a flux or *Dirac delta sheet* that sits just inside the boundary (at $z = z_b - \epsilon$ with $\epsilon \rightarrow 0$), which allows this data to be incorporated into the volume source data rather than be part of the boundary data. The specific form (4.107) can be generalized to the expression

$$\Lambda^*(\mathbf{x}) = \Lambda(\mathbf{x}) + \Sigma(\mathbf{x}) \delta[\hat{\mathbf{n}} \cdot (\mathbf{x} - \mathbf{x}_{\partial\mathcal{R}})] = \Lambda(\mathbf{x}) + \hat{\mathbf{n}} \cdot \nabla\psi(\mathbf{x}) \delta[\hat{\mathbf{n}} \cdot (\mathbf{x} - \mathbf{x}_{\partial\mathcal{R}})], \quad (4.108)$$

where the argument to the Dirac delta picks out the coordinates in the direction of the outward unit normal. The transformed Neumann problem thus takes the generic form

$$-\nabla^2\psi = \Lambda^*, \quad \text{for } \mathbf{x} \in \mathcal{R} \quad \text{and} \quad \hat{\mathbf{n}} \cdot \nabla\psi = 0, \quad \text{for } \mathbf{x} \in \partial\mathcal{R}. \quad (4.109)$$

Again, the solution to the boundary value problem (4.109) is identical to the solution of the original problem (4.99).

Notably, the same data, Σ , is needed for both equations (4.109) and (4.99), so there is nothing

fundamentally special or efficient about one formulation or the other. Rather, it is a matter of convenience. For example, the formulation using Λ^* has found some favor in the study of quasi-geostrophic potential vorticity ([Bretherton, 1966](#)). We also make use of a similar construct in Section 65.4.3 for studies of boundary buoyancy fluxes in water mass transformation analysis.

4.7.5 Verifying the solution

We verify that the solution (4.105) solves the Poisson boundary value problem (4.99). First consider a point in the interior of the region, $\mathbf{x} \in \mathcal{R}$, and apply $-\nabla_{\mathbf{x}}^2$ on equation (4.105) to find

$$-\nabla_{\mathbf{x}}^2 \psi(\mathbf{x}) = \int_{\mathcal{R}} \Lambda(\mathbf{x}_0) [-\nabla_{\mathbf{x}}^2 G(\mathbf{x}|\mathbf{x}_0)] dV_0 + \oint_{\partial\mathcal{R}} \Sigma(\mathbf{x}_0) [-\nabla_{\mathbf{x}}^2 G(\mathbf{x}|\mathbf{x}_0)] dS_0 = \Lambda(\mathbf{x}). \quad (4.110)$$

To reach this result we used $-\nabla_{\mathbf{x}}^2 G(\mathbf{x}|\mathbf{x}_0) = \delta(\mathbf{x} - \mathbf{x}_0)$ and noted that the boundary integral vanishes for $\mathbf{x} \notin \partial\mathcal{R}$.

To verify the boundary condition, act with the gradient, $\nabla_{\mathbf{x}}$, on the solution (4.105)

$$\nabla_{\mathbf{x}} \psi(\mathbf{x}) = \int_{\mathcal{R}} \Lambda(\mathbf{x}_0) [\nabla_{\mathbf{x}} G(\mathbf{x}|\mathbf{x}_0)] dV_0 + \oint_{\partial\mathcal{R}} \Sigma(\mathbf{x}_0) [\nabla_{\mathbf{x}} G(\mathbf{x}|\mathbf{x}_0)] dS_0. \quad (4.111)$$

Now move the field point onto the boundary, $\mathbf{x} \rightarrow \mathbf{x}_{\partial\mathcal{R}} \in \partial\mathcal{R}$, and project the gradient onto the unit normal direction, $\hat{\mathbf{n}}_{\mathbf{x}}$, at the point $\mathbf{x}_{\partial\mathcal{R}}$. This projection leads to $\hat{\mathbf{n}}_{\mathbf{x}} \cdot \nabla_{\mathbf{x}} \psi(\mathbf{x}) = \Sigma(\mathbf{x})$ on the left hand side, and it annihilates the volume term on the right hand side since $\hat{\mathbf{n}}_{\mathbf{x}} \cdot \nabla_{\mathbf{x}} G(\mathbf{x}|\mathbf{x}_0) = 0$ for $\mathbf{x} \in \partial\mathcal{R}$. We are thus left with

$$\hat{\mathbf{n}} \cdot \nabla_{\mathbf{x}} \psi(\mathbf{x}) = \Sigma(\mathbf{x}) = \oint_{\partial\mathcal{R}} \Sigma(\mathbf{x}_0) [\hat{\mathbf{n}}_{\mathbf{x}} \cdot \nabla_{\mathbf{x}} G(\mathbf{x}|\mathbf{x}_0)] dS_0 \quad \text{for } \mathbf{x} \in \partial\mathcal{R}. \quad (4.112)$$

Again, both arguments of the Green's function are on the boundary, $\mathbf{x}, \mathbf{x}_0 \in \partial\mathcal{R}$, with the Dirac source point, \mathbf{x}_0 , integrated around the boundary whereas the field point, \mathbf{x} , is an arbitrary point on the boundary. Equation (4.94) is the analogous integral equation for the solution with Dirichlet boundary conditions. As for the Dirichlet case, we are ensured a solution to the integral equation (4.112) if the Green's function satisfies the property

$$\hat{\mathbf{n}}_{\mathbf{x}} \cdot \nabla_{\mathbf{x}} G(\mathbf{x}|\mathbf{x}_0) = \delta^{(2)}(\mathbf{x} - \mathbf{x}_0) \quad \text{for } \mathbf{x}, \mathbf{x}_0 \in \partial\mathcal{R}, \quad (4.113)$$

which takes on the integral expression

$$\oint_{\partial\mathcal{R}} \hat{\mathbf{n}}_{\mathbf{x}} \cdot \nabla_{\mathbf{x}} G(\mathbf{x}|\mathbf{x}_0) dS_0 = \oint_{\partial\mathcal{R}} \delta^{(2)}(\mathbf{x} - \mathbf{x}_0) dS_0 \quad \text{for } \mathbf{x} \in \partial\mathcal{R}. \quad (4.114)$$

Table 4.3 compares the boundary properties of the respective Green's functions.

BOUNDARY CONDITION	GREEN'S FUNCTION PROPERTY	EQUATION
Dirichlet	$\partial G / \partial \hat{\mathbf{n}}_0 = \hat{\mathbf{n}}_{\mathbf{x}_0} \cdot \nabla_{\mathbf{x}_0} G(\mathbf{x} \mathbf{x}_0) = -\delta^{(2)}(\mathbf{x} - \mathbf{x}_0)$	(4.95)
Neumann	$\partial G / \partial \hat{\mathbf{n}} = \hat{\mathbf{n}}_{\mathbf{x}} \cdot \nabla_{\mathbf{x}} G(\mathbf{x} \mathbf{x}_0) = \delta^{(2)}(\mathbf{x} - \mathbf{x}_0)$	(4.113)

TABLE 4.3: Comparing the boundary normal derivatives for the Poisson equation Green's function with Dirichlet and Neumann boundary conditions. Each point is on the boundary, $\mathbf{x}, \mathbf{x}_0 \in \partial\mathcal{R}$, and the Dirac delta is two-dimensional so it has dimensions of inverse area. The properties satisfied by these Green's functions are realized by first placing the source point, \mathbf{x}_0 , on the boundary and then moving the field point to the boundary, $\mathbf{x} \rightarrow \mathbf{x}_{\partial\mathcal{R}} \in \partial\mathcal{R}$. For the Dirichlet condition, the normal derivative is computed at the source point, whereas the Neumann condition computes the normal derivative at the field point.

4.8 The diffusion equation

We continue building our understanding of Green's function methods by now studying the *diffusion equation*, also known as the *heat equation*. We first encountered the diffusion equation in Section 3.6, where it served as the canonical parabolic partial differential equation. It is more thoroughly explored in Chapter 61, with much of the current chapter a foundation for the Green's function treatment of the advection-diffusion equation in Section 61.10. Time dependence appearing in the diffusion equation is the new feature relative to the elliptic Poisson equation encountered thus far in this chapter.

The traditional Green's function formalism for the diffusion equation, and the one pursued in this chapter, assumes that the spatial domain, \mathcal{R} , is static. Doing so ensures that space and time operations commute, such as differentiation and integration. Although time independent domains are suitable for many applications, certain geophysical applications of interest in this book make use of time dependent boundaries, with the ocean free surface the key example. We examine time dependent boundaries when studying the advection-diffusion equation in Section 61.10, with that generality best confronted only after further exercising our Green's function brain muscle in the current chapter.

4.8.1 Causal free space Green's function

Consider a Dirac delta tracer source at (\mathbf{x}_0, t_0) and assume a continuous media where there is no advection, such as found in a stagnant fluid or elastic solid. The simplest solution to the diffusion equation is known as the *causal free space Green's function*, which is defined for $t \in (-\infty, \infty)$ and satisfies

$$(\partial_t - \kappa \nabla_{\mathbf{x}}^2) \mathcal{G}(\mathbf{x}, t | \mathbf{x}_0, t_0) = \delta(t - t_0) \delta(\mathbf{x} - \mathbf{x}_0) \quad \mathbf{x} \in \mathbb{R}^n \quad (4.115a)$$

$$\mathcal{G}(\mathbf{x}, t | \mathbf{x}_0, t_0) \rightarrow 0 \quad |\mathbf{x} - \mathbf{x}_0| \rightarrow \infty \quad (4.115b)$$

$$\mathcal{G}(\mathbf{x}, t | \mathbf{x}_0, t_0) = 0 \quad \mathbf{x} \in \mathbb{R}^n, \quad t < t_0, \quad (4.115c)$$

where \mathbb{R}^n is Euclidean space with $n = 1, 2, 3$ for a line, plane, and volume, respectively, and where $\kappa > 0$ is a constant diffusivity (dimensions $L^2 T^{-1}$). Equation (4.115b) ensures that the free space Green's function, \mathcal{G} , decays as the field point gets further away from the source point. The *causality condition* (4.115c) means that the Green's function vanishes for times prior to the time, t_0 , at which the Dirac source occurs. Given the dimensions of the Dirac source, we see that the Green's function has dimensions of L^{-n} .

The causal free-space Green's function is given by

$$\mathcal{G}(\mathbf{x}, t | \mathbf{x}_0, t_0) = \frac{H(t - t_0)}{[4 \pi \kappa (t - t_0)]^{n/2}} e^{-|\mathbf{x} - \mathbf{x}_0|^2 / [4 \kappa (t - t_0)]}, \quad (4.116)$$

where the Heaviside step function (equation (4.16)) enforces causality. The amplitude of the Green's function exponentially decays when moving away from the source location, thus satisfying the condition (4.115b). Additionally, as time progresses beyond the source time, the Green's function decays according to the pre-factor, $(t - t_0)^{-n/2}$. Each of these properties of the causal free space Green's function are reflected in solutions to more general diffusion processes.

4.8.2 Causal Green's function

Moving beyond the free space solution, we next introduce the *causal Green's function* for the diffusion equation. This Green's function is defined for $t \in (-\infty, \infty)$ and satisfies the following

equations when assuming Neumann boundary conditions

$$\frac{\partial[G(\mathbf{x}, t|\mathbf{x}_0, t_0)]}{\partial t} - \nabla_{\mathbf{x}} \cdot [\mathbb{K} \cdot \nabla_{\mathbf{x}} G(\mathbf{x}, t|\mathbf{x}_0, t_0)] = \delta(t - t_0) \delta(\mathbf{x} - \mathbf{x}_0) \quad \mathbf{x} \in \mathcal{R} \quad (4.117a)$$

$$\hat{\mathbf{n}} \cdot \mathbb{K} \cdot \nabla_{\mathbf{x}} G(\mathbf{x}, t|\mathbf{x}_0, t_0) = 0 \quad \mathbf{x} \in \partial\mathcal{R} \quad (4.117b)$$

$$G(\mathbf{x}, t|\mathbf{x}_0, t_0) = 0 \quad \mathbf{x} \in \mathcal{R}, \quad t < t_0. \quad (4.117c)$$

The Neumann boundary condition is relevant when one knows the boundary flux of heat or tracer concentration. Alternatively, Dirichlet conditions are used when knowing the boundary values for the field, in which case the corresponding causal Green's function satisfies

$$\frac{\partial[G(\mathbf{x}, t|\mathbf{x}_0, t_0)]}{\partial t} - \nabla_{\mathbf{x}} \cdot [\mathbb{K} \cdot \nabla_{\mathbf{x}} G(\mathbf{x}, t|\mathbf{x}_0, t_0)] = \delta(t - t_0) \delta(\mathbf{x} - \mathbf{x}_0) \quad \mathbf{x} \in \mathcal{R} \quad (4.118a)$$

$$G(\mathbf{x}, t|\mathbf{x}_0, t_0) = 0 \quad \mathbf{x} \in \partial\mathcal{R} \quad (4.118b)$$

$$G(\mathbf{x}, t|\mathbf{x}_0, t_0) = 0 \quad \mathbf{x} \in \mathcal{R}, \quad t < t_0. \quad (4.118c)$$

The Dirichlet condition is particularly relevant for passive tracers in the atmosphere and ocean, such as those studied in Section 61.10. In both the Neumann and Dirichlet cases, we generalized the free space solution from Section 4.8.1 by introducing a space-time dependent diffusivity tensor, $\mathbb{K}(\mathbf{x}, t)$, which is a symmetric second order tensor with dimensions $L^2 T^{-1}$ (we study such diffusion tensors in Chapter 61 and 63). The Green's function has dimensions of inverse volume, L^{-3} , which is implied since the Dirac delta source has dimensions of inverse volume times inverse time, $L^{-3} T^{-1}$.

In the presence of boundaries, the spatial position of the Dirac delta source impacts the value of the causal Green's function. In contrast, the causality condition (4.117c) means that the Green's function is dependent only on the time since the introduction of the source, $t - t_0$. Hence, there is no added generality afforded by setting the source time, t_0 , to be distinct from $t_0 = 0$. Even so, we retain t_0 to maintain symmetry with the spatial location \mathbf{x}_0 . Doing so also helps to distinguish the Dirac source time, t_0 , from the initial time, t_{init} , with the intitial time introduced in Section 4.8.6.

4.8.3 Adjoint causal Green's function

We make use of the *adjoint causal Green's function* for solving initial-boundary value problems for the diffusion equation. The adjoint causal Green's function is defined for $t \in (-\infty, \infty)$ and satisfies the following boundary value problem for the Neumann conditions, with these equations representing the adjoint to the Green's function equations (4.117a)-(4.117c)

$$-\frac{\partial[\tilde{G}(\mathbf{x}, t|\mathbf{x}_0, t_0)]}{\partial t} - \nabla_{\mathbf{x}} \cdot [\mathbb{K} \cdot \nabla_{\mathbf{x}} \tilde{G}(\mathbf{x}, t|\mathbf{x}_0, t_0)] = \delta(t - t_0) \delta(\mathbf{x} - \mathbf{x}_0) \quad \mathbf{x} \in \mathcal{R} \quad (4.119a)$$

$$\hat{\mathbf{n}} \cdot \mathbb{K} \cdot \nabla_{\mathbf{x}} \tilde{G}(\mathbf{x}, t|\mathbf{x}_0, t_0) = 0 \quad \mathbf{x} \in \partial\mathcal{R} \quad (4.119b)$$

$$\tilde{G}(\mathbf{x}, t|\mathbf{x}_0, t_0) = 0 \quad \mathbf{x} \in \mathcal{R}, \quad t > t_0. \quad (4.119c)$$

Similarly, the adjoint Green's function satisfying Dirichlet boundary conditions is determined by

$$-\frac{\partial[\tilde{G}(\mathbf{x}, t|\mathbf{x}_0, t_0)]}{\partial t} - \nabla_{\mathbf{x}} \cdot [\mathbb{K} \cdot \nabla_{\mathbf{x}} \tilde{G}(\mathbf{x}, t|\mathbf{x}_0, t_0)] = \delta(t - t_0) \delta(\mathbf{x} - \mathbf{x}_0) \quad \mathbf{x} \in \mathcal{R} \quad (4.120a)$$

$$\tilde{G}(\mathbf{x}, t|\mathbf{x}_0, t_0) = 0 \quad \mathbf{x} \in \partial\mathcal{R} \quad (4.120b)$$

$$\tilde{G}(\mathbf{x}, t|\mathbf{x}_0, t_0) = 0 \quad \mathbf{x} \in \mathcal{R}, \quad t > t_0. \quad (4.120c)$$

Note the sign change on the time derivative in equations (4.119a) and (4.120a) relative to equations (4.117a) and (4.118a). This change results since the single partial time derivative is not a self-adjoint operator, reflecting the lack of time symmetry of the diffusion equation (i.e., the diffusion equation distinguishes between past and future). Also note the backward causal condition, equations (4.119c) and (4.120c). Pondering the physics of these equations, we propose that the adjoint Green's function provides a solution to the *concentration equation*, which is the diffusion equation run backwards in time.

4.8.4 Reciprocity of the Green's function and its adjoint

When studying Poisson's equation we made use of reciprocity (4.75) satisfied by the Poisson equation Green's function, and we will require a corresponding reciprocity for the diffusion equation Green's function. Deriving reciprocity requires a bit more work for the diffusion equation due to the added time derivative term, which renders the adjoint diffusion operator distinct from the diffusion operator. That is, the diffusion operator is not *self-adjoint* due to sign change on the time derivative, whereas the Laplacian operator is self-adjoint (even with the symmetric diffusion tensor).

Before starting this derivation, note that we did not derive the adjoint in Section 4.8.3, instead we merely wrote it down. However, introduction of the adjoint Green's function is largely motivated by the following derivation of the reciprocity relation, where we see that the Green's function for the diffusion equation satisfies a reciprocity relation with the adjoint Green's function. Hence, as part of the following derivation we indirectly see how to construct the adjoint problem.

Setting up the derivation

To derive reciprocity, consider the partial differential equation (4.117a) with a Dirac delta source $\delta(t - t_1)\delta(\mathbf{x} - \mathbf{x}_1)$, and the adjoint partial differential equation (4.119a) with a distinct Dirac delta source $\delta(t - t_2)\delta(\mathbf{x} - \mathbf{x}_2)$. Multiply each of these equations by the complement Green's function and subtract

$$\begin{aligned} & \tilde{G}(\mathbf{x}, t | \mathbf{x}_2, t_2)(\partial_t G(\mathbf{x}, t | \mathbf{x}_1, t_1) - \nabla_{\mathbf{x}} \cdot [\mathbb{K} \cdot \nabla_{\mathbf{x}} G(\mathbf{x}, t | \mathbf{x}_1, t_1)]) \\ & - G(\mathbf{x}, t | \mathbf{x}_1, t_1)(-\partial_t \tilde{G}(\mathbf{x}, t | \mathbf{x}_2, t_2) - \nabla_{\mathbf{x}} \cdot [\mathbb{K} \cdot \nabla_{\mathbf{x}} \tilde{G}(\mathbf{x}, t | \mathbf{x}_2, t_2)]) \\ & = \tilde{G}(\mathbf{x}, t | \mathbf{x}_2, t_2)\delta(t - t_1)\delta(\mathbf{x} - \mathbf{x}_1) - G(\mathbf{x}, t | \mathbf{x}_1, t_1)\delta(t - t_2)\delta(\mathbf{x} - \mathbf{x}_2). \end{aligned} \quad (4.121)$$

The Dirac delta source locations, \mathbf{x}_1 and \mathbf{x}_2 , are arbitrary, so long as they are within the domain \mathcal{R} . Likewise, the source times, t_1 and t_2 , are arbitrary. In the following, we find it useful to introduce an arbitrarily large time, T , so that

$$-T < t_1, t_2 < T, \quad (4.122)$$

with T later dropping out from the results through use of the causality conditions.

Integration and use of the sifting property

An integral of the right hand side of equation (4.121) over the domain \mathcal{R} and over time, both for the observational space-time points (\mathbf{x}, t) , leads to

$$\begin{aligned} \int_{-T}^T \int_{\mathcal{R}} & \left[\tilde{G}(\mathbf{x}, t | \mathbf{x}_2, t_2) \delta(t - t_1) \delta(\mathbf{x} - \mathbf{x}_1) - G(\mathbf{x}, t | \mathbf{x}_1, t_1) \delta(t - t_2) \delta(\mathbf{x} - \mathbf{x}_2) \right] dV dt \\ & = \tilde{G}(\mathbf{x}_1, t_1 | \mathbf{x}_2, t_2) - G(\mathbf{x}_2, t_2 | \mathbf{x}_1, t_1). \end{aligned} \quad (4.123)$$

As shown in the following, the same integral of the left hand side of equation (4.121) vanishes, which then establishes the reciprocity property between the Green's function and the adjoint Green's function.

Moving the time derivative from G to \tilde{G} and picking up a minus sign

The left hand side of equation (4.121) requires us to massage just the first term since, as we will show, this term equals to the second so that the left hand side of equation (4.121) vanishes. To prove this assertion, start by examining the time derivative. Since the spatial domain, \mathcal{R} , is assumed to be static, we can swap the time and space derivatives to find

$$\begin{aligned} \int_{-T}^T & \tilde{G}(\mathbf{x}, t | \mathbf{x}_2, t_2) \partial_t G(\mathbf{x}, t | \mathbf{x}_1, t_1) dt \\ & = \int_{-T}^T \left[\partial_t \left(\tilde{G}(\mathbf{x}, t | \mathbf{x}_2, t_2) G(\mathbf{x}, t | \mathbf{x}_1, t_1) \right) - \partial_t \tilde{G}(\mathbf{x}, t | \mathbf{x}_2, t_2) G(\mathbf{x}, t | \mathbf{x}_1, t_1) \right] dt. \end{aligned} \quad (4.124)$$

We now set

$$G(\mathbf{x}, t = -T | \mathbf{x}_1, t_1) = 0 \quad \text{and} \quad \tilde{G}(\mathbf{x}, t = +T | \mathbf{x}_2, t_2) = 0, \quad (4.125)$$

which result from the causality conditions (4.117c) and (4.119c). Hence, in moving the time derivative from G to \tilde{G} we pick up a minus sign, which, again, means that the time derivative is not self-adjoint

$$\int_{-T}^T \tilde{G}(\mathbf{x}, t | \mathbf{x}_2, t_2) \partial_t G(\mathbf{x}, t | \mathbf{x}_1, t_1) dt = - \int_{-T}^T \partial_t \tilde{G}(\mathbf{x}, t | \mathbf{x}_2, t_2) G(\mathbf{x}, t | \mathbf{x}_1, t_1) dt. \quad (4.126)$$

The Laplacian is self-adjoint with a symmetric diffusion tensor

Consider next the spatial derivative term on the left hand side of equation (4.121)

$$\begin{aligned} & - \int_{\mathcal{R}} \tilde{G}(\mathbf{x}, t | \mathbf{x}_2, t_2) \nabla_{\mathbf{x}} \cdot [\mathbb{K} \cdot \nabla_{\mathbf{x}} G(\mathbf{x}, t | \mathbf{x}_1, t_1)] dV = \\ & \int_{\mathcal{R}} \left[-\nabla_{\mathbf{x}} \cdot \left(\tilde{G}(\mathbf{x}, t | \mathbf{x}_2, t_2) \mathbb{K} \cdot \nabla_{\mathbf{x}} G(\mathbf{x}, t | \mathbf{x}_1, t_1) \right) + \nabla_{\mathbf{x}} \tilde{G}(\mathbf{x}, t | \mathbf{x}_2, t_2) \cdot \mathbb{K} \cdot \nabla_{\mathbf{x}} G(\mathbf{x}, t | \mathbf{x}_1, t_1) \right] dV. \end{aligned} \quad (4.127)$$

Use of the divergence theorem and either the homogeneous Neumann boundary condition (4.117b) or homogeneous Dirichlet condition (4.118b) allow us to drop the total derivative term. The same manipulation, with either the Neumann condition (4.119b) or Dirichlet condition (4.120b) satisfied by the adjoint Green's function $\tilde{G}(\mathbf{x}, t | \mathbf{x}_2, t_2)$, allows us to seamlessly move the Laplacian operator from $G(\mathbf{x}, t | \mathbf{x}_1, t_1)$ onto $\tilde{G}(\mathbf{x}, t | \mathbf{x}_2, t_2)$, thus manifesting the self-adjoint nature of the Laplacian

operator even in the presence of a symmetric diffusion tensor

$$\begin{aligned} \int_{\mathcal{R}} \tilde{G}(\mathbf{x}, t | \mathbf{x}_2, t_2) \nabla_{\mathbf{x}} \cdot [\mathbb{K} \cdot \nabla_{\mathbf{x}} G(\mathbf{x}, t | \mathbf{x}_1, t_1)] dV \\ = \int_{\mathcal{R}} \nabla_{\mathbf{x}} \cdot [\mathbb{K} \cdot \nabla_{\mathbf{x}} \tilde{G}(\mathbf{x}, t | \mathbf{x}_2, t_2)] G(\mathbf{x}, t | \mathbf{x}_1, t_1) dV. \end{aligned} \quad (4.128)$$

Reciprocity of the Green's function and the adjoint Green's function

The above manipulations show that the space-time integral for the left hand side of equation (4.121) vanishes. Consequently, we are left with the reciprocity relation satisfied by the Green's function and adjoint Green's function for the diffusion equation

$$\tilde{G}(\mathbf{x}, t | \mathbf{x}_0, t_0) = G(\mathbf{x}_0, t_0 | \mathbf{x}, t). \quad (4.129)$$

The right hand side results from placing a Dirac source at (\mathbf{x}, t) and using the forward diffusion equation to determine the effect at (\mathbf{x}_0, t_0) with $t < t_0$. The left hand side results from placing a Dirac source at (\mathbf{x}_0, t_0) and using the adjoint diffusion equation to determine the effect at (\mathbf{x}, t) , again with $t < t_0$. The reciprocity relation (4.129) proves the two approaches are identical. We emphasize that reciprocity is the concerted property of the differential operator, the boundary conditions, and causality conditions.

Reciprocity in the form of equation (4.129) means we have no need to bother solving the adjoint Green's function equation for $\tilde{G}(\mathbf{x}, t | \mathbf{x}_0, t_0)$ since the adjoint Green's function equals to the Green's function after swapping the space-time points for the field and source. Hence, it is sufficient to determine the Green's function, $G(\mathbf{x}, t | \mathbf{x}_0, t_0)$, and then use reciprocity to determine $\tilde{G}(\mathbf{x}, t | \mathbf{x}_0, t_0)$. The simplicity of the reciprocity relation (4.129) is central to the practical use of the Green's function method for the diffusion equation.

4.8.5 Composition property of the Green's function

Following from the reciprocity relation derived in Section 4.8.4, we here derive the *composition property* satisfied by the Green's functions for the diffusion equation. This property connects the Green's function to Markov processes, in which the composition property is known as the *Chapman-Kolmogorov relation* (Gardiner, 1985). The derivation closely follows that given in Section 4.8.4 for reciprocity, though it is a bit simpler. Larson (1999) and Holzer (2009) discuss the composition property in the context of the advection-diffusion equation, to which we return to in Section 61.10.6. Holzer (2009) also provides further connections to probability theory, thus promoting the interpretation of the Green's function as a transition probability.

Setting up the derivation

Consider again the Green's function partial differential equation (4.117a) with a Dirac delta source at (t_1, \mathbf{x}_1) ,

$$\partial_t G(\mathbf{x}, t | \mathbf{x}_1, t_1) - \nabla_{\mathbf{x}} \cdot [\mathbb{K} \cdot \nabla_{\mathbf{x}} G(\mathbf{x}, t | \mathbf{x}_1, t_1)] = \delta(t - t_1) \delta(\mathbf{x} - \mathbf{x}_1), \quad (4.130)$$

and the adjoint Green's function partial differential equation (4.119a) with a distinct Dirac delta source at (t_2, \mathbf{x}_2)

$$\partial_t \tilde{G}(\mathbf{x}, t | \mathbf{x}_2, t_2) + \nabla_{\mathbf{x}} \cdot [\mathbb{K} \cdot \nabla_{\mathbf{x}} \tilde{G}(\mathbf{x}, t | \mathbf{x}_2, t_2)] = -\delta(t - t_2) \delta(\mathbf{x} - \mathbf{x}_2). \quad (4.131)$$

Multiply each of these equations by the complement Green's function and add the two equations.¹² Adding the time derivatives leads to

$$\begin{aligned} \tilde{G}(\mathbf{x}, t|\mathbf{x}_2, t_2) \partial_t G(\mathbf{x}, t|\mathbf{x}_1, t_1) + G(\mathbf{x}, t|\mathbf{x}_1, t_1) \partial_t \tilde{G}(\mathbf{x}, t|\mathbf{x}_2, t_2) \\ = \partial_t [\tilde{G}(\mathbf{x}, t|\mathbf{x}_2, t_2) G(\mathbf{x}, t|\mathbf{x}_1, t_1)], \end{aligned} \quad (4.132)$$

and adding the space derivatives leads to

$$\begin{aligned} -\tilde{G}(\mathbf{x}, t|\mathbf{x}_2, t_2) \nabla_{\mathbf{x}} \cdot [\mathbb{K} \cdot \nabla_{\mathbf{x}} G(\mathbf{x}, t|\mathbf{x}_1, t_1)] + G(\mathbf{x}, t|\mathbf{x}_1, t_1) \nabla_{\mathbf{x}} \cdot [\mathbb{K} \cdot \nabla_{\mathbf{x}} \tilde{G}(\mathbf{x}, t|\mathbf{x}_2, t_2)] \\ = \nabla_{\mathbf{x}} \cdot [-\tilde{G}(\mathbf{x}, t|\mathbf{x}_2, t_2) \mathbb{K} \cdot \nabla_{\mathbf{x}} G(\mathbf{x}, t|\mathbf{x}_1, t_1) + G(\mathbf{x}, t|\mathbf{x}_1, t_1) \mathbb{K} \cdot \nabla_{\mathbf{x}} \tilde{G}(\mathbf{x}, t|\mathbf{x}_2, t_2)]. \end{aligned} \quad (4.133)$$

Integrating over the full spatial domain and using the homogeneous Neumann or Dirichlet boundary conditions removes the space derivative terms, thus leaving

$$\begin{aligned} \int_{\mathcal{R}} \partial_t [\tilde{G}(\mathbf{x}, t|\mathbf{x}_2, t_2) G(\mathbf{x}, t|\mathbf{x}_1, t_1)] dV \\ = \tilde{G}(\mathbf{x}_1, t|\mathbf{x}_2, t_2) \delta(t - t_1) - G(\mathbf{x}_2, t|\mathbf{x}_1, t_1) \delta(t - t_2). \end{aligned} \quad (4.134)$$

Time integration and use of causality

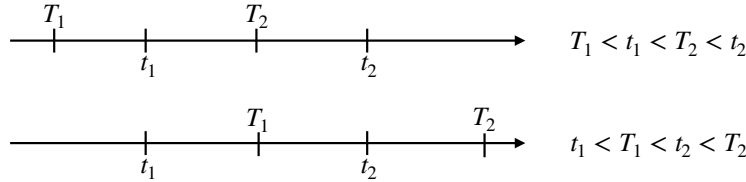


FIGURE 4.4: Two possible placements of the time steps used to derive the Green's function composition property.

Now integrate equation (4.134) over time, assuming the spatial domain is time independent as done for the reciprocity derivation, in which case

$$\begin{aligned} \int_{\mathcal{R}} [\tilde{G}(\mathbf{x}, T_2|\mathbf{x}_2, t_2) G(\mathbf{x}, T_2|\mathbf{x}_1, t_1) - \tilde{G}(\mathbf{x}, T_1|\mathbf{x}_2, t_2) G(\mathbf{x}, T_1|\mathbf{x}_1, t_1)] dV \\ = \int_{T_1}^{T_2} [\tilde{G}(\mathbf{x}_1, t|\mathbf{x}_2, t_2) \delta(t - t_1) - G(\mathbf{x}_2, t|\mathbf{x}_1, t_1) \delta(t - t_2)] dt, \end{aligned} \quad (4.135)$$

where $T_1 < T_2$ are time endpoints for the time integration. The causality conditions (4.117c) and (4.119c) lead to the following identities, depending on the placements of T_1, T_2 relative to t_1, t_2 as shown in Figure 4.4

$$\tilde{G}(\mathbf{x}_1, t_1|\mathbf{x}_2, t_2) = \int_{\mathcal{R}} \tilde{G}(\mathbf{x}, T_2|\mathbf{x}_2, t_2) G(\mathbf{x}, T_2|\mathbf{x}_1, t_1) dV \quad \text{if } T_1 < t_1 < T_2 < t_2 \quad (4.136a)$$

$$G(\mathbf{x}_2, t_2|\mathbf{x}_1, t_1) = \int_{\mathcal{R}} \tilde{G}(\mathbf{x}, T_1|\mathbf{x}_2, t_2) G(\mathbf{x}, T_1|\mathbf{x}_1, t_1) dV \quad \text{if } t_1 < T_1 < t_2 < T_2. \quad (4.136b)$$

¹²Recall that in Section 4.8.4 we subtracted the two equations to derive the reciprocity relation.

Use of the reciprocity relation (4.129) then leads to the composition relations

$$G(\mathbf{x}_2, t_2 | \mathbf{x}_1, t_1) = \int_{\mathcal{R}} G(\mathbf{x}_2, t_2 | \mathbf{x}, T_2) G(\mathbf{x}, T_2 | \mathbf{x}_1, t_1) dV \quad \text{if } T_1 < t_1 < T_2 < t_2 \quad (4.137a)$$

$$G(\mathbf{x}_2, t_2 | \mathbf{x}_1, t_1) = \int_{\mathcal{R}} G(\mathbf{x}_2, t_2 | \mathbf{x}, T_1) G(\mathbf{x}, T_1 | \mathbf{x}_1, t_1) dV \quad \text{if } t_1 < T_1 < t_2 < T_2. \quad (4.137b)$$

These equations are identical since both include an arbitrary intermediate time that is bounded by $t_1 < t_2$, thus allowing us to write the generic composition relation

$$G(\mathbf{x}_2, t_2 | \mathbf{x}_1, t_1) = \int_{\mathcal{R}} G(\mathbf{x}_2, t_2 | \mathbf{x}, \tau) G(\mathbf{x}, \tau | \mathbf{x}_1, t_1) dV \quad \text{if } t_1 < \tau < t_2 \quad (4.138)$$

Interpreting the Green's function composition property

The left hand side of the Green's function composition property (4.138) is the response from a Dirac source diffused from (\mathbf{x}_1, t_1) and measured at the field space-time point (\mathbf{x}_2, t_2) . The right hand side says that this response is identical to the composition of a Green's function feeling the source at (\mathbf{x}_1, t_1) but now sampled at an intermediate space-time position, (\mathbf{x}, τ) , and then further diffused to (\mathbf{x}_2, t_2) , with integration over all possible intermediate positions \mathbf{x} . Furthermore, note that the intermediate sampling can occur at an arbitrary intermediate time, τ , so long as $t_1 < \tau < t_2$. The composition property allows us to conceive of a long-time interval Green's function as the composition of an arbitrary number of shorter time interval Green's functions.

4.8.6 Integral solution

Having established reciprocity (4.129), we are now ready to derive an integral expression for the field, $\psi(\mathbf{x}, t)$, satisfying the diffusion equation initial-boundary value problem with either the Neumann boundary conditions

$$\frac{\partial \psi(\mathbf{x}, t)}{\partial t} - \nabla \cdot [\mathbb{K} \cdot \nabla_{\mathbf{x}} \psi(\mathbf{x}, t)] = \Lambda(\mathbf{x}, t) \quad \mathbf{x} \in \mathcal{R} \quad (4.139a)$$

$$\hat{\mathbf{n}} \cdot \mathbb{K} \cdot \nabla_{\mathbf{x}} \psi(\mathbf{x}, t) = \Sigma(\mathbf{x}, t) \quad \mathbf{x} \in \partial \mathcal{R} \quad (4.139b)$$

$$\psi(\mathbf{x}, t = t_{\text{init}}) = I(\mathbf{x}) \quad \mathbf{x} \in \mathcal{R}, \quad (4.139c)$$

or Dirichlet boundary conditions

$$\frac{\partial \psi(\mathbf{x}, t)}{\partial t} - \nabla \cdot [\mathbb{K} \cdot \nabla_{\mathbf{x}} \psi(\mathbf{x}, t)] = \Lambda(\mathbf{x}, t) \quad \mathbf{x} \in \mathcal{R} \quad (4.140a)$$

$$\psi(\mathbf{x}, t) = \sigma(\mathbf{x}, t) \quad \mathbf{x} \in \partial \mathcal{R} \quad (4.140b)$$

$$\psi(\mathbf{x}, t = t_{\text{init}}) = I(\mathbf{x}) \quad \mathbf{x} \in \mathcal{R}. \quad (4.140c)$$

In these equations we introduced the initial time, $t = t_{\text{init}}$, which is distinct from the Dirac delta source time, $t = t_0$. Correspondingly, the Dirac delta source is fired *after* the initial time,

$$t_{\text{init}} < t_0, \quad (4.141)$$

which follows since we are interested in the evolution of ψ after specification of the initial data, $\psi(\mathbf{x}, t = t_{\text{init}}) = I(\mathbf{x})$. Correspondingly, t_{init} defines the lower limit on time integrals in the following. Use of the $\nabla_{\mathbf{x}}$ notation is not needed for these equations, since there is no source point, \mathbf{x}_0 , in any of the expressions. However, writing $\nabla_{\mathbf{x}}$ helps us remain organized during the following

manipulations. Finally, note that the diffusion tensor appearing in these equations means that the source function, $\Lambda(\mathbf{x}, t)$, in equations (4.139a) and (4.140a), as well as the boundary data, $\Sigma(\mathbf{x}, t)$, in equation (4.139b), have different dimensions from their counterparts found in the Poisson boundary value problems (4.65) and (4.99).

The following derivation emulates that for the Poisson equation in Section 4.6.5, yet with distinct features arising from time evolution and the corresponding need to use the adjoint causal Green's function, \tilde{G} . We expose many details as doing so reveals general notions and tricks arising with Green's function methods for initial-boundary value problems.

Setting up the derivation

To start the derivation, multiply the diffusion equation (4.139a) by the adjoint Green's function, $\tilde{G}(\mathbf{x}, t|\mathbf{x}_0, t_0)$, and the adjoint Green's function equation (4.119a) by $\psi(\mathbf{x}, t)$. Subtracting and rearranging leads to

$$\partial_t[\tilde{G}\psi] + \nabla \cdot [\psi \mathbb{K} \cdot \nabla_{\mathbf{x}}\tilde{G} - \tilde{G} \mathbb{K} \cdot \nabla\psi] = \tilde{G}(\mathbf{x}, t|\mathbf{x}_0, t_0)\Lambda(\mathbf{x}, t) - \psi(\mathbf{x}, t)\delta(\mathbf{x} - \mathbf{x}_0)\delta(t - t_0), \quad (4.142)$$

where we temporarily suppressed arguments on the left hand side for brevity. Since the spatial domain is assumed to be static, we can integrate this equation over space and time without concern for the order of integration.

Time integration

A time integral of the first left hand side term in equation (4.142) leads to

$$\int_{t_{\text{init}}}^T \partial_t[\tilde{G}(\mathbf{x}, t|\mathbf{x}_0, t_0)\psi(\mathbf{x}, t)] dt = \tilde{G}(\mathbf{x}, T|\mathbf{x}_0, t_0)\psi(\mathbf{x}, T) - \tilde{G}(\mathbf{x}, t_{\text{init}}|\mathbf{x}_0, t_0)\psi(\mathbf{x}, t_{\text{init}}) \quad (4.143a)$$

$$= -\tilde{G}(\mathbf{x}, t_{\text{init}}|\mathbf{x}_0, t_0)I(\mathbf{x}), \quad (4.143b)$$

where we made use of the backward causal condition (4.119c) satisfied by the adjoint Green's function to set $\tilde{G}(\mathbf{x}, t = T|\mathbf{x}_0, t_0) = 0$, and used the initial condition (4.139c) to introduce the initial value data, $\psi(\mathbf{x}, t_{\text{init}}) = I(\mathbf{x})$.

Space integration

A space integral over all observation points, and use of the divergence theorem, brings the divergence term on the left side of equation (4.142) into

$$\begin{aligned} & \int_{\mathcal{R}} \nabla \cdot [\psi \mathbb{K} \cdot \nabla_{\mathbf{x}}\tilde{G} - \tilde{G} \mathbb{K} \cdot \nabla_{\mathbf{x}}\psi] dV \\ &= \oint_{\partial\mathcal{R}} [\psi(\mathbf{x}, t) \mathbb{K} \cdot \nabla_{\mathbf{x}}\tilde{G}(\mathbf{x}, t|\mathbf{x}_0, t_0) - \tilde{G}(\mathbf{x}, t|\mathbf{x}_0, t_0) \mathbb{K} \cdot \nabla_{\mathbf{x}}\psi] \cdot \hat{\mathbf{n}} d\mathcal{S}, \end{aligned} \quad (4.144)$$

where we kept both boundary terms pending specification of whether the fields satisfy Dirichlet or Neumann conditions. This boundary integral has the same appearance as found for the Poisson equation in Section 4.6.5, with the added feature here of the diffusion tensor.

Integrating the right hand side of equation (4.142)

A space and time integral for the right hand side of equation (4.142), along with the sifting properties of the Dirac delta, render

$$\begin{aligned} \int_{t_{\text{init}}}^T \left[\int_{\mathcal{R}} [\tilde{G}(\mathbf{x}, t | \mathbf{x}_0, t_0) \Lambda(\mathbf{x}, t) - \psi(\mathbf{x}, t) \delta(\mathbf{x} - \mathbf{x}_0) \delta(t - t_0)] dV \right] dt \\ = -\psi(\mathbf{x}_0, t_0) + \int_{t_{\text{init}}}^T \left[\int_{\mathcal{R}} \tilde{G}(\mathbf{x}, t | \mathbf{x}_0, t_0) \Lambda(\mathbf{x}, t) dV \right] dt. \end{aligned} \quad (4.145)$$

Notice how this integration over the observation space-time points, (\mathbf{x}, t) , serves to pick out the field, ψ , evaluated at the space-time point, (\mathbf{x}_0, t_0) , where the Dirac delta source is located.

Rearrangement and use of reciprocity

Bringing the above results together leads to the expression

$$\begin{aligned} \psi(\mathbf{x}_0, t_0) &= \int_{\mathcal{R}} \tilde{G}(\mathbf{x}, t_{\text{init}} | \mathbf{x}_0, t_0) I(\mathbf{x}) dV + \int_{t_{\text{init}}}^{t_0} \left[\int_{\mathcal{R}} \tilde{G}(\mathbf{x}, t | \mathbf{x}_0, t_0) \Lambda(\mathbf{x}, t) dV \right] dt \\ &+ \int_{t_{\text{init}}}^{t_0} \left[\oint_{\partial\mathcal{R}} [\tilde{G}(\mathbf{x}, t | \mathbf{x}_0, t_0) \mathbb{K} \cdot \nabla_{\mathbf{x}} \psi(\mathbf{x}, t) - \psi(\mathbf{x}, t) \mathbb{K} \cdot \nabla_{\mathbf{x}} \tilde{G}(\mathbf{x}, t | \mathbf{x}_0, t_0)] \cdot \hat{\mathbf{n}} d\mathcal{S} \right] dt. \end{aligned} \quad (4.146)$$

The time integrals are restricted to the range $t \in [t_{\text{init}}, t_0]$ through use of the causality condition (4.119c) for the adjoint Green's function. Hence, the arbitrary time, T , drops out from the solution and there is no dependence on fields at times later than t_0 nor before t_{init} .

Use of reciprocity (4.129) allows us to replace the adjoint Green's function with the Green's function to thus bring equation (4.146) to

$$\begin{aligned} \psi(\mathbf{x}_0, t_0) &= \int_{\mathcal{R}} G(\mathbf{x}_0, t_0 | \mathbf{x}, t_{\text{init}}) I(\mathbf{x}) dV + \int_{t_{\text{init}}}^{t_0} \left[\int_{\mathcal{R}} G(\mathbf{x}_0, t_0 | \mathbf{x}, t) \Lambda(\mathbf{x}, t) dV \right] dt \\ &+ \int_{t_{\text{init}}}^{t_0} \left[\oint_{\partial\mathcal{R}} [G(\mathbf{x}_0, t_0 | \mathbf{x}, t) \mathbb{K} \cdot \nabla_{\mathbf{x}} \psi(\mathbf{x}, t) - \psi(\mathbf{x}, t) \mathbb{K} \cdot \nabla_{\mathbf{x}} G(\mathbf{x}_0, t_0 | \mathbf{x}, t)] \cdot \hat{\mathbf{n}} d\mathcal{S} \right] dt. \end{aligned} \quad (4.147)$$

Finally, it is convenient to relabel $(\mathbf{x}_0, t_0) \leftrightarrow (\mathbf{x}, t)$ to write

$$\begin{aligned} \psi(\mathbf{x}, t) &= \underbrace{\int_{\mathcal{R}} G(\mathbf{x}, t | \mathbf{x}_0, t_{\text{init}}) I(\mathbf{x}_0) dV_0}_{\text{space integral of } G \text{ times } I \text{ on } \mathcal{R}} + \underbrace{\int_{t_{\text{init}}}^t \left[\int_{\mathcal{R}} G(\mathbf{x}, t | \mathbf{x}_0, t_0) \Lambda(\mathbf{x}_0, t_0) dV_0 \right] dt_0}_{\text{space-time integral of } G \text{ times } \Lambda \text{ over } \mathcal{R}} \\ &+ \underbrace{\int_{t_{\text{init}}}^t \left[\oint_{\partial\mathcal{R}} [G(\mathbf{x}, t | \mathbf{x}_0, t_0) \mathbb{K} \cdot \nabla_{\mathbf{x}_0} \psi(\mathbf{x}_0, t_0) - \psi(\mathbf{x}_0, t_0) \mathbb{K} \cdot \nabla_{\mathbf{x}_0} G(\mathbf{x}, t | \mathbf{x}_0, t_0)] \cdot \hat{\mathbf{n}}_{\mathbf{x}_0} d\mathcal{S}_0] dt_0}_{\text{space-time integral of boundary terms over } \partial\mathcal{R}}. \end{aligned} \quad (4.148)$$

Specializing to Neumann boundary conditions leads to

$$\begin{aligned} \psi^{\text{Neumann}}(\mathbf{x}, t) &= \int_{\mathcal{R}} G(\mathbf{x}, t | \mathbf{x}_0, t_{\text{init}}) I(\mathbf{x}_0) dV_0 + \int_{t_{\text{init}}}^t \left[\int_{\mathcal{R}} G(\mathbf{x}, t | \mathbf{x}_0, t_0) \Lambda(\mathbf{x}_0, t_0) dV_0 \right] dt_0 \\ &+ \int_{t_{\text{init}}}^t \left[\oint_{\partial\mathcal{R}} G(\mathbf{x}, t | \mathbf{x}_0, t_0) \Sigma(\mathbf{x}_0, t_0) d\mathcal{S}_0 \right] dt_0, \end{aligned} \quad (4.149)$$

whereas the solution with Dirichlet boundary conditions is

$$\begin{aligned}\psi^{\text{Dirichlet}}(\mathbf{x}, t) = & \int_{\mathcal{R}} G(\mathbf{x}, t | \mathbf{x}_0, t_{\text{init}}) I(\mathbf{x}_0) dV_0 + \int_{t_{\text{init}}}^t \left[\int_{\mathcal{R}} G(\mathbf{x}, t | \mathbf{x}_0, t_0) \Lambda(\mathbf{x}_0, t_0) dV_0 \right] dt_0 \\ & - \int_{t_{\text{init}}}^t \left[\oint_{\partial\mathcal{R}} \sigma(\mathbf{x}_0, t_0) \mathbb{K}(\mathbf{x}_0, t_0) \cdot \nabla_{\mathbf{x}_0} G(\mathbf{x}, t | \mathbf{x}_0, t_0) \cdot \hat{\mathbf{n}}_{\mathbf{x}_0} dS_0 \right] dt_0.\end{aligned}\quad (4.150)$$

4.8.7 Properties of the solution

Many of the properties of the solution (4.148) are also reflected in the Poisson equation solutions from Sections 4.6.6 and 4.7.4. In particular, the solution manifests the linear superposition principle, with the solution given by the sum of three terms arising from the initial conditions, distributed volume source, and spatial boundary conditions. We expect to have this connection given that the steady state diffusion equation satisfies a generalized Poisson equation (generalized by the presence of a diffusion tensor). A fundamentally new piece of physics and maths arises from time dependence. In this section we exhibit properties of the Green's function as inferred (through insisting on self-consistency) by the initial and boundary conditions.

Uniqueness of the solution

Uniqueness of a solution to the diffusion boundary value problem follows as in the discussion of the Poisson equation in Sections 4.6.2 and 4.7.2. Namely, consider two solutions to the diffusion equation and take their difference, $\Psi = \psi_A - \psi_B$. We readily see that Ψ satisfies the homogeneous diffusion equation with homogeneous boundary conditions along with a zero initial condition. Ψ thus remains zero for both the Dirichlet and Neumann cases, thus proving that the solution to both problems is unique.

Initial conditions

By sampling the solution (4.148) as time decreases towards the initial time, $t \rightarrow t_{\text{init}}$, and noting the initial condition $\psi(\mathbf{x}, t_{\text{init}}) = I(\mathbf{x})$, we are led to¹³

$$\lim_{t \rightarrow t_{\text{init}}} \psi(\mathbf{x}, t) = I(\mathbf{x}) = \lim_{t \rightarrow t_{\text{init}}} \int_{\mathcal{R}} G(\mathbf{x}, t | \mathbf{x}_0, t_{\text{init}}) I(\mathbf{x}_0) dV_0.\quad (4.151)$$

This temporal sampling of the field time is distinguished from the source time, t_0 , which here is fixed at the initial time, $t_0 = t_{\text{init}}$. Self-consistency in equation (4.151) implies that the Green's function for both Neumann and Dirichlet boundary conditions satisfies the initial condition

$$\lim_{t \rightarrow t_{\text{init}}} G(\mathbf{x}, t | \mathbf{x}_0, t_{\text{init}}) = \delta(\mathbf{x} - \mathbf{x}_0) \quad \text{with } \mathbf{x}, \mathbf{x}_0 \in \mathcal{R}.\quad (4.152)$$

That is, the Green's function is initialized by a Dirac delta pulse at the source point, \mathbf{x}_0 , which then leads to

$$\lim_{t \rightarrow t_{\text{init}}} \int_{\mathcal{R}} G(\mathbf{x}, t | \mathbf{x}_0, t_{\text{init}}) I(\mathbf{x}_0) dV_0 = \int_{\mathcal{R}} \delta(\mathbf{x} - \mathbf{x}_0) I(\mathbf{x}_0) dV_0 = I(\mathbf{x}).\quad (4.153)$$

¹³Since t_{init} is the initial time, the limit $t \rightarrow t_{\text{init}}$ is taken from above so that $t = t_{\text{init}} + \epsilon$ with $\epsilon \rightarrow 0$.

Neumann boundary conditions

Acting with $\mathbb{K}(\mathbf{x}, t) \cdot \nabla_{\mathbf{x}}$ on the Neumann solution (4.149); evaluating the expression on the boundary $\mathbf{x} = \mathbf{x}_{\partial\mathcal{R}} \in \partial\mathcal{R}$; and then projecting onto the outward unit normal, $\hat{\mathbf{n}}_{\mathbf{x}}$, serves to annihilate the volume integrals as per the homogeneous Neumann conditions satisfied by the Green's function. We are thus left with

$$\hat{\mathbf{n}}_{\mathbf{x}} \cdot \mathbb{K}(\mathbf{x}, t) \cdot \nabla_{\mathbf{x}} \psi(\mathbf{x}, t) = \Sigma(\mathbf{x}, t) = \int_{t_{\text{init}}}^t \left[\oint_{\partial\mathcal{R}} \hat{\mathbf{n}}_{\mathbf{x}} \cdot \mathbb{K}(\mathbf{x}, t) \cdot \nabla_{\mathbf{x}} G(\mathbf{x}, t | \mathbf{x}_0, t_0) \Sigma(\mathbf{x}_0, t_0) d\mathcal{S}_0 \right] dt_0. \quad (4.154)$$

Self-consistency implies that the Green's function for the Neumann problem, when evaluated on the spatial boundary, satisfies

$$\hat{\mathbf{n}}_{\mathbf{x}} \cdot \mathbb{K}(\mathbf{x}, t) \cdot \nabla_{\mathbf{x}} G(\mathbf{x}, t | \mathbf{x}_0, t_0) = \delta(t - t_0) \delta^{(2)}(\mathbf{x} - \mathbf{x}_0) \quad \text{with } \mathbf{x}, \mathbf{x}_0 \in \partial\mathcal{R}, \quad (4.155)$$

which is a generalization of the property (4.113) holding for the Poisson equation Green's function.

Transforming the Neumann boundary data to the interior

In Section 4.7.4, we saw how to transform the Neumann boundary condition into the interior by modifying the source function. The diffusion equation Neumann solution (4.149) allows for the same transformation by writing

$$\psi^{\text{Neumann}}(\mathbf{x}, t) = \int_{\mathcal{R}} G(\mathbf{x}, t | \mathbf{x}_0, t_{\text{init}}) I(\mathbf{x}_0) dV_0 + \int_{t_{\text{init}}}^t \left[\int_{\mathcal{R}} G(\mathbf{x}, t | \mathbf{x}_0, t_0) \Lambda^*(\mathbf{x}_0, t_0) dV_0 \right] dt_0, \quad (4.156)$$

where the modified source function follows from that used for the Poisson equation (4.108)

$$\Lambda^*(\mathbf{x}_0, t_0) = \Lambda(\mathbf{x}_0, t_0) + \Sigma(\mathbf{x}_0, t_0) \delta[\hat{\mathbf{n}} \cdot (\mathbf{x}_0 - \mathbf{x}_{\partial\mathcal{R}})]. \quad (4.157)$$

Dirichlet boundary conditions

Evaluating the Dirichlet solution (4.150) on a spatial boundary, $\mathbf{x} = \mathbf{x}_{\partial\mathcal{R}} \in \partial\mathcal{R}$, eliminates both of the volume integrals so that we are left with

$$\psi^{\text{dirichlet}}(\mathbf{x}_{\partial\mathcal{R}}, t) = \sigma(\mathbf{x}_{\partial\mathcal{R}}, t) = - \int_{t_{\text{init}}}^t \left[\oint_{\partial\mathcal{R}} \sigma(\mathbf{x}_0, t_0) \mathbb{K} \cdot \nabla_{\mathbf{x}_0} G(\mathbf{x}, t | \mathbf{x}_0, t_0) \cdot \hat{\mathbf{n}}_{\mathbf{x}_0} d\mathcal{S}_0 \right] dt_0. \quad (4.158)$$

Self-consistency implies that the Green's function for the Dirichlet problem, when evaluated on the spatial boundary, satisfies

$$\hat{\mathbf{n}}_{\mathbf{x}_0} \cdot \mathbb{K}(\mathbf{x}_0, t_0) \cdot \nabla_{\mathbf{x}_0} G(\mathbf{x}, t | \mathbf{x}_0, t_0) = -\delta(t - t_0) \delta^{(2)}(\mathbf{x} - \mathbf{x}_0) \quad \text{with } \mathbf{x}, \mathbf{x}_0 \in \partial\mathcal{R}, \quad (4.159)$$

which is a generalization of the property (4.95) holding for the Poisson equation Green's function.

4.8.8 Boundary propagator

In Sections 4.6.6 and 4.6.7 we studied the boundary Green's function for the Poisson equation. Here we extend those ideas to the *boundary propagator* for the diffusion equation, with the boundary propagator mediating the transfer of Dirichlet boundary information into the interior. Boundary propagators for diffusion and advection-diffusion (Section 61.10) have extensive use in geophysical fluids given that many tracers have no interior sources.

Defining the boundary propagator

To focus on the role of the boundary propagator, consider a tracer in which the initial conditions and interior source both vanish: $I(\mathbf{x}) = 0$ and $\Lambda(\mathbf{x}, t) = 0$. Assuming Dirichlet boundary conditions, the initial-boundary value problem (4.139a)-(4.139c) simplifies to

$$\frac{\partial \psi(\mathbf{x}, t)}{\partial t} - \nabla_{\mathbf{x}} \cdot [\mathbb{K} \cdot \nabla_{\mathbf{x}} \psi(\mathbf{x}, t)] = 0 \quad \mathbf{x} \in \mathcal{R} \quad (4.160a)$$

$$\psi(\mathbf{x}, t) = \sigma(\mathbf{x}, t) \quad \mathbf{x} \in \partial\mathcal{R} \quad (4.160b)$$

$$\psi(\mathbf{x}, t = t_{\text{init}}) = 0 \quad \mathbf{x} \in \mathcal{R}, \quad (4.160c)$$

with the corresponding Dirichlet Green's function solution (4.150) taking the form

$$\psi(\mathbf{x}, t) = - \int_{t_{\text{init}}}^t \left[\oint_{\partial\mathcal{R}} \sigma(\mathbf{x}_0, t_0) \mathbb{K}(\mathbf{x}_0, t_0) \cdot \nabla_{\mathbf{x}_0} G(\mathbf{x}, t | \mathbf{x}_0, t_0) \cdot \hat{\mathbf{n}}_{\mathbf{x}_0} d\mathcal{S}_0 \right] dt_0. \quad (4.161)$$

We define the *boundary propagator* as the kernel in this equation

$$G^{\text{bp}}(\mathbf{x}, t | \mathbf{x}_0, t_0) \equiv -\mathbb{K}(\mathbf{x}_0, t_0) \cdot \nabla_{\mathbf{x}_0} G(\mathbf{x}, t | \mathbf{x}_0, t_0) \cdot \hat{\mathbf{n}}_{\mathbf{x}_0} \quad \text{with } \mathbf{x}_0 \in \partial\mathcal{R}, \quad (4.162)$$

with this definition giving G^{bp} the dimensions of $L^{-2} T^{-1}$. Use of the boundary propagator brings the solution (4.161) into the succinct form

$$\psi(\mathbf{x}, t) = \int_{t_{\text{init}}}^t \left[\oint_{\partial\mathcal{R}} \sigma(\mathbf{x}_0, t_0) G^{\text{bp}}(\mathbf{x}, t | \mathbf{x}_0, t_0) d\mathcal{S}_0 \right] dt_0. \quad (4.163)$$

Boundary value problem for the boundary propagator

If we know the Green's function, $G(\mathbf{x}, t | \mathbf{x}_0, t_0)$, then we can compute the boundary propagator through the definition (4.162). Alternatively, we can directly determine the boundary propagator by solving its boundary value problem. Following from the definition (4.162) and the boundary condition (4.159), we know that

$$G^{\text{bp}}(\mathbf{x}, t | \mathbf{x}_0, t_0) = \delta(t - t_0) \delta^{(2)}(\mathbf{x} - \mathbf{x}_0) \quad \text{with } \mathbf{x}, \mathbf{x}_0 \in \partial\mathcal{R}. \quad (4.164)$$

Hence, the boundary propagator, when evaluated along the boundary, is a Dirac delta source that fires at time $t = t_0$ at the location $\mathbf{x} = \mathbf{x}_0 \in \partial\mathcal{R}$. To determine the partial differential equation satisfied by the boundary propagator, make use of the solution (4.163) and compute its time derivative

$$\frac{\partial \psi(\mathbf{x}, t)}{\partial t} = \oint_{\partial\mathcal{R}} \sigma(\mathbf{x}_0, t) G^{\text{bp}}(\mathbf{x}, t | \mathbf{x}_0, t) d\mathcal{S}_0 + \int_{t_{\text{init}}}^t \left[\oint_{\partial\mathcal{R}} \sigma(\mathbf{x}_0, t_0) \frac{\partial G^{\text{bp}}(\mathbf{x}, t | \mathbf{x}_0, t_0)}{\partial t} d\mathcal{S}_0 \right] dt_0. \quad (4.165)$$

The first right hand side term vanishes since the boundary propagator satisfies causality just like the Green's function when sampled at interior points

$$G^{\text{bp}}(\mathbf{x}, t | \mathbf{x}_0, t_0) = 0 \quad \text{if } t \leq t_0 \text{ and } \mathbf{x} \notin \partial\mathcal{R}. \quad (4.166)$$

We are thus left with

$$\begin{aligned} \frac{\partial\psi(\mathbf{x},t)}{\partial t} - \nabla_{\mathbf{x}} \cdot (\mathbb{K} \cdot \nabla_{\mathbf{x}}\psi) \\ = \int_{t_{\text{init}}}^t \left[\oint_{\partial\mathcal{R}} \sigma(\mathbf{x}_0, t_0) \left[\frac{\partial G^{\text{bp}}(\mathbf{x}, t|\mathbf{x}_0, t_0)}{\partial t} - \nabla_{\mathbf{x}} \cdot [\mathbb{K} \cdot \nabla_{\mathbf{x}} G^{\text{bp}}(\mathbf{x}, t|\mathbf{x}_0, t_0)] \right] dS_0 \right] dt_0. \end{aligned} \quad (4.167)$$

Since the left hand side vanishes via the partial differential equation (4.160a), and since the boundary data, σ , is arbitrary, we are led to the causal boundary value problem for the boundary propagator

$$\frac{\partial G^{\text{bp}}(\mathbf{x}, t|\mathbf{x}_0, t_0)}{\partial t} - \nabla_{\mathbf{x}} \cdot [\mathbb{K} \cdot \nabla_{\mathbf{x}} G^{\text{bp}}(\mathbf{x}, t|\mathbf{x}_0, t_0)] = 0 \quad \mathbf{x} \in \mathcal{R} \quad (4.168a)$$

$$G^{\text{bp}}(\mathbf{x}, t|\mathbf{x}_0, t_0) = 0 \quad \mathbf{x} \notin \partial\mathcal{R}, t \leq t_0 \quad (4.168b)$$

$$G^{\text{bp}}(\mathbf{x}, t|\mathbf{x}_0, t_0) = \delta(t - t_0) \delta^{(2)}(\mathbf{x} - \mathbf{x}_0) \quad \mathbf{x}, \mathbf{x}_0 \in \partial\mathcal{R}. \quad (4.168c)$$

In words, we see that upon firing the Dirac delta source on the boundary at time $t = t_0$ and point $\mathbf{x} = \mathbf{x}_0 \in \partial\mathcal{R}$, the boundary propagator diffuses the Dirac source into the region interior. We thus see that whereas the Dirichlet Green's function, $G(\mathbf{x}, t|\mathbf{x}_0, t_0)$, is zero along the boundary and yet feels the Dirac delta sources within the interior, the boundary propagator, $G^{\text{bp}}(\mathbf{x}, t|\mathbf{x}_0, t_0)$, places the Dirac delta sources just on the boundary and feels no sources within the interior. Just as the causality condition means that the Green's function is a function of $t - t_0$, so too is the boundary propagator. Furthermore, a focus on the boundary propagator rather than the Green's function allows us to dispense with the need to compute the normal gradient of the Green's function at the boundary, with that calculation rather awkward in practice.

Normalization of the boundary propagator

Consider the special case of a uniform constant Dirichlet boundary data, $\sigma = \sigma_{\text{constant}}$ in the solution (4.163). Diffusion will act on this constant boundary value to spread it throughout the region. After sufficient time the solution will reach a steady state whereby $\psi = \sigma_{\text{constant}}$ at every point within the domain. This result means that the boundary Green's function satisfies the normalization condition

$$\lim_{t_{\text{init}} \rightarrow -\infty} \int_{t_{\text{init}}}^t \left[\oint_{\partial\mathcal{R}} G^{\text{bp}}(\mathbf{x}, t|\mathbf{x}_0, t_0) dS_0 \right] dt_0 = 1, \quad (4.169)$$

where the lower time limit is meant to indicate some arbitrary time sufficiently far in the past so that a steady state has been reached. Again, this normalization condition holds for every point within the domain and for any time. It corresponds to the normalization condition (4.98) satisfied by the boundary Green's function for the Poisson equation.

4.9 Initial value problems and response functions

In this section we focus on initial value problems and study the response functions that help to characterize a dynamical system. For this purpose, consider the first order ordinary differential equation

$$[d/dt + \lambda(t)] \psi(t) = F(t) \quad \text{with } \psi(t \leq t_{\text{init}}) = 0, \quad (4.170)$$

where ψ is some geophysical field, such as the anomalous sea surface temperature, λ is a feedback parameter that is positive for a damped system, and F is a forcing function such as that introduced by atmospheric variability on the surface ocean. We are only concerned with temporal behavior so that all spatial information is ignored. This equation has found widespread use in the climate dynamics community, largely following the work from [Hasselmann \(1976\)](#).

The material in this section could well have been used near the start of this chapter since it only involves ordinary differential equations. However, placing it at the end helps to tie together some of the material sprinkled throughout this chapter, and to connect to applications of Green's function technology for studies of climate dynamics.

4.9.1 Impulse response function

Consider the system (4.170) with $\lambda > 0$ a time-independent feedback parameter damping the system back to zero, and with the forcing given by a Dirac delta

$$[d/dt + \lambda] G(t|t_0) = \alpha \delta(t - t_0) \quad \text{with } G(t|t_0) = 0 \text{ for } t < t_0, \quad (4.171)$$

where $\alpha > 0$ is a constant dimensionless scaling coefficient. We refer to the resulting causal Green's function, $G(t|t_0)$, as the *impulse response function* since it represents the response of the dynamical system to an impulse provided by the Dirac delta.¹⁴

Initial condition for the impulse response function

To determine the initial condition for the Green's function, integrate equation (4.171) over an interval containing the source time, t_0 , to render

$$\lim_{\epsilon \rightarrow 0} \left[G(t_0 + \epsilon|t_0) - G(t_0 - \epsilon|t_0) + \int_{t_0 - \epsilon}^{t_0 + \epsilon} \lambda G(t|t_0) dt \right] = \alpha. \quad (4.172)$$

Causality means that $G(t_0 - \epsilon|t_0) = 0$ so that

$$\lim_{\epsilon \rightarrow 0} G(t_0 + \epsilon|t_0) + \lim_{\epsilon \rightarrow 0} \int_{t_0 - \epsilon}^{t_0 + \epsilon} \lambda G(t|t_0) dt = \alpha. \quad (4.173)$$

We assume that the integral vanishes in the limit of $\epsilon \rightarrow 0$, which is a sensible assumption since the only means to have a nonzero integral is if the Green's function had a singularity similar to a Dirac delta. We are thus led to the initial condition for the Green's function

$$G(t = t_0|t_0) = \alpha. \quad (4.174)$$

Solution for the impulse response function

The causality condition $G(t < t_0|t_0) = 0$ can be satisfied by introducing the Heaviside step function from Section 4.3.5

$$G(t|t_0) = \mathcal{H}(t - t_0) g(t) \quad \text{with} \quad [d/dt + \lambda] g = 0 \quad \text{and} \quad g(t = t_0) = \alpha, \quad (4.175)$$

with the solution readily determined to be the damped exponential

$$G(t|t_0) = \mathcal{H}(t - t_0) \alpha e^{-\lambda(t-t_0)}. \quad (4.176)$$

¹⁴Recall our discussion of impulse in Section 4.3.7.

We verify this function satisfies the initial value problem (4.171) by noting that

$$\frac{dG(t|t_0)}{dt} = \alpha \delta(t - t_0) e^{-\lambda(t-t_0)} - \lambda G(t|t_0) = \alpha \delta(t - t_0) - \lambda G(t|t_0) \quad (4.177)$$

as per the discussion leading to equation (4.15). As illustrated in Figure 4.5, the impulse response function (4.176) has a particularly simple interpretation as the damped exponential response of the dynamical system to a Dirac impulse fired at $t = t_0$.

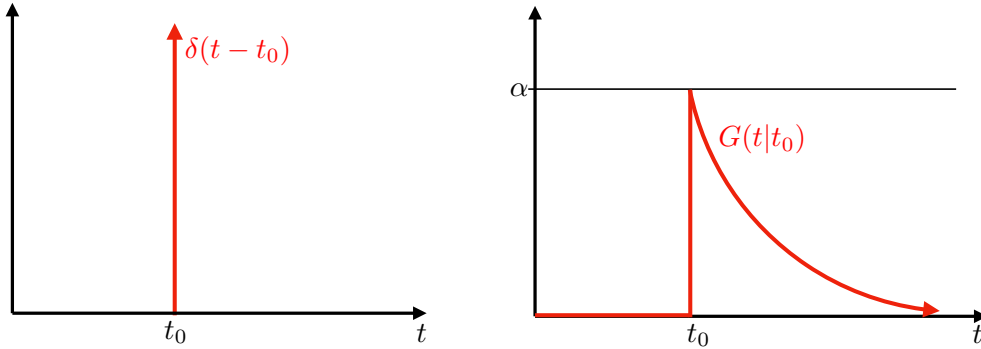


FIGURE 4.5: Left panel: Dirac delta that is fired at time $t = t_0$. Right panel: The impulse response function (4.176) resulting from the Dirac delta impulse as realized for the damped linear system (4.171).

4.9.2 Step response function

Rather than hit the system at a particular moment in time with a Dirac delta, we may choose to impose a force that turns on and remains on after some initial time, as per a Heaviside step function. The *step response function*, $S(t|t_0)$, measures the response of the dynamical system to this step forcing and it satisfies the differential equation

$$[d/dt + \lambda] S(t|t_0) = \alpha \mathcal{H}(t - t_0) \quad \text{with } S(t|t_0) = 0 \text{ for } t < t_0. \quad (4.178)$$

Note that in the steady state at $t \rightarrow \infty$, the step response function asymptotes to the constant

$$\lim_{t \rightarrow \infty} S(t|t_0) = \alpha/\lambda. \quad (4.179)$$

Connection to the impulse response function

The time derivative d/dt_0 acting on the step response function equation (4.178) leads to

$$[d/dt + \lambda] dS(t|t_0)/dt_0 = \alpha d\mathcal{H}(t - t_0)/dt_0. \quad (4.180)$$

The derivative of the Heaviside step function equals to the Dirac delta as per equation (4.19), in which

$$d\mathcal{H}(t - t_0)/dt_0 = -d\mathcal{H}(t - t_0)/dt = -\delta(t - t_0). \quad (4.181)$$

Use of this result in equation (4.180), and comparison to the impulse response function equation (4.171), yields the identity

$$\frac{dS(t|t_0)}{dt_0} = -G(t|t_0). \quad (4.182)$$

This identity holds even when the feedback parameter is a function of time, $\lambda = \lambda(t)$, since the time derivative operator, d/dt_0 , has no effect on $\lambda(t)$.

Initial condition for the step response function

To determine the initial condition for the step response function, integrate equation (4.178) over an interval bounding t_0 and take the limit as that interval vanishes

$$\lim_{\epsilon \rightarrow 0} \left[S(t_0 + \epsilon|t_0) - S(t_0 - \epsilon|t_0) + \int_{t_0 - \epsilon}^{t_0 + \epsilon} \lambda S(t|t_0) dt \right] = \int_{t_0 - \epsilon}^{t_0 + \epsilon} \mathcal{H}(t - t_0) dt. \quad (4.183)$$

Causality means that $S(t_0 - \epsilon|t_0) = 0$. Furthermore, the integral of the Heaviside is given by

$$\lim_{\epsilon \rightarrow 0} \int_{t_0 - \epsilon}^{t_0 + \epsilon} \mathcal{H}(t - t_0) dt = \lim_{\epsilon \rightarrow 0} \int_{t_0}^{t_0 + \epsilon} \mathcal{H}(t - t_0) dt = \lim_{\epsilon \rightarrow 0} \epsilon = 0, \quad (4.184)$$

so that

$$\lim_{\epsilon \rightarrow 0} S(t_0 + \epsilon|t_0) = \epsilon \lambda \implies S(t = t_0|t_0) = 0. \quad (4.185)$$

That is, the step response function starts at zero and then grows in time in response to the Heaviside step function forcing.

Solution for the step response function

It is straightforward to show that the causal step response function is given by the saturating exponential

$$S(t|t_0) = \frac{\alpha}{\lambda} \left[1 - e^{-\lambda(t-t_0)} \right] \mathcal{H}(t - t_0). \quad (4.186)$$

Figure 4.6 depicts this function along with the Heaviside step forcing. Furthermore, we verify the connection between $S(t|t_0)$ and $G(t|t_0)$ by computing

$$dS(t|t_0)/dt_0 = -\alpha \mathcal{H}(t - t_0) e^{-\lambda(t-t_0)} - \frac{\alpha}{\lambda} \left[1 - e^{-\lambda(t-t_0)} \right] \delta(t - t_0) \quad (4.187a)$$

$$= -G(t|t_0) - \frac{\alpha}{\lambda} \left[1 - e^{-\lambda(t-t_0)} \right] \delta(t - t_0). \quad (4.187b)$$

The second term on the right hand side vanishes since

$$\int_{t_0 - \epsilon}^{t_0 + \epsilon} \left[1 - e^{-\lambda(t-t_0)} \right] \delta(t - t_0) dt = 0, \quad (4.188)$$

in which case we have

$$dS(t|t_0)/dt_0 = -G(t|t_0). \quad (4.189)$$

4.9.3 Reciprocity relation

The initial value problem (4.170) is not self-adjoint. Hence, we need to develop a reciprocity condition for the impulse response function and its adjoint, following the procedure used for the diffusion equation in Section 4.8.4. Again, the impulse response function satisfies

$$[d/dt + \lambda] G(t|t_1) = \alpha \delta(t - t_1) \quad \text{with } G(t|t_1) = 0 \text{ for } t < t_1 \text{ and } G(t_1|t_1) = \alpha, \quad (4.190)$$

and the adjoint impulse response function satisfies

$$[-d/dt + \lambda] \tilde{G}(t|t_2) = \alpha \delta(t - t_2) \quad \text{with } \tilde{G}(t|t_2) = 0 \text{ for } t > t_2 \text{ and } \tilde{G}(t_2|t_2) = \alpha. \quad (4.191)$$

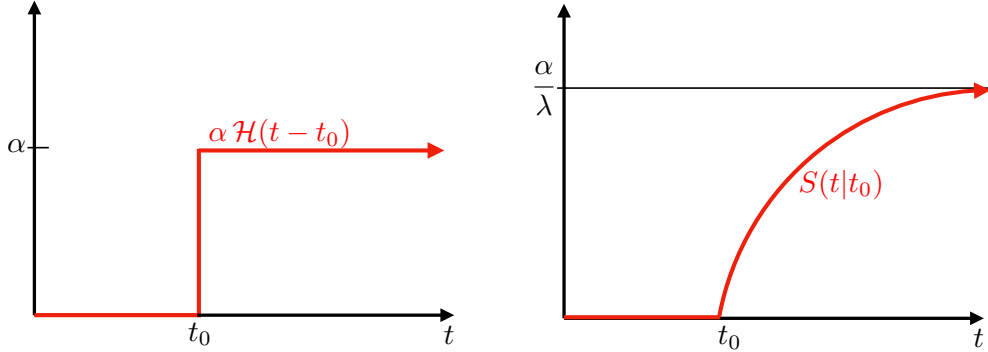


FIGURE 4.6: Left panel: Heaviside step function is fired at time $t = t_0$ and stays on afterward. Right panel: The step response function (4.186) resulting from the Heaviside step forcing impulse as realized for the damped linear system (4.171).

We here introduced two Dirac delta source times, t_1, t_2 , which both occur after the initial time and before the end time

$$t_{\text{init}} < t_1, t_2 < T. \quad (4.192)$$

As we will see, causality eliminates the final time, T , from the solution for ψ . We retain it merely for bookkeeping.

Determining the reciprocity relation between \tilde{G} and G follows by multiplying equation (4.190) by $\tilde{G}(t|t_2)$ and multiplying equation (4.191) by $G(t|t_1)$ and then subtracting

$$\frac{d}{dt} [G(t|t_1) \tilde{G}(t|t_2)] = \alpha [\tilde{G}(t|t_2) \delta(t - t_1) - G(t|t_1) \delta(t - t_2)]. \quad (4.193)$$

Now integrate this equation over the time range $t_{\text{init}} \leq t \leq T$. For the right hand side we assume α to be a constant, which then leads to the difference $\tilde{G}(t_1|t_2) - G(t_2|t_1)$. For the left hand side, use of the causality conditions in equations (4.190) and (4.191) render

$$\int_{t_{\text{init}}}^T \frac{d}{dt} [G(t|t_1) \tilde{G}(t|t_2)] dt = 0, \quad (4.194)$$

thus yielding the reciprocity relation

$$\tilde{G}(t|t_0) = G(t_0|t). \quad (4.195)$$

The feedback parameter, λ , dropped out from the derivation, with the reciprocity relation holding even if λ is time dependent. However, we again needed to assume the coefficient α to be constant.

4.9.4 Response function for general forcing

We now return to the initial value problem (4.170) and determine the response, ψ , to a general forcing function, $F(t)$, that turns on at some initial time $t = t_0 > t_{\text{init}}$. As for our earlier discussions of Green's functions, we express the general response function as an integral over impulse responses. For this purpose, multiply equation (4.170) by $\tilde{G}(t|t_0)$ and the adjoint equation (4.191) by $\psi(t)$, subtract, and then integrate to find

$$\alpha \psi(t_0) = \int_{t_{\text{init}}}^T \tilde{G}(t|t_0) F(t) dt - \int_{t_{\text{init}}}^T \frac{d}{dt} [\tilde{G}(t|t_0) \psi(t)] dt. \quad (4.196)$$

Making use of the causality condition $\tilde{G}(t|t_0) = 0$ for since $t > t_0$ leads to

$$\alpha \psi(t_0) = \tilde{G}(t_{\text{init}}|t_0) \psi(t_{\text{init}}) + \int_{t_{\text{init}}}^{t_0} \tilde{G}(t|t_0) F(t) dt, \quad (4.197)$$

where we retained the possibility of $\psi(t_{\text{init}}) \neq 0$ for a bit of generality. The reciprocity condition (4.195) brings this equation to the form

$$\alpha \psi(t_0) = G(t_0|t_{\text{init}}) \psi(t_{\text{init}}) + \int_{t_{\text{init}}}^{t_0} G(t_0|t) F(t) dt, \quad (4.198)$$

and swapping symbols, $t \leftrightarrow t_0$, yields

$$\alpha \psi(t) = G(t|t_{\text{init}}) \psi(t_{\text{init}}) + \int_{t_{\text{init}}}^t G(t|t_0) F(t_0) dt_0. \quad (4.199)$$

As anticipated, the general response is written as an initial response plus the integral of the general forcing with the impulse response function. Causality ensures that ψ is dependent only on forcing that is active between the initial time, t_{init} , and current time, t . To garner further insights into the general expression (4.199), consider the special case of constant feedback parameter, λ , in which the impulse response function is (4.176) so that

$$\psi(t) = e^{-\lambda(t-t_{\text{init}})} \psi(t_{\text{init}}) + \int_{t_{\text{init}}}^t e^{-\lambda(t-t_0)} F(t_0) dt_0. \quad (4.200)$$

4.9.5 Connection to the boundary propagator

Recall our discussion in Section 4.8.8 of the boundary propagator for the diffusion equation, which solves the causal boundary value problem (4.168a)-(4.168c). Again, the boundary propagator, $G^{\text{bp}}(\mathbf{x}, t|\mathbf{x}_0, t_0)$, measures the response of the system at (\mathbf{x}, t) to a Dirac delta space-time source imposed along the surface boundary. The details of the diffusion process are encoded into the boundary propagator so that the propagator is able to build up the response, ψ , to a general boundary forcing function, σ , as per equation (4.163). The discussion in the current section thus prompts us to consider the boundary propagator as an impulse response function for spatially distributed sources whose influence is mediated by diffusion.

4.9.6 Comments and further study

Many applications of Green's function methods in geophysical fluid mechanis and climate dynamics do not make use of analytical methods to solve for the Green's function. Instead, they make use of numerical estimates based on time stepping passive tracers in ocean and atmospheric models, with source functions approximating Dirac delta sources. Many applications have focused on boundary propagators, which as shown in this section are equivalent to impulse response functions for boundary sources. We return to this point when discussing the passive tracer equation in Section 61.10.

Hasselmann et al. (1993) introduced the impulse response function and step response function to the study of climate model drift. *Marshall et al. (2014)* and *Zanna et al. (2019)* presented further studies using this framework. Some of the mathematical formulation of impulse response and step response functions as presented here follow that offered in Exercise 1.52 of *Stakgold (2000a)*.



Chapter 5

FOURIER ANALYSIS

In this chapter we survey salient features of Fourier analysis of use for a variety of purposes. In particular, we employ Fourier analysis for the study of wave mechanics in Part IX of this book, thus motivating us to introduce some language from wave mechanics in this chapter. We are only concerned in this book with classical physical systems, in which all physical quantities are real numbers. Hence, our use of complex numbers, common in Fourier analysis, is solely for convenience, with the convenience a result of the remarkable Euler identity. This situation in classical physics contrasts with the wave function in quantum mechanics, which is fundamentally complex and satisfies the Schrödinger equation.

We here highlight conventions for Fourier analysis followed in this book, with clarification of these conventions provided later in the chapter.

- P is the period for functions represented using a Fourier series. Some treatments instead write the period as $P = 2L$.
- A factor of $1/2\pi$ is placed on the inverse Fourier transform as per equation (5.59c), whereas there is unity for the Fourier transform. An alternative convention, commonly used in quantum mechanics, is to place $1/\sqrt{2\pi}$ for both Fourier transform and its inverse. We have more to say on this convention in Section 5.4.6.
- Fourier space is referred to as *k-space* or *wavevector space*, which is a dual vector space (through the Fourier integral transform) to *x-space* or *position space*. Some treatments refer to *x-space* as “physical space”. We avoid that language since for describing a physical system, *x-space* is no more or less physical than *k-space*. Rather, they emphasize complementary features and both offer physical insights.

CHAPTER GUIDE

Fourier analysis is particularly relevant to the study of wave mechanics considered in Part IX of this book, thus motivating the use of wave mechanics terminology in this chapter. We follow standard treatments found in physics and applied maths texts, such as Chapters 2 and 5 of [Spiegel \(1974b\)](#), Appendix A of [Gasiorowicz \(1974\)](#), Appendix I of [Cohen-Tannoudji et al. \(1977\)](#), Sections 5.10-5.15 of [Hildebrand \(1976\)](#), and Section 6.4.2 of [Thorne and Blandford \(2017\)](#). However, as noted above, there are slight inconsistencies in conventions that warrant care if taking results from the literature, such as integral tables for Fourier transforms. [This video from 3Blue1Brown](#) provides an insightful introduction to Fourier series, and [and this video, also from 3Blue1Brown](#) provides a corresponding introduction to Fourier transforms.

5.1	Loose threads	118
5.2	Complex numbers	118
5.2.1	Modulus and phase	118
5.2.2	Phase averaging	119
5.2.3	Euler's identity motivates the use of complex numbers	120
5.3	Fourier series	121
5.3.1	Fourier series of sines and cosines	122
5.3.2	Functions with a particular parity	123
5.3.3	Complex Fourier series of exponentials	124
5.3.4	Bessel-Parseval relations	125
5.4	Fourier integrals	126
5.4.1	Fourier's integral theorem	126
5.4.2	Fourier transform	127
5.4.3	Integrals over a symmetric interval	128
5.4.4	Fourier cosine and sine transforms	129
5.4.5	Parseval-Plancherel formulas	131
5.4.6	Concerning the placement of $1/2\pi$	131
5.4.7	Fourier transform and derivatives	132
5.5	Time-frequency Fourier transforms	132
5.5.1	How to interpret negative frequency for waves	133
5.5.2	Frequency versus angular frequency	133
5.6	Example Fourier transform pairs	134
5.6.1	Dirac delta	134
5.6.2	Gaussian	135
5.7	Exercises	135

5.1 Loose threads

- Figures for the example Fourier transforms

5.2 Complex numbers

All physical fields are real in the classical physics considered in this book. Even so, we sometimes make use of complex numbers for convenience, particularly when studying linear waves since manipulating exponentials is simpler than the alternative sines and cosines. We here summarize a few salient points for working with complex numbers in classical physics.

5.2.1 Modulus and phase

A complex number, \mathcal{A} , is the sum of its real and imaginary parts, which we write as¹

$$\mathcal{A} = \text{Re}[\mathcal{A}] + i \text{Im}[\mathcal{A}], \quad (5.1)$$

and its complex conjugate is given by²

$$\mathcal{A}^* = \text{Re}[\mathcal{A}] - i \text{Im}[\mathcal{A}]. \quad (5.2)$$

¹In this book, we generally use the L^AT_EX *mathcal* notation for complex numbers.

²The star is the symbol commonly used in mathematics to represent the complex conjugate of a complex number.

Making use of the *Euler identity*³

$$e^{i\alpha} = \cos \alpha + i \sin \alpha \quad (5.3)$$

allows us to write a complex number as

$$\mathcal{A} = \sqrt{\mathcal{A} \mathcal{A}^*} e^{i\alpha} = |\mathcal{A}| (\cos \alpha + i \sin \alpha) \quad \text{with } \tan \alpha = \text{Im}[\mathcal{A}] / \text{Re}[\mathcal{A}]. \quad (5.4)$$

The term

$$|\mathcal{A}| = \sqrt{\mathcal{A} \mathcal{A}^*} = \sqrt{\text{Re}[\mathcal{A}]^2 + \text{Im}[\mathcal{A}]^2} \quad (5.5)$$

is the *modulus* of the complex number \mathcal{A} . The notation $|\mathcal{A}|$ is motivated since the modulus is a generalization of the absolute value used for real numbers. The angle, α , is called the *argument* in the maths literature, whereas we refer to it as the *phase* to correspond to its use in wave mechanics.

When we write a complex number in classical physics, it is the real part that is of physical interest

$$\text{Re}[\mathcal{A}] = \sqrt{\mathcal{A} \mathcal{A}^*} \cos \alpha. \quad (5.6)$$

Hence, we generally interpret the product, $\mathcal{A} \mathcal{A}$, as

$$\text{Re}[\mathcal{A}] \text{Re}[\mathcal{A}] = |\mathcal{A}|^2 \cos^2 \alpha. \quad (5.7)$$

Likewise, with $\mathcal{B} = |\mathcal{B}| e^{i\beta}$, we interpret the product $\mathcal{A} \mathcal{B}$ as

$$\text{Re}[\mathcal{A}] \text{Re}[\mathcal{B}] = |\mathcal{A}| |\mathcal{B}| \cos \alpha \cos \beta. \quad (5.8)$$

These considerations are particularly important when computing energetics of linear wave fields.

5.2.2 Phase averaging

There are many occasions in the study of waves where it is useful to average over the extent of a wave, either in space or time. Doing so provides a measure for the “wave averaged” properties. We here add precision to this notion. For this purpose, consider two real wave fields written in the form of a traveling plane wave

$$A = \text{Re}[\mathcal{A} e^{i(\mathbf{k} \cdot \mathbf{x} - \omega t)}] = |\mathcal{A}| \cos(\mathbf{k} \cdot \mathbf{x} - \omega t + \alpha) \quad (5.9a)$$

$$B = \text{Re}[\mathcal{B} e^{i(\mathbf{k} \cdot \mathbf{x} - \omega t)}] = |\mathcal{B}| \cos(\mathbf{k} \cdot \mathbf{x} - \omega t + \beta), \quad (5.9b)$$

where $\mathbf{k} \cdot \mathbf{x} - \omega t$ is the space-time dependence found for a traveling plane wave, with \mathbf{k} the wavevector and ω the angular frequency (e.g., Section 43.5). We wrote the complex wave amplitudes as

$$\mathcal{A} = |\mathcal{A}| e^{i\alpha} \quad \text{and} \quad \mathcal{B} = |\mathcal{B}| e^{i\beta}, \quad (5.10)$$

where α and β are phase shifts relative to $\mathbf{k} \cdot \mathbf{x} - \omega t$. To introduce the notion of a *phase average*, introduce a constant phase shift, φ , according to

$$\alpha = \alpha' + \varphi \quad \text{and} \quad \beta = \beta' + \varphi, \quad (5.11)$$

in which case we define a *phase average* as

$$\langle \dots \rangle \equiv \frac{1}{2\pi} \int_0^{2\pi} (\dots) d\varphi, \quad (5.12)$$

³There are few equations in mathematics that are more elegant and powerful than Euler’s identity.

so that a phase average is computed by sampling over the extent of a single wavelength or single wave period. The phase average of a traveling plane wave is zero

$$\langle A \rangle = \frac{1}{2\pi} \int_0^{2\pi} |\mathcal{A}| \cos(\mathbf{k} \cdot \mathbf{x} - \omega t + \alpha' + \varphi) d\varphi = 0, \quad (5.13)$$

whereas the phase average for the product of two real wave fields does not generally vanish

$$\langle A B \rangle = \frac{1}{2\pi} \int_0^{2\pi} |\mathcal{A}| |\mathcal{B}| \cos(\mathbf{k} \cdot \mathbf{x} - \omega t + \alpha' + \varphi) \cos(\mathbf{k} \cdot \mathbf{x} - \omega t + \beta' + \varphi) d\varphi \quad (5.14a)$$

$$= \frac{1}{4\pi} \int_0^{2\pi} |\mathcal{A}| |\mathcal{B}| [\cos(\alpha' - \beta') + \cos(2\mathbf{k} \cdot \mathbf{x} - 2\omega t + 2\varphi + \alpha' - \beta')] d\varphi \quad (5.14b)$$

$$= \frac{1}{2} |\mathcal{A}| |\mathcal{B}| \cos(\alpha' - \beta') \quad (5.14c)$$

$$= \frac{1}{2} \operatorname{Re}[\mathcal{A}^* \mathcal{B}] \quad (5.14d)$$

$$= \frac{1}{2} \operatorname{Re}[\mathcal{A} \mathcal{B}^*]. \quad (5.14e)$$

We see that the phase average of a product acts to remove information about the common phase, leaving only information about the modulus of the wave amplitudes and their phase difference. For example,

$$\langle A^2 \rangle = |\mathcal{A}|^2 / 2, \quad (5.15)$$

so that the phase average for the square of a real wave field is one-half the squared modulus of the wave amplitude. Similarly, if $\mathcal{B} = i\mathcal{A}$ then

$$\langle A B \rangle = \frac{1}{2\pi} \int_0^{2\pi} |\mathcal{A}| |\mathcal{B}| \cos(\pi/2) d\varphi = 0, \quad (5.16)$$

in which we say that the real wave fields A and B are *out of phase*.

5.2.3 Euler's identity motivates the use of complex numbers

As noted earlier, there is no physical reason to introduce complex numbers in classical physics. However, there are many mathematical reasons. In particular, it is generally more convenient to use complex Fourier analysis than real Fourier analysis when establishing various theoretical results in wave mechanics.

The central reason to employ complex numbers is the shear elegance and power of Euler's identity 5.3. We encountered examples in Section 5.2.2 when discussing phase averaging. One more example concerns the sum of two waves, such as the sum of the two real wave fields (5.9a) and (5.9b)

$$C = A + B = |\mathcal{A}| \cos(\mathbf{k} \cdot \mathbf{x} - \omega t + \alpha) + |\mathcal{B}| \cos(\mathbf{k} \cdot \mathbf{x} - \omega t + \beta). \quad (5.17)$$

It is certainly possible to determine an expression for the combined wave, C , through the use of trigonometric identities. However, it is far less tedious to compute the sum via Euler's identity,

in which case

$$C = |\mathcal{A}| \cos(\mathbf{k} \cdot \mathbf{x} - \omega t + \alpha) + |\mathcal{B}| \cos(\mathbf{k} \cdot \mathbf{x} - \omega t + \beta) \quad (5.18a)$$

$$= \operatorname{Re}[|\mathcal{A}| e^{i(\mathbf{k} \cdot \mathbf{x} - \omega t + \alpha)} + |\mathcal{B}| e^{i(\mathbf{k} \cdot \mathbf{x} - \omega t + \beta)}] \quad (5.18b)$$

$$= \operatorname{Re}[(|\mathcal{A}| e^{i\alpha} + |\mathcal{B}| e^{i\beta}) e^{i(\mathbf{k} \cdot \mathbf{x} - \omega t)}] \quad (5.18c)$$

$$\equiv \operatorname{Re}[|\mathcal{C}| e^{i(\mathbf{k} \cdot \mathbf{x} - \omega t + \gamma)}] \quad (5.18d)$$

$$= |\mathcal{C}| \cos(\mathbf{k} \cdot \mathbf{x} - \omega t + \gamma), \quad (5.18e)$$

where we introduced the complex amplitude

$$|\mathcal{C}| e^{i\gamma} \equiv |\mathcal{A}| e^{i\alpha} + |\mathcal{B}| e^{i\beta}. \quad (5.19)$$

We can further use Euler's identity and some trigonometric identities to determine the real amplitude and phase shift for the combined wave

$$|\mathcal{C}|^2 = |\mathcal{A}|^2 + |\mathcal{B}|^2 + 2 |\mathcal{A}| |\mathcal{B}| \cos(\alpha - \beta) \quad (5.20a)$$

$$\tan \gamma = \frac{|\mathcal{A}| \sin \alpha + |\mathcal{B}| \sin \beta}{|\mathcal{A}| \cos \alpha + |\mathcal{B}| \cos \beta}. \quad (5.20b)$$

The curious reader is encouraged to compute the expression (5.18e), along with the real amplitude (5.20a) and phase shift (5.20b), using only real analysis.

5.3 Fourier series

Consider an arbitrary real function, $F(x)$, defined over the real line and that is piecewise continuous on every finite interval, as is its first derivative.⁴ We also assume the function satisfies the periodicity condition⁵

$$F(x + P) = F(x), \quad (5.21)$$

where $P > 0$ is the period.⁶ The periodicity condition (5.21) holds for every point on the real line so that

$$F(x + nP) = F(x) \quad \text{for arbitrary positive or negative integer } n. \quad (5.22)$$

How general are periodic functions defined over the full real line? To answer this question, consider a function defined only over a finite domain, $x \in [\alpha, \beta]$, and that is periodic over that domain

$$G(\alpha) = G(\beta). \quad (5.23)$$

Quite trivially, we can construct the extended function, $F(x)$, that equals to $G(x)$ for $x \in [\alpha, \beta]$ and that is periodic over the real line, $F(x) = F(x + P)$, with period $P = \beta - \alpha$. For this reason, it is sufficient to focus on periodic functions defined over the full real line, $x \in (-\infty, \infty)$.

⁴These properties for $F(x)$ are commonly satisfied for functions considered in this book.

⁵We use the notation x as for a spatial coordinate. Yet everything that follows holds if x is interpreted as time.

⁶Some treatments, such as Chapter 2 of [Spiegel \(1974b\)](#), assume the function has period $F(x) = F(x + 2L)$, in which case $P = 2L$. In general, care is needed when making use of expressions from the literature to account for slight differences in conventions.

5.3.1 Fourier series of sines and cosines

A *Fourier series* decomposes an arbitrary periodic function⁷ in terms of the function's mean value over a period, plus an infinite series of sines and cosines

$$F(x) = a_0 + \sum_{n=1}^{\infty} [a_n \cos(k_n x) + b_n \sin(k_n x)], \quad (5.24)$$

where we introduced the discrete *wavenumber*

$$k_n = 2\pi n/P. \quad (5.25)$$

Clearly the Fourier series (5.24) satisfies the periodicity condition, $F(x) = F(x + nP)$. Mathematically, the Fourier series is enabled by completeness of the trigonometric functions as a basis for periodic functions over a finite interval. Furthermore, the real coefficients, a_n and b_n , are determined through use of orthonormality conditions satisfied by the sine and cosine functions

$$\frac{2}{P} \int_{x_0}^{x_0+P} \cos(k_n x) \sin(k_m x) dx = 0 \quad (5.26a)$$

$$\frac{2}{P} \int_{x_0}^{x_0+P} \cos(k_n x) \cos(k_m x) dx = \delta_{mn} \quad (5.26b)$$

$$\frac{2}{P} \int_{x_0}^{x_0+P} \sin(k_n x) \sin(k_m x) dx = \delta_{mn}, \quad (5.26c)$$

where δ_{mn} is the Kronecker delta tensor, which is unity if $m = n$ and vanishes otherwise.⁸ Furthermore, note that the constant, x_0 is arbitrary, with the equalities holding for any value.⁹ The orthonormality conditions (5.26a)-(5.26c) directly lead to the following expressions for the Fourier series expansion coefficients

$$a_0 = \frac{1}{P} \int_{x_0}^{x_0+P} F(x) dx \quad (5.27a)$$

$$a_{n>0} = \frac{2}{P} \int_{x_0}^{x_0+P} \cos(k_n x) F(x) dx \quad (5.27b)$$

$$b_{n>0} = \frac{2}{P} \int_{x_0}^{x_0+P} \sin(k_n x) F(x) dx. \quad (5.27c)$$

⁷There are certain mathematical conditions required of $F(x)$ that allow for the Fourier series to be an identity. These conditions are typically satisfied by functions encountered in physics. See Section 5.10 of [Hildebrand \(1976\)](#) for more details.

⁸As seen in Section 1.3, the Kronecker tensor is the metric for Euclidean space using Cartesian coordinates. For equations (5.26b) and (5.26c), we use the Kronecker merely as a signal of orthonormality of the trigonometric functions.

⁹We make use of this arbitrariness in Section 5.4.1 where we choose a particularly useful value for developing the notion of a Fourier integral.

Note that a_0 is the mean value of $F(x)$ over a single period. As an exercise, we verify equation (5.27b) by multiplying the Fourier series (5.24) by $\cos(k_m x)$ for $m > 0$ and integrating

$$\int_{x_0}^{x_0+P} \cos(k_m x) F(x) dx = \int_{x_0}^{x_0+P} \cos(k_m x) \left[a_0 + \sum_{n=1}^{\infty} [a_n \cos(k_n x) + b_n \sin(k_n x)] \right] dx \quad (5.28a)$$

$$= (P/2) a_n \delta_{mn}, \quad (5.28b)$$

where the second equality used the orthogonality conditions (5.26a)-(5.26c). Analogous steps are used to verify equation (5.27c)

$$\int_{x_0}^{x_0+P} \sin(k_m x) F(x) dx = \int_{x_0}^{x_0+P} \sin(k_m x) \left[a_0 + \sum_{n=1}^{\infty} [a_n \cos(k_n x) + b_n \sin(k_n x)] \right] dx \quad (5.29a)$$

$$= (P/2) b_n \delta_{mn}. \quad (5.29b)$$

5.3.2 Functions with a particular parity

A function is said to have even or odd *parity* if it maintains the following behavior under the transformation $x \rightarrow -x$

$$F(-x) = -F(x) \quad \text{odd parity} \quad (5.30a)$$

$$F(-x) = F(x) \quad \text{even parity.} \quad (5.30b)$$

We can show that the corresponding coefficients in the Fourier series satisfy the following relations for such functions

$$a_n = 0 \quad \text{if } F(x) = -F(-x) \quad \text{odd parity} \quad (5.31a)$$

$$b_n = 0 \quad \text{if } F(x) = F(-x) \quad \text{even parity.} \quad (5.31b)$$

To verify these identities, consider the following combinations

$$\frac{F(x) + F(-x)}{2} = a_0 + \sum_{n=1}^{\infty} a_n \cos(k_n x) \quad (5.32a)$$

$$\frac{F(x) - F(-x)}{2} = \sum_{n=1}^{\infty} b_n \sin(k_n x), \quad (5.32b)$$

which follow from the parity of the sine and cosine functions. Now multiply equation (5.32a) by $\sin(k_m x)$, integrate, and use orthogonality to find

$$\int_{x_0}^{x_0+P} \sin(k_m x) [F(x) + F(-x)] dx = \int_{x_0}^{x_0+P} \sin(k_m x) [a_0 + \sum_{n=1}^{\infty} a_n \cos(k_n x)] dx = 0. \quad (5.33)$$

If $F(x) = F(-x)$ then $\int_{x_0}^{x_0+P} \sin(k_m x) [F(x) + F(-x)] dx = 2 L b_m$, which we have just seen equals to zero due to the even parity of $F(x)$. We have thus verified relation (5.31b). Likewise, if we multiply equation (5.32b) by $\cos(k_m x)$ and integrate, we find

$$\int_{x_0}^{x_0+P} \cos(k_m x) [F(x) - F(-x)] dx = \int_{x_0}^{x_0+P} \cos(k_m x) \sum_{n=1}^{\infty} b_n \sin(k_n x) dx = 0. \quad (5.34)$$

If $F(x)$ has odd parity, the left hand side equals to $2P a_n$, which we have just shown vanishes. We have thus verified relation (5.31a).

5.3.3 Complex Fourier series of exponentials

Rather than a sum of sines and cosines, we can use the Euler identity (5.3) to decompose a periodic function into a series of exponentials by introducing the complex expansion coefficients

$$c_0 = a_0 \tag{5.35a}$$

$$c_{-n} = (a_n + i b_n)/2 \quad \text{for } n > 0 \tag{5.35b}$$

$$c_n = (a_n - i b_n)/2 \quad \text{for } n > 0. \tag{5.35c}$$

Making use of the expressions (5.27b) and (5.27c) yields

$$c_n = \frac{1}{P} \int_{x_0}^{x_0+P} e^{-ik_n x} F(x) dx. \tag{5.36}$$

The reality condition, sometimes referred to as *conjugate symmetry*

$$c_{-n} = c_n^* \tag{5.37}$$

holds since we are only considering real functions, $F(x)$. Inverting the relations (5.35a)-(5.35c)

$$a_0 = c_0 \tag{5.38a}$$

$$a_n = c_n + c_{-n} \quad \text{for } n > 0 \tag{5.38b}$$

$$b_n = i(c_n - c_{-n}) \quad \text{for } n > 0 \tag{5.38c}$$

then allows us to write the Fourier series (5.24) in the form

$$F(x) = a_0 + \sum_{n=1}^{\infty} [a_n \cos(k_n x) + b_n \sin(k_n x)] \tag{5.39a}$$

$$= c_0 + \sum_{n=1}^{\infty} [(c_n + c_{-n}) \cos(k_n x) + i(c_n - c_{-n}) \sin(k_n x)] \tag{5.39b}$$

$$= c_0 + \sum_{n=1}^{\infty} c_n [\cos(k_n x) + i \sin(k_n x)] + \sum_{n=1}^{\infty} c_{-n} [\cos(k_n x) - i \sin(k_n x)] \tag{5.39c}$$

$$= c_0 + \sum_{n=1}^{\infty} c_n e^{ik_n x} + \sum_{n=1}^{\infty} c_{-n} e^{-ik_n x} \tag{5.39d}$$

$$= \sum_{n=-\infty}^{\infty} c_n e^{ik_n x}. \tag{5.39e}$$

This exponential form is commonly more convenient for manipulations, with the reality condition (5.37) of fundamental importance when working with real fields. Importantly, note that the real coefficients, a_n and b_n , are defined only for $n \geq 0$, whereas the complex coefficients are defined by arbitrary integers.

5.3.4 Bessel-Parseval relations

Making use of the reality condition (5.37) allows us to write the square of a real periodic function as

$$F(x) F(x) = \left[\sum_{n=-\infty}^{\infty} c_n e^{ik_n x} \right] \left[\sum_{m=-\infty}^{\infty} c_m e^{ik_m x} \right] \quad \text{equation (5.39e)} \quad (5.40a)$$

$$= \left[\sum_{n=-\infty}^{\infty} c_n e^{ik_n x} \right] \left[\sum_{m=-\infty}^{\infty} c_{-m} e^{-ik_m x} \right] \quad \text{swap } m \text{ summation order} \quad (5.40b)$$

$$= \left[\sum_{n=-\infty}^{\infty} c_n e^{ik_n x} \right] \left[\sum_{m=-\infty}^{\infty} c_m^* e^{-ik_m x} \right] \quad \text{reality condition (5.37)} \quad (5.40c)$$

$$= \sum_{n,m=-\infty}^{\infty} c_n c_m^* e^{i(k_n - k_m)x} \quad \text{combining sums.} \quad (5.40d)$$

The *Bessel-Parseval relation* (sometimes just referred to as *Parseval's identity*) results from performing an average of this expression over a single period

$$\frac{1}{P} \int_{x_0}^{x_0+P} F(x) F(x) dx = \sum_{n=-\infty}^{\infty} c_n c_n^* = \sum_{n=-\infty}^{\infty} |c_n|^2 = \sum_{n=-\infty}^{\infty} c_n c_{-n}, \quad (5.41)$$

where we used the orthonormality condition holding for the exponentials

$$\frac{1}{P} \int_{x_0}^{x_0+P} e^{i(k_n - k_m)x} dx = \delta_{mn}, \quad (5.42)$$

and the final equality in equation (5.41) follows from the reality condition (5.37) holding since F is real. The analogous form of Parseval's identity holds when using the sine/cosine version of the Fourier series (5.24), whereby

$$F(x) F(x) = \left[a_0 + \sum_{n=1}^{\infty} [a_n \cos(k_n x) + b_n \sin(k_n x)] \right] \left[a_0 + \sum_{m=1}^{\infty} [a_m \cos(k_m x) + b_m \sin(k_m x)] \right], \quad (5.43)$$

with integration and the orthonormality relations (5.26a)-(5.26c) resulting in

$$\frac{1}{P} \int_{x_0}^{x_0+P} F(x) F(x) dx = a_0^2 + \frac{1}{2} \sum_{n=1}^{\infty} [a_n^2 + b_n^2]. \quad (5.44)$$

We find it useful to double-check this form of Parseval's identity while confirming we are consistently using both the real and complex forms of the Fourier series. For this purpose, substitute the expressions (5.35a)-(5.35c) for c_n into the final form of Parseval's identity (5.41) to yield

$$\sum_{n=-\infty}^{\infty} c_n c_{-n} = c_0^2 + \sum_{n=-\infty}^{-1} c_n c_{-n} + \sum_{n=1}^{\infty} c_n c_{-n} = c_0^2 + 2 \sum_{n=1}^{\infty} c_n c_{-n} = a_0^2 + \frac{1}{2} \sum_{n=1}^{\infty} [a_n^2 + b_n^2], \quad (5.45a)$$

which agrees with equation (5.44).

We can go one further step by introducing a second real and periodic function, $H(x) =$

$H(x + mP)$, in which case

$$H(x) = \sum_{n=-\infty}^{\infty} d_n e^{ik_n x}. \quad (5.46)$$

The Bessel-Parseval relation (5.41) can thus be generalized to

$$\frac{1}{P} \int_{x_0}^{x_0+P} F(x) H(x) dx = \sum_{n=-\infty}^{\infty} c_n d_n^* = \sum_{n=-\infty}^{\infty} c_n d_{-n}. \quad (5.47)$$

5.4 Fourier integrals

We develop *Fourier integrals* as the limit of a Fourier series and then derive some properties of these integrals. Our treatment is heuristic.¹⁰

5.4.1 Fourier's integral theorem

Consider a real periodic function, $F(x) = F(x + nP)$ with n and integer, and decompose it according to the Fourier series (5.24). Also, insert the expressions (5.27a)-(5.27c) for the expansion coefficients and specify the arbitrary constant $x_0 = -P/2$ in order to symmetrize the integral limits. The resulting Fourier series is given by

$$F(x) = \frac{2}{P} \int_{-P/2}^{P/2} F(u) \left[\frac{1}{2} + \sum_{n=1}^{\infty} [\cos(k_n u) \cos(k_n x) + \sin(k_n u) \sin(k_n x)] \right] du. \quad (5.48)$$

We now consider the limit as $P \rightarrow \infty$, in which case the period becomes infinite so that the function, $F(x)$, is no longer periodic over a finite interval. Precisely, we make the following assumptions and conversions.

- FINITE INTEGRAL: We assume the absolute value of the function has a finite integral for arbitrary P , which in turn means that its average tends to zero as P becomes infinite:

$$\int_{-P/2}^{P/2} |F(u)| du < \infty \implies \lim_{P \rightarrow \infty} \frac{1}{P} \int_{-P/2}^{P/2} F(u) du = 0. \quad (5.49)$$

- INFINITESIMAL WAVENUMBER INCREMENT: We introduce the wavenumber increment

$$k_{n+1} - k_n = \Delta k = 2\pi/P, \quad (5.50)$$

which becomes infinitesimal as P becomes large. As a result, the infinite sum over discrete wavenumbers transitions to an integral over continuous wavenumbers

$$\lim_{P \rightarrow \infty} \sum_{n=1}^{\infty} \frac{2}{P} = \frac{1}{\pi} \int_0^{\infty} dk. \quad (5.51)$$

Making use of these results in equation (5.48) leads to

$$F(x) = \frac{1}{\pi} \int_0^{\infty} \left[\cos(k x) \int_{-\infty}^{\infty} F(u) \cos(k u) du + \sin(k x) \int_{-\infty}^{\infty} F(u) \sin(k u) du \right] dk, \quad (5.52)$$

¹⁰The derivation of the Fourier transform equations in this section follows that given by Chapter 5 of *Spiegel (1974b)*, particularly worked exercise 5.11, yet note that L in *Spiegel (1974b)* is given by $L = P/2$.

which is known as *Fourier's integral theorem*. We can bring Fourier's integral theorem a bit closer to the discrete Fourier sum (5.24) by introducing the real amplitude functions

$$A(k) \equiv \frac{1}{\pi} \int_{-\infty}^{\infty} F(u) \cos(k u) du \quad \text{and} \quad B(k) \equiv \frac{1}{\pi} \int_{-\infty}^{\infty} F(u) \sin(k u) du, \quad (5.53)$$

thus resulting in the tidy expression of the Fourier integral theorem

$$F(x) = \int_0^{\infty} [A(k) \cos(k x) + B(k) \sin(k x)] dk. \quad (5.54)$$

This is the key result that forms the foundation for the remainder of this section. Indeed, the remainder of this section largely consists of rewriting this identity in a variety of forms. Before doing so, we emphasize the following points about Fourier's integral theorem (5.54).

All physical fields produce real numbers

As noted at the start of this chapter, all physical fields in this book are real. Hence, every term in equation (5.54) are real, including the amplitude functions $A(k)$ and $B(k)$. So although many versions of Fourier analysis involve complex numbers, as we do in Section 5.4.2, the introduction of complex numbers is not fundamental.

Concerning the functional degrees of freedom

For each function, $F(x)$, there are two amplitude functions, $A(k)$ and $B(k)$. However, there is no explosion of functional degrees of freedom since $F(x)$ is defined over the full real line, $-\infty < x < \infty$ whereas $A(k)$ and $B(k)$ are defined with $k \geq 0$. The equal functional degrees of freedom manifest when using the complex version of the Fourier integral theorem in Section 5.4.2.

Parity properties of the amplitude functions

The parity properties of the amplitude functions, $A(k)$ and $B(k)$, are directly inherited from the cosine and sine functions appearing in their definition (5.53), so that we find

$$A(k) = A(-k) \quad \text{and} \quad B(k) = -B(-k). \quad (5.55)$$

As shown in Section 5.4.4, these properties are reflected in the nature of the integral theorem when expressing functions, $F(x)$, with a particular parity.

Allowing the wavenumber to range over the full real line

The integral over wavenumber, k , in equation (5.53) extends from $k = 0$ to $k = \infty$. When moving to a complex representation that involves the Fourier transform in Section 5.4.2, the integral will extend from $-\infty < k < \infty$. As discussed in Section 4.3.6.3, the extension to $k < 0$ can be interpreted as a plane wave moving in the direction opposite to the wave with $k > 0$.

5.4.2 Fourier transform

To connect to the complex Fourier series from Section (5.3.3) we introduce the *Fourier transform*

$$\mathcal{F}(k) \equiv \pi [A(k) - i B(k)] = \int_{-\infty}^{\infty} F(u) e^{-iku} du \quad \Leftarrow \text{Fourier transform.} \quad (5.56)$$

In terms of $\mathcal{F}(k)$ we can write the Fourier integral theorem (5.54) as

$$F(x) = \int_0^\infty [A(k) \cos(kx) + B(k) \sin(kx)] dk \quad (5.57a)$$

$$= \frac{1}{2\pi} \int_0^\infty [\cos(kx) [\mathcal{F}(k) + \mathcal{F}^*(k)] + i \sin(kx) [\mathcal{F}(k) - \mathcal{F}^*(k)]] dk \quad (5.57b)$$

$$= \frac{1}{2\pi} \int_0^\infty [\mathcal{F}(k) e^{ikx} + [\mathcal{F}(k) e^{ikx}]^*] dk. \quad (5.57c)$$

From its definition (5.56), we know that the complex conjugate of the Fourier transform satisfies the *conjugate symmetry* identity

$$\mathcal{F}^*(k) = \int_{-\infty}^\infty F(u) e^{iku} du = \mathcal{F}(-k). \quad (5.58)$$

This identity is directly analogous to the discrete Fourier transform identity (5.37), both of which hold due to the reality of the function, $F(x)$. We are thus led to the complex version of the Fourier integral theorem

$$F(x) = \frac{1}{2\pi} \int_0^\infty \mathcal{F}(k) e^{ikx} dk + \frac{1}{2\pi} \int_0^\infty \mathcal{F}(-k) e^{-ikx} dk \quad (5.59a)$$

$$= \frac{1}{2\pi} \int_0^\infty \mathcal{F}(k) e^{ikx} dk - \frac{1}{2\pi} \int_0^{-\infty} \mathcal{F}(k) e^{ikx} dk \quad (5.59b)$$

$$= \frac{1}{2\pi} \int_{-\infty}^\infty \mathcal{F}(k) e^{ikx} dk. \quad (5.59c)$$

With $\mathcal{F}(k)$ referred to as the Fourier transform we sometimes refer to $F(x)$ as the *inverse Fourier transform*. Correspondingly, $\mathcal{F}(k)$ and $F(x)$ are *Fourier transform pairs*.

5.4.3 Integrals over a symmetric interval

As for the Fourier series, we can derive some reality and parity properties of the Fourier integral theorem. Before doing so we develop some results holding for functions of a particular parity. Consider the integral of a function, $F(x)$, defined over an arbitrary, but symmetric, interval $x \in [-L, L]$. Decomposing this function into its even and odd components leads to

$$\int_{-L}^L F(x) dx = \frac{1}{2} \int_{-L}^L [F(x) + F(-x)] dx + \frac{1}{2} \int_{-L}^L [F(x) - F(-x)] dx \quad (5.60a)$$

$$\equiv \int_{-L}^L F_{\text{even}}(x) dx + \int_{-L}^L F_{\text{odd}}(x) dx. \quad (5.60b)$$

The integral of the even parity component can be written

$$\int_{-L}^L F_{\text{even}}(x) dx = \int_{-L}^0 F_{\text{even}}(x) dx + \int_0^L F_{\text{even}}(x) dx \quad (5.61a)$$

$$= - \int_L^0 F_{\text{even}}(-x) dx + \int_0^L F_{\text{even}}(x) dx \quad (5.61b)$$

$$= 2 \int_0^L F_{\text{even}}(x) dx. \quad (5.61c)$$

Evidently, the integral of an even parity function over a symmetric interval equals to twice the integral over half the interval

$$\int_{-L}^L F_{\text{even}}(x) dx = 2 \int_0^L F_{\text{even}}(x) dx. \quad (5.62)$$

In a similar manner we find that the integral of an odd parity function over a symmetric interval vanishes

$$\int_{-L}^L F_{\text{odd}}(x) dx = \int_{-L}^0 F_{\text{odd}}(x) dx + \int_0^L F_{\text{odd}}(x) dx \quad (5.63a)$$

$$= - \int_L^0 F_{\text{odd}}(-x) dx + \int_0^L F_{\text{odd}}(x) dx \quad (5.63b)$$

$$= \int_0^L [F_{\text{odd}}(-x) + F_{\text{odd}}(x)] dx \quad (5.63c)$$

$$= 0. \quad (5.63d)$$

We thus find that the integral of an arbitrary function over a symmetric interval is given by twice the integral of the even component over half the interval

$$\int_{-L}^L F(x) dx = 2 \int_0^L F_{\text{even}}(x) dx = \int_0^L [F(x) + F(-x)] dx. \quad (5.64)$$

We make use of these relations in developing parity conditions for Fourier transforms, in which case the integral limits are infinity, $L = \infty$.

5.4.4 Fourier cosine and sine transforms

The Fourier integral theorem simplifies when acting on functions of a particular parity. As any function can be decomposed into its even and odd parity components (see Section 5.4.3), it is common to make use of the simplification by introducing the cosine and sine transforms. These transforms allow one to work with all real valued functions when convenient, rather than the complex valued functions used with the standard Fourier transform of Section 5.4.2.

Fourier cosine transform for even functions: $F(x) = F(-x)$

Consider an even function, $F(x) = F(-x)$, and expand it in terms of the Fourier integral theorem (5.54)

$$F(x) = \int_0^\infty [A(k) \cos(kx) + B(k) \sin(kx)] dk = \int_0^\infty [A(k) \cos(kx) - B(k) \sin(kx)] dk, \quad (5.65)$$

which follows from the odd parity of the sine function and even parity of $F(x)$. For this relation to hold requires $B(k) = 0$, which indeed follows from its definition

$$\pi B(k) = \int_{-\infty}^{\infty} F(u) \sin(k u) du \quad (5.66a)$$

$$= \int_{-\infty}^0 F(u) \sin(k u) du + \int_0^{\infty} F(u) \sin(k u) du \quad (5.66b)$$

$$= \int_0^{\infty} [-F(u) + F(u)] \sin(k u) du \quad (5.66c)$$

$$= 0. \quad (5.66d)$$

These simplification of Fourier's integral theorem motivate us to define the *Fourier cosine transform* for functions with even parity

$$F_C(k) \equiv (\pi/2) A(k) = \frac{1}{2} \int_{-\infty}^{\infty} F(u) \cos(k u) du = \int_0^{\infty} F(u) \cos(k u) du, \quad (5.67)$$

so that Fourier's integral theorem (5.65) for an even parity function takes the form

$$F(x) = \int_0^{\infty} A(k) \cos(k x) dk = \frac{2}{\pi} \int_0^{\infty} F_C(k) \cos(k x) dk \quad (5.68)$$

Fourier sine transform for odd functions: $F(x) = -F(-x)$

We now consider the case of an odd function, $F(x) = -F(-x)$, and expand it in terms of the Fourier integral theorem (5.54)

$$F(x) = \int_0^{\infty} [A(k) \cos(k x) + B(k) \sin(k x)] dk, = \int_0^{\infty} [-A(k) \cos(k x) + B(k) \sin(k x)] dk. \quad (5.69)$$

This relation is consistent only if $A(k) = 0$ for odd functions, which indeed follows from its definition

$$\pi A(k) = \int_{-\infty}^{\infty} F(u) \cos(k u) du \quad (5.70a)$$

$$= \int_{-\infty}^0 F(u) \cos(k u) du + \int_0^{\infty} F(u) \cos(k u) du \quad (5.70b)$$

$$= \int_0^{\infty} [F(-u) + F(u)] \cos(k u) du \quad (5.70c)$$

$$= 0. \quad (5.70d)$$

We are thus motivated to define the *Fourier sine transform* for functions with odd parity

$$F_S(k) \equiv (\pi/2) B(k) = \frac{1}{2} \int_{-\infty}^{\infty} F(u) \sin(k u) du = \int_0^{\infty} F(u) \sin(k u) du, \quad (5.71)$$

so that Fourier's integral theorem (5.69) for an odd parity function takes the form

$$F(x) = \int_0^{\infty} B(k) \sin(k x) dk = \frac{2}{\pi} \int_0^{\infty} F_S(k) \sin(k x) dk \quad (5.72)$$

5.4.5 Parseval-Plancherel formulas

In Section 5.3.4 we showed that a Fourier series expansion of a periodic function satisfies the Parseval identities (5.41) and (5.47). Here we derive the analog for Fourier transforms. For this purpose, consider the integral of the product of two real functions

$$\int_{-\infty}^{\infty} G(x) F(x) dx = \frac{1}{2\pi} \int_{-\infty}^{\infty} G(x) \left[\int_{-\infty}^{\infty} \mathcal{F}(k) e^{ikx} dk \right] dx, \quad (5.73)$$

where we expressed $F(x)$ in terms of its inverse Fourier transform (5.59c). Now swap the integration order and rearrange to render

$$\int_{-\infty}^{\infty} G(x) F(x) dx = \frac{1}{2\pi} \int_{-\infty}^{\infty} \left[\int_{-\infty}^{\infty} G(x) e^{-ikx} dx \right]^* \mathcal{F}(k) dk, \quad (5.74)$$

where we noted that

$$\left[e^{ikx} \right]^* = e^{-ikx} \quad \text{and} \quad G^* = G. \quad (5.75)$$

We recognize the bracketed term in equation (5.74) as the complex conjugate Fourier transform of G , thus bringing us to the identity

$$\int_{-\infty}^{\infty} G(x) F(x) dx = \frac{1}{2\pi} \int_{-\infty}^{\infty} [\mathcal{G}(k)]^* \mathcal{F}(k) dk. \quad (5.76)$$

For the special case with $G = F$ we recover the *Parseval-Plancherel formula*, commonly referred to as *Parseval's identity*

$$\int_{-\infty}^{\infty} [F(x)]^2 dx = \frac{1}{2\pi} \int_{-\infty}^{\infty} |\mathcal{F}(k)|^2 dk. \quad (5.77)$$

If $[F(x)]^2$ is proportional to the energy, then Parseval's identity expresses the identity of energy when expressed in either x -space or k -space.¹¹

5.4.6 Concerning the placement of $1/2\pi$

There is no universal convention for the pre-factors appearing in the Fourier transform pairs (5.56) and (5.59c). That is, the unity for the Fourier transform pre-factor in equation (5.56), versus the $1/2\pi$ pre-factor for the inverse Fourier transform (5.59c), could just as well be swapped, or alternatively they could both be equal to $1/\sqrt{2\pi}$. However these factors are chosen, their product must equal to $1/2\pi$.

Furthermore, the $1/2\pi$ factor in the inverse Fourier transform (5.59c) can be eliminated through use of the *reduced wavenumber*, \tilde{k} , defined as

$$\tilde{k} = k/2\pi, \quad (5.78)$$

in which case the inverse Fourier transform (5.59c) is given by

$$F(x) = \int_{-\infty}^{\infty} \mathcal{F}(\tilde{k}) e^{i2\pi\tilde{k}x} d\tilde{k} \quad (5.79)$$

An analogous approach is used when working in the time-frequency domain and using the fre-

¹¹The $1/2\pi$ factor in the Parseval identity (5.77) can be eliminated by distributing a $1/\sqrt{2\pi}$ equally between the Fourier transform and the inverse Fourier transform. That convention is generally followed in the quantum mechanics literature but not in the fluid mechanics literature. See Section 5.4.6 for more on the 2π factor.

quency, f , rather than the angular frequency, ω , where $f = \omega/2\pi$ (see Section 5.5). Even though k is somewhat more elegant, we generally work with the wavenumber, k , thus necessitating care to properly place the $1/2\pi$ factor.

5.4.7 Fourier transform and derivatives

Consider a function, $G(x)$, defined by the p 'th derivative of $F(x)$

$$G(x) = \frac{d^p F}{dx^p}. \quad (5.80)$$

From the expression for the inverse Fourier transform in equation (5.59c), we know that

$$G(x) = \frac{d^p}{dx^p} \left[\frac{1}{2\pi} \int_{-\infty}^{\infty} \mathcal{F}(k) e^{ikx} dk \right] \quad (5.81a)$$

$$= \frac{1}{2\pi} \int_{-\infty}^{\infty} (ik)^p \mathcal{F}(k) e^{ikx} dk \quad (5.81b)$$

$$\equiv \frac{1}{2\pi} \int_{-\infty}^{\infty} \mathcal{G}(k) e^{ikx} dk. \quad (5.81c)$$

We thus find that the Fourier transform of the derivative of a function is given by

$$\mathcal{G}(k) = (ik)^p \mathcal{F}(k). \quad (5.82)$$

The k^p factor means that $\mathcal{G}(k)$ has more structure at high wavenumbers than $\mathcal{F}(k)$. This result has far reaching implications for the structure of fluid mechanical fields. Namely, when acting on a field with a derivative, the resulting differentiated field has more fine scale structure than the undifferentiated field. The nutshell notion is that differentiation adds fine scales whereas integration smooths fields.

5.5 Time-frequency Fourier transforms

Our notation has thus far been based on space, x , and wavenumber, k . However, all formula hold whatever interpretation one gives to these coordinates, with time and frequency commonly used as well as space and wavenumber. For time, we write the Fourier transform and its inverse according to

$$\mathcal{F}(\omega) = \int_{-\infty}^{\infty} F(t) e^{-i\omega t} dt \quad (5.83a)$$

$$F(t) = \frac{1}{2\pi} \int_{-\infty}^{\infty} \mathcal{F}(\omega) e^{i\omega t} d\omega, \quad (5.83b)$$

where ω is the angular frequency. The time integral extends from $-\infty$ to ∞ , meaning that it extends arbitrarily far in the past into the future. The negative angular frequency arises from the same symmetrization of the integral limits made when moving to the complex Fourier transform in Section 5.4.2. As in Section 43.6.3, we here find it important to interpret the negative angular frequency, $\omega < 0$, which we do next.

5.5.1 How to interpret negative frequency for waves

As noted at the start of this chapter, we generally make use of Fourier analysis for waves. When working in x -space and k -space, we can consider the components of a wavevector to be positive or negative given that the wavevector determines the direction of a wave. We considered this point in Section 43.6.3. Since information about the direction of the wave is fully carried by the wavevector, we consider the angular frequency of a wave to be a non-negative number, $\omega \geq 0$ (Section 43.4), which corresponds to a non-negative wave period, $2\pi/\omega$. Hence, when working with waves, we interpret the expression (5.83b) for the inverse Fourier transform, with its negative frequency integral limits, as a convenient means to bring the Fourier sine and cosine functions together into a single integral. We do not give any physical meaning to $\omega < 0$.

To provide details to support the above words, return to the Fourier integral theorem (5.54), only now interpreted for time and angular frequency

$$F(t) = \int_0^\infty [A(\omega) \cos(\omega t) + B(\omega) \sin(\omega t)] d\omega. \quad (5.84)$$

Note that the frequency integral extends only over non-negative frequencies, consistent with ω as a frequency. In contrast, the amplitude functions are built from integrals over all time according to equation (5.53)

$$A(\omega) = \frac{1}{\pi} \int_{-\infty}^\infty F(t) \cos(\omega t) dt \quad \text{and} \quad B(\omega) = \frac{1}{\pi} \int_{-\infty}^\infty F(t) \sin(\omega t) dt. \quad (5.85)$$

We have no problem with negative time simply because the origin of time is arbitrary. In contrast, we ascribe no physical meaning to a negative frequency, but instead interpret a negative frequency as a mathematical expedient enabling us to write equation (5.83b) in a compact form. We emphasize this point by writing

$$F(t) = \int_0^\infty [A(\omega) \cos(\omega t) + B(\omega) \sin(\omega t)] d\omega \quad \text{equation (5.84)} \quad (5.86a)$$

$$= \frac{1}{2} \int_{-\infty}^\infty [A(\omega) \cos(\omega t) + B(\omega) \sin(\omega t)] d\omega \quad \text{parity properties} \quad (5.86b)$$

$$= \frac{1}{2} \int_{-\infty}^\infty [\cos(\omega t) + i \sin(\omega t)] [A(\omega) - i B(\omega)] d\omega \quad \text{parity properties} \quad (5.86c)$$

$$= \frac{1}{2\pi} \int_{-\infty}^\infty e^{i\omega t} \mathcal{F}(\omega) d\omega \quad \text{Euler + equation (5.56).} \quad (5.86d)$$

So again, we compute the inverse Fourier transform as in equation (5.83b) with a frequency interval including negative frequencies. Yet there is no physical meaning given to the negative frequencies. Instead, they simply offer the means to unify the Fourier cosine and sine amplitude functions according to the above identities.

5.5.2 Frequency versus angular frequency

As noted in Section 5.4.6, we can eliminate the $1/2\pi$ factor appearing in the inverse Fourier transform (5.83b) through using the frequency, f , rather than the angular frequency

$$f = \omega/2\pi, \quad (5.87)$$

in which case the Fourier transform partners (5.83a) and (5.83b) take the form

$$\mathcal{F}(f) = \int_{-\infty}^{\infty} F(t) e^{-i2\pi f t} dt \quad (5.88a)$$

$$F(t) = \int_{-\infty}^{\infty} \mathcal{F}(f) e^{i2\pi f t} df. \quad (5.88b)$$

Even though f is rather elegant from this perspective, we generally use the angular frequency, ω (along with the angular wavenumber, k), thus necessitating care with the placement of the $1/2\pi$ factor for the Fourier transform pair given by equations (5.83a) and (5.83b).

5.6 Example Fourier transform pairs

In this section we offer a few examples of Fourier transform pairs.

5.6.1 Dirac delta

We introduced the Dirac delta in Section 4.3

$$F(x) = \delta(x). \quad (5.89)$$

Following from its sifting property (4.7), we find that the Fourier transform (equation (5.56)) of the Dirac delta is given by

$$\mathcal{F}(k) = \int_{-\infty}^{\infty} \delta(x) e^{-ikx} dx = 1. \quad (5.90)$$

This result provides an extreme example of the *complementarity* relation maintained between the Fourier transform and its inverse. Namely, if a function is concentrated in x -space then its Fourier transform is widely distributed in k -space. The Dirac delta is infinitely concentrated in x -space at the origin, whereas it has a uniform and constant distribution in k -space. That is, the x -space distribution is infinitesimally narrow whereas the k -space distribution is infinitely broad. As a consistency check, we note the physical dimensionality of the terms in equation (5.90). Namely, the Dirac delta, $\delta(x)$, as dimensions of inverse length (Section 4.3.3), so that $\delta(x) dx$ is non-dimensional. We thus expect its Fourier transform, $\mathcal{F}(k)$, to be non-dimensional.

It follows that the inverse Fourier transform (equation (5.59c)) of the Dirac delta is given by

$$\delta(x - x_0) = \frac{1}{2\pi} \int_{-\infty}^{\infty} e^{ik(x-x_0)} dk = \frac{1}{2\pi} \int_{-\infty}^{\infty} \cos[k(x - x_0)] dk, \quad (5.91)$$

where we introduced an arbitrary shift from the origin, x_0 . We also noted that

$$\int_{-\infty}^{\infty} \sin[k(x - x_0)] dk = 0, \quad (5.92)$$

which follows since the k -space integral is over a symmetric domain yet the integrand has odd k -space parity. Equation (5.91) is a rather remarkable expression that can be heuristically explained by noting that for all values of $x - x_0 \neq 0$, the cosine function oscillates so that any positive values are exactly matched by negative values, thus yielding a zero integral. However, when $x - x_0 = 0$, the integral diverges since the integrand becomes unity and the integral limits are infinite.

5.6.2 Gaussian

Consider a Gaussian function,

$$F(x) = (2\pi\sigma)^{-1/2} e^{-x^2/4\sigma}, \quad (5.93)$$

where $\sigma > 0$ determines the standard deviation. Its Fourier transform is given by

$$\mathcal{F}(k) = (2\pi\sigma)^{-1/2} \int_{-\infty}^{\infty} e^{-x^2/4\sigma} e^{-ikx} dx = e^{-\sigma k^2}, \quad (5.94)$$

with evaluation of this integral following from the calculus of residues.¹² We expect the Fourier transform to be real since the Gaussian has even parity so that the Fourier sine transform vanishes (see Section 5.4.4). It is remarkable that the Fourier transform of a Gaussian function is itself a Gaussian, with this property unique to the Gaussian. We also note the inverse placement of σ between the two Gaussians. Hence, if the Gaussian is narrow in x -space, as per a small value of σ , then it is broad in k -space, and vice versa. This behavior again reflects the complementarity property of Fourier transform pairs.



5.7 Exercises

EXERCISE 5.1: SOLVING AN ODE (PROBLEM 9.8 OF *Fetter and Walecka* (2003))

In this exercise we find a general expression for a forced ordinary differential equation using Fourier transform methods to determine the Green's function.

- (a) Use a Fourier transform to solve the one-dimensional ordinary differential equation

$$\frac{d^2H(x)}{dx^2} - \lambda^2 H(x) = -F(x), \quad (5.95)$$

for $\lambda > 0$ and assuming that $H(x)$ vanishes as $|x| \rightarrow \infty$. Express your answer in the form of a Green's function (see Chapter 4)

$$H(x) = \int_{-\infty}^{\infty} G(x, x') F(x') dx'. \quad (5.96)$$

- (b) Find an explicit expression for the Green's function, $G(x, x')$. Hint: you might wish to make use of an integral table.
- (c) What are the physical dimensions of G ? And relative to F , what are the dimensions of H ?
- (d) Discuss the limit as $\lambda \rightarrow 0$.



¹²We discuss a few of the steps in Section 43.6.5 when studying Gaussian wave packets.

Chapter 6

CURVES AND SURFACES

We encounter curves and surfaces throughout the study of geophysical fluid mechanics, with fluid particle pathlines through space-time and isopycnal/isentropic surfaces providing two examples. Indeed, curves and surfaces are encountered throughout physics. Hence, there is a well developed mathematical framework to describe the geometric properties of these objects. Our goal in this chapter is to introduce some of the basics of curves and surfaces embedded in Euclidean space.

Although the curves and surfaces of geophysical fluid mechanics are commonly moving as part of the fluid flow, we are concerned in this chapter with describing their instantaneous spatial properties. Hence, time does not appear in this chapter. Furthermore, although curves and surfaces can overturn and intersect themselves, we restrict attention to orientable curves and surfaces whose normal direction has a nonzero projection onto the vertical; i.e., they have no overhangs and no wrapping (Figure 6.1). This constraint is satisfied by the surfaces of constant generalized vertical coordinates (e.g., isopycnal surfaces) considered in Chapter 56 and in many other places in this book. It allows us to make use of coordinates known as the *Monge gauge* in condensed matter physics

READER'S GUIDE TO THIS CHAPTER

This chapter requires an understanding of the Cartesian calculus of Chapter 2. The differential geometry presented here is of some use throughout this book, and yet the casual reader need not penetrate the material. Conversely, the interested reader can find far more development of the mathematics, along with physical applications, by studying the physics of fluctuating membranes, with Section 10.4 of the condensed matter physics textbook from [Chaikin and Lubensky \(1995\)](#) providing a starting point.

6.1	Definitions and notation	138
6.1.1	Definitions	138
6.1.2	Notation	138
6.1.3	Surfaces with $x = \gamma(y, z)$ or $y = \psi(x, z)$	139
6.2	Planar curves in 2D Euclidean space	140
6.2.1	Differential increments along the curve	140
6.2.2	Length along the curve	141
6.2.3	Curvature of a curve	142
6.3	Surfaces embedded in 3D Euclidean space	143
6.3.1	Area on the surface	144
6.3.2	Curvature of a surface	144
6.3.3	Curves on the surface $z = \eta(x, y)$	146
6.4	Exercises	147

6.1 Definitions and notation

The basic notions of curves and surfaces embedded in Euclidean space are rather intuitive. Nonetheless, it is important to be precise in our usage. For this purpose we here offer some notation and definitions.

6.1.1 Definitions

We assume the notion of a curve and surface embedded in Euclidean space to be self-evident, offering analytical expressions for curves in Section 6.2 and surfaces in Section 6.3. Given such, we here define some related notions used in our study of fluid mechanics.

- **ORIENTABLE:** An *orientable curve* is a curve that allows for normal and tangent directions to specify directions and sides to the curve. Likewise, an *orientable surface* has two sides, allowing one to choose a positive side and a negative side. A Möbius strip is the canonical surface that is not orientable since it only has one side. Likewise, the boundary of a Möbius strip is a non-orientable curve. We only consider orientable objects in this book.
- **PATH or CONTOUR:** A path or contour is a continuous piecewise smooth oriented curve. A *simple path* or *simple contour* does not cross itself. We already encountered contours when considering path integrals in Chapter 2.
- **CIRCUIT:** A circuit is a path that closes, and a *simple circuit* is a circuit that does not cross itself. Finally, a *reducible circuit* is a circuit that can be continuously deformed to a point within the domain without leaving the domain. For example, a circuit within the ocean that encloses an island or continent cannot be deformed to a point since doing so requires the circuit to cross onto land and thus to leave the ocean.

6.1.2 Notation

In this chapter we write the Cartesian position of a point on a surface as

$$\mathbf{S} = x \hat{\mathbf{x}} + y \hat{\mathbf{y}} + \eta(x, y) \hat{\mathbf{z}} \quad \text{position on surface,} \quad (6.1)$$

with the vertical position written as

$$z = \eta(x, y) \quad \text{vertical position on surface.} \quad (6.2)$$

If we are instead referring to a point on a planar curve in the x - z -plane, then we drop the y -dependence to have

$$\mathbf{S} = x \hat{\mathbf{x}} + \eta(x) \hat{\mathbf{z}} \quad \text{position on planar curve.} \quad (6.3)$$

Time dependence is dropped throughout this chapter since we focus on the spatial geometry of curves and surfaces at a particular time instance.

We assume the outward normal direction on the curve or the surface has a nonzero projection into the vertical as shown in Figure 6.1. Indeed, we are only able to write the vertical position as $z = \eta(x, y)$ so long as there are no overturns in the surface, in which case the outward unit normal direction is

$$\hat{\mathbf{n}} = \frac{\nabla(z - \eta)}{|\nabla(z - \eta)|} = \frac{\hat{\mathbf{z}} - \nabla\eta}{\sqrt{1 + |\nabla\eta|^2}}. \quad (6.4)$$

Figure 6.2 provides an example surface along with the notation.

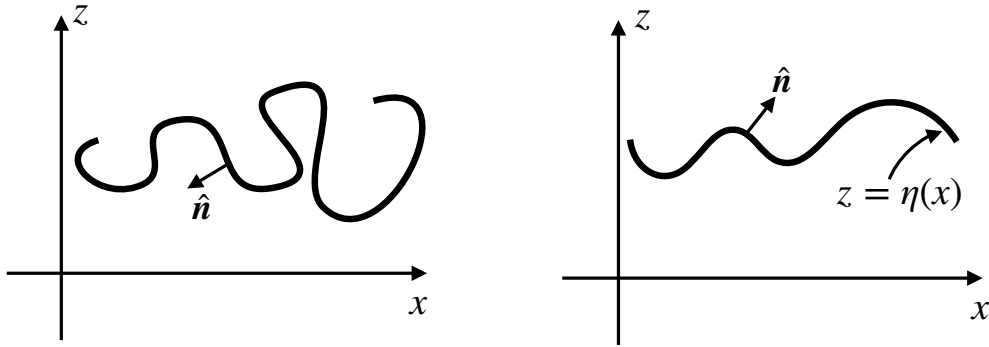


FIGURE 6.1: Two sample curves on the x - z plane. The left panel shows a curve whose outward unit normal, \hat{n} , encounters points where $\hat{n} \cdot \hat{z} = 0$ and where $\hat{n} \cdot \hat{z}$ changes sign. This curve, and its generalization to a surface, are not treated in this chapter. The right panel shows a more gently undulating curve where $\hat{n} \cdot \hat{z} \neq 0$ everywhere, and thus where $\hat{n} \cdot \hat{z}$ is single signed. For curves such as the right panel, we can express the vertical position as a 1-to-1 function of the horizontal position, $z = \eta(x)$. Again, this curve has its natural generalization to a gently undulating surface whereby $z = \eta(x, y)$ provides a unique mapping between horizontal position and vertical. The assumption regarding no overhanging curves and surfaces is consistent with our study of surfaces defined by a constant generalized vertical coordinate (e.g., isopycnals or isentropes) in Chapter 56.

6.1.3 Surfaces with $x = \gamma(y, z)$ or $y = \psi(x, z)$

We generally find it most useful to specify a point on a surface according to equation (6.1), whereby we write $z = \eta(x, y)$ for the vertical position as a function of the horizontal position. This approach is typical for our applications since the surfaces we encounter most commonly in stratified geophysical flows have a normal direction that has a non-zero projection into the \hat{z} direction. However, there are occasions where it is more convenient to define a point on a surface according to

$$\mathbf{S} = \gamma(y, z) \hat{x} + y \hat{y} + z \hat{z} \quad \text{alternative specification.} \quad (6.5)$$

Here, we specify the x position on the surface as a function of y and z via the function $\gamma(y, z)$. The unit normal is thus specified by

$$\hat{n} = \frac{\nabla(x - \gamma)}{|\nabla(x - \gamma)|} = \frac{\hat{x} - \hat{y} \partial_y \gamma - \hat{z} \partial_z \gamma}{1 + \sqrt{(\partial_y \gamma)^2 + (\partial_z \gamma)^2}}. \quad (6.6)$$

Hence, this specification is useful for those surfaces with normal direction having a non-zero \hat{x} component everywhere on the surface, in which case we are afforded the ability to define $\gamma(y, z)$. Alternatively, if the surface instead has a normal direction with a non-zero \hat{y} component everywhere, then we would find it more suitable to define a point on the surface according to

$$\mathbf{S} = x \hat{x} + \psi(x, z) \hat{y} + z \hat{z}, \quad (6.7)$$

where $y = \psi(x, z)$ provides the y position of a point on the surface as a function of x, z .

For the remainder of this chapter we return to the specification (6.1) whereby $z = \eta(x, y)$. However, there are occasions when we find it more suitable to define the surface using either equation (6.5) or (6.7). For example, we make use of the specification (6.5) in Section 18.6 when studying the meridional-depth overturning streamfunction.

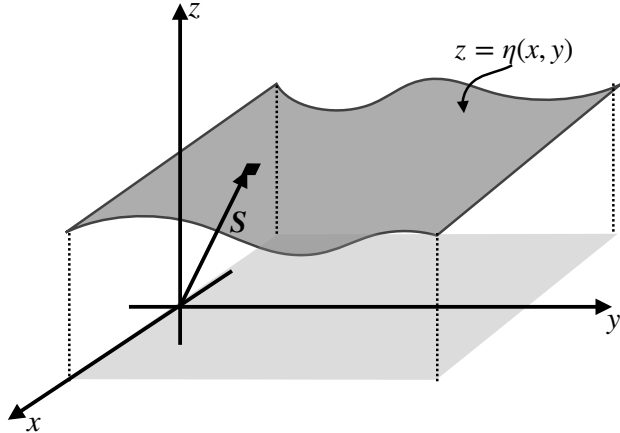


FIGURE 6.2: An example of a surface embedded in Euclidean space. The position of a point on the surface is given by the Cartesian position vector $\mathbf{S} = x \hat{\mathbf{x}} + y \hat{\mathbf{y}} + \eta(x, y) \hat{\mathbf{z}}$. The relation $z = \eta(x, y)$ provides a 1-to-1 mapping between the horizontal position and the vertical position of a point on the surface. Correspondingly, the surface is uniquely specified by finding the envelope of points where $z - \eta(x, y) = 0$. The lightly shaded region represents the projection of the curved surface onto the flat horizontal x - y plane below.

6.2 Planar curves in 2D Euclidian space

We here describe the geometry of a curve on the x - z -plane (a *planar curve*) as depicted in Figure 6.3. These curves are one-dimensional objects living in a two-dimensional Euclidean space. Extensions to curves on non-Euclidean surfaces, such as the sphere or an isopycnal, are straightforward when those surfaces are embedded in a background Euclidean space (which is typical for Newtonian physics).

6.2.1 Differential increments along the curve

As a one-dimensional geometric object, an arbitrary curve can be parameterized by a single coordinate, referred to here as φ . Let $\mathbf{S}(\varphi)$ specify the position of a point along the curve. Correspondingly, the differential increment between two infinitesimally close points on the curve is given by

$$\mathbf{S}(\varphi + d\varphi) - \mathbf{S}(\varphi) = d\mathbf{S} = \frac{d\mathbf{S}}{d\varphi} d\varphi \equiv \mathbf{t} d\varphi, \quad (6.8)$$

where

$$\mathbf{t} = \frac{d\mathbf{S}}{d\varphi} \quad (6.9)$$

is tangent to the curve. If $\varphi = s$ is the arc length along the curve, then $\mathbf{t} = \hat{\mathbf{t}}$ is a unit vector

$$\hat{\mathbf{t}} \cdot \hat{\mathbf{t}} = \frac{d\mathbf{S}}{ds} \cdot \frac{d\mathbf{S}}{ds} = 1. \quad (6.10)$$

In some treatments in this book we also write

$$\hat{s} = \hat{\mathbf{t}} \quad (6.11)$$

to correspond to s for arc length. Recall we made use of the arc length along a curve in Section 2.4 when describing path integration.

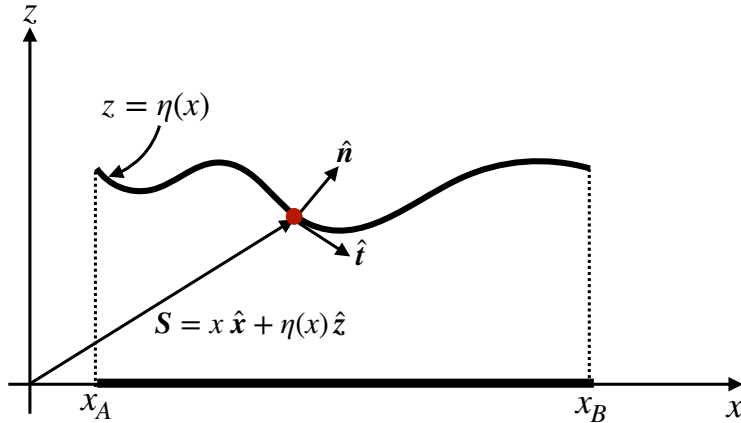


FIGURE 6.3: An orientable path in the x - z plane defined by a planar curve that does not intersect itself. The Cartesian position of a point on the curve is given by $\mathbf{S} = x \hat{\mathbf{x}} + \eta(x) \hat{\mathbf{z}}$, where $z = \eta(x)$ provides the vertical position of the point as a function of the horizontal position. The projection of the curve onto the horizontal x -axis occupies a range $x_A \leq x \leq x_B$. One way to define the curve is by finding the envelope of points where $z - \eta(x) = 0$, in which case we can readily find the unit normal direction pointing upward as $\hat{\mathbf{n}} = \nabla(z - \eta)/|\nabla(z - \eta)| = [\hat{\mathbf{z}} - (\mathrm{d}\eta/\mathrm{d}x) \hat{\mathbf{x}}] [1 + (\mathrm{d}\eta/\mathrm{d}x)^2]^{-1/2}$, and the unit tangent vector $\hat{\mathbf{t}} = [\hat{\mathbf{x}} + (\mathrm{d}\eta/\mathrm{d}x) \hat{\mathbf{z}}] [1 + (\mathrm{d}\eta/\mathrm{d}x)^2]^{-1/2}$.

6.2.2 Length along the curve

As in equation (6.3) we can represent the position of a point along the curve using Cartesian coordinates

$$\mathbf{S} = x \hat{\mathbf{x}} + \eta(x) \hat{\mathbf{z}}. \quad (6.12)$$

Hence, letting $\varphi = x$ parameterize the curve leads to the representation of the tangent direction

$$\mathbf{t} = \frac{\mathrm{d}\mathbf{S}}{\mathrm{d}x} = \hat{\mathbf{x}} + \frac{\mathrm{d}\eta}{\mathrm{d}x} \hat{\mathbf{z}}, \quad (6.13)$$

which has the magnitude

$$\mathbf{t} \cdot \mathbf{t} = 1 + (\mathrm{d}\eta/\mathrm{d}x)^2, \quad (6.14)$$

so that the unit tangent vector is

$$\hat{\mathbf{t}} = \frac{\hat{\mathbf{x}} + (\mathrm{d}\eta/\mathrm{d}x) \hat{\mathbf{z}}}{\sqrt{1 + (\mathrm{d}\eta/\mathrm{d}x)^2}}. \quad (6.15)$$

Likewise, the curve's unit normal vector is given by

$$\hat{\mathbf{n}} = \frac{\nabla(z - \eta)}{|\nabla(z - \eta)|} = \frac{\hat{\mathbf{z}} - (\mathrm{d}\eta/\mathrm{d}x) \hat{\mathbf{x}}}{\sqrt{1 + (\mathrm{d}\eta/\mathrm{d}x)^2}}, \quad (6.16)$$

with orthogonality manifest

$$\hat{\mathbf{t}} \cdot \hat{\mathbf{n}} = 0. \quad (6.17)$$

The squared length of an infinitesimal segment along the curve is given by

$$(\mathrm{d}s)^2 = \mathrm{d}\mathbf{S} \cdot \mathrm{d}\mathbf{S} = \left[\frac{\mathrm{d}\mathbf{S}}{\mathrm{d}x} \cdot \frac{\mathrm{d}\mathbf{S}}{\mathrm{d}x} \right] \mathrm{d}x \mathrm{d}x, \quad (6.18)$$

so that the finite length of the curve is determined by the integral

$$L = \int_0^L \mathrm{d}s = \int_{x_A}^{x_B} |\mathrm{d}\mathbf{S}/\mathrm{d}x| \mathrm{d}x = \int_{x_A}^{x_B} \sqrt{1 + (\mathrm{d}\eta/\mathrm{d}x)^2} \mathrm{d}x, \quad (6.19)$$

where $x_A \leq x \leq x_B$ is the range over which x runs for the projection of the curve onto the x -axis (see Figure 6.3).

6.2.3 Curvature of a curve

Curvature measures the amount that the unit normal changes along the curve. For a planar curve, the curvature at a point equals to the inverse radius of a circle that shares the same tangent plane to the curve at the point (see Figure 6.4). We refer to the radius as the *radius of curvature* and the corresponding circle as the *curvature circle*. To formulate an analytic expression for the radius of curvature at a point on a curve, orient the Cartesian coordinate axes so that the point is at the origin and the tangent plane sits along the x -axis as in Figure 6.4. Consequently, the outward unit normal, \hat{n} , is parallel to the \hat{z} direction.

A Taylor series expansion about the origin tells us that the vertical position of a point along the curve and near to the origin can be written

$$\eta(x) = \eta(0) + x \left[\frac{d\eta}{dx} \right]_{x=0} + \frac{x^2}{2} \left[\frac{d^2\eta}{dx^2} \right]_{x=0} + \mathcal{O}(x^3) \quad (6.20a)$$

$$= \frac{x^2}{2} \left[\frac{d^2\eta}{dx^2} \right]_{x=0} + \mathcal{O}(x^3). \quad (6.20b)$$

This result follows since we placed the origin so that $\eta(0) = 0$, and aligned the x -axis so that it is tangent at the origin, in which case $d\eta/dx = 0$ at $x = 0$. Hence, η has a quadratic behavior near the origin.

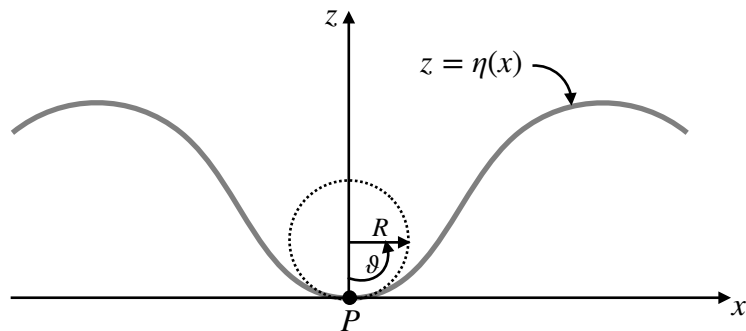


FIGURE 6.4: The radius of curvature at a point on a curve, P , equals to the radius of the curvature circle that shares the same tangent plane as the curve at the point P . When constructing the curvature circle we make use of the angle, ϑ , to measure the height of a point along the circle, $h(x) = R(1 - \cos \vartheta) \approx R\vartheta^2/2 \approx x^2/(2R)$. Setting $R^{-1} = d^2\eta/dx^2$ provides a second order accurate fit of the curvature circle to the curve at the point P .

Now place a circle with center along the z -axis so that it is tangent to the curve at the origin, as depicted in Figure 6.4. What is the radius, R , of the circle that best fits the curve at the origin? To answer this question note that the height of a point on the circle is given by $h(x) = R(1 - \cos \vartheta)$, where $\vartheta = 0$ for a point at the origin and $\vartheta = \pi$ at the diametrically opposite point. For small ϑ this height takes the form

$$h(x) \approx R[1 - 1 + \vartheta^2/2] = x^2/(2R), \quad (6.21)$$

where $\vartheta = x/R$ near the origin. For the height of a point on the curve (equation (6.20b)) to match the height along the circle, to second order accuracy, requires us to set the circle's radius to

$$\frac{1}{R} = \frac{d^2\eta}{dx^2}. \quad (6.22)$$

Equation (6.22) thus provides an expression for the radius of curvature, R , whose inverse is the

curvature

$$\text{curvature} = \frac{1}{R}. \quad (6.23)$$

This result supports our expectation that the second derivative measures the curvature. As radius, R , gets larger the curvature decreases since local regions along the circle appear more flat. In the opposite limit the curvature grows as R decreases. Note that we could have chosen to orient the circle on the opposite side of the tangent (on the convex side), in which case the radius of curvature is negative. That is, $R > 0$ when the unit normal points towards the concave side (side where the curve rises towards $\hat{\mathbf{n}}$), whereas $R < 0$ when the unit normal points towards the convex side (side where the curve falls away from $\hat{\mathbf{n}}$).

In closing this section we note that

$$-\nabla \cdot \hat{\mathbf{n}} = \frac{d^2\eta/dx^2}{[1 + (d\eta/dx)^2]^{3/2}}. \quad (6.24)$$

When evaluated at the point of interest along the curve, we set $d\eta/dx = 0$ so that

$$-\nabla \cdot \hat{\mathbf{n}} = \frac{d^2\eta}{dx^2} = \frac{1}{R}. \quad (6.25)$$

This result supports our earlier statement that curvature measures the change in the normal direction along the curve. In fact, the identity

$$-\nabla \cdot \hat{\mathbf{n}} = \frac{1}{R} \quad (6.26)$$

holds for an arbitrary point along the curve since it is a coordinate invariant statement.

Equation (6.25) provides a useful means to check the sign of the radius of curvature. Namely, the point of interest in Figure 6.4 is a local minimum, so that $d^2\eta/dx^2 > 0$ and the radius of curvature is thus positive, $R > 0$. In contrast, the radius of curvature is negative at points where $d^2\eta/dx^2 < 0$.

6.3 Surfaces embedded in 3D Euclidean space

We now extend the previous discussion to a two-dimensional surface embedded in three-dimensional Euclidean space such as in Figure 6.2. In general, a 2D surface in 3D space can be parameterized by two variables, φ_1 and φ_2 , so that infinitesimal increments along the surface satisfy

$$d\mathbf{S} = \frac{\partial \mathbf{S}}{\partial \varphi_1} d\varphi_1 + \frac{\partial \mathbf{S}}{\partial \varphi_2} d\varphi_2 = \mathbf{t}_1 d\varphi_1 + \mathbf{t}_2 d\varphi_2. \quad (6.27)$$

The vectors \mathbf{t}_1 and \mathbf{t}_2 are tangent to the surface at the point (φ_1, φ_2) , and yet they are not generally orthogonal to one another.

Making use of the Cartesian expression (6.1)

$$\mathbf{S} = x \hat{\mathbf{x}} + y \hat{\mathbf{y}} + \eta(x, y) \hat{\mathbf{z}} \quad (6.28)$$

brings the two tangent directions and the unit tangent directions into the form

$$\mathbf{t}_1 = \frac{\partial \mathbf{S}}{\partial x} = \hat{\mathbf{x}} + \frac{\partial \eta}{\partial x} \hat{\mathbf{z}} \quad \text{and} \quad \hat{\mathbf{t}}_1 = \frac{\hat{\mathbf{x}} + (\partial \eta / \partial x) \hat{\mathbf{z}}}{\sqrt{1 + (\partial \eta / \partial x)^2}} \quad (6.29a)$$

$$\mathbf{t}_2 = \frac{\partial \mathbf{S}}{\partial y} = \hat{\mathbf{y}} + \frac{\partial \eta}{\partial y} \hat{\mathbf{z}} \quad \text{and} \quad \hat{\mathbf{t}}_2 = \frac{\hat{\mathbf{y}} + (\partial \eta / \partial y) \hat{\mathbf{z}}}{\sqrt{1 + (\partial \eta / \partial y)^2}}. \quad (6.29b)$$

Likewise, the surface unit normal vector is given by

$$\hat{\mathbf{n}} = \frac{\nabla(z - \eta)}{|\nabla(z - \eta)|} = \frac{\hat{\mathbf{z}} - \nabla \eta}{|\hat{\mathbf{z}} - \nabla \eta|} = \frac{\hat{\mathbf{z}} - \nabla \eta}{\sqrt{1 + |\nabla \eta|^2}}, \quad (6.30)$$

and it is straightforward to show orthogonality with the two tangent vectors

$$\hat{\mathbf{t}}_1 \cdot \hat{\mathbf{n}} = \hat{\mathbf{t}}_2 \cdot \hat{\mathbf{n}} = 0. \quad (6.31)$$

6.3.1 Area on the surface

Recall from Section 1.4.5 that the magnitude of a vector product of two vectors equals to the area of the parallelogram subtended by the vectors. Hence, the area of an infinitesimal surface element with sides $d\varphi_1$ and $d\varphi_2$ is given by

$$d\mathcal{S} = \left| \frac{\partial \mathbf{S}}{\partial \varphi_1} \times \frac{\partial \mathbf{S}}{\partial \varphi_2} \right| d\varphi_1 d\varphi_2. \quad (6.32)$$

Making use of Cartesian coordinates brings the area element to

$$d\mathcal{S} = \sqrt{1 + |\nabla \eta|^2} dx dy = \sqrt{1 + |\nabla \eta|^2} dA, \quad (6.33)$$

where

$$dA = dx dy \quad (6.34)$$

is the area of the surface projected onto the horizontal plane. Hence, the area of a finite region is given by the integral

$$\mathcal{S} = \int d\mathcal{S} = \int |\nabla(z - \eta)| dA = \int \sqrt{1 + |\nabla \eta|^2} dx dy, \quad (6.35)$$

where the second and third integrals extend over the region defined by the projection of the surface onto the horizontal (see Figure 6.2).

6.3.2 Curvature of a surface

We now seek an expression for the curvature of a point on the surface. Since the surface has two dimensions, we expect the curvature to be measured by two numbers rather than the single curvature for the curve discussed in Section 6.2.3. The method for developing the curvature is analogous to that used for a curve, yet with a bit more mathematics needed to allow for the extra dimension. Figure 6.5 depicts the situation.

Let $\mathbf{x} = (x_1, x_2) = (x, y)$ be Cartesian coordinates on a tangent plane local to an arbitrary point on the surface, with the origin of the coordinate system taken at the point. Near to the point, we can estimate the vertical distance of a point on the surface from the tangent plane

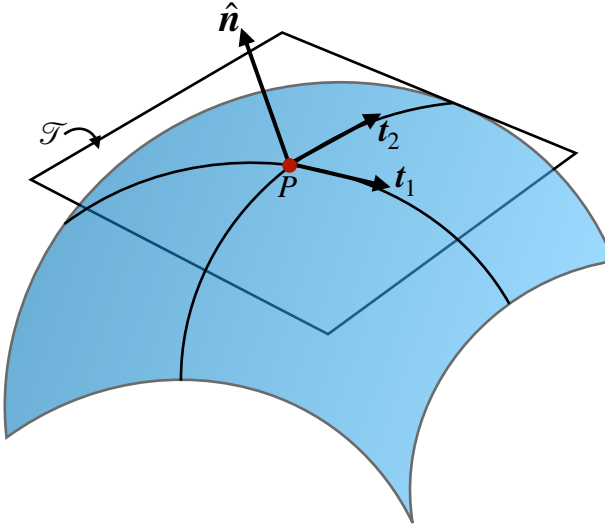


FIGURE 6.5: Depicting the elements needed to construct the curvature of a surface at an arbitrary point, P . The local unit normal direction is given by \hat{n} , along with the two tangent vectors t_1 and t_2 . The tangent vectors span the space of the tangent plane, \mathcal{T} , shown as a flat surface that is tangent at the chosen point on the surface. In this case the surface falls away from the normal direction, as per a convex surface, so that the two radii of curvature are negative. Other surfaces can be concave, whereby both radii of curvature are positive, or hyperbolic (saddle), whereby one is positive and another negative.

according to the quadratic form

$$\eta \approx \frac{1}{2} x_m \mathbb{C}_{mn} x_n, \quad (6.36)$$

where \mathbb{C} is the matrix of second partial derivatives evaluated at the point

$$\mathbb{C} = \begin{bmatrix} \frac{\partial^2 \eta}{\partial x_1^2} & \frac{\partial^2 \eta}{\partial x_1 \partial x_2} \\ \frac{\partial^2 \eta}{\partial x_1 \partial x_2} & \frac{\partial^2 \eta}{\partial x_2^2} \end{bmatrix}. \quad (6.37)$$

As a symmetric matrix, \mathbb{C} is diagonalizable and it has two eigenvalues, R_1^{-1} and R_2^{-1} , along with its associated eigenvectors, e_1 and e_2 . The quadratic form (6.36) can thus be written as

$$\eta \approx \frac{1}{2} R_1^{-1} (\mathbf{x} \cdot e_1)^2 + \frac{1}{2} R_2^{-1} (\mathbf{x} \cdot e_2)^2. \quad (6.38)$$

R_1 and R_2 are the principle radii of curvature for the surface at the point P . They correspond, respectively, to the radii of the curvature circles in the $\hat{n}\text{-}e_1$ and $\hat{n}\text{-}e_2$ planes. If the radius of curvature R_m is positive, then the surface curves towards \hat{n} along the $\hat{n}\text{-}e_i$ plane, and conversely if R_m is negative. The surface takes the shape of a saddle when the two radii of curvature have opposite signs.

There are two scalar invariants of the matrix \mathbb{C} that commonly arise in applications.

- $\text{Tr}(\mathbb{C}) = R_1^{-1} + R_2^{-1}$, which is twice the mean curvature for the surface. With the unit normal vector given by equation (6.4), one can show that

$$-\nabla \cdot \hat{n} = \frac{\nabla^2 \eta}{[1 + (\nabla \eta)^2]^{3/2}}. \quad (6.39)$$

A bit of algebra leads us to conclude that

$$-\nabla \cdot \hat{\mathbf{n}} = \frac{\nabla^2 \eta}{[1 + (\nabla \eta)^2]^{3/2}} = \frac{1}{R_1} + \frac{1}{R_2}, \quad (6.40)$$

for any point along the surface, thus generalizing the result (6.25) found for a curve. Furthermore, if $|\nabla \eta| \ll 1$ then we have

$$\nabla^2 \eta \approx \frac{1}{R_1} + \frac{1}{R_2}, \quad (6.41)$$

with this result proving useful in the study of surface tension in Section 22.11.

- $\det(\mathbb{C}) = 1/(R_1 R_2)$ is known as the *Gaussian curvature*, which is the product of the two curvatures.

6.3.3 Curves on the surface $z = \eta(x, y)$

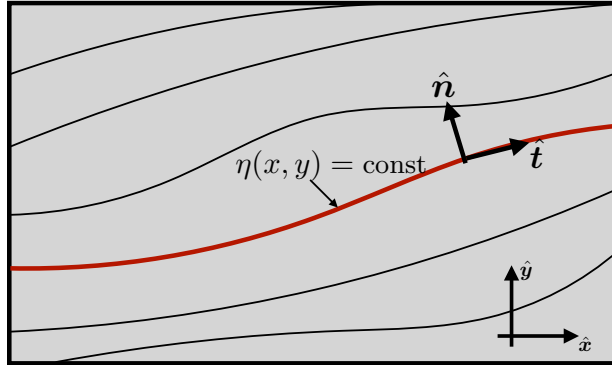


FIGURE 6.6: Geometry depicting a contour along a particular line of constant $z = \eta(x, y)$, such as for a constant elevation path along a mountain or valley. The along-contour unit tangent direction is $\hat{\mathbf{t}} = d\mathbf{x}/ds$, with s the arc length along the contour. The unit normal direction pointing to the left of the contour direction is $\hat{\mathbf{n}}$, with $\hat{\mathbf{n}} \cdot \hat{\mathbf{t}} = 0$ and $\hat{\mathbf{t}} \times \hat{\mathbf{n}} = \hat{\mathbf{z}}$. Both $\hat{\mathbf{n}}$ and $\hat{\mathbf{t}}$ are horizontal unit vectors.

We now consider a curve, as in Section 6.2, defined along a two dimensional surface, $z = \eta(x, y)$, with the curve defined by lines of constant $z = \eta(x, y)$. For example, if $\eta(x, y)$ is the solid earth topography, then lines of constant η are contours of constant topography. By definition, these contours have no projection into the vertical direction (i.e., they do not go uphill or downhill), and they are determined by

$$d\eta = 0 = \nabla \eta \cdot d\mathbf{x}, \quad (6.42)$$

where $d\mathbf{x} = \hat{\mathbf{x}} dx + \hat{\mathbf{y}} dy$ is the horizontal space increment along the contour. Following the introduction of arc length in Section 6.2.1, we write

$$d\eta = 0 = \nabla \eta \cdot d\mathbf{x} = \nabla \eta \cdot \frac{d\mathbf{x}}{ds} ds = \nabla \eta \cdot \hat{\mathbf{t}} ds, \quad (6.43)$$

where $\hat{\mathbf{t}}$ is a unit vector pointing in the direction of the contour. To build an orthogonal triad of coordinates, we then define an orthogonal unit vector, $\hat{\mathbf{n}}$, that points to the left of the contour direction so that

$$\hat{\mathbf{n}} \cdot \hat{\mathbf{t}} = 0 \quad \text{and} \quad \hat{\mathbf{t}} \times \hat{\mathbf{n}} = \hat{\mathbf{z}}, \quad (6.44)$$

as depicted in Figure 6.6. We provide an example use of this formalism in Exercise 6.1.



6.4 Exercises

EXERCISE 6.1: JACOBIAN EVALUATED ALONG A CONTOUR

Consider the vector cross product of two functions, $\psi(x, y)$ and $Q(x, y)$

$$\hat{z} \cdot (\nabla \psi \times \nabla Q) = \partial_x \psi \partial_y Q - \partial_y \psi \partial_x Q \equiv J(\psi, Q), \quad (6.45)$$

where the final equality defined the Jacobian operator. Show that when evaluated along a contour of constant Q , the Jacobian is given by

$$J(\psi, Q) = -(\hat{n} \cdot \nabla Q) (\hat{t} \cdot \nabla \psi) \quad (6.46)$$

where \hat{t} is the unit tangent along the contour and \hat{n} is a unit vector pointing to the left of the tangent (e.g., see Figure 6.6).

EXERCISE 6.2: CURVATURE OF A CIRCLE

Make use of equation (6.26), as well as the polar coordinates from Section 9.3, to show that for a circle of radius r we have

$$-\nabla \cdot \hat{n} = \frac{1}{r}, \quad (6.47)$$

where $\hat{n} = -\hat{r}$ points to the left when moving around the circle in a counterclockwise direction. Hence, the radius of curvature for the circle equals to the circle's radius.



Chapter 7

GENERAL TENSORS IN BRIEF

Vector calculus, as formalized by the Cartesian tensor analysis of Chapters 1 and 2, is sufficient for many areas of geophysical fluid mechanics. However, there are a number of applications where general tensors prove of use to ensure that the physics shines through the maths. We thus go beyond Cartesian tensor analysis to here consider general tensors, thus enabling a more versatile and precise mathematical formalism for the study of geophysical fluid mechanics. Besides enhancing our tools for geophysical fluid mechanics, general tensor analysis is found throughout physics so that understanding the formalism, if only its rudiments, can greatly help to understand the literature.

Geophysical fluid mechanics applications require only a modest level of new formalism in the transition from Cartesian tensors to general tensors. The key reason is that geophysical fluids are assumed to be embedded within Euclidean space, where Euclidean space is the flat space familiar from Newtonian mechanics. Notably, Euclidean space has zero intrinsic curvature so we say that it is a *flat space*. So although we are concerned with fluid motion on curved manifolds (e.g., spherical planets); motion on curved and fluctuating manifolds (e.g., isopycnals); and in describing that motion using non-orthogonal coordinates (e.g., generalized vertical coordinates), the fluid remains embedded within a background Euclidean space. Through this embedding, the local geometry inherits features from the Euclidean space such as how to measure distance between points via the Pythagorean theorem. A further simplification for geophysical fluid mechanics arises since we make use of universal Newtonian time. Hence, time is measured the same by all observers and reference frames. That is, the spatial coordinates used by geophysical fluid mechanics can be a function of time, but the time coordinate is always independent of space. Each of these features of the space and time used for geophysical fluid mechanics means that our mathematical needs are far simpler than the general relativist who studies fluids moving in strong gravity fields and/or over galactic distances.

Throughout our study of general tensor analysis it is useful to keep in mind the central goal is to uncover objective statements about how physical systems operate. In particular, we aim to make use of a formalism that

- supports computations to allow for the comparison of theory with measurements;
- provides a systematic technology to transform between coordinate systems, since there are many occasions where such transformations are useful to develop physical insight and support calculations;
- provides equations that are independent of specific coordinate system.

These goals are realized by general tensor analysis so that the technology reflects the underlying objective nature of physical relationships while allowing for a quantitative realization of those relationships in particular situations.

READER'S GUIDE TO THIS CHAPTER

This brief chapter offers an overview sufficient to appreciate why we need general tensors for certain subjects in this book. We do so by offering a conceptual platform for general tensor analysis, with details of the technology presented in Chapter 8. We focus on tensor analysis on spatial manifolds endowed with a metric, thus touching on the rudiments of *Riemannian differential geometry*. Furthermore, we restrict attention to manifolds embedded in Euclidean space, thus providing a natural extension of the Cartesian tensor analysis from Chapters 1 and 2.

7.1	Coordinate independent physical relations	150
7.1.1	Tensor operations	151
7.1.2	Comments	152
7.2	Points, trajectories, and coordinates	152
7.2.1	Time as a parameter and time as a coordinate	152
7.2.2	The importance of index placement	153
7.3	Example coordinate descriptions	153
7.3.1	Locally orthogonal coordinates	153
7.3.2	Isopycnal coordinates	154
7.3.3	Lagrangian or material coordinates	154
7.3.4	Tracer coordinates	155
7.4	The velocity vector and basis vectors	155
7.4.1	Coordinate representation	156
7.4.2	Basis vectors	156
7.5	Notational conventions	156
7.5.1	Placement of tensor labels	156
7.5.2	Covariant, contravariant, and Einstein summation	156
7.5.3	The boldface notation	157
7.5.4	Space-time approach	158

7.1 Coordinate independent physical relations

Physical relations are independent of subjective choices for their mathematical representations. This principle motivates us to seek mathematical expressions between objects whose meaning transcends a particular coordinate representation. At its most profound level, there is no *a priori* notion of the underlying geometry, with an insistence on such generalities leading to general relativity and the notion of *general covariance*. General covariance means that the physical equations take on the same form regardless the coordinates, even though when unpacked into coordinate components the terms in these equations generally are effected by coordinate choice. We are not going to insist on general covariance in this book, given that we accept the notion of a background Euclidean space on which the fluid moves, and we make use of a universal Newtonian time measured by all observers. Nonetheless, within the restricted class of Euclidean space and Newtonian time, we do insist that the mathematical expression of a physical relation in an inertial reference frame be independent of the choice of coordinates.

We refer to this property of the physical equations as *Newtonian covariance*, or more specifically *coordinate invariance*. This property is ensured when the equations of mathematical physics are relations between geometric objects such as points, vectors, and tensors. We thus focus in this chapter and in Chapter 8 with the operational goal of expressing the continuum equations of fluid mechanics in a form that exposes their underlying geometric foundation. Doing so allows

us to avoid being distracted by coordinate dependent statements, while also offering a framework for the practice of using specific coordinates as well as non-inertial reference frames.

Although physics does not care about coordinates, physicists often do. Namely, it is convenient, and sometimes necessary, to work with specific coordinates suited to the symmetry of the physical system, particularly when comparing theory to experiment. After deriving a physical law in one set of coordinates, it is often of interest to establish the form of the law in another set of coordinates. How does the physical law, typically represented as a differential equation, transform into other coordinates? So long as the equations are written in a proper tensorial form then the equations are form invariant. What constitutes “proper tensorial form” is a topic for this chapter and Chapter 8.

When the equations do not manifest form invariance, then that signals either a mistake or, more relevant to our study, a subjective view that arises when describing motion from a non-inertial reference frame. In Part II, we study the accelerations that result from viewing physical systems from a non-inertial reference frame, with such accelerations (centrifugal and Coriolis) fundamental to geophysical fluid mechanics. For this chapter and Chapter 8, we focus on coordinate invariance as a statement that the equations look the same regardless the choice of coordinates. Consequently, “physics as geometry” has a major practical implication. Namely, we can establish the validity of a physical relation in any convenient set of coordinates, and then extend that relation to all coordinates so long as we respect the basic rules of tensor analysis.

7.1.1 Tensor operations

Extending a mathematical equation to all coordinates requires the equations to respect certain tensor rules. In brief, all tensor indices are properly matched and each derivative is covariant as specified in Section 8.10. In chapter 8, we provide the details needed to understand general coordinate invariance. In this chapter we outline the procedure. The elegance and power rendered by coordinate invariance is the key reason that tensor analysis is ubiquitous in theoretical physics.

To ensure an equation respects coordinate invariance requires us to understand certain properties of tensors and operations with tensors that produce components of new tensors. We here summarize the specific properties characterizing coordinate invariance (taken after page 153 of *Schutz, 1985*):

1. Manipulations of tensor components are called *permissible tensor operations* if they produce components of new tensors. The following are permissible operations:
 - (a) Multiplication of a tensor by a scalar produces a new tensor of the same type.
 - (b) Addition of components of two tensors of the same type gives components of a new tensor of the same type. In particular, only tensors of the same type can be equal.
 - (c) Multiplication of components of two tensors of arbitrary type gives components of a new tensor whose type is given by the sum of the types for the individual tensors. This operation is called the *outer product* or *tensor product* and is denoted by the operator \otimes . For example, $\mathbf{A} \otimes \mathbf{B}$ is a second order tensor built from the outer product of two vectors, \mathbf{A} and \mathbf{B} .
 - (d) Covariant differentiation (Sections 8.10 and 8.11) increases by one the order of a tensor, with the covariant derivative operator denoted by ∇ .
 - (e) Contraction on a pair of indices of the components of a tensor reduces by one the order of a tensor.

- (f) A corollary of the multiplication rule is that if the inner product of two objects yields a tensor, and if one of these objects is itself a tensor then so too is the other. This result is known as the *quotient* rule.
2. If two tensors of the same type have equal components in a given coordinate system, then they have equal components in all coordinate systems. Hence, the tensors are identical. As a corollary, if a tensor is zero in one coordinate system, then it is zero in all coordinate systems.
 3. If a mathematical equation consists of tensors combined only by the permissible tensor operations, and if the equation is true in one coordinate system, then it is true in any coordinate system. If the equations involve covariant derivatives, then the equations remain form invariant under changes in coordinates. For the partial differential equations of geophysical fluid mechanics, covariant differentiation is the key to coordinate invariance.

7.1.2 Comments

The remainder of this chapter, as well as Chapter 8, provide the details needed for unpacking the notions of coordinate invariance and specifying particular tensor operations. Even without penetrating these details, the reader should be able to appreciate why coordinate invariance is so central to physics.

7.2 Points, trajectories, and coordinates

Consider a point in space, \mathcal{P} , at a particular time τ . As time progresses, the point traces out a curve in space-time. We call that curve a *trajectory*. The trajectory could be of a point particle following the fluid flow, thus defining the Lagrangian reference frame (Section 14.3). Or it could trace the path of something else such as a fish, balloon, boat, or airplane. As the trajectory is a one-dimensional curve, it is specified mathematically by a single parameter (see Section 6.2.1). We choose the time measured by an observer on the trajectory for this parameter, in which case the trajectory is written $\mathcal{P}(\tau)$.

A point in the fluid as well as the trajectory in space-time are both geometric objects that exist independently of any coordinate representation. Even so, we find the need to represent points, trajectories, vectors, and other geometric objects using coordinates. For example, coordinates are needed to make quantitative statements about fluid flow in relation to observers. What is its speed and direction relative to a chosen reference frame? What is the distance from an origin or from another particle? Tensor analysis provides a formalism that enables us to answer such quantitative questions while maintaining a clear view on the underlying physics and geometry.

7.2.1 Time as a parameter and time as a coordinate

In special and general relativity, there is a mixing of space and time that warrants the use of four-dimensional space-time tensor analysis. In contrast, for classical mechanics forming the foundation of geophysical fluid mechanics, time remains numerically the same throughout space. We thus make use of the same universal (or Newtonian) time since the fluid velocity and wave speeds are far smaller than the speed of light. Hence, for our studies we generally restrict attention to the space + time formalism of classical mechanics rather than the space-time formalism of relativity. See Section 7.5.4 for one qualification to this usage.

The time parameter, τ , specifies a point along a trajectory. The coordinate time, t , measures time for all positions throughout space. This distinction between the time parameter and

time coordinate is pedantic given that $\tau = t$ (up to a constant offset) in a Newtonian universe. Nonetheless, it is convenient to make the distinction when measuring how fluid properties change since these changes are subject to motion of the observer. For example, changes following a trajectory, found by computing the trajectory time derivative $\partial/\partial\tau$, are generally distinct from changes found by computing the time derivative $\partial/\partial t$, in which the spatial coordinates are held fixed.

When the trajectory is defined by a fluid particle, we refer to $\partial/\partial\tau$ as the *material or Lagrangian time derivative*. This time derivative is the same as when working with Newtonian particle mechanics as in Part II of this book. In contrast, if the spatial coordinates are fixed in space, then $\partial/\partial t$ is an Eulerian time derivative. When alternative spatial coordinates are used, some of which can move (see Section 7.2.2), then $\partial/\partial t$ can be a mixture of Lagrangian and Eulerian or perhaps neither.

7.2.2 The importance of index placement

Much of the formalism of general tensor analysis builds from Cartesian representations of vector and matrix analysis, with generalizations that provide objective statements independent of coordinates. One key point of distinction from Cartesian tensors is that the position (up or down) of a tensor label has significance in general tensor analysis, whereas there is no significance with Cartesian tensors. We follow the standard convention by labeling an arbitrary coordinate with indices upstairs in their *contravariant* position, ξ^α . It is furthermore common to express each of the coordinates in an ordered list according to

$$\xi^\alpha = (\xi^0, \xi^1, \xi^2, \xi^3). \quad (7.1)$$

We emphasize that the index is a label for the coordinate; it is not an exponent or power. We use a convention whereby Greek labels run from $\alpha = 0, 1, 2, 3$ with $\alpha = 0$ the time coordinate and $\alpha = a = 1, 2, 3$ the three coordinates used to locate a point in the Euclidean space of Newtonian mechanics. The following shorthand notations are commonly used in this book

$$\xi^\alpha = (\xi^0, \xi^1, \xi^2, \xi^3) = (\xi^0, \xi^a) = (\xi^0, \xi). \quad (7.2)$$

7.3 Example coordinate descriptions

We here offer a few examples of coordinates used for describing geophysical fluid systems. As the time coordinate remains universal in our study, we are here only concerned with the spatial coordinates, $a = 1, 2, 3$.

7.3.1 Locally orthogonal coordinates

In Chapter 9 we detail three sets of commonly used locally orthogonal coordinates: Cartesian, spherical, and cylindrical-polar. We here briefly summarize these coordinates.

In Cartesian coordinates, (x, y, z) , the position vector for a point in space is written

$$\mathbf{x} = x \hat{\mathbf{x}} + y \hat{\mathbf{y}} + z \hat{\mathbf{z}} \quad \text{Cartesian.} \quad (7.3)$$

For spherical coordinates (λ, ϕ, r) the position vector is (see Figure 9.1)

$$\mathbf{x} = r \hat{\mathbf{r}} \quad \text{spherical,} \quad (7.4)$$

and cylindrical-polar coordinates (r, ϑ, z) (see Figure 9.2) we have

$$\mathbf{x} = r \hat{\mathbf{r}} + z \hat{\mathbf{z}} \quad \text{cylindrical-polar.} \quad (7.5)$$

Note that in spherical coordinates, r is the distance from the origin to the point and $\hat{\mathbf{r}}$ points from the origin to the point. In contrast, for cylindrical-polar coordinates, r is the distance from the z -axis and $\hat{\mathbf{r}}$ is the horizontal vector pointing from the z -axis to the point. Each of these coordinate representations identify positions in space relative to a fixed coordinate origin. We can use these coordinates to mark the trajectory, $\mathbf{X}(t)$, as it crosses the spatial coordinate, $\mathbf{X}(t) = \mathbf{x}$, at time t .

As shown in Section 7.4, Cartesian coordinates have basis vectors that maintain a fixed direction throughout space. This feature lends simplicity to Cartesian coordinates and its corresponding Cartesian tensor analysis (Chapters 1 and 2). In contrast, the spherical basis vectors are spatially dependent. Likewise, the radial and angular basis vectors for polar cylindrical coordinates are spatially dependent, whereas the vertical direction is the same as the fixed Cartesian vertical direction. Additionally, the spherical and cylindrical coordinates do not all have the same physical dimensions. Each of these features of spherical and cylindrical coordinates places them outside the purview of Cartesian tensor analysis.

7.3.2 Isopycnal coordinates

In geophysical fluids that are stably stratified in the vertical, it is common to measure the vertical position of a fluid element by specifying its entropy, buoyancy, or potential density depending on the application. We generically write these *isentropic*, *buoyancy*, or *isopycnal* coordinates as

$$\xi^a = (x, y, b) \quad \text{with} \quad b = b(x, y, z, t) \quad \text{isopycnal coordinates,} \quad (7.6)$$

where $b = b(x, y, z, t)$ is a generic symbol for entropy, buoyancy, or potential density. Entropy, buoyancy, and potential density are materially invariant for perfect fluid flow (flow absent irreversible processes such as mixing or heating). Hence, all fluid particle motion occurs on surfaces of constant b . Under such perfect fluid conditions, isopycnal coordinates are of great use for describing fluid mechanics of stably stratified geophysical flows.

The isopycnal coordinates are generally not orthogonal since the direction normal to a buoyancy surface is not generally vertical. Hence, even if the horizontal coordinates are Cartesian, the use of b to measure the vertical precludes the use of Cartesian tensor analysis. Furthermore, we note the distinct physical dimensions of the three spatial coordinates (x, y, b) , again necessitating the use of general tensor analysis.

7.3.3 Lagrangian or material coordinates

We often conceive of a fluid as a continuum of constant mass fluid elements distinguished by continuum marker coordinates or labels. The initial position for a fluid element offers a suitable (and common) choice for these *material coordinates*. The fluid dynamical equations of motion (i.e., Newton's Law of motion) can be formulated using material coordinates so long as the material coordinate maintains a 1-to-1 relation to points in space. This kinematical framework is termed *Lagrangian* or *material*. The resulting dynamical equations share much in common with Newtonian particle mechanics, though with the added feature of contact forces acting between the fluid elements. We formally describe Lagrangian coordinates in Section 14.4 and encounter Lagrangian descriptions throughout this book.

If we represent material coordinates by the Cartesian positions of fluid elements at an arbitrary

initial time, then we can make use of Cartesian tensor analysis. However, it is sometimes useful to make use of alternative markers. One example is the isopycnal coordinate mentioned above, whose value remains invariant under perfect fluid motion. In this manner, we refer to the isopycnal coordinates as “quasi-Lagrangian” since its vertical coordinate follows the vertical position of a perfect fluid parcel whereas its horizontal coordinates are Eulerian.

7.3.4 Tracer coordinates

Consider a triplet of linearly independent tracer concentrations $C^a = C^a(x, y, z, t)$ that spans \mathbb{R}^3 . Hence, at any point in space there is a unique intersection of three constant tracer surfaces, so that we can uniquely determine a point in space by specifying the value for the three tracer concentrations. We can thus use tracer concentrations as the spatial coordinates

$$\xi^a = (C^1, C^2, C^3). \quad (7.7)$$

In some cases there are only two linearly independent tracers, in which case the two may be used in combination with a third spatial coordinate such as depth or pressure. Furthermore, the case of one tracer coordinate formally reduces to the isopycnal coordinate system described above.¹

7.4 The velocity vector and basis vectors

Consider two points in space that sit along a particular trajectory separated by an infinitesimal time increment, $d\tau$. The velocity vector for this trajectory is defined by

$$\vec{v}(\tau) = \lim_{\Delta\tau \rightarrow 0} \frac{\mathcal{P}(\tau + \Delta\tau/2) - \mathcal{P}(\tau - \Delta\tau/2)}{\Delta\tau} = \frac{d\mathcal{P}(\tau)}{d\tau}. \quad (7.8)$$

The velocity is a vector pointing in the direction determined by the difference between two points on a trajectory, in the limit as the time separation between the points vanishes. Consequently, the velocity points in a direction tangent to the trajectory. Notably, the above definition for the velocity makes no use of coordinates. Rather, the velocity vector is determined by the geometry of the trajectory and the specification of the trajectory’s time parameter. Hence, velocity is fundamentally an arrow with a length and direction and as such, the velocity is a geometric object with this fact emphasized by exposing the arrow.

The definition of velocity as a vector tangent to the trajectory is a general property of all vectors living on a manifold. Namely, a vector at a point on a manifold lives within the tangent space to the manifold at that point. This observation signals to us the need to be very careful when comparing vectors on a curved manifold such as the sphere or an isopycnal surface. Namely, the comparison of two vectors can only occur when they live on the same tangent space. So before comparing two vectors, they must be brought to the same tangent space so they can be compared. Herein lies the fundamental reason we need to extend our definition of partial derivative to covariant derivative when acting on vectors and higher order tensors.

¹See [Nurser et al. \(2022\)](#) for an elaboration of a description of fluid flow in the space defined by arbitrary continuous properties.

7.4.1 Coordinate representation

We now establish an arbitrary set of spatial coordinates, ξ^a , to represent points in space. These coordinates are used to measure the spatial position of the trajectory according to

$$\mathcal{P}(\tau) = \mathcal{P}[\xi^a(\tau)], \quad (7.9)$$

where $\xi^a(\tau)$ is the coordinate position on the trajectory at time τ . This coordinate representation for the trajectory induces a coordinate representation for the velocity through use of the chain rule

$$\vec{v}(\tau) = \frac{d\mathcal{P}(\tau)}{d\tau} = \frac{\partial \mathcal{P}}{\partial \xi^a} \frac{d\xi^a}{d\tau} \equiv \vec{e}_a v^a. \quad (7.10)$$

The expansion coefficients

$$v^a = \frac{d\xi^a}{d\tau} \quad (7.11)$$

provide a representation for the velocity vector $\vec{v}(\tau)$ within the coordinate system ξ^a .

7.4.2 Basis vectors

As seen by equation (7.10), for each number, v^a , there is a corresponding basis vector, \vec{e}_a , whose value at the point \mathcal{P} is given by

$$\vec{e}_a(\mathcal{P}) = \frac{\partial \mathcal{P}}{\partial \xi^a}. \quad (7.12)$$

Abstracting this expression allows us to identify the basis vector as the partial derivative

$$\vec{e}_a = \frac{\partial}{\partial \xi^a}. \quad (7.13)$$

The basis vectors are generally a function of space and time, with Cartesian coordinates a notable exception whereby they are space-time constants.

7.5 Notational conventions

We here introduce notational conventions that help to simplify many of the manipulations, sometimes referred to as *index gymnastics*, encountered with general tensors.

7.5.1 Placement of tensor labels

As indicated in Section 7.2.2, the placement of tensor labels has specific meaning with general tensor analysis. It is therefore critical to maintain proper usage to ensure *conservation of indices* across an equal sign. As a first example of this usage, notice how the basis vectors in equation (7.12) inherit a lowered tensor label. This placement follows from the partial derivative operator that carries an upper coordinate label in the denominator of the operator.

7.5.2 Covariant, contravariant, and Einstein summation

For general tensors, the Einstein summation convention assumes that labels are summed over their range when a lower *covariant* label matches an upper *contravariant* label. In this way we

have an arbitrary vector in space written as

$$\vec{F}(\tau) = \sum_{a=1}^3 \vec{e}_a F^a = \vec{e}_a F^a. \quad (7.14)$$

This form of the summation convention generalizes that used for Cartesian tensors in Chapter 1. Importantly, for general tensors we form the contraction (summation) between a lower and an upper label.

The names *covariant* and *contravariant* originate from their relation to the labels placed on a coordinate basis vectors (Section 7.4.2), and thus how they change under coordinate transformations relative to how basis vectors change (Section 8.1). The covariant tensor label accords with the downstairs label placement for a coordinate basis, whereas the upstairs contravariant label is contrary to the coordinate basis (e.g., see Section 2.26 of [Schutz \(1980\)](#)). A useful mnemonic is “co-low” to signal that the covariant label is downstairs (“low”). The names covariant and contravariant are used infrequently in modern tensor analysis, which instead considers tensors as geometric objects and so is not primarily concerned with the coordinate representations of tensors.

7.5.3 The boldface notation

In Cartesian tensor analysis we have no need to distinguish \vec{F} from the boldface \mathbf{F} . One means to extend this notation to general tensors is to organize the contravariant representation F^a into an ordered list (F^1, F^2, F^3) and to use the boldface notation

$$\mathbf{F} = (F^1, F^2, F^3). \quad (7.15)$$

Likewise, we can organize the basis vectors according to

$$\vec{\mathbf{e}} = (\vec{e}_1, \vec{e}_2, \vec{e}_3) \quad (7.16)$$

and the coordinates as

$$\boldsymbol{\xi} = (\xi^1, \xi^2, \xi^3). \quad (7.17)$$

With this notation the velocity vector representation from equation (7.10) takes on the form

$$\vec{v} = \vec{e}_a v^a = \vec{e} \cdot \mathbf{v}. \quad (7.18)$$

Likewise, a trajectory can be represented in terms of a chosen set of coordinates according to

$$\mathcal{P} = \vec{e}_a \xi^a = \vec{e} \cdot \boldsymbol{\xi}. \quad (7.19)$$

Notice that the arrow symbol over the basis vector remains even when using the boldface. This usage is required since the arrow carries information about the vector nature of the object, whereas the boldface is merely a shorthand for an ordered list.

Although the above notation makes good sense, we more generally allow the boldface to be synonymous with the vector arrow notation

$$\mathbf{F} = \vec{F} = \vec{e}_a F^a. \quad (7.20)$$

Though corrupting the convention in equation (7.18), this notation is readily used in the literature and as such will be employed in this book where the meaning is clear and after our tensor brain-muscle has been exercised.

7.5.4 Space-time approach

As introduced in Section 7.2.2, we make use of a Greek label when incorporating time to the tensor indices, with $\alpha = 0$ denoting the time coordinate. Time remains universal in the Newtonian world of geophysical fluid mechanics. However, many coordinates are functions of both space and time. Therefore, when measuring time changes in one coordinate system it will differ from time changes in another. Following equation (7.2) used for coordinates, we make use of the following index notation and ordered list for contravariant components of 4-vectors

$$F^\alpha = (F^0, F^1, F^2, F^3) = (F^0, F^a) = (F^0, \mathbf{F}). \quad (7.21)$$

In Cartesian coordinates, the time component of the velocity 4-vector is unity

$$v^\alpha = (1, v^1, v^2, v^3) = (1, v^a) = (1, \mathbf{v}) \quad \text{4-velocity in Cartesian coordinates.} \quad (7.22)$$

We make use of the 4-vector formalism in Section 8.9 when performing the transformation of partial derivatives. In that discussion we note that the time coordinate is not a function of space and yet the space coordinates are generally a function of time, which makes the 4-vector formalism of use to transform partial derivatives. Otherwise, we retain the space plus time approach (3+1) of classical mechanics.



Chapter 8

GENERAL TENSOR ANALYSIS

In this chapter we generalize the Cartesian algebra of Chapter 1 and Cartesian calculus of Chapter 2 to general tensors. We focus on space tensors so that time typically remains outside of the tensor formalism. The single exception is that we consider a space-time transformation of the partial time derivative operator (Section 8.9), since the time derivative cares about the motion of space coordinates even though the time itself is universal.

Cartesian tensor analysis provides a systematic formulation of vector analysis. The Euclidean metric provided by the Kronecker tensor (i.e., the identity tensor) underlies Cartesian tensors. Here, we extend the formalism of Cartesian tensors by allowing for an arbitrary spatial metric, and in so doing move into the realm of *Riemannian differential geometry*. A more mathematically deductive approach would be to first study calculus on differential manifolds that are not endowed with a metric, which constitutes the subject matter of *differential forms* or the *exterior calculus*. Doing so in the current book is beyond our scope.

READER'S GUIDE TO THIS CHAPTER

This chapter is necessary for understanding the mathematics of generalized vertical coordinates in Chapters 56, 57, and 58, as well as general curvilinear coordinates such as those in Chapter 9. Otherwise, this chapter can be skimmed or returned to later if the need arises. Some material in this chapter is an updated version of Chapters 20 and 21 from [Griffies \(2004\)](#), along with some streamlining. Other resources include the treatment of tensors for fluid mechanics as given by [Aris \(1962\)](#) as well as the classical physics treatment by [Thorne and Blandford \(2017\)](#).

8.1	The metric tensor and coordinate transformations	160
8.1.1	Cartesian coordinates in Euclidean space	160
8.1.2	The metric as a symmetric second order tensor	161
8.1.3	Coordinate representation of the metric tensor	161
8.1.4	Transforming the coordinate representation of the metric tensor	162
8.1.5	Basis vectors	163
8.1.6	Finite distance between points	163
8.2	One-forms	163
8.2.1	Coordinate representation of a one-form	163
8.2.2	Basis one-forms and the bi-orthogonality relation	164
8.2.3	Metric as a mapping between vectors and one-forms	164
8.2.4	Transformation of the coordinate representation	165
8.2.5	Arbitrary coordinate representation of inverse metric	165
8.2.6	Functions versus scalars	165
8.3	Scalar product	166

8.4	Worked example: oblique coordinates	166
8.4.1	Turning the crank	167
8.4.2	Comments	168
8.5	The volume element and Jacobian of transformation	168
8.5.1	Jacobian of transformation	169
8.5.2	Relating the Jacobian to the determinant of the metric	169
8.6	The permutation symbol and the determinant	170
8.6.1	Connecting the permutation symbol to the determinant	170
8.6.2	Further identities satisfied by the determinant	170
8.7	The Levi-Civita tensor and the volume element	171
8.7.1	General coordinate representation of the Levi-Civita tensor	171
8.7.2	The Levi-Civita tensor and the volume element	172
8.8	Vector cross product	172
8.9	Coordinate transformation of partial derivatives	172
8.9.1	The space-time transformation matrix	172
8.9.2	Determinant of the transformation matrix	173
8.9.3	Multiplying the transformation matrix and its inverse	174
8.9.4	Transformation of space and time partial derivatives	174
8.10	Covariant derivative of a scalar	175
8.11	Covariant derivative of a vector	175
8.11.1	Derivative of a vector and Christoffel symbols	175
8.11.2	An alternative derivation	176
8.11.3	Christoffel symbols as the metric connection	176
8.12	Covariant derivative of a one-form	176
8.13	Covariant derivative of the metric tensor	177
8.14	Christoffel symbols in terms of the metric	177
8.15	Covariant divergence of a vector	177
8.15.1	Contraction of the Christoffel symbols	178
8.15.2	Exponential of the determinant	178
8.16	Covariant Laplacian of a scalar	178
8.17	Covariant curl of a vector	179
8.18	Gauss's divergence theorem	179
8.19	Stokes' curl theorem	179

8.1 The metric tensor and coordinate transformations

In the study of fluid mechanics we find the need to measure the distance between two points in space at a particular time instance. Since we assume all points live on a smooth and orientable manifold (e.g., a sphere, an isopycnal), it is sufficient to consider the distance between two infinitesimally close points and use integration to measure finite distances. The measurement of distance requires a metric tensor, which is the subject of this section.

8.1.1 Cartesian coordinates in Euclidean space

Consider a Cartesian coordinate representation for the spatial position of two points, with point \mathcal{P} having space coordinates $\xi^a = x^a$ and the other point \mathcal{Q} an infinitesimal distance away at $x^a + dx^a$. Furthermore, let

$$d\mathbf{x} = dx^a \vec{e}_a \quad (8.1)$$

be the infinitesimal space vector pointing from \mathcal{P} to \mathcal{Q} . Since the space is Euclidean, the squared distance between the two points is based on the Euclidean norm; i.e., the familiar scalar or dot product (Section 1.3)

$$ds^2 = d\mathbf{x} \cdot d\mathbf{x} = \vec{e}_a \cdot \vec{e}_b dx^a dx^b = \delta_{ab} dx^a dx^b. \quad (8.2)$$

In this expression,

$$(ds)^2 \equiv ds^2 \quad (8.3)$$

is the squared infinitesimal arc-length separating the two points. The Kronecker symbol, δ_{ab} , is symmetric

$$\delta_{ab} = \delta_{ba}, \quad (8.4)$$

and vanishes when $a \neq b$ and is unity when $a = b$

$$\delta_{ab} = \begin{cases} 0 & \text{if } a \neq b \\ 1 & \text{if } a = b. \end{cases} \quad (8.5)$$

The Kronecker symbol is a representation of the identity tensor.

8.1.2 The metric as a symmetric second order tensor

As defined by equation (8.2), δ_{ab} forms the Cartesian representation of the *metric tensor* for Euclidean space. The metric is a second order tensor, meaning that its coordinate representation carries two tensor labels. Contracting the metric tensor with two vectors leads to a number, namely the squared distance between the two points. Hence, the metric establishes the means to measure the distance between two points that live on a manifold.

We write this distance-measuring property of the metric tensor in a geometric manner through

$$\text{distance}(\vec{P}, \vec{Q}) = \sqrt{\mathfrak{g}(\vec{P}, \vec{Q})}. \quad (8.6)$$

Here, \mathfrak{g} is the metric tensor with coordinate representation g_{ab} and \vec{P}, \vec{Q} are infinitesimally close vectors with coordinate representations

$$\vec{P} = \xi^a \vec{e}_a \quad \text{and} \quad \vec{Q} = \vec{P} + d\xi^a \vec{e}_a. \quad (8.7)$$

Equation (8.6) indicates that the metric tensor takes two vectors as argument and produces a scalar. Furthermore, since

$$\text{distance}(\vec{P}, \vec{Q}) = \text{distance}(\vec{Q}, \vec{P}) \geq 0, \quad (8.8)$$

the metric tensor is a symmetric and positive tensor that produces zero only when $\vec{P} = \vec{Q}$.

8.1.3 Coordinate representation of the metric tensor

Given the geometric expression (8.6) for the metric, we determine its representation in an arbitrary coordinate system by considering the squared distance between the coordinate basis vectors

$$\text{distance}(\vec{e}_a, \vec{e}_b) = \sqrt{\mathfrak{g}(\vec{e}_a, \vec{e}_b)}. \quad (8.9)$$

This relation determines the coordinate components of the metric tensor

$$\mathfrak{g}(\vec{e}_a, \vec{e}_b) \equiv g_{ab}. \quad (8.10)$$

Furthermore, for a manifold embedded in Euclidean space (as considered in this book) this relation is written

$$g_{ab} = \vec{e}_a \cdot \vec{e}_b = \sum_{i=1}^3 (e_a)_i (e_b)_i. \quad (8.11)$$

In this manner, we see that the metric tensor components are determined by computing the Euclidean scalar product between the basis vectors. We also see that if the basis vectors are orthogonal, then the metric tensor components vanish for $a \neq b$.

8.1.4 Transforming the coordinate representation of the metric tensor

We find opportunities to represent the metric tensor in various coordinate systems. Here, we consider the transformation from Cartesian coordinates $\xi^a = x^a$ to arbitrary coordinates $\xi^{\bar{a}}$. Use of the chain rule along with some index gymnastics leads to the equivalent expression for the squared infinitesimal length between two points

$$ds^2 = \delta_{ab} d\xi^a d\xi^b = \delta_{ab} \frac{\partial \xi^a}{\partial \xi^{\bar{a}}} \frac{\partial \xi^b}{\partial \xi^{\bar{b}}} d\xi^{\bar{a}} d\xi^{\bar{b}} \equiv \delta_{ab} \Lambda_{\bar{a}}^a \Lambda_{\bar{b}}^b d\xi^{\bar{a}} d\xi^{\bar{b}} \equiv g_{\bar{a}\bar{b}} d\xi^{\bar{a}} d\xi^{\bar{b}}, \quad (8.12)$$

where

$$g_{\bar{a}\bar{b}} = \delta_{ab} \Lambda_{\bar{a}}^a \Lambda_{\bar{b}}^b \quad (8.13)$$

defines the components to the metric tensor as represented by the new set of coordinates $\xi^{\bar{a}}$. We also introduced elements to the *transformation matrix*

$$\Lambda_{\bar{a}}^a = \frac{\partial \xi^a}{\partial \xi^{\bar{a}}}. \quad (8.14)$$

This matrix of partial derivatives has a non-zero entry when a coordinate in one representation changes while moving along the direction of a coordinate in the other representation. As for any partial derivative, the complement coordinates are held fixed when performing the derivative. Although carrying indices, the numbers $\Lambda_{\bar{a}}^a$ are *not* components of a tensor. Instead, they are components of a matrix used to transform tensor representations from one coordinate system to another. Organized as a matrix, we follow a convention whereby the row is denoted by a and the column by \bar{a}

$$\Lambda_{\bar{a}}^a = \begin{bmatrix} (\partial \xi^1 / \partial \xi^{\bar{1}})_{\bar{2},\bar{3}} & (\partial \xi^1 / \partial \xi^{\bar{2}})_{\bar{1},\bar{3}} & (\partial \xi^1 / \partial \xi^{\bar{3}})_{\bar{1},\bar{2}} \\ (\partial \xi^2 / \partial \xi^{\bar{1}})_{\bar{2},\bar{3}} & (\partial \xi^2 / \partial \xi^{\bar{2}})_{\bar{1},\bar{3}} & (\partial \xi^2 / \partial \xi^{\bar{3}})_{\bar{1},\bar{2}} \\ (\partial \xi^3 / \partial \xi^{\bar{1}})_{\bar{2},\bar{3}} & (\partial \xi^3 / \partial \xi^{\bar{2}})_{\bar{1},\bar{3}} & (\partial \xi^3 / \partial \xi^{\bar{3}})_{\bar{1},\bar{2}} \end{bmatrix}. \quad (8.15)$$

Note that the lower index is displaced to the right to delineate which index refers to the column. The transformation matrix is nonsingular for one-to-one invertible coordinate transformations, in which case its determinant, called the *Jacobian of the transformation*, is nonvanishing and single signed. Finally, we sometimes find it useful to write the un-barred coordinates as an ordered list in a column, $\xi = (\xi^1, \xi^2, \xi^3)^T$, in which case the transformation matrix takes on the abbreviated form

$$\Lambda_{\bar{a}}^a = \begin{bmatrix} (\partial \xi / \partial \xi^{\bar{1}})_{\bar{2},\bar{3}} & (\partial \xi / \partial \xi^{\bar{2}})_{\bar{1},\bar{3}} & (\partial \xi / \partial \xi^{\bar{3}})_{\bar{1},\bar{2}} \end{bmatrix}. \quad (8.16)$$

Use of this expression for the transformation matrix leads to the arbitrary coordinate representation of the metric tensor

$$g_{\bar{a}\bar{b}} = \vec{e}_{\bar{a}} \cdot \vec{e}_{\bar{b}} = \begin{bmatrix} \frac{\partial \xi}{\partial \xi^{\bar{1}}} \cdot \frac{\partial \xi}{\partial \xi^{\bar{1}}} & \frac{\partial \xi}{\partial \xi^{\bar{1}}} \cdot \frac{\partial \xi}{\partial \xi^{\bar{2}}} & \frac{\partial \xi}{\partial \xi^{\bar{1}}} \cdot \frac{\partial \xi}{\partial \xi^{\bar{3}}} \\ \frac{\partial \xi}{\partial \xi^{\bar{2}}} \cdot \frac{\partial \xi}{\partial \xi^{\bar{1}}} & \frac{\partial \xi}{\partial \xi^{\bar{2}}} \cdot \frac{\partial \xi}{\partial \xi^{\bar{2}}} & \frac{\partial \xi}{\partial \xi^{\bar{2}}} \cdot \frac{\partial \xi}{\partial \xi^{\bar{3}}} \\ \frac{\partial \xi}{\partial \xi^{\bar{3}}} \cdot \frac{\partial \xi}{\partial \xi^{\bar{1}}} & \frac{\partial \xi}{\partial \xi^{\bar{3}}} \cdot \frac{\partial \xi}{\partial \xi^{\bar{2}}} & \frac{\partial \xi}{\partial \xi^{\bar{3}}} \cdot \frac{\partial \xi}{\partial \xi^{\bar{3}}} \end{bmatrix}. \quad (8.17)$$

8.1.5 Basis vectors

We transform the basis vectors from Cartesian into arbitrary coordinates through the transformation

$$\vec{e}_{\bar{a}} = \Lambda_{\bar{a}}^a \vec{e}_a. \quad (8.18)$$

Use of the transformation matrix (8.16) renders the arbitrary coordinate basis vectors

$$\vec{e}_{\bar{1}} = \frac{\partial \xi}{\partial \xi^{\bar{1}}} \quad \text{and} \quad \vec{e}_{\bar{2}} = \frac{\partial \xi}{\partial \xi^{\bar{2}}} \quad \text{and} \quad \vec{e}_{\bar{3}} = \frac{\partial \xi}{\partial \xi^{\bar{3}}}, \quad (8.19)$$

which corresponds to the metric tensor written as in equation (8.17).

8.1.6 Finite distance between points

Once the metric is determined, the distance along a curve between two finitely separated points is given by integration

$$L = \int \sqrt{ds^2} = \int_{\varphi_1}^{\varphi_2} \left| g_{ab} \frac{d\xi^a}{d\varphi} \frac{d\xi^b}{d\varphi} \right|^{1/2} d\varphi, \quad (8.20)$$

where φ is a parameter specifying the curve (e.g., the arc length as in Section 2.4), with φ_1 and φ_2 specifying the endpoints of the curve.

8.2 One-forms

The metric tensor, g , is a function of two vectors, so that when the metric “eats” the two vectors the result is the scalar distance between the vectors (equation (8.6))

$$\text{distance}(\vec{A}, \vec{B}) = \sqrt{g(\vec{A}, \vec{B})}. \quad (8.21)$$

What if the metric only eats one vector? The resulting geometric object is known as a *one-form*

$$\tilde{A} \equiv g(\vec{A},), \quad (8.22)$$

with the tilde used to distinguish a one-form from a vector.

8.2.1 Coordinate representation of a one-form

We can determine the coordinate representation of a one-form by eating a basis vector

$$\tilde{A}(\vec{e}_b) = g(\vec{A}, \vec{e}_b) = g(A^a \vec{e}_a, \vec{e}_b) = g(\vec{e}_a, \vec{e}_b) A^a = g_{ab} A^a. \quad (8.23)$$

To reach this result we pulled the coordinate representation A^a outside of the metric tensor since the tensor eats vectors rather than numbers. This equation defines the coordinate representation of the one-form \tilde{A} in terms of its *dual* vector \vec{A} and the metric tensor

$$A_b = g_{ab} A^a. \quad (8.24)$$

We thus see that the metric tensor provides the means to lower an index on the representation of a vector, thus producing the representation of a one-form. We return to this important point in Section 8.2.3.

8.2.2 Basis one-forms and the bi-orthogonality relation

Just as for vectors, we find use for a basis of one-forms to specify their coordinate representation. The basis of one-forms, \tilde{e}^a , are defined through the bi-orthogonality relation

$$g(\tilde{e}^a, \vec{e}_b) = \tilde{e}^a \cdot \vec{e}_b = \delta_b^a, \quad (8.25)$$

where

$$\delta_b^a = g^{ac} g_{cb} \quad (8.26)$$

are components to the Kronecker tensor, taking the value of unity when $a = b$ and zero otherwise

$$\delta_b^a = \begin{bmatrix} 1 & 0 & 0 \\ 0 & 1 & 0 \\ 0 & 0 & 1 \end{bmatrix}. \quad (8.27)$$

Note that it is only for Cartesian coordinates that we have

$$\delta_c^a = g^{ab} \delta_{bc} \quad \text{Cartesian coordinates}, \quad (8.28)$$

which follows since $g^{ab} = \delta^{ab}$ in Cartesian coordinates.

We can obtain an explicit expression for the basis one-forms in arbitrary coordinates by transforming from Cartesian coordinates through use of the inverse transformation

$$\tilde{e}^{\bar{a}} = \Lambda_a^{\bar{a}} \tilde{e}^a, \quad (8.29)$$

which renders

$$\tilde{e}^{\bar{1}} = \hat{x} \frac{\partial \xi^{\bar{1}}}{\partial x} + \hat{y} \frac{\partial \xi^{\bar{1}}}{\partial y} + \hat{z} \frac{\partial \xi^{\bar{1}}}{\partial z} = \nabla \xi^{\bar{1}} \quad (8.30a)$$

$$\tilde{e}^{\bar{2}} = \hat{x} \frac{\partial \xi^{\bar{2}}}{\partial x} + \hat{y} \frac{\partial \xi^{\bar{2}}}{\partial y} + \hat{z} \frac{\partial \xi^{\bar{2}}}{\partial z} = \nabla \xi^{\bar{2}} \quad (8.30b)$$

$$\tilde{e}^{\bar{3}} = \hat{x} \frac{\partial \xi^{\bar{3}}}{\partial x} + \hat{y} \frac{\partial \xi^{\bar{3}}}{\partial y} + \hat{z} \frac{\partial \xi^{\bar{3}}}{\partial z} = \nabla \xi^{\bar{3}}. \quad (8.30c)$$

In Section 8.9.3 we verify that the basis one-forms satisfy the orthogonality relation (8.25) with the basis vectors

$$\tilde{e}^{\bar{a}} \cdot \vec{e}_{\bar{b}} = \delta_{\bar{b}}^{\bar{a}}. \quad (8.31)$$

8.2.3 Metric as a mapping between vectors and one-forms

We can contract the expression (8.24) with components of the inverse metric tensor, g^{ab} , to render

$$g^{ab} A_b = g^{ab} g_{bc} A^c = \delta_c^a A^c = A^a. \quad (8.32)$$

This identity, as well as equation (8.24), show that the metric provides a map between coordinate representations of one-forms and vectors.

To every vector \vec{A} there is a corresponding one-form \tilde{A} . We say that the one-forms and vectors are *dual*, with the mapping between one-forms and vectors rendered by the metric tensor. Abstractly, we say that a vector at a point on a manifold lives on the tangent space at that point, whereas a one-form lives on the cotangent space. The metric tensor attaches the tangent space to the co-tangent space. For Cartesian tensor analysis, the duality between one-forms and vectors

is the duality between row vectors and column vectors. Furthermore, as for Cartesian tensors, we construct an inner product by contracting one-forms and vectors to produce a scalar. Finally, the duality relation given by equation (8.24) offers us the means to raise and lower tensor indices in a manner akin to the transpose operation in linear algebra that produces a row vector from a column vector.

8.2.4 Transformation of the coordinate representation

The transformation matrix (8.14) provides the means to convert any arbitrary coordinate representation of a tensor from one coordinate system to another. For example, consider the coordinate representation of a vector, which is realized by letting the vector eat one of the basis one-forms

$$\vec{F}(\tilde{e}^a) = F^a. \quad (8.33)$$

Now consider another coordinate system with basis one-forms $\tilde{e}^{\bar{a}}$, so that the vector has a representation

$$\vec{F}(\tilde{e}^{\bar{a}}) = F^{\bar{a}}. \quad (8.34)$$

Transforming the basis one-form using the transformation matrix leads to

$$F^{\bar{a}} = \vec{F}(\tilde{e}^{\bar{a}}) = \vec{F}(\Lambda_a^{\bar{a}} \tilde{e}^a) = \Lambda_a^{\bar{a}} \vec{F}(\tilde{e}^a) = \Lambda_a^{\bar{a}} F^a. \quad (8.35)$$

Transformation of an arbitrary one-form representation takes place with the inverse transformation matrix

$$F_{\bar{a}} = \tilde{F}(\tilde{e}_{\bar{a}}) = \tilde{F}(\Lambda_{\bar{a}}^a \tilde{e}_a) = \Lambda_{\bar{a}}^a \tilde{F}(\tilde{e}_a) = \Lambda_{\bar{a}}^a F_a. \quad (8.36)$$

8.2.5 Arbitrary coordinate representation of inverse metric

The inverse metric tensor has an arbitrary coordinate representation given by

$$g^{\bar{a}\bar{b}} = \tilde{e}^{\bar{a}} \cdot \tilde{e}^{\bar{b}} = \begin{bmatrix} \nabla\xi^{\bar{1}} \cdot \nabla\xi^{\bar{1}} & \nabla\xi^{\bar{1}} \cdot \nabla\xi^{\bar{2}} & \nabla\xi^{\bar{1}} \cdot \nabla\xi^{\bar{3}} \\ \nabla\xi^{\bar{2}} \cdot \nabla\xi^{\bar{1}} & \nabla\xi^{\bar{2}} \cdot \nabla\xi^{\bar{2}} & \nabla\xi^{\bar{2}} \cdot \nabla\xi^{\bar{3}} \\ \nabla\xi^{\bar{3}} \cdot \nabla\xi^{\bar{1}} & \nabla\xi^{\bar{3}} \cdot \nabla\xi^{\bar{2}} & \nabla\xi^{\bar{3}} \cdot \nabla\xi^{\bar{3}} \end{bmatrix}. \quad (8.37)$$

Proof that $g^{\bar{a}\bar{b}} g_{\bar{b}\bar{c}} = \delta_{\bar{c}}^{\bar{a}}$ requires use of the chain rule relations derived in Section 8.9.3.

8.2.6 Functions versus scalars

A scalar field carries no tensor labels and as such it does not transform under coordinate transformations. That is, a scalar is coordinate invariant and it is the simplest type of tensor field. Temperature, kinetic energy, and specific entropy are example scalar fields considered in this book. Now consider the first component of a vector field, F^1 , whose value at a point, \mathcal{P} , and time, τ , is written $F^1(\mathcal{P}, \tau)$. Now change the coordinates so that the first component to the vector field at the same (\mathcal{P}, τ) is written $F^{\bar{1}}(\mathcal{P}, \tau)$. Yet under a coordinate transformation we generally have $F^{\bar{1}}(\mathcal{P}, \tau) \neq F^1(\mathcal{P}, \tau)$, so that the individual components to a vector field, though functions of space and time, *do not* individually transform as a scalar field. Instead, they transform as components to a vector field. This very basic example illustrates the distinction between functions of space and time, which includes any component of any tensor field, from scalar fields, which are coordinate invariant.

8.3 Scalar product

In Section 1.3.2 we defined the scalar product between two Cartesian vectors. The natural generalization is given by

$$\vec{P} \cdot \vec{Q} = P^a Q^b \vec{e}_a \cdot \vec{e}_b = P^a Q^b g_{ab} = P^a Q_a = P_b Q^b, \quad (8.38)$$

where the second equality made use of the metric tensor coordinate representation given by equation (8.11). We can conceive of the scalar product in a somewhat more general manner by recalling that a one-form operates on a vector, $\tilde{P}(\vec{Q})$. Conversely, a vector operates on a one-form, $\vec{Q}(\tilde{P})$. Exposing components leads to

$$\tilde{P}(\vec{Q}) = \tilde{P}(Q^a \vec{e}_a) = Q^a \tilde{P}(\vec{e}_a) = Q^a P_a, \quad (8.39)$$

which equals to

$$\vec{Q}(\tilde{P}) = \vec{Q}(P_a \tilde{e}^a) = P_a \vec{Q}(\tilde{e}^a) = P_a Q^a. \quad (8.40)$$

The scalar product is invariant to coordinate changes, as seen through

$$\vec{Q}(\tilde{P}) = \vec{Q}(P_a \tilde{e}^a) = P_a Q^a = \vec{Q}(P_{\bar{a}} \tilde{e}^{\bar{a}}) = P_{\bar{a}} Q^{\bar{a}}. \quad (8.41)$$

The invariance is also revealed by working just with the coordinate representations and introducing the transformation matrix elements

$$P_a Q^a = (\Lambda^{\bar{a}}_a P_{\bar{a}}) (\Lambda^a_{\bar{b}} Q^{\bar{b}}) = \Lambda^{\bar{a}}_a \Lambda^a_{\bar{b}} P_{\bar{a}} Q^{\bar{b}} = \delta^{\bar{a}}_{\bar{b}} P_{\bar{a}} Q^{\bar{b}} = P_{\bar{a}} Q^{\bar{a}}. \quad (8.42)$$

8.4 Worked example: oblique coordinates

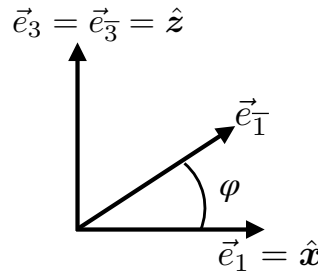


FIGURE 8.1: Oblique basis vectors for the x - z plane where $\vec{e}_{\bar{1}} = \vec{e}_1 \cos \varphi + \vec{e}_3 \sin \varphi$ and $\vec{e}_{\bar{3}} = \vec{e}_3$, with $\vec{e}_1 = \hat{x}$ and $\vec{e}_3 = \hat{z}$. These coordinate basis vectors are related to those used for generalized vertical coordinates shown in the left panel of Figure 56.2.

We pause in our development to work through some of the formalism for *oblique coordinates* for the x - z plane as specified by the basis vectors

$$\vec{e}_{\bar{1}} = \vec{e}_1 \cos \varphi + \vec{e}_3 \sin \varphi = \hat{x} \cos \varphi + \hat{z} \sin \varphi \quad \text{and} \quad \vec{e}_{\bar{3}} = \vec{e}_3 = \hat{z}. \quad (8.43)$$

The oblique coordinate basis vectors, $\vec{e}_{\bar{a}}$, are orthogonal when the angle $\varphi = 0, \pi$; otherwise they are non-orthogonal. Also note that if $\varphi = \pi/2, 3\pi/2$ then $\vec{e}_{\bar{1}} = \pm \vec{e}_{\bar{3}}$, in which case the vectors no longer form a basis for the x - z plane. So in the following we assume $\varphi \in (-\pi/2, \pi/2)$. These coordinates are oriented so that they correspond to the generalized vertical coordinate basis vectors depicted in Figure 56.2. Finally, for the purposes of this section we ignore the 2 direction

and just work within the x - z plane. Hence, tensor indices carry values 1 and 3 with 2 ignored.

8.4.1 Turning the crank

We here exhibit the results of turning the crank for the oblique coordinates.

Transformation matrix and its inverse

We can construct the transformation matrix through $\vec{e}_{\bar{a}} = \Lambda_{\bar{a}}^a \vec{e}_a$, and use of the coordinate basis definition (8.43)

$$\vec{e}_{\bar{1}} = \Lambda_{\bar{1}}^1 \vec{e}_1 + \Lambda_{\bar{1}}^3 \vec{e}_3 \implies \Lambda_{\bar{1}}^1 = \cos \varphi, \quad \Lambda_{\bar{1}}^3 = \sin \varphi \quad (8.44a)$$

$$\vec{e}_{\bar{3}} = \Lambda_{\bar{3}}^1 \vec{e}_1 + \Lambda_{\bar{3}}^3 \vec{e}_3 \implies \Lambda_{\bar{3}}^1 = 0, \quad \Lambda_{\bar{3}}^3 = 1, \quad (8.44b)$$

so that the transformation matrix is

$$\Lambda_{\bar{a}}^a = \begin{bmatrix} \Lambda_{\bar{1}}^1 & \Lambda_{\bar{1}}^3 \\ \Lambda_{\bar{3}}^1 & \Lambda_{\bar{3}}^3 \end{bmatrix} = \begin{bmatrix} \cos \varphi & 0 \\ \sin \varphi & 1 \end{bmatrix}, \quad (8.45)$$

and a matrix inversion yields the inverse transformation matrix

$$\Lambda^{\bar{a}}_a = \begin{bmatrix} \Lambda^{\bar{1}}_1 & \Lambda^{\bar{1}}_3 \\ \Lambda^{\bar{3}}_1 & \Lambda^{\bar{3}}_3 \end{bmatrix} = \frac{1}{\cos \varphi} \begin{bmatrix} 1 & 0 \\ -\sin \varphi & \cos \varphi \end{bmatrix}. \quad (8.46)$$

Basis one-forms

The basis one-forms using oblique coordinates are determined by

$$\tilde{e}^{\bar{a}} = \Lambda^{\bar{a}}_a \tilde{e}^a = \Lambda^{\bar{a}}_1 \tilde{e}^1 + \Lambda^{\bar{a}}_3 \tilde{e}^3 \quad (8.47)$$

with $\tilde{e}^1 = \hat{x}$ and $\tilde{e}^3 = \hat{z}$ for Cartesian coordinates. Making use of the inverse transformation matrix (8.46) leads to

$$\tilde{e}^{\bar{1}} = \Lambda^{\bar{1}}_1 \tilde{e}^1 + \Lambda^{\bar{1}}_3 \tilde{e}^3 = \frac{\hat{x}}{\cos \varphi} \quad (8.48a)$$

$$\tilde{e}^{\bar{3}} = \Lambda^{\bar{3}}_1 \tilde{e}^1 + \Lambda^{\bar{3}}_3 \tilde{e}^3 = -\hat{x} \tan \varphi + \hat{z}. \quad (8.48b)$$

We can readily verify the bi-orthogonality relation (8.25) whereby

$$\vec{e}_{\bar{a}} \cdot \tilde{e}^{\bar{b}} = \delta_{\bar{a}}^{\bar{b}}. \quad (8.49)$$

Representing a vector

The inverse transformation matrix (8.46) can be used to relate the Cartesian coordinate representation of an arbitrary vector, $\vec{P} = P^a \vec{e}_a$, to the oblique coordinate representation, $\vec{P} = P^{\bar{a}} \vec{e}_{\bar{a}}$. Doing so leads to the contravariant components written using oblique coordinates

$$P^{\bar{a}} = \Lambda^{\bar{a}}_a P^a = \Lambda^{\bar{a}}_1 P^1 + \Lambda^{\bar{a}}_3 P^3 \implies P^{\bar{1}} = \frac{1}{\cos \varphi} P^1 \quad \text{and} \quad P^{\bar{3}} = -\tan \varphi P^1 + P^3. \quad (8.50)$$

Likewise, the covariant representation can be found by using the transformation matrix (8.45) to render

$$P_{\bar{a}} = \Lambda_{\bar{a}}^a P_a = \Lambda_{\bar{a}}^1 P_1 + \Lambda_{\bar{a}}^3 P_3 \implies P_{\bar{1}} = P_1 \cos \varphi + P_3 \sin \varphi \text{ and } P_{\bar{3}} = P_3, \quad (8.51)$$

where $P^a = P_a$ for the Cartesian coordinate representation.

Representing the metric tensor

The covariant representation of the metric tensor is given by

$$g_{\bar{a}\bar{b}} = \delta_{ab} \Lambda_{\bar{a}}^a \Lambda_{\bar{b}}^b = \begin{bmatrix} g_{\bar{1}\bar{1}} & g_{\bar{1}\bar{3}} \\ g_{\bar{3}\bar{1}} & g_{\bar{3}\bar{3}} \end{bmatrix} = \begin{bmatrix} 1 & \sin \varphi \\ \sin \varphi & 1 \end{bmatrix}, \quad (8.52)$$

and its inverse is

$$g^{\bar{a}\bar{b}} = \delta^{ab} \Lambda_{\bar{a}}^a \Lambda_{\bar{b}}^b = \begin{bmatrix} g^{\bar{1}\bar{1}} & g^{\bar{1}\bar{3}} \\ g^{\bar{3}\bar{1}} & g^{\bar{3}\bar{3}} \end{bmatrix} = \frac{1}{(\cos \varphi)^2} \begin{bmatrix} 1 & -\sin \varphi \\ -\sin \varphi & 1 \end{bmatrix}. \quad (8.53)$$

Squared magnitude

The squared magnitude of a vector is given by

$$\vec{P} \cdot \vec{P} = g_{\bar{a}\bar{b}} P^{\bar{a}} P^{\bar{b}} \quad (8.54a)$$

$$= P_{\bar{b}} P^{\bar{b}} \quad (8.54b)$$

$$= (P_1 \cos \varphi + P_3 \sin \varphi) \frac{1}{\cos \varphi} P^1 + P_3 (P^3 - \tan \varphi P^1) \quad (8.54c)$$

$$= P_1 P^1 + P_3 P^3 \quad (8.54d)$$

$$= \delta_{ab} P^a P^b. \quad (8.54e)$$

8.4.2 Comments

Oblique coordinate offer a pedagogical step towards the more complex case of generalized vertical coordinates studied in Chapter 56. Indeed, much of the tensor algebra needed for generalized vertical coordinates is concisely summarized in the above steps using oblique coordinates.

8.5 The volume element and Jacobian of transformation

Recall from Section 1.5.2 that we derived an expression for the volume of an infinitesimal region of Euclidean space, \mathbb{R}^3 , using Cartesian coordinates

$$dV = dx dy dz (\hat{x} \times \hat{y}) \cdot \hat{z} = dx dy dz. \quad (8.55)$$

This volume element is used for integrating over a region of \mathbb{R}^3 when using Cartesian coordinates. Furthermore, its material fluid expression measures the volume of a fluid element. We now generalize this result to arbitrary coordinates.

8.5.1 Jacobian of transformation

From multi-variate calculus, the relation between $d\xi^1 d\xi^2 d\xi^3$ and $d\xi^{\bar{1}} d\xi^{\bar{2}} d\xi^{\bar{3}}$ for two sets of co-ordinates is given by

$$d\xi^1 d\xi^2 d\xi^3 = \frac{\partial \xi}{\partial \xi} d\xi^{\bar{1}} d\xi^{\bar{2}} d\xi^{\bar{3}} \quad (8.56a)$$

$$= \frac{\partial(\xi^1, \xi^2, \xi^3)}{\partial(\xi^{\bar{1}}, \xi^{\bar{2}}, \xi^{\bar{3}})} d\xi^{\bar{1}} d\xi^{\bar{2}} d\xi^{\bar{3}} \quad (8.56b)$$

$$= \left[\frac{\partial \xi}{\partial \xi^{\bar{1}}} \times \frac{\partial \xi}{\partial \xi^{\bar{2}}} \right] \cdot \frac{\partial \xi}{\partial \xi^{\bar{3}}} d\xi^{\bar{1}} d\xi^{\bar{2}} d\xi^{\bar{3}} \quad (8.56c)$$

$$= \det(\Lambda^a_{\bar{a}}) d\xi^{\bar{1}} d\xi^{\bar{2}} d\xi^{\bar{3}}, \quad (8.56d)$$

where $\det(\Lambda^a_{\bar{a}})$ is the determinant of the transformation matrix, also known as the *Jacobian of transformation*. The transformation is well defined so long as the Jacobian does not vanish. We maintain labels on the transformation matrix inside the determinant symbol to help indicate the sense for the transformation. This notation also helps maintain proper conservation of tensor indices.

8.5.2 Relating the Jacobian to the determinant of the metric

Recall the expression (8.12) for the transformation of the metric

$$g_{\bar{a}\bar{b}} = \Lambda^a_{\bar{a}} \Lambda^b_{\bar{b}} g_{ab}. \quad (8.57)$$

We can write this expression as a matrix equation

$$\bar{g} = \Lambda^T g \Lambda \quad (8.58)$$

where Λ^T is the transposed matrix. Taking determinants of both sides yields

$$\det(\bar{g}) = \det(\Lambda^T g \Lambda) = \det(\Lambda^T) \det(g) \det(\Lambda) = [\det(\Lambda)]^2 \det(g). \quad (8.59)$$

To reach this result we used the property of determinants that $\det(A B) = \det(A) \det(B)$ for any two matrices, and $\det(\Lambda^T) = \det(\Lambda)$. Consequently,

$$\det(\Lambda^a_{\bar{a}}) = \frac{\sqrt{\det(g_{\bar{a}\bar{b}})}}{\sqrt{\det(g_{ab})}} = \frac{\sqrt{\det(\bar{g})}}{\sqrt{\det(g)}}. \quad (8.60)$$

We are thus led to the equivalent expressions for the volume element

$$dV \equiv \sqrt{\det(g)} d\xi^1 d\xi^2 d\xi^3 = \sqrt{\det(\bar{g})} d\xi^{\bar{1}} d\xi^{\bar{2}} d\xi^{\bar{3}}. \quad (8.61)$$

This relation provides us with our desired general coordinate expression for the volume element. For the special case when the unbarred coordinates are Cartesian, $g_{ab} = \delta_{ab}$ so that $\det(g) = 1$ and

$$\det(\Lambda^a_{\bar{a}}) = \sqrt{\det(g_{\bar{a}\bar{b}})} \quad \text{unbarred coordinates are Cartesian.} \quad (8.62)$$

This is a rather useful expression for our purposes, since we can always use Cartesian as the unbarred coordinates given that geophysical fluids move in a background Euclidean space.

8.6 The permutation symbol and the determinant

As discussed in Section 1.4.1, the Cartesian components of the Levi-Civita tensor are given by the permutation symbol, ϵ_{abc} . To help determine the general coordinate representation of the Levi-Civita tensor, we here develop some identities satisfied by the determinant of the transformation matrix.

8.6.1 Connecting the permutation symbol to the determinant

Consider a two-dimensional space with a transformation matrix $\Lambda^a_{\bar{a}}$ between two sets of coordinates. The determinant of the transformation is given by

$$\det(\Lambda^a_{\bar{a}}) = \Lambda^1_{\bar{1}} \Lambda^2_{\bar{2}} - \Lambda^1_{\bar{2}} \Lambda^2_{\bar{1}}. \quad (8.63)$$

Introducing the permutation symbol ϵ_{ab} allows us to write this expression in a more tidy manner

$$\det(\Lambda^a_{\bar{a}}) = \epsilon_{ab} \Lambda^a_{\bar{1}} \Lambda^b_{\bar{2}} \quad (8.64)$$

with

$$\epsilon_{12} = 1 \quad \text{and} \quad \epsilon_{21} = -1. \quad (8.65)$$

The permutation symbol is defined to have numerically the same values whether the labels are raised or lowered: $\epsilon^{ab} = \epsilon_{ab}$.

We can generalize the above to any number of dimensions, each of which adds one more label to the permutation symbol and one more number added to the permutation string. We already encountered the three dimensional version in Section 1.4.1 when discussing the vector cross product, in which case the permutation symbol is

$$\epsilon_{123} = 1 \quad (8.66a)$$

$$\epsilon_{abc} = \begin{cases} 0 & \text{if any two labels are the same,} \\ 1 & \text{if } a, b, c \text{ is an even permutation of 1, 2, 3,} \\ -1 & \text{if } a, b, c \text{ is an odd permutation of 1, 2, 3.} \end{cases} \quad (8.66b)$$

Likewise, the determinant of the transformation matrix takes the form

$$\det(\Lambda^a_{\bar{a}}) = \frac{\partial \xi}{\partial \bar{\xi}} = \frac{\partial(\xi^1, \xi^2, \xi^3)}{\partial(\xi^{\bar{1}}, \xi^{\bar{2}}, \xi^{\bar{3}})} = \epsilon_{abc} \Lambda^a_{\bar{1}} \Lambda^b_{\bar{2}} \Lambda^c_{\bar{3}}. \quad (8.67)$$

8.6.2 Further identities satisfied by the determinant

The following identity in two dimensions can be readily verified through enumeration

$$\epsilon_{ab} \Lambda^a_{\bar{a}} \Lambda^b_{\bar{b}} = \epsilon_{\bar{a}\bar{b}} \det(\Lambda^a_{\bar{a}}), \quad (8.68)$$

which follows directly from the definition of the determinant and can be explicitly verified so long as we assume the permutation symbol $\epsilon_{\bar{a}\bar{b}}$ is numerically identical to ϵ_{ab} . Now contract both sides of this relation with $\epsilon^{\bar{a}\bar{b}}$ to isolate the determinant

$$\frac{1}{2} \epsilon^{\bar{a}\bar{b}} \epsilon_{ab} \Lambda^a_{\bar{a}} \Lambda^b_{\bar{b}} = \det(\Lambda^a_{\bar{a}}), \quad (8.69)$$

where we used

$$\epsilon^{\bar{a}\bar{b}} \epsilon_{ab} = \epsilon^{\bar{1}\bar{2}} \epsilon_{12} + \epsilon^{\bar{2}\bar{1}} \epsilon_{21} = 2. \quad (8.70)$$

The three dimensional version takes the form

$$\epsilon_{abc} \Lambda^a_{\bar{a}} \Lambda^b_{\bar{b}} \Lambda^c_{\bar{c}} = \epsilon_{\bar{a}\bar{b}\bar{c}} \det(\Lambda^a_{\bar{a}}), \quad (8.71)$$

so that

$$\frac{1}{3!} \epsilon^{\bar{a}\bar{b}\bar{c}} \epsilon_{abc} \Lambda^a_{\bar{a}} \Lambda^b_{\bar{b}} \Lambda^c_{\bar{c}} = \det(\Lambda^a_{\bar{a}}). \quad (8.72)$$

8.7 The Levi-Civita tensor and the volume element

The metric tensor introduced in Section 8.1 provides a means to measure distance between two points. The Levi-Civita tensor allows us to compute volumes (or areas for two dimensional manifolds). We make particular use of this tensor to compute the volume element used for integration. This section generalizes the Cartesian coordinate discussion provided in Section 1.5.3.

8.7.1 General coordinate representation of the Levi-Civita tensor

The relations (8.68) and (8.71) indicate that the permutation symbol *does not* transform as the components to a second order covariant tensor, unless the determinant of the transformation is unity. Unit determinants occur for special transformations, such as rotations (i.e., Cartesian to Cartesian coordinate transformation as in Chapter 1) and the identity transformation. Indeed, we have already noted that the permutation symbol has the same representation regardless the coordinate choice. As we now show, the permutation symbol is the Cartesian coordinate representation of the Levi-Civita tensor.

The above relations for the determinant motivate us to introduce the general coordinate form of the *Levi-Civita tensor*

$$\varepsilon_{abc} \equiv \sqrt{\det(g)} \epsilon_{abc}. \quad (8.73)$$

We highlight the distinct symbols in this definition, with ε the Levi-Civita tensor and ϵ the permutation symbol. By construction, the components to the Levi-Civita tensor transform as

$$\Lambda^a_{\bar{a}} \Lambda^b_{\bar{b}} \Lambda^c_{\bar{c}} \varepsilon_{abc} = \Lambda^a_{\bar{a}} \Lambda^b_{\bar{b}} \Lambda^c_{\bar{c}} \sqrt{\det(g)} \epsilon_{abc} \quad (8.74a)$$

$$= \sqrt{\det(g)} \epsilon_{\bar{a}\bar{b}\bar{c}} \det(\Lambda^a_{\bar{a}}) \quad (8.74b)$$

$$= \sqrt{\det(g)} \epsilon_{\bar{a}\bar{b}\bar{c}} \quad (8.74c)$$

$$= \varepsilon_{\bar{a}\bar{b}\bar{c}}, \quad (8.74d)$$

where equations (8.60) and (8.68) were used. Therefore, ε_{abc} transforms as components to a third order covariant tensor. Likewise,

$$\varepsilon^{abc} = \frac{\epsilon^{abc}}{\sqrt{\det(g)}} \quad (8.75)$$

transforms as the components to a third order contravariant tensor. These transformation rules allow us to identify ε as a tensor rather than just a combination of numbers.

8.7.2 The Levi-Civita tensor and the volume element

As a third order tensor, the Levi-Civita tensor takes three vectors as its argument. In particular, for three infinitesimal vectors we have

$$\varepsilon(\vec{e}_1 d\xi^1, \vec{e}_2 d\xi^2, \vec{e}_3 d\xi^3) = d\xi^1 d\xi^2 d\xi^3 \varepsilon(\vec{e}_1, \vec{e}_2, \vec{e}_3) \quad (8.76a)$$

$$= d\xi^1 d\xi^2 d\xi^3 \varepsilon_{123} \quad (8.76b)$$

$$= d\xi^1 d\xi^2 d\xi^3 \sqrt{\det(g)} \epsilon_{123} \quad (8.76c)$$

$$= dV, \quad (8.76d)$$

where we used equation (8.61) for the final step. This result means that geometrically, the Levi-Civita tensor measures the volume defined by three vectors

$$\varepsilon(\vec{A}, \vec{B}, \vec{C}) = \text{volume}(\vec{A}, \vec{B}, \vec{C}). \quad (8.77)$$

This interpretation accords with the Cartesian coordinate discussion of the Levi-Civita tensor in Section 1.5.3.

8.8 Vector cross product

The vector cross product of two Cartesian basis vectors yields the third, so that

$$\hat{x} \times \hat{y} = \hat{z} \quad \text{and cyclic permutations.} \quad (8.78)$$

The coordinate invariant generalization of this relation is given by

$$\vec{e}_a \times \vec{e}_b \equiv \varepsilon_{abc} \tilde{e}^c. \quad (8.79)$$

As defined, the vector cross product of two vectors leads to a one-form. We are thus led to the general coordinate expression for the vector cross product of two arbitrary vectors

$$\vec{P} \times \vec{Q} = P^a Q^b \vec{e}_a \times \vec{e}_b \quad (8.80a)$$

$$= P^a Q^b \varepsilon_{abc} \tilde{e}^c. \quad (8.80b)$$

8.9 Coordinate transformation of partial derivatives

Throughout this book, the background space is Euclidean and time is universal. We are thus concerned with space tensors rather than the space-time tensors of special and general relativity. Nonetheless, our description of points in space generally makes use of curved surfaces that are time dependent. Curved surfaces motivate the use of general tensors. Time dependence motivates a space-time formulation (Section 7.5.4) for the purpose of transforming the partial time derivative operator. In this section we establish some properties of the space-time transformation matrix and then exhibit the transformation of space and time partial time derivatives. We have further use of a space-time formulation in Sections 14.7 and 14.8, also for considering the transformation of partial derivatives.

8.9.1 The space-time transformation matrix

As discussed in Section 8.1.4, transformations between coordinate representations are enabled by the transformation matrix built from partial derivatives of the coordinate transformations.

The transformation matrix with a universal Newtonian time plus spatial coordinates (that are functions of space and time) takes on the form

$$\Lambda^{\alpha}_{\bar{\alpha}} = \frac{\partial \xi^{\alpha}}{\partial \xi^{\bar{\alpha}}} = \begin{bmatrix} \frac{\partial \xi^0}{\partial \xi^0} & \frac{\partial \xi^0}{\partial \xi^1} & \frac{\partial \xi^0}{\partial \xi^2} & \frac{\partial \xi^0}{\partial \xi^3} \\ \frac{\partial \xi^1}{\partial \xi^0} & \frac{\partial \xi^1}{\partial \xi^1} & \frac{\partial \xi^1}{\partial \xi^2} & \frac{\partial \xi^1}{\partial \xi^3} \\ \frac{\partial \xi^2}{\partial \xi^0} & \frac{\partial \xi^2}{\partial \xi^1} & \frac{\partial \xi^2}{\partial \xi^2} & \frac{\partial \xi^2}{\partial \xi^3} \\ \frac{\partial \xi^3}{\partial \xi^0} & \frac{\partial \xi^3}{\partial \xi^1} & \frac{\partial \xi^3}{\partial \xi^2} & \frac{\partial \xi^3}{\partial \xi^3} \\ \frac{\partial \xi^0}{\partial \xi^0} & \frac{\partial \xi^1}{\partial \xi^1} & \frac{\partial \xi^2}{\partial \xi^2} & \frac{\partial \xi^3}{\partial \xi^3} \end{bmatrix} = \begin{bmatrix} 1 & 0 & 0 & 0 \\ \frac{\partial \xi^1}{\partial \xi^0} & \frac{\partial \xi^1}{\partial \xi^1} & \frac{\partial \xi^1}{\partial \xi^2} & \frac{\partial \xi^1}{\partial \xi^3} \\ \frac{\partial \xi^2}{\partial \xi^0} & \frac{\partial \xi^2}{\partial \xi^1} & \frac{\partial \xi^2}{\partial \xi^2} & \frac{\partial \xi^2}{\partial \xi^3} \\ \frac{\partial \xi^3}{\partial \xi^0} & \frac{\partial \xi^3}{\partial \xi^1} & \frac{\partial \xi^3}{\partial \xi^2} & \frac{\partial \xi^3}{\partial \xi^3} \\ \frac{\partial \xi^0}{\partial \xi^0} & \frac{\partial \xi^1}{\partial \xi^1} & \frac{\partial \xi^2}{\partial \xi^2} & \frac{\partial \xi^3}{\partial \xi^3} \end{bmatrix}. \quad (8.81)$$

The final equality made use of our assumption that $\xi^0 = \xi^0$ since the time coordinate remains universal. Hence, when computing $\partial \xi^0 / \partial \xi^{\bar{\alpha}}$ we keep ξ^0 fixed so that the derivative vanishes as in the specific case of

$$\left[\frac{\partial \xi^0}{\partial \xi^1} \right]_{\xi^0, \xi^2, \xi^3} = \left[\frac{\partial \xi^0}{\partial \xi^1} \right]_{\xi^0, \xi^2, \xi^3} = 0. \quad (8.82)$$

Zero elements in the first row of the transformation matrix (8.81) reveals that time is not a function of space

$$\frac{\partial \xi^0}{\partial \xi^{\bar{\alpha}}} = 0, \quad (8.83)$$

which is expected since we are assuming universal Newtonian time in which time is independent of space. In contrast, nonzero elements in the first column indicate that our description of space is generally a function of time

$$\frac{\partial \xi^a}{\partial \xi^0} \neq 0. \quad (8.84)$$

We see the same overall structure in the inverse space-time transformation matrix

$$\Lambda^{\bar{\alpha}}_{\alpha} = \frac{\partial \xi^{\bar{\alpha}}}{\partial \xi^{\alpha}} = \begin{bmatrix} \frac{\partial \xi^0}{\partial \xi^0} & \frac{\partial \xi^0}{\partial \xi^1} & \frac{\partial \xi^0}{\partial \xi^2} & \frac{\partial \xi^0}{\partial \xi^3} \\ \frac{\partial \xi^1}{\partial \xi^0} & \frac{\partial \xi^1}{\partial \xi^1} & \frac{\partial \xi^1}{\partial \xi^2} & \frac{\partial \xi^1}{\partial \xi^3} \\ \frac{\partial \xi^2}{\partial \xi^0} & \frac{\partial \xi^2}{\partial \xi^1} & \frac{\partial \xi^2}{\partial \xi^2} & \frac{\partial \xi^2}{\partial \xi^3} \\ \frac{\partial \xi^3}{\partial \xi^0} & \frac{\partial \xi^3}{\partial \xi^1} & \frac{\partial \xi^3}{\partial \xi^2} & \frac{\partial \xi^3}{\partial \xi^3} \\ \frac{\partial \xi^0}{\partial \xi^0} & \frac{\partial \xi^1}{\partial \xi^1} & \frac{\partial \xi^2}{\partial \xi^2} & \frac{\partial \xi^3}{\partial \xi^3} \end{bmatrix} = \begin{bmatrix} 1 & 0 & 0 & 0 \\ \frac{\partial \xi^1}{\partial \xi^0} & \frac{\partial \xi^1}{\partial \xi^1} & \frac{\partial \xi^1}{\partial \xi^2} & \frac{\partial \xi^1}{\partial \xi^3} \\ \frac{\partial \xi^2}{\partial \xi^0} & \frac{\partial \xi^2}{\partial \xi^1} & \frac{\partial \xi^2}{\partial \xi^2} & \frac{\partial \xi^2}{\partial \xi^3} \\ \frac{\partial \xi^3}{\partial \xi^0} & \frac{\partial \xi^3}{\partial \xi^1} & \frac{\partial \xi^3}{\partial \xi^2} & \frac{\partial \xi^3}{\partial \xi^3} \\ \frac{\partial \xi^0}{\partial \xi^0} & \frac{\partial \xi^1}{\partial \xi^1} & \frac{\partial \xi^2}{\partial \xi^2} & \frac{\partial \xi^3}{\partial \xi^3} \end{bmatrix}. \quad (8.85)$$

8.9.2 Determinant of the transformation matrix

The determinant of the space-time transformation and its inverse remains identical to the determinant of their purely space portions

$$\det(\Lambda^{\alpha}_{\bar{\alpha}}) = \det(\Lambda^a_{\bar{a}}) \quad \text{and} \quad \det(\Lambda^{\bar{\alpha}}_{\alpha}) = \det(\Lambda^{\bar{a}}_a), \quad (8.86)$$

which follows since the first row in both transformations has only a single non-zero value, $\Lambda^0_{\bar{0}} = 1$ and $\Lambda^{\bar{0}}_0 = 1$. Hence, the relations developed in Sections 8.5 and 8.6 for the volume element and Jacobian of transformation remain unchanged when adding the universal time coordinate.

8.9.3 Multiplying the transformation matrix and its inverse

We here verify that the transformation matrix (8.81) indeed has its inverse given by (8.85). For this purpose we must prove that

$$\delta_{\beta}^{\alpha} = \Lambda_{\beta}^{\alpha} \Lambda_{\beta}^{\bar{\beta}} \quad \text{and} \quad \delta_{\bar{\beta}}^{\bar{\alpha}} = \Lambda_{\bar{\beta}}^{\bar{\alpha}} \Lambda_{\bar{\beta}}^{\beta}, \quad (8.87)$$

where δ_{β}^{α} and $\delta_{\bar{\beta}}^{\bar{\alpha}}$ are components to the identity tensor. The proof relies on writing the space-time coordinate transformation as a composite function

$$\xi^{\bar{\alpha}} = \xi^{\bar{\alpha}}(\xi^{\alpha}) = \xi^{\bar{\alpha}}[\xi^{\alpha}(\xi^{\bar{\beta}})]. \quad (8.88)$$

Taking partial derivatives and using the chain rule renders

$$\delta_{\bar{\beta}}^{\bar{\alpha}} = \frac{\partial \xi^{\bar{\alpha}}}{\partial \xi^{\bar{\beta}}} = \frac{\partial \xi^{\bar{\alpha}}}{\partial \xi^{\alpha}} \frac{\partial \xi^{\alpha}}{\partial \xi^{\bar{\beta}}} = \Lambda_{\alpha}^{\bar{\alpha}} \Lambda_{\beta}^{\alpha} \quad \text{and} \quad \delta_{\beta}^{\alpha} = \frac{\partial \xi^{\alpha}}{\partial \xi^{\beta}} = \frac{\partial \xi^{\alpha}}{\partial \xi^{\bar{\alpha}}} \frac{\partial \xi^{\bar{\alpha}}}{\partial \xi^{\beta}} = \Lambda_{\bar{\alpha}}^{\alpha} \Lambda_{\beta}^{\bar{\alpha}}. \quad (8.89)$$

Furthermore, the space subcomponents decouple from time, which can be seen by considering a few representative cases

$$1 = \delta_0^0 = \Lambda_{\alpha}^0 \Lambda_{\alpha}^{\bar{\alpha}} = \Lambda_{\bar{\alpha}}^0 \Lambda_{\alpha}^{\bar{\alpha}} \quad (8.90a)$$

$$1 = \delta_1^1 = \Lambda_{\alpha}^1 \Lambda_{\alpha}^{\bar{\alpha}} = \Lambda_{\bar{\alpha}}^1 \Lambda_{\alpha}^{\bar{\alpha}} \quad (8.90b)$$

$$0 = \delta_1^0 = \Lambda_{\alpha}^0 \Lambda_{\alpha}^{\bar{\alpha}} = \Lambda_{\bar{\alpha}}^0 \Lambda_{\alpha}^{\bar{\alpha}} \quad (8.90c)$$

$$0 = \delta_2^1 = \Lambda_{\alpha}^1 \Lambda_{\alpha}^{\bar{\alpha}} = \Lambda_{\bar{\alpha}}^1 \Lambda_{\alpha}^{\bar{\alpha}}. \quad (8.90d)$$

Consequently, the spatial components satisfy

$$\delta_b^a = \Lambda_{\bar{b}}^a \Lambda_{\bar{b}}^{\bar{b}} \quad \text{and} \quad \delta_{\bar{b}}^{\bar{a}} = \Lambda_{\bar{b}}^{\bar{a}} \Lambda_{\bar{b}}^b, \quad (8.91)$$

which allows for a splitting of the spatial components from the time component.

8.9.4 Transformation of space and time partial derivatives

Application of the chain rule leads to the transformation of the partial derivative operator

$$\partial_{\bar{\alpha}} = \frac{\partial}{\partial \xi^{\bar{\alpha}}} = \frac{\partial \xi^{\alpha}}{\partial \xi^{\bar{\alpha}}} \frac{\partial}{\partial \xi^{\alpha}} = \Lambda_{\bar{\alpha}}^{\alpha} \partial_{\alpha}. \quad (8.92)$$

Extracting the time and space components from the transformation matrix (8.81) yields

$$\partial_{\bar{0}} = \Lambda_{\bar{0}}^{\alpha} \partial_{\alpha} = \partial_0 + \Lambda_{\bar{0}}^a \partial_a \quad (8.93a)$$

$$\partial_{\bar{a}} = \Lambda_{\bar{a}}^{\alpha} \partial_{\alpha} = \Lambda_{\bar{a}}^a \partial_a. \quad (8.93b)$$

Notably, the time derivative operator in one coordinate system transforms into both space and time derivative operators in the new coordinate system. We expect this result since time derivatives in one coordinate system are computed with its spatial coordinates held fixed, but these coordinates are generally moving with respect to the other coordinate system. In contrast, the spatial components to the partial derivative operator transform among just the other spatial components; there is no mixing with the time derivative operator. This property of the spatial derivative operator follows from the use of universal Newtonian time. It allows us to focus on space tensors in the following sections.

8.10 Covariant derivative of a scalar

We now return to a focus on space tensor analysis by considering the contraction of spatial components to the partial derivative operator with the basis of one-forms. This contraction renders the geometric expression of the gradient operator acting on a scalar

$$\text{grad}(\psi) = \nabla\psi = \tilde{e}^a \partial_a \psi = \tilde{e}^{\bar{a}} \partial_{\bar{a}} \psi. \quad (8.94)$$

From this expression we define the *covariant derivative operator*

$$\nabla = \tilde{e}^a \partial_a \quad (8.95)$$

so that we refer to equation (8.94) as either the gradient acting on a scalar or the covariant derivative acting on a scalar.

8.11 Covariant derivative of a vector

The covariant derivative operator can act on a vector, in which case we consider $\nabla \vec{F}$. To perform calculations requires us to unpack the manifestly covariant expression $\nabla \vec{F}$ by introducing a coordinate representation

$$\nabla \vec{F} = (\tilde{e}^b \partial_b) (F^a \vec{e}_a). \quad (8.96)$$

8.11.1 Derivative of a vector and Christoffel symbols

The chain rule leads to the expression for the partial derivative operator acting on a vector field

$$\partial_b \vec{F} = \partial_b (\vec{e}_a F^a) \quad \text{coordinate representation of the vector } \vec{F} \quad (8.97a)$$

$$= (\partial_b F^a) \vec{e}_a + F^a \partial_b \vec{e}_a \quad \text{chain rule} \quad (8.97b)$$

$$= (\partial_b F^a) \vec{e}_a + F^a \Gamma_{ba}^c \vec{e}_c \quad \text{define Christoffel symbols} \quad (8.97c)$$

$$= (\partial_b F^a + F^c \Gamma_{bc}^a) \vec{e}_a \quad \text{reorganize} \quad (8.97d)$$

$$= (\nabla_b F^a) \vec{e}_a \quad \text{define covariant derivative acting on vector component.} \quad (8.97e)$$

In the third equality we introduced the *Christoffel symbols*

$$\partial_b \vec{e}_a = \Gamma_{ba}^c \vec{e}_c. \quad (8.98)$$

The Christoffel symbols carry information about the partial derivatives of the basis vectors. They vanish in Cartesian coordinates yet are generally nonzero. In the final equality we introduced components to the covariant derivative acting on the vector components

$$\nabla_b F^a = \partial_b F^a + \Gamma_{bc}^a F^c. \quad (8.99)$$

Contracting $\partial_b \vec{F}$ with the basis one-form \tilde{e}^b leads to the coordinate invariant expression for the covariant derivative of a vector field

$$\nabla \vec{F} = \tilde{e}^b (\partial_b \vec{F}) = (\tilde{e}^b \nabla_b F^a) \vec{e}_a. \quad (8.100)$$

8.11.2 An alternative derivation

A heuristic explanation of these ideas follows by applying the elementary calculus notions to a vector field \vec{F} as represented by arbitrary coordinates ξ^a , in which case

$$\partial_b \vec{F} = \lim_{\Delta \rightarrow 0} \frac{\vec{F}(\vec{P} + \Delta \vec{e}_b) - \vec{F}(\vec{P})}{\Delta}, \quad (8.101)$$

where $\vec{P} = \vec{e}_a \xi^a$ is the position vector for an arbitrary point and \vec{e}_b specifies the direction for computing the partial derivative. The basis vectors \vec{e}_a are spatially independent for Cartesian coordinates, so that the derivative of a vector is computed merely by taking the derivative of each Cartesian component

$$\partial_b \vec{F} = (\partial_b F^a) \vec{e}_a \quad \text{Cartesian coordinates.} \quad (8.102)$$

For general coordinates, however, both the vector components and the basis vectors are spatially dependent, in which case

$$\vec{F}(\vec{P} + \Delta \vec{e}_b) - \vec{F}(\vec{P}) = [F^a + \Delta \partial_b F^a] [\vec{e}_a + \Delta \partial_b \vec{e}_a] - F^a \vec{e}_a \quad (8.103a)$$

$$= \Delta \partial_b (F^a \vec{e}_a) + \mathcal{O}(\Delta^2). \quad (8.103b)$$

This is the same result as found in the first step of the chain rule used in equation (8.97a). Following through that derivation then leads to the same coordinate expression for the covariant derivative acting on a vector field.

8.11.3 Christoffel symbols as the metric connection

Recall from elementary calculus that the derivative of a function is computed by comparing the function at two points in space, dividing by the distance between those points, and taking the limit as the points get infinitesimally close. This operation is well defined for scalar fields on arbitrary manifolds. However, it is problematic for vectors since the vectors live on distinct tangent spaces and so cannot be directly compared. For example, how do we compare two vectors at distinct points on a sphere? To do so we must provide a method to move one vector to the position of the other before comparing. As seen through the above discussion of covariant derivative of a vector, the Christoffel symbols provide the means to move vectors. Namely, they connect the two vectors by carrying information about how the basis vectors change in space. It is for this reason that some refer to the Christoffel symbols as the *metric connection*.

There is a distinct coordinate dependence of Christoffel symbols. For example, the Christoffel symbols all vanish in Euclidean space when using Cartesian coordinates whereas they are nonzero with other coordinates. As discussed in Section 7.1, a tensor that vanishes in one coordinate system remains zero for all coordinate systems. We thus conclude that the Christoffel symbols are *not* components to a tensor. Rather, they carry information regarding the partial derivatives of the coordinate basis vectors and as such they are fundamentally tied to a chosen coordinate system.

8.12 Covariant derivative of a one-form

The product of a one-form and a vector is a scalar. As seen in Section 8.10, the covariant derivative of a scalar field is given by the gradient operator

$$\nabla(\tilde{E} \cdot \vec{F}) = \tilde{e}^b \partial_b (E_a F^a). \quad (8.104)$$

Expanding the partial derivative yields

$$\partial_b(E_a F^a) = F^a \partial_b E_a + E_a \partial_b F^a \quad (8.105a)$$

$$= F^a \partial_b E_a + E_a (\nabla_b F^a - \Gamma_{bc}^a F^c) \quad (8.105b)$$

$$= F^a (\partial_b E_a - \Gamma_{ba}^c E_c) + E_a \nabla_b F^a \quad (8.105c)$$

$$\equiv F^a \nabla_b E_a + E_a \nabla_b F^a. \quad (8.105d)$$

The last equality defines the covariant derivative when acting on the components to a one form

$$\nabla_b E_a = \partial_b E_a - \Gamma_{ba}^c E_c, \quad (8.106)$$

which leads to the coordinate invariant expression for the covariant derivative of a one-form

$$\nabla \tilde{E} = (\tilde{e}^b \partial_b) \tilde{E} = (\tilde{e}^b \nabla_b E_a) \tilde{e}^a. \quad (8.107)$$

8.13 Covariant derivative of the metric tensor

When written in Cartesian coordinates, the covariant derivative of components to the metric tensor for Euclidean space vanishes,

$$\nabla g_{ab} = \nabla \delta_{ab} = 0, \quad (8.108)$$

because the Cartesian representation of the metric is the unit tensor, δ_{ab} , in which case all Christoffel symbols vanish. Previous results establish the tensorial nature of the covariant derivative. Hence, $\nabla g_{ab} = 0$ is a valid result for *all* coordinates. This result is often called the *metricity* condition. It represents a self-consistency condition required for the manifolds considered in this book.

8.14 Christoffel symbols in terms of the metric

We can develop an expression for the covariant derivative when acting on the components to a second order tensor. When applied to the metric tensor, its vanishing covariant derivative (equation (8.108)) then leads to the identity

$$0 = \nabla_c g_{ab} = \partial_c g_{ab} - \Gamma_{ca}^d g_{db} - \Gamma_{cb}^d g_{ad}. \quad (8.109)$$

We can solve this equation for the Christoffel symbols

$$\Gamma_{ab}^c = \frac{1}{2} g^{cd} (\partial_b g_{da} + \partial_a g_{db} - \partial_d g_{ab}). \quad (8.110)$$

This expression exhibits the symmetry property of the lower two indices on the Christoffel symbols

$$\Gamma_{ab}^c = \Gamma_{ba}^c. \quad (8.111)$$

8.15 Covariant divergence of a vector

The covariant divergence of the components to a vector results in a scalar

$$\nabla_a F^a = \partial_a F^a + \Gamma_{ab}^a F^b. \quad (8.112)$$

We now bring this expression into a form more convenient for practical calculations.

8.15.1 Contraction of the Christoffel symbols

Expression (8.110) for the Christoffel symbols yields the contraction

$$\Gamma_{ab}^a = \frac{1}{2} g^{ad} (\partial_b g_{da} + \partial_a g_{db} - \partial_d g_{ab}) = \frac{1}{2} g^{ad} \partial_b g_{ad} \quad (8.113)$$

where symmetry of the metric tensor and its inverse was used.

8.15.2 Exponential of the determinant

For the matrix representation of a symmetric positive definite tensor, such as the metric tensor, we can write

$$\det(A) = e^{\ln \det(A)} \quad \text{simple identity} \quad (8.114a)$$

$$= e^{\ln(\Pi_i \Lambda_i)} \quad \text{determinant related to product of eigenvalues} \quad (8.114b)$$

$$= e^{\Sigma_i \ln \Lambda_i} \quad \text{simple identity} \quad (8.114c)$$

$$= e^{\text{Tr}(\ln A)} \quad \text{sum of eigenvalues related to trace of matrix.} \quad (8.114d)$$

Each of these identities is trivial to verify using a set of coordinates in which the matrix is diagonal. For any symmetric and positive definite matrix, such a set of coordinates always exists, in which case

$$\partial_c \ln \det(A) = \partial_c [\text{Tr}(\ln A)] = \text{Tr}(\partial_c \ln A) = \text{Tr}(A^{-1} \partial_c A). \quad (8.115)$$

With A now set equal to the metric tensor \mathbf{g} with components g_{ab} , this result yields

$$\partial_c \ln \det(\mathbf{g}) = g^{ab} \partial_c g_{ab} \quad (8.116)$$

which in turn yields for the contracted Christoffel symbol

$$\Gamma_{ac}^a = \partial_c \ln \sqrt{\det(\mathbf{g})}. \quad (8.117)$$

This result brings the covariant divergence of a vector to the form

$$\nabla_a F^a = \partial_a F^a + F^a \partial_a \ln \sqrt{\det(\mathbf{g})} = \frac{1}{\sqrt{\mathbf{g}}} \partial_a [\sqrt{\mathbf{g}} F^a]. \quad (8.118)$$

This is a very convenient result since it only requires partial derivatives in the chosen coordinate system, with all of the coordinate dependent properties summarized by $\sqrt{\det(\mathbf{g})}$.

8.16 Covariant Laplacian of a scalar

Making use of equation (8.118) with

$$F^a = g^{ab} \partial_b \psi \quad (8.119)$$

leads to the covariant Laplacian of a scalar field

$$\nabla_a (g^{ab} \partial_b \psi) = \frac{1}{\sqrt{\mathbf{g}}} \partial_a [\sqrt{\mathbf{g}} g^{ab} \partial_b \psi]. \quad (8.120)$$

This expression is fundamental to the evolution of scalar fields under the impacts from diffusion (Chapter 61).

8.17 Covariant curl of a vector

The Levi-Civita tensor

$$\varepsilon_{abc} = \sqrt{\det(\mathfrak{g})} \epsilon_{abc} \quad (8.121)$$

from Section 8.7 is useful for generalizing the curl operation from Cartesian coordinates in Euclidean space to arbitrary coordinates on a curved manifold embedded in Euclidean space. Consequently, we define the curl according to the coordinate invariant expression

$$\text{curl}(\vec{F}) = \vec{e}_a \varepsilon^{abc} (\nabla_b F_c) = \vec{e}^a \varepsilon_{abc} (\nabla^b F^c). \quad (8.122)$$

This expression simplifies by making use of equation (8.106) for the covariant derivative $\nabla_b F_c = \partial_b F_c - \Gamma_{cb}^a F_a$. Conveniently, the contraction $\varepsilon^{abc} \Gamma_{cb}^a$ vanishes identically since $\varepsilon^{abc} = -\varepsilon^{acb}$ whereas $\Gamma_{cb}^a = \Gamma_{bc}^a$. Hence, we are left with a general expression for the covariant curl that involves just the partial derivatives

$$\text{curl}(\vec{F}) = \vec{e}_a \varepsilon^{abc} (\partial_b F_c) = \vec{e}_a \varepsilon^{abc} [\partial_b (g_{cd} F^d)]. \quad (8.123)$$

The second equality made use of the identity $F_c = g_{cd} F^d$.

8.18 Gauss's divergence theorem

The integral theorems from Cartesian vector analysis transform in a straightforward manner to arbitrary coordinates in arbitrary smooth and oriented spaces. An easy way to prove the theorems is to invoke the ideas of general coordinate invariance from Section 7.1, in which the integral theorems are written in a tensorially proper manner with partial derivatives changed to covariant derivatives. The divergence theorem offers a particularly simple example. For this purpose, we make use of the volume element (8.61)

$$dV = \sqrt{\det(\mathfrak{g})} d\xi^1 d\xi^2 d\xi^3, \quad (8.124)$$

multiplied by the covariant divergence (8.118). Hence, the volume integral of the divergence is given by

$$\int_{\mathcal{R}} (\nabla_a F^a) dV = \int_{\mathcal{R}} \partial_a [\sqrt{\det(\mathfrak{g})} F^a] d\xi^1 d\xi^2 d\xi^3 = \oint_{\partial\mathcal{R}} F^a \hat{n}_a d\mathcal{S}. \quad (8.125)$$

In this equation, \hat{n} is the outward normal one-form for the boundary, $\partial\mathcal{R}$, with $d\mathcal{S}$ the invariant area element on the boundary, and \hat{n}_a the covariant components of the outward normal.

8.19 Stokes' curl theorem

The Cartesian form of Stokes' Theorem from Section 2.6 is generalized in a manner similar to the divergence theorem

$$\oint_{\partial\mathcal{S}} \vec{F} \cdot d\vec{x} = \int_{\mathcal{S}} \text{curl}(\vec{F}) \cdot \hat{n} d\mathcal{S}, \quad (8.126)$$

where $d\vec{x}$ is the vector line element along the path and $\partial\mathcal{S}$ is the closed path defining the boundary to a simply connected two-dimensional surface \mathcal{S} . For the circulation on the left hand side we

have

$$\vec{F} \cdot d\vec{x} = F^a \vec{e}_a \cdot \vec{e}_b dx^b = F_b dx^b = F_{\bar{b}} d\xi^{\bar{b}}. \quad (8.127)$$

For the curl on the right hand side we have

$$\text{curl}(\vec{F}) \cdot \hat{\mathbf{n}} = \varepsilon^{abc} (\partial_b F_c) \vec{e}_a \cdot \hat{\mathbf{n}} = \varepsilon^{abc} (\partial_b F_c) \hat{n}_a = \varepsilon^{\bar{a}\bar{b}\bar{c}} (\partial_{\bar{b}} F_{\bar{c}}) \hat{n}_{\bar{a}}, \quad (8.128)$$

thus leading to the expression of Stokes' theorem in arbitrary coordinates

$$\oint_{\partial\mathcal{S}} F_{\bar{b}} d\xi^{\bar{b}} = \int_{\mathcal{S}} \varepsilon^{\bar{a}\bar{b}\bar{c}} (\partial_{\bar{b}} F_{\bar{c}}) \hat{n}_{\bar{a}} d\mathcal{S}. \quad (8.129)$$



Chapter 9

ORTHOGONAL COORDINATES

READER'S GUIDE TO THIS CHAPTER

This chapter provides a compendium of mathematical results for Cartesian, spherical, and cylindrical-polar coordinates, thus providing explicit examples of the general tensor analysis machinery from Chapter 8. These coordinates are commonly used in geophysical fluid studies. They are time independent and locally orthogonal, and as such they are simpler than the non-orthogonal generalized vertical coordinates detailed in Part XI.

9.1	Cartesian coordinates	181
9.1.1	The basics	182
9.1.2	Summary	182
9.2	Spherical coordinates	183
9.2.1	Cartesian and spherical transformation	183
9.2.2	Basis vectors	185
9.2.3	Basis one-forms	185
9.2.4	Position and velocity	185
9.2.5	Metric tensor	186
9.2.6	Components of a vector field	187
9.2.7	Differential operators	187
9.2.8	Summary	188
9.3	Cylindrical-polar coordinates	188
9.3.1	Cartesian and cylindrical-polar transformation	190
9.3.2	Basis vectors	190
9.3.3	Basis one-forms	190
9.3.4	Position and velocity	191
9.3.5	Metric tensor	191
9.3.6	Volume element and Levi-Civita tensor	191
9.3.7	Vector cross product of basis vectors	191
9.3.8	Components of a vector field	192
9.3.9	Differential operators	192
9.3.10	Summary	193
9.4	General orthogonal coordinates	193

9.1 Cartesian coordinates

Whenever developing a general tensor relation it is useful to check its validity by considering Cartesian coordinates, in which case we can make use of familiar rules from vector calculus. We here summarize some results from our discussion of Cartesian tensors in Chapters 1 and 2.

9.1.1 The basics

We start by expressing the trajectory of a point through space in the following equivalent forms

$$\mathcal{P}(\tau) = \vec{e}_1 x(\tau) + \vec{e}_2 y(\tau) + \vec{e}_3 z(\tau) \quad (9.1a)$$

$$= \hat{\mathbf{x}} x(\tau) + \hat{\mathbf{y}} y(\tau) + \hat{\mathbf{z}} z(\tau) \quad (9.1b)$$

$$= \vec{x}(\tau) \quad (9.1c)$$

$$= \mathbf{x}(\tau), \quad (9.1d)$$

with the basis vectors written

$$\vec{e}_1 = \hat{\mathbf{x}} \quad \text{and} \quad \vec{e}_2 = \hat{\mathbf{y}} \quad \text{and} \quad \vec{e}_3 = \hat{\mathbf{z}}. \quad (9.2)$$

The boldface notation is used for the position vector in the final equality of equation (9.1d), with the boldface commonly used throughout this book. Notably, the orthogonal unit vectors for Cartesian coordinates are normalized so that

$$\vec{e}_1 \cdot \vec{e}_1 = \vec{e}_2 \cdot \vec{e}_2 = \vec{e}_3 \cdot \vec{e}_3 = 1. \quad (9.3)$$

Furthermore, the basis vectors are identical to the basis one-forms

$$\vec{e}_1 = \tilde{e}^1 = \hat{\mathbf{x}} \quad \text{and} \quad \vec{e}_2 = \tilde{e}^2 = \hat{\mathbf{y}} \quad \text{and} \quad \vec{e}_3 = \tilde{e}^3 = \hat{\mathbf{z}}, \quad (9.4)$$

in which we see there is no importance placed on whether a tensor index is up or down. Since the Cartesian basis vectors are independent of both space and time, we compute the coordinate representation of the velocity vector through taking the time derivative as

$$\vec{v}(\tau) = \mathbf{v}(\tau) = \frac{d\mathcal{P}}{d\tau} = \frac{d\mathbf{x}}{d\tau}, \quad (9.5)$$

which takes on the expanded expressions

$$\vec{v}(\tau) = \vec{e}_1 \frac{dx(\tau)}{d\tau} + \vec{e}_2 \frac{dy(\tau)}{d\tau} + \vec{e}_3 \frac{dz(\tau)}{d\tau} \quad (9.6a)$$

$$= \hat{\mathbf{x}} v^1(\tau) + \hat{\mathbf{y}} v^2(\tau) + \hat{\mathbf{z}} v^3(\tau). \quad (9.6b)$$

$$= \hat{\mathbf{x}} u(\tau) + \hat{\mathbf{y}} v(\tau) + \hat{\mathbf{z}} w(\tau), \quad (9.6c)$$

where (u, v, w) is the notation commonly used in this book for the three velocity components.

9.1.2 Summary

In Cartesian coordinates, mathematical operators and integral theorems take their familiar form from vector calculus. We here list the key ones in forms that are encountered throughout this

book.

$\mathbf{x} = (x^1, x^2, x^3) = (x, y, z)$	Cartesian coordinates	(9.7)
$\mathbf{F} = \hat{\mathbf{x}}F^1 + \hat{\mathbf{y}}F^2 + \hat{\mathbf{z}}F^3 = \hat{\mathbf{x}}F_1 + \hat{\mathbf{y}}F_2 + \hat{\mathbf{z}}F_3$	covariant = contravariant	(9.8)
$\frac{\partial}{\partial x^a} = \partial_a$ or $(\partial_x, \partial_y, \partial_z)$	partial derivative operator	(9.9)
$\nabla = \hat{\mathbf{x}}\partial_x + \hat{\mathbf{y}}\partial_y + \hat{\mathbf{z}}\partial_z$	gradient = covariant derivative	(9.10)
$\nabla_z = \hat{\mathbf{x}}\partial_x + \hat{\mathbf{y}}\partial_y$	horizontal gradient operator	(9.11)
$\nabla \cdot \mathbf{F} = \partial_x F_x + \partial_y F_y + \partial_z F_z$	divergence of a vector	(9.12)
$\nabla_z \cdot \mathbf{F} = \partial_x F_x + \partial_y F_y$	horizontal divergence of a vector	(9.13)
$(\nabla \times \mathbf{F})_a = \epsilon_{abc} \partial_b F_c$	components to the curl	(9.14)
$\nabla \cdot \nabla \psi = \nabla^2 \psi = (\partial_{xx} + \partial_{yy} + \partial_{zz}) \psi$	Laplacian of a scalar	(9.15)
$\int_{\mathcal{R}} \nabla \cdot \mathbf{F} dV = \oint_{\partial \mathcal{R}} \mathbf{F} \cdot \hat{\mathbf{n}} dS$	Gauss's divergence theorem	(9.16)
$\oint_{\partial S} \mathbf{F} \cdot d\mathbf{x} = \int_S (\nabla \times \mathbf{F}) \cdot \hat{\mathbf{n}} dS.$	Stokes' curl theorem.	(9.17)

9.2 Spherical coordinates

We now consider spherical coordinates defined by Figure 9.1 and related to Cartesian coordinates through the transformation

$$x = r \cos \phi \cos \lambda \quad (9.18a)$$

$$y = r \cos \phi \sin \lambda \quad (9.18b)$$

$$z = r \sin \phi. \quad (9.18c)$$

The radial coordinate

$$r = |\mathbf{x}| = \sqrt{\mathbf{x} \cdot \mathbf{x}} = \sqrt{x^2 + y^2 + z^2} \quad (9.19)$$

measures the distance from the center of the sphere to the position of the point. The spherical angle coordinates

$$0 \leq \lambda \leq 2\pi \quad \text{longitude} \quad (9.20)$$

$$-\pi/2 \leq \phi \leq \pi/2 \quad \text{latitude} \quad (9.21)$$

specify the longitude, measuring the radians of the position east of the prime meridian, and latitude, measuring the radians north ($\phi > 0$) or south ($\phi < 0$) from the equator. To streamline notation in the following, we introduce the unbarred and barred labels for the Cartesian and spherical coordinates, respectively

$$(x, y, z) = (\xi^1, \xi^2, \xi^3) \equiv \xi^a \quad \text{and} \quad (\lambda, \phi, r) = (\bar{\xi}^1, \bar{\xi}^2, \bar{\xi}^3) \equiv \bar{\xi}^a. \quad (9.22)$$

9.2.1 Cartesian and spherical transformation

Following the general discussion in Section 8.1.4, we consider the infinitesimal distance along one of the Cartesian coordinate axes, $d\xi^a$. The chain rule allows us to relate this distance to those

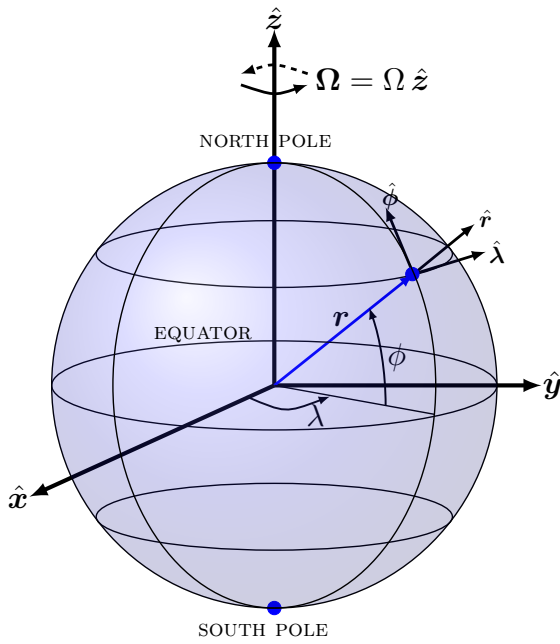


FIGURE 9.1: Geometry and notation for motion around a rotating sphere. For geophysical applications, the sphere rotates counter-clockwise when looking down from the north polar axis and it has an angular speed Ω . The planetary Cartesian triad of orthonormal basis vectors, $(\hat{x}, \hat{y}, \hat{z})$ points along the orthogonal axes and rotates with the sphere. The planetary spherical triad (also rotating with the sphere) of orthonormal basis vectors, $(\hat{\lambda}, \hat{\phi}, \hat{r})$, makes use of the longitudinal unit vector $\hat{\lambda}$, which points in the longitudinal direction (positive eastward), the latitudinal unit vector $\hat{\phi}$, which points in the latitudinal direction (positive northward) and the radial unit vector \hat{r} , which point in the radial direction (positive away from the center).

along the axes of the spherical coordinate system

$$d\xi^a = \frac{\partial \xi^a}{\partial \xi^{\bar{a}}} d\xi^{\bar{a}} = \Lambda_{\bar{a}}^a d\xi^{\bar{a}}. \quad (9.23)$$

The partial derivatives $\partial \xi^a / \partial \xi^{\bar{a}}$ form components to the transformation matrix that transforms between coordinate representations. For the coordinate transformation (9.18a)-(9.18c), the transformation matrix is given by

$$\Lambda_{\bar{a}}^a = \begin{bmatrix} \partial \xi^1 / \partial \xi^{\bar{1}} & \partial \xi^1 / \partial \xi^{\bar{2}} & \partial \xi^1 / \partial \xi^{\bar{3}} \\ \partial \xi^2 / \partial \xi^{\bar{1}} & \partial \xi^2 / \partial \xi^{\bar{2}} & \partial \xi^2 / \partial \xi^{\bar{3}} \\ \partial \xi^3 / \partial \xi^{\bar{1}} & \partial \xi^3 / \partial \xi^{\bar{2}} & \partial \xi^3 / \partial \xi^{\bar{3}} \end{bmatrix} = \begin{bmatrix} -r \cos \phi \sin \lambda & -r \sin \phi \cos \lambda & \cos \phi \cos \lambda \\ r \cos \phi \cos \lambda & -r \sin \phi \sin \lambda & \cos \phi \sin \lambda \\ 0 & r \cos \phi & \sin \phi \end{bmatrix}. \quad (9.24)$$

The determinant of the transformation (Jacobian) is given by

$$\det(\Lambda_{\bar{a}}^a) = r^2 \cos \phi. \quad (9.25)$$

The Jacobian vanishes at the north and south poles ($\phi = \pm\pi/2$), where the transformation is singular. Methods familiar from linear algebra render the inverse transformation matrix

$$\Lambda_{\bar{a}}^a = \frac{1}{r^2 \cos \phi} \begin{bmatrix} -r \sin \lambda & r \cos \lambda & 0 \\ -r \cos \phi \sin \phi \cos \lambda & -r \cos \phi \sin \phi \sin \lambda & r \cos^2 \phi \\ r^2 \cos^2 \phi \cos \lambda & r^2 \cos^2 \phi \sin \lambda & r^2 \cos \phi \sin \phi \end{bmatrix}. \quad (9.26)$$

9.2.2 Basis vectors

The spherical coordinate basis vectors, $\vec{e}_{\bar{a}}$, are related to the Cartesian coordinate basis vectors, \vec{e}_a , through the transformation

$$\vec{e}_{\bar{a}} = \Lambda_{\bar{a}}^a \vec{e}_a. \quad (9.27)$$

The transformation matrix (9.24) leads to

$$\vec{e}_\lambda = r \cos \phi (-\hat{x} \sin \lambda + \hat{y} \cos \lambda) \quad (9.28a)$$

$$\vec{e}_\phi = r (-\hat{x} \sin \phi \cos \lambda - \hat{y} \sin \phi \sin \lambda + \hat{z} \cos \phi) \quad (9.28b)$$

$$\vec{e}_r = \hat{x} \cos \phi \cos \lambda + \hat{y} \cos \phi \sin \lambda + \hat{z} \sin \phi. \quad (9.28c)$$

We can introduce the orthonormal unit vectors $(\hat{\lambda}, \hat{\phi}, \hat{r})$ through

$$\vec{e}_\lambda = r \cos \phi \hat{\lambda} \quad \text{and} \quad \vec{e}_\phi = r \hat{\phi} \quad \text{and} \quad \vec{e}_r = \hat{r}, \quad (9.29)$$

so that

$$\hat{\lambda} = -\hat{x} \sin \lambda + \hat{y} \cos \lambda \quad (9.30a)$$

$$\hat{\phi} = -\hat{x} \cos \lambda \sin \phi - \hat{y} \sin \lambda \sin \phi + \hat{z} \cos \phi \quad (9.30b)$$

$$\hat{r} = \hat{x} \cos \lambda \cos \phi + \hat{y} \sin \lambda \cos \phi + \hat{z} \sin \phi \quad (9.30c)$$

along with the inverse relations

$$\hat{x} = -\hat{\lambda} \sin \lambda - \hat{\phi} \cos \lambda \sin \phi + \hat{r} \cos \lambda \cos \phi \quad (9.31a)$$

$$\hat{y} = \hat{\lambda} \cos \lambda - \hat{\phi} \sin \lambda \sin \phi + \hat{r} \sin \lambda \cos \phi \quad (9.31b)$$

$$\hat{z} = \hat{\phi} \cos \phi + \hat{r} \sin \phi. \quad (9.31c)$$

9.2.3 Basis one-forms

Since spherical coordinates are locally orthogonal, we can readily derive the one-form basis through inverting the vector basis

$$\tilde{e}^\lambda = (r \cos \phi)^{-1} \hat{\lambda} \quad \text{and} \quad \tilde{e}^\phi = r^{-1} \hat{\phi} \quad \text{and} \quad \tilde{e}^r = \hat{r}, \quad (9.32)$$

which satisfy the bi-orthogonality relation with the basis vectors (Section 8.2.2)

$$\tilde{e}^{\bar{b}} \cdot \vec{e}_{\bar{a}} = \delta^{\bar{b}}_{\bar{a}}. \quad (9.33)$$

9.2.4 Position and velocity

In spherical coordinates, the position of a point is fully specified by the radial position

$$\mathcal{P}(\tau) = r \vec{e}_r = r \hat{r}. \quad (9.34)$$

However, the velocity requires all three spherical coordinates since the radial basis vector is a function of the angular positions, which are functions of time. Use of the chain rule renders

$$\vec{v}(\tau) = \vec{v} \quad (9.35a)$$

$$= \frac{d\vec{v}}{d\tau} \quad (9.35b)$$

$$= \vec{e}_r \frac{dr}{d\tau} + r \frac{d\vec{e}_r}{d\tau} \quad (9.35c)$$

$$= \vec{e}_r \frac{dr}{d\tau} + r \frac{\partial \vec{e}_r}{\partial \lambda} \frac{d\lambda}{d\tau} + r \frac{\partial \vec{e}_r}{\partial \phi} \frac{d\phi}{d\tau} \quad (9.35d)$$

$$\equiv \vec{e}_r \frac{dr}{d\tau} + \vec{e}_\lambda \frac{d\lambda}{d\tau} + \vec{e}_\phi \frac{d\phi}{d\tau} \quad (9.35e)$$

$$= \vec{e}_r v^r + \vec{e}_\lambda v^\lambda + \vec{e}_\phi v^\phi. \quad (9.35f)$$

To reach this result we made use of the identities satisfied by the spherical basis vectors

$$\vec{e}_\lambda = r \frac{\partial \vec{e}_r}{\partial \lambda} \quad \text{and} \quad \vec{e}_\phi = r \frac{\partial \vec{e}_r}{\partial \phi}, \quad (9.36)$$

which can be readily verified by equations (9.28a)-(9.28c).

9.2.5 Metric tensor

Since spherical coordinates are orthogonal, the metric tensor is diagonal and it is given by

$$g_{\bar{a}\bar{b}} = \vec{e}_{\bar{a}} \cdot \vec{e}_{\bar{b}} = \begin{bmatrix} (r \cos \phi)^2 & 0 & 0 \\ 0 & r^2 & 0 \\ 0 & 0 & 1 \end{bmatrix}, \quad (9.37)$$

along with the inverse metric tensor

$$g^{\bar{a}\bar{b}} = \vec{e}^{\bar{a}} \cdot \vec{e}^{\bar{b}} = \begin{bmatrix} (r \cos \phi)^{-2} & 0 & 0 \\ 0 & r^{-2} & 0 \\ 0 & 0 & 1 \end{bmatrix}. \quad (9.38)$$

Volume element and Levi-Civita tensor

The square root of the determinant of the metric tensor written in spherical coordinates (from equation (9.37)) is given by

$$\sqrt{\det(\mathcal{G})} = r^2 \cos \phi \quad (9.39)$$

so that the volume element is

$$dV = r^2 \cos \phi dr d\lambda d\phi. \quad (9.40)$$

The covariant Levi-Civita tensor has the spherical representation

$$\varepsilon_{\bar{a}\bar{b}\bar{c}} = (r^2 \cos \phi) \epsilon_{\bar{a}\bar{b}\bar{c}}, \quad (9.41)$$

where $\epsilon_{\bar{a}\bar{b}\bar{c}}$ are components to the permutation symbol (i.e., the Cartesian components to the Levi-Civita tensor) from Section 1.4.1.

Vector cross product of basis vectors

As a check on the formalism for cross products, let us verify the relation (8.79) for the vector cross product of two basis vectors using spherical coordinates

$$\vec{e}_{\bar{a}} \times \vec{e}_{\bar{b}} = \epsilon_{\bar{a}\bar{b}\bar{c}} \tilde{e}^{\bar{c}} \implies \vec{e}_{\bar{a}} \times \vec{e}_{\bar{b}} = (r^2 \cos \phi) \epsilon_{\bar{a}\bar{b}\bar{c}} \tilde{e}^{\bar{c}}. \quad (9.42)$$

Making use of the spherical coordinate basis vectors and one-forms renders

$$\vec{e}_r \times \vec{e}_{\lambda} = (r \cos \phi) (\hat{r} \times \hat{\lambda}) = (r \cos \phi) \hat{\phi} = (r^2 \cos \phi) \tilde{e}^{\phi} = \epsilon_{r\lambda\phi} \tilde{e}^{\phi} \quad (9.43a)$$

$$\vec{e}_{\lambda} \times \vec{e}_{\phi} = (r^2 \cos \phi) (\hat{\lambda} \times \hat{\phi}) = (r^2 \cos \phi) \hat{r} = (r^2 \cos \phi) \tilde{e}^r = \epsilon_{\lambda\phi r} \tilde{e}^r \quad (9.43b)$$

$$\vec{e}_{\phi} \times \vec{e}_r = r (\hat{\phi} \times \hat{r}) = r \hat{\lambda} = (r^2 \cos \phi) \tilde{e}^{\lambda} = \epsilon_{\phi r \lambda} \tilde{e}^{\lambda}. \quad (9.43c)$$

To reach these results we made use of the cross products for the spherical coordinate unit vectors

$$\hat{r} \times \hat{\lambda} = \hat{\phi} \quad \text{and} \quad \hat{\lambda} \times \hat{\phi} = \hat{r} \quad \text{and} \quad \hat{\phi} \times \hat{r} = \hat{\lambda}. \quad (9.44)$$

9.2.6 Components of a vector field

A vector field \vec{F} has Cartesian components, F^a , related to spherical components, $F^{\bar{a}}$, via the transformation matrix, $F^{\bar{a}} = \Lambda^{\bar{a}}_a F^a$. This transformation leads to

$$F^{\bar{1}} = (r \cos \phi)^{-1} [-F^x \sin \lambda + F^y \cos \lambda] \quad (9.45a)$$

$$F^{\bar{2}} = r^{-1} [-F^x \sin \phi \cos \lambda - F^y \sin \phi \sin \lambda + F^z \cos \phi] \quad (9.45b)$$

$$F^{\bar{3}} = F^x \cos \phi \cos \lambda + F^y \cos \phi \sin \lambda + F^z \sin \phi. \quad (9.45c)$$

Making use of the spherical unit vector (9.30a)-(9.30c) leads to the more tidy relations

$$(r \cos \phi) F^{\bar{1}} = \hat{\lambda} \cdot \mathbf{F} \quad (9.46a)$$

$$r F^{\bar{2}} = \hat{\phi} \cdot \mathbf{F} \quad (9.46b)$$

$$F^{\bar{3}} = \hat{r} \cdot \mathbf{F}, \quad (9.46c)$$

where \mathbf{F} is the Cartesian representation.

9.2.7 Differential operators

In spherical coordinates the gradient operator $\nabla = \tilde{e}^a \partial_a$ takes on the form

$$\nabla = \hat{\lambda} (r \cos \phi)^{-1} \partial_{\lambda} + \hat{\phi} r^{-1} \partial_{\phi} + \hat{r} \partial_r \quad (9.47)$$

and the covariant divergence of a vector field is given by

$$\nabla_{\bar{a}} F^{\bar{a}} = (r^2 \cos \phi)^{-1} \partial_{\bar{a}} [r^2 \cos \phi F^{\bar{a}}] \quad (9.48a)$$

$$= (r^2 \cos \phi)^{-1} \left(\partial_{\lambda} [r^2 \cos \phi F^{\bar{1}}] + \partial_{\phi} [r^2 \cos \phi F^{\bar{2}}] + \partial_r [r^2 \cos \phi F^{\bar{3}}] \right) \quad (9.48b)$$

$$= \frac{1}{r \cos \phi} \frac{\partial (\hat{\lambda} \cdot \mathbf{F})}{\partial \lambda} + \frac{1}{r \cos \phi} \frac{\partial (\hat{\phi} \cdot \mathbf{F} \cos \phi)}{\partial \phi} + \frac{1}{r^2} \frac{\partial (\hat{r} \cdot \mathbf{F} r^2)}{\partial r}. \quad (9.48c)$$

The covariant Laplacian of a scalar, $\nabla^2\psi = \nabla \cdot \nabla\psi$, is given by

$$\nabla^2\psi = \nabla \cdot [\hat{\lambda}(r \cos \phi)^{-1} \partial_\lambda \psi + \hat{\phi} r^{-1} \partial_\phi \psi + \hat{r} \partial_r \psi] \quad (9.49a)$$

$$= \frac{1}{(r \cos \phi)^2} \frac{\partial^2 \psi}{\partial \lambda^2} + \frac{1}{r^2 \cos \phi} \frac{\partial}{\partial \phi} \left[\cos \phi \frac{\partial \psi}{\partial \phi} \right] + \frac{1}{r^2} \frac{\partial}{\partial r} \left[r^2 \frac{\partial \psi}{\partial r} \right]. \quad (9.49b)$$

The covariant curl (Section 8.17) takes the form

$$(\text{curl } \vec{F})^{\bar{1}} = (r^2 \cos \phi)^{-1} [\partial_\phi F^{\bar{3}} - \partial_r (r^2 F^{\bar{2}})] \quad (9.50a)$$

$$(\text{curl } \vec{F})^{\bar{2}} = (r^2 \cos \phi)^{-1} [\partial_r (r^2 \cos^2 \phi F^{\bar{1}}) - \partial_\lambda F^{\bar{3}}] \quad (9.50b)$$

$$(\text{curl } \vec{F})^{\bar{3}} = (r^2 \cos \phi)^{-1} [\partial_\lambda (r^2 F^{\bar{2}}) - \partial_\phi (r^2 \cos^2 \phi F^{\bar{1}})], \quad (9.50c)$$

which can be written in the more conventional form (e.g., equation (2.33) of [Vallis \(2017\)](#))

$$r \cos \phi (\text{curl } \vec{F})^{\bar{1}} = \frac{1}{r} \left[\frac{\partial(\hat{r} \cdot \mathbf{F})}{\partial \phi} - \frac{\partial(r \hat{\phi} \cdot \mathbf{F})}{\partial r} \right] \quad (9.51a)$$

$$r (\text{curl } \vec{F})^{\bar{2}} = \frac{1}{r} \left[\frac{\partial(r \hat{\lambda} \cdot \mathbf{F})}{\partial r} - \frac{1}{\cos \phi} \frac{\partial(\hat{r} \cdot \mathbf{F})}{\partial \lambda} \right] \quad (9.51b)$$

$$(\text{curl } \vec{F})^{\bar{3}} = \frac{1}{r \cos \phi} \left[\frac{\partial(\hat{\phi} \cdot \mathbf{F})}{\partial \lambda} - \frac{\partial(\cos \phi \hat{\lambda} \cdot \mathbf{F})}{\partial \phi} \right]. \quad (9.51c)$$

9.2.8 Summary

We here summarize the spherical coordinate version of some common mathematical operators.

$$(\lambda, \phi, r) = (x^{\bar{1}}, x^{\bar{2}}, x^{\bar{3}}) \quad \text{spherical coordinates} \quad (9.52)$$

$$(r \cos \phi) F^{\bar{1}} = \hat{\lambda} \cdot \mathbf{F} \quad r F^{\bar{2}} = \hat{\phi} \cdot \mathbf{F} \quad F^{\bar{3}} = \hat{r} \cdot \mathbf{F} \quad \text{vector components} \quad (9.53)$$

$$\nabla = \hat{\lambda} (r \cos \phi)^{-1} \partial_\lambda + \hat{\phi} r^{-1} \partial_\phi + \hat{r} \partial_r \quad \text{gradient operator} \quad (9.54)$$

$$\nabla_{\bar{a}} F^{\bar{a}} = \frac{1}{r \cos \phi} \frac{\partial(\hat{\lambda} \cdot \mathbf{F})}{\partial \lambda} + \frac{1}{r \cos \phi} \frac{\partial(\hat{\phi} \cdot \mathbf{F} \cos \phi)}{\partial \phi} + \frac{1}{r^2} \frac{\partial(\hat{r} \cdot \mathbf{F} r^2)}{\partial r} \quad \text{divergence of vector} \quad (9.55)$$

$$\nabla^2 \psi = \frac{1}{(r \cos \phi)^2} \frac{\partial^2 \psi}{\partial \lambda^2} + \frac{1}{r^2 \cos \phi} \frac{\partial}{\partial \phi} \left[\cos \phi \frac{\partial \psi}{\partial \phi} \right] + \frac{1}{r^2} \frac{\partial}{\partial r} \left[r^2 \frac{\partial \psi}{\partial r} \right] \quad \text{Laplacian of scalar} \quad (9.56)$$

$$(\nabla \times \mathbf{F})_{\bar{a}} = \epsilon_{\bar{a}\bar{b}\bar{c}} \partial_b F^{\bar{c}} \quad \text{see equations (9.51a) -- (9.51c)} \quad \text{curl of vector.} \quad (9.57)$$

9.3 Cylindrical-polar coordinates

Many physical systems exhibit circular symmetry in two-dimensions or cylindrical symmetry in three-dimensions. The primary example encountered in this book is the laboratory motion of liquid in a rotating circular tank. In the following, we emulate the discussion presented for the spherical coordinates in Section 9.2, here focusing on cylindrical-polar coordinates as shown in Figure 9.2. Our task here is somewhat simpler than for the spherical coordinates since the vertical/axial position, z , remains unchanged from its Cartesian value. In a slight corruption of notation, we use the symbol r for the radial distance from the vertical axis in cylindrical-polar coordinates (Figure 9.2), which is distinct from the radial distance, r , used to measure the distance from the origin in spherical coordinates (Figure 9.1).

The coordinate transformation between Cartesian coordinates and cylindrical-polar coordi-

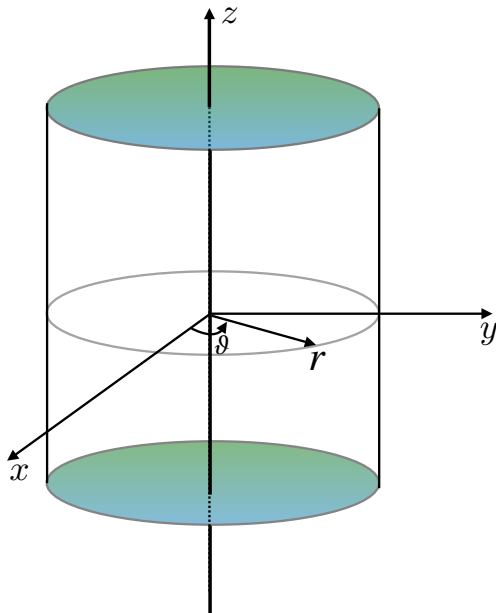


FIGURE 9.2: This schematic illustrates the geometry and notation for cylindrical-polar coordinates. The Cartesian triad of orthonormal basis vectors, $(\hat{x}, \hat{y}, \hat{z})$ points along the orthogonal axes. The cylindrical-polar triad of orthonormal basis vectors, $(\hat{r}, \hat{\vartheta}, \hat{z})$, makes use of the radial unit vector \hat{r} , which points outward from the vertical axis, the angular unit vector $\hat{\vartheta}$, which points in the counter-clockwise direction around the circle, and the vertical unit vector \hat{z} . Note that the radial unit vector used for cylindrical-polar coordinates is distinct from that radial vector used in spherical coordinates shown in Figure 9.1.

nates is given by

$$x = r \cos \vartheta \equiv \xi^1 \cos \xi^2 \quad (9.58a)$$

$$y = r \sin \vartheta \equiv \xi^1 \sin \xi^2 \quad (9.58b)$$

$$z = \xi^3. \quad (9.58c)$$

The radial coordinate for cylindrical-polar coordinates

$$r = \sqrt{x^2 + y^2} \quad (9.59)$$

measures the distance from the vertical z -axis, and the angular coordinate $0 \leq \vartheta \leq 2\pi$ measures the angle counter-clockwise from the positive x -axis. We introduce the unbarred and barred labels for the Cartesian and cylindrical polar coordinates

$$(x, y, z) = (\xi^1, \xi^2, \xi^3) \equiv \xi^a \quad \text{and} \quad (r, \vartheta, z) = (\xi^1, \xi^2, \xi^3) \equiv \xi^{\bar{a}}. \quad (9.60)$$

Although the vertical position z remains the same in both coordinates, and it is orthogonal to the other coordinates, we find it useful to introduce a distinct symbols, ξ^3 and $\xi^{\bar{3}}$, to specify what other coordinates are held fixed when performing derivative operations.

9.3.1 Cartesian and cylindrical-polar transformation

The coordinate transformation (9.58a)-(9.58c) leads to the transformation matrix

$$\Lambda_{\bar{a}}^a = \begin{bmatrix} \partial\xi^1/\partial\xi^{\bar{1}} & \partial\xi^1/\partial\xi^{\bar{2}} & \partial\xi^1/\partial\xi^{\bar{3}} \\ \partial\xi^2/\partial\xi^{\bar{1}} & \partial\xi^2/\partial\xi^{\bar{2}} & \partial\xi^2/\partial\xi^{\bar{3}} \\ \partial\xi^3/\partial\xi^{\bar{1}} & \partial\xi^3/\partial\xi^{\bar{2}} & \partial\xi^3/\partial\xi^{\bar{3}} \end{bmatrix} = \begin{bmatrix} \cos\vartheta & -r\sin\vartheta & 0 \\ \sin\vartheta & r\cos\vartheta & 0 \\ 0 & 0 & 1 \end{bmatrix} \quad (9.61)$$

and the inverse transformation is given by

$$\Lambda^{\bar{a}}_a = \frac{1}{r} \begin{bmatrix} r\cos\vartheta & r\sin\vartheta & 0 \\ -\sin\vartheta & \cos\vartheta & 0 \\ 0 & 0 & r \end{bmatrix}. \quad (9.62)$$

The determinant of the transformation (Jacobian) is given by

$$\det(\Lambda_{\bar{a}}^a) = r, \quad (9.63)$$

which vanishes along the vertical axis, which is where the transformation is singular.

9.3.2 Basis vectors

The cylindrical-polar coordinate basis vectors, $\vec{e}_{\bar{a}}$, are related to the Cartesian coordinate basis vectors, \vec{e}_a , through the transformation $\vec{e}_{\bar{a}} = \Lambda_{\bar{a}}^a \vec{e}_a$. The transformation matrix (9.61) leads to

$$\vec{e}_r = \hat{x}\cos\vartheta + \hat{y}\sin\vartheta \quad (9.64a)$$

$$\vec{e}_\vartheta = r(-\hat{x}\sin\vartheta + \hat{y}\cos\vartheta) \quad (9.64b)$$

$$\vec{e}_{\bar{z}} = \hat{z}. \quad (9.64c)$$

We sometimes make use of the following orthonormal unit vectors $(\hat{r}, \hat{\vartheta}, \hat{z})$

$$\vec{e}_r = \hat{r} \quad \text{and} \quad \vec{e}_\vartheta = r\hat{\vartheta} \quad \text{and} \quad \vec{e}_{\bar{z}} = \hat{z} \quad (9.65)$$

along with the inverse relations

$$\hat{x} = \hat{r}\cos\vartheta - \hat{\vartheta}\sin\vartheta \quad (9.66a)$$

$$\hat{y} = \hat{r}\sin\vartheta + \hat{\vartheta}\cos\vartheta \quad (9.66b)$$

$$\hat{z} = \hat{z}. \quad (9.66c)$$

9.3.3 Basis one-forms

Since cylindrical-polar coordinates are orthogonal, we can readily derive the one-form basis through inverting the vector basis

$$\tilde{e}^r = \hat{r} \quad \text{and} \quad \tilde{e}^\vartheta = r^{-1}\hat{\vartheta} \quad \text{and} \quad \tilde{e}^{\bar{z}} = \hat{z}, \quad (9.67)$$

which satisfy the orthogonality relation (Section 8.2.2)

$$\tilde{e}^{\bar{b}} \cdot \vec{e}_{\bar{a}} = \delta_{\bar{a}}^{\bar{b}}. \quad (9.68)$$

9.3.4 Position and velocity

In cylindrical-polar coordinates, the position of a point is specified by the radial position plus the vertical position

$$\mathcal{P}(\tau) = r \vec{e}_r + z \vec{e}_{\bar{z}}. \quad (9.69)$$

The velocity requires all three coordinates since the radial basis vector is a function of the angular positions, which are in turn functions of time. Use of the chain rule renders

$$\vec{v}(\tau) = \frac{d\mathcal{P}}{d\tau} \quad (9.70a)$$

$$= \vec{e}_r \frac{dr}{d\tau} + r \frac{d\vec{e}_r}{d\tau} + \vec{e}_{\bar{z}} \frac{dz}{d\tau} \quad (9.70b)$$

$$= \vec{e}_r \frac{dr}{d\tau} + r \frac{\partial \vec{e}_r}{\partial \vartheta} \frac{d\vartheta}{d\tau} + \vec{e}_{\bar{z}} \frac{dz}{d\tau} \quad (9.70c)$$

$$= \vec{e}_r \frac{dr}{d\tau} + \vec{e}_{\vartheta} \frac{d\vartheta}{d\tau} + \vec{e}_{\bar{z}} \frac{dz}{d\tau} \quad (9.70d)$$

$$= \vec{e}_r v^r + \vec{e}_{\vartheta} v^{\vartheta} + \vec{e}_{\bar{z}} v^{\bar{z}}. \quad (9.70e)$$

To reach this result we made use of the identity

$$\vec{e}_{\vartheta} = r \frac{\partial \vec{e}_r}{\partial \vartheta} = r \hat{\boldsymbol{\vartheta}}. \quad (9.71)$$

9.3.5 Metric tensor

Cylindrical-polar coordinates are orthogonal with the metric tensor and its inverse represented by the diagonal matrices

$$g_{\bar{a}\bar{b}} = \vec{e}_{\bar{a}} \cdot \vec{e}_{\bar{b}} = \begin{bmatrix} 1 & 0 & 0 \\ 0 & r^2 & 0 \\ 0 & 0 & 1 \end{bmatrix} \quad \text{and} \quad g^{\bar{a}\bar{b}} = \vec{e}^{\bar{a}} \cdot \vec{e}^{\bar{b}} = \begin{bmatrix} 1 & 0 & 0 \\ 0 & r^{-2} & 0 \\ 0 & 0 & 1 \end{bmatrix}. \quad (9.72)$$

9.3.6 Volume element and Levi-Civita tensor

The square root of the determinant of the metric tensor written in cylindrical-polar coordinates (from equation (9.72)) is given by

$$\sqrt{\det(\bar{\mathcal{G}})} = r \quad (9.73)$$

so that the volume element is

$$dV = r dr d\vartheta dz. \quad (9.74)$$

The covariant Levi-Civita tensor has the cylindrical-polar representation

$$\varepsilon_{\bar{a}\bar{b}\bar{c}} = r \epsilon_{\bar{a}\bar{b}\bar{c}}. \quad (9.75)$$

9.3.7 Vector cross product of basis vectors

As a check on the formalism for vector cross products, let us verify the relation (8.79) for the cross product of two basis vectors using cylindrical-polar coordinates

$$\vec{e}_{\bar{a}} \times \vec{e}_{\bar{b}} = \varepsilon_{\bar{a}\bar{b}\bar{c}} \vec{e}^{\bar{c}} \implies \vec{e}_{\bar{a}} \times \vec{e}_{\bar{b}} = r \epsilon_{\bar{a}\bar{b}\bar{c}} \vec{e}^{\bar{c}}. \quad (9.76)$$

Making use of the cylindrical-polar coordinate basis vectors and one-forms renders

$$\vec{e}_r \times \vec{e}_\vartheta = r(\hat{\mathbf{r}} \times \hat{\boldsymbol{\vartheta}}) = r\tilde{e}^z = \varepsilon_{r\vartheta z}\tilde{e}^z \quad (9.77a)$$

$$\vec{e}_\vartheta \times \vec{e}_{\bar{z}} = r(\hat{\boldsymbol{\vartheta}} \times \hat{\mathbf{z}}) = r\hat{\mathbf{r}} = r\tilde{e}^r = \varepsilon_{\vartheta\bar{z}r}\tilde{e}^r \quad (9.77b)$$

$$\vec{e}_{\bar{z}} \times \vec{e}_r = \hat{\mathbf{z}} \times \hat{\mathbf{r}} = \hat{\boldsymbol{\vartheta}} = r\tilde{e}^\vartheta = \varepsilon_{\bar{z}r\vartheta}\tilde{e}^\vartheta. \quad (9.77c)$$

To reach these results we made use of the cross products for the unit vectors

$$\hat{\mathbf{r}} \times \hat{\boldsymbol{\vartheta}} = \hat{\mathbf{z}} \quad \text{and} \quad \hat{\boldsymbol{\vartheta}} \times \hat{\mathbf{z}} = \hat{\mathbf{r}} \quad \text{and} \quad \hat{\mathbf{z}} \times \hat{\mathbf{r}} = \hat{\boldsymbol{\vartheta}}. \quad (9.78)$$

9.3.8 Components of a vector field

A vector field \vec{F} has Cartesian components, F^a , related to cylindrical-polar components, $F^{\bar{a}}$, via the transformation matrix, $F^{\bar{a}} = \Lambda_a^{\bar{a}} F^a$. This transformation leads to

$$F^{\bar{1}} = F^x \cos \vartheta + F^y \sin \vartheta \quad (9.79a)$$

$$F^{\bar{2}} = r^{-1} [-F^x \sin \vartheta + F^y \cos \vartheta] \quad (9.79b)$$

$$F^{\bar{3}} = F^z. \quad (9.79c)$$

Introducing the cylindrical-polar unit vectors (9.65) leads to the more tidy expressions

$$F^{\bar{1}} = \hat{\mathbf{r}} \cdot \mathbf{F} \quad (9.80a)$$

$$r F^{\bar{2}} = \hat{\boldsymbol{\vartheta}} \cdot \mathbf{F} \quad (9.80b)$$

$$F^{\bar{3}} = \hat{\mathbf{z}} \cdot \mathbf{F}, \quad (9.80c)$$

where \mathbf{F} is the Cartesian representation.

9.3.9 Differential operators

In cylindrical-polar coordinates, the gradient operator $\nabla = \tilde{e}^a \partial_a$ takes on the form

$$\nabla = \hat{\mathbf{r}} \frac{\partial}{\partial r} + \frac{\hat{\boldsymbol{\vartheta}}}{r} \frac{\partial}{\partial \vartheta} + \hat{\mathbf{z}} \frac{\partial}{\partial z} \quad (9.81)$$

and the covariant divergence of a vector field is given by

$$\nabla_{\bar{a}} F^{\bar{a}} = r^{-1} \partial_{\bar{a}} (r F^{\bar{a}}) \quad (9.82a)$$

$$= r^{-1} \left(\partial_r [r F^{\bar{1}}] + \partial_\vartheta [r F^{\bar{2}}] + \partial_z [r F^{\bar{3}}] \right) \quad (9.82b)$$

$$= \frac{1}{r} \frac{\partial (r \hat{\mathbf{r}} \cdot \mathbf{F})}{\partial r} + \frac{1}{r} \frac{\partial (\hat{\boldsymbol{\vartheta}} \cdot \mathbf{F})}{\partial \vartheta} + \frac{\partial (\hat{\mathbf{z}} \cdot \mathbf{F})}{\partial z}. \quad (9.82c)$$

The covariant Laplacian of a scalar, $\nabla^2 \psi = \nabla \cdot \nabla \psi$, is given by

$$\nabla^2 \psi = \nabla \cdot \left[\hat{\mathbf{r}} \frac{\partial \psi}{\partial r} + \frac{\hat{\boldsymbol{\vartheta}}}{r} \frac{\partial \psi}{\partial \vartheta} + \hat{\mathbf{z}} \frac{\partial \psi}{\partial z} \right] \quad (9.83a)$$

$$= \frac{1}{r} \frac{\partial}{\partial r} \left[r \frac{\partial \psi}{\partial r} \right] + \frac{1}{r^2} \frac{\partial^2 \psi}{\partial \vartheta^2} + \frac{\partial^2 \psi}{\partial z^2}. \quad (9.83b)$$

The covariant curl (Section 8.17) takes the form

$$(\text{curl} \vec{F})^{\bar{1}} = r^{-1} [\partial_{\vartheta} F^{\bar{3}} - \partial_{\bar{z}} (r^2 F^{\bar{2}})] \quad (9.84a)$$

$$(\text{curl} \vec{F})^{\bar{2}} = r^{-1} [\partial_{\bar{z}} F^{\bar{1}} - \partial_r F^{\bar{3}}] \quad (9.84b)$$

$$(\text{curl} \vec{F})^{\bar{3}} = r^{-1} [\partial_r (r^2 F^{\bar{2}}) - \partial_{\vartheta} F^{\bar{1}}], \quad (9.84c)$$

which can be written more conventionally as

$$(\text{curl} \vec{F})^{\bar{1}} = \frac{1}{r} \frac{\partial(\hat{z} \cdot \mathbf{F})}{\partial \vartheta} - \frac{\partial(\hat{\vartheta} \cdot \mathbf{F})}{\partial z} \quad (9.85a)$$

$$r (\text{curl} \vec{F})^{\bar{2}} = \frac{\partial(\hat{r} \cdot \mathbf{F})}{\partial z} - \frac{\partial(\hat{z} \cdot \mathbf{F})}{\partial r} \quad (9.85b)$$

$$(\text{curl} \vec{F})^{\bar{3}} = \frac{1}{r} \frac{\partial(r \hat{\vartheta} \cdot \mathbf{F})}{\partial r} - \frac{1}{r} \frac{\partial(\hat{r} \cdot \mathbf{F})}{\partial \vartheta}. \quad (9.85c)$$

9.3.10 Summary

We here summarize the cylindrical coordinate version of some common mathematical operators.

$$(r, \vartheta, z) = (x^{\bar{1}}, x^{\bar{2}}, x^{\bar{3}}) \quad \text{cylindrical coordinates} \quad (9.86)$$

$$F^{\bar{1}} = \hat{r} \cdot \mathbf{F} \quad r F^{\bar{2}} = \hat{\vartheta} \cdot \mathbf{F} \quad F^{\bar{3}} = \hat{z} \cdot \mathbf{F} \quad \text{vector components} \quad (9.87)$$

$$\nabla = \hat{r} \frac{\partial}{\partial r} + \frac{\hat{\vartheta}}{r} \frac{\partial}{\partial \vartheta} + \hat{z} \frac{\partial}{\partial z} \quad \text{gradient} \quad (9.88)$$

$$\nabla_{\bar{a}} F^{\bar{a}} = \frac{1}{r} \frac{\partial(r \hat{r} \cdot \mathbf{F})}{\partial r} + \frac{1}{r} \frac{\partial(\hat{\vartheta} \cdot \mathbf{F})}{\partial \vartheta} + \frac{\partial(\hat{z} \cdot \mathbf{F})}{\partial z}. \quad \text{divergence} \quad (9.89)$$

$$\nabla^2 \psi = \frac{1}{r} \frac{\partial}{\partial r} \left[r \frac{\partial \psi}{\partial r} \right] + \frac{1}{r^2} \frac{\partial^2 \psi}{\partial \vartheta^2} + \frac{\partial^2 \psi}{\partial z^2} \quad \text{Laplacian of scalar} \quad (9.90)$$

$$(\nabla \times \mathbf{F})_{\bar{a}} = \varepsilon_{\bar{a}\bar{b}\bar{c}} \partial_b F^{\bar{c}} \quad \text{see equations (9.84a) -- (9.84c).} \quad \text{curl of a vector} \quad (9.91)$$

9.4 General orthogonal coordinates

We can generalize the spherical and cylindrical-polar coordinates by considering a nonsingular and orthogonal set of coordinates defined such that the metric tensor takes on the diagonal form

$$g_{\bar{a}\bar{b}} = \vec{e}_{\bar{a}} \cdot \vec{e}_{\bar{b}} = \begin{bmatrix} h_{\bar{1}} & 0 & 0 \\ 0 & h_{\bar{2}} & 0 \\ 0 & 0 & h_{\bar{3}} \end{bmatrix}, \quad (9.92)$$

where $h_{\bar{a}} > 0$ are “stretching” functions. The corresponding volume element is expressed as

$$dV = h_{\bar{1}} h_{\bar{2}} h_{\bar{3}} d\xi^{\bar{1}} d\xi^{\bar{2}} d\xi^{\bar{3}}. \quad (9.93)$$

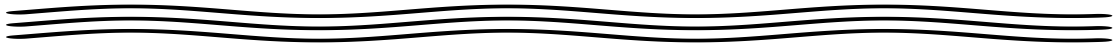
These *generalized orthogonal curvilinear coordinates* have a corresponding orthogonal set of basis vectors

$$\vec{e}_{\bar{a}} = h_{\bar{a}} \hat{\mathbf{e}}_{(\bar{a})} \quad \text{no implied sum.} \quad (9.94)$$

The objects $\hat{\mathbf{e}}_{(\bar{a})}$ are the dimensionless unit directions. The corresponding one-form basis is given by

$$\tilde{e}^{\bar{a}} = (h_{\bar{a}})^{-1} \hat{\mathbf{e}}_{(\bar{a})}. \quad (9.95)$$

The index on the unit directions is enclosed in parentheses to advertise that it is not tensorial; i.e., the unit directions do not transform as tensors. Rather, the functions $h_{\bar{a}}$ carry the tensorial properties of the basis vectors $\vec{e}_{\bar{a}}$. Results for the trajectory and velocity are straightforward generalizations of the spherical results in Section 9.2 and cylindrical-polar results from Section 9.3. A detailed presentation of generalized orthogonal coordinates is found in Section 21.11 of [Griffies \(2004\)](#), with these coordinates commonly used for ocean and atmospheric models.



Part II

Particle mechanics

Planetary rotation and gravitation are two defining features of geophysical fluid mechanics. Furthermore, geophysical fluids exhibit motions whose speed is small relative to that of the rotating planet. We thus say that geophysical fluids are in near solid-body motion, making it convenient to use a rotating (non-inertial) terrestrial reference frame for a physical description. Rotating and gravitating motion around a sphere introduce new physical ideas beyond the more familiar non-rotating system. Rather than study rotating physics within the context of fluid mechanics, we first focus on the point particle system as a venue to establish a foundation for rotating physics. In the process, we also review key facets of classical mechanics necessary for fluid mechanics.

There is a payoff for studying these chapters on *geophysical particle mechanics*, even for the experienced physics student. Namely, topics familiar from classical mechanics are presented from the viewpoint of what later proves to be central to the study of geophysical fluid mechanics. In particular, we encounter Newton's laws of motion, trajectories, reference frames, linear momentum, angular momentum, body forces, non-inertial accelerations (Coriolis and centrifugal), symmetries, center of mass coordinates, planetary Cartesian coordinates, and planetary spherical coordinates. We start by reviewing foundational elements of Newtonian particle mechanics in Chapter 10, considering both a single point particle as well as a system of particles. Thereafter, in Chapters 11 and 12 we focus on the geophysically relevant case of a classical massive point particle moving around a rotating and gravitating sphere as described from the rotating terrestrial reference frame.

Chapter 10

NEWTONIAN PARTICLE MECHANICS

Before diving into the mechanics of a particle moving around a rotating sphere in Chapters 11 and 12, we here summarize foundational elements of Newtonian particle mechanics for a single particle and for a system of particles. Doing so exposes some basic concepts such as space, time, mass, and force. Notably, within the bounds of classical physics, many concepts remain intuitive in that they are based on common experience rather than deduced from more fundamental notions. This perspective is sufficient for this book.

Newtonian mechanics is summarized by Newton's three laws of motion:

- NEWTON'S FIRST LAW: In an inertial reference frame, every body remains at rest or in uniform motion unless acted on by a net force.
- NEWTON'S SECOND LAW: In an inertial reference frame, application of a net force alters the linear momentum.
- NEWTON'S THIRD LAW: To each action there is an equal and opposite reaction.

The first and second laws offer definitions for an inertial reference frame and for a force, and as such they alone render little physical insight.¹ In contrast, the third law provides a statement about how forces act between physical systems, which then provides physical substance to the first and second laws. The third law holds for central forces, such as arise in Newtonian gravity and electrostatics. However, it does not hold for all forces, with an example being the Lorentz force acting on a moving charged particle.

CHAPTER GUIDE

Although the study of fluid mechanics is concerned with continuum matter rather than discrete matter, the study of Newtonian particle mechanics provides core physical notions that extend to our study of fluid mechanics. In this chapter we provide mathematical statements for the three laws of Newton as they manifest for the description of a single point particle as well as for a system of many point particles. Every classical mechanics textbook has some form of the material presented in this chapter. The books from [Goldstein \(1980\)](#) and [Fetter and Walecka \(2003\)](#) are targeted at the entering physics graduate student, whereas [Marion and Thornton \(1988\)](#), [Symon \(1971\)](#), and [Landau and Lifshitz \(1976\)](#) are targeted at second or third year undergraduates.

¹For more on this perspective of Newton's laws, see Chapter 1 of [Symon \(1971\)](#) or Chapter 2 of [Marion and Thornton \(1988\)](#).

10.1	Newtonian mechanics of a point particle	198
10.1.1	Linear momentum and Newton's second law	198
10.1.2	Galilean invariance of inertial reference frames	199
10.1.3	Inertial and non-inertial reference frames	200
10.1.4	Angular velocity and angular momentum	200
10.1.5	Mechanical work and kinetic energy	201
10.1.6	Kinetic energy of rotational motion	202
10.1.7	Mechanical energy conservation	202
10.1.8	Friction as a non-conservative force	203
10.2	Newtonian mechanics for a system of particles	204
10.2.1	Forces on the particles	204
10.2.2	Weak and strong form of Newton's third law	205
10.2.3	Newton's second law of motion	206
10.2.4	Angular momentum	206
10.2.5	Center of mass coordinates	207
10.2.6	Angular momentum in center of mass coordinates	207
10.2.7	Energy in center of mass coordinates	208
10.2.8	Comments and further reading	210

10.1 Newtonian mechanics of a point particle

In this section we study the Newtonian mechanics of a single point particle.

10.1.1 Linear momentum and Newton's second law

Let $\mathbf{X}(t)$ be the position in Euclidean space of a point particle at a particular Newtonian time instance, t . The spatial position is measured relative to an arbitrary origin, with the vector \mathbf{X} pointing from the origin to the particle. As the particle moves in time it traces out a *trajectory* through space plus time. The velocity of the particle at any time instance is measured by the time derivative

$$\mathbf{V} = \frac{d\mathbf{X}}{dt} = \dot{\mathbf{X}}, \quad (10.1)$$

where the second equality introduced a common “dot” notation for time derivatives that is sometimes used in this book. Geometrically, the velocity at each point in space and time is tangent to the trajectory.

The *linear momentum* of the particle equals to the mass of the particle, m , times its velocity

$$\mathbf{P} = m \dot{\mathbf{X}}. \quad (10.2)$$

The linear momentum changes when it experiences a net force. The vector sum of all forces is written \mathbf{F} , and Newton's second law of motion states that there exists *inertial reference frames* where motion of the particle is described by the differential equation

$$\frac{d\mathbf{P}}{dt} = \mathbf{F}. \quad (10.3)$$

If the particle mass is fixed, then this equation becomes a second order differential equation for the particle position or trajectory

$$\mathbf{A} = \frac{d\mathbf{V}}{dt} = \frac{d^2\mathbf{X}}{dt^2} = \mathbf{F}/m. \quad (10.4)$$

We refer to $\mathbf{A} = \dot{\mathbf{V}}$ as the *acceleration*.

Many conclusions in mechanics are expressed in terms of conservation laws (Chapter 12), which provide relations or conditions whereby mechanical properties of a physical system remain time invariant (i.e., time independent). Newton's second law provides our first conservation law since, in the absence of a net force, the linear momentum of a physical system remains unchanged: $d\mathbf{P}/dt = 0$. Depending on the nature of the forces, this conservation law might hold for one, two, or all three of the vector components to the linear momentum. Note that for a constant mass particle, a fixed linear momentum means that the velocity remains constant, which is Newton's first law.

10.1.2 Galilean invariance of inertial reference frames

If the forces acting on the particle are not directly dependent on the particle velocity, then the inertial frame equation of motion (10.4) is unchanged if shifting the velocity by a constant. Such velocity-independent forces (such as Newton's gravitational force) are commonly found in conservative (non-dissipative) motion of charge-free particles. This arbitrariness in the velocity reflects a *symmetry* respected by the equation of motion, where symmetry refers to an operation that can be performed on the system without changing any physics. We give the symmetry the name *Galilean invariance*, with Galilean invariance a property of all inertial reference frames in Newtonian mechanics.

These considerations indicate that there is no experiment that can distinguish between two arbitrary inertial reference frames, so long as the experiments are described by Newton's equation of motion (10.4) and the force is independent of the velocity. The reason we cannot make a distinction is that the equation of motion is indistinguishable in the two inertial frames. As a corollary, two inertial reference frames can at most be moving relative to one another by a constant velocity. Otherwise, at least one of the reference frames must be accelerating, which in turn would mean that it is not an inertial frame.

This discussion offers an example of the mathematical transformation theory introduced in Part I of this book. Mathematically, the Galilean transformation is written

$$\bar{t} = t \quad \text{and} \quad \bar{\mathbf{X}} = \mathbf{X} + \mathbf{U}t, \quad (10.5)$$

where the barred position vector is measured in the moving reference frame. Time remains unchanged since we make use of Newtonian universal time. In contrast, the position of the particle in the new frame equals to that in the original reference frame plus a contribution from the constant velocity, \mathbf{U} . We may sometimes refer to the barred reference frame as a *Galilean boosted* frame. The particle velocity in the moving (boosted) reference frame is given by

$$\bar{\mathbf{V}} = \frac{d\bar{\mathbf{X}}}{d\bar{t}} = \frac{d\mathbf{X}}{dt} + \frac{d(\mathbf{U}t)}{dt} = \mathbf{V} + \mathbf{U}, \quad (10.6)$$

where we set $d\mathbf{U}/dt = 0$ since \mathbf{U} has a fixed magnitude and direction (as per our assumption that it is a constant vector). As expected, the velocity is shifted by the constant reference frame velocity \mathbf{U} . Consequently, the acceleration in the two reference frames is identical

$$\bar{\mathbf{A}} = \frac{d^2\bar{\mathbf{X}}}{d\bar{t}^2} = \frac{d\mathbf{V}}{dt} = \mathbf{A}. \quad (10.7)$$

10.1.3 Inertial and non-inertial reference frames

As seen above, inertial reference frames (also called *absolute* reference frames) have a special status in Newtonian mechanics since it is in these reference frames that Newton's second law holds as per equations (10.3) or (10.4). In practice, inertial reference frames are an idealization never met exactly. For experiments taking place within many laboratories, the earth or *laboratory reference frame* provide a good approximation to an inertial reference frame. However, when the scale of the physical system under study increases, then it can become untenable to ignore the earth's rotation. In such cases the rotating earth reference frame is no longer a good approximation to an inertial frame, in which case the Coriolis and centrifugal accelerations become important. This is the situation holding for the geophysical fluid motions of concern in this book, and more fully explored for the point particle in Chapters 11 and 12.

10.1.4 Angular velocity and angular momentum

The *angular momentum* of a particle is defined relative to an arbitrary chosen origin and is given by the vector cross product

$$\mathbf{L} = \mathbf{X} \times \mathbf{P}. \quad (10.8)$$

Making use of Newton's second law (10.3) leads to the equation of motion for the angular momentum

$$\frac{d\mathbf{L}}{dt} = \mathbf{X} \times \mathbf{F}, \quad (10.9)$$

where we set $\dot{\mathbf{X}} \times \mathbf{P} = \dot{\mathbf{X}} \times m \dot{\mathbf{X}} = 0$. The cross product, $\mathbf{X} \times \mathbf{F}$, is the *torque* acting on the system relative to the chosen origin, with torques having dimensions of a force times a length. Equation (10.9) leads to our second conservation law: a particle has a constant angular momentum when experiencing zero torques, with this statement dependent on the choice of origin for the angular momentum and the corresponding torques.

The utility and relevance of angular momentum stems from its conservation for systems exhibiting rotational symmetry about special points or special directions. For example, motion on a smooth sphere exhibits rotational symmetry with respect to the center of the sphere. Consequently, all components of angular momentum for a particle are constant in the absence of externally applied torques. Likewise, for motion on a smooth rotating sphere, we show in Section 12.6 that the component of angular momentum about the rotation axis is a constant of the motion.

Angular velocity and moment of inertia

Whereas linear momentum has physical dimensions of

$$[\mathbf{P}] \equiv \text{mass} * \text{length} * \text{time}^{-1}, \quad (10.10)$$

angular momentum has dimensions of

$$[\mathbf{L}] \equiv \text{mass} * \text{length}^2 * \text{time}^{-1}. \quad (10.11)$$

We can pursue the analog by introducing the *angular velocity* of a particle relative to a chosen origin

$$\boldsymbol{\Omega} = \frac{\mathbf{X} \times \mathbf{V}}{|\mathbf{X}|^2}. \quad (10.12)$$

The angular velocity has physical dimensions of inverse time, and it is defined with respect to the chosen coordinate origin. By construction, the angular velocity vector is orthogonal to both the velocity and to the position

$$\boldsymbol{\Omega} \cdot \mathbf{X} = \boldsymbol{\Omega} \cdot \mathbf{V} = 0. \quad (10.13)$$

The angular velocity is not defined at the origin where $|\mathbf{X}| = 0$.

Inserting the definition of the angular velocity (10.12) into the angular momentum (10.8) renders

$$\mathbf{L} = m(\mathbf{X} \times \mathbf{V}) \quad (10.14a)$$

$$= m|\mathbf{X}|^2 \boldsymbol{\Omega} \quad (10.14b)$$

$$\equiv I\boldsymbol{\Omega}. \quad (10.14c)$$

In the final equality we introduced the moment of inertia for a point particle

$$I = m|\mathbf{X}|^2. \quad (10.15)$$

The moment of inertia measures the inertia appropriate for determining angular momentum relative to a chosen coordinate origin. The moment of inertia scalar, I , generalizes to the moment of inertia tensor, I_{mn} , when considering angular momentum for extended matter, such as a rigid body or a material fluid region (Section 34.8.4).

The cross product of the position vector with the angular velocity (10.12) is given by

$$\boldsymbol{\Omega} \times \mathbf{X} = \mathbf{V} - \mathbf{X} \frac{\mathbf{V} \cdot \mathbf{X}}{|\mathbf{X}|^2}. \quad (10.16)$$

For the special case of velocity \mathbf{V} orthogonal to the position vector, \mathbf{X} , we have

$$\mathbf{V} = \boldsymbol{\Omega} \times \mathbf{X} \quad \text{when } \mathbf{V} \cdot \mathbf{X} = 0. \quad (10.17)$$

In particular, for circular motion, the velocity vector is orthogonal to the position vector. The solid-body motion of a point on a rotating spherical planet provides another example where $\mathbf{V} = \boldsymbol{\Omega} \times \mathbf{X}$.

10.1.5 Mechanical work and kinetic energy

When a force is applied to a particle as it moves along its trajectory, the force does *mechanical work* on the particle. This force affects the motion, with the work performed by the force computed by the line integral along the trajectory

$$W = \int_{\mathbf{x}_1}^{\mathbf{x}_2} \mathbf{F} \cdot d\mathbf{x}, \quad (10.18)$$

where

$$\mathbf{x}_1 = \mathbf{X}(t = t_1) \quad \text{and} \quad \mathbf{x}_2 = \mathbf{X}(t = t_2) \quad (10.19)$$

are the spatial coordinates of the endpoints for the trajectory at times t_1 and t_2 , and $d\mathbf{x}$ is the differential vector increment along the trajectory. Since the particle is moving along its dynamical trajectory, we can write

$$d\mathbf{x} = \mathbf{V} dt \quad (10.20)$$

and make use of Newton's equation of motion (10.4) to reach

$$W = \int_{\mathbf{x}_1}^{\mathbf{x}_2} \mathbf{F} \cdot d\mathbf{x} = \int_{t_1}^{t_2} m \frac{d\mathbf{V}}{dt} \cdot \mathbf{V} dt = \frac{m}{2} \int_{t_1}^{t_2} \frac{d(\mathbf{V} \cdot \mathbf{V})}{dt} dt = K(t_2) - K(t_1), \quad (10.21)$$

where we defined the kinetic energy of the particle

$$K = \frac{m}{2} \mathbf{V} \cdot \mathbf{V}. \quad (10.22)$$

We conclude that the work done on the particle over a time interval is equal to its change in kinetic energy. The result (10.21) is called the *work-energy theorem*.

10.1.6 Kinetic energy of rotational motion

If the particle is undergoing rotational motion so that $\mathbf{V} = \boldsymbol{\Omega} \times \mathbf{X}$ (equation (10.17)), then the kinetic energy of the particle takes on the form

$$(2/m) K = V_i V_i \quad (10.23a)$$

$$= \epsilon_{ijk} \Omega_j X_k \epsilon_{ist} \Omega_s X_t \quad (10.23b)$$

$$= \epsilon_{ijk} \epsilon_{ist} \Omega_j X_k \Omega_s X_t \quad (10.23c)$$

$$= (\delta_{js} \delta_{kt} - \delta_{jt} \delta_{ks}) \Omega_j X_k \Omega_s X_t \quad (10.23d)$$

$$= (\mathbf{X} \cdot \mathbf{X}) (\boldsymbol{\Omega} \cdot \boldsymbol{\Omega}), \quad (10.23e)$$

where we set $\boldsymbol{\Omega} \cdot \mathbf{X} = 0$ as per equation (10.13), and made use of the epsilon tensor identity (1.38). Hence, the kinetic energy for purely rotational particle motion is

$$K = \frac{I}{2} \boldsymbol{\Omega} \cdot \boldsymbol{\Omega}, \quad (10.24)$$

where $I = m \mathbf{X} \cdot \mathbf{X}$ is the moment of inertia for the point particle as defined by equation (10.15).

10.1.7 Mechanical energy conservation

Consider the work done on a particle as it moves between two points in space. Now compute the work done on the particle as it moves along another path between the same initial and final positions. If the work done on the particle is independent of the path taken between the points, then the force is said to be *conservative*.

Conservation of mechanical energy

Recalling our discussion of exact differentials in Section 2.8, we know that a conservative force can be written as the gradient of a *force potential*²

$$\mathbf{F} = -\nabla V, \quad (10.25)$$

where V is called the *potential* or the *potential energy*. Inserting the potential into the work equation (10.21) leads to an expression of *mechanical energy* conservation

$$W = \int_{\mathbf{x}_1}^{\mathbf{x}_2} \mathbf{F} \cdot d\mathbf{x} = \Delta K = -\Delta V \implies K(t_2) + V(t_2) = K(t_1) + V(t_1). \quad (10.26)$$

²Do not confuse the potential, V , in equation (10.25) with the magnitude of the velocity, $|\mathbf{V}|$. They are distinct.

That is, the sum of the kinetic energy plus potential energy remains constant for a particle moving in a conservative force field. The conservation of kinetic plus potential energy within a conservative force field offers our third conservation law: the conservation of *mechanical energy*.

As a result of mechanical energy conservation (10.26), we see that if a particle takes a closed trajectory within a conservative force field, then there is zero work applied to the particle

$$W = \oint_C \mathbf{F} \cdot d\mathbf{x} = 0, \quad (10.27)$$

where C is an arbitrary closed trajectory. Another way to see that $W = 0$ for a closed trajectory is to write

$$W = \oint_C \mathbf{F} \cdot d\mathbf{x} = \oint_C m \frac{d\mathbf{V}}{dt} \cdot \mathbf{V} dt = \frac{m}{2} \oint_C d(\mathbf{V} \cdot \mathbf{V}) = 0, \quad (10.28)$$

with the zero resulting since $d(\mathbf{V} \cdot \mathbf{V})$ is an exact differential (see Section 2.8 for exact differentials).

Conservative force from the effective gravity field

The earth's gravitational field as well as the planetary centrifugal acceleration (due to motion on a rotating planet) both give rise to conservative forces. We discuss these ideas in Section 11.11.4, where we see that the combined accelerations from gravity and centrifugal are encapsulated by the gradient of the geopotential, Φ . In this case, the effective gravitational force acting on a point particle of mass, m , is given by

$$\mathbf{F} = -m \nabla \Phi. \quad (10.29)$$

Consequently, the work done on the particle by the effective gravitational field is

$$W = \int_{\mathbf{x}_1}^{\mathbf{x}_2} \mathbf{F} \cdot d\mathbf{x} = -m \int_{\mathbf{x}_1}^{\mathbf{x}_2} \nabla \Phi \cdot d\mathbf{x} = -m [\Phi(\mathbf{x}_2) - \Phi(\mathbf{x}_1)]. \quad (10.30)$$

The effective gravitational force field does positive work on the particle if $\Phi(\mathbf{x}_1) > \Phi(\mathbf{x}_2)$. That is, work is applied to the particle as it moves from a high geopotential at \mathbf{x}_1 to a lower geopotential at \mathbf{x}_2 , in which case the work-energy theorem (10.21) means that the kinetic energy increases. Conversely, if $\Phi(\mathbf{x}_1) < \Phi(\mathbf{x}_2)$, then gravity does negative work on the particle. In this case the potential energy of the particle increases as it moves to a higher geopotential, while, through the work-energy theorem, the kinetic energy of the particle decreases.

10.1.8 Friction as a non-conservative force

Friction is the canonical non-conservative force that typically depends on the velocity field. For example, a common form of the frictional force is given by *Rayleigh drag*

$$\mathbf{F}_{\text{Rayleigh}} = -\gamma m \mathbf{V}, \quad (10.31)$$

where $\gamma > 0$ is a constant with dimensions of inverse time. Newton's equation of motion with Rayleigh drag (and no other forces) takes the form

$$\frac{d\mathbf{V}}{dt} = -\gamma \mathbf{V}. \quad (10.32)$$

Notably, Rayleigh drag is not Galilean invariant since it is dependent on the velocity. We can understand this lack of invariance by noting that the friction force distinguishes the state of rest ($\mathbf{V} = 0$) with respect to a particular reference frame from motion in a Galilean boosted reference frame.

The solution to the first order ordinary differential equation (10.32) is the exponential decay

$$\mathbf{V}(t) = \mathbf{V}(0) e^{-\gamma t}, \quad (10.33)$$

with $\mathbf{V}(0)$ the velocity at time $t = 0$. We thus see that Rayleigh drag exponentially drives the velocity towards zero. Correspondingly, Rayleigh drag dissipates the kinetic energy according to twice the exponential decay

$$\frac{dK}{dt} = m \mathbf{V} \cdot \frac{d\mathbf{V}}{dt} = -2\gamma K \implies K(t) = K(0) e^{-2\gamma t}, \quad (10.34)$$

where $K(0) = \mathbf{V}(0) \cdot \mathbf{V}(0)/2$.

10.2 Newtonian mechanics for a system of particles

We here extend the single particle mechanics from Section 10.1 to the case of N particles with mass, $m_{(i)}$, position, $\mathbf{X}_{(i)}(t)$, and velocity, $\mathbf{V}_{(i)}(t) = d\mathbf{X}_{(i)}/dt$, where i is an integer labeling the particles and we assume the particle mass remains fixed in time.³ In the following, we find it useful to introduce the total mass of the system as well as the vector center of mass according to

$$M = \sum_{i=1}^N m_{(i)} \quad \text{and} \quad \mathbf{X} = \frac{1}{M} \sum_{i=1}^N m_{(i)} \mathbf{X}_{(i)}. \quad (10.35)$$

10.2.1 Forces on the particles

We conceive of two contributions to the forces acting on each particle. The first arises from *external force* fields that are independent of the N particles, $\mathbf{F}_{(i)}^{(\text{ext})}$. For example, we may consider a system of particles moving in the gravitational field of the planet, with the planet's gravitational field assumed to be independent of the particles. The second force arises from the interactions between the particles, which we refer to as an *internal force*. We write the internal force vector as $\mathbf{F}_{(ji)}$, which is taken to be the force on particle i due to interactions with particle j . We furthermore assume that there are no self-forces so that

$$\mathbf{F}_{(ii)} = 0. \quad (10.36)$$

The net force acting on particle i is thus written

$$\mathbf{F}_{(i)} = \mathbf{F}_{(i)}^{(\text{ext})} + \sum_{j=1}^N \mathbf{F}_{(ji)}, \quad (10.37)$$

and the net force acting on the full system of particles is

$$\sum_{i=1}^N \mathbf{F}_{(i)} = \sum_{i=1}^N \mathbf{F}_{(i)}^{(\text{ext})} + \sum_{i=1}^N \sum_{j=1}^N \mathbf{F}_{(ji)}. \quad (10.38)$$

³We place the particle index within parentheses to emphasize that it is not a tensor index. Correspondingly, particle indices do not follow the summation convention of tensor indices.

The final sum can be written

$$\sum_{i=1}^N \sum_{j=1}^N \mathbf{F}_{(ji)} = \frac{1}{2} \sum_{i=1}^N \sum_{j=1}^N (\mathbf{F}_{(ji)} + \mathbf{F}_{(ij)}), \quad (10.39)$$

where, again, $\mathbf{F}_{(ji)}$ is the force on particle i due to interactions with particle j , and $\mathbf{F}_{(ij)}$ is the force on particle j due to interactions with particle i . This identity follows since the sums are finite so that limits on double sums can be swapped.

10.2.2 Weak and strong form of Newton's third law

Newton's third law states that the force acting on particle i due to particle j is equal to, yet oppositely directed, the force acting on particle j due to particle i :

$$\mathbf{F}_{(ij)} = -\mathbf{F}_{(ji)}. \quad (10.40)$$

For those forces satisfying Newton's third law, the total force acting on the N particle system arises from just the external force, since the internal forces cancel pairwise

$$\sum_{i=1}^N \sum_{j=1}^N \mathbf{F}_{(ij)} = \sum_{i=1}^N \mathbf{F}_{(i)}^{(\text{ext})} = \mathbf{F}^{(\text{ext})}. \quad (10.41)$$

As discussed in Section 11.11.2, the gravitational force acting between two point masses offers an example force that satisfies Newton's third law, in which case the force is given by the inverse square expression

$$\mathbf{F}_{(ji)} = -\frac{G m_{(i)} m_{(j)} (\mathbf{X}_{(i)} - \mathbf{X}_{(j)})}{|\mathbf{X}_{(i)} - \mathbf{X}_{(j)}|^3} = -\mathbf{F}_{(ji)}, \quad (10.42)$$

where G is Newton's gravitational constant discussed in Section 11.11.1. Notice how the gravitational force acts along the line connecting the two particles, so that

$$(\mathbf{X}_{(i)} - \mathbf{X}_{(j)}) \times \mathbf{F}_{(ji)} = 0 \quad (10.43)$$

The electrostatic force acting on charged particles in an electric field is given by Coulombs law, which is also an inverse squared force and that acts along the line between the two particles.

Newton's gravity force and the Coulomb electrostatic force are known as *central forces*. Central forces are said to satisfy the *strong form* of Newton's third law, in that both $\mathbf{F}_{(ij)} = -\mathbf{F}_{(ji)}$ and $(\mathbf{X}_{(i)} - \mathbf{X}_{(j)}) \times \mathbf{F}_{(ji)} = 0$. Slightly more general forces arise that satisfy $\mathbf{F}_{(ji)} = -\mathbf{F}_{(ij)}$ and yet $(\mathbf{X}_{(i)} - \mathbf{X}_{(j)}) \times \mathbf{F}_{(ji)} \neq 0$, with such forces said to satisfy the *weak form* of Newton's third law:

$$\mathbf{F}_{(ij)} = -\mathbf{F}_{(ji)} \quad \text{and} \quad (\mathbf{X}_{(i)} - \mathbf{X}_{(j)}) \times \mathbf{F}_{(ji)} = 0 \implies \text{central force; strong 3rd law} \quad (10.44a)$$

$$\mathbf{F}_{(ij)} = -\mathbf{F}_{(ji)} \quad \text{and} \quad (\mathbf{X}_{(i)} - \mathbf{X}_{(j)}) \times \mathbf{F}_{(ji)} \neq 0 \implies \text{non-central force; weak 3rd law.} \quad (10.44b)$$

Any force that depends on the velocity of the particle is not a central force.⁴ The distinction between the weak and strong form of Newton's third law becomes important when studying particle angular momentum in Section 10.2.4. When studying stresses in fluids in Chapter 22, we assume the strong form of Newton's third law.

⁴The force acting on a classical charged particle moving in an electromagnetic field is known as the Lorentz force. The Lorentz force depends on the velocity of the charged particle and so it is not a central force, with the Lorentz force only satisfying the weak form of Newton's third law. See page 45 of *Marion and Thornton* (1988) for more discussion.

10.2.3 Newton's second law of motion

The linear momentum of a particle is its mass times the velocity

$$\mathbf{P}_{(i)} = m_{(i)} \mathbf{V}_{(i)} \quad \text{no implied summation.} \quad (10.45)$$

Assuming the mass of the particle is constant, the corresponding equation of motion is given by Newton's second law

$$\dot{\mathbf{P}}_{(i)} = m_{(i)} \dot{\mathbf{V}}_{(i)} = \mathbf{F}_{(i)}^{(\text{ext})} + \sum_{j=1}^N \mathbf{F}_{(ji)}. \quad (10.46)$$

Assuming the internal forces satisfy either the weak or strong form of Newton's third law as in equations (10.44a)-(10.44b), we find that the total momentum for the N particle system evolves according to just the total external force

$$\dot{\mathbf{P}} = \sum_{i=1}^N \dot{\mathbf{P}}_{(i)} = \frac{d^2}{dt^2} \sum_{i=1}^N m_{(i)} \mathbf{X}_{(i)} = M \ddot{\mathbf{X}} = \mathbf{F}^{(\text{ext})}. \quad (10.47)$$

That is, the time change in the total linear momentum is given by the total mass times the acceleration of the center of mass, which equals, through Newton's second and third laws, to the total external force acting on the system. We thus find that the center of mass maintains a fixed velocity if there is no net external force acting on the many particle system. This result accords with common experience whereby we cannot lift ourselves up by our own bootstraps.

10.2.4 Angular momentum

The total angular momentum for the many particle system is given by

$$\mathbf{L} = \sum_{i=1}^N \mathbf{L}_{(i)} = \sum_{i=1}^N \mathbf{X}_{(i)} \times \mathbf{P}_{(i)} = \sum_{i=1}^N m_{(i)} \mathbf{X}_{(i)} \times \mathbf{V}_{(i)}, \quad (10.48)$$

and its time derivative is given by

$$\dot{\mathbf{L}} = \sum_{i=1}^N m_{(i)} \mathbf{X}_{(i)} \times \dot{\mathbf{V}}_{(i)} = \sum_{i=1}^N \mathbf{X}_{(i)} \times \mathbf{F}_{(i)}^{(\text{ext})} + \sum_{i=1}^N \sum_{j=1}^N \mathbf{X}_{(i)} \times \mathbf{F}_{(ji)}, \quad (10.49)$$

where we set $\dot{\mathbf{X}}_{(i)} \times \mathbf{V}_{(i)} = \dot{\mathbf{X}}_{(i)} \times \dot{\mathbf{X}}_{(i)} = 0$, and made use of the particle equation of motion (10.46). We identify the term

$$\boldsymbol{\Gamma}^{(\text{ext})} \equiv \sum_{i=1}^N \mathbf{X}_{(i)} \times \mathbf{F}_{(i)}^{(\text{ext})} \quad (10.50)$$

as the total torque acting on the N particle system arising from the external force acting on each particle. The internal torque contribution can be written

$$\sum_{i=1}^N \sum_{j=1}^N \mathbf{X}_{(i)} \times \mathbf{F}_{(ji)} = \frac{1}{2} \sum_{i=1}^N \sum_{j=1}^N (\mathbf{X}_{(i)} \times \mathbf{F}_{(ji)} + \mathbf{X}_{(j)} \times \mathbf{F}_{(ij)}) = \frac{1}{2} \sum_{i=1}^N \sum_{j=1}^N (\mathbf{X}_{(i)} - \mathbf{X}_{(j)}) \times \mathbf{F}_{(ji)}, \quad (10.51)$$

where the first equality follows from interchanging particle indices, and the second equality follows from the weak form of Newton's third law given by equation (10.44b). If we furthermore assume the force satisfies the strong form of Newton's third law (10.44a), as for a central force, then the

total angular momentum evolves according to just the total external torque

$$\dot{\mathbf{L}} = \mathbf{\Gamma}^{(\text{ext})}. \quad (10.52)$$

That is, we require the strong form of Newton's third law to ensure that the total angular momentum is only affected by the torques created by external forces. If the forces only satisfy the weak form of Newton's third law, then evolution of the total angular momentum is generally affected by internal torques. Such torques arise in the presence of nonmechanical forces, such as a magnetic force between charged particles when the electromagnetic field contains intrinsic angular momentum. We have no occasion to study internal torques in this book, so that all physical systems are assumed to satisfy the strong form of Newton's third law.

10.2.5 Center of mass coordinates

It is sometimes preferable to move to an internal set of coordinates that dispenses with the arbitrary fixed origin. In this case we place the coordinate origin at the moving center of mass,

$$\mathbf{X}_{(i)} = \mathbf{X} + \mathbf{X}'_{(i)}, \quad (10.53)$$

with a corresponding velocity expression

$$\mathbf{V}_{(i)} = \mathbf{V} + \mathbf{V}'_{(i)}. \quad (10.54)$$

Making use of the definition of the center of mass coordinate (10.35), we readily find that the relative position and relative velocity each have a vanishing mass weighted sum over all the particles

$$\sum_{i=1}^N m_{(i)} \mathbf{X}'_{(i)} = 0 \quad \text{and} \quad \sum_{i=1}^N m_{(i)} \mathbf{V}'_{(i)} = 0. \quad (10.55)$$

10.2.6 Angular momentum in center of mass coordinates

The total angular momentum of the N particle system, expressed in the center of mass coordinates, is given by

$$\mathbf{L} = \sum_{i=1}^N m_{(i)} \mathbf{X}_{(i)} \times \mathbf{V}_{(i)} \quad (10.56a)$$

$$= \sum_{i=1}^N m_{(i)} (\mathbf{X} + \mathbf{X}'_{(i)}) \times (\mathbf{V} + \mathbf{V}'_{(i)}) \quad (10.56b)$$

$$= M \mathbf{X} \times \mathbf{V} + \sum_{i=1}^N m_{(i)} \mathbf{X}'_{(i)} \times \mathbf{V}'_{(i)} \quad (10.56c)$$

$$= \mathbf{L}^{(\text{cm})} + \mathbf{L}', \quad (10.56d)$$

where we used equation (10.55) to reach the third equality. The first term is the angular momentum of the center of mass relative to the fixed origin

$$\mathbf{L}^{(\text{cm})} = M \mathbf{X} \times \mathbf{V}, \quad (10.57)$$

whereas the second term is the internal angular momentum measured relative to the center of mass

$$\mathbf{L}' = \sum_{i=1}^N m_{(i)} \mathbf{X}'_{(i)} \times \mathbf{V}'_{(i)}. \quad (10.58)$$

Evolution of the center of mass angular momentum takes on the form

$$\dot{\mathbf{L}}^{(\text{cm})} = M \mathbf{X} \times \dot{\mathbf{V}} = \mathbf{X} \times \mathbf{F}^{(\text{ext})}, \quad (10.59)$$

with the right hand side the torque from the net external force computed relative to the center of mass position. Correspondingly, evolution of the total angular momentum is

$$\dot{\mathbf{L}} = \sum_{i=1}^N m_{(i)} \mathbf{X}_{(i)} \times \dot{\mathbf{V}}_{(i)} \quad (10.60\text{a})$$

$$= \sum_{i=1}^N (\mathbf{X} + \mathbf{X}'_{(i)}) \times \mathbf{F}_{(i)}^{\text{ext}} \quad (10.60\text{b})$$

$$= \mathbf{X} \times \mathbf{F}^{\text{ext}} + \sum_{i=1}^N \mathbf{X}'_{(i)} \times \mathbf{F}_{(i)}^{\text{ext}} \quad (10.60\text{c})$$

$$= \dot{\mathbf{L}}^{(\text{cm})} + \dot{\mathbf{L}}'. \quad (10.60\text{d})$$

We thus see that the rate of change for the angular momentum computed relative to the center of mass is given by the torques from the external forces applied to each particle, computed relative to the center of mass

$$\dot{\mathbf{L}}' = \sum_{i=1}^N \mathbf{X}'_{(i)} \times \mathbf{F}_{(i)}^{\text{ext}}. \quad (10.61)$$

10.2.7 Energy in center of mass coordinates

Making use of the identity (10.55), we find that the total kinetic energy is given by

$$K = \frac{1}{2} \sum_{i=1}^N m_{(i)} \mathbf{V}_{(i)} \cdot \mathbf{V}_{(i)} = \frac{M}{2} \mathbf{V} \cdot \mathbf{V} + \frac{1}{2} \sum_{i=1}^N m_{(i)} \mathbf{V}'_{(i)} \cdot \mathbf{V}'_{(i)} = K^{(\text{cm})} + K', \quad (10.62)$$

which is the sum of the center of mass kinetic energy, $K^{(\text{cm})}$, plus the kinetic energy of the internal motions relative to the center of mass, K' .

Consider two configurations of the N particle system, configuration A at time t_A and configuration B at time t_B . Let $\mathbf{X}_{(iA)}$ be the position of particle i in configuration A , and $\mathbf{X}_{(iB)}$ the position of this particle in configuration B , and assume the two configurations are connected by trajectories determined by the equation of motion for each particle. Extending our discussion of work in Section 10.1.5, we see that the work done by forces acting on the N particle system as it

moves between these two configurations is given by

$$W_{AB} = \sum_{i=1}^N \int_{\mathbf{X}_{(iA)}}^{\mathbf{X}_{(iB)}} \mathbf{F}_{(i)} \cdot d\mathbf{x}_{(i)} \quad (10.63a)$$

$$= \sum_{i=1}^N \int_{t_A}^{t_B} \mathbf{F}_{(i)} \cdot \mathbf{V}_{(i)} dt \quad (10.63b)$$

$$= \sum_{i=1}^N \int_{t_A}^{t_B} m_{(i)} \dot{\mathbf{V}}_{(i)} \cdot \mathbf{V}_{(i)} dt \quad (10.63c)$$

$$= \frac{1}{2} \sum_{i=1}^N \int_{t_A}^{t_B} m_{(i)} \frac{d}{dt} (\mathbf{V}_{(i)} \cdot \mathbf{V}_{(i)}) dt \quad (10.63d)$$

$$= K_A - K_B, \quad (10.63e)$$

where K_A and K_B are the kinetic energies in the two configurations.

Rather than making use of Newton's law of motion to introduce the kinetic energy, we can decompose the force vector in the expression for work, thus giving

$$W_{AB} = \sum_{i=1}^N \int_{\mathbf{X}_{(iA)}}^{\mathbf{X}_{(iB)}} \mathbf{F}_{(i)} \cdot d\mathbf{x}_{(i)} \quad (10.64a)$$

$$= \sum_{i=1}^N \int_{\mathbf{X}_{(iA)}}^{\mathbf{X}_{(iB)}} \mathbf{F}_{(i)}^{(\text{ext})} \cdot d\mathbf{x}_{(i)} + \frac{1}{2} \sum_{i=1}^N \sum_{j=1}^N \int_{\mathbf{X}_{(iA)}}^{\mathbf{X}_{(iB)}} \mathbf{F}_{(ji)} \cdot (d\mathbf{x}_{(i)} - d\mathbf{x}_{(j)}), \quad (10.64b)$$

where the minus sign on the final term arises from Newton's third law satisfied by the internal forces. Now assume that both the internal and external forces are conservative, so that they can separately be written as the gradient of respective potential energies. For the external potential energy acting on particle i , we assume it is a function just of the position of that particle

$$\mathbf{F}_{(i)}^{\text{ext}} = -\nabla_i V^{\text{ext}}(\mathbf{X}_{(i)}), \quad (10.65)$$

where ∇_i is the gradient operator acting on the position in space $\mathbf{x}_{(i)}$ of the trajectory at a particular time, $\mathbf{x}_{(i)} = \mathbf{X}_{(i)}(t)$. Furthermore, assume the interparticle potential energy between particles i and j is a function just of the distance between the two particles, which is a property of central forces. In this case we have

$$\mathbf{F}_{(ji)} = -\nabla_{ij} V(|\mathbf{X}_{(i)} - \mathbf{X}_{(j)}|), \quad (10.66)$$

where ∇_{ij} is the gradient operator acting on the relative position $\mathbf{x}_{(i)} - \mathbf{x}_{(j)}$ of the two particles at a particular time instance. These assumptions then, very nicely, bring the work into the form

$$W_{AB} = - \sum_{i=1}^N \int_{\mathbf{X}_{(iA)}}^{\mathbf{X}_{(iB)}} \nabla_i V^{\text{(ext)}} \cdot d\mathbf{x}_{(i)} - \frac{1}{2} \sum_{i=1}^N \sum_{j=1}^N \int_{\mathbf{X}_{(iA)}}^{\mathbf{X}_{(iB)}} \nabla_{ij} V \cdot (d\mathbf{x}_{(i)} - d\mathbf{x}_{(j)}) \quad (10.67a)$$

$$= - \sum_{i=1}^N \int_{\mathbf{X}_{(iA)}}^{\mathbf{X}_{(iB)}} dV_{(i)}^{\text{(ext)}} - \frac{1}{2} \sum_{i=1}^N \sum_{j=1}^N \int_{\mathbf{X}_{(iA)}}^{\mathbf{X}_{(iB)}} dV(|\mathbf{X}_{(i)} - \mathbf{X}_{(j)}|) \quad (10.67b)$$

$$\equiv -[V^{\text{(tot)}}(A) - V^{\text{(tot)}}(B)], \quad (10.67c)$$

where the total potential energy is

$$V^{(\text{tot})} = \sum_{i=1}^N V_{(i)}^{(\text{ext})} + \frac{1}{2} \sum_{i=1}^N \sum_{j=1}^N V(|\mathbf{X}_{(i)} - \mathbf{X}_{(j)}|). \quad (10.68)$$

Combining this result and the expression of work in terms of kinetic energy leads to the conservation of mechanical energy for the conservative N particle system

$$K + V^{(\text{tot})} = \text{constant}. \quad (10.69)$$

10.2.8 Comments and further reading

This section largely follows Section 2 of [Fetter and Walecka \(2003\)](#). Note that when considering a continuous fluid in Part V, the interparticle forces manifest as pressure and friction, whereas the external force is given by gravitation. Furthermore, we always assume the fluids in this book satisfy the strong form of Newton's third law.



Chapter 11

PARTICLE MECHANICS ON A ROTATING SPHERE

In this chapter we study the kinematics and dynamics of a point particle of fixed mass and zero electric charge moving around a rotating and gravitating sphere. The motion of the gravitating sphere is prescribed with a fixed kinetic energy and fixed angular momentum around its axis of rotation. Hence, our focus concerns just the mechanics of the moving particle. Notably, a particle at rest on the rotating sphere has both kinetic energy and angular momentum merely due to the rotation of the sphere. We examine the particle motion relative to the moving sphere from the perspective of a non-inertial rotating reference frame. This perspective is motivated by our interest in particle motion that is in near solid-body motion with the planet, with such motion relevant to the study of geophysical fluids.

The only inertial force acting on the particle arises from the gravitational field of the sphere (ignoring friction and other forces). Two non-inertial accelerations (planetary centrifugal and Coriolis) appear when viewing the motion from the rotating terrestrial reference frame. We make use of both the planetary Cartesian and planetary spherical coordinates to represent the position, velocity, and acceleration vectors, working through both the physics and the maths in support of later descriptions of geophysical fluid motions.

CHAPTER GUIDE

This chapter makes use of basic features of both Cartesian and general tensor algebra as presented in Chapters 1, 7, 8, and Section 9.2. We offer the salient features of tensor technology in this chapter where needed, thus providing a reasonably self-contained presentation. This chapter is notable for working through some relatively tedious algebra as part of developing the spherical coordinate representation of acceleration. This work is relevant also for geophysical fluids, although we rarely encounter the full spherical coordinate equations in later chapters. Even so, the reader is encouraged to read through the details, at least once, as they form part of the building blocks to numerical circulation models of planetary fluids.

Throughout this chapter, it can be useful to return to the general considerations presented Chapter 10, which summarizes the fundamental physical notions underlying Newtonian mechanics. These notions are quite simple in their essence. Such reminders are particularly useful when encountering the somewhat tedious mathematical manipulations with spherical coordinates in a rotating reference frame encountered in the present chapter.

Elements of this chapter can be found in various classical mechanics books, such as Chapter 12 of *French (1971)*, Chapter 1 of *Fetterer et al. (2009)* and Chapter 9 of *Marion and Thornton (1988)*.

11.1	The rotating earth	212
11.2	Reference frames and non-inertial accelerations	213
11.3	Rotation of a vector	215
11.3.1	Brief derivation	215
11.3.2	Detailed derivation for planar motion	216
11.3.3	Changes to Cartesian basis vectors under rotation	216
11.3.4	Changes to polar coordinate unit vectors under rotation	216
11.4	Some tensor algebra	217
11.4.1	Why we need general tensors	217
11.4.2	The coordinate representation of a vector	217
11.4.3	Transformation of a coordinate representation	218
11.5	The velocity vector	219
11.5.1	Coordinate velocity	219
11.5.2	Changes to the basis vectors	219
11.6	Inertial acceleration and its decomposition	220
11.7	Representing the position vector	221
11.8	Representing the velocity vector	221
11.8.1	Planetary Cartesian coordinate representation	221
11.8.2	Planetary spherical coordinate representation	222
11.8.3	Transforming from Cartesian to spherical	223
11.8.4	Axial angular momentum	224
11.9	Planetary Cartesian representation of acceleration	224
11.9.1	Planetary Cartesian representation	224
11.9.2	Summary of acceleration representation	226
11.9.3	Further study	226
11.10	Spherical representation of acceleration	227
11.10.1	Transforming from Cartesian to spherical	228
11.10.2	Decomposing the acceleration	228
11.10.3	Spherical coordinate acceleration	229
11.10.4	Metric acceleration	229
11.10.5	Centrifugal acceleration	229
11.10.6	Coriolis acceleration	230
11.10.7	Coriolis acceleration for large-scale motions	230
11.11	Newtonian gravity	231
11.11.1	Newtonian gravity from Poisson's equation	231
11.11.2	Gravitational field for a spherical earth	232
11.11.3	Approximate gravitational acceleration	233
11.11.4	Effective gravitational force from the geopotential	233
11.11.5	Further study	234
11.12	Newton's law of motion	234
11.12.1	Cartesian coordinate representation	234
11.12.2	Spherical coordinate representation	235
11.12.3	Geopotential coordinate representation	236
11.12.4	Comments	237
11.12.5	Further study	238
11.13	Exercises	238

11.1 The rotating earth

The earth's angular velocity is comprised of two main contributions: the spin of the earth about its axis and the orbit of the earth about the sun (see Figure 11.1). Other astronomical motions can be neglected for geophysical fluid mechanics. Therefore, in the course of a single period of 24 hours, or $24 \times 3600 = 86400$ seconds, the earth experiences an angular rotation of $(2\pi + 2\pi/365.24)$

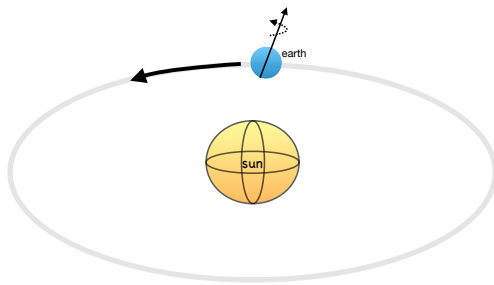


FIGURE 11.1: The angular frequency of the earth arises from the spin about the polar axis plus the orbit of the planet around the sun. This angular frequency determines the strength of the Coriolis acceleration and the planetary centrifugal acceleration.

radians. As such, the angular rotation rate (*angular frequency*) is given by

$$\Omega = \frac{2\pi + 2\pi/365.24}{86400\text{s}} = \left[\frac{\pi}{43082} \right] \text{s}^{-1} = 7.2921 \times 10^{-5} \text{ s}^{-1}. \quad (11.1)$$

The earth's angular frequency, both its direction through the polar axis and its magnitude, is assumed constant in time for purposes of geophysical fluid mechanics

$$\frac{d\Omega}{dt} = 0. \quad (11.2)$$

The angular frequency (11.1) seems quite small. However, a terrestrial reference frame on the earth surface, undergoing *solid body motion*, moves with linear speed

$$U_{\text{solid-body}}(\phi) = \Omega R_e \cos \phi \approx 465 \text{ m s}^{-1} \cos \phi = 1672 \text{ km hr}^{-1} \cos \phi, \quad (11.3)$$

where we set the earth's radius to

$$R_e = 6.371 \times 10^6 \text{ m}. \quad (11.4)$$

This speed is quite large relative to a fixed frame outside the planet (see Figure 11.2)

$$U_{\text{solid-body}}(0) = 1672 \text{ km hr}^{-1} \quad (11.5a)$$

$$U_{\text{solid-body}}(30^\circ) = 1448 \text{ km hr}^{-1} \quad (11.5b)$$

$$U_{\text{solid-body}}(60^\circ) = 826 \text{ km hr}^{-1}. \quad (11.5c)$$

Even so, motion of the atmosphere and ocean are generally quite close to the solid-body motion, so that their speeds relative to the planet are much smaller than the speed of the rotating planet itself. Hence, the preferred frame for studying geophysical motion is the rotating planetary frame (a non-inertial frame) rather than a frame fixed relative to the stars (an approximate inertial frame). Figure 11.3 illustrates the case for the position vector of a particle relative to the origin of a rotating sphere.

11.2 Reference frames and non-inertial accelerations

We need to choose a set of basis vectors from which we determine coordinates to represent vectors. The basis vectors hold two key pieces of information. The first detail concerns the coordinates relative to an origin; e.g., Cartesian, spherical. The second detail concerns the reference frame,

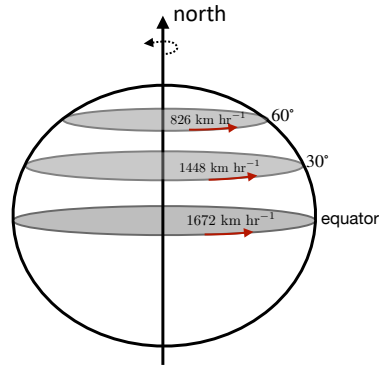


FIGURE 11.2: For an observer at rest on the earth's surface, the solid body speed is $\Omega R_e \cos \phi = 7.2921 \times 10^{-5} \text{ s}^{-1} \times 6.371 \times 10^6 \text{ m} \cos \phi \approx 465 \text{ m s}^{-1} \cos \phi = 1672 \text{ km hr}^{-1} \cos \phi$. We here display solid-body speeds for motion at the equator, 30° latitude, and 60° latitude. These speeds are much larger than motion of the ocean and atmosphere relative to the earth, thus motivating a description of geophysical fluid motion from the rotating terrestrial frame moving with the solid-body.

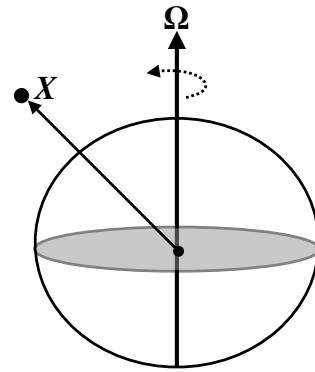


FIGURE 11.3: The position vector, $\mathbf{X}(t)$, for a particle moving around a rotating sphere with coordinate origins at the center of the sphere. The rotation axis is through the north pole, with angular velocity vector $\boldsymbol{\Omega}$. The sphere rotates in a positive right hand sense through the north polar axis (counter-clockwise from above). As given by equation (11.33), the rotating frame has a solid-body velocity $\mathbf{U}_{\text{solid}} = \boldsymbol{\Omega} \times \mathbf{X}$.

whereby non-inertial accelerations arise from time dependence to the basis vectors. When represented in terms of non-inertial reference frame coordinates, the inertial acceleration (a vector) is decomposed into the sum of relative acceleration (relative to the non-inertial reference frame), plus the centrifugal acceleration as well as the Coriolis acceleration.

When multiplied by mass, non-inertial accelerations can be interpreted as non-inertial forces. However, these forces are not imparted by an external force field. Rather, they arise from accelerated motion of the non-inertial reference frame. In this sense, non-inertial accelerations are often termed “fictitious” or “kinematic”. Nonetheless, a terrestrial observer interprets motion that is affected by non-inertial accelerations, so that non-inertial accelerations are central to rationalizing observed planetary fluid motions. Furthermore, as seen in Section 12.7, the Coriolis acceleration that appears in a non-inertial reference frame has its counterpart in axial angular momentum conservation, with angular momentum conservation the natural means to describe rotating motion from the perspective of an inertial frame.

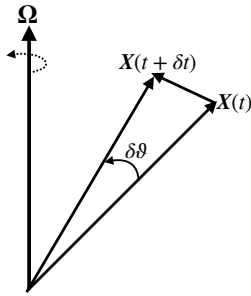


FIGURE 11.4: The change in a vector under a pure rotation leaves its origin fixed and the vector magnitude unchanged, $|\mathbf{X}(t)| = |\mathbf{X}(t + \delta t)|$. Only the vector direction changes by the angle $\delta\vartheta = \boldsymbol{\Omega} \delta t$. Infinitesimal changes generated by the angular velocity $\boldsymbol{\Omega}$ lead to the vector differences $\mathbf{X}(t + \delta t) - \mathbf{X}(t) = \delta t \boldsymbol{\Omega} \times \mathbf{X}(t)$.

11.3 Rotation of a vector

How does a vector change under a rotation such as that shown in Figure 11.4? That is, when a vector is assumed to not translate nor to change its magnitude, how does it change as a result of a pure rotation? To answer this question, observe that a pure rotation does not change the magnitude of a vector so that

$$|\mathbf{X}(t)| = |\mathbf{X}(t + \delta t)|. \quad (11.6)$$

The condition (11.6) can be written as

$$\frac{d(\mathbf{X} \cdot \mathbf{X})}{dt} = 0, \quad (11.7)$$

which leads to the constraint

$$\mathbf{X} \cdot \frac{d\mathbf{X}}{dt} = 0. \quad (11.8)$$

That is, the velocity vector generated by a pure rotation is itself perpendicular to the position vector. We encountered this result in Section 2.1.4 when showing that unit vectors (vectors of a fixed unit length) can only change through a translation or through a rotation. Likewise, any vector of fixed magnitude and fixed origin can change only through the rotation of its direction, in which case the instantaneous time change of the vector is itself perpendicular to the vector. We next determine the instantaneous time change as a function of the angular velocity vector, $\boldsymbol{\Omega}$.

11.3.1 Brief derivation

Referring to Figure 11.4, we see that the infinitesimal difference, $\mathbf{X}(t + \delta t) - \mathbf{X}(t)$, equals to the vector cross product of the angular velocity with the position vector

$$\mathbf{X}(t + \delta t) - \mathbf{X}(t) = \delta t \boldsymbol{\Omega} \times \mathbf{X}(t). \quad (11.9)$$

Dividing by δt leads to

$$\frac{d\mathbf{X}}{dt} = \boldsymbol{\Omega} \times \mathbf{X} \quad \text{pure rotation.} \quad (11.10)$$

Note that this evolution equation satisfies the constraint (11.8) since $\mathbf{X} \cdot (\boldsymbol{\Omega} \times \mathbf{X}) = 0$, meaning that the magnitude of the vector indeed remains fixed. We sometimes say that $\boldsymbol{\Omega}$ is the generator of rotations of \mathbf{X} .

11.3.2 Detailed derivation for planar motion

To determine the change in direction generated by a pure rotation, first consider the simplified case of planar rotation. Let $\boldsymbol{\Omega}$ be entirely in the vertical, and let \mathbf{X} be confined to the horizontal plane. In a time increment δt , the vector $\mathbf{X}(t)$ is rotated by an angle

$$\delta\vartheta = |\boldsymbol{\Omega}| \delta t \quad (11.11)$$

relative to $\mathbf{X}(t + \delta t)$. In the limit of small $\delta\vartheta$, the difference vector, $\mathbf{X}(t + \delta t) - \mathbf{X}(t)$, is perpendicular to $\mathbf{X}(t)$ and is of magnitude equal to the arc length

$$\delta s = |\mathbf{X}(t)| \delta\vartheta = |\mathbf{X}(t)| |\boldsymbol{\Omega}| \delta t. \quad (11.12)$$

We observe that the vector $\boldsymbol{\Omega} \times \mathbf{X}(t)$ points in the same direction as $\mathbf{X}(t + \delta t) - \mathbf{X}(t)$ and is of length $|\mathbf{X}(t)| |\boldsymbol{\Omega}|$. We conclude that

$$\mathbf{X}(t + \delta t) - \mathbf{X}(t) = \boldsymbol{\Omega} \times \mathbf{X}(t) \delta t. \quad (11.13)$$

Dividing through by δt and taking the limit $\delta t \rightarrow 0$ gives

$$\frac{d\mathbf{X}}{dt} = \boldsymbol{\Omega} \times \mathbf{X} \quad \text{pure rotation.} \quad (11.14)$$

The proof for the case in which $\boldsymbol{\Omega}$ has a component along \mathbf{X} is a straightforward generalization. The trajectory is still confined to a plane, but only the component of $\boldsymbol{\Omega}$ normal to the trajectory generates rotation.

11.3.3 Changes to Cartesian basis vectors under rotation

We make use of the result (11.10) in many places when working with rotating physics. One place of particular note concerns the changes to unit vectors under rotation. Cartesian unit vectors exhibit changes solely due to pure rotations since the unit vectors have fixed magnitude. With $\boldsymbol{\Omega} = \Omega \hat{z}$ as for a rotating spherical earth, the change in planetary Cartesian unit vectors under rotation is given by

$$\frac{d\hat{x}}{dt} = \boldsymbol{\Omega} \times \hat{x} = \Omega \hat{y} \quad \text{and} \quad \frac{d\hat{y}}{dt} = \boldsymbol{\Omega} \times \hat{y} = -\Omega \hat{x} \quad \text{and} \quad \frac{d\hat{z}}{dt} = \boldsymbol{\Omega} \times \hat{z} = 0. \quad (11.15)$$

11.3.4 Changes to polar coordinate unit vectors under rotation

As another example of how unit vectors change under rotation, consider the polar coordinates from Section 9.3 with rotation assumed to be about the vertical axis, \hat{z} . In the horizontal plane we have the radial and angular unit vectors

$$\hat{r} = \hat{x} \cos \vartheta + \hat{y} \sin \vartheta \quad (11.16a)$$

$$\hat{\vartheta} = -\hat{x} \sin \vartheta + \hat{y} \cos \vartheta. \quad (11.16b)$$

We can directly verify that the time derivative of these unit vectors is given by

$$\frac{d\hat{r}}{dt} = (\Omega + \dot{\vartheta}) \hat{\vartheta} = (\Omega + \dot{\vartheta}) (\hat{z} \times \hat{r}) \quad (11.17a)$$

$$\frac{d\hat{\vartheta}}{dt} = -(\Omega + \dot{\vartheta}) \hat{r} = (\Omega + \dot{\vartheta}) (\hat{z} \times \hat{\vartheta}). \quad (11.17b)$$

Notice how these unit vectors change both due to the rotation of the reference frame, Ω , plus the change in the angular position relative to the reference frame, $\dot{\vartheta}$. We thus see that unit vectors, such as those for spherical coordinates and cylindrical-polar coordinates, change due to the solid-body rotation, just like the Cartesian unit vectors. Additionally, non-Cartesian unit vectors change when their orientation is modified relative to the Cartesian coordinate axes at a rate distinct from the solid-body. This situation occurs when a trajectory moves relative to the solid-body. We further discuss this notion in Section 11.5.2 and detail the spherical coordinate case in Sections 11.8.2 and 11.10.

11.4 Some tensor algebra

In Part I of this book, we detailed the use of tensor analysis for geophysical motions. We here summarize some of the salient points that are of use in this chapter for manipulating spherical coordinates.

11.4.1 Why we need general tensors

Cartesian tensors are sufficient for many purposes of fluid mechanics, such as when using Cartesian coordinates for a tangent plane approximation to study geophysical fluid motion (e.g., Section 21.3.4). However, we make routine use of spherical coordinates when describing geophysical motion, and cylindrical-polar coordinates for studies of rotating tank experiments (see Section 33.8). Finally, we use generalized vertical coordinates in the description of stratified flows (Part XI). The basis vectors for curvilinear coordinates and generalized vertical coordinates change direction when moving through space. In contrast, Cartesian basis vectors always point in the same direction. This distinction between the basis vectors is the key reason curvilinear coordinates and generalized vertical coordinates require a more general formalism than afforded by Cartesian tensors.

11.4.2 The coordinate representation of a vector

The coordinate representation of a vector follows from decomposing the vector into components aligned according to a set of basis vectors. In particular, the coordinate representation of the position vector is given by

$$\vec{X} = \sum_{a=1}^3 \xi^a \vec{e}_a = \xi^a \vec{e}_a, \quad (11.18)$$

where the Einstein summation convention is defined by the final equality. In this equation,

$$\vec{e}_a = (\vec{e}_1, \vec{e}_2, \vec{e}_3) \quad (11.19)$$

is a set of linearly independent basis vectors, and ξ^a are the corresponding coordinate representations of the position vector \vec{X} . The basis vectors may be normalized to unit magnitude, as in the case of Cartesian coordinates, or may be unnormalized as for spherical coordinates (see Section 9.2.2). Note that we commonly make use of the boldface notation for a vector rather than the arrowed symbol (Section 7.5)

$$\mathbf{X} = \vec{X} = \xi^a \vec{e}_a. \quad (11.20)$$

The basis vectors in equation (11.18) have a lower index while the coordinate representation of a vector has an upper index. Why? For arbitrary coordinates (e.g., spherical), we make a distinction between a coordinate representation with an index upstairs (contravariant) versus the

downstairs (covariant) representation. Moving between the covariant and contravariant representations requires a metric tensor. For much of this book we can keep this mathematical framework at a modest distance, with exposure only in selected places. The key crutch we rely on is that the planet is assumed to be embedded in a background three-dimensional Euclidean space. That is, we are not considering the curved space-time of general relativity nor the marriage of space and time afforded by special relativity. These assumptions simplify our use of general tensors.

When working with general coordinates, it is necessary to distinguish between a basis vector, \vec{e}_a , and its dual partner known as a *one-form*, \tilde{e}^a . Duality is here defined by the familiar (Euclidean) inner product that leads to the bi-orthogonality relation

$$\vec{e}_a \cdot \tilde{e}^b = \delta_a^b, \quad (11.21)$$

with δ_a^b the Kronecker delta tensor

$$\delta_a^b = \begin{cases} 1 & \text{if } b = a \\ 0 & \text{if } b \neq a. \end{cases} \quad (11.22)$$

In linear algebra, a row vector is dual to its column vector, with that analog appropriate for the present context. Cartesian basis vectors equal to the basis one-forms, in which case there is no distinction between contravariant and covariant. However, the distinction is important for more general coordinates used in geophysical fluids.

11.4.3 Transformation of a coordinate representation

A vector is a geometric object; i.e., a line determined by its length and direction. More general tensors are also geometric objects. The coordinate representation of a tensor is a subjective description of the object. More specifically, the coordinate representation of a vector as given by equation (11.18) does not alter the vector, it only alters the representation of the vector. Hence, we can represent the vector using arbitrary coordinates

$$\vec{X} = \xi^a \vec{e}_a = \xi^{\bar{a}} \vec{e}_{\bar{a}}, \quad (11.23)$$

where $\xi^{\bar{a}}$ is the representation of the vector in a coordinate system defined by the basis vector $\vec{e}_{\bar{a}}$, whereas ξ^a is the representation in the unbarred coordinate system with basis vectors \vec{e}_a . In this chapter we choose the unbarred coordinates as planetary Cartesian and the barred coordinates as planetary spherical

$$(\xi^1, \xi^2, \xi^3) = (x, y, z) \quad \text{and} \quad (\xi^{\bar{1}}, \xi^{\bar{2}}, \xi^{\bar{3}}) = (\lambda, \phi, r), \quad (11.24)$$

with the coordinates related by (see Section 9.2 and Figure 9.1)

$$x = r \cos \phi \cos \lambda \quad \text{and} \quad y = r \cos \phi \sin \lambda \quad \text{and} \quad z = r \sin \phi. \quad (11.25)$$

The transformation of coordinate representations for a vector and basis vectors is provided by the transformation matrix and its inverse. For example, the relation between the coordinate representation of the velocity vector and acceleration vector, as well as the coordinate basis vectors, are given by

$$V^{\bar{a}} = \Lambda_a^{\bar{a}} V^a \quad \text{and} \quad A^{\bar{a}} = \Lambda_a^{\bar{a}} A^a \quad \text{and} \quad \vec{e}_{\bar{a}} = \Lambda_a^{\bar{a}} \vec{e}_a, \quad (11.26)$$

where the transformation matrix and its inverse are given by (see Section 9.2.1)

$$\Lambda_a^{\bar{a}} = \begin{bmatrix} \partial\xi^1/\partial\xi^{\bar{1}} & \partial\xi^1/\partial\xi^{\bar{2}} & \partial\xi^1/\partial\xi^{\bar{3}} \\ \partial\xi^2/\partial\xi^{\bar{1}} & \partial\xi^2/\partial\xi^{\bar{2}} & \partial\xi^2/\partial\xi^{\bar{3}} \\ \partial\xi^3/\partial\xi^{\bar{1}} & \partial\xi^3/\partial\xi^{\bar{2}} & \partial\xi^3/\partial\xi^{\bar{3}} \end{bmatrix} = \begin{bmatrix} -r\cos\phi\sin\lambda & -r\sin\phi\cos\lambda & \cos\phi\cos\lambda \\ r\cos\phi\cos\lambda & -r\sin\phi\sin\lambda & \cos\phi\sin\lambda \\ 0 & r\cos\phi & \sin\phi \end{bmatrix} \quad (11.27)$$

$$\Lambda^{\bar{a}}_a = \frac{1}{r^2\cos\phi} \begin{bmatrix} -r\sin\lambda & r\cos\lambda & 0 \\ -r\cos\phi\sin\phi\cos\lambda & -r\cos\phi\sin\phi\sin\lambda & r\cos^2\phi \\ r^2\cos^2\phi\cos\lambda & r^2\cos^2\phi\sin\lambda & r^2\cos\phi\sin\phi \end{bmatrix}, \quad (11.28)$$

with

$$\Lambda_a^{\bar{a}} \Lambda_b^a = \delta_a^{\bar{a}} \quad \text{and} \quad \Lambda_a^{\bar{a}} \Lambda_b^{\bar{a}} = \delta_b^a. \quad (11.29)$$

Hence, if we have the Cartesian representation of a vector, such as the velocity or acceleration, then we can use the above transformation rules to derive the spherical representation.

11.5 The velocity vector

The velocity is the time derivative of the position vector

$$\mathbf{V} = \frac{d\mathbf{X}}{dt}. \quad (11.30)$$

This equation is manifestly geometric in that the velocity at a space-time point is the tangent vector to the trajectory at that point. When expressing this relation using a coordinate representation we note that time dependence lives with both the coordinate representation of the position vector as well as the basis vectors

$$\mathbf{V} = \frac{d\mathbf{X}}{dt} = \frac{d(\xi^a \vec{e}_a)}{dt} = \frac{d\xi^a}{dt} \vec{e}_a + \xi^a \frac{d\vec{e}_a}{dt}. \quad (11.31)$$

11.5.1 Coordinate velocity

The first term on the right hand side of equation (11.31) is the velocity as measured within the chosen reference frame using the chosen coordinates

$$\mathbf{V}_{\text{coord}} \equiv \frac{d\xi^a}{dt} \vec{e}_a. \quad (11.32)$$

This is the contribution to velocity as measured in the reference frame that moves with the basis vectors. In the context of geophysical motions, this is the velocity measured in the rotating terrestrial reference frame.

11.5.2 Changes to the basis vectors

The second term on the right hand side of equation (11.31) arises from changes to the basis vectors. There are three means for a basis vector to change, and we encounter them when considering coordinate representations later in this chapter. Two changes arise from rotations, each of which change the basis vector's direction without changing its magnitude. The third change leads to a modification of the basis vector's magnitude.

- SOLID-BODY ROTATION: For a solid-body rotation of the reference frame, the solid-body velocity is given by (see Section 11.3)

$$\mathbf{U}_{\text{solid}} = \boldsymbol{\Omega} \times \mathbf{X}. \quad (11.33)$$

- ROTATION RELATIVE TO SOLID-BODY: A vector can also rotate at a rate that differs from the solid-body.
- CHANGE IN MAGNITUDE: Finally, if the basis vectors are not normalized to have unit magnitude, then they can change their magnitude during motion (expanding or contraction).

11.6 Inertial acceleration and its decomposition

The inertial acceleration is given by the time derivative of the inertial velocity, which is the second derivative of the position vector

$$\mathbf{A} = \frac{d\mathbf{V}}{dt} = \frac{d^2\mathbf{X}}{dt^2}. \quad (11.34)$$

This equation is independent of any coordinate representation so that the physical and geometrical content are manifest. When introducing a coordinate representation, the resulting expression becomes subject to details of the chosen coordinates and those details possibly obscure the underlying geometric basis. Hence, it is important to keep the geometric form in mind when offering an interpretation for coordinate dependent terms.

Introducing a coordinate representation $\mathbf{X} = \xi^a \vec{e}_a$ into the acceleration (11.34), and making use of the chain rule, leads to

$$\mathbf{A} = \frac{d}{dt} \frac{d\mathbf{X}}{dt} \quad (11.35a)$$

$$= \frac{d}{dt} \frac{d(\xi^a \vec{e}_a)}{dt} \quad (11.35b)$$

$$= \frac{d}{dt} \left[\frac{d\xi^a}{dt} \vec{e}_a + \xi^a \frac{d\vec{e}_a}{dt} \right] \quad (11.35c)$$

$$= \frac{d^2\xi^a}{dt^2} \vec{e}_a + 2 \frac{d\xi^a}{dt} \frac{d\vec{e}_a}{dt} + \xi^a \frac{d^2\vec{e}_a}{dt^2}. \quad (11.35d)$$

The first term on the right hand side is the acceleration of the coordinate representation as measured in the rotating reference frame

$$\mathbf{A}_{\text{coord}} \equiv \frac{d^2\xi^a}{dt^2} \vec{e}_a. \quad (11.36)$$

It is the acceleration measured by an observer in the rotating frame using coordinates ξ^a . The remaining two terms arise from changes to the basis vectors, and they give rise to the Coriolis and centrifugal accelerations associated with the rotating reference frame. In non-Cartesian coordinates, they also give rise to a *metric acceleration* arising from the change in directions of the unit vectors associated with motion of the particle relative to the rotating reference frame (Section 11.5.2).

Some presentations of the kinematic result (11.35d) suggest that the factor of two on the middle term (the Coriolis term) is mysterious. In fact, there is nothing mysterious. Rather, the factor of two merely results from the need to take two time derivatives of the basis vectors as part of a representation of acceleration.

11.7 Representing the position vector

We make use of some results from Section 9.2 relating Cartesian and spherical coordinates and as defined by Figure 9.1. Starting with the position vector, we introduce the *planetary* Cartesian basis vectors, $(\hat{\mathbf{x}}, \hat{\mathbf{y}}, \hat{\mathbf{z}})$, and corresponding spherical basis vectors, $(\hat{\lambda}, \hat{\phi}, \hat{r})$, leads to the equivalent expressions for the position of a particle moving around the sphere

$$\mathbf{X} = x \hat{\mathbf{x}} + y \hat{\mathbf{y}} + z \hat{\mathbf{z}} \quad (11.37a)$$

$$= (r \cos \phi \cos \lambda) \hat{\mathbf{x}} + (r \cos \phi \sin \lambda) \hat{\mathbf{y}} + (r \sin \phi) \hat{\mathbf{z}} \quad (11.37b)$$

$$= r \hat{\mathbf{r}} \quad (11.37c)$$

$$= |\mathbf{X}| \hat{\mathbf{r}}. \quad (11.37d)$$

Note how the expression for the position vector is quite simple when written in spherical coordinates, as it is merely the distance from the origin with a direction that points radially from the origin to the particle.

11.8 Representing the velocity vector

As seen in Section 11.5, the inertial velocity vector has a coordinate representation written as

$$\mathbf{V} = \frac{d\mathbf{X}}{dt} = \frac{d(\xi^a \vec{e}_a)}{dt} = \frac{d\xi^a}{dt} \vec{e}_a + \xi^a \frac{d\vec{e}_a}{dt}. \quad (11.38)$$

Contributions arise from both the time changes in the coordinates, ξ^a , and time changes to the basis vectors, \vec{e}_a . We now consider the Cartesian and spherical forms for these changes.

11.8.1 Planetary Cartesian coordinate representation

The basis vectors for the Cartesian coordinates, $(\vec{e}_1, \vec{e}_2, \vec{e}_3) = (\hat{\mathbf{x}}, \hat{\mathbf{y}}, \hat{\mathbf{z}})$, are normalized, so they do not change their magnitude. Furthermore, they move only through solid-body motion of the rotating reference frame. We refer to these coordinates as *planetary Cartesian coordinates* since they are oriented according to the rotating planet with origin at the planet's center. In Section 21.3.4 we introduce the distinct *tangent plane Cartesian coordinates*. Tangent plane Cartesian coordinates are also moving with the rotating planet. Yet they are defined according to a tangent plane at a point on the surface of the sphere. It is important to distinguish these two uses for Cartesian coordinates in geophysical fluid mechanics.

The angular velocity is oriented around the polar axis

$$\boldsymbol{\Omega} = \Omega \hat{\mathbf{z}}, \quad (11.39)$$

so that the solid-body velocity only has components in the $\hat{\mathbf{x}}$ and $\hat{\mathbf{y}}$ directions

$$\mathbf{U}_{\text{solid}} = \boldsymbol{\Omega} \times \mathbf{X} = \Omega (-\hat{\mathbf{x}} y + \hat{\mathbf{y}} x). \quad (11.40)$$

The inertial velocity thus has the following representation in terms of planetary Cartesian coor-

dinates

$$\mathbf{V} = \frac{d}{dt} [\hat{\mathbf{x}} x + \hat{\mathbf{y}} y + \hat{\mathbf{z}} z] \quad (11.41a)$$

$$= \left[\hat{\mathbf{x}} \frac{dx}{dt} + \hat{\mathbf{y}} \frac{dy}{dt} + \hat{\mathbf{z}} \frac{dz}{dt} \right] + x \frac{d\hat{\mathbf{x}}}{dt} + y \frac{d\hat{\mathbf{y}}}{dt} + z \frac{d\hat{\mathbf{z}}}{dt} \quad (11.41b)$$

$$= \left[-y \Omega + \frac{dx}{dt} \right] \hat{\mathbf{x}} + \left[x \Omega + \frac{dy}{dt} \right] \hat{\mathbf{y}} + \frac{dz}{dt} \hat{\mathbf{z}} \quad (11.41c)$$

$$= \mathbf{V}_{\text{Cartesian}} + \boldsymbol{\Omega} \times \mathbf{X} \quad (11.41d)$$

$$= \mathbf{V}_{\text{Cartesian}} + \mathbf{U}_{\text{solid}}, \quad (11.41e)$$

where we defined the Cartesian velocity vector

$$\mathbf{V}_{\text{Cartesian}} \equiv \frac{dx}{dt} \hat{\mathbf{x}} + \frac{dy}{dt} \hat{\mathbf{y}} + \frac{dz}{dt} \hat{\mathbf{z}}, \quad (11.42)$$

which is the velocity as measured in the rotating reference frame when using planetary Cartesian coordinates. We also made use of equation (11.15) to express the time rate of change for the planetary Cartesian unit vectors, with this change arising solely from the planetary rotation. Note that the results here hold whether $\boldsymbol{\Omega}$ is constant or varying in time.

11.8.2 Planetary spherical coordinate representation

The position vector in the planetary spherical coordinate representation is given by

$$\mathbf{X} = r \hat{\mathbf{r}}. \quad (11.43)$$

The basis vector $\hat{\mathbf{r}}$ is normalized, so that its evolution arises just from rotations. It can rotate either through solid-body motion of the rotating reference frame, or through changes in the spherical angles, λ, ϕ relative to the rotating reference frame. We see these two forms of time changes by taking the time derivative of $\hat{\mathbf{r}}$ as given by equation (9.30c)

$$\frac{d\hat{\mathbf{r}}}{dt} = \frac{d}{dt} [\hat{\mathbf{x}} \cos \lambda \cos \phi + \hat{\mathbf{y}} \sin \lambda \cos \phi + \hat{\mathbf{z}} \sin \phi]. \quad (11.44)$$

Expanding the right hand side leads to

$$\frac{d}{dt} [\hat{\mathbf{x}} \cos \lambda \cos \phi] = \frac{d\hat{\mathbf{x}}}{dt} \cos \lambda \cos \phi - \hat{\mathbf{x}} \dot{\lambda} \sin \lambda \cos \phi - \hat{\mathbf{x}} \dot{\phi} \cos \lambda \sin \phi \quad (11.45a)$$

$$\frac{d}{dt} [\hat{\mathbf{y}} \sin \lambda \cos \phi] = \frac{d\hat{\mathbf{y}}}{dt} \sin \lambda \cos \phi + \hat{\mathbf{y}} \dot{\lambda} \cos \lambda \cos \phi - \hat{\mathbf{y}} \dot{\phi} \sin \lambda \sin \phi \quad (11.45b)$$

$$\frac{d}{dt} [\hat{\mathbf{z}} \sin \phi] = \hat{\mathbf{z}} \dot{\phi} \cos \phi. \quad (11.45c)$$

Making use of equation (11.15) for the change in planetary Cartesian unit vectors due to rotation, and substituting the expressions (9.30a)-(9.30c) for the spherical unit vectors, leads to¹

$$\frac{d\hat{\mathbf{r}}}{dt} = \cos \phi \left[\frac{d\lambda}{dt} + \Omega \right] \hat{\boldsymbol{\lambda}} + \frac{d\phi}{dt} \hat{\boldsymbol{\phi}}. \quad (11.46)$$

¹The reader is encouraged to work through the details to derive equation (11.46).

Consequently, the inertial velocity has the following spherical coordinate representation

$$\mathbf{V} = \frac{d\mathbf{X}}{dt} \quad (11.47a)$$

$$= \frac{d(r\hat{\mathbf{r}})}{dt} \quad (11.47b)$$

$$= \frac{dr}{dt}\hat{\mathbf{r}} + r\frac{d\hat{\mathbf{r}}}{dt} \quad (11.47c)$$

$$= r_{\perp} \left[\frac{d\lambda}{dt} + \Omega \right] \hat{\lambda} + r \frac{d\phi}{dt} \hat{\phi} + \frac{dr}{dt} \hat{\mathbf{r}} \quad (11.47d)$$

$$= (u + r_{\perp} \Omega) \hat{\lambda} + v \hat{\phi} + w \hat{\mathbf{r}} \quad (11.47e)$$

$$= \mathbf{V}_{\text{spherical}} + \mathbf{U}_{\text{solid}}. \quad (11.47f)$$

In this equation we introduced the spherical coordinate velocity vector

$$\mathbf{V}_{\text{spherical}} = r_{\perp} \frac{d\lambda}{dt} \hat{\lambda} + r \frac{d\phi}{dt} \hat{\phi} + \frac{dr}{dt} \hat{\mathbf{r}} = u \hat{\lambda} + v \hat{\phi} + w \hat{\mathbf{r}}, \quad (11.48)$$

where

$$u = r_{\perp} \frac{d\lambda}{dt} \quad \text{and} \quad v = r \frac{d\phi}{dt} \quad \text{and} \quad w = \frac{dr}{dt}, \quad (11.49)$$

are components to the spherical velocity vector, and with

$$r_{\perp} = r \cos \phi \quad (11.50)$$

the distance to the polar axis. The spherical velocity, $\mathbf{V}_{\text{spherical}}$, is the velocity measured in the rotating reference frame when using planetary spherical coordinates. We also noted that the solid-body velocity has the spherical coordinate representation

$$\mathbf{U}_{\text{solid}} = \boldsymbol{\Omega} \times \mathbf{X} = r_{\perp} \Omega \hat{\lambda}. \quad (11.51)$$

That is, the solid-body velocity is purely zonal.

11.8.3 Transforming from Cartesian to spherical

We can make use of the tensor algebra from Section 11.4 to transform from the Cartesian representation of the velocity vector to the spherical representation. This approach leads to an equivalent result to that pursued thus far in this section, but it is somewhat more systematic and it offers useful experience with the formalities of coordinate transformations. In particular, we make use of the transformation rule (11.26) along with the transformation matrix (11.27) and its inverse (11.28) to have

$$V^{\bar{1}} = V^r = \Lambda_1^{\bar{1}} V^1 + \Lambda_2^{\bar{1}} V^2 + \Lambda_3^{\bar{1}} V^3 \quad (11.52a)$$

$$V^{\bar{2}} = V^{\lambda} = \Lambda_1^{\bar{2}} V^1 + \Lambda_2^{\bar{2}} V^2 + \Lambda_3^{\bar{2}} V^3 \quad (11.52b)$$

$$V^{\bar{3}} = V^{\phi} = \Lambda_1^{\bar{3}} V^1 + \Lambda_2^{\bar{3}} V^2 + \Lambda_3^{\bar{3}} V^3, \quad (11.52c)$$

where the Cartesian components are

$$V^1 = \dot{x} - \Omega y = \dot{r} \cos \phi \cos \lambda - r \dot{\phi} \sin \phi \cos \lambda - r (\dot{\lambda} + \Omega) \cos \phi \sin \lambda \quad (11.53a)$$

$$V^2 = \dot{y} + \Omega x = \dot{r} \cos \phi \sin \lambda - r \dot{\phi} \sin \phi \sin \lambda + r (\dot{\lambda} + \Omega) \cos \phi \cos \lambda \quad (11.53b)$$

$$V^3 = \dot{z} = \dot{r} \sin \phi + r \dot{\phi} \cos \phi. \quad (11.53c)$$

Making use of the inverse transformation matrix components $\Lambda_{\bar{b}}^{\bar{a}}$ given by equation (11.28), as well as the relation (11.26) between the coordinate basis vectors, leads to

$$\vec{V} = \mathbf{V} = V^{\bar{a}} \vec{e}_{\bar{a}} = r_{\perp} (\dot{\lambda} + \Omega) \hat{\lambda} + r \dot{\phi} \hat{\phi} + \dot{r} \hat{r}, \quad (11.54)$$

which is the same expression (11.47f) determined without the formalism of tensor algebra.

11.8.4 Axial angular momentum

As seen in Section 12.6, the zonal component of the inertial velocity equals to the axial angular momentum per unit mass

$$L^z = m \hat{\lambda} \cdot \mathbf{V} = m (u + r_{\perp} \Omega). \quad (11.55)$$

The distance to the rotational axis is given by r_{\perp} , and this is the *moment arm* for the axial angular momentum. For cases with rotational symmetry around polar axis, as for motion of a particle around a smooth sphere, the axial angular momentum is a constant of the motion. As discussed in Section 12.6, this conservation law provides a constraint on the particle trajectory and it plays a role in the motion of geophysical fluids (Section 21.5).

11.9 Planetary Cartesian representation of acceleration

The inertial acceleration vector is given by the second time derivative of the position vector

$$\mathbf{A} = \frac{d\mathbf{V}}{dt} = \frac{d^2\mathbf{X}}{dt^2}. \quad (11.56)$$

We here consider its representation using planetary Cartesian coordinates (x, y, z) and the Cartesian basis $(\vec{e}_1, \vec{e}_2, \vec{e}_3) = (\hat{x}, \hat{y}, \hat{z})$.

11.9.1 Planetary Cartesian representation

For our study of geophysical fluid motion, we assume the planetary angular velocity, $\boldsymbol{\Omega}$, is a constant in time

$$\frac{d\boldsymbol{\Omega}}{dt} = 0. \quad (11.57)$$

Making use of the results from Section 11.3 leads to

$$\frac{d\vec{e}_a}{dt} = \boldsymbol{\Omega} \times \vec{e}_a \quad (11.58)$$

and

$$\frac{d^2\vec{e}_a}{dt^2} = \frac{d}{dt} (\boldsymbol{\Omega} \times \vec{e}_a) = \boldsymbol{\Omega} \times \frac{d\vec{e}_a}{dt} = \boldsymbol{\Omega} \times (\boldsymbol{\Omega} \times \vec{e}_a), \quad (11.59)$$

which yields the inertial acceleration

$$\mathbf{A} = \frac{d}{dt} \frac{d\mathbf{X}}{dt} \quad (11.60a)$$

$$= \frac{d^2 \xi^a}{dt^2} \vec{e}_a + 2 \frac{d\xi^a}{dt} (\boldsymbol{\Omega} \times \vec{e}_a) + \xi^a \boldsymbol{\Omega} \times (\boldsymbol{\Omega} \times \vec{e}_a) \quad (11.60b)$$

$$= \hat{\mathbf{x}} [\ddot{x} - 2\Omega \dot{y} - \Omega^2 x] + \hat{\mathbf{y}} [\ddot{y} + 2\Omega \dot{x} - \Omega^2 y] + \hat{\mathbf{z}} \ddot{z} \quad (11.60c)$$

$$= \ddot{x} \hat{\mathbf{x}} + \ddot{y} \hat{\mathbf{y}} + \ddot{z} \hat{\mathbf{z}} + 2\Omega (-\dot{y} \hat{\mathbf{x}} + \dot{x} \hat{\mathbf{y}}) - \Omega^2 (x \hat{\mathbf{x}} + y \hat{\mathbf{y}}) \quad (11.60d)$$

$$= \mathbf{A}_{\text{Cartesian}} + 2\boldsymbol{\Omega} \times \mathbf{V}_{\text{Cartesian}} + \boldsymbol{\Omega} \times (\boldsymbol{\Omega} \times \mathbf{X}) \quad (11.60e)$$

$$= \mathbf{A}_{\text{Cartesian}} - \mathbf{A}_{\text{Coriolis}} - \mathbf{A}_{\text{centrifugal}}. \quad (11.60f)$$

The inertial acceleration is thus decomposed into three terms. The first contribution is the Cartesian expression

$$\mathbf{A}_{\text{Cartesian}} = \frac{d^2 x}{dt^2} \hat{\mathbf{x}} + \frac{d^2 y}{dt^2} \hat{\mathbf{y}} + \frac{d^2 z}{dt^2} \hat{\mathbf{z}} = \ddot{x} \hat{\mathbf{x}} + \ddot{y} \hat{\mathbf{y}} + \ddot{z} \hat{\mathbf{z}}, \quad (11.61)$$

which is the coordinate acceleration measured in the rotating frame using planetary Cartesian coordinates. The second contribution on the right hand side of equation (11.60f) leads to the Coriolis acceleration

$$\mathbf{A}_{\text{Coriolis}} = -2\boldsymbol{\Omega} \times \mathbf{V}_{\text{Cartesian}}. \quad (11.62)$$

One key feature of the Coriolis acceleration is that it vanishes when there is no motion relative to the rotating reference frame. The Coriolis acceleration plays a fundamental role in geophysical fluid mechanics and is central to our studies in this book. The third contribution is the *centripetal acceleration*, which is also minus the *centrifugal acceleration*

$$\mathbf{A}_{\text{centripetal}} = -\mathbf{A}_{\text{centrifugal}} = \boldsymbol{\Omega} \times (\boldsymbol{\Omega} \times \mathbf{X}) = -\Omega^2 \mathbf{X}. \quad (11.63)$$

The centrifugal acceleration points outward from (perpendicular to) the polar axis of rotation whereas the centripetal acceleration points inward; they are action/reaction pairs. They can be written as the gradient of a potential

$$\mathbf{A}_{\text{centrifugal}} = -\nabla \Phi_{\text{centrifugal}} \quad (11.64)$$

with

$$-\Phi_{\text{centrifugal}} \equiv \frac{(\boldsymbol{\Omega} \times \mathbf{x}) \cdot (\boldsymbol{\Omega} \times \mathbf{x})}{2} = \frac{\Omega^2 r_\perp^2}{2} = \frac{(\Omega r \cos \phi)^2}{2} = \frac{\Omega^2 (x^2 + y^2)}{2}. \quad (11.65)$$

The centripetal acceleration (pointing towards the rotational axis) is that part of the inertial acceleration that keeps the rotating particle from flying away from the rotational axis. On a massive rotating sphere, the centripetal acceleration is provided by that component of the gravitational force (Section 11.11) directed towards the rotation axis. The centripetal acceleration's opposing partner, the centrifugal acceleration, is a non-inertial acceleration that accounts for the slight equatorial bulge of the planet. The centrifugal acceleration pulls a person outward from the center of a rotating merry-go-round, whereas the person's arms provide the opposing centripetal acceleration to keep from flying outward.

11.9.2 Summary of acceleration representation

For the purpose of formulating the equation of motion in the rotating terrestrial frame, we write the rotating frame acceleration as

$$\mathbf{A}_{\text{Cartesian}} = \mathbf{A} + \mathbf{A}_{\text{Coriolis}} + \mathbf{A}_{\text{centrifugal}} \quad (11.66a)$$

$$= \mathbf{A} - 2\boldsymbol{\Omega} \times \mathbf{V}_{\text{Cartesian}} - \nabla\Phi_{\text{centrifugal}} \quad (11.66b)$$

and summarize the following accelerations (force per unit mass).

- **INERTIAL:** Newton's law of motion is formulated within an inertial reference frame. It is the inertial acceleration, \mathbf{A} , that is directly affected by forces such as gravitation.
- **CORIOLIS:** The Coriolis acceleration

$$\mathbf{A}_{\text{Coriolis}} = -2\boldsymbol{\Omega} \times \mathbf{V}_{\text{Cartesian}} = -2\Omega \hat{\mathbf{z}} \times \mathbf{V}_{\text{Cartesian}} = -2\Omega \left[-\frac{dy}{dt} \hat{\mathbf{x}} + \frac{dx}{dt} \hat{\mathbf{y}} \right], \quad (11.67)$$

arises from our choice to describe motion within the rotating reference frame. The Coriolis acceleration gives rise to a rich suite of fundamentally new phenomena relative to non-rotating motion. It has components only in the horizontal planetary Cartesian plane spanned by the unit vectors $(\hat{\mathbf{x}}, \hat{\mathbf{y}})$. That is, the Coriolis acceleration occurs in a plane parallel to the equatorial plane. This geometric result is to be expected since the Coriolis acceleration arises from rotation about the polar, $\hat{\mathbf{z}}$, axis.

- **CENTRIFUGAL:** The centrifugal acceleration

$$\mathbf{A}_{\text{centrifugal}} = -\nabla\Phi_{\text{centrifugal}} = \Omega^2 \mathbf{r}_\perp = \Omega^2 (x \hat{\mathbf{x}} + y \hat{\mathbf{y}}) \quad (11.68)$$

is another term arising from the rotating reference frame. As for the Coriolis acceleration, the centrifugal acceleration has components only in the horizontal planetary Cartesian plane spanned by the unit vectors $(\hat{\mathbf{x}}, \hat{\mathbf{y}})$; i.e., the centrifugal acceleration occurs in a plane parallel to the equatorial plane, which is again expected since the centrifugal acceleration arises from rotation about the polar axis. The centrifugal acceleration is directed outward from (perpendicular to) the polar axis of rotation. We see this orientation in Figure 11.6 to be discussed later. Furthermore, the centrifugal acceleration is nonzero even when the particle is fixed relative to the rotating planet, whereas the Coriolis acceleration is zero when the particle has zero motion relative to the planet.

The centrifugal acceleration can be written as the gradient of a scalar potential, $\mathbf{A}_{\text{centrifugal}} = -\nabla\Phi_{\text{centrifugal}}$ where $\Phi_{\text{centrifugal}} = -\Omega^2(x^2 + y^2)/2$ (equation (11.65)). Hence, the centrifugal acceleration can be combined with the gravitational acceleration in the equation of motion (see Section 11.11). The resulting “effective gravity” leads to a conservative force field that is modified relative to the central gravitational field of the non-rotating spherical planet. We detail these points in Section 11.11.4.

11.9.3 Further study

Section 3.5 of [Apel \(1987\)](#) offers an insightful presentation of the Coriolis acceleration. Visualizations from rotating tank experiments are useful to garner an intuitive understanding of the Coriolis acceleration. The first few minutes of [this video from Prof. Fultz of the University of Chicago](#) is particularly insightful. We further build up our understanding of the Coriolis acceleration as the book develops.

11.10 Spherical representation of acceleration

The spherical representation of the inertial velocity is given by equation (11.47f)

$$\mathbf{V} = \frac{d\mathbf{X}}{dt} = (u + r_{\perp} \Omega) \hat{\lambda} + v \hat{\phi} + w \hat{r} = \mathbf{V}_{\text{sphere}} + r_{\perp} \Omega \hat{\lambda}, \quad (11.69)$$

where we introduced the spherical velocity from equation (11.49)

$$\mathbf{V}_{\text{sphere}} \equiv u \hat{\lambda} + v \hat{\phi} + w \hat{r}. \quad (11.70)$$

We also make use of the notation for the zonal component of the inertial velocity,

$$u_I = u + r_{\perp} \Omega. \quad (11.71)$$

Just as for computing the inertial velocity vector, the inertial acceleration must take into account changes in both the spherical coordinates and spherical basis vectors

$$\mathbf{A} = \frac{d}{dt} (u_I \hat{\lambda} + v \hat{\phi} + w \hat{r}) \quad (11.72a)$$

$$= \frac{du_I}{dt} \hat{\lambda} + \frac{dv}{dt} \hat{\phi} + \frac{dw}{dt} \hat{r} + u_I \frac{d\hat{\lambda}}{dt} + v \frac{d\hat{\phi}}{dt} + w \frac{d\hat{r}}{dt}. \quad (11.72b)$$

The spherical unit vectors change due to both the solid-body rotation of the rotating reference frame, plus motion of the particle relative to the rotating frame. Making use of the expressions given in Section (9.2.2), a bit of algebra yields the time derivatives

$$\frac{d\hat{\lambda}}{dt} = \left[\Omega + \frac{d\lambda}{dt} \right] (\hat{\phi} \sin \phi - \hat{r} \cos \phi) \quad (11.73)$$

$$\frac{d\hat{\phi}}{dt} = -\hat{\lambda} \left[\Omega + \frac{d\lambda}{dt} \right] \sin \phi - \hat{r} \dot{\phi} \quad (11.74)$$

$$\frac{d\hat{r}}{dt} = \hat{\lambda} \left[\frac{d\lambda}{dt} + \Omega \right] \cos \phi + \frac{d\phi}{dt} \hat{\phi}. \quad (11.75)$$

We are thus led to the inertial acceleration components

$$\mathbf{A} \cdot \hat{\lambda} = \frac{du_I}{dt} + \left[\frac{d\lambda}{dt} + \Omega \right] (w \cos \phi - v \sin \phi) \quad (11.76a)$$

$$\mathbf{A} \cdot \hat{\phi} = \frac{dv}{dt} + \left[\frac{d\lambda}{dt} + \Omega \right] u_I \sin \phi + w \frac{d\phi}{dt} \quad (11.76b)$$

$$\mathbf{A} \cdot \hat{r} = \frac{dw}{dt} - \left[\frac{d\lambda}{dt} + \Omega \right] u_I \cos \phi - v \frac{d\phi}{dt}. \quad (11.76c)$$

Use of the identities

$$u = r_{\perp} \frac{d\lambda}{dt} \quad \text{and} \quad u_I = u + r_{\perp} \Omega \quad \text{and} \quad \frac{du_I}{dt} = \frac{du}{dt} + \Omega (w \cos \phi - v \sin \phi) \quad (11.77)$$

and some reorganization leads to the spherical coordinate representation of the inertial acceleration

$$\begin{aligned} \mathbf{A} = & \hat{\lambda} \left[\frac{du}{dt} + \frac{u(w - v \tan \phi)}{r} + 2\Omega(w \cos \phi - v \sin \phi) \right] \\ & + \hat{\phi} \left[\frac{dv}{dt} + \frac{v w + u^2 \tan \phi}{r} + 2\Omega u \sin \phi + r_\perp \Omega^2 \sin \phi \right] \\ & + \hat{r} \left[\frac{dw}{dt} - \frac{u^2 + v^2}{r} - 2\Omega u \cos \phi - r_\perp \Omega^2 \cos \phi \right]. \end{aligned} \quad (11.78)$$

When encountering this expression for the first time it can be rather intimidating. The reader is encouraged to remember the underlying kinematic origin of the various terms, in which case we understand the terms in this expression so that it can be seen as aesthetically pleasing.

11.10.1 Transforming from Cartesian to spherical

As in Section 11.8.3, we can make use of the tensor algebra from Section 11.4 to transform from the Cartesian representation of the acceleration vector to the spherical representation. Following the same steps as for the velocity leads to

$$A^{\bar{a}} = \Lambda_{\bar{a}}^a A^a \quad (11.79)$$

where the Cartesian components to the inertial acceleration are

$$A^1 = \ddot{x} - 2\Omega \dot{y} - \Omega^2 x \quad (11.80a)$$

$$A^2 = \ddot{y} + 2\Omega \dot{x} - \Omega^2 y \quad (11.80b)$$

$$A^3 = \ddot{z}. \quad (11.80c)$$

Making use of the coordinate transformation (11.25) allows us to express these Cartesian components of the acceleration in terms of spherical coordinates. Then we make use of the inverse transformation matrix components $\Lambda_{\bar{a}}^a$ given by equation (11.28), as well as the relation (11.26) between the coordinate basis vectors, which leads to

$$\vec{A} = \mathbf{A} = A^a \vec{e}_a = A^{\bar{a}} \vec{e}_{\bar{a}} \quad (11.81)$$

with the spherical coordinate representation given by equation (11.78) as derived without the formalism of tensor algebra. Both approaches require algebraic manipulations, so that it is useful to have two approaches to double-check results.

11.10.2 Decomposing the acceleration

We decompose the inertial acceleration (11.78) into the following terms

$$\mathbf{A} = \mathbf{A}_{\text{sphere}} + \mathbf{A}_{\text{metric}} - \mathbf{A}_{\text{Coriolis}} - \mathbf{A}_{\text{centrifugal}}, \quad (11.82)$$

with signs chosen so that in the rotating frame the acceleration is written

$$\underbrace{\mathbf{A}_{\text{sphere}} + \mathbf{A}_{\text{metric}}}_{\text{net spherical acceleration}} = \mathbf{A} + \mathbf{A}_{\text{Coriolis}} + \mathbf{A}_{\text{centrifugal}}. \quad (11.83)$$

We identify the net spherical acceleration as the sum of the coordinate acceleration and metric acceleration. In the absence of rotation, this sum provides an expression for the inertial accel-

eration as represented by spherical coordinates. The Coriolis and centrifugal terms arise from rotation.

11.10.3 Spherical coordinate acceleration

The spherical coordinate acceleration is given by the time change in the spherical velocity components

$$\mathbf{A}_{\text{sphere}} = \frac{du}{dt} \hat{\lambda} + \frac{dv}{dt} \hat{\phi} + \frac{dw}{dt} \hat{r}. \quad (11.84)$$

This term has no contribution from changes to the spherical unit vectors.

11.10.4 Metric acceleration

We define the metric acceleration as that contribution to the acceleration arising from the time dependence of the spherical unit vectors that appears when taking the time derivative of the velocity vector. For spherical coordinates we have

$$\mathbf{A}_{\text{metric}} = \hat{\lambda} \left[\frac{u(w - v \tan \phi)}{r} \right] + \hat{\phi} \left[\frac{v w + u^2 \tan \phi}{r} \right] - \hat{r} \left[\frac{u^2 + v^2}{r} \right] \quad (11.85a)$$

$$= \hat{\lambda} \left[\frac{u(w \cos \phi - v \sin \phi)}{r \cos \phi} \right] + \hat{\phi} \left[\frac{v w \cos \phi + u^2 \sin \phi}{r \cos \phi} \right] - \hat{r} \left[\frac{u^2 + v^2}{r} \right] \quad (11.85b)$$

$$= \frac{1}{r} [u \tan \phi (\hat{r} \times \mathbf{V}_{\text{sphere}}) + w \mathbf{U}_{\text{sphere}} - \hat{r} \mathbf{U}_{\text{sphere}} \cdot \mathbf{U}_{\text{sphere}}], \quad (11.85c)$$

where we wrote the horizontal (angular) and vertical (radial) components of the spherical velocity according to

$$\mathbf{V}_{\text{sphere}} = \mathbf{U}_{\text{sphere}} + \hat{r} w = \hat{\lambda} u + \hat{\phi} v + \hat{r} w. \quad (11.86)$$

Note that

$$\mathbf{V}_{\text{sphere}} \cdot \mathbf{A}_{\text{metric}} = 0, \quad (11.87)$$

so that the metric acceleration is orthogonal to the spherical velocity, in which case with (see equation (11.47f)) $\mathbf{V} = \mathbf{V}_{\text{sphere}} + r_{\perp} \Omega \hat{\lambda}$ we have

$$\mathbf{V} \cdot \mathbf{A}_{\text{metric}} = \Omega u (-v \sin \phi + w \cos \phi). \quad (11.88)$$

Furthermore, the metric acceleration vanishes when the curvature of the sphere vanishes (i.e., $r \rightarrow \infty$), as per a flat plane.

11.10.5 Centrifugal acceleration

The spherical coordinate representation of the centrifugal acceleration is given by

$$\mathbf{A}_{\text{centrifugal}} = -\nabla \Phi_{\text{centrifugal}} = \Omega^2 (x \hat{x} + y \hat{y}) = r_{\perp} \Omega^2 (-\hat{\phi} \sin \phi + \hat{r} \cos \phi). \quad (11.89)$$

The centrifugal acceleration points outward from the axis of rotation (see Figure 11.6 to be discussed later), so that it has no component in the longitudinal direction. Furthermore, note that

$$\mathbf{V} \cdot \mathbf{A}_{\text{centrifugal}} = \mathbf{V}_{\text{sphere}} \cdot \mathbf{A}_{\text{centrifugal}} = r_{\perp} \Omega^2 (-v \sin \phi + w \cos \phi). \quad (11.90)$$

11.10.6 Coriolis acceleration

The spherical coordinate representation of the Coriolis acceleration makes use of the spherical representation of the earth's angular velocity

$$\boldsymbol{\Omega} = \Omega \hat{\mathbf{z}} = \Omega (\hat{\phi} \cos \phi + \hat{\mathbf{r}} \sin \phi). \quad (11.91)$$

We here emphasize that although $\boldsymbol{\Omega} = \Omega \hat{\mathbf{z}}$ is assumed to be fixed in absolute space, its component representation using spherical coordinates is a function of position on the sphere. This spatial dependence, especially the dependence on latitude, gives rise to much of the characteristic features of geophysical flows associated with the *beta*-effect studied in Section 37.6.2.

We use the representation (11.91) to write the Coriolis acceleration as

$$\mathbf{A}_{\text{Coriolis}} = -2 \boldsymbol{\Omega} \times \mathbf{V}_{\text{sphere}} \quad (11.92a)$$

$$= -2 \Omega (\hat{\phi} \cos \phi + \hat{\mathbf{r}} \sin \phi) \times (u \hat{\lambda} + v \hat{\phi} + w \hat{\mathbf{r}}) \quad (11.92b)$$

$$= -2 \Omega [\hat{\lambda} (w \cos \phi - v \sin \phi) + \hat{\phi} u \sin \phi - \hat{\mathbf{r}} u \cos \phi]. \quad (11.92c)$$

As for the metric acceleration, we note that the Coriolis acceleration is orthogonal to the spherical velocity

$$\mathbf{V}_{\text{sphere}} \cdot \mathbf{A}_{\text{Coriolis}} = 0, \quad (11.93)$$

so that

$$\mathbf{V} \cdot \mathbf{A}_{\text{Coriolis}} = 2 r_{\perp} \Omega^2 (v \sin \phi - w \cos \phi). \quad (11.94)$$

We find it convenient to introduce a shorthand notation

$$\mathbf{f} = (2 \Omega \sin \phi) \hat{\mathbf{r}} \quad \text{and} \quad \mathbf{f}^* = (2 \Omega \cos \phi) \hat{\phi}, \quad (11.95)$$

so that the Coriolis acceleration takes the form

$$\mathbf{A}_{\text{Coriolis}} = -(\mathbf{f} + \mathbf{f}^*) \times \mathbf{V}_{\text{sphere}}. \quad (11.96)$$

There are two contributions to the Coriolis acceleration: one from the radial and one from the meridional component of the earth's rotation vector.

11.10.7 Coriolis acceleration for large-scale motions

Let us again write the Coriolis acceleration in equation (11.92c), only now underlining two terms

$$\mathbf{A}_{\text{Coriolis}} = -2 \Omega [\hat{\lambda} (\underline{w \cos \phi} - \underline{v \sin \phi}) + \hat{\phi} \underline{u \sin \phi} - \hat{\mathbf{r}} \underline{u \cos \phi}]. \quad (11.97)$$

For many applications in geophysical fluid mechanics, the term $\hat{\mathbf{r}} (2 \Omega u \cos \phi)$ is much smaller than the competing gravitational acceleration that also contributes to the radial acceleration, thus prompting $\hat{\mathbf{r}} (2 \Omega u \cos \phi)$ to be dropped from the $\hat{\mathbf{r}}$ equation of motion.² Furthermore, the vertical velocity term is generally much smaller than the horizontal velocity term appearing in the $\hat{\lambda}$ component. Dropping these two terms results in the form for the Coriolis acceleration used for large-scale dynamics, such as when considering the hydrostatic primitive equations for geophysical fluids (Section 24.1)

$$\mathbf{A}_{\text{Coriolis}}^{\text{large-scale}} \equiv -2 \Omega \sin \phi (-\hat{\lambda} v + \hat{\phi} u) \equiv -f \hat{\mathbf{r}} \times \mathbf{V}_{\text{sphere}}. \quad (11.98)$$

²The term $\hat{\mathbf{r}} (2 \Omega u \cos \phi)$ is called the Eötvös correction in the study of marine gravity.

For the last equality we introduced the Coriolis parameter

$$f \equiv 2\Omega \sin \phi. \quad (11.99)$$

As illustrated in Figure 11.5, we see that it is the radial (i.e., the local vertical) component of the earth's angular rotation that plays the most important role in large-scale geophysical fluid mechanics

$$\boldsymbol{\Omega} \cdot \hat{\mathbf{r}} = \Omega \hat{\mathbf{z}} \cdot \hat{\mathbf{r}} = \Omega (\hat{\phi} \cos \phi + \hat{r} \sin \phi) \cdot \hat{\mathbf{r}} = \Omega \sin \phi = f/2. \quad (11.100)$$

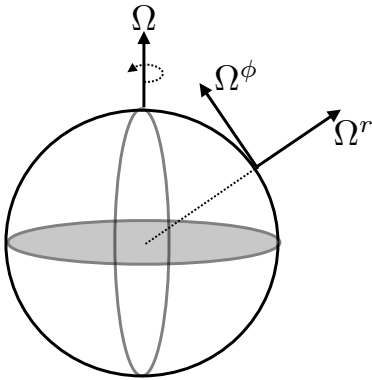


FIGURE 11.5: This figure illustrates the two components of the earth's rotational velocity, $\boldsymbol{\Omega} = \Omega \hat{\mathbf{z}} = \Omega (\hat{\phi} \cos \phi + \hat{r} \sin \phi)$. The radial component (also known as the local vertical component), $\boldsymbol{\Omega} \cdot \hat{\mathbf{r}} = \Omega \sin \phi \hat{\mathbf{r}}$, is the most important component for large scale geophysical fluid dynamics.

11.11 Newtonian gravity

Thus far we have focused on the kinematics of a particle moving around a rotating sphere. We now acknowledge that the particle is moving in the gravitational field of the planet. The gravitational force acting on the particle is the only inertial force felt by the point particle. Since the point particle contains no internal structure and it has no surface area, the total energy for the particle equals to the mechanical energy (Chapter 12). We here discuss the gravitational potential energy and the associated gravitational force, all within the context of Newtonian mechanics.

11.11.1 Newtonian gravity from Poisson's equation

The Newtonian gravitational potential, Φ , in the presence of a mass distribution with density, ρ , satisfies Poisson's equation (see Section 3.5)

$$\nabla^2 \Phi = 4\pi G \rho, \quad (11.101)$$

where

$$G = 6.674 \times 10^{-11} \text{ N m}^2 \text{ kg}^{-2} = 6.674 \times 10^{-11} \text{ m}^3 \text{ kg}^{-1} \text{ s}^{-2} \quad (11.102)$$

is Newton's gravitational constant. Gravity is a conservative force, so that the gradient of the gravitational potential gives the gravitational acceleration

$$\mathbf{g} = -\nabla \Phi. \quad (11.103)$$

The gravitational potential has dimensions of $\text{L}^2 \text{ T}^{-2}$ so that its gradient indeed has the dimensions of acceleration, L T^{-2} . Note that the gravitational potential responds instantaneously to any

changes in the mass distribution. It took a few centuries, and the genius of Einstein, to provide a local connection between mass and gravity as rendered by space-time curvature and gravitational waves.

A volume integral of Poisson's equation (11.101), computed over a region in space, leads to

$$\int_{\mathcal{R}} \nabla^2 \Phi \, dV = 4\pi G \int_{\mathcal{R}} \rho \, dV. \quad (11.104)$$

The integral on the right hand side is the mass contained in the region,

$$M = \int_{\mathcal{R}} \rho \, dV, \quad (11.105)$$

whereas the divergence theorem (Section 2.7) allows us to write the left hand side as a surface integral

$$\int_{\partial\mathcal{R}} \nabla \Phi \cdot \hat{\mathbf{n}} \, dS = 4\pi G M. \quad (11.106)$$

We now consider the special case of a spherical mass distribution as viewed from a point outside of the mass.

11.11.2 Gravitational field for a spherical earth

In this book we assume the mass density of the planet to be spherically symmetric, in which case the gravitational potential is a function only of the radial distance from the center of the mass distribution, $\Phi = \Phi(r)$. Letting the integration region, \mathcal{R} , be a sphere of radius $r > R_e$, where R_e is the radius of the planet, and making use of spherical coordinates from Section 9.2.8, brings equation (11.106) to

$$4\pi r^2 \frac{\partial \Phi}{\partial r} = 4\pi G M. \quad (11.107)$$

Integration leads to the gravitational potential for an arbitrary point outside the spherically symmetric mass distribution

$$\Phi_e = -\frac{GM}{r}, \quad (11.108)$$

where we set the integration constant to zero. We see that when sampling the gravity field at a radius equal to or larger than the spherical planet radius, the gravitational potential is identical to that of a point mass at the origin. The gradient of the gravitational potential (11.108) yields the inverse-squared dependence of the gravitational acceleration

$$\mathbf{g}_e = -\nabla \Phi_e = -\frac{GM}{r^2} \hat{\mathbf{r}} = -\frac{GM}{r^3} \mathbf{r}, \quad (11.109)$$

along with the gravitational force acting on a point particle of mass m

$$\mathbf{F}_{\text{gravity}} = m \mathbf{g}_e = -m \nabla \Phi_e. \quad (11.110)$$

Furthermore, the gravitational potential energy of the particle (dimensions $M L^2 T^{-2}$) is given by

$$P = m \Phi_e. \quad (11.111)$$

11.11.3 Approximate gravitational acceleration

For most applications of atmospheric and oceanic fluid dynamics, it is sufficient to assume the gravitational acceleration is constant and equal to its value at the earth's surface. This assumption holds so long as the radial position of the particle is a distance from the earth surface that is small relative to the earth radius. We generally make this assumption throughout this book.³ In this case we can assume the earth's gravitational acceleration, g_e , is a constant so that

$$\mathbf{g}_e = -g_e \hat{\mathbf{r}}, \quad (11.112)$$

where

$$g_e = \frac{GM_e}{R_e^2} \approx 9.8 \text{ m s}^{-2}. \quad (11.113)$$

To reach this value, we assumed a sphere of mass equal to the earth mass

$$M_e = 5.977 \times 10^{24} \text{ kg}, \quad (11.114)$$

and radius

$$R_e = 6.371 \times 10^6 \text{ m} \quad (11.115)$$

determined so that the sphere has the same volume as the earth.

The corresponding gravitational potential for the particle is given by

$$\Phi_e = g_e r, \quad (11.116)$$

with the gravitational acceleration

$$\mathbf{g}_e = -\nabla\Phi_e = -g_e \hat{\mathbf{r}}, \quad (11.117)$$

and the gravitational potential energy

$$m\Phi_e = m g_e r. \quad (11.118)$$

We emphasize that the expression for the gravitational potential, (11.116), and potential energy, (11.118), are accurate only so long as the radial position of the particle is a distance from the earth surface that is small relative to the earth radius. Furthermore, note that the approximate gravitational potential (11.116) is positive whereas the unapproximated potential (11.108) is negative. However, the absolute zero of the potential has no physical significance. Instead, what is relevant is the change between two points in space. As defined, both of the geopotentials increase when moving away from the earth center.

11.11.4 Effective gravitational force from the geopotential

We can combine the potential for the planetary centrifugal acceleration as given by equation (11.65) with the gravitational potential (11.108), thus resulting in the *geopotential*

$$\Phi = r [g_e - \mathbf{U}_{\text{solid}}^2/(2r)]. \quad (11.119)$$

³The assumption of constant gravitational field is not appropriate when considering details of oceanic or atmospheric tidal motions or when aiming for precise measures of sea level. We consider more general gravitational fields in Chapter 31.

Again, this form for the geopotential is relevant for motion that is close enough to the earth surface that we can assume the earth's gravitational acceleration, g_e , is constant as discussed in Section 11.11.3. In Exercise 11.6 we examine the geopotential when this assumption is not made.

The contribution from the planetary centrifugal term in the geopotential (11.119) can be estimated by making use of terrestrial values, in which $R = R_e = 6.371 \times 10^6$ m (equation (11.115)), and $\Omega_e = 7.292 \times 10^{-5}$ s⁻¹ (Section 11.1). The planetary centrifugal term is its largest at the equator, $\phi = 0$, where

$$\frac{\mathbf{U}_{\text{solid}}^2}{2R_e} \approx 0.017 \text{ m s}^{-2}, \quad (11.120)$$

so that the ratio of the gravitational to centrifugal accelerations is (at most)

$$\frac{g_e}{\mathbf{U}_{\text{solid}}^2/(2R_e)} = \frac{M_e G / R_e^2}{\Omega_e^2 R_e / 2} \approx 576. \quad (11.121)$$

The geopotential is thus dominated by the earth's gravitational potential. Even so, the centrifugal acceleration leads to a slight equatorial bulge on the earth. To account for this slight non-sphericity, geophysical fluid models generally interpret the radial direction, $\hat{\mathbf{r}}$, as pointing parallel to $\nabla\Phi$ rather than parallel to $\nabla\Phi_e$. We have more to say on this topic in Section 11.12.3.

11.11.5 Further study

Newton's gravitational law is standard material from freshman physics. Some commonly used physical properties of the earth are summarized in Appendix Two of [Gill \(1982\)](#).

11.12 Newton's law of motion

As seen in Section 10.1, Newton's law of motion says that in an inertial reference frame, temporal changes to the linear momentum arise only from externally applied forces. With gravity the only inertial force acting on the constant mass particle, Newton's equation of motion says that

$$m \mathbf{A} = -m \nabla\Phi_e. \quad (11.122)$$

This is a relatively simple equation of motion. However, it becomes more complex, yet useful for practical purposes, when moving to the rotating reference frame of terrestrial observers and furthermore when represented using spherical coordinates.

11.12.1 Cartesian coordinate representation

The inertial acceleration using planetary Cartesian coordinates is given by equation (11.66b)

$$\mathbf{A} = \mathbf{A}_{\text{Cartesian}} - \mathbf{A}_{\text{Coriolis}} - \mathbf{A}_{\text{centrifugal}} \quad (11.123a)$$

$$= \mathbf{A}_{\text{Cartesian}} + 2\boldsymbol{\Omega} \times \mathbf{V}_{\text{Cartesian}} + \nabla\Phi_{\text{centrifugal}}, \quad (11.123b)$$

so that the rotating frame Cartesian equation of motion is given by

$$\mathbf{A}_{\text{Cartesian}} = \mathbf{A} - 2\boldsymbol{\Omega} \times \mathbf{V}_{\text{Cartesian}} - \nabla\Phi_{\text{centrifugal}} \quad (11.124a)$$

$$= -\nabla\Phi_e - 2\boldsymbol{\Omega} \times \mathbf{V}_{\text{Cartesian}} - \nabla\Phi_{\text{centrifugal}} \quad (11.124b)$$

$$= -2\boldsymbol{\Omega} \times \mathbf{V}_{\text{Cartesian}} - \nabla\Phi, \quad (11.124c)$$

where the geopotential is the sum of the gravitational and centrifugal potentials (equation (11.119))

$$\Phi = \Phi_e + \Phi_{\text{centrifugal}}. \quad (11.125)$$

We can write the equation of motion in component form by exposing indices (Cartesian tensors) and using a dot for time derivative

$$\ddot{X}_a + 2\epsilon_{abc}\Omega_b\dot{X}_c = -\partial_a\Phi, \quad (11.126)$$

which takes on the vector form within the rotating reference frame

$$\frac{d^2\mathbf{X}}{dt^2} + 2\boldsymbol{\Omega} \times \dot{\mathbf{X}} = -\nabla\Phi. \quad (11.127)$$

Note that the basis vectors need not be time differentiated again since their change has already been taken care of when exposing the Coriolis and centrifugal accelerations. This equation of motion is the standard form that recurs for a fluid, with the addition of contact forces from pressure and friction (Chapter 21).

Since the rotation of the reference frame is assumed to be constant in time, the equation of motion (11.127) can be written

$$\frac{d\mathbf{M}}{dt} = \frac{d}{dt}(\mathbf{V}_{\text{Cartesian}} + 2\boldsymbol{\Omega} \times \mathbf{X}) = -\nabla\Phi, \quad (11.128)$$

where we introduced the *potential momentum* per mass

$$\mathbf{M} = \mathbf{V}_{\text{Cartesian}} + 2\boldsymbol{\Omega} \times \mathbf{X}. \quad (11.129)$$

We further discuss potential momentum in Section 12.4.

11.12.2 Spherical coordinate representation

We now make use of the acceleration written in planetary spherical coordinates given in Section 11.10

$$\mathbf{A}_{\text{sphere}} + \mathbf{A}_{\text{metric}} = \mathbf{A}_{\text{Coriolis}} + \mathbf{A} + \mathbf{A}_{\text{centrifugal}} = -2\boldsymbol{\Omega} \times \mathbf{V}_{\text{sphere}} - \nabla\Phi. \quad (11.130)$$

The effective gravitational force is not a central force due to the contribution from the centrifugal acceleration. We see this fact more explicitly by using the equations in Section 11.10 to write the spherical equations of motion

$$\dot{u} + \frac{u(w - v \tan \phi)}{r} + 2\Omega(w \cos \phi - v \sin \phi) = 0 \quad (11.131)$$

$$\dot{v} + \frac{v w + u^2 \tan \phi}{r} + 2\Omega u \sin \phi = -r_\perp \Omega^2 \sin \phi \quad (11.132)$$

$$\dot{w} - \frac{u^2 + v^2}{r} - 2\Omega u \cos \phi = r_\perp \Omega^2 \cos \phi - g_e. \quad (11.133)$$

The Ω^2 term in both the meridional equation, (11.132), and the radial equation, (11.133), are the two components of the planetary centrifugal acceleration, $\mathbf{A}_{\text{centrifugal}} = r_\perp \Omega^2 (-\hat{\phi} \sin \phi + \hat{r} \cos \phi)$. The centrifugal acceleration is directed outward from the planetary axis of rotation, and it is balanced by an inward directed planetary centripetal acceleration provided by that portion of the gravitational acceleration directed oppositely to the centrifugal. Notably, a particle initially at rest on a smooth spherical planet accelerates meridionally toward the equator due to the meridional

component of the centrifugal acceleration (from equation (11.132) we find $\dot{v} = -r_\perp \Omega^2 \sin \phi$).

Imagine setting the centripetal acceleration to zero, in which case the particle would still feel the central force from gravity but its trajectory would differ. As seen in Section 11.11.4, the earth's gravitational acceleration is much larger than the planetary centrifugal acceleration, so that in the absence of the planetary centrifugal acceleration the particle would still be bound to the planet. But in more extreme conditions where the rotational rate is much higher (e.g., a rotating neutron star), removing the centripetal acceleration causes a huge modification to the particle trajectory. Indeed, with enough rotation, the particle can overcome gravitational effects from the planet to leave its orbit.

11.12.3 Geopotential coordinate representation

As we saw in Section 11.11.2, the radius of a sphere that best fits the volume of the earth is given by $R_e = 6.371 \times 10^6$ m. The non-central nature of the effective gravitational force (arising from central gravity plus planetary centrifugal) leads to an oblate spheroidal shape for planets such as the earth. The result is a distinction between the earth's equatorial and polar radii (Appendix Two of [Gill \(1982\)](#))

$$R_{\text{equator}} = 6.378 \times 10^6 \text{ m} \quad \text{and} \quad R_{\text{pole}} = 6.357 \times 10^6 \text{ m}, \quad (11.134)$$

with a corresponding ratio

$$1 - \frac{R_{\text{pole}}}{R_{\text{equator}}} \approx 3 \times 10^{-3}. \quad (11.135)$$

An oblate spheroid shape does a better job fitting the actual earth shape than a sphere, thus motivating the use of oblate spheroid coordinates for describing planetary scale mechanics. In this case, the radial coordinate is constant on the oblate spheroid shaped geopotential, and the effective gravitational acceleration is precisely aligned with the geopotential direction.

Even though oblate spheroidal coordinates are better than spherical for describing geopotentials, it is possible, to a high degree of accuracy, to describe the earth's geometry as spherical. Doing so simplifies the mathematics since oblate spheroidal coordinates are less convenient and less familiar than standard spherical coordinates. We are thus led to assume that the radial coordinate measures distances perpendicular to the geopotential, yet to use geometric/metric functions based on spherical coordinates. The error in this approach is small for the earth, and well worth the price since there is no component to the effective gravitational force that is within the geopotential surface.

We illustrate the change in coordinates in Figure 11.6, with the figure caption also explaining how the force balances are reorganized. Absorbing the centrifugal term into an effective gravitational potential then leads to the effective gravitational acceleration vector

$$-\nabla\Phi = -g \hat{\mathbf{r}}, \quad (11.136)$$

with g the effective gravitational acceleration. Using this convention, the particle equations of motion take the following form

$$\dot{u} + \frac{u(w - v \tan \phi)}{r} + 2\Omega(w \cos \phi - v \sin \phi) = 0 \quad (11.137a)$$

$$\dot{v} + \frac{v w + u^2 \tan \phi}{r} + 2\Omega u \sin \phi = 0 \quad (11.137b)$$

$$\dot{w} - \frac{u^2 + v^2}{r} - 2\Omega u \cos \phi = -g. \quad (11.137c)$$

Notably, in geopotential vertical coordinates the effective gravitational acceleration only impacts the radial equation of motion.

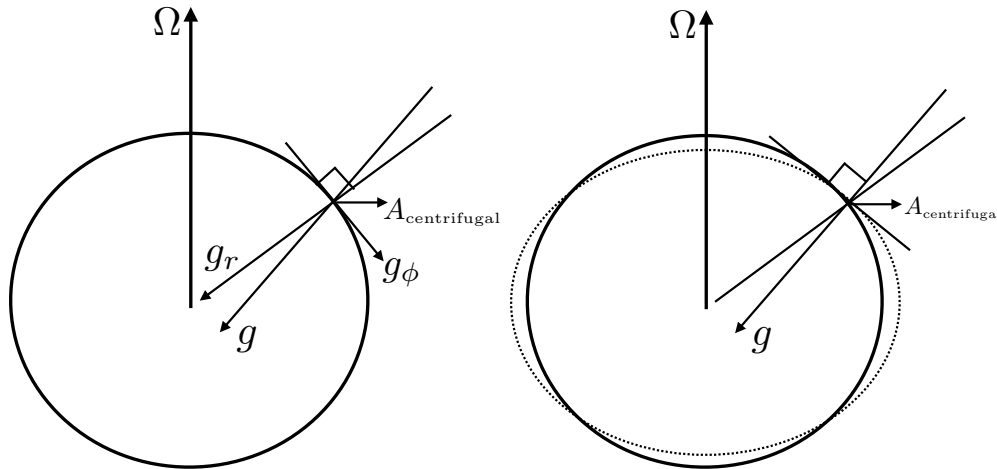


FIGURE 11.6: This figure illustrates the spherical (left panel) versus geopotential (right panel) coordinate systems used to study geophysical fluids. The left panel shows the non-central nature of the effective gravitational acceleration \mathbf{g} on a rotating spherical planet, with the effective gravity given by the sum of the gravitational acceleration, $\mathbf{g}_r = -g_e \hat{\mathbf{r}}$, plus centrifugal acceleration (equation (11.89)), $\mathbf{A}_{\text{centrifugal}} = r_\perp \Omega^2 (-\dot{\phi} \sin \phi + \hat{\mathbf{r}} \cos \phi)$. The gravitational acceleration points radially to the center of the sphere whereas the centrifugal acceleration points outward away from the polar axis of rotation. A particle initially at rest on a smooth spherical planet accelerates meridionally toward the equator due to the meridional component of the centrifugal acceleration (from equation (11.132) we have $\dot{v} = -r_\perp \Omega^2 \sin \phi$). The right panel shows a *geopotential vertical coordinate*, $r = R + z$, that measures the distance perpendicular to the oblate spheroid shaped geopotential surface (dotted surface). The geopotential vertical coordinate precisely aligns the effective gravitational force with the vertical coordinate, so that there is no component of the effective gravity along the surface directions ($g_\phi = 0$). Equivalently, the central gravitational acceleration now has a meridional component on the oblate spheroid that exactly balances the meridional component to the centrifugal acceleration, leaving an effective gravity that is only vertical. Hence, a frictionless oblate spheroidal planet allows for a particle at rest on the planet's surface to remain at rest (see equation (11.137b)). Note that this figure is not drawn to scale, with the oblate nature highly exaggerated compared to the real earth system (see equation (11.135)), and the centrifugal acceleration much smaller than the gravitational (see equation (11.121)). This figure is taken after Figure 2.2 of [Vallis \(2017\)](#) and Figure 2.8 of [Olbers et al. \(2012\)](#).

11.12.4 Comments

Figure 11.6, including its caption, offers a view on the transition from spherical coordinates to geopotential coordinates. The use of geopotential coordinates is rather accurate and extremely convenient for most purposes of geophysical fluid mechanics, with a notable exception being the study of tides and sea level, in which detailed models of the earth's mass distribution and gravity field are used (e.g., see [Gregory et al. \(2019\)](#) for a review). Although precise, the transition to geopotential coordinates is somewhat subtle in principle since we are reorganizing how the centrifugal acceleration appears. It is through this reorganization that we can largely ignore the centrifugal acceleration in our further studies of geophysical fluid mechanics since it is absorbed by the geopotential. The single exception for our studies concerns the rotating laboratory tank experiments in Section 24.3, where we find it more convenient to expose the centrifugal acceleration. We observe that the transition from spherical to geopotential coordinates for geophysical fluid dynamics remains a topic of some confusion, as evidenced by the clarification papers from [Stewart and McWilliams \(2022\)](#) and [Chang and Wolfe \(2022\)](#), both of which correct a confusion within the literature.

11.12.5 Further study

Section 4.12 of [Gill \(1982\)](#) and section 2.2.1 of [Vallis \(2017\)](#) present the terrestrial scaling needed to justify spherical coordinates with a radial effective gravitational potential. [Morse and Feshbach \(1953\)](#) and [Veronis \(1973\)](#) present details of oblate spheroidal coordinates.

11.13 Exercises

EXERCISE 11.1: INERTIAL ACCELERATION WITH $d\Omega/dt \neq 0$

Geophysical applications warrant taking the planetary rotation to be a constant vector, $d\Omega/dt = 0$, and that assumption is made throughout this book. However, for some applications, such as for rotating machines, we cannot make that assumption. What extra term appears in the inertial acceleration vector (11.60e) when $d\Omega/dt \neq 0$?

EXERCISE 11.2: WORKING THROUGH THE SPHERICAL ACCELERATION

Convince yourself that the spherical form of the acceleration given by equation (11.78) is indeed correct.

EXERCISE 11.3: VELOCITY AND ACCELERATION IN CYLINDRICAL-POLAR COORDINATES

In Section 9.3 we worked through the transformation from Cartesian coordinates to cylindrical-polar coordinates for describing motion in a rotating reference frame. We also made use of polar coordinates in Section 11.3.4 to illustrate how polar unit vectors change under rotations. Here we develop an expression for the position, velocity, and acceleration vectors in a reference frame rotating with a constant rate about the vertical axis ($\Omega = \Omega \hat{z}$) using rotating cylindrical-polar coordinates. The cylindrical-polar coordinates are useful when describing physical systems such as rotating fluid columns (e.g., fluids in a rotating circular tank as in Section 33.8) or when studying cyclostrophically balanced flow (Section 29.5).

- Determine the representation of the inertial velocity vector, $\mathbf{V} = d\mathbf{X}/dt$, in terms of cylindrical-polar coordinates. Hint: do not forget to include the solid body motion of the rotating reference frame, which was discussed in Section 11.3.4.
- Determine the representation of the inertial acceleration vector, $\mathbf{A} = d\mathbf{V}/dt$, in terms of cylindrical-polar coordinates.
- Writing the inertial acceleration in the form

$$\mathbf{A} = \mathbf{A}_{\text{cylindrical-polar}} + \mathbf{A}_{\text{metric}} - \mathbf{A}_{\text{centrifugal}} - \mathbf{A}_{\text{Coriolis}}, \quad (11.138)$$

give the mathematical expressions for these terms:

- $\mathbf{A}_{\text{cylindrical-polar}}$ = acceleration in the rotating reference frame using cylindrical-polar coordinates;
- $\mathbf{A}_{\text{metric}}$ = acceleration due to motion of the cylindrical-polar unit vectors relative to the rotating reference frame;
- $\mathbf{A}_{\text{centrifugal}}$ = centrifugal acceleration;
- $\mathbf{A}_{\text{Coriolis}}$ = Coriolis acceleration.

EXERCISE 11.4: VELOCITY PROJECTED ONTO ACCELERATION

The kinetic energy per mass of a particle is given by

$$\mathcal{K} = \mathbf{V} \cdot \mathbf{V}/2, \quad (11.139)$$

where \mathbf{V} is the inertial velocity of a particle. In an inertial reference frame it is trivial to show that

$$\frac{d\mathcal{K}}{dt} = \mathbf{V} \cdot \mathbf{A} \quad (11.140)$$

through use of the chain rule, where $\mathbf{A} = d\mathbf{V}/dt$ is the inertial acceleration. Verify that this identity also holds in the rotating reference frame. For simplicity make use of planetary Cartesian coordinates.

EXERCISE 11.5: GEOMETRY OF CONSTANT GEOPOTENTIAL SURFACES

Here we examine some properties of the geopotential given by equation (11.119), where the squared solid-body speed is $\mathbf{U}_{\text{solid}}^2 = (\Omega r \cos \phi)^2$. We only consider geopotentials that are close to the radius of the planet, so that we can assume the gravitational acceleration, g_e , is constant and takes on its value at R_e as in Sections 11.11.2 and 11.11.4.

- (A) Sketch surfaces of constant geopotential according to the expression (11.119). Draw both meridional (north-south) lines and zonal (east-west) lines.
- (B) By equating the geopotential going around the pole to that going around the equator, show that the polar radius is less than the equatorial radius when $\Omega > 0$.
- (C) Taking the terrestrial values of g_e , R_{equator} , and Ω , what is the polar radius R_{pole} ? Compare to the measured value of the polar radius given by equation (11.134).

EXERCISE 11.6: GENERAL FORM OF THE GEOPOTENTIAL

In Exercise 11.5, as in Sections 11.11.3 and 11.11.4, we only considered geopotentials that are close to the radius of the planet. Show that geopotentials have larger radius at the equator than at the poles even when not making this assumption. Hint: maintain the general form of the gravitational potential as given by equation (11.108), then add to the potential for the centrifugal acceleration (11.65). Evaluate the geopotential at the pole and then show that this same geopotential has a larger radial position anywhere equatorward of the pole.

EXERCISE 11.7: SCALING TO JUSTIFY USE OF GEOPOTENTIAL COORDINATES

Summarize the argument that justifies the use of geopotential coordinates while retaining the spherical geometry. Make use of your favorite textbook discussion such that given in Chapter 2 of *Vallis* (2017).

EXERCISE 11.8: ACCELERATIONS ACTING ON A RESTING PARTICLE

In this exercise we consider the accelerations acting on a particle at rest (in the rotating frame) on a smooth/frictionless rotating spherical planet and a rotating oblate spheroidal planet. We also consider similar questions in Section 12.9.

- (A) Motion of a particle on a rotating spherical planet is described using the spherical coordinates from Section 11.12.2 with the corresponding equations of motion (11.131)-(11.133). Suppose that we drop a particle on a rotating sphere and that we describe its motion using the spherical coordinates. Discuss the initial acceleration of the particle that is released from rest.
- (B) Motion of a particle on a rotating oblate spheroid planet is described using the geopotential coordinates from Section 11.12.3 with the corresponding equations of motion (11.137a)-(11.137c). Suppose that we drop a particle on a rotating oblate spheroid and that we describe its motion using the geopotential coordinates. Discuss the initial acceleration of the particle that is released from rest. Note that we return to this freely falling particle in Section 12.9.3.

EXERCISE 11.9: GRAVITATIONAL POTENTIAL INSIDE A SPHERE

In Section 11.11.1 we found the gravitational, Φ , for a point outside of the spherical earth. Here we find the gravitational potential inside of the earth. That is, solve the Poisson equation

$$\nabla^2 \Phi = 4\pi G \rho, \quad (11.141)$$

for a radial position $r < R_e$. Hint: follow the approach in Section 11.11.1 and then match the potential at $r = R_e$. Note: the solution can be found in many undergraduate physics texts.



Chapter 12

SYMMETRY AND CONSERVATION

A symmetry is a discrete or continuous operation that leaves a physical system unchanged. For example, let \mathbf{X} be a trajectory satisfying Newton's equation of motion and \mathcal{A} be an operation. If $\mathcal{A}[\mathbf{X}]$ also satisfies Newton's equation of motion then \mathcal{A} is a symmetry of the physical system. Noether's theorem provides a connection between symmetries and conservation laws and these connections are explored in this chapter. These ideas are fundamental to how we garner a qualitative understanding of motion in which, for many purposes, it is more useful to know the dynamically conserved properties shared by all trajectories rather than details of any particular trajectory. Furthermore, conservation laws provide predictive capabilities and guidance for designing analytical and numerical solution methods.

CHAPTER GUIDE

This chapter relies on the particle mechanics material studied in Chapter 11, and here we explore many facets of rotational physics that are central to geophysical fluid motions. We make use of ideas from this chapter throughout the book.

12.1	Loose threads	242
12.2	Trajectories and dynamical constraints	242
12.2.1	Connecting symmetries to conservation laws	243
12.2.2	Further study	243
12.3	Time reversal symmetry	243
12.4	Potential momentum	244
12.4.1	Basics	244
12.4.2	Comment about terminology	245
12.5	Inertial oscillations	245
12.5.1	Oscillator equation for inertial oscillations	246
12.5.2	Particle trajectory and velocity	246
12.5.3	Period of inertial oscillations	247
12.5.4	Comments and further study	247
12.6	Axial angular momentum conservation	248
12.6.1	Angular momentum	248
12.6.2	Conservation of axial angular momentum	249
12.7	Constraints from axial angular momentum conservation	250
12.7.1	Deriving the constraints	250
12.7.2	Axial angular momentum conservation and zonal Coriolis acceleration	251
12.7.3	Zonal acceleration induced by meridional motion	251
12.7.4	Zonal acceleration induced by radial motion	252
12.7.5	Zonal acceleration derived from axial angular momentum conservation	252
12.7.6	Coriolis acceleration from meridional motion	253

12.7.7	When lateral motions dominate vertical motions	254
12.7.8	Comments	254
12.8	Mechanical energy conservation	255
12.8.1	Some properties of kinetic energy	255
12.8.2	Planetary Cartesian mechanical energy	257
12.8.3	Planetary spherical mechanical energy	257
12.8.4	Geopotential mechanical energy	259
12.9	Sample particle trajectories	259
12.9.1	Free fall from rest in inertial frame	259
12.9.2	Free fall with constant zonal velocity	260
12.9.3	Free fall from rest in rotating frame	260
12.10	Summary of the dynamical constraints from spatial symmetries	261
12.10.1	Linear momentum conservation	261
12.10.2	Potential momentum conservation	262
12.10.3	Angular momentum conservation	262
12.11	Exercises	262

12.1 Loose threads

- Equations for inertial oscillations on a sphere.
- Discuss inertial oscillations as per [Durran \(1993\)](#) as well as [Early \(2012\)](#).

12.2 Trajectories and dynamical constraints

Newton's law of motion provides the trajectory of a particle so long as we know the forces acting on the particle, as well as the particle's initial position and initial velocity. The trajectory encapsulates all dynamical information about the moving particle. However, it is often difficult to unpack that information to understand the nature of the motion. Knowledge of the trajectory is not always the best route to dynamical insight nor to predictive capabilities.

For dynamical insight it is generally more useful to develop an understanding of constraints respected by the motion, with dynamical constraints manifesting as conservation laws. For example, does the motion conserve mechanical energy? What about angular momentum? If dynamical constraints are present, then all trajectories, regardless their complexity, satisfy the constraints. Knowledge of the constraints can reveal information often hidden when just having knowledge of the trajectory. Constraints also provide predictive statements of value when studying the stability of motion and for developing numerical methods for simulations.

An example is useful to illustrate the points noted above. Consider the following two situations and ask what is more useful.

- We have the analytic expression for the trajectory of a particle moving around a rotating sphere. We thus know the trajectory for an arbitrarily long time.
- We know that all particles, no matter what their trajectory, conserve both the axial angular momentum around the rotational axis and the mechanical energy.

Knowledge of the trajectory for a single particle is useful if we are interested in the details of a particular particle. For example, the particle might be the idealization of a satellite orbiting the planet, with an accurate description of the trajectory needed to predict its location at an arbitrary point in the future. However, for many purposes, we may prefer to know that all particles, no matter what trajectory, conserve angular momentum and mechanical energy. This

information offers the ability to understand basic properties of the motion and to predict its response to perturbations. Dynamical constraints imposed by conservation laws are especially relevant for fluids since it is rare to determine the analytical expression for fluid motion, making the knowledge of constraints incredibly valuable.

12.2.1 Connecting symmetries to conservation laws

The discovery of conservation laws often comes from inspired manipulations of the equations of motion. However, there is a more robust and fundamental means to deduce conservation laws through their connection to symmetries, with a symmetry manifesting as an operation that leaves the physical system unchanged. For example, does the physical system remain unchanged when shifting the origin of time? If so, then mechanical energy is a constant of the motion. Likewise, if there is rotational symmetry around an axis, then the associated angular momentum is a constant of the motion.

The connection between symmetries (kinematics) and conservation laws (dynamics) was made by [Noether \(1918\)](#) (see [Noether and Tavel \(2018\)](#) for an English translation). Noether's theorem is fundamental to nearly all areas of theoretical physics. It is sufficient for our study to make use of this theorem as a conceptual framework for understanding conservation laws and their connections to symmetries. Quite simply, if there is a symmetry then there is a corresponding conservation law, and vice versa.

It is very useful to identify conserved quantities as a means to understand and to constrain the motion. This perspective holds even when the symmetries giving rise to conserved quantities are broken in realistic cases. For example, as seen in Section 10.1.8, friction breaks time translation symmetry and so leads to the dissipation of mechanical energy. Nonetheless, understanding the frictionless motion, and the associated energy conservation law, offers insights for the frictional case. Indeed, for many purposes, knowledge of the trajectory is less important than knowledge of conserved, or partially conserved, dynamical quantities. In this chapter, we offer two examples to support this point: the case of mechanical energy conservation and axial angular momentum conservation. These conservation laws also hold in a modified form when moving to the continuum fluid (e.g., Chapter 21). Additional conservation properties also arise that are unique to the continuum, with conservation of potential vorticity the most notable one for geophysical fluids (Chapter 38).

12.2.2 Further study

Conservation laws and symmetries in classical mechanics are lucidly discussed in Chapters 1 and 2 of [Landau and Lifshitz \(1976\)](#). Pedagogical presentations on these topics can be found in this [online lecture from the Space Time series](#) and this [online lecture from Physics with Elliot](#). This [essay about Emmy Noether](#) provides insights into this mathematician whose work, conducted under some very unfortunate circumstances, forever connected symmetry and conservation laws, with this connection providing the basis for nearly all modern theories of physics.

12.3 Time reversal symmetry

A deterministic process is time-reversible if the time-reversed process satisfies the same dynamic equations as the forward-time process. That is, the dynamical equations are symmetric under a change in the sign of time so that the time-reversed evolution of one state is equivalent to the forward-time evolution of a corresponding state. We here discuss time reversal symmetry in the context of the point particle with trajectory, $\mathbf{X}(t)$, and velocity, $\mathbf{V}(t) = d\mathbf{X}(t)/dt$.

If $\mathbf{X}(t)$ is a solution to the equations of motion, then what is needed for

$$\mathbf{X}^*(t^*) = \mathbf{X}(-t) \quad \text{and} \quad \mathbf{V}^*(t^*) = d\mathbf{X}^*(t^*)/dt^* = -d\mathbf{X}(-t)/dt \quad (12.1)$$

to define the same trajectory traversed backwards in time, where $t^* = -t$? We answer this question by recalling from Section 11.12.1 that with planetary rotation a constant in time then the Cartesian coordinate equation of motion is given by

$$\frac{d}{dt} \left[\frac{d\mathbf{X}(t)}{dt} + 2\boldsymbol{\Omega} \times \mathbf{X}(t) \right] = -\nabla\Phi(t). \quad (12.2)$$

We are interested in the constraints that ensure the following equation is satisfied

$$\frac{d}{dt^*} \left[\frac{d\mathbf{X}^*(t^*)}{dt^*} + 2\boldsymbol{\Omega}^* \times \mathbf{X}^*(t^*) \right] = -\nabla\Phi(t^*). \quad (12.3)$$

The effective gravitational acceleration remains time reversible if

$$\Phi^*(t^*) = \Phi(t), \quad (12.4)$$

which is trivially satisfied for $\Phi = g z$. The Coriolis acceleration is velocity dependent so that it generally breaks time reversal symmetry. However, we can recover time symmetry by assuming that the rotation direction switches when time reverses so that

$$\boldsymbol{\Omega}^* = -\boldsymbol{\Omega}. \quad (12.5)$$

With this transformation, a trajectory, $\mathbf{X}(t)$, that solves the forward equation (12.2) yields a trajectory $\mathbf{X}(-t)$ that solves the same equation but with time reversed. We return to this question of time reversal symmetry for the Euler equations of perfect fluid mechanics in Exercise 21.3.

12.4 Potential momentum

In Section 11.12.1 we introduced the *potential momentum*, and we here further study its conservation properties. Recall that it is a constant of the motion when a particle moves on a time independent geopotential in a direction where the geopotential does not change. That is, the conservation of potential momentum arises from a spatial symmetry of the geopotential.

12.4.1 Basics

Start with the Cartesian coordinate equation of motion

$$\frac{d}{dt} \left[\dot{\mathbf{X}} + 2\boldsymbol{\Omega} \times \mathbf{X} \right] = -\nabla\Phi. \quad (12.6)$$

Now introduce the *potential momentum* per mass

$$\mathbf{M} \equiv \dot{\mathbf{X}} + 2\boldsymbol{\Omega} \times \mathbf{X} = \hat{\mathbf{x}}(u - 2\Omega y) + \hat{\mathbf{y}}(v + 2\Omega x) + \hat{\mathbf{z}}w, \quad (12.7)$$

in which case the equation of motion takes the form

$$\dot{\mathbf{M}} = -\nabla\Phi. \quad (12.8)$$

Now let $\hat{\mathbf{s}}$ be a unit vector tangent to the geopotential surface so that $\hat{\mathbf{s}} \cdot \nabla \Phi = 0$. Assuming the geopotential surface is time independent so that $\hat{\mathbf{s}}$ is also time independent, then the equation of motion (12.8) leads to

$$\frac{d(\hat{\mathbf{s}} \cdot \mathbf{M})}{dt} = 0. \quad (12.9)$$

That is, the projection of the potential momentum onto a static geopotential surface is a constant of motion. This dynamical constraint arises since we cannot distinguish one point on the geopotential from another; i.e., there is a symmetry associated with motion along the static geopotential. Noether's theorem (Section 12.2.1) then says that this geometric symmetry leads to a constant of the motion, here given by that component of potential momentum within the geopotential surface. We illustrate this situation in Figure 12.1 with a horizontal geopotential surface.

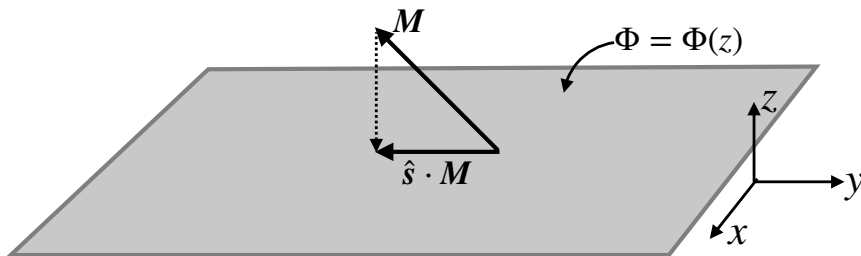


FIGURE 12.1: The projection of the potential momentum onto the geopotential surface is a constant of the motion, $d(\hat{\mathbf{s}} \cdot \mathbf{M})/dt = 0$. Here the geopotential surface is the x - y -plane so that $\hat{\mathbf{x}} \cdot \mathbf{M} = u - 2\Omega y$ and $\hat{\mathbf{y}} \cdot \mathbf{M} = v + 2\Omega x$ are the two conserved components of potential momentum.

Consider a particle with potential momentum \mathbf{M} and move it from an arbitrary point to a reference position with $\mathbf{X} = 0$. Upon reaching the reference position, the horizontal velocity of the particle must equal to \mathbf{M} in order to maintain the same potential momentum. This example motivates the name “potential momentum”, since \mathbf{M} measures the potential for relative motion contained in the particle as it moves along a geopotential.

12.4.2 Comment about terminology

As noted on page 51 of [Markowski and Richardson \(2010\)](#), one might see potential momentum referred to as *pseudo angular momentum*, with some dropping the “pseudo” portion to the name. In either case, it is important to note that potential momentum is distinct from angular momentum. In particular, there is no moment-arm as part of the potential momentum, nor is there any axial symmetry corresponding to the conservation law.

Many authors use the term *absolute momentum* rather than potential momentum, perhaps in reference to the momentum measured in the absolute or inertial reference frame. However, that connection is incorrect since the inertial velocity is (Section 11.8.1)

$$\mathbf{V} = \mathbf{V}_{\text{Cartesian}} + \mathbf{U}_{\text{solid-body}} = \mathbf{V}_{\text{Cartesian}} + \boldsymbol{\Omega} \times \mathbf{X}. \quad (12.10)$$

The factor of two multiplying the rotation rate in the potential momentum arises from the Coriolis acceleration. In contrast, solid-body rotation velocity contributes to the inertial velocity and it has a factor of unity multiplying the rotation rate.

12.5 Inertial oscillations

In Section 21.3.4 we introduce the tangent plane approximation for motion on a rotating sphere. In this approximation, motion occurs on a rotating geopotential surface with the surface approx-

imated as horizontal. Furthermore, we use local tangent plane Cartesian coordinates (which are distinct from the planetary Cartesian coordinates used in Chapter 11 and illustrated in Figure 9.1). The f -plane approximation furthermore sets the Coriolis parameter to a constant,

$$f = 2\Omega \sin \phi_0, \quad (12.11)$$

where ϕ_0 is a chosen latitude. Consequently, a free particle moving on the f -plane maintains a constant horizontal potential momentum

$$\frac{dM_x}{dt} = \frac{d(u - f y)}{dt} = 0 \quad (12.12a)$$

$$\frac{dM_y}{dt} = \frac{d(v + f x)}{dt} = 0, \quad (12.12b)$$

where we introduced the horizontal velocity components $(u, v) = (\dot{x}, \dot{y})$. These two conservation laws greatly constrain the motion of the particle moving on a constant geopotential surface.

12.5.1 Oscillator equation for inertial oscillations

Taking the time derivative of the zonal equation (12.12a) and using the meridional equation (12.12b) leads to

$$\ddot{u} - f \dot{v} = \ddot{u} + f^2 u = 0. \quad (12.13)$$

Similar manipulations for the meridional velocity equation render the free oscillator equation for each component of the horizontal velocity

$$\frac{d^2u}{dt^2} + f^2 u = 0 \quad \text{and} \quad \frac{d^2v}{dt^2} + f^2 v = 0. \quad (12.14)$$

Motions that satisfy this equation are termed *inertial oscillations*.

12.5.2 Particle trajectory and velocity

Time integrating the equation of motion (12.14) renders the particle trajectory and its velocity

$$\mathbf{X}(t) = (U/f) [\hat{\mathbf{x}} \sin(ft) + \hat{\mathbf{y}} \cos(ft)] \quad (12.15a)$$

$$\mathbf{U}(t) = U [\hat{\mathbf{x}} \cos(ft) - \hat{\mathbf{y}} \sin(ft)], \quad (12.15b)$$

where $U > 0$ is the particle speed, which is a constant, and we assumed the initial conditions

$$\mathbf{X}(0) = (U/f) \hat{\mathbf{y}} \quad \text{and} \quad \mathbf{U}(0) = U \hat{\mathbf{x}}. \quad (12.16)$$

From the particle trajectory equation (12.15a), we see that motion of a particle exhibiting inertial oscillations is circular with radius

$$R = U/|f|. \quad (12.17)$$

As depicted in Figure 12.2, northern hemisphere ($f > 0$) inertial oscillations occur in the clockwise direction whereas southern hemisphere motion is counter-clockwise. Consequently, particle motion undergoing inertial oscillations occurs in an anti-cyclonic sense (opposite to the sense of the rotating reference frame). As we discuss in more detail in Section 29.4, inertial oscillations arise from a balance between the Coriolis acceleration of the rotating frame and the centrifugal acceleration arising from the particle's circular motion.¹ The only way to realize this balance

¹This centrifugal acceleration is distinct from the planetary centrifugal acceleration absorbed into the geopo-

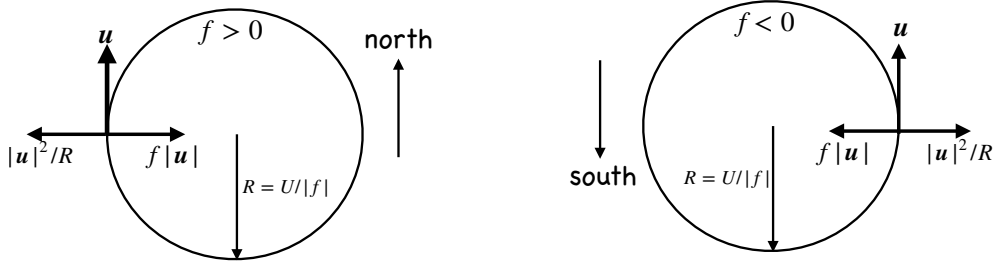


FIGURE 12.2: Inertial oscillation of a particle on a plane occurs when the centrifugal acceleration balances the Coriolis acceleration. Left panel: $f > 0$ for the northern hemisphere, revealing that inertial motion is an anti-cyclonic (clockwise) circular motion with radius $|R| = U/|f|$. The Coriolis acceleration is to the right, pointing into the center of the inertial circle, whereas the centrifugal acceleration points away from the center. Right panel: Counterclockwise inertial motion in the southern hemisphere with the same balance between Coriolis and centrifugal accelerations.

is for the particle to move anti-cyclonically, with the Coriolis acceleration pointing towards the inside of the inertial circle and the centrifugal acceleration pointing outside. Finally, note that the potential momentum for inertial oscillations vanishes since

$$\mathbf{M}(t) = \mathbf{U}(t) + f \hat{z} \times \mathbf{X}(t) = 0. \quad (12.18)$$

Adding an arbitrary constant to the initial position makes the potential momentum equal to a nonzero constant.

12.5.3 Period of inertial oscillations

Inertial oscillations possess a constant speed and move around the inertial circle with a period

$$T_{\text{inertial}} = \frac{2\pi}{f} = \frac{11.97}{|\sin \phi_0|} \text{ hour}, \quad (12.19)$$

where we set $\Omega = 7.292 \times 10^{-5} \text{ s}^{-1}$ (equation (11.1)). This period is the time it takes to go around the circle. It is smallest at the poles, where the latitude $\phi_0 = \pm\pi/2$ and $T_{\text{smallest}} \approx 12$ hour. At the equator, $\phi_0 = 0$, so that the radius of the inertial circle is infinite and inertial oscillations are unavailable. Furthermore, T_{inertial} is the time for a Foucault pendulum to turn through π radians, so that T_{inertial} is sometimes referred to as one-half a pendulum day.

12.5.4 Comments and further study

Inertial oscillations of fluid elements are described by the above constant potential momentum equation of motion. Such oscillations are commonly measured by ocean current meters, especially in higher latitude regions where diurnal (day-night) variations in wind forcing have a strong projection onto the inertial period. This resonant forcing puts energy into inertial or near-inertial motions. It is quite amazing that such oscillations are indeed found in the ocean, given that we have ignored pressure and friction, which are two forces that impact on fluid elements (as opposed to point particles). The main reason we can observe this motion in the ocean is that upper ocean currents are often generated by winds even in the absence of horizontal pressure gradients, so that there are occasions when the motion is not affected much by pressure gradients.

We study inertial waves in Section 46.2 as part of our study of rapidly rotating fluid motion. We also encounter inertial motions in Section 29.4 as part of our characterization of horizontal potential (Section 11.11.4). The planetary centrifugal acceleration plays no role in inertial oscillations.

fluid motion according to the balance between forces. As noted above, we arrive at inertial motion by balancing the Coriolis acceleration with the centrifugal acceleration due to the curved motion of a fluid particle. The name “inertial” does not here refer to motion in an inertial reference frame (Section 11.2). Instead, it refers to the balance between accelerations arising only when the particle is in motion (i.e., has inertia), with these accelerations being the Coriolis and centrifugal.

A rotating tank fluid experiment offers a useful controlled setting to observe inertial waves in a fluid, such as shown near the 18 minute mark in [this video from Prof. Fultz](#).

12.6 Axial angular momentum conservation

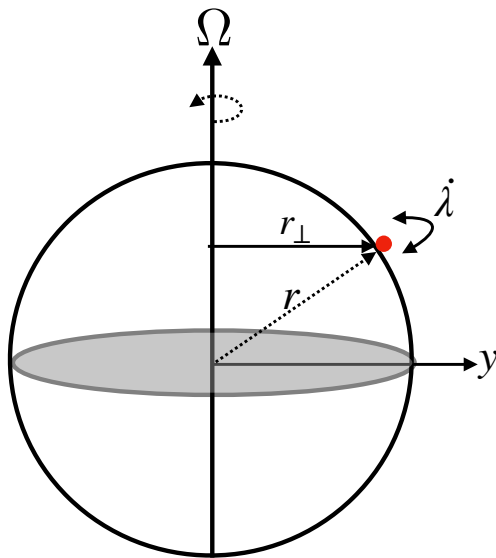


FIGURE 12.3: Axial angular momentum, $L^z = m r_{\perp}^2 (\dot{\lambda} + \Omega)$, is the moment of the zonal momentum around the sphere, with $r_{\perp} = r \cos \phi = \sqrt{x^2 + y^2}$ the moment-arm length; i.e., the distance of the particle to the axis of rotation, whereas $r^2 = \sqrt{x^2 + y^2 + z^2}$ is the radial distance to the center of the sphere. L^z is a constant of the motion for the particle moving in the absence of friction.

Does the particle know anything about the longitudinal angle, λ (Figure 12.3)? If we assume the sphere is smooth (i.e., no mountains), and the sphere rotates around the polar axis, there is an arbitrariness in how we choose the zero for the longitudinal angle. That is, the physical system remains unchanged if we shift the longitudinal angle by a constant. Noether’s theorem then says that this rotational symmetry leads to a corresponding angular momentum conservation. Hence, the particle’s angular momentum around the rotational axis remains fixed by the initial conditions. We here prove that axial angular momentum is constant by manipulating the equations of motion. Many of the same manipulations also occur when considering angular conservation for a continuous fluid (see Section 21.5).

12.6.1 Angular momentum

The angular momentum of the particle, computed with respect to the origin of the sphere, is given by

$$\mathbf{L} = m \mathbf{X} \times \mathbf{V}. \quad (12.20)$$

This is the moment of the linear momentum computed relative to the origin. We write the angular momentum computed along the polar axis as

$$L^z = \mathbf{L} \cdot \hat{\mathbf{z}} \quad (12.21a)$$

$$= m (\mathbf{X} \times \mathbf{V}) \cdot \hat{\mathbf{z}} \quad (12.21b)$$

$$= m (\hat{\mathbf{z}} \times \mathbf{X}) \cdot \mathbf{V} \quad (12.21c)$$

$$= m r \cos \phi (\hat{\boldsymbol{\lambda}} \cdot \mathbf{V}) \quad (12.21d)$$

$$= m r_{\perp} (\hat{\boldsymbol{\lambda}} \cdot \mathbf{V}). \quad (12.21e)$$

Hence, the angular momentum about the polar axis equals to the component of the linear momentum in the longitudinal direction, multiplied by the distance to the polar rotational axis (the moment-arm)

$$r_{\perp} = r \cos \phi. \quad (12.22)$$

In deriving equation (12.21e), we made use of the identity

$$\hat{\mathbf{z}} \times \mathbf{X} = r_{\perp} \hat{\boldsymbol{\lambda}}, \quad (12.23)$$

which is useful below for proving that axial angular momentum is a constant of the motion.

We now write the axial angular momentum in equation (12.21e) in terms of the rotating frame quantities. To do so, introduce the inertial velocity written using spherical coordinates according to equation (11.47f), which yields

$$L^z = m r_{\perp} (\hat{\boldsymbol{\lambda}} \cdot \mathbf{V}) = m r_{\perp}^2 (\dot{\lambda} + \Omega) = m r_{\perp} (u + r_{\perp} \Omega). \quad (12.24)$$

When measured from the rotating terrestrial frame, the axial angular momentum consists of two terms: one from the zonal velocity of the particle relative to the planet and another from the solid-body motion of the planet.

12.6.2 Conservation of axial angular momentum

The time derivative of the axial angular momentum is given by

$$m^{-1} dL^z/dt = d/dt [(\mathbf{X} \times \mathbf{V}) \cdot \hat{\mathbf{z}}] \quad \text{definition of axial angular momentum} \quad (12.25a)$$

$$= d/dt [(\hat{\mathbf{z}} \times \mathbf{X}) \cdot \mathbf{V}] \quad \text{cyclically permute terms} \quad (12.25b)$$

$$= (\hat{\mathbf{z}} \times \mathbf{V}) \cdot \mathbf{V} + (\hat{\mathbf{z}} \times \mathbf{X}) \cdot \mathbf{A} \quad d\mathbf{X}/dt = \mathbf{V}, d\mathbf{V}/dt = \mathbf{A}, \text{ and } d\hat{\mathbf{z}}/dt = 0 \quad (12.25c)$$

$$= (\hat{\mathbf{z}} \times \mathbf{V}) \cdot \mathbf{A} \quad (\hat{\mathbf{z}} \times \mathbf{V}) \cdot \mathbf{V} = 0 \quad (12.25d)$$

$$= r_{\perp} \hat{\boldsymbol{\lambda}} \cdot \mathbf{A}. \quad \text{from equation (12.23).} \quad (12.25e)$$

The inertial acceleration arises just from the central-force gravitational field (equation (11.122))

$$\mathbf{A} = -\nabla \Phi_e = -g_e \hat{\mathbf{r}}. \quad (12.26)$$

Since $\hat{\boldsymbol{\lambda}} \cdot \hat{\mathbf{r}} = 0$, we are led to axial angular momentum conservation

$$\frac{dL^z}{dt} = 0. \quad (12.27)$$

12.7 Constraints from axial angular momentum conservation

Axial angular momentum conservation constrains the particle motion and in turn it offers a means for interpreting and predicting motion on the sphere. It is also a natural means for describing the motion when viewed from a non-rotating inertial reference frame. We here explore how these constraints manifest through thought experiments illustrated in Figure 12.4. In doing so, we show that the acceleration induced by axial angular momentum conserving motion corresponds to the Coriolis acceleration that is part of a rotating non-inertial reference frame description. That is, angular momentum constrained motion described in an inertial reference frame corresponds to the Coriolis acceleration appearing in a rotating non-inertial frame description.

Throughout the following we write the axial angular momentum as

$$L^z = m l^z = m r_{\perp}^2 (\dot{\lambda} + \Omega) = m r_{\perp} (u + r_{\perp} \Omega), \quad (12.28)$$

where

$$l^z = L^z/m \quad \text{and} \quad u = r_{\perp} \dot{\lambda} \quad (12.29)$$

are the axial angular momentum per mass and zonal velocity component. Since the mass of the particle is constant, conservation of $L^z = m l^z$ implies conservation of l^z . Note that for most geophysical applications, $l^z > 0$ since solid-body motion dominates over the relative zonal velocity:

$$r_{\perp} \Omega > |u| \quad \text{for most terrestrial motions,} \quad (12.30)$$

with $r_{\perp} \Omega = 465 \text{ m s}^{-1}$ at the equator (see Figure 11.2). In Exercise 12.1 we consider the interesting, but geophysically uncommon, case where $l^z \leq 0$.

12.7.1 Deriving the constraints

Conservation of axial angular momentum says that it is not possible to change u or $\dot{\lambda}$ without also changing r_{\perp} in such a manner to ensure that l^z remains fixed. To determine the relation between these changes we set $\delta l^z = 0$, where δ refers to any small change. When writing $l^z = r_{\perp}^2 (\dot{\lambda} + \Omega)$ we have

$$\delta l^z = 2 r_{\perp} \delta r_{\perp} (\dot{\lambda} + \Omega) + r_{\perp}^2 \delta \dot{\lambda} = 2 l^z \frac{\delta r_{\perp}}{r_{\perp}} + r_{\perp}^2 \delta \dot{\lambda}, \quad (12.31)$$

where we set $\delta \Omega = 0$ since the earth's rotation rate is assumed to be fixed. Furthermore, we find it useful to write the changes in terms of l^z since it is a constant of the motion. Likewise, when writing $l^z = r_{\perp} (u + r_{\perp} \Omega)$ we have

$$\delta l^z = \delta r_{\perp} (u + r_{\perp} \Omega) + r_{\perp} (\delta u + \Omega \delta r_{\perp}) = \Omega r_{\perp} \delta r_{\perp} \left[1 + \frac{l^z}{\Omega r_{\perp}^2} \right] + r_{\perp} \delta u. \quad (12.32)$$

Setting $\delta l^z = 0$ then leads to the constraints

$$\delta \dot{\lambda} = -\frac{2 l^z}{r_{\perp}^2} \frac{\delta r_{\perp}}{r_{\perp}} \iff \delta u = -\Omega \delta r_{\perp} \left[1 + \frac{l^z}{\Omega r_{\perp}^2} \right]. \quad (12.33)$$

As noted above, $l^z > 0$ is generally the case for geophysical fluid motion. Consequently, axial angular momentum conserving motion that brings the particle closer to the rotation axis ($\delta r_{\perp} < 0$) leads to an eastward velocity change (angular velocity $\delta \dot{\lambda} > 0$ and zonal velocity $\delta u > 0$). The opposite occurs for motion with $\delta r_{\perp} > 0$. These results hold in both the northern and southern hemispheres.

Since $r_{\perp} = r \cos \phi$, the distance to the rotational axis can change either by changing the radial position or the meridional position

$$\delta r_{\perp} = (\cos \phi) \delta r - (r \sin \phi) \delta \phi. \quad (12.34)$$

Assuming these changes occur over a small time increment δt allows us to write

$$\delta r_{\perp}/\delta t = w \cos \phi - v \sin \phi, \quad (12.35)$$

where

$$v = r \delta \phi / \delta t = r \dot{\phi} \quad \text{and} \quad w = \delta r / \delta t = \dot{r} \quad (12.36)$$

introduced the meridional and vertical components to the particle velocity according to equation (11.49). For geophysical fluid motion, changes in vertical distance δr are far smaller than the distance to the earth's center, $\delta r \ll r$. In this case, when $\phi \neq 0$, then δr_{\perp} is affected much more by meridional motion at constant radial position (second term on right hand side of equation (12.35)) than by vertical motion at constant latitude (first term on right hand side of equation (12.35)). We return to this observation in Section 12.7.7 when discussing the shallow fluid approximation used to develop the primitive equations for the atmosphere and ocean in Section 24.1.2.

12.7.2 Axial angular momentum conservation and zonal Coriolis acceleration

Consider the zonal acceleration felt by a particle at rest (in the rotating frame) whose angular momentum per mass equals $l^z = r_{\perp}^2 \Omega$. In this case the zonal acceleration in equation (12.33) is

$$\delta \lambda = -2 \Omega \frac{\delta r_{\perp}}{r_{\perp}} \iff \dot{u} = -2 \Omega (\delta r_{\perp}/\delta t) = -2 \Omega (w \cos \phi - v \sin \phi), \quad (12.37)$$

where we used equation (12.35) for $\delta r_{\perp}/\delta t$. The expression for \dot{u} is precisely the same as the Coriolis acceleration appearing in the zonal momentum equation (11.137a)

$$\dot{u} + \frac{u (w - v \tan \phi)}{r} = \underbrace{-2 \Omega (w \cos \phi - v \sin \phi)}_{\text{Coriolis acceleration}}. \quad (12.38)$$

Hence, the Coriolis acceleration appearing in the zonal momentum equation is identical to the zonal acceleration induced by constraining the motion to conserve axial angular momentum. That is, by unpacking the constraint of axial angular momentum conservation to reveal the zonal momentum equation, the Coriolis acceleration is revealed as part of that package. We pursue this connection in Section 12.7.5 by deriving the zonal momentum equation from the axial angular momentum equation.

12.7.3 Zonal acceleration induced by meridional motion

Consider a particle moving meridionally ($\delta \phi \neq 0$) while maintaining a constant radial position ($\delta r = 0$). The axial angular momentum constraint (12.37) induces a zonal acceleration

$$\dot{u} = 2 \Omega v \sin \phi, \quad (12.39)$$

which, as seen by equation (12.38), is the Coriolis acceleration appearing in the zonal momentum equation arising from the meridional motion. For poleward motion in either hemisphere, the product $v \sin \phi$ is always positive: $v \sin \phi > 0$. Hence, axial angular momentum conserving motion towards either pole induces an eastward acceleration, whereas a westward acceleration is induced

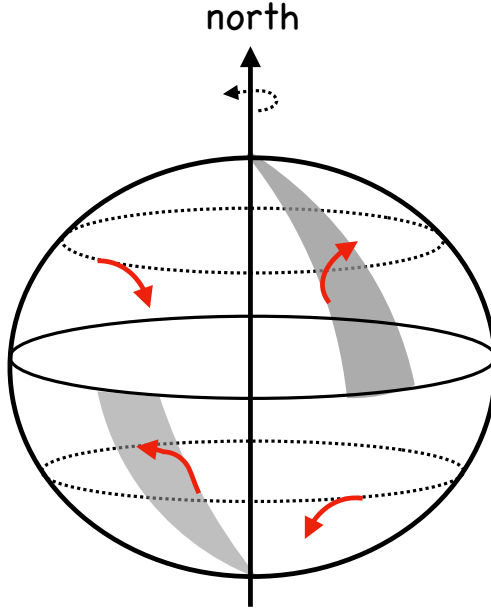


FIGURE 12.4: In the northern hemisphere, the Coriolis acceleration viewed from the rotating reference frame deflects a particle to its right whereas it deflects a particle to the left in the southern hemisphere. This deflection is also a result of axial angular momentum conservation, which is the natural way to describe the motion from a non-rotating inertial reference frame. We can summarize the ideas developed in Section 12.7 as follows. For a meridionally displaced trajectory, the spinning earth causes the trajectory to pick up motion relative to the earth surface, zonally to the right in the northern hemisphere and zonally to the left in the southern hemisphere. Equivalently, consider a projectile (say a cannon ball) shot poleward. As the projectile started from the ground closer to the equator, it has a zonal velocity component that is larger than the more poleward ground underneath it as it flies away from the equator. Hence, as it moves poleward it also picks up an eastward velocity component, which is to the right of the poleward motion in the northern hemisphere and to the left in the southern. For a zonally displaced trajectory to conserve angular momentum, the particle must pick up meridional motion; poleward if the zonal displacement is westward and equatorward if the displacement is eastward.

for equatorward motion. For the northern hemisphere, the induced acceleration deflects the particle to the right when looking downstream whereas in the southern hemisphere the induced acceleration deflects the particle to the left. These deflections are illustrated in Figure 12.4.

12.7.4 Zonal acceleration induced by radial motion

Now consider a particle moving radially while holding the latitude fixed ($\delta r \neq 0$ and $\delta\phi = 0$). The axial angular momentum constraint (12.37) induces a zonal acceleration

$$\dot{u} = -2\Omega w \cos \phi, \quad (12.40)$$

which, as seen by equation (12.38), is the Coriolis acceleration appearing in the zonal momentum equation arising from the vertical motion. Hence, for vertically downward motion ($w < 0$), axial angular momentum conservation induces a positive zonal acceleration, $\dot{u} > 0$, which we expect from axial angular momentum conservation since the particle is moving closer to the rotation axis.

12.7.5 Zonal acceleration derived from axial angular momentum conservation

The above discussion can be formalized by analyzing how the conservation of axial angular momentum leads to an expression for the zonal acceleration. For this purpose, compute the time

derivative of the first form of the axial angular momentum in equation (12.28), in which case

$$\frac{1}{m} \frac{dL^z}{dt} = \frac{d[(r \cos \phi)^2 (\dot{\lambda} + \Omega)]}{dt} \quad (12.41a)$$

$$= 2(\dot{r} \cos \phi - r \dot{\phi} \sin \phi)(\dot{\lambda} r \cos \phi + r \Omega \cos \phi) + (r \cos \phi)^2 \ddot{\lambda} \quad (12.41b)$$

$$= 2(w \cos \phi - v \sin \phi)(u + r \Omega \cos \phi) + (r \cos \phi)^2 \ddot{\lambda}, \quad (12.41c)$$

where we introduced the (u, v, w) velocity components according to equation (11.49). With the zonal velocity $u = \dot{\lambda} r_{\perp} = \dot{\lambda} r \cos \phi$, we have

$$r \cos \phi \ddot{\lambda} = \dot{u} + \frac{u}{r \cos \phi} (v \sin \phi - w \cos \phi), \quad (12.42)$$

so that equation (12.41c) takes the form

$$\frac{1}{m} \frac{dL^z}{dt} = 2(w \cos \phi - v \sin \phi)(u + r \Omega \cos \phi) + (r \cos \phi)^2 \ddot{\lambda} \quad (12.43a)$$

$$= (w \cos \phi - v \sin \phi)(u + 2r \Omega \cos \phi) + \dot{u} r \cos \phi. \quad (12.43b)$$

Setting $dL^z/dt = 0$ and rearranging then leads to a prognostic equation for the zonal velocity

$$\frac{du}{dt} = \left[\frac{u}{r \cos \phi} + 2\Omega \right] (v \sin \phi - w \cos \phi). \quad (12.44)$$

The first term in the bracket arises from curvature of the sphere (the “metric acceleration”) whereas the second term is the Coriolis acceleration.

The same result can be obtained by performing the time derivative on the second form of the axial angular momentum in equation (12.28), in which case

$$\frac{1}{m} \frac{dL^z}{dt} = \frac{d[u r \cos \phi + \Omega(r \cos \phi)^2]}{dt} \quad (12.45a)$$

$$= \dot{u} r \cos \phi + u \dot{r} \cos \phi - u r \dot{\phi} \sin \phi + 2\Omega r \cos \phi (\dot{r} \cos \phi - r \dot{\phi} \sin \phi). \quad (12.45b)$$

Again, setting $dL^z/dt = 0$ and rearranging leads to the zonal acceleration (12.44).

12.7.6 Coriolis acceleration from meridional motion

What happens when zonal motion is perturbed in the meridional direction? Following the angular momentum constraint (12.37), a poleward perturbation, $\delta\phi > 0$, to a northern hemisphere particle will have $\dot{u} > 0$, with this zonal acceleration corresponding to a rightward deflection relative to the $\delta\phi > 0$ perturbation. Likewise, for $\delta\phi < 0$ a northern hemisphere particle will have $\dot{u} < 0$, which corresponds to a rightward deflection relative to the $\delta\phi < 0$ perturbation.

We see the correspondence to the Coriolis acceleration when viewed in the rotating reference frame by examining the meridional momentum equation (11.137b)

$$\dot{v} + \frac{v w + u^2 \tan \phi}{r} = -2\Omega u \sin \phi, \quad (12.46)$$

with the Coriolis acceleration underlined on the right hand side. In the northern hemisphere ($\sin \phi > 0$), the Coriolis acceleration gives rise to a rightward (equatorward) acceleration, $-2\Omega u \sin \phi < 0$, when the particle is moving eastward, $u > 0$, thus inducing a negative meridional acceleration, $\dot{v} < 0$. Conversely, if the particle is moving to the west so that $u < 0$, then the Coriolis acceleration

is again to the right, only this time it deflects the particle in the poleward direction with $\dot{v} > 0$. The analogous considerations hold in the southern hemisphere where the particle is deflected to the left by the Coriolis acceleration. These motions are reflected in Figure 12.4.

12.7.7 When lateral motions dominate vertical motions

We here consider two approximations relevant to large scale geophysical fluid motions.

1. The particle kinetic energy is dominated by lateral motions on the sphere (i.e., motion at constant radial position).
2. Vertical (radial) excursions are much smaller than the earth radius.

When applied to a fluid, the first assumption leads to the hydrostatic approximation (Section 24.2), and the second assumption leads to the shallow fluid approximation (Section 24.1.2). Self-consistency of the equations of motion means that these two assumptions must be applied together.

Dropping the vertical velocity component to the kinetic energy leads to

$$K \approx \frac{m}{2} [(u + r_{\perp} \Omega)^2 + v^2]. \quad (12.47)$$

The second assumption means that the axial angular momentum takes the approximate form

$$L^z \approx m R_{\perp} (u + \Omega R_{\perp}) = m R_{\perp}^2 (\dot{\lambda} + \Omega), \quad (12.48)$$

where

$$r = R + z \approx R \quad \text{and} \quad R_{\perp} = R \cos \phi. \quad (12.49)$$

The approximate angular momentum (12.48) ignores contributions from vertical motion in changing the moment-arm. Indeed, as noted in Section 12.7.1, vertical movements within the atmosphere and ocean (relatively thin fluid layers over the earth's surface) lead to a relatively small modification to the moment-arm, so the assumption that $r_{\perp} \approx R \cos \phi$ is reasonable. With $r \approx R$, the zonal acceleration (12.44) is modified to the form

$$\frac{du}{dt} = v \left[\frac{u \tan \phi}{R} + f \right] \quad \text{where} \quad f = 2 \Omega \sin \phi. \quad (12.50)$$

That is, we dropped the vertical velocity component, w , from the general form of the acceleration (12.44). Correspondingly, the meridional momentum equation takes the form

$$\frac{dv}{dt} = -u \left[\frac{u \tan \phi}{R} + f \right]. \quad (12.51)$$

These approximate forms for the zonal and meridional accelerations appear in the primitive equations developed in Section 24.1.

12.7.8 Comments

To orient oneself according to the Coriolis acceleration, one needs to remember one fact: in the northern hemisphere motion on the sphere at constant radius ($\delta r = 0$) leads to a rightward deflection whereas in the southern hemisphere the particle experiences a leftward deflection. Figure 12.4 depicts some sample deflections.

A concise summary of many features of rotating physics is provided by [this video from SciencePrimer](#).

12.8 Mechanical energy conservation

Does the particle know anything about the origin of time? Since the angular velocity of the planet and the gravitational acceleration are both assumed constant in time, then changing the time will leave the physical system unaltered. That is, the physical system remains unchanged if we shift all clocks by a constant amount. Through Noether's theorem, this symmetry in time leads to mechanical energy conservation. That is, the particle's mechanical energy is fixed by the initial conditions. We here prove that mechanical energy is constant in time by manipulating the equations of motion. Many of the manipulations also occur when considering the mechanical energy conservation laws for a continuum fluid discussed in Chapter 21.

12.8.1 Some properties of kinetic energy

In this subsection we establish some basic properties of kinetic energy for a particle. As we saw in Section 10.1.5, changes in the kinetic energy of a particle equal to the *mechanical work* done on the particle as it moves along its trajectory

$$K(t_2) - K(t_1) = \int_{\mathbf{x}_1}^{\mathbf{x}_2} \mathbf{F} \cdot d\mathbf{x} = \int_{t_1}^{t_2} \mathbf{F} \cdot \mathbf{V} dt, \quad (12.52)$$

where $\mathbf{V} dt = d\mathbf{x}$ defines the vector increment along the trajectory, and $\mathbf{x}_{1,2}$ are the endpoints of the trajectory at times $t_{1,2}$. The integrand, $\mathbf{F} \cdot \mathbf{V}$, is known as the *power*. Hence, equation (12.52) says that the time integral of the power equals to the difference in kinetic energy between the final and initial times.

The kinetic energy is *not* Galilean invariant since movement to another inertial reference frame leads to the kinetic energy change

$$\bar{\mathbf{V}} = \mathbf{V} + \mathbf{U} \implies \bar{K} = K + \frac{m}{2} (2 \mathbf{V} \cdot \mathbf{U} + \mathbf{U} \cdot \mathbf{U}), \quad (12.53)$$

where \mathbf{U} is a constant boost velocity so that $d\mathbf{U}/dt = 0$. We do not expect kinetic energy to be Galilean invariant since kinetic energy measures energy of motion relative to a chosen reference frame. Even so, the time change of the kinetic energy in a different inertial frame is given by the power in the new frame

$$\frac{d\bar{K}}{dt} = \frac{dK}{dt} + m \mathbf{A} \cdot \mathbf{U} = \mathbf{F} \cdot \mathbf{V} + \mathbf{F} \cdot \mathbf{U} = \mathbf{F} \cdot \bar{\mathbf{V}}. \quad (12.54)$$

Hence, we can directly connect kinetic energy changes to forces within an arbitrary inertial reference frame.

Cartesian expression for kinetic energy

Consider the expression for kinetic energy when introducing the velocity of the rotating reference frame. Writing the inertial velocity in the planetary Cartesian form

$$\mathbf{V} = \mathbf{V}_{\text{Cartesian}} + \mathbf{U}_{\text{solid}}, \quad (12.55)$$

leads to

$$K = \frac{m}{2} [\mathbf{V}_{\text{Cartesian}} \cdot \mathbf{V}_{\text{Cartesian}} + 2 \mathbf{V}_{\text{Cartesian}} \cdot \mathbf{U}_{\text{solid}} + \mathbf{U}_{\text{solid}} \cdot \mathbf{U}_{\text{solid}}] \quad (12.56)$$

The first term arises from motion of the particle relative to the rotating sphere; the second arises from coupling between relative velocity and solid-body velocity; and the third arises from solid-

body motion of the sphere.

Spherical expression for kinetic energy: Part I

To expose spherical symmetry of the physical system, we express the kinetic energy in terms of the planetary spherical coordinates defined in Figure 9.1. Doing so for the solid body velocity leads to equation (11.51)

$$\mathbf{U}_{\text{solid}} = \Omega r \cos \phi (-\sin \lambda \hat{\mathbf{x}} + \cos \lambda \hat{\mathbf{y}}). \quad (12.57)$$

Likewise, the velocity components measured in the rotating frame are given by

$$\dot{X} = \frac{d(r \cos \phi \cos \lambda)}{dt} = \dot{r} \cos \phi \cos \lambda - r \dot{\phi} \sin \phi \cos \lambda - r \dot{\lambda} \cos \phi \sin \lambda \quad (12.58a)$$

$$\dot{Y} = \frac{d(r \cos \phi \sin \lambda)}{dt} = \dot{r} \cos \phi \sin \lambda - r \dot{\phi} \sin \phi \sin \lambda + r \dot{\lambda} \cos \phi \cos \lambda \quad (12.58b)$$

$$\dot{Z} = \frac{d(r \sin \phi)}{dt} = \dot{r} \sin \phi + r \dot{\phi} \cos \phi. \quad (12.58c)$$

Bringing terms together then leads to the kinetic energy in terms of spherical coordinates

$$K = \frac{m}{2} \left[(\dot{r}^2 + r^2 \dot{\phi}^2 + \dot{\lambda}^2 r^2 \cos^2 \phi) + (2 \Omega r^2 \dot{\lambda} \cos^2 \phi) + (\Omega r \cos \phi)^2 \right]. \quad (12.59)$$

Spherical expression for kinetic energy: Part II

An alternative means for deriving the kinetic energy in equation (12.59) makes use of the spherical coordinate form of the inertial velocity given by equation (11.47f), in which case

$$\mathbf{V} = (u + r_{\perp} \Omega) \hat{\mathbf{\lambda}} + v \hat{\mathbf{\phi}} + w \hat{\mathbf{r}}, \quad (12.60)$$

so that

$$K = \frac{m}{2} [(u + r_{\perp} \Omega)^2 + v^2 + w^2], \quad (12.61)$$

where $r_{\perp} = r \cos \phi$. Additionally, as discussed in Section 12.6, the axial angular momentum is given by

$$L^z = m r_{\perp} (u + r_{\perp} \Omega) \equiv m l^z, \quad (12.62)$$

and this property is a constant of the motion when there is azimuthal (zonal) symmetry. It is thus convenient to write the kinetic energy as

$$K = \frac{m}{2} \left[(l^z / r_{\perp})^2 + v^2 + w^2 \right]. \quad (12.63)$$

Geopotential expression for mechanical energy

As seen in Section 12.8.4, the conserved form of the mechanical energy using geopotential coordinates takes on the form

$$M_{\text{geop}} = \frac{m}{2} [u^2 + v^2 + w^2 + 2 g r], \quad (12.64)$$

where each of these symbols takes on their geopotential interpretation.

12.8.2 Planetary Cartesian mechanical energy

The time derivative of the kinetic energy is given by

$$\frac{dK}{dt} = m \mathbf{V} \cdot \frac{d\mathbf{V}}{dt} = m \mathbf{V} \cdot \mathbf{A} = -m \mathbf{V} \cdot \nabla \Phi_e. \quad (12.65)$$

For the final equality we introduced the gravitational potential given that the particle only feels an external force from gravity as per equation (11.122). The gravitational potential is given by (see equation (11.116))

$$\Phi_e = g_e r, \quad (12.66)$$

so that

$$\frac{dK}{dt} = -m \mathbf{V} \cdot \nabla \Phi_e = -m g_e \dot{r}. \quad (12.67)$$

This result means that kinetic energy is reduced when moving the particle away from the earth center ($\dot{r} > 0$). Moving away from the earth requires work to overcome the gravitational acceleration pointing towards the earth. This work to overcome the gravitational attraction is taken away from the kinetic energy of the particle. Furthermore, the work is added to the gravitational potential energy, whose evolution is given by (see equation (11.118))

$$\frac{dP_e}{dt} = m g_e \dot{r}, \quad (12.68)$$

where we assumed a constant gravitational acceleration g_e . Consequently, as the particle moves away from the earth center, its reduction in kinetic energy is exactly compensated by an increase in potential energy. Hence, the mechanical energy for the particle remains constant throughout the motion

$$\frac{d(K + P_e)}{dt} = 0, \quad (12.69)$$

where the mechanical energy is the sum of the inertial kinetic energy plus the gravitational potential energy

$$M = K + P_e \quad (12.70a)$$

$$= \frac{m}{2} \mathbf{V} \cdot \mathbf{V} + m \Phi_e \quad (12.70b)$$

$$= \frac{m}{2} [(u + r_\perp \Omega)^2 + v^2 + w^2] + m g_e r \quad (12.70c)$$

$$= \frac{m}{2} [(l^z/r_\perp)^2 + v^2 + w^2] + m g_e r. \quad (12.70d)$$

12.8.3 Planetary spherical mechanical energy

It is physically revealing to expose the exchange of mechanical energy between kinetic and gravitational potential energies. Furthermore, knowledge of the total mechanical energy at any time affords knowledge for all time since the mechanical energy (in the absence of dissipation) remains constant. Following from the discussion in Section 12.7, where we examined the constraints on particle motion due to conservation of axial angular momentum, we here ask similar questions about mechanical energy conservation. We make use of the spherical form of the equations of motion, equations (11.131)-(11.133), which expose the planetary centrifugal and Coriolis accelerations, and pursue the calculation for geopotential coordinates in Section 12.8.4.

We find it convenient to write the momentum equations (11.131)-(11.133) in terms of the

distance to the polar axis, $r_{\perp} = r \cos \phi$, and its time derivative, $\dot{r}_{\perp} = w \cos \phi - v \sin \phi$

$$\frac{d}{dt} [r_{\perp} u + \Omega r_{\perp}^2] = 0 \quad (12.71a)$$

$$\dot{v} = -\frac{v w}{r} - \frac{u \tan \phi}{r} (u + 2 \Omega r_{\perp}) - r_{\perp} \Omega^2 \sin \phi \quad (12.71b)$$

$$\dot{w} = \frac{u^2 + v^2}{r} + 2 \Omega u \cos \phi + r_{\perp} \Omega^2 \cos \phi - g_e. \quad (12.71c)$$

Equation (12.71a) expresses the conservation of axial angular momentum, $\dot{l}^z = 0$, where the axial angular momentum per mass is $l^z = r_{\perp} (u + r_{\perp} \Omega)$ (Section 12.6). For the mechanical energy, we have

$$\dot{M} = 0 \quad \text{with} \quad M = \frac{m}{2} [(l^z/r_{\perp})^2 + v^2 + w^2] + m g_e r, \quad (12.72)$$

where $l^z/r_{\perp} = u + r_{\perp} \Omega$ is the zonal component to the inertial velocity (equation (11.47f)). We now show that $\dot{M} = 0$ arises from the momentum equations. Performing the time derivative, and setting $dl^z/dt = 0$, leads to

$$\frac{1}{m} \dot{M} = \frac{1}{2} \frac{d}{dt} [(l^z/r_{\perp})^2 + v^2 + w^2 + 2 g_e r] = -\frac{(l^z)^2 \dot{r}_{\perp}}{(r_{\perp})^3} + v \dot{v} + w (\dot{w} + g_e). \quad (12.73)$$

Use of the meridional momentum equation (12.71b) renders

$$v \dot{v} = -v \left[\frac{v w}{r} + \frac{u \tan \phi}{r} (u + 2 \Omega r_{\perp}) + r_{\perp} \Omega^2 \sin \phi \right] \quad (12.74a)$$

$$= -\frac{v^2 w}{r} - \frac{v \tan \phi}{r} (u + r_{\perp} \Omega)^2. \quad (12.74b)$$

Likewise, the vertical momentum equation (12.71c) renders

$$w (\dot{w} + g_e) = \frac{v^2 w}{r} + \frac{w}{r} [u^2 + 2 \Omega u r_{\perp} + (r_{\perp} \Omega)^2] \quad (12.75a)$$

$$= \frac{v^2 w}{r} + \frac{w}{r} (u + r_{\perp} \Omega)^2, \quad (12.75b)$$

so that

$$v \dot{v} + w (\dot{w} + g_e) = r^{-1} (-v \tan \phi + w) (u + r_{\perp} \Omega)^2 = \frac{(l^z)^2 \dot{r}_{\perp}}{(r_{\perp})^3}. \quad (12.76)$$

Combining this result with equation (12.73) leads to the expected $\dot{M} = 0$, so that angular momentum conservation combined with the meridional and vertical momentum equations is equivalent to mechanical energy conservation.

12.8.4 Geopotential mechanical energy

Now consider the mechanical energy conservation when using geopotential coordinates with the equations of motion (11.137a)-(11.137c)

$$\dot{u} + \frac{u(w - v \tan \phi)}{r} + 2\Omega(w \cos \phi - v \sin \phi) = 0 \quad (12.77a)$$

$$\dot{v} + \frac{v w + u^2 \tan \phi}{r} + 2\Omega u \sin \phi = 0 \quad (12.77b)$$

$$\dot{w} - \frac{u^2 + v^2}{r} - 2\Omega u \cos \phi = -g. \quad (12.77c)$$

Multiplying each equation by its respective velocity component and summing yields

$$\frac{1}{m} \dot{M}_{\text{geop}} = \frac{1}{2} \frac{d}{dt} [u^2 + v^2 + w^2 + 2gr] = 0. \quad (12.78)$$

The conserved mechanical energy for the particle written in geopotential coordinates

$$M_{\text{geop}} = m(u^2 + v^2 + w^2)/2 + m gr \quad (12.79)$$

is compared to that written using spherical coordinates in equation (12.72). We note that since the coordinates are different (spherical versus geopotential), the velocity components (u, v, w) are slightly different in the two coordinate systems, as is the radial position.

12.9 Sample particle trajectories

Here we examine some relatively simple trajectories to illustrate how the dynamical properties discussed in this chapter, particularly angular momentum conservation, help to determine trajectories. The discussion complements that considered in Exercise 11.8.

12.9.1 Free fall from rest in inertial frame

A particle freely falling to the center of the sphere has a trajectory determined by the spherical equations

$$u = -r_\perp \Omega \quad \text{and} \quad v = 0 \quad \text{and} \quad \dot{w} = -g_e \implies w = -g_e t + w_0. \quad (12.80)$$

A zonal velocity of $u = -r_\perp \Omega$ (to the west) means that the particle has zero zonal inertial velocity; i.e., the particle has a fixed longitude in absolute space. It also means there is zero axial angular momentum, $l^z = 0$. To verify that axial angular momentum remains zero, note that

$$\dot{l}^z = 0 \implies \dot{u} r_\perp = -\dot{r}_\perp (u + 2\Omega r_\perp), \quad (12.81)$$

which is satisfied since $u = -r_\perp \Omega$ means that $\dot{u} = -\dot{r}_\perp \Omega$. Furthermore, note that the zonal acceleration is given by

$$\ddot{u} = -\Omega \dot{r}_\perp = -\Omega(w \cos \phi - v \sin \phi) = -\Omega w \cos \phi = (\Omega g_e \cos \phi) t > 0, \quad (12.82)$$

where we assumed the particle is released with $w_0 = 0$. As the particle falls, and thus reduces its distance from the polar axis, it zonally accelerates with $\ddot{u} > 0$ to maintain zero angular momentum. This acceleration slows the particle's relative speed, which is expected since $u = -r_\perp \Omega$ means

the relative zonal velocity goes to zero as the particle approaches the axis of rotation.

12.9.2 Free fall with constant zonal velocity

Now consider a trajectory, again using spherical coordinates, with a constant zonal velocity, in which case $\dot{u} = 0$ so that the angular momentum equation (12.71a) leads to

$$\dot{r}_\perp (u + 2\Omega r_\perp) = 0. \quad (12.83)$$

There are two ways to satisfy this constraint, one being to set $u = -2\Omega r_\perp$. We here choose to instead examine the case with a fixed moment-arm,

$$\dot{r}_\perp = 0 \implies w \cos \phi = v \sin \phi. \quad (12.84)$$

This relation couples vertical and meridional motion in a manner that keeps the distance to the rotational axis fixed. For example, if the particle is falling towards the earth center so that $w \cos \phi < 0$, then there is an equatorward meridional velocity to keep the distance from the rotational axis fixed. In this manner, the particle is freely falling not towards the earth center but instead towards the equatorial plane, all while maintaining a fixed zonal velocity with $\dot{u} = 0$.

Use of the relation (12.84) between v and w leads to the meridional acceleration

$$r_\perp \dot{v} = -v w \cos \phi - u \sin \phi (u + 2\Omega r_\perp) - (r_\perp \Omega)^2 \sin \phi = -\sin \phi [v^2 + (l^z/r_\perp)^2], \quad (12.85)$$

which is negative in the northern hemisphere and positive in the southern; i.e., it is always directed to lower latitudes. Similarly, the vertical momentum equation leads to

$$r (\dot{w} + g_e) = v^2 + (l^z/r_\perp)^2 > 0, \quad (12.86)$$

which is always positive, meaning the vertical acceleration is always dominated by the earth's gravitational acceleration. Finally, the meridional and vertical accelerations are related by

$$\dot{v} \cos \phi + (\dot{w} + g_e) \sin \phi = 0. \quad (12.87)$$

When the particle reaches the equator at $\phi = 0$, both the meridional acceleration and the vertical velocity vanish. In contrast, at the poles where $\phi = \pm\pi/2$, the vertical acceleration is $\dot{w} = -g_e$ whereas the meridional velocity vanishes.

12.9.3 Free fall from rest in rotating frame

We here consider the case of a particle initially at rest in the rotating reference frame that is allowed to freely fall. As in Exercise 11.8(B), we make use of geopotential coordinates since the particle will initially fall parallel to the effective gravity direction; i.e., the *plumb line*. We consider the trajectory just in the zonal and vertical plane, assuming $v = 0$ throughout the free fall. Setting $v = \dot{v} = 0$ in the geopotential coordinate equations of motion (11.137a) and (11.137c) yields

$$\dot{u} + \frac{u w}{r} + 2\Omega w \cos \phi = 0 \quad (12.88a)$$

$$\dot{w} - \frac{u^2}{r} - 2\Omega u \cos \phi = -g. \quad (12.88b)$$

We now linearize by dropping the uw/r and u^2/r terms to render

$$\dot{u} = -2\Omega w \cos \phi \quad (12.89a)$$

$$\dot{w} = 2\Omega u \cos \phi - g. \quad (12.89b)$$

We can write $w = w_0 + w_1$, where

$$\dot{w}_0 = -g \quad \text{and} \quad \dot{w}_1 = 2\Omega u \cos \phi, \quad (12.90)$$

so that $w_0 = -gt$. To first order in Ω , the zonal velocity satisfies

$$\dot{u} = 2\Omega gt \cos \phi \implies u = \Omega gt^2 \cos \phi. \quad (12.91)$$

We are thus left with the free fall particle velocity valid to first order in Ω

$$\mathbf{v} = (\Omega gt^2 \cos \phi) \hat{\mathbf{\Lambda}} - gt \hat{\mathbf{r}}. \quad (12.92)$$

The eastward velocity component arises from the need for the particle to conserve axial angular momentum as it falls closer to the polar axis.

12.10 Summary of the dynamical constraints from spatial symmetries

We close this chapter by summarizing the conservation laws described here that arise from spatial symmetries. These conservation laws complement the discussion in Section 12.8 for mechanical energy conservation arising from time symmetry.

12.10.1 Linear momentum conservation

As seen in Section 10.1.1, linear momentum remains constant for a particle moving without any forces acting on it; i.e., a *free particle*. This type of motion is not common for geophysical particles or fluids since they feel gravity and so are not free. Even so, we consider this limiting case as a point of comparison for the other conservation laws.

The conservation of linear momentum is simply viewed within the particle's inertial reference frame, where a vanishing inertial acceleration leads to a constant inertial velocity

$$\mathbf{A} = d\mathbf{V}/dt = 0. \quad (12.93)$$

In a Euclidean space, a vanishing acceleration means the particle is moving in a straight line with constant velocity. When viewed from a rotating frame using Cartesian coordinates, a vanishing inertial acceleration means that the Cartesian acceleration balances Coriolis and centrifugal accelerations

$$\ddot{\mathbf{X}} = -2\boldsymbol{\Omega} \times \dot{\mathbf{X}} - \nabla \Phi_{\text{centrifugal}}. \quad (12.94)$$

This equation is clearly not a very useful means to describe unaccelerated free particle motion. We can provide a bit more compactness to this equation by introducing the potential momentum (12.7) so that

$$d\mathbf{M}/dt = -\nabla \Phi_{\text{centrifugal}}. \quad (12.95)$$

While the inertial acceleration vanishes ($\mathbf{A} = d\mathbf{V}/dt = 0$), time changes to the potential momentum are balanced by the gradient of the centrifugal potential.

12.10.2 Potential momentum conservation

Conservation of potential momentum arises from symmetry of particle motion on a constant geopotential surface. The conservation law is most readily viewed within the rotating frame, whereby (equation (12.9))

$$\frac{d(\hat{s} \cdot \mathbf{M})}{dt} = 0. \quad (12.96)$$

A geopotential is a two-dimensional surface so that this conservation law corresponds to two dynamical constraints such as shown in Figure 12.1.

12.10.3 Angular momentum conservation

As detailed in Section 12.6, the angular momentum computed with respect to the axis of rotation is a constant of the motion (Figure 12.3). This conservation law arises from rotational symmetry of the system about the rotational axis. Axial (z -axis) angular momentum conservation takes the form

$$dL^z/dt = 0, \quad (12.97)$$

where the axial angular momentum is

$$L^z = m r_{\perp}^2 (\dot{\lambda} + \Omega) \quad \text{with} \quad r_{\perp} = \sqrt{x^2 + y^2} = r \cos \phi. \quad (12.98)$$

The distance from the rotation axis, r_{\perp} , is the *moment arm* for the axial angular momentum. The longitude, λ , measures the angle in the counter-clockwise direction from the positive x -axis, and $\dot{\lambda}$ is the time change of the longitude.



12.11 Exercises

EXERCISE 12.1: NEGATIVE AXIAL ANGULAR MOMENTUM

In Section 12.7 we assume the axial angular momentum is positive, which is geophysically the common situation since axial angular momentum from the solid-body motion is so large relative to motion of geophysical fluids. But let us consider the uncommon case where the particle moves zonally westward at a speed greater than the planetary rotation speed so that

$$\dot{\lambda} + \Omega < 0 \iff u + \Omega r_{\perp} < 0, \quad (12.99)$$

which means the axial angular momentum per mass of the particle is negative

$$l^z = r_{\perp} (u + r_{\perp} \Omega) = -|l^z| < 0. \quad (12.100)$$

Throughout this exercise we seek answers based on conservation of axial angular momentum. When checking to see whether an answer agrees with common sense, be careful since motion of this sort is not commonly experienced by terrestrial observers. Correspondingly, it is useful to check answers by viewing the motion from the perspective of an inertial reference frame rather than the rotating terrestrial reference frame. For example, the particular case where $\dot{\lambda} = -\Omega$, in which case the particle has zero angular momentum, corresponds to a particle that is stationary in the inertial reference frame while the planet rotates underneath.

- (A) Discuss what happens to $\delta\dot{\lambda}$ for the particle that is deflected poleward poleward with con-

stant radius while conserving axial angular momentum. Hint: consider the first form of equation (12.33).

- (B) Discuss what happens to δu for the particle as it is deflected poleward with constant radius while conserving axial angular momentum. Separately discuss the three cases where

- (i) $|l^z| = 0$
- (ii) $|l^z| < \Omega r_{\perp}^2$.
- (iii) $|l^z| > \Omega r_{\perp}^2$

Hint: consider the second form of equation (12.33).

- (C) Is fluid particle motion with $u + \Omega r_{\perp} < 0$ relevant for the terrestrial atmosphere and ocean? Why? To help answer this question, what is Ωr_{\perp} for $\phi = \pi/4$ and $r = R_e$? Note, we already provided the result for the equator just after equation (12.30). Compare these speeds to that of a category 5 tropical cyclone (Google it).



Part III

Fluid kinematics

In this part of the book we move from the discrete particle mechanics studied in Part II to now focus on continuous fluid media. We motivate the study of continuous media in Chapter 13 by noting the huge space and time scale separation between molecular motions and the motion of macroscopic fluid elements. Thereafter we develop kinematics for classical non-relativistic fluid flow. Quite conveniently, key kinematic properties of non-rotating flows also hold for the fluid flow on steady rotating planets such as considered in this book. The reason is that steady solid-body rotation does not directly impart any strain to the flow, where strain refers to the relative motion between fluid elements (Chapter 14). Rotation does impart a planetary component to the vorticity of geophysical fluids, with implications for our study of vorticity in Part VII. However, for the purpose of fluid kinematics studied in this part of the book, we can ignore planetary rotation.

EULERIAN AND LAGRANGIAN REFERENCE FRAMES

The *Eulerian and Lagrangian reference frames* provide dual kinematic descriptions of fluid flows. The Eulerian frame describes fluid motion relative to a frame fixed in the laboratory whereas the Lagrangian frame follows a moving fluid particle. The Eulerian frame is inertial (when the laboratory is not accelerating), whereas the Lagrangian is non-inertial since fluid particles generally accelerate. Having two descriptions of the same motion provides a synergy that is missing with either alone. We require skills to move between the Eulerian and Lagrangian descriptions, with tools from mathematical transformation theory of Part I used for this purpose. Elements of Eulerian and Lagrangian kinematics are the focus of Chapter 14, and Chapter 15 further develops the kinematics of material lines, areas, and volumes.

We acknowledge that for most flows encountered in geophysical fluid mechanics, a Lagrangian description has severe practical limitations. These limitations arise from the chaotic and turbulent nature of the flow that render a description based on fluid particle trajectories of little use after even a brief time. Nevertheless, Lagrangian formulations offer deep insights to the fundamental theorems of fluid mechanics, thus motivating us to study and to use Lagrangian kinematics in this book.

MASS AND MATTER CONSERVATION ARE PART OF FLUID KINEMATICS

The conservation of mass plays a central role in physics. For fluids, mass conservation constrains the flow regardless what forces act on the fluid. Hence, we include mass conservation as a part of fluid kinematics rather than fluid dynamics. Mass conservation, and its expression as volume conservation for incompressible flows, are the topics of Chapters 16 and 18. Chapter 17 develops the allied study of matter conservation and matter flow, with this study forming the foundations for *tracer mechanics* that we return to in earnest within Part XII in this book.

FLUID KINEMATICS + FLUID DYNAMICS = FLUID MECHANICS

Kinematics is concerned with the intrinsic properties of motion, including properties of the space and time in which motion occurs. It is the complement to dynamics, which is concerned with the causes of motion that arise through the action of forces. In one sense, kinematics deduces the acceleration whereas dynamics deduces the forces, with Newton's second law linking the two via the equation of motion: $\mathbf{F} = m \mathbf{a}$. In fluid mechanics, kinematics studies the flow of a fluid and its matter constituents, whereas dynamics studies the forces causing the motion. Furthermore, as discussed in Chapter 12, symmetries of a mechanical system lead, through Noether's Theorem, to dynamical conservation laws. That is, symmetries, which embody kinematic properties, lead to dynamical invariants maintained by the motion, with these invariants constraining the motion.

The intellectual avenues pursued in developing a mechanical description of fluid motion are many and varied, with fluid kinematics and fluid dynamics intimately woven into the fabric of that description.

Chapter 13

CONTINUUM APPROXIMATION

In any study of fluid motion, we start by understanding the nature of the fluid media. Viewed macroscopically, a fluid deforms continuously when applying a force so that a fluid has no preferred shape. Correspondingly, a fluid responds to a shearing stress by moving. Ordinary gases and liquids are canonical examples of fluids, with gases filling any container with its molecules widely separated whereas molecules in liquids are much closer together so that liquids are far less compressible than gases.

For geophysical fluid mechanics, we are concerned with the atmosphere (mostly a gas) and the ocean (mostly a liquid). We are furthermore interested in macroscopic properties of fluid motion, with no interest in describing molecular degrees of freedom. Nor do we consider rarefied gas dynamics, which is a subject appropriate for the upper bounds of the atmosphere where pressures are extremely low and the molecular mean free path relatively large. For these reasons we pursue a phenomenological approach that makes use of conservation laws describing the motion of a continuous fluid media. This treatment is based on the *continuum approximation*, which assumes that mathematical limits for fluid volumes tending to zero are reached on length and time scales very large compared to molecular scales.¹ The temporal version of the continuum approximation corresponds to *quasi-static processes*, which forms the basis for our study of quasi-equilibrium thermodynamics in Part IV of this book. Quasi-static processes refer to macroscopic motion that evolves with time scales far larger than time scales of molecular motions, so that when treated thermodynamically a fluid element evolves smoothly from one local thermodynamic equilibrium state to another.

The huge space and time scale separation that supports the continuum approximation allows us to make use of differential calculus for describing the mechanics of fluid motion. That is, the continuum approximation makes fluid mechanics a continuous field theory. Correspondingly, the conservation laws describing fluid motion are partial differential equations and whose finite volume expression are integral equations.

READER'S GUIDE TO THIS CHAPTER

This chapter presents salient points supporting our use of a space and time continuous description of fluid mechanics. Section 13.2 summarizes the key results and Section 13.3 provides a bit more detail by quoting from kinetic theory. Our overall goal here is to unpack the dictum *macroscopically small yet microscopically large*, which summarizes the regime considered by the continuum approximation and the quasi-static approximation. For this purpose, we borrow from the kinetic theory of gases as treated in statistical physics books such as [Reif \(1965\)](#) and [Huang \(1987\)](#). Chapter 1 of [Salmon \(1998\)](#) also provides a compelling discussion with

¹The continuum approximation used for continuum mechanics is not to be confused with the *continuum hypothesis* found in mathematical set theory.

application to geophysical fluid mechanics. No prior exposure to these treatments is necessary nor do we dive into the details.

13.1	Loose ends	270
13.2	A variety of length scales	270
13.2.1	Molecular and macroscopic length scales	270
13.2.2	Continuous fields rather than discrete molecules	271
13.2.3	Reynolds number and the continuum length scale	272
13.2.4	Resolution of measurements and simulations	273
13.2.5	Comments	274
13.3	Results from kinetic theory	274
13.3.1	A mole and Avogadro's number	274
13.3.2	Ideal gas law	274
13.3.3	Molecular mean free path	275
13.3.4	Root mean square molecular speed	276
13.3.5	Basis for the quasi-static approximation	276
13.3.6	Macroscopically small and microscopically large	277
13.3.7	Whence a rigorous treatment?	277
13.3.8	Further study	278

13.1 Loose ends

- Add a figure for Section 13.2.4.
- Can one be more precise about the scale in Figure 13.2 where measurements become fuzzy?

13.2 A variety of length scales

Matter is comprised of molecules. However, fluid mechanics is not concerned with the motion of individual molecular degrees of freedom. Rather, fluid mechanics is concerned with phenomenological conservation laws satisfied by a continuous fluid material. This approach represents an idealization that is supported by centuries of successful descriptions of macroscopic fluid motion.

We here outline the essential features of the continuum approximation. This approximation supports our macroscopic description of a fluid in terms of continuous fields rather than discrete molecules. More details are offered in Section 13.3, although a full discussion is outside the subject of fluid mechanics, instead resting deep within the field of statistical physics and kinetic theory.

13.2.1 Molecular and macroscopic length scales

A fluid mechanical description focuses on fluid regions that are macroscopically small (e.g., $L_{\text{macro}} \sim 10^{-3}$ m) yet microscopically large (e.g., $L_{\text{macro}} \gg L_{\text{mfp}} \sim 10^{-7}$ m, where L_{mfp} is the molecular mean free path). A region of air with volume L_{macro}^3 contains roughly 10^{16} air molecules at standard temperature ($T_{\text{stand}} = 0^\circ\text{C} = 273.15$ K) and standard atmospheric pressure ($p_{\text{stand}} = 101.325 \times 10^3$ Pa), whereas that same volume contains roughly 10^{19} water molecules. These numbers (justified in Section 13.3) illustrate the notions of macroscopically small yet microscopically large. It is only when reaching length scales on the order of the molecular mean free path that we need to be concerned with the discrete nature of matter. Figure 13.1 offers a schematic to illustrate these quite distinct length scales.

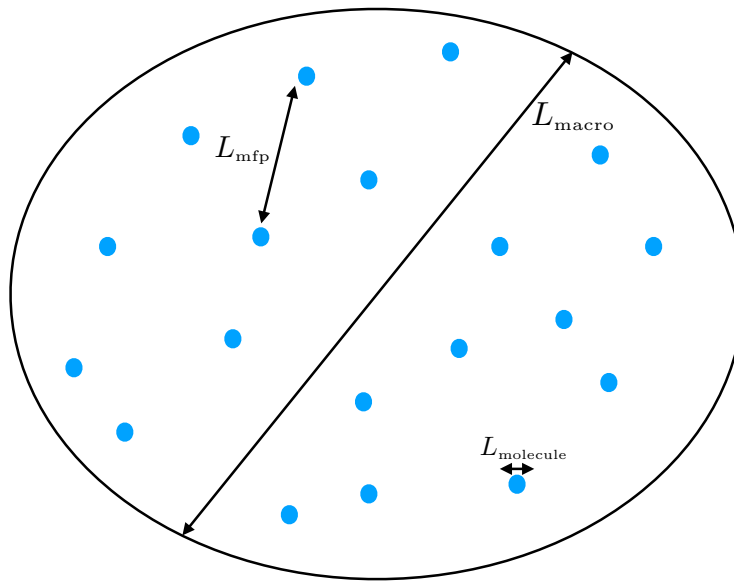


FIGURE 13.1: Schematic to illustrate the three length scales considered when making the continuum approximation. The blue circles represent molecules with diameter L_{molecule} . On average, molecules are separated by the mean free path, $L_{\text{mfp}} \approx 1000 L_{\text{molecule}}$. The smallest macroscopic length scale of interest for fluid mechanics is $L_{\text{macro}} \sim 10^{-3}$ m, which is roughly $L_{\text{macro}} = 10^4 L_{\text{mfp}}$ for an ideal gas at standard conditions. A region of air with volume L_{macro}^3 contains roughly 10^{16} air molecules, whereas that same volume contains roughly 10^{19} water molecules. For either case, the Law of Large Numbers greatly helps in taking the continuum limit. Note that this schematic is not drawn to scale!

The huge number of molecules within a macroscopically tiny region justifies our assumption that physical properties are homogeneous over regions of size L_{macro} . In essence, this *continuum approximation* works with small but finite sized fluid elements whose mean dynamical properties (e.g., velocity, vorticity) and thermodynamical properties (e.g., mass density, matter concentration, temperature, specific entropy) are defined locally at any point within the continuous fluid media.

13.2.2 Continuous fields rather than discrete molecules

When measured on length scales of the mean free path, material properties exhibit very large fluctuations on time scales of order $L_{\text{mfp}}/v_{\text{rms}}$, where v_{rms} is the root-mean-square speed of a fluid molecule (see Section 13.3.4). However, on macroscopic scales encompassing many molecular degrees of freedom, fluid matter appears continuous in both space and time.

Let us be a bit more precise by considering the measurement of mass density for a prescribed region of fluid, δV . To compute the mass density we simply take the ratio of the mass of fluid in the region, δm , to the region volume. When the region volume is sizable and thus containing many molecules, we can maintain a relatively fixed mass since molecular fluctuations have a relatively tiny effect on δm . Hence, we can maintain a precise measurement of the mass density, $\delta m/\delta V$. However, when the volume of the region reaches down to the order of $\delta V \sim L_{\text{mfp}}^3$, then molecular fluctuations lead to a relatively large fluctuation in the region mass. We thus lose the notion of a smooth and continuous mass density when the volume approaches that set by the molecular mean free path. This situation is depicted in Figure 13.2.

The ratio of the mean free path to the macroscopic length scale is known as the Knudsen number

$$\text{Kn} = \frac{L_{\text{mfp}}}{L_{\text{macro}}}. \quad (13.1)$$

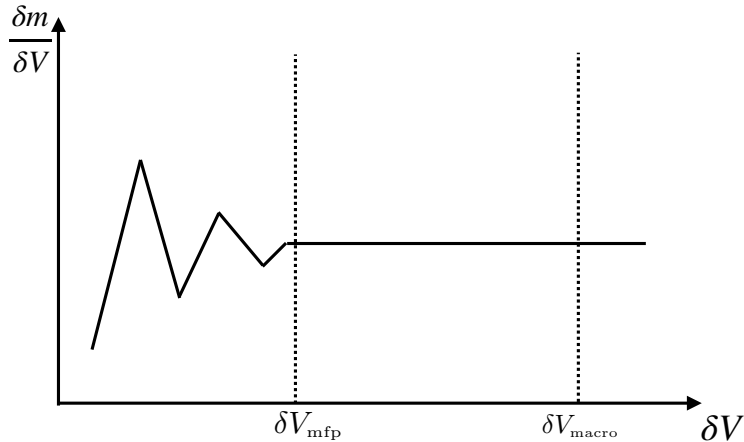


FIGURE 13.2: The measurement of mass density of a fluid becomes erratic for volumes smaller than that determined by the molecular mean free path, $\delta V_{\text{mfp}} \sim L_{\text{mfp}}^3$. For fluid mechanics we are concerned with macroscopic length scales much larger than the mean free path, $L_{\text{macro}} \gg L_{\text{mfp}}$, in which case the density is a smooth function of space and time. This figure is adapted from Figure 1.2.1 of [Batchelor \(1967\)](#).

For our purposes, we are concerned only with fluid conditions where the mean free path is microscopic so that the Knudsen number is tiny

$$\text{Kn} \ll 1. \quad (13.2)$$

For tiny Knudsen numbers, we are led to make use of the continuum approximation. The continuum approximation allows us to employ fluid properties that take values at each point within a space and time continuum, (\mathbf{x}, t) . For example, we make use of the mass density, $\rho(\mathbf{x}, t)$, fluid velocity, $\mathbf{v}(\mathbf{x}, t)$, pressure $p(\mathbf{x}, t)$, temperature $T(\mathbf{x}, t)$, tracer concentration, $C(\mathbf{x}, t)$, and other thermodynamic fields.

We contrast the above to the study of a rarefied gas, such as in the outer reaches of the earth's atmosphere. With a relatively small number density of molecules, rarefied gases have macroscopic mean free paths so that there are relatively few molecular collisions in a given time increment. Correspondingly, a rarefied gas is far from thermodynamic equilibrium and the continuum approximation is not well suited to its description.

13.2.3 Reynolds number and the continuum length scale

The continuum field equations of fluid mechanics are formally established for fluid motions with length scales on the order of L_{macro} and larger. We stated earlier that L_{macro} is on the order of a millimetre, with that length loosely based on noting that there are a huge number of molecules in a volume with this size. Furthermore, most macroscopic measurements in a fluid cannot distinguish features much smaller than a millimetre. We here describe another means to determine this length scale.

Namely, we set L_{macro} to the length scale at which the Reynolds number is order unity

$$\text{Re}_{\text{macro}} = \frac{U L_{\text{macro}}}{\nu} \sim 1. \quad (13.3)$$

In this equation, $\nu > 0$ is the kinematic viscosity (dimensions squared length per time), and U is the scale for a macroscopic fluid velocity fluctuation. The Reynolds number measures the ratio of inertial accelerations (accelerations felt by fluid elements) to frictional accelerations from viscous forces (forces due to the rubbing of fluid elements against one another in the presence of viscosity).

We provide more details concerning the Reynolds number when studying fluid stresses in Chapter 22. For present purposes, we note that when the Reynolds number is on the order of unity, viscous forces play a leading role in the acceleration of the fluid. In particular, it is at this scale that viscous accelerations act to dissipate kinetic energy, with this dissipation an important process in fluid turbulence. We are thus motivated to let the length scale where viscosity is important determine L_{macro} .

The kinematic viscosity is the ratio of the *dynamic viscosity* and the mass density. For air, the kinematic viscosity is (page 75 of [Gill \(1982\)](#))

$$\nu_{\text{air}} = \frac{1.7 \times 10^{-5} \text{ kg m}^{-1} \text{ s}^{-1}}{1.3 \text{ kg m}^{-3}} = 1.3 \times 10^{-5} \text{ m}^2 \text{ s}^{-1}, \quad (13.4)$$

and a typical fluid velocity fluctuation has a scale 10^{-1} m s^{-1} , so that

$$L_{\text{macro}} \approx 10^{-4} \text{ m} = 0.1 \text{ mm}. \quad (13.5)$$

Water has a kinematic viscosity (page 75 of [Gill \(1982\)](#))

$$\nu_{\text{water}} = \frac{10^{-3} \text{ kg m}^{-1} \text{ s}^{-1}}{1000 \text{ kg m}^{-3}} \approx 10^{-6} \text{ m}^2 \text{ s}^{-1}, \quad (13.6)$$

and a fluid velocity fluctuation about 10 times smaller than air. Hence, the macroscopic length scale for water is on the order of that for air, both of which are roughly 10^{-4} m . The Reynolds number based macroscale length is not too far from the millimetre scale proposed earlier. We are thus further compelled to consider the macroscopic length scale to be on the order $10^{-4} - 10^{-3} \text{ m}$.

13.2.4 Resolution of measurements and simulations

When we measure fluid motions in the laboratory or field, we generally do not measure the motions at scales on the order of L_{macro} . That is, our measurement devices generally have a spatial resolution much coarser than L_{macro} , so that $L_{\text{measure}} \gg L_{\text{macro}}$. Likewise, numerical simulations are generally made with discrete grids with length scales $L_{\text{numerical}} \gg L_{\text{macro}}$. The equations describing motions at the measurement/simulation length scales involve effects from coupled and nonlinear fluctuations occurring at the smaller (unmeasured) scales. These fluctuations, generally associated with turbulent or chaotic motions, have statistical correlations that can play a role, sometimes a dominant role, in the evolution of flow features at the measured/simulated scales. The parameterization of these correlations in terms of measured/simulated motions constitutes the *turbulence closure* problem. We do not study turbulence closure in this book though we do identify the role of turbulence at certain points.

It is important to acknowledge the limited ability of macroscopic measurements to accurately characterize fine scale motions. For this purpose define a gradient length scale

$$L_{\text{gradient}} = \frac{|\boldsymbol{v}|}{|\nabla \boldsymbol{v}|}, \quad (13.7)$$

where \boldsymbol{v} is the velocity of a fluid element relative to some mean velocity, and $|\nabla \boldsymbol{v}|$ is the magnitude of velocity gradients. Decomposing fluctuations into Fourier modes allows us to see that an accurate measurement of velocity fluctuations with length scales L_{gradient} requires a measurement length scale that satisfies

$$2\pi L_{\text{measure}} \leq L_{\text{gradient}}. \quad (13.8)$$

This constraint means that to measure velocity fluctuations on a scale L_{gradient} requires a finer

measurement sampling with $L_{\text{measure}} = L_{\text{gradient}}/(2\pi)$.

13.2.5 Comments

The above discussion of length scales transfers seamlessly over to time scales through dividing the length scale by the velocity scale. Correspondingly, fluctuations with time scales shorter than $2\pi T_{\text{measure}}$ cannot be accurately measured.

13.3 Results from kinetic theory

If the reader is content to accept the continuum approximation on face value, then the material in this section can be readily skipped. For others, this section outlines results from the kinetic theory of ideal gases in support of the continuum approximation. Deductive treatments that transition from molecular mechanics to macroscopic fluid mechanics is a topic of the kinetic theory of gases and liquids, which is well outside our scope. In Section 13.3.8, we provide literature pointers for those wishing more rigor.

13.3.1 A mole and Avogadro's number

There are a tremendous number of molecules in the tiniest drop of water or puff of air. Just how many? To answer this question, we introduce the notion of a mole of matter. A mole is defined as the mass of a material substance that contains Avogadro's number of that substance, where

$$A^v = 6.022 \times 10^{23} \text{ mole}^{-1}. \quad (13.9)$$

Avogadro's number, A^v , is the proportionality constant converting from one molar mass of a substance to the mass of a substance. Avogadro's number is conventionally specified so that one mole of the carbon isotope ^{12}C contains exactly 12 grams. Hence, 12 grams of ^{12}C contains 6.022×10^{23} atoms of ^{12}C . Avogadro's number provides a connection between scales active in the microscopic world of molecules to the macroscopic world of everyday experience.

Dry air (air with no water vapor) is comprised of oxygen molecules O_2 , at roughly 22% by molecular mass, and nitrogen molecules N_2 , at roughly 78% molecular mass.² The molar mass of dry air is thus

$$M^{\text{air}} = 0.22 * 32 \text{ g mole}^{-1} + 0.78 * 28 \text{ g mole}^{-1} \approx 28.8 \text{ g mole}^{-1}. \quad (13.10)$$

Pure (fresh) water is comprised of two hydrogen atoms and one oxygen atom. The molar mass of pure water is thus given by

$$M^{\text{water}} = 2 * 1 \text{ g mole}^{-1} + 16 \text{ g mole}^{-1} = 18 \text{ g mole}^{-1}. \quad (13.11)$$

13.3.2 Ideal gas law

The ideal gas law is given by

$$pV = nR^gT, \quad (13.12)$$

²We here ignore the presence of other trace gases, such as CO_2 and H_2O , although these gases are critical for understanding atmospheric radiation and hence the earth's energy budget.

where p is the pressure, V is the volume, n is the number of moles, R^g is the universal gas constant,³ and T is the absolute or thermodynamic temperature (temperature relative to absolute zero). Measuring the temperature in Kelvin leads to the universal gas constant

$$R^g = 8.314 \text{ J mole}^{-1} \text{ K}^{-1} = 8.314 \text{ kg m}^2 \text{ s}^{-2} \text{ mole}^{-1} \text{ K}^{-1}, \quad (13.13)$$

where the second equality replaced the energy unit, Joule, by its MKS equivalent,

$$\text{J} = \text{kg m}^2 \text{ s}^{-2}. \quad (13.14)$$

Use of the ideal gas law (13.12) says that one mole of ideal gas at standard temperature ($T_{\text{stand}} = 0^\circ\text{C} = 273.15 \text{ K}$) and standard atmospheric pressure ($p_{\text{stand}} = 101.325 \times 10^3 \text{ Pa}$) occupies the following volume

$$V = \frac{n R^g T_{\text{stand}}}{p_{\text{stand}}} \quad (13.15a)$$

$$= \frac{(1 \text{ mole})(8.314 \text{ kg m}^2 \text{ s}^{-2} \text{ mole}^{-1} \text{ K}^{-1})(273.15 \text{ K})}{101.325 \times 10^3 \text{ kg m}^{-1} \text{ s}^{-2}} \quad (13.15b)$$

$$\approx 2.25 \times 10^{-2} \text{ m}^3, \quad (13.15c)$$

where we introduced the MKS units for pressure (force per unit area)

$$\text{Pa} = \text{N m}^{-2} = \text{kg m}^{-1} \text{ s}^{-2}. \quad (13.16)$$

Hence, the number density (number of molecules per volume) for a mole of ideal gas is given by

$$n^{\text{gas}} = \frac{\text{number per mole}}{\text{volume per mole}} \quad (13.17a)$$

$$= \frac{A^v}{V} \quad (13.17b)$$

$$= \frac{6.022 \times 10^{23}}{2.25 \times 10^{-2} \text{ m}^3} \quad (13.17c)$$

$$= 2.68 \times 10^{25} \text{ m}^{-3}. \quad (13.17d)$$

Specializing to air, we compute the mass density of air at standard temperature and pressure as

$$\rho^{\text{air}} = \frac{M^{\text{air}}}{V} = \frac{28.8 \times 10^{-3} \text{ kg}}{2.25 \times 10^{-2} \text{ m}^3} = 1.28 \text{ kg m}^{-3}, \quad (13.18)$$

where we set $M^{\text{air}} = 28.8 \times 10^{-3} \text{ kg}$ according to equation (13.10). This ideal gas density is close to the 1.225 kg m^{-3} density measured for air at standard conditions, thus giving us confidence for using the ideal gas law for dry air. Differences arise from trace constituents in air as well as inter-molecular forces (an ideal gas has no inter-molecular forces).

13.3.3 Molecular mean free path

We are in search of length scales relevant for molecular motion. One length scale is that of the molecule itself. Another is set by the distance between molecular collisions. The molecular mean free path is the mean distance that a molecule travels before colliding with another molecule.

³We write R^g rather than the more conventional R to distinguish from R commonly used in this book for the radius of a spherical earth.

Arguments from kinetic theory of gases, applied to an ideal gas, lead to the expression

$$L_{\text{mfp}} = \frac{1}{\pi \sqrt{2} n^{\text{gas}} d^2} \quad (13.19)$$

where d is the diameter of the molecule. The mean diameter of air molecules is roughly

$$d_{\text{molecule air}} \approx 2 \times 10^{-10} \text{ m.} \quad (13.20)$$

Hence, the mean free path for air molecules at standard temperature and pressure is

$$L_{\text{mfp}} = \frac{1}{\pi \sqrt{2} n^{\text{gas}} d_{\text{molecule air}}^2} \quad (13.21a)$$

$$= \frac{1}{\pi \sqrt{2} (2.68 \times 10^{25} \text{ m}^{-3}) (2 \times 10^{-10} \text{ m})^2} \quad (13.21b)$$

$$= 2 \times 10^{-7} \text{ m.} \quad (13.21c)$$

The mean free path for an air molecule is roughly 1000 times larger than the molecular diameter (e.g., Figure 13.1).

13.3.4 Root mean square molecular speed

What is the mean speed for molecules moving through a gas? Again, kinetic theory for ideal gases offers an explicit expression, here written in terms of the pressure and density of the gas

$$v_{\text{rms}} = \sqrt{\frac{3p}{\rho}} = \sqrt{\frac{3R^g T}{M}}. \quad (13.22)$$

Note the direct relation between pressure, temperature, and speed. That is, molecules move faster at higher temperature, and thus impart larger pressure on their surrounding environment. At standard pressure and temperature, the root-mean-square speed for an air molecule is given by

$$v_{\text{rms}} = \sqrt{\frac{3p_{\text{stand}}}{\rho^{\text{air}}}} \quad (13.23a)$$

$$= \sqrt{\frac{3(101.325 \times 10^3 \text{ kg m}^{-1} \text{ s}^{-2})}{1.28 \text{ kg m}^{-3}}} \quad (13.23b)$$

$$= 487 \text{ m s}^{-1}. \quad (13.23c)$$

To get a sense for the relative scale of this speed, note that the speed of sound in air at standard temperature and pressure is 331 m s^{-1} . So these molecules are moving faster than sound! These speeds are correspondingly much higher than the speeds typical for fluid elements in the atmosphere and ocean.

13.3.5 Basis for the quasi-static approximation

Assuming one collision occurs within a mean free path, and the molecules are moving at the root-mean-square speed, we can estimate the time between collision according to

$$t_{\text{collision}} = \frac{L_{\text{mfp}}}{v_{\text{rms}}} \quad (13.24)$$

The corresponding time for air is given by

$$t_{\text{air}} = \frac{2 \times 10^{-7} \text{ m}}{487 \text{ m s}^{-1}} = 4.1 \times 10^{-10} \text{ s.} \quad (13.25)$$

Inverting this number, we see that there are roughly $t_{\text{air}}^{-1} = 2.5 \times 10^9 \text{ s}^{-1}$ collisions per second.

The huge number of collisions per second means that for all macroscopic processes, including geophysical fluid flow, the dynamical time scales for the macroscopic motion are much larger than the time scales for molecular equilibration. We are thus led to define a *quasi-static macroscopic process* as one that occurs through a series of thermodynamic equilibrium states. Consequently, we can use equilibrium thermodynamic relations while allowing for time evolution of the macroscopic system. We have more to say on this topic in Chapter 23 when studying thermodynamics of a moving fluid, with particular emphasis on the implications of the quasi-static approximation presented in Section 19.1.3.

13.3.6 Macroscopically small and microscopically large

For environmental measurements of the atmosphere and ocean, or for conventional measurements in laboratories, we can detect differences in fluid properties (e.g., mass density, velocity, tracer concentration, thermodynamic state properties) for length scales on the order of

$$L_{\text{macro}} = 10^{-3} \text{ m.} \quad (13.26)$$

For macroscopic purposes, fluid properties are homogeneous over regions with length scales on the order of L_{macro} . Although macroscopically rather tiny, a fluid region of volume L_{macro}^3 is huge microscopically. We can see so by computing the number of molecules in this region.

At standard conditions, a volume of air of size L_{macro}^3 contains

$$N_{\text{air molecules}} = V n^{\text{gas}} = (10^{-3} \text{ m})^3 (2.68 \times 10^{25} \text{ m}^{-3}) \approx 3 \times 10^{16} \text{ air molecules.} \quad (13.27)$$

To compute the number of water molecules in this same volume, we first use the water mass density of

$$\rho^{\text{water}} \approx 10^3 \text{ kg m}^{-3} \quad (13.28)$$

to determine the water mass in this region

$$M^{\text{water}} = \rho^{\text{water}} V = (1000 \text{ kg m}^{-3}) (10^{-9} \text{ m}^3) = 10^{-6} \text{ kg.} \quad (13.29)$$

Water has a molar mass of $0.018 \text{ kg mole}^{-1}$, so a volume of $(10^{-3} \text{ m})^3$ contains⁴

$$N_{\text{water molecules}} = \left(\frac{10^{-6} \text{ kg}}{0.018 \text{ kg mole}^{-1}} \right) \times 6.022 \times 10^{23} \text{ molecules mole}^{-1} = 3 \times 10^{19} \text{ water molecules.} \quad (13.30)$$

Water thus has roughly 10^3 more molecules in this volume than air at standard pressure, which reflects the roughly 10^3 times larger mass density for water. Regardless, both water and air contain a huge number of molecules in this macroscopically tiny region.

13.3.7 Whence a rigorous treatment?

A rigorous derivation of continuum field theory, starting from molecular dynamics, is nontrivial even for an ideal gas, and largely non-existent for liquids. Indeed, some say a Nobel Prize awaits

⁴The calculation on page 9 of [Griffies \(2004\)](#) has a factor of 10^6 error.

the person providing a fully deductive theory. For our purpose, we remain satisfied to postulate that a continuum description is suited for fluid mechanics of the atmosphere and ocean. A means for evaluating this postulate is to perform experimental measures and compare to the continuum theory. Centuries of experiments with fluid motions in the environment and laboratory lend credence to the continuum description. We consider these tests to be sufficient motivation to pursue the continuum approach for fluid mechanics and geophysical fluid dynamics.

13.3.8 Further study

Pedagogical treatments of the ideal gas law and kinetic theory can be found in most books on introductory physics or chemistry. [Vallis \(2017\)](#) provides extensions of the ideal gas law for an atmosphere with moisture.

For discussions of the continuum approximation reflecting that given here, see the discussion on page 1 of [Olbers et al. \(2012\)](#), or the more thorough treatments given in Section 1.2 of [Batchelor \(1967\)](#) and Section 1.4 of [Kundu et al. \(2016\)](#). Chapter 1 of [Salmon \(1998\)](#) offers an even more thorough treatment, touching on elements from kinetic theory and details for how to coarse grain average over molecular degrees of freedom (see his pages 3 and 4 and Sections 9, 10, and 11). A rigorous account of kinetic theory is offered in many treatments of statistical mechanics. That given by [Reif \(1965\)](#) and [Huang \(1987\)](#) are accessible to those with a physics undergraduate training. When reading the statistical mechanics literature, look for discussions of the “hydrodynamical limit,” which concerns the transition from discrete particle mechanics to continuum mechanics.



Chapter 14

FUNDAMENTALS OF FLUID KINEMATICS

Fluid motion is very complex and it is useful to access more than one means to describe the motion and its constraints. In understanding this motion, we find it useful to view the motion through the dual lenses offered by the Eulerian and Lagrangian reference frames, where the Eulerian frame is fixed in the laboratory and the Lagrangian frame moves with a fluid particle. These dual (fixed versus comoving) descriptions form the foundation for fluid kinematics.

Although the Eulerian frame is more familiar to many, and often the only kinematics needed for many purposes, a Lagrangian description offers insights into the conceptual foundations of the subject. It does so by providing the natural reference frame to formulate dynamical laws given that it follows seamlessly from the formulation of Newtonian point particle mechanics from Part II of this book. The Lagrangian approach also offers deep insights into some of the most important and useful theorems of fluid mechanics. Lagrangian or quasi-Lagrangian methods are also becoming ubiquitous in numerical modeling and are important for certain field and laboratory methods. We thus give attention to the needs of both Eulerian and Lagrangian kinematics in this chapter and elsewhere in this book.

READER'S GUIDE TO THIS CHAPTER

This chapter introduces many concepts and tools used in nearly every subsequent chapter of this book. For simplicity, we assume that spatial positions and fluid particle trajectories are represented using Cartesian coordinates. Even so, we require elements of the tensor analysis from Part I to systematically transform between the Eulerian and Lagrangian descriptions. We review the salient formalism in this chapter to keep the discussion self-contained.

Key references for this chapter include the text by [Salmon \(1998\)](#), who provides an elegant and accessible treatment of Eulerian and Lagrangian fluid mechanics. Chapter 4 of [Aris \(1962\)](#) offers a lucid treatment of fluid kinematics in the context of tensor analysis. Much of the treatment here follows Chapters 1 and 2 of the ocean fluid mechanics book of [Olbers et al. \(2012\)](#).

14.1 Loose ends	280
14.2 Strong and weak formulations	280
14.3 Conceptually partitioning the continuum	281
14.3.1 Fluid particle	281
14.3.2 Material fluid parcel in perfect fluids	282
14.3.3 Finite sized material objects in perfect fluids	283
14.3.4 Fluid elements in real fluids	283
14.3.5 Test fluid element in real fluids	283
14.3.6 Finite sized fluid region in real fluids	284
14.3.7 Comments	284

14.4	Lagrangian and Eulerian reference frames	284
14.5	Material and position coordinates	285
14.5.1	Trajectories of fluid particles	285
14.5.2	Material coordinates	286
14.5.3	Transforming between material and position coordinates	287
14.5.4	The transformation matrix	287
14.5.5	A discrete algorithm to compute the transformation matrix	288
14.5.6	Jacobian of the transformation as the ratio of volumes	290
14.5.7	Further study	291
14.6	Lagrangian and Eulerian time derivatives	291
14.6.1	Infinitesimal space-time increment of a function	291
14.6.2	Total time derivative of a function	291
14.6.3	Eulerian: evolution measured in the laboratory frame	292
14.6.4	Lagrangian: evolution measured in the material frame	292
14.6.5	Lagrangian time derivative formulated from the material frame	293
14.6.6	Sample material time derivative operations	294
14.6.7	Worked example: velocity and acceleration from a trajectory	295
14.6.8	Summarizing some terminology	295
14.7	Galilean invariance	296
14.7.1	Galilean transformation	296
14.7.2	Transformation matrix	296
14.7.3	Transforming the differential operators	297
14.7.4	Comments	298
14.8	Invariance of the material time derivative	298
14.8.1	Invariance based on definition of the material time derivative	298
14.8.2	Invariance for a rotating reference frame	299
14.8.3	Invariance using space-time tensors	301
14.8.4	Comments	301
14.9	Fluid flow lines	301
14.9.1	Material pathlines from fluid particle trajectories	302
14.9.2	Fluid streamlines and streamtubes	302
14.9.3	Distinguishing streamlines and pathlines	303
14.9.4	Fluid streaklines	304
14.9.5	An analytic example of flow lines	305
14.9.6	Further study	306
14.10	Exercises	307

14.1 Loose ends

- Maxey-Riley equations

14.2 Strong and weak formulations

The continuum approximation (Chapter 13) allows us to consider fluid flow from a field theoretic perspective, whereby physical properties are described by fields that take on values at each point of a space and time continuum. Consequently, we make use of a differential equation formulation of the governing fluid equations as well as an integral formulation. The differential equation formulation is sometimes referred to as the *strong* formulation. This name is motivated by the need to make “strong” assumptions about the smoothness of the continuum fields. Without such smoothness assumptions the differential equations lack predictive skill. Even so, some fluid phenomena (e.g., shocks) do not satisfy the necessary smoothness assumptions, thus making the strong formulation unsuitable for their description. The integral formulation is essential for such

non-smooth flows, with the integral formulation known as the *weak* formulation since it requires fewer assumptions about smoothness.

In this book, we are not concerned with shocks or other discontinuities within the fluid continuum, though we do study discontinuities at boundaries. Consequently, we can make use of both the strong and weak formulations. Smooth fluid flows are afforded a connection between the weak and strong formulations through the Leibniz-Reynolds transport theorem derived in Section 17.3.4. Each formulation is suited for particular needs. For example, the strong formulation provides a more concise view of the fluid equations and allows for familiar manipulations/transformations based on the rules of differential calculus studied in Part I. In contrast, the weak formulation is needed to develop budgets over finite fluid regions. Correspondingly, the weak formulation provides a starting point for the derivation of finite volume budgets that serve as the basis for certain numerical methods (e.g., [Griffies et al. \(2020\)](#)).

14.3 Conceptually partitioning the continuum

As part of a continuum description of fluid motion, we make use of conceptual physical systems to frame the mechanics and describe the motion. These physical systems are bounded by imagined partitions that help to organize questions about forces and transport within the continuum, and the partitions can be either open or closed to matter and energy exchange depending on the character of the fluid. There is no pretense that these partitions can be experimentally determined, nor are the fluid systems to be considered discrete molecules or solid objects. Rather, partitions are drawn within the continuum fluid by the theorist for purposes of formulation and conceptualization. We are afforded the ability to draw these partitions through our use of the continuum approach to fluid mechanics.¹

14.3.1 Fluid particle

A *fluid particle* is a zero dimensional mathematical point that follows the fluid flow as specified by the velocity field (left panel in Figure 14.1). Since it has zero spatial extent, a fluid particle has no impact on the flow. Notably, a fluid particle is not a molecule since even a molecule has nonzero spatial extent and impacts surrounding molecules.

The position of a fluid particle in space and time is uniquely specified by its material coordinate plus time (we discuss material coordinates in Section 14.5.1). The trajectory or pathline of a fluid particle is an *integral curve* of the velocity field, where each point along a trajectory has a tangent that is parallel to the velocity vector (Section 14.9).² The accumulation of a continuum of fluid particle trajectories define the pathlines that prescribe the Lagrangian reference frame (Section 14.4).

Fluid particles are directly analogous to *test mass particles* in Newtonian gravitation that are used to map gravitational field lines, and *test electric charges* in electromagnetism used for mapping the electromagnetic field. However, fluid particles have zero mass and are fully defined kinematically through specifying the velocity field. Fluid particles can be used to study perfect fluids, which necessarily have a single matter constituent, as well as real fluids with multiple matter constituents. For the perfect fluid, fluid particles trace out integral curves of the velocity

¹This conceptual formulation of fluid mechanics, namely as a continuous collection of infinitesimally small fluid elements, originates from the work of Leonard Euler (1707-1783). Indeed, as detailed by [Truesdell \(1953\)](#), both the Eulerian and Lagrangian formulation of fluid kinematics originates with Euler!

²When orienting time along the vertical axis, then the tangent to the trajectory is actually the inverse velocity: slope = $dt/dx = 1/u$. We follow the convention used in special relativity, where the trajectory is known as the *world line*, and world lines live within the cone bounded by the world line of photons.

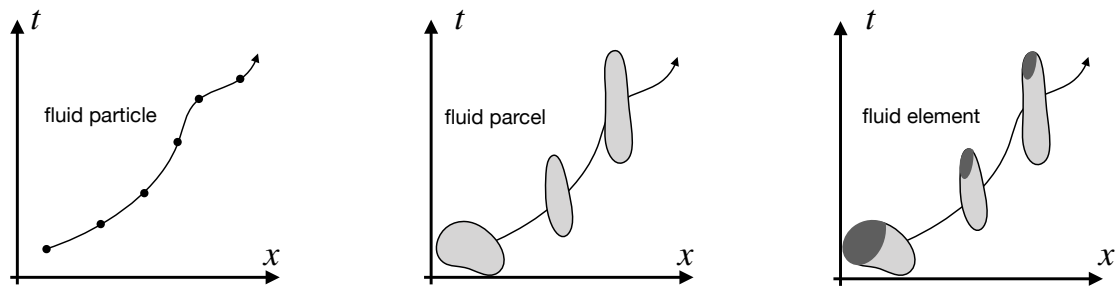


FIGURE 14.1: Schematic of the motion in space-time for the conceptual systems used in our considerations of fluid kinematics. Left panel: a fluid particle has zero spatial extent and has zero impact on the flow. Its motion in space-time defines a path/trajetory as determined by integral curves of the velocity field, $\mathbf{v}(\mathbf{x}, t)$. Note that slope of the curve on this space-time diagram is the inverse of the velocity: slope = $dt/dx = 1/u$. The trajectories of fluid particles define the Lagrangian reference frame. Middle panel: a material fluid parcel is comprised of a fixed material content (and thus a fixed mass) and fixed thermodynamic properties. Fluid parcels are infinitesimal deformable regions of a perfect fluid whose motion within a straining velocity field changes the parcel's shape. The center of mass for the fluid parcel follows a path that is approximated by that of a fluid particle at the center of mass. Right panel: a fluid element is comprised of a fixed mass but with matter and thermodynamic properties exchanged across its boundary, here depicted by the loss of dark gray matter and increase of light gray matter through exchanges with the surrounding fluid. The fluid element moves with the barycentric velocity (see Section 17.1), which is the center of mass velocity for the constituents contained in the fluid element. Both fluid parcels and fluid elements change their shape in the presence of fluid strain. Over time, a fluid parcel and a fluid element change their shape so much that their practical use requires a reinitialization of their boundaries to maintain coherency as identifiable fluid regions.

field, whereas for a real fluid the fluid particles provide integral curves for the *barycentric velocity* studied in Section 17.1.

Some books define fluid particles as finite sized fluid regions, much like the fluid parcel described in Section 14.3.2 or the fluid element in Section 14.3.4. Some treatments also suggest that a fluid particle is akin to a fluid molecule. We instead find it conceptually simpler and less troubling to define a fluid particle as a mathematical point with zero spatial extent and zero mass, thus serving solely as a conceptual probe for the flow and as a means to specify the Lagrangian reference frame.

14.3.2 Material fluid parcel in perfect fluids

For many purposes we find it useful to study fluid mechanics in the absence of irreversible processes such as friction, heat exchange, and diffusive mixing. In this case the fluid is referred to as an *ideal fluid* or equivalently a *perfect fluid*. We prefer the term *perfect fluid* for our studies in order to avoid confusions with an ideal gas often found useful in studying the atmosphere. Namely, ideal gases can possess irreversible processes so that they need not be perfect fluids.

Perfect fluid mechanics is concerned with motion of a homogeneous fluid (e.g., pure water) with zero viscosity (no friction), and in the absence of any heat exchange (adiabatic).³ In describing perfect fluids we follow Euler by making use of *material fluid parcels*, which are infinitesimal deformable fluid regions (middle panel in Figure 14.1) comprised of many fluid particles. A material fluid parcel maintains a fixed matter content so that it has a fixed mass. Furthermore, it does not experience irreversible exchanges of momentum arising from friction since the perfect fluid has zero viscosity. Hence, its only interaction with the surrounding fluid environment is through reversible mechanical exchanges from pressure. The material fluid parcel is thus a closed

³We study frictional stresses arising from viscosity in Chapter 22, with viscosity the means for the irreversible transfer of momentum within a non-perfect fluid. We study enthalpy in the Chapter 19, with a perfect fluid maintaining constant enthalpy since it is entirely adiabatic.

thermodynamic system that is open to reversible mechanical interactions.

A material parcel is not a point. Rather, it has an infinitesimal volume that deforms with the flow. Conceptually we can imagine the material fluid parcel as a tiny region of fluid surrounded by a perfectly slippery bag that is also perfectly insulating. This bag is closed to matter exchange but it deforms in response to the pressure of the surrounding fluid. Additionally, the bag expands or contracts according to the density of the fluid within the bag. This conceptual picture is qualified by noting that we never have occasion to precisely specify the boundary of a material fluid parcel. Rather, we make use of the conceptual framework provided by fluid parcels as a means to formulate the differential equations of perfect fluid mechanics.

14.3.3 Finite sized material objects in perfect fluids

Any extended region in a perfect fluid, either infinitesimal or finite, open or closed, remains exactly coherent (fixed matter content) as the region moves through the fluid. The reason for such coherency is that a perfect fluid supports no mixing or other irreversible processes that would act to diffuse the matter content. A closed material region in a perfect fluid is a finite volume generalization of a material fluid parcel. Conversely, a material fluid parcel is the infinitesimal limit of a closed material fluid region. Likewise, we can define finite sized material regions of any shape, each of which retains a fixed mass and fixed matter content as it moves through a perfect fluid. We study the kinematics of perfect fluid material lines, surfaces, and volumes in Chapter 15.

14.3.4 Fluid elements in real fluids

A fluid element is an infinitesimal and deformable fluid region of fixed mass yet non-fixed matter and non-fixed thermodynamic properties (right panel in Figure 14.1). For a homogeneous fluid comprised of a single matter constituent and no irreversible processes, then a fluid element reduces to a material fluid parcel. However, there is a distinction for real fluids such as the ocean and atmosphere, both of which have multiple constituents and support irreversible processes.

The exchange of matter across the boundary of a fluid element arises from the irreversible mixing of matter constituents within the fluid (Sections 17.1 and 61.3). As detailed in Section 17.1, diffusive matter exchange leaves the mass of the fluid element unchanged since the fluid element velocity is determined by its center of mass (*barycentric velocity*). Just as for a material fluid parcel, we have no need to experimentally specify the boundary of a fluid element. Instead, fluid elements are conceptual systems used to formulate the differential equations of a real fluid. Much of the kinematics in the current chapter holds for both material fluid parcels and fluid elements. However, in Chapter 16 and elsewhere, we make the distinction when studying the kinematics of multi-constituent fluids.

Many authors do not distinguish between material fluid parcels and fluid elements, choosing instead to retain a single overloaded term for both a perfect fluid and real fluid. However, this overloaded terminology can lead to confusion. We are thus motivated to maintain a distinction between fluid parcel (single component perfect fluid with no mixing) and fluid element (multi-component real fluid with mixing).⁴ The distinction offers an added signal for when the fluid under study is perfect (fluid parcel) or real (fluid element).

14.3.5 Test fluid element in real fluids

A *test fluid element* is a fluid element that has no effect on the surrounding fluid environment and it is used as a conceptual probe of the fluid much like the fluid particle in Section 14.3.1. Unlike

⁴We were inspired to introduce the term “fluid element” from page 3 of [Olbers et al. \(2012\)](#).

the fluid particle, the test fluid element has nonzero spatial extent and it can exchange matter and energy with its surrounding environment. The test fluid element is of particular use when studying buoyancy in Chapter 27.

14.3.6 Finite sized fluid region in real fluids

A finite sized region within a real fluid is the most general subsystem we consider, with the region having boundaries that are open to the exchange of matter, mechanical forces, and thermodynamic properties with the surrounding environment. Here, we are often concerned with details of the region boundary and study the transport of properties across that boundary.

14.3.7 Comments

Throughout the study of fluid kinematics, it is important to maintain an appreciation of the continuum approximation. In particular, the continuum approximation affords information about the continuous velocity field at each point of space and each instance of time. The velocity field allows us to determine fluid particle trajectories, as well as the motion of fluid parcels in perfect fluids and fluid elements in real fluids. As part of a diagnostic framework for laboratory or field experiments, it can be useful to seed the fluid flow with a large number of tiny objects that approximate fluid particles and thus whose motion approximate fluid particle trajectories. Similarly, in numerical experiments we may seed the flow with numerical fluid particles and compute their trajectories ([van Sebille et al., 2018](#)). If we initially seed these particles in a tiny region, then deformation of the region provides the means to study deformation of fluid parcels and fluid elements as they move through the fluid. Likewise, seeding particles over larger regions allows one to study how finite sized regions are deformed.

When thinking about fluids parcels and elements, we should acknowledge that they are convenient concepts, and yet we do not delineate their boundaries either conceptually or in practice. This situation contrasts the study of other areas of continuum mechanics, where discrete regions of the media are identifiable. For a fluid, the notion of identifying a fluid element, such as by wrapping a tiny region of fluid with an imaginary permeable sack, is a fiction that works for some thought experiments, but it is not taken literally. The perspective leads us to discount (i.e., consider incorrect) a description of continuum mechanics that depends on fluid elements as distinct and identifiable objects. Rather, we aim for a theoretical description independent of details for the fluid element boundaries. In this case, we are afforded the ability to describe a fluid as continuum matter with properties that are unambiguously defined at every point in the fluid.

14.4 Lagrangian and Eulerian reference frames

There are two reference frames commonly used as the basis for describing motion of a fluid continuum. These reference frames retain a 1-to-1 relation that allows for the transformation of descriptions between the frames.

- **LAGRANGIAN OR MATERIAL REFERENCE FRAME:** This reference frame is defined by that of fluid particles (Section 14.3.1). A mechanical description in this reference frame aims to determine the trajectory for each fluid element within the continuum. The material approach is commonly termed *Lagrangian*. Since fluid particles generally experience accelerations (i.e., they change their speed and/or direction), the Lagrangian frame is a non-inertial reference frame.

- EULERIAN OR LABORATORY REFERENCE FRAME: The second reference frame is based on observing the fluid from a fixed spatial position, \mathbf{x} , within a “laboratory”. This *Eulerian* approach measures fluid properties as the fluid streams by a fixed observer. It is not concerned with determining trajectories. Instead, the focus of Eulerian kinematics is on fluid properties determined as a function of position \mathbf{x} and time t .

The Eulerian and Lagrangian approaches complement one another. For example, the Lagrangian approach lends itself to fruitful physical insights since we can borrow freely from the point particle mechanics of Part II in this book. In contrast, the Eulerian approach is often more straightforward when developing numerical methods for simulations and it is typically simpler when making laboratory or field measurements. In general, we make use of both Eulerian and Lagrangian kinematics. A goal of this chapter is to provide the foundation for these two perspectives and to develop tools for transforming from one to the other.

In non-geophysical treatments of fluid mechanics, it is typical to assume that the laboratory reference frame is fixed in space and thus is an inertial reference frame. However, for geophysical fluid mechanics we generally consider an Eulerian reference frame fixed with respect to the rotating planet (a rotating laboratory frame), and as such the earth laboratory frame is not inertial. However, the discussion in this chapter is not concerned with the non-inertial features that give rise to planetary centrifugal and Coriolis accelerations (see Chapter 11). Instead, we note that the constant rotation of the planet does not impart any new strain to the fluid.⁵ Consequently, non-rotating fluid kinematics is sufficient for most purposes of geophysical fluid kinematics.

14.5 Material and position coordinates

A material description is suggested by the Lagrangian reference frame, whereby fluid particles are labeled with a material coordinate, \mathbf{a} , and sometimes referred to as the \mathbf{a} -space description. This description complements the Eulerian or \mathbf{x} -space description, whereby each point in space is labeled by its position relative to a fixed origin. The trajectory of a fluid particle provides the mathematical point transformation between the material coordinates and position coordinates. We explore this transformation in this section.

14.5.1 Trajectories of fluid particles

In describing the motion of a classical point particle (Chapter 11), we specify its spatial position according to a time dependent position vector, \mathbf{X} , that is a function of time, t . At a given time, t , the position vector is located at a space point denoted by the Cartesian position, \mathbf{x} , in which case we write

$$\mathbf{x} = \mathbf{X}(t) \quad \text{point particle.} \quad (14.1)$$

A sample trajectory is shown in Figure 14.2. We emphasize the notation convention used here, which may seem pedantic but in later discussions proves essential. Namely, the time dependent position of a particle is denoted with the capital, $\mathbf{X}(t)$, whose instantaneous space position is denoted by the lowercase, \mathbf{x} . This convention aims to distinguish time dependent functions, such as $\mathbf{X}(t)$, from the value of these functions evaluated at a time instance, \mathbf{x} .

When there are N discrete particles, we distinguish the various particle trajectories by introducing a discrete label. The position of particle n at time t is thus written

$$\mathbf{x} = \mathbf{X}(n, t). \quad (14.2)$$

⁵This point is made more formally when studying the kinematics of fluid strain in Section 15.3.

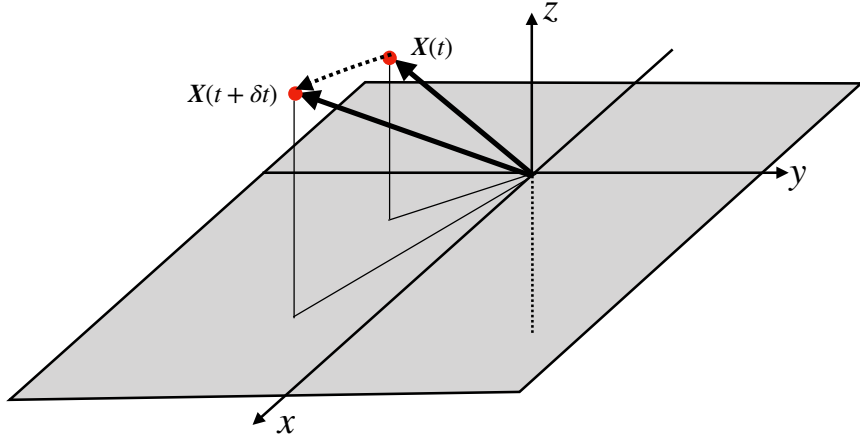


FIGURE 14.2: Sample trajectory of a fluid particle with endpoints $\mathbf{X}(t)$ and $\mathbf{X}(t + \delta t)$. The trajectory passes through the point $\mathbf{x} = \mathbf{X}(t)$ at time t and $\mathbf{x} + \delta\mathbf{x} = \mathbf{X}(t + \delta t)$ at time $t + \delta t$. Eulerian kinematics describes the fluid flow from the perspective of an observer fixed with respect to the laboratory frame. Lagrangian kinematics describes the fluid flow from the perspective of an observer moving in the frame of fluid particles.

When the matter is a continuum, such as for a rigid body, an elastic solid, or a fluid, then the discrete label becomes a continuous vector, \mathbf{a} , which is referred to as the *material coordinate*. At time t , the position of a fluid particle labelled by the material coordinate, \mathbf{a} , is written

$$\mathbf{x} = \mathbf{X}(\mathbf{a}, t) \quad \text{continuum of matter.} \quad (14.3)$$

The continuous vector, \mathbf{a} , labels a point of matter within the continuum fluid. Correspondingly, $\mathbf{X}(\mathbf{a}, t)$ is the trajectory for the center of mass for a fluid element labelled by the material coordinate, \mathbf{a} .

14.5.2 Material coordinates

In this book we ignore special relativistic effects of fluid particles. Consequently, both the material reference frame and the laboratory reference frame measure the same universal Newtonian time, t . In contrast, the spatial coordinates are distinct for the Eulerian and Lagrangian references frames. Again, the spatial coordinates for the Eulerian frame are given by the position relative to a fixed laboratory frame, whereas the three components of a material Lagrangian coordinate remains unchanged as the fluid particle moves. Additionally, the three coordinates for both the Eulerian and Lagrangian description must be linearly independent to allow for a unique specification of the fluid particle.

One common choice for material coordinate is to define it as the spatial position of a fluid particle at an arbitrary time

$$\mathbf{a} = \mathbf{X}(\mathbf{a}, t = t_0). \quad (14.4)$$

As a slightly more refined example, consider a perfect fluid (single material component with no irreversible processes). For this fluid, the specific entropy of each fluid parcel remains fixed at its initial value. When the fluid is placed in a gravitational field, layers of constant specific entropy are generally found to be monotonically stacked, or *stratified*, in the vertical direction (Chapter 27). As a result, we can uniquely specify a fluid parcel by giving its horizontal coordinate position, (x, y) , as well as the specific entropy. The material coordinates for a parcel can thus be written as

$$\mathbf{a} = (X, Y, \theta)_{t=t_0}, \quad (14.5)$$

where we write θ as a measure of the specific entropy (or potential temperature as discussed in Section 20.3). As indicated by this example, the physical dimensions of material coordinates can generally differ. It is this generality that necessitates the use of general tensor methods when developing the mechanical equations using arbitrary Lagrangian coordinates. The mathematical physics of these *generalized vertical coordinates* are detailed in Part XI of this book. For the current chapter we assume the Lagrangian coordinates are Cartesian, as given by the initial Cartesian positions as in equation (14.4).

14.5.3 Transforming between material and position coordinates

Motion of a fluid continuum is described by a *point transformation*. A point transformation is a mathematical way of saying that the fluid motion causes a fluid particle labeled by \mathbf{a} to continuously move from an initial position, $\mathbf{x}_0 = \mathbf{X}(\mathbf{a}, t_0)$, to another position, $\mathbf{x} = \mathbf{X}(\mathbf{a}, t)$, at time $t > t_0$. The point transformation is defined by the vector relation

$$\mathbf{x} = \mathbf{X}(\mathbf{a}, t), \quad (14.6)$$

which is written in component form as⁶

$$x^m = X^m(a^i, t). \quad (14.7)$$

The relation (14.6) defines a single-valued and invertible transformation from material coordinates (\mathbf{a}, t) to position coordinates (\mathbf{x}, t) . That is, for each material coordinate \mathbf{a} and time t , there is a unique spatial point \mathbf{x} , with this point specified by the trajectory $\mathbf{X}(\mathbf{a}, t)$. Conversely, for each space-time point (\mathbf{x}, t) there exists a unique material coordinate found by inverting equation (14.6)⁷

$$\mathbf{a} = \mathbf{A}(\mathbf{x}, t). \quad (14.8)$$

In this equation, \mathbf{A} is the inverse function that specifies the material coordinate \mathbf{a} given (\mathbf{x}, t) .

The single-valued property of the point transformation means that a fluid particle trajectory does not split, nor do two trajectories occupy the same point at the same time. This assumption is fundamental to the continuum approximation and the associated use of fluid particles to map out pathlines of the fluid flow. We acknowledge that fluid particle trajectories generally become increasingly complex in turbulent flow, thus making the Lagrangian description less convenient after a certain time (thus motivating the reinitialization of trajectories). However, so long as trajectories do not split or merge, the trajectories are well defined in principle, and so is the corresponding Lagrangian formulation.

14.5.4 The transformation matrix

In our analysis of fluid motions, we make routine use of the position coordinates (\mathbf{x} -space) of an Eulerian description and material coordinates (\mathbf{a} -space) of a Lagrangian description. We here introduce the transformation matrix allowing us to transform from one description to the other. Recall that in Section 9.2.1 we encountered the transformation matrix between Cartesian and spherical coordinates. We later consider a transformation matrix for moving between different references frames in Sections 14.7 and 14.8. Here, we develop the transformation matrix between \mathbf{x} -space and \mathbf{a} -space.

⁶We choose tensor labels m, n, p for spatial coordinates and trajectories, and i, j, k for material coordinates.

⁷The use of \mathbf{A} for the inverse function in equation (14.8) should not be confused with the acceleration, also written as \mathbf{A} elsewhere in this book. We will not have much use for equation (14.8), thus minimizing the opportunity for confusion.

The fluid particle trajectories, $\mathbf{X}(\mathbf{a}, t)$, are fundamental to this transformation. Namely, the trajectories given by equation (14.6) provide a transformation between position coordinates, (\mathbf{x}, t) , and material coordinates, (\mathbf{a}, t) . The transformation is invertible so long as the Jacobian (determinant) of the transformation matrix remains nonzero. Since the transformation has one foot in \mathbf{x} -space and another in \mathbf{a} -space, it is sometimes referred to as a *two-point transformation*.

The transformation matrix is given by the matrix of partial derivatives, and we organize this matrix according to the following convention⁸

$$F_i^m = \frac{\partial X^m}{\partial a^i} \equiv \begin{bmatrix} \partial X^1 / \partial a^1 & \partial X^1 / \partial a^2 & \partial X^1 / \partial a^3 \\ \partial X^2 / \partial a^1 & \partial X^2 / \partial a^2 & \partial X^2 / \partial a^3 \\ \partial X^3 / \partial a^1 & \partial X^3 / \partial a^2 & \partial X^3 / \partial a^3 \end{bmatrix}. \quad (14.9)$$

The upper label, m , denotes the row and the lower label, i , is the column. The transformation matrix F_i^m is also known as the *deformation gradient tensor*, as it provides a means to measure how trajectories are deformed by the flow. That is, each element of the tensor measures how much the m -component of the trajectory is modified when altering the i -component of the material coordinate.

To help understand the partial derivatives in the transformation matrix, assume the material coordinate is the initial position, $\mathbf{a} = \mathbf{X}(\mathbf{a}, t = 0)$. In this case, the partial derivatives measure how trajectories are modified when altering the initial position. If the fluid has no deformation, then the trajectory remains unaffected if changing the material coordinate (i.e., the initial position), in which case the deformation gradient tensor is the identity tensor

$$F_i^m = \delta_i^m \quad \text{if there is no flow deformation.} \quad (14.10)$$

Generally each component of the deformation gradient tensor is nonzero so that trajectories are deformed by the flow and as such they are dependent on the initial position.

The Jacobian determinant of the transformation matrix can be written in either of the following ways

$$\det(F_i^m) = \frac{\partial \mathbf{X}}{\partial \mathbf{a}} = \det \begin{bmatrix} \partial X^1 / \partial a^1 & \partial X^1 / \partial a^2 & \partial X^1 / \partial a^3 \\ \partial X^2 / \partial a^1 & \partial X^2 / \partial a^2 & \partial X^2 / \partial a^3 \\ \partial X^3 / \partial a^1 & \partial X^3 / \partial a^2 & \partial X^3 / \partial a^3 \end{bmatrix}. \quad (14.11)$$

We make use of the notation $\partial \mathbf{X} / \partial \mathbf{a}$ for the Jacobian as it offers a useful means to distinguish between the determinant of the transformation (14.9), and the determinant of the inverse transformation, written as $\partial \mathbf{a} / \partial \mathbf{X}$.

14.5.5 A discrete algorithm to compute the transformation matrix

To help further our understanding of the transformation matrix (14.9), we here sketch an algorithm for its discrete approximation. For this purpose, consider two-dimensional flow and write the trajectory using Cartesian coordinates

$$\mathbf{X}(t) = X^1(t) \hat{\mathbf{x}} + X^2(t) \hat{\mathbf{y}}, \quad (14.12)$$

and use a Cartesian representation for the material coordinate

$$\mathbf{a} = a^1 \hat{\mathbf{x}} + a^2 \hat{\mathbf{y}}. \quad (14.13)$$

⁸The use of covariant and contravariant notation in equation (14.9), with the upstairs and downstairs tensor labels, is strictly not needed since we assume in this chapter that both the \mathbf{x} -space and \mathbf{a} -space coordinates are Cartesian. However, the notation is quite helpful in keeping track of the ordering of partial derivatives and the corresponding coordinate transformations.

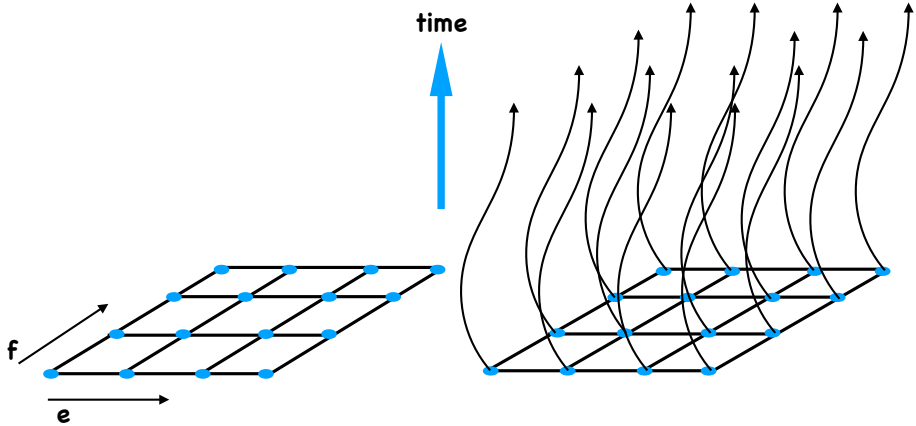


FIGURE 14.3: Illustrating the computational algorithm of Section 14.5.5 used to approximate the transformation matrix (also known as the deformation gradient tensor) F_i^m . The left panel shows the two-dimensional grid with nodal points defining the initial positions for fluid particles. Each position on the grid is labeled by a unique integer (e, f) . The initial position of each particle is taken as the material coordinate, with the discrete label (e, f) maintained by the particles as they evolve. The right panel shows the pathlines for the fluid particles after time $t > 0$. When working on a discrete grid, the position of the fluid particles is not generally at a nodal point. Hence, the position must be found by interpolating between the node points.

Now lay down a two-dimensional lattice with discrete indices (e, f) for each of the nodal points (grid points) on the lattice, and with corresponding spatial coordinates

$$\mathbf{x}(e, f) = x(e, f) \hat{\mathbf{x}} + y(e, f) \hat{\mathbf{y}}. \quad (14.14)$$

Initialize fluid particles at each of the lattice grid points,

$$\mathbf{X}(e, f; t = 0) = \mathbf{x}(e, f) = \mathbf{a}(e, f), \quad (14.15)$$

with the discrete material coordinates defined by the initial positions. Then time step the trajectories using the velocity field to compute the particle pathlines, $\mathbf{X}[\mathbf{a}(e, f); t]$, as illustrated in Figure 14.3. At any particular time, the position of a fluid particle is found by interpolating from the lattice grid points. Setting the material coordinates equal to the initial position then leads to the finite difference approximation to the transformation matrix

$$F_i^m = \begin{bmatrix} F_1^1 & F_2^1 \\ F_1^2 & F_2^2 \end{bmatrix} \approx \begin{bmatrix} \frac{X^1(e+1,f;t) - X^1(e-1,f;t)}{X^1(e+1,f;0) - X^1(e-1,f;0)} & \frac{X^1(e,f+1;t) - X^1(e,f-1;t)}{X^2(e,f+1;0) - X^2(e,f-1;0)} \\ \frac{X^2(e+1,f;t) - X^2(e-1,f;t)}{X^1(e+1,f;0) - X^1(e-1,f;0)} & \frac{X^2(e,f+1;t) - X^2(e,f-1;t)}{X^2(e,f+1;0) - X^2(e,f-1;0)} \end{bmatrix}. \quad (14.16)$$

If the grid is regular in both directions, then the initial positions have a separation, Δ , given by the grid spacing so that

$$F_i^m \approx \frac{1}{2\Delta} \begin{bmatrix} X^1(e+1,f;t) - X^1(e-1,f;t) & X^1(e,f+1;t) - X^1(e,f-1;t) \\ X^2(e+1,f;t) - X^2(e-1,f;t) & X^2(e,f+1;t) - X^2(e,f-1;t) \end{bmatrix}. \quad (14.17)$$

This expression illustrates how the transformation matrix provides a measure of trajectory spreading as fluid particles move away from their initial positions. As a check on the formulation, consider the case without any deformation. In this case $X^1(e, f; t) = X^1(e; t)$ and $X^2(e, f; t) = X^2(f; t)$ so that the transformation matrix is diagonal, and furthermore, $X^1(e+1; t) - X^1(e-1; t) = 2\Delta$ and $X^2(f+1; t) - X^2(f-1; t) = 2\Delta$, so that the transformation matrix is the identity.

14.5.6 Jacobian of the transformation as the ratio of volumes

We here establish the Jacobian of the transformation matrix as the ratio of the coordinate volume of fluid parcels as written using position space coordinates and material space coordinates. This property holds at each point within the continuum fluid so that it also holds on fluid elements.

Volume of an infinitesimal region of space within the fluid continuum

Consider the volume of an infinitesimal region of space. For simplicity, write this volume in terms of Cartesian coordinates

$$dV(\mathbf{x}) = dx \, dy \, dz. \quad (14.18)$$

The \mathbf{x} argument is introduced on the left hand side to distinguish this volume, which has dimensions L^3 , from the volume written in material coordinates

$$dV(\mathbf{a}) = da \, db \, dc, \quad (14.19)$$

where $\mathbf{a} = (a^1, a^2, a^3) = (a, b, c)$ are coordinates in material space. Note that $dV(\mathbf{a})$ does not generally have dimension L^3 , since the dimension for each component of the material coordinates is not necessarily length (e.g., see the example in equation (14.5)).

The two volumes are related by the Jacobian of transformation between \mathbf{x} -space coordinates and \mathbf{a} -space coordinates

$$dV(\mathbf{x}) = \frac{\partial \mathbf{X}}{\partial \mathbf{a}} dV(\mathbf{a}). \quad (14.20)$$

This relation indicates that the Jacobian measures the ratio of the volume written in terms of position coordinates to the volume written in terms of material coordinates

$$\frac{\partial \mathbf{X}}{\partial \mathbf{a}} = \frac{dV(\mathbf{x})}{dV(\mathbf{a})}. \quad (14.21)$$

Hence, the Jacobian is a function of space according to the ratio of the volume of a fluid element in \mathbf{x} -space to the volume in \mathbf{a} -space. This is a key kinematic result of great practical value for transforming between Eulerian and Lagrangian coordinates.

Volume of an infinitesimal fluid element

The above results have been formulated for an arbitrary region of the fluid continuum. Hence, the expressions also hold when evaluated on an arbitrary material fluid parcel or fluid element. We use the notation δV for the parcel/element volume, in terms of which the above relations take the form

$$\delta V(\mathbf{x}) = \frac{\partial \mathbf{X}}{\partial \mathbf{a}} \delta V(\mathbf{a}) \implies \frac{\partial \mathbf{X}}{\partial \mathbf{a}} = \frac{\delta V(\mathbf{x})}{\delta V(\mathbf{a})}. \quad (14.22)$$

Hence, when evaluated on a moving material parcel, the Jacobian measures the ratio of the parcel volume written in terms of position coordinates to the parcel volume written in terms of material coordinates. In the particular case where the material coordinates are the initial fluid particle positions, then the Jacobian measures the ratio of the instantaneous volume of a fluid element at a point $\mathbf{X}(\mathbf{a}, t) = \mathbf{x}$, to its initial volume

$$\frac{\partial \mathbf{X}}{\partial \mathbf{X}(0)} = \frac{\delta V(\mathbf{x})}{\delta V(0)}. \quad (14.23)$$

14.5.7 Further study

This video from the *National Committee for Fluid Mechanics Films* offers insightful visualizations to help understand Eulerian and Lagrangian fluid descriptions. This lecture from Prof. Brunton provides a lucid discussion of fluid kinematics related to finite time Lyapunov exponents, whose calculation requires estimating the transformation matrix in Section 14.5.5 along with its eigenvalues and eigenvectors.

14.6 Lagrangian and Eulerian time derivatives

As noted in Section 14.5.2, we assume non-relativistic motion so that the material reference frame and the laboratory reference frame both measure the same universal time, t . However, when computing time derivatives, the laboratory frame does so by fixing the space coordinate, \mathbf{x} , whereas the material frame computes time derivatives by fixing the material coordinate, \mathbf{a} . These two time derivatives generally measure distinct changes in the fluid since one is computed in the laboratory frame and the other from the material frame. Relating their changes constitutes a key result of fluid kinematics.

14.6.1 Infinitesimal space-time increment of a function

Consider a fluid property as represented by a space-time dependent field, Π . For example, Π could be the temperature, mass density, or velocity component. When measured at a point in space this fluid property is written mathematically as

$$\Pi = \Pi(\mathbf{x}, t). \quad (14.24)$$

The difference between $\Pi(\mathbf{x}, t)$ and $\Pi(\mathbf{x} + d\mathbf{x}, t + dt)$ delivers the differential space and time increment, computed to leading order via a Taylor series expansion

$$d\Pi = \Pi(\mathbf{x} + d\mathbf{x}, t + dt) - \Pi(\mathbf{x}, t) \quad (14.25a)$$

$$= dt \partial_t \Pi + d\mathbf{x} \cdot \nabla \Pi. \quad (14.25b)$$

In this equation, dt is the infinitesimal time increment, and $d\mathbf{x}$ is the vector of infinitesimal space increments. For example, making use of Cartesian coordinates leads to the increment

$$d\mathbf{x} = \hat{\mathbf{x}} dx + \hat{\mathbf{y}} dy + \hat{\mathbf{z}} dz. \quad (14.26)$$

We ignore higher order terms in equation (14.25b) since the space and time increments are infinitesimal.

14.6.2 Total time derivative of a function

In fluid mechanics, it is common to sample properties of the fluid from moving reference frames. In this case, the sampling position is a function of time. Consequently, the total time derivative of Π is determined by dividing both sides of equation (14.25b) by the infinitesimal time increment

$$\frac{d\Pi}{dt} = \frac{\partial \Pi}{\partial t} + \frac{d\mathbf{x}}{dt} \cdot \nabla \Pi. \quad (14.27)$$

The first term measures the time derivative of Π at the specific space point, \mathbf{x} . The second term accounts for changes in Π arising from movement of the reference frame relative to a point, \mathbf{x} ,

according to the velocity, $d\mathbf{x}/dt$. Expression (14.27) holds in general since the velocity of the moving frame is arbitrary. We next specialize to the two common cases in fluid mechanics.

14.6.3 Eulerian: evolution measured in the laboratory frame

The Eulerian time derivative considers the evolution of a fluid property when sampled at a fixed space point

$$\text{Eulerian time derivative} = \frac{\partial \Pi(\mathbf{x}, t)}{\partial t}. \quad (14.28)$$

This result follows from specializing the total time derivative in equation (14.27) to the case of fixed spatial points, so that $d\mathbf{x}/dt = 0$. In the geophysical fluids literature, the Eulerian time derivative is often termed the *time tendency* and flows with a nonzero time tendency are said to be *developing flows* or *evolving flows*. When the Eulerian time derivative vanishes everywhere the flow is said to be in a *steady state* or in a *steady flow* condition, with all points in the laboratory (inertial) frame measuring a zero time change for fluid properties. Note that steady flows are not generally static; rather, they are simply unchanging locally.

14.6.4 Lagrangian: evolution measured in the material frame

The Lagrangian or material time derivative measures the evolution of a fluid property sampled along the trajectory of a moving fluid particle. The Lagrangian time derivative for a field is thus written

$$\text{Lagrangian time derivative} = \frac{D\Pi}{Dt} = \frac{\partial \Pi}{\partial t} + \mathbf{v} \cdot \nabla \Pi. \quad (14.29)$$

The second equality follows by setting $d\mathbf{x}/dt = \mathbf{v}$ in equation (14.27) since we are sampling points along the fluid particle trajectory $\mathbf{x} = \mathbf{X}(\mathbf{a}, t)$. The operator $\partial/\partial t$ is the Eulerian time derivative from equation (14.28), whereas $\mathbf{v} \cdot \nabla$ is referred to as the *advection* operator. Use of the capital D for the material time operator

$$\frac{D}{Dt} = \frac{\partial}{\partial t} + \mathbf{v} \cdot \nabla \quad (14.30)$$

signals that the time derivative is computed along a fluid particle trajectory. This notation distinguishes the material time derivative from the more generic total time derivative of equation (14.27). In some texts the material time derivative is referred to as the *convective time derivative*, since the term “convection” is often used rather than our preferred term “advection”.⁹ It is also sometimes referred to as the *substantial time derivative* since it refers to the time changes following a material substance.

Equation (14.30) provides an Eulerian expression (right hand side) to the material time derivative, D/Dt . There are two Eulerian contributions: the local (fixed space point) time tendency $\partial/\partial t$ and advection, $\mathbf{v} \cdot \nabla$. Advection arises in the Eulerian reference frame due to the fluid passing by the fixed laboratory observer, whereas it is absent from the material reference frame since the material frame moves with the fluid particles. Figure 14.4 illustrates the differences between the Eulerian and Lagrangian perspectives.

A *steady flow* is one with zero Eulerian time derivatives so that a steady flow does not imply a vanishing Lagrangian time derivative. Rather, a steady flow is a statement that the flow is time independent when viewed from the Eulerian (laboratory) reference frame. Hence, a steady flow generally has changing properties when sampled along a fluid particle trajectory. That is, there

⁹In the geophysical fluids literature, “convection” generally refers to gravitationally unstable vertical motion initiated by buoyancy forces. In contrast, the engineering literature often refers to “convection” in the same manner as we refer to “advection.”

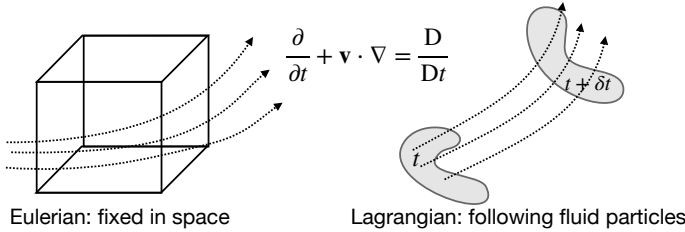


FIGURE 14.4: Illustrating the distinctions between the Eulerian (laboratory) and Lagrangian (material) reference frames for describing fluid motion. For the Eulerian description we consider a fixed control volume in the laboratory frame and measure properties as the fluid moves through the volume. For the Lagrangian description we tag fluid particles and measure fluid properties as sampled along the particle trajectories. The Eulerian representation of the material time derivative has two terms, one due to time changes local to the fixed laboratory point, and one due to the advection of properties that are swept by the local position.

can be a nonzero Lagrangian evolution (via advection) even when the Eulerian time tendency vanishes.

14.6.5 Lagrangian time derivative formulated from the material frame

Rather than start from the total time derivative (14.27), it is instructive to work in the moving material frame *a priori*. For this purpose, we measure the function, Π , on a fluid particle, in which case we introduce the shorthand notation

$$\Pi[\mathbf{X}(\mathbf{a}, t), t] \equiv \Pi^L(\mathbf{a}, t) \iff \text{sampling } \Pi \text{ on a trajectory } \mathbf{x} = \mathbf{X}(\mathbf{a}, t) \text{ at time } t. \quad (14.31)$$

In words, $\Pi^L(\mathbf{a}, t)$ is the function, Π , evaluated on a fluid particle trajectory $\mathbf{x} = \mathbf{X}(\mathbf{a}, t)$. That is, $\Pi^L(\mathbf{a}, t)$ is the Lagrangian version of the function, $\Pi(\mathbf{x}, t)$. For example, the Lagrangian velocity is given by

$$\mathbf{v}^L(\mathbf{a}, t) \equiv \mathbf{v}[\mathbf{X}(\mathbf{a}, t), t] = \left[\frac{\partial \mathbf{X}(\mathbf{a}, t)}{\partial t} \right]_{\mathbf{a}}. \quad (14.32)$$

The \mathbf{a} subscript emphasizes that the partial time derivative is computed while holding the material coordinate, \mathbf{a} , fixed.

The time derivative along a fluid particle trajectory is the material derivative, and we introduce a finite difference along the trajectory to estimate the derivative

$$\left[\frac{\partial \Pi[\mathbf{X}(\mathbf{a}, t), t]}{\partial t} \right]_{\mathbf{a}} = \lim_{\Delta t \rightarrow 0} \left[\frac{\Pi[\mathbf{X}(\mathbf{a}, t + \Delta t/2), t + \Delta t/2] - \Pi[\mathbf{X}(\mathbf{a}, t - \Delta t/2), t - \Delta t/2]}{\Delta t} \right]. \quad (14.33)$$

Expanding the numerator in a Taylor series, and keeping just the leading terms, yields

$$\left[\frac{\partial \Pi[\mathbf{X}(\mathbf{a}, t), t]}{\partial t} \right]_{\mathbf{a}} = \lim_{\Delta t \rightarrow 0} \left[\frac{\Pi[\mathbf{X}(\mathbf{a}, t + \Delta t/2), t + \Delta t/2] - \Pi[\mathbf{X}(\mathbf{a}, t - \Delta t/2), t - \Delta t/2]}{\Delta t} \right] \quad (14.34a)$$

$$= \left[\left(\frac{\partial}{\partial t} \right)_{\mathbf{X}} + \left(\frac{\partial \mathbf{X}(\mathbf{a}, t)}{\partial t} \right)_{\mathbf{a}} \cdot \nabla \right] \Pi[\mathbf{X}(\mathbf{a}, t), t] \quad (14.34b)$$

$$= \left[\left(\frac{\partial}{\partial t} \right)_{\mathbf{X}} + \mathbf{v}[\mathbf{X}(\mathbf{a}, t), t] \cdot \nabla \right] \Pi[\mathbf{X}(\mathbf{a}, t), t]. \quad (14.34c)$$

We included a subscript on the derivative operators on the right hand side to be explicit about what variables are held fixed during differentiation. This extra notation can generally be dropped,

since a partial derivative operation is based on holding all variables fixed except for the variable being differentiated. Evaluating the trajectory at the spatial point, $\mathbf{X}(\mathbf{a}, t) = \mathbf{x}$, allows us to dispense with the trajectory notation to recover the more succinct expression (14.29). Even so, it is useful to keep in mind the underlying trajectory basis for the material time derivative.

14.6.6 Sample material time derivative operations

The material time derivative operator is perhaps the most important operator in fluid mechanics, and its relation to the Eulerian time derivative plus advection is a key result of fluid kinematics. Therefore, it is critical to develop experience with this operator and its generalizations. The examples here offer a starting point.

Material invariant

Consider a scalar function that remains constant on a material trajectory so that its material time derivative vanishes

$$\frac{D\Pi}{Dt} = 0. \quad (14.35)$$

Material constancy is generally referred to as *material invariance* in this book. We may also say that the property, Π , is materially conserved. At a fixed point in space, a materially invariant property has its Eulerian time derivative arising only via advection

$$\frac{\partial\Pi}{\partial t} = -\mathbf{v} \cdot \nabla\Pi. \quad (14.36)$$

Recall the case of a wave characteristic whereby $\partial\Pi/\partial t = \omega$. Wave characteristics are material if the fluid particle velocity satisfies $\mathbf{k} \cdot \mathbf{v} = \omega$.¹⁰

We garner geometric insight into relation (14.36) by introducing the unit normal vector to the surface of constant Π

$$\hat{\mathbf{n}} = \frac{\nabla\Pi}{|\nabla\Pi|}. \quad (14.37)$$

Material invariance of Π thus means that the normalized Eulerian time tendency equals to the negative of the projection of the velocity into the direction normal to constant Π surfaces

$$\frac{\partial\Pi/\partial t}{|\nabla\Pi|} = -\mathbf{v} \cdot \hat{\mathbf{n}}. \quad (14.38)$$

That is, the fluid particle velocity, \mathbf{v} , is matched precisely to the velocity of the moving surface of constant Π . We return to this result in Section 16.4.2 when studying the kinematic boundary conditions at a variety of surfaces.

Time derivative measured in a general moving frame

Now consider a reference frame moving at an arbitrary velocity, $\mathbf{v}^{(s)}$. Examples include the quasi-Lagrangian reference frames of a float in the ocean or balloon in the atmosphere. Due to their finite size and associated drag effects, these objects only approximate material particle motion, so

¹⁰In one space dimension and for linear non-rotating gravity waves (Section 48.5), the wave phase speed is given by ω/k so that the wave characteristics are material if the fluid particle speed matches the wave speed, $|\mathbf{v}| = \omega/k$. The ratio of the particle speed to the wave speed is known as the Froude number. The Froude number is typically much less than unity, though highly nonlinear behavior (e.g., hydraulic jumps as discussed in [Pratt and Whitehead \(2008\)](#)) occurs when the Froude number reaches unity or larger (see Exercise 32.3).

that $\mathbf{v}^{(s)} \neq \mathbf{v}$. Returning to the general expression (14.27) for the total time derivative, we have the time derivative operator as measured in this non-material moving reference frame

$$\frac{D^{(s)}}{Dt} = \frac{\partial}{\partial t} + \mathbf{v}^{(s)} \cdot \nabla. \quad (14.39)$$

A function that remains constant within this general moving frame thus satisfies

$$\frac{D^{(s)}\Pi}{Dt} = 0 \implies \frac{\partial\Pi}{\partial t} = -\mathbf{v}^{(s)} \cdot \nabla\Pi. \quad (14.40)$$

Introducing the normal direction $\hat{\mathbf{n}} = |\nabla\Pi|^{-1} \nabla\Pi$ leads to

$$\frac{\partial\Pi/\partial t}{|\nabla\Pi|} = -\mathbf{v}^{(s)} \cdot \hat{\mathbf{n}}, \quad (14.41)$$

which is an analog to the material invariance condition (14.38).

14.6.7 Worked example: velocity and acceleration from a trajectory

Following example 3.2 from [Kundu et al. \(2016\)](#), we here consider a one-dimensional fluid motion whereby the trajectory of a fluid particle is given by

$$\mathbf{X}(t) = \hat{\mathbf{x}} X(t) = \hat{\mathbf{x}} [K(t - t_0) + x_0^3]^{1/3}, \quad (14.42)$$

where K is a constant with dimensions volume per time and x_0 is the particle position at time $t = t_0$. The particle velocity and particle acceleration are determined through time differentiation

$$\frac{d\mathbf{X}}{dt} = \hat{\mathbf{x}} \frac{K}{3X^2} \quad \text{and} \quad \frac{d^2\mathbf{X}}{dt^2} = -\hat{\mathbf{x}} \frac{2K^2}{9X^5}. \quad (14.43)$$

The Eulerian velocity field is then determined by

$$\mathbf{v}(\mathbf{x}, t) \equiv \left[\frac{d\mathbf{X}}{dt} \right]_{\mathbf{x}=\mathbf{X}(t)} = \hat{\mathbf{x}} \frac{K}{3x^2}, \quad (14.44)$$

which reveals that the flow is steady since there is no time dependence to the Eulerian velocity field. The Eulerian acceleration is given by the material time derivative of the Eulerian velocity, which is equal to the second time derivative of the trajectory evaluated at the field point

$$\frac{Du}{Dt} = \frac{\partial u}{\partial t} + \mathbf{v} \cdot \nabla u = 0 + u \partial_x u = -[K/(3x^2)] [(2K)/(3x^3)] = -\frac{2K^2}{9x^5} = \left[\frac{d^2X(t)}{dt^2} \right]_{\mathbf{x}=\mathbf{X}(t)}. \quad (14.45)$$

14.6.8 Summarizing some terminology

We here summarize certain terminology used in this book in reference to the variety of equations in geophysical fluid mechanics. Some of this terminology was introduced in this chapter, whereas others will be encountered in subsequent development.

- PROGNOSTIC: This is an equation that determines the time tendency (Eulerian evolution) of a quantity such as the temperature or velocity.
- DIAGNOSTIC: This is an equation that determines the value of a field at a particular instance in time. An example is the non-divergence condition satisfied by velocity in an incompress-

ible flow (Chapter 18) as well in a Boussinesq ocean (Chapter 26). There are generally no time derivatives appearing in diagnostic equations.

- **STEADY STATE:** All Eulerian time derivatives vanish, so that all fluid properties are time independent when measured in the laboratory frame.
- **MATERIAL INVARIANCE:** The Lagrangian time derivative vanishes for a property that is a material invariant.

14.7 Galilean invariance

Galilean invariance means that the laws of motion are the same in all inertial reference frames. Furthermore, two inertial reference frames can only be moving with a constant velocity relative to one another. We discussed Galilean invariance for a point particle in Section 10.1.2. Here we consider its expression for a fluid. As for the particle, Galilean invariance means that the material acceleration of a fluid particle remains the same when viewed in an arbitrary inertial reference frame. Some care is required when translating this invariance into a mathematical statement when decomposing the material acceleration into its Eulerian components. Our considerations here provide a useful warmup to the more general discussion in Section 14.8, where we transform space and time derivative operators between an inertial frame and a rotating frame.

The notions of Galilean invariance hold in free space. In the presence of boundaries we do not expect the physical system to respect Galilean invariance since boundaries generally distinguish between reference frames.

14.7.1 Galilean transformation

A Galilean transformation is given by the linear space-time transformation

$$\bar{t} = t \quad \text{and} \quad \bar{\mathbf{x}} = \mathbf{x} + \mathbf{U}t \quad \text{and} \quad \bar{\mathbf{v}} = \mathbf{v} + \mathbf{U}. \quad (14.46)$$

By convention, we say that the barred coordinates are those measured in the moving (boosted) reference frame and the unbarred are measured in the rest frame. However, since both reference frames are inertial, there is no experiment on a Galilean invariant physical system that can determine which frame is at rest or which is moving. Instead, what is relevant is that the two inertial frames are moving relative to one another. Furthermore, note that time remains unchanged (universal Newtonian time), whereas the position of a point in the new frame equals to that in the original reference frame plus a contribution from the constant velocity, \mathbf{U} . The inverse transformation is trivially given by

$$t = \bar{t} \quad \text{and} \quad \mathbf{x} = \bar{\mathbf{x}} - \mathbf{U}\bar{t} \quad \text{and} \quad \mathbf{v} = \bar{\mathbf{v}} - \mathbf{U}. \quad (14.47)$$

14.7.2 Transformation matrix

We take this opportunity to make use of the transformation matrix formalism to derive relations between the partial differential operators. Details of this formalism were presented in Section 8.9. However, the reader skipping that section should still be able to understand the gist of the following. For simplicity we work in the 1+1 dimensional case with time along with one space dimension.

Writing the space and time coordinates as $(t, x) = (x^0, x^1)$ and $(\bar{t}, \bar{x}) = (x^{\bar{0}}, x^{\bar{1}})$ renders the transformation of partial derivatives (following the chain rule)

$$\frac{\partial}{\partial x^{\bar{\alpha}}} = \frac{\partial x^\alpha}{\partial x^{\bar{\alpha}}} \frac{\partial}{\partial x^\alpha}, \quad (14.48)$$

where $\alpha = 0, 1$ is a tensor index that has $\alpha = 0$ for the time coordinate. The transformation matrix for the Galilean transformation is thus given by the 2×2 matrix

$$\frac{\partial x^{\bar{\alpha}}}{\partial x^\alpha} = \begin{bmatrix} \partial x^{\bar{0}}/\partial x^0 & \partial x^{\bar{0}}/\partial x^1 \\ \partial x^{\bar{1}}/\partial x^0 & \partial x^{\bar{1}}/\partial x^1 \end{bmatrix} = \begin{bmatrix} 1 & 0 \\ U & 1 \end{bmatrix}, \quad (14.49)$$

and the inverse is

$$\frac{\partial x^\alpha}{\partial x^{\bar{\alpha}}} = \begin{bmatrix} 1 & 0 \\ -U & 1 \end{bmatrix}. \quad (14.50)$$

The Jacobian determinant of the transformation matrix is unity, so that the Galilean transformation always has an inverse.

14.7.3 Transforming the differential operators

Given the transformation matrix, we can compute the Eulerian time derivative as measured in the moving frame as

$$\frac{\partial}{\partial x^{\bar{0}}} = \frac{\partial x^0}{\partial x^{\bar{0}}} \frac{\partial}{\partial x^0} + \frac{\partial x^1}{\partial x^{\bar{0}}} \frac{\partial}{\partial x^1} = \frac{\partial}{\partial x^0} - U \frac{\partial}{\partial x^1} = \frac{\partial}{\partial t} - U \frac{\partial}{\partial x}. \quad (14.51)$$

In words, this identity says that the time derivative computed between two inertial reference frames differs due to an advective term (with the constant Galilean boost velocity) arising from the relative motion of the two inertial observers. The space derivatives are related by

$$\frac{\partial}{\partial x^{\bar{1}}} = \frac{\partial x^0}{\partial x^{\bar{1}}} \frac{\partial}{\partial x^0} + \frac{\partial x^1}{\partial x^{\bar{1}}} \frac{\partial}{\partial x^1} = \frac{\partial}{\partial x^1}, \quad (14.52)$$

so that the space derivative operator remains form invariant under a Galilean transformation. This result holds also for the other two space dimensions. We thus find that the material time derivative operator is form invariant under a Galilean transformation

$$\frac{D}{Dt} = \frac{\partial}{\partial t} + \mathbf{v} \cdot \nabla \quad (14.53a)$$

$$= \frac{\partial}{\partial \bar{t}} + \mathbf{U} \cdot \bar{\nabla} + (\bar{\mathbf{v}} - \mathbf{U}) \cdot \bar{\nabla} \quad (14.53b)$$

$$= \frac{\partial}{\partial \bar{t}} + \bar{\mathbf{v}} \cdot \bar{\nabla} \quad (14.53c)$$

$$= \frac{\bar{D}}{D\bar{t}}, \quad (14.53d)$$

where we used the shorthand

$$\bar{\mathbf{v}} \cdot \bar{\nabla} = \bar{u} \frac{\partial}{\partial x^{\bar{1}}} + \bar{v} \frac{\partial}{\partial x^{\bar{2}}} + \bar{w} \frac{\partial}{\partial x^{\bar{3}}}. \quad (14.54)$$

So although the individual pieces to the material time operator are modified by a Galilean transformation, the material time derivative operator is form invariant. Hence, if a function has

a material time derivative $D\Pi/dt$ in one inertial reference frame, it has the same material time operator in any other inertial reference frame. That is, all properties sampled from a boosted fluid particle reference frame have the same material time evolution.

14.7.4 Comments

There are many features of geophysical fluid flows that break Galilean invariance. For example, a solid boundary breaks Galilean invariance since it establishes a special reference frame and thus breaks symmetry of the space. Additionally, a rotating planet distinguishes between longitude and latitude even if the planet is perfectly smooth. Nonetheless, as a starting point in our study of the equations of fluid mechanics, it is useful to establish their properties under a Galilean transformation. In general, if space is Galilean invariant and yet the equations of motion are not, then we question the physical relevance of the equations. Exercise 35.8 provides an example of this reasoning.

There are further symmetries of the equations of fluid mechanics, especially when there is no dissipation (inviscid). Section 2.2 of [Frisch \(1995\)](#) and Section 1.4 of [Badin and Crisciani \(2018\)](#) provide a discussion of such symmetries.

14.8 Invariance of the material time derivative

In our discussion of Galilean invariance in Section 14.7, we showed that the material time derivative operator remains form invariant under changes to the inertial reference frame. Consequently, the acceleration of a fluid particle is identical when measured in any inertial reference frame. We here consider the more general case of non-inertial reference frames that differ by both rotations and translations. We already know that the form for fluid particle accelerations differs between an inertial frame and a non-inertial frame. Nonetheless, we show here that the material time derivative operator remains form invariant. This is a result of great practical relevance, as it means that the scalar equations of fluid mechanics (e.g., mass continuity and tracer equations) remain form-invariant when changing reference frames.

14.8.1 Invariance based on definition of the material time derivative

We first determine invariance by focusing on the conceptual definition of the material time derivative. Namely, the material time derivative measures time changes of a fluid property in the reference frame of a moving fluid particle. The Lagrangian reference frame follows fluid particles, so it is the natural reference frame for measuring material time changes. In contrast, the Eulerian reference frame is fixed in a laboratory. The material time derivative computed from the laboratory reference frame consists of an Eulerian time tendency plus an advection operator

$$\frac{D}{Dt} = \frac{\partial}{\partial t} + \mathbf{v} \cdot \nabla. \quad (14.55)$$

Importantly, this expression holds regardless the choice of laboratory reference frames, either inertial or non-inertial. Our choice of laboratory frames only impacts on the form of the Eulerian time derivative and on the advection operator. The sum of the two terms returns the same material time derivative operator, no matter what laboratory frame is chosen.

Again for emphasis, the reason for the form invariance is that the material time derivative operator is, by definition, computed in the fluid particle reference frame. The particle reference frame is unconcerned with the subjective choice made by the observer in the laboratory reference frame. In the following, we exhibit how the mathematics respects this invariance. Namely, we

show how the Eulerian expression for the material time derivative remains form invariant when changing reference frames.

14.8.2 Invariance for a rotating reference frame

Consider two reference frames. The first is at rest and so serves as an inertial frame, whereas the second is rotating with rotational axis aligned with the vertical direction as in Figure 9.1. Introduce Cartesian coordinates for the inertial frame, with corresponding basis vectors $(\hat{\bar{x}}, \hat{\bar{y}}, \hat{\bar{z}})$. Let these inertial frame unit vectors be related to rotating frame unit vectors according to

$$\hat{\bar{x}} = \hat{x} \cos \vartheta - \hat{y} \sin \vartheta \quad (14.56a)$$

$$\hat{\bar{y}} = \hat{x} \sin \vartheta + \hat{y} \cos \vartheta \quad (14.56b)$$

$$\hat{\bar{z}} = \hat{z}, \quad (14.56c)$$

and let time be the same in the two reference frames. The angle ϑ measures the counter-clockwise angle between the inertial frame direction $\hat{\bar{x}}$ and the moving frame direction \hat{x} , with this angle a linear function of time

$$\vartheta = \Omega t. \quad (14.57)$$

The above relations between the two sets of basis vectors translates into the same relations between the corresponding coordinate representations for an arbitrary vector. Including time, we have the relation between inertial coordinates (the barred frame) and rotating coordinates (unbarred frame)

$$\bar{t} = t \quad (14.58a)$$

$$\bar{x} = x \cos \vartheta - y \sin \vartheta \quad (14.58b)$$

$$\bar{y} = x \sin \vartheta + y \cos \vartheta \quad (14.58c)$$

$$\bar{z} = z. \quad (14.58d)$$

The inverse transformation can be easily found

$$t = \bar{t} \quad (14.59a)$$

$$x = \bar{x} \cos \vartheta + \bar{y} \sin \vartheta \quad (14.59b)$$

$$y = -\bar{x} \sin \vartheta + \bar{y} \cos \vartheta \quad (14.59c)$$

$$z = \bar{z}. \quad (14.59d)$$

We are now prepared to make use of the transformation formalism generally considered in Section 8.9, and specifically applied for the Galilean transformation in Section 14.7. We include time as part of the formalism by introducing the Greek label $\alpha = 0, 1, 2, 3$ so that the transformation matrix between the inertial frame and rotating frame is given by

$$\frac{\partial x^{\bar{\alpha}}}{\partial x^{\alpha}} = \begin{bmatrix} \partial x^{\bar{0}}/\partial x^0 & \partial x^{\bar{0}}/\partial x^1 & \partial x^{\bar{0}}/\partial x^2 & \partial x^{\bar{0}}/\partial x^3 \\ \partial x^{\bar{1}}/\partial x^0 & \partial x^{\bar{1}}/\partial x^1 & \partial x^{\bar{1}}/\partial x^2 & \partial x^{\bar{1}}/\partial x^3 \\ \partial x^{\bar{2}}/\partial x^0 & \partial x^{\bar{2}}/\partial x^1 & \partial x^{\bar{2}}/\partial x^2 & \partial x^{\bar{2}}/\partial x^3 \\ \partial x^{\bar{3}}/\partial x^0 & \partial x^{\bar{3}}/\partial x^1 & \partial x^{\bar{3}}/\partial x^2 & \partial x^{\bar{3}}/\partial x^3 \end{bmatrix} = \begin{bmatrix} 1 & 0 & 0 & 0 \\ -\Omega \bar{y} & \cos \vartheta & -\sin \vartheta & 0 \\ \Omega \bar{x} & \sin \vartheta & \cos \vartheta & 0 \\ 0 & 0 & 0 & 1 \end{bmatrix}. \quad (14.60)$$

Similarly, the inverse transformation is given by

$$\frac{\partial x^\alpha}{\partial \bar{x}^{\bar{\alpha}}} = \begin{bmatrix} \partial x^0/\partial \bar{x}^0 & \partial x^0/\partial \bar{x}^1 & \partial x^0/\partial \bar{x}^2 & \partial x^0/\partial \bar{x}^3 \\ \partial x^1/\partial \bar{x}^0 & \partial x^1/\partial \bar{x}^1 & \partial x^1/\partial \bar{x}^2 & \partial x^1/\partial \bar{x}^3 \\ \partial x^2/\partial \bar{x}^0 & \partial x^2/\partial \bar{x}^1 & \partial x^2/\partial \bar{x}^2 & \partial x^2/\partial \bar{x}^3 \\ \partial x^3/\partial \bar{x}^0 & \partial x^3/\partial \bar{x}^1 & \partial x^3/\partial \bar{x}^2 & \partial x^3/\partial \bar{x}^3 \end{bmatrix} = \begin{bmatrix} 1 & 0 & 0 & 0 \\ \Omega y & \cos \vartheta & \sin \vartheta & 0 \\ -\Omega x & -\sin \vartheta & \cos \vartheta & 0 \\ 0 & 0 & 0 & 1 \end{bmatrix}. \quad (14.61)$$

The derivative operators transform according to

$$\frac{\partial}{\partial x^\alpha} = \frac{\partial x^{\bar{\alpha}}}{\partial x^\alpha} \frac{\partial}{\partial \bar{x}^{\bar{\alpha}}}, \quad (14.62)$$

in which case

$$\frac{\partial}{\partial t} = \frac{\partial}{\partial \bar{t}} + (\boldsymbol{\Omega} \times \bar{\boldsymbol{x}}) \cdot \bar{\nabla} \quad (14.63a)$$

$$\frac{\partial}{\partial x} = \cos \vartheta \frac{\partial}{\partial \bar{x}} + \sin \vartheta \frac{\partial}{\partial \bar{y}} \quad (14.63b)$$

$$\frac{\partial}{\partial y} = -\sin \vartheta \frac{\partial}{\partial \bar{x}} + \cos \vartheta \frac{\partial}{\partial \bar{y}} \quad (14.63c)$$

$$\frac{\partial}{\partial z} = \frac{\partial}{\partial \bar{z}}. \quad (14.63d)$$

The velocity vector components transform according to

$$v^\alpha = \frac{\partial x^\alpha}{\partial \bar{x}^{\bar{\alpha}}} v^{\bar{\alpha}}, \quad (14.64)$$

so that

$$v^0 = v^{\bar{0}} \quad (14.65a)$$

$$u = \Omega y + \bar{u} \cos \vartheta + \bar{v} \sin \vartheta \quad (14.65b)$$

$$v = -\Omega x - \bar{u} \sin \vartheta + \bar{v} \cos \vartheta \quad (14.65c)$$

$$w = \bar{w}, \quad (14.65d)$$

where

$$v^0 = v^{\bar{0}} = 1. \quad (14.66)$$

Bringing these result together leads to the transformation of the horizontal advection operator

$$u \frac{\partial}{\partial x} + v \frac{\partial}{\partial y} = (\bar{\boldsymbol{u}} - \boldsymbol{\Omega} \times \bar{\boldsymbol{x}}) \cdot \bar{\nabla}. \quad (14.67)$$

Combining this result with the transformed Eulerian time derivative leads to the material time

derivative

$$\frac{D}{Dt} = \frac{\partial}{\partial t} + \mathbf{v} \cdot \nabla \quad (14.68a)$$

$$= \frac{\partial}{\partial t} + u \frac{\partial}{\partial x} + v \frac{\partial}{\partial y} + w \frac{\partial}{\partial z} \quad (14.68b)$$

$$= \frac{\partial}{\partial \bar{t}} + (\boldsymbol{\Omega} \times \bar{\mathbf{x}}) \cdot \bar{\nabla} + (\bar{\mathbf{u}} - \boldsymbol{\Omega} \times \bar{\mathbf{x}}) \cdot \bar{\nabla} + \bar{w} \frac{\partial}{\partial \bar{z}} \quad (14.68c)$$

$$= \frac{\partial}{\partial \bar{t}} + \bar{\mathbf{v}} \cdot \bar{\nabla}. \quad (14.68d)$$

As advertised, the operator is form invariant under time dependent transformations to a non-inertial reference frame.

14.8.3 Invariance using space-time tensors

We can generalize the previous result by writing the material time derivative operator using space-time tensor notation from Section 7.5.4, in which case

$$\frac{D}{Dt} = \frac{\partial}{\partial t} + \mathbf{v} \cdot \nabla \quad (14.69a)$$

$$= \frac{\partial}{\partial x^0} + v^m \frac{\partial}{\partial x^m} \quad (14.69b)$$

$$= v^\alpha \frac{\partial}{\partial x^\alpha}, \quad (14.69c)$$

where we introduced the velocity 4-vector

$$(v^0, v^1, v^2, v^3) = (1, v^1, v^2, v^3). \quad (14.70)$$

All space-time indices are contracted in equation (14.69c), which means the material time derivative is a space-time scalar. Consequently, we can change coordinates or change reference frames without changing the material time operator.

14.8.4 Comments

As argued at the start of this section, the invariance of the material time derivative to changes in the laboratory reference frame is rather obvious: why would a time derivative computed in a material frame be concerned with the nature of the laboratory frame? Even so, it is satisfying to see the tools of coordinate transformations put to use verifying this result. It is this sort of exercise that nurtures trust in tensor analysis, thus allowing it becomes a reliable tool for exploration where the answer is not *a priori* known.

14.9 Fluid flow lines

There are three types of flow lines commonly used to visualize fluid motion: *pathlines*, *streamlines*, and *streaklines*. These flow lines are identical for time independent (steady) flow, where steady flow means that all fields are constant in time when observed in the Eulerian reference frame. However, these flow lines differ for unsteady flow. They each offer complementary information about the flow field, and have uses in both theoretical and experimental contexts. We have use for pathlines and streamlines in this book, yet also introduce streaklines for completeness.

14.9.1 Material pathlines from fluid particle trajectories

As introduced in Section 14.5.1, a fluid particle traces out a *trajectory* as it moves through space and time (Figure 14.2). We use the term material *pathline* for a fluid particle trajectory, with a collection of pathlines providing a means to visualize fluid particle motion throughout the flow. In this book we are only concerned with *smooth velocity fields*, which allow for an unambiguous specification of the particle trajectory at each point of the fluid.

Mathematically, a fluid particle trajectory is a curve, $\mathbf{X}(\mathbf{a}, t)$, in space that is traced by fixing the material coordinate, \mathbf{a} , and letting time advance. Trajectories are computed by time integrating the ordinary differential equation

$$\frac{\partial \mathbf{X}(\mathbf{a}, t)}{\partial t} = \mathbf{v}[\mathbf{X}(\mathbf{a}, t), t] \quad (14.71a)$$

$$\mathbf{X}(\mathbf{a}, t = 0) = \mathbf{a}, \quad (14.71b)$$

where the Lagrangian velocity of the fluid particle (see equation (14.32)) is written

$$\mathbf{v}[\mathbf{X}(\mathbf{a}, t), t] = \mathbf{v}^L(\mathbf{a}, t), \quad (14.72)$$

and we have assumed the material coordinates are determined by the initial position. Again, the partial time derivative is computed with the material coordinate held fixed, so that the material coordinate distinguishes between particle trajectories. In a mathematical context we refer to a particle trajectory as the *integral curve* for the velocity vector.

In the laboratory, we can insert tiny particles into the fluid to offer a means for visualizing the flow, with a time exposed photograph providing an estimate of fluid particle pathlines. Experimental particles provide an accurate estimate of fluid particle pathlines if the particles do not disperse through diffusion (see Chapter 61). As another example, consider cars moving at night with a time exposed photograph revealing pathlines formed by car head and tail lights. Like cars, the material pathlines in a fluid can intersect, cross, and become quite complex, particularly when the flow is turbulent.

14.9.2 Fluid streamlines and streamtubes

Streamlines are curves whose tangent is parallel to the instantaneous fluid velocity field. Streamlines can intersect only at a stagnation point; i.e., a point where the fluid is not moving. Let

$$d\mathbf{x} = \hat{\mathbf{x}} dx + \hat{\mathbf{y}} dy + \hat{\mathbf{z}} dz \quad (14.73)$$

be an infinitesimal increment along a streamline written using Cartesian coordinates. The family of streamlines at a given time, t , satisfy the tangent constraint

$$\mathbf{v} \times d\mathbf{x} = 0, \quad (14.74)$$

which is equivalent to

$$\frac{dx}{u(\mathbf{x}, t)} = \frac{dy}{v(\mathbf{x}, t)} = \frac{dz}{w(\mathbf{x}, t)}. \quad (14.75)$$

Alternatively, we can introduce a pseudo-time parameter, s , that determines a position along a streamline. Streamlines are the curves $\mathbf{x} = \mathbf{X}(s; \mathbf{a}, t)$ computed with (\mathbf{a}, t) held fixed, but with

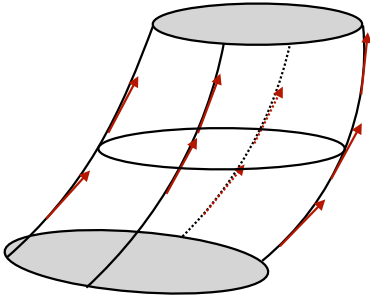


FIGURE 14.5: This image shows an example streamtube. The side boundaries of a streamtube consist of streamlines. At each point of a streamline, the local tangent vector equals to the velocity field (see equation (14.74)). Streamlines are identical to pathlines only for steady flow; they differ for unsteady flows. Hence, for unsteady flows, particle trajectories generally cross through the streamtube boundary.

the pseudo-time varied

$$\frac{\partial \mathbf{X}(s; \mathbf{a}, t)}{\partial s} = \mathbf{v}[\mathbf{X}(s; \mathbf{a}, t), t] \quad (14.76a)$$

$$\mathbf{X}(s = 0; \mathbf{a}, t) = \mathbf{a}. \quad (14.76b)$$

Again, both the material coordinate \mathbf{a} and time t are held fixed when determining streamlines, so that (\mathbf{a}, t) act as parameters to distinguish streamlines. Streamlines thus do not know about the time evolution of unsteady flow. Instead, streamlines only sample a snapshot of the velocity field; they are freshly computed at each time instance.

A *streamtube* is a bundle of streamlines crossing through an arbitrary closed curve (see Figure 14.5). Hence, at each time instance, streamtube sides are parallel to the velocity vector. Furthermore, when the flow is steady then streamlines are identical to material particle pathlines. Hence, a streamtube is a material tube for steady flow, in which case no fluid particles cross the streamtube boundary.

14.9.3 Distinguishing streamlines and pathlines

The tangent to a streamline gives the velocity at a single point in time, whereas the tangent to a material pathline (i.e., a trajectory) gives the velocity at subsequent times. These tangents are identical when the flow is steady. However, if the flow is time dependent (unsteady), then streamlines differ from material pathlines. Furthermore, for unsteady flow, the pseudo-time parameter, s , determining the streamlines in equation (14.76a) is not equal to the time, t , used to compute fluid particle trajectories in equation (14.71a). Consequently, the condition $\mathbf{v} \cdot \hat{\mathbf{n}} = 0$ satisfied at each instance by a streamline does not ensure that fluid particles do not cross streamlines. The reason is that a material pathline moves with the fluid in such a way that

$$(\mathbf{v} - \mathbf{v}^{\text{line}}) \cdot \hat{\mathbf{n}} = 0 \implies \mathbf{v} \cdot \hat{\mathbf{n}} = \mathbf{v}^{\text{line}} \cdot \hat{\mathbf{n}} \quad \text{material lines,} \quad (14.77)$$

where \mathbf{v}^{line} is the velocity of a point on the material pathline. The material pathline thus moves so that no fluid particles cross it. Only when the flow is steady, so that $\mathbf{v}^{\text{line}} \cdot \hat{\mathbf{n}} = 0$, will material pathlines and streamlines be equal. That is, the streamline constraint $\mathbf{v} \cdot \hat{\mathbf{n}} = 0$ is not a material constraint when $\mathbf{v}^{\text{line}} \cdot \hat{\mathbf{n}} \neq 0$. The key point is that streamlines do not probe the time behavior of the flow, so they do not know whether the velocity is steady or unsteady.

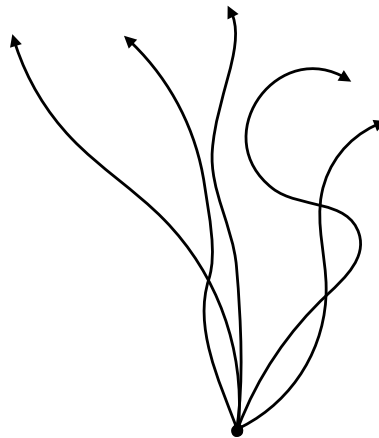


FIGURE 14.6: A suite of trajectories emanating from a single point. Common approximate realizations include the paths of fluid particles that leave a chimney, or the smoke from a source like a burning stick or torch. A streakline is defined as the accumulation of positions at time t of particles that passed through the common point at some earlier time $s < t$.

14.9.4 Fluid streaklines

A *streakline* is a curve obtained by connecting the positions for all fluid particles that emanate from a fixed point in space (see Figure 14.6). Streaklines are simple to define conceptually and to realize experimentally. However, they are a bit convoluted to specify mathematically. We thus present two formulations.

At any time t , the streakline passing through a fixed point \mathbf{y} is a curve going from \mathbf{y} to $\mathbf{X}(\mathbf{y}, t)$, the position reached by the particle initialized at $t = 0$ at the point \mathbf{y} . A particle is on the streakline if it passed the fixed point \mathbf{y} at some time between 0 and t . If this time was s , then the material coordinate of the particle would be given by $\mathbf{a}(\mathbf{y}, s)$ (see equation (14.8) relating the material coordinate to its corresponding laboratory position). Furthermore, at time t , this particle is at \mathbf{x} , so that the equation of the streakline at time t is

$$\mathbf{x} = \mathbf{X}[\mathbf{a}(\mathbf{y}, s), t] \quad 0 \leq s \leq t. \quad (14.78)$$

We can connect the streakline specification to that given for a pathline and streamline through the following. A streakline at some time instance \tilde{t} is a curve defined by fixing \tilde{t} and varying s over $s \leq \tilde{t}$ in the function $\mathbf{X}(s; \mathbf{a}, \tilde{t})$. We determine the curves $\mathbf{x} = \mathbf{X}(s; \mathbf{a}, \tilde{t})$ by solving the following set of initial value problems for trajectories with initial conditions imposed at $t = s$ rather than $t = 0$

$$\frac{\partial \mathbf{X}(s; \mathbf{a}, t)}{\partial t} = \mathbf{v}[\mathbf{X}(s; \mathbf{a}, t), t] \quad (14.79a)$$

$$\mathbf{X}(t = s; \mathbf{a}, t) = \mathbf{a}. \quad (14.79b)$$

Note that \mathbf{a} remains fixed, as we start all trajectories determining a streakline from the same initial point (e.g., the chimney does not move). A streakline can thus be generated by emitting a dye from a point over a time interval equal to the range of s , with the dye following fluid particle trajectories.

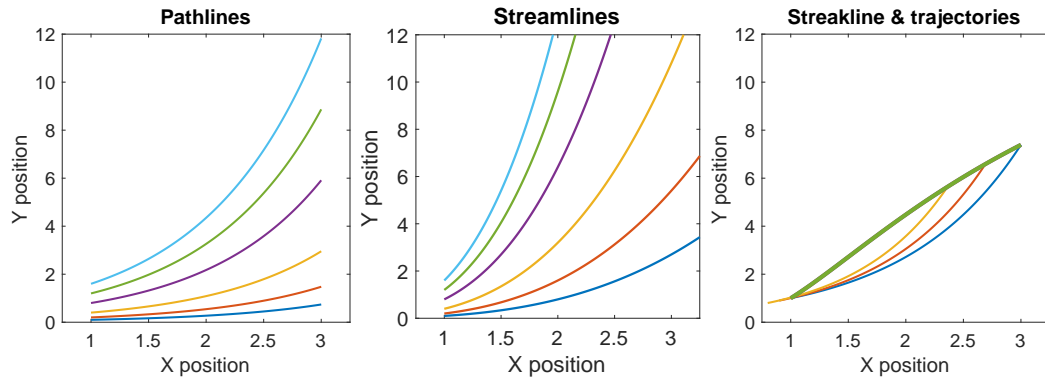


FIGURE 14.7: Left panel: sample pathlines $X(t) = X_0(1 + t/\tau)$ and $Y(t) = Y_0 e^{t/\tau}$ (see equations (14.82a) and (14.82b)) during times $t \in [0, 2]$. The trajectories drawn here all start at $X_0 = 1$ and set the parameter $\tau = 1$. Note that those pathlines with $X_0 = 0$ remain on the y-axis, and those with $Y_0 = 0$ remain on the x-axis. Middle panel: Sample streamlines $X(s; t) = X_0 e^{s/(\tau+t)}$ and $Y(s; t) = Y_0 e^{s/\tau}$ (see equations (14.85a) and (14.85b)). We set $t = 2$ and let the pseudo-time run from $s \in [0, 4]$. All streamlines shown here start at $X_0 = 1$. Note that those that start with $X_0 = 0$ remain on the y-axis, and those that start with $Y_0 = 0$ remain on the x-axis. Right panel: sample analytic streakline (dark bold line) at $t = 2$ according to equations (14.88a) and (14.88b). This streakline is determined by the position of particles at $t = 2$ that pass through $(X, Y) = (1, 1)$ during times $t \in (-\infty, 2)$. We show three sample trajectories that fall onto the streakline. The longest trajectory starts at $(X, Y) = (1, 1)$ at $t = 0$, whereas the two shorter trajectories pass through $(X, Y) = (1, 1)$ at some time $0 < t < 2$. Notice the distinction between all three flow lines, which is to be expected since the flow field is unsteady.

14.9.5 An analytic example of flow lines

Consider the following two-dimensional example as taken from Section 4.13 of [Aris \(1962\)](#). Let the Eulerian velocity field be given by

$$u = \frac{x}{\tau + t} \quad \text{and} \quad v = \frac{y}{\tau} \quad \text{and} \quad w = 0, \quad (14.80)$$

where $\tau > 0$ is a constant with the dimensions of time.

Pathlines

Pathlines are determined by solving the trajectory equations

$$\frac{dX(t)}{dt} = \frac{X(t)}{\tau + t} \quad \text{and} \quad \frac{dY(t)}{dt} = \frac{Y(t)}{\tau} \quad \text{and} \quad \frac{dZ(t)}{dt} = 0, \quad (14.81)$$

which are found to be

$$X(t) = X_0(1 + t/\tau) \quad (14.82a)$$

$$Y(t) = Y_0 e^{t/\tau} \quad (14.82b)$$

$$Z(t) = Z_0, \quad (14.82c)$$

where $\mathbf{X}(t = 0) = \mathbf{X}_0$. Sample trajectories are shown in Figure 14.7 over time $t \in [0, 2]$. We can eliminate time to yield a curve in the horizontal (x, y) plane

$$y = Y_0 e^{(x-X_0)/X_0}. \quad (14.83)$$

Streamlines

Streamlines are determined by solving the differential equations

$$\frac{dX(s; t)}{ds} = \frac{X(s; t)}{\tau + t} \quad \text{and} \quad \frac{dY(s; t)}{ds} = \frac{Y(s; t)}{\tau} \quad \text{and} \quad \frac{dZ(s; t)}{ds} = 0, \quad (14.84)$$

where time, t , is a fixed parameter whereas the pseudo-time, s , is varied. Integration renders the streamlines

$$X(s; t) = X_0 e^{s/(\tau+t)} \quad (14.85a)$$

$$Y(s; t) = Y_0 e^{s/\tau} \quad (14.85b)$$

$$Z(s; t) = Z_0. \quad (14.85c)$$

Sample streamlines are shown in Figure 14.7. Note that we can eliminate the pseudo-time s to render a curve in the horizontal (x, y) plane

$$y = Y_0 \left[\frac{x}{X_0} \right]^{(\tau+t)/\tau} \quad (14.86a)$$

$$z = Z_0. \quad (14.86b)$$

Streaklines

For streaklines, invert the trajectory expressions (14.82a)-(14.82b) to find the material coordinates $\mathbf{a}(\mathbf{y}, s)$ in the form

$$a_1 = \frac{y_1}{1 + s/\tau} \quad \text{and} \quad a_2 = y_2 e^{-s/\tau} \quad \text{and} \quad a_3 = y_3. \quad (14.87)$$

We next evaluate the trajectory expressions (14.82a)-(14.82b) with \mathbf{a} as the initial positions to find the streaklines

$$X(s; \mathbf{a}, t) = \frac{y_1 (1 + t/\tau)}{1 + s/\tau} \quad (14.88a)$$

$$Y(s; \mathbf{a}, t) = y_2 e^{(t-s)/\tau} \quad (14.88b)$$

$$Z(s; \mathbf{a}, t) = y_3. \quad (14.88c)$$

Figure 14.7 illustrates the streakline for a particular point $(X, Y) = (1, 1)$.

14.9.6 Further study

A discussion of flow lines can be found in most books on fluid mechanics. The presentation here borrows from Sections 4.11-4.13 of [Aris \(1962\)](#), Section 3.3 of [Kundu et al. \(2016\)](#), and online lecture notes on fluid kinematics from Professor McIntyre of Cambridge University.



14.10 Exercises

EXERCISE 14.1: FLUID VELOCITY AND ACCELERATION DERIVED FROM A TRAJECTORY

Following the example in Section 14.6.7, consider the one-dimensional fluid particle trajectory

$$\mathbf{X}(t) = \hat{\mathbf{x}} X(t) = \hat{\mathbf{x}} [k(t - t_0)^2 + x_0^3]^{1/3}, \quad (14.89)$$

where k is a constant with dimensions $\text{L}^3 \text{T}^{-2}$, x_0 is the particle position at time t_0 , and $\hat{\mathbf{x}}$ is the fixed Cartesian unit vector.

- (a) Determine the velocity of the fluid particle.
- (b) Determine the acceleration of the fluid particle.
- (c) Determine the Eulerian velocity field.
- (d) Determine the Eulerian acceleration field and show that it equals to the particle acceleration when evaluated at the field point, $\mathbf{x} = \mathbf{X}(t)$.

EXERCISE 14.2: MATERIAL EVOLUTION OF THE PARTIAL DERIVATIVE OF A FUNCTION

In this exercise we establish some properties of the material time derivative operator when acting on spatial derivatives of a scalar field.

- (a) If a scalar field Π is materially constant, prove that the material evolution of its spatial derivative is given by

$$\frac{D(\partial_m \Pi)}{Dt} = -\partial_m \mathbf{v} \cdot \nabla \Pi. \quad (14.90)$$

For example, if $D\Pi/Dt = 0$, then the zonal partial derivative $\partial_x \Pi$ has a material time derivative given by

$$\frac{D(\partial \Pi / \partial x)}{Dt} = -\frac{\partial \mathbf{v}}{\partial x} \cdot \nabla \Pi. \quad (14.91)$$

- (b) What is the material time derivative of $\nabla \Pi$ for the case that Π is not materially constant? Write your answer in a manner that clearly shows that the partial space derivative does not commute with the material time derivative. That is,

$$\frac{D(\partial_m \Pi)}{Dt} \neq \partial_m \frac{D\Pi}{Dt}. \quad (14.92)$$

Show what term appears on the right hand side to produce an equality.

Hint: Some might find it more suitable to first solve the general case in part (a) and then specialize to $D\Pi/Dt = 0$ in part (b). Also, use Cartesian tensors for convenience.



Chapter 15

MATERIAL FLUID OBJECTS

Draw an imaginary line, area, or volume within a perfect fluid. Since the fluid is perfect, all fluid particles that start on the geometric object remain on the object, even as the shape of the geometric object is deformed by the moving fluid. We say that the geometric object is a perfectly *coherent structure*. We study the kinematics of such objects in this chapter by using both Lagrangian and Eulerian descriptions, with the two offering complementary insights. Some extra attention is given to the kinematics of two-dimensional flow due to the relative mathematical ease and the associated intuition that proves useful for more general three dimensional flows.

The kinematic ideas developed in this chapter for a perfect fluid have use in the study of mixing and transport within real fluids (e.g., [Ottino \(1989\)](#)). That is, for a real fluid we also find it useful to study geometric objects that follow the flow. However, in a real fluid such objects are not perfectly coherent since matter generally crosses all surfaces through diffusive mixing. The question then becomes whether there are special surfaces where such mixing is suppressed, with this question forming a key part of the study of coherent structures in real fluids (e.g., [Haller \(2015\)](#)).

READER'S GUIDE FOR THIS CHAPTER

This chapter builds from the kinematics of Chapter 14 and makes some use of Section 3.1 of [Batchelor \(1967\)](#). The discussion of the Helmholtz decomposition in Section 15.7 assumes an understanding of elliptic partial differential equations from Section 3.5, as well as Stokes' curl theorem and Gauss's divergence theorem from Chapter 2. The presentation is restricted to Cartesian tensors to reduce the math overhead. Consequently, all tensor labels are downstairs with no distinction between covariant and contravariant. Extensions to arbitrary coordinates follow the methods of Chapter 8.

15.1	Loose threads	310
15.2	Increments operators in material and position space	310
15.2.1	Eulerian/position space increments	310
15.2.2	Lagrangian/material space increments	311
15.2.3	Duality between Eulerian and Lagrangian perspectives	311
15.3	Evolution of material curves	312
15.3.1	Deformation gradient tensor	312
15.3.2	Cauchy-Green strain tensor	313
15.3.3	Kinematic evolution equation	313
15.3.4	Cauchy's solution	313
15.3.5	Velocity gradient tensor	315
15.3.6	Stretching and tilting of a material lines	316
15.3.7	Rate of strain tensor	316

15.3.8	Rotation tensor	317
15.3.9	Cauchy-Stokes decomposition	318
15.4	Evolution of material surfaces	318
15.4.1	Surfaces in three-dimensional flow	318
15.4.2	Evolution of the area	319
15.4.3	Evolution of the normal vector	321
15.4.4	Material area in two-dimensional flow	322
15.5	Volume, thickness, and the Jacobian	322
15.5.1	Material parcel volume	322
15.5.2	Evolution of the column thickness	323
15.5.3	Evolution of the Jacobian of transformation	324
15.6	Kinematics of two-dimensional flow	324
15.6.1	Diverging flow	325
15.6.2	Rotational flow with nonzero vorticity	325
15.6.3	Flow with nonzero deformation	325
15.6.4	Further study	326
15.7	Helmholtz decomposition	327
15.7.1	Summarizing the Helmholtz decomposition	327
15.7.2	Concerning a harmonic contribution	328
15.7.3	Self-consistency conditions	331
15.7.4	Orthogonality with the L^2 inner product	332
15.7.5	Uniqueness of the decomposition	333
15.8	Exercises	335

15.1 Loose threads

- Convert Figure 15.2 into Keynote and gray shade the color.

15.2 Increments operators in material and position space

We here develop expressions for the differential increment of a function in both position/Eulerian space (\mathbf{x} -space) and in material/Lagrangian space (\mathbf{a} -space). These relations are of use for the subsequent development.

15.2.1 Eulerian/position space increments

In Section 14.6.1, we considered the space-time increment of a function. Here we consider just the space increment, as defined by the differential increment of a function evaluated at the same time but at two infinitesimally close points in space

$$d\Pi(\mathbf{x}, t) = \Pi(\mathbf{x} + d\mathbf{x}, t) - \Pi(\mathbf{x}, t) \quad (15.1a)$$

$$= (d\mathbf{x} \cdot \nabla)\Pi. \quad (15.1b)$$

The dimensionless increment operator

$$d\mathbf{x} \cdot \nabla = dx_m \frac{\partial}{\partial x_m} \quad (15.2)$$

is a scalar since it remains form invariant when switching to another set of position coordinates.¹

¹The operator (15.2) is represented using Cartesian coordinates. However, $d\mathbf{x} \cdot \nabla$ is the form of the operator for arbitrary coordinates, as found by making use of the general tensor analysis developed in Chapter 8.

15.2.2 Lagrangian/material space increments

Consider the same function, Π , evaluated on a material fluid particle trajectory, and write this Lagrangian function as in Section 14.6.5

$$\Pi^L(\mathbf{a}, t) \equiv \Pi[\mathbf{X}(\mathbf{a}, t), t], \quad (15.3)$$

where the notation $\Pi^L(\mathbf{a}, t)$ is a shorthand defined by this equality. Now consider an infinitesimal increment of $\Pi^L(\mathbf{a}, t)$ within material coordinate space. This increment represents the difference of Π when evaluated on two separate fluid particles labelled by \mathbf{a} and $\mathbf{a} + \delta\mathbf{a}$. Note that we use the δ symbol to signal material increments. Just like when working in \mathbf{x} -space, we can take a Taylor series and truncate to leading order, in which case

$$\delta\Pi^L(\mathbf{a}, t) = \Pi[\mathbf{X}(\mathbf{a} + \delta\mathbf{a}, t), t] - \Pi[\mathbf{X}(\mathbf{a}, t), t] \quad (15.4a)$$

$$= \Pi^L(\mathbf{a} + \delta\mathbf{a}, t) - \Pi^L(\mathbf{a}, t) \quad (15.4b)$$

$$= (\delta\mathbf{a} \cdot \nabla_{\mathbf{a}})\Pi^L(\mathbf{a}, t). \quad (15.4c)$$

The dimensionless operator

$$\delta\mathbf{a} \cdot \nabla_{\mathbf{a}} = \delta a_j \frac{\partial}{\partial a_j} \quad (15.5)$$

is a scalar since it remains form invariant when switching to another set of material coordinates.² We use the notation $\nabla_{\mathbf{a}}$ to emphasize that the gradient operator is in material space rather than position space.

15.2.3 Duality between Eulerian and Lagrangian perspectives

By construction, the value of a function at a postion \mathbf{x} (Eulerian perspective) equals to the function evaluated on a moving fluid particle (Lagrangian perspective) at the instance the particle trajectory passes through \mathbf{x} . Mathematically, this identity takes the form

$$\Pi^L(\mathbf{a}, t) = \Pi[\mathbf{X}(\mathbf{a}, t), t] = \Pi(\mathbf{x}, t) \quad \text{if } \mathbf{X}(\mathbf{a}, t) = \mathbf{x}. \quad (15.6)$$

Likewise, if the infinitesimal increment in space, $\delta\mathbf{x}$, equals to the vector increment of the two fluid particles,

$$\delta\mathbf{X}(\mathbf{a}, t) = \mathbf{X}(\mathbf{a} + \delta\mathbf{a}, t) - \mathbf{X}(\mathbf{a}, t), \quad (15.7)$$

then the functional increments are identical

$$\delta\Pi^L(\mathbf{a}, t) = \delta\Pi(\mathbf{x}, t) \quad \text{if } \delta\mathbf{X}(\mathbf{a}, t) = \delta\mathbf{x}, \quad (15.8)$$

where

$$\delta\Pi(\mathbf{x}, t) = \Pi(\mathbf{x} + \delta\mathbf{x}, t) - \Pi(\mathbf{x}, t). \quad (15.9)$$

These identities allow us to develop relations using either a Lagrangian or an Eulerian perspective, and then to interpret them in the complementary perspective. It is very useful in studying fluid mechanics to become versed in the routine use of this Eulerian/Lagrangian duality.

²As for the position space (\mathbf{x} -space), this invariance holds when using arbitrary material coordinates by making use of the general tensor analysis formalism of Chapter 8.

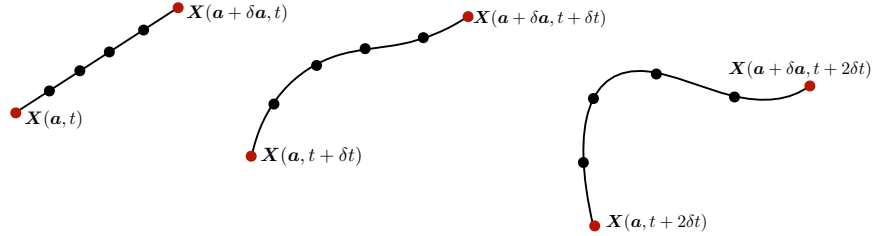


FIGURE 15.1: Three time instances of a material curve with endpoints determined by the trajectories of two fluid particles, $\mathbf{X}(\mathbf{a}, t)$ and $\mathbf{X}(\mathbf{a} + \delta\mathbf{a}, t)$. All points between the endpoints are part of the material curve, and the curve moves through the fluid by following the trajectories of the fluid particles. Kinematics of the curve are determined by properties of the velocity gradient tensor discussed in Section 15.3.5.

15.3 Evolution of material curves

Material curves are one-dimensional geometric objects that follow fluid particles in a perfect fluid. We initialize a material curve by drawing a line in the fluid and then following the fluid particles contained on the initial line. The material curve is stretched and folded by the fluid flow (see Figure 15.1). But since the fluid is perfect, the same fluid particles remain on the curve so that it retains exact coherency. We here develop the rudimentary kinematics of material curves.

15.3.1 Deformation gradient tensor

Assume the material curve is initially infinitesimal with endpoints given by fluid particles with trajectories $\mathbf{X}(\mathbf{a}, t)$ and $\mathbf{X}(\mathbf{a} + \delta\mathbf{a}, t)$ (see Figure 15.1). At time t , the vector displacement between these two particles is written

$$\delta\mathbf{X}(\mathbf{a}, t) = \mathbf{X}(\mathbf{a} + \delta\mathbf{a}, t) - \mathbf{X}(\mathbf{a}, t). \quad (15.10)$$

Expanding this expression to leading order yields an expression of *Cauchy's solution* (further explored in Section 15.3.4)

$$\delta\mathbf{X}(\mathbf{a}, t) = \mathbf{X}(\mathbf{a} + \delta\mathbf{a}, t) - \mathbf{X}(\mathbf{a}, t) \approx (\delta\mathbf{a} \cdot \nabla_{\mathbf{a}}) \mathbf{X}(\mathbf{a}, t), \quad (15.11)$$

where again $\nabla_{\mathbf{a}}$ is the gradient operator acting on the material coordinates. Writing this equation in component form leads to

$$\delta X_m = \delta a_j \frac{\partial X_m}{\partial a_j}. \quad (15.12)$$

As in Chapter 14, we assign the labels m, n, p for position/Eulerian coordinates, \mathbf{x} , and the labels i, j, k for material/Lagrangian coordinates, \mathbf{a} .

The components

$$F_{mj} \equiv \frac{\partial X_m}{\partial a_j} \quad (15.13)$$

appearing in equation (15.12) form elements of the transformation matrix linking position space (\mathbf{x} -space) to material space (\mathbf{a} -space). We already encountered this object in Section 14.5.3 (see equation (14.9)). In the continuum mechanics literature, the object (15.13) is known as the *displacement gradient tensor* or the *deformation gradient tensor*.³

³The deformation gradient tensor is a two-point tensor, connecting points in \mathbf{x} -space to points in \mathbf{a} -space.

15.3.2 Cauchy-Green strain tensor

The deformation gradient tensor plays a role in measuring the length of material curves. We see this role by considering the squared length of an infinitesimal portion of a material curve

$$\delta \mathbf{X} \cdot \delta \mathbf{X} = \frac{\partial \mathbf{X}}{\partial a_i} \cdot \frac{\partial \mathbf{X}}{\partial a_j} \delta a_i \delta a_j \equiv C_{ij} \delta a_i \delta a_j. \quad (15.14)$$

Algebraically, this expression is a quadratic form, and the symmetric tensor

$$C_{ij} \equiv \frac{\partial \mathbf{X}}{\partial a_i} \cdot \frac{\partial \mathbf{X}}{\partial a_j} = F_{mi} F_{mj} \quad (15.15)$$

is the metric tensor that provides the means to measure distance along an infinitesimal material curve. This metric tensor is called the *Cauchy-Green strain* tensor.

15.3.3 Kinematic evolution equation

Now consider the material time derivative of the material increment

$$\frac{\partial[\delta \mathbf{X}(\mathbf{a}, t)]}{\partial t} = \frac{\partial \mathbf{X}(\mathbf{a} + \delta \mathbf{a}, t)}{\partial t} - \frac{\partial \mathbf{X}(\mathbf{a}, t)}{\partial t} \quad (15.16a)$$

$$= \mathbf{v}^L(\mathbf{a} + \delta \mathbf{a}, t) - \mathbf{v}^L(\mathbf{a}, t) \quad (15.16b)$$

$$\equiv \delta \mathbf{v}^L(\mathbf{a}, t). \quad (15.16c)$$

In these equations, we introduced the Lagrangian velocity

$$\mathbf{v}^L(\mathbf{a}, t) = \mathbf{v}[\mathbf{X}(\mathbf{a}, t), t] \quad (15.17)$$

as per equation (14.32) and the discussion in Section 15.2.2. As for the manipulations in Section 15.3.1, we can massage the expression (15.16c) by performing a Taylor series expansion and truncating to leading order

$$\frac{\partial[\delta \mathbf{X}(\mathbf{a}, t)]}{\partial t} = \delta \mathbf{v}^L(\mathbf{a}, t) = (\delta \mathbf{a} \cdot \nabla_{\mathbf{a}}) \mathbf{v}^L(\mathbf{a}, t). \quad (15.18)$$

Alternatively, we can choose to evaluate this expression using an Eulerian perspective (see Section 15.2.3), in which case

$$\frac{D(\delta \mathbf{x})}{Dt} = \delta \mathbf{v}(\mathbf{x}, t) = (\delta \mathbf{x} \cdot \nabla_{\mathbf{x}}) \mathbf{v}(\mathbf{x}, t). \quad (15.19)$$

15.3.4 Cauchy's solution

We can determine a general solution to the kinematic evolution equation (15.19) following the method used by Cauchy⁴ to solve the perfect fluid barotropic vorticity equation discussed in Section 37.5. Indeed, we already encountered the Cauchy solution in Section 15.3.1. We rederive it here following a more laborious route. Doing so exposes formalism that can be of general use when working with Lagrangian coordinates, and it offers further insight into the meaning of the solution.

⁴See [Frisch and Villone \(2014\)](#) for an insightful discussion of the enduring impact of Cauchy's solution.

Derivation

The derivation that follows involves strategic uses of the transformation between \mathbf{a} -space and \mathbf{x} -space, which we start by writing

$$\frac{D(\delta x_n)}{Dt} = (\delta \mathbf{x} \cdot \nabla_{\mathbf{x}}) v_n \quad \text{kinematic evolution} \quad (15.20a)$$

$$= \delta x_m \frac{\partial}{\partial x_m} \left[\frac{Dx_n}{Dt} \right] \quad v_n = Dx_n/Dt \quad (15.20b)$$

$$= \delta x_m \frac{\partial a_j}{\partial x_m} \frac{\partial}{\partial a_j} \left[\frac{Dx_n}{Dt} \right] \quad \text{chain rule} \quad (15.20c)$$

$$= \delta x_m \frac{\partial a_j}{\partial x_m} \frac{D}{Dt} \frac{\partial x_n}{\partial a_j} \quad \text{commute } \partial/\partial a_j \text{ and } D/Dt \quad (15.20d)$$

$$= \delta x_m \frac{D}{Dt} \left[\frac{\partial a_j}{\partial x_m} \frac{\partial x_n}{\partial a_j} \right] - \delta x_m \frac{D}{Dt} \left[\frac{\partial a_j}{\partial x_m} \right] \frac{\partial x_n}{\partial a_j} \quad \text{move } D/Dt \quad (15.20e)$$

$$= -\delta x_m \frac{D}{Dt} \left[\frac{\partial a_j}{\partial x_m} \right] \frac{\partial x_n}{\partial a_j}. \quad \frac{\partial a_j}{\partial x_m} \frac{\partial x_n}{\partial a_j} = \delta_{mn} = \text{constant.} \quad (15.20f)$$

The commutation in equation (15.20d) follows since the material coordinates are fixed on a fluid particle so that

$$\frac{\partial}{\partial a_j} \frac{D}{Dt} = \frac{D}{Dt} \frac{\partial}{\partial a_j}. \quad (15.21)$$

Contracting the identity (15.20f) with $\partial a_k / \partial x_n$ yields

$$\frac{\partial a_k}{\partial x_n} \frac{D(\delta x_n)}{Dt} = -\delta x_m \frac{D}{Dt} \left[\frac{\partial a_j}{\partial x_m} \right] \frac{\partial x_n}{\partial a_j} \frac{\partial a_k}{\partial x_n} \quad \text{contraction (inner product)} \quad (15.22a)$$

$$= -\delta x_m \frac{D}{Dt} \left[\frac{\partial a_k}{\partial x_m} \right] \quad \frac{\partial x_n}{\partial a_j} \frac{\partial a_k}{\partial x_n} = \delta_{jk} \quad (15.22b)$$

$$= -\delta x_n \frac{D}{Dt} \left[\frac{\partial a_k}{\partial x_n} \right] \quad \text{change indices from } m \text{ to } n. \quad (15.22c)$$

We can thus identify the material invariant

$$\frac{D}{Dt} \left[\delta x_n \frac{\partial a_k}{\partial x_n} \right] = 0 \implies \delta \mathbf{x} \cdot \nabla_{\mathbf{x}} a_k = \text{material invariant.} \quad (15.23)$$

This result follows rather trivially by recognizing the coordinate transformation

$$\delta \mathbf{x} \cdot \nabla_{\mathbf{x}} a_k = \delta x_n \frac{\partial a_k}{\partial x_n} = \delta a_k, \quad (15.24)$$

and noting that δa_k is a material invariant, in which case $\delta \mathbf{x} \cdot \nabla_{\mathbf{x}} a_k$ must also be materially invariant.

If we choose the material coordinates as the initial positions of fluid particles,

$$\mathbf{a} = \mathbf{x}(t = 0), \quad (15.25)$$

then the inverse transformation matrix element at the initial time is given by the unit tensor

$$\frac{\partial a_k}{\partial x_m} = \delta_{km} \quad \text{at } t = 0, \quad (15.26)$$

so that the material invariance in equation (15.23) leads to

$$\delta\mathbf{x}(t) \cdot \nabla_{\mathbf{x}} a_k = \delta x_k(t=0) \iff \delta x_m \frac{\partial a_k}{\partial x_m} = \delta x_k(t=0). \quad (15.27)$$

Inverting this equation by contracting with $\partial x_n / \partial a_k$ and using $(\partial x_n / \partial a_k)(\partial a_k / \partial x_m) = \delta_{mn}$ leads to *Cauchy's solution*

$$\delta x_n(t) = \delta x_k(t=0) \frac{\partial x_n}{\partial a_k}. \quad (15.28)$$

Discussion and extension to vorticity

The Cauchy solution (15.28) says that the increment along a line segment defined by fluid particles, $\delta\mathbf{x}(t)$, expands or contracts according to the time and space dependent transformation matrix, $\partial x_n / \partial a_k$. This result follows from our assumption that the increment is defined by fixed \mathbf{a} -space coordinates (fixed fluid particles), which then constrains the increment's \mathbf{x} -space evolution. It is also an expression that we wrote down, rather trivially, in equation (15.11) when performing a truncated Taylor series expansion of the spatial increment between two material fluid particles. The ability to derive certain kinematic results using either simple (indeed trivial) methods versus more long-winded methods is somewhat exemplary of fluid kinematics. Both approaches offer distinct insights as well as confidence in the validity of the result.⁵

As seen in Section 37.3, the relative vorticity, $\boldsymbol{\omega} = \nabla \times \mathbf{v}$, for a homogeneous inviscid, barotropic fluid satisfies the same kinematic equation (15.19) as for a material line increment

$$\frac{D\boldsymbol{\omega}}{Dt} = (\boldsymbol{\omega} \cdot \nabla_{\mathbf{x}}) \mathbf{v}(\mathbf{x}, t). \quad (15.29)$$

We can thus invoke the Cauchy solution to write the vorticity

$$\omega_n(t) = \omega_k(t=0) \frac{\partial x_n}{\partial a_k}, \quad (15.30)$$

which is one form of Kelvin's circulation theorem detailed in Section 37.2.

15.3.5 Velocity gradient tensor

Writing the Eulerian result (15.19) in component form leads to

$$\frac{D(\delta x_m)}{Dt} = \frac{D(x_m + \delta x_m - x_m)}{Dt} = v_m(\mathbf{x} + \delta\mathbf{x}) - v_m(\mathbf{x}) = \delta x_n \frac{\partial v_m}{\partial x_n}. \quad (15.31)$$

The derivatives $\partial v_m / \partial x_n$ form components to the second-order *velocity gradient* tensor whose dimensions are inverse time (i.e., a rate). The velocity gradient tensor determines how an infinitesimal material line is deformed as it moves through the flow field.

As with any matrix, a second-order tensor can be decomposed into its symmetric and anti-symmetric components

$$\frac{\partial v_m}{\partial x_n} = \frac{1}{2} \left[\frac{\partial v_m}{\partial x_n} + \frac{\partial v_n}{\partial x_m} \right] + \frac{1}{2} \left[\frac{\partial v_m}{\partial x_n} - \frac{\partial v_n}{\partial x_m} \right] \equiv \mathbb{S}_{mn} + \mathbb{R}_{mn}, \quad (15.32)$$

⁵If there is more than one way to solve a problem, then do so, even if one of those ways is much more tedious!

where⁶

$$\mathbb{S}_{mn} = \frac{1}{2} \left[\frac{\partial v_m}{\partial x_n} + \frac{\partial v_n}{\partial x_m} \right] = \mathbb{S}_{nm} \quad \text{rate of strain tensor} \quad (15.33a)$$

$$\mathbb{R}_{mn} = \frac{1}{2} \left[\frac{\partial v_m}{\partial x_n} - \frac{\partial v_n}{\partial x_m} \right] = -\mathbb{R}_{nm} \quad \text{rotation tensor.} \quad (15.33b)$$

As seen in the following, these tensors affect the motion of a line element in very distinct manners.

15.3.6 Stretching and tilting of a material lines

Consider a material line that is initially aligned with the vertical axis

$$\delta \mathbf{x}_{t=0} = \hat{\mathbf{z}} \delta Z_0. \quad (15.34)$$

Consequently, the initial evolution of this material line takes on the form

$$\underbrace{\frac{D(\delta x)}{Dt}}_{\text{tilting}} = \delta Z_0 \underbrace{\left[\frac{\partial u}{\partial z} \right]}_{\text{tilting}} \quad \text{and} \quad \underbrace{\frac{D(\delta y)}{Dt}}_{\text{tilting}} = \delta Z_0 \underbrace{\left[\frac{\partial v}{\partial z} \right]}_{\text{tilting}} \quad \text{and} \quad \underbrace{\frac{D(\delta z)}{Dt}}_{\text{stretching}} = \delta Z_0 \underbrace{\left[\frac{\partial w}{\partial z} \right]}_{\text{stretching}}. \quad (15.35)$$

In the presence of a vertical derivative in the horizontal velocity field (vertical shear), the first and second terms create a non-zero projection of the material line onto the horizontal plane. That is, these terms *tilt* the material line. Additionally, in the presence of a vertical derivative in the vertical velocity, the material line is expanded or compressed along its initial axis. This term is called *stretching*. We return to the tilting and stretching mechanisms when discussing the dynamics of vorticity in Chapter 37. There, we see that vortex lines in a perfect fluid flow are material lines. Consequently, vortex lines are also affected by tilting and stretching just like a material line.

15.3.7 Rate of strain tensor

Recall the expression (15.14) for the squared length of a line element

$$\delta \mathbf{X} \cdot \delta \mathbf{X} = \frac{\partial \mathbf{X}}{\partial a_i} \cdot \frac{\partial \mathbf{X}}{\partial a_j} \delta a_i \delta a_j. \quad (15.36)$$

Its material time derivative is given by

$$\left[\frac{\partial (\delta \mathbf{X} \cdot \delta \mathbf{X})}{\partial t} \right]_a = 2 \frac{\partial \mathbf{v}^L}{\partial a_i} \cdot \frac{\partial \mathbf{X}}{\partial a_j} \delta a_i \delta a_j. \quad (15.37)$$

We can express this result using Eulerian \mathbf{x} -space coordinates by making use of the duality described in Section 15.2.3, which leads to

$$\frac{\partial \mathbf{v}^L}{\partial a_i} \delta a_i = \frac{\partial \mathbf{v}}{\partial x_n} \delta x_n \quad (15.38a)$$

$$\frac{\partial \mathbf{X}}{\partial a_j} \delta a_j = \delta \mathbf{x}, \quad (15.38b)$$

⁶The rate of strain tensor, \mathbb{S}_{mn} , is sometimes called the *deformation* tensor in the literature. We do not use this nomenclature to avoid confusion with the *deformation gradient* tensor defined by equation (15.13).

so that

$$\frac{D(\delta\mathbf{x} \cdot \delta\mathbf{x})}{Dt} = 2 \frac{\partial v_m}{\partial x_n} \delta x_n \delta x_m. \quad (15.39)$$

Since the product $\delta x_n \delta x_m$ is symmetric on the labels m, n , it projects out the symmetric portion of the velocity gradient tensor, thus yielding

$$\frac{1}{2} \frac{D(\delta\mathbf{x} \cdot \delta\mathbf{x})}{Dt} = \mathbb{S}_{mn} \delta x_n \delta x_m. \quad (15.40)$$

Consequently, the rate of strain tensor, \mathbb{S}_{mn} , determines the rate at which a material curve changes its length.

To help understand the result (15.40), consider two fluid particles initialized very close together. Equation (15.40) says that the distance between the two particles is modified so long as there are nonzero strains in the fluid flow, with strains measured by the rate of strain tensor. In the special case of a zero of strain tensor, then the curve retains a constant length.

As a symmetric matrix, the rate of strain tensor can be diagonalized, with the diagonal elements equal to the eigenvalues (e.g., see section 2.2 of [Segel \(1987\)](#)). Each eigenvalue measures the rate that material lines oriented according to the principle axes (eigenvectors) expand/contract under the impacts of straining motion in the fluid. According to equation (15.40), the expansion/contraction is exponential when aligned along the principle axes, with the exponential rate determined by the eigenvalues of \mathbb{S} . Furthermore, as shown in Section 15.5, the sum of these eigenvalues (given by the trace of the rate of strain tensor) measures the rate that a material volume changes through the divergence of the velocity

$$\mathbb{S}_{mm} = \nabla \cdot \mathbf{v}. \quad (15.41)$$

15.3.8 Rotation tensor

The rotation tensor is given by

$$\mathbb{R}_{mn} = (1/2) (\partial_n v_m - \partial_m v_n) = (1/2) (v_{m,n} - v_{n,m}), \quad (15.42)$$

with the second equality introducing the commonly used comma notation for the partial derivative; a notation that is helpful to keep the signs properly sorted with the definition. Notably, the rotation tensor is anti-symmetric:

$$\mathbb{R}_{mn} = -\mathbb{R}_{nm}. \quad (15.43)$$

Its components are related to the vorticity vector $\boldsymbol{\omega} = \nabla \times \mathbf{v}$ according to

$$\mathbb{R}_{mn} = -\epsilon_{mnp} \omega_p / 2 \iff \mathbb{R} = \frac{1}{2} \begin{bmatrix} 0 & -\omega_3 & \omega_2 \\ \omega_3 & 0 & -\omega_1 \\ -\omega_2 & \omega_1 & 0 \end{bmatrix} \iff \omega_p = -\epsilon_{pmn} \mathbb{R}_{mn}, \quad (15.44)$$

where the final expression made use of the identity (1.38) in the form

$$\epsilon_{mns} \epsilon_{mnp} = 2 \delta_{sp}. \quad (15.45)$$

We see that the squared rotation tensor equals to half the squared vorticity

$$\mathbb{R}^2 = \mathbb{R}_{mn} \mathbb{R}_{mn} = |\boldsymbol{\omega}|^2 / 2. \quad (15.46)$$

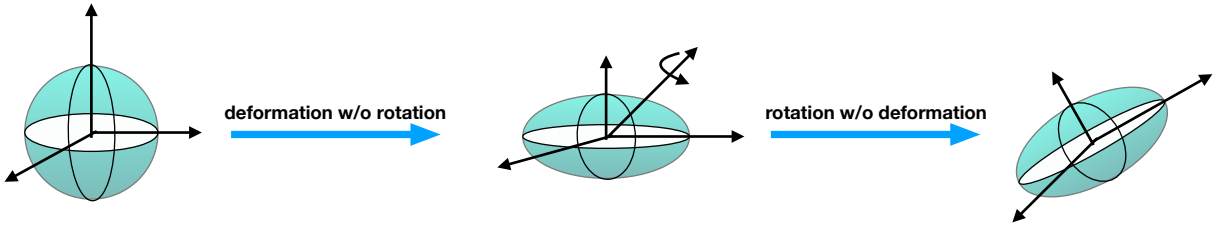


FIGURE 15.2: Schematic illustrating the Cauchy-Stokes decomposition of how fluid flow can modify a material region according to equation (15.48). First the sphere can be deformed without rotation, with this process encompassed by the rate of strate tensor, \mathbb{S}_{mn} . Next it can be rigidly rotated without changing its shape, as encompassed by the rotation tensor, \mathbb{R}_{mn} . The axes shown represent the principle axes so that deformation corresponds to expansion or contraction along the principle axes directions.

The contribution of the rotation matrix to evolution of the material curve is given by

$$\left[\frac{D(\delta x_m)}{Dt} \right]_{\text{rot}} = \mathbb{R}_{mn} \delta x_n = -(\epsilon_{mnp} \omega_p/2) \delta x_n \implies \left[\frac{D(\delta \mathbf{x})}{Dt} \right]_{\text{rot}} = \frac{1}{2} (\boldsymbol{\omega} \times \delta \mathbf{x}). \quad (15.47)$$

This relation is in the form of a pure rotation of the vector $\delta \mathbf{x}$ generated by the vector $\boldsymbol{\omega}/2$ (recall the discussion of rotations in Section 11.3). We thus conclude that the anti-symmetric rotation tensor, \mathbb{R} , provides a rigid body rotation to a material curve (or any infinitesimal fluid region) about the axis defined by the vorticity vector. It rotates the objects without altering the size (length, area, volume). Notably, when acting on vorticity the rotation tensor has no affect since $\boldsymbol{\omega} \times \boldsymbol{\omega} = 0$. We return to this point when discussing vortex filaments in Section 37.5.

15.3.9 Cauchy-Stokes decomposition

The above discussion of how fluid motion impacts on a material curve falls under the more general insights from the *Cauchy-Stokes decomposition theorem*. This theorem says that the arbitrary motion of a body can be decomposed into a uniform translation, dilation along three perpendicular axes, plus a rigid body rotation. Mathematically, this decomposition can be written by expanding equation (15.31) to read

$$v_m(\mathbf{x}, t) = v_m(\mathbf{x}_0, t) + \mathbb{S}_{mn} \delta x_n + \mathbb{R}_{mn} \delta x_n \iff \mathbf{v}(\mathbf{x}, t) = \mathbf{v}(\mathbf{x}_0, t) + \mathbb{S} \cdot \delta \mathbf{x} + \mathbb{R} \cdot \delta \mathbf{x}. \quad (15.48)$$

Figure 15.2 illustrates the deformation and rotation portion of this decomposition. A more thorough discussion of these fundamental kinematic notions can be found in Chapter 4 of [Aris \(1962\)](#), Section 3.1 of [Segel \(1987\)](#), and with a brief summary in Section 1.1 of [Olbers et al. \(2012\)](#).

15.4 Evolution of material surfaces

We here extend the discussion of material curves in Section 15.3 to a material surface such as that shown in Figure 15.3, with consideration given to both three-dimensional and two-dimensional flows.

15.4.1 Surfaces in three-dimensional flow

Following from the geometric interpretation of the vector product in Section 1.4.5, we here define a material surface by (see Figure 15.3)

$$\delta \mathcal{S} = \delta \mathbf{A} \times \delta \mathbf{B} \Rightarrow \delta \mathcal{S}_m = \epsilon_{mnp} \delta A_n \delta B_p \quad (15.49)$$

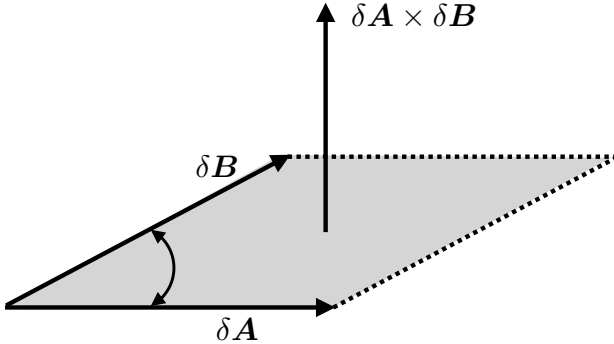


FIGURE 15.3: A material surface as defined by the cross product of two material line elements, $\delta\mathcal{S} = \delta\mathbf{A} \times \delta\mathbf{B}$. In the special case of $\delta\mathbf{A} = \hat{\mathbf{x}} \delta x$ and $\delta\mathbf{B} = \hat{\mathbf{y}} \delta y$, then $\delta\mathcal{S} = \delta x \delta y \hat{\mathbf{z}}$.

where $\delta\mathbf{A}$ and $\delta\mathbf{B}$ are non-parallel infinitesimal material lines. The surface projected onto the unit normal direction, $\hat{\mathbf{n}}$, is given by

$$\hat{\mathbf{n}} \cdot \delta\mathcal{S} = \hat{\mathbf{n}} \cdot (\delta\mathbf{A} \times \delta\mathbf{B}). \quad (15.50)$$

The evolution of the material surface is given by

$$\frac{D(\delta\mathcal{S})}{Dt} = \frac{D(\delta\mathbf{A})}{Dt} \times \delta\mathbf{B} + \delta\mathbf{A} \times \frac{D(\delta\mathbf{B})}{Dt} \quad (15.51a)$$

$$= [(\delta\mathbf{A} \cdot \nabla) \mathbf{v}] \times \delta\mathbf{B} + \delta\mathbf{A} \times [(\delta\mathbf{B} \cdot \nabla) \mathbf{v}], \quad (15.51b)$$

where the second equality made use of the material line evolution equation (15.19). To proceed we expose indices and make use of some tensor identities

$$\frac{D(\delta\mathcal{S}_m)}{Dt} = \epsilon_{mnp} [(\delta A_q \partial_q) v_n] \delta B_p + \epsilon_{mnp} \delta A_n [(\delta B_q \partial_q) v_p] \quad (15.52a)$$

$$= \epsilon_{mnp} [\delta A_q \delta B_p \partial_q v_n + \delta A_n \delta B_q \partial_q v_p] \quad (15.52b)$$

$$= \epsilon_{mnp} \partial_q v_n [\delta A_q \delta B_p - \delta A_p \delta B_q] \quad (15.52c)$$

$$= \epsilon_{mnp} \partial_q v_n \epsilon_{rqp} \delta\mathcal{S}_r \quad (15.52d)$$

$$= (\delta_{mr} \delta_{nq} - \delta_{mq} \delta_{nr}) \partial_q v_n \delta\mathcal{S}_r \quad (15.52e)$$

$$= (\nabla \cdot \mathbf{v}) \delta\mathcal{S}_m - (\partial_m \mathbf{v}) \cdot \delta\mathcal{S}. \quad (15.52f)$$

To reach this result we made use of the following identities available for the permutation symbol from Chapter 1

$$\delta A_q \delta B_p - \delta A_p \delta B_q = \epsilon_{rqp} \delta\mathcal{S}_r \quad (15.53a)$$

$$\epsilon_{mnp} \epsilon_{rqp} = \delta_{mr} \delta_{nq} - \delta_{mq} \delta_{nr} \quad (15.53b)$$

where δ_{mn} is the Kronecker tensor.

15.4.2 Evolution of the area

Now orient the material surface area according to its outward unit normal vector

$$\delta\mathcal{S} = \hat{\mathbf{n}} \delta\mathcal{S} \implies \delta\mathcal{S}_m = \hat{n}_m \delta\mathcal{S}, \quad (15.54)$$

where the magnitude of the area element is written

$$\delta\mathcal{S} = |\delta\mathcal{S}|. \quad (15.55)$$

Doing so brings equation (15.52f) to the form

$$\frac{1}{\delta\mathcal{S}} \frac{D(\hat{n}_m \delta\mathcal{S})}{Dt} = (\nabla \cdot \mathbf{v}) \hat{n}_m - (\partial_m \mathbf{v}) \cdot \hat{\mathbf{n}}. \quad (15.56)$$

We can thus develop evolution equations for the surface area, $\delta\mathcal{S}$, and the unit normal vector, $\hat{\mathbf{n}}$.

For the surface area evolution we take the inner product of equation (15.56) with \hat{n}_m to yield

$$\frac{1}{\delta\mathcal{S}} \frac{D\delta\mathcal{S}}{Dt} = \nabla \cdot \mathbf{v} - [(\hat{\mathbf{n}} \cdot \nabla) \mathbf{v}] \cdot \hat{\mathbf{n}} \quad (15.57)$$

where we set $\hat{\mathbf{n}} \cdot \hat{\mathbf{n}} = 1$ and followed the discussion in Section 2.1.5 to find that

$$\hat{\mathbf{n}} \cdot \hat{\mathbf{n}} = 1 \implies \hat{\mathbf{n}} \cdot \frac{D\hat{\mathbf{n}}}{Dt} = 0, \quad (15.58)$$

so that the normal vector is always perpendicular to its material time derivative. Rearrangement of equation (15.57) then leads to the kinematic evolution equation for the area

$$\frac{1}{\delta S} \frac{D\delta S}{Dt} = [\partial_m - \hat{n}_m (\hat{\mathbf{n}} \cdot \nabla)] v_m. \quad (15.59)$$

We next provide some interpretation of this result.

Surface derivative operator

The derivative operator on the right hand side of equation (15.59),

$$\partial_m^{\text{surf}} \equiv \partial_m - \hat{n}_m (\hat{\mathbf{n}} \cdot \nabla), \quad (15.60)$$

is a *surface derivative operator* since it subtracts from the gradient operator the projection onto the local normal, thus leaving a gradient operator just in the tangent plane of the surface. The area evolution equation (15.59) can thus be written in the tidy form

$$\frac{1}{\delta S} \frac{D\delta S}{Dt} = \nabla^{\text{surf}} \cdot \mathbf{v}, \quad (15.61)$$

so that the relative area of the material surface changes according to the surface divergence of the velocity field.

Special case of a horizontal surface

To help understand the kinematic equation (15.61), consider the special case of a horizontal surface with a vertical unit normal vector, $\hat{\mathbf{n}} = \hat{z}$, so that

$$\frac{1}{\delta S} \frac{D\delta S}{Dt} = \nabla \cdot \mathbf{v} - \hat{z} \cdot \partial_z \mathbf{v} = \nabla_z \cdot \mathbf{u}. \quad (15.62)$$

In this case we see that the area of a horizontal surface increases when the horizontal velocity diverges, and the area decreases when the horizontal velocity converges. We expect this behavior since the surface is material and is thus moving with the flow. We encounter this result again in Section 15.4.4 for two-dimensional flow, in which the area is always horizontal.

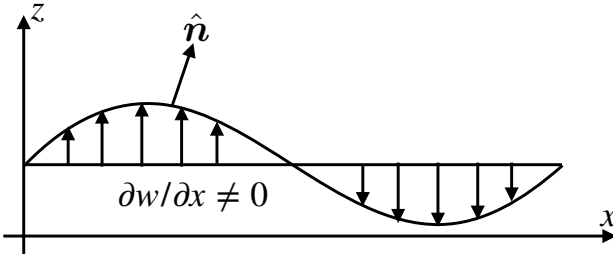


FIGURE 15.4: Horizontal shear in the vertical velocity, $\nabla_z w$, creates undulations in an initially horizontal material surface that leads to a horizontal component in the normal vector. We here show the case where $\partial w / \partial x \neq 0$, thus leading to a zonal component to the normal vector according to $D\hat{n}_x/Dt = -\partial_x w$.

As another special case, consider a three dimensional flow that is non-divergent, $\nabla \cdot \mathbf{v} = 0$ (see Chapter 18). In this case the area changes are only due to the projection of the normal gradient onto the normal direction. So again considering a horizontal area with $\hat{\mathbf{n}} = \hat{\mathbf{z}}$, the area evolution in a non-divergent flow is given by

$$\frac{1}{\delta S} \frac{D\delta S}{Dt} = -\hat{\mathbf{z}} \cdot (\hat{\mathbf{z}} \cdot \nabla) \mathbf{v} = -\partial_z w, \quad (15.63)$$

which follows from equation (15.62) with $\nabla_x u + \partial_y v + \partial_z w = \nabla_z \mathbf{u} + \partial_z w = 0$.

15.4.3 Evolution of the normal vector

We make use of the area evolution equation (15.61) within equation (15.56) to derive an evolution equation for the normal vector

$$\frac{D\hat{n}_m}{Dt} = -\hat{n}_m \frac{1}{\delta S} \frac{D\delta S}{Dt} + (\partial_p v_p) \hat{n}_m - (\partial_m v_p) \hat{n}_p \quad (15.64a)$$

$$= -\hat{n}_m [\partial_p v_p - \hat{n}_p (\hat{n}_q \partial_q) v_p] + (\partial_p v_p) \hat{n}_m - (\partial_m v_p) \hat{n}_p \quad (15.64b)$$

$$= -\hat{n}_p [\partial_m - \hat{n}_m \hat{n}_q \partial_q] v_p \quad (15.64c)$$

$$= -\hat{n}_p \partial_m^{\text{surf}} v_p \quad (15.64d)$$

$$= -\hat{\mathbf{n}} \cdot \partial_m^{\text{surf}} \mathbf{v}. \quad (15.64e)$$

Equation (15.64c) provides a simple means to verify that the kinematic constraint (15.58) is satisfied, in which $\hat{\mathbf{n}} \cdot D\hat{\mathbf{n}}/Dt = 0$.

To help understand the evolution equation (15.64e), consider again a horizontal area with its normal vector initially in the vertical. The evolution of this normal vector is thus given by

$$\frac{D\hat{n}_m}{Dt} = -(\partial_m - \hat{z}_m \partial_z) w, \quad (15.65)$$

with each component evolving according to

$$\frac{D\hat{n}_1}{Dt} = -\partial_x w \quad \text{and} \quad \frac{D\hat{n}_2}{Dt} = -\partial_y w \quad \text{and} \quad \frac{D\hat{n}_3}{Dt} = 0. \quad (15.66)$$

Hence, an initially vertical normal vector tilts into the horizontal direction according to minus the horizontal shear in the vertical velocity. We understand this result by noting that such a shear creates undulations in the initially horizontal surface that render a horizontal component to the normal vector (Figure 15.4).

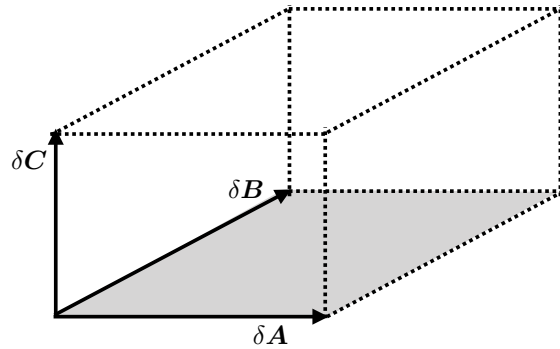


FIGURE 15.5: A parallelepiped defined by three material lines with volume (to within a sign) given by $\delta V = (\delta \mathbf{A} \times \delta \mathbf{B}) \cdot \delta \mathbf{C}$. See also the discussion surrounding Figure 1.4.

15.4.4 Material area in two-dimensional flow

Now consider a material area for two-dimensional fluid flow with velocity, $\mathbf{v} = (u, v, 0)$, and $\delta \mathbf{A} = \hat{x} \delta x$, $\delta \mathbf{B} = \hat{y} \delta y$, with zero dependence on z . In this case, the area of an infinitesimal material region is

$$\delta \mathcal{S} = (\delta \mathbf{A} \times \delta \mathbf{B}) \cdot \hat{z} = \delta x \delta y, \quad (15.67)$$

and its evolution is given by

$$\frac{D(\delta \mathcal{S})}{Dt} = (\delta \mathbf{B} \times \hat{z}) \cdot (\delta \mathbf{A} \cdot \nabla) \mathbf{u} + (\hat{z} \times \delta \mathbf{A}) \cdot (\delta \mathbf{B} \cdot \nabla) \mathbf{u} \quad (15.68a)$$

$$= \delta x \delta y \nabla \cdot \mathbf{u}, \quad (15.68b)$$

so that

$$\frac{1}{\delta \mathcal{S}} \frac{D(\delta \mathcal{S})}{Dt} = \nabla \cdot \mathbf{u}. \quad (15.69)$$

Hence, the area of the material region evolves according to the divergence of the horizontal velocity. Correspondingly, the area remains constant in a horizontally non-divergent flow. This result follows from specializing the three-dimensional result (15.52f) to the case of two-dimensional flow by assuming no dependence on the vertical direction.

15.5 Volume, thickness, and the Jacobian

The mass of a material parcel is constant. However, the volume is not generally constant since the fluid density is not generally uniform. We here derive the expression for how volume evolves for a material parcel. We also derive the material evolution equation for the Jacobian of transformation between position space and material space. We will see that the relative change for both the parcel volume and the Jacobian are determined by the divergence of the velocity field.

15.5.1 Material parcel volume

Consider a material region with a volume δV spanned by the infinitesimal material lines $\delta \mathbf{A}$, $\delta \mathbf{B}$, and $\delta \mathbf{C}$ (see Figure 15.5). To within a sign the volume is given by

$$\delta V = (\delta \mathbf{A} \times \delta \mathbf{B}) \cdot \delta \mathbf{C}. \quad (15.70)$$

Making use of the material line evolution equation (15.19) renders

$$\frac{D(\delta V)}{Dt} = (\delta \mathbf{B} \times \delta \mathbf{C}) \cdot (\delta \mathbf{A} \cdot \nabla) \mathbf{v} + (\delta \mathbf{C} \times \delta \mathbf{A}) \cdot (\delta \mathbf{B} \cdot \nabla) \mathbf{v} + (\delta \mathbf{A} \times \delta \mathbf{B}) \cdot (\delta \mathbf{C} \cdot \nabla) \mathbf{v}. \quad (15.71)$$

Now specialize to the case where the parcel is a parallelepiped oriented according to the coordinate axes

$$\delta \mathbf{A} = \hat{\mathbf{x}} \delta x \quad \text{and} \quad \delta \mathbf{B} = \hat{\mathbf{y}} \delta y \quad \text{and} \quad \delta \mathbf{C} = \hat{\mathbf{z}} \delta z, \quad (15.72)$$

so that

$$\delta V = \delta x \delta y \delta z. \quad (15.73)$$

Plugging into equation (15.71) leads to

$$\frac{1}{\delta V} \frac{D(\delta V)}{Dt} = \nabla \cdot \mathbf{v}. \quad (15.74)$$

This result is a three-dimensional generalization of the material area equation derived in Section 15.4.4.

We offer an alternative derivation of equation (15.74) in Section 16.2, where no assumptions are made concerning the shape of the material region. That derivation leads us to conclude that the relative volume of a material parcel increases when the parcel moves through a region where the velocity diverges ($\nabla \cdot \mathbf{v} > 0$). We think of a diverging velocity field as “spreading out” the material parcel boundary, thus increasing its volume. In contrast, the volume of a material parcel decreases where the fluid velocity converges ($\nabla \cdot \mathbf{v} < 0$)

$$\nabla \cdot \mathbf{v} > 0 \Rightarrow \text{material volume increases in diverging flow} \implies \text{parcel expands} \quad (15.75a)$$

$$\nabla \cdot \mathbf{v} < 0 \Rightarrow \text{material volume decreases in converging flow} \implies \text{parcel contracts.} \quad (15.75b)$$

15.5.2 Evolution of the column thickness

A material volume, δV , evolves according to the divergence of the velocity (equation (15.74)), whereas the material area, $\delta \mathcal{S}$, evolves according to the surface divergence of the velocity (equation (15.61)). Now consider a material volume whose cross-sectional area is $\delta \mathcal{S}$ and whose thickness is δh , with δh measuring the thickness in a direction defined by the unit normal, $\hat{\mathbf{n}}$. That is, the material volume is cylindrical. We can deduce the evolution of the thickness since we know the evolution of the volume and area

$$\frac{1}{\delta V} \frac{D(\delta V)}{Dt} = \frac{1}{\delta h \delta \mathcal{S}} \frac{D(\delta h \delta \mathcal{S})}{Dt} = \frac{1}{\delta h} \frac{D(\delta h)}{Dt} + \frac{1}{\delta \mathcal{S}} \frac{D(\delta \mathcal{S})}{Dt}. \quad (15.76)$$

Use of equations (15.74) and (15.61) render

$$\frac{1}{\delta h} \frac{D(\delta h)}{Dt} = \nabla \cdot \mathbf{v} - \nabla^{\text{surf}} \cdot \mathbf{v} = \hat{\mathbf{n}}_i (\hat{\mathbf{n}} \cdot \nabla) v_i. \quad (15.77)$$

For example, consider the special case with $\hat{\mathbf{n}} = \hat{\mathbf{z}}$, in which

$$\frac{1}{\delta h} \frac{D(\delta h)}{Dt} = \frac{\partial w}{\partial z}, \quad (15.78)$$

so that the column thickness evolves according to the vertical derivative of the vertical velocity. This result accords with our discussion of stretching in Section 15.3.6.

15.5.3 Evolution of the Jacobian of transformation

Recall the discussion in Section 14.5.6, where we showed that the Jacobian of transformation between material space (\mathbf{a} -space) and position space (\mathbf{x} -space) is related to the ratio of the volume elements written in the two coordinate systems. In particular, equation (14.22) is given by

$$\delta V(\mathbf{x}) = \frac{\partial \mathbf{X}}{\partial \mathbf{a}} \delta V(\mathbf{a}) \implies \frac{\partial \mathbf{X}}{\partial \mathbf{a}} = \frac{\delta V(\mathbf{x})}{\delta V(\mathbf{a})}. \quad (15.79)$$

The material coordinate volume $\delta V(\mathbf{a})$ is time independent when following the flow. Consequently, the material evolution of the Jacobian is given by

$$\frac{D}{Dt} \frac{\partial \mathbf{X}}{\partial \mathbf{a}} = \frac{1}{\delta V(\mathbf{a})} \frac{D(\delta V(\mathbf{x}))}{Dt} \quad (15.80a)$$

$$= \frac{\delta V(\mathbf{x})}{\delta V(\mathbf{a})} \nabla \cdot \mathbf{v} \quad (15.80b)$$

$$= \frac{\partial \mathbf{X}}{\partial \mathbf{a}} \nabla \cdot \mathbf{v}. \quad (15.80c)$$

The second equality made use of the equation (15.74), which expresses the material time change for the volume of a material fluid parcel, as measured in position space, in terms of the velocity divergence. We thus see that the relative change of the Jacobian is determined by the divergence of the velocity

$$\left[\frac{\partial \mathbf{X}}{\partial \mathbf{a}} \right]^{-1} \frac{D}{Dt} \left[\frac{\partial \mathbf{X}}{\partial \mathbf{a}} \right] = \nabla \cdot \mathbf{v}. \quad (15.81)$$

This equation is identical to the parcel volume equation (15.74), which is expected given the relation between the Jacobian and the parcel volume. In Exercise 15.5, we derive this result using the explicit expression for the Jacobian in terms of the permutation symbol ϵ .

15.6 Kinematics of two-dimensional flow

In this section we consider the rudiments of two-dimensional flow as a venue to illustrate certain topics presented earlier in this chapter such as dilation, rotation, and strains. In so doing we expose kinematic properties commonly used to characterize two-dimensional flow, with generalizations to three-dimensions available though with a bit more maths.

Our starting point is Figure 15.6, which shows a square region of fluid exposed to a variety of flow regimes. We can kinematically describe these changes by making use of the velocity gradient tensor introduced in Section 15.3.5, here written for the two-dimensional flow with horizontal velocity components, (u, v)

$$\frac{\partial v_m}{\partial x_n} = \begin{bmatrix} \partial u / \partial x & \partial u / \partial y \\ \partial v / \partial x & \partial v / \partial y \end{bmatrix} \quad (15.82a)$$

$$= \begin{bmatrix} \partial u / \partial x & (1/2)(\partial u / \partial y + \partial v / \partial x) \\ (1/2)(\partial u / \partial y + \partial v / \partial x) & \partial v / \partial y \end{bmatrix} + \frac{\zeta}{2} \begin{bmatrix} 0 & -1 \\ 1 & 0 \end{bmatrix} \quad (15.82b)$$

$$= \mathbb{S}_{mn} + \mathbb{R}_{mn}, \quad (15.82c)$$

where

$$\zeta = \hat{\mathbf{z}} \cdot \nabla \times \mathbf{v} = \partial v / \partial x - \partial u / \partial y \quad (15.83)$$

is the vertical component to the vorticity.

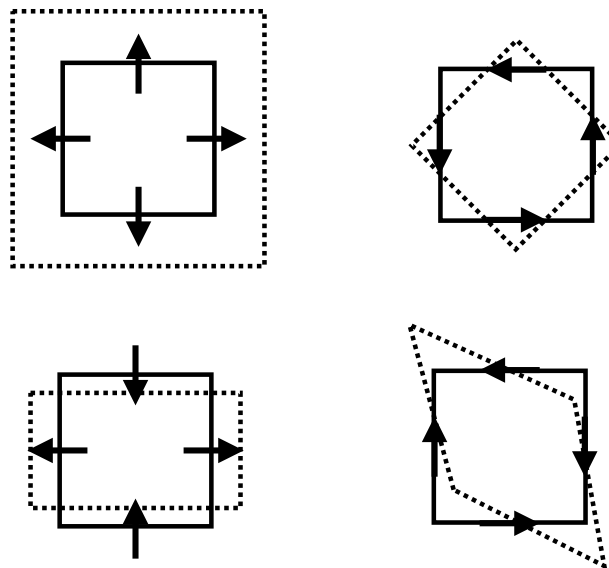


FIGURE 15.6: Illustrating the varieties of shape changes for a square material fluid region. Upper left: purely divergent flow, whereby $\nabla \cdot \mathbf{u} > 0$ yet with zero vorticity, thus leading to an increase in the area. Upper right: rotational flow with nonzero vorticity, $\zeta = \hat{\mathbf{z}} \cdot (\nabla \times \mathbf{u})$, yet zero divergence, thus leading to a pure rotation of the square patch. Lower left: result of a pure tension/compression straining flow with zero divergence and zero vorticity, leading to compression in one direction and dilation in the orthogonal direction. This flow is realized by the velocity field $\mathbf{u} = \hat{\mathbf{z}} \times \nabla \psi$, which is generated by the streamfunction $\psi = -\gamma xy$. Lower right: pure shearing strain flow with zero divergence and zero vorticity, as as realized by the flow $\mathbf{u} = \hat{\mathbf{z}} \times \nabla \psi$ generated by the streamfunction $\psi = -(\gamma/2)(x^2 - y^2)$. This figure is adapted from Figure 2.4 of [Hoskins and James \(2014\)](#).

15.6.1 Diverging flow

Recall from Section 15.4.4 that a material surface in two-dimensional flow changes its area according to the divergence. The upper left panel of Figure 15.6 thus illustrates equation (15.69)

$$\frac{1}{\delta S} \frac{D(\delta S)}{Dt} = \nabla \cdot \mathbf{u} = \mathbb{S}_{mm}, \quad (15.84)$$

where δS is the area and \mathbb{S}_{mm} is the trace of the rate of strain tensor. That is, a diverging flow as depicted by this figure, with $\nabla \cdot \mathbf{u} > 0$, leads to an expansion of the area. The opposite occurs for a converging flow, where the area compresses.

15.6.2 Rotational flow with nonzero vorticity

The upper right panel of Figure 15.6 illustrates the effects from flow with a non-zero vorticity, $\zeta = \partial v / \partial x - \partial u / \partial y$. We provide extensive discussion of vorticity in Part VII of this book. For now we simply note that vorticity measures the spin at a point within a fluid. The nonzero spin imparts a rotation to an area element, in this case bringing about a counter-clockwise rotation. All components of the strain tensor vanish for a purely rotational flow, so that there is no deformation of the square as it rotates.

15.6.3 Flow with nonzero deformation

The lower left panel of Figure 15.6 shows the square within a deformational flow whereby it contracts along the y -axis and dilates along the x -axis. This flow is non-divergent, $\nabla \cdot \mathbf{u} = 0$, and has zero vorticity, $\zeta = 0$, so that the area remains constant and the orientation is fixed. However, it has shear that acts to deform the area. This particular non-divergent deformational flow is

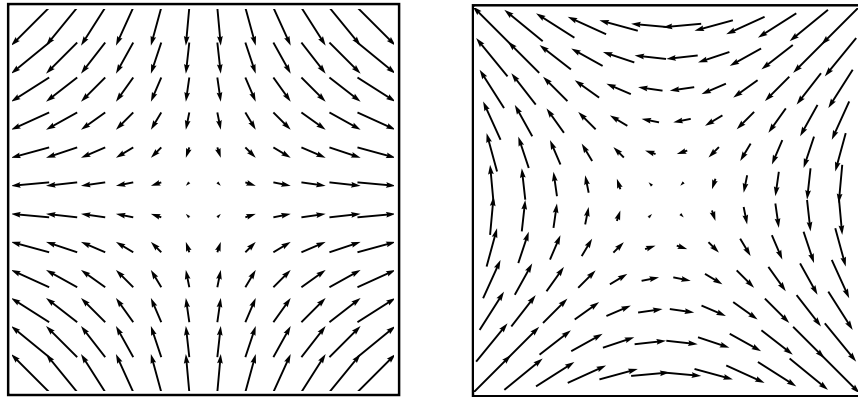


FIGURE 15.7: Two-dimensional non-divergent and irrotational flow with nonzero deformation/strain. Left panel: pure tension strain as determined by the streamfunction, $\psi = -\gamma xy$, so that the velocity components are $u = -\partial\psi/\partial y = \gamma x$ and $v = \partial\psi/\partial x = -\gamma y$. The vertical axis orients the direction along which flow contracts (compression) whereas the horizontal axis is the dilation axis (tension). Right panel: pure shearing flow as determined by the streamfunction $\psi = -(\gamma/2)(x^2 - y^2)$ so that the velocity components are $u = -\gamma y$ and $v = -\gamma x$. We set $\gamma = 1$ for both examples.

determined by

$$\mathbf{u} = \hat{\mathbf{z}} \times \nabla\psi, \quad (15.85)$$

with the streamfunction, $\psi = -\gamma xy$ where γ is a constant inverse time scale and hence the strength of the strain. The resulting velocity components are $u = -\partial\psi/\partial y = \gamma x$ and $v = \partial\psi/\partial x = -\gamma y$.

There are two combinations of the rate of strain tensor elements that are useful in describing deformational flows:

$$\text{tension strain} = S_T = \mathbb{S}_{11} - \mathbb{S}_{22} = \partial u / \partial x - \partial v / \partial y \quad (15.86a)$$

$$\text{shearing strain} = S_S = 2\mathbb{S}_{12} = \partial u / \partial y + \partial v / \partial x. \quad (15.86b)$$

The tension strain and shearing strain are also known as tension and shearing *deformation rates*. Note that negative tension is known as *compression*. For the deformation flow with streamfunction $\psi = -\gamma xy$, we have

$$S_T = 2\gamma \quad \text{and} \quad S_S = 0, \quad (15.87)$$

so that this velocity leads to a purely tension straining flow. In contrast, the following non-divergent irrotational flow is a purely shearing strain flow

$$\psi = -(\gamma/2)(x^2 - y^2) \quad u = -\gamma y \quad v = -\gamma x \quad S_T = 0 \quad S_S = -2\gamma, \quad (15.88)$$

as depicted by the right panel of Figure 15.7. This pure shearing flow leads to the deformation of the fluid square shown in the lower right panel of Figure 15.6.

15.6.4 Further study

Elements of this section can be found in Section 2.3 of [Hoskins and James \(2014\)](#). More detailed examinations of two-dimensional flow kinematics are offered by [Weiss \(1991\)](#) and [Lilly \(2018\)](#).

15.7 Helmholtz decomposition

In characterizing the kinematic properties of vector fields, such as the velocity vector for a moving fluid, [Helmholtz \(1867\)](#) introduced a method to decompose any vector into two distinct components whose properties are readily analyzed: one component vector has a zero divergence and the second vector has a zero curl. This *Helmholtz decomposition* has extensive applications throughout fluid mechanics (see [Bhatia et al. \(2013\)](#) for a review). We make particular use of the decomposition when introducing a scalar or vector potential for studying the kinematics of non-divergent fluid flows (Chapter 18). In this section we provide further insights into features of the Helmholtz decomposition, with much of the discussion following [Denaro \(2003\)](#) and [Bhatia et al. \(2013\)](#).

To introduce the Helmholtz decomposition, consider a vector field, \mathbf{F} , in free space (i.e., no boundaries) that decays to zero outside of a finite domain. In this case we can decompose \mathbf{F} into

$$\mathbf{F} = -\nabla D + \nabla \times \mathbf{R}, \quad (15.89)$$

where

$$D(\mathbf{x}) = \frac{1}{4\pi} \int_{\mathcal{R}} \frac{\nabla \cdot \mathbf{F}(\mathbf{x}')}{|\mathbf{x} - \mathbf{x}'|} dV' \quad (15.90a)$$

$$\mathbf{R}(\mathbf{x}) = \frac{1}{4\pi} \int_{\mathcal{R}} \frac{\nabla \times \mathbf{F}(\mathbf{x}')}{|\mathbf{x} - \mathbf{x}'|} dV'. \quad (15.90b)$$

The scalar potential, D , and vector potential, \mathbf{R} , are here given by the Green's function solutions derived in Section 4.6.5.

The Helmholtz decomposition (15.90a) and (15.90b) is both elegant and straightforward. It offers motivation to seek a similar decomposition for domains of relevance to geophysical fluids, where boundaries play a fundamental role. However, there are many mathematical nuances associated with Helmholtz decompositions in more general situations, each depending on the domain topology and nature of the prescribed boundary conditions. Our goal in this section is to explore the mathematics for a few common boundary conditions for a fluid on simply connected manifolds.⁷ We offer rather brief comments for the more general non-simply connected case as the mathematics is beyond our scope.⁸

15.7.1 Summarizing the Helmholtz decomposition

The Helmholtz decomposition on a simply connected manifold, \mathcal{R} , states that a vector field, \mathbf{F} , is fully determined by specifying its divergence, $\nabla \cdot \mathbf{F}$, and curl, $\nabla \times \mathbf{F}$, for points $\mathbf{x} \in \mathcal{R}$, along with the normal component, $\hat{\mathbf{n}} \cdot \mathbf{F}$, or the tangential component⁹, $\hat{\mathbf{n}} \times \mathbf{F}$, along the domain boundary, $\partial\mathcal{R}$. Here, $\hat{\mathbf{n}}$ is the outward normal along the boundary. Expressed with equations, the Helmholtz decomposition is given by

$$\mathbf{F} = -\nabla D + \nabla \times \mathbf{R} = \text{gradient term (curl-free)} + \text{rotation term (divergence-free)}. \quad (15.91)$$

⁷A manifold is simply connected if a closed curve can be continuously shrunk to a point while remaining on the manifold. For example, the domain of the global ocean on a water covered planet is a simply connected manifold. Adding land masses in the form of islands or continents makes the ocean domain non-simply connected.

⁸Section 5.2 of [Bhatia et al. \(2013\)](#) provides a few comments on the non-simply connected case, whereas chapter 14 of [Frankel \(2012\)](#) provides details for the mathematically experienced reader.

⁹[Helmholtz \(1867\)](#) only considered vector fields with a specified normal component along boundaries. This situation is most common in fluid mechanical applications. [Denaro \(2003\)](#) showed how specification of the tangential component along the boundary also allows for a Helmholtz decomposition. We explore both boundary conditions in this section.

The scalar potential, D , is arbitrary up to a constant, and the vector potential, \mathbf{R} , is arbitrary up to the gradient of a scalar field. This ambiguity in specifying D and \mathbf{R} is referred to as *gauge invariance* or *gauge freedom*, and we encounter it in other contexts within this book. For present purposes, gauge freedom allows us to choose the *Coulomb gauge* that is commonly used in electromagnetics ([Jackson, 1975](#)), whereby \mathbf{R} is prescribed to be divergence-free

$$\nabla \cdot \mathbf{R} = 0. \quad (15.92)$$

As seen next, this constraint simplifies the boundary value problem satisfied by \mathbf{R} .

Taking the divergence of (15.91) reveals that the scalar potential satisfies the Poisson equation

$$-\nabla^2 D = \nabla \cdot \mathbf{F} \quad \text{for } \mathbf{x} \in \mathcal{R}. \quad (15.93)$$

Taking the curl of the decomposition (15.91), and using the curl identity (2.37c) along with the Coulomb gauge (15.92)

$$\nabla \times (\nabla \times \mathbf{R}) = \nabla(\nabla \cdot \mathbf{R}) - \nabla^2 \mathbf{R} = -\nabla^2 \mathbf{R}, \quad (15.94)$$

leads to the vector Poisson equation

$$-\nabla^2 \mathbf{R} = \nabla \times \mathbf{F} \quad \text{for } \mathbf{x} \in \mathcal{R}. \quad (15.95)$$

The two elliptic equations, (15.93) and (15.95), are supplemented by boundary conditions for points $\mathbf{x} \in \partial\mathcal{R}$. The choice of boundary conditions depend on information available about the vector \mathbf{F} along the boundary. We here consider the following three sets of boundary conditions, with $\hat{\mathbf{n}}$ the outward unit normal along $\partial\mathcal{R}$:

$$\text{normal component} \quad -\hat{\mathbf{n}} \cdot \nabla D = \hat{\mathbf{n}} \cdot \mathbf{F} \quad \text{and} \quad \hat{\mathbf{n}} \cdot (\nabla \times \mathbf{R}) = 0 \quad (15.96a)$$

$$\text{tangential component} \quad \hat{\mathbf{n}} \times \nabla D = 0 \quad \text{and} \quad \hat{\mathbf{n}} \times (\nabla \times \mathbf{R}) = \hat{\mathbf{n}} \times \mathbf{F} \quad (15.96b)$$

$$\text{vanishing boundary} \quad \hat{\mathbf{n}} \cdot \nabla D = 0 \quad \text{and} \quad \hat{\mathbf{n}} \times (\nabla \times \mathbf{R}) = 0 \implies \mathbf{F} = 0. \quad (15.96c)$$

The homogeneous Neumann boundary condition $\hat{\mathbf{n}} \cdot (\nabla \times \mathbf{R}) = 0$ in equation (15.96a) means that $(\nabla \times \mathbf{R})$ is parallel to the boundary. Likewise, $\hat{\mathbf{n}} \times \nabla D = 0$ in equation (15.96b) means that ∇D is parallel to the boundary. If $\mathbf{F} = \mathbf{v}$ is the fluid velocity field, then $\mathbf{v} \cdot \hat{\mathbf{n}} = 0$ is the no-normal flow kinematic condition that holds for static solid boundaries (Section 16.4.1). Furthermore, the vanishing boundary condition (15.96c) holds for the velocity with the dynamic no-slip boundary condition discussed in Section 22.10.3.

15.7.2 Concerning a harmonic contribution

Consider a vector \mathbf{H} that is both divergent-free and curl-free

$$\nabla \cdot \mathbf{H} = 0 \quad \text{and} \quad \nabla \times \mathbf{H} = 0. \quad (15.97)$$

\mathbf{H} is a harmonic vector function (Section 3.5.1), which is seen by noting that with $\nabla \cdot \mathbf{H} = 0$ then (see equation (2.37c)) \mathbf{H} satisfies the vector Laplace equation

$$\nabla \times (\nabla \times \mathbf{H}) = -\nabla^2 \mathbf{H} = 0, \quad (15.98)$$

so that each component of \mathbf{H} is a harmonic function.

An arbitrary vector, \mathbf{F} , generally contains a portion that is harmonic, in which case we consider

the three-component decomposition

$$\mathbf{F} = -\nabla E + \nabla \times \mathbf{S} + \mathbf{H} = \text{gradient term} + \text{rotation term} + \text{harmonic term}. \quad (15.99)$$

However, as we show in this section, there are many physically interesting cases in which the original two-component Helmholtz decomposition (15.91) is sufficient. That is, for many cases the two-component Helmholtz decomposition is able to include contributions from the harmonic portion of \mathbf{F} as part of either ∇D or $\nabla \times \mathbf{R}$.

Normal component boundary condition

The constraint $\nabla \times \mathbf{H} = 0$ can be satisfied by writing $\mathbf{H} = -\nabla \phi$, which then brings the decomposition (15.99) into the form

$$\mathbf{F} = -(\nabla E + \nabla \phi) + \nabla \times \mathbf{S}. \quad (15.100)$$

We connect this decomposition to the original form of the Helmholtz decomposition in equation (15.91) by identifying

$$\nabla E + \nabla \phi \equiv \nabla D \quad \text{and} \quad \nabla \times \mathbf{S} \equiv \nabla \times \mathbf{R}. \quad (15.101)$$

In so doing, the harmonic term, here captured by $\nabla \phi$, is absorbed into the scalar potential, D . This method for absorbing the harmonic term is suited to the normal component boundary condition (15.96a), in which

$$-\hat{\mathbf{n}} \cdot \mathbf{F} = \hat{\mathbf{n}} \cdot (\nabla E + \nabla \phi) = \hat{\mathbf{n}} \cdot \nabla D \implies \hat{\mathbf{n}} \cdot \nabla E = -\hat{\mathbf{n}} \cdot (\mathbf{F} + \nabla \phi). \quad (15.102)$$

In practice, we determine D and \mathbf{R} as per the two-component decomposition (15.91), with the harmonic contribution to \mathbf{F} contained as part of the scalar potential, D .

Tangential component boundary condition

The constraint $\nabla \cdot \mathbf{H} = 0$ is satisfied by writing $\mathbf{H} = \nabla \times \mathbf{A}$, so that the decomposition (15.99) takes on the form

$$\mathbf{F} = -\nabla E + \nabla \times (\mathbf{S} + \mathbf{A}). \quad (15.103)$$

We connect this decomposition to the original form of the Helmholtz decomposition of equation (15.91) by identifying

$$\nabla E \equiv \nabla D \quad \text{and} \quad \nabla \times (\mathbf{S} + \mathbf{A}) \equiv \nabla \times \mathbf{R}. \quad (15.104)$$

In so doing, the harmonic term, here captured by $\nabla \times \mathbf{A}$, is included in the vector potential, \mathbf{R} . This method for absorbing the harmonic term is suited for the tangential component boundary condition (15.96b), in which case

$$\hat{\mathbf{n}} \times \mathbf{F} = \hat{\mathbf{n}} \times (\mathbf{S} + \mathbf{A}) = \hat{\mathbf{n}} \times \mathbf{R} \implies \hat{\mathbf{n}} \times \mathbf{S} = \hat{\mathbf{n}} \times (\mathbf{F} - \mathbf{A}). \quad (15.105)$$

Non-divergent velocity vector with no-normal flow boundary condition

As discussed in Chapters 18 and 26, many geophysical fluid flows maintain a non-divergent velocity field. Such velocity fields also maintain the no-normal flow boundary condition at static material boundaries (Section 16.4.1). For this vector field the scalar potential is harmonic and satisfies the

vanishing Neumann boundary condition

$$-\nabla^2 D = 0 \quad \text{for } \mathbf{x} \in \mathcal{R} \quad (15.106a)$$

$$\hat{\mathbf{n}} \cdot \nabla D = 0 \quad \text{for } \mathbf{x} \in \partial\mathcal{R}. \quad (15.106b)$$

The solution to this boundary value problem is a spatially constant D , so that the velocity field is fully specified by a vector potential

$$\mathbf{F} = \nabla \times \mathbf{R}. \quad (15.107)$$

In the presence of a time dependent boundary condition, such as a fluctuating free surface, the scalar potential is not generally a spatial constant. We encounter an example when studying surface gravity waves in Section 45.3.

Vanishing boundary condition

The case with $\mathbf{F} = 0$ on the boundary means that

$$\mathbf{F} \cdot \hat{\mathbf{n}} = 0 \quad \text{and} \quad \hat{\mathbf{n}} \times \mathbf{F} = 0 \quad \text{for } \mathbf{x} \in \partial\mathcal{R}. \quad (15.108)$$

We proceed with both of the previous boundary condition constraints whereby

$$\nabla E + \nabla \phi = \nabla D \quad \text{and} \quad \nabla \times \mathbf{S} = \nabla \times \mathbf{R} \quad (15.109a)$$

$$\nabla E = \nabla D \quad \text{and} \quad \nabla \times (\mathbf{A} + \mathbf{S}) = \nabla \times \mathbf{R}. \quad (15.109b)$$

These two sets of constraints are mutually satisfied only when

$$\nabla \phi = 0 \quad \text{and} \quad \nabla \times \mathbf{A} = 0, \quad (15.110)$$

so that the harmonic term vanishes identically for the case of $\mathbf{F} = 0$ along the boundary.

Summary comments

We have shown that for a simply connected domain, it is possible to absorb an arbitrary harmonic portion of \mathbf{F} into either the scalar potential D (for the normal component boundary conditions (15.96a)) or vector potential, \mathbf{R} (for tangential component boundary conditions (15.96b)). Furthermore, the harmonic term vanishes altogether for the vanishing boundary condition (e.g., no-slip velocity boundary condition).

We infer from this discussion that if both the normal and tangential components of \mathbf{F} are specified nonzero values on the boundary, then the harmonic term cannot be fully absorbed into one of the potentials D or \mathbf{R} . Rather, the harmonic term must be explicitly computed, in which case the three-component decomposition (15.99) is referred to as the *Helmholtz-Hodge decomposition*.

These considerations are analogous to the Cauchy-Stokes decomposition summarized by Figure 15.2. That is, Cauchy-Stokes decomposes the motion of a fluid element into three processes: a deformation plus a rigid rotation plus a uniform translation. The deformation corresponds to the curl-free vector in the Helmholtz decomposition ($-\nabla D$), the rotation corresponds to the divergent free vector ($\nabla \times \mathbf{R}$), and the uniform translation corresponds to the harmonic vector.

15.7.3 Self-consistency conditions

We here establish existence conditions for the scalar potential, D , and vector potential, \mathbf{R} , that satisfy the decomposition (15.91). We separately do so for the two sets of boundary conditions (15.96a) and (15.96b). The proof consists of showing that the source term on the right hand side of the Poisson equation is self-consistent with the boundary condition.

Normal component boundary condition

Consider the scalar Poisson equation with Neumann boundary conditions

$$-\nabla^2 \chi = \Lambda \quad \text{for } \mathbf{x} \in \mathcal{R} \quad (15.111\text{a})$$

$$-\hat{\mathbf{n}} \cdot \nabla \chi = \sigma \quad \text{for } \mathbf{x} \in \partial\mathcal{R}. \quad (15.111\text{b})$$

As discussed in Section 3.5.6, this elliptic boundary value problem has a solution so long as the source, Λ , and boundary condition, σ , satisfy a self-consistency condition given by equation (3.48)

$$\int_{\mathcal{R}} \Lambda \, dV = \oint_{\partial\mathcal{R}} \sigma \, d\mathcal{S}. \quad (15.112)$$

Now specialize to the Helmholtz decomposition (15.91) whereby $\chi = D$ is the scalar potential with source $\Lambda = \nabla \cdot \mathbf{F}$ and boundary condition $\sigma = \hat{\mathbf{n}} \cdot \mathbf{F}$. Gauss's divergence theorem (2.68) readily verifies self-consistency

$$\int_{\mathcal{R}} \Lambda \, dV = \int_{\mathcal{R}} \nabla \cdot \mathbf{F} \, dV = \oint_{\partial\mathcal{R}} \mathbf{F} \cdot \hat{\mathbf{n}} \, d\mathcal{S} = \oint_{\partial\mathcal{R}} \sigma \, d\mathcal{S}. \quad (15.113)$$

As noted in Section 3.5.6, self-consistency ensures the existence of a solution to the Neumann problem that is unique up to an arbitrary constant. Hence, ∇D is unique so that

$$\nabla \times \mathbf{R} = \mathbf{F} + \nabla D \quad (15.114)$$

is also unique (we further discuss uniqueness in Section 15.7.5). Finally, the inhomogeneous Neumann boundary condition satisfied by the scalar potential, $-\hat{\mathbf{n}} \cdot \nabla D = \hat{\mathbf{n}} \cdot \mathbf{F}$, means that the curl satisfies the homogeneous Neumann boundary condition

$$\hat{\mathbf{n}} \cdot (\nabla \times \mathbf{R}) = \hat{\mathbf{n}} \cdot (\mathbf{F} + \nabla D) = 0, \quad (15.115)$$

so that $(\nabla \times \mathbf{R})$ is parallel to the boundary.

Tangential component boundary condition

Consider the vector Poisson equation

$$-\nabla^2 \Psi = \Lambda \quad \text{for } \mathbf{x} \in \mathcal{R} \quad (15.116\text{a})$$

$$\hat{\mathbf{n}} \times (\nabla \times \Psi) = \hat{\mathbf{n}} \times \Sigma \quad \text{for } \mathbf{x} \in \partial\mathcal{R}, \quad (15.116\text{b})$$

with an assumed non-divergence condition (Coulomb gauge) placed on Ψ

$$\nabla \cdot \Psi = 0. \quad (15.117)$$

The region \mathcal{R} is assumed to be a bounded three-dimensional volume with a closed boundary surface, $\partial\mathcal{R}$. Now let \mathcal{S} be an arbitrary simply connected portion of $\partial\mathcal{R}$, and write $\partial\mathcal{S}$ for the

closed contour that bounds \mathcal{S} . Integrate the normal projection of the vector Poisson equation over \mathcal{S} and make use of Stokes' theorem (Section 2.6) to render

$$\int \boldsymbol{\Lambda} \cdot \hat{\mathbf{n}} d\mathcal{S} = - \int \nabla^2 \boldsymbol{\Psi} \cdot \hat{\mathbf{n}} d\mathcal{S} = \int \nabla \times (\nabla \times \boldsymbol{\Psi}) \cdot \hat{\mathbf{n}} d\mathcal{S} = \oint_{\partial\mathcal{S}} (\nabla \times \boldsymbol{\Psi}) \cdot \hat{\mathbf{t}} ds, \quad (15.118)$$

with $\hat{\mathbf{t}}$ the unit tangent vector pointing counter-clockwise along the closed contour, and ds the increment of arc-length along the contour (see Section 2.4). The assumed boundary condition (15.116b) means that for $\mathbf{x} \in \partial\mathcal{R}$ we can write

$$\nabla \times \boldsymbol{\Psi} = \boldsymbol{\Sigma} + \mathbf{m}, \quad (15.119)$$

where \mathbf{m} is parallel to $\hat{\mathbf{n}}$ so that $\hat{\mathbf{n}} \times \mathbf{m} = 0$. In turn, with \mathbf{m} parallel to $\hat{\mathbf{n}}$ then it is also perpendicular to the unit tangent vector, $\hat{\mathbf{t}} \cdot \mathbf{m} = 0$, so that

$$\oint_{\partial\mathcal{S}} (\nabla \times \boldsymbol{\Psi}) \cdot \hat{\mathbf{t}} ds = \oint_{\partial\mathcal{S}} \boldsymbol{\Sigma} \cdot \hat{\mathbf{t}} ds. \quad (15.120)$$

We are thus led to the self-consistency condition between the source, $\boldsymbol{\Lambda}$, and boundary condition, $\boldsymbol{\Sigma}$

$$\int \boldsymbol{\Lambda} \cdot \hat{\mathbf{n}} d\mathcal{S} = \oint_{\partial\mathcal{S}} \boldsymbol{\Sigma} \cdot \hat{\mathbf{t}} ds, \quad (15.121)$$

with this condition holding for any arbitrary simply connected region, \mathcal{S} , that lives on the boundary, $\partial\mathcal{R}$.

Now apply the self-consistency condition (15.121) to the Helmholtz decomposition (15.91), in which case $\boldsymbol{\Psi} = \mathbf{R}$, $\boldsymbol{\Lambda} = \nabla \times \mathbf{F}$, and $\boldsymbol{\Sigma} = \mathbf{F}$. Making use of Stokes' theorem readily verifies self-consistency

$$\int \boldsymbol{\Lambda} \cdot \hat{\mathbf{n}} d\mathcal{S} = \int (\nabla \times \mathbf{F}) \cdot \hat{\mathbf{n}} d\mathcal{S} = \oint_{\partial\mathcal{S}} \mathbf{F} \cdot \hat{\mathbf{t}} ds = \oint_{\partial\mathcal{S}} \boldsymbol{\Sigma} \cdot \hat{\mathbf{t}} ds. \quad (15.122)$$

We appeal to the scalar Poisson equation to conclude that self-consistency between the source and boundary conditions ensures the existence of a vector potential, \mathbf{R} , that is unique up to the gradient of a scalar. Hence, the gradient of the scalar potential is itself unique. Finally, we note that the assumed boundary condition (15.96b) for the vector potential, $\hat{\mathbf{n}} \times (\nabla \times \mathbf{R}) = \hat{\mathbf{n}} \times \mathbf{F}$, means that the scalar potential satisfies the homogeneous boundary condition

$$\hat{\mathbf{n}} \times \mathbf{F} = \hat{\mathbf{n}} \times (\nabla \times \mathbf{R}) = \hat{\mathbf{n}} \times (\mathbf{F} - \nabla D) \implies \hat{\mathbf{n}} \times \nabla D = 0. \quad (15.123)$$

We thus see that ∇D is aligned parallel to $\hat{\mathbf{n}}$ along the boundary.

15.7.4 Orthogonality with the L^2 inner product

Consider an L^2 inner product for vector functions defined according to the volume integral of their scalar product

$$\langle \mathbf{A}, \mathbf{B} \rangle \equiv \int_{\mathcal{R}} \mathbf{A} \cdot \mathbf{B} dV. \quad (15.124)$$

We here show that $\langle \nabla D, (\nabla \times \mathbf{R}) \rangle = 0$. That is, the Helmholtz decomposition (15.91) serves to decompose a vector into two orthogonal component vectors, where orthogonality is defined over the L^2 inner product (15.124). This orthogonality property is of great importance for the practical use of the Helmholtz decomposition.

Orthogonality with the normal component boundary condition

Assuming the normal component boundary conditions (15.96a), we readily find that the two vectors ∇D and $\nabla \times \mathbf{R}$ have a vanishing inner product

$$\langle \nabla D, \nabla \times \mathbf{R} \rangle = \int_{\mathcal{R}} \nabla D \cdot (\nabla \times \mathbf{R}) \, dV = \int_{\mathcal{R}} \nabla \cdot (D \nabla \times \mathbf{R}) \, dV = \int_{\partial\mathcal{R}} D (\nabla \times \mathbf{R}) \cdot \hat{\mathbf{n}} \, dS = 0, \quad (15.125)$$

where the final equality made use of the homogeneous boundary condition $(\nabla \times \mathbf{R}) \cdot \hat{\mathbf{n}} = 0$.

Orthogonality with the tangential boundary condition

Now assume the tangential component boundary conditions (15.96b). For this case we make use of the following identities

$$\nabla D \cdot (\nabla \times \mathbf{R}) = \partial_i D (\nabla \times \mathbf{R})_i \quad \text{expose Cartesian tensor indices} \quad (15.126a)$$

$$= \partial_i D \epsilon_{ijk} \partial_j R_k \quad \text{vector product as per equation (1.20d)} \quad (15.126b)$$

$$= \partial_j (\epsilon_{ijk} \partial_i D R_k) \quad \text{since } \epsilon_{ijk} \partial_i \partial_j D = 0 \text{ and } \partial_j \epsilon_{ijk} = 0 \quad (15.126c)$$

$$= -\partial_j (\epsilon_{jik} \partial_i D R_k) \quad \epsilon_{ijk} = -\epsilon_{jik} \quad (15.126d)$$

$$= -\nabla \cdot (\nabla D \times \mathbf{R}) \quad \text{reintroduce Cartesian vector notation.} \quad (15.126e)$$

As a result we have orthogonality

$$\langle \nabla D, \nabla \times \mathbf{R} \rangle = \int_{\mathcal{R}} \nabla \cdot (\mathbf{R} \times \nabla D) \, dV = \int_{\mathcal{R}} (\mathbf{R} \times \nabla D) \cdot \hat{\mathbf{n}} \, dS = \int_{\partial\mathcal{R}} (\nabla D \times \hat{\mathbf{n}}) \cdot \mathbf{R} \, dS = 0, \quad (15.127)$$

where the final equality made use of the homogeneous boundary condition $(\nabla D \times \hat{\mathbf{n}}) = 0$.

Comments

We have shown that the set of boundary conditions (15.96a) and (15.96b) are sufficient to produce an L^2 -orthogonal Helmholtz decomposition on a simply connected domain. However, we have *not* shown that these boundary conditions are necessary for orthogonality, with other boundary conditions generally available. Since orthogonality is central to the practical use of the Helmholtz decomposition, it is important to verify whether orthogonality property holds when using alternative boundary conditions.

15.7.5 Uniqueness of the decomposition

We already commented on the uniqueness of the scalar and vector potentials in Section 15.7.3. We here further that discussion by offering a uniqueness proof following a “proof by contradiction” method. For this approach we write the Helmholtz decomposition as

$$\mathbf{F} = -\nabla D_1 + \nabla \times \mathbf{R}_1 = -\nabla D_2 + \nabla \times \mathbf{R}_2, \quad (15.128)$$

and show that the only consistent solution has $D_1 = D_2$ and $\mathbf{R}_1 = \mathbf{R}_2$. Note that uniqueness is a function of the boundary conditions. That is, the normal component boundary conditions (15.96a) generally lead to a decomposition that is distinct from the tangential component boundary conditions (15.96b).

Uniqueness with the normal component boundary condition

From the assumed relation (15.128) we have

$$0 = -\nabla(D_1 - D_2) + \nabla \times (\mathbf{R}_1 - \mathbf{R}_2). \quad (15.129)$$

Taking the scalar product of this equality with $\nabla \times (\mathbf{R}_1 - \mathbf{R}_2)$ and then integrating over the domain leads to

$$0 = - \int_{\mathcal{R}} [\nabla(D_1 - D_2) \cdot \nabla \times (\mathbf{R}_1 - \mathbf{R}_2)] dV + \int_{\mathcal{R}} [\nabla \times (\mathbf{R}_1 - \mathbf{R}_2)]^2 dV. \quad (15.130)$$

The first integral vanishes, as seen by

$$-\int_{\mathcal{R}} [\nabla(D_1 - D_2) \cdot \nabla \times (\mathbf{R}_1 - \mathbf{R}_2)] dV = \int_{\mathcal{R}} [\nabla D_1 \cdot (\nabla \times \mathbf{R}_2) + \nabla D_2 \cdot (\nabla \times \mathbf{R}_1)] dV \quad (15.131a)$$

$$= \int_{\mathcal{R}} \nabla \cdot [D_1 (\nabla \times \mathbf{R}_2) + D_2 (\nabla \times \mathbf{R}_1)] dV \quad (15.131b)$$

$$= \int_{\partial \mathcal{R}} [D_1 (\nabla \times \mathbf{R}_2) + D_2 (\nabla \times \mathbf{R}_1)] \cdot \hat{\mathbf{n}} d\mathcal{S} \quad (15.131c)$$

$$= 0, \quad (15.131d)$$

where the first equality follows from orthogonality as per equation (15.125); the second equality holds since the divergence of the curl vanishes (Section 2.3.4); the third equality follows from Gauss's divergence theorem (Section 2.7); and the fourth equality follows from the homogeneous boundary conditions, $\hat{\mathbf{n}} \cdot (\nabla \times \mathbf{R}_1) = \hat{\mathbf{n}} \cdot (\nabla \times \mathbf{R}_2) = 0$, satisfied with the normal component boundary conditions (15.96a). We are thus left with the equality

$$\int_{\mathcal{R}} [\nabla \times (\mathbf{R}_1 - \mathbf{R}_2)]^2 dV = 0, \quad (15.132)$$

which is generally satisfied only when $\nabla \times \mathbf{R}_1 = \nabla \times \mathbf{R}_2$ so that $\nabla D_1 = \nabla D_2$. We have thus shown that the Helmholtz decomposition $\mathbf{F} = -\nabla D + \nabla \times \mathbf{R}$ is unique with the normal component boundary conditions (15.96a).

Uniqueness with the tangential component boundary condition

Now consider the tangential component boundary conditions (15.96b). The proof proceeds much like above, only now we take the scalar product of equation (15.129) with $\nabla(D_1 - D_2)$ and integrate over the domain. In doing so we encounter the term

$$-\int_{\mathcal{R}} [\nabla(D_1 - D_2) \cdot \nabla \times (\mathbf{R}_1 - \mathbf{R}_2)] dV = \int_{\mathcal{R}} [\nabla D_1 \cdot (\nabla \times \mathbf{R}_2) + \nabla D_2 \cdot (\nabla \times \mathbf{R}_1)] dV \quad (15.133a)$$

$$= \int_{\mathcal{R}} \nabla \cdot [\nabla D_1 \times \mathbf{R}_2 + \nabla D_2 \times \mathbf{R}_1] dV \quad (15.133b)$$

$$= \int_{\partial \mathcal{R}} [\mathbf{R}_2 \cdot (\hat{\mathbf{n}} \times \nabla D_1) + \mathbf{R}_1 \cdot (\hat{\mathbf{n}} \times \nabla D_2)] d\mathcal{S} \quad (15.133c)$$

$$= 0, \quad (15.133d)$$

where the second equality made use of the identity (15.126e) derived when examining orthogonality, the third equality made of the divergence theorem, and the fourth equality holds according to the homogenous boundary conditions $\hat{\mathbf{n}} \times \nabla D = 0$ following from equation (15.96b). We are

thus led to

$$\int_{\mathcal{R}} [\nabla(D_1 - D_2)]^2 dV = 0, \quad (15.134)$$

which generally holds only if $\nabla D_1 = \nabla D_2$ and hence $\nabla \times \mathbf{R}_1 = \nabla \times \mathbf{R}_2$. We have thus shown that the Helmholtz decomposition is unique with the tangential component boundary conditions (15.96b).



15.8 Exercises

EXERCISE 15.1: MATERIAL EVOLUTION OF THE ACCELERATION DIVERGENCE

This exercise is based on problem 10(a) from Section 3.1 of [Segel \(1987\)](#). Here, we derive the relation

$$\nabla \cdot \frac{D\mathbf{v}}{Dt} = \frac{D(\nabla \cdot \mathbf{v})}{Dt} + \mathcal{S}^2 - \mathcal{A}^2, \quad (15.135)$$

where $\mathcal{S}^2 = \mathcal{S}_{mn}\mathcal{S}_{mn}$ and $\mathcal{A}^2 = \mathcal{A}_{mn}\mathcal{A}_{mn}$ are the squared rate of strain and squared rotation tensors (Sections 15.3.7 and 15.3.8). Make use of Cartesian tensors for your solution.

EXERCISE 15.2: VELOCITY FIELD WITH ZERO STRAIN ([Aris \(1962\)](#) EXERCISE 4.41.1)

If the rate of strain tensor vanishes, show that the velocity field can be written

$$\mathbf{v} = \mathbf{U} + \boldsymbol{\Omega} \times \mathbf{x}, \quad (15.136)$$

where $\boldsymbol{\Omega}$ is a constant angular rotation rate and \mathbf{U} is a constant velocity. That is, a fluid velocity equal to a constant rotation plus translation renders zero strain. Hint: if $\mathbb{S}_{mn} = 0$, what does that imply about the velocity field? You may also wish to make use of the general decomposition (15.48).

EXERCISE 15.3: RATE OF STRAIN AND ROTATION TENSORS ([Aris \(1962\)](#) EXERCISE 4.43.3)

Consider a two-dimensional flow with horizontal velocity

$$\mathbf{u} = (F/r)(\hat{\mathbf{x}}y - \hat{\mathbf{y}}x), \quad (15.137)$$

where $F = F(r)$ is an arbitrary function of the radial distance $r = \sqrt{x^2 + y^2}$ and with dimensions of L T^{-1} . Throughout this exercise, be sure your solution is dimensionally consistent.

- (a) Show that the velocity field is non-divergent.
- (b) Determine an analytic expression for the streamlines and draw a picture.
- (c) Determine the elements to the rate of strain tensor, \mathbb{S} , given by equation (15.82c). Write the expression using polar coordinates $x = r \cos \varphi$ and $y = r \sin \varphi$ (see Section 9.3) and the structure function

$$G(r) = r \frac{d(F/r)}{dr} = (F' - F/r)/2 \quad \text{with } F' = dF/dr. \quad (15.138)$$

- (d) Determine elements to the rotation tensor, \mathbb{R} , given by equation (15.82c), also written in polar coordinates.

EXERCISE 15.4: RATE OF STRAIN AND ROTATION FOR PARALLEL SHEAR FLOW
 Consider a two-dimensional parallel shear flow with horizontal velocity

$$\mathbf{u} = a x \hat{\mathbf{y}}, \quad (15.139)$$

where a is a constant with dimension inverse time.

- (a) Compute the rate of strain tensor, \mathbb{S} (equation (15.82c)) for this velocity field.
- (b) Compute the rotation tensor, \mathbb{R} (equation (15.82c)) for this velocity field.
- (c) Decompose the velocity field according to equation (15.48), and show that each of the velocity components is non-divergent. That is, write

$$\mathbf{u} = \mathbf{u}^0 + \mathbf{u}^{(S)} + \mathbf{u}^{(A)} \quad \text{with} \quad \nabla \cdot \mathbf{u}^{(S)} = \nabla \cdot \mathbf{u}^{(A)} = 0, \quad (15.140)$$

with u_m^0 the velocity at the point where $\delta x_m = x_m - x_m^0 = 0$. The velocity $\mathbf{u}^{(S)}$ has a constant strain but no vorticity whereas $\mathbf{u}^{(A)}$ has a constant vorticity but no strain. Hint: both $\mathbf{u}^{(S)}$ and $\mathbf{u}^{(A)}$ have nonzero \hat{x} and \hat{y} components.

- (d) Determine the streamfunctions for $\mathbf{u}^{(S)}$ and $\mathbf{u}^{(A)}$.
- (e) Sketch the velocity vectors $\mathbf{u}^{(S)}$ and $\mathbf{u}^{(A)}$.

EXERCISE 15.5: EVOLUTION OF THE JACOBIAN USING ϵ -TENSOR GYMNASTICS

There is another way to derive the identity (15.81) for the evolution of the Jacobian. This other method is somewhat more tedious. However, it exercises some useful methods of index gymnastics involving the ϵ -tensor. It also has a natural generalization to curved spaces. This exercise is only for aficionados of tensor analysis.

An explicit expression for the Jacobian of transformation is given by

$$\frac{\partial \mathbf{X}}{\partial \mathbf{a}} = \frac{1}{3!} \epsilon_{mnp} \epsilon_{ijk} \frac{\partial X_m}{\partial a_i} \frac{\partial X_n}{\partial a_j} \frac{\partial X_p}{\partial a_k}. \quad (15.141)$$

Take the material derivative of this expression and show that we get the same expression as equation (15.81). Hint: make use of the identity

$$\frac{D}{Dt} \frac{\partial X_m}{\partial a_i} = \frac{\partial V_m}{\partial a_i}, \quad (15.142)$$

which holds since the material time derivative is taken with the material coordinates, \mathbf{a} , held fixed.



Chapter 16

MASS CONSERVATION

Throughout this book, we assume that matter is neither created nor destroyed anywhere within the continuous fluid domain, and that the fluid remains in a single phase.¹ Since this assumption holds independently of the forces acting on the fluid, we consider mass conservation a topic within fluid kinematics. In this chapter, we derive a variety of mathematical expressions for mass conservation in a single component fluid (materially homogeneous fluid), along with associated kinematic constraints placed on fluid motion. These constraints are examined both in the interior of the fluid as well as at fluid boundaries. We explore these results from the Eulerian and Lagrangian viewpoints.

READER'S GUIDE TO THIS CHAPTER

In this chapter we are concerned with single-component fluids, with generalizations to multiple-component fluids given in Chapter 17. Spatial positions and trajectories are represented using Cartesian coordinates to simplify the maths, with generalizations following the tensor analysis methods of Chapter 8. We here build on our understanding of the Eulerian and Lagrangian kinematic descriptions developed in Chapters 14 and 15.

16.1 Eulerian fluid regions	338
16.1.1 Finite volume expression	338
16.1.2 Arbitrary Eulerian region	339
16.2 Material fluid parcels	340
16.2.1 Lagrangian expression for mass conservation	340
16.2.2 Alternative derivation based on the Jacobian	341
16.2.3 Summary of material kinematic equations	341
16.3 Material fluid regions	341
16.3.1 Evolution of volume	342
16.3.2 Mass conservation	342
16.3.3 Mass conservation using Lagrangian methods	343
16.3.4 Reynolds transport theorem	344
16.3.5 Comments on notation for the time derivative	345
16.4 Kinematic boundary conditions	346
16.4.1 Static material surface	346
16.4.2 Moving material surface	347
16.4.3 Dynamic and permeable surface	350
16.5 Volume and mass budgets for an ocean column	354
16.5.1 Kinematic free surface equation	354

¹Chemical reactions transform matter from one form to the another. Nuclear reactions convert between matter and nuclear energy. Phases change matter from one form to another. These processes are all outside the scope of this book.

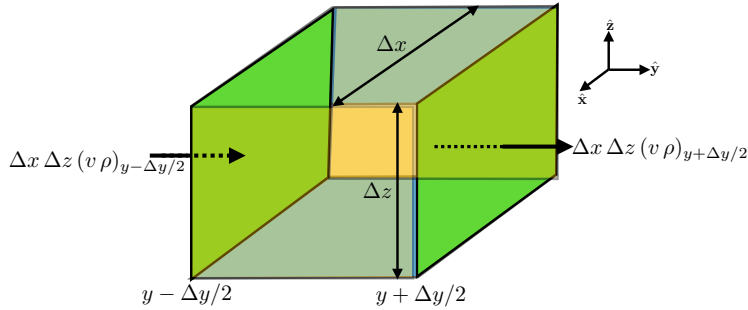


FIGURE 16.1: A finite sized cube or cell region with fixed dimensions and position (an Eulerian region) used to formulate the Eulerian form of mass conservation. We highlight two cell faces with area $\Delta x \Delta z$ and with meridional mass transport crossing the faces given by $\Delta x \Delta z (v \rho)_{y-\Delta y/2}$ and $\Delta x \Delta z (v \rho)_{y+\Delta y/2}$. To establish signs we assume the meridional velocity is positive, $v > 0$, so that mass enters the face at $y - \Delta y/2$ and leaves the face at $y + \Delta y/2$. Differences between these two transports leads to an accumulation of mass within the cell. The resulting mass budget holds regardless the direction of the flow velocity.

16.5.2 Budget for mass per horizontal area	355
16.6 Exercises	356

16.1 Eulerian fluid regions

We here develop expressions for the mass budget within an Eulerian region, both infinitesimal and finite. Recall that Eulerian regions are fixed in space and thus have constant volumes.

16.1.1 Finite volume expression

Consider a finite sized cubic region that is fixed in space as shown in Figure 16.1. The mass contained within the cube is given by

$$\Delta M = \rho \Delta V = \rho \Delta x \Delta y \Delta z, \quad (16.1)$$

where the cube volume,

$$\Delta V = \Delta x \Delta y \Delta z, \quad (16.2)$$

is constant in time as per an Eulerian region. As we will be taking the limit as the size of the cube gets smaller, it is sufficient to approximate the density as that at the cube center, $\rho = \rho(x, y, z, t)$. In the absence of mass sources within the fluid, the mass within the cube changes only through the accumulation or depletion of mass transported across the six cube faces.

Focusing on the mass transport in the meridional direction as illustrated in Figure 16.1, the accumulation of mass within the cube through this transport is determined by the difference in mass transport crossing the two adjacent cell faces

$$\text{mass change from meridional transport} = (\Delta x \Delta z) [(v \rho)_{y-\Delta y/2} - (v \rho)_{y+\Delta y/2}]. \quad (16.3)$$

Expanding the difference into a Taylor series and truncating after leading order yields

$$\text{mass change from meridional transport} \approx -(\Delta x \Delta y \Delta z) \frac{\partial(v \rho)}{\partial y}. \quad (16.4)$$

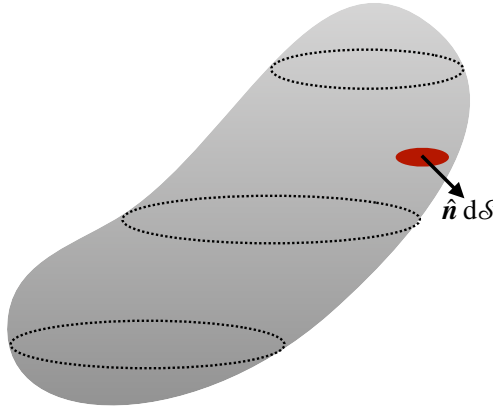


FIGURE 16.2: An arbitrarily shaped simply closed region, \mathcal{R} , within the fluid. If the region is fixed in space, then it represents a general Eulerian region for considering mass budgets. A surface area element, $d\mathcal{S}$, is oriented according to the outward normal, $\hat{\mathbf{n}}$.

The same analysis for the zonal and vertical directions leads to the mass budget for the cube

$$\frac{\partial(\rho \Delta V)}{\partial t} = -\Delta V \left[\frac{\partial(u \rho)}{\partial x} + \frac{\partial(v \rho)}{\partial y} + \frac{\partial(w \rho)}{\partial z} \right]. \quad (16.5)$$

Hence, the cube mass changes according to convergence of mass across the cube boundaries. Cancelling the constant volume ΔV (again, the volume is assumed fixed as per an Eulerian region) renders the *flux-form* Eulerian mass continuity equation

$$\frac{\partial \rho}{\partial t} + \nabla \cdot (\rho \mathbf{v}) = 0. \quad (16.6)$$

The mass continuity equation (16.6) is in the form of a *flux-form conservation law*, in which the local time tendency of a field is determined by the convergence of a flux

$$\frac{\partial \rho}{\partial t} = -\nabla \cdot (\rho \mathbf{v}). \quad (16.7)$$

The *mass flux*, $\rho \mathbf{v}$, with dimensions $M L^{-2} T^{-1}$, measures the mass per time of matter crossing a unit area oriented with an outward normal in each of the three Cartesian directions. If more mass flux comes into a point than leaves, then the density increases (mass converges), and vice versa for a mass flux that diverges from a point. It is notable that the mass flux also serves as a measure of the *momentum flux*, which we discuss in Chapter 21.

16.1.2 Arbitrary Eulerian region

The discussion for the infinitesimal cube can be generalized by making use of the divergence theorem. For that purpose, consider an arbitrary static and simply closed region within the fluid such as in Figure 16.2. Integrating the continuity equation (16.6) over that region leads to

$$\int_{\mathcal{R}} \frac{\partial \rho}{\partial t} dV = - \int_{\mathcal{R}} \nabla \cdot (\rho \mathbf{v}) dV. \quad (16.8)$$

Since the region is static we can move the partial time derivative outside on the left hand side. Furthermore, the divergence theorem can be applied to the right hand side to convert the volume integral to a surface integral over the boundaries of the static domain. The resulting mass budget

is given by

$$\frac{d}{dt} \int_{\mathcal{R}} \rho dV = - \oint_{\partial\mathcal{R}} \rho \mathbf{v} \cdot \hat{\mathbf{n}} d\mathcal{S}, \quad (16.9)$$

where $\hat{\mathbf{n}}$ is the outward unit normal vector along the closed boundary of the region, and $d\mathcal{S}$ is the surface area element along that boundary. This equation says that the mass within a fixed region of the fluid changes in time (left hand side) according to the accumulation of mass crossing the region boundary (right hand side). The minus sign means that the mass decreases in the region if there is a net mass transport leaving the domain in the direction of the outward normal.

16.2 Material fluid parcels

We here derive the differential expressions for mass conservation of a constant mass fluid parcel within a Lagrangian reference frame. The differential expressions for volume and density arise as a corollary. This discussion complements the Eulerian discussion from Section 16.1. To motivate the derivations we expand the Eulerian flux-form mass continuity equation (16.6) to have

$$\frac{1}{\rho} \frac{D\rho}{Dt} = -\nabla \cdot \mathbf{v}, \quad (16.10)$$

where $D/Dt = \partial_t + \mathbf{v} \cdot \nabla$ is the material time derivative operator. We now derive this form of the mass continuity using Lagrangian methods.

16.2.1 Lagrangian expression for mass conservation

The mass of an infinitesimal fluid parcel that moves with the fluid flow is written²

$$\delta M = \rho \delta V, \quad (16.11)$$

where δV is the volume and

$$\rho = \frac{\delta M}{\delta V} \quad (16.12)$$

is the mass density of the parcel. By definition, the fluid parcel has a constant mass as it moves with the flow, so that its material time derivative vanishes

$$\frac{D(\delta M)}{Dt} = 0. \quad (16.13)$$

Equation (16.13) is the most basic form of mass conservation for a fluid parcel. However, one often has need to express this result in terms of parcel density and parcel volume

$$\frac{D(\delta M)}{Dt} = \frac{D(\rho \delta V)}{Dt} \quad (16.14a)$$

$$= \delta M \left[\frac{1}{\rho} \frac{D\rho}{Dt} + \frac{1}{\delta V} \frac{D(\delta V)}{Dt} \right]. \quad (16.14b)$$

Comparing to the mass continuity equation (16.10) leads to³

$$\frac{1}{\delta M} \frac{D(\delta M)}{Dt} = \frac{1}{\rho} \frac{D\rho}{Dt} + \nabla \cdot \mathbf{v}. \quad (16.15)$$

²Recall that we use the δ symbol to signal a property measured in the Lagrangian reference frame.

³In Section 15.5.1 we derived the material evolution of volume, and will again see this result in equation (16.26).

Setting $D(\delta M)/Dt = 0$ renders the continuity equation (16.10) derived from the Eulerian expression

$$\frac{1}{\rho} \frac{D\rho}{Dt} = -\nabla \cdot \mathbf{v}. \quad (16.16)$$

The parcel volume contracts in regions where the velocity converges (we prove that property in Sections 15.5.1 and 16.3.1). The continuity equation (16.16) then says that regions of volume contraction are where the parcel density increases whereas the opposite occurs for regions where the velocity diverges.

16.2.2 Alternative derivation based on the Jacobian

An alternative approach to deriving the mass conservation equation makes use of the material time evolution of the Jacobian. We detail this approach for integrals in Section 16.3.3, and discussed it for fluid parcels in Section 15.5.3. Making use of those results, in particular equation (15.81), allows us to write the material evolution for the fluid parcel mass in the form

$$\frac{D}{Dt} [\rho \delta V(\mathbf{x})] = \frac{D}{Dt} \left[\rho \frac{\partial \mathbf{X}}{\partial \mathbf{a}} \delta V(\mathbf{a}) \right] \quad (16.17a)$$

$$= \left[\frac{D\rho}{Dt} + \rho \nabla \cdot \mathbf{v} \right] \left[\frac{\partial \mathbf{X}}{\partial \mathbf{a}} \right] \delta V(\mathbf{a}) \quad (16.17b)$$

$$= \left[\frac{D\rho}{Dt} + \rho \nabla \cdot \mathbf{v} \right] \delta V(\mathbf{x}). \quad (16.17c)$$

We recover the mass conservation equation (16.16) when noting that the mass of a material parcel is constant so that $D\rho/Dt = -\rho \nabla \cdot \mathbf{v}$.

16.2.3 Summary of material kinematic equations

Let us now summarize the variety of differential evolution equations for mass, volume, and density as viewed from a material reference frame

$$\frac{D(\delta M)}{Dt} = 0 \quad \text{parcel mass is constant} \quad (16.18)$$

$$\frac{1}{\delta V} \frac{D(\delta V)}{Dt} = \nabla \cdot \mathbf{v} \quad \text{parcel volume increases in divergent flow} \quad (16.19)$$

$$\frac{1}{\rho} \frac{D\rho}{Dt} = -\nabla \cdot \mathbf{v} \quad \text{parcel density increases in convergent flow.} \quad (16.20)$$

To help remember the signs on the right hand side, recall that as the fluid diverges from a point ($\nabla \cdot \mathbf{v} > 0$), it expands the boundaries of the material parcel and so increases the parcel volume as per equation (16.19). Since the parcel has a fixed mass, the diverging velocity field causes the material parcel density to decrease ($-\nabla \cdot \mathbf{v} < 0$) as per equation (16.20).

16.3 Material fluid regions

We now extend the kinematics of material fluid parcels in Section 16.2 to finite sized material fluid regions. Just as for material fluid parcels, the finite sized material fluid region retains the same matter content, and thus maintains a constant mass.⁴ We contrast the discussion here with

⁴Recall that throughout this chapter we are focused on single-component fluids, so there is no diffusion of matter considered here. We relax this restriction in Chapter 17.

that for the Eulerian regions (fixed in space) considered in Section 16.1. One key operational distinction between the Eulerian and Lagrangian domains is that partial time derivative operators commute with integration over a fixed Eulerian domain, whereas material time derivative operators commute with integration over a Lagrangian domain as per Reynolds transport theorem derived in Section 16.3.4.

16.3.1 Evolution of volume

Consider a finite material region, $\mathcal{R}(\mathbf{v})$, whose volume is given by the integral

$$V = \int_{\mathcal{R}(\mathbf{v})} dV, \quad (16.21)$$

with dV the volume element. The region changes its shape according to motion of the fluid particles fixed to the boundary of the material region. We designate this volume as

$$\mathcal{R}(\mathbf{v}) = \text{region following flow}, \quad (16.22)$$

with the \mathbf{v} argument emphasizing that the volume moves with the flow velocity. The material region expands when the flow moves outward and contracts when the flow moves inward. These statements take on the following mathematical expression

$$\frac{d}{dt} \int_{\mathcal{R}(\mathbf{v})} dV = \oint_{\partial\mathcal{R}(\mathbf{v})} \mathbf{v} \cdot \hat{\mathbf{n}} d\mathcal{S}, \quad (16.23)$$

where $\hat{\mathbf{n}}$ is the outward normal on the region's closed boundary, $d\mathcal{S}$ is the area element on the boundary, and

$$\mathbf{v} \cdot \hat{\mathbf{n}} d\mathcal{S} = \text{volume transport (volume per time) at the boundary } \partial\mathcal{R}. \quad (16.24)$$

Use of the divergence theorem then leads to the equivalent expression

$$\frac{d}{dt} \int_{\mathcal{R}(\mathbf{v})} dV = \int_{\mathcal{R}(\mathbf{v})} \nabla \cdot \mathbf{v} dV. \quad (16.25)$$

We now take the limit as the material region becomes a material parcel, in which case we recover the differential expression

$$\frac{1}{\delta V} \frac{D(\delta V)}{Dt} = \nabla \cdot \mathbf{v}, \quad (16.26)$$

where we make use of D/Dt since the infinitesimal volume is moving with the fluid. This equation is also derived in Section 15.5.1 using different methods.

16.3.2 Mass conservation

The mass of fluid contained in a finite material region is given by

$$M = \int_{\mathcal{R}(\mathbf{v})} \rho dV. \quad (16.27)$$

As a material fluid region, it maintains a constant mass as it moves through the fluid so that

$$\frac{d}{dt} \int_{\mathcal{R}(\mathbf{v})} \rho dV = 0. \quad (16.28)$$

Just as for the volume in Section 16.3.1, taking the limit as the material region becomes infinitesimally small, the region mass conservation statement (16.28) becomes the parcel mass conservation statement (16.13)

$$\frac{D(\delta M)}{Dt} = \frac{D(\rho \delta V)}{Dt} = 0. \quad (16.29)$$

16.3.3 Mass conservation using Lagrangian methods

Rather than take the limit as the finite material region $\mathcal{R}(\mathbf{v})$ becomes infinitesimal, we develop a formalism for moving the time derivative across an integral of the mass within a finite sized material region, as in equation (16.28). As part of this discussion we introduce two coordinate representations of the mass within a material region. The first is the Cartesian \mathbf{x} -space representation

$$\int_{\mathcal{R}(\mathbf{v})} \rho dV = \int_{x_1(t)}^{x_2(t)} \int_{y_1(t)}^{y_2(t)} \int_{z_1(t)}^{z_2(t)} \rho dx dy dz \equiv \int_{\mathcal{R}[\mathbf{v}(\mathbf{x}, t)]} \rho dV(\mathbf{x}). \quad (16.30)$$

The first equality expresses the integral with bounds that are functions of time, with the time dependence needed since the material region is moving with the fluid. The second equality uses a notation that emphasizes the region bounds and volume element are moving with the fluid velocity, \mathbf{v} , as specified using the \mathbf{x} -space representation, $\mathbf{v}(\mathbf{x}, t)$.

An alternative representation of mass in a material fluid region makes use of \mathbf{a} -space material coordinates. For this representation we perform a coordinate transformation from the \mathbf{x} -space representation to the \mathbf{a} -space representation, with this coordinate transformation requiring the Jacobian of transformation. To capture the gist of this transformation let us consider the one-dimensional case in which

$$\int_{x_1(t)}^{x_2(t)} \rho dx = \int_{a[x_1(t)]}^{a[x_2(t)]} \rho \frac{\partial X}{\partial a} da = \int_{a_1}^{a_2} \rho \frac{\partial X}{\partial a} da. \quad (16.31)$$

The first equality introduced the Jacobian, $\partial X / \partial a$, for the one-dimensional coordinate transformation from \mathbf{x} -space to \mathbf{a} -space, with corresponding changes to the limits of integration. We can make this coordinate transformation since there is a 1-to-1 relation between the \mathbf{a} -space and \mathbf{x} -space representation of a material fluid parcel. The second equality wrote the integral bounds in terms of the material coordinate. Since we are considering a material region that follows fluid particles, the integral bounds have fixed material coordinate values, $a[x_1(t)] = a_1$ and $a[x_2(t)] = a_2$. Generalizing to three dimensions then renders

$$\int_{\mathcal{R}[\mathbf{v}(\mathbf{x}, t)]} \rho dV(\mathbf{x}) = \int_{\mathcal{R}[\mathbf{v}(\mathbf{a})]} \rho \frac{\partial \mathbf{X}}{\partial \mathbf{a}} dV(\mathbf{a}). \quad (16.32)$$

Again, we distinguish the \mathbf{x} and \mathbf{a} arguments for the material region, with the \mathbf{x} representation also requiring a time argument whereas the material \mathbf{a} representation has no time dependence since it is attached to the moving fluid particles.

We now make use of the equality (16.32) to take the time derivative of the mass contained in the material region. Since the time derivative follows the material region, we can make use of the

material space coordinate representation as part of the manipulations

$$\frac{d}{dt} \left[\int_{\mathcal{R}[\mathbf{v}(\mathbf{x},t)]} \rho dV(\mathbf{x}) \right] = \frac{d}{dt} \left[\int_{\mathcal{R}[\mathbf{v}(\mathbf{a})]} \rho \frac{\partial \mathbf{X}}{\partial \mathbf{a}} dV(\mathbf{a}) \right] \quad (16.33a)$$

$$= \int_{\mathcal{R}[\mathbf{v}(\mathbf{a})]} \frac{D}{Dt} \left[\rho \frac{\partial \mathbf{X}}{\partial \mathbf{a}} \right] dV(\mathbf{a}) \quad (16.33b)$$

$$= \int_{\mathcal{R}[\mathbf{v}(\mathbf{x},t)]} \left[\frac{D\rho}{Dt} + \rho \nabla \cdot \mathbf{v} \right] dV(\mathbf{x}) \quad (16.33c)$$

$$= \int_{\mathcal{R}[\mathbf{v}(\mathbf{x},t)]} \left[\frac{1}{\rho} \frac{D\rho}{Dt} + \nabla \cdot \mathbf{v} \right] \rho dV(\mathbf{x}), \quad (16.33d)$$

where we used equation (15.81) for the equality (16.33c). When expressing the integral bounds using \mathbf{a} -space coordinates, the integral bounds have no time dependence since they are fixed on fluid particles. We can thus move the time derivative inside of the integral sign to reach the second equality. Upon entering the integral, the time derivative is written as a material time derivative, D/Dt , since it is a time derivative computed by following the fluid particles that define the material region. The third equality made use of equation (16.17c) and converted back to \mathbf{x} -space. As the material region \mathcal{R} has a materially constant mass, we recover the mass continuity equation (16.16) by setting the integrand in equation (16.33d) to zero.

16.3.4 Reynolds transport theorem

On first encounter, the method from Section 16.3.3 that involves moving between Eulerian (\mathbf{x} -space) and Lagrangian (\mathbf{a} -space) representations is clumsy at best and a black box at worse. However, with some practice it becomes an elegant means to study the time evolution of fluid properties integrated over a material region. The method is formalized by the *Reynolds transport theorem*.

Manipulations leading to the mass conservation statement (16.33d) can be generalized by considering the material time derivative of a mass-weighted field ψ (e.g., a tracer concentration as in Section 17.1)

$$\frac{D(\psi \rho \delta V)}{Dt} = \frac{D\psi}{Dt} \rho \delta V + \psi \frac{D(\rho \delta V)}{Dt} \quad (16.34a)$$

$$= \rho \delta V \left[\frac{D\psi}{Dt} + \frac{\psi}{\rho} \frac{D\rho}{Dt} + \psi \nabla \cdot \mathbf{v} \right] \quad (16.34b)$$

$$= \delta V \left[\frac{\partial(\rho \psi)}{\partial t} + \nabla \cdot (\rho \psi \mathbf{v}) \right]. \quad (16.34c)$$

The first equality used the product rule, which holds for material time derivatives. Mass conservation means that the material derivative $D(\rho \delta V)/Dt = 0$. However, we choose to write mass conservation in the form of equation (16.17c), which allows us to introduce the flux-form Eulerian expression after replacing the material time derivative with its Eulerian form from equation

(14.29). Another means to derive this result is to write

$$\rho \frac{D\psi}{Dt} = \rho \left[\frac{\partial \psi}{\partial t} + \mathbf{v} \cdot \nabla \psi \right] \quad (16.35a)$$

$$= \rho \left[\frac{\partial \psi}{\partial t} + \mathbf{v} \cdot \nabla \psi \right] + \psi \left[\frac{\partial \rho}{\partial t} + \nabla \cdot (\mathbf{v} \rho) \right] \quad (16.35b)$$

$$= \frac{\partial(\rho \psi)}{\partial t} + \nabla \cdot (\rho \mathbf{v} \psi). \quad (16.35c)$$

Following the discussion in Section 16.3.3, we can extend the material parcel result (16.34c) to a finite size material region. Again, each point in the material region is following a fluid particle. The result is known as the *Reynolds transport theorem*, which can be written in the following equivalent manners

$$\frac{d}{dt} \int_{\mathcal{R}(\mathbf{v})} \psi \rho dV = \int_{\mathcal{R}(\mathbf{v})} \frac{D\psi}{Dt} \rho dV \quad \text{material region} \quad (16.36a)$$

$$= \int_{\mathcal{R}(\mathbf{v})} \left[\frac{\partial(\rho \psi)}{\partial t} + \nabla \cdot (\rho \psi \mathbf{v}) \right] dV \quad \text{identity (16.35c)} \quad (16.36b)$$

$$= \int_{\mathcal{R}(\mathbf{v})} \frac{\partial(\rho \psi)}{\partial t} dV + \oint_{\partial \mathcal{R}(\mathbf{v})} \rho \psi \mathbf{v} \cdot \hat{\mathbf{n}} d\mathcal{S} \quad \text{divergence theorem (2.68).} \quad (16.36c)$$

Note that we returned to the notation $\mathcal{R}(\mathbf{v})$ for material region as introduced in Section 16.3.1. This notation is sufficient to designate that the region is following fluid particles along with the fluid velocity, \mathbf{v} . The surface integral term, $\mathbf{v} \cdot \hat{\mathbf{n}}$, generally does not vanish. Rather, it is given by $\mathbf{v} \cdot \hat{\mathbf{n}} = \mathbf{v}^{(s)} \cdot \hat{\mathbf{n}}$, where $\mathbf{v}^{(s)}$ is the velocity of a point on the boundary of the material region. Only when the material boundary is static can we set $\mathbf{v} \cdot \hat{\mathbf{n}} = 0$. We further consider this issue in Section 16.4 when studying kinematic boundary conditions.

16.3.5 Comments on notation for the time derivative

In this book we write d/dt for the time derivative operator acting on an integral. Furthermore, when the domain is specialized to follow fluid particles, we identify the special nature of such domains by introducing the fluid velocity argument to the domain name, $\mathcal{R}(\mathbf{v})$. This notation designates that all points in the domain, \mathcal{R} , move with the fluid velocity, \mathbf{v} , since all points have fluid particles attached. However, many authors choose an alternative notation by using the material time derivative, D/Dt , when acting on an integral over a material region. We thus have the following equality across the two notational conventions

$$\frac{D}{Dt} \int_{\mathcal{R}} \psi \rho dV = \frac{d}{dt} \int_{\mathcal{R}(\mathbf{v})} \psi \rho dV. \quad (16.37)$$

The use of one convention versus the other is a matter of taste. We follow Section 2.1 of [Batchelor \(1967\)](#) by restricting the D/Dt operator to act only on space-time fields, such as $\psi(\mathbf{x}, t)$. Hence, the D/Dt operator is not used when acting on integrals over spatial regions. Following this convention leads us to write $\mathcal{R}(\mathbf{v})$ for a region that moves with the fluid flow and to retain d/dt when acting on the integral over that region.

The $\mathcal{R}(\mathbf{v})$ notation is not generally used in the literature, with authors generally dropping the \mathbf{v} and thus letting words designate whether a region follows the flow or otherwise. As we have occasion in this book to consider a variety of fluid regions, we find it essential to introduce the somewhat more explicit notation, $\mathcal{R}(\mathbf{v})$, to denote a region moving with the flow velocity, \mathbf{v} . This

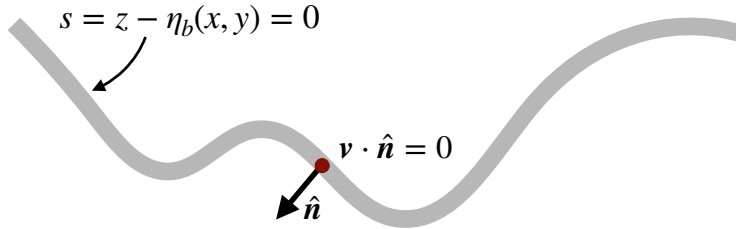


FIGURE 16.3: Illustrating the no-normal flow boundary condition maintained for a solid material boundary, on which $\mathbf{v} \cdot \hat{\mathbf{n}} = 0$ (equation (16.38)). When the solid boundary denotes the solid-earth (ground or ocean bottom), and when the boundary does not overturn (i.e., $\hat{\mathbf{n}} \cdot \hat{\mathbf{z}}$ is single-signed), then the position of the interface can be written $s(x, y, z) = z - \eta_b(x, y) = 0$ (equation (16.39)). Correspondingly, the outward unit normal is given by $\hat{\mathbf{n}} = -\nabla s/|\nabla s| = -(\hat{\mathbf{z}} - \nabla \eta_b)/\sqrt{1 + |\nabla \eta_b|^2}$ (equation (16.40)).

usage aims to help the reader freely swim along with the mathematical flow rather than struggling to stay afloat in a turbulent sea driven by confused or non-specific notation.

16.4 Kinematic boundary conditions

When a fluid encounters a boundary, either at the edge of the fluid region or an imaginary boundary within the fluid itself, the fluid must accommodate the boundary. Conversely, the boundary must accommodate the fluid flow. Some boundaries are impermeable, so that they do not allow matter to cross. For material boundaries, any fluid originally in contact with the boundary stays in contact; at most the fluid can move tangential to the boundary without leaving it. Other boundaries are permeable, thus allowing matter to cross. In this section we develop kinematic boundary conditions appropriate for the variety of cases encountered in fluid mechanics.

16.4.1 Static material surface

Consider a moving fluid that encounters a static material surface, such as the solid-earth. At the boundary, we can decompose the fluid velocity into a component that moves in the plane locally tangent to the boundary and another component that is normal to the boundary. To ensure that no fluid crosses the static boundary, the normal component must vanish at the boundary surface. Hence, the kinematic boundary condition for a moving fluid that encounters a static material boundary is (see Figure 16.3)

$$\mathbf{v} \cdot \hat{\mathbf{n}} = 0 \quad \text{no-normal flow condition on static material boundary.} \quad (16.38)$$

Recall our discussion of streamlines in Section 14.9.2, where $\mathbf{v} \cdot \hat{\mathbf{n}} = 0$ along a streamline. We thus see that the static material boundary is a flow streamline. That is, fluid that is in contact with the boundary remains in contact. This result holds even in the case of a time dependent flow. Note that specification of the tangential velocity along a material boundary requires dynamical information unavailable from the purely kinematic analysis considered here.

For many cases in practice, the material surface is monotonic in the vertical, meaning there are no overturns. In this case, it is useful to introduce some differential geometry (at the level of introductory calculus) to unpack the boundary condition (16.38). Doing so helps to develop a geometric formalism especially useful for the more complicated moving boundary conditions in Sections 16.4.2 and 16.4.3. For this purpose, introduce a coordinate expression for the boundary according to

$$s(x, y, z) = z - \eta_b(x, y) = 0 \quad \text{static material boundary,} \quad (16.39)$$

with $z = \eta_b(x, y)$ the vertical position of the boundary. The outward unit normal vector at the boundary is thus given by

$$\hat{\mathbf{n}} = -\frac{\nabla s}{|\nabla s|} = -\frac{\nabla(z - \eta_b)}{|\nabla(z - \eta_b)|} = -\frac{\hat{\mathbf{z}} - \nabla \eta_b}{\sqrt{1 + |\nabla \eta_b|^2}}. \quad (16.40)$$

Consequently, the no-flux boundary condition (16.38) takes the form

$$\nabla(z - \eta_b) \cdot \mathbf{v} = w - \mathbf{u} \cdot \nabla \eta_b = 0 \quad \text{at } z = \eta_b(x, y), \quad (16.41)$$

where the velocity is decomposed into its horizontal and vertical components, $\mathbf{v} = (\mathbf{u}, w)$. Hence, to maintain the no-flux boundary condition requires the vertical velocity component to precisely balance the projection of the horizontal velocity onto the slope of the material surface. If the material surface is flat, so that $\nabla \eta_b = 0$, then the kinematic boundary condition reduces to $w = 0$. Alternatively, if the flow is purely horizontal and thus moves along a constant η_b isoline, then $\mathbf{u} \cdot \nabla \eta_b = 0$ so that $w = 0$.

16.4.2 Moving material surface

We next consider the kinematic constraints imposed by a moving surface that does not allow matter to cross the surface.⁵

General expression of the kinematic boundary condition

To ensure that no matter crosses the surface, the normal component of the velocity for a point on the surface must match the normal component of the fluid at the surface. We are thus led to the kinematic boundary condition for a moving material surface

$$(\mathbf{v} - \mathbf{v}^{(s)}) \cdot \hat{\mathbf{n}} = 0 \quad \text{moving material boundary condition.} \quad (16.42)$$

We illustrate this boundary condition in Figure 16.4, where $\mathbf{v}^{(s)}$ is the velocity of a point fixed on the moving material surface and \mathbf{v} is the velocity of the fluid particles.

As for the static material boundary, there is no constraint on the tangential component of the velocities, since it is only the normal component that measures the flow of matter across the boundary. Hence, the boundary condition (16.42) does not mean \mathbf{v} and $\mathbf{v}^{(s)}$ are identical. It only says that their normal components are the same when evaluated on the material surface. As a Corollary, we see that $\mathbf{v} \cdot \hat{\mathbf{n}}$ is not generally zero so that a moving material boundary does *not* coincide with a flow streamline (see discussion in Sections 14.9.2 and 14.9.3).

Specialized expression of the boundary condition

Now specialize the kinematic condition (16.42) to the case of a material surface determined by a function that takes on a constant value on the surface

$$s(\mathbf{x}, t) = s_0. \quad (16.43)$$

An example of such a function is the Archimedean buoyancy (Chapter 27) or the Conservative Temperature (Section 23.9). Correspondingly, the surface unit normal vector is given by

$$\hat{\mathbf{n}} = |\nabla s|^{-1} \nabla s. \quad (16.44)$$

⁵As we discuss in Chapter 17, with multiple matter components a surface that follows the flow and so allows for zero net mass to cross it can still allow for the exchange of component matter in the presence of matter diffusion.

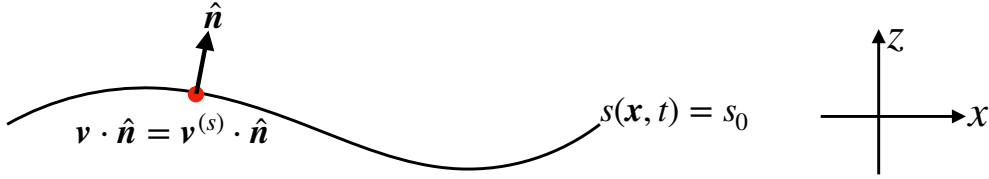


FIGURE 16.4: Illustrating the boundary condition for a moving material surface, on which $\hat{\mathbf{n}} \cdot (\mathbf{v} - \mathbf{v}^{(s)}) = 0$ (equation (16.42)), so that no fluid particles cross the surface. The boundary condition means that the velocity of the surface, $\mathbf{v}^{(s)}$, has the same normal component as the velocity of a fluid particle, \mathbf{v} . The material nature of the surface is not compromised if $\mathbf{v} \neq \mathbf{v}^{(s)}$, so long as their normal components are identical, $\hat{\mathbf{n}} \cdot \mathbf{v} = \hat{\mathbf{n}} \cdot \mathbf{v}^{(s)}$. For many cases, we can specify the surface by the value of a function that is a constant on the surface: $s(\mathbf{x}, t) = s_0$ for some constant s_0 (equation (16.43)), in which case the unit normal direction is given by $\hat{\mathbf{n}} = |\nabla s|^{-1} \nabla s$ (equation (16.44)). For example, s could represent a surface of constant buoyancy (Chapter 27) in a buoyancy stratified fluid.

From Section 14.6.6, we know that a point fixed on an arbitrary surface has a velocity that satisfies (see equation (14.41))

$$\frac{\partial s}{\partial t} + \mathbf{v}^{(s)} \cdot \nabla s = 0 \quad \text{on an iso-surface } s(\mathbf{x}, t) = s_0. \quad (16.45)$$

Use of the identity

$$\frac{\partial s}{\partial t} = \frac{Ds}{Dt} - \mathbf{v} \cdot \nabla s \quad (16.46)$$

renders

$$\frac{Ds}{Dt} - \mathbf{v} \cdot \nabla s + \mathbf{v}^{(s)} \cdot \nabla s = \frac{Ds}{Dt} + (\mathbf{v}^{(s)} - \mathbf{v}) \cdot \nabla s = 0. \quad (16.47a)$$

Since $(\mathbf{v}^{(s)} - \mathbf{v}) \cdot \nabla s = 0$ from the boundary condition (16.42), we are left with the material constancy condition

$$\frac{Ds}{Dt} = \frac{\partial s}{\partial t} + \mathbf{v} \cdot \nabla s = 0 \quad \text{on material surface } s(\mathbf{x}, t) = s_0. \quad (16.48)$$

Consequently, no matter crosses a surface of constant s as long as s is materially constant. This is an important kinematic property that reappears in many forms throughout fluid mechanics.

Boundary condition for a material interface

Consider the interface between two immiscible fluids. Assume this surface interface has an outward normal that has a nonzero vertical component, so that there are no breaking waves, for example. In this case we can express its vertical position of a point on the interface as

$$s(x, y, z, t) = z - \eta(x, y, t) = s_0. \quad (16.49)$$

The function $\eta(x, y, t)$ is the vertical deviation of the interface relative to the horizontal. The kinematic boundary condition (16.48) thus takes the form

$$\frac{Ds}{Dt} = \frac{D(z - \eta)}{Dt} = 0. \quad (16.50)$$

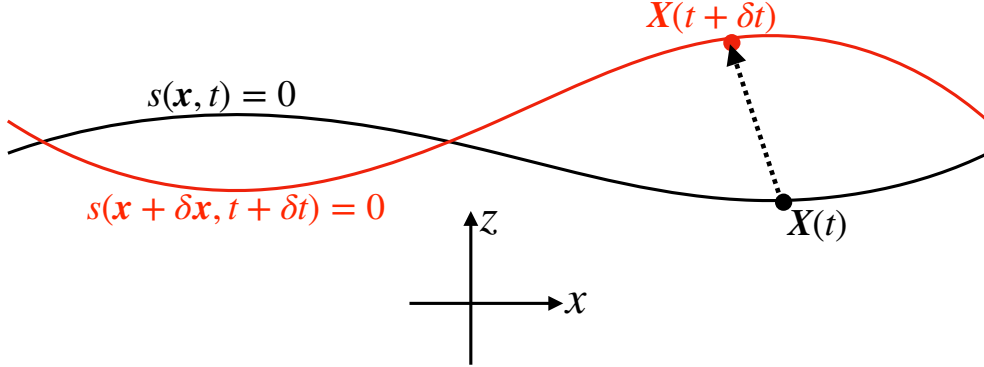


FIGURE 16.5: A surface that separates two fluid regions as realized at two time instants, along with the position of a sample point on the surface located at $\mathbf{X}(t)$ and $\mathbf{X}(t + \delta t)$. The velocity of a point on the surface is given by $\mathbf{v}^{(s)} = [\mathbf{X}(t + \delta t) - \mathbf{X}(t)]/\delta t = \delta \mathbf{X}/\delta t$. The equation $s(\mathbf{x}, t) = z - \eta(x, y, t) = 0$ specifies the vertical position for points on the surface as a function of horizontal position and time. At both time instances the vertical position is determined by $s(\mathbf{x}, t) = s(\mathbf{x} + \delta \mathbf{x}, t + \delta t) = 0$.

Hence, the vertical velocity component at the interface equals to the material time derivative of the interface displacement

$$\frac{Dz}{Dt} = \frac{D\eta}{Dt} \implies w = \frac{\partial \eta}{\partial t} + \mathbf{u} \cdot \nabla \eta \quad \text{material b.c. at interface } z = \eta(x, y, t). \quad (16.51)$$

This boundary condition can be equivalently written in the form

$$\mathbf{v} \cdot \hat{\mathbf{n}} = \frac{\partial \eta / \partial t}{\sqrt{1 + |\nabla \eta|^2}}, \quad (16.52)$$

where

$$\hat{\mathbf{n}} = \frac{\nabla(z - \eta)}{|\nabla(z - \eta)|} = \frac{-\nabla \eta + \hat{\mathbf{z}}}{\sqrt{1 + |\nabla \eta|^2}} \quad (16.53)$$

is the outward unit normal at the material surface. These equations provide kinematic relations for the motion of an interface between two immiscible fluid layers. A particular example concerns the boundary condition placed on the ocean free surface when there is no water penetrating the surface (i.e., no rain or evaporation).

A geometric derivation of the material boundary condition

The material invariance condition $Ds/Dt = 0$ is a key kinematic result. We thus offer yet another derivation to help solidify its meaning. As before, define the surface according to

$$s(\mathbf{x}, t) = z - \eta(x, y, t) = s_0, \quad (16.54)$$

which specifies the vertical position of a point on the surface at time t . Now consider the position of the surface after a small time interval, $t + \delta t$ (see Figure 16.5). The vertical position of the surface at the new time is determined by the same condition

$$s(\mathbf{x} + \delta \mathbf{x}, t + \delta t) = s_0, \quad (16.55)$$

where $\mathbf{X}(t + \delta t) = \mathbf{x} + \delta \mathbf{x}$ is the displaced position of a point on the surface that started at $\mathbf{X}(t) = \mathbf{x}$, and

$$\mathbf{v}^{(s)} = [\mathbf{X}(t + \delta t) - \mathbf{X}(t)]/\delta t = \delta \mathbf{x}/\delta t \quad (16.56)$$

is the velocity of a point stuck to the surface. Expanding equation (16.55) in a Taylor series to leading order yields

$$s(\mathbf{x}, t) + \delta\mathbf{x} \cdot \nabla s + \delta t \partial_t s = s_0. \quad (16.57)$$

Since $s(\mathbf{x}, t) = s_0$ from equation (16.54) we thus have

$$\frac{\partial s}{\partial t} + \frac{\delta\mathbf{x}}{\delta t} \cdot \nabla s = \frac{\partial s}{\partial t} + \frac{\delta\mathbf{x}}{\delta t} \cdot \hat{\mathbf{n}} |\nabla s| = 0, \quad (16.58)$$

where $\hat{\mathbf{n}} = |\nabla s|^{-1} \nabla s$ is the surface unit normal direction. This result means that when positioned at a fixed point in space, it is the normal component of the displacement that corresponds to a temporal modification of $s(\mathbf{x}, t)$

$$\frac{\partial s}{\partial t} = -\mathbf{v}^{(s)} \cdot \hat{\mathbf{n}} |\nabla s|. \quad (16.59)$$

In contrast, any tangential displacement along an s -isosurface leaves $s(\mathbf{x}, t)$ unchanged. Hence, when following motion of points on the surface, we are only concerned with motion along the direction set by the normal component of the velocity of that point, $\hat{\mathbf{n}} (\mathbf{v}^{(s)} \cdot \hat{\mathbf{n}})$. It is this velocity component that corresponds to movement of the surface normal to itself, thus leading to nonzero motion through space.

Writing equation (16.59) in a more conventional form leads to the differential equation satisfied by a point fixed on the moving surface

$$\frac{\partial s}{\partial t} + \mathbf{v}^{(s)} \cdot \nabla s = 0. \quad (16.60)$$

Again, assuming the surface is material means that

$$\mathbf{v}^{(s)} \cdot \hat{\mathbf{n}} = \mathbf{v} \cdot \hat{\mathbf{n}}, \quad (16.61)$$

so that motion of the surface normal to itself is identical to that of the fluid in the same direction. Use of the boundary condition (16.61) in equation (16.60) renders the material invariance condition

$$\frac{Ds}{Dt} = \frac{\partial s}{\partial t} + \mathbf{v} \cdot \nabla s = 0. \quad (16.62)$$

16.4.3 Dynamic and permeable surface

We now consider the kinematic boundary condition for a moving permeable surface that separates two fluid media (e.g., ocean and atmosphere) or two regions within a single media (e.g., surface of constant buoyancy within the ocean or within the atmosphere). As before, the kinematic boundary condition is a statement about the mass transport through the boundary. Whereas the previous conditions enforced a zero mass transport through the boundary at each point of the boundary, here we allow for a generally non-zero transport (mass per time). We write this transport condition as

$$\rho (\mathbf{v} - \mathbf{v}^{(s)}) \cdot \hat{\mathbf{n}} d\mathcal{S} = -\mathcal{Q}_m d\mathcal{S} \quad \text{moving non-material boundary condition.} \quad (16.63)$$

In this equation, $d\mathcal{S}$ is an infinitesimal area element on the surface, and \mathcal{Q}_m measures the mass per time per surface area (mass flux) crossing the boundary. The minus sign is a convention that will be motivated in the following. We now massage this kinematic boundary condition into alternative forms.

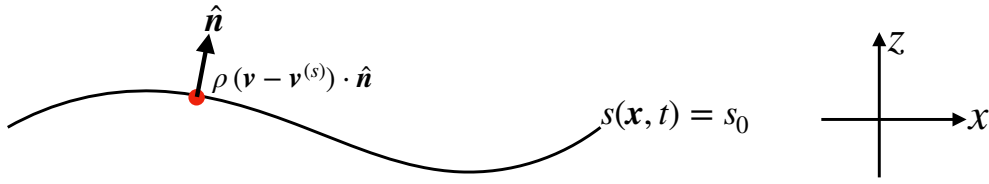


FIGURE 16.6: Illustrating the boundary condition for a moving permeable surface, such as the interface between two miscible fluid layers. On this surface, the boundary condition states that $\rho(\mathbf{v} - \mathbf{v}^{(s)}) \cdot \hat{\mathbf{n}} d\mathcal{S} = -Q_m d\mathcal{S}$ (equation (16.63)). In the special case of an ocean free surface with no overturns, this boundary condition reduces to the surface kinematic boundary condition (16.79).

Coordinate representation of the permeable surface

The expression (16.45) for $\mathbf{v}^{(s)} \cdot \hat{\mathbf{n}}$ holds for a point on an arbitrary surface so that

$$\mathbf{v}^{(s)} \cdot \hat{\mathbf{n}} = -\frac{\partial s / \partial t}{|\nabla s|}. \quad (16.64)$$

Furthermore, the projection of the fluid velocity onto the normal direction can be written

$$\frac{Ds}{Dt} = \frac{\partial s}{\partial t} + \mathbf{v} \cdot \nabla s \implies \mathbf{v} \cdot \hat{\mathbf{n}} = \frac{1}{|\nabla s|} \left[\frac{Ds}{Dt} - \frac{\partial s}{\partial t} \right]. \quad (16.65)$$

Bringing these results together leads to

$$\rho(\mathbf{v} - \mathbf{v}^{(s)}) \cdot \hat{\mathbf{n}} d\mathcal{S} = \frac{\rho d\mathcal{S}}{|\nabla s|} \frac{Ds}{Dt} \implies Q_m = -\frac{\rho}{|\nabla s|} \frac{Ds}{Dt}. \quad (16.66)$$

This equation says that the mass transport crossing the surface is proportional to the material time derivative of the surface coordinate. The material time derivative vanishes when there is no mass transport across the surface (see discussion in Section 16.4.2).

In terms of the horizontal projection of the surface area

Assume that the surface is not vertical, so that its normal direction has a nonzero component in the vertical (e.g., waves that do not overturn). This assumption means that

$$\frac{\partial s}{\partial z} \neq 0, \quad (16.67)$$

so that we can further massage the boundary condition (16.66) by writing the area factor in the form

$$\frac{d\mathcal{S}}{|\nabla s|} = \frac{d\mathcal{S}}{\sqrt{(\partial s/\partial x)^2 + (\partial s/\partial y)^2 + (\partial s/\partial z)^2}} \quad (16.68a)$$

$$= \frac{d\mathcal{S}}{|\partial s/\partial z| \sqrt{[(\partial s/\partial x)/(\partial s/\partial z)]^2 + [(\partial s/\partial y)/(\partial s/\partial z)]^2 + 1}} \quad (16.68b)$$

$$= \frac{d\mathcal{S}}{|\partial s/\partial z| \sqrt{1 + \tan^2 \vartheta}} \quad (16.68c)$$

$$= \left| \frac{\partial z}{\partial s} \right| |\cos \vartheta| d\mathcal{S} \quad (16.68d)$$

$$= \left| \frac{\partial z}{\partial s} \right| dA. \quad (16.68e)$$

The equality (16.68c) introduced the angle, ϑ , between the boundary surface and the horizontal plane. The squared slope of this surface is given by

$$\tan^2 \vartheta = \frac{\nabla_z s \cdot \nabla_z s}{(\partial s/\partial z)^2} = \nabla_s z \cdot \nabla_s z \quad (16.69)$$

with

$$\nabla_z = \hat{x} \left[\frac{\partial}{\partial x} \right]_{y,z} + \hat{y} \left[\frac{\partial}{\partial y} \right]_{x,z} \quad (16.70)$$

the horizontal gradient operator on constant z surfaces, and

$$\nabla_s = \hat{x} \left[\frac{\partial}{\partial x} \right]_{y,s} + \hat{y} \left[\frac{\partial}{\partial y} \right]_{x,s} \quad (16.71)$$

the horizontal gradient operator on constant s surfaces, along with $z(x, y, s, t)$ for the vertical position of the constant s surface.⁶ The equality (16.68d) made use of a trigonometric identity, and the equality (16.68e) introduced the horizontal projection of the area,

$$dA = |\cos \vartheta| d\mathcal{S}. \quad (16.72)$$

These results bring the kinematic boundary condition (16.66) into the form

$$\rho (\mathbf{v} - \mathbf{v}^{(s)}) \cdot \hat{\mathbf{n}} d\mathcal{S} = -Q_m d\mathcal{S} \quad (16.73a)$$

$$= \rho \frac{Ds}{Dt} \left| \frac{\partial z}{\partial s} \right| dA \quad (16.73b)$$

$$\equiv -Q_m dA. \quad (16.73c)$$

As defined, the flux Q_m is the net mass per time per horizontal area crossing the boundary surface

$$Q_m = -\rho (\mathbf{v} - \mathbf{v}^{(s)}) \cdot \hat{\mathbf{n}} \frac{d\mathcal{S}}{dA} = -\rho \frac{Ds}{Dt} \left| \frac{\partial z}{\partial s} \right|. \quad (16.74)$$

We motivate the minus sign through the ocean free surface case in the following.

⁶We study in detail such operators in Chapter 56 when developing the mathematics of generalized vertical coordinates.

Kinematic boundary condition at the ocean free surface

Consider the ocean free surface located at

$$s(x, y, z, t) = z - \eta(x, y, t) = 0 \quad \text{ocean free surface.} \quad (16.75)$$

For this boundary, $\partial s / \partial z = 1$ so that the area elements are related by

$$d\mathcal{S} = |\nabla(z - \eta)| dA = \sqrt{1 + |\nabla\eta|^2} dA. \quad (16.76)$$

The normal projection for the velocity of a point fixed on the free surface is given by

$$\mathbf{v}^{(\eta)} \cdot \hat{\mathbf{n}} = -\frac{\partial s / \partial t}{|\nabla s|} = \frac{\partial \eta / \partial t}{|\nabla(z - \eta)|} = \frac{\partial \eta / \partial t}{\sqrt{1 + |\nabla\eta|^2}} \implies \mathbf{v}^{(\eta)} \cdot \hat{\mathbf{n}} d\mathcal{S} = \partial_t \eta dA, \quad (16.77)$$

so that the mass flux crossing the free surface is

$$-\mathcal{Q}_m = \rho (\mathbf{v} - \mathbf{v}^{(\eta)}) \cdot \hat{\mathbf{n}}. \quad (16.78)$$

The boundary condition (16.74) thus takes the form

$$\rho (\mathbf{v} - \mathbf{v}^{(\eta)}) \cdot \hat{\mathbf{n}} \frac{d\mathcal{S}}{dA} = \rho \left[\frac{D(z - \eta)}{Dt} \right] = -Q_m \implies w + \rho^{-1} Q_m = \frac{\partial \eta}{\partial t} + \mathbf{u} \cdot \nabla \eta. \quad (16.79)$$

We now motivate the sign convention chosen for equation (16.73c) by considering the special case of a flat free surface and a resting fluid with $\mathbf{v} = 0$. Adding mass to the ocean raises the free surface, so that $\partial \eta / \partial t > 0$. Hence, the chosen sign convention means that $Q_m > 0$ corresponds to mass added to the ocean.

Kinematic boundary condition on a buoyancy surface

Now consider the boundary surface to be a surface of constant potential density in the ocean (or analogously a surface of constant specific entropy in the atmosphere). These buoyancy isosurfaces are also known as isopycnals, and we use the symbol⁷

$$s = \sigma(x, y, z, t) \quad (16.80)$$

for a particular isopycnal, σ . The mass transport crossing the isopycnal is written

$$Q_m = \rho \frac{D\sigma}{Dt} \left| \frac{\partial z}{\partial \sigma} \right| \equiv \rho w^{(\dot{\sigma})}, \quad (16.81)$$

where we introduced the *diapycnal transport velocity*

$$w^{(\dot{\sigma})} \equiv \frac{D\sigma}{Dt} \left| \frac{\partial z}{\partial \sigma} \right|. \quad (16.82)$$

A key aspect of physical oceanography concerns the development of theories for processes that cause a non-zero diapycnal transport. Examples include breaking waves, which act to mix matter across density surfaces; i.e., to *entrain* water from one density class to another.

⁷In this book, we use σ as an arbitrary generalized vertical coordinate, here chosen to be an isopycnal.

16.5 Volume and mass budgets for an ocean column

We close this chapter by deriving the budget for the volume per horizontal area in a column of ocean fluid such as that shown in Figure 16.7, as well as the budget for the mass per horizontal area in this column. Since the upper boundary of the domain is the free surface, and since the free surface is a function of time, the region is not strictly Eulerian even though the sides are fixed in space. Furthermore, the free surface is permeable, as are the sides, so that the region is not material. The derivation here thus offers us with experience working with the kinematic boundary conditions, as well as some exposure to the use of Leibniz's rule from calculus.

16.5.1 Kinematic free surface equation

We here derive an equation for the free surface evolution, with this equation providing a budget for the volume per horizontal area in the column. In outline form, the derivation proceeds by vertically integrating the mass continuity equation (16.16) over the depth of an ocean column, from $z = \eta_b(x, y)$ at the bottom to $z = \eta(x, y, t)$ at the free surface. Use of the bottom and surface kinematic boundary conditions renders a kinematic expression for the free surface time tendency.

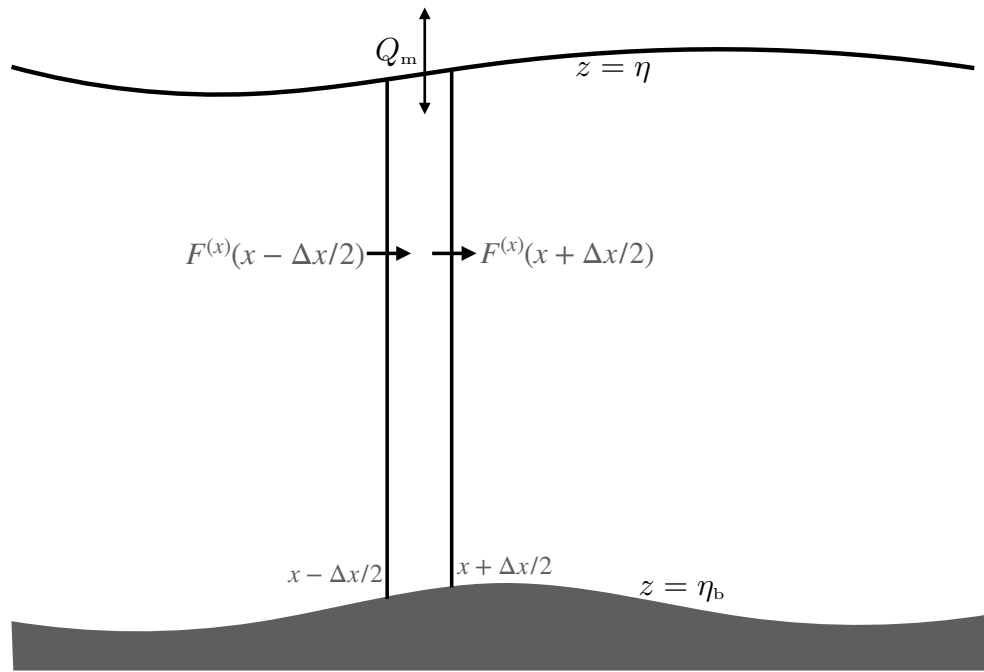


FIGURE 16.7: A longitudinal-vertical slice of ocean fluid from the surface at $z = \eta(x, y, t)$ to bottom at $z = \eta_b(x, y)$. The horizontal boundaries of the column at $x - \Delta x/2$ and $x + \Delta x/2$ are static and are penetrated by zonal mass transport, $F^{(x)}$. The zonal mass transport is computed by integrating the zonal mass flux, ρu over the area of the column sides. A similar transport acts in the meridional direction as well. The free surface is time dependent thus making the fluid column's horizontal cross-sectional area time independent. The ocean bottom at the solid-earth boundary, $z = \eta_b(x, y)$, is static with no mass crossing this interface. The ocean surface at $z = \eta(x, y, t)$ is time dependent with mass flux, Q_m , crossing this interface.

Vertically integrating the continuity equation (16.16) for a compressible fluid renders

$$-\int_{\eta_b}^{\eta} \frac{1}{\rho} \frac{D\rho}{Dt} dz = \int_{\eta_b}^{\eta} \nabla \cdot \mathbf{v} dz \quad (16.83a)$$

$$= w(\eta) - w(\eta_b) + \int_{\eta_b}^{\eta} \nabla_z \cdot \mathbf{u} dz \quad (16.83b)$$

$$= w(\eta) - w(\eta_b) + \nabla_z \cdot \left[\int_{\eta_b}^{\eta} \mathbf{u} dz \right] - \mathbf{u}(\eta) \cdot \nabla_z \eta + \mathbf{u}(\eta_b) \cdot \nabla_z \eta_b \quad (16.83c)$$

$$= [w(\eta) - \mathbf{u}(\eta) \cdot \nabla_z \eta] - [w(\eta_b) - \mathbf{u}(\eta_b) \cdot \nabla_z \eta_b] + \nabla_z \cdot \left[\int_{\eta_b}^{\eta} \mathbf{u} dz \right], \quad (16.83d)$$

where we made use of *Leibniz's rule* from calculus in order to move the horizontal divergence outside of the integral. Also note that $\nabla \cdot \mathbf{u} = \nabla_z \cdot \mathbf{u}$ since \mathbf{u} is the horizontal velocity, and likewise for $\nabla \eta_b$ and $\nabla \eta$ since η_b and η are both functions of horizontal space and time, and so have no z dependence.

Use of the surface kinematic boundary condition (16.79) and no-normal flow bottom boundary condition yield

$$\frac{\partial \eta}{\partial t} = \frac{Q_m}{\rho(\eta)} - \nabla \cdot \mathbf{U} - \int_{\eta_b}^{\eta} \frac{1}{\rho} \frac{D\rho}{Dt} dz \quad (16.84)$$

where

$$\mathbf{U} = \int_{\eta_b}^{\eta} \mathbf{u} dz \quad (16.85)$$

is the depth integrated horizontal transport. Hence, as deduced from the mass continuity equation, the ocean free surface time tendency is affected by the passage of mass across the surface boundary (as normalized by the surface density), the convergence of depth integrated flow, and the depth integral of the material changes in density. The density term contributes to a positive sea surface height tendency when density decreases, and vice versa when density increases. [Griffies and Greatbatch \(2012\)](#) provide a more complete analysis of the sea surface height budget (16.84) by unpacking the physical processes leading to the material evolution of density, which they refer to as the *non-Boussinesq steric effect*.

16.5.2 Budget for mass per horizontal area

The mass per horizontal area in the fluid column is given by $\int_{\eta_b}^{\eta} \rho dz$. Use of Leibniz's rule, the bottom kinematic boundary condition, (16.41), surface kinematic boundary condition (16.79), and the mass continuity equation (16.6), leads to

$$\frac{d}{dt} \left[\int_{\eta_b}^{\eta} \rho dz \right] = \rho(\eta) \frac{\partial \eta}{\partial t} + \int_{\eta_b}^{\eta} \frac{\partial \rho}{\partial t} dz \quad (16.86a)$$

$$= \rho(\eta) \frac{\partial \eta}{\partial t} - \int_{\eta_b}^{\eta} \nabla \cdot (\rho \mathbf{v}) dz \quad (16.86b)$$

$$= \rho(\eta) \left[\frac{\partial \eta}{\partial t} - w(\eta) \right] + \rho(\eta_b) w(\eta_b) - \int_{\eta_b}^{\eta} \nabla_z \cdot (\rho \mathbf{u}) dz \quad (16.86c)$$

$$= \rho(\eta) \left[\frac{\partial \eta}{\partial t} + \mathbf{u} \cdot \nabla \eta - w(\eta) \right] + \rho(\eta_b) [w(\eta_b) - \mathbf{u}(\eta_b) \cdot \nabla \eta_b] - \nabla_z \cdot \mathbf{U}^\rho \quad (16.86d)$$

$$= Q_m - \nabla_z \cdot \mathbf{U}^\rho, \quad (16.86e)$$

where

$$\mathbf{U}^\rho = \int_{\eta_b}^{\eta} \rho \mathbf{u} dz. \quad (16.87)$$

Hence, the mass per horizontal area within a column evolves according to

$$\frac{d}{dt} \left[\int_{\eta_b}^{\eta} \rho dz \right] = Q_m - \nabla \cdot \mathbf{U}^\rho, \quad (16.88)$$

with terms on the right hand side representing the convergence of mass onto the column either through the sides or surface. We consider an alternative derivation of this budget in Exercise 16.3.



16.6 Exercises

EXERCISE 16.1: VELOCITY THAT DOES NOT PENETRATE A SURFACE

Consider a static surface defined by

$$s(x, y) = xy = \text{constant}. \quad (16.89)$$

Provide an example velocity, $\mathbf{v} = u \hat{x} + v \hat{y} + w \hat{z}$, that has nonzero horizontal components and that satisfies $\mathbf{v} \cdot \hat{n} = 0$, where \hat{n} is the unit normal to the surface. Hint: see Section 35.5.5.

EXERCISE 16.2: CENTER OF MASS MOTION

Consider a material fluid region, $\mathcal{R}(\mathbf{v})$, with constant mass written as

$$M = \int_{\mathcal{R}(\mathbf{v})} \rho dV. \quad (16.90)$$

Assume Cartesian coordinates throughout this exercise.

- (a) Show mathematically that the center of mass for the region moves with the region's total linear momentum

$$\frac{d}{dt} \left[\frac{1}{M} \int_{\mathcal{R}(\mathbf{v})} \mathbf{x} \rho dV \right] = \frac{1}{M} \int_{\mathcal{R}(\mathbf{v})} \frac{D\mathbf{x}}{Dt} \rho dV = \frac{1}{M} \int_{\mathcal{R}(\mathbf{v})} \mathbf{v} \rho dV. \quad (16.91)$$

Precisely describe the reasoning behind each step. Note: a brief solution is sufficient, so long as the reasoning is sound.

- (b) Show mathematically (or precisely describe why) that the time change in the linear momentum for the region is given by

$$\frac{d}{dt} \left[\int_{\mathcal{R}(\mathbf{v})} \rho \mathbf{v} dV \right] = \int_{\mathcal{R}(\mathbf{v})} \frac{D\mathbf{v}}{Dt} \rho dV. \quad (16.92)$$

Precisely describe the reasoning behind each step. Note: a brief solution is sufficient, so long as the reasoning is sound.

EXERCISE 16.3: MASS BUDGET FOR A FLUID COLUMN

We here provide an alternative derivation of equation (16.88), the budget for the mass per horizontal area over a column of fluid.

The mass within an arbitrary fluid region is given by

$$M = \int \rho dV. \quad (16.93)$$

Consider the fluid mass within the column shown in Figure 16.7. In this column, the vertical side-walls are fixed in time, the bottom surface, $z = \eta_b(x, y)$, is at the solid-earth boundary, and the top, $z = \eta(x, y, t)$, is the fluctuating ocean free surface. Convince yourself that the mass for this column can be written

$$M = \iint \left[\int_{\eta_b(x, y)}^{\eta(x, y, t)} \rho dz \right] dx dy, \quad (16.94)$$

where the horizontal (x, y) integrals extend over the horizontal extent of the column. Mass conservation for this column means that the change in mass arises just through boundary fluxes, so that

$$\frac{dM}{dt} = - \int \rho \Delta \mathbf{v} \cdot \hat{\mathbf{n}} d\mathcal{S}, \quad (16.95)$$

where $\hat{\mathbf{n}}$ is the outward normal to the surface of the fluid region, $d\mathcal{S}$ is the area of an infinitesimal element on the surface, and the minus sign means that fluid leaving the region contributes to a reduction in mass within the region. The term

$$\Delta \mathbf{v} = \mathbf{v} - \mathbf{v}^{(s)} \quad (16.96)$$

is the velocity of the fluid relative to the velocity of the boundary; e.g., see the kinematic boundary condition discussion in Section 16.4.3. We also derive a general form of this relation in equation (17.47), though this exercise can be solved without knowing the details of that derivation.

- (a) Mass transported in the zonal direction (\hat{x}) that crosses the column's vertical boundary at x is given by

$$F^{(x)}(x, y, t) = \int_{y-\Delta y/2}^{y+\Delta y/2} \left[\int_{\eta_b(x, y')}^{\eta(x, y', t)} u(x, y', z', t) \rho(x, y', z', t) dz' \right] dy' \quad (16.97a)$$

$$\equiv \int_{y-\Delta y/2}^{y+\Delta y/2} U^\rho(x, y', t) dy', \quad (16.97b)$$

and similarly for mass transport in the meridional direction

$$F^{(y)}(x, y, t) = \int_{x-\Delta x/2}^{x+\Delta x/2} \left[\int_{\eta_b(x', y)}^{\eta(x', y, t)} v(x', y, z', t) \rho(x', y, z', t) dz' \right] dx' \quad (16.98a)$$

$$\equiv \int_{x-\Delta x/2}^{x+\Delta x/2} V^\rho(x', y, t) dx', \quad (16.98b)$$

where

$$U^\rho(x, y, t) = \int_{\eta_b(x, y)}^{\eta(x, y, t)} \mathbf{u}(x, y, z', t) \rho(x, y, z', t) dz' = \hat{x} U^\rho + \hat{y} V^\rho. \quad (16.99)$$

What are the physical dimensions [in terms of length (L), mass (M), and time (T)] for the

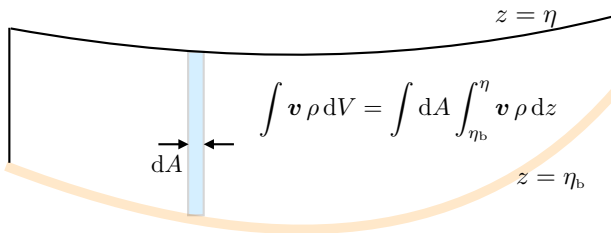


FIGURE 16.8: Cross-section of the integration region for Exercise 16.4, with the region extending from the ocean bottom at $z = \eta_b(x, y)$ and the free surface at $z = \eta(x, y, t)$. The sides are assumed to be vertical and rigid. An infinitesimal column is shown with cross-sectional area dA , extending from the bottom to the surface. The cross-sectional area for the column is time independent, so that a time derivative passes across the area integral to act only on the upper limit $z = \eta$ and the integrand in equation (16.104).

mass transports, $F^{(x)}$ and $F^{(y)}$?

- (b) Using these expressions for the mass crossing the vertical side boundaries of a fluid column, take the limit as the horizontal cross-sectional area of the column becomes infinitesimally small to show that the evolution equation for the mass per unit area of the column is given by

$$\frac{d}{dt} \left[\int_{\eta_b}^{\eta} \rho dz \right] = -\nabla \cdot \mathbf{U}^\rho + Q_m, \quad (16.100)$$

where Q_m is the mass transport entering the ocean through the surface, per horizontal area, as defined by equation (16.73c), so that

$$\int Q_m dA = - \int \rho \Delta \mathbf{v} \cdot \hat{\mathbf{n}} d\mathcal{S} \quad \text{at } z = \eta. \quad (16.101)$$

The derivation of equation (16.100) is part of this exercise, using methods distinct from those used in Section 16.5.2.

- (c) In words, the mass budget in equation (16.100) says that mass changes in a column of fluid if there is a convergence of mass into the column across its vertical boundaries (first term on right hand side), and a mass flux entering the column across the ocean surface (second term on right hand side). What are the physical dimensions of all terms in equation (16.100)?

EXERCISE 16.4: CHANGE IN LINEAR MOMENTUM OF A FLUID REGION

Consider a closed ocean basin with zero boundary fluxes of matter; i.e., zero precipitation/evaporation and zero mass fluxes through the solid-earth bottom. Consequently, this region is bounded by material surfaces and so it maintains constant matter content with fixed mass

$$M = \int_{\mathcal{R}} \rho dV. \quad (16.102)$$

Show that the time change in the linear momentum for this ocean basin is given by

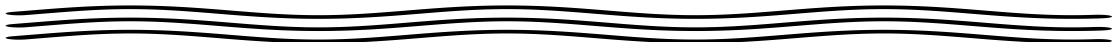
$$\frac{d}{dt} \left[\int_{\mathcal{R}} \rho \mathbf{v} dV \right] = \int_{\mathcal{R}} \frac{D\mathbf{v}}{Dt} \rho dV. \quad (16.103)$$

This result is identical to that derived in Exercise 16.2. Rather than just repeating the solution method used there, make use of Leibniz's rule, the kinematic boundary condition detailed in Section 16.4.2, and mass conservation.

Hint: Refer to Figure 16.8 for a schematic of the integration where we have expanded the volume integral into the form

$$\frac{d}{dt} \left[\int_{\mathcal{R}} \rho \mathbf{v} dV \right] = \frac{d}{dt} \left[\int \left(\int_{\eta_b}^{\eta} \rho \mathbf{v} dz \right) dA \right], \quad (16.104)$$

where the horizontal integral extends over the rigid and fixed horizontal area of the basin, $dA = dx dy$ is the time independent horizontal area element, $z = \eta_b(x, y)$ is the solid-earth bottom and $z = \eta(x, y, t)$ is the ocean free surface. Time dependence appears in the upper boundary at $z = \eta$ and within the integrand. Perform the time derivative operation and make use of mass continuity and the kinematic boundary condition. Also make use of the trigonometry presented in Section 16.4.3 (in particular equation (16.72)). Unlike the formulation in Exercise 16.2, there is no use of a material time derivative in this approach. Rather, it is a straightforward use of integration over a domain with fixed horizontal/bottom boundaries and a time dependent free surface boundary.



Chapter 17

TRACER CONSERVATION

As seen in Chapter 16, the assumption of *mass conservation* has many implications for the motion of single-component fluids. In this chapter we extend that discussion to the case of a fluid comprised of multiple matter constituents (e.g., seawater comprised of fresh water, salt, nitrogen, oxygen, carbon, nutrients, biogeochemicals). In so doing we develop differential and integral budget equations for extensive properties, such as mass or tracer content, along with *continuity equations* for intensive properties, such as mass density and tracer concentration. The Leibniz-Reynolds transport theorem provides the link between the differential and integral formulations.

A key element in the formulation of mass budgets concerns the *barycentric velocity*, which is the center of mass velocity for a fluid element. The barycentric velocity is the extension to multi-component fluids of the fluid parcel velocity used in single-component fluids. Differences between the barycentric velocity and the velocity of a specific fluid constituent lead to the diffusion of matter constituents across the boundary of the fluid element.

READER'S GUIDE TO THIS CHAPTER

The formulation pursued in this chapter is inspired by similar treatments in the chemical physics literature (e.g., Chapter 11 of [Aris \(1962\)](#), Chapter II of [DeGroot and Mazur \(1984\)](#), or Section 2.1 of [Kreuzer \(1981\)](#)), who develop a theory for transport processes in multi-component fluids. For this chapter, we assume an understanding of the Eulerian and Lagrangian kinematic descriptions detailed in Chapter 14 and the mass conservation analysis in Chapter 16. Much of the material from this chapter is used for the study of scalar fields such as potential enthalpy and material tracers. Furthermore, the Leibniz-Reynolds transport theorem of Section 17.3.4 is a kinematic result central to all finite volume budgets in fluid mechanics.

17.1 The tracer equation	362
17.1.1 Mass conservation for each constituent	362
17.1.2 Total mass conservation	363
17.1.3 The tracer equation	364
17.1.4 Compatibility between total mass and tracer mass	366
17.1.5 Summary of some conceptual points	366
17.1.6 Further study	367
17.2 Passive tracers	368
17.3 Budgets for arbitrary fluid regions	368
17.3.1 Extensive and intensive fluid properties	369
17.3.2 General form of the finite domain integral	370
17.3.3 Eulerian (static) domain	370
17.3.4 Deriving the Leibniz-Reynolds transport theorem	370
17.3.5 Interpreting the Leibniz-Reynolds transport theorem	373

17.3.6	Revisiting Reynolds transport theorem	374
17.3.7	Summary of the time derivatives acting on integrals	376
17.4	Brute force illustration of Leibniz-Reynolds	377
17.4.1	Leibniz's rule plus kinematic boundary conditions	377
17.4.2	Summarizing the result	378
17.5	Evolution of region mean scalar	379
17.5.1	Formulation	379
17.5.2	Application to a numerical ocean model grid cell	379
17.6	Boundary conditions	380
17.6.1	Interior layer boundary conditions	380
17.6.2	Solid-earth boundary conditions	380
17.6.3	Upper ocean surface boundary conditions	382
17.7	Exercises	383

17.1 The tracer equation

As defined in Section 14.3, a fluid element is an infinitesimal region of constant mass within the fluid continuum. Although possessing a constant mass, it generally has a non-constant material composition. That is, a fluid element is a non-material fluid parcel. Fluid element boundaries are open to the exchange of matter (i.e., tracers) with adjacent fluid elements. They are also open to the exchange of thermodynamic properties such as temperature and specific entropy.

The kinematics of fluid elements share certain features with material fluid parcels. For example, we can uniquely specify the position of a fluid element's center of mass by providing a material coordinate and time. Correspondingly, we can generalize the Reynolds transport theorem for integration over a constant mass fluid region (Section 17.3.4). We make use of fluid elements to develop the mass budgets for multi-component fluids such as the ocean and atmosphere. The constituent mass budgets are commonly referred to as *tracer equations*.

17.1.1 Mass conservation for each constituent

In this subsection we formulate the mass conservation equation for each constituent within the fluid. The mass equation is formulated by taking an integral (or weak formulation) approach over a fixed (Eulerian) region.

Density and velocity for each matter constituent

Consider a fluid with $n = 1, N$ matter constituents. For example, seawater has $N = 2$ when concerned just with its freshwater and salt content, whereas $N > 2$ when also concerned with other material constituents such as CO_2 and biogeochemical species. Now focus on a fixed (Eulerian) region of the fluid with volume V and total mass M . Inside of the region, count the number of molecules of each constituent and determine (at least, in principle) their corresponding velocities. This information can be used to construct the molecular center of mass velocity for each constituent, $\mathbf{v}^{(n)}$, as well as the mass density,

$$\rho^{(n)} = V^{-1} M^{(n)}. \quad (17.1)$$

In the continuum limit, the volume and mass in the region get tiny ($V \rightarrow dV$ and $M \rightarrow dM$), yet the mass density remains smooth and finite (see Figure 13.2). Correspondingly, the constituent velocity and mass density are continuous fields whose values are available at each point within the continuum fluid.

Integral formulation of the constituent mass budget

Consider an arbitrary region, \mathcal{R} , assumed to be fixed in space (an Eulerian region). The mass of component n within \mathcal{R} is given by the integral

$$M^{(n)} = \int_{\mathcal{R}} \rho^{(n)} dV, \quad (17.2)$$

and it changes in time according to the finite volume budget equation (there is no implied summation on the right hand side)

$$\frac{d}{dt} \int_{\mathcal{R}} \rho^{(n)} dV = - \int_{\partial\mathcal{R}} \rho^{(n)} \mathbf{v}^{(n)} \cdot \hat{\mathbf{n}} d\mathcal{S}. \quad (17.3)$$

This equation is a constituent form of the finite volume mass budget given for a single-component fluid by equation (16.9). Since the region, \mathcal{R} , is assumed to be fixed in space, we can move the time derivative across the integral to reveal

$$\int_{\mathcal{R}} \left[\frac{\partial \rho^{(n)}}{\partial t} + \nabla \cdot (\rho^{(n)} \mathbf{v}^{(n)}) \right] dV = 0, \quad (17.4)$$

where we also used the divergence theorem to convert the surface integral to a volume integral. Arbitrariness of the region means that this integral expression must be satisfied at each point of the continuum, thus leading to the Eulerian form of the constituent mass continuity equation

$$\frac{\partial \rho^{(n)}}{\partial t} + \nabla \cdot (\rho^{(n)} \mathbf{v}^{(n)}) = 0. \quad (17.5)$$

This equation can also be written using a material time derivative

$$\frac{D^{(n)} \rho^{(n)}}{Dt} = -\rho^{(n)} \nabla \cdot \mathbf{v}^{(n)} \quad \text{for each of the } n = 1, N \text{ constituents}, \quad (17.6)$$

where the constituent material time derivative is given by

$$\frac{D^{(n)}}{Dt} = \frac{\partial}{\partial t} + \mathbf{v}^{(n)} \cdot \nabla. \quad (17.7)$$

We thus have N statements of mass conservation corresponding to each constituent material fluid parcel moving according to the velocity $\mathbf{v}^{(n)}$.

17.1.2 Total mass conservation

Summing the Eulerian mass continuity equation (17.5) over all constituents leads to the continuity equation for the total mass

$$\frac{\partial \rho}{\partial t} + \nabla \cdot (\rho \mathbf{v}) = 0, \quad (17.8)$$

where the total mass density and *barycentric velocity* are given by

$$\rho = \sum_{n=1}^N \rho^{(n)} \quad \text{and} \quad \mathbf{v} = \rho^{-1} \sum_{n=1}^N \rho^{(n)} \mathbf{v}^{(n)}. \quad (17.9)$$

Introducing the material time derivative following the barycentric velocity, $D/Dt = \partial/\partial t + \mathbf{v} \cdot \nabla$, leads to the equivalent material form for the mass conservation equation

$$\frac{D\rho}{Dt} = -\rho \nabla \cdot \mathbf{v}. \quad (17.10)$$

The *barycenter* of a distribution of matter is the center of inertia for that matter. We choose the term *barycentric velocity* to distinguish \mathbf{v} from the molecular *center of mass velocity*, $\mathbf{v}^{(n)}$, of each constituent. The barycentric velocity plays a key role in the conservation laws for multi-component fluids.

17.1.3 The tracer equation

Rather than keep track of each constituent velocity, $\mathbf{v}^{(n)}$, and the corresponding material parcels, it is generally more convenient to focus on the fluid element that moves with the barycentric velocity. For this purpose, we consider again the constituent mass continuity equation (17.5)

$$\left[\frac{\partial}{\partial t} + \mathbf{v}^{(n)} \cdot \nabla \right] \rho^{(n)} = -\rho^{(n)} \nabla \cdot \mathbf{v}^{(n)} \quad (17.11)$$

and insert the barycentric velocity to both sides by adding $0 = \mathbf{v} - \mathbf{v}$

$$\left[\frac{\partial}{\partial t} + (\mathbf{v} - \mathbf{v} + \mathbf{v}^{(n)}) \cdot \nabla \right] \rho^{(n)} = -\rho^{(n)} \nabla \cdot [\mathbf{v} - \mathbf{v} + \mathbf{v}^{(n)}]. \quad (17.12)$$

Rearrangement leads to

$$\left[\frac{\partial}{\partial t} + \mathbf{v} \cdot \nabla \right] \rho^{(n)} = -\rho^{(n)} \nabla \cdot \mathbf{v} - \nabla \cdot [\rho^{(n)} (\mathbf{v}^{(n)} - \mathbf{v})], \quad (17.13)$$

which can be written

$$\frac{D\rho^{(n)}}{Dt} = -\rho^{(n)} \nabla \cdot \mathbf{v} - \nabla \cdot \mathbf{J}^{(n)}, \quad (17.14)$$

where we defined the constituent *tracer mass flux*

$$\mathbf{J}^{(n)} = \rho^{(n)} (\mathbf{v}^{(n)} - \mathbf{v}), \quad (17.15)$$

which arises from the difference between the constituent velocity and the barycentric velocity. The dimensions of $\mathbf{J}^{(n)}$ are mass of constituent n per time per area.

The material mass conservation equation (17.14) takes on the Eulerian form

$$\frac{\partial \rho^{(n)}}{\partial t} + \nabla \cdot (\mathbf{v} \rho^{(n)}) = -\nabla \cdot \mathbf{J}^{(n)}. \quad (17.16)$$

Introducing the tracer concentration $C^{(n)}$ according to

$$C^{(n)} = \frac{\rho^{(n)}}{\rho} = \frac{\delta M^{(n)}}{\delta M} = \frac{\text{mass of constituent } n \text{ in fluid element}}{\text{mass of fluid element}}, \quad (17.17)$$

leads to the tracer flux

$$\mathbf{J}^{(n)} = \rho C^{(n)} (\mathbf{v}^{(n)} - \mathbf{v}), \quad (17.18)$$

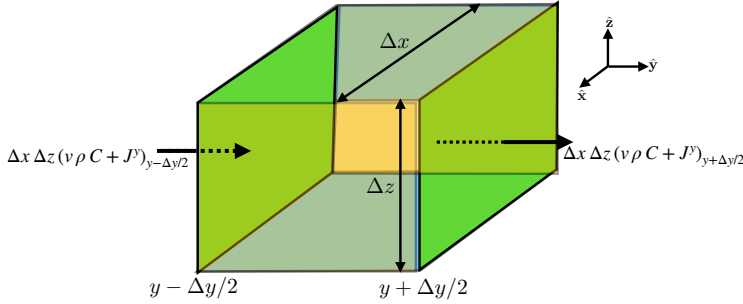


FIGURE 17.1: A finite sized cube as in Figure 16.1, here used to illustrate the budget of tracer mass over an Eulerian region. In addition to the advective flux of tracer moving with the barycentric velocity, \mathbf{v} , there is a diffusive flux, \mathbf{J} , that contributes to the transfer of tracer across the cell face.

the Eulerian flux-form tracer budget

$$\frac{\partial(\rho C^{(n)})}{\partial t} + \nabla \cdot [\mathbf{v} \rho C^{(n)} + \mathbf{J}^{(n)}] = 0. \quad (17.19)$$

In Figure 17.1 we illustrate the contributions to the tracer evolution according to this Eulerian flux-form equation (17.19).

Eulerian and Lagrangian forms of the tracer equation

The Eulerian flux-form equation (17.19) has a corresponding material time derivative form derived by expanding the derivatives

$$\begin{aligned} C^{(n)} \frac{\partial \rho}{\partial t} + \rho \frac{\partial C^{(n)}}{\partial t} + \rho \mathbf{v} \cdot \nabla C^{(n)} + C^{(n)} \nabla \cdot (\rho \mathbf{v}) \\ = C^{(n)} \left[\frac{\partial \rho}{\partial t} + \nabla \cdot (\rho \mathbf{v}) \right] + \rho \left[\frac{\partial C^{(n)}}{\partial t} + \mathbf{v} \cdot \nabla C^{(n)} \right]. \end{aligned} \quad (17.20)$$

The first term on the right hand side vanishes through mass continuity in the form of equation (17.8). The second term on the right hand side is the material time derivative of the tracer concentration. We are thus led to the equivalent forms for the tracer equation¹

$$\frac{\partial(\rho C^{(n)})}{\partial t} + \nabla \cdot [\mathbf{v} \rho C^{(n)}] = \rho \frac{DC^{(n)}}{Dt} = -\nabla \cdot \mathbf{J}^{(n)}. \quad (17.21)$$

Advection plus diffusive tracer fluxes

The above definitions allow us to decompose an advective tracer flux defined according to the tracer velocity into an advective flux based on the barycentric velocity plus a *diffusive flux*

$$\rho C^{(n)} \mathbf{v}^{(n)} = \rho C^{(n)} (\mathbf{v}^{(n)} - \mathbf{v} + \mathbf{v}) = \mathbf{J}^{(n)} + \rho C^{(n)} \mathbf{v}. \quad (17.22)$$

The diffusive flux vanishes when the tracer velocity equals to the barycentric velocity. Correspondingly, the diffusive flux also vanishes for a single-component fluid, since in that case there is only one matter component and so the constituent velocity equals to the barycentric velocity.

¹The same result was also derived in equation (16.35c) when discussing Reynolds transport theorem for a single-component fluid.

We refer to this flux as “diffusive” since it is common in practice to parameterize this term as a downgradient diffusive flux. However, as seen in Section 23.8.2, not all diffusion processes are downgradient. We also offer further discussion of diffusion due to turbulent processes in Chapter 63.

17.1.4 Compatibility between total mass and tracer mass

By construction, the Eulerian flux-form of the tracer equation (17.19) is compatible with the flux-form continuity equation

$$\frac{\partial(\rho C^{(n)})}{\partial t} + \nabla \cdot [\rho \mathbf{v} C^{(n)} + \mathbf{J}^{(n)}] = 0 \iff \frac{\partial \rho}{\partial t} + \nabla \cdot (\rho \mathbf{v}) = 0. \quad (17.23)$$

Compatibility is manifest by summing the tracer equation over all constituents and using the identities

$$\sum_{n=1}^N C^{(n)} = 1 \quad \text{and} \quad \sum_{n=1}^N \mathbf{J}^{(n)} = 0. \quad (17.24)$$

Furthermore, through use of the barycentric velocity (17.9), we are ensured that the continuity equation (17.8) for the total density of a fluid element is only transported by the barycentric velocity. There is no contribution from $\mathbf{J}^{(n)}$ since $\sum_{n=1}^N \mathbf{J}^{(n)} = 0$.

17.1.5 Summary of some conceptual points

What is a fluid element? How does it maintain constant mass but not constant matter? Here we aim to review some of the conceptual points to help answer these puzzles, building from our initial specification of fluid elements and fluid parcels in Section 14.3.

Revisiting a fluid element

The mass continuity equation (17.10) motivates us to define a fluid element as an infinitesimal fluid parcel that moves with barycentric velocity, \mathbf{v} , and maintains a constant total mass

$$\delta M = \sum_{n=1}^N \delta M^{(n)}. \quad (17.25)$$

The fluid element does not maintain a constant mass for each constituent, since the fluid element moves at the barycentric velocity, \mathbf{v} , which generally differs from the constituent velocities $\mathbf{v}^{(n)}$. Consequently, a fluid element boundary is permeable to matter transport that leaves its mass constant but allows for exchanges of matter constituents with adjacent fluid elements. Hence, if some matter leaves the fluid element, then an equal amount must enter the element in order to maintain a constant mass.

The exchange of matter across a fluid element’s boundary can arise from the direct motion of matter crossing the boundary, or from the motion of the fluid element boundary relative to the matter. This point is central to resolving some conundrums associated with the notion of matter exchange constrained to retain constant mass. We have more to say on this point in the following.

Conceptual summary of the formulation

The formulation pursued in this section is based on considering the multi-component fluid to be a continuum with distinct matter constituents (e.g., salt and freshwater for the ocean or water

vapor and dry air for the atmosphere). Furthermore, the mass concentration for each constituent is represented by a scalar field whose value at any point in space-time gives the mass of tracer per mass of fluid. We then formulate mass conservation equations (i.e., continuity equations) for each matter constituent following methods used for the single-component fluid in Chapter 16. By choosing to use the *barycentric* (center of mass) velocity for describing fluid flow, the mass continuity equation for the total mass in a fluid element takes on the same form as for a single-component fluid. The resulting constituent mass budgets (i.e., tracer equations) have “diffusive” fluxes since the velocity of each matter constituent is generally distinct from the barycentric velocity.

To expose a bit of the details, we saw in this section that the tracer equation expresses the balance of mass for each trace constituent in the fluid. Furthermore, a nonzero tracer flux, $\mathbf{J}^{(n)} = \rho C^{(n)} (\mathbf{v}^{(n)} - \mathbf{v})$, arises when the barycentric velocity, \mathbf{v} , differs from the constituent velocity, $\mathbf{v}^{(n)}$. In that case, matter and thermodynamic properties are exchanged between fluid elements, with the exchange made without altering the mass of a fluid element. In the presence of random motion within a turbulent fluid, or in the presence of random interactions with molecular degrees of freedom, tracer exchange is akin to a random walk. Such exchange is commonly parameterized by a diffusion process (see Section 61.3). Correspondingly, the mass of tracers in a fluid element is altered in the presence of differences in tracer concentration between fluid elements (i.e., tracer concentration gradients). However, the total mass of the element remains fixed.

How to maintain constant mass

As defined, a fluid element provides a generalization to multi-component fluids of the notion of a constant mass material fluid parcel that we used in describing a single-component fluid (see Section 14.3). Later in this chapter we encounter a finite volume extension of the fluid element, which we refer to as a *Lagrangian region*. A Lagrangian region has boundaries that follow the barycentric velocity, \mathbf{v} , so that the region maintains constant mass as per our discussion of Reynolds transport theorem in Section 17.3.6.

To maintain constant mass, any matter that leaves the fluid element by crossing its boundary is compensated by an equal mass that enters the boundary. Kinematically, there are two means for matter to cross a boundary. First, the matter itself can move across the boundary, with the limiting case being a stationary boundary with matter moving across. Second, the boundary can move relative to the matter, with the limiting case being stationary matter with the boundary moving. In either case, by choosing to follow the barycentric velocity, a fluid element’s boundary (or a corresponding Lagrangian region’s boundary) adjusts so that mass remains constant.

The strategic choice to formulate the kinematics of multi-component fluids using the barycentric velocity is directly analogous to the choice in Newtonian mechanics to describe motion relative to the center of mass for a system of many moving objects such as planets or point particles (see Section 10.2). In particular, by describing the motion of a multi-component fluid using the barycentric velocity, we simplify the kinematics by linking to the kinematics of single-component fluids while also supporting a generalization in the form of constituent tracer equations. As seen in Part V of this book, a dynamical description of fluid motion is also facilitated by working with constant mass fluid elements/regions.

17.1.6 Further study

We used many words in this section to help develop the mass budget for fluid elements in a multi-component fluid. The reason for such verbosity is that elements of the formulation can be confusing on first encounter. Even so, it is important to keep in mind that the basic notions

are quite simple. Further extension of these ideas incorporates chemical reactions that transfer mass from one matter constituent to others, while retaining fixed net mass. This extension is relevant for studies of atmospheric chemistry and ocean biogeochemistry. Development of these extensions, using nomenclature similar to that used here, is provided in Chapter 11 of [Aris \(1962\)](#), Chapter II of [DeGroot and Mazur \(1984\)](#), and Section 2.1 of [Kreuzer \(1981\)](#).

The tracer fluxes introduced when formulating the tracer equation are typically parameterized by downgradient diffusion. However, as discussed in our study of the ocean entropy budget in Section 23.8, the transport of a scalar field can arise both from spatial gradients in that field as well as gradients in other fluid properties. Such cross-diffusion effects have been found to be relevant in certain quiescent regions of the ocean, though they are generally washed-out by turbulent processes.

17.2 Passive tracers

As defined in equation (17.17), the concentration of a material tracer is the mass of the trace constituent per mass of a fluid element. Such material tracers modify the barycentric velocity (17.9) since they carry mass and thus affect the mass density. We here define the idealized construct known as a *passive tracer*. A passive tracer satisfies the advection-diffusion equation, but it has zero impact on the velocity and is thus dynamically passive. Mathematically, we conceive of a passive tracer as a material tracer in the limit where the tracer mass and mass of the fluid element together go to zero. The passive tracer is thus analogous to the massless fluid particle of Section 14.3 whose trajectories define the Lagrangian reference frame. However, the passive tracer is transported both via advection and diffusion. Hence, we make use of passive tracers to probe the advective and diffusive features of the flow without modifying the flow. For example, a passive tracer can be used to define tracer pathways and time scales for transport between fluid regions, such as reviewed by [Haine et al. \(2022\)](#) for ocean applications.

In Chapter 15 and Section 16.4.2, we discussed the notion of a material fluid object, which is an object comprised of fluid particles that follow the velocity, \mathbf{v} . In a single-component fluid, such material objects are impenetrable to matter, by construction. For a multi-component fluid, trace matter will generally cross the material object through diffusion since $\mathbf{v}^{(n)} \neq \mathbf{v}$. Hence, there is no perfectly impenetrable fluid object in a fluid with any form of diffusion, including molecular diffusion. However, we can conceive of a passive tracer that follows the barycentric velocity and is either acted on by diffusion or is unaffected by diffusion. Again, these features are afforded the passive tracer given that it is a massless conceptual idealization used to probe the fluid flow properties. Hence, the passive tracer is not subject to the same physical constraints as a material tracer.

17.3 Budgets for arbitrary fluid regions

Thus far in this chapter we have considered the evolution of mass within a variety of fluid regions, including infinitesimal and finite domains either moving with the fluid or fixed in space. We have also considered similar domains in Chapter 16 where the fluid domains were typically material regions. In this section we synthesize these presentations by considering mass budgets over an arbitrary finite sized domain within multi-component fluids. The resulting mass equations form the basis for matter budgets used in geophysical fluid mechanics.

17.3.1 Extensive and intensive fluid properties

Consider a bucket of seawater that has homogeneous temperature and salinity. Removing a cup of water from this bucket does not alter the temperature or salinity, but it does alter the enthalpy, salt mass, and freshwater mass. We are thus motivated to characterize physical properties as *extensive* or *intensive*. For the bucket of seawater, temperature and salinity are intensive quantities, whose value does not change when removing seawater from the bucket. Further intensive properties include number density (number of particles per volume), mass density (mass of substance per volume), tracer concentration (mass of tracer per mass of fluid), temperature, velocity (linear momentum per mass), kinetic energy per mass, entropy per mass, and enthalpy per mass. An extensive property changes when the size of the sample changes, with examples including particle number, mass, length, volume, kinetic energy, entropy, enthalpy, and linear momentum.²

We are concerned in this section with how scalar extensive properties change as a function of time.³ Determining the evolution of such properties constitutes a budget analysis for the scalar property. What are the processes responsible for these changes? Where are the changes coming from? Those are basic questions asked when performing a budget analysis. In addition to physical and biogeochemical processes active within the fluid, details of the region over which one performs a budget have an important impact on the budget. Is the region open to matter and energy transport, or is it closed? Is the region static (Eulerian) or do boundaries move? If the boundaries move, do they move with fluid elements (Lagrangian) or are they moving in some other manner (arbitrary)?

In the following, let Π represent an intensive scalar fluid property of a fluid element so that $\Pi \rho \delta V$ is the corresponding extensive property

$$\Pi = \text{intensive fluid property such as tracer concentration} \quad (17.26a)$$

$$\Pi \rho \delta V = \text{extensive fluid property such as tracer mass}. \quad (17.26b)$$

For example, if Π is the tracer concentration in a fluid element (i.e., mass of tracer per mass of fluid), then the corresponding extensive property, $\Pi \rho \delta V$, is the mass of tracer in the fluid element. Anticipating our discussion in Section 23.9, then if Π is the Conservative Temperature, Θ , of a fluid element, then the corresponding extensive property, $\Theta c_p \rho \delta V$, is the potential enthalpy with c_p the specific heat capacity.

We furthermore assume that Π satisfies the scalar conservation equation, written here in both its material form and Eulerian flux-form

$$\rho \frac{D\Pi}{Dt} = -\nabla \cdot \mathbf{J} \iff \frac{\partial(\rho \Pi)}{\partial t} + \nabla \cdot (\rho \Pi \mathbf{v} + \mathbf{J}) = 0, \quad (17.27)$$

where \mathbf{J} is a flux such as that associated with the tracer equation derived in Section 17.1.3. Depending on the context, the budget equation (17.27) is sometimes referred to as a *conservation law* for Π . Notably, satisfaction of a conservation law does not mean that Π is constant either at a point in space nor following a fluid particle. Instead, there are two cases of “constancy” that naturally arise. First, with $-\nabla \cdot \mathbf{J} = 0$, the scalar field is constant following a material fluid particle

$$-\nabla \cdot \mathbf{J} = 0 \implies \frac{D\Pi}{Dt} = 0. \quad (17.28)$$

In this case we say that Π is a *material invariant* or a *material constant*. Second, if the Eulerian time derivative vanishes, $\partial_t \Pi = 0$, then Π remains constant at a fixed spatial point in the fluid

²We again encounter intensive and extensive properties when studying thermodynamics in Chapter 19.

³We consider budget equations for vector linear momentum in Chapter 21.

and we say that Π is in a *steady state*. Furthermore, recall that the Eulerian reference frame is stationary with respect to a laboratory frame, with the laboratory frame inertial when connected by a Galilean transformation to the universal Newtonian reference frame (Section 14.4). Hence, if the flow in one laboratory frame is steady, then flow in all laboratory frames is steady so long as the laboratory frames are connected by a Galilean transformation (see Section 14.7).

17.3.2 General form of the finite domain integral

We are concerned here with the evolution of extensive fluid properties integrated over an arbitrary region. Let us make use of the following notation for such integrals

$$\mathcal{I}[\mathcal{R}(t), t] = \int_{\mathcal{R}(t)} \Pi \rho dV \equiv \int_{\mathcal{R}(t)} \varphi dV, \quad (17.29)$$

where we introduced the shorthand

$$\varphi = \rho \Pi. \quad (17.30)$$

The integrand in equation (17.29) is a function of space and time, $\varphi = \varphi(\mathbf{x}, t)$, and the integration region is generally a function of time, $\mathcal{R}(t)$. In previous sections, \mathcal{R} was a material region of fixed matter content (Section 16.3) or a constant mass fluid region open to the exchange of matter with the surroundings (Section 17.1). In both of these cases the region was denoted by $\mathcal{R}(\mathbf{v})$ since it moved with the fluid flow. Here we make no *a priori* assumption about the region.

The total time derivative of \mathcal{I} can be written as

$$\frac{d\mathcal{I}}{dt} = \left[\frac{\partial \mathcal{I}}{\partial t} \right]_{\mathcal{R}} + \frac{d\mathcal{R}}{dt} \left[\frac{\partial \mathcal{I}}{\partial \mathcal{R}} \right]_t. \quad (17.31)$$

The first term on the right hand side is the time derivative of the integral when holding the region fixed in space as per an Eulerian time derivative. The second term accounts for changes due to evolution of the region as weighted by dependence of the integral on the region itself. How the integral changes in time depends on both the evolution of the fluid property relative to the chosen region and evolution of the fluid region itself. Equation (17.31) is directly analogous to the total time derivative of a field in a moving fluid as given by equation (14.27).

17.3.3 Eulerian (static) domain

We first consider an Eulerian domain, which is fixed in space and thus static so that

$$\frac{d\mathcal{I}}{dt} = \left[\frac{\partial \mathcal{I}}{\partial t} \right]_{\mathcal{R}} = \frac{\partial}{\partial t} \left[\int_{\mathcal{R}} \Pi \rho dV \right] = \int_{\mathcal{R}} \left[\frac{\partial(\rho \Pi)}{\partial t} \right] dV. \quad (17.32)$$

Movement of the time derivative across the integral sign is available since the domain boundaries are static; i.e., the second term on the right hand side of equation (17.31) vanishes. Furthermore, since the domain is static, the volume element, dV , provides a static partition of the total domain volume so that dV does not appear inside the time derivative. This case corresponds to the Eulerian budgets depicted in Figures 16.1, 16.2, and 17.1.

17.3.4 Deriving the Leibniz-Reynolds transport theorem

We now allow the domain boundaries to be time dependent so that both terms in the total time derivative (17.31) contribute. The resulting *Leibniz-Reynolds transport theorem* is a general expression of conservation over an arbitrary region. We derive this theorem here using two

methods, one naive and another a bit more rigorous. Interpretation and application of this theorem are then presented in Section 17.3.5.

A rectangular region

Consider a one-dimensional domain with time dependent endpoints. Integrals of this type commonly arise when integrating over the depth of the atmosphere or ocean, in which case the boundary terms are replaced by the kinematic boundary conditions studied in Section 16.4. The chain rule for differentiating integrals is known as *Leibniz's rule*. It results in the time derivative acting on the upper integral limit, the lower limit, and the integrand

$$\frac{d}{dt} \left[\int_{x_1(t)}^{x_2(t)} \varphi(x, t) dx \right] = \int_{x_1(t)}^{x_2(t)} \frac{\partial \varphi}{\partial t} dx + \frac{d}{dt} \left[\int_{x_1(t)}^{x_2(t)} \right] \varphi(x, t) dx \quad (17.33a)$$

$$= \int_{x_1(t)}^{x_2(t)} \frac{\partial \varphi}{\partial t} dx + \frac{dx_2(t)}{dt} \varphi(x_2, t) - \frac{dx_1(t)}{dt} \varphi(x_1, t), \quad (17.33b)$$

with the terms $dx_{1,2}/dt$ the velocities of the endpoints.

We can generalize the one-dimensional result (17.33b) to three dimensions by assuming the three dimensional domain is expressible by Cartesian coordinates whose extents are mutually independent. That is, we assume the domain, $\mathcal{R}(t)$, is rectangular. In this case we can immediately generalize equation (17.33b) to

$$\frac{d}{dt} \left[\int_{\mathcal{R}} \varphi dV \right] = \int_{\mathcal{R}} \frac{\partial \varphi}{\partial t} dV + \oint_{\partial \mathcal{R}} \varphi \mathbf{v}^{(b)} \cdot \hat{\mathbf{n}} d\mathcal{S}, \quad (17.34)$$

where we introduced the shorthand for the velocity of a point on the region boundary

$$\mathbf{v}^{(b)} = \frac{d\mathbf{x}}{dt}. \quad (17.35)$$

The identity (17.34) is the *Leibniz-Reynolds transport theorem*.

An arbitrary simply connected region

We now present the derivation for an arbitrary simply connected domain, $\mathcal{R}(t)$, thus generalizing the domain geometry while offering further insight into the transport theorem. For this purpose, again let the region boundary, $\partial \mathcal{R}$, have an outward unit normal, $\hat{\mathbf{n}}$, and let points on the boundary move with the velocity, $\mathbf{v}^{(b)}$. In Figure 17.2 we depict the region geometry as it evolves over a time step of size, Δt . In particular, this figure illustrates the identity⁴

$$\mathcal{R}(t + \Delta t/2) = \mathcal{R}(t - \Delta t/2) + [\mathcal{R}(t + \Delta t/2) - \mathcal{R}(t - \Delta t/2)], \quad (17.36)$$

with the corresponding equation for the region volume given by

$$\int_{\mathcal{R}(t + \Delta t/2)} dV = \int_{\mathcal{R}(t - \Delta t/2)} dV + \int_{\mathcal{R}(t + \Delta t/2) - \mathcal{R}(t - \Delta t/2)} dV. \quad (17.37)$$

⁴For those familiar with numerical methods, note that we make use of centered finite time differences in this discussion. Doing so offers a second order accurate expression of the finite difference approximations to the time derivative, whereas forward or backward differences are only first order accurate. Central differences also provides an intuitive centering of the time differences around the central time, t .

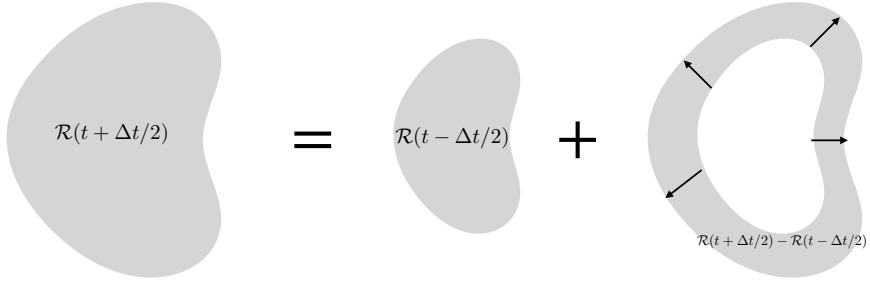


FIGURE 17.2: Illustrating the geometry of the Leibniz-Reynolds transport theorem. The region at time $t + \Delta t/2$, is written as $\mathcal{R}(t + \Delta t/2)$, which results from changing $\mathcal{R}(t - \Delta t/2)$ by the increment $\mathcal{R}(t + \Delta t/2) - \mathcal{R}(t - \Delta t/2)$. We here depict the case with an expanding boundary that renders a larger volume at $t + \Delta t/2$. At each point along the boundary the velocity of the boundary, $\mathbf{v}^{(b)}$, has an outward normal projection, $\mathbf{v}^{(b)} \cdot \hat{\mathbf{n}}$, with this projection measuring the rate that the boundary moves at that point. Area integrating $\mathbf{v}^{(b)} \cdot \hat{\mathbf{n}}$ over the boundary yields the rate that the region volume changes.

From Figure 17.2 we see that the volume of the time incremented region, $\mathcal{R}(t + \Delta t/2) - \mathcal{R}(t - \Delta t/2)$, in the limit $\Delta t \rightarrow 0$, is given by

$$\lim_{\Delta t \rightarrow 0} \frac{1}{\Delta t} \int_{\mathcal{R}(t + \Delta t/2) - \mathcal{R}(t - \Delta t/2)} dV = \lim_{\Delta t \rightarrow 0} \frac{1}{\Delta t} \left[\int_{\mathcal{R}(t + \Delta t/2)} dV - \int_{\mathcal{R}(t - \Delta t/2)} dV \right] \quad (17.38a)$$

$$= \frac{d}{dt} \left[\int_{\mathcal{R}(t)} dV \right] \quad (17.38b)$$

$$= \oint_{\partial\mathcal{R}(t)} \mathbf{v}^{(b)} \cdot \hat{\mathbf{n}} d\mathcal{S}. \quad (17.38c)$$

The final equality follows since $\mathbf{v}^{(b)} \cdot \hat{\mathbf{n}}$ measures the rate that the boundary is moving normal to itself, so that its area integral over $\partial\mathcal{R}(t)$ measures the rate that the volume of $\mathcal{R}(t)$ changes. It is the analog to the Lagrangian result (16.23) measuring the change in volume of a material region following the fluid flow.

The above ideas used to derive the volume budget equation (17.38c) are now applied when $\varphi(\mathbf{x}, t)$ is included within the integral, in which case we consider

$$\frac{d}{dt} \left[\int_{\mathcal{R}(t)} \varphi(t) dV \right] = \lim_{\Delta t \rightarrow 0} \frac{1}{\Delta t} \left[\int_{\mathcal{R}(t + \Delta t/2)} \varphi(t + \Delta t/2) dV - \int_{\mathcal{R}(t - \Delta t/2)} \varphi(t - \Delta t/2) dV \right], \quad (17.39)$$

where we suppress the \mathbf{x} functional dependence for brevity. Expanding the first integral on the right hand side around the central time leads to the expression, which is accurate to $\mathcal{O}(\Delta t)^2$,

$$\begin{aligned} & \int_{\mathcal{R}(t + \Delta t/2)} \varphi(t + \Delta t/2) dV \\ &= \int_{\mathcal{R}(t)} \left[\varphi(t) + \frac{\Delta t}{2} \frac{\partial \varphi(t)}{\partial t} \right] dV + \int_{\mathcal{R}(t + \Delta t/2) - \mathcal{R}(t)} \left[\varphi(t) + \frac{\Delta t}{2} \frac{\partial \varphi(t)}{\partial t} \right] dV. \end{aligned} \quad (17.40)$$

We have a similar expansion for the second integral in equation (17.39)

$$\begin{aligned} \int_{\mathcal{R}(t-\Delta t/2)} \varphi(t - \Delta t/2) dV \\ = \int_{\mathcal{R}(t)} \left[\varphi(t) - \frac{\Delta t}{2} \frac{\partial \varphi(t)}{\partial t} \right] dV + \int_{\mathcal{R}(t-\Delta t/2)-\mathcal{R}(t)} \left[\varphi(t) - \frac{\Delta t}{2} \frac{\partial \varphi(t)}{\partial t} \right] dV, \end{aligned} \quad (17.41)$$

thus leading to the finite difference

$$\begin{aligned} \int_{\mathcal{R}(t+\Delta t/2)} \varphi(t + \Delta t/2) dV - \int_{\mathcal{R}(t-\Delta t/2)} \varphi(t - \Delta t/2) dV \\ = \Delta t \int_{\mathcal{R}(t)} \frac{\partial \varphi(t)}{\partial t} dV + \int_{\mathcal{R}(t+\Delta t/2)-\mathcal{R}(t-\Delta t/2)} \varphi(t) dV, \end{aligned} \quad (17.42)$$

which is again accurate to $\mathcal{O}(\Delta t)^2$. Following our derivation of equation (17.38c) leads us to

$$\int_{\mathcal{R}(t+\Delta t/2)-\mathcal{R}(t-\Delta t/2)} \varphi(t) dV = \Delta t \oint_{\partial \mathcal{R}(t)} \varphi \mathbf{v}^{(b)} \cdot \hat{\mathbf{n}} d\mathcal{S}, \quad (17.43)$$

where all terms on the right hand side are evaluated at the central time, t . Bringing the pieces together, and taking the limit as $\Delta t \rightarrow 0$, leads to the Leibniz-Reynolds transport theorem

$$\frac{d}{dt} \left[\int_{\mathcal{R}(t)} \varphi(t) dV \right] = \int_{\mathcal{R}(t)} \frac{\partial \varphi}{\partial t} dV + \oint_{\partial \mathcal{R}(t)} \varphi \mathbf{v}^{(b)} \cdot \hat{\mathbf{n}} d\mathcal{S}, \quad (17.44)$$

which agrees with the earlier result given by equation (17.34).

17.3.5 Interpreting the Leibniz-Reynolds transport theorem

The Leibniz-Reynolds transport theorem (17.34) is a central kinematic result in fluid mechanics since it forms the starting point for all finite volume budgets. Although we made use of Cartesian coordinates for both derivations, the result is a coordinate invariant measure of how an extensive fluid property evolves within a region. Hence, by the rules of tensor analysis from Chapter 8, the result holds for arbitrary coordinates. Furthermore, we can extend it to multiply connected domains for which one sums over the distinct sub-domains to render the complete budget. These results confirm our notions regarding extensive properties, such as fluid mass, tracer mass, and enthalpy, and how they are budgeted throughout the fluid. Namely, these quantities are simply counted over the various regions of the fluid.

Comments on the boundary velocity

The appearance of the boundary velocity, $\mathbf{v}^{(b)}$, warrants some comment. As defined by equation (17.35), it measures the velocity of a point on the domain boundary. However, the resulting budget only requires information about the normal component to that velocity, $\mathbf{v}^{(b)} \cdot \hat{\mathbf{n}}$. For example, the domain boundary could be exhibiting arbitrary motion in the direction tangent to the bounding surface. However, such tangential motion is of no concern for a budget developed over the domain since we are only concerned with transport across the boundary. Indeed, information concerning the tangential component is not available without making dynamical assumptions that go beyond the kinematics considered here. We encountered the same ideas when studying the kinematic boundary conditions in Section 16.4.

Transport theorem for region volume

As part of the general derivation, we derived the expression (17.38c) for the volume changes of the region, which is recovered by setting $\varphi = 1$ in the transport theorem (17.34)

$$\frac{d}{dt} \left[\int_{\mathcal{R}} dV \right] = \oint_{\partial\mathcal{R}} \mathbf{v}^{(b)} \cdot \hat{\mathbf{n}} d\mathcal{S}. \quad (17.45)$$

This result says that the volume for an arbitrary region changes in time so long as there is motion of the region boundary normal to itself. As noted above, we can compare this expression to that for a material region given by equation (16.23), with the expressions identical when $\mathbf{v}^{(b)} \cdot \hat{\mathbf{n}} = \mathbf{v} \cdot \hat{\mathbf{n}}$ for a material region. Note that the general volume budget (17.45) holds for both compressible and incompressible flows, with further specialization to the incompressible case considered in Section 18.5.2.

Transport theorem for a scalar field

We here derive a corollary to the transport theorem (17.34) that proves useful for budget analyses over moving regions. For this purpose, make use of the Eulerian flux-form of the scalar conservation equation (17.27) so that the transport theorem is written

$$\frac{d}{dt} \left[\int_{\mathcal{R}} \rho \Pi dV \right] = - \oint_{\partial\mathcal{R}} [\rho \Pi (\mathbf{v} - \mathbf{v}^{(b)}) + \mathbf{J}] \cdot \hat{\mathbf{n}} d\mathcal{S}. \quad (17.46)$$

Setting $\Pi = 1$ gives an expression for the change in mass for the region

$$\frac{d}{dt} \left[\int_{\mathcal{R}} \rho dV \right] = - \oint_{\partial\mathcal{R}} \rho (\mathbf{v} - \mathbf{v}^{(b)}) \cdot \hat{\mathbf{n}} d\mathcal{S}. \quad (17.47)$$

The transport theorem (17.46) has a straightforward interpretation. Namely, the left hand side is the time tendency for the total Π -stuff within the moving region. The right hand side is the surface area integral of the flux of Π -stuff through the boundary of the region. The first right hand side term arises from the difference between the barycentric fluid velocity and the velocity of the boundary, and the second term arises from the diffusive flux. Both fluxes are projected onto the outward normal at the boundary and then integrated over the surface area. Hence, the budget is not affected by fluxes tangential to the boundary. Finally, for the mass budget (17.47), the diffusive flux vanishes since the mass of a fluid element moves according to the barycentric velocity of Section (17.1.2).

In Figure 17.3 we illustrate the transport theorem (17.46) for the special case of a discrete numerical model grid cell. This cell has fixed positions for the vertical sides whereas the top and bottom interfaces are time dependent. This application of the transport theorem provides the framework for finite volume methods in numerical models (e.g., [Griffies et al. \(2020\)](#)). We offer further discussion of the kinematics of such *general vertical coordinate* models in Chapter 57 and their dynamics in Chapter 58.

17.3.6 Revisiting Reynolds transport theorem

We here consider the special case of a region that is moving with the fluid flow, in which case we provide a more general derivation of the *Reynolds transport theorem* than originally given for material regions in Section 16.3.4. The following results are special cases of the general expression (17.46).

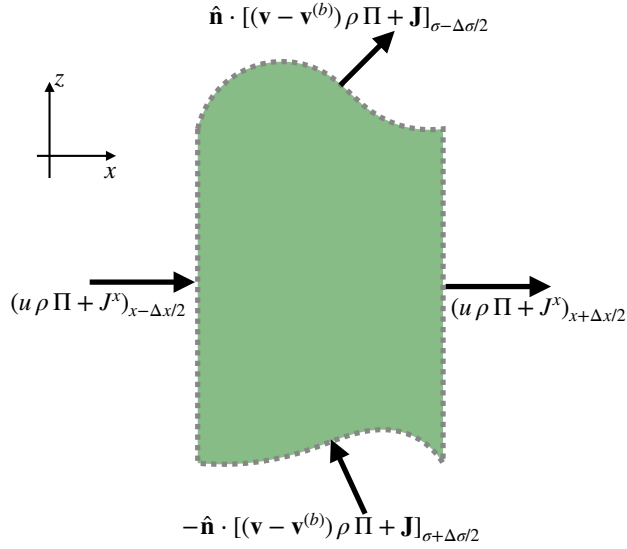


FIGURE 17.3: This figure depicts the contributions to the Leibniz-Reynolds transport theorem (17.46). The theorem is applied to a domain corresponding to a numerical model grid cell with the top and bottom interfaces defined by generalized vertical coordinates of Chapters 56, 57, and 58. In particular, the vertical cell faces are assumed to have fixed positions, so that $(\mathbf{v} - \mathbf{v}^{(b)}) \cdot \hat{\mathbf{n}} = \mathbf{v} \cdot \hat{\mathbf{n}}$ for these cell faces. Hence, the fluxes crossing these faces are due to advection by the barycentric velocity plus the diffusive flux. However, the top and bottom faces of the cell are allowed to move according to the generalized vertical coordinate surfaces. Hence, transport through these faces must take into account the nonzero velocity of the boundaries. Note that numerical models generally assume the top and bottom interfaces have a nonzero projection in the vertical direction so that they never overturn (e.g., Griffies et al. (2020)).

Reynolds Transport Theorem

Let us apply the result (17.34) to a region that follows the fluid flow as defined by the barycentric velocity, \mathbf{v} . For this moving region, the time derivative of the region boundaries in equation (17.34) is given by the fluid velocity thus leading to

$$\frac{d}{dt} \left[\int_{\mathcal{R}(\mathbf{v})} \varphi dV \right] = \int_{\mathcal{R}(\mathbf{v})} \left[\frac{\partial \varphi}{\partial t} + \nabla \cdot (\mathbf{v} \varphi) \right] dV = \int_{\mathcal{R}(\mathbf{v})} \left[\frac{D\varphi}{Dt} + \varphi \nabla \cdot \mathbf{v} \right] dV. \quad (17.48)$$

This result is the Reynolds transport theorem. The derivation given here is more general than that in Section 16.3.4, with that derivation assuming the region to be material (i.e., no matter crosses the region boundary). For the present derivation we only assumed that the region boundaries move so that $(\mathbf{v} - \mathbf{v}^{(b)}) \cdot \hat{\mathbf{n}} = 0$, where again \mathbf{v} is the barycentric velocity. We did not assume the region boundaries are material. We can thus make use of Reynolds transport theorem (17.48) for constant mass regions of a multi-component fluid so long as $(\mathbf{v} - \mathbf{v}^{(b)}) \cdot \hat{\mathbf{n}} = 0$. Furthermore, the region boundary is generally permeable via the diffusion of tracers.

Alternative form of Reynolds Transport Theorem

We can put the Reynolds Transport Theorem (17.48) into another useful form by reintroducing $\varphi = \rho \Pi$ and making use of mass continuity

$$\frac{1}{\rho} \frac{D\rho}{Dt} = -\nabla \cdot \mathbf{v}. \quad (17.49)$$

Doing so yields the rather tidy result

$$\frac{d}{dt} \left[\int_{\mathcal{R}(\mathbf{v})} \Pi \rho dV \right] = \int_{\mathcal{R}(\mathbf{v})} \left[\frac{D\varphi}{Dt} + \varphi \nabla \cdot \mathbf{v} \right] dV \quad \text{Reynolds (17.48)} \quad (17.50a)$$

$$= \int_{\mathcal{R}(\mathbf{v})} \left[\frac{D(\rho\Pi)}{Dt} + \rho\Pi \nabla \cdot \mathbf{v} \right] dV \quad \varphi = \rho\Pi \quad (17.50b)$$

$$= \int_{\mathcal{R}(\mathbf{v})} \left[\Pi \left(\frac{D\rho}{Dt} + \rho \nabla \cdot \mathbf{v} \right) + \rho \frac{D\Pi}{Dt} \right] dV \quad \text{product rule} \quad (17.50c)$$

$$= \int_{\mathcal{R}(\mathbf{v})} \frac{D\Pi}{Dt} \rho dV. \quad \text{mass continuity (17.10)} \quad (17.50d)$$

Heuristically, this result follows since ρdV is a constant when following the flow, so that passage of the time derivative across the material integral only picks up the material derivative of Π .

We can take the result (17.50d) one more step by inserting the material form of the scalar conservation equation (17.27) so that

$$\frac{d}{dt} \left[\int_{\mathcal{R}(\mathbf{v})} \Pi \rho dV \right] = - \oint_{\partial\mathcal{R}(\mathbf{v})} \mathbf{J} \cdot \hat{\mathbf{n}} d\mathcal{S}, \quad (17.51)$$

which is a special case of the general transport theorem (17.46) found by setting $(\mathbf{v} - \mathbf{v}^{(b)}) \cdot \hat{\mathbf{n}} = 0$ along the region boundary. This result says that the change in Π -stuff within a region moving with the barycentric velocity arises only from the area integrated diffusive flux crossing normal to the boundary. It is a finite volume generalization of the mass conservation statement for a fluid element as discussed in Section 17.1.3. We can set $\Pi = 1$ to render a statement of mass conservation for a Lagrangian region

$$\frac{d}{dt} \left[\int_{\mathcal{R}(\mathbf{v})} \rho dV \right] = 0, \quad (17.52)$$

where the diffusive flux, \mathbf{J} , vanishes for the mass.

17.3.7 Summary of the time derivatives acting on integrals

We here summarize the variety of time derivatives acting on integrals of scalar fields

$$\frac{d}{dt} \int_{\mathcal{R}} \rho \Pi dV = \begin{cases} \int_{\mathcal{R}} \frac{\partial(\rho\Pi)}{\partial t} dV = - \oint_{\partial\mathcal{R}} (\rho \mathbf{v} \Pi + \mathbf{J}) \cdot \hat{\mathbf{n}} d\mathcal{S} & \text{Eulerian } \mathcal{R} \\ \int_{\mathcal{R}(\mathbf{v})} \rho \frac{D\Pi}{Dt} dV = - \oint_{\partial\mathcal{R}(\mathbf{v})} \mathbf{J} \cdot \hat{\mathbf{n}} d\mathcal{S} & \text{Lagrangian } \mathcal{R}(\mathbf{v}) \\ - \oint_{\partial\mathcal{R}} [\rho \Pi (\mathbf{v} - \mathbf{v}^{(b)}) + \mathbf{J}] \cdot \hat{\mathbf{n}} d\mathcal{S} & \text{arbitrary } \mathcal{R}, \end{cases} \quad (17.53)$$

with the scalar fields assumed to satisfy the source-free differential equation

$$\rho \frac{D\Pi}{Dt} = - \nabla \cdot \mathbf{J} \iff \frac{\partial(\rho\Pi)}{\partial t} + \nabla \cdot (\rho \mathbf{v} \Pi + \mathbf{J}) = 0. \quad (17.54)$$

As discussed in Section 14.2, the partial differential equation (17.54) is referred to as the *strong formulation* of the scalar budget, whereas the integral expressions in equation (17.53) provide a variety of *weak formulations*.

17.4 Brute force illustration of Leibniz-Reynolds

The Leibniz-Reynolds transport theorem

$$\frac{d}{dt} \left[\int_{\mathcal{R}} \rho \Pi dV \right] = - \int_{\partial \mathcal{R}} [\rho \Pi (\mathbf{v} - \mathbf{v}^{(b)}) + \mathbf{J}] \cdot \hat{\mathbf{n}} dS, \quad (17.55)$$

is an incredibly useful and elegant expression of the scalar budget over an arbitrary domain. Correspondingly, we make great use of it throughout this book. To further our understanding, we here consider the scalar budget for an ocean domain such as in Figure 17.4. Rather than make direct use of Leibniz-Reynolds, we use a brute force approach by expanding the volume integral according to

$$\frac{d}{dt} \left[\int_{\mathcal{R}} \rho \Pi dV \right] = \frac{d}{dt} \left[\int_{A(t)} dA \int_{\eta_b}^{\eta} \rho \Pi dz \right]. \quad (17.56)$$

In this equation, $\int_{A(t)} dA$ is an integral over the horizontal area of the domain, with the lateral boundaries of the domain generally a function of time. This exercise requires the use of various kinematic boundary conditions and provides further practice with the Leibniz rule.

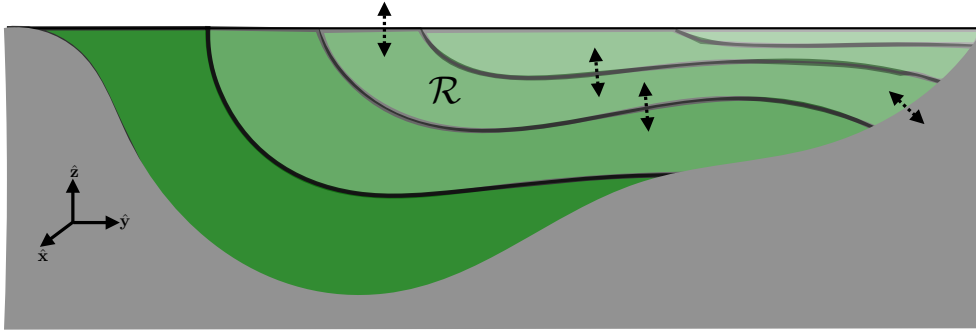


FIGURE 17.4: A depiction of fluid layers in which we formulate the budget for the total mass of scalar (e.g., tracer or potential enthalpy). The scalar mass within the layer, such as that one denoted by \mathcal{R} , is modified by dia-surface transport across interior layer interfaces, as well as transport across the surface and bottom boundaries. Note that an arbitrary layer might never intersect the bottom or surface boundaries. However, the layers depicted here each intersect boundaries, with such layers requiring extra care in formulating their budgets.

17.4.1 Leibniz's rule plus kinematic boundary conditions

Performing the time derivative in equation (17.56) and using Leibniz's rule yields

$$\frac{d}{dt} \left[\int_{\mathcal{R}} \rho \Pi dV \right] = \frac{dA}{dt} \left[\int_{\eta_b}^{\eta} \rho \Pi dz \right]_{\text{bounds}} + \int_{A(t)} [\partial_t \eta (\rho \Pi)_{z=\eta}] dA + \int_{A(t)} dA \int_{\eta_b}^{\eta} \frac{\partial (\rho \Pi)}{\partial t} dz. \quad (17.57)$$

The first term on the right hand side is evaluated along the lateral boundaries of the domain. If the boundaries are fixed in time, as in a rectangular box of seawater or a periodic channel, then $dA/dt = 0$. The more general case has a lateral boundary that is time dependent such as along a beach where fluid moves up and down the sloping shoreline. However, in that case the thickness of fluid vanishes at the lateral boundary, $\eta - \eta_b = 0$, thus again revealing that the first term on the right hand side drops from the budget to render

$$\frac{d}{dt} \left[\int_{\mathcal{R}} \rho \Pi dV \right] = \int_{A(t)} [\partial_t \eta (\rho \Pi)_{z=\eta}] dA + \int_{A(t)} dA \int_{\eta_b}^{\eta} \frac{\partial (\rho \Pi)}{\partial t} dz. \quad (17.58)$$

For the second term on the right hand side of equation (17.58) we make use of the scalar equation (17.54) and Leibniz's rule to write

$$\int_{\eta_b}^{\eta} \frac{\partial(\rho\Pi)}{\partial t} dz = - \int_{\eta_b}^{\eta} \nabla_z \cdot (\rho\Pi \mathbf{u} + \mathbf{J}_h) dz - \int_{\eta_b}^{\eta} \frac{\partial(\rho\Pi w + J^z)}{\partial z} dz \quad (17.59a)$$

$$\begin{aligned} &= -\nabla_z \cdot \int_{\eta_b}^{\eta} (\rho\Pi \mathbf{u} + \mathbf{J}_h) dz + \nabla(\eta - z) \cdot (\rho\Pi \mathbf{v} + \mathbf{J})_{z=\eta} \\ &\quad + \nabla(z - \eta_b) \cdot (\rho\Pi \mathbf{v} + \mathbf{J})_{z=\eta_b} \end{aligned} \quad (17.59b)$$

where we wrote $\mathbf{J} = \mathbf{J}_h + \hat{z} J^z$. The surface terms ($z = \eta$) combine with the $\partial_t \eta$ term appearing in equation (17.58) to yield

$$\rho\Pi \left[\frac{\partial\eta}{\partial t} + \mathbf{u} \cdot \nabla\eta - w \right] = \Pi Q_m, \quad (17.60)$$

where we used the surface kinematic boundary condition (16.79) to introduce the surface boundary mass flux Q_m . The bottom kinematic boundary condition eliminates the advective contribution at the bottom, $z = \eta_b$, via the no normal flow condition (16.41)

$$\nabla(z - \eta_b) \cdot \mathbf{v} = w - \mathbf{u} \cdot \nabla\eta_b = 0 \quad \text{at } z = \eta_b(x, y). \quad (17.61)$$

Finally, when integrated over the horizontal extent of the domain, the horizontal convergence term from equation (17.59b) vanishes. The reason it vanishes is because either the thickness of fluid vanishes at the horizontal boundaries (as along a beach); there is a no flux boundary condition if the boundary is a vertical wall; or the domain is periodic.

17.4.2 Summarizing the result

Bringing the results together yields the budget equation

$$\frac{d}{dt} \left[\int_{\mathcal{R}} \rho\Pi dV \right] = \int_{z=\eta} (\Pi Q_m + \nabla(\eta - z) \cdot \mathbf{J}) dA + \int_{z=\eta_b} \nabla(z - \eta_b) \cdot \mathbf{J} dA. \quad (17.62)$$

We now use the identity (16.68e) between horizontal area element, $dA = dx dy$, and area element on the surface

$$\hat{\mathbf{n}} d\mathcal{S} = -\nabla(\eta - z) dA \quad \text{at } z = \eta \quad (17.63a)$$

$$\hat{\mathbf{n}} d\mathcal{S} = -\nabla(z - \eta_b) dA \quad \text{at } z = \eta_b, \quad (17.63b)$$

to write

$$\frac{d}{dt} \left[\int_{\mathcal{R}} \rho\Pi dV \right] = - \int_{z=\eta} (-\Pi Q_m + \hat{\mathbf{n}} \cdot \mathbf{J}) d\mathcal{S} - \int_{z=\eta_b} \hat{\mathbf{n}} \cdot \mathbf{J} d\mathcal{S}, \quad (17.64)$$

where

$$Q_m dA = Q_m d\mathcal{S} = -\rho(\mathbf{v} - \mathbf{v}^{(\eta)}) \cdot \hat{\mathbf{n}} d\mathcal{S} \quad (17.65)$$

according to equation (16.73c). The budget for fluid mass is realized by setting Π to a constant and thus dropping the non-advectional flux

$$\frac{d}{dt} \left[\int_{\mathcal{R}} \rho dV \right] = \int_{z=\eta} Q_m d\mathcal{S} = - \int_{z=\eta} \rho(\mathbf{v} - \mathbf{v}^{(\eta)}) \cdot \hat{\mathbf{n}} d\mathcal{S}. \quad (17.66)$$

The manipulations in this section have succeeded in bringing the scalar and mass budgets into the form of the Leibniz-Reynolds transport theorem (17.55). The process of doing so required far

more tedium as compared to the elegance of merely starting from equation (17.55). Even so, our efforts provide a useful means to ground the formalism by unpacking the many steps summarized by Leibniz-Reynolds. Furthermore, many of these steps are encountered in practical calculations of finite volume budgets.

17.5 Evolution of region mean scalar

We here consider a brief application of the formalism developed in this chapter by developing the evolution equations for the averaged scalar defined by

$$\langle \Pi \rangle = \frac{1}{M} \int_{\mathcal{R}} \rho \Pi dV \quad \text{with} \quad M = \int_{\mathcal{R}} \rho dV, \quad (17.67)$$

where the region domain, \mathcal{R} , is arbitrary.

17.5.1 Formulation

Use of the product rule leads to

$$\frac{d[\langle \Pi \rangle M]}{dt} = M \frac{d\langle \Pi \rangle}{dt} + \langle \Pi \rangle \frac{dM}{dt} = M \frac{d\langle \Pi \rangle}{dt} - \langle \Pi \rangle \oint_{\partial\mathcal{R}} \rho (\mathbf{v} - \mathbf{v}^{(b)}) \cdot \hat{\mathbf{n}} d\mathcal{S}, \quad (17.68)$$

where the second equality made use of the mass budget (17.47). Inserting the transport theorem (17.46) for the left hand side yields

$$M \frac{d\langle \Pi \rangle}{dt} = - \oint_{\partial\mathcal{R}} [\rho [\Pi - \langle C \rangle] (\mathbf{v} - \mathbf{v}^{(b)}) + \mathbf{J}] \cdot \hat{\mathbf{n}} d\mathcal{S}. \quad (17.69)$$

The first term on the right hand side vanishes if the averaged concentration equals to the boundary concentration. That is, the region averaged tracer concentration is unchanged if the boundary fluxes of mass have a tracer concentration that matches the region average.

17.5.2 Application to a numerical ocean model grid cell

If the region is an ocean model grid cell that is adjacent to the ocean surface (see Figure 17.3 or 17.6), then use of the surface boundary condition (17.85) leads to

$$M \frac{d\langle \Pi \rangle}{dt} = \int_{z=\eta} [\Pi - \langle \Pi \rangle] Q_m dA - \int_{\partial\mathcal{R}_{\text{int}}} [\rho [\Pi - \langle \Pi \rangle] (\mathbf{v} - \mathbf{v}^{(b)}) + \mathbf{J}] \cdot \hat{\mathbf{n}} d\mathcal{S} - \oint_{\partial\mathcal{R}} \mathbf{J} \cdot \hat{\mathbf{n}} d\mathcal{S}, \quad (17.70)$$

where $\partial\mathcal{R}_{\text{int}}$ is the interior boundary to the grid cell. As noted above, the first term on the right hand side vanishes if $\Pi(z = \eta) = \langle \Pi \rangle$. This situation is commonly assumed for temperature in the surface grid cell of an ocean model. That is, the temperature of evaporation, precipitation, and river runoff is commonly taken as the temperature in the surface model grid cell. In contrast, $\Pi(z = \eta) = 0$ is commonly the case for material tracers such as salt, whose concentration is commonly close to zero within boundary water fluxes.

17.6 Boundary conditions

We here study the boundary conditions relevant at the variety of boundaries encountered by a fluid. To be specific, consider Π to be a tracer concentration,

$$\Pi = C, \quad (17.71)$$

though note that the formalism holds for an arbitrary scalar satisfying the budget equation

$$\frac{\partial(\rho C)}{\partial t} + \nabla \cdot (\rho C \mathbf{v} + \mathbf{J}) = 0. \quad (17.72)$$

We continue to focus on a fluid layer such as shown in Figure 17.4, paying particular interest to fluid layers that intersect surface (as for the ocean) and/or bottom boundaries (as for the ocean or atmosphere). We commonly think of this layer as defined by isosurfaces of generalized vertical coordinates whose layers are monotonically stacked in the vertical according to the discussion from Sections 56.9.1 and 57.3. However, the treatment given here allows for the layers to be non-monotonic in the vertical (e.g., overturns are allowed), so that these results can be used for the water mass transformation analysis discussed in Chapter 65. For example, the layers can be defined by surfaces of constant Conservative Temperature or salinity within the ocean, with these fields generally exhibiting regions of non-monotonic vertical stratification.

The Leibniz-Reynolds transport theorem (17.46) provides the starting point

$$\frac{d}{dt} \left[\int_{\mathcal{R}} \rho C dV \right] = - \int_{\partial\mathcal{R}} [\rho C (\mathbf{v} - \mathbf{v}^{(b)}) + \mathbf{J}] \cdot \hat{\mathbf{n}} d\mathcal{S}, \quad (17.73)$$

The left hand side of equation (17.73) is the time tendency for the mass of tracer within the region, such as the region \mathcal{R} shown in Figure 17.4. This tendency is affected by transport across the layer boundaries, with three boundaries considered here. We ignore interior sources, though note that the formalism can be readily extended in their presence.

17.6.1 Interior layer boundary conditions

The boundary transport across interior layer interfaces,

$$\text{interior boundary transport} = [\rho C (\mathbf{v} - \mathbf{v}^{(b)}) + \mathbf{J}] \cdot \hat{\mathbf{n}} d\mathcal{S}, \quad (17.74)$$

measures the tracer mass transport due to advective fluxes across the moving layer boundaries (first term) and subgrid scale fluxes (second term). The advective flux is sometimes known as the *dia-surface transport*, with the kinematics of this transport discussed in Section 57.4.

17.6.2 Solid-earth boundary conditions

At the static material bottom boundary, the no-normal flow condition means that

$$\mathbf{v} \cdot \hat{\mathbf{n}} = 0. \quad (17.75)$$

Consider the velocity of a point attached to the layer interface, $\mathbf{v}^{(b)}$, and focus on where the interface intersects the bottom boundary. At this point, $\mathbf{v}^{(b)}$ tracks the position of the interface as it intersects the bottom boundary. By construction, the movement of this intersection point is tangential to the bottom boundary so that it too is orthogonal to the boundary outward normal

direction

$$\mathbf{v}^{(b)} \cdot \hat{\mathbf{n}} = 0. \quad (17.76)$$

Hence, the only contribution to the tracer budget at the bottom boundary comes through the non-advection flux \mathbf{J}

$$\text{bottom boundary transport} = -\mathbf{J} \cdot \hat{\mathbf{n}} d\mathcal{S}. \quad (17.77)$$

This equation says that if there is any transport through the bottom boundary (left hand side), then it induces a non-advection transport within the ocean whose normal component at the boundary equals to the bottom transport (right hand side).

Geothermal heating is the canonical solid-earth transport in the ocean. Assuming a known geothermal heat flux, $\mathcal{Q}_{\text{geo-heat}}$, it leads to a non-advection ocean boundary flux

$$\mathcal{Q}_{\text{geo-heat}} = -c_p \mathbf{J}(\Theta) \cdot \hat{\mathbf{n}}, \quad (17.78)$$

where c_p is the ocean heat capacity and Θ is the Conservative Temperature (discussed in Section 23.9 and Chapter 64). Furthermore, if we assume the non-advection flux is parameterized as the downgradient diffusive flux (as in equation (64.54) in Chapter 64), then the geothermal boundary condition (17.78) takes the form

$$\mathcal{Q}_{\text{geo-heat}} = c_p \rho (\mathbb{K} \cdot \nabla \Theta) \cdot \hat{\mathbf{n}}, \quad (17.79)$$

where \mathbb{K} is the diffusion tensor (Chapter 63).

For those cases where the geothermal heating vanishes, or more generally for tracers that have zero bottom boundary flux, then the tracer must satisfy the following no-normal flux (Neumann) boundary condition

$$\text{no flux bottom boundary} = (\mathbb{K} \cdot \nabla \Theta) \cdot \hat{\mathbf{n}} = 0. \quad (17.80)$$

In the case where diffusion next to the boundary is isotropic, as per molecular diffusion, then we reach the simpler result

$$\text{no flux bottom boundary} = \nabla C \cdot \hat{\mathbf{n}} = 0. \quad (17.81)$$

Namely, in this case, tracer isosurfaces are oriented normal to the boundary as depicted in Figure 17.5. Notably, this kinematic boundary condition holds at each point in time. For the dynamical tracers like temperature and salinity, this boundary condition affects flow near the boundary by modifying the density field and thus the pressure.

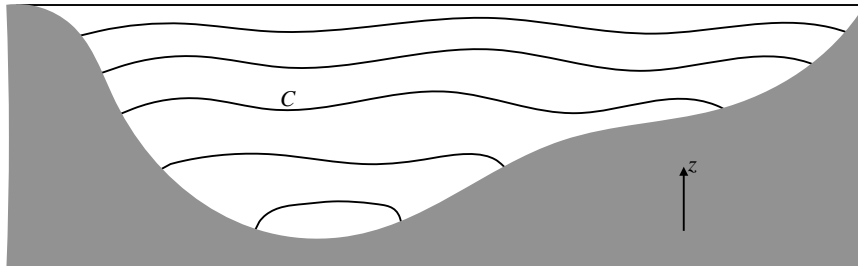


FIGURE 17.5: In the absence of a boundary tracer flux, and in the presence of isotropic downgradient diffusion, the isosurfaces of tracer, C , intersect solid boundaries normal to the boundary as per equation (17.81): $\nabla C \cdot \hat{\mathbf{n}} = 0$, where $\hat{\mathbf{n}}$ is the outward normal direction. This constraint holds at each time instance.

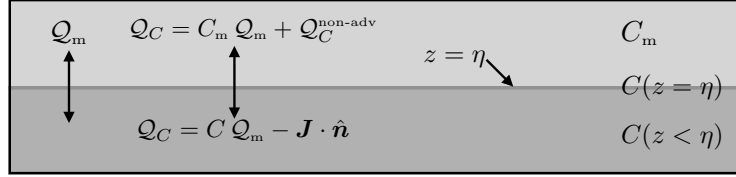


FIGURE 17.6: A schematic of an infinitesimal region of the ocean surface boundary at $z = \eta(x, y, t)$, with $z < \eta$ the ocean region. $\mathcal{Q}_m d\mathcal{S}$ is the mass transport (mass per time) that crosses the interface and carries a tracer concentration C_m . $\mathcal{Q}_C d\mathcal{S}$ is the tracer mass transport that crosses the ocean surface. Continuity across the $z = \eta$ boundary means that the tracer mass transport at $z = \eta - \epsilon$ (ocean side) equals to that at $z = \eta + \epsilon$ (atmospheric side), with $\epsilon > 0$ a tiny number. The tracer concentration at the interface, $C(z = \eta)$, is not determined by kinematics. Many analyses and numerical model applications approximate $C(z = \eta)$ as the bulk tracer concentration within the upper few meters of the ocean, depending on details of the upper ocean turbulence. However, as model vertical grid spacing is refined to be finer than a meter, this assumption must be reconsidered.

17.6.3 Upper ocean surface boundary conditions

Let us write the upper ocean surface boundary tracer transport as

$$\mathcal{Q}_C d\mathcal{S} = \text{net tracer mass per time crossing ocean surface.} \quad (17.82)$$

The surface boundary transport is generally comprised of two terms: a non-advection term just like at the solid-earth in Section 17.6.2, plus an advective term afforded since the ocean surface is permeable. If we assume that the tracer transported via the advected matter is either a dissolved tracer, such as salinity, or a thermodynamic tracer, such as Conservative Temperature, then we can write the net tracer flux as

$$\mathcal{Q}_C = C_m \mathcal{Q}_m + \mathcal{Q}_C^{\text{non-adv}}, \quad (17.83)$$

where $\mathcal{Q}_C^{\text{non-adv}}$ is the non-advection tracer flux, C_m is the tracer concentration within the mass transported across the surface, and \mathcal{Q}_m the mass per time per surface area of matter that crosses the boundary, as defined according to the kinematic boundary condition (16.63)

$$\mathcal{Q}_m = -\rho \hat{n} \cdot (\mathbf{v} - \mathbf{v}^{(\eta)}) \quad \text{surface ocean boundary.} \quad (17.84)$$

As for the solid-earth boundary condition, specification of \mathcal{Q}_C requires information concerning the flux of tracer mass into or out of the ocean, and this flux equals to the net flux on the ocean side of the surface

$$\mathcal{Q}_C = C_m \mathcal{Q}_m + \mathcal{Q}_C^{\text{non-adv}} \equiv -[\rho C (\mathbf{v} - \mathbf{v}^{(b)}) + \mathbf{J}] \cdot \hat{n} = C \mathcal{Q}_m - \mathbf{J} \cdot \hat{n}, \quad (17.85)$$

We thus see that the surface transport of tracer mass induces the following non-advection flux within the ocean at $z = \eta$

$$-\mathbf{J} \cdot \hat{n} = \mathcal{Q}_C - C \mathcal{Q}_m = \mathcal{Q}_C^{\text{non-adv}} + (C_m - C) \mathcal{Q}_m. \quad (17.86)$$

Figure 17.6 offers a schematic to summarize these results. We make use of these results when discussing the surface ocean boundary conditions in Sections 64.5 and 65.8.3.



17.7 Exercises

EXERCISE 17.1: EQUATION FOR TRACER MASS PER FLUID VOLUME

In some treatments it can be suitable to define a volumetric tracer concentration as the mass of tracer per volume of fluid

$$\phi = \frac{\text{mass of constituent } n \text{ in fluid element}}{\text{volume of fluid element}} = C \rho, \quad (17.87)$$

where C is the mass concentration defined by equation (17.17) and satisfying the tracer equation (17.21). Derive the corresponding equation satisfied by ϕ .



Chapter 18

NON-DIVERGENT FLOWS

In this chapter, we study the kinematics of a non-divergent fluid velocity field.¹ In many areas of fluid mechanics, fluid flows with a non-divergent velocity, $\nabla \cdot \mathbf{v} = 0$, are referred to as *incompressible* since the density is assumed to be constant everywhere; i.e., “incompressible”.² However, as seen when studying the Boussinesq ocean in Chapter 26, a non-divergent flow can still admit compressibility effects and the associated density variations. This discussion emphasizes the distinction between a *fluid property* versus a *flow property*. Namely, the Boussinesq ocean allows for an expression of compressibility (a property of the fluid), whereas the flow admitted by a Boussinesq ocean is non-divergent (a property of the flow). In this chapter we focus on the non-divergent nature of the flow and the attendant kinematics.

READER’S GUIDE TO THIS CHAPTER

We presume an understanding of the kinematics of mass conservation from Chapter 16 as well as many of the results from Cartesian tensor analysis in Chapter 2. This chapter introduces many concepts and tools of use in the remainder of the book.

18.1	Introduction to non-divergent flow	386
18.2	Kinematic boundary conditions	387
18.3	Streamfunction for two-dimensional flow	387
18.3.1	Streamfunction isolines are streamlines	388
18.3.2	Streamfunction is constant on material boundaries	388
18.3.3	The streamfunction and fluid transport	388
18.3.4	Gauge symmetry	389
18.3.5	Exact differential formulation	390
18.3.6	Concerning the Helmholtz decomposition	390
18.3.7	A caveat: transport with curl-free + divergent flow	391
18.4	Vector streamfunction for three-dimensional flow	391
18.4.1	Gauge symmetry	392
18.4.2	Vector streamfunction in the vertical gauge	392
18.4.3	The streamfunction and transport through a surface	393
18.4.4	Scalar streamfunctions and transport	393
18.4.5	Concerning a harmonic velocity potential	395
18.5	Evolution of volume and area	395
18.5.1	Material volumes and areas	395

¹A somewhat trivial example of a non-divergent fluid flow is given by $\mathbf{v}(x, y, z) = u(y, z) \hat{\mathbf{x}} + v(x, z) \hat{\mathbf{y}} + w(x, y) \hat{\mathbf{z}}$. However, there are far less trivial flows that are non-divergent, such as realized by the Boussinesq ocean studied in Chapter 26.

²In some presentations, $\nabla \cdot \mathbf{v} = 0$ is referred to as a *solenoidal velocity*, in analog to the non-divergent or solenoidal magnetic field occurring in classical electrodynamics.

18.5.2	Arbitrary volume and area	396
18.6	Meridional-depth overturning circulation	396
18.6.1	Specifying the zonal position as a function of (y, z)	396
18.6.2	The zonally integrated transport is non-divergent	397
18.6.3	Defining the meridional-depth overturning streamfunction	398
18.7	Kinematic free surface equation	399
18.7.1	Derivation	399
18.7.2	Comments	400
18.8	Exercises	400

18.1 Introduction to non-divergent flow

For many purposes in fluid mechanics, we can make the simplifying assumption regarding the fluid kinematics whereby the volume of a fluid element is approximated as a constant. In particular, this situation holds for the Boussinesq ocean discussed in Chapter 26. Recalling the expression

$$\frac{1}{\delta V} \frac{D(\delta V)}{Dt} = \nabla \cdot \mathbf{v} \quad (18.1)$$

from Section 15.5.1, we see that a constant volume for a fluid element constrains the velocity field to be non-divergent

$$\frac{1}{\delta V} \frac{D(\delta V)}{Dt} = 0 \implies \nabla \cdot \mathbf{v} = 0. \quad (18.2)$$

Flow satisfying $\nabla \cdot \mathbf{v} = 0$ is said to be *incompressible* since the volume of a fluid element is materially invariant. We illustrate this situation in Figure 18.1.

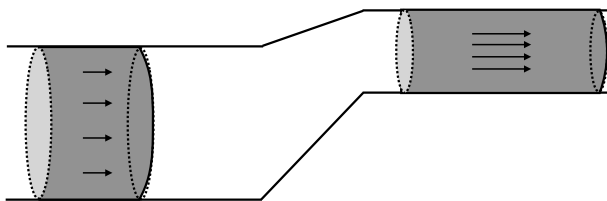


FIGURE 18.1: Illustrating volume continuity for a non-divergent velocity flow in a pipe. On the left the pipe has a relatively large diameter whereas on the right the pipe is narrower. A plug of water on the left moves through the pipe and becomes longer when it moves into the narrower region so that the volume of the plug remains the same. Correspondingly, the speed of the flow increases when moving into the narrower portion of the pipe.

A slightly less onerous constraint arises from the *anelastic approximation*, whereby

$$\nabla \cdot (\rho \mathbf{v}) = 0. \quad (18.3)$$

The anelastic approximation is sometimes motivated for the atmosphere. However, it is less commonly used for atmospheric dynamics than the Boussinesq ocean is used for the ocean. We thus focus on the Boussinesq case here, whereby $\nabla \cdot \mathbf{v} = 0$.

The non-divergence constraint (18.2) reduces by one the number of functional degrees of freedom possessed by the velocity field. What that means in practice is that we need one fewer velocity component to determine the flow since one component can be diagnosed from the other two components. This property manifests by our ability to introduce a streamfunction to specify the velocity, as further developed in this chapter.

18.2 Kinematic boundary conditions

For non-divergent flow, there are slight modifications to the compressible boundary conditions detailed in Section 16.4. Whereas the material conditions remain identical, the non-material conditions are applied with a constant reference density, ρ_0 , rather than the local *in situ* density, ρ . The reason is that we switch from specifying a mass transport condition as per equation (16.63) to a volume transport condition

$$\rho_0 (\mathbf{v} - \mathbf{v}^{(s)}) \cdot \hat{\mathbf{n}} dS = -\mathcal{Q}_m dS = -Q_m dA \quad \text{moving non-material boundary condition, (18.4)}$$

where the second equality introduced the mass flux per unit horizontal area, Q_m , according to equation (16.73c). Correspondingly, the kinematic boundary condition (16.79) applied at the ocean free surface takes on the form

$$\rho_0 \frac{D(z - \eta)}{Dt} = -Q_m \implies w + \frac{Q_m}{\rho_0} = \frac{\partial \eta}{\partial t} + \mathbf{u} \cdot \nabla \eta. \quad (18.5)$$

Making use of the non-divergence condition on the velocity allows us to write this equation in the equivalent forms³

$$\partial_t \eta - Q_m / \rho_0 = (\hat{\mathbf{z}} - \nabla \eta) \cdot \mathbf{v} = \nabla(z - \eta) \cdot \mathbf{v} = \nabla \cdot [(z - \eta) \mathbf{v}]. \quad (18.6)$$

In Section 18.7 we derive the kinematic free surface equation (18.78), which also shows that $\partial_t \eta - Q_m / \rho_0$ is a total divergence.

18.3 Streamfunction for two-dimensional flow

Vertical stratification of buoyancy plus the effects from planetary rotation inhibit vertical motion in geophysical flows. Therefore, as an idealization it is sometimes useful to assume the geophysical fluid flow is horizontal (two-dimensional) as well as non-divergent. The non-divergent constraint for two-dimensional flow can be satisfied by writing the horizontal velocity in the form

$$\mathbf{u} = \nabla \times (z \nabla \psi) = \hat{\mathbf{z}} \times \nabla \psi = \hat{\mathbf{z}} \times \nabla_z \psi = -\hat{\mathbf{x}} \frac{\partial \psi}{\partial y} + \hat{\mathbf{y}} \frac{\partial \psi}{\partial x}, \quad (18.7)$$

where

$$\nabla_z = \hat{\mathbf{x}} \partial_x + \hat{\mathbf{y}} \partial_y \quad (18.8)$$

is the horizontal gradient operator. The constraint $\nabla_z \cdot \mathbf{u} = 0$ is satisfied since the partial derivative operators commute

$$\frac{\partial^2 \psi}{\partial x \partial y} = \frac{\partial^2 \psi}{\partial y \partial x}. \quad (18.9)$$

We refer to ψ as the *streamfunction*, with this name motivated by the following considerations.

Note that in this section we can relax notation by dispensing with the z subscript on the horizontal gradient operator, ∇_z , since we are here concerned only with two-dimensional horizontal flow. Even so, we find it useful to be pedantic in order to distinguish the two-dimensional formulations in this section from the analogous three-dimensional case considered in Section 18.4.

³In equation (18.6), we set $z = \eta$ after applying the gradient operator in the penultimate expression and the divergence in the final expression.

18.3.1 Streamfunction isolines are streamlines

At any fixed time instance, the exact differential of the streamfunction is

$$d\psi = \frac{\partial\psi}{\partial x} dx + \frac{\partial\psi}{\partial y} dy = v dx - u dy, \quad (18.10)$$

where the second equality follows from equation (18.7). Instantaneous lines along which ψ is a constant satisfy

$$d\psi = 0 \implies \frac{dx}{u} = \frac{dy}{v}. \quad (18.11)$$

Furthermore, the normal direction to constant ψ lines

$$\hat{\mathbf{n}} = \frac{\nabla_z \psi}{|\nabla_z \psi|} = \frac{v \hat{\mathbf{x}} - u \hat{\mathbf{y}}}{|\mathbf{u}|} \quad (18.12)$$

is normal to the velocity

$$\mathbf{u} \cdot \nabla_z \psi = u v - v u = 0. \quad (18.13)$$

Consequently, at each time instance, lines of constant ψ are streamlines (see Section 14.9.2 for a general discussion of streamlines). This property motivates the name *streamfunction*. Furthermore, through each point of a two-dimensional non-divergent flow and at any particular time instance, there is one and only one streamline passing through that point.

18.3.2 Streamfunction is constant on material boundaries

As a corollary to the results from Section 18.3.1, we know that the streamfunction is a spatial constant when evaluated along static material boundaries where $\mathbf{u} \cdot \hat{\mathbf{n}} = 0$. This property follows from equation (18.13). We can also see it from

$$0 = \mathbf{u} \cdot \hat{\mathbf{n}} = (\hat{\mathbf{z}} \times \nabla_z \psi) \cdot \hat{\mathbf{n}} = (\hat{\mathbf{n}} \times \hat{\mathbf{z}}) \cdot \nabla_z \psi = \hat{\mathbf{t}} \cdot \nabla_z \psi, \quad (18.14)$$

where $\hat{\mathbf{t}}$ a unit vector pointing tangent to the boundary. The operator $\hat{\mathbf{t}} \cdot \nabla_z \psi$ is the derivative of ψ computed along the boundary tangent at any given boundary point. Hence, $\hat{\mathbf{t}} \cdot \nabla_z \psi = 0$ means that ψ is a spatial constant along the boundary. Even though spatially constant, ψ along the boundary is generally a function of time.

We emphasize that a constant streamfunction along a boundary, $\hat{\mathbf{t}} \cdot \nabla_z \psi = 0$, is distinct from a vanishing normal derivative at the boundary. Indeed, the streamfunction for a two-dimensional non-divergent flow generally has a nonzero normal derivative at boundaries, $\hat{\mathbf{n}} \cdot \nabla_z \psi \neq 0$.

18.3.3 The streamfunction and fluid transport

Consider an arbitrary curve in the fluid with endpoints \mathbf{x}_1 and \mathbf{x}_2 as depicted in Figure 18.2. At any particular time instance, the difference in streamfunction between these two points is given by

$$\psi(\mathbf{x}_2) - \psi(\mathbf{x}_1) = \int_{\mathbf{x}_1}^{\mathbf{x}_2} d\psi = \int_{\mathbf{x}_1}^{\mathbf{x}_2} \left[dx \frac{\partial\psi}{\partial x} + dy \frac{\partial\psi}{\partial y} \right] = \int_{\mathbf{x}_1}^{\mathbf{x}_2} \nabla_z \psi \cdot d\mathbf{x} = \int_{\mathbf{x}_1}^{\mathbf{x}_2} \nabla_z \psi \cdot \hat{\mathbf{t}} ds. \quad (18.15)$$

For the final equality we wrote

$$d\mathbf{x} = \hat{\mathbf{t}} ds, \quad (18.16)$$

where

$$ds = |\mathbf{dx}| \quad (18.17)$$

is the element of arc length along the curve, and $\hat{\mathbf{t}}$ is the unit tangent vector that points in the direction along the curve from \mathbf{x}_1 to \mathbf{x}_2 . Now introduce the unit normal vector along the curve according to

$$\hat{\mathbf{t}} = \hat{\mathbf{n}} \times \hat{\mathbf{z}}, \quad (18.18)$$

where $\hat{\mathbf{n}}$ points to the left when facing in the $\hat{\mathbf{t}}$ direction. We thus have

$$\psi(\mathbf{x}_2) - \psi(\mathbf{x}_1) = \int_{\mathbf{x}_1}^{\mathbf{x}_2} \nabla_z \psi \cdot (\hat{\mathbf{n}} \times \hat{\mathbf{z}}) ds = \int_{\mathbf{x}_1}^{\mathbf{x}_2} (\hat{\mathbf{z}} \times \nabla_z \psi) \cdot \hat{\mathbf{n}} ds = \int_{\mathbf{x}_1}^{\mathbf{x}_2} \mathbf{u} \cdot \hat{\mathbf{n}} ds, \quad (18.19)$$

with the final equality an expression for the net area transport of fluid normal to the curve (dimensions of area per time). As the chosen curve connecting the points is arbitrary, we conclude that the difference in streamfunction values between two points measures the transport across any curve connecting the points. Correspondingly, the stronger the gradient in the streamfunction, the larger the transport since

$$|\mathbf{u}| = |\nabla_z \psi|. \quad (18.20)$$

Connecting the transport between two points and the value of the streamfunction at those two points prompts the name *transport streamfunction*. More specifically, this term is used when the streamfunction is computed for the depth integrated flow (18.79), in the special case when that flow has no divergence, $\nabla \cdot \mathbf{U} = 0$. In this case we can write

$$\mathbf{U} = \nabla \times (z \nabla \Psi) = \hat{\mathbf{z}} \times \nabla \Psi, \quad (18.21)$$

where Ψ is the transport streamfunction with dimensions $L^3 T^{-1}$.

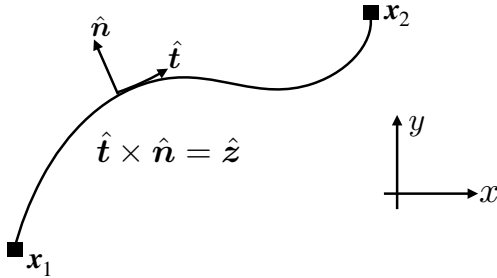


FIGURE 18.2: Depicting the transport between two points in a two-dimensional fluid. The transport is the line integral, $\int_{\mathbf{x}_1}^{\mathbf{x}_2} \mathbf{u} \cdot \hat{\mathbf{n}} ds$, from point \mathbf{x}_1 to \mathbf{x}_2 , with the unit normal, $\hat{\mathbf{n}}$, pointing to the left when facing in the direction of the local unit tangent vector, $\hat{\mathbf{t}}$. By construction, $\hat{\mathbf{t}} \times \hat{\mathbf{n}} = \hat{\mathbf{z}}$, where $\hat{\mathbf{z}}$ points vertically out of the page. For a two-dimensionally non-divergent flow, $\nabla_z \cdot \mathbf{u} = 0$, the transport between any two points is the streamfunction difference at these two points, $\int_{\mathbf{x}_1}^{\mathbf{x}_2} \mathbf{u} \cdot \hat{\mathbf{n}} ds = \psi(\mathbf{x}_1) - \psi(\mathbf{x}_2)$. This result holds regardless the path taken between these two points, so long as the path remains simple; i.e., it does not intersect itself.

18.3.4 Gauge symmetry

For a two-dimensional non-divergent flow, the constraint $\nabla_z \cdot \mathbf{u} = 0$ reduces the functional degrees of freedom from two (the two velocity components (u, v)) to one (the streamfunction). However, the streamfunction is arbitrary up to a constant, k , since

$$\psi' = \psi + k \Rightarrow \mathbf{u}' = \mathbf{u}. \quad (18.22)$$

So the value of the streamfunction at a particular point has no unambiguous physical meaning. Rather, only the difference in streamfunction between two points is physically relevant. The ability to add a constant to the streamfunction is termed a *gauge symmetry*.

18.3.5 Exact differential formulation

We here connect our discussion of velocity streamfunction to the discussion of exact differentials in Section 2.8. For that purpose introduce the differential

$$\mathbf{A} \cdot d\mathbf{x} \equiv (\mathbf{u} \times \hat{\mathbf{z}}) \cdot d\mathbf{x} = v dx - u dy. \quad (18.23)$$

By construction

$$\hat{\mathbf{z}} \cdot (\nabla_z \times \mathbf{A}) = 0 \quad \text{since} \quad \nabla_z \cdot \mathbf{u} = 0, \quad (18.24)$$

which means that $\mathbf{A} \cdot d\mathbf{x}$ is an exact differential (Section 2.8.1). Consequently, we can write

$$\mathbf{A} \cdot d\mathbf{x} = (\mathbf{u} \times \hat{\mathbf{z}}) \cdot d\mathbf{x} = \nabla_z \psi \cdot d\mathbf{x} = d\psi, \quad (18.25)$$

which then leads to the results derived earlier in this section where ψ is the transport streamfunction.

18.3.6 Concerning the Helmholtz decomposition

We close our discussion in this section by tidying up some mathematical niceties concerning the Helmholtz decomposition studied in Section 15.7. For two-dimensional flows the decomposition takes the form

$$\mathbf{u} = \hat{\mathbf{z}} \times \nabla_z \Gamma + \nabla_z \Phi, \quad (18.26)$$

for some functions Γ and Φ . For non-divergent flows, Φ is constrained to be harmonic⁴

$$\nabla \cdot \mathbf{u} = 0 \implies \nabla_z^2 \Phi = \nabla_z \cdot \nabla_z \Phi = 0. \quad (18.27)$$

As summarized in Table 18.1, it is sufficient to make use of just a streamfunction, ψ , for vortical flow and just a *velocity potential*, ϕ , for irrotational flow.⁵ In the following we verify why it is sufficient to make use of this truncated version of the Helmholtz decomposition for non-divergent two-dimensional flows.

NON-DIVERGENT VORTICAL FLOW	NON-DIVERGENT IRROTATIONAL FLOW
$\nabla_z \cdot \mathbf{u} = 0$	$\nabla_z \cdot \mathbf{u} = 0$
$\nabla_z \times \mathbf{u} \neq 0$	$\nabla_z \times \mathbf{u} = 0$
$\mathbf{u} = \hat{\mathbf{z}} \times \nabla_z \psi$	$\mathbf{u} = \nabla_z \phi$
$\hat{\mathbf{z}} \cdot (\nabla_z \times \mathbf{u}) = \nabla_z^2 \psi$	$\nabla_z^2 \phi = 0$

TABLE 18.1: Summarizing some mathematical properties of non-divergent two-dimensional velocity fields, $\nabla \cdot \mathbf{u} = 0$. The streamfunction is ψ whereas the harmonic velocity potential is ϕ .

Non-divergent vortical flow

Return to the exact differential formulation from Section 18.3.5. In that formulation we noted that $\nabla_z \cdot \mathbf{u} = 0$ means that the differential $\mathbf{A} \cdot d\mathbf{x} = (\mathbf{u} \times \hat{\mathbf{z}}) \cdot d\mathbf{x}$ is exact. Making use of the

⁴Recall our discussion of harmonic functions in Sections 2.2.2 and 3.5.1.

⁵The vorticity, $\nabla_z \times \mathbf{u}$, is a measure of the spin in the fluid and is the focus of Part VII of this book.

Helmholtz decomposition (18.26) renders

$$\mathbf{A} \cdot d\mathbf{x} = (\mathbf{u} \times \hat{\mathbf{z}}) \cdot d\mathbf{x} \quad (18.28a)$$

$$= [(\hat{\mathbf{z}} \times \nabla_z \Gamma) \times \hat{\mathbf{z}} + \nabla_z \Phi \times \hat{\mathbf{z}}] \cdot d\mathbf{x} \quad (18.28b)$$

$$= [\nabla_z \Gamma + \nabla_z \Phi \times \hat{\mathbf{z}}] \cdot d\mathbf{x}. \quad (18.28c)$$

To reveal the exactness of the right hand side requires the harmonic property of Φ so that we can write

$$\hat{\mathbf{z}} \cdot [\nabla_z \times (\nabla_z \Phi \times \hat{\mathbf{z}})] = -\nabla_z^2 \Phi = 0 \implies \nabla_z \Phi \times \hat{\mathbf{z}} \equiv \nabla_z \Upsilon, \quad (18.29)$$

in which case

$$\mathbf{A} \cdot d\mathbf{x} \equiv v dx - u dy = d(\Gamma + \Upsilon) \equiv d\psi. \quad (18.30)$$

We conclude that for non-divergent vortical flow, we lose no generality by working just with the streamfunction, ψ , of Section 18.3.3. There is no need to also include a harmonic function.

Non-divergent irrotational flow

Consider now non-divergent and irrotational flow. The irrotational condition holds so long as Γ is harmonic

$$\hat{\mathbf{z}} \cdot [\nabla_z \times (\hat{\mathbf{z}} \times \nabla_z \Gamma)] = \nabla_z^2 \Gamma = 0. \quad (18.31)$$

Consequently, we can write

$$\hat{\mathbf{z}} \times \nabla_z \Gamma = \nabla_z \gamma, \quad (18.32)$$

in which case

$$\mathbf{u} = \hat{\mathbf{z}} \times \nabla_z \Gamma + \nabla_z \Phi = \nabla_z (\gamma + \Phi) \equiv \nabla_z \phi. \quad (18.33)$$

Hence, for non-divergent irrotational flow, it is sufficient to work just with the harmonic velocity potential, ϕ .

18.3.7 A caveat: transport with curl-free + divergent flow

Consider a horizontal velocity that has a non-zero divergence, $\nabla \cdot \mathbf{u} \neq 0$, and yet it has a zero curl, $\nabla \times \mathbf{u} = 0$. The zero curl allows us to write $\mathbf{u} = \nabla_z \phi$, with ϕ the velocity potential. Hence, $d\Phi = \nabla_z \phi \cdot d\mathbf{x}$ is an exact differential and so its closed loop integral vanishes: $\oint d\Phi = 0$. However, there is no connection between velocity potential and transport. That is, we cannot conclude anything about the net transport across a closed curve based on properties of ϕ .

18.4 Vector streamfunction for three-dimensional flow

A three-dimensional non-divergent velocity, $\nabla \cdot \mathbf{v} = 0$, can be specified by a vector streamfunction

$$\mathbf{v} = \nabla \times \Psi. \quad (18.34)$$

The constraint $\nabla \cdot \mathbf{v} = 0$ is trivially satisfied since the divergence of the curl vanishes

$$\nabla \cdot (\nabla \times \Psi) = 0. \quad (18.35)$$

As we see next, the non-divergence condition reduces the three functional degrees of freedom for \mathbf{v} to two degrees of freedom plus a gauge function.

18.4.1 Gauge symmetry

For three-dimensional non-divergent flow, the constraint $\nabla \cdot \mathbf{v} = 0$ reduces the three functional degrees of freedom down to two, meaning that one of the velocity components can be diagnosed from the other two. Gauge symmetry manifests through the ability to add the gradient of an arbitrary function to the streamfunction, Ψ , without altering \mathbf{v} :

$$\Psi' = \Psi + \nabla \lambda \Rightarrow \mathbf{v}' = \mathbf{v}, \quad (18.36)$$

which follows since $\nabla \times \nabla \lambda = 0$. Hence, the vector streamfunction has no absolute physical meaning since it can be modified by adding an arbitrary gauge function. Even so, we find it useful to consider certain vector streamfunctions that have direct connection to fluid transport, as discussed in Section 18.4.3.

18.4.2 Vector streamfunction in the vertical gauge

We here choose a particular gauge so that the streamfunction measures the horizontal volume transport of fluid beneath a chosen depth. For this purpose, write the component expression for the velocity

$$u = \frac{\partial \Psi_3}{\partial y} - \frac{\partial \Psi_2}{\partial z} \quad \text{and} \quad v = \frac{\partial \Psi_1}{\partial z} - \frac{\partial \Psi_3}{\partial x} \quad \text{and} \quad w = \frac{\partial \Psi_2}{\partial x} - \frac{\partial \Psi_1}{\partial y}, \quad (18.37)$$

where the Cartesian components to the vector streamfunction are

$$\Psi = \hat{\mathbf{x}} \Psi_1 + \hat{\mathbf{y}} \Psi_2 + \hat{\mathbf{z}} \Psi_3. \quad (18.38)$$

We here choose the *vertical gauge*⁶ whereby $\nabla \lambda$ is set to precisely cancel the third component of the vector streamfunction

$$\Psi_3 = 0 \iff \text{vertical gauge}, \quad (18.39)$$

which then renders

$$u = -\frac{\partial \Psi_2}{\partial z} \quad \text{and} \quad v = \frac{\partial \Psi_1}{\partial z} \quad \text{and} \quad w = \frac{\partial \Psi_2}{\partial x} - \frac{\partial \Psi_1}{\partial y}. \quad (18.40)$$

Vertically integrating the u, v equations from the bottom at $z = \eta_b(x, y)$ up to an arbitrary geopotential leads to

$$\Psi = \int_{\eta_b}^z \mathbf{u} dz' \times \hat{\mathbf{z}} \equiv \mathbf{U}(z) \times \hat{\mathbf{z}}, \quad (18.41)$$

where $\mathbf{U}(z) = \int_{\eta_b}^z \mathbf{u} dz'$ is the horizontal transport of fluid from the bottom to a chosen vertical position. By construction, $u = -\partial \Psi_2 / \partial z$ and $v = \partial \Psi_1 / \partial z$. We verify that this streamfunction also renders w through noting that

$$\frac{\partial \Psi_2}{\partial x} = u(\eta_b) \partial_x \eta_b - \int_{\eta_b}^z \partial_x u dz' \quad \text{and} \quad \frac{\partial \Psi_1}{\partial y} = \int_{\eta_b}^z \partial_y v dz' - v(\eta_b) \partial_y \eta_b, \quad (18.42)$$

so that

$$\frac{\partial \Psi_2}{\partial x} - \frac{\partial \Psi_1}{\partial y} = \mathbf{u}(\eta_b) \cdot \nabla \eta_b - \int_{\eta_b}^z \left[\frac{\partial u}{\partial x} + \frac{\partial v}{\partial y} \right] dz' = w(\eta_b) + \int_{\eta_b}^z \frac{\partial w}{\partial z'} dz' = w(z), \quad (18.43)$$

⁶The vertical gauge is commonly used in studies of ocean mesoscale eddy parameterizations, such as discussed in Sections 61.7.1 and 63.1.

where we used the bottom kinematic boundary condition (16.41) to write $w - \mathbf{u} \cdot \nabla \eta_b = 0$ at $z = \eta_b(x, y)$. Hence, knowledge of the vector streamfunction (18.41) offers a means to compute the three velocity components. Of course, the velocity is needed to compute the vector streamfunction! Even though the logic is circular, we are satisfied that the circle closes to reveal self-consistency of the formalism. Furthermore, in some contexts it is more suitable to first compute the transport than the velocity, such as in ocean mesoscale eddy parameterizations (e.g., Chapter 9 of Griffies (2004)). We also note that the transport is a smoother field than the velocity given that it is computed as an integral of the velocity.

We close by noting that the transport through the solid-earth bottom, $z = \eta_b(x, y)$, vanishes according to equation (18.46). We can trivially verify this result for the vertical gauge since

$$\Psi(z = \eta_b) = 0, \quad (18.44)$$

so that $\oint_{\partial\mathcal{S}} \Psi \cdot \hat{\mathbf{t}} \, ds = 0$ on the bottom.

18.4.3 The streamfunction and transport through a surface

The volume transport (volume per time) of fluid crossing a surface is defined by the area integral

$$\mathcal{T}(\mathcal{S}) = \int_{\mathcal{S}} \mathbf{v} \cdot \hat{\mathbf{n}} \, d\mathcal{S}, \quad (18.45)$$

where $\hat{\mathbf{n}}$ is the outward unit normal vector on the surface. Introducing the vector streamfunction and making use of Stokes' Theorem (Section 2.6) then leads to

$$\mathcal{T}(\mathcal{S}) = \int_{\mathcal{S}} \mathbf{v} \cdot \hat{\mathbf{n}} \, d\mathcal{S} = \int_{\mathcal{S}} (\nabla \times \Psi) \cdot \hat{\mathbf{n}} \, d\mathcal{S} = \oint_{\partial\mathcal{S}} \Psi \cdot \hat{\mathbf{t}} \, ds, \quad (18.46)$$

where $\hat{\mathbf{t}} \, ds$ is the oriented arc distance increment along the boundary of \mathcal{S} , and $\oint_{\partial\mathcal{S}}$ is the oriented line integral around the boundary $\partial\mathcal{S}$. Hence, the volume transport of fluid through the surface depends only on the vector streamfunction on the perimeter of the surface. Furthermore, if the transport through the surface vanishes (e.g., no-flux material surface such as a solid earth boundary), then on the surface the vector streamfunction can be written as the gradient of an arbitrary scalar field, $\Psi = \nabla \chi$, since

$$\oint_{\partial\mathcal{S}} \Psi \cdot \hat{\mathbf{t}} \, ds = \oint_{\partial\mathcal{S}} \nabla \chi \cdot \hat{\mathbf{t}} \, ds = \oint_{\partial\mathcal{S}} \nabla \chi \cdot d\mathbf{x} = \oint_{\partial\mathcal{S}} d\chi = 0. \quad (18.47)$$

Because Ψ has a connection to fluid transport, we sometimes refer to it as the *transport streamfunction*, just as for the streamfunction ψ in two-dimensional non-divergent flows (Section 18.3.3).

18.4.4 Scalar streamfunctions and transport

We can expose the two degrees of freedom of the vector streamfunction by writing it as the product

$$\Psi = \gamma \nabla \psi \quad (18.48)$$

so that the velocity is given by

$$\mathbf{v} = \nabla \times \Psi = \nabla \gamma \times \nabla \psi. \quad (18.49)$$

By construction the velocity satisfies

$$\mathbf{v} \cdot \nabla \gamma = \mathbf{v} \cdot \nabla \psi = 0, \quad (18.50)$$

so that the velocity is parallel to surfaces of constant γ and ψ . Correspondingly, the velocity streamlines are intersections of the γ and ψ isosurfaces, as depicted in Figure 18.3. We thus refer to γ and ψ as the two *scalar streamfunctions* for the three dimensional non-divergent flow. However, note that γ and ψ have different dimensions. By convention, we choose γ to have dimensions of length, so that it is not a traditional streamfunction, whereas ψ to has the typical streamfunction dimensions of squared length per time.

As a check that the formalism is sensible, consider the special case of two-dimensional flow so that all streamlines are in the horizontal x - y plane. Taking $\gamma = z$ then renders

$$\Psi = z \nabla \psi \quad \text{and} \quad \mathbf{v} = \nabla \times \Psi = \hat{\mathbf{z}} \times \nabla \psi, \quad (18.51)$$

which agrees with the scalar streamfunction in equation (18.7) for two dimensional non-divergent flow.

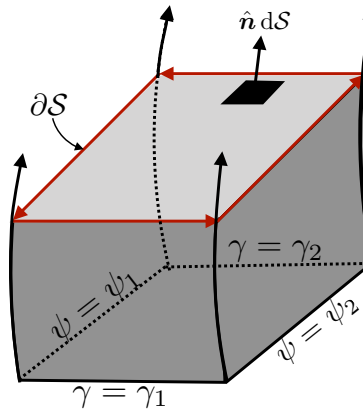


FIGURE 18.3: Isosurfaces of constant scalar streamfunctions, γ and ψ , for a three dimensional non-divergent flow. Streamlines are defined by the intersections of the γ and ψ isosurfaces, as shown by four streamlines along the corners of this particular volume. The volume transport of fluid through the surface, \mathcal{S} , is determined by the line integral, $\oint_{\partial\mathcal{S}} \gamma d\psi = -\oint_{\partial\mathcal{S}} \psi d\gamma = (\gamma_1 - \gamma_2)(\psi_2 - \psi_1)$, around the boundary circuit.

The volume transport through a surface defined by the two streamfunction isosurfaces takes the form

$$\mathcal{T}(\mathcal{S}) = \int_{\mathcal{S}} \mathbf{v} \cdot \hat{\mathbf{n}} d\mathcal{S} = \oint_{\partial\mathcal{S}} \Psi \cdot \hat{\mathbf{t}} ds = \oint_{\partial\mathcal{S}} \gamma \nabla \psi \cdot \hat{\mathbf{t}} ds = \oint_{\partial\mathcal{S}} \gamma d\psi = -\oint_{\partial\mathcal{S}} \psi d\gamma. \quad (18.52)$$

To reach the penultimate step we set

$$d\psi = \nabla \psi \cdot d\mathbf{x} = \nabla \psi \cdot \hat{\mathbf{t}} ds, \quad (18.53)$$

and for the final step we used the identity

$$\oint_{\partial\mathcal{S}} \gamma d\psi = \oint_{\partial\mathcal{S}} d(\gamma \psi) - \oint_{\partial\mathcal{S}} \psi d\gamma = -\oint_{\partial\mathcal{S}} \psi d\gamma, \quad (18.54)$$

which follows since $\oint_{\partial\mathcal{S}} d(\gamma \psi) = 0$. The volume transport for the particular surface shown in Figure 18.3 is given by

$$\mathcal{T}(\mathcal{S}) = \oint_{\partial\mathcal{S}} \gamma d\psi = \gamma_1 (\psi_2 - \psi_1) + \gamma_2 (\psi_1 - \psi_2) = (\gamma_1 - \gamma_2)(\psi_2 - \psi_1). \quad (18.55)$$

Hence, the volume transport through a streamtube defined by isosurfaces of γ and ψ is given by

the product of the difference between the isosurfaces.

18.4.5 Concerning a harmonic velocity potential

As for the two-dimensional case discussed in Section 18.3.6, we consider the relevance of an arbitrary harmonic velocity potential, χ , so that the velocity takes the form

$$\mathbf{v} = \nabla \times \boldsymbol{\Gamma} + \nabla \chi \quad \text{with} \quad \nabla^2 \chi = 0. \quad (18.56)$$

Since $\nabla \cdot \nabla \chi = 0$ we can write $\nabla \chi$ as the curl of another vector

$$\nabla \cdot \nabla \chi = 0 \implies \nabla \chi = \nabla \times \boldsymbol{\Lambda}, \quad (18.57)$$

in which case the velocity takes the form

$$\mathbf{v} = \nabla \times \boldsymbol{\Gamma} + \nabla \chi = \nabla \times (\boldsymbol{\Gamma} + \boldsymbol{\Lambda}) \equiv \nabla \times \boldsymbol{\Psi}. \quad (18.58)$$

Consequently, just as for the two-dimensional case, we are at liberty to work with the transport streamfunction $\boldsymbol{\Psi}$ if that suits our needs. Otherwise, we can work with the harmonic potential, χ , which is commonly used when the velocity is both non-divergent and irrotational, such as for our studies of surface gravity waves in Chapter 45.

18.5 Evolution of volume and area

In this section we develop kinematic equations for the evolution of volume and area within a non-divergent flow. We start by considering a material region and then study an arbitrary region.

18.5.1 Material volumes and areas

As shown by equation (18.2), the volume of a fluid element remains constant in a non-divergent flow. Correspondingly, a fluid region moving with the velocity field maintains a constant volume

$$\frac{d}{dt} \int_{\mathcal{R}(\mathbf{v})} dV = \int_{\mathcal{R}(\mathbf{v})} \frac{D(\delta V)}{Dt} = \int_{\mathcal{R}(\mathbf{v})} (\nabla \cdot \mathbf{v}) dV = \oint_{\partial \mathcal{R}(\mathbf{v})} \mathbf{v} \cdot \hat{\mathbf{n}} d\mathcal{S} = 0. \quad (18.59)$$

The appearance of a material time derivative on the inside of the integral arises since the integral is computed following fluid particles whose trajectories define integral curves of the flow (see Section 17.3.7). Likewise, following from the area element equation (15.69), the area of a region moving with a two-dimensional non-divergent flow remains materially constant

$$\frac{d}{dt} \int_{\mathcal{S}(\mathbf{v})} d\mathcal{S} = \int_{\mathcal{S}(\mathbf{v})} \frac{D(\delta \mathcal{S})}{Dt} = \int_{\mathcal{S}(\mathbf{v})} (\nabla \cdot \mathbf{u}) d\mathcal{S} = \oint_{\partial \mathcal{S}(\mathbf{v})} \mathbf{u} \cdot \hat{\mathbf{n}} ds = 0. \quad (18.60)$$

This area preservation property is illustrated in Figure 18.4, in which a two-dimensional non-divergent flow is seen to deform an initially square patch of fluid.



FIGURE 18.4: Illustrating the stretching and straining of an initially square patch of fluid in a two-dimensional non-divergent flow field. As discussed in Section 18.5, the area of a region moving with the flow remains fixed.

18.5.2 Arbitrary volume and area

We make use of the Leibniz-Reynolds transport theorem from Section 17.3.4 to develop the evolution equation for the volume of an arbitrary region. In particular, equation (17.45) gives

$$\frac{d}{dt} \left[\int_{\mathcal{R}} dV \right] = \oint_{\partial\mathcal{R}} \mathbf{v}^{(b)} \cdot \hat{\mathbf{n}} d\mathcal{S}. \quad (18.61)$$

This result holds for both divergent and non-divergent flows. But for non-divergent flows we can go one step further by noting that

$$0 = \int_{\mathcal{R}} \nabla \cdot \mathbf{v} dV = \oint_{\partial\mathcal{R}} \mathbf{v} \cdot \hat{\mathbf{n}} d\mathcal{S}. \quad (18.62)$$

Importantly, this result holds only when integrating around the boundary of the closed volume, $\partial\mathcal{R}$. It does not necessarily mean that $\mathbf{v} \cdot \hat{\mathbf{n}} = 0$ holds at every point along the boundary. Indeed, when the boundary is time dependent, then $\mathbf{v} \cdot \hat{\mathbf{n}} \neq 0$ generally holds along the boundary.

Making use of equation (18.62) allows us to write

$$\frac{d}{dt} \left[\int_{\mathcal{R}} dV \right] = \oint_{\partial\mathcal{R}} \mathbf{v}^{(b)} \cdot \hat{\mathbf{n}} d\mathcal{S} = - \oint_{\partial\mathcal{R}} (\mathbf{v} - \mathbf{v}^{(b)}) \cdot \hat{\mathbf{n}} d\mathcal{S}. \quad (18.63)$$

This result is identical to the mass budget equation (17.47) for the special case of a constant reference density appropriate for a Boussinesq ocean. The dia-surface transport, $(\mathbf{v} - \mathbf{v}^{(b)}) \cdot \hat{\mathbf{n}} d\mathcal{S}$, measures the volume per time crossing the boundary of the region, whether that region has a static or moving boundary. For example, if the boundary is the ocean free surface, then we can make use of the surface kinematic boundary condition (18.4).

18.6 Meridional-depth overturning circulation

Geophysical fluid flow is generally three-dimensional. However, it is sometimes useful to summarize aspects of that flow by integrating the mass transport over one of the directions. A common approach is to integrate over the zonal direction either between two solid-wall boundaries (as in an ocean basin) or over a periodic domain (as in the atmosphere or within the Southern Ocean). Doing so leaves a two-dimensional transport in the (y, z) plane known as the meridional-depth overturning circulation

$$V^\rho = \int_{x_1}^{x_2} \rho v dx \quad \text{and} \quad W^\rho = \int_{x_1}^{x_2} \rho w dx. \quad (18.64)$$

where

$$x_1 = x_1(y, z) \quad \text{and} \quad x_2 = x_2(y, z) \quad (18.65)$$

are expressions for the zonal boundaries as a function of (y, z) . As we show in this section, we can introduce a streamfunction for the meridional-depth circulation if the zonally integrated flow is non-divergent.

18.6.1 Specifying the zonal position as a function of (y, z)

In Section 6.1.3 we introduced the geometry of surfaces specified by the zonal position as in equation (18.65). There, we noted that by writing the functions $x_1(y, z)$ and $x_2(y, z)$, we must assume that the normal direction along the boundary everywhere has a nonzero and single-signed

projection in the $\hat{\mathbf{x}}$ direction.⁷ If that is indeed the case, then we can write the normal direction as

$$\hat{\mathbf{n}}_i = \frac{\nabla(x - x_i)}{|\nabla(x - x_i)|} = \frac{\hat{\mathbf{x}} - \hat{\mathbf{y}} \partial_y x_i - \hat{\mathbf{z}} \partial_z x_i}{|\sqrt{1 + (\partial_y x_i)^2 + (\partial_z x_i)^2}|}, \quad (18.66)$$

for boundaries $i = 1, 2$. Furthermore, the no-normal flow boundary condition at the bottom (Section 16.4.1) takes on the form

$$\mathbf{v} \cdot \hat{\mathbf{n}}_i = 0 \implies u = v \partial_y x_i - w \partial_z x_i \quad \text{at } x = x_i(y, z). \quad (18.67)$$

We make use of this boundary condition in the following to prove that the zonally integrated flow is non-divergent.

18.6.2 The zonally integrated transport is non-divergent

To see how to create an overturning streamfunction, consider the zonal integrated area transport for a non-divergent flow⁸

$$V(y, z, t) = \int_{x_1(y, z)}^{x_2(y, z)} v(x', y, z, t) dx' \quad \text{and} \quad W(y, z, t) = \int_{x_1(y, z)}^{x_2(y, z)} w(x', y, z, t) dx'. \quad (18.68)$$

Taking the meridional derivative of the meridional transport, and making use of Leibniz's rule and the non-divergence condition, leads to

$$\frac{\partial V}{\partial y} = \frac{\partial}{\partial y} \left[\int_{x_1}^{x_2} v(x', y, z) dx' \right] \quad (18.69a)$$

$$= v(x_2) \partial_y x_2 - v(x_1) \partial_y x_1 + \int_{x_1}^{x_2} \frac{\partial v}{\partial y} dx \quad (18.69b)$$

$$= v(x_2) \partial_y x_2 - v(x_1) \partial_y x_1 - \int_{x_1}^{x_2} \left[\frac{\partial u}{\partial x} + \frac{\partial w}{\partial z} \right] dx \quad (18.69c)$$

$$= -[u - v \partial_y x - w \partial_z x]_{x=x_2} + [u - v \partial_y x - w \partial_z x]_{x=x_1} - \frac{\partial}{\partial z} \int_{x_1}^{x_2} w(x', y, z) dx \quad (18.69d)$$

$$= -\frac{\partial W}{\partial z}. \quad (18.69e)$$

To reach the final equality we made use of the no-normal flow boundary condition in the form of equation (18.67), so that the boundary terms vanish identically. We thus conclude that the zonally integrated transport is non-divergent

$$\frac{\partial V}{\partial y} + \frac{\partial W}{\partial z} = 0. \quad (18.70)$$

⁷That is, we do not admit any embayments along the coast with a headland where the boundary outward normal has zero projection in the $\hat{\mathbf{x}}$ direction.

⁸The case for a steady compressible flow follows analogously since in that case $\nabla \cdot (\rho \mathbf{v}) = 0$, in which case we would consider $(\rho v, \rho w)$ rather than (v, w) .

18.6.3 Defining the meridional-depth overturning streamfunction

As a consequence of the non-divergence condition (18.70), we can introduce a meridional-depth overturning streamfunction

$$\Psi(y, z, t) = - \int_{\eta_b^{\min}}^z V(y, z', t) dz' = - \int_{\eta_b^{\min}}^z \left[\int_{x_1(y, z')}^{x_2(y, z')} v(x', y, z', t) dx' \right] dz', \quad (18.71)$$

which can be used to specify the zonally integrated flow. Note that the z dependence for the streamfunction arises just from the upper limit of the vertical integral. Furthermore, the lower limit of $z = \eta_b^{\min}$ is a spatial constant that is chosen so that the lower limit on the integral is beneath the fluid anywhere in the full domain, with the convention that there is zero transport for any region below the fluid bottom (i.e., no fluid transport in rock). This specification for the lower integration limits ensures that the streamfunction has a spatial dependence just on (y, z) . If we choose, for some reason, the lower limit on the integral as $\eta_b(x, y)$, then we would have Ψ as a function of all three spatial coordinates, (x, y, z) , in which case it cannot be a streamfunction for the zonally integrated flow.

It is a useful exercise to verify that Ψ as defined by equation (18.71) is indeed a streamfunction. Suppressing the time dependence for notational brevity, we first show that

$$\frac{\partial \Psi}{\partial z} = - \frac{\partial}{\partial z} \left[\int_{\eta_b^{\min}}^z V(y, z') dz' \right] = -V(y, z), \quad (18.72)$$

where we used Leibniz's rule and noted that only the upper integration limit is a function of z . For the meridional derivative we have

$$\frac{\partial \Psi}{\partial y} = - \frac{\partial}{\partial y} \left[\int_{\eta_b^{\min}}^z V(y, z') dz' \right] \quad (18.73a)$$

$$= - \int_{\eta_b^{\min}}^z \frac{\partial V(y, z')}{\partial y} dz' \quad (18.73b)$$

$$= \int_{\eta_b^{\min}}^z \frac{\partial W(y, z')}{\partial z} dz' \quad (18.73c)$$

$$= W(y, z), \quad (18.73d)$$

where we used the non-divergent condition (18.70), and we also set

$$W(z = \eta_b^{\min}) = 0, \quad (18.74)$$

which follows from our convention that η_b^{\min} is below the deepest fluid region. Also, we are able to move the $\partial/\partial y$ derivative across the lower limit of the integral since η_b^{\min} is a constant. An idealized version of the meridional-depth circulation is shown in Figure 18.5.

The overturning streamfunction at the ocean surface

To evaluate the overturning streamfunction (18.71) at the ocean surface, $z = \eta(x, y, t)$, we follow a method similar to how we deal with the bottom. Namely, introduce a constant η^{\max} that is larger than any value of $\eta(x, y, t)$ and with the convention that the transport is zero in regions above the ocean surface. In this case the streamfunction computed across the full depth of the domain

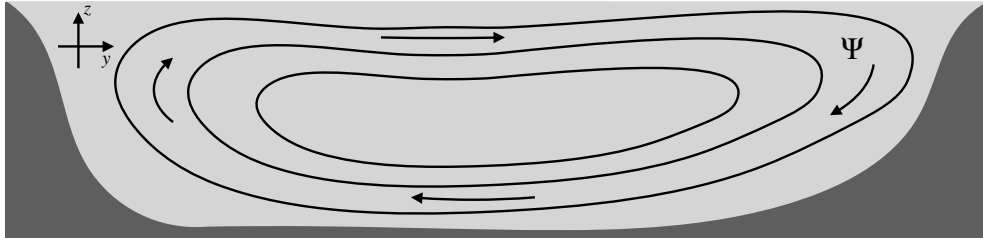


FIGURE 18.5: An idealized depiction of a steady meridional-depth overturning circulation. Shown here are streamlines (isolines of constant Ψ) for the zonally integrated flow between two solid boundaries or over a zonally periodic domain. The flow is assumed to be non-divergent, as per equation (18.70). In the upper reaches of the fluid, flow moves northward (positive y), with downward motion as it reaches the northern boundary, then southward motion at depth and eventual return towards the surface near the southern boundary.

is given by minus the net meridional transport across the chosen latitude

$$\Psi(y, z = \eta^{\max}) = - \int_{\eta_b^{\min}}^{\eta^{\max}} V \, dz' = - \int_{\eta_b^{\min}}^{\eta^{\max}} \left[\int_{x_1}^{x_2} v \, dx \right] \, dz', \quad (18.75)$$

Volume conservation means that this transport vanishes in the steady state but it is generally nonzero in the presence of transients.

18.7 Kinematic free surface equation

We here derive the volume budget over a column of fluid. This budget provides a kinematic expression for the free surface evolution in a non-divergent flow.

18.7.1 Derivation

Vertically integrate the constraint, $\nabla \cdot \mathbf{v} = 0$, over the depth of an ocean column, from $z = \eta_b(x, y)$ at the bottom to $z = \eta(x, y, t)$ at the free surface and use the bottom and surface kinematic boundary conditions. This calculation yields

$$0 = \int_{\eta_b}^{\eta} \nabla \cdot \mathbf{v} \, dz \quad (18.76a)$$

$$= w(\eta) - w(\eta_b) + \int_{\eta_b}^{\eta} \nabla \cdot \mathbf{u} \, dz \quad (18.76b)$$

$$= w(\eta) - w(\eta_b) + \nabla \cdot \left[\int_{\eta_b}^{\eta} \mathbf{u} \, dz \right] - \mathbf{u}(\eta) \cdot \nabla \eta + \mathbf{u}(\eta_b) \cdot \nabla \eta_b \quad (18.76c)$$

$$= [w(\eta) - \mathbf{u}(\eta) \cdot \nabla \eta] - [w(\eta_b) - \mathbf{u}(\eta_b) \cdot \nabla \eta_b] + \nabla \cdot \left[\int_{\eta_b}^{\eta} \mathbf{u} \, dz \right], \quad (18.76d)$$

where we made use of Leibniz's Rule to move the horizontal divergence outside of the integral. We now make use of the surface kinematic boundary condition (18.5) and the bottom no-flow condition

$$w(\eta) - \mathbf{u} \cdot \nabla \eta = -Q_m / \rho_0 + \partial_t \eta \quad z = \eta \quad (18.77a)$$

$$w = \mathbf{u} \cdot \nabla \eta_b \quad z = \eta_b \quad (18.77b)$$

to render the free surface equation for a fluid with a non-divergent flow

$$\partial_t \eta = Q_m / \rho_0 - \nabla \cdot \mathbf{U}, \quad (18.78)$$

where

$$\mathbf{U} = \int_{\eta_b}^{\eta} \mathbf{u} dz \quad (18.79)$$

is the depth integrated horizontal transport. For the special case of a steady state with zero boundary mass flux, the depth integrated flow is non-divergent

$$\nabla \cdot \mathbf{U} = 0 \quad \text{if } Q_m = 0 \text{ and } \partial \eta / \partial t = 0. \quad (18.80)$$

18.7.2 Comments

Comparing to the surface kinematic boundary condition

Recall that we can write the surface kinematic boundary condition for a non-divergent flow in the special form of equation (18.6). Comparing to the free surface equation (18.78) renders the identity

$$\partial_t \eta - Q_m / \rho_0 = -\nabla \cdot \mathbf{U} = \nabla \cdot [(z - \eta) \mathbf{v}], \quad (18.81)$$

where the final expression is evaluated at $z = \eta$ after evaluating the divergence.

Concerning the evolution of sea level

Comparing the free surface equation (18.78) holding for a non-divergent flow to the free surface equation (16.84) holding for a divergent flow indicates that the non-divergent case is missing a contribution from the material changes in density

$$\frac{\partial \eta}{\partial t} = \frac{Q_m}{\rho_0} - \nabla \cdot \mathbf{U} \quad \text{Boussinesq ocean } (\nabla \cdot \mathbf{v} = 0) \quad (18.82a)$$

$$\frac{\partial \eta}{\partial t} = \frac{Q_m}{\rho(\eta)} - \nabla \cdot \mathbf{U} - \int_{\eta_b}^{\eta} \frac{1}{\rho} \frac{D\rho}{Dt} dz \quad \text{non-Boussinesq ocean } (\nabla \cdot \mathbf{v} \neq 0). \quad (18.82b)$$

The material time changes to density arise from mixing and boundary fluxes of buoyancy. The particular absence of an impact from surface buoyancy fluxes means that the free surface in a Boussinesq ocean is not impacted by global thermal expansion, such as that arising from ocean warming. [Greatbatch \(1994\)](#) and [Griffies and Greatbatch \(2012\)](#) provide a recipe for diagnostically addressing this formulation limitation, thus enabling a study of global mean sea level with Boussinesq ocean models.



18.8 Exercises

EXERCISE 18.1: STREAMLINES FOR CELLULAR FLOW

Sketch the velocity field for this streamfunction

$$\psi(x, y) = A \sin(kx) \sin ly, \quad (18.83)$$

where (k, l) are the zonal and meridional components to the wavevector, respectively. Hint: assume any convenient value for k, l and the amplitude, A , but indicate what values were chosen. Furthermore, show vectors so that the sense of the flow is clear.

EXERCISE 18.2: ZERO NET AREA TRANSPORT THROUGH STATIC CLOSED CURVE

For a two-dimensional non-divergent flow, show that there is zero net transport of fluid crossing an arbitrary static and simply connected closed curve. Note that in two space dimensions, the transport of fluid across a line has dimensions $L^2 T^{-1}$, thus representing an area transport.

EXERCISE 18.3: ZERO NET VOLUME TRANSPORT THROUGH STATIC CLOSED SURFACE

For a three-dimensional non-divergent flow, show that there is zero net transport of fluid crossing an arbitrary static and simply connected closed surface within the fluid interior. Note that in three space dimensions, the transport of fluid across a surface has dimensions $L^3 T^{-1}$, thus representing a volume transport.

EXERCISE 18.4: NET FLUID TRANSPORT ACROSS AN ARBITRARY SURFACE

Consider flow in a container with static sides/bottom. Draw an arbitrary static surface, \mathcal{S} , within the fluid from one side of the container to the other as in Figure 18.6. Integrate the fluid transport over the surface, $\int_{\mathcal{S}} \mathbf{v} \cdot \hat{\mathbf{n}} d\mathcal{S}$.

- For a non-divergent flow, show that the transport $\int_{\mathcal{S}} \mathbf{v} \cdot \hat{\mathbf{n}} d\mathcal{S}$ vanishes. That is, the net transport across the surface is zero.
- Specialize the above result to a horizontal surface so that we see there is zero integrated vertical transport across the surface, $\int_{\mathcal{S}} w dx dy = 0$. Discuss these results. Note: see Section 57.4.8 for the more general case of a non-static surface.
- Rework part (a) for the case of a compressible fluid so that fluid elements conserve their mass rather than their volume, in which case mass continuity is given by equation (16.10)

$$\frac{1}{\rho} \frac{D\rho}{Dt} = -\nabla \cdot \mathbf{v}. \quad (18.84)$$

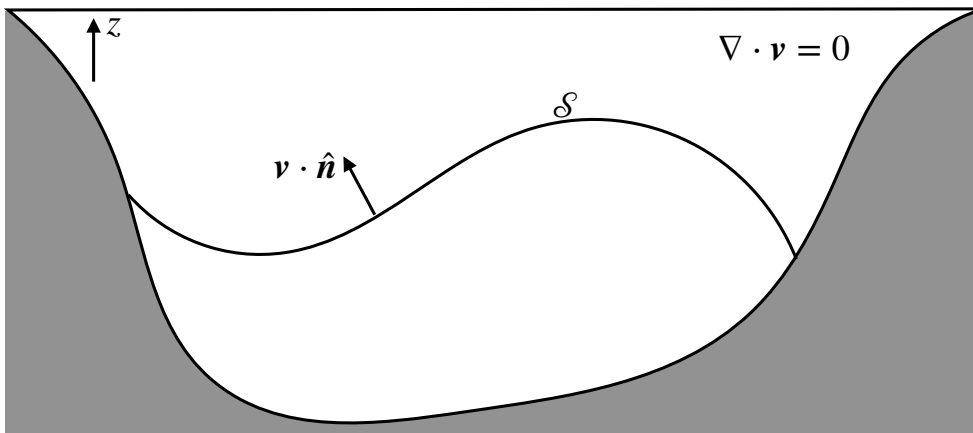


FIGURE 18.6: Schematic for exercise 18.4, whereby we show that the net flow vanishes across a static surface, \mathcal{S} , that extends from one boundary to the other within a non-divergent flow.

EXERCISE 18.5: SOLID BODY ROTATION

Consider a velocity field corresponding to a time-independent solid-body rotation on a plane

$$\mathbf{u} = \Omega \hat{z} \times \mathbf{x} = \Omega (-y \hat{x} + x \hat{y}), \quad (18.85)$$

where $\Omega > 0$ is a constant rotation rate.

- Compute the relative vorticity, $\boldsymbol{\omega} = \nabla \times \mathbf{u}$.
- Compute the streamfunction $\mathbf{u} = \hat{\mathbf{z}} \times \nabla \psi$. Draw streamfunction contours; i.e., lines of constant streamfunction. Put arrows to orient the flow along the streamlines.
- Describe the geometry of material lines. Hint: since the velocity field is time-independent, material parcel trajectories are coincident with streamlines.

EXERCISE 18.6: ALTERNATIVE FORM OF MERIDIONAL-DEPTH STREAMFUNCTION

In equation (18.71), we introduced the meridional-depth overturning streamfunction

$$\Psi(y, z, t) = - \int_{\eta_b^{\min}}^z V(y, z', t) dz'. \quad (18.86)$$

Show that an alternative streamfunction is given by

$$\Gamma(y, z, t) = \int_{y_s}^y W(y', z, t) dy', \quad (18.87)$$

where y_s is a constant latitude southward of the southern-most latitude where fluid exists. That is, show that

$$\frac{\partial \Gamma}{\partial y} = W \quad \text{and} \quad \frac{\partial \Gamma}{\partial z} = -V. \quad (18.88)$$

EXERCISE 18.7: VOLUME TRANSPORT THROUGH STREAMTUBE ENDS

Recall our discussion of streamtubes in Section 14.9.2 (see in particular Figure 14.5). For a steady non-divergent three-dimensional flow, show that the volume transport (volume per time) through the two streamtube ends balances

$$\int_{\mathcal{S}_1} \mathbf{v} \cdot \hat{\mathbf{n}}_1 d\mathcal{S} + \int_{\mathcal{S}_2} \mathbf{v} \cdot \hat{\mathbf{n}}_2 d\mathcal{S} = 0, \quad (18.89)$$

where $\hat{\mathbf{n}}_1$ and $\hat{\mathbf{n}}_2$ are the outward normals at the two end caps \mathcal{S}_1 and \mathcal{S}_2 . Since the end caps have oppositely directed outward normals, equation (18.89) says that the volume transport entering one streamtube end equals to that leaving the other end. Furthermore, the area of the streamtube is inversely proportional to the local normal velocity, so that flow speeds up when moving through a narrower region of the tube.

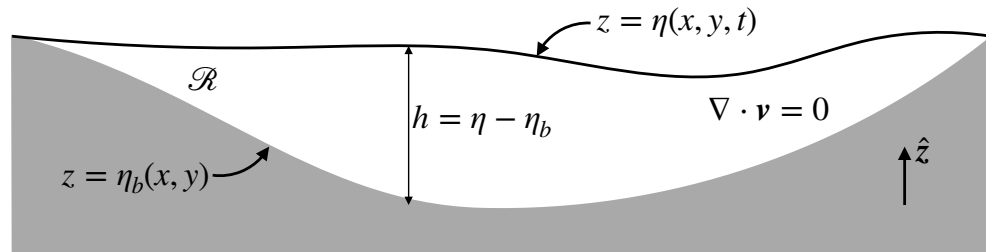


FIGURE 18.7: Schematic for exercise 18.8 with $z = \eta(x, y, t)$ the free surface at the top of the fluid. This exercise shows that the area integrated time tendency for the free surface vanishes in the absence of mass transport across the free surface.

EXERCISE 18.8: AREA AVERAGE OF FREE SURFACE TIME TENDENCY

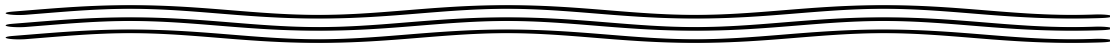
Consider a non-divergent ocean flow bounded by a free upper surface and a solid bottom. Let $z = \eta_b(x, y)$ be the vertical position of the static bottom, and $z = \eta(x, y, t)$ be the position of the transient free surface, so that the thickness of the layer is $h = -\eta_b + \eta$ (see Figure 18.7). The horizontal extent of the layer is a function of time, and is defined by a vanishing thickness $h = -\eta_b + \eta = 0$ (e.g., ocean water reaching the shoreline). Assume no material crosses either the surface or bottom boundaries, so that both boundaries are material surfaces. Show that the free surface has a time derivative, $\partial\eta/\partial t$, whose area average vanishes. Discuss this result.

EXERCISE 18.9: VOLUME INTEGRAL OF THE NON-DIVERGENT CARTESIAN VELOCITY FIELD

Consider a non-divergent ocean flow in Cartesian coordinates bounded by a free upper surface and a solid bottom over a domain \mathcal{R} . Let $z = \eta_b(x, y)$ be the vertical position of the static bottom, and $z = \eta(x, y, t)$ be the position of the transient free surface as in Figure 18.7. Prove that the domain integral of the velocity is given by

$$\int_{\mathcal{R}} \mathbf{v} dV = \int_{z=\eta} \mathbf{x} (\mathbf{v} \cdot \hat{\mathbf{n}}) dS = \int_{z=\eta} \mathbf{x} (\partial_t \eta - Q_m / \rho_0) dx dy. \quad (18.90)$$

Hint: make use of the results from Section 2.7.6 and then use the kinematic boundary conditions from Section 18.2. Note that to enable this exercise we assume Cartesian coordinates, which is required when integrating a vector.



Part IV

Equilibrium thermodynamics

Thermodynamics is a phenomenological discipline focused on relations between macroscopic properties of physical systems, in particular how those properties change as the system transitions from one state to another. Thermodynamics is a necessary ingredient for understanding the stability, evolution, and transformation of macroscopic systems, with such topics at the heart of geophysical fluid mechanics. In this part of the book we develop elements of equilibrium thermodynamics relevant to a multi-component fluid. We limit concern to a single phase of matter (liquid or gas), noting that a more complete treatment relevant to geophysical fluids must consider multiple phases and their transitions.

We focus on classical thermodynamics, which means we are generally concerned with macroscopic states of a fluid system; i.e., a *macrostate* that is specified by a few macroscopic properties such as temperature, pressure, and matter concentration. For our purposes, a macrostate is synonymous with *thermodynamic state*. This nomenclature must be modified when discussing statistical mechanics and quantum mechanics, whereby the complementary notion of a microstate takes on a far more central role than considered in this book.

The name “thermodynamics” suggests that the discipline concerns how heat moves through a system. Indeed, that topic formed the focus of the subject in the 19th century, as exemplified by [Maxwell \(1872\)](#). However, treatments following the formulation from Gibbs generally focus on energy and entropy, from which temperature is derived. Energy and entropy are logically distinct concepts that together form the basis for thermodynamics. Energy is a concept borrowed from mechanics. *Internal energy* refers to the energy of microscopic degrees of freedom, with this energy the concern of Chapter 19, where we focus on transitions between thermodynamic equilibrium states in the absence of gravity. In Chapter 20 we extend the equilibrium theory to include a geopotential, with this study directly relevant to geophysical fluid mechanics.

Our study of thermodynamics is only partly addressed in this part of the book. The next stage concerns the melding of thermodynamics with the mechanics describing macroscopic fluid motion. After introducing the basics of momentum and mechanical energy for macroscopic motion in Chapter 21, we return to thermodynamics in Chapter 23 as applied to a moving fluid. That study necessarily moves beyond the restrictions of equilibrium thermodynamics considered in Chapters 19 and 20, but only slightly. The key assumption we make in Chapter 23 is that each fluid element is locally within thermodynamic equilibrium. The assumption of local thermodynamic equilibrium allows us to bring forward the key facets of equilibrium thermodynamics to the nonequilibrium thermodynamics required for moving fluids.

Thermodynamics is a deep subject whose subtleties rarely cease to puzzle and amaze both the novice and expert. For some perspective, consider the following reflections from two giants of physics on the enduring and profound nature of thermodynamics.

Thermodynamics is a funny subject. The first time you go through it, you do not understand it at all. The second time you go through it, you think you understand it, except for one or two points. The third time you go through it, you know you do not understand it, but by that time you are so used to the subject it does not bother you anymore. *Attributed to Arnold Sommerfeld, unknown source*

A theory is the more impressive the greater the simplicity of its premises, the more different kinds of things it relates, and the more extended is its area of applicability. Therefore the deep impression which classical thermodynamics made upon me. It is the only physical theory of universal content concerning which I am convinced that, within the framework of the applicability of its basic concepts, it will never be overthrown. [Einstein \(1949\)](#)

Chapter 19

EQUILIBRIUM THERMODYNAMICS

We here study equilibrium thermodynamics following classical treatments, with emphasis on the needs for atmosphere and ocean fluid mechanics. Thermodynamics is conceptually subtle but technically straightforward, thus making this chapter relatively long on words yet brief on equations.

CHAPTER GUIDE

Our treatment follows [Callen \(1985\)](#), [Reif \(1965\)](#), chapter 2 of [Landau and Lifshitz \(1980\)](#), and chapter 2 of [Ebeling and Feistel \(2011\)](#). Mathematical tools required for thermodynamics include the basics of partial differential calculus from Chapter 2.

19.1 Conceptual foundations	408
19.1.1 Thermodynamic equilibrium	408
19.1.2 Exchanges between thermodynamic systems	409
19.1.3 Quasi-static processes	410
19.1.4 Extensive and intensive properties	410
19.1.5 Thermodynamic configuration space	411
19.1.6 Internal energy and total energy	411
19.1.7 Postulates of thermodynamics	412
19.2 Materially closed systems	413
19.2.1 First law of thermodynamics	413
19.2.2 The nature of working and heating	413
19.2.3 Mechanical work from pressure	414
19.2.4 Entropy and the quasi-static transfer of internal degrees of freedom	415
19.2.5 Gibbs' fundamental thermodynamic relation	415
19.2.6 Partial derivatives	416
19.2.7 Entropy and thermodynamic processes	417
19.2.8 Properties of thermodynamic equilibrium	418
19.3 Characterizing materially open systems	419
19.3.1 Euler's theorem for homogeneous functions	419
19.3.2 Homogeneous functions of degree one	420
19.3.3 Chemical potential and the Euler form	420
19.3.4 Molar mass and molar chemical potential	421
19.3.5 Chemical work and the Gibbs-Duhem relation	422
19.3.6 Gibbs potential	422
19.3.7 Extensive functions of (T, p, M_n)	423
19.4 Thermodynamic equilibrium with matter flow	424
19.5 Materially open systems with fixed total mass	425
19.5.1 Matter concentrations	425
19.5.2 Fundamental thermodynamic relation per unit mass	425

19.5.3	Seawater as a binary fluid	426
19.5.4	Further study	427
19.6	Thermodynamic potentials	427
19.6.1	Equations of state	427
19.6.2	Internal energy	428
19.6.3	Entropy	428
19.6.4	Enthalpy	429
19.6.5	Helmholtz free energy	430
19.6.6	Gibbs potential	430
19.6.7	Chemical potential and the Gibbs potential	431
19.7	Response functions	432
19.7.1	Specific heat capacities	433
19.7.2	Thermal expansion coefficient	433
19.7.3	Haline contraction coefficient	434
19.7.4	Speed of sound (acoustic) waves	434
19.8	Maxwell relations for single component fluids	434
19.8.1	Maxwell relation from internal energy	434
19.8.2	Summary of the Maxwell relations	435
19.9	Exercises	435

19.1 Conceptual foundations

In our study of thermodynamics, we are concerned with macroscopic fluid systems whose evolution tends toward states in which its properties are determined by intrinsic factors rather than depending on memory of previous external influences. These particular *macrostates* are known as *thermodynamic equilibria*. One aim for thermodynamics is the determination of a new thermodynamic equilibrium after the removal of a constraint. When a constraint is removed, the system moves through a sequence of macrostates as it evolves towards its new equilibrium, with the time evolution through such macrostates referred to as a *process*. Any macrostate is comprised of a huge number of microscopic degrees of freedom; i.e., *microstates*. The allure of thermodynamics is that we can describe macroscopic systems, and the process of moving from one thermodynamic equilibria to another, using just a handful of macroscopically measurable properties.

19.1.1 Thermodynamic equilibrium

Equilibrium thermodynamics is the study of physical systems in *thermodynamic equilibrium* and how these systems transit from one thermodynamic equilibrium state to another through quasi-static processes. We explore the defining characteristics of thermodynamic equilibrium within this chapter. At a basic level, a system in thermodynamic equilibrium will remain in that state for all time, with equilibrium dependent on the constraints imposed on the system. When such constraints are removed, then a system generally transitions to another equilibrium state. Note that “for all time” is a loaded term. More precisely, we mean “for a time extremely long compared to any time scale relevant to the physical system under consideration”, with such time scales considered in Section 19.1.3.

A system in thermodynamic equilibrium experiences no time changes to the system’s macroscopic properties. However, all dynamically steady states are not necessarily in thermodynamic equilibrium. For example, consider a region of fluid with nonzero heat fluxes yet with no heat flux convergence so the temperature of the region does not change. As we see in this chapter, a temporally constant temperature is a signature of a steady state whereas the flow of heat is the sign of thermodynamic disequilibrium. The distinction is sometimes subtle and always important.

To provide motivation for the study of thermodynamic equilibrium, consider an isolated system, defined as a physical system that does not exchange heat, matter, or mechanical forces with its surroundings, though possibly experiencing body forces such as from gravity.¹ Given sufficient time, all isolated systems will reach their thermodynamic equilibrium consistent with the constraints on that system. Geophysical fluids are routinely exposed to mechanical and thermal interactions with their surrounding environment, and as such as they are not isolated. Even so, it is useful to understand the basic properties of isolated systems and their corresponding thermodynamic equilibrium, as doing so provides the starting point for understanding how systems deviate from thermodynamic equilibrium. Furthermore, a fundamental assumption of thermodynamics applied to moving fluids (Chapter 23) is that each fluid element is in a local thermodynamic equilibrium, even while the macroscopic fluid does not reach a global thermodynamic equilibrium. Hence, we are motivated to study equilibrium thermodynamics since it forms the foundations for a study of moving fluids, even when those moving fluids are globally far from thermodynamic equilibrium.

19.1.2 Exchanges between thermodynamic systems

In the study of thermodynamics it is important to characterize how a physical system interacts with its surrounding environment through mechanical, thermal, and material interactions and exchanges. Infinitesimal fluid elements, and their accumulation into finite fluid regions, constitute the physical systems we are concerned with in this book.² We are concerned with systems that routinely interact mechanically with their surroundings so that the systems are mechanically open; i.e., they feel pressure from the surrounding environment. Hence, we here focus on characterizing how a physical system interacts thermally and materially with its surroundings.

- **THERMALLY OPEN (DIABATIC) AND MATERIALLY OPEN:** An open physical system exchanges matter, thermodynamic properties, and mechanical forces with its surrounding environment. All naturally occurring fluid systems are open in this manner.
- **THERMALLY OPEN (DIABATIC) AND MATERIALLY CLOSED:** We have occasion to consider a thermodynamic system that is mechanically and thermally open yet materially closed. Such systems maintain a fixed matter content yet exchange thermal and mechanical energy with their surrounding environment.
- **THERMALLY CLOSED (ADIABATIC) AND MATERIALLY CLOSED:** We sometimes consider a thermodynamic system that is both materially and thermally closed and yet mechanically open. In fluid mechanics, such systems constitute *material fluid parcels* (Section 14.3), defined as infinitesimal regions that maintain fixed matter and thermal properties yet move according to the mechanical forces acting on the parcel. A *perfect fluid* is a continuum of infinitesimal material fluid parcels.

Each of the above interactions is mechanically open, so that the thermodynamic system is exposed to mechanical forces, either contact forces such as pressure and friction or body forces such as gravity and Coriolis. For pedagogical purposes we first study the thermodynamics of fluid elements that are thermally open yet materially closed and then extend to fluid elements that are both thermally and materially open. As a somewhat overloaded terminology, “adiabatic” in fluid mechanics is often used for a system that is *both* thermally closed *and* materially closed. However, we maintain the distinction in our treatment to maintain consistency with the physics literature.

¹We define body and contact forces in Section 21.2 when studying Newton’s second law.

²See Section 14.3.4 for a reminder of how we define fluid elements.

19.1.3 Quasi-static processes

When extending equilibrium thermodynamics to the linear irreversible thermodynamics of moving fluid systems in Chapter 23, we make use of the huge time scale separation between molecular degrees of freedom and macroscopic degrees of freedom. We are led to define a *quasi-static process* as one that proceeds via an arbitrary number of intermediate equilibrium states. In fact, as formally defined (e.g., Section 4.2 of [Callen \(1985\)](#)), a quasi-static process is a locus of equilibrium states that can only be approximated by realistic processes occurring through steps that are each arbitrarily close to thermodynamic equilibrium. By formulating the notion of a quasi-static process, we are afforded a precise definition for intensive properties such as its temperature, pressure, and chemical potential, whereas such intensive properties are fuzzy concepts for systems out of thermodynamic equilibrium.³

A quasi-static process is a relevant idealization for our study of macroscopic fluid motion. We recognize this relevance by considering the time scale separation between macroscopic and microscopic motions. Recall from Section 13.3.5 that the time between molecular collisions is on the order of $t_{\text{collision}} \approx 10^{-9}$ s, with this time scale setting the time scale for molecular equilibration. In contrast, typical macroscopic processes occur on time increments on the order of $\Delta\tau_{\text{macro}} \sim 1$ s. Hence, we can safely assume that any macroscopic process arising in fluid flows, even turbulent flows, evolves through time increments that are much longer than the molecular collision time

$$\Delta\tau_{\text{macro}} \ggg t_{\text{collision}} \approx 10^{-9} \text{ s.} \quad (19.1)$$

We are thus led to the following conceptual framework for our treatment of fluid motion. Namely, we assume that the macroscopic motion of a fluid is comprised of the motion of a continuum of fluid elements that are, individually, in a thermodynamically equilibrated state on the time scale of the macroscopic motion. Hence, each fluid element evolves quasi-statically. So although any finite region of fluid is not necessarily in thermodynamic equilibrium (e.g., nonuniform temperature over macroscopic length scales), the individual fluid elements comprising any finite fluid region are in thermodynamic equilibrium. The justification for this foundational assumption is that the time scales for macroscopic fluid motion, even for highly turbulent motion, are many orders of magnitude longer than the molecular time scales that bring about local thermodynamic equilibrium.

19.1.4 Extensive and intensive properties

In describing thermodynamic systems we characterize properties according to whether they are *extensive* or *intensive*. Extensive properties scale with the size of the system, with examples including mass, internal energy and entropy. Mathematically, we say that extensive properties scale with a power 1 with the size of the system (we return to this point in Section 19.3.1).

A *homogeneous fluid* is one in which all *intensive properties* are identical, with temperature, pressure, and chemical potential the canonical examples. This characteristic of intensive properties contrasts to extensive properties. Hence, intensive properties do not scale with the size of a system. That is, intensive properties are scale invariant and thus scale with power 0 as the size of the system changes. Intensive properties describe possible gradients within a thermodynamic system. In the absence of an externally imposed force field such as gravity, intensive properties are

³Some authors do not make a distinction between a quasi-static process and a reversible process. Our treatment follows [Callen \(1985\)](#) (see his sections 4.2 and 4.3) and [Reif \(1965\)](#) (see his sections 2.9 and 2.10), whereby reversible processes are subsets of quasi-static processes. Namely, a reversible process is a quasi-static process that occurs without net entropy change (see Section 19.2.7), and yet not all quasi-static processes are reversible since entropy can increase in a quasi-static process.

uniform for systems in thermodynamic equilibrium (we show this property in Sections 19.2.8 and 20.1.2). However, as discussed in Section 20.1, hydrostatic balance is realized in thermodynamic equilibrium for a fluid in an externally imposed gravity field, in which case pressure is not uniform.

Extensive and intensive properties come as conjugate pairs in thermodynamics, whereby intensive properties always multiply their conjugate extensive property (e.g., pressure-volume and temperature-entropy) when appearing in the various forms of the first law of thermodynamics. In this chapter, extensive properties are labeled with a superscript e (except for the mass and volume), with this label *not* a tensor index. In Section 19.5 we introduce the internal energy per mass and entropy per mass, as doing so is most convenient when studying thermodynamic systems of fixed mass. In this manner we can convert the extensive properties to their specific (per mass) form in which case we drop the e superscript. It is the specific form of extensive properties that provides a straightforward transfer to the study of constant mass fluid elements.

19.1.5 Thermodynamic configuration space

Equilibrium thermodynamics is not concerned with points in geographical space. Rather, it characterizes a physical system through specifying a suite of continuous thermodynamic properties, and studying how those processes change under changes in the constraints. Thermodynamic properties define coordinates for a point within *thermodynamic configuration space*. Even though one commonly encounters thermodynamic diagrams with orthogonal axes specifying values of thermodynamic properties, there is no notion of distance or angle between points in thermodynamic configuration space since there is no metric structure. Mathematically, we say that thermodynamic configuration space comprises a *differentiable manifold*.⁴

19.1.6 Internal energy and total energy

As discussed in Chapter 13, there are a huge number of microscopic (molecular) degrees of freedom that are averaged over when describing a fluid as a continuous media. *Internal energy* embodies the energy of microscopic degrees of freedom not explicitly considered in a macroscopic continuum treatment. Internal energy is not readily accessed or harnessed, which contrasts to the mechanical energy of the macroscopic motion.

For a simple ideal gas (Section 20.4), internal energy arises from the translational kinetic energy of molecular motion, as well as degrees of freedom associated with rotation and vibration. Kinetic theory studies of a simple ideal gas suggests that we conceive of internal energy as *thermal energy*. That is, we idealize molecules as point masses whose kinetic energy is directly related to temperature, and with the internal energy of an ideal gas directly proportional to temperature. However, for a general fluid, particularly for liquids, the internal energy is far more than a measure of the kinetic energy of molecules, as real molecules exhibit intermolecular potential energy arising from molecular interactions. In general, the concept of internal energy is rather slippery. We are thus motivated to sidestep internal when getting serious about quantitative notions, such as when studying energetics of fluid flow in Chapter 23. We do so by appealing to the conservation of *total energy* as postulated in Section 19.1.7. Even so, to lay the foundations we largely focus on internal energy in this chapter.

⁴A summary of the mathematical structure of equilibrium thermodynamics can be found in [this online tutorial from Salamon et al.](#) Note that there are some formulations of thermodynamics that do introduce a metric through properties of the entropy. In so doing, these formulations transform the differentiable manifold to a Riemannian manifold. There are tradeoffs when doing so, with [Andresen et al. \(1988\)](#) offering a survey of the tradeoffs. Here, we follow the approach of Gibbs as articulated in the books by [Reif \(1965\)](#) and [Callen \(1985\)](#).

19.1.7 Postulates of thermodynamics

Thermodynamics is not a first principles theory, though it does have its roots in statistical mechanics. We follow [Callen \(1985\)](#) by building thermodynamics from a set of postulates from which deductive results are derived. The following postulates render a logical basis for the subject, with the bulk of this chapter exemplifying these postulates and developing implications.

- * **THERMODYNAMIC EQUILIBRIUM:** There exists states of thermodynamic equilibrium that are completely characterized macroscopically by a few extensive properties, including internal energy, volume, and mass (or mole number). For each thermodynamic equilibrium there exists a scalar intensive property, called the *thermodynamic temperature*, or more briefly the temperature, that is uniquely defined. Furthermore, the temperature has the same value for two systems in thermodynamic equilibrium with one another.
- * **ZEROTH LAW OF THERMODYNAMICS:** When two systems, A and B , are each separately in thermodynamic equilibrium with a third system, C , then the systems A and B are also in thermodynamic equilibrium with one another.
- * **MAXIMUM ENTROPY:** *Entropy* is an extensive property of a macrostate. The values assumed by the other extensive properties are those that maximize the entropy over the manifold of constrained thermodynamic equilibrium states. This postulate is fundamental to how we determine properties of thermodynamic equilibria.
- * **ENTROPY INCREASES:** The entropy of a composite macroscopic system is additive over the constituent subsystems. Furthermore, entropy is a continuous and differential function that is a monotonically increasing function of the internal energy. This postulate is fundamental to how we use thermodynamics for composite systems such as a fluid.
- * **TOTAL ENERGY IS CONSERVED:** The total energy of a thermodynamic system is locally (in space and time) conserved while undergoing a thermodynamic process. This property constitutes the *first law of thermodynamics*. For a macroscopic fluid, total energy is the sum of the internal energy arising from microscopic degrees of freedom plus the mechanical energy of macroscopic degrees of freedom. In this chapter, as well as Chapter 20, we are mostly concerned with internal energy, whereas Chapters 21 and 23 extend the discussion to include mechanical energy. Space and time locality of total energy conservation means that physical processes are not allowed in which total energy disappears from one point in space or time only to reappear at a distant point. As a corollary, we are afforded a local budget equation for total energy whereby energy transferred from one form to another, with particular forms of this budget equation a topic of Chapter 23. Note that energy is well defined for both microstates and macrostates, whereas entropy is only defined for macrostates.
- * **THIRD LAW OF THERMODYNAMICS:** Internal energy and entropy are extensive scalar quantities that are finite for finite systems and bounded from below. In the limit of zero thermodynamic temperature for single-phase systems (single state of matter), the derivatives of entropy with respect to extensive variables disappear asymptotically. Many take the zero temperature limit to have zero entropy, though statistical fluctuations break this assumption (see page 51 of [Ebeling and Feistel \(2011\)](#) for discussion). We have little direct use for the third law, though it takes on an important role when considering quantum statistical mechanics.

The two postulates concerning entropy (entropy maximum and entropy increasing) constitute the *second law of thermodynamics*. Statistical mechanics reveals the statistical nature of entropy and the second law. In Sections 19.2.8 and 20.1.2, we see how it provides the basis for determining properties at thermodynamic equilibrium, and for how systems approach equilibrium. We make further use of the second law in Chapter 23 to constrain fundamental processes acting in a multi-component fluid.

19.2 Materially closed systems

We are now ready to apply the above foundational concepts by studying the thermodynamics of a physical system that is closed materially.

19.2.1 First law of thermodynamics

The first law of thermodynamics for a materially closed system establishes a relationship between infinitesimal changes of internal energy of a physical system, the work done to or by the system, and the thermal energy transferred between the system and its surrounding environment. The first law takes on the mathematical form

$$dJ^e = dW + dQ \quad \Leftarrow \text{materially closed.} \quad (19.2)$$

In this equation, dJ^e is the exact differential of the internal energy; dW is the change in internal energy due to work applied to the system (*working*); and dQ is the internal energy change due to thermal energy transferred to the system (*heating*). We only have occasion to study mechanical work in this book, though note that there are other forms such as those arising from electromagnetic forces.

The first law of thermodynamics is a statement of energy conservation for a physical system, where energy changes arise from working and heating applied to the system or by the system. We are only interested in changes to the energy, with the absolute value of the energy of no concern. For the present consideration, the relevant energy is just the internal energy since we here ignore mechanical energy associated with moving fluids. We relax that assumption in Chapter 23 where we add mechanical energy of macroscopic motion (Section 23.3) to internal energy, thus forming the total energy of a moving fluid.

19.2.2 The nature of working and heating

Working and heating are both path-dependent thermodynamic processes that transform a system from one thermodynamic state to another. That is, working and heating represent *path functions* whose value depends on their history. They are mathematically represented by inexact differentials as denoted by the \tilde{d} symbol. It is remarkable that the first law in equation (19.5) shows that the sum of two inexact differentials equals to an exact differential which, in the absence of macroscopic motion, is the exact differential of the internal energy.

The internal energy is a *state function* that is a property of the thermodynamic state of a system and not a function of the path history taken to reach that state. The term *thermodynamic potential* is synonymous with state function. It follows that if the internal energy change occurs in the absence of heating then the working process must occur as a path independent process. The converse holds if internal energy changes without any working. Furthermore, the first law (19.5) allows us to decompose changes to internal energy according to mechanical and thermal contributions. However, it is not possible to perform that decomposition for the internal energy itself.

Working and heating denote actions applied to a system (verbs) rather than properties of a system (nouns). They are energy *in transition* that arise at the boundary of a thermodynamic system. We raise this somewhat pedantic yet subtle point since the terms “work” and “heat” are often used instead of “working” and “heating”. Indeed, we will often make use of that language in this book. However, such usage should be used with care as it can spuriously lead one to seek information concerning the “work content” or “heat content” of a physical system; i.e., to incorrectly consider work and heat as state properties (i.e., nouns). Rather, in thermodynamics we only consider the work imparted to change a system’s energy (working), or likewise the thermal energy used to change a system (heating).

These conceptual points are particularly relevant when asking questions about the heat transported by a fluid (with dimensions energy per time and SI units of Watt = Joule per second). In the analysis of a heat budget, it is tempting to define the “heat content” of a fluid element or fluid region according to its temperature, mass, and heat capacity. But the notion of heat content spuriously conflates a thermodynamic process whereby a system moves from one state to another (heating) with a thermodynamic state property (e.g., enthalpy, which is a property of the state; see Section 19.6.4). Furthermore, any definition of heat content is ambiguous due to the arbitrariness of the temperature scale; i.e., heat content based on the Celsius scale is distinct from that based on the Kelvin scale. Therefore, when working with heat transport, care should be exercised if also including the notion of heat content. One way to detect an error is to ask whether a particular conclusion is modified by changing the temperature scale. If so, then one should revisit assumptions of the analysis since the results might be unphysical.

19.2.3 Mechanical work from pressure

As forces do work on a physical system they change its internal energy and mechanical energy. We are here concerned only with the effects on internal energy, though note that mechanical changes that alter internal energy are generally balanced by compensating changes to mechanical energy (see Section 23.5). One way to perform mechanical work is via changes to the volume of a fluid element through the action of pressure (a contact force per area) on the boundary of the fluid element. For example, if a fluid element increases its volume, it must do work against the surrounding environment to overcome the compressive force from pressure.

When volume changes occur quasi-statically, then we can write the *pressure work* in the mathematical form

$$dW = -p dV, \quad (19.3)$$

where p is the pressure that acts on the boundaries of the fluid element. The assumption that the mechanical process is quasi-static allows us to unambiguously define pressure acting on the system, and thus to write equation (19.3) for the work. The negative sign arises since the compression of a fluid element into a smaller volume, $dV < 0$, requires positive mechanical work be applied to the fluid element, $dW > 0$. The mathematical form of pressure work derives from the general form of mechanical work given by

$$\text{work} = \text{force} \times \text{distance} = \text{force}/\text{area} \times \text{distance} \times \text{area} = \text{force}/\text{area} \times \text{volume}. \quad (19.4)$$

Stated alternatively, we note that pressure is a force per unit area acting on a surface, and the product of the surface area and its normal displacement is the volume swept out during a time increment.

We offer the following points in regards to this form of mechanical work.

- Pressure is an intensive property that measures the *intensity* of a force (per area) that is conjugate to the extensive property, V . In general, work applied to a thermodynamic

system, thus leading to a change in the internal energy, takes on the form of an intensive property multiplying the change of an extensive property.

- From a mathematical perspective, pressure is the *integrating factor* that connects the inexact (path dependent) differential dW to the exact differential dV . We studied the mathematics of inexact differentials in Section 2.8.
- For a quasi-static process, pressure changes the internal energy of a fluid through the pressure work according to equation (19.3). As seen in Section 23.3.1, pressure also changes the kinetic energy of a moving fluid by changing the fluid speed. When combining the internal energy and mechanical energy budgets in Section 23.5, we see how pressure affects the total energy of a fluid element.
- Surface tension acting on fluid interfaces can give rise to mechanical work. However, we generally ignore surface tension in this book since it is negligible for scales larger than a few centimeters (see Section 22.11).

19.2.4 Entropy and the quasi-static transfer of internal degrees of freedom

The internal energy of a thermodynamic system can change when the molecular degrees of freedom are energized. For a materially closed system whose internal energy changes in a quasi-static manner, we consider the thermal energy change as relates to entropy changes via

$$dQ = T dS^e \quad \text{materially closed system.} \quad (19.5)$$

T is the thermodynamic temperature (measured relative to absolute zero) and it is an intensive variable whereas S^e is the extensive form of entropy. Entropy is an extensive state function so that T provides the integrating factor connecting the inexact differential dQ to the exact differential dS^e . A nonzero dQ in a geophysical fluid can arise from radiative fluxes external to the fluid element; internal sources from friction; and the exchange of thermal energy through the mixing of fluid properties. Since heating has dimensions of energy, the entropy has dimensions of energy per temperature.

19.2.5 Gibbs' fundamental thermodynamic relation

We summarize the discussion of this section by writing the first law for quasi-static materially closed processes

$$dJ^e = -p dV + T dS^e \iff \text{quasi-static materially closed processes.} \quad (19.6)$$

This equation is known as the *Gibbs relation* or more commonly the *fundamental thermodynamic relation* for quasi-static materially closed processes moving from one thermodynamic equilibrium state to another. This relation suggests that we interpret minus the pressure as the amount of internal energy required to add one unit of volume to the system while holding entropy fixed. Likewise, temperature is the internal energy required to add one unit of entropy to the system while holding volume fixed.

The fundamental thermodynamic relation (19.6) is an integrable differential equation, with a solution found by performing a path integral within thermodynamic configuration space. The solution provides one of the extensive properties, such as internal energy or entropy, as a function of the other extensive properties. However, we generally do not require this solution since it is the differentials, as determined by the Gibbs relation, that are sufficient for determining practical thermodynamic properties such as temperature, pressure, and chemical potential.

All differentials within the fundamental thermodynamic relation (19.6) are exact differentials of state functions. This property is a result of assuming the thermodynamic processes are quasi-static, in which case we can determine the integrating factors pressure and temperature to thus replace the inexact differentials dW and dQ with exact differentials. Even with the quasi-static restriction, equation (19.6) offers great utility (with its extension to materially open systems given in Section 19.5). Since we are only concerned with quasi-static changes to fluid elements in this book, the fundamental thermodynamic relation (19.6) provides the central expression of the first law of thermodynamics for our purposes.

It follows from the first law expression in equation (19.6) that the internal energy is a natural function of volume and entropy

$$d\mathcal{I}^e = -p dV + T dS^e \implies \mathcal{I}^e = \mathcal{I}^e(V, S^e). \quad (19.7)$$

Conversely, the entropy for a materially closed system is naturally a function of volume and internal energy

$$T dS^e = d\mathcal{I}^e + p dV \implies S^e = S^e(V, \mathcal{I}^e). \quad (19.8)$$

We see that both of the extensive state functions, \mathcal{I}^e and S^e , are functions of extensive properties, with such dependence having implications for the scaling discussed in Section 19.3.2. Furthermore, we note that both \mathcal{I}^e and S^e are functions of the volume of a system, but not of the shape. This behavior is strictly only appropriate for fluids, and it ignores effects from interfaces. Both of these assumptions are suitable for our study of geophysical fluids.

19.2.6 Partial derivatives

The fundamental thermodynamic relation (19.7) appears in terms of internal energy, which is written as a natural function of the extensive properties volume and entropy. We arrive at two partial derivative identities by expanding the exact derivative of internal energy

$$d\mathcal{I}^e = \left[\frac{\partial \mathcal{I}^e}{\partial V} \right]_{S^e, M} dV + \left[\frac{\partial \mathcal{I}^e}{\partial S^e} \right]_{V, M} dS^e \quad (19.9)$$

and then identifying this expression with the fundamental thermodynamic relation (19.7) to reveal

$$\left[\frac{\partial \mathcal{I}^e}{\partial S^e} \right]_{V, M} = T \quad (19.10)$$

$$\left[\frac{\partial \mathcal{I}^e}{\partial V} \right]_{S^e, M} = -p. \quad (19.11)$$

Each equation relates an intensive property (right hand side) to the partial derivative of internal energy with respect to an extensive property. Furthermore, since each of the extensive properties is a homogeneous function of degree one, then it follows that the intensive properties are homogeneous functions of degree zero. That is, the intensive properties, T and p , do not scale with the size of the system. Rather, intensive properties are scale invariant. We arrive at analogous partial derivative identities for entropy, $S^e(V, \mathcal{I}^e)$, by expanding its exact differential and then comparing

to equation (19.8)

$$\left[\frac{\partial S^e}{\partial J^e} \right]_{V,M} = \frac{1}{T} \quad (19.12)$$

$$\left[\frac{\partial S^e}{\partial V} \right]_{J^e,M} = \frac{p}{T}. \quad (19.13)$$

Recall that partial derivatives are defined with the complement variables held fixed during the differentiation. Hence, so long as we are clear about functional dependence, extra subscripts such as those exposed in equations (19.10)-(19.11) are not needed for the partial derivatives. Nonetheless, traditional thermodynamic notation exposes all of the subscripts in order to remain explicit about the dependent and independent variables. Such notation, though clumsy, can be essential when in the midst of manipulations with thermodynamic potentials and their derivatives.

19.2.7 Entropy and thermodynamic processes

A *reversible process* can, at each stage, go either forward or backward in time so that there is symmetry in time. In the absence of non-conservative forces (e.g., dissipation such as friction), Newton's dynamical laws are reversible. For example, one observes nothing unphysical about the motion of an ideal pendulum with time moving backward rather than forward.⁵

From a thermodynamic perspective, a reversible process does not alter the net entropy of a physical system plus its surrounding environment. Reversible thermodynamic processes are quasi-static and yet not all quasi-static processes are reversible. For example, a process that involves friction can evolve quasi-statically and yet frictional processes, as with any dissipative process, increases entropy. When the net entropy changes, we say the process occurs *irreversibly*, with the second law of thermodynamics stating that the net entropy change is positive. Quasi-static is a property of how a system changes, whereas reversibility is a statement about how both the system and its surrounding environment change. Any natural process is irreversible, with irreversibility providing an arrow for the evolution of physical systems; i.e., it breaks the symmetry between past and future.

The entropy differential for a quasi-static process in a materially closed system is given by $dS^e = dQ/T$, with $T > 0$ (recall T is the Kelvin thermodynamic temperature) so that the entropy differential has the same sign as the heating differential, and entropy for a materially closed system remains unchanged in the absence of heating. The idealization of a heat bath allows us to perform reversible heating; i.e., heating without change in net entropy for a thermodynamic system plus the heat bath. Heat baths are held at a fixed temperature, which is the idealization of the case when the surrounding environment is arbitrarily larger than the thermodynamic system under consideration. Now imagine exchanging heat between a thermodynamic system and a series of heat baths to progressively alter the system's temperature by differential dT . In each exchange of heat, the entropy of the system plus heat bath is constructed to remain unchanged since we are exchanging an equal magnitude of entropy between them

$$dS_{\text{net}}^e = dS_{\text{system}}^e + dS_{\text{bath}}^e = dQ/T - dQ/T = 0. \quad (19.14)$$

To reverse the process, we merely reverse the heat exchanges between the thermodynamic system and the heat baths.

As noted above, when any thermodynamic process occurs irreversibly there is a net increase in entropy of the universe, which is a statement of the second law of thermodynamics. In statistical

⁵We briefly discussed time-reversal symmetry in Section 12.3.

mechanics, entropy is computed by counting the number of microstates accessible to any given macrostate. Reversible processes do not modify the number of accessible microstates so there is zero change in the entropy. In contrast, irreversible processes increase entropy by increasing the number of accessible microstates.

19.2.8 Properties of thermodynamic equilibrium

Consider two systems labelled⁶ by α and β that are separately in thermodynamic equilibrium with internal energies, \mathcal{I}_α^e , \mathcal{I}_β^e , and volumes, V_α , V_β . Allow these two systems to interact mechanically and thermally, but do not allow for any exchange of matter. Furthermore, assume that the interactions conserve the total internal energy and volume of the combined system so that the system maintains the following constraints during the interaction process

$$d(\mathcal{I}_\alpha^e + \mathcal{I}_\beta^e) = 0 \quad \text{and} \quad d(V_\alpha + V_\beta) = 0. \quad (19.15)$$

When the composite system reaches thermodynamic equilibrium, the entropy maximum postulate forming the second law of thermodynamics (Section 19.1.7) means that

$$d\mathcal{S}^e = d(\mathcal{S}_\alpha^e + \mathcal{S}_\beta^e) = 0 \quad (19.16)$$

for the combined composite system. Importantly, this condition holds only at equilibrium, whereas the constraints (19.15) hold throughout the process of reaching equilibrium. From equation (19.8) we know that entropy is naturally a function of volume and internal energy so that

$$d\mathcal{S}^e = \left[\frac{\partial \mathcal{S}_\alpha^e}{\partial \mathcal{I}_\alpha^e} \right]_{V_\alpha, M_\alpha} d\mathcal{I}_\alpha^e + \left[\frac{\partial \mathcal{S}_\alpha^e}{\partial V_\alpha} \right]_{\mathcal{I}_\alpha^e, M_\alpha} dV_\alpha + \left[\frac{\partial \mathcal{S}_\beta^e}{\partial \mathcal{I}_\beta^e} \right]_{V_\beta, M_\beta} d\mathcal{I}_\beta^e + \left[\frac{\partial \mathcal{S}_\beta^e}{\partial V_\beta} \right]_{\mathcal{I}_\beta^e, M_\beta} dV_\beta \quad (19.17a)$$

$$= \frac{1}{T_\alpha} d\mathcal{I}_\alpha^e + \frac{p_\alpha}{T_\alpha} dV_\alpha + \frac{1}{T_\beta} d\mathcal{I}_\beta^e + \frac{p_\beta}{T_\beta} dV_\beta \quad (19.17b)$$

$$= \left[\frac{1}{T_\alpha} - \frac{1}{T_\beta} \right] d\mathcal{I}_\alpha^e + \left[\frac{p_\alpha}{T_\alpha} - \frac{p_\beta}{T_\beta} \right] dV_\alpha, \quad (19.17c)$$

where we used the partial derivative identities (19.12) and (19.13) for the second equality, and the constraints (19.15) for the final equality. Again, $d\mathcal{S}^e = 0$ at thermodynamic equilibrium, and this condition holds for arbitrary and independent $d\mathcal{I}_\alpha^e$ and dV_α . We are thus led to the thermal and mechanical equilibrium conditions

$$T_\alpha = T_\beta \quad \text{and} \quad p_\alpha = p_\beta \quad \text{at thermodynamic equilibrium.} \quad (19.18)$$

That is, the temperature and pressure are uniform when the composite system reaches thermodynamic equilibrium.⁷

To understand how the two systems thermally approach thermodynamic equilibrium, assume the volumes of the two systems are fixed so that there is no mechanical work from pressure. Furthermore, assume the two systems are initially separated by an adiabatic wall with initial temperatures $T_\alpha^{\text{init}} > T_\beta^{\text{init}}$. Now allow for the flow of heat by switching from an adiabatic wall to a diathermal wall. Since the temperature differs for the two systems, they are mutually out of equilibrium. Heat flows in a manner to bring the two systems into equilibrium, during which time entropy of the composite system increases. At the new equilibrium, temperature is uniform

⁶The labels α and β are not tensor labels. Instead, they merely label the system under consideration.

⁷As seen in Chapter 20, pressure at thermodynamic equilibrium is not a uniform constant for a system within a gravity field.

and entropy has reached its maximum within the constraints imposed on the composite system. At a time instant after the wall changes from adiabatic to diathermal, the infinitesimal entropy change takes the form

$$dS^e = \left[\frac{1}{T_\alpha^{\text{init}}} - \frac{1}{T_\beta^{\text{init}}} \right] dJ_\alpha^e > 0, \quad (19.19)$$

where the inequality follows from the second law of thermodynamics (Section 19.1.7). If $T_\alpha^{\text{init}} > T_\beta^{\text{init}}$, then an increase in entropy requires $dJ_\alpha^e < 0$, which means that heat leaves the system α and flows to the system β . That is, as the composite system approaches thermodynamic equilibrium, heat flows from the region with higher temperature to the region with lower temperature. This result, deduced from the second law of thermodynamics, accords with common experience.

Further to the time scale for equilibration, we note that mechanical equilibrium (pressure equality) generally arises much sooner than thermal equilibrium (temperature equality). The reason is that mechanical equilibrium is facilitated by force imbalances that lead to macroscopic motion (e.g., acoustic waves), whereas thermal equilibrium arises from microscopic motion (e.g., molecular diffusion). This time scale separation means that real fluid systems are far closer to mechanical equilibrium than thermal equilibrium.

19.3 Characterizing materially open systems

A thermodynamic system is generally open to the transfer of matter across its boundaries. We here summarize methods used to characterize systems and processes that allow for the movement of matter.

19.3.1 Euler's theorem for homogeneous functions

Consider a suite of Q independent variables, X_1, X_2, \dots, X_Q , and an arbitrary function of these variables, $F(X_1, X_2, \dots, X_Q)$. We say that this function is a *homogeneous function* of degree γ if the following property holds

$$F(\lambda X_1, \lambda X_2, \dots, \lambda X_Q) = \lambda^\gamma F(X_1, X_2, \dots, X_Q), \quad (19.20)$$

with λ an arbitrary scalar. The left hand side is the function evaluated with each of the independent variables scaled by the same number, λ . The right hand side is the function evaluated with the unscaled variables, but multiplied by the scale raised to the power γ . A particularly remarkable and useful property of such functions can be found by taking $\partial/\partial\lambda$ on both sides of the identity (19.20). The left hand side has the following partial derivative, as found through the chain rule

$$\begin{aligned} \frac{\partial F(\lambda X_1, \lambda X_2, \dots, \lambda X_Q)}{\partial \lambda} &= \frac{\partial F(X_1, X_2, \dots, X_Q)}{\partial X_1} \frac{\partial(\lambda X_1)}{\partial \lambda} + \dots + \frac{\partial F(X_1, X_2, \dots, X_Q)}{\partial X_Q} \frac{\partial(\lambda X_Q)}{\partial \lambda} \\ &= \sum_{q=1}^Q \left[\frac{\partial F(X_1, X_2, \dots, X_Q)}{\partial X_q} \right]_{X_r \neq q} X_q \end{aligned} \quad (19.21)$$

The derivative of the right hand side of equation (19.20) is given by

$$\frac{\partial[\lambda^\gamma F(X_1, X_2, \dots, X_Q)]}{\partial \lambda} = \gamma \lambda^{\gamma-1} F(X_1, X_2, \dots, X_Q). \quad (19.22)$$

Bringing these results together leads to *Euler's theorem* for homogeneous functions

$$\sum_{q=1}^Q X_q \left[\frac{\partial F(X_1, X_2, \dots, X_Q)}{\partial X_q} \right]_{X_r \neq q} = \gamma \lambda^{\gamma-1} F(X_1, X_2, \dots, X_Q). \quad (19.23)$$

Intensive thermodynamic properties are homogeneous functions of degree $\gamma = 0$, meaning they are scale invariant. For example, a bucket of homogeneous water has the same temperature whether or not we remove an arbitrary sample of the water. In contrast, as discussed below, extensive thermodynamic properties are homogeneous functions of degree $\gamma = 1$.

19.3.2 Homogeneous functions of degree one

Both the internal energy, \mathcal{I}^e , and entropy, \mathcal{S}^e , are extensive properties of a fluid system. Consequently, the transfer of matter across the system boundaries leads to an additive change in \mathcal{I}^e and \mathcal{S}^e . The internal energy and entropy thus have their natural functional dependencies (19.7) and (19.8) extended to include the matter content

$$\mathcal{I}^e = \mathcal{I}^e(V, \mathcal{S}^e, M_n) \quad \text{and} \quad \mathcal{S}^e = \mathcal{S}^e(V, \mathcal{I}^e, M_n), \quad (19.24)$$

where the M_n argument is shorthand for M_1, M_2, \dots, M_N for the N matter constituents.⁸

What happens when we scale the system by an arbitrary parameter λ ? Under this scale operation, the extensive variables, \mathcal{I}^e , \mathcal{S}^e , as well as the volume, V , and masses, M_n , scale by the same scale factor. The relation (19.24) thus leads to the scaling

$$\lambda \mathcal{I}^e(V, \mathcal{S}^e, M_n) = \mathcal{I}^e(\lambda V, \lambda \mathcal{S}^e, \lambda M_n) \quad \text{and} \quad \lambda \mathcal{S}^e(V, \mathcal{I}^e, M_n) = \mathcal{S}^e(\lambda V, \lambda \mathcal{I}^e, \lambda M_n), \quad (19.25)$$

thus revealing that $\mathcal{I}^e(V, \mathcal{S}^e, M_n)$ and $\mathcal{S}^e(\lambda V, \lambda \mathcal{I}^e, \lambda M_n)$ are homogeneous functions of degree one. Making use of Euler's theorem (19.23) with $\gamma = 1$ leads to

$$\mathcal{I}^e(V, \mathcal{S}^e, M_n) = V \left[\frac{\partial \mathcal{I}^e}{\partial V} \right]_{\mathcal{S}^e, M_n} + \mathcal{S}^e \left[\frac{\partial \mathcal{I}^e}{\partial \mathcal{S}^e} \right]_{V, M_n} + \sum_{n=1}^N M_n \left[\frac{\partial \mathcal{I}^e}{\partial M_n} \right]_{V, \mathcal{S}^e, M_{m \neq n}} \quad (19.26a)$$

$$\mathcal{S}^e(V, \mathcal{I}^e, M_n) = V \left[\frac{\partial \mathcal{S}^e}{\partial V} \right]_{\mathcal{I}^e, M_n} + \mathcal{I}^e \left[\frac{\partial \mathcal{S}^e}{\partial \mathcal{I}^e} \right]_{V, M_n} + \sum_{n=1}^N M_n \left[\frac{\partial \mathcal{S}^e}{\partial M_n} \right]_{V, \mathcal{I}^e, M_{m \neq n}}. \quad (19.26b)$$

These are very special expressions for the internal energy and entropy that are of great use throughout thermodynamics.

19.3.3 Chemical potential and the Euler form

We can further massage the results (19.26a) and (19.26b) by making use of the partial derivative identities from Section 19.2.6 to render

$$\mathcal{I}^e = -pV + T\mathcal{S}^e + \sum_{n=1}^N M_n \left[\frac{\partial \mathcal{I}^e}{\partial M_n} \right]_{V, \mathcal{S}^e, M_{m \neq n}} \quad (19.27)$$

$$T\mathcal{S}^e = pV + \mathcal{I}^e + \sum_{n=1}^N T M_n \left[\frac{\partial \mathcal{S}^e}{\partial M_n} \right]_{V, \mathcal{I}^e, M_{m \neq n}}. \quad (19.28)$$

⁸Note that in this subsection the subscript refers to the matter constituents, $n = 1, \dots, N$, whereas in Section 19.3.1 we used $q = 1, \dots, Q$ to label the number of independent variables.

Self-consistency requires

$$\left[\frac{\partial \mathcal{J}^e}{\partial M_n} \right]_{V,S^e} = -T \left[\frac{\partial S^e}{\partial M_n} \right]_{V,\mathcal{J}^e, M_{m \neq n}}, \quad (19.29)$$

which motivates defining the *chemical potential*

$$\mu_n \equiv \left[\frac{\partial \mathcal{J}^e}{\partial M_n} \right]_{V,S^e, M_{m \neq n}} = -T \left[\frac{\partial S^e}{\partial M_n} \right]_{V,\mathcal{J}^e, M_{m \neq n}} \quad (19.30)$$

thus leading to

$$\mathcal{J}^e = T S^e - p V + \sum_{n=1}^N \mu_n M_n \iff T S^e = \mathcal{J}^e + p V - \sum_{n=1}^N \mu_n M_n. \quad (19.31)$$

These are the *Euler forms* for the internal energy and entropy.

By definition, the chemical potential, μ_n , is an intensive property that measures the change in the internal energy, \mathcal{J}^e , when altering the mass, M_n , of the constituent n , while fixing the entropy, volume, and mass of the other components. Equivalently, it is minus the temperature weighted change in the entropy, S^e , when altering the mass, M_n while fixing the volume, internal energy, and mass of the other components. We can define a chemical potential for a single component system, in which it is the change arising from altering the mass of the system. Despite its name, the chemical potential does not necessarily refer to the existence of chemical reactions, though we note that it does appear prominently in the thermodynamics of chemical reactions ([Atkins and de Paula, 2006](#)).

19.3.4 Molar mass and molar chemical potential

It is sometimes convenient to write the mass of a constituent as the product of the number of moles, N_n , and the mass per mole, \mathfrak{M}_n (the *molar mass*), so that

$$M_n = N_n \mathfrak{M}_n \quad \text{no implied sum.} \quad (19.32)$$

In this way, an infinitesimal mass change is given by

$$dM = \sum_{n=1}^N dM_n = \sum_{n=1}^N d(N_n \mathfrak{M}_n) = \sum_{n=1}^N \mathfrak{M}_n dN_n, \quad (19.33)$$

so that mass changes are signalled by changes in the number of moles. We furthermore note the identity (no implied sum)

$$M_n \mu_n = M_n \left[\frac{\partial \mathcal{J}^e}{\partial M_n} \right]_{V,S^e, M_{m \neq n}} = N_n \mathfrak{M}_n \left[\frac{\partial \mathcal{J}^e}{\partial (N_n \mathfrak{M}_n)} \right]_{V,S^e, N_{m \neq n}} = N_n \tilde{\mu}_n, \quad (19.34)$$

where we defined the molar chemical potential determined according to mole number

$$\tilde{\mu}_n = \left[\frac{\partial \mathcal{J}^e}{\partial N_n} \right]_{V,S^e, N_{m \neq n}} = \mathfrak{M}_n \mu_n. \quad (19.35)$$

We are similarly led to the identities (no implied sum)

$$M_n d\mu_n = N_n d\tilde{\mu}_n \quad \text{and} \quad \mu_n dM_n = \tilde{\mu}_n dN_n. \quad (19.36)$$

19.3.5 Chemical work and the Gibbs-Duhem relation

Changes to the matter composition of a system changes the internal energy through *chemical work*, written as $d\mathcal{C}$. If the changes to the matter composition occur quasi-statically then the chemical work is written

$$d\mathcal{C} = \sum_{n=1}^N \mu_n dM_n = \sum_{n=1}^N \tilde{\mu}_n dN_n \quad (19.37)$$

so that the chemical potential is the integrating factor connecting the inexact differential measuring the chemical work to the exact differential change in matter content. The chemical potential is the energy absorbed or released due to an infinitesimal change in the matter content. As shown in Section 20.1.2, matter in a mixture tends to move from regions of high chemical potential to lower chemical potential, thus motivating the name “potential” in analog to the gravitational potential.

The inclusion of chemical work brings the first law of thermodynamics to the form

$$d\mathcal{I}^e = d\mathcal{W} + d\mathcal{Q} + d\mathcal{C} \quad \text{materially open} \quad (19.38a)$$

$$d\mathcal{I}^e = -p dV + T d\mathcal{S}^e + \sum_{n=1}^N \mu_n dM_n \quad \text{quasi-static and materially open.} \quad (19.38b)$$

Use of the quasi-static form of the first law (19.38b) along with the differential of the result (19.31) leads to the *Gibbs-Duhem* relation⁹

$$\mathcal{S}^e dT - V dp + \sum_{n=1}^N M_n d\mu_n = 0. \quad (19.39)$$

As a corollary we see that for processes occurring at constant temperature and pressure that

$$\sum_{n=1}^N M_n d\mu_n = \sum_{n=1}^N N_n d\tilde{\mu}_n = 0 \quad \text{constant } T, p. \quad (19.40)$$

19.3.6 Gibbs potential

We offer a formal study of thermodynamic potentials in Section 19.6. Among those, we find Gibbs potential most useful for geophysical fluid mechanics and thus introduce it here

$$\mathcal{G}^e = \mathcal{I}^e - T \mathcal{S}^e + p V = \sum_{n=1}^N \mu_n M_n. \quad (19.41)$$

The reason that the Gibbs potential is so useful is that it is a natural function of temperature, pressure, and matter content,

$$\mathcal{G}^e = \mathcal{G}^e(T, p, M_n), \quad (19.42)$$

with T, p, M_n readily measured properties. This convenient functional dependence is confirmed by taking the differential, $d\mathcal{G}^e$, and using the fundamental thermodynamic relation (19.38b) to find

$$d\mathcal{G}^e = -\mathcal{S}^e dT + V dp + \sum_{n=1}^N \mu_n dM_n. \quad (19.43)$$

⁹In Exercise 19.1 we work through the derivation of Gibbs-Duhem (19.39) in a bit more detail.

In turn, we can derive the following partial derivatives,

$$\left[\frac{\partial \mathcal{G}^e}{\partial T} \right]_{p, M_n} = -\mathcal{S}^e \quad \text{and} \quad \left[\frac{\partial \mathcal{G}^e}{\partial p} \right]_{T, M_n} = V \quad \text{and} \quad \left[\frac{\partial \mathcal{G}^e}{\partial M_n} \right]_{p, T, M_{m \neq n}} = \mu_n \quad (19.44)$$

along with the second derivative identities

$$\left[\frac{\partial \mu_n}{\partial p} \right]_{T, M_n} = \frac{\partial}{\partial p} \left[\frac{\partial \mathcal{G}^e}{\partial M_n} \right]_{p, T, M_{m \neq n}} = \frac{\partial}{\partial M_n} \left[\frac{\partial \mathcal{G}^e}{\partial p} \right]_{p, T, M_{m \neq n}} = \left[\frac{\partial V}{\partial M_n} \right]_{p, T, M_{m \neq n}} \quad (19.45a)$$

$$\left[\frac{\partial \mu_n}{\partial T} \right]_{p, M_n} = \frac{\partial}{\partial T} \left[\frac{\partial \mathcal{G}^e}{\partial M_n} \right]_{p, T, M_{m \neq n}} = \frac{\partial}{\partial M_n} \left[\frac{\partial \mathcal{G}^e}{\partial T} \right]_{p, M_n} = - \left[\frac{\partial \mathcal{S}^e}{\partial M_n} \right]_{p, T, M_{m \neq n}}. \quad (19.45b)$$

The second derivative identities are particular *Maxwell relations*. Maxwell relations result from commutativity of the partial derivative operation.

19.3.7 Extensive functions of (T, p, M_n)

Just as for the internal energy and entropy, the Gibbs function, $\mathcal{G}^e(T, p, M_n)$, is an extensive function. Since the temperature and pressure are both intensive properties, we follow the scale analysis from Section 19.3.2 to arrive at the Euler form of the Gibbs function

$$\mathcal{G}^e(T, p, M_n) = \sum_{n=1}^N M_n \left[\frac{\partial \mathcal{G}^e}{\partial M_n} \right]_{p, T, M_{m \neq n}} = \sum_{n=1}^N \mu_n M_n, \quad (19.46)$$

which is consistent with the definition (19.41). Indeed, any extensive property written as a function of (T, p, M_n) can be written in the same fashion. For example, the internal energy, entropy, and volume take the form

$$\mathcal{I}^e(T, p, M_n) = \sum_{n=1}^N M_n \left[\frac{\partial \mathcal{I}^e}{\partial M_n} \right]_{p, T, M_{m \neq n}} = \sum_{n=1}^N N_n \left[\frac{\partial \mathcal{I}^e}{\partial N_n} \right]_{p, T, N_{m \neq n}} \quad (19.47a)$$

$$\mathcal{S}^e(T, p, M_n) = \sum_{n=1}^N M_n \left[\frac{\partial \mathcal{S}^e}{\partial M_n} \right]_{p, T, M_{m \neq n}} = \sum_{n=1}^N N_n \left[\frac{\partial \mathcal{S}^e}{\partial N_n} \right]_{p, T, N_{m \neq n}} \quad (19.47b)$$

$$V(T, p, M_n) = \sum_{n=1}^N M_n \left[\frac{\partial V}{\partial M_n} \right]_{p, T, M_{m \neq n}} = \sum_{n=1}^N N_n \left[\frac{\partial V}{\partial N_n} \right]_{p, T, N_{m \neq n}}. \quad (19.47c)$$

The partial derivatives, $[\partial(\mathcal{G}^e, \mathcal{I}^e, \mathcal{S}^e, V)/\partial N_n]_{p, T, N_{m \neq n}}$, are intensive properties known as the *partial Gibbs potential*, *partial internal energy*, *partial entropy*, and *partial volume*. These relations mean that we can regard each of the extensive quantities as the sum of contributions from each of the material components as determined by their partial properties. For the particular case of a single

matter component we have

$$\mathcal{G}^e(T, p, M) = M \left[\frac{\partial \mathcal{G}^e}{\partial M} \right]_{p,T} = \mu M \quad (19.48a)$$

$$\mathcal{I}^e(T, p, M) = M \left[\frac{\partial \mathcal{I}^e}{\partial M} \right]_{p,T} = N \left[\frac{\partial \mathcal{I}^e}{\partial N} \right]_{p,T} \quad (19.48b)$$

$$\mathcal{S}^e(T, p, M) = M \left[\frac{\partial \mathcal{S}^e}{\partial M} \right]_{p,T} = N \left[\frac{\partial \mathcal{S}^e}{\partial N} \right]_{p,T} \quad (19.48c)$$

$$V(T, p, M) = M \left[\frac{\partial V}{\partial M} \right]_{p,T} = N \left[\frac{\partial V}{\partial N} \right]_{p,T}. \quad (19.48d)$$

19.4 Thermodynamic equilibrium with matter flow

Consider a single-component fluid ($N = 1$) that consists of two regions or systems, labelled by α and β , with each of these two systems separately in thermodynamic equilibrium. Assume the composite system is enclosed in a container with fixed volume, $V_\alpha + V_\beta = V$. Allow the two systems to interact thermally, mechanically, and materially. What are the properties of thermodynamic equilibrium for the composite system, $\alpha \oplus \beta$?

To answer this question, we follow the procedure in Section 19.2.8, only here considering the case where matter flows between the systems in addition to thermal transfer and mechanical interactions. Such interactions occur as the composite system approaches thermodynamic equilibrium. Initially, the α and β systems are separately in thermodynamic equilibrium with internal energies, $(\mathcal{I}_\alpha^e, \mathcal{I}_\beta^e)$, volumes, (V_α, V_β) , and masses, (M_α, M_β) . During the process of reaching equilibrium, the internal energy, volume, and mass of the composite system remains constant so that¹⁰

$$d(\mathcal{I}_\alpha^e + \mathcal{I}_\beta^e) = 0 \quad \text{and} \quad d(V_\alpha + V_\beta) = 0 \quad \text{and} \quad d(M_\alpha + M_\beta) = 0. \quad (19.49)$$

From equation (19.24) we know that entropy is a natural function of volume, internal energy, and mass of each matter constituent. With only a single matter constituent we have

$$d\mathcal{S}^e = \frac{1}{T_\alpha} d\mathcal{I}_\alpha^e + \frac{p_\alpha}{T_\alpha} dV_\alpha - \frac{\mu_\alpha}{T_\alpha} dM_\alpha + \frac{1}{T_\beta} d\mathcal{I}_\beta^e + \frac{p_\beta}{T_\beta} dV_\beta - \frac{\mu_\beta}{T_\beta} dM_\beta \quad (19.50a)$$

$$= \left[\frac{1}{T_\alpha} - \frac{1}{T_\beta} \right] d\mathcal{I}_\alpha^e + \left[\frac{p_\alpha}{T_\alpha} - \frac{p_\beta}{T_\beta} \right] dV_\alpha - \left[\frac{\mu_\alpha}{T_\alpha} - \frac{\mu_\beta}{T_\beta} \right] dM_\alpha, \quad (19.50b)$$

where we used the partial derivative identities (19.12), (19.13), and (19.30). As before, $d\mathcal{S}^e = 0$ at thermodynamic equilibrium, and this condition holds for arbitrary and independent $d\mathcal{I}_\alpha^e$, dV_α , and dM_α . We are thus led to the thermal, mechanical, and material conditions for thermodynamic equilibrium

$$T_\alpha = T_\beta \quad \text{and} \quad p_\alpha = p_\beta \quad \text{and} \quad \mu_\alpha = \mu_\beta. \quad (19.51)$$

That is, the temperature, pressure, and chemical potential are uniform when the composite system reaches thermodynamic equilibrium. Note that this condition for thermodynamic equilibrium means that each term in the Gibbs-Duhem relation (19.39) separately vanishes. Furthermore, since the Gibbs potential equals to the mass times the chemical potential for a single component

¹⁰We here assume there is no macroscopic mechanical energy, so that the total energy is the internal energy. In Section 23.6 we relax this assumption by considering macroscopic motion.

system (equation (19.46)), equality of the chemical potentials at equilibrium means that

$$\mu_\alpha = \mu_\beta \implies \frac{G_\alpha^e}{M_\alpha} = \frac{G_\beta^e}{M_\beta}. \quad (19.52)$$

As for the direction of heat flow discussed in Section 19.2.8, we can determine the direction for matter flow as $\alpha \oplus \beta$ approaches thermodynamic equilibrium. For this purpose, assume the temperature and volumes are already uniform, but the matter content initially differs. At the instance the two systems start interacting, the entropy differential is given by

$$T dS^e = -(\mu_\alpha - \mu_\beta) dM_\alpha > 0, \quad (19.53)$$

where T is the equilibrium temperature of the two systems, and where the inequality holds according to the second law of thermodynamics (Section 19.1.7). If $\mu_\alpha > \mu_\beta$, then this inequality requires $dM_\alpha < 0$. Hence, in the process of approaching thermodynamic equilibrium, matter flows from regions of high chemical potential to regions of low chemical potential. This behavior allows us to consider the chemical potential in a manner directly akin to temperature. That is, temperature differences measure the potential for heat to be fluxed, and likewise chemical potential differences measure the potential for matter to be fluxed. The chemical potential is central to the study of changes in matter states (e.g., solid to liquid, liquid to gas), as well as for chemical reactions (e.g., *Guggenheim*, 1967; *Atkins and de Paula*, 2006).

19.5 Materially open systems with fixed total mass

In our study of geophysical fluids, we make use of a continuum of fluid elements. Each fluid element is open mechanically, thermally, and materially while maintaining constant mass as it quasi-statically evolves through local thermodynamic equilibrium states. Hence, when formulating the equations of linear irreversible thermodynamics in Chapter 23, we make use of thermodynamic equations written in their “per unit mass” form. Here we present these equations, as well as extend our understanding of the formalism.

19.5.1 Matter concentrations

We generally make use of matter or tracer concentration as written

$$C_n = M_n/M \implies \sum_{n=1}^N C_n = 1, \quad (19.54)$$

with the constant mass constraint $\sum_{n=1}^N C_n = 1$ meaning that only $N - 1$ of the concentrations are linearly independent. We also introduced tracer concentrations in Section 17.1 when developing the tracer equation.

19.5.2 Fundamental thermodynamic relation per unit mass

We scale away the mass of the system by setting the scale factor $\lambda = M^{-1}$ in our discussion in Section 19.3.2 of how extensive properties scale. The result is the *specific* (per mass) versions of

the extensive properties

$$\mathcal{J}^e = M \mathcal{J} \quad (19.55a)$$

$$\mathcal{S}^e = M \mathcal{S} \quad (19.55b)$$

$$V = M/\rho = M \nu_s \quad (19.55c)$$

$$M_n = M C_n, \quad (19.55d)$$

where

$$\nu_s = 1/\rho \quad (19.56)$$

is the *specific volume* and the total mass, M , is held fixed. In the equality (19.55d), C_n is the mass fraction or concentration of species n in the fluid (Section 19.5.1). Substituting the specific quantities (19.55a)-(19.55d) into the fundamental thermodynamic relation (19.38b) leads to the fundamental thermodynamic relation in terms of specific thermodynamic quantities

$$d\mathcal{J} = T d\mathcal{S} - p d\rho^{-1} + \sum_n \mu_n dC_n. \quad (19.57)$$

This is the form of the fundamental thermodynamic relation most commonly used in this book. Again, this relation holds for quasi-static processes that hold the total mass of the system fixed, thus making it relevant for our study of constant mass fluid elements in Chapter 23.

19.5.3 Seawater as a binary fluid

The atmosphere is a multi-component and multi-phase fluid that is well approximated as a mixture of water vapor and dry air. However, we do not consider moist atmospheric processes in this book nor do we consider phases changes. In contrast, there are many occasions in this book that require us to consider seawater as a binary fluid system of salt dissolved in fresh water so that their concentrations satisfy the constraint¹¹

$$C_{\text{salt}} + C_{\text{water}} = 1 \implies dC_{\text{water}} = -dC_{\text{salt}}. \quad (19.58)$$

We are thus able to write the Gibbs fundamental thermodynamic relation (19.57) in the form

$$d\mathcal{J} = T d\mathcal{S} - p d\rho^{-1} + \mu_{\text{water}} dC_{\text{water}} + \mu_{\text{salt}} dC_{\text{salt}} \quad (19.59a)$$

$$= T d\mathcal{S} - p d\rho^{-1} + \mu dC, \quad (19.59b)$$

where

$$C = C_{\text{salt}} \quad (19.60)$$

is the concentration of salt (mass of salt per mass of seawater), and

$$\mu = \mu_{\text{salt}} - \mu_{\text{water}} \quad (19.61)$$

is the *relative chemical potential*, often referred to as the *seawater chemical potential*. We return in Section 19.6.1 to discuss how the chemical potentials are computed according to partial derivatives

¹¹Salt in the ocean is largely comprised of chloride ions, sodium ions, sulphate ions, magnesium ions, calcium ions, potassium ions, and hydro-carbonate ions. The composition of the principal ions in seawater is roughly a constant, thus allowing us to be concerned only with the “salt” content and concentration rather than that for the individual components. In turn, we can accurately consider seawater as a two-component fluid comprised of fresh water and salt. See Section 1.4 of [Kamenkovich \(1977\)](#), Section 3.1 of [Gill \(1982\)](#), Section 1.2 of [Olbers et al. \(2012\)](#), or Section 1.4 of [Vallis \(2017\)](#) for more details.

of the Gibbs potential, which is the preferred method for the ocean and atmosphere.

The *absolute salinity* S , with units parts per thousand (gram per kilogram), is related to C_{salt} via

$$S = 1000 C_{\text{salt}}. \quad (19.62)$$

The range of absolute salinity in the ocean (roughly $0 \leq S \leq 40$) is more convenient than the range of C_{salt} , making salinity more commonly used in oceanography.

19.5.4 Further study

Chapters 1 and 2 of [Olbers et al. \(2012\)](#) provide a more complete suite of thermodynamic relations for seawater.

19.6 Thermodynamic potentials

Internal energy and entropy are referred to as state functions (functions only of the current state) as well as *thermodynamic potentials*, and they are related by equation (19.31), here written in its specific form as appropriate for constant mass fluid elements

$$\mathcal{I} = TS - p\nu_s + \sum_{n=1}^N \mu_n C_n \iff TS = \mathcal{I} + p\nu_s - \sum_{n=1}^N \mu_n C_n. \quad (19.63)$$

Each thermodynamic potential is a natural function of certain other thermodynamic properties, as determined by the fundamental thermodynamic relation.

It is useful to have access to a suite of thermodynamic potentials (internal energy, entropy, enthalpy, Gibbs potential, Helmboltz free energy) that have different functional dependencies, which in turn yield distinct expressions for the fundamental equation of state. Thermodynamic potentials are related mathematically through a *Legendre transformation*. Motivation for their introduction comes from the distinct laboratory and environmental conditions whereby the controlling parameters may differ. In this section we introduce the variety of thermodynamic potentials commonly used for fluid mechanics, and exhibit their natural functional dependencies. We specialize to the case of a binary fluid, which is most commonly the case for the ocean and atmosphere. Generalization to more components is straightforward.

We emphasize the importance of committing to a single choice for the thermodynamic potential when manipulating thermodynamic equations. The reason to adhere to a single choice is that functional dependencies change when switching to a different thermodynamic potential, thus exposing oneself to mistakes when swapping midstream to another formulation.

19.6.1 Equations of state

Equations (19.10), (19.11), and (19.30) provide expressions for intensive properties, T , p , and μ_n , in terms of the partial derivatives of the internal energy in terms of extensive functions \mathcal{S}^e , V , and M_m . We thus conclude that we can write T , p , and μ_n in the functional form

$$T = T(\mathcal{S}^e, V, M_m) \quad \text{and} \quad p = p(\mathcal{S}^e, V, M_m) \quad \text{and} \quad \mu_n = \mu_n(\mathcal{S}^e, V, M_m). \quad (19.64)$$

These equations are known as *equations of state*. Knowledge of all the equations of state is equivalent to knowledge of the fundamental thermodynamic relation (19.38b). In the following, we develop similar equations of state based on other thermodynamic potentials.

19.6.2 Internal energy

Recall the fundamental thermodynamic relation (19.59b) written for a binary fluid¹²

$$d\mathcal{J} = T dS - p d\nu_s + \mu dC. \quad (19.65)$$

Equation (19.65) identifies the specific internal energy, \mathcal{J} , as a natural function of specific entropy, S , specific volume, ν_s , and matter concentration, C

$$\mathcal{J} = \mathcal{J}(S, \nu_s, C). \quad (19.66)$$

Knowledge of the fundamental thermodynamic relation (19.65) allows us to derive a variety of thermodynamic relations via partial differentiation. For example, we can identify

$$\left[\frac{\partial \mathcal{J}}{\partial S} \right]_{\nu_s, C} = T \quad \text{and} \quad \left[\frac{\partial \mathcal{J}}{\partial \nu_s} \right]_{S, C} = -p \quad \text{and} \quad \left[\frac{\partial \mathcal{J}}{\partial C} \right]_{S, \nu_s} = \mu, \quad (19.67)$$

which are the specific (per mass) forms of equations (19.10), (19.11), and (19.30).

We see that equations (19.67) provide a relation between T, p, μ as derivatives of a function, the internal energy, which is itself a function $\mathcal{J}(S, \nu_s, C)$. Hence, we may consider T, p, μ each as a function of (S, ν_s, C) , and thus write the equations of state

$$T = T(S, \nu_s, C) \quad \text{and} \quad p = p(S, \nu_s, C) \quad \text{and} \quad \mu = \mu(S, \nu_s, C), \quad (19.68)$$

which are the equations of state (19.64) written in terms of specific (per mass) quantities. In turn, the exact differentials of the intensive properties are

$$dT = \left[\frac{\partial T}{\partial S} \right]_{\nu_s, C} dS + \left[\frac{\partial T}{\partial \nu_s} \right]_{C, S} d\nu_s + \left[\frac{\partial T}{\partial C} \right]_{S, \nu_s} dC \quad (19.69)$$

$$dp = \left[\frac{\partial p}{\partial S} \right]_{\nu_s, C} dS + \left[\frac{\partial p}{\partial \nu_s} \right]_{C, S} d\nu_s + \left[\frac{\partial p}{\partial C} \right]_{S, \nu_s} dC \quad (19.70)$$

$$d\mu = \left[\frac{\partial \mu}{\partial S} \right]_{\nu_s, C} dS + \left[\frac{\partial \mu}{\partial \nu_s} \right]_{C, S} d\nu_s + \left[\frac{\partial \mu}{\partial C} \right]_{S, \nu_s} dC. \quad (19.71)$$

19.6.3 Entropy

Rearrangement of the fundamental thermodynamic relation (19.65) leads to the exact differential for specific entropy

$$dS = \frac{1}{T} d\mathcal{J} + \frac{p}{T} d\nu_s - \frac{\mu}{T} dC. \quad (19.72)$$

In this form, specific entropy has the functional dependence

$$S = S(\mathcal{J}, \nu_s, C), \quad (19.73)$$

¹²If there are more than two matter constituents, then the term μdC appearing in these formula become $\sum_{n=1}^N \mu_n dC_n$. Partial derivatives are also modified accordingly. We choose the binary case since it is typically sufficient for the earth's atmosphere and ocean.

whose knowledge provides yet another form of the fundamental equation of state. This functional dependence, along with equation (19.72), lead to the following identities

$$\left[\frac{\partial S}{\partial J} \right]_{\nu_s, C} = \frac{1}{T} \quad \text{and} \quad \left[\frac{\partial S}{\partial \nu_s} \right]_{J, C} = \frac{p}{T} \quad \text{and} \quad \left[\frac{\partial S}{\partial C} \right]_{J, \nu_s} = -\frac{\mu}{T}. \quad (19.74)$$

As for internal energy in Section 19.6.2, equation (19.74) provides a relation between T, p, μ as derivatives of a function, the entropy, which is itself a function $S(J, \nu_s, C)$. Hence, we may consider T, p, μ as each a function of (J, ν_s, C) to thus write the equations of state

$$T = T(J, \nu_s, C) \quad \text{and} \quad p = p(J, \nu_s, C) \quad \text{and} \quad \mu = \mu(J, \nu_s, C). \quad (19.75)$$

19.6.4 Enthalpy

Thus far we have worked only with the fundamental thermodynamic relation (19.65). We now introduce the specific enthalpy

$$\mathcal{H} = J + p \nu_s = T S + \sum_{n=1}^N \mu_n C_n, \quad (19.76)$$

where the second equality made use of equation (19.63). Specializing to the case of a binary fluid, such as the ocean or atmosphere, and use of the fundamental thermodynamic relation (19.65), leads to the exact differential for enthalpy

$$d\mathcal{H} = dJ + d(p \nu_s) \quad (19.77a)$$

$$= T dS - p d\nu_s + \mu dC + p d\nu_s + \nu_s dp \quad (19.77b)$$

$$= T dS + \nu_s dp + \mu dC \quad (19.77c)$$

Recalling that for quasi-static processes, $T dS$ equals to the thermal energy added to a fluid element. Hence, for processes occurring at constant pressure and constant matter content, changes in enthalpy are determined by the thermal energy added to the system. This connection motivates the name *heat function* sometimes applied to enthalpy (e.g., page 4 of [Landau and Lifshitz \(1987\)](#)).

Equation (19.77c) provides the fundamental thermodynamic relation with enthalpy rather than internal energy. Consequently, the *Legendre transformation* (19.76) renders a functional dependence for enthalpy

$$\mathcal{H} = \mathcal{H}(S, p, C), \quad (19.78)$$

which in turn leads to the following partial derivative identities

$$\left[\frac{\partial \mathcal{H}}{\partial S} \right]_{p, C} = T \quad \text{and} \quad \left[\frac{\partial \mathcal{H}}{\partial p} \right]_{S, C} = \nu_s \quad \text{and} \quad \left[\frac{\partial \mathcal{H}}{\partial C} \right]_{S, p} = \mu. \quad (19.79)$$

As for internal energy in Section 19.6.2, equations (19.79) provide a relation between T, ν_s, μ as derivatives of a function, the enthalpy, which is itself a function $\mathcal{H}(S, p, C)$. Hence, we may consider T, ν_s, μ as each a function of (S, p, C) to thus render the following equations of state

$$T = T(S, p, C) \quad \text{and} \quad \nu_s = \nu_s(S, p, C) \quad \text{and} \quad \mu = \mu(S, p, C). \quad (19.80)$$

Enthalpy's functional dependence (19.78) is more convenient for studies of geophysical fluids than that for internal energy, $J(S, \nu_s, C)$, or for entropy $S(J, \nu_s, C)$.

- In the laboratory or field, we generally have direct mechanical means for measuring pressure

in a fluid, whereas specific volume requires indirect methods involving the equation of state for density discussed in Section 27.3.

- Correspondingly, the interaction between fluid elements typically occurs at near constant pressure. Hence, fluid elements exchange both their entropy and enthalpy when the exchange occurs as constant pressure.
- Specific entropy remains constant on a fluid element in the absence of mixing or other irreversible effects. Correspondingly, enthalpy remains constant for constant pressure motion without mixing. Conversely, in the presence of mixing at constant pressure, fluid elements mix their specific enthalpy, specific entropy, and tracer concentration.

19.6.5 Helmholtz free energy

The Helmholtz free energy is defined by the Legendre transformation

$$\mathcal{F} = \mathcal{I} - T \mathcal{S} = -p \nu_s + \sum_{n=1}^N \mu_n C_n, \quad (19.81)$$

where the second equality made use of equation (19.63). The exact differential of the Helmholtz free energy is given by

$$d\mathcal{F} = d\mathcal{I} - d(T \mathcal{S}) \quad (19.82a)$$

$$= d\mathcal{I} - T d\mathcal{S} - \mathcal{S} dT \quad (19.82b)$$

$$= -\mathcal{S} dT - p d\nu_s + \mu dC, \quad (19.82c)$$

where we used the fundamental thermodynamic relation (19.59b) for the final equality. Isothermal and constant concentration processes render the changes to the free energy equal to the pressure work applied to the system.

The Helmholtz free energy has the functional dependence

$$\mathcal{F} = \mathcal{F}(T, \nu_s, C), \quad (19.83)$$

which then leads to the partial derivatives identities

$$\left[\frac{\partial \mathcal{F}}{\partial T} \right]_{\nu_s, C} = -\mathcal{S} \quad \text{and} \quad \left[\frac{\partial \mathcal{F}}{\partial \nu_s} \right]_{T, C} = -p \quad \text{and} \quad \left[\frac{\partial \mathcal{F}}{\partial C} \right]_{T, \nu_s} = \mu. \quad (19.84)$$

As for internal energy in Section 19.6.2, equations (19.84) provide a relation between \mathcal{S}, p, μ as derivatives of a function, the Helmholtz free energy, which is itself a function $\mathcal{F}(T, \nu_s, C)$. Hence, we may consider \mathcal{S}, p, μ each as a function of (T, ν_s, C) to render the functional relations

$$\mathcal{S} = \mathcal{S}(T, \nu_s, C) \quad \text{and} \quad p = p(T, \nu_s, C) \quad \text{and} \quad \mu = \mu(T, \nu_s, C). \quad (19.85)$$

19.6.6 Gibbs potential

The Gibbs potential is defined by the Legendre transformation

$$\mathcal{G} = \mathcal{I} + p \nu_s - T \mathcal{S} = \mathcal{H} - T \mathcal{S} = \sum_{n=1}^N \mu_n C_n, \quad (19.86)$$

where the final equality made use of equation (19.63). The exact differential of the Gibbs potential is given by

$$d\mathcal{G} = d\mathcal{H} - d(T\mathcal{S}) \quad (19.87a)$$

$$= T d\mathcal{S} + \nu_s dp + \mu dC - T d\mathcal{S} - \mathcal{S} dT \quad (19.87b)$$

$$= -\mathcal{S} dT + \nu_s dp + \mu dC, \quad (19.87c)$$

where we made use of the fundamental thermodynamic relation (19.77c) written in terms of enthalpy. The Gibbs potential has the functional dependence

$$\mathcal{G} = \mathcal{G}(T, p, C), \quad (19.88)$$

which leads to the partial derivatives identities

$$\left[\frac{\partial \mathcal{G}}{\partial T} \right]_{p,C} = -\mathcal{S} \quad \text{and} \quad \left[\frac{\partial \mathcal{G}}{\partial p} \right]_{T,C} = \nu_s \quad \text{and} \quad \left[\frac{\partial \mathcal{G}}{\partial C} \right]_{T,p} = \mu. \quad (19.89)$$

As for internal energy in Section 19.6.2, equations (19.89) provide a relation between \mathcal{S}, ν_s, μ as derivatives of a function, the Gibbs potential, which is itself a function $\mathcal{G}(T, p, C)$. Hence, we may consider \mathcal{S}, ν_s, μ each as a function of (T, p, C) to render the following functional relations

$$\mathcal{S} = \mathcal{S}(T, p, C) \quad \text{and} \quad \nu_s = \nu_s(T, p, C) \quad \text{and} \quad \mu = \mu(T, p, C). \quad (19.90)$$

The form of the fundamental dependencies (19.88), and the associated equations of state (19.90), are often used in fluid mechanics and physical chemistry. The reason is that temperature, pressure, and concentration are readily measured in the laboratory and the environment. We can thus readily measure the partial derivatives of \mathcal{G} , and the functional dependence (19.90) provides a convenient means to express \mathcal{S}, ν_s , and μ (e.g., see the adiabatic lapse rate discussion in Section 20.2).

Given its convenient functional dependence, the Gibbs potential plays a central role in developing the thermodynamics of seawater as formulated by *Feistel* (1993) and codified by *IOC et al.* (2010). We thus endeavor to exhibit how quantities (e.g., response functions as in Section 19.7) can be computed based on knowledge of the Gibbs potential and its partial derivatives. For example, use of equation (19.89) renders the expression for the enthalpy

$$\mathcal{H} = \mathcal{G} + T\mathcal{S} = \mathcal{G} - T \left[\frac{\partial \mathcal{G}}{\partial T} \right]_{p,C}. \quad (19.91)$$

19.6.7 Chemical potential and the Gibbs potential

Throughout this section we have displayed equations for the chemical potential of a binary fluid in terms of the partial derivatives of the thermodynamic potentials, such as equation (19.89) using the Gibbs potential. Here we consider some details that lead to further understanding of the partial derivatives. We start by writing the chemical potential of fresh water and salt as contained within seawater in terms of the partial derivatives of the extensive Gibbs potential

$$\mu_{\text{water}} = \left[\frac{\partial \mathcal{G}^e}{\partial M_{\text{water}}} \right]_{T,p,M_{\text{salt}}} \quad \text{and} \quad \mu_{\text{salt}} = \left[\frac{\partial \mathcal{G}^e}{\partial M_{\text{salt}}} \right]_{T,p,M_{\text{water}}}. \quad (19.92)$$

The total mass of a sample of seawater is given by $M = M_{\text{water}} + M_{\text{salt}}$. Consequently, to compute these partial derivatives requires us to alter the mass of the sample as we hold the mass of one

component fixed while varying the mass of the other component. This sort of partial derivative is less convenient for our purposes since we prefer to work with constant mass samples, such as we encounter with constant mass fluid elements. For that purpose we introduce the specific Gibbs potential, in which case the chemical potential of fresh water is

$$\mu_{\text{water}} = \left[\frac{\partial \mathcal{G}^e}{\partial M_{\text{water}}} \right]_{T,p,M_{\text{salt}}} = \left[\frac{\partial(M \mathcal{G})}{\partial M_{\text{water}}} \right]_{T,p,M_{\text{salt}}} = \mathcal{G} + M \left[\frac{\partial \mathcal{G}}{\partial M_{\text{water}}} \right]_{T,p,M_{\text{salt}}}. \quad (19.93)$$

The specific Gibbs potential is a natural function of T, p, C_n , and since $C_{\text{water}} + C_{\text{salt}} = 1$ we can write the Gibbs potential in terms of just one of the concentrations, typically chosen as C_{salt} . We are thus led to

$$\mu_{\text{water}} = \mathcal{G} + M \left[\frac{\partial \mathcal{G}}{\partial M_{\text{water}}} \right]_{T,p,M_{\text{salt}}} \quad (19.94a)$$

$$= \mathcal{G} + M \left[\frac{\partial \mathcal{G}}{\partial C_{\text{water}}} \right]_{T,p} \left[\frac{\partial C_{\text{water}}}{\partial M_{\text{water}}} \right]_{M_{\text{salt}}} \quad (19.94b)$$

where the concentration partial derivative is given by

$$\left[\frac{\partial C_{\text{water}}}{\partial M_{\text{water}}} \right]_{M_{\text{salt}}} = \left[\frac{\partial}{\partial M_{\text{water}}} \right]_{M_{\text{salt}}} \left[\frac{M_{\text{water}}}{M_{\text{water}} + M_{\text{salt}}} \right] = \frac{C_{\text{salt}}}{M}, \quad (19.95)$$

thus leading to the chemical potential of fresh water within seawater

$$\mu_{\text{water}} = \mathcal{G} + C_{\text{salt}} \left[\frac{\partial \mathcal{G}}{\partial C_{\text{water}}} \right]_{T,p} = \mathcal{G} - C_{\text{salt}} \left[\frac{\partial \mathcal{G}}{\partial C_{\text{salt}}} \right]_{T,p}. \quad (19.96)$$

We are thus able to work with the specific Gibbs function for a constant mass fluid element and compute its concentration partial derivative. Similar manipulations lead to the chemical potential for salt within seawater

$$\mu_{\text{salt}} = \mathcal{G} + C_{\text{water}} \left[\frac{\partial \mathcal{G}}{\partial C_{\text{salt}}} \right]_{T,p} = \mathcal{G} + (1 - C_{\text{salt}}) \left[\frac{\partial \mathcal{G}}{\partial C_{\text{salt}}} \right]_{T,p}. \quad (19.97)$$

We are thus led to the seawater chemical potential

$$\mu = \mu_{\text{salt}} - \mu_{\text{water}} = \left[\frac{\partial \mathcal{G}}{\partial C_{\text{salt}}} \right]_{T,p}, \quad (19.98)$$

which agrees with equation (19.89).

19.7 Response functions

Response functions measure the change in a thermodynamic property as the system is forced in some manner. We here introduce the heat capacity, thermal expansion coefficient, and haline contraction coefficient, which are three response functions commonly encountered in ocean and atmospheric fluid mechanics.

19.7.1 Specific heat capacities

The heat capacity measures the change in heat associated with a change in temperature at constant matter composition. There are two distinct heat capacities generally considered in fluid mechanics: one with specific volume held fixed and the other with pressure held fixed

$$c_v \equiv \frac{1}{M} \left[\frac{d\Omega}{dT} \right]_{\nu_s, C} \quad \text{SI units m}^2 \text{ s}^{-2} \text{ K}^{-1}. \quad (19.99)$$

$$c_p \equiv \frac{1}{M} \left[\frac{d\Omega}{dT} \right]_{p, C} \quad \text{SI units m}^2 \text{ s}^{-2} \text{ K}^{-1}. \quad (19.100)$$

Each of these quantities are specific heat capacities since we have divided by the mass. If heating occurs quasi-statically, we can make use of the equation (19.5) that relates heating and entropy, applied here in its specific (per mass) form $M^{-1} d\Omega = T dS$. The result is a state function form of the specific heat capacities

$$c_v = T \left[\frac{\partial S}{\partial T} \right]_{\nu_s, C} = -T \left[\frac{\partial}{\partial T} \right]_{\nu_s, C} \left[\frac{\partial G}{\partial T} \right]_{p, C} \quad (19.101)$$

$$c_p = T \left[\frac{\partial S}{\partial T} \right]_{p, C} = -T \left[\frac{\partial}{\partial T} \right]_{p, C} \left[\frac{\partial G}{\partial T} \right]_{p, C} \quad (19.102)$$

where the second equalities in both of the above equations introduced the Gibbs potential according to equation (19.89). Furthermore, we can make use of the fundamental thermodynamic relation (19.57) with specific volume and matter concentration held fixed to yield

$$c_v = T \left[\frac{\partial S}{\partial T} \right]_{\nu_s, C} = \left[\frac{\partial J}{\partial T} \right]_{\nu_s, C}. \quad (19.103)$$

The second form of c_v motivates the name *internal energy capacity* rather than heat capacity at fixed volume. Likewise, making use of the fundamental thermodynamic relation (19.77c) written in terms of enthalpy leads to the constant pressure heat capacity

$$c_p = T \left[\frac{\partial S}{\partial T} \right]_{p, C} = \left[\frac{\partial J}{\partial T} \right]_{p, C} + p \left[\frac{\partial \nu_s}{\partial T} \right]_{p, C} = \left[\frac{\partial H}{\partial T} \right]_{p, C}. \quad (19.104)$$

That is, the constant pressure heat capacity is equivalently referred to as the *enthalpy capacity*.

19.7.2 Thermal expansion coefficient

The thermal expansion coefficient measures relative changes in density as temperature changes at constant pressure and concentration

$$\alpha_T = -\frac{1}{\rho} \left[\frac{\partial \rho}{\partial T} \right]_{p, C} = \frac{1}{\nu_s} \left[\frac{\partial \nu_s}{\partial T} \right]_{p, C} = \frac{1}{(\partial G / \partial p)_{T, C}} \left[\frac{\partial}{\partial T} \right]_{p, C} \left[\frac{\partial G}{\partial p} \right]_{T, C} \quad (19.105)$$

where the final equality introduced the Gibbs function according to equation (19.89). The minus sign in the definition is introduced since density typically reduces when temperature increases, so that for most substances $\alpha_T > 0$. Freshwater near its freezing point is an important counter-example, with $\alpha_T < 0$ allowing for solid ice to float on liquid water.

19.7.3 Haline contraction coefficient

A similar response function measures changes to density arising from changes in the salt concentration (salinity) in seawater

$$\beta_s = \frac{1}{\rho} \left[\frac{\partial \rho}{\partial S} \right]_{p,T} = -\frac{1}{\nu_s} \left[\frac{\partial \nu_s}{\partial S} \right]_{p,T} = -\frac{1}{(\partial \mathcal{G}/\partial p)_{T,S}} \left[\frac{\partial \mathcal{G}}{\partial S} \right]_{T,p} \left[\frac{\partial \mathcal{G}}{\partial p} \right]_{T,S} \quad (19.106)$$

where $S = 1000 C$ is the salinity (19.62). Seawater density typically increases (fluid element volume contracts) when salinity increases, so that $\beta_s > 0$.

19.7.4 Speed of sound (acoustic) waves

Changes in density with respect to pressure at a fixed entropy define the inverse squared sound speed¹³

$$\frac{1}{c_s^2} = \left[\frac{\partial \rho}{\partial p} \right]_s = -\frac{1}{(\nu_s)^2} \left[\frac{\partial \nu_s}{\partial p} \right]_s = -\frac{1}{[(\partial \mathcal{G}/\partial p)_{T,S}]^2} \left[\frac{\partial \mathcal{G}}{\partial p} \right]_s \left[\frac{\partial \mathcal{G}}{\partial p} \right]_{T,S}. \quad (19.107)$$

The sound speed is a strong function of pressure, generally increasing with higher pressure, as well as temperature, generally decreasing with lower temperature. For the ocean, these two effects compete when moving into the ocean interior. In the upper 500 m to 1000 m, decreasing temperatures cause the sound speed to reduce whereas at deeper regions the higher pressures overcome the temperature effect thus increasing the sound speed. The result is a sound speed minimum between 500 m and 1000 m. The sound speed minimum and the associated acoustic waveguide play an important role in ocean acoustics, in particular for how certain whales are able to communicate across ocean basins. We consider the sound speed for an ideal gas in Section 20.4.8.

19.8 Maxwell relations for single component fluids

Thermodynamics makes use of basic properties of exact differentials for the purpose of developing identities between partial derivatives. Maxwell relations refer to a suite of partial derivative identities that follow from the equality of mixed second partial derivatives of thermodynamic potentials. We already made use of some Maxwell relations in Section 19.3.6 when discussing the Gibbs potential, and we use another in Section 20.2 for expressing the adiabatic lapse rate in terms of readily measurable thermo-mechanical properties. In this section we develop the Maxwell relations encountered with single component fluids, with similar relations readily derived for multi-component fluids.

19.8.1 Maxwell relation from internal energy

As seen from Section 19.6.2, the natural functional dependence for internal energy in a single-component fluid is given by its fundamental thermodynamic relation (19.65)

$$d\mathcal{I} = \left[\frac{\partial \mathcal{I}}{\partial S} \right]_{\nu_s} dS + \left[\frac{\partial \mathcal{I}}{\partial \nu_s} \right]_S d\nu_s = T dS - p d\nu_s \implies \mathcal{I} = \mathcal{I}(S, \nu_s). \quad (19.108)$$

¹³We study sound waves in Chapter 44.

The mixed second partial derivatives are equal

$$\left[\frac{\partial}{\partial \nu_s} \right]_{S,C} \left[\frac{\partial}{\partial S} \right]_{\nu_s,C} \mathcal{I} = \left[\frac{\partial}{\partial S} \right]_{\nu_s,C} \left[\frac{\partial}{\partial \nu_s} \right]_{S,C} \mathcal{I}, \quad (19.109)$$

so that, via the fundamental thermodynamic relation (19.108), we have the Maxwell relation

$$\left[\frac{\partial T}{\partial \nu_s} \right]_S = - \left[\frac{\partial p}{\partial S} \right]_{\nu_s}. \quad (19.110)$$

19.8.2 Summary of the Maxwell relations

The other thermodynamic potentials, and their associated fundamental thermodynamical relations, lead to further Maxwell relations as summarized here

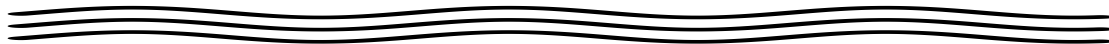
$$d\mathcal{J} = T dS - p d\nu_s \implies \left[\frac{\partial T}{\partial \nu_s} \right]_S = - \left[\frac{\partial p}{\partial S} \right]_{\nu_s} \quad (19.111)$$

$$d\mathcal{H} = T dS + \nu_s dp \implies \left[\frac{\partial T}{\partial p} \right]_S = \left[\frac{\partial \nu_s}{\partial S} \right]_p \quad (19.112)$$

$$d\mathcal{G} = -S dT + \nu_s dp \implies \left[\frac{\partial S}{\partial p} \right]_T = - \left[\frac{\partial \nu_s}{\partial T} \right]_p. \quad (19.113)$$

$$d\mathcal{F} = -S dT - p d\nu_s \implies \left[\frac{\partial S}{\partial \nu_s} \right]_T = \left[\frac{\partial p}{\partial T} \right]_{\nu_s}. \quad (19.114)$$

These four Maxwell relations for single-component fluids involve permutations on cross derivatives of (T, S) and (p, ν_s) . In statistical mechanics, (T, S) determine the density of accessible microscopic states forming the thermodynamic system, whereas (p, ν_s) involves an external control parameter and its corresponding generalized force.



19.9 Exercises

EXERCISE 19.1: DERIVATION OF THE GIBBS-DUHEM RELATION

Show all of the steps leading to the Gibbs-Duhem relation (19.39).

EXERCISE 19.2: CHEMICAL POTENTIAL IDENTITY

As seen in Section 23.4.6, we have need to consider the partial derivative

$$\left[\frac{\partial \mathcal{H}}{\partial C} \right]_{T,p} \quad (19.115)$$

when determining the chemical work done by mixing within a fluid. Prove the identity

$$\left[\frac{\partial \mathcal{H}}{\partial C} \right]_{T,p} = \left[\frac{\partial \mathcal{H}}{\partial C} \right]_{S,p} - T \left[\frac{\partial \mu}{\partial T} \right]_{C,p} = \mu - T \left[\frac{\partial \mu}{\partial T} \right]_{C,p}. \quad (19.116)$$

Hint: as seen in Section 19.6.4, the natural functional dependence for enthalpy is $\mathcal{H}(S, p, C)$, whereas in Section 19.6.6 we found the natural function dependence of the Gibbs potential to be $\mathcal{G}(T, p, C)$. Equate the exact differential expressions for enthalpy using the two functional depen-

dencies $\mathcal{H}(S, p, C)$ and $\mathcal{H}(T, p, C)$, and then derive a Maxwell relation based on the fundamental thermodynamic relation written in terms of the Gibbs potential.

EXERCISE 19.3: CONSTANT OF MOTION FOR ADIABATIC PROCESSES

Show that for a simple ideal gas, isentropic processes (i.e., both adiabatic and of constant matter concentration) maintain

$$p \nu_s^{c_p/c_v} = \text{constant}, \quad (19.117)$$

where $\nu_s = \rho^{-1}$ is the specific volume.



Chapter 20

EQUILIBRIUM THERMODYNAMICS WITH A GEOPOTENTIAL

We here extend the equilibrium thermodynamics from Chapter 19 to allow for gravitational effects as embodied by the geopotential (which also includes the planetary centrifugal acceleration). Thermodynamic equilibrium of a fluid in a constant gravitational field is consistent with mechanical equilibrium; i.e., the fluid is in hydrostatic balance. We develop certain properties of hydrostatic fluids, such as the adiabatic lapse rate, potential temperature, and a variety of identities holding for an ideal gas (which offers a useful approximation to the atmosphere).

CHAPTER GUIDE

This chapter develops the rudiments of equilibrium thermodynamics in the presence of gravity, building on the foundations established in Chapter 19. There are relatively few presentations of gravity within standard thermodynamic texts. However, Chapter 9 of *Guggenheim (1967)* and §25 of *Landau and Lifshitz (1980)* are notable exceptions, along with Section 1.8 of the oceanography text from *Kamenkovich (1977)*.

20.1 Thermodynamic equilibrium with a geopotential	438
20.1.1 The first law	438
20.1.2 Thermodynamic equilibrium with varying volume	438
20.1.3 Thermodynamic equilibrium with fixed volume	439
20.1.4 Vertical salinity gradient at thermodynamic equilibrium	440
20.1.5 Comments and further study	441
20.2 Adiabatic lapse rate	441
20.2.1 Isentropic rearrangement	441
20.2.2 Thermodynamic formulation	442
20.2.3 Adiabatic lapse rate for pressure changes	442
20.2.4 Adiabatic lapse rate for height changes	443
20.2.5 Further study	443
20.3 Potential temperature	443
20.3.1 Motivating the definition of potential properties	444
20.3.2 Temperature changes from pressure changes	444
20.3.3 Defining the potential temperature	445
20.3.4 Potential temperature and specific entropy	446
20.4 Thermodynamic relations for a simple ideal gas	447
20.4.1 Equation of state	447
20.4.2 Internal energy	448
20.4.3 Heat capacity	448
20.4.4 Enthalpy	449
20.4.5 Thermal expansion coefficient	449
20.4.6 Fundamental thermodynamic relations	450

20.4.7 Isothermal compressibility	450
20.4.8 Sound speed	450
20.4.9 Adiabatic lapse rate	450
20.4.10 Geopotential thickness	451
20.4.11 Potential temperature	452
20.4.12 Further study	453
20.5 Exercises	453

20.1 Thermodynamic equilibrium with a geopotential

What does thermodynamic equilibrium look like in the presence of a gravity field? To answer this question, we here consider a single-component system in the presence of a static gravity field. To further connect to geophysical fluids, we let the geopotential, Φ , represent the effects from central gravity plus the planetary centrifugal acceleration (Section 11.11.4). Throughout this analysis, we assume the acceleration from the geopotential is prescribed and is thus not affected by the mass of the thermodynamic system that feels the geopotential. Furthermore, we assume the force from the geopotential is terrestrial, so that it is weak enough to ignore general relativistic effects.¹

20.1.1 The first law

As seen in Section 19.2.3, a thermodynamic system subjected to a pressure field undergoes pressure work as its volume changes. Analogously, when the mass of a thermodynamic system changes within a geopotential field, then it is subjected to geopotential work, which takes the form

$$dW_{\text{geopotential}} = \Phi dM. \quad (20.1)$$

We thus see that the geopotential is an intensive property with mass its corresponding extensive property. Consequently, the first law for a quasi-static process is modified from equation (19.38b) to now read

$$dJ^e = -p dV + T dS^e + (\mu + \Phi) dM \iff dS^e = T^{-1} [p dV + dJ^e - (\mu + \Phi) dM], \quad (20.2)$$

where μ is the chemical potential in the absence of a geopotential

$$\left[\frac{\partial J^e}{\partial M} \right]_{V,S^e} = \mu + \Phi \quad \text{and} \quad \left[\frac{\partial J^e}{\partial M} \right]_{V,S^e,\Phi=0} = \mu. \quad (20.3)$$

The corresponding Gibbs-Duhem relation (19.39) now takes on the form

$$-V dp + S^e dT + M d(\mu + \Phi) = 0. \quad (20.4)$$

20.1.2 Thermodynamic equilibrium with varying volume

Following our discussion in Section 19.4, we consider two adjoining fluid regions that are allowed to adjust toward thermodynamic equilibrium in the presence of a geopotential field. The entropy

¹The relevant non-dimensional ratio is given by Φ/c^2 , with c the speed of light. See [Santiago and Visser \(2018\)](#) for a concise review of how gravity leads to a spatially dependent temperature in thermal equilibrium through Tolman's temperature gradient. These considerations are important when Φ/c^2 is order unity. For terrestrial purposes, $\Phi/c^2 \lll 1$, so that relativistic gravitational effects are entirely negligible.

differential in equation (19.50b) now takes on the form

$$dS^e = \left[\frac{1}{T_\alpha} - \frac{1}{T_\beta} \right] dJ_\alpha^e + \left[\frac{p_\alpha}{T_\alpha} - \frac{p_\beta}{T_\beta} \right] dV_\alpha - \left[\frac{\mu_\alpha + \Phi_\alpha}{T_\alpha} - \frac{\mu_\beta + \Phi_\beta}{T_\beta} \right] dM_\alpha, \quad (20.5)$$

which follows from the constraints (19.49) that assume fixed internal energy, mass, and volume for the composite system $\alpha \oplus \beta$. Equilibrium is characterized by $dS^e = 0$, which leads to a uniform temperature, as for the case with uniform Φ . A further extension of Section 19.4 suggests that $dp = 0$ and $d(\mu + \Phi) = 0$ at equilibrium. However, our understanding of fluid statics leads us to expect pressure to vary according to the hydrostatic balance discussed in Section 21.4. That is, a uniform pressure does not arise for equilibrium with a nonuniform geopotential. For that purpose we consider different constraints as seen below.

20.1.3 Thermodynamic equilibrium with fixed volume

To recover hydrostatic balance at thermodynamic equilibrium, consider the case with each volume remaining fixed. In this manner we have

$$d(J_\alpha^e + J_\beta^e) = 0 \quad \text{and} \quad dV_\alpha = dV_\beta = 0 \quad \text{and} \quad d(M_\alpha + M_\beta) = 0. \quad (20.6)$$

An example consists of two vertically positioned fluid boxes, with $\nabla\Phi$ defining the local vertical direction and with adjustment towards equilibrium consisting of mass moving from one box to the other. By fixing each of the region volumes, pressure does no work so that internal energy changes only through entropy and mass changes

$$dJ^e = T dS^e + (\mu + \Phi) dM \iff dS^e = T^{-1} [dJ^e - (\mu + \Phi) dM]. \quad (20.7)$$

Correspondingly, we find that thermodynamic equilibrium results when

$$dT = 0 \quad \text{and} \quad d(\mu + \Phi) = 0. \quad (20.8)$$

To interpret the equilibrium condition, $d(\mu + \Phi) = 0$, take the derivative with respect to geopotential, holding temperature and mass fixed, to render

$$\left[\frac{\partial \mu}{\partial \Phi} \right]_{T,M} = -1. \quad (20.9)$$

Anticipating the hydrostatic balance, we assume that pressure at thermodynamic equilibrium is a monotonic function of Φ , so that

$$\left[\frac{\partial \mu}{\partial \Phi} \right]_{T,M} = \left[\frac{\partial \mu}{\partial p} \right]_{T,M} \left[\frac{dp}{d\Phi} \right]_{T,M} = -1. \quad (20.10)$$

Making use of the Maxwell relation (19.45a) and the identity (19.48d) leads to

$$\left[\frac{dp}{d\Phi} \right]_{T,M} = -M/V = -\rho, \quad (20.11)$$

where $\rho = M/V$ is the mass density. We thus recover the exact hydrostatic balance²

$$dp = -\rho d\Phi. \quad (20.12)$$

That is, thermodynamic equilibrium in a gravity field consists of a uniform temperature with pressure satisfying the exact hydrostatic balance.

20.1.4 Vertical salinity gradient at thermodynamic equilibrium

Consider the case of seawater as approximated as a two-component fluid, so that the entropy exact differential is given by

$$dS^e = T^{-1} [p dV + dJ^e - (\mu_{\text{salt}} + \Phi) dM_{\text{salt}} - (\mu_{\text{water}} + \Phi) dM_{\text{water}}]. \quad (20.13)$$

Separately holding the salt and freshwater masses fixed,³ we apply the same formalism as pursued in Section 20.1.3 for a single component fluid, thus leading to

$$dT = 0 \quad \text{and} \quad d(\mu_{\text{salt}} + \Phi) = 0 \quad \text{and} \quad d(\mu_{\text{water}} + \Phi) = 0. \quad (20.14)$$

Subtracting the second and third equilibrium condition leads to the equilibrium condition for the seawater chemical potential,

$$d(\mu_{\text{salt}} - \mu_{\text{water}}) = d\mu = 0. \quad (20.15)$$

Now recall the seawater chemical potential is given by equation (19.98) in terms of the salinity derivative of the specific Gibbs potential

$$\mu = \mu_{\text{salt}} - \mu_{\text{water}} = \left[\frac{\partial \mathcal{G}}{\partial S} \right]_{T,p}, \quad (20.16)$$

where $S = C_{\text{salt}}$ is the salt concentration. Hence, we may consider the seawater chemical potential to be a function of the temperature, pressure, and salt concentration

$$\mu = \mu(T, p, S). \quad (20.17)$$

The equilibrium conditions $dT = 0$ and $d\mu = 0$ lead to

$$\frac{\partial \mu}{\partial S} dS + \frac{\partial \mu}{\partial p} dp = 0. \quad (20.18)$$

The hydrostatic relation $dp = -\rho d\Phi$ leads to

$$\frac{\partial \mu}{\partial S} \frac{dS}{d\Phi} = \rho \frac{\partial \mu}{\partial p}. \quad (20.19)$$

Of when the geopotential takes on the simple form, $\Phi = g z$, then

$$\frac{\partial \mu}{\partial S} \frac{dS}{dz} = g \rho \frac{\partial \mu}{\partial p}. \quad (20.20)$$

We thus conclude that at thermodynamic equilibrium, the salinity maintains a nonzero geopo-

²We discuss the exact hydrostatic balance in Section 21.4, and discuss the approximate hydrostatic balance in Chapter 24.

³This constraint is appropriate since we are looking for the entropy extrema for an isolated system with no boundary fluxes of either salt or freshwater.

tential gradient whereas the *in situ* temperature is uniform.

20.1.5 Comments and further study

A depth independent *in situ* temperature is not observed in the ocean or atmosphere. Likewise, as noted on page 28 of [Kamenkovich \(1977\)](#), the vertical salinity gradient implied by the equilibrium relation (20.19) is not observed in the ocean. Both results point to the absence of thermodynamic equilibrium for the macroscale atmosphere and ocean. The absence of global thermodynamic equilibrium is expected since both the atmosphere and ocean are not isolated systems. Furthermore, the fluids are both turbulently mixed rather than mixed solely by molecular processes, with turbulent mixing not leading to thermodynamic equilibrium.⁴

Although we do not generally observe temperature close to thermodynamic equilibrium, we do find a horizontally local hydrostatic balance to be well maintained by the large-scale atmosphere and ocean. In addition to being a thermodynamic equilibrium state, hydrostatic balance is a mechanical equilibrium state (Section 21.4). We thus conclude that for a moving and turbulent geophysical fluid, the mechanical equilibrium state of hydrostatic balance is far more robust than full thermodynamic equilibrium of *in situ* temperature and material tracers. The reason is that mechanical equilibrium is enabled by macroscopic motion (e.g., acoustic waves), whereas thermodynamic equilibrium required for uniform *in situ* temperature is enabled by the far slower molecular diffusion.

The presentation in this section largely follows §25 of [Landau and Lifshitz \(1980\)](#) and Section 1.8 of [Kamenkovich \(1977\)](#).

20.2 Adiabatic lapse rate

The temperature of a fluid can change without the transfer of heat. This *adiabatic* temperature change arises when the fluid pressure changes. We here introduce the *adiabatic lapse rate*, which measures the vertical variations in temperature for a static fluid placed in a gravity field. There are two lapse rates commonly considered: one related to height and one related to pressure. We introduce some manipulations commonly performed with thermodynamic state functions and their partial derivatives, with the goal of expressing the lapse rate in terms of commonly measured response functions.

The *in situ* temperature is globally uniform for a fluid in thermodynamic equilibrium. Hence, a fluid with a nonzero lapse rate is globally out of thermodynamic equilibrium. However, we again assume that each fluid element is locally in thermodynamic equilibrium so that we can make use of equilibrium thermodynamic relations to derive the lapse rate. Furthermore, we note that the atmosphere is observed to have an *in situ* temperature profile closer to the adiabatic lapse rate than to a uniform *in situ* temperature, thus further indicating that global thermodynamic equilibrium is not realized in geophysical fluids.

20.2.1 Isentropic rearrangement

Consider a finite region of a static fluid in a gravitational field. Assume the fluid is initially in a horizontal layer in thermodynamic equilibrium so that it has a uniform *in situ* temperature. Now rearrange the fluid into a vertical column, and do so without changing the entropy; i.e., without the transfer of heat across the fluid boundary (adiabatically) and without mixing any of its matter constituents. Performing this rearrangement raises the center of mass of the fluid and

⁴As emphasized in Section 19.1 and in Chapter 23, the macroscale atmosphere and ocean are not in thermodynamic equilibrium, and yet these fluids maintain local thermodynamic equilibrium at the scale of fluid elements.

thus increases the gravitational potential energy. This process requires mechanical work against the gravitational field.

Gravity makes pressure at the bottom of the vertical fluid column greater than at the top. This pressure difference modifies the temperature in the column, thus putting the fluid out of global thermodynamic equilibrium. We seek a general expression for how changes in pressure affects changes in temperature for a static fluid, with the pressure changes imparted reversibly and adiabatically so that entropy does not change. Mathematically, we seek an expression for the partial derivative

$$\hat{\Gamma} \equiv \left[\frac{\partial T}{\partial p} \right]_{C,S}, \quad (20.21)$$

which is known as the *adiabatic lapse rate*. The adiabatic lapse rate can be measured directly, with empirical expressions fit to laboratory measurements. Additionally, it is convenient to express it in terms of other thermodynamic response functions in order to garner further physical insight. The necessary manipulations form the bulk of this section.

20.2.2 Thermodynamic formulation

When the matter concentration is held fixed, the equation of state (19.90) allows us to consider entropy as a function of temperature and pressure so that

$$dS = \left[\frac{\partial S}{\partial T} \right]_p dT + \left[\frac{\partial S}{\partial p} \right]_T dp. \quad (20.22)$$

Substituting the definition of heat capacity from equation (19.102) leads to

$$T dS = c_p dT + T \left[\frac{\partial S}{\partial p} \right]_T dp. \quad (20.23)$$

It is useful to eliminate $(\partial S / \partial p)_T$ in favor of a more easily measurable quantity. For that purpose we make use of the Maxwell relation (19.113) to write

$$\left[\frac{\partial S}{\partial p} \right]_T = - \left[\frac{\partial \nu_s}{\partial T} \right]_p. \quad (20.24)$$

Introducing the thermal expansion coefficient (19.105) yields an expression for changes in entropy in terms of changes in temperature and pressure

$$T dS = c_p dT - T \left[\frac{\partial \nu_s}{\partial T} \right]_p dp = c_p dT - \left[\frac{T \alpha_T}{\rho} \right] dp. \quad (20.25)$$

Since c_p and α_T are readily measurable response functions, the expression (20.25) is a useful means to compute infinitesimal entropy changes when matter concentration is held constant.

20.2.3 Adiabatic lapse rate for pressure changes

Equation (20.25) means that the change in temperature associated with changes in pressure, with $dS = 0$ and $dC = 0$, can be written

$$\hat{\Gamma} = \left[\frac{\partial T}{\partial p} \right]_{C,S} = \frac{T \alpha_T}{\rho c_p}. \quad (20.26)$$

This relation holds for any form of pressure changes, such as those due to hydrostatic pressure changes or pressure fluctuations in an acoustic wave (see Section 44.5.4). Temperature indeed changes when pressure changes, even though there has been no heat exchanged with the environment. With $\hat{\Gamma}$ so defined, we can write the entropy change in equation (20.25) as

$$T dS = c_p (dT - \hat{\Gamma} dp). \quad (20.27)$$

The term $dT - \hat{\Gamma} dp$ subtracts from the *in situ* temperature differential the pressure induced changes in temperature. In Section 20.3 we introduce the *potential temperature*, which is defined just for the purpose of removing changes due to pressure.

20.2.4 Adiabatic lapse rate for height changes

A static fluid in a gravity field is in exact hydrostatic balance, whereby the pressure at a point equals to the weight per area above that point (Section 21.4). Hydrostatic balance in a constant gravity field maintains the following relation between the pressure differential and the vertical differential

$$dp = -g \rho dz. \quad (20.28)$$

Use of the chain rule within the lapse rate expression (20.26) leads to

$$\Gamma = \left[\frac{\partial T}{\partial z} \right]_{C,S} = \left[\frac{\partial T}{\partial p} \right]_{C,S} \left[\frac{\partial p}{\partial z} \right] = -\rho g \left[\frac{T \alpha_T}{\rho c_p} \right] = -\frac{g T \alpha_T}{c_p}. \quad (20.29)$$

This form for the lapse rates measures the change in temperature (the *lapse*) within a constant composition fluid element as it is isentropically moved vertically through a hydrostatic pressure field.

20.2.5 Further study

In Section 20.4.9 we consider the adiabatic lapse rate for the special case of a simple ideal gas. For this gas, the internal energy of a fluid element is represented entirely by its temperature, and pressure is caused solely by molecular thermal motion. For water, however, molecular interaction energies are important, and pressure arises not only from thermal motion but also from interaction forces of the densely packed molecules. It is these differences between the behavior of water and a perfect gas that were examined by [McDougall and Feistel \(2003\)](#) in terms of molecular dynamics. In particular, they note that the lapse rate, being proportional to the thermal expansion coefficient, can be negative when the thermal expansion is negative. A negative thermal expansion coefficient occurs in cool fresh water, such as the Baltic Sea. Hence, although work is done on the fluid element under increasing pressure, its temperature decreases in these cases.

The addition of water to the atmosphere modifies the lapse rate, as the air is then no longer well approximated by an ideal gas. Chapter 18 of [Vallis \(2017\)](#) offers a pedagogical discussion of the thermodynamics of a moist tropical atmosphere.

20.3 Potential temperature

As discussed in Section 20.1, thermodynamic equilibrium of a fluid in a geopotential field sees the hydrostatic pressure balancing the weight of fluid. Thermodynamic equilibrium is also characterized by a uniform *in situ* temperature, T , which requires removal of the temperature gradient associated with the adiabatic lapse rate discussed in Section 20.2. The molecular diffusive processes (see Section 23.9) that homogenize *in situ* temperature are very slow, so that geophysical

fluids are rarely in thermodynamic equilibrium. We here introduce the notion of *potential temperature*, which offers a measure of temperature that removes the adiabatic lapse rate. With some qualifiers discussed below, turbulent mixing processes active in geophysical fluids lead to a nearly homogenous potential temperature. As such, potential temperature is a more practical thermodynamic tracer than *in situ* temperature.

20.3.1 Motivating the definition of potential properties

We observe that the processes of heating and cooling of the ocean occur predominantly near the ocean surface. In contrast, transport in the ocean interior is nearly adiabatic and isohaline (i.e., nearly isentropic). The physical picture is suggested whereby the surface ocean boundary layer experiences irreversible processes that set characteristics of water masses that move quasi-reversibly within the ocean interior. As a means to characterize and thus to label these *water masses*, oceanographers prefer to use properties that maintain constant values when moving within the quasi-isentropic ocean interior. Salinity is a good label for this purpose since it is only altered by mixing between waters of varying concentrations, and in turn it is materially constant in the absence of mixing.⁵ This behavior constitutes a basic property of material tracers (tracers that measure the mass per mass of a constituent as discussed in Section 17.1). However, it is *not* a property of the *in situ* temperature, T , which changes even in the absence of mixing due to pressure effects. We are thus motivated to seek a thermodynamic property that evolves analogously to material tracers, so that it can be used as a second material label for fluid elements. A similar motivation stems from the analysis of atmospheric motions.

A thermodynamic property that remains constant when a fluid element is moved from one pressure to another, without the transfer of heat or matter and without any kinetic energy dissipation, is said to be a *potential property*. The *potential temperature* is the example that concerns us in this section. As we will see, in some special cases the potential temperature is directly proportional to the specific entropy. More practically, it offers a means to estimate the heat transport within a geophysical fluid.

Conservative Temperature, Θ , is another potential property discussed in Section 23.9, with Conservative Temperature defined as the potential enthalpy divided by a constant heat capacity. As detailed in [McDougall \(2003\)](#), Conservative Temperature provides a more convenient and accurate measure of heat transport in a geophysical fluid than potential temperature. As such, Θ is now more commonly used in applications than potential temperature, θ , ([McDougall et al., 2021](#)).

20.3.2 Temperature changes from pressure changes

Motion of a fluid element, without exchange of heat (adiabatic) or matter (constant concentration), generally changes the pressure of the fluid element. In turn, this motion causes the *in situ* temperature to have a differential that is in proportion to the adiabatic lapse rate given by (Section 20.2)

$$dT = \hat{\Gamma} dp. \quad (20.30)$$

Consequently, and as already noted, the *in situ* temperature is not a useful thermodynamic variable to label fluid elements since it changes even in the absence of irreversible mixing processes.

⁵There are nuances concerning what we mean by “salinity”, with details given by [IOC et al. \(2010\)](#) (in particular, see Sections A.8 and A.9). We are not directly concerned with these nuances in this book, though note that they are important for ocean measurements and the interpretation of salinity as used in numerical ocean models ([McDougall et al., 2021](#)).

Instead, it is more useful to remove the adiabatic pressure effects. This is the key reason for introducing potential temperature.

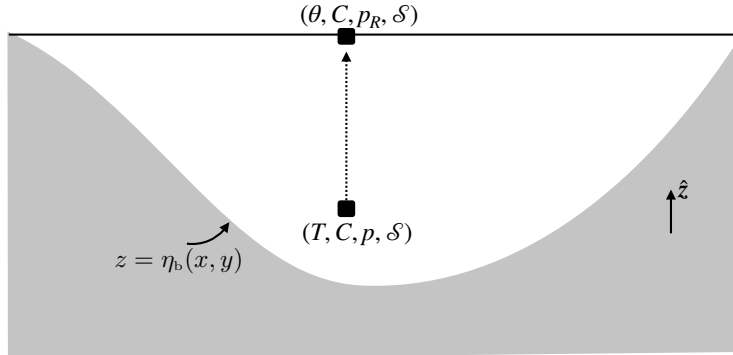


FIGURE 20.1: Potential temperature is the *in situ* temperature that a fluid element of fixed material composition would have if isentropically displaced from its *in situ* pressure to a reference pressure, p_R . The schematic here depicts that displacement for a seawater fluid element with *in situ* temperature, T , salinity, $S = 1000\text{C}$, pressure, p , and specific entropy, S . The element is moved to the ocean surface with the standard sea level atmospheric pressure providing the reference pressure.

20.3.3 Defining the potential temperature

Operationally, the potential temperature is based on removing adiabatic pressure effects from *in situ* temperature. That is, potential temperature is defined as the *in situ* temperature that a fluid element of fixed material composition would have if it were isentropically transported from its *in situ* pressure to a reference pressure p_R , with the reference pressure typically taken at the ocean/land surface (see Figure 20.1). Mathematically, the potential temperature, θ , is the reference temperature obtained via integration of $dT = \hat{\Gamma} dp$ for an isentropic *in situ* temperature change with respect to pressure

$$\int_{\theta}^T dT' = \int_{p_R}^p \hat{\Gamma}(T, p', C) dp' \implies T = \theta(T, p_R, C) + \int_{p_R}^p \hat{\Gamma}(T, p', C) dp', \quad (20.31)$$

with $\hat{\Gamma}$ the lapse rate defined in terms of pressure changes (equation (20.26)). By definition, the *in situ* temperature, T , equals the potential temperature, θ , at the reference pressure, $p = p_R$. Elsewhere, they differ by an amount determined by the adiabatic lapse rate. Furthermore, we see that

$$\left[\frac{\partial T}{\partial p} \right]_{C,S} = \left[\frac{\partial \theta}{\partial p} \right]_{C,S} + \hat{\Gamma}. \quad (20.32)$$

However, by definition

$$\left[\frac{\partial T}{\partial p} \right]_{C,S} = \hat{\Gamma} \quad (20.33)$$

so that

$$\left[\frac{\partial \theta}{\partial p} \right]_{C,S} = 0. \quad (20.34)$$

That is, by construction, the potential temperature depends explicitly on the concentration, C , and *in situ* temperature, T , and has a parametric dependence on the reference pressure. It has no explicit dependence on the *in situ* pressure when holding tracer concentration and entropy

fixed. Finally, we emphasize that the potential temperature is a function of tracer concentration, C . Hence, the potential temperature generally changes if the tracer concentration changes. For example, potential temperature in the ocean changes if the salinity changes.

20.3.4 Potential temperature and specific entropy

An alternative definition of the potential temperature follows by noting that the entropy of a fluid element remains unchanged as it is reversibly moved to the reference pressure. Consequently, writing entropy as a function of the *in situ* temperature, pressure, and matter concentration as in equation (19.90)

$$\mathcal{S} = \mathcal{S}(T, p, C) \quad (20.35)$$

leads to the defining identity for potential temperature

$$\mathcal{S} = \mathcal{S}(T, p, C) = \mathcal{S}(\theta, p_R, C). \quad (20.36)$$

This relation directly connects changes in entropy to changes in potential temperature

$$d\mathcal{S} = \left[\frac{\partial \mathcal{S}(\theta, p_R, C)}{\partial \theta} \right]_C d\theta. \quad (20.37)$$

Consequently, the reversible transport of a fluid element with constant matter concentration ($dC = 0$) occurs with both a constant specific entropy and constant potential temperature.

We can go even further than the relation (20.37) by recalling that equation (20.27) relates the differential of specific entropy to temperature and pressure

$$T d\mathcal{S} = c_p (dT - \hat{\Gamma} dp), \quad (20.38)$$

where $\hat{\Gamma}$ is the adiabatic lapse rate defined in terms of pressure changes (equation (20.26)), and we set $dC = 0$. To relate $dT - \hat{\Gamma} dp$ to $d\theta$ we write the potential temperature equation (20.31) in the form

$$\theta(T, p_R, C) = T - \int_{p_R}^p \hat{\Gamma}(T, p', C) dp' = T - \Psi(T, p, C, p_R), \quad (20.39)$$

so that the differentials are related by

$$d\theta = dT - d\Psi. \quad (20.40)$$

We evaluate $d\Psi$ using the chain rule and then specialize to the case of constant composition and with a fixed reference pressure

$$d\Psi = \frac{\partial \Psi}{\partial T} dT + \frac{\partial \Psi}{\partial p} dp + \frac{\partial \Psi}{\partial C} dC + \frac{\partial \Psi}{\partial p_R} dp_R \quad (20.41a)$$

$$= \frac{\partial \Psi}{\partial T} dT + \frac{\partial \Psi}{\partial p} dp \quad (20.41b)$$

$$\equiv \int_{p_R}^p \frac{\partial \hat{\Gamma}(T, p', C)}{\partial T} dp' + \hat{\Gamma}(T, p, C) dp. \quad (20.41c)$$

Evaluating this differentials at the reference pressure removes the integral so that

$$d\Psi = \hat{\Gamma}(T, p_R, C) dp, \quad (20.42)$$

in which case the potential temperature differential is

$$d\theta = dT - \hat{\Gamma}(T, p_R, C) dp. \quad (20.43)$$

Making use of this relation in equation (20.38) renders an expression for the entropy differential in terms of the potential temperature differential

$$dS = c_p \theta^{-1} d\theta \quad p = p_R \text{ and } dC = 0. \quad (20.44)$$

Although evaluated at the reference pressure, as part of exercise 23.4 we see that this relation holds for an ideal gas at all pressures. Furthermore, as part of exercise 23.5 we see that this relation also holds for all pressures in certain liquids.

20.4 Thermodynamic relations for a simple ideal gas

In an ideal gas, we ignore the potential energy of intermolecular interaction forces between molecules. Also, the molecules in an ideal gas are assumed to occupy zero volume (i.e., they are point particles), although they do collide elastically. As a result, the internal energy of an ideal gas is just due to translation, rotation, and vibration of molecules. We refer to a *simple ideal gas* as an ideal gas where the internal energy is a linear function of temperature. In this section we develop a variety of thermodynamic relations for a simple ideal gas atmosphere in exact hydrostatic balance. Although the real atmosphere is moving, and thus not in exact hydrostatic balance, and the real atmosphere is not a simple ideal gas, it turns out that many of the relations established here are rather accurate approximations to the real atmosphere. Furthermore, by exposing these relations for the ideal gas, we further our understanding of the more general thermodynamic relations established earlier in this chapter.

20.4.1 Equation of state

An ideal gas satisfies the following equation of state (see Section 13.3.2)

$$PV = n R^g T, \quad (20.45)$$

where p is the pressure, V is the volume, n is the number of moles,

$$R^g = 8.314 \text{ J mole}^{-1} \text{ K}^{-1} = 8.314 \text{ kg m}^2 \text{ s}^{-2} \text{ mole}^{-1} \text{ K}^{-1} \quad (20.46)$$

is the *universal gas constant*, and T is the absolute temperature in Kelvin (see Section 13.3.2). The number of moles equals to the mass, M , of the gas divided by the mass per mole, M_{mole}

$$n = M/M_{\text{mole}}. \quad (20.47)$$

The mass density, $\rho = M/V$, is thus given by

$$\rho = \frac{p M_{\text{mole}}}{T R^g} \equiv \frac{p}{T R^M}, \quad (20.48)$$

where

$$R^M = R^g / M_{\text{mole}} \quad (20.49)$$

is the *specific gas constant* as defined by the universal gas constant normalized by the molar mass for the constituent. For air we have (Section 13.3.2)

$$M^{\text{air}} = 28.8 \times 10^{-3} \text{ kg mole}^{-1} \quad (20.50)$$

so that air's specific gas constant is

$$R^{\text{air}} = \frac{R^g}{M^{\text{air}}} = \frac{8.314 \text{ kg m}^2 \text{ s}^{-2} \text{ mole}^{-1} \text{ K}^{-1}}{28.8 \times 10^{-3} \text{ kg mole}^{-1}} = 2.938 \times 10^2 \text{ m}^2 \text{ s}^{-2} \text{ K}^{-1}. \quad (20.51)$$

The relation (20.48) is known as a *thermal equation of state*, or more succinctly just an equation of state (see Section 27.3 for more discussion). It shows that the mass density of an ideal gas is directly proportional to the pressure: increasing pressure increases density. In contrast, mass density is inversely proportional to the temperature: increases in temperature lead to lower mass density. This behavior for the ideal gas density is reflected in certain real gases and liquids.⁶

20.4.2 Internal energy

An ideal gas is comprised of molecules that interact only through elastic collisions. There are no inter-molecular forces. Furthermore, the volume of the individual molecules is ignored in comparison to the volume of empty space between the molecules, so they are approximated as point masses. Consequently, the internal energy for an ideal gas is independent of density and of the matter concentration. It is hence a function only of the temperature, which measures the kinetic energy of the elastic point molecules

$$\mathcal{I} = \mathcal{I}(T) \quad \text{ideal gas.} \quad (20.52)$$

Consequently, the exact differential of internal energy for an ideal gas is

$$d\mathcal{I} = c_v dT. \quad (20.53)$$

The appearance of c_v , the constant volume specific heat capacity discussed in Section 19.7.1, arises in order for the ideal gas internal energy to satisfy the general equation (19.103). The heat capacity for an ideal gas is generally a function of temperature. However, for many applications it is sufficient to consider a simple ideal gas, in which c_v is a constant so that

$$\mathcal{I} = c_v T + \text{constant} \quad \text{simple ideal gas.} \quad (20.54)$$

The arbitrary constant of integration is generally set to zero so that the internal energy vanishes at absolute zero.

20.4.3 Heat capacity

The heat capacity is a constant for a simple ideal gas (equation 20.54). Results from statistical mechanics show that the thermal/internal energy per molecule equals to $k_B T/2$ per excited molecular degree of freedom, where

$$k_B = 1.3806 \times 10^{-23} \text{ m}^2 \text{ kg s}^{-2} \text{ K}^{-1} \quad (20.55)$$

⁶A notable counter-example is water near its freezing point, which becomes more dense as temperature rises. This anomalous behavior is why a body of water freezes from the top down rather than from the bottom up.

is the *Boltzmann constant*. Dry air is mostly comprised of the diatomic molecules N_2 and O_2 . Diatomic molecules at temperatures of the lower atmosphere have two rotational and three translational degrees of freedom,⁷ so that $\mathcal{I}_{\text{molecule}} = 5 k_B T/2$.

We convert this energy per molecule to an energy per mole of diatomic molecules by multiplying by Avogadro's number (equation (13.9))

$$\mathcal{I}_{\text{mole diatomic}} = 5 A^v k_B T/2 = 5 R^g T/2, \quad (20.56)$$

where the gas constant is given by

$$R^g = A^v k_B \quad (20.57\text{a})$$

$$= (6.022 \times 10^{23} \text{ mole}^{-1}) (1.3806 \times 10^{-23} \text{ m}^2 \text{ kg s}^{-2} \text{ K}^{-1}) \quad (20.57\text{b})$$

$$= 8.314 \text{ kg m}^2 \text{ s}^{-2} \text{ mole}^{-1} \text{ K}^{-1}. \quad (20.57\text{c})$$

Finally, dividing by the molar mass for dry air (equation (13.10))

$$M^{\text{air}} = 0.028 \text{ kg mole}^{-1} \quad (20.58)$$

leads to the simple ideal gas approximation to the dry air heat capacity

$$c_v = \frac{5 R^g}{2 M^{\text{air}}} = 742 \text{ m}^2 \text{ s}^{-2} \text{ K}^{-1}. \quad (20.59)$$

The measured heat capacity for dry air at standard temperature (300 K) is $718 \text{ m}^2 \text{ s}^{-2} \text{ K}^{-1}$, so the simple ideal gas estimate is only $(742 - 718)/718 = 3.3\%$ too large.

20.4.4 Enthalpy

The enthalpy is generally given by equation (19.76), which for a simple ideal gas takes the form

$$\mathcal{H} = \mathcal{I} + p/\rho = c_v T + \frac{T R^g}{M_{\text{mole}}} = T(c_v + R^M) \quad (20.60)$$

where $R^M = R^g/M_{\text{mole}}$ (equation (20.49)) is the specific gas constant for the gas. Recall that the constant pressure heat capacity is given by equation (19.104)

$$c_p = T \left[\frac{\partial \mathcal{S}}{\partial T} \right]_{p,C} = \left[\frac{\partial \mathcal{H}}{\partial T} \right]_{p,C}. \quad (20.61)$$

Consequently, for a simple ideal gas we have

$$c_p = c_v + R^M \quad \text{and} \quad \mathcal{H} = c_p T. \quad (20.62)$$

20.4.5 Thermal expansion coefficient

The thermal expansion coefficient for an ideal gas is given by

$$\alpha_T = -\frac{1}{\rho} \frac{\partial \rho}{\partial T} = \frac{1}{T}, \quad (20.63)$$

so that as temperature increases the thermal expansion decreases.

⁷At high temperatures, two vibrational degrees of freedom are also excited so that $\mathcal{I}_{\text{molecule}} = 7 k_B T/2$ at high temperatures.

20.4.6 Fundamental thermodynamic relations

The fundamental thermodynamic relation, written in terms of internal energy (equation (19.59b)) and enthalpy (equation (19.76)), are given by

$$d\mathcal{J} = T dS - p d\nu_s + \mu dC \quad (20.64)$$

$$d\mathcal{H} = T dS + \nu_s dp + \mu dC. \quad (20.65)$$

For a simple ideal gas these relations take the form

$$c_v dT = T dS - p d\nu_s + \mu dC \quad (20.66)$$

$$c_p dT = T dS + \nu_s dp + \mu dC. \quad (20.67)$$

20.4.7 Isothermal compressibility

The isothermal compressibility measures the change in volume when holding the temperature and matter concentration fixed and it is determined by the partial derivatives

$$-\frac{1}{V} \left[\frac{\partial V}{\partial p} \right]_{T,C} = \frac{1}{\rho} \left[\frac{\partial \rho}{\partial p} \right]_{T,C}. \quad (20.68)$$

For an ideal gas the compressibility is given by

$$-\frac{1}{V} \left[\frac{\partial V}{\partial p} \right]_{T,C} = \frac{1}{p}, \quad (20.69)$$

so that the compressibility decreases when pressure increases.

20.4.8 Sound speed

As studied in Chapter 44, sound travels through a fluid through compression and expansion of the fluid media. So we expect the sound speed to be related to the compressibility. But rather than the isothermal compressibility considered above, sound waves are largely adiabatic waves so that the entropy is constant. We are thus in need of the isentropic compressibility to compute the sound speed. That is, as defined by equation (19.107), the sound speed is the pressure derivative of density computed with entropy and matter concentration held fixed. We make use of the fundamental relations (20.66) and (20.67), with $dS = 0$ and $dC = 0$ to have

$$\frac{c_v}{c_p} = \frac{p}{\rho} \left[\frac{\partial \rho}{\partial p} \right]_{S,C} = (p/\rho) c_s^{-2} \implies c_s^2 = (p/\rho)(c_p/c_v) = T R^M (c_p/c_v). \quad (20.70)$$

For an ideal diatomic gas, such as nitrogen and oxygen, the ratio $c_p/c_v = 7/5$. Taking $R^M = 2.938 \times 10^2 \text{ m}^2 \text{ s}^{-2} \text{ K}^{-1}$ for air from equation (20.51) then leads to

$$c_s \approx 350 \text{ m s}^{-1} \quad \text{for } T = 300 \text{ K.} \quad (20.71)$$

20.4.9 Adiabatic lapse rate

For an ideal gas, the thermal expansion coefficient is given by (equation (20.63)) $\alpha_T = T^{-1}$ so that the lapse rates are

$$\hat{\Gamma} = \frac{1}{\rho c_p} \quad \text{and} \quad \Gamma = -\frac{g}{c_p}. \quad (20.72)$$

The measured specific heat capacity for a dry atmosphere at standard temperature (300 K) is

$$c_p = 1005 \text{ m}^2 \text{ s}^{-2} \text{ K}^{-1} \quad (20.73)$$

so that the adiabatic lapse rate for a dry atmosphere is roughly

$$\Gamma_d = -9.8 \text{ K}/(1000 \text{ m}). \quad (20.74)$$

Hence, temperature decreases by nearly 10 K when rising 1000 m in a dry and ideal gas atmosphere.

20.4.10 Geopotential thickness

We now establish basic relations for a static atmosphere satisfying the hydrostatic balance. These relations also hold to a very good approximation for the large-scale atmosphere given the dominance of approximate hydrostatic balance for these scales (see Section 24.2).

From the hydrostatic equation (21.52) we know that the pressure on a geopotential, Φ_1 , equals to

$$p(\Phi_1) = \int_{\Phi_1}^{\infty} \rho(\Phi) d\Phi \quad (20.75)$$

where we assumed that $p(\Phi_2 = \infty) = 0$. Equation (21.51) allows us to write the integrand as

$$d\Phi = -\rho^{-1} dp = -\frac{T R^{\text{air}} dp}{p}, \quad (20.76)$$

where the second equality assumed an ideal gas atmosphere. Vertical integration of equation (20.76) leads to the *hypsometric equation*, which provides the geopotential thickness between two pressure isosurfaces

$$\Phi(z_2) - \Phi(z_1) = -R^{\text{air}} \int_{p_1}^{p_2} T d(\ln p). \quad (20.77)$$

Recall that $dp < 0$ if $dz > 0$ since the hydrostatic pressure decreases when moving up in the atmosphere. We define the *geopotential height* according to

$$Z = \Phi/g, \quad (20.78)$$

where g is the gravitational acceleration at sea level. The geopotential height is close to the geometric height in the troposphere and lower stratosphere. The hypsometric equation (20.77) says that the geopotential thickness between two isobars is

$$Z_2 - Z_1 = \frac{R^{\text{air}}}{g} \int_{p_2}^{p_1} T d(\ln p). \quad (20.79)$$

Defining the layer mean temperature

$$\langle T \rangle = \frac{\int_{p_2}^{p_1} T d(\ln p)}{\int_{p_2}^{p_1} d(\ln p)} \quad (20.80)$$

and the layer mean *scale height*

$$H = \frac{R^{\text{air}} \langle T \rangle}{g} \quad (20.81)$$

leads to the geopotential thickness

$$Z_2 - Z_1 = -H \ln(p_2/p_1) \quad (20.82)$$

The geopotential thickness is thus directly proportional to the mean temperature within the pressure layer, with thicker layers, for example, with higher mean temperatures.

We can invert the geopotential thickness relation (20.82) for the pressures to render

$$p_1 = p_2 e^{-(Z_1 - Z_2)/H}. \quad (20.83)$$

This relation, or more commonly its simplified version (20.87) discussed below, is sometimes referred to as the *law of atmospheres* or the *barometric law*. The scale height is a function of pressure through its dependence on the layer averaged temperature in equation (20.81). For the special case of an atmosphere with a constant temperature, T , then the scale height is a constant⁸

$$H_{\text{const}} = \frac{R^{\text{air}} T_{\text{const}}}{g}. \quad (20.84)$$

Setting $T_{\text{const}} = 300$ K and using the specific gas constant for air from equation (20.51) leads to the scale height

$$H_{\text{const}} = \frac{2.938 \times 10^2 \text{ m}^2 \text{ s}^{-2} \text{ K}^{-1} \times 300 \text{ K}}{9.8 \text{ m s}^{-2}} \approx 9 \times 10^3 \text{ m}. \quad (20.85)$$

It is furthermore convenient to set $Z_2 = 0$ with $p_2 = p_{\text{slp}}$ the sea level pressure, whose global average is

$$\langle p_{\text{slp}} \rangle = 101.325 \times 10^3 \text{ N m}^{-2}. \quad (20.86)$$

The pressure in an isothermal atmosphere thus decreases exponentially with geopotential height according to the scale height

$$p(Z) = \langle p_{\text{slp}} \rangle \exp(-Z/H_{\text{const}}). \quad (20.87)$$

20.4.11 Potential temperature

The fundamental thermodynamic relation for a simple ideal gas (20.67) takes on the following form for an isentropic change

$$c_p dT = \nu_s dp. \quad (20.88)$$

Dividing both sides by temperature and using the ideal gas relation

$$\frac{\nu_s}{T} = \frac{R^M}{p} \quad (20.89)$$

leads to

$$c_p d(\ln T) = R^M d(\ln p). \quad (20.90)$$

Since c_p and R^M are constants, we can integrate this relation from the reference pressure to an arbitrary pressure

$$c_p \int_{\theta}^T d(\ln T) = R^M \int_{p_R}^p d(\ln p), \quad (20.91)$$

⁸As we saw earlier in this chapter, a fluid has uniform temperature at thermodynamic equilibrium. However, the effects from turbulent motions, even very modest turbulent motions, readily break thermodynamic equilibrium. This topic was first discussed starting on page 299 by [Maxwell \(1872\)](#), where he also credits input from Lord Kelvin.

which renders the explicit expression for the potential temperature of a simple ideal gas

$$\theta = T \left[\frac{p_R}{p} \right]^{R^M/c_p} \quad \text{where} \quad c_p = \frac{7 R^M}{2}, \quad (20.92)$$

with c_p the constant pressure heat capacity of a simple ideal gas of diatomic molecules (Section 20.4.3). In some treatments (e.g., Exercise 20.3) it is useful to introduce the *Exner function*

$$\Pi = \frac{c_p T}{\theta} = c_p \left[\frac{p}{p_R} \right]^{R^M/c_p}. \quad (20.93)$$

In Exercise 20.2 we show that $\partial\theta/\partial p = 0$ for the ideal gas, thus exemplifying the removal of explicit pressure effects from the potential temperature. Furthermore, it follows from equation (20.92) that the potential temperature differential is related to temperature and pressure differentials via

$$\frac{\delta\theta}{\theta} = \frac{\delta T}{T} - \frac{\delta p}{p}. \quad (20.94)$$

In particular, if the differential is computed between points in space within a fluid at a particular time instance, then we are led to the relationship between spatial gradients

$$\frac{\nabla\theta}{\theta} = \frac{\nabla T}{T} - \frac{\nabla p}{p}. \quad (20.95)$$

20.4.12 Further study

Atmospheric sciences and dynamic meteorology books have thorough discussions of ideal gas thermodynamics. Some of the material in section 1.6 of Holton (1992) was used in the present section.



20.5 Exercises

EXERCISE 20.1: GEOPOTENTIAL HEIGHT

The *geopotential height* is the height above the earth of a chosen pressure surface.

- (a) Show that an ideal gas atmosphere in exact hydrostatic balance with a uniform lapse rate

$$\frac{dT}{dz} = -|\Gamma| = \text{constant} \quad (20.96)$$

has a geopotential height at a pressure p given by

$$z = \frac{T_0}{|\Gamma|} \left[1 - \left[\frac{p_0}{p} \right]^{-R^M |\Gamma| / g} \right], \quad (20.97)$$

where T_0 is the temperature at $z = 0$.

- (b) For an isothermal atmosphere, obtain an expression for the geopotential height as a function of pressure, and show that this result is consistent with the expression (20.97) in the appropriate limit.

EXERCISE 20.2: POTENTIAL TEMPERATURE FOR AN IDEAL GAS

Show that $\partial\theta/\partial p = 0$ for the potential temperature of an ideal gas given by equation (20.92)

$$\theta = T \left[\frac{p_R}{p} \right]^{R^M/c_p}. \quad (20.98)$$

Hint: remember that $\partial T/\partial p \neq 0$ since the partial derivative is computed with other variables fixed.

EXERCISE 20.3: THERMODYNAMIC RELATIONS FOR AN ATMOSPHERE

In this exercise, we establish some relations for an ideal gas atmosphere, and one relation holding for an arbitrary equation of state. We assume that the gravitational acceleration is constant throughout the full depth of the atmosphere. This assumption becomes questionable when integrating to the top of the atmosphere. We furthermore ignore differences in the horizontal cross-sectional area of a fluid column at the bottom and top of the atmosphere arising from the spherical nature of the planet. These two assumptions are sufficient for our purposes.

- (a) PRESSURE-HEIGHT IDENTITY: Prove the following identity and state your assumptions

$$\int_0^{p_s} z dp = \int_{z=0}^{z_{top}} p dz. \quad (20.99)$$

This identity will be of use for some of the following questions.

- (b) IDEAL GAS $\mathcal{I} + \Phi$ INTEGRATED OVER DEPTH OF A HYDROSTATIC ATMOSPHERE: For an ideal gas atmosphere in exact hydrostatic balance, show that the integral of the gravitational potential energy plus internal energy from the surface to the top of the atmosphere is equal to the integral of the enthalpy of the atmosphere

$$\int_0^{z_{top}} (\Phi + \mathcal{I}) \rho dz = \int_0^{z_{top}} \mathcal{H} \rho dz, \quad (20.100)$$

where

$$\mathcal{H} = p \alpha + \mathcal{I} \quad (20.101)$$

is the enthalpy per mass,

$$\Phi = g z \quad (20.102)$$

is the simple form of the geopotential, which is also the gravitational potential energy per mass (Section 11.11.4), and \mathcal{I} is the internal energy per mass. The height integral extends from the surface where $z = 0$, to the top of the atmosphere where $z = z_{top}$.

- (c) VERTICAL DERIVATIVE OF DRY STATIC ENERGY: For an ideal gas atmosphere in hydrostatic balance, show that

$$\frac{d\sigma}{dz} = \Pi \frac{d\theta}{dz}, \quad (20.103)$$

where

$$\sigma = \mathcal{H} + \Phi \quad (20.104)$$

is the dry static energy and

$$\Pi = c_p (T/\theta) \quad (20.105)$$

is the *Exner function* introduced in equation (20.93).

- (d) FIRST IDENTITY FOR HORIZONTAL PRESSURE GRADIENT: For an ideal gas atmosphere

(either hydrostatic or non-hydrostatic), derive the following expression for the pressure gradient acceleration

$$-\frac{1}{\rho} \nabla p = -\theta \nabla \Pi. \quad (20.106)$$

It then follows that for any instant in time, we have the relation between differentials

$$\rho^{-1} dp = \theta d\Pi. \quad (20.107)$$

- (e) SECOND IDENTITY FOR HORIZONTAL PRESSURE GRADIENT: For an ideal gas atmosphere (either hydrostatic or non-hydrostatic), derive the following expression for the pressure gradient acceleration

$$-\frac{1}{\rho} \nabla p = -\frac{c_s^2}{\rho \theta} \nabla(\rho \theta), \quad (20.108)$$

where c_s is the sound speed.

- (f) $\mathcal{I} + \Phi$ INTEGRATED OVER DEPTH OF A HYDROSTATIC ATMOSPHERE: Show that for a hydrostatic atmosphere with an arbitrary equation of state

$$\int_0^{p_s} (\Phi + \mathcal{I}) dp = \int_0^{p_s} \mathcal{H} dp. \quad (20.109)$$

That is, show that the relation in the first part of this problem holds even without making the ideal gas assumption.

EXERCISE 20.4: UNIT KNUDSEN NUMBER

Recall from Section 13.2.2 that the Knudsen number is the ratio $\text{Kn} = L_{\text{mfp}}/L_{\text{macro}}$, where $L_{\text{macro}} \approx 10^{-4}$ m is the macroscopic length scale used in the discussion of the continuum approximation, and L_{mfp} is the molecular mean free path (Section 13.3.3). Throughout this exercise make use of $p_{\text{stand}} = 101.325 \times 10^3$ Pa for standard atmospheric pressure.

- (a) Consider a mole of an isothermal and ideal gas atmosphere of $T = 300\text{K}$ with a constant gravitational acceleration. At what pressure is the Knudsen number unity? Write your answer as a fraction of standard sea atmospheric pressure, p_{stand} .
- (b) Compute the altitude corresponding to the above pressure, assuming the sea level pressure is p_{slp} and the geopotential is $\Phi = g z$. Hint: make use of results from Section 20.4.10.
- (c) Assuming $p = p_{\text{stand}}$, at what temperature is $\text{Kn} = 1$? Hint: assume the ideal gas law holds regardless the temperature.
- (d) Comment on what is the least atmospherically relevant assumption made during this exercise.



Part V

Dynamics of geophysical flows

Dynamics is the area of mechanics that examines the causes of motion. For a Newtonian system, such as a geophysical fluid, the cause of motion is understood when we understand the forces acting on the fluid. In this part of the book, we encounter a suite of theoretical concepts that form the foundations of geophysical fluid mechanics. Our presentation typically moves from the general to the specific, with each chapter written in a manner that allows it to be picked up without relying too much on other chapters. The *general to specific* presentation allows us to establish general principles based on foundational concepts and to then see how they manifest in specific contexts.

Forces of concern in geophysical fluid mechanics include the body force acting on a fluid element from the earth's gravity field along with the contact forces from pressure and friction that act between adjacent fluid elements. Additionally, by choosing to work in a non-inertial rotating terrestrial reference frame, we encounter body forces from the Coriolis and planetary centrifugal accelerations, just as encountered for geophysical particle mechanics in Part II. Each of these forces play important roles in determining the diversity of geophysical fluid motion, and their analysis leads to dynamical insights into the nature and causes of fluid motion. We observe that forces in fluids are commonly inferred from kinematic properties of the motion, thus making use of the fluid kinematics from Part III.

SUMMARY OF THE DYNAMICS CHAPTERS

We start the development of dynamics by formulating the equations of motion (linear momentum and angular momentum) in Chapter 21. In subsequent chapters we study the forces appearing in these equations, including friction (Chapter 22), pressure (Chapter 25), and buoyancy (Chapter 27). Buoyancy is the vertical pressure force, arising from density inhomogeneities, that are not balanced by gravity. As such, our study of buoyancy focuses on vertical forces, which contrasts to our study of pressure form stresses in Chapter 25, which focus on horizontal forces.

When studying buoyancy in Chapter 27, we make use of an equation of state that provides the mass density of a fluid element as a function of thermodynamical properties such as temperature, pressure, and matter concentration. In Chapter 23 we study the flow of energy through the fluid, including both mechanical energy of the macroscopic fluid and the internal energy of the molecular degrees of freedom. We thus study how mechanical energy is exchanged with internal energy in the presence of work done by pressure and heat generated by friction.

Chapters 24 and 26 introduce a variety of approximate equations that allow us to focus on selected dynamical regimes by filtering away uninteresting phenomena. It is here that we encounter the hydrostatic approximation and the Boussinesq approximation, both of which are commonly used for large-scale models of the ocean and atmosphere. Approximate balances are further examined in Chapter 28, where we study the mechanics of a rapidly rotating fluid. We here encounter the geostrophic balance, which is a diagnostic balance appropriate for describing large-scale geophysical flows in which the horizontal pressure acceleration is balanced by the Coriolis acceleration. Geostrophic balance is one of the variety of balances considered in Chapter 29, which introduces balanced flow regimes pertaining to horizontal motions. We close this part of the book in Chapter 30, which examines the physics of an Ekman boundary layer in which the Coriolis acceleration balances vertical friction.

Throughout the previous chapters we assumed a constant effective gravitational acceleration. However, much of the observed motion of the ocean arises from the spatial-temporal variations of the gravity field that give rise to tides, thus motivating our brief look at the subject in Chapter 31. Finally, in Chapter 45 we briefly visit the topic of gravity waves on the surface of a homogenous and non-hydrostatic fluid. Such waves have a vertical extent that decays exponentially, thus leading to the transport of particles through Stokes drift. Stokes drift appears in many guises in

fluid mechanics, with the presentation in this chapter rather standard but helping to support the later view in Chapter 62 from the basis of the generalized Lagrangian mean.

Chapter 21

MOMENTUM DYNAMICS

We here formulate the fluid mechanical equations for linear and axial angular momentum for geophysical fluid motions. These equations of geophysical fluid dynamics (GFD) are based on Newton's laws of motion applied to a stratified fluid continuum moving on a rotating spherical planet where the rotation rate is constant in time. Relative to the point particle, the new dynamical feature afforded to the continuum concerns contact forces between fluid elements, which lead to pressure and frictional forces from mechanical interactions.

READER'S GUIDE TO THIS CHAPTER

We make liberal use of results from point particle mechanics studied in Part II as well as fluid kinematics from Part III.

21.1	Loose threads	461
21.2	Linear momentum equation	462
21.2.1	Body forces	462
21.2.2	Contact forces	462
21.2.3	Equation of motion	464
21.2.4	Euler equation for perfect fluid motion	465
21.2.5	Further study	465
21.3	Special forms for the momentum equation	466
21.3.1	Spherical coordinates	466
21.3.2	Vector-invariant velocity equation	467
21.3.3	Dynamic pressure and the Magnus acceleration	467
21.3.4	The f -plane and β -plane	469
21.4	Exact hydrostatic balance	470
21.4.1	Properties of exact hydrostatic balance	470
21.4.2	Comparison to approximate hydrostatic balance	471
21.5	Axial angular momentum	472
21.5.1	Axial angular momentum conserving motion of a ring of air	472
21.5.2	Sketching the atmospheric angular momentum budget	473
21.5.3	Further study	475
21.6	Exercises	475

21.1 Loose threads

- Figures needed

21.2 Linear momentum equation

We here summarize elements of classical continuum mechanics and in turn apply Newton's second law to derive the linear momentum budget for a fluid continuum. We present the momentum budget over both a finite volume region of the fluid (weak formulation) and for an infinitesimal fluid element (strong formulation).

21.2.1 Body forces

Forces acting on an arbitrary volume, \mathcal{R} , of a continuous media are of two general types. The first involves *external* or *body* forces, such as gravitation (including astronomical tidal forces), Coriolis, planetary centrifugal, and electromagnetic forces. These forces act throughout the extent of the media. Consequently, the total body force acting on a volume of fluid is the integral of the body force per unit mass, \mathbf{f}_{body} , multiplied by the mass of the media and then integrated over the volume

$$\mathbf{F}_{\text{body}} = \int_{\mathcal{R}} \mathbf{f}_{\text{body}} \rho dV. \quad (21.1)$$

For example, the effective gravitational force (combination of central gravity plus planetary centrifugal) acting on a volume of fluid is given by

$$\mathbf{F}_{\text{effective gravity}} = \int_{\mathcal{R}} \mathbf{g} \rho dV, \quad (21.2)$$

where $\mathbf{g} = -\nabla\Phi$ is the effective acceleration of gravity with Φ the geopotential (Section 11.11.4). Likewise, the Coriolis force acting on the volume is given by

$$\mathbf{F}_{\text{Coriolis}} = -2 \int_{\mathcal{R}} (\boldsymbol{\Omega} \times \mathbf{v}) \rho dV. \quad (21.3)$$

These body forces have the same appearance as for the point particle in Chapter 11, with the only difference being the material is now a continuous media rather than a point mass, thus requiring us to integrate over the region.

21.2.2 Contact forces

The second kind of forces are *internal* or *contact* forces, such as pressure forces and frictional forces. These forces act on a region of a continuous media through the area integrated stresses acting on the boundary enclosing the region. Mathematically, we compute the contact force exerted on the region by area integrating the *stress tensor* projected onto the normal direction along the region boundary

$$\mathbf{F}_{\text{contact}} = \oint_{\partial\mathcal{R}} \mathbb{T} \cdot \hat{\mathbf{n}} d\mathcal{S}, \quad (21.4)$$

where $\hat{\mathbf{n}}$ is the outward normal direction orienting the domain boundary with $d\mathcal{S}$ the associated area element, and \mathbb{T} is the second order stress tensor. We have more to say about the stress tensor in the following as well as in Chapter 22.

Contact forces affect continuous media and they do so through the nonzero spatial extent of elements within the media, with this spatial extent allowing for interactions between adjacent fluid elements. Point particles (Part II) do not experience contact forces since point particles have no spatial extent. Hence, contact forces represent a fundamentally new feature, conceptually and operationally, to the fluid dynamical equations relative to the equations of point particles.

Stresses from friction and pressure

As studied in detail in Chapter 22, there are two types of stress that concern us: diagonal stresses associated with reversible momentum exchange through pressure, and stresses associated with the irreversible exchange of momentum through friction. Hence, it is convenient to decompose the stress tensor components according to

$$\mathbb{T}^{ab} = \tau^{ab} - p g^{ab}. \quad (21.5)$$

In this equation, p is the pressure, which is a force per unit area acting in a compressive manner on the area of a surface. The second order tensor, g^{ab} , is a chosen coordinate representation of the inverse metric tensor and it equals to the Kronecker or unit tensor when choosing Cartesian coordinates in Euclidean space (Section 8.1). The frictional stress tensor is written τ^{ab} . It is also known as the *deviatoric* stress tensor as it represents deviations from the static case when stress is due solely to pressure. The friction stress tensor generally has zero trace, with pressure comprising the trace portion of the full stress tensor.

Substitution of the stress tensor (21.5) into the contact force expression (21.4) leads to

$$\mathbf{F}_{\text{contact}} = \oint_{\partial\mathcal{R}} (\tau \cdot \hat{\mathbf{n}} - p \hat{\mathbf{n}}) dS, \quad (21.6)$$

where the integral is taken over the bounding surface of the domain whose outward normal is $\hat{\mathbf{n}}$. Given this expression for contact forces acting on the boundary of a fluid domain, it is seen that positive pressure ($p > 0$) acts in the direction opposite to the surface's outward normal so that pressure always acts in a compressive manner. Deviatoric stresses create more general forces on the bounding surface, which can have compressive, expansive, shearing, and/or rotational characteristics.

Exchange of momentum between fluid elements

We mathematically represent the exchange of momentum between fluid elements via a symmetric stress tensor, with symmetry implied by statements about angular momentum conservation (detailed in Section 22.4). The divergence of the stress tensor then leads to a force acting on the fluid element. The forces arising from molecular viscosity provide an irreversible exchange of momentum that reduce the kinetic energy of fluid elements (Section 23.3.2). This process is dissipative and thus referred to as friction. Furthermore, when averaging over turbulent realizations of a fluid, the impacts on the mean flow are generally far larger than those associated with molecular viscosity, with these exchanges commonly parameterized via a symmetric stress tensor.

A gauge symmetry of pressure force

The contribution from pressure in the contact force (21.6) remains invariant if pressure is shifted by an arbitrary function of time

$$p(\mathbf{x}, t) \rightarrow p(\mathbf{x}, t) + F(t). \quad (21.7)$$

We see this invariance by noting that

$$\oint_{\partial\mathcal{R}} F(t) \hat{\mathbf{n}} dS = F(t) \oint_{\partial\mathcal{R}} \hat{\mathbf{n}} dS = 0, \quad (21.8)$$

where the final equality follows from a corollary of the divergence theorem as discussed in Section 2.7.3. Briefly, through the divergence theorem in Section 2.7.2 we know that

$$\oint_{\partial\mathcal{R}} p \hat{\mathbf{n}} d\mathcal{S} = \int_{\mathcal{R}} \nabla p dV, \quad (21.9)$$

so that if pressure is shifted by a spatial constant then the pressure gradient body force remains unchanged, as will the pressure contact force.

We refer to this invariance of the pressure force as a *gauge symmetry*. It means that motion of the fluid remains unchanged if pressure is modified by a spatial constant that can generally be a function of time.

21.2.3 Equation of motion

The linear momentum of a fluid region is given by

$$\mathbf{P} = \int_{\mathcal{R}} \mathbf{v} \rho dV. \quad (21.10)$$

Applying Newton's law of motion to the continuum leads to the finite volume equation of motion

$$\frac{d}{dt} \int_{\mathcal{R}} \mathbf{v} \rho dV = \int_{\mathcal{R}} \rho \mathbf{f}_{\text{body}} dV + \oint_{\partial\mathcal{R}} \mathbb{T} \cdot \hat{\mathbf{n}} d\mathcal{S}. \quad (21.11)$$

The time derivative can be material, as for a constant mass fluid region moving with the barycentric velocity. Or it could be Eulerian, as for a fixed region in space (see Section 17.3), or it could be a time derivative following an arbitrary fluid region. Applying the divergence theorem (Section 2.7.2) to the area integral yields

$$\frac{d}{dt} \int_{\mathcal{R}} \rho \mathbf{v} dV = \int_{\mathcal{R}} (\rho \mathbf{f}_{\text{body}} + \nabla \cdot \mathbb{T}) dV, \quad (21.12)$$

where we brought the contact forces into the volume integral through exposing the divergence of the stress tensor.

General form of the equation of motion for a fluid element

Since the volume under consideration is arbitrary, the integral relation (21.12) is satisfied for an arbitrary region. We apply the result to an infinitesimal fluid element moving with the flow

$$\frac{D(\rho \mathbf{v} \delta V)}{Dt} = \delta V (\rho \mathbf{f}_{\text{body}} + \nabla \cdot \mathbb{T}). \quad (21.13)$$

Assuming the mass for the fluid element is constant then reveals the strong form of the equation of motion

$$\rho \frac{D\mathbf{v}}{Dt} = \rho \mathbf{f}_{\text{body}} + \nabla \cdot \mathbb{T} \iff \rho \frac{D\mathbf{v}_a}{Dt} = \rho \mathbf{f}_a + \partial_b \mathbb{T}_{ba}. \quad (21.14)$$

This equation is a continuum expression of Newton's equation of motion, and it is sometimes referred to as *Cauchy's equation of motion*. The right expression exposes the Cartesian tensor labels, with the "body" label dropped for brevity.

Momentum equation for a rotating fluid in a gravitational field

We now specialize the momentum equation (21.14) to suit the needs of geophysical fluid mechanics. We first write the stress tensor in terms of the deviatoric component from friction and a diagonal component from pressure (equation (21.6))

$$\rho \frac{D\mathbf{v}}{Dt} = \rho \mathbf{f}_{\text{body}} - \nabla p + \nabla \cdot \boldsymbol{\tau}. \quad (21.15)$$

Next, move to a rotating terrestrial reference frame and thus expose the Coriolis acceleration and the effective gravitational force (Section 11.12)

$$\rho \frac{D\mathbf{v}}{Dt} + 2\rho \boldsymbol{\Omega} \times \mathbf{v} = -\rho \nabla \Phi - \nabla p + \nabla \cdot \boldsymbol{\tau}. \quad (21.16)$$

This form of the equation of motion arises from extracting the solid-body motion of the basis vectors to define the Coriolis acceleration (see Section 11.10). Any remaining changes to the basis vectors arise from motion of the fluid relative to the solid-body rotating reference frame, and thus appear when expanding the material time derivative. The form (21.16) for the equation of motion offers a suitable starting point for studies of geophysical fluid dynamics. It sometimes goes by the name of *Navier-Stokes* equation. However, that name is more commonly applied to the non-rotating case with a specific form for the friction operator (see Section 22.8.7). We thus refer to equation (21.16) as Newton's law of motion for a rotating fluid.¹

21.2.4 Euler equation for perfect fluid motion

The inviscid form of the momentum equation (21.15) is known as the *Euler equation* of perfect fluid mechanics

$$\rho \frac{D\mathbf{v}}{Dt} = \rho \mathbf{f}_{\text{body}} - \nabla p, \quad (21.17)$$

where the body force is conservative. That is, the Euler equation is concerned just with fluid motion in the absence of dissipative processes. The inviscid form of the momentum equation (21.16) leads to the Euler equation in the presence of rotation and gravitation

$$\rho \frac{D\mathbf{v}}{Dt} + 2\rho \boldsymbol{\Omega} \times \mathbf{v} = -\rho \nabla \Phi - \nabla p. \quad (21.18)$$

We have many occasions in this book to ignore dissipation, in which case we work with a particular form of the Euler equation. We further comment on the Euler equation in Section 22.8.7.

21.2.5 Further study

Chapter 5 of [Aris \(1962\)](#) offers an insightful discussion of continuum mechanics as applied to a fluid. Section 2.2 [Vallis \(2017\)](#) provides a thorough derivation of the dynamical equations of motion for the atmosphere and ocean. We offer further discussion of the mathematics and physics of stress in fluids in Chapters 22 and 25.

¹The Navier-Stokes equations were first derived by Claude-Louis Navier in 1822 and later independently derived by George Stokes in 1845.

21.3 Special forms for the momentum equation

We here display some special forms of the momentum equation that will be of use in our studies throughout this book.

21.3.1 Spherical coordinates

Geophysical fluids move on a rotating planet with the planet commonly assumed to have an oblate spherical geometry, though with the equations approximated by their spherical form using the geopotential vertical coordinate. To display the equations of motion, we make use of the acceleration as derived in Section 11.12.3 for the point particle, using the geopotential coordinate to measure radial distances from the center of the sphere, as well as the longitude and latitude angular coordinates defined by Figure 9.1. The point particle time derivative, which is computed following the particle, translates into a material time derivative for fluid elements. We are thus led to the spherical equations of motion in their full glory

$$\frac{Du}{Dt} + \frac{u(w - v \tan \phi)}{r} + 2\Omega(w \cos \phi - v \sin \phi) = -\frac{1}{\rho r \cos \phi} \frac{\partial p}{\partial \lambda} + F^\lambda \quad (21.19)$$

$$\frac{Dv}{Dt} + \frac{v w + u^2 \tan \phi}{r} + 2\Omega u \sin \phi = -\frac{1}{\rho r} \frac{\partial p}{\partial \phi} + F^\phi \quad (21.20)$$

$$\frac{Dw}{Dt} - \frac{u^2 + v^2}{r} - 2\Omega u \cos \phi = -g - \frac{1}{\rho} \frac{\partial p}{\partial r} + F^r, \quad (21.21)$$

where we introduced the spherical components to the friction acceleration

$$\mathbf{F} = F^\lambda \hat{\lambda} + F^\phi \hat{\phi} + F^r \hat{r}, \quad (21.22)$$

which is determined by the divergence of the frictional stress tensor. We also note the spherical coordinate form for the gradient operator (Section 9.2.8)

$$\nabla = \frac{\hat{\lambda}}{r \cos \phi} \frac{\partial}{\partial \lambda} + \frac{\hat{\phi}}{r} \frac{\partial}{\partial \phi} + \hat{r} \frac{\partial}{\partial r}, \quad (21.23)$$

as well as the material time derivative operator

$$\frac{D}{Dt} = \frac{\partial}{\partial t} + \mathbf{v} \cdot \nabla = \frac{\partial}{\partial t} + \frac{u}{r \cos \phi} \frac{\partial}{\partial \lambda} + \frac{v}{r} \frac{\partial}{\partial \phi} + w \frac{\partial}{\partial r}. \quad (21.24)$$

We can write the spherical momentum equations in a bit more compact form by introducing the spherical coordinate velocity field (see equation (11.48))

$$\mathbf{v} = \mathbf{u} + \hat{r} w = u \hat{\lambda} + v \hat{\phi} + w \hat{r} \quad (21.25)$$

and the corresponding spherical coordinate acceleration

$$\mathbf{A}_{\text{sphere}} = \frac{Du}{Dt} \hat{\lambda} + \frac{Dv}{Dt} \hat{\phi} + \frac{Dw}{Dt} \hat{r}. \quad (21.26)$$

We also introduce the expression (11.85c) for the metric acceleration to render

$$\rho \frac{D\mathbf{v}}{Dt} + 2\rho \boldsymbol{\Omega} \times \mathbf{v} = -\rho \nabla \Phi - \nabla p + \rho \mathbf{F}, \quad (21.27)$$

where we have the acceleration relative to the rotating frame

$$\frac{D\mathbf{v}}{Dt} = \mathbf{A}_{\text{sphere}} + \frac{1}{r} [u \tan \phi (\hat{\mathbf{r}} \times \mathbf{v}) + w \mathbf{u} - \hat{\mathbf{r}} \mathbf{u} \cdot \mathbf{u}]. \quad (21.28)$$

For some purposes it is convenient to combine one piece of the metric acceleration to the Coriolis acceleration to yield

$$\mathbf{A}_{\text{sphere}} + \frac{1}{r} [w \mathbf{u} - \hat{\mathbf{r}} \mathbf{u} \cdot \mathbf{u}] + \left[2\Omega + \frac{u \tan \phi \hat{\mathbf{r}}}{r} \right] \times \mathbf{v} = -\nabla \Phi - \rho^{-1} \nabla p + \mathbf{F}. \quad (21.29)$$

21.3.2 Vector-invariant velocity equation

The metric terms appearing in the momentum equation (21.29) are those terms proportional to r^{-1} that arise from spatial dependence of the spherical unit vectors. An alternative formulation removes these terms in favor of the vorticity and kinetic energy. For that purpose we make use of the identity (equation (2.38)) for the nonlinear self-advection term

$$(\mathbf{v} \cdot \nabla) \mathbf{v} = \boldsymbol{\omega} \times \mathbf{v} + \nabla(\mathbf{v} \cdot \mathbf{v})/2, \quad (21.30)$$

where $\boldsymbol{\omega} = \nabla \times \mathbf{v}$ is the vorticity from Part VII of this book. We derive the corresponding *vector-invariant* form of the velocity equation using Cartesian coordinates and then invoke general coordinate invariance (Section 7.1) to extend the result to arbitrary coordinates.² Making use of equation (21.30) thus leads to the material acceleration

$$\frac{D\mathbf{v}}{Dt} = \frac{\partial \mathbf{v}}{\partial t} + \boldsymbol{\omega} \times \mathbf{v} + \nabla(\mathbf{v} \cdot \mathbf{v})/2 \quad (21.31)$$

so that the momentum equation (21.16) becomes the vector-invariant velocity equation

$$\frac{\partial \mathbf{v}}{\partial t} + (2\Omega + \boldsymbol{\omega}) \times \mathbf{v} = -\nabla(\Phi + \mathbf{v} \cdot \mathbf{v}/2) + (1/\rho) (-\nabla p + \nabla \cdot \tau). \quad (21.32)$$

The name *vector-invariant* is motivated since the form of this equation remains unchanged when using Cartesian or spherical coordinates. However, this name seems rather unnecessary since when formulated using the tensor formalism from Chapters 7 and 8, any mathematical physics equation remains form invariant.

21.3.3 Dynamic pressure and the Magnus acceleration

The *velocity equation* (21.32) is mathematically equivalent to the momentum equation (21.16). Even so, it provides a more convenient means to derive Bernoulli's theorem in Section 23.7.3 and the vorticity equation in Chapter 37. Furthermore, it highlights certain physical processes affecting accelerations that are not obviously seen from the momentum equation. We here consider two such processes.

Dynamic pressure

The velocity equation (21.32) reveals that gradients in the kinetic energy per mass contribute a *dynamical pressure gradient* that accelerates the fluid down the kinetic energy gradient, from regions of high kinetic energy per mass to regions of low kinetic energy per mass. To help understand this process, consider a Boussinesq fluid (Chapter 26), in which case the density

²See Section 4.4.4 of [Griffies \(2004\)](#) for a detailed derivation using general coordinates.

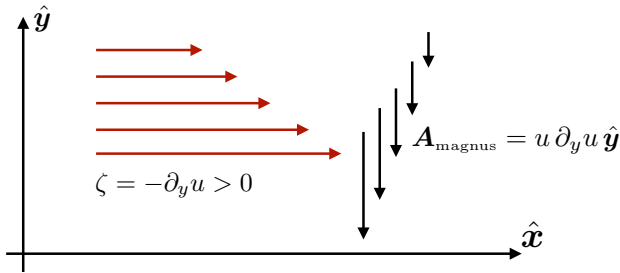


FIGURE 21.1: The Magnus acceleration, $\mathbf{A}_{\text{magnus}} = -\boldsymbol{\omega} \times \mathbf{v}$, acting on a fluid element with nonzero vorticity. In this case the fluid element has a zonal velocity with a linear meridional shear, $\mathbf{v} = u(y) \hat{x}$, so that the relative vorticity is $\boldsymbol{\omega} = \zeta \hat{z} = -(\partial_y u) \hat{z}$ and the Magnus acceleration is $\mathbf{A}_{\text{magnus}} = u \partial_y u \hat{y}$. When the fluid has a negative meridional shear, $\partial_y u < 0$, its relative vorticity is positive (cyclonic), $\zeta = -\partial_y u > 0$, so that the Magnus acceleration deflects the fluid element to the right of the motion, just as for the Coriolis acceleration in the northern hemisphere.

factor is a constant, $\rho = \rho_0$, so that we can write the accelerations from pressure and kinetic energy as

$$-(1/\rho_0) \nabla p - \nabla(\mathbf{v} \cdot \mathbf{v}/2) = -\rho_0^{-1} \nabla(p + \rho_0 \mathbf{v} \cdot \mathbf{v}/2) \equiv -\rho_0^{-1} \nabla p_{\text{stagnation}}. \quad (21.33)$$

In this equation we defined the *stagnation pressure*

$$p_{\text{stagnation}} \equiv p + \rho_0 \mathbf{v} \cdot \mathbf{v}/2, \quad (21.34)$$

which is the sum of the mechanical pressure, p , plus the dynamic pressure, $\rho_0 \mathbf{v} \cdot \mathbf{v}/2$.

The stagnation pressure is the pressure required to keep the local acceleration unchanged if the dynamic pressure is set to zero as per a stagnant fluid. This situation arises in practice in a device known as a *Pitot tube* used to measure the speed of flow in a pipe, with the Pitot tube making use of the Bernoulli theorem formulated in Section 23.7. Stagnation points also arise at special points along solid objects within a moving fluid, such as wings. The dynamic pressure, $\rho_0 \mathbf{v} \cdot \mathbf{v}/2$, provides an isotropic force per area in addition to mechanical pressure, p . Hence, the stagnation pressure is the total isotropic contact force per area, thus motivating some treatments to refer the stagnation pressure as the *total pressure*.³

Magnus acceleration

The acceleration $-\boldsymbol{\omega} \times \mathbf{v}$ appearing in the velocity equation (21.32) couples vorticity and velocity. This acceleration is known as the *Magnus effect* or *Magnus acceleration*. Since it acts only when there is both motion and vorticity, it is sometimes referred to as a *vortex force*, with the force increasing in magnitude where the velocity and/or vorticity are larger in magnitude. As discussed in Chapter 34, vorticity is a measure of the spin of a fluid element, so that the Magnus acceleration deflects a spinning fluid element in a direction perpendicular to its trajectory just like the Coriolis acceleration. We illustrate a particular case in Figure 21.1 for a zonal flow with a negative meridional shear that creates a positive vertical relative vorticity. Besides causing a moving and spinning fluid element to deflect, the Magnus acceleration provides the mechanism whereby a solid spinning body immersed in a moving fluid is deflected, such as commonly experienced by spinning balls used for baseball, tennis, and cricket. Notably, as per Newton's third law, the spinning ball is deflected in a direction opposite to that of the spinning fluid element.

³In many engineering applications, the mechanical pressure, p , is referred to as the *static pressure* so that the total/stagnation pressure is the sum of the static plus dynamic pressures. See section 4.9 of [Kundu et al. \(2016\)](#) for more discussion.

21.3.4 The f -plane and β -plane

Spherical coordinates are suited for the study of planetary fluid dynamics for cases where the fluid samples the earth's sphericity. However, spherical coordinates remain more complicated to work with than Cartesian coordinates. We are thus led to consider the utility of an idealized tangent plane configuration as part of a hierarchy of theoretical models to help understand geophysical fluid motion. This motivation leads to the f -plane and β -plane approximations, which are the two cases considered as part of the tangent plane approximations. We here expose these equations, with further use encountered later in the book.

Tangent plane approximation

Consider a tangent plane located at latitude $\phi = \phi_0$ and introduce a Cartesian set of coordinates according to

$$(x, y, z) = (R_e \lambda \cos \phi_0, R_e (\phi - \phi_0), z) \quad (21.35)$$

$$(\hat{x}, \hat{y}, \hat{z}) = (\hat{\lambda}, \hat{\phi}, \hat{r}). \quad (21.36)$$

Use of these Cartesian coordinates leads to the following inviscid (i.e., no friction) equations of motion

$$\frac{Du}{Dt} + 2(\Omega^y w - \Omega^z v) = -\frac{1}{\rho} \frac{\partial p}{\partial x} \quad (21.37)$$

$$\frac{Dv}{Dt} + 2(\Omega^z u - \Omega^x w) = -\frac{1}{\rho} \frac{\partial p}{\partial y} \quad (21.38)$$

$$\frac{Dw}{Dt} + 2(\Omega^x v - \Omega^y u) = -\frac{1}{\rho} \frac{\partial p}{\partial z} - g, \quad (21.39)$$

with rotational vector components

$$\boldsymbol{\Omega} = \Omega (\cos \phi_0 \hat{y} + \sin \phi_0 \hat{z}). \quad (21.40)$$

Note the absence of metric terms due to the use of Cartesian coordinates on a flat planar geometry.

The tangent plane approximation originates from the geopotential vertical coordinate system (Section 11.12.3). In that coordinate system, the effective gravitational acceleration (gravity plus planetary centrifugal) is aligned with the local vertical direction. Correspondingly, the resulting tangent plane equations have the effective gravitational force aligned in the \hat{z} direction. As seen in Section 24.3, these equations are slightly different from those describing a fluid in a rotating tank, in which the effective gravity is not aligned with the vertical.

Traditional approximation and the f -plane

The *traditional approximation* is discussed in Section 24.1.3, where we justify retaining only the local vertical component of the rotation vector for the study of large-scale planetary flows, thus resulting in

$$\mathbf{D}\mathbf{u}/Dt + f \hat{z} \times \mathbf{u} = -\rho^{-1} \nabla_z p \quad \text{and} \quad D w/Dt = -\rho^{-1} \partial_z p - g. \quad (21.41)$$

The f -plane makes further use of a constant Coriolis parameter

$$f = 2\Omega \sin \phi_0 \equiv f_0. \quad (21.42)$$

The f -plane approximation is the simplest model for a rotating fluid, and as such it provides an end member in the hierarchy of theoretical models for geophysical fluid flows.

β -plane approximation

As seen in Section 47.3, *Rossby waves* are planetary scale waves that sample the earth's spherical geometry. The essential ingredient for their existence is the latitudinal dependence of the Coriolis parameter. To capture Rossby waves on a tangent plane requires the meridional gradient of the Coriolis parameter, with a linear dependence sufficient

$$f = f_0 + R_e^{-1} (2\Omega \cos \phi_0) (y - y_0). \quad (21.43)$$

For many purposes the β -plane approximation only depends on the meridional gradient of the Coriolis parameter, in which case we generally set

$$f = f_0 + \beta y \quad (21.44)$$

$$\beta = \partial f / \partial y = (2\Omega / R_e) \cos \phi_0, \quad (21.45)$$

thus ignoring the constant $-(2\Omega \cos \phi_0) y_0 / R_e$. The β -plane approximation is formally valid so long as the horizontal scale of motion, L , is not too large, in which case we require

$$\beta L \ll |f_0|. \quad (21.46)$$

21.4 Exact hydrostatic balance

We are mostly interested in moving fluids within this book. Even so, it is useful to expose the signature of a static fluid supporting the trivial solution, $\mathbf{v} = 0$. The equation of motion (21.16) has an exact static solution so long as the pressure gradient force balances the effective gravitational force

$$\nabla p = -\rho \nabla \Phi, \quad (21.47)$$

and where the frictional stress tensor has zero divergence. Equation (21.47) constitutes the *exact hydrostatic balance*. As justified in Section 24.2, the hydrostatic balance is a very good approximation for the vertical momentum equation in large-scale geophysical fluids even when those fluids are moving. We will thus commonly make the *hydrostatic approximation* for moving fluids. For the current considerations, we are interested in a static fluid, in which case the hydrostatic balance (21.47) is an exact solution to the equation of motion.

21.4.1 Properties of exact hydrostatic balance

We make the following observations of the exact hydrostatic balance.

- Since ∇p is directly proportional to $\nabla \Phi$, surfaces of constant pressure (*isobars*) in a static fluid correspond to surfaces of constant geopotential.
- Since the curl of the pressure gradient vanishes, a static fluid maintains its density gradients parallel to geopotential gradients

$$\nabla \rho \times \nabla \Phi = 0, \quad (21.48)$$

which in turn means that density surfaces are parallel to geopotentials so that

$$\rho = \rho(\Phi) \quad \text{static fluid.} \quad (21.49)$$

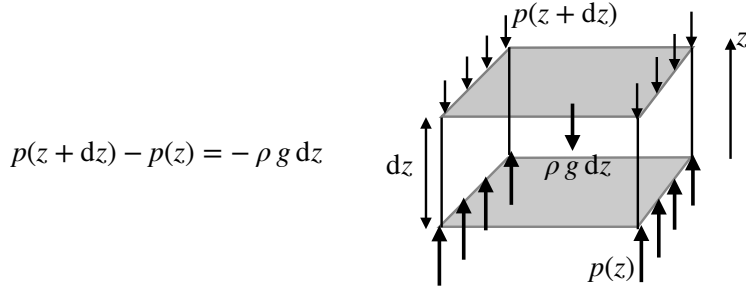


FIGURE 21.2: Illustrating the forces acting in a hydrostatically balanced fluid layer placed in a geopotential field $\Phi = g z$ with g constant. The layer has an infinitesimal thickness $dz > 0$, density ρ , and horizontal cross-sectional area dA . The pressure force acting on the top and bottom of the layer are compressive. Hence, the pressure force at the top of the layer acts downward, $\mathbf{F}^{\text{press}}(z + dz) = -\hat{z} p(z + dz) dA$, whereas the pressure force at the bottom of the layer acts upward, $\mathbf{F}^{\text{press}}(z) = +\hat{z} p(z) dA$. In a hydrostatically balanced fluid, the difference in pressure across the layer is exactly balanced by the weight per area of fluid within the layer. Consequently, $p(z + dz) - p(z) = -g \rho(z) dz$, so that pressure at the top of the layer is less than that at the bottom.

For the geopotential $\Phi = g z$, a static fluid is realized if the density depends only on the vertical position

$$\rho = \rho(z) \quad \text{static fluid with } \Phi = g z. \quad (21.50)$$

If the density gradient has any component perpendicular to $\nabla\Phi$, then pressure forces will affect fluid flow thus implying that the fluid is not in an exact hydrostatic balance.

- Projecting both sides of equation (21.47) onto an infinitesimal space increment, $d\mathbf{x}$, renders

$$d\mathbf{x} \cdot \nabla p = -\rho d\mathbf{x} \cdot \nabla\Phi \implies \frac{dp}{d\Phi} = -\rho. \quad (21.51)$$

Hence, the difference in hydrostatic pressure between any two geopotentials is given by the integral

$$p(\Phi_2) - p(\Phi_1) = - \int_{\Phi_1}^{\Phi_2} \rho(\Phi) d\Phi. \quad (21.52)$$

If $\Phi = g z$ then we recover

$$p(z_2) - p(z_1) = -g \int_{z_1}^{z_2} \rho(z) dz, \quad (21.53)$$

so that the difference in hydrostatic pressure between two geopotentials is given by the weight per horizontal area of fluid between the two geopotentials. This relation is illustrated for an infinitesimally thin layer in Figure 21.2.

21.4.2 Comparison to approximate hydrostatic balance

A static fluid in a gravitational field exhibits hydrostatic balance whereby pressure at a point is a function solely of the geopotential, in which case $p = p(z)$ when $\Phi = g z$. Correspondingly, $dp/dz = -\rho g$, which means that we determine hydrostatic pressure at a point by computing the weight per horizontal area of fluid above that point. Likewise, density is just a function of geopotential since $\nabla\rho \times \nabla\Phi = 0$.

For an approximate hydrostatic fluid, pressure is a function of space and time, $p = p(\mathbf{x}, t)$, as is density, $\rho = \rho(\mathbf{x}, t)$. Hence, we are no longer ensured that pressure and density isolines are

parallel. However, the approximate hydrostatic fluid retains a vertical pressure gradient given by

$$\frac{\partial p}{\partial z} = -\rho g \quad \text{approximate hydrostatic.} \quad (21.54)$$

Hence, column by column, the pressure at a point in an approximate hydrostatic fluid is determined by the weight per horizontal area of fluid above that point. This key property is thus shared between fluids in exact and approximate hydrostatic balance. We have more to say regarding approximate hydrostatic balance in Chapter 24.

21.5 Axial angular momentum

Following our discussion of a point particle in Section 12.6, the axial angular momentum of a fluid element is given by

$$L^z = (\rho \delta V) r_{\perp} (u + r_{\perp} \Omega) \equiv (\rho \delta V) l^z \quad (21.55)$$

where

$$l^z = r_{\perp} (u + r_{\perp} \Omega) \quad (21.56)$$

is the axial angular momentum per unit mass, and the distance to the polar rotation axis,

$$r_{\perp} = r \cos \phi \quad (21.57)$$

is the moment-arm for determining the torques acting on a fluid element. Making use of the zonal momentum equation (21.19) we find the material time change

$$\frac{Dl^z}{Dt} = (u + 2\Omega r_{\perp}) \frac{Dr_{\perp}}{Dt} + r_{\perp} \frac{Du}{Dt} \quad (21.58a)$$

$$= (u + 2\Omega r_{\perp}) \frac{Dr_{\perp}}{Dt} + (u + 2\Omega r_{\perp}) (v \sin \phi - w \cos \phi) - \frac{1}{\rho} \frac{\partial p}{\partial \lambda} \quad (21.58b)$$

$$= (u + 2\Omega r_{\perp}) \left[\frac{Dr_{\perp}}{Dt} + v \sin \phi - w \cos \phi \right] - \frac{1}{\rho} \frac{\partial p}{\partial \lambda} \quad (21.58c)$$

$$= -\frac{1}{\rho} \frac{\partial p}{\partial \lambda}, \quad (21.58d)$$

so that

$$\rho \frac{Dl^z}{Dt} = -\frac{\partial p}{\partial \lambda} \implies \frac{\partial(\rho l^z)}{\partial t} + \nabla \cdot (\rho l^z \mathbf{v}) = -\frac{\partial p}{\partial \lambda}. \quad (21.59)$$

It is only in the absence of a zonal pressure gradient that the axial angular momentum for a fluid element is materially invariant just like for the point particle discussed in Section 12.6. The physical constraints for motion of the point particle, as described in Section 12.7, also hold for the fluid element. In particular, we can equate the zonal Coriolis acceleration to the zonal acceleration induced by axial angular momentum conservation. For example, a fluid element initially at rest in a fluid with zero zonal pressure gradient will zonally accelerate when moved meridionally (e.g., as from a meridional pressure gradient) according to the needs of axial angular momentum conservation.

21.5.1 Axial angular momentum conserving motion of a ring of air

Atmospheric and oceanic flows rarely experience a zero zonal pressure gradient. However, on a smooth spherical planet without meridional boundaries there is a zero zonally integrated zonal

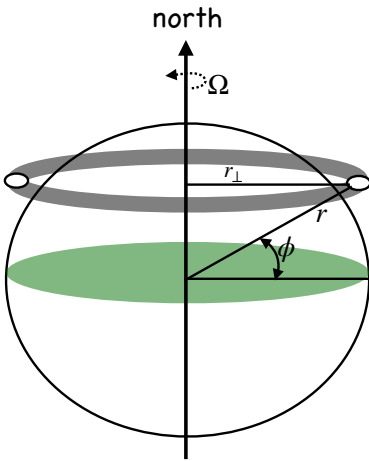


FIGURE 21.3: A ring of inviscid air circulating around a constant latitude circle over a smooth planet. This ring conserves is axial angular momentum. Consequently, axial angular momentum conserving motion of the ring induces a zonal acceleration if the ring alters its distance from the rotation axis, r_{\perp} , by moving meridionally or vertically.

pressure gradient

$$\oint_{\text{ring}} \frac{\partial p}{\partial \lambda} d\lambda = 0. \quad (21.60)$$

Hence, a constant mass material ring of fluid circling the smooth planet (Figure 21.3) will preserve its axial angular momentum in the absence of friction

$$\frac{d}{dt} \oint_{\text{ring}} \rho l^z dV = \oint_{\text{ring}} \rho \frac{Dl^z}{Dt} dV = - \oint_{\text{ring}} \frac{\partial p}{\partial \lambda} dV = 0. \quad (21.61)$$

For example, consider a latitudinal ring of constant mass inviscid fluid circling around the equator at radius R_e , and assume it is at rest relative to the rotating earth. The angular momentum per mass for this ring is $l^z = \Omega R_e^2$. Moving the ring vertically to $r \neq R_e$ while maintaining constant axial angular momentum induces a zonal velocity given by

$$u = \frac{\Omega (R_e^2 - r^2)}{r}. \quad (21.62)$$

Movement downward to $r < R_e$ leads to an eastward flow, $u > 0$, (westerly winds), whereas upward motion leads to the opposite. Likewise, moving the ring latitudinally while keeping $r = R_e$ leads to the zonal velocity

$$u = \frac{\Omega R_e \sin^2 \phi}{\cos \phi}. \quad (21.63)$$

Since $\cos \phi \geq 0$ on the sphere, latitudinal motion away from the equator while preserving axial angular momentum leads to eastward flow ($u > 0$) whether the ring is moved northward or southward.

21.5.2 Sketching the atmospheric angular momentum budget

How realistic is it to have coherent rings of inviscid air circulating around the planet at all latitudes? To answer this question we insert some numbers for a ring of radius R_e that starts with zero relative velocity at the equator. Equation (21.63) says that the westerly winds induced by

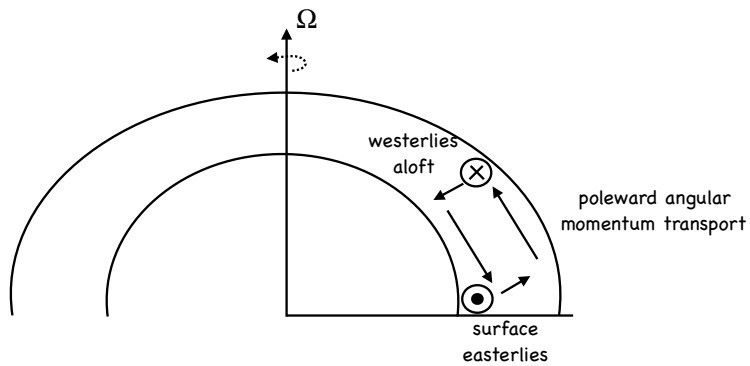


FIGURE 21.4: A sketch of the Hadley circulation. At the low latitudes, low level winds are predominantly easterly (blowing to the west) and so the atmosphere gains positive axial angular momentum from the earth via frictional boundary layer processes. As air rises and moves poleward it zonally accelerates according to conservation of axial angular momentum, thus becoming the mid-latitude westerlies (blowing to the east). The westerlies are generally unstable thus producing baroclinic eddies that vertically transfer axial angular momentum via form stress, thus depositing axial angular momentum back to the earth to close the axial angular momentum cycle.

axial angular momentum conserving motion have the following speeds at a selection of latitudes

$$u(10^\circ) = 14 \text{ m s}^{-1} \quad u(20^\circ) = 58 \text{ m s}^{-1} \quad u(30^\circ) = 134 \text{ m s}^{-1}. \quad (21.64)$$

The values at higher latitudes grow unbounded since $\cos \phi \rightarrow 0$ as the poles are approached. So there is a problem with an idealized theory of atmospheric circulation based on axial angular momentum conserving rings of air. It turns out that inviscid axial angular momentum conserving ideas extend only so far as the Hadley circulation is concerned, with the latitude extents of the Hadley Cell extending only to the middle latitudes. There are two missing ingredients to a more realistic theory: (i) frictional dissipation between the atmosphere and land; (ii) baroclinic eddies that contribute to poleward transport of angular momentum. It is outside of our scope to detail these physical processes and the corresponding atmospheric circulation. Instead, we here simply sketch the scene following Section 10.3 of [Holton \(1992\)](#) and Section 8.2 of [Marshall and Plumbe \(2008\)](#).

Given that the earth has a near constant rotation rate, we can examine a zonally integrated axial momentum budget for the atmosphere and assume that the axial angular momentum of the earth is fixed.⁴ Rather than an inviscid fluid, we consider the dissipation due to boundary layer friction and/or vertical eddy form stress from baroclinic eddies (we study form stress in Chapter 25). In the tropical atmosphere, the atmosphere generally has less angular momentum per mass than the earth given that the winds are predominantly easterly (lower branch of the Hadley Cell). In this region, boundary layer interactions transfer angular momentum per mass from the earth to the atmosphere. In contrast, the presence of middle latitude westerlies aloft (upper branch of the Hadley Cell) signal that the atmosphere has more angular momentum per mass than the earth at these latitudes. There is an implied transfer of angular momentum per mass from the atmosphere to the earth, largely mediated through vertical form stresses due to baroclinic eddies.

As sketched in Figure 21.4, a steady state axial angular momentum budget is realized through a meridional transport of axial angular momentum from the lower latitude atmosphere to the middle latitudes. This transport is mediated partly through an atmospheric overturning circulation (Hadley Cell) and partly through the vertical transfer of momentum via synoptic scale baroclinic eddies (see Section 63.3.5). Furthermore, dissipation by eddies and boundary layer interactions

⁴In fact, the length of a day fluctuates by roughly 10^{-3} s over a seasonal cycle due to transfer of axial angular momentum between the atmosphere and land.

is crucial to realize the observed zonal wind profile. Namely, as seen above, a non-dissipative angular momentum conserving atmosphere exhibits winds that are far larger in magnitude than observed, particularly when moving to higher latitudes.

21.5.3 Further study

In Section 25.5 we consider the zonally integrated axial angular momentum budget for the ocean with sloping solid-earth bottom boundary as well as the upper surface (ocean) boundary. In particular, we see how boundary form stresses (Section 25.1) affect the angular momentum in addition to boundary frictional stresses. That analysis is analogous to that for the atmosphere given in Section 10.3 of [Holton \(1992\)](#).

21.6 Exercises

EXERCISE 21.1: CONDITIONS FOR UNIFORM FLOW WITHOUT GRAVITY AND ROTATION

Consider the Euler equation (21.18) in the absence of rotation (zero Coriolis) and gravitation (free space fluid)

$$\rho \frac{D\mathbf{v}}{Dt} = -\nabla p. \quad (21.65)$$

Ignore all boundaries throughout this exercise, and assume density is a uniform constant.

- What equation does the pressure need to satisfy to ensure $\mathbf{v} \equiv \mathbf{v}_0$, where \mathbf{v}_0 is a constant in space and time?
- What equation does the pressure need to satisfy to ensure $\partial_t(\nabla \cdot \mathbf{v}) = 0$?

EXERCISE 21.2: THEOREM OF STRESS MEANS ([Aris \(1962\)](#)) EXERCISE 5.12.2

Make use of Cauchy's equation of motion (21.14) and the divergence theorem to prove the *theorem of stress means*

$$\oint_{\partial\mathcal{R}} \Psi \mathbb{T}_{pq} \hat{n}_q d\mathcal{S} = \int_{\mathcal{R}} \left[\mathbb{T}_{pq} \partial_q \Psi + \rho \Psi \left(\frac{Dv_p}{Dt} - f_p \right) \right] dV, \quad (21.66)$$

where Ψ is an arbitrary differentiable function, and \hat{n}_q is the q 'th component of the outward normal vector on $\partial\mathcal{R}$. This theorem finds use in certain formulations of continuum mechanics. Assume Cartesian tensors.

EXERCISE 21.3: TIME SYMMETRY OF THE EULER EQUATION

In Section 12.3 we studied the needs for time reversal symmetry in the equations of a point particle. Here we ask the same question for the Euler equation (21.18) in a rotating reference frame. Consider a solution, $\mathbf{v}(\mathbf{x}, t)$, to the Euler equation (21.18) in a rotating reference frame in either free space (i.e., no boundaries) or with fixed material boundaries. What transformation properties are needed for $p(\mathbf{x}, t)$, $\rho(\mathbf{x}, t)$, $\Phi(\mathbf{x}, t)$, and $\boldsymbol{\Omega}$ to ensure that $\mathbf{v}^*(\mathbf{x}, t^*) = -\mathbf{v}(\mathbf{x}, -t)$ is also a solution? That is, what time symmetry properties ensure that the velocity is reversible so that if $\mathbf{v}(\mathbf{x}, t)$ is a solution then so is $-\mathbf{v}(\mathbf{x}, -t)$? Discuss your answer.

EXERCISE 21.4: AREA OF A STEADY 1D LAMINAR JET EMANATING FROM A DOWNWARD NOZZLE

Consider a steady state laminar jet of constant density and inviscid water emanating from a downward facing nozzle with a constant prescribed volume flow rate, Q (dimensions volume per time). Ignore surface tension and assume the air pressure acting on the surface of the jet is constant all along the jet. You can solve this exercise by making use of the steady vertical momentum equation and the steady mass continuity equation.

- (a) Explain why we can set $dp/dz = 0$ within the jet once it leaves the nozzle.
- (b) Determine an expression for the area of the jet, $A(z)$, as a function of distance, z , from the nozzle, with the nozzle placed at $z = 0$ and $z < 0$ a position beneath the nozzle. In addition to z , your expression will contain Q , g , and $A(0)$.
- (c) Is the area of the jet getting smaller or larger as the water moves downward away from the nozzle? Does this answer agree with your experience?
- (d) If the downward speed of water at the nozzle is $w(0) = 0.5 \text{ m s}^{-1}$, then at what vertical position, z , is the area of the jet four times different than at $z = 0$?

EXERCISE 21.5: ROSSBY EFFECT

Consider a horizontal region of fluid whose velocity is rotationally symmetric and depth independent

$$\mathbf{u} = \boldsymbol{\Gamma} \times \mathbf{r}, \quad (21.67)$$

where

$$\boldsymbol{\Gamma} = \Gamma(r) \hat{\mathbf{z}} \quad (21.68)$$

is an angular velocity, $\hat{\mathbf{z}}$ is the vertical direction, and r is the radial distance to the origin. Furthermore, let $\Gamma(r)$ vanish for radial distances $r \geq R$ for some radius R . Let the fluid be moving on a β -plane with Coriolis parameter $f = f_0 + \beta y = f_0 + \beta r \sin \vartheta$, where ϑ is the polar angle relative to the x -axis (see Section 9.3 for definition of polar coordinates). Derive an integral expression for the Coriolis acceleration integrated over this fluid region. Discuss the direction of the acceleration.

You may find the following hints of use.

- The resulting integrated Coriolis acceleration is solely in the $\hat{\mathbf{y}}$ direction, and it vanishes when $\beta = 0$.
- The answer is given in [Rossby \(1948\)](#), and is sometimes known as the *Rossby effect*.
- We further consider such interactions between rotating fluid motion and the Coriolis parameter in Section 35.6.4 when studying the *beta drift* of axially symmetric vortices. We there find that the beta drift leads to a northwestward drift rather than the northward drift from the Rossby effect. The reason for the discrepancy is that [Rossby \(1948\)](#) ignored pressure effects that set up a secondary flow that induces westward drift, in addition to Rossby's northward drift.

EXERCISE 21.6: CENTER OF MASS TRANSPORT THEOREM

Consider a field, ψ , that satisfies the standard conservation law

$$\rho \frac{D\psi}{Dt} = -\nabla \cdot \mathbf{J}, \quad (21.69)$$

within a region, \mathcal{R} , that moves with the fluid flow. We here derive some results that hold for Cartesian coordinates.

- (a) Prove the transport theorem valid for Cartesian tensors

$$\frac{d}{dt} \int_{\mathcal{R}} \psi \mathbf{x} \rho dV = \int_{\mathcal{R}} (\mathbf{J} + \rho \psi \mathbf{v}) dV - \oint_{\partial\mathcal{R}} \mathbf{x} (\hat{\mathbf{n}} \cdot \mathbf{J}) d\mathcal{S}. \quad (21.70)$$

Hint: multiply both sides of equation (21.69) by x_m .

- (b) Offer an interpretation of equation (21.70). Hint: first consider the special case that the total ψ -stuff, defined by $\Psi \equiv \int_{\mathcal{R}} \psi \rho dV$, is constant when following the flow. Further hint: consider the more specialized case of $\psi = 1$ and $\mathbf{J} = 0$, and then make use of Exercise 16.2.



Chapter 22

STRESS IN FLUIDS

As an extended continuous region of matter, a fluid element experiences two kinds of forces: *external* or *body* forces and *internal* or *contact* forces. Body forces act throughout the fluid element and arise from sources external to the matter acted upon. The accumulated effects from body forces within a fluid region result from volume integrating the body forces over the region. In geophysical fluid mechanics, we are concerned with body forces from the effective gravitational acceleration (central gravity plus planetary centrifugal) plus the body force from the Coriolis acceleration. Body forces are also experienced by the point particles studied in Part II in this book.

Contact forces act on a fluid element due to local intermolecular forces within the fluid media. Contact forces signal a fundamental distinction between the dynamics of a fluid element (an infinitesimal portion of a continuous media) and the dynamics of a point particle. Contact forces give rise to the local exchange of dynamical properties between fluid elements. Dividing the contact force by the area upon which it acts leads to the stress vector acting on the surface. As a force per unit area, stresses are associated with two directions: the direction of the force and the direction normal to the area acted upon by the force. Correspondingly, stresses acting on a fluid element are naturally organized into a second order *stress tensor*. Contact forces, which are given by the stress times an area element, satisfy Newton's third law, also known as the action/reaction law. Hence, the net contact force acting on a finite region arises just from the contact forces acting at the region boundary. This property of contact forces means that a mechanically isolated region of a continuous media (i.e., a region unaffected by external forces or boundary contact forces) does not spontaneously translate its center of mass.

Surface tension is a rather unique kind of stress acting on fluid boundaries such as oil and water or air and water. As shown in Section 22.11, surface tension is generally negligible for length scales larger than a few centimeters. It is for this reason that surface tension is commonly absent from books on geophysical fluid mechanics, where most concern is with larger length scales. Nevertheless, the effects are important if studying physical processes associated with air-sea interactions, such as tracer, heat, and momentum exchange through bubbles, droplets, and capillary waves.

CHAPTER GUIDE

We introduced contact forces in Chapter 21 when deriving the fluid equations of motion. In this chapter we dive deeper into contact forces and their corresponding stresses. We also discuss conditions placed on stress and velocity at boundaries. The material in this chapter builds from our study of forces, acceleration, and Newton's laws as applied to a fluid continuum in Chapter 21. Fluid stresses can be organized into a second order tensor and further decomposed into pressure stresses and viscous/frictional stresses. Understanding the mathematical and physical aspects of stress is important for the suite of fluid models studied in this book. Because the subject involves vectors and tensors, it can require a bit more patience from the reader than analogous chapters that discuss scalar fields. To make the formalism less mathematically intense, we employ Cartesian tensors as discussed in Chapters 1 and 2. Results can be generalized to arbitrary coordinates through the general tensor analysis detailed in Chapter 8.

22.1	Loose threads	481
22.2	Cauchy's stress principle and Newton's laws	481
22.2.1	Cauchy's stress principle	481
22.2.2	Newton's third law and local equilibrium of stresses	482
22.2.3	Comments on the local equilibrium relation	482
22.3	The stress tensor	484
22.4	Angular momentum and stress tensor symmetry	486
22.4.1	Basic formulation	487
22.4.2	Physical interpretation	487
22.4.3	Symmetry of the stress tensor	488
22.5	Forces and torques in an exact hydrostatic fluid	489
22.5.1	Force balance	489
22.5.2	Pressure force balance for a homogeneous fluid	490
22.5.3	Torque balance	492
22.6	Flux-form Eulerian momentum equation	493
22.7	Linear momentum for arbitrary regions	494
22.8	Constitutive relation between stress and rate of strain	495
22.8.1	Thermodynamic pressure and mechanical pressure	495
22.8.2	Couette flow and the viscous tensor	496
22.8.3	D'Alembert's theorem for perfect fluids	497
22.8.4	Guidance from Galilean invariance	497
22.8.5	A comment on Rayleigh drag	498
22.8.6	Constitutive relation for Newtonian fluids	498
22.8.7	Navier-Stokes and Euler equations	500
22.8.8	Laplacian friction in terms of vorticity and divergence	501
22.8.9	Frictional stresses in a sheared flow	501
22.8.10	The net stress tensor	502
22.8.11	Comments and further study	503
22.9	Reynolds number and flow regimes	503
22.9.1	Non-dimensional Navier-Stokes	503
22.9.2	Ratio of inertial to frictional accelerations	503
22.9.3	Reynolds numbers for some example flows	504
22.10	Stress on an interface	505
22.10.1	General formulation	505
22.10.2	Solid material boundary	506
22.10.3	No-slip boundary condition	507
22.10.4	Lagrangian interface	507

22.10.5 Permeable interface	508
22.10.6 Summary comments	508
22.10.7 Comments on boundary layers	509
22.11 Surface tension	509
22.11.1 Capillary tube	509
22.11.2 Force balance on an air-water interface	510
22.11.3 Young-Laplace formula	511
22.11.4 Soluble gas bubbles inside water	514
22.11.5 When we can ignore surface tension	514
22.11.6 Further study	515
22.12 Exercises	515

22.1 Loose threads

- Schematic of viscous transfer as in Figure 12.6 of *Kundu et al. (2016)*
- More on existence and uniqueness of Navier-Stokes as per *Doering and Gibbon (1995)*.

22.2 Cauchy's stress principle and Newton's laws

We here develop some general properties of contact forces and the associated stresses. For that purpose, consider an arbitrary smooth closed region, \mathcal{R} , of fluid with volume $V = \int_{\mathcal{R}} dV$ and mass $M = \int_{\mathcal{R}} \rho dV$ (Figure 22.1). Furthermore, let $\partial\mathcal{R}$ be the bounding surface for the region, and let $\hat{\mathbf{n}}$ be the outward normal at a point on the boundary.

22.2.1 Cauchy's stress principle

The bounding surface of the region experiences mechanical interactions with the surrounding fluid continuum and these interactions lead to contact forces acting on the boundary. Let $\boldsymbol{\tau}$ be the stress vector (force per unit area) acting at a point on $\partial\mathcal{R}$. Cauchy's stress principle asserts that the stress vector is a function of the position, time, and boundary normal

$$\boldsymbol{\tau} = \boldsymbol{\tau}(\mathbf{x}, t, \hat{\mathbf{n}}). \quad (22.1)$$

The dependence on boundary normal means that the stress acting on a surface is generally a function of the orientation of that surface. This form of the stress trivially holds for an exactly hydrostatic fluid where the stress vector is proportional to the pressure (Section 21.4). Furthermore, the stress from pressure is oriented along the inward normal, thus reflecting the purely compressive nature of pressure

$$\boldsymbol{\tau} = -p(\mathbf{x}, t) \hat{\mathbf{n}} \quad \text{static fluid in hydrostatic balance.} \quad (22.2)$$

Cauchy's stress principle is sensible for points within the fluid media, and its relevance has been supported by experimental studies over the time since Cauchy made this assertion in the year 1823. Furthermore, it holds for pressure and viscous stresses at the interface between fluid media or at solid-earth boundaries. However, Cauchy's stress principle does not hold for surface tension, which is proportional to the curvature of the surface separating two fluid media (e.g., atmosphere and ocean), where curvature involves spatial gradients of the normal vector. As discussed in Section 22.11, surface tension effects are important for relatively small scales (order centimeters), and as such play a minor role in this book. Hence, with the single exception of surface tension, we rely on Cauchy's stress principle to formulate the fluid dynamical equations.

22.2.2 Newton's third law and local equilibrium of stresses

Newton's second law says that in an inertial reference frame, unbalanced forces acting on a physical system affect a time change to the linear momentum. Consider a region, $\mathcal{R}(\mathbf{v})$, whose fluid elements follow the barycentric velocity. Newton's second law then states that the material time evolution of the region's linear momentum is given by

$$\frac{d}{dt} \int_{\mathcal{R}(\mathbf{v})} \mathbf{v} \rho dV = \int_{\mathcal{R}(\mathbf{v})} \mathbf{f} \rho dV + \oint_{\partial\mathcal{R}(\mathbf{v})} \boldsymbol{\tau} d\mathcal{S}, \quad (22.3)$$

where $\int_{\mathcal{R}(\mathbf{v})} \mathbf{f} \rho dV$ is the domain integrated body force (from central gravity, planetary centrifugal, and Coriolis). To develop a general property for the contact forces, consider this balance for a region whose size gets infinitesimally small. Assuming the integrands for the two volume integrals are well behaved (i.e., smooth and bounded) as the region size goes to zero, we see that the volume integrals are proportional to L^3 , where L is a length scale measuring the size of the region (e.g., side for a cubical region or diameter for a spherical region). In the same manner, we assume the stresses are well behaved in the case of an infinitesimal region. However, the integral of the contact forces goes to zero at the slower rate that is proportional to L^2 . Self-consistency for the balance (22.3) over a region of infinitesimal size thus requires the contact forces to satisfy the limiting behavior

$$\lim_{L \rightarrow 0} \frac{1}{L^2} \oint_{\partial\mathcal{R}(\mathbf{v})} \boldsymbol{\tau} d\mathcal{S} = 0. \quad (22.4)$$

This behavior means that contact forces at a point in the fluid must be in local equilibrium. Equation (22.4) is sometimes referred to as *Cauchy's fundamental lemma*.

A direct implication of the local equilibrium statement is that stress vectors that respect Cauchy's principle (22.1) satisfy

$$\boldsymbol{\tau}(\mathbf{x}, t, \hat{\mathbf{n}}) = -\boldsymbol{\tau}(\mathbf{x}, t, -\hat{\mathbf{n}}). \quad (22.5)$$

For example, the stress vector on one side of a surface is equal and oppositely directed to the stress vector acting on the other side. This equation is an expression of Newton's third law of mechanics (the action/reaction law; see Section 10.2), here written in terms of the stresses acting in a continuous media. It is of fundamental importance throughout our study of contact forces and their associated stresses acting within the fluid and at boundaries. We thus see how an application of Newton's second law, the linear momentum principle (22.3) for a continuous media, leads to a statement of Newton's third law, (22.5), for contact forces.

As an example of the above ideas, the simplest stress we consider in this chapter is that from pressure, with pressure acting solely in a compressive manner so that the stress vector takes the form

$$\boldsymbol{\tau}^{\text{press}}(\mathbf{x}, t, \hat{\mathbf{n}}) = -p(\mathbf{x}, t) \hat{\mathbf{n}}. \quad (22.6)$$

This stress trivially satisfies the Newton's third law relation (22.5) since

$$\boldsymbol{\tau}^{\text{press}}(\mathbf{x}, t, \hat{\mathbf{n}}) = -\boldsymbol{\tau}^{\text{press}}(\mathbf{x}, t, -\hat{\mathbf{n}}). \quad (22.7)$$

22.2.3 Comments on the local equilibrium relation

The local equilibrium relation (22.4), and the corresponding expression of Newton's third law, (22.5), might suggest that stresses cannot lead to motion. However, that suggestion is incorrect since stresses integrated over a finite region can lead to a net force that causes motion. Since con-

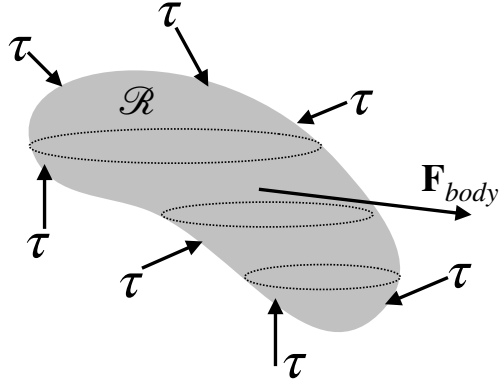


FIGURE 22.1: Schematic of the net body force, \mathbf{F}_{body} , acting on a finite region of fluid, plus the accumulation of stress vectors, τ , acting on the region boundaries. The net body force is determined by a volume integral of the body force (gravity, centrifugal, and Coriolis) at each point within the volume. In contrast, since the stresses are in local equilibrium, the volume integral of the stress divergence reduces to an area integral of the stress over the region boundary. Stress arises from pressure (compressive and normal) and strains (which then lead to viscous stresses when there is viscosity). The area integrated contribution from pressure to horizontal accelerations is referred to as *form stress*. The form stress coming from the bottom boundary is called the *topographic form stress*. The form stress appearing at the air-sea boundary is the *atmospheric form stress* if considering ocean dynamics and *oceanic form stress* if considering atmospheric dynamics. We study form stress in Chapter 25.

tact forces within the domain interior cancel pointwise, the local equilibrium relation (22.4) says that the net contact force acting on the region arises only from the area integrated stresses acting on the region boundary. Local or pointwise mechanical equilibrium does not imply mechanical equilibrium for finite regions.

To further emphasize the above point, consider an ocean region bounded at its bottom by the solid earth and its upper surface by a massive atmosphere. Variations (divergences) in stresses over finite regions within the ocean fluid lead to accelerations; e.g., ocean circulation. However, when integrated over the full ocean domain, all stresses cancel pointwise. Consequently, the net contact force acting on the full ocean domain reduces to the contact force acting just on the ocean boundaries. The boundary contact forces arise from mechanical interactions with the solid-earth and the overlying atmosphere. The center of mass for the ocean basin remains static if the accumulation of forces sum to zero, which includes the contact forces acting over its boundaries plus the volume integrated body forces from effective gravity (central gravity plus planetary centrifugal) and Coriolis.

In Figure 22.2 we illustrate the net pressure force acting on an arbitrary fluid domain. Pressure acts solely in a compressive manner as directed along the inward normal to the domain. Area integration over a domain boundary renders the net pressure force acting on the domain

$$\mathbf{F}^{\text{pressure}} = - \oint_{\partial\mathcal{R}} p \hat{\mathbf{n}} d\mathcal{S} = - \int_{\mathcal{R}} \nabla p dV, \quad (22.8)$$

where the second equality follows from application of Gauss's divergence theorem for a scalar field (Section 2.7.2). When decomposed according to coordinate axes, the pressure force acting on the boundary has a component in both the vertical and horizontal directions, thus contributing to both vertical and horizontal accelerations. The vertical accelerations are closely balanced by the weight of fluid, with exact balance in the case of a hydrostatic fluid. The horizontal stresses from pressure are known as *form stress*. This name arises since the stress depends on the form, or shape, of the interface on which pressure acts.

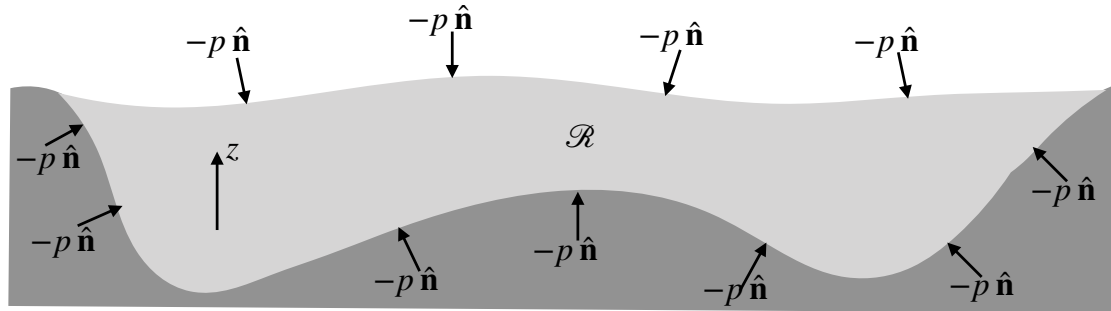


FIGURE 22.2: Schematic of contact forces from pressure acting on the boundaries to an ocean domain. Pressure forces are directed according to minus the local normal since pressure is a compressive force aligned with the inward normal direction. As with all contact forces, the pressure forces acting in the interior of the ocean are locally in mechanical equilibrium. Hence, when integrated over the global domain the net pressure forces only arise at the domain boundaries. That is, the net pressure force acting on the full ocean domain arises only at the interface between the solid-earth and the ocean, plus the interface between the atmosphere and the ocean. Note that the pressure force has a component in both the vertical and horizontal directions as per the orientation of the local normal vector. Further boundary stresses arise from viscous exchange, which generally have components perpendicular to the boundary normal; i.e., tangential to the boundary. Such stresses also satisfy Newton's third law.

22.3 The stress tensor

Cauchy's stress principle reduces the mathematical complexity of describing stress vectors. A further implication of this principle leads to *Cauchy's theorem*, which states that the stress vector, which is a function of space, time, and normal direction, can be expressed in terms of a stress tensor (a function of space and time) projected into the direction of the normal. The purpose of this section is to provide arguments supporting this theorem.

For this purpose, consider the tetrahedron fluid region shown in Figure 22.3, where three of the four sides are aligned according to the Cartesian coordinate axes and the fourth side has an outward normal, $\hat{n} = (\hat{n}_1, \hat{n}_2, \hat{n}_3)$, projecting into all three directions. The results developed for this rather contrived region hold for an arbitrary region using arbitrary coordinates. The reason for this generality is that once we derive a tensorially correct result using one choice of coordinates, such as Cartesian used here, we can make use of general tensor analysis (Chapters 7 and 8) to move from specific coordinates to arbitrary coordinates.

In the limit that the tetrahedron size goes to zero, local equilibrium of the contact forces means that

$$-\sum_{m=1}^3 \tau_{(m)} dA_m + \tau_{\hat{n}} dA = 0, \quad (22.9)$$

where we use the shorthand expression for the outward normal directed stress vector

$$\tau(\mathbf{x}, t, \hat{n}) = \tau_{\hat{n}}. \quad (22.10)$$

In equation (22.9), $\tau_{(m)} dA_m$ (no implied summation) is the contact force vector acting on the face with outward normal parallel to the corresponding coordinate axis and $\tau_{\hat{n}} dA$ is the contact force acting on the slanted face with outward normal \hat{n} . The minus sign arises for the summation term since the outward normals for these three faces point in the negative coordinate directions, and our convention is for $\tau_{(m)}$ to align with the positive coordinate directions. The areas for each

face are related to the slanted face area through

$$dA_m = \hat{n}_m dA, \quad (22.11)$$

so that the local equilibrium relation (22.9) becomes

$$\tau_{\hat{n}} = \sum_{m=1}^3 \hat{n}_m \tau_{(m)}. \quad (22.12)$$

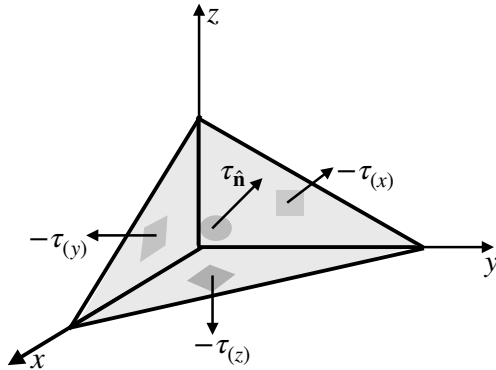


FIGURE 22.3: Tetrahedron region of fluid with stresses acting on the four faces. Note that the stresses are not necessarily directed normal to the faces. Local equilibrium of stresses means that the accumulation of these four stresses around the region adds to zero as the region volume goes to zero.

Equation (22.12) can be organized into a matrix-vector equation

$$\begin{bmatrix} (\tau_{\hat{n}})_1 \\ (\tau_{\hat{n}})_2 \\ (\tau_{\hat{n}})_3 \end{bmatrix} = [\hat{n}_1 \quad \hat{n}_2 \quad \hat{n}_3] \begin{bmatrix} \tau_{(1)1} & \tau_{(1)2} & \tau_{(1)3} \\ \tau_{(2)1} & \tau_{(2)2} & \tau_{(2)3} \\ \tau_{(3)1} & \tau_{(3)2} & \tau_{(3)3} \end{bmatrix}, \quad (22.13)$$

where each matrix element is the n -component of the m -stress $\tau_{(m)}$. We introduce a less cumbersome notation by writing

$$\begin{bmatrix} (\tau_{\hat{n}})_1 \\ (\tau_{\hat{n}})_2 \\ (\tau_{\hat{n}})_3 \end{bmatrix} = [\hat{n}_1 \quad \hat{n}_2 \quad \hat{n}_3] \begin{bmatrix} \mathbb{T}_{11} & \mathbb{T}_{12} & \mathbb{T}_{13} \\ \mathbb{T}_{21} & \mathbb{T}_{22} & \mathbb{T}_{23} \\ \mathbb{T}_{31} & \mathbb{T}_{32} & \mathbb{T}_{33} \end{bmatrix}, \quad (22.14)$$

so that \mathbb{T}_{mn} measures the force per area in the n -direction along a surface whose outward normal points in the m -direction, as depicted in Figure 22.4. Making use of \mathbb{T}_{mn} in the expression (22.12) leads to

$$(\tau_{\hat{n}})_n = \sum_{m=1}^3 \hat{n}_m \mathbb{T}_{mn}, \quad (22.15)$$

which can be written more succinctly as

$$\tau_{\hat{n}} = \hat{n} \cdot \mathbb{T}. \quad (22.16)$$

We thus see that the stress vector that acts on a surface that is oriented according to a normal vector, \hat{n} , equals to the projection of the *stress tensor*, \mathbb{T} , onto the normal vector. We emphasize that $\tau_{\hat{n}}$ is a vector with components within the tangent plane of the surface, as well as normal

to the surface. Exposing functional dependence reveals

$$\tau_{\hat{n}}(\mathbf{x}, t, \hat{\mathbf{n}}) = \hat{\mathbf{n}} \cdot \mathbb{T}(\mathbf{x}, t), \quad (22.17)$$

which manifests Cauchy's theorem. Namely, the stress vector $\tau_{\hat{n}}$, which is a function of $(\mathbf{x}, t, \hat{\mathbf{n}})$, has been decomposed into a stress tensor, \mathbb{T} , which is a function of (\mathbf{x}, t) , as well as the projection of the stress tensor into a direction $\hat{\mathbf{n}}$.

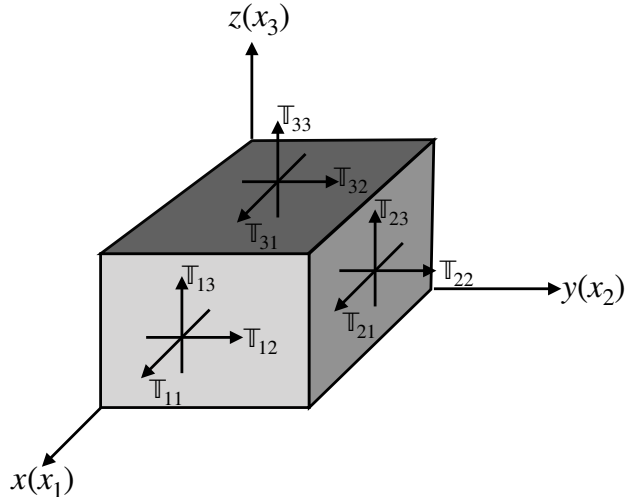


FIGURE 22.4: Illustrating the components to the stress tensor, \mathbb{T}_{mn} and how they are organized according to the coordinate axes. The component \mathbb{T}_{mn} is the stress that points in the n -direction along the face with outward normal in the m -direction.

How do we know that \mathbb{T}_{mn} form the components to a tensor rather than just being elements of a 3×3 matrix? To answer this question we note that each component of \mathbb{T} is a force per area, with force a vector and area orientable by its outward normal. As it is built from vectors, which are first order tensors, we suspect that \mathbb{T} should be a proper second order tensor. This suspicion is supported by the quotient rule from tensor analysis (Section 7.1.1). Namely, the quotient rule means that equation (22.15) indeed yields \mathbb{T}_{mn} that are components to a second order tensor. As components to a second order tensor, the tensor components, \mathbb{T}_{mn} , transform under a coordinate transformation according to the rules developed in Chapter 1 for Cartesian tensors and in Chapter 8 for general tensors. Through the power of tensor analysis, we thus see that our considerations, based on the rather contrived tetrahedron region in Figure 22.3, hold for an arbitrary region described by an arbitrary coordinate system.

22.4 Angular momentum and stress tensor symmetry

The linear momentum principle afforded by Newton's law of motion allowed us to deduce the local equilibrium property (22.4) of the stress. We here derive a constraint placed on the stress tensor that is imposed by studying angular momentum. Phenomenologically, we observe that geophysical fluids, as with most common fluids, experience torques only as the moments of body forces acting throughout the volume of a fluid region, or as moments of contact forces acting on the surface bounding the fluid region. We now make use of this observation to deduce symmetry of the stress tensor.¹

¹Page 11 of [Batchelor \(1967\)](#) and Section 5.13 of [Aris \(1962\)](#) offer brief discussions of fluids in which internal force couplets lead to torques distinct from those considered here, and in which the stress tensor has an anti-

22.4.1 Basic formulation

Consider a constant mass fluid element that has a Cartesian position \mathbf{x} relative to an arbitrary origin. The angular momentum of the fluid element with respect to the origin is

$$\mathbf{L} = \rho \delta V (\mathbf{x} \times \mathbf{v}), \quad (22.18)$$

and its material time evolution is

$$\frac{D\mathbf{L}}{Dt} = \rho \delta V \mathbf{x} \times \frac{D\mathbf{v}}{Dt}, \quad (22.19)$$

which follows since $D(\rho \delta V)/Dt = 0$, $D\mathbf{x}/Dt = \mathbf{v}$, and $\mathbf{v} \times \mathbf{v} = 0$. Making use of Cauchy's form for the equation of motion (21.14)

$$\rho \frac{D\mathbf{v}}{Dt} = \rho \mathbf{f} + \nabla \cdot \mathbb{T} \quad (22.20)$$

allows us to write the angular momentum evolution as

$$\frac{D\mathbf{L}}{Dt} = \delta V \mathbf{x} \times (\rho \mathbf{f} + \nabla \cdot \mathbb{T}). \quad (22.21)$$

The first term arises from body forces (e.g., central gravity, planetary centrifugal, and Coriolis) and the second term arises from the divergence of stresses. Expanding the stress divergence term renders

$$\left[\frac{D\mathbb{T}_m}{Dt} \right]_{\text{stress}} = \delta V \epsilon_{mnp} x_n (\nabla \cdot \mathbb{T})_p \quad (22.22a)$$

$$= \delta V \epsilon_{mnp} x_n \partial_q \mathbb{T}_{pq} \quad (22.22b)$$

$$= \delta V \epsilon_{mnp} [\partial_q (x_n \mathbb{T}_{pq}) - (\partial_q x_n) \mathbb{T}_{pq}] \quad (22.22c)$$

$$= \delta V \epsilon_{mnp} [\partial_q (x_n \mathbb{T}_{pq}) - \mathbb{T}_{pn}], \quad (22.22d)$$

where the final equality follows since $\partial_q x_n = \delta_{qn}$. Bringing this result back into the full expression (22.21) leads to

$$\frac{D\mathbb{T}_m}{Dt} = \delta V \epsilon_{mnp} [\rho x_n f_p + \partial_q (x_n \mathbb{T}_{pq}) - \mathbb{T}_{pn}]. \quad (22.23)$$

22.4.2 Physical interpretation

To facilitate a physical interpretation of the terms appearing in equation (22.23), integrate over an arbitrary Lagrangian region (region moving with the barycentric velocity, \mathbf{v}) so that

$$\frac{d}{dt} \int_{\mathcal{R}(\mathbf{v})} L_m = \int_{\mathcal{R}(\mathbf{v})} \epsilon_{mnp} [\rho x_n f_p + \partial_q (x_n \mathbb{T}_{pq}) - \mathbb{T}_{pn}] dV. \quad (22.24)$$

As noted earlier, the first term on the right hand side arises from torques due to body forces acting over the region

$$\int_{\mathcal{R}(\mathbf{v})} \epsilon_{mnp} (\rho x_n f_p) dV = \int_{\mathcal{R}(\mathbf{v})} (\mathbf{x} \times \mathbf{f})_m \rho dV. \quad (22.25)$$

symmetric component. [Dahler and Scriven \(1961\)](#) provide a more thorough account.

The second term on the right hand side of equation (22.24) can be transferred into a surface integral using the divergence theorem

$$\int_{\mathcal{R}(\mathbf{v})} \epsilon_{mnp} \partial_q (x_n \mathbb{T}_{pq}) dV = \int_{\partial\mathcal{R}(\mathbf{v})} \epsilon_{mnp} x_n \mathbb{T}_{pq} \hat{n}_q dS = \int_{\partial\mathcal{R}(\mathbf{v})} (\mathbf{x} \times \boldsymbol{\tau})_m dS, \quad (22.26)$$

where \hat{n}_q is the q 'th component of the normal vector on the region boundary, $\partial\mathcal{R}(\mathbf{v})$, and

$$\tau_p = \mathbb{T}_{pq} \hat{n}_q \quad (22.27)$$

is the p 'th component to the stress vector that is normal to $\hat{\mathbf{n}}$ (see equation (22.16)). Hence, the second term is the contribution to angular momentum evolution due to torques arising from the moment of contact forces acting on the region boundary.

22.4.3 Symmetry of the stress tensor

As noted at the start of this section, geophysical fluids have their angular momentum affected by torques arising from the moment of body forces acting throughout the fluid region, plus the moment of contact forces acting on the region boundary. There is a third term in equation (22.23) that does not fit into either category, and it is given by the volume integral

$$-\int_{\mathcal{R}(\mathbf{v})} \epsilon_{mnp} \mathbb{T}_{pn} dV = \int_{\mathcal{R}(\mathbf{v})} \epsilon_{mpn} \mathbb{T}_{pn} dV \equiv \int_{\mathcal{R}(\mathbf{v})} T_m^\times dV, \quad (22.28)$$

where we defined

$$T_m^\times = \epsilon_{mpn} \mathbb{T}_{pn}. \quad (22.29)$$

This term contributes a volume source to angular momentum and yet it is *not* associated with body forces. We might refer to it as a *torque density* (torque source per volume). As already noted, such torque sources are *not* relevant for geophysical fluids, in which case we conclude that geophysical fluids are affected only by symmetric stress tensors

$$\mathbb{T}_{mn} = \mathbb{T}_{nm} \implies \epsilon_{mnp} \mathbb{T}_{np} = 0. \quad (22.30)$$

Symmetry of the stress tensor is a central property of the stresses acting on most fluids, including geophysical fluids. We thus only consider symmetric stress tensors throughout this book.

To further support the above conclusion concerning a symmetric stress tensor, consider a particular component of the torque density, such as the vertical

$$T_3^\times = \epsilon_{3pn} \mathbb{T}_{pn} = \mathbb{T}_{12} - \mathbb{T}_{21}, \quad (22.31)$$

with the corresponding torque applied to a fluid element given by

$$T_3^\times \delta V = (\mathbb{T}_{12} - \mathbb{T}_{21}) \delta x \delta y \delta z. \quad (22.32)$$

What sort of angular acceleration is induced by this torque when computed relative to the fluid element center? To answer this question, assume the fluid element is moving as a rigid body so that we can compute its angular acceleration by dividing the torque by the moment of inertia for the fluid element. The moment of inertia depends on the shape of the element, which is unspecified. Even so, we can estimate the moment of inertia computed relative to a vertical axis through the center of the element

$$I_3 = \alpha [(\delta x)^2 + (\delta y)^2] \rho \delta x \delta y \delta z, \quad (22.33)$$

where α is a dimensionless geometric factor. Dividing the torque (22.32) by the moment of inertia thus leads to an estimate of the angular acceleration

$$\text{angular acceleration} \approx \frac{T_3^x}{I_3} \approx \frac{\mathbb{T}_{12} - \mathbb{T}_{21}}{[(\delta x)^2 + (\delta y)^2] \rho \alpha}. \quad (22.34)$$

Now consider the continuum limit, found as δx and δy are reduced to zero. In the absence of an unspecified counteracting torque, a finite angular acceleration in the continuum limit (where $(\delta x)^2 + (\delta y)^2 \rightarrow 0$) is ensured only if the stress tensor is symmetric so that the numerator vanishes.

22.5 Forces and torques in an exact hydrostatic fluid

In this section we return to the study of a static fluid in a gravitational field originally considered in Section 21.4. The exact solution is known as *exact hydrostatic balance*, which distinguishes it from the approximate hydrostatic balance appropriate for moving geophysical fluids under certain scaling regimes (Section 24.2). For a static fluid, all forces and all torques sum to zero at any point. Similarly, the integrated forces and integrated torques acting on any finite fluid region also vanish. The static fluid, although trivial dynamically, offers useful practice in applying the formalism of continuum mechanics to a system where we know the answer. Furthermore, there are interesting and important applications of these ideas, such as in the building of dams and underwater structures, both of which we certainly hope will remain static!

22.5.1 Force balance

The force balance in an exact hydrostatic fluid was addressed in Section 21.4 where we deduced the following relation between the pressure gradient and geopotential gradient

$$\nabla p = -\rho \nabla \Phi. \quad (22.35)$$

This equality holds at every point within the fluid, and as such it is a strong form of the hydrostatic balance.² Integrating over a finite fluid region, \mathcal{R} , and using the divergence theorem for scalar fields, (2.73), renders the finite volume or weak form of hydrostatic balance

$$\int_{\mathcal{R}} \rho \nabla \Phi \, dV = - \int_{\mathcal{R}} \nabla p \, dV = - \oint_{\partial \mathcal{R}} p \hat{n} \, d\mathcal{S}. \quad (22.36)$$

Expanding the above relations for the special case of $\Phi = g z$ leads to the differential statements

$$0 = \hat{x} \cdot \nabla p = \hat{y} \cdot \nabla p \quad \text{and} \quad \rho g = -\hat{z} \cdot \nabla p, \quad (22.37)$$

with the first two equations implying that the exact hydrostatic pressure is only a function of z . The corresponding weak form of hydrostatic balance reads

$$g M = - \int_{\mathcal{R}} \nabla p \cdot \hat{z} \, dV = - \oint_{\partial \mathcal{R}} p (\hat{n} \cdot \hat{z}) \, d\mathcal{S}, \quad (22.38)$$

²Recall the discussion of weak and strong formulation in Section 14.2. In brief, the weak formulation provides integral relations whereas the strong formulation provides differential relations.

where $M = \int_{\mathcal{R}} \rho dV$ is the mass in the fluid region, and the weak form of horizontal balances are

$$0 = \int_{\mathcal{R}} \nabla p \cdot \hat{\mathbf{x}} dV = \oint_{\partial\mathcal{R}} p (\hat{\mathbf{n}} \cdot \hat{\mathbf{x}}) d\mathcal{S} \quad (22.39a)$$

$$0 = \int_{\mathcal{R}} \nabla p \cdot \hat{\mathbf{y}} dV = \oint_{\partial\mathcal{R}} p (\hat{\mathbf{n}} \cdot \hat{\mathbf{y}}) d\mathcal{S}. \quad (22.39b)$$

We emphasize that these finite volume balances hold for any arbitrarily shaped region within a static fluid.

22.5.2 Pressure force balance for a homogeneous fluid

To further our understanding of the pressure force balances in a static fluid, consider a constant density static ocean sitting under a massless atmosphere, in which case the hydrostatic pressure is

$$p = -\rho g z, \quad (22.40)$$

where $z < 0$ for the ocean. Now examine the pressure forces acting on the three sides of the triangle in Figure 22.5. This geometry is simple enough to explicitly compute the pressure forces, thus confirming the general properties in equations (22.38), (22.39a), and (22.39b).

The outward normal vectors along the three triangle faces are given by

$$\hat{\mathbf{n}}_A = +\hat{\mathbf{y}} \quad \text{and} \quad \hat{\mathbf{n}}_B = -\hat{\mathbf{z}} \quad \text{and} \quad \hat{\mathbf{n}}_C = \hat{\mathbf{z}} \cos \varphi - \hat{\mathbf{y}} \sin \varphi, \quad (22.41)$$

where

$$\tan \varphi = \frac{z_2 - z_1}{y_2 - y_1} = \frac{\Delta z}{\Delta y} \quad (22.42)$$

is the slope of the hypotenuse relative to the horizontal. The integrated pressure force along the vertical face is thus given by

$$\mathbf{F}_A^{\text{press}} = - \int p \hat{\mathbf{n}}_A d\mathcal{S} = \hat{\mathbf{y}} \Delta x \int_{z_1}^{z_2} \rho g z dz = \hat{\mathbf{y}} (\rho g / 2) (z_2 + z_1) \Delta z \Delta x, \quad (22.43)$$

where Δx is the thickness of the triangle in the $\hat{\mathbf{x}}$ direction into the page. Note that $\mathbf{F}_A^{\text{press}}$ points in the $-\hat{\mathbf{y}}$ direction since $z_2 + z_1 < 0$. Likewise, the integrated pressure force along the horizontal face is given by

$$\mathbf{F}_B^{\text{press}} = - \int p \hat{\mathbf{n}}_B d\mathcal{S} = -\hat{\mathbf{z}} \Delta x \int_{y_1}^{y_2} \rho g z_1 dy = -\hat{\mathbf{z}} \rho g z_1 \Delta y \Delta x, \quad (22.44)$$

which points upward since $z_1 < 0$.

The integrated pressure force along the sloped hypotenuse face, C , requires a bit of trigonometry. For this purpose we make use of the formalism from Section 16.4.3, in which the vertical position along the hypotenuse is written

$$z = \eta(y) = z_2 - (y_2 - y) \tan \varphi, \quad (22.45)$$

so that the horizontal projection of the surface area is given by equation (25.4)

$$d\mathcal{S} = |\nabla(z - \eta)| dx dy = \frac{dx dy}{|\cos \varphi|}. \quad (22.46)$$

Hence, the integrated pressure force on the hypotenuse is given by

$$\mathbf{F}_C^{\text{press}} = - \int p \hat{\mathbf{n}}_C d\mathcal{S} \quad (22.47a)$$

$$= \frac{\hat{\mathbf{n}}_C}{\cos \varphi} \Delta x \int_{y_1}^{y_2} \rho g \eta(y) dy \quad (22.47b)$$

$$= (\hat{\mathbf{z}} - \hat{\mathbf{y}} \tan \varphi) \rho g \Delta x [z_2 \Delta y - y_2 \Delta z - (1/2)(y_1 + y_2) \Delta y \tan \varphi] \quad (22.47c)$$

$$= (\hat{\mathbf{z}} - \hat{\mathbf{y}} \tan \varphi) \rho g \Delta x [z_2 \Delta y - y_2 \Delta z + (y_1 + y_2) \Delta z / 2] \quad (22.47d)$$

$$= (\hat{\mathbf{z}} - \hat{\mathbf{y}} \tan \varphi) \rho g \Delta x \Delta y (z_1 + z_2) / 2. \quad (22.47e)$$

Bringing these results together renders the net pressure forces in the two directions

$$\hat{\mathbf{y}} \cdot (\mathbf{F}_A^{\text{press}} + \mathbf{F}_B^{\text{press}} + \mathbf{F}_C^{\text{press}}) = (\rho g \Delta x / 2) [(z_1 + z_2) \Delta z - \tan \varphi (z_1 + z_2) \Delta y] = 0 \quad (22.48a)$$

$$\hat{\mathbf{z}} \cdot (\mathbf{F}_A^{\text{press}} + \mathbf{F}_B^{\text{press}} + \mathbf{F}_C^{\text{press}}) = \rho g \Delta x \Delta y \Delta z / 2 = M g, \quad (22.48b)$$

where the mass of the triangle is given by

$$M = \rho \Delta x \Delta y \Delta z / 2. \quad (22.49)$$

We thus see that the area integrated horizontal pressure forces vanish, whereas the area integrated vertical pressure force balances the weight of the fluid. Again, these results are expected given the general expressions (22.38), (22.39a), and (22.39b) of force balance. Even so, being able to explicitly compute the pressure forces acting around a region, and to confirm the general force balances, is a useful means to become familiar with hydrostatic pressure.

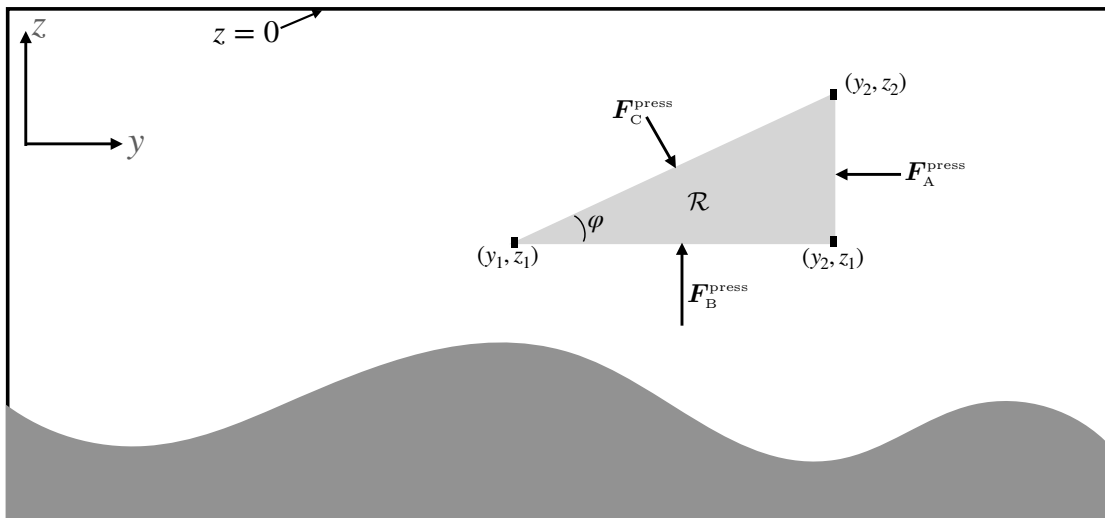


FIGURE 22.5: A right triangle region of fluid in a static ocean where $z < 0$. The positions for the three corners are shown as (y_1, z_1) , (y_2, z_1) , and (y_2, z_2) , along with the pressure forces acting on the three sides. In exact hydrostatic balance, the area integrated pressure force acting over the triangle boundary vanishes, $-\oint_{\partial\mathcal{R}} p \hat{\mathbf{n}} d\mathcal{S} = 0$. If the density of the fluid is assumed constant, then we can analytically compute the force balance as detailed in Section 22.5.2.

22.5.3 Torque balance

Torques arise in the presence of force *couplets*, which in turn lead to time changes in the angular momentum. In our discussion of the stress tensor in Section 22.4, we saw that a symmetric stress tensor removes volume sources of torque; i.e., there are no internal sources of force couplets. So the only means to impart a nonzero torque is for force couplets to arise from body forces (forces originating outside of the fluid region) and from contact forces that act between fluid elements within the region. In this section, we show that for a static fluid then the net torque vanishes both at an arbitrary point in the fluid as well as when integrated over an arbitrary region.

Strong form: zero torques acting on a fluid element

The torque is the moment of a force computed about a chosen origin. For a static geophysical fluid, the torque acting on a fluid element is given by the moment of the pressure force plus the moment of the effective gravity force (central gravity plus planetary centrifugal)

$$\mathbf{x} \times \mathbf{f} \rho \delta V = \mathbf{x} \times (-\rho^{-1} \nabla p - \nabla \Phi) \rho \delta V. \quad (22.50)$$

As seen in Section 22.5.1, the pressure and effective gravitational forces exactly balance at each point with a static fluid so that $\nabla p = -\rho \nabla \Phi$. Hence, there can be no torques at each point since there are no net forces at each point.

Weak form: zero torques acting on a finite fluid region

To show that the torque vanishes for a finite fluid region, we can merely integrate the fluid element result (22.50) over the finite region. Since the integral of zero is still zero, there are no torques on the region. An alternative approach makes use of the weak formulation by following the discussion in Section 22.4.2. In this approach, we start by writing the time change in angular momentum acting on a static fluid region

$$\frac{d}{dt} \int_{\mathcal{R}} \mathbf{L} = \int_{\mathcal{R}} [\mathbf{x} \times (-\rho \nabla \Phi)] dV + \oint_{\partial \mathcal{R}} [\mathbf{x} \times (-\hat{\mathbf{n}} p)] d\mathcal{S}. \quad (22.51)$$

Note that although the discussion in Section 22.4.2 focused on a Lagrangian region, $\mathcal{R}(\mathbf{v})$, there is no distinction here between Lagrangian and Eulerian since the fluid is static.

The pressure contribution in equation (22.51) is written in its contact force form, which is appropriate for a weak formulation. However, to compare its contribution to the torque with that from effective gravity requires us to convert the area integral to a volume integral. For that

purpose we use Cartesian tensor notation and expose full details for clarity

$$\begin{aligned}
 \oint_{\partial\mathcal{R}} (\hat{\mathbf{n}} \times \mathbf{x})_a p dS &= \epsilon_{abc} \oint_{\partial\mathcal{R}} \hat{n}_b x_c p dS && \text{permutation symbol (Section 1.4.1)} \quad (22.52a) \\
 &= \epsilon_{abc} \int_{\mathcal{R}} \partial_b (x_c p) dV && \text{divergence theorem} \quad (22.52b) \\
 &= \epsilon_{abc} \int_{\mathcal{R}} (\delta_{bc} p + x_c \partial_b p) dV && \text{product rule} \quad (22.52c) \\
 &= \epsilon_{abc} \int_{\mathcal{R}} x_c \partial_b p dV && \epsilon_{abc} \delta_{bc} = 0 \quad (22.52d) \\
 &= -\epsilon_{acb} \int_{\mathcal{R}} x_c \partial_b p dV && \epsilon_{abc} = -\epsilon_{acb} \quad (22.52e) \\
 &= - \int_{\mathcal{R}} (\mathbf{x} \times \nabla p)_a dV && \text{vector cross product notation.} \quad (22.52f)
 \end{aligned}$$

This result then brings the angular momentum equation (22.51) to the form

$$\frac{d}{dt} \int_{\mathcal{R}} \mathbf{L} = \int_{\mathcal{R}} [\mathbf{x} \times (-\rho \nabla \Phi - \nabla p)] dV. \quad (22.53)$$

At this point we can invoke the strong form force balance in equation (22.35), thus revealing that the integrand on the right hand side vanishes at each point in the fluid. However, this approach is no different than starting from the strong formulation of the torques in equation (22.50) and integrating over a finite region. An alternative approach, remaining fully within the weak formulation, states that if the region's angular momentum remains constant, then that defines a region experiencing zero net torque. This approach is the same as taken for the force balance, whereby we say that a fluid region experiencing no acceleration is one that has zero net forces acting on it. Hence, for a region with time invariant angular momentum we are led to the finite volume (weak form) torque balance

$$\int_{\mathcal{R}} [\mathbf{x} \times (\rho \nabla \Phi + \nabla p)] dV = 0 \implies \int_{\mathcal{R}} (\mathbf{x} \times \rho \nabla \Phi) dV = - \int_{\partial\mathcal{R}} (\mathbf{x} \times \hat{\mathbf{n}} p) dS, \quad (22.54)$$

with this balance the direct analog for torques of the weak form of the force balances given by equations (22.38), (22.39a), and (22.39b).

22.6 Flux-form Eulerian momentum equation

We often find it useful to consider Cauchy's form of the momentum equation (22.20) in its flux-form Eulerian expression. Making use of Cartesian tensors, we expand the material time derivative acting on the velocity and introduce the mass conservation equation (16.6) so that

$$\rho \frac{D\mathbf{v}}{Dt} = \rho [\partial_t \mathbf{v} + (\mathbf{v} \cdot \nabla) \mathbf{v}] \quad (22.55a)$$

$$= \rho [\partial_t \mathbf{v} + (\mathbf{v} \cdot \nabla) \mathbf{v}] + \mathbf{v} (\partial_t \rho + \nabla \cdot (\rho \mathbf{v})) \quad (22.55b)$$

$$= \partial_t (\rho \mathbf{v}) + \nabla \cdot [\rho \mathbf{v} \otimes \mathbf{v}], \quad (22.55c)$$

where $\mathbf{v} \otimes \mathbf{v}$ is the outer product of the velocity vector and it has Cartesian tensor components written as

$$(\mathbf{v} \otimes \mathbf{v})_{mn} = v_m v_n. \quad (22.56)$$

Consequently, the momentum equation (22.20) takes on the flux-form Eulerian expression

$$\partial_t(\rho \mathbf{v}) + \nabla \cdot [\rho \mathbf{v} \otimes \mathbf{v}] = \rho \mathbf{f} + \nabla \cdot \mathbb{T}. \quad (22.57)$$

Alternatively, we can move the advection of momentum term onto the right hand side so that

$$\partial_t(\rho \mathbf{v}) = \rho \mathbf{f} + \nabla \cdot [\mathbb{T} - \rho \mathbf{v} \otimes \mathbf{v}], \quad (22.58)$$

which takes on the component form

$$\partial_t(\rho v_m) = \rho f_m + \partial_n[\mathbb{T}_{mn} - \rho v_m v_n]. \quad (22.59)$$

In this form we see that momentum advection can be interpreted as a stress that modifies the linear momentum per volume at a point in space. We refer to the stress,

$$\mathbb{T}_{mn}^{\text{kinetic}} = -\rho (\mathbf{v} \otimes \mathbf{v})_{mn} = -\rho v_m v_n, \quad (22.60)$$

as the *mechanical stress* or *kinetic stress*, which arises from the mechanical interactions between moving fluid elements. The turbulent contribution to the mechanical stress is known as the *Reynolds stress*.

For a rotating fluid in a gravity field we set the body force to

$$\rho \mathbf{f} = -2 \rho \boldsymbol{\Omega} \times \mathbf{v} - \rho \nabla \Phi, \quad (22.61)$$

and the divergence of the stress tensor is

$$\nabla \cdot \mathbb{T} = -\nabla p + \rho \mathbf{F}, \quad (22.62)$$

with \mathbf{F} the frictional acceleration (see Section 22.8). In this case, Cauchy's equation (22.57) takes on the form

$$\frac{\partial(\rho \mathbf{v})}{\partial t} + \nabla \cdot (\rho \mathbf{v} \otimes \mathbf{v}) + 2 \rho \boldsymbol{\Omega} \times \mathbf{v} = -\nabla p - \rho \nabla \Phi + \rho \mathbf{F}. \quad (22.63)$$

22.7 Linear momentum for arbitrary regions

Consider the budget of linear momentum for an arbitrary region, \mathcal{R} , moving in an arbitrary manner within the fluid. For this purpose we make use of the Leibniz-Reynolds Transport Theorem (17.34)

$$\frac{d}{dt} \left[\int_{\mathcal{R}} \varphi dV \right] = \int_{\mathcal{R}} \frac{\partial \varphi}{\partial t} dV + \oint_{\partial \mathcal{R}} \varphi \mathbf{v}^{(b)} \cdot \hat{\mathbf{n}} dS, \quad (22.64)$$

where $\mathbf{v}^{(b)}$ is the velocity of the region boundary, $\partial \mathcal{R}$, with $\hat{\mathbf{n}}$ the outward normal along the boundary. Applying this result to a component of the linear momentum per volume, $\varphi = \rho v_m$,

and making use of the flux-form Eulerian momentum equation (22.59) leads to

$$\frac{d}{dt} \left[\int_{\mathcal{R}} \rho v_m dV \right] = \int_{\mathcal{R}} \partial_t (\rho v_m) dV + \oint_{\partial \mathcal{R}} (\rho v_m) \mathbf{v}^{(b)} \cdot \hat{\mathbf{n}} dS \quad (22.65a)$$

$$= \int_{\mathcal{R}} [\rho f_m + \partial_n (\mathbb{T}_{mn} - \rho v_m v_n)] dV + \oint_{\partial \mathcal{R}} (\rho v_m) \mathbf{v}^{(b)} \cdot \hat{\mathbf{n}} dS \quad (22.65b)$$

$$= \int_{\mathcal{R}} \rho f_m dV + \oint_{\partial \mathcal{R}} (\mathbb{T}_{mn} - \rho v_m v_n) \hat{\mathbf{n}}_n dS + \oint_{\partial \mathcal{R}} (\rho v_m) \mathbf{v}^{(b)} \cdot \hat{\mathbf{n}} dS \quad (22.65c)$$

$$= \int_{\mathcal{R}} \rho f_m dV + \oint_{\partial \mathcal{R}} [\mathbb{T}_{mn} + \rho v_m (v_n^{(b)} - v_n)] \hat{\mathbf{n}}_n dS. \quad (22.65d)$$

We can write this relation in the more elegant geometric form as

$$\frac{d}{dt} \left[\int_{\mathcal{R}} \rho \mathbf{v} dV \right] = \int_{\mathcal{R}} \rho \mathbf{f} dV + \oint_{\partial \mathcal{R}} [\mathbb{T} + \rho \mathbf{v} \otimes (\mathbf{v}^{(b)} - \mathbf{v})] \cdot \hat{\mathbf{n}} dS. \quad (22.66)$$

As a relation between geometric objects (vectors and tensors), the momentum budget (22.66) is independent of coordinate representation. We conclude that the evolution of linear momentum over an arbitrary region is affected by the volume integrated body force acting over the region, plus the impacts from stresses acting on the region boundary. Notably, the stresses have a contribution from the advection of linear momentum across the region boundary, with advection computed relative to motion of the boundary. In Section 22.10 we specialize the budget (22.66) to an infinitesimally thin interface. That analysis is then used to develop stress conditions for a surface within a single fluid media, and the stress condition at the boundary between two fluids.

We refer to a *Lagrangian region* as one that moves with the barycentric velocity so that $\mathbf{v}^{(b)} = \mathbf{v}$, in which case the mechanical stress is eliminated from the finite volume momentum budget (22.66). In fact, to eliminate the mechanical stress only requires the normal components of the boundary velocity to equal that of a fluid element, $(\mathbf{v} - \mathbf{v}^{(b)}) \cdot \hat{\mathbf{n}} = 0$. In either case we distinguish a Lagrangian region by writing $\mathcal{R}(\mathbf{v})$ to emphasize that the region moves with the barycentric fluid velocity, \mathbf{v} . For this case the linear momentum is only affected by body forces as well as stresses contained in the stress tensor

$$(\mathbf{v} - \mathbf{v}^{(b)}) \cdot \hat{\mathbf{n}} = 0 \implies \frac{d}{dt} \left[\int_{\mathcal{R}(\mathbf{v})} \rho \mathbf{v} dV \right] = \int_{\mathcal{R}(\mathbf{v})} \rho \mathbf{f} dV + \oint_{\partial \mathcal{R}(\mathbf{v})} \mathbb{T} \cdot \hat{\mathbf{n}} dS. \quad (22.67)$$

This relation is Reynold's transport theorem (Section 17.3.6) as applied to linear momentum.

22.8 Constitutive relation between stress and rate of strain

Thus far we have offered a rather general treatment of stress, developing its properties according to the conservation of linear momentum and angular momentum. We now develop *constitutive relations*, which relate stress to properties of the fluid as well as properties of the fluid flow.

22.8.1 Thermodynamic pressure and mechanical pressure

Consider a fluid in which the stress on an area element is always normal to the area element and is independent of the orientation. This fluid is in hydrostatic balance and the corresponding stress tensor and stress vector are written

$$\mathbb{T}_{mn} = -p \delta_{mn} \iff \mathbb{T} \cdot \hat{\mathbf{n}} = -p \hat{\mathbf{n}}, \quad (22.68)$$

where p is the hydrostatic pressure field. Since the pressure introduced here arises from purely mechanical considerations, we refer to it as the *mechanical pressure*. For a compressible fluid at rest, we can identify the mechanical pressure with the *thermodynamic pressure* encountered in our study of equilibrium thermodynamics (Chapter 19). Furthermore, if we assume that local thermodynamic equilibrium is maintained for fluid elements within a moving fluid, then we are motivated to continue making this identification between mechanical pressure and thermodynamical pressure (see Section 4.5 of [Kundu et al. \(2016\)](#) or Section 1.10 of [Salmon \(1998\)](#)). However, we note that there is no fully deductive theory supporting this equality of pressures. The reader in search of a deductive theory likely will need to penetrate nonequilibrium statistical mechanics, which is outside our scope.

When the fluid flow is non-divergent (Chapter 18), we lose the equality between mechanical pressure and thermodynamical pressure, even when the fluid is at rest. The reason is that a non-divergent fluid flow is unable to do pressure work on a fluid element since the flow cannot change the fluid element's volume. Hence, for non-divergent flow there is no connection between pressure and changes to internal energy as per the first law of thermodynamics (Section 19.2). A non-divergent flow only has access to the mechanical pressure as revealed through the measurement of stresses. Furthermore, the mechanical pressure instantaneously conforms to the needs of non-divergence throughout the fluid (see Section 26.3 and Section 35.5). Correspondingly, energetic consistency requires us to make use of the geopotential in the equation of state for *in situ* density in an oceanic Boussinesq fluid (in which the velocity is non-divergent), rather than the thermodynamic pressure. We explore this point in Section 26.8.

22.8.2 Couette flow and the viscous tensor

Couette flow arises when fluid is placed between two long and straight concentric cylinders that can rotate. Relative motion between the two cylinders leads to fluid motion. For example, if the inner surface rotates, then fluid next to the cylinder wall will move with the cylinder. Any normal stresses on the fluid imparted by the cylinders are directed toward the cylinder axis and so cannot render any tangential motion. This elegant experiment proves that fluid motion can be induced by purely tangential stresses. Furthermore, the tangential stress imparted by the inner cylinder transfers through the fluid to the outer cylinder. Indeed, if the inner cylinder rotates at a constant rate, then eventually the whole fluid-cylinder system rotates as a solid body. Couette flow thus exhibits how real fluids can support tangential stresses in response to tangential strains, thus providing a clear distinction from a perfect fluid where only normal stresses (i.e., pressure) are supported.

As evidenced by the Couette flow, a moving fluid has a more complex stress relation than a static fluid. In particular, the presence of tangential stresses in the fluid provides evidence for an additional piece to the stress tensor that we write as

$$\mathbb{T}_{mn} = -p\delta_{mn} + \tau_{mn} \iff \mathbb{T} = -p\mathbb{I} + \tau. \quad (22.69)$$

The pressure term remains isotropic as for a fluid at rest, thus imparting normal stresses. The additional tensor, τ , is referred to as the *friction tensor* or *viscous tensor*. The viscous tensor captures the irreversible exchanges of momentum between moving (relative to one another) fluid elements, such as in Couette flow, with the irreversible momentum exchange supported by fluid viscosity. Viscosity is assumed to be identically zero in a perfect fluid, so that a perfect fluid can only support normal stresses from pressure even when the perfect fluid has relative motion.

As noted above, we assume the viscous tensor vanishes when there is zero relative motion

within the fluid.³ The physical idea is that fluid strains are needed to generate friction between fluid elements to support the transfer of momentum through the presence of viscosity. The determination of frictional stresses from kinematic properties (such as strain) requires a constitutive relation. The constitutive relation commonly used for geophysical fluids follows that for a *Newtonian fluid*, which is a particular type of *Stokesian fluid* whose frictional stresses are assumed to be linearly proportional to the rate of strain.

The diagonal stresses, \mathbb{T}_{11} , \mathbb{T}_{22} , and \mathbb{T}_{33} , are known as the *direct stresses* or *normal stresses*, whereas the off-diagonal stresses are *shear stresses*. The sum of the direct stresses forms the trace of the stress tensor and is given by

$$\mathbb{T}_{qq} = \mathbb{T}_{11} + \mathbb{T}_{22} + \mathbb{T}_{33} = -3p + \tau_{qq}. \quad (22.70)$$

If $\tau_{qq} = 0$ then it is known as the *deviatoric friction tensor*. As argued in Section 22.8.6, a deviatoric friction tensor is consistent with the assumption of equal mechanical and thermodynamical pressures.

22.8.3 D'Alembert's theorem for perfect fluids

Consider a finite impermeable solid body placed in a steady fluid flow, with the flow assumed to be uniform upstream and downstream. A particular realization is an arbitrarily long pipe flow with a solid object in the middle of the pipe. *D'Alembert's theorem* says that the force exerted by a perfect fluid on the solid body has no component along the direction of the pipe's central axis. A proof of this theorem, as provided in Section 13 of [Meyer \(1971\)](#), makes use of basic insights into momentum balances. Remarkably, D'Alembert's theorem suggests a behavior that is contrary to common experience, whereby an object placed in a real fluid flow experiences a net force in the direction of the flow, so that there is a transfer of momentum between the fluid and the solid body. Consequently, D'Alembert's theorem became known as *D'Alembert's paradox*, thus motivating research during the 19th and early 20th centuries to understand stresses acting between a fluid and solid. It further put into question the ability to approximate a fluid with arbitrarily small, but nonzero, viscosity with a perfect fluid where the viscosity identically vanishes. Namely, a real fluid supports tangential stresses, through the action of viscosity, in addition to normal (pressure) stresses. It is the tangential stresses, no matter how small in magnitude but nonzero, that lead to a net force on the solid body.

22.8.4 Guidance from Galilean invariance

Consider a fluid in uniform motion in free space. Boosting the reference frame allows us to move to a reference frame where the fluid is static. Through Galilean invariance (Section 14.7) we expect the dynamics to remain unchanged. Since we assume friction vanishes when the fluid is static (as per a Stokesian fluid), Galilean invariance implies that the frictional stresses vanish when the fluid undergoes uniform motion in any direction.

Uniform motion of fluid elements is reflected in zero velocity gradients, which offers a key insight into how friction depends on strains. Namely, these considerations suggest that the friction tensor is a function of gradients in the velocity field, $\partial_m v_n$. Furthermore, as the stress tensor must be symmetric (Section 22.4), the simplest expression for the friction tensor is one that is linearly proportional to the rate of strain tensor introduced in Section 15.3.5. Fluids that satisfy this linear stress-rate of strain constitutive relation are known as *Newtonian fluids*. Furthermore, this constitutive relation takes the same mathematical form as *Hooke's Law* used in the study of elastic materials or simple harmonic oscillators (see Section 44.3).

³This assumption follows those for a Stokes fluid as discussed in Section 5.21 of [Aris \(1962\)](#).

22.8.5 A comment on Rayleigh drag

Rayleigh drag is a particular form of friction that makes use of the acceleration

$$\mathbf{F}_{\text{Rayleigh}} = -\gamma \mathbf{v}, \quad (22.71)$$

where $\gamma > 0$ is an inverse time scale. Rayleigh drag does *not* satisfy the Galilean principle since it decelerates all flows, even uniformly moving flows, towards rest where rest is defined by the laboratory frame. Furthermore, Rayleigh drag is not equal to the divergence of a frictional stress tensor, and so it does not arise from a contact stress. Even so, it has found some use for rudimentary purposes, particularly when aiming to derive analytic expressions for how friction acts on flows in a bulk sense. We provide one example in our discussion of Ekman dynamics in Section 30.2.3.

22.8.6 Constitutive relation for Newtonian fluids

There are many details involved with deriving the Newtonian fluid constitutive relation, with discussions provided in Chapter 5 of [Aris \(1962\)](#), Section 3.1 of [Segel \(1987\)](#), and Section 4.5 of [Kundu et al. \(2016\)](#) for general fluids, and Chapter 17 and 18 of [Griffies \(2004\)](#) for stratified fluids with particular focus on the ocean. We here offer a taste of these considerations by starting with the constitutive relation

$$\tau_{mn} = \rho (2\nu \mathbb{S}_{mn} + \lambda \nabla \cdot \mathbf{v} \delta_{mn}), \quad (22.72)$$

with \mathbb{S}_{mn} the components to the rate of strain tensor introduced in Section 15.3.7 and whose trace equals to the velocity divergence

$$\mathbb{S}_{qq} = \nabla \cdot \mathbf{v}. \quad (22.73)$$

The first contribution to the frictional stress (22.72) includes the strain tensor multiplied by the *first kinematic viscosity*, $\nu > 0$ (dimensions of squared length per time). The second contribution arises just from flow divergence as scaled by a *second kinematic viscosity*, λ . The sum

$$\nu_{\text{bulk}} = \rho (\lambda + 2\nu/3) \quad (22.74)$$

is known as the *bulk viscosity*, which, as discussed in the following, will be set to zero. Finally, one sometimes finds it more convenient to work with the *dynamic viscosity*

$$\mu_{\text{vsc}} = \rho \nu. \quad (22.75)$$

Note that we set ρ to the constant Boussinesq reference density, ρ_0 (Chapter 26), when working with a Boussinesq fluid.

Deviatoric friction tensor

As noted in Section 22.8.1, the pressure appearing in the stress tensor is a mechanical pressure that equals to minus one-third the trace of the stress tensor when the fluid is at rest

$$\mathbb{T}_{qq}^{\text{static}} = -3p. \quad (22.76)$$

We assume that the friction stress tensor does *not* alter this trace, so that the friction tensor has zero trace and is known as a *deviatoric friction tensor*⁴

$$\tau_{qq} = 0 = 3 \nu_{\text{bulk}} \nabla \cdot \mathbf{v} \implies \lambda = -2\nu/3, \quad (22.77)$$

so that the total stress tensor is given by

$$\mathbb{T}_{mn} = -\delta_{mn} p + 2\mu_{\text{vsc}} \mathbb{S}_{mn}^{\text{dev}} \quad \text{with} \quad \mathbb{S}_{mn}^{\text{dev}} = \mathbb{S}_{mn} - \delta_{mn} \mathbb{S}_{qq}/3, \quad (22.78)$$

where \mathbb{S}^{dev} is the *deviatoric rate of strain tensor*. We next offer arguments for why the friction tensor used for geophysical flows should have zero trace.

Equality of the mechanical and thermodynamic pressures

The frictional stress tensor (22.72) is not the precise form typically used in geophysical fluid modeling. Instead, the velocity divergence term is generally dropped even for compressible flows, and the viscosity is anisotropic and more generally takes the form of a fourth order tensor (see Chapter 17 and 18 of [Griffies \(2004\)](#) for the ocean). Furthermore, what is generally respected in most geophysical applications is the deviatoric nature of the friction tensor. That property is maintained since it is consistent with our assumption in Section 22.8.1 that the mechanical pressure equals to the thermodynamic pressure.

To see this equality between the pressures, introduce the mechanical pressure, p^{mech} , according to the trace of the stress tensor

$$\mathbb{T}_{qq} = -3p^{\text{mech}}. \quad (22.79)$$

That is, mechanical pressure is minus one-third the trace of the stress tensor whether the fluid is at rest or in motion. We can, in principle, measure this pressure by measuring the stresses. If we now return to the general form of the stress tensor

$$\mathbb{T}_{mn} = -\delta_{mn} p + \rho(\lambda \nabla \cdot \mathbf{v} \delta_{mn} + 2\nu \mathbb{S}_{mn}), \quad (22.80)$$

with p here given by the thermodynamic pressure, then the trace is

$$\mathbb{T}_{qq} = -3p + \rho(3\lambda + 2\nu) \nabla \cdot \mathbf{v}. \quad (22.81)$$

Setting the two traces (22.79) and (22.81) equal then leads to

$$p - p^{\text{mech}} = \nu_{\text{bulk}} \nabla \cdot \mathbf{v}. \quad (22.82)$$

In principle, one can measure the difference in pressures, but in practice this measurement is rather difficult. Stokes assumed $p - p^{\text{mech}} = 0$ by taking a zero bulk viscosity, and he used arguments from kinetic theory of gases to support that choice. This choice is generally taken for geophysical fluid applications, largely based on the assumption of local thermodynamic equilibrium mentioned in Section 22.8.1.

Local thermodynamical equilibrium is not a good assumption in supersonic flows, in which case $p - p^{\text{mech}} \neq 0$ and the bulk viscosity is nonzero. Correspondingly, the divergence term and the second kinematic viscosity, $\lambda \neq -2\nu/3$, are important. Additionally, the second viscosity is important when concerned with the damping of acoustic waves. Neither topics are considered in this book so that we have no further concern for the second viscosity.

⁴A second order tensor in 3-dimensions, \mathbb{D} , has a *deviator* with components given by $\mathbb{D}_{mn}^{\text{dev}} = \mathbb{D}_{mn} - (1/3) \delta_{mn} \mathbb{D}_{qq}$. By construction, the trace of the deviator vanishes: $\mathbb{D}_{qq}^{\text{dev}} = 0$.

Frictional force per volume

The viscous force per volume is given by the divergence of the frictional stress tensor

$$\rho F_n = \partial_m \tau_{mn} = 2 \partial_m (\mu_{vsc} S_{mn}^{\text{dev}}). \quad (22.83)$$

For a Boussinesq fluid this friction simplifies to

$$\rho_0 F_n = 2 \rho_0 \partial_m (\nu S_{mn}), \quad (22.84)$$

where we set the dynamic viscosity to $\mu_{vsc} = \rho_0 \nu$, with ρ_0 the constant Boussinesq reference density. Finally, for the case of a constant kinematic viscosity, such as for molecular viscous effects, we have the Boussinesq result reducing to the Laplacian form

$$\mathbf{F} = \nu \nabla^2 \mathbf{v}. \quad (22.85)$$

This form is commonly used in scale analysis, such as when determining the Reynolds number in Section 22.9.

22.8.7 Navier-Stokes and Euler equations

The *Navier-Stokes* equation is a special form of the momentum equation found by assuming a Newtonian fluid constitutive relation. In this case the Navier-Stokes momentum equation (21.16), in the presence of rotation and gravity, takes on the form

$$\rho \frac{D\mathbf{v}}{Dt} + 2\rho \boldsymbol{\Omega} \times \mathbf{v} = -\rho \nabla \Phi - \nabla p + \nabla \cdot (2\mu_{vsc} S^{\text{dev}}), \quad (22.86)$$

where we set the friction tensor equal to $\tau = 2\mu_{vsc} S^{\text{dev}}$. Quite often when examining the mathematical properties of the Navier-Stokes equation, one assumes the flow to be non-divergent, in which case $S^{\text{dev}} = S$ since $S_{qq} = \nabla \cdot \mathbf{v} = 0$. A further simplification occurs by assuming a constant density, ρ , and constant kinematic viscosity, ν , in which case the friction tensor reduces to the Laplacian form 22.85 so that the Navier-Stokes equation becomes

$$\frac{D\mathbf{v}}{Dt} + 2\boldsymbol{\Omega} \times \mathbf{v} = -\nabla \Phi - \rho^{-1} \nabla p + \nu \nabla^2 \mathbf{v}. \quad (22.87)$$

This form, or even simpler when ignoring rotation and gravity, is commonly studied by mathematicians concerned with existence and uniqueness properties of fluid flow solutions (e.g., see *Doering and Gibbon (1995)*). When assuming the fluid to be perfect, so that there are no viscous forces, the momentum equation is referred to as the *Euler equation*⁵

$$\frac{D\mathbf{v}}{Dt} + 2\boldsymbol{\Omega} \times \mathbf{v} = -\nabla \Phi - \rho^{-1} \nabla p. \quad (22.88)$$

It is tempting to consider the Euler equations to be a continuous limit of the Navier-Stokes equation as the viscosity goes to zero. However, there is a key distinction between the two equations. Namely, the Navier-Stokes equations admit solutions that display statistically equilibrated turbulent motions, whereby energy cascades to the small scales through vortex stretching in three dimensional flows. This energy is ultimately dissipated by viscosity at the small spatial scales, and this mechanism holds no matter how small the viscosity, so long as it is nonzero. In contrast,

⁵Note that some authors refer to the Euler equations only in the case of a perfect fluid that has no body force, so that both rotation and gravitation vanish.

for the Euler equations, with identically zero viscosity, energy cannot be dissipated at the small scales so that an equilibrium turbulent flow is not available.

Another fundamental distinction between the Euler equation and Navier-Stokes equation concerns the boundary conditions. For the Navier-Stokes equations, the presence of a second order operator (the Laplacian), weighted by the viscosity, signals a very distinct behavior of the flow next to boundaries. The Euler equation can only maintain a no-normal flow condition at a boundary, with the kinematics detailed in Section 16.4. The viscous fluid described by the Navier-Stokes equation must satisfy an additional boundary condition. Evidence based on research in the 19th and 20th centuries suggests that that fluids, such as air and water, adhere to solid boundaries and thus satisfy the *no-slip* boundary condition. This boundary condition has basic implications for how stress acts between fluids and solids. We have more to say concerning this boundary condition in Section 22.10.⁶

22.8.8 Laplacian friction in terms of vorticity and divergence

The Laplacian friction operator with a constant viscosity is afforded the following decomposition

$$\nu^{-1} F_n = \partial_m (\partial_m v_n) \quad (22.89a)$$

$$= \partial_m (\partial_m v_n - \partial_n v_m + \partial_n v_m) \quad (22.89b)$$

$$= \partial_m (\partial_m v_n - \partial_n v_m) + \partial_n (\partial_m v_m) \quad (22.89c)$$

$$= -2 \partial_m \mathbb{R}_{mn} + \partial_n \nabla \cdot \mathbf{v} \quad (22.89d)$$

$$= \partial_m (\epsilon_{mnp} \omega_p) + \partial_n \nabla \cdot \mathbf{v} \quad (22.89e)$$

$$= -\epsilon_{nmp} \partial_m \omega_p + \partial_n \nabla \cdot \mathbf{v} \quad (22.89f)$$

$$= -(\nabla \times \boldsymbol{\omega})_n + \partial_n \nabla \cdot \mathbf{v}. \quad (22.89g)$$

In the fourth equality we introduced the rotation tensor (15.42)

$$\mathbb{R}_{mn} = (1/2) (\partial_n v_m - \partial_m v_n), \quad (22.90)$$

which is related to the vorticity, $\boldsymbol{\omega} = \nabla \times \mathbf{v}$, via equation (15.44)

$$\mathbb{R}_{mn} = -\epsilon_{mnp} \omega_p / 2. \quad (22.91)$$

These manipulations have served to decompose the Laplacian viscous acceleration, with a constant viscosity, into the two terms

$$\mathbf{F} = \nu [-\nabla \times \boldsymbol{\omega} + \nabla (\nabla \cdot \mathbf{v})]. \quad (22.92)$$

The Laplacian friction acceleration is thus due to the curl of the vorticity plus gradients in the velocity divergence. Many geophysical flows are dominated by vorticity since the divergence is quite small. Indeed, the Boussinesq ocean discussed in Chapter 26 has $\nabla \cdot \mathbf{v} = 0$, in which case frictional acceleration arises only when the vorticity has a nonzero curl. Correspondingly, irrotational flows (where $\boldsymbol{\omega} = 0$) that are also non-divergent have zero Laplacian frictional acceleration.

22.8.9 Frictional stresses in a sheared flow

As a means to connect the above ideas in this section to the Couette flow discussed in Section 22.8.2, consider a non-divergent velocity that only has a zonal component with a vertical shear (Figure 22.6)

$$\mathbf{v} = u(z) \hat{x}. \quad (22.93)$$

⁶See also the comments and footnote on page 86 of [Segel \(1987\)](#) as well as pages 83-84 of [Meyer \(1971\)](#).

In this case the only nonzero components to the rate of strain tensor are due to the vertical shear, $\mathbb{S}_{13} = \mathbb{S}_{31} = \partial_z u / 2$. Now consider a horizontal area whose outward normal is parallel to the $\hat{\mathbf{z}}$ direction. The frictional force acting on that area is given by the area integral of the frictional stress

$$\mathbf{F}_{\text{area}} = \int \tau \cdot \hat{\mathbf{n}} dS = \int \tau \cdot \hat{\mathbf{z}} dx dy = \rho_0 \frac{\hat{\mathbf{x}}}{2} \nu A \frac{\partial u}{\partial z}, \quad (22.94)$$

where $A = \int dx dy$ is the horizontal area, and where we used the constant reference density, ρ_0 , for a Boussinesq fluid. Hence, the zonal stress arises from the nonzero vertical shear.

Momentum is deposited in regions where there is a divergence in the stress, in which case momentum is transferred from regions of high vertical shear to low vertical shear. At a point, the momentum is affected by the divergence of the viscous stress at that point. For $\mathbf{v} = u(z) \hat{\mathbf{x}}$ we have

$$\left[\frac{\partial(\rho v_m)}{\partial t} \right]_{\text{viscous}} = \partial_n \tau_{nm} \implies \left[\frac{\partial(\rho u)}{\partial t} \right]_{\text{viscous}} = \partial_z (\mu_{\text{vsc}} \partial_z u), \quad (22.95)$$

so that zonal momentum is preferentially deposited to or removed from regions with high vertical curvature in the zonal velocity. Spatial variations in the dynamic viscosity, $\mu_{\text{vsc}} = \rho_0 \nu$, also contribute to friction.

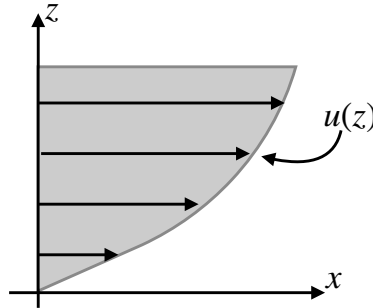


FIGURE 22.6: Sample profile of zonal velocity possessing a vertical shear: $\mathbf{v} = u(z) \hat{\mathbf{x}}$ and with a no-slip boundary condition at $z = 0$. The resulting zonal frictional stress arises from the nonzero vertical shear and viscosity.

22.8.10 The net stress tensor

Combining the frictional stress tensor with pressure and kinetic stress yields the flux-form momentum equation (22.63)

$$\frac{\partial(\rho \mathbf{v})}{\partial t} + 2\rho \boldsymbol{\Omega} \times \mathbf{v} + \rho \nabla \Phi = \nabla \cdot \mathbb{T}^{\text{net}}, \quad (22.96)$$

where we introduced the net stress tensor

$$\mathbb{T}^{\text{net}} = -p \mathbb{I} - \rho \mathbf{v} \otimes \mathbf{v} + \tau = \begin{bmatrix} -p - \rho u^2 + \tau_{11} & -\rho u v + \tau_{12} & -\rho u w + \tau_{13} \\ -\rho u v + \tau_{21} & -p - \rho v^2 + \tau_{22} & -\rho v w + \tau_{23} \\ -\rho u w + \tau_{31} & -\rho v w + \tau_{32} & -p - \rho w^2 + \tau_{33} \end{bmatrix}. \quad (22.97)$$

The left hand side of the momentum equation (22.96) includes the local time tendency plus the body forces from Coriolis and effective gravity. The right hand side is the divergence of the net stress tensor, with this tensor combining the pressure stress, kinetic stress, and frictional stress. Varieties of the net stress tensor appear in subsequent chapters of this book, with details dependent on the chosen approximations.

22.8.11 Comments and further study

There are more elaborate relations between the frictional stress and rate of strain tensors than those considered here. The most general form for a Newtonian fluid introduces a fourth-order viscosity tensor as in Section 4.5 of [Kundu et al. \(2016\)](#) and Chapter 17 in [Griffies \(2004\)](#). We also suggest the treatment of stress in Chapter 5 of [Aris \(1962\)](#).

Geophysical fluids such as air and water are generally well treated using Newtonian constitutive relations. However, there are some geophysical turbulence theories that propose a non-Newtonian constitutive relation for part of their closures, whereby the constitutive relation makes use of products of the rate of strain tensor for computing stress. [Anstey and Zanna \(2017\)](#) offer a compelling approach with a subgrid scale stress tensor that is non-Newtonian and furthermore contains a non-zero trace, thus resulting in a modification to the mechanical pressure. Additional nonlinear relations can arise when the viscous tensor is a function of the flow, such as with the Smagorinsky scheme commonly used for Large Eddy Simulations (LES) (see [Smagorinsky \(1993\)](#) or Chapter 18 of [Griffies \(2004\)](#)).

22.9 Reynolds number and flow regimes

How important is friction relative to other terms in the momentum equation? In particular, how does it compare to the material acceleration? We consider that question in the context of the non-rotating and constant density Navier-Stokes equations with a constant viscosity

$$\frac{\partial \mathbf{v}}{\partial t} + (\mathbf{v} \cdot \nabla) \mathbf{v} = -\rho^{-1} \nabla p + \nu \nabla^2 \mathbf{v}, \quad (22.98)$$

with ρ the constant density.

22.9.1 Non-dimensional Navier-Stokes

We non-dimensionalize the Navier-Stokes equation (22.98) to garner an understanding of relative magnitudes of the various terms. For that purpose, introduce the dimensional scales and corresponding non-dimensional fields

$$L = \text{length scale} \quad U = \text{velocity scale} \quad P = \text{pressure scale} \quad T = \text{time scale}, \quad (22.99)$$

so that equation (22.98) takes the form

$$\frac{\partial \hat{\mathbf{v}}}{\partial \hat{t}} + \frac{V T}{L} (\hat{\mathbf{v}} \cdot \hat{\nabla}) \hat{\mathbf{v}} = -\frac{T P}{\rho V L} \hat{\nabla} \hat{p} + \frac{T \nu}{L^2} \hat{\nabla}^2 \hat{\mathbf{v}}, \quad (22.100)$$

where the hat fields are non-dimensional and defined according to

$$\nabla = L \hat{\nabla} \quad \partial_t = T^{-1} \partial_{\hat{t}} \quad \mathbf{v} = U \hat{\mathbf{v}} \quad p = P \hat{p} \quad (22.101)$$

22.9.2 Ratio of inertial to frictional accelerations

We are concerned with three dimensional flows with only a single length and velocity scale, L and U . For the time scale we assume that it is determined by fluid particle time scale; i.e., the advective time

$$T \sim L/U. \quad (22.102)$$

Furthermore, we assume that the scale of mechanical pressure is comparable to the stress induced by the flow itself

$$P \sim \rho U^2. \quad (22.103)$$

These assumed scales for time and pressure bring the non-dimensional Navier-Stokes equation (22.100) into the rather tidy form

$$\frac{\partial \hat{\mathbf{v}}}{\partial \hat{t}} + (\hat{\mathbf{v}} \cdot \hat{\nabla}) \hat{\mathbf{v}} = -\hat{\nabla} \hat{p} + \frac{1}{\text{Re}} \hat{\nabla}^2 \hat{\mathbf{v}}. \quad (22.104)$$

Flow regimes of the non-dimensional Navier-Stokes equation are specified by the non-dimensional number, $\text{Re} = L, U/\nu$, which is the *Reynolds number*. By definition, the Reynolds number is the ratio of scales for material (inertial) acceleration to frictional acceleration

$$\text{Re} = \frac{\text{inertial accelerations}}{\text{frictional accelerations}} = \frac{U/T}{\nu U/L^2} = \frac{L^2/T}{\nu} = \frac{LU}{\nu}. \quad (22.105)$$

22.9.3 Reynolds numbers for some example flows

Laboratory experiments with flow around and within various objects indicates the following regimes of flow as a function of the Reynolds number:

$$\text{Re} \sim \begin{cases} \leq 10^2 & \text{laminar} \\ 10^2 - 10^3 & \text{quasi-periodic flow} \\ 10^3 - 10^4 & \text{transition to turbulence} \\ \geq 10^4 & \text{fully turbulent.} \end{cases} \quad (22.106)$$

These numbers are fuzzy given dependence on the geometry of the objects placed in the flow and their characteristic length scale. What is more general concerns the behavior of the flow, with a transition from laminar to turbulent typically occurring as the flow moves from relatively low to high Reynolds number.

For a given molecular kinematic viscosity, the Reynolds number is dependent on the velocity and length scales. Let us consider some examples. First, put your finger into a flowing stream of water, such as in a gentle mountain creek. Let the length scale for the finger be 10^{-2} m and the stream flow at a speed of $U \approx 0.1 - 1$ m s⁻¹. With the kinematic viscosity of water given by (page 75 of [Gill \(1982\)](#))

$$\nu_{\text{water}} = 10^{-6} \text{ m}^2 \text{ s}^{-1}, \quad (22.107)$$

we see that our finger poking into the mountain stream is associated with a flow Reynolds number on the order of

$$\text{Re}_{\text{finger in stream}} = 10^3 - 10^4. \quad (22.108)$$

Hence, mountain stream flow around a finger is at the lower end of the turbulent regime. Hence, we might expect to see slightly turbulent whirls and eddies downstream from our finger.

Now consider an oceanographic length scale given by a Gulf Stream ring (see Figure 28.1) in which $L \approx 10^5$ m. Assuming the flow speed is on the same order as the mountain stream (good assumption) leads to a huge Reynolds number for Gulf Stream flow

$$\text{Re}_{\text{Gulf Stream}} = 10^{10} - 10^{11}. \quad (22.109)$$

For the atmosphere, we take $L = 10^6$ m for a typical atmospheric weather system, $U = 10$ m s⁻¹ for the speed, and

$$\nu_{\text{air}} = 1.4 \times 10^{-5} \text{ m}^2 \text{ s}^{-1}, \quad (22.110)$$

for the kinematic viscosity of air at standard pressure (page 75 of [Gill \(1982\)](#)). Given the larger length and velocity scales, the Reynolds number for large-scale atmospheric circulation features is

$$\text{Re}_{\text{weather system}} = 10^{12}. \quad (22.111)$$

These values for the Reynolds number are huge relative to typical values found in engineering flows. They signal the minor role that molecular friction plays in large-scale geophysical fluid flows. Even so, molecular friction is the process leading to mechanical energy dissipation at the small scales. A fundamental feature of large Reynolds number flow is the presence of turbulent motions. Turbulent flows are highly nonlinear and affect a transfer of mechanical energy across length and time scales. This cascade leads to the dissipation of mechanical energy at the small scales. It is at the small scales that flow curvature can be large enough for the relatively tiny values of molecular viscosity to dissipate the energy, thus preventing an *ultraviolet catastrophe*; i.e., preventing the unbounded pile up of mechanical energy at the smallest scales.⁷

The ocean and atmosphere exhibit a huge variety of turbulent regimes, from the macroturbulence of quasi-geostrophic eddies to the microturbulence of boundary layers. Turbulence is not directly considered in this book. However, certain of its implications are identified in various places given that it is so basic to the ocean and atmosphere flows. [Vallis \(2017\)](#) offers a pedagogical entry point for the physics and maths of geophysical turbulence.

22.10 Stress on an interface

In this section we study the stress acting on an interface. This analysis applies to an arbitrary surface within a single media as well as for the boundary interface separating a liquid and a gas (air-sea boundary) or between a fluid and a rigid boundary (air-land or ocean-land). We ignore the effects from surface tension discussed in Section 22.11 since we are interested in length scales on the order of meters or larger (see in particular Section 22.11.5).

22.10.1 General formulation

Formulation of the stress boundary conditions follows from applying the finite volume momentum equation (22.66) to a cylindrical region straddling a moving interface such as that shown in Figure 22.7. The sides of the cylinder have thickness h and the top and bottom have area $\delta\mathcal{S}$. In the limit that the cylinder thickness goes to zero, the volume integrals in equation (22.66) vanish under the assumption of a smooth velocity field on both sides of the interface as well as smooth body forces. We are thus left with the constraint that the area integrated contact forces must vanish when integrated around the cylinder boundary

$$\oint_{\partial\text{cylinder}} [\mathbb{T} + \rho \mathbf{v} \otimes (\mathbf{v}^{(b)} - \mathbf{v})] \cdot \hat{\mathbf{n}} d\mathcal{S} = \oint_{\partial\text{cylinder}} [-p \mathbb{I} + \tau + \rho \mathbf{v} \otimes (\mathbf{v}^{(b)} - \mathbf{v})] \cdot \hat{\mathbf{n}} d\mathcal{S} = 0. \quad (22.112)$$

The end-caps on the cylinder vanish as $h \rightarrow 0$, in which case we have no constraint based on the stresses acting on the end-caps. Instead, the $h \rightarrow 0$ limit leads us to conclude that the contact force on one side of the interface is equal and opposite to that on the other side. This condition is a direct statement of the Newton's third law as manifest via the local equilibrium of stresses discussed in Section 22.2.2. For the stresses acting on the interface in Figure 22.7 we have

$$[-p_A \mathbb{I} + \tau_A + \rho_A \mathbf{v}_A \otimes (\mathbf{v}^{(b)} - \mathbf{v}_A)] \cdot \hat{\mathbf{n}}_A + [-p_B \mathbb{I} + \tau_B + \rho_B \mathbf{v}_B \otimes (\mathbf{v}^{(b)} - \mathbf{v}_B)] \cdot \hat{\mathbf{n}}_B = 0. \quad (22.113)$$

⁷Ultraviolet refers to the high wavenumber end of the flow spectrum, as in the violet part of the visible electromagnetic spectrum.

Setting $\hat{\mathbf{n}} = \hat{\mathbf{n}}_B = -\hat{\mathbf{n}}_A$ leads to

$$[-p_A \mathbb{I} + \tau_A + \rho_A \mathbf{v}_A \otimes (\mathbf{v}^{(b)} - \mathbf{v}_A)] \cdot \hat{\mathbf{n}} = [-p_B \mathbb{I} + \tau_B + \rho_B \mathbf{v}_B \otimes (\mathbf{v}^{(b)} - \mathbf{v}_B)] \cdot \hat{\mathbf{n}}, \quad (22.114)$$

which is an expanded expression of Newton's third law given in equation (22.5). Recall that we are ignoring surface tension, which means there is no pressure jump across the interface (see Section 22.11). Hence, setting $p_A = p_B$ allows us to cancel pressure thus leaving an interface stress condition involving just the frictional stress and kinetic stress

$$[\tau_A + \rho_A \mathbf{v}_A \otimes (\mathbf{v}^{(b)} - \mathbf{v}_A)] \cdot \hat{\mathbf{n}} = [\tau_B + \rho_B \mathbf{v}_B \otimes (\mathbf{v}^{(b)} - \mathbf{v}_B)] \cdot \hat{\mathbf{n}}. \quad (22.115)$$

We now consider a variety of examples to illustrate this condition.

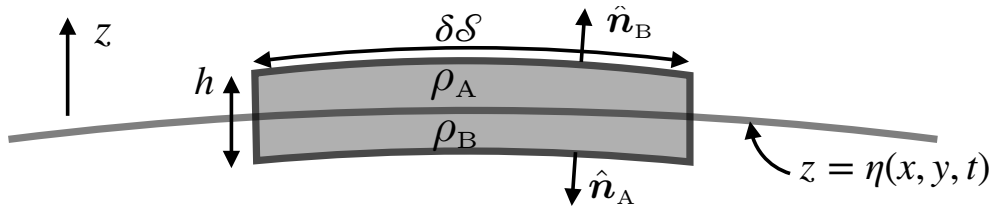


FIGURE 22.7: An infinitesimal cylindrical region used in formulating the stress boundary condition at an interface. The interface can be one that separates two fluid regions with densities ρ_A and ρ_B . It can also represent the boundary between a fluid (region A) and solid (region B). The interface generally moves with velocity $\mathbf{v}^{(b)}$. We orient the interface through the outward normals according to $\hat{\mathbf{n}} = \hat{\mathbf{n}}_B = -\hat{\mathbf{n}}_A$. The outward normal for region A points into region B whereas the outward normal for region B points into region A. For this particular interface, the normal direction has a nonzero projection in the vertical, $\hat{\mathbf{n}} \cdot \hat{\mathbf{z}} \neq 0$, thus allowing us to define the interface vertical position according to $z = \eta(x, y, t)$. This interface represents an idealized geometry useful to formulate the stress condition at the boundary between fluid media, such as the air-sea interface, fluid-land interface, or interior fluid interface (e.g., buoyancy surface). The single geometric assumption is that there are no overturning motions so that $\hat{\mathbf{n}} \cdot \hat{\mathbf{z}} \neq 0$, with this assumption based on convenience. The stress condition is general and so does not require this assumption.

22.10.2 Solid material boundary

Consider a solid material boundary through which no matter crosses. Let region B be the solid side of the interface and region A the fluid side (region A is either the ocean or atmosphere). The material nature of the boundary means that no matter crosses it, in which case (see Section 16.4.2)

$$(\mathbf{v}_A - \mathbf{v}^{(b)}) \cdot \hat{\mathbf{n}} = (\mathbf{v}_B - \mathbf{v}^{(b)}) \cdot \hat{\mathbf{n}} = 0. \quad (22.116)$$

A nonzero $\mathbf{v}^{(b)}$ corresponds here to a moving solid boundary, such as the region next to the grounding line of an ice-shelf. More commonly, in geophysical fluid applications we have $\mathbf{v}^{(b)} = 0$ for solid boundaries. Since there is no contribution from the kinetic stress, the stress condition (22.115) reduces to

$$\tau_A \cdot \hat{\mathbf{n}} = \tau_B \cdot \hat{\mathbf{n}}. \quad (22.117)$$

This identity is consistent with

$$\tau_A \cdot \hat{\mathbf{n}} = \boldsymbol{\tau}^{\text{friction } A}(\mathbf{x}, t, \hat{\mathbf{n}}) = -\boldsymbol{\tau}^{\text{friction } A}(\mathbf{x}, t, -\hat{\mathbf{n}}) = \tau_B \cdot \hat{\mathbf{n}} = \boldsymbol{\tau}^{\text{friction } B}(\mathbf{x}, t, \hat{\mathbf{n}}), \quad (22.118)$$

which expresses Newton's third law in the form of equation (22.5). Hence, the frictional force imparted by the land on the fluid is equal and opposite to that imparted by the fluid on the land.

22.10.3 No-slip boundary condition

At solid boundaries, the kinematic boundary condition from Section 16.4.1 sets the normal component of the velocity to zero

$$\mathbf{v} \cdot \hat{\mathbf{n}} = 0 \quad \text{kinematic no-flux condition on static material boundary.} \quad (22.119)$$

However, no place have we specified the tangential component of the velocity along a solid boundary. What is it?

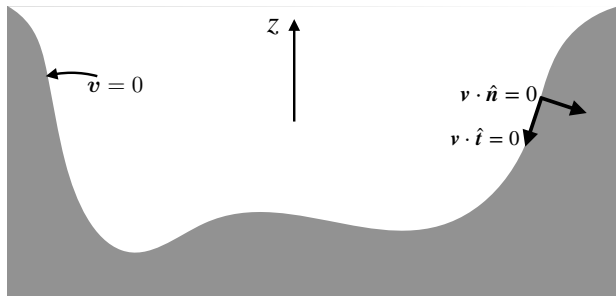


FIGURE 22.8: The no-slip boundary condition means that fluid exhibits zero relative motion at the solid-fluid boundary, $\mathbf{v} \cdot \hat{\mathbf{t}} = 0$. That is, the fluid sticks to the solid boundary. The kinematic no-normal flow boundary condition, $\mathbf{v} \cdot \hat{\mathbf{n}} = 0$, plus the dynamic no-slip boundary condition together mean that both the normal and tangential components of the velocity vanish at solid boundaries. For both the normal and tangential components of the velocity to vanish at a solid boundary requires the velocity to fully vanish at this boundary.

Laboratory experiments over the 19th and 20th centuries indicate that there is no relative motion of molecules at solid-fluid interfaces.⁸ That is, a fluid at the solid-fluid interface has a velocity matching that of the solid so that the fluid sticks to the solid boundary as depicted in Figure 22.8. The no-slip boundary condition means that both the normal and tangential components of the fluid velocity vanish next to static solid boundaries

$$\mathbf{v} \cdot \hat{\mathbf{n}} = \mathbf{v} \cdot \hat{\mathbf{t}} = 0 \quad \text{no-slip condition on static solid boundaries.} \quad (22.120)$$

The no-slip boundary condition gives rise to an exchange of momentum between the solid and fluid, with this exchange mediated by viscosity. This boundary condition is the origin of the tangential stresses found in the Couette flow discussed in Section 22.8.2. In the absence of viscous friction, as per an inviscid perfect fluid, the no-slip boundary condition cannot be imposed since doing so would mathematically over-specify the flow. Consequently, for inviscid fluids the tangential component of the velocity remains unspecified at solid boundaries.

22.10.4 Lagrangian interface

Consider a Lagrangian interface within the fluid, with this interface defined so that

$$(\mathbf{v}_A - \mathbf{v}^{(b)}) \cdot \hat{\mathbf{n}} = (\mathbf{v}_B - \mathbf{v}^{(b)}) \cdot \hat{\mathbf{n}} = 0. \quad (22.121)$$

Again the kinetic stress contribution to equation (22.115) vanishes. We thus have the frictional stress condition (22.117) and a Newton's third law interpretation (22.118), yet now the frictional transfer takes place between two regions of the same fluid.

⁸As discussed in the historical essay by [Anderson \(2005\)](#), it was the work of Prandtl in 1905 that first exposed the fundamental nature of the no-slip boundary condition, and its role in establishing boundary layers around solid bodies immersed in a fluid flow.

22.10.5 Permeable interface

Now allow for the interface to be permeable and introduce the dia-surface transport defined by equation (57.41)

$$(\mathbf{v}_A - \mathbf{v}^{(b)}) \cdot \hat{\mathbf{n}} = (\mathbf{v}_B - \mathbf{v}^{(b)}) \cdot \hat{\mathbf{n}} = w^{\text{dia}}, \quad (22.122)$$

where we assumed continuous dia-surface transport across the interface; i.e., what leaves one side enters the other. The kinetic stress thus adds to the frictional contribution in the stress boundary condition (22.115), with the kinetic stress providing a transfer of momentum across the interface through the dia-surface advection of fluid elements

$$\tau_A \cdot \hat{\mathbf{n}} + \rho_A \mathbf{v}_A w^{\text{dia}} = \tau_B \cdot \hat{\mathbf{n}} + \rho_B \mathbf{v}_B w^{\text{dia}}. \quad (22.123)$$

We consider two cases.

Single continuous fluid media

If the interface is within a single continuous fluid media, then $\rho_A = \rho_B$ and $\mathbf{v}_A = \mathbf{v}_B$, in which case the advection of momentum from region A to B is equal to that from region B to A . Consequently, the frictional condition (22.117) again holds.

Air-sea boundary interface

Consider now the air-sea boundary where region B is the ocean and region A the atmosphere. Introduce the dia-surface mass flux according to equation (16.63)

$$\rho_A w^{\text{dia}} = \rho_B w^{\text{dia}} = -\mathcal{Q}_m, \quad (22.124)$$

where \mathcal{Q}_m is the mass per time per surface area crossing the boundary. The minus sign is implied by the convention that $\mathcal{Q}_m > 0$ means that mass enters the ocean side of the interface and leaves the atmosphere side. Even though the densities and velocities on the two sides of the interface are unequal, mass conservation means that the mass transport entering the ocean must leave the atmosphere, and vice versa. Consequently, the stress boundary condition (22.123) takes the form

$$\tau_{\text{atm}} \cdot \hat{\mathbf{n}} - \mathbf{v}_{\text{atm}} \mathcal{Q}_m = \tau_{\text{ocn}} \cdot \hat{\mathbf{n}} - \mathbf{v}_{\text{ocn}} \mathcal{Q}_m \implies (\tau_{\text{atm}} - \tau_{\text{ocn}}) \cdot \hat{\mathbf{n}} = (\mathbf{v}_{\text{atm}} - \mathbf{v}_{\text{ocn}}) \mathcal{Q}_m. \quad (22.125)$$

There is generally a jump in the frictional stress in the presence of mass transport across the air-sea interface. However, when introducing the dia-surface transport (22.122) we see that $\mathbf{v}_A \cdot \hat{\mathbf{n}} = \mathbf{v}_B \cdot \hat{\mathbf{n}}$ at the interface. So a nonzero $\mathbf{v}_{\text{atm}} - \mathbf{v}_{\text{ocn}}$ arises just from differences in the tangential velocities at the air-sea interface. If those velocities are equal so that $(\mathbf{v}_{\text{atm}} - \mathbf{v}_{\text{ocn}}) \mathcal{Q}_m = 0$, then we are again left with the friction boundary condition (22.117).

22.10.6 Summary comments

There are three terms in the general expression for the stress boundary condition (22.114), with contributions from pressure, friction, and kinetic stress. In the absence of surface tension, pressure is continuous at the interface; i.e., its value is the same on both sides of the interface. In the absence of mass transport across the interface, then we find a continuous kinetic stress at the interface that then leads to a continuous frictional stress. However, mass transport crossing the interface leads to a jump in the friction for those case where the tangential velocity has a jump across the interface. Assuming no such jump then leads again to a continuous frictional stress.

22.10.7 Comments on boundary layers

A fundamental advance in the relevance of fluid mechanics for describing observed flows came from the 20th century work of Prandtl and others who noted the central role of viscosity, even the tiny molecular values, in forming boundary layers when fluids flow next to rigid bodies.⁹ Prandtl's work focused on flows around airplane wings, thus supporting the development of aerodynamics as a scientific and engineering discipline. The key ideas transfer to geophysical flows where boundary layers form in the atmosphere and ocean as these fluids interact with the solid earth. Boundary layers also form where the atmosphere and ocean interact with one another.

A key facet of geophysical boundary layers concerns the dominance of turbulence in producing an eddy viscosity that is many orders larger than molecular viscosity. Indeed, molecular viscosity plays a role only in a very small region (the *laminar subregion*) immediately adjacent to the boundary, where as the bulk of the boundary layer is dominated by turbulence. The study of boundary layers is well outside our scope, as it is largely a topic of turbulence. However, in Chapter 30 we dive into the details of geophysical boundary layers that are affected by pressure, Coriolis, and turbulence induced friction. The leading role of rotation distinguishes geophysical boundary layers from engineering applications. The associated *Ekman boundary layers* are crucial for understanding circulation and transport in both the atmosphere and ocean.

22.11 Surface tension

Surface tension is present on surfaces between two immiscible liquids, between a liquid and gas, or between a fluid and a solid. It arises from the anisotropic forces acting on molecules that are within a mean free path distance from the surface. Surface tension has many consequences that are part of our common experience. For example, it allows certain insects to walk on water even though their body density is greater than water. It also accounts for the predominantly spherical shape of rain drops and gas bubbles in liquids. Surface tension also gives rise to capillary waves when there is a very slight breeze on the ocean surface, or when a tiny stone is thrown into a still pond (gravity waves dominate for larger stones). We further discuss capillary waves in Section 45.7. In the present section we focus on the classical physics of surface tension.¹⁰

22.11.1 Capillary tube

As an introduction to surface tension, consider that atmospheric pressure at the earth's surface is roughly $p_{\text{atm}} = 10^5 \text{ N m}^{-2}$. As we saw in Section 22.8, pressure acts normal to a surface regardless the surface orientation. So fill a container of water whose weight per horizontal area is less than the atmospheric pressure, $\rho g h < p_{\text{atm}}$ and turn the container upside-down as in Figure 22.9. Does the water spill from the container? Common experience with drinking glasses indicate that water will spill. But what about containers with a very small cross-sectional area such as the pipettes used in chemistry laboratories? Pipettes, or more generally capillary tubes, hold the liquid regardless the orientation. They do so since their cross-sectional area is small enough to allow forces from surface tension to overcome gravitational instabilities acting at the liquid-gas interface. We return to this point in Section 51.3.3 when studying the *Rayleigh-Taylor* instability in the presence of

⁹For a historical treatment of boundary layer theory see [Anderson \(2005\)](#), or for a pedagogical study see [Tennekes and Lumley \(1972\)](#). The associated mathematical methods of singular perturbation theory and matched asymptotic expansions (e.g., [Dyke \(1975\)](#)) offer an example of how the study of physical systems can spawn the development of new mathematical methods.

¹⁰A first principles understanding of surface tension involves tools from physical chemistry that are outside of our scope. Instead, we here develop the subject heuristically.

surface tension. In the remainder of this section we discuss elements of surface tension with the goal to develop intuition as well as to determine the length scales where it becomes important.

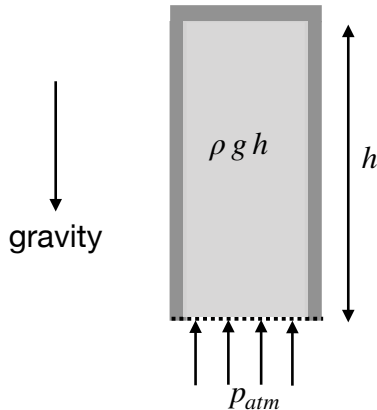


FIGURE 22.9: A container of water with density ρ and height h is placed upside-down. Atmospheric pressure, p_{atm} , will support water with thickness $h < p_{atm}/(\rho g) \approx 10$ m if the cross-sectional area of the container is small enough to allow for surface tension to overcome the gravitationally unstable waves that otherwise allow water to spill from the container. The liquid-gas interface supports both gravity waves (Section 45.3) and capillary waves (Section 45.7). If the wavelength is small enough then surface tension suppresses the growth of unstable gravity waves so that the liquid remains within the *capillary tube*. However, for longer waves allowed by increasing the cross-sectional area, then fluctuations will allow the gravitational instability to overcome surface tension, thus breaking the interface and releasing water.

22.11.2 Force balance on an air-water interface

Consider two fluids with distinct densities. Air and water provide one example of special importance to understanding physics at the ocean-atmosphere boundary. Another example concerns two immiscible layers of water within the ocean or two layers of air within the atmosphere. For molecules well within either of the fluid regions, the intermolecular forces are statistically isotropic. In contrast, intermolecular forces are not isotropic for molecules within a mean free path distance from the interface.¹¹ Attractive (cohesive) intermolecular (van der Waals) forces dominate within a liquid whereas gas molecules generally feel more repulsive forces. Hence, a liquid molecule within the liquid-gas interface preferentially experiences an attractive force towards the liquid side of the interface, as depicted in Figure 22.10. Surface tension arises from the cohesive force per area acting between molecules in a direction that parallels the interface, with surface tension acting to resist perturbations to the interface shape.

Anisotropic attractive intermolecular forces cause the interface between the two fluids to behave as a stretched membrane that experiences a tensile force resisting any stretching of the interface. The magnitude of the tensile force per unit length (or energy per unit area) is the *surface tension*, γ (SI units $N\ m^{-1} = kg\ s^{-2}$). The surface tension is a property of the two fluids, including their temperature, as well as any impurities that might be included on the interface; e.g., oil on the surface of water effects properties of the capillary waves found on the air-sea interface (see Section 45.7). In the following we focus on the liquid-gas example to be specific and to expose issues that arise in studies of the air-sea interface. For a liquid-gas interface surrounding a liquid drop, the tensile force acts to curve the interface towards the liquid into a spherical shape.

¹¹As discussed in Section 13.2, the mean free path is a statistical measure of the distance a molecule moves before hitting another molecule.

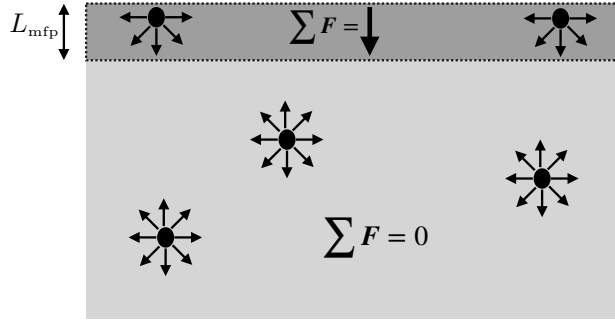


FIGURE 22.10: Surface tension at a liquid-gas interface arises from the anisotropic cohesive forces acting on liquid molecules within a mean-free-path distance, L_{mfp} , from the interface, which contrasts to the isotropic cohesive forces acting away from the interface. The net intermolecular force vanishes for interior molecules, whereas the net force acts inward on molecules at the interface. Surface tension refers to the cohesive force per area acting between molecules in a direction that is parallel to the interface.

The tensile force along a line segment is directed normal to the line and tangent to the interface

$$\mathbf{f}_{\text{interface}} = -\gamma \hat{\mathbf{n}} \times \delta \mathbf{x}, \quad (22.126)$$

where $\hat{\mathbf{n}}$ is a normal vector pointing towards the center of the curved interface, and $\delta \mathbf{x}$ is a line element oriented so that the normal $\hat{\mathbf{n}}$ points to the left facing in the direction of the line increment. Figure 22.11 depicts the surface tensile forces acting on the surface of a spherical bubble of water. Note that it is sometimes useful to consider the product γdS as the work (units of N m^{-1} = Joule) required to create an area, dS , on the interface. We make use of this energetic perspective in Section 22.11.3.

To develop an expression for the pressure jump across the liquid-gas interface, consider a spherical droplet of radius R shown in Figure 22.11 and focus on the circular cross-section cut through the center of the sphere. The net tensile force acting on the circumference of the circle is

$$\mathbf{F}_{\text{circle}} = \oint_{\text{circle}} \mathbf{f}_{\text{interface}} = - \oint_{\text{circle}} \gamma \hat{\mathbf{n}} \times \delta \mathbf{x} = -2\pi R \gamma \hat{\mathbf{z}}. \quad (22.127)$$

Equilibrium of the spherical droplet is realized by a pressure jump across the circular cross-sectional area

$$\pi R^2 (p_{\text{in}} - p_{\text{out}}) = 2\pi R \gamma \implies (p_{\text{in}} - p_{\text{out}}) = 2\gamma/R. \quad (22.128)$$

Hence, the pressure jump is determined by the surface tension (a property of the two fluids) and the curvature of the sphere, R , which is also the radius of curvature for the sphere. Pressure is higher inside of the sphere (i.e., on the concave side of the interface), with this pressure required to balance the pressure outside the sphere plus the surface tension. Notably, equilibrium for smaller bubbles (with $R \rightarrow 0$) requires a larger pressure difference than for larger bubbles.

The pressure jump is known as the *capillary pressure*. It arises from surface tension and curvature of the interface. The relation (22.128) is a special case of the *Young-Laplace formula*, specialized here to a sphere.

22.11.3 Young-Laplace formula

We garner added insight into the physics of surface tension by considering the energetics required to enable a virtual displacement of a surface through a pressure field along with the work required

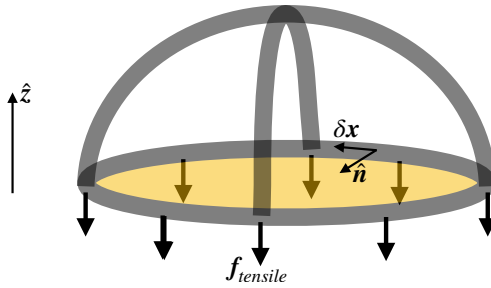


FIGURE 22.11: Surface tension on a spherical water droplet, with water on the inside of the sphere and air on the outside. The tensile forces act parallel to the spherical interface between the water and air. When cutting a circular cross-section as shown here, the surface tensile force acts downward. In equilibrium, the net tensile forces acting downward along the circumference of the hemisphere ($2\pi R \gamma$) are balanced by a pressure jump across the droplet, with the interior pressure larger than the exterior pressure. Focusing on the circular cross-section, this area remains static so long as $2\pi R \gamma = \pi R^2 (p_{\text{in}} - p_{\text{out}})$, leading to a pressure jump across the droplet interface $p_{\text{in}} - p_{\text{out}} = 2\gamma/R$. This result is general: namely, according to the Young-Laplace formula (22.138), pressure is greater on the concave side of the interface than on the convex side.

to change the area of the surface. The resulting equation for the pressure jump across the surface is referred to as the *Young-Laplace formula*, which expresses the pressure jump in terms of the surface tension and the principle radii of curvature for the surface.

Consider a horizontal surface depicted in Figure 22.12 that represents the interface separating fluid-A from fluid-B, with \hat{n} a unit normal vector oriented from fluid-A to fluid-B. Now consider a virtual displacement of each point along the interface by an infinitesimal distance, $\delta h = \eta(x, y, t)$, with $\hat{n} \delta h$ connecting points on the initial position of the interface to the displaced position, where $\delta h > 0$ if the displacement is directed towards fluid-B and $\delta h < 0$ if directed towards fluid-A. The (signed) volume swept out by an infinitesimal area dA is given by $\delta h dA$. There are two forms of work required to move the surface: pressure work required to change the fluid volume and area work required to change the surface area. The pressure work is given by

$$W_{\text{volume}} = -p_A \delta V_A - p_B \delta V_B = (p_B - p_A) \delta V_A = (p_B - p_A) \delta h dA, \quad (22.129)$$

where we set $\delta V_A = -\delta V_B = \delta h dA$. For example, if $p_B > p_A$ and the displacement is into fluid-B ($\delta h > 0$), then $W_{\text{volume}} > 0$. We thus find that $W_{\text{volume}} > 0$ to displace the surface into the fluid region with higher pressure, whereas $W_{\text{volume}} < 0$ if displacing the interface into a region with lower pressure.

In the presence of surface tension, work is needed to change to the interface area

$$W_{\text{area}} = \gamma \delta A, \quad (22.130)$$

where δA is the change in area of an infinitesimal element on the interface

$$\delta A = d\mathcal{S} - dA \quad (22.131a)$$

$$= dA \left[\sqrt{1 + (\nabla \delta h)^2} - 1 \right] \quad (22.131b)$$

$$\approx dA (\nabla \delta h)^2 / 2. \quad (22.131c)$$

To reach this result we made use of equation (6.33) that relates the area of an infinitesimal element on a curved surface to the area of its horizontal projection (see Section 6.3.1). We next make use of the surface curvature detailed in Section 6.3.2, where equation (6.38) shows that the vertical

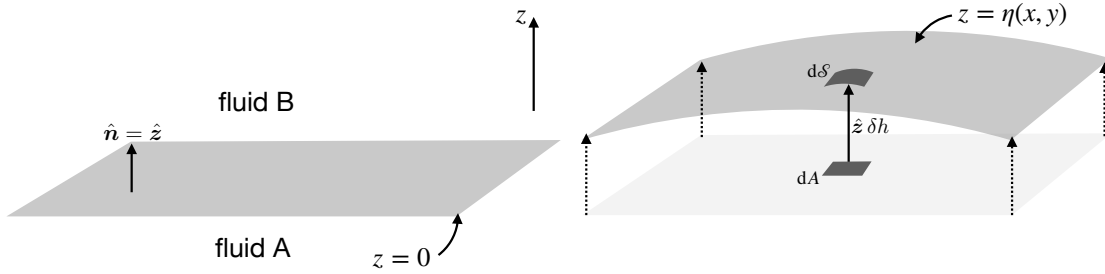


FIGURE 22.12: Left panel: initial position of a material interface separating two fluid regions, fluid-A and fluid-B. Right panel: infinitesimal displacement of the interface sweeps out a volume in space, here depicted with the interface moving upward. To determine the volume, extend a unit normal vector, \hat{n} , from the initial interface position and pointing towards fluid-B. For this example, $\hat{n} = \hat{z}$. Let $\delta h = \eta$ be the distance along that normal to the new position, with $\delta h > 0$ if the displacement moves towards fluid-B and $\delta h < 0$ for displacements pointing to fluid-A. We assume that displacements at each interface point can move independently of adjacent points, so that the interface area generally changes. The Young-Laplace formula (22.138) says that the pressure jumps when crossing an interface that is subject to surface tension, with pressure higher on the concave side. In this example, Young-Laplace says pressure is higher on the Fluid-A side since that it is the concave side.

displacement is given, for small displacements, by

$$-\delta h \approx \frac{1}{2} R_1^{-1} (\mathbf{x} \cdot \mathbf{e}_1)^2 + \frac{1}{2} R_2^{-1} (\mathbf{x} \cdot \mathbf{e}_2)^2. \quad (22.132)$$

R_1^{-1}, R_2^{-1} are the eigenvalues and $\mathbf{e}_1, \mathbf{e}_2$ are the corresponding eigenvectors of the matrix of second partial derivatives of $\delta h(x, y)$, whereas the inverse eigenvalues, R_1, R_2 , are the radii of curvature of the displaced surface. To get signs correct, it is important to note that the radius of curvature is positive if the surface curves towards the outward normal direction, and negative otherwise (see Figure 6.5). For the example depicted in the right panel of Figure 22.12, and both radii of curvature are negative since the surface curves away from the outward normal (pointing from A to B). This convention explains the minus sign on the left side of equation (22.132).

Orienting the Cartesian axes along the eigenvector directions renders

$$(\nabla \delta h)^2 \approx (x/R_1)^2 + (y/R_2)^2 = (-\delta h) \left[\frac{1}{R_1} + \frac{1}{R_2} \right], \quad (22.133)$$

where we set

$$(-\delta h)/R_1 = (x/R_1)^2 \quad \text{and} \quad (-\delta h)/R_2 = (y/R_2)^2. \quad (22.134)$$

We are thus led to the area difference

$$\delta A \approx dA (-\delta h) \left[\frac{1}{R_1} + \frac{1}{R_2} \right]. \quad (22.135)$$

Note that $\delta A > 0$ whether displacing the surface into a concave or convex direction, since the sign of δh accounts for the sign of the radii of curvature. For small displacements of the surface from its horizontal position, equation (6.41) allows us to connect the radii of curvature for a surface with the Laplacian of the displacement of the surface, in which case equation (22.135) takes on the form

$$\delta A \approx -dA \delta h \nabla^2(\delta h). \quad (22.136)$$

Total work for the interface displacement is given by the sum of the area work and volume

work

$$W_{\text{area}} + W_{\text{volume}} = dA \delta h \left[-\gamma (R_1^{-1} + R_2^{-1}) + p_B - p_A \right] = dA \delta h \left[-\gamma \nabla^2 \eta + p_B - p_A \right], \quad (22.137)$$

and equilibrium results if the net work vanishes, in which case

$$p_B - p_A = \gamma (R_1^{-1} + R_2^{-1}) = \gamma \nabla^2 \eta, \quad (22.138)$$

where we set $\delta h = \eta$ as per Figure 22.12. This equation is the *Young-Laplace* formula, which reduces to equation (22.128) if $R_1 = R_2$ as for a sphere. It says that there is a pressure jump, known as the *capillary pressure*, across an interface as given by the surface tension times the sum of the inverse principle radii of curvature, or equivalently the surface tension times the Laplacian of the displacement. To help remember signs, note that the Young-Laplace formula (22.138) says that the pressure on the concave side of an interface is higher than on the convex side. Hence, pressure is higher on the inside of a bubble/droplet. For the example depicted in Figure 22.12, $\nabla^2 \eta < 0$ since the surface is a local maximum, in which case $p_A > p_B$ since fluid A is on the concave side of the interface.

22.11.4 Soluble gas bubbles inside water

The previous considerations hold whether there is liquid or gas inside a spherical bubble or drop. As an example, consider a spherical gas bubble of radius $R = 10^{-6}$ m inside water and make use of the air-water surface tension $\gamma = 0.072 \text{ N m}^{-1} = 0.072 \text{ kg s}^{-2}$. We thus find the pressure jump is

$$p_{\text{in}} - p_{\text{out}} = 2 \gamma / R \approx 144 \times 10^3 \text{ N m}^{-2} = 1.42 p_{\text{atm}}, \quad (22.139)$$

where $p_{\text{atm}} = 1.01 \times 10^5 \text{ N m}^{-2}$ is standard atmospheric pressure. If the gas inside the bubble is water soluble, then the enhanced pressure inside the bubble will induce more gas to dissolve in the water, which in turn will cause the bubble to shrink and thus increase the pressure inside the bubble. Small bubbles of soluble gases can thus be squeezed towards zero radius by the effects of surface tension induced pressure.

22.11.5 When we can ignore surface tension

The sizable pressure jump (22.139) arises from the tiny radius of curvature of the bubble, with the pressure jump decreasing as the bubble radius increases. Rather than a bubble, consider an ocean surface capillary-gravity wave, such as those observed from a boat (e.g., Sections 45.3 and 45.7). Such waves may have wavelength on the order of 10^{-2} m or longer. If we set the radius of curvature to $R \sim 10^{-2}$ m, then equation (22.139) finds an entirely negligible pressure jump of $\Delta p \approx 10^{-4} p_{\text{a}}$.

Most geophysical fluid motion of concern in this book is associated with material interfaces having a radius of curvature on the order of meters or larger. It is for this reason that surface tension is generally ignored when studying geophysical fluid motion. That is, we can safely assume there is no pressure jump when approaching an interface between two fluid media, or between a fluid and a solid boundary. This discussion then justifies the approach considered in Section 22.10 when studying stresses at interfaces, in which we made use of Newton's third law at the interface.

Even so, the role of surface tension is central to the fundamental mechanisms of how matter, momentum, and energy are transferred across the air-sea interface. Relatedly, as we show in Section 45.7, capillary waves arise from surface tension, with capillary waves the initial response of the ocean free surface upon the imposition of a wind stress.

22.11.6 Further study

This [30-minute video](#) from Prof. Trefethen provides a pedagogical summary of surface tension. The upside-down container of water in Figure 22.9 is based on a discussion of capillary-gravity waves in Section 3.1.3 of [Falkovich \(2011\)](#). Section 1.9 of [Batchelor \(1967\)](#) discusses how surface tension acts between two fluid media, with that discussion extended into his Section 3.3 to develop boundary conditions for velocity and stress. The bubble example in Section 22.11.4 is taken from Section 1.3 of [Kundu et al. \(2016\)](#). Section 4.10 of [Kundu et al. \(2016\)](#) provides a detailed accounting of the force balance at an interface, offering more details than found in [Batchelor \(1967\)](#). The energetic arguments used to derive the Young-Laplace formula follows Section 61 of [Landau and Lifshitz \(1987\)](#). Section 46 of [Fetter and Walecka \(2003\)](#) discuss the dynamics of membranes under tension.

22.12 Exercises

EXERCISE 22.1: FORCE BALANCE FOR A NON-ACCELERATING OCEAN

Consider an ocean basin, \mathcal{R} , on the rotating earth as in Figure 22.2, with bottom interface separating the ocean fluid from the solid-earth, and upper interface separating the ocean fluid from the atmosphere, and where the atmosphere has a nonzero mass.¹² Assume no matter crosses the ocean boundaries; i.e., no evaporation, precipitation, nor river runoff. Hence, the ocean domain maintains a fixed mass

$$M = \int_{\mathcal{R}} \rho dV \quad (22.140)$$

as well as fixed matter. In this case, the ocean domain is materially closed and so its center of mass position

$$\mathbf{X}^{\text{com}} = M^{-1} \int_{\mathcal{R}} \mathbf{x} \rho dV \quad (22.141)$$

has a velocity given by

$$\frac{d\mathbf{X}^{\text{com}}}{dt} = M^{-1} \int_{\mathcal{R}} \mathbf{v} \rho dV, \quad (22.142)$$

and corresponding acceleration

$$\frac{d^2 \mathbf{X}^{\text{com}}}{dt^2} = M^{-1} \int_{\mathcal{R}} \frac{D\mathbf{v}}{Dt} \rho dV. \quad (22.143)$$

Apply a turbulent stress over the ocean surface with a horizontal stress vector $\boldsymbol{\tau}^{\text{surf}}$, with this stress leading to motion of the ocean fluid. Allow for the ocean bottom to exchange momentum with the static solid-earth through a horizontal bottom turbulent stress, $\boldsymbol{\tau}^{\text{bott}}$. Assume there are no vertical components to $\boldsymbol{\tau}^{\text{surf}}$ and $\boldsymbol{\tau}^{\text{bott}}$.

- (a) What is the force balance for the full ocean domain if the center of mass experiences no acceleration. Express the corresponding force balance in words and in equations. Expose the contact forces arising from pressure and from turbulent stresses, as well as the body forces from Coriolis and gravity. The answer should be generally stated, with no need for specific details. Hint: consider Figure 22.2 and include the missing forces to this diagram. Mathematically express the force balance as an integral expression as per the weak formulation of fluid mechanics (see Section 14.2).

¹²In some applications it is suitable to assume a zero mass atmosphere. For this exercise, however, we do not make that assumption.

- (b) Express the vertical component of the force balance assuming the fluid is in an approximate hydrostatic balance, meaning that the pressure and gravitational forces are balanced.¹³
- (c) Consider an ocean without any turbulent contact stresses at the boundaries, $\tau^{\text{surf}} = \tau^{\text{bott}} = 0$ and assume there is no motion anywhere in the fluid. What integral constraints are satisfied by the horizontal components of the pressure contact force? Hint: recall equations equations (22.39a) and (22.39b). Also note assume that the free surface is flat, which is consistent with the absence of motion.
- (d) Assume the ocean is on an f -plane (Section 21.3.4) so that $\Omega = \hat{z}\Omega = \hat{z}(f/2)$ is a constant vector. Also assume that the center of mass velocity vanishes, $\int_{\mathcal{R}} \rho \mathbf{v} dV = 0$. Discuss the resulting zonal and meridional force balance. Hint: one of the forces appearing in part (a) now vanishes.



¹³In Section 24.2 we provide a discussion of when this approximation is appropriate for moving fluids. That discussion is not needed for the current exercise. Instead, we merely assume the vertical momentum balance is hydrostatic.

Chapter 23

Thermodynamics and Energetics

In this chapter we study the energetics of fluid flow. In particular, we are concerned with how energy is partitioned between the mechanical energy of macroscopic motion and the internal energy associated with internal degrees of freedom. To fully specify energy in fluid flows requires us to study the flow of entropy and the associated constraints arising from the second law of thermodynamics. For this purpose we extend the equilibrium thermodynamics of Chapters 19 and 20 to include time dependent moving fluid phenomena. Making this transition requires us to assume that moving fluid elements are in *local thermodynamic equilibrium*. This assumption is based on the quasi-static nature of macroscopic motions (Section 19.1.3) whereby microscopic motions have a much shorter equilibration time scale relative to the slower macroscopic processes of interest for fluid mechanics, including advection, waves, turbulence, and turbulent mixing. The extremely wide space and time scale separation between the microscopic and macroscopic allows us to use phenomenological thermodynamic laws to develop evolution equations for continuous thermodynamic properties of moving continuum fluid elements. Consistent with the time scale separation, we can assume that the macroscopic motion of a fluid element does not alter its entropy. That is, advective transport in the absence of mixing is a reversible process. In contrast, mixing of properties between fluid elements, whether through molecular or turbulent processes, is irreversible and thus increases entropy.

The application of thermodynamics to a moving fluid is known as *quasi-equilibrium thermodynamics* or *linear irreversible thermodynamics*. The fundamentals of this subject are developed in [DeGroot and Mazur \(1984\)](#) and [Landau and Lifshitz \(1987\)](#). The term “linear” in the name refers to an assumption that the system is close to thermodynamic equilibrium throughout its motion. This assumption is very accurate for the atmosphere and ocean motions studied in this book, whereby local thermodynamic equilibrium is maintained for fluid elements even as those elements move as a result of imbalances in macroscopic forces. Thermodynamic fluxes are thus linear functions of the gradients of the thermodynamic state variables. The assumption of local thermodynamic equilibrium breaks down in the rarefied gas dynamics of the upper atmosphere, which is a subject outside the scope of this book.

READER'S GUIDE FOR THIS CHAPTER

This chapter builds from the momentum dynamics of Chapter 21 and the thermodynamics of Chapters 19 and 20. In addition to developing the budgets for mechanical energy and total energy (mechanical plus internal), we derive budgets for entropy and potential enthalpy. A particularly important practical outcome of this chapter concerns the derivation of the equation for potential enthalpy or Conservative Temperature, with this equation completing the suite of fundamental equations describing the evolution of a geophysical fluid.

23.1	Loose threads	519
23.2	Gravitational potential energy	519
23.2.1	Material evolution	519
23.2.2	Eulerian flux-form potential energy equation	520
23.2.3	Reference geopotential	520
23.2.4	Regionally integrated gravitational potential energy	520
23.2.5	Potential energy and vertical stratification	521
23.2.6	Gravitational potential energy and mixing	522
23.3	Mechanical energy of macroscopic motion	523
23.3.1	Kinetic energy	523
23.3.2	Frictional dissipation of kinetic energy	524
23.3.3	Mechanical energy budget	526
23.3.4	Mechanical energy for a finite volume	526
23.3.5	Further study	528
23.4	Thermodynamics of a moving fluid	528
23.4.1	Concerning the transition to a continuous fluid	529
23.4.2	Space-time derivatives and thermodynamic partial derivatives	529
23.4.3	A caution for thermodynamic partial derivatives	530
23.4.4	First law for a moving fluid element	531
23.4.5	Enthalpy budget	532
23.4.6	Thermal and chemical processes and fluxes	532
23.4.7	First law in terms of potential temperature	533
23.4.8	Materially constant specific entropy for a perfect fluid	533
23.4.9	Further study	534
23.5	Budget for total energy	534
23.5.1	Postulating the budget for total energy	534
23.5.2	First law of thermodynamics for a moving fluid	535
23.5.3	Joule heating from friction	535
23.5.4	Comments on gauge symmetry	535
23.5.5	Further study	536
23.6	Thermodynamic equilibrium with macroscopic motion	536
23.6.1	Deriving the equilibrium conditions	536
23.6.2	Further study	537
23.7	Bernoulli theorem	537
23.7.1	Bernoulli potential	538
23.7.2	Mechanical injection work	538
23.7.3	Bernoulli's theorem for a steady perfect fluid	539
23.7.4	Traditional derivation of Bernoulli's theorem	539
23.7.5	Steady flow in a pipe	540
23.7.6	Steady flow over a topographic bump	542
23.7.7	Further study	543
23.8	Entropy budget for the ocean	543
23.8.1	Non-advective entropy flux and entropy source	544
23.8.2	Constraints from the second law of thermodynamics	545
23.8.3	A summary presentation	547
23.8.4	Comments	548
23.8.5	Further study	548
23.9	Temperature evolution	549
23.9.1	Evolution of <i>in situ</i> temperature	549
23.9.2	Evolution of potential temperature	550
23.9.3	Conservative Temperature for the ocean	550
23.9.4	Alternative functional dependencies for specific enthalpy	552
23.9.5	Further study	552

23.10 Conservation laws and potential properties	553
23.10.1 Flux-form conservation laws	553
23.10.2 Conservation laws that are not flux-form	553
23.10.3 Non-material or wave-like transport of properties	554
23.10.4 Material and non-material conservation laws	554
23.10.5 Concerning potential properties	555
23.10.6 Further study	555
23.11 Summary of the equations for rotating and stratified fluids	555
23.12 Exercises	557

23.1 Loose threads

- Figures needed
- Potential energy as per Section 108 of *Landau and Lifshitz* (1980)

23.2 Gravitational potential energy

Geophysical fluids move within a gravitational field created by the mass of the planet, including the mass of the fluid itself. We typically focus on a rather simple form for the effective gravitational acceleration exemplified by the geopotential $\Phi = g z$, where g is the gravitational acceleration that includes effects from both central gravity plus planetary centrifugal (Section 11.11.4). However, we offer some discussion of astronomical tide producing forces in Chapter 31, whereby the geopotential is a more complicated function of space and time, $\Phi(\mathbf{x}, t)$. In this section we study the potential energy of a fluid element due to its presence in a gravitational field, with the geopotential providing the effective gravitational potential energy per mass of fluid elements.¹

23.2.1 Material evolution

The gravitational potential energy per mass of a fluid element is given by the geopotential, Φ , so that the gravitational potential energy is $\Phi \rho \delta V$. Hence, the evolution of potential energy for a constant mass fluid element is given by

$$\frac{D(\Phi \rho \delta V)}{Dt} = \rho \delta V \frac{D\Phi}{Dt}, \quad (23.1)$$

where $D(\rho \delta V)/Dt = 0$ since the fluid element has a constant mass. The material time derivative for the geopotential

$$\frac{D\Phi}{Dt} = \frac{\partial \Phi}{\partial t} + \mathbf{v} \cdot \nabla \Phi, \quad (23.2)$$

contains a local time dependence that arises from astronomical tide forcing or movement of mass on the planet (Chapter 31). As further explored in Section 23.3, the advective term represents an exchange of mechanical energy between the kinetic energy contained in fluid motion and the gravitational potential energy due to the fluid being within a gravitational field. This energy exchange arises from fluid motion across constant geopotential surfaces. For example, motion up the geopotential gradient, $\mathbf{v} \cdot \nabla \Phi > 0$, increases gravitational potential energy and motion down

¹In the following we generally refer to the more concise “gravitational potential energy” or even briefer “potential energy” rather than “potential energy from the effective gravitational field.”

the geopotential gradient decreases potential energy. With the geopotential $\Phi = g z$, we have

$$\mathbf{v} \cdot \nabla \Phi = g w, \quad (23.3)$$

so that vertically upward motion ($w > 0$) increases potential energy.

23.2.2 Eulerian flux-form potential energy equation

Another way to reveal the same ideas in Section 23.2.1 is to make use of the kinematic identity (16.35c), so that the density weighted material time derivative of the geopotential is given by

$$\rho \frac{D\Phi}{Dt} = \partial_t(\rho \Phi) + \nabla \cdot (\rho \mathbf{v} \Phi). \quad (23.4)$$

For the simple geopotential, $\Phi = g z$, we thus find

$$\rho \frac{D\Phi}{Dt} = \rho g w \iff \partial_t(\rho \Phi) + \nabla \cdot (\rho \mathbf{v} \Phi) = \rho g w. \quad (23.5)$$

23.2.3 Reference geopotential

There is no change to the energetics if we modify the gravitational reference state by modifying the geopotential

$$\Phi \rightarrow \Phi + \Phi_r \quad (23.6)$$

with Φ_r an arbitrary constant. In particular, this offset has no effect on the evolution of gravitational potential energy of the constant mass fluid element since

$$\frac{D(\Phi_r \rho \delta V)}{Dt} = \Phi_r \frac{D(\rho \delta V)}{Dt} = 0. \quad (23.7)$$

Hence, as is well known from classical mechanics, it is not the value of the gravitational potential energy that is important, but instead it is the space and time changes that affect energetics.

23.2.4 Regionally integrated gravitational potential energy

Now consider the evolution of the gravitational potential energy integrated over a finite region \mathcal{R} . If the fluid region is closed to mass transport, as per a material boundary, then we can make use of the Leibniz-Reynolds transport theorem in the form of equation (17.50d) to write

$$\frac{d}{dt} \int_{\mathcal{R}} \Phi \rho dV = \int_{\mathcal{R}} \frac{D\Phi}{Dt} \rho dV, \quad (23.8)$$

which is an extension of the material evolution equation (23.1). If the region is open to material mass transport, we make use Leibniz-Reynolds transport theorem in the form of equation (17.34) to find

$$\frac{d}{dt} \int_{\mathcal{R}} \rho \Phi dV = \int_{\mathcal{R}} \frac{\partial(\rho \Phi)}{\partial t} dV + \oint_{\partial \mathcal{R}} \rho \Phi \mathbf{v}^{(b)} \cdot \hat{\mathbf{n}} d\mathcal{S} \quad (23.9a)$$

$$= \int_{\mathcal{R}} \left[\rho \frac{D\Phi}{Dt} - \nabla \cdot (\rho \Phi \mathbf{v}) \right] dV + \oint_{\partial \mathcal{R}} \rho \Phi \mathbf{v}^{(b)} \cdot \hat{\mathbf{n}} d\mathcal{S} \quad (23.9b)$$

$$= \int_{\mathcal{R}} \rho \frac{D\Phi}{Dt} dV + \oint_{\partial \mathcal{R}} \rho \Phi (\mathbf{v}^{(b)} - \mathbf{v}) \cdot \hat{\mathbf{n}} d\mathcal{S}, \quad (23.9c)$$

where $\mathbf{v}^{(b)}$ is the velocity of a point on the boundary of the domain. The evolution thus consists of the mass integrated material time evolution of the geopotential, plus a surface term that contributes to the transport of the geopotential across the regional boundaries.

If the region is a vertical column of ocean fluid with fixed horizontal cross-section, extending from the ocean surface to the ocean bottom, then there is horizontal transport across the vertical column bounds, plus vertical transport of mass across the ocean free surface. For the free surface we make use of the surface kinematic boundary condition (16.73c) to write

$$\int_{z=\eta} \rho \Phi (\mathbf{v}^{(b)} - \mathbf{v}) \cdot \hat{\mathbf{n}} d\mathcal{S} = \int_{z=\eta} Q_m \Phi dA. \quad (23.10)$$

In this equation, Q_m is the mass per time per horizontal area of matter crossing the ocean free surface at $z = \eta$ where $Q_m > 0$ for matter entering the ocean domain, and $d\mathcal{S}$ is the area element on the free surface with dA its horizontal projection. As noted in Section 23.2.3, we can add a constant to the geopotential without affecting the energetics, which is here seen by noting that mass conservation means that

$$\frac{d}{dt} \int \rho dV = - \int_{\mathcal{R}} \nabla \cdot [\rho (\mathbf{v} - \mathbf{v}^{(b)})] dV, \quad (23.11)$$

which results from setting $\Phi = 1$ in equation (23.9c). In general, we expect the transfer of mass across the surface boundary to affect the gravitational potential energy both because it adds or removes mass to the ocean domain, and because it affects the geopotential. To help interpret the sign from the boundary term, it is useful to define the reference state geopotential so that $\Phi > 0$ at the ocean surface, no matter what the value of η . We can do so by defining the reference geopotential at or below the ocean bottom. In this case, adding mass increases the gravitational potential energy and removing mass reduces it.

Consider the special case of a geopotential $\Phi = g z$, so returning to a $z = 0$ reference state, in which case the global ocean potential energy equation is written

$$\frac{d}{dt} \int \rho z dV = \int \rho w dV + \int Q_m \eta dA, \quad (23.12)$$

where we cancelled the constant gravitational acceleration. Now decompose Q_m and η into their global area means and deviations

$$Q_m = \overline{Q_m} + Q'_m \quad \text{and} \quad \eta = \bar{\eta} + \eta', \quad (23.13)$$

so that

$$g \int Q_m \eta dA = g \overline{Q_m} \bar{\eta} A + g \int Q'_m \eta' dA. \quad (23.14)$$

As before, the $\overline{Q_m} \bar{\eta}$ term alters potential energy relative to the arbitrary reference state, here taken as $z = 0$. The area correlation term increases potential energy in regions where $Q'_m \eta' > 0$, which acts to increase the relative deviation of the free surface from its mean value. That is, $Q'_m \eta' > 0$ in regions where $Q'_m > 0$ and $\eta' > 0$ as well as in regions where $Q'_m < 0$ and $\eta' < 0$. Conversely, the correlation term reduces potential energy where Q'_m and η' are anti-correlated, which acts to decrease the relative deviation of the free surface height.

23.2.5 Potential energy and vertical stratification

Consider the potential energy of a region of horizontally homogeneous fluid centered at a vertical position, $z = z_c$, and with constant horizontal cross-sectional area, A . Assuming we do not move

vertically far away from the central position, we can write the density in the linear form

$$\rho(z) = \rho(z_c) + \frac{d\rho(z_c)}{dz} (z - z_c) \equiv \rho_c - K(z - z_c), \quad (23.15)$$

where $K = -d\rho(z_c)/dz > 0$ is a shorthand for the vertical density gradient at the central point. The potential energy per volume ($\Delta V = A \Delta z$) for fluid in the vertical region $z \in [z_c - \Delta z/2, z_c + \Delta z/2]$ is given by

$$(g/\Delta z) \int z \rho dz = (g/\Delta z) \int_{z_c - \Delta z/2}^{z_c + \Delta z/2} [\rho_c - K(z - z_c)] z dz \quad (23.16a)$$

$$= g \rho_c z_c - g K (\Delta z)^2 / 12. \quad (23.16b)$$

We thus see that the gravitational potential energy decreases as the vertical stratification, $K > 0$, increases, with the maximum potential energy when the stratification vanishes, $K = 0$. As seen in Section 23.2.6, potential energy is maximized when $K = 0$ since the center of mass moves vertically upward as the stratification reduces to zero.

23.2.6 Gravitational potential energy and mixing

Consider a fluid in exact hydrostatic balance (Section 21.4) with a gravitationally stable vertical stratification where light fluid is above heavy fluid.² Now introduce a physical process, such as vertical mixing associated with a kinetic energy source, that reduces the vertical stratification. Reducing vertical stratification requires mixing to move heavy fluid up and light fluid down. In so doing, the kinetic energy supporting the mixing is converted into gravitational potential energy since the center of mass for the fluid column rises.

We can formulate this thought experiment by considering a column of seawater that is vertically stratified in salinity, S , and Conservative Temperature, Θ , and another column that is vertically unstratified with constant values S_m and Θ_m .³ We assume the mass of the two columns is the same so that the bottom pressure is the same. However, the volumes will generally differ since the density differs, so that the two free surfaces, η and η_m , are different. Assuming a geopotential, $\Phi = g z$, leads to the difference between the gravitational potential energies per horizontal area in the two columns

$$g \int_{\eta_b}^{\eta_m} \rho(S_m, \Theta_m, p) z dz - g \int_{\eta_b}^{\eta} \rho(S, \Theta, p) z dz = \int_{p_a}^{p_b} (z_m - z) dp \quad (23.17a)$$

$$= (p_b - p_a) (\bar{z}_m - \bar{z}). \quad (23.17b)$$

To reach this result we used the same pressure differential, dp , when integrating over both columns, which we can do since mass is conserved. Furthermore, we used the hydrostatic balance to convert from a depth integral into a pressure integral

$$dp = -g \rho(S, \Theta, p) dz = -g \rho(S_m, \Theta_m, p) dz_m \implies z \rho(S, \Theta, p) dz = z_m \rho(S_m, \Theta_m, p) dz_m. \quad (23.18)$$

We also introduced the center of mass positions for the vertically homogeneous column, \bar{z}_m , and

²See Section 27.5 for a more precise discussion of gravitational stability.

³See Section 27.3 for discussion of the seawater equation of state. For present purposes it is sufficient to know that seawater density is a function of the material tracer S , the thermodynamic tracer, Θ , and pressure, p . When a column is vertically homogenized that means S and Θ are constant throughout the column. However, pressure remains hydrostatic and thus is not vertically constant. Since density is a function of pressure, it too retains a vertical gradient.

the stratified column, \bar{z}

$$\bar{z}_m = \frac{1}{p_b - p_a} \int_{p_a}^{p_b} z_m dp \quad \text{and} \quad \bar{z} = \frac{1}{p_b - p_a} \int_{p_a}^{p_b} z dp. \quad (23.19)$$

There are two terms in the potential energy difference in equation (23.17b). The first is the mass per horizontal area, as measured by the difference in bottom pressure and applied surface pressure, $p_b - p_a$. The second is the difference between the center of mass for the two columns, $\bar{z}_m - \bar{z}$, which is a positive number since homogenizing a fluid column moves heavier water up and lighter water down so that $\bar{z}_m > \bar{z}$. Hence, we see that the potential energy of the mixed column is larger than the stratified column. We develop more experience with these ideas in Exercise 23.1.

23.3 Mechanical energy of macroscopic motion

Mechanical energy is a dynamical property formed by adding the energy due to motion of fluid elements (kinetic energy) to the energy arising from the position of a fluid element within the gravitational field (gravitational potential energy). We studied the gravitational potential energy budget in Section 23.2. Here, we develop the budget for kinetic energy and then the full mechanical energy (kinetic plus gravitational potential) of the macroscopic fluid motion. In Section 23.5 we then add the mechanical energy to the internal energy to study the budget for total energy.

More precisely, we develop the mechanical energy budget for the macroscopic motion of a fluid in a rotating reference frame. For this purpose we make use of the momentum equation (21.16), repeated here for convenience

$$\rho \frac{D\mathbf{v}}{Dt} + 2\rho \boldsymbol{\Omega} \times \mathbf{v} = -\rho \nabla \Phi + \nabla \cdot (-p \mathbb{I} + \tau) \quad (23.20a)$$

$$= -\rho \nabla \Phi - \nabla p + \rho \mathbf{F}, \quad (23.20b)$$

where we wrote

$$\mathbf{F} = \rho^{-1} \nabla \cdot \tau \quad (23.21)$$

for acceleration due to friction arising from the divergence of the frictional stress tensor.

23.3.1 Kinetic energy

Following our discussion of mechanical energy of a point particle in Section 12.8, consider the kinetic energy per mass of a fluid element

$$\mathcal{K} = \mathbf{v} \cdot \mathbf{v}/2. \quad (23.22)$$

Use of the momentum equation in the form of equations (23.20a) and (23.20b) reveals that the material evolution of the kinetic energy per mass is given by

$$\rho \frac{D\mathcal{K}}{Dt} = -\rho \mathbf{v} \cdot \nabla \Phi - \mathbf{v} \cdot \nabla p + \rho \mathbf{v} \cdot \mathbf{F}. \quad (23.23)$$

We thus see that the kinetic energy of a fluid element is affected by work done by the geopotential, $-\rho \mathbf{v} \cdot \nabla \Phi$, along with work done by stresses through both pressure and friction. We detail these processes in the following.

Contribution from the geopotential

Kinetic energy increases for motion directed down the geopotential gradient

$$\mathbf{v} \cdot \nabla \Phi < 0 \implies \text{increases kinetic energy.} \quad (23.24)$$

For example, with a simple geopotential, $\Phi = g z$, kinetic energy increases where the vertical velocity is downward,

$$w < 0 \implies -w g \rho > 0 \longleftrightarrow \text{downward motion increases } \mathcal{K} \text{ of a fluid element.} \quad (23.25)$$

As seen in Section 23.2.1, this increase in kinetic energy due to motion down the geopotential gradient is exactly balanced by a decrease in gravitational potential energy. This exact conversion between kinetic energy and potential energy is also seen in Section 12.8 for motion of the point particle.

Contribution from the pressure gradient body force

Kinetic energy increases in regions where the velocity projects down the pressure gradient,

$$\mathbf{v} \cdot \nabla p < 0 \implies \text{increase kinetic energy,} \quad (23.26)$$

thus resulting in an increase in fluid speed imparted by the pressure gradient force. Conversely, kinetic energy is reduced in regions where the flow is directed up the pressure gradient. It is notable that geostrophic flows, studied in Section 28.4, have a velocity given by

$$\mathbf{v}_g = (g \rho)^{-1} \hat{\mathbf{z}} \times \nabla p. \quad (23.27)$$

Consequently, geostrophic flows have $\mathbf{v}_g \cdot \nabla p = 0$, so that the pressure gradient force has no impact on the horizontal kinetic energy of a geostrophic fluid.

Contribution from friction

Kinetic energy is reduced in regions where the velocity has a negative projection onto the direction of the friction vector, $\rho \mathbf{v} \cdot \mathbf{F} < 0$. As detailed in Section 23.3.2, the friction arising from a viscous stress tensor appropriate for a Newtonian fluid gives rise to two contributions to kinetic energy: the divergence of a viscous flux plus a sign-definite sink.

23.3.2 Frictional dissipation of kinetic energy

We here detail the role of friction on kinetic energy

$$\text{friction power per volume} = \rho \mathbf{v} \cdot \mathbf{F}, \quad (23.28)$$

where friction is determined by the stress-rate of strain relation (22.78). We interpret $\rho \mathbf{v} \cdot \mathbf{F}$ as the frictional power (energy per time) per volume acting to alter the kinetic energy per volume

of a fluid element. To proceed, we expose Cartesian tensor labels to have

$$\rho \mathbf{v} \cdot \mathbf{F} = v_m \rho F_m \quad (23.29a)$$

$$= v_m \partial_n \tau_{nm} \quad (23.29b)$$

$$= 2 v_m \partial_n (\rho \nu S_{mn}^{\text{dev}}) \quad (23.29c)$$

$$= 2 \partial_n (\rho \nu v_m S_{mn}^{\text{dev}}) - 2 \rho \nu \partial_n v_m S_{mn}^{\text{dev}} \quad (23.29d)$$

$$= 2 \nabla \cdot (\rho \nu \mathbf{v} \cdot \mathbb{S}^{\text{dev}}) - 2 \rho \nu S_{mn} S_{mn}^{\text{dev}}, \quad (23.29e)$$

where we recall from Section 22.8.6 that the *deviatoric rate of strain tensor* has elements given by

$$S_{mn}^{\text{dev}} = S_{mn} - \delta_{mn} S_{qq}/3 \quad \text{with} \quad S_{qq} = \nabla \cdot \mathbf{v}. \quad (23.30)$$

To reach equation (23.29e) required the identity

$$2 \partial_n v_m S_{mn}^{\text{dev}} = (\partial_n v_m + \partial_m v_n) S_{mn}^{\text{dev}} + (\partial_n v_m - \partial_m v_n) S_{mn}^{\text{dev}} = 2 S_{mn} S_{mn}^{\text{dev}}, \quad (23.31)$$

where

$$(\partial_n v_m - \partial_m v_n) S_{mn}^{\text{dev}} = 2 A_{mn} S_{mn}^{\text{dev}} = 0 \quad (23.32)$$

due to symmetry of the deviatoric rate of strain tensor, $S_{mn}^{\text{dev}} = S_{nm}^{\text{dev}}$, and anti-symmetry of the rotation tensor, A_{mn} (see Section 15.3.5 as well as Exercise 1.2). We can show that the second term in equation (23.29e) is sign-definite by noting that

$$S_{mn}^{\text{dev}} S_{mn}^{\text{dev}} = (S_{mn} - \delta_{mn} S_{qq}/3)^2 \quad (23.33a)$$

$$= S_{mn} S_{mn} + \delta_{mn} \delta_{mn} S_{qq} S_{qq}/9 - 2 S_{mn} \delta_{mn} S_{qq}/3 \quad (23.33b)$$

$$= S_{mn} S_{mn} + (S_{qq})^2/3 - 2 (S_{qq})^2/3 \quad (23.33c)$$

$$= S_{mn} (S_{mn} - \delta_{mn} S_{qq}/3) \quad (23.33d)$$

$$= S_{mn} S_{mn}^{\text{dev}}. \quad (23.33e)$$

We are thus left

$$\rho \mathbf{v} \cdot \mathbf{F} = 2 \nabla \cdot (\rho \nu \mathbf{v} \cdot \mathbb{S}^{\text{dev}}) - 2 \rho \nu \mathbb{S}^{\text{dev}} \cdot \mathbb{S}^{\text{dev}}, \quad (23.34)$$

with

$$\mathbb{S}^{\text{dev}} \cdot \mathbb{S}^{\text{dev}} = S_{mn}^{\text{dev}} S_{mn}^{\text{dev}}. \quad (23.35)$$

We interpret the two contributions to the frictional power in equation (23.34) as

$$\rho \mathbf{v} \cdot \mathbf{F} = \text{divergence of viscous flux} - \text{kinetic energy dissipation}. \quad (23.36)$$

The divergence theorem means that when integrated over the full domain, the flux divergence becomes a contribution from boundary stresses, and boundary stresses can either increase or decrease kinetic energy according to the boundary processes. In contrast, the sign-definite dissipation term provides a sink to the kinetic energy at each point in the fluid interior. This frictional dissipation is commonly written

$$\epsilon \equiv [\mathbf{v} \cdot \mathbf{F}]_{\text{dissipate}} = 2 \nu \mathbb{S}^{\text{dev}} \cdot \mathbb{S}^{\text{dev}} \geq 0. \quad (23.37)$$

The dimensions of ϵ are $\text{L}^2 \text{T}^{-3}$, which in SI units are $\text{m}^2 \text{s}^{-3} = \text{W kg}^{-1}$. We thus refer to ϵ as the kinetic energy dissipation per mass due to viscous effects.

23.3.3 Mechanical energy budget

Adding the material time evolution equations for kinetic energy per mass and gravitational potential energy per mass leads to the material form of the mechanical energy per mass

$$\rho \frac{Dm}{Dt} = -\mathbf{v} \cdot \nabla p + 2 \nabla \cdot (\rho \nu \mathbf{v} \cdot \mathbb{S}^{\text{dev}}) + \rho (-\epsilon + \partial_t \Phi) \quad (23.38a)$$

$$= -\nabla \cdot (p \mathbf{v} - 2 \rho \nu \mathbf{v} \cdot \mathbb{S}^{\text{dev}}) + p \nabla \cdot \mathbf{v} + \rho (-\epsilon + \partial_t \Phi) \quad (23.38b)$$

$$= -\nabla \cdot \mathbf{J}_{\text{mech}} + p \nabla \cdot \mathbf{v} + \rho (-\epsilon + \partial_t \Phi), \quad (23.38c)$$

where

$$m = \mathcal{K} + \Phi \quad (23.39)$$

is the mechanical energy per mass of a fluid element. Equation (23.40) can be written as an Eulerian flux-form conservation equation

$$\partial_t(\rho m) + \nabla \cdot (\rho m \mathbf{v} + \mathbf{J}_{\text{mech}}) = p \nabla \cdot \mathbf{v} + \rho (-\epsilon + \partial_t \Phi). \quad (23.40)$$

As already anticipated, there is a cancellation of the mechanical energy exchanged between kinetic and potential energy due to motion through the gravitational field. However, the time-dependent geopotential provides a source of mechanical energy arising from processes external to the fluid; e.g., astronomical effects such as those driving tides.

Equation (23.40) introduced the mechanical energy flux

$$\mathbf{J}_{\text{mech}} = p \mathbf{v} - 2 \rho \nu \mathbf{v} \cdot \mathbb{S}^{\text{dev}} = -\mathbf{v} \cdot (-p \mathbb{I} + \tau) = -\mathbf{v} \cdot \mathbb{T}. \quad (23.41)$$

We see from equation (23.40) that the material evolution of mechanical energy per mass arises from the convergence of the mechanical energy flux, \mathbf{J}_{mech} , plus the work done by pressure, effects from frictional dissipation (more discussed in Section 23.5.3), and time changes to the geopotential. Furthermore, as shown when studying total energy in Section 23.5, mechanical energy is exchanged with internal energy through pressure work and frictional dissipation. This exchange provides the fundamental link between the mechanical energy of macroscopic motion and the internal energy of microscopic degrees of freedom.

23.3.4 Mechanical energy for a finite volume

We here examine the mechanical energy integrated over a finite volume, \mathcal{R} .

Gravitational potential energy budget

We start with the gravitational potential energy as it is a bit simpler. Using the Leibniz-Reynolds transport theorem in the form of equation (17.44) yields

$$\frac{d}{dt} \left[\int_{\mathcal{R}} \rho \Phi dV \right] = \int_{\mathcal{R}} \partial_t(\rho \Phi) dV + \oint_{\partial \mathcal{R}} \rho \Phi \mathbf{v}^{(b)} \cdot \hat{\mathbf{n}} d\mathcal{S}, \quad (23.42)$$

where $\mathbf{v}^{(b)}$ is the velocity of a point on the region boundary, $\partial \mathcal{R}$, and $\hat{\mathbf{n}}$ is the boundary outward normal. Next we replace the partial time derivative with

$$\partial_t(\rho \Phi) = \rho \frac{D\Phi}{Dt} - \nabla \cdot (\rho \mathbf{v} \Phi), \quad (23.43)$$

in which case

$$\frac{d}{dt} \left[\int_{\mathcal{R}} \rho \Phi dV \right] = \int_{\mathcal{R}} \rho \frac{D\Phi}{Dt} dV - \oint_{\partial\mathcal{R}} \rho \Phi (\mathbf{v} - \mathbf{v}^{(b)}) \cdot \hat{\mathbf{n}} d\mathcal{S}. \quad (23.44)$$

For the case of the full ocean domain we use the surface kinematic boundary condition (16.73a), and no-flux boundary condition on the bottom, to yield

$$\frac{d}{dt} \left[\int_{\mathcal{R}} \rho \Phi dV \right] = \int_{\mathcal{R}} \rho \frac{D\Phi}{Dt} dV + \oint_{\partial\mathcal{R}} \Phi Q_m dA, \quad (23.45)$$

with Q_m the mass flux crossing the upper boundary at $z = \eta$, and dA the horizontal area element. For the simple geopotential, $\Phi = g z$, this equation takes the form

$$\frac{d}{dt} \left[\int_{\mathcal{R}} \rho \Phi dV \right] = \int_{\mathcal{R}} \rho g w dV + \oint_{\partial\mathcal{R}} \Phi Q_m dA. \quad (23.46)$$

This budget says that the gravitational potential energy for the global ocean domain changes due to the domain integrated vertical motion, plus contributions from the transfer of mass across the free surface boundary.

Mechanical energy budget

For the mechanical energy we make use of the Leibniz-Reynolds transport theorem in the form of equation (17.46), as well as the Eulerian flux-form mechanical energy budget (23.40), which lead to the finite volume budget

$$\begin{aligned} \frac{d}{dt} \left[\int_{\mathcal{R}} \rho m dV \right] &= - \oint_{\partial\mathcal{R}} \left[\rho (m + p/\rho) (\mathbf{v} - \mathbf{v}^{(b)}) - 2\rho\nu(\mathbf{v} - \mathbf{v}^{(b)}) \cdot \mathbb{S}^{\text{dev}} \right] \cdot \hat{\mathbf{n}} d\mathcal{S} \\ &\quad + \int_{\mathcal{R}} [p \nabla \cdot \mathbf{v} + \rho (-\epsilon + \partial_t \Phi)] dV, \end{aligned} \quad (23.47)$$

The first term on the right hand side arises from the advective transport of $m + p/\rho$ across the boundary, whereas the next boundary term arises from viscous stresses integrated around the boundary. Then there is a volume integral of the pressure work acting to modify the volume of a fluid element, along with viscous dissipation and a time dependent geopotential.

Non-divergent flow of a perfect fluid in a material region

Consider the particular case of a non-divergent flow, so that pressure does no work on fluid elements since each element maintains a constant volume (see Chapter 18). Furthermore, assume the fluid is perfect, so that there are no effects from viscosity. Finally, assume the geopotential is constant. These assumptions bring the mechanical energy equation (23.47) to the simpler form

$$\frac{d}{dt} \left[\int_{\mathcal{R}} \rho m dV \right] = - \oint_{\partial\mathcal{R}} \rho (m + p/\rho) (\mathbf{v} - \mathbf{v}^{(b)}) \cdot \hat{\mathbf{n}} d\mathcal{S}. \quad (23.48)$$

For this fluid, mechanical energy of a region changes only via the advective transport of $m + p/\rho$ across the region boundary. If the region is material, then there is no material transport across the boundary so that $(\mathbf{v} - \mathbf{v}^{(b)}) \cdot \hat{\mathbf{n}} = 0$. We conclude that the mechanical energy remains time invariant for the non-divergent flow of a perfect fluid in a material region

$$\text{non-divergent flow of perfect fluid in a material region} \implies \frac{d}{dt} \left[\int_{\mathcal{R}} \rho m dV \right] = 0. \quad (23.49)$$

Consequently, there is a direct exchange between the kinetic energy and gravitational potential energy

$$\frac{d}{dt} \left[\int_{\mathcal{R}} \rho \mathcal{K} dV \right] = - \frac{d}{dt} \left[\int_{\mathcal{R}} \rho \Phi dV \right], \quad (23.50)$$

so that their sum remains constant. The energetics described for this particular example provides a direct analog to a frictionless point particle from Section 12.8, whose mechanical energy also remains constant.

23.3.5 Further study

The study of physical processes contributing to mechanical energy dissipation is central to the study of ocean mixing. The review by [MacKinnon et al. \(2013\)](#) provides a pedagogical starting point for this area of physical oceanography.

As shown in Section 17.8 of [Griffies \(2004\)](#), we can relate the global integral of the kinetic energy dissipation to the friction vector by taking the functional derivative of the dissipation with respect to the velocity field. This connection follows from the self-adjoint nature of the friction operator and it can be a useful mathematical framework for developing numerical discretizations of the viscous friction operator (e.g., [Griffies and Hallberg \(2000\)](#)). In Section 61.4.4 we consider a similar connection between the tracer diffusion operator and tracer variance.

23.4 Thermodynamics of a moving fluid

We here extend the formalism of equilibrium thermodynamics from Chapters 19 and 20 to the case of a moving fluid. One practical outcome of this development is a framework to understand how the internal energy of microscopic degrees of freedom is exchanged with the mechanical energy of macroscopic fluid motion. For that purpose, recall the fundamental thermodynamic relation (19.59b) for a two-component fluid such as seawater or the atmosphere

$$d\mathcal{I} = T d\mathcal{S} - p d(1/\rho) + \mu dC. \quad (23.51)$$

This equation expresses the first law of thermodynamics for a quasi-static process, thus relating the exact differential of specific internal energy, \mathcal{I} , to the specific entropy, \mathcal{S} , specific volume, $1/\rho$, and matter concentration, C , along with the thermodynamic temperature, T , the pressure, p , and the relative chemical potential, μ .

Now consider a finite region of fluid comprised of a continuum of fluid elements. The fluid region is generally exposed to mechanical and thermal processes that support macroscopic fluid motion. However, we assume that each fluid element is in local thermodynamic equilibrium and separately satisfies the fundamental thermodynamic relation (23.51). This assumption is supported by noting that the equilibrium time scale for the microscopic degrees of freedom within an individual fluid element is extremely tiny compared to the equilibrium time scales of the macroscopic motion. We discussed this extremely large time scale separation in Section 19.1.3 when presenting the notion of a quasi-static process. Within this regime, we are justified in making use of quasi-equilibrium thermodynamics, which consists of using equilibrium thermodynamics locally yet allowing for macroscopic gradients in fluid properties. In effect, each fluid element is locally in thermodynamic equilibrium while it is out of equilibrium with its neighbors.

We furthermore assume that the thermodynamic potentials have the same functional relation across all of the fluid elements. This assumption is basic to our ability to maintain a field theoretic description of the continuum. Namely, there is no objective definition of a fluid element. Instead, they are infinitesimal regions of a continuum. So we must make use of the same functional

expression for thermodynamic potentials across all of the fluid elements. This further assumption allows us to take space and time derivatives of thermodynamic potentials as considered next.

23.4.1 Concerning the transition to a continuous fluid

For a continuum fluid, each of the thermodynamic properties in the fundamental thermodynamic relation (23.51) are continuous functions of space and time. Furthermore, equation (23.51) provides a relation between exact differentials as detailed in Section 2.8. As exact differentials of continuous fields, we can make use of the space and time differentials detailed in Section 14.6.1 to write

$$d\Psi = \Psi(\mathbf{x} + d\mathbf{x}, t + dt) - \Psi(\mathbf{x}, t) = dt \partial_t \Psi + d\mathbf{x} \cdot \nabla \Psi, \quad (23.52)$$

where Ψ is one of the thermodynamic properties, dt is the time differential, and $d\mathbf{x}$ is the vector of space differentials. Following the discussion in Section 14.6.2, we are led to the total time derivative for a property following an arbitrary trajectory $\mathbf{x} = \mathbf{X}(t)$

$$\frac{d\Psi}{dt} = \frac{\partial \Psi}{\partial t} + \frac{d\mathbf{X}}{dt} \cdot \nabla \Psi. \quad (23.53)$$

Restricting the trajectory to that defined by a fluid particle, so that $\mathbf{v} = d\mathbf{X}/dt$, renders the material time derivative as in Section 14.6.4

$$\frac{D\Psi}{Dt} = \frac{\partial \Psi}{\partial t} + \mathbf{v} \cdot \nabla \Psi. \quad (23.54)$$

We make use of this result in Section 23.4.4 to transition the quasi-static relation (23.51) to a moving fluid.

23.4.2 Space-time derivatives and thermodynamic partial derivatives

We need one more piece of formalism prior to transitioning the quasi-static relation (23.51) to a moving fluid. For this purpose, consider the particular case of specific enthalpy, in which case

$$\mathcal{H} = \mathcal{H}(\mathbf{x}, t) = \mathcal{H}[\mathcal{S}(\mathbf{x}, t), p(\mathbf{x}, t), C(\mathbf{x}, t)], \quad (23.55)$$

where the second equality exposed the natural functional dependence based on the fundamental thermodynamic relation (19.77c)

$$d\mathcal{H} = T d\mathcal{S} + (1/\rho) dp + \mu dC, \quad (23.56)$$

which holds for transitions between equilibrium states (Section 19.6.4). Again, this same functional dependence is assumed to hold for the case of an evolving fluid, so long as the evolution time scales are much slower than the time scales for reaching local thermodynamic equilibrium. We next make use of the chain-rule to render the spatial gradient

$$\nabla \mathcal{H} = \left[\frac{\partial \mathcal{H}}{\partial \mathcal{S}} \right]_{p,C} \nabla \mathcal{S} + \left[\frac{\partial \mathcal{H}}{\partial p} \right]_{S,C} \nabla p + \left[\frac{\partial \mathcal{H}}{\partial C} \right]_{S,p} \nabla C. \quad (23.57)$$

This spatial gradient probes properties of the field, $\mathcal{H}(\mathbf{x}, t)$, which is a function of three other fields, $\mathcal{S}(\mathbf{x}, t), p(\mathbf{x}, t), C(\mathbf{x}, t)$. From this field theory perspective, the thermodynamic partial derivatives are computed by holding the value of the complement thermodynamic properties fixed at a point in space and time. For example, exposing space and time positions renders the awkward, yet

unambiguous, expression

$$\left[\frac{\partial \mathcal{H}}{\partial S} \right]_{p,C} = \left[\frac{\partial \mathcal{H}[S(\mathbf{x}, t), p(\mathbf{x}, t), C(\mathbf{x}, t)]}{\partial S(\mathbf{x}, t)} \right]_{p(\mathbf{x}, t), C(\mathbf{x}, t)}. \quad (23.58)$$

We next apply the thermodynamic partial derivative identities (19.79) to write

$$\left[\frac{\partial \mathcal{H}}{\partial S} \right]_{p,C} = \left[\frac{\partial \mathcal{H}[S(\mathbf{x}, t), p(\mathbf{x}, t), C(\mathbf{x}, t)]}{\partial S(\mathbf{x}, t)} \right]_{p(\mathbf{x}, t), C(\mathbf{x}, t)} = T(\mathbf{x}, t) \quad (23.59a)$$

$$\left[\frac{\partial \mathcal{H}}{\partial p} \right]_{S,C} = \left[\frac{\partial \mathcal{H}[S(\mathbf{x}, t), p(\mathbf{x}, t), C(\mathbf{x}, t)]}{\partial p(\mathbf{x}, t)} \right]_{S(\mathbf{x}, t), C(\mathbf{x}, t)} = 1/\rho(\mathbf{x}, t) \quad (23.59b)$$

$$\left[\frac{\partial \mathcal{H}}{\partial C} \right]_{S,p} = \left[\frac{\partial \mathcal{H}[S(\mathbf{x}, t), p(\mathbf{x}, t), C(\mathbf{x}, t)]}{\partial C(\mathbf{x}, t)} \right]_{S(\mathbf{x}, t), p(\mathbf{x}, t)} = \mu(\mathbf{x}, t), \quad (23.59c)$$

thus leading to⁴

$$\nabla \mathcal{H} = T \nabla S + \rho^{-1} \nabla p + \mu \nabla C. \quad (23.60)$$

An analogous relation also holds for time derivatives, in which case

$$\partial_t \mathcal{H} = T \partial_t S + \rho^{-1} \partial_t p + \mu \partial_t C. \quad (23.61)$$

We thus find a direct connection between exact differentials satisfied by the fundamental thermodynamic relations in equilibrium thermodynamics (Chapters 19 and 20), and partial derivatives in both space and time. Such connections prove particularly useful in connecting between the mechanical force from pressure and gradients in thermodynamic properties. That is, the identity (23.60) offers an alternative means to express the pressure gradient acceleration appearing in the momentum equation (e.g., equation (21.15))⁵

$$-\rho^{-1} \nabla p = -\nabla \mathcal{H} + T \nabla S + \mu \nabla C. \quad (23.62)$$

23.4.3 A caution for thermodynamic partial derivatives

One common confusion arises when not being clear on whether a mathematical expression refers to an equilibrium thermodynamic relation between thermodynamic variables, as in the fundamental thermodynamic relation (23.51), or whether it expresses a relation involving space-time field representations of thermodynamic properties. The distinction is particularly important when considering derivatives and integrals since it is necessary to know what variables are held fixed in the process of performing the operations.

For example, consider the middle relation in equation (19.89), which says that the partial derivative of the Gibbs potential with respect to pressure, holding temperature and concentration

⁴Equation (23.60) is used on page 193 of *Landau and Lifshitz* (1987) as part of their derivation of the entropy budget for a moving fluid in the presence of heat conduction. It is also used on their page 229 to derive energetics for a fluid with both heat conduction and matter diffusion. See also their page 4 for more general discussion of how equilibrium thermodynamic relations imply relations between the space and time structure of thermodynamic functions in a moving fluid. Other treatments in the literature typically gloss over the transition of the fundamental thermodynamic relation of equilibrium thermodynamics to the quasi-equilibrium thermodynamics needed for moving fluids.

⁵We make use of the identity (23.62) for studies of circulation in Section 37.2.5 and for potential vorticity in Section 38.6.

fixed, equals to the specific volume

$$\left[\frac{\partial \mathcal{G}}{\partial p} \right]_{T,C} = \nu_s = \rho^{-1}. \quad (23.63)$$

However, if we encounter the Gibbs potential as a space-time function, and we use pressure as a generalized vertical coordinate, then we might find need to compute the distinct partial derivative

$$\left[\frac{\partial \mathcal{G}}{\partial p} \right]_{x,y,t} \neq \left[\frac{\partial \mathcal{G}}{\partial p} \right]_{T,C}. \quad (23.64)$$

When appropriate, we offer reminders to help avoid a cascade of misunderstandings. One point where this reminder is particularly useful is when discussing energetics for a Boussinesq fluid in Section 26.7.

23.4.4 First law for a moving fluid element

Sections 23.4.1 and 23.4.2 provide the key operational means for developing the equations of quasi-equilibrium thermodynamics, in which we apply the equilibrium thermodynamic relations to moving and evolving fluid elements. Consequently, the fundamental thermodynamic relation (23.51), which is the first law for a quasi-static process transitioning between thermodynamic equilibrium, takes the form for a moving fluid element

$$\frac{D\mathcal{J}}{Dt} = T \frac{D\mathcal{S}}{Dt} + \frac{p}{\rho^2} \frac{D\rho}{Dt} + \mu \frac{DC}{Dt}. \quad (23.65)$$

Making use of the space and time derivative results from Section 23.4.2 leads to the gradient and Eulerian time derivative identities

$$\nabla \mathcal{J} = T \nabla \mathcal{S} + p \rho^{-2} \nabla \rho + \mu \nabla C \quad (23.66a)$$

$$\partial_t \mathcal{J} = T \partial_t \mathcal{S} + p \rho^{-2} \partial_t \rho + \mu \partial_t C. \quad (23.66b)$$

We can further massage the first law (23.65) by recalling that mass conservation as discussed in Section 16.2 means that changes in the volume of a fluid element are related to density changes via

$$\frac{1}{\delta V} \frac{D\delta V}{Dt} = \frac{1}{\nu_s} \frac{D\nu_s}{Dt} = -\frac{1}{\rho} \frac{D\rho}{Dt}. \quad (23.67)$$

Hence, equation (23.65) can be written

$$\delta M \frac{D\mathcal{J}}{Dt} = T \delta M \frac{D\mathcal{S}}{Dt} - p \frac{D\delta V}{Dt} + \mu \delta M \frac{DC}{Dt}, \quad (23.68)$$

where $\delta M = \rho \delta V$ is the mass of the fluid element. Since the mass of the fluid element is constant, equation (23.68) is the fluid element extension of the first law given by equation (23.51). Alternatively, we can use the further result from mass conservation (equation (16.26))

$$\frac{1}{\delta V} \frac{D\delta V}{Dt} = \nabla \cdot \mathbf{v} \quad (23.69)$$

to write

$$\frac{D\mathcal{J}}{Dt} = T \frac{D\mathcal{S}}{Dt} - (p/\rho) \nabla \cdot \mathbf{v} + \mu \frac{DC}{Dt}. \quad (23.70)$$

Processes affecting internal energy that appear on the right hand side are (i) entropy production,

whose form is developed in Sections 23.8 and 23.5, (ii) mechanical work from pressure modifying the volume of the fluid element, and (iii) mixing (chemical work) through the exchange of matter constituents between fluid elements. We provide further details for the first law in Section 23.5 when considering the budget for the total energy of a fluid element.

23.4.5 Enthalpy budget

It is often more convenient to consider the specific enthalpy (Section 19.6.4),

$$\mathcal{H} = \mathcal{I} + p/\rho = \mathcal{I} + \mu \nu_s. \quad (23.71)$$

The mass continuity equation (16.20) and the internal energy equation (23.70) yield

$$\frac{D\mathcal{H}}{Dt} = \frac{D\mathcal{I}}{Dt} + \frac{1}{\rho} \frac{Dp}{Dt} - \frac{p}{\rho^2} \frac{D\rho}{Dt} \implies \frac{D\mathcal{H}}{Dt} = T \frac{D\mathcal{S}}{Dt} + \frac{1}{\rho} \frac{Dp}{Dt} + \mu \frac{DC}{Dt}, \quad (23.72)$$

with the second expression consistent with equations (23.60) and (23.61) for the gradient and local time tendency of the specific enthalpy.

The specific enthalpy equation (23.72) says that for constant pressure processes, changes to specific enthalpy of a moving fluid element arise just from those processes that give rise to changes in specific entropy and changes in matter concentration

$$\frac{Dp}{Dt} = 0 \implies \frac{D\mathcal{H}}{Dt} = T \frac{D\mathcal{S}}{Dt} + \mu \frac{DC}{Dt}. \quad (23.73)$$

Since many boundary processes occur approximately at near constant pressure (e.g., air-sea fluxes), this result motivates formulating boundary fluxes of matter and thermal energy in terms of enthalpy fluxes rather than internal energy fluxes. Also, the mixing of fluid elements occurs locally in space so that pressure of fluid elements is the same when they mix, again making enthalpy a useful thermodynamic potential for the study of mixing.

23.4.6 Thermal and chemical processes and fluxes

The internal energy of a fluid element is modified by the diabatic transfer of thermal energy. We are generally concerned with two thermal fluxes, one due to conduction and one due to radiation

$$\mathbf{J}_{\text{therm}} = \mathbf{J}_{\text{cond}} + \mathbf{J}_{\text{rad}}. \quad (23.74)$$

Details of the radiant flux require topics outside our scope so we leave it unspecified. However, we consider forms for heat conduction in Section 23.8, with the simplest form being *Fourier's law* whereby \mathbf{J}_{cond} is directed down the temperature gradient.

The internal energy of a fluid element also changes through changes in the matter concentration. This change occurs when fluid elements mix at constant pressure. As mentioned in Section 23.4.5, enthalpy is the proper thermodynamic potential to consider for examining the mixing of matter concentrations. We thus assume that the transfer of chemical energy associated with a matter flux, \mathbf{J}_C , leads to a corresponding chemical energy flux given by

$$\mathbf{J}_{\text{chem}} = \left[\frac{\partial \mathcal{H}}{\partial C} \right]_{T,p} \mathbf{J}_C. \quad (23.75)$$

The enthalpy partial derivative is computed at constant pressure and temperature so to isolate the energy change associated just with mixing of matter. It is important to distinguish this partial

derivative with the distinct derivative that leads to the chemical potential as in equation (19.79)

$$\left[\frac{\partial \mathcal{H}}{\partial C} \right]_{S,p} = \mu. \quad (23.76)$$

As shown by Exercise 19.2, the two partial derivatives are related by

$$\left[\frac{\partial \mathcal{H}}{\partial C} \right]_{T,p} = \mu - T \left[\frac{\partial \mu}{\partial T} \right]_{p,C}, \quad (23.77)$$

so that

$$\mathbf{J}_{\text{chem}} = \left[\mu - T \left[\frac{\partial \mu}{\partial T} \right]_{p,C} \right] \mathbf{J}_C. \quad (23.78)$$

We make use of this relation when studying the entropy budget in Section 23.8.

Details of the thermal and chemical fluxes are undetermined at this point. We garner further insights through studying the entropy budget and second law of thermodynamics in Section 23.8 and the budget for total energy in Section 23.5. It is remarkable how far the laws of thermodynamics can be used to constrain the molecular flux laws. Even so, we note that the conductive and chemical fluxes are those that arise from molecular motions rather than turbulent motions, with turbulent fluxes determined by properties of the flow whereas \mathbf{J}_{cond} and \mathbf{J}_{chem} are determined by properties of the fluid.

23.4.7 First law in terms of potential temperature

Equation (20.44) says that the change in entropy for a fluid element moving with constant matter concentration and at the reference pressure is given in terms of the potential temperature

$$\frac{D\mathcal{S}}{Dt} = \frac{c_p}{\theta} \frac{D\theta}{Dt} \quad (23.79)$$

For a single-component fluid, the potential temperature equals to the *in situ* temperature when $p = p_R$, in which case

$$c_p \frac{D\theta}{Dt} = \theta \frac{D\mathcal{S}}{Dt} \quad \text{at } p = p_R \text{ and } dC = 0. \quad (23.80)$$

In general, this relation has little practical value since a fluid element generally does not maintain pressure at the reference pressure. Even so, in Exercise 23.4 we see that the relations hold for all pressures for the special case of an ideal gas, and in Exercise 23.5 we see they also hold for some liquids at all pressures.

23.4.8 Materially constant specific entropy for a perfect fluid

Each material fluid parcel within a perfect fluid maintains a constant specific entropy given that it experiences no dissipation (friction is absent), maintains a constant composition (mixing is absent), and encounters no heating (adiabatic). Consequently, specific entropy for each fluid parcel is reversibly stirred through advection

$$\frac{D\mathcal{S}}{Dt} = \frac{\partial \mathcal{S}}{\partial t} + \mathbf{v} \cdot \nabla \mathcal{S} = 0. \quad (23.81)$$

Notably, a perfect fluid generally admits nonzero gradients of specific entropy even as each fluid element moves without altering its specific entropy.

23.4.9 Further study

DeGroot and Mazur (1984) provide an authoritative accounting of quasi-equilibrium thermodynamics as applied to continuum matter such as a fluid. *Gregg* (1984) and *Davis* (1994) apply these methods to small-scale mixing in the ocean. Slightly different formulations can be found in *Landau and Lifshitz* (1987) and *Batchelor* (1967).

23.5 Budget for total energy

Recall from Section 12.8 that a point particle conserves its mechanical energy in the absence of friction. In contrast, the mechanical energy for a fluid element is not materially constant even when only conservative forces act on the element. The reason is that for the continuum fluid, there is (i) a conversion between mechanical energy and internal energy as pressure does work to alter the volume of fluid elements, and (ii) frictional dissipation of kinetic energy irreversibly converts some kinetic energy to internal energy through Joule heating (Section 23.5.3). In this section we combine the mechanical energy budget from Section 23.3 to the internal energy budget from Section 23.4, thus rendering the budget for total energy of a fluid element. We furthermore postulate that the domain integrated total energy changes only due to boundary effects, as well as possible changes in the geopotential such as via astronomical effects. This assumption then leads to further specifications of the processes contributing to the internal energy and enthalpy budgets.

23.5.1 Postulating the budget for total energy

In their specific (per mass) forms, the total energy of a fluid element is the sum of the internal energy, \mathcal{I} , of internal degrees of freedom, plus the mechanical energy, \mathcal{M} , from macroscopic motion, with the mechanical energy the sum of the kinetic energy plus potential energy

$$\mathcal{E} = \mathcal{I} + \mathcal{M} = \mathcal{I} + \mathcal{K} + \Phi. \quad (23.82)$$

We postulate that this total energy per mass satisfies a conservation law whereby it is affected only by the convergence of a total energy flux, plus a source due to temporal changes in the geopotential

$$\rho \frac{D\mathcal{E}}{Dt} = -\nabla \cdot \mathbf{J}_{\mathcal{E}} + \rho \partial_t \Phi. \quad (23.83)$$

Correspondingly, the Eulerian flux form equation for total energy is

$$\frac{\partial(\rho \mathcal{E})}{\partial t} + \nabla \cdot (\rho \mathbf{v} \mathcal{E} + \mathbf{J}_{\mathcal{E}}) = \rho \partial_t \Phi. \quad (23.84)$$

The flux of total energy is given by

$$\rho \mathbf{v} \mathcal{E} + \mathbf{J}_{\mathcal{E}} = \rho \mathbf{v} \mathcal{E} + \mathbf{J}_{\text{therm}} + \mathbf{J}_{\text{chem}} + \mathbf{J}_{\text{mech}} \quad (23.85a)$$

$$= \rho \mathbf{v} \mathcal{E} + \mathbf{J}_{\text{therm}} + \mathbf{J}_{\text{chem}} - \mathbf{v} \cdot (-p \mathbb{I} + \boldsymbol{\tau}) \quad (23.85b)$$

$$= \rho \mathbf{v} (\mathcal{E} + p/\rho) + \mathbf{J}_{\text{therm}} + \mathbf{J}_{\text{chem}} - \mathbf{v} \cdot \boldsymbol{\tau}, \quad (23.85c)$$

where $\mathbf{J}_{\text{therm}}$ and \mathbf{J}_{chem} were discussed in Section 23.4.6, and \mathbf{J}_{mech} was derived in Section 23.3.3. We have more to say concerning the flux of total energy in Section 23.7 when studying the Bernoulli potential.

We are led to postulate the total energy equation (23.83) through assuming that $\int_{\mathcal{R}} \rho \mathcal{E} dV$ remains constant in time for a region, \mathcal{R} , that is closed to thermal, material, and mechanical

interactions, and one where the geopotential is constant in time. This assumption is based on our understanding of molecular and atomic mechanics.

23.5.2 First law of thermodynamics for a moving fluid

We now have the total energy budget as postulated in the form of equation (23.83), along with the mechanical energy budget derived in equation (23.40). Subtracting the two yields the internal energy budget

$$\rho \frac{D(\mathcal{E} - m)}{Dt} = \rho \frac{DJ}{Dt} = -\nabla \cdot (\mathbf{J}_{\text{therm}} + \mathbf{J}_{\text{chem}}) - p \nabla \cdot \mathbf{v} + \rho \epsilon. \quad (23.86)$$

This equation provides yet another expression for the first law of thermodynamics for a moving fluid element. It says that the internal energy of a fluid element is modified through the convergence of thermal and chemical fluxes, pressure work that alters the volume of a fluid element, and frictional dissipation through viscosity. Both the pressure work and frictional dissipation are exchanged with mechanical energy, and so they appear with opposite signs in the budget for mechanical energy. We specify the thermal and chemical fluxes in Section 23.8 when studying the entropy budget.

We can make use of the enthalpy equation (23.72) to render the enthalpy budget

$$\rho \frac{D\mathcal{H}}{Dt} - \frac{Dp}{Dt} = -\nabla \cdot (\mathbf{J}_{\text{therm}} + \mathbf{J}_{\text{chem}}) + \rho \epsilon. \quad (23.87)$$

This equation is used in Section 23.9 when studying the evolution of temperature.

23.5.3 Joule heating from friction

Frictional dissipation, $\epsilon > 0$, measures the conversion of kinetic energy into heat, and it is thus a conversion from mechanical energy to internal energy

$$\dot{Q}_{\text{Joule}} \equiv \epsilon. \quad (23.88)$$

This term is referred to as *Joule heating* in analog to the process that occurs in electrical circuits. The Joule heating of a fluid by molecular viscosity is larger in regions where the fluid strains are larger, signalling a more efficient transfer of power to the microscales where molecular viscosity can act on the flow.

In the ocean interior, measurements indicate that $\epsilon \approx 10^{-9} \text{ W kg}^{-1}$. Dividing by $c_p = 3900 \text{ J kg}^{-1} \text{ K}^{-1}$ leads to a heating rate of less than $10^{-3} \text{ K century}^{-1}$, which is a very small rate of ocean heating. Consequently, ocean Joule heating has a negligible role in the ocean heat budget and as such is generally ignored. Atmospheric flows are roughly two orders faster so that the kinetic energy per mass is four orders larger. The larger flow speeds lead to larger shears thus creating larger viscous dissipation that reaches roughly $\epsilon \approx 2 \text{ W m}^{-2}$ globally averaged. Hence, Joule heating is an important part of the global atmosphere enthalpy budget (Becker, 2003).

23.5.4 Comments on gauge symmetry

Consider again the Eulerian flux equation for total energy (23.84). It is notable that the time tendency for the total energy remains unchanged if we shift the flux of total energy by a curl,

$$\rho \mathcal{E} \mathbf{v} + \mathbf{J}_{\mathcal{E}} \rightarrow \rho \mathcal{E} \mathbf{v} + \mathbf{J}_{\mathcal{E}} + \nabla \times \mathbf{G}, \quad (23.89)$$

with \mathbf{G} referred to as a *gauge function*. This arbitrariness in the definition of total energy flux is ubiquitous in physics; e.g., see the discussion of the electromagnetic field energy flux in Section

27-4 in Volume II of [Feynman et al. \(1963\)](#).⁶ We conclude that the energy flux has no unique local physical meaning. Instead, it is only the convergence of the energy flux that has an unambiguous meaning given by its role in affecting a time change to the energy at a point in space.

We also encounter such *gauge symmetry* in the potential vorticity flux discussed in Chapter 39, as well as the vector streamfunction for an incompressible fluid in Section 18.4.1. In some cases we can exploit the symmetry to our subjective desires, such as discussed in Section 39.5.6 for potential vorticity. However, we know of no strategic use of gauge symmetry for the study of energy budgets.

23.5.5 Further study

The postulate of globally integrated total energy conservation in Section 23.5.1, and the associated discussion of energy budgets, follow that from Chapter 14 of [Callen \(1985\)](#), Sections 49 and 58 of [Landau and Lifshitz \(1987\)](#), Section II.4 of [DeGroot and Mazur \(1984\)](#), Chapters 3 and 4 of [Müller \(2006\)](#), Appendix B of [IOC et al. \(2010\)](#), Section 2.4 of [Olbers et al. \(2012\)](#), Chapter 1 of [Vallis \(2017\)](#), and Section 13.5.5 of [Thorne and Blandford \(2017\)](#).

23.6 Thermodynamic equilibrium with macroscopic motion

We derived the properties of thermodynamic equilibria in Section 19.2.8 for a single component fluid, and in Section 20.1 for a binary fluid in the presence of a geopotential. We here extend those discussions to the case of a finite region of a fluid undergoing macroscopic motion in the absence of gravity. We assume no external forces or torques, so that the total linear momentum and total angular momentum remain constant. As in our earlier discussions, we derive the properties of thermodynamic equilibrium by assuming entropy is an extremum at equilibrium. Furthermore, the extremum must be consistent with the variety of conserved quantities, thus motivating the use of Lagrange multipliers as part of the formalism needed to determine the extremum.

23.6.1 Deriving the equilibrium conditions

To focus on the allowed macroscopic motion, we ignore external fields such as from gravity, in which case the total energy is the sum of the internal energy plus kinetic energy

$$\mathcal{E}^e = \mathcal{I}^e + P^2/(2M), \quad (23.90)$$

where $\mathbf{P} = M\mathbf{v}$ is the linear momentum of the system with velocity \mathbf{v} and mass M , and $P^2 = \mathbf{P} \cdot \mathbf{P}$ is the squared momentum. If the macroscopic system is materially and mechanically closed then total energy remains constant, as does the linear momentum and angular momentum. Thermodynamic equilibrium is realized by maximizing the function

$$\Psi = \mathcal{S}^e + \mathbf{A} \cdot \mathbf{P} + \mathbf{B} \cdot (\mathbf{x} \times \mathbf{P}), \quad (23.91)$$

where \mathbf{x} is the position of the macroscopic system, and the vectors \mathbf{A} and \mathbf{B} are constant Lagrange multipliers. Note that for convenience we assume the system to be macroscopically small but microscopically large (e.g., a fluid element) so that we can assign a single position vector to the system.

Should entropy be a function of the total energy (which is a constant of the motion) or remain a function of just the internal energy? To answer this question we appeal to the statistical interpretation of entropy whereby the number of microstates corresponding to a particular macrostate

⁶The Feynman lectures are available online through the California Institute of Technology.

is Galilean invariant.⁷ The local rest state, where total energy equals to internal energy, is thus sufficient for defining the functional dependence⁸

$$\mathcal{S}^e = \mathcal{S}^e(V, \mathcal{I}^e) = \mathcal{S}^e[V, \mathcal{E}^e - P^2/(2M)]. \quad (23.92)$$

Hence, maximizing Ψ with respect to the linear momentum component, P_m , requires the derivative

$$\left[\frac{\partial \mathcal{S}^e}{\partial P_m} \right]_V = \left[\frac{\partial \mathcal{S}^e}{\partial \mathcal{I}^e} \right]_V \frac{\partial \mathcal{I}^e}{\partial P_m} = -\frac{1}{T} \frac{P_m}{M} = -\frac{v_m}{T}, \quad (23.93)$$

so that the macroscopic velocity at equilibrium is

$$\frac{\partial \Psi}{\partial P_m} = 0 \implies \mathbf{v} = T(\mathbf{A} + \mathbf{B} \times \mathbf{x}). \quad (23.94)$$

With temperature uniform throughout the macroscopic system at thermodynamic equilibrium, then we find a velocity decomposed into a uniform translation plus a solid-body rotation. That is, a closed macroscopic system in thermodynamic equilibrium can, at most, exhibit uniform translation plus solid-body rotation. More general macroscopic motion is not possible when the system is in thermodynamic equilibrium. Furthermore, note that each component of the rate of strain tensor vanishes for uniform translation plus a solid-body rotation (see Exercise 15.2). For the Newtonian fluids considered in this book, a zero rate of strain means there are no frictional stresses (Section 22.8.6), thus ensuring no frictionally generated entropy.

The Cauchy-Stokes decomposition from Section 15.3.9 shows that at each time instance, motion of a fluid element can be kinematically decomposed into translation, rotation, and dilation. Dilation occurs through mechanical work. In its absence, and without heating or mixing, the fluid element moves through sequences of translations and rotations that maintain thermodynamic equilibrium. With dilation, heating, and/or matter mixing, we conceive of a moving fluid as a continuum of fluid elements that, on a time scale that is tiny relative to macroscopic processes, adjusts to thermodynamic equilibrium in response to interactions with the surrounding fluid environment.

23.6.2 Further study

We here followed the discussion of §10 in *Landau and Lifshitz* (1980). See also a complementary discussion in Section 1.8 of *Kamenkovich* (1977), who considers a two-component fluid in the presence of gravity. *Kamenkovich* (1977) finds that although *in situ* temperature is a uniform constant in thermodynamic equilibrium, the salinity is not constant.

23.7 Bernoulli theorem

The total energy equation (23.83) reveals that the material time change for the total energy of a fluid element is affected by the convergence of pressure times velocity. Hence, even in the absence of irreversible processes (i.e., a perfect fluid) and with a time-independent geopotential, the total energy of a fluid element is not materially invariant. The energy source term, $p\mathbf{v}$, is fundamental to energy within the continuum. As shown in this section, it is the pressure work required for the fluid element to mechanically exist within the continuum. We thus refer to $p\mathbf{v}$ as the mechanical *injection work*. This conceptualization of $p\mathbf{v}$ arises in the context of exploring

⁷Recall our discussion of Galilean invariance in Section 14.7.

⁸See footnote on page 36 of *Landau and Lifshitz* (1980) for more discussion.

the remarkably versatile Bernoulli theorem, which is particularly useful in diagnosing energetic properties of steady flows.

23.7.1 Bernoulli potential

Consider the Eulerian flux form equation for the total energy, (23.84), written here in the form

$$\frac{\partial(\rho \mathcal{E})}{\partial t} + \nabla \cdot [\rho \mathbf{v} (\mathcal{E} + p/\rho) + \mathbf{J}_{\text{therm}} + \mathbf{J}_{\text{chem}} - \mathbf{v} \cdot \boldsymbol{\tau}] = \rho \partial_t \Phi. \quad (23.95)$$

The left hand side indicates that total energy of a fluid element is locally modified by the advective transport of the quantity

$$\mathcal{E} + p/\rho = (\mathcal{K} + \Phi) + (\mathcal{I} + p/\rho) = \mathcal{M} + \mathcal{H} \equiv \mathcal{B}, \quad (23.96)$$

where we introduced the *Bernoulli potential*, which is the sum of the mechanical energy per mass plus the enthalpy per mass

$$\mathcal{B} = \mathcal{M} + \mathcal{H} = \mathcal{K} + \Phi + \mathcal{I} + p/\rho. \quad (23.97)$$

For a perfect fluid there is no irreversible transfer of heat, matter, or momentum so that

$$\text{perfect fluid} \implies \mathbf{J}_{\text{therm}} = 0 \quad \text{and} \quad \mathbf{J}_{\text{chem}} = 0 \quad \text{and} \quad \boldsymbol{\tau} = 0. \quad (23.98)$$

Hence, we see that integration over a region with zero boundary transfer of $\mathbf{v} \mathcal{B}$ leads to the conservation of total energy for a perfect fluid with a time independent geopotential. Note that for some purposes it can be useful to write the total energy equation (23.95) as an equation for the Bernoulli function, which takes the form

$$\frac{\partial(\rho \mathcal{B})}{\partial t} + \nabla \cdot [\rho \mathbf{v} \mathcal{B} + \mathbf{J}_{\text{therm}} + \mathbf{J}_{\text{chem}} - \mathbf{v} \cdot \boldsymbol{\tau}] = \partial_t p + \rho \partial_t \Phi. \quad (23.99)$$

23.7.2 Mechanical injection work

Why is $\rho \mathcal{E}$ affected by the convergence of $\rho \mathbf{v} \mathcal{B}$ rather than the convergence of $\rho \mathbf{v} \mathcal{E}$? To answer this question,⁹ again note that the Bernoulli potential is the sum of the total energy per mass of a fluid element, \mathcal{E} , plus the term $p/\rho = p/\rho$. So what is p/ρ ? Imagine carving out a tiny region from within a continuous fluid with pressure p and specific volume $1/\rho$, leaving behind a “hole”. The mechanical work required to carve out this hole is precisely equal to p/ρ . Correspondingly, we interpret p/ρ as the mechanical work required to inject a unit mass of fluid with specific volume $1/\rho$ into a region with pressure p . We thus refer to p/ρ as the *injection work*, and we in turn see that specific enthalpy, $\mathcal{H} = \mathcal{I} + p/\rho$ (equation (23.71)), measures the internal energy plus the mechanical work required for a fluid element to exist within a continuum.

We can support the above interpretation by considering the flux, $\rho \mathbf{v} \mathcal{B}$, in a perfect fluid that penetrates a static closed fluid region

$$\oint_{\partial \mathcal{R}} \rho \mathbf{v} \mathcal{B} \cdot \hat{\mathbf{n}} dS = \oint_{\partial \mathcal{R}} \rho \mathbf{v} \mathcal{E} \cdot \hat{\mathbf{n}} dS + \oint_{\partial \mathcal{R}} p \mathbf{v} \cdot \hat{\mathbf{n}} dS. \quad (23.100)$$

The first term on the right hand side is the flux of total energy (mechanical plus internal) that penetrates the region boundary, $\partial \mathcal{R}$. The second term is the mechanical work done by pressure acting on the boundary. The pipe flow example in Section 23.7.3 further supports this perspective.

⁹This argument follows Section 13.5.4 of [Thorne and Blandford \(2017\)](#) as well as Section 6 of [Landau and Lifshitz \(1987\)](#).

23.7.3 Bernoulli's theorem for a steady perfect fluid

Consider a perfect fluid flow in steady state (vanishing Eulerian time derivatives). Steady state mass conservation means that

$$\frac{\partial \rho}{\partial t} = -\nabla \cdot (\rho \mathbf{v}) = 0. \quad (23.101)$$

This relation, along with a steady state energy in equation (23.95) (absent friction, heating, mixing, and with a time-independent geopotential), means that the steady state velocity field is locally tangent to isosurfaces of the Bernoulli potential

$$\mathbf{v} \cdot \nabla \mathcal{B} = 0. \quad (23.102)$$

We thus see that for the perfect fluid to be in a steady state, the Bernoulli potential is constant along streamlines, which is a result known as *Bernoulli's theorem*. Hence, as the fluid moves along a streamline, there is an exchange between the total energy per mass, \mathcal{E} , and the injection work, p/ρ , such that their sum remains constant.

A constant Bernoulli potential for steady flow is used frequently in engineering fluid dynamics to interpret flow around objects, such as for flow around a wing, in which case the sum $p + \rho \mathbf{v}^2/2$ is sometimes referred to as the *total pressure* or *stagnation pressure*. It leads to a realization of *Bernoulli's principle*, whereby in regions of low pressure the energy per mass is relatively large, whereas the converse holds in regions of high pressure. The change in energy is largely due to a change in the kinetic energy, so that flow is fast in regions of low pressure (e.g., top of the wing, flow around a train moving through a tunnel) and slow in regions of high pressure (e.g., bottom of the wing).¹⁰

That is, the Bernoulli principle provides an energetic expression for why a fluid slows down when moving into a region of relatively high pressure, and speeds up when moving to a region of low pressure.

23.7.4 Traditional derivation of Bernoulli's theorem

For completeness we offer a second derivation of Bernoulli's theorem that follows a more traditional route and reveals some useful manipulations. For this purpose, convert the advective-form momentum equation (21.16) into its vector-invariant form by making use of the vector identity (see Section 2.3.4)

$$\boldsymbol{\omega} \times \mathbf{v} = -\mathcal{K} + (\mathbf{v} \cdot \nabla) \mathbf{v}. \quad (23.103)$$

This identity allows us to eliminate velocity self-advection in favor of the vorticity and kinetic energy per mass

$$\frac{\partial \mathbf{v}}{\partial t} + \boldsymbol{\omega}_a \times \mathbf{v} = -\frac{1}{\rho} \nabla p - \nabla m, \quad (23.104)$$

where

$$\boldsymbol{\omega}_a = \boldsymbol{\omega} + 2 \boldsymbol{\Omega} \quad (23.105)$$

is the absolute vorticity (see Chapter 37) and we set the irreversible terms to zero since we are assuming a perfect fluid. The Eulerian time evolution for the kinetic energy per mass is therefore given by

$$\frac{\partial \mathcal{K}}{\partial t} = -\frac{1}{\rho} \mathbf{v} \cdot \nabla p - \mathbf{v} \cdot \nabla m, \quad (23.106)$$

where we set $\mathbf{v} \cdot (\boldsymbol{\omega}_a \times \mathbf{v}) = 0$.

¹⁰See [this video](#) for why it is incorrect to use Bernoulli's theorem for explaining the lift on an airplane wing.

For Bernoulli's theorem we are interested in the steady state, with a steady kinetic energy per mass realized by the balance

$$\rho^{-1} \mathbf{v} \cdot \nabla p = -\mathbf{v} \cdot \nabla m. \quad (23.107)$$

We can connect this steady state balance to the Bernoulli potential by noting that for a steady perfect and single-component fluid, equation (23.62) allows us to write

$$\rho^{-1} \mathbf{v} \cdot \nabla p = \mathbf{v} \cdot (\nabla \mathcal{H} - T \nabla \mathcal{S}). \quad (23.108)$$

Combining with equation (23.107) renders

$$\mathbf{v} \cdot (\nabla \mathcal{H} + \nabla m - T \nabla \mathcal{S}) = \mathbf{v} \cdot (\nabla \mathcal{B} - T \nabla \mathcal{S}) = 0. \quad (23.109)$$

A perfect fluid maintains materially constant specific entropy (Section 23.4.8), which in a steady state means that

$$\mathbf{v} \cdot \nabla \mathcal{S} = 0 \quad \text{and} \quad \mathbf{v} \cdot \nabla \mathcal{B} = 0 \quad \Longleftarrow \text{steady state perfect fluid.} \quad (23.110)$$

That is, for a steady perfect fluid the velocity is aligned with isosurfaces of specific entropy and Bernoulli potential.

23.7.5 Steady flow in a pipe

To help further understand Bernoulli's theorem and the contribution from the mechanical work provided by pressure forces, consider the steady flow of a constant density perfect fluid in a frictionless pipe as depicted in Figure 23.1. For this system, Bernoulli's theorem says that the following simplified form of the Bernoulli potential is constant for flow along a streamline

$$\mathcal{B} = \mathbf{v}^2/2 + p/\rho + g z = \text{constant}. \quad (23.111)$$

Note that internal energy dropped out since for a constant density fluid the internal energy is a constant and so plays no role in the energetics. This equation means that there is a precise balance between the kinetic energy per mass, injection work, and geopotential for a steady and constant density fluid. For example, for flow following a constant geopotential, pressure is relatively low in regions of large kinetic energy whereas pressure is relatively high in regions of small kinetic energy. We further pursue this understanding by showing that the statement (23.111) of Bernoulli's theorem can be derived through traditional energetic arguments, whereby the mechanical work done on the fluid system equals to the system's change in kinetic energy (see Section 10.1.5 for the particle mechanics version of this *work-energy theorem*).

For this purpose, let the system under examination be a control volume of fluid as described in the caption to Figure 23.1, and examine the work done on the control volume over an arbitrary time increment, Δt . During this time, a mass of fluid given by

$$M = \rho A_1 u_1 \Delta t = \rho A_2 u_2 \Delta t \quad (23.112)$$

moves through the pipe, with $A_1 u_1 = A_2 u_2$ following from volume conservation, and we assumed that the $u_{1,2} = \Delta x_{1,2}/\Delta t$ measures the average velocity across the pipe cross-section. Mechanical work is applied to the fluid in the control volume by pressure acting on the end caps (contact force) and by gravity acting throughout the fluid (body force).

- **PRESSURE WORK:** At the left end cap, pressure from fluid to the left of the control volume does work on the control volume by the amount $p_1 A_1 \Delta x_1 = p_1 M/\rho$. On the right end,

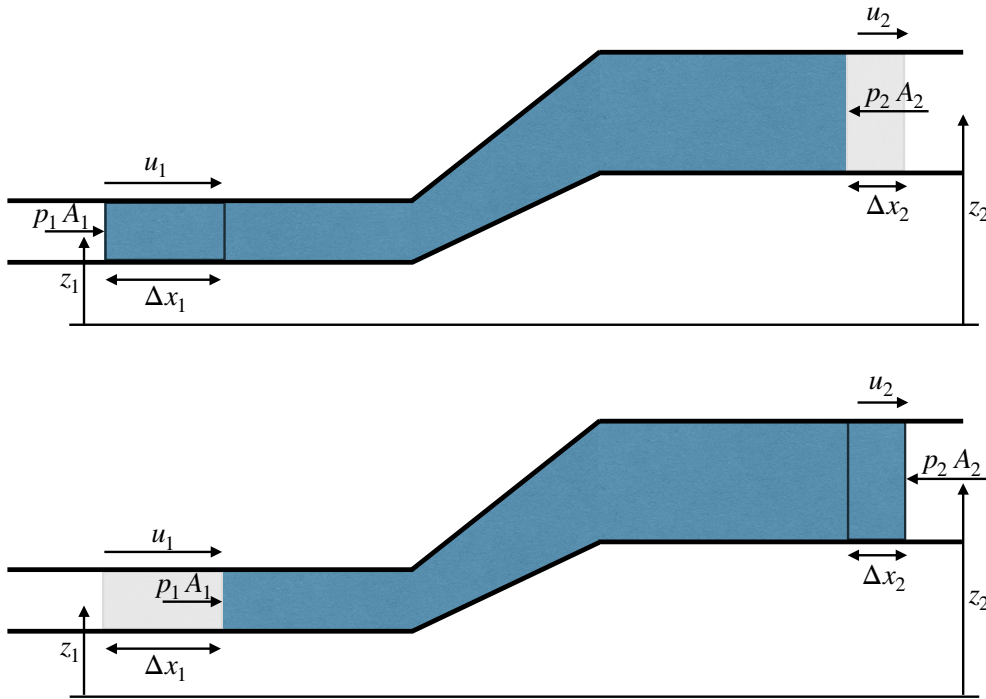


FIGURE 23.1: An example to illustrate the basic physics of Bernoulli's theorem and pressure work, whereby we depict the flow of a perfect and constant density fluid from left to right in a pipe of variable cross-section and variable height. We study the energetics of a control volume (dark blue region) moving with the fluid. The top panel shows the control volume at one time and the lower panel shows the control volume at a time Δt later, after which a mass of fluid, M , has moved through the system. Volume conservation means that $(u_1 \Delta t) A_1 = (u_2 \Delta t) A_2$, where $\Delta x_{1,2}$ is the horizontal displacement of the fluid plug over time Δt , $u_{1,2}$ is the cross-sectional area average velocity, $A_{1,2}$ is the pipe cross-sectional area, and $M = \rho \Delta x_1 A_1 = \rho \Delta x_2 A_2$ is the mass of fluid moving over the Δt time increment. Pressure forces, $p_{1,2}$, at the end caps point inward (compressive), with pressure on the left larger than that on the right to support the fluid moving to the right. As the fluid moves upward it increases its gravitational potential energy and in so doing the fluid does work against gravity.

the control volume does work on the fluid to its right, which means that a negative work is applied to the control volume in the amount $-p_2 A_2 \Delta x_2 = -p_2 M/\rho$.

- **GRAVITATIONAL WORK:** Fluid downstream at the right end is higher than fluid upstream on the left end. The control volume must do work against gravity to achieve this altitude increase and this work is given by $-g M (z_2 - z_1)$.

As the fluid moves from left to right, the control volume changes its kinetic energy by the amount $(M/2)(u_2^2 - u_1^2)$. Equating this kinetic energy change to the work applied to the control volume renders

$$(1/2)(u_2^2 - u_1^2) = (1/\rho)(p_1 - p_2) - g(z_2 - z_1), \quad (23.113)$$

where the mass, M , dropped out. Rearrangement then leads to

$$u^2/2 + p/\rho + g z = \text{constant}, \quad (23.114)$$

which is a statement of Bernoulli's theorem (23.111). Furthermore, the pressure difference between the left and right end of the pipe is given by

$$p_1 - p_2 = \rho g (z_2 - z_1) + (\rho/2) u_1^2 [1 - (A_1/A_2)^2] > 0. \quad (23.115)$$

We expect $p_1 > p_2$ given the assumed fluid motion from left to right, whereby pressure on the

left end must be larger than the right end to support this flow. This example thus supports our understanding of how pressure provides a mechanical work on fluid control volume boundaries. Indeed, taking the control volume to be a tiny fluid element furthers our interpretation of the p/ρ contribution to the Bernoulli potential (23.96).

23.7.6 Steady flow over a topographic bump

We build from the discussion of steady pipe flow in Section 23.7.5 by describing a more geophysically relevant case of steady single-component perfect fluid flowing over a topographic bump. In Figure 23.2 we illustrate this flow in the absence of rotation. As the fluid moves over the bump, it speeds up in order to maintain volume continuity. In regions of faster flow, Bernoulli's theorem (23.111) says that the pressure is lower, which is realized here by a lowering of the sea surface height over the bump. For a small bump, we can imagine that the flow remains symmetric with respect to the bump, so that the flow downstream of the bump is a reflection of the upstream flow. To maintain steady flow in the presence of a larger bump requires a larger pressure drop, which will eventually break the symmetry between downstream and upstream. For an even larger topographic bump, we find there is no way to satisfy Bernoulli's theorem, in which case the flow transitions into at time dependent *hydraulic jump*.

As for the pipe flow, the steady flow maintains two flow constants: the volume flow rate and the simplified form of the Bernoulli potential in equation (23.111)

$$\mathcal{T} = v h \Delta \quad \text{and} \quad \mathcal{B} = v^2/2 + p/\rho + g z, \quad (23.116)$$

where h is the thickness of the layer and Δ the width in the direction perpendicular to the flow. Also, recall that the Bernoulli potential is a constant along a particular streamline. However, for a constant density layer the Bernoulli potential is independent of depth, as we illustrate below. For simplicity we assume the flow is only a function of the along-stream coordinate, y , and furthermore assume the pressure on the upper interface is a uniform constant p_a . We also assume the top and bottom interfaces of the layer are material, which then means they are each streamlines.

We can eliminate the velocity, v , from the Bernoulli potential to write

$$\mathcal{B} = \mathcal{T}^2/(2 h^2 \Delta^2) + p/\rho + g z. \quad (23.117)$$

Far upstream of the bump the layer thickness takes on its unperturbed value, H , so that the Bernoulli potential along the surface streamline at $z = H$ is given by

$$\mathcal{B} = \mathcal{T}^2/(2 H^2 \Delta^2) + p_a/\rho + g H. \quad (23.118)$$

Notice how every term on the right hand side is positive, so that $\mathcal{B} > 0$. Also notice that the Bernoulli potential along the bottom streamline takes the same value

$$\mathcal{B} = \mathcal{T}^2/(2 H^2 \Delta^2) + p_b/\rho = \mathcal{T}^2/(2 H^2 \Delta^2) + (p_a + \rho h H)/\rho, \quad (23.119)$$

which results since the layer has constant density. Now express the Bernoulli potential in a region affected by the bump, in which case

$$\mathcal{B} = \mathcal{T}^2/(2 h^2 \Delta^2) + p_a/\rho + g \eta = \mathcal{T}^2/(2 h^2 \Delta^2) + p_a/\rho + g (h + \eta_b). \quad (23.120)$$

We observe that

$$\mathcal{B} - g \eta_b = \mathcal{T}^2/(2 h^2 \Delta^2) + p_a/\rho + g h \geq 0, \quad (23.121)$$

with this quantity referred to as the *Bernoulli head*. The condition $\mathcal{B} - g \eta_b \geq 0$ holds so long

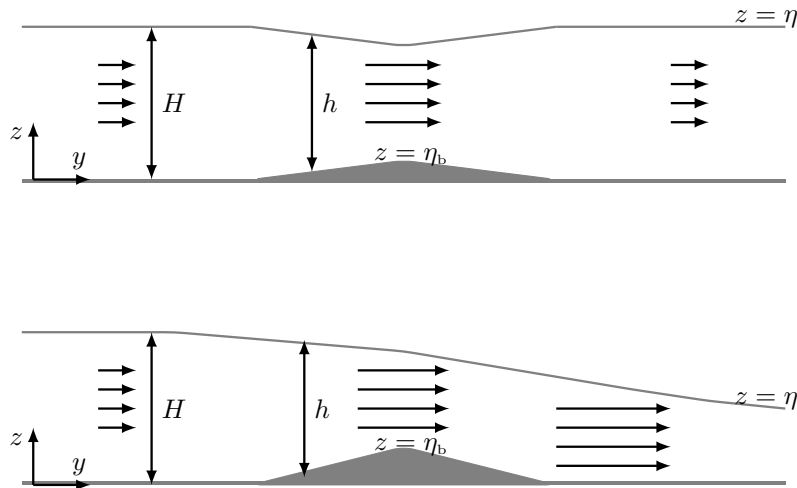


FIGURE 23.2: Depicting steady flow of a non-rotating single-component fluid with constant density, ρ , flowing over a topographic bump. We assume all properties are a function only of the along-stream position, y , and $z = 0$ is taken at the position of a flat topography. For steady flow of a constant density fluid, the volume transport, \mathcal{T} , is constant and given by $\mathcal{T} = v h \Delta x$, where Δx is the width of the flow in the direction perpendicular to the page, and $h = \eta - \eta_b$ is the layer thickness. The simplified form of the Bernoulli potential given by equation (23.111) is also constant along any streamline, $\mathcal{B} = \mathbf{v}^2/2 + p/\rho + g z = \text{constant}$. The top panel shows the flow for a very small topographic bump, so that the flow is symmetric around the bump. The lower panel show flow for a larger bump that requires more fluid upstream of the bump to support enough pressure drop for steady flow to make it over the bump.

as the flow maintains the assumptions of Bernouli's theorem. However, if the topography is too tall, then $\mathcal{B} - g \eta_b \leq 0$, in which case the flow can no longer satisfy the Bernoulli theorem. This result leads us to define a critical topography height

$$\eta_b^{\text{crit}} = \mathcal{B}/g = \mathcal{T}^2/(2 H^2 \Delta^2 g) + p_a/(\rho g) + H. \quad (23.122)$$

When topography is larger than this height, the flow cannot reach a steady state and/or the flow develops a dependence on the direction perpendicular to the page.

23.7.7 Further study

For an examination of Bernoulli's theorem for non-rotating flows, such as flow in laminar boundary layers, see [this video](#) from Prof. Shapiro. The text from [Pratt and Whitehead \(2008\)](#) makes use of Bernoulli's theorem for understanding non-rotating and rotating geophysical flows over obstacles. Their Section 1.4 forms the basis for the discussion in Section 23.7.6. See also Exercise 8.6 of [Klinger and Haine \(2019\)](#).

23.8 Entropy budget for the ocean

In this section we consider the entropy budget for the ocean and make use of the second law of thermodynamics to infer specific forms for the thermal and chemical fluxes introduced in Section 23.4.6. The discussion also holds for the atmosphere in the absence of phase transitions, though we focus on the ocean application to be specific. Hence, the matter concentration in this section is the salt concentration for seawater.

The entropy budget follows by rearranging the enthalpy equation (23.72)

$$T \rho \frac{D\mathcal{S}}{Dt} = \rho \frac{D\mathcal{H}}{Dt} - \frac{Dp}{Dt} - \mu \rho \frac{DC}{Dt}, \quad (23.123)$$

with the enthalpy budget in the form (23.87) yielding

$$T \rho \frac{D\mathcal{S}}{Dt} = -\nabla \cdot (\mathbf{J}_{\text{therm}} + \mathbf{J}_{\text{chem}}) + \rho \epsilon + \mu \nabla \cdot \mathbf{J}_C, \quad (23.124)$$

where we wrote the tracer equation as

$$\rho \frac{DC}{Dt} = -\nabla \cdot \mathbf{J}_C, \quad (23.125)$$

following Section 17.1.3. Through manipulations pursued in Section 23.8.1, we identify a non-advection entropy flux and a corresponding entropy source. This form of the entropy budget is useful since we can then invoke the second law to insist that the entropy source is non-negative, and that statement renders some constraints on the thermal and chemical fluxes.

23.8.1 Non-advection entropy flux and entropy source

To start the manipulations, divide equation (23.124) by T and rewrite in terms of a flux convergence plus a source

$$\rho \frac{D\mathcal{S}}{Dt} = -\nabla \cdot \left[\frac{\mathbf{J}_{\text{therm}} + \mathbf{J}_{\text{chem}} - \mu \mathbf{J}_C}{T} \right] + \nabla(1/T) \cdot (\mathbf{J}_{\text{therm}} + \mathbf{J}_{\text{chem}} - \mu \mathbf{J}_C) - (\mathbf{J}_C/T) \cdot \nabla \mu + \frac{\rho \epsilon}{T}. \quad (23.126)$$

Recall from the identity (23.77) that we can write the chemical energy flux as

$$\mathbf{J}_{\text{chem}} = \left[\frac{\partial \mathcal{H}}{\partial C} \right]_{T,p} \mathbf{J}_C = \left[\mu - T \left[\frac{\partial \mu}{\partial T} \right]_{C,p} \right] \mathbf{J}_C = (\mu - T \mu_T) \mathbf{J}_C, \quad (23.127)$$

where we introduced a shorthand for the third equality. This identity then leads to

$$\mathbf{J}_{\text{chem}} - \mu \mathbf{J}_C = -T \mu_T \mathbf{J}_C, \quad (23.128)$$

in which case the entropy equation (23.126) becomes

$$\rho \frac{D\mathcal{S}}{Dt} = -\nabla \cdot \left[\frac{\mathbf{J}_{\text{therm}} - T \mu_T \mathbf{J}_C}{T} \right] + \nabla(1/T) \cdot (\mathbf{J}_{\text{therm}} - T \mu_T \mathbf{J}_C) - (\mathbf{J}_C/T) \cdot \nabla \mu + \frac{\rho \epsilon}{T}. \quad (23.129)$$

We thus identify the non-advection entropy flux

$$\mathbf{J}_{\mathcal{S}} = \frac{\mathbf{J}_{\text{therm}}}{T} - \left[\frac{\partial \mu}{\partial T} \right]_{p,C} \mathbf{J}_C = \frac{\mathbf{J}_{\text{therm}}}{T} + \left[\frac{\partial \mathcal{S}}{\partial C} \right]_{T,p} \mathbf{J}_C, \quad (23.130)$$

where the second equality made use of the Maxwell relation

$$-\left[\frac{\partial \mathcal{S}}{\partial C} \right]_{T,p} = \left[\frac{\partial \mu}{\partial T} \right]_{p,C}, \quad (23.131)$$

which is derived as part of the solution to Exercise 19.2. The additional terms comprise the entropy source

$$\Sigma_S = \frac{\rho \epsilon}{T} + \nabla(1/T) \cdot (\mathbf{J}_{\text{therm}} - T \mu_T \mathbf{J}_C) - (\mathbf{J}_C \cdot \nabla \mu)/T \quad (23.132a)$$

$$= \frac{\rho \epsilon}{T} + \frac{\nabla T}{T^2} \cdot (T \mu_T \mathbf{J}_C - \mathbf{J}_{\text{therm}}) - (\mathbf{J}_C \cdot \nabla \mu)/T \quad (23.132b)$$

$$= \frac{\rho \epsilon}{T} - \frac{\nabla T \cdot \mathbf{J}_{\text{therm}}}{T^2} + \frac{\mathbf{J}_C \cdot (\mu_T \nabla T - \nabla \mu)}{T} \quad (23.132c)$$

$$= \frac{\rho \epsilon}{T} - \frac{\nabla T \cdot \mathbf{J}_{\text{therm}}}{T^2} - \frac{\mathbf{J}_C \cdot (\mu_C \nabla C + \mu_p \nabla p)}{T} \quad (23.132d)$$

$$= \frac{\rho \epsilon}{T} - \frac{\nabla T \cdot \mathbf{J}_{\text{therm}}}{T^2} - \frac{\mathbf{J}_C}{T} \cdot \left[\left[\frac{\partial \mu}{\partial C} \right]_{T,p} \nabla C + \left[\frac{\partial \mu}{\partial p} \right]_{T,C} \nabla p \right], \quad (23.132e)$$

where we wrote the gradient of the chemical potential, $\mu(T, p, C)$, as

$$\nabla \mu = \left[\frac{\partial \mu}{\partial T} \right]_{p,C} \nabla T + \left[\frac{\partial \mu}{\partial p} \right]_{T,C} \nabla p + \left[\frac{\partial \mu}{\partial C} \right]_{T,p} \nabla C = \mu_T \nabla T + \mu_p \nabla p + \mu_C \nabla C. \quad (23.133)$$

The non-advective entropy flux (23.130) arises from the thermal and chemical fluxes, and the entropy source (23.132e) includes contributions from those fluxes as well as the frictional dissipation of mechanical energy.

23.8.2 Constraints from the second law of thermodynamics

The second law of thermodynamics states that the entropy source is non-negative

$$\Sigma_S \geq 0 \iff \text{second law of thermodynamics}. \quad (23.134)$$

This condition imposes constraints on the frictional dissipation, thermal flux, and tracer flux. Since frictional dissipation in Newtonian fluids (equation (23.37)) is non-negative, $\epsilon \geq 0$, we make use of the second law to constrain just the thermal flux and tracer flux. Furthermore, recall from equation (23.74) that the thermal flux is comprised of a radiant flux and conductive flux. We assume that radiant flux is determined by processes external to the fluid. We thus use the second law to constrain just the conductive portion of the thermal flux along with the tracer flux. That is, from the entropy source (23.132e) we have the second law constraint

$$-\nabla T \cdot \mathbf{J}_{\text{cond}} - T \mu_C \mathbf{J}_C \cdot \left[\nabla C + \frac{\mu_p}{\mu_C} \nabla p \right] \geq 0. \quad (23.135)$$

This constraint can be satisfied by assuming the conductive and tracer fluxes are of the form

$$\rho^{-1} \mathbf{J}_{\text{cond}} = -c_p \kappa_T \nabla T - \kappa_{TC} \left[\nabla C + \frac{\mu_p}{\mu_C} \nabla p \right] \quad (23.136a)$$

$$\rho^{-1} \mathbf{J}_C = -\kappa_C \left[\nabla C + \frac{\mu_p}{\mu_C} \nabla p \right] - \kappa_{CT} \nabla T. \quad (23.136b)$$

The variety of molecular fluxes

The first term in the conductive thermal flux (23.136a) is known as *Fourier's law of conduction*

$$\mathbf{J}_{\text{cond}}^{\text{Fourier}} = -\rho c_p \kappa_T \nabla T, \quad (23.137)$$

in which case the conductive thermal flux is directed down the gradient of the *in situ* temperature. The second term leads to a conductive thermal flux in the presence of matter concentration gradients and pressure gradients, and this process is known as the *Dufour effect*

$$\mathbf{J}_{\text{cond}}^{\text{Dufour}} = -\rho \kappa_{TC} \left[\nabla C + \frac{\mu_p}{\mu_C} \nabla p \right]. \quad (23.138)$$

The first term in the matter flux (23.136b) is known as *Fick's law of diffusion*

$$\mathbf{J}_C^{\text{Fick}} = -\rho \kappa_C \nabla C. \quad (23.139)$$

The second term in the matter flux (23.136b) is known as *barodiffusion*

$$\mathbf{J}_C^{\text{barodiff}} = -(\rho \kappa_{CT} \mu_p / \mu_C) \nabla p, \quad (23.140)$$

which is a matter flux arising from a pressure gradient. Finally, the matter flux arising from temperature gradients is known as the *Soret effect*

$$\mathbf{J}_C^{\text{Soret}} = -\rho \kappa_{CT} \nabla T. \quad (23.141)$$

Thermodynamic equilibrium and the vertical gradient of salinity

In Section 20.1, we learned that thermodynamic equilibrium for a fluid in a gravity field leads to a uniform temperature, T , and a pressure in exact hydrostatic balance. The salt flux must vanish in thermodynamic equilibrium, but in the presence of a pressure gradient we have a nonzero vertical salinity gradient from equation (23.136b) given by

$$\frac{dC}{dz} = -\frac{\mu_p}{\mu_C} \frac{dp}{dz} = \frac{\mu_p \rho g}{\mu_C}. \quad (23.142)$$

This relation is identical to equation (20.20) resulting from our study of conditions for thermodynamic equilibrium of a binary fluid in a gravity field. It is satisfying to see the same thermodynamic equilibrium condition arise from the rather different path taken here.

Invoking Onsager reciprocity condition

The Onsager reciprocity conditions¹¹ are now invoked to relate the two off-diagonal coefficients according to

$$T \mu_C \kappa_{CT} = \kappa_{TC}, \quad (23.143)$$

which brings the entropy condition to the form

$$c_p \kappa_T |\nabla T|^2 + \kappa_C \mu_C T \left| \nabla C + \frac{\mu_p}{\mu_C} \nabla p \right|^2 + 2 \kappa_{TC} \nabla T \cdot \left[\nabla C + \frac{\mu_p}{\mu_C} \nabla p \right] \geq 0. \quad (23.144)$$

This condition then constrains the phenomenological constants κ_C , κ_T and κ_{TC} so that

$$|\kappa_{TC}|^2 \leq \kappa_T \kappa_C c_p T \mu_S. \quad (23.145)$$

¹¹See Chapter 14 of [Callen \(1985\)](#) for these conditions and their underlying dynamical connections.

Comments on measurements

The cross-diffusion coefficients, κ_{TC} and κ_{CT} , are both measured to be very small for seawater, so that the Dufour effect and Soret effect are commonly ignored. Furthermore, in an ocean in thermodynamic equilibrium, the vertical salinity gradient implied by equation (23.142) is roughly 3 g kg^{-1} per 1000 m. This vertical salinity gradient is far larger than measured in the ocean, thus providing evidence that turbulent fluxes, even in the ocean interior, dominate over molecular fluxes. That is, the observed ocean has sufficient turbulence to keep it well away from thermodynamic equilibrium.

23.8.3 A summary presentation

We here summarize the previous material by skipping details for the entropy flux, thermal flux, and matter flux. For this purpose, write the budget for the total energy in the form

$$\rho \frac{D\mathcal{E}}{Dt} = -\nabla \cdot (p \mathbf{v} - \mathbf{v} \cdot \tau) + \rho \left[-\epsilon + T \frac{DS}{Dt} + \mu \frac{DC}{Dt} \right] + \rho \partial_t \Phi. \quad (23.146)$$

Now assume that the specific entropy and matter concentration satisfy the evolution equations

$$\rho \frac{DS}{Dt} = -\nabla \cdot \mathbf{J}_S + \Sigma_S \quad \text{and} \quad \rho \frac{DC}{Dt} = -\nabla \cdot \mathbf{J}_C, \quad (23.147)$$

thus rendering

$$\rho \left[T \frac{DS}{Dt} + \mu \frac{DC}{Dt} \right] = -T \nabla \cdot \mathbf{J}_S + T \Sigma_S - \mu \nabla \cdot \mathbf{J}_C \quad (23.148a)$$

$$= -\nabla \cdot (T \mathbf{J}_S + \mu \mathbf{J}_C) + \nabla T \cdot \mathbf{J}_S + \nabla \mu \cdot \mathbf{J}_C + T \Sigma_S, \quad (23.148b)$$

which then brings the total energy equation (23.146) into the form

$$\rho \frac{D\mathcal{E}}{Dt} = -\nabla \cdot (p \mathbf{v} - \mathbf{v} \cdot \tau + T \mathbf{J}_S + \mu \mathbf{J}_C) + [-\rho \epsilon + \nabla T \cdot \mathbf{J}_S + \nabla \mu \cdot \mathbf{J}_C + T \Sigma_S] + \rho \partial_t \Phi. \quad (23.149)$$

We now postulate that the globally integrated total energy is constant in the absence of boundary processes and with a time independent geopotential. In the presence of mechanical dissipation and matter constituent mixing, a necessary condition for such global energy conservation is for the specific entropy source to take the form

$$T \Sigma_S = \rho \epsilon - \nabla T \cdot \mathbf{J}_S - \nabla \mu \cdot \mathbf{J}_C. \quad (23.150)$$

That is, the entropy source arises from frictional dissipation, entropy mixing, and matter mixing. With this form for the entropy source, the total energy budget (23.149) is given by the material form and the equivalent Eulerian flux-form expressions

$$\rho \frac{D\mathcal{E}}{Dt} = -\nabla \cdot (p \mathbf{v} - \mathbf{v} \cdot \tau + T \mathbf{J}_S + \mu \mathbf{J}_C) + \rho \partial_t \Phi \quad (23.151a)$$

$$\frac{\partial(\rho \mathcal{E})}{\partial t} = -\nabla \cdot (\mathcal{E} \mathbf{v} + p \mathbf{v} - \mathbf{v} \cdot \tau + T \mathbf{J}_S + \mu \mathbf{J}_C) + \rho \partial_t \Phi. \quad (23.151b)$$

The modified form of the internal energy budget (23.70) is found by subtracting the mechanical energy budget (23.40) from the total energy budget (23.151a)

$$\rho \frac{D\mathcal{J}}{Dt} = \rho \frac{D(\mathcal{E} - \mathcal{M})}{Dt} = -p \nabla \cdot \mathbf{v} - \nabla \cdot (T \mathbf{J}_S + \mu \mathbf{J}_C) + \rho \epsilon. \quad (23.152)$$

The corresponding enthalpy budget (23.72) is given by

$$\rho \frac{D\mathcal{H}}{Dt} - \frac{Dp}{Dt} = -\nabla \cdot (T \mathbf{J}_S + \mu \mathbf{J}_C) + \rho \epsilon = -\nabla \cdot \mathbf{J}_{\mathcal{H}} + \rho \epsilon. \quad (23.153)$$

In the second equality we defined the enthalpy flux

$$\mathbf{J}_{\mathcal{H}} = T \mathbf{J}_S + \mu \mathbf{J}_C \quad (23.154a)$$

$$= \mathbf{J}_{\text{therm}} - T \left[\frac{\partial \mu}{\partial T} \right]_{p,C} \mathbf{J}_C + \mu \mathbf{J}_C \quad (23.154b)$$

$$= \mathbf{J}_{\text{therm}} + \left[\frac{\partial \mathcal{H}}{\partial C} \right]_{T,p} \mathbf{J}_C \quad (23.154c)$$

$$= \mathbf{J}_{\text{therm}} + \mathbf{J}_{\text{chem}}, \quad (23.154d)$$

where we used equation (23.130) for the entropy flux, \mathbf{J}_S , equation (23.127) for the chemical flux, \mathbf{J}_{chem} , and the thermodynamic identity (23.77) for the third equality. Furthermore, recall that the thermal flux, $\mathbf{J}_{\text{therm}}$, is the sum of a conductive plus radiative contribution as per equation (23.74).

23.8.4 Comments

It is remarkable how the second law of thermodynamics is able to predict new physical processes through considering the various forms that the thermal and matter fluxes can take to ensure a positive entropy source. [Caldwell \(1973\)](#) and [Caldwell and Eide \(1981\)](#) estimate the Soret effect for seawater, where they propose some relevance of this effect in quiescent ocean regions with strong gradients. In contrast, for liquids the Dufour effect is about 1000 times smaller than Fickian heat conduction and so it is safely ignored throughout the ocean. [McDougall and Turner \(1982\)](#) and [McDougall \(1983\)](#) studied double-diffusive convection in the presence of cross-diffusion, extending the oceanographic applications to arbitrary solutions with a pair of solutes. None of these studies consider the role of pressure gradients in generating fluxes.

For most purposes of oceanography, the fluxes considered in this section are far smaller than those induced by turbulent flow processes. In this case, the flux relations reduce to the Fickian and Fourier expressions yet with turbulent exchange coefficients rather than their molecular values. Turbulence thus makes molecular diffusive processes generally negligible for the ocean. Indeed, we already made this conclusion when noting that thermodynamic equilibrium implies a sizable vertical salinity gradient as given by equation (23.142). Whereas turbulence acts to produce a homogenous salinity (as well as potential temperature and potential enthalpy), molecular diffusion leads to a rather large vertical salinity gradient. Since the vertical salinity gradient implied by thermodynamic equilibrium is much larger than that measured in the ocean, we conclude that the ocean is far from a thermodynamic equilibrium state.

23.8.5 Further study

Much of our presentation in this section followed that from Sections 2.4 and 2.5 from [Olbers et al. \(2012\)](#) and Appendix B of [IOC et al. \(2010\)](#). [Graham and McDougall \(2013\)](#) extend these ideas

to a turbulent ocean. The physical ideas underlying the Onsager reciprocity conditions are lucidly discussed in Chapter 14 of [Callen \(1985\)](#).

23.9 Temperature evolution

In specifying the state of a fluid element it is sensible to make use of the temperature, pressure, and tracer concentration given that these state properties are readily measured in the laboratory and environment. Furthermore, these properties are the natural variables for the Gibbs potential (Section 19.6.6). Hence, given values for (T, p, C) we can determine the Gibbs potential and then determine all other thermodynamic properties by taking partial derivatives.

How do we specify the evolution of (T, p, C) for a fluid element? Evolution of the matter concentration follows from the tracer equation (an advection-diffusion equation) as developed in Section 17.1. Pressure measures the compressive stress acting on each fluid element (Section 22.8), with its specification depending on the dominant dynamical balances (see Section 23.11). Temperature reflects the energy of the internal microscopic degrees of freedom within a fluid element, with its evolution the subject of this section. We show how Conservative Temperature, Θ , rather than *in situ* temperature, T , or potential temperature, θ , offers the simplest prognostic equation of the three temperature variables. The key reason is that Θ evolves almost precisely like a material tracer, driven by the convergence of fluxes, whereas the equations for T and θ contain extra source terms in addition to flux convergences.

23.9.1 Evolution of *in situ* temperature

In developing the temperature equation it is useful to start from the prognostic equation for enthalpy as developed in Sections 23.4.5. For that purpose we write the enthalpy equation (23.153) as

$$\rho \frac{D\mathcal{H}}{Dt} = \frac{Dp}{Dt} - \nabla \cdot \mathbf{J}_{\mathcal{H}} + \rho \epsilon, \quad (23.155)$$

with the enthalpy flux, $\mathbf{J}_{\mathcal{H}}$, written in terms of the entropy and tracer fluxes as per equation (23.154d).

To reveal a prognostic equation for temperature, we write enthalpy as a function of (T, p, C) so that

$$\frac{D\mathcal{H}}{Dt} = \left[\frac{\partial \mathcal{H}}{\partial T} \right]_{p,C} \frac{DT}{Dt} + \left[\frac{\partial \mathcal{H}}{\partial p} \right]_{T,C} \frac{Dp}{Dt} + \left[\frac{\partial \mathcal{H}}{\partial C} \right]_{T,p} \frac{DC}{Dt}. \quad (23.156)$$

The partial derivatives can be related to response functions via the following. First, the specific heat capacity at constant pressure is given by equation (19.104)

$$\left[\frac{\partial \mathcal{H}}{\partial T} \right]_{p,C} = c_p. \quad (23.157)$$

Next, we make use of the Gibbs potential identities in Section 19.6.6 to write

$$\left[\frac{\partial \mathcal{H}}{\partial p} \right]_{T,C} = \left[\frac{\partial \mathcal{G}}{\partial p} \right]_{T,C} - T \left[\frac{\partial}{\partial p} \right]_{T,C} \left[\frac{\partial \mathcal{G}}{\partial T} \right]_{p,C} \quad (23.158a)$$

$$= \nu_s - T \left[\frac{\partial}{\partial T} \right]_{p,C} \left[\frac{\partial \mathcal{G}}{\partial p} \right]_{T,C} \quad (23.158b)$$

$$= \nu_s - T \left[\frac{\partial \nu_s}{\partial T} \right]_{p,C} \quad (23.158c)$$

$$= \nu_s (1 - T \alpha_T), \quad (23.158d)$$

where α_T is the thermal expansion coefficient given by equation (19.105). Use of these identities in the enthalpy equation (23.156) and rearrangement leads to the *in situ* temperature equation

$$c_p \rho \frac{DT}{Dt} = -\nabla \cdot \mathbf{J}_{\mathcal{H}} + \left[\frac{\partial \mathcal{H}}{\partial C} \right]_{T,p} \nabla \cdot \mathbf{J}_C + \alpha_T T \frac{Dp}{Dt} + \rho \epsilon. \quad (23.159)$$

The *in situ* temperature of a fluid element thus evolves according to convergence of the enthalpy fluxes, divergence of matter concentration fluxes, material time changes to pressure, and frictional dissipation. We can massage this expression a bit more by introducing the enthalpy flux (23.154c) so that

$$c_p \rho \frac{DT}{Dt} = -\nabla \cdot \mathbf{J}_{\text{therm}} - \mathbf{J}_C \cdot \nabla \left[\frac{\partial \mathcal{H}}{\partial C} \right]_{T,p} + \alpha_T T \frac{Dp}{Dt} + \rho \epsilon, \quad (23.160)$$

where constraints on the conductive portion of the thermal flux were discussed in Section 23.8.2.

23.9.2 Evolution of potential temperature

We can convert the *in situ* temperature equation (23.159) into a version of the potential temperature equation by recalling the expression (20.26) for the lapse rate

$$\hat{\Gamma} = \left[\frac{\partial T}{\partial p} \right]_{C,S} = \frac{T \alpha_T}{\rho c_p} \quad (23.161)$$

so that equation (23.159) takes the form

$$c_p \rho \left[\frac{DT}{Dt} - \hat{\Gamma} \frac{Dp}{Dt} \right] = -\nabla \cdot \mathbf{J}_{\mathcal{H}} + \left[\frac{\partial \mathcal{H}}{\partial C} \right]_{T,p} \nabla \cdot \mathbf{J}_C + \rho \epsilon. \quad (23.162)$$

Making use of the definition (20.31) for potential temperature renders

$$c_p \rho \frac{D\theta}{Dt} = -\nabla \cdot \mathbf{J}_{\mathcal{H}} + \left[\frac{\partial \mathcal{H}}{\partial C} \right]_{T,p} \nabla \cdot \mathbf{J}_C + \rho \epsilon. \quad (23.163)$$

As expected, pressure changes are removed from the evolution equation for potential temperature.

23.9.3 Conservative Temperature for the ocean

Rather than expressing enthalpy as a function $\mathcal{H}(T, p, C)$, we make use of its natural coordinate dependence $\mathcal{H}(S, p, C)$ from Section 19.6.4, which leads to the enthalpy equation in the form (23.153)

$$\rho \frac{D\mathcal{H}}{Dt} = \frac{Dp}{Dt} - \nabla \cdot \mathbf{J}_{\mathcal{H}} + \rho \epsilon. \quad (23.164)$$

The pressure term arises just like for *in situ* temperature. Its presence suggests we introduce the *potential enthalpy*.

Potential enthalpy and Conservative Temperature

The potential enthalpy is defined to be the enthalpy of a fluid element moved to a reference pressure, p_R , while maintaining fixed specific entropy and fixed tracer concentration

$$\mathcal{H}^{\text{pot}}(\mathcal{S}, C) = \mathcal{H}(\mathcal{S}, p_R, C). \quad (23.165)$$

As for potential temperature (Section 20.3.3), it is most convenient to take p_R as the standard atmospheric pressure, thus corresponding to the standard pressure at the air-sea interface. This definition parallels that for potential temperature given by equation (20.36). It is also motivated by the exchange of enthalpy (heat) across the air-sea boundary, thus providing a natural means to study coupled air-sea processes.

By construction, the material time derivative of potential enthalpy is given by

$$\rho \frac{D\mathcal{H}^{\text{pot}}}{Dt} = \rho \left[\frac{\partial \mathcal{H}^{\text{pot}}}{\partial \mathcal{S}} \right]_C \frac{D\mathcal{S}}{Dt} + \rho \left[\frac{\partial \mathcal{H}^{\text{pot}}}{\partial C} \right]_S \frac{DC}{Dt} \quad (23.166a)$$

$$= \theta (-\nabla \cdot \mathbf{J}_S + \Sigma_S) - \mu_R \nabla \cdot \mathbf{J}_C \quad (23.166b)$$

$$= (\theta/T) [\rho \epsilon - \nabla \cdot \mathbf{J}_H] - [\mu_R - (\theta/T) \mu] \nabla \cdot \mathbf{J}_C, \quad (23.166c)$$

where we set

$$\theta = \left[\frac{\partial \mathcal{H}^{\text{pot}}}{\partial \mathcal{S}} \right]_C \quad \text{and} \quad \mu_R = \left[\frac{\partial \mathcal{H}^{\text{pot}}}{\partial C} \right]_S \quad (23.167)$$

and used equation (23.150) for the entropy source, Σ_S . Now define the Conservative Temperature, Θ , via

$$c_p^{\text{ref}} \Theta \equiv \mathcal{H}^{\text{pot}}(\mathcal{S}, C) = \mathcal{H}(\mathcal{S}, p_R, C), \quad (23.168)$$

where c_p^{ref} is an arbitrary reference specific heat capacity. For the ocean, [McDougall \(2003\)](#) suggested that c_p^{ref} be chosen so that $\Theta = \theta$ at a salinity of 35 parts per thousand. [McDougall \(2003\)](#) furthermore argued that the terms appearing in the potential enthalpy equation (23.166c) are well approximated for the ocean by just the convergence of the enthalpy flux. Hence, the Conservative Temperature satisfies, to a very good approximation, the source-free tracer equation

$$\rho c_p^{\text{ref}} \frac{D\Theta}{Dt} = -\nabla \cdot \mathbf{J}_H. \quad (23.169)$$

Key points regarding the Conservative Temperature equation

The Conservative Temperature equation (23.169) is mathematically identical to the material tracer equation, and as such it offers an elegant means to prognose thermodynamic properties of the fluid and to perform budget analyses. We further emphasize two points in regards to this equation relative to the potential temperature equation (23.163).

- The source terms (those not associated with flux convergences) on the right hand side of the potential temperature equation are much larger than those in the Conservative Temperature equation. In particular, [McDougall \(2003\)](#) and [Graham and McDougall \(2013\)](#) showed that the potential temperature sources are roughly 100 times larger in certain regions of the ocean than the Conservative Temperature sources.

- The heat capacity appearing in the Conservative Temperature equation is a fixed constant, by construction. This feature contrasts to the space-time variable heat capacity, c_p , appearing in both the *in situ* temperature equation (23.159) and potential temperature equation (23.163). The space-time variations of c_p are not negligible (e.g., order 5% for the global ocean), thus making the non-constant heat capacity required for the T and θ equations very inconvenient for purposes of budget analyses (see [McDougall et al. \(2021\)](#) for more on this point).

We close by noting that the enthalpy flux, \mathbf{J}_H , is related to the entropy flux and concentration flux as per equation (23.154d). As discussed in Section 2.6 of [Olbers et al. \(2012\)](#), the dominant terms appearing in this flux arise from entropy, which itself is largely due to fluxes of temperature. Consequently, the flux \mathbf{J}_H is well approximated as a flux just of Θ .

23.9.4 Alternative functional dependencies for specific enthalpy

Thus far in this section, we have considered specific enthalpy to be a function of (T, p, C) as well as its natural functional dependence, (\mathcal{S}, p, C) . The introduction of potential temperature and Conservative Temperature allow us to consider two more functional dependencies

$$\mathcal{H} = \mathcal{H}^{\text{natural}}(\mathcal{S}, p, C) = \mathcal{H}^T(T, p, C) = \mathcal{H}^\theta(\theta, p, C) = \mathcal{H}^\Theta(\Theta, p, C). \quad (23.170)$$

We use distinct notations for the functions since they each return specific enthalpy yet when fed distinct input. Given the more common use of either potential temperature or Conservative Temperature in atmosphere and ocean sciences, the final two functional dependencies are most commonly used in practice. Note that for brevity, we often drop the extra notation adorning the specific enthalpy symbol, except where confusion may arise. As an example of the above functional dependence, consider the exact differential of specific enthalpy when written using the (Θ, p, C) dependence, in which

$$d\mathcal{H} = \left[\frac{\partial \mathcal{H}^\Theta}{\partial \Theta} \right]_{p,C} d\Theta + \left[\frac{\partial \mathcal{H}^\Theta}{\partial p} \right]_{\Theta,C} dp + \left[\frac{\partial \mathcal{H}^\Theta}{\partial C} \right]_{\Theta,p} dC \quad (23.171a)$$

$$= \left[\frac{\partial \mathcal{H}^\Theta}{\partial \Theta} \right]_{p,C} d\Theta + \rho^{-1} dp + \left[\frac{\partial \mathcal{H}^\Theta}{\partial C} \right]_{\Theta,p} dC, \quad (23.171b)$$

where we set

$$\rho^{-1} = \left[\frac{\partial \mathcal{H}^\Theta}{\partial p} \right]_{\Theta,C}, \quad (23.172)$$

which is a generalization of the partial derivative (19.79) holding for the natural functional dependence. Further discussion of the other partial derivatives are provided in [Graham and McDougall \(2013\)](#) as well as Appendices A.10 and A.11 of [IOC et al. \(2010\)](#).

23.9.5 Further study

The discussion in this section largely followed the more complete ocean discussion given in Section 2.6 of [Olbers et al. \(2012\)](#), which is itself based on [McDougall \(2003\)](#) and [Graham and McDougall \(2013\)](#).

Considerations for a realistic atmosphere involve phase changes (liquid-vapor and liquid-solid), with the associated latent heat exchanges are leading order contributions to the enthalpy budget (see [Lauritzen et al. \(2022\)](#) for a comprehensive review). Additionally, the role of frictional

dissipation is not negligible in the atmosphere whereas it is negligible in the ocean (see Section 23.5.3).

23.10 Conservation laws and potential properties

A central facet of theoretical physics concerns the development of concepts and tools to expose conservation laws and their underlying symmetries.¹² We routinely make use of such laws in geophysical fluid mechanics to provide constraints on the fluid motion and to study budgets of corresponding properties to help understand fundamental processes. As such, conservation laws offer great physical insight and predictive utility. We close this chapter by summarizing some conceptual points concerning conservation laws. In particular, we identify the need to distinguish laws that involve just the convergence of a flux from those that also include non-conservative “source” terms. We also distinguish between material and non-material conservation laws, in which properties satisfying material conservation laws are materially invariant in the absence of local mixing processes.

23.10.1 Flux-form conservation laws

Certain scalar properties studied in fluid mechanics satisfy conservation laws that are written as

$$\rho \frac{D\psi}{Dt} = -\nabla \cdot \mathbf{J} \iff \frac{\partial(\rho\psi)}{\partial t} = -\nabla \cdot (\rho \mathbf{v}\psi + \mathbf{J}). \quad (23.173)$$

The right hand side of the Eulerian flux-form expression (second equation) involves a flux that is comprised of an advective term, $\rho \mathbf{v}\psi$, plus a non-advective term, \mathbf{J} . Examples of conservation laws of this type include the material tracer concentration, $\psi = C$, as in equation (23.179); the Conservative Temperature, $\psi = \Theta$, as in equation (23.180); the total energy, $\psi = \mathcal{E}$, in the absence of astronomical forces, as in equation (23.151b); and the potential vorticity, $\psi = Q$, as in equation (38.49). In Chapter 17, we saw how this differential equation leads to finite volume conservation properties for the integral of ψ -stuff within a region, $\int_{\mathcal{R}} \psi \rho dV$, with the evolution of this integral only affected by area integrated fluxes, $\rho \mathbf{v}\psi + \mathbf{J}$, penetrating the region boundary (mathematically seen by applying the divergence theorem).

Conservation laws of the form (23.173) are a direct consequence of the *local* conservation of ψ -stuff within the fluid. That is, the amount of ψ -stuff changes at a point only through the local convergence of fluxes onto that point, and likewise for a finite region. Such conservation laws are consistent with basic notions of causality and locality that appear throughout physics, with a discussion of such conservation laws offered in Section 27-1 of [Feynman et al. \(1963\)](#).

23.10.2 Conservation laws that are not flux-form

The presence of source/sinks are relevant for chemical or biogeochemical reactions, whereby matter is converted from one form to another. Such processes are not mathematically represented as the convergence of a flux. As such, they are not contained in the conservation law (23.173) and they are correspondingly referred to as *non-conservative processes*. Even without chemical reactions, not all fluid properties satisfy flux-form conservation laws of the form (23.173). For example, linear momentum of a fluid element is affected by pressure, Coriolis, and effective gravity, and these processes are not represented as the convergence of a flux.

¹²See Chapter 12 for the connection between conservation laws and symmetries, as embodied by Noether’s theorem.

As discussed in Chapter 12, conservation laws are associated with symmetries of the physical system. Correspondingly, non-conservative terms appearing in an evolution equation often reflect the breaking of a symmetry. For example, motion around a sphere does not conserve linear momentum even in the absence of forces, whereas linear momentum is conserved for free motion in a planar geometry.

23.10.3 Non-material or wave-like transport of properties

Pressure is of particular note since pressure perturbations travel through a compressible fluid via acoustic waves (Chapter 44), or, in the case of an incompressible flow, a pressure perturbation is felt globally and instantaneously as reflected in the elliptic Poisson equation satisfied by pressure (Section 26.3). More generally, the wave mediated transfer of forces, or other fluid properties such as momentum or mechanical energy, is an example of a non-material transfer; i.e., a transfer of information not arising from the transfer of matter. Non-material wave mediated transfer often occurs much faster than material transfer, with matter transport only mediated through advection and diffusion. Correspondingly, material substances (and potential enthalpy) are not directly affected by wave transport. Rather, waves affect material substances only so far as they affect advection and diffusion.

23.10.4 Material and non-material conservation laws

Mass invariance for a fluid element reflects matter conservation in classical physics, which in turn motivates the kinematic perspective pursued throughout this book that follows fluid elements whose mass remains constant. Relatedly, in the absence of irreversible mixing, the matter content of the fluid element remains invariant so that its tracer concentration is materially constant

$$\rho \frac{DC}{Dt} = 0. \quad (23.174)$$

For example, in the absence of mixing, the salt content of seawater and the water content of moist air are materially invariant, so that the salt concentration and water concentration in a fluid element remains invariant. Correspondingly, in the presence of mixing between two fluid elements, the net material tracer in the combined fluid element equals to the sum of the tracer content in the contributing elements. We refer to fluid properties satisfying such conservation laws as *materially conservative properties*.

What about fluid properties that satisfy a local flux-form conservation law of the form (23.173), and yet do not remain materially invariant in the absence of mixing? For example, consider the total energy, \mathcal{E} , from Section 23.5. Even in the absence of entropy sources (i.e., no mixing) and astronomical forces (i.e., constant gravity), mechanical work from pressure modifies the internal energy of the fluid element via the energy equation (23.151a)

$$\rho \frac{D\mathcal{E}}{Dt} = -\nabla \cdot (p \mathbf{v}). \quad (23.175)$$

Pressure work means that when two fluid elements are combined, the total energy of the combined fluid, \mathcal{E}_{12} , is not generally equal to the sum of their separate total energies,

$$\mathcal{E}_{12} \neq \mathcal{E}_1 + \mathcal{E}_2. \quad (23.176)$$

So although total energy is locally conserved in the sense that it is affected by a local flux convergence, it does not satisfy a material-like conservation law. We say that total energy is a *non-materially conservative* fluid property. Notably, when integrated globally over a domain

closed to energy fluxes, including mechanical energy fluxes (meaning there is no pressure work applied to the domain boundaries), and when there are no time dependent astronomical forces, then the domain integrated total energy, $\int \rho \mathcal{E} dV$, remains constant. This *global* conservation law means that the total energy is conserved globally. Conservation laws for non-materially conserved properties, such as total energy, offer a less powerful constraint on fluid motion than the material conservation laws. Even so, global conservation can be of great use when studying energy transformations within a closed domain.

We summarize the above discussion by noting that for a fluid property to be locally conservative, it is necessary that the density weighted material derivative of that property be given by the convergence of a flux as in equation (23.173). To be materially conservative, a property must have its flux convergence vanish in the absence of mixing processes that are local in space and time. A diffusive flux satisfies this property (see Chapter 61 for more on diffusion). In contrast, the pressure flux convergence acting to modify total energy, $-\nabla \cdot (p \mathbf{v})$, can be nonzero even in regions where there is no mixing since pressure is transported by waves (Section 23.10.3). So although total energy is locally conserved, its flux is dependent on non-local processes as mediated by waves, so that total energy satisfies a non-material conservation law.

23.10.5 Concerning potential properties

As introduced in Sections 20.3 and 23.9.3, to study fluid mixing it is useful to work with scalar fields that are not affected by adiabatic and isentropic pressure work. For this reason, rather than *in situ* temperature, we prefer to work with potential temperature, θ , or Conservative Temperature, Θ , both of which are potential properties as discussed in Section 20.3.1. Some potential properties are also endowed with the local conservation property discussed above, which makes local budgets available just like for a material tracer. For example, Conservative Temperature is very well approximated as a conservative property, with its non-flux form sources far smaller than potential temperature (Section 23.9.3). In contrast, neither *in situ* temperature nor total energy are potential properties since an adiabatic and isentropic change in pressure alters the *in situ* temperature and total energy of a fluid element.

23.10.6 Further study

Much from this section is motivated by the more extensive discussion in Sections A.8 and A.9 of *IOC et al. (2010)*.

23.11 Summary of the equations for rotating and stratified fluids

We close this chapter by summarizing the physical content of the suite of partial differential equations describing rotating and stratified fluids.

$$\rho \frac{D\mathbf{v}}{Dt} + 2\rho \boldsymbol{\Omega} \times \mathbf{v} = -\rho \nabla \Phi - \nabla p + \nabla \cdot \tau \quad \text{momentum} \quad (23.177)$$

$$\frac{D\rho}{Dt} = -\rho \nabla \cdot \mathbf{v} \quad \text{mass continuity} \quad (23.178)$$

$$\rho \frac{DC}{Dt} = -\nabla \cdot \mathbf{J}(C) \quad \text{matter conservation} \quad (23.179)$$

$$\rho \frac{D\Theta}{Dt} = -\nabla \cdot \mathbf{J}(\Theta) \quad \text{potential enthalpy conservation} \quad (23.180)$$

$$\rho = \rho(C, \Theta, p) \quad \text{equation of state.} \quad (23.181)$$

It is a testament to the success of classical continuum mechanics that these equations are of use for describing fluid phenomena from the millimetre scale to the astrophysical scale. We summarize the following terms in these equations.

- **LINEAR MOMENTUM AND VELOCITY:** Newton's second law of motion, as developed for a fluid in Chapter 21, provides the prognostic equation for the velocity field, \mathbf{v} . Each of the three velocity components evolves according to its respective dynamical equation (23.177). As noted at the end of Section 21.2.3, we write the momentum equation in the form (23.177) by separating the time dependence of the basis vectors into a term arising from solid-body rotation (which leads to planetary Coriolis and planetary centrifugal accelerations) and a term arising from the motion of the fluid relative to the rotating sphere (which leads to the metric acceleration when using non-Cartesian coordinates).
- **MASS CONSERVATION:** Kinematics provides a constraint on the velocity field according to the needs of mass conservation for a fluid element (Section 16.2). This constraint leads to the continuity equation (23.178).
- **MATERIAL TRACER CONSERVATION:** Kinematic constraints from the conservation of matter (Section 17.1) leads to the material tracer equation (23.179). Evolution is determined by the convergence of tracer fluxes, \mathbf{J} , with this flux specified by molecular diffusion as discussed in Section 61.3, or through other parameterized processes when sampling flow on scales larger than millimetres (see Chapter 63).
- **THERMODYNAMIC TRACER:** The Conservative Temperature, Θ , (Section 23.9.3), evolves according to the convergence of fluxes, just like a material tracer.
- **DENSITY:** The *in situ* density can be updated in time via mass continuity (equation (23.178)) or via knowledge of (C, Θ, p) . We discussed the many forms of density for the ocean and atmosphere in Section 27.3.
- **PRESSURE:** There is no prognostic equation for pressure. Rather, pressure is diagnosed based on knowledge of other fields. Here are sketches of how that diagnostic calculation is performed.
 - For an ideal gas, pressure is diagnosed from the ideal gas relation (20.48) using the density and temperature.
 - For fluid flow maintaining an approximate hydrostatic balance (Section 24.2), pressure is diagnosed at a point through knowledge of the weight per area above the point.
 - For an incompressible flow as per the oceanic Boussinesq fluid (Chapter 26), pressure is no longer connected thermodynamically to partial derivatives of the thermodynamic potentials (Section 19.6). Instead, pressure is determined kinematically by the incompressibility constraint. In particular, for a non-hydrostatic Boussinesq fluid, pressure is diagnosed by solving a Poisson equation derived from taking the divergence of the momentum equation (see Section 26.3).
- **GEOPOTENTIAL:** The geopotential, Φ , is specified once the height above an arbitrary reference level is known, as well as the effective gravitational acceleration (Section 11.11.4). For geophysical fluid studies, the reference level is generally taken at the level of a resting sea surface. We thus often write the radial coordinate as

$$r = R_e + z \tag{23.182}$$

where $R_e = 6.371 \times 10^6$ m is the earth radius (equation (11.115)), and z is the geopotential coordinate measuring the height above sea level.

- EARTH'S SPIN: The earth's angular velocity, Ω , is constant for geophysical fluid studies of concern here. Its value is discussed in Section 11.1.
- FRICTION: The friction vector,

$$\rho \mathbf{F} = \nabla \cdot \tau, \quad (23.183)$$

is the divergence of a symmetric and trace-free deviatoric stress tensor, τ (Section 22.8). The stress tensor is determined through a constitutive relation as a function of the strain and viscous properties.

- BOUNDARY CONDITIONS: Boundary conditions consist of the exchange of matter, momentum, and enthalpy with the surrounding media, such as the solid earth or another fluid component (e.g., atmosphere-ocean exchange). We discuss the boundary conditions for matter in Section 16.4; for momentum in Section 22.10; and for ocean buoyancy in Section 64.6.



23.12 Exercises

EXERCISE 23.1: ENERGETICS OF OCEAN MIXING

In this exercise we develop some basics for the energetics of mixing, thus providing more experience with the ideas developed in Section 23.2.6. We do so by examining a vertical column of seawater with uniform horizontal cross-sectional area, A . Let the initial conditions consist of two homogeneous regions stacked vertically, with thickness h_n , mass M_n , density ρ_n , Conservative Temperature Θ_n , and salinity S_n , where $n = 1$ is the lower region and $n = 2$ the upper region. Assume this column to be stably stratified so that $\Delta\rho = \rho_1 - \rho_2 > 0$. We then completely mix the two regions to produce a homogeneous column of fluid of mass M , salinity S , and Conservative Temperature Θ . We ignore pressure effects on density, so that the density is uniform in the two regions prior to mixing, and uniform in the full column after mixing. The conservation of mass, conservation of salt, and conservation of potential enthalpy (heat), mean that these scalar properties remain the same before and after the mixing, thus allowing us to compute the properties of the homogenized column

$$M = M_1 + M_2 \quad \text{and} \quad M\Theta = M_1\Theta_1 + M_2\Theta_2 \quad \text{and} \quad MS = M_1S_1 + M_2S_2. \quad (23.184)$$

- Compute the gravitational potential energy of the initial seawater column, taking the bottom of the column as the zero reference level.
- Compute the gravitational potential energy of the fluid column after homogenization. Verify that the gravitational potential energy of the homogenized column is greater than the initial column. For this question, assume the final thickness of the column equals to the sum of the initial thicknesses. This assumption is not exact but is very accurate for our purposes. For an exact calculation see equation (64.112) in our study of sea level in Section 64.7.7.
- If the same amount of energy used to increase in gravitational potential energy was instead used to increase kinetic energy of the homogenized fluid, what is the expression for the

change in squared velocity? Write your expression in terms of the thicknesses, h_n , and densities, ρ_n .

- (d) If the change in gravitational potential energy were converted to potential enthalpy of the homogenized fluid, what is the expression for the increase in Conservative Temperature, Θ ? Again, write your expression in terms of the thicknesses, h_n , and densities, ρ_n .
- (e) Compute the change in speed and change in Conservative Temperature for the previous parts of this exercise using the following values for a region of seawater: $c_p = 3992.1 \text{ J kg}^{-1} \text{ K}^{-1}$, $\rho_1 = 1020 \text{ kg m}^{-3}$, $\Delta\rho = 1 \text{ kg m}^{-3}$, $h_1 = 1 \text{ m}$, and $h_2 = 1 \text{ m}$.

EXERCISE 23.2: FRICTIONAL DISSIPATION FROM VISCOSITY

This exercise works through a simple case of the more general considerations from Section 23.3.2. Here, assume the friction in the momentum equation takes the form

$$\rho \mathbf{F} = \nabla \cdot (\rho \nu \nabla \mathbf{v}) = \partial_n (\rho \nu \partial_n \mathbf{v}), \quad (23.185)$$

with $\nu > 0$ a scalar kinematic viscosity (generally non-constant). Show that when integrated over the full domain

$$\int \mathbf{F} \cdot \mathbf{v} \rho dV < 0, \quad (23.186)$$

where boundary terms are dropped. Hence, the global integrated kinetic energy is dissipated (reduced) through the impacts of viscosity. This dissipation of mechanical energy is converted to an increase in internal energy through Joule heating. Hint: for this exercise, it is sufficient to assume Cartesian tensors so that

$$\rho \mathbf{F} \cdot \mathbf{v} = \rho F_m v_m = \partial_n (\rho \nu \partial_n v_m) v_m. \quad (23.187)$$

EXERCISE 23.3: INTEGRATED FRICTIONAL DISSIPATION FOR AN INCOMPRESSIBLE FLUID

Consider an incompressible fluid ($\nabla \cdot \mathbf{v} = 0$ along with ρ is constant). Assume the fluid is contained in a region, \mathcal{R} , whose boundary, $\partial\mathcal{R}$, is static. Also assume the velocity satisfies the no-slip condition on $\partial\mathcal{R}$, as relevant for a viscous fluid. Show that the frictional dissipation of kinetic energy (Section 23.3.2) has a global integral

$$\int_{\mathcal{R}} \mathbf{v} \cdot \mathbf{F} \rho dV = -\rho \nu \int_{\mathcal{R}} |\boldsymbol{\omega}|^2 dV, \quad (23.188)$$

where $\boldsymbol{\omega} = \nabla \times \mathbf{v}$ is the vorticity. Hint: derive equation (15.135) from exercise 15.1, and specialize that equation to the case of an incompressible fluid.

EXERCISE 23.4: THERMODYNAMIC MANIPULATIONS FOR IDEAL GASES

This question develops some manipulations with the potential temperature.

- (a) Beginning with the expression (20.92) for potential temperature of an ideal gas, show that

$$d\theta = \frac{\theta}{T} \left[dT - \frac{\nu_s}{c_p} dp \right]. \quad (23.189)$$

- (b) Given the result (23.189), show that an ideal gas satisfies the following relation

$$T dS = \frac{c_p T}{\theta} d\theta. \quad (23.190)$$

Whereas the relation (20.44) holds for a general fluid only at the reference pressure, this exercise shows that it holds for an ideal gas at all pressures. As a result, a moving fluid of ideal gas satisfies the material time relation

$$T \frac{D\mathcal{S}}{Dt} = \frac{c_p T}{\theta} \frac{D\theta}{Dt} \Rightarrow \frac{c_p T}{\theta} \frac{D\theta}{Dt} = \dot{Q}. \quad (23.191)$$

EXERCISE 23.5: THERMODYNAMIC MANIPULATIONS FOR A LIQUID

Consider seawater with specific entropy given by (see Section 1.7.2 of [Vallis \(2017\)](#))

$$\mathcal{S}(S, T, p) = S_0 + c_{p0} \ln(T/T_o) [1 + \beta_s^*(S - S_o)] - \alpha_o p \left[\beta_T + \beta_T \gamma^* \frac{p}{2} + \beta_T^* (T - T_o) \right], \quad (23.192)$$

and corresponding specific heat capacity at constant pressure

$$c_p(S, T, p) = c_{p0} [1 + \beta_s^*(S - S_o)] - \alpha_o p \beta_T^* T. \quad (23.193)$$

In these equations, T is the *in situ* temperature, S is the salinity, and p is the *in situ* pressure. All other terms on the right hand side to these expressions are empirical constants. Verify that the specific entropy differential for a fluid element with constant composition is given by

$$\theta d\mathcal{S} = c_p(S, \theta, p_R) d\theta, \quad (23.194)$$

where θ is the potential temperature and p_R is the corresponding reference pressure. Consequently, we can write for a moving fluid element

$$\dot{Q} = \frac{c_p T}{\theta} \frac{D\theta}{Dt}, \quad (23.195)$$

where we evaluate the non-constant heat capacity at $c_p(S, \theta, p_R)$. We see that certain liquids have an expression for heating that is analogous to that for an ideal gas, with the ideal gas case discussed in Exercise 23.4. Hint: Make use of the identity (20.36).

EXERCISE 23.6: DYNAMICALLY INCONSISTENT VELOCITY

Consider the two dimensional vector field

$$\mathbf{u} = \Gamma (y^2 \hat{\mathbf{x}} + x^2 \hat{\mathbf{y}}), \quad (23.196)$$

with Γ a constant of dimensions $L^{-1} T^{-1}$.

- (a) Assuming \mathbf{u} is a velocity field, then determine the pressure field giving rise to this velocity assuming constant density, non-rotating reference frame, zero friction, and no boundary effects. Do so by making use of the Bernoulli theorem in equation (23.111) for horizontal (constant z) flow.
- (b) Now make use of the momentum equation and integrating the pressure gradient. You should reach an inconsistency condition. What can you conclude about the physical realizability of the given velocity field? Hint: recall the discussion of exact differentials in Section 2.8.

EXERCISE 23.7: CROCCO'S THEOREM

Prove that the spatial gradient of the Bernoulli potential for a single-component steady state perfect fluid can be written

$$\mathcal{B} = T \nabla \mathcal{S} + \mathbf{v} \times \boldsymbol{\omega}_a. \quad (23.197)$$

This result is known as Crocco's Theorem ([Crocco, 1937](#)). We derive two conclusions from this theorem. First, in a steady state, there is a nonzero vorticity non-parallel to the velocity whenever $\mathcal{B} - T \nabla \mathcal{S}$; i.e.,

$$\mathbf{v} \times \boldsymbol{\omega}_a = \mathcal{B} - T \nabla \mathcal{S}. \quad (23.198)$$

Second, it means that the velocity for a single-component perfect fluid in steady state is aligned parallel to isosurfaces of both the Bernoulli potential and the specific entropy

$$\mathbf{v} \cdot \nabla \mathcal{B} = T \mathbf{v} \cdot \nabla \mathcal{S}. \quad (23.199)$$

We encounter another form of this theorem for the steady state shallow water equations in Exercise [36.6](#).

Hint: to help formulate the proof, study the discussion in Section [23.7.3](#) where we showed that the Bernoulli potential is constant along a steady flow streamline in a perfect fluid. Also recall equation [\(23.108\)](#), which is valid for a steady state and applied here to a single-component fluid.



Chapter 24

APPROXIMATE HYDROSTATIC FLOW

The ocean and atmosphere thermo-hydrodynamical equations (23.177)-(23.181) explain a huge range of phenomena. Yet by encapsulating so many physical scales of motion and associated dynamical processes, the equations are difficult to manage when studying a focused dynamical regime. Therefore, it is common to approximate or filter the equations to remove scales of little interest, thus enabling a more telescopic view of the dynamics. In this chapter, we develop the hydrostatic primitive equations, which have been quite useful in the study of ocean and atmospheric circulation since their introduction in the 1950s.

READER'S GUIDE TO THIS CHAPTER

The equations developed in this chapter, and their associated approximations, are used extensively throughout the remainder of this book.

24.1	The hydrostatic primitive equations	562
24.1.1	Hydrostatic approximation	562
24.1.2	Shallow fluid approximation	562
24.1.3	Traditional approximation	563
24.1.4	Summary of the hydrostatic primitive equations	563
24.1.5	Flux-form mechanical energy budget	564
24.1.6	Depth integrated mechanical energy budget	565
24.1.7	Comments and further study	565
24.2	Physics of approximate hydrostatic balanced flow	566
24.2.1	Expressions for the hydrostatic pressure	566
24.2.2	Evolution of hydrostatic pressure	566
24.2.3	Heuristic scaling	568
24.2.4	Removal of a dynamically irrelevant background state	569
24.2.5	Decomposing the horizontal pressure gradient	570
24.2.6	Horizontal hydrostatic pressure gradient in a mass conserving fluid	572
24.2.7	Ocean dynamic topography	573
24.2.8	Surfaces of atmospheric geopotential height and pressure	574
24.2.9	Concerning vertical motion	575
24.2.10	Further study	575
24.3	Homogeneous fluid in a rotating tank	575
24.3.1	What about the planet's rotation?	575
24.3.2	Formulating the equations of motion	576
24.3.3	Solid-body rotation and parabolic free surface shape	577
24.3.4	Further study	578
24.4	Exercises	578

24.1 The hydrostatic primitive equations

The hydrostatic *primitive equations* provide a set of approximate equations for use in studying large-scale atmospheric and oceanic phenomena. Indeed, nearly all numerical models of the large-scale atmospheric and oceanic circulation are based on the primitive equations. They make use of the following three approximations.

24.1.1 Hydrostatic approximation

As discussed in Section 21.4, a static fluid in a gravity field maintains an exact hydrostatic balance, whereby the pressure at a point equals to the weight per area of fluid above that point. As shown in Section 24.2, the hydrostatic balance is very closely maintained column-by-column for the large scales in a moving geophysical fluid. Hence, it is appropriate for many purposes to take the *hydrostatic approximation* for the vertical momentum equation, with this approximation central to the study of geophysical fluid dynamics.

The hydrostatic approximation results in a balance within the vertical momentum equation (21.21) between the vertical pressure gradient and the effective gravitational force

$$\frac{\partial p}{\partial r} = -\rho g, \quad (24.1)$$

with this balance holding separately for each vertical column. Notably, there are no viscous or turbulent terms appearing in the hydrostatic balance.

Vertical integration of this equation, while assuming g is constant, renders a diagnostic expression for the hydrostatic pressure at a point as a function of the weight per horizontal area above the point

$$p(r, \lambda, \phi, t) = p(r_0, \lambda, \phi, t) + g \int_r^{r_0} \rho(r', \lambda, \phi, t) dr'. \quad (24.2)$$

Note that we exposed the horizontal space dependence along with the time dependence for the density and hence the hydrostatic pressure. That is, an approximate hydrostatic fluid has horizontal pressure gradients as well as time dependence.

We emphasize that in making the hydrostatic approximation that we are *not* assuming that vertical motion vanishes. In fact, there is vertical motion. But with the hydrostatic approximation, the vertical motion is not prognosed by the vertical momentum equation. Instead, it must be diagnosed via the constraints imposed on the motion. We have more comment on this point in Section 24.2.9. Furthermore, there are no other terms appearing in the vertical momentum equation, so that we retain just the vertical pressure gradient and the gravity term. Friction or boundary turbulent stresses do not appear in the hydrostatic balance.

24.1.2 Shallow fluid approximation

The ocean and atmosphere each form a fluid shell that envelopes the outer portion of the planet. The thickness of the these fluids is small relative to the earth's radius. The shallow fluid approximation¹ builds this scale separation into the equations of motion by setting the radial coordinate equal to the earth's radius

$$r = R_e + z \approx R_e. \quad (24.3)$$

¹The shallow fluid approximation is distinct from the *shallow water approximation* treated in Part VI of this book.

This approximation is made where r appears as a multiplier, but not as a derivative operator. For example, the spherical coordinate gradient operator (21.23) takes the approximate form

$$\nabla = \frac{\hat{\lambda}}{r \cos \phi} \frac{\partial}{\partial \lambda} + \frac{\hat{\phi}}{r} \frac{\partial}{\partial \phi} + \hat{r} \frac{\partial}{\partial r} \approx \frac{\hat{\lambda}}{R_e \cos \phi} \frac{\partial}{\partial \lambda} + \frac{\hat{\phi}}{R_e} \frac{\partial}{\partial \phi} + \hat{r} \frac{\partial}{\partial r}. \quad (24.4)$$

24.1.3 Traditional approximation

The *traditional approximation* comprises three approximations that come as a package.

Coriolis acceleration

The traditional approximation sets to zero the Coriolis terms in the horizontal momentum equations involving the vertical velocity. We are thus concerned only with the local vertical component of the earth's angular rotation vector (see discussion in Section 11.10.7)

$$\boldsymbol{\Omega} = \Omega \hat{\mathbf{Z}} = \Omega (\hat{\phi} \cos \phi + \hat{r} \sin \phi) \rightarrow \Omega \sin \phi \hat{r} = \mathbf{f}/2, \quad (24.5)$$

where

$$\mathbf{f} = (2 \Omega \sin \phi) \hat{r} \quad (24.6)$$

is the Coriolis parameter and $\hat{\mathbf{Z}}$ is the spherical earth unit vector pointing out of the north pole (Figure 9.1).²

Metric terms

The traditional approximation also drops the metric terms, uw/r and vw/r , associated with the vertical velocity as they appear in the horizontal momentum equations (21.19) and (21.20). These terms are generally smaller than the other terms since w is much smaller than the horizontal velocity for large-scale geophysical fluid flow.

Self consistency

The shallow fluid approximation and both parts of the traditional approximation must be taken together in order to maintain a consistent energy and angular momentum conservation principle for the resulting equations. As shown in Exercise 24.1, taking one but not the other leads to an inconsistent set of equations

24.1.4 Summary of the hydrostatic primitive equations

The above approximations lead to the primitive equations written in spherical coordinates

$$\frac{Du}{Dt} - \frac{uv \tan \phi}{R_e} - fv = -\frac{1}{\rho R_e \cos \phi} \frac{\partial p}{\partial \lambda} + F^\lambda \quad (24.7)$$

$$\frac{Dv}{Dt} + \frac{u^2 \tan \phi}{R_e} + fu = -\frac{1}{\rho R_e} \frac{\partial p}{\partial \phi} + F^\phi \quad (24.8)$$

$$\frac{\partial p}{\partial z} = -g \rho, \quad (24.9)$$

²We use the capital $\hat{\mathbf{Z}}$ to distinguish this north pole unit vector from the local $\hat{\mathbf{z}} = \hat{r}$ unit vector pointing vertical relative to a tangent plane discussed in Section 21.3.4.

where the gradient operator is given by equation (24.4). We can write these equations in the vector form

$$\rho \frac{D\mathbf{u}}{Dt} + (f + u \tan \phi / R_e) \hat{\mathbf{z}} \times \rho \mathbf{u} = -\rho \nabla \Phi - \nabla p + \rho \mathbf{F}, \quad (24.10)$$

where

$$\mathbf{F} = \hat{\boldsymbol{\lambda}} F^\lambda + \hat{\boldsymbol{\phi}} F^\phi \quad (24.11)$$

is the horizontal friction acceleration, and the vertical component of equation (24.10) is the hydrostatic balance. Furthermore, the material time derivative in this equation signifies the relative acceleration

$$\frac{D\mathbf{u}}{Dt} = \hat{\boldsymbol{\lambda}} \frac{Du}{Dt} + \hat{\boldsymbol{\phi}} \frac{Dv}{Dt}. \quad (24.12)$$

24.1.5 Flux-form mechanical energy budget

For the approximate hydrostatic fluid, the kinetic energy is dominated by the horizontal motions. Indeed, as we now show, the proper form of the kinetic energy is precisely that contained just in the horizontal motions. We do so by taking the scalar product of the horizontal velocity with the momentum equation (24.10) to render

$$\rho \frac{D\mathcal{K}^{\text{hyd}}}{Dt} = -\rho \mathbf{u} \cdot \nabla \Phi - \mathbf{u} \cdot \nabla p + \rho \mathbf{u} \cdot \mathbf{F}, \quad (24.13)$$

where we introduced the hydrostatic kinetic energy per mass

$$\mathcal{K}^{\text{hyd}} = \mathbf{u} \cdot \mathbf{u} / 2. \quad (24.14)$$

Making use of the hydrostatic balance in the presence of a simple geopotential, $\Phi = gz$ (so that $\mathbf{u} \cdot \nabla \Phi = 0$), leads to

$$\rho \frac{D\mathcal{K}^{\text{hyd}}}{Dt} = -(\mathbf{v} \cdot \nabla p - w \partial_z p) + \rho \mathbf{u} \cdot \mathbf{F} \quad (24.15a)$$

$$= -\nabla \cdot (\mathbf{v} p) + p \nabla \cdot \mathbf{v} - w g \rho + \rho \mathbf{u} \cdot \mathbf{F}, \quad (24.15b)$$

which leads to the Eulerian flux-form conservation equation for kinetic energy

$$\partial_t(\rho \mathcal{K}^{\text{hyd}}) + \nabla \cdot [\mathbf{v} (\rho \mathcal{K}^{\text{hyd}} + p)] = p \nabla \cdot \mathbf{v} - \rho g w + \rho \mathbf{u} \cdot \mathbf{F}. \quad (24.16)$$

Furthermore, $\Phi = gz$ means that

$$\rho D\Phi/Dt = \partial_t(\rho \Phi) + \nabla \cdot (\rho \mathbf{v} \Phi) = \rho g w, \quad (24.17)$$

in which case the flux-form equation for the mechanical energy per mass, \mathcal{M}^{hyd} , is given by

$$\partial_t(\rho \mathcal{M}^{\text{hyd}}) + \nabla \cdot [\rho \mathbf{v} (\mathcal{M}^{\text{hyd}} + p/\rho)] = p \nabla \cdot \mathbf{v} + \rho \mathbf{u} \cdot \mathbf{F}, \quad (24.18)$$

where

$$\mathcal{M}^{\text{hyd}} = \mathcal{K}^{\text{hyd}} + \Phi = \mathbf{u} \cdot \mathbf{u} / 2 + g z. \quad (24.19)$$

Equation (24.18) compares to the non-hydrostatic mechanical energy equation (23.40). The key difference is that the kinetic energy per mass is here just given by the horizontal flow (24.14). Additionally, the friction vector for the hydrostatic flow is horizontal. Otherwise, the physical interpretation of the mechanical energy budget accords with that for the non-hydrostatic fluid given in Section 23.3.3.

24.1.6 Depth integrated mechanical energy budget

We here extend the analysis from Section 24.1.5 to derive the depth integrated mechanical energy budget for the hydrostatic primitive equations. The kinetic energy per area contained in the horizontal flow as integrated over a column is given by

$$\int_{\eta_b}^{\eta} \rho \mathcal{K}^{\text{hyd}} dz = \frac{1}{2} \int_{\eta_b}^{\eta} \rho \mathbf{u} \cdot \mathbf{u} dz. \quad (24.20)$$

Leibniz's rule leads to the time tendency

$$\frac{d}{dt} \int_{\eta_b}^{\eta} \rho \mathcal{K}^{\text{hyd}} dz = \partial_t \eta [\rho \mathcal{K}^{\text{hyd}}]_{z=\eta} + \int_{\eta_b}^{\eta} \partial_t (\rho \mathcal{K}^{\text{hyd}}) dz. \quad (24.21)$$

Making use of the kinetic energy equation (24.16) as well as Leibniz's rule gives the budget

$$\begin{aligned} \frac{d}{dt} \int_{\eta_b}^{\eta} \rho \mathcal{K}^{\text{hyd}} dz &= [\rho \mathcal{K}^{\text{hyd}} + p_a]_{z=\eta} (\partial_t \eta - w + \mathbf{u} \cdot \nabla \eta)_{z=\eta} + [\rho \mathcal{K}^{\text{hyd}} + p_b]_{z=\eta_b} (w - \mathbf{u} \cdot \nabla \eta_b)_{z=\eta_b} \\ &\quad - \nabla_z \cdot \int_{\eta_b}^{\eta} (\rho \mathbf{u} \mathcal{K}^{\text{hyd}} + \mathbf{u} p) dz + \int_{\eta_b}^{\eta} (p \nabla \cdot \mathbf{v} - \rho g w + \rho \mathbf{u} \cdot \mathbf{F}) dz. \end{aligned} \quad (24.22)$$

The bottom kinematic boundary condition (16.41) and surface boundary condition (16.79) then give the budget

$$\begin{aligned} \frac{d}{dt} \int_{\eta_b}^{\eta} \rho \mathcal{K}^{\text{hyd}} dz &= \\ Q_m [\mathcal{K}^{\text{hyd}} + p_a/\rho]_{z=\eta} - \nabla_z \cdot \int_{\eta_b}^{\eta} (\rho \mathbf{u} \mathcal{K}^{\text{hyd}} + \mathbf{u} p) dz + \int_{\eta_b}^{\eta} (p \nabla \cdot \mathbf{v} - \rho g w + \rho \mathbf{u} \cdot \mathbf{F}) dz. \end{aligned} \quad (24.23)$$

The first term on the right hand side arises from the mass transport across the ocean surface, along with the applied surface pressure. The second term is the convergence of the depth integrated flux of kinetic energy plus pressure. The final term is the depth integral of the buoyancy conversion term plus frictional work. Similar manipulations starting from the flux-form mechanical energy budget (24.18) lead to the depth integrated budget

$$\begin{aligned} \frac{d}{dt} \int_{\eta_b}^{\eta} \rho m^{\text{hyd}} dz &= \\ Q_m [m^{\text{hyd}} + p_a/\rho]_{z=\eta} - \nabla_z \cdot \int_{\eta_b}^{\eta} (\rho \mathbf{u} m^{\text{hyd}} + \mathbf{u} p) dz + \int_{\eta_b}^{\eta} (p \nabla \cdot \mathbf{v} + \rho \mathbf{u} \cdot \mathbf{F}) dz. \end{aligned} \quad (24.24)$$

24.1.7 Comments and further study

The primitive equations make use of the momentum equations, which contrasts to *non-primitive* equation methods that develop evolution equations for the vorticity and divergence. [Smagorinsky \(1963\)](#) was an early proponent of the hydrostatic primitive equations for use in studying the large-scale ocean and atmospheric circulation. These equations form the basis for many general circulation models of the atmosphere and ocean. However, it is notable that finer resolution simulations, that admit strong vertical motions, must make use of the non-hydrostatic equations. Non-hydrostatic simulations are particularly relevant when studying clouds in the atmosphere and fine-scale mixing in the ocean, with both of these processes involving nontrivial vertical accelerations that break the hydrostatic approximation. These models sometimes also time step

the momentum equations, and as such are referred to as *non-hydrostatic primitive equation* models.

24.2 Physics of approximate hydrostatic balanced flow

For a static fluid with identically zero net acceleration, the vertical pressure gradient precisely balances the weight of fluid in thus realizing exact hydrostatic balance. We discussed this static solution to the equations of motion in Sections 21.4 and 22.5. For a moving fluid with scales of motion that maintain a small vertical to horizontal aspect ratio, the presentation in this section reveals that the vertical pressure gradient and gravitational acceleration individually remain far larger than other accelerations acting on a fluid element. In this case, the vertical momentum equation, even for the moving fluid, remains approximately in hydrostatic balance column-by-column. We thus have a fluid state whereby each vertical fluid column is in hydrostatic balance, and yet there are horizontal pressure gradients that drive motion. In this section we study aspects of such approximately hydrostatic fluids.

For simplicity in this section we make use of Cartesian coordinates rather than the spherical coordinates used in Section 24.1.

24.2.1 Expressions for the hydrostatic pressure

Making the hydrostatic approximation in the vertical momentum equation leads to the local balance

$$\frac{\partial p}{\partial z} = -\rho g. \quad (24.25)$$

Vertically integrating upward from a point within the ocean to the ocean surface leads to the hydrostatic pressure

$$p(x, y, z, t) = p_a(x, y, t) + g \int_z^\eta \rho(x, y, z', t) dz'. \quad (24.26)$$

In this equation we wrote $p(\eta) = p_a$ for the pressure at the ocean free surface, $z = \eta(x, y, t)$, arising from the weight of the overlying atmosphere or sea ice; i.e., this is the applied pressure acting on the top of the ocean fluid. A similar integration applies to the atmosphere

$$p(x, y, z, t) = g \int_z^{z_{\text{top}}} \rho(x, y, z', t) dz', \quad (24.27)$$

where $z = z_{\text{top}}$ is the top of the atmosphere, sometimes approximated by $z_{\text{top}} = \infty$. For both the ocean and the atmosphere, we assume g remains a constant over the vertical extent of the fluid, which is a sensible approximation even for the top of the atmosphere.

In both the ocean and atmosphere, the hydrostatic pressure at a vertical position, z , equals to the weight per horizontal area of matter above that position, with equations (24.26) and (24.27) providing explicit expressions in terms of *in situ* density and boundary contributions. These expressions offer a huge simplification for how we determine pressure, with the remainder of this section providing example implications.

24.2.2 Evolution of hydrostatic pressure

We expect that hydrostatic pressure evolves according to the convergence of mass onto the column of fluid above that point. The ocean hydrostatic pressure also changes due to time changes in the applied upper boundary pressure. Here we derive mathematical expressions that support these expectations, with Figure 24.1 providing a schematic.

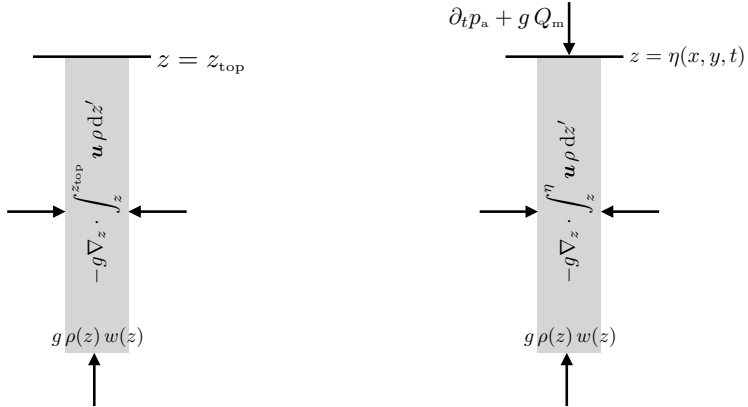


FIGURE 24.1: Evolution of hydrostatic pressure for a vertical position in the atmosphere (left panel) and ocean (right panel) according to equations (24.30) and (24.33a). Hydrostatic pressure at a vertical position, z , which here is the bottom of the fluid column, arises from the convergence of mass onto the column over the region above z . The ocean column also has a contribution from the time tendency of applied surface pressure plus the mass of coming across the top boundary. For the atmosphere as assume the top boundary is at $z_{\text{top}} = \infty$ and so there is no mass coming across that boundary.

Hydrostatic pressure in the atmosphere

A time derivative of the atmospheric hydrostatic pressure expression (24.27) renders

$$\partial_t p = g \int_z^{z_{\text{top}}} \partial_t \rho(x, y, z', t) dz'. \quad (24.28)$$

Note the absence of a time derivative on z_{top} . We ensure this time derivative is not relevant by setting z_{top} to a constant value well above anything of physical relevance; e.g., $z_{\text{top}} \approx \infty$. Now insert the mass continuity equation (16.6) and make further use of Leibniz's rule to write

$$\partial_t p = -g \int_z^{z_{\text{top}}} \nabla \cdot (\mathbf{v} \rho) dz' \quad (24.29a)$$

$$= g \rho(z) w(z) - g \int_z^{z_{\text{top}}} \nabla_z \cdot (\mathbf{u} \rho) dz', \quad (24.29b)$$

where we set $w(z_{\text{top}}) \rho(z_{\text{top}}) = 0$. The first term on the right hand side arises from the vertical mass flux into the fluid column from below. The second term arises from the horizontal convergence of mass as integrated over the column above the position, z . If the vertical position of the bottom limit on the integral is independent of horizontal position, then we can pull the horizontal divergence operator outside of the integral to render

$$\partial_t p = g \rho(z) w(z) - g \nabla_z \cdot \int_z^{z_{\text{top}}} \mathbf{u} \rho dz'. \quad (24.30)$$

In Exercise 24.3 we derive an expression for the bottom pressure, $p(x, y, z = \eta_b(x, y, t))$, where we must use Leibnitz's rule to pull the horizontal derivative outside of the integral.

Hydrostatic pressure in the ocean

The derivation for the ocean requires some more work since the ocean free surface is a permeable space and time dependent function. A time derivative of the ocean pressure expression (24.26)

renders

$$\partial_t p = \partial_t p_a + g \rho(\eta) \partial_t \eta + g \int_z^\eta \partial_t \rho(x, y, z', t) dz', \quad (24.31)$$

where we made use of Leibniz's rule to take the time derivative of the upper limit at $z = \eta(x, y, t)$, and with the shorthand $\rho(\eta) = \rho(x, y, z = \eta, t)$. Now insert the mass continuity equation (16.6) and make further use of Leibniz's rule to write

$$\partial_t(p - p_a) - g \rho(\eta) \partial_t \eta = g \int_z^\eta \partial_t \rho(x, y, z', t) dz' \quad (24.32a)$$

$$= -g \int_z^\eta \nabla \cdot (\mathbf{v} \rho) dz' \quad (24.32b)$$

$$= -g [\rho(\eta) w(\eta) - \rho(z) w(z)] - g \int_z^\eta \nabla_z \cdot (\mathbf{u} \rho) dz' \quad (24.32c)$$

$$= g \rho(z) w(z) + g [(-w + \mathbf{u} \cdot \nabla \eta) \rho]_{z=\eta} - g \nabla_z \cdot \int_z^\eta \mathbf{u} \rho dz' \quad (24.32d)$$

$$= g \rho(z) w(z) + g (Q_m - \rho(\eta) \partial_t \eta) - g \nabla_z \cdot \int_z^\eta \mathbf{u} \rho dz', \quad (24.32e)$$

where the last step made use of the kinematic boundary condition (16.79) for the ocean free surface, with Q_m the mass flux entering the ocean across the free surface. Rearrangement, and cancellation of the $\rho(\eta) \partial_t \eta$ term appearing on both sides, leads to

$$\partial_t p = \partial_t p_a + g \rho(z) w(z) + g Q_m - g \nabla_z \cdot \int_z^\eta \mathbf{u} \rho dz'. \quad (24.33a)$$

The first term on the right hand side arises from time fluctuations of the applied pressure at $z = \eta$. The second and third terms measure the vertical convergence of mass onto the column of fluid sitting above the vertical position, with $\rho(z) w(z)$ the mass flux entering the column from below and Q_m the mass flux entering from across the free surface. The final term arises from the vertically integrated horizontal mass transport converging onto the column above the position of interest.

24.2.3 Heuristic scaling

We here present a scale analysis to justify the hydrostatic approximation. This analysis serves to introduce a common method used in fluid mechanics to identify those processes that may be dominant for a particular flow regime. In particular, the flow regime of interest here occurs with a small vertical to horizontal aspect ratio

$$\alpha_{\text{aspect}} \equiv \frac{H}{L} \ll 1, \quad (24.34)$$

with H a typical length scale for vertical motion and L the horizontal length scale. This regime is fundamental to the large-scale circulation of the ocean and atmosphere. As the hydrostatic approximation is concerned with the force balances in a fluid column, it is sufficient to ignore rotation when performing a scale analysis.

Consider the vertical momentum equation (21.39) from the tangent plane and traditional

approximations (Section 21.3.4), along with the associated scales for the various terms

$$\frac{Dw}{Dt} = -\frac{1}{\rho} \frac{\partial p}{\partial z} - g \quad (24.35a)$$

$$\frac{W}{T} + \frac{UW}{L} + \frac{WW}{H} = -\frac{1}{\rho} \frac{\partial p}{\partial z} - g. \quad (24.35b)$$

In the second equation we introduced the following scales for the terms appearing on the left hand side of the first equation.

- L is the horizontal scale of the motion.
- H is the vertical scale of the motion.
- W is the vertical velocity scale.
- U is the horizontal velocity scale. For this analysis we do not distinguish between the zonal and meridional velocity scales, writing U for both. This assumption is not always valid, such as when scaling for jet stream or equatorial flows, both of which have larger zonal speeds than meridional.
- T is the time scale of the motion. We assume that the time scale is determined by horizontal advection³ so that $T \sim L/U$.

To get a sense for the numbers, consider large-scale atmospheric flows with $W = 10^{-2}$ m s⁻¹, $L = 10^5$ m, $H = 10^3$ m, $U = 10$ m s⁻¹. These numbers lead to $T = L/U = 10^4$ s and to the values for the vertical momentum equation

$$10^{-6} \text{ m s}^{-2} \sim -\frac{1}{\rho} \frac{\partial p}{\partial z} - g. \quad (24.36)$$

With $g \sim 10$ m s⁻², the only term that can balance the gravitational acceleration is the vertical pressure gradient. A similar analysis holds for large-scale ocean flows where we set $W = 10^{-3}$ m s⁻¹, $L = 10^3$ m, $H = 10^1$ m, $U = 10^{-1}$ m s⁻¹. These numbers lead to $T = L/U = 10^4$ s and to

$$10^{-7} \text{ m s}^{-2} \sim -\frac{1}{\rho} \frac{\partial p}{\partial z} - g. \quad (24.37)$$

In either case, large scale motion maintains an approximate hydrostatic balance whereby $\partial p/\partial z = -\rho g$.

We offer a more formal scale analysis in Section 26.2, making use of the oceanic Boussinesq equations derived in Chapter 26. For the remainder of this section we explore certain properties of a fluid maintaining an approximate hydrostatic balance.

24.2.4 Removal of a dynamically irrelevant background state

The previous analysis pointed to the dominance of the hydrostatic balance in the vertical momentum equation for large scale motions. However, is that analysis sufficient to understand what causes motion? To help answer that question, consider a density field that is decomposed into a constant, ρ_0 , plus a deviation

$$\rho(\mathbf{x}, t) = \rho_0 + \delta\rho(\mathbf{x}, t), \quad (24.38)$$

³This assumption for time scale is not always appropriate, such as for studies of waves where we may instead consider time scales according to a wave speed and wave length.

with a corresponding decomposition of the pressure field

$$p(\mathbf{x}, t) = p_0(z) + p'(\mathbf{x}, t) \quad \text{with} \quad \frac{dp_0}{dz} = -\rho_0 g. \quad (24.39)$$

That is, the pressure is decomposed into a background *static pressure* field that is just a function of z , plus a deviation from the background pressure. In this case, the non-rotating vertical momentum equation takes the form

$$\rho \frac{Dw}{Dt} = -\frac{\partial p'}{\partial z} - \left[\frac{dp_0}{dz} + \rho_0 g \right] = -\frac{\partial p'}{\partial z}. \quad (24.40)$$

We thus see that the exact hydrostatically balanced background pressure, $p_0(z)$, has no dynamical implications. Correspondingly, to garner a more relevant scaling for the hydrostatic balance it is appropriate to ask whether the dynamically active pressure, p' , is approximately hydrostatic.

For flows with small aspect ratios, the vertical momentum equation remains approximately hydrostatic even when removing the dynamically inactive background pressure field. So our intuition about hydrostatic dominance holds unchanged even for the dynamical pressure. The formal justification of this approximation is nicely framed within the Boussinesq equations of Chapter 26 since the pressure force in these equations exposes just the dynamically active pressure. We thus postpone further discussion of hydrostatic scaling until Section 26.2.

24.2.5 Decomposing the horizontal pressure gradient

In contrast to an exact hydrostatic fluid, where there is no motion, there are generally horizontal pressure gradients in an approximate hydrostatic fluid, and these horizontal gradients drive horizontal motion. Such horizontal gradients in the hydrostatic pressure can arise from horizontal differences in the fluid mass density. We refer to such pressure gradients as *internal pressure gradients* since they arise from density gradients internal to the fluid. Horizontal pressure gradients can also arise from horizontal gradients in the total mass of a fluid column, with such pressure gradients referred to as *external pressure gradients*. In developing an understanding of the horizontal pressure gradients in an approximate hydrostatic fluid, it can be useful to examine the mathematical expressions for the pressure gradient. We do so in this section, considering the specific case of a column of ocean fluid.⁴

Starting from the top and integrating down

Recall equation (24.26), which expresses the hydrostatic pressure at a point within the ocean

$$p(x, y, z, t) = p_a(x, y, t) + g \int_z^\eta \rho(x, y, z', t) dz'. \quad (24.41)$$

In this equation, $p_a = p[x, y, z = \eta(x, y, t), t]$ is the pressure applied to the ocean free surface at $z = \eta(x, y, t)$ from any mass above the ocean, such as the atmosphere or cryosphere. In many idealized cases we assume the media above the ocean is massless, in which case $p_a = 0$. Nonetheless, we maintain $p_a \neq 0$ for generality. Now introduce the globally referenced Archimedean buoyancy (see Chapter 27) as defined by

$$b = -g(\rho - \rho_0)/\rho_0, \quad (24.42)$$

⁴Note that some authors refer to *baroclinic* and *barotropic* pressure gradients rather than the *internal* and *external* used here.

in which case the hydrostatic pressure is

$$p = -g \rho_0 z + g \rho_0 [\eta + p_a/(g \rho_0)] - \rho_0 \int_z^\eta b dz'. \quad (24.43)$$

The first term is a background pressure that increases moving downward. However, this background pressure has no horizontal dependence and so it does not contribute to the horizontal pressure gradient. In contrast, the second and third terms have horizontal gradients and are thus sometimes referred to as the *dynamical pressure*. The second term arises from the free surface height plus the applied surface pressure. This term is uniformly felt throughout the fluid column since it has no vertical dependence. The free surface term is the product of the large number, $g \rho_0$, times a small free surface undulation, η . The third term arises from buoyancy within the fluid computed relative to the constant background density, ρ_0 , and this term is a function of vertical position. Furthermore, it is the vertical integral over a generally large depth range of the buoyancy. In this manner, the second and third terms can be of comparable magnitude.

The horizontal gradient of the hydrostatic pressure (24.43) is given by

$$\nabla_z p = \underbrace{\nabla_z p_a + g \rho(\eta) \nabla_z \eta}_{\text{external contribution}} - \underbrace{\rho_0 \int_z^\eta \nabla_z b dz'}_{\text{internal contribution}} = \underbrace{\nabla_z p_a + g \rho(\eta) \nabla_z \eta}_{\text{external contribution}} + \underbrace{g \int_z^\eta \nabla_z \rho dz'}_{\text{internal contribution}}. \quad (24.44)$$

The internal contribution to the pressure gradient arises from horizontal gradients in Archimedean buoyancy that are integrated vertically over the region above the point of interest. The external contribution acts throughout the vertical fluid column since it is only a function of horizontal position and time. Every point within the fluid column instantly feels this term whenever there is a gradient in the applied surface pressure, the surface height, or the surface buoyancy, with $\rho_0[g - b(\eta)] = g \rho(\eta)$.

Note that the external contributions in equation (24.44) are all functions of horizontal position and time, so there is no z dependence to hold fixed when computing ∇_z on these terms. In contrast, the buoyancy is a function $b(x, y, z, t)$, so that it is important to specify that the buoyancy gradient is indeed computed with fixed z .

Starting from the bottom and integrating up

We can invert the above formulation by introducing the bottom pressure

$$p_b = p_a + g \int_{\eta_b}^\eta \rho dz, \quad (24.45)$$

in which case

$$p = p_b - g \rho_0 (z - \eta_b) + \rho_0 \int_{\eta_b}^z b dz', \quad (24.46)$$

so that the corresponding expression for the horizontal hydrostatic pressure gradient is

$$\nabla_z p = \underbrace{\nabla_z p_b + g \rho(\eta_b) \nabla_z \eta_b}_{\text{external contribution}} + \underbrace{\rho_0 \int_{\eta_b}^z \nabla_z b dz'}_{\text{internal contribution}}. \quad (24.47)$$

The bottom pressure contribution is dominated by gradients in the bottom topography so that it can be useful to write

$$\nabla_z p_b = -\rho_0 g \nabla_z \eta_b + \nabla_z p'_b, \quad (24.48)$$

in which case the external contribution takes the form

$$\nabla_z p = \underbrace{\nabla_z p'_b - \rho_0 b(\eta_b) \nabla_z \eta_b}_{\text{external contribution}} + \underbrace{\rho_0 \int_{\eta_b}^z \nabla_z b \, dz'}_{\text{internal contribution}}. \quad (24.49)$$

As for the expression (24.44), we have decomposed the horizontal pressure gradient into an external and internal contribution. Here, the external contributions arise from gradients in the bottom pressure, which measures the mass per area of fluid within the column, plus gradients in the bottom topography as weighted by the difference between the gravitational acceleration and bottom buoyancy, with $\rho_0[g - b(\eta_b)] = g\rho(\eta_b)$. The internal term arises from gradients in the buoyancy as integrated below the depth of interest.

24.2.6 Horizontal hydrostatic pressure gradient in a mass conserving fluid

We here consider a specific example that is emblematic of how one determines the sign for horizontal gradients in a mass conserving fluid that maintains an approximate hydrostatic balance, and thus to determine the direction for the pressure force. In so doing, we further our understanding of the pressure field driving motion in a hydrostatic fluid. The example is posed for a bounded column of fluid, as in the ocean, but analogous considerations hold for the atmosphere where the upper boundary is the top of the atmosphere (i.e., effectively unbounded). Furthermore, the fluid is assumed to be compressible so that fluid elements conserve their mass. In Section 26.2.5 we reconsider this example for a volume conserving oceanic Boussinesq fluid.

Two columns with equal mass yet different densities

Consider two adjacent columns of seawater with equal mass but with distinct density; assume the density in each column is constant throughout the respective columns; and assume the atmospheric pressure is equal above the two water columns. Figure 24.2 offers a schematic, where we make the additional assumption that the two columns sit on a flat bottom. We can imagine setting up this configuration by starting with uniform density water, then warming the water in column B more than column A while maintaining constant mass in the two columns. This process sets up a horizontal density gradient with an associated horizontal gradient in the hydrostatic pressure. Furthermore, the less dense water in column B occupies more volume so that its free surface sits higher

$$\rho_B < \rho_A \implies \eta_B > \eta_A. \quad (24.50)$$

What is the sign of the horizontal hydrostatic pressure gradient? As we show in the following, column B (the low density column) has larger hydrostatic pressure than column A (the high density column) for every point in the column, except at the bottom where the two bottom pressures are identical since the two columns have equal mass.

Computing pressure starting from the equal bottom pressures

Since the two columns have equal mass and equal cross-sectional area, the hydrostatic pressures (weight per unit area) at the bottom of the two columns are equal and given by

$$p_{\text{bot}} = g \rho_A (\eta_A - \eta_b) = g \rho_B (\eta_B - \eta_b), \quad (24.51)$$

where $z = \eta_b(x, y)$ is the vertical position at the bottom, $z = \eta_A(x, y, t)$ is the top of column A, and $z = \eta_B(x, y, t)$ top of column B. Since the bottom pressures are identical, there is no horizontal pressure gradient at the bottom so that all pressure gradients exist above the bottom.

The hydrostatic pressure at an arbitrary position within column A is given by

$$p_A(z) = g \rho_A (\eta_A - z) = p_{\text{bot}} - g \rho_A (-\eta_b + z). \quad (24.52)$$

The second equality arose by substituting the bottom pressure from equation (24.51) to eliminate the surface height η_A . Likewise, the pressure in column B is given by

$$p_B(z) = g \rho_B (\eta_B - z) = p_{\text{bot}} - g \rho_B (-\eta_b + z). \quad (24.53)$$

We can now take the difference between the two hydrostatic pressures to find

$$p_B(z) - p_A(z) = g (-\eta_b + z) (\rho_A - \rho_B) > 0. \quad (24.54)$$

Since $\rho_A > \rho_B$ and $z \geq \eta_b$ we see that at any point above the bottom, the hydrostatic pressure in column B (the lighter column) is greater than that in column A (the denser column). This horizontal difference in the hydrostatic pressure renders a force pointing from column B to column A . Vertically integrating this pressure difference over the thickness of column A leads to the net force per horizontal length

$$F_{\text{pressure } B \text{ to } A} = \int_{\eta_b}^{\eta_A} [p_B(z) - p_A(z)] dz = (g/2) (\rho_A - \rho_B) (\eta_A - \eta_b)^2 > 0. \quad (24.55)$$

Inferring pressure gradients starting from the top

Another way to understand why the pressure force points from column B to column A is to note that at the top of both columns the pressures are the same (and equal to the uniform atmospheric pressure). However, since column B sits higher than column A , as we move down from $z = \eta_B$ the pressure increases in column B immediately, whereas the pressure in column A remains at the atmospheric pressure until entering the water column at $z = \eta_A < \eta_B$. So it is clear that the pressure in column B is greater than A starting from the surface and moving down. Since the two bottom pressures are equal, then one can infer the pressure isolines as drawn in Figure 24.2.

24.2.7 Ocean dynamic topography

There are occasions in oceanography where it is useful to study the thickness of a layer bounded by isobars. For example, it is often assumed in dynamical oceanography that there is a pressure at which baroclinic currents vanish (*level of no motion*), with the reduced gravity model of Section 32.3 studying the associated dynamical implications.⁵ We are thus led to consider the thickness of fluid extending from the ocean free surface to a chosen pressure level in the ocean interior as given by

$$D(p) = \eta - z(p). \quad (24.56)$$

Assuming a hydrostatic balance for each fluid column allows us to relate this expression to the vertical integral between two pressure surfaces of the specific volume, ρ^{-1}

$$D(p) = \int_{z(p)}^{\eta} dz = g^{-1} \int_{p_a}^p \frac{dp'}{\rho}, \quad (24.57)$$

where the second step used the hydrostatic balance and absorbed a minus sign by swapping integral limits. We refer to the thickness $D(p)$ as the *dynamic topography* with respect to a

⁵Baroclinic refers to a fluid state with pressure and density surfaces distinct, whereas these surfaces are parallel in a *barotropic* fluid state. We discuss *baroclinicity* in the context of vorticity in Section 37.4.

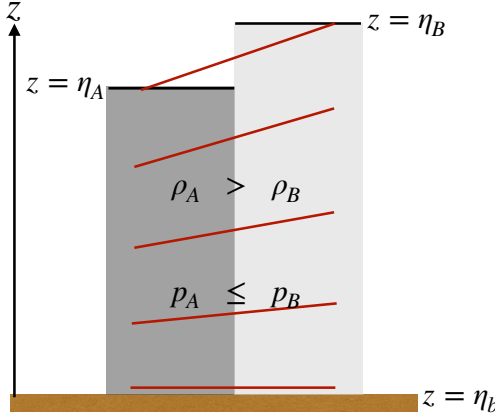


FIGURE 24.2: Two seawater columns on a flat bottom with equal mass but different densities with $\rho_A > \rho_B$. We assume the atmosphere above the columns has the same pressure over both columns, thus offering zero horizontal pressure force. Furthermore, the horizontal cross-sectional area of the two columns are the same so that the less dense water in column B has more volume and thus a greater thickness: $\eta_B > \eta_A$. Since the column masses are the same, the hydrostatic pressures (weight per horizontal area) at the bottom of the two columns are equal: $p_A(z = \eta_b) = p_B(z = \eta_b) = p_{\text{bot}}$. In oceanographic parlance, the bottom offers a “level of no motion” from which to reference the pressure field. At any position z above the bottom, equation (24.54) shows that the hydrostatic pressure in column B is greater than A : $p_B(z) - p_A(z) = g(-\eta_b + z)(\rho_A - \rho_B) > 0$. The horizontal gradient in hydrostatic pressure thus points from column B towards column A . The red lines show lines of constant pressure (isobars), which are horizontal next to the bottom but which slope upward to the right moving towards the surface. This configuration provides salient points about hydrostatic pressure relevant for the slightly more complex reduced gravity example in Figure 32.5. Also, it is useful to compare this schematic to Figure 28.4, which discusses the depth dependence of the horizontal gradient in hydrostatic pressure as per $\partial(\nabla_z p)/\partial z = -g \nabla_z \rho$.

reference pressure p . Note that it is sometimes also called the *steric sea level*. Evolution of the dynamic topography arises from changes in the pressure applied to the free surface as well as changes in the specific volume

$$g \frac{\partial D(p)}{\partial t} = -\frac{1}{\rho(\eta)} \frac{\partial p_a}{\partial t} + \int_{p_a}^p \frac{\partial \rho^{-1}}{\partial t} dp. \quad (24.58)$$

Note that the time derivative acts on the specific volume when computed on surfaces of constant pressure. If the depth $z(p)$ of the constant pressure surface is static, then the evolution of layer thickness, $D(p)$, is identical to the sea surface, η . In general, there is no such static pressure level, thus making the time tendencies differ, though certain situations warrant this approximation.

24.2.8 Surfaces of atmospheric geopotential height and pressure

In Section 20.4.10 we computed the geopotential height within an exact hydrostatic and ideal gas atmosphere. We here apply those results to the case of approximate hydrostatic and ideal gas columns, making use of equation (20.82) for the difference in geopotential height between two isobars

$$Z_2 - Z_1 = -(R^{\text{atm}} \langle T \rangle / g) \ln(p_2/p_1). \quad (24.59)$$

In this equation, $\langle T \rangle$ is the mean temperature within the column as computed according equation (20.80), and R^{atm} is the specific gas constant for air given by equation (20.51). The geopotential thickness of a column is positive when the isobars have $p_2 < p_1$; i.e., p_2 is higher in the atmosphere than p_1 . Furthermore, the geopotential thickness of a column is directly proportional to the column mean temperature so that a warmer column is thicker. This result is expected since for a

given mass of air, a warmer column is less dense and so isobars are higher over warmer hydrostatic air columns than cooler columns. Correspondingly, when moving horizontally along a constant geopotential surface, we encounter higher pressure when moving into a region of warmer air. This situation is entirely analogous to that in Figure 24.2 when studying the horizontal pressure difference between two hydrostatic and equal mass columns of seawater.

24.2.9 Concerning vertical motion

Unbalanced vertical accelerations still exist in an approximate hydrostatic fluid. Yet these vertical accelerations are not needed for the prognostic equations since the vertical momentum equation reduces to a local hydrostatic balance. Hence, rather than compute vertical motion prognostically, vertical motion in an approximate hydrostatic fluid is diagnosed through constraints on the fluid motion.

For example, an important constraint on the large-scale ocean circulation arises from vorticity and potential vorticity conservation, which are topics considered in Part VII of this book. Mass continuity discussed in Section 26.1.4 provides another constraint. In particular, horizontal velocity divergence in an incompressible flow is balanced by vertical velocity convergence as per equation (26.17). The vertical pressure forces required to produce the vertical motion are those precisely needed to maintain volume continuity. In a hydrostatic fluid, we do not directly compute these forces for the purpose of prognosing vertical accelerations. Rather, the vertical acceleration is inferred through kinematic constraints. The associated forces, if desired, can be diagnosed given the velocity and the accelerations.

24.2.10 Further study

Section 2.7.4 in [Vallis \(2017\)](#) provides examples of scales over which the hydrostatic relation remains a useful approximation in geophysical fluids. Our discussion of the hydrostatic pressure in Section 24.2.6 is motivated by similar considerations presented in Chapter 2 of the oceanography text from [Tomczak and Godfrey \(1994\)](#). Further discussion of dynamic topography is given in Appendix B.4 of [Griffies et al. \(2014\)](#) as well as in [Tomczak and Godfrey \(1994\)](#). Finally, this [8-minute video](#) from Prof. Hogg offers an introduction to hydrostatic pressure.

24.3 Homogeneous fluid in a rotating tank

As an application of the ideas developed in this chapter and in earlier chapters, we develop the equations for a homogeneous fluid in a rotating tank such as occurs in laboratory studies of rotating fluids. One point of departure from planetary applications concerns the choice of vertical coordinate. Recall we introduced geopotential surfaces in Section 11.11.4, on which the effective gravitational force (sum of central gravity plus planetary centrifugal) is constant. Correspondingly, we introduced geopotential coordinates in Section 11.12.3 to simplify the equations for planetary fluid dynamics. In contrast, for the rotating tank we do not make use of geopotential coordinates. Instead, we expose the centrifugal acceleration (due to rotation of the tank), which allows for a clear display of the parabolic shape for the free surface when the fluid is in solid-body motion.

24.3.1 What about the planet's rotation?

Do we need to worry about the planet's rotation? To answer this question, consider a typical record player with an angular speed of 45 revolutions per minute

$$\Omega_{\text{record}} = 0.75 \text{ s}^{-1}. \quad (24.60)$$

This angular speed is roughly 10^4 times faster than the earth's angular speed of $7.29 \times 10^{-5} \text{ s}^{-1}$ (equation (11.1)). For a tank rotating at a rate on the same order as a record player, we are justified ignoring the rotating earth in comparison to the rotating tank. That is, we can safely ignore planetary Coriolis and planetary centrifugal accelerations, allowing us to instead focus on non-inertial accelerations just from the rotating tank.

24.3.2 Formulating the equations of motion

In an inertial reference frame, a fluid element feels the gravitational force, pressure force, and friction, thus leading to the Cartesian coordinate equations of motion

$$\frac{Du_I}{Dt} = -\frac{1}{\rho} \frac{\partial p}{\partial x} + F^x \quad (24.61)$$

$$\frac{Dv_I}{Dt} = -\frac{1}{\rho} \frac{\partial p}{\partial y} + F^y \quad (24.62)$$

$$\frac{Dw_I}{Dt} = -\frac{1}{\rho} \frac{\partial p}{\partial z} - g_e + F^z, \quad (24.63)$$

where \mathbf{v}_I is the inertial velocity, ρ is the constant density, and we orient the coordinates so that the z -axis extends vertically upward from the center of the tank and parallel to the gravity acceleration. Correspondingly, the rotation vector for the tank is

$$\boldsymbol{\Omega} = \Omega \hat{\mathbf{z}} = (f/2) \hat{\mathbf{z}}. \quad (24.64)$$

To derive the rotating frame equations, return to some of the kinematics from Chapter 11, in which we write the position of a fluid particle as

$$\mathbf{X}(t) = X \hat{\mathbf{x}} + Y \hat{\mathbf{y}} + Z \hat{\mathbf{z}}. \quad (24.65)$$

We assume that the Cartesian unit vectors are fixed in the rotating frame and thus move as a solid body with the rotating tank. The inertial velocity is thus given by

$$\frac{d\mathbf{X}}{dt} = \left[\frac{dX}{dt} \right] \hat{\mathbf{x}} + \left[\frac{dY}{dt} \right] \hat{\mathbf{y}} + \left[\frac{dZ}{dt} \right] \hat{\mathbf{z}} + \boldsymbol{\Omega} \times \mathbf{X}. \quad (24.66)$$

Correspondingly, the acceleration is given by

$$\frac{d^2\mathbf{X}}{dt^2} = \left[\frac{d^2X}{dt^2} \right] \hat{\mathbf{x}} + \left[\frac{d^2Y}{dt^2} \right] \hat{\mathbf{y}} + \left[\frac{d^2Z}{dt^2} \right] \hat{\mathbf{z}} + 2 \boldsymbol{\Omega} \times \mathbf{v} + \boldsymbol{\Omega} \times (\boldsymbol{\Omega} \times \mathbf{X}), \quad (24.67)$$

where we defined the rotating frame Cartesian velocity as

$$\mathbf{v} = \left[\frac{dX}{dt} \right] \hat{\mathbf{x}} + \left[\frac{dY}{dt} \right] \hat{\mathbf{y}} + \left[\frac{dZ}{dt} \right] \hat{\mathbf{z}}. \quad (24.68)$$

Setting the inertial acceleration equal to the inertial force per mass leads to the equations of

motion in the rotating frame

$$\frac{Du}{Dt} - 2\Omega v = -\frac{1}{\rho} \frac{\partial p}{\partial x} + \Omega^2 x + F^x \quad (24.69)$$

$$\frac{Dv}{Dt} + 2\Omega u = -\frac{1}{\rho} \frac{\partial p}{\partial y} + \Omega^2 y + F^y \quad (24.70)$$

$$\frac{Dw}{Dt} = -\frac{1}{\rho} \frac{\partial p}{\partial z} - g_e + F^z, \quad (24.71)$$

which take on the vector form

$$\frac{D\mathbf{v}}{Dt} + f \hat{\mathbf{z}} \times \mathbf{v} = -\nabla [p/\rho + g_e z - \Omega^2 (x^2 + y^2)/2] + \mathbf{F}. \quad (24.72)$$

As expected, we encounter both a Coriolis and centrifugal acceleration due to the rotation of the tank.

24.3.3 Solid-body rotation and parabolic free surface shape

Consider a fluid at rest in a non-rotating tank, and then start the tank rotating. As in our discussion of Couette flow in Section 22.8.2, viscous effects transfer motion from the outside tank wall (where a no-slip boundary condition makes the fluid move with the wall) into the interior of the fluid. Given sufficient time and a constant rotation rate, the fluid will move as a solid-body. As an application of the above equations of motion, we here determine the shape of the upper free surface for this solid-body motion, offering two related derivations. Note that when the fluid reaches solid-body motion, all strains vanish within the fluid so that frictional stresses vanish (see Section 22.8). Hence, the steady force balance is fully inviscid although the steady state required viscosity to reach it.

Component equations of motion

The velocity and acceleration in the rotating frame are zero when the fluid is in solid-body rotation. The vertical momentum equation (24.71) thus reduces to the approximate hydrostatic balance

$$\frac{\partial p}{\partial z} = -\rho g_e. \quad (24.73)$$

In general we do not have hydrostatic balance for motion in a tank that deviates from solid-body. However, when that motion is close to a solid-body rotation, then the fluid is in an approximate hydrostatic balance. As seen in Section 24.2, this situation corresponds to the large-scale ocean and atmosphere.

Hydrostatic balance with a constant density means that the pressure is a linear function of depth

$$p(x, y, z) = \rho g_e (\eta - z), \quad (24.74)$$

where $z = \eta(x, y)$ is the vertical position of the free surface. The horizontal momentum equations (24.69)-(24.70) reduce to a balance between the pressure gradient and centrifugal accelerations

$$\frac{\partial p}{\partial x} = \rho x \Omega^2 \quad \text{and} \quad \frac{\partial p}{\partial y} = \rho y \Omega^2. \quad (24.75)$$

Pressure thus increases when moving radially away from the center. Substituting in the pressure as given by the hydrostatic relation (24.74) leads to relations satisfied by the solid-body free

surface

$$g_e \frac{\partial \eta}{\partial x} = x \Omega^2 \quad \text{and} \quad g_e \frac{\partial \eta}{\partial y} = y \Omega^2. \quad (24.76)$$

Integration leads to the quadratic expression for the free surface

$$\eta = \eta(0) + \frac{\Omega^2 (x^2 + y^2)}{2 g_e}, \quad (24.77)$$

where $\eta(0)$ is the free surface at the center of the tank where $x = y = 0$. The solid-body rotating fluid thus has a quadratic free surface with the height of the surface increasing away from the center. Notice how the fluid density dropped out from the problem, so that this parabolic shape holds for any fluid in solid-body motion.

Vector force balance

A more telescopic means to determine the free surface shape is to set the forces to zero on the right hand side of the vector equation of motion (24.72) so that

$$p/\rho + g_e z - \Omega^2 (x^2 + y^2)/2 = p_0/\rho, \quad (24.78)$$

where p_0 is a constant pressure to be specified below. Furthermore, we set friction to zero since the fluid is in solid-body motion. Everywhere along the free surface, with $z = \eta$, the pressure equals to that applied to the free surface by the overlying media, $p = p_a$ (e.g., atmospheric pressure). Hence, setting $z = \eta$ in equation (24.78) and solving for η yields

$$\eta = \frac{p_0 - p_a}{\rho g_e} + \frac{\Omega^2 (x^2 + y^2)}{2 g_e}. \quad (24.79)$$

For simplicity, assume the applied pressure is spatially constant. Hence, setting p_0 according to the free surface at $x = y = 0$ brings the free surface to the parabolic form in equation (24.77)

$$\frac{p_0 - p_a}{\rho g_e} = \eta(0) \implies \eta = \eta(0) + \frac{\Omega^2 (x^2 + y^2)}{2 g_e}. \quad (24.80)$$

24.3.4 Further study

We study the angular momentum for the shallow water version of this system in Section 33.8. See section 6.6.4 of [Marshall and Plumb \(2008\)](#) for more discussion of laboratory rotating tank experiments.



24.4 Exercises

EXERCISE 24.1: PRIMITIVE EQUATIONS AND AXIAL ANGULAR MOMENTUM

The axial angular momentum of a fluid element satisfying the primitive equations is given by

$$L^z = (\rho \delta V) R_\perp (u + R_\perp \Omega) \equiv (\rho \delta V) l^z \quad (24.81)$$

where

$$R_\perp = R_e \cos \phi \quad (24.82)$$

is the distance from the polar rotation axis to a point on the sphere with radius Re , and

$$l^z = R_\perp (u + R_\perp \Omega) \quad (24.83)$$

is the angular momentum per unit mass.

- (a) Consider a constant mass fluid element in the absence of friction. Show that the primitive equation zonal momentum equation (24.7) implies that the material evolution of axial angular momentum per mass is given by

$$\frac{Dl^z}{Dt} = -\frac{1}{\rho} \frac{\partial p}{\partial \lambda}. \quad (24.84)$$

- (b) Assume the zonal pressure gradient vanishes. Move the fluid element vertically while maintaining a fixed latitude. What happens to the zonal momentum of this primitive equation fluid element? Hint: be sure to remain within the “world” of the primitive equations.
- (c) Give a very brief symmetry argument for why the axial angular momentum is materially conserved when $\partial p / \partial \lambda = 0$. Hint: recall the discussion of Noether’s Theorem in Section 12.2.1.
- (d) Consider the material evolution of primitive equation axial angular momentum per mass in the case where the zonal momentum equation retains the unapproximated form of the Coriolis acceleration. Discuss the resulting material evolution equation. Does this equation make sense based on the symmetry argument given in the previous part of this exercise?

EXERCISE 24.2: MASS BALANCE FOR A HYDROSTATIC OCEAN COLUMN

Equation (16.88) provides a kinematic expression for the column mass budget. Show that for a hydrostatic fluid the mass balance for a fluid column (equation (16.100)) takes the form

$$\partial_t(p_b - p_a) = -g \nabla \cdot \mathbf{U}^\rho + g Q_m, \quad (24.85)$$

where

$$\mathbf{U}^\rho = \int_{\eta_b}^{\eta} \mathbf{u} \rho dz \quad (24.86)$$

is the depth integrated horizontal mass transport,

$$p_b = p_a + g \int_{\eta_b}^{\eta} \rho dz \quad (24.87)$$

is the hydrostatic pressure at the ocean bottom, and $p_a(x, y, t)$ is the pressure applied to the ocean surface from the overlying atmosphere or sea ice.

EXERCISE 24.3: EVOLUTION OF ATMOSPHERIC BOTTOM HYDROSTATIC PRESSURE

In deriving equation (24.30) we assumed the lower limit on the integral to be a horizontal constant. However, when integrating over the full atmospheric column, the lower limit varies horizontally given that the earth boundary is not flat. Return to equation (24.29b) and derive the evolution equation for the bottom pressure

$$\partial_t p_{\text{bot}} = -g \nabla_z \cdot \mathbf{U}^\rho, \quad (24.88)$$

where

$$p_{\text{bot}}(x, y, t) = p[x, y, z = \eta_b(x, y), t] \quad (24.89)$$

is the atmospheric pressure at the solid earth at $z = \eta_b(x, y)$,

$$\mathbf{U}^\rho = \int_{\eta_b}^{z_{\text{top}}} \mathbf{u} \rho dz' \quad (24.90)$$

is the depth integrated horizontal mass transport, and z_{top} is the vertical position of the atmospheric top that is assumed to be independent of horizontal position.



Chapter 25

PRESSURE FORM STRESS

As introduced in our discussion of Cauchy's stress principle in Section 22.2, pressure form stress is the horizontal stress arising from pressure that acts on a sloped surface or interface. As a contact force per area, Newton's third law describes how form stress renders a transfer of pressure forces across interfaces, with pressure form stress affecting a vertical transfer of horizontal pressure forces. Hence, it provides an inviscid/reversible mechanism for the vertical transfer of horizontal momentum, thus complementing the vertical transfer associated with viscosity in the presence of tangential shear stresses (Section 22.8.2).

In this chapter we study pressure form stresses on the variety of interfaces encountered in geophysical fluids. We then develop two case studies to expose the role of pressure form stress in the force balances affecting motion of an ocean fluid column. The first case study is concerned with the evolution of vertically integrated horizontal linear momentum per mass. The second case study focuses on the axial angular momentum budget as a framework to study the dominant force balances in ocean channel flow and ocean gyre flow.

CHAPTER GUIDE

In this chapter we build from the study of stresses in Chapter 22, with an understanding of pressure form stress greatly enhancing our understanding of horizontal forces acting in geophysical fluids. The focus on horizontal forces in this chapter complements our studies in Chapter 27, whereby the net vertical acceleration from pressure and gravitational forces is repackaged into the buoyancy force.

25.1 Pressure form stresses at an interface	582
25.1.1 Concerning the sign of a form stress	583
25.1.2 Mathematical expression for form stress	583
25.1.3 Comments	585
25.2 Form stresses on the ocean boundaries	585
25.2.1 Zonally symmetric ridge	586
25.2.2 Form stress transfer between the fluid and its boundaries	586
25.2.3 Decomposing topographic form stress	588
25.3 Interfacial form stress	588
25.3.1 Interfacial form stresses transferred between layers	588
25.3.2 Zonally integrated interfacial form stress	590
25.3.3 Comments	591
25.4 Evolution of depth integrated horizontal momentum	591
25.4.1 Flux-form horizontal momentum equation	591
25.4.2 Leibniz's rule for the inertial and Coriolis accelerations	592
25.4.3 External and internal decomposition of the kinetic stress	592

25.4.4	Decomposing the depth integrated horizontal pressure gradient	593
25.4.5	Depth integrated momentum equation	595
25.4.6	Balances when $\nabla \cdot \mathbf{U}^P = 0$	595
25.5	Axial angular momentum budget for an ocean domain	596
25.5.1	Anticipating the budget	597
25.5.2	Axial angular momentum	597
25.5.3	Depth integrated budget	598
25.5.4	Atmospheric and topographic form stresses	598
25.5.5	Turbulent stresses at the surface and bottom	598
25.5.6	Summary budget for column integrated axial angular momentum .	599
25.5.7	Zonal domain topology/geometry and zonal integration	600
25.5.8	Steady domain integrated balance	601
25.5.9	Form stress versus dual form stress	602
25.5.10	Steady zonal and depth integrated budget	602
25.5.11	Southern Ocean balances	602
25.5.12	Topographic form stress and ocean gyres	603
25.5.13	Further study	604

25.1 Pressure form stresses at an interface

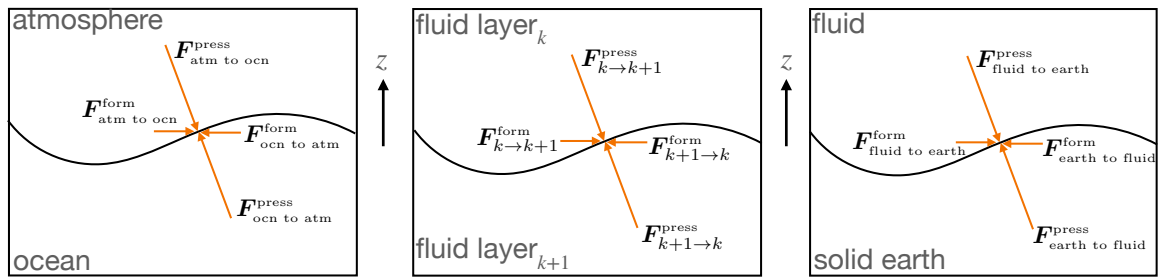


FIGURE 25.1: Illustrating the three interfaces of concern in geophysical fluid mechanics for the discussion of form stresses. Continuity of pressure at the interface, through Newton's third law, means that the form stress on one side of the interface is equal and opposite to that acting on the other side. Left panel: a curved atmosphere-ocean interface leads to an atmospheric form stress acting on the ocean, $\mathbf{F}_{\text{atm to ocn}}^{\text{form}}$, and its equal and opposite oceanic form stress acting on the atmosphere, $\mathbf{F}_{\text{ocn to atm}}^{\text{form}} = -\mathbf{F}_{\text{atm to ocn}}^{\text{form}}$. Middle panel: a curved interior ocean interface (e.g., a buoyancy surface) leads to an interfacial form stress acting on the lower layer, $\mathbf{F}_{k \rightarrow k+1}^{\text{form}}$, and its equal and opposite interfacial form stress acting on the upper layer, $\mathbf{F}_{k+1 \rightarrow k}^{\text{form}} = -\mathbf{F}_{k \rightarrow k+1}^{\text{form}}$. Right panel: a curved fluid-solid earth interface leads to a fluid form stress acting on the solid earth, $\mathbf{F}_{\text{fluid to earth}}^{\text{form}}$, and its equal and opposite oceanic form stress acting on the fluid, $\mathbf{F}_{\text{earth to fluid}}^{\text{form}} = -\mathbf{F}_{\text{fluid to earth}}^{\text{form}}$. The magnitude of the form stresses is a function of the pressure acting at the interface as well as the slope of the interface (steeper slopes lead to larger magnitude).

As depicted in Figure 25.1, there are three surfaces or interfaces across which we commonly study form stresses in geophysical fluids.

- **ATMOSPHERE-OCEAN FORM STRESS:** A form stress occurs at the air-sea interface. From the perspective of the ocean, the nonzero atmospheric pressure applied to the sea surface (the *sea level pressure*) provides a pressure acting on the sloped upper ocean free surface, thus rendering an *atmospheric form stress* acting on the ocean. Through *Newton's third law* (see Section 10.2.2), this form stress is met by the equal in magnitude but oppositely directed *ocean form stress* acting on the atmosphere.
- **INTERIOR FLUID INTERFACIAL FORM STRESS:** A form stress occurs on an internal interface within the fluid, and we study such *interfacial form stresses* in Section 25.3. Although the

interface is arbitrary, it is dynamically very interesting to study form stresses acting on buoyancy isosurfaces. The reason is that buoyancy interfaces are directly connected to the geostrophic motion studied in Chapter 28. In particular, in Section 28.6 we study form stresses associated with buoyancy interfaces found in geostrophic flows.

- FLUID-TOPOGRAPHY FORM STRESS: A form stress exists at a solid/fluid boundary, at which the ocean or atmosphere impart a pressure force on the solid earth. Through Newton's third law, the pressure force imparted by the fluid on the solid earth is met equally in magnitude but oppositely in direction by a force provided by the solid earth onto the fluid. The horizontal projection of this force per area acting from the earth on the fluid is the *topographic form stress* and it is considered in Section 25.2.

25.1.1 Concerning the sign of a form stress

As a vector, pressure form stress has a direction and a magnitude, with three examples depicted in Figure 25.1. Even so, keeping track of the direction can be confusing if it is unclear who is the giver of the form stress and who is the receiver. To help in understanding the sign, imagine pushing against a rigid wall: you exert a force on the wall in one direction whereas, through Newton's third law, the wall exerts an equal and opposite force on you. One simply must specify the origin of the force in order to determine its sign. For example, as illustrated in Figure 25.2, is one concerned with the force applied by the ocean bottom pressure onto the earth (liquid ocean is giver and solid earth is receiver), or instead with the force from the earth applied onto the ocean fluid (earth is giver and ocean is receiver)? These forces have equal magnitude but opposite direction. Knowing the direction requires knowing the force giver and/or the force receiver.

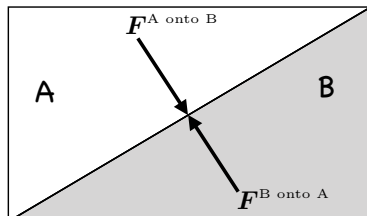


FIGURE 25.2: Contact forces, such as pressure, satisfy Newton's third law. Hence, the contact force at a point imparted by region A onto region B, $\mathbf{F}^A \text{ onto } B$, is equal and opposite to the force imparted by region B onto region A so that $\mathbf{F}^A \text{ onto } B = -\mathbf{F}^B \text{ onto } A$. In the case where A=fluid (ocean or atmosphere) and B=solid earth, we generally refer to the horizontal portion of $\mathbf{F}^{\text{earth}} \text{ onto } \text{fluid}$, per horizontal area, as the *topographic form stress*.

25.1.2 Mathematical expression for form stress

To expose the mathematics of form stress, consider a surface, \mathcal{S} , such as that shown in Figure 25.3. To develop a kinematic decomposition of the pressure force, we assume the surface has no vertical section, with this assumption commonly satisfied by surfaces of interest for geophysical flows.

Assuming the surface has no vertical sections allows us to write the vertical position of a point on the surface as¹

$$z = \eta(x, y, t). \quad (25.1)$$

¹See the geometry discussion in Chapter 6 for more on the maths of such surfaces. Also see the discussion of generalized vertical coordinates in Chapters 56 and 57.

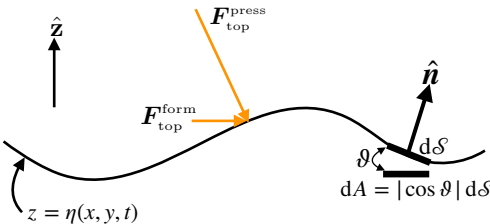


FIGURE 25.3: The pressure force acting on an arbitrary surface is given by $\mathbf{F}^{\text{press}} = -p \hat{\mathbf{n}} d\mathcal{S}$, where $d\mathcal{S}$ is the surface area element. We here depict the pressure acting on the top side of a surface, $\mathbf{F}_{\text{top}}^{\text{press}}$. Through Newton's third law, the pressure force vector acting on the top side of the interface is equal and opposite to the pressure force acting on the bottom side: $\mathbf{F}_{\text{top}}^{\text{press}} = -\mathbf{F}_{\text{b}}^{\text{press}}$. The horizontal component of this force vector arises from the slope; i.e., the geometric *form* of the surface. We thus refer to the horizontal pressure force per area as the *form stress*, $\mathbf{F}_{\text{top}}^{\text{form}} = -\mathbf{F}_{\text{b}}^{\text{form}}$. The area element on the surface, $d\mathcal{S}$, has a horizontal projection given by $dA = dx dy = \cos \vartheta d\mathcal{S}$, with the angle assumed to be within the range $-\pi/2 < \vartheta < \pi/2$ so that the surface is nowhere vertical.

The outward normal pointing away from the top side of the surface is given by

$$\hat{\mathbf{n}}_{\text{top}} = \frac{\nabla(z - \eta)}{|\nabla(z - \eta)|} = \frac{\hat{z} - \nabla\eta}{\sqrt{1 + |\nabla\eta|^2}}. \quad (25.2)$$

Multiplying the pressure times the horizontal area element on the surface, $d\mathcal{S}$, leads to the net pressure force acting at a point on the top side of the surface

$$\mathbf{F}^{\text{press}} = -p \hat{\mathbf{n}}_{\text{top}} d\mathcal{S} = -p (\hat{z} - \nabla\eta) dA = -p (-\partial_x \eta \hat{x} - \partial_y \eta \hat{y} + \hat{z}) dA. \quad (25.3)$$

In this equation we used the identity²

$$d\mathcal{S} = |\nabla(z - \eta)| dA = \sqrt{1 + |\nabla\eta|^2} dA, \quad (25.4)$$

with

$$dA = dx dy \quad (25.5)$$

the horizontal projection of the surface area element (see Figure 25.3). We identify the form stress acting on the top side of this interface as

$$\text{pressure form stress acting on top side of interface} \equiv p \nabla\eta. \quad (25.6)$$

The name follows since the stress is determined by the “form” of the surface as measured by its slope, $\nabla\eta$. We can thus write the pressure force acting on the top side of the surface as the sum of a vertical pressure force plus a horizontal pressure form stress

$$\mathbf{F}_{\text{top}}^{\text{press}} = \hat{z} [\hat{z} \cdot \mathbf{F}_{\text{top}}^{\text{press}}] + \mathbf{F}_{\text{top}}^{\text{form}} = p (-\hat{z} + \nabla\eta) dA \quad \text{pressure force on top of interface.} \quad (25.7)$$

Newton's third law, as manifested by Cauchy's Stress principle (Section 22.2) says that there is a local mechanical equilibrium of pressure contact forces within a fluid. Additionally, as seen in our discussion of stress on an interface in Section 22.10, this local equilibrium holds for pressure forces acting on interfaces separating two fluids, such as the atmosphere and ocean, as well as a fluid and the solid earth. Thus, the contact pressure force acting on the bottom side of the interface is equal in magnitude but oppositely directed to the contact force acting on the top side

²The identity (25.4) follows from trigonometry summarized in Figure 25.3. See further details in the kinematic boundary conditions of Section 16.4 and the analogous dia-surface transport in Section 57.4.

(see Section 22.8.2)

$$\mathbf{F}_{\text{bot}}^{\text{press}} = \hat{\mathbf{z}} [\hat{\mathbf{z}} \cdot \mathbf{F}_{\text{bot}}^{\text{press}}] + \mathbf{F}_{\text{bot}}^{\text{form}} = p (+\hat{\mathbf{z}} - \nabla \eta) \, dA \quad \text{pressure force on bottom of interface. (25.8)}$$

25.1.3 Comments

We here offer three comments in regards to pressure form stress.

- MYSTERIOUS NOTION: The form stress, particularly interfacial form stress, can appear mysterious in some presentations. Part of the reason is that it sometimes appears seemingly without prior motivation as part of mathematical manipulations of the momentum equation. We illustrate these manipulations in Sections 25.2, 25.3, and 25.5, yet aim to offer sufficient physical motivation to help guide the maths. Another reason for the mystery is that the signs ascribed to form stress are often not clearly specified, with such ambiguities motivating the somewhat pedantic discussion in Section 25.1.1.

- UNBALANCED FORM STRESSES AND MOTION

Consider a container filled with water at rest. The horizontal pressure forces acting on the container sides are pressure form stresses between the water and the container. As discussed in Section 22.5, without motion we know that the form stresses balance over the whole of the fluid-container boundary, whereas horizontal motion occurs if the form stresses are out of balance. Quite generally, when concerned with fluid motion, we are interested in processes that lead to unbalanced form stresses. For example, when studying bottom topographic form stresses in the ocean, the bulk of the form stress acts to support the ocean water within the ocean basin. The dynamically active portion of the topographic form stress, associated with the fluid motion, is a small residual of the total form stress. Careful analysis is required to diagnose dynamically relevant patterns, with [Molemaker et al. \(2015\)](#) and [Gula et al. \(2015\)](#) presenting one method, and we explore their method as part of Exercise 37.11.

- DUAL FORM STRESS OFTEN CONFUSED WITH FORM STRESS: It is notable that much of the literature refers to $-\eta \nabla p$ as a form stress. However, as noted in Section 25.4.4, $-\eta \nabla p$ is not a form stress but is a *dual form stress*. This confusion between form stress and dual form stress perhaps originates from the common application of zonal averages for studying atmospheric motions, whereby $\overline{\eta \partial_x p}^x = -\overline{p \partial_x \eta}^x$ so that the zonal average of the form stress equals to the zonal average of the dual form stress. Importantly, this identity does not hold for arbitrary averaging operators, such as the ensemble averages commonly used for turbulence studies. So it is generally necessary to distinguish the form stress from the dual form stress.

25.2 Form stresses on the ocean boundaries

In this section we focus on form stress arising from the shape of the solid earth interface with the atmosphere and ocean; i.e., the *fluid-topographic form stress*. As we are normally interested in the form stress applied to the fluid, we focus on the *topographic form stress*. We also encounter the form stress associated with undulations in the ocean free surface and the atmospheric pressure at that interface, with the *atmospheric form stress* the stress imparted to the ocean from the atmosphere.

25.2.1 Zonally symmetric ridge

In Figure 25.4 we depict an idealized ridge with an example oceanic pressure field to illustrate the nature of topographic form stress acting on a fluid. Rather than assuming exact hydrostatic equilibrium as in Figure 22.5, with zero horizontal pressure gradients, we here consider pressure to be higher to the west of the ridge than to the east. Since the ridge is assumed to be symmetric in the zonal direction, we conclude that the topographic form stress, which acts just at the fluid-solid interface, is higher on the west side of the ridge than on the east. In turn, the net topographic form stress acting on the fluid is to the west, whereas the net oceanic form stress acting on the solid earth is to the east. We encounter this situation in Section 25.5.11 when studying the force balances for steady circulation in a zonally periodic channel.

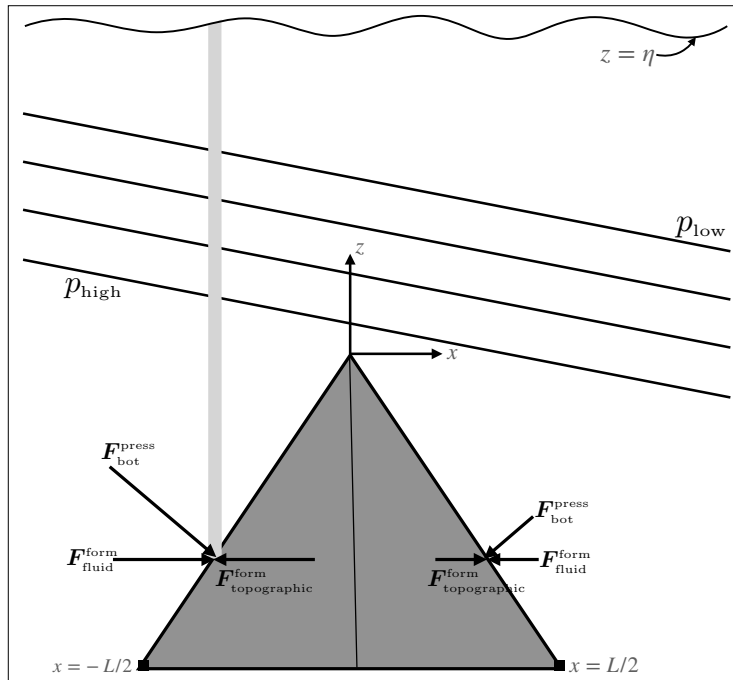


FIGURE 25.4: Depicting contact forces acting at a fluid-solid interface. The topographic form stress acts on the fluid and the equal in magnitude but oppositely directed fluid form stress acts on the solid earth. In this illustration the topography is assumed to be a ridge in the shape of an equilateral triangle. We also assume there is higher pressure to the west of the ridge than to the east as per the zonal balance discussed in Figure 25.8 for a Southern Ocean ridge. Hence, the topographic form stress has a larger magnitude on the western side of the ridge than on the eastern side. When integrated over the full ridge, there will be a net westward topographic form stress acting on the fluid and a net eastward fluid form stress acting on the solid earth. If the ridge was free to move, it would move to the east. The thin gray column extends from the solid earth bottom to the ocean free surface. As this column sits on the western side of the ridge, topographic form stress provides a westward acceleration at the column bottom. The net acceleration of the column is determined by integrating the contact forces around the column boundary and body forces throughout the column interior. We study the axial angular momentum budget for a fluid column in Section 25.5, with form stresses appearing in that budget.

25.2.2 Form stress transfer between the fluid and its boundaries

We now illustrate how topographic form stress appears mathematically in the study of momentum balances acting on a fluid. For definiteness, consider a column of ocean fluid extending from the bottom at $z = \eta_b(x, y)$ to the free surface at $z = \eta(x, y, t)$, and focus on the zonal force balance such as depicted in Figure 25.4. In computing the acceleration acting on this column at a particular

horizontal position, we need to determine the depth integrated zonal pressure gradient

$$\text{depth integrated zonal pressure gradient} = - \int_{\eta_b}^{\eta} \frac{\partial p}{\partial x} dz. \quad (25.9)$$

We expose the contact force version of the pressure force by making use of Leibniz's Rule (Section 16.5) to write

$$- \int_{\eta_b}^{\eta} \frac{\partial p}{\partial x} dz = \underbrace{- \frac{\partial}{\partial x} \int_{\eta_b}^{\eta} p dz}_{\text{zonal deriv depth integrated pressure}} + \underbrace{\frac{\partial \eta}{\partial x} p_a}_{\text{atmospheric form stress}} - \underbrace{\frac{\partial \eta_b}{\partial x} p_b}_{\text{topographic form stress}}, \quad (25.10)$$

where p_a is the pressure applied to the ocean at its surface, $z = \eta$, and p_b is the pressure at the ocean bottom, $z = \eta_b$. The decomposition identifies the following three pressure contributions to the pressure force acting on the fluid column.

- **ZONAL DERIVATIVE OF THE COLUMN INTEGRATED PRESSURE:** The first term arises from the zonal derivative of pressure across the vertical sides of the column

$$\text{zonal derivative of layer integrated pressure} = - \frac{\partial}{\partial x} \int_{\eta_b}^{\eta} p dz. \quad (25.11)$$

This term leads to a net eastward acceleration if the depth integrated pressure is higher to the west than the east.

- **ATMOSPHERIC FORM STRESS AT THE FREE SURFACE:** In the presence of a sloping free surface interface, $\partial \eta / \partial x \neq 0$, the atmospheric pressure, p_a , imparts an atmospheric form stress onto the ocean

$$\text{zonal atmospheric form stress acting on ocean} = \frac{\partial \eta}{\partial x} p_a. \quad (25.12)$$

For example, if the free surface slopes up to the east, $\partial \eta / \partial x > 0$, then the atmosphere provides a positive (eastward) zonal form stress onto the ocean. In turn, through Newton's third law, the ocean provides a westward zonal form stress to the atmosphere.

- **TOPOGRAPHIC FORM STRESS ON OCEAN:** The bottom pressure, p_b , present at $z = \eta_b$ imparts an oceanic form stress to the solid earth

$$\text{zonal oceanic form stress acting on solid earth} = \frac{\partial \eta_b}{\partial x} p_b. \quad (25.13)$$

In turn, through Newton's third law, the topographic form stress acting on the ocean is equal in magnitude but oppositely directed

$$\text{zonal topographic form stress acting on ocean} = - \frac{\partial \eta_b}{\partial x} p_b. \quad (25.14)$$

For example, if the bottom rises to the east, so that $\partial \eta_b / \partial x > 0$, then the oceanic form stress acting on the solid earth is eastward whereas the topographic form stress acting on the ocean is westward. As a check, we verify that the signs of these form stresses are consistent with those in Figure 25.4.

25.2.3 Decomposing topographic form stress

Assuming the fluid maintains an approximate hydrostatic balance, and focusing on the oceanic case, allows us to decompose the bottom pressure into the following terms

$$p_b = p_a + g \int_{\eta_b}^{\eta} \rho dz \quad (25.15a)$$

$$= \underbrace{g \rho_0 [\eta + p_a / (g \rho_0)]}_{\text{external}} - \underbrace{g \rho_0 \eta_b}_{\text{topog}} + \underbrace{g \int_{\eta_b}^{\eta} (\rho - \rho_0) dz}_{\text{internal}} \quad (25.15b)$$

$$\equiv p_{\text{ext}} + p_{\text{topog}} + p_{\text{int}}. \quad (25.15c)$$

We refer to the contribution from applied surface pressure plus surface height undulations as *external*, whereas those arising from density deviations relative to a constant reference density are termed *internal*. There is a final contribution from bottom topography itself. Multiplying this pressure by the bottom topography slope renders an expression for the various contributions to topographic form stress

$$-p_b \nabla \eta_b = -p_{\text{ext}} \nabla \eta_b - p_{\text{topog}} \nabla \eta_b - p_{\text{int}} \nabla \eta_b. \quad (25.16)$$

The topographic term is static whereas the other two terms are time dependent. External contributions arise from undulations in the free surface as well as the applied pressure. This contribution fluctuates due to motions occurring on the relatively rapid time scales associated with external gravity waves or atmospheric pressure fluctuations such as through synoptic weather patterns. Internal contributions arise from the relatively slow internal movements of density surfaces, such as from internal gravity waves or even slower motions due to advection and diffusion. The study from [McCabe et al. \(2006\)](#) pursues this decomposition of the topographic form stress as part of their analysis of flow around a headland.

25.3 Interfacial form stress

In this section we focus on the form stress acting at an interface within the fluid itself, which is known as the *interfacial form stress*. As part of this discussion we expose some of the common manipulations found when considering finite volume integrated momentum budgets, whereby we decompose the horizontal pressure gradient acceleration acting on an infinitesimal column of fluid within the layer, as depicted in Figure 25.5. These manipulations are analogous to those considered in Section 25.2 for the topographic and atmospheric form stresses.

25.3.1 Interfacial form stresses transferred between layers

When studying the momentum of a column of fluid within a chosen layer, we need to compute the depth integrated zonal pressure gradient over a layer at a particular horizontal point

$$\text{layer integrated zonal pressure gradient} = - \int_{\eta_{k+1/2}}^{\eta_{k-1/2}} \frac{\partial p}{\partial x} dz, \quad (25.17)$$

where $z = \eta_{k-1/2}(x, y, t)$ is the vertical position for the interface at the top of the fluid layer and $z = \eta_{k+1/2}(x, y, t)$ is the vertical position for the bottom interface. If the layer integrated pressure gradient points downgradient to the east, then pressure accelerates the column to the east.

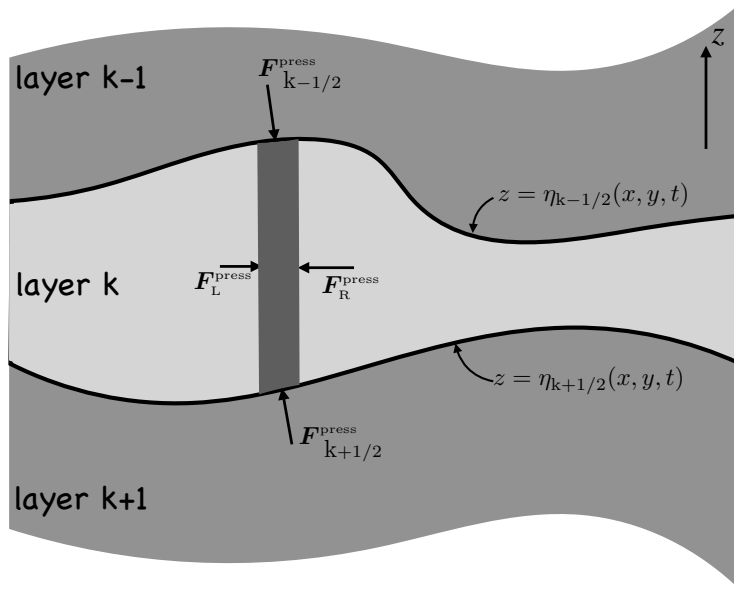


FIGURE 25.5: A schematic of the contact pressure force per area acting on the boundaries of a vertical column region within a fluid layer. The horizontal cross-sectional area of the column is depth independent. The interface at the lower boundary is at the vertical position $z = \eta_{k+1/2}$, and the upper interface is at $z = \eta_{k-1/2}$. In accordance with Newton's third law, pressures are continuous across each of the $\eta_{k\pm 1/2}$ layer interfaces so that the pressure forces are equal in magnitude yet oppositely directed on the opposite sides to the interfaces. The boundaries of the dark gray columnar region feel a contact pressure force acting inward. The left side of the column experiences a pressure p_L ; the right side experiences p_R ; the upper interface has a pressure $p_{k-1/2}$ acting between the layer $k-1$ and layer k , and the lower interface has a pressure $p_{k+1/2}$ acting between the layer $k+1$ and layer k . The interfacial form stress (IFS) is the name given to the horizontal pressure stress acting on the upper and lower layer interfaces. Through Newton's third law, the IFS imparted to layer k at the $z = \eta_{k-1/2}$ interface is equal and opposite to the IFS imparted to layer $k-1$ at this same interface. The same holds for the IFS at the $k+1/2$ interface. It is common to define the layers according to buoyancy (see Section 28.6) given its direct connection to pressure and dynamics. Even so, the ideas of pressure contact forces are generic and thus hold for layers defined arbitrarily.

Although the depth integrated pressure gradient expression (25.17) is straightforward to understand, we also find it useful to consider the complementary perspective by studying the contact force version of the pressure acceleration. Proceeding as in Section 25.2 for topographic and atmospheric form stresses, we make use of Leibniz's Rule for a fluid layer

$$-\int_{\eta_{k+1/2}}^{\eta_{k-1/2}} \frac{\partial p}{\partial x} dz = \underbrace{-\frac{\partial}{\partial x} \int_{\eta_{k+1/2}}^{\eta_{k-1/2}} p dz}_{\text{zonal deriv layer integrated pressure}} + \underbrace{\frac{\partial \eta_{k-1/2}}{\partial x} p_{k-1/2}}_{\text{IFS at } k-1/2 \text{ interface}} - \underbrace{\frac{\partial \eta_{k+1/2}}{\partial x} p_{k+1/2}}_{\text{IFS at } k+1/2 \text{ interface}}, \quad (25.18)$$

where we introduced the pressures acting at a point on the interfaces

$$p_{k-1/2} = p(x, y, z = \eta_{k-1/2}, t) \quad \text{and} \quad p_{k+1/2} = p(x, y, z = \eta_{k+1/2}, t). \quad (25.19)$$

The decomposition identifies the following three pressure contributions, analogous to the decomposition in Section 25.2 for the topographic and atmospheric form stresses.

- **ZONAL DERIVATIVE OF THE COLUMN INTEGRATED PRESSURE:** The first term arises from

the zonal derivative of pressure across the vertical sides of the column within the layer

$$\text{zonal derivative of layer integrated pressure} = -\frac{\partial}{\partial x} \int_{\eta_{k+1/2}}^{\eta_{k-1/2}} p dz. \quad (25.20)$$

- INTERFACIAL FORM STRESS AT UPPER INTERFACE: The pressure at the $z = \eta_{k-1/2}$ interface is given by $p_{k-1/2}$. In the presence of a sloping interface, $\partial\eta_{k-1/2}/\partial x \neq 0$, this pressure imparts the following interfacial form stress (IFS) to layer-k:

$$\text{IFS on layer-k from the } \eta_{k-1/2} \text{ interface} = \frac{\partial\eta_{k-1/2}}{\partial x} p_{k-1/2}. \quad (25.21)$$

For example, if the upper layer interface slopes up to the east, $\partial\eta_{k-1/2}/\partial x > 0$, then the interfacial form stress provides a positive (eastward) zonal force to layer-k. In turn, through Newton's third law, the layer above, labelled k-1, feels an interfacial form stress accelerating this layer to the west.

- INTERFACIAL FORM STRESS AT LOWER INTERFACE: The pressure, $p_{k+1/2}$ present at the $z = \eta_{k+1/2}$ interface imparts an interfacial form stress to layer-k given by

$$\text{IFS on layer-k from } \eta_{k+1/2} \text{ interface} = -\frac{\partial\eta_{k+1/2}}{\partial x} p_{k+1/2}. \quad (25.22)$$

For example, if the layer slopes down to the east, $\partial\eta_{k+1/2}/\partial x < 0$, then the interfacial form stress accelerates layer-k to the east. In turn, through Newton's third law, the interfacial form stress acts to accelerate the layer below, labelled k + 1, to the west.

Now apply the above to a column of ocean fluid, and extending the integration to include the full ocean column from the free upper surface to the solid earth bottom. Note that all the intermediate interfacial form stresses vanish in the depth integral, with this cancellation a result of Newton's third law. Hence, accumulation of the interfacial form stresses throughout the ocean column leaves only the interfacial form stress at the top and at the bottom, with those boundary form stresses arising from mechanical interactions with the atmosphere and solid earth as discussed in Section 25.2. This result was already encountered in a more general context of contact forces in Section 22.2. It will also be found in our analysis of the depth integrated axial angular momentum budget in Section 25.5.

25.3.2 Zonally integrated interfacial form stress

Besides studying the force acting on a column at a particular horizontal position, it is interesting to study the net zonal force acting on the layer. For pressure, we thus need to consider the zonal integral of the layer integrated zonal pressure gradient

$$-\int \left[\int_{\eta_{k+1/2}}^{\eta_{k-1/2}} \frac{\partial p}{\partial x} dz \right] dx = \int \left[-\frac{\partial}{\partial x} \int_{\eta_{k+1/2}}^{\eta_{k-1/2}} p dz + \frac{\partial\eta_{k-1/2}}{\partial x} p_{k-1/2} - \frac{\partial\eta_{k+1/2}}{\partial x} p_{k+1/2} \right] dx. \quad (25.23)$$

If the domain is zonally periodic or is bounded by sloping shorelines (see Figure 25.7 discussed in Section 25.5.7), then the first term vanishes so that the zonally integrated pressure acting on the layer arises just from the interfacial form stresses

$$-\int \left[\int_{\eta_{k+1/2}}^{\eta_{k-1/2}} \frac{\partial p}{\partial x} dz \right] dx = \int \left[\frac{\partial\eta_{k-1/2}}{\partial x} p_{k-1/2} - \frac{\partial\eta_{k+1/2}}{\partial x} p_{k+1/2} \right] dx. \quad (25.24)$$

This zonal integral is only affected by zonal anomalies for the layer vertical positions and pressures

$$-\int \left[\int_{\eta_{k+1/2}}^{\eta_{k-1/2}} \frac{\partial p}{\partial x} dz \right] dx = \int \left[\frac{\partial \eta'_{k-1/2}}{\partial x} p'_{k-1/2} - \frac{\partial \eta'_{k+1/2}}{\partial x} p'_{k+1/2} \right] dx \quad (25.25a)$$

$$= \int \left[-\eta'_{k-1/2} \frac{\partial p'_{k-1/2}}{\partial x} + \eta'_{k+1/2} \frac{\partial p'_{k+1/2}}{\partial x} \right] dx, \quad (25.25b)$$

where primes denote deviations from the zonal mean. We spend some time in Section 25.5.10 to prove that it is only the anomalies that matter for the zonally periodic channel, or for domains with sloping shorelines. Furthermore, note that for the second equality we introduced the alternative expressions for the form stresses afforded by zonal periodicity or zonal sloped shorelines. We offer some cautionary remarks in Section 25.5.9 regarding this second equality.

25.3.3 Comments

Interfacial form stress acts on any arbitrary surface drawn in a fluid. Interfaces defined by buoyancy surfaces make the connection between the general concepts presented here to geostrophic mechanics, and they do so given the connection between buoyancy slopes and thermal wind (Section 28.4.4). Most studies of interfacial form stress are thus concerned with isopycnal interfacial form stress, with a discussion given in Section 28.6.

25.4 Evolution of depth integrated horizontal momentum

In this section we develop the evolution equation for the depth integrated horizontal momentum per volume in a column of ocean fluid

$$\mathbf{U}^\rho = \int_{\eta_b}^{\eta} \rho \mathbf{u} dz, \quad (25.26)$$

extending from the ocean bottom at $z = \eta_b(x, y)$ to the ocean surface at $z = \eta(x, y, t)$. The evolution equation exposes how form stresses acting at the ocean surface and ocean bottom contribute to the column force balance. A study of the depth integrated momentum equation is commonly considered when the ocean fluid maintains an approximate hydrostatic balance, so we assume such in this section. We discussed the exact hydrostatic fluid in Section 21.4, which is realized by a static fluid in a gravity field. The approximate hydrostatic fluid, as studied in Sections 24.2 and 26.2, is more general since it applies to a moving fluid whose vertical momentum equation is well approximated by the hydrostatic balance.

25.4.1 Flux-form horizontal momentum equation

Our starting point is the flux-form horizontal momentum equation (22.63) as specialized to a simple geopotential, $\Phi = g z$,

$$\frac{\partial(\rho \mathbf{u})}{\partial t} + \nabla \cdot [\rho \mathbf{v} \otimes \mathbf{u}] + f \hat{z} \times (\rho \mathbf{u}) = -\nabla_z p + \rho \mathbf{F}. \quad (25.27)$$

In this equation, $\rho \mathbf{F}$ is the horizontal friction vector, and the outer product provides components to the kinetic stress (Section 22.6)

$$\rho [\mathbf{v} \otimes \mathbf{u}]_{mi} = \rho v_m u_i = -\mathbb{T}_{mi}^{\text{kinetic}}, \quad (25.28)$$

with $m = 1, 2, 3$ (for the full velocity vector, \mathbf{v}) extending over the full range whereas $i = 1, 2$ (for the horizontal velocity vector, \mathbf{u}) extending just over the horizontal range.

25.4.2 Leibniz's rule for the inertial and Coriolis accelerations

Leibniz's rule (Section 17.3.4) renders the following expressions for the depth integrated inertial acceleration and Coriolis acceleration

$$\int_{\eta_b}^{\eta} \frac{\partial(\rho \mathbf{u})}{\partial t} dz = \partial_t \mathbf{U}^\rho - [\rho \mathbf{u} \partial_t \eta]_{z=\eta} \quad (25.29a)$$

$$\int_{\eta_b}^{\eta} \frac{\partial(w \rho \mathbf{u})}{\partial z} dz = [w \rho \mathbf{u}]_{z=\eta} - [w \rho \mathbf{u}]_{z=\eta_b} \quad (25.29b)$$

$$\int_{\eta_b}^{\eta} \nabla_z \cdot [\rho \mathbf{u} \otimes \mathbf{u}] dz = \nabla_z \cdot \left[\int_{\eta_b}^{\eta} \rho \mathbf{u} \otimes \mathbf{u} dz \right] - [\mathbf{u} \cdot \nabla \eta (\rho \mathbf{u})]_{z=\eta} + [\mathbf{u} \cdot \nabla \eta_b (\rho \mathbf{u})]_{z=\eta_b} \quad (25.29c)$$

$$\int_{\eta_b}^{\eta} f \hat{\mathbf{z}} \times (\rho \mathbf{u}) dz = f \hat{\mathbf{z}} \times \mathbf{U}^\rho. \quad (25.29d)$$

Use of the surface and bottom kinematic boundary conditions from Section 16.4

$$\partial_t \eta + \mathbf{u} \cdot \nabla \eta = w + \rho^{-1} Q_m \quad \text{for } z = \eta \quad (25.30a)$$

$$\mathbf{u} \cdot \nabla \eta_b = w \quad \text{for } z = \eta_b \quad (25.30b)$$

leads to the depth integrated inertial and Coriolis accelerations

$$\begin{aligned} & \int_{\eta_b}^{\eta} [\partial_t(\rho \mathbf{u}) + \nabla \cdot [\mathbf{v} \otimes (\rho \mathbf{u})] + f \hat{\mathbf{z}} \times \rho \mathbf{u}] dz \\ &= (\partial_t + f \hat{\mathbf{z}} \times) \mathbf{U}^\rho - \mathbf{u}(\eta) Q_m - \nabla_z \cdot \int_{\eta_b}^{\eta} \mathbb{T}_{\text{hor}}^{\text{kinetic}} dz, \end{aligned} \quad (25.31)$$

where we introduced the horizontal kinetic stress tensor

$$\mathbb{T}_{\text{hor}}^{\text{kinetic}} = -\rho \mathbf{u} \otimes \mathbf{u}. \quad (25.32)$$

25.4.3 External and internal decomposition of the kinetic stress

For some applications it can be useful to introduce the density weighted depth averaged horizontal velocity

$$\bar{\mathbf{u}} = \frac{\int_{\eta_b}^{\eta} \rho \mathbf{u} dz}{\int_{\eta_b}^{\eta} \rho dz} = \frac{\mathbf{U}^\rho}{(p_b - p_a)/g}, \quad (25.33)$$

where p_b is the hydrostatic pressure at the ocean bottom, and p_a is the pressure applied to the ocean surface. The depth averaged velocity is referred to as the *external velocity*, whereas the deviation from the depth average

$$\mathbf{u}' = \mathbf{u} - \bar{\mathbf{u}}, \quad (25.34)$$

is referred to it as the *internal velocity*.³ It follows by definition that the internal velocity has a zero density weighted vertical integral

$$\int_{\eta_b}^{\eta} \rho \mathbf{u}' dz = \int_{\eta_b}^{\eta} \rho (\mathbf{u} - \bar{\mathbf{u}}) dz = 0. \quad (25.35)$$

Consequently, by making use of $\mathbf{u} = \bar{\mathbf{u}} + \mathbf{u}'$ we find the depth integrated kinetic stress

$$\int_{\eta_b}^{\eta} \mathbb{T}_{\text{hor}}^{\text{kinetic}} dz = -g^{-1} (p_b - p_a) [\bar{\mathbf{u}} \otimes \bar{\mathbf{u}} + \overline{\mathbf{u}' \otimes \mathbf{u}' }]. \quad (25.36)$$

Note that absence of cross-terms (i.e., no internal-external correlation terms) appearing in the depth integrated stress (25.36). In this manner we have separated the contributions from kinetic stresses due to depth averaged horizontal velocities from those arising from depth-dependent horizontal velocities.

25.4.4 Decomposing the depth integrated horizontal pressure gradient

We here consider the depth integrated pressure

$$P = \int_{\eta_b}^{\eta} p dz, \quad (25.37)$$

and the corresponding depth integrated horizontal pressure gradient

$$\int_{\eta_b}^{\eta} \nabla_z p dz. \quad (25.38)$$

Assuming each fluid column maintains an approximate hydrostatic balance allows us to decompose these integrals into elemental constituents.

Depth integrated pressure

For the pressure, write its depth integral as

$$P = \int_{\eta_b}^{\eta} p dz = \int_{\eta_b}^{\eta} [d(pz) - z dp] = p_a \eta - p_b \eta_b + \mathcal{P}, \quad (25.39)$$

where we used the hydrostatic balance for a vertical fluid column to write⁴ $dp = -g \rho dz$, and we introduced the potential energy per horizontal area of a fluid column

$$\mathcal{P} = \int_{\eta_b}^{\eta} g \rho z dz. \quad (25.40)$$

Evidently, equation (25.39) decomposes the depth integrated pressure into a contribution from the applied surface pressure acting at the free surface, the bottom pressure acting at the ocean bottom (recall that $\eta_b < 0$), and the potential energy per horizontal area of a fluid column.

³It is also common in the oceanography literature to refer to \mathbf{u}' as the *baroclinic velocity* and $\bar{\mathbf{u}}$ as the *barotropic velocity*. We avoid that nomenclature since we prefer to use baroclinic and barotropic in reference to vorticity mechanics in Section 37.4.

⁴More generally, the differential of pressure is given by $dp = \nabla p \cdot d\mathbf{x}$ when probing three-dimensional spatial increments, $d\mathbf{x}$. However, the integral in equation (25.39) is vertical, in which case $dp = (\partial p / \partial z) dz$. For the approximate hydrostatic fluid we thus have the transformation $dp = -g \rho dz$.

Depth integrated horizontal pressure gradient

For the depth integrated horizontal pressure gradient, we start by using Leibniz's rule to render

$$\nabla_z P = \nabla_z \int_{\eta_b}^{\eta} p \, dz = p_a \nabla \eta - p_b \nabla \eta_b + \int_{\eta_b}^{\eta} \nabla_z p \, dz. \quad (25.41)$$

Making use of the decomposition (25.39) leads to

$$-\int_{\eta_b}^{\eta} \nabla_z p \, dz = -\nabla_z P + p_a \nabla_z \eta - p_b \nabla_z \eta_b \quad (25.42a)$$

$$= -\nabla_z [p_a \eta - p_b \eta_b + \mathcal{P}] + p_a \nabla_z \eta - p_b \nabla_z \eta_b \quad (25.42b)$$

$$= -\nabla_z \mathcal{P} - \eta \nabla_z p_a + \eta_b \nabla_z p_b. \quad (25.42c)$$

Equation (25.42a) exposes contributions from surface and bottom form stresses,

$$\text{surface and bottom form stresses} = p_a \nabla_z \eta - p_b \nabla_z \eta_b, \quad (25.43)$$

along with the horizontal gradient of the depth integrated pressure. As a complement, equation (25.42c) exposes the *dual form stress*,

$$\text{surface and bottom dual form stresses} = -\eta \nabla_z p_a + \eta_b \nabla_z p_b, \quad (25.44)$$

plus the gradient of the potential energy. The role of these accelerations is further studied for the axial angular momentum budget in Section 25.5, and then within the column vorticity balance in Section 37.9.

Constraints when the fluid is exactly hydrostatic and thus motionless

As discussed in Section 21.4, the horizontal pressure gradient everywhere vanishes for a fluid in exact hydrostatic balance, $\nabla_z p = 0$. Correspondingly, the free surface and surface applied pressure are spatially constant in order to maintain zero pressure gradients throughout the fluid. For the depth integral pressure gradient, the decompositions (25.42a) and (25.42c) lead to the exact hydrostatic fluid identities maintained at each vertical fluid column

$$\nabla_z P = -p_b \nabla_z \eta_b \quad (25.45a)$$

$$\nabla_z \mathcal{P} = \eta_b \nabla_z p_b. \quad (25.45b)$$

The first identity says that the horizontal gradient of the depth integrated hydrostatic pressure exactly balances the topographic form stress. The second identity says that the horizontal gradient of the potential energy per area balances the dual topographic form stress.

Since the curl of the left hand side vanishes for both of equation (25.45a) and (25.45b), we find that the bottom pressure must be aligned with the bottom topography in order to maintain zero flow

$$\hat{z} \cdot (\nabla \eta_b \times \nabla p_b) = 0. \quad (25.46)$$

In the language of vorticity, we say that there is no bottom pressure torque when the flow is exactly hydrostatic (see Section 37.8.3). Conversely, nonzero flow is signaled by a misalignment of bottom pressure and bottom topography contours. We can also arrive at the identity (25.46) by taking the horizontal derivative of the bottom pressure. Since the fluid is static we have a spatially constant free surface and applied pressure, and a density that is horizontally uniform.

Consequently,

$$\nabla_z p_b = g \nabla_z \int_{\eta_b}^0 \rho dz = -g \rho(z = \eta_b) \nabla_z \eta_b, \quad (25.47)$$

thus revealing that bottom pressure contours are indeed parallel to bottom topography contours when the fluid is in exact hydrostatic balance.

25.4.5 Depth integrated momentum equation

Bringing the pieces together leads to the depth integrated horizontal momentum equation for an approximate hydrostatic fluid

$$(\partial_t + f \hat{z} \times) \mathbf{U}^\rho = \mathbf{u}(\eta) Q_m - \eta \nabla_z p_a + \eta_b \nabla_z p_b - \nabla_z \mathcal{P} + \nabla_z \cdot \left[\int_{\eta_b}^\eta \mathbb{T}_{\text{hor}}^{\text{kinetic}} dz \right] + \int_{\eta_b}^\eta \rho \mathbf{F} dz. \quad (25.48)$$

For many applications we focus on the vertical divergence of horizontal frictional stress plus a term arising from horizontal strains, in which case

$$\int_{\eta_b}^\eta \rho \mathbf{F} dz = \int_{\eta_b}^\eta (\rho \mathbf{F}_{\text{horz}} + \partial_z \boldsymbol{\tau}) dz = \mathbf{D} + \boldsymbol{\tau}^\eta - \boldsymbol{\tau}^{\eta_b} \equiv \mathbf{D} + \Delta \boldsymbol{\tau}, \quad (25.49)$$

where $\boldsymbol{\tau}^\eta$ is the horizontal stress at the surface (e.g., wind stress on the ocean surface), $\boldsymbol{\tau}^{\eta_b}$ is the horizontal stress at the bottom (e.g., turbulent drag at the fluid-solid earth boundary), and

$$\mathbf{D} = \int_{\eta_b}^\eta \rho \mathbf{F}_{\text{horz}} dz \quad (25.50)$$

is the depth integrated friction arising from horizontal stresses within the fluid interior (e.g., viscous stresses as in Section 22.8). In this case the horizontal momentum equation (25.48) takes on the form

$$(\partial_t + f \hat{z} \times) \mathbf{U}^\rho = \mathbf{u}(\eta) Q_m - \eta \nabla_z p_a + \eta_b \nabla_z p_b - \nabla_z \mathcal{P} + \mathbf{A} + \mathbf{D} + \Delta \boldsymbol{\tau}. \quad (25.51)$$

where we introduced the shorthand for the nonlinear kinetic stress term

$$\mathbf{A} \equiv \nabla_z \cdot \left[\int_{\eta_b}^\eta \mathbb{T}_{\text{hor}}^{\text{kinetic}} dz \right] = -\nabla_z \cdot \left[\int_{\eta_b}^\eta \rho \mathbf{u} \otimes \mathbf{u} dz \right]. \quad (25.52)$$

25.4.6 Balances when $\nabla \cdot \mathbf{U}^\rho = 0$

There are many occasions in which the depth integrated flow is close to non-divergent, $\nabla \cdot \mathbf{U}^\rho = 0$. Such occurs particularly at the large scale and for cases where we neglect the mass transport across the ocean surface, $Q_m = 0$. Following the kinematics from Section 18.3, we introduce a *transport streamfunction* so that

$$\mathbf{U}^\rho = \hat{z} \times \nabla \Psi, \quad (25.53)$$

with Ψ having dimensions of mass per time. Use of the transport streamfunction brings the Coriolis contribution to the form

$$f \hat{z} \times \mathbf{U}^\rho = f \hat{z} \times (\hat{z} \times \nabla \Psi) = -f \nabla \Psi, \quad (25.54)$$

so that the momentum equation (25.51) becomes

$$\partial_t \mathbf{U}^\rho = f \nabla_z \Psi - \eta \nabla_z p_a + \eta_b \nabla_z p_b - \nabla_z \mathcal{P} + \mathbf{A} + \mathbf{D} + \Delta\boldsymbol{\tau} \quad (25.55a)$$

$$= f \nabla_z \Psi + p_a \nabla_z \eta - p_b \nabla_z \eta_b - \nabla_z P + \mathbf{A} + \mathbf{D} + \Delta\boldsymbol{\tau}. \quad (25.55b)$$

Zonal integral of the depth integrated zonal momentum equation

For many purposes, we wish reduce the number of processes contributing to the momentum equations (25.55a) and (25.55b) by forming horizontal integrals along selected contours. For example, a zonal integral of the zonal equation, computed around a periodic domain, eliminates the Coriolis term as well as $\partial_x P$ and $\partial_x \mathcal{P}$, in which case

$$\partial_t \oint U^\rho dx = \oint [-\eta \partial_x p_a + \eta_b \partial_x p_b + \hat{\mathbf{x}} \cdot (\mathbf{A} + \mathbf{D} + \Delta\boldsymbol{\tau})] dx \quad (25.56a)$$

$$= \oint [p_a \partial_x \eta - p_b \partial_x \eta_b + \hat{\mathbf{x}} \cdot (\mathbf{A} + \mathbf{D} + \Delta\boldsymbol{\tau})] dx. \quad (25.56b)$$

As discussed in Section 25.5, this equation, or its analog for the axial angular momentum, provides a valuable framework for studies of the Southern Ocean momentum balances.

Steady balance

As another example, consider a steady balance in which

$$-f \nabla_z \Psi = p_a \nabla_z \eta - p_b \nabla_z \eta_b - \nabla_z P + \mathbf{A} + \mathbf{D} + \Delta\boldsymbol{\tau}. \quad (25.57)$$

Note that by projecting into the horizontal direction tangent to the bottom topography, denoted by the unit vector $\hat{\mathbf{t}}$, we eliminate the $p_b \nabla_z \eta_b$ term to have the steady along-topography balance

$$-f \hat{\mathbf{t}} \cdot \nabla_z \Psi = \hat{\mathbf{t}} \cdot (p_a \nabla_z \eta - \nabla_z P + \mathbf{A} + \mathbf{D} + \Delta\boldsymbol{\tau}). \quad (25.58)$$

25.5 Axial angular momentum budget for an ocean domain

We here develop the column integrated budget for axial angular momentum for a region of the ocean, such as shown in Figure 25.6. We then further specialize the budget by zonally integrating. The analysis shares features with the depth integrated linear momentum balance developed in Section 25.4. Similarity arises largely due to the connection between the axial angular momentum and the zonal linear momentum, with details provided in our study of geophysical particle dynamics in Sections 12.6 and 12.7. We choose to study axial angular momentum since it has a slightly simpler budget (equation (25.59) discussed below) than the corresponding budget equation (25.51) for zonal linear momentum. The simpler budget follows since axial angular momentum is directly connected to the axial symmetry of the rotating spherical planet (Sections 12.6 and 21.5).

To add a bit more generality to the analysis, we make use of spherical coordinates, though doing so offers only a modest degree of extra details beyond Cartesian coordinates. Although here focused on the ocean, many of the concepts and methods are directly relevant to a study of atmospheric axial angular momentum as introduced in Section 21.5 and lucidly discussed in Section 10.3 of Holton (1992).

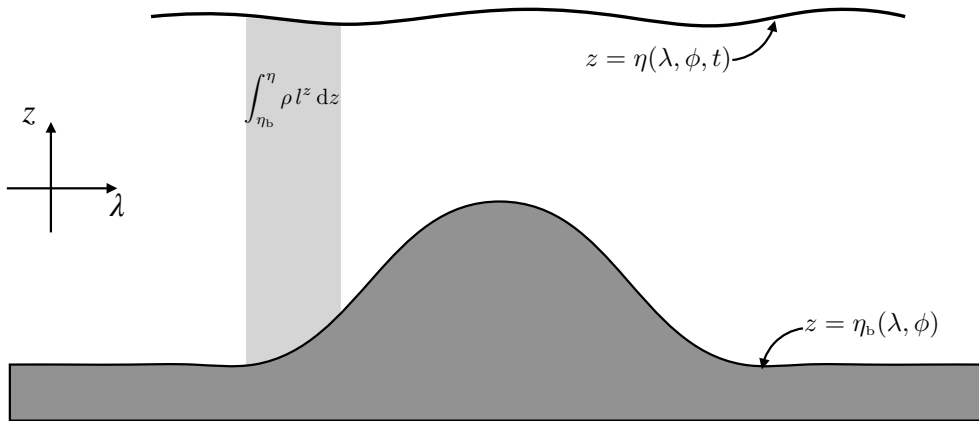


FIGURE 25.6: Schematic of the axial angular momentum for a fluid column, here depicted moving in an ocean with a topographic bump. In Section 25.5 we develop the budget for the depth and zonal integrated axial angular momentum in the ocean, where we see that the axial angular momentum is affected by a variety of boundary processes as well as interior transports and pressures.

25.5.1 Anticipating the budget

Before diving into the mathematical formulation, let us use some of the understanding gleaned from earlier sections of this chapter to anticipate the basic results. Doing so offers us a framework to guide the maths, and to double check that the maths indeed renders a physically sensible budget.

For this purpose, consider a column of fluid such as shown in Figure 25.6. The forces acting on that column arise from contact forces (pressure, kinetic, and frictional stresses) acting on the boundary (sides, top, and bottom), and body forces acting throughout the column (from effective gravity and Coriolis). There are further avenues for momentum to be transported across the ocean surface as part of the mass transported by rain, evaporation, and rivers. Each of these forces contribute a torque to the fluid column computed relative to the earth's rotational axis, thus modifying the axial angular momentum of the fluid column. In the following development, we mathematically express the variety of forces and corresponding torques, thus building up the axial angular momentum budget.

25.5.2 Axial angular momentum

The axial angular momentum budget for a fluid element follows that developed in Section 21.5, here written with zonal friction

$$\rho \frac{Dl^z}{Dt} = -\frac{\partial p}{\partial \lambda} + r_{\perp} \rho F^{\lambda}, \quad (25.59)$$

where

$$l^z = r_{\perp} (u + r_{\perp} \Omega) \quad (25.60)$$

is the axial angular momentum per unit mass, and

$$r_{\perp} = r \cos \phi \quad (25.61)$$

is the distance to the polar rotation axis (the moment arm). Use of the Eulerian form of mass conservation (equation (16.6)) leads to the Eulerian flux-form budget

$$\frac{\partial(\rho l^z)}{\partial t} + \nabla \cdot (\rho \mathbf{v} l^z) = -\frac{\partial p}{\partial \lambda} + r_{\perp} \rho F^{\lambda}, \quad (25.62)$$

with $l^z \rho dz$ the angular momentum per unit horizontal area. We use this form for the budget to develop the depth integrated axial angular momentum budget.

25.5.3 Depth integrated budget

Vertically integrating equation (25.62) over a column of ocean fluid renders a budget for the column-integrated axial angular momentum. As in Section 25.4.2, we here make use of Leibniz's Rule to reach the following identities that expose boundary contributions

$$\int_{\eta_b}^{\eta} \frac{\partial(\rho l^z)}{\partial t} dz = \frac{\partial}{\partial t} \left[\int_{\eta_b}^{\eta} \rho l^z dz \right] - \left[\rho l^z \frac{\partial \eta}{\partial t} \right]_{z=\eta} \quad (25.63a)$$

$$\int_{\eta_b}^{\eta} \nabla_z \cdot (\rho \mathbf{u} l^z) dz = \nabla_z \cdot \left[\int_{\eta_b}^{\eta} \rho \mathbf{u} l^z dz \right] - [\rho l^z \mathbf{u} \cdot \nabla \eta]_{z=\eta} + [\rho l^z \mathbf{u} \cdot \nabla \eta_b]_{z=\eta_b} \quad (25.63b)$$

$$\int_{\eta_b}^{\eta} \frac{\partial(\rho w l^z)}{\partial z} dz = [w \rho l^z]_{z=\eta} - [w \rho l^z]_{z=\eta_b}. \quad (25.63c)$$

The surface kinematic boundary condition (16.79) and bottom kinematic boundary condition (16.41) allow us to reach a reasonably tidy expression

$$\frac{\partial}{\partial t} \left[\int_{\eta_b}^{\eta} l^z \rho dz \right] = [l^z Q_m]_{z=\eta} - \nabla_z \cdot \left[\int_{\eta_b}^{\eta} l^z \mathbf{u} \rho dz \right] + \int_{\eta_b}^{\eta} \left[-\frac{\partial p}{\partial \lambda} + r_{\perp} \rho F^{\lambda} \right] dz. \quad (25.64)$$

The budget (25.64) says that the depth integrated axial angular momentum per horizontal area in a horizontally fixed fluid column has a time tendency (left hand side) arising from the convergence of horizontal advection of axial angular momentum plus torques due to surface boundary mass fluxes, depth integrated zonal pressure gradients, and depth integrated irreversible stresses. This mathematical expression of the budget meets our expectations based on our understanding of the physical principles discussed in Section 25.5.1.

25.5.4 Atmospheric and topographic form stresses

We can further unpack the contribution from pressure in the budget (25.64) by making use of Leibniz's rule to write

$$-\int_{\eta_b}^{\eta} \frac{\partial p}{\partial \lambda} dz = -\frac{\partial P}{\partial \lambda} + p_a \frac{\partial \eta}{\partial \lambda} - p_b \frac{\partial \eta_b}{\partial \lambda}, \quad (25.65a)$$

where P is the depth-integrated pressure given by equation (25.37). We studied this decomposition of the pressure force in Section 25.2 and encountered it in Section 25.4.4. Again, we see that the depth integrated zonal pressure gradient has been decomposed into three terms: (i) zonal pressure differences integrated across the depth of the column, (ii) form stress imparted to the ocean from the atmospheric pressure, (iii) form stress imparted by the solid earth bottom topography onto the ocean.

25.5.5 Turbulent stresses at the surface and bottom

For turbulent stresses, we focus on the vertical transfer of zonal momentum arising from the vertical shear of horizontal stresses

$$\rho F^{\lambda} = \frac{\partial \tau^{\lambda}}{\partial z}, \quad (25.66)$$

where τ^λ is the zonal component to the stress vector.⁵ When integrated vertically over an ocean column, $\int_{\eta_b}^{\eta_s} \rho F^\lambda dz$, this friction arises from stresses acting in the ocean surface and bottom boundary/Ekman layers (Chapter 30), where the stress arises from turbulent motions that transfer momentum vertically through these layers.

To slightly simplify the contribution from friction, we assume that the axial moment-arm is well approximated by its value at the ocean surface

$$r_\perp = r \cos \phi = (z + R) \cos \phi \approx R \cos \phi = R_\perp, \quad (25.67)$$

with this assumption holding for the shallow fluid approximation built into the hydrostatic primitive equations discussed in Section 24.1. This assumption allows us to write the frictional contribution to the angular momentum budget (25.64) in the form

$$\int_{\eta_b}^{\eta_s} r_\perp \rho F^\lambda dz \approx R_\perp \int_{\eta_b}^{\eta_s} \rho F^\lambda dz = R_\perp (\tau_a^\lambda - \tau_b^\lambda). \quad (25.68)$$

The final expression introduced τ_a^λ , which is the zonal component to the stress acting on the ocean surface imparted through interactions between the ocean and the overlying atmosphere and/or ice. The signs are such that $\tau_a^\lambda > 0$ transfers an eastward momentum to the ocean such as via a westerly wind stress. Likewise, the stress τ_b^λ is the zonal stress at the ocean bottom imparted through interactions between the ocean and the solid-earth. The signs are such that $\tau_b^\lambda > 0$ reflects the transfer of eastward momentum from the ocean to the solid-earth, or conversely the transfer of westward momentum from the earth to the ocean. The net contribution from vertical friction is thus given by the moment arm, R_\perp , multiplied by the difference in boundary stresses.

25.5.6 Summary budget for column integrated axial angular momentum

Bringing all the pieces together leads to the depth integrated axial angular momentum budget

$$\frac{\partial}{\partial t} \left[\int_{\eta_b}^{\eta_s} l^z \rho dz \right] = -\nabla_z \cdot \left[\int_{\eta_b}^{\eta_s} l^z u \rho dz \right] - \frac{\partial P}{\partial \lambda} + [l^z Q_m]_{z=\eta} + p_a \frac{\partial \eta}{\partial \lambda} - p_b \frac{\partial \eta_b}{\partial \lambda} + R_\perp (\tau_a^\lambda - \tau_b^\lambda). \quad (25.69)$$

Other than assuming the approximate form (25.67) for the moment-arm, and choosing a specific form of the frictional stress given by equation (25.66), this result is an exact budget for the axial angular momentum of a column of ocean fluid.

Removing zonal means

We further isolate the processes contributing to the budget (25.69) by introducing the zonal mean operator

$$\bar{A} \equiv \frac{1}{L(\phi)} \int A d\lambda, \quad (25.70)$$

where

$$L(\phi) = (R \cos \phi) \Delta \lambda = R_\perp \Delta \lambda \quad (25.71)$$

is the zonal length of the domain as a function of latitude, ϕ , and $\Delta \lambda$ is the zonal extent of the domain in radians. For a domain that circles the planet, then $\Delta \lambda = 2\pi$. Other domains are

⁵As seen in equation (25.50), there are other turbulent terms associated with interior Reynolds stresses arising from horizontal shears. We omit these terms for the present analysis since they are generally smaller than stresses arising from vertical strains, and smaller than the turbulent stresses associated with surface and bottom boundary processes.

possible when considering idealized theoretical models as in Figure 25.7. The corresponding zonal anomalies to the depth integrated pressure, sea surface height, and bottom topography are thus given by

$$P' = P - \bar{P} \quad \text{and} \quad \eta' = \eta - \bar{\eta} \quad \text{and} \quad \eta'_b = \eta_b - \bar{\eta}_b, \quad (25.72)$$

in which case equation (25.69) takes the form

$$\frac{\partial}{\partial t} \left[\int_{\eta_b}^{\eta} l^z \rho dz \right] = -\nabla_z \cdot \left[\int_{\eta_b}^{\eta} l^z \mathbf{u} \rho dz \right] - \frac{\partial P'}{\partial \lambda} + [l^z Q_m]_{z=\eta} + p_a \frac{\partial \eta'}{\partial \lambda} - p_b \frac{\partial \eta'_b}{\partial \lambda} + R_{\perp} (\tau_a^{\lambda} - \tau_b^{\lambda}). \quad (25.73)$$

Steady state balance

Steady state balances are of particular interest when studying the large-scale low frequency circulation. A steady state holds for the angular momentum budget (25.73) so long as the following balance is maintained

$$\nabla_z \cdot \left[\int_{\eta_b}^{\eta} l^z \mathbf{u} \rho dz \right] = -\frac{\partial P'}{\partial \lambda} + [l^z Q_m]_{z=\eta} + p_a \frac{\partial \eta'}{\partial \lambda} - p_b \frac{\partial \eta'_b}{\partial \lambda} + R_{\perp} (\tau_a^{\lambda} - \tau_b^{\lambda}). \quad (25.74)$$

Consequently, a steady state is realized if the horizontal divergence of depth integrated axial angular momentum advection (left hand side) is balanced by torques created by the variety of physical processes on the right hand side. We further examine these physical processes by studying the zonally integrated budget.

25.5.7 Zonal domain topology/geometry and zonal integration

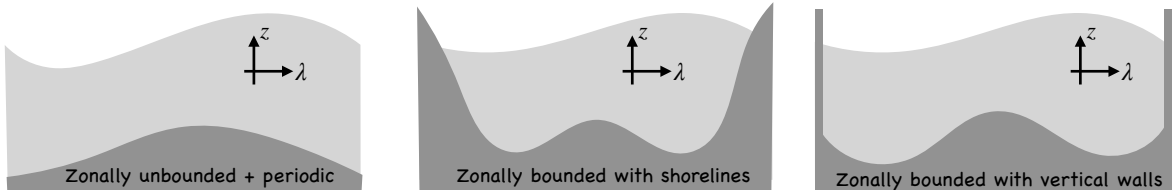


FIGURE 25.7: Three canonical zonal topologies/geometries considered in the study of fluid flow, particularly ocean flows. The light portion of each panel represents the fluid whereas the darker portion is the solid earth bottom topography. Left panel: zonally unbounded and periodic channel. Here, the topography, surface boundary forcing, and flow are zonally periodic. Middle panel: zonally bounded region where the zonal bounds occur along sloping shorelines at which the fluid thickness vanishes. The horizontal position of the vanishing thickness is time dependent since the fluid can move up and down the shoreline. Right panel: zonally bounded region where the fluid encounters a vertical sidewall so that the horizontal position of the fluid boundary is fixed, and so that there is no horizontal position where the fluid thickness vanishes. Fixed vertical sidewall boundaries are commonly found in numerical model simulations and yet they are uncommon in Nature.

Zonal integration and zonal averaging offer a common means to filter the three dimensional equations, particularly in the atmosphere where zonal motions are much stronger than meridional given the earth's rotation and the differential solar heating of the planet. Additionally, zonal averaging is of particular interest in the Southern Ocean, where the Drake Passage latitudes offer a zonally unbounded domain for ocean circulation. Even for zonally bounded ocean domains where gyre circulations occur, it is of interest to zonally integrate across the domain to study balances leading to meridional motion across the chosen latitude.

We are thus motivated to integrate zonally across the full extent of the domain, with the resulting boundary contributions dependent on the geometry and topology of the domain. We

illustrate three canonical domains in Figure 25.7. For the zonally periodic domain, the zonal integral of any zonal derivative vanishes so that

$$\oint \frac{\partial P}{\partial \lambda} d\lambda = 0, \quad (25.75)$$

where we write $\oint d\lambda$ for integration over a zonally periodic domain. Additionally, zonal derivatives vanish for a zonally bounded domain with sloping shorelines

$$\int_{\text{shorelines}} \frac{\partial P}{\partial \lambda} d\lambda = 0. \quad (25.76)$$

The reason this integral vanishes is that quantities such as P are depth integrated, and so $P = 0$ at the shoreline edge merely since the layer thickness vanishes at the shoreline edge. The same result holds for any other depth integrated quantity, such as the axial angular momentum.

It is only for the zonally bounded domain with vertical sidewalls (third panel in Figure 25.7) that we are unable to drop the zonal integral of zonal derivatives. We observe that vertical sidewalls are common for numerical models and many theories of the ocean circulation. However, vertical sidewalls are the exception in Nature. For this reason, in the following we focus on the more geophysically relevant periodic configuration and the sloping shoreline configuration.

25.5.8 Steady domain integrated balance

Consider the area integral of the steady state balance (25.74) over the full ocean domain that is either periodic and/or has sloping side boundaries. In this case the divergence of the angular momentum transport integrates to zero, so that we are left with the balance

$$\int_{\phi_s}^{\phi_n} \left(\int_{\lambda_w(\phi)}^{\lambda_e(\phi)} \left[[l^z Q_m]_{z=\eta} + p'_a \frac{\partial \eta'}{\partial \lambda} - p'_b \frac{\partial \eta'_b}{\partial \lambda} + R_\perp (\tau_a^\lambda - \tau_b^\lambda) \right] d\lambda \right) R^2 \cos \phi d\phi = 0. \quad (25.77)$$

In computing the area integral, we chose to first integrate over the longitudinal domain, $\lambda_w(\phi) \leq \lambda \leq \lambda_e(\phi)$, which is a function of latitude, and then to integrate over the full latitudinal domain, $\phi_s \leq \phi \leq \phi_n$. In most applications the surface mass term, $[l^z Q_m]_{z=\eta}$, is smaller than the other terms, in which case the balance is between the boundary form stresses and the boundary turbulent stresses.

In the angular momentum balance (25.77), we introduced the zonal anomalies for the applied surface pressure and the bottom pressure

$$p'_a(\lambda, \phi) = p_a(\lambda, \phi) - \bar{p}_a(\phi) \quad \text{and} \quad p'_b(\lambda, \phi) = p_b(\lambda, \phi) - \bar{p}_b(\phi). \quad (25.78)$$

We can introduce these anomalous fields since their zonal averages do not contribute to the budgets in either the periodic or sloping shoreline domains. To verify this property, note that

$$\int \bar{p}_a \frac{\partial \eta'}{\partial \lambda} d\lambda = \int \frac{\partial (\bar{p}_a \eta')}{\partial \lambda} d\lambda = 0. \quad (25.79)$$

For a periodic domain this term vanishes by inspection. For a zonally bounded domain with a sloping shoreline, it also vanishes since $\eta' = 0$ at the edge of the shoreline. Likewise, the bottom pressure term satisfies

$$\int \bar{p}_b \frac{\partial \eta'_b}{\partial \lambda} d\lambda = \int \frac{\partial (\bar{p}_b \eta'_b)}{\partial \lambda} d\lambda = 0, \quad (25.80)$$

which follows either by periodicity or since $\eta'_b = 0$ along the edge of a sloping shoreline. In conclusion, we see that it is only the zonal anomalies of the atmospheric and bottom pressures, and free surface and bottom topography, that impact the zonal mean zonal momentum balance (25.82) for the periodic and sloping shoreline domains.

25.5.9 Form stress versus dual form stress

We can further exploit the symmetries of the periodic and sloping shoreline domains by writing the form stresses in equation (25.82) in an alternative manner that makes use of the dual form stress

$$\int \left[p'_a \frac{\partial \eta'}{\partial \lambda} - p'_b \frac{\partial \eta'_b}{\partial \lambda} \right] d\lambda = \int \left[-\frac{\partial p'_a}{\partial \lambda} \eta' + \frac{\partial p'_b}{\partial \lambda} \eta'_b \right] d\lambda. \quad (25.81)$$

Diagnostics of zonally integrated form stress can be more convenient using one form or the other, depending on dataset or numerical model framework. We have a choice since the zonal integral is the same, and that freedom is afforded since the spatial integral removes local information that appears as a total zonal derivative. However, we offer two caveats in this regard.

- The identity (25.81) does not hold for the bounded domain with vertical sidewalls (third panel of Figure 25.7). If working in such a domain and if one chooses to study patterns based on the right hand side dual form stress, then its zonal integral will not agree with that of the form stress on the left hand side. Correspondingly, physical interpretations based on the dual form stress are questionable.
- Although the zonal integrals in equation (25.81) agree for the periodic domain and sloping shoreline domain, there is no local identity between terms on the left hand side and right hand side. So if one wishes to make a statement about patterns of local form stresses acting on the depth integrated axial angular momentum, then it is necessary to return to the form stress appearing on the left hand side of equation (25.81).

25.5.10 Steady zonal and depth integrated budget

Now consider just a zonal integral, again over a domain that is either periodic or has sloping shorelines (Figure 25.7). In both of these cases, we are left with the zonal and depth integrated steady angular momentum budget

$$\frac{1}{R \cos \phi} \int \frac{\partial}{\partial \phi} \left[\int_{\eta_b}^{\eta_a} l^z v \rho dz \right] d\lambda = \int \left[[l^z Q_m]_{z=\eta} + p'_a \frac{\partial \eta'}{\partial \lambda} - p'_b \frac{\partial \eta'_b}{\partial \lambda} + R_{\perp} (\tau_a^{\lambda} - \tau_b^{\lambda}) \right] d\lambda. \quad (25.82)$$

The meridional divergence of the advective transport of angular momentum is balanced, in the steady state, by the boundary terms on the right hand side.

25.5.11 Southern Ocean balances

Under certain cases the primary balance in equation (25.82) is between the form stress and boundary turbulent stress, whereby

$$\oint \left[p'_a \frac{\partial \eta'}{\partial \lambda} + R_{\perp} \tau_a^{\lambda} \right] d\lambda \approx \oint \left[p'_b \frac{\partial \eta'_b}{\partial \lambda} + R_{\perp} \tau_b^{\lambda} \right] d\lambda. \quad (25.83)$$

For much of the large-scale Southern Ocean circulation, the primary balance is even simpler: it is a balance between surface wind stress and topographic form stress

$$\oint \tau_a^\lambda d\lambda \approx \oint p'_b \frac{1}{R_\perp} \frac{\partial \eta'_b}{\partial \lambda} d\lambda = - \oint \eta'_b \frac{1}{R_\perp} \frac{\partial p'_b}{\partial \lambda} d\lambda, \quad (25.84)$$

with this balance exemplified in Figure 25.8. We now state in words what this balance means in the presence of a net eastward wind stress, $\oint \tau_a^\lambda d\lambda > 0$. The equivalent expressions on the right hand side allow complementary perspectives.

- For the first equality in equation (25.84) we see that a balance is realized if on the upwind side of a topographic bump there is an anomalously high bottom pressure, with the opposite on the downwind side. Correspondingly, there is a net westward topographic form stress imparted by the solid earth onto the ocean that balances the eastward surface wind stress imparted by the atmosphere onto the ocean.
- The second equality in equation (25.84) reveals that for $\eta'_b > 0$ (topographic ridge), a steady angular momentum balance is maintained so long as the bottom pressure decreases across the ridge from west to east, just as depicted in Figure 25.8.

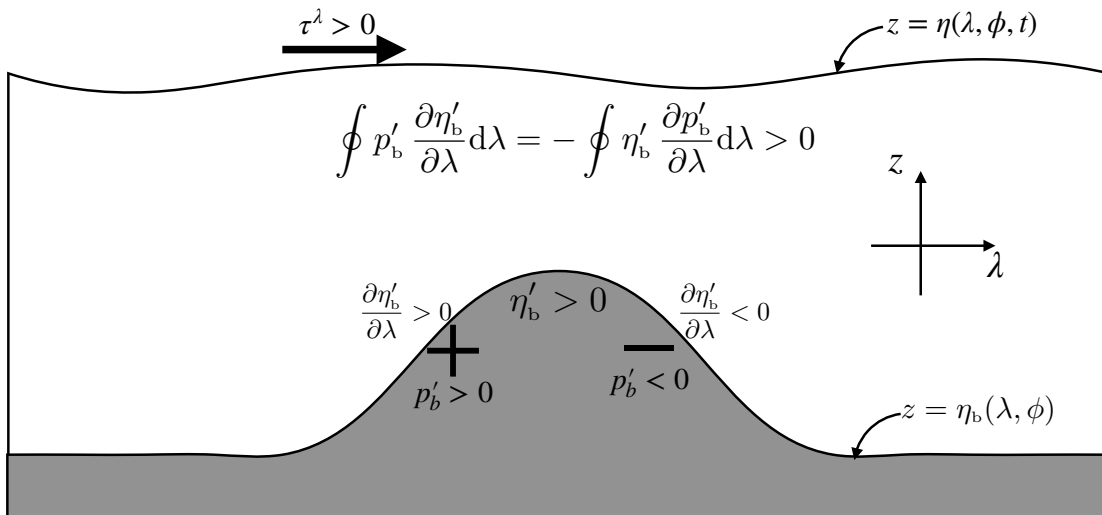


FIGURE 25.8: Depicting the balance between zonal wind stress and topographic form stress for a southern hemisphere zonally periodic ocean channel. For an eastward wind stress, the flow reaches a steady state if the upwind side of a topographic bump sees an anomalously high bottom pressure whereas on the downwind side it is anomalously low. The form stress imparted by the ocean onto the solid earth is eastward since the bottom pressure is higher in the west and lower in the east. Conversely, Newton's third law tells us that the topographic form stress imparted by the solid earth onto the ocean is westward. In this manner, the eastward force imparted by the atmosphere onto the ocean through wind stress is balanced by a westward topographic form stress imparted by the solid earth onto the ocean. Furthermore, the eastward bottom pressure gradient leads to a northward depth integrated geostrophic transport above the southern hemisphere ridge. Signs are swapped when flow moves over a depression, in which a westward bottom pressure gradient leads to southward geostrophic transport over the depression. We revisit these dynamical processes for the shallow water fluid in Figure 33.8.

25.5.12 Topographic form stress and ocean gyres

Hughes and de Cueves (2001) are notable for having emphasized the importance of bottom topographic form stress, and the associated bottom pressure torque appearing in the vorticity equation

(detailed in see Section 37.9). The key role for topographic form stress is well appreciated for channel flows since the work of *Munk and Palmén* (1951) who studied the Southern Ocean force balances. However, *Hughes and de Cueves* (2001) showed that it is central even for steady ocean gyre circulations when allowing for sloping sides rather than vertical sides. Hence, sloping sides for the gyre domain allow for a steady momentum balance to occur between bottom form stress and wind stress, and a steady vorticity balance to occur between bottom pressure torque and wind stress curl. As a result, topographic form stress and bottom pressure torques allow for a mostly inviscid balance in ocean gyres much like for the zonally re-entrant Southern Ocean.

The critical role of sloping sides was not appreciated by the pioneering studies of ocean gyres from *Stommel* (1948) and *Munk* (1950), who used vertical sidewalls and relied on friction to close the vorticity budget. That is, vertical sides hide the role of topographic form stresses, thus requiring frictional stresses to balance the wind stress. We return to these points in Section 36.7, in particular in Section 36.7.5, when studying gyre circulations in a shallow water fluid.

25.5.13 Further study

Elements of this section are based on *Hughes and de Cueves* (2001) and the analogous discussion of the global atmospheric axial angular momentum budget developed in Section 10.3 of *Holton* (1992). *Straub* (1993) provides an analogous analysis with a focus on the Southern Ocean. The physical processes establishing the balances noted for the Southern Ocean remain under investigation, with further resources to the literature including Section 21.7 of *Vallis* (2017), and the reviews by *Rintoul et al.* (2001), *Rintoul and Naveira Garabato* (2013), and *Rintoul* (2018). We further revisit this balance in Section 33.7 for the shallow water system.



Chapter 26

THE BOUSSINESQ OCEAN

In some areas of fluid mechanics the speed of fluid particles can approach the speed of sound. In that case, the *Mach number*, which is the ratio of the fluid particle speed to the speed of sound waves (Chapter 44), reaches unity or larger.¹ In such flows it is important to consider the influence of compressibility since the large flow speeds can lead to nontrivial local density changes through the convergence of advective mass fluxes.

Geophysical flows of interest in this book have Mach numbers well below unity. As such, their local density changes are generally much smaller than the mean density.² Yet even with a small Mach number, the impacts of pressure can play a nontrivial role in affecting density changes for those cases where motions extend over distances in the vertical that are comparable to the *scale height*. For the atmosphere, the scale height from Section 20.4.10 is roughly 10 km, whereas the ocean's scale height is generally deeper than the ocean. For this reason, compressibility effects are generally non-negligible for atmospheric motions, whereas they can be neglected for many purposes in ocean fluid mechanics.

The flow in many liquids, such as the ocean, is close to incompressible whereby the velocity is well approximated as non-divergent thus allowing for the volume conserving kinematics from Chapter 18. Even so, a strictly incompressible fluid is one where the density is uniform throughout, with this approximation not suitable for many purposes in ocean fluid mechanics when aiming to capture physical processes driving large-scale ocean circulation.³ In this chapter we study the *Boussinesq ocean*, whose formulation emphasizes the distinction between a property of the fluid versus a property of the flow. In effect, the Boussinesq ocean captures a middle ground between compressible fluids and incompressible flows, whereby the flow is non-divergent whereas the fluid is quasi-compressible. Since the flow is non-divergent, the associated Boussinesq pressure is not an independent field. Rather, pressure is a diagnosed via an elliptic partial differential equation with sources determined by the flow.

Operationally, the Boussinesq ocean measures the *inertial mass*⁴ of a fluid element by multiplying the materially constant volume of the element with a constant reference density, ρ_0 . In contrast, the *gravitational mass* of the Boussinesq fluid element is computed with the space and time dependent *in situ* density, $\rho(\mathbf{x}, t)$. Hence, in all places where density is multiplied by the gravitational acceleration, such as for the calculation of pressure and gravitational potential energy, we make use of the *in situ* density. A related detail concerns the mechanical energy budget for a Boussinesq fluid, which we show (see Section 26.8) is self-consistent so long as the *in situ*

¹When a jet airplane or rocket moves at a speed greater than Mach one, such super-sonic motion generates a spectacularly loud and powerful sonic boom.

²In Section 44.6.2 in our study of acoustics, we see precisely how a density fluctuation is related to the Mach number.

³The study of constant density fluid flow is sometimes referred to as *hydrodynamics*.

⁴The inertial mass is the mass used to measure the inertia of a fluid element, such as when considering Newton's law of motion.

density is determined with its pressure dependence set according to $\rho(S, \Theta, p_{\text{eos}} = -\rho_0 \Phi)$ where $\Phi(\mathbf{x}, t)$ is the geopotential (Chapter 31).

READER'S GUIDE TO THIS CHAPTER

The Boussinesq ocean comprises a quasi-compressible fluid in which density materially changes, yet with a non-divergent flow whereby the prognostic velocity is non-divergent. We here derive the oceanic Boussinesq approximation and explore certain of its physical properties including energetics. As part of this discussion we study the available potential energy, which measures that portion of the potential energy available for converting to kinetic energy. Available potential energy is a concept that also holds for compressible non-Boussinesq fluids, but it is more conveniently studied within the Boussinesq ocean. The Boussinesq ocean has broader application than just to the ocean, with many of its characteristics also holding for atmospheric flow satisfying the anelastic approximation (see Section 2.5 of [Vallis \(2017\)](#)). Furthermore, the Boussinesq ocean provides the starting point for many of the geophysical fluid models found later in this book.

26.1	The Boussinesq ocean approximation	607
26.1.1	Isolating the dynamically active pressure field	607
26.1.2	Boussinesq momentum equation	608
26.1.3	A vorticity motivation to set ρ_0 constant	609
26.1.4	Mass continuity	610
26.1.5	Dependence on reference density	610
26.1.6	Version I of the Boussinesq ocean equations	611
26.1.7	Version II of the Boussinesq ocean equations	612
26.1.8	Summary points	613
26.1.9	Further study	614
26.2	Scaling for the hydrostatic approximation	614
26.2.1	Stratified non-rotating Boussinesq ocean equations	615
26.2.2	Non-dimensionalization	615
26.2.3	Specifying scales	616
26.2.4	The role of the Froude number	617
26.2.5	Horizontal hydrostatic pressure gradient	618
26.2.6	Evolution of hydrostatic pressure	619
26.3	How pressure enforces non-divergent flow	619
26.3.1	Poisson equation for pressure	620
26.3.2	Boundary conditions	620
26.3.3	Characterizing the pressure sources	621
26.3.4	Comments and further study	623
26.4	Helmholtz decomposing the velocity equation	623
26.4.1	Helmholtz decomposition	624
26.4.2	The pressure equation	624
26.4.3	The vorticity equation	624
26.4.4	The velocity equation	625
26.4.5	Comments	625
26.5	Tracer budgets in Eulerian regions	625
26.5.1	Formulating the budget equation	625
26.5.2	Interpreting advective tracer contributions	626
26.5.3	A rectangular region example	627
26.5.4	Comments	628
26.6	Subgrid scale processes and boundary conditions	628
26.6.1	Material evolution of buoyancy	628
26.6.2	Mechanical forcing and dissipation	629

26.7 Mechanical energy analysis: Part I	630
26.7.1 Kinetic energy	630
26.7.2 Gravitational potential and mechanical energies	631
26.8 Mechanical energy analysis: Part II	632
26.8.1 Boussinesq dynamic enthalpy	633
26.8.2 Regionally integrated Boussinesq dynamic enthalpy	635
26.8.3 Vertical derivative of density	636
26.8.4 Comments	638
26.9 Available potential energy (APE)	638
26.9.1 Analytic continuation of buoyancy surfaces	639
26.9.2 The dual relation between height and buoyancy	642
26.9.3 Exact expression for APE	643
26.9.4 Approximate expression for APE	644
26.9.5 Comments	646
26.10 Exercises	647

26.1 The Boussinesq ocean approximation

For the ocean, density deviates no more than a few percent relative to the volume mean density. Although small, ocean density deviations act over large distances and are crucial for driving large-scale circulations. Such *thermohaline circulations* derive their driving force from variations in temperature and salinity that affect density and, in turn, modify the pressure. A key reason that small density changes can be so pivotal is that the density variations are multiplied by the relatively large gravitational acceleration when computing pressure. The oceanic Boussinesq approximation provides a systematic means to ignore small density deviations where it is safe to do so dynamically, while retaining density variations where they are critical such as when multiplied by gravity. In brief, the oceanic Boussinesq approximation makes use of (a slightly modified) compressible thermodynamics plus an incompressible kinematics. The use of compressible thermodynamics allows for thermohaline processes to modify density and thus pressure, while the incompressible kinematics removes sound waves and renders the volume of a fluid element materially invariant in the fluid interior.

26.1.1 Isolating the dynamically active pressure field

Pressure in a vertically stratified fluid can be decomposed into a static background hydrostatic pressure plus a deviation from the background pressure. We made use of this decomposition in Section 24.2.4 when developing the scaling for the hydrostatic approximation. The decomposition holds even when the fluid is non-hydrostatic. We consider the background pressure to be a function just of depth and as such it is determined by a static and horizontally homogeneous background density field. We are motivated to introduce this decomposition given that the background hydrostatic pressure field (again, it is just a function of depth) is dynamically inactive (we show this below). It is thus convenient to remove it from the dynamical equations. This decomposition is exact and motivated by the desire to isolate the dynamically active part of the equations of motion.

To achieve the pressure decomposition, start by decomposing density according to

$$\rho(\mathbf{x}, t) = \rho_0(z) + \rho'(\mathbf{x}, t) \tag{26.1}$$

where the deviation density is much smaller than the reference density

$$\rho' \ll \rho_0. \tag{26.2}$$

The following formulation for the momentum equation holds for the general case of $\rho_0(z)$. However, we note in Section 26.1.2 that setting $\rho_0(z) = \rho_0$ is motivated for studies of potential vorticity in the Boussinesq ocean. Indeed, a space and time constant reference density is generally synonymous with the oceanic Boussinesq approximation.⁵

The corresponding decomposition of pressure is given by the sum of a static and depth dependent background pressure, $p_0(z)$, and a deviation pressure, $p'(\mathbf{x}, t)$,

$$p(\mathbf{x}, t) = p_0(z) + p'(\mathbf{x}, t). \quad (26.3)$$

The background pressure is assumed to be in hydrostatic balance with the reference density

$$\frac{dp_0}{dz} = -\rho_0 g, \quad (26.4)$$

with p_0 and ρ_0 both static. We offer the following points to clarify the decomposition of pressure in equation (26.3).

- Assuming the background pressure, $p_0(z)$, to be hydrostatic does *not* imply that the full pressure, $p(\mathbf{x}, t)$, is also hydrostatic. Rather, the decomposition merely serves to remove that portion of the pressure field that plays no role in establishing motion (we see this property below). So this decomposition holds whether the full pressure is approximately hydrostatic or fully non-hydrostatic.
- Furthermore, if $p(\mathbf{x}, t)$ is in an approximate hydrostatic balance (Section 24.2), the decomposition (26.3) does *not* remove all of the hydrostatic pressure from $p(\mathbf{x}, t)$. Rather, $p'(\mathbf{x}, t)$ is generally nonzero whether $p(\mathbf{x}, t)$ is in an approximate hydrostatic balance or fully non-hydrostatic.

With the above density and pressure decompositions, the momentum equation

$$\rho \left[\frac{D\mathbf{v}}{Dt} + 2\boldsymbol{\Omega} \times \mathbf{v} \right] = -\nabla p - \hat{\mathbf{z}} g \rho \quad (26.5)$$

takes the equivalent form

$$(\rho_0 + \rho') \left[\frac{D\mathbf{v}}{Dt} + 2\boldsymbol{\Omega} \times \mathbf{v} \right] = -\nabla p' - g \rho' \hat{\mathbf{z}} - \left[\frac{dp_0}{dz} + \rho_0 g \right] \hat{\mathbf{z}} \quad (26.6a)$$

$$= -\nabla p' - g \rho' \hat{\mathbf{z}}, \quad (26.6b)$$

where we used the hydrostatic balance (26.4) for the second equality. We thus see that the background hydrostatic pressure, $p_0(z)$, leads to no motion since it drops out from the momentum equation. The gradient pressure force is thus determined solely by the gradient of p' .

26.1.2 Boussinesq momentum equation

To develop the Boussinesq momentum equation, divide the momentum equation (26.6b) by the density, $\rho = \rho_0 + \rho'$, and write the pressure and gravity terms as

$$\frac{\nabla p' + g \rho' \hat{\mathbf{z}}}{\rho_0 + \rho'} = \frac{\nabla p' + g \rho' \hat{\mathbf{z}}}{\rho_0 + \rho'} \left[\frac{\rho_0 - \rho'}{\rho_0 - \rho'} \right] = \frac{\nabla p' + g \rho' \hat{\mathbf{z}}}{\rho_0^2 - (\rho')^2} (\rho_0 - \rho') \approx \frac{\nabla p' + g \rho' \hat{\mathbf{z}}}{\rho_0}, \quad (26.7)$$

⁵Exercise 26.3 offers a modest means to generalize this assumption.

where the final approximation results from dropping all terms that are second order in deviation quantities. This approximation then leads to the Boussinesq momentum equation

$$\frac{D\mathbf{v}}{Dt} + 2\boldsymbol{\Omega} \times \mathbf{v} = -\frac{1}{\rho_0} \nabla p' + b \hat{\mathbf{z}}, \quad (26.8)$$

where we introduced the globally referenced *Archimedean buoyancy* (Chapter 27) as defined relative to the constant background density

$$b = -\frac{g \rho'}{\rho_0} = -\frac{g(\rho - \rho_0)}{\rho_0}. \quad (26.9)$$

Hence, the globally referenced Archimedean buoyancy is positive when the *in situ* density is less than the reference density so that $\rho' = \rho - \rho_0 < 0$. That is, $b > 0$ when the fluid element is lighter (more buoyant) than the background reference density. Buoyancy is the product of the gravitational acceleration, which is a relatively large term, and the small number ρ'/ρ_0 . Their product is generally not small so that it generally cannot be neglected from the momentum equation.

In the special case of a space and time constant reference density, $\rho_0(z) = \rho_0$, it is convenient to introduce the shorthand for the deviation pressure normalized by the reference density

$$\varphi = \frac{p'}{\rho_0} = \frac{p - p_0(z)}{\rho_0}. \quad (26.10)$$

In this case the Boussinesq momentum equation takes the form

$$\frac{D\mathbf{v}}{Dt} + 2\boldsymbol{\Omega} \times \mathbf{v} = -\nabla \varphi + b \hat{\mathbf{z}}. \quad (26.11)$$

26.1.3 A vorticity motivation to set ρ_0 constant

We now anticipate a later discussion of vorticity and potential vorticity to motivate setting $\rho_0(z)$ to a constant. This paragraph is not critical for the remainder of this chapter, but worth returning to after studying vorticity. For that purpose, we note that the form of the pressure gradient acceleration found in equation (26.11) is particularly useful given that the curl of the right hand side eliminates pressure from the vorticity equation (Section 37.7.1). In contrast, for the more general form with $\rho_0(z)$ in equation (26.8), the Boussinesq baroclinicity vector (equation (37.140)) has a contribution from both pressure and buoyancy (we derive equation (26.12) in Exercise 37.2)

$$\mathbf{B} = \nabla \left[b - \frac{p'}{\rho_0^2} \frac{d\rho_0}{dz} \right] \times \hat{\mathbf{z}}. \quad (26.12)$$

The additional pressure contribution complicates the development of potential vorticity whereby we wish to have $\mathbf{B} \cdot \nabla b = 0$ (see Section 38.5.1). We are thus motivated to use a space and time constant reference density so that $d\rho_0/dz = 0$. Following this motivation, we generally assume ρ_0 is a constant in this book. Even so, in Exercise 26.3 we discuss a middle ground by defining a slightly more general buoyancy field while retaining a constant ρ_0 .

26.1.4 Mass continuity

When decomposing density according to equation (26.1), the mass continuity equation

$$\frac{D\rho}{Dt} = -\rho \nabla \cdot \mathbf{v}, \quad (26.13)$$

takes the form

$$\frac{D\rho'}{Dt} = -(\rho_0 + \rho') (\nabla_z \cdot \mathbf{u} + \partial_z w). \quad (26.14)$$

For many geophysical flows, the material time derivative on the left hand side is much smaller than either of the two terms appearing on the right hand side. To help formalize this observation it is useful to introduce a time scale for the various terms in this equation

$$\left| \frac{1}{\rho} \frac{D\rho'}{Dt} \right| \sim \frac{1}{T_\rho} \quad |\partial_x u| \sim T_u^{-1} \quad |\partial_y v| \sim T_v^{-1} \quad |\partial_z w| \sim T_w^{-1}. \quad (26.15)$$

Quite often we find flows in which the time scales associated with the spatial deformations of the flow, in the direction of the flow, are much smaller than time scales for the material changes in density, whereby

$$T_u^{-1}, T_v^{-1}, T_w^{-1} \gg T_\rho^{-1}. \quad (26.16)$$

In this case the only way for the mass balance equation (26.14) to hold is for the three terms contributing to the divergence to balance one another

$$\partial_x u + \partial_y v + \partial_z w \approx 0. \quad (26.17)$$

Taking this balance to the limit motivates setting the velocity field for the Boussinesq ocean to be non-divergent

$$\nabla \cdot \mathbf{v} = 0. \quad (26.18)$$

Note that for stratified flows we generally find the horizontal divergence of the horizontal velocity balancing the vertical convergence of the vertical velocity. For a Boussinesq ocean this balance is exact

$$\nabla_z \cdot \mathbf{u} = -\partial_z w. \quad (26.19)$$

26.1.5 Dependence on reference density

How does the solution compare when considering two distinct reference densities, say $\rho_0 \neq \rho_1$? To answer this question, write the inviscid Boussinesq velocity equation in the form

$$(\partial_t + \mathbf{v}_0 \cdot \nabla) \mathbf{v}_0 + 2\boldsymbol{\Omega} \times \mathbf{v}_0 = -\nabla \varphi_0 + b_0 \hat{\mathbf{z}} \quad (26.20a)$$

$$(\partial_t + \mathbf{v}_1 \cdot \nabla) \mathbf{v}_1 + 2\boldsymbol{\Omega} \times \mathbf{v}_1 = -\nabla \varphi_1 + b_1 \hat{\mathbf{z}}. \quad (26.20b)$$

Consider an initial condition in which

$$\rho_0 \mathbf{v}_0 = \rho_1 \mathbf{v}_1, \quad (26.21)$$

and with pressure and buoyancy initialized so that

$$\rho_0 (-\nabla \varphi_0 + b_0 \hat{\mathbf{z}}) = \rho_1 (-\nabla \varphi_1 + b_1 \hat{\mathbf{z}}) = -\nabla p - g \rho \hat{\mathbf{z}}. \quad (26.22)$$

Hence, the difference between equations (26.20a) and (26.20b) takes the form

$$\partial_t(\rho_0 \mathbf{v}_0 - \rho_1 \mathbf{v}_1) = -(\rho_0 \mathbf{v}_0 \cdot \nabla) \mathbf{v}_0 + (\rho_1 \mathbf{v}_1 \cdot \nabla) \mathbf{v}_1 \quad (26.23a)$$

$$= -[(\rho_1 - \rho_0)/\rho_0] (\mathbf{v}_1 \cdot \nabla) \mathbf{v}_1. \quad (26.23b)$$

The difference in reference densities allows for the nonlinear self-advection to evolve the difference $\rho_0 \mathbf{v}_0 - \rho_1 \mathbf{v}_1$. This property of the oceanic Boussinesq equations must be kept in mind if comparing numerical solutions using distinct reference densities. Namely, a Boussinesq ocean is dependent on the reference density through the nonlinear advection term.

26.1.6 Version I of the Boussinesq ocean equations

The first form of the oceanic Boussinesq equations emphasizes the role of buoyancy computed relative to a reference state of constant density, $\rho = \rho_0$. This form facilitates a focus on that portion of the pressure field giving rise to internal or baroclinic pressure gradients; i.e., those pressure gradients that generate motion independent of free surface undulations. The oceanic Boussinesq equations thus take the form

$$\frac{D\mathbf{v}}{Dt} + 2\boldsymbol{\Omega} \times \mathbf{v} = -\nabla\varphi + b\hat{z} + \mathbf{F} \quad \text{velocity equation} \quad (26.24a)$$

$$\nabla \cdot \mathbf{v} = 0 \quad \text{continuity equation} \quad (26.24b)$$

$$\frac{Db}{Dt} = \dot{b} \quad \text{buoyancy equation} \quad (26.24c)$$

$$b = -\frac{g\rho'}{\rho_0} = -\frac{g(\rho - \rho_0)}{\rho_0} \quad \text{buoyancy defined} \quad (26.24d)$$

$$\varphi = \frac{p'}{\rho_0} = \frac{p - p_0(z)}{\rho_0} \quad \text{dynamic pressure defined} \quad (26.24e)$$

$$\rho = \rho_0(1 - \alpha\Theta + \beta S) \quad \text{linear equation of state} \quad (26.24f)$$

$$\frac{dp_0}{dz} = -\rho_0 g \quad \text{background hydrostatic pressure.} \quad (26.24g)$$

We offer the following comments on these equations.

- MATERIAL EVOLUTION OF BUOYANCY: The term \dot{b} on the right hand side of the buoyancy equation (26.24c) is a placeholder for any process leading to a material change in buoyancy. We discuss some explicit examples of $\dot{b} \neq 0$ in Section 26.6.1.
- EQUATION OF STATE: The equation of state, (26.24f), is written as a linear function of salinity and Conservative Temperature, with the thermal expansion coefficient, α , and haline contraction coefficient, β , assumed constant. This form of the equation of state eliminates processes such as cabbeling and thermobaricity (discussed in Section 64.3). These processes are important for certain features of the ocean, thus prompting the more general equation set in Section 26.1.7. However, for many studies the linear equation of state is sufficient, and we will at times make use of it, as well as the further simplified form with zero haline contraction, $\beta = 0$.
- HYDROSTATIC APPROXIMATION: Most numerical models of the large-scale ocean circulation are hydrostatic. Making the hydrostatic approximation in the velocity equation (26.24a)

leads to the split into a horizontal velocity equation plus a vertical hydrostatic balance

$$\frac{D\mathbf{u}}{Dt} + 2\boldsymbol{\Omega} \times \mathbf{v} = -\nabla_z \varphi + \mathbf{F}^h \quad \text{horizontal velocity equation} \quad (26.25a)$$

$$\frac{\partial \varphi}{\partial z} = b \quad \text{hydrostatic balance,} \quad (26.25b)$$

where ∇_z is the horizontal gradient operator and \mathbf{F}^h is the horizontal frictional acceleration. We emphasize that the vertical momentum equation, reduced to the hydrostatic approximation, has no friction. Rather, when making the hydrostatic approximation we have just a balance between the vertical pressure gradient and gravity/buoyancy.

26.1.7 Version II of the Boussinesq ocean equations

The non-hydrostatic Boussinesq equations (26.24a)-(26.24g) are suited for many purposes in this book. However, we find the following form more convenient when examining the equations used in a realistic non-hydrostatic Boussinesq ocean flows, with such flows involving prognostic equations for salinity and Conservative Temperature rather than for buoyancy. We are thus motivated to consider the Boussinesq ocean equations in the form

$$\frac{D\mathbf{v}}{Dt} + 2\boldsymbol{\Omega} \times \mathbf{v} = -(1/\rho_0) (\nabla p + \rho \nabla \Phi) + \mathbf{F} \quad \text{velocity equation} \quad (26.26a)$$

$$\nabla \cdot \mathbf{v} = 0 \quad \text{continuity equation} \quad (26.26b)$$

$$\frac{DS}{Dt} = \dot{S} \quad \text{salinity equation} \quad (26.26c)$$

$$\frac{D\Theta}{Dt} = \dot{\Theta} \quad \text{Conservative Temperature equation} \quad (26.26d)$$

$$\rho = \rho(S, \Theta, \Phi) \quad \text{equation of state.} \quad (26.26e)$$

We make the following comments concerning these equations.

- **GEOPOTENTIAL:** The geopotential is here considered to be a function of space and time, as relevant when studying the role of atmospheric tidal forcing or changes to the mass distribution of the planet (see Chapter 31)

$$\Phi = \Phi(\mathbf{x}, t). \quad (26.27)$$

- **EQUATION OF STATE:** The equation of state is a function of salinity, Conservative Temperature, and geopotential, thus allowing for processes such as cabelling and thermobaricity (see Section 64.3). Even so, the pressure dependence in the equation of state is computed as per a homogeneous and resting hydrostatic fluid

$$\rho(S, \Theta, \Phi) = \rho(S, \Theta, p = -\rho_0 \Phi). \quad (26.28)$$

In Section 26.8 we see why it is appropriate to take this functional form rather than the more general form discussed in Section 27.3, in which density is a function of the full *in situ* pressure rather than the geopotential: $\rho = \rho(S, \Theta, p)$.

- **HYDROSTATIC APPROXIMATION:** As for version I of the Boussinesq ocean equations, we here list the equations when making the hydrostatic approximation in the vertical momentum equation, in which case the velocity equation (26.26a) splits into a horizontal velocity

equation and hydrostatic balance

$$\frac{D\mathbf{u}}{Dt} + 2\boldsymbol{\Omega} \times \mathbf{v} = -(1/\rho_0) (\nabla_z p + \rho \nabla_z \Phi) + \mathbf{F}^h \quad \text{horizontal velocity equation} \quad (26.29a)$$

$$\frac{\partial p}{\partial z} = -g \rho \quad \text{hydrostatic balance.} \quad (26.29b)$$

26.1.8 Summary points

We close this section by summarizing a number of conceptual points characterizing the Boussinesq ocean. It is useful to return to this list to help avoid common conceptual confusions.

Divergent and non-divergent velocity components

The velocity that results from the Boussinesq momentum equation (i.e., the prognostic Boussinesq velocity) is non-divergent. This is the velocity used for transport as per the material time derivative operator. Additionally, there is a divergent velocity component, \mathbf{v}^d , that balances the material evolution of density

$$\frac{1}{\rho'} \frac{D\rho'}{Dt} = -\nabla \cdot \mathbf{v}^d \neq 0. \quad (26.30)$$

The divergent velocity is not used for any of the Boussinesq dynamical equations. Nonetheless, $\mathbf{v}^d \neq 0$, as its divergence balances the material evolution of density according to equation (26.30). Consequently, there are acoustic waves (Chapter 44) in the Boussinesq ocean.

Concerning density evolution and thermohaline circulation

The use of a non-divergent velocity for the Boussinesq ocean equations does not mean that the material time evolution of ρ vanishes. Instead, the scaling in Section 26.1.4 focuses just on the mass continuity equation. We must additionally acknowledge that as temperature and salinity evolve, so too does *in situ* density as determined through the equation of state. Indeed, equation (26.30) provides one expression for this evolution. Changes to density translate into changes in pressure, which in turn drive the large-scale *thermohaline circulation*.

The thermodynamic equation for Conservative Temperature or potential temperature is needed to determine density. There are various forms for the relation between temperature and density that depend on thermodynamic assumptions. We discuss the flavors for density in Section 27.3. For purposes of realistic ocean modeling, an accurate expression for density is critical, whereas for idealized modeling it is common to assume density equals to a constant times the temperature.

Buoyancy

We note the rather trivial point that there is identically zero buoyancy, $b = -g(\rho - \rho_0)/\rho_0$, in a fully homogeneous fluid where density is constant everywhere. Hence, for an exactly incompressible fluid, where density is a fixed and uniform constant, there are no buoyancy forces. Such fluids serve many purposes, as exemplified by studies of a single layer of shallow water fluid in Part VI of this book. However, buoyancy forces are of primary importance for many other purposes in geophysical fluid mechanics. The Boussinesq ocean accounts for buoyancy forces, and the changes arising from processes such as heating and freshening, while making use of the more convenient kinematics of an incompressible flow. We have far more to say concerning buoyancy in Chapter 27.

Distinction from traditional Boussinesq approximation

The Boussinesq equations are more general than the traditional Boussinesq approximation considered in other areas of fluid mechanics (e.g., [Chandrasekhar, 1961](#)). In particular, the traditional Boussinesq approximation typically assumes a linear equation of state. However, as we saw in Section 26.1.7, the Boussinesq ocean does not generally assume a linear equation of state, with a nonlinear equation of state essential for realistic ocean circulation studies.

Inertial mass is not equal to gravitational mass

A Boussinesq ocean fluid element materially conserves its volume, with this property forming the basis for Boussinesq kinematics. In turn, we measure the inertial mass of a Boussinesq ocean fluid element by multiplying its volume times the constant reference density, ρ_0 . However, whenever there is a gravitational acceleration multiplying density we retain the full *in situ* density to measure the weight of the fluid element. That is, for a Boussinesq ocean the inertial mass of a fluid element is not the same as its gravitational mass, so that

$$\text{inertial mass of Boussinesq fluid element} = \rho_0 \delta V \quad (26.31\text{a})$$

$$\text{linear momentum of Boussinesq fluid element} = \mathbf{v} \rho_0 \delta V \quad (26.31\text{b})$$

$$\text{tracer mass of Boussinesq fluid element} = C \rho_0 \delta V \quad (26.31\text{c})$$

$$\text{enthalpy content of Boussinesq fluid element} = c_p \Theta \rho_0 \delta V \quad (26.31\text{d})$$

$$\text{gravitational mass of Boussinesq fluid element} = \rho \delta V. \quad (26.31\text{e})$$

$$\text{weight of Boussinesq fluid element} = g \rho \delta V. \quad (26.31\text{f})$$

The use of the *in situ* density for the gravitational mass ensures a realistic calculation of the hydrostatic pressure (Section 26.2.6) and the gravitational potential energy (Sections 26.7 and 26.8), both of which require the *in situ* density, while maintaining the convenience of incompressible flow kinematics.

Connection to anelastic atmosphere

The atmosphere is far more compressible than the ocean, so that density variations cannot be neglected and the divergent nature of the velocity is important. However, there are some cases in which an atmospheric analog to the oceanic Boussinesq approximation can be useful. The analog is known as the *anelastic approximation* and it is mathematically isomorphic to the oceanic Boussinesq approximation, in which case $\nabla \cdot (\rho \mathbf{v}) = 0$ is assumed. Section 2.5 of [Vallis \(2017\)](#) offers more details for the atmospheric anelastic approximation.

26.1.9 Further study

Section 2.4 of [Vallis \(2017\)](#) offers more details to show that density variations are small within the ocean. Further discussion of the oceanic Boussinesq approximation also can be found in Section 9.3 of [Griffies and Adcroft \(2008\)](#). This video [from SciencePrimer](#) provides a concise summary of ocean circulation arising from differences in density created by both thermal and haline (salinity) processes.

26.2 Scaling for the hydrostatic approximation

Section 24.2 provided the rudiments of a scale analysis justifying the hydrostatic approximation for large-scale ocean and atmospheric flow. However, in that discussion we noted the need to

remove a dynamically inactive hydrostatic pressure before addressing the question of whether the dynamically active pressure field is approximately hydrostatic. That decomposition of pressure was performed in Section 26.1.1 as part of deriving the Boussinesq ocean equations. We thus here return to the question of hydrostatic scaling within the context of the perfect non-rotating Boussinesq ocean equations.

26.2.1 Stratified non-rotating Boussinesq ocean equations

The stratified non-rotating perfect Boussinesq equations are

$$\frac{Du}{Dt} = -\nabla_z \varphi \quad \text{and} \quad \frac{Dw}{Dt} = -\frac{\partial \varphi}{\partial z} + b \quad \text{and} \quad \nabla \cdot \mathbf{v} = 0 \quad \text{and} \quad \frac{Db}{Dt} = 0. \quad (26.32)$$

To help isolate the dynamically important portion of pressure, we proceed much like in Section 26.1.1 whereby buoyancy is written

$$b = b'(x, y, z, t) + \tilde{b}(z). \quad (26.33)$$

The static buoyancy $\tilde{b}(z)$ encompasses a background stratification that is in hydrostatic balance with its corresponding portion of the pressure field

$$\frac{d\tilde{\varphi}}{dz} = \tilde{b}(z). \quad (26.34)$$

The Boussinesq equations thus take the form

$$\frac{Du}{Dt} = -\nabla_z \varphi' \quad \text{and} \quad \frac{Dw}{Dt} = -\frac{\partial \varphi'}{\partial z} + b' \quad \text{and} \quad \nabla \cdot \mathbf{v} = 0 \quad \text{and} \quad \frac{Db'}{Dt} = -w N^2, \quad (26.35)$$

where

$$N^2 = \frac{d\tilde{b}}{dz} \quad (26.36)$$

is the squared buoyancy frequency from the background vertical stratification.⁶ The decomposition into a background stratification helps to isolate the dynamical portion of the horizontal pressure gradient by removing a static depth dependent background. It also allows us to consider the dynamically interesting, but simpler, case in which the background stratification dominates those perturbations around it.

26.2.2 Non-dimensionalization

Now introduce the dimensional scales (in uppercase) and corresponding non-dimensional quantities (with hats)

$$(x, y) = L(\hat{x}, \hat{y}) \quad z = H\hat{z} \quad \mathbf{u} = U\hat{\mathbf{u}} \quad w = W\hat{w} \quad (26.37)$$

$$t = T\hat{t} \quad \varphi' = \Phi\hat{\varphi}' \quad b' = B\hat{b}' \quad N^2 = \bar{N}^2\hat{N}^2, \quad (26.38)$$

⁶We discuss buoyancy frequency in Section 27.5.4. For present purposes, we merely note that it provides a measure of the vertical stratification, with $N^2 > 0$ signally a gravitationally stable situation.

which yields the equations of motion

$$\frac{U}{T} \frac{\partial \hat{u}}{\partial \hat{t}} + \frac{U^2}{L} \hat{u} \frac{\partial \hat{u}}{\partial \hat{x}} + \frac{U^2}{L} \hat{v} \frac{\partial \hat{u}}{\partial \hat{y}} + \frac{UW}{H} \hat{w} \frac{\partial \hat{u}}{\partial \hat{z}} = -\frac{\Phi}{L} \frac{\partial \hat{\varphi}'}{\partial \hat{x}} \quad (26.39a)$$

$$\frac{U}{T} \frac{\partial \hat{v}}{\partial \hat{t}} + \frac{U^2}{L} \hat{u} \frac{\partial \hat{v}}{\partial \hat{x}} + \frac{U^2}{L} \hat{v} \frac{\partial \hat{v}}{\partial \hat{y}} + \frac{UW}{H} \hat{w} \frac{\partial \hat{v}}{\partial \hat{z}} = -\frac{\Phi}{L} \frac{\partial \hat{\varphi}'}{\partial \hat{y}} \quad (26.39b)$$

$$\frac{W}{T} \frac{\partial \hat{w}}{\partial \hat{t}} + \frac{UW}{L} \hat{u} \frac{\partial \hat{w}}{\partial \hat{x}} + \frac{UW}{L} \hat{v} \frac{\partial \hat{w}}{\partial \hat{y}} + \frac{WW}{H} \hat{w} \frac{\partial \hat{w}}{\partial \hat{z}} = -\frac{\Phi}{H} \frac{\partial \hat{\varphi}'}{\partial \hat{z}} + B \hat{b}' \quad (26.39c)$$

$$\frac{B}{T} \frac{\partial \hat{b}'}{\partial \hat{t}} + \frac{UB}{L} \hat{u} \frac{\partial \hat{b}'}{\partial \hat{x}} + \frac{UB}{L} \hat{v} \frac{\partial \hat{b}'}{\partial \hat{y}} + \frac{WB}{H} \hat{w} \frac{\partial \hat{b}'}{\partial \hat{z}} = -W \bar{N}^2 \hat{w} \bar{N}^2 \quad (26.39d)$$

$$\frac{U}{L} \frac{\partial \hat{u}}{\partial \hat{x}} + \frac{U}{L} \frac{\partial \hat{v}}{\partial \hat{y}} + \frac{W}{H} \frac{\partial \hat{w}}{\partial \hat{z}} = 0. \quad (26.39e)$$

26.2.3 Specifying scales

We impose the following choices for scales based on the flow regimes of interest.

- **TIME SCALE:** Assume that the time scale is determined by the horizontal velocity and the horizontal length scale

$$T = L/U. \quad (26.40)$$

- **VERTICAL VELOCITY:** It is common to assume the vertical velocity scales according to the continuity equation

$$\nabla_z \cdot \mathbf{u} + \frac{\partial w}{\partial z} = 0 \implies W = U \frac{H}{L} \equiv U \alpha_{\text{aspect}}, \quad (26.41)$$

where the final equality introduced the vertical to horizontal aspect ratio, α_{aspect} . However, vertical stratification acts to suppress vertical motion so that we introduce a non-dimensional number ϵ so that

$$w = W \hat{w} = \epsilon \left[\frac{HU}{L} \right] \hat{w}. \quad (26.42)$$

In Section 26.2.4 we motivate choosing ϵ to be the squared Froude number.

- **PRESSURE:** Scale the pressure according to the non-rotating balance of the material time change in horizontal velocity and the horizontal pressure gradient

$$\frac{U}{T} + \frac{UU}{L} = \frac{\Phi}{L} \implies \Phi = U^2. \quad (26.43)$$

Note that for rotating flows in near geostrophic balance, we will see how pressure scales with the Coriolis acceleration as in Sections 30.3.2 and 41.2.

- **BUOYANCY:** Scale buoyancy according to the hydrostatic balance

$$B = \frac{\Phi}{H} = \frac{U^2}{H}. \quad (26.44)$$

With these choices, the equations of motion (26.39a)-(26.39e) take on form

$$\frac{D\hat{\mathbf{u}}}{Dt} = -\hat{\nabla}\hat{\varphi}' \quad (26.45)$$

$$\epsilon \alpha_{\text{aspect}}^2 \frac{D\hat{w}}{Dt} = -\frac{\partial \hat{\varphi}'}{\partial \hat{z}} + \hat{b}' \quad (26.46)$$

$$\left[\frac{U^2}{N^2 H^2} \right] \frac{D\hat{b}'}{Dt} + \epsilon \hat{N}^2 \hat{w} = 0 \quad (26.47)$$

$$\hat{\nabla} \cdot \hat{\mathbf{u}} + \epsilon \frac{\partial \hat{w}}{\partial \hat{z}} = 0 \quad (26.48)$$

where we introduced the non-dimensional material time derivative

$$\frac{D}{Dt} = \frac{\partial}{\partial \hat{t}} + \hat{\mathbf{u}} \cdot \hat{\nabla}_z + \epsilon \hat{w} \frac{\partial}{\partial \hat{z}}. \quad (26.49)$$

26.2.4 The role of the Froude number

At this point we make a choice for the parameter ϵ , noting that there are many choices that one could consider. For our interests it is suitable to set ϵ equal to the squared *Froude number*

$$\epsilon = \text{Fr}^2 = \frac{U^2}{N^2 H^2}. \quad (26.50)$$

The Froude number measures the relative strength of vertical shears of the horizontal velocity, U/H , versus the buoyancy stratification, N . Alternatively, it measures the ratio of the horizontal speed for a fluid particle, U , to an internal gravity wave speed, NH . Large Froude numbers indicate large fluid particle speeds relative to wave speeds, with $\text{Fr} > 1$ a common indicator of hydraulic instability (see Exercise 32.3 for a shallow water example). In contrast, a relatively strong stratification (N^2 large) corresponds to a small Froude number and to flow that is stabilized by vertical stratification. Note that the squared Froude number is the inverse of the *Richardson number*

$$\text{Ri} = \text{Fr}^{-2} = \frac{N^2 H^2}{U^2}. \quad (26.51)$$

It is a matter of taste whether one works with Fr or Ri .

The choice (26.50) leads to the vertical velocity scale

$$W = \text{Fr}^2 \left[\frac{HU}{L} \right]. \quad (26.52)$$

For $\text{Fr} < 1$, which is the case for stratified fluids, this result means that stratification reduces the scale for the vertical velocity. The corresponding non-dimensional Boussinesq equations take the

form

$$\frac{D\hat{u}}{Dt} = -\hat{\nabla}_z \hat{\varphi}' \quad (26.53)$$

$$Fr^2 \alpha_{\text{aspect}}^2 \frac{D\hat{w}}{Dt} = -\frac{\partial \hat{\varphi}'}{\partial \hat{z}} + \hat{b}' \quad (26.54)$$

$$\frac{\hat{D}\hat{b}'}{Dt} + \hat{N}^2 \hat{w} = 0 \quad (26.55)$$

$$\hat{\nabla} \cdot \hat{\mathbf{u}} + Fr^2 \frac{\partial \hat{w}}{\partial \hat{z}} = 0. \quad (26.56)$$

The condition for hydrostatic balance in a stratified fluid thus takes the form

$$Fr^2 \alpha_{\text{aspect}}^2 \ll 1. \quad (26.57)$$

This result supports our initial suspicion that stratification suppresses vertical motion, thus reducing the vertical acceleration terms that break hydrostatic balance. That is, hydrostatic balance is more readily achieved for a stratified flow than for an unstratified flow. Note also that the horizontal divergence of the horizontal flow is reduced by the presence of stratification, which thus leads to a nearly horizontally non-divergent flow

$$\left| \hat{\nabla} \cdot \hat{\mathbf{u}} \right| = \left| Fr^2 \frac{\partial \hat{w}}{\partial \hat{z}} \right| \ll \left| \frac{\partial \hat{w}}{\partial \hat{z}} \right|. \quad (26.58)$$

Finally, this scaling reveals how the hydrostatic approximation becomes less accurate when $Fr^2 \alpha_{\text{aspect}}^2 \sim 1$, which occurs when stratification is weak and/or the aspect ratio large.

26.2.5 Horizontal hydrostatic pressure gradient

In Section 26.2.5 we studied the horizontal pressure gradient between two columns of constant density for a hydrostatic fluid. In that example, the two columns were assumed to have equal mass and the fluid non-Boussinesq. Here, we reconsider that example for a Boussinesq ocean. The expression for the hydrostatic pressure at a point within the fluid takes on the same form as that for a compressible fluid (Section 24.2.1)

$$p_h(x, y, z, t) = p_a(x, y, t) + g \int_z^\eta \rho(x, y, z', t) dz', \quad (26.59)$$

and the horizontal pressure gradient is thus given by

$$\nabla_z p_h = \nabla_z p_a + g \rho(\eta) \nabla_z \eta + g \int_z^\eta \nabla_z \rho dz'. \quad (26.60)$$

For many studies with Boussinesq ocean, we are interested in the horizontal pressure gradients in the presence of a rigid lid ocean surface whereby $\eta = 0$. In this case we compute the *internal pressure gradient*

$$\nabla_z p_h = g \int_z^0 \nabla_z \rho dz' \quad \text{rigid lid ocean.} \quad (26.61)$$

Hence, the internal horizontal pressure gradient at a vertical position z equals to the horizontal density gradient vertically integrated above that point. For example, if density increases poleward, then so too does the internal hydrostatic pressure.

26.2.6 Evolution of hydrostatic pressure

In Section 24.2.2 we developed the Eulerian evolution equation for hydrostatic pressure in a mass conserving non-Boussinesq fluid. Here we discuss the evolution in a Boussinesq ocean, starting with the expression (24.26) for hydrostatic pressure at a point within the ocean

$$p(x, y, z, t) = p_a(x, y, t) + g \int_z^\eta \rho(x, y, z', t) dz', \quad (26.62)$$

and then taking the Eulerian time tendency

$$\partial_t p = \partial_t p_a + g \rho(\eta) \partial_t \eta + \int_z^\eta \partial_t \rho(x, y, z', t) dz'. \quad (26.63)$$

These expressions hold for both the Boussinesq and non-Boussinesq ocean. However, it is only for the mass conserving non-Boussinesq ocean that we can use mass continuity (16.6) to set $\partial_t \rho = -\nabla \cdot (\mathbf{v} \rho)$. Use of Leibniz's rule then reveals that the hydrostatic pressure evolves due to the convergence of mass onto the fluid column above that point (see Section 24.2.2 for the derivation). This result is expected since the hydrostatic pressure at a point is the weight per area of fluid above that point.

For a Boussinesq ocean, the volume conserving kinematics means that we cannot replace $\partial_t \rho$ with $-\nabla \cdot (\mathbf{v} \rho)$. Correspondingly, the weight of a fluid column can change merely through *in situ* density changes, so that the weight can change even if the matter content remains fixed; e.g., through heating. We expose details by noting that the energetic consistency ideas from Section 26.8 mean that the *in situ* density in a Boussinesq ocean has the functional dependence, $\rho(S, \Theta, \Phi)$, with Φ the geopotential. Hence, the Eulerian time derivative of density is given by

$$\partial_t \rho = (\partial \rho / \partial S) \partial_t S + (\partial \Theta / \partial t) \partial_t \Theta + (\partial \rho / \partial \Phi) \partial_t \Phi. \quad (26.64)$$

With a simple geopotential, $\Phi = g z$, we have $\partial_t \Phi = 0$ since the Eulerian time derivative is computed at fixed (x, y, z) . This result leads to the time changes in the hydrostatic pressure for a Boussinesq ocean

$$\partial_t p = \partial_t p_a + g \rho(\eta) \partial_t \eta + \int_z^\eta [(\partial \rho / \partial S) \partial_t S + (\partial \Theta / \partial t) \partial_t \Theta] dz'. \quad (26.65)$$

This equation reveals the direct dependence of the hydrostatic pressure on changes in S and Θ . Hence, heating and freshening, which alter the *in situ* density, directly alter the hydrostatic pressure in a Boussinesq ocean by altering the fluid's weight per area. This result contrasts to the mass conserving non-Boussinesq fluid, whose weight per area changes only through changes to its mass per area.

26.3 How pressure enforces non-divergent flow

We return now to the case of a non-hydrostatic fluid and consider the Boussinesq velocity equation (26.26a) written in the form

$$\rho_0 (\partial_t + \mathbf{v} \cdot \nabla) \mathbf{v} + f \mathbf{z} \times \rho_0 \mathbf{v} = -\nabla p - \rho g \hat{\mathbf{z}} + \rho_0 \mathbf{F}. \quad (26.66)$$

The non-divergence constraint on the velocity, $\nabla \cdot \mathbf{v} = 0$, must be maintained at each point in the fluid and at each time instance. How is that constraint maintained? As we show in this section, pressure enforces non-divergence of the velocity. Furthermore, pressure is determined

through solving an elliptic boundary value problem. As we discussed in Section 3.5, elliptic partial differential equations transfer information instantaneously. Physically, this situation corresponds to the transition from a compressible fluid, in which pressure signals propagate via acoustic waves (Chapter 44), to an incompressible flow, in which pressure adjusts instantaneously just as if the acoustic waves travel at infinite speed. The Boussinesq ocean sits between the compressible fluid and incompressible flow. That is, the Boussinesq prognostic velocity is non-divergent, and so it does not support acoustic waves, whereas the full velocity is divergent (Section 26.1.8), and this divergent portion supports acoustic waves, although such waves are never felt by the Boussinesq dynamical fields.

26.3.1 Poisson equation for pressure

To derive the pressure equation, we find it convenient to expose Cartesian tensor labels on the momentum equation (26.66)

$$\partial_t v_m + v_n \partial_n v_m + f \epsilon_{mnp} \delta_{3n} v_p = -\partial_m p / \rho_0 - \delta_{3m} g \rho / \rho_0 + F_m. \quad (26.67)$$

The time derivative is eliminated by taking the divergence through contracting with the operator ∂_m , thus leading to

$$-\nabla^2 p / \rho_0 = \partial_m (v_n \partial_n v_m + f \epsilon_{m3p} v_p + \delta_{3m} g \rho / \rho_0 - F_m), \quad (26.68)$$

where the Laplacian operator is

$$\nabla^2 = \partial_m \partial_m \quad (26.69)$$

and the non-divergence constraint eliminated the time derivative

$$\partial_m \partial_t v_m = \partial_t \partial_m v_m = 0. \quad (26.70)$$

Equation (26.68) can be written as the Poisson equation

$$-\nabla^2 p = \rho_0 \nabla \cdot \mathbf{G}, \quad (26.71)$$

with the vector \mathbf{G} given by

$$G_m = v_n \partial_n v_m + f \epsilon_{m3p} v_p + \delta_{3m} g \rho / \rho_0 - F_m \quad (26.72a)$$

$$\mathbf{G} = (\mathbf{v} \cdot \nabla) \mathbf{v} + f \hat{\mathbf{z}} \times \mathbf{v} + g (\rho / \rho_0) \hat{\mathbf{z}} - \mathbf{F}. \quad (26.72b)$$

As when studying Green's functions in Chapter 4, it is useful to maintain the minus sign on the left hand side of equation (26.71) so that a positive divergence ($\nabla \cdot \mathbf{G} > 0$) represents a positive source for p . Equivalently, for a wavelike pressure perturbation we have

$$-\nabla^2 p \propto p, \quad (26.73)$$

so that a positive source, $-\nabla^2 p = \rho_0 \nabla \cdot \mathbf{G} > 0$, leads to a local positive pressure anomaly, and conversely for a negative source.

26.3.2 Boundary conditions

To derive the boundary conditions to go along with the Poisson equation (26.71), we find it useful to write the velocity equation as

$$\partial_t \mathbf{v} = -\nabla p / \rho_0 - \mathbf{G}. \quad (26.74)$$

Static material surface

For a static material boundary we can make use of the no normal flow kinematic boundary condition (Section 16.4.1), in which case

$$\hat{\mathbf{n}} \cdot \partial_t \mathbf{v} = \partial_t (\hat{\mathbf{n}} \cdot \mathbf{v}) = 0 \implies (\nabla p + \rho_0 \mathbf{G}) \cdot \hat{\mathbf{n}} = 0 \quad \text{for static material boundaries.} \quad (26.75)$$

This boundary condition thus takes the form of a Neumann condition

$$\hat{\mathbf{n}} \cdot \nabla p = -\rho_0 \mathbf{G} \cdot \hat{\mathbf{n}} \quad \text{for static material boundaries.} \quad (26.76)$$

Hence, maintenance of the no normal flow condition along a static material boundary requires a corresponding *Neumann boundary condition* for pressure.

Upper ocean free surface

The ocean free surface is generally dynamic and permeable, so that the velocity does not satisfy a no normal flow condition along this surface (see Section 16.4). To develop the pressure boundary condition at the free surface, we invoke a dynamical principle rather than a kinematic principle. Namely, we invoke continuity of pressure across an interface, which follows from Newton's third law (recall our discussion of stress along an interface in Section 22.10). Hence, the pressure condition at the ocean free surface is the *Dirichlet boundary condition*

$$p = p_{\text{applied}} \quad \text{at } z = \eta(x, y, t), \quad (26.77)$$

where p_{applied} is the pressure applied to the ocean surface from the overlying atmosphere or cryosphere.

26.3.3 Characterizing the pressure sources

The right hand side of the Poisson equation (26.71) contains four sources for the pressure field. Linearity of the Poisson equation allows us to separately study these sources. We here summarize their basics, borrowing from the treatment given in Section 35.5 for the kinematically simpler non-divergent barotropic model. As we will see, three of the pressure sources contribute to non-hydrostatic pressures and one to hydrostatic pressure. Note that these pressure sources are diagnostically related to pressure perturbations. That is, the sources are *associated* with the pressure perturbations rather than *causing* the perturbations. Such is part of the nuance of pressure in a non-divergent flow.

Divergence of self-advection

The first source is given by the divergence of self-advection, which can be written

$$\nabla \cdot \mathbf{G}_{\text{self-advect}} = \partial_n(v_m \partial_m v_n) = (\partial_n v_m)(\partial_m v_n) + v_m(\partial_n \partial_m v_n) = (\partial_n v_m)(\partial_m v_n), \quad (26.78)$$

where we set

$$v_m \partial_n \partial_m v_n = v_m \partial_m \partial_n v_n = 0 \quad (26.79)$$

since $\partial_n v_n = 0$ follows from the non-divergent nature of the flow. Furthermore, introducing the rate of strain tensor (equation (15.33a)) and rotation tensor (equation (15.33b)), renders

$$2 \mathbb{S}_{mn} \mathbb{S}_{mn} = (\partial_m v_n) (\partial_m v_n) + (\partial_m v_n) (\partial_n v_m) \quad (26.80)$$

$$2 \mathbb{R}_{mn} \mathbb{R}_{mn} = (\partial_m v_n) (\partial_m v_n) - (\partial_m v_n) (\partial_n v_m), \quad (26.81)$$

so that

$$\nabla \cdot \mathbf{G}_{\text{self-advect}} = (\partial_n v_m) (\partial_m v_n) = \underbrace{\mathbb{S}_{mn} \mathbb{S}_{mn}}_{\text{splat}} - \underbrace{\mathbb{R}_{mn} \mathbb{R}_{mn}}_{\text{spin}}. \quad (26.82)$$

In this equation, \mathbb{S}_{mn} are components to the rate of strain tensor and \mathbb{R}_{mn} are components to the rotation tensor. The vorticity or spin source provides a negative source to $-\nabla^2 p$. In contrast, the contribution from strain, sometimes referred to as *splat*, provides a positive source.⁷ As detailed in Sections 35.5.3, 35.5.4, and 35.5.5 for non-divergent barotropic flow, we can understand the presence of a negative pressure source from vortical (spinning) motion due to the need for pressure to counteract the centrifugal acceleration associated with curved fluid motion. Likewise, the positive pressure source from straining motion counteracts the convergent acceleration induced by the strains.

Divergence of the Coriolis acceleration

The divergence of the Coriolis acceleration introduces a pressure source given by

$$-\nabla \cdot \nabla p_{\text{coriolis}} = \nabla \cdot \mathbf{G}_{\text{coriolis}} = \nabla \cdot (f \hat{\mathbf{z}} \times \mathbf{v}) = \beta u - f \zeta, \quad (26.83)$$

where $\zeta = \partial_x v - \partial_y u$ is the vertical component to the relative vorticity, and $\beta = \partial_y f$ is the planetary vorticity gradient. As an example, consider two-dimensional flow oriented cyclonically around a point as for geostrophic flow around a low pressure center. The cyclonic flow feels an associated centrifugal acceleration directed “outward”. To maintain a non-divergent two-dimensional flow requires an oppositely directed inward pressure force. Hence, such rotating flow induces a low pressure source as a means to counteract the centrifugal acceleration

$$-\nabla \cdot \nabla p_{\text{coriolis}} < 0. \quad (26.84)$$

See section 35.5.6 for more discussion of this source as found in the non-divergent barotropic fluid.

Divergence of the gravitational force per volume

The divergence of the gravitational force per volume is given by

$$-\nabla \cdot \nabla p_{\text{gravity}} = \rho_0 \nabla \cdot \mathbf{G}_{\text{gravity}} = \nabla \cdot (g \rho \hat{\mathbf{z}}) = g \partial_z \rho, \quad (26.85)$$

with this pressure source absent in the depth-independent barotropic fluid of Section 35.5. The associated pressure gradient is that arising from the local hydrostatic component of the pressure field in which

$$\nabla \cdot (-\nabla p_{\text{gravity}} + g \rho \hat{\mathbf{z}}) = 0. \quad (26.86)$$

In regions where density decreases upward, $\partial_z \rho < 0$, a compressible fluid element that conserves its mass will expand when moving upward into less dense fluid. For a non-divergent flow that

⁷The whimsically named *splat* source is so-named since it is large when a fluid element is squashed in a manner increasing fluid strains, akin to how strains appear when a fluid impacts or “splats” against a solid obstacle. Imagine a water balloon thrown against a wall.

conserves the volume of fluid elements, there must be a counteracting force from pressure to halt the expansion of a fluid element. This counteracting force arises from the hydrostatic component to the pressure field that acts inward to squeeze the fluid element, with this pressure force originating from the negative pressure source, $-\nabla^2 p_{\text{gravity}} = g \partial_z \rho < 0$.

Divergence of the friction vector

The third source arises from the divergence of friction,

$$-\nabla \cdot \nabla p_{\text{friction}} = \rho_0 \nabla \cdot \mathbf{G}_{\text{friction}} = -\rho_0 \nabla \cdot \mathbf{F}. \quad (26.87)$$

With interior fluid friction arising from a nonzero rate of strain (Section 22.8), we expect this pressure source to be most important in regions of large strains. Indeed, for an incompressible flow feeling only molecular viscosity, the friction operator is given by (see Section 22.8.7)

$$\mathbf{F} = \nu \nabla^2 \mathbf{v}, \quad (26.88)$$

where $\nu > 0$ is a constant molecular viscosity. In this case $\nabla \cdot \mathbf{F} = 0$, so that viscous friction does not contribute a pressure source. More general cases are considered in applications where the molecular viscosity is replaced by a flow dependent eddy viscosity so that $\nabla \cdot \mathbf{F} \neq 0$. For the case of a converging frictional acceleration, $\nabla \cdot \mathbf{F} < 0$, friction then leads to a positive pressure source to counteract the friction to thus maintain a non-divergent flow.

26.3.4 Comments and further study

The gravitational source contributes a local hydrostatic component to the pressure field, whereas the other three sources contribute non-hydrostatic pressure sources. In many applications, such as general circulation modeling of the ocean and atmosphere, the fluid is assumed to be approximately hydrostatic. In this case vertical motion is diagnosed rather than prognosed, and the non-hydrostatic component of pressure is never needed to evolve the fluid motion. Even so, vertical derivatives in the non-hydrostatic pressure provide the vertical force needed for vertical accelerations. We have more to say on vertical motion in Section 27.7.

[Markowski and Richardson \(2010\)](#) provide lucid discussions of pressure forces acting in geophysical fluids. In particular their Section 2.5 inspired much of the current section.

26.4 Helmholtz decomposing the velocity equation

In this section we introduce some mathematical properties of the velocity equation for a Boussinesq ocean in a simply connected ocean domain \mathcal{R} with boundary $\partial\mathcal{R}$. For this purpose we write the velocity equation (26.66) in the form

$$\partial_t \mathbf{v} = -\nabla p/\rho_0 - \mathbf{G}, \quad (26.89)$$

where \mathbf{G} , as given by equation (26.72b), contains the various accelerations sans the pressure gradient

$$\mathbf{G} = (\mathbf{v} \cdot \nabla) \mathbf{v} + f \hat{\mathbf{z}} \times \mathbf{v} + g(\rho/\rho_0) \hat{\mathbf{z}} - \mathbf{F}. \quad (26.90)$$

26.4.1 Helmholtz decomposition

The Helmholtz decomposition from Section 15.7 says that on a simply connected domain, an arbitrary vector, such as the acceleration \mathbf{G} , can be decomposed as

$$\mathbf{G} = \mathbf{G}^{\text{rot}} + \mathbf{G}^{\text{div}} \quad (26.91)$$

where the two vectors on the right hand side satisfy

$$\nabla \cdot \mathbf{G}^{\text{rot}} = 0 \quad \text{and} \quad \nabla \times \mathbf{G}^{\text{rot}} \neq 0 \quad \mathbf{G}^{\text{rot}} \text{ is divergent-free} \quad (26.92a)$$

$$\nabla \times \mathbf{G}^{\text{div}} = 0 \quad \text{and} \quad \nabla \cdot \mathbf{G}^{\text{div}} \neq 0 \quad \mathbf{G}^{\text{div}} \text{ is curl-free} \quad (26.92b)$$

We make use of the Helmholtz decomposition for a Boussinesq ocean by noting that the non-divergent velocity only has a rotational contribution

$$\mathbf{v} = \mathbf{v}^{\text{rot}}, \quad (26.93)$$

whereas the pressure gradient only has a divergent component

$$\nabla p = (\nabla p)^{\text{div}}. \quad (26.94)$$

In contrast, the acceleration, \mathbf{G} , generally has a rotational, a divergent, and a harmonic component as written in equation (26.91).

26.4.2 The pressure equation

Making use of the Helmholtz decomposition (26.91) brings the velocity equation (26.89) into the form

$$\partial_t \mathbf{v} = -\nabla p/\rho_0 - \mathbf{G}^{\text{rot}} - \mathbf{G}^{\text{div}}. \quad (26.95)$$

The accelerations, $\partial_t \mathbf{v}$, and \mathbf{G}^{rot} , are each divergent-free. In contrast, the accelerations, $-\nabla p/\rho_0$ and \mathbf{G}^{div} , each have nonzero divergence. Self-consistency is maintained if the sum, $\nabla p/\rho_0 + \mathbf{G}^{\text{div}}$, has zero divergence so that

$$\nabla \cdot (\nabla p/\rho_0 + \mathbf{G}^{\text{div}}) = 0 \implies -\nabla^2 p = \rho_0 \nabla \cdot \mathbf{G}^{\text{div}} = \rho_0 \nabla \cdot \mathbf{G}. \quad (26.96)$$

This is the Poisson equation for the pressure field already derived in Section 26.3.1. We go one further step by observing that $\nabla p/\rho_0 + \mathbf{G}^{\text{div}}$ is both curl-free and divergent-free, which we write as

$$\nabla p/\rho_0 + \mathbf{G}^{\text{div}} = \mathbf{H} \quad \text{with} \quad \nabla \cdot \mathbf{H} = \nabla \times \mathbf{H} = 0. \quad (26.97)$$

26.4.3 The vorticity equation

As for the pressure equation in Section 26.4.2, we note that the accelerations $\nabla p/\rho_0$, and \mathbf{G}^{div} , are each curl-free. In contrast, the accelerations, $\partial_t \mathbf{v}$ and \mathbf{G}^{rot} , each have nonzero curl. Self-consistency thus requires $\partial_t \mathbf{v} + \mathbf{G}^{\text{rot}}$ to be curl-free

$$\nabla \times (\partial_t \mathbf{v} + \mathbf{G}^{\text{rot}}) = 0 \implies \partial_t (\nabla \times \mathbf{v}) = -\nabla \times \mathbf{G}^{\text{rot}}, \quad (26.98)$$

which is the relative vorticity equation that we further study in Chapter 37. Going one step further we note that the vector $\partial_t \mathbf{v} + \mathbf{G}^{\text{rot}}$ is both curl-free and divergent-free, which we write as

$$\partial_t \mathbf{v} + \mathbf{G}^{\text{rot}} = \mathbf{I} \quad \text{with} \quad \nabla \cdot \mathbf{I} = \nabla \times \mathbf{I} = 0. \quad (26.99)$$

26.4.4 The velocity equation

The above considerations have led us to the pressure gradient equation (26.97) and the velocity tendency equation (26.99)

$$\nabla p/\rho_0 + \mathbf{G}^{\text{div}} = \mathbf{H} \quad (26.100)$$

$$\partial_t \mathbf{v} + \mathbf{G}^{\text{rot}} = \mathbf{I}, \quad (26.101)$$

where both \mathbf{H} and \mathbf{I} are divergent-free and curl-free. Adding these two equations leads to

$$\partial_t \mathbf{v} = -\nabla p/\rho_0 - \mathbf{G}^{\text{rot}} - \mathbf{G}^{\text{div}} + \mathbf{H} + \mathbf{I}, \quad (26.102)$$

with this form of the velocity equation equivalent to the original Helmholtz decomposed equation (26.95) if we set

$$\mathbf{H} + \mathbf{I} = 0. \quad (26.103)$$

26.4.5 Comments

This section was inspired by [Marshall and Pillar \(2011\)](#), who applied a Helmholtz decomposition to study the variety of accelerations appearing in the Boussinesq velocity equation. A particularly revealing result of this decomposition, when setting $\mathbf{H} = \mathbf{I} = 0$, is the ability to make a 1-to-1 connection between terms in the Helmholtz decomposed velocity equation with terms in the relative vorticity equation.

26.5 Tracer budgets in Eulerian regions

We are commonly interested in the tracer budget for a fluid region, and we examined a variety of regions in Section 17.3 for a compressible fluid. Here, we expose issues that arise for tracer budgets in a Boussinesq ocean, whereby the flow is non-divergent. We specialize to the study of an Eulerian region, \mathcal{R} , and emphasize how the non-divergent flow constrains how the advective tracer transport affects changes to the volume integrated tracer content.

26.5.1 Formulating the budget equation

Consider a tracer concentration, C , and compute its net content over an Eulerian region, \mathcal{R}

$$\rho_0 \int_{\mathcal{R}} C \, dV = \rho_0 V \langle C \rangle, \quad (26.104)$$

where C satisfies the tracer equation

$$\frac{\partial(\rho_0 C)}{\partial t} + \nabla \cdot (\rho_0 C \mathbf{v} + \mathbf{J}) = 0, \quad (26.105)$$

and

$$\langle C \rangle = \frac{\int_{\mathcal{R}} C \, dV}{\int_{\mathcal{R}} dV} = \frac{1}{V} \int_{\mathcal{R}} C \, dV \quad (26.106)$$

is the volume averaged tracer concentration within the region with fixed volume, $V = \int_{\mathcal{R}} dV$. Following from the discussion of tracer budgets in Section 17.3, we have

$$\rho_0 \frac{d(V \langle C \rangle)}{dt} = \rho_0 V \frac{d\langle C \rangle}{dt} \quad (26.107a)$$

$$= \rho_0 \frac{d}{dt} \int_{\mathcal{R}} C dV \quad (26.107b)$$

$$= \int_{\mathcal{R}} \frac{\partial(\rho_0 C)}{\partial t} dV \quad (26.107c)$$

$$= - \int_{\mathcal{R}} \nabla \cdot (\rho_0 C \mathbf{v} + \mathbf{J}) dV \quad (26.107d)$$

$$= - \oint_{\partial\mathcal{R}} (\rho_0 C \mathbf{v} + \mathbf{J}) \cdot \hat{\mathbf{n}} d\mathcal{S}, \quad (26.107e)$$

where we used the divergence theorem on the final equality with $\partial\mathcal{R}$ the boundary of \mathcal{R} and the outward normal $\hat{\mathbf{n}}$. Changes in the total tracer contained within the region arise from the convergence of boundary fluxes due to the non-advectional flux, \mathbf{J} , plus convergence of the advective tracer flux, $\rho_0 C \mathbf{v}$. Since the region volume is constant in time, changes in the total tracer content directly affect the volume averaged tracer concentration, $\langle C \rangle$.

At any point along the boundary, the tracer content is modified if there is a non-advectional flux, \mathbf{J} , directed across the boundary. There is no *a priori* constraint on \mathbf{J} , with local properties determining its sign and magnitude. In contrast, contributions from the boundary advective flux are constrained due to the non-divergent nature of the Boussinesq velocity, which we discuss next.

26.5.2 Interpreting advective tracer contributions

As seen by equation (26.107e), any advective flux, $\rho_0 \mathbf{v} C$, that is directed into the region adds tracer to the region, whereas a flux directed outward reduces the region's tracer content. However, because the velocity is non-divergent, the tracer contained within the region is unaffected if we modify the advective tracer flux along the boundary by adding a number than is constant over the region \mathcal{R} . We see this property for any closed Eulerian region by writing⁸

$$0 = \int_{\mathcal{R}} \nabla \cdot \mathbf{v} dV = \oint_{\partial\mathcal{R}} \mathbf{v} \cdot \hat{\mathbf{n}} d\mathcal{S}. \quad (26.108)$$

Hence, the velocity is, at each time instance, constrained so that the non-divergent flow cannot lead to the accumulation of fluid within any closed and static region. Correspondingly, the amount of fluid entering \mathcal{R} exactly and instantaneously balances the amount of fluid leaving \mathcal{R} . We can thus add any spatial constant, k , to the advective flux without affecting the net tracer content change

$$\oint_{\partial\mathcal{R}} (C + k) \mathbf{v} \cdot \hat{\mathbf{n}} d\mathcal{S} = \oint_{\partial\mathcal{R}} C \mathbf{v} \cdot \hat{\mathbf{n}} d\mathcal{S} + k \oint_{\partial\mathcal{R}} \mathbf{v} \cdot \hat{\mathbf{n}} d\mathcal{S} = \oint_{\partial\mathcal{R}} C \mathbf{v} \cdot \hat{\mathbf{n}} d\mathcal{S}. \quad (26.109)$$

Boundary advection occurring with $C = k$ has no effect on the net tracer within a region since an equal amount of fluid enters as leaves.

To help interpret the role of advective fluxes on integrated tracer content, we find it useful to set the arbitrary spatial constant to $k = -\langle C \rangle$. In this manner, the advective contribution to the

⁸We considered property (26.108) in Exercise 18.3.

tracer budget takes the form

$$V \left[\frac{d\langle C \rangle}{dt} \right]_{\text{advective}} = - \oint_{\partial\mathcal{R}} C \mathbf{v} \cdot \hat{\mathbf{n}} d\mathcal{S} = - \oint_{\partial\mathcal{R}} (C - \langle C \rangle) \mathbf{v} \cdot \hat{\mathbf{n}} d\mathcal{S}. \quad (26.110)$$

Hence, advective transport through the region boundary changes the region integrated C , and thus the volume mean $\langle C \rangle$, only if the boundary transport occurs with C values that differ from the region average, $\langle C \rangle$.

26.5.3 A rectangular region example

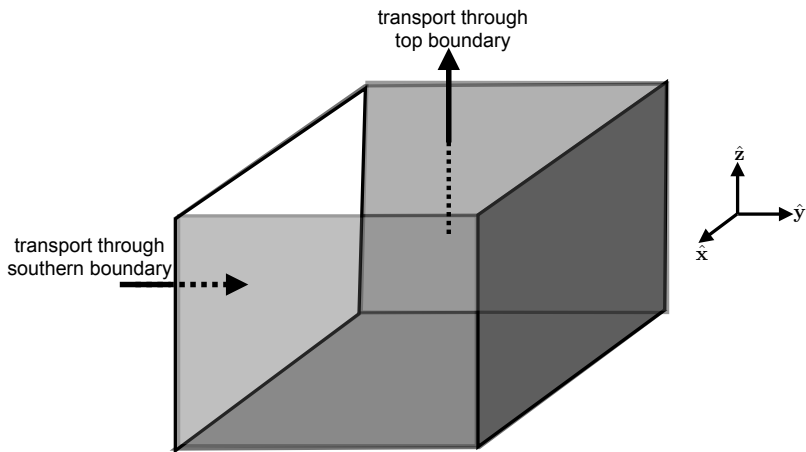


FIGURE 26.1: A rectangular ocean region for considering the tracer budget in a Boussinesq ocean. We assume the only open boundaries of the region are along the southern boundary and top boundary, with the remaining boundaries closed. Note that the top boundary can generally be within the ocean interior, and so does not need to be the top of the ocean. The non-divergent nature of the flow means that any fluid entering through the southern boundary must leave through the top boundary, and conversely. This constraint on the flow impacts on how the advective tracer transport affects changes to the volume integrated tracer within the region.

Consider the rectangular region of Figure 26.1 that is closed along its bottom, northern, eastern, and western boundaries, yet that is open along its top boundary and southern boundary. Specify flow along the southern boundary to be northward and let it bring fluid into the region with $C_{\text{south}} > \langle C \rangle$, thus acting to increase $\langle C \rangle$. Due to the non-divergent nature of the velocity, the northward transport of fluid through the southern boundary must be precisely balanced by a vertically upward transport of fluid out of the top boundary. What does that vertical transport of fluid imply about changes to $\langle C \rangle$? The answer depends on the tracer concentration on the top boundary.

- If $C_{\text{top}} > \langle C \rangle$, then the relatively high values of tracer that leave through the top boundary act to decrease the net C within the region, thus counteracting the contribution of $C_{\text{south}} > \langle C \rangle$ that enters through the southern boundary. For the special case of equal C transports through the two boundaries, then there is no accumulation of C within the region so that $\langle C \rangle$ remains unchanged.
- If $C_{\text{top}} = \langle C \rangle$, then $\langle C \rangle$ increases due to the transport of C through the southern boundary, with no net transport across the top boundary.
- If $C_{\text{top}} < \langle C \rangle$, then the vertical transport of $C_{\text{top}} < \langle C \rangle$ increases $\langle C \rangle$ acting just like the $C_{\text{south}} > \langle C \rangle$ fluid that enters through the southern boundary. That is, we can increase $\langle C \rangle$

in the region by bringing fluid into the domain with C greater than $\langle C \rangle$, or by exporting fluid with C less than $\langle C \rangle$.

26.5.4 Comments

Constraints introduced by the non-divergent nature of the Boussinesq ocean render subtleties to the physical interpretation of how tracer fluxes affect the budget of tracer within a region. These constraints are absent from the compressible fluid, whose flow is generally divergent. The discussion in this section was motivated by Appendix B of [Gregory \(2000\)](#), who studied heat (enthalpy) budgets within a numerical Boussinesq ocean circulation model.

26.6 Subgrid scale processes and boundary conditions

The Boussinesq ocean equations from Section 26.1 must be supplemented with boundary conditions as well as subgrid scale parameterizations. We examine boundary stresses in Chapter 22.10; study tracer subgrid scale parameterizations in Chapter 63; and detail the variety of boundary buoyancy fluxes in Section 64.6. Even so, there is far more to each of these stories than provided in this book. In this section we summarize facets sufficient to help work through exercises at the end of this chapter. One key point to emphasize here is that for all the subgrid scale and boundary conditions in a Boussinesq ocean, appearances of the *in situ* density are converted to the Boussinesq reference density, ρ_0 .

26.6.1 Material evolution of buoyancy

The term \dot{b} appearing in the buoyancy equation (26.24c) is a shorthand for any process leading to a material change in buoyancy, such as a boundary flux, parameterized turbulent mixing of salinity or Conservative Temperature, or vertical motion through a vertically stratified fluid. With a linear equation of state, we can write the material evolution as the convergence of a subgrid scale buoyancy flux

$$\frac{Db}{Dt} = -\nabla \cdot \mathbf{F}^b. \quad (26.111)$$

A particularly common form for this flux is given by

$$\mathbf{F}^b = -\kappa \frac{\partial b}{\partial z} \hat{z} + \mathbf{v}^* b. \quad (26.112)$$

The first term is a downgradient vertical diffusive flux with the vertical *eddy diffusivity*, $\kappa > 0$, a function of the flow state so that

$$\kappa = \kappa(x, y, z, t). \quad (26.113)$$

The second term is an advective flux, where the advective velocity, $\mathbf{v}^* = (\mathbf{u}^*, w^*)$, is assumed to be non-divergent

$$\nabla \cdot \mathbf{v}^* = \nabla_z \cdot \mathbf{u}^* + \frac{\partial w^*}{\partial z} = 0. \quad (26.114)$$

The velocity, \mathbf{v}^* , is commonly termed the *eddy-induced* velocity, with a particular choice for its parameterization discussed in Exercise 26.10 and further examined in Section 63.1.

Boundary conditions for buoyancy are commonly incorporated through the boundary conditions on the subgrid scale fluxes, with the following representing one form for these boundary

conditions

$$\hat{\mathbf{n}} \cdot \mathbf{F}^b = Q_{\text{surf}} \quad \text{at } z = \eta(x, y, t) \quad (26.115\text{a})$$

$$(-\hat{\mathbf{n}}) \cdot \mathbf{F}^b = Q_{\text{bot}} \quad \text{at } z = \eta_b(x, y) \quad (26.115\text{b})$$

$$\mathbf{v}^* \cdot \hat{\mathbf{n}} = 0 \quad \text{all boundaries,} \quad (26.115\text{c})$$

where Q_{surf} is the surface buoyancy flux, Q_{bot} is the bottom buoyancy flux (e.g., geothermal heating), and $\hat{\mathbf{n}}$ is the outward normal at the boundaries. Both Q_{surf} and Q_{bot} are positive upward. In Section 64.6 we detail the plethora of processes leading to boundary fluxes of buoyancy.

26.6.2 Mechanical forcing and dissipation

The ocean is a forced-dissipative system, with mechanical and buoyant forcing predominantly at the surface and bottom boundaries and mechanical dissipation via molecular viscosity. We must parameterize mechanical dissipation in the ocean interior arising from subgrid scale processes. A common form for this parameterization is via a vertical transfer of momentum through vertical shears that are weighted by a vertical *eddy viscosity*, $\nu^{\text{eddy}} > 0$, in which case the horizontal frictional acceleration in the ocean interior is written as the vertical divergence of a turbulent stress

$$\mathbf{F}^h = \frac{1}{\rho_0} \frac{\partial \boldsymbol{\tau}}{\partial z} = \frac{\partial}{\partial z} \left[\nu^{\text{eddy}} \frac{\partial \mathbf{u}}{\partial z} \right], \quad (26.116)$$

where $\boldsymbol{\tau}$ is a horizontal turbulent stress whose vertical derivative contributes to the vertical transfer of horizontal momentum. The eddy viscosity can be many orders of magnitude larger than the molecular viscosity in regions of strong turbulent mixing. Whereas the molecular viscosity is a function of the fluid composition (Section 22.8), the eddy viscosity is a function of the flow state, which in turn means that

$$\nu^{\text{eddy}} = \nu^{\text{eddy}}(\mathbf{x}, t). \quad (26.117)$$

We parameterize the turbulent mechanical forcing at the ocean boundaries via a boundary stress. This stress is introduced to the governing equations through the following surface and bottom boundary conditions placed on the turbulent stress

$$\boldsymbol{\tau} = \boldsymbol{\tau}^{\text{surf}} \quad \text{at } z = \eta(x, y, t) \quad (26.118)$$

$$\boldsymbol{\tau} = \boldsymbol{\tau}^{\text{bott}} \quad \text{at } z = \eta_b(x, y) \quad (26.119)$$

At the ocean surface, $z = \eta$, we introduce the turbulent stress, $\boldsymbol{\tau}^{\text{surf}}$, arising from the transfer of momentum between the ocean and atmosphere (or the ocean and ice). In practice, the stress is computed by a boundary layer parameterization that ingests the momentum from the atmosphere and computes a stress that is transferred to the ocean through these boundary conditions. As per Newton's third law (the action/reaction law; see Section 22.10), the stress imparted to the ocean is equal and opposite the stress imparted to the atmosphere at its lower boundary.

At the ocean bottom, $z = \eta_b$, we often parameterize subgrid scale interactions with bottom topography via a quadratic bottom drag

$$\boldsymbol{\tau}^{\text{bott}} = -C_D \mathbf{u} |\mathbf{u}|, \quad (26.120)$$

where $C_D > 0$ is a dimensionless *drag coefficient* that is sometimes assumed to be a function of the bottom topographic roughness. This bottom stress acts to drag the ocean bottom velocity towards a state of rest. It is equal and opposite to the frictional stress transferred to the solid earth from the ocean. Note that this bottom drag acts similarly to the linear Rayleigh drag

in equation (22.71). However, the bottom drag in equation (26.120) is nonlinear, whereas the Rayleigh drag

$$\mathbf{F}_{\text{Rayleigh}} = -\gamma \mathbf{v}, \quad (26.121)$$

is linear.

26.7 Mechanical energy analysis: Part I

The volume of a fluid element in a non-divergent flow remains materially invariant even as pressure acts on the element, which means that pressure can perform no mechanical work. In turn, non-divergent flow supports no pressure work conversion between internal energy and kinetic energy. So the mechanical energy budget closed in a Boussinesq ocean, whereas the non-Boussinesq ocean has a transfer of frictional heating to the internal energy. In this section we formulate a mechanical energy budget for the Boussinesq ocean that is closed for a perfect fluid so long as the geopotential is time-independent and there are no boundary effects.

We here develop the mechanical energy budget for an unforced non-hydrostatic Boussinesq ocean assuming density is a function only of salinity and Conservative Temperature,

$$\rho = \rho(S, \Theta). \quad (26.122)$$

The more general pressure-dependent equation of state is considered in Section 26.8. Furthermore, we choose to work with the velocity, density, and continuity equations in the form

$$\rho_0 \left[\frac{D\mathbf{v}}{Dt} + 2\boldsymbol{\Omega} \times \mathbf{v} \right] = -\nabla p - \rho \nabla \Phi \quad (26.123a)$$

$$\frac{D\rho}{Dt} = \frac{\partial \rho}{\partial S} \frac{DS}{Dt} + \frac{\partial \rho}{\partial \Theta} \frac{D\Theta}{Dt} = \dot{\rho} \quad (26.123b)$$

$$\nabla \cdot \mathbf{v} = 0. \quad (26.123c)$$

Note that the geopotential, Φ , is generally a function of space and time, $\Phi = \Phi(\mathbf{x}, t)$. This general dependence is appropriate when studying astronomical tides or mass inhomogeneities creating spatial variations in the gravity field, and we introduce some of these topics in Chapter 31.

26.7.1 Kinetic energy

To obtain a kinetic energy equation, start by taking the dot product of the velocity, \mathbf{v} , and the momentum equation (26.210a) and note that the Coriolis acceleration drops out since it is orthogonal to the velocity

$$\mathbf{v} \cdot (2\boldsymbol{\Omega} \times \mathbf{v}) = 0. \quad (26.124)$$

The material time derivative takes the form

$$v_i \left[\frac{\partial v_i}{\partial t} + v_j \frac{\partial v_i}{\partial x_j} \right] = \frac{D\mathcal{K}}{Dt} + \mathbf{v} \cdot \nabla \mathcal{K} = \frac{D\mathcal{K}}{Dt}, \quad (26.125)$$

where we introduced the kinetic energy per mass

$$\mathcal{K} = \mathbf{v} \cdot \mathbf{v} / 2. \quad (26.126)$$

The equation for the Boussinesq kinetic energy per volume thus takes the form

$$\rho_0 \frac{D\mathcal{K}}{Dt} = -\mathbf{v} \cdot \nabla p - \rho \mathbf{v} \cdot \nabla \Phi \quad (26.127)$$

Alternatively, we can write this equation in the Eulerian flux-form

$$\frac{\partial(\rho_0 \mathcal{K})}{\partial t} + \nabla \cdot [\mathbf{v} (\rho_0 \mathcal{K} + p)] = -\rho \mathbf{v} \cdot \nabla \Phi, \quad (26.128)$$

where we used $\nabla \cdot \mathbf{v} = 0$ to write $\mathbf{v} \cdot \nabla p = \nabla \cdot (\mathbf{v} p)$. Note that in Exercise 26.4 we show that the kinetic energy evolution derived here for the non-hydrostatic fluid holds also for the hydrostatic fluid, yet with the kinetic energy in the hydrostatic fluid determined solely by the horizontal velocity.

The term $-\rho \mathbf{v} \cdot \nabla \Phi$ in the kinetic energy equation (26.128) is a source/sink that arises from fluid motion crossing surfaces of constant geopotential. Moving a fluid element down the geopotential gradient ($\mathbf{v} \cdot \nabla \Phi < 0$) increases the kinetic energy, and conversely when the fluid moves up the geopotential gradient. We sometimes refer to this process as *buoyancy work*, particularly when considered in the context of a vertically stratified fluid. We can further exemplify this term by taking the simplified form of the geopotential, $\Phi = g z$, in which $\mathbf{v} \cdot \nabla \Phi = g w$.

26.7.2 Gravitational potential and mechanical energies

We here develop the gravitational energy budget and then add to the kinetic energy to derive the mechanical energy budget.

Gravitational potential energy

A fluid element has a gravitational potential energy per mass given by the geopotential, Φ , which has a material time derivative

$$\frac{D\Phi}{Dt} = \partial_t \Phi + \mathbf{v} \cdot \nabla \Phi. \quad (26.129)$$

The time-dependent geopotential provides an external source of potential energy to the system. Additionally, motion moving up the gradient of the geopotential ($\mathbf{v} \cdot \nabla \Phi > 0$) increases the potential energy per mass, and conversely for motion down the geopotential gradient.

Mechanical energy budget

Adding the gravitational potential energy equation (26.129) to the kinetic energy equation (26.127) renders the material evolution

$$\rho_0 \frac{D\mathcal{K}}{Dt} + \rho \frac{D\Phi}{Dt} = -\nabla \cdot (\mathbf{v} p) + \rho \partial_t \Phi. \quad (26.130)$$

Note how the buoyancy work source, $\rho \mathbf{v} \cdot \nabla \Phi$, dropped out from this budget. Consequently, this term provides a reversible transfer of mechanical energy between gravitational potential energy per volume and the kinetic energy per volume. We saw the same transfer in Section 23.3.3 when studying the mechanical energy budget for a compressible non-Boussinesq fluid.

Equation (26.130) has nearly the same form as that for the non-Boussinesq fluid given by equation (23.40). However, for the Boussinesq ocean it does not lead to a flux-form Eulerian conservation law for mechanical energy, even for the perfect fluid. Operationally, the derivations diverge at this point since for the non-Boussinesq fluid we make use of the mass continuity

equation (16.6) to write the material evolution of density. In contrast, material density evolution in a Boussinesq ocean is determined by material changes in temperature, salinity, and pressure.

To develop a closed Boussinesq mechanical energy budget, add $\Phi D\rho/Dt = \dot{\rho}$ to both sides of equation (26.130) to render the material evolution for the mechanical energy *per volume*

$$\frac{D}{Dt} [\rho_0 \mathcal{K} + \rho \Phi] = -\nabla \cdot (\mathbf{v} p) + \rho \partial_t \Phi + \dot{\rho} \Phi, \quad (26.131)$$

which has the Eulerian flux-form expression

$$\partial_t (\rho_0 m) + \nabla \cdot [\mathbf{v} (\rho_0 m + p)] = \rho \partial_t \Phi + \dot{\rho} \Phi, \quad (26.132)$$

where we defined the Boussinesq mechanical energy per volume as

$$\rho_0 m = \rho_0 \mathcal{K} + \rho \Phi. \quad (26.133)$$

Finite volume form of the mechanical energy bugdet

The Leibniz-Reynolds transport theorem in the form of equation (17.46) renders the finite volume mechanical energy budget

$$\frac{d}{dt} \left[\int_{\mathcal{R}} \rho_0 m dV \right] = - \oint_{\partial\mathcal{R}} (\rho_0 m + p) (\mathbf{v} - \mathbf{v}^{(b)}) \cdot \hat{\mathbf{n}} d\mathcal{S} + \int_{\mathcal{R}} [\rho \partial_t \Phi + \dot{\rho} \Phi] dV, \quad (26.134)$$

where \mathcal{R} is the finite volume region, $\partial\mathcal{R}$ is its boundary, $\mathbf{v}^{(b)}$ is the velocity of a point on the boundary, and $\hat{\mathbf{n}}$ is the outward normal on the boundary. The budget (26.134) for a Boussinesq fluid corresponds to the budget (23.47) for a non-Boussinesq fluid.

A material region is characterized by $(\mathbf{v} - \mathbf{v}^{(b)}) \cdot \hat{\mathbf{n}} = 0$ on the boundaries, in which case the mechanical energy budget (26.134) simplifies to

$$\frac{d}{dt} \left[\int_{\mathcal{R}} \rho_0 m dV \right] = \int_{\mathcal{R}} [\rho \partial_t \Phi + \dot{\rho} \Phi] dV, \quad (26.135)$$

Recall we are assuming $\rho = \rho(S, \Theta)$ in this section, so that

$$\dot{\rho} = (\partial\rho/\partial S) \dot{S} + (\partial\rho/\partial \Theta) \dot{\Theta}. \quad (26.136)$$

Hence, for a time-independent geopotential ($\partial_t \Phi = 0$) and in the absence of processes that contribute to a material evolution of S and Θ (i.e., $\dot{S} = 0$ and $\dot{\Theta} = 0$), then the finite volume Boussinesq mechanical energy for a material fluid region is time independent.⁹

26.8 Mechanical energy analysis: Part II

In this section we build on the analysis from Section 26.7, here allowing density to be a function of salinity, Conservative Temperature, and pressure so that

$$\frac{D\rho}{Dt} = \frac{\partial\rho}{\partial S} \frac{DS}{Dt} + \frac{\partial\rho}{\partial \Theta} \frac{D\Theta}{Dt} + \frac{\partial\rho}{\partial p} \frac{Dp}{Dt}. \quad (26.137)$$

⁹We find that \dot{S} and $\dot{\Theta}$ are nonzero in the presence of boundary processes (e.g., heat fluxes, fresh water fluxes) and in the presence of mixing (e.g., as parameterized by diffusion). We study diffusion in Chapter 61 and then in Chapter 65 we provide a detailed look at the suite of processes contributing to nonzero \dot{S} and $\dot{\Theta}$.

Density thus materially evolves even in the absence of mixing or diabatic processes since $D\rho/Dt$ is nonzero whenever flow crosses isobars. Hence, the Eulerian flux-form mechanical energy equation (26.132) now takes on the form

$$\partial_t(\rho_0\mathcal{K} + \rho\Phi) + \nabla \cdot [\mathbf{v}(\rho_0\mathcal{K} + \rho\Phi + p)] = \rho\partial_t\Phi + \Phi \left[\frac{\partial\rho}{\partial S}\dot{S} + \frac{\partial\rho}{\partial\Theta}\dot{\Theta} + \frac{\partial\rho}{\partial p}\dot{p} \right]. \quad (26.138)$$

The right hand side terms provide sources that contribute to the evolution of mechanical energy. In the absence of mixing, diabatic processes, and with a time independent geopotential, the sources reduce to a term arising from motion across pressure surfaces. Such motion can occur for either reversible or irreversible processes. This pressure source term is rather awkward since it means the mechanical energy budget is not closed even when the flow is reversible and with time independent astronomical forces. We now follow the approach of [Young \(2010\)](#) to recover a closed Boussinesq mechanical energy budget by making use of a modified form of the gravitational potential energy.

26.8.1 Boussinesq dynamic enthalpy

In this section we introduce a new thermodynamic function that, in effect, provides us with an integrating factor to render a closed form to the Boussinesq mechanical energy budget. This function is referred to as the *Boussinesq dynamic enthalpy*. Before considering that function we do a brief warm-up to refamiliarize ourself with the necessary thermodynamic formalism from Chapter 19.

Material time changes to a pressure integral of density

Consider a thermodynamic potential, $\tilde{\Pi}(S, \Theta, p | p_r)$, defined according to the pressure integral of the *in situ* density

$$\tilde{\Pi}(S, \Theta, p | p_r) \equiv \int_{p_r}^p \rho(S, \Theta, p') dp' \implies \left[\frac{\partial \tilde{\Pi}}{\partial p} \right]_{S, \Theta} = \rho(S, \Theta, p), \quad (26.139)$$

where p_r is an arbitrary constant reference pressure. The notation $\tilde{\Pi}(S, \Theta, p | p_r)$ emphasizes that p_r is a specified parameter whereas S, Θ, p are coordinates in thermodynamic configuration space (see Section 19.1.5). The integration in equation (26.139) is taken over pressure in a thermodynamic configuration space rather than an integral over a region in x -space.¹⁰ Accordingly, the infinitesimal increment of $\tilde{\Pi}$ is given by

$$\delta\tilde{\Pi} = \delta S \left[\frac{\partial \tilde{\Pi}}{\partial S} \right]_{\Theta, p} + \delta\Theta \left[\frac{\partial \tilde{\Pi}}{\partial \Theta} \right]_{S, p} + \delta p \left[\frac{\partial \tilde{\Pi}}{\partial p} \right]_{S, \Theta} \quad (26.140a)$$

$$= \delta S \left[\frac{\partial \tilde{\Pi}}{\partial S} \right]_{\Theta, p} + \delta\Theta \left[\frac{\partial \tilde{\Pi}}{\partial \Theta} \right]_{S, p} + \rho(S, \Theta, p) \delta p. \quad (26.140b)$$

¹⁰This is an example where the discussion in Section 23.4.3 is key, whereby we must distinguish between fields in a thermodynamic configuration space versus space and time dependent fields.

If the increment is computed following a moving fluid element then we are led to the material time derivative

$$\frac{D\tilde{\Pi}}{Dt} = \frac{DS}{Dt} \left[\frac{\partial \tilde{\Pi}}{\partial S} \right]_{\Theta,p} + \frac{D\Theta}{Dt} \left[\frac{\partial \tilde{\Pi}}{\partial \Theta} \right]_{S,p} + \rho(S, \Theta, p) \frac{Dp}{Dt}. \quad (26.141)$$

Material time changes to a geopotential integral of density

Using the same formalism as above, now consider a thermodynamic potential that is a function of salinity, Conservative Temperature, and geopotential

$$\Pi(S, \Theta, \Phi | \Phi_r) \equiv \int_{\Phi_r}^{\Phi} \rho(S, \Theta, \Phi') d\Phi' \implies \left[\frac{\partial \Pi}{\partial \Phi} \right]_{S, \Theta} = \rho(S, \Theta, \Phi), \quad (26.142)$$

where Φ_r is an arbitrary constant reference geopotential. We offer the following three comments concerning Π .

- For density that is independent of the geopotential, then $\Pi dV = (\Phi - \Phi_r) \rho dV$, which is the gravitational potential energy relative to a reference state. We thus interpret $\Pi(S, \Theta, \Phi)$ as a generalized gravitational potential energy per volume.
- One might consider Π to be the difference in hydrostatic pressure between Φ and Φ_r as per equation (21.52). However, the integral in equation (21.52) occurs in x -space between two geopotentials and holding the (x, y) coordinates fixed during the integration, so that this integration generally crosses surfaces of constant S and Θ . In contrast, integration in equation (26.142) is taken from Φ_r to Φ within thermodynamic configuration space so that S and Θ are fixed while performing the geopotential integral. In this manner, the geopotential, rather than pressure, provides a coordinate within a Boussinesq thermodynamic configuration space along with S and Θ .
- [Young \(2010\)](#) provides motivation for calling Π the *Boussinesq dynamic enthalpy*.¹¹

Following the same formalism used to derive $D\tilde{\Pi}/Dt$ in equation (26.141), we here compute the material time derivative of the Boussinesq dynamic enthalpy

$$\frac{D\Pi}{Dt} = \frac{DS}{Dt} \left[\frac{\partial \Pi}{\partial S} \right]_{\Theta, \Phi} + \frac{D\Theta}{Dt} \left[\frac{\partial \Pi}{\partial \Theta} \right]_{S, \Phi} + \rho(S, \Theta, \Phi) \frac{D\Phi}{Dt}. \quad (26.143)$$

We now create a mechanical energy budget in the form

$$\frac{D}{Dt} [\rho_0 \mathcal{K} + \Pi] = -[\mathbf{v} \cdot \nabla p + \rho \mathbf{v} \cdot \nabla \Phi] + \dot{S} \left[\frac{\partial \Pi}{\partial S} \right]_{\Theta, \Phi} + \dot{\Theta} \left[\frac{\partial \Pi}{\partial \Theta} \right]_{S, \Phi} + \rho \frac{D\Phi}{Dt} \quad (26.144a)$$

$$= -[\mathbf{v} \cdot \nabla p + \rho \mathbf{v} \cdot \nabla \Phi] + \dot{S} \left[\frac{\partial \Pi}{\partial S} \right]_{\Theta, \Phi} + \dot{\Theta} \left[\frac{\partial \Pi}{\partial \Theta} \right]_{S, \Phi} + \rho (\partial_t \Phi + \mathbf{v} \cdot \nabla \Phi) \quad (26.144b)$$

$$= -\mathbf{v} \cdot \nabla p + \rho \partial_t \Phi + \dot{S} \left[\frac{\partial \Pi}{\partial S} \right]_{\Theta, \Phi} + \dot{\Theta} \left[\frac{\partial \Pi}{\partial \Theta} \right]_{S, \Phi}, \quad (26.144c)$$

whose Eulerian flux-form expression is given by

$$\partial_t (\rho_0 \mathcal{K} + \Pi) + \nabla \cdot [\mathbf{v} \cdot (\rho_0 \mathcal{K} + \Pi + p)] = \rho \partial_t \Phi + \dot{S} \left[\frac{\partial \Pi}{\partial S} \right]_{\Theta, \Phi} + \dot{\Theta} \left[\frac{\partial \Pi}{\partial \Theta} \right]_{S, \Phi}. \quad (26.145)$$

¹¹Mention here the gist of the motivation.

We thus see that in the absence of irreversible effects, and with a time independent geopotential, we have succeeded in deriving a closed (i.e., flux-form) mechanical energy budget for a Boussinesq ocean, with

$$\rho_0 \mathcal{M} = \rho_0 \mathcal{K} + \Pi \xrightarrow{\rho=\rho(S,\Theta)} \rho_0 \mathcal{K} + \rho (\Phi - \Phi_r) \quad (26.146)$$

the appropriate Boussinesq expression for the mechanical energy per volume.

26.8.2 Regionally integrated Boussinesq dynamic enthalpy

Following the treatment for a compressible non-Boussinesq fluid in Section 23.2.4, we here study the evolution of the gravitational potential energy integrated over a finite region, \mathcal{R} , that is open to material mass transport. Rather than working with the geopotential as done for the non-Boussinesq fluid, we here follow the discussion in Section 26.8.1 by making use of the Boussinesq dynamic enthalpy, thus ensuring a closed mechanical energy budget.

Budget with the equation of state: $\rho = \rho(S, \Theta, \Phi)$

For this purpose we make use the Leibniz-Reynolds transport theorem in the form of equation (17.34) to find

$$\frac{d}{dt} \int_{\mathcal{R}} \Pi dV = \int_{\mathcal{R}} \left[\frac{\partial \Pi}{\partial t} + \nabla \cdot (\Pi \mathbf{v}^{(b)}) \right] dV \quad (26.147a)$$

$$= \int_{\mathcal{R}} \left[\frac{\partial \Pi}{\partial t} + \nabla \cdot (\Pi \mathbf{v}) - \nabla \cdot (\Pi \mathbf{v}) + \nabla \cdot (\Pi \mathbf{v}^{(b)}) \right] dV \quad (26.147b)$$

$$= \int_{\mathcal{R}} \left[\frac{D\Pi}{Dt} + \Pi \nabla \cdot \mathbf{v} + \nabla \cdot [\Pi (\mathbf{v}^{(b)} - \mathbf{v})] \right] dV \quad (26.147c)$$

$$= \int_{\mathcal{R}} \left[\frac{D\Pi}{Dt} + \nabla \cdot [\Pi (\mathbf{v}^{(b)} - \mathbf{v})] \right] dV, \quad (26.147d)$$

where $\mathbf{v}^{(b)}$ is the velocity of a point on the boundary of the domain, $\partial\mathcal{R}$, and we set $\nabla \cdot \mathbf{v} = 0$ as per a Boussinesq ocean. We expose the contributions from irreversible S and Θ processes by making use of the identity (26.143)

$$\frac{d}{dt} \int_{\mathcal{R}} \Pi dV = \int_{\mathcal{R}} \left[\frac{DS}{Dt} \left[\frac{\partial \Pi}{\partial S} \right]_{\Theta, \Phi} + \frac{D\Theta}{Dt} \left[\frac{\partial \Pi}{\partial \Theta} \right]_{S, \Phi} + \rho \frac{D\Phi}{Dt} + \nabla \cdot [\Pi (\mathbf{v}^{(b)} - \mathbf{v})] \right] dV. \quad (26.148)$$

Note that a constant can be added to the dynamic enthalpy without altering the energetics, which is seen by noting that volume conservation means that (equation (18.63))

$$\frac{d}{dt} \int dV = - \int_{\mathcal{R}} \nabla \cdot (\mathbf{v} - \mathbf{v}^{(b)}) dV = - \int_{\partial\mathcal{R}} (\mathbf{v} - \mathbf{v}^{(b)}) \cdot \hat{\mathbf{n}} d\mathcal{S}. \quad (26.149)$$

If the region is a vertical column of fluid with fixed horizontal cross-section, extending from the ocean surface to the ocean bottom, then there is horizontal transport across the vertical boundaries, plus vertical transport of mass across the ocean free surface. For the free surface we make use of the surface kinematic boundary condition (16.73c) to write

$$\int_{z=\eta} (\Pi/\rho) \rho (\mathbf{v}^{(\eta)} - \mathbf{v}) \cdot \hat{\mathbf{n}} d\mathcal{S} = \int_{z=\eta} (\Pi/\rho) Q_m dA. \quad (26.150)$$

In this equation, Q_m is the mass per time per horizontal area of matter crossing the ocean free

surface at $z = \eta$ where $Q_m > 0$ for matter entering the ocean domain, and $d\mathcal{S}$ is the area element on the free surface with dA its horizontal projection.

Budget with the equation of state: $\rho = \rho(S, \Theta)$

For the special case of an equation of state independent of pressure, $\rho = \rho(S, \Theta)$ (Section 26.7), we have $\Pi = \rho(\Phi - \Phi_r)$ so that equation (26.148) reduces to

$$\frac{d}{dt} \int_{\mathcal{R}} \rho (\Phi - \Phi_r) dV = \int_{\mathcal{R}} \left[(\Phi - \Phi_r) \frac{D\rho}{Dt} + \rho \frac{D\Phi}{Dt} + \nabla \cdot [\rho (\Phi - \Phi_r) (\mathbf{v}^{(b)} - \mathbf{v})] \right] dV. \quad (26.151)$$

Note that the reference geopotential, Φ_r , drops out since the Boussinesq form of the Leibniz-Reynolds transport theorem (i.e., equation (26.147d)) with ρ replacing Π) leads to the identity

$$\frac{d}{dt} \int_{\mathcal{R}} \rho dV = \int_{\mathcal{R}} \left[\frac{D\rho}{Dt} + \nabla \cdot [\rho (\mathbf{v}^{(b)} - \mathbf{v})] \right] dV. \quad (26.152)$$

This equation means that the mass for a region of Boussinesq ocean (left hand side) changes through boundary terms, as for a non-Boussinesq fluid, plus processes that lead to material time changes in S and Θ

$$\rho = \rho(S, \Theta) \implies \frac{D\rho}{Dt} = \frac{\partial \rho}{\partial S} \frac{DS}{Dt} + \frac{\partial \rho}{\partial \Theta} \frac{D\Theta}{Dt}. \quad (26.153)$$

We understand the presence of the \dot{S} and $\dot{\Theta}$ terms by noting that irreversible processes, such as mixing, do not alter volume in a Boussinesq ocean. Hence, if irreversible processes change density then there must be a corresponding change in mass.

26.8.3 Vertical derivative of density

When computing the vertical derivative of density, it is important to note whether the derivative is computed holding (Θ, S) fixed or holding (x, y) fixed. As seen here, this distinction can be confused for the oceanic Boussinesq ocean, especially when the geopotential takes the simple form $\Phi = gz$.

Vertical derivative of in situ density for a non-Boussinesq fluid

To motivate the discussion, recall the *in situ* density for a non-Boussinesq fluid is a function of the salinity, S , Conservative Temperature, Θ , and *in situ* pressure, p ,

$$\rho = \rho(S, \Theta, p), \quad (26.154)$$

so that its spatial gradient is

$$\nabla \rho = \left[\frac{\partial \rho}{\partial S} \right]_{\Theta, p} \nabla S + \left[\frac{\partial \rho}{\partial \Theta} \right]_{S, p} \nabla \Theta + \left[\frac{\partial \rho}{\partial p} \right]_{S, \Theta} \nabla p = \left[\frac{\partial \rho}{\partial S} \right]_{\Theta, p} \nabla S + \left[\frac{\partial \rho}{\partial \Theta} \right]_{S, p} \nabla \Theta + \frac{1}{c_s^2} \nabla p. \quad (26.155)$$

In the final step we introduced the inverse squared sound speed

$$\frac{1}{c_s^2} = \left[\frac{\partial \rho}{\partial p} \right]_{S, \Theta}, \quad (26.156)$$

which is the partial derivative of density holding S and Θ fixed. Equation (26.155) says that the spatial gradient of density on the left hand side is determined by the sum of three terms that

arise from spatial gradients of (S, Θ, p) , each multiplied by their respective functional derivative of the equation of state for density. The vertical component of this equation arises when measuring vertical stratification, in which case

$$\left[\frac{\partial \rho}{\partial z} \right]_{x,y} = \left[\frac{\partial \rho}{\partial S} \right]_{\Theta,p} \left[\frac{\partial S}{\partial z} \right]_{x,y} + \left[\frac{\partial \rho}{\partial \Theta} \right]_{S,p} \left[\frac{\partial \Theta}{\partial z} \right]_{x,y} + \frac{1}{c_s^2} \left[\frac{\partial p}{\partial z} \right]_{x,y}, \quad (26.157)$$

with $\partial p / \partial z = -\rho g$ for a hydrostatic fluid. Note that we exposed the (x, y) labels on the left hand side partial derivative. As seen next, these extra labels are especially important for the case of the Boussinesq ocean.

Vertical derivative of in situ density for a Boussinesq ocean

As seen earlier in this section, the *in situ* density for an energetically consistent Boussinesq ocean has the functional dependence

$$\rho = \rho(S, \Theta, \Phi). \quad (26.158)$$

That is, the geopotential, Φ , replaces pressure in the functional dependence, with the equation of state evaluated with a pressure $p_{\text{eos}} = -\rho_0 \Phi$. Hence, the spatial gradient of *in situ* density for a Boussinesq ocean is

$$\nabla \rho = \left[\frac{\partial \rho}{\partial S} \right]_{\Theta,\Phi} \nabla S + \left[\frac{\partial \rho}{\partial \Theta} \right]_{S,\Phi} \nabla \Theta + \left[\frac{\partial \rho}{\partial \Phi} \right]_{S,\Theta} \nabla \Phi, \quad (26.159)$$

so that the vertical stratification is measured by

$$\left[\frac{\partial \rho}{\partial z} \right]_{x,y} = \left[\frac{\partial \rho}{\partial S} \right]_{\Theta,\Phi} \left[\frac{\partial S}{\partial z} \right]_{x,y} + \left[\frac{\partial \rho}{\partial \Theta} \right]_{S,\Phi} \left[\frac{\partial \Theta}{\partial z} \right]_{x,y} + \left[\frac{\partial \rho}{\partial \Phi} \right]_{S,\Theta} \left[\frac{\partial \Phi}{\partial z} \right]_{x,y}. \quad (26.160a)$$

This relation is analogous to the non-Boussinesq expression (26.157). In particular, the inverse squared sound speed for a Boussinesq ocean is given by

$$\left[\frac{\partial \rho}{\partial \Phi} \right]_{S,\Theta} = -\frac{\rho_0 g}{c_s^2}. \quad (26.161)$$

Although the prognostic flow is non-divergent for the Boussinesq ocean, the full velocity field is divergent (Section 26.1.8), thus supporting acoustic waves.

Now consider the special (and common) case of a simple geopotential, $\Phi = g z$, whereby the Boussinesq sound speed is given by

$$\left[\frac{\partial \rho}{\partial z} \right]_{S,\Theta} = -\frac{\rho_0 g}{c_s^2}, \quad (26.162)$$

and the vertical stratification derivative is given by

$$\left[\frac{\partial \rho}{\partial z} \right]_{x,y} = \left[\frac{\partial \rho}{\partial S} \right]_{\Theta,z} \left[\frac{\partial S}{\partial z} \right]_{x,y} + \left[\frac{\partial \rho}{\partial \Theta} \right]_{S,z} \left[\frac{\partial \Theta}{\partial z} \right]_{x,y} + \left[\frac{\partial \rho}{\partial z} \right]_{S,\Theta}. \quad (26.163)$$

We here see why attachment of subscripts to the partial derivatives is essential to avoid confusion, since

$$\left[\frac{\partial \rho}{\partial z} \right]_{x,y} \neq \left[\frac{\partial \rho}{\partial z} \right]_{S,\Theta}. \quad (26.164)$$

The left hand side vertical derivative is computed holding the horizontal position fixed, as appro-

priate for computing the vertical stratification, whereas the right hand side vertical derivative is computed with (S, Θ) fixed, as appropriate for computing the sound speed. These two derivatives are conceptually distinct, with equation (26.163) exposing the mathematical distinction.

26.8.4 Comments

Decoupling mechanical energy from internal energy

There are further niceties required to unravel energetics of the Boussinesq ocean, with details provided by [Young \(2010\)](#). When encountering these details for the first time one may wonder why bother since the compressible energetics discussed in Sections 23.3 and 23.5 are rather straightforward. However, the difficulty with compressible energetics arises from the internal energy. Namely, since many geophysical flows, particularly those in the ocean, have speeds that are tiny compared to molecular speeds (see Section 13.3), the mechanical energy associated with geophysical flow is tiny relative to the internal energy arising from molecular motions. So when studying the total energy budget for a compressible fluid, that energy is dominated by the internal energy. As detailed in [Young \(2010\)](#), the oceanic Boussinesq approximation allows one to focus on the Boussinesq mechanical energy arising just from the fluid flow, and it does so by decoupling mechanical energy from the internal energy.

General form of the geopotential

The treatments in [Young \(2010\)](#) and Section 2.4.3 of [Vallis \(2017\)](#) focus on the simple form of the geopotential, $\Phi = g z$, in which case it appears that density in an energetically consistent Boussinesq ocean can at most have the space and time dependence

$$\rho = \rho[S(\mathbf{x}, t), \Theta(\mathbf{x}, t), p = -\rho_0 g z]. \quad (26.165)$$

However, the formalism developed by [Young \(2010\)](#) allows for a general geopotential, including those that arise from astronomical tidal forcing and from mass redistributions such as near ice shelves. In these cases we retain a consistent Boussinesq energetics with density of the more general form

$$\rho = \rho[S(\mathbf{x}, t), \Theta(\mathbf{x}, t), p = -\rho_0 \Phi(\mathbf{x}, t)]. \quad (26.166)$$

Distinct manifestations of irreversible processes

It is notable that the irreversible terms from \dot{S} and $\dot{\Theta}$ that appear in the mechanical energy equations (26.132), (26.144c) and (26.145) are absent from the non-Boussinesq budget in equation (23.40). Instead, for the non-Boussinesq fluid, the irreversible mixing processes manifest through their effects on flow convergence via the mass continuity equation

$$-\nabla \cdot \mathbf{v} = \frac{1}{\rho} \frac{D\rho}{Dt}. \quad (26.167)$$

Since the Boussinesq ocean has a zero flow divergence, the role of mixing on the potential energy budget appears elsewhere within the mechanical energy budget.

26.9 Available potential energy (APE)

As we have seen, the gravitational potential energy per mass of a fluid element as measured relative to the $z = 0$ geopotential is given by $g \rho z$. But how much of that potential energy is convertible

to kinetic energy? Clearly not all of it since a state of zero potential energy means all of the fluid sits at $z = 0$, which is not generally possible. In Section 26.7 we noted that $-g^{-1} b \Phi$ is the potential energy per mass relative to the constant density background state. Pursuing this idea one more step, consider a background buoyancy, $b_{\text{ref}}(z)$, that has a non-zero depth dependence but with no horizontal dependence. Without any horizontal buoyancy gradients there are zero horizontal internal pressure gradients so that an initially static fluid will remain static. As seen in the discussion of vorticity in Section 37.7.1, a fluid with zero baroclinicity does not generate vorticity since its pressure gradients are perpendicular to buoyancy gradients, which are vertical for a reference state with $b = b_{\text{ref}}(z)$ (see Section 26.1.2 for the Boussinesq baroclinicity vector). These ideas motivate us to compute the potential energy relative to a depth-dependent background buoyancy profile.

Lorenz (1955) suggested that a particularly relevant background buoyancy state is that obtained by a reversible rearrangement or “sorting” of the original buoyancy to a state that has zero baroclinicity. A reversible rearrangement means there is no mixing when moving between the original state and the background state. The difference in gravitational potential energy between these two states is termed the *available potential energy* (APE), with the APE measuring the potential energy accessible for generating reversible motion. Figure 26.2 illustrates these notions. In the remainder of this section we provide further details to support this conceptual description of APE. We restrict attention to the perfect Boussinesq ocean with a linear equation of state, thus ignoring the role of mixing processes and subtleties associated with the nonlinear equation of state.

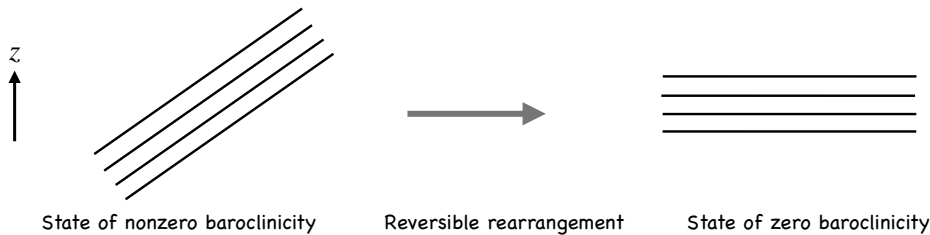


FIGURE 26.2: Isolines of constant buoyancy to illustrate the concept of available potential energy (APE) in a stably stratified Boussinesq ocean. The initial state (left panel) with non-zero baroclinicity is reversibly rearranged to have zero baroclinicity (right panel). The difference in gravitational potential energy between these two states defines the APE in the initial state. As shown in Section 26.9.3, the APE is a non-negative measure of the amount of gravitational potential energy that can, in principle, be reversibly converted to kinetic energy. Due to volume conservation and the absence of irreversible processes, the depth of a buoyancy surface in the background state shown in the right panel equals to the area average depth of the same buoyancy surface in the left panel (see Section 26.9.2).

26.9.1 Analytic continuation of buoyancy surfaces

We use the term *outcrop* to refer to the vanishing of a buoyancy surface at the upper boundary, and *incrop* when it vanishes at the lower boundary. Figure 26.3 illustrates such surfaces. When considering a fluid in a domain with geometric boundaries, and when describing properties of the fluid according to thermodynamic coordinates such as buoyancy, we must decide how to describe these surfaces in regions where they do not exist; i.e., where they are outcropped or incropped. We follow the *Lorenz convention* described in Lorenz (1955), Andrews (1983), Section 4 of Young (2012), and Appendix A of Ringler et al. (2017).

This goal might appear to be pointless; i.e., if the surface does not exist in a region, then why do we need to specify any of its properties. However, the “analytic continuation” of buoyancy

surfaces is very useful when developing their kinematics, with particular use for available potential energy in Section 26.9.3. Such concerns have further applications for studies of water mass transformation arising from boundary buoyancy fluxes (e.g., [Nurser et al. \(1999\)](#) as well as Chapter 65). Additionally, as we will see, the buoyancy frequency along these surfaces is formally infinite since the extended buoyancy surfaces are squeezed into a zero thickness layer. Doing so thus creates an infinite potential vorticity, which corresponds to the potential vorticity *delta sheets* as discussed by [Bretherton \(1966\)](#) and [Schneider et al. \(2003\)](#). In the following we limit our attention to domains with flat bottoms and vertical side-walls to minimize the niceties that arise with more general domains.

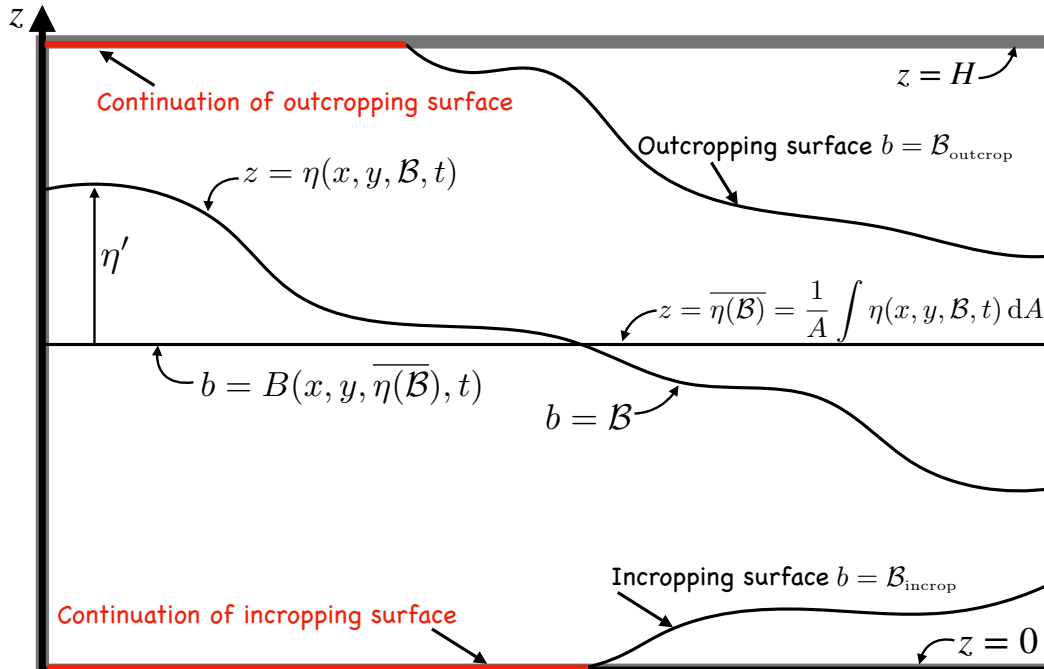


FIGURE 26.3: Geometry of buoyancy surfaces in a flat bottom box of perfect Boussinesq ocean with height H and horizontal area $\int dA = A$. Three representative buoyancy surfaces are shown: one that spans the full domain with $b = \mathcal{B}$, one that incrops at the bottom with $b = \mathcal{B}_{\text{incrop}}$, and one that outcrops at the surface with $b = \mathcal{B}_{\text{outcrop}}$. The vertical height of a buoyancy surface is $z = \eta(x, y, \mathcal{B}, t)$; its area average (which is time independent; see Section 26.9.2) is $\bar{\eta}(\mathcal{B}) = A^{-1} \int \eta(x, y, \mathcal{B}, t) dA$; and its corresponding anomalous height is $\eta'(x, y, \mathcal{B}, t) = \eta(x, y, \mathcal{B}, t) - \bar{\eta}(\mathcal{B})$. As a complement, a particular point on the $z = \bar{\eta}(\mathcal{B})$ height surface has buoyancy $b = B(x, y, \bar{\eta}(\mathcal{B}), t)$, which then leads to an anomalous buoyancy $b'(x, y, \bar{\eta}(\mathcal{B}), t) = B(x, y, \bar{\eta}(\mathcal{B}), t) - \mathcal{B}$, where $B(x, y, \bar{\eta}(\mathcal{B}), t) = \mathcal{B}$ (see equation (26.175)). To allow the formalism to be transparent across all buoyancy surfaces, we set $\eta(x, y, \mathcal{B}_{\text{outcrop}}, t) = H$ in regions where the surface has outcropped, and $\eta(x, y, \mathcal{B}_{\text{incrop}}, t) = 0$ where the surface has incropped (denoted by the red lines). As a complement, we set $\partial z / \partial b = 1/N^2 = 0$ for regions where the surface has either incropped or outcropped, thus formally imposing an infinitely stratified extension of the incropped and outcropped surfaces across the top and bottom domain boundaries. Through this analytic continuation of the buoyancy surfaces, we are ensured that the area mean height of all buoyancy surfaces forms a monotonic sequence from 0 to H , with $\bar{\eta}(\mathcal{B}_1) > \bar{\eta}(\mathcal{B}_2)$ if $\mathcal{B}_1 > \mathcal{B}_2$. When focused on a single buoyancy surface, we can reduce notational clutter by writing, for example, $\bar{\eta}$ rather than $\eta(\mathcal{B})$, as well as $b'(\bar{\eta}) = B(\bar{\eta}) - \mathcal{B}$, and $\eta' = \eta - \bar{\eta}$.

Buoyancy-area mean height of a buoyancy surface

A kinematic property that we make use of when formulating available potential energy is the area mean height of a buoyancy surface. One way to define this mean is to integrate the height over

the area of the buoyancy surface and then divide by the area of the buoyancy surface

$$\overline{\eta(\mathcal{B}, t)}^{\text{buoyancy}} = \frac{\int_{\mathcal{B}} \eta(x, y, \mathcal{B}, t) dS}{\int_{\mathcal{B}} dS}, \quad (26.168)$$

where $\int_{\mathcal{B}} dS$ is the area integral over the \mathcal{B} buoyancy surface. There are two problems with this area mean. First, the area of a buoyancy surface is rather complicated to compute in practice. Second, the buoyancy surface area is time dependent thus making the area mean also time dependent.

Domain-area mean height of a buoyancy surface

An alternative method to compute the area mean height is to integrate over the area of the fluid domain

$$\overline{\eta(\mathcal{B})} = \frac{\int \eta(x, y, \mathcal{B}, t) dA}{\int dA}, \quad (26.169)$$

where

$$A = \int dA = \int_{\text{fluid domain}} dx dy \quad (26.170)$$

is the time-independent horizontal area of the fluid domain. However, in choosing the domain area we must specify the height of a buoyancy surface in those horizontal regions where the surface does not exist; i.e., where the surface outcrops or incrops. By doing so, we see in Section 26.9.2 that the area mean height is time-independent for all buoyancy surfaces. Furthermore, this area mean height satisfies the monotonicity property

$$\overline{\eta(\mathcal{B}_1)} > \overline{\eta(\mathcal{B}_2)} \quad \text{if} \quad \mathcal{B}_1 > \mathcal{B}_2. \quad (26.171)$$

We make use of both the time-independence of the mean height and the monotonicity property when formulating the available potential energy in Section 26.9.3.

Analytic continuation of surface height at outcrops and incrops

So how do we specify the height in outcrop regions? Let us motivate a specification by considering a buoyancy surface that sits near the top of the domain; i.e., its buoyancy is near the domain maximum, b_{\max} . Assume this surface is not horizontal, with the surface $b = \mathcal{B}_{\text{outcrop}}$ in Figure 26.3 an example. Furthermore, let it cover less horizontal area than the full domain area. If we horizontally integrate just over regions where the surface does not outcrop, but still normalize by the total horizontal area of the domain, then the area mean height will be less than certain other buoyancy surfaces whose buoyancy is less and yet whose horizontal area is more. As a result we will not satisfy the monotonicity property (26.171). A way to recover monotonicity is to analytically continue the buoyancy surface along the upper boundary so that its height in the outcropped region is set to $\eta(x_{\text{outcrop}}, y_{\text{outcrop}}, \mathcal{B}_{\text{outcrop}}, t) = H$. Doing so then ensures that the domain-area mean height for buoyancy surfaces will approach H as their buoyancy approaches the maximum buoyancy. We provide an analogous continuation of the surface within the bottom boundary so that

$$\eta(x, y, \mathcal{B}, t) = \begin{cases} H & \text{if } (x, y) \in \text{outcrop region} \\ 0 & \text{if } (x, y) \in \text{incrop region} \\ \eta(x, y, \mathcal{B}, t) & \text{otherwise.} \end{cases} \quad (26.172)$$

These two continuations of the buoyancy surfaces ensures that the domain-area mean height of all buoyancy surfaces forms a monotonic sequence and that the sequency extends from $0 \leq \overline{\eta(\mathcal{B})} \leq H$.

Analytic continuation of buoyancy stratification at outcrops and incrops

What does the analytic continuation (26.172) imply for buoyancy? As described, we allow all outcropped buoyancy surfaces to continue along the surface at $\eta = H$. All outcropped surfaces are thus squeezed into the infinitesimal upper fluid layer with buoyancy in that layer bounded above by the domain maximum buoyancy, b_{\max} . Likewise, for the bottom of the domain we squeeze all incropped buoyancy surfaces into an infinitesimal layer bounded below by b_{\min} , the minimum buoyancy in the domain. Consequently, the upper and lower boundaries are formally capped by infinitely stratified shells in which the inverse squared buoyancy frequency vanishes.

26.9.2 The dual relation between height and buoyancy

In deriving an expression for the APE in Section 26.9.3, we will find it useful to have relations between the unsorted and sorted buoyancy fields. We will also make use of the dual relation between the height of a constant buoyancy surface and the buoyancy of a constant height surface. For this purpose we examine certain kinematic properties of buoyancy surfaces in a stably stratified box of a perfect Boussinesq ocean as in Figure 26.3.

Volume beneath a buoyancy surface using height coordinates

Making use of notation from Figure 26.3, the volume of fluid contained beneath an arbitrary buoyancy surface is

$$V(\mathcal{B}) = \int dA \int_0^{\eta(x,y,\mathcal{B},t)} dz = \int \eta(x, y, \mathcal{B}, t) dA = A \overline{\eta(\mathcal{B})}, \quad (26.173)$$

The following properties result from volume conservation in a perfect non-divergent flow (see Chapter 18).

- The volume of fluid beneath an arbitrary buoyancy surface is time-independent, as is the area mean height of this surface. This property allowed us to drop the time argument from $V(\mathcal{B})$ and $\overline{\eta(\mathcal{B})}$ in equation (26.173).
- The area mean height of a buoyancy surface is identical to the height of the surface when it is reversibly rearranged to be horizontal.

To verify these properties, recall that buoyancy surfaces are material in a perfect fluid so that no fluid crosses them even as they fluctuate. It follows that the volume of fluid beneath an arbitrary buoyancy surface is time-independent. Since the horizontal area of the domain is time-independent, equation (26.173) also means that the area averaged height of the buoyancy surface is time-independent. Furthermore, any motion of a buoyancy surface in a perfect fluid is reversible, including motion that flattens the surface. Since its area mean height remains fixed, the area mean equals to the height of the surface when it is flat.

Area mean buoyancy on a constant depth surface

As a further realization of the dual relation between height and buoyancy, note that the area average buoyancy, $b = B(x, y, z, t)$ along a constant height surface is also constant in time

$$\overline{B(z)} = A^{-1} \int B(x, y, z, t) dA = \text{time independent.} \quad (26.174)$$

This property follows since both buoyancy and volume are material constants following a fluid parcel in a perfect Boussinesq ocean. Hence, a fluid parcel carries both its buoyancy and volume unchanged so that the volume integrated buoyancy within any fluid region remains constant. Correspondingly, the area integrated buoyancy along any fixed height surface remains constant. It also follows that the area mean buoyancy at $z = \overline{\eta(\mathcal{B})}$ is \mathcal{B}

$$\overline{B[\overline{\eta(\mathcal{B})}]} = A^{-1} \int B(x, y, z = \overline{\eta(\mathcal{B})}, t) dA = \mathcal{B}. \quad (26.175)$$

Volume beneath a buoyancy surface using buoyancy coordinates

Let us return to the volume beneath a buoyancy surface, only now use buoyancy coordinates to write

$$V(\mathcal{B}) = \int dA \int_0^{\eta(x, y, \mathcal{B}, t)} dz = \int dA \int_{b(x, y, 0, t)}^{\mathcal{B}} \frac{\partial z}{\partial b} db = \int dA \int_{b(x, y, 0, t)}^{\mathcal{B}} \frac{db}{N^2} \quad (26.176)$$

where $b(x, y, 0, t)$ is the buoyancy at the bottom of the domain and

$$N^2 = \frac{\partial b}{\partial z} \quad (26.177)$$

is the squared buoyancy frequency. As noted in Section 26.9.1 and illustrated in Figure 26.3, we analytically continue the buoyancy surfaces into the surface and bottom boundaries so that

$$N^{-2}(x, y, \mathcal{B}) = \begin{cases} = 0 & \text{if } \mathcal{B} > b(x, y, H) \text{ (surface outcrop region)} \\ = 0 & \text{if } \mathcal{B} < b(x, y, 0) \text{ (bottom incrop region)} \\ = N^{-2}(x, y, \mathcal{B}) & \text{if } b(x, y, 0) \leq \mathcal{B} \leq b(x, y, H). \end{cases} \quad (26.178)$$

In this manner we can replace the lower limit in equation (26.176) with a constant buoyancy well below any buoyancy found in the domain, which we write as b_{\min} , so that

$$V(\mathcal{B}) = \int dA \int_{b_{\min}}^{\mathcal{B}} \frac{db}{N^2} = \int_{b_{\min}}^{\mathcal{B}} db \int \frac{dA}{N^2}. \quad (26.179)$$

Being able to commute the area and buoyancy integrals proves useful in the following.

26.9.3 Exact expression for APE

In this section we develop an expression for the APE of the perfect stably stratified Boussinesq ocean in a box. To start, consider the gravitational potential energy of the fluid in Figure 26.3 relative to a constant density background state with $\rho = \rho_0$

$$\mathcal{P} = - \int dA \int_0^H b z dz = -\frac{1}{2} \int dA \int_0^H b d(z^2). \quad (26.180)$$

Integration by parts leads to the equivalent expression

$$\mathcal{P} = -\frac{1}{2} \int dA \int_0^H d(b z^2) + \frac{1}{2} \int dA \int_{b(x,y,0)}^{b(x,y,H)} \eta^2(x, y, b) db \quad (26.181)$$

$$= -\frac{A H^2}{2} \overline{b(H)} + \frac{1}{2} \int dA \int_{b(x,y,0)}^{b(x,y,H)} \eta^2(x, y, b) db, \quad (26.182)$$

where $\overline{b(H)}$ is the area averaged buoyancy at the top of the fluid domain, $z = H$. As discussed in Section 26.9.1, integration over the finite domain using a buoyancy coordinate leads us to set $\overline{b(H)} = b_{\max}$, the domain maximum buoyancy. Likewise, the second expression in equation (26.182) has its buoyancy integral range extended to b_{\min} and b_{\max} . By doing so we can swap the area and buoyancy integrals to render

$$\mathcal{P} = \frac{A}{2} \left[-H^2 b_{\max} + \int_{b_{\min}}^{b_{\max}} \overline{\eta^2(b)} db \right], \quad (26.183)$$

where $\overline{\eta^2(b)}$ is the area mean of the squared height of a buoyancy surface. The same calculation for the reference buoyancy, $b_{\text{ref}}(z)$, leads to

$$\mathcal{P}_{\text{ref}} = \frac{A}{2} \left[-H^2 b_{\max} + \int_{b_{\min}}^{b_{\max}} \overline{\eta(b)^2} db \right], \quad (26.184)$$

where we noted that the height of a reference buoyancy surface equals to the area mean of the corresponding buoyancy surface

$$\eta(b_{\text{ref}}) = \overline{\eta}(b = b_{\text{ref}}), \quad (26.185)$$

and the reference buoyancy at the surface boundary equals to the maximum buoyancy, $b_{\text{ref}}(H) = b_{\max}$.

Subtracting the gravitational potential energy of the reference/background state from the potential energy of the full state renders an expression for the available potential energy

$$\mathcal{P}_{\text{APE}} = \mathcal{P} - \mathcal{P}_{\text{ref}} = \frac{A}{2} \left[\int_{b_{\min}}^{b_{\max}} [\overline{\eta^2(b)} - \overline{\eta(b)^2}] db \right] = \int_{b_{\min}}^{b_{\max}} \overline{(\eta')^2} db \geq 0, \quad (26.186)$$

where (see Figure 26.3)

$$\eta(x, y, b, t) = \overline{\eta(b)} + \eta'(x, y, b, t). \quad (26.187)$$

The positive definite nature of the APE arises since either a positive or negative buoyancy surface undulation gives rise to motion.

Equation (26.186) is an exact expression for the APE of a perfect Boussinesq ocean in a flat bottom domain. We encounter the same expression when studying the APE in a shallow water fluid in Section 33.5.6. It is the natural expression when working in buoyancy coordinates, whereby the APE is determined by height variations of constant buoyancy surfaces.

26.9.4 Approximate expression for APE

When working with geopotential coordinates it is useful to obtain an approximate expression for the APE in terms of buoyancy variations on constant height surfaces. That is the subject of this subsection.

Approximate version of APE in terms of buoyancy fluctuations

To develop an approximate expression for the APE we write the height of a buoyancy surface $\eta(\mathcal{B})$ in the form (see caption to Figure 26.3 if confused by signs)

$$\eta(\mathcal{B}) \approx \overline{\eta(\mathcal{B})} + \left[\frac{\partial z}{\partial b} \right]_{z=\bar{\eta}} [\mathcal{B} - B(\bar{\eta})] = \bar{\eta} - \frac{b'}{N^2} \approx \bar{\eta} - \frac{b'}{N_{\text{ref}}^2}, \quad (26.188)$$

where the final step set $N^2(x, y, \bar{\eta}) \approx N_{\text{ref}}^2(\bar{\eta})$, which is valid to the same order as the approximation. We are thus lead to the approximate expression

$$\eta' = \eta - \bar{\eta} \approx -\frac{b'}{N_{\text{ref}}^2} \quad (26.189)$$

so that the APE is given approximately by

$$\mathcal{P}_{\text{APE}} \approx A \left[\int_0^H \frac{(b')^2}{2 N_{\text{ref}}^2} dz \right], \quad (26.190)$$

This approximate expression is commonly used in practical calculations of APE, particularly when making use of field measurements (e.g., [Bishop et al. \(2020\)](#)).

Practical issues related to the sorted buoyancy profile

Figure 26.4 illustrates how to obtain the sorted buoyancy profile from a discretized version of a stably stratified fluid. The buoyancy of each cell is compared to that of all other cells and vertically stacked according to the relative buoyancy. The vertical position of the sorted grid cell is determined by accumulating the volume per horizontal area of the cell, starting from the bottom and moving up.

It is notable that cells with identical buoyancy lead to regions of zero vertical stratification in the sorted buoyancy profile. Such zero stratification regions commonly arise when sorting stratified fluid layers, where the buoyancy is constant within the layers. One is thus led to perform a vertical smoothing of the sorted profile to remove such unstratified regions, particularly if using the profile to define a background buoyancy frequency as required for the approximate APE calculation given by equation (26.190).

Budget for approximatae APE

To develop a budget for the approximate form of APE, start by considering the budget for buoyancy as decomposed as

$$b(x, y, z, t) = b_{\text{ref}}(z) + b'(x, y, z, t), \quad (26.191)$$

so that the perfect fluid buoyancy equation takes on the form

$$\frac{Db}{Dt} = 0 \implies \frac{Db'}{Dt} = -w N_{\text{ref}}^2. \quad (26.192)$$

Multiplying by b' leads to

$$\frac{D[(b')^2/2]}{Dt} = -w b' N_{\text{ref}}^2, \quad (26.193)$$

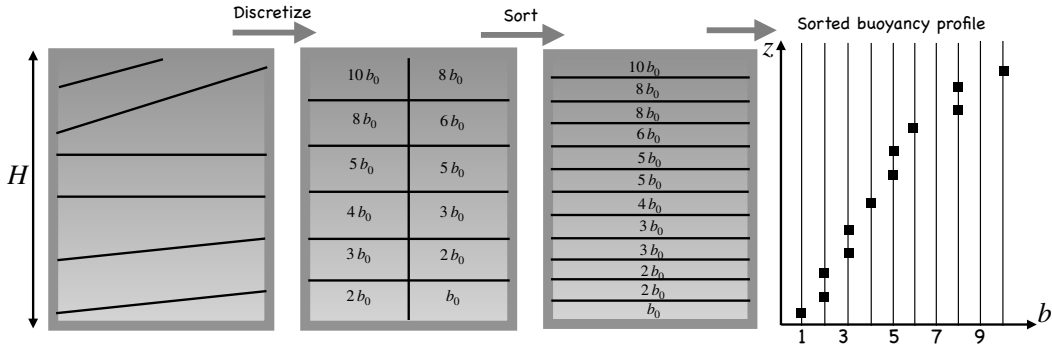


FIGURE 26.4: Illustrating how to sort buoyancy to determine the background or reference profile for computing APE. The first panel on the left shows a sample buoyancy field with black lines representing buoyancy isolines. The second panel shows a discretized version of the field, with b_0 a unit of buoyancy and each cell's buoyancy an integer multiple of b_0 . For simplicity we assume the horizontal area of the domain is depth independent and that each of the discrete grid cells has the same volume and horizontal area. The third panel shows the result of sorting the discrete buoyancy field, with the most buoyant fluid above the less buoyant fluid. During the sort, the cell's volume remains constant (Boussinesq ocean) and the accumulated volume per horizontal area determines the vertical position of the sorted cell. The final panel shows the sorted profile $b_{\text{ref}}(z)$. Note that regions of zero lateral buoyancy gradient in the unsorted buoyancy field lead to vertically unstratified regions in the sorted buoyancy.

and then dividing by N_{ref}^2 renders

$$\frac{\partial P_{\text{APE}}}{\partial t} + \mathbf{v} \cdot \nabla P_{\text{APE}} = -w b' \left[1 - \frac{b'}{2} \frac{\partial(1/N_{\text{ref}}^2)}{\partial z} \right], \quad (26.194)$$

where we defined the approximate APE per unit volume

$$P_{\text{APE}} = (1/2) [b'/N_{\text{ref}}]^2. \quad (26.195)$$

In the case of a depth-independent reference buoyancy frequency, we see that the APE per unit volume materially evolves with a source $-w b'$, which is analogous to the potential energy evolution where the source is $-w b$. Now adding equation (26.194) to the kinetic energy equation (26.128) with $\Phi = g z$ leads to

$$\frac{\partial(\mathcal{K} + P_{\text{APE}})}{\partial t} + \mathbf{v} \cdot \nabla(\mathcal{K} + P_{\text{APE}} + p/\rho_0) = -w \left[g - b_{\text{ref}} - \frac{(b')^2}{2} \frac{\partial(1/N_{\text{ref}}^2)}{\partial z} \right]. \quad (26.196)$$

Note that a global area average on any surface eliminates the $w(g - b_{\text{ref}})$ term since

$$\bar{w} = A^{-1} \int w \, dA = 0, \quad (26.197)$$

which follows from $\nabla \cdot \mathbf{v} = 0$ (see Exercise 18.4). Further simplifications arise with depth-independent N_{ref} , with the corresponding space and time spectra studied by [Bühler et al. \(2014\)](#).

26.9.5 Comments

Elements of this section follow from Section 3.11.1 of [Vallis \(2017\)](#). APE has remained a compelling notion throughout geophysical fluid studies. Unfortunately, for the ocean it has proven very difficult to extend its formalism beyond the perfect fluid Boussinesq system considered here. Particular difficulties arise from the nonlinear equation of state for seawater and the nontrivial ocean geometry with distinct basins and enclosed seas.



26.10 Exercises

EXERCISE 26.1: SYMMETRY UNDER A TIME-DEPENDENT TRANSLATION

In this exercise we consider the Euler equation in free space (no boundaries) where we focus only on the acceleration and the pressure gradient force. That is, we ignore any body forces from gravity and rotation so that the Euler equation takes on the form

$$\rho_0 \frac{D\mathbf{v}}{Dt} = -\nabla p, \quad (26.198)$$

where we assume a Boussinesq ocean so that $\nabla \cdot \mathbf{v} = 0$.

Consider a shift in the reference frame used to describe the flow so that a coordinate position shifts according to

$$\mathbf{x} \rightarrow \mathbf{x} + \mathbf{c}(t), \quad (26.199)$$

where the vector \mathbf{c} is time dependent but has the same value for all points in space.

- (a) Is the shift (26.199) a Galilean transformation? Hint: recall the discussion of Galilean transformation in Section 14.7.
- (b) What happens to pressure in the new reference frame? Hint: consider the elliptic problem for pressure as discussed in Section 26.3.1.
- (c) Write the equation of motion (26.198) in this new reference frame.

EXERCISE 26.2: STEADY PARALLEL SHEARED FLOW

Consider the non-divergent parallel sheared flow on a tangent plane

$$\mathbf{v} = \hat{\mathbf{x}} u(y). \quad (26.200)$$

That is, the steady velocity is zonal and has a meridional dependence.

- (a) Show that this flow is an exact solution to the β -plane inviscid Boussinesq velocity equation.
- (b) What is the corresponding pressure gradient?
- (c) Show that for an f -plane the stationary velocity can have an arbitrary orientation. Hint: it is sufficient to show that $\mathbf{v} = \hat{\mathbf{y}} v(x)$ is a stationary solution.

EXERCISE 26.3: A GENERALIZED BOUSSINESQ APPROXIMATION

In this exercise we derive a mild generalization to the Boussinesq approximation. This generalization facilitates a more accurate decomposition of pressure by introducing a new reference density, $\bar{\rho}(z)$, that is a static function of depth. The new decomposition also leads to a slightly modified buoyancy field.

The derivation starts with the usual decomposition of density using ρ_0 as a space and time constant

$$\rho(\mathbf{x}, t) = \rho_0 + \rho'(\mathbf{x}, t), \quad (26.201)$$

thus leading to the Boussinesq momentum equation

$$\frac{D\mathbf{v}}{Dt} + 2\boldsymbol{\Omega} \times \mathbf{v} = -\rho_0^{-1} (\nabla p + \hat{\mathbf{z}} g \rho). \quad (26.202)$$

But rather than take the traditional decomposition of the pressure and gravitational terms, we now write

$$\nabla p + \hat{z} g \rho = \nabla[p - \bar{p}(z) + \bar{p}(z)] + \hat{z} g [\rho - \bar{\rho}(z) + \bar{\rho}(z)] \quad (26.203a)$$

$$= \nabla[p - \bar{p}(z)] + \hat{z} g [\rho - \bar{\rho}(z)]. \quad (26.203b)$$

This step introduced the density, $\bar{\rho}(z)$, and the corresponding hydrostatically balanced pressure

$$\frac{d\bar{p}(z)}{dz} = -g \bar{\rho}(z). \quad (26.204)$$

- (a) Show that the pressure is decomposed as

$$p(\mathbf{x}, t) = [p(\mathbf{x}, t) - \bar{p}(z)] + \bar{p}(z) = \rho_0 \tilde{\varphi} + \bar{p}(z). \quad (26.205)$$

What is $\tilde{\varphi}$?

- (b) Introduce a buoyancy

$$\tilde{b} = -\frac{g(\rho - \bar{\rho})}{\rho_0}, \quad (26.206)$$

defined relative to the depth-dependent background density, $\bar{\rho}(z)$, rather than the globally constant density ρ_0 . Show that the momentum equation is given by

$$\frac{D\mathbf{v}}{Dt} + 2\boldsymbol{\Omega} \times \mathbf{v} = -\nabla \tilde{\varphi} + \hat{z} \tilde{b}. \quad (26.207)$$

- (c) Show that the baroclinicity vector appearing in the Boussinesq vorticity equation takes the form

$$\tilde{\mathbf{B}} = \nabla \tilde{b} \times \hat{z}, \quad (26.208)$$

which is mathematically the same as with the traditional Boussinesq approximation from Section 26.1.2. We have thus succeeded in generalizing the pressure decomposition and buoyancy field, yet without corrupting the familiar Boussinesq vorticity dynamics.

EXERCISE 26.4: KINETIC ENERGY FOR A PERFECT HYDROSTATIC BOUSSINESQ FLUID

Consider a perfect *hydrostatic* Boussinesq ocean. Show that the kinetic energy per mass contained in the horizontal velocity,

$$\mathcal{K}_{\text{horz}} = \frac{\mathbf{u} \cdot \mathbf{u}}{2}, \quad (26.209)$$

satisfies the same equation as that for a non-hydrostatic fluid given by equation (26.127). Assume the simple form for the geopotential, $\Phi = g z$.

EXERCISE 26.5: ENERGETICS FOR A PERFECT BOUSSINESQ OCEAN

In Section 26.7 we developed the energetic balances for a perfect Boussinesq ocean in a closed domain (domain where all boundary fluxes vanish). We here rederive the same energetics but using the momentum, buoyancy, and continuity equations in the form that exposes buoyancy

$$\frac{D\mathbf{v}}{Dt} + 2\boldsymbol{\Omega} \times \mathbf{v} = -\nabla \varphi + \hat{z} b \quad (26.210a)$$

$$\frac{Db}{Dt} = 0 \quad (26.210b)$$

$$\nabla \cdot \mathbf{v} = 0 \quad (26.210c)$$

$$b = b(S, \Theta). \quad (26.210d)$$

Assume the simple form for the geopotential, $\Phi = g z$, and assume a closed and static domain (i.e., an Eulerian domain with no boundary contributions). To help physically interpret terms, remember to isolate the total divergence terms and the remainder.

- (a) Derive the material time evolution equation for the kinetic energy.
- (b) Derive the material time evolution equation for $P^b = -g^{-1} \Phi b$, with $\Phi = g z$. Interpret P^b .
- (c) Derive the mechanical energy equation written in its Eulerian flux-form, where we define the mechanical energy per mass as $\mathcal{K} + P^b$. Discuss.
- (d) Integrate the mechanical energy equation to derive a global domain budget for mechanical energy. Discuss.

EXERCISE 26.6: ENERGETICS FOR A DISSIPATIVE BOUSSINESQ OCEAN

We here examine the energy budget for a Boussinesq ocean in a rotating frame under the Traditional approximation and including diabatic forcing, momentum mixing from molecular viscosity, and buoyancy mixing from molecular diffusivity. The equations for this fluid system are

$$\frac{D\mathbf{v}}{Dt} + f \hat{\mathbf{z}} \times \mathbf{v} = -\nabla\varphi + \hat{\mathbf{z}} b + \nu \nabla^2 \mathbf{v} \quad (26.211a)$$

$$\frac{Db}{Dt} = Q^b + \kappa \nabla^2 b \quad (26.211b)$$

$$\nabla \cdot \mathbf{v} = 0. \quad (26.211c)$$

In the above, $\nu > 0$ is the viscosity leading to irreversible mixing of velocity, and $\kappa > 0$ is the diffusivity leading to irreversible mixing of buoyancy.

- Assume both ν and κ are constant for this exercise; e.g., they are molecular values.
 - Assume a linear equation of state so that buoyancy is linearly related to temperature with a constant thermal expansion coefficient (equation (26.24f) with haline contraction coefficient $\beta = 0$).
 - Assume the domain has static boundaries so that it has a fixed volume.
 - When performing domain integrated budgets, ignore boundary terms that appear as a result of the divergence theorem. Even though boundary terms are generally important, we here are not focused on them.
 - Let Q^b be a three-dimensional buoyancy source and/or boundary term; e.g., surface buoyancy fluxes, geothermal heating, interior sources. That is, we choose to isolate the boundary and source terms in Q^b so that $\hat{\mathbf{n}} \cdot \nabla b = 0$ along all boundaries. This construct allows us to contemplate placing buoyancy sources at various places within the fluid column and determining how those sources affect the energy budget.
 - Hint: Elements of this exercise are discussed in Chapter 21 of [Vallis \(2017\)](#).
 - To help physically interpret terms, remember to isolate the total divergence terms and the remainder.
- (a) Derive the material evolution of kinetic energy per mass.

- (b) Derive the equation for domain integrated evolution of kinetic energy per mass. Make use of the identity

$$\nabla^2 \mathbf{v} = -\nabla \times \boldsymbol{\omega} \text{ if } \nabla \cdot \mathbf{v} = 0 \quad (26.212)$$

to express the viscosity contributions in terms of the vorticity

$$\boldsymbol{\omega} = \nabla \times \mathbf{v}. \quad (26.213)$$

- (c) Show that the domain integrated kinetic energy per mass is reduced (dissipated) by the viscosity in the presence of a nonzero vorticity. Discuss this result.
- (d) Derive the material evolution equation for $P^b = -g^{-1} \Phi b$ with $\Phi = g z$. Interpret P^b .
- (e) Derive the equation for domain integrated evolution of gravitational potential energy per mass.
- Discuss how downgradient vertical diffusion of buoyancy impacts on the domain integrated gravitational potential energy.
 - Discuss how diabatic heating impacts on the domain integrated gravitational potential energy.
- (f) Discuss the reversible conversion between kinetic and gravitational potential energy. For example, what happens to the kinetic and gravitational potential energies if a heavy fluid element moves upward?
- (g) Derive the equation for material evolution of mechanical energy per mass.
- (h) Derive the domain integrated evolution of mechanical energy per mass.
- (i) Over a closed volume (no boundary fluxes), show that the dissipation of domain integrated kinetic energy is balanced by the buoyancy source.
- (j) In a steady state (Eulerian time derivative vanishes) and absent buoyancy diffusion, show that diabatic heating from Q^b must occur at a lower level (lower gravitational geopotential) than cooling if a kinetic energy dissipating circulation is to be maintained.

EXERCISE 26.7: KINETIC ENERGY AND THE HYDROSTATIC BOUSSINESQ EQUATIONS

In this exercise we develop some properties of the kinetic energy for the hydrostatic Boussinesq equations listed in Section 26.1.6. We here assume the horizontal frictional acceleration is determined by vertical viscous friction in equation (26.116), and the stress boundary conditions are given by equations (26.118) and (26.120).

- (a) Derive the Eulerian flux-form expression for the kinetic energy budget.
- (b) Why does the kinetic energy only have contributions from the horizontal velocity components?
- (c) Discuss the role of vertical viscosity in transporting kinetic energy in the vertical.
- (d) Discuss the role of vertical viscosity in dissipating kinetic energy.
- (e) Discuss how wind stress and bottom drag impact the globally integrated kinetic energy. Assume bottom drag in the form of equation (26.120).

EXERCISE 26.8: POTENTIAL ENERGY AND THE HYDROSTATIC BOUSSINESQ EQUATIONS

In this exercise we develop some properties of the gravitational potential energy for the hydrostatic Boussinesq equations stated in Section 26.1.6.

- (a) Derive the Eulerian flux-form budget for gravitational potential energy written as $P^b = -g^{-1} \Phi b$ with $\Phi = g z$. Interpret P^b .
- (b) Discuss the role of the subgrid scale eddy-induced advection in this budget as given by equation (26.112). In particular, discuss its impact on the center of mass of the fluid.
- (c) Discuss the role of vertical diffusion in this budget as given by equation (26.112). In particular, discuss its impact on the center of mass of the fluid.
- (d) Integrate the gravitational potential energy budget over the global ocean. Discuss how the surface boundary buoyancy flux, Q_b , impacts on the global potential energy budget through impacts on the center of mass of the fluid. Ignore any bottom geothermal heating.

EXERCISE 26.9: SQUARED BUOYANCY AND THE OCEAN MODEL EQUATIONS

In this exercise we develop some properties of the squared buoyancy for the hydrostatic Boussinesq equations stated in Section 26.1.6 using the subgrid scale buoyancy flux in equation (26.112).

- (a) Write the Eulerian flux-form budget describing the evolution of b^2 , the squared buoyancy. Write the budget using the residual mean velocity defined by the sum

$$\mathbf{v}^\dagger = \mathbf{v} + \mathbf{v}^*. \quad (26.214)$$

Hint: start from the buoyancy equation (26.111).

- (b) Discuss the impacts from vertical diffusion on the b^2 budget.

EXERCISE 26.10: PARAMETERIZED EDDY VELOCITY AND THE OCEAN MODEL EQUATIONS

In this exercise we develop some implications of assuming a specific form for the parameterized eddy velocity for the hydrostatic Boussinesq equations stated in Section 26.1.6. Namely, we consider the specific form for the parameterized eddy-induced velocity proposed by [Gent et al. \(1995\)](#)

$$\mathbf{u}^* = -\partial_z(B \mathbf{S}) \quad (26.215a)$$

$$w^* = \nabla_z \cdot (B \mathbf{S}) \quad (26.215b)$$

$$\mathbf{S} = -\frac{\nabla_z b}{N^2} \quad (26.215c)$$

$$\mathbf{v}^* \cdot \hat{\mathbf{n}} = 0 \quad \text{at all ocean boundaries.} \quad (26.215d)$$

In this expression, $B > 0$ is an eddy diffusivity. To ensure $\mathbf{v}^* \cdot \hat{\mathbf{n}} = 0$ at all domain boundaries requires that $B = 0$ along these boundaries. The horizontal vector $\mathbf{S} = (S^{(x)}, S^{(y)}, 0)$ measures the slope of the buoyancy surfaces relative to the horizontal. We assume the ocean is stably stratified in the vertical, so that $\partial b / \partial z = N^2 > 0$.

- (a) Determine the vector streamfunction Ψ^* such that

$$\mathbf{v}^* = \nabla \times \Psi^*. \quad (26.216)$$

Choose the gauge with $\hat{\mathbf{z}} \cdot \Psi^* = 0$.

- (b) Show that

$$\int_{-H}^{\eta} \mathbf{u}^* dz = 0. \quad (26.217)$$

That is, the parameterized horizontal flow has a zero depth integral.

- (c) At any chosen meridional position y , the meridional buoyancy transport from advection (resolved plus parameterized) is computed by

$$\mathcal{B}^{(y)}(y, t) = \int_{x_1}^{x_2} dx \int_{-H}^{\eta} b(v + v^*) dz. \quad (26.218)$$

The zonal and vertical integrals are over the full zonal and vertical extent of the ocean domain. Show that the effects from v^* are to reduce the meridional gradients of buoyancy. That is, if buoyancy decreases poleward, then v^* will flux buoyancy poleward to reduce the gradient.

- (d) How does the introduction of \mathbf{v}^* to the buoyancy equation (26.24c) affect the global integrated *gravitational potential energy*? Discuss.
- (e) How does the introduction of \mathbf{v}^* to the buoyancy equation (26.24c) affect the global integrated *available potential energy*? Discuss.



Chapter 27

BUOYANCY

A large portion of the vertical pressure force acting on a geophysical fluid is balanced by the gravitational force, with precise balance holding for an exact hydrostatic fluid. If there are unbalanced density-induced pressure forces, then a fluid element experiences a *buoyant* acceleration that causes vertical motion. More precisely, *buoyancy* is the vertical pressure force acting on a fluid element that arises from inhomogeneities in the fluid density field. Correspondingly, there are no buoyant forces in a homogeneous fluid, even though each fluid element still feels a gravitational force.

If the vertical pressure forces acting on a fluid element are balanced by gravity, then the fluid element is said to be *neutrally buoyant*. If these forces are unbalanced then the fluid element has a net buoyancy that causes vertical acceleration. Buoyancy is a convenient packaging of the vertical forces from gravity that offers insights into the role of density inhomogeneities in creating vertical accelerations. There are various nuances to this packaging, with some of the nuances discussed in this chapter.

Our study of buoyancy starts by examining the buoyancy of a *test fluid element*, with a test fluid element probing properties of the surrounding fluid environment yet without altering the environment.¹ We refer to the buoyant force acting on the test fluid element as the *Archimedean buoyancy*, with Archimedean buoyancy providing a natural generalization of the familiar buoyancy force acting to keep extended bodies, like a ship, floating in a fluid. Examining the buoyancy of test fluid elements positioned within a fluid leads to the notions of gravitational stability and neutral directions.²

Most references to buoyancy in the geophysical literature refer to the Archimedean buoyancy. Even so, Archimedean buoyancy is an incomplete rendering of the forces acting in a fluid element arising from density inhomogeneities. To obtain a more complete description requires us to move beyond the notion of a test fluid element by acknowledging that a real fluid element affects the environment surrounding it. This description leads to the notion of *effective buoyancy*, with effective buoyancy accounting for the *static forces* that create vertical accelerations of a fluid element. More precisely, the effective buoyancy is the vertical acceleration acting on a fluid element that remains when setting all velocity dependent accelerations to zero. The effective buoyancy has a contribution from both Archimedean buoyancy acting on a test fluid element, plus the vertical derivative of a pressure perturbation that depends only on the density field. This extra pressure force can be interpreted as the *back-reaction* on a fluid element due to the

¹As defined in Section 14.3.5, a test fluid element is directly analogous to the point test mass particles that probe properties of the gravitational field and the point test electrical charges that probe the electromagnetic field. Like the test fluid element, neither of these test particles alter the force fields where they are placed.

²Archimedes was a Greek mathematician, inventor, engineer, physicist, and astronomer who lived in Syracuse, Sicily from roughly 287 B.C.E to 212 B.C.E. The Archimedean buoyancy of a test fluid element makes use of perhaps the most ancient of physical concepts used in modern fluid mechanics.

surrounding fluid environment. That is, it accounts for the distinction between a test fluid element and a fluid element.

CHAPTER GUIDE

This chapter builds from our study of pressure in Chapters 21, 22, and 25. We also make use of the equations for a Boussinesq fluid as derived in Chapter 26, in particular the Poisson equation satisfied by pressure in a non-divergent flow. An understanding of this chapter greatly supports an understanding of how pressure and gravity work within an inhomogeneous fluid to create vertical accelerations.

27.1	Loose threads	655
27.2	Archimedes' Principle for a fluid region	655
27.2.1	Hydrostatic pressure force	656
27.2.2	Archimedean buoyancy force	656
27.3	Mass density and its flavors	657
27.3.1	Equation of state for the atmosphere and ocean	657
27.3.2	Modified temperature variables	657
27.3.3	Infinitesimal density increments and material time changes	658
27.3.4	Potential density	659
27.3.5	Linear equation of state for the ocean	660
27.3.6	Comments on density in a hydrostatic ocean	660
27.3.7	Further study	660
27.4	Archimedean buoyancy of a test fluid element	661
27.4.1	Locally referenced Archimedean buoyancy	661
27.4.2	Globally referenced Archimedean buoyancy	661
27.5	Buoyancy stratification and neutral directions	662
27.5.1	General considerations	662
27.5.2	Comparing <i>in situ</i> densities	663
27.5.3	Neutral directions and the neutrality condition	663
27.5.4	Buoyancy frequency and gravitational stability	664
27.5.5	Locally referenced potential density	665
27.5.6	Gravitational stability of an ideal gas atmosphere	666
27.5.7	Comments and further study	668
27.6	Neutral helicity	668
27.6.1	Mathematical preliminaries	669
27.6.2	Neutral helicity is the reason neutral surfaces are ill-defined	670
27.6.3	Comments and further study	671
27.7	Effective buoyancy and vertical accelerations	671
27.7.1	Vertical motion in approximately hydrostatic fluids	671
27.7.2	Two decompositions of pressure and gravity forces	672
27.7.3	Boussinesq velocity equations	673
27.7.4	Poisson equations for $p' = p'_{\text{buoy}} + p'_{\text{flow}}$	673
27.7.5	Accelerations from effective buoyancy and fluid motion	675
27.7.6	Boundary value problems for the accelerations	676
27.7.7	Relative scales for effective and Archimedean buoyancies	677
27.7.8	Thought experiments for effective buoyancy	679
27.7.9	Comments and further study	680
27.8	Exercises	680

27.1 Loose threads

- Provide some examples of b_{eff} fields in Section 27.7 as taken from [Tarshish et al. \(2018\)](#).

27.2 Archimedes' Principle for a fluid region

The Archimedean buoyancy acting on a massive body immersed in a static fluid is the vertical acceleration due to the gravitational acceleration of the body relative to the gravitational acceleration of the fluid displaced by the body. A body's Archimedean buoyancy is proportional to its density relative to that of the displaced fluid. Hence, there is no Archimedean buoyancy without gravity nor is there a buoyant acceleration without density differences. These statements of *Archimedes' Principle* are a direct consequence of hydrostatics.

Archimedean buoyancy has wide applications for the study of bodies immersed within fluids; e.g. mechanics of marine organisms, ships, submarines, hot air balloons. Our interests concern the buoyancy of the fluid within itself, with this buoyancy fundamentally related to the density field. To extend the notions of Archimedean buoyancy to a fluid, we introduce the conceptual construct of a *test fluid element* originally defined in Section 14.3.5. A test fluid element does not alter the environment into which it is placed, so that it is an imaginary probe that allows us to map the Archimedean buoyancy of the fluid environment without modifying the environment.³

To help build toward an understanding of the Archimedean buoyancy of a test fluid element, consider an arbitrary finite region, \mathcal{R} , contained within a static fluid such as shown in Figure 27.1. For our studies, we are interested in an arbitrary region of the fluid itself, such as an infinitesimal fluid element or a finite fluid volume. The mass of the fluid region is given by the integral of the fluid density over the region

$$M_{\text{fluid}} = \int_{\mathcal{R}} \rho \, dV. \quad (27.1)$$

We seek an understanding of the forces acting on this region from the surrounding fluid.

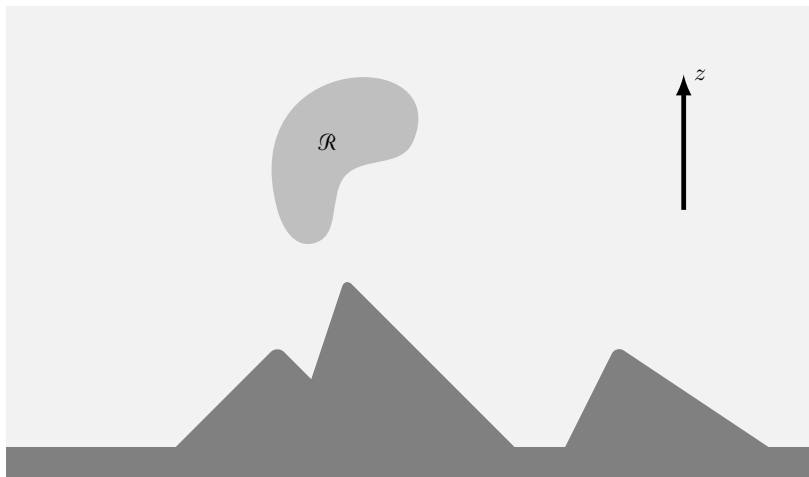


FIGURE 27.1: An arbitrary region of fluid, \mathcal{R} , within a density stratified fluid experiences a gravitational force acting down and a buoyant force acting up. The dark gray features represent the solid earth topography.

³We dispense with the “does not alter” assumption when considering the effective buoyancy acting on a fluid element in Section 27.7.

27.2.1 Hydrostatic pressure force

As discussed in Chapters 22 and 25, any surface, even an imaginary surface, within a fluid experiences a contact stress due to interactions between the fluid and the surface. For a fluid at rest in a gravitational field, the only contact stress arises from pressure. Pressure is a compressive stress, acting in the direction determined by minus the outward normal along the surface. Integrating the pressure over the closed boundary, $\partial\mathcal{R}$, leads to the pressure force acting on the region

$$\mathbf{F}_{\text{pressure}} = - \oint_{\partial\mathcal{R}} p \hat{\mathbf{n}} dS, \quad (27.2)$$

where p is the pressure, $\hat{\mathbf{n}}$ is the outward normal on the boundary, and dS is the area element.

Since the region, \mathcal{R} , is part of the fluid itself, then we can use Gauss's divergence theorem in the form of equation (2.73) to render the equivalent expression for $\mathbf{F}_{\text{pressure}}$ in terms of the volume integral of the pressure gradient

$$\mathbf{F}_{\text{pressure}} = - \int_{\mathcal{R}} \nabla p dV. \quad (27.3)$$

Furthermore, since the fluid is at rest, it is in an exact hydrostatic balance so that its pressure only has a dependence on the vertical position within the fluid, $p = p(z)$. The hydrostatic pressure equals to the weight per horizontal area of fluid sitting above any point in the fluid so that its vertical derivative given by

$$\frac{dp}{dz} = -\rho g. \quad (27.4)$$

Hence, the force acting on the region is

$$\mathbf{F}_{\text{pressure}} = - \int_{\mathcal{R}} \nabla p dV = - \int_{\mathcal{R}} \hat{\mathbf{z}} (dp/dz) dV = \hat{\mathbf{z}} g \int_{\mathcal{R}} \rho dV = \hat{\mathbf{z}} g M_{\text{fluid}}, \quad (27.5)$$

where we assumed a constant gravitational acceleration over \mathcal{R} . The hydrostatic pressure acting on the region imparts a vertical upward force equal to the weight of the fluid within the region. This result is a mathematical expression of *Archimedes' Principle* as applied to a fluid region.

Note that the net horizontal force acting over the region vanishes. The reason is that there are no horizontal pressure gradients within the fluid since, by assumption, the fluid is at rest and thus experiences no horizontal acceleration. So although the region \mathcal{R} experiences horizontal compressive pressure forces acting along its boundary, $\partial\mathcal{R}$, these forces balance when integrated over the body, thus leaving a zero net horizontal acceleration. We studied such static force balances in Section 22.5.

27.2.2 Archimedean buoyancy force

Imagine replacing the fluid in the region \mathcal{R} with another material whose density, ρ_{body} , generally differs from that of the displaced fluid, as does the mass of the region

$$M_{\text{body}} = \int_{\mathcal{R}} \rho_{\text{body}} dV. \quad (27.6)$$

If the material has a density less than the displaced fluid, $\rho_{\text{body}} < \rho_{\text{fluid}}$, then we say that \mathcal{R} has a net positive *buoyancy* force relative to the displaced fluid, in which case \mathcal{R} experiences an upward acceleration. The converse holds if \mathcal{R} is filled with matter that is more dense than the displaced fluid, in which case \mathcal{R} sinks downward.

Mathematically we write this buoyancy force as

$$\mathbf{F}_{\text{buoy}} = \hat{\mathbf{z}} g \int_{\mathcal{R}} (\rho_{\text{fluid}} - \rho_{\text{body}}) dV = \hat{\mathbf{z}} g (M_{\text{fluid}} - M_{\text{body}}). \quad (27.7)$$

In this manner, we define the Archimedean buoyancy as a relative force. The vertical buoyancy force is negative if the mass of the body is larger than that of the fluid it displaces, and conversely if the body is less massive. If the densities are equal, then the body is *neutrally buoyant* and thus experiences no net vertical force; i.e., it floats.

As we observed earlier, a nonzero buoyancy force that leads to vertical acceleration arises from an imbalance between the gravitational body force acting over the region, \mathcal{R} , with the pressure contact force acting on the region boundary, $\partial\mathcal{R}$. Furthermore, if \mathcal{R} is a region of fluid itself, then the buoyancy forces arise from non-hydrostatic pressure forces since any vertical acceleration breaks the hydrostatic balance. We further examine these non-hydrostatic pressure forces in Section 27.7.

27.3 Mass density and its flavors

The density of a fluid element is central to determining its buoyancy. The *thermal equation of state*, or *equation of state* to be more brief (Section 20.4.1), provides an expression for the mass density as a function of pressure, temperature, and material tracer concentration (salinity in the ocean and humidity in the atmosphere). In this section we discuss the equation of state as well as the related flavors of mass density used to study stratified fluids.

27.3.1 Equation of state for the atmosphere and ocean

The atmosphere and ocean are commonly approximated as two-component fluids (air and water vapor for the atmosphere; freshwater and salt for ocean). We thus write the *in situ* density as a function

$$\rho = \rho(S, T, p). \quad (27.8)$$

This *equation of state* is a function of the *in situ* temperature, T , the *in situ* pressure, p , and the *in situ* salinity (ocean) or humidity (atmosphere), S .⁴ The term *in situ* refers to a property measured locally at a point in the fluid. Such *in situ* properties contrast to *potential* properties, which are based on referencing to a chosen pressure (e.g., potential temperature described in Section 20.3).

Liquids such as seawater have rather complex equations of states obtained from empirical fits to measurements. Part of the complexity arises from the multi-component nature of seawater (salt plus freshwater) as well as the nontrivial inter-molecular forces commonly found in liquids. In contrast, the dry atmosphere can, for many purposes, be well approximated as an ideal gas, which has a rather simple equation of state (see Section 20.4.1). Furthermore, even a moist atmosphere has an equation of state that can be massaged to look like that of an ideal gas (e.g., see Section 18.1 of [Vallis \(2017\)](#)). Hence, much of our discussion in this section is biased toward the ocean, where niceties of the equation of state are most important.

27.3.2 Modified temperature variables

As discussed in Section 20.3, the *in situ* temperature of a fluid element changes even if there is no heating applied to the element nor any changes to its material composition. Pressure changes

⁴For our purposes when discussing the ocean, we set $S = 1000 C$ with C the salt concentration, with this specification referred to as the *absolute salinity* by [IOC et al. \(2010\)](#). C generally has values around 0.035 so that S has values around 35.

provide the mechanical means for temperature to change even with processes that are adiabatic and constant composition. Is it possible to remove such pressure effects and still have a field that describes the “temperature” of a fluid element? That is, can we define a temperature field that is only modified by irreversible processes such as heating and mixing? This question is answered by defining *potential temperature*, θ , as well as potential enthalpy or *Conservative Temperature*, Θ , with full discussions given for potential temperature in Section 20.3 and Conservative Temperature in Section 23.9. For now it is sufficient to note that the mass density can be written as a function salinity, potential temperature, and pressure

$$\rho = \rho(S, \theta, p), \quad (27.9)$$

or as a function of salinity, Conservative Temperature, and pressure

$$\rho = \rho(S, \Theta, p). \quad (27.10)$$

For our purposes throughout this book, it is not important to distinguish between potential temperature and Conservative Temperature. Hence, we use θ for brevity when referring to either of the two temperature fields.

One comment on notation is key here. Namely, the functions $\rho(S, T, p)$, $\rho(S, \theta, p)$, and $\rho(S, \Theta, p)$ have distinct coefficients and as such they are distinct functions. Hence, one may wish to introduce notation to distinguish the functions by writing, say,

$$\rho = \mathcal{F}(S, T, p) = \mathcal{G}(S, \theta, p) = \mathcal{H}(S, \Theta, p). \quad (27.11)$$

However, we choose brevity in notation by allowing the functional dependence to signal the distinction. This overloaded notation is standard in the oceanography literature, with care needed to ensure clarity in understanding.

27.3.3 Infinitesimal density increments and material time changes

When computing the buoyancy of a fluid element, we compare the density of that element with the density of its local surrounding fluid environment. To support that comparison, we here consider how density changes under infinitesimal changes in spatial position. Given the functional dependence for the equation of state written in terms of S, θ, p (equation (27.9)), the density differential is given by

$$d\rho = \left[\frac{\partial \rho}{\partial S} \right] dS + \left[\frac{\partial \rho}{\partial \theta} \right] d\theta + \left[\frac{\partial \rho}{\partial p} \right] dp \equiv \rho \beta dS - \rho \alpha d\theta + c_s^{-2} dp. \quad (27.12)$$

The second equality introduced the following thermodynamic properties of the fluid

$$\beta = \frac{1}{\rho} \left[\frac{\partial \rho}{\partial S} \right]_{\theta, p} \quad \text{haline contraction coefficient} \quad (27.13)$$

$$\alpha = -\frac{1}{\rho} \left[\frac{\partial \rho}{\partial \theta} \right]_{S, p} \quad \text{thermal expansion coefficient} \quad (27.14)$$

$$c_s^2 = \left[\frac{\partial p}{\partial \rho} \right]_{S, \theta} \quad \text{squared sound speed.} \quad (27.15)$$

The haline contraction coefficient, β , is considered for the ocean, where *haline* refers to salinity.⁵

The density differential (27.12) leads to the expression for the material change in the *in situ* density moving along a fluid particle trajectory

$$\frac{1}{\rho} \frac{D\rho}{Dt} = \beta \frac{DS}{Dt} - \alpha \frac{D\theta}{Dt} + \frac{1}{\rho c_s^2} \frac{Dp}{Dt}. \quad (27.16)$$

In the absence of mixing, the potential temperature and salinity are materially constant.⁶ In this case, the *in situ* density changes only through adiabatic processes that lead to pressure changes

$$\frac{D\rho}{Dt} = \frac{1}{c_s^2} \frac{Dp}{Dt} \quad \text{adiabatic and isohaline changes.} \quad (27.17)$$

27.3.4 Potential density

As discussed in Section 27.3.2, the reversible motion of a perfect fluid element generally occurs with materially constant potential temperature and materially constant tracer concentration. We thus find it convenient to combine the evolution of salinity and potential temperature into the evolution of a single variable. *Potential density* is one such combination, with it defined as the density a fluid element would have if reversibly moved to a reference pressure

$$\varrho = \varrho(S, \theta | p_{\text{ref}}) \equiv \rho(S, \theta, p = p_{\text{ref}}). \quad (27.18)$$

Hence, potential density is found by evaluating the equation of state for *in situ* density with the local value for S and θ , but with the pressure set to the fixed reference pressure, $p = p_{\text{ref}}$. Potential density is thus parametrically a function of the reference pressure. As for the potential temperature, the reference pressure is often taken as that at sea level. However, that choice is neither necessary nor universal.

Material evolution of potential density

With the definition (27.18), the material evolution of potential density is given by

$$\frac{1}{\varrho} \frac{D\varrho}{Dt} = \beta(S, \theta, p = p_{\text{ref}}) \frac{DS}{Dt} - \alpha(S, \theta, p = p_{\text{ref}}) \frac{D\theta}{Dt}, \quad (27.19)$$

where

$$\beta(S, \theta, p = p_{\text{ref}}) = \frac{1}{\varrho(S, \theta, p = p_{\text{ref}})} \left[\frac{\partial \rho(S, \theta, p_{\text{ref}})}{\partial S} \right]_{\theta} \quad \text{haline contraction at } p = p_{\text{ref}} \quad (27.20)$$

$$\alpha(S, \theta, p = p_{\text{ref}}) = -\frac{1}{\varrho(S, \theta, p = p_{\text{ref}})} \left[\frac{\partial \rho(S, \theta, p_{\text{ref}})}{\partial \theta} \right]_S \quad \text{thermal expansion at } p = p_{\text{ref}} \quad (27.21)$$

are the haline contraction and thermal expansion coefficients evaluated at the reference pressure $p = p_{\text{ref}}$. Since pressure is fixed at the reference value, there is no pressure derivative on the right hand side of equation (27.19). Potential temperature and salinity are materially constant for reversible processes; i.e., adiabatic motion that also maintains constant matter content (e.g., isohaline) for fluid elements. By construction, potential density is also materially constant for

⁵Note that in many chapters of this book, $\beta = \partial f / \partial y$ is the meridional derivative of the Coriolis parameter. We keep the two usages for β distinct so to avoid confusion.

⁶This statement has nuances that are detailed in IOC et al. (2010). For our purposes we can ignore those nuances.

reversible processes since both terms on the right hand side of equation (27.19) vanish. This behavior is in contrast to *in situ* density, whose evolution is affected by pressure changes as revealed by equations (27.16) and (27.17).

Reference pressures for ϱ and θ

The reference pressure for the potential density is commonly assumed to be the same as for the potential temperature. This assumption is particularly the norm for the atmosphere, where the reference pressure is generally taken at the sea level. Likewise for the ocean, the potential temperature is generally computed using a sea level reference pressure. However, there are many occasions in the ocean to consider potential density with larger reference pressures, such as when considering processes within the ocean interior. Doing so is motivated by the rather strong nonlinear effects associated with the seawater equation of state. In this case, pressure effects prompt one to choose a reference pressure closer to the *in situ* pressure near to the region of analysis. Even though it is common to choose a potential density reference pressure distinct from the surface pressure, the potential temperature reference pressure generally remains at the surface. There is no fundamental problem with the use of distinct reference pressures for ϱ and θ . In particular, all of the above properties of potential density remain unchanged.

27.3.5 Linear equation of state for the ocean

For certain purposes, it is useful to approximate the equation of state used to study ocean fluid mechanics. One common idealization is to compute density as a linear function of potential temperature and salinity

$$\rho = \rho_0 [1 - \alpha (\theta - \theta_0) + \beta (S - S_0)], \quad (27.22)$$

where α , β , ρ_0 , θ_0 , and S_0 are constants. An even further simplification is to set salinity to a constant, so that density is just a linear function of potential temperature.

27.3.6 Comments on density in a hydrostatic ocean

In an approximate hydrostatic fluid (Section 24.2), we only have access to the hydrostatic pressure so that density is computed as a function of hydrostatic pressure. Furthermore, density is generally a function of pressure whereas hydrostatic pressure is directly determined by the vertical integral of density. This self-referential situation is resolved for the Boussinesq ocean in which energetic consistency requires the seawater equation of state to use the geopotential defined pressure, $p_{\text{eos}} = -\rho_0 \Phi$, as the argument for density (Section 26.8), which takes on the static form, $p_{\text{eos}} = -\rho_0 g z$, for a simple geopotential. For the non-Boussinesq hydrostatic ocean, we can make use of pressure as the vertical coordinate, thus allowing for density to be evaluated at a pressure prescribed by the value of the vertical coordinate.

27.3.7 Further study

Chapter 1 of [Vallis \(2017\)](#) provides a pedagogical discussion of the equation of state for an ideal gas atmosphere and for seawater, as well as a discussion of the various flavors of density. See also Section 18.1 of [Vallis \(2017\)](#) for the equation of state for an ideal gas with water vapor. The seawater equation of state is detailed by [IOC et al. \(2010\)](#), with a pedagogical overview provided by [McDougall et al. \(2013\)](#).

27.4 Archimedean buoyancy of a test fluid element

We now return to the notions of Archimedean buoyancy (in brief, the fluid “buoyancy”) of a test fluid element. Again, buoyancy is the gravitational acceleration that acts on a massive body due to the difference between the density of the body and the density of the local fluid environment. For this section, we consider the massive body to be a test fluid element whose presence does not alter the density field.

27.4.1 Locally referenced Archimedean buoyancy

Consider a local definition of fluid buoyancy according to

$$b_{\text{local}} = -g(\rho_{\text{test}} - \rho_{\text{environ}})/\rho_{\text{environ}} = g(1 - \rho_{\text{test}}/\rho_{\text{environ}}), \quad (27.23)$$

where ρ_{environ} is the local density of the fluid environment, and ρ_{test} is the density of the test fluid element within that environment. If the fluid element has a density greater than the environment, then it has a negative locally referenced buoyancy, and vice versa.

We determine ρ_{test} by specifying its point of origin and specifying how it is moved (e.g., with or without mixing?) to the environment point. Conventional approaches are specified later in this section. A key notion is that buoyancy as defined by equation (27.23) is a function of the path that the test fluid element takes to reach the environment point. This subjectivity lends ambiguity in the definition of buoyancy. We remove this ambiguity by asking specific questions about local buoyancy. For example, if the fluid element moves an infinitesimal distance while mixing its temperature and salinity with the environment, what direction maintains a neutrally buoyant state for the fluid element? This question forms the basis for defining *neutral directions*.

Working with locally referenced Archimedean buoyancy requires a redefinition of a reference state when moving from point to point within a fluid. The continuum of reference states allows for an accounting of the gravitational stability and neutral directions. However, the re-referencing is not a process that can be seamlessly incorporated to the equations of motion since at each point one needs to redefine the reference state. As an alternative means to garner local information about forces associated with density gradients, we explicitly focus on the pressure force in our discussion of *effective buoyancy* in Section 27.7.

27.4.2 Globally referenced Archimedean buoyancy

The definition (27.23) accepts that buoyancy is a relative field. Hence, at each fluid point we redefine the environment to which to compare the density of the test fluid element. However, there are cases in which it is more convenient, and sufficient, to define a globally constant environment with a constant reference density, ρ_{ref} . In this case we consider the global buoyancy as

$$b_{\text{global}} = g(1 - \rho/\rho_{\text{ref}}), \quad (27.24)$$

where we compute ρ according to the local environmental density. This definition is particularly useful for idealized cases where the *in situ* density is not a function of pressure. In this case buoyancy is a function only of potential temperature and salinity so that we can make use of potential density to measure buoyancy (as explained below).

Although the numerical value of b_{global} is a function of the reference density, what is more relevant is the buoyancy of one fluid element relative to another

$$\Delta b_{\text{global}} = -\Delta\rho/\rho_{\text{ref}}. \quad (27.25)$$

The sign of this relative buoyancy does not depend on the reference density, with the sign all that we need to conclude whether one fluid element is more buoyant than another. Furthermore, with a globally constant environmental density, the buoyancy becomes a local function of space. That is, we no longer compare the fluid element density to a changing local density. Instead, we compute the local density and compare it to the reference density. We can thus determine b_{global} at a point through information available just at that point. Correspondingly, we can map b_{global} and determine the relative buoyancy of fluid elements anywhere in the fluid.

27.5 Buoyancy stratification and neutral directions

What are the Archimedean buoyant forces that act on a fluid element? Is the fluid gravitationally stable to small perturbations? We answer these questions by using a test fluid element to probe the local fluid environment without disturbing the environment. We do not consider time changes in this section, instead considering a snapshot of the fluid environment and using test fluid elements to probe the buoyant properties of the environment.

27.5.1 General considerations

As a fluid element moves through the fluid environment it is exposed to a suite of physical processes that can modify its thermal, material, and mechanical properties; i.e., its θ , S , and p . Modification of its pressure occurs through contact stresses with other fluid elements (Chapters 22 and 25). Modification of its thermal and material properties occurs through the mixing-induced exchange of heat and matter. The exchange of thermal and material properties occurs in the presence of irreversible processes whereas mechanical exchanges occur either reversibly (pressure exchange) or irreversibly (viscous exchange; Section 22.3).

The *in situ* density of a fluid element generally changes when it moves through the fluid, with the density change determined by how the element interacts with the surrounding environment. We conceive of two complementary interactions for the purpose of examining the local Archimedean buoyancy of the test fluid element.

- **UNMIXED TEST FLUID ELEMENT:** Displace the test fluid element without changing θ and S yet allowing p to equilibrate with the local environment. We imagine this adiabatic and isohaline displacement to occur by surrounding the test element with a thermally and materially impermeable elastic sack. In this case there is no mixing of the test element with the environment, yet it mechanically equilibrates its pressure with the surrounding fluid. Hence, the test fluid element's *in situ* density changes through the changing pressure of the local environment.
- **MIXED TEST FLUID ELEMENT:** Displace the test fluid element with θ , S , and p equilibrating with the local environment. Such equilibration requires a complete mixing of the test fluid element's θ and S with the local environment, as well as the mechanical equilibration of its pressure.

If we displace the unmixed test fluid element to a region where its *in situ* density differs from the local environment, then the fluid element feels a local Archimedean buoyant force. However, there are directions that the test fluid element can move that leave its local Archimedean buoyancy zero; i.e., where the test fluid element retains the same *in situ* density as the local environment and so remains neutrally buoyant. These directions are referred to as *neutral directions*, with a test fluid element displaced along a neutral direction maintaining zero local Archimedean buoyancy. It is as if the test fluid element floats along a neutral direction.

A complementary means to conceive of neutral directions is found by considering the mixed test fluid element that is displaced and equilibrates its θ , S , and p with the local environment. An arbitrary displacement leads to a change in the fluid element's *in situ* density due to changes in θ , S , and p . However, if the test element is displaced along the neutral direction, the mixing-induced changes from θ and S exactly balance (details given below). In this manner, the only change to the *in situ* density arises from changes to the pressure felt by the test fluid element, with these changes identical to those felt by the unmixed test fluid element.

27.5.2 Comparing *in situ* densities

To make the above ideas mathematically precise, consider an infinitesimal displacement, $d\mathbf{x}$, of a test fluid element and examine how its *in situ* density, $\rho = \rho(S, \theta, p)$, changes under the above two displacements. First consider the mixed fluid element so that it equilibrates θ , S , and p with the local environment. The *in situ* density of the test element at the new location equals to that of the local environment, $\rho(\mathbf{x} + d\mathbf{x})$. To leading order, the difference in density between the origin and the displaced position is computed according to the exact differential

$$d\rho = \rho(\mathbf{x} + d\mathbf{x}) - \rho(\mathbf{x}) \quad (27.26a)$$

$$= \rho[S(\mathbf{x} + d\mathbf{x}), \theta(\mathbf{x} + d\mathbf{x}), p(\mathbf{x} + d\mathbf{x})] - \rho[S(\mathbf{x}), \theta(\mathbf{x}), p(\mathbf{x})] \quad (27.26b)$$

$$= d\mathbf{x} \cdot \left[\frac{\partial \rho}{\partial \theta} \nabla \theta + \frac{\partial \rho}{\partial S} \nabla S + \frac{\partial \rho}{\partial p} \nabla p \right] \quad (27.26c)$$

$$= \rho d\mathbf{x} \cdot \left[-\alpha \nabla \theta + \beta \nabla S + \frac{1}{\rho c_s^2} \nabla p \right]. \quad (27.26d)$$

For the unmixed test fluid element there is no exchange (mixing) of θ and S with the surrounding environment. Hence, the test element's density changes just from pressure changes

$$(d\rho)_{(\text{no mix})} = \rho(\mathbf{x} + d\mathbf{x})_{(\text{no mix})} - \rho(\mathbf{x}) \quad (27.27a)$$

$$= \rho[S(\mathbf{x}), \theta(\mathbf{x}), p(\mathbf{x} + d\mathbf{x})] - \rho[S(\mathbf{x}), \theta(\mathbf{x}), p(\mathbf{x})] \quad (27.27b)$$

$$= \rho d\mathbf{x} \cdot \left[\frac{1}{\rho c_s^2} \nabla p \right]. \quad (27.27c)$$

Comparing the densities of the two displaced test fluid elements renders

$$\rho(\mathbf{x} + d\mathbf{x}) - \rho(\mathbf{x} + d\mathbf{x})_{(\text{no mix})} = [\rho(\mathbf{x} + d\mathbf{x}) - \rho(\mathbf{x})] - [\rho(\mathbf{x} + d\mathbf{x})_{(\text{no mix})} - \rho(\mathbf{x})] \quad (27.28a)$$

$$= \rho[S(\mathbf{x} + d\mathbf{x}), \theta(\mathbf{x} + d\mathbf{x}), p(\mathbf{x} + d\mathbf{x})] - \rho[S(\mathbf{x}), \theta(\mathbf{x}), p(\mathbf{x} + d\mathbf{x})] \quad (27.28b)$$

$$= \rho d\mathbf{x} \cdot [-\alpha \nabla \theta + \beta \nabla S]. \quad (27.28c)$$

We discuss this result in the following.

27.5.3 Neutral directions and the neutrality condition

As noted in Figure 27.2, if the density of the displaced unmixed test fluid element is the same as the local environment, then the particular displacement defines a neutral direction. From equation (27.28c) we see a displacement along a neutral direction satisfies

$$d\mathbf{x}_{\text{neutral}} \cdot [-\alpha \nabla \theta + \beta \nabla S] = d\mathbf{x}_{\text{neutral}} \cdot \hat{\gamma} | -\alpha \nabla \theta + \beta \nabla S | = 0, \quad (27.29)$$

where we introduced the *dianeutral direction*

$$\hat{\gamma} = \frac{-\alpha \nabla \theta + \beta \nabla S}{| -\alpha \nabla \theta + \beta \nabla S |}, \quad (27.30)$$

which points in the direction of increasing density.⁷ Infinitesimal displacements, $d\mathbf{x}_{\text{neutral}}$, that are orthogonal to the dianeutral direction, $\hat{\gamma}$, occur along a neutral direction

$$d\mathbf{x}_{\text{neutral}} \cdot \hat{\gamma} = 0 \implies \text{displacement along a neutral direction.} \quad (27.31)$$

These displacements of the unmixed test fluid element lead to no difference in the *in situ* density of the local environment and the fluid element. Hence, neutral displacements retain a vanishing local Archimedean buoyancy for the unmixed test fluid element. In contrast, displacements in the dianeutral direction alter the local buoyancy.

Let us write the neutral displacement in the form

$$d\mathbf{x}_{\text{neutral}} = \hat{\mathbf{t}}_{\text{neutral}} ds, \quad (27.32)$$

where ds is the arc-length along the displacement and $\hat{\mathbf{t}}_{\text{neutral}}$ is the unit vector pointing along the neutral displacement. We can thus write equation (27.29) as

$$\alpha \hat{\mathbf{t}}_{\text{neutral}} \cdot \nabla \theta = \beta \hat{\mathbf{t}}_{\text{neutral}} \cdot \nabla S, \quad (27.33)$$

which we refer to as the *neutrality condition*. The neutrality condition means that the α and β weighted derivatives of θ and S aligned along a neutral direction are precisely balanced. So when considering neutral directions from the perspective of the mixed test fluid element, the mixing-induced changes in θ precisely compensate mixing-induced changes in S as per the neutrality condition (27.33). As a result, the *in situ* density of the mixed test fluid element changes only via changes to the pressure (since θ and S changes are compensated), which is precisely how the unmixed test fluid element changes its *in situ* density.

27.5.4 Buoyancy frequency and gravitational stability

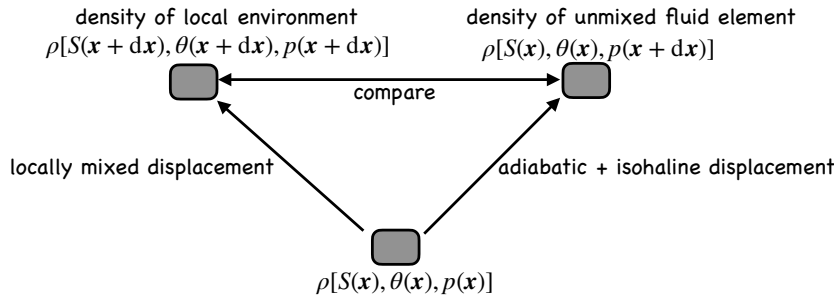
Thus far we have considered a general displacement, $d\mathbf{x}$, of two test fluid elements, and determined conditions for this displacement to keep the locally defined Archimedean buoyancy at zero. Here we specialize to the case of a vertical displacement (Figure 27.3) in which the difference between the environmental density and the unmixed test element's density is

$$\rho(z + dz) - \rho(z + dz)_{(\text{no mix})} = \rho dz \left[-\alpha \frac{\partial \theta}{\partial z} + \beta \frac{\partial S}{\partial z} \right]. \quad (27.34)$$

Now consider a vertically upward displacement so that $dz > 0$. If the surrounding environment has a lower density than the adiabatic and isohaline displaced test fluid element, $\rho(z + dz) < \rho(z + dz)_{(\text{no mix})}$, then the test element will feel a buoyancy force returning it to the original depth. The restorative buoyancy force per volume is written

$$g [\rho(z + dz) - \rho(z + dz)_{(\text{no mix})}] = g \rho dz \left[-\alpha \frac{\partial \theta}{\partial z} + \beta \frac{\partial S}{\partial z} \right] \equiv -N^2 \rho dz, \quad (27.35)$$

⁷Equation (4) in [McDougall et al. \(2014\)](#) makes use of the opposite convention so that their dianeutral direction points towards decreasing density. We instead follow the water mass transformation convention as in equation (65.38), so that $\hat{\gamma}$ points in the direction of increasing density.



$$\rho[S(\mathbf{x} + d\mathbf{x}), \theta(\mathbf{x} + d\mathbf{x}), p(\mathbf{x} + d\mathbf{x})] = \rho[S(\mathbf{x}), \theta(\mathbf{x}), p(\mathbf{x} + d\mathbf{x})] \implies \text{neutral direction}$$

$$\alpha \hat{\mathbf{t}}_{\text{neutral}} \cdot \nabla \theta = \beta \hat{\mathbf{t}}_{\text{neutral}} \cdot \nabla S \implies \text{neutrality condition}$$

FIGURE 27.2: Schematic of the complementary thought experiments used to determine neutral directions. For the right pathway we imagine a test fluid element that is thermally and materially closed but is mechanically open. Hence, as the test fluid element is displaced from its original location, \mathbf{x} , to a new position, $\mathbf{x} + d\mathbf{x}$, it equilibrates to the local pressure but retains the θ and S of the origin. If the *in situ* density of the fluid element is displaced along a direction where it maintains the same density as the local environment, then the locally defined Archimedean buoyancy vanishes and this displacement is aligned along a neutral direction. The complement perspective is shown by the left pathway whereby we follow the mixed test fluid element. If the mixing-induced changes in θ precisely compensate mixing-induced changes in S , according to the neutrality condition (27.33), then the *in situ* density changes for this test fluid element arise only from pressure changes, just like for the unmixed test element on the right pathway.

where we defined the squared buoyancy frequency

$$N^2 = g \left[\alpha \frac{\partial \theta}{\partial z} - \beta \frac{\partial S}{\partial z} \right]. \quad (27.36)$$

Stable vertical motion results from a background density profile with $N^2 > 0$. An unstable profile occurs when $N^2 < 0$, in which case motion of the test fluid element results in an exponential growth associated with a *gravitational instability*. That is, when the fluid column is unstably stratified in the vertical, an initially tiny vertical displacement of a test element will lead to an even larger displacement, thus causing the perturbation to grow unbounded, which is the sign of an instability. We illustrate these cases in Figure 27.4 for the case of linear density profiles.

27.5.5 Locally referenced potential density

Equation (27.36) defines the squared buoyancy frequency in terms of the vertical temperature and salinity gradients. This expression is identical to the vertical gradient of the potential density (27.18), when the reference pressure for density is taken local to the point where the buoyancy frequency is computed. That is, the vertical gradient of the *locally referenced potential density* provides a measure of the vertical stratification

$$N^2 = -g \left[\frac{1}{\varrho} \frac{\partial \varrho}{\partial z} \right]_{p_{\text{ref}}=p} = g \left[\alpha \frac{\partial \theta}{\partial z} - \beta \frac{\partial S}{\partial z} \right]. \quad (27.37)$$

Note that at a point in the fluid, the locally referenced potential density equals to the *in situ* density. However, when probing nearby points by displacing test fluid elements, and thus to take spatial gradients into account, the two densities have distinct gradients. Namely, the *in situ* density is modified by pressure gradients, whereas spatial gradients of the locally referenced potential density remove pressure effects.

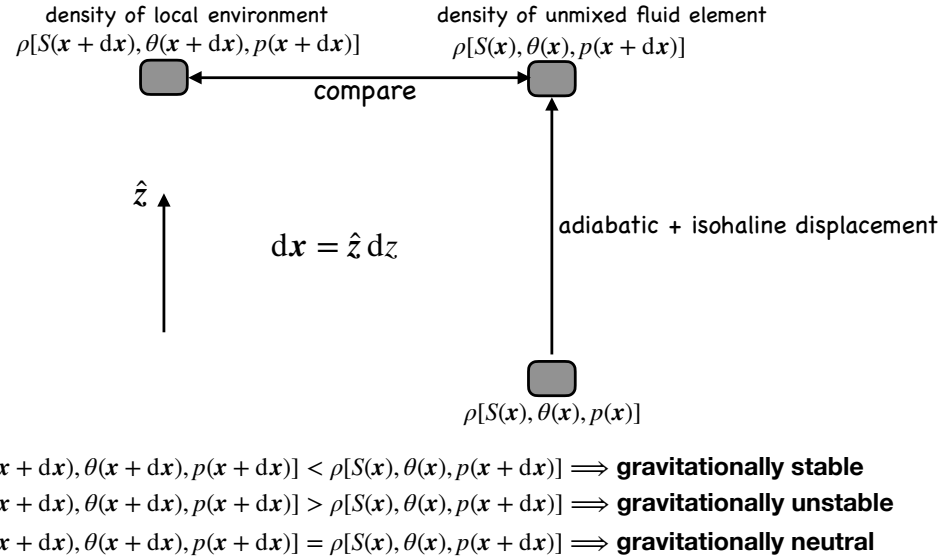


FIGURE 27.3: Schematic of the calculation used to examine whether a fluid column is gravitationally stable under vertical displacement of a test fluid element, here realized by specializing the general displacement in Figure 27.2. A test fluid element is displaced from its original location at a position \mathbf{x} to a position $\mathbf{x} + d\mathbf{x}$, with $d\mathbf{x} = \hat{z} dz$ and $dz > 0$ in this figure. We compare the density of the displaced unmixed test fluid element with the local environment to determine whether the density stratification of the fluid environment is gravitationally stable, unstable, or neutral.

27.5.6 Gravitational stability of an ideal gas atmosphere

We introduced the adiabatic lapse rate in Section 20.2 as a measure of how temperature varies as a function of pressure or depth. For an ideal gas atmosphere (Section 20.4), the squared buoyancy frequency can be written (Exercise 27.2)

$$N^2 = \frac{g}{\theta} \frac{\partial \theta}{\partial z}. \quad (27.38)$$

The potential temperature for an ideal gas is given by equation (20.92)

$$\theta = T \left[\frac{p_{\text{ref}}}{p} \right]^{\varphi} \quad (27.39)$$

where

$$\varphi = R^M/c_p \quad (27.40)$$

is a dimensionless constant for a simple ideal gas. Consequently, the squared buoyancy frequency takes the form

$$g^{-1} N^2 = \frac{\partial \ln \theta}{\partial z} = \frac{\partial \ln T}{\partial z} - \varphi \frac{\partial \ln p}{\partial z}. \quad (27.41)$$

For a hydrostatic fluid with a constant gravitational acceleration, the vertical derivative of pressure is given by (Section 24.2)

$$\frac{\partial p}{\partial z} = -\rho g, \quad (27.42)$$

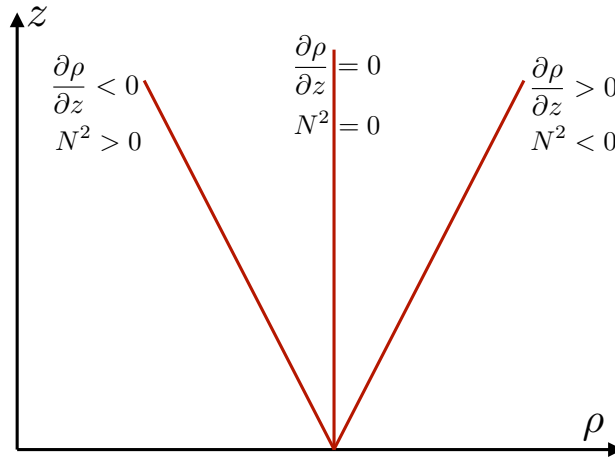


FIGURE 27.4: Sample vertical “soundings” of density in the atmosphere or density profiles in the ocean, with the density assumed to be a linear function of z . If the density decreases upward, the squared buoyancy frequency is positive, $N^2 > 0$, and the fluid is gravitationally stable. If the density does not change when moving vertically, then the fluid is said to be neutrally buoyant with $N^2 = 0$. If the density increases moving upward, then the fluid is gravitationally unstable, with this instability signaled by $N^2 < 0$.

so that pressure at a point in the fluid equals to the weight per area above that point. Using this result leads to the squared buoyancy frequency

$$g^{-1} N^2 = \frac{\partial \ln T}{\partial z} + \frac{\varphi g \rho}{p} = \frac{1}{T} \frac{\partial T}{\partial z} + \frac{g}{c_p T}, \quad (27.43)$$

where we used the ideal gas relation $p = \rho T R^M$ for the final step.

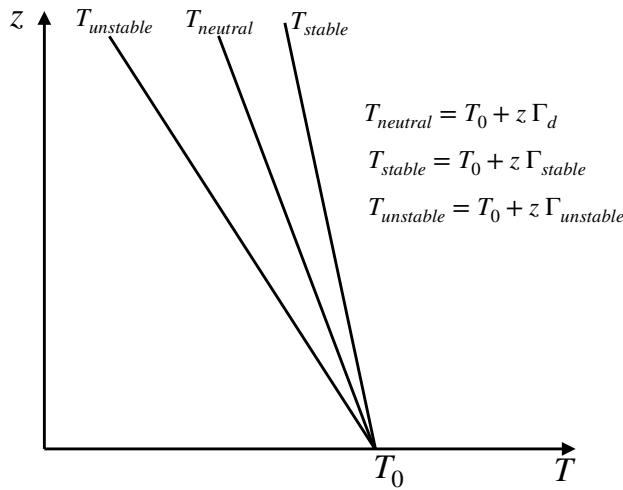


FIGURE 27.5: Three vertical profiles of *in situ* temperature in a dry ideal gas atmosphere. The neutrally stable profile has $T_{neutral} = T_0 + z \Gamma_d$, where $\Gamma_d = -g/c_p \approx -9.8 \text{ K}/(1000 \text{ m})$. A vertically unstable profile (heavy over light) has $T_{unstable} = T_0 + z \Gamma_{unstable}$ where $\Gamma_{unstable} < \Gamma_d = -g/c_p$. In contrast, the gravitationally stable atmosphere has $T_{stable} = T_0 + z \Gamma_{stable}$ where $\Gamma_{stable} > \Gamma_d = -g/c_p$.

A vanishing buoyancy frequency, or equivalently a vanishing vertical derivative of potential

temperature, occurs when the vertical temperature gradient equals to the dry adiabatic lapse rate

$$N^2 = 0 \iff -\frac{\partial T}{\partial z} = \Gamma_d, \quad (27.44)$$

where (see equation (20.74))

$$\Gamma_d = -\frac{g}{c_p} \approx -9.8 \text{ K/(1000 m)}. \quad (27.45)$$

That is, if the *in situ* temperature decreases upon ascent more quickly than the dry adiabatic lapse rate, then the vertical column is gravitationally unstable. In effect, the column becomes top heavy and subject to overturning. We summarize this stability criteria as

$$\text{stable} \quad N^2 > 0 \iff -\frac{\partial T}{\partial z} < \frac{g}{c_p} \quad (27.46)$$

$$\text{unstable} \quad N^2 < 0 \iff -\frac{\partial T}{\partial z} > \frac{g}{c_p}, \quad (27.47)$$

with Figure 27.5 providing an illustration for three linear temperature profiles.

27.5.7 Comments and further study

Neutral directions were introduced to oceanography by [McDougall \(1987a\)](#) and [McDougall \(1987b\)](#), and they are the basis for how oceanographers think about buoyancy stratification. [McDougall et al. \(2014\)](#) offer another presentation of why neutral directions are relevant for the ocean, taking into account measurements of dianeutral mixing. Our discussion of neutral directions was inspired by the concise presentation in Section 2.7.2 of [Olbers et al. \(2012\)](#).

In deriving an algorithm to compute neutral directions, we have not presented an argument for dynamical processes favoring neutral displacements. That argument requires dynamical principles, such as the equations of motion and associated energetic constraints. Yet there is presently no dynamical argument for why the ocean prefers neutral displacements over arbitrary non-neutral displacements. However, robust empirical measures support the relevance of neutral directions for orienting tracer mixing within the ocean interior. More discussion of these points is given by [McDougall et al. \(2014\)](#).

Our study of vertical gravitational stability follows Section 3.6 of [Gill \(1982\)](#) as well as Section 2.10 of [Vallis \(2017\)](#). In an actual fluid, the movement of any fluid, even a tiny fluid element, modifies the surrounding fluid so that a perfect test fluid element is a fiction. We return to this point in Section 27.7 when studying effective buoyancy.

27.6 Neutral helicity⁸

In our study of neutral directions in Section 27.5 we introduced the notion of a neutral displacement. We here consider a particularly remarkable property of neutral displacements and the dianeutral direction, with this property first identified by [McDougall and Jackett \(1988\)](#).

⁸This section greatly benefited from input by Geoffrey Stanley.

27.6.1 Mathematical preliminaries

Consider a continuous vector field, $\mathbf{N}(\mathbf{x})$, and write its normalized version as

$$\hat{\mathbf{n}} = \mathbf{N}/|\mathbf{N}|. \quad (27.48)$$

Let this vector field define a smooth two-dimensional surface, \mathcal{S} , so that wherever \mathbf{N} is evaluated on \mathcal{S} then it is perpendicular to \mathcal{S} (see Figure 27.6 for an example). In general there is a continuum of such surfaces, yet we are here only interested in one of them. To be specific, assuming $\hat{\mathbf{n}} \cdot \hat{\mathbf{z}}$ is single-signed, let \mathcal{S} be defined by the accumulation of points $\mathbf{x}_{\mathcal{S}} = x\hat{\mathbf{x}} + y\hat{\mathbf{y}} + \psi(x, y)\hat{\mathbf{z}}$, where $\psi(x, y)$ provides the vertical position of the surface as a continuous function of horizontal position.⁹ In this case, $\mathbf{N} = \hat{\mathbf{z}} - \hat{\mathbf{x}}\partial_x\psi - \hat{\mathbf{y}}\partial_y\psi$ when evaluated on \mathcal{S} , so that $\mathbf{N} = \hat{\mathbf{z}} = 1$. In the following, we say that these sorts of surfaces are *well-defined* since they are both smooth and everywhere have an outward normal vector.

Consider a unit vector, $\hat{\mathbf{t}}$, that forms the tangent vector to an arbitrary closed region, Ω , that lives on the surface, $\Omega \in \mathcal{S}$. Let $\hat{\mathbf{t}}$ be oriented counterclockwise around the boundary, $\partial\Omega$, relative to \mathbf{N} (see Figure 27.6). Since $\mathbf{N} \cdot \hat{\mathbf{t}} = 0$ by construction, we can integrate this identity around $\partial\Omega$ to have

$$\oint_{\partial\Omega} \mathbf{N} \cdot \hat{\mathbf{t}} \, ds = 0 \implies \int_{\Omega} (\nabla \times \mathbf{N}) \cdot \hat{\mathbf{n}} \, d\mathcal{S} = 0, \quad (27.49)$$

where we used Stokes' theorem to reach the second identity. Since the region, Ω , is arbitrary, the area integral in equation (27.49) vanishes only if the integrand is identically zero for each point on \mathcal{S} . We thus conclude the following:

$$\text{well-defined surface } \mathcal{S} \implies \mathcal{H} \equiv \mathbf{N} \cdot (\nabla \times \mathbf{N}) = 0. \quad (27.50)$$

The contrapositive also holds so that¹⁰

$$\mathcal{H} \neq 0 \implies \text{ill-defined surface } \mathcal{S}. \quad (27.51)$$

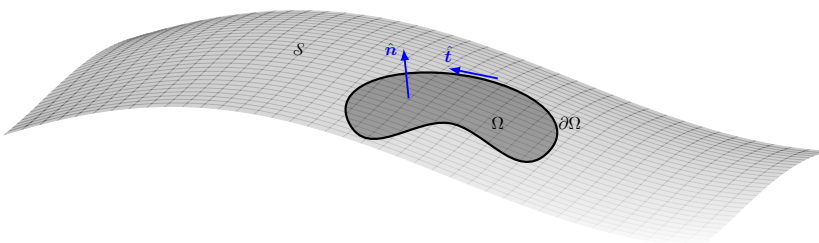


FIGURE 27.6: Illustrating a smooth and orientable two-dimensional surface, \mathcal{S} , which we refer to as a “well-defined surface”. At each point on \mathcal{S} we can unambiguously define an outward normal, $+\hat{\mathbf{n}}$, and inward normal, $-\hat{\mathbf{n}}$. Furthermore, we can consider an arbitrary simply connected closed region, Ω , with boundary $\partial\Omega$. The boundary is oriented by a unit tangent vector, $\hat{\mathbf{t}}$, that is perpendicular to the unit normal, $\hat{\mathbf{n}} \cdot \hat{\mathbf{t}} = 0$, and is oriented counterclockwise around $\partial\Omega$ according to an “outward” pointing $\hat{\mathbf{n}}$.

⁹We considered such surfaces in Section 16.4.2 when studying kinematic boundary conditions for flow encountering a material surface.

¹⁰A contrapositive is a proposition or theorem formed by contradicting both the subject and predicate or both the hypothesis and conclusion of a given proposition or theorem. More succinctly, the proposition “if A then B” has the contrapositive “if not-B then not-A”; it has the converse “if B then A”; and it has the inverse “if not-A then not-B”.

27.6.2 Neutral helicity is the reason neutral surfaces are ill-defined

Now apply the above general results to the question of whether a surface with its outward normal parallel to the dianeutral direction, $\hat{\gamma}$,

$$\mathbf{N} = -\alpha \nabla \theta + \beta \nabla S = \hat{\gamma} | -\alpha \nabla \theta + \beta \nabla S | \quad (27.52)$$

is a well-defined surface. We refer to this surface as a *neutral surface*, since at each point its local normal is $\hat{\gamma}$. From the discussion in Section 27.6.1 we know that neutral surfaces are well defined only if the *neutral helicity* vanishes, where the neutral helicity is

$$\mathcal{H}_{\text{neutral}} = \mathbf{N} \cdot (\nabla \times \mathbf{N}) = (-\alpha \nabla \theta + \beta \nabla S) \cdot [\nabla \times (-\alpha \nabla \theta + \beta \nabla S)], \quad (27.53)$$

which can be written

$$\mathcal{H}_{\text{neutral}} = (-\alpha \nabla \theta + \beta \nabla S) \cdot [\nabla \times (-\alpha \nabla \theta + \beta \nabla S)] \quad (27.54a)$$

$$= -\alpha \nabla \theta \cdot (\nabla \times \beta \nabla S) - \beta \nabla S \cdot (\nabla \times \alpha \nabla \theta) \quad (27.54b)$$

$$= -\alpha \nabla \theta \cdot (\nabla \beta \times \nabla S) - \beta \nabla S \cdot (\nabla \alpha \times \nabla \theta). \quad (27.54c)$$

Further expanding the spatial gradients of α and β

$$\nabla \alpha = \partial_\theta \alpha \nabla \theta + \partial_S \alpha \nabla S + \partial_p \alpha \nabla p \quad (27.55a)$$

$$\nabla \beta = \partial_\theta \beta \nabla \theta + \partial_S \beta \nabla S + \partial_p \beta \nabla p, \quad (27.55b)$$

then leads to

$$-\alpha \nabla \theta \cdot (\nabla \beta \times \nabla S) = -\alpha \nabla \theta \cdot (\partial_p \beta \nabla p \times \nabla S) = -\alpha \partial_p \beta \nabla p \cdot (\nabla S \times \nabla \theta) \quad (27.56a)$$

$$-\beta \nabla S \cdot (\nabla \alpha \times \nabla \theta) = -\beta \nabla S \cdot (\partial_p \alpha \nabla p \times \nabla \theta) = \beta \partial_p \alpha \nabla p \cdot (\nabla S \times \nabla \theta) \quad (27.56b)$$

which brings neutral helicity to the form

$$\mathcal{H}_{\text{neutral}} = \nabla p \cdot (\nabla S \times \nabla \theta) (\beta \partial_p \alpha - \alpha \partial_p \beta). \quad (27.57)$$

Introducing the thermobaricity parameter¹¹

$$\mathcal{T} = \beta \partial_p (\alpha / \beta) = \beta^{-1} (\beta \partial_p \alpha - \alpha \partial_p \beta) \quad (27.58)$$

renders the tidy result

$$\mathcal{H}_{\text{neutral}} = \beta \mathcal{T} \nabla p \cdot (\nabla S \times \nabla \theta). \quad (27.59)$$

A nonzero neutral helicity (27.59) is fundamentally related to a nonzero thermobaricity parameter \mathcal{T} . It is also associated with the non-zero volume for a parallelopiped in (θ, S, p) space (see Section 1.5)

$$\nabla p \cdot (\nabla S \times \nabla \theta) = \nabla \theta \cdot (\nabla p \times \nabla S) = \nabla S \cdot (\nabla \theta \times \nabla p), \quad (27.60)$$

with this volume a function of the (S, θ, p) arrangement.

Returning to the question of whether a neutral surface is well-defined, we see that with $\mathcal{H}_{\text{neutral}} \neq 0$ then neutral surfaces are ill-defined. What does this result mean in practice? Consider a stably stratified ocean where $\hat{\gamma} \cdot \hat{z} \neq 0$ everywhere. Even for this ocean we are unable to find any finite smooth surface, $\mathcal{S}_{\text{neutral}}$, whose outward normal is given by $\hat{\gamma}$. That is, we cannot find a single function, $\psi(x, y)$, where $\mathbf{N} = \hat{z} - \hat{x} \partial_x \psi - \hat{y} \partial_y \psi$ everywhere on $\mathcal{S}_{\text{neutral}}$.

¹¹We further discuss the thermobaricity parameter in Section 64.3.

27.6.3 Comments and further study

Figure 27.6 provides an example smooth surface; i.e., a canonical well-defined surface. What does an ill-defined surface look like? [McDougall and Jackett \(1988\)](#) answered by noting that neutral paths possess a helical structure, with each closed loop in (S, θ) space displaced vertically in pressure. Besides being rather novel mathematically, this helical structure provides a source for irreversible (dianeutral) transformation of seawater. [Klocker and McDougall \(2010a\)](#) and [Klocker and McDougall \(2010b\)](#) estimated the effects of this transformation on large-scale ocean overturning circulation. They found the effects from neutral helicity to be comparable to those from mixing, especially in the Southern Ocean.

[Bennett \(2019\)](#) discussed the geometry of neutral paths and made an elegant connection to a theorem of Carathéodory developed in the context of thermodynamics. Additionally, [Stanley \(2019\)](#) showed that S and θ (or ρ and p) on a neutral surface are functionally related but in a way that varies geographically. Stanley's topological analysis determined how different single-valued S - θ relations in different geographic regions mesh together to form a globally continuous S - θ relation. [Stanley et al. \(2021\)](#) then provided a corresponding method for determining approximate neutral surfaces. Such approximate neutral surfaces are globally well-defined, but with a local normal direction that is closely aligned with the dianeutral direction, $\hat{\gamma}$.

27.7 Effective buoyancy and vertical accelerations

We extend our discussion of Archimedean buoyancy in this section by focusing on the vertical forces acting on a fluid element, or more generally a finite sized fluid region, rather than on a test fluid element. To do so requires us to study, in some detail, the various forces appearing in the momentum equation. As a means to conceptually organize these forces, we introduce *static forces*, which are those forces not associated with fluid motion, plus *motional forces*, which are forces not associated with density inhomogeneities. Motional forces are specific to details of the velocity field, whereas static forces are deduced just from knowledge of the density field.

In analogy with Archimedean buoyancy, we use the term *effective buoyancy* for the static forces acting on a fluid element. Although the effective buoyancy is in part comprised of Archimedean buoyancy, there are distinctions that arise through interactions between the fluid element and its surrounding environment. These interactions depend on the shape of the fluid region. As we see in this section (see in particular Figure 27.7), effective buoyancy explains why fluid regions with the same Archimedean buoyancy generally have different net buoyant accelerations due to differences in their geometric shape.

To facilitate the analysis of this section, we consider a Boussinesq ocean, with the analysis also directly relevant to an anelastic atmosphere as considered by [Jeevanjee and Romps \(2015b\)](#). As already explored in Section 26.3, pressure in a Boussinesq ocean provides the needed constraint to maintain a non-divergent velocity field. Furthermore, pressure in a Boussinesq ocean satisfies an elliptic boundary value problem (Poisson equation from Section 3.5). This boundary value problem is linear for the pressure field. Linearity is exploited for conceptual purposes by decomposing the pressure sources into physically distinct processes. The mathematical task of this section is to derive the Poisson equations according to the various pressure sources and then discuss the physics of their associated vertical accelerations.

27.7.1 Vertical motion in approximately hydrostatic fluids

As introduced in Section 24.2 and further detailed in Section 26.2, an approximate hydrostatic fluid is one in which the vertical pressure gradient locally balances the gravitational accelera-

tion, with the horizontal gradient of hydrostatic pressure contributing to horizontal accelerations. Although vertical motion can occur in the approximately hydrostatic fluid, that motion is diagnosed rather than prognosed since the vertical momentum equation is reduced to local hydrostatic balance. For example, a diagnostic evaluation of the vertical velocity in a Boussinesq ocean is performed through vertically integrating the continuity equation, $\partial_z w = -\nabla \cdot \mathbf{u}$, along with the specification of w at one point within the vertical column.

As we see in equation (27.70c) below, the vertical gradient of the non-hydrostatic pressure is the only inviscid force contributing to a vertical acceleration. So even if the fluid is approximately hydrostatic, it is the non-hydrostatic pressure force that enables vertical accelerations. This situation is directly analogous to the oceanic Boussinesq approximation as derived in Section 26.1, whereby the fluid flow is incompressible so that $\nabla \cdot \mathbf{v} = 0$, yet the fluid itself is compressible so that $D\rho/Dt \neq 0$. For the approximately hydrostatic fluid we have the local hydrostatic balance, $\partial p/\partial z = -\rho g$, yet nonzero vertical acceleration, $Dw/Dt \neq 0$.

27.7.2 Two decompositions of pressure and gravity forces

Consider the momentum equation with the geopotential, $\Phi = g z$,

$$\rho (\partial_t + \mathbf{v} \cdot \nabla) \mathbf{v} + f \hat{\mathbf{z}} \times \rho \mathbf{v} = -\nabla p - \rho g \hat{\mathbf{z}} + \rho \mathbf{F}. \quad (27.61)$$

We are concerned with the pressure and gravity contributions on the right hand side, and we offer two means to organize these terms. The first follows that used to formulate the Boussinesq approximation in Section 26.1.1. Summarizing those steps for completeness, we introduce a constant reference density, ρ_0 , along with a corresponding hydrostatically balanced reference pressure

$$p = p' + p_0 \quad \text{with} \quad dp_0(z)/dz = -\rho_0 g. \quad (27.62)$$

This decomposition brings the pressure and gravity contributions on the right hand side of the momentum equation (27.61) into the form

$$\nabla p + \rho g \hat{\mathbf{z}} = \nabla p' - \rho_0 b \hat{\mathbf{z}}, \quad (27.63)$$

with

$$b = -g(\rho - \rho_0)/\rho_0 = -g \rho'/\rho_0 \quad (27.64)$$

the globally referenced Archimedean buoyancy computed relative to the globally constant reference density, ρ_0 , and

$$\rho' = \rho - \rho_0 \quad (27.65)$$

is the density deviation relative to the reference density. The second decomposition splits pressure into a local hydrostatic pressure, p_h , and a non-hydrostatic pressure, p_{nh} ,

$$p = p_h + p_{nh} \quad \text{with} \quad \partial p_h / \partial z = -\rho g, \quad (27.66)$$

in which case

$$\nabla p + \rho g \hat{\mathbf{z}} = \nabla p_{nh} + \nabla_z p_h = \nabla_z p + \hat{\mathbf{z}} \partial_z p_{nh}. \quad (27.67)$$

We retain both the global and local pressure decompositions in the following as doing so offers complementary perspectives on how pressure forces lead to vertical accelerations.

The following comments compare and contrast the two decompositions.

- By decomposing pressure as $p = p_0 + p'$, we expose the dynamically active portion of the pressure field, p' , by removing the dynamically irrelevant pressure, p_0 , from the momentum

equation. Notably, this decomposition results in a dynamical pressure, p' , that has both hydrostatic and non-hydrostatic contributions.

- The decomposition into local hydrostatic plus local non-hydrostatic pressures splits the pressure field into its two dynamically distinct portions, and as such it is useful when concerned with deviations from a local hydrostatic balance. However, it does not remove the global hydrostatic background pressure, which can be seen by the identity

$$\partial p_h / \partial z = dp_0(z) / dz - \rho' g = dp_0(z) / dz + \rho_0 b. \quad (27.68)$$

27.7.3 Boussinesq velocity equations

To further study how pressure and gravity lead to vertical motion, we find it convenient to make the Boussinesq approximation so that the velocity equation (27.61) takes the form of equation (26.66)

$$\rho_0 (\partial_t \mathbf{v} + \mathbf{v} \cdot \nabla) \mathbf{v} + f \hat{\mathbf{z}} \times \rho_0 \mathbf{v} = -\nabla p - \rho g \hat{\mathbf{z}} + \rho_0 \mathbf{F} \quad (27.69a)$$

$$= -\nabla p' + \rho_0 b \hat{\mathbf{z}} + \rho_0 \mathbf{F} \quad (27.69b)$$

$$= -\nabla p_{nh} - \nabla_z p_h + \rho_0 \mathbf{F}. \quad (27.69c)$$

We provide particular focus on the vertical velocity equation in studying processes leading to vertical acceleration of fluid elements (i.e., the vertical Lagrangian acceleration)

$$\rho_0 D w / D t = -\partial_z p - \rho g + \rho_0 \mathbf{F} \cdot \hat{\mathbf{z}} \quad (27.70a)$$

$$= -\partial_z p' + \rho_0 b + \rho_0 \mathbf{F} \cdot \hat{\mathbf{z}} \quad (27.70b)$$

$$= -\partial_z p_{nh} + \rho_0 \mathbf{F} \cdot \hat{\mathbf{z}}. \quad (27.70c)$$

Equation (27.70b) reveals that the vertical Lagrangian acceleration has contributions from vertical gradients in the dynamical pressure, p' , plus the globally referenced Archimedean buoyancy, b . From equation (27.70c) we see that the vertical Lagrangian acceleration has an inviscid contribution that arises solely from vertical derivatives in the non-hydrostatic pressure, p_{nh} .

27.7.4 Poisson equations for $p' = p'_{buoy} + p'_{flow}$

The two decompositions of pressure described in Section 27.7.2, as reflected in the Boussinesq velocity equations from Section 27.7.3, render two sets of corresponding Poisson equations for pressure. We here focus on the decomposition (27.69b), where the pressure and gravity accelerations appear in terms of the Archimedean buoyancy plus perturbation pressure. We defer until Section 27.7.6 an examination of the alternative decomposition into the local hydrostatic and non-hydrostatic pressures.

Boundary value problem for the perturbation pressure, p'

We start by considering the Boussinesq momentum equation (27.69b)

$$\rho_0 (\partial_t + \mathbf{v} \cdot \nabla) \mathbf{v} + f \hat{\mathbf{z}} \times \rho_0 \mathbf{v} = -\nabla p' + \rho_0 b \hat{\mathbf{z}} + \rho_0 \mathbf{F}. \quad (27.71)$$

As detailed in Section 26.3.1, the time tendency is eliminated by computing the divergence of this equation to render the Poisson equation for the perturbation pressure

$$-\nabla^2 p' = \rho_0 \nabla \cdot \mathbf{G}' = \rho_0 \nabla \cdot [(\mathbf{v} \cdot \nabla) \mathbf{v} + f \hat{\mathbf{z}} \times \mathbf{v} - b \hat{\mathbf{z}} - \mathbf{F}], \quad (27.72)$$

where we introduced the vector,

$$\mathbf{G}' = (\mathbf{v} \cdot \nabla) \mathbf{v} + f \hat{\mathbf{z}} \times \mathbf{v} - b \hat{\mathbf{z}} - \mathbf{F}, \quad (27.73)$$

whose divergence renders a source for the pressure field. We find it convenient to carry around a minus sign on the Laplacian operator since a positive source, $\rho_0 \nabla \cdot \mathbf{G}' > 0$, leads to a locally positive pressure signal (see Section 26.3.1 for more details on this point).

We require boundary conditions to fully specify the pressure, and for simplicity we assume material boundaries. In this case, the analysis considered in Section 26.3.2 renders the Neumann boundary condition

$$\hat{\mathbf{n}} \cdot \nabla p' = -\rho_0 \hat{\mathbf{n}} \cdot \mathbf{G}', \quad (27.74)$$

where $\hat{\mathbf{n}}$ is the outward normal along the boundary. We further simplify the analysis by assuming flat and rigid top and bottom boundaries along with horizontal boundaries that are either doubly periodic or infinite. Hence, along the top boundary, where $\hat{\mathbf{n}} = \hat{\mathbf{z}}$, the pressure satisfies the Neumann boundary condition

$$\partial_z p' = -\rho_0 \hat{\mathbf{z}} \cdot \mathbf{G}' = \rho_0 (b + \mathbf{F} \cdot \hat{\mathbf{z}}) \quad \text{top boundary.} \quad (27.75)$$

To reach this result we noted that

$$\hat{\mathbf{z}} \cdot [(\mathbf{v} \cdot \nabla) \mathbf{v}] = (\mathbf{v} \cdot \nabla) (\hat{\mathbf{z}} \cdot \mathbf{v}) = 0, \quad (27.76)$$

since $\hat{\mathbf{z}} \cdot \mathbf{v} = w = 0$ along a rigid and material flat surface. The analogous result holds along the bottom boundary where $\hat{\mathbf{n}} = -\hat{\mathbf{z}}$ so that

$$\partial_z p' = \rho_0 \hat{\mathbf{z}} \cdot \mathbf{G}' = -\rho_0 (b + \mathbf{F} \cdot \hat{\mathbf{z}}) \quad \text{bottom boundary.} \quad (27.77)$$

Buoyancy induced and flow induced pressures

The Laplacian operator is linear, with linearity affording the freedom to decompose the source in the Poisson equation (27.72), $\rho_0 \nabla \cdot \mathbf{G}'$, into physically distinct processes. For this purpose we choose the following decomposition

$$-\nabla^2 p' \equiv -\nabla^2(p'_{\text{buoy}} + p'_{\text{flow}}) \quad (27.78a)$$

$$-\nabla^2 p'_{\text{buoy}} = -\rho_0 \partial_z b \quad (27.78b)$$

$$-\nabla^2 p'_{\text{flow}} = \rho_0 \nabla \cdot [(\mathbf{v} \cdot \nabla) \mathbf{v} + f \hat{\mathbf{z}} \times \mathbf{v} - \mathbf{F}]. \quad (27.78c)$$

The source term for the buoyancy pressure, p'_{buoy} , only involves the vertical derivative of the Archimedean buoyancy. Hence, there is no direct contribution from fluid motion on p'_{buoy} , with fluid motion only affecting p'_{buoy} indirectly through effects on $\partial_z b$. The converse holds for the second pressure perturbation, p'_{flow} , which is sourced by fluid motion that gives rise to accelerations from self-advection, Coriolis, and friction. Hence, there is no direct impact from Archimedean buoyancy on p'_{flow} . The Neumann boundary conditions for these two pressures follows from the boundary conditions (27.75) and (27.77). For example, along the top boundary we have

$$\partial_z p'_{\text{buoy}} = \rho_0 b \quad \text{and} \quad \partial_z p'_{\text{flow}} = \rho_0 \hat{\mathbf{z}} \cdot \mathbf{F} \quad \text{top boundary conditions,} \quad (27.79)$$

with the same conditions holding along the bottom yet with a minus sign on the right hand side.

27.7.5 Accelerations from effective buoyancy and fluid motion

Having established the Poisson equations for the variety of pressures in Section 27.7.4, we now examine contributions to the vertical Lagrangian acceleration as given by equations (27.70b) and (27.70c). Emulating the decomposition used for pressure, we here decompose the vertical acceleration into conceptually distinct contributions from buoyancy and from fluid flow.

Vertical acceleration from effective buoyancy

Effective buoyancy is the first contribution to vertical Lagrangian acceleration, which is the vertical acceleration arising solely from the instantaneous mass/density field. Operationally, we deduce the effective buoyancy by instantaneously setting velocity to zero everywhere in the expression for the vertical acceleration

$$b_{\text{eff}} \equiv \left. \frac{Dw}{Dt} \right|_{\mathbf{v}=0}. \quad (27.80)$$

Two conclusions follow directly from the operational definition of b_{eff} in equation (27.80). First, as viscous friction only arises when there is relative fluid motions that lead to strains (Section 22.8.6), viscous friction does not contribute to the effective buoyancy. Next, we observe that any direct role for pressure in b_{eff} arises solely from the buoyancy pressure, p'_{buoy} . We make this conclusion since the Poisson equation (27.81) for the buoyancy pressure has a source that only depends on the instantaneous Archimedean buoyancy field, whereas it ignores all contributions from fluid flow. This dependence is precisely that defined for b_{eff} .

From the definition (27.80) we make use of equations (27.70b) and (27.70c) to unpack the variety of contributions to effective buoyancy

$$\rho_0 b_{\text{eff}} = \rho_0 b - \partial_z p' \Big|_{\mathbf{v}=0} = -\partial_z p_{\text{nh}} \Big|_{\mathbf{v}=0}. \quad (27.81)$$

The first equality identifies the difference between the effective buoyancy and the Archimedean buoyancy

$$\rho_0 (b_{\text{eff}} - b) = -\partial_z p'_{\text{buoy}}, \quad (27.82)$$

in which we set

$$\partial_z p' \Big|_{\mathbf{v}=0} = \partial_z p_{\text{buoy}} \quad (27.83)$$

as per the discussion below equation (27.80). So equation (27.82) states that in the presence of a vertical gradient in the buoyancy pressure, then the Archimedean buoyancy is an incomplete description of the vertical acceleration associated with the density field.

Equation (27.81) also reveals that the effective buoyancy is associated with that portion of the vertical gradient in the non-hydrostatic pressure that remains when $\mathbf{v} = 0$

$$\rho_0 b_{\text{eff}} = -\partial_z p_{\text{nh}} \Big|_{\mathbf{v}=0}. \quad (27.84)$$

This equation provides a generalization of the local hydrostatic balance, $\rho_0 b = \partial_z(p_h - p_0)$ (equation (27.68)), so that we have the correspondence

$$\underbrace{\rho_0 b}_{\text{hydrostatic}} = \partial_z(p_h - p_0) \longleftrightarrow \underbrace{\rho_0 b_{\text{eff}}}_{\text{non-hydrostatic}} = -\partial_z p_{\text{nh}} \Big|_{\mathbf{v}=0}. \quad (27.85)$$

Vertical acceleration from fluid flow

If one introduces an Archimedean buoyancy anomaly in a static fluid, then the initial vertical acceleration acting on the anomaly is given by its effective buoyancy, with this result following

from the definition of effective buoyancy in equation (27.80). However, as the anomaly evolves, fluid motion is generated, at which point effective buoyancy is an incomplete measure of vertical acceleration. So in the presence of fluid motion we must also consider another term that we refer to as the *flow induced or motional vertical acceleration*. Operationally, we deduce the motional vertical acceleration by setting the density to a constant within the expression for the vertical acceleration

$$A_{\text{flow}} \equiv \left. \frac{Dw}{Dt} \right|_{\rho=\rho_0}. \quad (27.86)$$

As for the effective buoyancy in equation (27.80), the right hand side of equation (27.86) is evaluated using the full flow field at an instant, but with the accelerations evaluated with constant density at that instance. Since the Archimedean buoyancy vanishes when density has the uniform value, we know that

$$\rho_0 A_{\text{flow}} = -\partial_z p' \Big|_{\rho=\rho_0} + \rho_0 \mathbf{F} \cdot \hat{\mathbf{z}} = -\partial_z p_{\text{nh}} \Big|_{\rho=\rho_0} + \rho_0 \mathbf{F} \cdot \hat{\mathbf{z}}. \quad (27.87)$$

Consequently, when the density field is uniform, $\rho = \rho_0$, then the vertical gradient of p' and p_{nh} are identical

$$\partial_z p' \Big|_{\rho=\rho_0} = \partial_z p_{\text{nh}} \Big|_{\rho=\rho_0}. \quad (27.88)$$

Furthermore, we identify the vertical gradient in $\partial_z p' \Big|_{\rho=\rho_0}$ with the vertical gradient in the flow induced pressure, p'_{flow} , that satisfies the Poisson equation (27.78c). We thus have the identities

$$\partial_z p' \Big|_{\rho=\rho_0} = \partial_z p'_{\text{flow}} = \partial_z p_{\text{nh}} \Big|_{\rho=\rho_0}. \quad (27.89)$$

27.7.6 Boundary value problems for the accelerations

Following from the discussion in Section 27.7.5, we here derive the boundary value problems for the effective buoyancy and the flow induced acceleration.

Poisson equations for b_{eff} and A_{flow}

From equation (27.82) for the effective buoyancy and from the Poisson equation (27.78b) for the buoyancy pressure we derive the Poisson equation for the effective buoyancy

$$\rho_0 b_{\text{eff}} = \rho_0 b - \partial_z p'_{\text{buoy}} \quad \text{and} \quad -\nabla^2 p'_{\text{buoy}} = -\rho_0 \partial_z b \implies -\nabla^2 b_{\text{eff}} = -\nabla_z^2 b. \quad (27.90)$$

Hence, the source for the effective buoyancy is the horizontal Laplacian of the Archimedean buoyancy. Correspondingly, the source for the difference, $b_{\text{eff}} - b$, is the vertical curvature of the Archimedean buoyancy

$$-\nabla^2(b_{\text{eff}} - b) = \partial_{zz} b. \quad (27.91)$$

We similarly derive the Poisson equation for the motional acceleration by making use of its operational definition (27.87) as well as the Poisson equation (27.78c) for the flow pressure

$$\begin{aligned} \rho_0 A_{\text{flow}} &= -\partial_z p'_{\text{flow}} + \rho_0 \mathbf{F} \cdot \hat{\mathbf{z}} \quad \text{and} \quad -\nabla^2 p'_{\text{flow}} = \rho_0 \nabla \cdot [(\mathbf{v} \cdot \nabla) \mathbf{v} + f \hat{\mathbf{z}} \times \mathbf{v} - \mathbf{F}] \\ &\implies -\nabla^2 A_{\text{flow}} = -\partial_z \nabla \cdot [(\mathbf{v} \cdot \nabla) \mathbf{v} + f \hat{\mathbf{z}} \times \mathbf{v} - \mathbf{F}] - \nabla^2(\mathbf{F} \cdot \hat{\mathbf{z}}). \end{aligned} \quad (27.92)$$

Boundary conditions

To completely specify the decomposition of vertical acceleration requires boundary conditions for the effective buoyancy, b_{eff} , and the motional acceleration, A_{flow} . Following our discussion of the

Poisson equations in Section 27.7.4, we here only consider rigid and flat material upper and lower boundaries with no boundaries for the horizontal domain (either periodic or infinite horizontal domain). At the upper and lower boundaries we have $Dw/Dt = 0$, and this boundary condition holds whether $\mathbf{v} = 0$ or $\rho = \rho_0$, so that

$$b_{\text{eff}} = 0 \quad \text{and} \quad A_{\text{flow}} = 0 \quad \text{on rigid and flat boundaries.} \quad (27.93)$$

We are thus ensured that the net vertical acceleration is indeed the sum

$$\rho_0 \frac{Dw}{Dt} = \rho_0 (A_{\text{flow}} + b_{\text{eff}}). \quad (27.94)$$

Poisson equation for the local non-hydrostatic pressure

We can also arrive at the above results by considering the momentum equation (27.69c) written using the decomposition of pressure into is local non-hydrostatic and local hydrostatic components

$$\rho_0 (\partial_t + \mathbf{v} \cdot \nabla) \mathbf{v} + f \hat{\mathbf{z}} \times \rho_0 \mathbf{v} = -\nabla p_{\text{nh}} - \nabla_z p_{\text{h}} + \rho_0 \mathbf{F}. \quad (27.95)$$

A divergence of this equation leads to the Poisson equation for the non-hydrostatic pressure

$$-\nabla^2 p_{\text{nh}} = \nabla_z^2 p_{\text{h}} + \rho_0 \nabla \cdot [(\mathbf{v} \cdot \nabla) \mathbf{v} + f \hat{\mathbf{z}} \times \mathbf{v} - \mathbf{F}]. \quad (27.96)$$

Taking a vertical derivative and use of the hydrostatic relation leads to the Poisson equation for the vertical derivative of the non-hydrostatic pressure

$$-\nabla^2 (\partial_z p_{\text{nh}}) = -g \nabla_z^2 \rho + \rho_0 \partial_z \nabla \cdot [(\mathbf{v} \cdot \nabla) \mathbf{v} + f \hat{\mathbf{z}} \times \mathbf{v} - \mathbf{F}]. \quad (27.97)$$

Setting $\mathbf{v} = 0$ in equation (27.96) renders the Poisson equation

$$-(\nabla^2 p_{\text{nh}})_{\mathbf{v}=0} = \nabla_z^2 p_{\text{h}}. \quad (27.98)$$

This equation says that the static portion of the non-hydrostatic pressure is sourced by the horizontal Laplacian of the hydrostatic pressure. Equivalently, the convergence of $(\nabla p_{\text{nh}})_{\mathbf{v}=0}$ is balanced by the divergence of the horizontal hydrostatic pressure gradient, $\nabla_z p_{\text{h}}$. Furthermore, setting $\mathbf{v} = 0$ in equation (27.97) yields the Poisson equation for the effective buoyancy

$$-\rho_0 \nabla^2 b_{\text{eff}} = g \nabla_z^2 \rho \iff \nabla^2 b_{\text{eff}} = \nabla_z^2 b, \quad (27.99)$$

which accords with equation (27.90).

27.7.7 Relative scales for effective and Archimedean buoyancies

One way to emphasize the distinction between the effective buoyancy equation (27.99) and that for the Archimedean buoyancy is to compare their two elliptic equations

$$-\rho_0 \nabla^2 b = g \nabla^2 \rho \quad \text{and} \quad -\rho_0 \nabla^2 b_{\text{eff}} = g \nabla_z^2 \rho, \quad (27.100)$$

with the first equality following trivially by definition of Archimedean buoyancy, $b = -(g/\rho_0)(\rho - \rho_0)$. The different Laplacian operators acting on the source terms for b_{eff} and b means that these two buoyancy fields scale differently.

As an example of the distinct scaling for b_{eff} and b , consider a cylindrically shaped Archimedean buoyancy anomaly (Figure 27.7) of scale B and with diameter D and height H . Given this

information we seek a corresponding scale for the effective buoyancy, B_{eff} . Using the relation (27.99), and the cylindrical-polar coordinate version of the Laplacian operator (equation (9.83b)), we have

$$\nabla^2 b_{\text{eff}} = \frac{1}{r} \frac{\partial}{\partial r} \left[r \frac{\partial b_{\text{eff}}}{\partial r} \right] + \frac{1}{r^2} \frac{\partial^2 b_{\text{eff}}}{\partial \vartheta^2} + \frac{\partial^2 b_{\text{eff}}}{\partial z^2} \quad \text{and} \quad \nabla_z^2 b = \frac{1}{r} \frac{\partial}{\partial r} \left[r \frac{\partial b}{\partial r} \right] + \frac{1}{r^2} \frac{\partial^2 b}{\partial \vartheta^2}, \quad (27.101)$$

where r is the radial distance from the cylinder axis, z the vertical coordinate along the cylinder axis, and ϑ the polar coordinate. We thus find the scalings

$$\nabla^2 b_{\text{eff}} \sim B_{\text{eff}} (D^{-2} + H^{-2}) \quad \text{and} \quad \nabla_z^2 b \sim B D^{-2}, \quad (27.102)$$

so that for a given Archimedean buoyancy anomaly scale, B , we find an associated effective buoyancy scale

$$B_{\text{eff}} = \frac{B}{1 + D^2/H^2}, \quad (27.103)$$

Hence, the effective buoyancy scale is smaller than the Archimedean buoyancy scale. The effective buoyancy scale is smaller due to the pressure contribution that slows down any buoyant fluid element, with this pressure induced environmental back-reaction missing from the Archimedean buoyancy. Also observe that the effective buoyancy decreases when the ratio D/H increases. As a result, wide and flat “pancake” shaped buoyancy anomalies rise slower (with $B > 0$) than narrow “rocket shaped” anomalies. This result follows since a pancake anomaly must push aside more surrounding fluid, whereas the narrow rocket shaped anomaly is more streamlined and thus more readily rises.

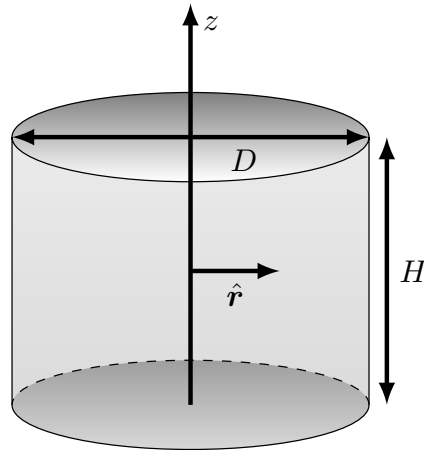


FIGURE 27.7: An Archimedean buoyancy anomaly of scale B here configured in the shape of a cylinder with diameter D and height H . Also shown are the vertical, z , and radial, r axes for cylindrical-polar coordinates. In equation (27.103) we find the effective buoyancy for this anomaly scales as $B_{\text{eff}} = B/(1 + D^2/H^2)$, so that the effective buoyancy has a smaller magnitude than the Archimedean buoyancy. Also note that the magnitude of the effective buoyancy decreases as the diameter increases. This behavior reflects the need for a wide and flat buoyancy anomaly to push aside more surrounding fluid as it rises (as with $B > 0$) than for a narrow and tall anomaly.

As a buoyant fluid element moves vertically, it must displace the surrounding environmental fluid. The pressure contribution to the effective buoyancy accounts for the back-reaction of the environmental fluid on the buoyant fluid element. Since the Archimedean buoyancy ignores the back-reaction, it generally over estimates the magnitude of the vertical acceleration. By account-

ing for the pressure forces acting on the element from the surrounding fluid, the effective buoyancy offers a more accurate measure of the static vertical forces arising from density inhomogeneities.

27.7.8 Thought experiments for effective buoyancy

We here present some thought experiments for the purpose of developing an understanding of effective buoyancy. The thought experiments are somewhat trivial physically and yet they require us to confront basic assumptions, which is generally a useful exercise.

Horizontally unstratified density

Consider a horizontally unstratified density, $\rho = \rho(z)$, on a horizontally periodic domain with the fluid in hydrostatic equilibrium. By construction, the Archimedean buoyancy, $b = -g(\rho - \rho_0)/\rho_0$, exactly balances the vertical pressure gradient, $d(p - p_0)/dz = b\rho_0$. In the absence of horizontal density gradients, the effective buoyancy is everywhere a harmonic function since $\nabla^2 b_{\text{eff}} = 0$. With vanishing Dirichlet boundary conditions at the rigid bottom and top of the domain, $z = 0, H$, then $b_{\text{eff}} = 0$ everywhere, signaling the absence of any vertical acceleration.

It is notable that this result holds for an arbitrary vertical profile of density, even if the density is gravitationally unstable (Section 27.5). The assumed horizontal symmetry is the key point. This assumption precludes any vertical motion since no fluid element at a single horizontal position can be vertically displaced without breaking the assumption of horizontal symmetry. The only way to maintain volume conservation ($\nabla \cdot \mathbf{v} = 0$) with vertical motion is for some fluid to move up while other fluid moves down, and for that to happen requires breaking horizontal symmetry. Once a tiny seed of horizontal asymmetry is presented to the fluid, effective buoyancy is sourced by $\nabla_z^2 \rho \neq 0$, which in turn allows the gravitational instability to grow.

Vertically unstratified density

Now consider a vertically unstratified density field, $\rho = \rho(x, y)$, so that the Archimedean buoyancy has no depth dependence. This vertically “neutrally buoyant” case commonly means that a fluid element can move vertically without feeling any buoyancy forces. Indeed, such is the case when referring to Archimedean buoyancy. What about effective buoyancy?

If density is a linear function of horizontal position then the effective buoyancy is a harmonic function so that $b_{\text{eff}} = 0$. If density is a nonlinear function of the horizontal then the effective buoyancy is nonzero. Yet is there vertical motion? Again we must confront the boundary conditions to answer this question. Here, the rigid top and bottom boundaries preclude movement of fluid across these boundaries by imparting a boundary pressure form stress (Chapter 25) acting throughout the fluid to counteract the effective buoyancy. As a result, the fluid remains static. If instead we allow for a free surface, then the effective buoyancy would cause vertical motion that then leads to horizontal convergences, thus leading to further motion. Alternatively, if we allow for depth dependence of the density, then fluid can move laterally as well as vertically.

Localized source of Archimedean buoyancy

Although useful to garner some understanding of effective buoyancy, the previous examples are not realistic. More realistic applications are concerned with Archimedean buoyancy sources localized in both the horizontal and vertical directions. In this case the buoyancy source, $\nabla_z^2 \rho \neq 0$, and boundary conditions lead to a nontrivial structure for the effective buoyancy through solving the Poisson equation. Studies listed below offer examples, both analytical and numerical, to further an understanding of how effective buoyancy offers a more complete description of vertical acceleration than Archimedean buoyancy.

27.7.9 Comments and further study

Studies from [Davies-Jones \(2003b\)](#), [Doswell and Markowski \(2004\)](#), [Jeevanjee and Romps \(2015a\)](#), [Jeevanjee and Romps \(2015b\)](#), and [Tarshish et al. \(2018\)](#), point to the use of the effective buoyancy and the limitations of Archimedean buoyancy when studying buoyancy dominated motion, such as the early stages of a buoyant thermal in the atmosphere. Much of the material in this section was gleaned from these papers, particularly from [Jeevanjee and Romps \(2015a\)](#) and [Jeevanjee and Romps \(2015b\)](#). Chapter 2 of [Markowski and Richardson \(2010\)](#) provides a pedagogical foundation for understanding pressure forces leading to vertical motion.

The structure of b_{eff} is distinct from the Archimedean buoyancy, b , with [Jeevanjee and Romps \(2015a\)](#) and [Tarshish et al. \(2018\)](#) providing examples where b and b_{eff} can even have opposite signs. Furthermore, [Tarshish et al. \(2018\)](#) made use of an elegant analogy between the Poisson equation for b_{eff} and the Poisson equation for certain magnetostatics problems. The analogy allowed them to derive analytical expressions for b_{eff} from spherical and elliptical Archimedean buoyancy sources.



27.8 Exercises

EXERCISE 27.1: EXAMPLES OF BUOYANCY PERIOD

Using approximate but realistic values for the observed stratification, determine the buoyancy period ($T_b = 2\pi/N$) for

- mid-latitude troposphere
- stratosphere
- ocean thermocline
- ocean abyss.

Express the period in units of minutes, and provide references for where you obtained the observed stratification. Hint: for both the atmosphere and ocean, it is sufficient to assume stratification is dominated by potential temperature.

EXERCISE 27.2: BUOYANCY FREQUENCY FOR AN IDEAL GAS

Derive equation (27.38) for the squared buoyancy frequency of an ideal gas. Hint: first derive the expression for the potential density and then take its vertical derivative as per equation (27.37).

EXERCISE 27.3: VERTICAL INTEGRAL OF N^2

The expression for squared buoyancy frequency

$$N^2 = -g \left[\frac{\partial \ln \varrho}{\partial z} \right]_{p_{\text{ref}}=p} \quad (27.104)$$

makes it tempting to consider its vertical integral according to

$$-g^{-1} \int_{-H}^{\eta} N^2 dz \stackrel{?}{=} [\ln \varrho]_{\eta} - [\ln \varrho]_{-H}. \quad (27.105)$$

Discuss what is wrong with this equation. Under what conditions is it correct?

EXERCISE 27.4: WATER LEVEL OF A BOAT WITH AND WITHOUT A STONE

Consider a boat of mass M_b floating in constant density water, ρ_w , contained in a tank with vertical sidewalls and cross-sectional area A . Place a stone of mass M_s and density $\rho_s > \rho_w$ in the boat and measure the water level on the tank wall, h_1 . Then throw the stone into the water. What is the new water level, h_2 , as a function of h_1 and the other properties listed above? Does the water level rise or fall along the sides of the tank as a result of throwing the stone over the side? Hint: Watch [this Physics Girl video](#).



Chapter 28

ROTATING FLUID FLOW

Large-scale and low frequency flows in the atmosphere and ocean are strongly affected by planetary rotation. The inviscid balance for such flows is termed *geostrophic*, in which the planetary Coriolis acceleration balances the pressure gradient acceleration. In this chapter, we introduce salient features of geostrophically balanced flow and the associated *thermal wind balance*. These two diagnostic relations involve no time derivatives, and so cannot be used to predict the fluid flow evolution. However, they provide a very powerful framework for interpreting large-scale and low frequency flow in the atmosphere and ocean.

After studying the basic elements of rotating flow, we study the distinctive nature of isopycnal form stresses associated with geostrophically balanced eddy motions. Such form stresses are a key feature of the earth's planetary energy balance, whereby positive buoyancy in the tropics is, in part, transported meridionally through the action of geostrophic eddies.

READER'S GUIDE TO THIS CHAPTER

This chapter assumes an understanding of the primitive equations from Chapter 24 and the Coriolis acceleration from Chapters 11 and 12. The material in this chapter is fundamental to understanding the nature and mechanisms of large-scale flow in the atmosphere and ocean, so that we make great use of this chapter in the remainder of this book. Throughout the discussion we are not explicitly concerned with sphericity, thus enabling the use of Cartesian vector calculus.

28.1 Loose threads	684
28.2 Primitive equations	684
28.3 The Rossby number	684
28.3.1 Scaling for the Rossby number	685
28.3.2 Ratio of material acceleration to Coriolis acceleration	685
28.3.3 Ratio of local time tendency to Coriolis acceleration	685
28.3.4 Rossby number for a kitchen sink	686
28.3.5 Rossby number for a Gulf Stream ring	686
28.4 Geostrophic balance	686
28.4.1 Geostrophic balance is distinctly fluid mechanical	687
28.4.2 Geostrophic relation in geopotential coordinates	687
28.4.3 Cyclonic and anti-cyclonic orientation	688
28.4.4 Density gradients and thermal wind balance	689
28.4.5 Geostrophic relation in pressure coordinates	690
28.4.6 Further study	690
28.5 Planetary geostrophic mechanics	690
28.5.1 Planetary geostrophic equations	690
28.5.2 Planetary geostrophic vorticity equation	691

28.5.3	Taylor-Proudman and vertical stiffening	692
28.5.4	Meridional motion in response to vortex stretching and stress curls	693
28.5.5	Sverdrup balance	694
28.5.6	Features of thermal wind balanced flows	694
28.5.7	Thermal wind balance for the atmosphere	696
28.5.8	Thermal wind for the ocean	698
28.5.9	Further study	700
28.6	Isopycnal form stress from geostrophic eddies	700
28.6.1	Zonal mean zonal form stress on an isopycnal surface	701
28.6.2	Zonal mean zonal form stress acting on an isopycnal layer	703
28.6.3	Comments and further study	704
28.7	Exercises	705

28.1 Loose threads

- NATT

28.2 Primitive equations

Throughout this chapter we make use of the inviscid hydrostatic primitive equations derived in Section 24.1

$$\partial \mathbf{u} / \partial t + (\mathbf{v} \cdot \nabla) \mathbf{u} + f \hat{\mathbf{z}} \times \mathbf{u} = -\rho^{-1} \nabla_z p \quad (28.1a)$$

$$\partial p / \partial z = -g \rho \quad (28.1b)$$

$$D\rho/Dt = -\rho \nabla \cdot \mathbf{v}, \quad (28.1c)$$

where the velocity vector is written using Cartesian coordinates

$$\mathbf{v} = \mathbf{u} + \hat{\mathbf{z}} w = \hat{\mathbf{x}} u + \hat{\mathbf{y}} v + \hat{\mathbf{z}} w, \quad (28.2)$$

and the horizontal gradient operator is

$$\nabla_z = \hat{\mathbf{x}} \partial_x + \hat{\mathbf{y}} \partial_y. \quad (28.3)$$

For some of the scale analysis in this chapter we assume an oceanic Boussinesq fluid (Section 26.1), in which case the mass continuity equation (28.1c) becomes the non-divergent condition on the velocity

$$\nabla \cdot \mathbf{v} = 0. \quad (28.4)$$

Furthermore, ρ in the Boussinesq horizontal momentum equation (28.1a) is converted to a constant reference density, ρ_0 , and yet it retains its full form when appearing in the hydrostatic equation since it is there multiplied by the gravitational acceleration.

28.3 The Rossby number

Large-scale geophysical fluid flows are strongly influenced by the earth's rotation. Indeed, the earth can be considered a rapidly rotating planet for much of the observed large-scale motion of the ocean and atmosphere. There are two points to emphasize in this regard. First, much of the ocean and atmosphere motion is close to solid-body rotation, in which weather patterns and ocean circulation are best viewed relative to the rotating earth rather than from an inertial frame.

Second, human scale horizontal length scales are generally far too small to take a direct notice of the planetary rotation. This point is quantified by considering the *Rossby number*, which includes a horizontal length scale, a velocity scale, and angular rotation speed.

28.3.1 Scaling for the Rossby number

The Rossby number measures the ratio of the material acceleration (acceleration of a fluid particle) to the Coriolis acceleration. The material acceleration has two contributions: one from local time tendencies and one from advection. We expose typical characteristic scales for the acceleration of a fluid particle by writing

$$\frac{\partial \mathbf{u}}{\partial t} + (\mathbf{v} \cdot \nabla) \mathbf{u} \sim \frac{U}{T} + \frac{U^2}{L} + \frac{WU}{H}, \quad (28.5)$$

where U, W are typical horizontal and vertical velocity scales, L, H are typical horizontal and vertical length scales, and T is a typical time scale (recall a similar scale analysis for the hydrostatic balance in Section 24.2). Likewise, the Coriolis acceleration scales as

$$f \hat{\mathbf{z}} \times \mathbf{u} \sim f_0 U, \quad (28.6)$$

where f_0 is the scale for the Coriolis parameter. From the continuity equation for non-divergent flow ($\nabla \cdot \mathbf{v} = 0$) we see that the vertical and horizontal velocity scales are related by¹

$$W/H \sim U/L \implies W \sim U(H/L). \quad (28.7)$$

In either non-divergent or divergent flows, we assume the vertical to horizontal grid aspect ratio is small

$$\alpha_{\text{aspect}} = H/L \ll 1, \quad (28.8)$$

as per the hydrostatic approximation discussed in Section 24.2. Consequently, the vertical velocity scale is much less than the horizontal

$$W \ll U. \quad (28.9)$$

28.3.2 Ratio of material acceleration to Coriolis acceleration

Taking the ratio of the advection scale to the Coriolis scale leads to our first expression for the Rossby number

$$\text{Ro} = \frac{U^2/L}{f_0 U} = \frac{U}{f_0 L}. \quad (28.10)$$

Due to the latitudinal variation of the Coriolis parameter, the Rossby number is generally small in magnitude near the poles and large in the tropics. This functional dependence is modified by noting that the length and velocity scales are not constant.

28.3.3 Ratio of local time tendency to Coriolis acceleration

A complementary way to understand the Rossby number is to consider it as the ratio of the local time tendency for the horizontal velocity to the Coriolis acceleration

$$\text{Ro} = \frac{U/T}{U f_0} = \frac{1/T}{f_0}. \quad (28.11)$$

¹For divergent flows we can replace W with the scale for motion across hydrostatic pressure surfaces.

Hence, the Rossby number is small for motions that have a frequency, T^{-1} , that is small compared to the *inertial frequency*, f_0 . In both ways of writing the Rossby number, we associate small Ro with regimes of flow where the earth's rotation plays a crucial role in the dynamics. With small Rossby number, both the local time derivative and the advective acceleration are smaller than the Coriolis acceleration.

28.3.4 Rossby number for a kitchen sink

Consider flow in a kitchen sink (left panel of Figure 28.1). Here, the length scale is $L = 1 \text{ m}$ (sink size) and the velocity scale is $U = 0.01 - 0.1 \text{ m s}^{-1}$, thus giving a typical time scale for sink motion of $L/U \approx 10 \text{ s} - 100 \text{ s}$. Hence, at 30° latitude, where $f = 2\Omega \sin \phi = \Omega$, the Rossby number for fluid motion in a sink is

$$\text{Ro}_{\text{sink}} \approx 10^2 - 10^3. \quad (28.12)$$

The effects from planetary rotation are tiny on these length scales, so that the Coriolis force is negligible for kitchen sink fluid dynamics. Hence, it is extremely difficult to experimentally determine a correlation between the hemisphere (northern or southern) to the rotational direction of water leaving a sink drain.

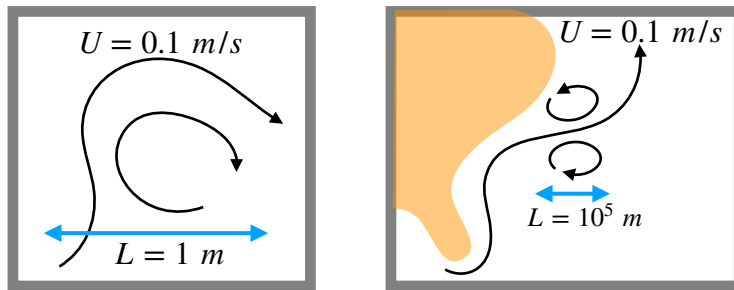


FIGURE 28.1: Estimating the Rossby number for flow in a kitchen sink (left panel) and rings spawned from the Gulf Stream (right panel). The kitchen sink has velocity scales on the order of $U \sim 0.01 - 0.1 \text{ m s}^{-1}$ whereas Gulf Stream rings have velocity scales on the order $U \sim 0.1 - 1.0 \text{ m s}^{-1}$. Their length scales are much more distinct, with the scale for a sink $L \sim 1 \text{ m}$ whereas for the Gulf Stream rings $L \sim 10^5 \text{ m}$. Taking the Coriolis parameter at 30° leads to $\text{Ro}_{\text{sink}} \sim 10^2 - 10^3$ and $\text{Ro}_{\text{ring}} \sim 10^{-2} - 10^{-1}$. The planetary Coriolis acceleration is central to Gulf Stream ring dynamics whereas it is utterly negligible for the kitchen sink.

28.3.5 Rossby number for a Gulf Stream ring

For a Gulf Stream ring (right panel of Figure 28.1), the typical length scale is $L = 10^5 \text{ m}$ and velocity scale is $U = 0.1 - 1.0 \text{ m s}^{-1}$, thus leading to a time scale $L/U \approx 10^5 - 10^6 \text{ s}$. At 30° latitude the Rossby number is

$$\text{Ro}_{\text{ring}} \approx 10^{-2} - 10^{-1}. \quad (28.13)$$

Flow features of such large length scales can feel the planetary rotation so that the Coriolis acceleration is central to dynamics of Gulf Stream rings, as reflected in the small magnitude of the associated Rossby number.

28.4 Geostrophic balance

Under the influence of horizontal pressure forces, a fluid accelerates down the pressure gradient (movement from high pressure to low pressure). In the presence of rotation, a nonzero horizontal

velocity couples to the Coriolis parameter, f , thus giving rise to a nonzero horizontally oriented Coriolis acceleration $-f \hat{z} \times \mathbf{u}$. The Coriolis acceleration acts perpendicular to the fluid motion

$$\mathbf{u} \cdot (\hat{z} \times \mathbf{u}) = 0, \quad (28.14)$$

and as such it affects the fluid motion but does not alter kinetic energy; i.e., it does zero work on the fluid.² In the northern hemisphere where $f > 0$, the Coriolis acceleration acts to the right of the parcel motion. It follows that if the Coriolis and pressure gradient accelerations are balanced, then a fluid particle moves counter-clockwise around low pressure centers and clockwise around high pressure centers (Figure 28.3). In the southern hemisphere, where $f < 0$, the Coriolis acceleration acts in the opposite direction so that geostrophically balanced flow is oppositely oriented in the southern hemisphere relative to the north. In Figure 28.2 we offer a heuristic model to help understand the geostrophic balance and to remember its orientation.

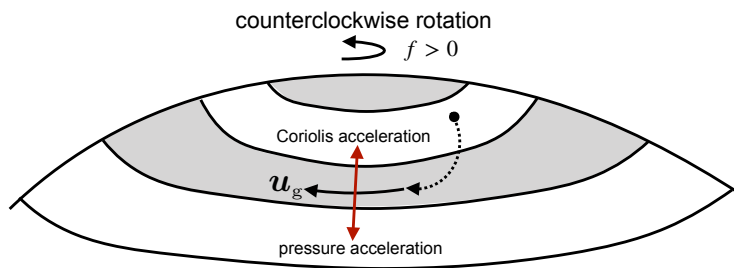


FIGURE 28.2: Geostrophy is a diagnostic relation where the pressure gradient acceleration balances the Coriolis acceleration so that the net acceleration acting on a fluid element is zero. Here we depict a particle on a rotating and frictionless hill (analogous to a high pressure center) as a conceptual model to help understand geostrophic balance. As the particle moves downhill (or down the pressure gradient) it picks up a rightward component to its trajectory as a result of the Coriolis acceleration that couples to motion. Equilibrium arises when the downhill acceleration (pressure gradient acceleration) balances the oppositely directed Coriolis acceleration.

28.4.1 Geostrophic balance is distinctly fluid mechanical

When pressure and Coriolis forces balance, fluid motion is said to be in *geostrophic* balance, whereby large-scale atmospheric winds and ocean currents generally follow isobars (lines of constant pressure). Recall from Chapter 11 that point particles also experience a Coriolis acceleration when viewed in a rotating reference frame. However, geostrophic balance is not afforded to particles since particles do not experience a pressure force that can balance the Coriolis force. Hence, the geostrophic balance is a distinctly fluid mechanical phenomena.

28.4.2 Geostrophic relation in geopotential coordinates

When the Rossby number is small and friction is negligible, the leading order dynamical balance in the horizontal momentum equation (28.1a) is between the Coriolis acceleration and horizontal pressure gradient acceleration

$$f \hat{z} \times \mathbf{u}_g = -\rho^{-1} \nabla_z p, \quad (28.15)$$

²These characteristics of the Coriolis acceleration are directly analogous to the Lorentz force in electrodynamics (Jackson, 1975).

which leads to the expression for the geostrophic velocity³

$$\mathbf{u}_g = \frac{\hat{z} \times \nabla p}{f\rho} \implies u_g = -\frac{1}{f\rho} \frac{\partial p}{\partial y} \quad \text{and} \quad v_g = \frac{1}{f\rho} \frac{\partial p}{\partial x}. \quad (28.16)$$

Note that the equator is special since the Coriolis parameter, $f = 2\Omega \sin \phi$, vanishes, thus precluding the relevance of geostrophy near the equator. Instead, at the equator flow generally moves down the horizontal pressure gradient since there is no Coriolis acceleration to turn the flow.

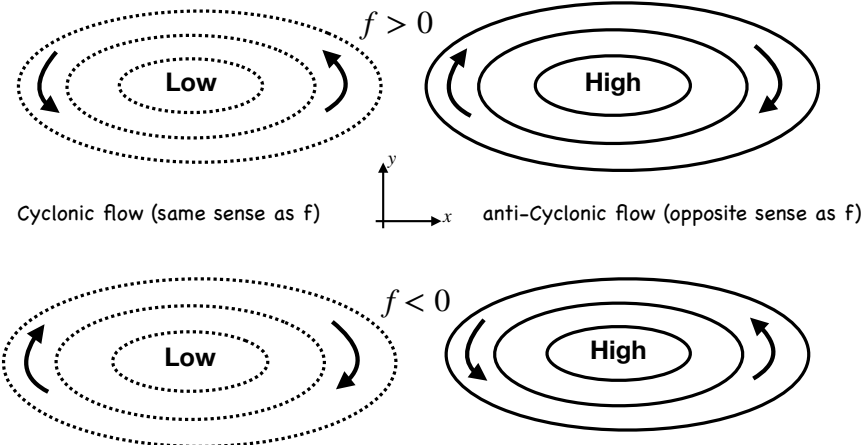


FIGURE 28.3: Geostrophic motion around low and high pressure centers in the northern hemisphere and southern hemisphere ($f = 2\Omega \sin \phi > 0$ in the north and $f < 0$ in the south). Upper panel: the counter-clockwise motion around the low pressure center in the northern hemisphere is in the same sense as the planetary rotation, and is thus termed cyclonic. Cyclonic motion in the southern hemisphere occurs in a clockwise direction, again corresponding to the planetary rotation direction as viewed from the south. Geostrophic motion around a high pressure center is counter to the planetary rotation in both hemispheres, and is thus termed anti-cyclonic.

Equation (28.16) for the geostrophic velocity can be written as

$$\rho f \mathbf{u}_g = \hat{z} \times \nabla_z p, \quad (28.17)$$

which suggests we interpret pressure as a streamfunction for $\rho f \mathbf{u}_g$. For the particular case of a Boussinesq ocean on an f -plane, in which we set ρ to the reference density ρ_0 and f is a constant, then we can write

$$\mathbf{u}_g = \hat{z} \times \nabla_z [p/(\rho_0 f)]. \quad (28.18)$$

In this case $p/(\rho_0 f)$ is referred to as the *geostrophic streamfunction* for the f -plane Boussinesq geostrophic flow.

28.4.3 Cyclonic and anti-cyclonic orientation

When oriented in the same sense as the earth's rotation (i.e., same sign of the Coriolis parameter) rotational motion is said to be in a *cyclonic* sense. Oppositely oriented motion is *anti-cyclonic*. For example, geostrophic motion around a low pressure center in the northern hemisphere is counter-clockwise (Figure 28.3). Using the right hand rule, this motion represents a positively oriented rotation. Hence, with $f > 0$ in the north, counter-clockwise motion is cyclonic. In the southern hemisphere, geostrophic motion around a low pressure center is clockwise, which is

³We can write either ∇ or ∇_z in equation (28.16). The reason is that the $\hat{z} \times$ operator selects only the horizontal portion of the gradient.

a negatively oriented rotational motion (again, recall the right hand rule). In the south where $f < 0$, clockwise motion around a low pressure center represents cyclonic motion (Figure 28.3).

28.4.4 Density gradients and thermal wind balance

Horizontal momentum is affected by horizontal pressure gradient forces. Furthermore, the hydrostatic balance says that the vertical derivative of the horizontal pressure gradient is determined by horizontal density gradients

$$\frac{\partial(\nabla_z p)}{\partial z} = -g \nabla_z \rho. \quad (28.19)$$

Hence, in the presence of horizontal density gradients, the horizontal pressure gradient forces are depth dependent. Correspondingly, the horizontal velocity field experiences a depth dependent pressure force.

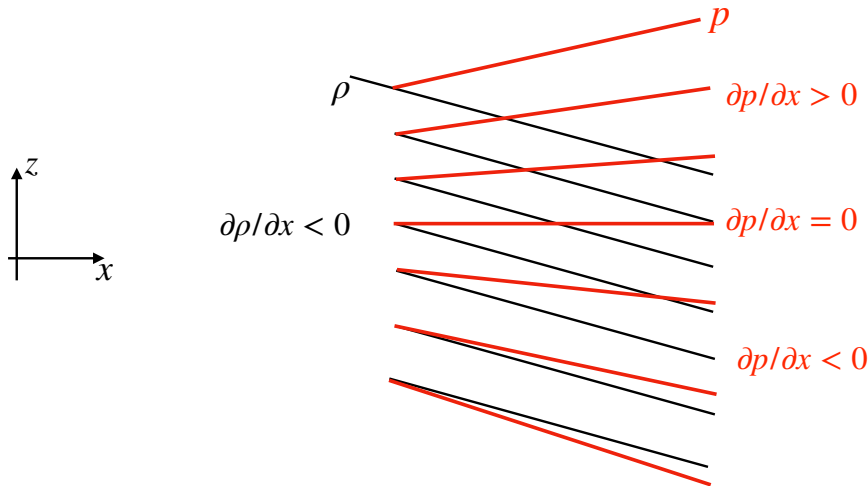


FIGURE 28.4: Horizontal density gradients support a vertical dependence to the horizontal gradient of the hydrostatic pressure via $\partial(\nabla_z p)/\partial z = -g \nabla_z \rho$. This figure depicts a constant horizontal density gradient with $\partial \rho / \partial x < 0$, thus leading to an increase in the zonal pressure gradient with height, $\partial(\partial p / \partial x) / \partial z > 0$. Depending on the thickness of the fluid column, the horizontal pressure gradient can change sign when moving up in the column, as shown here. Compare this figure to Figure 24.2, which discusses how to compute horizontal pressure gradients in a hydrostatic fluid.

We illustrate this depth dependence in Figure 28.4 with a depth independent horizontal density gradient, $\partial \rho / \partial x = \text{constant} < 0$, thus leading to a depth dependent horizontal gradient in the hydrostatic pressure. This figure also illustrates how the sign of the horizontal pressure gradient can change when moving in the vertical, depending on the value of the gradient at depth. It also illustrates how horizontal density gradients lead to a nonzero baroclinicity vector

$$\mathbf{B} = \frac{\nabla \rho \times \nabla p}{\rho^2}. \quad (28.20)$$

As shown in Section 37.4, a nonzero baroclinicity imparts a torque on fluid elements that acts as a source for vorticity.

The depth dependence to the horizontal pressure gradient leads to a vertical shear in the horizontal geostrophic velocity

$$\frac{\partial(\rho f \mathbf{u}_g)}{\partial z} = \hat{\mathbf{z}} \times \nabla(\partial p / \partial z) = -g \hat{\mathbf{z}} \times \nabla \rho. \quad (28.21)$$

This connection between horizontal density gradients and vertical shears in the geostrophic velocity is known as the *thermal wind balance*, which we return to in Section 28.5.6.

28.4.5 Geostrophic relation in pressure coordinates

The hydrostatic balance

$$\partial p / \partial z = -\rho g \quad (28.22)$$

can be used to eliminate density from the geostrophic balance (28.15) to render

$$f \hat{z} \times \mathbf{u}_g = \frac{g \nabla_z p}{\partial p / \partial z}. \quad (28.23)$$

The right hand side is minus the lateral gradient of the geopotential, $\Phi = g z$, as computed along surfaces of constant pressure⁴

$$f \hat{z} \times \mathbf{u}_g = -\nabla_p \Phi \implies f \mathbf{u}_g = \hat{z} \times \nabla_p \Phi. \quad (28.24)$$

This is a useful expression of geostrophy for the compressible atmosphere.

28.4.6 Further study

Visualizations from rotating tank experiments provide very useful illustrations of the Coriolis acceleration and geostrophic balance. One example occurs near the 10 minute mark in [this video from Prof. Fultz](#).

28.5 Planetary geostrophic mechanics

We here introduce the planetary geostrophic (PG) equations, which have found great use in describing elements of the large-scale laminar ocean circulation. We state the equations and discuss their physical implications, deferring a systematic derivation for later. In particular, the shallow water planetary geostrophic equations are derived in Section 40.4 and the continuously stratified planetary geostrophic equations are derived in Section 41.3.

28.5.1 Planetary geostrophic equations

The governing equations for planetary geostrophy are based on the hydrostatic Boussinesq equations stated in Section 26.1.7, with the assumption of a steady state linear and frictional-/geostrophic balance for the horizontal momentum

$$\rho_0 f (\hat{z} \times \mathbf{u}) = -\nabla p - \rho g \hat{z} + \partial \boldsymbol{\tau} / \partial z \quad (28.25a)$$

$$\nabla_z \cdot \mathbf{u} + \partial w / \partial z = 0 \quad (28.25b)$$

$$D b / D t = \dot{b}. \quad (28.25c)$$

The stress, $\boldsymbol{\tau}$, acts just in the horizontal directions so that the vertical component of the momentum equation (28.25a) is the hydrostatic balance

$$\partial p / \partial z = -\rho g. \quad (28.26)$$

⁴See Section 56.12.2 for details of computing derivatives using generalized vertical coordinates. In particular, the formalism in that section reveals that $(\partial p / \partial x)_{y,z} / (\partial p / \partial z)_{x,y} = -(\partial z / \partial x)_{y,p} = -g^{-1} (\partial \Phi / \partial x)_{x,p}$, and likewise for the meridional derivative.

We now list some of the key physical attributes captured by these equations.

Velocity is determined by buoyancy

The only time derivative appearing in the planetary geostrophic equations appears in the buoyancy equation (28.25c). All other equations are diagnostic. As the buoyancy evolves, the hydrostatic pressure changes and so too does the geostrophic velocity. Hence, the velocity is determined by the buoyancy field.

Planetary geostrophy admits no turbulence

The momentum equation is linear since planetary geostrophy drops the nonlinear advection of momentum. Hence, there is no turbulence in the planetary geostrophic fluid since turbulence relies on the nonlinear momentum advection. Instead, planetary geostrophy is used to describe laminar ocean circulation features at the large-scales.

Vertical transfer of horizontal momentum and subgrid scale parameterizations

We introduced a horizontal stress (dimensions of force per area) into the momentum equation

$$\boldsymbol{\tau} = (\tau^x, \tau^y, 0). \quad (28.27)$$

This stress is associated with vertical transfer of horizontal momentum in the ocean interior through vertical viscosity, as well as vertical transport of momentum from the atmosphere to the ocean. The vertical stress is enhanced by waves and turbulent features such as mesoscale eddies. However, such transient processes are not represented by planetary geostrophy. Hence, they must be parameterized, which generally leads to an enhanced vertical viscosity relative to that from molecular viscosity. In general, all models (analytical or numerical) of planetary scale circulations are too coarse to resolve the scales over which molecular viscosity dominates the frictional dissipation. Consequently, it is necessary to provide rational *subgrid-scale (SGS) parameterizations* for the variety of physical processes that are unresolved by the model. We have more to say about the parameterization of vertical transfer of horizontal momentum in Section 63.3.5.

28.5.2 Planetary geostrophic vorticity equation

The vertical component of relative vorticity is given by

$$\zeta = \partial v / \partial x - \partial u / \partial y, \quad (28.28)$$

with a thorough discussion of vorticity given in Chapter 37. Here, we form the relative vorticity budget for the planetary geostrophic system by taking the curl of the momentum equation.

Curl of the PG momentum equation

Taking the curl of the momentum equation (28.25a), and rearranging terms, leads to the planetary geostrophic vorticity equation

$$-\rho_0 f \frac{\partial \mathbf{u}}{\partial z} + \hat{z} \rho_0 \nabla \cdot (f \mathbf{u}) = -g \nabla \times (\hat{z} \rho) + \frac{\partial (\nabla \times \boldsymbol{\tau})}{\partial z}. \quad (28.29)$$

Note that $\nabla \cdot (f \mathbf{u}) = \nabla_z \cdot (f \mathbf{u})$ since \mathbf{u} is the horizontal velocity vector. Introducing the Archimedean buoyancy (Section 26.1.2)

$$b = -g(\rho - \rho_0)/\rho_0 \quad (28.30)$$

leads to

$$-f \frac{\partial \mathbf{u}}{\partial z} + \hat{z} \nabla_z \cdot (f \mathbf{u}) = \nabla \times (\hat{z} b) + \frac{1}{\rho_0} \frac{\partial(\nabla \times \boldsymbol{\tau})}{\partial z}. \quad (28.31)$$

Pressure gradients are removed from the vorticity equation

One of the key reasons to study vorticity is that its evolution equation is not explicitly affected by the pressure gradient since the curl of the pressure gradient vanishes. Eliminating the pressure force affords a simpler evolution equation for vorticity, and we pursue that evolution more thoroughly in Chapter 37. Pressure perturbations are rapidly transferred in a fluid, either by acoustic waves in divergent flows (Chapter 44) or instantaneously in non-divergent flows (Section 26.3). Hence, in the absence of pressure directly affecting the vorticity equation, contributions to vorticity evolution are more localized in space than contributions to velocity evolution.

Relative vorticity is absent from the PG vorticity equation

It is notable that there is no appearance of the relative vorticity, $\zeta = \partial_x v - \partial_y u$, in the planetary geostrophic vorticity equation (28.25a). The reason is that we dropped the material time derivative of velocity when forming the planetary geostrophic momentum equation (28.25a). By doing so, we drop all expressions of ζ in the vorticity equation. Planetary geostrophy is valid for those cases where

$$|\zeta| \ll |f|, \quad (28.32)$$

which means the absolute vorticity (sum of planetary vorticity plus relative vorticity) is dominated by the planetary vorticity. We encounter more complete versions of the vorticity equation in Chapter 37 where we do not make the planetary geostrophic assumption.

Rather than taking the curl of the planetary geostrophic momentum equation, we could have also derived the vorticity equation (28.31) by taking planetary geostrophic scaling in the full vorticity equation. We choose here the path through the planetary geostrophic momentum equation since we have yet to discuss the full vorticity equation (see Chapter 37).

28.5.3 Taylor-Proudman and vertical stiffening

Consider the vorticity equation (28.31) on an f -plane with zero friction, in which the horizontal geostrophic motion is horizontally non-divergent

$$\nabla_z \cdot \mathbf{u} = 0 \quad f\text{-plane geostrophy.} \quad (28.33)$$

Use of continuity (equation (28.25b)) means there is no vertical stretching of a vertical material line element (Section 15.3.6)

$$\partial w / \partial z = 0. \quad (28.34)$$

As shown in Chapter 37, a vortex tube exhibits the same kinematics as a material line element described in Section 15.3. Hence, $\partial w / \partial z = 0$ means there is no vertical stretching of a vortex tube in the planetary geostrophic fluid. This result has important implications that we now describe.

Flat bottom boundary and columnar motion

If there is a solid flat bottom to the domain, then the vertical velocity vanishes at that surface. With $\partial_z w = 0$ in the interior as well, then w vanishes throughout the domain. Hence, the fluid has zero vertical velocity, and motion occurs on horizontal planes perpendicular to the rotation axis; i.e., the flow is two-dimensional. We furthermore assume zero horizontal buoyancy gradients, so that the vorticity equation (28.31) implies that the horizontal velocity has zero vertical shear

$$\partial \mathbf{u} / \partial z = 0 \quad f\text{-plane and homogeneous density.} \quad (28.35)$$

This result is known as the *Taylor-Proudman effect*, with Figure 28.5 providing an illustration.

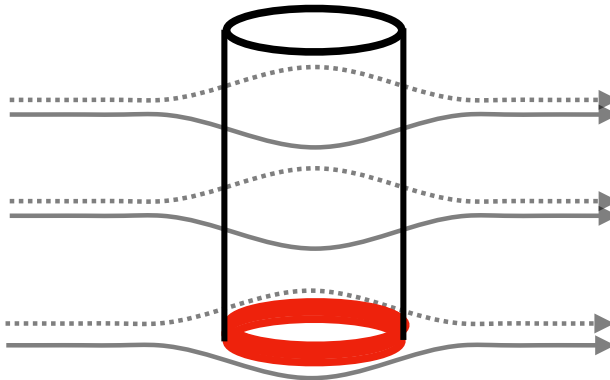


FIGURE 28.5: The Taylor-Proudman effect (28.35) says that horizontal flow in a homogeneous rapidly rotating fluid over a flat bottom (where $w = 0$) is depth-independent. Hence, when flow encounters an obstacle anywhere in the column, such as the red ring shown here at the bottom, then flow throughout the full depth coherently moves around the obstacle. The result is a vertically stiffened motion known as *Taylor columns*.

Relevance to the ocean and atmosphere

In the ocean and atmosphere, the assumptions leading to the Taylor-Proudman effect are rarely satisfied due to the presence of stratification (i.e., vertical density variations), and a sloping solid earth bottom. Nonetheless, there is a tendency for vertical velocities to be quite small due to the effects of rotation; even smaller than the non-divergent flow scaling $W/H \sim U/L$ would indicate (see Section 28.3.1). Additionally, for unstratified or linearly stratified fluids, there is a tendency for geostrophic turbulence to cascade energy into the *gravest vertical mode*; i.e., the largest vertical scale. This largest vertical scale mode is termed the *barotropic mode*, and motion of this mode is predominantly horizontal and depth independent. Smaller vertical scales of variation are captured by an infinite hierarchy of *baroclinic modes*. The process of moving energy to the barotropic mode is referred to as *barotropization*.

28.5.4 Meridional motion in response to vortex stretching and stresscurls

The vertical component to the vorticity balance (28.31) leads to

$$\nabla_z \cdot (f \mathbf{u}) = \frac{1}{\rho_0} \frac{\hat{\mathbf{z}} \cdot \partial (\nabla \times \boldsymbol{\tau})}{\partial z} \quad (28.36)$$

which can be written

$$\beta v = -f \nabla_z \cdot \mathbf{u} + \frac{1}{\rho_0} \frac{\hat{\mathbf{z}} \cdot \partial (\nabla \times \boldsymbol{\tau})}{\partial z} \quad (28.37)$$

where

$$\beta = \partial f / \partial y \quad (28.38)$$

is the gradient of planetary vorticity. The continuity equation (28.25b) can be used to remove the horizontal divergence, which yields the vorticity balance

$$\beta v = f \frac{\partial w}{\partial z} + \frac{1}{\rho_0} \frac{\hat{z} \cdot \partial (\nabla \times \boldsymbol{\tau})}{\partial z}. \quad (28.39)$$

The left hand side is the meridional advection of planetary vorticity. The first term on the right hand side arises from vortex stretching by planetary vorticity; i.e., planetary induction or the β -effect discussed in Section 37.6.2. The second term is the vertical divergence of the curl of the stress.

Reading the vorticity equation (28.39) from right to left indicates that any process leading to a vorticity source via vortex stretching or wind stress curls must be balanced by meridional motion. That is, the fluid responds to vortex stretching and wind curls by moving meridionally through the planet's vorticity field. In a fluid that maintains planetary geostrophic balance, meridional movement is the only means for it to respond to vorticity input since its vorticity is set by planetary vorticity. Conversely, reading the equality (28.39) from the left to the right reveals that any meridional motion itself must be balanced by vortex stretching plus wind stress curls. We study the depth integrated form of this vorticity equation in Section 41.5, where we see how the depth integrated meridional flow is affected by stretching created by boundary torques.

28.5.5 Sverdrup balance

Depth integrating the vorticity balance (28.39) over the full depth of an ocean column leads to

$$\beta V = f [(w(\eta) - w(\eta_b)) + \hat{z} \cdot \nabla \times [\boldsymbol{\tau}(\eta) - \boldsymbol{\tau}(\eta_b)]] / \rho_0, \quad (28.40)$$

where

$$V = \int_{\eta_b}^{\eta} v \, dz \quad (28.41)$$

is the depth integrated meridional velocity. For the large-scale we generally assume the surface vertical velocity is small, with $w(\eta) = 0$ when making the *rigid lid approximation*. Further assuming a flat bottom allows us to drop the vertical velocity at the ocean bottom, $w(\eta_b) = 0$. Additionally, the surface turbulent stress is often far larger than the bottom turbulent stress. These assumptions then lead to the *Sverdrup balance*, which is a balance between the depth integrated meridional motion and the curl of the surface turbulent stress

$$\rho_0 \beta V_{\text{Sverdrup}} = \hat{z} \cdot \nabla \times \boldsymbol{\tau}(\eta) \quad \text{Sverdrup balance.} \quad (28.42)$$

As further discussed in Section 37.9.4, the most problematic aspect of this balance concerns the assumption of vanishing $w(\eta_b)$, with $w(\eta_b)$ generally non-negligible in regions with sloping side boundaries. We also discuss a variant of this balance, known as the *geostrophic Sverdrup balance*, in Section 41.6.

28.5.6 Features of thermal wind balanced flows

Horizontal components to the inviscid vorticity equation (equation (28.31) with $\boldsymbol{\tau}$ set to zero) form the thermal wind balance

$$f \partial \mathbf{u} / \partial z = -\nabla \times (\hat{z} b) = \hat{z} \times \nabla b, \quad (28.43)$$

which takes on the component form

$$f \partial u / \partial z = -\partial b / \partial y \quad \text{and} \quad f \partial v / \partial z = \partial b / \partial x. \quad (28.44)$$

As seen already in Section 28.4.4, these relations can also be derived directly from taking the vertical derivative of the horizontal momentum equation (28.25a) and then using the horizontal gradient of the hydrostatic balance (28.26). In either case, the thermal wind balance (28.43) says that the horizontal geostrophic velocity possesses a vertical shear where the buoyancy field has a horizontal gradient. Buoyancy with a horizontal gradient is termed *baroclinic* since it leads to a nonzero baroclinicity vector that provides a source for vorticity (see Section 37.7.2). Correspondingly, it is only the baroclinic (depth dependent) piece of geostrophic velocity that is related to horizontal buoyancy gradients. The depth-independent flow is not constrained by horizontal buoyancy gradients.

Thermal wind, the atmospheric jet stream and the Antarctic Circumpolar Current

Due to the increased solar radiation reaching the equator relative to the poles, the zonal averaged temperature generally reduces poleward. This poleward reduction in temperature corresponds to a poleward reduction in buoyancy. Also, for a stably stratified fluid, density increases with depth so that buoyancy decreases. Figure 28.6 illustrates this situation.

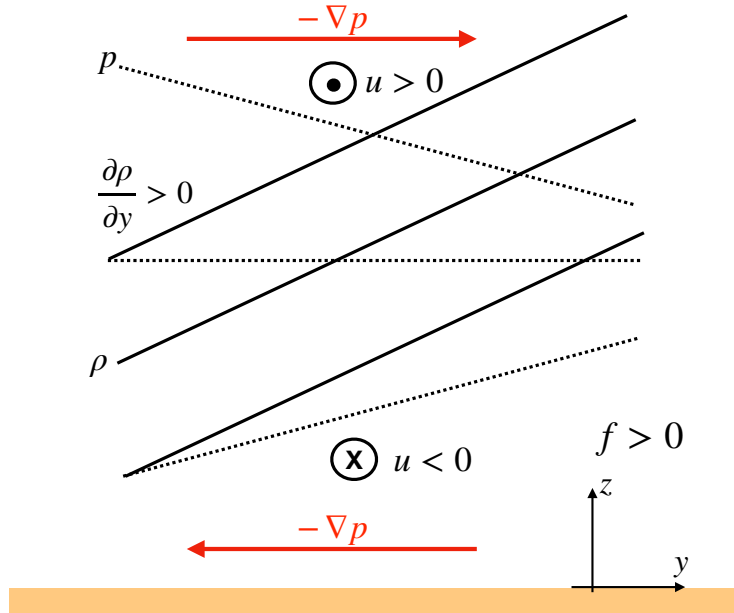


FIGURE 28.6: Schematic of the density and hydrostatic pressure fields and the associated thermal wind balanced flow in the northern hemisphere ($f > 0$) with north to the right and east out of the page. We show surfaces of constant density (solid lines) and constant pressure (isobars; dashed lines). Density increases poleward ($\partial \rho / \partial y > 0$) so that, according to the discussion surrounding Figure 28.4, the meridional pressure gradient decreases when moving upward, $\partial(\partial p / \partial y) / \partial z = -g \partial_y \rho < 0$. We illustrate isobars with an equatorward directed downgradient pressure force at lower elevations ($-\partial p / \partial y < 0$) and poleward directed pressure force at higher elevations ($-\partial p / \partial y > 0$). The zonal geostrophic wind is in geostrophic balance with these pressure gradients, with a westward zonal flow at lower elevations (easterly winds) and eastward flow at higher elevations (westerly winds). This flow configuration creates an eastward vertical shear of the zonal geostrophic winds, $\partial u_g / \partial z > 0$.

A zonal average around a zonally symmetric globe, such as in the Antarctic Circumpolar Current, removes all zonal variations, thus putting $\partial_x \rho = 0$ and so rendering the zonally averaged

thermal wind relation

$$f \frac{\partial \bar{u}}{\partial z} = \frac{g}{\rho_0} \frac{\partial \bar{b}}{\partial y} = -\frac{\partial \bar{b}}{\partial y} > 0, \quad (28.45)$$

where $\overline{(\)}$ is the zonal mean operator. In the northern hemisphere, $\partial_y \bar{b} < 0$, so that the zonal averaged thermal wind shear is positive, $\partial_z \bar{u} > 0$. For example, a westerly zonal wind (blowing to the east) strengthens with height (easterly thermal wind shear). In the Southern Hemisphere, $f < 0$ with poleward decreasing buoyancy, $\partial_y \bar{b} > 0$, means there is also an eastward thermal wind shear. Note that movement towards the poles, where $|f|$ increases, leads to a smaller thermal wind shear given the same buoyancy gradient.

Diagnosing geostrophic velocity from the buoyancy field

Vertical integration of the thermal wind relation (28.43) between two constant depth surfaces leads to

$$\mathbf{u}(z) = \mathbf{u}(z_{\text{ref}}) - f^{-1} \nabla \times \hat{\mathbf{z}} \int_{z_{\text{ref}}}^z b \, dz. \quad (28.46)$$

Hence, knowledge of the buoyancy field (e.g., through hydrographic measurements of temperature and salinity in the ocean), along with knowledge of the geostrophic velocity at a single depth, allows for determination of the full geostrophic velocity in terms of density. Unfortunately, specification of the unknown reference velocity is unavailable just from hydrographic measurements. This is the origin of the *depth of no motion* problem in oceanography.

28.5.7 Thermal wind balance for the atmosphere

The large-scale atmosphere is compressible and approximately in hydrostatic balance. The expression for geostrophic balance (28.24) in pressure coordinates is a suitable starting point to derive thermal wind for the atmosphere. For this purpose, we take the pressure derivative, $\partial/\partial p$, of (28.24) to render

$$f \frac{\partial \mathbf{u}}{\partial p} = \hat{\mathbf{z}} \times \nabla_p \left[\frac{\partial \Phi}{\partial p} \right], \quad (28.47)$$

with $\Phi = g z$ the geopotential. The hydrostatic relation $\partial p/\partial z = -\rho g$ takes the form

$$\frac{\partial p}{\partial \Phi} = -\rho \Rightarrow \frac{\partial \Phi}{\partial p} = -1/\rho \quad (28.48)$$

in which case

$$f \frac{\partial \mathbf{u}}{\partial p} = -\hat{\mathbf{z}} \times \nabla_p (1/\rho). \quad (28.49)$$

Ideal gas atmosphere

The specific volume takes the following form for an ideal gas atmosphere (see Section 20.4.1)

$$\rho^{-1} = R^M T/p. \quad (28.50)$$

Since the horizontal derivative in the thermal wind relation (28.49) is along pressure surfaces, we have

$$f \frac{\partial \mathbf{u}}{\partial p} = -\frac{R^M}{p} [\hat{\mathbf{z}} \times \nabla_p T]. \quad (28.51)$$

This expression gives rise to the name “thermal wind”, with vertical shears of the horizontal velocity generated by horizontal temperature gradients along isobars.

As for the ocean in equation (28.46), we vertically integrate the thermal wind expression (28.51), here between two pressure levels

$$\mathbf{u}(p_A) - \mathbf{u}(p_B) = f^{-1} R^M \hat{\mathbf{z}} \times \nabla_p \left[\int_{p_A}^{p_B} \frac{T dp}{p} \right], \quad (28.52)$$

where $p_A < p_B$, so that p_A is at a higher altitude than p_B . We define the thermal wind shear as the difference between the wind aloft (higher altitude and lower pressure) from that at a lower altitude (greater pressure)

$$\mathbf{u}_T = \mathbf{u}(p_A) - \mathbf{u}(p_B) \quad \text{with } p_A < p_B \quad (28.53)$$

so that

$$\mathbf{u}_T = \frac{R^M}{f} \hat{\mathbf{z}} \times \nabla_p \bar{T}^{\ln p}, \quad (28.54)$$

where we introduced the log-pressure weighted temperature between the two pressure surfaces

$$\bar{T}^{\ln p} = \int_{p_A}^{p_B} \frac{T dp}{p}. \quad (28.55)$$

The relation (28.54) means that on the f -plane, R^M/f times the log-pressure weighted temperature serves as a streamfunction for the thermal wind shear. Reconsider the previous example where the polar regions are colder than tropics, so that in the northern hemisphere on pressure surfaces, $\partial \bar{T}^{\ln p} / \partial y < 0$. Hence, the zonal westerly winds increase in magnitude with height. We depict this situation in Figure 28.7. Furthermore, the thermal wind shear points to the east. For a more general flow in the northern hemisphere, cold air sits on the left side of the thermal wind shear and warm air on the right. The opposite orientation holds for the southern hemisphere where the Coriolis parameter is negative, $f < 0$

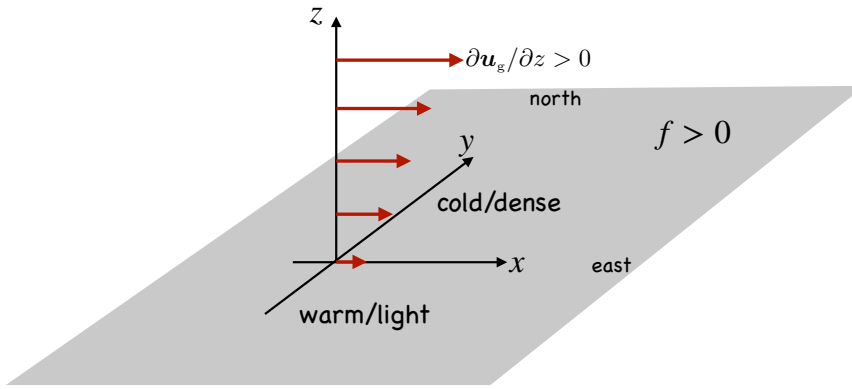


FIGURE 28.7: Thermal wind shear in the northern hemisphere ($f > 0$) middle latitude atmosphere, whereby cold/dense air sits to the north and warm/light air to the south. The zonal geostrophic winds increase to the east when rising in elevation, $\partial u_g / \partial z > 0$. We say that the zonal winds have an eastward thermal wind shear. In general, a geostrophic wind in the northern hemisphere atmosphere has cold/dense air to the left when facing downwind, whereas the opposite orientation holds for the southern hemisphere where $f < 0$.

Barotropic flow

Return to the thermal wind equation (28.49)

$$f \frac{\partial \mathbf{u}}{\partial p} = -\hat{\mathbf{z}} \times \nabla_p(1/\rho) = \frac{\hat{\mathbf{z}} \times \nabla_p \rho}{\rho^2}. \quad (28.56)$$

For the special case of density a function just of the pressure, $\rho = \rho(p)$, then $\nabla_p \rho = 0$. This situation defines a *barotropic* flow, which is characterized here by a horizontal geostrophic velocity with zero vertical variations. Note that we are here only concerned with the geostrophic flow. A density related to pressure through $\rho = \rho(p)$ can still support vertical variations of the ageostrophic flow.

We further discuss barotropic flow in Section 37.2 as part of our study of vorticity. As detailed in that discussion, the general definition of a barotropic flow is one whereby the *baroclinicity* vector vanishes, $\mathbf{B} = \nabla p \times \nabla(1/\rho) = 0$. The functional relation $\rho = \rho(p)$ (equivalently $p = p(\rho)$) is a sufficient condition for vanishing baroclinicity. As seen in Section 37.4, for a barotropic flow there is no generation of vorticity through the torques created when density isosurfaces deviate from pressure isosurfaces (isobars).

28.5.8 Thermal wind for the ocean

We here expose a few details for how to work with thermal wind in the ocean. To start, we write the most general form of thermal wind according to equation (28.21)

$$f \frac{\partial(\rho \mathbf{u}_g)}{\partial z} = -g \hat{\mathbf{z}} \times \nabla \rho. \quad (28.57)$$

Treatment of the *in situ* density depends on whether we consider a Boussinesq ocean, as done for most of this section, versus a non-Boussinesq ocean.

Thermal wind for a Boussinesq ocean

For a Boussinesq ocean, the *in situ* density on the left hand side of equation (28.57) is set to the constant reference density, ρ_0 , in which case the thermal wind relation is given by

$$f \rho_0 \frac{\partial \mathbf{u}_g}{\partial z} = -g \hat{\mathbf{z}} \times \nabla \rho. \quad (28.58)$$

Following from the discussion of Boussinesq energetics in Section 26.8.4, we know that the *in situ* density in a Boussinesq ocean takes the functional form of equation (26.166)

$$\rho = \rho[S(\mathbf{x}, t), \Theta(\mathbf{x}, t), p = -\rho_0 \Phi(\mathbf{x}, t)]. \quad (28.59)$$

For geostrophic flows we are generally only concerned with the simple geopotential, $\Phi(\mathbf{x}, t) = g z$, which defines the local vertical direction, $\hat{\mathbf{z}}$. Hence, $\hat{\mathbf{z}} \times \nabla \rho$ picks out horizontal derivatives of the *in situ* density along surfaces of constant geopotential

$$g \hat{\mathbf{z}} \times \nabla \rho = g \hat{\mathbf{z}} \times \nabla_z \rho. \quad (28.60)$$

We can thus express the horizontal *in situ* density gradient as

$$\nabla_z \rho = \left[\frac{\partial \rho}{\partial S} \right]_{\Theta, \Phi} \nabla_z S + \left[\frac{\partial \rho}{\partial \Theta} \right]_{S, \Phi} \nabla_z \Theta = \rho_0 (\beta \nabla_z S - \alpha \nabla_z \Theta), \quad (28.61)$$

where we introduced the Boussinesq form of the haline contraction and thermal expansion coefficients

$$\beta = \frac{1}{\rho_0} \left[\frac{\partial \rho}{\partial S} \right]_{\Theta, \Phi} \quad \text{and} \quad \alpha = -\frac{1}{\rho_0} \left[\frac{\partial \rho}{\partial \Theta} \right]_{S, \Phi}. \quad (28.62)$$

These results lead to the oceanic Boussinesq form of thermal wind relation

$$f \frac{\partial \mathbf{u}_g}{\partial z} = -g \hat{\mathbf{z}} \times (\beta \nabla_z S - \alpha \nabla_z \Theta), \quad (28.63)$$

which decomposes the thermal wind shear into a contribution from horizontal gradients in S and from Θ . In some treatments, the right hand side contribution is referred to as the horizontal gradient of the locally referenced potential density (see Section 27.5.5). Correspondingly, one generally finds that vertical sections of the potential density (referenced to a pressure near to that where computing thermal wind) provide a useful means to determine the magnitude and direction of the thermal wind shears; more useful than sections of *in situ* density.

Thermal wind for a non-Boussinesq hydrostatic ocean

Formulation of the thermal wind equation for a non-Boussinesq ocean follows quite closely to a Boussinesq, only now we start from the expression (28.49) for a compressible hydrostatic fluid using pressure as a vertical coordinate

$$\rho^2 f \frac{\partial \mathbf{u}}{\partial p} = \hat{\mathbf{z}} \times \nabla_p \rho. \quad (28.64)$$

For a non-Boussinesq ocean, we make use of the pressure dependence of the density so that

$$\rho = \rho[S(\mathbf{x}, t), \Theta(\mathbf{x}, t), p(\mathbf{x}, t)]. \quad (28.65)$$

The gradient operator is here computed along surfaces of constant pressure so that

$$\nabla_p \rho = \left[\frac{\partial \rho}{\partial S} \right]_{\Theta, p} \nabla_p S + \left[\frac{\partial \rho}{\partial \Theta} \right]_{S, p} \nabla_p \Theta = \rho (\beta \nabla_p S - \alpha \nabla_p \Theta), \quad (28.66)$$

where we introduced the non-Boussinesq form of the haline contraction and thermal expansion coefficients

$$\beta = \frac{1}{\rho} \left[\frac{\partial \rho}{\partial S} \right]_{\Theta, p} \quad \text{and} \quad \alpha = -\frac{1}{\rho} \left[\frac{\partial \rho}{\partial \Theta} \right]_{S, p}. \quad (28.67)$$

In this manner we can write the thermal wind relation (28.64) as

$$\rho f \frac{\partial \mathbf{u}}{\partial p} = \hat{\mathbf{z}} \times (\beta \nabla_p S - \alpha \nabla_p \Theta). \quad (28.68)$$

This expression is directly analogous to the Boussinesq form given by equation (28.63). Indeed, we can go one step further by using the chain rule and the hydrostatic relation to write

$$\frac{\partial \mathbf{u}}{\partial p} = \frac{\partial \mathbf{u}}{\partial z} \frac{\partial z}{\partial p} = -(\rho g)^{-1} \frac{\partial \mathbf{u}}{\partial z}, \quad (28.69)$$

in which case the non-Boussinesq thermal wind takes on the form

$$f \frac{\partial \mathbf{u}}{\partial z} = -g \hat{\mathbf{z}} \times (\beta \nabla_p S - \alpha \nabla_p \Theta). \quad (28.70)$$

Now, the key distinction from the Boussinesq form (28.63) is the appearance of a constant pressure derivative, ∇_p , for the non-Boussinesq case, in contrast to the constant geopotential derivative, ∇_z , appearing in the Boussinesq case. Additionally, the non-Boussinesq case uses the slightly distinct form of α and β given by equation (28.67) rather than the Boussinesq form in equation (28.62).

28.5.9 Further study

Much of the material in this section forms the basis for laminar theories of the large-scale ocean circulation. We further pursue these theories in Chapter 41 where we take a deeper dive into the study of planetary geostrophy. Further discussion of phenomenology is given in Chapter 7 of [Marshall and Plumb \(2008\)](#), whereas Chapters 19-22 of [Vallis \(2017\)](#) as well as [Samelson \(2011\)](#) present ocean circulation theory making use of fundamental concepts from geophysical fluid dynamics. A compelling discussion of the cascade of energy from the baroclinic modes to barotropic mode is offered by [Smith and Vallis \(2001\)](#). [Gill \(1982\)](#) provides a discussion of the depth of no motion problem in dynamic oceanography.

Rotating tank laboratory experiments offer a powerful means to explore the variety of rotating fluid mechanics relevant to the atmosphere and oceans. The following resources exemplify the Taylor-Proudman effect (28.35) and the associated vertical stiffening of rotating fluids.

- One means to test Taylor-Proudman is to insert a dye into a rapidly rotating tank of unstratified water. After a few rotation periods the dye forms vertical sheets known as *Taylor curtains* whose center is along the rotation axis. The fluid is said to have a *vertical stiffness* due to the effects of rotation. Vertical stiffening in turn means that flow over a small obstacle is deflected throughout the column rather than just near the bump. This situation is depicted in Figure 28.5 and more vividly illustrated in [this video from the UCLA SpinLab](#).
- Near the 20 minute mark of [this video, also from UCLA](#), we see how vortices in a rotating fluid maintain their coherency much more than in a non-rotating fluid.
- Another laboratory test shown in [this video from Prof. Fultz](#) shows that a buoyant object (a ping pong ball) placed into a rotating tank rises much slower than in a non-rotating tank. The reason for the slower rise is that the ball must push up against the vertically stiffened fluid column when rotating, thus slowing its rise relative to when in a non-rotating fluid. Later in the same video, near the 16 minute mark, we see Taylor curtains in rotating fluids.

28.6 Isopycnal form stress from geostrophic eddies

As introduced in Section 25.1, form stress is the horizontal stress arising from pressure acting on a sloped surface. The mathematical expression for the form stress acting on the top side of a surface is given by equation (25.6)

$$\Sigma^{\text{form}} = p \nabla \eta, \quad (28.71)$$

with the opposite sign for the form stress on the bottom side of the surface. Here, $z = \eta(x, y, t)$ is the depth of the surface (see Figure 25.3 or Figure 28.8). The net horizontal force from form stress is the area integral over the surface.

In this section we examine the zonal mean zonal form stress acting on an isopycnal surface (Section 28.6.1) and on an isopycnal layer (Section 28.6.2), each for an adiabatic, Boussinesq, hydrostatic fluid in geostrophic balance and within a zonally periodic channel of length L . As we

show, the zonal mean zonal form stress arising from geostrophically balanced fluctuations provide an eastward acceleration to the fluid. At the same time, these *geostrophic eddies* transport buoyancy and thickness/volume meridionally. Although the channel geometry is rather simple, it has applications to the middle latitude atmospheric circulation as well as for ocean circulation, particularly in the Southern Ocean where there is circumpolar channel-like flow within the Antarctic Circumpolar Current. Furthermore, the discussion exposes key elements of eddy-mean flow interactions, sharing points with the leading order generalized Lagrangian mean of Section 62.3 and the quasi-Stokes transport discussed in Section 63.3.

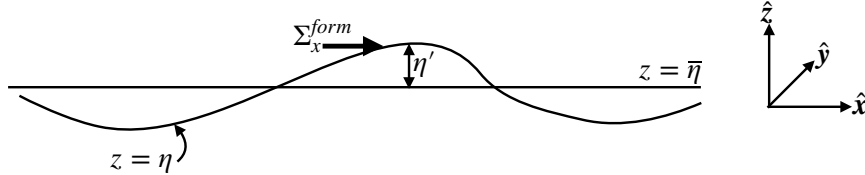


FIGURE 28.8: Schematic of the zonal form stress, Σ_x^{form} , acting on a surface whose zonal mean vertical position is $z = \bar{\eta}(y, t)$ and whose vertical position relative to the zonal mean is $z = \bar{\eta}(y, t) + \eta'(x, y, t)$.

28.6.1 Zonal mean zonal form stress on an isopycnal surface

We are here interested in the form stress acting on an isopycnal surface. Before specializing to an isopycnal, we decompose the form stress according to the zonal mean depth and its deviation from zonal mean (see Figure 28.8). Thereafter, specialization to an isopycnal surface in an adiabatic fluid connects the zonal mean form stress to the meridional eddy flux of buoyancy.

Zonal form stress on an arbitrary surface in a channel

The zonal mean vertical position of the surface is written

$$\bar{\eta} = \frac{1}{L} \int_0^L \eta \, dx \quad (28.72)$$

and its corresponding zonal fluctuation is

$$\eta' = \eta - \bar{\eta}. \quad (28.73)$$

The zonal component of the form stress is thus given by

$$p \partial_x \eta = p(x, \bar{\eta} + \eta') \partial_x (\bar{\eta} + \eta') \quad (28.74\text{a})$$

$$= p(x, \bar{\eta} + \eta') \partial_x \eta' \quad (28.74\text{b})$$

$$\approx [p(x, \bar{\eta}) + \partial_z p(x, \bar{\eta}) \eta'] \partial_x \eta' \quad (28.74\text{c})$$

$$= p(x, \bar{\eta}) \partial_x \eta' + \mathcal{O}(\eta')^2. \quad (28.74\text{d})$$

Hence, to second order in fluctuations, η' , the zonal form stress acting on the surface equals to $p(x, \bar{\eta}) \partial_x \eta'$, where it is important to note that pressure is evaluated at the zonal mean depth, $z = \bar{\eta}$.

To within the same accuracy, the zonal integral of the zonal form stress is given by

$$\int_0^L \Sigma_x^{\text{form}} \, dx \approx \int_0^L p(\bar{\eta}) (\partial \eta' / \partial x) \, dx = - \int_0^L \eta' [\partial p(\bar{\eta}) / \partial x] \, dx, \quad (28.75)$$

where the final equality follows from zonal periodicity. Now assume the zonal pressure gradient at $\bar{\eta}$ is balanced by a meridional geostrophic velocity

$$\partial p(\bar{\eta})/\partial x = f \rho_0 v(\bar{\eta}), \quad (28.76)$$

where

$$v(\bar{\eta}) = \bar{v}(\bar{\eta}) + v'(\bar{\eta}) \quad (28.77)$$

so that

$$\int_0^L \Sigma_x^{\text{form}} dx = -\rho_0 f \int_0^L \eta' v' dx, \quad (28.78)$$

where we noted that the Coriolis parameter is independent of zonal position. Hence, there is a nonzero zonal mean zonal form stress when there is a nonzero zonal correlation between fluctuations in the meridional velocity and the depth of the surface

$$\bar{\Sigma}_x^{\text{form}} = -\rho_0 f \bar{v}' \bar{\eta}'. \quad (28.79)$$

Zonal mean zonal form stress acting on an isopycnal surface

To further unpack the correlation appearing in equation (28.79), specialize to the case of an isopycnal surface in an adiabatic fluid. As shown in our discussion of generalized Lagrangian mean averaging in Sections 62.3.6 and 62.5.7, vertical fluctuations in the position of the isopycnal surfaces, relative to the zonal mean $\bar{\eta}$, are related to zonal fluctuations in the density

$$\eta' \approx -\frac{\rho'}{\partial \bar{\rho}/\partial z} = -\frac{b'}{N^2}, \quad (28.80)$$

where we introduced the squared buoyancy frequency of the zonal mean state as well as the fluctuating buoyancy

$$N^2 = -\frac{g}{\rho_0} \frac{\partial \bar{\rho}}{\partial z} \quad \text{and} \quad b' = -\frac{g \rho'}{\rho_0}. \quad (28.81)$$

The zonally averaged zonal form stress thus takes the form

$$\bar{\Sigma}_x^{\text{form}} = \frac{\rho_0 f}{N^2} \bar{v}' \bar{b}'. \quad (28.82)$$

Again, the assumptions rendering the result (28.82) are (i) zonal periodicity, (ii) adiabatic and Boussinesq fluid, (iii) geostrophically balanced flow. Under these assumptions, the zonal mean zonal form stress acting on an isopycnal surface is proportional to the zonal correlation between fluctuations in the meridional velocity and the buoyancy. It is a general statistical property of geostrophic eddies in the atmosphere and ocean to transport positive buoyancy (e.g., warm air/water) poleward and negative buoyancy (e.g., cold air/water) equatorward, thus ameliorating the equator-to-pole buoyancy difference setup by solar radiation that preferentially warms the tropics. In turn, this property of geostrophic eddies leads to a positive zonal mean zonal form stress

$$\bar{\Sigma}_x^{\text{form}} > 0. \quad (28.83)$$

Hence, in addition to transporting buoyancy poleward, geostrophic eddies provide a positive zonal mean force through zonal integrated form stress that accelerates the fluid in the eastward direction. These two properties of geostrophic eddies (poleward flux of positive buoyancy anomalies along with an eastward acceleration from form stress) are fundamental to the middle latitude atmospheric circulation as well as for ocean circulation, particularly within the channel-like Antarctic

Circumpolar Current.

28.6.2 Zonal mean zonal form stress acting on an isopycnal layer

We offer yet another means to understand the zonal mean zonal form stress by here examining the form stress acting on a constant density layer of adiabatic Boussinesq fluid such as shown in Figure 28.9. This layered/isopycnal analysis anticipates some of the development considered for the stacked shallow water model in Chapters 32 and 33 as well as for isopycnal models in Section 59.2.

The net form stress acting on the upper and lower layer interfaces in Figure 28.9 is given by

$$\Sigma^{\text{layer form}} = p_1 \nabla \eta_1 - p_2 \nabla \eta_2 \quad (28.84\text{a})$$

$$= p(\eta + h/2) \nabla(\eta + h/2) - p(\eta - h/2) \nabla(\eta - h/2) \quad (28.84\text{b})$$

$$\approx [p(\eta) - \rho g h/2] \nabla(\eta + h/2) - [p(\eta) + \rho g h/2] \nabla(\eta - h/2) \quad (28.84\text{c})$$

$$= p \nabla h - \rho g h \nabla \eta \quad (28.84\text{d})$$

$$= \nabla(p h) - h \nabla(p + \rho g \eta) \quad (28.84\text{e})$$

$$= \nabla(p h) - \rho_0 h \nabla M. \quad (28.84\text{f})$$

In this relation we set $z = \eta$ for the vertical position at the center of the layer, introduced the Montgomery potential from Section 59.2.1

$$M \rho_0 = p + \rho g \eta, \quad (28.85)$$

and noted that ρ is a uniform constant layer density so that it commutes with the horizontal gradient operator computed along ρ surfaces. We also made use of the hydrostatic balance to approximate the interface pressures as

$$p(\eta + h/2) \approx p(\eta) + \frac{\partial p}{\partial z} \frac{h}{2} = p(\eta) - \rho g h/2 \quad (28.86\text{a})$$

$$p(\eta - h/2) \approx p(\eta) - \frac{\partial p}{\partial z} \frac{h}{2} = p(\eta) + \rho g h/2. \quad (28.86\text{b})$$

The zonal mean of the zonal layer form stress is thus given by the correlation between the layer thickness fluctuations and fluctuations in the zonal derivative of the Montgomery potential

$$\bar{\Sigma}_x^{\text{layer form}} = -\rho_0 \bar{h'} \partial M'/\partial x, \quad (28.87)$$

where we set $\overline{\partial M/\partial x} = 0$ due to zonal periodicity. As seen in Section 59.2.1, the Montgomery potential is the geostrophic streamfunction in isopycnal coordinates, so that the fluctuating meridional geostrophic velocity is given by

$$f v' = \partial_x M'. \quad (28.88)$$

Consequently, the zonal mean zonal form stress acting on the layer equals to the correlation between the thickness fluctuations and fluctuations in the meridional geostrophic velocity

$$\bar{\Sigma}_x^{\text{layer form}} = -\rho_0 f \overline{v' h'}. \quad (28.89)$$

Hence, as the geostrophic eddies provide a net eastward acceleration to the layer (equation (28.83)), they also move volume meridionally within isopycnal layers, moving positive thickness fluctuations equatorward.

To further understand the physics of the form stress in equation (28.89), parameterize the

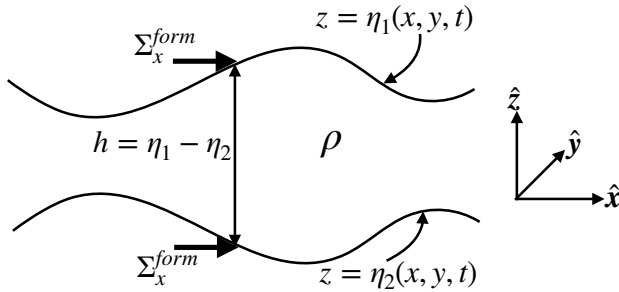


FIGURE 28.9: Schematic of a constant density layer of an adiabatic, hydrostatic, Boussinesq fluid with thickness $h(x, y, t) = \eta_1(x, y, t) - \eta_2(x, y, t) = (\eta + h/2) - (\eta - h/2)$, and uniform density $\rho = \text{constant}$. East points to the right and north is oriented into the page. The zonal form stress, Σ_x^{form} , acting on the upper and lower interfaces at a horizontal position (x, y) are shown by the thick horizontal vectors. The zonal form stress is the horizontal component of the pressure force per area acting on the layer interfaces, with the sign of the form stress determined by the slope of the layer interface. For a zonally periodic fluid layer, the net zonal pressure force acting on the layer arises from the zonal form stress integrated over the layer interfaces.

velocity-thickness eddy correlation, $\overline{v' h'}$, by downgradient diffusion of thickness

$$\overline{v' h'} = -\kappa \partial_y \bar{h}, \quad (28.90)$$

where $\kappa > 0$ is a nonzero kinematic diffusivity (dimensions of squared length per time). This parameterization is suggested by the work of [Gent and McWilliams \(1990\)](#) as discussed in Section 63.3.6. As noted there, thickness diffusion as a parameterization reflects the general tendency of geostrophic eddies to reduce horizontal gradients in layer thickness as they reduce the available potential energy of the flow. In this case the zonal mean zonal form stress is

$$\overline{\Sigma_x^{\text{layer form}}} = \rho_0 f \kappa \partial_y \bar{h}. \quad (28.91)$$

So in the northern hemisphere in regions where the zonal mean layer thickness increases to the north, $\partial_y \bar{h} > 0$, there is a corresponding eastward zonal mean zonal form stress arising from parameterized geostrophic eddies acting on layer thickness. This situation corresponds to the case in Section 28.6.1, where we saw that geostrophic eddies preferentially transport positive buoyancy anomalies poleward and negative buoyancy anomalies equatorward. In the present analysis, meridional changes to the layer thickness correspond to a nonzero thermal wind shear. If layer thickness increases poleward, as for the case of weaker vertical stratification in the high latitudes, then the zonal velocity has a positive vertical shear, thus contributing an eastward zonal mean form stress.

28.6.3 Comments and further study

A key feature of geostrophic eddies exposed by this discussion concerns the connection between zonal form stress (providing an eastward force on the zonally periodic channel flow) and meridional eddy transport of buoyancy (positive buoyancy anomalies are transported poleward) and thickness (positive thickness anomalies are transported equatorward). The periodic channel domain is highly idealized. Nonetheless, the basic ideas form the roots for much of how we think about geostrophic eddies in the middle latitude atmosphere and the Southern Ocean. Further generalizations lead to the generalized Lagrangian mean, whose kinematic rudiments are discussed in Section 62.3, as well as the thickness weighted average, discussed in Chapter 60.

The fundamental role of form stress in geostrophic turbulent flows is pedagogically treated by [Vallis \(2017\)](#). See, in particular, his Chapter 21 for a thorough and insightful discussion of

circulation in the Southern Ocean. We also return to form stress within the shallow water fluid in Section 33.4. That discussion complements the presentation given here, with a focus on a layer of shallow water fluid. We also touch on the notions of form stress when discussing the [Gent and McWilliams \(1990\)](#) mesoscale eddy parameterization in Section 63.3.

28.7 Exercises

EXERCISE 28.1: SMALL ROSSBY NUMBER AT HUMAN SCALES

Consider motion of a car at a speed $U \sim 10^5$ m hour $^{-1}$ and a length scale of $L \sim 10$ m. Furthermore, assume the car is moving at 30°N latitude so that $f_{\text{human}} = 2\Omega_{\text{human}} \sin \phi = \Omega_{\text{human}}$.

- (a) What is the rotation rate of the planet and corresponding rotation period, $T_{\text{human}} = 2\pi/\Omega_{\text{human}}$, required to render a unit Rossby number ($\text{Ro} = 1$) for the given “human” sized scales? Give resulting rotation rate in units of inverse seconds and period in seconds.
- (b) If the earth rotated at the angular speed Ω_{human} , what would be the solid-body speed for a point at rest on the earth’s surface at the equator? Give result in units of meter per second.
- (c) How does the solid-body speed compare to the speed of sound at standard atmospheric conditions? What about the root-mean-square speed for air molecules? Hint: read Section 13.3.4.
- (d) Discuss an astronomical object that has a very large rotational speed. Hint: 1993 Nobel Prize in physics.

EXERCISE 28.2: THE BETA SPIRAL

Consider a steady state Boussinesq planetary geostrophic fluid in the absence of mixing. Write the geostrophic velocity as

$$u = |\mathbf{u}| \cos \Delta \quad v = |\mathbf{u}| \sin \Delta, \quad (28.92)$$

where Δ is the angle measured counter-clockwise from east. Use thermal wind and the steady state perfect fluid buoyancy equation to determine an expression for $\partial \Delta / \partial z$. Show that for $f > 0$ (northern hemisphere) and $\partial b / \partial z = N^2 > 0$ (gravitationally stable fluid column; see Section 27.5), then $\partial \Delta / \partial z$ has opposite sign from the vertical velocity, w . This spiralling of the geostrophic velocity is known as the *beta spiral* in oceanography.

EXERCISE 28.3: ALTERNATIVE FORM OF THERMAL WIND

Consider a fluid with density a function of pressure and potential temperature

$$\rho = \rho(\theta, p). \quad (28.93)$$

A physical realization of this equation of state is a lake. Show that the thermal wind shear for a hydrostatic and *compressible* fluid with this equation of state can be written in the form

$$\frac{\partial \mathbf{u}}{\partial z} = \left[\frac{N^2}{f \rho g} \right] (\hat{\mathbf{z}} \times \nabla_\theta p), \quad (28.94)$$

where

$$N^2 = -\frac{g}{\rho} \frac{\partial \rho}{\partial \theta} \frac{\partial \theta}{\partial z} = g \alpha_\theta \frac{\partial \theta}{\partial z} > 0 \quad (28.95)$$

is the squared buoyancy frequency, assumed positive so that the fluid is gravitationally stable in the vertical (see Section 27.5.4). The term α_θ is the thermal expansion coefficient written in

terms of potential temperature (Section 27.3.4),

$$\alpha_\theta = -(1/\rho) \partial \rho / \partial \theta > 0. \quad (28.96)$$

Finally, the horizontal gradient projected onto constant θ surfaces is given by (see Section 56.12.2)

$$\nabla_\theta = \hat{\mathbf{x}} \left[\frac{\partial}{\partial x} \right]_{y,\theta} + \hat{\mathbf{y}} \left[\frac{\partial}{\partial y} \right]_{x,\theta} \quad (28.97a)$$

$$= \nabla_z - \left[\frac{\nabla_z \theta}{\partial \theta / \partial z} \right] \frac{\partial}{\partial z}. \quad (28.97b)$$

Hint: This exercise requires careful use of the chain rule and the hydrostatic relation, along with the equations given in the problem statement. Furthermore, assume the fluid is fully compressible.

Hint: Some may wish to “warm-up” by showing that the result holds for the simpler equation of state $\rho = \rho(\theta)$. Some of the steps used for the simpler case are relevant for the case with $\rho = \rho(\theta, p)$.



Chapter 29

TANGENT PLANE FLOW BALANCES

We here consider a variety of inviscid tangent plane (horizontal) flow regimes characterized by a balance between a subset of terms appearing in the horizontal momentum equation. This discussion allows us to directly compare the geostrophically balanced flow of Chapter 28 to a variety of other balanced flows such as gradient wind, inertial motion, and cyclostrophic balance. We provide a categorization of the flow following *natural coordinates*, where natural coordinates offer a concise means to compare the relative magnitudes of the Coriolis, pressure, and centrifugal accelerations acting on a fluid element moving horizontally.

READER'S GUIDE TO THIS CHAPTER

We make use of the Boussinesq momentum equation from Section 26.1 and assume an understanding of the geostrophic balance from Chapter 28. We also use of some geometric notions discussed in Chapter 6, though most of the salient points are revisited here so that Chapter 6 is an option rather than a requirement. Throughout this chapter we assume a tangent plane geometry and associated equations from Section 21.3.4, thus allowing for Cartesian coordinates. Also, we ignore all vertical motion. Some of this material is used in subsequent chapters, in particular Chapter 30 on Ekman dynamics as well as Chapters 40 and 42 on quasi-geostrophy.

29.1	Loose ends	708
29.2	Horizontal flow described by natural coordinates	708
29.2.1	Natural coordinates	708
29.2.2	Material acceleration	708
29.2.3	Centripetal and centrifugal accelerations	710
29.2.4	Coriolis and pressure gradient	711
29.2.5	Horizontal momentum equation and local Rossby number	711
29.2.6	Eulerian decomposition of the acceleration	712
29.2.7	Further study	713
29.3	Exact geostrophic balance	713
29.3.1	Steady f -plane flow	714
29.3.2	Steady β -plane flow	714
29.3.3	What about geostrophic balance with curved motion?	715
29.4	Inertial motion	715
29.4.1	Anti-cyclonic circular motion on f -plane	715
29.4.2	Period for inertial motion	716
29.4.3	Observing inertial motion	716
29.4.4	Inertial motion is Lagrangian	717
29.4.5	“Inertial” motion does not refer to an inertial reference frame	717
29.4.6	Inertial motion on a sphere	717
29.5	Cyclostrophic balance	717

29.6 Gradient wind balance	719
29.6.1 Constraints on gradient wind flow	720
29.6.2 The variety of gradient wind flows	721
29.6.3 Comments	722

29.1 Loose ends

- How to determine whether the velocity field is divergent or non-divergent for the cyclostrophic and gradient wind motions?
- Exercises needed for this chapter.

29.2 Horizontal flow described by natural coordinates

In this section we decompose the horizontal Boussinesq momentum equation into motion parallel to and motion perpendicular to the instantaneous trajectory of a fluid element moving along a constant geopotential surface. That is, we characterize the velocity and acceleration according to the local flow direction. Furthermore, we are only concerned with motion on a constant geopotential using the tangent plane approximation; i.e., horizontal motion. The *natural coordinates* arising from this description exposes the centripetal/centrifugal acceleration that arises from curvature in the trajectory as measured by the radius of curvature. This non-inertial acceleration is distinct from the centrifugal acceleration that arises from planetary rotation, with planetary centrifugal acceleration already contained within the effective gravitational acceleration that acts in the local vertical direction (see Section 11.9.1). We also decompose the accelerations from pressure, friction, and Coriolis into their natural coordinate components.

29.2.1 Natural coordinates

Natural coordinates for horizontal motion are defined by a locally orthogonal set of unit vectors (see Figure 29.1)

$$\hat{z} = \hat{u} \times \hat{n} = \text{vertical direction} \quad (29.1a)$$

$$\hat{u} = \hat{n} \times \hat{z} = \text{tangent to horizontal velocity} \quad (29.1b)$$

$$\hat{n} = \hat{z} \times \hat{u} = \text{normal direction to the left of motion.} \quad (29.1c)$$

The unit vector, \hat{u} , is tangent to the velocity vector (which is horizontal), so that

$$\mathbf{u} = |\mathbf{u}| \hat{u} = \frac{Ds}{Dt} \hat{u}, \quad (29.2)$$

where s is the arc-length measured along the trajectory as introduced in Section 2.4. The unit vector, \hat{n} , is perpendicular to the velocity and points to the left of the trajectory facing downstream.

29.2.2 Material acceleration

When writing the velocity according to equation (29.2), we decompose the acceleration into the change in speed and change in direction

$$\frac{D\mathbf{u}}{Dt} = \frac{D|\mathbf{u}|}{Dt} \hat{u} + |\mathbf{u}| \frac{D\hat{u}}{Dt}. \quad (29.3)$$

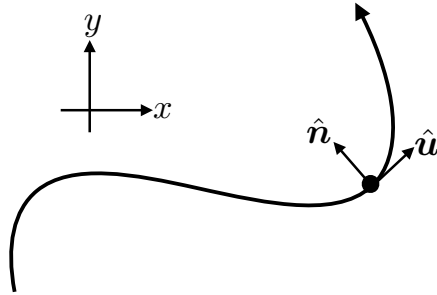


FIGURE 29.1: Illustrating the decomposition of horizontal motion of a fluid element into natural coordinate directions. These directions are defined by a unit tangent vector, \hat{u} , pointing in the direction of the fluid element motion, and a unit normal vector, \hat{n} , pointing to the left of the motion facing downstream.

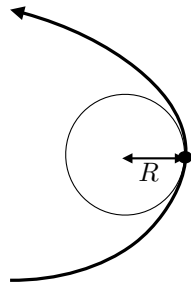


FIGURE 29.2: Illustrating the radius of curvature associated with turning motion of a fluid element. The radius of curvature equals to the radius of a tangent circle (the *curvature circle*) that approximates, to second order accuracy, the trajectory at a particular point. The radius is smaller in magnitude when the trajectory is highly curved, and $|R| = \infty$ when the trajectory is straight. The radius is positive when the trajectory turns into the normal direction as depicted here (to the left; concave as defined by \hat{n}) and negative when turning in the opposite direction (to the right; convex as defined by \hat{n}). See Section 6.2 for more details on curvature, with Figure 6.4 offering more details for how to determine the radius of curvature.

Following our discussion of rotation in Section 11.3 (see Figure 11.4), the magnitude of the direction change can be written in terms of the infinitesimal angle swept out by the motion as the fluid element moves along a trajectory

$$|\delta\hat{u}| = |\delta\vartheta|. \quad (29.4)$$

The infinitesimal angle swept out by the trajectory is related to the radius of curvature, R (Figure 29.2), and the arc-length increment, δs , traversed by the trajectory

$$\delta\vartheta = \frac{\delta s}{R}. \quad (29.5)$$

Finally, the infinitesimal change in tangent, $\delta\hat{u}$, is directed normal to the motion, which we see by noting

$$\hat{u} \cdot \hat{u} = 1 \implies \delta\hat{u} \cdot \hat{u} = 0. \quad (29.6)$$

That is, $\delta\hat{u}$ is orthogonal to \hat{u} , so that it points either parallel or anti-parallel to \hat{n} . We detailed this property of rotating unit vectors in Section 2.1.4 (see Figure 2.2). Our convention is that \hat{n} points to the left of \hat{u} , so that if the trajectory turns to the left, then $\delta\hat{u}$ points parallel to \hat{n} , whereas if the trajectory turns to the right then $\delta\hat{u}$ points anti-parallel to \hat{n} . That is, $\delta\hat{u}$ always points towards the center of the circle used to compute the radius of curvature as in Figure 29.2.

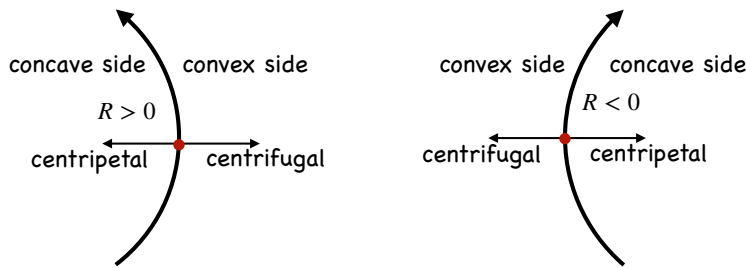


FIGURE 29.3: Centripetal acceleration of a turning fluid element, $\hat{\mathbf{n}} |\mathbf{u}|^2 / R$, points to the concave side of the curve (towards the center) whereas the centrifugal acceleration, $-\hat{\mathbf{n}} |\mathbf{u}|^2 / R$, points to the convex side (away from the center). The centripetal and centrifugal accelerations are paired action/reaction accelerations. The normal unit vector, $\hat{\mathbf{n}}$, always points to the left of the motion, whereas the radius of curvature, R , is positive or negative depending on the direction of the turning motion. For a left turning trajectory (in direction of $\hat{\mathbf{n}}$), the concave side is on the left and has positive radius of curvature, $R > 0$, whereas for the right turning trajectory (opposite direction of $\hat{\mathbf{n}}$) the concave side is to the right with $R < 0$. To help remember the signs, note that centrifugal means “away from the center” whereas centripetal means “towards the center”. It is the centrifugal acceleration that pulls one away from the center of a merry-go-round whereas one’s arms and hands provide the balancing centripetal acceleration.

Bringing these results together leads to the expression for the infinitesimal unit vector change

$$\delta \hat{\mathbf{u}} = \hat{\mathbf{n}} \frac{\delta s}{R}. \quad (29.7)$$

Our sign convention takes $R > 0$ for a fluid element turning in the direction of $\hat{\mathbf{n}}$ (to the left facing downstream) and $R < 0$ when turning opposite to $\hat{\mathbf{n}}$ (to the right facing downstream). Hence, the material time change is

$$\frac{D\hat{\mathbf{u}}}{Dt} = \frac{D\hat{\mathbf{u}}}{Ds} \frac{Ds}{Dt} = \frac{\hat{\mathbf{n}}}{R} \frac{Ds}{Dt} = \frac{\hat{\mathbf{n}}}{R} |\mathbf{u}|, \quad (29.8)$$

where the speed is given by the time change of the arc-length along the trajectory

$$|\mathbf{u}| = \frac{Ds}{Dt}. \quad (29.9)$$

Combining these results renders the acceleration

$$\frac{D\mathbf{u}}{Dt} = \frac{D|\mathbf{u}|}{Dt} \hat{\mathbf{u}} + \frac{|\mathbf{u}|^2}{R} \hat{\mathbf{n}}. \quad (29.10)$$

The acceleration has thus been decomposed into the change in speed of the fluid element along the direction of the motion, plus the centripetal acceleration due to curvature of the trajectory. In Section 29.2.3 we justify referring to $\hat{\mathbf{n}} |\mathbf{u}|^2 / R$ as the *centripetal* acceleration.

29.2.3 Centripetal and centrifugal accelerations

The centripetal acceleration points towards the concave side of a turning trajectory; “centripetal” means “towards the center.” Its opposing partner, the centrifugal (“away from center”) acceleration points to the convex side (see Figure 29.3). So how do we interpret $\hat{\mathbf{n}} |\mathbf{u}|^2 / R$? For motion turning to the left, towards $\hat{\mathbf{n}}$, the radius of curvature is positive, $R > 0$, so that $\hat{\mathbf{n}} |\mathbf{u}|^2 / R$ points to the concave side of the trajectory (left side). For a trajectory turning to the right then $R < 0$, which again means that $\hat{\mathbf{n}} |\mathbf{u}|^2 / R$ points to the concave side (now on the right). We conclude that the acceleration $\hat{\mathbf{n}} |\mathbf{u}|^2 / R$ indeed represents a centripetal acceleration and $-\hat{\mathbf{n}} |\mathbf{u}|^2 / R$ is the centrifugal acceleration.

29.2.4 Coriolis and pressure gradient

The Coriolis acceleration takes the following form in natural coordinates

$$-f\hat{z}\times\mathbf{u}=-(\hat{z}\times\hat{\mathbf{u}})f|\mathbf{u}|=-\hat{\mathbf{n}}f|\mathbf{u}|, \quad (29.11)$$

so that the Coriolis acceleration always points to the right of the flow direction for $f > 0$. In contrast, the pressure gradient has two components

$$\nabla p=\hat{\mathbf{u}}(\hat{\mathbf{u}}\cdot\nabla p)+\hat{\mathbf{n}}(\hat{\mathbf{n}}\cdot\nabla p)=\hat{\mathbf{u}}\frac{\partial p}{\partial s}+\hat{\mathbf{n}}\frac{\partial p}{\partial n}, \quad (29.12)$$

one pointing along the flow direction and one normal to the direction.

29.2.5 Horizontal momentum equation and local Rossby number

Bringing the above results together leads to the horizontal momentum equation as decomposed into natural coordinates

$$\frac{D|\mathbf{u}|}{Dt}=-\frac{1}{\rho_0}\frac{\partial p}{\partial s}+\mathbf{F}\cdot\hat{\mathbf{u}} \quad \text{motion in } \hat{\mathbf{u}} \text{ direction} \quad (29.13a)$$

$$\frac{|\mathbf{u}|^2}{R}+f|\mathbf{u}|=-\frac{1}{\rho_0}\frac{\partial p}{\partial n}+\mathbf{F}\cdot\hat{\mathbf{n}} \quad \text{motion in } \hat{\mathbf{n}} \text{ direction (perpendicular to } \hat{\mathbf{u}}), \quad (29.13b)$$

where \mathbf{F} is the frictional acceleration and ρ_0 is the reference density for the Boussinesq ocean. These equations decompose the accelerations into those acting parallel to and normal to the trajectory. It is notable that the equation for the normal component is purely diagnostic; there is no time derivative in equation (29.13b). Instead, it is a balance containing accelerations from centripetal, Coriolis, normal pressure gradient, and normal component of friction. In the next few sections we consider certain limiting cases as revealed by the equations of motion (29.13a) and (29.13b). Friction remains zero in this chapter but is nonzero for the discussion of Ekman mechanics in Chapter 30.

Steady frictionless flow

The frictionless balanced motions considered in this chapter all occur with a fixed velocity magnitude for the fluid element, so that the along-trajectory component of the momentum equation (29.13a) for frictionless motion reduces to

$$\frac{D|\mathbf{u}|}{Dt}=-\frac{1}{\rho_0}\frac{\partial p}{\partial s}=0. \quad (29.14)$$

Hence, there is no pressure gradient along the direction of the fluid element motion. Correspondingly, the frictionless fluid motion preserves its kinetic energy

$$\frac{1}{2}\frac{D(\mathbf{u}\cdot\mathbf{u})}{Dt}=|\mathbf{u}|\frac{D|\mathbf{u}|}{Dt}=0. \quad (29.15)$$

Local Rossby number

As discussed in Section 28.3, the Rossby number is the ratio of the acceleration from velocity advection to the Coriolis acceleration. In the normal component to the momentum equation (29.13b), we have the advection term manifest as the local centrifugal term. Following Chapter 1

of [van Heijst \(2010\)](#) we define the *local Rossby number* as the ratio of the centrifugal acceleration to the Coriolis acceleration

$$\text{Ro}_{\text{local}} = \frac{|\mathbf{u}|^2/R}{f/|\mathbf{u}|} = \frac{|\mathbf{u}|}{Rf}, \quad (29.16)$$

where, again, R is the radius of curvature for the motion. In this chapter we consider flow regimes as determined by values of the local Rossby number.

29.2.6 Eulerian decomposition of the acceleration

The horizontal equations of motion (29.13a) and (29.13b) offer a relatively simple and insightful Lagrangian description of the motion. In contrast, an Eulerian description requires us to expand the material time derivative. Although we focus in this chapter on the Lagrangian perspective, we here consider two Eulerian decompositions.

Advection form

The standard form of the material time derivative for horizontal motion is given by

$$\frac{\partial \mathbf{u}}{\partial t} + (\mathbf{u} \cdot \nabla) \mathbf{u} = \frac{\text{D}|\mathbf{u}|}{\text{D}t} \hat{\mathbf{u}} + \frac{|\mathbf{u}|^2}{R} \hat{\mathbf{n}}, \quad (29.17)$$

so that

$$\hat{\mathbf{u}} \cdot \left[\frac{\partial \mathbf{u}}{\partial t} + (\mathbf{u} \cdot \nabla) \mathbf{u} \right] = \frac{\text{D}|\mathbf{u}|}{\text{D}t} = -\frac{1}{\rho_0} \frac{\partial p}{\partial s} + \mathbf{F} \cdot \hat{\mathbf{u}} \quad (29.18a)$$

$$\hat{\mathbf{n}} \cdot \left[\frac{\partial \mathbf{u}}{\partial t} + (\mathbf{u} \cdot \nabla) \mathbf{u} \right] = \frac{|\mathbf{u}|^2}{R} = -f |\mathbf{u}| - \frac{1}{\rho_0} \frac{\partial p}{\partial n} + \mathbf{F} \cdot \hat{\mathbf{n}}. \quad (29.18b)$$

Depending on the information provided by a field measurement or numerical simulation, one might more readily diagnose the kinematic expressions on the left side of these equations or the force balances on the right side. For example, the inverse radius of curvature for the fluid flow can be diagnosed in either of the following ways

$$R^{-1} = \frac{\hat{\mathbf{n}} \cdot [\partial \mathbf{u} / \partial t + (\mathbf{u} \cdot \nabla) \mathbf{u}]}{|\mathbf{u}|^2} = \frac{-f |\mathbf{u}| - \rho_0^{-1} \partial p / \partial n + \mathbf{F} \cdot \hat{\mathbf{n}}}{|\mathbf{u}|^2}. \quad (29.19)$$

Vector invariant form

We can transform the self-advection term using the vector identity (see Section 2.3.4)

$$(\mathbf{u} \cdot \nabla) \mathbf{u} = \nabla K - \mathbf{u} \times \zeta \hat{\mathbf{z}}, \quad (29.20)$$

where $K = \mathbf{u} \cdot \mathbf{u} / 2$ is the kinetic energy per mass in the horizontal flow, and $\zeta = \partial_x v - \partial_y u$ is the vertical component to the relative vorticity (see Chapter 34). The deflecting acceleration, $\mathbf{u} \times \zeta \hat{\mathbf{z}}$, is known as the *Magnus acceleration* and was discussed in Section 21.3.3. Projecting into the $\hat{\mathbf{u}}$ and $\hat{\mathbf{n}}$ directions leads to

$$\hat{\mathbf{u}} \cdot \frac{\partial \mathbf{u}}{\partial t} = -\frac{\partial(p/\rho_0 + K)}{\partial s} + \mathbf{F} \cdot \hat{\mathbf{u}} \quad (29.21a)$$

$$\hat{\mathbf{n}} \cdot \frac{\partial \mathbf{u}}{\partial t} = -(f + \zeta) |\mathbf{u}| - \frac{\partial(p/\rho_0 + K)}{\partial n} + \mathbf{F} \cdot \hat{\mathbf{n}}. \quad (29.21b)$$

The gradient acceleration is affected by both pressure and the *dynamical pressure* afforded by the kinetic energy per mass. The Magnus acceleration appears only in the normal component equation, which is expected since it acts just as the Coriolis acceleration to deflect the fluid element perpendicular to its trajectory. Following the example in Figure 21.1, consider a positive relative vorticity, $\zeta > 0$. For this case, the Magnus acceleration deflects the fluid element to the right of its trajectory; i.e., opposite to the normal direction, which points to the left as per our convention in Figure 29.1.

29.2.7 Further study

Section 3.2 of [Holton \(1992\)](#) details the use of natural coordinates for geophysical flows, with a similar decomposition provided in Section 7.10 of [Gill \(1982\)](#) and Section 2.9 of [Vallis \(2017\)](#). Natural coordinates are also used in describing non-rotating flows as illustrated in [this video](#).

29.3 Exact geostrophic balance

Frictionless flow parallel to pressure contours experiences no pressure gradient ($\partial p / \partial s = 0$), so that the speed of a fluid element remains constant. Furthermore, if this motion occurs with an infinite radius of curvature (straight line motion parallel to pressure contours), then the force balance is between the normal pressure gradient and Coriolis. In this case the local Rossby number (29.16) vanishes

$$\text{Ro}_{\text{local}} = \frac{|\mathbf{u}|}{R f} = 0 \quad \text{if } |R| = \infty. \quad (29.22)$$

More precisely, exact geostrophic balance occurs under the following conditions.

- Fluid moves on a straight line so that the radius of curvature is infinite, $|R| = \infty$, thus making the centripetal acceleration and local Rossby number both vanish;
- Fluid moves along lines of constant pressure so that $\partial p / \partial s = 0$;
- Friction is zero.

In this case the equations of motion (29.13a) and (29.13b) take the form

$$\frac{D|\mathbf{u}|}{Dt} = 0 \quad (29.23a)$$

$$f |\mathbf{u}| = -\frac{1}{\rho_0} \frac{\partial p}{\partial n}. \quad (29.23b)$$

Equation (29.23a) says that the speed of a fluid element is constant, so that the horizontal kinetic energy likewise is constant. Equation (29.23b) says that the pressure gradient normal to the motion balances the Coriolis acceleration. We refer to this flow, depicted in Figure 29.4, as *exact geostrophic balance* since it is an exact solution under the above assumptions.

Writing the horizontal advection of speed in the form

$$\mathbf{u} \cdot \nabla |\mathbf{u}| = |\mathbf{u}| \hat{\mathbf{u}} \cdot \nabla |\mathbf{u}| = |\mathbf{u}| \frac{\partial |\mathbf{u}|}{\partial s}, \quad (29.24)$$

allows us to write the material constancy of the flow speed as

$$\frac{\partial |\mathbf{u}|}{\partial t} + |\mathbf{u}| \frac{\partial |\mathbf{u}|}{\partial s} = 0. \quad (29.25)$$

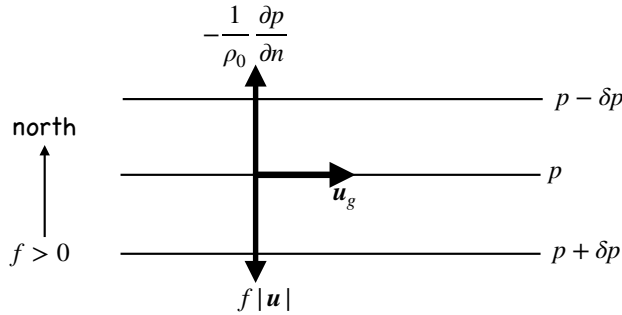


FIGURE 29.4: Exact geostrophic balance on a tangent plane occurs when the flow is horizontal, frictionless, straight, and follows contours of constant pressure. For this case the pressure gradient exactly balances the Coriolis acceleration so that the motion is perpendicular to both of these accelerations. We here depict motion assuming $f > 0$ as for the northern hemisphere. If flow is on an f -plane then the exact geostrophic balance is steady for any arbitrary flow direction. On a β -plane, steady exact geostrophic balance holds only for zonal flow.

Hence, a steady flow speed, with $\partial|\mathbf{u}|/\partial t = 0$, only holds for the exact geostrophic balance if the flow speed is fixed along each trajectory path

$$\frac{\partial|\mathbf{u}|}{\partial s} = 0 \implies \frac{\partial|\mathbf{u}|}{\partial t} = 0. \quad (29.26)$$

What is required for this condition to hold? We examine two cases, again restricted to a tangent plane.

29.3.1 Steady f -plane flow

Geostrophic motion on an f -plane is horizontally non-divergent (Section 28.4)

$$\nabla \cdot \mathbf{u} = \nabla \cdot (\hat{\mathbf{u}} |\mathbf{u}|) = 0. \quad (29.27)$$

Flow in a straight line, with each trajectory parallel to one another, has the trajectory direction independent of space. Hence, the non-divergent condition means that

$$0 = \nabla \cdot (\hat{\mathbf{u}} |\mathbf{u}|) = (\hat{\mathbf{u}} \cdot \nabla) |\mathbf{u}| = \frac{\partial |\mathbf{u}|}{\partial s}, \quad (29.28)$$

which proves that exact geostrophic flow on an f -plane is steady.

29.3.2 Steady β -plane flow

The geostrophic velocity in the presence of a meridional gradient of the Coriolis parameter, $f = f(y)$, satisfies (Section 28.4)

$$\nabla \cdot (f \mathbf{u}) = 0. \quad (29.29)$$

Making use of $\nabla \cdot \hat{\mathbf{u}} = 0$ for straight line trajectories leads to

$$\nabla \cdot (f \mathbf{u}) = \frac{\partial(f |\mathbf{u}|)}{\partial s} = 0. \quad (29.30)$$

We conclude that $\partial|\mathbf{u}|/\partial s = 0$ holds only for trajectories that are parallel to latitude lines, in which case $\partial f/\partial s = \partial f/\partial x = 0$. Therefore, exact geostrophic motion on the β -plane is steady only for trajectories that follow constant latitude lines; i.e., zonal trajectories as depicted in Figure 29.4.

29.3.3 What about geostrophic balance with curved motion?

The geostrophically balanced flows discussed in Chapter 28 generally have curvature, such as for the geostrophic motion around a pressure center as shown in Figure 28.3. But as emphasized by the natural coordinate decomposition as per equations (29.13a) and (29.13b), curved motion has an associated centrifugal acceleration. So when speaking of geostrophic balance for flow that has a nonzero curvature, then the local Rossby number (29.16) is not precisely zero. Rather, its magnitude is small but nonzero

$$|\text{Ro}_{\text{local}}| \ll 1 \quad \text{approximate geostrophic flow.} \quad (29.31)$$

In this limit it is accurate to ignore the centrifugal acceleration, which is commonly the case for large-scale flows. Even so, it is an approximation, with the centrifugal acceleration identically zero only for straight line motion on a plane.

29.4 Inertial motion

Inertial motion occurs under the following conditions:

- vanishing pressure gradient
- vanishing friction,

so that the equations of motion (29.13a) and (29.13b) take the form

$$\frac{\text{D}|\boldsymbol{u}|}{\text{D}t} = 0 \quad (29.32\text{a})$$

$$\frac{|\boldsymbol{u}|^2}{R} + f |\boldsymbol{u}| = 0. \quad (29.32\text{b})$$

Equation (29.32a) says that inertial motion occurs with constant speed, whereas equation (29.32b) says that the motion maintains the balance between Coriolis and centrifugal accelerations

$$f |\boldsymbol{u}| = -\frac{|\boldsymbol{u}|^2}{R}. \quad (29.33)$$

Hence, local Rossby number has a unit magnitude

$$|\text{Ro}_{\text{local}}| = \frac{|\boldsymbol{u}|}{|R| |f|} = 1. \quad (29.34)$$

29.4.1 Anti-cyclonic circular motion on f -plane

To further understand inertial motion, rearrange equation (29.33) so that

$$f = -\frac{|\boldsymbol{u}|}{R}, \quad (29.35)$$

in which case the radius for the inertial circle is

$$R = -|\boldsymbol{u}|/f. \quad (29.36)$$

Equation (29.35) can be satisfied in the northern hemisphere ($f > 0$) only for motion turning to the right (in which $R < 0$). The opposite orientation occurs in the southern hemisphere, where

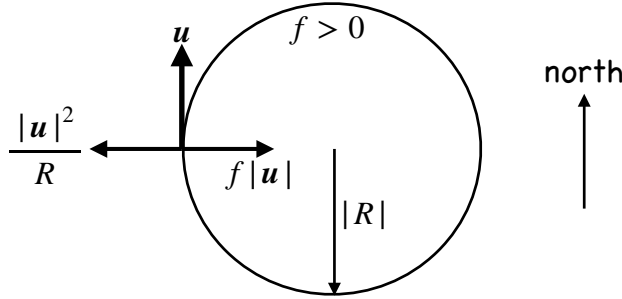


FIGURE 29.5: Inertial motion of a fluid on a plane occurs when the flow is horizontal, frictionless, and the centrifugal acceleration balances the Coriolis in the presence of zero pressure gradient. We here depict motion assuming $f > 0$ as for the northern hemisphere, revealing that inertial motion is an anti-cyclonic circular motion with radius $|R| = |\mathbf{u}|/|f|$. When turning to the right as in the northern hemisphere, the radius of curvature for the inertial circle is negative (see Figure 29.2 for sign convention), so that $R = -|\mathbf{u}|/f < 0$.

inertial motion turns to the left so that the radius of curvature is positive, $R = -|\mathbf{u}|/f > 0$ (see Figure 29.2 for the sign convention on the radius of curvature). Hence, inertial motion is oriented anti-cyclonically (orientated opposite to the earth's rotation). If the Coriolis parameter is constant, then the motion is circular, as depicted in Figure 29.5.

To emphasize the balance, return to equation (29.33) and recall that the Coriolis acceleration in the northern hemisphere points to the right when facing downstream, as per equation (29.11). Hence, the balance (29.33) is between the Coriolis acceleration pointing to the right and the centrifugal acceleration pointing to the left. That is, the Coriolis acceleration provides the centripetal acceleration to balance the centrifugal acceleration.

29.4.2 Period for inertial motion

Equation (29.36) says that the speed of a fluid element is given by the radius of curvature times the magnitude of the Coriolis parameter

$$|\mathbf{u}| = R|f|. \quad (29.37)$$

The time for a fluid element to traverse an inertial circle is given by the circumference of the circle, $2\pi R$, divided by the constant speed, thus yielding the inertial period

$$T_{\text{inertial}} = \frac{2\pi R}{|\mathbf{u}|} = \frac{2\pi}{|f|}. \quad (29.38)$$

We encountered this inertial period in Section 12.5 when considering inertial oscillations for a point particle.

29.4.3 Observing inertial motion

Inertial motion is rarely observed in the atmosphere since fluid motion nearly always occurs in the presence of a pressure gradient. In contrast, surface ocean flow is commonly generated by wind stresses that setup motion even in the absence of pressure gradients. The moving fluid then engenders a Coriolis acceleration, in which case there can be a balance between centrifugal and Coriolis for the moving ocean fluid. As a result, the observed surface ocean currents have nontrivial power within the inertial frequency band, rivaling energy contained in frequencies associated with astronomical tides (e.g., see Figure 3.3 of Holton (1992)).

How large is an inertial circle? Consider a surface ocean current speed of $|\mathbf{u}| \sim 0.1 \text{ m s}^{-1}$,

which is not atypical of current speeds outside of strong boundary currents or mesoscale eddies, and assume the Coriolis parameter $f = 10^{-4} \text{ s}^{-1}$. In this case the inertial radius is

$$R_{\text{inertial}} \approx 10^3 \text{ m.} \quad (29.39)$$

Observations of inertial motion, such as that reproduced in Figure 8.3 of [Gill \(1982\)](#), confirm that the radii are indeed on the order of a few kilometers.

29.4.4 Inertial motion is Lagrangian

The analysis in this section concerns a fluid element moving without feeling the impacts from pressure forces. The fluid thus exhibits the same force balance as the point particle discussed in Section 12.5. So although we can measure inertial motion at a fixed point in space, the present considerations are Lagrangian in nature, focusing on motion of fluid elements. Furthermore, the inertial period refers to the time it takes for a fluid element to move around the inertial circle at its constant speed. It does not refer to the period of a wave, for example, and yet there are inertial waves (Section 46.2) with this period as well as inertia-gravity waves that have periods close to the inertial period (Section 48.7),

29.4.5 “Inertial” motion does not refer to an inertial reference frame

We make use of the term “inertial” when referring to inertial motion since both the Coriolis and centrifugal accelerations are nonzero only in the presence of motion; i.e., they require the inertia obtained by a moving massive body. Hence, as noted in Section 12.5.4, “inertial motion” in this context does *not* refer to the motion viewed in the inertial reference frames discussed in Section 11.2.

29.4.6 Inertial motion on a sphere

In the analysis thus far, we have assumed an f -plane so that inertial motion is circular. Without solving the spherical equations for inertial motion we can anticipate what happens when such motion occurs on a sphere. As a fluid element moves to higher latitudes the magnitude of the Coriolis parameter increases, thus decreasing the radius of curvature. The opposite happens when moving equatorward. This effect of planetary sphericity leads to an egg-shaped pattern that does not close but instead drifts to the west. Now consider inertial motion that spans the equator. As the fluid crosses the equator, where $f = 0$, the radius of curvature is infinite so that the motion is straight. When moving away from the equator the Coriolis parameter increases in magnitude, which causes a fluid element to turn and close its path, again with a drift to the west. Motion north of the equator turns to the right whereas motion to the south turns left, so that inertial motion that spans the equator forms a figure-eight path. We illustrate this motion in Figure 29.6.

29.5 Cyclostrophic balance

Cyclostrophic balance occurs under the following conditions:

- fluid elements move along lines of constant pressure so that $\partial p / \partial s = 0$;
- vanishing Coriolis acceleration;
- vanishing friction.

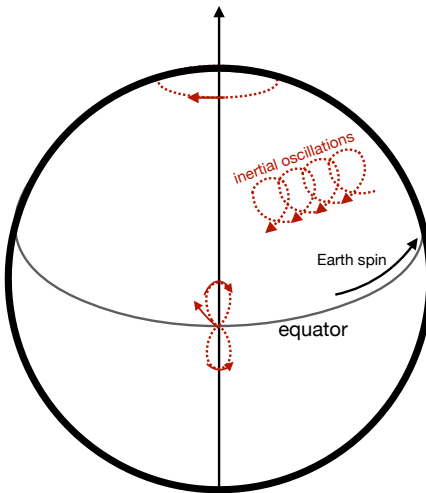


FIGURE 29.6: Depicting inertial motion on a sphere. As the fluid element moves poleward, f increases so that the radius of curvature decreases. Correspondingly, the fluid motion does not close, but instead the path drifts to the west. This westward drift holds for both hemispheres, where the sense of the motion is anti-cyclonic. The only closed and circular inertial motions are those that encircle the pole. Fluid elements that cross the equator exhibit a figure-eight pattern that also drifts to the west. This figure is taken after Figure 4-14 of [von Arx \(1962\)](#).

The resulting equations of motion (29.13a) and (29.13b) take the form

$$\frac{D|\mathbf{u}|}{Dt} = 0 \quad (29.40a)$$

$$\frac{|\mathbf{u}|^2}{R} = -\frac{1}{\rho_0} \frac{\partial p}{\partial n}. \quad (29.40b)$$

With a vanishing Coriolis acceleration we see that cyclostrophic balance corresponds to local Rossby number that has an infinite magnitude

$$|Ro_{local}| = \infty \quad \text{if } f = 0. \quad (29.41)$$

Approximate cyclostrophic balance holds when $|Ro_{local}| \gg 1$.

Again, equation (29.40a) says that the speed is constant following a material fluid element. Equation (29.40b) says that cyclostrophic flow occurs when the centrifugal acceleration balances the pressure gradient, with the squared speed given by

$$|\mathbf{u}|^2 = -\frac{R}{\rho_0} \frac{\partial p}{\partial n}. \quad (29.42)$$

This equation can be satisfied for either clockwise or counter-clockwise motion around a low pressure center, as shown in Figure 29.7. For clockwise flow, the radius of curvature is negative, $R < 0$, whereas $\partial p / \partial n > 0$. The signs are swapped for counter-clockwise flow. Cyclostrophic balance cannot be maintained around a high pressure center. The reason is that if both the pressure and centrifugal accelerations point away from the circle's center, then they are unable to balance one another.

Cyclostrophic balance is relevant for scales on the order of a tornado, with a radius on the order of 300 m where tangential speeds are on the order of 30 m s^{-1} (see Section 3.2.4 of [Holton \(1992\)](#)). For this flow scale, the Rossby number is on the order of 1000 at middle latitudes, thus justifying neglect of the Coriolis acceleration. Although tornadoes in cyclostrophic balance can rotate either clockwise or counter-clockwise, they are more often observed rotating cyclonically given that they

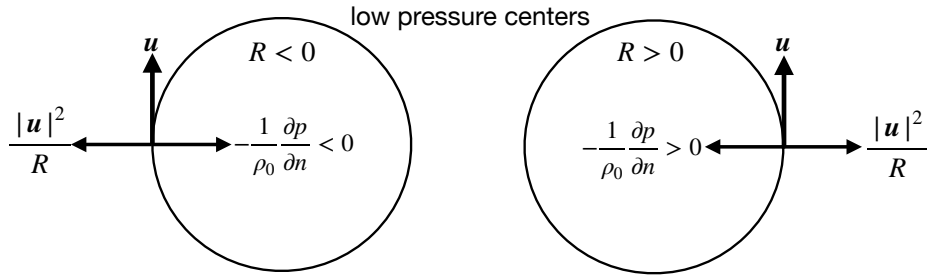


FIGURE 29.7: Cyclostrophic motion of a fluid element on a tangent plane occurs when the flow is horizontal, non-rotating, frictionless, with constant speed, and where the centrifugal acceleration balances the pressure gradient normal to the flow direction. We here depict motion for clockwise and counter-clockwise cyclostrophic flow, both around a low pressure center. Left panel: clockwise motion with radius of curvature, $R < 0$, and the pressure gradient pointing in the direction of the normal, $\partial p / \partial n > 0$. Right panel: counter-clockwise motion with radius of curvature, $R > 0$, and the pressure gradient pointing opposite to the direction of the normal, $\partial p / \partial n < 0$. Cyclostrophic balance does not occur for flow around a high pressure center. The reason is that if both the pressure and centrifugal accelerations point away from the center, then they are unable to balance one another.

are generally embedded within cyclonic storm systems. In contrast, smaller motions such as dust devils and water spouts are quite often seen rotating in either direction.

29.6 Gradient wind balance

Gradient wind balance occurs under the following conditions:

- fluid elements move along lines of constant pressure so that $\partial p / \partial s = 0$;
- vanishing friction.

The resulting equations of motion (29.13a) and (29.13b) take the form

$$\frac{D|\mathbf{u}|}{Dt} = 0 \quad (29.43a)$$

$$\frac{|\mathbf{u}|^2}{R} + f |\mathbf{u}| = -\frac{1}{\rho_0} \frac{\partial p}{\partial n}, \quad (29.43b)$$

Again, equation (29.43a) says that the speed is constant following a material fluid element. Equation (29.43b) says that gradient wind balanced flow occurs when the centrifugal and Coriolis accelerations balance the pressure gradient acting normal to the motion.

The local Rossby number is order unity for the gradient wind balance

$$|\text{Ro}_{\text{local}}| = \frac{|\mathbf{u}|}{|R| |f|} \sim 1, \quad (29.44)$$

meaning that both centrifugal and Coriolis accelerations are both important as they balance the pressure gradient. Recall that the inertial motion from Section 29.4 has $|\text{Ro}_{\text{local}}| = 1$, which arises when the pressure gradient vanishes so that the Coriolis and centrifugal terms have equal but opposite magnitudes. The nonzero pressure gradient makes gradient wind flow fundamentally distinct from inertial motion.

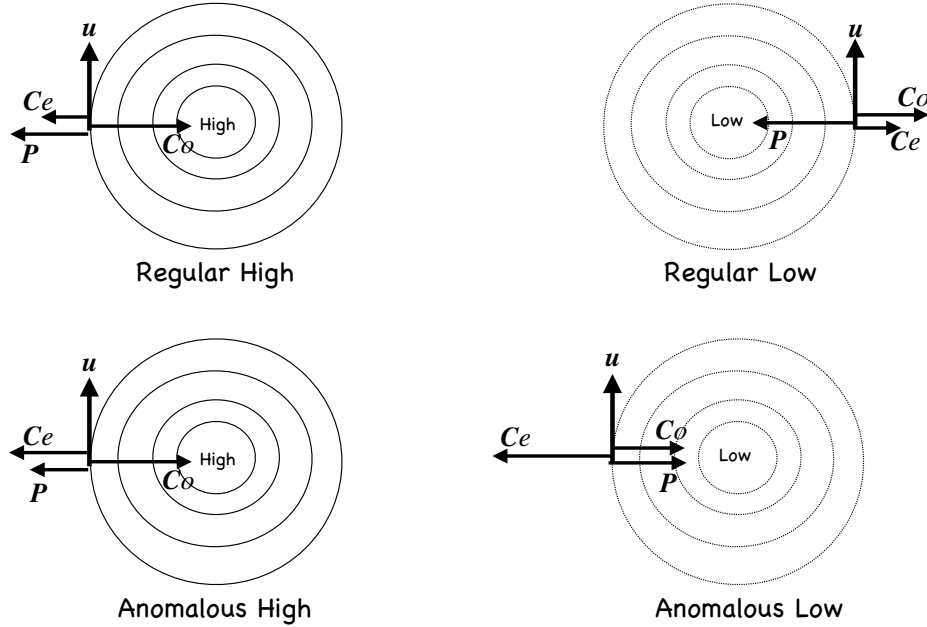


FIGURE 29.8: The variety of gradient wind balances available in the northern hemisphere ($f > 0$). Gradient wind balance occurs when the flow is horizontal, frictionless, with constant speed, and where the centrifugal, pressure, and Coriolis accelerations balance under a variety of magnitudes. To reduce clutter, we use the following shorthand for the accelerations: $P = -\rho_0^{-1} \partial p / \partial n$, $C_\phi = f |\mathbf{u}|$, and $C_e = |\mathbf{u}|^2 / R$. Upper left panel: motion around a regular high pressure center, whereby the centrifugal acceleration helps the pressure acceleration to balance the Coriolis acceleration. The pressure acceleration is larger in magnitude than the centrifugal. This flow is termed “regular” as it directly corresponds to geostrophic flow around a high pressure center. Lower left panel: motion around an anomalous high pressure center, whereby the centrifugal acceleration helps the pressure acceleration to balance the Coriolis acceleration, with the pressure acceleration smaller in magnitude than the centrifugal. This flow is termed “anomalous” as the pressure acceleration is subdominant to the centrifugal, in contrast to the case of geostrophic flow. Upper right panel: motion around a regular low pressure center, whereby the Coriolis and centrifugal accelerations balance the pressure acceleration. Lower right panel: motion around an anomalous low pressure center, whereby the Coriolis and pressure accelerations balance the centrifugal acceleration. Note the opposite flow orientation between the regular and anomalous lows, whereas the regular and anomalous highs have the same flow orientation.

29.6.1 Constraints on gradient wind flow

The quadratic formula leads to the following expression for the speed of gradient wind flow

$$|\mathbf{u}| = \frac{R}{2} \left[f \pm \sqrt{f^2 - \frac{4}{R} \frac{1}{\rho_0} \frac{\partial p}{\partial n}} \right]. \quad (29.45)$$

The speed is a real number if the pressure gradient, Coriolis parameter, and radius of curvature satisfy

$$f^2 > \frac{4}{R} \frac{1}{\rho_0} \frac{\partial p}{\partial n} \implies \frac{1}{\rho_0} \left| \frac{\partial p}{\partial n} \right| \leq \frac{|R| f^2}{4}. \quad (29.46)$$

This relation has direct implications for the structure of the pressure field depending on the sign of the radius of curvature. In particular, as seen in the following, this constraint implies that the pressure gradient at the center of a high pressure region must go to zero as the radius of curvature vanishes, which renders the pressure field relatively flat near the center of highs. In contrast, there is no analogous limit for the magnitude of the pressure gradient approaching a low pressure center. This asymmetry between high and low pressures manifests in atmospheric flow

with low pressure centers (cyclonic lows) having stronger magnitude than high pressure centers (anti-cyclonic highs).

29.6.2 The variety of gradient wind flows

We now identify the following force balances available with a gradient wind balance, with illustrations provided in Figure 29.8.

Regular high pressure center (right turn with high pressure on right)

A *regular high pressure* occurs with $R < 0$ and $\partial p/\partial n \leq 0$. This case occurs with the centrifugal and pressure accelerations pointing away from the center, and these balance the Coriolis acceleration pointing to the high pressure center (upper left panel of Figure 29.8).

The inequality (29.46) provides a bound to the size of the pressure gradient since

$$\frac{1}{\rho_0} \frac{\partial p}{\partial n} \leq \frac{R f^2}{4} \text{ with } R \leq 0 \text{ and } \frac{\partial p}{\partial n} \leq 0 \implies \frac{1}{\rho_0} \left| \frac{\partial p}{\partial n} \right|_{\max} = \frac{|R| f^2}{4}. \quad (29.47)$$

That is, the pressure gradient for a regular high cannot be larger than this bound in order for there to be a gradient wind solution. Since $R \rightarrow 0$ as the center is approached, the normal pressure gradient, $\partial p/\partial n$, in turn must vanish towards the center. Holton (1992) identifies two subcases for this balance depending on the relative size of the pressure and centrifugal accelerations, with the anomalous high the case where the pressure gradient acceleration is weaker than the centrifugal (lower left panel of Figure 29.8).

Regular low (left turn with low pressure on left)

This flow occurs with $R \geq 0$ and $\partial p/\partial n \leq 0$, so that the inequality (29.46) is always satisfied

$$\frac{1}{\rho_0} \frac{\partial p}{\partial n} \leq \frac{R f^2}{4} \text{ with } R \geq 0 \text{ and } \frac{\partial p}{\partial n} \leq 0 \implies \text{arbitrary size to } \left| \frac{\partial p}{\partial n} \right|. \quad (29.48)$$

Hence, there is no constraint imposed by gradient wind balance on the size of the pressure gradient magnitude, $|\partial p/\partial n|$. So the low pressure center can be arbitrarily strong and still maintain a gradient wind balance. Furthermore, the Coriolis and centrifugal accelerations point away from the low pressure center, and these two accelerations balance the pressure acceleration that points toward the center (upper right panel of Figure 29.8).

Anomalous low (right turn with low pressure on right)

This flow occurs with $R < 0$ and $\partial p/\partial n \geq 0$. This case occurs with the Coriolis and pressure accelerations pointing toward the low pressure center, and these two accelerations balance the centrifugal acceleration pointing away from the center (lower right panel of Figure 29.8). As with the regular low, the inequality (29.46) provides no bound to the magnitude of the low pressure. Note the opposite orientation for the flow around an anomalous low relative to the regular low.

Left turn with high pressure on left

In this case $R > 0$ and $\partial p/\partial n > 0$. There is no solution for the northern hemisphere since all accelerations point to the right of the motion thus disallowing any balance.

29.6.3 Comments

As noted in Section 3.2 of [Holton \(1992\)](#), the difference between gradient wind speeds and geostrophic wind speeds is no more than 10% to 20% in middle latitude synoptic atmosphere flow. In the tropics, where geostrophy becomes less relevant, it is important to apply the gradient wind relation to capture the balanced flow states. Furthermore, [van Heijst \(2010\)](#) and Chapter 18 of [Cushman-Roisin and Beckers \(2011\)](#) make use of a gradient wind analysis for the study of ocean vortices. The deviations from geostrophy become important when considering relatively small ocean vortices and/or tropical vortices.



Chapter 30

EKMAN MECHANICS

A *boundary layer* is a region of the fluid flow that is directly affected by boundaries. For geophysical applications we have in mind the solid-earth boundary that interacts with both the ocean and atmosphere; the ocean-atmosphere boundary; the ocean-cryosphere boundary; and the atmosphere-cryosphere boundary. The fluid flow in geophysical boundary layers is generally very turbulent, thus causing rapid mixing and the transfer of properties within the boundary layer, along with the transport of properties between the boundary layer and the less turbulent fluid interior. Boundary layer physics is a well developed discipline for geophysical as well as engineering applications. Our treatment is relatively superficial by comparison to the focused treatments given by books such as [Tennekes and Lumley \(1972\)](#), [Stull \(1988\)](#), and [Thorpe \(2005\)](#).

Here, we are particularly focused on the rudiments of *Ekman mechanics*, which is concerned with flow affected by accelerations from horizontal pressure gradients, vertical friction, and Coriolis, with particular attention given to regions near boundaries where friction is especially large and *Ekman boundary layers* form. The leading role for Coriolis acceleration causes Ekman boundary layers to exhibit behaviors quite distinct from their non-rotating cousins mentioned in Section 22.10.7. In particular, Ekman boundary layer flows are horizontally divergent, thus leading to the vertical exchange of mass, tracers, momentum, and vorticity between the boundary layer and the fluid region outside of the boundary layer (i.e., the fluid interior). In so doing, the Ekman layer flow imparts a stretching and squeezing of interior fluid columns that strongly couples the boundary layer to vorticity and circulation of the fluid interior. This role for Ekman layers is especially crucial for the ocean general circulation.

READER'S GUIDE TO THIS CHAPTER

To introduce the subject we exhibit the role of friction in producing a down pressure gradient component to the flow, making use of natural coordinates from Chapter 29 for this purpose. The remainder of the chapter focuses on the mechanics of Ekman boundary layers, with this study greatly extending our understanding of strongly rotating flows from Chapter 28. Indeed, the addition of friction to an otherwise geostrophically balanced flow provides a surprising level of richness that motivates the variety of perspectives presented in this chapter.

Ekman boundary layers are a key element in the study of ocean circulation, particularly the wind-driven circulation. We here borrow liberally from the material in Section 9.2 of [Gill \(1982\)](#), Section 6.2 of [Apel \(1987\)](#), Section 7.4 of [Marshall and Plumb \(2008\)](#), Chapter 8 of [Cushman-Roisin and Beckers \(2011\)](#), Section 5.7 of [Vallis \(2017\)](#), and materials from [Thorpe \(1988\)](#) and [Thorpe \(2005\)](#). A presentation consistent with engineering boundary layers can be found in Section 5.3 of [Tennekes and Lumley \(1972\)](#).

30.1	The dynamical balances	724
30.2	Horizontal balances in natural coordinates	725
30.2.1	Natural coordinates according to isobars	725
30.2.2	Geostrophic and Ekman balances	726
30.2.3	Rayleigh drag	727
30.2.4	Cross isobar flow driven by Rayleigh drag	727
30.2.5	Horizontal spiral plus vertical rising/sinking	729
30.2.6	Further study	729
30.3	Ekman number and Ekman layer thickness	729
30.3.1	Laplacian vertical friction	730
30.3.2	Non-dimensionalization	730
30.3.3	Defining the Ekman number and layer thickness	731
30.3.4	Estimates for the vertical eddy viscosity	731
30.4	Ocean surface Ekman layer	732
30.4.1	Horizontal mass transport within the Ekman layer	732
30.4.2	Example Ekman mass transports	733
30.4.3	Mass budget for the Ekman layer	734
30.4.4	Ekman layer coupled to the geostrophic interior	736
30.4.5	Further study	738
30.5	Bottom Ekman layer	739
30.5.1	Horizontal mass transport within the Ekman layer	739
30.5.2	Mass budget for the bottom Ekman layer	740
30.5.3	An analytic bottom Ekman spiral velocity	740
30.5.4	Comments	743
30.6	Arrested bottom Ekman flows	743
30.6.1	Description	743
30.6.2	Applications	744
30.7	Exercises	745

30.1 The dynamical balances

Throughout this chapter we make use of a steady, linear, Boussinesq, and hydrostatic fluid maintaining a balance between the horizontal accelerations from Coriolis, pressure, and friction

$$f \hat{z} \times \mathbf{u} = -\frac{1}{\rho_o} \nabla_z p + \mathbf{F}. \quad (30.1)$$

This balance is most relevant over large horizontal length scales as per the planetary geostrophic equations of Section 28.5.

The frictional acceleration, \mathbf{F} , of interest in this chapter arises from the vertical exchange of horizontal momentum between fluid layers. Turbulence induced viscous exchange is especially large in boundary regions such as the ocean surface, the atmospheric planetary boundary layer, and next to the ocean and atmosphere bottom where they interact with the solid earth. In such turbulent boundary layer regions we make use of the eddy viscosity, which is much larger than molecular values

$$\nu^{\text{eddy}} \gg \nu. \quad (30.2)$$

We have more to say regarding the frictional operator in Section 30.3.1.

For conceptual and mathematical convenience, we find it useful to separate the horizontal velocity into two components. The first is the geostrophic velocity defined by a balance between

pressure gradient and Coriolis accelerations

$$f \hat{z} \times \mathbf{u}_g = -\frac{1}{\rho_o} \nabla_z p \implies \mathbf{u}_g = \frac{1}{f \rho_0} \hat{z} \times \nabla_z p. \quad (30.3)$$

In some treatments, \mathbf{u}_g is referred to as the *pressure driven velocity*. The second is an *ageostrophic* or Ekman component defined by a balance between the frictional and Coriolis accelerations

$$f \hat{z} \times \mathbf{u}_e = \mathbf{F} \implies \mathbf{u}_e = -f^{-1} \hat{z} \times \mathbf{F}, \quad (30.4)$$

so that \mathbf{u}_e is the *frictional driven velocity*.

This velocity decomposition has the appearance of superposing linearly independent flows, one geostrophic (pressure driven) and one ageostrophic (friction driven). However, the flows are coupled and thus not linearly independent. Namely, ageostrophic motions alter the pressure field which in turn affects the geostrophic flow. So the presence of friction and the associated ageostrophic flows lead to geostrophic flows differing from the inviscid case. Conversely, geostrophic flows affect the level of friction. Hence, the above decomposition does not reflect a physical decoupling of geostrophic and ageostrophic flows. Rather, it is only meant to help conceptually understand and describe the flow and the various force balances.

30.2 Horizontal balances in natural coordinates

Motion in Ekman boundary layers is both horizontal and vertical. Here, we introduce the role of friction in rotating flows by just focusing on the horizontal. In particular, we study balances occurring in horizontal flows that maintain a frictional geostrophic balance. As per the definition (30.3), geostrophic motion occurs along lines of constant pressure, with frictionally induced deviations crossing isobars and providing a down pressure gradient component to the fluid trajectory. Motivated by the discussion in Chapter 29, we make use of natural coordinates for the kinematics.

30.2.1 Natural coordinates according to isobars

We represent the horizontal flow according to natural coordinates defined along an arbitrary geopotential surface. Instead of defining the natural coordinates according to the flow direction, as done in Section 29.2 for the frictionless case, we here decompose the motion according to pressure contours (isobars). The unit vector \hat{s} is defined tangent to isobars in the horizontal plane and directed along the direction of geostrophic flow. We define the direction, \hat{n} , to be perpendicular to isobars and oriented down the horizontal pressure gradient

$$\hat{n} = -\frac{\nabla_z p}{|\nabla_z p|}. \quad (30.5)$$

As illustrated in Figure 30.1, in the northern hemisphere \hat{n} points to the left of the geostrophic velocity, whereas it is to the right in the southern hemisphere. We thus have the northern hemisphere triplet of unit vectors

NORTHERN HEMISPHERE TRIPLET OF DIRECTIONS

$$\hat{z} = \hat{s} \times \hat{n} = \text{vertical direction} \quad (30.6a)$$

$$\hat{n} = \hat{z} \times \hat{s} = \text{down pressure gradient direction} \quad (30.6b)$$

$$\hat{s} = \hat{n} \times \hat{z} = \text{tangent to isobar in direction of geostrophic flow.} \quad (30.6c)$$

In the southern hemisphere, since $\hat{\mathbf{n}}$ points to the right of $\hat{\mathbf{s}}$, the triplet of directions becomes

SOUTHERN HEMISPHERE TRIPLET OF DIRECTIONS

$$\hat{\mathbf{z}} = \hat{\mathbf{n}} \times \hat{\mathbf{s}} = \text{vertical direction} \quad (30.7a)$$

$$\hat{\mathbf{n}} = \hat{\mathbf{s}} \times \hat{\mathbf{z}} = \text{down pressure gradient direction} \quad (30.7b)$$

$$\hat{\mathbf{s}} = \hat{\mathbf{z}} \times \hat{\mathbf{n}} = \text{tangent to isobar in direction of geostrophic flow.} \quad (30.7c)$$

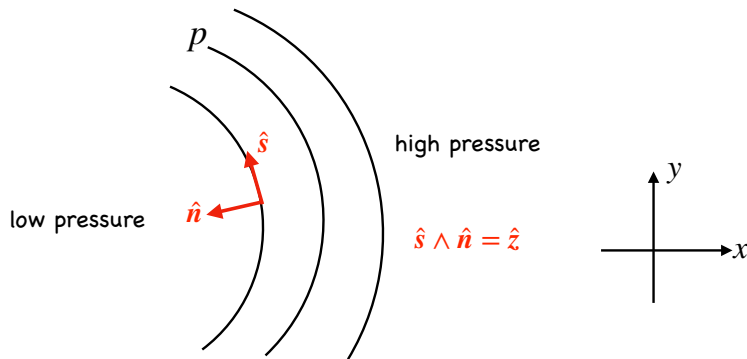


FIGURE 30.1: Natural coordinates defined along an arbitrary geopotential surface according to isobars in the horizontal plane, here depicted for the northern hemisphere. The normal direction, $\hat{\mathbf{n}} = -\nabla_z p / |\nabla_z p|$, is oriented down the horizontal pressure gradient so that it points to the left of the geostrophic velocity (facing downstream) in the northern hemisphere and to the right in the southern hemisphere. The tangent direction, $\hat{\mathbf{s}}$, points along the isobar in the direction of the geostrophic velocity.

30.2.2 Geostrophic and Ekman balances

As found when studying the geostrophic balance in Section 29.3, the geostrophic velocity flows along isobars and so only has a component in the $\hat{\mathbf{s}}$ direction

$$\hat{\mathbf{s}} \cdot \mathbf{u}_g = -\frac{1}{f\rho_0} \frac{\partial p}{\partial n} \quad \text{and} \quad \hat{\mathbf{n}} \cdot \mathbf{u}_g = 0 \quad (30.8)$$

In contrast, the Ekman velocity has a component both along and across isobars. For the northern and southern hemispheres we have

$$\hat{\mathbf{s}} \cdot \mathbf{u}_e = |f|^{-1} \hat{\mathbf{n}} \cdot \mathbf{F} \quad \text{and} \quad \hat{\mathbf{n}} \cdot \mathbf{u}_e = -|f|^{-1} \hat{\mathbf{s}} \cdot \mathbf{F}. \quad (30.9)$$

As expected, the Ekman velocity vanishes when the frictional acceleration vanishes, in which case the flow reduces to the geostrophic flow that moves along isobars so that $\hat{\mathbf{s}} = \hat{\mathbf{u}}$. However, when there is a nonzero friction aligned along isobars, that drives an Ekman velocity across isobars. Conversely, friction aligned across isobars drives Ekman velocities along isobars.

We arrive at a complementary perspective on the origin of cross-isobar flow through the following considerations. Without friction, the Coriolis and pressure gradient accelerations balance when the flow is geostrophic. In the presence of friction, the velocity is slowed so that the Coriolis acceleration weakens. If the pressure gradient acceleration is retained, as occurs if it is determined by large scale balances outside of the Ekman layer, then the Coriolis acceleration no longer balances the pressure gradient. Consequently, flow is diverted from isobars and develops a component down the pressure gradient.

30.2.3 Rayleigh drag

The relative simplicity of Rayleigh drag facilitates analytical expressions for the Ekman velocity using natural coordinates, written in terms of the geostrophic velocity (equation (30.8)). In doing so we are afforded an explicit illustration of how the Ekman flow provides a cross-isobar component to the flow in the direction down the pressure gradient. Before developing the Ekman flows we here summarize elements of Rayleigh drag.

In Section 23.3.2 we studied how Rayleigh drag affects the kinetic energy budget. As a reminder, consider a frictional acceleration in the form of a Rayleigh drag acting on the velocity field

$$\mathbf{F} = -\frac{U_{\text{fric}}}{\delta} \mathbf{u} = -\gamma \mathbf{u}, \quad (30.10)$$

where δ is a depth scale and U_{fric} is a friction velocity scale with dimensions L/T . The ratio

$$\gamma = \frac{U_{\text{fric}}}{\delta} \quad (30.11)$$

has dimensions T^{-1} and is an inverse spin-down time. That is, if only Rayleigh drag affected changes to the horizontal momentum, $\partial_t \mathbf{u} = -\gamma \mathbf{u}$, then the flow would exponentially come to a halt with an e-folding time γ^{-1} . The drag is relatively large over rough surfaces, thus leading to a small e-folding time. In particular, drag on the lower atmospheric winds is larger over land than over the ocean. The reason is that trees, cities, and mountains dissipate more of the atmosphere's mechanical energy than interactions with the relatively smooth ocean surface (see Section 22.10.7 for a discussion of roughness length).

Rayleigh drag dissipates all flow features regardless of their spatial structure. That is, Rayleigh drag does not prefer any particular length scales in the fluid flow. This lack of scale selectivity contrasts to the Laplacian friction discussed in Section 30.3.1, with Laplacian friction dissipating small spatial scales more strongly than large scales. Correspondingly, Rayleigh drag does not generally provide the means to produce a boundary layer.¹ Hence, when studying physics within the Ekman boundary layer in Section 30.3 we make use of Laplacian friction. But for now, Rayleigh drag provides a very useful means to analytically illustrate the role of friction in producing spiral flows with non-zero horizontal divergence.

30.2.4 Cross isobar flow driven by Rayleigh drag

Making use of the Rayleigh drag (30.10) brings the northern hemisphere expressions (30.9) for the Ekman velocity into the form

$$\hat{\mathbf{s}} \cdot \mathbf{u}_e = f^{-1} \hat{\mathbf{n}} \cdot \mathbf{F} = -(\gamma/f) \hat{\mathbf{n}} \cdot \mathbf{u} = -(\gamma/f) \hat{\mathbf{n}} \cdot \mathbf{u}_e \quad (30.12a)$$

$$\hat{\mathbf{n}} \cdot \mathbf{u}_e = -f^{-1} \hat{\mathbf{s}} \cdot \mathbf{F} = (\gamma/f) \hat{\mathbf{s}} \cdot \mathbf{u} = (\gamma/f) \hat{\mathbf{s}} \cdot (\mathbf{u}_e + \mathbf{u}_g). \quad (30.12b)$$

Similar considerations for the southern hemisphere lead to the general result for both hemispheres

$$\hat{\mathbf{s}} \cdot \mathbf{u}_e = -(\gamma/|f|) \hat{\mathbf{n}} \cdot \mathbf{u}_e \quad (30.13a)$$

$$\hat{\mathbf{n}} \cdot \mathbf{u}_e = (\gamma/|f|) \hat{\mathbf{s}} \cdot (\mathbf{u}_e + \mathbf{u}_g). \quad (30.13b)$$

¹In Section 30.3.3 we provide further discussion of what is needed mathematically and physically to produce a boundary layer.

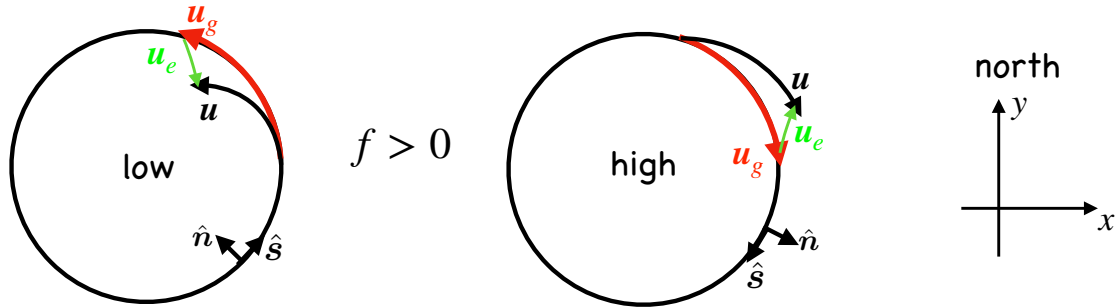


FIGURE 30.2: Illustrating frictional geostrophic flow in the northern hemisphere ($f > 0$). Left panel: geostrophic flow, \mathbf{u}_g , around a low pressure center is counter-clockwise and aligned with pressure isobars. Friction aligned along the isobars drives Ekman flow, \mathbf{u}_e , that has a component down the pressure gradient (normal to the geostrophic flow) as well as a component that is directed opposite the geostrophic flow. Consequently, the total velocity, $\mathbf{u}_g + \mathbf{u}_e$, spirals into the low pressure center. Right panel: the opposite oriented flow occurs around high pressure centers, where fluid spirals away from the high due to the cross-isobar flow driven by friction. By the definition given by equation (30.6b), the normal direction, $\hat{\mathbf{n}}$, is directed down the pressure gradient, whereas $\hat{\mathbf{s}}$ is tangent to the isobar and directed along the geostrophic flow direction.

Rearrangement of these equations allows us to express the Ekman velocity in terms of the geostrophic velocity (equation (30.8)), with results for both hemispheres given by

$$\hat{\mathbf{n}} \cdot \mathbf{u}_e = \hat{\mathbf{s}} \cdot \mathbf{u}_g \left[\frac{\gamma |f|}{f^2 + \gamma^2} \right] \quad (30.14a)$$

$$\hat{\mathbf{s}} \cdot \mathbf{u}_e = -\hat{\mathbf{s}} \cdot \mathbf{u}_g \left[\frac{\gamma^2}{\gamma^2 + f^2} \right], \quad (30.14b)$$

where equation (30.8) expresses the geostrophic velocity in terms of the normal pressure gradient. Equation (30.14a) says that the normal component to the Ekman velocity is directed down the pressure gradient. Equation (30.14b) says that the component of the Ekman velocity along the pressure isobar is directed opposite to the geostrophic velocity. We provide an example of an Ekman velocity in Figure 30.2 for the northern hemisphere.

Bringing all pieces together leads to the components for the total velocity, $\mathbf{u} = \mathbf{u}_g + \mathbf{u}_e$, and its squared magnitude

$$\hat{\mathbf{s}} \cdot \mathbf{u}_g = -\frac{1}{f\rho_0} \frac{\partial p}{\partial n} \quad \text{geostrophic velocity (aligned along isobars)} \quad (30.15a)$$

$$\hat{\mathbf{s}} \cdot \mathbf{u} = \hat{\mathbf{s}} \cdot \mathbf{u}_g \left[\frac{f^2}{f^2 + \gamma^2} \right] \quad \text{isobaric velocity component} \quad (30.15b)$$

$$\hat{\mathbf{n}} \cdot \mathbf{u} = (\gamma/|f|) \hat{\mathbf{s}} \cdot \mathbf{u} \quad \text{normal velocity component} \quad (30.15c)$$

$$(\hat{\mathbf{s}} \cdot \mathbf{u})^2 + (\hat{\mathbf{n}} \cdot \mathbf{u})^2 = \frac{(\hat{\mathbf{s}} \cdot \mathbf{u}_g)^2}{1 + (\gamma/f)^2} \quad \text{horizontal kinetic energy per mass.} \quad (30.15d)$$

The cross-isobar flow (equation (30.15c)) is directly driven by the Rayleigh drag, and it is directed down the pressure gradient so long as the flow has a positive projection onto the tangent direction

$$\hat{\mathbf{s}} \cdot \mathbf{u} > 0 \implies \hat{\mathbf{n}} \cdot \mathbf{u} > 0. \quad (30.16)$$

When flow is moving counter-clockwise around a low pressure in the northern hemisphere, where $\hat{\mathbf{n}}$ points towards the low pressure center, then Rayleigh drag causes the fluid to spiral into the low pressure center. Conversely, when flow is moving clockwise around a high pressure, with $\hat{\mathbf{n}}$ pointing

away from the high pressure center, then Rayleigh drag causes the fluid to spiral away from the high pressure center. We depict these cases in Figure 30.2. Furthermore, equation (30.15d) shows that when $\gamma \neq 0$ the magnitude of the total flow is reduced relative to the geostrophic flow, thus reflecting the dissipation of kinetic energy arising from Rayleigh drag (Section 23.3.2).

30.2.5 Horizontal spiral plus vertical rising/sinking

Thus far, we have focused on the horizontal spiral motion as shown in Figure 30.2. Through continuity we infer a corresponding vertical motion induced by the convergence of mass into the low pressure center and the divergence of mass away from the high pressure center. Figure 30.3 illustrates the vertical motion in a bottom Ekman boundary layer of either the atmosphere or ocean whereby mass rises above a low pressure center in response to the horizontal convergence of mass in the Ekman layer. Conversely, mass diverges from the high pressure Ekman layer, with this divergence inducing a sinking motion over the high pressure to replace the diverging mass. In subsequent sections of this chapter we develop the formalism needed to compute the mass transport into and out of the Ekman boundary layer.

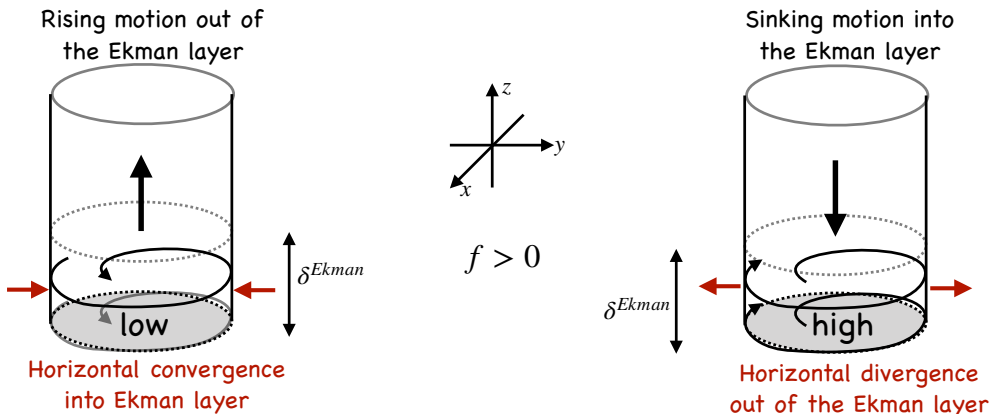


FIGURE 30.3: Illustrating the three-dimensional flow associated with Ekman layers in the northern hemisphere ($f > 0$) next to a bottom boundary. Left panel: flow spiralling into a low pressure center creates convergence of mass into the Ekman layer. Mass continuity means that flow must vertically leave the Ekman layer to thus enter the interior fluid above. Right panel: flow spiralling away from a high pressure center creates divergence of mass away from the Ekman layer. Mass continuity means that flow must vertically sink into the Ekman layer from above. The Ekman layer thickness is denoted by δ^{Ekman} (Section 30.3). An analogous picture holds for the surface Ekman layer in the ocean, yet with the Ekman layer at the top of the column rather than the bottom.

30.2.6 Further study

Our discussion of Ekman velocity arising from Rayleigh drag follows a similar treatment in Section 7.4 of *Marshall and Plumb* (2008).

30.3 Ekman number and Ekman layer thickness

Friction that is most prominent near surface and bottom boundaries arises from vertical shears in the horizontal velocity, with shears leading to flow instabilities and the development of turbulence and associated turbulent friction. There is no deductive theory for turbulent friction so we must rely on empirical expressions. These expressions are typically based on a Laplacian viscous operator, partly motivated by the form arising from kinetic theory of gases briefly mentioned in Chapter 13 (see also equation (22.85)). Most notably, this operator supports the development

of a boundary layer through maintenance of both the no-slip (homogeneous Dirichlet) and stress (Neumann) boundary conditions.

30.3.1 Laplacian vertical friction

We introduced the Laplacian friction operator in Section 22.8.6 when studying stress in fluids. The Laplacian friction operator considered here is given just in terms of the vertical shears of horizontal stresses

$$\mathbf{F}^{\text{viscous}} = \frac{1}{\rho_0} \frac{\partial \boldsymbol{\tau}}{\partial z} = \frac{\partial}{\partial z} \left[\nu^{\text{eddy}} \frac{\partial \mathbf{u}}{\partial z} \right], \quad (30.17)$$

with $\nu^{\text{eddy}} > 0$ a turbulent kinematic viscosity with dimensions $L^2 T^{-1}$. This form of the friction operator emulates the Laplacian operator representing molecular viscous friction (equation (22.85)). It is also the form most commonly used in theoretical and numerical models that focus on boundary layers where rotation is important.

Expanding the derivative in equation (30.17) reveals that the Laplacian friction is nonzero where there is curvature in the vertical profile of the horizontal velocity, and where there is depth dependence to the viscosity and velocity

$$\mathbf{F}^{\text{viscous}} = \frac{\partial \nu^{\text{eddy}}}{\partial z} \frac{\partial \mathbf{u}}{\partial z} + \nu^{\text{eddy}} \frac{\partial^2 \mathbf{u}}{\partial z^2}. \quad (30.18)$$

The turbulent viscosity generally has a depth dependence, with larger values in the boundary layer where turbulence is most energetic. This form of the friction preferentially acts on velocity exhibiting nontrivial vertical structure, thus acting to smooth any depth dependent behaviour. In Section 61.4 we discuss further mathematical properties of Laplacian friction.

30.3.2 Non-dimensionalization

We non-dimensionalize the equations to isolate important non-dimensional numbers affecting the flow regime. In particular, we identify the Ekman number as a measure of the importance of friction relative to rotation, with friction important where the Ekman number is order unity or larger, and unimportant where the Ekman number is much smaller than unity.²

We make use of the following scales and associated non-dimensional quantities

$$(x, y) = L(\hat{x}, \hat{y}) \quad z = H \hat{z} \quad (u, v) = U(\hat{u}, \hat{v}) \quad f = f_0 \hat{f} \quad p = P \hat{p} \quad (30.19)$$

where the hat terms are non-dimensional,³ and we introduced typical scales for horizontal length (L), vertical height (H), velocity (U), Coriolis parameter (f_0), and pressure (P). For the pressure scale we assume it follows geostrophic scaling so that it can be written⁴

$$P = f_0 \rho_0 U L. \quad (30.20)$$

Inserting the relations (30.19) into equation (30.1) leads to the non-dimensional frictional geostrophic equation

$$\hat{\mathbf{f}} \times \hat{\mathbf{u}} = -\hat{\nabla} \hat{p} + \frac{\mathbf{F}}{f_0 U}. \quad (30.21)$$

²For flows unaffected by rotation, the Reynolds number is the key non-dimensional number (Section 22.9) determining where viscous friction is important.

³In Section 29.2.1 we defined $\hat{\mathbf{u}}$ as the unit vector pointing along the trajectory of a fluid element. In contrast, we here let $\hat{\mathbf{u}}$ be the non-dimensional horizontal velocity.

⁴Recall that in Section 26.2.3 we considered pressure in a non-rotating system to scale according to the dynamical pressure scale, U^2 , where U is a horizontal flow speed scale.

30.3.3 Defining the Ekman number and layer thickness

The *Ekman number* is a non-dimensional measure of the relative importance of the frictional acceleration due to vertical shears versus the Coriolis acceleration

$$\text{Ek} = \frac{\text{frictional acceleration from vertical shears}}{\text{Coriolis acceleration}}. \quad (30.22)$$

The Ekman number increases when there is more boundary layer turbulence, in which case the eddy viscosity, ν^{eddy} , is large relative to its small values in the interior region outside of the boundary layer. Additionally, the Ekman number increases when moving towards the equator, where the Coriolis parameter reduces.⁵

For the viscous stress form of Laplacian vertical frictional acceleration (equation (30.17))

$$\mathbf{F}^{\text{viscous}} = \frac{\nu^{\text{eddy}} U}{H^2} \frac{\partial^2 \hat{\mathbf{u}}}{\partial z^2}, \quad (30.23)$$

the Ekman number is given by

$$\text{Ek} = \frac{\nu^{\text{eddy}}}{f_0 H^2}. \quad (30.24)$$

If we take the vertical scale, H , equal to the depth scale over which interior flow processes occur, then the Ekman number will be very small, even if the eddy viscosity is relatively large. In this case we conclude that friction is negligible, as indeed it is for many purposes where the boundary layer is not of concern.

However, the Ekman number multiplies the highest derivative in equation (30.21). So setting the Ekman number to zero represents a *singular limit*, whose mathematical meaning is that we change the order of the differential equation when setting $\text{Ek} = 0$. Reducing the order of the differential equation then means we can only satisfy a reduced number of boundary conditions relative to the $\text{Ek} > 0$ case. In particular, with $\text{Ek} = 0$ we can no longer satisfy the no-slip condition at the solid-fluid boundary. In contrast, with any non-zero value of $\text{Ek} > 0$, viscosity will drag the flow to zero towards the boundary within a *boundary layer* where friction is leading order. We expect a boundary layer to form within a boundary layer thickness, $H = \delta^{\text{Ekman}}$, in which the Ekman number is order unity so where friction is of leading order importance

$$H = \delta^{\text{Ekman}} \implies \text{Ek} = \frac{\nu^{\text{eddy}}}{f_0 (\delta^{\text{Ekman}})^2} = 1. \quad (30.25)$$

Turning this equation around we see that the vertical scale, δ^{Ekman} , defines the viscous Ekman boundary layer thickness as a function of the eddy viscosity and Coriolis parameter

$$\text{Ek} = 1 \implies \delta^{\text{Ekman}} = \delta^{\text{viscous}} = \sqrt{\nu^{\text{eddy}} / f_0}. \quad (30.26)$$

30.3.4 Estimates for the vertical eddy viscosity

The eddy viscosity is not readily available from direct measurements or first principles theory. However, measuring the boundary layer thickness provides a means to infer a bulk viscosity for the boundary layer

$$\nu^{\text{eddy}} = f_0 (\delta^{\text{Ekman}})^2. \quad (30.27)$$

⁵When getting very close to the equator, our assumption of a frictional geostrophic balance breaks down so that other terms in the momentum equation, such as advection, become important.

In the atmosphere, the boundary layer thickness is order 1000 m, so that at mid-latitudes, with $f_0 = 10^{-4} \text{ s}^{-1}$, we expect

$$\nu_{\text{atmos}}^{\text{eddy}} \sim 10^2 \text{ m}^2 \text{ s}^{-1}. \quad (30.28)$$

In the ocean, the upper ocean boundary layer depth, outside of the deep convection regions, is roughly 50 m, in which case

$$\nu_{\text{ocean}}^{\text{eddy}} \sim 0.25 \text{ m}^2 \text{ s}^{-1}. \quad (30.29)$$

30.4 Ocean surface Ekman layer

It is possible to establish integrated mass transport properties of the Ekman layer even without specifying details of the friction (i.e., the viscosity) or the stratification. The key ingredient is the boundary stress. This stress is commonly estimated for the surface ocean given information about the wind speed and atmospheric stratification. Hence, Ekman theory has found much application to studies of the wind-driven ocean circulation, with the integrated properties the most consequential results from Ekman theory. We here focus on the ocean surface Ekman layer and then consider bottom Ekman boundaries for the atmosphere and ocean in Section 30.5.

Before starting, we emphasize that the stress is the key ingredient in computing properties of the Ekman layer. And yet, determining the stress is a nontrivial exercise in boundary layer physics, which is far outside our scope. Additionally, the turbulent boundary stress exchanged between the fluid and its boundary (either another fluid, ice, or the solid earth) arises within Ekman boundary layers, where flow spirals relative to the interior geostrophic flow. So the boundary stress is generally rotated some amount relative to the interior geostrophic flow. We consider an analytic example of this rotation when studying the bottom Ekman layer in Section 30.5. For now, we simply recognize that the story is relatively simple when assuming the stress is given, but the stress itself can be difficult to obtain.

30.4.1 Horizontal mass transport within the Ekman layer

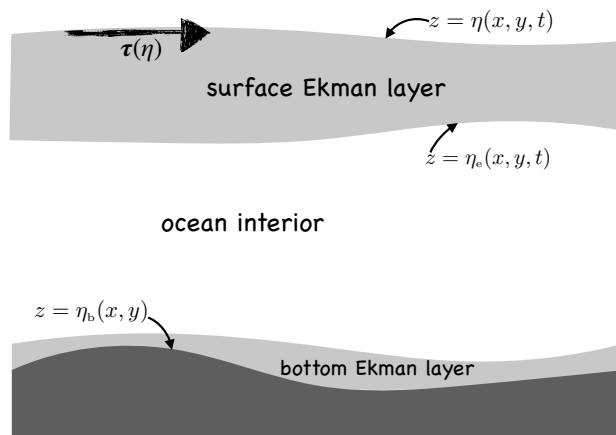


FIGURE 30.4: Ekman layer at the ocean surface, defined for vertical position $\eta_e(x, y, t) \leq z \leq \eta(x, y, t)$, with η_e specifying the Ekman layer bottom and η the free surface vertical position. Boundary stress from winds and/or sea ice imparts horizontal momentum to the upper ocean that is transmitted throughout the Ekman layer via the vertical divergence of turbulent horizontal shear stresses. As studied in Section 30.6, there is also a bottom Ekman layer created by stresses active next to the ocean bottom.

We are concerned with the mass budget for the ocean surface Ekman layer sitting between

the Ekman layer bottom and the ocean free surface

$$\eta_e(x, y, t) \leq z \leq \eta(x, y, t), \quad (30.30)$$

as depicted in Figure 30.4. Knowledge of the mass budget has implications for how mechanical energy imparted to the boundary layer drives circulation well within the interior of the ocean. This transport and associated circulation are how Ekman mechanics, limited to the boundary layer, affect large-scale ocean circulation throughout the fluid column.

Integrating the horizontal Ekman balance (30.4) over the depth of the Ekman layer leads to

$$\mathbf{M}_e = \int_{\eta_e}^{\eta} \rho_o \mathbf{u}_e dz \implies f \hat{z} \times \mathbf{M}_e = \int_{\eta_e}^{\eta} \rho_o \mathbf{F} dz, \quad (30.31)$$

with \mathbf{M}_e the depth integrated ageostrophic horizontal mass transport within the Ekman boundary layer. Assuming friction to be in the form of a vertical stress divergence as in equation (30.17) leads to the horizontal Ekman mass transport

$$\mathbf{M}_e = -f^{-1} \hat{z} \times [\boldsymbol{\tau}(\eta) - \boldsymbol{\tau}(\eta_e)]. \quad (30.32)$$

Stress at the bottom of the Ekman layer, $\boldsymbol{\tau}(\eta_e)$, matches to the stress in the ocean interior. The stress in the fluid interior is generally much smaller than stress in the turbulent upper ocean surface, $\boldsymbol{\tau}(\eta)$, so that we can neglect $\boldsymbol{\tau}(\eta_e)$ when computing the mass transport. We are thus led to the expression for the surface stress induced ageostrophic horizontal mass transport within the upper ocean Ekman layer

$$\mathbf{M}_e = -f^{-1} \hat{z} \times \boldsymbol{\tau}(\eta). \quad (30.33)$$

The surface stress induced mass transport given by equation (30.33) is very useful in practice. Notably, we do not need to know the depth of the Ekman layer nor details about the boundary layer turbulence. Rather, the mass transport is determined solely by the surface boundary stress.⁶ Furthermore, the horizontal mass transport within the Ekman layer is directed at right angles to the surface stress, as depicted in Figure 30.5, with mass transport to the right of the surface stress in the northern hemisphere and to the left in the southern hemisphere.

30.4.2 Example Ekman mass transports

A particularly relevant example is when zonal boundary stress is eastward, $\boldsymbol{\tau}(\eta) = |\tau| \hat{x}$, in which the Ekman transport is meridional

$$\mathbf{M}_e = -(|\tau|/f) \hat{y}, \quad (30.34)$$

which points equatorward in both hemispheres. Conversely, in the equatorial region where winds are easterly so that $\boldsymbol{\tau}(\eta) = -|\tau| \hat{x}$, the horizontal Ekman mass transport causes waters to move poleward away from the equator. Mass continuity is then satisfied by upwelling waters along the equator within the Ekman layer. We sketch the elements of this flow in Figure 30.6. Exercise 30.1 considers an analogous situation for a channel in the southern hemisphere, thus illustrating a basic feature of the wind-driven overturning circulation in the Southern Ocean.

A second example concerns the case of a wind stress with a component aligned with a coastline as depicted in Figure 30.7. When the horizontal Ekman mass transport is directed away from the coast, a steady mass balance in the Ekman layer is associated with the upwelling of waters from

⁶This statement is somewhat overloaded. Namely, determining the stress, $\boldsymbol{\tau}(\eta)$, transferred to the ocean requires information about the boundary layer processes. Nevertheless, by expressing the mass transport, \mathbf{M}_e , in terms of the boundary stress provides a clear delineation of the causes for boundary layer transport. It has thus offered an important foundation for theories of wind-driven ocean circulation.

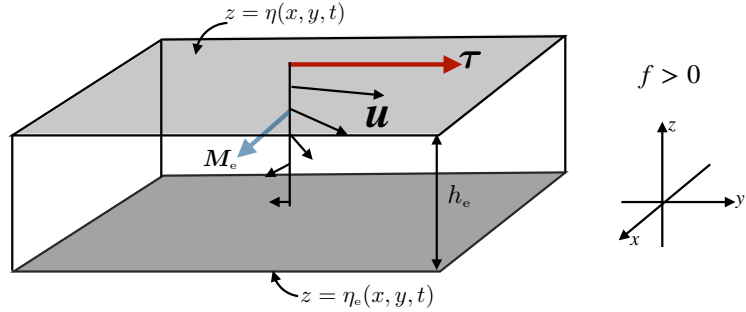


FIGURE 30.5: Horizontal transport integrated over the depth of the surface ocean Ekman layer in the region $\eta_e(x, y, t) \leq z \leq \eta(x, y, t)$. The net mass transport is directed perpendicular to the boundary stress, oriented to the right in the northern hemisphere and to the left in the southern hemisphere. Here, the boundary stress, τ , is shown directed to the north so that in the northern hemisphere ($f > 0$), the depth integrated horizontal Ekman transport, M_e , is to the east. This perpendicular mass transport is the result of the vertically spiralling Ekman flow. The Ekman mass transport resulting from boundary stress is independent of the assumptions made about ocean friction within the ocean boundary layer, and it is independent of the stratification assumed for the Ekman layer.

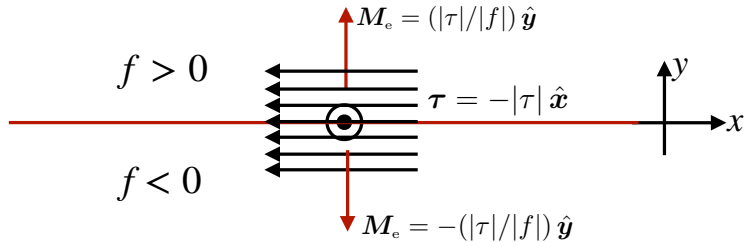


FIGURE 30.6: Easterly winds along the equator drive poleward horizontal mass transport within the upper ocean Ekman layer, as per equation (30.34). Furthermore, as discussed in Section 30.4.3, a steady state Ekman layer mass budget is typically realized by the upwelling of interior waters into the Ekman layer.

beneath the Ekman layer. Conversely when the horizontal mass transport is directed toward the coast, steady mass balance is realized by coastal downwelling. This process is very important for coastal physical and biological oceanography.

30.4.3 Mass budget for the Ekman layer

As seen in Figure 30.3, the horizontal transport of fluid within the Ekman layer induces a vertical transport into or out of the Ekman layer. To obtain a mathematical expression for the vertical transport, integrate the continuity equation $\nabla \cdot \mathbf{v} = 0$ over the vertical extent of the Ekman layer

$$\frac{\partial}{\partial x} \left[\int_{\eta_e}^{\eta} u \, dz \right] + \frac{\partial}{\partial y} \left[\int_{\eta_e}^{\eta} v \, dz \right] + [w(\eta) - \mathbf{u}(\eta) \cdot \nabla \eta] - [w(\eta_e) - \mathbf{u}(\eta_e) \cdot \nabla \eta_e] = 0. \quad (30.35)$$

For a Boussinesq fluid, the kinematic boundary condition at the ocean free surface is given by equation (18.5)

$$w + \frac{Q_m}{\rho_0} = \frac{\partial \eta}{\partial t} + \mathbf{u} \cdot \nabla \eta \quad \text{at } z = \eta(x, y, t). \quad (30.36)$$

Similarly, at the bottom of the Ekman layer we measure the volume transport through this layer by computing the dia-surface transport, $w^{(\dot{\eta}_e)}$, according to equation (57.38)

$$w^{(\dot{\eta}_e)} = w - (\partial_t z + \mathbf{u} \cdot \nabla z) \quad \text{at } z = \eta_e(x, y, t). \quad (30.37)$$

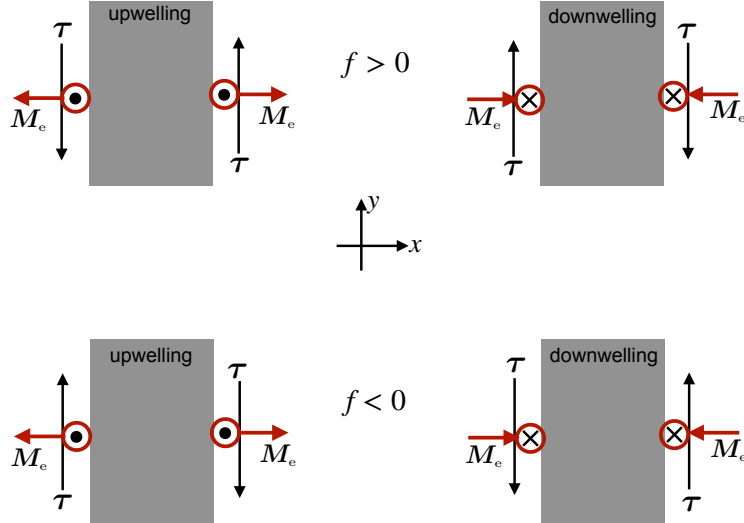


FIGURE 30.7: Wind stresses with a component that is parallel to coastlines lead to horizontal mass transport away from or towards the coast. Mass continuity then leads to coastal upwelling or downwelling of waters into or out of the Ekman layer. Here we depict the various scenarios for the northern hemisphere (top row) and southern hemisphere (bottom row), with the gray regions representing land, the black vectors the wind stresses, and the red arrows the horizontal wind induced mass transports in the Ekman layer. This figure is adapted from Figure 4-24 of [von Arx \(1962\)](#).

The sign convention is such that $w^{(\dot{\eta}_e)} > 0$ means that mass enters (entrains into) the surface Ekman layer through its base, whereas $w^{(\dot{\eta}_e)} < 0$ means that mass leaves (detrains from) the surface Ekman layer base.

Using the kinematic boundary conditions (30.36) and (30.37) in the depth integrated volume budget (30.35), and rearranging, leads to the Ekman layer mass budget

$$\rho_0 w^{(\dot{\eta}_e)} + Q_m = \rho_0 \partial h_e / \partial t + \nabla \cdot \mathbf{M}. \quad (30.38)$$

In this equation we wrote

$$h_e = \eta - \eta_e \quad (30.39)$$

for the thickness of the Ekman layer and

$$\mathbf{M} = \rho_0 \int_{\eta_e}^{\eta} \mathbf{u} dz \quad (30.40)$$

for the Ekman layer integrated horizontal mass transport. As a check on the above manipulations, let the Ekman layer go to the ocean bottom (so that $w^{(\dot{\eta}_e)} = 0$ and $\eta_e = \eta_b$), in which case the mass budget equation (30.38) correctly reduces to the kinematic free surface equation for the full ocean column as given by equation (18.78)

$$\rho_0 \frac{\partial \eta}{\partial t} = Q_m - \rho_0 \nabla \cdot \mathbf{U}, \quad (30.41)$$

with $\mathbf{U} = \int_{\eta_b}^{\eta} \mathbf{u} dz$ the depth integrated horizontal velocity.

The horizontal mass transport given by equation (30.40) has a contribution from both the Ekman transport and remaining processes, such as geostrophic flow and ageostrophic flows not associated with Ekman. We write this mass transport in the form

$$\mathbf{M} = \mathbf{M}_e + \mathbf{M}_{\text{other}}. \quad (30.42)$$

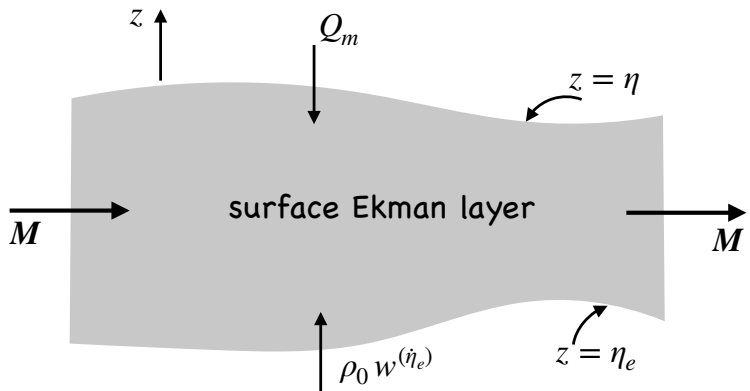


FIGURE 30.8: Mass budget over the surface Ekman layer of the ocean, with contributions from the surface mass flux, Q_m , flux through the bottom of the layer, $w^{(\eta_e)}$, and depth integrated horizontal flux, \mathbf{M} , within the layer. If there are any imbalances then the layer thickness will have a nonzero time tendency, $\partial h_e / \partial t \neq 0$. Our sign convention is such as $w^{(\eta_e)} > 0$ corresponds to water entering (entraining into) the Ekman layer (vertically upward motion) through the Ekman layer base at $z = \eta_e$, and likewise $Q_m > 0$ corresponds to water entering the Ekman layer through the free surface at $z = \eta$. Entrainment through the base of the Ekman layer is referred to as *Ekman suction* or *Ekman upwelling*. The opposite case is referred to as *Ekman pumping* or *Ekman downwelling* when water leaves the Ekman layer and enters the ocean interior.

The horizontal Ekman transport is determined by the boundary stress according to equation (30.33), with its divergence given by

$$\nabla \cdot \mathbf{M}_e = \hat{\mathbf{z}} \cdot [\nabla \times (\boldsymbol{\tau}/f)]. \quad (30.43)$$

This result brings the Ekman layer mass budget (30.38) into the form

$$\rho_0 w^{(\eta_e)} + Q_m = \rho_0 \frac{\partial h_e}{\partial t} + \nabla \cdot \mathbf{M}_{\text{other}} + \hat{\mathbf{z}} \cdot [\nabla \times (\boldsymbol{\tau}/f)]. \quad (30.44)$$

The left hand side measures the mass transport crossing the bottom of the Ekman layer, $\rho_0 w^{(\eta_e)}$, plus the transport crossing the free surface, Q_m . This transport balances a time change in the Ekman layer thickness (first right hand side term) plus the horizontal divergence of mass within the layer. A steady state Ekman layer thickness, $\partial h_e / \partial t = 0$, is realized if the horizontal divergence of mass within the Ekman layer is exactly balanced by mass entering the Ekman layer through the top and/or bottom of the layer. We illustrate this budget in Figure 30.8. For example, in the equatorial case of Figure 30.6, the diverging horizontal Ekman layer flow induced by easterly winds (poleward Ekman transport on both sides of the equator) is balanced by water upwelling into the Ekman layer through the base, $w^{(\eta_e)} > 0$, along with a generally smaller effects from surface mass fluxes through Q_m and possible other contributions through $\nabla \cdot \mathbf{M}_{\text{other}}$.

30.4.4 Ekman layer coupled to the geostrophic interior

The effects from boundary stress curl in equation (30.44) warrant particular attention whereby

$$\rho_0 w_{\text{Ekman}}^{(\eta_e)} \equiv \nabla \cdot \mathbf{M}_e = \hat{\mathbf{z}} \cdot [\nabla \times (\boldsymbol{\tau}/f)]. \quad (30.45)$$

The stress curl, as well as changes in f on the sphere, drive vertical motion through the base of the Ekman layer. The flow crossing the Ekman layer boundary acts to stretch or compress vertical fluid columns in the adjoining fluid interior. Interior fluid columns in a rotating fluid are stiffened through the effects of Taylor-Proudman (Section 28.5.3). From our understanding

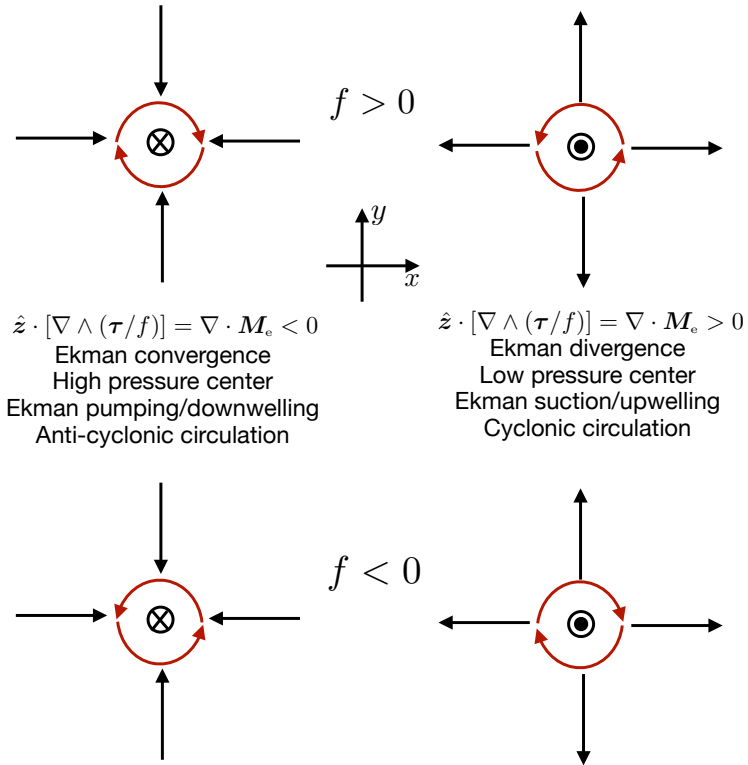


FIGURE 30.9: Plan view depicting the steady state horizontal and vertical transport in the surface Ekman layer (ignoring the possible transport across the ocean surface with Q_m). The left column shows horizontal wind-induced convergence in the Ekman layer that induces vertical pumping/downwelling, where $\nabla \cdot \mathbf{M}_e = \hat{z} \cdot [\nabla \times (\boldsymbol{\tau}/f)] < 0$. The right column shows the horizontal divergence within the Ekman layer that is balanced by suction/upwelling, where $\nabla \cdot \mathbf{M}_e = \hat{z} \cdot [\nabla \times (\boldsymbol{\tau}/f)] > 0$. The top row is for the northern hemisphere, with $f > 0$, and the bottom row is for the southern hemisphere. The red arrows depict the sense for the induced geostrophic circulation in the interior just below the Ekman layer. Note that the horizontal Ekman transport is to the right of the red circulating flow in the northern hemisphere and to the left in the southern. Ekman pumping is associated with anti-cyclonic circulation (clockwise in the northern hemisphere and anti-clockwise in southern hemisphere). In contrast, Ekman suction is associated with cyclonic circulation. The circulation is supported by pressure gradients, with high pressure in regions of Ekman convergence, $\nabla \cdot \mathbf{M}_e < 0$, due to the accumulation of mass towards the center, thus giving rise to anti-cyclonic geostrophic flow in the interior. The opposite holds for regions of Ekman divergence, $\nabla \cdot \mathbf{M}_e > 0$, where water leaves the region thus leaving a low pressure center and inducing a cyclonic interior geostrophic flow.

of vorticity (studied in Chapter 37), particularly the notions of vortex stretching, we see that the Ekman induced stretching/compression of interior fluid columns leads to a change in vorticity of the fluid interior, and can then lead to meridional motion due to the beta effect.

Consider an example with $\nabla \cdot \mathbf{M}_e = \hat{z} \cdot [\nabla \times (\boldsymbol{\tau}/f)] > 0$, so that winds induce a divergence within the Ekman layer. In a steady state, the interior flow accommodates this Ekman layer mass divergence by upwelling water through the Ekman layer base, $w^{(\eta_e)} > 0$. This process of entraining interior water into the Ekman layer is known as *Ekman suction* or *Ekman upwelling*. For the opposite case with $\hat{z} \cdot [\nabla \times (\boldsymbol{\tau}/f)] < 0$, water leaves (detains) from the Ekman layer and moves into the interior. Water detraining from the Ekman layer is known as *Ekman pumping* or *Ekman downwelling*. As water diverges it produces a local low pressure so that the induced flow in the geostrophic interior is cyclonic around a region of Ekman divergence/upwelling. Conversely, the induced interior geostrophic flow is anti-cyclonic around a region of Ekman convergence/downwelling. Figure 30.9 provides an illustration for the variety of cases found in the northern and southern hemispheres.

In the language of vorticity, developed in Part VII of this book, Ekman upwelling with

$w^{(\dot{\eta}_e)} > 0$ leads to vortex stretching of interior fluid columns, whereas Ekman downwelling with $w^{(\dot{\eta}_e)} < 0$ squashes the interior fluid columns. Vertical stiffening through Taylor-Proudman within the geostrophic interior, coupled to Ekman induced vortex stretching/squashing, makes what happens within the Ekman boundary layer of primary importance to the interior geostrophic flow. This boundary-interior coupling forms a key mechanism for how mechanical forcing from surface boundary stress creates the *wind driven* ocean circulation. It is notable that the coupling between boundary layer and interior flow is absent from non-rotating boundary layer flows. In Figure 30.10 we offer a highly idealized schematic of the circulation implied by Ekman dynamics in a homogeneous fluid on an f -plane, thus illustrating the coupling of the upper surface Ekman layer to the geostrophic interior and then to the bottom Ekman layer. We also briefly discuss the *geostrophic Sverdrup balance* in Section 30.4.4, which builds on the ideas in this section.

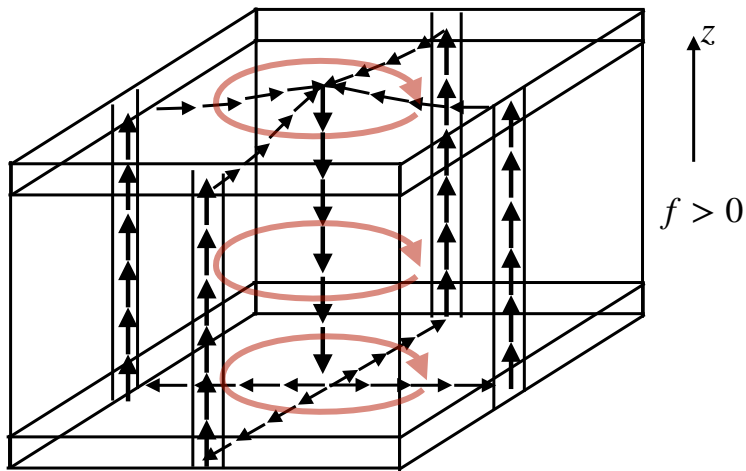


FIGURE 30.10: Schematic Ekman gyre circulation in a rectangular box in the northern hemisphere on an f -plane as forced by an anti-cyclonic wind stress curl. The wind stress curl causes fluid to pile up in the center of the gyre and develop an anti-cyclonic flow. The horizontal convergence of mass towards the center of the gyre leads to downwelling into the gyre interior below the Ekman layer (as per the upper left panel of Figure 30.9). This downwelling water enters the geostrophic interior and further into the bottom Ekman layer. As discussed in Section 30.5, the downwelling water in the bottom Ekman layer causes a horizontal divergence of mass. Assuming the domain has fixed vertical side walls, continuity requires an upwelling along the outer portion of the gyre. If the wind stress is symmetric about the center of the domain, then so is the flow. However, as studied in Section 36.7, the axial symmetry is broken on the β -plane, in which flow is stronger on the western side of the gyre even if the wind remains symmetric about the domain center. This figure is adapted from Figure 6-15 of [von Arx \(1962\)](#).

30.4.5 Further study

The following videos offer visuals to help develop further intuition for Ekman boundary flows.

- [This 4-minute video from Science Primer](#) provides an overview of how Ekman transport affects ocean circulation features near the coast and in open ocean gyres.
- [This video from MIT Earth, Atmospheric, and Planetary Sciences](#) illustrates the spiral flow found within an Ekman layer as realized in a rotating tank experiment.
- [This video from the UCLA SpinLab](#), near the 18 minute mark, shows how Ekman transport helps to explain the garbage patches found near the center of the ocean's sub-tropical gyres.
- [This video from the University of Chicago](#), starting near the 23 minute mark, provides examples of Ekman layers in a rotating tank. The other portions of this video exhibit many other novel aspects of rotating fluids and is highly recommended.

30.5 Bottom Ekman layer

In this section we study the mechanics of a bottom Ekman boundary layer. For the mass transport, we merely translate the results from the upper ocean Ekman layer considered in Section 30.4, whereby the mass transports are specified by the bottom boundary stress. We go further in this analysis by also providing an analytic expression for the velocity profile within the Ekman layer, with the velocity profile allowing us to diagnose the bottom boundary stress according to the Neumann boundary condition placed on the horizontal velocity (equation (30.58) below).

30.5.1 Horizontal mass transport within the Ekman layer

Turning the derivation from Section 30.4.1 upside-down leads to a bottom horizontal Ekman mass transport

$$\mathbf{M}_e = \int_{\eta_b}^{\eta_e} \rho_0 \mathbf{u}_e dz = -f^{-1} \hat{\mathbf{z}} \times [\boldsymbol{\tau}(\eta_e) - \boldsymbol{\tau}(\eta_b)] \approx f^{-1} \hat{\mathbf{z}} \times \boldsymbol{\tau}(\eta_b). \quad (30.46)$$

Note the sign swap relative to the upper Ekman layer transport in equation (30.33). Hence, the Ekman transport is directed to the left of the bottom stress in the northern hemisphere and to the right in the southern hemisphere. In general, care must be exercised when determining the stress, with examples given below, including an analytic example given in Section 30.5.3. In general, the stress is not aligned with the interior geostrophic flow, but instead is rotated by some amount.

Atmosphere-ocean Ekman layers

Consider the case where the bottom Ekman layer is the bottom of the atmosphere sitting over the ocean. The stress imparted to the bottom of the atmosphere is equal in magnitude yet oppositely directed to the stress acting on the upper ocean.⁷ Hence, the frictional stress induced mass transport (30.33) for the upper ocean Ekman layer is equal and opposite to the frictional stress induced mass transport in the atmosphere Ekman layer

$$\mathbf{M}_e^{\text{ocn}} = -\mathbf{M}_e^{\text{atm}} \implies \mathbf{M}_e^{\text{ocn}} + \mathbf{M}_e^{\text{atm}} = 0. \quad (30.47)$$

Since the density of the atmosphere and ocean are quite different, the equal Ekman mass transports correspond to very different volume transports.

Ocean-solid earth or atmosphere-solid earth Ekman layer

Consider the bottom Ekman layer next to the solid earth. Just like the atmosphere-ocean case, the stress imparted by the fluid on the earth is equal and opposite to the stress by the earth on the fluid. It is not generally simple to determine this stress, though we provide an example in Section 30.5.3 based on assuming information about the vertical viscosity profile within the boundary layer. From that example, we see that the stress is not directly aligned with the interior geostrophic flow just above the boundary layer. Instead, the stress is $\pi/4$ rotated to the left of the interior flow. The rotation is due to the spiralling structure of the boundary layer flow that gives rise to the stress.

⁷Recall our discussion of stress in Chapter 22, whereby stress on one side of an interface matches that on the other, which is a result following from Newton's third law.

30.5.2 Mass budget for the bottom Ekman layer

Following the derivation of the Ekman layer mass budget in Section 30.4.3, and assuming no mass enters through the solid earth, we are led to the mass budget for the bottom Ekman boundary layer⁸

$$\rho_0 w^{(\eta_e)} = \rho_0 \frac{\partial h_e}{\partial t} - \nabla \cdot \mathbf{M} \quad (30.48)$$

where $z = \eta_e(x, y, t)$ is the vertical position for the top of the bottom Ekman layer, and

$$h_e = \eta_e - \eta_b \quad (30.49)$$

is the Ekman layer thickness. For a steady state, the budget equation (30.48) says that the horizontal convergence of mass into the bottom Ekman boundary layer leads to a detrainment of mass from the Ekman layer into the interior fluid above (upwelling). Conversely, when fluid horizontally diverges from the bottom Ekman layer there is a balance from an entrainment (downwelling) of fluid from the interior into the Ekman layer. This orientation for the mass transport is illustrated in Figure 30.3 as part of our earlier discussion.

30.5.3 An analytic bottom Ekman spiral velocity

When studying the bottom boundary layer for the atmosphere or the surface boundary layer for the ocean, we are generally afforded an estimate of the frictional boundary stress, $\tau(\eta)$. In turn, we can estimate the boundary stress induced mass transport and its divergence, and we can do so without making assumptions about the density profile or viscous stresses within the boundary layer. However, this estimate is less directly accessible for the ocean bottom Ekman layer, where we need $\tau(\eta_b)$ to determine the mass transport. We here take an alternative approach that produces an analytic profile for the velocity within the Ekman layer, so long as we know the viscosity within the boundary layer. Knowing the velocity profile then affords an estimate of the boundary stress. This approach requires a few assumptions that are not always met, in particular it requires the viscosity. Even so, it provides physical insights that further our understanding of Ekman mechanics thus motivating the analysis.

Physical configuration

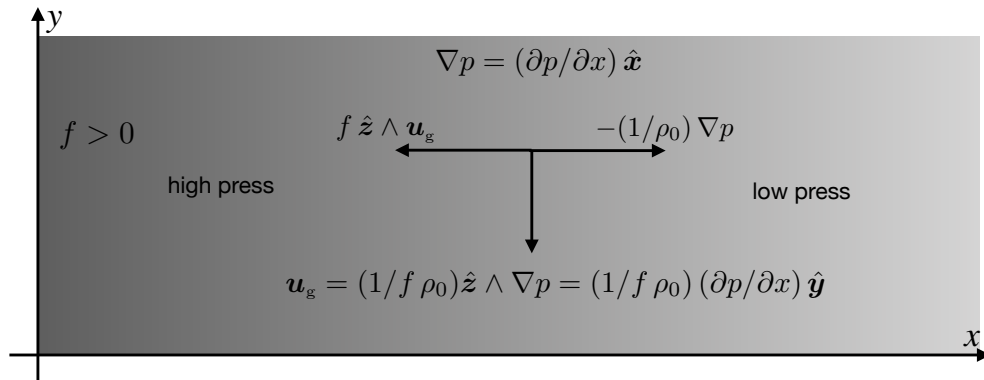


FIGURE 30.11: A southward geostrophic flow in the northern hemisphere ($f > 0$) induced by an eastward pressure gradient acceleration (low pressure to the east; $\partial p / \partial x < 0$) that balances a westward Coriolis acceleration.

⁸Note the sign swap in the budget (30.48) in front of the horizontal transport term as compared to the surface boundary layer mass budget (30.38).

We assume flow above the boundary layer is geostrophic and supported by a prescribed depth-independent pressure gradient

$$f \rho_0 \mathbf{u}_g = \hat{\mathbf{z}} \times \nabla p. \quad (30.50)$$

A specific example is given by Figure 30.11, where a southward geostrophic flow in the northern hemisphere has an eastward pressure gradient acceleration (low pressure to the east) balanced by a westward Coriolis acceleration.

For flow within the boundary layer, viscous stresses exchange horizontal momentum vertically between the inviscid interior and the bottom no-slip condition. This viscous exchange slows the boundary layer velocity relative to the interior velocity above the boundary layer. Since the pressure gradient is assumed to be depth-independent and prescribed, the slower velocity within the boundary layer means that the Coriolis acceleration is unable to balance the pressure gradient acceleration. This imbalance between pressure acceleration and Coriolis acceleration leads to a down pressure gradient component to the boundary layer velocity. As a result, the velocity spirals downward toward the bottom.

The key assumptions required to produce an analytic Ekman spiral velocity are: (i) the fluid within the Ekman layer has a constant density, ρ_0 ; (ii) the Coriolis parameter is a constant as per the f -plane; (iii) the prescribed pressure gradient is depth independent so that the associated geostrophic velocity is depth independent; (iv) the eddy viscosity is constant within the boundary layer and zero in the interior region above the boundary layer; (v) the flow is steady. The homogeneous density assumption is motivated by the rather small vertical scale of the bottom Ekman layer (tens of meters) relative to the horizontal scales over which density varies in the ocean bottom (tens to hundreds of kilometers). A constant viscosity is not always realistic since the turbulent viscosity is generally inhomogeneous within boundary layers. Even so, by assuming sufficient time for statistics to become stationary we can expect to make good use of the time averaged viscosity.

Velocity profile within the Ekman layer

Bringing the above assumptions into the frictional geostrophic equations (30.1) leads to

$$f \hat{\mathbf{z}} \times \mathbf{u} = -(1/\rho_0) \nabla p + \nu^{\text{eddy}} \partial_{zz} \mathbf{u} \quad \text{frictional geostrophic} \quad (30.51\text{a})$$

$$\partial_z (\nabla_z p) = 0 \quad z\text{-independent horizontal pressure gradient} \quad (30.51\text{b})$$

$$\mathbf{u}(\eta_b) = 0 \quad \text{no-slip bottom boundary condition} \quad (30.51\text{c})$$

$$\mathbf{u}(\infty) = \mathbf{u}_g \quad \text{matching to geostrophic interior.} \quad (30.51\text{d})$$

Decomposing the velocity into its geostrophic and ageostrophic components

$$\mathbf{u} = \mathbf{u}_g + \mathbf{u}_e, \quad (30.52)$$

leads to

$$f \hat{\mathbf{z}} \times \mathbf{u}_e = \nu^{\text{eddy}} \frac{\partial^2 \mathbf{u}_e}{\partial z^2} \quad (30.53\text{a})$$

$$\mathbf{u}_e(\eta_b) = 0 \quad (30.53\text{b})$$

$$\mathbf{u}_e(\infty) = 0. \quad (30.53\text{c})$$

To reach this result we noted that the geostrophic velocity is depth independent within the boundary layer where the density is constant, so that the geostrophic velocity does not contribute to the viscous friction operator. These coupled second order differential equations are equivalent

to the two uncoupled fourth order differential equations

$$(f^2 + \nu^2 \partial_{zzzz}) \mathbf{u}_e = 0 \quad (30.54a)$$

$$\mathbf{u}_e(\eta_b) = 0 \quad (30.54b)$$

$$\mathbf{u}_e(\infty) = 0. \quad (30.54c)$$

A solution to these equations renders the Ekman boundary layer profile

$$u = u_g \left[1 - e^{-\Delta z/h_e} \cos(\Delta z/h_e) \right] - v_g e^{-\Delta z/h_e} \sin(\Delta z/h_e) \quad (30.55a)$$

$$v = v_g \left[1 - e^{-\Delta z/h_e} \cos(\Delta z/h_e) \right] + u_g e^{-\Delta z/h_e} \sin(\Delta z/h_e) \quad (30.55b)$$

$$h_e^2 = 2 \nu^{\text{eddy}} / |f| \quad (30.55c)$$

$$\Delta z = z - \eta_b. \quad (30.55d)$$

Properties of the Ekman spiral

The spiral velocity profile (30.55a)-(30.55b) vanishes at the bottom, $\Delta z = 0$ or $z = \eta_b$, reflecting the no-slip bottom boundary condition. It also reduces to the interior geostrophic velocity at $\Delta z = \infty$. In moving downward through the boundary layer, the boundary layer current deflects to the left of the interior geostrophic current (deflection is to the right in the southern hemisphere). This deflection is consistent with the schematic in Figure 30.10. Making use of the integral identities

$$\int_{\eta_b}^{\infty} e^{-\Delta z/h_e} \cos(\Delta z/h_e) d\Delta z = h_e/2 \quad \text{and} \quad \int_{\eta_b}^{\infty} e^{-\Delta z/h_e} \sin(\Delta z/h_e) d\Delta z = -h_e/2 \quad (30.56)$$

leads to the frictionally induced mass transport within the Ekman layer

$$\mathbf{M}_e = \rho_0 \int_{\eta_b}^{\infty} \mathbf{u}_e dz \quad (30.57a)$$

$$= (h_e \rho_0/2) [-\hat{x}(u_g + v_g) + \hat{y}(u_g - v_g)] \quad (30.57b)$$

$$= f^{-1} \hat{z} \times \boldsymbol{\tau}(\eta_b), \quad (30.57c)$$

where we introduced the bottom stress according to equation (30.46). Furthermore, this stress is given by the Neumann boundary condition placed on the horizontal velocity

$$\boldsymbol{\tau}(\eta_b) = \rho_0 \nu^{\text{eddy}} \left[\frac{\partial \mathbf{u}_e}{\partial z} \right]_{z=\eta_b} = (f h_e/2) [\hat{x}(u_g - v_g) + \hat{y}(u_g + v_g)]. \quad (30.58)$$

Following from equation (30.48) we see that the bottom stress induced mass transport across the top of the bottom Ekman boundary layer is

$$\rho_0 w_{\text{Ekman}}^{(\eta_e)} = -\nabla \cdot \mathbf{M}_e = -\nabla \cdot [f^{-1} \hat{z} \times \boldsymbol{\tau}(\eta_b)] = (h_e/2) \zeta_g, \quad (30.59)$$

where we made use of the f -plane assumption to set $\nabla \cdot \mathbf{u}_g = 0$ and introduced the relative vorticity of the geostrophic flow

$$\zeta_g = \partial_x v_g - \partial_y u_g. \quad (30.60)$$

Hence, the relative vorticity of the interior geostrophic flow provides a divergence to the horizontal mass transport within the bottom Ekman layer. We illustrate the Ekman mass transport and bottom stress in Figure 30.12.

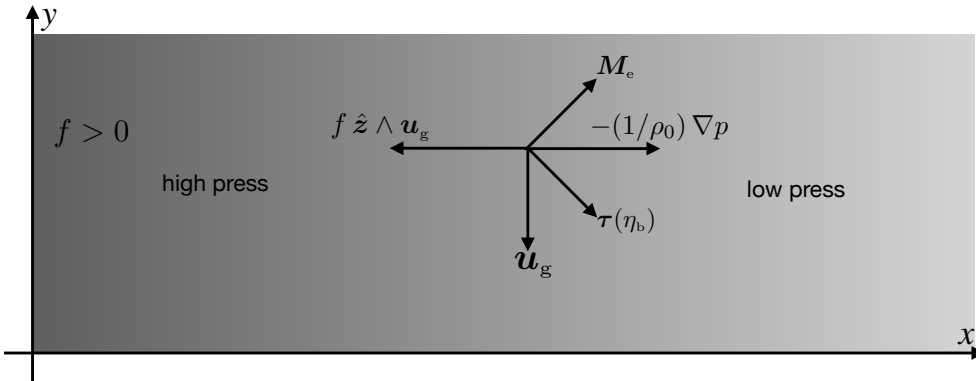


FIGURE 30.12: Mass transport and bottom stress in a homogeneous bottom Ekman layer on an f -plane in the northern hemisphere. Note how the boundary layer stress is directed $\pi/4$ radians to the left of the prescribed interior geostrophic velocity. Furthermore, the horizontal Ekman transport is itself $\pi/2$ radians to the left of the stress, which is then $3\pi/4$ to the left of the geostrophic velocity.

30.5.4 Comments

The Ekman spiral is a striking solution to the linear frictional geostrophic equations in a homogeneous fluid next to a flat no slip boundary. Section 5.7 of [Vallis \(2017\)](#) provides further discussion of the Ekman spiral solution discussed here. The spiral profile has been measured in the atmosphere and can be produced in the laboratory. However, it has proven difficult to measure in the ocean (see [Gnanadesikan and Weller \(1995\)](#) for an example). Even so, the effects from Ekman transport are robust features of the theory developed in this chapter, with those results independent of details for the vertical viscosity.

30.6 Arrested bottom Ekman flows

When studying the vertical velocity profile within the bottom boundary layer in Section 30.5, we assumed the density to be uniform within the boundary layer. A uniform density is commonly assumed for Ekman layers. However, [MacCready and Rhines \(1991\)](#), [MacCready and Rhines \(1993\)](#), and [Garrett et al. \(1993\)](#) examined that assumption in their study of bottom boundary layers in the presence of a nonzero vertical density stratification next to sloping topography. They point out the remarkable possibility of a vanishing frictional stress within the sloping bottom boundary layer. That is, rather than nonzero friction leading to a zero flow next to the bottom, flow is arrested by a compensation of pressure gradient accelerations. The vanishing frictional stress motivates the term *slippery Ekman layers*, whereas the equivalent term *arrested Ekman layer* refers to the zero boundary layer flow. We here briefly describe the arrested Ekman layer by studying Figure 30.13.

30.6.1 Description

In both panels of Figure 30.13 we depict a prescribed barotropic pressure acceleration that acts eastward and has a corresponding southward geostrophic flow ($f > 0$) and westward Coriolis acceleration. This configuration is identical to that shown in Figure 30.11 when studying the bottom Ekman spiral over a flat bottom. As the flow enters the bottom boundary layer it slows so that its Coriolis acceleration no longer balances the barotropic pressure gradient acceleration (we have seen this imbalance throughout this chapter). The bottom Ekman layer flow sends water cross-slope in the direction down the barotropic pressure gradient. In the configuration shown here, the cross-slope flow advects denser water upslope. In so doing, a horizontal baroclinic

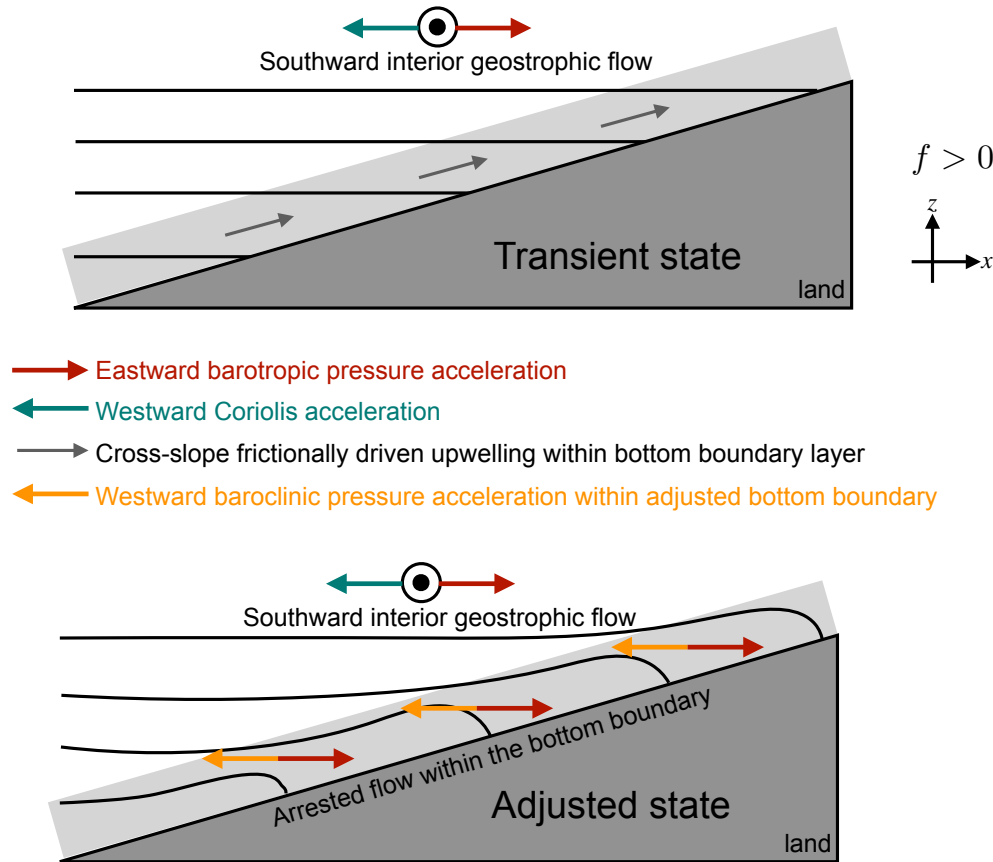


FIGURE 30.13: In both panels we depict a prescribed barotropic pressure acceleration that acts eastward and has a corresponding southward geostrophic flow and westward Coriolis acceleration. The solid lines depict lines of constant buoyancy, also known as isopycnals (see Chapter 27). Top panel: As the flow enters the bottom boundary layer it slows so that its Coriolis acceleration no longer balances the barotropic pressure, thus sending water cross slope in the down pressure gradient direction. Bottom panel: The cross-slope movement of density creates a baroclinic pressure acceleration that counteracts the barotropic pressure acceleration. The steady state is realized when the two pressure accelerations balance, in which case flow within the boundary layer halts. In this halted state there are no frictional stresses since the flow halts due to pressure effects rather than friction. Note that isopycnals are shown intersecting the solid boundary in a perpendicular direction, which is implied by the no-flux bottom boundary condition (in the absence of geothermal heating) as discussed in Section 17.6.2. Geostrophic flow in the opposite direction leads to downwelling along the bottom rather than upwelling. This figure is adapted from Figure 5 of [Wählin et al. \(2012\)](#).

pressure acceleration develops adjacent to the bottom boundary layer, with the baroclinic pressure acceleration pointing opposite to the barotropic pressure acceleration. A steady state is realized when the two pressure accelerations balance, in which case flow within the boundary layer halts.

It is remarkable that the dynamical balance for the arrested bottom boundary layer flow does not involve friction. Rather, arrest happens when the two pressure gradients balance and the Coriolis acceleration vanishes. That is, referring to the frictional geostrophic equation (30.1), each term separately vanishes in the arrested state.

30.6.2 Applications

[MacCready and Rhines \(1991, 1993\)](#) and [Garrett et al. \(1993\)](#) study the transient adjustment leading to the arrested state. They derive the expression for the time scale for adjustment to the

arrest state

$$T_{\text{arrest}} = \frac{|f|}{N^2 s^2}, \quad (30.61)$$

where s is the slope of the bottom and N^2 is the squared buoyancy frequency of the ambient water. The time is less in regions of strong stratification (N^2 relatively large), large topographic slopes (s^2 large), and low latitudes (f small). Conversely, the infinite time for either $N^2 = 0$ or $s^2 = 0$ indicates the need for both stratification and topographic slopes to render an arrest. Finally, we note the absence of any dissipation parameters (e.g., viscosity) from the time scale. Friction is needed to support the Ekman layer where flow crosses isobars, but the time to reach the arrest state is independent of friction.

[Wahlén et al. \(2012\)](#) interpreted observations from the Amundsen Sea according to the arrested Ekman boundary layer and found T_{arrest} to be just a few hours. Additionally, the numerical model studies from [Spence et al. \(2017\)](#) and [Webb et al. \(2019\)](#) point to the ability of barotropic shelf waves around Antarctica to provide an onshore directed barotropic pressure acceleration. Through the arrested Ekman layer mechanism described here, they find that the barotropic pressure is compensated through an upslope transport of relatively warm deep water in regions of the Antarctic Peninsula. Extensions and refinements of these ideas support an active area of ongoing research (e.g., [Ruan et al., 2021](#); [Peterson and Callies, 2022](#)).



30.7 Exercises

EXERCISE 30.1: EKMAN MASS TRANSPORT IN A SOUTHERN CHANNEL

Consider a southern hemisphere channel (e.g., an idealized Southern Ocean) with a zonal wind stress that has a meridional dependence such as shown in Figure 30.14. Following the discussion in Sections 30.4.1 and 30.4.4, sketch the sense for the horizontal and vertical Ekman mass transport arising from this wind stress. Show the transport for regions to the north and to the south of the wind stress maximum. Ignore the β contribution by assuming the channel is not very wide and by noting that β is smaller in the high latitudes (as relevant to the Southern Ocean).

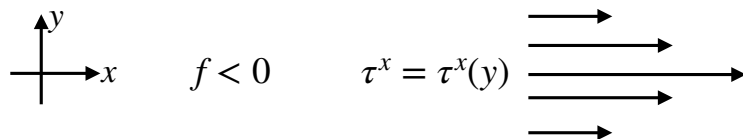


FIGURE 30.14: Zonal wind stress in a southern hemisphere channel with a maximum flanked by lower winds. What is the sense for the associated horizontal and vertical Ekman mass transport following from the discussion in Sections 30.4.1 and 30.4.4?

EXERCISE 30.2: RELATING EKMAN, ROSSBY, AND REYNOLDS NUMBERS

Under certain scalings, we can connect the Ekman number to the Rossby and Reynolds numbers. In detail, we have

$$\text{Ro} = \frac{U}{f_0 L} \quad \text{and} \quad \text{Ek} = \frac{\nu^{\text{eddy}}}{f_0 H^2} \quad \text{and} \quad \text{Re} = \frac{W H}{\nu^{\text{eddy}}}, \quad (30.62)$$

where

$$H = \text{vertical length scale} \quad (30.63\text{a})$$

$$L = \text{horizontal length scale} \quad (30.63\text{b})$$

$$U = \text{horizontal velocity scale} \quad (30.63\text{c})$$

$$W = \text{vertical velocity scale.} \quad (30.63\text{d})$$

and we defined the Reynolds number (Section 22.9) in terms of the vertical viscosity, vertical length scale, and vertical velocity scale. What is the ratio of the Rossby number to Reynolds if the flow is non-divergent?

EXERCISE 30.3: EKMAN BOUNDARY LAYERS AND RAYLEIGH DRAG

Rayleigh drag described in Section 30.2.3 allowed us to study the effects of friction on fluid trajectories. However, Rayleigh drag has no spatial derivatives, which contrasts to the Laplacian friction from Section 30.3.1 and used elsewhere in this chapter. Comment on whether Rayleigh drag can support the no-slip boundary condition and the corresponding development of a boundary layer.



Chapter 31

SPACE AND TIME DEPENDENT GRAVITY

We here formulate the dynamical equations for a geophysical fluid in the presence of a space and time dependent gravitational acceleration. This formulation has application to the study of astronomical tides in the ocean, thus motivating a discussion of the astronomical tidal forcing that follows the treatment given in Chapter 3 of [Pugh \(1987\)](#) and Section 5.15 of [Apel \(1987\)](#), with Chapter 2 of [Brown \(1999\)](#) and Section 17.4 of [Stewart \(2008\)](#) useful pedagogical supplements. Besides tides, a topic of interest to climate science concerns the study of how ocean sea level responds to changes in mass distributions associated with melting land ice. The nontrivial impact that melting land glaciers has on the earth's geoid and earth's rotation ([Farrell and Clark, 1976](#); [Mitrovica et al., 2001](#); [Kopp et al., 2010](#)) further motivates developing the dynamical equations of a liquid ocean in the presence of a space-time dependent gravity.

READER'S GUIDE TO THIS CHAPTER

This chapter assumes an understanding of the equations of motion derived in Chapter 21 as well as the gravitational and planetary centrifugal accelerations from Section 11.11. We dispense with tensor notation in this chapter, with subscripts used here as descriptive labels rather than tensor indices. No other chapter depends on the material in this chapter.

31.1 Gravitational potential	747
31.1.1 Simple geopotential	748
31.1.2 General geopotential	748
31.2 Momentum equation	748
31.3 Primitive equations	749
31.4 Depth independent perturbed geopotential	749
31.5 Forces contributing to ocean tides	750
31.5.1 Tidal acceleration in a spherically symmetric gravity field	750
31.5.2 Heuristics of tidal acceleration on the surface of a sphere	751
31.5.3 Gravitational potential for an idealized earth-moon system	753
31.5.4 Concerning realistic tides	757
31.5.5 Comments	758

31.1 Gravitational potential

In this section we summarize elements of the gravitational force, including the case with a non-constant gravitational acceleration such as occurs from astronomical tidal forcing and changes to the mass distribution of the planet.

31.1.1 Simple geopotential

As detailed in Section 11.11, the effective gravitational field incorporates the effects from the planetary centrifugal acceleration. The effective gravitational field is conservative, so that the gravitational acceleration of a fluid element can be represented as the gradient of a scalar (see Section 11.11.4),

$$\mathbf{g} = -\nabla \Phi, \quad (31.1)$$

with Φ the geopotential. In most applications of this book, the local vertical direction is denoted by

$$z = r - R_e, \quad (31.2)$$

with $z = 0$ the geopotential surface corresponding to a resting ocean and $R_e = 6.367 \times 10^6$ m the average radius of the earth (Section 11.1). The geopotential in this case is given by

$$\Phi = \Phi_0 = g z, \quad (31.3)$$

with $g \approx 9.8 \text{ m s}^{-2}$ the typical value used for the gravitational acceleration at the earth's surface.

31.1.2 General geopotential

Consider a generalized geopotential written in the form

$$\Phi = \Phi_0(r) + \Phi_1(r, \lambda, \phi, t), \quad (31.4)$$

where $\Phi_0(r)$ is the geopotential given by equation (31.3), and Φ_1 incorporates perturbations to the geopotential. For the study of ocean tides, the structure of Φ_1 arises from astronomical perturbations to the earth's gravity field. The calculation of ocean tides arising from astronomical forcing is formulated with a space-time dependent geopotential as in equation (31.4), with the radial dependence of Φ_1 neglected (e.g., Section 9.8 in [Gill, 1982](#)). [Arbic et al. \(2004\)](#) provide a discussion of global tide modelling.

Nontrivial Φ_1 variations also arise from perturbations in terrestrial masses, such as the melting of land ice such as that occurring on Greenland or Antarctica due to climate warming. These mass distribution changes lead to changes in the earth's gravitational field, its rotational moment of inertia, and the deformation of the crust (GRD as in [Gregory et al. \(2019\)](#)). Each of these effects lead to modifications in the *static equilibrium sea level*. In contrast to ocean tides, GRD perturbations associated with melting land ice are not periodic nor readily predictable. Furthermore, as evidenced by Figure 1 in [Mitrovica et al. \(2001\)](#), the amplitude of static equilibrium sea level changes can be far greater than typical open ocean tide fluctuations.

31.2 Momentum equation

As detailed in Section 21.2.3, the inviscid momentum equation for a rotating fluid in a gravitational field is given by

$$\rho \frac{D\mathbf{v}}{Dt} + 2\boldsymbol{\Omega} \times \rho \mathbf{v} = -\nabla p - \rho \nabla \Phi. \quad (31.5)$$

In writing the momentum equation in the form (31.5), we have chosen to retain an orientation afforded by the unperturbed geopotential, $\Phi_0(r)$, which are surfaces of constant z . This approach reflects that commonly used to study ocean tides. In the presence of a perturbed geopotential, Φ_1 , the "horizontal" directions defined by surfaces of constant z are no longer parallel to geopotential surfaces. We thus may interpret the sum $\nabla_z p + \rho \nabla_z \Phi$ as an orientation of the pressure gradient

along surfaces of constant geopotential, where the geopotential is determined by $\Phi = \Phi_0 + \Phi_1$, rather than just the unperturbed geopotential Φ_0 .

31.3 Primitive equations

As detailed in Section 24.1, the primitive equations reduce the vertical momentum equation to its static inviscid form, which is the hydrostatic balance

$$\frac{\partial p}{\partial z} = -\rho \frac{\partial \Phi}{\partial z} = -\rho(g + \partial_z \Phi_1). \quad (31.6)$$

The hydrostatic balance is modified from its traditional form for cases where the perturbation geopotential Φ_1 exhibits nontrivial depth dependence. Correspondingly, the horizontal momentum equation (making the Traditional Approximation from Section 24.1) takes the form

$$\rho \frac{D\mathbf{u}}{Dt} + \hat{\mathbf{z}} f \times \rho \mathbf{u} = -(\rho \nabla_z \Phi_1 + \nabla_z p) \quad (31.7)$$

where ∇_z is the horizontal gradient taken on surfaces of constant z . In their oceanic Boussinesq form (Chapter 26), the inviscid horizontal momentum equation becomes

$$\frac{D\mathbf{u}}{Dt} + \hat{\mathbf{z}} f \times \mathbf{u} = -(1/\rho_0) (\rho_0 \nabla_z \Phi_1 + \nabla_z p) \quad (31.8)$$

where ρ_0 is the constant reference density for a Boussinesq fluid. The Boussinesq form makes the addition of a perturbed geopotential quite straightforward, in which it is gradients in $\rho_0 \Phi_1 + p$ that take the place of gradients in pressure p .

31.4 Depth independent perturbed geopotential

A particularly simple form of Φ_1 occurs when it is depth independent,

$$\Phi_1 = \Phi_1(\lambda, \phi, t), \quad (31.9)$$

in which case the hydrostatic balance (31.6) returns to its traditional form $\partial_z p = -\rho g$. This form is motivated by the scale analysis in Section 31.5.3 where we find that the radial component of the earth's gravitational field greatly exceeds that from the moon or other celestial bodies, so that it is the lateral variation in the gravitational acceleration that drive tidal motions. In this case it is convenient to write the geopotential as

$$\Phi_1 = -g h, \quad (31.10)$$

with $h = h(\lambda, \phi, t)$ the perturbed geopotential height field. The full geopotential is thus written

$$\Phi = g(z - h), \quad (31.11)$$

with this form revealing that the zero of the geopotential is now set by $z = h$ rather than $z = 0$. In the study of ocean tides, h is referred to as the *equilibrium tide*. In geodesy, h is referred to as the *static equilibrium sea level*.

Since the perturbed geopotential is depth independent, it only affects the depth integrated

horizontal momentum, and it does so through the term

$$-\int_{\eta_b}^{\eta} \nabla_z \Phi_1 dz = g \int_{\eta_b}^{\eta} \nabla_z h dz = g (-\eta_b + \eta) \nabla_z h. \quad (31.12)$$

Hence, modifications to the geopotential as embodied by the perturbed geopotential height field, $h = h(\lambda, \phi, t)$, are isolated to their impacts on the horizontal pressure gradients acting on the depth integrated horizontal momentum.

31.5 Forces contributing to ocean tides

We here describe the rudiments of forces that contribute to ocean tides as well as solid-earth tides. For simplicity we focus just on the earth-moon system, though note that the sun also plays an analogous role for observed tidal motion.

31.5.1 Tidal acceleration in a spherically symmetric gravity field

Before considering the earth-moon system, we introduce the notion of *tidal acceleration*, which arises on a finite sized body placed within a non-uniform gravitational field. Figure 31.1 depicts this situation where the finite sized body is a narrow rod whose axis points towards the center of a spherically symmetric massive body. One end of the rod experiences a different gravitational acceleration than the other since the gravitational field falls off as the inverse squared distance from the center of the sphere. It is this differential gravitational acceleration that we refer to as the tidal acceleration. As we will see, its key property is that the tidal acceleration falls off as the inverse cube of the distance rather than the more familiar inverse square.

To develop a mathematical expression for the tidal acceleration, focus on the spherically symmetric gravitational field in which the gravitational acceleration at a point is given by (Section 11.11.2)

$$\mathbf{g} = -\frac{GM}{r^2} \hat{\mathbf{r}}, \quad (31.13)$$

where r is the distance from the sphere's center, G is Newton's gravitational constant, M is the mass of the sphere, and $\hat{\mathbf{r}}$ is the radial unit vector. The minus sign indicates that the gravitational acceleration points toward the center of the sphere. For the rod in Figure 31.1, the difference between the gravitational acceleration acting at a point nearest to the sphere (point B) and a point furthest from the sphere (point A) is given by

$$\mathbf{g}(r_B) - \mathbf{g}(r_A) = \mathbf{g}(r_0 - L/2) - \mathbf{g}(r_0 + L/2), \quad (31.14)$$

where r_0 is the distance from the sphere's center to the center of the rod. Assuming the rod is not long, we can expand this difference in a Taylor series about the rod center at r_0 , thus leading to an expression for the tidal acceleration

$$\mathbf{g}(r_B) - \mathbf{g}(r_A) \approx -L \frac{\partial \mathbf{g}}{\partial r} = -2L \frac{GM}{r_0^3} \hat{\mathbf{r}} = (2L/r_0) \mathbf{g}(r_0). \quad (31.15)$$

The key point to conclude from this example is that the tidal acceleration is proportional to the inverse cube of the distance to the center of the sphere. We see this property again when considering in Section 31.5.3 the gravitational acceleration generated from a remote body (e.g., the moon) acting on the surface of a sphere (e.g., the earth).

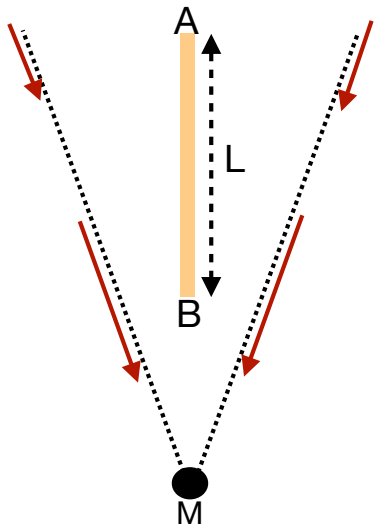


FIGURE 31.1: *Tidal acceleration* is the acceleration that acts on a finite sized object placed in a non-uniform gravitational field. The finite object is here depicted as a narrow rod of length L placed in the gravity field of a spherically symmetric body of mass M . That portion of the rod closer to the gravitating sphere (end B) experiences a stronger gravitational acceleration than the end that is further away (end A). The gradient in the gravitational acceleration constitutes the tidal acceleration acting on the rod.

31.5.2 Heuristics of tidal acceleration on the surface of a sphere

We now consider the tidal acceleration acting on the surface of a smooth massive sphere due to a spherically symmetric gravitational field generated by a neighboring massive body. Figure 31.2 depicts this system, which we consider an idealized earth-moon system where each body is assumed homogeneous and spherical. Given that they gravitationally attract one another, it is not astronomically possible for the two bodies to remain spatially fixed. Instead, they orbit around their common center of mass while conserving their angular momentum.

A central question of tidal studies is why there are generally two ocean tides per day (semi-diurnal tides) rather than just one (diurnal tides). We here offer two complementary arguments. The first is based on extending the tidal acceleration discussion of Section 31.5.1, whereas the second follows the more traditional account by considering a balance between gravitational and centrifugal accelerations.

General ideas

Every point on the surface of the earth is attracted to the earth's center by the earth's gravitational field. For a spherical earth, this attractive force is purely radial, so that it cannot lead to lateral motion on the surface of the perfect sphere. We thus conclude that the radial gravitational field is not the cause of tidal motion. Instead, tidal motion arises from a non-radial gravitational field.

The earth-moon gravitational field accelerates the earth and moon toward one another along the axis connecting their centers. Additionally, the spatial dependence of the moon's gravitational field over the earth leads to lateral forces along the earth's surface, thus providing the ingredient for ocean tidal motion. To capture the essence of this force, we examine how the moon's gravitational field acts on a point on the earth relative to its action at the center of the earth.

Sample tidal accelerations on the sphere

Again, we are tasked with computing the tidal acceleration from the moon's gravitational field for selected points on the earth, and we are computing these accelerations relative to the earth

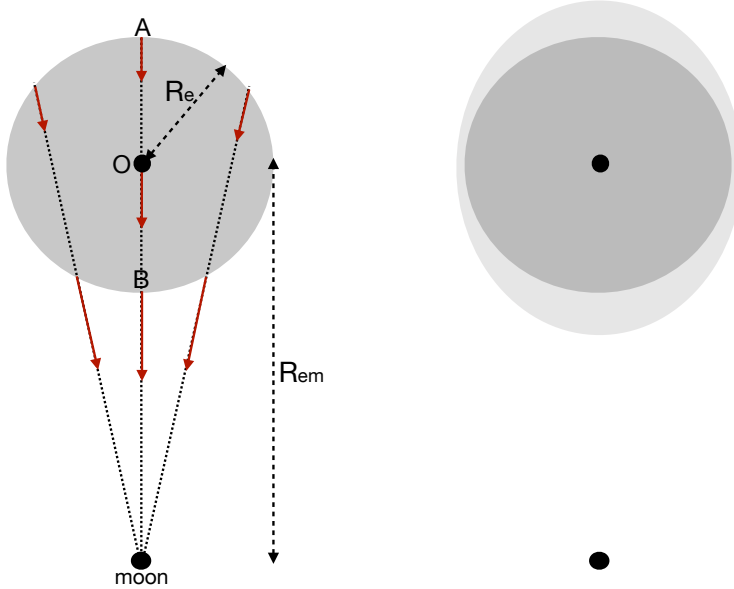


FIGURE 31.2: Illustrating the tidal force on the surface of a sphere. The sphere is an ideal depiction of the earth and the smaller massive object is the moon. The distance between the center of the earth and moon is R_{em} , and the radius of the earth is R_e . The left panel shows representative moon-generated gravitational field lines. Two points along these field lines on the surface of the earth represent the two ends of an imaginary rod as depicted in Figure 31.1. The tidal acceleration acting at point B, relative to the earth's center, points toward the moon (equation (31.16)). In contrast, the tidal acceleration at point A, relative to the earth's center, points in the opposite direction (equation (31.17)). Points on the earth surface between A and B have tidal accelerations with a non-zero component directed along the surface of the earth. Symmetry of the configuration allows us to conclude that a layer of water on the surface of the sphere will accumulate to produce two bulges as shown in the right panel. It is the lateral component of the gravitational acceleration that causes the water to accumulate to produce tidal bulges at points A and B. In contrast, the radial component to the moon's gravitational field has no contribution to the tides. Note that as shown in Section 31.5.3, the bulge shown in the right panel is greatly exaggerated.

center. As for the rod in Figure 31.1, the tidal acceleration at point B relative to the center of the earth is given by

$$\mathbf{g}(r_B) - \mathbf{g}(R_{\text{em}}) = (2R_e/R_{\text{em}}) \mathbf{g}(R_{\text{em}}). \quad (31.16)$$

This acceleration points towards the moon. In contrast, the tidal acceleration at point A relative to the center of the earth is given by

$$\mathbf{g}(r_A) - \mathbf{g}(R_{\text{em}}) = -(2R_e/R_{\text{em}}) \mathbf{g}(R_{\text{em}}), \quad (31.17)$$

which is of equal magnitude but points away from the moon.

The tidal accelerations at points A and B act radially away from the earth's center. Hence, as noted above, these radial forces do not directly lead to tidal motion at those points. However, through symmetry of the configuration, points on the surface of the sphere between A and B have a tidal acceleration from the moon's gravitational field with a nonzero lateral component. These lateral forces lead to the accumulation of water at points A and B . We can compute the gravitational acceleration at intermediate points. However, the trigonometry is somewhat complex and we prefer to compute the forces in Section 31.5.3 through use of the gravitational potential. For the current discussion we appeal to symmetry to conclude that the lateral tidal accelerations act to pile up water at both points A and B as depicted in the second panel of Figure 31.2. This argument, though heuristic, provides the means to understand how a water covered spherical planet has two bulges, rather than one, due to spatial gradients in the moon's gravitational field. We confirm this argument in Section 31.5.3 by explicitly computing the gravitational potential

for this idealized earth-moon system and then taking the gradient to compute the gravitational acceleration (see Figure 31.4).

Including orbital motion

Thus far we have ignored the orbital motion of the earth-moon system around their common center of mass. As we will see, there are no fundamental changes to the above arguments when allowing for orbital motion.

In the absence of dissipation, as assumed here, the earth-moon distance remains constant due to their angular momentum conserving orbital motion. From a force-balance perspective, the two spherical bodies remain in a fixed orbit since the gravitational acceleration acting at their centers is balanced by their respective centrifugal accelerations, where the centrifugal acceleration is computed relative to the center of mass of the two-body system. The gravitational acceleration from the moon, acting at the center of the earth, is given by the *free fall* value $\mathbf{g}(R_{\text{em}})$, which has magnitude $GM_{\text{m}}/R_{\text{em}}^2$ and is directed along the axis connecting the earth and moon centers.

Furthermore, when a body exhibits orbital motion, each point on the body exhibits the same orbital motion and has the same linear velocity. Consequently, each point on the earth possess the same centrifugal acceleration

$$\mathbf{a}_{\text{orbital centrifugal}} = -\mathbf{g}(R_{\text{em}}). \quad (31.18)$$

This property of orbital motion is distinct from the spinning motion of a planet rotating about its axis, whereby points further from the rotational axis have larger centrifugal acceleration (see Section 11.11). To help understand orbital motion, move your hand in a circle while maintaining the arm in a single direction so that the hand exhibits an orbital motion rather than a spinning motion. Notice that all parts of the hand move with the same linear velocity and exhibit the same orbital motion. Hence, each point on the hand has the same centrifugal acceleration.

We can now ask about the acceleration felt by a point on the surface of the earth. The acceleration giving rise to tidal motions is the sum of the gravitational acceleration from the moon plus the centrifugal acceleration due to orbital motion. However, this calculation is identical to that considered previously, which led, for example, to the tidal accelerations for points *B* and *A* as given by equations (31.16) and (31.17). We are thus led to the same result as before.

31.5.3 Gravitational potential for an idealized earth-moon system

We now perform a more thorough calculation of the gravitational acceleration by computing the gradient of the gravitational potential. First recall the discussion of Newton's gravitational law in Section 11.11.2, whereby the gravitational potential for a point at distance r from the center of a spherical earth is given by

$$\Phi_{\text{e}}(r) = -\frac{GM_{\text{e}}}{r}, \quad (31.19)$$

where M_{e} is the mass of the earth. The corresponding radial gravitational acceleration is given by

$$\mathbf{g}_{\text{e}} = -\nabla\Phi_{\text{e}} = -\frac{GM_{\text{e}}\hat{\mathbf{r}}}{r^2}. \quad (31.20)$$

The same considerations hold for the moon's gravitational potential. Hence, referring to Figure 31.3, the moon's gravitational potential evaluated at a distance L from the moon's center is given by

$$\Phi_{\text{m}}(L) = -\frac{GM_{\text{m}}}{L}. \quad (31.21)$$

Trigonometry leads to the law of cosines relation

$$L^2 = (R_{\text{em}} - r \cos \psi)^2 + (r \sin \psi)^2 = R_{\text{em}}^2 + r^2 - 2 r R_{\text{em}} \cos \psi, \quad (31.22)$$

where again r is the distance to the earth's center and ψ is the polar angle relative to the \hat{x} axis pointing between the earth and moon centers (see Figure 31.3).

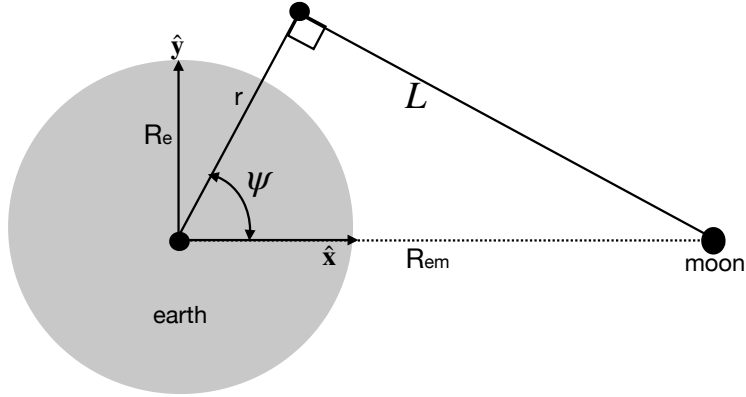


FIGURE 31.3: Geometry of an idealized earth-moon system. The center of the earth is a distance R_{em} from the center of the moon; the moon has a mass M_m ; and the earth has a radius R_e . An arbitrary test point is shown a distance L from the center of the moon, r from the center of the earth, and with a polar angle ψ relative to the \hat{x} axis, where the \hat{x} axis points from the earth center to the moon center. Relative to the earth's center, the test point has Cartesian coordinates $(x, y) = r(\cos \psi, \sin \psi)$. See Section 9.3 for details on relating polar and Cartesian coordinates.

Identifying the leading order contributions

Assuming the test point in Figure 31.3 is closer to the earth than to the moon, we can perform a Taylor series expansion in the small parameter r/R_{em} to render

$$\Phi_m(L) = -\frac{GM_m}{L} = -\frac{GM_m}{R_{\text{em}}} \left[1 + \frac{r \cos \psi}{R_{\text{em}}} + \frac{r^2}{2R_{\text{em}}^2} (3 \cos^2 \psi - 1) + \mathcal{O}(r/R_{\text{em}})^3 \right]. \quad (31.23)$$

We thus identify the leading three terms to the geopotential

$$\Phi_m^{(0)} = -\frac{GM_m}{R_{\text{em}}} \quad (31.24)$$

$$\Phi_m^{(1)} = -\frac{GM_m}{R_{\text{em}}^2} r \cos \psi \quad (31.25)$$

$$\Phi_m^{(2)} = -\frac{GM_m}{2R_{\text{em}}^3} r^2 (3 \cos^2 \psi - 1). \quad (31.26)$$

Assuming the distance between the earth and moon remains fixed, the zeroth order term $\Phi_m^{(0)}$ is a spatial constant and thus leads to no gravitational acceleration. We now examine the gravitational accelerations from the other two terms.

Acceleration maintaining the orbiting earth-moon system

For the first order term, $\Phi_m^{(1)}$, we introduce the Cartesian coordinate as in Figure 31.3 to write

$$\Phi_m^{(1)} = -\frac{GM_m x}{R_{em}^2}, \quad (31.27)$$

where $x = r \cos \psi$ is the distance along \hat{x} . Hence, the gradient of $\Phi_m^{(1)}$ leads to the gravitational acceleration

$$\mathbf{g}_m^{(1)} = -\nabla \Phi_m^{(1)} = \hat{x} \frac{GM_m}{R_{em}^2}. \quad (31.28)$$

This gravitational acceleration has a constant magnitude at every point in space and it everywhere points in a direction parallel to the earth-moon axis. Furthermore, the magnitude of $\mathbf{g}_m^{(1)}$ equals to that of the moon's gravitational acceleration, \mathbf{g}_m , when evaluated at the earth's center. As seen in Section 31.5.2, the acceleration $\mathbf{g}_m^{(1)}$ maintains the earth in orbit about the center of mass for the earth-moon system; i.e., this is the free fall acceleration towards the moon. Notably, at the earth's surface, the magnitude of $\mathbf{g}_m^{(1)}$ is tiny relative to the gravitational acceleration from the earth itself, with their ratios given by

$$\frac{M_m/R_{em}^2}{M_e/R_e^2} \approx 3.4 \times 10^{-6}, \quad (31.29)$$

where we set

$$M_e = 5.97 \times 10^{24} \text{ kg} \quad M_m = 7.35 \times 10^{22} \text{ kg} = (1/81.2) M_e \quad (31.30a)$$

$$R_e = 6.367 \times 10^6 \text{ m} \quad R_{em} = 3.84 \times 10^8 \text{ m} = 60.3 R_e. \quad (31.30b)$$

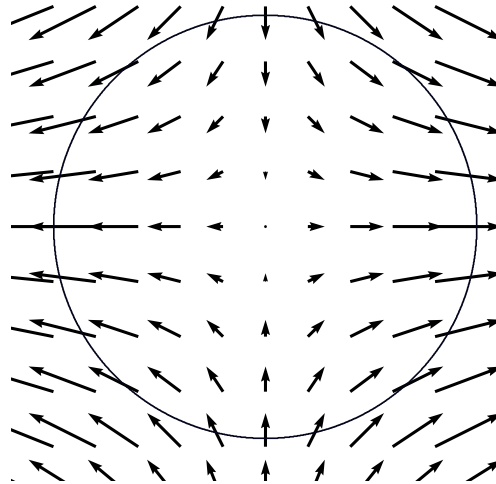


FIGURE 31.4: The tide producing gravitational acceleration $\mathbf{g}_m^{(2)}$ given by equation (31.34). The moon is assumed to be positioned in the equatorial plane of the earth.

Tide producing geopotential

The main tide producing acceleration results from $\Phi_m^{(2)}$. Introducing the second Cartesian coordinate, $y = r \sin \psi$, leads to

$$\Phi_m^{(2)} = -\frac{GM_m}{2R_{em}^3} r^2 (3 \cos^2 \psi - 1) = -\frac{GM_m}{2R_{em}^3} (2x^2 - y^2). \quad (31.31)$$

The corresponding perturbed geopotential height field (see equation (31.11)) is given by

$$h = -\frac{\Phi_m^{(2)}}{g} = \frac{R_e^2}{2R_{em}^3} \frac{M_m}{M_e} r^2 (3 \cos^2 \psi - 1). \quad (31.32)$$

Placing the test point on the earth surface, $r = R_e$, renders

$$h = \frac{R_e^4}{2R_{em}^3} \frac{M_m}{M_e} (3 \cos^2 \psi - 1) \approx 2.8 \times 10^{-8} R_e (3 \cos^2 \psi - 1). \quad (31.33)$$

Plugging in numbers for the earth-moon system suggests that the maximum perturbation to the geopotential height arising from the moon's gravity field is roughly 36 cm. Correspondingly, the bulge shown in Figure 31.2 is greatly exaggerated. Note that ocean tidal amplitudes can get much larger (order meters) than this "equilibrium tide" amplitude due to resonances from ocean geometry, with the Bay of Fundy in Nova Scotia a particularly striking example.

Tide producing acceleration

The gravitational acceleration arising from the tidal potential is determined by the gradient of the tidal geopotential

$$\mathbf{g}_m^{(2)} = -\nabla \Phi_m^{(2)} = \frac{GM_m}{R_{em}^3} (2x \hat{\mathbf{x}} - y \hat{\mathbf{y}}). \quad (31.34)$$

We illustrate the vector field $\mathbf{g}_m^{(2)}$ in Figure 31.4. Note how the accelerations lead to two bulges on opposite sides of the planet. We can write this acceleration using polar coordinates by introducing the polar unit vectors $\hat{\mathbf{r}}$ and $\hat{\psi}$ according to Section 9.3.2

$$\hat{\mathbf{r}} = \hat{\mathbf{x}} \cos \psi + \hat{\mathbf{y}} \sin \psi \quad (31.35a)$$

$$\hat{\psi} = -\hat{\mathbf{x}} \sin \psi + \hat{\mathbf{y}} \cos \psi \quad (31.35b)$$

thus rendering

$$\mathbf{g}_m^{(2)} = \frac{GM_m R_e}{R_{em}^3} \left[\hat{\mathbf{r}} (3 \cos^2 \psi - 1) - (3/2) \hat{\psi} \sin 2\psi \right], \quad (31.36)$$

where we evaluated the acceleration at the earth surface so that $r = R_e$. Evaluating the acceleration at $\psi = 0, \pi$ verifies the heuristic calculation performed in Section 31.5.2 for points on the earth surface nearest and furthest from the moon. We can further gauge the magnitude of the tidal acceleration by introducing the acceleration due to the earth's gravity field

$$\mathbf{g}_m^{(2)} = g_e \frac{M_m}{M_e} \frac{R_e^3}{R_{em}^3} \left[\hat{\mathbf{r}} (3 \cos^2 \psi - 1) - (3/2) \hat{\psi} \sin 2\psi \right], \quad (31.37)$$

where $g_e = GM_e/R_e^2$ is the acceleration at the earth's surface from the earth's gravity field. The dimensional prefactor has magnitude $\approx 5.6 \times 10^{-8} g_e$, so that the tidal acceleration is tiny relative to that from the earth's gravity field. It is for this reason that the radial component of the tidal

acceleration is largely irrelevant since it is dominated by the far larger radial component of the earth's gravity field. However, the angular component of the tidal acceleration, although small relative to the earth's radial gravitational acceleration, is able to move water along the surface of the planet as indicated by Figure 31.4, thus leading to tidal motion.

31.5.4 Concerning realistic tides

Our discussion of tides has been rather terse, aiming to identify key aspects of the tidal accelerations but giving little attention to details that impact real ocean tides. Here are a few points that must be considered for these purposes.

- As the earth spins under the tidal bulges, there are two high and two low tides per day. Additional orbital motion of the moon adds roughly 50 minutes per day to the diurnal (daily) tide and 25 minutes to the semi-diurnal (twice daily).
- The moon orbits the earth at a latitude of roughly $28.5^\circ N$ rather than within the equatorial plane, so that the tidal bulges are offset from the equator. As the earth spins under the bulges, one of the high tides is generally larger than the other due to the offset. This offset in turn introduces a diurnal component to the tides in addition to the semi-diurnal.
- The sun contributes to tides in a manner similar to the moon. The sun is more massive than the moon, yet it is further away, so that the ratio of the magnitudes for the tidal producing accelerations is given by

$$\frac{\text{moon tidal acceleration}}{\text{sun tidal acceleration}} = \frac{M_m/R_{em}^3}{M_s/R_{es}^3} \approx 2.2 \quad (31.38)$$

where we set

$$M_s = 1.99 \times 10^{30} \text{ kg} \quad R_{es} = 23460 R_e. \quad (31.39)$$

Hence, the moon has an impact on tides that is somewhat more than double that of the sun.

- The gravitational acceleration that leads to the tidal bulge moves around the mid-latitudes at roughly 330 m s^{-1} , which is faster than the $\approx 200 \text{ m s}^{-1}$ wave speed for shallow water gravity waves. Hence, the ocean tidal motion is never equilibrated to the *equilibrium tides* defined by the tidal acceleration. In contrast, solid-earth waves are much faster and so the solid-earth tidal motions are mostly equilibrated with the equilibrium tidal acceleration. Solid-earth tides have an amplitude on the order of 10 cm with wavelengths spanning the planet. Hence, an accurate treatment of ocean tides must take into account the solid-earth tides.
- The movement of ocean mass modifies the earth's gravity field and the domain within with the ocean moves, and these effects are referred to as *self attraction and loading* (SAL). The loading term arises from alterations in the mass felt by the solid earth that leads the crust to expand or compress. Self-attraction arises from modifications to the gravity field due to self-gravity of both the load-deformed solid earth and the ocean tide itself. Locally, SAL can contribute to roughly 20% of the ocean tide amplitude, so that accurate tide modeling must include SAL. [Barton et al. \(2022\)](#) provide an example of global ocean tide modeling that includes a discussion of how to compute the SAL terms online during a simulation.
- Geometry of the ocean plays a leading role in determining tides at a particular location. We have incomplete information about the geometry of ocean basins, such as the presence

of deep ridges, troughs, and seamounts. In lieu of such information we can garner useful information based on the analysis of past tides, with that information used to fit sinusoidal waves to the measured time series for use in projecting forward in time.

31.5.5 Comments

A key feature of the tidal producing forces is that it is the lateral (along-earth) component of the moon's tidal gravitational force that produces the earth's tides. These lateral forces cause water to accumulate at the point nearest to and furthest from the moon (points *A* and *B* in Figure 31.2), thus producing the characteristic double-bulge pattern. Notably, many common literature presentations make it appear that it is the radial (i.e., pointing to the earth's center) component of the moon's gravitational force, and its gradient across the earth, that leads to the earth's tidal bulges. But as discussed in Section 31.5.2, radial gravitational forces cannot lead to tidal motions; what is needed is a force that leads to lateral motion. These key notions are nicely emphasized in [this Space Time video](#).



Part VI

Shallow water mechanics

Adiabatic shallow water models consist of constant density homogeneous fluid layers whose interfaces are material (i.e., no matter is transferred between the immiscible layers). Thermodynamic processes are absent from the system, thus allowing us to focus on the dynamics of fluid layers. Pressure is hydrostatic, which means that motion occurs in columns whereby horizontal velocity is independent of the vertical position within a layer, whereas the column can expand and contract so that there is vertical motion within a layer. Horizontal momentum is transferred between shallow water layers via pressure form stresses that act on sloping layer interfaces. Our goal in this part of the book is to develop an understanding of the shallow water model fundamentals and to study some basic dynamical features as realized in the model. We have further use of the shallow water model in our study of vorticity in Part VII, balanced flows in Part VIII, waves in Chapter 48, and generalized vertical coordinates in Part XI.

The shallow water mode offers a suite of versatile theoretical models of use to deduce impacts on the flow from both rotation and (when multiple layers are used) stratification. Consequently, the shallow water model is featured in many areas of geophysical fluid mechanics as well as in ocean and atmosphere applications. Additionally, there is a direct analogy between shallow water flow and compressible fluid flow, in which the *in situ* density of a compressible fluid corresponds to the layer thickness of a shallow water fluid. Furthermore, the acoustic waves of compressible flow (Chapter 44) are directly analogous to the gravity waves of shallow water flow (Section 48.5). Shallow water flow is somewhat simpler, however, since it is horizontal within a layer. For these reasons, the shallow water model has found great use both inside and outside of geophysical fluid mechanics.

We offer a comment concerning the mathematics required for studying the shallow water model. Namely, the shallow water model is a vertically discrete realization of a continuously stratified fluid described by the isopyncal coordinates of Chapter 59. However, the mathematical formalism of generalized vertical coordinates developed in Part XI of this book is largely unnecessary when working with the shallow water model. The reason for the simplification is that columnar motion within a shallow water layer means that lateral gradients of properties need not be projected along the slope of the layer. In contrast, this projection is needed for a continuously stratified fluid described by generalized vertical coordinates (e.g., see Figure 56.4). So although we appreciate the beauty and power of generalized vertical coordinate mathematics for studying continuously stratified flows, it is liberating to avoid that formalism while still capturing much of the underlying physics associated with stratification (albeit discretely stratified). This feature of the shallow water model greatly adds to its allure and accessibility.

Chapter 32

FORMULATING SHALLOW WATER MODELS

In this chapter we formulate the kinematic and dynamic equations for a suite of shallow water models. For this purpose we develop the equations describing motion of a single shallow water layer; multiple shallow water layers (stacked shallow water); and reduced gravity models (models with one layer that is dynamically inactive). In formulating these models we also expose their underlying physical basis.

READER'S GUIDE TO THIS CHAPTER

We make use of fluid kinematics and dynamics described in earlier chapters. Our presentation was inspired by Chapter 3 of [Vallis \(2017\)](#) as well as various sections in [Salmon \(1998\)](#). We make use of the formulation here for further study of the shallow water fluid mechanics, including dynamical balances in Chapter 33, vorticity mechanics in Chapter 36, and wave mechanics Chapter 48.

The horizontal velocity is vertically uniform within a shallow water layer, whereas the vertical velocity and hydrostatic pressure are linear functions of vertical position within the layer. When acting on a property that is vertically uniform within a layer, the gradient operator, ∇ , results in a horizontal vector. To minimize notational clutter, we typically write ∇ for brevity, rather than the more clumsy ∇_k or ∇_z (with k the layer index). The meaning of the resulting vector equations will be clear from the functional dependencies of the fields present in the equations.

[This video](#) offers a pedagogical introduction to shallow water waves and to the general phenomenology of a shallow water layer.

32.1	Loose threads	762
32.2	A single shallow water layer	762
32.2.1	Pressure gradient force within the fluid layer	762
32.2.2	Effective sea level and the inverse barometer sea level	764
32.2.3	Further comments on pressure in a homogeneous layer	765
32.2.4	Momentum equation	766
32.2.5	Thickness equation	766
32.2.6	Bottom kinematic boundary condition	768
32.2.7	Surface kinematic boundary condition	769
32.2.8	Column stretching and vertical velocity	770
32.2.9	Tracer concentration equation	771
32.2.10	Summary comments	772
32.3	Reduced gravity model for the upper ocean	773
32.3.1	Momentum and thickness equations for the active layer	773
32.3.2	Relating undulations of the top and bottom layer interfaces	774

32.3.3	Momentum equation with reduced gravity	775
32.3.4	Reduced gravity and relative buoyancy	775
32.3.5	Further study	776
32.4	Stacked shallow water equations	776
32.4.1	Formulation of a 2-layer model	777
32.4.2	N -layer model equations	780
32.4.3	Dynamic pressure and the Montgomery potential	781
32.4.4	Properties of the vertical velocity	781
32.4.5	Rigid lid models	783
32.5	Vector-invariant velocity equation	784
32.5.1	Basic manipulations	784
32.5.2	Dynamical pressure and the Magnus acceleration	785
32.6	Non-conservative processes and boundary stresses	785
32.6.1	Di-a-surface volume fluxes	785
32.6.2	Frictional and boundary stresses	787
32.7	Exercises	788

32.1 Loose threads

- Internal and external mode as per Raymond's notes.

32.2 A single shallow water layer

Consider a homogeneous layer of fluid in a uniform effective gravitational field (gravity plus planetary centrifugal as in Section 11.11.4), contained on its side by solid boundaries. If there are no lateral force imbalances, then the fluid remains static. Now perturb the fluid so that it has a nonuniform layer thickness, say with a bump in a particular region. Conservation of fluid mass (which translates into volume conservation for a uniform density layer) means that thicker fluid regions must be exactly compensated by thinner fluid regions. Furthermore, layer thickness gradients create pressure differences (thicker water has larger hydrostatic pressure than thinner water), which in turn drives fluid motion. If the fluid has much larger lateral extent than vertical, then the lateral motion occurs as an expanding and contracting column with no depth dependence to the horizontal pressure forces and thus the horizontal motion is depth independent.

The essence of a perfect fluid (i.e., no irreversible processes such as mixing) shallow water flow concerns the motion of fluid columns accelerated by pressure gradients created by layer thickness undulations, and the associated conservation of mass ensuring that the accumulation of fluid in one region is balanced by the depletion of fluid in another. Pressure gradients act to homogenize the layer thickness. However, rotation allows for layer thickness to be non-constant even in a steady state.

32.2.1 Pressure gradient force within the fluid layer

Figure 32.1 shows a single shallow water layer with a generally non-flat bottom and an undulating free surface height. We assume that each column of fluid within the layer is in hydrostatic balance, so that the vertical momentum equation reduces to

$$\frac{\partial p}{\partial z} = -\rho g. \quad (32.1)$$

Recall from Section 24.2 that the hydrostatic balance is consistent with lateral length scales much larger than vertical (small vertical to horizontal aspect ratio), which is satisfied by large-

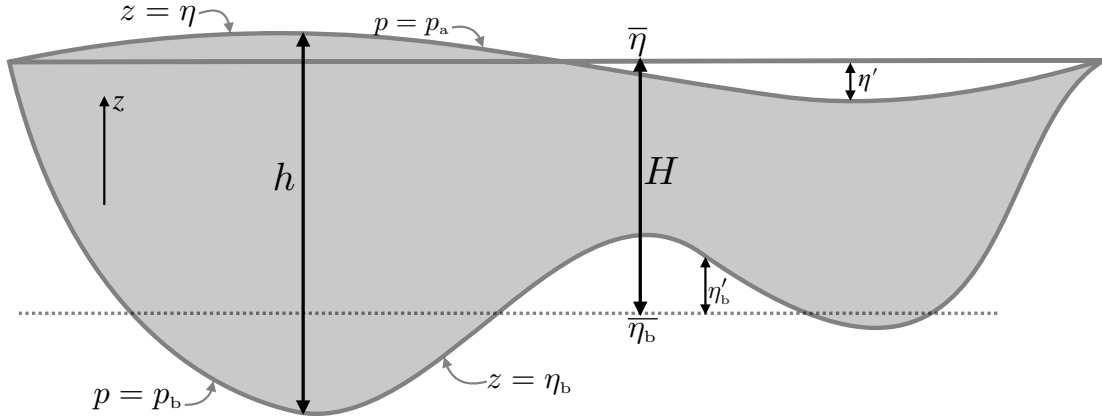


FIGURE 32.1: A single layer of shallow water fluid with thickness $h = \eta - \eta_b$ that extends from the bottom at $z = \eta_b$ to the free surface at $z = \eta$. The area averaged thickness is defined by $H = \bar{h} = A^{-1} \int h \, dx \, dy = A^{-1} \int (\eta - \eta_b) \, dx \, dy = \bar{\eta} - \bar{\eta}_b$, where $A = \int dx \, dy$ is the horizontal area of the layer. The deviation of the free surface from $\bar{\eta}$ is given by $\eta' = \eta - \bar{\eta} = \eta - (\bar{\eta}_b + H)$ so that $\eta(x, y, t) = \eta_b(x, y) + h(x, y, t) = \bar{\eta}_b + H + \eta'(x, y, t)$. Likewise, the deviation of the bottom from $\bar{\eta}_b$ is given by $\eta'_b = \eta_b - \bar{\eta}_b$, so that $h = \eta - \eta_b = H + \eta' - \eta'_b$. Volume conservation for the layer is maintained in the absence of volume boundary fluxes, in which case $\bar{\eta}' = 0$. Note that the position of the reference height, $z = 0$, is arbitrary. Atmospheric conventions typically set $z = 0$ so that $\bar{\eta}_b = 0$, $\eta = H + \eta'$, and $\bar{\eta} = H$. Oceanic conventions typically choose $\bar{\eta} = 0$ so that $\eta = \eta'$ and $\bar{\eta}_b = -H$. We are only concerned with fluctuations that leave the free surface monotonic; i.e., we do not consider overturns or breaking waves. This assumption is implied by assuming that each column extending from $\eta_b \leq z \leq \eta$ maintains hydrostatic balance.

scale geophysical fluid motion. Hence, a shallow water fluid is a relevant idealization if we are considering horizontal scales that are very large relative to vertical scales.

Since the fluid density is assumed constant (i.e., the fluid is a homogeneous layer), we can integrate the hydrostatic balance from the surface to an arbitrary vertical position within the layer

$$p(x, y, z, t) = p_a(x, y, t) + g \rho \int_z^\eta dz = p_a(x, y, t) + g \rho [\eta(x, y, t) - z], \quad (32.2)$$

where $p_a(x, y, t)$ is the pressure applied to the layer free surface, say from the overlying atmosphere. Furthermore, the horizontal pressure gradient thus takes the form

$$\nabla_z p = \nabla_z p_a + g \rho \nabla_z \eta. \quad (32.3)$$

This pressure gradient is depth independent within the layer, as depicted in Figure 32.2.

For the left hand side of the pressure gradient in equation (32.3), it is useful to write ∇_z since the pressure within a layer is a function of z (equation (32.2)), whereas for the horizontal momentum equation we only want the horizontal pressure gradient. For the right hand side, p_a and η are independent of z , so that there is no need to expose the z subscript on the gradient operator. We thus drop the subscript when no ambiguity results, as per our convention noted at the start of the chapter.

Layer depth independent pressure gradient force

We emphasize that although hydrostatic pressure within a shallow water layer is depth dependent as per equation (32.2), the horizontal pressure gradient, as given by equation (32.3), has no depth dependence within the layer. The acceleration from this hydrostatic pressure force points from highs in the effective sea level to lows in the effective sea level (see Figure 32.2). The depth-

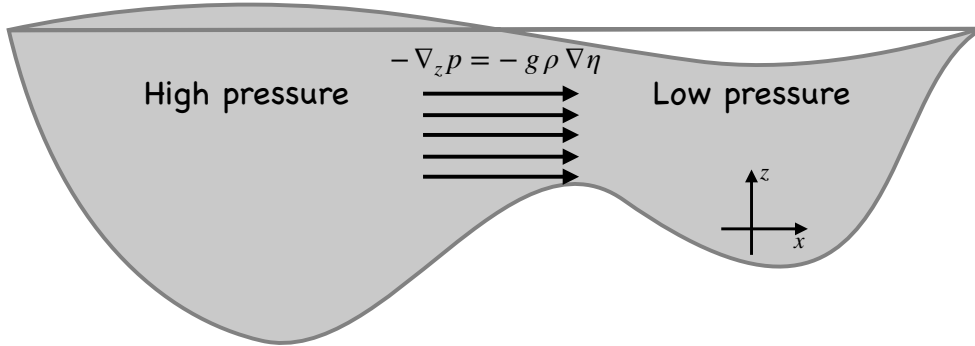


FIGURE 32.2: The horizontal pressure gradient within a shallow water layer is independent of the depth within that layer. In this schematic we assume here are zero horizontal gradients in the applied surface pressure, $\nabla p_a = 0$, in which case the horizontal acceleration from pressure within a single shallow water fluid layer is determined solely by the surface height, $-\nabla_z p = -g \rho \nabla \eta$. The acceleration is uniform throughout the layer and points from sea level highs towards sea level lows. Although bottom topography interacts with the flow and thus affects the shape of the free surface, the topography does not appear explicitly in the horizontal pressure gradient (though the bottom shape does affect bottom form stresses as per the discussion in Sections 25.1 and 33.4). Instead, we only need to know the shape of the free surface (and the applied pressure p_a) to know the horizontal pressure force throughout the layer.

independence of the pressure gradient within a shallow water layer holds also for multiple shallow water layers as discussed in Section 32.4, in which case the horizontal velocity has no vertical structure within any layer.

Pressure gradient force only depends on layer interface gradients

It is notable that the horizontal pressure gradient is solely determined by properties at the upper interface of the layer. That is, we only need to know the shape of the free surface, $z = \eta$, and the applied pressure, p_a , to know the horizontal pressure force acting throughout the layer. There is no explicit dependence on the shape of the bottom topography. The result also holds for the stacked shallow water model discussed in Section 32.4, whereby horizontal pressure gradients are determined by gradients in the layer interfaces and with no appearance of the bottom topography. This characteristic is specific to the use of a pressure gradient body force to describe the role of pressure on the layer momentum. As a complement, we saw in Chapter 25 how to formulate the pressure contact force. It is through the contact force perspective that we see, in Section 33.4, how bottom topography appears in the momentum balance of a shallow water layer. In particular, this perspective exposes the topographic form stresses that mechanically exchange momentum between the layer and the solid earth bottom.

32.2.2 Effective sea level and the inverse barometer sea level

When considering a nonzero atmospheric pressure, we sometimes find it useful to introduce an *effective free surface height*

$$\eta^{\text{eff}} = \eta + p_a / (\rho g), \quad (32.4)$$

with gradients in the effective sea level leading to horizontal motion. However, when considering motions on time scales longer than a few days, the ocean free surface adjusts under atmospheric loading towards an *inverse barometer sea level*. An inverse barometer sea level compensates to atmospheric pressure so that there is no horizontal pressure gradient, and so there is no motion induced by the atmospheric pressure. Hence, all that matters for motion are deviations from the

inverse barometer sea level.¹

We expose details to support the above comments by writing pressure within the shallow water layer as

$$p(z) = p_a + \rho g (\eta - z) \quad (32.5a)$$

$$= \bar{p}_a + (p_a - \bar{p}_a) + \rho g (\eta - z) \quad (32.5b)$$

$$= \bar{p}_a + \rho g (\eta - \eta^{ib} - z). \quad (32.5c)$$

In these equations we introduced the area mean atmospheric pressure, \bar{p}_a , as well as the inverse barometer sea level

$$\rho g \eta^{ib} = \bar{p}_a - p_a. \quad (32.6)$$

The inverse barometer sea level is defined according to deviations of the atmospheric pressure from its area mean. Hence, when the atmospheric pressure is higher than the area mean, $p_a > \bar{p}_a$, then the inverse barometer sea level is negative, $\eta^{ib} < 0$, reflecting the downward depression of the inverse barometer sea level. In contrast, $\eta^{ib} > 0$ for anomalously low pressures, $p_a < \bar{p}_a$.

Introducing the inverse barometer sea level brings the horizontal pressure gradient to the form

$$\nabla_z p = \nabla p_a + g \rho \nabla \eta = \rho g \nabla \eta^{\text{eff}} = \rho g \nabla(\eta - \eta^{ib}). \quad (32.7)$$

If sea level adjusts to the atmospheric pressure so that $\nabla \eta = \nabla \eta^{ib}$, then there is no horizontal pressure gradient in the shallow water layer, in which case there is no induced motion from the atmospheric pressure. It follows that for dynamical purposes, we can seamlessly incorporate atmospheric pressure into the formalism by working with deviations of sea level from the inverse barometer sea level, $\eta - \eta^{ib}$.

32.2.3 Further comments on pressure in a homogeneous layer

The depth independence of the horizontal pressure gradient within the shallow water layer is a direct result of the assumed hydrostatic nature of the pressure within the layer. To emphasize this point, we certainly can imagine a homogeneous fluid layer in which the horizontal velocity has a vertical shear. For example, in Section 45.3 we study surface gravity waves in a homogeneous fluid layer. Such waves have an amplitude that exponentially decays with depth, and so the horizontal and vertical fluid motion associated with the waves have a non-zero vertical shear. Such motion clearly cannot be caused by a hydrostatic pressure gradient since it has no vertical dependence throughout the layer, in which case

$$\partial_z(\nabla_z p_{\text{hydrostatic}}) = 0. \quad (32.8)$$

Hence, in a homogeneous fluid layer, hydrostatic pressure gradients can only drive a horizontal flow that is depth independent within that layer. So if the vertically sheared horizontal flow is found within a homogeneous fluid layer, and if pressure gradients cause this flow, then it can only be through gradients in the *non-hydrostatic pressure*. As discussed in Section 45.2.4, surface gravity waves indeed involve non-hydrostatic pressure forces that drive the vertical dependence to the wave amplitude.

Moving beyond the homogeneous layer assumption, we saw in Section 24.2.6 that a horizontal gradient in the density leads to a vertically dependent hydrostatic pressure gradient

¹The discussion in this section follows Appendix C to [Griffies and Greatbatch \(2012\)](#), where further details are provided. In particular, they allow for continuously stratified density rather than the shallow water model considered here. Even so, the key points from the shallow water discussion hold for the continuously stratified case.

$\partial_z(\nabla_z p_{\text{hydrostatic}}) \neq 0$. This hydrostatic pressure force can impart vertical shears to the horizontal flow. Thermal wind shear is the canonical example whereby vertical shears in the horizontal velocity are present in geostrophically balanced fluids as driven by horizontal density gradients (Section 28.4.4). We encounter the shallow water version of thermal wind in Section 33.2.2.

32.2.4 Momentum equation

If there is no friction anywhere in the fluid, including at the upper and lower boundaries, then the horizontal momentum is effected only by the Coriolis and pressure forces. Following our discussion of the Traditional Approximation in Section 24.1.3, we retain only the local vertical component to the Coriolis acceleration, which is compatible with the hydrostatic approximation. We are thus led to the horizontal velocity equation

$$\frac{D\mathbf{u}}{Dt} + f \hat{\mathbf{z}} \times \mathbf{u} = -\nabla(g\eta + p_a/\rho), \quad (32.9)$$

where

$$\mathbf{v} = (\mathbf{u}, w) \quad (32.10)$$

splits out the horizontal velocity vector, \mathbf{u} , from the vertical velocity component, w .

The Coriolis parameter, $f = f \hat{\mathbf{z}}$, is independent of depth, as is the horizontal pressure force from gradients in the free surface and applied pressure. Consequently, if the horizontal velocity is initially independent of depth, it will remain so for all time. The material time derivative thus only has contributions from the local time derivative and from horizontal advection

$$\frac{D\mathbf{u}}{Dt} = \left[\frac{\partial}{\partial t} + u \frac{\partial}{\partial x} + v \frac{\partial}{\partial y} \right] \mathbf{u} \quad (32.11)$$

so that the shallow water velocity equation (32.9) takes on the form

$$(\partial_t + u \partial_x + v \partial_y) \mathbf{u} + f \hat{\mathbf{z}} \times \mathbf{u} = -\nabla(g\eta + p_a/\rho). \quad (32.12)$$

32.2.5 Thickness equation

The mass of a shallow water layer is constant in the absence of sources, sinks, or boundary fluxes. Hence, changes in mass at a particular region in the fluid must arise from mass fluxed across the region boundaries, leaving one region and accumulating in another. For simplicity, we assume that no mass crosses the fluid top (the free surface) or the bottom (the solid earth). We consider the more general case of boundary mass transport in Section 32.6. Note that since the fluid density is constant, mass conservation is the same as volume conservation. Hence, the terms “mass conservation” and “volume conservation” are commonly used interchangeably when working with shallow water models.

Consider an infinitesimally thin (in horizontal cross-section) vertical column of shallow water fluid that is fixed in space and extending from $\eta_b \leq z \leq \eta$. Let the horizontal cross-sectional area be written as dA and the thickness be $h = \eta - \eta_b$ (see Figure 32.3). The total mass of fluid in this column is given by

$$M = \int_{\text{column}} \left[\int_{\eta_b}^{\eta} \rho dz \right] dA = \rho \int_{\text{column}} (\eta - \eta_b) dA = \rho \int_{\text{column}} h dA. \quad (32.13)$$

Time changes in the column mass thus arise from time changes in the layer thickness integrated

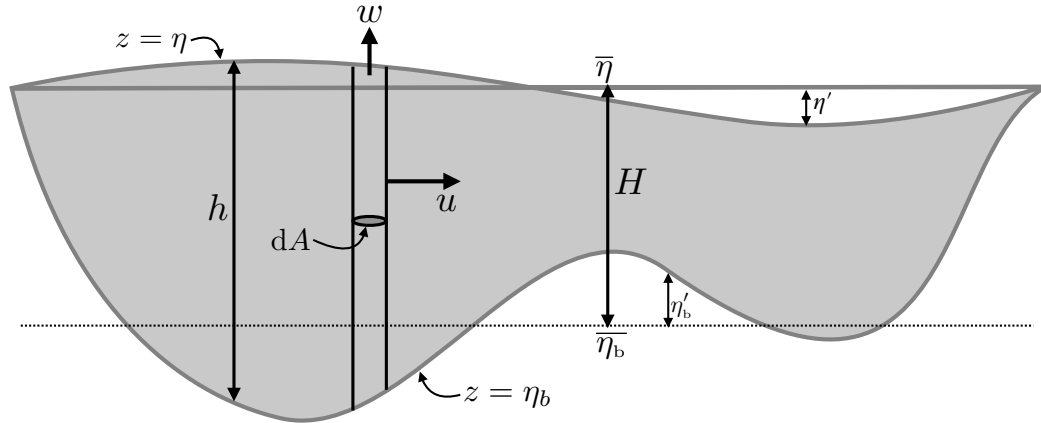


FIGURE 32.3: Mass budget for a column of shallow water fluid with fixed cross-sectional area, dA , constant density, ρ , and layer thickness, $h(x, y, t)$. The column mass is affected only by horizontal transport (transport within the layer) in the absence of boundary mass fluxes through the top, $z = \eta$, or bottom, $z = \eta_b$. Note that since the density of the layer is constant, then mass equals to the constant density times the volume.

over the horizontal area of the column

$$\frac{dM}{dt} = \rho \int_{\text{column}} \frac{\partial h}{\partial t} dA, \quad (32.14)$$

where

$$\frac{\partial h}{\partial t} = \frac{\partial (\eta - \eta_b)}{\partial t} = \frac{\partial \eta}{\partial t}, \quad (32.15)$$

since the bottom topography at $z = \eta_b(x, y)$ is static.

General derivation

The mass within a fluid column changes due to mass crossing the vertical column boundaries (again, we assume here that no mass crosses the top or bottom interfaces). The mass flux penetrating the vertical boundary is given by

$$\text{mass per time entering column} = -\rho \oint_{\text{column}} \mathbf{u} \cdot \hat{\mathbf{n}} d\mathcal{S}, \quad (32.16)$$

where $\hat{\mathbf{n}}$ is the outward normal at the column boundary, and $d\mathcal{S}$ is the area element along the column boundary. The area integral is computed over the boundary of the column, which involves a vertical integral and a circumferential line integral

$$\text{mass per time entering column} = -\rho \oint_{\text{column}} \left[\int \mathbf{u} \cdot \hat{\mathbf{n}} dz \right] dl, \quad (32.17)$$

where dl is the infinitesimal line element around the column circumference. Since $\hat{\mathbf{n}} \cdot \mathbf{u}$ is depth independent, we can perform the vertical integral to render

$$-\rho \oint_{\text{column}} \left[\int \mathbf{u} \cdot \hat{\mathbf{n}} dz \right] dl = -\rho \oint_{\text{column}} h \mathbf{u} \cdot \hat{\mathbf{n}} dl = -\rho \int_{\text{column}} \nabla \cdot (h \mathbf{u}) dA, \quad (32.18)$$

where the second equality follows from the divergence theorem applied to the horizontal cross-sectional area of the column. Equating this result to the mass time tendency (32.14), and noting

that the horizontal cross-sectional area is arbitrary, yields an equation for the layer thickness

$$\partial_t h + \nabla \cdot (h \mathbf{u}) = 0. \quad (32.19)$$

This result means that the thickness of fluid at a fixed location increases if there is a convergence of thickness onto that location, and decreases if thickness diverges from the location. We may also write the thickness equation (32.19) in the material time derivative form

$$\frac{Dh}{Dt} = -h \nabla \cdot \mathbf{u}. \quad (32.20)$$

Hence, thickness of a material fluid column increases in regions where the horizontal flow converges.

Special case with a rectangular column

To further our understanding of the second step in equation (32.18), consider the special case of a rectangular column, for which the mass per time of fluid entering the column is given by

mass per time entering column

$$= -\rho \int_{\text{column}} [(u h)_{\text{east}} - (u h)_{\text{west}}] dy - \rho \int_{\text{column}} [(v h)_{\text{north}} - (v h)_{\text{south}}] dx. \quad (32.21)$$

Taking the limit as the horizontal cross-section of the column becomes infinitesimal leads to

mass per time entering column

$$= -\rho \int_{\text{column}} \left[\frac{\partial(u h)}{\partial x} + \frac{\partial(v h)}{\partial y} \right] dx dy = -\rho \int_{\text{column}} \nabla \cdot (h \mathbf{u}) dA, \quad (32.22)$$

thus recovering the result (32.18).

32.2.6 Bottom kinematic boundary condition

Kinematic boundary conditions arise from geometric constraints placed on the fluid system. We consider here the kinematic boundary condition at the bottom interface in the case where there is no flow through this interface, and follow in Section 32.2.7 with the surface kinematic boundary condition.²

The ocean bottom is located at a vertical position, $z = \eta_b(x, y)$. This location can equivalently be specified mathematically by the surface

$$s(x, y, z) = z - \eta_b(x, y) = 0. \quad (32.23)$$

The outward normal (pointing from the fluid into the rock) at this surface is given by

$$\hat{\mathbf{n}} = -\frac{\nabla s}{|\nabla s|} = \frac{\nabla \eta_b - \hat{\mathbf{z}}}{\sqrt{1 + \nabla \eta_b \cdot \nabla \eta_b}}. \quad (32.24)$$

²From the discussion of fluid kinematics in Part III, we use the term *material surface* for any continuous surface or interface that is impenetrable to the flow of matter or thermal energy (mechanical energy can be transferred via pressure forces). In Section 16.4 we derived the kinematic boundary conditions for a fluid at interfaces. We here apply those ideas to the shallow water system, so that the presentation in Sections 32.2.6 and 32.2.7 offer a review of Section 16.4 as applied to a shallow water layer.

If the bottom is impenetrable to fluid then the velocity field is constrained to satisfy the no-normal flow boundary condition

$$\mathbf{v} \cdot \hat{\mathbf{n}} = 0 \quad \text{at } z = \eta_b. \quad (32.25)$$

Making use of the bottom outward normal (32.24) leads to

$$w = \mathbf{u} \cdot \nabla \eta_b \quad \text{at } z = \eta_b. \quad (32.26)$$

For a flat bottom, with $\nabla \eta_b = 0$, the no-normal flow condition means that $w(\eta_b) = 0$. For the case of nontrivial bottom topography, $w(\eta_b) = 0$ remains if flow occurs along lines of constant topography; i.e., along isobaths, in which case $\mathbf{u} \cdot \nabla \eta_b = 0$. But more generally, sloping bottoms lead to a nonzero vertical velocity component. Dynamically, a nonzero bottom vertical velocity arises from forces at the bottom that cause the horizontal velocity to cross isobaths, $\mathbf{u} \cdot \nabla \eta_b \neq 0$.

The kinematic result (32.26) is written in an Eulerian sense, with the velocity constrained to satisfy this relation at each point along the bottom interface. It has a dual material interpretation based on acknowledging that the bottom interface is a material surface. A fluid element on the bottom at $s = z - \eta_b = 0$ will thus remain there; it does not cross the bottom interface. Rather, it can at most move tangentially to the bottom.³ We can ensure the no-normal flow constraint by setting

$$\frac{Ds}{Dt} = \frac{D(z - \eta_b)}{Dt} = 0 \quad \text{at } z = \eta_b. \quad (32.27)$$

Rearrangement of this result leads to the Eulerian constraint (32.26). Equivalently, we can write this boundary condition in the form

$$w = \frac{D\eta_b}{Dt} \quad \text{at } z = \eta_b. \quad (32.28)$$

Since $\eta_b = \eta_b(x, y)$, this expression of the kinematic boundary condition is identical to equation (32.26).

32.2.7 Surface kinematic boundary condition

We here assume the surface boundary is a material surface to derive the surface kinematic boundary condition, with Section 32.6 considering the slightly more general case of volume crossing this surface. As a material surface, the surface kinematic boundary condition follows analogously to the bottom. However, there is a fundamentally new feature in that the layer's upper free surface is a time dependent moving boundary. We studied such boundaries in Section 16.4.2 when detailing the kinematic boundary conditions for a material surface. We here review some of that discussion.

The free surface is located at a vertical position $z = \eta(x, y, t)$. Equivalently, the free surface can be specified by a surface of constant s , where

$$s(x, y, z, t) = z - \eta(x, y, t) = 0. \quad (32.29)$$

The outward normal to the free surface is thus given by

$$\hat{\mathbf{n}} = \frac{\nabla s}{|\nabla s|} = \frac{\hat{\mathbf{z}} - \nabla \eta}{\sqrt{1 + \nabla \eta \cdot \nabla \eta}}. \quad (32.30)$$

We must account for motion of the surface when formulating the no-normal flow condition.

³Details of the tangential motion along a material boundary require dynamical information such as boundary stresses (see Chapter 22). We are not concerned with such dynamical information here, rather our concern is solely with kinematics.

To do so, write this no-normal flow condition as

$$(\mathbf{v} - \mathbf{v}^{(s)}) \cdot \hat{\mathbf{n}} = 0 \quad \text{at } z = \eta(x, y, t), \quad (32.31)$$

where $\mathbf{v}^{(s)}$ is the velocity of a point on the ocean surface. The velocity of a point fixed on an arbitrary surface with specified s satisfies

$$\frac{\partial s}{\partial t} + \mathbf{v}^{(s)} \cdot \nabla s = 0. \quad (32.32)$$

As defined, $\mathbf{v}^{(s)}$ advects a fluid element in a manner to always keep the element fixed on the constant s surface. With $\hat{\mathbf{n}} = \nabla s / |\nabla s|$, we have

$$\mathbf{v}^{(s)} \cdot \hat{\mathbf{n}} = -\frac{\partial_t s}{|\nabla s|} = \frac{\partial_t \eta}{\sqrt{1 + \nabla \eta \cdot \nabla \eta}}. \quad (32.33)$$

Hence, if the surface remains static, then $\mathbf{v}^{(s)} \cdot \hat{\mathbf{n}} = 0$. But more generally, the surface is moving, and that movement is fundamental to the surface kinematic boundary condition.

Making use of the result (32.33) in the no-normal flow constraint (32.31) then leads to the surface kinematic boundary condition

$$w - \mathbf{u} \cdot \nabla \eta = \frac{\partial \eta}{\partial t} \quad \text{at } z = \eta. \quad (32.34)$$

As for the bottom kinematic boundary condition written as (32.27), we can interpret the surface kinematic condition (32.34) materially, in which case

$$\frac{Ds}{Dt} = \frac{D(z - \eta)}{Dt} = 0 \quad \text{at } z = \eta. \quad (32.35)$$

That is, in the absence of flow across the surface boundary, that surface remains material. We can write this boundary condition in the equivalent form

$$w = \frac{D\eta}{Dt} = (\partial_t + \mathbf{u} \cdot \nabla) \eta \quad \text{at } z = \eta. \quad (32.36)$$

32.2.8 Column stretching and vertical velocity

Since the fluid has constant density, we know that the velocity has zero divergence

$$\nabla \cdot \mathbf{u} + \partial_z w = 0 \implies \partial_z w = -\nabla \cdot \mathbf{u}. \quad (32.37)$$

This result also follows since material fluid elements in the constant density shallow water layer maintain a constant volume (see Section 18.1). Furthermore, since the horizontal velocity has no depth dependence, we can vertically integrate the continuity equation from the bottom to an arbitrary depth within the layer to render

$$w(z) = w(\eta_b) - (z - \eta_b) \nabla \cdot \mathbf{u}, \quad (32.38)$$

so that the vertical velocity is a linear function of depth within a shallow water layer. Applying this equation at the ocean surface yields

$$w(\eta) = w(\eta_b) - (\eta - \eta_b) \nabla \cdot \mathbf{u}. \quad (32.39)$$

Eliminating the horizontal convergence between equations (32.38) and (32.39) leads to

$$w(z) - w(\eta_b) = \left[\frac{z - \eta_b}{\eta - \eta_b} \right] [w(\eta) - w(\eta_b)]. \quad (32.40)$$

Making use of the surface kinematic boundary condition (32.36) and bottom kinematic boundary condition (32.28) renders the material form

$$\frac{1}{z - \eta_b} \left[\frac{D(z - \eta_b)}{Dt} \right] = \frac{1}{\eta - \eta_b} \left[\frac{D(\eta - \eta_b)}{Dt} \right]. \quad (32.41)$$

Finally, introducing the layer thickness $h = \eta - \eta_b$ yields the material conservation law

$$\frac{D}{Dt} \left[\frac{z - \eta_b}{h} \right] = 0. \quad (32.42)$$

Again, $h = \eta - \eta_b$ is the layer thickness and $z - \eta_b$ is the height of a fluid element from the bottom interface (see Figure 32.1). Consequently, equation (32.42) means that the ratio of the fluid element height above the bottom to the layer thickness remains constant as the fluid element moves through the shallow water fluid. That is, a vertical column of shallow water fluid stretches or squeezes coherently within a shallow water layer, so that the relative vertical position remains fixed for a point within the column. Shallow water mechanics thus comprises the mechanics of coherent vertical fluid columns moving within a fluid layer. This constrained behavior results from the linear depth dependence of the vertical velocity, which itself is a result of the depth independence of the horizontal velocity, and which follows from the depth independence of the horizontal gradient of hydrostatic pressure.

32.2.9 Tracer concentration equation

Suppose there is a material substance, a tracer, contained within a shallow water layer.⁴ We expect the tracer concentration, ψ , to have a non-uniform vertical structure within the layer, in addition to having horizontal structure: $\psi = \psi(x, y, z, t)$. If the tracer is advected through the layer without any diffusion, then the concentration satisfies the perfect fluid tracer equation (i.e., the *advection equation*)

$$\frac{\partial \psi}{\partial t} + \mathbf{u} \cdot \nabla_z \psi + w \partial_z \psi = 0. \quad (32.43)$$

For a shallow water layer, where the horizontal velocity has no depth dependence within a layer, we find it sufficient to study the depth averaged tracer concentration within the layer,

$$C(x, y, t) \equiv \frac{1}{h} \int_{\eta_b}^{\eta} \psi(x, y, z, t) dz. \quad (32.44)$$

To develop the evolution equation for C , we vertically integrate the tracer equation (32.43) over

⁴We developed the theory of material tracers in Chapter 17.

the layer and make use of Leibniz's rule (Section 17.3.4)

$$\int_{\eta_b}^{\eta} \frac{\partial \psi}{\partial t} dz = \partial_t(h C) - \psi(\eta) \partial_t \eta \quad (32.45a)$$

$$\int_{\eta_b}^{\eta} \mathbf{u} \cdot \nabla \psi dz = \nabla \cdot (h C \mathbf{u}) - \psi(\eta) \mathbf{u}(\eta) \cdot \nabla \eta + \psi(\eta_b) \mathbf{u}(\eta_b) \cdot \nabla \eta_b - h C \nabla \cdot \mathbf{u} \quad (32.45b)$$

$$\int_{\eta_b}^{\eta} w \partial_z \psi dz = w(\eta) \psi(\eta) - w(\eta_b) \psi(\eta_b) - h C \partial_z w. \quad (32.45c)$$

For these equations we made use of the z independence of \mathbf{u} and $\partial_z w$ within the layer. Use of the kinematic boundary conditions from Sections 32.2.6 and 32.2.7, and the three dimensional continuity equation, $\nabla \cdot \mathbf{u} + \partial_z w = 0$, renders the equation for the layer depth averaged tracer concentration

$$\frac{\partial(h C)}{\partial t} + \nabla \cdot (h C \mathbf{u}) = 0 \iff \frac{\partial C}{\partial t} + \mathbf{u} \cdot \nabla C = \frac{DC}{Dt} = 0. \quad (32.46)$$

As a self-consistency check, note that if the tracer concentration has a horizontally uniform value, then the Eulerian flux-form of the tracer equation (32.46) reduces to the thickness equation (32.19).

32.2.10 Summary comments

Key physical assumptions for the shallow water fluid

The shallow water fluid model is based on the following two assumptions.

- The fluid layer has a uniform density, which then means the fluid is incompressible.
- The pressure is hydrostatic.

Since the pressure gradient is depth-independent within the layer, an initial horizontal velocity that is depth independent will remain depth independent. That is, the fluid moves as columns within the layer, with the columns stretching and squashing depending on the divergence or convergence of volume towards the column.

The term “shallow” refers to the small vertical to horizontal aspect ratio, $H/L \ll 1$, which in turn is consistent with the hydrostatic approximation (Section 24.2). The term “water” refers to the incompressible nature of the fluid, which is a more relevant approximation for the ocean than for the atmosphere (see Section 26.1). Nonetheless, the shallow water model has direct applications to many features of both the atmosphere and ocean circulation, and as such it is widely used across the atmosphere and ocean sciences.

Shallow water fluid columns are not Taylor columns

The columnar motion of fluid within a shallow water layer is reminiscent of the Taylor columns discussed in Section 28.5.3. However, the columnar motion of fluid within a Taylor column is fundamentally distinct from that of a column of shallow water fluid. Motion in a Taylor column holds for homogeneous fluids undergoing rapid rotation and moving over a flat surface. The horizontal fluid velocity within a Taylor column is non-divergent so that there is no vertical motion of the fluid. These properties allow one to interpret a Taylor column as a fluid mechanical realization of a column of rigid matter much like a solid body.

In contrast, shallow water fluid columns do not rely on rotation, but instead arise from the hydrostatic balance maintained within each homogeneous layer. Additionally, shallow water columns

are not rigid. Rather, they stretch and squash in the presence of nonzero divergence in the horizontal flow, thus leading to vertical motion of fluid within the column. Finally, shallow water columns remain coherent even as they move over topography, and yet, again, they can stretch and squash.

32.3 Reduced gravity model for the upper ocean

The *reduced gravity model* describes an active layer of uniform density, ρ_1 , above a stagnant layer of density, ρ_2 , and below a fluid of zero density, $\rho_0 = 0$. It is often referred to as the 1.5 layer model. This theoretical model has been used, to some success, as an idealization of the upper ocean circulation whereby an active layer (e.g., the region above the ocean pycnocline), sits above an inactive layer (the abyss) of much smaller motion (here assumed to be zero motion). In this way, we introduce the *level of no motion*, below which (baroclinic) currents vanish.

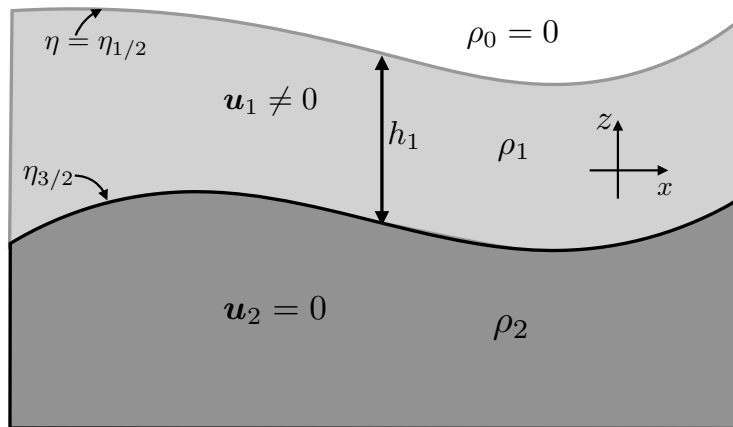


FIGURE 32.4: Reduced gravity model of shallow water fluid. The lower layer with density ρ_2 is dynamically inactive and thus has a zero velocity. The upper layer is dynamically active with thickness, $h = \eta_{1/2} - \eta_{3/2}$, and density, ρ_1 . The dynamically active layer is bounded above by a zero density atmosphere, $\rho_0 = 0$. The lower inactive layer is assumed to be infinitely deep so that its continuity equation can be ignored; i.e., even though there are zero currents within this layer, the layer thickness can still undulate. The reduced gravity between the two layers is defined by $g_{3/2}^r = g(\rho_2 - \rho_1)/\rho_{\text{ref}} \ll g$, whereas the reduced gravity at the top interface is given by $g_{1/2}^r = g$.

32.3.1 Momentum and thickness equations for the active layer

We develop the momentum equations for the reduced gravity model by making use of the hydrostatic balance, in which pressure at a depth, z , in the upper layer is computed as (see Figure 32.4)

$$p_1(x, y, z, t) = p_{1/2}(x, y, t) + g \rho_1 [\eta_{1/2}(x, y, t) - z], \quad (32.47)$$

where we denote an interface value by a half-index, so that $\eta_{1/2}$ and $p_{1/2}$ are the interface height and pressure at the upper layer interface.⁵ Since the fluid above the upper layer is assumed to have zero density, we set

$$p_{1/2} = 0. \quad (32.48)$$

⁵There is no general consensus on this notation, with some treatments, such as [Vallis \(2017\)](#) and [Cushman-Roisin and Beckers \(2011\)](#) using an integer to label an interface quantity, whereas some numerical model papers (e.g., [Griffies et al. \(2020\)](#)) use the half-index. We prefer the half-index since it removes any ambiguity concerning the ordering of the interfaces relative to the layer.

The horizontal momentum equation for the upper (active) layer is given by

$$\rho_{\text{ref}} \left[\frac{D\mathbf{u}_1}{Dt} + f \hat{\mathbf{z}} \times \mathbf{u}_1 \right] = -g \rho_1 \nabla \eta_{1/2}, \quad (32.49)$$

where the z dependent term in the pressure (32.47) drops out when computing the horizontal pressure gradient. Setting the reference density equal to the top layer density, $\rho_{\text{ref}} = \rho_1$, leads to the more tidy equation

$$\frac{D\mathbf{u}_1}{Dt} + f \hat{\mathbf{z}} \times \mathbf{u}_1 = -g \nabla \eta_{1/2}. \quad (32.50)$$

The equations for the upper layer are completed by volume conservation in the form of the thickness equation

$$\frac{Dh_1}{Dt} = -h_1 \nabla \cdot \mathbf{u}_1. \quad (32.51)$$

32.3.2 Relating undulations of the top and bottom layer interfaces

The pressure in the lower stagnant layer is given by the weight per horizontal area of fluid above it, and it can be written

$$p_2(x, y, z, t) = g \rho_1 (\eta_{1/2} - \eta_{3/2}) + g \rho_2 (\eta_{3/2} - z) \quad (32.52a)$$

$$= g \rho_1 \eta_{1/2} + g (\rho_2 - \rho_1) \eta_{3/2} - g \rho_2 z \quad (32.52b)$$

$$= \rho_{\text{ref}} (g_{1/2}^r \eta_{1/2} + g_{3/2}^r \eta_{3/2}) - g \rho_2 z. \quad (32.52c)$$

In this equation we introduced the *reduced gravities*

$$g_{1/2}^r = g \quad \text{and} \quad g_{3/2}^r = g (\rho_2 - \rho_1) / \rho_{\text{ref}} \ll g. \quad (32.53)$$

We employ the half-index notation for the reduced gravities since they are computed by differencing the densities between two adjacent layers, and as such they are considered an interface property. Additionally, the reduced gravities multiply a corresponding interface gradient, which also uses the half-integer notation.

For the reduced gravity model we assume the lower layer is motionless. To maintain zero motion in the lower layer requires the lower layer horizontal pressure gradient to vanish

$$\rho_{\text{ref}}^{-1} \nabla_z p_2 = g_{1/2}^r \nabla \eta_{1/2} + g_{3/2}^r \nabla \eta_{3/2} = 0. \quad (32.54)$$

This constraint links the undulations of the top and bottom interfaces of the dynamically active layer

$$\nabla \eta_{1/2} = -\frac{g_{3/2}^r}{g_{1/2}^r} \nabla \eta_{3/2} = -[(\rho_2 - \rho_1) / \rho_{\text{ref}}] \nabla \eta_{3/2} \implies \eta_{1/2} = -\eta_{3/2} [(\rho_2 - \rho_1) / \rho_{\text{ref}}] + \text{constant}. \quad (32.55)$$

The density ratio, $(\rho_2 - \rho_1) / \rho_{\text{ref}}$, is positive but typically much smaller than unity. Hence, the relation (32.55) means that undulations of the free surface, $\eta_{1/2}$, are of opposite sign and of much smaller amplitude than undulations in the lower interface, $\eta_{3/2}$. This behavior is typical for undulations of the pycnocline region of the ocean and the free surface as depicted in Figure 32.5.

32.3.3 Momentum equation with reduced gravity

Relation (32.54) can be used to write the momentum equation (32.50) in the form

$$\frac{D\mathbf{u}_1}{Dt} + f \hat{\mathbf{z}} \times \mathbf{u}_1 = g_{3/2}^r \nabla \eta_{3/2}. \quad (32.56)$$

It is common to make use of the momentum equation in the form (32.56), rather than the original form (32.50). The reason is that historically, ocean hydrography measurements⁶ have allowed for an estimate of the pycnocline slope, $\nabla \eta_{3/2}$, whereas it was not until precise satellite altimetry measurements starting in the 1990s that we could estimate the far smaller sea level slope, $\nabla \eta_{1/2}$.

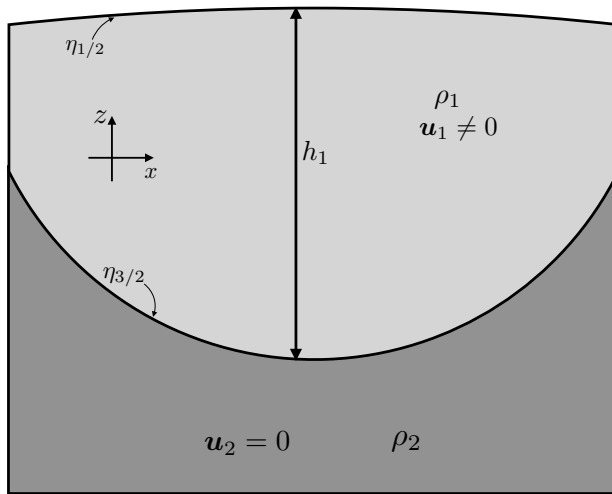


FIGURE 32.5: A vertical slice through a reduced gravity, or 1.5 layer, ocean in hydrostatic balance. Shown here is a plug of dynamically active light water, as may occur in a warm core eddy to the subtropical gyres, sitting on top of heavy water of zero motion. The free surface corresponds to $\eta_{1/2}$ in Figure 32.4, whereas the pycnocline (heavy black line) corresponds to the lower interface $\eta_{3/2}$ of Figure 32.4. The sea surface experiences an applied pressure $p = p_a$, assumed to be uniform for this idealized situation. Note how sea level is a maximum above the pycnocline minimum, with this geometry reflected in equation (32.55). In the ocean, the slope of the pycnocline is about 100-300 times larger than the slope of the sea level. That is, sea level may show undulations on the order of a metre, whereas the pycnocline undulations are on the order of 100-300 m.

32.3.4 Reduced gravity and relative buoyancy

Equation (32.54)

$$g \nabla \eta_{1/2} = -g_{3/2}^r \nabla \eta_{3/2}, \quad (32.57)$$

says that with $g_{3/2}^r \ll g$, the free surface slopes are much smaller than interior slopes

$$|\nabla \eta_{1/2}| \ll |\nabla \eta_{3/2}|. \quad (32.58)$$

We thus infer that the interior interface has less resistance to vertical motion than the free surface. To help understand this result, recall the study of Archimedean buoyancy in Section 27.4. We see that the reduced gravity, $g_{3/2}^r$, is the Archimedean buoyancy of layer 1 relative to layer 2, with normalization given by the reference density as per the Boussinesq approximation

$$\text{buoyancy layer 1 relative to layer 2} = -g (\rho_1 - \rho_2) / \rho_{\text{ref}} = g_{3/2}^r. \quad (32.59)$$

⁶In oceanography, hydrography refers to measurements of temperature, salinity, and pressure; see [Talley et al. \(2011\)](#).

For the upper free surface, the buoyancy of layer 0 (a zero mass atmosphere) relative to layer 1 equals to the full gravitational acceleration.

$$\text{buoyancy layer 0 relative to layer 1} = -g (\rho_0 - \rho_1)/\rho_{\text{ref}} = g, \quad (32.60)$$

where we assumed that $\rho_{\text{ref}} = \rho_1$ and $\rho_0 = 0$. A small relative buoyancy between two density layers renders little resistance for motion of the layer interface. Indeed, as the density difference vanishes, so too does the buoyant resistance to motion of the layer interface.

It is for this reason that the interior interface is more flexible than the free surface, as depicted in Figure 32.5. Even for an atmosphere with mass, so that $\rho_0 > 0$, the upper interface's reduced gravity is close to g since the atmosphere is roughly 1000 times less dense than seawater. This result holds in general, whereby increasing the reduced gravity between density layers, and thus increasing the vertical density stratification, increases the resistance to motion of the layer interface and thus reduces the interface flexibility.

32.3.5 Further study

The material in this section is inspired by Section 3.2 of [Vallis \(2017\)](#). [Tomczak and Godfrey \(1994\)](#) make use of the reduced gravity model for interpreting aspects of the observed ocean. Additional use is made by [Griffies et al. \(2014\)](#) for interpreting patterns of sea level in the ocean.

32.4 Stacked shallow water equations

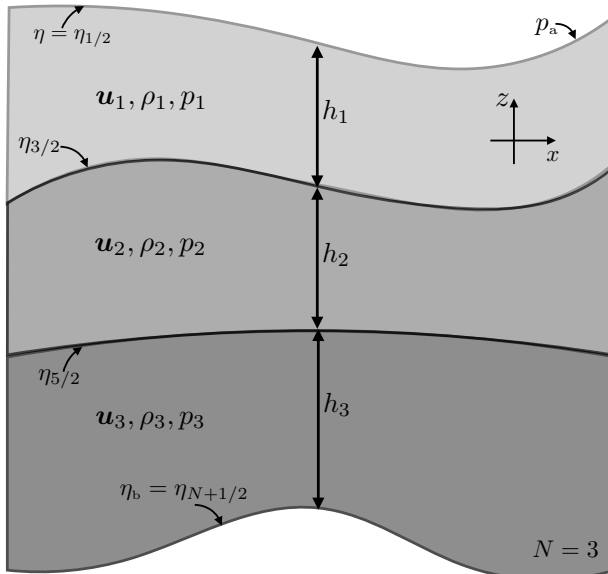


FIGURE 32.6: Three dynamically active layers of stacked shallow water fluid ($N = 3$). The notation corresponds to that for the reduced gravity model of Figure 32.4, yet here with three dynamically active layers. In particular, $\eta_{1/2}$ is the free surface, $\eta_{1/2} = \eta$, whereas $\eta_{N+1/2} = \eta_b$ is the bottom interface. Hence, the total thickness of a column is $h_1 + h_2 + h_3 = \eta_{1/2} - \eta_b$. The “atmosphere” above the layers is assumed to apply a pressure, p_a , to the upper surface. The horizontal velocity is depth-independent within each layer, as is the horizontal pressure gradient, so that both are discontinuous across a layer interface. In contrast, the pressure is a linear function of depth within a layer and is continuous across a layer interface. Finally, the vertical velocity is also a linear function of depth within a layer but it is discontinuous across a layer interface. The reduced gravity defined between each layer is given by $g_{k+1/2}^r = g (\rho_{k+1} - \rho_k)/\rho_{\text{ref}}$.

In studies of shallow water fluids, much of the formalism developed for a single layer can be readily extended to an arbitrary number of layers. We here pursue this extension and thereby expose the underlying kinematics and dynamics of stacked shallow water models. We assume the layers are immiscible so that matter and thermal properties are not exchanged between the layers. Consequently, the layers couple only through mechanical forces arising from pressure form stress. Furthermore, we continue to assume that the horizontal velocity has no depth-dependence within each shallow water layer, which in turn means the horizontal pressure gradient is depth independent within each layer. The notation for our derivations is depicted in Figure 32.6 in the case of three active layers.

In Section 59.2 we develop the equations for a continuously stratified Boussinesq fluid making use of isopycnal vertical coordinates. Although the vertical stratification is continuous in that case, we see in that discussion that the isopycnal equations are isomorphic to the stacked shallow water equations. Hence, besides being of intrinsic interest as a versatile theoretical model, the stacked shallow water model offers a suitable step towards studies of a continuously stratified fluid using isopycnal coordinates.

32.4.1 Formulation of a 2-layer model

We here display the equations for two layers, thus offering the seeds for an extension to N layers in Section 32.4.2.

Thickness and tracer equations

Each shallow water layer satisfies its own independent thickness equation and tracer equation, representing the conservation of volume and tracer content for each layer

$$\frac{\partial h_1}{\partial t} + \nabla \cdot (h_1 \mathbf{u}_1) = 0 \quad (32.61a)$$

$$\frac{\partial h_2}{\partial t} + \nabla \cdot (h_2 \mathbf{u}_2) = 0 \quad (32.61b)$$

$$\frac{\partial(h_1 C_1)}{\partial t} + \nabla \cdot (h_1 C_1 \mathbf{u}_1) = 0 \quad (32.61c)$$

$$\frac{\partial(h_2 C_2)}{\partial t} + \nabla \cdot (h_2 C_2 \mathbf{u}_2) = 0. \quad (32.61d)$$

We emphasize that there is no explicit coupling between these equations, as each layer separately must satisfy volume conservation and tracer conservation. However, the velocities are coupled through the pressure force, as we now discuss.

Pressure within a layer

To compute the pressure within a layer, we make use of the hydrostatic balance and integrate down from the surface, which results in the pressure fields

$$p_1 = \rho_1 g (\eta_{1/2} - z) + p_a \quad (32.62)$$

$$p_2 = \rho_1 g (\eta_{1/2} - \eta_{3/2}) + \rho_2 g (\eta_{3/2} - z) + p_a. \quad (32.63)$$

It is convenient to write pressure in layer-two using the reduced gravity, which leads to

$$p_2 - p_a = \rho_1 g (\eta_{1/2} - \eta_{3/2}) + \rho_2 g (\eta_{3/2} - z) \quad (32.64a)$$

$$= g \eta_{1/2} \rho_1 + g \eta_{3/2} (\rho_2 - \rho_1) - g \rho_2 z \quad (32.64b)$$

$$= g_{1/2}^r \rho_1 \eta_{1/2} + g_{3/2}^r \rho_{\text{ref}} \eta_{3/2} - g \rho_2 z \quad (32.64c)$$

with the reduced gravities given by

$$g_{1/2}^r = g \quad \text{and} \quad g_{3/2}^r = g (\rho_2 - \rho_1) / \rho_{\text{ref}} \ll g, \quad (32.65)$$

and with ρ_{ref} the Boussinesq reference density. Even though we include an atmospheric pressure, p_a , in the formulation, there is no dynamical equation for the atmosphere so that $g_{1/2}^r = g$ is the only choice available.

Boussinesq reference density and the reduced gravity

We are formulating the shallow water model according to Boussinesq ocean equations from Chapter 26, whereby fluid elements conserve their volume rather than their mass. According to our discussion of the Boussinesq momentum equation in Section 26.1.2, density is set to a constant reference density when measuring the inertial mass of a fluid element, yet density remains the *in situ* density when measuring weight of a fluid element. For the shallow water model, we multiply the inertial acceleration and Coriolis acceleration with a reference density,

$$\rho_{\text{ref}} = \text{shallow water reference density}, \quad (32.66)$$

whereas pressure and potential energy maintain the density, ρ_k , of the shallow water layer.

We further make use of the Boussinesq ocean when computing the buoyancy frequency (Section 27.5.4). Namely, with ϱ the potential density, the Boussinesq form of the squared buoyancy frequency is

$$N^2 = -g \left[\frac{1}{\rho_{\text{ref}}} \frac{\partial \varrho}{\partial z} \right] \approx -\frac{g}{\rho_{\text{ref}}} \frac{\Delta \rho}{\Delta z} = -g^r / \Delta z. \quad (32.67)$$

It is for this reason that we take ρ_{ref} for the denominator of the reduced gravity throughout all of the shallow water layers, thus defining

$$g_{k-1/2}^r = g (\rho_k - \rho_{k-1}) / \rho_{\text{ref}} \quad \text{and} \quad g_{1/2}^r = g. \quad (32.68)$$

Horizontal velocity equations

The horizontal velocity equations for the two layers take the form

$$\rho_{\text{ref}} \left[\frac{D_1 \mathbf{u}_1}{Dt} + f \hat{\mathbf{z}} \times \mathbf{u}_1 \right] = -\nabla p_1 \quad (32.69a)$$

$$\rho_{\text{ref}} \left[\frac{D_2 \mathbf{u}_2}{Dt} + f \hat{\mathbf{z}} \times \mathbf{u}_2 \right] = -\nabla p_2, \quad (32.69b)$$

where we introduced the layer material time derivatives

$$\frac{D_k}{Dt} = \frac{\partial}{\partial t} + \mathbf{u}_k \cdot \nabla \quad \text{for } k = 1, 2. \quad (32.70)$$

Making use of expressions (32.62) and (32.64c) for layer pressures leads to the horizontal momentum equations

$$\rho_{\text{ref}} \left[\frac{D_1 \mathbf{u}_1}{Dt} + f \hat{\mathbf{z}} \times \mathbf{u}_1 \right] = -g \rho_1 \nabla [\eta_{1/2} + p_a / (g \rho_1)] \quad (32.71\text{a})$$

$$\rho_{\text{ref}} \left[\frac{D_2 \mathbf{u}_2}{Dt} + f \hat{\mathbf{z}} \times \mathbf{u}_2 \right] = -g \rho_1 \nabla [\eta_{1/2} + p_a / (g \rho_1)] - g_{3/2}^r \rho_{\text{ref}} \nabla \eta_{3/2}. \quad (32.71\text{b})$$

It is convenient to express the interface heights in terms of layer thicknesses, h_1 and h_2 , since the layer thicknesses are the prognostic fields determined by time stepping the thickness equations (32.61a) and (32.61b). We thus write

$$\eta_{1/2} = \eta_b + h_1 + h_2 \quad \text{and} \quad \eta_{3/2} = \eta_b + h_2, \quad (32.72)$$

so that

$$p_1 - p_a = \rho_1 g (\eta_b + h_1 + h_2) - g \rho_1 z \quad (32.73\text{a})$$

$$p_2 - p_a = \rho_1 g (\eta_b + h_1 + h_2) + \rho_{\text{ref}} g_{3/2}^r (\eta_b + h_2) - g \rho_2 z, \quad (32.73\text{b})$$

thus resulting in the horizontal momentum equations

$$\rho_{\text{ref}} \left[\frac{D_1 \mathbf{u}_1}{Dt} + f \hat{\mathbf{z}} \times \mathbf{u}_1 \right] = -\rho_1 g \nabla [\eta_b + h_1 + h_2 + p_a / (g \rho_1)] \quad (32.74\text{a})$$

$$\rho_{\text{ref}} \left[\frac{D_2 \mathbf{u}_2}{Dt} + f \hat{\mathbf{z}} \times \mathbf{u}_2 \right] = -\rho_1 g \nabla [\eta_b + h_1 + h_2 + p_a / (g \rho_1)] - \rho_{\text{ref}} g_{3/2}^r \nabla (\eta_b + h_2). \quad (32.74\text{b})$$

Notice how layer thickness from one layer appears in the other layer's pressure gradient. In this way, changes in the thickness of one layer have a direct impact on pressure forces and flow in the adjacent layer. Also notice how the bottom topography appears in the bottom pressure gradient, which arises due to our switch from layer interfaces to layer thicknesses.

It is common for a stacked shallow water model to choose

$$\rho_{\text{ref}} = \rho_1. \quad (32.75)$$

In this case, we have the more tidy layer velocity equations

$$\frac{D_1 \mathbf{u}_1}{Dt} + f \hat{\mathbf{z}} \times \mathbf{u}_1 = -g \nabla [\eta_b + h_1 + h_2 + p_a / (g \rho_1)] \quad (32.76\text{a})$$

$$\frac{D_2 \mathbf{u}_2}{Dt} + f \hat{\mathbf{z}} \times \mathbf{u}_2 = -g \nabla [\eta_b + h_1 + h_2 + p_a / (g \rho_1)] - g_{3/2}^r \nabla (\eta_b + h_2). \quad (32.76\text{b})$$

Vertical shear in horizontal velocities between layers

The difference in layer velocities, $\mathbf{u}_1 - \mathbf{u}_2$, represents the vertical shear in the layers. This difference is affected by a pressure gradient arising just from bottom topography and the interior layer thickness, h_2

$$\frac{D_1 \mathbf{u}_1}{Dt} - \frac{D_2 \mathbf{u}_2}{Dt} + f \hat{\mathbf{z}} \times (\mathbf{u}_1 - \mathbf{u}_2) = g_{3/2}^r \nabla (\eta_b + h_2). \quad (32.77)$$

That is, the vertical shear does not directly feel undulations of the free surface, $\eta_{1/2}$, or the applied pressure, p_a . Rather, it feels these surface undulations only indirectly via nonlinear terms appearing in the advection on the left hand side. We further discuss this result in Section 33.2.2 by introducing thermal wind and the Margules' Relation.

32.4.2 N -layer model equations

The 2-layer equations from Section 32.4.1 can be generalized to N -layers. The thickness equation and tracer equation represent volume and tracer conservation for each layer

$$\frac{\partial h_k}{\partial t} + \nabla \cdot (\mathbf{u}_k h_k) = 0 \quad (32.78a)$$

$$\frac{\partial(h_k C_k)}{\partial t} + \nabla \cdot (\mathbf{u}_k h_k C_k) = 0, \quad (32.78b)$$

where $k = 1, N$ is the discrete layer index and there is no implied summation on this label.⁷

Expressions for the pressure

Some work is needed to generalize the pressure gradient appearing in the velocity equation. For that purpose, write the interface height as

$$\eta_{k+1/2} = \eta_b + \sum_{j=k+1}^N h_j \quad \text{with } \eta_{N+1/2} = \eta_b \text{ and } \eta_{1/2} = \eta. \quad (32.79)$$

For example, the layer interfaces with $N = 3$ layers are given by

$$\eta_{1/2} = \eta_b + h_1 + h_2 + h_3 \quad \eta_{3/2} = \eta_b + h_2 + h_3 \quad \eta_{5/2} = \eta_b + h_3 \quad \eta_{7/2} = \eta_b. \quad (32.80)$$

In turn, the hydrostatic pressure within layer- k is given by

$$p_k = -g \rho_k z + p_a + \rho_{\text{ref}} \sum_{j=0}^{k-1} g_{j+1/2}^r \eta_{j+1/2} = p_{k-1/2} + g \rho_k (\eta_{k-1/2} - z), \quad (32.81)$$

where the reduced gravities are defined according to equation (32.68)

$$g_{j-1/2}^r = g (\rho_j - \rho_{j-1}) / \rho_{\text{ref}} > 0 \quad \text{with} \quad g_{1/2}^r = g. \quad (32.82)$$

As an example, the layer pressures for $N = 3$ are given by

$$p_1 = p_a + g \rho_1 (\eta_{1/2} - z) \quad p_2 = p_{3/2} + g \rho_2 (\eta_{3/2} - z) \quad p_3 = p_{5/2} + g \rho_3 (\eta_{5/2} - z). \quad (32.83)$$

The half-integer pressures are evaluated on the corresponding interface, and the hydrostatic balance yields the pressure difference

$$p_{k+1/2} - p_{k-1/2} = g \rho_k h_k = g \rho_k (\eta_{k-1/2} - \eta_{k+1/2}). \quad (32.84)$$

Summary of the thickness weighted velocity equation

The velocity equation for an arbitrary layer- k is given by

$$\rho_{\text{ref}} \left[\frac{D_k \mathbf{u}_k}{Dt} + f \hat{z} \times \mathbf{u}_k \right] = -\nabla p_k \iff [\partial_t + (\mathbf{u}_k \cdot \nabla)] \mathbf{u}_k + f \hat{z} \times \mathbf{u}_k = -\rho_{\text{ref}}^{-1} \nabla p_k. \quad (32.85)$$

⁷To help distinguish the layer index, k , from a tensor index, k , we write the layer index using an upright Roman font whereas a tensor index is slanted.

Use of the layer thickness equation (32.78a) readily leads to the thickness-weighted momentum equation

$$\partial_t(h_k \mathbf{u}_k) + \nabla \cdot (h_k \mathbf{u}_k \otimes \mathbf{u}_k) + f \hat{\mathbf{z}} \times h_k \mathbf{u}_k = -(h_k / \rho_{\text{ref}}) \nabla p_k. \quad (32.86)$$

We study the thickness-weighted momentum equation in Section 33.3, where we find it offers a more suitable framework than the velocity equation for studying the pressure form stresses acting at layer interfaces.

32.4.3 Dynamic pressure and the Montgomery potential

The term $g \rho_k z$ appearing in the layer pressures (32.81) has a zero horizontal gradient. Hence, it does not contribute to the horizontal pressure gradient acceleration acting on a layer. As a result, it is a “do nothing” pressure that motivates us to introduce the *shallow water dynamic pressure* (e.g., equation (3.44) of [Vallis \(2017\)](#))

$$p_k + g \rho_k z = p_a + \rho_{\text{ref}} \sum_{j=0}^{k-1} g_{j+1/2}^r \eta_{j+1/2} \equiv p_a + p_k^{\text{dyn}} \implies \nabla p_k = \nabla p_a + \nabla p_k^{\text{dyn}}, \quad (32.87)$$

The term “dynamic” is motivated since p_k^{dyn} gradients directly lead to accelerations. Notably, the dynamic pressure is depth independent within a layer, so that it has a jump moving across a layer interface. Also note that p_k^{dyn} is related to the shallow water *Montgomery potential* via

$$M_k^{\text{dyn}} = \rho_{\text{ref}}^{-1} p_k^{\text{dyn}} = \sum_{j=0}^{k-1} g_{j+1/2}^r \eta_{j+1/2} \quad (32.88)$$

(e.g., Section 12.2 of [Cushman-Roisin and Beckers \(2011\)](#)), with the continuous Montgomery potential defined by equation (59.4). When studying the mechanical energy budget in Section 33.6, we find that p_k^{dyn} naturally appears since the energy budget is derived using the pressure gradient body force. The difference of the dynamic pressure between two layers is given by

$$p_k^{\text{dyn}} - p_{k+1}^{\text{dyn}} = -\rho_{\text{ref}} g_{k+1/2}^r \eta_{k+1/2} \iff M_k^{\text{dyn}} - M_{k+1}^{\text{dyn}} = -g_{k+1/2}^r \eta_{k+1/2}, \quad (32.89)$$

which is an expression of the hydrostatic balance for shallow water layers.

We often find it useful to study pressure contributions to the momentum equation via the duality between the pressure gradient body force and the pressure contact force as when studying form stress in Chapter 25, and further applied to the shallow water in Section 33.4 and in Chapter 60. For those purposes, we do not use p_k^{dyn} since it is not the hydrostatic pressure measured within a shallow water layer, so that p_k^{dyn} cannot be directly used to convert the pressure gradient body force to the pressure contact force. Instead, we use the pressure, p_k .

32.4.4 Properties of the vertical velocity

From Section 16.4.2 we know that

$$w = \frac{D\eta}{Dt} \quad (32.90)$$

provides an expression for the vertical velocity of a fluid parcel at a point on an impermeable surface, $z = \eta(x, y, t)$. We made use of this equation in Section (32.2.7) when studying the surface kinematic boundary condition for a single shallow water layer. We make use of this relation to further our understanding of the vertical velocity in a shallow water model. In particular, we find that the jump in horizontal velocity across the interface leads to a jump in the vertical velocity.

Jump condition for the vertical velocity across a layer interface

Consider two shallow water layers labelled by k and $k+1$ that are separated by an interface at $z = \eta_{k+1/2}(x, y, t)$. Define the vertical velocity at the $z = \eta_{k+1/2}$ interface according to the material kinematic condition

$$w^{(k)}(\eta_{k+1/2}) = w_{k+1/2}^{(k)} = (\partial_t + \mathbf{u}_k \cdot \nabla) \eta_{k+1/2}. \quad (32.91)$$

Evidently, $w_{k+1/2}^{(k)}$ is the vertical velocity for a fluid parcel on the top side of the $z = \eta_{k+1/2}$ interface. Similarly, define the vertical velocity for a fluid parcel on the lower side of the $z = \eta_{k+1/2}$ interface according to

$$w_{k+1/2}^{(k+1)} = (\partial_t + \mathbf{u}_{k+1} \cdot \nabla) \eta_{k+1/2}. \quad (32.92)$$

Taking the difference leads to the jump condition

$$w^{(k)}(\eta_{k+1/2}) - w^{(k+1)}(\eta_{k+1/2}) = (\mathbf{u}_k - \mathbf{u}_{k+1}) \cdot \nabla \eta_{k+1/2} \neq 0. \quad (32.93)$$

As advertised, the vertical velocity has a jump across the interface that arises from the jump in the horizontal velocity. In Section 33.2.2 we derive the shallow water expression (33.9) for thermal wind balance maintained by geostrophic flow, known as the *Margules' relation*. In that special case there is no jump in the vertical velocity since $\hat{\mathbf{z}} \times (\mathbf{u}_k - \mathbf{u}_{k+1})$ is parallel to $\nabla \eta_{k+1/2}$, so that $(\mathbf{u}_k - \mathbf{u}_{k+1}) \cdot \nabla \eta_{k+1/2} = 0$. We thus conclude that the vertical velocity arises from ageostrophic contributions to the flow.

It is tempting to introduce a sub-region that smoothly connects the horizontal velocity between the layers, thus removing the jump condition for both \mathbf{u} and w . Doing so enhances the realism of the stacked layers, since a physical realization of fluid layers will have a finite sized region that interpolates between the layer properties. However, adding this transition zone moves us beyond the stacked shallow water model, and so requires analysis that falls outside shallow water theory.

Preservation of the relative vertical position within a column

Following the approach from Section 32.2.8, we compute the vertical velocity within a layer by vertically integrating the non-divergence condition, $\nabla \cdot \mathbf{v} = 0$. For layer k we have

$$w^{(k)}(z) = w_{k+1/2}^{(k)} - (z - \eta_{k+1/2}) \nabla \cdot \mathbf{u}_k, \quad (32.94)$$

where $w^{(k)}(z)$ is the vertical velocity at a vertical position, z , that is located within layer, k so that $\eta_{k+1/2} \leq z \leq \eta_{k-1/2}$. Equation (32.94) generalizes the single-layer equation (32.38), thus revealing that the vertical velocity within an arbitrary shallow water layer is a linear function of the vertical position. Now evaluate equation (32.94) at the upper interface for the layer, $z = \eta_{k-1/2}$, in which case

$$w_{k-1/2}^{(k)} = w_{k+1/2}^{(k)} - h_k \nabla \cdot \mathbf{u}_k, \quad (32.95)$$

where

$$h_k = \eta_{k-1/2} - \eta_{k+1/2} \quad (32.96)$$

is the layer thickness. Eliminating the horizontal convergence between equations (32.94) and (32.95) renders

$$\frac{w_{k-1/2}^{(k)} - w_{k+1/2}^{(k)}}{h_k} = \frac{w^{(k)}(z) - w_{k+1/2}^{(k)}}{z - \eta_{k+1/2}}. \quad (32.97)$$

Making use of the kinematic boundary condition at the two interfaces allows us to write

$$w_{k-1/2}^{(k)} = \frac{D^{(k)}\eta_{k-1/2}}{Dt} = (\partial_t + \mathbf{u}_k \cdot \nabla) \eta_{k-1/2} \quad (32.98a)$$

$$w_{k+1/2}^{(k)} = \frac{D^{(k)}\eta_{k+1/2}}{Dt} = (\partial_t + \mathbf{u}_k \cdot \nabla) \eta_{k+1/2}, \quad (32.98b)$$

which then brings equation (32.97) to the form

$$\frac{1}{h_k} \frac{D^{(k)}h_k}{Dt} = \frac{1}{z - \eta_{k+1/2}} \frac{D^{(k)}(z - \eta_{k+1/2})}{Dt} \implies \frac{D^{(k)}}{Dt} \left[\frac{z - \eta_{k+1/2}}{h_k} \right] = 0 \quad (32.99)$$

Just like for a single layer of shallow water fluid, vertical columns within each layer are stretched and squeezed in a manner that preserves the relative vertical position for a point within the column.

Averaged vertical velocity for a layer

Since the vertical velocity is a linear function of depth within a layer, its layer averaged value is the average of the vertical velocity at the upper and lower layer interfaces. It is a useful exercise of the formalism to prove this result

$$\bar{w}_k = \frac{1}{h_k} \int_{\eta_{k+1/2}}^{\eta_{k-1/2}} w^{(k)}(z) dz \quad (32.100a)$$

$$= \frac{1}{h_k} \int_{\eta_{k+1/2}}^{\eta_{k-1/2}} \left[w_{k+1/2}^{(k)} - (z - \eta_{k+1/2}) \nabla \cdot \mathbf{u}_k \right] dz \quad (32.100b)$$

$$= w_{k+1/2}^{(k)} + \eta_{k+1/2} \nabla \cdot \mathbf{u}_k - (1/h_k) (\eta_{k-1/2}^2 - \eta_{k+1/2}^2) \nabla \cdot \mathbf{u}_k \quad (32.100c)$$

$$= w_{k+1/2}^{(k)} - (h_k/2) \nabla \cdot \mathbf{u}_k \quad (32.100d)$$

$$= (w_{k+1/2}^{(k)} + w_{k-1/2}^{(k)})/2, \quad (32.100e)$$

where the final step made use of the identity (32.95). Note that we can also write the layer averaged vertical velocity as

$$\bar{w}_k = (w_{k+1/2}^{(k)} + w_{k-1/2}^{(k)})/2 = \frac{D^{(k)}\bar{\eta}_k}{Dt}, \quad (32.101)$$

where

$$\bar{\eta}_k = (\eta_{k+1/2} + \eta_{k-1/2})/2 \quad (32.102)$$

is the average of the interface height for the layer.

32.4.5 Rigid lid models

Throughout this section we formulated the equations for an N-layer shallow water model where $\eta_{1/2}$ is the undulating free surface. For some applications of large-scale oceanography, it is useful to remove the external gravity waves from the model, where these gravity waves are associated with linear fluctuations of the upper free surface.⁸ To remove these gravity waves we can, by fiat, set the upper ocean interface to a rigid constant, conventionally taken as $\eta_{1/2} = 0$. This

⁸In Section 48.5 we study gravity waves in a single shallow water layer.

assumption is known as the *rigid lid*. If there is no applied pressure, $p_a = 0$, then there is no horizontal pressure gradient in the upper layer, much like an inverted reduced gravity model (see Exercise 32.5). A dynamically more interesting case arises when there is an applied pressure, $p_a \neq 0$, so that motion is generated in layer one, which in turn induces motion throughout all layers.

Note that velocity in the upper layer remains horizontally divergent since the $\eta_{3/2}$ interface is not generally rigid. Even so, by fixing the upper ocean to be rigid we remove the relatively fast external gravity waves from the model. We return to the rigid lid assumption when discussing the horizontal non-divergent barotropic model in Chapter 35 (see in particular Section 35.5).

32.5 Vector-invariant velocity equation

Following the discussion in Section 21.3.2 for a continuously stratified fluid, we here derive the vector-invariant form of the shallow water velocity equation. This formulation proves useful in the kinetic energy budget of Section 33.6.3 and for vorticity in Section 36.1.

32.5.1 Basic manipulations

The following manipulations hold for each shallow water layer, so it is convenient to drop layer indices to reduce clutter. To start, we introduce vorticity for the full velocity field

$$\boldsymbol{\omega} = \nabla \times \mathbf{v} \quad (32.103a)$$

$$= \hat{\mathbf{x}} (\partial_y w - \partial_z v) + \hat{\mathbf{y}} (\partial_z u - \partial_x w) + \hat{\mathbf{z}} (\partial_x v - \partial_y u) \quad (32.103b)$$

$$= \hat{\mathbf{x}} \partial_y w - \hat{\mathbf{y}} \partial_x u + \hat{\mathbf{z}} (\partial_x v - \partial_y u) \quad (32.103c)$$

$$= -\hat{\mathbf{z}} \times \nabla w + \hat{\mathbf{z}} (\partial_x v - \partial_y u), \quad (32.103d)$$

where we set

$$\partial_z u = \partial_z v = 0 \quad (32.104)$$

holding for the horizontal velocity within a shallow water layer. We also find it convenient to introduce the vorticity associated with the horizontal velocity field

$$\boldsymbol{\omega}^* = \nabla \times \mathbf{u} = -\hat{\mathbf{x}} \partial_z v + \hat{\mathbf{y}} \partial_z u + \hat{\mathbf{z}} (\partial_x v - \partial_y u) = \hat{\mathbf{z}} (\partial_x v - \partial_y u). \quad (32.105)$$

The vertical component to vorticity is particularly important for geophysical flows, in which case we write

$$\zeta = \hat{\mathbf{z}} \cdot \boldsymbol{\omega} = \hat{\mathbf{z}} \cdot \boldsymbol{\omega}^* = \partial_x v - \partial_y u. \quad (32.106)$$

The vector identity (see Section 2.3.4)

$$(\mathbf{u} \cdot \nabla) \mathbf{u} = (1/2) \nabla(\mathbf{u} \cdot \mathbf{u}) - \mathbf{u} \times (\nabla \times \mathbf{u}) = (1/2) \nabla(\mathbf{u} \cdot \mathbf{u}) + \boldsymbol{\omega}^* \times \mathbf{u} \quad (32.107)$$

brings the inviscid shallow water velocity equation (32.85)

$$\frac{\partial \mathbf{u}}{\partial t} + (\mathbf{u} \cdot \nabla) \mathbf{u} + f \hat{\mathbf{z}} \times \mathbf{u} = -\rho_{\text{ref}}^{-1} \nabla p \quad (32.108)$$

into its *vector invariant* form

$$\frac{\partial \mathbf{u}}{\partial t} + (f + \zeta) \hat{\mathbf{z}} \times \mathbf{u} = -\nabla (p/\rho_{\text{ref}} + \mathbf{u} \cdot \mathbf{u}/2). \quad (32.109)$$

Again, this equation holds separately for each layer, so that by reintroducing layer indices we have

$$\frac{\partial \mathbf{u}_k}{\partial t} + (f + \zeta_k) \hat{\mathbf{z}} \times \mathbf{u}_k = -\nabla(p_k/\rho_{\text{ref}} + \mathbf{u}_k \cdot \mathbf{u}_k/2). \quad (32.110)$$

32.5.2 Dynamical pressure and the Magnus acceleration

As in our discussion in Section 21.3.2 of the vector invariant velocity equation for continuously stratified flows, the velocity equation (32.110) exposes two physical processes that lend insight into the motion of a shallow water fluid column.

Dynamical pressure from kinetic energy per mass

The kinetic energy per mass, $\mathbf{u} \cdot \mathbf{u}/2$, adds a *dynamical pressure* to the mechanical pressure associated with the free surface undulations. Gradients in the kinetic energy thus drive accelerations towards regions of smaller kinetic energy; i.e., down the kinetic energy gradient.⁹

Magnus acceleration

As discussed in Sections 21.3.2 and 29.2.6, the Magnus acceleration is a body acceleration defined by the nonlinear term

$$\mathbf{A}_{\text{magnus}} = -\boldsymbol{\omega}^* \times \mathbf{u} = \zeta (\mathbf{u} \times \hat{\mathbf{z}}), \quad (32.111)$$

appearing in the vector-invariant velocity equation (32.110). There is a non-zero Magnus acceleration when a shallow water fluid column spins while it moves, with this acceleration acting to deflect the spinning column perpendicular to its trajectory. As for the example in Figure 21.1, consider a shallow water fluid column moving zonally, in which case the Magnus acceleration is

$$\mathbf{A}_{\text{magnus}} = u \zeta (\hat{\mathbf{x}} \times \hat{\mathbf{z}}) = -\hat{\mathbf{y}} u \zeta. \quad (32.112)$$

With a positive relative vorticity, $\zeta > 0$, the Magnus acceleration is directed to the right of the motion, which is in the same direction as the Coriolis acceleration in the northern hemisphere. For large-scale geophysical flows, the Magnus acceleration is sub-dominant to the Coriolis acceleration. However, the Magnus acceleration is a crucial facet of large (order unity or larger) Rossby number motions in which relative vorticity is sizable.

32.6 Non-conservative processes and boundary stresses

Much of our focus on shallow water mechanics concerns the adiabatic case in which the layers are immiscible and there are no frictional processes. Even so, we find occasion to consider non-conservative processes, such as the transfer of volume between layers via dia-surface fluxes, as well as irreversible momentum transfer associated with friction and boundary stresses. In this section we consider these processes for the single shallow water layer, with a straightforward extension to stacked shallow water.

32.6.1 Dia-surface volume fluxes

Consider the case of dia-surface transfer as occurs across the ocean surface through evaporation, precipitation, and river runoff, or as occurs for interior layers in the presence of irreversible mixing

⁹The dynamical pressure afforded by the kinetic energy should not be confused with the shallow water dynamic pressure introduced by equation (32.87). They are distinct.

processes. Let $w^{(\dot{\eta})}$ measure the volume per time per horizontal area of fluid entering across the surface interface of the shallow water layer, with $w^{(\dot{\eta})}$ having dimensions of length per time and a sign convention so that $w^{(\dot{\eta})} > 0$ means volume enters the shallow water layer.¹⁰ For example, $w^{(\dot{\eta})} > 0$ could represent the addition of rain to the surface layer. To keep the analysis simple, assume the mass contained in $w^{(\dot{\eta})} \neq 0$ has the same density and same velocity as the shallow water layer. Hence, there is no modification to the layer density. This assumption must be relaxed for realistic layered models.

Surface kinematic boundary condition

The kinematic boundary condition (32.35) expresses the material nature of the free surface in the absence of boundary volume flux. In the presence of a non-zero boundary flux, $w^{(\dot{\eta})} \neq 0$, we follow the formulation of the kinematic boundary condition for the ocean free surface with a mass flux (equation (16.79)), which renders the boundary condition

$$\frac{D(z - \eta)}{Dt} = -w^{(\dot{\eta})} \quad \text{at } z = \eta. \quad (32.113)$$

In effect, this relation defines the surface boundary flux, and this boundary condition can be written in the equivalent form

$$\frac{D\eta}{Dt} = w(\eta) + w^{(\dot{\eta})}. \quad (32.114)$$

Stretching of a vertical column

Equation (32.42) shows that in the absence of volume sources, a column of shallow water fluid stretches or squeezes uniformly. What happens when $w^{(\dot{\eta})} \neq 0$? Following through the derivation of the thickness equation in Section 32.2.5, we are trivially led to the following generalization

$$\frac{\partial h}{\partial t} + \nabla \cdot (h \mathbf{u}) = w^{(\dot{\eta})}, \quad (32.115)$$

or equivalently

$$\frac{Dh}{Dt} = -h \nabla \cdot \mathbf{u} + w^{(\dot{\eta})}. \quad (32.116)$$

Equation (32.40) is derived through assuming the horizontal velocity has no depth dependence within a shallow water layer, and the fluid has a three-dimensional non-divergent velocity. It holds whether the ocean surface is material or non-material, and thus forms a suitable starting point for generalization to the case of $w^{(\dot{\eta})} \neq 0$

$$w(z) - w(\eta_b) = \left[\frac{z - \eta_b}{\eta - \eta_b} \right] [w(\eta) - w(\eta_b)]. \quad (32.117)$$

We now make use of the new surface kinematic boundary condition (32.114) and the unmodified bottom kinematic boundary condition (32.28) to write the material form

$$\frac{1}{z - \eta_b} \left[\frac{D(z - \eta_b)}{Dt} \right] = \frac{1}{\eta - \eta_b} \left[\frac{D(\eta - \eta_b)}{Dt} - w^{(\dot{\eta})} \right]. \quad (32.118)$$

¹⁰This sign convention follows that used for water mass transformation as developed in Chapter 65 and defined by equation (65.38).

Rearrangement thus leads to the material conservation statement

$$\left[\frac{z - \eta_b}{h} \right]^{-1} \frac{D}{Dt} \left[\frac{z - \eta_b}{h} \right] = -\frac{w^{(\dot{\eta})}}{h}, \quad (32.119)$$

where $h = \eta - \eta_b$ is the layer thickness. This result can be written in the more concise form

$$\frac{D}{Dt} \left[\ln \left(\frac{z - \eta_b}{h} \right) \right] = -\frac{w^{(\dot{\eta})}}{h}. \quad (32.120)$$

Either way, we see that in the presence of a surface boundary volume flux, a column of shallow water fluid no longer stretches or squeezes uniformly. Instead, for $w^{(\dot{\eta})} > 0$, a fluid parcel moves down within the column as more water is added to the top of the layer.

32.6.2 Frictional and boundary stresses

As discussed in Chapter 22, accelerations from friction appear in the momentum equation via the divergence of the frictional stress tensor. For a shallow water fluid we may choose to include a frictional stress proportional to lateral shears within each layer much like the friction operators discussed in Section 22.8. Additionally, we may need to include boundary stresses such as those from winds and bottom friction. To incorporate boundary stresses, consider the Boussinesq form (Section 26.6.2) of the vertical stress divergence appearing in the momentum equation as a horizontal acceleration

$$\mathbf{F} = \frac{1}{\rho_0} \frac{\partial \boldsymbol{\tau}}{\partial z}, \quad (32.121)$$

where $\boldsymbol{\tau}$ is the horizontal stress imparted to the layer interface due to turbulent boundary layer processes. Since a shallow water layer is homogeneous, we can only apply this boundary stress uniformly throughout the layer (as a layer body stress) and so it appears as the horizontal acceleration

$$\mathbf{F}_k = \frac{1}{\rho_{\text{ref}}} \frac{\boldsymbol{\tau}_{k-1/2} - \boldsymbol{\tau}_{k+1/2}}{h_k}. \quad (32.122)$$

In this expression, h_k is the layer thickness, $\boldsymbol{\tau}_{k-1/2}$ is the stress at the upper layer interface and $\boldsymbol{\tau}_{k+1/2}$ is the stress at the lower interface.

Bottom drag is a common means to add dissipation in shallow water models. In this case the acceleration from bottom drag takes on the nonlinear form

$$\mathbf{F}_{\text{bot}} = -\frac{1}{\rho_{\text{ref}}} \frac{\boldsymbol{\tau}_{\text{bot}}}{h} = -\frac{C_D |\mathbf{u}| \mathbf{u}}{h}, \quad (32.123)$$

where C_D is a dimensionless drag coefficient (typically given values on the order of 10^{-3}), \mathbf{u} is the velocity in the layer adjacent to the bottom, and h is the bottom layer thickness. This friction is directed in the opposite direction of the velocity vector, just like the Rayleigh drag discussed in Sections 22.8.5 30.2.3. However, bottom drag is nonlinear whereas Rayleigh drag is linear.



32.7 Exercises

EXERCISE 32.1: RELATIONS FOR VERTICAL VELOCITY (EXERCISE (3.2) OF [Vallis \(2006\)](#))

Show that the vertical velocity within a shallow water system is given by

$$w = \left[\frac{z - \eta_b}{h} \right] \frac{Dh}{Dt} + \frac{D\eta_b}{Dt}, \quad (32.124)$$

where η_b is the position of the bottom topography (see Figure 32.1). Interpret the result, showing that it gives sensible answers at the top and bottom of the fluid layer.

EXERCISE 32.2: DERIVING THE SHALLOW WATER TRACER EQUATION ([32.46](#))

Show all steps needed to derive equations ([32.45a](#))-([32.45c](#)) and then show the steps leading to the shallow water tracer equation ([32.46](#)). Hint: use the z independence of \mathbf{u} and $\partial_z w$ within the shallow water layer.

EXERCISE 32.3: NON-ROTATING HYDRAULIC CONTROL

Consider the steady flow in a non-rotating shallow water layer where the flow is purely one-dimensional in the zonal direction, and with positive layer thickness, $h > 0$, throughout the domain.

- (a) Show that the steady flow satisfies the balance

$$[1 - Fr^2] \partial_x h = \partial_x \eta_b \quad (32.125)$$

where η_b is the position of the bottom topography (see Figure 32.1), and where the local Froude number is given by

$$Fr = \frac{u}{\sqrt{gh}}. \quad (32.126)$$

The Froude number is the local ratio of the speed for a fluid particle to the speed of a shallow water gravity wave.

- (b) Discuss the case in which $\partial_x \eta_b = 0$ yet $\partial_x h \neq 0$. This case is known as *hydraulic control*.

EXERCISE 32.4: SHALLOW WATER EQUATIONS WITH TIDES

In Chapter 31 we derive the equations for a primitive equation ocean in the presence of astronomical forcing that leads to tides. Specialize the general results from that chapter to derive the thickness and momentum equations for a single layer of shallow water fluid in the presence of astronomical tidal forcing. As in Section 31.4, assume the perturbation geopotential is depth independent.

EXERCISE 32.5: INVERTED REDUCED GRAVITY MODEL

Derive the shallow water equations for a single moving layer of fluid of density ρ_2 above a rigid floor, with this moving layer below a stagnant fluid of density ρ_1 , with $\rho_1 < \rho_2$. Assume $\nabla p_a = 0$. Discuss the constraint placed on the interface $\eta_{1/2}$ to maintain a stagnant upper layer. Show that as $\rho_1/\rho_2 \rightarrow 0$ with $\rho_{ref} = \rho_2$, then the single layer shallow water equations emerge. Make use of notation from the three-layer system shown in Figure 32.6. This model might be used to study flow in the atmosphere well above the boundary layer, or the abyssal ocean well below the pycnocline. Hint: invert the approach taken in Section 32.3 for the reduced gravity model of the upper ocean.



Chapter 33

SHALLOW WATER DYNAMICS

In this chapter we further our dynamical understanding of the shallow water fluid model. The study includes geostrophy, thermal wind (as expressed by Margules' relation), momentum budgets, form stress, kinetic energy, gravitational potential energy, available potential energy, and mechanical energy. We also develop the following case studies to exemplify the fundamentals: the steady force balance in a zonally reentrant channel, and the angular momentum dynamics of a rotating tank of shallow water fluid. We offer many details to support those aiming to become nimble with the equations describing the momentum and energy dynamics of a stacked shallow water model.

READER'S GUIDE TO THIS CHAPTER

This chapter builds from the formulations in Chapter 32 as well as the geostrophic mechanics from Chapter 28 and the pressure form stress from Chapter 25. We make use of the dynamical results in this chapter for many of the subsequent chapters. Notationally, we follow the same convention for the gradient operator noted at the start of Chapter 32.

33.1	Loose threads	790
33.2	Geostrophic balance and thermal wind	790
33.2.1	Geostrophy for a single layer	790
33.2.2	Geostrophy and thermal wind for two layers	791
33.2.3	Geostrophic transport within layers	792
33.2.4	Flow within a geostrophic eddy	793
33.3	Thickness weighted momentum equation	795
33.3.1	Single layer equations	795
33.3.2	Geostrophic and ageostrophic contributions	796
33.3.3	Form stresses acting on a shallow water column	796
33.3.4	Comments on the two pressure force formulations	799
33.4	Contact pressure forces in shallow water layers	799
33.4.1	Pressure contact force and pressure body force	800
33.4.2	N -layer equations	800
33.4.3	Contact pressure force along vertical sides	800
33.4.4	Contact pressure force along the top and bottom interfaces	802
33.4.5	Form stress	803
33.4.6	Net contact pressure force on a shallow water column	803
33.4.7	Contact pressure force summed over all layers	804
33.4.8	Horizontal pressure force with potential energy gradients	804
33.4.9	Momentum equation with contact pressure forces	805
33.4.10	Further reading	808
33.5	Energetics for a single layer	808
33.5.1	Gravitational potential energy	809

33.5.2	Kinetic energy and work from pressure gradients	810
33.5.3	Kinetic energy and buoyancy work	811
33.5.4	Kinetic energy and pressure form stress	812
33.5.5	Mechanical energy budget	813
33.5.6	Available potential energy	815
33.6	Energetics for N layers	816
33.6.1	Potential energy and available potential energy	816
33.6.2	Potential energy and buoyancy work	818
33.6.3	Kinetic energy	819
33.6.4	Comments and further study	820
33.7	Steady momentum balance in a zonal channel	820
33.7.1	Volume transport for steady flow	821
33.7.2	Steady meridional balances	822
33.7.3	Steady zonal balance	823
33.7.4	The role of frictional bottom drag	823
33.7.5	Correlation between surface height and topographic slope	824
33.7.6	Connection to meridional geostrophic transport	825
33.7.7	Sinusoidal example	825
33.7.8	Comments and further study	827
33.8	Angular momentum in a rotating tank	829
33.8.1	Angular momentum for a column of shallow water fluid	830
33.8.2	Material time evolution of the angular momentum	830
33.8.3	Materially invariant angular momentum	831
33.8.4	Comments	831
33.9	Exercises	832

33.1 Loose threads

- Some more interpretation of the N -layer mechanical energy equations and their connections to the continuous case.
- More schematics
- Consider adding a diabatic term to the energy budgets in Sections 33.5 and 33.6.
- Work through a two-layer example for the zonal channel in Section 33.7 to describe the features exhibited by Olbers and Hughes in their schematic of the Southern Ocean circulation. Discuss topographic form stress.

33.2 Geostrophic balance and thermal wind

As described in Chapter 28, geostrophic balance arises from neglecting the material time derivative in the inviscid horizontal momentum equation, which is a sensible assumption when the Rossby number is small. The resulting balance between Coriolis and pressure accelerations constitutes the geostrophic balance. We consider here the implications of geostrophy for one and two-layer shallow water systems.

33.2.1 Geostrophy for a single layer

Ignoring atmospheric pressure ($p_a = 0$) leads to the geostrophic balance for a single shallow water layer

$$f \hat{z} \times \mathbf{u}_g = -g \nabla \eta \implies f \mathbf{u}_g = g \hat{z} \times \nabla \eta, \quad (33.1)$$

or in component form

$$u_g = -\frac{g}{f} \frac{\partial \eta}{\partial y} \quad \text{and} \quad v_g = \frac{g}{f} \frac{\partial \eta}{\partial x}. \quad (33.2)$$

Consequently, the shallow water layer geostrophic current is balanced by the gradient of the free surface (sea level). In the northern hemisphere, where $f > 0$, geostrophic shallow water currents flow counter-clockwise around negative sea level anomalies (low pressure) and clockwise around positive sea level anomalies (high pressure). The opposite orientation holds in the southern hemisphere, where $f < 0$. Figure 33.1 shows a schematic of geostrophic balance for a single shallow water layer.

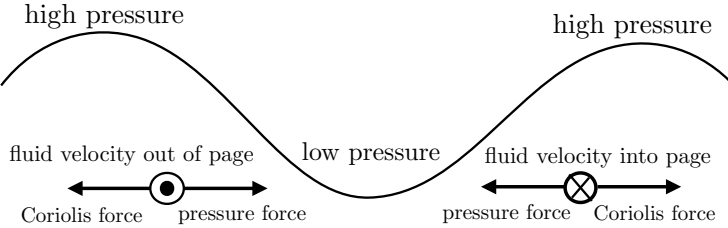


FIGURE 33.1: Side view of geostrophic balance for a single shallow water layer, here shown with two high pressure centers surrounding a low pressure center. The Coriolis force balances the pressure gradient force. In the northern hemisphere, where $f > 0$, geostrophic flow is counter-clockwise around a low pressure center and clockwise around a high pressure center.

33.2.2 Geostrophy and thermal wind for two layers

Now consider two shallow water layers as in Figure 32.6. Recall the layer pressure equations (32.62) and (32.63), which leads to the pressure difference

$$p_1 - p_2 = g \eta_{3/2} (\rho_1 - \rho_2) + g z (\rho_2 - \rho_1) = g_{3/2}^r \rho_{\text{ref}} (z - \eta_{3/2}), \quad (33.3)$$

where the reduced gravity is given by equation (32.68)

$$g_{3/2}^r = g (\rho_2 - \rho_1) / \rho_{\text{ref}} > 0, \quad (33.4)$$

where ρ_{ref} is the shallow water Boussinesq reference density (32.66). The density difference $\rho_2 - \rho_1$ is generally much smaller than either density, so that $g_{3/2}^r \ll g$. For the Boussinesq shallow water system, the momentum equations are given by

$$\frac{D^{(1)} \mathbf{u}_1}{Dt} + f \hat{z} \times \mathbf{u}_1 = -\rho_{\text{ref}}^{-1} \nabla p_1 \quad (33.5a)$$

$$\frac{D^{(2)} \mathbf{u}_2}{Dt} + f \hat{z} \times \mathbf{u}_2 = -\rho_{\text{ref}}^{-1} \nabla p_2, \quad (33.5b)$$

where we introduced the material time derivatives for each layer (we introduced this notation in Section 32.4.4)

$$\frac{D^{(k)}}{Dt} = \frac{\partial}{\partial t} + \mathbf{u}_k \cdot \nabla. \quad (33.6)$$

Making use of the pressure difference (33.3) renders

$$\frac{D_1 \mathbf{u}_1}{Dt} - \frac{D_2 \mathbf{u}_2}{Dt} + f \hat{z} \times \Delta \mathbf{u} = -\rho_{\text{ref}}^{-1} \nabla (p_1 - p_2) = g_{3/2}^r \nabla \eta_{3/2}, \quad (33.7)$$

where

$$\Delta \mathbf{u} = \mathbf{u}_1 - \mathbf{u}_2 \quad (33.8)$$

is the vertical difference of the layer horizontal velocities. We see that the difference in the geostrophic velocities for the two layers is proportional to the slope of the interface between the two layers

$$f \hat{\mathbf{z}} \times \Delta \mathbf{u}_g = g_{3/2}^r \nabla \eta_{3/2} \implies \Delta u_g = + (g_{3/2}^r / f) \partial_y \eta_{3/2} \quad \text{and} \quad \Delta v_g = - (g_{3/2}^r / f) \partial_x \eta_{3/2}. \quad (33.9)$$

These equations are known as the *Margules' relation*. It applies at any interface between two shallow water fluid layers. It says that the vertical difference between the layer geostrophic velocities is proportional to the interface slope. When the slope is large, the vertical difference in the geostrophic velocity is large. Also, the velocity difference is large when the reduced gravity is large; i.e., when the density difference is large. We illustrate this relation in Figure 33.2. The Margules relation is a discrete (two-layer) version of the thermal wind relation discussed in Section 28.5.6.

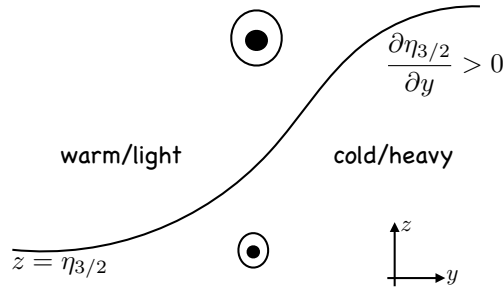


FIGURE 33.2: Illustrating Margules' relation for the northern hemisphere ($f > 0$). Here we show the interface between a two-layer shallow water model with a cold/heavy layer to the right and a warm/light layer to the left. The slope of the interface is positive, $\partial \eta_{3/2} / \partial y > 0$, thus leading to an increase in the eastward zonal geostrophic velocity moving upward, as depicted by the circles with a dot. This orientation corresponds to the northern hemisphere atmospheric jet stream, whereby the interface between cold/heavy air to the north and warm/light air to the south leads to a zonal thermal wind jet. This figure is directly comparable to the continuously stratified case shown in Figure 28.6.

33.2.3 Geostrophic transport within layers

We are often interested in computing the net volume transport within a layer of fluid in order to measure how much the fluid is moving across a particular region. For an N -layer shallow water fluid this transport is written

$$\mathbf{U} = \int \mathbf{u} dz = \sum_{k=1}^N \mathbf{u}_k h_k, \quad (33.10)$$

where \mathbf{u}_k is the layer horizontal velocity and h_k the layer thickness. For many purposes it is sufficient to compute the transport due to the geostrophic motion, in which case

$$\mathbf{u}_k = (\rho_{\text{ref}} f)^{-1} \hat{\mathbf{z}} \times \nabla p_k, \quad (33.11)$$

so that the geostrophic transport is

$$\mathbf{U}_g = \int_{\eta_b}^{\eta} \mathbf{u}_g dz = (\rho_{\text{ref}} f)^{-1} \hat{\mathbf{z}} \times \sum_{k=1}^N h_k \nabla p_k. \quad (33.12)$$

For the pressure gradient we can make use of the expression (32.87)

$$\nabla p_k = \nabla p_a + \nabla p_k^{\text{dyn}} = \nabla p_a + \rho_{\text{ref}} \sum_{j=1}^k g_{j-1/2}^r \nabla \eta_{j-1/2}, \quad (33.13)$$

thus revealing the cascade of contributions from each of the layer interfaces.

As an exercise, let us write the geostrophic transport for $N = 3$ layers (assuming $p_a = 0$), in which the layer pressure gradients are

$$\nabla p_1 = \rho_{\text{ref}} g \nabla \eta_{1/2} \quad (33.14a)$$

$$\nabla p_2 = \nabla p_1 + \rho_{\text{ref}} g_{3/2}^r \nabla \eta_{3/2} \quad (33.14b)$$

$$\nabla p_3 = \nabla p_1 + \nabla p_2 + \rho_{\text{ref}} g_{5/2}^r \nabla \eta_{5/2}. \quad (33.14c)$$

We see here the utility of setting

$$\rho_{\text{ref}} = \rho_1, \quad (33.15)$$

in which case the geostrophic transport within the three layers is

$$h_1 \mathbf{u}_{1g} = \frac{h_1}{f} \hat{\mathbf{z}} \times \nabla(g_{1/2}^r \eta_{1/2}) \quad (33.16a)$$

$$h_2 \mathbf{u}_{2g} = \frac{h_2}{f} \hat{\mathbf{z}} \times \nabla(g_{1/2}^r \eta_{1/2} + g_{3/2}^r \eta_{3/2}) \quad (33.16b)$$

$$h_3 \mathbf{u}_{3g} = \frac{h_3}{f} \hat{\mathbf{z}} \times \nabla(g_{1/2}^r \eta_{1/2} + g_{3/2}^r \eta_{3/2} + g_{5/2}^r \eta_{5/2}), \quad (33.16c)$$

in which case the depth integrated geostrophic transport is

$$\mathbf{U}_g = f^{-1} \hat{\mathbf{z}} \times \left[h_1 \nabla(g \eta) + h_2 \nabla(g \eta + g_{3/2}^r \eta_{3/2}) + h_3 \nabla(g \eta + g_{3/2}^r \eta_{3/2} + g_{5/2}^r \eta_{5/2}) \right]. \quad (33.17)$$

This expression for \mathbf{U}_g displays the cascade of contributions from each of the layer interfaces and their corresponding reduced gravities.

33.2.4 Flow within a geostrophic eddy

The ocean and atmosphere are highly turbulent fluids, with turbulent features extending from the small scales (millimeters) to large scales (hundreds to thousands of kilometers). The larger scale turbulent features feel the earth's rotation and thus maintain a force balance close to geostrophic.¹ We here outline some features of an ocean *geostrophic eddy* as idealized using the reduced gravity model of Section 32.3. Figure 33.3 shows a vertical-zonal slice through the upper portion of an ocean eddy in the middle latitude northern hemisphere ($f > 0$) ocean. The central region consists of a geostrophic eddy, sometimes also referred to as an *ocean mesoscale eddy*. The signature of the eddy is a depression in the free surface height and upward deformation of the pycnocline. The lateral scale of the eddy is on the order of the internal deformation scale (see Exercise 33.10).

The ocean eddy in Figure 33.3 is an anomalously dense cyclonic mesoscale eddy with the dense water causing the pycnocline to deviate upward. If density is dominated by temperature, as it typically is within the middle to lower latitude oceans, then the eddy is a *cold core eddy*, meaning

¹As noted in Section 29.6, the gradient wind balance provides a more accurate approximation to flows in ocean and atmospheric eddies by also including the centrifugal acceleration associated with the curved motion. Even so, the geostrophic balance provides a sufficient approximation for many purposes and it will be used here, along with thermal wind.

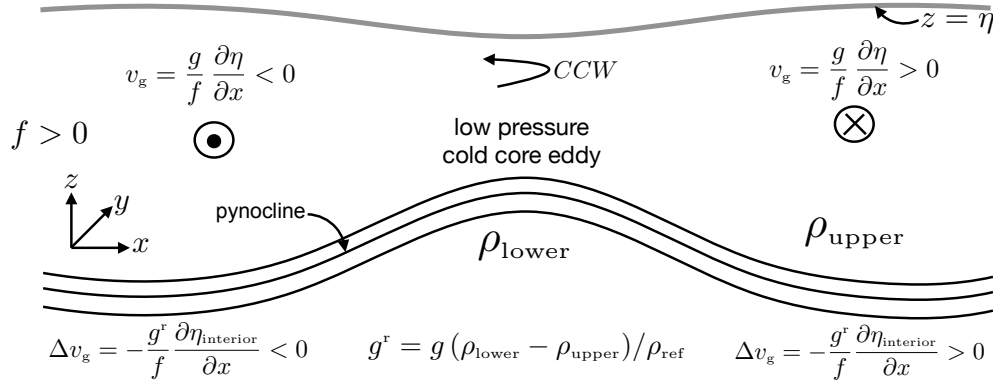


FIGURE 33.3: Vertical-zonal slice through a northern hemisphere mid-latitude cold-core ocean eddy looking from the south to the north (north is into the page). The ocean free surface is depressed down in the middle so that geostrophic flow is cyclonic (counter-clockwise in north) within the upper portion of the eddy where $\rho = \rho_{upper}$. The pycnocline (region of enhanced vertical density gradient) is deformed upward, and the baroclinic flow implied by Margules' relation (33.9) is indicated, making use of the reduced gravity $g^r = g(\rho_{lower} - \rho_{upper})/\rho_{ref}$. Note that $\Delta v_g = v_{upper} - v_{lower}$, so that $\Delta v_g > 0$ means that the meridional flow increases in the $+ŷ$ -direction when moving from the lower to upper layer, and conversely when $\Delta v_g < 0$.

that the core of the eddy is cold. Under geostrophic balance, water circulates counter-clockwise in the northern hemisphere within the upper portion of the cold core eddy, in the region where the pressure gradient force is dominated by the free surface undulation. In this case we see say the eddy is cyclonic. According to the reduced gravity model from Section 32.3 (see in particular Figure 32.5), the ratio of the free surface undulation to the pycnocline undulation scales like the reduced gravity, so that a meter undulation of the free surface corresponds to roughly 100 m undulation of the pycnocline. The same ideas hold for a *warm core eddy*, such as that depicted in Figure 33.4, with undulations complementing those in the cold core and thus supporting anti-cyclonic thermal wind flow.

In presenting the idealized rendition of an ocean eddy in Figure 33.3, we are assuming a reduced gravity model is sufficient and that the atmosphere has no significant horizontal pressure gradients over the scale of the eddy. Under these assumptions, we make use of the Margules' relation (33.9) to deduce the thermal wind flow in the upper layer relative to the layer below; i.e., the vertical shear in the geostrophic flow. For the left side of the eddy, where $\partial \eta_{interior}/\partial x > 0$, the vertical shear in the meridional geostrophic velocity is southward, consistent with orientation of the flow implied by the sea surface gradient. Conversely, on the right side of the eddy, where $\partial \eta_{interior}/\partial x < 0$, the vertical shear in the meridional flow is northward.

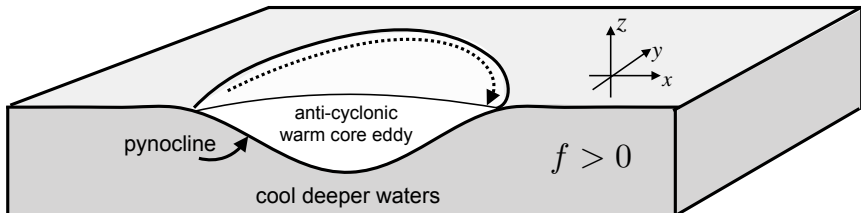


FIGURE 33.4: Schematic of a warm core (light water) geostrophic ocean eddy as idealized by a reduced gravity model. The geostrophic/thermal wind flow is anti-cyclonic within the eddy, which contrasts to the cyclonic flow for a cold core eddy as depicted in Figure 33.3. The eddy is characterized by a slight expansion of the free surface (high pressure) and a relatively larger depression of the pycnocline.

33.3 Thickness weighted momentum equation

Throughout our discussion of the shallow water model, we made use of the prognostic equation for the velocity of a layer. Here, we study the momentum equation as determined by the velocity as depth integrated within a shallow water layer. This formulation proves particularly useful when studying forces acting on the layer, such as those from pressure form stresses. It is also of use for studies of rotating hydraulics such as pursued in the book by [Pratt and Whitehead \(2008\)](#).

For a shallow water model with just a single layer, the water column extends from the surface to the bottom of the layer (see Figure 33.5)

$$\int_{\eta_b}^{\eta} \mathbf{u} dz = \mathbf{u} h, \quad (33.18)$$

so that the column momentum equals to $\mathbf{u} h \rho dx dy$. The resulting momentum equation is written in an Eulerian flux form. In Section 33.7 we illustrate the momentum budget for a zonal channel. We also show in Section 33.4.2 that the N -layer equations are isomorphic to the single layer, thus allowing for concepts developed for a single layer to be readily extended to multiple layers.

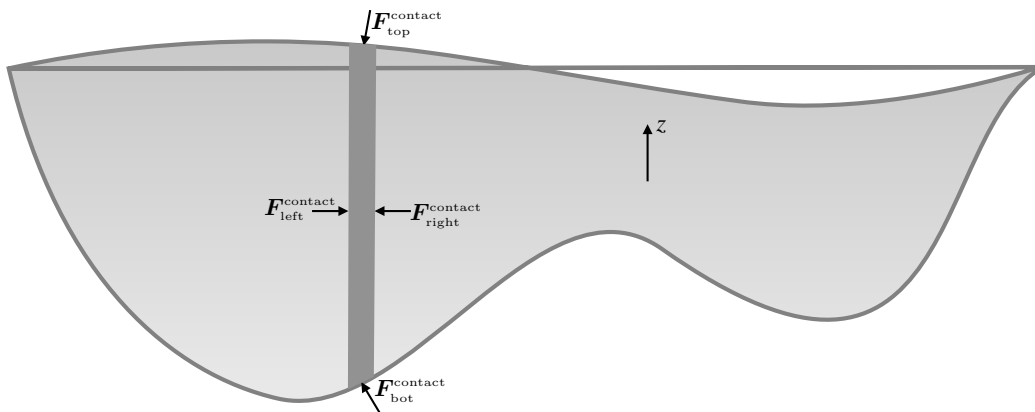


FIGURE 33.5: Momentum of a column of a single layer shallow water fluid is affected by contact forces at the column boundaries (pressure and friction), as well as body forces acting throughout the column (Coriolis and gravity).

33.3.1 Single layer equations

Recall the velocity and thickness equations written using the material time operator

$$\frac{D\mathbf{u}}{Dt} + f \hat{z} \times \mathbf{u} = -g \nabla \eta \quad \text{and} \quad \frac{Dh}{Dt} = -h \nabla \cdot \mathbf{u}. \quad (33.19)$$

Combining these two equations allows us to write the thickness weighted material acceleration as

$$h \frac{D\mathbf{u}}{Dt} = h \frac{D\mathbf{u}}{Dt} + \mathbf{u} \left[\frac{Dh}{Dt} + h \nabla \cdot \mathbf{u} \right] = \frac{\partial(h \mathbf{u})}{\partial t} + \nabla \cdot [h \mathbf{u} \otimes \mathbf{u}], \quad (33.20)$$

so that the thickness weighted equation takes the vector form

$$\frac{\partial(h \mathbf{u})}{\partial t} + \nabla \cdot [h \mathbf{u} \otimes \mathbf{u}] + f \hat{z} \times (h \mathbf{u}) = -g h \nabla \eta. \quad (33.21)$$

The Cartesian tensor form of the outer product is²

$$[\mathbf{u} \otimes \mathbf{u}]_{mn} = u_m u_n \quad \text{for } m, n = 1, 2, \quad (33.22)$$

with $h \mathbf{u} \otimes \mathbf{u}$ the specialization to the shallow water system of the *kinetic stress* appearing in the continuously stratified momentum equation (22.56). The component form of the thickness weighted momentum equation (33.21) is

$$\frac{\partial(h u)}{\partial t} + \partial_x(h u^2) + \partial_y(h u v) - v h f = -g h \partial_x \eta \quad (33.23a)$$

$$\frac{\partial(h v)}{\partial t} + \partial_x(h u v) + \partial_y(h v^2) + u h f = -g h \partial_y \eta. \quad (33.23b)$$

Note that when the bottom is flat then $\nabla h = \nabla \eta$ so that we have

$$\frac{\partial(h u)}{\partial t} + \partial_x(h u^2 + g h^2/2) + \partial_y(h u v) - v h f = 0 \quad (33.24a)$$

$$\frac{\partial(h v)}{\partial t} + \partial_x(h u v) + \partial_y(h v^2 + g h^2/2) + u h f = 0. \quad (33.24b)$$

33.3.2 Geostrophic and ageostrophic contributions

Bringing the Coriolis terms to the right hand side of equations (33.23a) and (33.23b) renders

$$\frac{\partial(h u)}{\partial t} + \partial_x(h u^2) + \partial_y(h u v) = h(-g \partial_x \eta + v f) \quad (33.25a)$$

$$\frac{\partial(h v)}{\partial t} + \partial_x(h u v) + \partial_y(h v^2) + u h f = h(-g \partial_y \eta - u f). \quad (33.25b)$$

In the absence of rotation, the right hand side has contributions only from the thickness weighted pressure gradient. For the case of rotation it sometimes proves useful to decompose velocity into its geostrophic and ageostrophic components

$$f u = f(u_a + u_g) = f u_a - g \partial \eta / \partial y \quad (33.26a)$$

$$f v = f(v_a + v_g) = f v_a + g \partial \eta / \partial x, \quad (33.26b)$$

in which case equations (33.25a) and (33.25b) become

$$\frac{\partial(h u)}{\partial t} + \partial_x(h u^2) + \partial_y(h u v) = h f v_a \quad (33.27a)$$

$$\frac{\partial(h v)}{\partial t} + \partial_x(h u v) + \partial_y(h v^2) = -h f u_a. \quad (33.27b)$$

One should be careful *not* to take the $f = 0$ limit of these equations since one might spuriously conclude there is no free surface contribution. Instead, equations (33.25a) and (33.25b) should be the basis for the $f = 0$ limit.

33.3.3 Form stresses acting on a shallow water column

The kinetic stress contributes to momentum evolution in equations (33.23a) and (33.23b) via its divergence. In contrast, the pressure stress contributes as a thickness weighted pressure gradient

²Equation (33.22) is the only place in this chapter where a subscript refers to a tensor label. Otherwise, subscripts refer to a shallow water layer index as in Section 33.4.2.

body stress. In this subsection, and in all of Section 33.4, we formulate pressure as a contact stress, in which case it also contributes to momentum evolution as a divergence. In so doing, we provide an Eulerian flux-form conservation law for momentum that supports analysis and interpretation.

Reintroducing atmospheric pressure to symmetrize the forces acting on the layer

To expose both the surface and bottom form stresses, we reintroduce the atmospheric pressure, p_a , and thus make use of the effective sea level (32.4)

$$\eta^{\text{eff}} = \eta + p_a/(\rho g) = \eta_b + h + p_a/(\rho g), \quad (33.28)$$

with the corresponding thickness weighted horizontal momentum equation

$$\frac{\partial(h \mathbf{u})}{\partial t} + \nabla \cdot [h \mathbf{u} \otimes \mathbf{u}] + f \hat{\mathbf{z}} \times (h \mathbf{u}) = -g h \nabla \eta^{\text{eff}}. \quad (33.29)$$

Exposing the contact pressure stresses

The free surface height equals $\eta = \eta_b + h$, in which case the momentum equation (33.29) is

$$\frac{\partial(h \mathbf{u})}{\partial t} + \nabla \cdot [h \mathbf{u} \otimes \mathbf{u}] + f \hat{\mathbf{z}} \times (h \mathbf{u}) = -(g/2) \nabla h^2 - g h \nabla [\eta_b + p_a/(\rho g)]. \quad (33.30)$$

To help interpret this equation it is convenient to write the boundary terms on the right hand side as

$$-g h \nabla [\eta_b + p_a/(\rho g)] = -\nabla(h p_a/\rho) + (p_a/\rho) \nabla(\eta - \eta_b) - g h \nabla \eta_b \quad (33.31a)$$

$$= -\nabla(h p_a/\rho) + (p_a/\rho) \nabla \eta - (g h + p_a/\rho) \nabla \eta_b \quad (33.31b)$$

$$= -\nabla(h p_a/\rho) + \rho^{-1} (p_a \nabla \eta - p_b \nabla \eta_b), \quad (33.31c)$$

so that

$$-(g/2) \nabla h^2 - g h \nabla [\eta_b + p_a/(\rho g)] = -\nabla[(g/2) h^2 + h p_a/\rho] + \rho^{-1} (p_a \nabla \eta - p_b \nabla \eta_b). \quad (33.32)$$

The first term on the right hand side is the gradient of the layer integrated hydrostatic pressure

$$P \equiv \int_{\eta_b}^{\eta} [p_a + \rho g (\eta - z)] dz = h (\rho g h/2 + p_a), \quad (33.33)$$

and the second term exposes the form stresses acting at the surface and bottom of the layer. With these expressions, the horizontal thickness weighted momentum equation (33.30) becomes

$$\frac{\partial(h \mathbf{u})}{\partial t} + \nabla \cdot [h \mathbf{u} \otimes \mathbf{u} + \mathbb{I} P/\rho] + f \hat{\mathbf{z}} \times (h \mathbf{u}) = (p_a \nabla \eta - p_b \nabla \eta_b)/\rho, \quad (33.34)$$

where \mathbb{I} is the unit tensor. Exposing the zonal and meridional components renders

$$\frac{\partial(h u)}{\partial t} + \partial_x(h u^2 + P/\rho) + \partial_y(h u v) - v h f = (p_a \partial_x \eta - p_b \partial_x \eta_b)/\rho \quad (33.35a)$$

$$\frac{\partial(h v)}{\partial t} + \partial_x(h u v) + \partial_y(h v^2 + P/\rho) + u h f = (p_a \partial_y \eta - p_b \partial_y \eta_b)/\rho. \quad (33.35b)$$

The horizontal pressure gradient appears as a continuous operator since we assumed an infinitesimal horizontal cross-sectional area for the fluid column. In contrast, the pressure form stresses appear as a vertical finite difference across the layer interfaces, which results since we are integrating over the thickness of a finite layer. Furthermore, note how the depth integrated pressure contributions appear in a flux-form, which contrasts to the body force version that appears as thickness weighted pressure gradient.

Kinetic stresses and contact pressure stresses combined into a momentum flux

To anticipate the thickness weighted momentum equation for the stacked shallow water model in Section 33.4, write the finite difference of the form stresses as

$$p_a \nabla \eta - p_b \nabla \eta_b = p_{1/2} \nabla \eta_{1/2} - p_{3/2} \nabla \eta_{3/2} \equiv \delta_k(p_{k-1/2} \nabla \eta_{k-1/2}). \quad (33.36)$$

We here introduced the layer interface difference operator

$$\delta_k(\Psi_{k-1/2}) = \Psi_{k-1/2} - \Psi_{k+1/2} = -(\Psi_{k+1/2} - \Psi_{k-1/2}), \quad (33.37)$$

with the backward difference motivated since k increases downward whereas \hat{z} points upward. In the following, we choose to define the difference operator to only act on interface fields. Hence, any layer quantity, such as the layer thickness, commutes with the interface operator

$$\delta_k(h A_{k-1/2}) = h (A_{k-1/2} - A_{k+1/2}). \quad (33.38)$$

Also note that the thickness itself is the difference between the layer interfaces

$$h = \eta - \eta_b = \delta_k \eta_{k-1/2}, \quad (33.39)$$

where $\eta_{1/2} = \eta$ and $\eta_{3/2} = \eta_b$.

With the above notation, the component momentum equations (33.35a) and (33.35b) take on the matrix-vector form

$$\begin{bmatrix} \partial_t(h u) - h f v \\ \partial_t(h v) + h f u \end{bmatrix} = - \begin{bmatrix} \partial_x & \partial_y & h^{-1} \delta_k \end{bmatrix} \begin{bmatrix} D_1^{(u)} & D_1^{(v)} & 0 \\ D_2^{(u)} & D_2^{(v)} & 0 \\ D_3^{(u)} & D_3^{(v)} & 0 \end{bmatrix}. \quad (33.40)$$

The 3×3 matrix is a second order tensor with the first and second columns consisting of the momentum fluxes

$$\mathbf{D}^{(u)} = (h u^2 + P/\rho) \hat{\mathbf{x}} + h u v \hat{\mathbf{y}} - (p_{k-1/2} \partial_x \eta_{k-1/2}/\rho) h \hat{\mathbf{z}} \quad (33.41a)$$

$$\mathbf{D}^{(v)} = h u v \hat{\mathbf{x}} + (h v^2 + P/\rho) \hat{\mathbf{y}} - (p_{k-1/2} \partial_y \eta_{k-1/2}/\rho) h \hat{\mathbf{z}}, \quad (33.41b)$$

where we suppressed unnecessary layer indices. The horizontal flux components are given by minus the thickness weighted kinetic stress, $h \mathbf{u} \otimes \mathbf{u}$, plus the depth integrated contact pressure acting on the vertical sides of the shallow water column. The vertical flux component contains the pressure form stresses acting on the top and bottom interfaces, with these interfacial form stresses leading to the vertical transfer of horizontal form stresses across the layer boundaries. These fluxes allow us to write the thickness weighted zonal and meridional momentum equations

as

$$\frac{\partial(h u)}{\partial t} - v h f = -(\hat{x} \partial_x + \hat{y} \partial_y + \hat{z} h^{-1} \delta_k) \cdot \mathbf{D}^{(u)} \quad (33.42a)$$

$$\frac{\partial(h v)}{\partial t} + u h f = -(\hat{x} \partial_x + \hat{y} \partial_y + \hat{z} h^{-1} \delta_k) \cdot \mathbf{D}^{(v)}. \quad (33.42b)$$

In this form of the momentum equation, contributions from contact stresses (kinetic stresses and form stresses) appear as the convergence of these stresses with the divergence operator built as combination of the continuous horizontal gradient operator along with a finite difference vertical operator. The third column of the tensor (33.40) is identically zero and so it can be readily dropped. However, we include it to connect with the *Eliassen-Palm flux tensor* as detailed by [Maddison and Marshall \(2013\)](#). We return to equations (33.42a) and (33.42b) in Section 33.4.9 for the stacked shallow water model.

33.3.4 Comments on the two pressure force formulations

The momentum equations (33.42a) and (33.42b) are written as a flux-form Eulerian conservation law, with only the Coriolis force appearing as a body force. This formulation follows that for Cauchy's equation of motion as discussed in Section 21.2.3. We make use of these flux-form momentum equations in Section 33.7 when discussing force balances in a zonally periodic channel, as well as in Chapter 60 when formulating the thickness weighted averaged shallow water equations. Before doing so, we focus in Section 33.4 by further unpacking the contact force version of pressure as it appears in the shallow water model.

What has been gained by writing the momentum equation as the thickness weighted forms (33.42a) and (33.42b) versus the non-flux form velocity equation (33.19)? Indeed, the thickness weighted formulation is arguably less elegant and takes more effort to derive. A key reason we consider the thickness weighted equations is that they provide a venue to study how pressure contact forces alter momentum of a shallow water fluid column through interactions with the bottom, the surface, and adjacent vertical columns. We put this perspective to use in Section 33.7 when studying the force balances on a zonally reentrant channel. Additionally, in Section 33.4 we further pursue the contact force perspective by studying how pressure form stresses appear within a stacked shallow water model.

33.4 Contact pressure forces in shallow water layers

For a finite region of fluid, if the boundary area integrated contact pressure stress is nonzero, then pressure accelerates the region. In this section we study the physics and maths of contact pressure forces as they appear in the stacked shallow water model. As revealed by this study, the columnar motion of the shallow water fluid is fundamental to the analysis. Namely, the contact pressure approach is realized by studying the thickness weighted velocity equations of motion, which determine evolution of the momentum per horizontal area of a shallow water fluid column. We introduced the thickness weighted approach in Section 33.3 for a single shallow water layer, and it led to the flux-form Eulerian momentum equations (33.42a) and (33.42b). The single layer results are reproduced here for the stacked shallow water model, yet only after furthering our understanding of how pressure forces act to move momentum through shallow water layers.

33.4.1 Pressure contact force and pressure body force

As discussed in Section 22.2.3, the connection between the body force and contact force expressions of the pressure force arise through an application of Gauss's divergence theorem to scalar fields (see Section 2.7.2)

$$\mathbf{F}_{\mathcal{R}}^{\text{press}} = - \int_{\mathcal{R}} \nabla p \, dV = - \oint_{\partial\mathcal{R}} p \hat{\mathbf{n}} \, dS. \quad (33.43)$$

The first expression on the right hand side is a volume integral of the pressure gradient over the fluid region, \mathcal{R} . This expression provides the body force version of the pressure force. The second expression is a surface area integral over the region boundary, $\partial\mathcal{R}$, whose outward normal is $\hat{\mathbf{n}}$. This second expression provides the contact force version of the pressure force. Neither expression is more or less fundamental. Instead, they offer complementary insights into how pressure acts to modify the momentum of a fluid, with general notions of this complementarity the topic of Chapter 25. We here pursue the contact force perspective as a means to understand the *pressure form stress* or *interfacial form stress* acting between layers of a shallow water fluid. There is also a pressure form stress acting between a fluid layer and the solid earth (topographic form stress), as well as between a fluid layer and the overlying atmosphere when the atmosphere has a non-zero mass (atmosphere form stress).

33.4.2 N -layer equations

Our starting point for the development in this section are the N -layer shallow water thickness and velocity equations derived in Section 32.4.2

$$\frac{\partial h_k}{\partial t} + \nabla \cdot (h_k \mathbf{u}_k) = 0 \quad \text{and} \quad [\partial_t + (\mathbf{u}_k \cdot \nabla)] \mathbf{u}_k + f \hat{z} \times \mathbf{u}_k = -(1/\rho_{\text{ref}}) \nabla p_k, \quad (33.44)$$

where $k = 1, N$ is the layer index with no implied summation over this index, ρ_{ref} is the the Boussinesq reference density (often chosen as $\rho_{\text{ref}} = \rho_1$), and equation (32.81) gives the horizontal pressure gradient acceleration. Equations (33.44) are isomorphic to the single layer equations considered in Section 33.3.1. Hence, the thickness weighted velocity equation is a simple generalization of the single layer equation (33.21)

$$\frac{\partial(h_k \mathbf{u}_k)}{\partial t} + \nabla \cdot [h_k \mathbf{u}_k \otimes \mathbf{u}_k] + f \hat{z} \times (h_k \mathbf{u}_k) = -(h_k/\rho_{\text{ref}}) \nabla p_k, \quad (33.45)$$

where, again, there is no implied summation over the layer index, k . We commonly refer to the thickness weighted equation (33.45) as the momentum equation since $\rho dx dy h_k \mathbf{u}_k$ is the horizontal momentum of a shallow water fluid column,

33.4.3 Contact pressure force along vertical sides

We now build up our understanding of pressure form stresses acting in a stacked shallow water fluid, with the essence of this discussion following that encountered for the single layer in Section 33.3. Our interest concerns the pressure acting on the boundaries of a fluid column within a shallow water layer, such as shown in Figure 33.6.

The pressure at a vertical position within the shallow water layer- k is given by

$$p_k(z) = \rho_k g (\eta_{k-1/2} - z) + p_{k-1/2}. \quad (33.46)$$

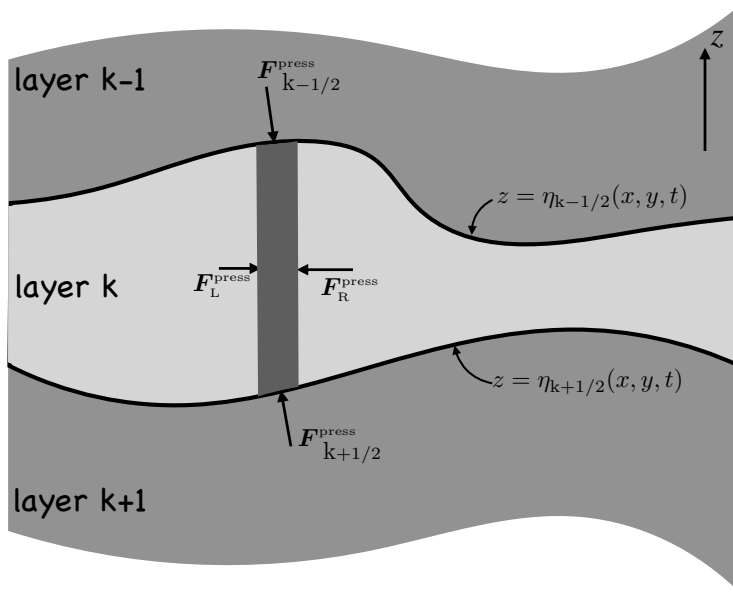


FIGURE 33.6: A schematic of the contact pressure force per area acting on the boundaries of a vertical column region within a shallow water layer of density ρ_k . Since fluid moves as vertical columns in a shallow water layer, we focus on the pressure forces acting on this column. The horizontal cross-sectional area of the column is depth independent. The interface at the lower boundary is at the vertical position $z = \eta_{k+1/2}$, and the upper interface is at $z = \eta_{k-1/2}$. In accordance with Newton's third law, pressures are continuous across each of the $\eta_{k\pm 1/2}$ layer interfaces so that the pressure forces are equal in magnitude yet oppositely directed on the opposite sides to the interfaces. The layer thickness is the difference between the interface positions, $h_k = \eta_{k-1/2} - \eta_{k+1/2}$. The boundaries of the columnar region feel a contact pressure force from the surrounding fluid that acts inward. The left side of the column experiences a pressure p_L ; the right side experiences p_R ; the upper interface has a pressure $p_{k-1/2}$ acting between the layer $k-1$ and layer k , and the lower interface has a pressure $p_{k+1/2}$ acting between the layer $k+1$ and layer k . The net pressure acting on the column is computed as the area integral of the pressure acting around the full extent of the column boundaries. The horizontal components of the stress are known as *interfacial form stresses*. This figure is identical to Figure 25.5 used to discuss the general notions of pressure form stress.

Integrating this pressure over the layer thickness yields

$$P_k \equiv \int_{\eta_{k+1/2}}^{\eta_{k-1/2}} p_k(z) dz \quad (33.47a)$$

$$= g \rho_k \left[\eta_{k-1/2} h_k - (1/2) (\eta_{k-1/2}^2 - \eta_{k+1/2}^2) \right] + p_{k-1/2} h_k \quad (33.47b)$$

$$= h_k (g \rho_k h_k / 2 + p_{k-1/2}). \quad (33.47c)$$

Since pressure is a linear function of z within a layer, the vertically averaged hydrostatic pressure within a layer, P_k/h_k , equals to the pressure at the upper interface, $p_{k-1/2}$, plus one-half the weight per area of the layer, $g \rho_k h_k / 2$.

The zonal pressure force acting on the column sides is the difference between the pressure integrated across the left and right zonal faces of the column. Assuming the fluid column to have

an infinitesimal horizontal cross-sectional area $dx dy$, we find the zonal pressure force is given by

$$dy \int_{\eta_{k+1/2}}^{\eta_{k-1/2}} (p_L - p_R) dz = -dx dy \left[(g/2) \rho_k \frac{\partial h_k^2}{\partial x} + \frac{\partial(h_k p_{k-1/2})}{\partial x} \right] \quad (33.48a)$$

$$= -dx dy \partial_x \left[(g/2) \rho_k h_k^2 + h_k p_{k-1/2} \right] \quad (33.48b)$$

$$= -dx dy \partial_x P_k. \quad (33.48c)$$

The analogous result holds for the meridional direction, thus rendering the net contact pressure force acting on the vertical sides of the column

$$\mathbf{F}_{\text{sides}}^{\text{press}} = -dx dy \nabla P_k. \quad (33.49)$$

Hence, the contact force on the vertical sides of the column is given by the gradient of the layer vertically integrated pressure, with the vertical integral given by equation (33.47c). It is notable that this semi-discrete exercise reveals no more information than already contained within the integral theorem (33.43). Nonetheless, it is useful to see how the integral theorem manifests within discrete shallow water layers.

33.4.4 Contact pressure force along the top and bottom interfaces

Now consider the contact pressure force acting on the top interface. This interface is generally sloped, so that the contact force has a component in both the vertical and horizontal directions. The vertical component to the pressure force maintains hydrostatic balance with the contact pressure at the lower boundary interface. The horizontal component provides a horizontal acceleration, with this acceleration (sign and magnitude) determined by the slope of the interface. Following our discussion in Section 25.3, we term the horizontal pressure acting on the sloped interface the *interfacial form stress*.

To mathematically characterize the pressure force on the top interface, $z = \eta_{k-1/2}$, requires the outward normal

$$\hat{\mathbf{n}}_{k-1/2} = \frac{\nabla(z - \eta_{k-1/2})}{|\nabla(z - \eta_{k-1/2})|} = \frac{\hat{\mathbf{z}} - \nabla\eta_{k-1/2}}{\sqrt{1 + (\nabla\eta_{k-1/2})^2}}. \quad (33.50)$$

Temporarily assume the interface slope to have a zero projection in the $\hat{\mathbf{y}}$ direction. In this case, the outward normal is

$$\hat{\mathbf{n}}_{k-1/2} = \frac{\hat{\mathbf{z}} - \hat{\mathbf{x}} \partial_x \eta_{k-1/2}}{\sqrt{1 + (\partial_x \eta_{k-1/2})^2}} \quad (33.51a)$$

$$= \frac{\hat{\mathbf{z}} - \hat{\mathbf{x}} \tan \varphi_{k-1/2}}{\sqrt{1 + \tan^2 \varphi_{k-1/2}}} \quad (33.51b)$$

$$= (\hat{\mathbf{z}} - \hat{\mathbf{x}} \tan \varphi_{k-1/2}) \cos \varphi_{k-1/2}, \quad (33.51c)$$

where we defined the interface slope as

$$\frac{\partial \eta_{k-1/2}}{\partial x} = \tan \varphi_{k-1/2}, \quad (33.52)$$

with $\varphi_{k-1/2}$ the angle between the horizontal plane and the interface. Trigonometry leads to an

expression for the area of the top of the column³

$$dS_{k-1/2} = \frac{dx dy}{\cos \varphi_{k-1/2}}, \quad (33.53)$$

so that the product of the area and the outward normal is given by

$$\hat{\mathbf{n}}_{k-1/2} dS_{k-1/2} = dx dy (\hat{\mathbf{z}} - \hat{\mathbf{x}} \partial_x \eta_{k-1/2}). \quad (33.54)$$

This result generalizes to an interface slope that projects into both horizontal directions

$$\hat{\mathbf{n}}_{k-1/2} dS_{k-1/2} = dx dy (\hat{\mathbf{z}} - \nabla \eta_{k-1/2}), \quad (33.55)$$

so that the contact pressure force acting on layer-k at its top interface is given by

$$\mathbf{F}_{\text{top}}^{\text{press}} = -dx dy (\hat{\mathbf{z}} - \nabla \eta_{k-1/2}) p_{k-1/2}. \quad (33.56)$$

Analogous considerations lead to the contact pressure force acting on layer-k at the bottom of the column

$$\mathbf{F}_{\text{bot}}^{\text{press}} = dx dy (\hat{\mathbf{z}} - \nabla \eta_{k+1/2}) p_{k+1/2}. \quad (33.57)$$

33.4.5 Form stress

As noted earlier, form stress is the horizontal projection of the contact pressure acting on the sloped top or bottom interface of the fluid column (Chapter 25). The corresponding forces acting on layer-k is the horizontal area element multiplied by the form stress

$$\mathbf{F}_{\text{top face}}^{\text{form stress}} = dx dy (p_{k-1/2} \nabla \eta_{k-1/2}) \quad (33.58)$$

$$\mathbf{F}_{\text{bot face}}^{\text{form stress}} = -dx dy (p_{k+1/2} \nabla \eta_{k+1/2}). \quad (33.59)$$

These forces render a mechanically reversible vertical exchange of horizontal momentum. This momentum exchange occurs without any exchange of matter. Rather, it an inviscid exchange that occurs according to Newton's third law principle of action/reaction.

For a specific case, consider a $k - 1/2$ interface that slopes upward in the $\hat{\mathbf{x}}$ direction (e.g., see Figure 33.6). Form stress acting at the interface provides a $+ \hat{\mathbf{x}}$ directed acceleration on the column. For the $k + 1/2$ interface, a negatively sloped interface also experiences a $+ \hat{\mathbf{x}}$ directed acceleration.

33.4.6 Net contact pressure force on a shallow water column

Summing the contact pressure forces (33.49), (33.56), and (33.57), and dividing by the horizontal area, leads to the net pressure force per horizontal area acting on a column within layer-k

$$\frac{\mathbf{F}_{\text{net},k}^{\text{press}}}{dx dy} = -\nabla P_k - (\hat{\mathbf{z}} - \nabla \eta_{k-1/2}) p_{k-1/2} + (\hat{\mathbf{z}} - \nabla \eta_{k+1/2}) p_{k+1/2} \quad (33.60a)$$

$$= \rho_k g \hat{\mathbf{z}} - \nabla P_k + p_{k-1/2} \nabla \eta_{k-1/2} - p_{k+1/2} \nabla \eta_{k+1/2}. \quad (33.60b)$$

³Equation (33.53) was also found in Section 16.4.3 when developing the kinematic boundary condition for a material interface.

To reach this result we made use of the hydrostatic relation for the vertical pressure difference across a layer

$$p_{k+1/2} - p_{k-1/2} = \rho_k g h_k, \quad (33.61)$$

and introduced the mass of a column within layer k

$$M_k = g \rho_k h_k dx dy. \quad (33.62)$$

The vertical component of the net contact pressure force balances the weight of the column within the layer, which is expected since the shallow water fluid is in hydrostatic balance. The horizontal contact pressure force arises from a horizontal gradient plus the form stress at the surface and bottom interfaces. The gradient term is removed when integrating horizontally over the full domain given that the thickness of the layer vanishes upon reaching the coastlines (e.g., see Figure 25.7). The resulting net force on the full domain arises just from the weight of the fluid acting in the vertical, plus form stress at the surface and bottom. We discuss this point more in Section 33.4.7.

33.4.7 Contact pressure force summed over all layers

Summing the contact pressure force (33.60b) over all layers reveals the contact forces on the interior layer interfaces vanish, as per Newton's third law (see Section 25.1), thus leaving just the form stress at the surface and bottom and the contact pressure force acting on the vertical sides. Dividing by the horizontal area of the column leads to the net pressure force per area

$$\frac{1}{dx dy} \sum_{k=1}^N \mathbf{F}_{\text{net},k}^{\text{press}} = \hat{\mathbf{z}} g \sum_{k=1}^N \rho_k h_k + p_a \nabla \eta_{1/2} - p_b \nabla \eta_b - \sum_{k=1}^N \nabla P_k \quad (33.63a)$$

$$= (p_b - p_a) \hat{\mathbf{z}} + p_a \nabla \eta_{1/2} - p_b \nabla \eta_b - \sum_{k=1}^N \nabla P_k, \quad (33.63b)$$

where we wrote the total mass per area within the column as the difference between the bottom pressure and applied surface pressure

$$g \sum_{k=1}^N \rho_k h_k = p_b - p_a. \quad (33.64)$$

The horizontal components to the applied and bottom pressure terms in equation (33.63b) arise from pressure form stresses applied to the interfaces at the top and bottom of the column. The vertical component arises from the net weight per area of the fluid. The summation term is the horizontal gradient of the depth integrated pressure form stress applied along the vertical sides of the column.

33.4.8 Horizontal pressure force with potential energy gradients

There is another means to express the horizontal pressure force. Here, we expose the gravitational potential energy per horizontal area for a column of fluid within a shallow water layer

$$\mathcal{P}_k = g \rho_k \int_{\eta_{k+1/2}}^{\eta_{k-1/2}} z dz = (g \rho_k / 2) (\eta_{k-1/2}^2 - \eta_{k+1/2}^2). \quad (33.65)$$

Use of the layer gravitational potential energy brings the layer vertical integral of the hydrostatic pressure from Section 33.4.3 into

$$\int_{\eta_{k+1/2}}^{\eta_{k-1/2}} p_k(z) dz = g \rho_k h_k^2 / 2 + h_k p_{k-1/2} = \mathcal{P}_k - g \rho_k h_k \eta_{k+1/2} + h_k p_{k-1/2}. \quad (33.66a)$$

Making use of this result in equation (33.60b), along with a few lines of algebra, yields the net horizontal contact pressure force acting on a shallow water column

$$-\nabla P_k + \delta_k(p_{k-1/2} \nabla \eta_{k-1/2}) = -\nabla \mathcal{P}_k - \delta_k(\eta_{k-1/2} \nabla p_{k-1/2}). \quad (33.67)$$

To reach the identity (33.67) requires the hydrostatic relation, $p_{k+1/2} - p_{k-1/2} = g \rho_k h_k$, and the layer thickness, $h_k = \eta_{k-1/2} - \eta_{k+1/2}$. A consistency check notes that the curl of both sides to equation (33.67) are the same. The identity (33.67) suggests we define the form stress and its dual

$$\mathbf{F}^{\text{form}} = p \nabla \eta \quad \text{and} \quad \mathbf{F}^{\text{dual form}} = -\eta \nabla p, \quad (33.68)$$

with both \mathbf{F}^{form} and $\mathbf{F}^{\text{dual form}}$ defined on layer interfaces. These two stresses have the same curl, and thus impart the same pressure torque on a column of fluid (Chapter 36)

$$\nabla \times (p \nabla \eta) = \nabla \times (-\eta \nabla p). \quad (33.69)$$

However, these stresses are distinct and as such cannot be arbitrarily interchanged.⁴

33.4.9 Momentum equation with contact pressure forces

Comparing the body force version and the contact force version

Recall that the thickness weighted velocity equation (33.45), as written in terms of the pressure gradient body force, is given by⁵

$$\frac{\partial(h_k \mathbf{u}_k)}{\partial t} + \nabla \cdot [h_k \mathbf{u}_k \otimes \mathbf{u}_k] + f \hat{\mathbf{z}} \times (h_k \mathbf{u}_k) = -(h_k / \rho_{\text{ref}}) \nabla_z p_k, \quad (33.70)$$

again with no implied summation over the layer label, k. Alternatively, we can make use of the net contact pressure force (33.60b) so that

$$\frac{\partial(h_k \mathbf{u}_k)}{\partial t} + \nabla \cdot (h_k \mathbf{u}_k \otimes \mathbf{u}_k + \mathbb{I} P_k / \rho_{\text{ref}}) + f \hat{\mathbf{z}} \times (h_k \mathbf{u}_k) = \delta_k(p_{k-1/2} \nabla \eta_{k-1/2}) / \rho_{\text{ref}}, \quad (33.71)$$

where \mathbb{I} is the identity tensor, P_k is the layer integrated pressure given by equation (33.47c), and δ_k is the difference operator defined by equation (33.37). Choosing the contact pressure force as in equation (33.67) to expose the potential energy brings the momentum equation (33.71) into

⁴As noted in Section 25.1.3, much of the literature refers to $-\eta \nabla p$ as the form stress rather than the dual form stress. This usage presumably originates from the common application of zonal averages for studying atmospheric motions, whereby $\eta \partial_x p = -p \partial_x \eta$. But this identity does not hold for arbitrary averaging operators, such as the ensemble averages commonly used for turbulence studies. So it is generally necessary to distinguish the form stress from the dual form stress.

⁵In equation (33.70) we wrote the gradient on the pressure as ∇_z since we are only interested in the horizontal gradient acting on $p_k(x, y, z)$. All other objects in equation (33.70) are just a function of horizontal position within a layer, so that ∇ acting on them reduces to ∇_z . Hence, the subscript on the gradient operator, ∇_z , is exposed only when it acts on a function of z , such as for $p_k(x, y, z)$. Since $p_k(x, y, z)$ is a linear function of z , its horizontal gradient is depth independent within the layer, as illustrated in Figure 32.1.

the alternative form

$$\frac{\partial(h_k \mathbf{u}_k)}{\partial t} + \nabla \cdot [h_k \mathbf{u}_k \otimes \mathbf{u}_k + \mathbb{I} \mathcal{P}_k / \rho_{\text{ref}}] + f \hat{\mathbf{z}} \times (h_k \mathbf{u}_k) = -\delta_k (\eta_{k-1/2} \nabla p_{k-1/2}) / \rho_{\text{ref}}. \quad (33.72)$$

Equations (33.70), (33.71), and (33.72) allow us to identify the body force and contact force versions of the thickness weighted horizontal pressure acceleration

$$-h_k \nabla_z p_k = -\nabla P_k + \delta_k (p_{k-1/2} \nabla \eta_{k-1/2}) = -\nabla \mathcal{P}_k - \delta_k (\eta_{k-1/2} \nabla p_{k-1/2}). \quad (33.73)$$

The balance of pressure torques acting on a shallow water column

A necessary (but not sufficient) check of the identity (33.73) can be found by verifying that the curl agrees for each expression

$$-\nabla \times \delta_k (\eta_{k-1/2} \nabla p_{k-1/2}) = \nabla \times \delta_k (p_{k-1/2} \nabla \eta_{k-1/2}) \quad (33.74a)$$

$$= \delta_k [\nabla \times (p_{k-1/2} \nabla \eta_{k-1/2})] \quad (33.74b)$$

$$= \delta_k [\nabla p_{k-1/2} \times \nabla \eta_{k-1/2}] \quad (33.74c)$$

$$= \nabla p_{k-1/2} \times \nabla \eta_{k-1/2} - \nabla (p_{k-1/2} + g \rho_k h_k) \times \nabla \eta_{k+1/2} \quad (33.74d)$$

$$= \nabla p_{k-1/2} \times \nabla h_k - g \rho_k \nabla h_k \times \nabla \eta_{k+1/2} \quad (33.74e)$$

$$= \nabla (p_{k-1/2} + g \rho_k \eta_{k+1/2}) \times \nabla h_k \quad (33.74f)$$

$$= \nabla (p_{k-1/2} - g \rho_k h_k + g \rho_k \eta_{k-1/2}) \times \nabla h_k \quad (33.74g)$$

$$= \nabla_z [p_{k-1/2} + g \rho_k (\eta_{k-1/2} - z)] \times \nabla h_k \quad (33.74h)$$

$$= \nabla_z p_k \times \nabla h_k \quad (33.74i)$$

$$= -\nabla \times (h_k \nabla_z p_k), \quad (33.74j)$$

which concurs with the curl of the left hand side of equation (33.73). To reach this result we set $h_k = \eta_{k-1/2} - \eta_{k+1/2}$ and used equation (33.46) for the pressure within a shallow water layer: $p_k(z) = \rho_k g (\eta_{k-1/2} - z) + p_{k-1/2}$.

Anticipating our discussion of vorticity for the shallow water fluid in Section 36.1, we observe that the identity derived above

$$\nabla \times \delta_k (p_{k-1/2} \nabla \eta_{k-1/2}) = -\nabla \times (h_k \nabla_z p_k) \quad (33.75)$$

says that the difference in interfacial pressure torques acting on the top and bottom of a shallow water layer precisely balances minus the torque arising from the thickness weighted horizontal pressure gradient acting within the layer. This rather remarkable fine tuning of the interfacial and interior pressure torques is a direct consequence of assuming that the fluid motion is restricted to extensible vertical columns within each shallow water layer. This balance is not maintained within a three dimensional fluid, where fluid columns can generally tilt and bend (Chapter 37).

Layer summed momentum equation

Taking the vertical sum of the layer-k momentum equation (33.71) leads to the column integrated horizontal momentum equation

$$\frac{\partial \mathbf{U}}{\partial t} + f \hat{\mathbf{z}} \times \mathbf{U} + \nabla \cdot \left[\sum_{k=1}^N (h_k \mathbf{u}_k \otimes \mathbf{u}_k + \mathbb{I} P_k / \rho_{\text{ref}}) \right] = [p_a \nabla \eta_{1/2} - p_b \nabla \eta_b] / \rho_{\text{ref}}, \quad (33.76)$$

where \mathbf{U} is the depth integrated horizontal velocity given by equation (33.10). The same vertical sum for equation (33.72) leads to

$$\frac{\partial \mathbf{U}}{\partial t} + f \hat{\mathbf{z}} \times \mathbf{U} + \nabla \cdot \left[\sum_{k=1}^N (h_k \mathbf{u}_k \otimes \mathbf{u}_k + \mathbb{I} \mathcal{P}_k / \rho_1) \right] = [-\eta_{1/2} \nabla p_a + \eta_b \nabla p_b] / \rho_{\text{ref}}. \quad (33.77)$$

The right hand side of equation (33.76) exposes the pressure form stresses acting on the ocean surface and bottom, whereas the right hand side of equation (33.77) exposes the dual form stress acting on the ocean surface and bottom.

Decomposing into depth averaged and depth deviation velocities

For detailed analyses of the depth integrated (layer summed) momentum and vorticity budgets, it is of interest to introduce the depth averaged operator and its deviation

$$\bar{\Phi}^z = \frac{\sum_{k=1}^N h_k \Phi_k}{\sum_{k=1}^N h_k} \quad \text{and} \quad \Phi'_k = \Phi_k - \bar{\Phi}^z \quad (33.78)$$

so that the depth integrated kinetic stress in equation (33.76) is

$$\sum_{k=1}^N h_k \mathbf{u}_k \otimes \mathbf{u}_k = D [\bar{\mathbf{u}}^z \otimes \bar{\mathbf{u}}^z + \bar{\mathbf{u}}' \otimes \bar{\mathbf{u}}'^z] \quad \text{where } D = \sum_{k=1}^N h_k. \quad (33.79)$$

The velocity \mathbf{u}'_k is the deviation of the layer- k velocity from the depth average velocity, and we refer to it as the *internal velocity*, whereas the depth averaged velocity, $\bar{\mathbf{u}}^z$, is the *external velocity*.⁶ The identity (33.79) reveals that the depth integrated kinetic stress can be decomposed into a stress arising from internal-internal velocity interactions plus external-external velocity interactions. By construction, there are no cross-terms (i.e., no internal-external terms) appearing in this depth integrated stress.

Momentum fluxes

Following the single layer discussion in Section 33.3.3, we write the momentum equation (33.71) in the form

$$\frac{\partial(h u)}{\partial t} - v h f = -(\hat{\mathbf{x}} \partial_x + \hat{\mathbf{y}} \partial_y + \hat{\mathbf{z}} h^{-1} \delta_k) \cdot \mathbf{D}^{(u)} \quad (33.80a)$$

$$\frac{\partial(h v)}{\partial t} + u h f = -(\hat{\mathbf{x}} \partial_x + \hat{\mathbf{y}} \partial_y + \hat{\mathbf{z}} h^{-1} \delta_k) \cdot \mathbf{D}^{(v)}, \quad (33.80b)$$

where we dropped the k label for brevity and introduced the layer momentum fluxes

$$\mathbf{D}^{(u)} = (h u^2 + P / \rho_{\text{ref}}) \hat{\mathbf{x}} + h u v \hat{\mathbf{y}} - (p_{k-1/2} \partial_x \eta_{k-1/2} / \rho_{\text{ref}}) h \hat{\mathbf{z}} \quad (33.81a)$$

$$\mathbf{D}^{(v)} = h u v \hat{\mathbf{x}} + (h v^2 + P / \rho_{\text{ref}}) \hat{\mathbf{y}} - (p_{k-1/2} \partial_y \eta_{k-1/2} / \rho_{\text{ref}}) h \hat{\mathbf{z}}. \quad (33.81b)$$

⁶It is also common in the oceanography literature to refer to \mathbf{u}'_k as the *baroclinic velocity* and $\bar{\mathbf{u}}^z$ as the *barotropic velocity*.

Likewise, we can write the momentum equation (33.72) in the component form

$$\frac{\partial(h u)}{\partial t} - v h f = -(\hat{x} \partial_x + \hat{y} \partial_y + \hat{z} h^{-1} \delta_k) \cdot \mathbf{E}^{(u)} \quad (33.82a)$$

$$\frac{\partial(h v)}{\partial t} + u h f = -(\hat{x} \partial_x + \hat{y} \partial_y + \hat{z} h^{-1} \delta_k) \cdot \mathbf{E}^{(v)}, \quad (33.82b)$$

where the dual layer momentum fluxes are given by

$$\mathbf{E}^{(u)} = (h u^2 + \mathcal{P}/\rho_{\text{ref}}) \hat{x} + h u v \hat{y} + (\eta_{k-1/2} \partial_x p_{k-1/2}/\rho_{\text{ref}}) h \hat{z} \quad (33.83a)$$

$$\mathbf{E}^{(v)} = h u v \hat{x} + (h v^2 + \mathcal{P}/\rho_{\text{ref}}) \hat{y} + (\eta_{k-1/2} \partial_y p_{k-1/2}/\rho_{\text{ref}}) h \hat{z}. \quad (33.83b)$$

Besides swapping the depth integrated pressure, P , for the potential energy, \mathcal{P} , the dual momentum fluxes, $\mathbf{E}^{(u)}$ and $\mathbf{E}^{(v)}$, make use of the dual form stress, $\eta_{k-1/2} \nabla p_{k-1/2}$, rather than the form stress, $-p_{k-1/2} \nabla \eta_{k-1/2}$. Upon performing an eddy-mean flow decomposition as in Section 60.6, the eddy correlation portion of the fluxes (33.83a) and (33.83b) lead to the shallow water *Eliassen-Palm* fluxes, which are rows in the Eliassen-Palm flux tensor.

33.4.10 Further reading

[Ward and Hogg \(2011\)](#) and [Barthel et al. \(2017\)](#) offer pedagogical treatments of the stacked shallow water equations in the context of idealized simulations that lend insight into the dynamical balances. [Maddison and Marshall \(2013\)](#) study the Eliassen-Palm flux tensor for continuously stratified quasi-geostrophy as well as the Boussinesq hydrostatic equations.

33.5 Energetics for a single layer

In this section we develop budgets for gravitational potential energy, kinetic energy, and mechanical energy for a single shallow water layer sitting on top of a non-flat bottom. Since the shallow water model has no internal energy, the total energy of the fluid is just that arising from the mechanical energy of the macroscopic motion. As part of this discussion we also consider the available potential energy (APE).

Motion within a shallow water layer occurs in vertical columns, so that we consider the energy of the layer integrated motion. The gravitational potential energy of a shallow water column is affected by vertical movement of the top and bottom of the column within the gravitational field. The kinetic energy is affected by pressure work, which, as we have seen in Sections 33.3 and 33.4, can be expressed either as a gradient body force or a contact force. Furthermore, pressure work leading to vertical motion manifests as buoyancy work. Our goal in this section is to study these energetic transformations and their mathematical expressions. We then extend the energetic analysis from the single layer to multiple layers in Section 33.6, though note that much of our work for the single layer is sufficient for multiple layers.

Before diving into details, we note that shallow water energetics can be derived from a layer integration of the continuously stratified Boussinesq energy equations from Section 26.7. That approach offers a somewhat more telescopic presentation than given here. However, we choose to present the derivations in a manner that supports skills in manipulating the shallow water equations, and further exposes the physical concepts arising from the motion of shallow water fluid columns.

33.5.1 Gravitational potential energy

The gravitational potential energy per horizontal area of a shallow water fluid is given by⁷

$$\mathcal{P}^{\text{sw}} = g \rho \int_{\eta_b}^{\eta} z \, dz = \frac{g \rho}{2} (\eta^2 - \eta_b^2) = \rho g h \bar{\eta}, \quad (33.84)$$

where the final equality introduced the layer thickness, h , and average of the layer interface heights

$$h = \eta - \eta_b \quad \text{and} \quad \bar{\eta} = (\eta + \eta_b)/2. \quad (33.85)$$

Notice how the gravitational potential energy vanishes when $\eta^2 = \eta_b^2$. For the case $\eta = \eta_b$, there is no fluid in the column and so we expect the potential energy to vanish. For the case $\eta = -\eta_b > 0$, there is the same amount of fluid above $z = 0$ as below, in which case the potential energy for the column vanishes since we are computing it relative to the $z = 0$ reference state. Furthermore, in the flat bottom case, $\eta_b = 0$ so that $h = \eta - \eta_b = \eta$, in which case the potential energy (33.84) reduces to $\mathcal{P}_{\text{flat}}^{\text{sw}} = g \rho \eta^2 / 2$.

Material time derivative of gravitational potential energy

Taking the material time derivative of the gravitational potential energy in equation (33.84) yields

$$\frac{D\mathcal{P}^{\text{sw}}}{Dt} = g \rho \left[\eta \frac{D\eta}{Dt} - \eta_b \frac{D\eta_b}{Dt} \right] \quad (33.86a)$$

$$= g \rho [\eta w(\eta) - \eta_b w(\eta_b)] \quad (33.86b)$$

$$= g \rho h [w(\eta_b) - \eta \nabla \cdot \mathbf{u}] \quad (33.86c)$$

$$= g \rho h [w(\eta) - \eta_b \nabla \cdot \mathbf{u}], \quad (33.86d)$$

where we used equations for the vertical velocity component from Section 32.2.8, and for the final equality we used equation (32.95) to write

$$w(\eta) - w(\eta_b) = -h \nabla \cdot \mathbf{u}. \quad (33.87)$$

Evidently, the potential energy changes according to how the thickness of the layer increases through vertical motion along the top and bottom interfaces, and as weighted by the position of these interfaces relative to $z = 0$. Finally, it is useful to write equation (33.86d) in its Eulerian flux-form, which is given by

$$\partial_t \mathcal{P}^{\text{sw}} + \nabla \cdot (\mathbf{u} \mathcal{P}^{\text{sw}}) = \mathcal{P}^{\text{sw}} \nabla \cdot \mathbf{u} + g \rho h [w(\eta) - \eta_b \nabla \cdot \mathbf{u}]. \quad (33.88)$$

The source term on the right hand side can be written as a buoyancy work term, which we show next.

⁷We include the “sw” superscript to distinguish the shallow water energetic terms, which we consider in their thickness weighted form so their dimensions are energy per area. In other areas of this book, we consider the energy per mass, such as in Chapters 23 and 26.

Exposing the role of buoyancy work

An alternative expression for the potential energy evolution is found by working with the final expression for potential energy in equation (33.84), whose material time derivative is

$$\frac{D\mathcal{P}^{sw}}{Dt} = g\rho\bar{\eta}\frac{Dh}{Dt} + g\rho h\frac{D\bar{\eta}}{Dt} = -\mathcal{P}^{sw}\nabla \cdot \mathbf{u} + \rho gh\bar{w}, \quad (33.89)$$

where we introduced the averaged vertical velocity for the layer according to equation (32.101)

$$\bar{w} = \frac{D\bar{\eta}}{Dt} = \frac{1}{2} \frac{D(\eta + \eta_b)}{Dt}. \quad (33.90)$$

The Eulerian flux-form version of the potential energy equation (33.89) thus takes on the form

$$\partial_t \mathcal{P}^{sw} + \nabla \cdot (\mathbf{u} \mathcal{P}^{sw}) = g\rho h \bar{w}. \quad (33.91)$$

This equation is the shallow water analog to the gravitational potential energy budget (23.5) for in a continuously stratified fluid. In particular, we see that the buoyancy work term, $g\rho h \bar{w}$, alters potential energy when there is vertical motion through the gravity field. As a check on the manipulations, we verify that the potential energy budgets (33.88) and (33.91) are indeed self-consistent by noting that

$$\mathcal{P}^{sw} \nabla \cdot \mathbf{u} + \rho gh [w(\eta) - \eta_b \nabla \cdot \mathbf{u}] = \rho gh [(\bar{\eta} - \eta_b) \nabla \cdot \mathbf{u} + w(\eta)] \quad (33.92a)$$

$$= \rho gh [(h/2) \nabla \cdot \mathbf{u} + w(\eta)] \quad (33.92b)$$

$$= \rho gh [-(1/2) Dh/Dt + w(\eta)] \quad (33.92c)$$

$$= \rho gh \bar{w}. \quad (33.92d)$$

33.5.2 Kinetic energy and work from pressure gradients

The kinetic energy per horizontal area is

$$\mathcal{K}^{sw} = \frac{1}{2} \int_{\eta_b}^{\eta} \rho \mathbf{u} \cdot \mathbf{u} dz = \frac{1}{2} \rho h \mathbf{u} \cdot \mathbf{u}. \quad (33.93)$$

Its material time derivative is given by

$$\frac{D\mathcal{K}^{sw}}{Dt} = \rho h \mathbf{u} \cdot \frac{Du}{Dt} + \frac{1}{2} \rho \mathbf{u} \cdot \mathbf{u} \frac{Dh}{Dt} \quad (33.94a)$$

$$= -h \mathbf{u} \cdot \nabla p + \rho h \mathbf{u} \cdot \mathbf{F} + \frac{\mathcal{K}^{sw}}{h} \frac{Dh}{Dt} \quad (33.94b)$$

$$= -h \mathbf{u} \cdot \nabla p + \rho h \mathbf{u} \cdot \mathbf{F} - \mathcal{K}^{sw} \nabla \cdot \mathbf{u}, \quad (33.94c)$$

where we made use of the velocity equation (32.9) along with the addition of a frictional acceleration, \mathbf{F} (see Section 32.6.2), and we used the thickness equation (32.20). Rearrangement of equation (33.94c) leads to the Eulerian flux-form budget for layer integrated kinetic energy

$$\partial_t \mathcal{K}^{sw} + \nabla \cdot (\mathbf{u} \mathcal{K}^{sw}) = -h \mathbf{u} \cdot \nabla p + \rho h \mathbf{u} \cdot \mathbf{F}. \quad (33.95)$$

The first term on the right hand side is the projection of the horizontal velocity onto the horizontal pressure gradient acceleration, thus indicating that kinetic energy for the fluid column increases if the velocity has a component that is directed down the horizontal pressure gradient. This term arises from the work done by the horizontal pressure gradient force acting on the moving fluid

columns. The second right hand side term is the projection of the velocity onto the thickness weighted horizontal friction, which accounts for work done by friction and/or boundary stresses on the moving fluid.

For a slight modification to the budget equation (33.95), write the layer pressure as

$$p = p_a + \rho g (\eta - z) = \rho g (\eta^{\text{eff}} - z), \quad (33.96)$$

where we introduced the effective free surface from equation (32.4)

$$\eta^{\text{eff}} = \eta + p_a / (\rho g). \quad (33.97)$$

The thickness weighted pressure work thus takes the form

$$-h \mathbf{u} \cdot \nabla p = -h \rho g \mathbf{u} \cdot \nabla \eta^{\text{eff}}, \quad (33.98)$$

so that the kinetic energy equation (33.95) becomes

$$\partial_t \mathcal{K}^{\text{sw}} + \nabla \cdot [\mathbf{u} (\mathcal{K}^{\text{sw}} + \rho g h \eta^{\text{eff}})] = \rho g \eta^{\text{eff}} \nabla \cdot (h \mathbf{u}) + \rho h \mathbf{u} \cdot \mathbf{F}. \quad (33.99)$$

33.5.3 Kinetic energy and buoyancy work

Following the second formulation of gravitational potential energy in Section 33.5.1, we here expose the buoyancy work that is contained in the term $\rho g \eta^{\text{eff}} \nabla \cdot (h \mathbf{u})$ appearing in equation (33.99). For this purpose, make use of the thickness equation, $\partial_t h = -\nabla \cdot (\mathbf{u} h)$, to write

$$\rho g \eta^{\text{eff}} \nabla \cdot (h \mathbf{u}) = -\rho g \eta^{\text{eff}} \partial_t h = -\rho g \eta^{\text{eff}} \partial_t (\delta_k \eta_{k-1/2}) = -\delta_k (\rho g \eta^{\text{eff}} \partial_t \eta_{k-1/2}). \quad (33.100)$$

For the final two equations we introduced the layer index, with $k = 1$ for the single layer and with the layer interfaces $\eta_{1/2} = \eta$ and $\eta_{3/2} = \eta_b$. Additionally, δ_k is the finite difference operator (33.37) so that

$$h = \eta - \eta_b = \eta_{1/2} - \eta_{3/2} = \delta_k \eta_{k-1/2}. \quad (33.101)$$

We inserted $\rho g \eta^{\text{eff}}$ into the difference operator in equation (33.100) since this term is depth independent across the layer.

For the next step, we make use of equation (33.96) for the layer pressure, $p = \rho g (\eta^{\text{eff}} - z)$, in which case⁸

$$-\delta_k (\rho g \eta^{\text{eff}} \partial_t \eta_{k-1/2}) = -\delta_k [(p + \rho g z) \partial_t \eta_{k-1/2}] \quad (33.102a)$$

$$= -\delta_k (p_{k-1/2} \partial_t \eta_{k-1/2}) - \delta_k (\rho g \eta_{k-1/2} \partial_t \eta_{k-1/2}). \quad (33.102b)$$

This step is somewhat subtle since we replaced $\rho g \eta^{\text{eff}}$, which is depth independent within a layer, with the sum $p + \rho g z$, where both p and $\rho g z$ are functions of depth. For equation (33.102b) we replaced p and z with their interface values since the argument of the difference operator is evaluated on the layer interfaces. Observe that $\partial_t \eta_b = 0$, and yet it is convenient to carry this term through the manipulations to retain symmetry of the equations, and to anticipate the same formulation for the stacked shallow water energetics in Section 33.6.

We now make use of the potential energy in Section 33.5.1 by writing

$$-\delta_k (\rho g \eta_{k-1/2} \partial_t \eta_{k-1/2}) = -(\rho g/2) \partial_t (\eta^2 - \eta_b^2) = -\partial_t \mathcal{P}^{\text{sw}} = \nabla \cdot (\mathbf{u} \mathcal{P}^{\text{sw}}) - g \rho h \bar{w}, \quad (33.103)$$

where the final step used the potential energy equation (33.91). As advertised, this formulation

⁸Equations (33.102a) and (33.102b) are inspired by some unpublished notes from Christopher Wolfe.

exposes the buoyancy work term, $-g \rho h \bar{w}$, which then allows us to bring the kinetic energy equation (33.99) to the form

$$\partial_t \mathcal{K}^{\text{sw}} + \nabla \cdot [\mathbf{u} (\mathcal{K}^{\text{sw}} - \mathcal{P}^{\text{sw}} + \rho g h \eta^{\text{eff}})] + \delta_k (p_{k-1/2} \partial_t \eta_{k-1/2}) = -g \rho h \bar{w} + \rho h \mathbf{u} \cdot \mathbf{F}. \quad (33.104)$$

We can simplify the advective flux by writing

$$-\mathcal{P}^{\text{sw}} + \rho g h \eta^{\text{eff}} = -\rho g h \bar{\eta} + \rho g \eta + h p_a = h (\rho g h / 2 + p_a) = P, \quad (33.105)$$

where the final equality introduced the layer integrated pressure

$$P = \int_{\eta_b}^{\eta} p(z) dz = \rho g \int_{\eta_b}^{\eta} (\eta^{\text{eff}} - z) dz = h (\rho g h / 2 + p_a). \quad (33.106)$$

The kinetic energy equation (33.104) thus takes the form

$$\partial_t \mathcal{K}^{\text{sw}} + \nabla \cdot [\mathbf{u} (\mathcal{K}^{\text{sw}} + P)] + \delta_k (p_{k-1/2} \partial_t \eta_{k-1/2}) = -g \rho h \bar{w} + \rho h \mathbf{u} \cdot \mathbf{F}. \quad (33.107)$$

The term $\delta_k (p_{k-1/2} \partial_t \eta_{k-1/2})$ on the left hand side is a vertical transfer that, as seen in Section 33.5.4, arises in part from pressure form stresses acting on the boundary of the fluid column.

33.5.4 Kinetic energy and pressure form stress

As a final form of the kinetic energy equation, we recombine the vertical transfer term and the buoyancy work term in equation (33.107) to have

$$-g \rho h \bar{w} - \delta_k (p_{k-1/2} \partial_t \eta_{k-1/2}) = -g \rho h \bar{w} - p_a [w(\eta) - \mathbf{u} \cdot \nabla \eta] + p_b [w(\eta_b) - \mathbf{u} \cdot \nabla \eta_b]. \quad (33.108)$$

Introducing the bottom pressure and depth integrated pressure

$$p_b = p_a + \rho g h \quad \text{and} \quad P = h (p_a + \rho g h / 2), \quad (33.109)$$

leads to

$$-g \rho h \bar{w} - \delta_k (p_{k-1/2} \partial_t \eta_{k-1/2}) = (P/h) [w(\eta_b) - w(\eta)] + \mathbf{u} \cdot (p_a \nabla \eta - p_b \nabla \eta_b) \quad (33.110a)$$

$$= \frac{P}{h} \frac{D(\eta_b - \eta)}{Dt} + \mathbf{u} \cdot (p_a \nabla \eta - p_b \nabla \eta_b) \quad (33.110b)$$

$$= -\frac{P}{h} \frac{Dh}{Dt} + \mathbf{u} \cdot (p_a \nabla \eta - p_b \nabla \eta_b) \quad (33.110c)$$

$$= P \nabla \cdot \mathbf{u} + \mathbf{u} \cdot (p_a \nabla \eta - p_b \nabla \eta_b), \quad (33.110d)$$

so that the kinetic energy equation (33.107) can be written

$$\partial_t \mathcal{K}^{\text{sw}} + \nabla \cdot (\mathbf{u} \mathcal{K}^{\text{sw}}) = \mathbf{u} \cdot (-\nabla P + p_a \nabla \eta - p_b \nabla \eta_b) + \rho h \mathbf{u} \cdot \mathbf{F}. \quad (33.111)$$

We have thus exposed the work done by pressure form stresses acting on the vertical side of an expanding or contracting shallow water column, plus those form stresses acting on the top and bottom layer interfaces. A direct way to derive equation (33.111) is to return to the kinetic energy equation (33.95) and make use of the identity (33.73). This identity equates the thickness weighted horizontal pressure gradient acting on a shallow water column, to the pressure form stresses acting over the boundary of the column, and for a single shallow water layer this identity

is

$$-h \nabla p = -\nabla P + p_a \nabla \eta - p_b \nabla \eta_b. \quad (33.112)$$

Nonetheless, we chose the more tedious derivation as it provides a check on the correctness of the transfer term and the buoyancy work term in the kinetic energy budget (33.107).

33.5.5 Mechanical energy budget

The mechanical energy per horizontal area for the shallow water layer is given by

$$m^{sw} = \mathcal{K}^{sw} + \mathcal{P}^{sw} = (\rho/2) [h \mathbf{u} \cdot \mathbf{u} + g(\eta^2 - \eta_b^2)] = \rho h (\mathbf{u} \cdot \mathbf{u}/2 + g \bar{\eta}). \quad (33.113)$$

To form a budget equation for the mechanical energy we simply add the budgets for the gravitational potential energy and kinetic energy.

Summary of the potential and kinetic energy budgets

We here summarize the Eulerian flux-form budgets for potential energy and kinetic energy (equations (33.91), (33.95), (33.99), (33.107), and (33.111)):

$$\partial_t \mathcal{P}^{sw} + \nabla \cdot (\mathbf{u} \mathcal{P}^{sw}) = g \rho h \bar{w} \quad (33.114a)$$

$$\partial_t \mathcal{K}^{sw} + \nabla \cdot (\mathbf{u} \mathcal{K}^{sw}) = -h \mathbf{u} \cdot \nabla p + \rho h \mathbf{u} \cdot \mathbf{F}. \quad (33.114b)$$

$$\partial_t \mathcal{K}^{sw} + \nabla \cdot [\mathbf{u} (\mathcal{K}^{sw} + \rho g h \eta^{\text{eff}})] = \rho g \eta^{\text{eff}} \nabla \cdot (h \mathbf{u}) + \rho h \mathbf{u} \cdot \mathbf{F}. \quad (33.114c)$$

$$\partial_t \mathcal{K}^{sw} + \nabla \cdot [\mathbf{u} (\mathcal{K}^{sw} + P)] + \delta_k(p_{k-1/2} \partial_t \eta_{k-1/2}) = -g \rho h \bar{w} + \rho h \mathbf{u} \cdot \mathbf{F} \quad (33.114d)$$

$$\partial_t \mathcal{K}^{sw} + \nabla \cdot (\mathbf{u} \mathcal{K}^{sw}) = \mathbf{u} \cdot (-\nabla P + p_a \nabla \eta - p_b \nabla \eta_b) + \rho h \mathbf{u} \cdot \mathbf{F}. \quad (33.114e)$$

Example forms of the mechanical energy budget

Adding equations (33.114a) and (33.114b) leads to the mechanical energy budget

$$\partial_t m^{sw} + \nabla \cdot (\mathbf{u} m^{sw}) = g \rho h \bar{w} - h \mathbf{u} \cdot \nabla p + \rho h \mathbf{u} \cdot \mathbf{F}, \quad (33.115)$$

whereas the sum of equations (33.114a) and (33.114d) leads to

$$\partial_t m^{sw} + \nabla \cdot [\mathbf{u} (m^{sw} + P)] + \delta_k(p_{k-1/2} \partial_t \eta_{k-1/2}) = \rho h \mathbf{u} \cdot \mathbf{F}. \quad (33.116)$$

As we discuss in Section 33.6, equations (33.115) and (33.116) hold also for the mechanical energy in a N -layer shallow water model.

Specializing to the single layer

Making use of the identity (see equation (33.105))

$$m^{sw} + P = \rho h (\mathbf{u} \cdot \mathbf{u}/2 + g \eta^{\text{eff}}), \quad (33.117)$$

brings the mechanical energy budget (33.116) to the form

$$\partial_t m^{sw} + \nabla \cdot [h \mathbf{u} (\rho \mathbf{u} \cdot \mathbf{u}/2 + \rho g \eta + p_a)] + \delta_k(p_{k-1/2} \partial_t \eta_{k-1/2}) = \rho h \mathbf{u} \cdot \mathbf{F}. \quad (33.118)$$

Further note that $\partial_t \eta_b = 0$ so that

$$\nabla \cdot (h \mathbf{u} p_a) + \delta_k(p_{k-1/2} \partial_t \eta_{k-1/2}) = \nabla \cdot (h \mathbf{u} p_a) + p_a \partial_t \eta = h \mathbf{u} \cdot \nabla p_a, \quad (33.119)$$

where $\partial_t \eta + \nabla \cdot (h \mathbf{u}) = 0$. We are thus led to single layer mechanical energy budget

$$\partial_t m^{\text{sw}} + \nabla \cdot [h \mathbf{u} (\mathbf{u} \cdot \mathbf{u}/2 + g \eta)] = -h \mathbf{u} \cdot \nabla p_a + \rho h \mathbf{u} \cdot \mathbf{F}. \quad (33.120)$$

which proves of use when studying the mechanical energy of shallow water waves in Section 48.3.2.

Shallow water form of the Bernoulli theorem

It is notable that in the steady state of an unforced perfect shallow water fluid (so with $p_a = 0$ and $\mathbf{F} = 0$), equation (33.118) becomes

$$\mathbf{u} \cdot \nabla (\mathbf{u} \cdot \mathbf{u} + g h) = 0, \quad (33.121)$$

which is an expression of the Bernoulli theorem (Section 23.7) for steady shallow water flow.

Domain integrated mechanical energy

The budget equations (33.115) or (33.116) have already been layer integrated. So to study the domain integrated energetics requires only an area integral. The budget equation (33.116) is ideally suited for this purpose since all terms, except the non-conservative acceleration, are written as a flux divergence and so they represent transfer processes. The domain integral of the Eulerian flux-form mechanical energy equation (33.116) is

$$\int \partial_t m^{\text{sw}} d\mathcal{S} = - \oint_{\partial\mathcal{S}} (m^{\text{sw}} + P) \mathbf{u} \cdot \hat{\mathbf{n}} dl + \int_{\mathcal{S}} (-p_a \partial_t \eta + h \rho \mathbf{u} \cdot \mathbf{F}) d\mathcal{S}, \quad (33.122)$$

where we set $\partial_t \eta_b = 0$. The boundary integral on the right hand side is computed as a line integral around the edge of the layer. We consider three options for the layer geometry as illustrated in Figure 25.7. First, the thickness vanishes at the edge of the domain as in the case of shorelines, in which case the boundary integral vanishes since each term in the integral is thickness weighted. Second, we assume the layer is bounded by vertical sidewalls, in which case $\mathbf{u} \cdot \hat{\mathbf{n}} = 0$ at the sidewall boundaries. Third, the domain has periodicity in one or both directions (e.g., a zonal channel), in which case the boundary integral again vanishes in the periodic directions.

Evidently, for either of the three types of domain boundaries considered above, the boundary integral in equation (33.122) vanishes, in which case the domain integrated mechanical energy budget reduces to

$$\int_{\mathcal{S}} \partial_t m^{\text{sw}} d\mathcal{S} = \int_{\mathcal{S}} (-p_a \partial_t \eta + h \rho \mathbf{u} \cdot \mathbf{F}) d\mathcal{S} = - \int_{\mathcal{S}} h \mathbf{u} \cdot (\nabla p_a - \rho \mathbf{F}) d\mathcal{S}. \quad (33.123)$$

To reach the second equality we wrote

$$- \int_{\mathcal{S}} p_a \partial_t \eta d\mathcal{S} = \int_{\mathcal{S}} p_a \nabla \cdot (h \mathbf{u}) d\mathcal{S} = - \int_{\mathcal{S}} h \mathbf{u} \cdot \nabla p_a d\mathcal{S}, \quad (33.124)$$

where we set

$$\int \nabla \cdot (p_a h \mathbf{u}) d\mathcal{S} = 0, \quad (33.125)$$

which follows from the same reasoning used for the boundary integral in equation (33.122). Evidently, there is a nonzero domain integrated atmospheric pressure work only if there is a nonzero time tendency for the layer thickness. Furthermore, if p_a is a spatial constant, volume conservation

for the full layer means that

$$\int_{\mathcal{S}} \partial_t \eta \, d\mathcal{S} = - \int_{\mathcal{S}} \nabla \cdot (h \mathbf{u}) \, d\mathcal{S} = 0, \quad (33.126)$$

in which case we find that equation (33.123) is indeed self-consistent.

If the domain is bounded by sloping sides, then the mechanical energy vanishes at the horizontal boundaries, so that the time derivative acting on m^{sw} commutes with the area integral on the left hand side of equation (33.122). Alternatively, if the layer is bounded by fixed vertical walls, or is periodic in one or both directions, then the horizontal domain boundaries are static, again meaning that the time derivative commutes with the horizontal integral. In each case we can write the domain integrated mechanical energy equation as

$$\frac{d}{dt} \int_{\mathcal{S}} m^{\text{sw}} \, d\mathcal{S} = - \int_{\mathcal{S}} h \mathbf{u} \cdot (\nabla p_a - \rho \mathbf{F}) \, d\mathcal{S}. \quad (33.127)$$

In the absence of work on the layer from atmospheric pressure, then the total mechanical energy is affected only via non-conservative forces, such as those from viscous friction or boundary stresses. It then follows that for a perfect and unforced shallow water fluid, then the domain integrated mechanical energy remains constant, in which case there is an exact exchange between the domain integrated gravitational potential and kinetic energies.

33.5.6 Available potential energy

As discussed in Section 26.9, a huge portion of the gravitational potential energy is not realizable as kinetic energy, merely because the minimum potential energy state is when the fluid is at rest with some fluid parcels sitting above others. Available potential energy measures the gravitational potential energy that can be converted to kinetic energy through a reversible rearrangement of the fluid. We here display the available potential energy for a single shallow water layer in a simply connected domain, thus specializing the more general discussion given in Section 26.9 for a continuously stratified Boussinesq ocean.

Taking $z = 0$ as the reference level, the domain integrated gravitational potential energy for a single shallow water layer is

$$\int \mathcal{P}^{\text{sw}} \, d\mathcal{S} = g \rho \int d\mathcal{S} \int_{\eta_b}^{\eta} z \, dz = \frac{g \rho}{2} \int (\eta^2 - \eta_b^2) \, d\mathcal{S}. \quad (33.128)$$

We define a background or reference state potential energy as the potential energy contained in the fluid at rest, so that the free surface interface has its uniform area average value. Write the area average free surface height as

$$\langle \eta \rangle = \frac{1}{A} \int \eta \, d\mathcal{S}, \quad (33.129)$$

where

$$A = \int d\mathcal{S} \quad (33.130)$$

is the horizontal area integral over the full domain of the fluid. Hence, the reference state gravitational potential energy is realized when the surface height is flat at $z = \langle \eta \rangle$, so that

$$\int \mathcal{P}_{\text{ref}}^{\text{sw}} \, d\mathcal{S} = \frac{g \rho}{2} \int (\langle \eta \rangle^2 - \eta_b^2) \, d\mathcal{S}. \quad (33.131)$$

The available potential energy is defined by the difference

$$E_{\text{APE}} = \int (\mathcal{P}^{\text{sw}} - \mathcal{P}_{\text{ref}}^{\text{sw}}) d\mathcal{S} = \frac{g\rho}{2} \int (\eta^2 - \langle \eta \rangle^2) d\mathcal{S} = \frac{g\rho}{2} \int (\eta')^2 d\mathcal{S} \geq 0, \quad (33.132)$$

where

$$\eta' = \eta - \langle \eta \rangle \quad (33.133)$$

is the anomalous free surface. Note how the bottom topography cancelled out from E_{APE} since η_b^2 appears in both \mathcal{P}^{sw} and $\mathcal{P}_{\text{ref}}^{\text{sw}}$. Also note that to reach the final equality in equation (33.132) required the identity

$$\int (\eta - \langle \eta \rangle^2) d\mathcal{S} = \int (\eta^2 - 2\langle \eta \rangle \eta + \langle \eta \rangle^2) d\mathcal{S} \quad (33.134a)$$

$$= \int \eta^2 d\mathcal{S} + A \langle \eta \rangle^2 - 2\langle \eta \rangle \int \eta d\mathcal{S} \quad (33.134b)$$

$$= \int \eta^2 d\mathcal{S} - \langle \eta \rangle^2 A \quad (33.134c)$$

$$= \int (\eta^2 - \langle \eta \rangle^2) d\mathcal{S}. \quad (33.134d)$$

Equation (33.132) shows that the available potential energy is non-negative for the shallow water layer. That is, any slope to the shallow water layer represents a store of positive available potential energy. We derive the available potential energy in Section 33.6.1 for the N -layer shallow water model, showing that it too is non-negative.

33.6 Energetics for N layers

We here generalize the single layer mechanical energy analysis from Section 33.5 to N -layers, making use of the N -layer equations from Section 32.4.

33.6.1 Potential energy and available potential energy

Here we develop the equation for potential energy in a form that naturally leads to the expression for the available potential energy.

Potential energy for N -layers

To derive the gravitational potential energy per horizontal area in a stacked shallow water model, first consider the case with $N = 3$ (Figure 32.6), in which the potential energy per horizontal area is

$$\mathcal{P}^{\text{sw}} = g \int_{\eta_b}^{\eta} z \rho dz = g \rho_3 \int_{\eta_b}^{\eta_{5/2}} z dz + g \rho_2 \int_{\eta_{5/2}}^{\eta_{3/2}} z dz + g \rho_1 \int_{\eta_{3/2}}^{\eta} z dz, \quad (33.135)$$

which then leads to

$$2\mathcal{P}^{\text{sw}} = g \rho_3 (\eta_{5/2}^2 - \eta_b^2) + g \rho_2 (\eta_{3/2}^2 - \eta_{5/2}^2) + g \rho_1 (\eta^2 - \eta_{3/2}^2) \quad (33.136a)$$

$$= g \eta_{5/2}^2 (\rho_3 - \rho_2) + g \eta_{3/2}^2 (\rho_2 - \rho_1) + g \eta_{1/2}^2 \rho_1 - g \rho_3 \eta_b^2 \quad (33.136b)$$

$$= \rho_{\text{ref}} (g_{5/2}^r \eta_{5/2}^2 + g_{3/2}^r \eta_{3/2}^2 + g_{1/2}^r \eta_{1/2}^2) - g \rho_3 \eta_b^2, \quad (33.136c)$$

where $g_{1/2}^r = g$ and $\eta_{1/2} = \eta$. Generalizing this expression to an arbitrary number of layers leads to

$$\mathcal{P}^{\text{sw}} = \frac{1}{2} \left[-g \rho_N \eta_b^2 + \rho_{\text{ref}} \sum_{k=0}^{N-1} g_{k+1/2}^r \eta_{k+1/2}^2 \right], \quad (33.137)$$

with $\eta_{N+1/2} = \eta_b$ (see Figure 32.6). The first term is a constant and so does not contribute to time changes of the potential energy, and so it is commonly ignored in the literature.

Available potential energy for N -layers

The transient terms in equation (33.137) are positive definite, so that potential energy increases when the reduced gravity increases and/or the layer interfaces deviate in either direction from their resting values. This behavior motivates us to introduce the available potential energy by decomposing the layer interface heights into their area mean and deviations, just as for the single layer in Section 33.5.6

$$\eta'_{k\pm 1/2} = \eta_{k\pm 1/2} - \langle \eta_{k\pm 1/2} \rangle. \quad (33.138)$$

Volume conservation for each layer implies that the area mean, $\langle \eta_{k-1/2} \rangle$, is a space and time constant. Substitution into equation (33.137) leads to

$$\begin{aligned} \mathcal{P}^{\text{sw}} = & \frac{1}{2} \left[-g \rho_N \eta_b^2 + \rho_{\text{ref}} \sum_{k=0}^{N-1} g_{k+1/2}^r \langle \eta_{k+1/2} \rangle^2 \right] \\ & + \frac{\rho_{\text{ref}}}{2} \left[2 \sum_{k=0}^{N-1} g_{k+1/2}^r \langle \eta_{k+1/2} \rangle \eta'_{k+1/2} + \sum_{k=0}^{N-1} g_{k+1/2}^r (\eta'_{k+1/2})^2 \right]. \end{aligned} \quad (33.139)$$

The first bracketed term is a constant in time, and it measures the potential energy of the system when all interfaces sit at their area mean values, for which $\eta'_{k1/2} = 0$. When performing an area integral over the full domain, the term with $\langle \eta_{k+1/2} \rangle \eta'_{k+1/2}$ vanishes since the area integral of $\eta'_{k+1/2}$ vanishes. We thus define the available potential energy for the N -layer shallow water fluid

$$E_{\text{APE}} = \frac{\rho_{\text{ref}}}{2} \int \sum_{k=0}^{N-1} g_{k+1/2}^r (\eta'_{k+1/2})^2 dS \geq 0. \quad (33.140)$$

This expression generalizes the single layer form given by equation (33.132). As expected, the available potential energy increases whether a layer interface moves up or down, and it vanishes when all interfaces heights equal to their area mean values.

Time evolution of the potential energy

To derive an evolution equation for the potential energy, we take the time derivative of equation (33.137)

$$\partial_t \mathcal{P}^{\text{sw}} = \rho_{\text{ref}} \sum_{k=0}^{N-1} g_{k+1/2}^r \eta_{k+1/2} \partial_t \eta_{k+1/2} = \rho_{\text{ref}} \sum_{k=0}^{N-1} g_{k+1/2}^r \eta_{k+1/2} \sum_{j=k+1}^N \partial_t h_j, \quad (33.141)$$

where the second equality made use of equation (32.79) to relate the interface height and the layer thickness. We can collapse the double sum through the following identities

$$\begin{aligned} & \sum_{k=0}^{N-1} g_{k+1/2}^r \eta_{k+1/2} \sum_{j=k+1}^N \partial_t h_j \\ &= \partial_t h_N \sum_{j=0}^{N-1} g_{j+1/2}^r \eta_{j+1/2} + \partial_t h_{N-1} \sum_{j=0}^{N-2} g_{j+1/2}^r \eta_{j+1/2} + \dots + \partial_t h_1 g_{1/2}^r \eta_{1/2}. \end{aligned} \quad (33.142)$$

The product of reduced gravity and interface height can be written in terms of the shallow water dynamic pressure from equation (32.87)

$$p_k^{\text{dyn}} = \rho_{\text{ref}} \sum_{j=0}^{k-1} g_{j+1/2}^r \eta_{j+1/2}, \quad (33.143)$$

in which case we have the potential energy budget

$$\partial_t \mathcal{P}^{\text{sw}} = \sum_{k=1}^N p_k^{\text{dyn}} \partial_t h_k = - \sum_{k=1}^N p_k^{\text{dyn}} \nabla \cdot (\mathbf{u}_k h_k), \quad (33.144)$$

where the second equality made use of the layer thickness equation (32.78a). Rearrangement brings this equation to its Eulerian flux-form expression

$$\partial_t \mathcal{P}^{\text{sw}} + \nabla \cdot \sum_{k=1}^N p_k^{\text{dyn}} h_k \mathbf{u}_k = \sum_{k=1}^N h_k \mathbf{u}_k \cdot \nabla p_k^{\text{dyn}}. \quad (33.145)$$

33.6.2 Potential energy and buoyancy work

Potential energy for N -layers

Following the method for the single layer in Section 33.5.1, we write the gravitational potential energy for a column of shallow water fluid as

$$\mathcal{P}^{\text{sw}} = g \int_{\eta_b}^{\eta} z \rho dz = g \sum_{k=1}^N \rho_k h_k \bar{\eta}_k = \sum_{k=1}^N \mathcal{P}_k^{\text{sw}}, \quad (33.146)$$

where, again,

$$h_k = \eta_{k-1/2} - \eta_{k+1/2} \quad \text{and} \quad \bar{\eta}_k = (\eta_{k-1/2} + \eta_{k+1/2})/2 \quad (33.147)$$

makes use of the layer thickness, h_k , and the average interface height, $\bar{\eta}_k$. We can think of equation (33.146) as building the potential energy using layer properties, whereas the alternative expression (33.137) is built using interface properties.

Time evolution of the potential energy

Taking the time derivative of the potential energy (33.146) leads to

$$\partial_t \mathcal{P}_k^{sw} = g \rho_k \partial_t (h_k \bar{\eta}_k) \quad (33.148a)$$

$$= g \rho_k (\partial_t h_k \bar{\eta}_k + h_k \partial_t \bar{\eta}_k) \quad (33.148b)$$

$$= g \rho_k [-\bar{\eta}_k \nabla \cdot (\mathbf{u}_k h_k) + h_k (\bar{w}_k - \mathbf{u}_k \cdot \nabla \bar{\eta}_k)] \quad (33.148c)$$

$$= g \rho_k h_k \bar{w}_k - g \nabla \cdot (\rho_k \bar{\eta}_k h_k \mathbf{u}_k) \quad (33.148d)$$

$$= g \rho_k h_k \bar{w}_k - \nabla \cdot (\mathbf{u}_k \mathcal{P}_k^{sw}), \quad (33.148e)$$

so that the Eulerian flux-form budget is given by

$$\partial_t \mathcal{P}_k^{sw} + \nabla \cdot (\mathbf{u} \mathcal{P}_k^{sw}) = g \rho_k h_k \bar{w}_k. \quad (33.149)$$

This budget is identical to equation (33.91) that we discussed for a single layer, with the buoyancy work term exposed on the right hand side.

33.6.3 Kinetic energy

Kinetic energy and work from pressure gradients

Following our treatment in Section 33.5.2, consider the kinetic energy per horizontal area contained in a shallow water layer

$$\mathcal{K}_k^{sw} = \frac{1}{2} \int_{\eta_{k+1/2}}^{\eta_{k-1/2}} \rho_{ref} \mathbf{u}_k \cdot \mathbf{u}_k dz = \frac{1}{2} \rho_{ref} h_k \mathbf{u}_k \cdot \mathbf{u}_k. \quad (33.150)$$

Note that we set the density equal to the reference density as per the Boussinesq ocean, whereby the inertial mass is determined by the reference density (Section 26.1).

To derive an evolution equation for kinetic energy, multiply the thickness equation (32.78a) by $\mathbf{u}_k \cdot \mathbf{u}_k$, and take the dot product of the vector-invariant velocity equation (32.110) with $h_k \mathbf{u}_k$,

$$(\mathbf{u}_k \cdot \mathbf{u}_k) \partial_t h_k = -(\mathbf{u}_k \cdot \mathbf{u}_k) \nabla \cdot (h_k \mathbf{u}_k) \quad (33.151a)$$

$$h_k \mathbf{u}_k \cdot \partial_t \mathbf{u}_k = -h_k \mathbf{u}_k \cdot \nabla (p_k / \rho_{ref} + \mathbf{u}_k \cdot \mathbf{u}_k / 2) + h_k \mathbf{u}_k \cdot \mathbf{F}_k, \quad (33.151b)$$

where we included an acceleration, \mathbf{F}_k , arising from friction or boundary stresses, as discussed in Section 32.6.2. Making use of these expressions leads to the time derivative of the kinetic energy per area, $\dot{\mathcal{K}}_k^{sw} = \rho_{ref} h_k \mathbf{u}_k \cdot \mathbf{u}_k / 2$, of a shallow water layer

$$(2/\rho_{ref}) \partial_t \mathcal{K}_k^{sw} = \partial_t (h_k \mathbf{u}_k \cdot \mathbf{u}_k) \quad (33.152a)$$

$$= (\mathbf{u}_k \cdot \mathbf{u}_k) \partial_t h_k + 2 h_k \mathbf{u}_k \cdot \partial_t \mathbf{u}_k \quad (33.152b)$$

$$= -(\mathbf{u}_k \cdot \mathbf{u}_k) \nabla \cdot (h_k \mathbf{u}_k) - 2 h_k \mathbf{u}_k \cdot \nabla (p_k / \rho_{ref} + \mathbf{u}_k \cdot \mathbf{u}_k / 2) + 2 h_k \mathbf{u}_k \cdot \mathbf{F}_k \quad (33.152c)$$

$$= -2 \nabla \cdot [\mathbf{u}_k \mathcal{K}_k^{sw} / \rho_{ref}] - 2 h_k \mathbf{u}_k \cdot \nabla (p_k / \rho_{ref}) + 2 h_k \mathbf{u}_k \cdot \mathbf{F}_k, \quad (33.152d)$$

which then leads to the equivalent forms for the layer integrated kinetic energy budget

$$\partial_t \mathcal{K}_k^{sw} + \nabla \cdot (\mathbf{u}_k \mathcal{K}_k^{sw}) = -h_k \mathbf{u}_k \cdot [\nabla p_k - \rho_{ref} \mathbf{F}_k], \quad (33.153a)$$

$$\partial_t \mathcal{K}_k^{sw} + \nabla \cdot [\mathbf{u}_k (\mathcal{K}_k^{sw} + h_k p_k)] = p_k \nabla \cdot (h_k \mathbf{u}_k) + \rho_{ref} h_k \mathbf{u}_k \cdot \mathbf{F}_k. \quad (33.153b)$$

Recall that the pressure gradient is given by equation (32.87)

$$\nabla p_k = \nabla p_a + \nabla p_k^{\text{dyn}} = \nabla p_a + \rho_{\text{ref}} \nabla M_k^{\text{dyn}} \quad (33.154)$$

which arises from gradients in the applied atmospheric pressure plus the dynamic pressure, and where $M_k^{\text{dyn}} = \rho_{\text{ref}} p_k^{\text{dyn}}$ is the Montgomery potential from Section 32.4.3. The budget equation (33.153b) corresponds to the single layer equation (33.99), where we identify the dynamic pressure for shallow water model with just a single layer

$$p_{k=1}^{\text{dyn}} = \rho g \eta^{\text{eff}} = p_a + \rho g \eta. \quad (33.155)$$

Kinetic energy and buoyancy work

The single layer discussion in Section 33.5.3 fully anticipated the N -layer case, so that we can immediately translate equation (33.107) to an arbitrary layer

$$\partial_t \mathcal{K}_k^{\text{sw}} + \nabla \cdot [\mathbf{u} (\mathcal{K}_k^{\text{sw}} + P_k)] + \delta_k (p_{k-1/2} \partial_t \eta_{k-1/2}) = -g \rho_k h_k \bar{w}_k + \rho_k h_k \mathbf{u}_k \cdot \mathbf{F}_k. \quad (33.156)$$

33.6.4 Comments and further study

The discussion of mechanical energy for the single shallow water layer in Section 33.5.5 directly transfers to the N -layer case, thus making it unnecessary for us to develop the theory any further.

Elements of the discussion in this section are motivated by the energetic analysis of [Loose et al. \(2022\)](#), who detail the mechanical energy in a stacked shallow water model and decompose the energy budget into mean and transient eddy contributions.

33.7 Steady momentum balance in a zonal channel

In this section we study the depth integrated steady momentum budget for a single shallow water layer of density ρ in a zonally re-entrant channel, such as depicted in Figure 33.7. Such shallow water models have been used to garner insights into adiabatic aspects of Southern Ocean circulation, and we keep this application in mind for the following (so that $f < 0$). We are particularly interested in the force balances required to reach a steady flow in the presence of a prescribed constant wind stress acceleration, τ/ρ . The channel has arbitrary topography, including northern and southern bounds with sloping shelves and shorelines. Applying a zonal surface stress inserts zonal momentum to the fluid through the ocean surface. For simplicity we set the atmospheric pressure to zero, $p_a = 0$, so that the bottom pressure is $p_b = \rho g h$, and there is no form stress acting on the layer's upper surface.

A similar analysis was presented in Section 25.5 for the depth integrated axial angular momentum budget in a continuously stratified fluid. Following from that analysis, we ignore the role of internal viscous friction. However, we consider bottom frictional stresses written as a quadratic bottom drag

$$\mathbf{F}^{\text{drag}} = -C_d \mathbf{u} |\mathbf{u}|, \quad (33.157)$$

where $C_d > 0$ is a dimensionless bottom drag coefficient.

The horizontal areal extent of the domain is a function of space and time since the shallow water layer rises up and down the northern and southern shorelines as motion occurs. Even so, since layer thickness vanishes at the shoreline edge, the horizontal boundary conditions for the shallow water layer are easy to apply when working with the thickness weighted equations. That is, all thickness weighted fields vanish at the shoreline edge merely since the thickness vanishes at the

edge. Indeed, working with thickness weighted fields allows us to handle any degree of vanishing layer thicknesses, including if the topography in the center of the channel becomes an island rather than a submerged seamount. We also made use of this property of thickness weighted budgets in Section 25.5 where we also considered sloping sides rather than the commonly considered, yet less realistic, vertical sides.

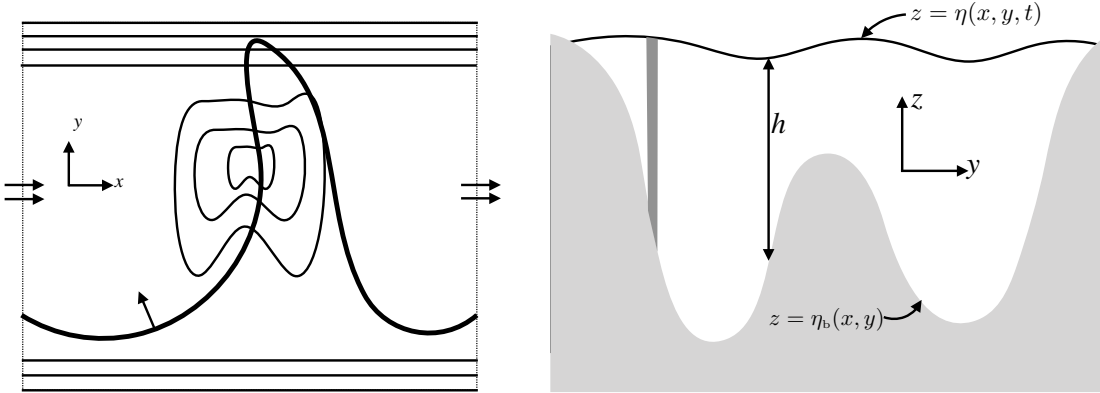


FIGURE 33.7: A zonally periodic/re-entrant southern hemisphere channel with northern and southern shelves and arbitrary seamount topography. Flow that leaves either the east or west boundary is assumed to re-enter the other side, so that the topology is periodic zonally. Left panel: horizontal (plan) view, showing the contours of the shelves and the topography, with flow leaving one of the zonal ends re-entering the other. The arbitrary dark solid contour extends across the zonal extent of the channel and is periodic, with a unit vector, \hat{n} , depicted normal to a point along the contour. In a steady state, the net fluid transport crossing this contour vanishes: $\oint h \mathbf{u} \cdot \hat{n} ds = 0$, meaning that there is no accumulation of fluid within any region of the channel. Right panel: meridional-depth view through an arbitrary longitude, along with a sample vertical column of water extending from the bottom to the surface. The shoreline edges occur where the layer thickness vanishes on the northern and southern shelves. So although the position of the shoreline edge is a function of space and time (since the fluid moves up and down the shoreline slope), the vanishing layer thickness found at the edge renders a simple treatment of boundary conditions for the thickness weighted equations.

33.7.1 Volume transport for steady flow

Before considering the steady force balance, we establish a constraint based on volume conservation by considering the steady thickness equation

$$\nabla \cdot (h \mathbf{u}) = 0. \quad (33.158)$$

As discussed for incompressible flow in Chapter 18, this non-divergence condition means that there is zero net steady transport crossing any simply connected closed contour in the fluid. A particularly interesting closed contour is one that is periodic and extends across the full zonal extent of the channel (see Figure 33.7), in which case

$$\oint h \mathbf{u} \cdot \hat{n} ds = 0, \quad (33.159)$$

where \oint denotes a periodic line integral across the zonal extent of the channel, \hat{n} is a unit vector normal to the contour, and ds is the arc-length line element along the contour. The constraint (33.159) reflects the inability of the steady flow to build up or deplete the fluid on one region of the channel at the expense of another. In particular, if the contour follows a constant latitude line, then we see that for a steady state there is no net meridional transport across a latitude

circle

$$\oint h \mathbf{u} \cdot \hat{\mathbf{y}} dx = \oint h v dx = 0 \quad \text{steady flow.} \quad (33.160)$$

This result means that the depth weighted Coriolis acceleration appearing in the zonal momentum equation vanishes when integrated zonally

$$\oint f h v dx = f \oint h v dx = 0 \quad \text{steady flow.} \quad (33.161)$$

We make use of this result in Section 33.7.3.

33.7.2 Steady meridional balances

Consider the thickness weighted meridional momentum equation (33.35b) in the presence of a wind stress and bottom drag

$$\frac{\partial(h v)}{\partial t} + \partial_x(h u v) + \partial_y(h v^2 + g h^2/2) + u h f = -(p_b/\rho) \partial_y \eta_b + \tau^y/\rho - C_d v |\mathbf{u}|. \quad (33.162)$$

Integrating zonally over the channel removes the zonal transport term, $\partial_x(h u v)$, due to periodicity

$$\oint \left[\frac{\partial(h v)}{\partial t} + \partial_y(h v^2 + g h^2/2) + u h f \right] dx = \oint [-(p_b/\rho) \partial_y \eta_b + \tau^y/\rho - C_d v |\mathbf{u}|] dx. \quad (33.163)$$

We can pull the time derivative outside of the zonal integral since the domain is zonally periodic, in which case the time changes to the net meridional transport across a latitude circle are given by

$$\frac{d}{dt} \oint v h dx = \oint [-\partial_y(h v^2 + g h^2/2) - u h f - (p_b/\rho) \partial_y \eta_b + \tau^y/\rho - C_d v |\mathbf{u}|] dx. \quad (33.164)$$

Correspondingly, a steady state along a latitude circle is realized by the balance

$$\oint [\partial_y(h v^2 + g h^2/2) + u h f] dx = \oint [-(p_b/\rho) \partial_y \eta_b + \tau^y/\rho - C_d v |\mathbf{u}|] dx. \quad (33.165)$$

The right hand side represents forcing by the topographic form stress, meridional wind stress, and bottom drag. That forcing, integrated over a latitude circle, balances the left hand side, which is the Coriolis acceleration arising from zonal motion, plus the meridional divergence of meridional momentum advection plus layer integrated pressure.

We can eliminate the nonlinear term on the left hand side of the balance (33.165) by integrating meridionally across the channel. Since $h = 0$ at the shoreline edges we know that $h v^2 + g h^2/2$ vanishes at the boundaries, thus leaving

$$\int \left[\oint u h f dx \right] dy = \int \left[\oint [-(p_b/\rho) \partial_y \eta_b + \tau^y/\rho - C_d v |\mathbf{u}|] dx \right] dy. \quad (33.166)$$

This is a balance between the integrated meridional Coriolis force on the left hand side with pressure form stress, winds, and bottom drag on the right hand side.

33.7.3 Steady zonal balance

Now consider the thickness weighted zonal momentum equation (33.35a), here with bottom drag and wind stress contributions

$$\frac{\partial(h u)}{\partial t} + \partial_x(h u^2 + g h^2/2) + \partial_y(h u v) - v h f = -(p_b/\rho) \partial_x \eta_b + \tau^x/\rho - C_d u |\mathbf{u}|. \quad (33.167)$$

Assuming a steady state and integrating along a latitude circle leads to

$$\rho \oint \partial_y(h u v) dx = \oint [-p_b \partial_x \eta_b + \tau^x - C_d \rho u |\mathbf{u}|] dx, \quad (33.168)$$

where we dropped the Coriolis acceleration as per volume conservation in equation (33.161). For flows that are quasi-linear, the nonlinear term $\partial_y(h u v)$ will be subdominant to the wind stress and topographic form stress, thus leading to the approximate balance along each latitude circle

$$\oint p_b \partial_x \eta_b dx \approx \oint [\tau^x - C_d \rho u |\mathbf{u}|] dx \quad \text{nonlinear term small.} \quad (33.169)$$

We realize an exact balance over the full channel domain by meridionally integrating the latitude balance (33.168), in which the nonlinear term $\partial_y(h u v)$ drops out since $h = 0$ at the northern and southern shoreline edges

$$\int \left[\oint \tau^x dx \right] dy = \int \left[\oint [p_b \partial_x \eta_b + C_d \rho u |\mathbf{u}|] dx \right] dy. \quad (33.170)$$

Again, this is an exact steady state balance realized by integrating the zonal thickness weighted momentum equation over the full domain channel. It is a balance between the zonal momentum input from the winds (left hand side) to the full domain, and the integrated bottom form stress plus bottom frictional drag (right hand side).

33.7.4 The role of frictional bottom drag

Consider a flat bottom channel, in which case the area integrated balance (33.170) is between winds and bottom drag

$$\int \left[\oint \tau^x dx \right] dy = \int \left[\oint C_d \rho u |\mathbf{u}| dx \right] dy \implies \rho^{-1} \langle \tau^x \rangle = C_d \langle u |\mathbf{u}| \rangle, \quad (33.171)$$

where the angle brackets denote a channel area mean. Typical empirical values for the dimensionless bottom drag coefficient are

$$C_d \approx 2 \times 10^{-3}. \quad (33.172)$$

An area mean eastward zonal wind stress of $\langle \tau^x \rangle = 0.1 \text{ N m}^{-2}$ leads to a root-mean-square zonal velocity of

$$\sqrt{\langle u |\mathbf{u}| \rangle} \approx \sqrt{\langle u^2 \rangle} \approx 0.2 \text{ m s}^{-1}, \quad (33.173)$$

where the first approximation follows from assuming the zonal velocity dominates over the meridional velocity. How realistic is this number for the Southern Ocean? Field measurements from the Southern Ocean suggest that depth and area averaged velocities are far smaller than this value. Furthermore, if this value occurred in a channel 4000 m deep and 2000 km wide (a rough idealization of the Antarctic Circumpolar Current), then this depth averaged velocity would yield a zonal volume transport of $\approx 1500 \times 10^6 \text{ m}^3 \text{ s}^{-1}$, which is about ten times larger than the measured

transport through the Drake Passage.

Munk and Palmén (1951) identified the problematic aspect of assuming a bottom frictional stress balance for the Southern Ocean. In brief, the field measurements do not support a frictional balance, either from bottom drag or from internal turbulent viscous friction. By inference, they proposed that topographic form stress is the dominant term that balances wind stress in the Southern Ocean. They supported that inference through estimates based on topographic features encountered by the Antarctic Circumpolar Current in its transit of the Southern Ocean. Subsequent studies, using theory, field measurements, and numerical models, support their conclusion. Indeed, in numerical models one finds that so long as there is only a modest degree of bottom slope, the bottom topographic form stress dominates over bottom drag. Given these considerations, we dispense with bottom drag for the remainder of this section.

33.7.5 Correlation between surface height and topographic slope

Given the minor role for bottom drag in establishing a steady channel flow in the Southern Ocean, the balance (33.170) says that an eastward wind stress must be balanced, in the area integral over the channel, by a westward topographic form stress

$$\int \left[\oint \tau^x dx \right] dy = \int \left[\oint p_b \partial_x \eta_b dx \right] dy. \quad (33.174)$$

What is required to establish a westward topographic form stress? Quite simply, in the area mean, there must be an anomalously large bottom pressure in regions where $\partial_x \eta_b > 0$ and an anomalously small bottom pressure in regions where $\partial_x \eta_b < 0$. Bottom pressure in a shallow water layer is determined by the column thickness. Hence, to establish the anomalous bottom pressures requires an anomalously thick fluid column upstream of topographic bumps and thin fluid column downstream. This situation is illustrated in Figure 33.8 described in Section 33.7.7.

To further reveal the correlation between surface height and bottom topography, write $p_b = \rho g h$ and use $\eta = h + \eta_b$ so that

$$p_{\text{bot}} \partial_x \eta_b = \rho g (\eta - \eta_b) \partial_x \eta_b = \rho g \eta \partial_x \eta_b - (g \rho/2) \partial_x \eta_b^2. \quad (33.175)$$

The balance (33.174) thus becomes

$$\langle \tau^x \rangle = \rho g \langle \eta \partial_x \eta_b \rangle. \quad (33.176)$$

Furthermore, due to zonal periodicity, it is only the zonal anomalies in η and η_b that contribute so that

$$\langle \tau^x \rangle = \rho g \langle \eta' \partial_x \eta'_b \rangle, \quad (33.177)$$

where

$$\eta = \eta' + L^{-1} \oint \eta dx \quad \text{and} \quad \eta_b = \eta'_b + L^{-1} \oint \eta_b dx, \quad (33.178)$$

with $L = \oint dx$ the zonal length of the channel. With $\langle \tau^x \rangle > 0$, we see that surface height anomalies must be positively correlated with the bottom slope, $\int \eta' \partial_x \eta'_b dx dy > 0$. That is, the surface height is high where topography slopes are positive and low where topography slopes are negative.

As noted above, we must have a positive correlation between surface height anomalies and topographic slope, as in equation (33.177). It follows that a nonzero zonal integrated topographic form stress requires a nonzero phase shift between surface height anomalies and the bottom topography anomalies. That is, if the surface height and bottom topography were perfectly

aligned along a latitude circle, then $\oint \eta' \partial_x \eta'_b dx = 0$, in which case there is a zero zonal integrated topographic form stress along that latitude. The required phase shift between the free surface and bottom topography has the free surface shifted ahead (i.e., to the west) of the topography. We consider an explicit example in Section 33.7.7 to help in our understanding.

33.7.6 Connection to meridional geostrophic transport

Zonal periodicity allows us to swap the zonal derivative in the balance (33.177) so that

$$\langle \tau^x \rangle = -\rho g \langle \partial_x \eta' \eta'_b \rangle \quad (33.179)$$

For the large scale flows under consideration here, we can assume that $g \partial_x \eta'$ is associated with an anomalous meridional geostrophic velocity

$$g \partial_x \eta' = f v'_g \quad (33.180)$$

so that the balance (33.179) is

$$\langle \tau^x \rangle = -\rho \langle f v'_g \eta'_b \rangle. \quad (33.181)$$

Hence, the steady balance is realized with anomalous meridional geostrophic transport correlated with topographic anomalies. Note that periodicity means that the steady meridional geostrophic transport has a zero zonal integral

$$\oint v'_g dx = (g/f) \oint \partial_x \eta' dx = 0, \quad (33.182)$$

which follows from the steady volume balance discussed in Section 33.7.1.

33.7.7 Sinusoidal example

To help further our understanding of the balance (33.177), and the phase shift required to develop nonzero zonal integrated topographic form stress, consider a sinusoidal topography that is a function only of the zonal direction. Also assume that the free surface has a sinusoidal shape (though we do not specify the dynamical mechanism for it to reach this shape). With these assumptions the anomalous surface height and bottom topography can be written

$$\eta' = \eta_o \sin(\kappa x + \varphi) \quad \text{and} \quad \eta'_b = D \sin(\kappa x) \quad (33.183)$$

where $\eta_o > 0$ is a constant amplitude for the free surface undulations, $D > 0$ is the constant amplitude for the bottom undulations, $\kappa = 2\pi n/L$ is the wavenumber for the undulations, $n > 0$ is an integer, L is the size of the zonal channel, and φ is a phase shift between the topography and the free surface. The corresponding meridional geostrophic flow is given by

$$f v'_g = g \partial_x \eta' = g \kappa \eta_o \cos(\kappa x + \varphi). \quad (33.184)$$

Plugging into the balance (33.177) leads to

$$\sin \varphi = \left[\frac{L \langle \tau^x \rangle}{D \rho g \eta_o \pi n} \right]. \quad (33.185)$$

For $\langle \tau^x \rangle > 0$ we see that the free surface undulations are, as expected, shifted to the west of the bottom topography undulations. As an explicit example from an idealized channel configuration,

set

$$L = 10^7 \text{ m} \quad D = 10^3 \text{ m} \quad \eta_o = 1 \text{ m} \quad \tau^x = 1 \text{ N m}^{-2}, \quad (33.186)$$

in which case

$$\sin \varphi \approx (\pi n)^{-1}. \quad (33.187)$$

For $n = 1$, which corresponds to just one topographic bump, then we have a phase shift of $\varphi \approx 18^\circ$, and this case is depicted in Figure 33.8 for the southern hemisphere. If there are two bumps, then the phase shift is reduced to $\varphi \approx 9^\circ$ since each bump shares half the burden of balancing the wind stress.

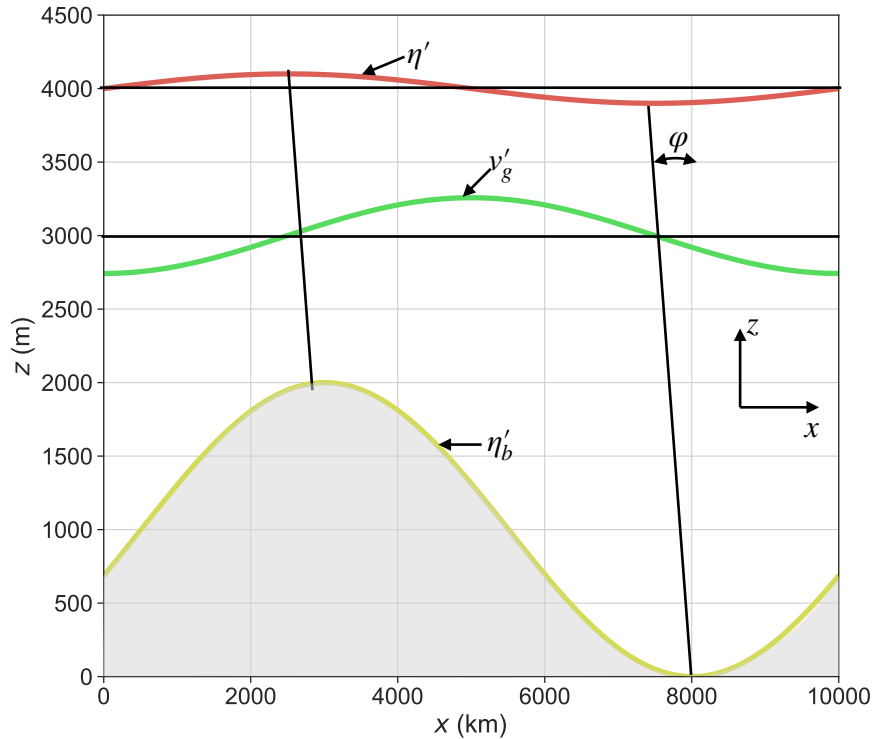


FIGURE 33.8: Zonal-depth view of the wind stress and bottom pressure acting on a steady state layer of shallow water fluid flowing over a sinusoidal bump (north is directed into the page and east is to the right). The eastward surface stress acts in the $+\hat{x}$ direction and it is balanced by a westward topographic form stress. To establish this form stress when integrated over the zonal extent of the channel requires the sea surface undulations to be phase shifted to the west of the bottom topography undulations, with the phase shift, φ , given by equation (33.185). To better visualize the sea surface, the surface undulations are in units of cm whereas the bottom topography undulations are in units of m. In general, for the topographic form stress to balance the wind stress, the bottom pressure must be anomalously large where $\partial\eta_b/\partial x > 0$ and small where $\partial\eta_b/\partial x < 0$, thus leading to the anomalously thick fluid column upstream of the bump and thin column downstream. This correlation also leads to a corresponding meridional geostrophic flow as shown here by the green curve for the southern hemisphere where $f < 0$, with $v_g > 0$ (northward) when shown above the horizontal line and $v_g < 0$ (southward) when below the line. Compare this figure to the analogous schematic in Figure 25.8.

Summarizing the dependencies

We here highlight the various dependencies in the phase equation (33.185).

- The phase shift increases with both larger wind stress and larger zonal extent to the domain. This dependency arises since with enhanced wind stress and an enhanced zonal *fetch* (distance over which the winds blow), there is an increase in zonal momentum inserted

to the ocean that must be absorbed by the bottom. The larger phase shift increases this topographic form stress, thus enabling the balance.

- Conversely, the phase shift decreases for larger topography D , and larger undulations in the free surface, η_o , in which case the free surface becomes more aligned with the topographic ridges. This result follows since the topographic form stress is larger for larger topography, thus requiring less phase shift in the surface wave patterns to affect a bottom pressure anomaly.
- Phase shifts decrease when there are more topographic bumps in the channel, with n the parameter setting the number of bumps. For the Southern Ocean, [Munk and Palmén \(1951\)](#) identified around four or five large-scale topographic features that provide the dominant balance for the zonal wind stress.
- What if the parameters are such that the right hand side of equation (33.185) has a magnitude larger than unity (e.g., huge winds, very long fetch, small topography, small surface height amplitude)? This situation signals that topographic form stress is insufficient to balance the winds. In a numerical model, one can merely increase the topographic wavenumber, n , to increase the topographic form stress. Yet where topography is fixed, such as in Nature, then bottom frictional stresses come into play to help reach a force balance (see Section 33.7.4).

Distinguishing steady motion from zero motion

Why is the phase shift (33.185) independent of the fluid depth? One might suspect that to reach a force balance would require more form stress if there is more fluid. Instead, the force balance, as reflected in the phase shift, depends on the zonal anomalies of the surface height and bottom topography. The depth of the fluid is absent.

The answer to this question is that we are seeking a force balance. When forces are balanced there is no acceleration and thus, as per Newton's second law, the fluid maintains a constant velocity relative to the laboratory reference frame. If we instead wished to stop the fluid, then we would need to decelerate all fluid elements to zero velocity. Determining the forces needed to stop the fluid requires the total fluid mass and thus its depth (as well as the time over which the fluid is to stop). If the fluid is in motion, then halting the motion requires a net force, and that is a very different consideration than the case of zero net force. So in brief, a steady state refers to the absence of time dependence in the fluid from the perspective of an Eulerian (laboratory) observer, with a steady state *not* necessarily a static state.

33.7.8 Comments and further study

Gyres and channels

The dominance of topographic form stress for the steady Southern Ocean balance contrasts to many of the frictional theories for gyre circulations, such as the classic solutions discussed in Section 36.7. In those theories, based on flat bottom and vertical side configurations, the curl of the wind stress is balanced by torques created by friction.⁹ One is thus led to conclude that zonally re-entrant channels exhibit a fundamentally distinct steady force balance from gyres. However, as discussed in Section 25.5.12, [Hughes and de Cueves \(2001\)](#) showed how topographic form stresses associated with sloping sides can lead to an inviscid balance for gyres. That is, friction is not needed so long as the bottom can support topographic torques. In this manner,

⁹We will encounter such balances in Chapter 36 when studying vorticity.

gyres and channels share much in common so long as they both contain topography and sloping sides.

The case with vertical stratification

The analysis of a single shallow water layer has direct relevance to flow in a stratified fluid. The reason is that when integrating over the full depth of the fluid, internal interfacial form stresses cancel pairwise.¹⁰ The resulting net balance for contact forces is concerned with just those acting on the boundaries at the surface and the bottom. This property of contact forces was also implicit in Section 25.5 where we developed the angular momentum budget for a continuously stratified fluid. In that discussion we encountered the correlation between bottom pressure and bottom topography slope for steady flow in a channel as realized by a balance between wind stress and bottom form stress (see Figure 25.8). This correlation also holds for the single shallow water layer.

Although the single layer provides a direct connection to the depth integrated momentum in a continuously stratified fluid, the direct connection between undulations in the sea surface height and bottom pressure is more nuanced when allowing for stratification. We here outline some of the considerations that arise with flow in a stratified channel with a topographic bump. Our presentation is rather incomplete, with a more thorough analysis supported by numerical simulations.

Following the analysis of Section 24.2, we decompose the horizontal gradient of bottom pressure according to equation (24.44)

$$\nabla_z p_b = \underbrace{\nabla_z p_a + g \rho(\eta) \nabla_z \eta}_{\text{external contribution}} - \underbrace{\rho_0 \int_{\eta_b}^{\eta} \nabla_z b \, dz'}_{\text{internal contribution}} \equiv \nabla_z p_{bext} + \nabla_z p_{bint}, \quad (33.188)$$

where $b = -g(\rho - \rho_0)/\rho_0$ is the Archimedean buoyancy from Chapter 27. The external pressure gradient is all that is available for a single shallow water layer, so that there is a direct correlation between bottom topography and surface pressure in the steady channel flow where bottom form stress balances wind stress. In contrast, for a continuously stratified fluid, or for a stacked shallow water fluid, the internal contribution to the pressure gradient is nonzero since buoyancy generally has a horizontal gradient.

As discussed in Section 16.4 of [Olbers et al. \(2012\)](#), watermasses in the Southern Ocean generally align themselves with lighter water on the upstream side of topographic features (to the west), and heavy water on the downstream side. This configuration means that the internal pressure is lower upstream of a topographic bump and higher downstream, thus leading to a westward internal pressure gradient force. To realize a steady flow with a balance between bottom pressure form stress and wind stress requires the external contribution to the bottom pressure gradient to counteract the internal contribution. Hence, the free surface height must have larger undulations in the presence of vertical stratification than without, with high values upstream of the bump and low values downstream. We depict this configuration in Figure 33.9, with the caption offering further details.

Meridional overturning circulation

The balances in this section are modified when allowing for the vertical transfer of volume between the layers as required to admit a meridional-depth overturning circulation. In this case, there can be net meridional motion along a latitude circle to thus add the Coriolis force to the steady force

¹⁰We discussed this property of interfacial form stresses in Sections 22.2, 25.3, and 33.4.

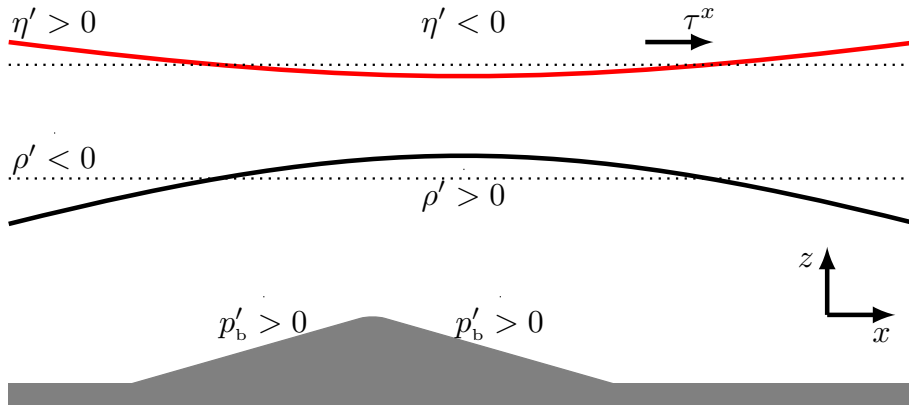


FIGURE 33.9: A schematic of steady flow in a two-layer zonally periodic channel with a topographic bump and with bottom pressure form stress balancing zonal wind stress. To realize this balance requires anomalously high bottom pressure on the upstream side of the bump and anomalously low bottom pressure on the downstream side, where anomalies are relative to the zonal mean. Such anomalous bottom pressure is just as for a single shallow water layer. However, for a stratified fluid the bottom pressure is established by the sum of effects from the external and internal pressure fields. The internal pressure field arises from density, here shown with anomalously light water on the upstream side of the bump and heavy water downstream, such as occurs in the Southern Ocean. This density field leads to a westward contribution to the bottom pressure gradient force; i.e., anomalously low bottom pressure on the upstream side of the bump and high bottom pressure on the downstream. The external pressure field arises from the free surface undulations (red line), with a high upstream of the bump and low downstream. This free surface field leads to an eastward contribution to the bottom pressure gradient force; i.e., anomalously high bottom pressure on the upstream side of the bump and low bottom pressure on the downstream. For the bottom pressure form stress to balance the wind stress, we must have the external pressure gradient dominate the internal pressure gradient. Note that undulations of the free surface height are roughly 100-300 times smaller than those of the density field, with the relative undulations set according to the reduced gravity as described in Section 32.3.

balance, including an Ekman transport (balance between Coriolis and surface stress as in Section 30.1) for the layer feeling the zonal surface stress. Realization of a steady state balance requires the surface stress imparted to the upper layer to be vertically transmitted through sloped layer interfaces to the bottom topography. Section 21.7 of [Vallis \(2017\)](#) as well as Chapter 16 of [Olbers et al. \(2012\)](#) provide pedagogical discussions of flow in the Antarctic Circumpolar Current, in which interfacial pressure form stress developed from baroclinic eddies provides a mechanism for transferring horizontal momentum from the surface stress to the solid-earth bottom.

33.8 Angular momentum in a rotating tank

As our second case study for this chapter, we study angular momentum for a layer of inviscid shallow water fluid in a rotating cylindrical tank. This system was first discussed in Section 24.3, where we developed the horizontal equation of motion

$$\frac{D\mathbf{u}}{Dt} + f \hat{\mathbf{z}} \times \mathbf{u} = -\nabla (p/\rho + g_e z - \Omega^2 r^2/2), \quad (33.189)$$

where $r^2 = x^2 + y^2$ is the radial distance from the rotational axis,

$$\Omega = f/2 \quad (33.190)$$

is the constant angular rotation rate, and the vertical component to the right hand side is the hydrostatic balance, $\partial p / \partial z = -\rho g_e$. Where convenient, we make use of the polar coordinates (see Chapter 9.3) in the following, whereby

$$x = r \cos \vartheta \quad (33.191a)$$

$$y = r \sin \vartheta, \quad (33.191b)$$

with the polar angle ϑ measured counter-clockwise from the positive x -axis.

33.8.1 Angular momentum for a column of shallow water fluid

The angular momentum for a column of shallow water fluid, computed with respect to the vertical rotational axis, is given by (see Sections 12.6 and 21.5)

$$L^z = \delta M [\mathbf{x} \times (\mathbf{u} + \mathbf{U}_{\text{solid}})] \cdot \hat{\mathbf{z}}, \quad (33.192)$$

where $\mathbf{x} = x \hat{\mathbf{x}} + y \hat{\mathbf{y}} = r \hat{\mathbf{r}}$ is the position vector relative to the rotational axis, $\delta M = \rho h \delta A$ is the constant mass for the fluid column, and the solid-body rotation velocity is

$$\mathbf{U}_{\text{solid}} = (f/2) \hat{\mathbf{z}} \times \mathbf{x} = r \Omega \hat{\boldsymbol{\theta}}, \quad (33.193)$$

where $\hat{\mathbf{z}} \times \hat{\mathbf{r}} = \hat{\boldsymbol{\theta}}$ is the azimuthal unit vector pointing counter-clockwise around the origin.

We can further massage the expression for the angular momentum by writing

$$\mathbf{x} \times \mathbf{u} = (x v - y u) \hat{\mathbf{z}} = r^2 \dot{\vartheta} \hat{\mathbf{z}}, \quad (33.194)$$

where $\dot{\vartheta} = D\vartheta/Dt$ is the angular velocity. Likewise, we have

$$\mathbf{x} \times \mathbf{U}_{\text{solid}} = r^2 \Omega \hat{\mathbf{z}}, \quad (33.195)$$

so that the angular momentum can be written

$$L^z = \delta M [\mathbf{x} \times (\mathbf{u} + \mathbf{U}_{\text{solid}})] \cdot \hat{\mathbf{z}} = \delta M r^2 (\dot{\vartheta} + \Omega). \quad (33.196)$$

33.8.2 Material time evolution of the angular momentum

The material time evolution for the angular momentum is given by

$$\frac{D L^z}{Dt} = \delta M [\mathbf{u} \times (\mathbf{u} + \mathbf{U}_{\text{solid}})] \cdot \hat{\mathbf{z}} + \delta M \left[\mathbf{x} \times \left(\frac{D \mathbf{u}}{Dt} + \frac{D \mathbf{U}_{\text{solid}}}{Dt} \right) \right] \cdot \hat{\mathbf{z}}. \quad (33.197)$$

Note that we set

$$\frac{D(\delta M)}{Dt} = \rho D(h \delta A) Dt = 0 \quad (33.198)$$

since the shallow water fluid columns each have constant volume as they move with the horizontal flow (Section 32.2.5). Using the solid-body rotation velocity given by equation (33.193), and with a constant rotation rate, yields

$$\mathbf{u} \times \mathbf{U}_{\text{solid}} + \mathbf{x} \times \frac{D \mathbf{U}_{\text{solid}}}{Dt} = \mathbf{u} \times (\boldsymbol{\Omega} \times \mathbf{x}) + \mathbf{x} \times (\boldsymbol{\Omega} \times \mathbf{u}) \quad (33.199a)$$

$$= (\mathbf{x} \cdot \mathbf{u}) f \hat{\mathbf{z}}. \quad (33.199b)$$

Making use of the material evolution of the horizontal velocity given by equation (33.189) renders

$$\left[\mathbf{x} \times \frac{D\mathbf{u}}{Dt} \right] \cdot \hat{\mathbf{z}} = (\mathbf{x} \times [-f \hat{\mathbf{z}} \times \mathbf{u} - \nabla (p/\rho + g_e z - \Omega^2 r^2/2)]) \cdot \hat{\mathbf{z}} \quad (33.200a)$$

$$= -f (\mathbf{x} \cdot \mathbf{u}) - (\mathbf{x} \times g \nabla \eta) \cdot \hat{\mathbf{z}}. \quad (33.200b)$$

The centrifugal term dropped out since

$$\mathbf{x} \times \nabla r^2 = 2 \mathbf{x} \times r \hat{\mathbf{r}} = 2 \mathbf{x} \times \mathbf{x} = 0. \quad (33.201)$$

The gravitational term dropped out since

$$(\mathbf{x} \times \nabla z) \cdot \hat{\mathbf{z}} = (\mathbf{x} \times \hat{\mathbf{z}}) \cdot \hat{\mathbf{z}} = 0, \quad (33.202)$$

as does the vertical component to the pressure gradient. We are thus left with

$$\frac{1}{\delta M} \frac{DL^z}{Dt} = -g (\mathbf{x} \times \nabla \eta) \cdot \hat{\mathbf{z}}. \quad (33.203)$$

Consequently, the axial angular momentum for a fluid column is modified by the torque from the horizontal pressure gradient caused by undulations in the free surface height. Note how there is no contribution from the Coriolis acceleration, so that the evolution of angular momentum is the same whether viewed in the laboratory frame or rotating frame.

We can bring the expression (33.203) into a more transparent form by switching to polar coordinates

$$\mathbf{x} \times \nabla \eta = r \hat{\mathbf{r}} \times \left[\hat{\mathbf{r}} \frac{\partial \eta}{\partial r} + \hat{\vartheta} \frac{1}{r} \frac{\partial \eta}{\partial \vartheta} \right] = \frac{\partial \eta}{\partial \vartheta} \hat{\mathbf{z}}, \quad (33.204)$$

so that

$$\frac{1}{\delta M} \frac{DL^z}{Dt} = -g \frac{\partial \eta}{\partial \vartheta}. \quad (33.205)$$

This result is directly analogous to the angular momentum evolution for a fluid moving around a sphere as derived in Section 21.5. Namely, in the presence of angular pressure gradients, the fluid experiences a torque that in turn leads to a change in the angular momentum relative to the vertical rotation axis.

33.8.3 Materially invariant angular momentum

The angular momentum for a fluid column is materially invariant (i.e., a constant on a material fluid parcel) if

$$\frac{DL^z}{Dt} = 0 \iff \frac{\partial \eta}{\partial \vartheta} = 0. \quad (33.206)$$

For a flat bottom, equation (24.80) says that the free surface takes on a radial parabolic shape when the fluid is in solid-body rotation. In this case, $\nabla \eta$ is in the radial direction, in which case $\mathbf{x} \times \nabla \eta = 0$. Consequently, when the fluid is in solid-body rotation, the angular momentum for each fluid column remains materially constant.

33.8.4 Comments

The material evolution equation (33.203) also holds for a fluid on the f -plane tangent to a sphere. The f -plane formulation is slightly simpler than the tank since the centrifugal term is absorbed into the geopotential (see Section 11.11.4). However, the tank is arguably more pedagogical as it

is simpler to visualize and to conduct laboratory experiments. See Section 6.6.4 of [Marshall and Plumb \(2008\)](#) for more discussion of rotating tank experiments. Also, we return to this physical system in Section 50.3 when studying centrifugal instability of cyclostrophically balanced flow.



33.9 Exercises

EXERCISE 33.1: POTENTIAL TEMPERATURE SLOPES IN ATMOSPHERE AND OCEAN

Use the two-layer thermal wind relations from Section 33.2.2, also known as Margules' relation, to estimate the slope of the potential temperature surfaces in the atmosphere and ocean. This question is based on exercise 3.2 of [Vallis \(2006\)](#).

- Model the atmosphere as two immiscible shallow water layers of different density stacked one above the other. Using reasonable values for any required physical parameters, estimate the vertical displacement of the interfacial surface associated with a pole-to-equator temperature difference of 40K. You may wish to consult [Wallace and Hobbs \(2006\)](#) or [Marshall and Plumb \(2008\)](#) for physical scales.
- Estimate a vertical interfacial displacement in the ocean thermocline associated with a temperature difference of 20K over a horizontal distance of 4000 km. The interface between the two shallow water layers offers a crude representation of the main oceanic thermocline. Ignore salinity effects so that temperature and density are directly proportional.

Double-check your results by examining some atmosphere and ocean latitude-height profiles for potential temperature (e.g., Figure 5.8 of [Marshall and Plumb \(2008\)](#)).

EXERCISE 33.2: CIRCULAR STEADY GEOSTROPHIC FLOW

Consider a single layer of shallow water fluid in steady geostrophic balance on a f -plane so that

$$f \hat{z} \times \mathbf{u}_g = -g \nabla \eta. \quad (33.207)$$

Assume $f > 0$ and that the free surface has a circular Gaussian shape

$$\eta = \eta_0 e^{-r^2/(2\sigma^2)} \quad (33.208)$$

where $r^2 = x^2 + y^2$ is the squared radial position and σ is the standard deviation of the Gaussian.

- Determine the horizontal geostrophic velocity components corresponding to this free surface undulation. Write the solution in both Cartesian coordinates and polar coordinates. Is the flow oriented cyclonic or anti-cyclonic?
- Determine the streamlines for the flow. Hint: recall the discussion in Section 14.9.2. What is the geometric shape of a streamline?

EXERCISE 33.3: STEADY STATE MOMENTUM AND GEOSTROPHY

Consider a single layer of shallow water fluid with zero boundary mass fluxes through the surface. Assume the lateral boundaries are solid. All boundaries are thus material. The domain integrated horizontal momentum (within the rotating reference frame) is defined by

$$\mathbf{P} = \int \rho \mathbf{u} dV = \int \rho h \mathbf{u} dS. \quad (33.209)$$

Show that for tangent plane motion (Section 21.3.4)

$$\frac{d\mathbf{P}}{dt} = 0 \quad (33.210)$$

can be realized either by (A) zero flow everywhere, (B) flow that is in geostrophic balance at each point, or (C) flow that is in geostrophic balance as a global integral.

EXERCISE 33.4: THICKNESS WEIGHTED MOMENTUM FOR TWO LAYERS

Following the methods from Section 33.3, derive the thickness weighted momentum equation for an inviscid two-layer stacked shallow water fluid. That is, derive the evolution equation for $h_1 \mathbf{u}_1 + h_2 \mathbf{u}_2$, thus providing the two-layer version of equation (33.21).

EXERCISE 33.5: CONTACT PRESSURE FORCE ON A SINGLE LAYER

As a check on our calculation of the contact pressure force (33.60b), consider a single shallow water layer under a massless atmosphere. Show that the contact pressure force per mass is given by

$$\frac{\mathbf{F}_{\text{net}}^{\text{press}}}{M} = g \hat{\mathbf{z}} - g \nabla \eta. \quad (33.211)$$

As expected, the horizontal component of this force equals to the pressure gradient body force per mass detailed in Section 32.2.1. The vertical pressure force balances the weight of the fluid as per the hydrostatic balance.

EXERCISE 33.6: TOPOGRAPHIC FORM STRESS FOR A RIDGE

As in Section 33.7, apply a constant eastward zonal wind to a zonally reentrant channel with a single shallow water layer. Let the layer flow over a topographic ridge of height H above the surrounding flat bottom, and let the ridge be a function just of zonal position, $\eta'_b(x)$. Furthermore, assume the ridge has a constant slope on both the upstream (west) side, S_{up} , and downstream (east) side, S_{dn} . An example is depicted in Figure 33.10. Following the force balance (33.177), derive an expression for the free surface height zonally averaged over the upstream side of the ridge, minus the free surface height zonally averaged over the downstream sides of the ridge,

$$\Delta\eta' = (\bar{\eta'})_{\text{up}} - (\bar{\eta'})_{\text{dn}}, \quad (33.212)$$

where

$$(\bar{\eta'})_{\text{up}} = \frac{\int_{x_{\text{up}}}^{x_0} \eta' dx}{L_{\text{up}}} \quad \text{and} \quad (\bar{\eta'})_{\text{dn}} = \frac{\int_{x_0}^{x_{\text{dn}}} \eta' dx}{L_{\text{dn}}}. \quad (33.213)$$

Show that the expression for $\Delta\eta'$ is independent of the two slopes. Instead, the only geometric property that determines $\Delta\eta'$ is the ridge height, H . Discuss this result.

EXERCISE 33.7: GEOSTROPHIC TRANSPORT

Consider a zonal-vertical section of shallow water flow in the middle latitude northern hemisphere. Let the section be 1000 m deep and away from side and bottom boundaries. Assume the sea level is 1 cm higher at the eastern end of the section than the western end. Estimate the mass transport (kg/sec) of constant density seawater going through the section. What direction is the transport? Hint: Assume geostrophic balance; choose a representative constant seawater density; and note that the zonal width of the section cancels out so it is not needed.

EXERCISE 33.8: APE FOR TWO SHALLOW WATER LAYERS

Compute the APE for two shallow water layers using the notation from Figure 32.6 with nontrivial bottom topography, $z = \eta_b(x, y)$. Show that the APE is non-negative. Assume the domain is simply connected. Hint: The answer is given by specializing the arbitrary N results in equation

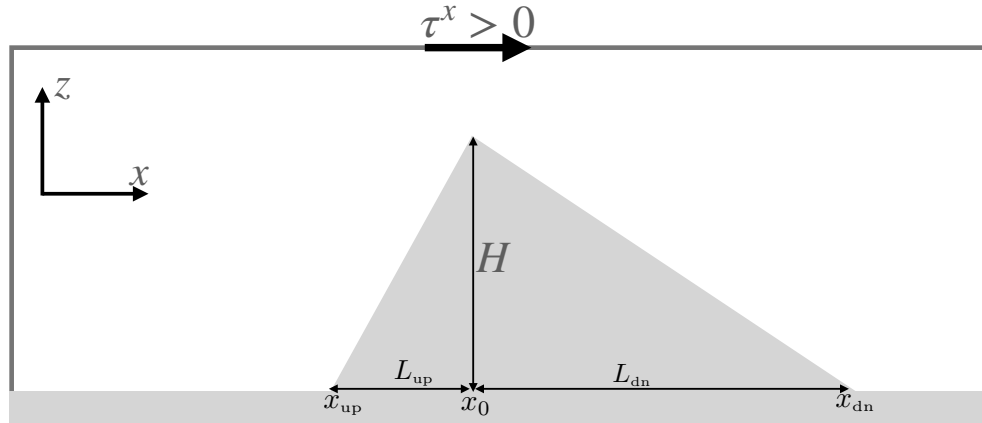


FIGURE 33.10: Zonal-vertical view of a single layer of shallow water fluid moving in a zonally re-entrant channel for use in Exercise 33.6. The domain has a topographic ridge that is a function just of the zonal direction and has constant slopes on its western and eastern sides. There is a constant eastward zonal wind stress.

(33.140) to the special case of the $N = 2$. However, for this exercise you should not merely quote that result. Instead, show all steps starting from the potential energy for an $N = 2$ layer model.

EXERCISE 33.9: RATIO OF KE TO APE FOR SINGLE LAYER f -PLANE GEOSTROPHY

Consider a single layer of shallow water fluid in geostrophic balance on an f -plane with a flat bottom. Show that the ratio of kinetic energy to available potential energy scales like

$$\frac{E_{\text{KE}}}{E_{\text{APE}}} \sim \left[\frac{L_d^{\text{ext}}}{L} \right]^2. \quad (33.214)$$

In this equation, L is the horizontal length scale for the fluctuation of the free surface η (i.e., $\nabla\eta \sim \eta'/L$), and

$$L_d^{\text{ext}} = \frac{\sqrt{gH}}{f} \quad (33.215)$$

is the external deformation radius. The scaling (33.214) means that for scales larger than the external deformation radius, L_d , the available potential energy is larger than the kinetic energy. The converse holds for scales smaller than L_d .

EXERCISE 33.10: RATIO OF KE TO APE FOR 1.5 LAYER f -PLANE GEOSTROPHY

Consider a reduced gravity system (Section 32.3) in geostrophic balance on an f -plane. Show that the ratio of kinetic energy to available potential energy scales like

$$\frac{E_{\text{KE}}}{E_{\text{APE}}} \sim \left[\frac{L_d^{\text{int}}}{L} \right]^2. \quad (33.216)$$

In this equation, L is the horizontal length scale for the fluctuation of the internal interface $\eta_{3/2}$ (i.e., $\nabla\eta_{3/2} \sim \eta'_{3/2}/L$), and

$$L_d^{\text{int}} = \frac{\sqrt{g_{3/2}^r h}}{f} \quad (33.217)$$

is the internal deformation radius with $g_{3/2}^r = g(\rho_2 - \rho_1)/\rho_{\text{ref}}$ the reduced gravity and $h = A^{-1} \int (\eta_{1/2} - \eta_{3/2}) dS$ the area averaged layer thickness (see Figure 32.4). The scaling (33.216) means that for scales larger than the internal deformation radius, L_d^{int} , the available potential

energy is larger than the kinetic energy, and conversely for scales smaller than L_d^{int} .

To solve this exercise you must make use of the following.

- Derive the APE for two layers with a flat bottom.
- Assume the contribution to the APE from free surface undulations, is much smaller than from the interior interface. So that the APE is roughly due just to undulations of the interior interface. This assumption follows from Figure 32.5.
- The scaling (33.216) is identical to that found for the quasi-geostrophic system in Section 42.6.4. However, to solve this exercise it is not sufficient to merely reproduce the scaling discussed in Section 42.6.4. Instead, use here the expressions for APE and KE appropriate for the shallow water system.

EXERCISE 33.11: NON-DIMENSIONALIZED LINEAR SHALLOW WATER EQUATIONS

For the linear equations (48.107a)-(48.107b), introduce

$$\mathbf{x} = L \hat{\mathbf{x}}, \quad \mathbf{u}' = U \hat{\mathbf{u}}, \quad t = \frac{L \hat{t}}{U}, \quad f = \hat{f} T^{-1}, \quad \eta' = H \hat{\eta}, \quad (33.218)$$

where L is a horizontal length scale, $T = L/U$ is an advective time scale, U is a velocity scale, and $H \ll L$ is the resting layer thickness. All variables with hats are non-dimensional and not to be confused with unit vectors. Substitute into equations (48.107a)-(48.107b) and identify the non-dimensional ratio of the advective velocity scale to the non-rotating gravity wave speed

$$\text{Fr} \equiv \frac{U}{\sqrt{g H}}. \quad (33.219)$$

This non-dimensional number is known as the *Froude number*. When the Froude number is larger than unity, the fluid can experience an instability known as an *hydraulic jump*, with some elements of jumps discussed in Exercise 32.3.



Part VII

Vorticity mechanics

Vorticity locally measures the spin of a fluid element. For geophysical flows, external forces, ultimately due to differential heating over the planet, resupply vorticity in the face of dissipation. The addition of planetary vorticity, arising from motion on a rotating spherical planet, also renders a nonzero vorticity to geophysical fluids even when the fluid is at rest in the rotating earth reference frame. Vorticity thus plays a central role in characterizing geophysical fluid motions, even for relatively sluggish and laminar flow, since motion on a rotating planet always involves vorticity.

Besides offering a key method for flow characterization, vorticity evolution and its steady balances provide the means to mechanically understand how flows respond under changes to forces. Surprisingly, it does so even without needing to directly compute forces acting on the fluid. We thus encounter examples where vorticity mechanics offers a more direct and focused explanation for flow behavior than momentum or energy mechanics. This practical feature of vorticity mechanics represents the central reason it is so essential to the theoretical machinery of geophysical fluid mechanics.

Potential vorticity is a strategically chosen component of vorticity whose evolution is simpler than the full vorticity vector, thus helping to identify key facets of geophysical flows, their forcing, and constraints. Indeed, under certain assumptions of balance (considered in Part VIII), knowledge of potential vorticity offers the means to deduce all prognostic information about the flow. For these and other reasons explored in this part of the book, potential vorticity has found great use for understanding and predicting geophysical fluid flows. Indeed, the central importance of potential vorticity for the study of atmospheric and oceanic flows helps to distinguish geophysical fluid mechanics from other areas of fluid mechanics, such as those motivated by engineering and biophysical applications.

OUTLINE FOR THIS PART OF THE BOOK

We start this part of the book by introducing vorticity and circulation in Chapter 34, making use of Stokes' Theorem to show that the area integral of vorticity over a finite region yields the circulation around the region's boundary. Chapter 35 considers the case where the horizontal flow is non-divergent, thus leading to the study of non-divergent barotropic flow. This flow is fully described by the vorticity field, and it offers many insights into large-scale vortical flows in the atmosphere and ocean. Chapter 36 then introduces the mechanics of vorticity and potential vorticity within a shallow water fluid. It was for the shallow water system that [Rossby \(1940\)](#) showed how powerful the notion of potential vorticity conservation is for understanding geophysical fluid flow patterns.

Chapter 37 then dives into the fundamentals of vorticity and circulation. It is here that we encounter Kelvin's circulation theorem, which identifies the materially conserved nature of circulation around an arbitrary simply closed loop in a perfect barotropic flow. Chapter 38 presents the foundations of potential vorticity and then Chapter 39 develops differential and integral potential vorticity budget equations. Our study of potential vorticity budgets exposes us to the remarkable impermeability property of the potential vorticity flux vector.

Chapter 34

VORTICITY AND CIRCULATION

Vorticity measures the angular motion contained in a fluid flow at each point within the fluid; i.e., it is a measure of spin. Vorticity generalizes to continuum mechanics the angular momentum that is central to the study of rigid body mechanics. We here relate the two, showing that flow strains available to a fluid lead to distinctions between vorticity and angular momentum. Circulation measures the fluid flow computed over a closed line integral (circuit) within the fluid. Helmholtz was an early proponent of vorticity whereas Kelvin was a proponent of circulation. These two flow properties are connected through Stokes' theorem, with the study of vortex lines and vortex tubes clearly exposing the connections.

CHAPTER GUIDE

In this chapter, we introduce kinematic properties of vorticity and circulation. We make use of vector calculus using Cartesian coordinates as detailed in Chapter 2. The concepts and methods introduced in this chapter are fundamental to the remaining chapters in this part of the book.

34.1	Vorticity	840
34.1.1	Rotation of line elements	840
34.1.2	Rotating reference frame	841
34.1.3	There are no vorticity sources	842
34.1.4	Further study	842
34.2	Irrational flows	842
34.2.1	Characterizing irrotational flows	842
34.2.2	Comments	843
34.3	Circulation of the velocity field	843
34.4	The free vortex	844
34.4.1	Motion of a fluid particle	844
34.4.2	Circulation	846
34.5	Translation and solid-body rotation	846
34.5.1	Absolute vorticity	846
34.5.2	Solid-body rotation on a plane	847
34.5.3	Circulation for solid-body rotation	847
34.5.4	Comments	848
34.6	Kinematics of vortex lines and vortex tubes	848
34.6.1	Vortex lines and vortex tubes	848
34.6.2	Kinematic properties	849
34.6.3	Helmholtz's theorems	850
34.6.4	Further study	851
34.7	Relative vorticity from curvature and shear	851

34.7.1	Circular flow	852
34.7.2	Generalization to natural coordinates	852
34.7.3	Example vorticities	853
34.8	Relating angular momentum to vorticity and strain	855
34.8.1	Linear momentum	855
34.8.2	Angular momentum	856
34.8.3	Taylor expanding the velocity	857
34.8.4	Angular momentum, rate of strain, and vorticity	858
34.8.5	Comments and further reading	859
34.9	Exercises	859

34.1 Vorticity

Vorticity is the curl of the velocity field

$$\boldsymbol{\omega} = \nabla \times \mathbf{v}. \quad (34.1)$$

Vorticity measures the rotation or spin of fluid flow at each point and, unlike angular momentum, it does so without reference to an origin. In addition to writing vorticity as the curl of the velocity, we may choose to use the equivalent expression

$$\boldsymbol{\omega} = [\nabla \cdot (\mathbf{v} \times \hat{\mathbf{x}})] \hat{\mathbf{x}} + [\nabla \cdot (\mathbf{v} \times \hat{\mathbf{y}})] \hat{\mathbf{y}} + [\nabla \cdot (\mathbf{v} \times \hat{\mathbf{z}})] \hat{\mathbf{z}}. \quad (34.2)$$

That is, a vorticity component in a particular coordinate direction is the divergence of the velocity field after being rotated by $-\pi/2$ around the coordinate axis direction. For example, the vector $\mathbf{v} \times \hat{\mathbf{z}}$ is the result of rotating the velocity by $-\pi/2$ radians around the $\hat{\mathbf{z}}$ axis, with the identity

$$\hat{\mathbf{z}} \cdot (\nabla \times \mathbf{v}) = \nabla \cdot (\mathbf{v} \times \hat{\mathbf{z}}) \quad (34.3)$$

leading to the vertical component of the vorticity in equation (34.2).

Being the curl of a vector, the vorticity transforms as a vector under coordinate rotations. However, vorticity changes sign under mirror symmetry, thus making it a pseudo-vector (Section 1.4.2). A simple means to understand this property is to note that the spinning earth rotates counter-clockwise when viewed from above the north pole and clockwise when viewed from below the south pole (see Figure 11.3).

Figure 34.1 provides an example zonal flow with a meridional strain (shear). The vertical component to the vorticity is negative for this flow, as per the right hand rule. Furthermore, an imaginary test “paddle wheel” placed anywhere within this flow spins clockwise about its axis. The nonzero spin of a test paddle wheel is a fundamental property of fluid flow with nonzero vorticity.

34.1.1 Rotation of line elements

In Section 15.3 we considered the kinematic evolution of a line element, $\delta\mathbf{x}$, separating two fluid particles, with that evolution provided by equation (15.31)

$$\frac{D(\delta x_m)}{Dt} = \delta x_n \frac{\partial v_m}{\partial x_n} \implies \frac{D(\delta \mathbf{x})}{Dt} = (\delta \mathbf{x} \cdot \nabla) \mathbf{v}. \quad (34.4)$$

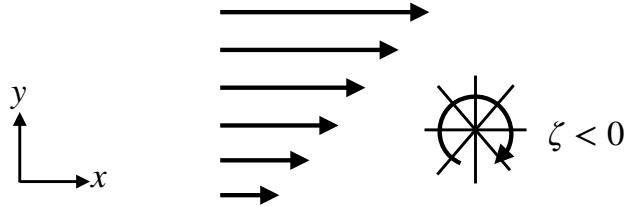


FIGURE 34.1: An example zonal flow with a meridional shear, $\mathbf{v} = u(y)\hat{x}$, and a corresponding vertical vorticity component that is negative: $\zeta = \hat{z} \cdot (\nabla \times \mathbf{v}) = \partial v / \partial x - \partial u / \partial y = -\partial u / \partial y < 0$. The clockwise arrow surrounds a test “paddle wheel” that exhibits a clockwise spin about its axis when placed in this flow. Such test paddle wheels only spin when there is nonzero vorticity. The right hand rule determines the sign of the vorticity, which for this example is into the page (negative \hat{z}).

This equation says that the material line element evolves according to the velocity gradient tensor $\partial_n v_m$. The symmetric portion of this tensor is the rate of strain tensor,

$$\mathbb{S}_{mn} = (\partial_n v_m + \partial_m v_n)/2, \quad (34.5)$$

whose action generates changes in the distance between the fluid particles (Section 15.3.7). The anti-symmetric portion to the velocity gradient tensor is known as the rotation tensor,

$$\mathbb{R}_{mn} = (\partial_n v_m - \partial_m v_n)/2. \quad (34.6)$$

The rotation tensor is related to vorticity via equation (15.44)

$$\mathbb{R}_{mn} = -\epsilon_{mnp} \omega_p/2 \iff \mathbb{R} = \frac{1}{2} \begin{bmatrix} 0 & -\omega_3 & \omega_2 \\ \omega_3 & 0 & -\omega_1 \\ -\omega_2 & \omega_1 & 0 \end{bmatrix}, \quad (34.7)$$

so that

$$2 \mathbb{R}_{mn} \delta x_n = -\epsilon_{mnp} \omega_p \delta x_n \implies 2 \mathbb{R} \cdot \delta \mathbf{x} = \boldsymbol{\omega} \times \delta \mathbf{x}. \quad (34.8)$$

From our discussion of rotation in Section 11.3, this equation means that vorticity in a fluid generates a rigid rotation of a material line element (Section 15.3.8). This result accords with Figure 34.1, whereby vorticity leads to the spin of a test paddle wheel; i.e., the rotation of line elements.

34.1.2 Rotating reference frame

As another means to understand the kinematics of vorticity, let us view the flow field from a reference frame that rotates with a constant angular velocity, $\boldsymbol{\Gamma}$, not unlike the case of observing geophysical flows from the non-inertial terrestrial reference frame. Following equation (11.41e), we know that the velocity observed in the non-rotating or absolute reference frame, \mathbf{v}_a , is related to the rotating reference frame velocity, \mathbf{v} , via

$$\mathbf{v}_a = \mathbf{v} + \boldsymbol{\Gamma} \times \mathbf{x}. \quad (34.9)$$

The vorticity measured in the absolute reference frame, $\boldsymbol{\omega}_a$, is related to the relative vorticity measured in the rotating reference frame, $\boldsymbol{\omega}$, via

$$\boldsymbol{\omega}_a = \nabla \times \mathbf{v}_a = \nabla \times \mathbf{v} + \nabla \times (\boldsymbol{\Gamma} \times \mathbf{x}) = \boldsymbol{\omega} + 2 \boldsymbol{\Gamma}. \quad (34.10)$$

If there is a point in the fluid whereby the rotating reference frame's angular velocity equals to one-half the absolute vorticity at that point, $\Gamma = \omega_a/2$, then the rotating reference frame's vorticity (the relative vorticity) vanishes at that point

$$\Gamma = \omega_a/2 \implies \omega = 0. \quad (34.11)$$

Hence, we may interpret $\omega_a/2$ as twice the local angular velocity of the fluid. Correspondingly, if the absolute vorticity, ω_a , is spatially constant, then we can move to a rotating reference frame in which the relative vorticity vanishes everywhere, with such flow referred to as *irrotational*.

34.1.3 There are no vorticity sources

Vorticity has zero divergence

$$\nabla \cdot \boldsymbol{\omega} = \nabla \cdot (\nabla \times \mathbf{v}) = 0. \quad (34.12)$$

This property is akin to the non-divergent nature of the velocity vector in an incompressible flow (see Chapter 18). However, vorticity is non-divergent for both compressible and incompressible flow. Consequently, there are no interior sources or sinks of vorticity for any fluid. This very basic property plays an important role in developing some further kinematic properties of vorticity in Chapter 37.

34.1.4 Further study

[This video from 3Blue1Brown](#) provides some compelling graphics to help develop intuition for the divergence and curl of a vector, with particular emphasis on fluid flow. In so doing, one learns much about vorticity.

34.2 Irrotational flows

Most geophysical flows have nonzero vorticity. Indeed, even when at rest on the earth, a geophysical fluid carries the vorticity of the rotating planet. However, if we can ignore the planetary vorticity component, as when focused on motions too small to feel the Coriolis acceleration, we can find some geophysically relevant flows with vanishing vorticity. Linear gravity waves in the absence of planetary rotation provide a particularly relevant example (Section 48.3.3).

34.2.1 Characterizing irrotational flows

Irrotational fluid flow is characterized by a zero vorticity

$$\boldsymbol{\omega} = 0 = \text{irrotational flow.} \quad (34.13)$$

Since the curl of a gradient vanishes, irrotational flow has a velocity field equal to the gradient of a velocity potential

$$\nabla \times \mathbf{v} = 0 \implies \mathbf{v} = \nabla \Psi. \quad (34.14)$$

Irrotational flow is therefore sometimes called *potential flow*. Figure 34.2 illustrates a two-dimensional flow field generated by taking the gradient of a scalar potential so that the flow has zero vorticity. In this case, the vertical component of the vorticity vanishes at each point since $\partial v / \partial x = \partial u / \partial y$.

If the flow is non-divergent (solenoidal), as in a Boussinesq ocean (Section 26.1), then the velocity potential is a harmonic function since it satisfies Laplace's equation

$$\nabla \cdot \mathbf{v} = 0 \implies \nabla^2 \Psi = 0. \quad (34.15)$$

The study of harmonic functions is a very mature area of mathematical physics, thus providing a great deal of analytic power towards the study of potential flow for non-divergent flows.

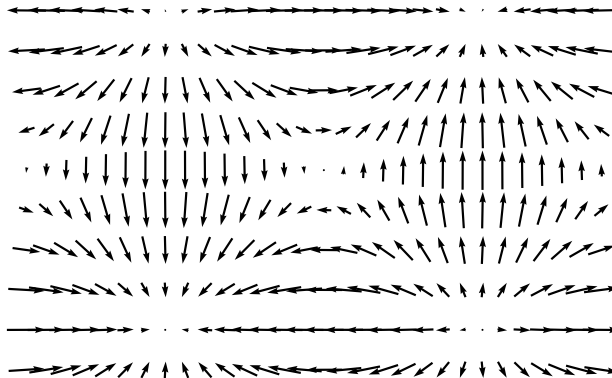


FIGURE 34.2: An example horizontal flow based on a potential, $\Psi = \sin(x/5) \sin(y/5)$. The flow has zero vorticity, $\boldsymbol{\omega} \cdot \hat{\mathbf{z}} = \zeta = \partial v / \partial x - \partial u / \partial y = 0$, since the flow is based on a scalar potential: $\boldsymbol{\omega} = \nabla \times \mathbf{v} = \nabla \times \nabla \Psi = 0$. This example illustrates how irrotational flow may have nontrivial structure even though a test paddle wheel will not spin since there is zero vorticity given that $\partial v / \partial x = \partial u / \partial y$.

34.2.2 Comments

This book does not discuss turbulence in any depth. Nevertheless, we here note that three dimensional turbulence fundamentally relies on vorticity. Hence, irrotational flows, though they may exhibit chaotic motions, are not turbulent since they do not allow for the nonlinear cascade of energy to small spatial scales, with this cascade a fundamental characteristic of three dimensional turbulence. As we will see in Section 37.3, vorticity evolves from sources that tilt and stretch vortex tubes. Vortex stretching is the key source for the turbulent cascade in three dimensional turbulence. Section 3.3 of [Tennekes and Lumley \(1972\)](#) provides a pedagogical discussion of vorticity in the context of three-dimensional turbulence.

34.3 Circulation of the velocity field

The velocity circulation, or more briefly the *circulation*, is defined as the oriented closed loop line integral of velocity as projected onto the unit tangent of the path

$$\mathcal{C} \equiv \oint_{\partial S} \mathbf{v} \cdot d\mathbf{x}, \quad (34.16)$$

with Figure 34.3 offering a schematic. The line element, $d\mathbf{x}$, is oriented in the counter-clockwise direction around the circuit ∂S . More precisely, let $\mathbf{x}(\varphi)$ be an expression for the position of a point on the circuit, with $\varphi(x, y, z, t)$ a parameter that measures the distance along the closed circuit (see Section 2.4). The difference between two very close positions along the circuit defines the increment

$$d\mathbf{x} = \mathbf{x}(\varphi + \delta\varphi) - \mathbf{x}(\varphi). \quad (34.17)$$

By construction, $d\mathbf{x}$ is tangent to the circuit so that $\mathbf{v} \cdot d\mathbf{x}$ picks out the component of the velocity that is tangent to the path.

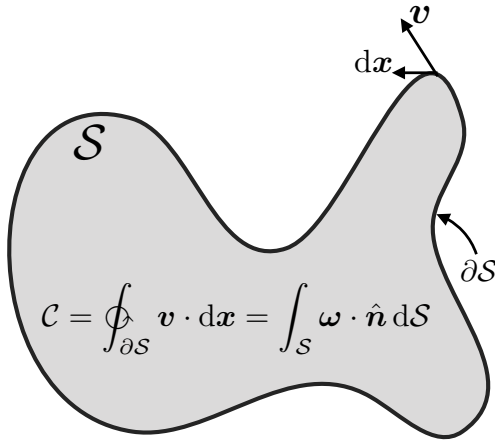


FIGURE 34.3: The velocity circulation around the boundary of a region, ∂S , is determined by the line integral of the velocity projected into the direction of the line integral, $\mathbf{v} \cdot d\mathbf{x}$. Stokes' theorem shows that the velocity circulation computed as a line integral is identical to the normal projection of the vorticity integrated over the area of the region, $C = \oint_{\partial S} \mathbf{v} \cdot d\mathbf{x} = \int_S \boldsymbol{\omega} \cdot \hat{\mathbf{n}} dS$.

Stokes' theorem (Section 2.6) renders the very important identity

$$C = \oint_{\partial S} \mathbf{v} \cdot d\mathbf{x} = \int_S (\nabla \times \mathbf{v}) \cdot \hat{\mathbf{n}} dS = \int_S \boldsymbol{\omega} \cdot \hat{\mathbf{n}} dS, \quad (34.18)$$

where $\hat{\mathbf{n}}$ is the outward unit normal vector orienting the area according to the right-hand rule applied to the bounding circuit. The area integral expression motivates interpreting velocity circulation as the “flux of vorticity” penetrating the area. Stokes' theorem provides the means to connect the vorticity theories promoted by Helmholtz to the circulation theories of Kelvin.

34.4 The free vortex

Consider a two-dimensional rotating fluid in the x - y plane with angular velocity given by

$$\boldsymbol{\Omega} = \frac{\mathbf{x} \times \mathbf{v}}{r^2} = \frac{K \hat{z}}{r^2}. \quad (34.19)$$

The constant K has dimensions $L^2 T^{-1}$, and $r^2 = x^2 + y^2$ is the squared distance from the axis of rotation with \hat{z} the unit vector normal to the x - y plane. The angular velocity falls off as the squared distance from the center, whereas it is singular at the origin. As shown in this section, the fluid flow associated with this *free vortex* has zero vorticity and zero circulation for all points except the origin. Yet the same points with zero vorticity and zero circulation have a constant angular momentum relative to the origin. As shown by Exercise 34.4, and pursued in more detail in Section 34.8, nonzero angular momentum can arise in a fluid with zero circulation so long as there is a nonzero strain within the fluid, such as the flow arising from the free vortex.

34.4.1 Motion of a fluid particle

A fluid particle moves in a circular orbit when in the free vortex flow field. Hence, the particle velocity is perpendicular to its position vector, $\mathbf{x} = x \hat{x} + y \hat{y}$, with respect to the origin

$$\mathbf{v} \cdot \mathbf{x} = 0. \quad (34.20)$$

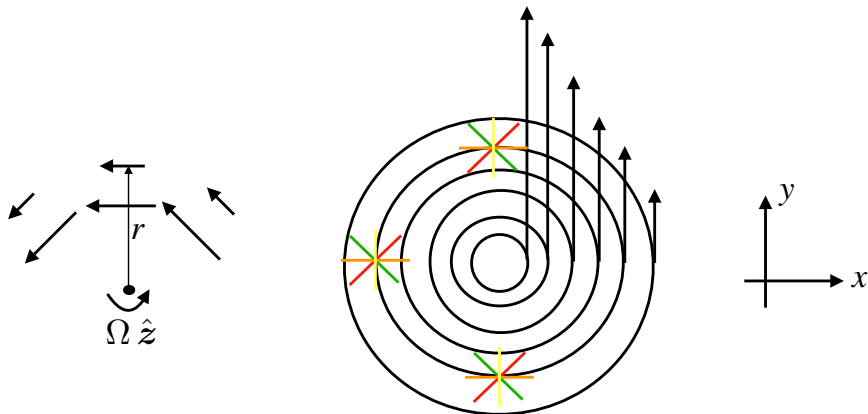


FIGURE 34.4: Irrotational counter-clockwise planar flow in the presence of a free vortex with velocity $\mathbf{v} = (K/r)\hat{\vartheta}$. The tangential velocity decays as $1/r$ from the origin and the vorticity, $\nabla \times \mathbf{v}$, vanishes for all points except the origin. Also, test paddle wheels (colored line segments) do not spin when not at the origin since there is zero vorticity. Notice also that the free vortex has constant angular momentum per mass (computed relative to the origin), since the tangential velocity falls off as $1/r$ thus canceling the moment-arm distance r .

The velocity for this pure rotational flow is given by (see Section 11.3)

$$\mathbf{v} = \boldsymbol{\Omega} \times \mathbf{x} = \frac{K(-y\hat{x} + x\hat{y})}{r^2} = \frac{K\hat{\vartheta}}{r}, \quad (34.21)$$

where $\hat{\vartheta}$ is the polar angle unit vector oriented in the counter-clockwise direction (see Section 9.3). Each component of the velocity falls off as $1/r$ when moving away from the origin. Away from the origin, the vorticity vector vanishes

$$\boldsymbol{\omega} = \nabla \times \mathbf{v} = 0, \quad (34.22)$$

whereas it is singular at the origin.

As noted above, although vorticity is zero everywhere (except at the origin), the angular momentum is nonzero, as expected since the fluid is rotating around the vortex center. The angular momentum for this system arises just from the nonzero strain in the flow field (see Exercise 34.4), with the strain causing fluid particles to move relative to one another. The angular momentum per unit mass, relative to the center of the vortex, is constant and pointed vertically

$$\mathbf{x} \times \mathbf{v} = r\hat{r} \times (K/r)\hat{\vartheta} = K\hat{z}. \quad (34.23)$$

This result follows since the velocity falls off as $1/r$ to cancel the moment-arm distance, r . Hence, the angular momentum per mass is the same for all fluid particles in the presence of a free vortex, no matter what radial distance the particles have from the vortex center.

We illustrate the free vortex velocity field (34.21) in Figure 34.4 along with test paddle wheels. As the paddle wheel centers move counter-clockwise with the flow, the marked paddle wheel blades remain oriented at the same angle. That is, the paddle wheels orbit around the vortex center but they do not spin since the vorticity vanishes in the region bounded away from the origin. Hence, the free vortex generates a flow with non-zero angular momentum yet with zero vorticity (except at the origin).

34.4.2 Circulation

The circulation vanishes for any circuit bounded away from the origin since vorticity vanishes away from the origin. However, the circulation is nonzero for any circuit enclosing the origin

$$\mathcal{C} = \oint_{\partial\mathcal{S}} \mathbf{v} \cdot d\mathbf{x} = \int_0^{2\pi} \mathbf{v} \cdot \hat{\boldsymbol{\vartheta}} r d\vartheta = 2\pi K. \quad (34.24)$$

To reach this result, we set the line element to

$$d\mathbf{x} = \hat{\boldsymbol{\vartheta}} r d\vartheta \quad (34.25)$$

and inserted the velocity (34.21) represented in cylindrical polar coordinates, $\mathbf{v} \cdot \hat{\boldsymbol{\vartheta}} = K/r$. Hence, the singular point vortex at $r = 0$ induces a nonzero circulation for all circuits that enclose the origin.

34.5 Translation and solid-body rotation

Rigid or solid-body fluid motion occurs when all fluid particles are rigidly locked into their relative positions, as if in a rigid solid body. There are two kinds of rigid body motion: translation and rotation. The velocity field for this motion is given by

$$\mathbf{v} = \mathbf{U} + \boldsymbol{\Gamma} \times \mathbf{x}, \quad (34.26)$$

where \mathbf{x} is the position vector relative to the origin, \mathbf{U} is a translation velocity, and $\boldsymbol{\Gamma}$ is an angular velocity. For rigid body motion, both \mathbf{U} and $\boldsymbol{\Gamma}$ are spatially uniform, but can in general be time dependent. The rate of strain tensor vanishes for uniform translation or solid-body motion (see Exercise 15.2)

$$S_{mn} = \frac{1}{2}(\partial_m v_n + \partial_n v_m) = 0. \quad (34.27)$$

A zero rate of strain tensor is expected since strain measures the relative motion between fluid particles, and for a solid-body motion there is no such motion. Even so, the vorticity for solid-body flow is nonzero (see Exercise 34.1)

$$\boldsymbol{\omega} = \nabla \times (\boldsymbol{\Gamma} \times \mathbf{x}) = 2\boldsymbol{\Gamma}. \quad (34.28)$$

We encountered this vorticity in Section 34.1.2 when connecting vorticity and angular velocity. In the remainder of this section, we set the rotation rate to that of the planet, $\boldsymbol{\Gamma} = \boldsymbol{\Omega}$, and assume it to be constant in space and time.

34.5.1 Absolute vorticity

For planetary fluid dynamics, rotation of the planet imparts *planetary vorticity* to fluids. Hence, the total or *absolute* vorticity of a fluid is the vector sum of the *relative vorticity*, $\boldsymbol{\omega}$, plus the planetary vorticity

$$\boldsymbol{\omega}_{\text{absolute}} = \boldsymbol{\omega}_{\text{planet}} + \boldsymbol{\omega}. \quad (34.29)$$

In this equation,

$$\boldsymbol{\omega}_{\text{planet}} = 2\boldsymbol{\Omega}_{\text{planet}} \quad (34.30)$$

is the planetary vorticity associated with solid-body motion of a fluid particle stationary with respect to the planet, and

$$\boldsymbol{\omega} = \nabla \times \mathbf{v} \quad (34.31)$$

is the relative vorticity. The relative vorticity measures the vorticity of the fluid due to motion relative to the rotating sphere, with \mathbf{v} the velocity relative to the rotating sphere.

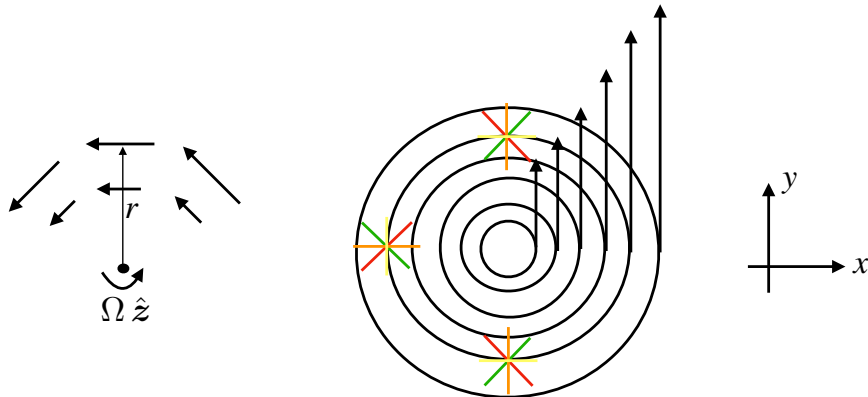


FIGURE 34.5: Rigid body fluid motion, whereby the fluid velocity is: (A) purely tangential and linearly proportional to the radial distance from the vortex center, $\mathbf{v} = |\Omega| r \hat{\vartheta}$; (B) fluid particles maintain a fixed relative position; (C) and vorticity is constant and points perpendicular to the page, $\boldsymbol{\omega} = 2\boldsymbol{\Omega} = 2|\Omega|\hat{z}$. Test paddle wheels rigidly move around the center, and they exhibit a spin about their axis that manifests the nonzero vorticity.

34.5.2 Solid-body rotation on a plane

Consider the circular solid-body rotation on a plane shown in Figure 34.5, in which the velocity is purely tangential and linearly proportional to the distance from the center

$$\mathbf{v} = \boldsymbol{\Omega} \times \mathbf{x} = |\Omega| (-y \hat{x} + x \hat{y}) = |\Omega| r \hat{\vartheta}. \quad (34.32)$$

Assuming the center of mass to be at the circle center, the angular momentum for the flow is the same as that for a solid-body. Even though the motion of each fluid particle is rigidly fixed relative to all other particles, there is a nonzero vorticity in this flow as illustrated by the spin of colored test paddle wheels in Figure 34.5.

34.5.3 Circulation for solid-body rotation

For solid-body rotation, the velocity circulation around a circular path of radius R is given by

$$C = \oint \mathbf{v} \cdot d\mathbf{x} = \oint (\boldsymbol{\Omega} \times \mathbf{x}) \cdot d\mathbf{x} = R^2 |\Omega| \oint d\vartheta = 2\pi R^2 |\Omega| = 2A |\Omega|, \quad (34.33)$$

where $A = \pi R^2$ is the area of the circle. Hence, the circulation per area for solid-body rotating fluid flow is twice the angular rotation rate, which is the magnitude of the vorticity

$$C/A = |\boldsymbol{\omega}| = 2 |\boldsymbol{\Omega}|. \quad (34.34)$$

34.5.4 Comments

As seen in Section 34.4, fluid flow in the presence of a free vortex has zero vorticity for all points except the origin of the vortex. However, the same points also have a constant angular momentum relative to the origin, and they experience a nonzero strain. In contrast, constant solid-body rotating fluid flow has a nonzero vorticity, nonzero angular momentum, yet a zero strain. Section 34.8 details the connection between vorticity, strain, and angular momentum, where we see that angular momentum can be nonzero if either vorticity or strain are nonzero. These ideas are illustrated in [this 3-minute video](#) as well as in this [10 minute video from the Open University](#).

34.6 Kinematics of vortex lines and vortex tubes

We here develop the basics of vorticity kinematics, with this discussion closely following from the kinematics of material line elements discussed in Section 15.3.3.

34.6.1 Vortex lines and vortex tubes

A *vortex line* is a line drawn through the fluid that is instantaneously tangent to the vorticity at each spatial point. A vortex line is mathematically parameterized just like any other line, whereby we write the spatial coordinates along the line as a function of a suitable parameter φ (e.g., the arc-length)

$$\mathbf{x}(\varphi) = x(\varphi) \hat{\mathbf{x}} + y(\varphi) \hat{\mathbf{y}} + z(\varphi) \hat{\mathbf{z}}. \quad (34.35)$$

Correspondingly, the tangent vector for the line is given by

$$\frac{d\mathbf{x}(\varphi)}{d\varphi} = \frac{dx(\varphi)}{d\varphi} \hat{\mathbf{x}} + \frac{dy(\varphi)}{d\varphi} \hat{\mathbf{y}} + \frac{dz(\varphi)}{d\varphi} \hat{\mathbf{z}}. \quad (34.36)$$

The three coordinates of the line are constrained so that the tangent is parallel to vorticity at each point

$$\frac{d\mathbf{x}(\varphi)}{d\varphi} \times \boldsymbol{\omega} = 0, \quad (34.37)$$

which is satisfied by the following constraint

$$\frac{dx/d\varphi}{\omega_x} = \frac{dy/d\varphi}{\omega_y} = \frac{dz/d\varphi}{\omega_z}. \quad (34.38)$$

These equations are directly analogous to those satisfied by velocity streamlines (Section 14.9.2)

$$\frac{dx/d\varsigma}{u} = \frac{dy/d\varsigma}{v} = \frac{dz/d\varsigma}{w}, \quad (34.39)$$

where ς is the parameter along the streamline. Notably, the velocity is not constant along a velocity streamline, nor is vorticity constant along a vortex line. In a steady state, streamlines map the trajectory of a fluid particle (see Section 14.9). However, a vortex line does not offer an interpretation in terms of trajectories.

A *vortex tube* is a bundle of vortex lines that pass through a simple closed curve such as illustrated in Figure 34.6. By definition, the sides of the vortex tube are parallel to the vorticity field, since the sides are constructed from vortex lines. We defined a similar notion, the streamtube, for a non-divergent velocity field in Figure 14.5.

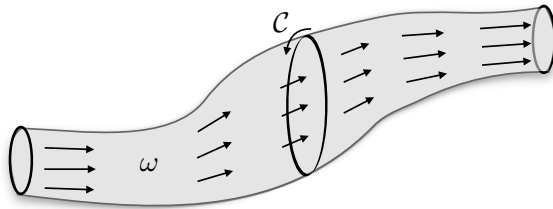


FIGURE 34.6: A vortex line is a line in the fluid that is everywhere tangent to the vorticity vector. A vortex tube is the accumulation of vortex lines passing through a closed loop. A vortex tube is sometimes referred to as a vortex filament. We here depict a vortex tube within the fluid and illustrate the circulation around the tube $C = \oint_{\partial S} \mathbf{v} \cdot d\mathbf{x} = \int \boldsymbol{\omega} \cdot \hat{\mathbf{n}} dS$. Since vorticity has zero divergence, the circulation is the same for any loop around the vortex tube (Helmholtz's first theorem from Section 34.6.3). A uniform circulation along the tube means that the magnitude of the vorticity is larger in regions where the tube has a small area and conversely the circulation magnitude is smaller where the tube has a large area.

34.6.2 Kinematic properties

Vorticity has zero divergence

$$\nabla \cdot \boldsymbol{\omega} = \nabla \cdot (\nabla \times \mathbf{v}) = 0, \quad (34.40)$$

which follows since the divergence of a curl vanishes. Integrating the non-divergence relation over an arbitrary closed volume within the fluid leads to

$$\int_{\mathcal{R}} \nabla \cdot \boldsymbol{\omega} dV = \oint_{\partial \mathcal{R}} \boldsymbol{\omega} \cdot \hat{\mathbf{n}} dS = 0, \quad (34.41)$$

where we made use of Gauss's divergence theorem to reach the surface integral expression, with $\hat{\mathbf{n}} dS$ the oriented area element on the boundary of the volume, $\partial \mathcal{R}$, and $\hat{\mathbf{n}}$ the outward normal on the boundary. This result means there is no net vorticity entering or leaving an arbitrary closed region. That is, there is a vanishing net integrated “flux” of vorticity across the closed region. Consequently, there are no sources or sinks of vorticity within the fluid. In turn, there is no accumulation of vorticity within any arbitrary closed region.

Now specialize the surface integral in equation (34.41) to a volume along a chosen vortex tube such as in Figure 34.6.¹ The two ends of the tube generally have different cross-sectional areas. The integral over the sides of the vortex tube vanishes, since the vorticity is parallel to the tube sides. Hence, the surface integral only picks up contributions from the two ends of the tube

$$\int_A \boldsymbol{\omega} \cdot \hat{\mathbf{n}} dS_A + \int_B \boldsymbol{\omega} \cdot \hat{\mathbf{n}} dS_B = 0. \quad (34.42)$$

The outward normals point in the opposite direction so that the flux of vorticity is independent of position along the tube. Stoke's theorem transfers the vorticity constraint to a constraint on the circulation around the circumference of the tube

$$\oint_A \mathbf{v} \cdot d\mathbf{x} + \oint_B \mathbf{v} \cdot d\mathbf{x} = 0. \quad (34.43)$$

¹In Exercise 18.7, we developed a similar set of results for a streamtube in a non-divergent flow.

Hence, the circulation around the vortex tube is the same no matter where it is computed. The circulation constraints (34.42) and (34.43) are kinematic, holding for any vorticity field. We now consider some consequences of this constraint.

34.6.3 Helmholtz's theorems

There are a few basic properties of vorticity that follow from its vanishing divergence. These properties are known as Helmholtz's theorems.

Helmholtz's first theorem

Since the cross-sectional slices used to derive the circulation constraint (34.43) are arbitrary, the constraint holds throughout the full extent of the vortex tube. Hence, as noted following equation (34.43), the circulation is the same for any position along the vortex tube; i.e., the strength of a vortex tube is constant along its length (see Figure 34.6). This result is known as *Helmholtz's first theorem*.

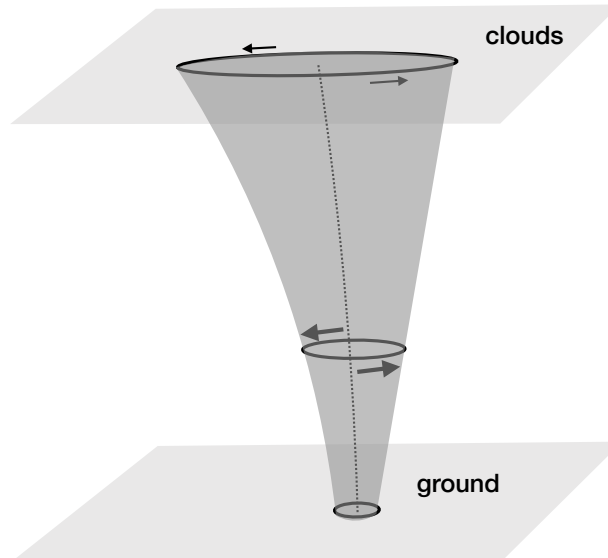


FIGURE 34.7: A vortex tube idealization of a tornado. Since the circulation around the tube is uniform (Helmholtz's first theorem), the tangential velocity of a fluid particle has a larger magnitude in regions where the vortex area is smaller, such as near the ground. As the tornado reaches into the clouds, it generally has a larger cross-sectional area and thus a smaller magnitude for the tangential velocity.

As a corollary, we refer to the vorticity constraint (34.42) to note that changes in the vortex tube cross-sectional area are compensated by changes in vorticity. For example, let the vortex tube shrink over some region. To maintain constant circulation along the tube, the vorticity magnitude must increase where the area decreases, which in turn means that the velocity circulating around the tube increases in magnitude as the area reduces. Think of a tornado as in Figure 34.7, which is a natural expression of a vortex tube. Near the ground, the cross-sectional area of the tornado is small, with the tangential velocity of a fluid particle within the tube relatively large. Near the tornado top, the cross-sectional area is large so the tangential velocity is relatively small.

Helmholtz's second theorem

The vorticity constraint (34.42) cannot be satisfied by a finite vorticity if the area of a vortex tube vanishes anywhere. Hence, a vortex tube cannot begin or end within the fluid. This result follows from the absence of vortex sources and sinks within the fluid. Hence, a vortex tube can only loop with itself (e.g., a smoke ring as in Figure 34.8), or intersect a boundary (as for a tornado in Figure 34.7, where the ground and clouds form the boundary).

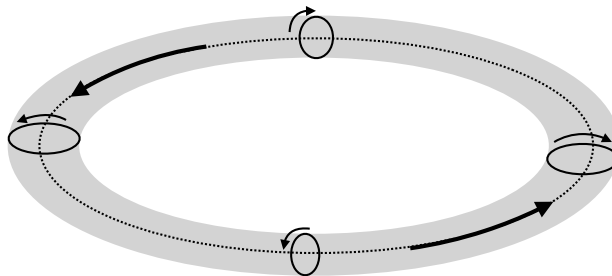


FIGURE 34.8: A vortex ring (torus) is a vortex tube that closes on itself. We here depict a vortex ring with vorticity pointing counter-clockwise around the ring. The tangential velocity is oriented as shown so that the vorticity points according to the right hand rule. That is, orient the fingers on the right hand according to the tangential velocity. The thumb of the right hand then points in the direction of the vorticity vector.

Helmholtz's third theorem

Helmholtz's third theorem states that an unforced inviscid barotropic fluid that has zero vorticity remains irrotational forever. This theorem is a special case of Kelvin's circulation theorem that is studied in Section 37.2.

34.6.4 Further study

A particularly insightful and pedagogical discussion of the ideas in this section can be found in Chapter 5 of [Acheson \(1990\)](#). Additionally, the following videos offer laboratory demonstrations of vorticity in non-rotating and rotating flows.

- Helmholtz's theorems are vividly exhibited [by this video](#) from the *Physics Girl* of flow generated by a paddle in a swimming pool. She also discusses vortex rings in [this video](#).
- Vorticity and Helmholtz's theorems are also described by [this classic video](#) from Prof. Shapiro.
- A rotating tank experiment shown near the 15 minute mark of [this video](#) from Prof. Fultz shows how vorticity is affected by vortex stretching.
- [This video](#) offers a classic tutorial on vorticity in non-rotating fluids from Prof. Shapiro.

34.7 Relative vorticity from curvature and shear

In this section we decompose the vorticity into two terms: one arising from curvature in the flow and another arising from shears in the direction normal to the flow. This decomposition is formulated for horizontal flows, but can be generalized to arbitrary flow. It offers yet another means to understand the kinematic properties of vorticity.

34.7.1 Circular flow

Before treating the general case, it is useful to consider a two-dimensional velocity that locally takes the form of an angular flow

$$\mathbf{u} = u^\vartheta(r, \vartheta) \hat{\boldsymbol{\vartheta}}, \quad (34.44)$$

where ϑ is the polar angle. Circulation around the circular wedge shown in Figure 34.9 has zero contributions from the two radial segments since these segments are perpendicular to the angular flow. The circulation is thus given by

$$\mathcal{C} = \oint_{\text{wedge}} \mathbf{u} \cdot d\mathbf{x} \quad (34.45a)$$

$$= \int_{\vartheta}^{\vartheta+\delta\vartheta} u^\vartheta(r + \delta r, \vartheta') (r + \delta r) d\vartheta' + \int_{\vartheta+\delta\vartheta}^{\vartheta} u^\vartheta(r, \vartheta') r d\vartheta' \quad (34.45b)$$

$$= \int_{\vartheta}^{\vartheta+\delta\vartheta} [u^\vartheta(r + \delta r, \vartheta') (r + \delta r) - r u^\vartheta(r, \vartheta')] d\vartheta' \quad (34.45c)$$

$$\approx \int_{\vartheta}^{\vartheta+\delta\vartheta} \left[u^\vartheta(r, \vartheta') \delta r + \frac{\partial u^\vartheta}{\partial r} r \delta r \right] d\vartheta' \quad (34.45d)$$

$$= r \delta r \int_{\vartheta}^{\vartheta+\delta\vartheta} \left[\frac{u^\vartheta}{r} + \frac{\partial u^\vartheta}{\partial r} \right] d\vartheta', \quad (34.45e)$$

where the approximation holds when $\delta r \rightarrow 0$. Taking the further limit $\delta\vartheta \rightarrow 0$ renders

$$\mathcal{C} \approx \zeta \delta A = \zeta r \delta r \delta\vartheta = \left[\frac{u^\vartheta}{r} + \frac{\partial u^\vartheta}{\partial r} \right] r \delta r \delta\vartheta \implies \zeta = \frac{u^\vartheta}{r} + \frac{\partial u^\vartheta}{\partial r}. \quad (34.46)$$

The first term in the vorticity arises from the nonzero radius of curvature of the circular flow whereas the second term arises from radial shear.

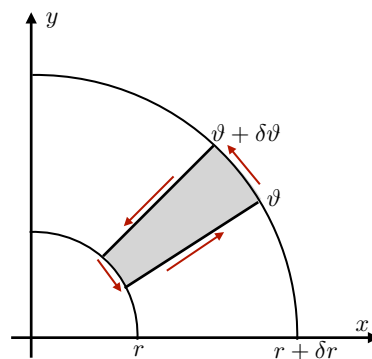


FIGURE 34.9: Circulation around the circular wedge $[r, r + \delta r] \otimes [\vartheta, \vartheta + \delta\vartheta]$.

34.7.2 Generalization to natural coordinates

The decomposition (34.46) can be generalized to arbitrary horizontal flow by making use of the natural coordinates from Section 29.2. Here, we introduce the locally orthogonal coordinates, (s, n) , with s the arc-length defined along the trajectory of a fluid element and n measuring the distance normal to the trajectory. We make the convention that the unit tangent direction, \hat{s} , is aligned along the local flow direction whereas the unit normal direction, \hat{n} , is to the left facing

downstream. Furthermore, the radius of curvature at a point along a trajectory (see Section 6.2.3) is positive if the flow turns into the positive \hat{n} direction (left turn) and negative for oppositely curved flow (right turn) (see Figures 29.2 and 29.3). Finally, the radius of curvature is infinite for straight flow.

For the counter-clockwise circuit in Figure 34.9, a left turn occurs with $\hat{n} = -\hat{r}$ so that equation (34.46) takes on the general form

$$\zeta = \underbrace{\frac{|\mathbf{u}|}{R}}_{\text{curvature}} - \underbrace{\frac{\partial |\mathbf{u}|}{\partial n}}_{\text{shear}} = \zeta_{\text{curv}} + \zeta_{\text{shear}}. \quad (34.47)$$

Again, the first term arises from curvature in the flow, with R the radius of curvature. This *curvature vorticity* is sometimes also called the *orbital vorticity*. A trajectory turning to the left has $R > 0$ and this curved trajectory contributes to a positive vorticity; conversely for a trajectory turning to the right. The second term in equation (34.47) arises from shears computed normal to the flow direction. If the flow speed decreases in the normal direction (e.g., towards the center of the circle in Figure 34.9), then that too contributes to a positive vorticity. Furthermore, flow with $\zeta = 0$ arises if there is an exact compensation between the curvature-induced vorticity with the shear-induced vorticity

$$\zeta = 0 \implies \frac{|\mathbf{u}|}{R} = \frac{\partial |\mathbf{u}|}{\partial n}. \quad (34.48)$$

34.7.3 Example vorticities

Rigid body vortex and free vortex

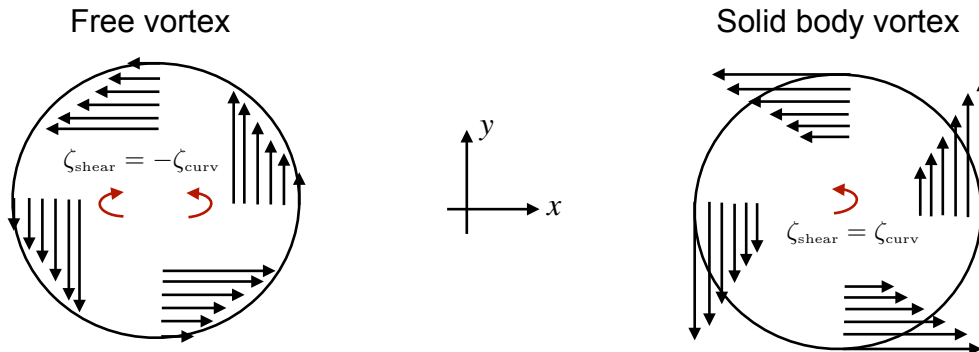


FIGURE 34.10: Decomposing the relative vorticity into its contributions from curvature and normal shear. Left panel: the free vortex from Figure 34.4 has $\zeta_{\text{curv}} = -\zeta_{\text{shear}} = K/r^2$ so that $\zeta = \zeta_{\text{curv}} + \zeta_{\text{shear}} = 0$. Right panel: the solid body vortex from Figure 34.5 has $\zeta_{\text{curv}} = \zeta_{\text{shear}} = \Omega$ so that $\zeta = 2\Omega$.

To help further understand the decomposition (34.47), consider the case of solid body rotation (Figure 34.5) where $\mathbf{v} = \Omega r \hat{\theta}$ and $\hat{n} = -\hat{r}$. For a circle the radius of curvature equals to the radius of the circle, so that

$$\zeta_{\text{curv}} = \frac{\Omega r}{r} = \Omega \quad \text{and} \quad \zeta_{\text{shear}} = -\partial_n |\mathbf{u}| = \partial_r (\Omega r) = \Omega, \quad (34.49)$$

in which case

$$\zeta = \zeta_{\text{curv}} + \zeta_{\text{shear}} = 2\Omega = \hat{z} \cdot (\nabla \times \mathbf{v}), \quad (34.50)$$

as depicted in the right panel of Figure 34.10. Likewise, for the free vortex (Figure 34.4) we have

$\mathbf{v} = (K/r) \hat{\vartheta}$ so that

$$\zeta_{\text{curv}} = K/r^2 \quad \text{and} \quad \zeta_{\text{shear}} = \partial|\mathbf{u}|/\partial r = -K/r^2, \quad (34.51)$$

which yields zero relative vorticity

$$\zeta = \zeta_{\text{curv}} + \zeta_{\text{shear}} = 0, \quad (34.52)$$

as depicted in the left panel of Figure 34.10.

Gaussian jet moving along a line and around a circle

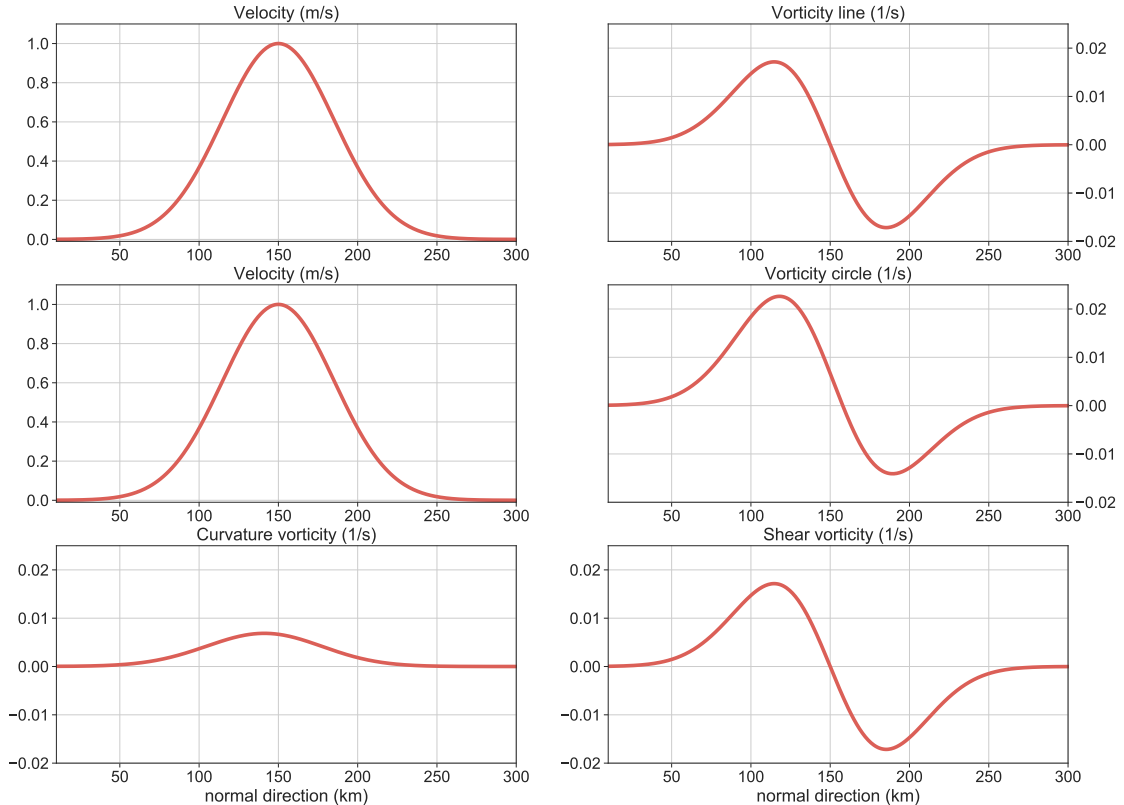


FIGURE 34.11: Top row: velocity and vorticity within a Gaussian jet that is moving along a straight line according to equations (34.53) and (34.54). We set the jet e-folding scale as $L = 50$ km, jet maximum at $x_{\max} = 150$ km, and velocity scale as $v_o = 1$ m s $^{-1}$. Note the symmetry of the vorticity relative to the jet maximum, with the vorticity extrema corresponding to the inflection points of the Gaussian velocity field. Middle left: the same Gaussian velocity profile only now for a jet that is moving counter-clockwise around a circle so that $\mathbf{v} = v(r) \hat{\vartheta}$ according to equation (34.55). To avoid a singularity of the curvature vorticity at $r = 0$ (infinite curvature) we assume the velocity field vanishes within a small distance from the origin. Middle right: vorticity for the Gaussian jet moving around the circle, with $\zeta = r^{-1} \partial_r(r v)$. Notice how the vorticity is not symmetric relative to the jet maximum. Rather, the zero vorticity occurs to the right of the jet maximum, and the vorticity on the inside of the jet maximum is larger in magnitude than the outer vorticity. Lower left: vorticity due to the curvature of the jet as it moves around the circle, $\zeta_{\text{curve}} = v(r)/r$. Lower right: vorticity due to the radial shear in the Gaussian jet, $\zeta_{\text{shear}} = -2(r - r_{\max}) v(r)/L^2$.

Next consider a Gaussian jet moving along a straight line in the meridional direction with velocity field

$$\mathbf{v}(x) = v(x) \hat{\mathbf{y}} = v_o \exp[-(x - x_{\max})^2/L^2] \hat{\mathbf{y}}, \quad (34.53)$$

where v_o is the velocity scale, L is the e-folding length scale for the jet, and x_{\max} is the position

of the jet maximum. The corresponding vorticity of the jet is given by

$$\zeta_{\text{line}} = \partial_x v = -2 [(x - x_{\max})/L^2] v(x). \quad (34.54)$$

We depict the velocity (34.53) and vorticity (34.54) in the top row of Figure 34.11. Note the symmetry of the vorticity around the jet maximum at $x = x_{\max}$, with the vorticity extrema corresponding to inflection points of the jet.²

Now assume the same jet is moving counter-clockwise around a circle so that the velocity field is given by

$$\mathbf{v}(r) = v(r) \hat{\vartheta} = v_o \exp[-(r - r_{\max})^2/L^2] \hat{\vartheta}, \quad (34.55)$$

where we made use of the polar coordinates from Section 9.3 with $r^2 = x^2 + y^2$ the squared radial distance from the center, and $\hat{\vartheta}$ the unit vector pointing in the counter-clockwise direction from the \hat{x} axis. Making use of the curl operation in polar coordinates given by equation (9.85c) renders the vorticity

$$\zeta = r^{-1} \partial_r(r v) = \frac{v}{r} - \frac{2(r - r_{\max}) v}{L^2} = \zeta_{\text{curve}} + \zeta_{\text{shear}}. \quad (34.56)$$

We depict these terms in the third row of Figure 34.11. Note how the vorticity, ζ , has the amplitude of its maximum increased, whereas the amplitude of its minimum is decreased. Correspondingly, the vorticity is not symmetric about the jet maximum, with its zero crossing to the outside of the jet maximum. Asymmetry of the vorticity arises from the curvature vorticity, $\zeta_{\text{curve}} = v/r$, which has its peak inside the jet maximum. So although the shear vorticity, ζ_{shear} , is symmetric around the jet axis, the curvature vorticity causes a movement of vorticity towards the center of the circle.

34.8 Relating angular momentum to vorticity and strain

As noted in Section 34.5.4, fluid flow in the presence of a free vortex (Section 34.4) has zero vorticity for all points except the origin of the vortex. However, the same points with zero vorticity also have a constant angular momentum relative to the origin, and they experience a nonzero strain. In contrast, solid-body fluid flow (Section 34.5) has a nonzero vorticity, nonzero angular momentum, yet a zero strain. In this section we study the connection between vorticity, rate of strain, and angular momentum for a fluid continuum. We here show that angular momentum and vorticity are fundamentally distinct in a fluid that has straining motion between fluid elements. In contrast, angular momentum and vorticity are directly proportional (through the moment of inertia tensor) when the fluid exhibits solid body motion in which the rate of strain tensor vanishes.

34.8.1 Linear momentum

To start the analysis, consider the velocity and linear momentum of a connected material fluid region denoted by $\mathcal{R}(\mathbf{v})$, with each point of the region moving with the local fluid velocity $\mathbf{v}(\mathbf{x}, t)$. Let an arbitrary fluid parcel within this region be marked with the material label \mathbf{a} so that its position vector is $\mathbf{X}(\mathbf{a}, t)$ and its velocity is

$$\mathbf{V}(\mathbf{a}, t) = \frac{\partial \mathbf{X}(\mathbf{a}, t)}{\partial t}, \quad (34.57)$$

²Inflection points are where the curvature changes sign.

where the time derivative is computed holding the material label fixed. Since the parcel is within a finite material region, we find it useful to decompose the motion of the parcel into the motion of the region's center of mass plus the motion of the parcel relative to the center of mass

$$\mathbf{V}(\mathbf{a}, t) = \frac{\partial \mathbf{X}(\mathbf{a}, t)}{\partial t} \quad (34.58a)$$

$$= \frac{\partial (\bar{\mathbf{X}} + \mathbf{X}')}{\partial t} \quad (34.58b)$$

$$= \bar{\mathbf{V}}(t) + \mathbf{V}'(\mathbf{a}, t). \quad (34.58c)$$

In this equation, we introduced the velocity \mathbf{V}' defined relative to the center of mass of the region. Furthermore, the center of mass velocity is given by

$$\bar{\mathbf{V}} = \frac{d\bar{\mathbf{X}}}{dt} \quad (34.59a)$$

$$= \frac{d}{dt} \left[\frac{\int_{\mathcal{R}(\mathbf{v})} \mathbf{x} \rho dV}{\int_{\mathcal{R}(\mathbf{v})} \rho dV} \right] \quad (34.59b)$$

$$= \frac{1}{M} \int_{\mathcal{R}(\mathbf{v})} \frac{D\mathbf{x}}{Dt} \rho dV \quad (34.59c)$$

$$= \frac{1}{M} \int_{\mathcal{R}(\mathbf{v})} \mathbf{v} \rho dV. \quad (34.59d)$$

The identity (34.59c) follows since the material region maintains a constant mass,

$$M = \int_{\mathcal{R}(\mathbf{v})} \rho dV \implies \frac{dM}{dt} = 0, \quad (34.60)$$

allowing the denominator to come outside the derivative. Additionally, each of the fluid parcels in the region maintains constant mass. As per Reynold's transport theorem (Section 16.3.4), the time derivative moves across the integral to act materially on the position vector. The final equality, (34.59d), follows since the material time derivative of a parcel trajectory when evaluated at a point, \mathbf{x} , equals to the velocity field at that point

$$\mathbf{v}(\mathbf{x}, t) = \frac{D\mathbf{x}}{Dt}. \quad (34.61)$$

It follows that the linear momentum for the material fluid region is given by

$$\mathbf{P} = \int_{\mathcal{R}(\mathbf{v})} \mathbf{v} \rho dV = M \bar{\mathbf{V}}. \quad (34.62)$$

We conclude that the total linear momentum of an extended body equals to that of a point particle of mass $M = \int_{\mathcal{R}(\mathbf{v})} \rho dV$ moving with the center of mass velocity, $\bar{\mathbf{V}}$.

34.8.2 Angular momentum

We here consider angular momentum for a material fluid region, which is determined by the material integral of the angular momentum for each fluid parcel

$$\mathbf{L} = \int_{\mathcal{R}(\mathbf{v})} (\mathbf{x} \times \mathbf{v}) \rho dV. \quad (34.63)$$

Our goal is to expose how physically distinct aspects of the fluid motion contribute to the angular momentum. To proceed, decompose the position vector of a point within the region into the center of mass position plus a deviation, $\mathbf{x} = \bar{\mathbf{x}} + \mathbf{x}'$, where $\bar{\mathbf{x}} = \bar{X}$ is the instantaneous position of the moving center of mass. The angular momentum thus takes the form

$$\mathbf{L} = \int_{\mathcal{R}(\mathbf{v})} (\mathbf{x} \times \mathbf{v}) \rho dV \quad (34.64a)$$

$$= \int_{\mathcal{R}(\mathbf{v})} [(\bar{\mathbf{x}} + \mathbf{x}') \times \mathbf{v}] \rho dV \quad (34.64b)$$

$$= \bar{\mathbf{X}} \times \left[\int_{\mathcal{R}(\mathbf{v})} \mathbf{v} \rho dV \right] + \int_{\mathcal{R}(\mathbf{v})} (\mathbf{x}' \times \mathbf{v}) \rho dV \quad (34.64c)$$

$$= (\bar{\mathbf{X}} \times \mathbf{P}) + \int_{\mathcal{R}(\mathbf{v})} (\mathbf{x}' \times \mathbf{v}) \rho dV. \quad (34.64d)$$

The final equality introduced the linear momentum, (34.62), for the fluid region. The first term in equation (34.64d) is the angular momentum of the region with respect to the position of the center of mass. The second term is associated with deviations of parcel positions relative to the center of mass.

We now focus on how the deviation term, $\int_{\mathcal{R}(\mathbf{v})} (\mathbf{x}' \times \mathbf{v}) \rho dV$, contributes to the angular momentum (34.63). As we will see, this analysis exposes how angular momentum of the extended material fluid region is affected by vorticity and rate of strain in the fluid flow. To facilitate some of the manipulations, we make use of basic Cartesian tensor analysis from Chapter 1, including the summation convention whereby repeated indices are summed over their range.

34.8.3 Taylor expanding the velocity

We perform a Taylor expansion of the velocity $\mathbf{v}(\mathbf{x})$ around the instantaneous center of mass position, $\bar{\mathbf{x}} = \bar{X}$, and truncate the expansion to the leading order term³

$$\mathbf{v}(\mathbf{x}) = \mathbf{v}(\bar{\mathbf{x}} + \mathbf{x}') \approx \mathbf{v}(\bar{\mathbf{x}}) + (\mathbf{x}' \cdot \nabla) \mathbf{v}|_{\mathbf{x}=\bar{\mathbf{x}}}. \quad (34.65)$$

We are thus left with

$$\mathbf{L} = (\bar{\mathbf{X}} \times \mathbf{P}) + \int_{\mathcal{R}(\mathbf{v})} (\mathbf{x}' \times \mathbf{v}) \rho dV \quad (34.66a)$$

$$= (\bar{\mathbf{X}} \times \mathbf{P}) + \int_{\mathcal{R}(\mathbf{v})} [\mathbf{x}' \times \mathbf{v}(\bar{\mathbf{x}})] \rho dV + \int_{\mathcal{R}(\mathbf{v})} [\mathbf{x}' \times (\mathbf{x}' \cdot \nabla) \mathbf{v}(\bar{\mathbf{x}})] \rho dV. \quad (34.66b)$$

The velocity $\mathbf{v}(\bar{\mathbf{x}})$ can be removed from the integration since it is evaluated at the center of mass point. Hence, the second term in equation (34.66b) vanishes

$$\int_{\mathcal{R}(\mathbf{v})} [\mathbf{x}' \times \mathbf{v}(\bar{\mathbf{x}})] \rho dV = \left[\int_{\mathcal{R}(\mathbf{v})} \mathbf{x}' \rho dV \right] \times \mathbf{v}(\bar{\mathbf{x}}) = 0, \quad (34.67)$$

³The velocity field evaluated at the center of mass position, $\mathbf{v}(\bar{\mathbf{x}})$, is not equal to the center of mass velocity: $\mathbf{v}(\bar{\mathbf{x}}) \neq \bar{\mathbf{v}}$.

where $\int_{\mathcal{R}(\mathbf{v})} \mathbf{x}' \rho dV = 0$ by definition of the center of mass. The angular momentum is thus given by the two terms

$$\mathbf{L} = (\bar{\mathbf{X}} \times \mathbf{P}) + \int_{\mathcal{R}(\mathbf{v})} [\mathbf{x}' \times (\mathbf{x}' \cdot \nabla) \mathbf{v}(\bar{\mathbf{x}})] \rho dV. \quad (34.68)$$

The m' th component of the second right hand side term can be written

$$\int_{\mathcal{R}(\mathbf{v})} [\mathbf{x}' \times (\mathbf{x}' \cdot \nabla) \mathbf{v}(\bar{\mathbf{x}})]_m \rho dV = \epsilon_{mnp} \int_{\mathcal{R}(\mathbf{v})} x'_n [(\mathbf{x}' \cdot \nabla) \mathbf{v}(\bar{\mathbf{x}})]_p \rho dV \quad (34.69a)$$

$$= \epsilon_{mnp} \int_{\mathcal{R}(\mathbf{v})} x'_n x'_q \partial_q v_p(\bar{\mathbf{x}}) \rho dV \quad (34.69b)$$

$$= \epsilon_{mnp} \left[\int_{\mathcal{R}(\mathbf{v})} x'_n x'_q \rho dV \right] \partial_q v_p(\bar{\mathbf{x}}). \quad (34.69c)$$

We removed the velocity derivatives

$$\partial_q v_p(\bar{\mathbf{x}}) = \left[\frac{\partial v_p}{\partial x_q} \right]_{\mathbf{x}=\bar{\mathbf{x}}} \quad (34.70)$$

from the integral, since they are evaluated at the center of mass point and so do not participate in the integration.

34.8.4 Angular momentum, rate of strain, and vorticity

Following from the discussion in Section 15.3.5, we know that the velocity derivatives, $\partial_q v_p$, appearing in equation (34.69c) form the components to a second order tensor known as the *velocity gradient tensor*, which can be decomposed into the rate of strain tensor, \mathbb{S} , and the rotation tensor, \mathbb{R} . Introducing these two tensors brings the angular momentum for a continuum fluid region into the form

$$L_m = (\bar{\mathbf{X}} \times \mathbf{P})_m + \epsilon_{mnp} \left[\int_{\mathcal{R}(\mathbf{v})} x'_n x'_q \rho dV \right] \mathbb{S}_{qp} + \epsilon_{mnp} \left[\int_{\mathcal{R}(\mathbf{v})} x'_n x'_q \rho dV \right] \mathbb{R}_{qp} \quad (34.71a)$$

$$= (\bar{\mathbf{X}} \times \mathbf{P})_m + \epsilon_{mnp} \left[\int_{\mathcal{R}(\mathbf{v})} x'_n x'_q \rho dV \right] \mathbb{S}_{qp} + \frac{1}{2} \epsilon_{mnp} \epsilon_{sqp} \left[\int_{\mathcal{R}(\mathbf{v})} x'_n x'_q \rho dV \right] \omega_s \quad (34.71b)$$

$$= \underbrace{(\bar{\mathbf{X}} \times \mathbf{P})_m}_{\text{center of mass}} + \underbrace{\epsilon_{mnp} \left[\int_{\mathcal{R}(\mathbf{v})} x'_n x'_q \rho dV \right]}_{\text{strain contribution}} \mathbb{S}_{qp} + \underbrace{\frac{1}{2} \left[\int_{\mathcal{R}(\mathbf{v})} (\mathbf{x}' \cdot \mathbf{x}' \delta_{ms} - x'_m x'_s) \rho dV \right]}_{\text{vorticity contribution}} \omega_s. \quad (34.71c)$$

Since each point in the fluid continuum can be considered the center of mass for an arbitrary material region, the decomposition (34.71c) holds in general.

- **CENTER OF MASS ANGULAR MOMENTUM:** The first term on the right hand side of equation (34.71c) arises from the angular momentum of the material region as measured with respect to the center of mass position. It has the form of that for a point particle (see equation (10.14a)).
- **STRAINS:** The second contribution is proportional to fluid deformations studied in Section 15.3.5. At each point of the fluid, deformations are measured by the rate of strain tensor,

\mathbb{S}_{qp} . A rigid body moves by uniform translations and/or solid-body rotations, with the rate of strain tensor vanishing for rigid body motions (see Section 34.5). The contribution from strains is weighted by an integral of deviations of parcel position from the center of mass position. A closed form expression for this integral is available only for special shapes.

- **VORTICITY:** The third contribution to angular momentum (34.71c) contains the vorticity as weighted by the moment of inertia tensor

$$I_{ms} \equiv \int_{\mathcal{R}(\mathbf{v})} (\mathbf{x}' \cdot \mathbf{x}' \delta_{ms} - x'_m x'_s) \rho dV. \quad (34.72)$$

Since the material region is evolving and is not rigid, the moment of inertia tensor is time dependent. Even so, the contribution

$$L_m^{\text{vorticity}} \equiv \frac{1}{2} I_{ms} \omega_s \quad (34.73)$$

has the same form as angular momentum for a rigid body, with one-half the vorticity playing the role of angular velocity (see equation (10.14c) for the point particle expression). Fluid vorticity hence contributes to angular momentum for a material region via its product with the moment of inertia tensor.

34.8.5 Comments and further reading

Angular momentum is computed relative to a chosen origin, whereas vorticity is an intrinsic property measuring the spin of the fluid at a point. So although they both offer measures of the rotational properties of fluid motion, they are distinct when the fluid experiences a nonzero rate of strain. It is only for the special case of a solid-body motion that the rate of strain vanishes, in which case the angular momentum of a fluid region is directly related to vorticity.

Further discussion of the material in this section can be found in [Chatwin \(1973\)](#), Section 2.3.1 of [Davidson \(2015\)](#), and the online notes “The Vorticity Equation and Conservation of Angular Momentum” from A.J. DeCaria.



34.9 Exercises

EXERCISE 34.1: VORTICITY FOR SOLID-BODY ROTATION

Show that a fluid in solid-body rotation with angular velocity

$$\mathbf{v}_{\text{solid-body}} = \boldsymbol{\Omega} \times \mathbf{x}, \quad (34.74)$$

has a vorticity given by

$$\nabla \times \mathbf{v}_{\text{solid-body}} = 2 \boldsymbol{\Omega}. \quad (34.75)$$

EXERCISE 34.2: PLANETARY ROTATION IS NON-DIVERGENT

Show that a fluid in solid-body rotation with angular velocity

$$\mathbf{v}_{\text{solid-body}} = \boldsymbol{\Omega} \times \mathbf{x}, \quad (34.76)$$

has zero divergence

$$\nabla \cdot \mathbf{v}_{\text{solid-body}} = 0. \quad (34.77)$$

Consequently, rotation of the planet imparts zero divergence to fluid motion. We make use of this result in part to justify our study of non-rotating fluid kinematics in Part III of this book.

EXERCISE 34.3: VELOCITY POTENTIAL FOR THE FREE VORTEX

What is the velocity potential (34.14) for the free vortex whose velocity field is given by (34.21)?

Hint: The problem is two-dimensional and rotationally symmetric, so it is convenient to make use of polar coordinates $x = r \cos \vartheta$ and $y = r \sin \vartheta$ as in Appendix 9.3.

EXERCISE 34.4: STRAIN TENSOR FOR THE FREE VORTEX

Determine all components to the strain tensor

$$S_{pq} = \begin{bmatrix} S_{11} & S_{12} \\ S_{21} & S_{22} \end{bmatrix} = \begin{bmatrix} \frac{\partial u}{\partial x} & \frac{1}{2} \left[\frac{\partial u}{\partial y} + \frac{\partial v}{\partial x} \right] \\ \frac{1}{2} \left[\frac{\partial v}{\partial x} + \frac{\partial u}{\partial y} \right] & \frac{\partial v}{\partial y} \end{bmatrix} \quad (34.78)$$

for the free vortex as specified by the velocity field (34.21). Present the answer in the form of a 2×2 matrix.

EXERCISE 34.5: VANISHING VISCOSIVE FRICTION FOR SOLID-BODY MOTION

As discussed in Section 22.8.6, viscous effects from molecular viscosity in an incompressible fluid appear in the momentum equation as a Laplacian weighted by a constant molecular viscosity

$$\text{viscous force per mass} = \nu \nabla^2 \mathbf{v}, \quad (34.79)$$

where $\nu > 0$ is the molecular kinematic viscosity, which is a constant that is a property of the fluid. Show that the viscous operator vanishes for a fluid in solid-body rotation. That is, solid-body motion engenders no frictional dissipation. This result reflects the lack of frictional interaction in a strain-free fluid flow.

EXERCISE 34.6: VORTICITY FOR A C-GRID NUMERICAL MODEL

Vorticity is commonly diagnosed in numerical model simulations. In this exercise we consider how one might determine a discrete equation for the vertical vorticity when the horizontal velocity is arranged according to the Arakawa C-grid ([Arakawa and Lamb, 1977](#)) commonly used in ocean models, and as depicted in Figure 34.12. Derive an expression for the area averaged vorticity over the shaded grid cell region centered at the vorticity point, $q_{i,j}$. Make use of Stokes' theorem with the surrounding C-grid velocity components and the corresponding grid distances.



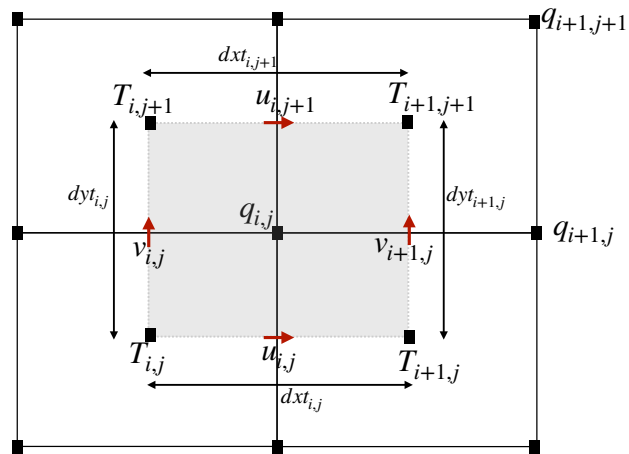


FIGURE 34.12: Layout for velocity on a discrete Arakawa C-grid for use in Exercise 34.6. The central T-point is labeled $T_{i,j}$ and its corresponding vorticity point, $q_{i,j}$, is located to its northeast. This exercise aims to determine the area averaged vorticity for the shaded region. The zonal velocity, $u_{i,j}$, is arranged on the east face of the T-cell, whereas the meridional velocity, $v_{i,j}$, is on the north face. The zonal and meridional grid distances are indicated, thus measuring distances between adjacent tracer points and so measuring the sides of the shaded region.

Chapter 35

NON-DIVERGENT BAROTROPIC FLOW

A single layer of homogeneous shallow water fluid is among the simplest conceptual models available for the study of fluid motion. In the language of vorticity as described in Chapter 37, a shallow water layer is a barotropic fluid since it has zero baroclinicity (Section 37.4). Consequently, the shallow water model is often referred to as a divergent barotropic model, with divergence referring to the nonzero divergence of the horizontal velocity that occurs when the layer thickness varies.

For some geophysical studies, we are interested in the low frequency vortical (Rossby wave) motions rather than the divergent and higher frequency gravity wave motions (Section 48.5). The *non-divergent barotropic model* focuses on vortical motion by assuming the horizontal velocity has zero divergence. We here study the non-divergent barotropic model with a flat free surface (i.e., rigid lid). For this flow the vertical fluid columns have a fixed thickness, which contrasts to the extensible columns in the shallow water model. To remain flat, the free surface feels an externally imposed *lid pressure*, with the lid pressure in turn generating motion. We study the variety of sources for this pressure associated with flow processes active in the non-divergent model, thus rendering an understanding of how pressure forces activate the flow.

For many purposes, we do not need to compute the lid pressure since the relative vorticity is the primary dynamical field, with knowledge of the vorticity sufficient to determine the streamfunction and the velocity. Furthermore, the absolute vorticity is materially invariant in the absence of irreversible processes such as friction. Hence, meridional motion of the fluid parcel is associated with an exchange of vorticity between the fluid and the rotating reference frame. This exchange provides a key constraint on the flow, and we consider some case studies to illustrate how this constraint affects motion. In particular, this constraint, in its linearized form, provides the physical mechanism for Rossby waves (Section 47.3).

CHAPTER GUIDE

We here develop some properties of the non-divergent barotropic model, and use this model to exemplify basic features of geophysical flows constrained by conservation of absolute vorticity. The model served as the basis for the pioneering numerical weather prediction model described by [Charney et al. \(1950\)](#), and it has become a valued theoretical model for large-scale dynamics. It is also useful for studies of coherent vortex structures, with Chapter 3 of [McWilliams \(2006\)](#) exploring analytical vortex solutions. We return to this model in Sections 47.2 and 47.3 when studying Rossby waves.

Since all fields in this chapter are a spatial function only of the horizontal position, the vector gradient operator is itself two-dimensional; e.g., $\nabla\psi = \nabla_z\psi$. Furthermore, we retain the use of Cartesian coordinates here, with extensions to general coordinates following the tensor analysis methods from Chapter 8.

35.1	Loose threads	864
35.2	Basic equations and their properties	864
35.2.1	Velocity equation	865
35.2.2	Kinematics of rigid fluid columns	865
35.2.3	Vertical velocity	866
35.2.4	Velocity self-advection and the kinetic stress tensor	867
35.2.5	Further reading	868
35.3	Vorticity	868
35.3.1	Vorticity equation	868
35.3.2	Absolute vorticity is the potential vorticity	869
35.3.3	Jacobian forms of vorticity advection	870
35.3.4	Taylor-Bretherton identity	870
35.3.5	Poisson equation for the streamfunction	871
35.3.6	Zonal flow as an exact geostrophic solution	871
35.4	Connection to equivalent barotropic flow	872
35.4.1	Vorticity equation for the depth averaged flow	872
35.4.2	Comments	873
35.5	The externally applied lid pressure	873
35.5.1	Poisson equation for pressure	873
35.5.2	Gradient wind balance	874
35.5.3	Pressure source from self-advection	875
35.5.4	Pressure source from solid-body flow	875
35.5.5	Pressure source from irrotational flow	877
35.5.6	Pressure source from Coriolis acceleration	877
35.5.7	Pressure source from friction	878
35.5.8	Comments and further study	878
35.6	Constraints from absolute vorticity invariance	879
35.6.1	Relative vorticity from curvature and planetary beta	879
35.6.2	Relative vorticity from curvature and normal shears	880
35.6.3	Curvature, shear, and planetary contributions	881
35.6.4	Beta drift	882
35.6.5	Understanding and prediction	884
35.7	Exercises	884

35.1 Loose threads

- NATT

35.2 Basic equations and their properties

The non-divergent barotropic model arises from the following assumptions.

- The flow occurs in a single homogeneous fluid layer, as for the shallow water model from Chapter 32.
- The horizontal velocity is non-divergent: $\nabla \cdot \mathbf{u} = \partial_x u + \partial_y v = 0$, which means that the thickness of the layer is time independent.

The second property provides some rather strict constraints on the flow relative to flow in the horizontally divergent shallow water layer. In this section we exhibit the governing equations and derive some of their properties.

35.2.1 Velocity equation

The velocity equation for the non-divergent barotropic model follows in a manner akin to the shallow water model from Chapter 32. Namely, the fluid is a homogeneous (uniform and constant density) layer so that the horizontal velocity satisfies

$$\frac{D\mathbf{u}}{Dt} + f \hat{\mathbf{z}} \times \mathbf{u} = -\nabla \varphi \quad \text{and} \quad \nabla \cdot \mathbf{u} = 0, \quad (35.1)$$

where the pressure is normalized according to

$$\varphi = p/\rho \quad (35.2)$$

with ρ the constant layer density, and where material evolution occurs with the two-dimensional non-divergent flow

$$\frac{D}{Dt} = \frac{\partial}{\partial t} + \mathbf{u} \cdot \nabla. \quad (35.3)$$

All fields are depth independent and there is no vertical motion, so that the flow occurs in rigid fluid columns. We can make use of the vector identity (2.38)

$$(\mathbf{u} \cdot \nabla) \mathbf{u} = \zeta \hat{\mathbf{z}} \times \mathbf{u} + \nabla(\mathbf{u}^2/2), \quad (35.4)$$

so that the velocity equation (35.1) can be written in its vector-invariant form

$$\partial_t \mathbf{u} + (f + \zeta) \hat{\mathbf{z}} \times \mathbf{u} = -\nabla(\varphi + \mathbf{u} \cdot \mathbf{u}/2). \quad (35.5)$$

The horizontal non-divergent flow can be described by a streamfunction

$$\mathbf{u} = \hat{\mathbf{z}} \times \nabla \psi \implies u = -\partial_y \psi \quad \text{and} \quad v = \partial_x \psi. \quad (35.6)$$

Making use of the identities

$$\nabla \psi = -\hat{\mathbf{z}} \times \mathbf{u} \implies \mathbf{u} \cdot \nabla \psi = 0 \quad (35.7)$$

brings the vector-invariant velocity equation (35.5) into the form

$$\partial_t \mathbf{u} - (f + \zeta) \nabla \psi = -\nabla(\varphi + \mathbf{u} \cdot \mathbf{u}/2), \quad (35.8)$$

and then quickly yields the kinetic energy equation

$$(\partial_t + \mathbf{u} \cdot \nabla) \mathcal{K} = -\mathbf{u} \cdot \nabla \varphi, \quad (35.9)$$

where we introduced the kinetic energy per mass

$$\mathcal{K} = \mathbf{u} \cdot \mathbf{u}/2 = (u^2 + v^2)/2. \quad (35.10)$$

35.2.2 Kinematics of rigid fluid columns

Recall the thickness equation (32.20) for a shallow water layer

$$\frac{Dh}{Dt} = -h \nabla \cdot \mathbf{u}, \quad (35.11)$$

where $h = \eta - \eta_b$ is the column thickness, $z = \eta(x, y, t)$ is the upper layer interface (the free surface), and $z = \eta_b(x, y)$ is the lower interface (the bottom topography) (see Figure 32.1). With

zero divergence in the horizontal velocity, the thickness of a fluid column is constant when moving with the horizontal flow

$$(\partial_t + \mathbf{u} \cdot \nabla) h = \partial_t(\eta - \eta_b) + \mathbf{u} \cdot \nabla(\eta - \eta_b) = 0. \quad (35.12)$$

We choose to satisfy this equation by setting the upper surface to be static and flat

$$\eta = 0, \quad (35.13)$$

and furthermore by constraining the horizontal flow to follow the bottom topography

$$\mathbf{u} \cdot \nabla \eta_b = (\nabla \psi \times \nabla \eta_b) \cdot \hat{\mathbf{z}} = 0. \quad (35.14)$$

As formulated, we study horizontally non-divergent flow within a homogeneous fluid layer, for which a fluid column does not expand or contract, thus constraining the flow to move along lines of constant topography.

For the case of a flat bottom domain that is bounded on its side by a vertical wall, then the no-flow boundary condition takes the form

$$\mathbf{u} \cdot \hat{\mathbf{n}} = (\hat{\mathbf{z}} \times \nabla \psi) \cdot \hat{\mathbf{n}} = \hat{\mathbf{t}} \cdot \nabla \psi = 0, \quad (35.15)$$

where $\hat{\mathbf{n}}$ is the horizontal outward unit vector at the boundary, and $\hat{\mathbf{t}} = \hat{\mathbf{n}} \times \hat{\mathbf{z}}$ is the unit tangent vector along the boundary. The kinematic condition (35.15) means that the streamfunction is a constant along the solid vertical sidewall boundary. We encountered this boundary condition in Section 18.3.2 when studying two-dimensional non-divergent flow. A zonally reentrant channel is an example considered in Section 47.3 when introducing Rossby waves, whereby ψ is a constant along the northern and southern walls.

35.2.3 Vertical velocity

Vanishing vertical velocity

Without horizontal divergence and with a flat free surface ($\eta = 0$), there is identically zero vertical motion within the layer

$$w = 0. \quad (35.16)$$

Another manner to deduce this property is by noting that the surface kinematic boundary condition for a static and flat free surface leads to

$$w(\eta) = \partial_t \eta + \mathbf{u} \cdot \nabla \eta = 0 + 0, \quad (35.17)$$

so that the vertical velocity at $z = \eta = 0$ vanishes. With $w(0) = 0$, and with $\nabla \cdot \mathbf{u} = 0$ for the horizontal velocity, then $w = 0$ throughout the layer. Correspondingly, this constraint means that the no-normal flow bottom kinematic condition (Section 16.4.1) renders a horizontal velocity that is aligned with the topography, $\mathbf{u} \cdot \nabla \eta_b = 0$, which is a property we already encountered in Section 35.2.2. Since the vertical velocity is zero, the gravitational potential energy is a uniform constant, so that the mechanical energy arises just from kinetic energy.

What about a non-vanishing vertical velocity?

In Section 35.2.2 we chose to satisfy the thickness equation kinematics by setting $\partial_t \eta = \nabla \eta = 0$, in which case the vertical velocity vanishes so long as the horizontal flow follows the bottom

topography. However, a static and flat upper boundary is a sufficient condition but it is not necessary.

Another approach to satisfying the thickness equation (35.12) is to consider a static yet non-flat free surface ($\eta \neq 0$) with horizontal flow constrained so that

$$\mathbf{u} \cdot \nabla(\eta - \eta_b) = 0. \quad (35.18)$$

The surface and bottom kinematic boundary conditions then result in a vertical velocity at the surface and bottom

$$w(\eta) = -\mathbf{u} \cdot \nabla \eta \quad \text{and} \quad w(\eta_b) = -\mathbf{u} \cdot \nabla \eta_b. \quad (35.19)$$

Now these two boundary velocities are equal, thus satisfying $\partial_z w = 0$. If the bottom topography is flat, $\nabla \eta_b = 0$, then $w(\eta_b) = w(\eta) = 0$, in which case $\nabla \eta = 0$, so that the upper surface is flat. If the bottom is not flat, then the kinematic constraints lead to

$$\nabla \eta = \nabla \eta_b, \quad (35.20)$$

so that the upper surface slope equals to the slope of the bottom topography. In the ocean, it is generally the case that the upper ocean surface undulations are far less than the bottom topography. Hence, $\nabla \eta = \nabla \eta_b$ is not generally a realistic behavior, though one may study this case particularly with weakly sloping bottom topography.

For the remainder of this chapter we follow the conventional approach whereby $w = 0$. Hence, the upper boundary is static and flat, and we set $\eta = 0$. In the presence of a non-flat bottom, then the horizontal flow follows lines of constant bottom topography, $\mathbf{u} \cdot \nabla \eta_b = 0$.

35.2.4 Velocity self-advection and the kinetic stress tensor

The velocity self-advection appearing in the velocity equation (35.1) can be written as the divergence of a 2×2 symmetric tensor

$$-(\mathbf{u} \cdot \nabla) \mathbf{u} = \nabla \cdot \mathbb{E} \iff -u_m \partial_m u_n = \partial_m \mathbb{E}_{mn}, \quad (35.21)$$

where

$$\mathbb{E} = \begin{bmatrix} -u^2 & -uv \\ -uv & -v^2 \end{bmatrix}, \quad (35.22)$$

thus bringing the momentum equation (35.1) to the Eulerian form

$$\partial_t \mathbf{u} + f \hat{\mathbf{z}} \times \mathbf{u} = -\nabla \varphi + \nabla \cdot \mathbb{E}. \quad (35.23)$$

The tensor,

$$\rho \mathbb{E} = -\rho \mathbf{u} \otimes \mathbf{u} \quad (35.24)$$

is the *kinetic stress tensor*, whose three-dimensional form was introduced in Section 22.6.

In anticipation of our study of vorticity in Section 35.3, we find it useful to decompose the kinetic stress tensor into its horizontally isotropic and horizontally anisotropic components¹

$$\mathbb{E} = \begin{bmatrix} -u^2 & -uv \\ -uv & -v^2 \end{bmatrix} = -\mathcal{K} \begin{bmatrix} 1 & 0 \\ 0 & 1 \end{bmatrix} + \begin{bmatrix} -(u^2 - v^2)/2 & -uv \\ -uv & (u^2 - v^2)/2 \end{bmatrix} \equiv -\mathcal{K} \mathbb{I} + \mathbb{F}, \quad (35.25)$$

where we introduced the kinetic energy per mass according to equation (35.10), as well as the

¹Recall our discussion of isotropy in Section 1.8.

trace-free anisotropic portion of the kinetic stress tensor

$$\mathbb{F} = \mathcal{K} \mathbb{I} + \mathbb{E} = \begin{bmatrix} -(u^2 - v^2)/2 & -uv \\ -uv & (u^2 - v^2)/2 \end{bmatrix} \iff \mathbb{F}_{mn} = \mathcal{K} \delta_{mn} - u_m u_n. \quad (35.26)$$

Making use of the decomposition (35.25) brings the velocity equation (35.27) to the form

$$\partial_t \mathbf{u} + f \hat{\mathbf{z}} \times \mathbf{u} = \nabla \cdot [\mathbb{F} - \mathbb{I}(\mathcal{K} + \varphi)]. \quad (35.27)$$

Comparing to the vector-invariant velocity equation (35.5) allows us to infer the identity

$$\nabla \cdot \mathbb{F} = -\zeta (\hat{\mathbf{z}} \times \mathbf{u}). \quad (35.28)$$

We provide an explicit derivation of this identity in Exercise (35.1).

35.2.5 Further reading

As discussed by [Hoskins et al. \(1983\)](#), [Waterman and Hoskins \(2013\)](#) and [Waterman and Lilly \(2015\)](#), the decomposition (35.25) is useful for developing a geometric interpretation of eddying flow features.

35.3 Vorticity

For the two-dimensional non-divergent flow with a vanishing vertical velocity, the vertical component of the relative vorticity is the only nonzero vorticity component, and it is given by the Laplacian of the streamfunction

$$\zeta = \hat{\mathbf{z}} \cdot (\nabla \times \mathbf{u}) = \partial_x v - \partial_y u = \nabla^2 \psi. \quad (35.29)$$

We here derive basic features of the vorticity for this fluid on the β -plane whereby the Coriolis parameter is

$$f = f_0 + \beta (y - y_0). \quad (35.30)$$

35.3.1 Vorticity equation

To form the dynamical equation for the vorticity, take the zonal derivative of the meridional momentum equation (see equation (35.1)) and meridional derivative of the zonal momentum equation

$$\frac{\partial}{\partial t} \left(\frac{\partial v}{\partial x} - \frac{\partial u}{\partial y} \right) + \frac{\partial}{\partial x} [\nabla \cdot (\mathbf{u} v)] - \frac{\partial}{\partial y} [\nabla \cdot (\mathbf{u} u)] + f \nabla \cdot \mathbf{u} + \beta v = 0. \quad (35.31)$$

Notice how the pressure gradient dropped out since there is zero baroclinicity for a barotropic flow (see Section 37.4 for a discussion of baroclinicity). We now make use of the identity

$$\frac{\partial}{\partial x} [\nabla \cdot (\mathbf{u} v)] - \frac{\partial}{\partial y} [\nabla \cdot (\mathbf{u} u)] = \frac{\partial \mathbf{u}}{\partial x} \cdot \nabla v - \frac{\partial \mathbf{u}}{\partial y} \cdot \nabla u + \mathbf{u} \cdot \nabla \zeta = \mathbf{u} \cdot \nabla \zeta, \quad (35.32)$$

where we used the non-divergence condition, $\partial_x u + \partial_y v = 0$, to write

$$\frac{\partial \mathbf{u}}{\partial x} \cdot \nabla v - \frac{\partial \mathbf{u}}{\partial y} \cdot \nabla u = \frac{\partial u}{\partial x} \frac{\partial v}{\partial x} + \frac{\partial v}{\partial x} \frac{\partial v}{\partial y} - \frac{\partial u}{\partial y} \frac{\partial u}{\partial x} - \frac{\partial v}{\partial y} \frac{\partial u}{\partial y} \quad (35.33a)$$

$$= -\frac{\partial v}{\partial y} \frac{\partial v}{\partial x} + \frac{\partial v}{\partial x} \frac{\partial v}{\partial y} + \frac{\partial u}{\partial y} \frac{\partial v}{\partial y} - \frac{\partial v}{\partial y} \frac{\partial u}{\partial y} \quad (35.33b)$$

$$= 0. \quad (35.33c)$$

We are thus led to the vorticity equation

$$\frac{\partial \zeta}{\partial t} + \nabla \cdot (\mathbf{u} \zeta) = -\beta v \quad \text{and} \quad \frac{D\zeta}{Dt} = -\beta v. \quad (35.34)$$

Hence, the material evolution of relative vorticity in the non-divergent barotropic fluid is only affected by meridional advection of planetary vorticity. Since $\beta > 0$ over the globe, northward flow ($v > 0$) produces a negative source (clockwise tendency) for relative vorticity following a fluid parcel. This source term is the *beta effect* that we study in Section 37.6.

35.3.2 Absolute vorticity is the potential vorticity

Since f is time independent, we can write the vorticity equation (35.34) in the form

$$(\partial_t + \mathbf{u} \cdot \nabla) \zeta_a = 0, \quad (35.35)$$

where

$$\zeta_a = \zeta + f \quad (35.36)$$

is the vertical component of the absolute vorticity. Hence, there is no stretching or tilting of fluid columns in the non-divergent barotropic fluid. Again, we conceive of the flow as that of rigid fluid columns of constant thickness. Furthermore, the material conservation of ζ_a allows us to identify the potential vorticity with the absolute vorticity for the non-divergent barotropic fluid

$$q = \zeta_a = \zeta + f \implies (\partial_t + \mathbf{u} \cdot \nabla) q = 0 \implies Dq/Dt = 0. \quad (35.37)$$

We return to this connection in equation (38.24), showing that the absolute vorticity is indeed the Ertel potential vorticity for a two-dimensional non-divergent barotropic fluid with $w = 0$.

To maintain a materially constant absolute vorticity requires the relative vorticity to change oppositely to that of the planetary vorticity. For example, in the northern hemisphere, the relative vorticity must decrease ($\zeta \downarrow$) for fluid particles moving northward. This change in the relative vorticity is needed to counteract the increasing planetary vorticity ($f \uparrow$) when moving northward. This result accords with the $-\beta v$ source found in the relative vorticity equation (35.34). Furthermore, it is a reflection of the beta effect studied in Section 37.6.2.

The presence of topography adds further richness to the flow. According to the kinematic boundary condition (35.14), horizontal flow is aligned with isobaths (lines of constant bathymetry or topography). Flow moving along constant isobaths generally crosses latitude lines, and in so doing the relative vorticity must change precisely to maintain $f + \zeta$ materially constant.

35.3.3 Jacobian forms of vorticity advection

In some contexts it is convenient to write the advection operator acting on relative vorticity as

$$\mathbf{u} \cdot \nabla \zeta = u \partial_x \zeta + v \partial_y \zeta \quad (35.38a)$$

$$= -\partial_y \psi \partial_x \zeta + \partial_x \psi \partial_y \zeta \quad (35.38b)$$

$$= \hat{\mathbf{z}} \cdot (\nabla \psi \times \nabla \zeta) \quad (35.38c)$$

$$\equiv J(\psi, \zeta), \quad (35.38d)$$

where J is the Jacobian operator

$$J(A, B) = \hat{\mathbf{z}} \cdot (\nabla A \times \nabla B) = \frac{\partial A}{\partial x} \frac{\partial B}{\partial y} - \frac{\partial A}{\partial y} \frac{\partial B}{\partial x}. \quad (35.39)$$

We can also make use of the Jacobian for the advection of absolute vorticity²

$$\mathbf{u} \cdot \nabla \zeta_a = \hat{\mathbf{z}} \cdot (\nabla \psi \times \nabla \zeta_a) \equiv J(\psi, \zeta + f). \quad (35.40)$$

35.3.4 Taylor-Bretherton identity

An equivalent means to write the vorticity equation is to start from the velocity equation in the form (35.27). Taking the curl and projecting onto the vertical direction then leads to

$$\partial_t \zeta = -\beta v + \hat{\mathbf{z}} \cdot [\nabla \times \nabla \cdot \mathbb{F}]. \quad (35.41)$$

The nonlinear forcing from the anisotropic kinetic stress can be written

$$\hat{\mathbf{z}} \cdot [\nabla \times \nabla \cdot \mathbb{F}] = \hat{\mathbf{z}}_n \epsilon_{npq} \partial_p (\partial_m \mathbb{F}_{mq}) \quad (35.42a)$$

$$= \partial_m \partial_p (\epsilon_{npq} \hat{\mathbf{z}}_n \mathbb{F}_{mq}) \quad (35.42b)$$

$$= -\partial_m \partial_p (\epsilon_{pnq} \hat{\mathbf{z}}_n \mathbb{F}_{qm}) \quad (35.42c)$$

$$= -\partial_m \partial_p (\hat{\mathbf{z}} \times \mathbb{F})_{pm} \quad (35.42d)$$

$$= -\nabla \cdot [\nabla \cdot (\hat{\mathbf{z}} \times \mathbb{F})], \quad (35.42e)$$

where we used symmetry of the anisotropic kinetic tensor, $\mathbb{F}_{mq} = \mathbb{F}_{qm}$.

Taylor-Bretherton identity for relative vorticity

Comparing to the vorticity equation in the form (35.34) reveals the identity

$$\nabla \cdot (\mathbf{u} \zeta) = \nabla \cdot [\nabla \cdot (\hat{\mathbf{z}} \times \mathbb{F})] \implies \mathbf{u} \zeta = \nabla \cdot (\hat{\mathbf{z}} \times \mathbb{F}). \quad (35.43)$$

This equation says that the advective vorticity flux equals to the divergence of the counter-clockwise rotated anisotropic kinetic stress tensor. Equation (35.43) is a special form of the *Taylor-Bretherton identity* that provides a connection between the vorticity flux and the momentum flux. We encounter the shallow water form of this identity Chapter 60 when studying the decomposition of eddy and mean flows.

²The Jacobian operator corresponds to the Poisson bracket used in Hamiltonian mechanics.

Verifying the Taylor-Bretherton identity

The divergence expression on the left hand side of equation (35.43) can be satisfied by $\hat{\mathbf{z}} \times \nabla \Upsilon + \nabla \cdot (\hat{\mathbf{z}} \times \mathbb{F})$, with Υ an arbitrary gauge function. However, $\Upsilon = 0$ is zero for the anisotropic kinetic tensor (35.26), as seen by

$$[\nabla \cdot (\hat{\mathbf{z}} \times \mathbb{F})]_1 = \partial_m (\epsilon_{mnp} \hat{\mathbf{z}}_n \mathbb{F}_{p1}) \quad (35.44a)$$

$$= \epsilon_{m3p} \partial_m \mathbb{F}_{p1} \quad (35.44b)$$

$$= -\epsilon_{3mp} \partial_m \mathbb{F}_{p1} \quad (35.44c)$$

$$= -\epsilon_{312} \partial_1 \mathbb{F}_{21} - \epsilon_{321} \partial_2 \mathbb{F}_{11} \quad (35.44d)$$

$$= -\partial_x \mathbb{F}_{21} + \partial_y \mathbb{F}_{11} \quad (35.44e)$$

$$= \partial_x (u v) + \partial_y (-u^2 + v^2)/2 \quad (35.44f)$$

$$= v \partial_x u + u \partial_x v - u \partial_y u + v \partial_y v \quad (35.44g)$$

$$= u \zeta, \quad (35.44h)$$

and likewise

$$[\nabla \cdot (\hat{\mathbf{z}} \times \mathbb{F})]_2 = \partial_y \mathbb{F}_{12} - \partial_x \mathbb{F}_{22} = v \zeta. \quad (35.45)$$

Taylor-Bretherton identity for potential vorticity

Building from the development for relative vorticity, we can readily connect the potential vorticity flux, $\mathbf{u} q$, to the anisotropic kinetic stress. We do so by considering the two equivalent forms for the potential vorticity equation

$$\frac{\partial q}{\partial t} = -\nabla \cdot (\mathbf{u} q) \quad \text{and} \quad \frac{\partial q}{\partial t} = -\nabla \cdot [\mathbf{u} f + \nabla \cdot (\hat{\mathbf{z}} \times \mathbb{F})]. \quad (35.46)$$

Hence, the Taylor-Bretherton identity for potential vorticity in the two dimensional non-divergent flow is given by

$$\mathbf{u} q = \mathbf{u} f + \nabla \cdot (\hat{\mathbf{z}} \times \mathbb{F}). \quad (35.47)$$

35.3.5 Poisson equation for the streamfunction

Given boundary conditions, the barotropic vorticity equation (35.35) allows us to determine the evolution of vorticity. We can in turn invert the Poisson equation (see Section 3.5 for discussion of the Poisson equation)

$$\nabla^2 \psi = \zeta \quad (35.48)$$

to determine the streamfunction and then the velocity field $\mathbf{u} = \hat{\mathbf{z}} \times \nabla \psi$. This inversion requires information about the boundary conditions for the streamfunction, as discussed in Section 35.2.2. By this method, time integration of the absolute vorticity equation is sufficient to fully specify time evolution of the horizontal velocity. Notably, we do not need to explicitly determine pressure to determine the flow.

35.3.6 Zonal flow as an exact geostrophic solution

An arbitrary zonal velocity with a meridional shear, $\mathbf{u} = U(y) \hat{\mathbf{x}}$, is an exact solution of the perfect fluid non-divergent barotropic model. We see this property by plugging into the velocity equation (35.1) and noting that $D\mathbf{u}/Dt = 0$. Hence, this flow is an exact geostrophic solution whose pressure field is itself also just a function of latitude and whose meridional gradient is

determined by

$$f \hat{z} \times \mathbf{u} = -\nabla \varphi \implies \partial_y \varphi = -f(y) U(y). \quad (35.49)$$

Furthermore, each term in the vorticity equation (35.34) identically vanishes, so that the vorticity

$$\zeta = -\partial_y U \quad (35.50)$$

remains constant in time at each point in space.

35.4 Connection to equivalent barotropic flow

In many cases, flows respecting the quasi-geostrophic assumptions (Section 40.5) possess a vertical profile that can be separated from the horizontal. In this case we write the horizontal velocity as

$$\mathbf{u}(x, y, z, t) = \Gamma(z) \mathbf{u}^{\text{eb}}(x, y, t), \quad (35.51)$$

where $\Gamma > 0$ is a single-signed non-dimensional structure function that has a unit vertical average, $\langle \Gamma \rangle = 1$, when computed over the fluid layer thickness, and where $\mathbf{u}^{\text{eb}}(x, y, t)$ carries the horizontal spatial dependence of the flow. With $\Gamma > 0$, the horizontal flow remains in the same direction throughout the fluid column; i.e., eastward flow at the top of the column remains eastward at the bottom. This orientation of the flow is generally referred to as *equivalent barotropic*.

35.4.1 Vorticity equation for the depth averaged flow

To connect the very particular form (35.51) for the flow with the non-divergent barotropic model, we anticipate a discussion in Section 42.2.2 in which the quasi-geostrophic vorticity equation is shown to be

$$\frac{\partial \zeta_g}{\partial t} + \mathbf{u}_g \cdot \nabla \zeta_g = -\beta \zeta_g + f_0 \frac{\partial w}{\partial z}, \quad (35.52)$$

where \mathbf{u}_g is the horizontally non-divergent geostrophic velocity, and $\zeta_g = \hat{z} \cdot (\nabla \times \mathbf{u}_g)$ is the geostrophic relative vorticity. We see that the quasi-geostrophic vorticity is affected by both the beta-effect and by vertical stretching of fluid columns (the $\partial w / \partial z$ term), whereas vertical stretching is absent from the non-divergent barotropic vorticity equation (35.34). There are occasions in which it is sensible to assume the vertical velocity for a quasi-geostrophic flow vanishes at the top and bottom of the fluid domain, such as when considering flow in the absence of topography. In this case, performing the decomposition (35.51) for the horizontal flow and then taking a vertical average of the quasi-geostrophic vorticity equation (35.52) leads to

$$\frac{\partial \zeta_g^{\text{eb}}}{\partial t} + \langle \Gamma^2 \rangle \mathbf{u}_g^{\text{eb}} \cdot \nabla \zeta_g^{\text{eb}} = -\beta v_g^{\text{eb}}. \quad (35.53)$$

This equation motivates us to define

$$\mathbf{u}^* = \langle \Gamma^2 \rangle \mathbf{u}_g^{\text{eb}} \quad \text{and} \quad \zeta^* = \langle \Gamma^2 \rangle \zeta_g^{\text{eb}}, \quad (35.54)$$

which are the original geostrophic fields, $\mathbf{u}_g(x, y, z, t)$ and $\zeta_g(x, y, z, t)$, when evaluated at a depth where $\Gamma(z^*) = \langle \Gamma^2 \rangle$. The depth, z^* , is known as the *equivalent barotropic depth*. Introduction of the starred fields then brings the vorticity equation (35.53) into the form of the non-divergent barotropic vorticity equation

$$\frac{\partial \zeta^*}{\partial t} + \mathbf{u}^* \cdot \nabla \zeta^* = -\beta v^*. \quad (35.55)$$

35.4.2 Comments

[Charney et al. \(1950\)](#) justified their study of the non-divergent barotropic vorticity model by noting its connection to the commonly observed equivalent barotropic structure of the large-scale middle latitude atmosphere. The equivalent barotropic model has been a very useful analysis and prediction tool for meteorologists, and it formed the basis of many numerical weather prediction models into the 1980s. Section 7.1 of [Haltiner and Williams \(1980\)](#) offers further details on such numerical models.

One hypothesis for why quasi-geostrophic flows tend towards an equivalent barotropic profile relates to movement of energy in rotationally dominant turbulent flows, whereby energy cascades to the larger scales. As discussed in [Smith and Vallis \(2001\)](#) and [Venaille et al. \(2012\)](#), among others, this *inverse* energy cascade pumps mechanical energy into a vertically uniform or “barotropic” structure. In a realistic flow, including topography, stratification, and variable forcing, this cascade is never realized completely, thus rendering a flow that approaches the equivalent barotropic structure.

The case of $f = 0$ with flat bottom is referred to as *two-dimensional turbulence* ([Kraichnan and Montgomery, 1980](#)). This model has a history of key theoretical results that presaged their analog in quasi-geostrophic turbulence. See chapters 11 and 12 of [Vallis \(2017\)](#) for further discussion of this model and its relevance to geostrophic turbulence of the ocean and atmosphere.

35.5 The externally applied lid pressure

As noted in Section 35.3.5, we do not need to determine the lid pressure to determine the evolution of the non-divergent barotropic flow. Instead, we can determine the flow by time stepping vorticity and then inverting the elliptic problem to get the streamfunction. Furthermore, the free surface is absolutely flat even in the presence of topography. Hence, there is no pressure generated by undulations of the free surface. So how is there flow in this model?

As we see in this section, the non-divergent barotropic model maintains a flat *rigid lid* upper surface due to an externally imposed *lid pressure*. In turn, it is the lid pressure that provides the force that drives flow in this model. We here expose details to understand the fundamental, yet somewhat hidden, role for the lid pressure.

To further motivate the analysis, we again emphasize the strong constraints placed on the velocity field, which must satisfy the following conditions at each space and time point

$$\nabla \cdot \mathbf{u} = 0 \quad \text{and} \quad \mathbf{u} \cdot \nabla \eta_b = 0 \quad \text{and} \quad w = 0. \quad (35.56)$$

Kinematics of the constrained flow induce a depth-independent pressure that enforces these constraints. Examining the resulting pressure field furthers our understanding of the forces acting in the fluid. This role for pressure as an enforcer of non-divergence is shared by the three-dimensional non-divergent flow found in a Boussinesq ocean (see Section 26.3). It is simpler to visualize fields in the two dimensional non-divergent barotropic model, thus facilitating understanding and insights that are also useful for the three dimensional case.

35.5.1 Poisson equation for pressure

We derive the pressure equation by using the two-dimensional non-divergence property of the horizontal flow and then developing a diagnostic relation. We can eliminate the time derivative from equation (35.1) by taking $\partial/\partial x$ on the zonal equation and $\partial/\partial y$ on the meridional equation,

then adding. The result is a diagnostic relation for the Laplacian of the pressure³

$$-\nabla^2\varphi = \partial_x[\nabla \cdot (\mathbf{u} u)] + \partial_y[\nabla \cdot (\mathbf{u} v)] - f\zeta + \beta u, \quad (35.57)$$

where we set

$$\nabla \cdot \partial_t \mathbf{u} = \partial_t \nabla \cdot \mathbf{u} = 0 \implies \partial_x(\partial_t u) = -\partial_y(\partial_t v). \quad (35.58)$$

Making use of the boundary conditions discussed in Section 35.2.2, the elliptic partial differential equation (35.57) can be inverted to find the pressure field (Section 3.5). As for the three-dimensional Boussinesq ocean, or for a three-dimensional incompressible fluid, we see that the pressure is instantaneously constrained to satisfy the non-divergence condition placed on the velocity.

Numerically inverting an elliptic operator in equation (35.57) is straightforward on simple domains, such as flat bottom rectangular regions or a smooth sphere. However, when the bottom is not flat, or when there are islands (i.e., the domain is not simply connected), then the elliptic inversion can be numerically difficult to perform. This algorithmic complexity is one reason numerical barotropic models are less commonly used for realistic numerical experimentation than the more general shallow water models. Even so, as pursued in the remainder of this section, we can make use of idealized configurations to garner insight into how pressure maintains the flow constraints.

35.5.2 Gradient wind balance

For two-dimensional non-divergent flow we can write the self-advection in terms of the streamfunction, or equivalently as the Jacobian of the velocity field, through the following manipulations

$$\partial_x[\nabla \cdot (\mathbf{u} u)] + \partial_y[\nabla \cdot (\mathbf{u} v)] = \nabla \cdot (\partial_x \mathbf{u} u) + \nabla \cdot (\mathbf{u} \partial_x u) + \nabla \cdot (\partial_y \mathbf{u} v) + \nabla \cdot (\mathbf{u} \partial_y v) \quad (35.59a)$$

$$= \partial_x \mathbf{u} \cdot \nabla u + \partial_y \mathbf{u} \cdot \nabla v \quad (35.59b)$$

$$= (\partial_x u)^2 + (\partial_y v)^2 + 2 \partial_x v \partial_y u \quad (35.59c)$$

$$= 2[(\partial_x u)^2 + \partial_x v \partial_y u] \quad (35.59d)$$

$$= 2[(\partial_{xy}\psi)^2 - \partial_{xx}\psi \partial_{yy}\psi] \quad (35.59e)$$

$$= 2\hat{\mathbf{z}} \cdot (\partial_x \nabla \psi \times \partial_y \nabla \psi) \quad (35.59f)$$

$$= -2J(\partial_x \psi, \partial_y \psi), \quad (35.59g)$$

$$= 2J(v, u), \quad (35.59h)$$

where we introduced the Jacobian operator from equation (35.34). The pressure equation (35.57) thus takes on the form

$$-\nabla^2\varphi = 2J(u, v) - \nabla \cdot (f \nabla \psi), \quad (35.60)$$

where we also wrote

$$-\nabla \cdot (f \nabla \psi) = -f \nabla^2 \psi - \beta \partial_y \psi = -f \zeta + \beta u. \quad (35.61)$$

We refer to this equation as a *gradient wind balance* in analog to the gradient wind balance discussed in Section 29.6. Here, the Jacobian term accounts for the centrifugal acceleration of the curved fluid motion, and the $\nabla \cdot (f \nabla \psi)$ term accounts for the Coriolis acceleration, both for

³We maintain the minus sign on the left hand side of equation (35.57) so that a positive source on the right hand side leads to a positive φ . We can readily understand the sign by taking a Fourier transform, whereby the Laplacian operator picks up a minus sign when converted to Fourier space. We follow the same sign convention when studying the Green's function for the Poisson equation in Chapter 4.

the f -plane and β -plane. Equation (35.60) thus offers a more accurate diagnostic relation for the pressure field than provided by assuming a geostrophically balanced flow.

35.5.3 Pressure source from self-advection

We here introduce yet another way to examine the self-advection source appearing in the pressure equation (35.57) by writing it as

$$\partial_x[\nabla \cdot (\mathbf{u} u)] + \partial_y[\nabla \cdot (\mathbf{u} v)] = \mathbb{S}_{mn} \mathbb{S}_{mn} - \mathbb{R}_{mn} \mathbb{R}_{mn}, \quad (35.62)$$

where the rate of strain tensor, \mathbb{S} , and rotation tensor, \mathbb{R} , have components given by equations (15.33a) and (15.33b)

$$\mathbb{S}_{mn} = \frac{1}{2} \left[\frac{\partial v_m}{\partial x_n} + \frac{\partial v_n}{\partial x_m} \right] = \mathbb{S}_{nm} \quad \text{rate of strain tensor} \quad (35.63)$$

$$\mathbb{R}_{mn} = \frac{1}{2} \left[\frac{\partial v_m}{\partial x_n} - \frac{\partial v_n}{\partial x_m} \right] = -\mathbb{R}_{nm} \quad \text{rotation tensor.} \quad (35.64)$$

For two-dimensional flow the rotation tensor is related to the relative vorticity via

$$\mathbb{R}_{mn} = -\epsilon_{mn} \zeta / 2 = -\epsilon_{mn} \nabla^2 \psi / 2, \quad (35.65)$$

where ϵ_{mn} is the anti-symmetric Levi-Civita permutation symbol (see Section 1.4.1)

$$\epsilon_{mn} = \begin{bmatrix} \epsilon_{11} & \epsilon_{12} \\ \epsilon_{21} & \epsilon_{22} \end{bmatrix} = \begin{bmatrix} 0 & 1 \\ -1 & 0 \end{bmatrix}, \quad (35.66)$$

which leads to

$$\mathbb{R}_{mn} \mathbb{R}_{mn} = \zeta^2 / 2. \quad (35.67)$$

The identity (35.62) indicates that the squared strain (sometimes referred to as the *splat*) provides a positive source to the Poisson equation (35.57) whereas squared vorticity provides a negative source. Bringing these results together leads us to write the pressure equation as

$$-\nabla^2 \varphi = \mathbb{S}_{mn} \mathbb{S}_{mn} - \zeta^2 / 2 - \nabla \cdot (f \nabla \psi) = 2[(\partial_{xy}\psi)^2 - \partial_{xx}\psi \partial_{yy}\psi] - \nabla \cdot (f \nabla \psi), \quad (35.68)$$

where the second equality made use of equation (35.59e) to write the pressure source fully in terms of the streamfunction.

In the following sections, we present two examples to help support understanding of how pressure gradients arise in a 2d-barotropic flow to maintain, at each time instance, a non-divergent two-dimensional velocity field. For simplicity we just consider the non-rotating case so that it is sufficient to examine how pressure responds to the nonlinear source term $\mathbb{S} \cdot \mathbb{S} - \zeta^2 / 2$.

35.5.4 Pressure source from solid-body flow

Consider a velocity field in a flat domain that is initialized in circular solid-body motion (Figure 35.1)

$$\mathbf{u} = \boldsymbol{\Omega} \times \mathbf{x} = \Omega (-y \hat{\mathbf{x}} + x \hat{\mathbf{y}}), \quad (35.69)$$

where $\boldsymbol{\Omega} = \Omega \hat{\mathbf{z}}$ is a constant angular velocity. This flow has zero strain and non-zero vorticity

$$\hat{\mathbf{z}} \cdot (\nabla \times \mathbf{u}) = \zeta = 2\Omega \implies -\mathbb{R}_{mn} \mathbb{R}_{mn} = -\Omega^2. \quad (35.70)$$

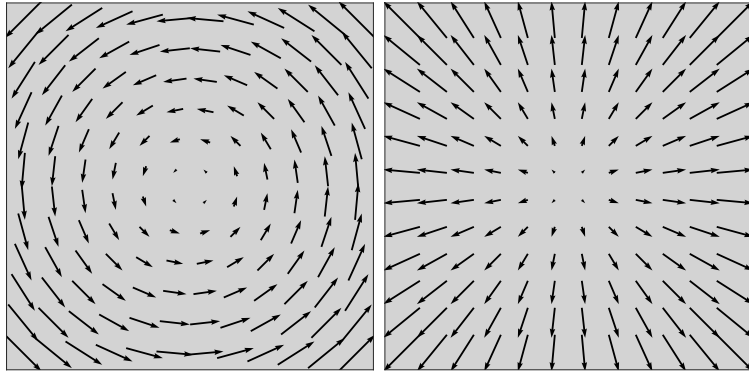


FIGURE 35.1: Left panel: example flow field from solid-body rotation, $\mathbf{u} = \boldsymbol{\Omega} \times \mathbf{x} = (-y, x)$, which has vorticity $\nabla \times \mathbf{u} = 2\boldsymbol{\Omega}$ and zero strain. Right panel: corresponding acceleration from self-advection, $-(\mathbf{u} \cdot \nabla) \mathbf{u} = \boldsymbol{\Omega}^2 \mathbf{x}$. The acceleration from self-advection is exactly compensated by the pressure gradient force: $-(\mathbf{u} \cdot \nabla) \mathbf{u} - \nabla \varphi = 0$, thus allowing for the solid-body motion to be an exact solution to two-dimensional non-divergent flow. The units are arbitrary.

The velocity time tendency from the self-advection acceleration is

$$-(\mathbf{u} \cdot \nabla) \mathbf{u} = \boldsymbol{\Omega}^2 \mathbf{x}, \quad (35.71)$$

which is the outward directed centrifugal acceleration associated with the circular solid-body motion.⁴ The centrifugal acceleration generates a velocity field that diverges from the origin. However, the velocity is constrained to remain non-divergent at each instance, so the centrifugal acceleration cannot be the full story. Indeed, to maintain the non-divergent constraint, a pressure gradient is instantaneously established that exactly counteracts the centrifugal acceleration. Hence, there is a low pressure established at the origin so that the pressure gradient force points inward. This example illustrates how vorticity provides a source of low pressure in a non-divergent flow. Furthermore, since the pressure gradient exactly counteracts the centrifugal acceleration from the velocity self-advection, the solid-body flow is an exact steady solution for the non-divergent and non-rotating barotropic system. This result holds even in the presence of viscosity, since the solid-body flow has no strain and hence it does not support viscous stresses (see Section 22.8).

In the absence of planetary rotation ($f = 0$), the pressure field is found by solving the Poisson equation

$$-\nabla^2 \varphi = -\boldsymbol{\Omega}^2. \quad (35.72)$$

Assuming circular symmetry allows us to let φ be a function just of the radial distance from the origin, in which case the pressure field is parabolic and the pressure gradient acceleration is radial

$$\varphi = (\boldsymbol{\Omega} r)^2 / 2 \quad \text{and} \quad -\nabla \varphi = -\boldsymbol{\Omega}^2 \mathbf{x} = (\mathbf{u} \cdot \nabla) \mathbf{u}. \quad (35.73)$$

To reach this result, we used the cylindrical expression for the Laplacian operator (equation (9.83b)) and set $\varphi(r = 0) = 0$. To help understand the physics of this parabolic pressure field, recall the analysis in Section 24.3 of a solid-body rotating homogeneous fluid layer in a cylindrical tank. In contrast to the barotropic system, the horizontal velocity in a homogeneous fluid layer, such as in a shallow water fluid, is divergent so that the layer thickness is not constrained to remain flat. Hence, the centrifugal acceleration causes the velocity to diverge from the center so

⁴We considered the more general case in Section 29.2.2 when decomposing the material acceleration for two-dimensional flow into natural coordinates.

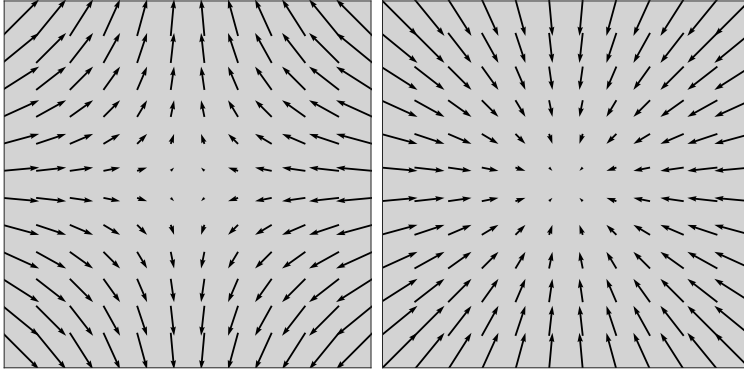


FIGURE 35.2: Left panel: example purely strained flow field with zero vorticity, $\mathbf{u} = \Omega(-x\hat{\mathbf{x}} + y\hat{\mathbf{y}})$. Right panel: corresponding converging acceleration from self-advection, $-(\mathbf{u} \cdot \nabla) \mathbf{u} = -\Omega^2 \mathbf{x}$. The units are arbitrary.

that the layer thickness increases radially outward, with the layer bounded by the tank wall. At steady state, the homogeneous fluid layer has a parabolic free surface with a minimum at the center (see equation (24.80)). The parabolic free surface creates a pressure field that precisely corresponds to the pressure field (35.73) in the non-divergent barotropic system. The adjustment of a homogeneous fluid layer, such as a shallow water fluid, contains linear fluctuations in the form of gravity waves such as discussed in Chapter 33. In contrast, the adjustment required to reach a steady state occurs instantaneously in the non-divergent barotropic fluid.

35.5.5 Pressure source from irrotational flow

Now consider the following pure strain flow (Figure 35.2)

$$\mathbf{u} = \Omega(-x\hat{\mathbf{x}} + y\hat{\mathbf{y}}), \quad (35.74)$$

whose vorticity vanishes and whose self-advection acceleration is given by

$$-(\mathbf{u} \cdot \nabla) \mathbf{u} = -\Omega^2 \mathbf{x} \implies \mathbb{S}_{mn} \mathbb{S}_{mn} = \Omega^2. \quad (35.75)$$

This acceleration is exactly the opposite of that produced by the solid-body motion studied in the previous example. Hence, to maintain the non-divergent nature of the barotropic flow, a pressure (again, assuming $f = 0$) is established with a high pressure at the center that exactly counteracts the converging self-advection acceleration arising in the strained flow

$$\varphi = -(\Omega r)^2/2 \quad \text{and} \quad -\nabla \varphi = \Omega^2 \mathbf{x} = (\mathbf{u} \cdot \nabla) \mathbf{u}. \quad (35.76)$$

This example illustrates how strain provides a source for high pressure in a non-divergent flow. Furthermore, we see that this flow, in the absence of viscosity, is an exact steady solution for non-rotating non-divergent barotropic flow. However, in contrast to the solid-body flow in Section 35.5.4, the purely strained flow (35.74) supports viscous friction, so that this flow does not remain steady in the presence of viscosity.

35.5.6 Pressure source from Coriolis acceleration

In addition to the self-advection source, pressure is affected by a source from the Coriolis acceleration

$$-\nabla^2 \varphi_{\text{geostrophy}} \equiv \nabla \cdot (f \hat{\mathbf{z}} \times \mathbf{u}) = -\nabla \cdot (f \nabla \psi) = \beta u - \zeta f. \quad (35.77)$$

As such, we can write the pressure gradient as⁵

$$-\nabla\varphi_{\text{geostrophy}} = f \hat{\mathbf{z}} \times \mathbf{u}. \quad (35.78)$$

Consider cyclonic flow around an arbitrary point. What is the pressure field induced by this flow? As in our discussion in Section 35.5.4 of the solid body rotating flow, a cyclonic flow has an associated centrifugal acceleration that points outward. To counteract the centrifugal acceleration, and thus to maintain a non-divergent flow, requires an inward pointing pressure force; i.e., a low pressure center. Hence, cyclonic circulation induces, through the Coriolis acceleration, a negative pressure source whereas anti-cyclonic circulation induces a positive pressure source.

35.5.7 Pressure source from friction

Consider flow with friction, in which case the velocity equation (35.1) takes the form

$$\frac{D\mathbf{u}}{Dt} + f \hat{\mathbf{z}} \times \mathbf{u} = -\nabla\varphi + \mathbf{F}, \quad (35.79)$$

with \mathbf{F} a frictional acceleration. In this case we have yet another source for pressure given by

$$-\nabla^2\varphi_{\text{friction}} \equiv -\nabla \cdot \mathbf{F} \implies -\nabla\varphi_{\text{friction}} = -\mathbf{F}. \quad (35.80)$$

As discussed in Section 22.8, viscous friction is generally associated with a nonzero rate of strain. We see that the frictional acceleration induces a high pressure source in regions where frictional accelerations converge, $-\nabla \cdot \mathbf{F} > 0$, with this source acting to maintain non-divergent flow in the presence of converging frictional acceleration.

35.5.8 Comments and further study

- The pressure equation (35.57) is elliptic, and elliptic equations need boundary conditions. In the presence of topography the boundary conditions are modified relative to the flat bottom case. Hence, pressure knows about topography through its boundary conditions. The resulting pressure force keeps the flow non-divergent and the flow aligned with topography as per the kinematic conditions in Section 35.2.2.
- The discussion of pressure induced by self-advection in Sections 35.5.4 and 35.5.5 is based on a similar presentation in Appendix B of *Jeevanjee and Romps (2015a)*.
- *Bryan (1969)* provided the first working numerical algorithm to simulate the ocean general circulation. Bryan's method made use of the rigid lid approximation of Section 35.5 so that the depth integrated velocity is non-divergent. However, the vorticity in Bryan's ocean model is affected by more than just the beta-effect. The reason is that the depth integrated velocity equation includes contributions from baroclinic processes, and such processes affect the barotropic vorticity in a baroclinic fluid. We detail such effects in Sections 41.7 and 41.8.

The rigid lid method was used for large-scale ocean circulation modeling until the late 1990s. Free surface methods, allowing divergence in the depth integrated flow, have largely displaced the rigid lid as a practical method for time stepping ocean models (e.g., see chapter 12 of *Griffies (2004)*).

⁵Formally, we can add an arbitrary gauge function to the right hand side of equation (35.78), with this term of the form $\hat{\mathbf{z}} \times \nabla\chi$. However, since we derived the pressure Poisson equation from the velocity equation, then we know there is no gauge function arising in equation (35.78).

35.6 Constraints from absolute vorticity invariance

We here examine constraints on the flow imposed by material invariance of absolute vorticity, which holds for two-dimensional non-divergent flow when there is no dissipation

$$\frac{D(\zeta + f)}{Dt} = 0. \quad (35.81)$$

These constraints offer insights into the flow behavior and allow us to predict responses to perturbations. Notably, these predictions arise even without direct information about the forces giving rise to the responses. Rather, we deduce the responses based on vorticity constraints rather than force imbalances.

We frame the discussion in terms of the decomposition (34.47) of relative vorticity into a curvature (or orbital) term and normal shear term

$$\zeta = \frac{|\mathbf{u}|}{R} - \frac{\partial |\mathbf{u}|}{\partial n} \equiv \zeta_{\text{curv}} + \zeta_{\text{shear}}, \quad (35.82)$$

so that

$$\frac{D(\zeta_{\text{curv}} + \zeta_{\text{shear}} + f)}{Dt} = 0. \quad (35.83)$$

When the flow turns, the curvature term contributes with R the radius of curvature.⁶ If the flow develops shears in the direction normal to the flow, then the shear term contributes. In the presence of $\beta = \partial_y f$, meridional motion through the planetary vorticity field requires a compensating response from relative vorticity. In general each of the three terms contribute to the relative vorticity, though in the following we consider cases where one is subdominant.

35.6.1 Relative vorticity from curvature and planetary beta

According to the decomposition (35.82), fluid that curves to the left (facing downstream) picks up a positive relative vorticity from flow curvature, $R > 0 \Rightarrow \zeta > 0$, as depicted in Figure 35.3. The oppositely curved flow has a negative radius of curvature so flow curving to the right picks up a negative relative vorticity, $R < 0 \Rightarrow \zeta < 0$. We focus here on the case where the normal shear induced relative vorticity can be neglected so that we are only concerned with curvature induced vorticity plus planetary vorticity (beta effect).

Consider a flow that is initially zonal with zero relative vorticity. If the flow turns meridionally then it experiences a change in relative vorticity both through the curvature term plus a change in planetary vorticity since f changes. To maintain constant absolute vorticity, a fluid column that moves meridionally requires the relative vorticity induced by the curved flow path to counteract the change in planetary vorticity. As we now discuss, the constraint of fixed absolute vorticity, in the absence of induced normal shears, means that eastward flow (westerly winds) cannot turn meridionally while maintaining fixed absolute vorticity, whereas westward flow (easterly winds) can turn (see Figure 35.3).

Consider westward flow in the northern hemisphere ($f > 0$). If the flow turns to the north (to the right facing downstream) then this flow picks up a curvature-induced negative relative vorticity, $\zeta < 0$, and an increase in the planetary vorticity (f increases). Likewise, a westward flowing fluid column that turns equatorward (to the left) has a positive curvature-induced relative vorticity ($\zeta > 0$) and a reduction in planetary vorticity (f decreases). Hence, westward flow in

⁶As discussed in Section 29.2, we take the convention whereby the normal direction is to the left of flow when facing downstream. Flow turning into the normal direction (to the left) has a positive radius of curvature, $R > 0$, and flow turning opposite to the normal direction (to the right) has $R < 0$.

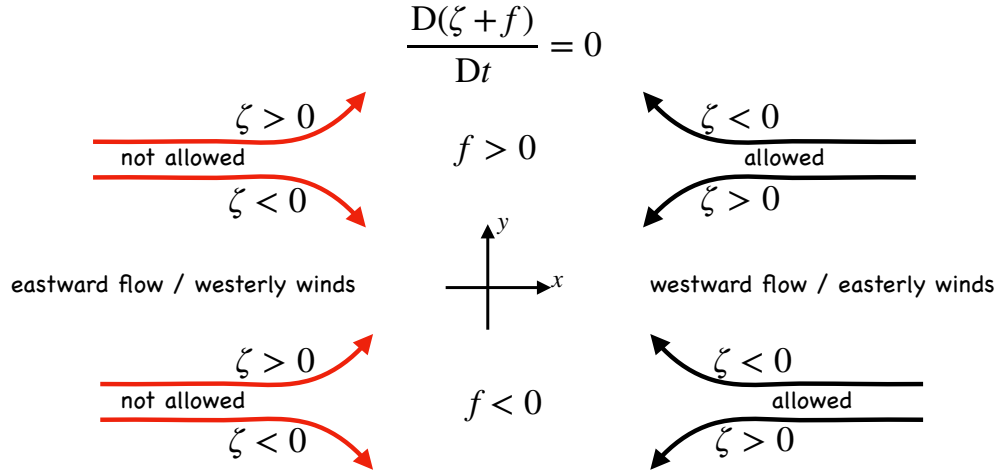


FIGURE 35.3: Illustrating the constraints on a two dimensional non-divergent flow imposed by material invariance of absolute vorticity: $\zeta + f = \text{constant}$. We assume flow is over a flat region and assume there is only curvature induced relative vorticity (no shear-induced relative vorticity; $\partial|\mathbf{u}|/\partial n = 0$) as per the decomposition in equation (35.82). In each of the four cases depicted, the entering flow has zero relative vorticity, which means that absolute vorticity must remain constant at the initial Coriolis parameter, $\zeta + f = f_{\text{initial}}$. The red eastward flow (westerly winds) that turns meridionally picks up a curvature vorticity that supports the change in planetary vorticity, thus precluding material invariance of absolute vorticity. Hence, the meridional turning of eastward flow is not allowed so that flow must remain zonal for absolute vorticity to remain invariant. In contrast, the oppositely directed westward flow (easterly winds) can deviate either to the north or south and still retain a constant absolute vorticity. We illustrate flows for both the northern and southern hemispheres. Note that the allowed westward flow is consistent with the westward phase propagation of Rossby waves as detailed in Section 47.3. This figure is adapted from Figure 4.8 of [Holton \(1992\)](#).

the northern hemisphere can turn either poleward (to the north) or equatorward (to the south) and still maintain constant absolute vorticity, so long as the curved motion induces the proper relative vorticity to counteract the changes to f . The same arguments also hold in the southern hemisphere, so that the general scenarios are depicted in Figure 35.3.

The situation is different for eastward flow. Consider again flow in the northern hemisphere. A poleward (to the left) turning fluid column is associated with a positive curvature-induced relative vorticity, $\zeta > 0$, as well as an increase in the planetary vorticity. Hence, this motion changes the absolute vorticity and as such it is not allowed if the absolute vorticity is constrained to remain constant. Likewise, an equatorward (to the right) turning eastward fluid column induces a negative curvature-induced relative vorticity, $\zeta < 0$, and a decrease in planetary vorticity, again leading to a change in absolute vorticity. Hence, eastward flow (westerly winds) in either hemisphere must remain zonal to maintain a constant absolute vorticity.

As an application of these results, consider the situation depicted in Figure 35.4, whereby inviscid flow in the interior of an ocean domain moves westward into a frictional western boundary layer. The constraints imposed by absolute vorticity invariance allow for this flow to occur, whereas the opposite is disallowed whereby eastward inviscid flow cannot enter an eastern boundary. We return to this example in Section 36.7 when discussing western intensification of ocean gyres.

35.6.2 Relative vorticity from curvature and normal shears

Now consider the case in which the meridional displacements are small so that the beta effect can be neglected. In this case there is an exchange between relative vorticity arising from curvature

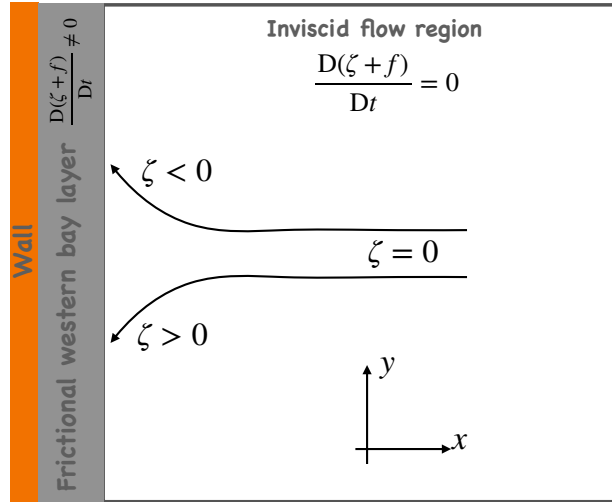


FIGURE 35.4: Illustrating the constraints on a homogeneous and constant thickness fluid layer imposed by material invariance of absolute vorticity: $\zeta + f = \text{constant}$. As per the results from Figure 35.3, inviscid flow with initially zero relative vorticity can enter a western boundary layer as depicted here, whereas it cannot enter an eastern boundary layer. This conclusion assumes that there is no shear-induced relative vorticity ($\partial|\mathbf{u}|/\partial n = 0$) that can overcome changes in the vorticity induced by changes to f and by curvature-induced relative vorticity (see Section 34.7.2). This figure is adapted from Figure 19.12 of [Vallis \(2017\)](#).

and relative vorticity from normal shears, thus leaving their sum materially invariant

$$\frac{D(\zeta_{\text{curv}} + \zeta_{\text{shear}})}{Dt} = 0. \quad (35.84)$$

We depict an example in Figure 35.5 whereby a vortex undergoes a left turn facing downstream. While on the curve, the relative vorticity of the vortex is in part due to the positive curvature vorticity, $\zeta_{\text{curv}} > 0$. If the relative vorticity is positive on the straight portion of the trajectory, then when on the curve the shear vorticity must lose some of its strength in order to compensate for the curvature vorticity. Conversely, if the relative vorticity is negative on the straight portion of the trajectory, then when on the curve the shear vorticity gains in strength to allow for the positive curvature vorticity.

35.6.3 Curvature, shear, and planetary contributions

We now consider all three terms appearing in the vorticity equation (35.83). Let us consider again the eastward flow that turns to the north in the northern hemisphere. Such flow is not allowed if the only source for relative vorticity is curvature. However, if the eastward flow, as it turns, picks up a shear that induces a nonzero negative relative vorticity, then such flow can turn so long as the shear-induced negative relative vorticity balances the positive absolute vorticity from increases in f and the curvature-induced vorticity. Writing this condition for the shear-induced relative vorticity yields

$$\zeta_{\text{shear}} = -\Delta f - \zeta_{\text{curv}} = -(f_{\text{final}} - f_{\text{init}}) - \zeta_{\text{curv}} < 0, \quad (35.85)$$

where f_{init} and f_{final} are the initial and final Coriolis parameters. Conversely, if the flow deviates towards the equator then it can do so only if there is a positive shear-induced relative vorticity

$$\zeta_{\text{shear}} = -(f_{\text{final}} - f_{\text{init}}) - \zeta_{\text{curv}} > 0. \quad (35.86)$$

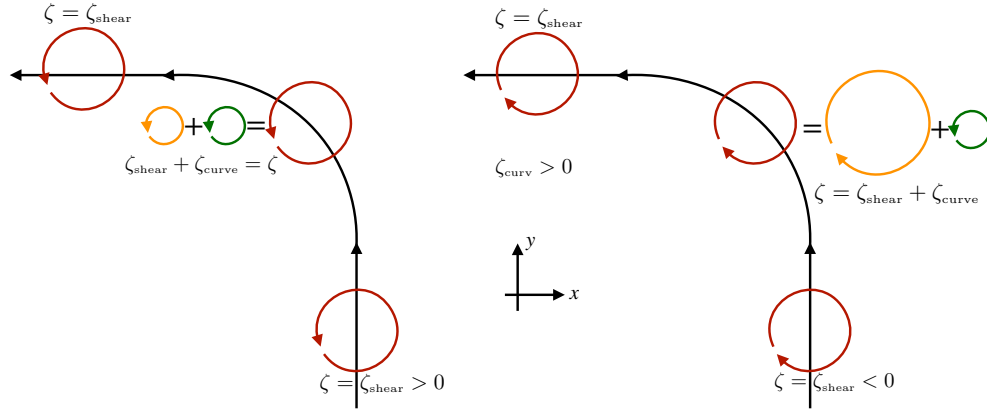


FIGURE 35.5: Material invariance of relative vorticity, $D\zeta/Dt = D(\zeta_{curv} + \zeta_{shear})/Dt = 0$, means that as a vortex moves around a curve its shear vorticity is modified to keep the total relative vorticity invariant. On the straight portion of these trajectories, the relative vorticity is due only to shear vorticity, $\zeta = \zeta_{shear}$ since $\zeta_{curv} = 0$. However, when the vortex enters the curve, maintaining a constant relative vorticity requires an exchange of shear vorticity with the curvature vorticity. In this example we illustrate a steady flow that turns to the left so that the vortex picks up a positive curvature vorticity, $\zeta_{curv} > 0$. Left panel: a vortex that enters the left turn with a positive relative vorticity must give some of its shear vorticity to the curvature vorticity in order to maintain ζ constant along the trajectory. Right panel: a vortex that enters the curve with a negative relative vorticity sees its shear vorticity increase in magnitude to compensate for the positive curvature vorticity.

35.6.4 Beta drift

In Exercise 21.5 we introduced the *Rossby effect* (Rossby, 1948), in which a circular cyclonic vortex experiences an area integrated Coriolis acceleration that is directed poleward, and with the integrated acceleration vanishing on the f -plane. Hence, this poleward drift arises from the beta effect. Following Rossby (1948), we did not consider the pressure field associated with the vortex, so it is unclear whether such a vortex would actually drift due northward. Indeed, subsequent studies showed that motion of an initially circular vortex sets up a secondary flow that renders a poleward+westward *beta drift*; i.e., northwestward in the northern hemisphere and southwestward in the southern hemisphere. As for the other motions considered in this section, we describe the mechanism for beta drift by invoking conservation of absolute vorticity respected by an inviscid non-divergent barotropic flow. This discussion reflects similar ideas encountered when studying Rossby waves in Section 47.3.

Consider a circularly symmetric northern hemisphere cyclonic monopole as shown in Figure 35.6. The monopole flow has positive circulation and thus positive relative vorticity. On an f -plane this circulation is stationary, whereas on the β -plane parcels moving around the monopole pick up anomalous relative vorticity according to the beta effect: $D\zeta/Dt = -\beta v$. On the west side of the monopole, fluid elements are moving southward and thus pick up a positive anomalous relative vorticity ($-\beta v > 0$), whereas on the east side the northward flow picks up a negative relative vorticity anomaly. We note that the material evolution of relative vorticity is also reflected in the local time changes, since for an initially circular monopole, the only contribution to the local evolution is given by the beta effect. We see this property by writing the vorticity equation using polar coordinates (see Section 9.3)

$$\partial_t \zeta = -\beta v - \mathbf{u} \cdot \nabla \zeta = -\beta v - (\dot{r} \partial_r + \dot{\vartheta} \partial_\vartheta) \zeta, \quad (35.87)$$

where r is the radial coordinate and ϑ is the angular coordinate measured counter-clockwise from the x -axis. By assumption, the flow is initially moving only in the angular direction, so that $\dot{r} = 0$. Additionally, the monopole is symmetric in the angular direction, so that $\partial_\vartheta \zeta = 0$. As a

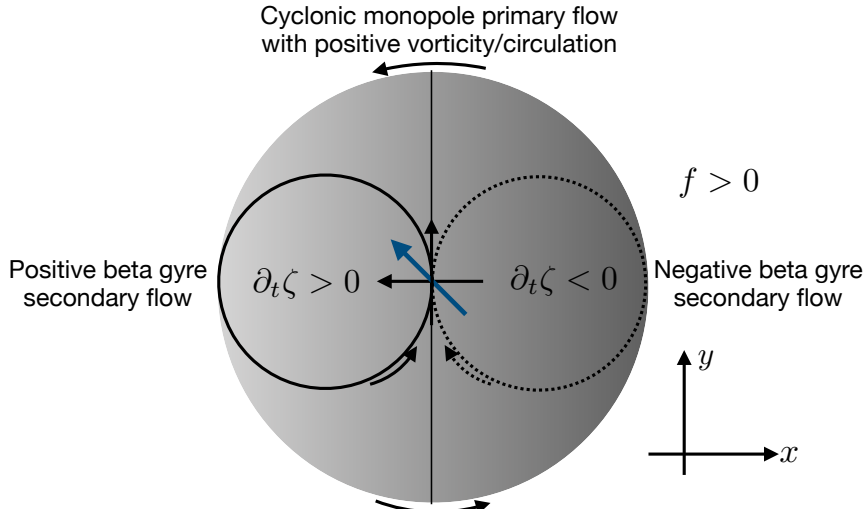


FIGURE 35.6: Schematic cyclonic and circularly symmetric northern hemisphere ($f > 0$) monopole flow in a two-dimensional non-divergent barotropic fluid. The monopole has positive circulation and thus positive relative vorticity. On the β -plane, parcels moving around the monopole pick up anomalous relative vorticity according to the beta effect: $D\zeta/Dt = -\beta v$. On the western side, fluid elements are moving southward and thus pick up a positive relative vorticity anomaly ($-\beta v > 0$), whereas on the eastern side the northward flow picks up a negative relative vorticity anomaly. The beta effect thus induces a westward drift of the monopole maximum, towards where the relative vorticity is increasing. Additionally, the positive anomaly on the western side of the monopole induces a secondary circulation known as a *beta gyre*, with this gyre rotating counter-clockwise, whereas there is an oppositely oriented beta gyre on the eastern side. The secondary circulation from the counter-rotating beta gyres induces a northward drift to the monopole. The combined effect of the westward beta induced drift and the northward drift from the beta gyres leads to a net northwestward *beta drift* for the monopole.

result, $\partial_t \zeta = -\beta v$.

From the above analysis, we see that throughout the western side of the monopole, beta induces a positive anomalous vorticity, whereas beta induces a negative vorticity anomaly throughout the eastern side. When combined with the vorticity from the monopole, we see that the beta induced anomalous vorticity leads to a westward drift of the location for the maximum vorticity; i.e., the monopole maximum drifts to the west. Yet that is not the full story. Additionally, the positive vorticity anomaly on the western side induces a positive gyre-like circulation referred to as a *beta gyre*, whereas the negative vorticity on the eastern side induces a negative beta gyre. The beta gyre circulations are referred to as *secondary circulations* since they arise in response to the anomalies induced by motion through the primary monopole circulation. Furthermore, the counter-rotating beta gyres induce a northward drift of the monopole. The combined westward drift induced by beta acting on the primary monopole circulation, plus the northward drift from the secondary beta gyre circulations, leads to an overall northwestward drift of the monopole. More generally, a cyclonic monopole experiences a poleward and westward beta drift, whereas for anti-cyclonic monopoles the beta drift is equatorward and westward.

The extent to which beta drift is respected by more realistic monopoles depends on many factors, such as the strength and radius of the monopole, strength of the background planetary vorticity gradient, and stability of the monopole. The literature on these topics makes use of numerical models to probe the nonlinearities associated with these relatively strong, and sometimes unstable, flow regimes. Some of the papers are motivated by motion of coherent ocean eddies (e.g., [McWilliams and Flierl, 1979](#); [Carnevale et al., 1991](#)), and others are motivated by motion of atmospheric tropical cyclones (e.g., [Holland, 1983](#); [Smith, 1993](#)). For tropical cyclones born off the coast of Africa in the tropical Atlantic, beta drift gives the cyclones a general tendency to move northwestward toward North America (absent environmental flows that can counteract the

beta drift). More recently, [Gavriel and Kaspi \(2021\)](#) employed these concepts to help understand vortices found in the polar regions of the Jovian atmosphere.

35.6.5 Understanding and prediction

The examples in this section illustrate the power of vorticity constraints for the purpose of predicting flow responses. The power largely rests on our ability to determine flow responses without directly determining forces causing the response. Even so, without determining the forces acting in the fluid, our understanding of the dynamics remains incomplete even if our ability to predict is complete. So when one can determine the forces (it is not always as simple as the examples in Section 35.5), then doing so offers further physical insights into the nature of the flow.



35.7 Exercises

EXERCISE 35.1: VORTICITY IDENTITY IN TWO-DIMENSIONAL BAROTROPIC MODEL

Directly prove the identity (35.28) holding for the two-dimensional non-divergent barotropic model.

EXERCISE 35.2: INTEGRAL PROPERTIES OF THE INVISCID 2D NON-DIVERGENT FLOW

In this exercise, we establish some global conservation properties for inviscid two-dimensional non-divergent flow on a β -plane. Assume the geometry is a flat plane defined over a region, \mathcal{S} , with static material boundary, $\partial\mathcal{S}$. Many of the properties derived here are discussed in Section 3.1 of [McWilliams \(2006\)](#).

- (a) Show that the domain integrated kinetic energy per mass remains constant in time

$$\frac{d}{dt} \int_{\mathcal{S}} \mathcal{K} d\mathcal{S} = \frac{1}{2} \frac{d}{dt} \int_{\mathcal{S}} \mathbf{u} \cdot \mathbf{u} d\mathcal{S} = 0, \quad (35.88)$$

where the horizontal integral extends over the full fluid domain \mathcal{S} .

- (b) Why is the mechanical energy budget only associated with kinetic energy? What about the gravitational potential energy?
- (c) Show that the domain integrated relative vorticity (equal also to the relative circulation) is constant in time

$$\frac{dC}{dt} = \frac{d}{dt} \int_{\mathcal{S}} \zeta d\mathcal{S} = 0. \quad (35.89)$$

- (d) Show that the domain integrated enstrophy is constant in time for f -plane motion ($\beta = 0$)

$$\frac{dZ^{(\zeta)}}{dt} = \frac{d}{dt} \int_{\mathcal{S}} \zeta^2 d\mathcal{S} = 0. \quad (35.90)$$

- (e) Show that the domain integrated potential enstrophy is constant in time even with $\beta \neq 0$

$$\frac{dZ^{(q)}}{dt} = \frac{d}{dt} \int_{\mathcal{S}} q^2 d\mathcal{S} = 0. \quad (35.91)$$

EXERCISE 35.3: ALTERNATIVE EXPRESSION FOR THE GLOBALLY INTEGRATED KINETIC ENERGY
 For a simply connected region, \mathcal{S} , with static material boundary, $\partial\mathcal{S}$, show that the globally integrated kinetic energy per mass can be written

$$\int_{\mathcal{S}} \mathcal{K} d\mathcal{S} = \frac{1}{2} \int_{\mathcal{S}} \mathbf{u} \cdot \mathbf{u} d\mathcal{S} = \frac{1}{2} \int_{\mathcal{S}} \zeta (\psi_b - \psi) d\mathcal{S} = \frac{1}{2} [\psi_b C - \int_{\mathcal{S}} \psi \zeta d\mathcal{S}], \quad (35.92)$$

where $\mathbf{u} = \hat{\mathbf{z}} \times \nabla \psi$ is the horizontally non-divergent velocity, ψ is the streamfunction, ψ_b is the streamfunction on the boundary, and $\zeta = \nabla^2 \psi$ is the vorticity. Hint: recall from Section 18.3.2 that the streamfunction for two-dimensional non-divergent flow is a constant on material boundaries.

EXERCISE 35.4: CIRCULATION IN A 2D BAROTROPIC FLOW

Consider a non-divergent barotropic flow on a β -plane in the presence of a biharmonic friction operator, where the governing vorticity equation is

$$\frac{\partial \zeta}{\partial t} + J(\psi, \zeta + \beta y) = -\nu \nabla^4 \zeta, \quad (35.93)$$

with $\nu > 0$ a constant biharmonic viscosity with dimensions of $L^4 T^{-1}$. Show that the circulation around a fixed material area, \mathcal{S} , in the fluid evolves according to

$$\frac{dC}{dt} = - \oint_{\partial\mathcal{S}} \left[\psi \frac{\partial q}{\partial s} + \nu \frac{\partial(\nabla^2 \zeta)}{\partial n} \right] ds, \quad (35.94)$$

where s is the arc-length along the boundary of the region and n is a coordinate normal to the boundary.

EXERCISE 35.5: KINEMATICS OF VORTICITY GRADIENTS

For many purposes it is of interest to develop equations describing the evolution of scalar gradients. We developed a general expression in Exercise 14.2. Here, we derive a similar equation for the gradient of relative vorticity in a non-divergent barotropic flow. For this purpose, consider the inviscid barotropic vorticity equation on an f -plane

$$\frac{\partial \zeta}{\partial t} + J(\psi, \zeta) = 0. \quad (35.95)$$

- (a) Show that the material evolution of the vorticity gradient is given by

$$\frac{D(\nabla \zeta)}{Dt} = -J(\nabla \psi, \zeta). \quad (35.96)$$

- (b) Show that the material evolution of the squared vorticity gradient is given by

$$\frac{D|\nabla \zeta|^2}{Dt} = 2 J(\zeta, \nabla \psi) \cdot \nabla \zeta. \quad (35.97)$$

EXERCISE 35.6: ANGULAR MOMENTUM FOR BAROTROPIC FLOW IN A BASIN

The exercise derives some equations presented in [Holloway and Rhines \(1991\)](#), who offer a specialized example of the shallow water angular momentum discussed in Section 33.8.

As in Section 33.8.1, the relative angular momentum for a region of fluid is given by

$$\mathbf{L} = \int d\mathcal{S} \int (\mathbf{x} \times \mathbf{v}) \rho dz, \quad (35.98)$$

where \mathbf{x} is the position vector and the relative angular momentum is that due to the motion of the fluid with respect to the solid body. For a barotropic fluid of constant density and constant thickness, and correspondingly a zero vertical velocity, the relative angular momentum reduces to

$$\mathbf{L} = \rho H \int_{\mathcal{S}} (\mathbf{x} \times \mathbf{u}) d\mathcal{S}, \quad (35.99)$$

with \mathbf{u} the horizontal velocity and \mathcal{S} the horizontal region. For barotropic motion on a tangent plane we are interested in the vertical component of the relative angular momentum

$$L^z = \rho H \int_{\mathcal{S}} \hat{\mathbf{z}} \cdot (\mathbf{x} \times \mathbf{u}) d\mathcal{S}. \quad (35.100)$$

Show for a simply connected and bounded region, L^z can be written

$$L^z = 2\rho H \int_{\mathcal{S}} (\psi_b - \psi) d\mathcal{S} \quad (35.101)$$

where ψ is the streamfunction satisfying $\mathbf{u} = \hat{\mathbf{z}} \times \nabla \psi$, and ψ_b is the value of the streamfunction evaluated on the region boundary. Hint: note that $\nabla \cdot \mathbf{x} = 2$ for a horizontal position vector. Also recall from Section 18.3.2 that the streamfunction equals to a spatial constant when evaluated along the domain boundary.

EXERCISE 35.7: STEADY AXIALLY SYMMETRIC FLOW

Consider a two-dimensional non-divergent velocity

$$\mathbf{v} = \hat{\mathbf{z}} \times \nabla \psi. \quad (35.102)$$

Assume the streamfunction is static and depends only on the radial distance from an arbitrary origin,

$$\psi = \psi(r), \quad (35.103)$$

where $r = \sqrt{x^2 + y^2}$, and assume the velocity is a solution to the steady inviscid non-divergent barotropic dynamics on an f -plane.

- (a) Show that the velocity only has an angular component

$$\mathbf{v} = v^\varphi \hat{\boldsymbol{\varphi}}, \quad (35.104)$$

where $\hat{\boldsymbol{\varphi}}$ is the angular unit vector oriented counter-clockwise from the $\hat{\mathbf{x}}$ axis.⁷ Express v^φ in terms of the streamfunction ψ . Hint: see Figure 9.2 and Section 9.3 for a reminder of polar coordinates.

- (b) Write the relative vorticity in terms of the streamfunction using polar coordinates.

- (c) Consider the circulation

$$\mathcal{C} = \oint_{\partial\mathcal{S}} \mathbf{v} \cdot d\mathbf{r}, \quad (35.105)$$

where \mathcal{S} is a circular region in the x - y plane centered at $r = 0$. Express the circulation in terms of v^φ and the radius of the circle.

⁷The azimuthal angular coordinate, φ , that appears in $\mathbf{v} = v^\varphi \hat{\boldsymbol{\varphi}}$, is not the same as the density normalized pressure, $\varphi = p/\rho$, defined by equation (35.2) and used throughout this chapter.

- (d) Write the pressure gradient acceleration in terms of v^φ , f , and r . Hint: remember that $\hat{\varphi}$ is a function of the polar angle φ .
- (e) Interpret the steady balance of accelerations in terms of the balanced dynamics in Chapter 29.
- (f) Why is this axial symmetric solution only valid for an f -plane? Hint: show that if $\beta \neq 0$ that there is an inconsistency in the velocity equation.

EXERCISE 35.8: GALILEAN TRANSFORMATION OF PV ADVECTION AND THE APV METHOD

In Section 14.7 we established the invariance of the material time derivative operator under a Galilean transformation

$$\bar{\mathbf{x}} = \mathbf{x} + \mathbf{U} t \quad \text{and} \quad \bar{\mathbf{u}} = \mathbf{u} + \mathbf{U}, \quad (35.106)$$

where \mathbf{U} is a constant. Here we study the Galilean transformation properties of the non-divergent barotropic model on a β -plane.

- (a) Determine the Galilean transformation properties of the potential vorticity equation (35.37)

$$\frac{\partial q}{\partial t} + \mathbf{u} \cdot \nabla q = \frac{\partial q}{\partial t} + J(\psi, q) = 0, \quad (35.107)$$

where $q = \zeta + f$, $\hat{\mathbf{z}} \times \psi = \mathbf{u}$, and J is the Jacobian operator.

- (b) Determine the Galilean transformation properties of the relative vorticity equation (35.34)

$$\frac{\partial \zeta}{\partial t} + \mathbf{u} \cdot \nabla \cdot \zeta = -\beta v. \quad (35.108)$$

Discuss why there is Galilean invariance *only* for zonal Galilean boosts, $\mathbf{U} = \hat{\mathbf{x}} U$.

- (c) An Euler forward time stepping scheme for the PV equation leads to

$$q^{n+1} = q^n - \Delta t \mathbf{u}^n \cdot \nabla q^n, \quad (35.109)$$

where Δt is the discrete time step and the integer n represents the discrete time label. Inspired by this time discrete expression, [Sadourny and Basdevant \(1985\)](#) proposed the *anticipated potential vorticity* (APV) method for parameterizing subgrid scale processes. The simplest form of APV is given by

$$\frac{\partial q}{\partial t} = -\mathbf{u} \cdot \nabla [q - \tau \mathbf{u} \cdot \nabla q] = -J[\psi, q - \tau J(\psi, q)], \quad (35.110)$$

with τ a constant time scale. From the time discrete expression (35.109), we see that the APV method makes use of an estimate for the future value of PV in computing the advection operator, thus motivating the term “anticipated” in the method’s name.

Show that $\tau \neq 0$ breaks Galilean invariance for the equation (35.110). Provide a discussion of why invariance is broken. Hint: [Vallis and Hua \(1988\)](#) offer a technical reason for why Galilean invariance is broken, making use of the streamfunction and Jacobian form. You do not necessarily need to follow their approach. Rather, it is sufficient to merely note how velocity appears in the APV operator.

EXERCISE 35.9: ELEMENTS OF THE FOFONOFF GYRE

A Fofonoff gyre is an unforced inviscid solution in a flat bottom bounded domain with a rigid lid.

For a single layer of homogeneous fluid with constant thickness, the absolute vorticity is materially invariant, $D(\zeta + f)/Dt = 0$. An explicit solution is derived in Section 19.5.3 of [Vallis \(2017\)](#) for quasi-geostrophic flow using the method of matched asymptotics. We depict elements of a double Fofonoff gyre in Figure 35.7. Provide a narrative for this flow based on material conservation of absolute vorticity. In particular, discuss how the flow enters and leaves the side boundaries and conversely how it leaves and enters the interior region. We are not concerned with how this flow is established. Instead, assume the flow exists and discuss how its existence is consistent with $D(\zeta + f)/Dt = 0$. Hint: recall our discussion of Figure 35.3.

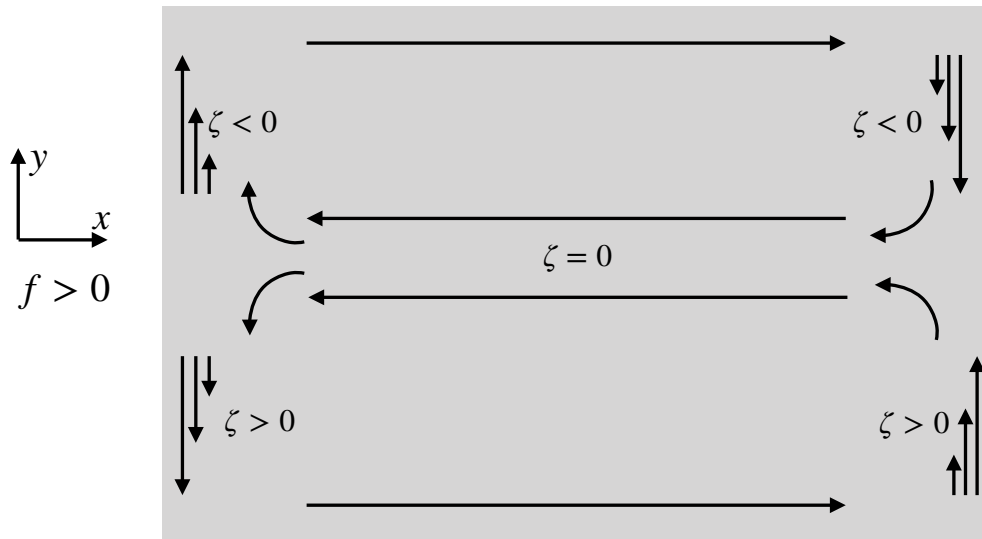


FIGURE 35.7: A Fofonoff gyre is an unforced inviscid flow in a bounded domain where $D(\zeta + f)/Dt = 0$. We here depict elements of this double-gyre flow in the northern hemisphere as part of Exercise 35.9.

EXERCISE 35.10: PRESSURE EQUATION WITH $w \neq 0$

Equation (35.57) or equation (35.60) provide equivalent expressions for the pressure Poisson equation with $\nabla \eta = 0$ and, correspondingly, with $w = 0$. However, in Section 35.2.3 we considered the possibility of $\nabla \eta = \nabla \eta_b$, thus providing a solution with $w \neq 0$. In this case, derive the Poisson equation for pressure as decomposed according to $\varphi = g\eta + \varphi'$.



Chapter 36

SHALLOW WATER VORTICITY AND POTENTIAL VORTICITY

In this chapter we study vorticity and potential vorticity within the shallow water system. We start by deriving the evolution equation for vorticity by taking the curl of the velocity equation. Combining vorticity evolution with mass continuity then renders the evolution equation for potential vorticity. Potential vorticity is a material invariant for inviscid shallow water motion, thus providing a mechanical constraint on the fluid flow. After developing the basic concepts and equations, we consider a variety of flow regimes and case studies, mostly with an ocean focus. These case studies illustrate where the study of vorticity, potential vorticity, and circulation enhances our understanding of geophysical fluid mechanics.

CHAPTER GUIDE

The shallow water fluid offers a fruitful conceptual model to introduce the dynamics of vorticity and potential vorticity while requiring a relatively modest level of mathematical sophistication. Even so, we require vector calculus identities for Cartesian coordinates as detailed in Chapter 2. We also require an understanding of shallow water mechanics from Chapters 32 and 33, as well as the vorticity kinematics introduced in Chapter 34. The concepts and methods developed in this chapter are fundamental to the remaining chapters in this part of the book.

36.1 Shallow water vorticity equation	890
36.1.1 Vorticity equation for a single layer	891
36.1.2 Vorticity equation for N -layers	891
36.1.3 Vorticity flux divergence and curl of nonlinear advection	892
36.2 Potential vorticity for a solid-body rotating cylinder	892
36.2.1 Mass conservation	893
36.2.2 Angular momentum conservation	893
36.2.3 Potential vorticity conservation	894
36.2.4 Connecting angular momentum and vorticity	894
36.2.5 Comments and further study	895
36.3 Shallow water potential vorticity	895
36.3.1 Mass conservation plus the vorticity equation	895
36.3.2 Motivating the name	896
36.3.3 Mass conservation + Kelvin's circulation theorem	897
36.3.4 A fluid column with constant $f \neq 0$	898
36.3.5 Material conservation of an arbitrary function of PV	899
36.3.6 N -layer potential vorticity	900
36.3.7 Further study	900
36.4 Potential vorticity with non-conservative processes	900
36.4.1 Material time evolution of PV	900

36.4.2	The potential vorticity flux	901
36.5	Example implications of PV material invariance	902
36.5.1	Topographic beta effect	902
36.5.2	Planetary geostrophic PV and f/H contours	903
36.5.3	Spin up of converging flow	904
36.5.4	Further study	905
36.6	Circulation with non-conservative processes	905
36.6.1	Circulation around a closed streamline in steady flow	906
36.6.2	Circulation from wind stress and Rayleigh drag	907
36.7	A primer on steady ocean gyres	908
36.7.1	Steady and large-scale vorticity balance	908
36.7.2	Planetary geostrophic flow and the Sverdrup balance	908
36.7.3	Sverdrup flow in a closed domain with anti-cyclonic wind stress	909
36.7.4	Western intensification and the role of beta	909
36.7.5	A role for bottom pressure torques	911
36.7.6	Properties of area integrated bottom pressure torques	914
36.7.7	Advection-diffusion of the steady streamfunction	914
36.7.8	Comments and further study	915
36.8	Free surface patterns in steady ocean gyres	916
36.8.1	Formulating the free surface equation	917
36.8.2	Advecting the free surface	917
36.8.3	Rayleigh drag and free surface diffusion	918
36.9	Column vorticity	919
36.9.1	Formulating the column vorticity equation	920
36.9.2	Summary of the column vorticity equation	921
36.9.3	Steady linear column vorticity balance and the island rule	922
36.9.4	Further study	923
36.10	Exercises	923

36.1 Shallow water vorticity equation

In this section we formulate the vorticity equation for the shallow water fluid, starting with a single layer and then extending to multiple layers. We sometimes make use of the vertical component to the absolute vorticity from equation (32.105)

$$\boldsymbol{\omega}^* = (\zeta + f) \hat{z} = \zeta_a \hat{z} \quad (36.1)$$

which is the sum of the relative vorticity of the horizontal flow, $\boldsymbol{\omega}^* = \zeta \hat{z}$, plus the solid-body vorticity, $f \hat{z}$, due to motion of the rotating reference frame (recall Section 34.5.1). The absolute vorticity appears in the vector-invariant velocity equation (32.110), which is valid for each of the layers in a shallow water fluid

$$\partial_t \mathbf{u} + \boldsymbol{\omega}_a^* \times \mathbf{u} = -\nabla(p/\rho_{\text{ref}} + \mathbf{u} \cdot \mathbf{u}/2). \quad (36.2)$$

This equation forms the starting point for deriving the shallow water vorticity equation.

36.1.1 Vorticity equation for a single layer

We make use of the vector identity from Section 2.3.4 to express the curl of the Magnus acceleration plus Coriolis acceleration in the form

$$\nabla \times (\boldsymbol{\omega}_a^* \times \mathbf{u}) = \boldsymbol{\omega}_a^* (\nabla \cdot \mathbf{u}) + (\mathbf{u} \cdot \nabla) \boldsymbol{\omega}_a^* - \mathbf{u} (\nabla \cdot \boldsymbol{\omega}_a^*) - (\boldsymbol{\omega}_a^* \cdot \nabla) \mathbf{u} \quad (36.3a)$$

$$= \boldsymbol{\omega}_a^* (\nabla \cdot \mathbf{u}) + (\mathbf{u} \cdot \nabla) \boldsymbol{\omega}_a^*, \quad (36.3b)$$

so that

$$\hat{z} \cdot [\nabla \times (\boldsymbol{\omega}_a^* \times \mathbf{u})] = \nabla \cdot (\mathbf{u} \zeta_a) \quad (36.4)$$

Equation (36.3b) required setting

$$\nabla \cdot \boldsymbol{\omega}_a^* = \nabla \cdot \boldsymbol{\omega}^* + \nabla \cdot (f \hat{z}) = 0, \quad (36.5)$$

which follows since this expression involves the divergence of a curl (first right hand side term) and since f has no z dependence. We furthermore set

$$(\boldsymbol{\omega}_a^* \cdot \nabla) \mathbf{u} = |\boldsymbol{\omega}_a^*| \partial_z \mathbf{u} = 0, \quad (36.6)$$

which follows since the horizontal velocity in a shallow water fluid is depth independent within a layer (see Section 32.2).

Applying the operator $\hat{z} \cdot (\nabla \times)$ onto the vector-invariant velocity equation (36.2) annihilates the gradient of pressure and kinetic energy, with the identity (36.4) leading to the Eulerian flux-form evolution equation for absolute vorticity

$$\frac{\partial \zeta_a}{\partial t} + \nabla \cdot (\mathbf{u} \zeta_a) = 0. \quad (36.7)$$

This equation says that the vertical component to the absolute vorticity, ζ_a , at a point in the inviscid shallow water fluid changes according to the horizontal convergence of vorticity advected to that point

$$\frac{\partial \zeta_a}{\partial t} = -\nabla \cdot (\mathbf{u} \zeta_a). \quad (36.8)$$

We can write the vorticity equation (36.7) in the material form

$$\frac{D\zeta_a}{Dt} = -\zeta_a \nabla \cdot \mathbf{u}, \quad (36.9)$$

where the material time derivative for the shallow water fluid is determined just by the horizontal flow

$$\frac{D}{Dt} = \frac{\partial}{\partial t} + \mathbf{u} \cdot \nabla = \frac{\partial}{\partial t} + u \partial_x + v \partial_y. \quad (36.10)$$

The material evolution equation (36.9) means that the absolute vorticity of a shallow water fluid column, moving with the horizontal flow, changes according to the horizontal convergence of the fluid flow as multiplied by the absolute vorticity.

36.1.2 Vorticity equation for N -layers

The previous results for a single layer are readily extended to N -layers, simply because the velocity for layer- k evolves according to equation (36.2), now with a subscript k to denote the layer

$$\partial_t \mathbf{u}_k + (f + \zeta_k) \hat{z} \times \mathbf{u}_k = -\nabla(p_k/\rho_{ref} + \mathbf{u}_k \cdot \mathbf{u}_k/2), \quad (36.11)$$

where $\zeta_k = \hat{z} \cdot (\nabla \times \mathbf{u}_k)$ is the vertical component to the layer-k relative vorticity. Taking the curl and making use of the mathematical identities used for single layer in Section 36.1.1 renders the vorticity equation for layer-k

$$\frac{\partial \zeta_{ak}}{\partial t} + \nabla \cdot (\mathbf{u}_k \zeta_{ak}) = 0 \iff \frac{D_k \zeta_{ak}}{Dt} = -\zeta_{ak} \nabla \cdot \mathbf{u}_k \quad (36.12)$$

where

$$\zeta_{ak} = f + \zeta_k \quad (36.13)$$

is the vertical component to the absolute vorticity of layer-k. Hence, the vorticity equation for an arbitrary layer in a stacked shallow water model is the same as that for a single shallow water layer.

36.1.3 Vorticity flux divergence and curl of nonlinear advection

We revisit the manipulations from Section 36.1.1 to explicitly identify a connection between the nonlinear terms in the vorticity equation. Start by writing the velocity equation in the advective form and the vector invariant form

$$\frac{\partial \mathbf{u}}{\partial t} + (\mathbf{u} \cdot \nabla) \mathbf{u} + f \hat{z} \times \mathbf{u} = -g \nabla \eta \quad (36.14a)$$

$$\frac{\partial \mathbf{u}}{\partial t} + (f + \zeta) \hat{z} \times \mathbf{u} = -\nabla (g \eta + \mathbf{u} \cdot \mathbf{u}/2). \quad (36.14b)$$

Taking their curl yields two expressions of the vorticity equation

$$\frac{\partial \boldsymbol{\omega}^*}{\partial t} + \nabla \times [(\mathbf{u} \cdot \nabla) \mathbf{u}] + \nabla \times [f \hat{z} \times \mathbf{u}] = 0 \quad (36.15a)$$

$$\frac{\partial \boldsymbol{\omega}^*}{\partial t} + \nabla \times [(f + \zeta) \hat{z} \times \mathbf{u}] = 0, \quad (36.15b)$$

whose equality leads to

$$\nabla \times [(\mathbf{u} \cdot \nabla) \mathbf{u} - \zeta \hat{z} \times \mathbf{u}] = 0. \quad (36.16)$$

Making use of the identity

$$\hat{z} \cdot [\nabla \times (\zeta \hat{z} \times \mathbf{u})] = \nabla \cdot (\mathbf{u} \zeta) \quad (36.17)$$

renders the relation

$$\hat{z} \cdot \nabla \times [(\mathbf{u} \cdot \nabla) \mathbf{u}] = \nabla \cdot (\mathbf{u} \zeta). \quad (36.18)$$

We thus see that the divergence of the advective vorticity flux (right hand side) equals to the curl of the nonlinear advection (left hand side). This identity holds for each layer in an N -layer shallow water model.

36.2 Potential vorticity for a solid-body rotating cylinder

To introduce the concept of shallow water potential vorticity, consider a fluid cylinder of constant mass M , constant density ρ , variable radius R , and variable height h , and assume the cylinder exhibits solid-body rotation about its central axis. This analysis offers a useful conceptual picture for a rotating column of a shallow water layer, in which time derivatives in the following are interpreted as material derivatives.

36.2.1 Mass conservation

With a constant density, mass conservation for the cylinder means that its volume is fixed. Hence, mass conservation constrains the relative changes to the radius and height of the cylinder. A materially constant cylinder mass

$$M = \pi R^2 h \rho \quad (36.19)$$

implies

$$\frac{2}{R} \frac{DR}{Dt} = -\frac{1}{h} \frac{Dh}{Dt}. \quad (36.20)$$

That is, mass conservation means that the relative height decreases as twice the relative radius increases. That is, if the cylinder is squashed (h decreases) it thickens (R increases) and conversely the cylinder thins (R decreases) as it extends (h increases).

36.2.2 Angular momentum conservation

A second constraint arises from angular momentum conservation. Since the cylinder is rotating as a solid-body, angular momentum is straightforward to compute. For simplicity, choose the center of mass coordinate axes through the center of the cylinder, with the z -axis along the central line of the cylinder and with $z = 0$ at the cylinder mid-point. The angular rotation vector is thus given by

$$\boldsymbol{\Omega} = \Omega \hat{\mathbf{z}}. \quad (36.21)$$

With this axis orientation, the solid-body rotation occurs about the center of mass so that the angular momentum of the center of mass vanishes. The moment of inertia tensor for a cylinder with this axis orientation is given by¹

$$I_{mn} = \delta_{mn} \frac{MR^2}{2}. \quad (36.22)$$

The moment of inertia is a measure of the rotational inertia of a moving continuous body. For the cylinder it is directly related to the cylinder mass (assumed fixed here) and the radius (which can change). Notably, the moment of inertia about the central vertical axis is not a function of the cylinder height. The reason is that the moment measures the inertia relative to the rotational axis, which is here along the central vertical axis. The angular momentum for the cylinder is thus given by

$$\mathbf{L} = \frac{MR^2}{2} \boldsymbol{\Omega} \hat{\mathbf{z}}. \quad (36.23)$$

The familiar *ice skater* example occurs when the cylinder radius changes and thus changes the moment of inertia (e.g., the ice skater's arms are brought in toward the central axis of the body or out away from the body). Maintaining constant angular momentum and constant mass means that the angular velocity, Ω , increases in magnitude (rotates faster) when the cylinder radius decreases, and vice versa. Explicitly for the cylinder we have $d\mathbf{L}/dt = 0$ and $dM/dt = 0$ thus rendering

$$\frac{2}{R} \frac{DR}{Dt} = -\frac{1}{\Omega} \frac{D\Omega}{Dt}. \quad (36.24)$$

We see that reducing the moment of inertia for a constant mass body by bringing its mass distribution towards the central axis (converging mass) leads, through angular momentum conservation, to an increase in rotation speed. The opposite occurs when mass diverges from a region, thus

¹See Marion and Thornton (1988) or many other classical mechanics texts for a discussion of the moment of inertia for a variety of solid bodies.

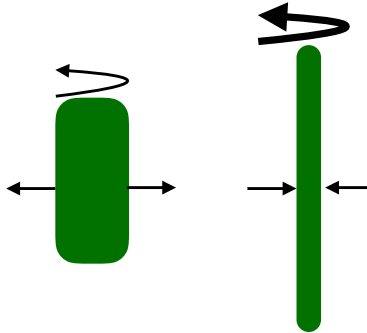


FIGURE 36.1: Illustrating the conservation of angular momentum for a spinning cylinder of constant mass undergoing solid-body rotation around its central axis. The moment of inertia (relative to the central axis) for the left cylinder is larger since more of its mass is distributed away from the central axis than in the right configuration. If the initial spin for the left cylinder is counterclockwise, then for the two configurations to have identical angular momentum means that the right cylinder spins more rapidly since its moment of inertia is smaller. This example exemplifies the familiar ice skater experience, whereby the skater's spin rate increases when bringing arms (mass) inward towards the central axis of the body (depicted by the inward arrows on the right panel), and the skater slows when extending the arms outward (depicted by the outward arrows on the left panel).

reducing the rotation speed.

Although the angular momentum constraint means that the spin rate changes when changing the moment of inertia, it does not impose a preferred direction. For example, no matter what direction a skater is rotating, decreasing the moment of inertia increases the spin rate in that particular direction. Yet when placing the spinning column on a rotating planet, the planetary rotation breaks the symmetry and thus prescribes the direction for the spin changes. The reason is that planetary rotation contributes to the spin of the column, even if the column has no spin relative to the rotating planetary reference frame. We encounter this additional part of the story in Section 36.3.

36.2.3 Potential vorticity conservation

Combining angular momentum conservation (36.24) with mass conservation (36.20) leads to the conservation law

$$\frac{D}{Dt} \frac{\Omega}{h} = 0. \quad (36.25)$$

Equation (36.25) is a statement of potential vorticity conservation for the material fluid column, with potential vorticity given by

$$Q \equiv \frac{\Omega}{h}. \quad (36.26)$$

For example, if the column thickens then the rotational velocity increases to maintain $Q = \Omega/h$ constant. Equivalently, if the column cross-sectional area decreases, the column thickness increases according to volume conservation, which in turn results in an increase in the spin according to angular momentum conservation.

36.2.4 Connecting angular momentum and vorticity

When allowing the fluid to exhibit motion that is more general than a solid-body, then the angular rotation rate appearing in the potential vorticity (36.26) is generalized to the absolute vorticity, and we consider this generalization in Section 36.3. Furthermore, as shown in Section 34.5, the

vorticity for solid body motion equals to twice the rotation rate, 2Ω . Hence, the numerator for the potential vorticity of the solid-body rotating cylinder equals to one-half the vorticity.

36.2.5 Comments and further study

The discussion in this section is motivated by Section 2.4 of [Salmon \(1998\)](#). The solid-body rotating cylinder succinctly identifies the two mechanical properties contributing to the potential vorticity conservation law (36.25): a kinematic property (mass conservation) and a dynamic property (angular momentum conservation). For the solid-body rotating cylinder, the implications of PV conservation are well gleaned from the separate mass and angular momentum conservation principles. Hence, PV conservation lends little novel insight for the cylinder. However, PV conservation is of fundamental use for studies of rotating and stratified fluids where the flow generally has strains that make vorticity distinct from angular momentum (Section 34.8).

We also note that an important element missing from this discussion is the *beta effect*, which accounts for the changes in planetary vorticity when moving on a rotating spherical planet. We encounter this effect in the following sections.

36.3 Shallow water potential vorticity

We now consider the potential vorticity for a single layer of shallow water fluid. The result is directly analogous to that derived for the solid-body rotating cylinder in Section 36.2. However, the derivation here makes use of fluid mechanical equations rather than those from rigid body mechanics, thus allowing for the added feature of strains in the fluid that distinguish vorticity from angular momentum. We present two derivations: one based on manipulations of the mass and momentum equations, and one based on the small aspect ratio limit of Kelvin's circulation theorem, with Kelvin's theorem more thoroughly studied in Chapter 37.

Figure 36.2 summarizes key elements leading to PV conservation for a shallow water fluid layer. Namely, as shown in this section, shallow water PV conservation arises from combining the kinematic constraint of mass conservation (material conservation of $h A$) with either the vorticity equation or Kelvin's circulation theorem for a small aspect ratio fluid.

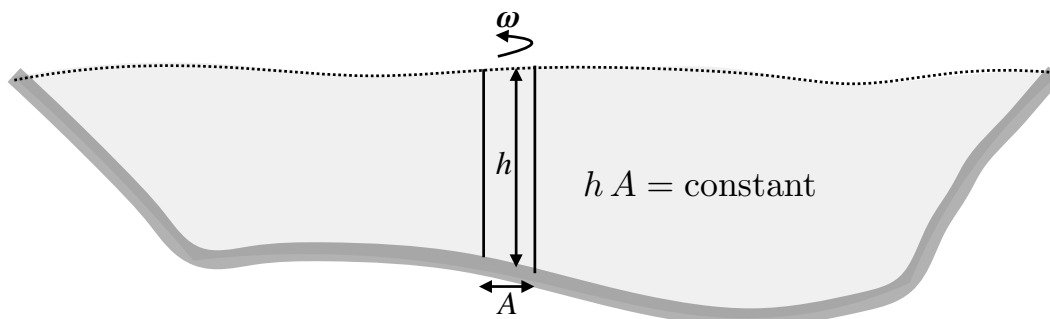


FIGURE 36.2: Illustrating the conservation of PV for a layer of shallow water fluid column. PV conservation results from merging mass conservation (material conservation of the column volume, $h A$), to either the vorticity equation or Kelvin's circulation theorem for a small aspect ratio fluid (material conservation of ζA).

36.3.1 Mass conservation plus the vorticity equation

To derive the potential vorticity equation, we here make use of the vorticity equation (36.9) and combine it with mass conservation.

Shallow water vorticity and vortex stretching

Mass conservation in the form of the material thickness equation (32.20) leads to the following expression for the divergence of the horizontal velocity

$$\nabla \cdot \mathbf{u} = -\frac{1}{h} \frac{Dh}{Dt}. \quad (36.27)$$

Making use of this result in the vorticity equation (36.9) allows us to eliminate the horizontal convergence

$$\frac{D\zeta_a}{Dt} = -\zeta_a \nabla \cdot \mathbf{u} = \frac{\zeta_a}{h} \frac{Dh}{Dt}. \quad (36.28)$$

This equation says that material changes in shallow water absolute vorticity arise only from material changes in the layer thickness; i.e., absolute vorticity increases in magnitude if the column stretches and decreases if the column compresses. We refer to this process as *vortex stretching*. We see in Section 37.5.3 that vorticity in more general fluids is affected by vortex stretching as well as *vortex tilting* and torques from baroclinicity. In contrast, equation (36.28) says that the material evolution of absolute vorticity for a shallow water fluid is affected only through vortex stretching. This behavior is a result of the depth independence of the horizontal velocity within a shallow water layer and the associated vertical columnar motion of fluid within the layer.

Material invariance of PV

Equation (36.28) can be written as an expression of the material invariance of the shallow water potential vorticity

$$\frac{DQ}{Dt} = 0, \quad (36.29)$$

where

$$Q = \frac{\zeta_a}{h} = \frac{\zeta + f}{h} \quad (36.30)$$

is the shallow water potential vorticity. As defined, shallow water potential vorticity is the ratio of absolute vorticity to the thickness of the fluid layer. The material conservation law (36.29) says that this ratio remains constant for the shallow water layer in the absence of irreversible processes. Much of the remainder of this chapter explores the many implications of potential vorticity conservation.

36.3.2 Motivating the name

Material invariance of the shallow water potential vorticity in equation (36.30) is most practically a statement about how the relative vorticity, ζ , changes when changing column thickness or latitude. That is, by maintaining Q fixed, ζ must change when either the column thickness, h , changes or when the column moves meridionally to thus alter the Coriolis parameter, f . By focusing on relative vorticity we are offered insights into how the fluid motion is constrained and thus a means to predict changes in that motion. In turn, these changes in ζ motivate the name “potential vorticity” as we now see.

Potential vorticity measures the ability for a shallow water fluid column to either spin up or spin down (change its relative vorticity) relative a standard configuration. For example, let the standard configuration be defined by an arbitrary standard thickness, h_s , at the equator (where $f = 0$). Now move an off-equatorial shallow water fluid column with zero relative vorticity to the equator and stretch/compress the column to the standard thickness. Material invariance of the column’s potential vorticity allows us to deduce the column’s relative vorticity at the equator,

given information about the initial column thickness and initial Coriolis parameter (see Figure 36.3). Hence, potential vorticity, as an invariant material property, provides the “potential” for a fluid column to manifest a particular value of the relative vorticity when moved and stretched into a standard configuration. In this manner, the use of “potential” in “potential vorticity” is directly analogous to the use of “potential” in “potential temperature” as described in Section 20.3, or gravitational potential energy as discussed in Section 23.2.

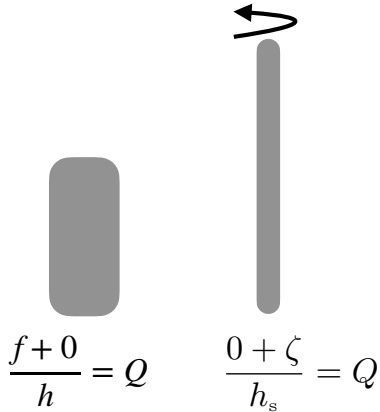


FIGURE 36.3: Left panel: an arbitrary shallow water column with zero relative vorticity and potential vorticity $Q = f/h$, with $f > 0$ assumed for this figure (northern hemisphere). Right panel: the same fluid column moved to the equator (where $f = 0$) and stretched to have the standard thickness, $h_s > h$. The relative vorticity of the column at the equator is given by $\zeta = f(h_s/h)$, where f is the Coriolis parameter at the original latitude where $f > 0$. Potential vorticity thus provides a means to deduce the relative vorticity that can be realized by moving any particular configuration to a standard location and with a standard thickness. This property motivates the “potential” used in the name.

36.3.3 Mass conservation + Kelvin's circulation theorem

Although we have yet to discuss Kelvin's theorem (Section 37.2), we here invoke it to illustrate another way to derive shallow water PV conservation. As we will see, this derivation lends itself to direct analog of the rotating cylinder discussed in Section 36.2.

When applied to an infinitesimal circuit in an inviscid and constant density fluid, Kelvin's theorem says that

$$\frac{D(\omega_a \cdot \hat{n} \delta S)}{Dt} = 0, \quad (36.31)$$

where ω_a is the absolute vorticity

$$\omega_a = \omega + f \hat{z}, \quad (36.32)$$

$\hat{n} \delta S$ is the infinitesimal surface area enclosed by the closed circuit, with \hat{n} the unit outward normal to the surface. Hence, equation (36.31) says that the projection of the absolute vorticity onto the local normal of an area element, multiplied by that area element, remains materially constant. This identity offers a very strong constraint on the flow.

To make use of equation (36.31) for the shallow water layer, decompose absolute vorticity into

$$\omega_a = \hat{z} (\zeta + f) + \omega_h, \quad (36.33)$$

where (see equation (32.103d))

$$\zeta = \hat{z} \cdot (\nabla \times \mathbf{v}) \quad (36.34)$$

is the vertical component to the relative vorticity, and

$$\boldsymbol{\omega}_h = -\hat{z} \times \nabla w = \hat{x} \partial_y w - \hat{y} \partial_x w \quad (36.35)$$

is the horizontal component to the shallow water relative vorticity from equation (32.103d) (recall the expression for $\boldsymbol{\omega}_h$ follows since the horizontal velocity components have no vertical dependence within a shallow water layer: $\partial u / \partial z = \partial v / \partial z = 0$). Inserting the absolute vorticity (36.33) into Kelvin's theorem (36.31) leads to

$$\frac{D}{Dt} [(\zeta + f) \delta A + \boldsymbol{\omega}_h \cdot \hat{n} \delta S] = 0, \quad (36.36)$$

where the horizontal area element, δA , is the projection of the surface area element onto the vertical direction

$$\delta A = \hat{z} \cdot \hat{n} dS. \quad (36.37)$$

Shallow water fluid mechanics arises from considering a constant density fluid layer under the small aspect ratio limit ($H/L \ll 1$, with H the vertical length scale and L the horizontal length scale). Under this limit, the second term in equation (36.36) is much smaller than the first. Ignoring this small term then leads to²

$$\frac{D}{Dt} \left[\left(\frac{\zeta + f}{h} \right) h \delta A \right] = 0, \quad (36.38)$$

where h is the layer thickness and $h \delta A$ is the volume of an infinitesimal fluid column. Given the incompressible nature of the shallow water layer, the column volume is materially constant

$$\frac{D(h \delta A)}{Dt} = 0, \quad (36.39)$$

so that equation (36.38) yields the material invariance of shallow water PV

$$\frac{D}{Dt} \left[\frac{\zeta + f}{h} \right] = \frac{DQ}{Dt} = 0, \quad (36.40)$$

where $Q = (\zeta + f)/h$ is the same shallow water potential vorticity derived above in Section 36.3.1.

36.3.4 A fluid column with constant $f \neq 0$

Some of the essential features of shallow water potential vorticity conservation are depicted in Figure 36.4 for the case of a fluid column with constant $f \neq 0$. In the left panel, the column thickness increases (column is stretched). Volume conservation means that the column radius decreases. As the material in the column moves radially inward toward the center, it experiences a Coriolis deflection to the right in the northern hemisphere and to the left in the southern. Both of these deflections renders a cyclonic tendency to the relative vorticity, creating a positive relative vorticity tendency in the north and negative relative vorticity tendency in the south.

An equivalent way to understand the cyclonic tendency is to consider the angular momentum of the fluid column, assuming the column moves coherently as a solid-body. As the radius of the column decreases so too does its moment of inertia. Angular momentum conservation means that the column picks up a tendency that causes its spin to increase. The direction of this spin increase accords with the background f of the environment. Returning to the skater analog in

²Since $|\boldsymbol{\omega}_h| \ll |\zeta|$ for the shallow water, a vortex tube in a shallow water layer never closes. Rather, it is nearly vertical, running from the bottom of the layer to the top.

Figure 36.1, we consider f to be the initial spin of the skater so that when the moment of inertia decreases the column picks up a spin in the same direction as f ; i.e., a cyclonic tendency.³

In both hemispheres, the Coriolis deflection, or equivalently angular momentum conservation, creates a cyclonic relative vorticity tendency when the column stretches, thus maintaining $Q = (f + \zeta)/h$ fixed. Again, the cyclonic relative vorticity adds to the magnitude of the planetary vorticity to ensure that the absolute vorticity magnitude increases in accord with the column thickness increase, thus keeping $Q = \zeta_a/h$ constant. The converse holds when the column is flattened/squashed, whereby the relative vorticity picks up an anti-cyclonic tendency (negative relative vorticity tendency in the northern hemisphere and positive relative vorticity tendency in the southern). Doing so reduces the magnitude of the absolute vorticity in accord with the reduced column thickness.

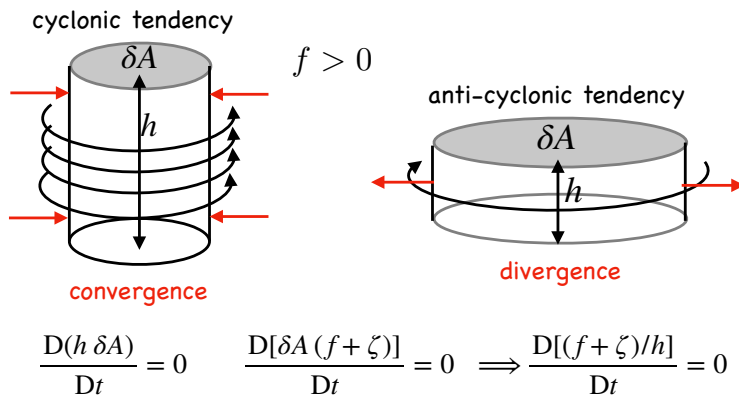


FIGURE 36.4: Material invariance for PV in a shallow water layer results from combining material invariance of the volume of a coherent fluid column with the material invariance of the area weighted absolute vorticity. As the cross-sectional area of the column decreases, as in a converging flow, the thickness of the fluid must increase in order to maintain constant volume. Furthermore, PV invariance can be maintained by changing the fluid spin, as measured by the relative vorticity, or by changing the latitude and thus changing its planetary vorticity (the β -effect discussed in Section 37.6). We here depict the case with $f > 0$ constant (so that $\beta = 0$). Flow converging toward the center of the column picks up a Coriolis acceleration that creates a cyclonic tendency in the relative vorticity, just like the spinning cylinder in Figure 36.1. Equivalently, as the radius of the column decreases so too does its moment of inertia so that the column must pick up a cyclonic tendency to conserve angular momentum. Conversely, as the cross-sectional area increases, the diverging flow creates an anti-cyclonic tendency in the relative vorticity.

36.3.5 Material conservation of an arbitrary function of PV

The material conservation law for PV, equation (36.29), means that any function, $F(Q)$ is also materially constant. We see this property through the chain rule

$$\frac{DF}{Dt} = \frac{dF}{dQ} \frac{DQ}{Dt} = 0. \quad (36.41)$$

Since F is arbitrary, there are an infinite number of material invariants corresponding to distinct functions F . This result holds for all materially invariant scalar properties of the fluid.

³The connection between the Coriolis acceleration and angular momentum conservation was discussed for particle mechanics in Section 12.7.

36.3.6 N -layer potential vorticity

The thickness equation (32.78a) and the vorticity equation (36.12) for an N -layer shallow water model are given by

$$\frac{D_k h_k}{Dt} = -h_k \nabla \cdot \mathbf{u}_k \quad \text{and} \quad \frac{D_k \zeta_{ak}}{Dt} = -\zeta_{ak} \nabla \cdot \mathbf{u}_k, \quad (36.42)$$

where there is no implied summation over the layer index k . These forms are isomorphic to the single layer equations so that the potential vorticity of layer- k is given by

$$Q_k = \frac{f + \zeta_k}{h_k}, \quad (36.43)$$

and for a perfect shallow water fluid this layer potential vorticity is materially constant

$$\frac{D_k Q_k}{Dt} = \frac{\partial Q_k}{\partial t} + \mathbf{u}_k \cdot \nabla Q_k = 0, \quad (36.44)$$

where, again, there is no implied summation over k .

36.3.7 Further study

The shallow water potential vorticity (36.30) was introduced by [Rossby \(1940\)](#) and as such it is sometimes referred to as the *Rossby potential vorticity*. Non-rotating shallow water potential vorticity, ζ/h , is illustrated in this [video from Prof. Shapiro at around the 11 minute mark](#). Note that he does not use the term “potential vorticity”, instead invoking mass conservation and angular momentum conservation to describe the motion.

36.4 Potential vorticity with non-conservative processes

In this section we consider the role of a non-conservative force per mass, \mathbf{F} , with this term arising from friction and boundary stresses (Section 32.6.2). Additionally, we allow for the presence of a boundary volume source, $w^{(\dot{\eta})}$ (as in precipitation minus evaporation), thus changing the volume in the layer. We introduced such processes in Section 32.6, in which case the shallow water equations take on the form

$$\frac{D\mathbf{u}}{Dt} + f \hat{\mathbf{z}} \times \mathbf{u} = -g \nabla \eta + \mathbf{F} \quad \text{and} \quad \frac{Dh}{Dt} + h \nabla \cdot \mathbf{u} = w^{(\dot{\eta})}. \quad (36.45)$$

36.4.1 Material time evolution of PV

In the presence of friction, the absolute vorticity equation (36.7) becomes

$$\frac{\partial \zeta_a}{\partial t} + \nabla \cdot (\mathbf{u} \zeta_a) = \hat{\mathbf{z}} \cdot (\nabla \times \mathbf{F}) \implies \frac{D\zeta_a}{Dt} + \zeta_a \nabla \cdot \mathbf{u} = \hat{\mathbf{z}} \cdot (\nabla \times \mathbf{F}), \quad (36.46)$$

so that vorticity is now affected by the curl of friction. As before, we make use of the thickness equation to replace the horizontal divergence according to

$$\nabla \cdot \mathbf{u} = \frac{1}{h} \left[-\frac{Dh}{Dt} + w^{(\dot{\eta})} \right]. \quad (36.47)$$

The presence of $w^{(\dot{\eta})}$ modifies the divergence of the horizontal velocity beyond that for a conservative fluid. We are thus led to the PV equation

$$h \frac{DQ}{Dt} = -Q w^{(\dot{\eta})} + \hat{z} \cdot (\nabla \times \mathbf{F}). \quad (36.48)$$

Hence, with $w^{(\dot{\eta})} \neq 0$ and/or $\hat{z} \cdot (\nabla \times \mathbf{F}) \neq 0$, shallow water potential vorticity is no longer materially invariant.

36.4.2 The potential vorticity flux

Deriving the Eulerian flux-form equation

We can convert the potential vorticity equation (36.48) into an Eulerian flux-form conservation equation by making use of the thickness equation

$$h \frac{DQ}{Dt} = h \left[\frac{\partial Q}{\partial t} + \mathbf{u} \cdot \nabla Q \right] + Q \left[\frac{\partial h}{\partial t} + \nabla \cdot (h \mathbf{u}) - w^{(\dot{\eta})} \right] = \frac{\partial(h Q)}{\partial t} + \nabla \cdot (h \mathbf{u} Q) - Q w^{(\dot{\eta})}, \quad (36.49)$$

thus rendering

$$\frac{\partial(h Q)}{\partial t} + \nabla \cdot (h \mathbf{u} Q) = \hat{z} \cdot (\nabla \times \mathbf{F}). \quad (36.50)$$

As a final step, make use of the identity

$$\hat{z} \cdot (\nabla \times \mathbf{F}) = -\nabla \cdot (\hat{z} \times \mathbf{F}), \quad (36.51)$$

so that the thickness weighted PV equation (36.50) can be written

$$\frac{\partial(h Q)}{\partial t} = -\nabla \cdot (h Q \mathbf{u} + \hat{z} \times \mathbf{F}). \quad (36.52)$$

Note how the volume source term, $w^{(\dot{\eta})}$, does not explicitly appear in the flux-form equation (36.52) since the effects from $w^{(\dot{\eta})}$ are captured by the divergence, $\nabla \cdot \mathbf{u}$, as per equation (36.47).

For the shallow water fluid, the thickness weighted potential vorticity equals to the absolute vorticity

$$h Q = \zeta_a. \quad (36.53)$$

Consequently, the flux-form conservation form of the PV equation (36.52) is identical to equation (36.46) for the absolute vorticity

$$\frac{\partial(h Q)}{\partial t} = -\nabla \cdot (h Q \mathbf{u} + \hat{z} \times \mathbf{F}) \iff \frac{\partial \zeta_a}{\partial t} = -\nabla \cdot (\zeta_a \mathbf{u} + \hat{z} \times \mathbf{F}). \quad (36.54)$$

Potential vorticity flux vector

It is remarkable that even with non-conservative forcing, the thickness weighted potential vorticity (equivalently, the absolute vorticity) has its Eulerian evolution determined by the convergence of a flux,

$$\mathbf{J}_Q = h Q \mathbf{u} + \hat{z} \times \mathbf{F}. \quad (36.55)$$

Observe that this potential vorticity flux is oriented in the horizontal direction. As detailed in Chapters 39 and 59, the PV flux never crosses the interface between two shallow water layers, even in the presence of irreversible processes such as mixing and friction. This result is a special case

of the more general *impermeability theorem* that holds for continuously stratified fluids (Section 39.2).

The flux convergence evolution for the potential vorticity equation (36.54) is a kinematic result of the definition of potential vorticity. Namely,

$$h Q - f = \zeta = \nabla \cdot (\mathbf{u} \times \hat{\mathbf{z}}) \quad (36.56)$$

so that

$$\partial_t(h Q) = \nabla \cdot (\partial_t \mathbf{u} \times \hat{\mathbf{z}}) \equiv -\nabla \cdot \mathbf{J}^{\text{kin}}, \quad (36.57)$$

where we defined the kinematic potential vorticity flux vector

$$\mathbf{J}^{\text{kin}} \equiv -\partial_t \mathbf{u} \times \hat{\mathbf{z}} = \mathbf{J} - \nabla \times (g \eta + \mathbf{u} \cdot \mathbf{u}/2). \quad (36.58)$$

Since the two potential vorticity fluxes differ by a curl; i.e., a rotational term, their divergences are identical

$$\nabla \cdot \mathbf{J}^{\text{kin}} = \nabla \cdot \mathbf{J}, \quad (36.59)$$

so that their convergence leads to the same evolution of $h Q$. Stated more formally, \mathbf{J}^{kin} and \mathbf{J} differ by a gauge, with the gauge function given by $g \eta + \mathbf{u} \cdot \mathbf{u}/2$.

36.5 Example implications of PV material invariance

The material conservation properties of shallow water PV provide nontrivial constraints on the fluid motion by stating that f, h, ζ cannot change independently of the other. Rather, the combination $Q = (f + \zeta)/h$ must remain materially invariant (in the absence of friction and mixing). There are a variety of situations that induce changes in one or two of the terms, with the third term constrained to ensure Q remains unchanged. We here consider some thought experiments to garner experience with shallow water PV-thinking.

36.5.1 Topographic beta effect

Changes in the topography affect the potential vorticity by changing the thickness of a fluid column via (see Figure 32.1)

$$h = H + \Delta\eta - \Delta\eta_b, \quad (36.60)$$

with $H = \bar{h}$ the area mean layer thickness, $\Delta\eta = \eta - \bar{\eta}$ the deviation of the free surface from its area mean, and $\Delta\eta_b = \eta_b - \bar{\eta}_b$ the deviation of the bottom from its area mean. For relative vorticity, we note that spatial changes in the topography act to drive a vertical velocity at the layer bottom as per equation (32.28),

$$w = \frac{D\eta_b}{Dt} \quad \text{at } z = \eta_b, \quad (36.61)$$

which then leads to vortex stretching and hence to a change in relative vorticity. In this subsection we highlight the analog between topographic slopes and planetary beta to thus motivate the term *topographic beta effect*.

To mathematically exhibit the topographic beta effect, consider a fluid column whose vorticity is dominated by planetary vorticity and with bottom topography having a small and linear slope in the meridional direction

$$\Delta\eta_b = \delta y, \quad (36.62)$$

where $|\delta| \ll 1$ is the topographic slope. Assuming the free surface undulations are small relative to the resting layer thickness, $\Delta\eta \ll H$, we can expand the potential vorticity according to

$$Q = \frac{f + \zeta}{h} \quad (36.63a)$$

$$= \frac{f_0 + \beta y + \zeta}{H + \Delta\eta - \delta y} \quad (36.63b)$$

$$\approx \frac{f_0 + \beta y + \zeta}{H} [1 - H^{-1}(\Delta\eta - \delta y)] \quad (36.63c)$$

$$\approx \frac{f_0 + \beta y + \zeta}{H} - \frac{f_0}{H^2} (\Delta\eta - \delta y). \quad (36.63d)$$

Setting $DQ/Dt = 0$ and rearranging leads to the material evolution of relative vorticity

$$\frac{D\zeta}{Dt} = -v(\beta + f_0\delta/H) + \frac{f_0 w(\eta)}{H}. \quad (36.64)$$

The second term on the right hand side is the vortex stretching associated with vertical motion at the top of the layer, where

$$w(\eta) = D\Delta\eta/Dt = D\eta/Dt \quad (36.65)$$

according to the surface kinematic boundary condition (32.36). The first term on the right hand side is vortex stretching arising from both planetary beta and topographic slopes. It is written in a form revealing the parallels between these two contributions, and it is readily generalized to the following for arbitrary topography

$$\beta_{\text{eff}} = (H - \eta_b) \nabla[f/(H - \eta_b)] \approx \beta \hat{\mathbf{y}} + (f_0/H) \nabla\eta_b. \quad (36.66)$$

One of the more prominent roles for topographic beta is in supporting topographic Rossby waves, which are analogous to the Rossby waves supported by planetary beta (see Section 47.3). We also encounter the topographic beta effect in Section 40.6.1 in our study of the quasi-geostrophic shallow water model.

36.5.2 Planetary geostrophic PV and f/H contours

As introduced in Section 28.5, planetary geostrophy (PG) is used to study the large-scale laminar ocean circulation where relative vorticity is ignored. Furthermore, as shown in Section 40.4, the inviscid and adiabatic PG system materially preserves the PG potential vorticity, $Q = f/h$, so that

$$\frac{D(f/h)}{Dt} = 0. \quad (36.67)$$

Consequently, fluid particles respecting the inviscid planetary geostrophic equations follow contours of constant f/h . These contours are referred to as *geostrophic contours* since the flow is under geostrophic balance.

If we assume the free surface undulations are negligible compared to the bottom topography (a useful assumption for planetary geostrophic flow), then shallow water columns follow contours of constant f/H , where $z = -H(x, y) = \eta_b(x, y)$ is the vertical position of the bottom topography. In Figure 36.5 we illustrate f/H contours for a topographic seamount (bump), a topographic depression (bowl), and a shelf/slope along the western boundary. We see that f/H contours are diverted equatorward when the depth decreases, whereas they are diverted poleward when they encounter deeper water. Furthermore, those contours that are near to either the bump or basin are closed, so that fluid columns following these contours are trapped around the topographic

feature. For the shelf/slope region, the f/H contours are horizontal where the topography is flat, which is on the shelf and in the open ocean, whereas they are steered toward the equator as they pass from the shelf toward the coast.

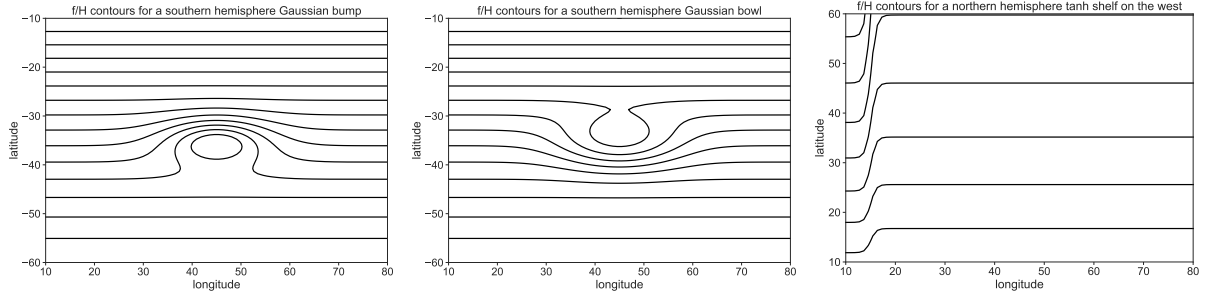


FIGURE 36.5: When a shallow water fluid is governed by the inviscid and adiabatic planetary geostrophic equations and there is no external forcing, then shallow water fluid columns maintain fixed planetary geostrophic potential vorticity, $D(f/h)/Dt = 0$. Ignoring free surface undulations relative to changes in the bottom depth means that f/H remains fixed following the inviscid geostrophic flow, where $z = -H(x, y) = \eta_b(x, y)$ is the bottom topography. We illustrate these *geostrophic contours* for three topographic features: a Gaussian seamount or bump and a Gaussian bowl, both in the southern hemisphere; and a western boundary continental slope and shelf in the northern hemisphere. Contours of f/H follow lines of constant latitude when H is constant, f/H contours are steered equatorward when moving into a region of shoaling water (H decreases), and steered poleward when moving into deeper water (H increases). Furthermore, note that contours near the seamount and bowl can close, in which case the associated geostrophic contours are trapped next to the topographic features.

The shelf example in Figure 36.5 reveals that for a given change in depth, the latitudinal diversion of an f/H contour is larger in magnitude for poleward contours relative to equatorward contours. We can understand this property by noting that along a contour, the latitude and depth change so as to keep f/H fixed, which means that

$$\delta(f/H) = 0, \quad (36.68)$$

where δ is a deviation taking place along a contour. With $f = 2\Omega \sin \phi$, this constraint leads to the relation between deviations in latitude, $\delta\phi$, and deviations in depth, δH , along a constant f/H contour

$$\delta\phi = (\delta H/H) \tan \phi = \frac{f/H}{2\Omega \cos \phi} = \frac{\delta H}{H} \frac{f}{R_e \beta}, \quad (36.69)$$

where for the final equality we introduced

$$\beta = \partial_y f = (2\Omega/R_e) \cos \phi. \quad (36.70)$$

As the equator is approached, f is smaller in magnitude yet β is larger. Hence, for a given change in the depth, δH , the change in latitude, $\delta\phi$, is smaller in magnitude for an f/H contour that is closer to the equator.

36.5.3 Spin up of converging flow

Consider the flow shown in Figure 36.6, whereby mass in the shallow water layer converges into a region. Just as described in the PV derivation Figure 36.4, increasing the column thickness, without substantially altering the planetary vorticity (e.g., f -plane), requires $\partial\zeta/\partial t > 0$ in order to maintain $Q = (\zeta + f)/h$ materially constant. Following our discussion of the rotating column in Section 36.2, note that convergence of mass reduces the moment of inertia relative to the center of

the region. Angular momentum conservation requires the fluid to rotate faster thus picking up a positive relative vorticity. This dynamical process is embedded in the material invariance of PV. Finally, note that the opposite occurs in a region of diverging fluid, whereby the PV invariance implies that the relative vorticity has a negative tendency ($\partial\zeta/\partial t < 0$) (see also Figure 36.4).

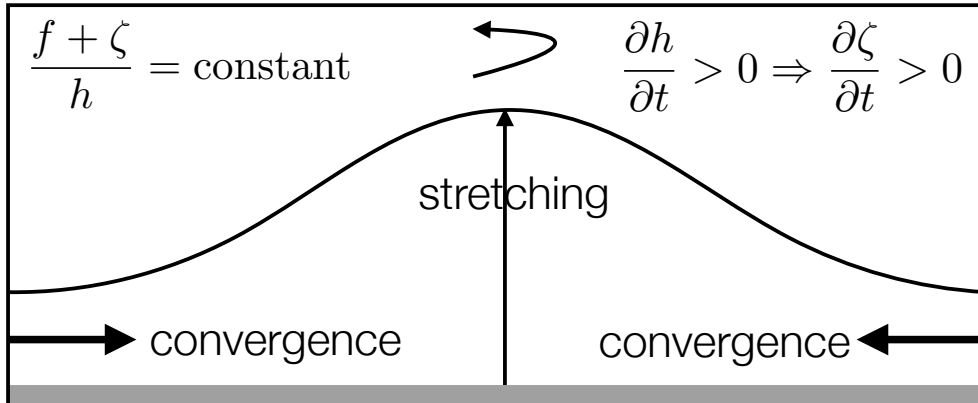


FIGURE 36.6: Illustrating the implications of material PV invariance for a shallow water fluid on an f -plane. If mass converges into a region, thus stretching the fluid column, then PV invariance implies the relative vorticity increases, $\partial\zeta/\partial t > 0$. This result is directly analogous to the rotating cylinder example considered in Figures 36.1 and 36.4. Namely, converging a region of constant mass reduces its moment of inertia so that angular momentum conservation leads to an increase in spin.

36.5.4 Further study

Section 4.3 of [Holton \(1992\)](#) discusses the case of flow over topography where the full shallow water PV is materially invariant, $D(f + \zeta)/Dt = 0$. In that case there is a dramatic difference between easterly and westerly flows. In the northern hemisphere, westerly winds (eastward flow) deflects over the topography and downstream it undulates as topographic leewaves. A rotating tank offers a useful controlled setting to observe leewaves, such as shown near the 20 minute mark in [this video from Prof. Fultz of the University of Chicago](#). Easterly winds (westward flow) do not exhibit a wavelike pattern, instead following a trajectory similar to the f/H contours of planetary geostrophic case, though modified by relative vorticity. In general, the study of flow near topography, either in the shallow water or continuously stratified, introduces a wealth of dynamical behaviors where material invariance of potential vorticity provides an important tool to help unravel mechanisms.

36.6 Circulation with non-conservative processes

We follow the discussion in Section 36.4 to study the evolution of circulation in the presence of non-conservative processes such as dia-surface transport and boundary stresses (Section 32.6). For this purpose, consider the velocity circulation around a closed horizontal area, S (see Figure 36.7)

$$C = \int_S \zeta dS = \oint_{\partial S} \mathbf{u} \cdot \hat{\mathbf{t}} d\ell. \quad (36.71)$$

In this equation, $\hat{\mathbf{t}} d\ell$ is the vector line increment around the contour, and $\hat{\mathbf{t}}$ is the tangent vector orienting the contour integral in a counterclockwise direction. We assume the circulation contour extends vertically through the layer so that the unit outward normal, $\hat{\mathbf{n}}$, to the contour is strictly

horizontal, as is the tangent vector, $\hat{\mathbf{t}}$. We now seek an evolution equation for this circulation by making use of the vorticity equation (36.54).

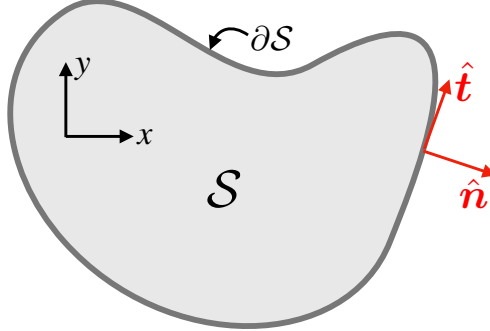


FIGURE 36.7: Illustrating the calculation of circulation around the contour, $\partial\mathcal{S}$, of a static horizontal area, \mathcal{S} , within a layer of shallow water fluid. The circulation theorem (36.75) provides the means to compute the time changes in circulation as a function of the advection of absolute vorticity crossing the contour plus the circulation of friction. Note that the contour has a vertical extent throughout the shallow water layer, so that the unit outward normal, $\hat{\mathbf{n}}$, and the unit tangent direction, $\hat{\mathbf{t}}$, are both horizontal vectors.

To develop an evolution equation for \mathcal{C} , integrate the vorticity equation (36.54) over the area \mathcal{S} to yield

$$\int_{\mathcal{S}} \frac{\partial \zeta}{\partial t} d\mathcal{S} = \int_{\mathcal{S}} [-\nabla \cdot (\zeta_a \mathbf{u} + \hat{\mathbf{z}} \times \mathbf{F})] d\mathcal{S} = - \oint_{\partial\mathcal{S}} [\zeta_a \mathbf{u} + \hat{\mathbf{z}} \times \mathbf{F}] \cdot \hat{\mathbf{n}} d\ell, \quad (36.72)$$

where \oint symbolizes an integral around the contour. To reach this equation we used the divergence theorem on the right hand side, with $\hat{\mathbf{n}}$ the *horizontal* unit outward normal vector along the contour, $\partial\mathcal{S}$, and $d\ell$ is the line increment along the contour. We also set $\partial f / \partial t = 0$ as part of the time derivative of the absolute vorticity. The non-conservative forcing term can be written

$$(\hat{\mathbf{z}} \times \mathbf{F}) \cdot \hat{\mathbf{n}} = (\hat{\mathbf{n}} \times \hat{\mathbf{z}}) \cdot \mathbf{F} = -\hat{\mathbf{t}} \cdot \mathbf{F}, \quad (36.73)$$

thus leading to

$$\int_{\mathcal{S}} \frac{\partial \zeta}{\partial t} d\mathcal{S} = - \oint_{\partial\mathcal{S}} \zeta_a \mathbf{u} \cdot \hat{\mathbf{n}} d\ell + \oint_{\partial\mathcal{S}} \mathbf{F} \cdot \hat{\mathbf{t}} d\ell, \quad (36.74)$$

where \oint is the counter-clockwise oriented closed contour integral. We next assume the area \mathcal{S} is constant in time, so that the Eulerian time derivative can be pulled across the integral to render

$$\frac{d\mathcal{C}}{dt} = - \oint_{\partial\mathcal{S}} \zeta_a \mathbf{u} \cdot \hat{\mathbf{n}} d\ell + \oint_{\partial\mathcal{S}} \mathbf{F} \cdot \hat{\mathbf{t}} d\ell. \quad (36.75)$$

The first term on the right hand side arises from the horizontal advection of absolute vorticity across the contour. This term is not oriented and so the integral sign has no arrow. The second term arises from the counter-clockwise oriented circulation of any non-conservative accelerations. We refer to equation (36.75) as a *circulation theorem*. It has many uses under specific cases, some of which are described in the remainder of this chapter.

36.6.1 Circulation around a closed streamline in steady flow

As a particular example of the circulation theorem (36.75), consider a steady flow in the absence of boundary volume sources ($w^{(i)} = 0$). In this case, the thickness equation (32.19) reduces to

$\nabla \cdot (h \mathbf{u}) = 0$ so that we can introduce a transport streamfunction, Ψ (with dimensions of $L^3 T^{-1}$)

$$h \mathbf{u} = \hat{\mathbf{z}} \times \nabla \Psi. \quad (36.76)$$

In a bounded domain, the streamlines (contours of constant Ψ) are closed. Furthermore, the unit outward normal to a closed streamline is perpendicular to the velocity, $\mathbf{u} \cdot \hat{\mathbf{n}} = 0$. We thus see that the steady state expression of the circulation theorem (36.75), computed around a closed streamline, leads to the following constraint on the non-conservative forces

$$\oint_{\text{streamline}} \mathbf{F} \cdot \hat{\mathbf{t}} d\ell = \int_{\text{streamline area}} (\nabla \times \mathbf{F}) \cdot \hat{\mathbf{z}} dS = 0, \quad (36.77)$$

where the second equality follows from Stokes' theorem applied over the area bounded by the streamline. Equation (36.77) provides a constraint on the non-conservative forcing that must be satisfied to enable a steady flow. For example, when integrated around a closed streamline, the wind stress forcing must balance dissipation. If the constraint (36.77) is not satisfied, then the flow cannot reach a steady state. Although we may not know explicit details of the streamlines, we can still make use of this constraint if we assume the flow is steady. The analysis in Section 36.7 offers an example application of these ideas for studies of circulation in steady ocean gyres.

36.6.2 Circulation from wind stress and Rayleigh drag

A particularly simple form for the non-conservative acceleration is given by

$$\mathbf{F} = -\gamma \mathbf{u} + \boldsymbol{\tau}^{\text{wind}} / (h \rho) \equiv -\gamma \mathbf{u} + \mathbf{F}^{\text{wind}}. \quad (36.78)$$

The first term is referred to as *Rayleigh drag* with $\gamma > 0$ a constant with dimensions of inverse time.⁴ Rayleigh drag damps all flow to rest with γ^{-1} the e-folding time for the damping. The second term in equation (36.78) is the acceleration on the layer from wind stress,

$$\mathbf{F}^{\text{wind}} = \frac{\boldsymbol{\tau}^{\text{wind}}}{h \rho}, \quad (36.79)$$

with this form following from our discussion in Section 32.6.2. Namely, the homogeneity of the shallow water layer renders the contact stress from winds into a body stress applied throughout the layer.

Plugging the acceleration (36.78) into the time dependent circulation theorem (36.75) leads to

$$\frac{dC}{dt} + \gamma C = - \int_{\partial S} \zeta_a \mathbf{u} \cdot \hat{\mathbf{n}} d\ell + \oint_{\partial S} \mathbf{F}^{\text{wind}} \cdot \hat{\mathbf{t}} d\ell. \quad (36.80)$$

Specializing to a steady state and choosing the contour as a closed streamline (along which $\mathbf{u} \cdot \hat{\mathbf{n}} = 0$), renders

$$C = \gamma^{-1} \oint_{\text{streamline}} \mathbf{F}^{\text{wind}} \cdot \hat{\mathbf{t}} d\ell = (\gamma \rho)^{-1} \oint_{\text{streamline}} (\boldsymbol{\tau}^{\text{wind}} / h) \cdot \hat{\mathbf{t}} d\ell. \quad (36.81)$$

This equation says that velocity circulation around a closed streamline is determined by wind stress circulation around that streamline plus knowledge of the Rayleigh drag damping time scale γ^{-1} . This result supports our expectation that the steady circulation around a closed streamline is oriented with the same sense as the applied wind stress.

⁴See Section 30.2.4 for more discussion of Rayleigh drag in the context of Ekman mechanics.

36.7 A primer on steady ocean gyres

Ocean gyres are a prominent feature of ocean circulation, with the North Atlantic and North Pacific middle-latitude gyres two canonical examples. A characteristic feature of ocean gyres is that they are not symmetric in the east-west direction, with a prominent western side where flow is stronger than the more sluggish interior flow. As shown in this section, gyre asymmetry is not a response to the wind forcing, with the asymmetry found even without any zonal variations in the winds. Instead, it is a manifestation of the beta effect present for flow on a rotating spherical planet (or idealized as the β -plane from Section 21.3.4). We discuss the beta effect more formally in Section 37.6, but for now it is sufficient to know that it arises from the meridional derivative of the planetary vorticity:

$$\beta = \partial_y f. \quad (36.82)$$

We have the basic tools in hand to understand the physical balances leading to western intensification in steady ocean gyres. For that purpose, we make use of vorticity balances as they offer a more direct path towards western intensification than the linear momentum or axial angular momentum balances used to explore channel flow in Sections 25.5 and 33.7.

36.7.1 Steady and large-scale vorticity balance

The steady circulation theorem (36.81) holds regardless the bottom topography or surface height undulations. Again, it says that circulation around a closed streamline is in the same sense as the wind circulation. However, we need more information to see how western intensification emerges as a property of ocean gyres. For that purpose, consider the steady absolute vorticity equation (36.54), again in the presence of wind forcing and Rayleigh drag

$$\nabla \cdot (\mathbf{u} \zeta_a) = -\gamma \zeta + \hat{\mathbf{z}} \cdot (\nabla \times \mathbf{F}^{\text{wind}}). \quad (36.83)$$

Introducing the shallow water potential vorticity, $Q = \zeta_a/h$, allows us to write

$$\nabla \cdot (\mathbf{u} \zeta_a) = \nabla \cdot (h \mathbf{u} Q). \quad (36.84)$$

The steady state thickness equation (32.19) means that $\nabla \cdot (h \mathbf{u}) = 0$, so that the vorticity equation (36.83) takes the form

$$h \mathbf{u} \cdot \nabla Q = -\gamma \zeta + \hat{\mathbf{z}} \cdot (\nabla \times \mathbf{F}^{\text{wind}}). \quad (36.85)$$

This equation says that in the absence of the irreversible terms on the right hand side, the steady horizontal flow follows contours of constant potential vorticity. This result follows directly from the material invariance of PV in the absence of non-conservative processes. However, in the presence of Rayleigh drag and/or wind stress curl, PV is modified when following the flow so that $\mathbf{u} \cdot \nabla Q \neq 0$; i.e., circulation does not follow Q contours.

36.7.2 Planetary geostrophic flow and the Sverdrup balance

For large-scale flow away from lateral boundaries, the flow has an absolute vorticity that is dominated by planetary vorticity so that

$$Q \approx Q_{\text{PG}} = f/h, \quad (36.86)$$

which is the PV for planetary geostrophic flow (Section 28.5 and 40.4). Correspondingly, we assume the Rayleigh drag term is negligible in this region since the relative vorticity is small, so

that the PV equation (36.85) takes the form

$$h \mathbf{u} \cdot \nabla Q_{\text{PG}} = \hat{\mathbf{z}} \cdot (\nabla \times \mathbf{F}^{\text{wind}}). \quad (36.87)$$

Expanding the left hand side and introducing the planetary vorticity gradient renders the *shallow water Sverdrup balance*

$$\beta v = Q_{\text{PG}} \mathbf{u} \cdot \nabla h + \hat{\mathbf{z}} \cdot (\nabla \times \mathbf{F}^{\text{wind}}) \quad \text{shallow water Sverdrup balance.} \quad (36.88)$$

This balance states how horizontal advection of layer thickness (first right hand side term) plus the wind stress curl (second term) balance meridional motion for flow on a rotating sphere (beta effect on left hand side). Gradients in the layer thickness arise from free surface undulations as well as gradients in the bottom topography (see Figure 32.1). The traditional *Sverdrup balance* arises when we assume the flow takes place over a flat bottom and the free surface undulations are negligible, in which case $\nabla h = 0$ so that

$$\beta v = \hat{\mathbf{z}} \cdot (\nabla \times \mathbf{F}^{\text{wind}}) \quad \text{traditional Sverdrup balance.} \quad (36.89)$$

This balance is also suited to a stratified ocean in regions where the upper ocean flow does not interact with the bottom, such as in regions far from the continental shelves.

36.7.3 Sverdrup flow in a closed domain with anti-cyclonic wind stress

Consider a closed northern hemisphere middle latitude β -plane domain driven by an anti-cyclonic wind stress

$$\hat{\mathbf{z}} \cdot (\nabla \times \mathbf{F}^{\text{wind}}) < 0 \quad \text{northern hemisphere anti-cyclonic wind stress.} \quad (36.90)$$

This situation is depicted in Figure 36.8, where we also illustrate a commonly used wind stress profile that is purely zonal and has a co-sinusoidal meridional structure that is symmetric about the central latitude of the domain

$$\mathbf{F}^{\text{wind}} = -\hat{\mathbf{x}} A \cos[\pi(y - y_0 + L/2)/L] \quad (36.91a)$$

$$\hat{\mathbf{z}} \cdot (\nabla \times \mathbf{F}^{\text{wind}}) = -(\pi A/L) \sin[\pi(y - y_0 + L/2)/L]. \quad (36.91b)$$

In these equations, $A > 0$ is the magnitude of the wind stress acceleration applied to the layer, and the domain extends meridionally from $y_0 - L/2 \leq y \leq y_0 + L/2$ with $y = y_0$ the central latitude. This wind stress has westerlies on the poleward side of the domain and easterlies (trade winds) on the equatorward side so that $\hat{\mathbf{z}} \cdot (\nabla \times \boldsymbol{\tau}) < 0$ throughout the domain.

The Sverdrup balance (36.89) indicates that an anti-cyclonic wind stress curl drives an equatorward Sverdrup flow. We emphasize that this flow is *not* the result of meridional winds pushing the fluid to the south. Instead, it arises in response to the constraints of vorticity balance with an anti-cyclonic wind stress curl in the presence of the beta effect. Indeed, for the idealized wind stress (36.91a) there is no meridional wind component. Although water satisfying Sverdrup balance flows south, all the water in the domain cannot be moving to the south. Rather, volume conservation requires a poleward return flow somewhere outside the region of Sverdrup balance.

36.7.4 Western intensification and the role of beta

Volume conservation is a kinematic constraint that requires a return flow on either the eastern or western side of the domain, outside the region of Sverdrup balance. But what side? We offer the

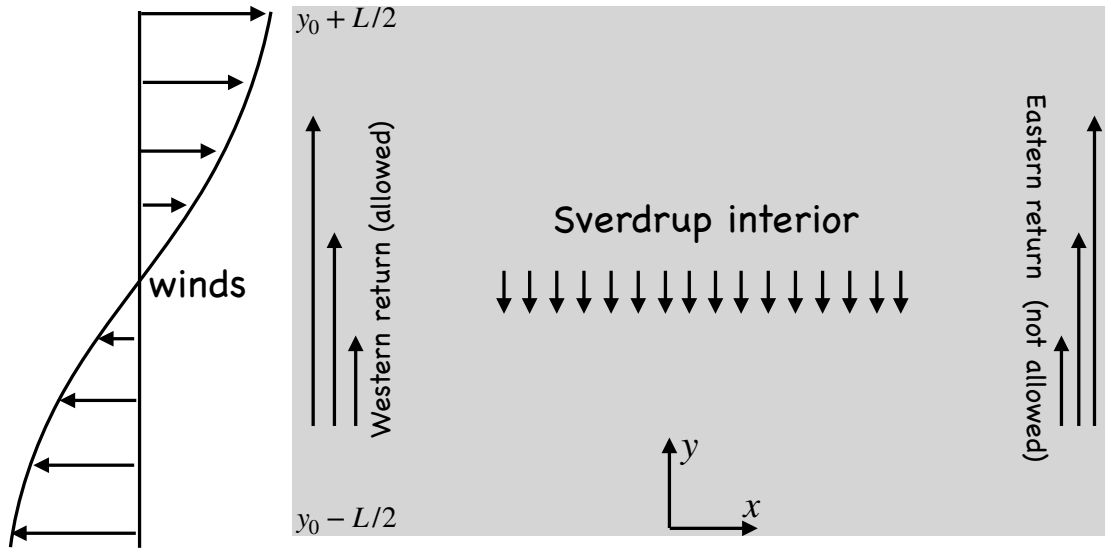


FIGURE 36.8: Illustrating the southward Sverdrup flow in response to an anti-cyclonic wind stress forcing in a bounded northern hemisphere domain. A northward return flow is required to satisfy volume conservation. As seen in Section 36.7.4, a linear vorticity balance between beta, winds, and friction lead to a western boundary return flow and corresponding western intensification.

following arguments for the western side.

Inertial entry into a boundary layer region

Recall the discussion of Figure 35.4 where we considered how inviscid flow in a homogeneous fluid over a flat bottom region materially preserves absolute vorticity in the presence of a meridional barrier. To materially preserve absolute vorticity (and ignoring free surface undulations relative to the depth of the fluid), the flow can deviate meridionally, either northward or southward, when encountering a western wall. In contrast, such meridional deviation is prohibited for absolute vorticity preserving flow that encounters an eastern wall. So in referring to Figure 36.8, southward flow can make a turn westward towards the western boundary, enter the boundary layer, and move northward within the boundary layer. It cannot do so for the eastern side.

Steady velocity circulation follows wind circulation

The steady circulation theorem (36.81) means that the flow circulation is in the same sense as the wind circulation. With an anti-cyclonic wind forcing, the circulation also must be anti-cyclonic. This result again leads us to conclude that the western boundary is the region for the return flow, in which case the full gyre circulation will be anti-cyclonic.

Steady vorticity balance and a role for dissipation

The two previous arguments point to the western side as the return flow region. But we have yet to provide an argument for western boundary intensification. For that purpose, recall that the return flow region is not in traditional Sverdrup balance. To see what terms can break that balance, consider again the steady vorticity balance (36.85). Continuing to assume a flat bottom and rigid lid surface leads to

$$\beta v = -\gamma \zeta + \hat{z} \cdot (\nabla \times \mathbf{F}^{\text{wind}}), \quad (36.92)$$

where we dropped the nonlinear advection term $\mathbf{u} \cdot \nabla \zeta$ (the “inertial” term) since we wish to determine whether a linear balance can give rise to western intensification (we return to this assumption in Section 36.7.8). The Rayleigh drag on the right hand side breaks the Sverdrup balance in regions where the relative vorticity is nontrivial. Since we know there must be a return flow somewhere in the domain, we know there must be a region where dissipation is sufficiently strong to break Sverdrup balance.

What is required for the steady and linear dissipative vorticity balance (36.92) to be maintained in the northward return flow region? To answer this question, expose the signs on the terms in equation (36.92)

$$\underbrace{\beta v}_{\text{positive}} + \underbrace{\gamma \zeta}_{\text{unspecified}} = \underbrace{\hat{\mathbf{z}} \cdot (\nabla \times \mathbf{F}^{\text{wind}})}_{\text{negative}}. \quad (36.93)$$

We have $\beta v > 0$ since we are concerned with the region of northward return flow, and $\hat{\mathbf{z}} \cdot (\nabla \times \mathbf{F}^{\text{wind}}) < 0$ by assumption of anti-cyclonic wind stress over the full domain. Hence, for the balance (36.93) to be realized requires $\zeta < 0$, with the value large enough to balance both the winds and the meridional advection of planetary vorticity

$$\underbrace{\gamma \zeta}_{\text{negative}} = \underbrace{-\beta v}_{\text{negative}} + \underbrace{\hat{\mathbf{z}} \cdot (\nabla \times \mathbf{F}^{\text{wind}})}_{\text{negative}}. \quad (36.94)$$

For anti-cyclonic gyre flow, as required by the circulation condition (36.81), the only way to realize $\zeta < 0$ of sufficient magnitude is to have an intensified flow along the western side of the gyre. In this region, $\zeta \approx \partial v / \partial x < 0$ can become sufficiently large in magnitude. Furthermore, since the wind stress is applied throughout the domain, all streamlines feel the winds and must pass through the western boundary region where vorticity is enhanced and Rayleigh drag is able to balance the winds and planetary advection. The required boundary current flow is depicted in Figure 36.8.

The importance of beta

In the absence of beta, there would be no interior region in Sverdrup balance driving southward flow. The flow would thus only be subject to the circulation condition (36.81) whereby linear flow can symmetrically dissipate the wind stress. Hence, the beta effect is the fundamental element that causes poleward flow to intensify along the western side of the gyre in response to the equatorward interior flow.

36.7.5 A role for bottom pressure torques

Recall the shallow water Sverdrup balance (36.88), here with the addition of Rayleigh drag

$$\beta v = Q_{\text{PG}} \mathbf{u} \cdot \nabla h - \gamma \zeta + \hat{\mathbf{z}} \cdot (\nabla \times \mathbf{F}^{\text{wind}}). \quad (36.95)$$

For the right hand side, we have thus far considered a flat bottom and ignored free surface undulations, in which case $\nabla h = 0$. In this case, the only way to balance meridional motion on a beta plane is to invoke irreversible processes either from wind stress or Rayleigh drag.

Spatial variations in the bottom topography open up the possibility for an inviscid balance

$$\beta v = Q_{\text{PG}} \mathbf{u} \cdot \nabla h, \quad (36.96)$$

or more generally a balance where frictional vorticity sinks are unimportant except for regions very close to the boundary. For example, consider northward flow in the northern hemisphere

along a shallow western continental shelf. Assume the bottom topography only has variations in the zonal direction, with $\partial_x h > 0$ reflecting deeper water to the east of the shelf. The inviscid vorticity balance (36.96) thus takes the form

$$\beta v = (f/h) u \partial_x h. \quad (36.97)$$

Since $\beta v > 0$ and $(f/h) \partial_x h > 0$, we must have $u > 0$. Hence, flow departs from purely northward motion by leaving the shelf and moving into deeper waters. This behavior is also revealed by the western shelf example in Figure 36.5, where the f/H contours deviate from contours of constant depth when there is a nonzero β . As examined in this section, the bottom pressure torque, arising from bottom topographic form stress, plays the lead role in the corresponding vorticity balance.

Curl of the form stresses

In the present analysis, we are only concerned with that portion of $\mathbf{u} \cdot \nabla h$ directly arising from pressure gradients. We thus consider just the geostrophic flow to arrive at

$$\mathbf{u} \cdot \nabla h = (g/f) \nabla h \cdot (\hat{\mathbf{z}} \times \nabla \eta) = (g/f) \hat{\mathbf{z}} \cdot (\nabla \eta \times \nabla h). \quad (36.98)$$

It is this term that contains the various pressure torques arising from form stresses. But before unpacking those torques, briefly return to the above shelf example and note that with $\nabla h = \hat{\mathbf{x}} \partial_x h$ then there is a nonzero $\mathbf{u} \cdot \nabla h$ only with a nonzero $\partial_y \eta$, which in turn means there is a nonzero zonal geostrophic flow. As noted above, this zonal flow is a consequence of the sloping bottom topography.

Pressure torques

Returning to the general situation, we determine the expressions for the pressure torques contained in the term $\mathbf{u} \cdot \nabla h$ by making use of the hydrostatic relation $p_b = p_a + \rho g h$, and the layer thickness, $h = \eta - \eta_b$ (see Figure 32.1), in which case

$$\mathbf{u} \cdot \nabla h = (g/f) \hat{\mathbf{z}} \cdot (\nabla \eta \times \nabla h) \quad (36.99a)$$

$$= 1/(\rho f) \hat{\mathbf{z}} \cdot [\nabla \times (p_a \nabla \eta) + \nabla \eta \times \nabla p_b] \quad (36.99b)$$

$$= 1/(\rho f) \hat{\mathbf{z}} \cdot [\nabla \times (p_a \nabla \eta) - \nabla \times (p_b \nabla \eta_b) + \nabla h \times \nabla p_b] \quad (36.99c)$$

$$= 1/(\rho f) \hat{\mathbf{z}} \cdot [\nabla \times (p_a \nabla \eta) - \nabla \times (p_b \nabla \eta_b) + \nabla p_b \times \nabla p_a / (\rho g)]. \quad (36.99d)$$

The first and second terms are the curls of the pressure form stresses applied to the surface (atmospheric) and bottom boundaries (Section 25.2), respectively, which we refer to as the atmospheric and bottom pressure torques. The third term is a torque arising from misalignment of the applied pressure and bottom pressure. Inserting equation (36.99d) in the vorticity balance (36.95) leads to the steady balance

$$\beta \rho h v = \hat{\mathbf{z}} \cdot [\nabla \times (p_a \nabla \eta) - \nabla \times (p_b \nabla \eta_b) + \nabla p_b \times \nabla p_a / (\rho g)] + \rho h [-\gamma \zeta + \hat{\mathbf{z}} \cdot (\nabla \times \mathbf{F}^{\text{wind}})]. \quad (36.100)$$

We consider a few special cases to see how the pressure torques affect the meridional flow in a gyre circulation, with a focus on bottom pressure torque since this term is generally far larger than those torques involving the atmospheric pressure.

Inviscid balance between meridional flow and bottom pressure torque

In the absence of friction and wind forcing, and with a uniform atmospheric pressure ($\nabla p_a = 0$), then β times the depth integrated meridional mass transport in equation (36.100) is balanced by the bottom pressure torque (i.e., curl of the topographic form stress)

$$\beta \rho h v = -\hat{z} \cdot (\nabla \times p_b \nabla \eta_b) \quad \text{linear inviscid and unforced.} \quad (36.101)$$

Again consider the example of northward flow along a western continental shelf. In this case, $\nabla \eta_b = \hat{x} \partial_x \eta_b < 0$, so that the balance (36.101) reduces to

$$\beta \rho h v = \partial_y p_b \partial_x \eta_b. \quad (36.102)$$

This balance says that if the bottom depth increases eastward away from the shelf, so that $\partial_x \eta_b < 0$, then northward flow corresponds to a northward decrease in the bottom pressure, $\partial_y p_b < 0$. That is, the northward flow is directed down the bottom pressure gradient.

Association rather than causality

The inviscid planetary geostrophic balance (36.101) does not express causality. Rather, it expresses a balance or association that is maintained by steady linear flows in the presence of sloping topography. Hence, it is incorrect to say that bottom pressure torque gives rise to (i.e., causes) inviscid planetary geostrophic flow. Rather, the balance (36.101) says for planetary geostrophic flow, there is no bottom pressure torque without a meridional flow, and conversely there is no meridional flow without bottom pressure torque.

Vanishing topographic form stress curl for geostrophic *f*-plane motion

As a corollary of the balance (36.101), a linear inviscid and unforced geostrophic flow on an *f*-plane satisfies $\hat{z} \cdot (\nabla \times p_b \nabla \eta_b) = \hat{z} \cdot (\nabla p_b \times \nabla \eta_b) = 0$, so that the isolines of surface height align with isolines of bottom topography since $p_b = g \rho h = g \rho (\eta - \eta_b)$ when $p_a = 0$. Conversely, surface height contours that deviate from bottom topography contours signal the role of friction and/or β acting on the planetary geostrophic flow.

Local generation of bottom pressure torque

The beta effect provides an inviscid means to balance a misalignment between the surface height and the bottom topography, with misalignment required to generate a nonzero topographic form stress curl, which we have been referring to as the bottom pressure torque. We discussed an analogous misalignment in Section 33.7 when studying the force balances in a steady zonally re-entrant channel with bottom topography. Wind stress forcing and dissipation offer another means to balance (η, η_b) -misalignment, as seen merely by rewriting the vorticity balance (36.100) as an expression for the bottom pressure torque

$$\begin{aligned} \hat{z} \cdot (\nabla \times p_b \nabla \eta_b) = \\ -\beta \rho h v + \hat{z} \cdot [\nabla \times (p_a \nabla \eta) + \nabla p_b \times \nabla p_a / (\rho g)] + \rho h [-\gamma \zeta + \hat{z} \cdot (\nabla \times \mathbf{F}^{\text{wind}})]. \end{aligned} \quad (36.103)$$

In our discussion of western intensification in Section 36.7.4, we ignored the role of bottom pressure torque. However, as seen by this balance, bottom pressure torque plays a role when topography and surface height are misaligned, with that role in some locations more important than friction

(see [Becker and Salmon \(1997\)](#), [Hughes and de Cueves \(2001\)](#), [Jackson et al. \(2006\)](#) and [Patmore et al. \(2019\)](#) for examples).

36.7.6 Properties of area integrated bottom pressure torques

Consider a simply connected fluid domain bounded by an isobath. Stokes' theorem reveals that the integral of the bottom pressure torque, $\hat{\mathbf{z}} \cdot (\nabla \times p_b \nabla \eta_b)$, vanishes when computed over the area bounded by any isobath

$$\int_{\mathcal{S}} \hat{\mathbf{z}} \cdot (\nabla \times p_b \nabla \eta_b) d\mathcal{S} = \oint_{\partial\mathcal{S}} p_b \nabla \eta_b \cdot \hat{\mathbf{t}} d\ell = 0. \quad (36.104)$$

The integrand for the line integral vanishes pointwise since, by construction, the boundary, $\partial\mathcal{S}$, is determined by an isobath so its the tangent vector, $\hat{\mathbf{t}}$, is orthogonal to $\nabla \eta_b$. The identical argument holds for an area bounded by an isobar of bottom pressure since, for any region,

$$\int_{\mathcal{S}} \hat{\mathbf{z}} \cdot (\nabla \times p_b \nabla \eta_b) d\mathcal{S} = - \int_{\mathcal{S}} \hat{\mathbf{z}} \cdot (\nabla \times \eta_b \nabla p_b) d\mathcal{S} = - \oint_{\partial\mathcal{S}} \eta_b \nabla p_b \cdot \hat{\mathbf{t}} d\ell. \quad (36.105)$$

Now if the region is bounded by an isobar, then $\nabla p_b \cdot \hat{\mathbf{t}} = 0$ at each point along the region boundary. With a bit more work, we can show that the area integral of the bottom pressure torque vanishes for an annular region bounded by any two isobaths or any two bottom pressure isobars. The proof is presented in the caption to Figure 36.9.

These mathematical identities mean that bottom pressure torque plays no role in the area integrated vorticity budget for regions bounded by isobaths or bottom pressure isobars. In particular, taking a contour that encircles the global ocean reveals that bottom pressure torque does not alter the global area integrated vorticity. Equivalently, topographic form stresses integrated around a closed contour defined by an isobath or isobar do not alter the circulation around that contour. Evidently, topographic form stress cannot spin-up or spin-down the circulation around a contour determined by isobaths or bottom pressure isobars. Other processes, such as flow nonlinearities, viscous friction, and/or boundary stresses, must play role in determining the circulation since their contour integrals are unconstrained. As studied by [Stewart et al. \(2021\)](#), these very special properties of bottom pressure torque and topographic form stress introduce a variety of nuances when interpreting the area integrated vorticity budget.

36.7.7 Advection-diffusion of the steady streamfunction⁵

Since the steady state flow satisfies $\nabla \cdot (h \mathbf{u}) = 0$, we can introduce a streamfunction

$$h \mathbf{u} = \hat{\mathbf{z}} \times \nabla \Psi, \quad (36.106)$$

in which case the relative vorticity becomes

$$\zeta = \hat{\mathbf{z}} \cdot (\nabla \times \mathbf{u}) = \nabla \cdot (h^{-1} \nabla \psi), \quad (36.107)$$

and the steady vorticity equation (36.85) can be written

$$\hat{\mathbf{z}} \cdot (\nabla \Psi \times \nabla Q) = -\gamma \nabla \cdot (h^{-1} \nabla \Psi) + \hat{\mathbf{z}} \cdot (\nabla \times \mathbf{F}^{\text{wind}}). \quad (36.108)$$

⁵We study the physics of advection and diffusion in Chapter 61. For Section 36.7.7 we only require a few basic features of this equation.

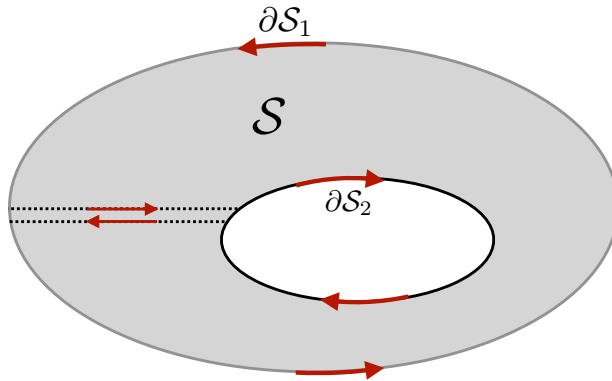


FIGURE 36.9: Stokes' theorem is generally applicable in a simply connected region. However, an annulus region, \mathcal{S} , is not simply connected since it has a hole. To apply Stokes' theorem over an annulus we imagine snipping the outer contour, $\partial\mathcal{S}_1$, and inner contour, $\partial\mathcal{S}_2$, and then connecting the two ends of the snipped contours as shown here. In this manner we convert the non-simply connected annulus into a simply connected region, over which we can apply Stokes' theorem in the naive manner. Importantly, we see that the two segments connecting the inner and outer contour are traversed in opposite directions when performing the contour integral. Assuming all functions are smooth, we can take the limit as these two contours get infinitesimally close, in which they cancel identically. This limit also recovers the connected outer and inner contours. If the outer and inner contours are defined by isobaths or bottom pressure isobars, then the bottom pressure torque identically vanishes on the contours. In this manner we have proven that the bottom pressure torque vanishes within the annulus region. We make use of this method in Exercise 37.7 when considering the circulation in an ocean domain with islands.

Following [Welander \(1968\)](#), we interpret equation (36.108) as a steady advection-diffusion equation for Ψ . Namely, introduce the horizontally non-divergent vector

$$\mathbf{u}^{(Q)} = \hat{\mathbf{z}} \times \nabla Q, \quad (36.109)$$

in which case the streamfunction equation (36.108) becomes

$$\mathbf{u}^{(Q)} \cdot \nabla \Psi = \gamma \nabla \cdot (h^{-1} \nabla \Psi) - \hat{\mathbf{z}} \cdot (\nabla \times \mathbf{F}^{\text{wind}}). \quad (36.110)$$

With zero wind stress curl and zero Rayleigh drag, the contours of the steady streamfunction are aligned with $\mathbf{u}^{(Q)}$; that is, Ψ and Q contours are parallel. In the presence of Rayleigh drag, the streamfunction deviates from the Q contours, as it does in the presence of a wind stress curl.

These results represent a mere repackaging of results found earlier. Even so, the advection-diffusion interpretation offers complementary insights into the patterns of the steady streamfunction. Indeed, as we see in Section 36.8, the advective-diffusive interpretation proves very useful when studying patterns of steady sea level in planetary geostrophic gyres.

36.7.8 Comments and further study

Friction is needed to close the vorticity budget in a flat bottom linear ocean

The study of ocean gyres originates [Stommel \(1948\)](#). This video from [SciencePrimer](#) provides a concise summary of the dynamics of ocean gyres and western boundary intensification due to the beta effect. Chapter 19 of [Vallis \(2017\)](#) provides a lucid treatment of ocean gyre dynamics by working through the key features of Stommel's model as well as variants such as that from [Munk \(1950\)](#), who considered a viscous closure (most important next to side boundaries) rather than Rayleigh drag. The Stommel model and its variants are themselves very idealized renditions of the ocean gyres occurring in Nature. Notable further factors become important in studying Nature's

gyres, such as topography (briefly discussed in Section 36.7.5), nonlinearities and instabilities (recall we dropped the inertial term in Section 36.7.4, thus focusing on linear balances), turbulent boundary layers, and coupled air-sea processes. Each of these processes render the study of western boundary currents one of the most complex and timeless areas of physical oceanography.

Topographic form stress from sloping shelves reduces the need for friction

Friction plays a central role in the Stommel and Munk models of western intensification. As described in Chapter 19 of [Vallis \(2017\)](#), there have been attempts to produce an inviscid (and unforced) gyre solution, with the study from [Fofonoff \(1954\)](#) of particular note. We consider elements of the Fofonoff gyre in Exercise 35.9. Additionally, we raised the importance of sloping sides in Section 36.7.5 and in the earlier discussion of axial angular momentum in Section 25.5. Sloping sides enable bottom topographic form stress and bottom pressure torques to dominate over bottom turbulent stresses and turbulent torques. In so doing, sloping sides play a leading role in gyre balances, though we did note in the discussion surrounding equation (36.104) that friction remains essential to close the vorticity balance integrated around the gyre. The role of sloping sides for gyre circulations was emphasized by [Hughes and de Cueves \(2001\)](#), with [Stewart et al. \(2021\)](#) identifying further nuances related to the integrated properties in Section 36.7.6.

Flow nonlinearities also reduce the need for frictional closures of the vorticity budget

Furthermore, we ignored the role of nonlinearities, which generally require the use of numerical models to investigate. Indeed, one of the first numerical simulations was from [Bryan \(1963\)](#), who showed that western boundary currents in a flat bottom gyre generally experience hydrodynamical instabilities when the flows become strong enough. [Becker and Salmon \(1997\)](#); [Becker \(1999\)](#) further studied the case of a nonlinear gyre circulation in the presence of a sloping side shelf, thus allowing for both nonlinearities and topography form stresses to play leading roles in the vorticity balance. These, and many other, studies allow for inviscid contributions to the vorticity balance, thus alleviating the need for invoking strong frictional effects found in the models of Stommel and Munk.

Distinguishing western intensification from western boundary layers

Finally, we emphasize that the western intensification of the gyre, implied by β , is distinct from a frictional boundary layer implied by a no-slip side boundary (e.g., Section 22.8). The two are very distinct flow regimes. Namely, a frictional western boundary layer next to the solid earth boundary leads to cyclonic flow in the boundary layer (since there is no-slip at the western boundary), whereas the β -induced western intensification gives rise to anti-cyclonic flow.

36.8 Free surface patterns in steady ocean gyres

We here consider basic features of steady free surface patterns realized by a shallow water fluid, with inspiration from [Minobe et al. \(2017\)](#), [Wise et al. \(2018\)](#), [Wise et al. \(2020a\)](#) and [Wise et al. \(2020b\)](#), and making use of the advection-diffusion interpretation of [Welander \(1968\)](#) introduced in Section 36.7.7. The basic question is how to relate the free surface near the coast to that in the interior of an ocean gyre. We formulate the steady linear case following [Wise et al. \(2018\)](#), who considered sloping bottom topography rather than the vertical walls assumed by [Minobe et al. \(2017\)](#). The transient case, which involves coastal boundary waves, is considered by [Hughes et al. \(2019\)](#), [Wise et al. \(2020a\)](#) and [Wise et al. \(2020b\)](#).

36.8.1 Formulating the free surface equation

We make use of the steady frictional geostrophic equations, with the velocity equation given by the linearized version of equation (36.126)

$$f \hat{z} \times h \mathbf{u} = -g h \nabla \eta + \mathbf{f}^{\text{nc}}. \quad (36.111)$$

Here, \mathbf{f}^{nc} is the thickness weighted acceleration from non-conservative processes, such as the wind stress, viscous friction, and bottom drag, with details provided in Section 36.9.1. Since the flow is steady, the layer thickness equation (32.20) leads to the non-divergence condition

$$\nabla \cdot (h \mathbf{u}) = 0. \quad (36.112)$$

We now formulate a vorticity-like equation. Yet rather than taking the curl of equation (36.111), thus emulating the work from Section 36.9, we first divide by the Coriolis parameter to write

$$\hat{z} \times h \mathbf{u} = -(g h/f) \nabla \eta + \mathbf{f}^{\text{nc}}/f, \quad (36.113)$$

so that the curl leads to

$$\hat{z} \cdot [\nabla(g h/f) \times \nabla \eta] = \hat{z} \cdot \nabla \times (\mathbf{f}^{\text{nc}}/f), \quad (36.114)$$

where we used the non-divergence condition (36.112). Dividing by the Coriolis parameter limits the analysis to regions bounded away from the equator, which is not a problem for our focus on middle or high latitude planetary geostrophic ocean gyres. We are motivated to pursue this formulation since it supports the use of equation (36.114) next to sloping boundaries, in which the layer thickness vanishes ($h = 0$) at the shoreline edge of the domain.

36.8.2 Advectiong the free surface

To help interpret the conservative portion of the free surface equation (36.114), we introduce the streamfunction⁶

$$\psi^{(\eta)} \equiv -g h/f, \quad (36.115)$$

so that equation (36.114) takes the form

$$\mathbf{u}^{(\eta)} \cdot \nabla \eta = -\hat{z} \cdot \nabla \times (\mathbf{f}^{\text{nc}}/f), \quad \text{with} \quad \mathbf{u}^{(\eta)} = \hat{z} \times \nabla \psi^{(\eta)} = -\hat{z} \times \nabla(g h/f). \quad (36.116)$$

The left hand side is written as the advection of the free surface by the horizontally non-divergent velocity, $\mathbf{u}^{(\eta)}$. That is, the velocity, $\mathbf{u}^{(\eta)}$, advects the free surface, whereas the fluid velocity, \mathbf{u} , advects matter. In the absence of non-conservative forces ($\mathbf{f}^{\text{nc}} = 0$), the free surface is aligned with isolines of $h/f = 1/Q_{\text{PG}}$, or equivalently with lines of constant planetary geostrophic potential vorticity, Q_{PG} (recall that $Q_{\text{PG}} = f/h$ as defined by (36.86)). For free surface contours to deviate from Q_{PG} contours requires non-conservative forces, such as those from wind stresses and frictional dissipation. This discussion is related to that given in Section 36.5.2 where we introduced the notion of f/H contours for planetary geostrophic flow.

⁶We follow the sign convention of Wise et al. (2018) by introducing $\psi^{(\eta)} = -g h/f$ in equation (36.115). The alternative choice of $\psi^{(\eta)} = +g h/f$ is less convenient for interpreting the direction of the velocity induced by topographic slopes. Additionally, in equation (36.123) we introduce Rayleigh drag and interpret the resulting equation as an advective-diffusion balance. If we take $\psi^{(\eta)} = +g h/f$ then it would be an advective-anti-diffusive balance, which is far less physically satisfying.

The advection operator

The layer thickness is the difference between the free surface and bottom topography, $h = \eta - \eta_b \geq 0$ (see Figure 32.1), in which case the advection operator takes on the form

$$\nabla\psi \times \nabla\eta = -(g/f) \nabla(\eta - \eta_b) \times \nabla\eta + (g h/f^2) \beta \hat{\mathbf{y}} \times \nabla\eta \quad (36.117a)$$

$$= (g/f) [\nabla\eta_b + (h\beta/f) \hat{\mathbf{y}}] \times \nabla\eta. \quad (36.117b)$$

This result motivates decomposing $\mathbf{u}^{(\eta)}$ into two terms

$$\mathbf{u}^{(b)} = (g/f) \hat{\mathbf{z}} \times \nabla\eta_b = (g/f) (-\hat{\mathbf{x}} \partial_y \eta_b + \hat{\mathbf{y}} \partial_x \eta_b) \quad (36.118a)$$

$$\mathbf{u}^{(\beta)} = \hat{\mathbf{z}} \times (g h \beta/f^2) \hat{\mathbf{y}} = -(g h \beta/f^2) \hat{\mathbf{x}}, \quad (36.118b)$$

so that the free surface equation (36.116) takes on the form

$$(\mathbf{u}^{(b)} + \mathbf{u}^{(\beta)}) \cdot \nabla\eta = -\hat{\mathbf{z}} \cdot \nabla \times (\mathbf{f}^{nc}/f). \quad (36.119)$$

As so defined, $\mathbf{u}^{(b)}$ arises from gradients in the bottom topography and it is directed with shallow water to the right in the northern hemisphere and to the left in the southern hemisphere (just as the phase velocity for a coastally trapped Kelvin wave; see Section 48.8). The velocity, $\mathbf{u}^{(\beta)}$, arises from the planetary vorticity gradient and is always directed to the west, just as the phase velocity of a Rossby wave (Section 48.11). Notably, $\mathbf{u}^{(\eta)}$ has a meridional component only so long as there is a zonal topographic slope, $\partial_x \eta_b \neq 0$.

Free surface trajectories in the absence of non-conservative forcing

In the absence of non-conservative forces the steady free surface equation (36.119) is

$$(\mathbf{u}^{(b)} + \mathbf{u}^{(\beta)}) \cdot \nabla\eta = 0 \implies [\hat{\mathbf{z}} \times \nabla\eta_b - (h\beta/f) \hat{\mathbf{x}}] \cdot \nabla\eta = 0. \quad (36.120)$$

For the case of a flat bottom domain, so that $\mathbf{u}^{(b)} = 0$, free surface contours are purely zonal ($\partial_x \eta = 0$). Conversely, on an f -plane, so that $\mathbf{u}^{(\beta)} = 0$, free surface contours are aligned with the bottom topography, $\hat{\mathbf{z}} \cdot (\nabla\eta_b \times \nabla\eta) = 0$. In the general case, the unforced steady free surface contours are aligned according to the interplay between planetary beta and bottom topography according to equation (36.120).

It is instructive to imagine a free surface “trajectory” as defined by integral curves of $\mathbf{u}^{(\eta)}$. Consider one such trajectory that moves from the interior of a northern hemisphere gyre onto the continental shelf, such as in the example depicted in Figure 36.5. In the interior we assume the bottom topography is nearly flat, so that $\mathbf{u}^{(b)} \approx 0$ and the corresponding free surface trajectory is along a constant latitude line. As we reach the continental slope, the trajectory becomes southwestward with a trajectory slope determined by the zonal slope of the topography. Finally, as the continental shelf is reached, which is relatively flat, the trajectory returns to a near constant latitude contour.

36.8.3 Rayleigh drag and free surface diffusion

The free surface equation (36.119) indicates that any non-conservative acceleration, \mathbf{f}^{nc} , causes the free surface to deviate from contours of constant streamfunction, $\psi^{(\eta)} = -g h/f$. The dominant contribution to \mathbf{f}^{nc} arises from wind stress. Here, we consider the role of a thickness weighted

Rayleigh drag assumed to take the form given by equation (36.128)

$$\mathbf{f}^{\text{nc}} = -\gamma h \mathbf{u}_g, \quad (36.121)$$

where γ has dimensions of inverse time and \mathbf{u}_g is the geostrophic flow given by

$$\mathbf{u}_g = (g/f) \hat{\mathbf{z}} \times \nabla \eta. \quad (36.122)$$

Substituting into the free surface equation (36.119) leads to

$$\underbrace{(\mathbf{u}^{(b)} + \mathbf{u}^{(\beta)}) \cdot \nabla \eta}_{\text{advection}} = \underbrace{\nabla \cdot [(\gamma h g/f^2) \nabla \eta]}_{\text{diffusion}} - \underbrace{\hat{\mathbf{z}} \cdot \nabla \times [\boldsymbol{\tau}^{\text{wind}} / (\rho f)]}_{\text{source from } \nabla \times \boldsymbol{\tau}^{\text{wind}}/f}. \quad (36.123)$$

In the absence of a wind stress, the free surface satisfies an advective-diffusive balance.⁷ Evidently, the Rayleigh drag, acting as a sink to the geostrophic momentum also acts to diffuse the free surface and so to cause the free surface contours to deviate from contours of constant gh/f . Notice that the diffusion coefficient,

$$\kappa = \gamma h g/f^2 = -(\gamma/f) \psi^{(\eta)}, \quad (36.124)$$

gets larger moving toward the equator. Hence, free surface contours can more readily deviate from contours of constant $\psi^{(\eta)}$ when moving towards the equator.

36.9 Column vorticity

Throughout this chapter we have focused on vorticity as defined by the curl of the horizontal velocity, $\zeta = \hat{\mathbf{z}} \cdot (\nabla \times \mathbf{u})$. Since flow within a shallow water layer moves in coherent and extensible vertical columns (Section 32.2), the shallow water vorticity measures the spin of a shallow water column.

We can also measure the column spin by considering the curl of the thickness weighted velocity

$$\Sigma = \hat{\mathbf{z}} \cdot \nabla \times (h \mathbf{u}) = h \zeta + \hat{\mathbf{z}} \cdot \nabla h \times \mathbf{u}. \quad (36.125)$$

We refer to Σ as the *column vorticity*, though note that it has the dimensions of a velocity due to the thickness weighting. In addition to the thickness weighted relative vorticity, the column vorticity measures the misalignment between the layer thickness gradient and the velocity, with $\hat{\mathbf{z}} \cdot \nabla h \times \mathbf{u}$ generally nonzero especially for geostrophic flows. Hence, the second term offers an extra measure of the spin for the fluid column beyond the relative vorticity measure.⁸ The layer thickness factor ensures that Σ directly probes stresses acting at the layer interfaces, as well as stresses within the fluid layer. Besides its intrinsic interest, this analysis is motivated by studies of the depth integrated flow commonly pursued in oceanography, with examples studied in Chapter 41.

⁷We study advection and diffusion in Chapter 61.

⁸Exercise 36.7 offers a particular example of a geostrophic flow that is aligned perpendicular to ∇h , as found in a geostrophic shallow water front.

36.9.1 Formulating the column vorticity equation

To formulate the dynamical equation for Σ , we start from the momentum equation (33.29)

$$\frac{\partial(h \mathbf{u})}{\partial t} + \nabla \cdot (h \mathbf{u} \otimes \mathbf{u}) + f \hat{\mathbf{z}} \times (h \mathbf{u}) = -g h \nabla \eta^{\text{eff}} + \mathbf{f}^{\text{nc}} \quad (36.126)$$

where

$$\mathbf{f}^{\text{nc}} = h \mathbf{F} \quad (36.127)$$

is the thickness weighted acceleration (dimension of squared velocity) arising from non-conservative processes, such as from horizontal strains in the presence of viscosity and the boundary transfer of turbulent momentum such as through winds and bottom drag (see Section 32.6). For example, recall the acceleration given by equation (36.78), which is built from Rayleigh drag plus wind stress, in which case

$$\mathbf{f}^{\text{nc}} = -\gamma h \mathbf{u} + \boldsymbol{\tau}^{\text{wind}}/\rho = -\gamma h \mathbf{u} + h \mathbf{F}^{\text{wind}}. \quad (36.128)$$

Taking the vertically projected curl of equation (36.126) leads to

$$\partial_t \Sigma + \hat{\mathbf{z}} \cdot \nabla \times [\nabla \cdot (h \mathbf{u} \otimes \mathbf{u})] + \nabla \cdot (f h \mathbf{u}) = -g \hat{\mathbf{z}} \cdot (\nabla h \times \nabla \eta^{\text{eff}}) + \hat{\mathbf{z}} \cdot (\nabla \times \mathbf{f}^{\text{nc}}). \quad (36.129)$$

Let us now examine each of these terms and offer physical interpretations.

Frictional torques and boundary pressure torques

The term $\hat{\mathbf{z}} \cdot (\nabla \times \mathbf{f}^{\text{nc}})$ in equation (36.129) provides a torque from boundary stresses and interior viscous stresses. The term $g \nabla h \times \nabla \eta^{\text{eff}}$ provides a torque whenever the thickness gradients are not aligned with the gradients in the effective surface height. We can write this term in the equivalent form based on the following identities

$$\rho g \nabla h \times \nabla \eta^{\text{eff}} = \rho g \nabla h \times \nabla \eta + \nabla h \times \nabla p_a \quad (36.130a)$$

$$= -\nabla p_a \times \nabla \eta + \nabla p_b \times \nabla \eta + \nabla(p_b - p_a) \times \nabla p_a / (\rho g) \quad (36.130b)$$

$$= -\nabla p_a \times \nabla \eta + \nabla p_b \times \nabla[\eta + p_a / (\rho g)] \quad (36.130c)$$

$$= -\nabla p_a \times \nabla \eta + \nabla p_b \times \nabla[\eta_b + h + p_a / (\rho g)] \quad (36.130d)$$

$$= -\nabla p_a \times \nabla \eta + \nabla p_b \times \nabla \eta_b \quad (36.130e)$$

$$= \nabla \times (-p_a \nabla \eta + p_b \nabla \eta_b), \quad (36.130f)$$

where we made use of the hydrostatic relation $p_b = p_a + \rho g h$. We thus see that $-g \nabla h \times \nabla \eta^{\text{eff}} = \rho^{-1} \nabla \times (p_a \nabla \eta - p_b \nabla \eta_b)$ arises from pressure torques acting on the surface and bottom of the shallow water column. These torques spin the column if there is a misalignment between the boundary pressure gradients and the boundary surface slopes. Notably, it is commonly the case that the torque associated with the applied surface pressure is far smaller than that from the bottom pressure, in which case

$$-g \nabla h \times \nabla \eta^{\text{eff}} \approx -\rho^{-1} \nabla \times (p_b \nabla \eta_b) = -\rho^{-1} \nabla p_b \times \nabla \eta_b. \quad (36.131)$$

Torque from the nonlinear transport

The nonlinear term $\hat{\mathbf{z}} \cdot \nabla \times [\nabla \cdot (h \mathbf{u} \otimes \mathbf{u})]$ can be written

$$\hat{\mathbf{z}} \cdot \nabla \times [\nabla \cdot (h \mathbf{u} \otimes \mathbf{u})] = \hat{z}_m \epsilon_{mst} \partial_s [\partial_n (h u_n u_t)] \quad (36.132a)$$

$$= \partial_n \partial_s [(h u_n) \epsilon_{mst} \hat{z}_m u_t] \quad (36.132b)$$

$$= \partial_n [\partial_s (h u_n) \epsilon_{mst} \hat{z}_m u_t + h u_n \zeta] \quad (36.132c)$$

$$= -\partial_n [\epsilon_{smt} \hat{z}_m u_t \partial_s (h u_n)] + \nabla \cdot (h \zeta \mathbf{u}), \quad (36.132d)$$

which exposes the divergence of the thickness weighted advective flux of relative vorticity. Further manipulations lead to

$$-\partial_n [\epsilon_{smt} \hat{z}_m u_t \partial_s (h u_n)] = -\partial_n [\epsilon_{smt} \hat{z}_m u_t u_n \partial_s h + \epsilon_{smt} \hat{z}_m u_t h \partial_s u_n] \quad (36.133a)$$

$$= \partial_n [\hat{z}_m (\epsilon_{mst} \partial_s h u_t) u_n - h \epsilon_{smt} \hat{z}_m u_t \partial_s u_n] \quad (36.133b)$$

$$= \nabla \cdot [\hat{\mathbf{z}} \cdot (\nabla h \times \mathbf{u}) \mathbf{u}] - \partial_n [h (\hat{\mathbf{z}} \times \mathbf{u}) \cdot \nabla u_n] \quad (36.133c)$$

$$= \nabla \cdot [\hat{\mathbf{z}} \cdot (\nabla h \times \mathbf{u}) \mathbf{u}] + \nabla \cdot [h (v \partial_x - u \partial_y) \mathbf{u}], \quad (36.133d)$$

so that the nonlinear term takes the form

$$\hat{\mathbf{z}} \cdot \nabla \times [\nabla \cdot (h \mathbf{u} \otimes \mathbf{u})] = \nabla \cdot [\Sigma \mathbf{u} + h (v \partial_x - u \partial_y) \mathbf{u}] = \nabla \cdot [\Sigma \mathbf{u} + h (\mathbf{u}_{\text{clock}} \cdot \nabla) \mathbf{u}] \quad (36.134)$$

The first term inside the square bracket is the advective flux of Σ . The second term is the thickness weighted transport of \mathbf{u} by the clockwise rotated horizontal velocity

$$\mathbf{u}_{\text{clock}} = -\hat{\mathbf{z}} \times \mathbf{u}. \quad (36.135)$$

36.9.2 Summary of the column vorticity equation

The above manipulations bring the Σ equation (36.129) into the Eulerian flux-form

$$\partial_t \Sigma = -\nabla \cdot \mathbf{J}^\Sigma + \rho^{-1} \hat{\mathbf{z}} \cdot \nabla \times [-p_a \nabla \eta + p_b \nabla \eta_b + \rho \mathbf{f}^{\text{nc}}], \quad (36.136)$$

where

$$\mathbf{J}^\Sigma \equiv [h f + \Sigma + h (v \partial_x - u \partial_y)] \mathbf{u} = h \zeta_a \mathbf{u} + [v (\partial_x h + h \partial_x) - u (\partial_y h + h \partial_y)] \mathbf{u} \quad (36.137)$$

is the total flux of Σ . The corresponding material time derivative form of equation (36.136) is given by

$$\frac{D\Sigma}{Dt} + \Sigma \nabla \cdot \mathbf{u} + \nabla \cdot [h f \mathbf{u} + h (v \partial_x - u \partial_y) \mathbf{u}] = \rho^{-1} \hat{\mathbf{z}} \cdot \nabla \times [-p_a \nabla \eta + p_b \nabla \eta_b + \rho \mathbf{f}^{\text{nc}}]. \quad (36.138)$$

The thickness equation (32.116)

$$\frac{Dh}{Dt} = -h \nabla \cdot \mathbf{u} + w^{(\dot{\eta})}, \quad (36.139)$$

brings equation (36.138) into the form

$$h \frac{D(\Sigma/h)}{Dt} + \nabla \cdot [h f \mathbf{u} - h \hat{\mathbf{z}} \cdot (\mathbf{u} \times \nabla) \mathbf{u}] = -\frac{\Sigma w^{(\dot{\eta})}}{h} + \rho^{-1} \hat{\mathbf{z}} \cdot \nabla \times [-p_a \nabla \eta + p_b \nabla \eta_b + \rho \mathbf{f}^{\text{nc}}], \quad (36.140)$$

where we wrote

$$v \partial_x - u \partial_y = -\hat{\mathbf{z}} \cdot (\mathbf{u} \times \nabla). \quad (36.141)$$

36.9.3 Steady linear column vorticity balance and the island rule

To garner experience with the column vorticity equation (36.136), consider the steady state and assume \mathbf{J}^Σ is dominated by the planetary vorticity

$$\mathbf{J}^\Sigma \approx h f \mathbf{u}, \quad (36.142)$$

in which case the budget equation (36.136) reduces to the balance

$$\nabla \cdot (h f \mathbf{u}) = \rho^{-1} \hat{\mathbf{z}} \cdot \nabla \times [-p_a \nabla \eta + p_b \nabla \eta_b + \rho \mathbf{f}^{nc}]. \quad (36.143)$$

Hence, torques due to interface pressures and turbulent stresses are balanced by the divergence of the thickness weighted advective flux of planetary vorticity. Furthermore, since $\nabla \cdot (h \mathbf{u}) = 0$ in the steady state, equation (36.143) takes the form

$$\rho h \beta v = \hat{\mathbf{z}} \cdot \nabla \times (-p_a \nabla \eta + p_b \nabla \eta_b + \rho \mathbf{f}^{nc}), \quad (36.144)$$

which connects to the discussion of pressure torques given in Section 36.7.5. It says that for planetary geostrophic flow, meridional transport in the presence of $\beta \neq 0$ is balanced by the torques arising from form atmospheric and bottom form stresses, as well as from non-conservative processes such as wind stress, viscous friction, and bottom drag.

Formulating an integral balance

The local balance (36.143) holding for planetary geostrophic flow leads to an integral balance through an area integral over an arbitrary closed domain

$$\oint_{\mathcal{S}} \nabla \cdot (h f \mathbf{u}) d\mathcal{S} = \rho^{-1} \oint_{\mathcal{S}} \hat{\mathbf{z}} \cdot \nabla \times [-p_a \nabla \eta + p_b \nabla \eta_b + \rho \mathbf{f}^{nc}] d\mathcal{S}. \quad (36.145)$$

Making use of Gauss' divergence theorem on the left hand side and Stokes' theorem on the right hand side renders

$$\oint_{\partial\mathcal{S}} h f \mathbf{u} \cdot \hat{\mathbf{n}} d\ell = \rho^{-1} \oint_{\partial\mathcal{S}} [-p_a \nabla \eta + p_b \nabla \eta_b + \rho \mathbf{f}^{nc}] \cdot \hat{\mathbf{t}} d\ell. \quad (36.146)$$

The left hand side is a contour integral with $\hat{\mathbf{n}}$ the unit outward normal along the contour. The right hand side is also a contour integral, yet with $\hat{\mathbf{t}}$ the unit tangent along the contour oriented in the counter-clockwise sense. The integral balance (36.146) says that the advective transport of planetary vorticity leaving the closed region (left hand side) is balanced by the oriented contour integral of the pressure and turbulent stresses. If the contour follows a closed streamline, on which $\mathbf{u} \cdot \hat{\mathbf{n}} = 0$, then the right hand side contour integral must vanish.

The integral balance (36.146) is a rather remarkable statement that equates the transport leaving a region to pressure and turbulent stresses integrated along the region boundary. [Godfrey \(1989\)](#) chose a particularly clever contour, such as that depicted in Figure 36.10, and made some assumptions about the stresses that then allowed for an estimate of the transport. We here present the arguments.

Assumptions about the stresses

A portion of the red contour in Figure 36.10 traverses the eastern boundary on both Island A and Island B. As shown in Section 36.7, friction in the eastern boundary region of an ocean gyre is much less than the western boundary, motivating us to ignore friction (either viscous or

bottom drag) along the eastern boundary portions of the contour. Likewise, friction is generally small for the open ocean portion along the two latitudinal lines. Hence, wind stress is the only non-conservative process that affects the right hand side of equation (36.146).

[Godfrey \(1989\)](#) furthermore ignored pressure form stresses and their associated torques. This assumption is reasonable for the atmospheric form stress, $-p_a \nabla \eta$, which is generally quite small (it is zero for a rigid lid approximation). However, the bottom form stress, $p_b \nabla \eta_b$, and the associated bottom pressure torque, can be larger than the wind stress and wind stress curl, especially near the continental margins and with strong currents. Hence, ignoring bottom pressure torque is an unsatisfying assumption.

The island rule

The islands are material surfaces so that $\mathbf{u} \cdot \hat{\mathbf{n}} = 0$ along those portions of the contour that are adjacent to the coasts. Integrating along the northern latitude, with $\hat{\mathbf{n}} = \hat{\mathbf{y}}$, yields

$$f_{\text{north}} \int_{y_{\text{north}}} h v \, dx \equiv f_{\text{north}} \mathcal{T}, \quad (36.147)$$

where \mathcal{T} is the meridional transport. Ignoring any volume transport through the layer surface (e.g., $w^{(\dot{\eta})} = 0$), the steady transport crossing the northern boundary equals to that crossing the southern boundary, so that

$$f_{\text{south}} \int_{y_{\text{south}}} h v \, dx \equiv f_{\text{south}} \mathcal{T}. \quad (36.148)$$

Making use of these results in the integral balance (36.146), and following the above assumptions about the boundary stresses, leads to *Godfrey's island rule*

$$\rho \mathcal{T} = \frac{1}{f_{\text{north}} - f_{\text{south}}} \oint_{\partial S} \boldsymbol{\tau}^{\text{wind}} \cdot \hat{\mathbf{t}} \, d\ell, \quad (36.149)$$

where $\boldsymbol{\tau}^{\text{wind}}$ is the wind stress, and where the minus sign on f_{south} arises since $\hat{\mathbf{n}} = -\hat{\mathbf{y}}$ along the southern latitude contour. This expression provides an approximation to the flow around Island A, noting that the only nonzero flow normal to the contour is through the two latitudinal segments.

36.9.4 Further study

[Godfrey \(1989\)](#) applied the island rule (36.149) to estimate transport around Austral-Asia, New Zealand, and Malagasy. Further discussion of Godfrey's island rule can be found in [Tomczak and Godfrey \(1994\)](#), [Pedlosky et al. \(1997\)](#), and [Klinger and Haine \(2019\)](#).



36.10 Exercises

EXERCISE 36.1: FLOW NEAR A TOPOGRAPHIC BUMP IN A REDUCED GRAVITY MODEL

Elements of this exercise are motivated by Figure 2 from [Adcock and Marshall \(2000\)](#) and Figure 1 from [Marshall et al. \(2012\)](#), where we consider a reduced gravity model with a dynamic lower layer and stagnant upper layer. Place a topographic bump (e.g., seamount or mountain) fully within the lower layer as shown in Figure 36.11.

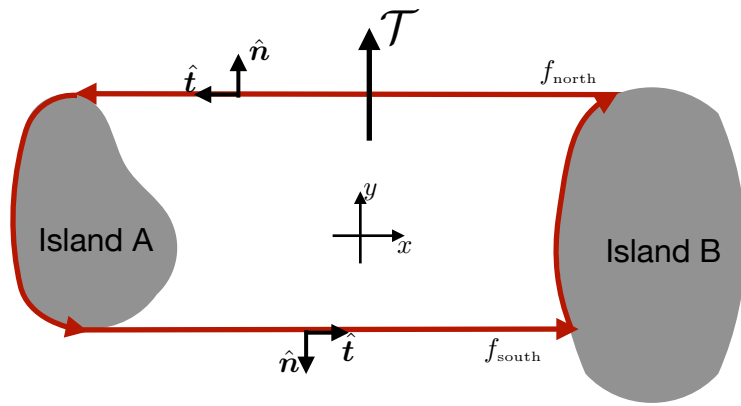


FIGURE 36.10: Illustrating the island rule with two land masses (“islands”). The red contour surrounds all of Island A and traverses along the eastern side of both Island A and Island B. The northern contour extends along a constant latitude line with a corresponding Coriolis parameter f_{north} , whereas the southern contour has Coriolis parameter f_{south} . Ignoring any precipitation or evaporation crossing the surface, steady state volume conservation means that the same meridional transport, \mathcal{T} , crosses both the southern and northern contours. Godfrey’s island rule (36.149) provides an estimate for this transport when given the wind stress along the contour.

- Following Exercise 32.5, derive the momentum and thickness equations for a reduced gravity model with a stagnant upper layer. Then derive the potential vorticity equation for the dynamical layer.
- Now assume an f -plane. If the lower layer potential vorticity is (somehow) horizontally homogenized (e.g., some form of mixing produces a horizontally constant PV), draw the resulting layer interface $\eta_{3/2}$. Assume the relative vorticity is negligible compared to the planetary vorticity so that the flow satisfies the planetary geostrophic scaling introduced in Section 36.5.2 and further pursued in Section 40.4. Also, ignore any non-steady processes; we are only interested here in the steady flow.
- For the case of horizontally homogenized potential vorticity from the previous part, what is the direction for a geostrophically balanced flow: cyclonic or anti-cyclonic? Hint: make use of Exercise 32.5 for the momentum equation of an inverted reduced gravity model.

EXERCISE 36.2: PV FOR TWO SHALLOW WATER LAYERS

Consider the inviscid Boussinesq two-layer shallow water model as discussed in Section 32.4. Derive the potential vorticity equation for each layer, showing the mathematical steps used in the derivation. Hint: the answer is given in Section 36.3.6.

EXERCISE 36.3: AVERAGE VORTICITY IN A SHALLOW WATER LAYER

Consider a single layer of shallow water fluid on a rotating plane with rotation rate $\Omega = \hat{z}\Omega$. Assume the fluid is contained in an arbitrary horizontal region and that it has a constant total volume given by

$$\mathcal{V} = \int \left[\int dz \right] d\mathcal{S} = \int h d\mathcal{S} = \int (H + \Delta\eta - \eta_b) d\mathcal{S} = H \mathcal{S}, \quad (36.150)$$

where \mathcal{S} is the horizontal area of the domain, $h(x, y, t) = H + \Delta\eta(x, y, t) - \eta_b(x, y)$ is the layer thickness, H is the resting depth relative to $z = 0$, $\Delta\eta$ is the sea level deviation from resting, and η_b is the undulation of the bottom topography (see Figure 32.1). Additionally, recall that $z = 0$

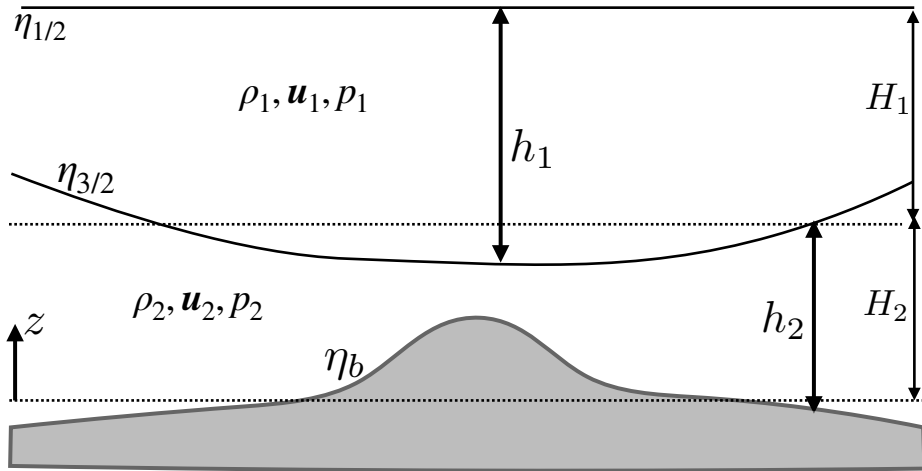


FIGURE 36.11: A reduced gravity model (see Section 32.3) with a stagnant upper layer and a dynamic lower layer as in Exercise 32.5. A seamount sits fully within the lower layer.

is set according to

$$\int \eta_b \, d\mathcal{S} = 0, \quad (36.151)$$

and volume conservation ensures that

$$\int \Delta\eta \, d\mathcal{S} = 0. \quad (36.152)$$

- (a) Determine the volume average of the vorticity $\hat{\mathbf{z}} \cdot \boldsymbol{\omega}_{\text{solid}}$ arising from the solid-body rotation

$$\langle \hat{\mathbf{z}} \cdot \boldsymbol{\omega}_{\text{solid}} \rangle = V^{-1} \int \hat{\mathbf{z}} \cdot \boldsymbol{\omega}_{\text{solid}} \, dV. \quad (36.153)$$

- (b) Determine the area average of the relative vorticity,

$$\bar{\zeta} = \mathcal{S}^{-1} \int \hat{\mathbf{z}} \cdot \boldsymbol{\omega} \, d\mathcal{S}, \quad (36.154)$$

in terms of the circulation around the boundary of the domain.

- (c) Determine the volume average of the relative vorticity

$$\langle \zeta \rangle = V^{-1} \int \hat{\mathbf{z}} \cdot \boldsymbol{\omega} \, dV. \quad (36.155)$$

Write the expression in terms of the area average vorticity, $\bar{\zeta}$, and the correlation, $\overline{\zeta' h'}$, where primes are deviations from the area mean.

EXERCISE 36.4: APPLICATIONS OF SHALLOW WATER PV CONSERVATION

In an adiabatic shallow water fluid in a rotating reference frame, show that the potential vorticity conservation law is

$$\frac{D}{Dt} \left[\frac{\zeta + f}{\eta - \eta_b} \right] = 0, \quad (36.156)$$

where η is the height of the free surface and η_b is the height of the bottom topography (see Figure

32.1). For both of the following questions, assume constant volume for the fluid column. Also, assume the column rotates about its axis as a solid-body.

- (a) A cylindrical column of air at 30° latitude with radius 100 km expands horizontally to twice its original radius. If the air is initially at rest, what is the mean tangential velocity at the perimeter after the expansion?
- (b) An air column at 60°N with zero relative vorticity ($\zeta = 0$) stretches from the surface to the tropopause, which we assume is a rigid lid at 10 km. The air column moves zonally onto a plateau 2.5 km high. What is its relative vorticity? Suppose it then moves southward along the plateau to 30°N , starting from the relative vorticity it obtained from the plateau. What is its new relative vorticity?

EXERCISE 36.5: APPLICATION OF SHALLOW WATER PV CONSERVATION

An air column at 60°N with $\zeta = 0$ initially reaches from the surface to a fixed tropopause at 10 km height. If the air column moves across a mountain 2.5 km high at 45°N , what is its absolute vorticity and relative vorticity as it passes the mountaintop? Hint: Use PV conservation for a shallow-water fluid, and assume the top of the column remains at 10 km.

EXERCISE 36.6: PROPERTIES OF THE STEADY STATE SHALLOW WATER FLUID

Consider a single layer of shallow water fluid in steady state (i.e., all Eulerian time derivatives vanish).

- (a) Show that there exists a streamfunction for the steady state thickness weighted horizontal flow

$$h \mathbf{u} = \hat{\mathbf{z}} \times \nabla \Psi. \quad (36.157)$$

- (b) What are the physical dimensions of Ψ ?

- (c) Show that the shallow water potential vorticity is a constant along the steady state streamlines of the thickness weighted flow

$$Q = Q(\Psi). \quad (36.158)$$

- (d) Show that the Bernoulli function,

$$B = g \eta + \mathbf{u} \cdot \mathbf{u} / 2 \quad (36.159)$$

is also a constant along the same streamlines; i.e.,

$$B = B(\Psi). \quad (36.160)$$

- (e) What is the functional relation between the Bernoulli function and the potential vorticity?
Hint: make use of the physical dimensions for Q , B , and Ψ to be sure that your solution is dimensionally consistent.

EXERCISE 36.7: ZONALLY SYMMETRIC SHALLOW WATER FRONT

Consider a single layer of shallow water fluid on a β -plane with a flat bottom. Assume all fields possess zonal symmetry as in the zonal front shown in Figure 36.12. Since the zonal pressure gradient vanishes under the assumption of zonal symmetry, the geostrophic portion of the meridional velocity vanishes. However, there is generally a non-zero ageostrophic component to this velocity, and we retain that possibility throughout this exercise.

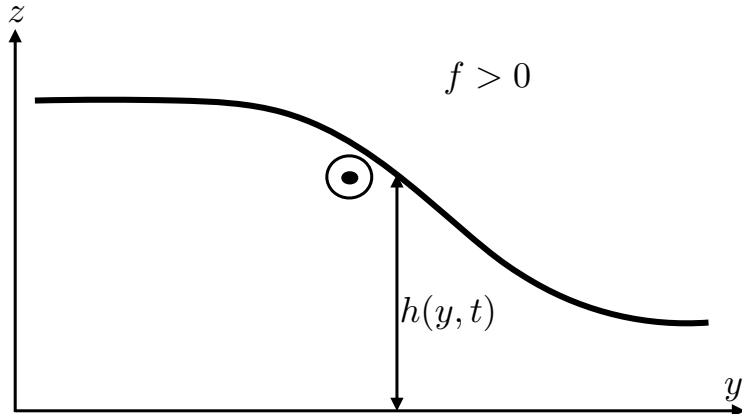


FIGURE 36.12: Schematic of a zonally symmetric front in a shallow water layer in the northern hemisphere ($f > 0$), here used for Exercise 36.7. The thickness decreases to the north. If the zonal flow is in geostrophic balance, then the northward pressure gradient is in geostrophic balance with a southward Coriolis acceleration arising from an eastward (out of the page) geostrophic current (see also Figure 33.1). The geostrophic component of the meridional flow vanishes due to zonal symmetry, but the full meridional flow need not vanish if there are ageostrophic processes. We allow for the possibility of a nonzero meridional velocity throughout this exercise.

- (a) Write the potential vorticity, Q , assuming the zonal flow is in geostrophic balance. Write Q terms of meridional derivatives of the layer thickness.
- (b) From the shallow water equations, explicitly show that the PV is materially constant (i.e., it is a Lagrangian invariant). To do so, work through the usual shallow water PV conservation derivation yet make use of the zonally symmetric equations of motion. Allow for a nonzero ageostrophic meridional flow. Show all relevant steps.
- (c) Show that the potential vorticity can be written as $Q = -(\partial_y M)/h$, where h is the layer thickness. What is the expression for M ? Hint: recall our discussion of potential momentum in Section 12.4.
- (d) Potential vorticity is not the only material constant for this system. Due to the zonal symmetry, Noether's Theorem indicates there is another. Show that M is materially constant. Again, continue to allow for a nonzero meridional velocity component.

EXERCISE 36.8: RAYLEIGH DRAG AND GALILEAN INVARIANCE

Recall the discussion of Galilean invariance from Section 14.7. Is the Rayleigh drag used in equation (36.78) Galilean invariant? Why? If not, then should that be of concern for its use in studying flow in a closed and bounded domain?

EXERCISE 36.9: GYRES IN THE PRESENCE OF CYCLONIC WINDS

Consider the ocean gyre discussion in Section 36.7. Rather than anti-cyclonic winds, now apply a cyclonic wind stress to the domain. As per the circulation theorem (36.81), the gyre flow will have a cyclonic sense. Will the resulting gyre exhibit eastern intensification or western? Appeal to whatever arguments you wish.

EXERCISE 36.10: SHALLOW WATER EQUATIONS WITH DIVERGENCE-DAMPING

When breaking the continuous symmetry of the equations of motion, a discretized numerical simulation admits unphysical flow features sometimes referred to as *computational modes*. Some computational modes can evolve in time with energy accumulating at high wave numbers, in which case the numerical simulation produces unphysical grid noise and becomes of little physical use. To suppress grid noise, numerical models commonly introduce numerical dissipation, even

if the continuous equations have zero dissipation. The formulation of numerical dissipation is largely an art guided by the dual needs of suppressing grid noise without otherwise damaging physical properties of the simulated flow. We here consider physical properties of a specific form of numerical dissipation known as *divergence-damping*. We work within the framework of the continuous equations so to develop generic physical properties of the divergence-damping operator. No knowledge of numerical methods is required to solve this problem.

Divergence-damping is motivated by the desire to leave the vorticity equation untouched while damping divergent motion that can arise in numerical simulations. This motivation is based on noting that much of the large-scale circulation in a rotating fluid has a nontrivial absolute vorticity yet a relatively small horizontal divergence. For example, geostrophic flow on an f -plane has vorticity dominated by planetary vorticity f , while it has zero horizontal divergence (see Section 28.4 or the 2d barotropic equation in Section 35.2). The divergence-damping operator is thus designed to reduce the magnitude of the horizontal divergence while leaving the vorticity untouched.

We here examine the impacts of divergence-damping on mechanical energy and angular momentum. For this purpose, consider a single layer of shallow water fluid with divergence-damping. This system is described by the momentum and thickness equations

$$\frac{D\mathbf{u}}{Dt} + f \hat{\mathbf{z}} \times \mathbf{u} = -\nabla(g\eta + \alpha\Gamma) \quad (36.161a)$$

$$\frac{Dh}{Dt} = -h\nabla \cdot \mathbf{u}. \quad (36.161b)$$

The parameter $\alpha > 0$ is a constant and the field Γ is given by the Laplacian of the horizontal flow divergence

$$\Gamma = \nabla^2 \mathcal{D}, \quad (36.162)$$

where

$$\mathcal{D} = \nabla \cdot \mathbf{u}. \quad (36.163)$$

The divergence has physical dimensions of inverse time (T^{-1}), so that its Laplacian, Γ , has dimensions of $L^{-2} T^{-1}$, and the coefficient α has dimensions $L^4 T^{-1}$.

Divergence damping leads to a modification to the horizontal pressure gradient. We may think of this modification as arising from the horizontal gradient of a modified free surface height

$$\tilde{\eta} = \eta + \frac{\alpha\Gamma}{g}. \quad (36.164)$$

Notably, mass conservation remains the same since the thickness equation is unchanged. Hence, momentum evolution is modified by changing the pressure gradient, yet the thickness equation remains the same.

- (a) Show that the vorticity equation (36.9) remains unchanged in the presence of divergence-damping.
- (b) Show that the potential vorticity equation (36.29) remains unchanged in the presence of divergence-damping.
- (c) Show that the horizontal divergence evolves according to

$$\frac{\partial \mathcal{D}}{\partial t} = \left[\frac{\partial \mathcal{D}}{\partial t} \right]_{\alpha=0} - \alpha \nabla^2 \Gamma. \quad (36.165)$$

- (d) Show that the evolution of gravitational potential energy per horizontal area

$$\mathcal{P} = g \rho \int_{\eta_b}^{\eta} z \, dz \quad (36.166)$$

remains unchanged from that determined in Section 33.5.1.

- (e) Show that the kinetic energy per horizontal area evolves according to

$$\frac{\partial \mathcal{K}}{\partial t} + \nabla \cdot (\mathbf{u} \mathcal{K}) = -h \rho g \mathbf{u} \cdot \nabla \tilde{\eta}, \quad (36.167)$$

where

$$\mathcal{K} = \frac{1}{2} \int_{\eta_b}^{\eta} \rho \mathbf{u}^2 \, dz = \rho h \mathbf{u}^2 / 2, \quad (36.168)$$

is the horizontal kinetic energy per area (Section 33.5.2).

- (f) Determine the evolution equation for global integrated kinetic energy

$$\frac{\partial}{\partial t} \left[\int \mathcal{K} \, dA \right] = \frac{\partial}{\partial t} \left[\int \int_{\eta_b}^{\eta} (\rho \mathbf{u} \cdot \mathbf{u} / 2) \, dz \, dA \right]. \quad (36.169)$$

Hint: drop all lateral boundary terms by assuming either solid lateral walls or periodicity.

- (g) Consider a single shallow water layer in a rotating tank as in Section 33.8. Show that the material evolution of angular momentum relative to the vertical rotational axis is given by

$$\frac{1}{\delta M} \frac{D L^z}{Dt} = -g \frac{\partial \eta}{\partial \phi} + \mathcal{T}. \quad (36.170)$$

What is the mathematical form for \mathcal{T} ? Hint: check your answer with the next part of this exercise.

- (h) Show that the domain integrated angular momentum satisfies the equation

$$\frac{\partial}{\partial t} \int L^z = \alpha \rho \int \Gamma \frac{\partial \eta}{\partial \phi} \, dA. \quad (36.171)$$

where we assume the bottom topography is flat so that $h = \eta$.

- (i) The linearized thickness equation (see Section 48.5) for a flat bottom is given by

$$\frac{\partial \eta}{\partial t} + H \nabla \cdot \mathbf{u} = 0, \quad (36.172)$$

where H is the thickness of the resting fluid layer. Show that the time change for the global integrated angular momentum is given by

$$\frac{\partial}{\partial t} \int L^z = -\frac{\alpha \rho}{H} \int \left[\frac{\partial}{\partial t} \nabla^2 \eta \right] \frac{\partial \eta}{\partial \phi} \, dA. \quad (36.173)$$



Chapter 37

VORTICITY AND CIRCULATION MECHANICS

In this chapter we study the kinematics and dynamics of vorticity and circulation, extending our introductory study in Chapter 34 and shallow water study in Chapter 36. An understanding of vorticity mechanics offers many insights into the nature of fluid flow and how that flow is constrained. Hence, vorticity is a central feature in nearly all theories of geophysical fluid mechanics. To ground the conceptual presentation, we include sample applications of particular importance to atmosphere and ocean flows.

In making use of vorticity for geophysical fluids, it is common to move beyond the vorticity of a fluid element as defined by the curl of the velocity field. For example, as a means to summarize facets of the vorticity contained within a three-dimensional fluid, we study the depth integral of the vorticity equation in Section 37.8 for a hydrostatic and Boussinesq fluid and in Section 41.5 for a planetary geostrophic flow. This analysis has its most common application to the ocean where the vertical domain is bounded and with vertical columns extending from the bottom at $z = \eta_b$ to the surface at $z = \eta$. Relatedly, there are occasions to study vorticity of the depth integrated or depth averaged flow, and we do so in Section 37.9. Such studies emphasize the importance of boundary forces and their curls (“torques”) for the vorticity of a fluid column.

CHAPTER GUIDE

This chapter assumes an understanding of vorticity developed in earlier chapters in this part of the book. We also make use of fluid kinematics from Part III and fluid dynamics from Part V. As for the shallow water vorticity discussed in Chapter 36, we here make use of vector calculus identities for Cartesian coordinates as detailed in Chapter 2. The concepts and methods developed in this chapter are fundamental to the notions of vorticity and circulation, with some encountered in the remainder of this part of the book as well as the balanced models considered in Part VIII.

Throughout this chapter, when considering spherical geometry, we make use of the planetary Cartesian coordinates from Figure 9.1. Since the sphere is assumed to be embedded in Euclidean space, we can naively perform integrals of vectors over the Euclidean space.

37.1	Loose threads	932
37.2	Kelvin’s circulation theorem	933
37.2.1	Formulation	933
37.2.2	Two processes affecting circulation	934
37.2.3	Barotropic flow	935
37.2.4	Pressure contribution to circulation in an ideal gas	935
37.2.5	Circulation around a loop with constant entropy and concentration	936
37.2.6	Circulation around a loop with constant S and Θ	937

37.2.7	Comments and further reading	937
37.3	Vorticity dynamics	938
37.3.1	Vector-invariant velocity equation	938
37.3.2	Basic form of the vorticity equation	938
37.3.3	Massaged form of the vorticity equation	939
37.3.4	Evolution of Cartesian vorticity components	939
37.3.5	Evolution of the normal component of absolute vorticity	941
37.3.6	Vorticity, angular momentum, and torques	942
37.4	Mechanics of baroclinicity	942
37.4.1	Curl of the pressure gradient body force	942
37.4.2	Kelvin's circulation theorem and contact pressure forces	943
37.4.3	Bottom pressure contributions at the solid-earth boundary	944
37.4.4	Further study	945
37.5	Vorticity filaments and material line elements	946
37.5.1	Vortex filaments evolve through the rate of strain	946
37.5.2	Frozen-in nature of vorticity	946
37.5.3	Stretching and tilting of vortex tubes	947
37.5.4	Shallow water vorticity revisited	949
37.5.5	Concerning three-dimensional turbulence	951
37.6	Circulation for rotating fluids	951
37.6.1	Material evolution of absolute circulation	952
37.6.2	The beta effect	953
37.6.3	The case of two-dimensional non-divergent flow	955
37.6.4	Further study	956
37.7	Vorticity budget in a primitive equation ocean	956
37.7.1	Deriving the vorticity equation	957
37.7.2	Boussinesq baroclinicity	958
37.7.3	Vertical vorticity equation	959
37.8	Depth integral of the vertical vorticity equation	961
37.8.1	Comments on the role of baroclinicity	961
37.8.2	Leibniz rule expressions	961
37.8.3	Bottom boundary contribution	962
37.8.4	Surface boundary contribution	963
37.8.5	Comments	964
37.9	Vorticity for the depth integrated horizontal flow	964
37.9.1	Comparing the two vorticities	965
37.9.2	Evolution of vorticity for the depth integrated horizontal flow	965
37.9.3	Boundary pressure torques	966
37.9.4	Steady state vorticity budget	968
37.9.5	Integral balances satisfied by steady flows	969
37.9.6	Formulation based on the vector-invariant velocity equation	970
37.9.7	Vorticity of the depth averaged flow	971
37.9.8	Comments and further study	972
37.10	Exercises	972

37.1 Loose threads

- Rewrite Section 37.8 using the full vertical vorticity equation derived in Section 37.3.4. The only difference is the presence of a component of baroclinicity, $-\hat{z} \times \rho^{-1} \nabla p$.

37.2 Kelvin's circulation theorem

Kelvin's circulation theorem is concerned with the evolution of circulation around a closed loop that follows the flow, or equivalently (through Stokes' theorem) with the change in vorticity penetrating the area enclosed by the loop

$$\frac{dC}{dt} = \frac{d}{dt} \oint_{\partial\mathcal{S}(\mathbf{v})} \mathbf{v} \cdot d\mathbf{x} = \frac{d}{dt} \int_{\mathcal{S}(\mathbf{v})} \boldsymbol{\omega} \cdot \hat{\mathbf{n}} d\mathcal{S}, \quad (37.1)$$

where $\mathcal{S}(\mathbf{v})$ designates a surface whose points all move with the fluid flow. We here consider the case of non-rotating flow, with the straightforward extension to rotating fluids studied in Section 37.6.

We emphasize that our concern is with circulation computed around closed loops that follow the flow. For homogeneous fluids, such loops are material (i.e., the same fluid particles are fixed to the loop). For multi-component fluids there is no perfectly material loop in the presence of diffusion, and yet we can still consider loops that follow the barycentric velocity, \mathbf{v} .

37.2.1 Formulation

Since the circulation is computed following the flow, the time derivative in equation (37.1) moves inside the integral as a material/Lagrangian time derivative¹

$$\frac{dC}{dt} = \frac{d}{dt} \oint_{\partial\mathcal{S}(\mathbf{v})} \mathbf{v} \cdot d\mathbf{x} = \oint_{\partial\mathcal{S}(\mathbf{v})} \frac{D(\mathbf{v} \cdot d\mathbf{x})}{Dt}. \quad (37.2)$$

The material evolution of \mathbf{v} is determined by Newton's law of motion, which for a non-rotating flow is given by (see Section 23.11)

$$\frac{D\mathbf{v}}{Dt} = -\frac{1}{\rho} \nabla p - \nabla \Phi + \mathbf{F}. \quad (37.3)$$

In this equation, p is the pressure, ρ is the mass density, Φ is the geopotential (and/or the potential for any conservative force), and \mathbf{F} is the acceleration from any non-conservative forces such as from viscous stresses and/or boundary interactions.

The material time derivative of the differential line element moving around the circuit equals to the differential of the velocity on the circuit

$$\frac{D(d\mathbf{x})}{Dt} = d\mathbf{v}. \quad (37.4)$$

This result follows since all points along the circuit follow the flow, by construction. Consequently,

¹In Section 17.3, we studied how to take derivatives of flow-following integrals.

evolution of circulation following a loop becomes

$$\frac{dC}{dt} = \oint_{\partial S(v)} [(-\rho^{-1} \nabla p - \nabla \Phi + \mathbf{F}) \cdot d\mathbf{x} + \mathbf{v} \cdot dv] \quad (37.5a)$$

$$= \oint_{\partial S(v)} [(-\rho^{-1} \nabla p + \mathbf{F}) \cdot d\mathbf{x} + d(-\Phi + \mathbf{v} \cdot \mathbf{v}/2)] \quad (37.5b)$$

$$= \oint_{\partial S(v)} (-\rho^{-1} \nabla p + \mathbf{F}) \cdot d\mathbf{x} \quad (37.5c)$$

$$= \int_{S(v)} [-\nabla \times (\rho^{-1} \nabla p) + \nabla \times \mathbf{F}] \cdot \hat{\mathbf{n}} dS \quad (37.5d)$$

$$= \int_{S(v)} (\mathbf{B} + \nabla \times \mathbf{F}) \cdot \hat{\mathbf{n}} dS. \quad (37.5e)$$

We noted that when integrating over space at a particular time, $\nabla \Phi \cdot d\mathbf{x} = d\Phi$ is an exact spatial differential, and so is dv^2 . Hence, they both have a zero line integral around a closed circuit in space²

$$\oint_{\partial S(v)} d\Phi = 0 \quad \text{and} \quad \oint_{\partial S(v)} dv^2 = 0. \quad (37.6)$$

37.2.2 Two processes affecting circulation

Equation (37.5e) says that the circulation around a flow-following loop is affected by two processes, whose form depends on whether considering their line integral or surface integral expressions. The irreversible process arises from frictional acceleration

$$\oint_{\partial S(v)} \mathbf{F} \cdot d\mathbf{x} = \int_{S(v)} (\nabla \times \mathbf{F}) \cdot \hat{\mathbf{n}} dS, \quad (37.7)$$

with the line integral form expressing the mechanical work per unit mass (acceleration times distance) done by friction around the closed loop.³ Friction dissipates kinetic energy, so that friction generally reduces the magnitude of the circulation. The surface integral form expresses the curl of friction as integrated over the surface.

The reversible process affecting circulation in equation (37.5e) arises from the pressure gradient acceleration

$$\oint_{\partial S(v)} (-\rho^{-1} \nabla p) \cdot d\mathbf{x} = \int_{S(v)} \rho^{-2} (\nabla \rho \times \nabla p) \cdot \hat{\mathbf{n}} dS = \int_{S(v)} \mathbf{B} \cdot \hat{\mathbf{n}} dS. \quad (37.8)$$

As for friction, the line integral form expresses the mechanical work per unit mass (acceleration times distance) done by the pressure gradient acceleration as integrated around the circuit. The vector \mathbf{B} is referred to as the *baroclinicity*

$$\mathbf{B} = -\nabla \times (\rho^{-1} \nabla p) = \rho^{-2} \nabla \rho \times \nabla p, \quad (37.9)$$

and it has physical dimensions of inverse squared time, T^{-2} . Its appearance in the circulation theorem arises from the non-alignment of density and pressure isolines.

Work done by pressure around an arbitrary loop does not generally vanish, nor does it have a specific sign. However, there are a variety of special loops around which the pressure work

²See Section 2.8 for more on exact differentials.

³We introduced the notions of mechanical work in Section 10.1.5.

does vanish. For example, the pressure work vanishes for closed contours on surfaces of constant density or constant pressure. However, such contours are generally not flow-following, and so their circulation is less interesting dynamically. In the remainder of this section, we consider some more relevant cases where baroclinicity vanishes.

37.2.3 Barotropic flow

The solenoidal/baroclinicity vector vanishes for a constant density fluid, in which $\nabla\rho = 0$ such as for a single layer of shallow water fluid. More generally, the baroclinicity vector vanishes for barotropic flow, in which

$$p = p(\rho) \implies \text{barotropic flow.} \quad (37.10)$$

Kelvin's circulation theorem then follows, which states that for inviscid barotropic flow the circulation around any closed flow-following circuit remains constant

$$\frac{d\mathcal{C}}{dt} = \frac{d}{dt} \oint_{\partial\mathcal{S}(\mathbf{v})} \mathbf{v} \cdot d\mathbf{x} = \frac{d}{dt} \int_{\mathcal{S}(\mathbf{v})} \boldsymbol{\omega} \cdot \hat{\mathbf{n}} d\mathcal{S} = 0 \quad \iff \text{inviscid barotropic flow.} \quad (37.11)$$

That is, the circulation around any vortex tube in a perfect barotropic fluid moves in a manner that keeps the circulation materially constant. This remarkable result greatly constrains the motion of a perfect barotropic fluid.

Another way to recognize that baroclinicity vanishes for a barotropic flow is to note that the curl of the pressure gradient acceleration vanishes

$$\nabla \times (\rho^{-1} \nabla p) = 0. \quad (37.12)$$

Hence, there is a scalar potential whereby

$$\nabla \Phi_p = \rho^{-1} \nabla p, \quad (37.13)$$

with integration leading to

$$\Phi_p = \int_{p_0}^p \frac{dp'}{\rho(p')}, \quad (37.14)$$

where p_0 is an arbitrary reference pressure.⁴ The identity (37.13) means that the pressure gradient acceleration for a barotropic flow is an exact spatial differential

$$\rho^{-1} \nabla p \cdot d\mathbf{x} = \rho^{-1} dp \equiv d\Phi_p. \quad (37.15)$$

Since the closed loop integral of an exact differential vanishes, we again see that the pressure gradient acceleration has no impact on circulation around flow-following loops in a barotropic flow.

37.2.4 Pressure contribution to circulation in an ideal gas

Building on the notions from a barotropic flow in Section 37.2.3, we here determine an important class of contours for an ideal gas where baroclinicity vanishes even if the flow is not barotropic. To start, recall from Exercise 20.3 that we derived equation (20.106) for an ideal gas

$$\rho^{-1} \nabla p = \theta \nabla \Pi, \quad (37.16)$$

⁴We make use of the scalar potential, Φ_p , in Exercise 37.9.

where θ is the potential temperature (equation (20.92)) and Π is the Exner function (equation (20.93)). This equation says that the pressure gradient acceleration, for an ideal gas, is equal to the potential temperature times the gradient of the Exner function. We can thus write the pressure gradient acceleration contribution in equation (37.5c) as

$$-\oint_{\partial S(v)} \rho^{-1} \nabla p \cdot d\mathbf{x} = -\oint_{\partial S(v)} \theta \nabla \Pi \cdot d\mathbf{x} = -\oint_{\partial S(v)} \theta d\Pi = \oint_{\partial S(v)} \Pi d\theta, \quad (37.17)$$

where the final step noted that the closed loop integral of an exact differential vanishes

$$\oint_{\partial S(v)} d(\theta \Pi) = 0. \quad (37.18)$$

Hence, the contribution from baroclinicity (i.e., pressure gradient acceleration) vanishes for closed contours drawn either on a constant Π surface or a constant θ surface. For an ideal gas, changes in θ are directly related to changes in specific entropy (see equation (23.190) from Exercise 23.4). Hence, for a perfect fluid flow of an ideal gas, where specific entropy is materially invariant, so too is potential temperature: $D\theta/Dt = 0$. It follows that a contour drawn on a potential temperature surface remains a flow-following contour for a perfect fluid. We have thus deduced that isentropic flow of an ideal gas has a flow-following circulation that is unaffected by baroclinicity.

37.2.5 Circulation around a loop with constant entropy and concentration

We here make use of the expression (23.62) for the pressure gradient acceleration in terms of thermodynamic functions

$$-\rho^{-1} \nabla p = -\nabla \mathcal{H} + T \nabla \mathcal{S} + \mu \nabla C, \quad (37.19)$$

where \mathcal{H} is the specific enthalpy, \mathcal{S} is the specific entropy, T is the thermodynamic (Kelvin) *in situ* temperature, and μ is the chemical potential for a binary fluid such as commonly assumed for the ocean (freshwater and salt) and atmosphere (dry air and water vapor). Equation (37.19) holds for a compressible fluid, in which the thermodynamic pressure and mechanical pressure are the same (Section 22.8.1).

The identity (37.19) brings the pressure gradient contribution to Kelvin's circulation theorem (37.5e) into

$$-\oint_{\partial S(v)} \rho^{-1} \nabla p \cdot d\mathbf{x} = \oint_{\partial S(v)} (T \nabla \mathcal{S} + \mu \nabla C) \cdot d\mathbf{x}, \quad (37.20)$$

where we set

$$\oint_{\partial S(v)} \nabla \mathcal{H} \cdot d\mathbf{x} = 0, \quad (37.21)$$

which holds since \mathcal{H} is a state function so that

$$\nabla \mathcal{H} \cdot d\mathbf{x} = d\mathcal{H} \quad (37.22)$$

is an exact spatial differential. The decomposition (37.20) reveals that the pressure contribution to circulation vanishes when computing circulation for an isentropic and constant concentration loop⁵

$$\oint_{\partial S(v)} \rho^{-1} \nabla p \cdot d\mathbf{x} = 0 \quad \text{if } d\mathcal{S} = 0 \text{ and } dC = 0. \quad (37.23)$$

⁵For the ocean, an isentropic and constant salt concentration process maintains a constant Conservative Temperature.

Such loops follow the flow in those cases where specific entropy and matter concentration are materially invariant

$$\frac{D\delta}{Dt} = 0 \quad \text{and} \quad \frac{DC}{Dt} = 0. \quad (37.24)$$

It follows that for the special case of a homogeneous fluid ($C = \text{constant}$) undergoing isentropic quasi-static changes, pressure plays no role in the circulation computed around an isentropic loop.

37.2.6 Circulation around a loop with constant S and Θ

Rather than invoking the gradient form of the fundamental thermodynamic relation (37.19), consider an ocean application where equation (27.10) says that the *in situ* density, ρ , takes on the functional form

$$\rho = \rho(S, \Theta, p), \quad (37.25)$$

with S the salinity and Θ the Conservative Temperature. It follows that along a contour that maintains fixed S and Θ , the pressure gradient acceleration is a function just of the pressure, in which case we write

$$\rho^{-1} \nabla p \cdot d\mathbf{x} = \rho^{-1}(S_{\text{const}}, \Theta_{\text{const}}, p) dp \equiv d\Psi_p \quad \text{if } S \text{ and } \Theta \text{ are fixed,} \quad (37.26)$$

where we followed the barotropic case of equation (37.14) to write

$$\Psi_p(S_{\text{const}}, \Theta_{\text{const}}, p) = \int_{p_0}^p \frac{dp'}{\rho(S_{\text{const}}, \Theta_{\text{const}}, p')}, \quad (37.27)$$

with p_0 an arbitrary reference pressure. As in Section 37.2.5, we conclude that pressure plays no role in affecting circulation around loops with fixed S and Θ

$$\oint_{\partial\mathcal{S}(\mathbf{v})} \rho^{-1} \nabla p \cdot d\mathbf{x} = \oint_{\partial\mathcal{S}(\mathbf{v})} d\Psi_p(S, \Theta, p) = 0 \quad \text{if } S = S_{\text{const}} \text{ and } \Theta = \Theta_{\text{const}}, \quad (37.28)$$

which follows since $d\Psi_p$ is an exact spatial differential. Such closed loop contours follow the flow if S and Θ are materially invariant

$$\frac{DS}{Dt} = 0 \quad \text{and} \quad \frac{D\Theta}{Dt} = 0, \quad (37.29)$$

which is the case in the absence of mixing and/or sources of S and Θ .

37.2.7 Comments and further reading

There is no guarantee that the closed loops discussed in Sections 37.2.5 and 37.2.6 exist in any particular flow. All we showed that *if* such closed contours exist, and if the flow maintains materially invariant specific entropy and concentration (Section 37.2.5) or salinity and Conservative Temperature (Section 37.2.6), then the circulation around such loops is unaffected by the pressure gradient acceleration.

Our presentation of Kelvin's circulation theorem anticipates analogous considerations encountered with potential vorticity in Chapter 38, with portions of the discussion motivated by [Kooloth et al. \(2022\)](#).

37.3 Vorticity dynamics

We now move from the circulation around a macroscopic circuit to the vorticity at a point. In particular, we seek information for how vorticity changes in time. What physical processes lead to these changes? As for Kelvin's theorem, we make use of Newton's law of motion, written here in the form for a rotating fluid (see Section 23.11)

$$\frac{D\mathbf{v}}{Dt} + 2\boldsymbol{\Omega} \times \mathbf{v} = -\rho^{-1} \nabla p - \nabla \Phi + \mathbf{F}, \quad (37.30)$$

where $\boldsymbol{\Omega}$ is the angular velocity of the rotating reference frame.

37.3.1 Vector-invariant velocity equation

As for the shallow water fluid in Section 36.1, we find it useful to convert the advective-form momentum equation to vector-invariant velocity equation. For this purpose, make use of the vector identity (see Section 2.3.4)

$$\boldsymbol{\omega} \times \mathbf{v} = -(1/2) \nabla(\mathbf{v} \cdot \mathbf{v}) + (\mathbf{v} \cdot \nabla) \mathbf{v} \quad (37.31)$$

to eliminate velocity self-advection in favor of vorticity

$$\frac{\partial \mathbf{v}}{\partial t} + \boldsymbol{\omega}_a \times \mathbf{v} = -\frac{1}{\rho} \nabla p - \nabla \left[\frac{1}{2} \mathbf{v}^2 + \Phi \right] + \mathbf{F}. \quad (37.32)$$

We here introduced the absolute vorticity

$$\boldsymbol{\omega}_a = \boldsymbol{\omega} + 2\boldsymbol{\Omega}, \quad (37.33)$$

which is the sum of the relative vorticity plus the planetary vorticity (see Section 34.5.1).

37.3.2 Basic form of the vorticity equation

Taking the curl of the vector-invariant momentum equation (37.32) removes the mechanical energy per mass, $\mathbf{v}^2/2 + \Phi$, thus leaving

$$\frac{\partial \boldsymbol{\omega}}{\partial t} + \nabla \times (\boldsymbol{\omega}_a \times \mathbf{v}) = \frac{1}{\rho^2} (\nabla \rho \times \nabla p) + \nabla \times \mathbf{F}. \quad (37.34)$$

For geophysical fluids we generally assume that $\boldsymbol{\Omega}$ has zero time tendency, so that

$$\frac{\partial \boldsymbol{\omega}_a}{\partial t} = \frac{\partial (\boldsymbol{\omega} + 2\boldsymbol{\Omega})}{\partial t} = \frac{\partial \boldsymbol{\omega}}{\partial t}, \quad (37.35)$$

in which case equation (37.34) can be written as an equation for absolute vorticity

$$\frac{\partial \boldsymbol{\omega}_a}{\partial t} + \nabla \times (\boldsymbol{\omega}_a \times \mathbf{v}) = \mathbf{B} + \nabla \times \mathbf{F}, \quad (37.36)$$

where \mathbf{B} is the baroclinicity vector given by equation (37.9).

37.3.3 Massaged form of the vorticity equation

Physical interpretation of the term $\nabla \times (\boldsymbol{\omega}_a \times \mathbf{v})$ appearing in the prognostic equation (37.36) can be made more transparent by using the following vector identity

$$\nabla \times (\boldsymbol{\omega}_a \times \mathbf{v}) = (\mathbf{v} \cdot \nabla) \boldsymbol{\omega}_a - (\boldsymbol{\omega}_a \cdot \nabla) \mathbf{v} + \boldsymbol{\omega}_a \nabla \cdot \mathbf{v} - \mathbf{v} \nabla \cdot \boldsymbol{\omega}_a \quad (37.37a)$$

$$= (\mathbf{v} \cdot \nabla) \boldsymbol{\omega}_a - (\boldsymbol{\omega}_a \cdot \nabla) \mathbf{v} - \frac{\boldsymbol{\omega}_a}{\rho} \frac{D\rho}{Dt}. \quad (37.37b)$$

The second equality required the continuity equation

$$\frac{D\rho}{Dt} = -\rho \nabla \cdot \mathbf{v}, \quad (37.38)$$

and the non-divergent nature of the absolute vorticity

$$\nabla \cdot \boldsymbol{\omega}_a = \nabla \cdot (\nabla \times \mathbf{v} + 2\boldsymbol{\Omega}) = 0. \quad (37.39)$$

Equation (37.36) thus takes the form

$$\frac{D\boldsymbol{\omega}_a}{Dt} - \frac{\boldsymbol{\omega}_a}{\rho} \frac{D\rho}{Dt} = (\boldsymbol{\omega}_a \cdot \nabla) \mathbf{v} + \frac{1}{\rho^2} (\nabla \rho \times \nabla p) + \nabla \times \mathbf{F}, \quad (37.40)$$

which can be written

$$\rho \frac{D(\boldsymbol{\omega}_a/\rho)}{Dt} = (\boldsymbol{\omega}_a \cdot \nabla) \mathbf{v} + \mathbf{B} + \nabla \times \mathbf{F}. \quad (37.41)$$

Each term on the right hand side of the material evolution equation (37.41) represents a distinct physical process that affects $\boldsymbol{\omega}_a/\rho$ of a fluid element. The first term, $(\boldsymbol{\omega}_a \cdot \nabla) \mathbf{v}$, embodies stretching and twisting and is explored in Section 37.5 in the simplified context of a barotropic fluid. The second term arises from baroclinicity as introduced in equation (37.9) and given a mechanical interpretation in Section 37.4. The third term arises from the curl of the friction vector, which contributes especially in boundary layer regions where friction curls are relatively large in magnitude.

37.3.4 Evolution of Cartesian vorticity components

The terms appearing on the right hand side of the vorticity equation (37.41) provide sources for the vorticity of a fluid element. However, these sources are quite special in that they can be written as the convergence of a flux corresponding to each component of the vorticity. We here expose that property by deriving Eulerian flux-form conservation equations that are separately satisfied by each of the vorticity components.

For this purpose, consider the equation for the vertical component of the absolute vorticity

$$\rho \frac{D(\zeta_a/\rho)}{Dt} = (\boldsymbol{\omega}_a \cdot \nabla) w + \hat{\mathbf{z}} \cdot (\mathbf{B} + \nabla \times \mathbf{F}) \quad \text{with } \zeta_a = \hat{\mathbf{z}} \cdot \boldsymbol{\omega}_a. \quad (37.42)$$

Making use of the identities

$$\rho \frac{D(\zeta_a/\rho)}{Dt} = \frac{\partial \zeta_a}{\partial t} + \nabla \cdot (\mathbf{v} \zeta_a) \quad (37.43a)$$

$$(\boldsymbol{\omega}_a \cdot \nabla) w = \nabla \cdot (\boldsymbol{\omega}_a w) \quad (37.43b)$$

$$\hat{\mathbf{z}} \cdot \mathbf{B} = -\hat{\mathbf{z}} \cdot [\nabla \times (\rho^{-1} \nabla p)] = \nabla \cdot (\hat{\mathbf{z}} \times \rho^{-1} \nabla p) \quad (37.43c)$$

$$\hat{\mathbf{z}} \cdot (\nabla \times \mathbf{F}) = -\nabla \cdot (\hat{\mathbf{z}} \times \mathbf{F}), \quad (37.43d)$$

brings equation (37.42) into the Eulerian flux-form

$$\frac{\partial \zeta_a}{\partial t} = -\nabla \cdot \mathbf{J}_\zeta \quad \text{with} \quad \mathbf{J}_\zeta = \mathbf{v} \zeta_a - \boldsymbol{\omega}_a w - \hat{\mathbf{z}} \times \rho^{-1} \nabla p + \hat{\mathbf{z}} \times \mathbf{F}. \quad (37.44)$$

This budget equation says that ζ_a evolves at a point according to the convergence of a flux, \mathbf{J}_ζ . There are no source terms appearing outside of the flux. This vorticity flux is comprised of an advective flux of vertical vorticity, $\mathbf{v} \zeta_a$; a contribution from absolute vorticity transported vertically, $-\boldsymbol{\omega}_a w$; a contribution from the pressure gradient acceleration rotated clockwise by $\pi/2$ radians around the vertical axis, $-\hat{\mathbf{z}} \times \rho^{-1} \nabla p$; and the $\pi/2$ counter-clockwise rotated friction acceleration, $\hat{\mathbf{z}} \times \mathbf{F}$. Note that there is no vertical component to the vorticity flux:

$$\hat{\mathbf{z}} \cdot \mathbf{J}_\zeta = \hat{\mathbf{z}} \cdot [\mathbf{v} \zeta_a - \boldsymbol{\omega}_a w - \hat{\mathbf{z}} \times \rho^{-1} \nabla p + \hat{\mathbf{z}} \times \mathbf{F}] = 0, \quad (37.45)$$

so that ζ_a is only affected by the convergence of a purely horizontal flux. We offer a schematic of this property in Figure 37.1.

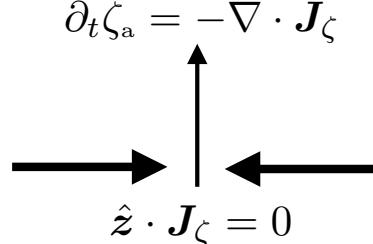


FIGURE 37.1: Tendency for the vertical component to the absolute vorticity arises from the convergence of the vorticity flux, \mathbf{J}_ζ , given by equation (37.44). This vorticity flux is strictly horizontal, $\mathbf{J}_\zeta \cdot \hat{\mathbf{z}} = 0$. This result generalizes for any arbitrary Cartesian component of the absolute vorticity, whereby the corresponding vorticity flux is orthogonal to its vorticity component. Generalization of this result leads to the impermeability theorem of potential vorticity studied in Section 39.2.

Mathematically, there is nothing special about the vertical vorticity component. Hence, we readily find that the horizontal vorticity components also satisfy their own respective Eulerian flux-form conservation equations, thus leading to the general result

$$\frac{\partial(\hat{\mathbf{e}} \cdot \boldsymbol{\omega}_a)}{\partial t} = -\nabla \cdot [\mathbf{v}(\hat{\mathbf{e}} \cdot \boldsymbol{\omega}_a) - \boldsymbol{\omega}_a(\hat{\mathbf{e}} \cdot \mathbf{v}) - \hat{\mathbf{e}} \times \rho^{-1} \nabla p + \hat{\mathbf{e}} \times \mathbf{F}], \quad (37.46)$$

where $\hat{\mathbf{e}}$ is any one of the Cartesian unit vectors $\hat{\mathbf{x}}, \hat{\mathbf{y}}, \hat{\mathbf{z}}$. Furthermore, we readily see that the vorticity flux satisfies

$$\hat{\mathbf{e}} \cdot [\mathbf{v}(\hat{\mathbf{e}} \cdot \boldsymbol{\omega}_a) - \boldsymbol{\omega}_a(\hat{\mathbf{e}} \cdot \mathbf{v}) - \hat{\mathbf{e}} \times \rho^{-1} \nabla p + \hat{\mathbf{e}} \times \mathbf{F}] = 0, \quad (37.47)$$

so that the time tendency for $\hat{\mathbf{e}} \cdot \boldsymbol{\omega}_a$ is affected by a flux in the directions orthogonal to $\hat{\mathbf{e}}$. This

property of the vorticity flux is generalized via the impermeability theorem of potential vorticity studied in Section 39.2, with particular connection to the present discussion given in Section 39.2.2.

37.3.5 Evolution of the normal component of absolute vorticity

As a further examination of vorticity components, we here consider the material evolution of vorticity projected onto the unit normal vector, $\hat{\mathbf{n}}$, for an infinitesimal material area, $\delta\mathcal{S}$. This discussion leads to an infinitesimal version of Kelvin's circulation theorem, thus explicitly linking the evolution equations for vorticity and circulation. In the process we make use of some kinematics from Chapter 15.

The unit normal vector to a material surface evolves according to equation (15.64e)

$$\frac{D\hat{n}_m}{Dt} = -\hat{\mathbf{n}} \cdot \partial_m^{\text{surf}} \mathbf{v}, \quad (37.48)$$

where the surface derivative, and corresponding surface divergence, are given from equation (15.60)

$$\partial_m^{\text{surf}} = \partial_m - \hat{n}_m (\hat{\mathbf{n}} \cdot \nabla) \quad \text{and} \quad \nabla^{\text{surf}} = \nabla - \hat{\mathbf{n}} (\hat{\mathbf{n}} \cdot \nabla). \quad (37.49)$$

Making use of the vorticity equation in the form (37.40), along with the continuity equation (37.38), leads to

$$\hat{\mathbf{n}} \cdot \frac{D\omega_a}{Dt} - (\hat{\mathbf{n}} \cdot \omega_a) \nabla \cdot \mathbf{v} + \hat{n}_j (\omega_a \cdot \nabla) v_j + \hat{\mathbf{n}} \cdot (\mathbf{B} + \nabla \times \mathbf{F}). \quad (37.50)$$

Likewise, taking the dot product of ω_a with the evolution equation (37.48) yields

$$\omega_a \cdot \frac{D\hat{\mathbf{n}}}{Dt} = \hat{n}_j [-(\omega_a \cdot \nabla) + (\hat{\mathbf{n}} \cdot \omega_a) (\hat{\mathbf{n}} \cdot \nabla)] v_j. \quad (37.51)$$

Adding these two equations renders the material time evolution

$$\frac{D(\omega_a \cdot \hat{\mathbf{n}})}{Dt} = -(\omega_a \cdot \hat{\mathbf{n}}) \nabla^{\text{surf}} \cdot \mathbf{v} + \hat{\mathbf{n}} \cdot (\mathbf{B} + \nabla \times \mathbf{F}). \quad (37.52)$$

The surface divergence of the velocity measures, via equation (15.61), the evolution of the material surface area

$$\frac{1}{\delta S} \frac{D\delta\mathcal{S}}{Dt} = \nabla^{\text{surf}} \cdot \mathbf{v}, \quad (37.53)$$

so that the material evolution equation for the $\hat{\mathbf{n}}$ component of absolute vorticity is

$$\frac{D(\omega_a \cdot \hat{\mathbf{n}})}{Dt} = -\frac{(\omega_a \cdot \hat{\mathbf{n}})}{\delta S} \frac{D\delta\mathcal{S}}{Dt} + \hat{\mathbf{n}} \cdot (\mathbf{B} + \nabla \times \mathbf{F}). \quad (37.54)$$

The area term arises from the familiar “ice-skater” effect reflecting angular momentum conservation for the column (Section 36.2.2), whereas the other terms are the projection of the baroclinicity and friction curl onto $\hat{\mathbf{n}}$. Bringing the area term onto the left hand side then renders the infinitesimal form of Kelvin's circulation theorem (37.5e)

$$\frac{D}{Dt} (\omega_a \cdot \hat{\mathbf{n}} d\mathcal{S}) = (\mathbf{B} + \nabla \times \mathbf{F}) \cdot \hat{\mathbf{n}} d\mathcal{S}. \quad (37.55)$$

Note the presence of the absolute vorticity, ω_a , in equation (37.54) rather than the relative vorticity considered in Section 37.2. We return in Section 37.6 to the question of circulation arising from

planetary rotation, where we derive the finite version of the circulation theorem (37.54).

37.3.6 Vorticity, angular momentum, and torques

Both vorticity and angular momentum offer measures of the rotational motion of a fluid flow. However, there are key distinctions as detailed in Section 34.8. Perhaps the most fundamental distinction is that vorticity measures the rotation or spin without reference to an origin, whereas angular momentum is computed relative to a subjectively chosen origin. Vorticity is thus an intrinsic property of the fluid flow, whereas angular momentum depends on the chosen origin and is affected by fluid strains in the region between the point and the origin. Consequently, there is a direct connection between angular momentum and vorticity only for the special case of flow exhibiting solid-body motion.

Angular momentum of motion relative to an origin changes in the presence of torques computed about the chosen origin, with the torque equal to the cross product of the position vector of a point and the force vector acting at that point. In contrast, vorticity at a point is affected by the curl of the force per mass acting at the point. Furthermore, angular momentum is a property of any mechanical system, including point particles and rigid bodies, whereas vorticity is a property only of a continuous media where we can compute spatial derivatives.

When the curl of a force per mass is applied to a fluid and thus changes its vorticity, we commonly use the term “torque” in reference to this force curl. For example, in Section 37.4 we explore baroclinicity, which is the key mechanism for how inviscid torques from pressure modify vorticity. In that discussion, we see that baroclinicity provides a vorticity source when the pressure force acting on a fluid element does not pass through the center of mass of that element. When there is baroclinicity, the pressure force spins the fluid element thus affecting vorticity. Analogous inviscid and viscous force curls act on boundaries, such as when a fluid interacts with the solid earth. It is within this context that we use the term “torque” when referring to a vorticity source. Correspondingly, the torques providing a vorticity source have the dimension of force per mass per length, whereas the torques altering angular momentum have the dimension of force times length.

37.4 Mechanics of baroclinicity

Baroclinicity is present in most geophysical flows, thus affecting the material evolution of circulation and vorticity. Flow with a nonzero baroclinicity vector is generally referred to as *baroclinic flow*, whereas *barotropic* flows have zero baroclinicity. We illustrate the basic distinction between barotropic and baroclinic fluids in Figure 37.2. We observe that a baroclinic fluid is associated with fluid motion that is a function of depth. In contrast, a barotropic fluid in the special case of pressure and density surfaces aligned with geopotentials, supports no motion. We further develop these points as we explore the mechanics of baroclinicity in the following.

37.4.1 Curl of the pressure gradient body force

Baroclinicity is the curl of the pressure gradient body force

$$\mathbf{B} = \nabla \times \mathbf{F}_{\text{press}} = \nabla \times (-\rho^{-1} \nabla p) = -\nabla \rho^{-1} \times \nabla p = \frac{\nabla \rho \times \nabla p}{\rho^2}. \quad (37.56)$$

As discussed in Section 37.3.6, the curl of a force provides a torque that spins the fluid, thus rendering a vorticity source. Geometrically, baroclinicity arises when there is nonzero change in pressure along contours of constant density, or conversely changes in density along contours of

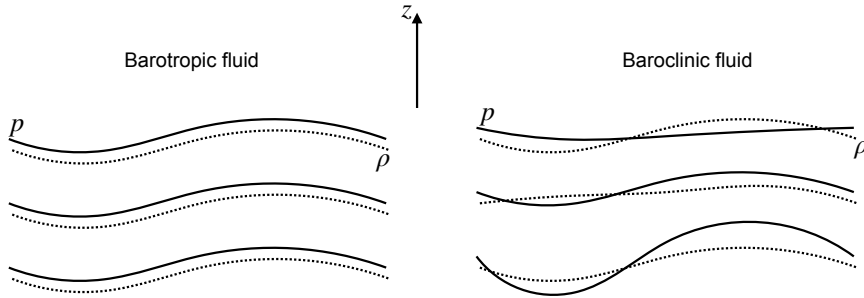


FIGURE 37.2: Left panel: a barotropic fluid, whereby density is a function just of pressure, $\rho = \rho(p)$, so that density surfaces (dashed lines) and pressure surfaces (solid lines) are parallel. Horizontal density and pressure surfaces in a barotropic fluid support no motion. Right panel: a baroclinic fluid, whereby density and pressure surfaces generally differ so that density is a function of more than just the pressure. A baroclinic fluid is associated with fluid motion.

constant pressure.⁶ It can be useful to introduce the notion of a *solenoid*, which is a tube region in the fluid that is perpendicular to both $\nabla\rho$ and ∇p . There are no solenoids for barotropic flows, whereby $p = p(\rho)$ (see equation (37.10)). For baroclinic flow, solenoids are associated with a torque that affects vorticity.

To further understand the mechanical interpretation of solenoids in terms of a torque, consider the cross product

$$\rho \mathbf{B} = \mathbf{F}^{\text{press}} \times \nabla\rho = (-\rho^{-1} \nabla p) \times \nabla\rho. \quad (37.57)$$

The first term on the right hand side is the pressure gradient force that acts down the pressure gradient. Now consider a tiny fluid element such as shown in Figure 37.3. By construction, the pressure force acts at the geometric center of the element. However, the nonzero density gradient means that the center of mass for the fluid element is not at the geometric center. Since the pressure force does not pass through the center of mass, it imparts a torque to the fluid element. This torque then modifies the vorticity and hence the circulation around the boundary of the element. Only when the pressure force is aligned with the density gradient (barotropic flow), or if the density is spatially uniform (e.g., constant density homogeneous fluid) does the pressure force pass through the center of mass, thus creating no torque and inducing no vorticity.

37.4.2 Kelvin's circulation theorem and contact pressure forces

We are afforded another means to understand baroclinicity by returning to the formulation of Kelvin's circulation theorem in Section 37.2.1. Focusing just on the baroclinicity contribution in equation (37.5e) we have

$$\left[\frac{dC}{dt} \right]_{\text{baroclinicity}} = \oint_{\partial S(v)} -\rho^{-1} \nabla p \cdot d\mathbf{x} = \oint_{\partial S(v)} \rho^{-2} (-p \nabla\rho) \cdot d\mathbf{x}, \quad (37.58)$$

which follows since

$$\oint_{\partial S(v)} \nabla(p/\rho) \cdot d\mathbf{x} = \oint_{\partial S(v)} d(p/\rho) = 0. \quad (37.59)$$

The term $-p \nabla\rho$ in equation (37.58) is proportional to the compressive contact pressure force (Section 22.2) acting normal to a constant density surface. Consequently, if the material surface on which we are computing circulation happens to be parallel to a constant density surface, then pressure cannot generate any circulation around that material circuit. The left circuit in Figure

⁶See Exercise 6.1 for a two-dimensional example of this geometry.

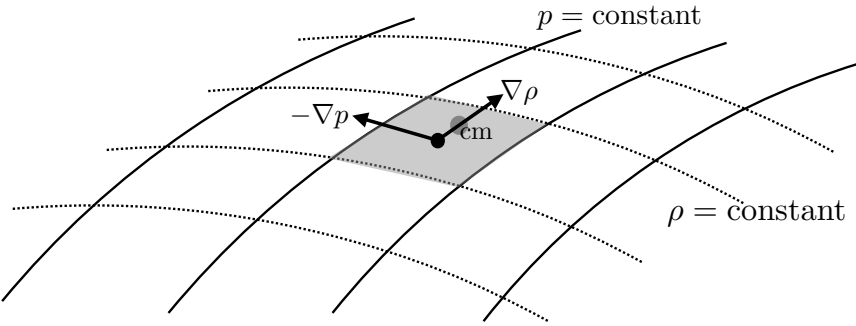


FIGURE 37.3: A mechanical interpretation of the baroclinicity vector. We consider a tiny fluid element bounded by surfaces of constant pressure and density. By construction, the pressure force acts at the geometric center of the element, whereas the center of mass for the element is off-center due to the density gradient across the element. The pressure force thus provides a torque for the fluid element, with the moment-arm for the torque determined by the distance between the geometric center and the center of mass. This torque modifies the vorticity of the fluid element, and in turn modifies the circulation computed around the element's boundary. As depicted here, the baroclinicity vector points into the page (right hand rule for $(-\rho^{-1} \nabla p) \times \nabla \rho$), so that this baroclinicity spins-up a clockwise circulation around the element, or equivalently a clockwise vorticity. This figure is adapted from Figure 14.9 of [Thorne and Blandford \(2017\)](#).

37.4 illustrates this situation. For the more general case where a material surface crosses constant density surfaces, pressure modifies circulation computed around such circuits (right circuit in Figure 37.4).

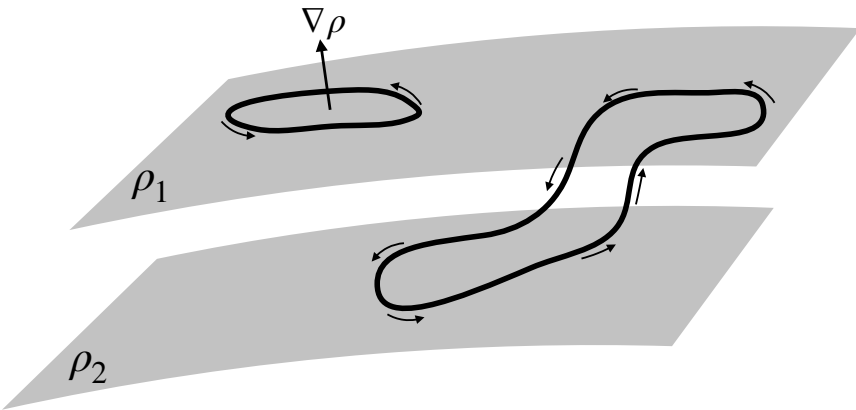


FIGURE 37.4: The material circuit on the left is assumed to be within a constant density surface. In this case, $\nabla \rho \cdot d\mathbf{x} = 0$ so that pressure cannot modify the circulation around this circuit. However, if a material circuit is not contained fully within constant density surface, such as depicted on the right, then pressure is able to modify the circulation computed around the circuit.

37.4.3 Bottom pressure contributions at the solid-earth boundary

As an application of the above ideas, consider a fluid region that intersects the solid-earth boundary. The solid-earth boundary is material so that we can apply Kelvin's circulation theorem to a circuit on the boundary. Consider the situation in Figure 37.5, which shows a vertical slice next to a sloping bottom with constant density surfaces intersecting the bottom. As in our considerations in Section 37.4.2, any material circuit that sits within the bottom boundary crosses density surfaces, in which case circulation is affected by the bottom pressure. Indeed, even if the bottom

is flat, so long as density is not constant along the bottom, then a material circuit within the bottom has circulation modified by bottom pressure.

To develop the mathematics of the above ideas, write the differential line element within the bottom circuit as

$$d\mathbf{x} = \hat{\mathbf{x}} dx + \hat{\mathbf{y}} dy + \hat{\mathbf{z}} dz = (\hat{\mathbf{x}} + \hat{\mathbf{z}} \partial_x \eta_b) dx + (\hat{\mathbf{y}} + \hat{\mathbf{z}} \partial_y \eta_b) dy. \quad (37.60)$$

To reach this result we set $z = \eta_b(x, y)$ since the circuit is along the bottom boundary, which in turn means that⁷

$$dz = d\eta_b = \nabla \eta_b \cdot (\hat{\mathbf{x}} dx + \hat{\mathbf{y}} dy) = \nabla \eta_b \cdot d\mathbf{x}_{\text{horz}}. \quad (37.61)$$

Consequently, the projection of the density gradient onto the circuit is given by

$$\nabla \rho \cdot d\mathbf{x} = (\nabla_z \rho + \partial_z \rho \nabla \eta_b) \cdot d\mathbf{x}_{\text{horz}}. \quad (37.62)$$

Making use of this result in Kelvin's circulation theorem and focusing on the pressure contribution, as in equation (37.58), leads to

$$\left[\frac{dC}{dt} \right]_{\text{bottom}} = - \oint_{\partial S_{\text{bottom}}} p \rho^{-2} \nabla \rho \cdot d\mathbf{x} = - \oint_{\partial S_{\text{bottom}}} \frac{p_b}{\rho^2} (\nabla_z \rho + \partial_z \rho \nabla \eta_b) \cdot d\mathbf{x}_{\text{horz}}. \quad (37.63)$$

There are two contributions to the circulation changes revealed by equation (37.63). The first arises from the sloped density surfaces next to the bottom, and the second arises from the sloped bottom multiplied by the vertical density gradient. These two contributions are weighted by the bottom pressure, p_b , which is normalized by the squared density. Circulation modifications are enhanced by increased horizontal density gradients next to the bottom, as well as increased topographic slopes. For the special case of flat topography and flat density there are no bottom pressure-induced changes to the circulation around a bottom material circuit.

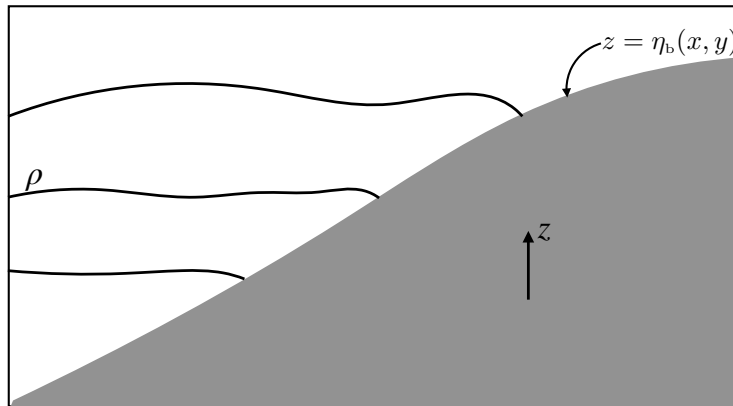


FIGURE 37.5: Constant density surfaces intersecting a sloped solid-earth boundary. Any circuit that sits along the boundary is material since the bottom is material. For circuits that cross density surfaces, the bottom pressure acts to modify circulation computed for this circuit.

37.4.4 Further study

[This video from Prof. Shapiro](#) provides a lucid discussion of baroclinicity and its role in affecting vorticity and circulation.

⁷Since $\eta_b = \eta_b(x, y)$, its gradient is horizontal: $\nabla \eta_b = \hat{\mathbf{x}} \partial_x \eta_b + \hat{\mathbf{y}} \partial_y \eta_b$.

37.5 Vorticity filaments and material line elements

We here study the physics of the source term

$$(\boldsymbol{\omega}_a \cdot \nabla) \mathbf{v} = f \partial_z \mathbf{v} + (\boldsymbol{\omega} \cdot \nabla) \mathbf{v} \quad (37.64)$$

appearing in the vorticity equation (37.41). The contribution from $\hat{z} f \partial_z w$ to the first term is further explored when studying the planetary geostrophic equations in Sections 28.5 and 41.4, given its importance for large-scale meridional motion on a spherical planet. The second term, $(\boldsymbol{\omega} \cdot \nabla) \mathbf{v}$, is the focus of this section.

37.5.1 Vortex filaments evolve through the rate of strain

To help unpack the physics of the source, $(\boldsymbol{\omega} \cdot \nabla) \mathbf{v}$, write it in the following form found by exposing Cartesian tensor labels

$$\omega_m \partial_m v_n = (\omega_m/2) [(\partial_m v_n + \partial_n v_m) + (\partial_m v_n - \partial_n v_m)] \quad (37.65a)$$

$$= \omega_m \mathbb{S}_{mn} - \omega_m \mathbb{R}_{mn}, \quad (37.65b)$$

where $\mathbb{S}_{mn} = (1/2)(\partial_n v_m + \partial_m v_n)$ are components to the rate of strain tensor and $\mathbb{R}_{mn} = (1/2)(\partial_n v_m - \partial_m v_n)$ are components to the rotation tensor. These tensors were introduced in Section 15.3 when studying the kinematics of line elements. As shown in that discussion, the rotation tensor is related to the vorticity by the identity (15.44), whose use leads to

$$2\omega_m \mathbb{R}_{mn} = -\omega_m \epsilon_{mnp} \omega_p = \epsilon_{nmp} \omega_m \omega_p = (\boldsymbol{\omega} \times \boldsymbol{\omega})_n = 0. \quad (37.66)$$

Recalling that the rotation tensor generates rotations about the axis defined by vorticity, we can understand why $\boldsymbol{\omega} \cdot \mathbb{R} = 0$. Namely, there is no rotation generated when a vector is rotated about its own axis. We are thus left just with

$$(\boldsymbol{\omega} \cdot \nabla) \mathbf{v} = \boldsymbol{\omega} \cdot \mathbb{S}. \quad (37.67)$$

That is, the source, $(\boldsymbol{\omega} \cdot \nabla) \mathbf{v}$, appearing in the vorticity equation is determined by the projection of the vorticity onto the rate of strain tensor. This result highlights the fundamental role of flow strains in affecting vorticity.

37.5.2 Frozen-in nature of vorticity

Consider an inviscid, non-rotating barotropic fluid whose flow is non-divergent, in which case the vorticity equation (37.41) reduces to

$$\frac{D\boldsymbol{\omega}}{Dt} = (\boldsymbol{\omega} \cdot \nabla) \mathbf{v}, \quad (37.68)$$

and recall the evolution equation for a material line element as detailed in Section 15.3

$$\frac{D(\delta\mathbf{x})}{Dt} = (\delta\mathbf{x} \cdot \nabla) \mathbf{v}. \quad (37.69)$$

Now recall from Section 34.6.1 that a vortex line is a line drawn through the fluid that is everywhere parallel to the vorticity. Such a line connects material fluid particles, so that a vortex line constitutes a particular case of a material line. At some initial time, $t = 0$, let the vorticity on an

infinitesimal vortex line be related to the material line element according to

$$\delta\mathbf{x}(0) = \Gamma \boldsymbol{\omega}(\mathbf{x}, 0), \quad (37.70)$$

where Γ has dimensions LT and is determined by the initial vorticity and initial line element. Since the vorticity equation (37.68) has precisely the same mathematical form as the material line element equation (37.69), the difference vector

$$\mathbf{A} \equiv \delta\mathbf{x} - \Gamma \boldsymbol{\omega}, \quad (37.71)$$

evolves according to

$$\frac{D\mathbf{A}}{Dt} = (\mathbf{A} \cdot \nabla) \mathbf{v}. \quad (37.72)$$

But since \mathbf{A} vanishes at $t = 0$, we conclude that it vanishes for all time

$$\frac{D\mathbf{A}}{Dt} = 0. \quad (37.73)$$

Consequently, the relation (37.70) holds for all time with Γ a constant. That is, the vortex filament and its corresponding line element remain parallel as they both evolve according to their projection onto the rate of strain tensor. We thus say that vorticity is a *frozen-in* property as illustrated by Figure 37.6. Although we established this property only for the case of an inviscid, barotropic fluid with non-divergent flow, it offers insight into the more general situation occurring in real fluids.

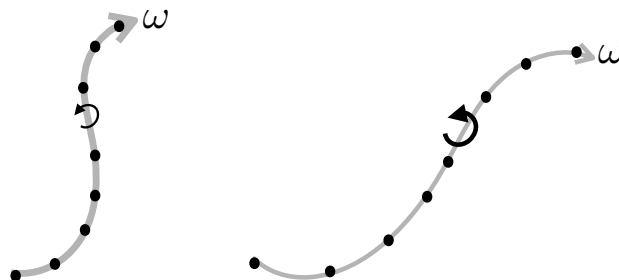


FIGURE 37.6: For the non-divergent flow of a perfect barotropic fluid, vortex lines (also known as vortex filaments) are also material lines. This property means that for an arbitrary vortex line drawn in the fluid, the fluid particles that are initially on the vortex line remain on the line as it moves through the fluid according to the rate of strain tensor. We here show two instances of the same vortex line along with sample test fluid particles. The left configuration stretches into the right configuration, with the vorticity increasing as the vortex line stretches according to the discussion in Section 37.5.3. This property of a vortex line is known as its *frozen-in nature*. The frozen-in nature of vortex lines strictly holds only for perfect barotropic fluid exhibiting non-divergent flow, yet it offers useful insights into the vortex dynamics of more general fluids.

37.5.3 Stretching and tilting of vortex tubes

Vorticity responds when vortex lines or tubes are stretched or bent by the rate of strain tensor. To help understand the response, consider again the perfect fluid barotropic vorticity equation with a non-divergent flow (equation (37.68)) and focus on the material evolution of the vertical vorticity component

$$\frac{D\omega_z}{Dt} = \omega_x \frac{\partial w}{\partial x} + \omega_y \frac{\partial w}{\partial y} + \omega_z \frac{\partial w}{\partial z} = \boldsymbol{\omega} \cdot \nabla w = \nabla \cdot (w \boldsymbol{\omega}). \quad (37.74)$$

The following discussion closely emulates that given for a material line element in Section 15.3.6.

Stretching

Consider the vortex tube to be initially aligned with the \hat{z} -axis, so that $\omega_x = \omega_y = 0$, in which case there is only a single term impacting the material evolution of vertical vorticity⁸

$$\frac{D\omega_z}{Dt} = \omega_z \frac{\partial w}{\partial z}. \quad (37.75)$$

Since the flow is non-divergent, the volume of an infinitesimal portion of the vortex tube is materially constant

$$\frac{D(\delta V)}{Dt} = 0, \quad (37.76)$$

which means that the vertical extent, δz , and cross-sectional area, δA , are constrained

$$\frac{1}{\delta z} \frac{D(\delta z)}{Dt} + \frac{1}{\delta A} \frac{D(\delta A)}{Dt} = 0. \quad (37.77)$$

As the tube stretches vertically, its horizontal area reduces, and vice versa. Making use of the expression for the evolution of a material line segment (equation (37.69)) allows us to write

$$\frac{1}{\delta z} \frac{D(\delta z)}{Dt} = \frac{\partial w}{\partial z}, \quad (37.78)$$

so that the vorticity equation (37.75) becomes

$$\frac{D\omega_z}{Dt} = \omega_z \frac{\partial w}{\partial z} = \omega_z \left[\frac{1}{\delta z} \frac{D(\delta z)}{Dt} \right] = -\omega_z \left[\frac{1}{\delta A} \frac{D(\delta A)}{Dt} \right]. \quad (37.79)$$

Rearrangement leads to

$$\frac{D(\omega_z \delta A)}{Dt} = 0, \quad (37.80)$$

which is an expression of Kelvin's circulation theorem (equation (37.11)) for a horizontal cross-section of the vortex tube.

The above manipulations suggest the following interpretation for the *stretching* term, $\omega_z (\partial w / \partial z)$, appearing in the vertical vorticity equation (37.74) and illustrated in Figure 37.7. Namely, as the vortex tube is stretched and its cross-sectional area is compressed, the vorticity magnitude increases so to maintain a constant circulation around the tube, as per Kelvin's theorem (or equivalently as per Helmholtz's first theorem discussed in Section 34.6.3). Stretching a vortex tube increases the magnitude of the vorticity in the direction of the stretching whereas compressing a tube reduces the vorticity magnitude. This result accords with our understanding of angular momentum conservation as discussed for the rotating cylinder in Section 36.2.2 and depicted by Figure 36.1.

Tilting

Now consider an initially horizontal vortex tube as in the lower left panel of Figure 37.7 so that $\omega_z = 0$. Furthermore, to focus on just one of the two horizontal directions we set $\omega_y = 0$ so that

⁸Be mindful to distinguish the symbols for the vertical component of vorticity, ω_z , and the vertical component of velocity, w .

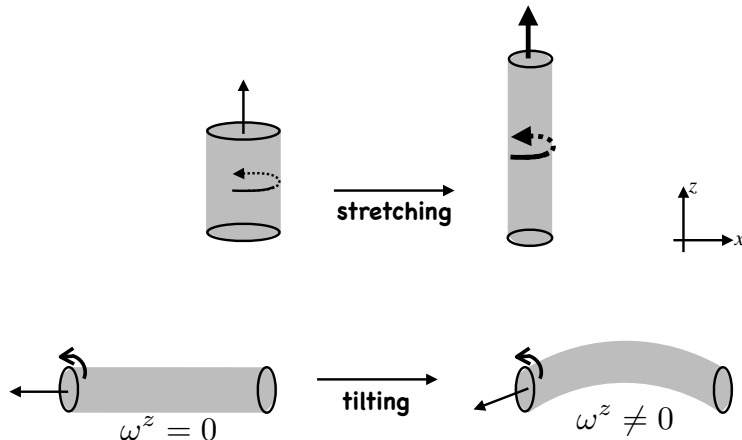


FIGURE 37.7: Illustrating how stretching and tilting of a vortex tube impacts on the vorticity. Top panels: As the cross-sectional area of the vortex tube shrinks, and the vertical extent of the tube stretches, the magnitude of the vorticity along the axis of the tube increases. This result accords with our understanding of angular momentum conservation as discussed for the rotating cylinder in Section 36.2.2 and depicted by Figure 36.1, as well as with Helmholtz's first theorem in Section 34.6.3 and Figure 34.7. Lower panels: The initial vortex tube is assumed to be aligned parallel to the x -axis, so that it has zero projection in the vertical direction. A horizontal shear of the vertical velocity ($\partial w / \partial x \neq 0$) deforms the vortex tube. Upon deforming (or tilting), the tube picks up a nonzero projection in the vertical, which means that it now has a nonzero vertical component to vorticity.

equation (37.74) for the vertical vorticity becomes

$$\frac{D\omega_z}{Dt} = \omega_x \frac{\partial w}{\partial x}. \quad (37.81)$$

If there is no horizontal shear in the vertical velocity ($\partial w / \partial x = 0$), then the vortex tube remains horizontal. However, in the presence of $\partial w / \partial x \neq 0$, the vorticity vector picks up a nonzero vertical projection. To help visualize this process, recall the frozen-in nature of vortex lines, and consider the evolution of an infinitesimal line segment on the vortex tube. With the vortex tube initially aligned parallel to the x -axis, the evolution of a material line segment (equation (37.69)) is given by

$$\frac{D(\delta x)}{Dt} = \delta x \frac{\partial v}{\partial x}. \quad (37.82)$$

The initially horizontal line segment thus picks up a projection in the vertical so long as $\partial w / \partial x \neq 0$. Correspondingly, the vorticity picks up a vertical component. We can think of this process as a tilting or deforming of the initially horizontal vortex tube, with the tilted tube having a nonzero vertical projection.

37.5.4 Shallow water vorticity revisited

We here revisit our discussion of the shallow water vorticity from Chapter 36 in light of the vorticity equation (37.41). Notably, an inviscid shallow water fluid has zero baroclinicity, so that only stretching and tilting affect shallow water vorticity.

Vortex tubes never close in a shallow water layer

The absolute vorticity vector in a shallow water layer is given by equation (32.103d)

$$\boldsymbol{\omega}_a = \nabla \times \mathbf{v} + \hat{z} f = \boldsymbol{\omega}_h + \hat{z} (\zeta + f) = \hat{x} \partial_y w - \hat{y} \partial_x w + \hat{z} \zeta_a = -\hat{z} \times \nabla w + \hat{z} \zeta_a, \quad (37.83)$$

where we set $\partial_z u = \partial_z v = 0$ for the horizontal velocity within a shallow water layer. Since the shallow water fluid is hydrostatic, the horizontal vorticity component is much smaller in magnitude than the vertical component,

$$|\partial_x w, \partial_y w| \ll |\zeta|. \quad (37.84)$$

Vortex tubes in a shallow water fluid do not close, since to close requires breaking this inequality. Hence, shallow water vortex tubes reach from the bottom of the layer to the top, with only a slight tilt relative to the vertical.

Material time evolution of shallow water vorticity

To determine how shallow water vorticity evolves, we make use of the stretching and tilting term in the form of equation (37.67) so that

$$\frac{D\omega_a}{Dt} = (\boldsymbol{\omega}_a \cdot \nabla) \mathbf{v} \implies \frac{D\omega_{an}}{Dt} = \omega_{am} \mathbb{S}_{mn}. \quad (37.85)$$

The rate of strain tensor for the shallow water fluid is

$$\mathbb{S} = \frac{1}{2} \begin{bmatrix} 2\partial_x u & \partial_y u + \partial_x v & \partial_z u + \partial_x w \\ \partial_x v + \partial_y u & 2\partial_y v & \partial_z v + \partial_y w \\ \partial_x w + \partial_z u & \partial_y w + \partial_z v & 2\partial_z w \end{bmatrix} = \frac{1}{2} \begin{bmatrix} 2\partial_x u & \partial_y u + \partial_x v & \partial_x w \\ \partial_x v + \partial_y u & 2\partial_y v & \partial_y w \\ \partial_x w & \partial_y w & 2\partial_z w \end{bmatrix}, \quad (37.86)$$

so that material time evolution of the vertical vorticity component, is given by

$$\frac{D(\zeta + f)}{Dt} = \omega_1 \mathbb{S}_{13} + \omega_2 \mathbb{S}_{23} + \omega_{a3} \mathbb{S}_{33} \quad (37.87a)$$

$$= (1/2)(\omega_1 \partial_x w + \omega_2 \partial_y w) + \omega_{a3} \partial_z w \quad (37.87b)$$

$$= (\zeta + f) \partial_z w \quad (37.87c)$$

$$= -(\zeta + f) \nabla \cdot \mathbf{u}, \quad (37.87d)$$

which agrees with the shallow water vorticity equation (36.9). For the zonal vorticity component we have

$$\frac{D\omega_1}{Dt} = \omega_1 \mathbb{S}_{11} + \omega_2 \mathbb{S}_{21} + \omega_{a3} \mathbb{S}_{31} \quad (37.88a)$$

$$= \omega_1 \partial_x u + \omega_2 (\partial_x v + \partial_y u)/2 + \omega_3 \partial_x w, \quad (37.88b)$$

and a similar expression for the meridional component.

Eulerian flux-form evolution of Cartesian vorticity components

In Section 37.3.4, we showed how each of the three Cartesian vorticity components evolves according to a flux-form Eulerian equation. For the vertical component to the vorticity, the vorticity flux, \mathbf{J}_ζ , is given by equation (37.44) and it takes on the following form for a shallow water layer

$$\mathbf{J}_\zeta = \mathbf{v} \zeta_a - w \boldsymbol{\omega}_a = \mathbf{u} \zeta_a - w \boldsymbol{\omega}_h = \mathbf{u} \zeta_a + w \hat{\mathbf{z}} \times \nabla w = \mathbf{u} \zeta_a + \hat{\mathbf{z}} \times \nabla w^2/2. \quad (37.89)$$

The term

$$\hat{\mathbf{z}} \times \nabla w^2/2 = -\nabla \times \hat{\mathbf{z}} w^2/2 \quad (37.90)$$

has a zero divergence and so has no contribution to the convergence of the vorticity flux. Hence, the vorticity flux, \mathbf{J}_ζ , derived here differs by a gauge from the purely advective flux, $\mathbf{u} \zeta_a$, considered

in the shallow water vorticity equation (36.7).

For the zonal component to the vorticity, the vorticity flux, \mathbf{J}_{ω_1} , is given by equation (37.46) and it takes on the following form for a shallow water layer

$$\mathbf{J}_{\omega_1} = \mathbf{v} \omega_{a1} - u \boldsymbol{\omega}_a = (\hat{\mathbf{y}} v + \hat{\mathbf{z}} w) \omega_1 - \hat{\mathbf{y}} \omega_2 - \hat{\mathbf{z}} (\zeta + f) = \hat{\mathbf{y}} (v \omega_1 - u \omega_2) + \hat{\mathbf{z}} [w \omega_1 - u (\zeta + f)], \quad (37.91)$$

with a similar form for the flux of the meridional vorticity component, \mathbf{J}_{ω_2} .

37.5.5 Concerning three-dimensional turbulence

As a vortex tube is stretched in the presence of straining motion, it spins faster as its radius decreases. Hence, its kinetic energy moves from larger to smaller spatial scales. This process of downscale energy cascade (i.e., the movement of kinetic energy from large to small scales) is a fundamental property of three dimensional turbulence, and vortex stretching is the dominant mechanism for the cascade. In contrast, two dimensional turbulence, which occurs in horizontal non-divergent flows, does not support vortex stretching and consequently does not support the downscale energy cascade. Instead, two dimensional turbulence supports an inverse cascade whereby there is a net flow of energy to larger scales, with that flow related to the material conservation of vorticity in two dimensional non-divergent flows (see Chapter 35). [Vallis \(2017\)](#) provides a lucid discussion of energy cascades in both two and three dimensional turbulence.

37.6 Circulation for rotating fluids

We here tie up an important loose end by studying circulation and vorticity for rotating fluids, such as those on a rotating planet. It turns out that incorporating rotation is straightforward, and yet the implications are quite profound for the motion of geophysical fluids.

Start by recalling the expression from Section 11.8.1 for the inertial or absolute velocity (i.e., velocity measured in an inertial frame)

$$\mathbf{v}_a = \mathbf{v} + \boldsymbol{\Omega} \times \mathbf{x}, \quad (37.92)$$

where \mathbf{v} is the velocity measured in the rotating frame (relative velocity), and \mathbf{x} is the position vector relative to the origin (e.g., center of earth). The absolute circulation around an arbitrary circuit (a circuit that is not necessarily material) is thus given by

$$C_a = \oint_{\partial S} (\mathbf{v} + \boldsymbol{\Omega} \times \mathbf{x}) \cdot d\mathbf{x} = C + C_{\text{planet}}, \quad (37.93)$$

where the circulation measured in the rotating frame is

$$C = \oint_{\partial S} \mathbf{v} \cdot d\mathbf{x} \quad (37.94)$$

and the circulation associated with the rotating planet is

$$C_{\text{planet}} = \oint_{\partial S} (\boldsymbol{\Omega} \times \mathbf{x}) \cdot d\mathbf{x}. \quad (37.95)$$

A fluid element at rest in the rotating frame still has a nonzero absolute circulation as given by the planetary circulation. Making use of Stokes' theorem leads to the equivalent forms for the

circulations

$$\mathcal{C} = \oint_{\partial\mathcal{S}} \mathbf{v} \cdot d\mathbf{x} = \int_{\mathcal{S}} \boldsymbol{\omega} \cdot \hat{\mathbf{n}} d\mathcal{S} \quad \text{relative circulation} \quad (37.96a)$$

$$\mathcal{C}_{\text{planet}} = \oint_{\partial\mathcal{S}} (\boldsymbol{\Omega} \times \mathbf{x}) \cdot d\mathbf{x} = \int_{\mathcal{S}} \boldsymbol{\omega}_{\text{planet}} \cdot \hat{\mathbf{n}} d\mathcal{S} \quad \text{planetary circulation} \quad (37.96b)$$

$$\mathcal{C}_a = \oint_{\partial\mathcal{S}} \mathbf{v}_a \cdot d\mathbf{x} = \int_{\mathcal{S}} \boldsymbol{\omega}_a \cdot \hat{\mathbf{n}} d\mathcal{S} \quad \text{absolute circulation,} \quad (37.96c)$$

where

$$\boldsymbol{\omega} = \nabla \times \mathbf{v} \quad \text{relative vorticity} \quad (37.97a)$$

$$\boldsymbol{\omega}_{\text{planet}} = \nabla \times (\boldsymbol{\Omega} \times \mathbf{x}) = 2\boldsymbol{\Omega} \quad \text{planetary vorticity} \quad (37.97b)$$

$$\boldsymbol{\omega}_a = \nabla \times (\mathbf{v} + \boldsymbol{\Omega} \times \mathbf{x}) = \boldsymbol{\omega} + \boldsymbol{\omega}_{\text{planet}} \quad \text{absolute vorticity.} \quad (37.97c)$$

Thus far we have merely substituted in the expression (37.92) for the inertial velocity and then decomposed the vorticity and circulation into its relative and planetary components. Next we consider how circulation evolves, in which case we see how the relative and planetary circulations interact.

37.6.1 Material evolution of absolute circulation

We now consider how the absolute circulation evolves for a material circuit that moves with the fluid

$$\frac{d\mathcal{C}_a}{dt} = \frac{d}{dt} \oint_{\partial\mathcal{S}(\mathbf{v})} \mathbf{v}_a \cdot d\mathbf{x} = \frac{d}{dt} \oint_{\partial\mathcal{S}(\mathbf{v})} (\mathbf{v} + \boldsymbol{\Omega} \times \mathbf{x}) \cdot d\mathbf{x}. \quad (37.98)$$

We measure fluid motion in the rotating frame so that the material time derivative is computed with the velocity, \mathbf{v} , rather than the absolute velocity, \mathbf{v}_a . We now follow the derivation of the non-rotating Kelvin's circulation theorem in Section 37.2 so that

$$\frac{d\mathcal{C}_a}{dt} = \frac{d}{dt} \oint_{\partial\mathcal{S}(\mathbf{v})} (\mathbf{v} + \boldsymbol{\Omega} \times \mathbf{x}) \cdot d\mathbf{x} \quad (37.99a)$$

$$= \oint_{\partial\mathcal{S}(\mathbf{v})} \left[\frac{D\mathbf{v}}{Dt} + \boldsymbol{\Omega} \times \frac{D\mathbf{x}}{Dt} \right] \cdot d\mathbf{x} + \oint_{\partial\mathcal{S}(\mathbf{v})} (\mathbf{v} + \boldsymbol{\Omega} \times \mathbf{x}) \cdot d\mathbf{v} \quad (37.99b)$$

$$= \oint_{\partial\mathcal{S}(\mathbf{v})} \left[\frac{D\mathbf{v}}{Dt} + \boldsymbol{\Omega} \times \mathbf{v} \right] \cdot d\mathbf{x} + \oint_{\partial\mathcal{S}(\mathbf{v})} (\boldsymbol{\Omega} \times \mathbf{x}) \cdot d\mathbf{v} \quad (37.99c)$$

$$= \oint_{\partial\mathcal{S}(\mathbf{v})} \left[\frac{D\mathbf{v}}{Dt} + 2\boldsymbol{\Omega} \times \mathbf{v} \right] \cdot d\mathbf{x}. \quad (37.99d)$$

To reach this result we set

$$\mathbf{v} = \frac{D\mathbf{x}}{Dt}, \quad (37.100)$$

for the velocity of a fluid particle on the circuit. We also used the identity

$$\oint_{\partial\mathcal{S}(\mathbf{v})} \mathbf{v} \cdot d\mathbf{v} = \frac{1}{2} \oint_{\partial\mathcal{S}(\mathbf{v})} d(\mathbf{v} \cdot \mathbf{v}) = 0 \quad (37.101)$$

as well as

$$\oint_{\partial S(\mathbf{v})} (\boldsymbol{\Omega} \times \mathbf{x}) \cdot d\mathbf{v} = \oint_{\partial S(\mathbf{v})} d[(\boldsymbol{\Omega} \times \mathbf{x}) \cdot \mathbf{v}] - \oint_{\partial S(\mathbf{v})} (\boldsymbol{\Omega} \times d\mathbf{x}) \cdot \mathbf{v} = \oint_{\partial S(\mathbf{v})} (\boldsymbol{\Omega} \times \mathbf{v}) \cdot d\mathbf{x}, \quad (37.102)$$

where we set

$$\oint_{\partial S(\mathbf{v})} d[(\boldsymbol{\Omega} \times \mathbf{x}) \cdot \mathbf{v}] = 0 \quad (37.103)$$

since, as for equation (37.101), the closed loop integral of an exact spatial differential vanishes. We also noted that $\boldsymbol{\Omega}$ is a constant vector so that $d\boldsymbol{\Omega} = 0$. Now insert the momentum equation (37.30) into equation (37.99d) to yield

$$\frac{dC_a}{dt} = \oint_{\partial S(\mathbf{v})} \left[\frac{D\mathbf{v}}{Dt} + 2\boldsymbol{\Omega} \times \mathbf{v} \right] \cdot d\mathbf{x}. \quad (37.104a)$$

$$= \oint_{\partial S(\mathbf{v})} \left[-\frac{1}{\rho} \nabla p - \nabla \Phi + \mathbf{F} \right] \cdot d\mathbf{x}. \quad (37.104b)$$

$$= \oint_{\partial S(\mathbf{v})} \left[-\frac{dp}{\rho} + \mathbf{F} \cdot d\mathbf{x} \right]. \quad (37.104c)$$

Making use of Stokes' theorem leads to the evolution of absolute circulation around a material loop

$$\frac{dC_a}{dt} = \oint_{\partial S(\mathbf{v})} \left[-\frac{dp}{\rho} + \mathbf{F} \cdot d\mathbf{x} \right] = \int_{S(\mathbf{v})} (\mathbf{B} + \nabla \times \mathbf{F}) \cdot \hat{\mathbf{n}} dS, \quad (37.105)$$

where $\mathbf{B} = \rho^{-2} \nabla \rho \times \nabla p$ is the baroclinicity vector from equation (37.56).

The circulation theorem (37.105) is the same as obtained for the non-rotating Kelvin's circulation theorem discussed in Section 37.2 (see equation (37.5e)). As such, we find that time changes to the absolute circulation are affected by pressure and friction work around the material circuit. We find it satisfying that the formalism confirms the expected result that absolute circulation is an objective (frame invariant) property of the fluid, in which its evolution is unchanged when moving to a non-inertial rotating frame.

37.6.2 The beta effect

As given by equation (37.93), the absolute circulation around an arbitrary circuit equals to the circulation of fluid measured in the rotating frame (relative circulation) plus circulation of the rotating frame itself (planetary circulation)

$$C_a = C + C_{\text{planet}} = C + 2 \int_S \boldsymbol{\Omega} \cdot \hat{\mathbf{n}} dS \iff \frac{dC_a}{dt} = \frac{dC}{dt} + \frac{dC_{\text{planet}}}{dt}. \quad (37.106)$$

We can determine the processes that affect the absolute circulation around a material loop by using the circulation theorem (37.105)

$$\frac{dC}{dt} = -\frac{dC_{\text{planet}}}{dt} + \frac{dC_a}{dt} \quad (37.107a)$$

$$= -2 \frac{d}{dt} \left[\int_{S(\mathbf{v})} \boldsymbol{\Omega} \cdot \hat{\mathbf{n}} dS \right] + \int_{S(\mathbf{v})} (\mathbf{B} + \nabla \times \mathbf{F}) \cdot \hat{\mathbf{n}} dS. \quad (37.107b)$$

We generally assume that the planetary rotation is a constant in time and points through the north pole of the sphere⁹ $\boldsymbol{\Omega} = \Omega \hat{\mathbf{Z}}$, so that

$$\int_{\mathcal{S}(\mathbf{v})} \boldsymbol{\Omega} \cdot \hat{\mathbf{n}} d\mathcal{S} = \Omega \int_{\mathcal{S}(\mathbf{v})} \hat{\mathbf{Z}} \cdot \hat{\mathbf{n}} d\mathcal{S} = \Omega A_{\perp}. \quad (37.108)$$

The area, A_{\perp} , is the projection of the spherical area enclosed by the circuit onto the horizontal equatorial plane, with Figure 37.8 illustrating the geometry. This result has profound impact on large scale geophysical fluid motion, whereby relative circulation around a material circuit in the rotating frame changes according to

$$\frac{dC}{dt} = \underbrace{-2\Omega \frac{dA_{\perp}}{dt}}_{\text{beta effect}} + \underbrace{\int_{\mathcal{S}} (\mathbf{B} + \nabla \times \mathbf{F}) \cdot \hat{\mathbf{n}} d\mathcal{S}(\mathbf{v})}_{\text{baroclinicity plus friction curl}}. \quad (37.109)$$

Equation (37.109) is sometimes referred to as the *Bjerknes circulation theorem* (see Holton (1992) equation (4.5)). The second term, comprised of baroclinicity and friction, also appears in the non-rotating case. It has already been studied in Sections 37.2 and 37.4.

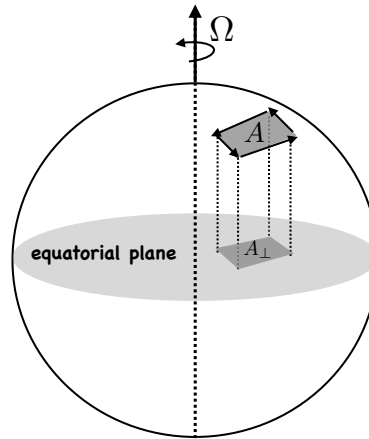


FIGURE 37.8: Geometry of the beta effect. According to the Bjerknes circulation theorem (37.109), the circulation for a material loop on the surface of a rotating sphere is affected by baroclinicity and friction, as for a non-rotating sphere, as well as latitudinal motion of the loop. The latitudinal motion alters the area of the loop as projected onto the equatorial plane, with the projected area increasing as the loop moves poleward. When multiplied by the magnitude of the planetary vorticity, 2Ω , the area contribution is termed *planetary induction* (i.e., relative circulation is induced by latitudinal motion), or more commonly it is called the *beta effect*. The beta effect requires both rotation (2Ω) and curvature of the sphere ($\partial_y f = \beta$); it is therefore absent on the *f*-plane.

The first term in the circulation theorem (37.109) is fundamentally new. It is nonzero in the presence of both rotation and curvature of the sphere. The spherical effect arises from latitudinal movement of a material circuit, with the area, A_{\perp} , changing under such motion. When the circuit moves poleward, the projected area A_{\perp} increases whereas it decreases to zero as it moves equatorward. The material change in A_{\perp} , when multiplied by the planetary vorticity, modifies the relative circulation around the material circuit. We refer to *planetary induction* as the process whereby relative circulation changes due to latitudinal motion of a material circuit on a rotating sphere. Or more commonly, planetary induction is referred to as the *beta effect*, given its connec-

⁹We follow the notational conventions of Figure 9.1 with one exception. Here, the vertical Cartesian direction through the north pole is written $\hat{\mathbf{Z}}$ to avoid confusion with the local vertical direction $\hat{\mathbf{z}}$ determined by the geopotential.

tion to the latitudinal gradient of the Coriolis parameter, $\beta = \partial_y f$. Notably, longitudinal motion of the circuit has no impact on A_{\perp} , so that longitudinal motion imparts no planetary induction of relative circulation.

In theories of large-scale laminar planetary flows, the baroclinicity and friction terms are typically sub-dominant. For these flows, the material evolution of relative circulation is dominated by the beta effect. Planetary geostrophic flow is the canonical example of such flow, as studied in Section 28.5 as well as Chapters 40 and 41. In such flows, forces that lead to meridional motion also give rise to changes in the relative circulation. Conversely, forces that change the circulation around a material loop affect meridional motion of the loop.

37.6.3 The case of two-dimensional non-divergent flow

To garner further insight into the nature of the beta effect, consider a perfect two-dimensional and non-divergent flow (zero vertical velocity) on a rotating sphere. In this case there is only a vertical component to vorticity and both baroclinicity and friction have no role in vorticity dynamics. Hence, vorticity is affected only via the beta effect. In addition, the fluid flow materially preserves the area of any material region. This *two-dimensional non-divergent barotropic flow* is discussed in more detail in Chapter 35. We here use it as an example to expose essential features of the beta effect (see also Section 35.3.2).

In the rotating frame, circulation around an infinitesimal closed material loop is

$$\mathcal{C} = A \zeta, \quad (37.110)$$

where ζ is the relative vorticity and A is the area enclosed by the loop. Because the fluid flow is non-divergent, the loop area A remains constant even as the loop becomes contorted (see Section 18.5). This area preservation property simplifies the evolution equation for the circulation, which is given by

$$\frac{D\mathcal{C}}{Dt} = \frac{D(A\zeta)}{Dt} = A \frac{D\zeta}{Dt}. \quad (37.111)$$

Equating this result to the circulation change implied by Bjerknes' circulation theorem (37.109) renders

$$\frac{D\mathcal{C}}{Dt} = A \frac{D\zeta}{Dt} = -2\Omega \frac{DA_{\perp}}{Dt}. \quad (37.112)$$

Let the material circuit be at a latitude, ϕ , so that the projection of the loop area onto the equatorial plane is (see Figure 37.8)

$$A_{\perp} = A \sin \phi. \quad (37.113)$$

Hence, material evolution of the circulation is

$$\frac{D\mathcal{C}}{Dt} = A \frac{D\zeta}{Dt} \quad (37.114a)$$

$$= -2\Omega \frac{DA_{\perp}}{Dt} \quad (37.114b)$$

$$= -2A\Omega \frac{D \sin \phi}{Dt} \quad (37.114c)$$

$$= -2A\Omega \cos \phi \frac{D\phi}{Dt} \quad (37.114d)$$

$$= -A \left[\frac{2\Omega \cos \phi}{R} \right] \left[R \frac{D\phi}{Dt} \right] \quad (37.114e)$$

$$= -A\beta v, \quad (37.114f)$$

where we introduced the meridional velocity component

$$v = R \frac{D\phi}{Dt} \quad (37.115)$$

and the meridional derivative of the planetary vorticity

$$\beta = \frac{df}{dy} = \frac{1}{R} \frac{d}{d\phi} (2\Omega \sin \phi) = \frac{2\Omega \cos \phi}{R}. \quad (37.116)$$

The result (37.114f)

$$\frac{1}{A} \frac{DC}{Dt} = \frac{D\zeta}{Dt} = -\beta v, \quad (37.117)$$

shows how meridional motion on a rotating sphere induces relative circulation, and thus relative vorticity. It furthermore motivates the name *beta effect* for the planetary induction.

37.6.4 Further study

The beta effect and its role in vorticity is nicely summarized in [this video from Science Primer](#) in the context of Rossby waves.

37.7 Vorticity budget in a primitive equation ocean

In this section we develop the vorticity budget for a hydrostatic Boussinesq primitive equation ocean (Section 24.1) in the presence of diabatic sources and frictional forcing. This system is of particular importance for models of the ocean circulation with the governing equations given by (see Section 26.1.6)

$$\frac{D\mathbf{u}}{Dt} + f \hat{\mathbf{z}} \times \mathbf{v} = -\nabla_z \varphi + \mathbf{F} \quad (37.118a)$$

$$\frac{\partial \varphi}{\partial z} = b \quad (37.118b)$$

$$\nabla \cdot \mathbf{v} = 0 \quad (37.118c)$$

$$\frac{Db}{Dt} = \dot{b}, \quad (37.118d)$$

with the non-divergent velocity field written

$$\mathbf{v} = (\mathbf{u}, w) = \mathbf{u} + w \hat{\mathbf{z}}. \quad (37.119)$$

The perturbation pressure is given by

$$\rho_0 \varphi = \delta p = p - p_0, \quad (37.120)$$

with the reference pressure, $p_0 = p_0(z)$, in hydrostatic balance with the constant reference density

$$\frac{dp_0}{dz} = -g \rho_0, \quad (37.121)$$

and p the hydrostatic pressure satisfying the local hydrostatic balance

$$\frac{\partial p}{\partial z} = -g \rho. \quad (37.122)$$

The globally referenced Archimedean buoyancy is given by

$$b = -g(\rho - \rho_0)/\rho_0, \quad (37.123)$$

with this field discussed in Section 27.4.2. We assume the Coriolis acceleration of the form relevant to the Traditional approximation, (Section 24.1.3), in which case we are only concerned with the local vertical component of planetary rotation so that

$$f \hat{z} \times \mathbf{v} = f \hat{z} \times \mathbf{u}. \quad (37.124)$$

Finally, the horizontal friction acceleration vector is given by

$$\mathbf{F} = (F^x, F^y, 0) \quad (37.125)$$

and the gradient operator is

$$\nabla = \nabla_z + \hat{z} \partial_z. \quad (37.126)$$

37.7.1 Deriving the vorticity equation

Vector invariant velocity equation

To derive the vorticity equation, it is useful to combine the horizontal momentum equation with the hydrostatic balance, in which case

$$\frac{D\mathbf{u}}{Dt} + f \hat{z} \times \mathbf{v} = -\nabla\varphi + b \hat{z} + \mathbf{F}. \quad (37.127)$$

As for the non-hydrostatic case (Section 37.3.1), we rewrite the self-advection operator, $(\mathbf{v} \cdot \nabla) \mathbf{u}$, before taking the curl. In turn, we introduce the hydrostatic relative vorticity given by the curl of the horizontal velocity

$$\boldsymbol{\omega}^{\text{hy}} = \nabla \times \mathbf{u} = \hat{z} \times \partial_z \mathbf{u} + \hat{z} \zeta = -\hat{x} \partial_z v + \hat{y} \partial_z u + \hat{z} \zeta, \quad (37.128)$$

where

$$\zeta = \partial_x v - \partial_y u \quad (37.129)$$

is the vertical component to the relative vorticity, and the hydrostatic vorticity is non-divergent

$$\nabla \cdot \boldsymbol{\omega}^{\text{hy}} = 0. \quad (37.130)$$

It is then straightforward to show that

$$\boldsymbol{\omega}^{\text{hy}} \times \mathbf{v} = \hat{x} (w \partial_z u - v \partial_x u + v \partial_y u) + \hat{y} (w \partial_z v - u \partial_y u + u \partial_x v) - \hat{z} \partial_z (u^2 + v^2)/2 \quad (37.131a)$$

$$= w \partial_z \mathbf{u} + \zeta (-v \hat{x} + u \hat{y}) - \hat{z} \partial_z (u^2 + v^2)/2, \quad (37.131b)$$

in which case

$$\nabla(u^2/2) + \boldsymbol{\omega}^{\text{hy}} \times \mathbf{v} = \nabla(u^2 + v^2)/2 - \hat{z} \partial_z (u^2 + v^2)/2 + w \partial_z \mathbf{u} + \zeta (-v \hat{x} + u \hat{y}) \quad (37.132a)$$

$$= (u \partial_x + v \partial_y + w \partial_z) \mathbf{u} \quad (37.132b)$$

$$= (\mathbf{v} \cdot \nabla) \mathbf{u}. \quad (37.132c)$$

The material time derivative of the horizontal velocity can thus be written

$$\frac{D\mathbf{u}}{Dt} = \frac{\partial \mathbf{u}}{\partial t} + (\mathbf{v} \cdot \nabla) \mathbf{u} = \frac{\partial \mathbf{u}}{\partial t} + \boldsymbol{\omega}^{\text{hy}} \times \mathbf{v} + \nabla(\mathbf{u}^2/2), \quad (37.133)$$

which then leads to the vector invariant horizontal velocity equation

$$\partial_t \mathbf{u} + (f \hat{\mathbf{z}} + \boldsymbol{\omega}^{\text{hy}}) \times \mathbf{v} = -\nabla(\varphi + \mathbf{u}^2/2) + b \hat{\mathbf{z}} + \mathbf{F}, \quad (37.134)$$

which can be written in the equivalent form¹⁰

$$(\partial_t + w \partial_z) \mathbf{u} + (f + \zeta) \hat{\mathbf{z}} \times \mathbf{u} = -\nabla_z (\varphi + \mathbf{u}^2/2) - (\partial_z \varphi - b) \hat{\mathbf{z}} + \mathbf{F}. \quad (37.135)$$

Curl of the velocity equation to render the vorticity equation

Now take the curl of the vector invariant velocity equation (37.134), and make use of the identity

$$\nabla \times (\boldsymbol{\omega}_a^{\text{hy}} \times \mathbf{v}) = (\mathbf{v} \cdot \nabla) \boldsymbol{\omega}_a^{\text{hy}} - (\boldsymbol{\omega}_a^{\text{hy}} \cdot \nabla) \mathbf{v}, \quad (37.136)$$

where we introduced the absolute vorticity for a hydrostatic fluid

$$\boldsymbol{\omega}_a^{\text{hy}} = f \hat{\mathbf{z}} + \boldsymbol{\omega}^{\text{hy}}. \quad (37.137)$$

The result is the vorticity equation

$$\partial_t \boldsymbol{\omega}^{\text{hy}} + (\mathbf{v} \cdot \nabla) \boldsymbol{\omega}_a^{\text{hy}} = (\boldsymbol{\omega}_a^{\text{hy}} \cdot \nabla) \mathbf{v} + \nabla \times \hat{\mathbf{z}} b + \nabla \times \mathbf{F}. \quad (37.138)$$

Since the Coriolis parameter is time independent, we can add it to the time derivative to yield an equation for absolute vorticity

$$\frac{D\boldsymbol{\omega}_a^{\text{hy}}}{Dt} = \underbrace{(\boldsymbol{\omega}_a^{\text{hy}} \cdot \nabla) \mathbf{v}}_{\text{stretching + tilting}} + \underbrace{\nabla \times \hat{\mathbf{z}} b}_{\text{baroclinicity}} + \underbrace{\nabla \times \mathbf{F}}_{\text{friction curl}}. \quad (37.139)$$

37.7.2 Boussinesq baroclinicity

Equation (37.139) is the vorticity equation for a hydrostatic Boussinesq ocean. We can compare this equation to the vorticity equation for a non-hydrostatic and non-Boussinesq fluid (equation (37.41)). Both equations have a vorticity source due to stretching and tilting, and both have a source due to the curl of friction. However, the baroclinicity vector for the Boussinesq ocean is given by¹¹

$$\mathbf{B}_{\text{bouss}} = \nabla \times \hat{\mathbf{z}} b = \nabla b \times \hat{\mathbf{z}}, \quad (37.140)$$

which is simpler than baroclinicity in a compressible fluid

$$\mathbf{B} = (\nabla \rho \times \nabla p)/\rho^2 = -\nabla \times (\rho^{-1} \nabla p) \quad (37.141)$$

(equation (37.56)). This form of Boussinesq baroclinicity arises since the pressure gradient acceleration is annihilated by the cross product in the Boussinesq vorticity equation, thus leaving only the buoyancy to affect a baroclinicity source. Consequently, we can diagnose the presence

¹⁰As discussed in [Griffies et al. \(2020\)](#), the form (37.135) is commonly used for Boussinesq and hydrostatic ocean models.

¹¹We see in Exercise 38.2 that the baroclinicity vector (37.140) also applies for the non-hydrostatic Boussinesq ocean.

of baroclinicity for the Boussinesq ocean (either non-hydrostatic or hydrostatic) merely by noting whether there is a slope to the buoyancy surfaces relative to the horizontal plane, such as in Figure 37.9. A sloping buoyancy surface provides a vorticity source for the Boussinesq ocean by providing a spin to fluid elements (see Section 37.4).

While the Boussinesq baroclinicity is somewhat simpler than the non-Boussinesq fluid, we lose certain aspects of the physical interpretation offered in Section 37.4 based on baroclinicity as the curl of the pressure acceleration. Since the curl of the non-Boussinesq pressure acceleration has components in all three directions, the non-Boussinesq baroclinicity vector, \mathbf{B} , affects a source for each of the three vorticity components. In contrast, the Boussinesq baroclinicity is the curl of the Archimedean buoyant acceleration and this acceleration acts only in the vertical. Consequently, the Boussinesq baroclinicity has no direct affect on the vertical component to absolute vorticity

$$\hat{\mathbf{z}} \cdot \mathbf{B}_{\text{bouss}} = \hat{\mathbf{z}} \cdot (\nabla \times \hat{\mathbf{z}} b) = 0. \quad (37.142)$$

That is, Boussinesq baroclinicity only acts directly as a source for horizontal vorticity. Thus, Boussinesq baroclinicity can only indirectly affect vertical vorticity through its effects on vertical velocity and the corresponding vertical stretching.

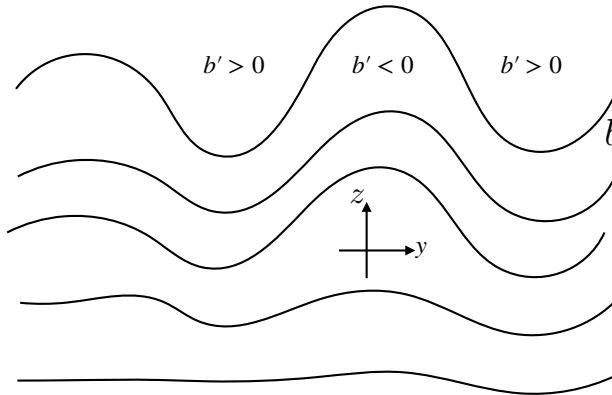


FIGURE 37.9: Baroclinicity in a Boussinesq ocean is manifest by nonzero horizontal gradients in the buoyancy field. Here we depict a region of relatively strong baroclinicity above a region of weaker baroclinicity. A sloping buoyancy surface is therefore synonymous with a nontrivial baroclinic structure. We label anomalously positive ($b' > 0$) and negative buoyancy ($b' < 0$), where the prime denotes anomalies relative to a horizontal average. Furthermore, as per equation (37.142), baroclinicity in a Boussinesq ocean only acts as a source for horizontal vorticity.

37.7.3 Vertical vorticity equation

Following the discussion in Section 37.3.4 for the unapproximated vorticity, we here examine the vertical component of the hydrostatic and Boussinesq vorticity equation (37.139)

$$\frac{D\zeta_a}{Dt} = (\boldsymbol{\omega}_a^{\text{hy}} \cdot \nabla) w + \hat{\mathbf{z}} \cdot (\nabla \times \mathbf{F}), \quad (37.143)$$

with the absence of baroclinicity noted above in Section 37.7.2. The stretching, tilting, and friction curl appearing on the right hand side provide vorticity sources that affect the left hand side's material time evolution. We see this evolution more fully by expanding the terms to render

$$\frac{\partial \zeta_a}{\partial t} + (\mathbf{v} \cdot \nabla) \zeta + \beta v = \hat{\mathbf{z}} \cdot (\partial_z \mathbf{u} \times \nabla_z w) + (\zeta + f) \partial_z w + \hat{\mathbf{z}} \cdot (\nabla \times \mathbf{F}). \quad (37.144)$$

Planetary geostrophic limit

The linearized, inviscid, and steady version of the vorticity equation (37.144) leads to the linear vorticity balance studied in Section 28.5.4 and Chapter 41

$$\beta v = f \partial_z w \quad (37.145)$$

with this relation comprising the inviscid vorticity equation for a flow respecting planetary geostrophic scaling. It represents a kinematic balance since no forces are exposed here to explicitly cause motion, though such forces do appear in the momentum equation. Reading the balance from right to left indicates that any process generating vorticity via vortex stretching must be balanced by meridional motion. That is, the fluid responds to vortex stretching by moving meridionally through the planet's vorticity field. Since the vorticity of a planetary geostrophic fluid is solely determined by planetary vorticity, meridional movement is the only means for the fluid to balance vortex sources. Conversely, reading the equality from left to right reveals that any meridional motion itself must be balanced by vortex stretching.

Vorticity flux vector

We can write the vorticity equation (37.144) in an alternative form by making use of $\nabla \cdot \mathbf{v} = \nabla \cdot \boldsymbol{\omega}_a^{hy} = 0$ to yield

$$\frac{\partial \zeta_a}{\partial t} = -\nabla \cdot (\mathbf{v} \zeta_a - w \boldsymbol{\omega}_a^{hy}) + \hat{z} \cdot (\nabla \times \mathbf{F}). \quad (37.146)$$

Furthermore, we can write the friction curl in the form

$$\hat{z} \cdot (\nabla \times \mathbf{F}) = \nabla z \cdot (\nabla \times \mathbf{F}) \quad (37.147a)$$

$$= \nabla \cdot [z \nabla \times \mathbf{F}] \quad (37.147b)$$

$$= \nabla \cdot [\nabla \times (z \mathbf{F}) - \nabla z \times \mathbf{F}] \quad (37.147c)$$

$$= -\nabla \cdot (\hat{z} \times \mathbf{F}). \quad (37.147d)$$

Hence, the vertical component of the Boussinesq vorticity evolves according to the convergence of the vorticity flux

$$\frac{\partial \zeta_a}{\partial t} = -\nabla \cdot \mathbf{J}_\zeta \quad \text{with} \quad \mathbf{J}_\zeta = \mathbf{v} \zeta_a - w \boldsymbol{\omega}_a^{hy} + \hat{z} \times \mathbf{F}, \quad (37.148)$$

which can be compared to the vorticity flux (37.44) for the compressible nonhydrostatic fluid. Again, the main difference arises from the absence of a baroclinicity contribution for the hydrostatic Boussinesq ocean.

The identity $\boldsymbol{\omega}_a^{hy} = \hat{z} \times \partial_z \mathbf{u} + \hat{z} \zeta_a$ allows us to write

$$\mathbf{v} \zeta_a - w \boldsymbol{\omega}_a^{hy} = \mathbf{u} \zeta_a - w \hat{z} \times \partial_z \mathbf{u}, \quad (37.149)$$

which is a horizontal vector. Furthermore, note that $\hat{z} \times \mathbf{F}$ is a horizontal vector, which then means that there is no vertical contribution to the vorticity flux vector, $\mathbf{J}_\zeta \cdot \hat{z} = 0$. We previously encountered this property in Section 37.3.4 when discussing the vorticity flux for the non-Boussinesq fluid, with Figure 37.1 providing a schematic.

37.8 Depth integral of the vertical vorticity equation

In this section we study the depth integral of the vertical vorticity equation (37.44)

$$\frac{\partial \zeta_a}{\partial t} = -\nabla \cdot \mathbf{J}_\zeta \quad \text{with} \quad \mathbf{J}_\zeta = \mathbf{v} \zeta_a - \boldsymbol{\omega}_a w - \hat{\mathbf{z}} \times \rho^{-1} \nabla p + \hat{\mathbf{z}} \times \mathbf{F}. \quad (37.150)$$

We perform the depth integral over the full depth of the ocean from its bottom at $z = \eta_b(x, y)$ to the ocean surface at $z = \eta(x, y, t)$ (see Figure 32.1). Studies of the depth integrated vorticity equation allow us to focus on the two dimensional budgets with particular attention to how boundary torques alter the budget. This section anticipates analysis of the depth integrated planetary geostrophic vorticity equation in Section 41.5, with that analysis of use for understanding the role of topography in forcing the large-scale ocean circulation. We also consider the vorticity of the depth integrated flow in Section 37.9, which is commonly considered in numerical applications.

37.8.1 Comments on the role of baroclinicity

Results of the analysis in this section can be readily specialized to the Boussinesq and hydrostatic case given by equation (37.148). The key distinction, as noted in Section 37.7.2, is that Boussinesq baroclinicity does not directly affect changes to the vertical component of the Boussinesq vorticity (whether hydrostatic or non-hydrostatic; see Exercise 38.2). This property of the Boussinesq baroclinicity means that the boundary pressure torques discussed in Sections 37.8.3 and 37.8.4 play no direct role in the Boussinesq vorticity equation. However, these boundary pressure torques play a direct role in vertical motion next to the boundaries, especially next to the bottom, with such motion affecting a source to vorticity through stretching. We have much to say in Section 41.5 concerning how boundary pressure torques affect vertical motion for vorticity for the planetary geostrophic fluid. Additionally, as seen in Section 37.9, boundary pressure torques do play a direct role in affecting vorticity of the depth integrated flow in both the Boussinesq and non-Boussinesq fluids.

This discussion exemplifies the sometimes subtle differences between vorticity sources depending on the precise nature of the vorticity, whether it be vorticity for a fluid element as discussed in this section, vorticity of the depth integrated flow in Section 37.9, or vorticity of the depth averaged flow in Section 37.9.7. When studying flavors of vorticity, it is important to be clear on details of their evolution equations since the details color the physical interpretations.

37.8.2 Leibniz rule expressions

The necessary manipulations are typical for the analysis of depth integrated budgets, such as considered for the depth integrated momentum in Section 25.4 and depth integrated angular momentum in Section 25.5. For vorticity we are interested in manipulating following equation

$$\int_{\eta_b}^{\eta} \frac{\partial \zeta_a}{\partial t} dz = - \int_{\eta_b}^{\eta} \nabla \cdot \mathbf{J}_\zeta dz, \quad (37.151)$$

where \mathbf{J}_ζ is the vorticity flux given by equation (37.150). We make use of Leibniz's rule (Section 17.3.4) to move the time and space derivatives from inside the integrals to outside

$$\int_{\eta_b}^{\eta} \frac{\partial \zeta_a}{\partial t} dz = -[\zeta_a \partial_t \eta]_{z=\eta} + \frac{\partial}{\partial t} \int_{\eta_b}^{\eta} \zeta_a dz \quad (37.152)$$

$$-\int_{\eta_b}^{\eta} \nabla_z \cdot \mathbf{J}_\zeta dz = [\nabla_z \eta \cdot \mathbf{J}_\zeta]_{z=\eta} - [\nabla_z \eta_b \cdot \mathbf{J}_\zeta]_{z=\eta_b} - \nabla_z \cdot \int_{\eta_b}^{\eta} \mathbf{J}_\zeta dz \quad (37.153)$$

$$-\int_{\eta_b}^{\eta} \frac{\partial (\hat{\mathbf{z}} \cdot \mathbf{J}_\zeta)}{\partial z} dz = -[\hat{\mathbf{z}} \cdot \mathbf{J}_\zeta]_{z=\eta} + [\hat{\mathbf{z}} \cdot \mathbf{J}_\zeta]_{z=\eta_b}. \quad (37.154)$$

These results then lead to

$$\frac{\partial}{\partial t} \int_{\eta_b}^{\eta} \zeta_a dz = [\zeta_a \partial_t \eta - \nabla(z - \eta) \cdot \mathbf{J}_\zeta]_{z=\eta} + [\nabla(z - \eta_b) \cdot \mathbf{J}_\zeta]_{z=\eta_b} - \nabla_z \cdot \int_{\eta_b}^{\eta} \mathbf{J}_\zeta dz. \quad (37.155)$$

The time tendency for the depth integrated absolute vorticity for a fluid column at a fixed horizontal position (left hand side) is determined by a suite of boundary contributions due to baroclinicity, vortex stretching and friction, plus the convergence of the depth integrated vorticity flux (final term on right hand side). We next massage the boundary contributions to expose their associated physical processes.

37.8.3 Bottom boundary contribution

The bottom boundary contribution to the vorticity equation (37.155) takes on the form

$$\nabla(z - \eta_b) \cdot \mathbf{J}_\zeta = \nabla(z - \eta_b) \cdot [\mathbf{v} \zeta_a - \boldsymbol{\omega}_a w - \hat{\mathbf{z}} \times \rho^{-1} \nabla p + \hat{\mathbf{z}} \times \mathbf{F}]_{z=\eta_b} \quad (37.156a)$$

$$= -|\nabla(z - \eta_b)| \hat{\mathbf{n}} \cdot [-\boldsymbol{\omega}_a w - \hat{\mathbf{z}} \times \rho^{-1} \nabla p + \hat{\mathbf{z}} \times \mathbf{F}]_{z=\eta_b}, \quad (37.156b)$$

where we made use of the no-normal flow bottom kinematic boundary condition, $\hat{\mathbf{n}} \cdot \mathbf{v} = 0$ (Section 16.4.1), and where

$$\hat{\mathbf{n}} = -\left[\frac{\nabla(z - \eta_b)}{|\nabla(z - \eta_b)|} \right] = -\left[\frac{\hat{\mathbf{z}} - \nabla_z \eta_b}{\sqrt{1 + \nabla_z \eta_b \cdot \nabla_z \eta_b}} \right] \quad (37.157)$$

is the outward unit normal at the bottom.

Vortex stretching by vertical flow along a sloping bottom

The first term in the bottom boundary flux (37.156b) provides an inviscid vertical transport of the normal component of the absolute vorticity at the boundary. This term contributes through the action of vertical motion next to a sloping bottom, thus providing a vertical transfer of the vorticity component that is perpendicular to the bottom. This motion provides a form of vortex stretching that vanishes for a flat bottom, in which case $w(\eta_b) = 0$. It also vanishes for flow that parallels the bottom, whereby $\mathbf{u} \cdot \nabla \eta_b = 0$ so that $w(\eta_b) = 0$ according to the bottom kinematic boundary condition (16.41).

Bottom pressure torques

The second term in the bottom boundary flux (37.156b) arises from baroclinicity next to the bottom, in which case we consider the following term

$$\hat{\mathbf{n}} \cdot [\hat{\mathbf{z}} \times (\rho^{-1} \nabla p_b)] = \rho^{-1} \nabla p_b \cdot (\hat{\mathbf{n}} \times \hat{\mathbf{z}}) \equiv \rho^{-1} \nabla p_b \cdot \mathbf{t} \quad \text{with} \quad \mathbf{t} = \hat{\mathbf{n}} \times \hat{\mathbf{z}} = \left[\frac{\nabla \eta_b \times \hat{\mathbf{z}}}{|\nabla(z - \eta_b)|} \right]. \quad (37.158)$$

The vector \mathbf{t} is horizontal and it points along isolines of constant topography in a direction with land to the left pointing in the direction of \mathbf{t} , as depicted in Figure 37.10. Since $\hat{\mathbf{z}}$ and $\hat{\mathbf{n}}$ are not orthogonal, \mathbf{t} is not normalized so that it is not adorned with a hat. We thus find the contribution from baroclinicity takes the form

$$\nabla(z - \eta_b) \cdot \mathbf{J}_\zeta^{\text{baroclinicity}} = \rho^{-1} \nabla p_b \cdot (\nabla \eta_b \times \hat{\mathbf{z}}) = \rho^{-1} \hat{\mathbf{z}} \cdot [\nabla p_b \times \nabla \eta_b] = \rho^{-1} \hat{\mathbf{z}} \cdot [\nabla \times (p_b \nabla \eta_b)]. \quad (37.159)$$

Hence, the contribution from baroclinicity next to the bottom arises from the bottom pressure torque due to bottom pressure isolines that are not parallel to bottom topography isolines. We have more to say concerning boundary pressure torques in Section 37.9.3 as they also affect vorticity of the depth integrated flow.

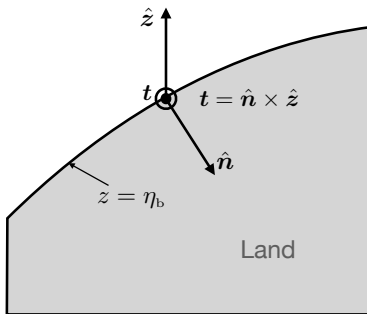


FIGURE 37.10: Orientation of the unit vectors next to the bottom of the fluid. The vertical unit vector, $\hat{\mathbf{z}}$, points vertically upward and the outward unit vector, $\hat{\mathbf{n}}$, points downward into the rock (shaded gray). The along-topography horizontal vector, $\mathbf{t} = \hat{\mathbf{n}} \times \hat{\mathbf{z}}$, points along lines of constant topography with land to the left when facing in the direction of \mathbf{t} ; in this figure it points out from the page. The vector \mathbf{t} is not necessarily a unit vector since it is not orthogonal to $\hat{\mathbf{n}}$.

Torques from bottom friction

The third term in the boundary flux (37.156b) is the contribution from friction along the bottom

$$-\hat{\mathbf{n}} \cdot (\hat{\mathbf{z}} \times \mathbf{F}) = -\mathbf{F} \cdot (\hat{\mathbf{n}} \times \hat{\mathbf{z}}) \equiv -\mathbf{F} \cdot \mathbf{t}. \quad (37.160)$$

Hence, contributions to the vertical vorticity evolution arise from the component of friction that projects onto the direction that parallels isobaths. To further our understanding of this result, consider a bottom friction written as a Rayleigh drag (e.g., Section 30.2.3) so that $\mathbf{F} = -\gamma \mathbf{u}$ and

$$-\mathbf{F} \cdot \mathbf{t} = \gamma \mathbf{u} \cdot \mathbf{t}, \quad (37.161)$$

with γ an inverse time scale. If the flow is oriented with shallow water to the right; e.g., into the page in Figure 37.10, then $-\mathbf{F} \cdot \mathbf{t} < 0$, thus contributing a negative vorticity tendency. In general, the bottom friction acts to damp the depth integrated vorticity, which is expected since bottom friction does not spontaneously spin-up the flow.

37.8.4 Surface boundary contribution

The surface boundary contribution to the vorticity equation (37.155) takes on a similar form to the bottom, with the new feature that the free surface is both moving and permeable (Section

16.4.3). This boundary term is given by

$$\zeta_a \partial_t \eta - \nabla(z - \eta) \cdot \mathbf{J}_\zeta = \zeta_a \partial_t \eta - \nabla(z - \eta) \cdot [\mathbf{v} \zeta_a - w \boldsymbol{\omega}_a - \hat{\mathbf{z}} \times \rho^{-1} \nabla p + \hat{\mathbf{z}} \times \mathbf{F}]_{z=\eta} \quad (37.162a)$$

$$= \zeta_a [\partial_t \eta + \mathbf{u} \cdot \nabla_z \eta - w]_{z=\eta} + \nabla(z - \eta) \cdot [w \boldsymbol{\omega}_a + \hat{\mathbf{z}} \times \rho^{-1} \nabla p - \hat{\mathbf{z}} \times \mathbf{F}]_{z=\eta} \quad (37.162b)$$

$$= \zeta_a Q_m / \rho + |\nabla(z - \eta)| \hat{\mathbf{n}} \cdot [w \boldsymbol{\omega}_a + \hat{\mathbf{z}} \times \rho^{-1} \nabla p - \hat{\mathbf{z}} \times \mathbf{F}]_{z=\eta}, \quad (37.162c)$$

where we made use of the surface kinematic boundary condition (16.79) to introduce the surface mass flux Q_m , and where

$$\hat{\mathbf{n}} = \frac{\nabla(z - \eta)}{|\nabla(z - \eta)|} = \frac{\nabla_z \eta + \hat{\mathbf{z}}}{\sqrt{1 + \nabla_z \eta \cdot \nabla_z \eta}} \quad (37.163)$$

is the outward unit normal at the surface. The first term in the surface boundary flux (37.162c) provides transport of boundary vorticity due to the transfer of mass across the boundary. The second term provides an inviscid vertical transport of absolute vorticity at the surface boundary, thus acting as a vortex stretching contribution. The third term provides a torque due to misalignments between the applied pressure isobars and the free surface isolines

$$|\nabla(z - \eta)| \hat{\mathbf{n}} \cdot (\hat{\mathbf{z}} \times \rho^{-1} \nabla p_a) = \rho^{-1} \nabla p_a \cdot (\nabla \eta \times \hat{\mathbf{z}}) = \rho^{-1} \hat{\mathbf{z}} \cdot \nabla p_a \times \nabla \eta = \rho^{-1} \hat{\mathbf{z}} \cdot \nabla \times (p_a \nabla \eta), \quad (37.164)$$

where the density, ρ , is evaluated at the ocean surface. The fourth term provides the corresponding contribution from the friction along the upper surface, with friction acting to reduce the magnitude of the surface boundary vorticity. For a rigid lid surface, $w(0) = 0$, $\eta = 0$, and $Q_m = 0$ so that the only surface boundary contribution arises from friction.

37.8.5 Comments

The depth integrated vorticity budget as derived in this section is perhaps the most physically straightforward of the suite of depth integrated vorticity budgets. However, in the practice of ocean modeling, this budget is generally not used since it requires an online coding of the vorticity equation and then its depth integral. As ocean models generally time step the velocity rather than the vorticity, it is common to form a vorticity budget based on the depth integrated flow or the depth averaged flow. We develop these budgets in the following section.

37.9 Vorticity for the depth integrated horizontal flow

In this section we develop dynamical equations for vorticity of the depth integrated flow in a hydrostatic fluid. A compelling application of these ideas comes from the study of large-scale ocean circulation. The leading order impacts from bottom pressure torques has emerged from research during recent decades, thus pointing to the fundamental role of bottom topography and flows next to sloping bottom (rather than vertical sidewalls) in affecting the ocean circulation. This recognition contrasts to traditional theories whereby the wind stress curl balances meridional motion through the beta effect. In particular, numerical model studies reveal that wind stress curl is sub-dominant in any region with nontrivial bottom velocities.¹² In this section we introduce the basics and provide more discussion in Sections 41.7 and 41.8 when studying vorticity dynamics for the planetary geostrophic system.

¹²The natural ocean has no distinction between side and bottom. Rather, as discussed in Figure 25.7, the ocean has a sloping bottom that reaches to the surface along its boundary at the “beach.” *Hallberg and Rhines* (1996), *Hughes and de Cueves* (2001), and many subsequent studies emphasize that theoretical and numerical models using vertical sides and a flat bottom exhibit somewhat unnatural dynamical balances, whereas models with sloping bottoms better capture key effects from topography.

37.9.1 Comparing the two vorticities

In Section 37.8 we derived the evolution equation for the depth integral of the vertical component to the absolute vorticity,

$$\int_{\eta_b}^{\eta} \zeta_a dz = \int_{\eta_b}^{\eta} (f + \hat{z} \cdot \nabla \times \mathbf{u}) dz. \quad (37.165)$$

In this section we study the evolution equation for the relative vorticity in the depth integrated horizontal flow

$$\hat{z} \cdot \nabla \times \mathbf{U}^\rho = \hat{z} \cdot \nabla \times \int_{\eta_b}^{\eta} \mathbf{u} \rho dz, \quad (37.166)$$

where we introduced the depth integrated horizontal mass flux

$$\mathbf{U}^\rho = \int_{\eta_b}^{\eta} \rho \mathbf{u} dz. \quad (37.167)$$

For a Boussinesq ocean we set the density to a constant, in which case the difference between the two relative vorticities is

$$\hat{z} \cdot \nabla \times \left[\int_{\eta_b}^{\eta} \mathbf{u} dz \right] - \int_{\eta_b}^{\eta} \hat{z} \cdot \nabla \times \mathbf{u} dz = \hat{z} \cdot [\nabla \eta \times \mathbf{u}(\eta) - \nabla \eta_b \times \mathbf{u}(\eta_b)]. \quad (37.168)$$

Flows along boundaries generally have a nontrivial projection in the direction parallel to boundary isosurfaces, in which case the cross products are nonzero thus leading to differences in the two relative vorticities.

37.9.2 Evolution of vorticity for the depth integrated horizontal flow

In Section 25.4 we developed the horizontal momentum equation for a hydrostatic fluid, as given by equation (25.48)

$$(\partial_t + f \hat{z} \times) \mathbf{U}^\rho = \mathbf{u}(\eta) Q_m - \eta \nabla_z p_a + \eta_b \nabla_z p_b - \nabla_z \mathcal{P} + \mathbf{D} + \nabla_z \cdot \left[\int_{\eta_b}^{\eta} \mathbb{T}_{\text{hor}}^{\text{kinetic}} dz \right]. \quad (37.169)$$

We here introduced the potential energy per horizontal area of the fluid column (equation (25.40)), the depth integrated horizontal friction (equation (25.49)), and the divergence of the horizontal kinetic stress tensor (equation (25.32))

$$\mathcal{P} = \int_{\eta_b}^{\eta} g \rho z dz \quad \text{and} \quad \mathbf{D} = \int_{\eta_b}^{\eta} \rho \mathbf{F}_{\text{horz}} dz. \quad \text{and} \quad \mathbb{T}_{\text{hor}}^{\text{kinetic}} = -\rho \mathbf{u} \otimes \mathbf{u}. \quad (37.170)$$

All terms on the right hand side of equation (37.169) provide a stress that drives changes in \mathbf{U}^ρ . Hence, the curl of these terms provides a torque, in which case we have

$$\begin{aligned} \hat{z} \cdot \partial_t (\nabla \times \mathbf{U}^\rho) &= -\nabla \cdot (f \mathbf{U}^\rho) \\ &+ \hat{z} \cdot \nabla \times \left[\mathbf{u}(\eta) Q_m - \eta \nabla_z p_a + \eta_b \nabla_z p_b + \Delta \boldsymbol{\tau} + \mathbf{D} + \nabla_z \cdot \left(\int_{\eta_b}^{\eta} \mathbb{T}_{\text{hor}}^{\text{kinetic}} dz \right) \right], \end{aligned} \quad (37.171)$$

where we used the vector identity

$$\hat{z} \cdot \nabla \times (f \hat{z} \times \mathbf{U}^\rho) = \nabla \cdot (f \mathbf{U}^\rho), \quad (37.172)$$

as well as $\nabla \times \nabla_z \varphi = 0$. We now discuss the various physical processes appearing in the vorticity equation (37.171).

Beta effect

The first term on the right hand side of the vorticity equation (37.171) arises from the convergence of mass within a fluid column due to depth integrated horizontal flow. We can further decompose the effects from this term by performing the product rule

$$-\nabla \cdot (f \mathbf{U}^\rho) = -f \nabla \cdot \mathbf{U}^\rho - \beta V^\rho. \quad (37.173)$$

The contribution from βV^ρ arises from the beta effect as discussed in Section 37.6.2. For the first term, the weighting by the Coriolis parameter means that mass convergence at higher latitudes has more impact on vorticity changes than at lower latitudes. We can understand this weighting by noting that vertical fluid columns are more aligned with the planetary rotation at the high latitudes. Hence, when the mass of vertical columns converges at the higher latitudes, there is more impact on changes to the vorticity of the depth integrated flow.

Mass transfer, turbulent momentum transfer, and nonlinear effects

The term $\nabla \times [\mathbf{u}(\eta) Q_m]$ appearing in equation (37.174) accounts for vorticity crossing the ocean surface as affected by the mass flux. The term $\nabla \times \Delta\tau$ is the torque from turbulent stresses at the ocean surface and bottom, and $\hat{\mathbf{z}} \cdot \nabla \times \mathbf{D}$ is the torque from horizontal frictional stresses in the fluid interior. The final term arises from the nonlinear kinetic stresses, $\mathbb{T}_{\text{hor}}^{\text{kinetic}}$, that account for curls in the self-advection operator.

37.9.3 Boundary pressure torques

The pressure terms in equation¹³ (37.171)

$$\hat{\mathbf{z}} \cdot \nabla \times (-\eta \nabla p_a + \eta_b \nabla p_b) = \hat{\mathbf{z}} \cdot \nabla \times (p_a \nabla \eta - p_b \nabla \eta_b) \quad (37.174)$$

arise from curls of the pressure form stresses (see Chapter 25) at the ocean surface and bottom, and these contributions are referred to as *pressure torques*. When the fluid is a column of ocean water, then the surface pressure contribution is the *atmospheric pressure torque* and the bottom pressure term is the *bottom pressure torque*.

Geometry of boundary pressure torques

Geometrically, there is a nonzero atmospheric pressure torque when the applied pressure, p_a , has a gradient when moving along contours of constant free surface. Likewise, there is a nonzero bottom pressure torque when bottom pressure, p_b , changes along contours of constant bottom topography. Mathematically, we reveal these properties through use of either Exercise 6.1 or 37.11. For example, the bottom pressure torque along an isobath (contour of constant η_b) can be written

$$\hat{\mathbf{z}} \cdot \nabla \eta_b \times \nabla p_b = -(\hat{\mathbf{n}} \cdot \nabla \eta_b) (\hat{\mathbf{t}} \cdot \nabla p_b), \quad (37.175)$$

where $\hat{\mathbf{t}}$ is a unit tangent vector directed along the isobath, and $\hat{\mathbf{n}}$ is a unit vector that points to the left of $\hat{\mathbf{t}}$ (see Figure 37.11). Both $\hat{\mathbf{t}}$ and $\hat{\mathbf{n}}$ are horizontal vectors. Hence, $\hat{\mathbf{n}} \cdot \nabla \eta_b$ measures

¹³To reduce notational clutter, we sometimes write ∇ rather than ∇_z when operating on functions that are independent of z , such as η , p_a , η_b and p_b . Since these fields are independent of z , we have $\nabla_z \eta = \nabla \eta$, and likewise for the other fields.

the slope of the bottom topography in the direction normal to an isobath, and $\hat{\mathbf{t}} \cdot \nabla p_b$ measures the change of the bottom pressure along the isobath. There is a nonzero bottom pressure torque along an isobath so long as there is a slope to the bottom pressure along the isobath, and there is a change in bottom pressure moving along the isobath.

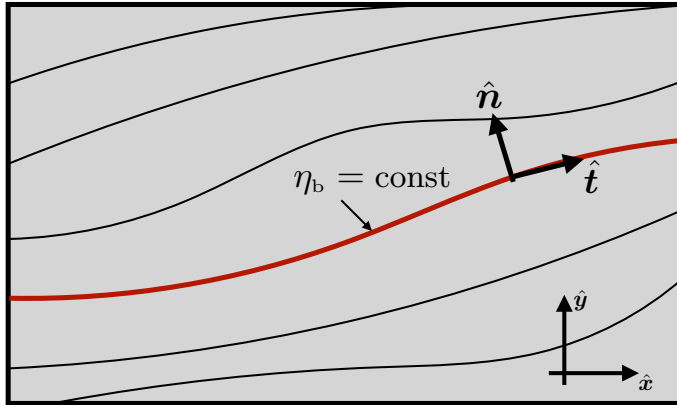


FIGURE 37.11: Geometry depicting a contour along a particular line of constant topography (i.e., an isobath), $\eta_b(x, y)$. The along-contour direction is $\hat{\mathbf{t}} = d\mathbf{x}/ds$, with s the arc length along the contour. The unit direction pointing to the left of $\hat{\mathbf{t}}$ is written $\hat{\mathbf{n}}$, with $\hat{\mathbf{n}} \cdot \hat{\mathbf{t}} = 0$ and $\hat{\mathbf{t}} \times \hat{\mathbf{n}} = \hat{\mathbf{z}}$. Both $\hat{\mathbf{n}}$ and $\hat{\mathbf{t}}$ are horizontal unit vectors. There is a nonzero bottom pressure torque if bottom pressure changes when following an isobath.

Geostrophic velocity associated with the bottom pressure torque

To further our understanding of the pressure torques in equation (37.174), focus on the bottom pressure and introduce a geostrophic velocity

$$\rho_0 f \mathbf{u}_g = \hat{\mathbf{z}} \times \nabla p_b, \quad (37.176)$$

so that the bottom pressure torque takes the form

$$\hat{\mathbf{z}} \cdot \nabla \times (\eta_b \nabla p_b) = \hat{\mathbf{z}} \cdot \nabla \eta_b \times \nabla p_b = \rho_0 f \mathbf{u}_g \cdot \nabla \eta_b. \quad (37.177)$$

This equation is merely a replacement of the bottom pressure gradient with a corresponding geostrophic velocity. However, if this geostrophic velocity is assumed to satisfy the kinematic boundary condition (16.41), then we reach the equality¹⁴

$$\hat{\mathbf{z}} \cdot \nabla \eta_b \times \nabla p_b = \rho_0 f w_g, \quad (37.178)$$

which links the bottom pressure torque to vertical vortex stretching by the vertical component to the geostrophic velocity.

The equality (37.178) is sometimes used to infer the bottom pressure torque by diagnosing the bottom vertical velocity, $w(\eta_b)$ (Spence et al., 2012). Although this diagnostic is suitable for some studies, there are important caveats. Namely, the bottom vertical velocity is generally affected by bottom frictional effects and thus can have a nontrivial Ekman component.¹⁵ Nonlinear effects

¹⁴The velocity, \mathbf{v} , satisfies the kinematic boundary condition (16.41), in which $\mathbf{v}(\eta_b) \cdot \hat{\mathbf{n}} = 0$. Decomposing the velocity into its geostrophic and ageostrophic components, $\mathbf{v} = \mathbf{v}_g + \mathbf{v}_a$, does not generally imply that \mathbf{v}_g and \mathbf{v}_a separately satisfies the kinematic boundary condition. Rather, we must make that assumption in order to reach the equality (37.178).

¹⁵Recall our discussion of Ekman boundary layers in Chapter 30.

can also be important especially when considering motions with sizable Rossby numbers. Neither the Ekman component nor nonlinear terms are directly related to the bottom pressure torque. We thus expect $\rho_0 f w(\eta_b)$ to be distinct from $\hat{z} \cdot \nabla \eta_b \times \nabla p_b$ in regions of sizable deep flows where bottom friction and/or nonlinear effects are of leading order importance.¹⁶ The studies from [Gula et al. \(2015\)](#) and [LeCorre et al. \(2020\)](#) illustrate these points from numerical simulations of the subpolar North Atlantic circulation.

37.9.4 Steady state vorticity budget

The steady state form of the vorticity budget (37.171) leads to the balance

$$\beta V^\rho = -f \nabla \cdot \mathbf{U}^\rho + \hat{z} \cdot \nabla \times \left[\mathbf{u}(\eta) Q_m - \eta \nabla_z p_a + \eta_b \nabla_z p_b + \Delta \boldsymbol{\tau} + \mathbf{D} + \nabla_z \cdot \left(\int_{\eta_b}^{\eta} \mathbb{T}_{\text{hor}}^{\text{kinetic}} dz \right) \right]. \quad (37.179)$$

Writing the balance in this manner reveals how the beta effect affords a steady meridional mass transport as a balance with the variety of terms on the right hand side.

Specializing the budget to expose a variety of balanced flow regimes

Let us further specialize to the case appropriate for many studies of the large-scale circulation, whereby we make the following assumptions.

- Uniform mass atmosphere so that p_a is a constant.
- The frictional stresses from horizontal strains within the fluid interior, \mathbf{D} , can be neglected.
- Zero boundary mass transport so that $Q_m = 0$ and, correspondingly, the steady depth integrated mass budget (16.88) means that $\nabla \cdot \mathbf{U}^\rho = 0$ when $Q_m = 0$.

These simplifications bring the balance (37.179) to the form

$$\beta V^\rho = \hat{z} \cdot \nabla \times \left[\eta_b \nabla_z p_b + \Delta \boldsymbol{\tau} + \nabla_z \cdot \left(\int_{\eta_b}^{\eta} \mathbb{T}_{\text{hor}}^{\text{kinetic}} dz \right) \right] \quad (37.180a)$$

$$\text{MERIDIONAL TRANSPORT} = \text{BOTTOM PRESS TORQUE} + \text{BOUNDARY STRESS} + \text{NONLINEAR}. \quad (37.180b)$$

This steady balance reveals distinct flow regimes depending on which of the terms dominate, and as such it serves as a useful framework for analysis.

Topographic nonlinear balance

[Jackson et al. \(2006\)](#), [Patmore et al. \(2019\)](#), and [LeCorre et al. \(2020\)](#) emphasize the importance of the nonlinear term in equation (37.180b) when flows are especially strong. The bottom pressure torque contribution is particularly strong where flows are strong near the bottom. Such nonlinear flow regimes generally have variations over length scales much smaller than that of the wind stress. Hence, if the horizontal friction is small, as it is even for strong flows not directly adjacent to

¹⁶In addition to the Ekman and nonlinear effects noted here, diagnosing $w(\eta_b)$ in a numerical model can be fraught with difficulties related to the discrete grid stencil given that grids can be quite coarse in the deep ocean with many ocean model configurations.

solid boundaries, and the bottom frictional drag is small, then the vorticity balance (37.180a) in the nonlinear inviscid regime takes on the form

$$\beta V^\rho = \hat{z} \cdot \nabla \times \left[\eta_b \nabla_z p_b + \nabla_z \cdot \left(\int_{\eta_b}^{\eta} \mathbb{T}_{\text{hor}}^{\text{kinetic}} dz \right) \right] \quad \text{topographic nonlinear balance.} \quad (37.181)$$

Observe that the nonlinear term and bottom pressure torque have derivatives whereas there are none on the βV^ρ term. These derivatives make the right hand side terms have variations at smaller scales than βV^ρ . We infer that the smaller scales present in the bottom pressure torque and the nonlinear term nearly balance, and with any residual leading to the broader scale meridional transport. Figure 6 in [LeCorre et al. \(2020\)](#) provides a striking example of this balance in a numerical simulation of the North Atlantic subpolar gyre.

Linear regime of planetary geostrophy

For the linear regime of planetary geostrophic flow (Chapter 41), the nonlinear term from the kinetic stress is small, so that the balance is between meridional transport, bottom pressure torque, and curl of turbulent boundary stresses. The *Sverdrup balance* is one particular example of a planetary geostrophic balance, with Sverdrup balance ignoring the bottom pressure torque and bottom turbulent stresses, and thus focuses just on the balance between meridional transport with the turbulent surface stresses largely arising from winds

$$\beta V^\rho = \hat{z} \cdot \nabla \times \boldsymbol{\tau}^\eta \quad \text{Sverdrup balance.} \quad (37.182)$$

However, as emphasized by [Hallberg and Rhines \(1996\)](#) and [Hughes and de Cueves \(2001\)](#), as well as more recent studies, contributions from bottom pressure torques are of leading order importance in the presence of flow next to sloping side boundaries, thus making the traditional Sverdrup balance mostly relevant in the open ocean away from boundaries. A more general balance is known as *topographic Sverdrup balance*

$$\beta V^\rho = \hat{z} \cdot \nabla \times (\eta_b \nabla_z p_b + \boldsymbol{\tau}^\eta) \quad \text{topographic Sverdrup balance.} \quad (37.183)$$

We further study these balances of planetary geostrophy in Sections 41.5, 41.7, and 41.8.

37.9.5 Integral balances satisfied by steady flows

Reconsider the steady vorticity balance (37.179), here written in the form

$$\nabla \cdot (f \mathbf{U}^\rho) = \hat{z} \cdot \nabla \times \mathbf{M} \quad (37.184)$$

where we introduced the stress vector

$$\mathbf{M} = \mathbf{u}(\eta) Q_m - \eta \nabla_z p_a + \eta_b \nabla_z p_b + \Delta \boldsymbol{\tau} + \mathbf{D} + \nabla_z \cdot \left(\int_{\eta_b}^{\eta} \mathbb{T}_{\text{hor}}^{\text{kinetic}} dz \right). \quad (37.185)$$

Now integrate equation (37.184) over an area, \mathcal{S} , with Gauss's divergence theorem on the left hand side leading to

$$\int_{\mathcal{S}} \nabla \cdot (f \mathbf{U}^\rho) d\mathcal{S} = \oint_{\partial\mathcal{S}} f \mathbf{U}^\rho \cdot \hat{\mathbf{n}} ds, \quad (37.186)$$

where $\hat{\mathbf{n}}$ is the horizontal outward unit normal on the boundary, $\partial\mathcal{S}$, and ds is the arc-length increment along the boundary. This term is the mass transport crossing the boundary as weighted by the Coriolis parameter.

Use of Stokes' curl theorem on the right hand side of equation (37.184) leads to

$$\int_{\mathcal{S}} \hat{\mathbf{z}} \cdot \nabla \times \mathbf{M} d\mathcal{S} = \oint_{\partial\mathcal{S}} \mathbf{M} \cdot \hat{\mathbf{t}} ds, \quad (37.187)$$

where $\hat{\mathbf{t}}$ is the horizontal unit tangent vector along the boundary, and the integral is oriented in the counter-clockwise direction. To help interpret the closed loop integral in equation (37.187), consider just the contribution from bottom pressure

$$\oint_{\partial\mathcal{S}} \mathbf{M}_{\text{bottom press}} \cdot \hat{\mathbf{t}} ds = \oint_{\partial\mathcal{S}} \eta_b \nabla p_b \cdot \hat{\mathbf{t}} ds = - \oint_{\partial\mathcal{S}} p_b \nabla \eta_b \cdot \hat{\mathbf{t}} ds, \quad (37.188)$$

which is the work done by bottom topographic form stress around the closed contour. The other terms in equation (37.184) have interpretations as the work arising from integrating stresses from mass transport through the surface, atmospheric form stress, turbulent boundary stresses, interior frictional stresses, and nonlinear kinetic stress. Observe that the integral of bottom pressure torque in equation (37.188) vanishes if the closed contour follows either an isobath or a bottom pressure isobar. The vanishing of this integral means that bottom pressure torques have zero net circulation around isobaths or bottom isobars. An analogous property is satisfied by the atmospheric pressure torque when integrated around closed contours of constant atmospheric pressure, p_a , or constant surface height, η .

Bringing the above results together renders the general balance around the boundary of an arbitrary closed region

$$\oint_{\partial\mathcal{S}} f \mathbf{U}^\rho \cdot \hat{\mathbf{n}} ds = \oint_{\partial\mathcal{S}} \mathbf{M} \cdot \hat{\mathbf{t}} ds. \quad (37.189)$$

We thus see that transport across the closed boundary, as weighted by the Coriolis parameter, arises from a nonzero net work around the boundary by the variety of stresses comprising \mathbf{M} . We are afforded a key simplification if $\mathbf{U}^\rho \cdot \hat{\mathbf{n}} = 0$ at each point along the boundary. For example, if $\nabla \cdot \mathbf{U}^\rho = 0$, which generally also requires $Q_m = 0$, then contours along which $\mathbf{U}^\rho \cdot \hat{\mathbf{n}} = 0$ correspond to closed streamlines of the steady \mathbf{U}^ρ . Hence, we find the following balance holds around any closed streamline

$$\oint_{\partial\mathcal{S}} \mathbf{M} \cdot \hat{\mathbf{t}} ds = 0. \quad \text{for } \partial\mathcal{S} \text{ a closed streamline of } \mathbf{U}^\rho. \quad (37.190)$$

Closed streamlines do not always exist. But when they do, such as for steady ocean gyre circulations, this balance holds. In Section 41.7.3, we consider the planetary geostrophic version of this balance.

37.9.6 Formulation based on the vector-invariant velocity equation

In formulating the budget equation (37.171) for vorticity of the depth integrated flow, we started with the depth integrated momentum in Section 25.4.5. However, many numerical models are formulated using the vector invariant form of the horizontal velocity equation (37.135), here written in the equivalent form for a Boussinesq ocean

$$\underbrace{\partial_t \mathbf{u} + f \hat{\mathbf{z}} \times \mathbf{u} + \nabla_z p / \rho_0 - \mathbf{F}}_{\text{linear terms plus friction}} = \underbrace{-\zeta \hat{\mathbf{z}} \times \mathbf{u} - w \partial_z \mathbf{u} - \nabla_z \mathbf{u}^2 / 2}_{\text{Magnus + vertical advection + kinetic energy}}. \quad (37.191)$$

The three nonlinear terms on the right hand side arise from expanding the nonlinear self-advection term, $(\mathbf{v} \cdot \nabla) \mathbf{u}$, following the manipulations in Section 37.7.1. Much of the formulation to follow emulates that considered thus far, with the exception of the nonlinear terms and elements of the boundary contributions.

We take the vertical integral of equation (37.191)

$$\int_{\eta_b}^{\eta} [\partial_t \mathbf{u} + f \hat{\mathbf{z}} \times \mathbf{u} + \nabla_z p / \rho_0 - \mathbf{F}] dz = - \int_{\eta_b}^{\eta} (\zeta \hat{\mathbf{z}} \times \mathbf{u} + w \partial_z \mathbf{u} + \nabla_z \mathbf{u}^2 / 2) dz, \quad (37.192)$$

and then the curl

$$\nabla \times \int_{\eta_b}^{\eta} (\partial_t \mathbf{u} + f \hat{\mathbf{z}} \times \mathbf{u} + \nabla_z p / \rho_0 - \mathbf{F}) dz = - \nabla \times \int_{\eta_b}^{\eta} (\zeta \hat{\mathbf{z}} \times \mathbf{u} + w \partial_z \mathbf{u} + \nabla_z \mathbf{u}^2 / 2) dz. \quad (37.193)$$

Making use of the following identities

$$\hat{\mathbf{z}} \cdot \left[\nabla \times \int_{\eta_b}^{\eta} \partial_t \mathbf{u} dz \right] = \hat{\mathbf{z}} \cdot \partial_t (\nabla \times \mathbf{U}) - \hat{\mathbf{z}} \cdot \nabla \times [\mathbf{u}(\eta) \partial_t \eta] \quad (37.194a)$$

$$\hat{\mathbf{z}} \cdot \left[\nabla \times \int_{\eta_b}^{\eta} f \hat{\mathbf{z}} \times \mathbf{u} dz \right] = \nabla \cdot (f \mathbf{U}) \quad (37.194b)$$

$$\hat{\mathbf{z}} \cdot \left[\nabla \times \int_{\eta_b}^{\eta} \nabla_z p dz \right] = \hat{\mathbf{z}} \cdot \nabla \times (\eta \nabla p_a - \eta_b \nabla p_b) \quad (37.194c)$$

$$\hat{\mathbf{z}} \cdot \left[\nabla \times \int_{\eta_b}^{\eta} \zeta \hat{\mathbf{z}} \times \mathbf{u} dz \right] = \nabla \cdot \left[\int_{\eta_b}^{\eta} \zeta \mathbf{u} dz \right] \quad (37.194d)$$

$$\hat{\mathbf{z}} \cdot \left[\nabla \times \int_{\eta_b}^{\eta} \rho_0 \mathbf{F} dz \right] = \hat{\mathbf{z}} \cdot \nabla \times (\Delta \boldsymbol{\tau} + \mathbf{D}), \quad (37.194e)$$

leads to

$$\begin{aligned} \hat{\mathbf{z}} \cdot \partial_t (\nabla \times \mathbf{U}) &= - \nabla \cdot \left[f \mathbf{U} + \int_{\eta_b}^{\eta} \zeta \mathbf{u} dz \right] \\ &+ \hat{\mathbf{z}} \cdot \nabla \times \left[\mathbf{u}(\eta) \partial_t \eta - \eta \nabla p_a + \eta_b \nabla p_b + (\Delta \boldsymbol{\tau} + \mathbf{D}) / \rho_0 - \int_{\eta_b}^{\eta} (w \partial_z \mathbf{u} + \nabla_z \mathbf{u}^2 / 2) dz \right]. \end{aligned} \quad (37.195)$$

The left hand side is the time tendency of the vorticity of the depth integrated horizontal flow, with this time tendency driven by the various linear and nonlinear terms on the right hand side. This evolution equation should be compared to equation (37.171) as derived from the advective form of the momentum equation. Likewise, we derive a steady state balance by setting the time tendencies to zero to yield

$$\begin{aligned} \beta V &= -f \nabla \cdot \mathbf{U} - \nabla \cdot \left[\int_{\eta_b}^{\eta} \zeta \mathbf{u} dz \right] \\ &+ \hat{\mathbf{z}} \cdot \nabla \times \left[\mathbf{u}(\eta) \partial_t \eta - \eta \nabla p_a + \eta_b \nabla p_b + (\Delta \boldsymbol{\tau} + \mathbf{D}) / \rho_0 - \int_{\eta_b}^{\eta} (w \partial_z \mathbf{u} + \nabla_z \mathbf{u}^2 / 2) dz \right], \end{aligned} \quad (37.196)$$

which should be compared to equation (37.179).

37.9.7 Vorticity of the depth averaged flow

The vorticity of the depth averaged flow is given by $\hat{\mathbf{z}} \cdot \nabla \times \bar{\mathbf{u}}$, where $\bar{\mathbf{u}}$ is given by equation (25.33) for a compressible non-Boussinesq fluid, and which takes on the following form for a Boussinesq ocean

$$\bar{\mathbf{u}} = \frac{\int_{\eta_b}^{\eta} \mathbf{u} dz}{\eta - \eta_b} = \frac{\mathbf{U}}{\eta - \eta_b}. \quad (37.197)$$

The difference is given by

$$\nabla \times \mathbf{U} - (\eta - \eta_b) \nabla \times \bar{\mathbf{u}} = \nabla(\eta - \eta_b) \times \bar{\mathbf{u}}, \quad (37.198)$$

so that the two vorticities are the same in the special case of a depth averaged flow that is parallel to $\nabla(\eta - \eta_b)$. Quite trivially, $\nabla(\eta - \eta_b) \times \bar{\mathbf{u}} = 0$ occurs for a rigid lid and flat bottom ocean, in which $\nabla\eta = \nabla\eta_b = 0$. More generally, $\nabla(\eta - \eta_b) \times \bar{\mathbf{u}} \neq 0$, particularly in the presence of topography. We further study the budgets for these two vorticities, for planetary geostrophic flow, in Sections 41.7 and 41.8.

37.9.8 Comments and further study

The diagnostic budgets derived in this section have appeared in many studies of ocean vorticity. When diagnosing the budget terms in a numerical model, the choice for how to mathematically formulate the diagnostic balances is largely driven by physical transparency as well as by numerical precision. Concerning numerical precision, it is useful to note that vorticity, as the derivative of velocity, has more power at the high spatial wave numbers than does velocity. In a numerical model, such power can manifest as grid scale noise. It is thus of use to perform much of the calculation online to enable the most accurate available diagnostic. Even so, further spatial smoothing is generally required, especially in realistic models, to extract physically interpretable signals.



37.10 Exercises

EXERCISE 37.1: STRAIN AND ROTATION FOR STRETCHING AND TILTING

In this exercise we write the 3×3 rate of strain tensor, \mathbb{S} , and rotation tensor, \mathbb{R} , for the examples of vortex stretching and vortex tilting considered in Section 37.5.3. Recall that elements of \mathbb{S} are given by equation (15.33a) and \mathbb{R} have elements given by equation (15.33b). Hint: there is no unique answer for the rate of strain tensors, so offer a simple example that renders the desired behavior of a vortex filament.

- (a) Write a rate of strain tensor corresponding to vortex stretching as per equation (37.75) along with $\omega^x = \omega^y = 0$, and write the corresponding vorticity source term $\boldsymbol{\omega} \cdot \mathbb{S}$.
- (b) Write the rotation tensor for vortex stretching as per equation (37.75) and verify that $\omega_m \cdot \mathbb{R}_{mn} = 0$.
- (c) Write a rate of strain tensor corresponding to vortex tilting as per equation (37.81) along with $\omega^y = \omega^z = 0$.
- (d) Write the rotation tensor for vortex tilting as per equation (37.81) and verify that $\omega_m \mathbb{R}_{mn} = 0$.

EXERCISE 37.2: BAROCLINICITY WITH $\rho_0(z)$

Recall the discussion of the Boussinesq momentum equation in Section 26.1.2. The form given by equation (26.8) is written with the reference density, $\rho_0 = \rho_0(z)$. We then stated that the form of the baroclinicity vector appearing in the Boussinesq vorticity equation is greatly simplified by

setting ρ_0 to a global constant, and thus dropping the z dependence. Derive the second term in the baroclinicity

$$\mathbf{B} = \nabla \left[b - \frac{\delta p}{\rho_0^2} \frac{d\rho_0}{dz} \right] \times \hat{\mathbf{z}}, \quad (37.199)$$

so that $\mathbf{B} = \nabla b \times \hat{\mathbf{z}}$ when ρ_0 is assumed to be a global constant. Hint: write the vector-invariant form of equation (26.8) with $\rho_0(z)$. Then take the curl.

EXERCISE 37.3: FRICTION IN THE VORTICITY EQUATION

Assume a viscous friction operator of the form

$$\mathbf{F} = \nu \nabla^2 \mathbf{v}, \quad (37.200)$$

with ν a constant molecular kinematic viscosity. Assuming Cartesian coordinates, write the vorticity equation (37.41) with this term included.

EXERCISE 37.4: FRICTION FOR NON-DIVERGENT FLOWS

Consider a non-divergent flow with a Laplacian frictional acceleration

$$\mathbf{F} = \nu \nabla^2 \mathbf{v} \quad \text{with} \quad \nabla \cdot \mathbf{v} = 0, \quad (37.201)$$

with ν a constant molecular kinematic viscosity. Write this expression in terms of the vorticity. Hint: check that $\nabla \times \mathbf{F}$ equals to the friction appearing in the vorticity equation derived in exercise 37.3. Further hint: the derivation is given in Section 22.8.8.

EXERCISE 37.5: GENERATION OF VORTICITY BY BAROCLINICITY

Consider an initially resting body of water with a flat bottom and rigid sides. Let the top surface be at $z = 0$ and bottom at $z = -H$, and assume zero pressure applied at the top surface. Let the density have a horizontal structure given by

$$\rho(x) = \rho_0 (1 - \gamma x) \quad (37.202)$$

where ρ_0 and γ are positive constants (with dimensions of density and inverse length, respectively). We furthermore assume that $\gamma|x| \ll 1$ so that the density is strictly positive. Note that a study of Figure 37.3 helps with this exercise.

- (a) Compute the density gradient $\nabla \rho$ and draw a schematic.
- (b) Compute the pressure gradient, ∇p , assuming approximate hydrostatic balance so that $\partial p / \partial z = -\rho g$. Draw a schematic at $x = 0$.
- (c) Compute the baroclinicity/solenoidal vector $\mathbf{B} = \rho^{-2} (\nabla \rho \times \nabla p)$. Draw a schematic.
- (d) Describe the vorticity induced by the baroclinicity vector.

EXERCISE 37.6: GENERATION OF CIRCULATION BY BAROCLINICITY IN AN IDEAL GAS

In this exercise we examine the baroclinicity vector for a simple ideal gas, which is described by the equation of state (20.48)

$$\rho = \frac{p M_{\text{mole}}}{T R^g} \equiv \frac{p}{T R^M}, \quad (37.203)$$

where R^g is the universal gas constant and R^M is the specific gas constant. We also assume the atmosphere is in approximate hydrostatic balance (Section 24.2), and we ignore rotation (relatively small lateral region of the atmosphere). For further hints to this exercise, see Section 4.1 of Holton (1992) or Section 2.4.3 of Markowski and Richardson (2010), where they discuss circulation generated by differences in land-sea temperatures, thus leading to a sea breeze.

- (a) Express the baroclinicity vector, \mathbf{B} , in terms of pressure and temperature gradients.
- (b) Express the baroclinicity vector in terms of pressure and potential temperature gradients.
Hint: see Section 20.4.11 for potential temperature in an ideal gas.
- (c) Consider an ideal gas atmosphere straddling the ocean and flat land as in Figure 37.12. Let the daytime air be relatively cool over the ocean and relatively warm over the land. Furthermore, assume the sea level pressure is the same value over land and ocean. Ignoring rotation, draw isolines of constant temperature and constant pressure. Assume the horizontal temperature gradient is constant with height. Here are some hints.
- Temperature decreases from land to ocean and decreases when ascending into the atmosphere.
 - Pressure is assumed to be horizontally constant at sea level and it decreases upward. Use the ideal gas law to determine the sense for the horizontal pressure gradient as one ascends. Consult the discussion in Section 20.4.10 for geopotentials in an ideal gas atmosphere.
 - We are only concerned with a qualitative sense for the isolines in the lower atmosphere and over a horizontal region small enough that rotation can be ignored.
- (d) Describe the sense for the circulation induced by the baroclinicity. Does circulation correspond to your experience at a sunny beach day as the air warms over the land faster than over the adjacent ocean? What force causes air to rise and to fall?

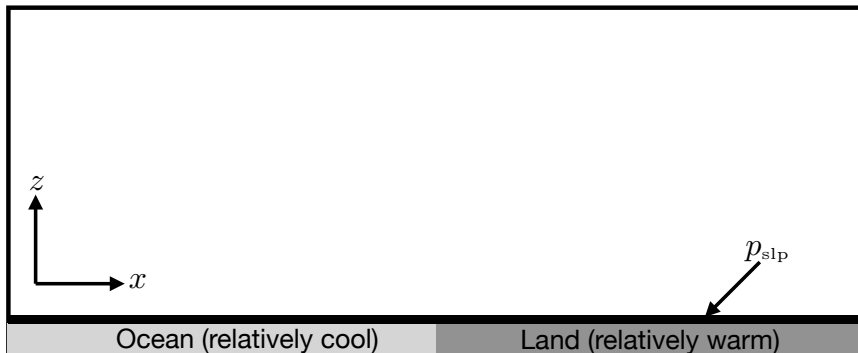


FIGURE 37.12: Setup for the sea breeze Exercise 37.6. We here depict a vertical-zonal cross-section of the atmosphere where the lower boundary straddles the ocean and land. The atmosphere over the ocean is assumed to be cooler than the atmosphere over the land, as typically occurs on a sunny afternoon with solar radiation warming land faster than the ocean.

EXERCISE 37.7: CIRCULATION WITH ISLANDS

Our discussion of Stokes' theorem has been thus far restricted to a simply connected domain, in which

$$\oint_{\partial S} \mathbf{v} \cdot d\mathbf{x} = \int_S \boldsymbol{\omega} \cdot \hat{\mathbf{n}} dS. \quad (37.204)$$

For a simply connected domain, the closed contour can be shrunk to a point without leaving the domain.

A more general topology consists of a region with holes, whereby closed contours cannot in general be shrunk to a point without leaving the region. In an oceanographic context, the “holes” are islands or continents and the circulation is that for the depth integrated flow. Figure 37.13

shows a region of the ocean containing three arbitrarily shaped impenetrable islands, with the three islands surrounded by a contour. The contour cannot be shrunk to a point without crossing over the islands, thus making this region of the ocean multiply-connected. The presence of islands thus adds a level of complexity to the World Ocean that is absent an AquaPlanet or the global atmosphere.

Derive the following expression for the circulation in multiply-connected regions

$$\oint_{\partial\mathcal{S}} \mathbf{v} \cdot d\mathbf{x} = \sum_{n=1}^N \left(\oint_{\partial\mathcal{S}_n} \mathbf{v} \cdot d\mathbf{x} \right) + \int_{\mathcal{S}} \boldsymbol{\omega} \cdot \hat{\mathbf{n}} dS, \quad (37.205)$$

where N is the number of islands, \mathcal{S}_n is the contour surrounding each island, and \mathcal{S} is the region of water that excludes the islands. In words, this result says that the circulation around a region equals to the circulation around the islands within the region, plus the normal component of the vorticity integrated over the area within the fluid region. Removing the islands allows the island contours to be shrunk to zero size, in which case we recover the simply connected result (37.204). As part of your solution, make use of the contour integral method detailed in Figure 36.9.

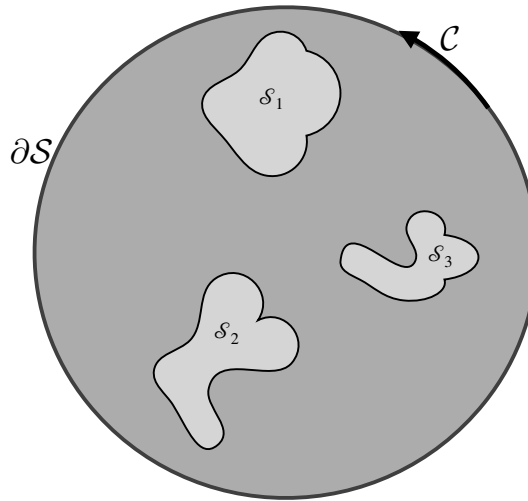


FIGURE 37.13: A region of the ocean consisting of three islands, \mathcal{S}_1 , \mathcal{S}_2 , and \mathcal{S}_3 , each with boundaries $\partial\mathcal{S}_n$ and with the closed contour, $\partial\mathcal{S}$, drawn around the three islands. The contour $\partial\mathcal{S}$ cannot be shrunk to a point without crossing over the islands, thus indicating that the domain is multiply connected. Exercise 37.7 is concerned with deriving an expression for the circulation of the depth-integrated flow as defined along the closed contour, $\partial\mathcal{S}$. In that derivation we can make use of the contour integral method detailed in Figure 36.9.

EXERCISE 37.8: EVOLUTION OF CIRCULATION AROUND ISLANDS

The momentum equation for a homogeneous layer of inviscid shallow water on a tangent plane is given by

$$\frac{\partial \mathbf{u}}{\partial t} + (\mathbf{u} \cdot \nabla) \mathbf{u} + f \hat{\mathbf{z}} \times \mathbf{u} = -g \nabla \eta. \quad (37.206)$$

In this equation, $\mathbf{u} = (u, v)$ is the horizontal velocity, f is the Coriolis parameter (need not be constant), g is the effective gravitational acceleration, and η is the deviation of the free surface from its horizontal resting position. All spatial derivatives are horizontal, so that

$$\mathbf{u} \cdot \nabla = u \partial_x + v \partial_y. \quad (37.207)$$

Use of a vector identity allows us to write

$$\frac{\partial \mathbf{u}}{\partial t} + (f + \zeta) \hat{\mathbf{z}} \times \mathbf{u} = -\nabla (\mathbf{u}^2/2 + g \eta), \quad (37.208)$$

where

$$\zeta = \hat{\mathbf{z}} \cdot (\nabla \times \mathbf{u}) \quad (37.209)$$

is the vorticity of the shallow water fluid.

Consider an island, such as one shown in Figure 37.13. Each island is static and impenetrable to fluid flow, which means that

$$\mathbf{u} \cdot \hat{\mathbf{n}} = 0 \quad (37.210)$$

where $\hat{\mathbf{n}}$ is the outward normal on an island boundary. This no-normal flow constraint means that the velocity just next to an island is parallel to the island¹⁷

$$\mathbf{u} \times d\mathbf{x} = 0. \quad (37.211)$$

Equivalently, the island represents a solid material boundary across which no flow passes. Show that the inviscid shallow-water circulation around an island remains constant in time

$$\frac{d}{dt} \oint_I \mathbf{u} \cdot d\mathbf{x} = 0. \quad (37.212)$$

Recall that Kelvin's circulation theorem is formulated for a material contour in an inviscid fluid. This exercise shows that the circulation theorem also holds for a material contour enclosing a static solid boundary.

EXERCISE 37.9: HELICITY FOR A PERFECT BAROTROPIC FLUID IN A GRAVITY FIELD AND NON-ROTATING REFERENCE FRAME

Consider a closed material volume, \mathcal{R} , of a perfect homogenous barotropic fluid ($\rho = \rho(p)$) in a gravity field ($\mathbf{g} = -\nabla\Phi$) and in a non-rotating reference frame ($\boldsymbol{\Omega} = 0$). Let this material volume have a boundary that is always tangent to the fluid vorticity, $\boldsymbol{\omega}$. Hence, the outward normal to the region boundary is orthogonal to the vorticity,

$$\hat{\mathbf{n}} \cdot \boldsymbol{\omega} = 0. \quad (37.213)$$

Such volumes define closed vortex tubes, such as a smoke ring or linked smoke rings. The *helicity* of the fluid within the vortex tube volume is defined as the integration of the helicity density, $\mathbf{v} \cdot \boldsymbol{\omega}$, over the closed volume

$$\mathbb{H} = \int_{\mathcal{R}(v)} \mathbf{v} \cdot \boldsymbol{\omega} dV, \quad (37.214)$$

where the volume $\mathcal{R}(v)$ is material. In Cartesian coordinates, the helicity density takes the form

$$\mathbf{v} \cdot \boldsymbol{\omega} = u(\partial_y w - \partial_z v) + v(\partial_z u - \partial_x w) + w(\partial_x v - \partial_y u). \quad (37.215)$$

Although the helicity density vanishes for some common examples, such as for a fluid in solid-body rotation, it need not vanish in general.

¹⁷This boundary condition is valid only for inviscid fluids such as that considered here. For a real fluid with nonzero viscosity, all components of the velocity vector vanish at solid boundaries due to the no-slip condition.

- (a) Show that helicity is materially constant following the material volume

$$\frac{d\mathbb{H}}{dt} = 0. \quad (37.216)$$

- (b) Discuss why helicity is not defined for a shallow water fluid.

Use the following hints.

- Make use of Φ_p that satisfies equation (37.13).
- The shallow water fluid model is based on the small aspect ratio limit, in which the fluid depth is much smaller than its lateral extent. In this limit, the vertical component of vorticity dominates over the horizontal. See further discussion in Section 37.5.4.

EXERCISE 37.10: DISCRETE CALCULATION OF BOTTOM PRESSURE TORQUE

In many diagnostic studies with numerical models it is of interest to compute pressure torques affecting vorticity. One particularly common diagnostic concerns the bottom pressure torque arising in equation (37.174). Derive a discrete expression for the area averaged bottom pressure torque

$$\overline{\text{BPT}} = A^{-1} \int_S \hat{z} \cdot \nabla \times (\eta_b \nabla p_b) dS = A^{-1} \oint_{\partial S} \eta_b \nabla p_b \cdot \hat{t} d\ell, = -A^{-1} \oint_{\partial S} p_b \nabla \eta_b \cdot \hat{t} d\ell, \quad (37.217)$$

over the shaded region depicted in Figure 37.14, with $A = \int_S dS$ the horizontal area of this region. Hint: this exercise shares much with the area averaged vorticity in Exercise 34.6, although the final result is distinct. Note: given that the bottom pressure torque is generally the small difference between large numbers, it is very useful to perform the diagnostic calculation online so that full computational precision can be maintained.

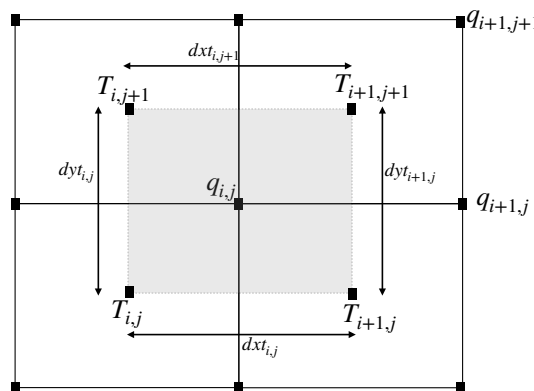


FIGURE 37.14: Discrete grid layout for variables needed to compute the bottom pressure torque as averaged over the shaded vorticity region. The bottom topography and bottom pressure are both known at the tracer points.

EXERCISE 37.11: DYNAMICAL PORTION OF THE TOPOGRAPHIC FORM STRESS

We discussed bottom topographic form stress in Chapter 25, with its curl leading to the bottom pressure torque in equation (37.174). As noted in Section 25.1.3, the dominant portion of the bottom topographic form stress acting on the ocean has little to do with fluid motion. Rather, it merely holds the ocean fluid within the basin, much as water is held within a drinking container through pressure imparted by the container sides.

- (a) To help isolate the dynamically relevant portion of the bottom bottom pressure, show that we can write the horizontal gradient of the bottom pressure for a hydrostatic fluid according to

$$\nabla_z p_b = g [\rho(\eta) \nabla_z \eta - \rho(\eta_b) \nabla_z \eta_b] + g \int_{\eta_b}^{\eta} \nabla_z \rho dz. \quad (37.218)$$

where we ignore the applied surface pressure, p_a , for simplicity.

- (b) Hence, show that the bottom pressure torque takes the form

$$\hat{z} \cdot \nabla_z \eta_b \times \nabla_z p_b = g \hat{z} \cdot \nabla_z \eta_b \times \left[\rho(\eta) \nabla_z \eta + \int_{\eta_b}^{\eta} \nabla_z \rho dz \right] \equiv \hat{z} \cdot \nabla \eta_b \times \nabla p_b^*, \quad (37.219)$$

where

$$\nabla_z p_b^* = g \rho(\eta) \nabla_z \eta + g \int_{\eta_b}^{\eta} \nabla_z \rho dz. \quad (37.220)$$

Note how $\nabla_z p_b^*$ has no contribution from the potentially very large term, $-g \rho(\eta_b) \nabla_z \eta_b$, arising from gradients in the bottom topography.

- (c) [Molemaker et al. \(2015\)](#) and [Gula et al. \(2015\)](#) assume knowledge of the bottom pressure torque along contours of constant topography. Given that knowledge they then make use of the following diagnostic expression for p_b^*

$$p_b^*(s) - p_b^*(s_0) = - \int_{s_0}^s \frac{\hat{z} \cdot (\nabla \eta_b \times \nabla p_b)}{\hat{n} \cdot \nabla \eta_b} ds, \quad (37.221)$$

with $p_b^*(s_0)$ the value at the arbitrary starting point for the contour. Derive equation (37.221), with the following information of possible use.

- As depicted in Figure 37.11, s is the arc length along the chosen contour of constant η_b , with s increasing in the tangent direction, \hat{t} . Likewise, \hat{n} is a unit vector pointing to the left of the contour so that $\hat{n} \cdot \hat{t} = 0$ and $\hat{t} \times \hat{n} = \hat{z}$.
- Along any contour of constant $\eta_b(x, y)$ we have

$$0 = d\eta_b = \nabla \eta_b \cdot dx = \nabla \eta_b \cdot \frac{dx}{ds} ds = \nabla \eta_b \cdot \hat{t} ds. \quad (37.222)$$

- The main mathematics of this exercise are contained in Exercise 6.1.

Equation (37.221) provides a means to compute the anomalous p_b^* [anomalous relative to $p_b^*(s_0)$] along a constant topography contour. Mapping $p_b^*(s) - p_b^*(s_0)$ for a suite of contours then provides the means to determine the dynamically relevant portion of the bottom pressure and then, when multiplying by the bottom slope, compute the dynamically relevant portion of the form stress.



Chapter 38

POTENTIAL VORTICITY MECHANICS

Potential vorticity (PV) is a dynamical tracer of immense importance to the study of geophysical fluid mechanics. One application of potential vorticity concerns its direct connection to the flow field in certain balanced models (e.g., geostrophically balanced models), with [Hoskins \(1991\)](#) providing an insightful starting point for this perspective. Potential vorticity is also useful as a tracer whose structure signals a variety of dynamical interactions, particularly with boundaries, and that can be directly tied to flow stability properties.

In this chapter we establish fundamental properties of potential vorticity and its time evolution. The potential vorticity we consider here is sometimes referred to as *Ertel* potential vorticity ([Ertel, 1942](#)), which is the most basic of the many potential vorticities encountered in geophysical fluids mechanics. The barotropic fluid forms a pedagogically useful starting point for our study. However, realistic geophysical flows are baroclinic, which are fluids where “PV thinking” is arguably the most useful. The general method exploited for the construction of potential vorticity is to choose a scalar field to strategically orient the absolute vorticity. If the scalar is a material invariant, and it annihilates the baroclinicity vector, then the corresponding potential vorticity is a material invariant in the absence of irreversible processes.

For a barotropic fluid, the choice of scalar field is rather arbitrary, with preference given to one that is materially invariant. For a baroclinic fluid we are more restricted since the scalar must orient vorticity in a direction that annihilates the torque from baroclinicity and, ideally, be itself materially invariant in the absence of irreversible processes. Even in the presence of irreversible processes, potential vorticity remains an important fluid property that constrains the fluid motion and provides insights into the fluid dynamics of that motion.

CHAPTER GUIDE

This chapter requires an understanding of vorticity from Chapter 37 as well as skills with vector calculus identities for Cartesian coordinates as detailed in Chapter 2. The concepts and methods developed in this chapter are fundamental to the notions of potential vorticity, and are essential for the budget equations developed in Chapter 39. We also encounter potential vorticity when studying balanced models in Part VIII.

38.1 Material invariance of PV in perfect fluids	980
38.1.1 Perfect barotropic fluid	980
38.1.2 Region between two constant χ surfaces	980
38.1.3 Material invariance	981
38.1.4 Perfect baroclinic fluid	982
38.1.5 A variety of materially invariant potential vorticities	983
38.1.6 Some remarks	984

38.2	PV and the seawater equation of state	986
38.2.1	Baroclinicity vector	986
38.2.2	PV based on potential density, ϱ	986
38.2.3	An example EOS admitting a materially invariant PV	987
38.2.4	Further reading	988
38.3	PV evolution with non-conservative processes	988
38.4	Eulerian flux-form PV budget	989
38.4.1	Deriving the Eulerian flux-form PV budget	990
38.4.2	PV-substance and the PV flux	990
38.4.3	Gauge freedom	991
38.5	PV budget for a hydrostatic Boussinesq ocean	992
38.5.1	Potential vorticity	993
38.5.2	Potential vorticity flux vector	993
38.5.3	Kinematic derivation of the PV-substance flux	994
38.5.4	A potential vorticity flux vector suited to steady flows	995
38.6	Conservation of pancake potential vorticity	997
38.7	Exercises	999

38.1 Material invariance of PV in perfect fluids

In this section we derive the material invariance of potential vorticity (PV) for a perfect homogeneous fluid.¹ We make use of Kelvin's circulation theorem for an infinitesimal closed loop, in which case the primary object of interest is a particular component of the absolute vorticity.

38.1.1 Perfect barotropic fluid

Consider a perfect barotropic fluid. As for the shallow water discussion in Section 36.3.3, we can apply Kelvin's circulation theorem (Section 37.2.3) to an infinitesimal material circuit within the fluid (Figure 38.1) to render the material invariance

$$\frac{D}{Dt}(\boldsymbol{\omega}_a \cdot \hat{\mathbf{n}} \delta\mathcal{S}) = 0, \quad (38.1)$$

with $\delta\mathcal{S}$ the area enclosed by the circuit. The conservation of PV is built from specializing this result. For that purpose, introduce a materially invariant field

$$\frac{D\chi}{Dt} = 0. \quad (38.2)$$

In most applications, χ is a scalar field such as tracer concentration, globally referenced Archimedean buoyancy, Conservative Temperature, or specific entropy. However, in equation (38.21) we consider the non-standard case of $\chi = z$, which is relevant for two-dimensional non-divergent barotropic fluids. So at this point in the discussion χ can be considered general.

38.1.2 Region between two constant χ surfaces

We make use of isosurfaces of χ to orient the material circuit and hence to orient the vorticity. In particular, referring to Figure 38.2, let the circuit bound a small cylinder whose ends sit on

¹A perfect homogeneous fluid has zero viscosity (inviscid) and a single material component. There can be no mixing of matter in this fluid since every fluid element has the same homogeneous concentration. So without viscosity, the homogeneous fluid is perfect.

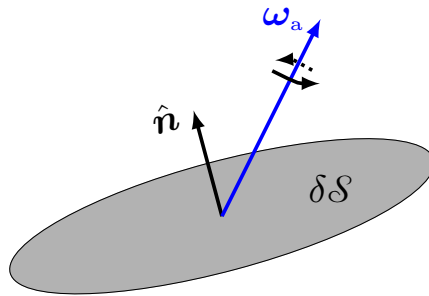


FIGURE 38.1: The projection of the absolute vorticity, ω_a , onto the normal direction for an infinitesimal moving surface, $\hat{n} \delta S$.

isosurfaces with concentrations $\chi - \delta\chi/2$ and $\chi + \delta\chi/2$. The cylinder's volume is given by

$$\delta V = \delta S \delta h, \quad (38.3)$$

where δh is the distance between the isosurfaces. The unit normal direction orienting the area δS is given by

$$\hat{n} = \nabla \chi / |\nabla \chi|. \quad (38.4)$$

The separation between the two isosurfaces is related to the increment $\delta\chi$ through

$$\delta\chi = \nabla \chi \cdot \delta x = |\nabla \chi| \hat{n} \cdot \delta x = |\nabla \chi| \delta h. \quad (38.5)$$

This result takes on the equivalent form

$$\delta\chi = |\nabla \chi| \delta h = (\hat{n} \cdot \nabla \chi) \delta h, \quad (38.6)$$

so that the distance (or thickness) between the two isosurfaces is

$$\delta h = \delta\chi / |\nabla \chi|. \quad (38.7)$$

As seen in Figure 38.2, the spatial separation between the two isosurfaces is reduced in regions of strong scalar gradients and increased in regions of weak gradients, thus verifying that this expression accords with common sense.

38.1.3 Material invariance

We now have the necessary pieces to write the normal projection of the absolute vorticity as

$$\omega_a \cdot \hat{n} \delta S = \frac{\omega_a \cdot \nabla \chi}{|\nabla \chi|} \delta S \quad \text{equation (38.4)} \quad (38.8a)$$

$$= \frac{\omega_a \cdot \nabla \chi}{|\nabla \chi|} \frac{\delta V}{\delta h} \quad \text{equation (38.3)} \quad (38.8b)$$

$$= (\omega_a \cdot \nabla \chi) \frac{\delta V}{\delta \chi} \quad \text{equation (38.7)} \quad (38.8c)$$

$$= \frac{\omega_a \cdot \nabla \chi}{\rho} \frac{\rho \delta V}{\delta \chi} \quad \text{multiply by } \rho/\rho. \quad (38.8d)$$

Mass is materially invariant so that

$$\frac{D(\rho \delta V)}{Dt} = 0. \quad (38.9)$$

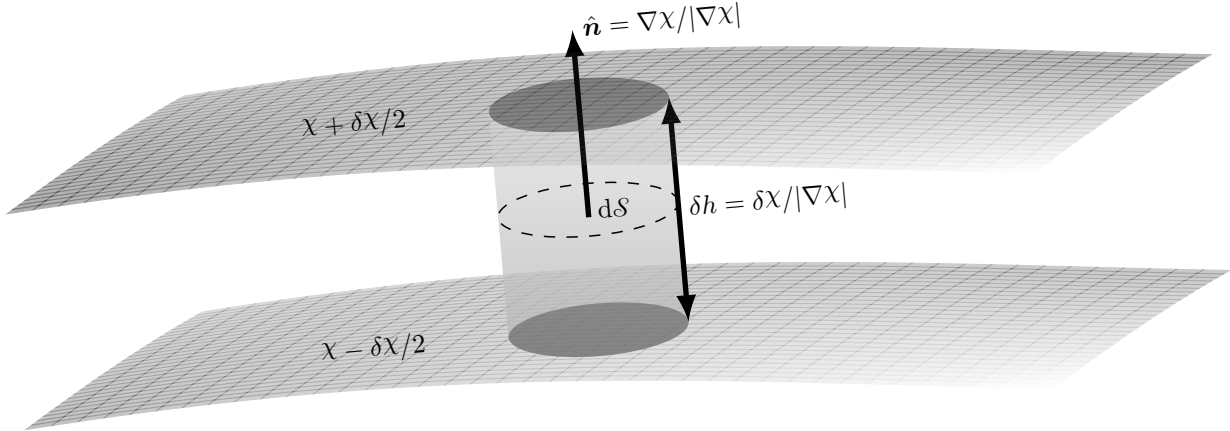


FIGURE 38.2: Illustrating the geometry of a cylindrical region of fluid between two iso-surfaces of a field χ , separated by the infinitesimal amount $\delta\chi$. The volume of the region is $\delta V = \delta\mathcal{S} \delta h$, with δh the thickness and $\delta\mathcal{S}$ the area. By convention, the unit normal vector, $\hat{\mathbf{n}} = \nabla\chi/|\nabla\chi|$, points towards larger values of χ . It is here depicted at the center of the cylinder, which differs by an infinitesimal amount from the normal computed on either $\chi + \delta\chi/2$ or $\chi - \delta\chi/2$. If χ is a material invariant so that $D\chi/Dt = 0$, then so too is its infinitesimal increment, $D(\delta\chi)/Dt = 0$. As per equation (38.7), the geometric thickness between the isosurfaces is related to the field increment by $\delta h = \delta\chi/|\nabla\chi|$, so that the larger the magnitude of the gradient in the scalar field, the smaller the layer thickness. For a baroclinic fluid, material invariance of PV in a perfect fluid holds if we can find a field such that $\hat{\mathbf{n}} \cdot \mathbf{B} = 0$, with baroclinicity $\mathbf{B} = (\nabla\rho \times \nabla p)/\rho^2$.

Likewise, by assumption χ is materially invariant so that the increment between two χ isosurfaces is materially invariant

$$\frac{D(\delta\chi)}{Dt} = 0. \quad (38.10)$$

Bringing these elements into Kelvin's circulation theorem (38.1) leads us to conclude that the potential vorticity, Q , is also materially invariant

$$Q \equiv \frac{\omega_a \cdot \nabla\chi}{\rho} = \frac{\nabla \cdot (\omega_a \chi)}{\rho} \quad \text{with} \quad \frac{DQ}{Dt} = 0. \quad (38.11)$$

This expression for the potential vorticity is the most general form and it is often referred to as the *Ertel PV* ([Ertel, 1942](#)). The first expression shows the numerator as the projection of the absolute vorticity into the direction normal to χ isosurfaces. Conversely, it is a measure of the χ stratification in the direction of the absolute vorticity vector. The second expression follows since the absolute vorticity has zero divergence so that the numerator is a total divergence. This divergence form of the potential vorticity numerator has important implications for the potential vorticity budgets studied in Section 38.4 and throughout Chapter 39.

38.1.4 Perfect baroclinic fluid

Consider the case of a perfect baroclinic fluid, in which Kelvin's circulation theorem for an infinitesimal circuit takes the form

$$\frac{D}{Dt}(\omega_a \cdot \hat{\mathbf{n}} \delta\mathcal{S}) = \mathbf{B} \cdot \hat{\mathbf{n}} \delta\mathcal{S}. \quad (38.12)$$

The source on the right hand side involves the baroclinicity vector, \mathbf{B} , discussed in Sections 37.2 and 37.4, which is the curl of the pressure gradient acceleration

$$\mathbf{B} = \nabla \times (-\rho^{-1} \nabla p) = \rho^{-2} \nabla\rho \times \nabla p. \quad (38.13)$$

Now assume there exists a materially invariant field, $D\chi/Dt = 0$, that also annihilates the baroclinicity vector as in Figure 38.3, so that

$$\mathbf{B} \cdot \hat{\mathbf{n}} = \frac{\mathbf{B} \cdot \nabla \chi}{|\nabla \chi|} = 0. \quad (38.14)$$

In that case, the derivation detailed earlier for the barotropic fluid follows directly for the baroclinic case, in which case we conclude that PV remains materially invariant

$$\frac{DQ}{Dt} = 0 \quad \text{where} \quad Q = \frac{\boldsymbol{\omega}_a \cdot \nabla \chi}{\rho}. \quad (38.15)$$

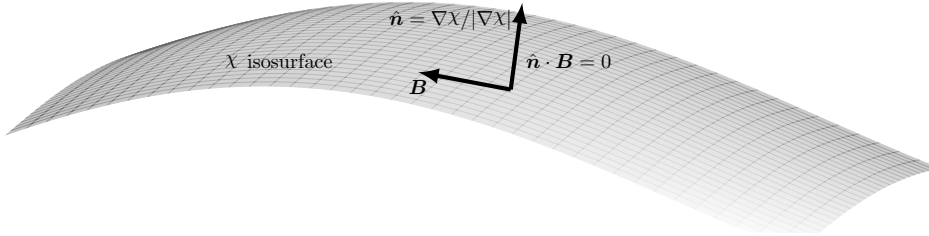


FIGURE 38.3: Material invariance of PV is ensured for perfect fluids that admit a materially invariant field that also annihilates the baroclinicity vector. Mathematically, this property means that $\hat{\mathbf{n}} \cdot \mathbf{B} = 0$ where $\hat{\mathbf{n}} = \nabla \chi / |\nabla \chi|$ is the unit normal direction for the surface. In this figure we depict the baroclinicity vector, \mathbf{B} , that is aligned with χ isosurfaces.

Existence of a materially invariant potential vorticity for perfect baroclinic fluids depends on the existence of a materially invariant field that annihilates the baroclinicity vector. Buoyancy is the most common choice for this field in geophysical fluid applications, with buoyancy typically measured by specific entropy or potential temperature in the atmosphere and potential density or buoyancy in the ocean. We have more to say on the chosen field in the remainder of this chapter as well as in Section 39.3.

38.1.5 A variety of materially invariant potential vorticities

The material invariant statement

$$\frac{DQ}{Dt} = \frac{D(\rho^{-1} \boldsymbol{\omega}_a \cdot \nabla \chi)}{Dt} = 0 \quad (38.16)$$

generates a number of further materially invariant fields. First, consider any function of Q , whereby

$$\frac{D\mathcal{F}(Q)}{Dt} = \frac{d\mathcal{F}}{dQ} \frac{DQ}{Dt} = 0, \quad (38.17)$$

which follows since $DQ/Dt = 0$. Among the infinite number of possible functions, $\mathcal{F}(Q)$, the most commonly considered is $\mathcal{F}(Q) = Q^2$, whose global integral is referred to as the *potential enstrophy*.

Second, consider the *iterated potential vorticity* defined according to

$$Q^{(1)} = \rho^{-1} \boldsymbol{\omega}_a \cdot \nabla \chi \quad \text{and} \quad Q^{(n)} = \boldsymbol{\omega}_a \cdot \nabla Q^{(n-1)} \quad \text{for } n = 2, 3, 4\dots \quad (38.18)$$

As defined, $Q^{(1)}$ is the familiar Ertel potential vorticity, whereas higher iterations replace the

field, χ , with $Q^{(n-1)}$. Since $Q^{(n-1)}$ is materially invariant, so too is $Q^{(n)}$. Consider the example

$$Q^{(2)} = \boldsymbol{\omega}_a \cdot \nabla Q^{(1)} = \boldsymbol{\omega}_a \cdot \nabla(\rho^{-1} \boldsymbol{\omega}_a \cdot \nabla \chi) = \nabla \cdot (\boldsymbol{\omega}_a \rho^{-1} \boldsymbol{\omega}_a \cdot \nabla \chi), \quad (38.19)$$

which reveals that there are n powers of absolute vorticity for $Q^{(n)}$.

38.1.6 Some remarks

Perfect fluid PV material invariance \leftrightarrow Kelvin's circulation theorem

Kelvin's circulation theorem from Section 37.2.3 is at the heart of the derivations presented in this section, with the theorem applied to a strategically chosen infinitesimal loop. Because the loop is tiny, we use Stokes' theorem to convert the line integral expression of Kelvin's theorem into a statement about the material evolution of absolute vorticity projected onto the normal direction of the loop, and multiplied by the loop area. We further specialize the theorem to a cylindrical region between two isosurfaces of a materially invariant field. For the perfect barotropic fluid, we merely require that both the mass of the cylinder and the field to be materially invariant in order to realize a potential vorticity that is also materially invariant. Material invariance of potential vorticity for a baroclinic fluid requires a field that is both materially invariant *and* that annihilates the baroclinicity vector. We have more to say in regards to the availability of such fields when considering entropic PV in the remainder of this chapter, whereby potential temperature is the chosen field.

There are numerous forms for potential vorticity

The expression (38.11) is, on first glance, quite distinct from the shallow water potential vorticity, $Q = (\zeta + f)/h$, studied in Chapter 36 (see equation (36.30)). However, as shown in Section 59.3, they are closely related for the special case of entropic potential vorticity in a Boussinesq ocean when formulated using isopycnal/isentropic coordinates. Even so, there are a variety of other forms for potential vorticity, with the forms (and physical dimensions) depending on the dynamical and thermodynamical properties. We encounter some further forms of potential vorticity in the remainder of this chapter, as well as in the oceanic potential vorticity discussions of Chapter 59 and in our study of balanced models in Part VIII. The review paper by Müller (1995) offers a lucid presentation of potential vorticity and its many forms encountered in physical oceanography.

Motivating the adjective "potential"

In Section 36.3.2 we motivated the advective "potential" for the shallow water potential vorticity. We do so here for Ertel's potential vorticity. For that purpose, write potential vorticity in the form

$$Q = \frac{\boldsymbol{\omega}_a \cdot \hat{\mathbf{n}}}{\rho} |\nabla \chi| \quad \text{with} \quad \hat{\mathbf{n}} = \frac{\nabla \chi}{|\nabla \chi|}. \quad (38.20)$$

As noted in Section 2.1 of Müller (1995), in cases where ρ is roughly a constant, and when Q is materially invariant, the component of the absolute vorticity in the direction parallel to $\nabla \chi$ increases when the fluid parcel moves into a region where $|\nabla \chi|$ decreases. There is hence a "release" of absolute vorticity aligned with $\nabla \chi$ in regions where χ isosurfaces are spread, and a withdrawal of absolute vorticity where χ isosurfaces are tightly packed. We thus conceive of potential vorticity as the "potential" for releasing absolute vorticity oriented in the direction parallel to $\nabla \chi$.

Potential vorticity as a dynamical tracer

We refer to potential vorticity as a *dynamical tracer* since it depends directly on the velocity field through the vorticity. It also depends on the scalar field, χ , which is commonly taken as a thermodynamic tracer such as the potential temperature, θ . In these cases, potential vorticity marries dynamical and thermodynamical information into a single package. In contrast, material tracers such as salinity, and thermodynamic tracers such as θ , are properties of the fluid whose distribution depends on the velocity field but whose local measurement does not require knowledge of velocity.

Entropic potential vorticity as the grand unifier

Entropic potential vorticity provides a connection between vorticity (mechanics) and stratification (thermodynamics). By connecting these two basic facets of geophysical fluid flows, the study of potential vorticity and its conservation properties provides a powerful and unique lens to help rationalize the huge variety of geophysical flow regimes, and to predict their response to changes in forcing. It is for this reason that potential vorticity is sometimes considered the grand unifying concept in geophysical fluid mechanics.

Potential vorticity as a diagnostic tracer

Suppose we have an initial flow field in which $Q = 0$ so that the absolute vorticity lives within constant χ surfaces. In an inviscid and adiabatic fluid, material conservation of Q means that ω_a remains within constant χ surfaces for all time. Hence, if we know the evolution of χ , then we know the evolution of vortex lines defined by ω_a , which in turn allows for the inference of a number of further flow properties. This particular example offers a hint at the multiple applications of “PV thinking” to understand and predict fluid motion, with [Hoskins \(1991\)](#) providing an elegant survey of such thinking.

Potential vorticity versus momentum

Momentum is affected by pressure, and pressure fluctuations propagate at the speed of sound (Chapter 44) for compressible flows and oceanic Boussinesq flows, whereas they move with infinite speed for fully incompressible fluids. In contrast, potential vorticity, for those cases where we can remove the effects of the baroclinicity vector, does not directly feel the impacts from pressure fluctuations. Hence, potential vorticity, much like vorticity in a barotropic fluid, evolves much slower and more locally than momentum. This dynamical difference offers a key reason that potential vorticity offers added insights into fluid flows beyond that afforded by momentum.

Potential vorticity for non-divergent barotropic flow

A non-standard, but relevant, choice for the function χ used to define potential vorticity is given by the vertical coordinate

$$\chi = z, \tag{38.21}$$

in which case

$$\rho Q = \omega_a \cdot \hat{z} = \zeta_a. \tag{38.22}$$

In Chapter 35, we consider the two-dimensional non-divergent barotropic model, in which case ρ is a constant and

$$w = \frac{Dz}{Dt} = 0. \tag{38.23}$$

The corresponding materially invariant potential vorticity is the vertical component of the absolute vorticity divided by the constant density. Ignoring the constant density leads to the potential vorticity in this flow given by the absolute vorticity

$$q = \zeta_a = \zeta + f. \quad (38.24)$$

In Chapter 35 we study the variety of constraints based on material invariance of absolute vorticity.

38.2 PV and the seawater equation of state

As seen in Section 38.1, material invariance of potential vorticity for a perfect fluid requires a materially invariant scalar field to annihilate the baroclinicity vector. In the ocean with a realistic seawater equation of state, there is generally no such scalar. Nonetheless, there are important approximate cases that allow for material potential vorticity invariance, and we explore such cases in this section.

38.2.1 Baroclinicity vector

Recall the baroclinicity vector given by (Sections 37.2 and 37.4)

$$\mathbf{B} = \frac{\nabla\rho \times \nabla p}{\rho^2}. \quad (38.25)$$

If we take the *in situ* density as the scalar field to define potential vorticity, then $\mathbf{B} \cdot \nabla\rho = 0$. However, *in situ* density is not a conserved scalar in the ocean due to pressure effects. Namely, with *in situ* density having the function dependence $\rho = \rho(S, \Theta, p)$ (see Section 27.3), its material time derivative is

$$\frac{D\rho}{Dt} = \frac{\partial\rho}{\partial S} \frac{DS}{Dt} + \frac{\partial\rho}{\partial\Theta} \frac{D\Theta}{Dt} + \frac{\partial\rho}{\partial p} \frac{Dp}{Dt}. \quad (38.26)$$

Even when salinity and Conservative Temperature are materially constant, $DS/Dt = 0$ and $D\Theta/Dt = 0$, the *in situ* density has a nonzero material time derivative due to material pressure changes, $Dp/Dt \neq 0$. Material changes in the pressure of a fluid element arise even in the absence of irreversible mixing. In general, such *mechanical changes* arise due to the gradients in the pressure field that the fluid element feels. Given that pressure affects *in situ* density, with such effects occurring even in a perfect fluid, we conclude that *in situ* density is not an appropriate scalar for developing a materially invariant PV.

38.2.2 PV based on potential density, ϱ

Potential density is commonly used in oceanography (see Section 27.3.4), with potential density the *in situ* density referenced to a chosen pressure.² We write potential density as in equation (27.18)

$$\varrho(S, \Theta) = \rho(S, \Theta, p = p_{\text{ref}}), \quad (38.27)$$

so that its material time derivative is

$$\frac{D\varrho}{Dt} = \frac{\partial\varrho}{\partial S} \frac{DS}{Dt} + \frac{\partial\varrho}{\partial\Theta} \frac{D\Theta}{Dt}, \quad (38.28)$$

²Oceanographers often choose the reference pressure as the standard atmospheric sea level pressure. However, that is not required for the following formalism to hold; any reference pressure is suitable.

which vanishes in the absence of irreversible material changes to salinity and Conservative Temperature. When using potential density as the scalar field for PV, the baroclinicity vector projects onto the diapycnal direction according to

$$\rho^2 \mathbf{B} \cdot \nabla \varrho = (\nabla \rho \times \nabla p) \cdot \nabla \varrho \quad (38.29a)$$

$$= (\nabla \varrho \times \nabla \rho) \cdot \nabla p \quad (38.29b)$$

$$= [(\varrho_S \nabla S + \varrho_\Theta \nabla \Theta) \times (\rho_S \nabla S + \rho_\Theta \nabla \Theta + \rho_p \nabla p)] \cdot \nabla p \quad (38.29c)$$

$$= [(\varrho_S \nabla S + \varrho_\Theta \nabla \Theta) \times (\rho_S \nabla S + \rho_\Theta \nabla \Theta)] \cdot \nabla p \quad (38.29d)$$

$$= [\varrho_S \nabla S \times \rho_\Theta \nabla \Theta + \varrho_\Theta \nabla \Theta \times \rho_S \nabla S] \cdot \nabla p \quad (38.29e)$$

$$= (\varrho_S \rho_\Theta - \varrho_\Theta \rho_S) (\nabla S \times \nabla \Theta) \cdot \nabla p, \quad (38.29f)$$

where we used the shorthand notation for partial derivatives

$$\rho_S = \frac{\partial \rho}{\partial S} \quad \text{and} \quad \varrho_S = \frac{\partial \varrho}{\partial S} \quad (38.30a)$$

$$\rho_\Theta = \frac{\partial \rho}{\partial \Theta} \quad \text{and} \quad \varrho_\Theta = \frac{\partial \varrho}{\partial \Theta}. \quad (38.30b)$$

Note that the triple product, $(\nabla S \times \nabla \Theta) \cdot \nabla p$, also appears in the discussion of neutral helicity in Section 27.6 (see equation (27.59)). Equation (38.29f) allows us to identify cases where the baroclinicity vector is annihilated, $\mathbf{B} \cdot \nabla \varrho = 0$, thus yielding a materially invariant potential vorticity in the absence of irreversible processes.

- UNIFORM SALINITY OR UNIFORM CONSERVATIVE TEMPERATURE: If salinity or Conservative Temperature are spatially uniform, then $\mathbf{B} \cdot \nabla \varrho = 0$.
- ADDITIVE PRESSURE DEPENDENCE TO THE *in situ* DENSITY: There is a materially invariant potential vorticity with a vanishing thermodynamic pre-factor in equation (38.29f), $\varrho_S \rho_\Theta - \varrho_\Theta \rho_S$. This term does not generally vanish since the ocean has a pressure dependent equation of state, and this pressure dependence generally means that $\mathbf{B} \cdot \nabla \varrho \neq 0$. Even so, we can annihilate the baroclinicity vector if the *in situ* density has a pressure dependence that is additive, in which case we can write

$$\rho(S, \Theta, p) = \varrho(S, \Theta) + F(p) - F(p_{\text{ref}}) \implies \varrho_S \rho_\Theta - \varrho_\Theta \rho_S = 0. \quad (38.31)$$

Notably, we did not assume a linear equation of state; only that it has the special functional form in equation (38.31). For some cases, we may assume F to be a constant, in which case there is no pressure dependence so that *in situ* density is the same as potential density.

38.2.3 An example EOS admitting a materially invariant PV

An explicit realization of the equation of state (38.31) can be found by taking a Taylor series expansion of the *in situ* density around the reference pressure, and evaluating the derivatives in the expansion in terms of a chosen reference pressure, reference salinity, and reference Conservative Temperature

$$\rho(S, \Theta, p) \approx \varrho(S, \Theta) + (p - p_{\text{ref}}) \underbrace{\left[\frac{\partial \rho}{\partial p} \right]_{S=S_{\text{ref}}, \Theta=\Theta_{\text{ref}}, p=p_{\text{ref}}} + H.O.T.}_{F(p) - F(p_{\text{ref}})} \quad (38.32)$$

where

$$\varrho(S, \Theta) = \rho(S, \Theta, p_{\text{ref}}) \quad (38.33)$$

is the potential density referenced to $p = p_{\text{ref}}$, and where *H.O.T.* symbolizes higher order terms. This approach ignores the salinity and Conservative Temperature dependence of terms in the Taylor series expansion. Ignoring this dependence is a rather good approximation for many purposes since the ocean sound speed is not far from a constant

$$c_s^{-2} = \frac{\partial \rho}{\partial p} \approx \text{constant}. \quad (38.34)$$

In this case, the equation of state takes the form

$$\rho(S, \Theta, p) \approx \varrho(S, \Theta) + \frac{p - p_{\text{ref}}}{c_s^2}, \quad (38.35)$$

38.2.4 Further reading

The presentation given here follows that given in Section 4.5.4 of [Vallis \(2017\)](#). [Straub \(1999\)](#) presents a discussion of ocean potential vorticity with a focus on the source of potential vorticity arising from a nonzero thermobaricity parameter, $\mathcal{T} = \partial_p(\alpha/\beta)$ (see Section [64.3.4](#)). In Section [38.6](#) reconsider the notions presented here by suggesting the relevance of an alternative potential vorticity field that is attached to a finite sized region rather than a fluid particle.

38.3 PV evolution with non-conservative processes

Thus far we have considered perfect fluids, with the use of Kelvin's circulation theorem a suitable framework to derive the material invariance of potential vorticity. In this section we consider a real fluid that contains non-conservative processes. Potential vorticity is no longer materially invariant when exposed to non-conservative processes such as mixing, friction, and diabatic sources.

To develop the potential vorticity budget in the presence of non-conservative processes, we pursue an algebraic approach that starts from the vorticity equation ([37.41](#))

$$\rho \frac{D(\boldsymbol{\omega}_a/\rho)}{Dt} = (\boldsymbol{\omega}_a \cdot \nabla) \mathbf{v} + \mathbf{B} + \nabla \times \mathbf{F}, \quad (38.36)$$

where \mathbf{F} is the acceleration from non-conservative forces and \mathbf{B} the baroclinicity vector. Furthermore, we introduce a scalar field that generally has a nonzero material evolution

$$\frac{D\chi}{Dt} = \dot{\chi}, \quad (38.37)$$

with $\dot{\chi}$ arising from diffusion, sources, or other processes.

As part of the manipulations in this section, we make use of the identity

$$(\boldsymbol{\omega}_a \cdot \nabla) \frac{D\chi}{Dt} = \boldsymbol{\omega}_a \cdot \frac{D(\nabla\chi)}{Dt} + [(\boldsymbol{\omega}_a \cdot \nabla) \mathbf{v}] \cdot \nabla\chi, \quad (38.38)$$

which is readily proven by expanding terms and assuming Cartesian coordinates. Rearrangement, and use of the scalar equation ([38.37](#)), leads to

$$\boldsymbol{\omega}_a \cdot \frac{D(\nabla\chi)}{Dt} = (\boldsymbol{\omega}_a \cdot \nabla) \dot{\chi} - [(\boldsymbol{\omega}_a \cdot \nabla) \mathbf{v}] \cdot \nabla\chi. \quad (38.39)$$

Now project the vorticity equation (38.36) onto the direction normal to the χ isosurfaces

$$\rho \nabla \chi \cdot \frac{D(\boldsymbol{\omega}_a/\rho)}{Dt} = \nabla \chi \cdot [(\boldsymbol{\omega}_a \cdot \nabla) \mathbf{v}] + \nabla \chi \cdot (\mathbf{B} + \nabla \times \mathbf{F}). \quad (38.40)$$

The sum of equations (38.39) and (38.40) leads to

$$\rho \frac{D(\nabla \chi \cdot \boldsymbol{\omega}_a/\rho)}{Dt} = (\boldsymbol{\omega}_a \cdot \nabla) \dot{\chi} + \nabla \chi \cdot (\mathbf{B} + \nabla \times \mathbf{F}). \quad (38.41)$$

This equation is general so that it applies to any scalar field.

To simplify the source terms on the right hand side of equation (38.41), follow the discussion from Section 38.1.4 by assuming that χ annihilates the baroclinicity vector.³ This scalar field is typically given by potential temperature, specific entropy, buoyancy, or potential density. We thus have

$$\nabla \chi \cdot \mathbf{B} = 0, \quad (38.42)$$

which in turn leads to the potential vorticity equation in the presence of irreversible processes such as friction and mixing

$$\rho \frac{DQ}{Dt} = (\boldsymbol{\omega}_a \cdot \nabla) \dot{\chi} + \nabla \chi \cdot (\nabla \times \mathbf{F}), \quad (38.43)$$

where the potential vorticity is again given by

$$Q = \frac{\boldsymbol{\omega}_a \cdot \nabla \chi}{\rho}. \quad (38.44)$$

If χ is a thermodynamic scalar such as potential entropy, then the material evolution of potential vorticity is affected by diabatic processes (heating and cooling) as well as friction. Hence, the potential vorticity of a fluid element can be either generated or destroyed depending on details of these irreversible process. Such processes are often localized to areas of mixing as well as to boundaries where strong mechanical and/or buoyancy processes are active. The study of how potential vorticity is materially modified by irreversible processes forms an important area of research in potential vorticity dynamics. We have more to say on this notion when studying budgets of potential vorticity in Chapter 39.

38.4 Eulerian flux-form PV budget

The material invariance of potential vorticity is an example of a material or Lagrangian conservation property of perfect fluids, with the material conservation statement $\rho DQ/Dt = 0$ having its Eulerian flux-form expression

$$\frac{\partial(\rho Q)}{\partial t} + \nabla \cdot (\rho \mathbf{v} Q) = 0 \quad \text{perfect fluid.} \quad (38.45)$$

Following the formalism established for material tracers in Section 17.3, the flux-form local conservation law (38.45) leads to conservation properties over finite regions, which we refer to as *global conservation* laws. In this section we examine the Eulerian flux-form budget in the presence of non-conservative processes. We shown here, the Eulerian evolution of potential vorticity continues to be determined by the convergence of a flux, thus allowing for natural extensions to global conservation laws and budget analyses.

³In Section 39.3 we study what happens when no such scalar exists.

38.4.1 Deriving the Eulerian flux-form PV budget

To transform the material evolution equation (38.43) into a flux-form Eulerian equation we make use of the following identities

$$\frac{D}{Dt} = \frac{\partial}{\partial t} + \mathbf{v} \cdot \nabla \quad \text{relating material and Eulerian time changes} \quad (38.46a)$$

$$\frac{D\rho}{Dt} = -\rho \nabla \cdot \mathbf{v} \quad \text{mass conservation} \quad (38.46b)$$

$$(\boldsymbol{\omega}_a \cdot \nabla) \dot{\chi} = \nabla \cdot (\boldsymbol{\omega}_a \dot{\chi}) \quad \text{absolute vorticity is non-divergent: } \nabla \cdot \boldsymbol{\omega}_a = 0 \quad (38.46c)$$

$$\nabla \chi \cdot (\nabla \times \mathbf{F}) = \nabla \cdot (\mathbf{F} \times \nabla \chi) \quad \text{divergence of curl vanishes.} \quad (38.46d)$$

The identity (38.46d) follows from

$$\nabla \chi \cdot (\nabla \times \mathbf{F}) = \nabla \cdot (\chi \nabla \times \mathbf{F}) = \nabla \cdot [\nabla \times (\chi \mathbf{F}) - \nabla \chi \times \mathbf{F}] = \nabla \cdot (\mathbf{F} \times \nabla \chi), \quad (38.47)$$

where a vanishing divergence of a curl is needed to reach the first and third equalities. These identities then lead to the material evolution equation

$$\rho \frac{DQ}{Dt} = \nabla \cdot (\boldsymbol{\omega}_a \dot{\chi} + \mathbf{F} \times \nabla \chi). \quad (38.48)$$

Now converting the material time derivative into its Eulerian expression, and making use of mass conservation, renders the flux-form Eulerian PV budget equation

$$\frac{\partial(\rho Q)}{\partial t} + \nabla \cdot [\rho Q \mathbf{v} - \boldsymbol{\omega}_a \dot{\chi} - \mathbf{F} \times \nabla \chi] = 0. \quad (38.49)$$

38.4.2 PV-substance and the PV flux

The budget equation (38.49) says that the density-weighted potential vorticity

$$\rho Q = \boldsymbol{\omega}_a \cdot \nabla \chi \quad (38.50)$$

has a local time tendency determined by the convergence of the PV flux vector

$$\frac{\partial(\rho Q)}{\partial t} = -\nabla \cdot \mathbf{J}_Q \quad \text{with} \quad \mathbf{J}_Q = \rho Q \mathbf{v} - \boldsymbol{\omega}_a \dot{\chi} - \mathbf{F} \times \nabla \chi. \quad (38.51)$$

The budget (38.49) follows a form similar to material tracers detailed in Chapter 17, though with some specific terms in the flux vector, \mathbf{J}_Q . The correspondence suggests that one consider equation (38.49) as the local budget for *PV-substance*, with Q the concentration of PV-substance and \mathbf{J}_Q its flux. This interpretation is pursued further in Chapter 39 when exposing the rather novel properties of budgets for PV-substance when integrated over regions bounded by isentropes.

The first term in the PV-substance flux vector (38.51) arises from the advection of PV-substance; the second contribution arises from processes leading to material evolution of χ ; and the third from the curl of the friction vector. Note that there is a nonzero friction contribution only when the frictional acceleration has a component that is not parallel to $\nabla \chi$. In this manner we can think of the friction vector as contributing to a “torque” that rotates the χ isosurfaces as it contributes to the evolution of PV-substance (see Figure 38.4).

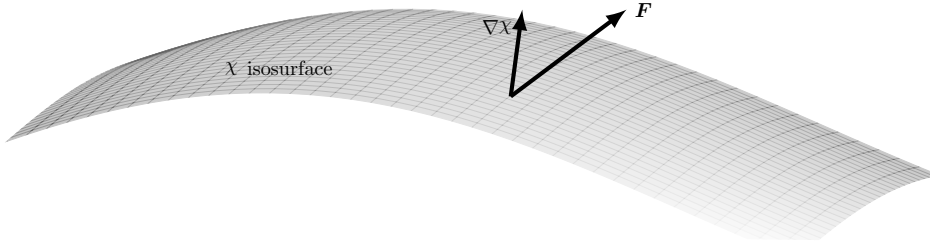


FIGURE 38.4: The contribution from friction to the PV flux is given by $\mathbf{J}_{\text{friction}} = \nabla\chi \times \mathbf{F}$. This cross product is nonzero only when the frictional acceleration is not fully aligned with $\nabla\chi$. Friction creates PV by rotating χ isosurfaces. Hence, if friction is aligned with $\nabla\chi$, or when there is no spatial structure to $\nabla\chi \times \mathbf{F}$ (i.e., zero divergence), then friction does not contribute to PV evolution. This interpretation is analogous to that given to the effects from baroclinicity on vorticity given in Section 37.4.

38.4.3 Gauge freedom

As seen by the potential vorticity equation (38.51), the time tendency for PV-substance, $\partial_t(\rho Q)$, is unchanged by adding the curl of a vector to the PV-substance flux \mathbf{J}_Q . This ambiguity manifests a *gauge freedom*. We here exhibit the gauge freedom associated with \mathbf{J}_Q , and expose yet another gauge freedom associated with the potential vorticity itself. We offer more discussion of gauge freedom in Section 18.4.1 and further the use of gauge freedom for the study of potential vorticity in Section 38.5 as well as throughout Chapter 39.

Gauge freedom associated with the PV-substance flux

One way to further expose gauge freedom is by writing

$$\rho Q = \nabla\chi \cdot \boldsymbol{\omega}_a = \nabla \cdot (\chi \boldsymbol{\omega}_a), \quad (38.52)$$

so that

$$\partial_t(\rho Q) = \partial_t[\nabla \cdot (\chi \boldsymbol{\omega}_a)] = \nabla \cdot [\partial_t(\chi \boldsymbol{\omega}_a)], \quad (38.53)$$

where the time derivative commutes with the divergence operator. We can thus write the potential vorticity equation (38.51) in the form

$$\nabla \cdot [\partial_t(\chi \boldsymbol{\omega}_a) + \mathbf{J}_Q] = 0. \quad (38.54)$$

This equation means that $\partial_t(\chi \boldsymbol{\omega}_a)$ and \mathbf{J}_Q differ by the curl of a vector

$$\partial_t(\chi \boldsymbol{\omega}_a) + \mathbf{J}_Q = -\nabla \times \mathbf{A}, \quad (38.55)$$

with \mathbf{A} referred to as a *gauge function*. The minus sign is arbitrary and is introduced to correspond to the discussion in Section 38.5.

Gauge freedom arising from the non-divergent nature of vorticity

The divergence form of PV-substance given by equation (38.52) reveals that ρQ remains unchanged if we add a total curl to the argument of the divergence operator. In particular, consider

the identities⁴

$$\chi \boldsymbol{\omega}_a = \chi (\nabla \times \mathbf{v} + 2\boldsymbol{\Omega}) \quad \text{since } \boldsymbol{\omega}_a = \boldsymbol{\omega} + 2\boldsymbol{\Omega} \quad (38.56a)$$

$$= \nabla \times (\chi \mathbf{v}) - \nabla \chi \times \mathbf{v} + \chi 2\boldsymbol{\Omega} \quad \text{move gradient operator.} \quad (38.56b)$$

We have thus moved the curl operation acting on the velocity field (to compute relative vorticity) onto a gradient of the scalar field, with a total curl making up the difference. Since $\nabla \cdot [\nabla \times (\chi \mathbf{v})] = 0$, we are led to the equivalent expressions for PV-substance

$$\rho Q = \nabla \chi \cdot \boldsymbol{\omega}_a = \nabla \cdot (\chi 2\boldsymbol{\Omega} + \chi \boldsymbol{\omega}) = \nabla \cdot (2\boldsymbol{\Omega} \chi - \nabla \chi \times \mathbf{v}) = \nabla \chi \cdot (2\boldsymbol{\Omega}) - \nabla \cdot (\nabla \chi \times \mathbf{v}). \quad (38.57)$$

The resulting formulation is an expression for the Ertel potential vorticity that does not involve the relative vorticity, but is instead written as the convergence of a flux

$$\rho Q = -\nabla \cdot (-2\boldsymbol{\Omega} \chi + \nabla \chi \times \mathbf{v}). \quad (38.58)$$

This form involves the component of the velocity that is parallel to χ isosurfaces since

$$(\nabla \chi \times \mathbf{v}) \cdot \nabla \chi = 0. \quad (38.59)$$

Besides offering a curious expression for potential vorticity that does not require the relative vorticity, we show in Section 39.4 how the formulation (38.58) can be especially useful for developing budgets of integrated PV-substance.

In the manipulations (38.56a)-(38.56b), we did not touch the planetary vorticity term. We certainly could do so, in which case

$$\chi 2\boldsymbol{\Omega} = \chi \nabla \times (\boldsymbol{\Omega} \times \mathbf{x}) = \nabla \times (\chi \boldsymbol{\Omega} \times \mathbf{x}) - \nabla \chi \times (\boldsymbol{\Omega} \times \mathbf{x}). \quad (38.60)$$

The term $\nabla \times (\chi \boldsymbol{\Omega} \times \mathbf{x})$ drops out when taking the divergence. However, the term $\boldsymbol{\Omega} \times \mathbf{x}$ requires us to evaluate the position vector, \mathbf{x} , for each point in the fluid, and doing so is not generally convenient. For this reason, we do not modify the planetary vorticity contribution to the potential vorticity, preferring to keep the form $\chi 2\boldsymbol{\Omega}$ in equation (38.58).

38.5 PV budget for a hydrostatic Boussinesq ocean

Building on the vorticity budget in Section 37.7, we here develop the potential vorticity substance budget for a hydrostatic Boussinesq ocean in the presence of diabatic and frictional forcing. For that purpose, recall the vorticity equation for a hydrostatic and Boussinesq ocean (37.139)

$$\frac{D\boldsymbol{\omega}_a^{\text{hy}}}{Dt} = \underbrace{(\boldsymbol{\omega}_a^{\text{hy}} \cdot \nabla) \mathbf{v}}_{\text{stretching + tilting}} + \underbrace{\nabla \times \hat{\mathbf{z}} b}_{\text{baroclinicity}} + \underbrace{\nabla \times \mathbf{F}}_{\text{friction curl}}, \quad (38.61)$$

where b is the Archimedean buoyancy used in our discussion of the Boussinesq ocean in Chapter 26.

⁴We encounter similar mathematical manipulations in Section 61.6 when studying the connection between advection and skew diffusion in the tracer equation.

38.5.1 Potential vorticity

Baroclinicity is eliminated from the potential vorticity equation (38.61) by projecting the absolute vorticity onto the direction normal to buoyancy surfaces

$$\nabla b \cdot \frac{D\omega_a^{\text{hy}}}{Dt} = \nabla b \cdot [(\omega_a^{\text{hy}} \cdot \nabla) \mathbf{v}] + \nabla b \cdot (\nabla \times \mathbf{F}), \quad (38.62)$$

where we used

$$\nabla b \cdot (\nabla \times \hat{\mathbf{z}} b) = \nabla b \cdot (\nabla b \times \hat{\mathbf{z}}) = 0. \quad (38.63)$$

We next make use of the identity

$$\frac{D(\partial b / \partial x^i)}{Dt} = \frac{\partial}{\partial x^i} \left[\frac{Db}{Dt} \right] - \nabla b \cdot \frac{\partial \mathbf{v}}{\partial x^i} = \frac{\partial \dot{b}}{\partial x^i} - \nabla b \cdot \frac{\partial \mathbf{v}}{\partial x^i}, \quad (38.64)$$

so that

$$\omega_a^{\text{hy}} \cdot \left[\frac{D \nabla b}{Dt} \right] = \omega_a^{\text{hy}} \cdot \nabla \dot{b} - \nabla b \cdot [(\omega_a^{\text{hy}} \cdot \nabla) \mathbf{v}]. \quad (38.65)$$

Making use of this result in equation (38.62) renders

$$\nabla b \cdot \frac{D\omega_a^{\text{hy}}}{Dt} + \omega_a^{\text{hy}} \cdot \frac{D\nabla b}{Dt} = \omega_a^{\text{hy}} \cdot \nabla \dot{b} + \nabla b \cdot (\nabla \times \mathbf{F}), \quad (38.66)$$

which leads to

$$\frac{DQ}{Dt} = \omega_a^{\text{hy}} \cdot \nabla \dot{b} + \nabla b \cdot (\nabla \times \mathbf{F}) \quad (38.67)$$

where

$$Q = \omega_a^{\text{hy}} \cdot \nabla b = \omega^{\text{hy}} \cdot \nabla b + f \partial_z b \quad (38.68)$$

is the potential vorticity for a rotating hydrostatic Boussinesq ocean. Potential vorticity is materially invariant for the inviscid and adiabatic case, in which $\mathbf{F} = 0$ and $\dot{b} = 0$.

It is sometimes useful to split the hydrostatic vorticity into its vertical and horizontal terms as per equation (37.128). In this way, PV takes on the form

$$Q = \frac{\partial u}{\partial z} \frac{\partial b}{\partial y} - \frac{\partial v}{\partial z} \frac{\partial b}{\partial x} + (\zeta + f) \frac{\partial b}{\partial z} = \hat{\mathbf{z}} \cdot \left[\frac{\partial \mathbf{u}}{\partial z} \times \nabla b \right] + (\zeta + f) \frac{\partial b}{\partial z}. \quad (38.69)$$

This expression plays an important role in characterizing flows with order unity Rossby number, where the term $\hat{\mathbf{z}} \cdot (\partial_z \mathbf{u} \times \nabla b)$, can become comparable to $(\zeta + f) \partial_z b$, particularly in regions of strong horizontal buoyancy fronts such as those studied by [Thomas et al. \(2008\)](#) and [Thomas et al. \(2013\)](#).

38.5.2 Potential vorticity flux vector

The material form of the PV equation (38.67) is converted into its Eulerian flux-form via

$$\frac{\partial Q}{\partial t} + \nabla \cdot (\mathbf{v} Q) = \omega_a^{\text{hy}} \cdot \nabla \dot{b} + \nabla b \cdot (\nabla \times \mathbf{F}) \quad (38.70a)$$

$$= \nabla \cdot [\dot{b} \omega_a^{\text{hy}} + b (\nabla \times \mathbf{F})] \quad (38.70b)$$

$$= \nabla \cdot [\dot{b} \omega_a^{\text{hy}} + \nabla \times (b \mathbf{F}) - \nabla b \times \mathbf{F}] \quad (38.70c)$$

$$= \nabla \cdot (\dot{b} \omega_a^{\text{hy}} - \nabla b \times \mathbf{F}), \quad (38.70d)$$

where we used

$$\nabla \cdot \mathbf{v} = 0 \quad \text{Boussinesq flow is non-divergent} \quad (38.71\text{a})$$

$$\nabla \cdot \boldsymbol{\omega}_a^{\text{hy}} = 0 \quad \text{vorticity always has zero divergence} \quad (38.71\text{b})$$

$$\nabla \cdot (\nabla \times \mathbf{F}) = 0 \quad \text{divergence of curl vanishes} \quad (38.71\text{c})$$

$$\nabla \cdot [\nabla \times (b \mathbf{F})] = 0 \quad \text{divergence of curl vanishes.} \quad (38.71\text{d})$$

The conservation equation (38.70d) allows us to identify a potential vorticity flux vector

$$\mathbf{J}_Q = \mathbf{v} Q - \dot{b} \boldsymbol{\omega}_a^{\text{hy}} + \nabla b \times \mathbf{F} + \nabla \times \mathbf{A}, \quad (38.72)$$

so that the potential vorticity equation takes the form

$$\partial_t Q + \nabla \cdot \mathbf{J}_Q = 0. \quad (38.73)$$

The potential vorticity flux (38.72) is comprised of an advective term

$$\mathbf{J}_{\text{advective}} = \mathbf{v} Q, \quad (38.74)$$

and non-advective terms arising from diabatic and frictional forcing,

$$\mathbf{J}_{\text{non-advective}} = -\dot{b} \boldsymbol{\omega}_a^{\text{hy}} + \nabla b \times \mathbf{F}, \quad (38.75)$$

as well as a gauge term,

$$\mathbf{J}_{\text{gauge}} = \nabla \times \mathbf{A}, \quad (38.76)$$

whose form remains unspecified.

38.5.3 Kinematic derivation of the PV-substance flux

Following the discussion in Section 38.4.3, we consider a purely kinematic derivation of the PV flux vector. For that purpose write the hydrostatic Boussinesq PV in the form

$$Q = \boldsymbol{\omega}_a^{\text{hy}} \cdot \nabla b = \nabla \cdot (b \boldsymbol{\omega}_a^{\text{hy}}), \quad (38.77)$$

which follows since $\nabla \cdot \boldsymbol{\omega}_a^{\text{hy}} = 0$. Taking the Eulerian time derivative then leads to

$$\frac{\partial Q}{\partial t} = \nabla \cdot \left[\frac{\partial b}{\partial t} \boldsymbol{\omega}_a^{\text{hy}} + b \frac{\partial \boldsymbol{\omega}_a^{\text{hy}}}{\partial t} \right] = \nabla \cdot \left[\frac{\partial b}{\partial t} \boldsymbol{\omega}_a^{\text{hy}} + \frac{\partial \mathbf{u}}{\partial t} \times \nabla b \right], \quad (38.78)$$

which made use of the identities

$$\frac{\partial \boldsymbol{\omega}_a^{\text{hy}}}{\partial t} = \frac{\partial \boldsymbol{\omega}^{\text{hy}}}{\partial t} = \frac{\partial (\nabla \times \mathbf{u})}{\partial t} \quad \text{and} \quad \nabla \cdot [\nabla \times (b \mathbf{u})] = 0. \quad (38.79)$$

The PV thus evolves according to

$$\frac{\partial Q}{\partial t} = -\nabla \cdot \tilde{\mathbf{J}}_Q \quad (38.80)$$

where the PV flux is given by

$$\tilde{\mathbf{J}}_Q = -\frac{\partial b}{\partial t} \boldsymbol{\omega}_a^{\text{hy}} - \frac{\partial \mathbf{u}}{\partial t} \times \nabla b. \quad (38.81)$$

This form of the PV flux manifests the impermeability property of Chapter 39 since

$$\hat{\mathbf{n}} \cdot (\tilde{\mathbf{J}}_Q/Q) = -\frac{1}{|\nabla b|} \frac{\partial b}{\partial t} = \hat{\mathbf{n}} \cdot \mathbf{v}_{b\perp}, \quad (38.82)$$

where $\hat{\mathbf{n}} = \nabla b |\nabla b|^{-1}$ is the unit normal for a buoyancy surface, and with $\mathbf{v}_{b\perp}$ the velocity of a point on the isopycnal that satisfies

$$\frac{\partial b}{\partial t} + \mathbf{v}_{b\perp} \cdot \nabla b = 0. \quad (38.83)$$

We return in Chapter 39 to help clarify this particular point about impermeability.

38.5.4 A potential vorticity flux vector suited to steady flows

[Schär \(1993\)](#) provided a generalization of Bernoulli's Theorem for understanding steady geophysical flows, with [Marshall \(2000\)](#), [Marshall et al. \(2001\)](#), and [Polton and Marshall \(2007\)](#) applying this theorem to oceanic contexts within a hydrostatic and Boussinesq ocean.⁵ We here derive the potential vorticity flux vector for a hydrostatic and Boussinesq ocean. The manipulations offer experience with the variety of gauge choices available when studying potential vorticity fluxes, with certain gauge choices aligned with particular analysis goals. The presentation here is a warm-up to the non-Boussinesq and non-hydrostatic case studied in Section 39.3.1, where we also provide example uses for the formulation.

Momentum equation

We start by exposing the Boussinesq form of the Bernoulli potential within the vector-invariant velocity equation. For this purpose, return to the horizontal momentum equation (37.134), and expand the expressions for the perturbation pressure and the buoyancy

$$\frac{\partial \mathbf{u}}{\partial t} + (\mathbf{f} + \boldsymbol{\omega}^{\text{hy}}) \times \mathbf{v} = -\nabla(\varphi + |\mathbf{u}|^2/2) + \hat{\mathbf{z}} b + \mathbf{F} \quad (38.84a)$$

$$= -\nabla(|\mathbf{u}|^2/2) - \frac{1}{\rho_0} \nabla(p - p_0) - \hat{\mathbf{z}} \left[\frac{g(\rho - \rho_0)}{\rho_0} \right] + \mathbf{F} \quad (38.84b)$$

$$= -\nabla(|\mathbf{u}|^2/2) - \frac{1}{\rho_0} \nabla p - \hat{\mathbf{z}} \frac{g\rho}{\rho_0} + \mathbf{F} \quad (38.84c)$$

$$= -\nabla \left[\frac{|\mathbf{u}|^2}{2} + \frac{p}{\rho_0} \right] - \hat{\mathbf{z}} \left[\frac{g\rho - g\rho_o + g\rho_o}{\rho_0} \right] + \mathbf{F} \quad (38.84d)$$

$$= -\nabla \left[\frac{|\mathbf{u}|^2}{2} + \frac{p}{\rho_0} + gz \right] - \hat{\mathbf{z}} \left[\frac{g(\rho - \rho_o)}{\rho_0} \right] + \mathbf{F} \quad (38.84e)$$

$$= -\nabla \mathcal{B} + \hat{\mathbf{z}} b + \mathbf{F}, \quad (38.84f)$$

where we introduced the Bernoulli potential for a hydrostatic and Boussinesq fluid⁶

$$\mathcal{B} = \frac{|\mathbf{u}|^2}{2} + \frac{p}{\rho_0} + gz. \quad (38.85)$$

⁵Recall that we introduced the Bernoulli potential and Bernoulli theorem in Section 23.7.3.

⁶See Section 23.7 for the non-Boussinesq Bernoulli potential.

Potential vorticity flux

The flux-form potential vorticity conservation statement remains as given by equation (38.70d), and the PV-substance flux is given by equation (38.72). However, we can make use of the gauge invariance of the PV-substance flux to write it in a manner conducive to analyzing steady state conditions. For this purpose, operate with $\nabla b \times$ on the velocity equation (38.84f) to have

$$\nabla b \times \frac{\partial \mathbf{u}}{\partial t} + \nabla b \times (\boldsymbol{\omega}_a^{hy} \times \mathbf{v}) = -\nabla b \times \nabla \mathcal{B} + \nabla b \times \hat{\mathbf{z}} b + \nabla b \times \mathbf{F}. \quad (38.86)$$

Now make use of the identity

$$\nabla b \times (\boldsymbol{\omega}_a^{hy} \times \mathbf{v}) = (\nabla b \cdot \mathbf{v}) \boldsymbol{\omega}_a^{hy} - (\boldsymbol{\omega}_a^{hy} \cdot \nabla b) \mathbf{v} \quad (38.87)$$

in equation (38.86) to yield

$$(\mathbf{v} \cdot \nabla b) \boldsymbol{\omega}_a^{hy} - (\boldsymbol{\omega}_a^{hy} \cdot \nabla b) \mathbf{v} = -\nabla b \times \frac{\partial \mathbf{u}}{\partial t} - \nabla b \times \nabla \mathcal{B} + \nabla b \times \hat{\mathbf{z}} b + \nabla b \times \mathbf{F}. \quad (38.88)$$

We next make use of this identity for the purpose of manipulating the potential vorticity flux given by equation (38.72)

$$\mathbf{J}_Q = \mathbf{v} Q - \dot{b} \boldsymbol{\omega}_a^{hy} + \nabla b \times \mathbf{F} + \nabla \times \mathbf{A} \quad (38.89a)$$

$$= \mathbf{v} (\boldsymbol{\omega}_a^{hy} \cdot \nabla b) - \left[\frac{\partial b}{\partial t} + \mathbf{v} \cdot \nabla b \right] \boldsymbol{\omega}_a^{hy} + \nabla b \times \mathbf{F} + \nabla \times \mathbf{A} \quad (38.89b)$$

$$= [\mathbf{v} (\boldsymbol{\omega}_a^{hy} \cdot \nabla b) - (\mathbf{v} \cdot \nabla b) \boldsymbol{\omega}_a^{hy}] - \frac{\partial b}{\partial t} \boldsymbol{\omega}_a^{hy} + \nabla b \times \mathbf{F} + \nabla \times \mathbf{A} \quad (38.89c)$$

$$= \left[\nabla b \times \frac{\partial \mathbf{u}}{\partial t} + \nabla b \times \nabla \mathcal{B} - \nabla b \times \hat{\mathbf{z}} b - \nabla b \times \mathbf{F} \right] - \frac{\partial b}{\partial t} \boldsymbol{\omega}_a^{hy} + \nabla b \times \mathbf{F} + \nabla \times \mathbf{A} \quad (38.89d)$$

$$= \nabla b \times \frac{\partial \mathbf{u}}{\partial t} - \frac{\partial b}{\partial t} \boldsymbol{\omega}_a^{hy} + \nabla b \times \nabla \mathcal{B} - \nabla b \times \hat{\mathbf{z}} b + \nabla \times \mathbf{A}. \quad (38.89e)$$

$$= \nabla b \times \left[\frac{\partial \mathbf{u}}{\partial t} + \nabla \mathcal{B} \right] - \frac{\partial b}{\partial t} \boldsymbol{\omega}_a^{hy} + \nabla \times (\mathbf{A} - \hat{\mathbf{z}} b^2/2). \quad (38.89f)$$

Choosing the gauge function

$$\mathbf{A} = \hat{\mathbf{z}} (b^2/2) \quad (38.90)$$

renders the flux vector

$$\mathbf{J}_Q^{ss} = \nabla b \times \left(\frac{\partial \mathbf{u}}{\partial t} + \nabla \mathcal{B} \right) - \frac{\partial b}{\partial t} \boldsymbol{\omega}_a^{hy} \quad (38.91)$$

We have now reached our goal whereby the steady state version of the PV flux (38.91) takes the rather elegant form

$$\mathbf{J}_Q^{ss} = \nabla b \times \nabla \mathcal{B} = \nabla \times b \nabla \mathcal{B} = -\nabla \times \mathcal{B} \nabla b \quad \text{steady state.} \quad (38.92)$$

Hence, the steady state potential vorticity flux is aligned with the intersection of surfaces of constant buoyancy and Bernoulli potential

$$\nabla b \cdot \mathbf{J}_Q^{ss} = 0 \quad \text{and} \quad \nabla \mathcal{B} \cdot \mathbf{J}_Q^{ss} = 0 \quad \text{steady state.} \quad (38.93)$$

Recalling our discussion of vector streamfunctions in Section 18.4.4, where here see that the buoyancy and Bernoulli potential serve as the two scalar functions that build the vector streamfunction

for the steady state potential vorticity flux. Mapping surfaces of constant buoyancy and constant Bernoulli potential, and determining their intersections, then determine the potential vorticity flux pathways operating in a steady state. Figure 38.5 offer a schematic based on the analogous situation for a velocity streamfunction shown in Figure 18.3. This result is the Boussinesq/hydrostatic form of the more general non-Boussinesq/non-hydrostatic case derived in Section 39.3.3.

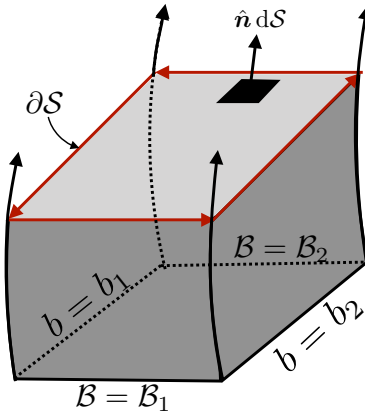


FIGURE 38.5: Isosurfaces of constant buoyancy, b , and Bernoulli potential, \mathcal{B} , serving as the two scalar functions building the vector streamfunction for potential vorticity flux, \mathbf{J}_Q^{ss} , in the steady state (see equation (38.93)). Streamlines are defined by the intersections of the b and \mathcal{B} isosurfaces, as shown by four streamlines along the corners of this particular volume. The transport of PV-substance through the surface, S , is determined by the line integral, $\oint_{\partial S} \mathcal{B} db = -\oint_{\partial S} b d\mathcal{B} = (\mathcal{B}_1 - \mathcal{B}_2)(b_2 - b_1)$, around the boundary circuit.

38.6 Conservation of pancake potential vorticity

In Section 38.2, we detailed why there is no materially invariant potential vorticity for a realistic equation of state for seawater, in which $\rho = \rho(S, \Theta, p)$. A similar limitation holds for the atmosphere, where the specific entropy is a function of pressure, density, and moisture concentration. We here build from our discussion of Kelvin's circulation theorem in Section 37.2 to consider a finite volume *pancake potential vorticity*. Rather than being a property carried by each fluid particle, the pancake potential vorticity is carried by a finite fluid region and it is materially invariant for perfect fluid flows, even for a realistic equation of state. The discussion here follows that given by [Kooloth et al. \(2022\)](#).

Our starting point is the potential vorticity equation written as in equation (38.41)

$$\rho \frac{DQ}{Dt} = (\boldsymbol{\omega}_a \cdot \nabla) \dot{\chi} + \nabla \chi \cdot [\nabla \times (-\rho^{-1} \nabla p)] + \nabla \chi \cdot (\nabla \times \mathbf{F}) \quad \text{with} \quad Q = \rho^{-1} \nabla \chi \cdot \boldsymbol{\omega}_a. \quad (38.94)$$

The key step in the derivation is to replace the pressure gradient acceleration with its equivalent in terms of specific enthalpy and its partial derivatives.⁷ For this purpose we write the specific enthalpy as a function of Conservative Temperature, salt concentration (i.e., absolute salinity), and pressure

$$\mathcal{H} = \mathcal{H}(\Theta, S, p), \quad (38.95)$$

⁷We made use of a similar approach when studying circulation in Section 37.2.

which leads to the spatial gradient⁸

$$\nabla \mathcal{H} = \rho^{-1} \nabla p + \left[\frac{\partial \mathcal{H}}{\partial \Theta} \right]_{p,S} \nabla \Theta + \left[\frac{\partial \mathcal{H}}{\partial S} \right]_{\Theta,p} \nabla S, \quad (38.96)$$

which then leads to the expression for the pressure gradient acceleration

$$-\rho^{-1} \nabla p = -\nabla \mathcal{H} + \mathcal{H}_\Theta \nabla \Theta + \mathcal{H}_S \nabla S, \quad (38.97)$$

where we introduced the shorthand notation

$$\mathcal{H}_\Theta = \left[\frac{\partial \mathcal{H}}{\partial \Theta} \right]_{p,S} \quad \text{and} \quad \mathcal{H}_S = \left[\frac{\partial \mathcal{H}}{\partial S} \right]_{\Theta,p}. \quad (38.98)$$

Use of the identity (38.97) within the potential vorticity equation (38.94) leads to

$$\rho \frac{DQ}{Dt} = (\boldsymbol{\omega}_a \cdot \nabla) \dot{\chi} + \nabla \chi \cdot \nabla \times [\mathcal{H}_\Theta \nabla \Theta + \mathcal{H}_S \nabla S + \mathbf{F}], \quad (38.99)$$

where we set $\nabla \times \nabla \mathcal{H} = 0$. Now make use of the following vector identity

$$\nabla \chi \cdot (\nabla \times \mathbf{A}) = \nabla \cdot (\chi \nabla \times \mathbf{A}) = \nabla \cdot [\nabla \times (\chi \mathbf{A}) - \nabla \chi \times \mathbf{A}] = -\nabla \cdot (\nabla \chi \times \mathbf{A}), \quad (38.100)$$

to bring the potential vorticity equation (38.99) to

$$\rho \frac{DQ}{Dt} = \nabla \cdot [\boldsymbol{\omega}_a \dot{\chi} - \nabla \chi \times (\mathcal{H}_\Theta \nabla \Theta + \mathcal{H}_S \nabla S + \mathbf{F})]. \quad (38.101)$$

Equation (38.101) is quite general. To reduce by one the terms on the right hand side, we can either choose $\chi = \Theta$ or $\chi = S$. Let us choose $\chi = \Theta$, in which case

$$\rho \frac{DQ^{(\Theta)}}{Dt} = \nabla \cdot [\mathcal{H}_S \nabla S \times \nabla \Theta + \mathbf{F} \times \nabla \Theta + \boldsymbol{\omega}_a \dot{\Theta}] \quad \text{with} \quad Q^{(\Theta)} = \rho^{-1} \nabla \Theta \cdot \boldsymbol{\omega}_a. \quad (38.102)$$

We still have the reversible term, $\mathcal{H}_S \nabla S \times \nabla \Theta$, contributing to the material time evolution of $Q^{(\Theta)}$, and this term vanishes only for particularly idealized forms of the fluid thermodynamics. Rather than pursue material invariance for potential vorticity along a fluid particle, consider an integration of $Q^{(\Theta)}$ over a finite region that moves with the flow, and take its time derivative

$$\frac{d}{dt} \int_{\mathcal{S}(\mathbf{v})} \rho Q^{(\Theta)} dV = \int_{\mathcal{S}(\mathbf{v})} \rho \frac{DQ^{(\Theta)}}{Dt} dV \quad (38.103a)$$

$$= \int_{\mathcal{S}(\mathbf{v})} \nabla \cdot [\mathcal{H}_S \nabla S \times \nabla \Theta + \mathbf{F} \times \nabla \Theta + \boldsymbol{\omega}_a \dot{\Theta}] dV \quad (38.103b)$$

$$= \oint_{\partial \mathcal{S}(\mathbf{v})} [\mathcal{H}_S \nabla S \times \nabla \Theta + \mathbf{F} \times \nabla \Theta + \boldsymbol{\omega}_a \dot{\Theta}] \cdot \hat{\mathbf{n}} d\mathcal{S}. \quad (38.103c)$$

The first and second terms on the right hand side vanish if we choose a volume whose boundary has an outward unit normal vector, $\hat{\mathbf{n}}$, parallel to $\nabla \Theta$ at every point around the closed region. This sort of Θ -bubble is uncommon in a stably stratified fluid, though it may occur over relatively small scales in turbulent flows. Another arrangement to consider is where salinity has a closed contour on Conservative Temperature surfaces. We thus take a pancake/disk region with $\hat{\mathbf{n}}$ parallel to

⁸We performed a similar manipulation in Section 23.4.2.

$\nabla\Theta$ on its top and bottom and $\hat{\mathbf{n}}$ parallel to ∇S on the sides. For this region, the $\nabla S \times \nabla\Theta$ contribution vanishes along all the boundaries, and the contribution from friction only appears on the sides where $\hat{\mathbf{n}}$ is parallel to ∇S . We can take a complementary approach by setting $\chi = S$, in which case the previous discussion holds yet with Θ and S interchanged. Either of these pancake regions preserves the materially integrated potential vorticity for inviscid flows with S and Θ both materially invariant.



38.7 Exercises

EXERCISE 38.1: PV FOR A PERFECT NON-HYDROSTATIC BOUSSINESQ OCEAN

Consider a perfect rotating Boussinesq ocean whose governing equations are given by

$$\frac{D\mathbf{v}}{Dt} + f(\hat{\mathbf{z}} \times \mathbf{v}) = -\nabla\varphi + b\hat{\mathbf{z}} \quad (38.104)$$

$$\nabla \cdot \mathbf{v} = 0 \quad (38.105)$$

$$\frac{Db}{Dt} = 0 \quad (38.106)$$

$$b = -\frac{g(\rho - \rho_0)}{\rho_0} = g\alpha\theta, \quad (38.107)$$

where θ is the potential temperature and $\alpha > 0$ is a constant thermal expansion coefficient. Further details are provided in Section 26.1.6. Some of this exercise follows the hydrostatic Boussinesq discussion in Section 38.5, though they differ in important places so be careful!

- (a) Derive the equation for the material time evolution of potential vorticity in this fluid system. Show all steps in the derivation.
- (b) The baroclinicity vector appearing in the Boussinesq vorticity equation is $\mathbf{B} = \nabla \times \hat{\mathbf{z}} b = \nabla b \times \hat{\mathbf{z}}$ (see Section 37.7.1 to check the derivation in part (a) above). Show that this vector results upon making the Boussinesq approximation to the non-Boussinesq expression $\mathbf{B} = (\nabla\rho \times \nabla p)/\rho^2$. Hint: drop the $\delta\rho$ and δp product given that it is a higher order quantity.
- (c) Show that the vertical portion of Q^{bouss} can be written

$$Q_{\text{vert}}^{\text{bouss}} = (\zeta + f) N^2 \quad (38.108)$$

where $\zeta = \partial_x v - \partial_y u$ is the vertical component to the relative vorticity and $N^2 = \partial b / \partial z$ is the squared buoyancy frequency (Section 27.5.4). Hint: this is not tough to show; there is no trick here.

- (d) If flow maintains hydrostatic and geostrophic balance, show that the horizontal portion of Q^{bouss} can be written

$$Q_{\text{horz}}^{\text{bouss}} = \boldsymbol{\omega} \cdot \nabla_z b \approx -f^{-1} |\nabla_z b|^2. \quad (38.109)$$

Hint: recall that for hydrostatic and geostrophic flow, the vertical velocity is much smaller than horizontal.

EXERCISE 38.2: PV FOR DIABATIC AND FRICTIONAL NON-HYDROSTATIC BOUSSINESQ OCEAN
 Reconsider Exercise 38.1 in the presence of irreversible friction and buoyancy sources so that the governing equations are

$$\frac{D\mathbf{v}}{Dt} + f(\hat{\mathbf{z}} \times \mathbf{v}) = -\nabla\varphi + b\hat{\mathbf{z}} + \mathbf{F} \quad (38.110)$$

$$\nabla \cdot \mathbf{v} = 0 \quad (38.111)$$

$$\frac{Db}{Dt} = \dot{b} \quad (38.112)$$

$$b = -\frac{g(\rho - \rho_0)}{\rho_0} = g\alpha\theta, \quad (38.113)$$

where $\dot{\theta}$ is a diabatic heating source/sink, α is a constant thermal expansion coefficient, and \mathbf{F} is a non-conservative acceleration such as from friction or boundary stresses.

- (a) Derive the equation for the material time evolution of potential vorticity in this fluid system, including the irreversible contributions from friction and heating.
- (b) Derive an equation for the potential vorticity time tendency (i.e., Eulerian time derivative), written in the form

$$\frac{\partial Q}{\partial t} = -\nabla \cdot \mathbf{J}_Q. \quad (38.114)$$

What is the PV flux \mathbf{J}_Q ? Note that your answer is unique up to the curl of an arbitrary vector (gauge symmetry). Also note that for a Boussinesq flow we drop the constant reference density in the definition of \mathbf{J}_Q .

- (c) A common diabatic process is written in the form of a damping source

$$\dot{b} = -\mu(b - b^*), \quad (38.115)$$

where μ is a constant Newtonian damping coefficient (dimensions of inverse time), and b^* is a specified buoyancy profile. This form of a buoyancy source acts to damp the buoyancy towards a specified profile b^* . Show that Newtonian damping of buoyancy corresponds to potential vorticity damping towards $Q^* = \boldsymbol{\omega}_a \cdot \nabla b^*$.

- (d) A form for the friction operator is given by Rayleigh drag

$$\mathbf{F} = -\gamma\mathbf{v}, \quad (38.116)$$

with γ a constant Rayleigh damping coefficient with dimension of inverse time. Show that Rayleigh drag in the momentum equation, which acts to damp velocity towards zero, corresponds to a damping of potential vorticity towards its planetary geostrophic form, $Q^{pg} = fN^2$, where $N^2 = \partial b / \partial z$ is the squared buoyancy frequency.

- (e) Discuss the balance needed between forcing terms in \mathbf{J}_Q to arrive at a steady state (i.e., zero Eulerian time tendency). Continue to assume the friction is in the form of Rayleigh drag and heating is in the form of Newtonian damping.



Chapter 39

POTENTIAL VORTICITY BUDGETS

In Chapter 38 we studied properties of potential vorticity, Q , with $\rho Q = \omega_a \cdot \nabla \chi$ the projection of the absolute vorticity, ω_a , onto a direction determined by a smooth scalar field, χ . If χ annihilates the baroclinicity vector and is materially invariant, then Q is materially invariant: $DQ/Dt = 0$. In geophysical fluid mechanics, it is common to define potential vorticity with χ equal to the specific entropy (for the atmosphere) or Archimedean buoyancy (for the ocean), in which case Q is referred to as the *Ertel potential vorticity*. Specific entropy and buoyancy are preferred given their intimate connection to dynamics, and since they annihilate baroclinicity in interesting and relevant special cases.

In this chapter we develop finite volume budgets for potential vorticity substance, with such budgets fundamentally affected by the *impermeability theorem* respected by potential vorticity fluxes. Impermeability says that for potential vorticity defined according to a scalar field, χ , there is identically zero potential vorticity flux crossing χ -isosurfaces. This property holds even when there are mass and thermal fluxes crossing χ -isosurfaces. Such generality signals its kinematic nature, which ultimately follows from the non-divergent nature of vorticity. It offers further insight into why, as developed in Section 39.4, the volume integrated PV-substance, ρQ , changes only when χ surfaces intersect a boundary.

These points are fundamental to potential vorticity and yet easily confused, thus motivating us to summarize them here.

- Material invariance of potential vorticity, Q , holds for a perfect fluid and for Q that is defined according to a materially invariant scalar field, χ , that annihilates baroclinicity.
- Impermeability of the flux of ρQ (PV-substance) holds for potential vorticity defined according to an arbitrary scalar, χ , even in the presence of irreversible processes. This property is purely kinematic and it follows from the non-divergent nature of absolute vorticity.

CHAPTER GUIDE

The goal of this chapter is to fill in the conceptual and technical details needed to understand the above points about impermeability, and in turn to develop an understanding of finite volume budgets of potential vorticity. We build from the potential vorticity mechanics introduced in Chapter 38, and make use of many elements of vector calculus summarized in Chapter 2. This chapter is an essential read for those interested in potential vorticity theory and potential vorticity budgets.

39.1 Loose threads	1002
39.2 Variations on the impermeability theorem	1002

39.2.1	Impermeability for the Haynes-McIntyre PV flux	1002
39.2.2	A kinematic derivation of impermeability	1004
39.2.3	Comments	1006
39.3	Impermeability theorem for seawater	1006
39.3.1	Ocean PV in terms of potential density	1006
39.3.2	A modified PV-substance flux	1007
39.3.3	Integral constraints for steady state	1008
39.3.4	Further study	1009
39.4	Integrated potential vorticity substance	1009
39.4.1	The primary role of boundaries	1009
39.4.2	Region bounded by a single buoyancy surface	1010
39.4.3	Region bounded by two buoyancy surfaces	1011
39.4.4	Region bounded by land and a buoyancy surface	1012
39.4.5	A layer outcropping at the ocean surface	1013
39.4.6	Further study	1014
39.5	Boundary fluxes of PV-substance	1014
39.5.1	Layer integrated budget	1015
39.5.2	Impermeability across interior layer interfaces	1016
39.5.3	PV flux at a land-sea boundary	1016
39.5.4	PV flux at the air-sea boundary	1017
39.5.5	Thought experiments	1019
39.5.6	Is there a preferred form of the PV-substance flux?	1019
39.5.7	Further study	1020

39.1 Loose threads

- *Callies and Ferrari (2018)* and bottom mixing induced circulation. Connect the thermal wind next to the bottom, inducing flow counter to Kelvin waves, to the potential vorticity boundary fluxes in Section 39.5.3. Discuss the spin up experiment in Section 4 of *Callies and Ferrari (2018)* from a potential vorticity perspective. Note the role of bottom friction in enabling the bottom buoyancy mixing to impart potential vorticity to the flow. without friction then there would be no way to introduce potential vorticity to the flow. That then couples the buoyancy mixing to the friction. *Callies and Ferrari (2018)* also note that to satisfy $\hat{\mathbf{n}} \cdot \nabla b = 0$ requires friction. I do not understand that fully, but must be related to this potential vorticity argument.

39.2 Variations on the impermeability theorem

In this section we derive the impermeability theorem satisfied by the potential vorticity flux vector. We illustrate the theorem for a variety of potential vorticity flux vectors that differ by a gauge function. So although these fluxes have identical divergences, the physical content of the fluxes is distinct. Consequently, one may choose to use a particular flux depending on the context of their use. We return to this point in Section 39.5.6.

39.2.1 Impermeability for the Haynes-McIntyre PV flux

We start with the Eulerian flux-form evolution equation for PV-substance given by equation (38.49)

$$\frac{\partial(\rho Q)}{\partial t} + \nabla \cdot \mathbf{J}_Q = 0 \quad \text{with} \quad \mathbf{J}_Q = \rho \mathbf{v} Q - \dot{\chi} \boldsymbol{\omega}_a + \nabla \chi \times \mathbf{F}, \quad (39.1)$$

with $\dot{\chi} = D\chi/Dt$, and with the PV-substance flux vector, \mathbf{J}_Q , given in the form examined in [Haynes and McIntyre \(1987\)](#).¹ Following the derivation in [Haynes and McIntyre \(1987\)](#), we decompose the velocity into two components, one oriented parallel to constant χ surfaces and one oriented perpendicular

$$\mathbf{v}_{\parallel} = \mathbf{v} - \hat{\mathbf{n}}(\mathbf{v} \cdot \hat{\mathbf{n}}) \quad \text{and} \quad \mathbf{v}_{\perp} = -\frac{\hat{\mathbf{n}} \partial \chi / \partial t}{|\nabla \chi|} \quad \Rightarrow \mathbf{v} = \mathbf{v}_{\parallel} + \mathbf{v}_{\perp} + \frac{\hat{\mathbf{n}} \dot{\chi}}{|\nabla \chi|} \quad (39.2)$$

where

$$\hat{\mathbf{n}} = \nabla \chi / |\nabla \chi| \quad (39.3)$$

is the unit normal vector for χ -isosurfaces. By construction, the velocity \mathbf{v}_{\perp} satisfies

$$\frac{\partial \chi}{\partial t} + \mathbf{v}_{\perp} \cdot \nabla \chi = 0. \quad (39.4)$$

Hence, according to the kinematics detailed in Section 16.4.2,

$$\mathbf{v}_{\perp} \cdot \hat{\mathbf{n}} = \mathbf{v}_{\chi} \cdot \hat{\mathbf{n}}, \quad (39.5)$$

where \mathbf{v}_{χ} is the velocity of a point fixed on a constant χ surface. That is, \mathbf{v}_{\perp} provides a measure of the velocity for a point following a constant χ surface, even as that surface moves through the fluid. We make use of this key identity below.

With the velocity decomposition (39.2), the PV-substance flux vector takes the form

$$\mathbf{J}_Q = \rho \mathbf{v} Q - \dot{\chi} \boldsymbol{\omega}_a + \nabla \chi \times \mathbf{F} \quad (39.6a)$$

$$= \left[\mathbf{v}_{\parallel} + \mathbf{v}_{\perp} + \frac{\dot{\chi} \nabla \chi}{|\nabla \chi|^2} \right] \rho Q - \dot{\chi} \boldsymbol{\omega}_a + \nabla \chi \times \mathbf{F} \quad (39.6b)$$

$$= (\mathbf{v}_{\parallel} + \mathbf{v}_{\perp}) \rho Q - \dot{\chi} [\boldsymbol{\omega}_a - (\boldsymbol{\omega}_a \cdot \hat{\mathbf{n}}) \hat{\mathbf{n}}] + \nabla \chi \times \mathbf{F} \quad (39.6c)$$

$$= (\mathbf{v}_{\parallel} + \mathbf{v}_{\perp}) \rho Q - \dot{\chi} (\boldsymbol{\omega}_a)_{\parallel} + \nabla \chi \times \mathbf{F} \quad (39.6d)$$

$$= \underbrace{\mathbf{v}_{\perp} \rho Q}_{\mathbf{J}_{\perp}} + \underbrace{\left[\rho Q \mathbf{v}_{\parallel} - \dot{\chi} (\boldsymbol{\omega}_a)_{\parallel} \right]}_{\mathbf{J}_{\parallel}} + \nabla \chi \times \mathbf{F} \quad (39.6e)$$

$$\equiv \mathbf{J}_{\perp} + \mathbf{J}_{\parallel}, \quad (39.6f)$$

where

$$(\boldsymbol{\omega}_a)_{\parallel} = \boldsymbol{\omega}_a - (\boldsymbol{\omega}_a \cdot \hat{\mathbf{n}}) \hat{\mathbf{n}} = \boldsymbol{\omega}_a - \left[\frac{\boldsymbol{\omega}_a \cdot \nabla \chi}{|\nabla \chi|^2} \right] \nabla \chi = \boldsymbol{\omega}_a - \frac{\rho Q}{|\nabla \chi|} \hat{\mathbf{n}}. \quad (39.7)$$

The above results motivate us to write the PV-substance budget equation (39.1) in the form

$$\frac{\partial(\rho Q)}{\partial t} + \nabla \cdot (\mathbf{v}_Q \rho Q) = 0, \quad (39.8)$$

¹Following [Haynes and McIntyre \(1987\)](#), we set the gauge function, \mathbf{A} , to zero in equation (39.1).

where

$$\mathbf{v}_Q \equiv \frac{\mathbf{J}_Q}{\rho Q} \quad \text{definition of } \mathbf{v}_Q \quad (39.9a)$$

$$= \mathbf{v} + \frac{-\dot{\chi} \boldsymbol{\omega}_a + \nabla \chi \times \mathbf{F}}{\rho Q} \quad \text{equation (39.1)} \quad (39.9b)$$

$$= \mathbf{v}_\perp + \mathbf{v}_\parallel + \frac{-\dot{\chi} (\boldsymbol{\omega}_a)_\parallel + \nabla \chi \times \mathbf{F}}{\rho Q} \quad \text{equation (39.6e),} \quad (39.9c)$$

so that \mathbf{v}_Q is the velocity that advects the PV-substance through the fluid. A direct calculation shows that \mathbf{v}_Q satisfies the following property

$$\mathbf{v}_Q \cdot \hat{\mathbf{n}} = \mathbf{v}_\perp \cdot \hat{\mathbf{n}} = \mathbf{v}_\chi \cdot \hat{\mathbf{n}}, \quad (39.10)$$

where the final equality made use of the identity (39.5). As a result, the velocity, \mathbf{v}_Q , has a normal component that is identical to that of the velocity of a point fixed on the χ surface

$$\frac{\partial \chi}{\partial t} + \mathbf{v}_Q \cdot \nabla \chi = 0. \quad (39.11)$$

We depict this result in Figure 39.1, whereby the PV-substance flux never crosses the χ -isosurface, even as the surface moves and even in the presence of processes that allow for matter and thermal properties to cross the surface. This result holds since the χ -isosurface moves in a way to precisely track the PV-substance flux. In general, χ surfaces are permeable to matter and thermal properties but, as we have just shown, are impermeable to PV-substance. This is a rather remarkable kinematic result that has important implications for budgets of PV-substance within regions bounded by constant χ surfaces.

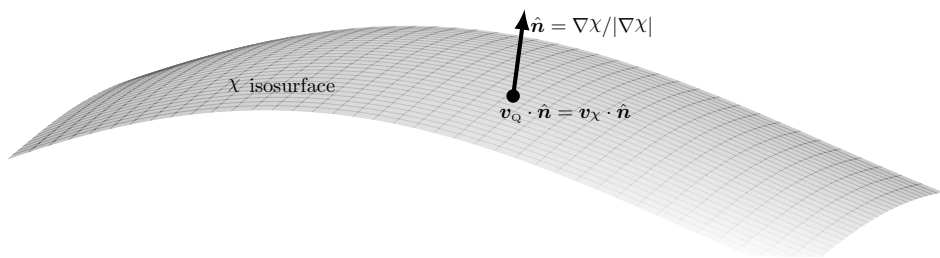


FIGURE 39.1: The flux, \mathbf{J}_Q , of PV-substance, $\rho Q = \nabla \cdot (\chi \boldsymbol{\omega}_a)$, does not penetrate a surface of constant χ . This kinematic result follows since the effective velocity of PV-substance, $\mathbf{v}_Q = \mathbf{J}_Q/(\rho Q)$, has the same normal component as a point fixed on a χ surface, $\mathbf{v}_Q \cdot \hat{\mathbf{n}} = \mathbf{v}_\chi \cdot \hat{\mathbf{n}}$. Consequently, the χ surface moves in a manner so that no flux of PV-substance crosses the surface, even in the presence of irreversible processes. This result is known as the impermeability theorem since χ surfaces are impermeable to the flux of PV-substance, even though they are permeable to matter and thermal properties.

39.2.2 A kinematic derivation of impermeability

The derivation of impermeability in Section 39.2.1 follows that given by [Haynes and McIntyre \(1987\)](#). We now complement that derivation by an alternative that emphasizes the kinematic

origins of impermeability. For that purpose, we make no use of the vorticity equation or the equation for χ . Instead, we merely use the definition of potential vorticity and the non-divergence property of absolute vorticity. This derivation follows our discussion of gauge freedom introduced in Section 38.4.3, as well as the discussion of potential vorticity for a hydrostatic Boussinesq ocean in Section 38.5.

The key identity we need was already given by equation (38.11)

$$\rho Q = \boldsymbol{\omega}_a \cdot \nabla \chi = \nabla \cdot (\boldsymbol{\omega}_a \chi), \quad (39.12)$$

thus revealing that ρQ is a pure divergence. Taking the Eulerian time derivative then leads to

$$\frac{\partial(\rho Q)}{\partial t} = -\nabla \cdot \mathbf{J}_Q^{\text{kin}}, \quad (39.13)$$

where

$$\mathbf{J}_Q^{\text{kin}} = -\frac{\partial(\boldsymbol{\omega}_a \chi)}{\partial t} \quad (39.14)$$

is the kinematic form of the PV-substance flux. By construction, this flux vanishes in the steady state

$$\mathbf{J}_Q^{\text{kin}} = 0 \quad \text{in steady state}, \quad (39.15)$$

which certainly contrasts to the steady state Haynes-McIntyre flux given by equation (39.1).

Introducing the velocity seen from an inertial reference frame (also called the absolute velocity (Section 11.8.1))

$$\mathbf{v}_a = \mathbf{v} + \boldsymbol{\Omega} \times \mathbf{x} \quad (39.16)$$

leads to

$$-\frac{\partial \boldsymbol{\omega}_a}{\partial t} \chi = -\frac{\partial(\nabla \times \mathbf{v}_a)}{\partial t} \chi = -\left[\nabla \times \frac{\partial \mathbf{v}_a}{\partial t} \right] \chi = -\nabla \times \left[\frac{\partial \mathbf{v}_a}{\partial t} \chi \right] + \nabla \chi \times \frac{\partial \mathbf{v}_a}{\partial t}. \quad (39.17)$$

Dropping the total curl (which amounts to choosing a gauge function) yields the modified kinematic form for the PV-substance flux

$$\tilde{\mathbf{J}}_Q^{\text{kin}} = -\frac{\partial \mathbf{v}_a}{\partial t} \times \nabla \chi - \boldsymbol{\omega}_a \frac{\partial \chi}{\partial t}. \quad (39.18)$$

It follows that

$$\tilde{\mathbf{v}}_Q^{\text{kin}} \cdot \hat{\mathbf{n}} = \frac{\tilde{\mathbf{J}}_Q^{\text{kin}} \cdot \hat{\mathbf{n}}}{\rho Q} = -\frac{\boldsymbol{\omega}_a \cdot \nabla \chi}{\rho Q} \frac{\partial \chi}{\partial t} \frac{1}{|\nabla \chi|} = -\frac{\partial \chi}{\partial t} \frac{1}{|\nabla \chi|} = \mathbf{v}_\chi \cdot \hat{\mathbf{n}}, \quad (39.19)$$

which is the same result (39.10) as found for the Haynes-McIntyre flux. This result allows us to conclude that $\tilde{\mathbf{J}}_Q^{\text{kin}}$ satisfies the impermeability theorem. We again emphasize that there has been no use of the dynamical equations for vorticity or for χ . Instead, this expression of impermeability only used the definition of potential vorticity, along with the non-divergent nature of vorticity, $\nabla \cdot \boldsymbol{\omega}_a = 0$.

Throughout this discussion, we assumed χ to be an arbitrary smooth scalar field. Hence, *any* scalar field used to project out a component of the absolute vorticity has its iso-surfaces impenetrable to the flux of the corresponding component of absolute vorticity. This result trivializes the impermeability theorem from a mathematical perspective. In Section 37.3.4 we somewhat anticipated this result when studying the Cartesian components of the absolute vorticity (see also Section 5 of [Haynes and McIntyre \(1987\)](#)). However, this result does not reduce the importance

of the entropic potential vorticity impermeability theorem for studying stratified flows. The importance holds since this particular potential vorticity has direct connection to dynamics and thermodynamics.

39.2.3 Comments

The impermeability theorem was introduced by [Haynes and McIntyre \(1987\)](#). Their paper was met by some confusion thus prompting them to write [Haynes and McIntyre \(1990\)](#). Besides exposing the purely kinematic aspects of impermeability, the presentation in this section reveals that there are multiple potential vorticity flux vectors that satisfy impermeability, with the vectors differing by a gauge transformation. Which flux vector is preferred depends on the application, with [Bretherton and Schär \(1993\)](#), [Davies-Jones \(2003a\)](#), and [Marshall et al. \(2001\)](#) proposing criteria favoring one form over another. We pursue such considerations in Section 39.3.

39.3 Impermeability theorem for seawater

As seen from Section 39.2.2, impermeability holds for any component of vorticity and the corresponding scalar isosurface. In contrast, material invariance of potential vorticity requires a materially conserved scalar to annihilate the baroclinicity vector (e.g., Section 38.1.4). Consequently, material invariance is much tougher to satisfy than impermeability. Indeed, as shown in Section 38.2, there is no materially invariant potential vorticity for an ocean with a realistic nonlinear equation of state (EOS). Hence, there is no materially invariant potential vorticity for the ocean even in the absence of irreversible processes. Nevertheless, one can define an ocean potential vorticity according to any scalar field, such as potential density, and still make use of the impermeability theorem when performing a potential vorticity budget. We here expose the details.

39.3.1 Ocean PV in terms of potential density

Following [Marshall et al. \(2001\)](#), we introduce an ocean potential vorticity field according to

$$Q^{\text{ocn}} = \frac{\nabla b \cdot \omega_a}{\rho}, \quad (39.20)$$

where the Archimedean buoyancy field, b , is approximated by a chosen potential density (see Section 27.3.4). As shown in Section 38.2, a globally defined buoyancy does not annihilate the baroclinicity vector for a realistic seawater equation of state

$$\mathbf{B} \cdot \nabla b = [-\nabla(1/\rho) \times \nabla p] \cdot \nabla b \neq 0. \quad (39.21)$$

Consequently, $DQ^{\text{ocn}}/Dt \neq 0$ even in the absence of irreversible processes. Nonetheless, the Eulerian budget for PV-substance satisfies

$$\frac{\partial(\rho Q^{\text{ocn}})}{\partial t} = -\nabla \cdot \tilde{\mathbf{J}}_Q^{\text{ocn}}, \quad (39.22)$$

and $\tilde{\mathbf{J}}_Q^{\text{ocn}}$ satisfies the impermeability theorem for b -surfaces. A flux-form budget equation greatly facilitates the study of budgets for PV-substance even within an ocean with a realistic equation of state. Derivation of the flux-form equation (39.22) follows from the discussion in Section 39.2.2,

where we know that the kinematic flux

$$\tilde{\mathbf{J}}_Q^{\text{ocn}} = -\frac{\partial \mathbf{v}_a}{\partial t} \times \nabla b - \boldsymbol{\omega}_a \frac{\partial b}{\partial t} = -\frac{\partial \mathbf{v}}{\partial t} \times \nabla b - \boldsymbol{\omega}_a \frac{\partial b}{\partial t} \quad (39.23)$$

satisfies the impermeability theorem for b -surfaces and whose convergence drives the time tendency for the PV-substance. Note that the second equality in equation (39.23) follows since

$$\frac{\partial \mathbf{v}_a}{\partial t} = \frac{\partial(\mathbf{v} + \boldsymbol{\Omega} \times \mathbf{x})}{\partial t} = \frac{\partial \mathbf{v}}{\partial t}, \quad (39.24)$$

given that the Eulerian time derivative is computed at a fixed position, \mathbf{x} , and the planetary rotation is assumed constant.

39.3.2 A modified PV-substance flux

The kinematic flux (39.23) vanishes in the steady state. We here motivate a gauge transformed flux that leads to the same flux divergence yet that renders a nonzero steady state flux. For this purpose, make use of the vector-invariant velocity equation (equation (37.32))

$$\frac{\partial \mathbf{v}}{\partial t} + \boldsymbol{\omega}_a \times \mathbf{v} = -\rho^{-1} \nabla p - \nabla m + \mathbf{F}, \quad (39.25)$$

where

$$m = \frac{1}{2} \mathbf{v} \cdot \mathbf{v} + \Phi \quad (39.26)$$

is the mechanical energy per mass of a fluid element. Bringing the pressure term inside of the gradient operator leads to

$$\frac{\partial \mathbf{v}}{\partial t} + \boldsymbol{\omega}_a \times \mathbf{v} = p \nabla(1/\rho) - \nabla(m + p/\rho) + \mathbf{F}. \quad (39.27)$$

Following our treatment of the hydrostatic Boussinesq ocean in Section 38.5.4, we introduce the Bernoulli function²

$$B = m + p/\rho. \quad (39.28)$$

The vector-invariant velocity equation (39.27) thus leads to the cross-product

$$\frac{\partial \mathbf{v}}{\partial t} \times \nabla b = -(\boldsymbol{\omega}_a \times \mathbf{v}) \times \nabla b + [p \nabla(1/\rho) - \nabla(m + p/\rho) + \mathbf{F}] \times \nabla b \quad (39.29a)$$

$$= -(\nabla b \cdot \boldsymbol{\omega}_a) \mathbf{v} + (\nabla b \cdot \mathbf{v}) \boldsymbol{\omega}_a + [p \nabla(1/\rho) - \nabla(m + p/\rho) + \mathbf{F}] \times \nabla b \quad (39.29b)$$

$$= -\mathbf{v} \rho Q^{\text{ocn}} + (\dot{b} - \partial_t b) \boldsymbol{\omega}_a + [p \nabla(1/\rho) - \nabla(m + p/\rho) + \mathbf{F}] \times \nabla b. \quad (39.29c)$$

Use of this result leads to the flux (39.23)

$$\tilde{\mathbf{J}}_Q^{\text{ocn}} = -\frac{\partial \mathbf{v}}{\partial t} \times \nabla b - \boldsymbol{\omega}_a \frac{\partial b}{\partial t} \quad (39.30a)$$

$$= \mathbf{v} \rho Q^{\text{ocn}} - \dot{b} \boldsymbol{\omega}_a - \mathbf{F} \times \nabla b + [\nabla(m + p/\rho) - p \nabla(1/\rho)] \times \nabla b \quad (39.30b)$$

$$= \mathbf{J}_Q + [\nabla(m + p/\rho) - p \nabla(1/\rho)] \times \nabla b, \quad (39.30c)$$

²The Bernoulli potential, \mathcal{B} , arises from an analysis of the total energy budget as in equation (23.97), where we see that the Bernoulli potential in a compressible (non-Boussinesq) fluid, $\mathcal{B} = m + p/\rho + \mathcal{I}$, also includes the internal energy per mass, \mathcal{I} . However, the internal energy is missing from equation (39.28), thus motivating our use of the terminology “a Bernoulli function” rather than “the Bernoulli potential”.

where \mathbf{J}_Q is the Haynes-McIntyre form of the PV-substance flux given by equation (39.1). The term

$$\nabla(m + p/\rho) \times \nabla b = \nabla \times [(m + p/\rho) \nabla b] \quad (39.31)$$

is a total curl and as such it can be moved around without altering the evolution of PV-substance; i.e., it is a “do nothing” flux. Furthermore, since it is parallel to buoyancy isosurfaces it does not alter the impermeability properties of the PV-substance flux.

Marshall et al. (2001) focused attention on the flux

$$\mathbf{J}_Q^{\text{marshall}} = \tilde{\mathbf{J}}_Q^{\text{ocn}} - \nabla(m + p/\rho) \times \nabla b = - \left[\frac{\partial \mathbf{v}}{\partial t} + \nabla(m + p/\rho) \right] \times \nabla b - \boldsymbol{\omega}_a \frac{\partial b}{\partial t}. \quad (39.32)$$

Diagnostically desirable features of $\mathbf{J}_Q^{\text{marshall}}$ include the following:

- $\nabla b \cdot \mathbf{J}_Q^{\text{marshall}} / (\rho Q) = \partial_t b$, thus satisfying the impermeability theorem.
- $\mathbf{J}_Q^{\text{marshall}}$ has no explicit reference to irreversible processes. Consequently, in some cases it can be simpler to diagnose than the Haynes-McIntyre flux, \mathbf{J}_Q .
- In a steady state, the flux is given by

$$\mathbf{J}_Q^{\text{marshall}} = \nabla b \times \nabla(m + p/\rho) = \nabla \times [b \nabla(m + p/\rho)]. \quad (39.33)$$

Consequently, $m + p/\rho$ provides a streamfunction for the steady state flux on buoyancy surfaces. As emphasized by *Schär (1993)*, this result holds even when there are irreversible processes, thus providing useful diagnostics even in the presence of dissipation.

39.3.3 Integral constraints for steady state

The steady state PV-substance flux in the form (39.33) can be used to develop some integral constraints on the steady flow. For this purpose consider the steady form of $\mathbf{J}_Q^{\text{marshall}}$ and integrate over an arbitrary simply connected area making use of Stokes' theorem

$$\int_S \nabla \times [b \nabla B] \cdot \hat{\mathbf{n}} dS = \oint_{\partial S} b \nabla B \cdot d\mathbf{r} = \oint_{\partial S} b dB = - \oint_{\partial S} B db. \quad (39.34a)$$

The first equality made use of Stokes' theorem; the second make use of the identity for exact differentials

$$\nabla B \cdot d\mathbf{r} = dB; \quad (39.35)$$

and the final equality made use of

$$b dB = d(bB) - B db \quad (39.36)$$

and noted that the closed loop integral of an exact differential vanishes, so that

$$\oint_{\partial S} d(Bb) = 0. \quad (39.37)$$

If we can find a closed contour where either B is a constant ($dB = 0$), or the buoyancy is a constant ($db = 0$), then we have the steady state constraint

$$\int_S \mathbf{J}_Q^{\text{marshall}} \cdot \hat{\mathbf{n}} dS = 0 \quad \text{area enclosed by contour with } m + p/\rho \text{ constant or } b \text{ constant.} \quad (39.38)$$

In regions where there are such closed contours, this constraint offers useful insight into the steady state balances. [Marshall \(2000\)](#) and [Polton and Marshall \(2007\)](#) make particular use of closed B contours on constant depth surfaces (so that $\hat{\mathbf{n}} = \hat{\mathbf{z}}$) in a Boussinesq ocean.

39.3.4 Further study

[Marshall et al. \(2001\)](#) builds from the generalized Bernoulli theorem of [Schär \(1993\)](#) and [Bretherton and Schär \(1993\)](#). We also consider these topics for a hydrostatic Boussinesq ocean in Section 38.5.4.

39.4 Integrated potential vorticity substance

In this section we derive some properties of integrated potential vorticity, with these properties merely the result of how potential vorticity is defined. We write potential vorticity using a global buoyancy field, b , as in our discussion of ocean potential vorticity in Section 39.3

$$\rho Q = \boldsymbol{\omega}_a \cdot \nabla b = \nabla \cdot (\boldsymbol{\omega}_a b) = \nabla \cdot [(\boldsymbol{\omega} + 2\boldsymbol{\Omega}) b]. \quad (39.39)$$

The following points are central to the results derived in this section, and they all follow from the non-divergent nature of the absolute vorticity.

- The divergence form given in the second and third equalities of equation (39.39) is the starting point for the derivations in this section. Indeed, as emphasized by [Morel et al. \(2019\)](#), the divergence form is appropriate for deriving discrete approximations since in this case the discrete potential vorticity also satisfies the properties developed in this section.
- As emphasized in Section 39.2, the properties in this section hold for any smooth scalar field that is used to define the potential vorticity.
- The properties in this section hold even when there is no materially invariant potential vorticity since we only make use of the non-divergent nature of the absolute vorticity.

39.4.1 The primary role of boundaries

Integral in terms of boundary vorticity and boundary buoyancy

We consider Q to be an intensive fluid property measuring the amount of PV-substance per unit mass (i.e., the concentration of PV-substance), and correspondingly with ρQ the amount of PV-substance per volume.³ With this interpretation, the amount of PV-substance within an arbitrary finite region is determined by the volume integral of ρQ

$$\mathcal{I} = \int_{\mathcal{R}} Q \rho dV = \int_{\mathcal{R}} \nabla \cdot (\boldsymbol{\omega}_a b) dV = \oint_{\partial\mathcal{R}} b \boldsymbol{\omega}_a \cdot \hat{\mathbf{n}} d\mathcal{S}, \quad (39.40)$$

where the final equality used Gauss's divergence theorem. Hence, the volume integrated PV-substance in a region is determined solely by values of the absolute vorticity and buoyancy on the region boundary. This property is strikingly distinct from material tracers. In practice it can be useful to decompose the absolute vorticity into the relative vorticity plus planetary vorticity

$$\mathcal{I} = \int_{\mathcal{R}} Q \rho dV = \oint_{\partial\mathcal{R}} b \boldsymbol{\omega}_a \cdot \hat{\mathbf{n}} d\mathcal{S} = \oint_{\partial\mathcal{R}} b \boldsymbol{\omega} \cdot \hat{\mathbf{n}} d\mathcal{S} + \oint_{\partial\mathcal{R}} b 2\boldsymbol{\Omega} \cdot \hat{\mathbf{n}} d\mathcal{S}. \quad (39.41)$$

³Recall our discussion of extensive and intensive fluid properties in Section 17.3.1.

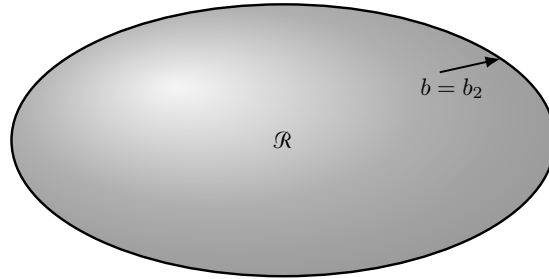


FIGURE 39.2: Integrating PV-substance over regions bounded by constant buoyancy surfaces that do not intersect the ground. Here we show a single buoyancy surface, $b = b_2$, bounding the bubble-like fluid region \mathcal{R} . Notably, the region inside the bubble generally has nontrivial buoyancy distribution. The only assumption is that it is wholly contained inside the $b = b_2$ contour. There is identically zero domain integrated potential vorticity in \mathcal{R} . Hence, if there is any nontrivial distribution of PV in either domain, there must be as much integrated positive values as there are negative.

Integral in terms of boundary velocity and boundary buoyancy gradient

We follow [Morel et al. \(2019\)](#) by deriving an alternative expression for \mathcal{I} in equation (39.41), with this alternative expression more convenient in some cases. For this purpose we write

$$b\boldsymbol{\omega} = b\nabla \times \mathbf{v} = \nabla \times (b\mathbf{v}) - \nabla b \times \mathbf{v}, \quad (39.42)$$

and use the divergence theorem to eliminate the total curl term (see Section 2.7.5)

$$\oint_{\partial\mathcal{R}} \nabla \times (b\mathbf{v}) \cdot \hat{\mathbf{n}} dS = \int_{\mathcal{R}} \nabla \cdot [\nabla \times (b\mathbf{v})] dV = 0. \quad (39.43)$$

We are thus led to the equivalent expressions for the integrated potential vorticity substance

$$\mathcal{I} = \int_{\mathcal{R}} Q\rho dV = \oint_{\partial\mathcal{R}} b\boldsymbol{\omega} \cdot \hat{\mathbf{n}} dS + 2 \oint_{\partial\mathcal{R}} b\boldsymbol{\Omega} \cdot \hat{\mathbf{n}} dS = - \oint_{\partial\mathcal{R}} (\nabla b \times \mathbf{v}) \cdot \hat{\mathbf{n}} dS + 2 \oint_{\partial\mathcal{R}} b\boldsymbol{\Omega} \cdot \hat{\mathbf{n}} dS. \quad (39.44)$$

In effect, the alternative forms move the derivative operator between the boundary velocity (for computing the relative vorticity) and the boundary buoyancy. One formulation may be more convenient than the other, depending on the boundary conditions. We emphasize that once a particular formulation is chosen, it is necessary to use that formulation for all of the domain boundaries. We must do so since the curl term that moves us from one form to the other vanishes only when integrating over the full domain boundary.

39.4.2 Region bounded by a single buoyancy surface

Consider a volume of fluid bounded by a single buoyancy surface as shown in the bubble-like region in Figure 39.2. Since the outer boundary of the region is set by a constant b -surface, we can pull b outside of the surface integral in equation (39.44) so that

$$\mathcal{I} = \oint_{\partial\mathcal{R}} \boldsymbol{\omega}_a \cdot \hat{\mathbf{n}} dS = b_2 \oint_{\partial\mathcal{R}} \boldsymbol{\omega}_a \cdot \hat{\mathbf{n}} dS. \quad (39.45)$$

We can now use the divergence theorem to return to the volume integral, only now with b outside of the integral

$$\mathcal{I} = b_2 \int_{\mathcal{R}} \nabla \cdot \boldsymbol{\omega}_a dV = 0, \quad (39.46)$$

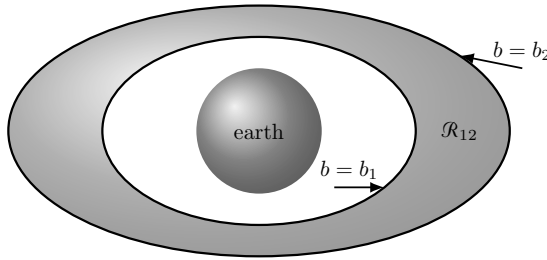


FIGURE 39.3: Integrating PV-substance over regions bounded by constant buoyancy surfaces that do not intersect the ground. Here we show a buoyancy layer or shell, \mathcal{R}_{12} , bounded by two buoyancy isosurfaces, $b_1 < b_2$, surrounding the earth, with neither surface intersecting the ground. There is identically zero domain integrated potential vorticity in \mathcal{R}_{12} . Hence, if there is any nontrivial distribution of potential vorticity in either domain, there must be as much integrated positive values as there are negative.

where $\nabla \cdot \boldsymbol{\omega}_a = 0$ led to the final equality. Equivalently, we can use Stokes' theorem to convert the closed area integral, $\oint_{\partial\mathcal{R}} \boldsymbol{\omega}_a \cdot \hat{\mathbf{n}} dS$, to a line integral around the boundary. However, there is no boundary for the closed area since it covers the sphere, thus again showing that $\mathcal{I} = 0$ (see also Section 2.7.5).

Yet another way to derive the identity (39.46) is to make use of the alternative expression for \mathcal{I} given by equation (39.44)

$$\mathcal{I} = - \oint_{\partial\mathcal{R}} (\nabla b \times \mathbf{v}) \cdot \hat{\mathbf{n}} dS + 2 \oint_{\partial\mathcal{R}} b \boldsymbol{\Omega} \cdot \hat{\mathbf{n}} dS. \quad (39.47)$$

Since the domain is bounded by a constant b surface, the outward normal is parallel to ∇b so that the first integral vanishes. Furthermore, since b is a constant in the second integral we are led to consider

$$\oint_{\partial\mathcal{R}} 2 \boldsymbol{\Omega} \cdot \hat{\mathbf{n}} dS = \oint_{\partial\mathcal{R}} [\nabla \times (\boldsymbol{\Omega} \times \mathbf{x})] \cdot \hat{\mathbf{n}} dS = \int_{\mathcal{R}} \nabla \cdot [\nabla \times (\boldsymbol{\Omega} \times \mathbf{x})] dV = 0, \quad (39.48)$$

which made use of the divergence theorem and the vanishing divergence of a curl.

The identity (39.46) says that there is zero integrated PV-substance contained within any region bounded by a single buoyancy surface; i.e., a bubble. The result holds whether there are reversible or irreversible processes acting on the buoyancy surface, and it holds if the b -surface is moving in space. Hence, within the domain there is just as much positive PV-substance as there is negative PV-substance. So if potential vorticity changes locally within the domain, then somewhere else it must experience an oppositely signed change so to leave a zero net integrated PV-substance. We emphasize that this result holds at each time instance.

39.4.3 Region bounded by two buoyancy surfaces

The identity (39.46) has a corollary, in which we consider a region bounded by two b -surfaces such as the region \mathcal{R}_{12} shown in Figure 39.3. The above arguments hold for that region as well, since we can decompose the surface integral into two integrals separately over b_1 and b_2

$$\mathcal{I} = \int_{\mathcal{R}_{12}} \nabla \cdot (\boldsymbol{\omega}_a b) dV = \int_{\mathcal{R}_2} \nabla \cdot (\boldsymbol{\omega}_a b) dV - \int_{\mathcal{R}_1} \nabla \cdot (\boldsymbol{\omega}_a b) dV, \quad (39.49)$$

where the domain \mathcal{R}_1 extends from the ground up to b_1 and \mathcal{R}_2 extends from the ground up to b_2 . Integration over the region below b_1 cancels through the subtraction. Indeed, the region below b_1

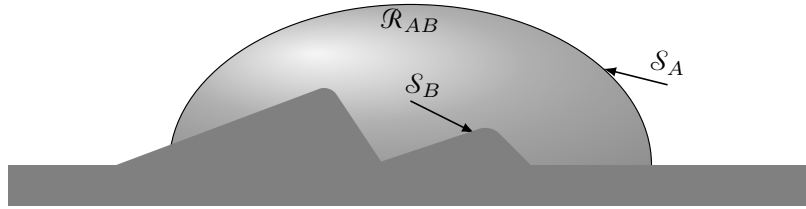


FIGURE 39.4: A fluid region, \mathcal{R}_{AB} , bounded by two buoyancy surfaces, \mathcal{S}_A and \mathcal{S}_B . The upper surface, \mathcal{S}_A , is defined by a buoyancy isosurface, $b = b_A$, with this surface intersecting the ground. The lower surface, \mathcal{S}_B , is along the ground (which is generally not flat, as shown here) and has a buoyancy that is a function of space and time, $b = b_B(\mathbf{x}, t)$.

could be anything without changing the result. So let that region be filled with fluid throughout (i.e., ignore the earth) to allow us to extend both integrals throughout the spherical region just like in the buoyancy bubble \mathcal{R} in Figure 39.3. Invoking the buoyancy bubble result we see that both integrals separately vanish. We are thus led to a vanishing integral for the layer

$$\mathcal{I} = \int_{\mathcal{R}_{12}} \nabla \cdot (\boldsymbol{\omega}_a b) dV = 0. \quad (39.50)$$

Again, the key assumption is that no buoyancy surface intersects land, in which case we are able to ignore the presence of land altogether and thus make use of the buoyancy bubble result. The identity (39.50) also follows from the second form of equation (39.44).

39.4.4 Region bounded by land and a buoyancy surface

We now consider a domain consisting of fluid bounded by a buoyancy surface that intersects (incrops) the ground, such as the region shown in Figure 39.4. This atmospheric example can be turned over to produce an ocean example with buoyancy surfaces outcropping at the ocean surface. Using the vorticity form of the integrated potential vorticity in equation (39.44) leads to

$$\mathcal{I} = \int_{\mathcal{R}_{AB}} \nabla \cdot (\boldsymbol{\omega}_a b) dV \quad (39.51a)$$

$$= \int_{\mathcal{S}_A} \boldsymbol{\omega}_a b \cdot \hat{\mathbf{n}} d\mathcal{S} + \int_{\mathcal{S}_B} \boldsymbol{\omega}_a b \cdot \hat{\mathbf{n}} d\mathcal{S} \quad (39.51b)$$

$$= b_A \int_{\mathcal{S}_A} \boldsymbol{\omega}_a \cdot \hat{\mathbf{n}} d\mathcal{S} + \int_{\mathcal{S}_B} b \boldsymbol{\omega}_a \cdot \hat{\mathbf{n}} d\mathcal{S} \quad (39.51c)$$

$$= b_A \left[\int_{\mathcal{S}_A} \boldsymbol{\omega}_a \cdot \hat{\mathbf{n}} d\mathcal{S} + \int_{\mathcal{S}_B} \boldsymbol{\omega}_a \cdot \hat{\mathbf{n}} d\mathcal{S} - \int_{\mathcal{S}_B} \boldsymbol{\omega}_a \cdot \hat{\mathbf{n}} d\mathcal{S} \right] + \int_{\mathcal{S}_B} b \boldsymbol{\omega}_a \cdot \hat{\mathbf{n}} d\mathcal{S} \quad (39.51d)$$

$$= b_A \int_{\mathcal{R}_{AB}} \nabla \cdot \boldsymbol{\omega}_a dV + \int_{\mathcal{S}_B} (b - b_A) \boldsymbol{\omega}_a \cdot \hat{\mathbf{n}} d\mathcal{S} \quad (39.51e)$$

$$= \int_{\mathcal{S}_B} (b - b_A) (\boldsymbol{\omega} + 2\boldsymbol{\Omega}) \cdot \hat{\mathbf{n}} d\mathcal{S}, \quad (39.51f)$$

where we made use of $\nabla \cdot \boldsymbol{\omega}_a = 0$ to reach the final equality. As both the ground and the ocean surface have buoyancy gradients, they contribute to the PV-substance within the region they bound.

For this domain it can be quite useful to use the second form of the integral in equation

(39.44). For this purpose we write

$$\int_{\mathcal{S}_B} (b - b_A) \boldsymbol{\omega} \cdot \hat{\mathbf{n}} d\mathcal{S} = \int_{\mathcal{S}_B + \mathcal{S}_A} (b - b_A) \boldsymbol{\omega} \cdot \hat{\mathbf{n}} d\mathcal{S} \quad (39.52a)$$

$$= - \int_{\mathcal{S}_B + \mathcal{S}_A} (\nabla b \times \mathbf{v}) \cdot \hat{\mathbf{n}} d\mathcal{S} \quad (39.52b)$$

$$= - \int_{\mathcal{S}_B} (\nabla b \times \mathbf{v}) \cdot \hat{\mathbf{n}} d\mathcal{S}. \quad (39.52c)$$

Equation (39.52a) follows from

$$\int_{\mathcal{S}_A} (b - b_A) \boldsymbol{\omega} \cdot \hat{\mathbf{n}} d\mathcal{S} = 0 \quad \text{since } b = b_A \text{ on } \mathcal{S}_A. \quad (39.53)$$

Equation (39.52b) follows from the divergence theorem

$$\int_{\mathcal{S}_B + \mathcal{S}_A} \nabla \times [(b - b_A) \mathbf{v}] \cdot \hat{\mathbf{n}} d\mathcal{S} = \int_{\mathcal{R}_{AB}} \nabla \cdot (\nabla \times [(b - b_A) \mathbf{v}]) dV = 0. \quad (39.54)$$

And equation (39.52c) holds since $\hat{\mathbf{n}} \times \nabla b = 0$. The expression (39.52c) is particularly convenient for the case of a no-slip boundary condition (Section 22.10.3), whereby the velocity vanishes along \mathcal{S}_B so that we are left with the rather tidy expression

$$\mathcal{I} = 2 \int_{\mathcal{S}_B} (b - b_A) \boldsymbol{\Omega} \cdot \hat{\mathbf{n}} d\mathcal{S} \quad \text{no-slip condition on } \mathcal{S}_B. \quad (39.55)$$

39.4.5 A layer outcropping at the ocean surface

Figure 39.5 depicts a buoyancy layer that outcrops at the ocean surface at both of its ends. Following the derivation in Section 39.4.4 leads to the integrated PV-substance

$$\mathcal{I}_A \equiv \int_{\mathcal{S}_1 + \mathcal{S}_2 + \mathcal{S}_3 + \mathcal{S}_A} b \boldsymbol{\omega}_a \cdot \hat{\mathbf{n}} d\mathcal{S} = \int_{\mathcal{S}_1 + \mathcal{S}_2 + \mathcal{S}_3} (b - b_A) \boldsymbol{\omega}_a \cdot \hat{\mathbf{n}} d\mathcal{S} \quad (39.56a)$$

$$\mathcal{I}_B \equiv \int_{\mathcal{S}_2 + \mathcal{S}_B} b \boldsymbol{\omega}_a \cdot \hat{\mathbf{n}} d\mathcal{S} = \int_{\mathcal{S}_2} (b - b_B) \boldsymbol{\omega}_a \cdot \hat{\mathbf{n}} d\mathcal{S}, \quad (39.56b)$$

with the difference leading to the integrated potential vorticity within the layer \mathcal{R}_{AB}

$$\mathcal{I}_{AB} \equiv \mathcal{I}_A - \mathcal{I}_B = \int_{\mathcal{R}_{AB}} \rho Q dV = \int_{\mathcal{S}_1 + \mathcal{S}_3} (b - b_A) \boldsymbol{\omega}_a \cdot \hat{\mathbf{n}} d\mathcal{S} + (b_B - b_A) \int_{\mathcal{S}_2} \boldsymbol{\omega}_a \cdot \hat{\mathbf{n}} d\mathcal{S}. \quad (39.57)$$

The relation (39.57) requires information about the absolute vorticity over the region \mathcal{S}_2 that lies outside the outcrop regions. To instead only make use of information over the outcrop areas, \mathcal{S}_1 and \mathcal{S}_3 , we consider buoyancy gradients when considering the contributions from the relative vorticity

$$\begin{aligned} & \int_{\mathcal{S}_1 + \mathcal{S}_2 + \mathcal{S}_3 + \mathcal{S}_A} b \boldsymbol{\omega} \cdot \hat{\mathbf{n}} d\mathcal{S} - \int_{\mathcal{S}_2 + \mathcal{S}_B} b \boldsymbol{\omega} \cdot \hat{\mathbf{n}} d\mathcal{S} \\ &= - \int_{\mathcal{S}_1 + \mathcal{S}_2 + \mathcal{S}_3 + \mathcal{S}_A} (\nabla b \times \mathbf{v}) \cdot \hat{\mathbf{n}} d\mathcal{S} + \int_{\mathcal{S}_2 + \mathcal{S}_B} (\nabla b \times \mathbf{v}) \cdot \hat{\mathbf{n}} d\mathcal{S}. \end{aligned} \quad (39.58)$$

We can drop the integrals along \mathcal{S}_A and \mathcal{S}_B since their respective normals are parallel to ∇b , in

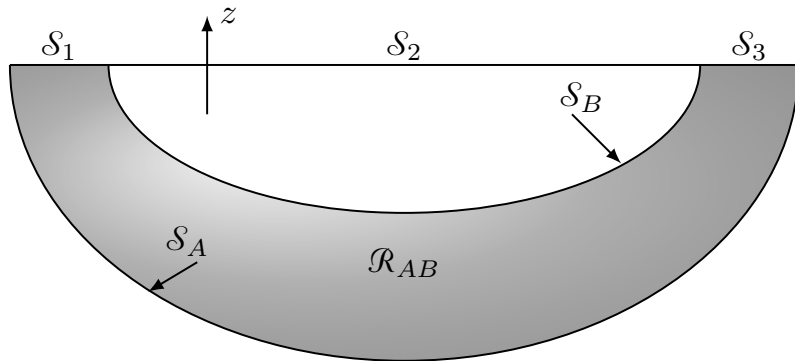


FIGURE 39.5: This figure depicts a buoyancy layer in the ocean that outcrops at both ends of the layer. The boundaries for the layer are given by the following surfaces. Surfaces \mathcal{S}_A and \mathcal{S}_B are defined by buoyancy isosurfaces with $b_A < b_B$. The sea surface is decomposed into three regions, \mathcal{S}_1 , \mathcal{S}_2 , and \mathcal{S}_3 according to the outcrop locations of \mathcal{S}_A and \mathcal{S}_B .

which case

$$\int_{\mathcal{S}_1+\mathcal{S}_2+\mathcal{S}_3+\mathcal{S}_A} b \boldsymbol{\omega} \cdot \hat{\mathbf{n}} d\mathcal{S} - \int_{\mathcal{S}_2+\mathcal{S}_B} b \boldsymbol{\omega} \cdot \hat{\mathbf{n}} d\mathcal{S} = - \int_{\mathcal{S}_1+\mathcal{S}_3} (\nabla b \times \mathbf{v}) \cdot \hat{\mathbf{n}} d\mathcal{S}. \quad (39.59)$$

We are thus led to write the layer integrated PV-substance in the form

$$\mathcal{I}_{AB} = - \int_{\mathcal{S}_1+\mathcal{S}_3} (\nabla b \times \mathbf{v}) \cdot \hat{\mathbf{n}} d\mathcal{S} + \int_{\mathcal{S}_1+\mathcal{S}_3} (b - b_A) 2 \boldsymbol{\Omega} \cdot \hat{\mathbf{n}} d\mathcal{S} + (b_B - b_A) \int_{\mathcal{S}_2} 2 \boldsymbol{\Omega} \cdot \hat{\mathbf{n}} d\mathcal{S}. \quad (39.60)$$

As desired, this alternative formulation only requires information about the flow field and buoyancy field over the outcrop surfaces, \mathcal{S}_1 and \mathcal{S}_3 . For the region between the outcrops, we only need to know its area and outward normal, with $\hat{\mathbf{n}} \approx \hat{\mathbf{z}}$ an accurate approximation.

39.4.6 Further study

Section 4.8 of [Vallis \(2017\)](#) discusses the integrated PV-substance in terms of the vorticity formulation, whereas [Morel et al. \(2019\)](#) introduced the dual perspective based on the buoyancy gradient formulation. [Morel et al. \(2019\)](#) also provide details for the practical diagnosis of potential vorticity in a numerical ocean model or from observational based measurements.

39.5 Boundary fluxes of PV-substance

In Section 39.4 we developed kinematic expressions for the PV-substance integrated over a selection of volumes. That discussion illustrated how the volume integrated potential vorticity has contributions only from boundaries; e.g., where an atmospheric region intersects the ground or ocean, and where an oceanic region intersects the ground or the atmosphere. In this section we further our understanding of budgets for PV-substance by examining a buoyancy layer within the ocean that intersects the bottom on one side and the atmosphere on the other (Figure 39.6). We garner further understanding of the physical processes affecting changes to the PV-substance by here unpacking the boundary fluxes.

A buoyancy layer generally moves as it expands and contracts due to both reversible and irreversible processes (waves, currents, mixing). The impermeability theorem means that the total potential vorticity substance for the layer changes only through exchanges at the boundaries,

including the bottom (boundary between the solid earth and the fluid) and air-sea boundaries. Removing interior interfaces from the layer PV-substance budget simplifies the budget analysis, as already revealed in Section 39.4. As per the discussion of Section 39.3, the results in this section apply even when there is no materially invariant potential vorticity. All we require is an Eulerian flux-form budget along with the impermeability theorem, which holds for potential vorticity defined according to an arbitrary smooth scalar field (Section 39.2.2).

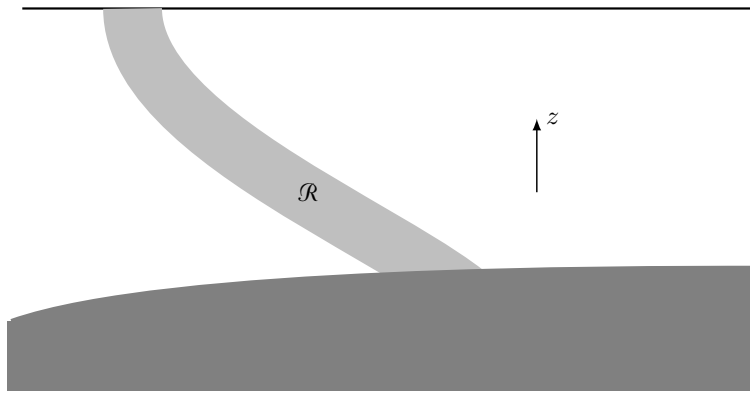


FIGURE 39.6: A buoyancy layer of seawater denoted by \mathcal{R} , with the layer intersecting bottom topography on one side and the atmosphere on the other. The interior boundaries of the layer are formed by constant buoyancy surfaces.

39.5.1 Layer integrated budget

In addition to waves, currents, mixing, and sources affecting the layer interfaces, there is movement of the intersection of the layer with the side boundaries, thus changing the vertical and horizontal extents of these intersections. As a formulation framework, we derive the layer potential vorticity budget making use of the Leibniz-Reynolds transport theorem derived in Section 17.3.4. Just as for the layer integrated tracer budget considered in Section 17.6, applying Leibniz-Reynolds to the layer integrated potential vorticity budget renders

$$\frac{d}{dt} \left[\int_{\mathcal{R}} \rho Q dV \right] = \int_{\mathcal{R}} \frac{\partial(\rho Q)}{\partial t} dV + \oint_{\partial\mathcal{R}} \rho Q \dot{\mathbf{x}} \cdot \hat{\mathbf{n}} d\mathcal{S}, \quad (39.61)$$

where \mathcal{R} is the domain defined by the layer (Figure 39.6), $\partial\mathcal{R}$ is its boundary, and

$$\dot{\mathbf{x}} = \frac{d\mathbf{x}}{dt} \quad (39.62)$$

is the velocity for a point on the boundary. Making use of the PV equation,

$$\partial(\rho Q)/\partial t = -\nabla \cdot \mathbf{J}_Q, \quad (39.63)$$

and the divergence theorem renders

$$\frac{d}{dt} \left[\int_{\mathcal{R}} \rho Q dV \right] = \oint_{\partial\mathcal{R}} (-\mathbf{J}_Q + \rho Q \dot{\mathbf{x}}) \cdot \hat{\mathbf{n}} d\mathcal{S}. \quad (39.64)$$

This result holds around the full domain boundary. Now we decompose that boundary into portions defined by layer interfaces and those along the air-sea and land-sea boundaries.

39.5.2 Impermeability across interior layer interfaces

Rather than invoking the impermeability theorem derived in Section 39.2, we rederive it within the present context to further our confidence in its use. We thus consider the following for interior layer interfaces, here making use of the Haynes-McIntyre form (39.1) of the PV flux vector

$$[-\mathbf{J}_Q + \rho Q \dot{\mathbf{x}}] \cdot \hat{\mathbf{n}} = \left[\rho Q (\dot{\mathbf{x}} - \mathbf{v}) + \dot{b} \boldsymbol{\omega}_a - \nabla b \times \mathbf{F} \right] \cdot \hat{\mathbf{n}} \quad (39.65a)$$

$$= \left[(\boldsymbol{\omega}_a \cdot \nabla b) (\dot{\mathbf{x}} - \mathbf{v}) + \dot{b} \boldsymbol{\omega}_a \right] \cdot \hat{\mathbf{n}} \quad (39.65b)$$

$$= [(\boldsymbol{\omega}_a \cdot \nabla b) (\dot{\mathbf{x}} - \mathbf{v}) + (\partial b / \partial t + \mathbf{v} \cdot \nabla b) \boldsymbol{\omega}_a] \cdot \hat{\mathbf{n}} \quad (39.65c)$$

$$= [(\boldsymbol{\omega}_a \cdot \nabla b) \dot{\mathbf{x}} + (\partial b / \partial t) \boldsymbol{\omega}_a] \cdot \hat{\mathbf{n}}, \quad (39.65d)$$

where

$$\hat{\mathbf{n}} = \nabla b / |\nabla b| \quad (39.66)$$

is the outward unit normal vector pointing to regions of higher buoyancy. Now recall that the velocity of a point fixed on an layer interface has a normal component that satisfies equation (39.10) (here applied to buoyancy surfaces)

$$\dot{\mathbf{x}} \cdot \hat{\mathbf{n}} = -(\partial b / \partial t) / |\nabla b|. \quad (39.67)$$

This result then leads to the impermeability statement for isopycnal interfaces in the fluid interior

$$(-\mathbf{J}_Q + \rho Q \dot{\mathbf{x}}) \cdot \hat{\mathbf{n}} = 0. \quad (39.68)$$

We thus conclude that changes to the layer integrated potential vorticity occur only via transfer across the land-sea boundary and the air-sea boundary

$$\frac{d}{dt} \left[\int_{\mathcal{R}} \rho Q dV \right] = \int_{\text{land-sea}} [-\mathbf{J}_Q + \rho Q \dot{\mathbf{x}}] \cdot \hat{\mathbf{n}} d\mathcal{S} + \int_{\text{air-sea}} [-\mathbf{J}_Q + \rho Q \dot{\mathbf{x}}] \cdot \hat{\mathbf{n}} d\mathcal{S}. \quad (39.69)$$

We now separately consider these two boundaries.

39.5.3 PV flux at a land-sea boundary

We here evaluate the potential vorticity flux from equation (39.6a) at a land-sea boundary

$$-\mathbf{J}_Q + \rho Q \dot{\mathbf{x}} = \rho Q (\dot{\mathbf{x}} - \mathbf{v}) + \dot{b} \boldsymbol{\omega}_a - \nabla b \times \mathbf{F}. \quad (39.70)$$

At a solid and static boundary, the no-normal flow boundary condition (Section 16.4.1) means that $\hat{\mathbf{n}} \cdot \mathbf{v} = 0$. Likewise, the velocity of a point along the boundary moves along the tangent to the boundary so that $\dot{\mathbf{x}} \cdot \hat{\mathbf{n}} = 0$. Hence, the bottom boundary condition is solely comprised of irreversible processes

$$(-\mathbf{J}_Q + \rho Q \dot{\mathbf{x}}) \cdot \hat{\mathbf{n}} = (\dot{b} \boldsymbol{\omega}_a - \nabla b \times \mathbf{F}) \cdot \hat{\mathbf{n}}. \quad (39.71)$$

If this boundary flux is positive, then it acts to increase the integrated PV-substance of the region, and conversely if the boundary flux is negative.

In many parts of the ocean bottom, geothermal heating is negligible so that there is no

buoyancy input at the bottom, thus leaving just the contribution from friction

$$\text{no geothermal heating} \implies (-\mathbf{J}_Q + \rho Q \dot{\mathbf{x}}) \cdot \hat{\mathbf{n}} = -(\nabla b \times \mathbf{F}) \cdot \hat{\mathbf{n}} = (\nabla b \times \hat{\mathbf{n}}) \cdot \mathbf{F}. \quad (39.72)$$

Furthermore, in the absence of geothermal heating the buoyancy satisfies a no-flux boundary condition, which can be ensured by having the buoyancy satisfying

$$\text{no geothermal heating} \implies \hat{\mathbf{n}} \cdot \nabla b = 0. \quad (39.73)$$

Buoyancy isolines thus intersect the bottom parallel to the bottom outward normal, as shown in Figure 39.7.⁴ Correspondingly, $(\nabla b \times \hat{\mathbf{n}}) \cdot \mathbf{F}$ projects onto that component of the friction vector pointing parallel to the bottom. Assuming buoyancy increases upward along the sloping bottom, as per a stably stratified fluid, then $\nabla b \times \hat{\mathbf{n}}$ points counter-clockwise around bowls and clockwise around bumps (see Figure 39.7).

Within the bottom boundary layer, quadratic bottom drag is a common parameterization of the acceleration associated with turbulent frictional processes

$$\mathbf{F} = -C_d |\mathbf{u}| \mathbf{u}, \quad (39.74)$$

where C_d is a non-dimensional drag coefficient and \mathbf{u} is the horizontal velocity. In this case the boundary condition for potential vorticity takes the form

$$(-\mathbf{J}_Q + \rho Q \dot{\mathbf{x}}) \cdot \hat{\mathbf{n}} = (\nabla b \times \hat{\mathbf{n}}) \cdot \mathbf{F} = -C_d |\mathbf{u}| (\nabla b \times \hat{\mathbf{n}}) \cdot \mathbf{u}. \quad (39.75)$$

We see that the sign of the bottom boundary potential vorticity flux depends on the relative orientation of the bottom flow and the vector $\nabla b \times \hat{\mathbf{n}}$. To help understand the sign, consider an abyssal bowl with buoyancy increasing upward along the sloping bottom, in which case $\nabla b \times \hat{\mathbf{n}}$ points counter-clockwise around the bowl. A bottom boundary flow that is also oriented counter-clockwise carries a positive curvature relative vorticity (Section 34.7). This positive relative vorticity is damped by the bottom friction, which corresponds to the negative potential vorticity source as per equation (39.75). Conversely, a bottom boundary flow that is oriented clockwise around the abyssal bowl carries a negative curvature relative vorticity. This negative relative vorticity is damped by the bottom friction, which corresponds to the positive potential vorticity source as per equation (39.75).

Consider a component to the bottom flow that is parallel to ∇b . This flow provides a zero potential vorticity source since $\nabla b \times \mathbf{F} = 0$ (again, assuming $\mathbf{F} = -C_d |\mathbf{u}| \mathbf{u}$). This result is expected from the discussion in Section 38.4 and Figure 38.4, where we note that friction changes PV by rotating buoyancy surfaces, with that rotation realized only when friction is not aligned with ∇b .

39.5.4 PV flux at the air-sea boundary

For the permeable air-sea boundary, we make use of the kinematic boundary condition derived in Section 16.4.3, where the boundary condition (16.63) leads to

$$\rho \hat{\mathbf{n}} \cdot (\dot{\mathbf{x}} - \mathbf{v}) = \mathcal{Q}_m \quad \text{air-sea boundary}, \quad (39.76)$$

⁴There is ongoing research aimed at determining the thickness of the region over which the boundary condition (39.73) is accurate. The boundary condition presumably holds within a molecular sublayer. But the question is whether larger scale motions near the ocean bottom allow for this condition to hold over a thicker region. See the review chapter by [Polzin and McDougall \(2021\)](#) for discussion.

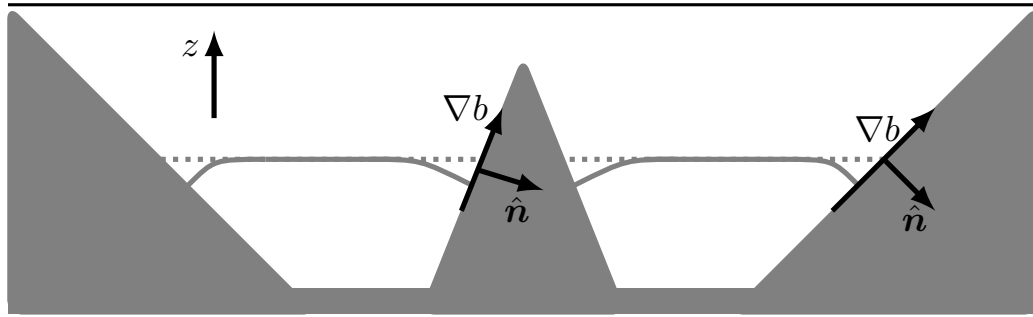


FIGURE 39.7: Depicting a buoyancy isosurface that intersects the bottom. As discussed in Section 17.6 and depicted in Figure 17.5, in the absence of geothermal heating, a buoyancy isosurface satisfies the no-normal flux bottom boundary condition, $\hat{\mathbf{n}} \cdot \nabla b = 0$. This boundary condition requires buoyancy isosurfaces to be orthogonal to the bottom. Assuming buoyancy increases upward along the sloping bottom, then $\nabla b \times \hat{\mathbf{n}}$ points counterclockwise around bowls and clockwise around bumps (when viewed from above). This structure for the buoyancy surfaces affects how friction impacts on the layer-integrated potential vorticity budget, with details provided in Section 39.5.3.

with \mathcal{Q}_m the mass per time per surface area of matter that crosses the air-sea boundary. We are thus led to the air-sea boundary condition

$$(-\mathbf{J}_Q + \rho Q \dot{\mathbf{x}}) \cdot \hat{\mathbf{n}} = Q \mathcal{Q}_m + (\dot{b} \boldsymbol{\omega}_a - \nabla b \times \mathbf{F}) \cdot \hat{\mathbf{n}}. \quad (39.77)$$

Besides the irreversible processes, potential vorticity is affected at the air-sea interface by the transfer of matter across the boundary via the term $Q \mathcal{Q}_m$. We can think of this term as an advection of potential vorticity across the boundary via the boundary mass transport. More generally, we can think of the full boundary flux (39.77) as acting to stretch/compress the fluid column so to alter vorticity and hence the potential vorticity.

To help interpret the friction term appearing in the flux (39.77), write

$$(\dot{b} \boldsymbol{\omega}_a - \nabla b \times \mathbf{F}) \cdot \hat{\mathbf{n}} = (\boldsymbol{\omega}_a \cdot \hat{\mathbf{n}}) (\partial_t b + \mathbf{v} \cdot \nabla b) + (\hat{\mathbf{n}} \times \mathbf{F}) \cdot \nabla b \quad (39.78a)$$

$$= (\boldsymbol{\omega}_a \cdot \hat{\mathbf{n}}) [\partial_t b + (\mathbf{v} - \mathbf{v}_E) \cdot \nabla b], \quad (39.78b)$$

where we introduced the *generalized Ekman velocity*

$$\mathbf{v}_E \equiv \frac{\mathbf{F} \times \hat{\mathbf{n}}}{\boldsymbol{\omega}_a \cdot \hat{\mathbf{n}}}, \quad (39.79)$$

thus bringing the air-sea boundary potential vorticity flux (39.77) to the form

$$(-\mathbf{J}_Q + \rho Q \dot{\mathbf{x}}) \cdot \hat{\mathbf{n}} = Q \mathcal{Q}_m + (\boldsymbol{\omega}_a \cdot \hat{\mathbf{n}}) [\partial_t b + (\mathbf{v} - \mathbf{v}_E) \cdot \nabla b]. \quad (39.80)$$

Note that for the special case of a vertical outward normal, $\hat{\mathbf{n}} = \hat{z}$, and weak relative vorticity, $f + \zeta \approx f$, we have

$$\mathbf{v}_E \approx f^{-1} \mathbf{F} \times \hat{z}, \quad (39.81)$$

which is the Ekman velocity given by equation (30.4). We thus see that the sign of the $(\boldsymbol{\omega}_a \cdot \hat{\mathbf{n}})$ portion of the potential vorticity flux is determined by whether the surface buoyancy is increasing or decreasing in time following the velocity difference, $\mathbf{v} - \mathbf{v}_E$, along the air-sea boundary. We can interpret $\mathbf{v} - \mathbf{v}_E$ as the inviscid portion of the velocity since it removes that portion arising from

friction.⁵

39.5.5 Thought experiments

The surface potential vorticity flux (39.77), or its rewritten form in equation (39.80), provide an explicit expression for how surface boundary fluxes affect the potential vorticity budget within a buoyancy layer outcropping at the ocean surface. It contains a wealth of physics that can be explored via thought experiments.

PV generation in a fluid with zero initial baroclinicity

Consider a fluid region initially with zero baroclinicity and zero flow so that the initial potential vorticity is given by $f N^2$, with N^2 the squared buoyancy frequency. The surface potential vorticity flux (39.77) creates potential vorticity via the mass flux term and through heating/cooling. If this term alone affected the PV, and it did so uniformly in space, then it would alter potential vorticity only via changes in the vertical stratification. More generally, both the mass term and the diabatic term create horizontal buoyancy gradients, which then generate currents and vorticity that generate further contributions to the PV flux.

PV generation in a fluid that is initially homogeneous

Consider an initially homogenous box of seawater with zero PV. In this case it is only the buoyancy term, $\dot{b} f$, that contributes to initial changes in PV. Northern hemisphere ($f > 0$) surface cooling ($\dot{b} < 0$) adds negative potential vorticity to the box. Cooling also initiates gravitational instability that mixes the water and in turn spreads the negative potential vorticity boundary source throughout the fluid. Cooling adds structure to the buoyancy field by inflating the formerly zero thickness buoyancy layers, with layer inflation originating from the boundary. Once inflated, the impermeability theorem dictates that the layer integrated PV-substance changes only via boundary interactions, whereas stirring and mixing transport potential vorticity into the fluid interior. Notably, a region with $f Q < 0$ is locally unstable to symmetric instability, with the generated symmetric instability acting to locally bring the flow towards a state with zero potential vorticity. However, the constraints from impermeability mean that the net PV-substance remains unchanged within a buoyancy layer, even in the presence of mixing.

39.5.6 Is there a preferred form of the PV-substance flux?

Analysis in this section made use of the Haynes-McIntyre form of the PV-substance flux (equation (39.1))

$$\mathbf{J}_Q = \rho \mathbf{v} Q - \dot{b} \boldsymbol{\omega}_a + \nabla b \times \mathbf{F}. \quad (39.82)$$

We could have instead chosen to work with the Marshall form (equation (39.32))

$$\mathbf{J}_Q^{\text{marshall}} = - \left[\frac{\partial \mathbf{v}}{\partial t} + \nabla(m + p/\rho) \right] \times \nabla b - \boldsymbol{\omega}_a \frac{\partial b}{\partial t}, \quad (39.83)$$

or the modified kinematic form (equation (39.18))

$$\tilde{\mathbf{J}}_Q^{\text{kin}} = - \frac{\partial \mathbf{v}_a}{\partial t} \times \nabla b - \boldsymbol{\omega}_a \frac{\partial b}{\partial t}. \quad (39.84)$$

⁵The velocity difference, $\mathbf{v} - \mathbf{v}_E$, is not equal to the inviscid velocity that would appear in an inviscid (perfect) fluid. Rather, $\mathbf{v} = \mathbf{v}_E + (\mathbf{v} - \mathbf{v}_E)$ is an interpretational decomposition akin to that studied in Chapter 30 for Ekman mechanics. See the comment after equation (30.4) for more on this point.

These fluxes differ by a gauge choice and yet they each satisfy the impermeability theorem. Subjective choices determine which one is preferred. Importantly, once chosen, we can use only a single form of the flux throughout the budget analysis in order to remain self-consistent with the form of the total curl that is removed by the divergence operator.

The PV-substance budget, though invariant to the choice of flux, has distinct physical pictures depending on the choice of the flux. As a particularly clear example consider a steady state budget in which the fluxes take the form

$$\mathbf{J}_Q = \rho \mathbf{v} Q - (\mathbf{v} \cdot \nabla b) \boldsymbol{\omega}_a + \nabla b \times \mathbf{F} \quad (39.85)$$

$$\mathbf{J}_Q^{\text{marshall}} = -\nabla(m + p/\rho) \times \nabla b \quad (39.86)$$

$$\tilde{\mathbf{J}}_Q^{\text{kin}} = 0. \quad (39.87)$$

The physical picture for $\tilde{\mathbf{J}}_Q^{\text{kin}}$ is rather trivial, whereby the PV-substance stays constant within buoyancy layers and there are zero PV-substance fluxes across *all* boundaries of the layer. In contrast, a steady state budget when working with \mathbf{J}_Q or $\mathbf{J}_Q^{\text{marshall}}$ afford a physical picture of PV-substance entering, leaving, and transported through the buoyancy layers. [Marshall et al. \(2001\)](#) developed a rather elegant analysis framework using $\mathbf{J}_Q^{\text{marshall}}$ for steady budgets, and we explore facets of that approach in Section 38.5 for the special case of a Boussinesq hydrostatic fluid.

Nevertheless, our use of the Haynes-McIntyre PV-substance flux in the present section is motivated by its utility for describing how boundary forcing can change the sign of the PV. Such forcing exposes the flow to a variety of local instabilities (e.g., symmetric, centrifugal, gravitational). [Thomas et al. \(2008\)](#) offer a pedagogical review for the ocean; [Thomas et al. \(2013\)](#) provides a thorough study of the upper reaches of the Gulf Stream; and [Naveira Garabato et al. \(2019\)](#) provide evidence for such boundary forcing in regions of strong abyssal flows. Each of these studies points to the need to further understand details of the boundary PV flux and to furthermore ensure it is properly formulated within numerical models (e.g., [Hallberg and Rhines \(1996\)](#)).

39.5.7 Further study

The study of boundary potential vorticity fluxes is incredibly rich and generally requires careful analysis of the multitude of processes active in the boundary layer. The interested reader can find ocean examples of these analyses in [Benthuyzen and Thomas \(2012\)](#) and [Wenegrat et al. \(2018\)](#), and the references therein.



Part VIII

Mechanics of nearly geostrophic flows

Fluid motion dominated by rotation is characterized by a small Rossby number. To zeroth order in an asymptotic expansion in Rossby number, the flow maintains geostrophic balance, which is a balance between the Coriolis acceleration and pressure gradient acceleration. As seen in Chapter 28, the geostrophic balance is diagnostic so that it offers no means to compute the time evolution of the fluid. To obtain a prognostic equation requires going to next order in Rossby number within the asymptotic expansion. The resulting prognostic equation makes use of ageostrophic motions, though only as an intermediate step towards an evolution equation involving just zeroth order geostrophically balanced fields.

The nuts and bolts of this part of the book involve methods of scaling analysis and asymptotic analysis via perturbation series. In Chapter 40, we use these tools to derive equations for planetary geostrophy (PG) and quasi-geostrophy (QG) within the shallow water system, and then PG and QG for continuously stratified flows in Chapters 41 and 42 . PG and QG are useful theoretical models lending insights into ocean and atmosphere fluid mechanics. In particular, PG is commonly used to study features of the large-scale laminar ocean circulation, and QG is ubiquitous in studies of both oceanic and atmospheric flows at or near the deformation radius.

One central property of balanced flow is that knowledge of the relevant balanced version of potential vorticity is sufficient to determine the flow field. A way to appreciate this property is to consider a horizontally non-divergent flow, in which the Laplacian of the streamfunction gives the relative vorticity, $\zeta = \nabla^2\psi$. Turning this equation around, we see that knowledge of the vorticity field, through inversion of the Laplace equation (with suitable boundary conditions), yields the streamfunction and hence the velocity. In our discussion of quasi-geostrophy in Chapter 42, we extend this result to three-dimensional quasi-geostrophic flow, where the prognostic fields are the horizontal components to the geostrophic flow, plus the buoyancy field. Such methods of *potential vorticity inversion* are routinely used to study atmospheric flows given maps of potential vorticity.

Chapter 40

SHALLOW WATER PLANETARY AND QUASI-GEOSTROPHY

In this chapter we develop the mechanical equations for planetary geostrophy (PG) and quasi-geostrophy (QG) within the shallow water fluid. The derivations require elements from dimensional analysis and asymptotic methods. Salient details are introduced and the many mathematical steps exposed.

READER'S GUIDE FOR THIS CHAPTER

This chapter is largely technical in nature, aiming to provide the necessary tools from dimensional analysis, scale analysis, and asymptotic methods to derive approximate geostrophic equations. We assume an understanding of the equations for a single layer of shallow water fluid as derived in Chapter 32. We follow this work with further studies of the continuously stratified systems in Chapters 41 and 42.

40.1	Loose threads	1024
40.2	Scaling analysis and the Buckingham-II theorem	1024
40.3	Shallow water equations	1024
40.3.1	Dimensional scales	1025
40.3.2	Physical dimensions	1026
40.3.3	Number of non-dimensional parameters	1026
40.3.4	Choosing the non-dimensional parameters	1026
40.3.5	Assumed values for the non-dimensional parameters	1028
40.3.6	Deformation radius and the free surface undulation scale	1029
40.3.7	Non-dimensional shallow water equations	1030
40.4	Shallow water planetary geostrophy	1031
40.5	Shallow water quasi-geostrophy	1032
40.5.1	Quasi-geostrophic scaling	1032
40.5.2	Outlining the asymptotic method	1033
40.5.3	Order Ro^0 asymptotic equations	1035
40.5.4	Order Ro^1 asymptotic equations	1035
40.6	Physical elements of the theory	1037
40.6.1	Dimensional potential vorticity and streamfunction	1037
40.6.2	Contributions to the QG potential vorticity	1038
40.6.3	Connecting to rest state potential vorticity	1039
40.6.4	Summarizing the equations of quasi-geostrophy	1039
40.6.5	Connecting quasi-geostrophic PV to shallow water PV	1040
40.6.6	Considering topography to be $\mathcal{O}(\text{Ro}^0)$	1041
40.6.7	Two layer quasi-geostrophy	1042
40.7	Exercises	1043

40.1 Loose threads

- External and internal modes for QG two layers in Section 40.6.7.

40.2 Scaling analysis and the Buckingham-II theorem

Scale analysis is ubiquitous in physics, with the Buckingham-II theorem providing a useful framework. The theorem states that the number of dimensionless parameters in a physical system is a function of the number of dimensional parameters or scales K (e.g., scales for the velocity, rotation rate, pressure force, friction force, gravitational acceleration) and the number of physical dimensions R (e.g., time, length, mass). Precisely, Buckingham-II states that the number of dimensionless parameters is

$$N_{\text{dimensionless}} = K - R. \quad (40.1)$$

Different physical systems possessing the same suite of dimensionless parameters are isomorphic. For example, a laboratory study of flow around a cylinder contains two dimensionless parameters: the drag coefficient, C_d , and the Reynolds number, Re . If the problem is scaled up to a building with the same shape, then so long as the values for the dimensionless parameters are the same (e.g., same drag coefficient and same Reynolds number), one can make use of the laboratory analog for determining suitability of the building architecture. Similar isomorphisms exist between flows in a rotating tank and flows in the ocean and atmosphere.

The Buckingham-II theorem does not provide the form of the dimensionless parameters. Nor does the theorem determine their values. This information comes only after introducing physical prejudices surrounding a regime of chosen interest. Additionally, Buckingham-II does not offer information about how the dimensionless parameters might be related. Instead, any such relations arise from the mechanical and thermodynamical equations describing the system. Consequently, mechanical and thermodynamical equations generally mean that fewer than $N_{\text{dimensionless}}$ non-dimensional numbers are independent.

We focus in this chapter on the regime of large-scale atmospheric and oceanic flow where the shallow water fluid is close to geostrophic balance. That choice then guides the length and time scales, which in turn determines the size of the dimensionless parameters. In many cases, one is able to identify dimensionless parameters that are large or small in particular regimes, which in turn suggests asymptotic analyses to render equations specific to the regime of interest.

40.3 Shallow water equations

A single-layer of inviscid shallow water fluid of thickness h is governed by the velocity and thickness equations (Chapter 32)

$$\frac{\partial \mathbf{u}}{\partial t} + (\mathbf{u} \cdot \nabla) \mathbf{u} + \mathbf{f} \times \mathbf{u} = -g \nabla \eta \quad (40.2a)$$

$$\frac{\partial h}{\partial t} + \nabla \cdot (h \mathbf{u}) = 0, \quad (40.2b)$$

where \mathbf{u} is the horizontal velocity that is independent of depth within the layer. The geometry of the layer is specified by the free surface height, $z = \eta(x, y, t)$, and bottom topography, $z = \eta_b(x, y)$ (see Figure 32.1). They are related according to

$$\eta = \eta_b + h = H + \bar{\eta}_b + \eta' = \bar{h} + \bar{\eta}_b + \eta', \quad (40.3)$$

where $H = \bar{h}$ is the area average layer thickness, $\bar{\eta}_b$ is the area average of the bottom topography, $\eta' = \eta - \bar{\eta}$ is the deviation of the surface height from its area average $\bar{\eta} = \bar{\eta}_b + H$. We also find occasion to write the layer thickness in the form

$$h = \eta - \eta_b = H + (\bar{\eta}_b - \eta_b) + \eta' = \bar{h} - \eta'_b + \eta' = \bar{h} + h', \quad (40.4)$$

where $\eta'_b = \eta_b - \bar{\eta}_b$ is the deviation of the bottom topography from its area mean, and we introduced the thickness deviation from the area mean

$$h' = h - \bar{h} = \eta' - \eta'_b. \quad (40.5)$$

Dexterity with these geometrical relations is assumed in the following.

40.3.1 Dimensional scales

We identify nine dimensional parameters for the shallow water system.

- LENGTH SCALES

- ★ H = depth scale of the fluid, which we take equal to the area average layer thickness (see Figure 32.1).
- ★ L = horizontal/lateral length scale of motions under consideration. We assume both horizontal directions to have the same length scale. This assumption is not necessarily valid on a rotating planet, where flows in the zonal (east-west) direction can have length scales longer than meridional (north-south) flow scales. Nonetheless, this choice does not preclude the dynamical emergence of anisotropic length scales.
- ★ R = radius of the planet. We include this scale anticipating that for length scales small compared to the earth's radius, the Coriolis parameter may be approximated by a constant (f -plane) or linear function of latitude (β -plane).
- ★ \mathcal{H} = scale for deviations of the free surface height, η , relative to its area average, $\bar{\eta}$, so that $\eta' = \eta - \bar{\eta} \sim \mathcal{H}$.
- ★ \mathcal{B} = scale for deviations of the bottom topography, η_b , relative to its area average, $\bar{\eta}_b$, so that $\eta'_b = \eta_b - \bar{\eta}_b \sim \mathcal{B}$.

- VELOCITY SCALES

- ★ U = velocity scale for horizontal fluid particle motion; i.e., the speed for horizontal currents or winds.
- ★ c = wave speed scale. For the shallow water model, the wave speed scale is given by the shallow water gravity wave (Section 48.5.1)

$$c = \sqrt{g H}. \quad (40.6)$$

We introduce the wave speed anticipating the presence of distinct flow regimes depending on whether the fluid particle speed is larger or smaller than the wave speed. The ratio of the wave speed to particle speed is known as the *Froude number* (Section 40.3.4).

- BODY FORCES: There are two body forces acting on the fluid; one from gravity and one from Coriolis.

- ★ g = gravitational acceleration.
- ★ f = Coriolis frequency.

If we were interested in other forces, such as electromagnetic or frictional forces, then we would have other dimensional parameters corresponding to these forces.

40.3.2 Physical dimensions

There are two physical dimensions in the shallow water system: length, L , and time, T . Notably, there is no mass in the shallow water system. The reason is that the fluid density is assumed uniform within a shallow water layer so that mass is described by area times thickness

$$M = \int \rho dV \quad [\equiv] \quad L^2 H \rho, \quad (40.7)$$

where $[\equiv]$ is read “has dimensions”.

40.3.3 Number of non-dimensional parameters

The Buckingham-II theorem then says there are

$$N_{\text{dimensionless}} = 9 - 2 = 7 \quad (40.8)$$

non-dimensional parameters. What if we incorrectly count the physical dimensions or the dimensional scales/parameters? Fortunately, the process of determining the non-dimensional parameters is largely self-correcting. Namely, in the process of non-dimensionalizing the shallow water equations, the seven non-dimensional parameters arise as part of the analysis. Hence, making use of Buckingham-II is useful but it is not essential. If one left out a physical dimension or a physical parameter, then it would appear somewhere in the subsequent analysis, often not until near the end where something mathematically or physically inconsistent appears. One must always be cognizant of the need to self-correct when performing dimensional analysis.

40.3.4 Choosing the non-dimensional parameters

There is no unique choice for the non-dimensional parameters. Our choice is guided by experience, interest, and what parameters might be available to experimental control or measurement.

1. VERTICAL TO HORIZONTAL/LATERAL ASPECT RATIO: The ratio of the vertical scale to the horizontal/lateral¹ scale defines the aspect ratio

$$\delta_{\text{vertical/horizontal}} = \frac{\text{vertical length scale}}{\text{horizontal length scale}} = \frac{H}{L}. \quad (40.9)$$

2. RATIO OF HORIZONTAL/LATERAL SCALE TO PLANETARY SCALE: The ratio of the horizontal length scale to the planet radius is

$$\delta_{\text{horizontal/planet}} = \frac{\text{horizontal length scale}}{\text{planetary length scale}} = \frac{L}{R}. \quad (40.10)$$

¹The terms “lateral” and “horizontal” are used interchangeably, referring to motion at constant vertical position either on the sphere or on the plane.

3. RATIO OF FREE SURFACE UNDULATION TO VERTICAL LENGTH SCALE: The ratio of the free surface undulation scale to the vertical length scale is

$$\delta_{\text{free surface/depth}} = \frac{\text{free surface undulation scale}}{\text{vertical length scale}} = \frac{\mathcal{H}}{H}. \quad (40.11)$$

4. RATIO OF BOTTOM TOPOGRAPHY UNDULATION TO VERTICAL LENGTH: The ratio of the bottom topography undulation scale to the vertical length scale is

$$\delta_{\text{bottom/depth}} = \frac{\text{bottom topography undulation scale}}{\text{vertical length scale}} = \frac{\mathcal{B}}{H}. \quad (40.12)$$

5. FROUDE NUMBER: The Froude number is the ratio of the fluid particle speed to the wave speed. For the shallow water system, this ratio is

$$\text{Fr} = \frac{U}{c} = \frac{U}{\sqrt{g H}}. \quad (40.13)$$

6. ROSSBY NUMBER: The Rossby number is the ratio of the fluid particle acceleration scale to the Coriolis acceleration

$$\text{Ro} = \frac{\text{particle acceleration}}{\text{Coriolis acceleration}}. \quad (40.14)$$

The particle acceleration scale is determined by the local time tendency plus advection

$$\text{particle acceleration} = \frac{\partial \mathbf{u}}{\partial t} + (\mathbf{u} \cdot \nabla) \mathbf{u} \sim \frac{U}{T} + \frac{U^2}{L}. \quad (40.15)$$

The local time tendency and advection generally have distinct scales, thus leading to the potential for two Rossby numbers

$$\text{Ro}^{\text{local}} = \frac{1}{T f} \quad \text{and} \quad \text{Ro}^{\text{adv}} = \frac{U}{L f}. \quad (40.16)$$

In the following we consider these two Rossby numbers to have the same scale, which is realized by advective contributions to material time evolution being comparable to local time changes. We refer to this choice as an *advection time scale*, whereby

$$T = \frac{L}{U} \implies \frac{U^2}{L} = \frac{U}{T}, \quad (40.17)$$

so that there is only one Rossby number

$$\text{Ro} = \frac{1}{f T} = \frac{U}{f L}. \quad (40.18)$$

Another interpretation for the Rossby number is the ratio of the relative vorticity to the planetary vorticity

$$\text{Ro} = \frac{\text{relative vorticity}}{\text{planetary vorticity}} \quad (40.19)$$

With the relative vorticity scaling as U/L and the planetary vorticity scaling as f , we recover the expression (40.18) for the Rossby number.

7. GEOSTROPHIC NUMBER: We define the geostrophic number as the ratio of the Coriolis

acceleration to the pressure gradient acceleration

$$Ge = \frac{\text{Coriolis acceleration}}{\text{pressure gradient acceleration}}. \quad (40.20)$$

The Coriolis acceleration scales as

$$\text{Coriolis acceleration} \sim f U \quad (40.21)$$

whereas the pressure gradient acceleration, $-g \nabla \eta$, scales as

$$\text{pressure gradient acceleration} \sim \frac{g \mathcal{H}}{L}, \quad (40.22)$$

so that

$$Ge = \frac{\text{Coriolis acceleration}}{\text{pressure gradient acceleration}} = \frac{f U}{(g/L) \mathcal{H}}. \quad (40.23)$$

40.3.5 Assumed values for the non-dimensional parameters

We now enumerate the assumed values for the non-dimensional parameters. These values are based on the chosen physical regime of flow that is of interest for the analysis.

1. SMALL VERTICAL TO HORIZONTAL ASPECT RATIO: The aspect ratio is generally small for large-scale atmospheric and oceanic fluid systems

$$\delta_{\text{vertical/horizontal}} = H/L \ll 1. \quad (40.24)$$

This assumption was made when formulating the shallow water system, which is based on hydrostatic balance (see Section 32.2). We thus retain this assumption as we further scale the shallow water system.

2. SMALL OR ORDER ONE RATIO OF HORIZONTAL/LATERAL TO PLANETARY SCALES: The ratio of the lateral length scale to the planet radius is small for quasi-geostrophic systems and order unity for planetary geostrophy

$$\delta_{\text{horizontal/planet}} = L/R \ll 1 \quad \text{quasi-geostrophy} \quad (40.25a)$$

$$\delta_{\text{horizontal/planet}} = L/R \sim 1 \quad \text{planetary geostrophy}. \quad (40.25b)$$

3. RATIO OF FREE SURFACE UNDULATION TO VERTICAL LENGTH SCALE: The ratio \mathcal{H}/H is implied by assuming a unit geostrophic number below.
4. RATIO OF BOTTOM TOPOGRAPHY UNDULATION TO VERTICAL LENGTH SCALE: For quasi-geostrophy, we assume that undulations in the bottom topography are small relative to the vertical length scale, whereas there is no restriction for planetary geostrophy. “Small” in the present context is determined by the Rossby number, in which case

$$\delta_{\text{bottom/depth}} = \mathcal{B}/H = Ro \quad \text{for quasi-geostrophy}. \quad (40.26)$$

5. FROUDE NUMBER: We find that the Froude number is implied by scales assumed for the other non-dimensional numbers.

6. SMALL ROSSBY NUMBER: The Rossby number is assumed small

$$\text{Ro} = U/(f L) \ll 1, \quad (40.27)$$

which means that the Coriolis acceleration is a leading order term in the horizontal velocity equation (40.2a).

7. UNIT GEOSTROPHIC NUMBER: The geostrophic number is assumed to be order unity

$$\text{Ge} \sim 1. \quad (40.28)$$

This assumption means that the Coriolis acceleration and pressure gradient acceleration scale together

$$f U \sim (g/L) \mathcal{H}. \quad (40.29)$$

Making use of the velocity equation (40.2a), we see that this scaling is consistent only so long as the Rossby number is small, $\text{Ro} \ll 1$. Furthermore, this scaling constrains the scale of the free surface undulation, \mathcal{H} , as we discuss in Section 40.3.6.

40.3.6 Deformation radius and the free surface undulation scale

We determine the scale for the free surface height undulation, \mathcal{H} , by making use of the assumed order unity geostrophy number. For this purpose, start from the geostrophic scaling of Coriolis and pressure gradient accelerations, (40.29), to express the free surface undulation scale according to

$$\eta' \sim \mathcal{H} = \frac{f U L}{g} = \text{Ro} \frac{f^2 L^2}{g} = \text{Ro} H \frac{f^2 L^2}{g H} = \text{Ro} H \left[\frac{L}{L_d} \right]^2. \quad (40.30)$$

In the final equality we introduced the *deformation radius*

$$L_d = \sqrt{g H}/f = c_{\text{grav}}/f, \quad (40.31)$$

where c_{grav} is the gravity wave speed (Section 48.5.1). We previously encountered the deformation radius when discussing geostrophic adjustment in Section 48.9. In Section 40.6.2 we further discuss its role as a regime boundary (between relative vorticity and vortex stretching) for the quasi-geostrophic potential vorticity. The deformation radius decreases toward the poles, so that rotational effects are felt by smaller scales in the high latitudes than in the tropics.

We can use L_d to rewrite the Froude number as the ratio of the advection speed to the rotation speed

$$\text{Fr} = \frac{U}{\sqrt{g H}} = \frac{U}{f L_d} = \text{Ro} \frac{L}{L_d}. \quad (40.32)$$

Furthermore, the squared ratio of the deformation radius to the lateral length scale is termed the *Burger number*

$$\text{Bu} = \left[\frac{L_d}{L} \right]^2. \quad (40.33)$$

Use of the Burger number allows us to write the Froude number in terms of the Rossby number and Burger number

$$\text{Fr} = \frac{\text{Ro}}{\sqrt{\text{Bu}}}. \quad (40.34)$$

Likewise, the free surface height undulation scale can be written

$$\mathcal{H} = H \text{Ro} \left[\frac{L}{L_d} \right]^2 = H \frac{\text{Ro}}{\text{Bu}} = H \frac{\text{Fr}^2}{\text{Ro}}. \quad (40.35)$$

Hence, the ratio of the free surface undulations to the layer thickness (depth) scale is given by

$$\delta_{\text{free surface/depth}} = \frac{\mathcal{H}}{H} = \text{Ro} \left[\frac{L}{L_d} \right]^2 = \frac{\text{Ro}}{\text{Bu}} = \frac{\text{Fr}^2}{\text{Ro}}. \quad (40.36)$$

Again, this scaling is implied by making the dynamical assumption of a unit geostrophic number, which means that the pressure gradient acceleration scales according to the Coriolis acceleration.

40.3.7 Non-dimensional shallow water equations

To non-dimensionalize the shallow water equations we introduce non-dimensional variables for space, time, velocity, and Coriolis parameter as adorned with a widehat²

$$t = T \widehat{t} \quad (x, y) = L (\widehat{x}, \widehat{y}) \quad \partial_t = \partial_{\widehat{t}}/T \quad \nabla = \widehat{\nabla}/L \quad (u, v) = U (\widehat{u}, \widehat{v}) \quad f = f_0 \widehat{f}, \quad (40.37)$$

where f_0 is the Coriolis parameter at the central latitude for the β -plane approximation (Section 21.3.4). We also require non-dimensional variables for the surface and bottom undulations

$$\eta' = \mathcal{H} \widehat{\eta} \quad \eta'_b = \mathcal{B} \widehat{\eta}_b \quad h = H + \eta' - \eta'_b = H + \mathcal{H} \widehat{\eta} - \mathcal{B} \widehat{\eta}_b, \quad (40.38)$$

where we used equation (40.4) for the layer thickness. Importantly, we assume that the non-dimensional variables (the widehat variables) are order unity.

Non-dimensional velocity equation

Introducing the above variables into the shallow water velocity equation (40.2a) renders

$$\frac{U}{T} \frac{\partial \widehat{\mathbf{u}}}{\partial \widehat{t}} + \frac{U^2}{L} (\widehat{\mathbf{u}} \cdot \widehat{\nabla}) \widehat{\mathbf{u}} + f_0 U (\widehat{\mathbf{f}} \times \widehat{\mathbf{u}}) = - \frac{g \mathcal{H}}{L} \widehat{\nabla} \widehat{\eta}. \quad (40.39)$$

As before, we assume the time scale is given by the advection time

$$T = L/U = 1/(\text{Ro} f_0), \quad (40.40)$$

so that dividing by $f_0 U$ leads to

$$\text{Ro} \left[\frac{\partial \widehat{\mathbf{u}}}{\partial \widehat{t}} + (\widehat{\mathbf{u}} \cdot \widehat{\nabla}) \widehat{\mathbf{u}} \right] + (\widehat{\mathbf{f}} \times \widehat{\mathbf{u}}) = - \left[\frac{g H}{f_0 L U} \frac{\text{Ro}}{\text{Bu}} \right] \widehat{\nabla} \widehat{\eta}, \quad (40.41)$$

where we set $\mathcal{H} = H (\text{Ro}/\text{Bu})$ according to equation (40.36). We reduce the factor on the right hand side according to

$$\frac{g H}{f_0 L U} \frac{\text{Ro}}{\text{Bu}} = \frac{g H}{f_0 L U} \frac{U}{f_0 L} \frac{L^2}{L_d^2} = \frac{g H}{f_0 L U} \frac{U}{f_0 L} \frac{L^2 f_0^2}{g H} = 1. \quad (40.42)$$

²The L^AT_EX widehat symbol is used for non-dimensional variables, such as the non-dimensional velocity, $\widehat{\mathbf{u}}$. The widehat is distinguished from the hat used for unit vectors, such as for the vertical unit vector, $\widehat{\mathbf{z}}$. We also use widehats for thickness weighted means in Chapter 60, but that usage is completely distinct from the non-dimensionalization usage in the present chapter.

Hence, the non-dimensional inviscid shallow water velocity equation takes on the rather elegant form

$$\text{Ro} \left[\frac{\partial \hat{\mathbf{u}}}{\partial \hat{t}} + (\hat{\mathbf{u}} \cdot \hat{\nabla}) \hat{\mathbf{u}} \right] + \hat{\mathbf{f}} \times \hat{\mathbf{u}} = -\hat{\nabla} \hat{\eta}. \quad (40.43)$$

Introducing the non-dimensional material time derivative

$$\frac{D}{Dt} = \frac{\partial}{\partial \hat{t}} + \hat{\mathbf{u}} \cdot \hat{\nabla} \quad (40.44)$$

brings the velocity equation to

$$\text{Ro} \frac{D \hat{\mathbf{u}}}{Dt} + \hat{\mathbf{f}} \times \hat{\mathbf{u}} = -\hat{\nabla} \hat{\eta}. \quad (40.45)$$

We see that the velocity equation is consistent with a unit geostrophy number (i.e., Coriolis acceleration balances pressure gradient acceleration) if and only if the Rossby number is small, thus eliminating the material acceleration.

Non-dimensional thickness equation

The thickness equation (40.2b) can be written

$$\frac{\partial \eta'}{\partial t} + \nabla \cdot [(H + \eta' - \eta'_b) \mathbf{u}] = 0, \quad (40.46)$$

which takes on the non-dimensional form

$$\frac{\mathcal{H}}{T} \frac{\partial \hat{\eta}}{\partial \hat{t}} + \frac{U H}{L} \hat{\nabla} \cdot [(1 + \hat{\eta} \mathcal{H}/H - \hat{\eta}_b \mathcal{B}/H) \hat{\mathbf{u}}] = 0. \quad (40.47)$$

The advective time scaling $T = L/U$ brings the thickness equation to

$$\frac{\mathcal{H}}{H} \frac{\partial \hat{\eta}}{\partial \hat{t}} + \hat{\nabla} \cdot [(1 + \hat{\eta} \mathcal{H}/H - \hat{\eta}_b \mathcal{B}/H) \hat{\mathbf{u}}] = 0. \quad (40.48)$$

40.4 Shallow water planetary geostrophy

We make use of the non-dimensional equations derived in Section 40.3.7 to derive the dynamical equations for planetary geostrophy. Our presentation is brief since the derivation is technically trivial. In Chapter 41 we develop the theory of planetary geostrophic flows, with this theory of particular use for understanding the large-scale ocean circulation. We also already studied facets of planetary geostrophy flow for the continuously stratified case in Section 28.5 and for the shallow water in Sections 36.7, 36.9, and 36.8.

Planetary geostrophy is realized by dropping the fluid particle acceleration from the momentum equation (40.45), given that it is one order of Rossby number smaller than the Coriolis and pressure gradient accelerations. This assumption means that the velocity equation reduces to the geostrophic balance

$$\hat{\mathbf{f}} \times \hat{\mathbf{u}} = -\hat{\nabla} \hat{\eta}. \quad (40.49)$$

We furthermore assume that the Rossby number and Burger numbers scale together

$$\text{Ro} \sim \text{Bu} = (L_d/L)^2 \ll 1, \quad (40.50)$$

so that the horizontal length scale for the planetary geostrophic flow is much larger than the

deformation radius

$$L \gg L_d. \quad (40.51)$$

This assumption is consistent with dropping the material acceleration term in the velocity equation. Although the velocity equation is greatly simplified, we make no assumption concerning the thickness equation. Consequently, the free surface and bottom undulations are unconstrained with planetary geostrophic flows, so long as the flow maintains the hydrostatic balance.

In summary, the thickness equation for the planetary geostrophic fluid retains its full unapproximated form, whereas the velocity equation reduces to geostrophy. Reintroducing dimensions leads to the planetary geostrophic equations

$$f \hat{\mathbf{z}} \times \mathbf{u} = -g \nabla \eta \quad \text{and} \quad \frac{Dh}{Dt} = -h \nabla \cdot \mathbf{u} \quad \text{and} \quad h = \eta - \eta_b. \quad (40.52)$$

Since the Coriolis parameter retains its spatial dependence, and so includes the beta effect, the horizontal velocity field is divergent

$$f \nabla \cdot \mathbf{u} = -\beta (g/f) \partial_x \eta = -\beta v. \quad (40.53)$$

As shown in Exercise 40.1, the shallow water planetary geostrophic equations are equivalent to

$$f \hat{\mathbf{z}} \times \mathbf{u} = -g \nabla \eta \quad \text{and} \quad \frac{DQ}{Dt} = 0 \quad \text{with} \quad Q = \frac{f}{h}. \quad (40.54)$$

We encountered this form for the potential vorticity in Section 36.3, in which the shallow water potential vorticity, $(f + \zeta)/h$, is approximated by f/h in the small Rossby number limit.

40.5 Shallow water quasi-geostrophy

In this section we develop the quasi-geostrophic equations for a single shallow water fluid layer. Doing so requires more work than for the planetary geostrophic equations. In particular, we use rudimentary asymptotic methods with the Rossby number the small parameter.

40.5.1 Quasi-geostrophic scaling

Quasi-geostrophic scaling is based on the following assumptions, with the first and second shared with planetary geostrophy whereas the remaining are distinct.

1. SMALL ROSSBY NUMBER: $\text{Ro} \ll 1$, which is fundamental to geostrophic scaling.
2. ADVECTIVE TIME SCALE: $T \sim L/U$; that is, the time scale is determined by advection, which is how time scales throughout this chapter.
3. ORDER ROSSBY NUMBER BETA EFFECT: $|\beta L| \ll |f_0|$, which means that the Coriolis frequency does not vary much from its central value. To incorporate this assumption into the asymptotics, we expand the non-dimensional Coriolis parameter in terms of the Rossby number³

$$\hat{\mathbf{f}} = \mathbf{f}/f_0 = (1 + \beta y/f_0) \hat{\mathbf{z}} \equiv (\hat{f}_0 + \text{Ro} \beta \hat{y}) \hat{\mathbf{z}}. \quad (40.55)$$

³One could conceive of another small parameter that scales the beta effect, but the resulting asymptotics would be more difficult to manage given the need to keep track of two small parameters.

In this equation, $\hat{\mathbf{z}}$ is the unit vector in the vertical, and the time scaling in equation (40.40) renders⁴

$$\hat{\beta} \hat{y} = \beta y / (\text{Ro } f_0) = T \beta y \quad \text{and} \quad \hat{f}_0 = f_0 / f_0 = 1. \quad (40.56)$$

The Coriolis expression (40.55) and the scaling (40.56) are motivated by assuming the horizontal scales of motion are on the same order as the deformation radius, and that the Coriolis frequency does not vary much from its central value. Quasi-geostrophy is thus formulated within the beta plane approximation discussed in Section 21.3.4.

4. BURGER NUMBER ORDER ONE: $Bu \sim 1$, which means that the horizontal scales of motion for the quasi-geostrophic flows are on the order as the deformation radius, $L \sim L_d$.
5. ORDER ROSSBY NUMBER FREE SURFACE UNDULATIONS: From equation (40.36), an order unity Burger number means that undulations of the free surface height scale according to the Rossby number: $\mathcal{H}/H = \text{Ro}$, so that free surface height undulations are small.
6. ORDER ROSSBY NUMBER BOTTOM TOPOGRAPHY UNDULATIONS: As seen in Section 40.6.5, for the quasi-geostrophic potential vorticity to correspond to the small Rossby number version of the shallow water potential vorticity requires the topography undulations to scale as $\mathcal{B}/H = \text{Ro}$. The assumed scaling for the bottom topography undulation pairs with that for the free surface, so that the layer thickness undulations, $h' = \eta' - \eta'_b$, also scale as Ro . We are thus able to take a sensible Ro expansion of the $1/h$ factor appearing in the shallow water potential vorticity (Section 40.6.5). It is useful to maintain a direct connection to the shallow water model as doing so helps to ensure that the resulting asymptotic theory is self-consistent. In particular, it ensures that quasi-geostrophic energetics are physically sensible since there is a direct lineage to the shallow water energetics.

The $\mathcal{B}/H = \text{Ro}$ scaling is consistent with the assumption that the planetary beta effect is small. Together, the two scalings $\mathcal{B}/H = \text{Ro}$ and $\mathcal{H}/H = \text{Ro}$ mean that the effective beta effect (arising from both planetary and topographic variations; see Section 40.6.1 below) are small.

40.5.2 Outlining the asymptotic method

To derive the quasi-geostrophic shallow water model, we employ an asymptotic series method with the Rossby number as the small parameter and stop at the first nontrivial order. For this purpose, recall the non-dimensional shallow water equations from Section 40.3.7, and make use of the assumed $Bu \sim 1$ scaling

$$\text{Ro} \frac{D\hat{\mathbf{u}}}{Dt} + (\hat{\mathbf{f}} \times \hat{\mathbf{u}}) = -\hat{\nabla} \hat{\eta} \quad (40.57a)$$

$$\text{Ro} \left[\frac{\partial(\hat{\eta} - \hat{\eta}_b)}{\partial t} + \hat{\nabla} \cdot [(\hat{\eta} - \hat{\eta}_b) \hat{\mathbf{u}}] \right] = -\hat{\nabla} \cdot \hat{\mathbf{u}}. \quad (40.57b)$$

Note that we brought the time independent bottom topography, $\hat{\eta}_b$, into the time derivative for the thickness equation as doing so provides some symmetry with $\hat{\eta}$.

Asymptotic expansion of prognostic fields

Asymptotic methods are ideally suited for non-dimensional equations since we can unambiguously determine scales via the size of non-dimensional parameters. We here assume the Rossby number

⁴Although $\hat{f}_0 = 1$ in equation (40.56), it is useful to retain this term as a placeholder in the manipulations to follow.

to be small, in which case we are led to perform an asymptotic expansion of the prognostic fields in terms of the Rossby number. There are three prognostic fields, \hat{u} , \hat{v} , $\hat{\eta}$, and corresponding vertical velocity, \hat{w} , which we assume can be written as an asymptotic series

$$\hat{u} = \hat{u}_0 + \text{Ro} \hat{u}_1 + \text{Ro}^2 \hat{u}_2 + \dots \quad (40.58a)$$

$$\hat{v} = \hat{v}_0 + \text{Ro} \hat{v}_1 + \text{Ro}^2 \hat{v}_2 + \dots \quad (40.58b)$$

$$\hat{w} = \hat{w}_0 + \text{Ro} \hat{w}_1 + \text{Ro}^2 \hat{w}_2 + \dots \quad (40.58c)$$

$$\hat{\eta} = \hat{\eta}_0 + \text{Ro} \hat{\eta}_1 + \text{Ro}^2 \hat{\eta}_2 + \dots \quad (40.58d)$$

We thus refer to the zeroth, first, second, etc. “order” of the asymptotic expansion. The three components of the velocity satisfy the non-divergence condition at each order of Rossby number

$$\nabla \cdot \hat{\mathbf{v}}_n = 0 \quad \forall n. \quad (40.59)$$

Practical goal

The practical goal of asymptotic analysis is to develop a closed set of prognostic equations for functions appearing in the asymptotic expansions (40.58a)-(40.58d). For our purposes, we are content to stop at the lowest nontrivial order, meaning the point at which there is a prognostic equation that provides a means to move the system forward in time. Motivation for asymptotic analysis is to produce an equation set offering a means to focus analysis on dynamics most active under the regime determined by the chosen non-dimensional parameters. Each higher order in asymptotic expansion generally requires more complex algebraic manipulations. Hence, pursuit of higher order expansions should be undertaken only after first determining that the lower order equation set remains physically lacking.

Enabling the machinery

At this point we enable the machinery by “turning the crank”. To do so, we insert the asymptotic expansions (40.58a)-(40.58d) into the non-dimensional partial differential equations (40.57a) and (40.57b). Since Ro is arbitrarily small, and all non-dimensional fields are order unity regardless their order, the only means to maintain self-consistency is for terms to balance at equal order in Rossby number. Hence, we do not mix terms from different orders of Rossby number. This point is basic to asymptotic methods.

Again, our goal is to establish a set of prognostic equations that allows us to evolve a state that is arbitrarily close to geostrophic balance. We anticipate that at zeroth order the asymptotic method offer just the geostrophic balance, which has no prognostic value. Hence, we need to go at least to order Ro^1 , and hopefully no further as the algebraic tedium increases with order. With that anticipation and hope, we only keep track of terms of order Ro^0 and Ro^1 , in which the momentum and continuity equations become

$$\text{Ro} \frac{D\hat{\mathbf{u}}_0}{Dt} + (\hat{f}_0 + \text{Ro} \beta \hat{y}) \hat{z} \times (\hat{\mathbf{u}}_0 + \text{Ro} \hat{\mathbf{u}}_1) = -\hat{\nabla}(\hat{\eta}_0 + \text{Ro} \hat{\eta}_1) \quad (40.60a)$$

$$\text{Ro} \left[\frac{\partial \hat{\eta}_0}{\partial \hat{t}} + \hat{\nabla} \cdot [(\hat{\eta}_0 - \hat{\eta}_b) \hat{\mathbf{u}}_0] + \hat{\nabla} \cdot \hat{\mathbf{u}}_1 \right] = -\hat{\nabla} \cdot \hat{\mathbf{u}}_0. \quad (40.60b)$$

40.5.3 Order Ro^0 asymptotic equations

Terms in equations (40.60a) and (40.60b) balancing at order Ro^0 are given by

$$\hat{\mathbf{f}}_0 \times \hat{\mathbf{u}}_0 = -\hat{\nabla} \hat{\eta}_0 \quad (40.61\text{a})$$

$$\hat{\nabla} \cdot \hat{\mathbf{u}}_0 = 0. \quad (40.61\text{b})$$

The zeroth order velocity equation (40.61a) is the f -plane geostrophic balance. The vertical component to the curl of this equation leads to the horizontal non-divergence condition

$$\hat{\nabla} \cdot \hat{\mathbf{u}}_0 = 0, \quad (40.62)$$

which is identical to the zeroth order thickness equation (40.61b). Hence, the zeroth order horizontal velocity is given by f -plane geostrophy.

Given the non-divergence condition (40.61b), the zeroth order velocity field can be written in terms of a *geostrophic streamfunction*

$$\hat{u}_0 = -\frac{\partial \hat{\psi}_0}{\partial \hat{y}} \quad \text{and} \quad \hat{v}_0 = \frac{\partial \hat{\psi}_0}{\partial \hat{x}} \quad \text{and} \quad \hat{\zeta}_0 = \hat{\nabla}^2 \hat{\psi}_0, \quad (40.63)$$

where the zeroth order streamfunction is the ratio of the zeroth order surface height to zeroth order Coriolis parameter

$$\hat{\psi}_0 = \hat{\eta}_0 / \hat{f}_0. \quad (40.64)$$

We also introduced the zeroth order vorticity, $\hat{\zeta}_0$, which plays a role in the order Ro^1 equations. The corresponding dimensionful quantities are

$$\psi = (U L) \hat{\psi}_0 \quad \text{and} \quad \zeta = (U/L) \hat{\zeta}_0. \quad (40.65)$$

We dropped the asymptotic label on the dimensional quantities to reduce clutter and since we only evolve the zeroth order fields. In the following, the higher order fields are referred to as *ageostrophic* fields, whereas the zeroth order fields are the geostrophic fields.

40.5.4 Order Ro^1 asymptotic equations

The zeroth order equations do not render a prognostic equation, prompting us to consider equations at order Ro^1

$$\frac{D_0 \hat{\mathbf{u}}_0}{Dt} + \hat{f}_0 \hat{z} \times \hat{\mathbf{u}}_1 + \hat{\beta} \hat{y} \hat{z} \times \hat{\mathbf{u}}_0 = -\hat{\nabla} \hat{\eta}_1 \quad (40.66\text{a})$$

$$\frac{D_0 (\hat{\eta}_0 - \hat{\eta}_b)}{Dt} = -\hat{\nabla} \cdot \hat{\mathbf{u}}_1. \quad (40.66\text{b})$$

At this order, the material time derivative makes use of *only* the zeroth order geostrophic horizontal velocity

$$\frac{D_0}{Dt} = \frac{\partial}{\partial \hat{t}} + \hat{\mathbf{u}}_0 \cdot \hat{\nabla}. \quad (40.67)$$

The set of first order equations (40.66a) and (40.66b) appear to be unclosed because the evolution equation for zeroth order (geostrophic) terms is dependent on first order (ageostrophic) terms. However, the ageostrophic terms can be eliminated using two steps. First, we produce the vorticity equation from the momentum equation, which removes the ageostrophic pressure gradient $-\hat{\nabla} \hat{\eta}_1$. Second, combine the vorticity equation and continuity equation to eliminate the

horizontal convergence of the ageostrophic velocity, $-\hat{\nabla} \cdot \hat{\mathbf{u}}_1$. The second step leads to the quasi-geostrophic potential vorticity equation. Although details are specific to our study of shallow water quasi-geostrophy, similar steps are frequently encountered in other balanced geophysical fluid systems.

The geostrophic vorticity equation

Taking the curl of the momentum equation (40.66a) eliminates the ageostrophic pressure gradient, $\hat{\nabla} \hat{\eta}_1$, thus producing the vorticity equation

$$\frac{\partial \hat{\zeta}_0}{\partial \hat{t}} + (\hat{\mathbf{u}}_0 \cdot \hat{\nabla}) (\hat{\zeta}_0 + \hat{\beta} \hat{y}) = -\hat{f}_0 \hat{\nabla} \cdot \hat{\mathbf{u}}_1. \quad (40.68)$$

The right hand side term arises from stretching in the presence of rotation. To this order, stretching arises just from the planetary vorticity, with stretching due to relative vorticity appearing at a higher order. Since $\hat{\beta} \hat{y}$ is time independent, we can write the vorticity equation using the geostrophic material time derivative

$$\frac{D_0 (\hat{\zeta}_0 + \hat{\beta} \hat{y})}{D \hat{t}} = -\hat{f}_0 \hat{\nabla} \cdot \hat{\mathbf{u}}_1. \quad (40.69)$$

The quasi-geostrophic potential vorticity equation

As anticipated, we need one more step to close the system since the evolution of zeroth order vorticity in equations (40.68) and (40.69) are a function of vortex stretching induced by convergence of the first order velocity. To eliminate $\hat{\nabla} \cdot \hat{\mathbf{u}}_1$, we substitute from the thickness equation (40.66b), thus leading to a prognostic equation involving just zeroth order terms

$$\frac{\partial [\hat{\zeta}_0 + \hat{\beta} \hat{y} - \hat{f}_0 (\hat{\eta}_0 - \hat{\eta}_b)]}{\partial \hat{t}} + \hat{\mathbf{u}}_0 \cdot \hat{\nabla} [\hat{\zeta}_0 + \hat{\beta} \hat{y} - \hat{f}_0 (\hat{\eta}_0 - \hat{\eta}_b)] = 0, \quad (40.70)$$

which can be written in the material form

$$\frac{D_0}{D \hat{t}} [\hat{\zeta}_0 + \hat{\beta} \hat{y} - \hat{f}_0 (\hat{\eta}_0 - \hat{\eta}_b)] = 0. \quad (40.71)$$

Finally, we introduce the geostrophic streamfunction $\hat{\psi}_0 = \hat{\eta}_0 / \hat{f}_0$ (equation (40.64)) to render

$$\frac{D_0}{D \hat{t}} [\hat{\nabla}^2 \hat{\psi}_0 + \hat{\beta} \hat{y} + \hat{f}_0 \hat{\eta}_b - \hat{f}_0^2 \hat{\psi}_0] = 0. \quad (40.72)$$

Equation (40.72) is a statement of the material conservation of quasi-geostrophic potential vorticity, where material evolution is defined by the horizontal geostrophic currents (equation (40.67)). This equation is the culmination of our quest to derive a prognostic equation for the evolution of geostrophic flow. It enables us to evolve the geostrophic velocity and geostrophic free surface by probing, but not explicitly determining, the leading order ageostrophic motions. Practical use of the quasi-geostrophic method is based on time stepping the quasi-geostrophic potential vorticity, and then inverting the potential vorticity equation to diagnose the streamfunction to then determine the geostrophic velocity and free surface. That inversion requires solving an elliptic boundary value problem.

40.6 Physical elements of the theory

The asymptotic analysis of Section 40.5 worked with non-dimensional quantities, which are suitable for determining the scales required for asymptotic methods. Now that we have worked through the details, we can make use of that effort to both further the theory and to understand its physical content. For that purpose we find it essential to reintroduce physical dimensions.

40.6.1 Dimensional potential vorticity and streamfunction

To introduce physical dimensions, we invert the relations used in Section 40.3.7

$$\hat{t} = t/T \quad (\hat{x}, \hat{y}) = (x, y)/L \quad \partial_{\hat{t}} = T \partial_t \quad \hat{\nabla} = L \nabla \quad (\hat{u}, \hat{v}) = (u, v)/U \quad (40.73a)$$

$$\hat{\eta} = \eta'/\mathcal{H} \quad \hat{\eta}_b = \eta'_b/\mathcal{B} \quad \mathcal{H} = H \text{Ro} \quad \mathcal{B} = H \text{Ro} \quad (40.73b)$$

$$\hat{f}_0 = f_0/f_0 \quad \hat{\beta} \hat{y} = \beta y/(Ro f_0) = (L/U) \beta y \quad \hat{\zeta} = (L/U) \zeta = L^2 \nabla^2 \psi. \quad (40.73c)$$

We generally drop asymptotic subscripts on dimensional terms to help reduce clutter.

For the potential vorticity we start from the non-dimensional quasi-geostrophic potential vorticity (40.71) and find

$$\hat{q} = \hat{\zeta}_0 + \hat{\beta} \hat{y} + \hat{f}_0 \hat{\eta}_b - \hat{f}_0 \hat{\eta}_0 \quad (40.74a)$$

$$= \frac{L}{U} (\zeta + \beta y) + \frac{\eta'_b}{\mathcal{B}} - \frac{\eta'}{\mathcal{H}} \quad (40.74b)$$

$$= \frac{L}{U} (\zeta + \beta y) + \frac{\eta'_b}{H \text{Ro}} - \frac{\eta'}{H \text{Ro}} \quad (40.74c)$$

$$= \frac{L}{U} \left[\zeta + \beta y - \frac{f_0 (\eta' - \eta'_b)}{H} \right] \quad (40.74d)$$

$$= \frac{L}{U} \left[\zeta + \beta y - \frac{g (\eta' - \eta'_b)}{f_0} \frac{1}{L_d^2} \right] \quad (40.74e)$$

$$= \frac{L}{U} [\zeta + \beta y - L_d^{-2} (\psi - \psi_b)], \quad (40.74f)$$

where $L_d = \sqrt{g H}/f$ is the shallow water deformation radius (equation (40.31)), and we introduced the geostrophic streamfunction⁵

$$\psi = (g/f_0) \eta'. \quad (40.75)$$

We also wrote the contribution from topography as

$$\psi_b = (g/f_0) \eta'_b, \quad (40.76)$$

which is a static field. We are thus led to the dimensionful quasi-geostrophic potential vorticity for a single shallow water layer

$$q = f_0 (1 + \text{Ro} \hat{q}) = (\zeta + f) - L_d^{-2} (\psi - \psi_b) = f + \psi_b L_d^{-2} + (\nabla^2 - L_d^{-2}) \psi. \quad (40.77)$$

We took the liberty of adding the constant, f_0 , to the QG potential vorticity, which does not alter the dynamics but does allow us to introduce the planetary vorticity, $f = f_0 + \beta y$. The dynamically relevant portions of q appear at order Ro.

⁵ Vallis (2017) defines the geostrophic streamfunction in his equation (5.69) as $\psi_{\text{vallis}} = g \eta/f_0 = \psi + g H/f_0$, which differs by the constant $g H/f_0$. However, there is no difference in the dynamics since a streamfunction is unique only up to a constant.

40.6.2 Contributions to the QG potential vorticity

The quasi-geostrophic potential vorticity (40.77) has three main contributions

$$q = f + \zeta - f_0 h'/H, \quad (40.78)$$

where we wrote

$$L_d^{-2} (\psi - \psi_b) = f_0^2 / (g H) (g/f_0) (\eta' - \eta'_b) = f_0 h'/H, \quad (40.79)$$

with h' the undulations in the layer thickness due to undulations in the free surface and bottom topography. Heuristically, we can connect q to the shallow water $Q = (f + \zeta)/h$ by

$$(f + \zeta)/h \approx (f + \zeta) (1 - h'/H) \approx H^{-1} (f + \zeta - f_0 h'/H), \quad (40.80)$$

where we assumed βy , ζ , and h' are order Ro whereas f_0 is order unity. We pursue this expansion more formally in Section 40.6.5. But for present purposes we can use it to summarize the various contributions to potential vorticity.

- **PLANETARY VORTICITY:** The contribution $f = f_0 + \beta y$ arises from planetary vorticity, with the dynamically relevant contribution for QG arising just from the βy term.
- **GEOSTROPHIC RELATIVE VORTICITY:** $\nabla^2 \psi = (g/f_0) \nabla^2 \eta$ is the relative vorticity of the geostrophic flow. Given the Laplacian operator emphasizes small spatial scales, the relative vorticity is most important at scales at or smaller than the deformation radius.
- **EFFECTIVE BETA:** The contribution from the gradient of planetary vorticity is given by $\beta y = \mathbf{x} \cdot \nabla f$. Likewise, the contribution from topography is given by

$$\psi_b L_d^{-2} = f_0 \eta'_b / H = (f_0/H) (\eta_b - \bar{\eta}_b) \approx (f_0/H) \mathbf{x} \cdot \nabla \eta_b, \quad (40.81)$$

where the approximate expression made use of a Taylor series. These two contributions can be combined into an effective beta

$$\beta y + \psi_b L_d^{-2} = \mathbf{x} \cdot \nabla (f + f_0 \eta_b / H) \approx \mathbf{x} \cdot (H - \eta_b) \nabla [f/(H - \eta_b)], \quad (40.82)$$

with the final approximate expression connecting to the effective beta discussed in Section 36.5.1.

- **VERTICAL STRETCHING:** As discussed in Section 32.2, shallow water fluids move as vertical extensible columns. Hence, the term $(f_0/H) h'$ accounts for the contribution to potential vorticity from column stretching and squashing. It is most important for scales at or larger than those where the relative vorticity is important; i.e., at or larger than the deformation radius.
- **FLOW REGIMES RELATIVE TO THE DEFORMATION RADIUS:** As noted above, the term $(\nabla^2 - L_d^{-2}) \psi$ signals two regimes as determined by the deformation radius. For lateral scales on the order of the deformation radius, both the relative vorticity and vortex stretching make equal contributions to the potential vorticity. For smaller scales relative vorticity is more important whereas for larger scales vortex stretching dominates.

40.6.3 Connecting to rest state potential vorticity

For some purposes, particularly when studying Rossby waves in Section 48.11, we find it useful to unpack the material time derivative

$$\mathrm{D}q/\mathrm{D}t = \partial_t q + \hat{\mathbf{z}} \cdot (\nabla \psi \times \nabla q) \quad (40.83)$$

to expose the role of the potential vorticity contained in a resting fluid. For this purpose, expand the gradient

$$\nabla q = \nabla(\nabla^2 \psi) - \nabla \psi / L_d^2 + \nabla f + \nabla \psi_b / L_d^2, \quad (40.84)$$

so that

$$\nabla \psi \times \nabla q = \nabla \psi \times \nabla(\nabla^2 \psi) + \nabla \psi \times (\nabla f + \nabla \psi_b / L_d^2). \quad (40.85)$$

The second term on the right hand side can be written in terms of the resting state potential vorticity

$$\nabla f + \nabla \psi_b / L_d^2 = \nabla f + (f_0/H) \nabla \eta'_b = \nabla f - (f_0/H) \nabla(H - \eta'_b) \approx H \nabla(f/H_r) = H \nabla Q_r, \quad (40.86)$$

where $H_r = H - \eta'_b$ is the thickness of the resting fluid, and Q_r is the potential vorticity of the resting fluid. The approximation in the penultimate step above follows from assuming $\eta'_b/H = \mathcal{O}(\text{Ro})$, as per the quasi-geostrophic scaling in Section 40.5.1.

Bringing the pieces together leads us to write the material time evolution of quasi-geostrophic potential vorticity as

$$(f_0/g) \mathrm{D}q/\mathrm{D}t = \partial_t [(L_d^{-2} - \nabla^2) \eta'] - H \hat{\mathbf{z}} \cdot (\nabla \eta' \times \nabla Q_r) - (g/f_0) \hat{\mathbf{z}} \cdot [\nabla \eta' \times \nabla(\nabla^2 \eta')]. \quad (40.87)$$

The second term on the right hand side arises from the geostrophic advection of the potential vorticity in the resting fluid. This linear term is fundamental to the Rossby wave dispersion relation studied in Section 48.11. The nonlinear term on the right hand side arises from advection by the geostrophic velocity of the geostrophic relative vorticity. This term is generally ignored when studying small amplitude wave fluctuations. It is notable, however, that this term vanishes identically for plane waves. We discuss this point further in Section 48.11.2.

40.6.4 Summarizing the equations of quasi-geostrophy

The following fields are the key pieces of the single layer shallow water quasi-geostrophic theory

$$\mathbf{u} = \hat{\mathbf{z}} \times \nabla \psi \quad \text{and} \quad \zeta = \hat{\mathbf{z}} \cdot \nabla \times \mathbf{u} = \nabla^2 \psi \quad \text{and} \quad q = f + \zeta - L_d^{-2} (\psi - \psi_b) \quad (40.88a)$$

$$\psi = (g/f_0) \eta' \quad \text{and} \quad \psi_b = (g/f_0) \eta'_b \quad \text{and} \quad L_d = \sqrt{g H} / f_0. \quad (40.88b)$$

Evolution of the geostrophic flow

Evolution of the geostrophic flow is determined by material time changes to the QG potential vorticity following the horizontal geostrophic flow

$$\frac{\mathrm{D}q}{\mathrm{D}t} = \frac{\partial q}{\partial t} + \mathbf{u} \cdot \nabla q = \frac{\partial q}{\partial t} + \hat{\mathbf{z}} \cdot (\nabla \psi \times \nabla q) = \frac{\partial q}{\partial t} + J(\psi, q), \quad (40.89)$$

where the final equality introduced the Jacobian operator

$$J(\psi, q) = \partial_x \psi \partial_y q - \partial_y \psi \partial_x q. \quad (40.90)$$

For a perfect fluid, the quasi-geostrophic PV is materially constant, whereas more general flows have forcing and dissipation so that

$$\frac{Dq}{Dt} = \text{forcing} - \text{dissipation}. \quad (40.91)$$

As an algorithm, we first update the potential vorticity to a new time step, then diagnose the streamfunction, $\psi = g\eta/f_0$, by solving the elliptic boundary value problem

$$(\nabla^2 - L_d^{-2})\psi = q - f - \psi_b/L_d^2, \quad (40.92)$$

at which point we know the updated free surface and updated velocity. This same algorithm was outlined for time stepping the two-dimensional non-divergent barotropic model in Section 35.3.5.

Velocity and free surface equations

In the above algorithm we are not concerned with the velocity and free surface equations, but instead we are concerned with inverting the potential vorticity equation (40.92) to find the streamfunction. Even so, it can be of interest to consider these equations, which are determined by the order Ro^1 equations in Section 40.5.4

$$\partial_t \mathbf{u}_g + (\mathbf{u}_g \cdot \nabla) \mathbf{u}_g + (f_0 + \beta y) \hat{\mathbf{z}} \times \mathbf{u}_g + f_0 \hat{\mathbf{z}} \times \mathbf{u}_{ag} = -g \nabla(\eta_g + \eta_{ag}) \quad (40.93a)$$

$$\partial_t(\eta_g - \eta_b) + (\mathbf{u}_g \cdot \nabla)(\eta_g - \eta_b) = -\nabla \cdot \mathbf{u}_{ag}. \quad (40.93b)$$

In these equations we temporarily introduced subscripts to distinguish the geostrophic velocity and corresponding surface height

$$f_0 \hat{\mathbf{z}} \times \mathbf{u}_g = -g \nabla \eta_g \quad (40.94)$$

from the ageostrophic free surface height, η_{ag} , and ageostrophic velocity, \mathbf{u}_{ag} . Since the ageostrophic velocity generally has a nonzero horizontal convergence, but it is three dimensionally non-divergent (since the fluid layer has constant density), then we can identify a corresponding vertical component to the ageostrophic velocity that satisfies

$$\mathbf{v}_{ag} = \mathbf{u}_{ag} + \hat{\mathbf{z}} w_{ag} \quad \text{with} \quad \nabla \cdot \mathbf{v}_{ag} = \partial_x u_{ag} + \partial_y v_{ag} + \partial_z w_{ag} = 0. \quad (40.95)$$

40.6.5 Connecting quasi-geostrophic PV to shallow water PV

We here determine how potential vorticity for shallow water quasi-geostrophy relates to the full shallow water potential vorticity studied in Chapter 36. For that purpose, recall that the potential vorticity for a single layer of shallow water fluid is (Section 36.3)

$$Q = \frac{f + \zeta}{h}, \quad (40.96)$$

where $h = H + \eta' - \eta'_b$ (equation (40.4)) is the layer thickness.

To connect to the quasi-geostrophic potential vorticity, we non-dimensionalize the potential vorticity prior to performing an asymptotic expansion to order Ro^1 . For this purpose, use the scaling relations from Section 40.3.7 to write the geostrophic relative vorticity as

$$\zeta = \nabla^2 \psi = (g/f_0) \nabla^2 \eta' = (g \mathcal{H})/(f_0 L^2) \widehat{\nabla}^2 \widehat{\eta} = (g H \text{Ro})/(f_0 L^2) \widehat{\zeta}_0 = f_0 \text{Ro} (L_d/L)^2 \widehat{\zeta}_0 \quad (40.97)$$

as well as

$$h = H + H \text{Ro} (\hat{\eta} - \hat{\eta}_b) \quad (40.98\text{a})$$

$$f = f_0 (\hat{f}_0 + \text{Ro} \hat{\beta} \hat{y}). \quad (40.98\text{b})$$

Taking the ratio and expanding to order Ro^1 leads to

$$\frac{\zeta + f}{h} = \frac{f_0}{H} \left[\frac{\hat{f}_0 + \text{Ro} (L_d/L)^2 \hat{\zeta}_0 + \text{Ro} \hat{\beta} \hat{y}}{1 + \text{Ro} (\hat{\eta} - \hat{\eta}_b)} \right] \quad (40.99\text{a})$$

$$\approx \frac{f_0}{H} + \frac{f_0 \text{Ro}}{H} \left[-\hat{f}_0 (\hat{\eta} - \hat{\eta}_b) + (L_d/L)^2 \hat{\zeta}_0 + \hat{\beta} \hat{y} \right] \quad (40.99\text{b})$$

$$= \frac{f_0}{H} + \frac{f_0 \text{Ro}}{H} \left[(L_d/L)^2 \hat{\zeta}_0 + \hat{\beta} \hat{y} - \hat{f}_0 (\hat{\eta} - \hat{\eta}_b) \right] \quad (40.99\text{c})$$

$$= \frac{f_0}{H} + \frac{f_0 \text{Ro}}{H} \left[\frac{\zeta}{f_0 \text{Ro}} + \frac{\beta y}{f_0 \text{Ro}} - \frac{\eta'}{\mathcal{H}} + \frac{\eta'_b}{\mathcal{B}} \right] \quad (40.99\text{d})$$

$$= \frac{1}{H} \left[\zeta + f_0 + \beta y - \frac{f_0 (\eta' - \eta'_b)}{H} \right] \quad (40.99\text{e})$$

$$= \hat{q} U / (H L) \quad (40.99\text{f})$$

$$= q / H. \quad (40.99\text{g})$$

We are thus led to the relation between the shallow water potential vorticity and the quasi-geostrophic shallow water potential vorticity

$$\frac{f + \zeta}{h} = \frac{q}{H} + \mathcal{O}(\text{Ro}^2). \quad (40.100)$$

As noted in Section 40.5.1, this connection between the potential vorticities only holds when assuming deviations in *both* the bottom topography and free surface scale according to the Rossby number, $\eta' = \mathcal{H} \text{Ro}$ and $\eta'_b = \mathcal{B} \text{Ro}$, thus allowing us to combine $\hat{\eta}$ and $\hat{\eta}_b$ in the thickness equation (40.98a).

The identity (40.100) is a consequence of the asymptotic expansion of the velocity and thickness equations. We could alternatively invert our development of quasi-geostrophy by using the quasi-geostrophic potential vorticity as the basis for deriving the governing equations. We pursue that approach to derive the layered quasi-geostrophic equations in Section 40.6.7.

40.6.6 Considering topography to be $\mathcal{O}(\text{Ro}^0)$

We here briefly consider topography to be arbitrarily large, in which case we are no longer ensured asymptotic consistency since we can no longer combine η' and η'_b into an order Rossby number fluctuation of the layer thickness. Even so, it is not uncommon to examine how an asymptotic theory performs when outside of its formal regime of validity, particularly with the advent of numerical codes to facilitate such studies. In many cases the theories continue to provide provocative, and sometimes physically relevant, information.

To see what happens, consider the quasi-geostrophic PV equation

$$(\partial_t + \mathbf{u} \cdot \nabla) [\zeta + \beta y + L_d^{-2} (\psi_b - \psi)] = 0. \quad (40.101)$$

If ψ_b is order unity whereas the other terms are order Ro , then to leading order the potential vorticity is given by the static term, $L_d^{-2} \psi_b$, so that material conservation of potential vorticity

reduces to

$$\mathbf{u} \cdot \nabla \psi_b = 0 \implies \mathbf{u} \cdot \nabla \eta_b = 0. \quad (40.102)$$

This constraint means that the f -plane geostrophic flow is constrained to flow along lines of constant topography (isobaths), in which case the geostrophic streamfunction satisfies

$$(f/g) \mathbf{u} \cdot \nabla \eta_b = \hat{\mathbf{z}} \cdot (\nabla \eta \times \nabla \eta_b) \equiv J(\eta, \eta_b) = 0. \quad (40.103)$$

The order one bottom topography undulations thus provide a strong constraint on the f -geostrophic flow, making the flow align with the bottom topography and in turn aligning surface height undulations with bottom undulations. We uncovered this constraint in our analysis of topographic form stress in Section 36.7.5. We also discussed this flow as a particular realization of the two-dimensional non-divergent barotropic flow in Section 35.2.3.

40.6.7 Two layer quasi-geostrophy

In Section 32.4 we developed the equations for an adiabatic stacked shallow water model. We here specialize those equations to a two-layer quasi-geostrophic model, with extensions to multiple layers following straightforwardly. Rather than pursue the formal asymptotic methods used previously, we here make use of our observation in Section 40.6.5 concerning the connection between shallow water and quasi-geostrophic potential vorticities.

To get started, recall from Section 36.3.6 that the shallow water potential vorticity for an arbitrary layer, labelled by the index k , is given by

$$Q_k = \frac{f + \zeta_k}{h_k}, \quad (40.104)$$

As in Section 40.6.2, we assume βy , ζ_k , and h'_k scale as Ro , in which case we have the quasi-geostrophic potential vorticity for each layer

$$q_k = f + \zeta_k - f_0 h'_k / H, \quad (40.105)$$

where ζ_k is here the geostrophic relative vorticity.

From our asymptotic analysis earlier in this section, the toughest part of that analysis concerned the derivation of the quasi-geostrophic potential vorticity equation. In the present approach, we already have the potential vorticity for each layer via equation (40.105). What we need is the velocity field to advect it. Again, we know what that velocity is: it is the f -plane geostrophic velocity for each layer. The 2-layer velocity equations are given by equations (32.74a) and (32.74b), with their geostrophic components determined by

$$f_0 \hat{\mathbf{z}} \times \mathbf{u}_1 = -g \nabla (\eta'_b + h'_1 + h'_2) \quad (40.106a)$$

$$f_0 \hat{\mathbf{z}} \times \mathbf{u}_2 = -\nabla \left[g_{1/2}^r (\eta'_b + h'_1 + h'_2) + g_{3/2}^r (\eta'_b + h'_2) \right]. \quad (40.106b)$$

In these equations we set the applied atmospheric pressure to a constant, and made use of the reduced gravities at the layer interfaces are

$$g_{1/2}^r = g (\rho_1 - \rho_a) / \rho_{ref} \approx g \quad \text{and} \quad g_{3/2}^r = g (\rho_2 - \rho_1) / \rho_{ref}, \quad (40.107)$$

with the Boussinesq reference density taken as $\rho_{ref} = \rho_1$. Furthermore, we assume $\rho_a \ll \rho_{ref}$ so that the top interface reduced gravity is well approximated by the full gravity. From equations

(40.106a) and (40.106b) we can identify the geostrophic streamfunctions

$$\psi_1 = (g/f_0)(\eta'_b + h'_1 + h'_2) \quad (40.108a)$$

$$\psi_2 = (1/f_0) \left[g_{1/2}^r (\eta'_b + h'_1 + h'_2) + g_{3/2}^r (\eta'_b + h'_2) \right], \quad (40.108b)$$

so that the layer geostrophic velocities are given by

$$\mathbf{u}_1 = \hat{\mathbf{z}} \times \nabla \psi_1 \quad \text{and} \quad \mathbf{u}_2 = \hat{\mathbf{z}} \times \nabla \psi_2. \quad (40.109)$$

We thus proceed with the usual quasi-geostrophic algorithm, whereby evolution is determined by the material time changes of the potential vorticity with advection given by the layer geostrophic flow

$$(\partial_t + \mathbf{u}_k \cdot \nabla) q_k = 0. \quad (40.110)$$



40.7 Exercises

EXERCISE 40.1: PV CONSERVATION FOR PLANETARY GEOSTROPHY

Show that the planetary geostrophic equations

$$\mathbf{f} \times \mathbf{u} = -g \nabla \eta \quad \text{and} \quad \frac{Dh}{Dt} = -h \nabla \cdot \mathbf{u} \quad \text{with} \quad \eta = \eta_b + h \quad (40.111)$$

are equivalent to

$$\mathbf{f} \times \mathbf{u} = -g \nabla \eta \quad \text{and} \quad \frac{DQ}{Dt} = 0 \quad \text{with} \quad Q = \frac{f}{h}. \quad (40.112)$$

This result shows that the shallow water PG equations may be written as an evolution equation for an approximated version of the shallow water potential vorticity, $(f + \zeta)/h \approx f/h$. This limit holds when the Rossby number is small.

EXERCISE 40.2: CONSTRAINTS ON STEADY STATE PLANETARY GEOSTROPHIC FLOW

Consider a shallow water fluid satisfying the planetary geostrophic equations developed in Section 40.4. Assume the flow is in steady state.

- (a) In what manner does potential vorticity conservation constrain the velocity field?
- (b) Consider an initially zonal geostrophic flow. In what direction (poleward or equatorward) will a fluid parcel deviate when encountering a seamount (i.e., a region of relatively shallow depth)?
- (c) Describe the geostrophic contours (i.e., path of fluid particles following the geostrophic flow) for the case where the ocean sea surface height undulations, η' , are far smaller than undulations in the bottom topography, η'_b (see Figure 32.1 for notation).
- (d) For the special case of an f -plane, show that the velocity is aligned with isolines of bottom topography.
- (e) For the special case of a flat bottom and latitudinally dependent Coriolis parameter, $f(y)$, show that there is no meridional geostrophic velocity. That is, the flow is zonally aligned.



Chapter 41

CONTINUOUSLY STRATIFIED PLANETARY GEOSTROPHY

The planetary geostrophic equations consist of linear steady geostrophic balance (commonly also with friction) plus the full nonlinear buoyancy equation. Circulation is thus determined by the mass field given that the flow is diagnostic whereas buoyancy is prognostic. Given that the momentum equation is linear, there is no turbulence in planetary geostrophy. Instead, the equation set allows the analyst to focus on large-scale flow of a stratified laminar fluid dominated by rotation in the presence of planetary and topographic beta.

We already encountered many physical properties of planetary geostrophic flow in Chapter 28, where we studied geostrophy, vorticity, thermal wind, and Taylor-Proudman. We also made use of planetary geostrophy when studying western boundary current intensification for a shallow water layer in Section 36.7. In this chapter we fill in certain of the mathematical details left out from those early discussions by deriving, through non-dimensionalization and scale analysis, the planetary geostrophic equations.

As an application of the planetary geostrophic equations, we examine a variety of vorticity budgets formed from this equation set. We start by examining the potential vorticity budget and studying how the impermeability theorem (Chapter 39.2) manifests. We then discuss a variety of vorticity budgets used to describe the depth integrated or depth averaged flow. Each of these two-dimensional vorticity budgets offers insights into how the large-scale flow is constrained by rotation and the β -effect present on a sphere. In particular, these budgets offer insights into how forces and the curl of forces generate both vertical flow next to the boundaries as well as meridional flow for the full fluid column. The stratified planetary geostrophic equations form the foundation for many theories of the large-scale ocean circulation. Constraints provided by the vorticity theorems developed in this chapter provide the key reasons for why these theories are so physically compelling.

CHAPTER GUIDE

We here extend the shallow water discussions from Chapter 40 to derive the continuously stratified planetary geostrophic equations. We make use of stratified geophysical fluid dynamics from Chapters 21 and 28, vorticity and the planetary beta effect from Chapter 37, and potential vorticity from Chapter 38. Physical properties of stratified geostrophic mechanics were considered in Chapter 28, with an understanding of that material assumed here. We follow the non-dimensionalization used to derive the shallow water planetary geostrophic equations in Chapter 40, and further extend this material to continuously stratified quasi-geostrophy in Chapter 42.

41.1 Loose threads	1046
41.2 Non-dimensionalizing the stratified Boussinesq equations	1046

41.2.1	Dimensional parameters	1047
41.2.2	Physical dimensions and non-dimensional parameters	1048
41.2.3	Choosing the non-dimensional parameters	1048
41.2.4	Relating the buoyancy scale to the Coriolis acceleration scale	1049
41.2.5	Richardson number and QG/PG flow regimes	1050
41.2.6	The Rossby deformation radius	1051
41.2.7	Assumed values for the non-dimensional parameters	1051
41.2.8	Non-dimensional Boussinesq equations	1053
41.3	Summary of the planetary geostrophic equations	1054
41.3.1	Common form of the equations	1054
41.3.2	Planetary geostrophic energetics	1055
41.4	Planetary geostrophic potential vorticity	1056
41.4.1	Derivation	1056
41.4.2	Impermeability theorem	1057
41.4.3	Kinematic fluxes satisfying impermeability	1058
41.5	Depth integrated vorticity budget	1059
41.5.1	The β -effect, stretching, and meridional transport	1059
41.5.2	Bottom kinematics and dynamics	1060
41.5.3	Surface kinematics and dynamics	1063
41.5.4	Summary of force curls driving depth integrated meridional flow .	1064
41.5.5	Integral constraints	1065
41.6	Sverdrup balance and geostrophic Sverdrup balance	1066
41.7	Vorticity of the depth integrated velocity	1067
41.7.1	Depth integrated velocity equation	1068
41.7.2	Vorticity budget	1068
41.7.3	Integral balances for steady flows	1069
41.8	Vorticity equation for the depth averaged velocity	1070
41.8.1	Relating the depth average velocity to boundary velocities	1070
41.8.2	Formulation of the vorticity equation	1071
41.8.3	Rigid lid approximation and the role of JEBAR	1071
41.8.4	Further study	1074

41.1 Loose threads

- Consider a new small chapter with the material in Section 41.2, since this material is also relevant to QG.
- Reintroduce the bottom topography to the derivation in Section 41.2 as per the shallow water discussion in Chapter 40.
- More figures throughout the chapter
- Exercises

41.2 Non-dimensionalizing the stratified Boussinesq equations

In this section we non-dimensionalize the continuously stratified Boussinesq equations. As part of this process we identify a variety of non-dimensional numbers that characterize the flow. Planetary geostrophy is a rather simple asymptotic theory. Nonetheless, our work to non-dimensionalize the Boussinesq equations supports the work needed for the more complicated derivations of continuously stratified quasi-geostrophy in Chapter 42.

The starting point is the perfect fluid stratified hydrostatic Boussinesq equations (Section 26.1)

$$\frac{D\mathbf{u}}{Dt} + f \hat{\mathbf{z}} \times \mathbf{u} = -\nabla_z \varphi \quad (41.1a)$$

$$\frac{\partial \varphi}{\partial z} = b \quad (41.1b)$$

$$\frac{Db}{Dt} = 0 \quad (41.1c)$$

$$\nabla \cdot \mathbf{v} = 0, \quad (41.1d)$$

where $\mathbf{v} = (\mathbf{u}, w)$ is the three-dimensional velocity written using Cartesian coordinates, $b = -g(\rho - \rho_0)/\rho_0$ is the Archimedian buoyancy relative to a constant reference density, ρ_0 , with ρ the density. We also write $\varphi = \delta p/\rho_0$ for the dynamic pressure (dimensions of $L^2 T^{-2}$), and $\nabla_z = (\partial_x, \partial_y, 0)$ for the horizontal gradient operator. We separate a background vertical buoyancy profile from a space-time fluctuating buoyancy

$$b = \tilde{b}(z) + b'(x, y, z, t), \quad (41.2)$$

and introduce the corresponding background squared buoyancy frequency

$$N^2 = \frac{d\tilde{b}}{dz}. \quad (41.3)$$

With this decomposition, the buoyancy equation (41.1c) takes the form

$$\frac{Db'}{Dt} + w N^2 = 0. \quad (41.4)$$

We also introduce an associated decomposition of the hydrostatic pressure

$$\varphi = \tilde{\varphi}(z) + \varphi'(x, y, z, t) \quad (41.5)$$

where $\tilde{\varphi}$ is hydrostatically balanced by \tilde{b}

$$\frac{d\tilde{\varphi}}{dz} = \tilde{b}, \quad (41.6)$$

and the fluctuating pressure, φ' , is hydrostatically balanced by b'

$$\frac{\partial \varphi'}{\partial z} = b'. \quad (41.7)$$

41.2.1 Dimensional parameters

Following the shallow water discussion in Section 40.3.1, we have the following dimensional parameters for the perfect Boussinesq fluid.

- LENGTH SCALES

- ★ H = length scale of a typical vertical structure in the fluid (e.g., the depth of the thermocline).
- ★ L = horizontal/lateral length scale of motions under consideration.
- ★ R = radius of the planet.

- VELOCITY SCALES

- ★ U = horizontal velocity scale for fluid motion.
 - ★ W = vertical velocity scale for fluid motion.

- PRESSURE AND BUOYANCY SCALES: Pressure is a contact force, acting on the boundary of an arbitrary fluid region, and buoyancy arises from the gravitational force that acts to raise or lower a fluid element depending on its density relative to the environment. They have scales given by the following.

- ★ Φ = scale for pressure fluctuations φ' (dimensions of pressure divided by density = length scale \times acceleration).
 - ★ B = scale of buoyancy fluctuations b' (dimensions of acceleration).

- BODY FORCES: There are two body forces acting on the fluid, one from gravity and one from Coriolis.

- ★ g = gravitational acceleration
 - ★ f = Coriolis frequency

Contrary to the shallow water discussion in Section 40.3.1, we do not introduce a wave speed since it does not affect the asymptotics considered here. We also dropped the bottom topography scale, assuming it is small for present purposes.

41.2.2 Physical dimensions and non-dimensional parameters

There are two physical dimensions in the Boussinesq system: length, L , and time, T . As for the shallow water system, there no mass since mass is determined by the density (buoyancy) and volume. The Buckingham-II theorem then says there are

$$N_{\text{dimensionless}} = 9 - 2 = 7 \quad (41.8)$$

non-dimensional parameters.

41.2.3 Choosing the non-dimensional parameters

Following the shallow water discussion in Section 40.3.4, we choose the following non-dimensional parameters.

1. VERTICAL TO HORIZONTAL ASPECT RATIO: The ratio of the vertical scale to the horizontal length scales defines the aspect ratio

$$\delta_{\text{vertical/horizontal}} = \frac{\text{vertical length scale}}{\text{horizontal length scale}} = \frac{H}{L}. \quad (41.9)$$

2. RATIO OF HORIZONTAL SCALE TO PLANETARY SCALE: The ratio of the horizontal length scale to the planet radius is given by

$$\delta_{\text{horizontal/planet}} = \frac{\text{horizontal length scale}}{\text{planetary length scale}} = \frac{L}{R}. \quad (41.10)$$

3. RATIO VERTICAL TO HORIZONTAL VELOCITY SCALES: The ratio of the vertical to horizontal velocity scales is given by

$$\frac{\text{vertical velocity scale}}{\text{horizontal velocity scale}} = \frac{W}{U}. \quad (41.11)$$

4. HYDROSTATIC NUMBER: The hydrostatic number is the ratio of the pressure gradient scale to the buoyancy scale. For the hydrostatic fluid fluctuations

$$\Phi/H = B, \quad (41.12)$$

where B is the scale for the buoyancy fluctuations.

5. ROSSBY NUMBER: The Rossby number is the ratio of the fluid particle acceleration scale to the Coriolis acceleration

$$\text{Ro} = \frac{\text{particle acceleration}}{\text{Coriolis acceleration}} = \frac{U}{fL}. \quad (41.13)$$

As in Section 40.3.4, we assume that the time scale is advective

$$T \sim L/U \implies \text{Ro} = U/(fL) = (fT)^{-1}. \quad (41.14)$$

6. GEOSTROPHIC NUMBER: The ratio of the Coriolis acceleration to the pressure gradient acceleration defines the geostrophic number

$$\text{Ge} = \frac{\text{Coriolis acceleration}}{\text{pressure gradient acceleration}}. \quad (41.15)$$

The Coriolis acceleration scales as

$$\text{Coriolis acceleration} \sim fU \quad (41.16)$$

whereas the pressure gradient acceleration from the fluctuating pressure, φ' , scales as

$$\text{pressure gradient acceleration} \sim \Phi/L, \quad (41.17)$$

so that

$$\text{Ge} = \frac{\text{Coriolis acceleration}}{\text{pressure gradient acceleration}} = \frac{fU}{(\Phi/L)}. \quad (41.18)$$

7. RATIO OF FLUCTUATING STRATIFICATION TO BACKGROUND STRATIFICATION: The ratio of the buoyancy frequency arising from the fluctuating buoyancy, B/H , to the background squared buoyancy frequency, N^2 , is given by

$$\frac{\text{fluctuating squared buoyancy frequency}}{\text{background squared buoyancy frequency}} = \frac{B/H}{N^2}. \quad (41.19)$$

41.2.4 Relating the buoyancy scale to the Coriolis acceleration scale

The fluctuating buoyancy, b' , and fluctuating pressure, φ' , have scales related through the hydrostatic balance. From equation (41.12) we have

$$B = \Phi/H. \quad (41.20)$$

Additionally, assuming geostrophic scaling, equation (41.18) means that the fluctuating pressure has a scale related to the Coriolis acceleration scale according to

$$\Phi = f U L. \quad (41.21)$$

Hence, the scale for the fluctuating buoyancy is given by

$$B = f U (L/H). \quad (41.22)$$

41.2.5 Richardson number and QG/PG flow regimes

The *Richardson number* is the non-dimensional ratio of the squared buoyancy frequency to the squared vertical shear of the horizontal velocity

$$Ri = \frac{N^2}{|\partial_z \mathbf{u}|^2}. \quad (41.23)$$

In regions where $Ri \ll 1$, the vertical shear is stronger than the stabilizing effects from vertical stratification. In regions with small Richardson numbers, there is enough kinetic energy in the vertical shear to extract potential energy from the stratification, and this extraction process occurs via a dynamical instability known as *Kelvin-Helmholtz instability*. In contrast, for large-scale highly stratified flow, the Richardson number is quite large, with $Ri \sim 100$ common. Large Richardson number flow regimes are where quasi-geostrophy is relevant (Chapter 42).

In our choice for dimensionless parameters, we could choose one determined by the scale for the Richardson number

$$Ri = \frac{N^2}{(U/H)^2}, \quad (41.24)$$

where we set the vertical scale equal to H , the horizontal velocity scale to U , and the squared buoyancy frequency to a scale N^2 . Alternatively, the Richardson number can be related to the Rossby and Burger numbers through

$$Bu = \left[\frac{L_d}{L} \right]^2 = \left[\frac{NH}{fL} \right]^2 = \frac{U^2 Ri}{U^2/(Ro)^2} = (Ro)^2 Ri. \quad (41.25)$$

One further way to write the Burger number is by introducing the angle φ defined by the vertical and horizontal length scales

$$\tan \varphi \equiv H/L \quad (41.26)$$

in which case

$$Bu = \left[\frac{L_d}{L} \right]^2 = \left[\frac{NH}{fL} \right]^2 = (Ro)^2 Ri = [(N/f) \tan \varphi]^2. \quad (41.27)$$

When $\tan^2 \varphi$ is set according to the slope of the ocean bottom, then $[(N/f) \tan \varphi]^2$ is known as the *slope Burger number* ([MacCready and Rhines, 1993](#); [Peterson and Callies, 2022](#)).

For QG flows, the horizontal length scales, L , are assumed to be on the order of the deformation radius, L_d , in which case the Burger number is close to unity. The relation (41.25) thus means that the Richardson number scales as

$$Ri \sim (Ro)^{-2} \quad \text{QG flow regime.} \quad (41.28)$$

For atmospheric flows with a Rossby number order 1/10, QG flow regimes are realized with a Richardson number ~ 100 . For the ocean, the Rossby number can be even smaller, in which case

QG flows are characterized by an even larger Richardson number. For planetary geostrophy, the Burger number is small. Hence, PG flows are characterized by somewhat smaller Richardson numbers than QG flows.

41.2.6 The Rossby deformation radius

The combined effects of buoyancy and rotation yield the richness of continuously stratified planetary geostrophic and quasi-geostrophic motions. Hence, the buoyancy frequency and the Coriolis parameter play central role in characterizing these flow regimes. The ratio of these two frequencies, N/f , in regions of nontrivial vertical stratification is typically around 100. Hence, rotational inertial oscillations (usually just called *inertial oscillations*; Section 12.5) have about 100 times longer period, $2\pi/f$, than buoyancy oscillations with period $2\pi/N$.

Letting the squared buoyancy frequency, N^2 , refer to a value typical of a particular flow regime, one can define the Rossby deformation radius

$$L_d = H(N/f). \quad (41.29)$$

As defined, the deformation radius is the vertical length scale multiplied by the ratio of the buoyancy frequency to the Coriolis frequency. The ratio f/N appears frequently in rotating/stratified fluids, and is sometimes called the Prandtl ratio

$$\text{Prandtl ratio} = f/N. \quad (41.30)$$

With $H \approx 1$ km and $N/f \approx 100$, the Rossby deformation radius is roughly 100 km. This length scale measures the relative importance of stratification and rotation. Depending on the ratio L/L_d , we can have large or small stratification fluctuations relative to the background stratification. Furthermore, the deformation radius sets the scale for unstable baroclinic waves leading to baroclinically unstable flow (see Chapter 6 of [Vallis \(2017\)](#)). For some context, recall the shallow water deformation radius is given by equation (40.31), $L_d = \sqrt{gH}/f$, which is the ratio of the gravity wave speed to Coriolis frequency. With $N = 100$ $f = 10^{-2}$ s $^{-1}$ and $H = 10^3$ m, the shallow water deformation radius is about an order of magnitude larger than the internal deformation radius. This scale difference means that the characteristic length scales, as set by L_d , are much larger in a single layer of shallow water fluid than in a stratified fluid.

41.2.7 Assumed values for the non-dimensional parameters

We now enumerate the assumed values for the non-dimensional parameters, again largely following the choices made for the shallow water layer in Section 40.3.5. These assumptions are guided by the regimes of interest to our analysis.

1. SMALL VERTICAL TO HORIZONTAL ASPECT RATIO: The aspect ratio is generally small for large-scale atmospheric and oceanic fluid systems

$$\delta_{\text{vertical/horizontal}} \ll 1. \quad (41.31)$$

This assumption is part of the hydrostatic approximation (Section 24.2).

2. SMALL OR ORDER ONE RATIO OF HORIZONTAL TO PLANETARY SCALES: The ratio of the horizontal length scale to the planet radius is small for quasi-geostrophic systems, and order

unity for planetary geostrophy

$$\delta_{\text{horizontal/planet}} \ll 1 \quad \text{quasi-geostrophy} \quad (41.32\text{a})$$

$$\delta_{\text{horizontal/planet}} \sim 1 \quad \text{planetary geostrophy.} \quad (41.32\text{b})$$

3. SMALL RATIO VERTICAL TO HORIZONTAL VELOCITY SCALE: The continuity equation implies

$$W/H = U/L, \quad (41.33)$$

so that

$$W = U(H/L). \quad (41.34)$$

As noted above, for a hydrostatic fluid the vertical to horizontal aspect ratio H/L is small, so that the vertical velocity scale is smaller than the horizontal velocity scale. Furthermore, when the fluid is close to geostrophically balanced, the vertical velocity scale is even smaller, by a factor of Ro . We will see that factor emerge in the following scale analysis.

4. UNIT HYDROSTATIC NUMBER: As already noted, the hydrostatic balance (41.1b) means that the scales for a buoyancy fluctuation and pressure fluctuation are related by (see equation (41.12))

$$\Phi = H B. \quad (41.35)$$

5. SMALL ROSSBY NUMBER: The Rossby number is assumed small

$$\text{Ro} = U/(f L) = (f T)^{-1} \ll 1, \quad (41.36)$$

where we set the time scale according to advection, $T = L/U$.

6. UNIT GEOSTROPHIC NUMBER: The geostrophic number is assumed to be order unity

$$\text{Ge} \sim 1, \quad (41.37)$$

which means that the Coriolis acceleration and pressure gradient acceleration scale together

$$f U \sim \Phi/L. \quad (41.38)$$

This scaling is consistent with the momentum equation (41.1a) so long as the Rossby number is small, $\text{Ro} \ll 1$.

7. STRATIFICATION FLUCTUATIONS COMPARED TO BACKGROUND STRATIFICATION: Making use of the assumed unit geostrophic number, the ratio of the buoyancy frequency arising from the fluctuating buoyancy to the background buoyancy frequency is given by

$$\frac{B/H}{N^2} = \frac{\Phi}{H^2 N^2} = \frac{f U L}{H^2 N^2} = \frac{U}{f L} \frac{L^2 f^2}{H^2 N^2} = \text{Ro} \frac{L^2}{L_d^2}, \quad (41.39)$$

where we introduced the deformation radius (41.29) $L_d = H N/f$. It is important to keep the depth dependence of N^2 when returning to dimensional fields, particularly for the QG system in Section 42.3.7.

41.2.8 Non-dimensional Boussinesq equations

Following the shallow water approach in Section 40.3.7, we introduce non-dimensional variables according to

$$t = T \hat{t} \quad (x, y) = L(\hat{x}, \hat{y}) \quad \partial_t = \partial_{\hat{t}}/T \quad \nabla_z = \hat{\nabla}_z/L \quad \partial_z = \partial_{\hat{z}}/H \quad f = f_0 \hat{f} \quad (41.40a)$$

$$(u, v) = U(\hat{u}, \hat{v}) \quad w = W \hat{w} \quad \varphi' = f_0 U L \hat{\varphi} \quad b' = B \hat{b} = (f_0 U L / H) \hat{b}. \quad (41.40b)$$

For the second equality in the buoyancy scale, we made use of equation (41.22) to connect the buoyancy fluctuation scale to the Coriolis acceleration scale. We also make use of the following relations between scales

$$T = L/U \quad \text{advective scaling for } T \quad (41.41)$$

$$W = U(H/L) \quad \text{continuity scaling for } W \quad (41.42)$$

$$\text{Ro} = U/(f_0 L) = (T f_0)^{-1} \quad \text{advective scaling for } T. \quad (41.43)$$

The first relation assumes the time scale is determined by the advection time, $T = L/U$, which then means that the Rossby number is the ratio of the advective frequency, $1/T$, to the Coriolis frequency, f_0 . Furthermore, we assume vertical velocity scales according to the continuity equation, $W = U(H/L)$. This continuity scaling for W will be seen to be an over-estimate in the following, where we find that W instead scales like $W = \text{Ro} U (H/L)$.

Non-dimensional momentum equation

Introducing the above dimensionless variables and dimensionful scales into the Boussinesq momentum equation (41.1a) renders

$$\frac{U}{T} \frac{\partial \hat{\mathbf{u}}}{\partial \hat{t}} + \frac{U^2}{L} (\hat{\mathbf{u}} \cdot \hat{\nabla}_z) \hat{\mathbf{u}} + \frac{W U}{H} \hat{w} \frac{\partial \hat{\mathbf{u}}}{\partial \hat{z}} + f_0 U (\hat{\mathbf{f}} \times \hat{\mathbf{u}}) = -f_0 U \hat{\nabla}_z \hat{\varphi}, \quad (41.44)$$

and dividing by $f_0 U$ leads to

$$\text{Ro} \left[\frac{\partial \hat{\mathbf{u}}}{\partial \hat{t}} + (\hat{\mathbf{u}} \cdot \hat{\nabla}_{\hat{z}}) \hat{\mathbf{u}} + \hat{w} \frac{\partial \hat{\mathbf{u}}}{\partial \hat{z}} \right] + (\hat{\mathbf{f}} \times \hat{\mathbf{u}}) = -\hat{\nabla}_z \hat{\varphi}. \quad (41.45)$$

The momentum equation is consistent with a unit geostrophy number (i.e., Coriolis acceleration balances pressure gradient acceleration) if and only if the Rossby number is small, thus eliminating the material acceleration. Likewise, the non-dimensional hydrostatic balance is given by

$$\frac{\partial \hat{\varphi}}{\partial \hat{z}} = \hat{b}, \quad (41.46)$$

and the non-dimensional continuity equation is

$$\hat{\nabla} \cdot \hat{\mathbf{v}} = 0. \quad (41.47)$$

Non-dimensional buoyancy equation

The buoyancy equation (41.4) requires a bit more work to non-dimensionalize. The material time derivative takes the form

$$\frac{D b'}{D t} = \frac{B}{T} \frac{D \hat{b}}{D \hat{t}} = \frac{U}{L} \frac{f_0 U L}{H} \frac{D \hat{b}}{D \hat{t}} = \frac{f_0 U^2}{H} \frac{D \hat{b}}{D \hat{t}}, \quad (41.48)$$

where we made use of the advective scaling $T = L/U$ and continuity scaling $W = U(H/L)$. The vertical advection of background stratification is given by

$$N^2 w = N^2 W \hat{w} = N^2 U (H/L) \hat{w} = L_d^2 \frac{U f_0^2}{H L} \hat{w}, \quad (41.49)$$

where we introduced the deformation radius, $L_d = H(N/f)$, from equation (41.29). Bringing these two pieces together leads to

$$\text{Ro} \frac{D\hat{b}}{Dt} + \text{Bu} \hat{w} = 0, \quad (41.50)$$

where we introduced the Burger number $\text{Bu} = (L_d/L)^2$.

41.3 Summary of the planetary geostrophic equations

Just like for the shallow water model in Section 40.4, the planetary geostrophic system for the stratified Boussinesq ocean is a rather simple asymptotic theory. For this case, we assume the horizontal scales are large compared to the deformation radius, so that

$$\text{Ro}/\text{Bu} \sim 1 \implies \text{Ro} L^2 \sim L_d^2. \quad (41.51)$$

With this scaling, and with a small Rossby number, the momentum equation (41.45) reduces to geostrophic balance. However, the continuity and buoyancy equations retain their unapproximated Boussinesq form. Hence, in dimensional form, the perfect (adiabatic and inviscid) planetary geostrophic equations for a stratified Boussinesq ocean are

$$\frac{Db'}{Dt} + w N^2 = 0 \quad (41.52a)$$

$$f \hat{\mathbf{z}} \times \mathbf{u} = -\nabla_z \varphi' \quad (41.52b)$$

$$\frac{\partial \varphi'}{\partial z} = b' \quad (41.52c)$$

$$\nabla \cdot \mathbf{v} = 0. \quad (41.52d)$$

41.3.1 Common form of the equations

We could just as well write the above planetary geostrophic equations in terms of the full buoyancy

$$b = \tilde{b}(z) + b', \quad (41.53)$$

and full pressure,

$$p = p_0(z) + \rho_0 \varphi. \quad (41.54)$$

Additionally, we can include non-conservative terms such as buoyancy mixing, \dot{b} , as well as horizontal frictional accelerations and/or boundary accelerations, \mathbf{F} . The following frictional and

diabatic planetary geostrophic equations form the basis for discussions in this chapter

$$f \hat{z} \times \mathbf{u} = -\rho_0^{-1} \nabla_z p + \mathbf{F} \quad \text{frictional geostrophy} \quad (41.55a)$$

$$\frac{\partial b}{\partial t} + \mathbf{u} \cdot \nabla_z b + N^2 w = \dot{b} \quad \text{diabatic buoyancy equation} \quad (41.55b)$$

$$\frac{\partial p}{\partial z} = -\rho g \quad \text{hydrostatic balance} \quad (41.55c)$$

$$\nabla \cdot \mathbf{v} = \nabla_z \cdot \mathbf{u} + \frac{\partial w}{\partial z} = 0 \quad \text{non-divergent flow} \quad (41.55d)$$

$$N^2 = \frac{\partial b}{\partial z} \quad \text{squared buoyancy frequency} \quad (41.55e)$$

$$b = -g(\rho - \rho_0)/\rho_0 \quad \text{Archimedean buoyancy.} \quad (41.55f)$$

Note that the material time derivative in planetary geostrophy makes use of advection by the three velocity components, $\mathbf{v} = (\mathbf{u}, w)$, as seen in the buoyancy equation (41.55b), with the horizontal velocity components determined by the frictional geostrophic balance (41.52b). This situation contrasts to quasi-geostrophy, where it is only the horizontal advection by the geostrophic flow that contributes to material time evolution (Section 42.2).

As for the Boussinesq ocean equations discussed in Section 26.1.6, we sometimes find it convenient to combine the horizontal velocity equation with the hydrostatic balance to write

$$f \hat{z} \times \mathbf{u} = -\nabla \varphi + b \hat{z} + \mathbf{F}. \quad (41.56)$$

Furthermore, it is common to assume an equation of state that is independent of pressure, so that material time changes in buoyancy arise only from changes in potential temperature and/or salinity

$$\dot{b} = \frac{\partial b}{\partial S} \dot{S} + \frac{\partial b}{\partial \Theta} \dot{\Theta}. \quad (41.57)$$

The buoyancy partial derivatives, $\partial b / \partial \Theta$ and $\partial b / \partial S$, are often assumed constant for idealized studies.

41.3.2 Planetary geostrophic energetics

Since the velocity is diagnostic in planetary geostrophy, it is a slave to the buoyancy field. In turn, there is a prognostic equation for potential energy that arises from the buoyancy equation, whereas kinetic energy is diagnostic. The energetics are thus a special case of the Boussinesq energetics studied in Section 26.7. We here consider just the basics.

General considerations

Multiplying the buoyancy equation (41.55b) by z leads to the potential energy equation

$$\partial_t P + \nabla \cdot (\mathbf{v} P) + w b = -z \dot{b}, \quad (41.58)$$

where we introduced the potential energy per mass relative to the reference density

$$P = -z b = z g(\rho - \rho_0)/\rho_0. \quad (41.59)$$

Equation (41.58) says that the potential energy at a point in the planetary geostrophic fluid is affected by advective transport, buoyancy work, and diabatic processes. As we will see, diabatic processes, such as diffusion, provide a local source for potential energy, whereas buoyancy work

transfers potential energy to kinetic energy.

Projecting the geostrophic/hydrostatic balance equation (41.56) onto the velocity leads to the diagnostic balance between pressure work, buoyancy work, and friction

$$\mathbf{v} \cdot \nabla \varphi - w b = \mathbf{u} \cdot \mathbf{F}. \quad (41.60)$$

We can add this balance to the potential energy equation (41.58) to eliminate the buoyancy work term, $w b$, thus yielding

$$\partial_t P + \nabla \cdot (\mathbf{v} P + \mathbf{v} \varphi) = \mathbf{u} \cdot \mathbf{F} - z \dot{b}, \quad (41.61)$$

where we used $\nabla \cdot \mathbf{v} = 0$ to bring $\mathbf{v} \varphi$ inside the divergence. We thus see that potential energy at a point in the planetary geostrophic fluid is affected by reversible transport processes from advection and pressure work, along with irreversible processes from friction and material buoyancy changes.

Diffusively driven flow

It is revealing to consider the special case of a rigid domain with no boundary fluxes and with buoyancy irreversibly modified through diffusion

$$\dot{b} = \nabla \cdot (\kappa \nabla b), \quad (41.62)$$

with $\kappa > 0$ a kinematic eddy diffusivity that is generally a function of the flow. Integrating the potential energy equation (41.61) over the domain leads to

$$\partial_t \langle P \rangle = \langle \mathbf{u} \cdot \mathbf{F} \rangle + \langle \kappa N^2 \rangle, \quad (41.63)$$

where the angle brackets signify volume means. To reach this identity we made use of

$$z \dot{b} = z \nabla \cdot (\kappa \nabla b) = \nabla \cdot (z \kappa \nabla b) - \kappa \partial_z b = \nabla \cdot (z \kappa \nabla b) - \kappa N^2, \quad (41.64)$$

with $\nabla \cdot (z \kappa \nabla b)$ integrating to zero in the absence of boundary fluxes. The global mean potential energy equation (41.63) indicates that vertical diffusion increases volume mean potential energy for a stably stratified fluid ($N^2 > 0$), whereas friction generally dissipates potential energy since $\mathbf{u} \cdot \mathbf{F} < 0$ (Section 23.3.2). So diffusion is the only source for potential energy, with spatial variations in potential energy leading to motion through the geostrophic balance. In the steady state this *diffusively driven flow* leads to the global mean balance between diffusion and friction

$$\langle \kappa N^2 \rangle = -\langle \mathbf{u} \cdot \mathbf{F} \rangle \quad \text{steady state.} \quad (41.65)$$

41.4 Planetary geostrophic potential vorticity

In Section 38.5 we developed the potential vorticity equation for the hydrostatic Boussinesq ocean in the presence of horizontal friction in the momentum equation and diabatic terms in the buoyancy equation. Here we specialize that result to the case of planetary geostrophic system written in the form of equations (41.55a)-(41.55e).

41.4.1 Derivation

Derivation of the potential vorticity equation proceeds much like that for the hydrostatic Boussinesq ocean. The first step requires the planetary geostrophic vorticity equation as determined by taking the curl of the momentum equation (41.55a). The vertical component of this vorticity

equation is given by (see also Section 28.5.2)

$$\beta v = f \partial_z w + \hat{z} \cdot (\nabla_z \times \mathbf{F}) \quad \text{with} \quad \beta = \partial_y f. \quad (41.66)$$

Next, make use of the thermal wind relation in the presence of friction

$$f \frac{\partial \mathbf{u}}{\partial z} = \hat{z} \times \nabla_z b - \frac{\partial(\hat{z} \times \mathbf{F})}{\partial z} \quad (41.67)$$

as well as the identities

$$N^2 \frac{Df}{Dt} = N^2 \beta v \quad (41.68a)$$

$$f \frac{DN^2}{Dt} = f \frac{\partial \dot{b}}{\partial z} - f \nabla b \cdot \frac{\partial \mathbf{v}}{\partial z} \quad (41.68b)$$

$$f \nabla b \cdot \frac{\partial \mathbf{v}}{\partial z} = f N^2 \frac{\partial w}{\partial z} - \frac{\partial(\hat{z} \times \mathbf{F})}{\partial z} \cdot \nabla_z b, \quad (41.68c)$$

to render

$$\frac{D(f N^2)}{Dt} = N^2 \beta v + f \frac{\partial \dot{b}}{\partial z} - f \nabla b \cdot \frac{\partial \mathbf{v}}{\partial z} \quad (41.69a)$$

$$= N^2 \left[f \frac{\partial w}{\partial z} + \hat{z} \cdot (\nabla_z \times \mathbf{F}) \right] + f \frac{\partial \dot{b}}{\partial z} - f N^2 \frac{\partial w}{\partial z} + \frac{\partial(\hat{z} \times \mathbf{F})}{\partial z} \cdot \nabla_z b \quad (41.69b)$$

$$= f \frac{\partial \dot{b}}{\partial z} + \nabla b \cdot (\nabla \times \mathbf{F}) \quad (41.69c)$$

$$= \nabla \cdot (f \dot{b} \hat{z} + \mathbf{F} \times \nabla b). \quad (41.69d)$$

We thus identify the planetary geostrophic potential vorticity

$$Q_{PG} = f N^2, \quad (41.70)$$

which is materially invariant in the absence of both diabatic processes and friction

$$\frac{DQ_{PG}}{Dt} = 0 \quad \text{when } \dot{b} = 0 \text{ and } \mathbf{F} = 0. \quad (41.71)$$

We can write the general budget equation in the form of an Eulerian flux-form expression

$$\partial_t Q_{PG} + \nabla \cdot \mathbf{J}_{PG} = 0, \quad (41.72)$$

where the potential vorticity flux is given by

$$\mathbf{J}_{PG} = \mathbf{v} Q_{PG} - \dot{b} f \hat{z} + \nabla b \times \mathbf{F} + \nabla \times \mathbf{A}. \quad (41.73)$$

The vector \mathbf{A} is an arbitrary gauge function that has no impact on the potential vorticity evolution. Comparing to the hydrostatic Boussinesq ocean expression (38.72), we see that the planetary geostrophic result follows by approximating the absolute vorticity by just the planetary vorticity.

41.4.2 Impermeability theorem

Following the discussion in Section 39.2.2, we verify that the potential vorticity flux vector (41.73) satisfies the impermeability theorem for buoyancy isosurfaces. We do so for the particular case of

a zero gauge function ($\mathbf{A} = 0$), in which case

$$\mathbf{v}_{\text{PG}} \cdot \nabla b = \frac{\mathbf{J}_{\text{PG}} \cdot \nabla b}{Q} = \mathbf{v} \cdot \nabla b - \dot{b} = -\frac{\partial b}{\partial t}, \quad (41.74)$$

so that

$$\frac{\partial b}{\partial t} + \mathbf{v}_{\text{PG}} \cdot \nabla b = 0. \quad (41.75)$$

Hence, there is zero flux of PV-substance crossing buoyancy isosurfaces, even in the presence of irreversible processes that allow matter and heat to cross those surfaces. As shown in the next subsection, we identify two more forms of the PV-substance flux vector that also satisfy impermeability, with these alternative forms differing by gauge transformations.

41.4.3 Kinematic fluxes satisfying impermeability

Following the discussion of impermeability for the Ertel potential vorticity in Section 39.2.2, we expose a purely kinematic means to derive the impermeability theorem for the planetary geostrophic potential vorticity. This derivation follows by computing the time tendency of the potential vorticity

$$\frac{\partial Q}{\partial t} = \frac{\partial}{\partial t} \nabla \cdot (f b \hat{\mathbf{z}}) = \nabla \cdot \left[f \frac{\partial b}{\partial t} \hat{\mathbf{z}} \right] \equiv -\nabla \cdot \tilde{\mathbf{J}}_{\text{PG}}, \quad (41.76)$$

where

$$\tilde{\mathbf{J}}_{\text{PG}} = -f \frac{\partial b}{\partial t} \hat{\mathbf{z}}. \quad (41.77)$$

This form of the PV-substance flux also satisfies impermeability since

$$\tilde{\mathbf{v}}_{\text{PG}} \cdot \nabla b = \frac{\tilde{\mathbf{J}}_{\text{PG}} \cdot \nabla b}{Q} = -\frac{\partial b}{\partial t}, \quad (41.78)$$

so that

$$\frac{\partial b}{\partial t} + \tilde{\mathbf{v}}_{\text{PG}} \cdot \nabla b = 0. \quad (41.79)$$

The flux $\tilde{\mathbf{J}}_{\text{PG}}$ vanishes in the steady state, whereas the steady state form of \mathbf{J}_{PG} does not vanish. Following the discussion in Section 39.3.2, we may choose to introduce a gauge transformation to the kinematic flux, $\tilde{\mathbf{J}}_{\text{PG}}$, so that it does not vanish in the steady state. Taking the small Rossby number limit of the flux (39.32) renders

$$\mathbf{J}_Q^{\text{marshall PG}} = -\nabla(g z + \varphi) \times \nabla b - f \frac{\partial b}{\partial t} \hat{\mathbf{z}}. \quad (41.80)$$

This flux differs from $\tilde{\mathbf{J}}_{\text{PG}}$ by a curl

$$\nabla(g z + \varphi) \times \nabla b = \nabla \times [(g z + \varphi) \nabla b], \quad (41.81)$$

and it also satisfies the impermeability theorem. As discussed in Section 39.5.6, there are a variety of motivations for using one form of the PV-substance flux versus another. Some applications prefer a nonzero steady flux that also does not involve any irreversible processes, with $\mathbf{J}_Q^{\text{marshall PG}}$ satisfying these desires.

41.5 Depth integrated vorticity budget

In a planetary geostrophic flow, vorticity arises just from planetary rotation since relative vorticity is assumed to be negligible. With planetary vorticity a function just of latitude, a budget for the planetary geostrophic vorticity reveals how the curl of forces imparted to the fluid cause meridional motion as the fluid meets the constraints imposed by the vorticity equation. As per our discussion in Section 37.3.6, we commonly refer to a force curl as a “torque” in our study of vorticity sources, with that terminology common in the study of vorticity budgets. However, one must keep in mind that more common usage in physics refers to a torque as affecting changes to angular momentum, with angular momentum generally distinct from vorticity (see Section 34.8 for a discussion of the distinction).

In this section we study the depth integrated vorticity budget for the planetary geostrophic fluid and derive implications for the meridional flow. For this purpose we focus on frictional and boundary accelerations that take the form of a vertical divergence of horizontal turbulent stresses

$$\mathbf{F} = \frac{\partial \boldsymbol{\tau}}{\partial z}. \quad (41.82)$$

The curl of this stress, as well as pressure forces, provide sources or torques that generate meridional motion as revealed by the planetary geostrophic vorticity budget.

41.5.1 The β -effect, stretching, and meridional transport

In Section 28.5.2 we derived the vorticity equation for the planetary geostrophic system. We also encountered this equation when deriving the potential vorticity budget in Section 41.4.1. With friction written as a vertical divergence of horizontal turbulent stresses (equation (41.82)), the vertical component of the planetary geostrophic vorticity equation takes the form

$$\rho_0 \beta v = \frac{\partial}{\partial z} [\rho_0 f w + \hat{z} \cdot (\nabla \times \boldsymbol{\tau})]. \quad (41.83)$$

Vertical integration from the ocean bottom at $z = \eta_b(x, y)$ to sea surface at $z = \eta(x, y, t)$ leads to¹

$$\rho_0 \beta V = \underbrace{\rho_0 f [w(\eta) - w(\eta_b)]}_{\text{column stretching}} + \underbrace{\hat{z} \cdot (\nabla \times \Delta \boldsymbol{\tau})}_{\text{boundary stresses}}, \quad (41.84)$$

where

$$V = \int_{\eta_b}^{\eta} v dz \quad (41.85)$$

is the depth-integrated meridional flow, and

$$\Delta \boldsymbol{\tau} = \boldsymbol{\tau}(\eta) - \boldsymbol{\tau}(\eta_b) \quad (41.86)$$

is the difference in boundary stresses applied at the ocean surface and ocean bottom. Note that $\Delta \boldsymbol{\tau}$ is just a function of horizontal position and time.

For a planetary geostrophic flow, absolute vorticity is approximated by just the planetary vorticity

$$\zeta_a = \zeta + f \approx f. \quad (41.87)$$

As revealed by the vorticity equation (41.84), vorticity sources in a planetary geostrophic fluid

¹As a means to unclutter notation, we write ∇ , rather than ∇_z , whenever acting on a field that is just a function of horizontal position, such as p_a, p_b, η_b and $\Delta \boldsymbol{\tau}$. We can do so since, for example, $\nabla p_b = \nabla_z p_b$ since $\partial_z p_b = 0$.

lead to meridional motion. The sources lead to meridional motion since that is the only way a planetary geostrophic fluid can modify its vorticity in response to sources.

The first term on the right hand side of the vorticity equation (41.84) arises from vertical stretching of the depth integrated column as measured by differences in the vertical velocity at the ocean surface and bottom. For example, vertical stretching caused by positive surface velocity, $w(\eta) > 0$, or a negative bottom velocity, $w(\eta_b) < 0$, lead to poleward motion of the fluid column. Conversely, vertical squashing leads to equatorward motion. We emphasize that the vertical stretching term arises from the difference in the boundary vertical velocity rather than the vertical velocity within the interior of the fluid.

The second term in the vorticity equation (41.84) arises from differences in the vorticity imparted by surface and bottom boundary stresses. Positive vorticity imparted to the fluid through the curl of wind stresses, $\hat{z} \cdot [\nabla \times \boldsymbol{\tau}(\eta)] > 0$, or by the curl of bottom stresses, $\hat{z} \cdot [\nabla \times \boldsymbol{\tau}(\eta_b)] < 0$, lead to poleward motion of the fluid column, with opposite motion for the converse curls.

The β -effect (Section 37.6.2) is a fundamental element of the depth integrated vorticity equation (41.84). Namely, as fluid columns are stretched or squashed, they must move meridionally to maintain vorticity balance for a planetary geostrophic fluid on a rotating spherical earth. The planetary geostrophic vorticity equation restricts attention to vertical stretching through vertical motion (the w terms) and through the vorticity imparted by the curl of boundary stresses. Notably, the curl of boundary stresses also imparts vertical motion through surface and bottom Ekman layer dynamics (see Chapter 30). Hence, the right hand side of the vorticity equation (41.84) is fundamentally related to vortex stretching.

Equation (41.84) is central to mechanical descriptions of large-scale ocean circulation. For many flow regimes, the curl of the surface wind stress dominates, thus allowing us to ignore the vertical velocity terms as well as bottom frictional stresses. Formally, we isolate the wind stress when studying a flat bottom rigid lid model, whereby $w(\eta) = w(\eta_b) = 0$. However, there can be nontrivial impacts from bottom pressure torques when flow interacts with sloping topography, with the North Atlantic and Southern Ocean providing important case studies. Other processes can be important in various flow regimes, thus prompting us to derive a full diagnostic framework to identify where these processes are important. To pursue that framework, we make use of the kinematic boundary conditions and the horizontal momentum equation to unpack the vertical velocity terms. Doing so reveals the forces and their curls that drive vertical motion at the boundaries for a planetary geostrophic flow. By doing so, we capture how these force curls contribute, through the β -effect, to meridional motion of the depth integrated flow.

41.5.2 Bottom kinematics and dynamics

The bottom kinematic boundary condition applied at $z = \eta_b(x, y)$ (Section 16.4.1) is given by

$$w = \mathbf{u} \cdot \nabla \eta_b \quad \text{at } z = \eta_b(x, y). \quad (41.88)$$

This relation expresses the no-normal flow condition $\hat{\mathbf{n}} \cdot \mathbf{v} = 0$ at the ocean bottom, with

$$\hat{\mathbf{n}} = -\frac{\nabla(z - \eta_b)}{|\nabla(z - \eta_b)|} = -\left[\frac{\hat{z} - \nabla \eta_b}{\sqrt{1 + \nabla \eta_b \cdot \nabla \eta_b}} \right] \quad (41.89)$$

the outward unit normal to the bottom. The boundary condition constrains the flow so that any horizontal motion next to a sloping bottom that is oriented either up or down the slope must have an associated vertical motion. As we see in this section, such vertical motion next to the bottom boundary arises from force curls acting to stretch or squash a fluid column. In turn, through the vorticity equation (41.84), vertical motion at the bottom leads to meridional motion of the full

fluid column.

Expressions for bottom vertical velocity

The bottom kinematic boundary condition holds for all dynamical flow regimes. For the particular case of planetary geostrophy, we garner insight into the forces that drive vertical flow near the bottom by making use of the planetary geostrophic momentum equation (41.55a). Evaluating the horizontal components of this equation at the ocean bottom yields²

$$\rho_0 f \hat{z} \times \mathbf{u} = -\nabla p_b + \mathbf{F}_b, \quad (41.90)$$

where $p_b(x, y, t)$ is the bottom pressure and $\mathbf{F}_b(x, y, t)$ is the bottom friction. For the special case of a no-slip bottom, all velocity components vanish at $z = \eta_b$. In that case, we consider \mathbf{u} in equation (41.90) to be the horizontal velocity averaged within the bottom boundary layer, and w the corresponding vertical velocity leaving the boundary layer.

It is convenient to decompose the bottom horizontal velocity into its geostrophic and Ekman³ components via

$$\rho_0 f \hat{z} \times \mathbf{u}_g = -\nabla p_b \quad \text{and} \quad \rho_0 f \hat{z} \times \mathbf{u}_e = \mathbf{F}_b, \quad (41.91)$$

so that

$$\mathbf{u}_g = \frac{\hat{z} \times \nabla p_b}{\rho_0 f} \quad \text{and} \quad \mathbf{u}_e = -\frac{\hat{z} \times \mathbf{F}_b}{\rho_0 f}. \quad (41.92)$$

The corresponding bottom vertical velocity components are determined by inserting equations (41.92) into the bottom kinematic boundary condition (41.88)

$$w_g = \frac{\hat{z} \cdot (-\nabla \eta_b \times \nabla p_b)}{\rho_0 f} \quad \text{and} \quad w_e = \frac{\hat{z} \cdot (\nabla \eta_b \times \mathbf{F}_b)}{\rho_0 f}. \quad (41.93)$$

These equations reveal how the curl of inviscid pressure forces and boundary frictional forces drive a nonzero vertical motion next to the bottom, all while maintaining the bottom kinematic boundary condition (41.88). As seen by these equations, is only the projection of ∇p_b and \mathbf{F}_b onto the isobath direction that contributes to a nonzero vertical velocity. These along-isobath forces are needed to render a horizontal velocity that is itself misaligned with isobaths, thus satisfying the kinematic requirement for vertical motion.

To further understand the bottom pressure term, we write it as

$$w_g = \frac{\hat{z} \cdot (-\nabla \eta_b \times \nabla p_b)}{\rho_0 f} = \frac{\hat{z} \cdot [\nabla \times p_b \nabla \eta_b]}{\rho_0 f}. \quad (41.94)$$

The numerator is the curl of the horizontal projection of the pressure contact force along the bottom, $p_b \nabla \eta_b$. This term is the topographic form stress discussed in Section 25.2 for a general fluid and in Section 36.7.5 for the shallow water. We thus conclude that vertical geostrophic motion next to the bottom arises from the curl of the topographic form stress. This is an important result that will appear again within this section as well as in Sections 41.7 and 41.8.

Comments on the bottom vertical geostrophic velocity

A large part of the bottom pressure gradient driving the horizontal geostrophic flow in equation (41.92) arises from changes in bottom depth. However, that portion of the bottom pressure

²Recall that since $p_b = p_b(x, y, t)$, we have $\nabla p_b = \nabla_z p_b$. As noted in the footnote on page 1059, we drop the z script to reduce notational clutter.

³Recall our discussion of Ekman mechanics in Chapter 30.

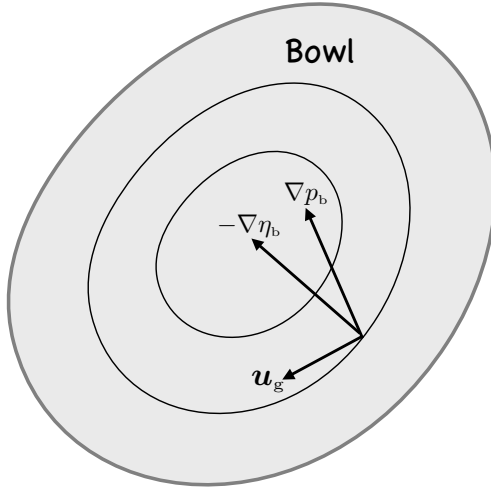


FIGURE 41.1: Depicting how bottom pressure gradients create vertical motion in planetary geostrophic flow next to a sloping bottom according to equations (41.93) and (41.95). Here we show a bowl or depression (local maximum in the depth) with $-\nabla \eta_b$ increasing inward toward the bowl center. Only those portions of ∇p_b and \mathbf{F}_b that are aligned parallel to the topographic slope contribute to vertical motion. We illustrate here a case where the bottom pressure gradient leads to $-\nabla \eta_b \cdot \mathbf{u}_g > 0$ so that $w_g < 0$ in the northern hemisphere and $w_g > 0$ in the southern hemisphere (see equations (41.93) and (41.95)).

gradient has no impact on w_g , since it only drives horizontal flow along isobaths. We see this property by writing

$$p_b = -\rho_0 g \eta_b + p'_b \implies w_g = \frac{\hat{z} \cdot (-\nabla \eta_b \times \nabla p'_b)}{\rho_0 f}. \quad (41.95)$$

When there is misalignment between isolines of bottom pressure and bottom topography, the geostrophic flow in a fluid column will cross isobaths. Correspondingly, with the pressure force misaligned with topographic gradients, the fluid column experiences a twisting action akin to how baroclinicity spins a fluid element if the pressure force does not act through the fluid element's center of mass (see Section 37.4).

To illustrate the above, consider the topographic bowl in Figure 41.1, with sides steep enough so that the bottom pressure gradient is dominated by the topographic slopes. Along the bottom the pressure increases moving down (increasing depth) towards the bowl center. The corresponding bottom geostrophic flow is anti-cyclonic within the bowl and largely follows isobaths. As already noted, if the geostrophic flow exactly follows isobaths, then there is no corresponding vertical component to the bottom velocity. A vertical velocity arises only in the presence of an anomalous bottom pressure gradient, $\nabla p'_b$, that is misaligned with the bottom slope, $\nabla \eta_b$. This bottom pressure gradient balances a geostrophic flow that deviates from isobaths thus giving rise to a nonzero w_g . Similar geometric analysis holds for the bottom friction vector, \mathbf{F}_b , and how it gives rise to a nonzero vertical Ekman velocity, w_e .

What causes misalignment between p_b and η_b ?

As we just discussed, misalignment of p_b and η_b lead to vertical geostrophic motion along the bottom. In Section 41.5.3 we will see a similar relation for vertical geostrophic motion at the ocean surface. But what causes such misalignment? The answer to this question is circular when working within the planetary geostrophic whose momentum equation is diagnostic. Even so, we can offer some insight by returning to the depth-integrated vorticity balance (41.84) and rewriting

it as an expression for vertical motion

$$\rho_0 f [w(\eta_b) - w(\eta)] = -\rho_0 \beta V + \hat{z} \cdot (\nabla \times \Delta \boldsymbol{\tau}). \quad (41.96)$$

Hence, vertical motion at the surface and bottom arise from meridional motion in the presence of planetary beta, plus the curl of surface and bottom stresses. The absence of planetary beta, and the absence of boundary stress curls, realizes $w(\eta_b) = w(\eta)$, with zero vertical motion the typical case.

41.5.3 Surface kinematics and dynamics

For purposes of large-scale circulation studies using the PG equations, it is generally sufficient to assume a rigid lid upper boundary condition, whereby $w(\eta) = w(0) = 0$. Even so, we find it revealing to present the results for a free surface in which there is the possibility of nonzero surface mass fluxes. The surface kinematic boundary condition for a Boussinesq fluid (Section 18.2) is given by

$$w = -\frac{Q_m}{\rho_0} + \frac{\partial \eta}{\partial t} + \mathbf{u} \cdot \nabla \eta \quad \text{at } z = \eta(x, y, t). \quad (41.97)$$

We retain the sea surface time tendency, $\partial_t \eta$, even though for transient solutions the time tendency is many orders of magnitude smaller than the typical vertical velocity under the planetary geostrophic regime.⁴ Evaluating the horizontal planetary geostrophic momentum equation (28.25a) at the ocean surface renders

$$\rho_0 f \hat{z} \times \mathbf{u} = -\nabla p_a + \mathbf{F}_\eta, \quad (41.98)$$

where p_a is the pressure applied to the ocean surface and \mathbf{F}_η is the corresponding horizontal friction vector. Like the bottom, we decompose the horizontal velocity into a geostrophic component and an Ekman component via

$$\rho_0 f \hat{z} \times \mathbf{u}_g = -\nabla p_a \quad \text{and} \quad \rho_0 f \hat{z} \times \mathbf{u}_e = \mathbf{F}_\eta, \quad (41.99)$$

so that

$$\mathbf{u}_g = \frac{\hat{z} \times \nabla p_a}{\rho_0 f} \quad \text{and} \quad \mathbf{u}_e = -\frac{\hat{z} \times \mathbf{F}_\eta}{\rho_0 f}. \quad (41.100)$$

The corresponding vertical velocity components are determined by inserting into the surface kinematic boundary condition (41.97)

$$w_{Q\eta} = -\frac{Q_m}{\rho_0} + \frac{\partial \eta}{\partial t} \quad \text{and} \quad w_g = \frac{\hat{z} \cdot (-\nabla \eta \times \nabla p_a)}{\rho_0 f} \quad \text{and} \quad w_e = \frac{\hat{z} \cdot (\nabla \eta \times \mathbf{F}_\eta)}{\rho_0 f}, \quad (41.101)$$

where we introduced a vertical velocity, $w_{Q\eta}$, associated with the boundary mass flux and transient sea level fluctuations. As for the bottom, the second and third of these equations reveal how the curl of inviscid pressure forces and boundary frictional forces drive a nonzero vertical motion at the ocean surface, all while maintaining the surface kinematic boundary condition (41.97). Furthermore, it is only the projection of ∇p_a and \mathbf{F}_η onto the direction parallel to sea surface height contours that contributes to a nonzero vertical velocity. This orientation of the surface forces is needed to render a horizontal velocity that is itself misaligned with sea surface height contours, thus satisfying the kinematics required to render vertical motion.

⁴See Section 3.3 of [Samelson \(2011\)](#) for more details on this scaling of the planetary geostrophic system.

41.5.4 Summary of force curls driving depth integrated meridional flow

Plugging expressions (41.93), (41.95), and (41.101) into equation (41.84) renders the depth integrated planetary vorticity balance

$$\rho_0 \beta V = f (-Q_m + \rho_0 \partial_t \eta) + \hat{z} \cdot [\nabla \eta \times (\mathbf{F}_\eta - \nabla p_a) - \nabla \eta_b \times (\mathbf{F}_b - \nabla p'_b) + \nabla \times \Delta \boldsymbol{\tau}] . \quad (41.102)$$

We see how the force curls are symmetrically applied at the surface and bottom, which is part of the motivation for exposing the surface terms even though they are generally subdominant. In general, equation (41.102) shows that the depth integrated meridional flow, within the planetary geostrophic regime, is driven by the following processes.

Surface mass transport plus sea surface fluctuations

The term $f (-Q_m + \rho_0 \partial_t \eta)$ arises from mass transport across the ocean surface plus fluctuations in the sea surface height. For example, as sea surface height increases or as water leaves the ocean surface, they impart a positive surface vertical velocity, $w(\eta) > 0$, thus causing column stretching and poleward meridional depth integrated flow. In the steady state, where it is just the mass flux term that contributes, the meridional circulation is known as the Goldsbrough-Stommel circulation (see [Huang and Schmitt \(1993\)](#) for a review).

Curl of turbulent boundary stresses

The term $\hat{z} \cdot (\nabla \times \Delta \boldsymbol{\tau})$ arises from the curl of the turbulent wind stress and turbulent bottom stress. The wind stress term is generally larger than the bottom turbulent stress, with many theories for ocean circulation, particularly those with a flat bottom, almost exclusively focused on the role of surface stress in forcing the planetary geostrophic vorticity budget. We comment more on this case in Section 41.6 where we discuss the *Sverdrup balance*.

Atmospheric pressure torque

The term

$$\nabla p_a \times \nabla \eta = \nabla \times (p_a \nabla \eta) = -\nabla \times (\eta \nabla p_a) \quad (41.103)$$

arises from differences in lines of constant atmospheric pressure and lines of constant sea surface height. Such misalignments create a torque akin to the baroclinicity detailed in Section 37.4, with these misalignments driving vertical motion and a corresponding depth integrated meridional flow.

Bottom pressure torque

The term

$$\nabla p'_b \times (-\nabla \eta_b) = \nabla \times (-p'_b \nabla \eta_b) = \nabla \times (\eta_b \nabla p'_b) \quad (41.104)$$

arises from differences in lines of constant bottom pressure and lines of constant bottom topography. That is, bottom pressure torque requires a gradient of bottom pressure along isobaths, thus producing a bottom geostrophic flow that deviates from isobaths. As for the atmospheric pressure torques, such misalignments create a torque that drives a depth integrated meridional flow, with this term vanishing when the bottom topography is flat. In many cases with strong flow next to sloping bottoms, this term can contribute more to the vorticity budget than the turbulent bottom stress. Indeed, in some cases it can rival contributions from the surface wind stress. We sketched out such cases for the shallow water when discussing western boundary currents in Section 36.7.5.

Surface frictional acceleration

The term

$$\hat{\mathbf{z}} \cdot (\nabla \eta \times \mathbf{F}_\eta) = \hat{\mathbf{z}} \cdot \left[\nabla \eta \times \frac{\partial \boldsymbol{\tau}_\eta}{\partial z} \right] \quad (41.105)$$

arises from evaluating the vertical divergence of the frictional stress at the sea surface. A finite volume boundary layer treatment of this term prompts us to integrate the stress divergence over the extent of the surface Ekman layer to render the alternative expression

$$\hat{\mathbf{z}} \cdot \int_{-h_{e\text{-surf}}}^{\eta} \left[\nabla \eta \times \frac{\partial \boldsymbol{\tau}}{\partial z} \right] dz = \hat{\mathbf{z}} \cdot [\nabla \eta \times \boldsymbol{\tau}(\eta)], \quad (41.106)$$

where we assumed $\boldsymbol{\tau}$ is negligible at the base of the surface Ekman layer, $z = -h_{e\text{-surf}}(x, y, t)$. The term $\hat{\mathbf{z}} \cdot [\nabla \eta \times \boldsymbol{\tau}(\eta)]$ creates a torque from that component of the surface turbulent stress that is aligned with isolines of the sea surface height.

Bottom frictional acceleration

The term

$$\hat{\mathbf{z}} \cdot (-\nabla \eta_b \times \mathbf{F}_b) = \hat{\mathbf{z}} \cdot \left[-\nabla \eta_b \times \frac{\partial \boldsymbol{\tau}_b}{\partial z} \right] \quad (41.107)$$

arises from evaluating the vertical divergence of the frictional stress at the ocean bottom. As for the analogous term for the surface, we offer a finite volume Ekman boundary layer treatment to render the alternative expression

$$\hat{\mathbf{z}} \cdot \int_{\eta_b}^{h_{e\text{-bot}}} \left[-\nabla \eta_b \times \frac{\partial \boldsymbol{\tau}}{\partial z} \right] dz = \hat{\mathbf{z}} \cdot [-\nabla \eta_b \times \boldsymbol{\tau}(\eta_b)], \quad (41.108)$$

where we assumed $\boldsymbol{\tau}$ is negligible at the top of the bottom Ekman layer, $z = -\eta_b + h_{e\text{-bot}}$. The term $\hat{\mathbf{z}} \cdot [-\nabla \eta_b \times \boldsymbol{\tau}(\eta_b)]$ creates a torque from that component of the bottom turbulent stress that is aligned with isobaths.

41.5.5 Integral constraints

The atmospheric and bottom pressure torques appearing in the depth integrated planetary vorticity balance (41.102) satisfy an integral constraint that follows from Stokes' curl theorem. To illustrate this constraint, consider the bottom pressure torque integrated over an arbitrary area

$$\int (\nabla \eta_b \times \nabla p'_b) \cdot \hat{\mathbf{z}} dA = \int [\nabla \times (\eta_b \nabla p'_b)] \cdot \hat{\mathbf{z}} dA \quad (41.109a)$$

$$= \oint_{\partial A} \eta_b \nabla p'_b \cdot \hat{\mathbf{t}} ds \quad (41.109b)$$

$$= - \oint_{\partial A} p'_b \nabla \eta_b \cdot \hat{\mathbf{t}} ds. \quad (41.109c)$$

We see that the bottom pressure torque vanishes when integrated around a closed loop that follows either an isobath or a bottom isobar, since the integrand vanishes identically. A similar constraint holds for the atmospheric pressure torque, whereas there is generally no analogous constraint satisfied by the turbulent boundary stresses.

One exception for the turbulent stresses occurs for f -plane flow ($\beta = 0$) where the depth

integrated flow is non-divergent

$$\partial_t \eta - Q_m / \rho_0 = -\nabla \cdot \mathbf{U} = 0, \quad (41.110)$$

and where the interior friction vanishes at the surface and bottom boundaries, $\mathbf{F}_\eta = \mathbf{F}_b = 0$. From equation (41.102), we see that a steady state is realized only if there is a balance between pressure torques and turbulent boundary stresses

$$\hat{\mathbf{z}} \cdot (\nabla \eta \times \nabla p_a - \nabla \eta_b \times \nabla p'_b) = \hat{\mathbf{z}} \cdot (\nabla \times \Delta \boldsymbol{\tau}). \quad (41.111)$$

Consider even further specialization in which the atmospheric pressure torque vanishes, and the bottom turbulent stress is negligible, in which case a steady state balance requires a balance between bottom pressure torques and torques from surface turbulent wind stress

$$-\hat{\mathbf{z}} \cdot (\nabla \eta_b \times \nabla p'_b) = \hat{\mathbf{z}} \cdot [\nabla \times \boldsymbol{\tau}(\eta)]. \quad (41.112)$$

Integration over either an isobath or bottom pressure isobar then requires, for a steady state, the following identity

$$\int [\nabla \times \boldsymbol{\tau}(\eta)] \cdot \hat{\mathbf{z}} \, dA = \oint \boldsymbol{\tau}(\eta) \cdot \hat{\mathbf{t}} \, ds = 0 \quad f\text{-plane closed isobath or closed isobar.} \quad (41.113)$$

Deviation from this identity leads to non-steady flow on the f -plane. In contrast, the β -plane has no such steady state constraint since meridional flow can balance the circulation imparted by turbulent wind stresses.

41.6 Sverdrup balance and geostrophic Sverdrup balance

The balance (41.102) exposes many processes that affect meridional flow in a planetary geostrophic fluid. However, for many purposes, particularly when confronted with minimal information from ocean measurements, we examine just the main contributors to this balance.

The *Sverdrup balance* is a very simplified form of the balance (41.102), and it was first encountered in Section 28.5.5

$$\rho_0 \beta V_{\text{Sverdrup}} = \hat{\mathbf{z}} \cdot [\nabla \times \boldsymbol{\tau}(\eta)] \quad \text{Sverdrup balance.} \quad (41.114)$$

This balance arises from dropping the vertical velocity at both the surface and bottom; ignoring horizontal frictional stresses, and assuming $\partial_t \eta = -Q_m / \rho_0$ as per a rigid lid flow in which $\nabla \cdot \mathbf{U} = 0$. It offers a null hypothesis for the large-scale and low frequency meridional ocean circulation away from sloping sides; i.e., in regions where bottom pressure torques can be ignored.

To derive the Sverdrup balance (41.114), we performed a depth integral of the planetary geostrophic vorticity equation (41.83) from the ocean bottom to the free surface. This integral encompasses both the geostrophic interior and the ageostrophic Ekman flow in the top and bottom Ekman layers. In some treatments we focus exclusively on contributions from the geostrophic interior, in which case the depth integral extends from the top of the bottom Ekman layer, $z = \eta_{eb}$, to the bottom of the top Ekman layer, $z = \eta_{et}$, thus leading to the depth integrated geostrophic transport

$$V_g \equiv \int_{\eta_{eb}}^{\eta_{et}} v \, dz. \quad (41.115)$$

Integrating the planetary geostrophic vorticity balance (41.83) over this depth range, and ignoring

contributions from friction since we are concerned just with the geostrophic interior, leads to

$$\rho_0 \beta V_g = f [w(\eta_{et}) - w(\eta_{eb})]. \quad (41.116)$$

This equation provides a balance between the depth integrated meridional transport within the geostrophic interior (left hand side), with the vertical vortex stretching within this depth range (right hand side).

We now make use of the Ekman theory from Chapter 30 to approximate the vertical velocities in equation (41.116). For this purpose we neglect both the time tendency for the vertical position of the Ekman layer and the slope of the Ekman layer, in which case the kinematic identity (30.37), applied at the Ekman base, $z = \eta_e(x, y, t)$, is approximated by

$$w^{(\dot{\eta}_e)} = w - (\partial_t z + \mathbf{u} \cdot \nabla z) \approx w \quad \text{at } z = \eta_e(x, y, t), \quad (41.117)$$

where $z = \eta_e$ is the vertical position of the Ekman layer. We now make use of the Ekman layer mass budgets to determine the entrainment velocity, $w^{(\dot{\eta}_e)}$. In particular, equation (30.44) is used for $w(\eta_{et})$ to give

$$w(\eta_{et}) \approx w_{\text{Ekman-top}}^{(\dot{\eta}_e)} = (1/\rho_0) \hat{\mathbf{z}} \cdot [\nabla \times (\boldsymbol{\tau}(\eta)/f)]. \quad (41.118)$$

with a similar treatment for the bottom leading to

$$w(\eta_{eb}) \approx w_{\text{Ekman-bot}}^{(\dot{\eta}_e)} = (1/\rho_0) f \hat{\mathbf{z}} \cdot [\nabla \times (\boldsymbol{\tau}(\eta_b)/f)]. \quad (41.119)$$

Bringing these results into equation (41.116) leads to

$$\rho_0 \beta V_g = \hat{\mathbf{z}} \cdot \nabla \times [\boldsymbol{\tau}(\eta)/f - \boldsymbol{\tau}(\eta_b)/f]. \quad (41.120)$$

Since the bottom turbulent stress is generally much smaller than the surface, it can be readily ignored, in which case we reach the *geostrophic Sverdrup balance*

$$\rho_0 \beta V_g = \hat{\mathbf{z}} \cdot \nabla \times [\boldsymbol{\tau}(\eta)/f] \quad \text{geostrophic Sverdrup balance.} \quad (41.121)$$

The geostrophic Sverdrup balance relates the meridional geostrophic transport to the curl of $\boldsymbol{\tau}/f$ due to upper ocean mechanical stresses from boundary processes; i.e., wind stress and ice-ocean stresses. [Gray and Riser \(2014\)](#) assess the geostrophic Sverdrup balance based on ocean measurements.

41.7 Vorticity of the depth integrated velocity

In Section 41.5 we studied the depth integrated vorticity budget for planetary geostrophic flow. We were led to see how boundary torques (i.e., the curl of boundary forces) lead to vertical motion and in turn, through the β -effect, lead to meridional motion of the depth integrated flow. In this section we present another analysis of vorticity in the planetary geostrophic regime, here focusing on vorticity of the depth integrated velocity. Elements of this material were discussed in Section 37.9 without making the planetary geostrophic assumption. By assuming planetary geostrophy we can further constrain the flow through studies of the vorticity balances.

41.7.1 Depth integrated velocity equation

The depth integrated horizontal velocity equation (41.55a) is given by

$$\rho_0 f \hat{z} \times \mathbf{U} = - \int_{\eta_b}^{\eta} \nabla_z p dz + \Delta\tau \quad (41.122)$$

where

$$\mathbf{U} = \int_{\eta_b}^{\eta} \mathbf{u} dz \quad (41.123)$$

is the depth integrated horizontal velocity, and we assumed friction in the form of the vertical divergence of a horizontal turbulent stress as in equation (41.82). For the depth integrated pressure gradient, we follow the decomposition in Section 25.4.4 by writing

$$\int_{\eta_b}^{\eta} p dz = \int_{\eta_b}^{\eta} [d(p z) - z dp] = p_a \eta - p_b \eta_b + \mathcal{P}, \quad (41.124)$$

where we used the hydrostatic balance to write $dp = -g \rho dz$, which is valid for each fluid column. We also introduced the potential energy per horizontal area of a fluid column

$$\mathcal{P} = \int_{\eta_b}^{\eta} g \rho z dz = (g \rho_0/2) (\eta^2 - \eta_b^2) + \int_{\eta_b}^{\eta} g \rho' z dz, \quad (41.125)$$

where

$$\rho' = \rho - \rho_0 \quad (41.126)$$

is the density deviation from the background reference density. These results then lead to the depth integrated horizontal pressure gradient

$$\int_{\eta_b}^{\eta} \nabla_z p dz = \nabla_z \left[\int_{\eta_b}^{\eta} p dz \right] - p_a \nabla_z \eta + p_b \nabla_z \eta_b \quad (41.127a)$$

$$= \nabla_z [p_a \eta - p_b \eta_b + \mathcal{P}] - p_a \nabla_z \eta + p_b \nabla_z \eta_b \quad (41.127b)$$

$$= \eta \nabla_z p_a - \eta_b \nabla_z p_b + \nabla_z \mathcal{P}, \quad (41.127c)$$

$$= \eta \nabla p_a - \eta_b \nabla p_b + \nabla \mathcal{P}, \quad (41.127d)$$

where the final equality follows since p_a , η_b , p_b , and \mathcal{P} , are functions just of horizontal position and time. We are thus led to the depth integrated planetary geostrophic momentum balance

$$\rho_0 f \hat{z} \times \mathbf{U} = -\eta \nabla p_a + \eta_b \nabla p_b - \nabla \mathcal{P} + \Delta\tau. \quad (41.128)$$

The depth integrated balance is here written in terms of gradients in the surface and bottom pressures, the gradient of the potential energy per area, and the difference in turbulent stresses at the top and bottom boundaries, $\Delta\tau = \tau(\eta) - \tau(\eta_b)$.

41.7.2 Vorticity budget

Taking the curl of the depth integrated balance (41.128) annihilates the potential energy term, thus leaving

$$\rho_0 \beta V = -\rho_0 f \nabla \cdot \mathbf{U} + \hat{z} \cdot \nabla \times [p_a \nabla \eta + \tau(\eta) - p_b \nabla \eta_b - \tau(\eta_b)]. \quad (41.129)$$

From Section 18.7, we know that the divergence of the depth-integrated flow for a steady Boussinesq fluid is given by

$$\rho_0 \nabla \cdot \mathbf{U} = Q_m, \quad (41.130)$$

so that

$$\rho_0 \beta V = -f Q_m + \hat{\mathbf{z}} \cdot \nabla \times [p_a \nabla \eta + \boldsymbol{\tau}(\eta) - p_b \nabla \eta_b - \boldsymbol{\tau}(\eta_b)]. \quad (41.131)$$

This is the vorticity equation for the depth integrated planetary geostrophic fluid. It is quite similar to the vorticity balance for a shallow water fluid as given by equation (36.100) (which considered zero atmospheric pressure). In the presence of β , meridional mass transport for the fluid column is generated by surface mass fluxes, $Q_m \neq 0$; the curl of surface form stresses and surface turbulent stresses; and the curl of topographic form stresses and bottom turbulent stresses. This result follows quite naturally when recognizing that the forces acting on a depth integrated fluid column arise from the depth integrated stresses acting in the column sides plus those acting on the top and bottom boundaries. In the absence of interior friction stresses due to horizontal strains, it is only the depth integrated pressure that acts on the column sides, and this term has zero curl. We are thus left with the curl of the form stresses and turbulent stresses on the surface and bottom boundaries, along with the contribution from mass transport.

The Sverdrup balance (41.114) is a special case of the more complete vorticity budget (41.129). Furthermore, the *topographic Sverdrup balance* results when meridional transport balances the curl of the wind plus bottom pressure form stress

$$\rho_0 \beta V_{\text{topo-Sverdrup}} = \hat{\mathbf{z}} \cdot \nabla \times (\boldsymbol{\tau}(\eta) - p_b \nabla \eta_b) \quad \text{topographic Sverdrup balance.} \quad (41.132)$$

In the presence of flows interacting with topography, where bottom pressure torques are sizable, this balance is generally much more accurate than the Sverdrup balance.

41.7.3 Integral balances for steady flows

Following the discussion in Section 37.9.5, we write the vorticity balance (41.129) in the form

$$\rho_0 \nabla \cdot (f \mathbf{U}) = \hat{\mathbf{z}} \cdot \nabla \times [p_a \nabla \eta + \boldsymbol{\tau}(\eta) - p_b \nabla \eta_b - \boldsymbol{\tau}(\eta_b)]. \quad (41.133)$$

Integrating over a horizontal area, \mathcal{S} , leads to

$$\rho_0 \oint_{\partial\mathcal{S}} f \mathbf{U} \cdot \hat{\mathbf{n}} \, ds = \oint_{\partial\mathcal{S}} [p_a \nabla \eta + \boldsymbol{\tau}(\eta) - p_b \nabla \eta_b - \boldsymbol{\tau}(\eta_b)] \cdot \hat{\mathbf{t}} \, ds, \quad (41.134)$$

where we used Gauss's divergence theorem for the left hand side and Stokes' curl theorem for the right hand side. The unit vector $\hat{\mathbf{n}}$ points horizontally outward from the boundary of the area, whereas the unit vector $\hat{\mathbf{t}}$ is the counter-clockwise oriented tangent to the closed contour around the boundary. For the special case of $Q_m = 0$ we are afforded a steady state streamfunction for the depth-integrate flow since $\nabla \cdot \mathbf{U} = 0$. Choosing the area, \mathcal{S} , to be bounded by a closed streamline allows us to set $\mathbf{U} \cdot \hat{\mathbf{n}} = 0$ along that streamline. We thus see that for steady planetary geostrophic flow with $\nabla \cdot \mathbf{U} = 0$, any closed streamline of the flow must maintain the following work balance around the streamline

$$\oint_{\partial\mathcal{S}} [p_a \nabla \eta + \boldsymbol{\tau}(\eta) - p_b \nabla \eta_b - \boldsymbol{\tau}(\eta_b)] \cdot \hat{\mathbf{t}} \, ds = 0. \quad (41.135)$$

This equation is a simplified form of equation (37.190) that was formulated for a more general flow. We can rearrange equation (41.135) to display an integrated balance between the work done

by boundary pressure form stresses and work done by boundary turbulent stresses

$$\oint_{\partial S} (p_a \nabla \eta - p_b \nabla \eta_b) \cdot \hat{\mathbf{t}} \, ds = - \oint_{\partial S} [\boldsymbol{\tau}(\eta) - \boldsymbol{\tau}(\eta_b)] \cdot \hat{\mathbf{t}} \, ds. \quad (41.136)$$

41.8 Vorticity equation for the depth averaged velocity

In some numerical models, it is more common to have access to the depth averaged velocity

$$\bar{\mathbf{u}} = \frac{1}{D} \int_{\eta_b}^{\eta} \mathbf{u} \, dz \quad \text{with} \quad D = \eta - \eta_b. \quad (41.137)$$

We thus find it useful to derive the budget for the vorticity of the depth averaged velocity. In this discussion we encounter a distinct means for describing how bottom topography, in the presence of baroclinicity, generates meridional flow.

41.8.1 Relating the depth average velocity to boundary velocities

Before studying the vorticity equation, we here relate the depth averaged velocity, $\bar{\mathbf{u}}(x, y, t)$, to the surface velocity, $\mathbf{u}(x, y, z = \eta, t)$, and bottom velocity, $\mathbf{u}(x, y, z = \eta_b, t)$. This analysis exposes some general features of how the boundary flows are driven away from the depth average.

The starting point is the identity

$$\int_{\eta_b}^{\eta} \mathbf{u} \, dz = (\eta - \eta_b) \mathbf{u}(\eta) - \int_{\eta_b}^{\eta} \frac{\partial \mathbf{u}}{\partial z} (z - \eta_b) \, dz, \quad (41.138)$$

which, along with the analogous identity for the bottom flow, leads to

$$\bar{\mathbf{u}} - \mathbf{u}(\eta) = - \int_{\eta_b}^{\eta} \frac{\partial \mathbf{u}}{\partial z} \left[\frac{z - \eta_b}{\eta - \eta_b} \right] \, dz \quad \text{and} \quad \bar{\mathbf{u}} - \mathbf{u}(\eta_b) = \int_{\eta_b}^{\eta} \frac{\partial \mathbf{u}}{\partial z} \left[\frac{\eta - z}{\eta - \eta_b} \right] \, dz. \quad (41.139)$$

Note that $\mathbf{u}(\eta) - \mathbf{u}(\eta_b) = \int_{\eta_b}^{\eta} (\partial \mathbf{u} / \partial z) \, dz$ serves as a useful check on the manipulations leading to equation (41.139). We see that the difference between the depth averaged flow and the surface flow, $\bar{\mathbf{u}} - \mathbf{u}(\eta)$, is determined by the integral of the weighted vertical shear, with the weight linearly decreasing from unity at the surface to zero at the bottom. The minus sign in front of the integral is sensible because if the flow increases in the positive direction from the bottom to the surface, then the depth averaged flow will have a smaller magnitude than the surface flow. The converse weighting holds for computing the difference $\bar{\mathbf{u}} - \mathbf{u}(\eta_b)$.

The identities (41.139) hold for arbitrary horizontal velocity fields. Assuming the flow satisfies frictional geostrophy as per equation (41.55a) leads to the frictional thermal wind relation

$$f \mathbf{u} = \rho_0^{-1} \hat{\mathbf{z}} \times \nabla p - \hat{\mathbf{z}} \times \mathbf{F} \implies f \partial_z \mathbf{u} = -(g/\rho_0) \hat{\mathbf{z}} \times \nabla \rho - \hat{\mathbf{z}} \times \partial_z \mathbf{F}, \quad (41.140)$$

so that the velocity differences are given by

$$f [\bar{\mathbf{u}} - \mathbf{u}(\eta)] = \int_{\eta_b}^{\eta} [(g/\rho_0) \hat{\mathbf{z}} \times \nabla \rho - \hat{\mathbf{z}} \times \partial_z \mathbf{F}] \left[\frac{z - \eta_b}{\eta - \eta_b} \right] \, dz \quad (41.141a)$$

$$f [\bar{\mathbf{u}} - \mathbf{u}(\eta_b)] = - \int_{\eta_b}^{\eta} [(g/\rho_0) \hat{\mathbf{z}} \times \nabla \rho - \hat{\mathbf{z}} \times \partial_z \mathbf{F}] \left[\frac{\eta - z}{\eta - \eta_b} \right] \, dz. \quad (41.141b)$$

Hence, differences between the depth averaged flow and the boundary flows are determined by

weighted integrals of the baroclinicity and vertical friction shears.

41.8.2 Formulation of the vorticity equation

To develop the vorticity equation, we start by deriving the momentum equation for the depth averaged flow. For that purpose, rearrange the depth integrated momentum budget (41.128) according to

$$\rho_0 f \hat{z} \times \mathbf{U} = -\eta \nabla_z (p_a - p_b) - D \nabla p_b - \nabla \mathcal{P} + \Delta \boldsymbol{\tau} \quad (41.142)$$

and then divide by the thickness, $D = \eta - \eta_b$, of the ocean column to render

$$\rho_0 f \hat{z} \times \bar{\mathbf{u}} = -(\eta/D) \nabla (p_a - p_b) - \nabla p_b + (1/D) (-\nabla \mathcal{P} + \Delta \boldsymbol{\tau}). \quad (41.143)$$

Taking the curl then leads to

$$\rho_0 \nabla \cdot (f \bar{\mathbf{u}}) = -\hat{z} \cdot \nabla \times [(\eta/D) \nabla (p_a - p_b)] + D^{-2} \hat{z} \cdot [\nabla \times (D \nabla \mathcal{P})] + \hat{z} \cdot [\nabla \times (D^{-1} \Delta \boldsymbol{\tau})] \quad (41.144a)$$

$$= \hat{z} \cdot \nabla \times [(p_a - p_b) \nabla (\eta/D)] - D^{-2} \hat{z} \cdot [\nabla \times (\mathcal{P} \nabla D)] + \hat{z} \cdot [\nabla \times (D^{-1} \Delta \boldsymbol{\tau})]. \quad (41.144b)$$

The vorticity budget (41.144) is a bit less tidy than that for the depth integrated budget (41.131). Nonetheless, it offers some useful insights concerning the flow. For that purpose, write the left hand side in the suggestive form

$$\nabla \cdot (f \bar{\mathbf{u}}) = \nabla \cdot [(f/D) \mathbf{U}], \quad (41.145)$$

with f/D reminiscent of the shallow water potential vorticity for the planetary geostrophic flow (Section 40.4). Motivated by this analog, we write the vorticity equation (41.144) in the form

$$\begin{aligned} \rho_0 \mathbf{U} \cdot \nabla (f/D) &= -\rho_0 (f/D) \nabla \cdot \mathbf{U} + \hat{z} \cdot \nabla \times [(p_a - p_b) \nabla (\eta/D)] \\ &\quad - D^{-2} \hat{z} \cdot [\nabla \times (\mathcal{P} \nabla D)] + \hat{z} \cdot [\nabla \times (D^{-1} \Delta \boldsymbol{\tau})]. \end{aligned} \quad (41.146)$$

Contrary to the shallow water case, we here see that even for a perfect planetary geostrophic fluid, the depth-integrated flow does not generally follow contours of constant f/D . Even so, it is of interest to examine how the processes on the right hand side contribute to flow deviations from f/D contours. For that purpose we simplify the flow even more by making the rigid lid approximation.

41.8.3 Rigid lid approximation and the role of JEBAR

The rigid lid approximation is commonly made for studies of large-scale circulation. Indeed, it was the basis for many ocean general circulation models following the work of [Bryan \(1969\)](#). A fluid satisfying the rigid lid approximation has a vanishing horizontal divergence for the depth integrated flow

$$\text{rigid lid approximation} \implies \nabla \cdot \mathbf{U} = 0. \quad (41.147)$$

Furthermore, as part of the rigid lid approximation we assume the free surface undulations are much smaller than the resting ocean depth so that⁵

$$|\eta| \ll |\eta_b| \implies \eta/D \approx 0 \quad (41.148a)$$

$$1/(\eta - \eta_b) \approx 1/(-\eta_b) = 1/H. \quad (41.148b)$$

Hence, with the rigid lid approximation the vorticity equation (41.146) takes the simplified form

$$\rho_0 \mathbf{U} \cdot \nabla(f/H) = \hat{\mathbf{z}} \cdot [\nabla \times \mathcal{P} \nabla(1/H) + \nabla \times (H^{-1} \Delta \boldsymbol{\tau})]. \quad (41.149)$$

JEBAR drives deviations from f/H aligned flow

The first term on the right hand side of the vorticity equation (41.149) is referred to as the Joint Effect of Baroclinicity and Relief (JEBAR)

$$\text{JEBAR} = \hat{\mathbf{z}} \cdot [\nabla \times \mathcal{P} \nabla(1/H)] = \hat{\mathbf{z}} \cdot [\nabla \mathcal{P} \times \nabla(1/H)]. \quad (41.150)$$

This name arises since JEBAR is nonzero only in the presence of non-flat topography (“relief”) and (as shown below) when density is not a constant (i.e., for baroclinic flow). In addition to contributions from boundary stresses, equation (41.149) says that misalignment of f/H contours with the depth-integrated steady rigid lid flow is driven by misalignments of isobaths and isolines of the depth integrated potential energy.

Contributions to JEBAR arise only from the component of the potential energy that deviates from a constant density reference state. To show that property, note that in the rigid lid approximation, the potential energy in a column, as given by equation (41.125), takes the form

$$\mathcal{P} = (1/2) g \rho_0 H^2 + g \int_{-H}^0 \rho' z dz, \quad (41.151)$$

where $\rho' = \rho - \rho_0$. With $\nabla H^2 \times \nabla(1/H) = 0$, we are left with just the contribution from ρ'

$$\text{JEBAR} = \hat{\mathbf{z}} \cdot \left[\nabla \left(g \int_{-H}^0 \rho' z dz \right) \times \nabla(1/H) \right]. \quad (41.152)$$

JEBAR vanishes for a homogeneous density field, where ρ' is a constant, but is nonzero with a nonzero ρ' , which is typically associated with baroclinicity.

Relating JEBAR to pressure

JEBAR as given by equation (41.150) has the appearance of the curl of a form stress, and yet it is not. The reason is that \mathcal{P} is the potential energy of the fluid column rather than bottom pressure. We make this point explicit by recalling the decomposition (41.124), here specialized to the rigid lid in which

$$\mathcal{P} = H(\bar{p} - p_b) \quad \text{with} \quad \bar{p} = H^{-1} \int_{-H}^0 p dz = (-\eta_b)^{-1} \int_{\eta_b}^0 p dz. \quad (41.153)$$

⁵We use the notation $\eta_b = -H$ in this subsection to correspond to the literature for rigid lid models and the JEBAR term. Note that H is the vertical depth scale, which is a constant, and it is distinct from $H(x, y) = -\eta_b(x, y)$, which is a function of horizontal position.

Plugging into the vorticity equation (41.149) leads to

$$\rho_0 \mathbf{U} \cdot \nabla(f/\mathbb{H}) = \mathbb{H}^{-1} \hat{\mathbf{z}} \cdot [\nabla \mathbb{H} \times \nabla(\bar{p} - p_b)] + \hat{\mathbf{z}} \cdot \nabla \times (\mathbb{H}^{-1} \Delta \boldsymbol{\tau}). \quad (41.154)$$

The JEBAR term thus arises from deviations of the depth averaged pressure from the bottom pressure

$$\text{JEBAR} = \hat{\mathbf{z}} \cdot [\nabla \mathcal{P} \times \nabla(1/\mathbb{H})] = \mathbb{H}^{-1} \hat{\mathbf{z}} \cdot [\nabla \mathbb{H} \times \nabla(\bar{p} - p_b)]. \quad (41.155)$$

We can go one more step in exposing this pressure difference through use of equation (41.139), here applied to hydrostatic pressure, in which case

$$\bar{p} - p_b = \int_{\eta_b}^0 \frac{\partial p}{\partial z} \frac{z}{\eta_b} dz = (g/\mathbb{H}) \int_{-\mathbb{H}}^0 z \rho dz = \mathbb{H}^{-1} \mathcal{P} \quad (41.156)$$

so that

$$g^{-1} \nabla(\bar{p} - p_b) = -\rho(z = \eta_b) \nabla \mathbb{H} - \int_{-\mathbb{H}}^0 \nabla(\rho z/\mathbb{H}) dz. \quad (41.157)$$

The first term arises from slopes in the bottom topography as weighted by the bottom density, whereas the second term arises from the density integral of the horizontal gradients in the depth-weighted density.

Alternatively, we can introduce a geostrophic velocity associated with the gradient of the bottom pressure as well as the vertically averaged pressure

$$\rho_0 f \hat{\mathbf{z}} \times \mathbf{u}_{gb} = -\nabla p_b \quad \text{and} \quad \rho_0 f \hat{\mathbf{z}} \times \bar{\mathbf{u}}_g = -\nabla \bar{p}. \quad (41.158)$$

Doing so brings JEBAR from equation (41.155) into the form

$$\text{JEBAR} = \mathbb{H}^{-1} \hat{\mathbf{z}} \cdot [\nabla \mathbb{H} \times \nabla(\bar{p} - p_b)] = -\rho_0 f \mathbb{H}^{-1} \nabla \mathbb{H} \cdot (\mathbf{u}_{gb} - \bar{\mathbf{u}}_g). \quad (41.159)$$

JEBAR thus arises from a nonzero projection onto the bottom slope of the difference between the geostrophic velocity arising from the bottom pressure and the geostrophic velocity arising from the depth averaged pressure.

Equation (41.131) provides the budget for vorticity of the depth integrated flow, in which we find the curl of the topographic form stress leads to vortex stretching. For the vorticity of the depth averaged flow, we instead encounter the JEBAR term in equation (41.154), which is not a pure vortex stretching term. Instead, it accounts for the fact that it is the horizontal velocity flowing across isobaths, $\mathbf{u}(z = \eta_b)$, rather than depth averaged horizontal velocity, $\bar{\mathbf{u}}$, that leads to vortex stretching. Hence, when studying vorticity of the depth averaged velocity, $\bar{\mathbf{u}}$, accounting for the role of vortex stretching requires us to include JEBAR.

Integral balances

Since the depth integrated flow is assumed to be non-divergent in the rigid lid approximation, $\nabla \cdot \mathbf{U} = 0$, we know there exists a streamfunction for this flow. Consider a region where there are closed streamlines. Following the steps in Section (41.7.3), we integrate the steady vorticity equation (41.149) around the streamline. Noting that $\mathbf{U} \cdot \hat{\mathbf{n}} = 0$ along the streamline, where $\hat{\mathbf{n}}$ is the horizontal unit normal to the streamline, thus renders the steady balance

$$\oint_{\partial S_{\text{streamline}}} (\mathcal{P} \nabla \mathbb{H}^{-1} + \mathbb{H}^{-1} \Delta \boldsymbol{\tau}) \cdot \hat{\mathbf{t}} ds = 0. \quad (41.160)$$

41.8.4 Further study

Chapter 3 in [Samelson \(2011\)](#) studies the large-scale ocean circulation based on planetary geostrophy. [Mertz and Wright \(1992\)](#) discuss the physics of how JEBAR relates to the curl of the topographic form stress as well as other mathematically equivalent forms. [Cane et al. \(1998\)](#) as well as Section 2.5 of [Drijfhout et al. \(2013\)](#) offer critical remarks concerning how JEBAR can be physically confusing. [Yeager \(2015\)](#) connects torques acting on the depth integrated horizontal flow in the North Atlantic and buoyancy forces affecting the Atlantic meridional overturning circulation.



Chapter 42

CONTINUOUSLY STRATIFIED QUASI-GEOSTROPHY

Quasi-geostrophy (QG) is the canonical *balanced model* in geophysical fluid mechanics whereby the potential vorticity is the sole prognostic field; all other fields, such as the velocity and buoyancy, are diagnosed from potential vorticity. The process of diagnosing the allied fields requires the inversion of an elliptic operator to compute the geostrophic streamfunction from the potential vorticity. Some authors refer to this connection between potential vorticity and streamfunction as *invertibility*, with the mathematical technology required for inversion shared with many other elliptic problems in mathematical physics (see Section 3.5 for more on elliptic partial differential equations).

Quasi-geostrophy is an elegant theory of mathematical physics offering great physical and mathematical insights into the workings of geophysical fluid motions where rotation and stratification play leading roles in the dynamics. Giving the theory full justice requires a book the size of the current one. Instead, we here aim to provide a taste of its continuously stratified realization, offering a detailed derivation that builds from Chapters 40 and 41, and sampling some of its physical and mathematical content.

CHAPTER GUIDE

In this chapter we extend to continuously stratified fluids the shallow water discussions of quasi-geostrophy in Chapter 40. Continuously stratified quasi-geostrophy is not concerned with the processes that affect stratification, but instead with the processes that slightly perturb that stratification. We make use of stratified geophysical fluid dynamics from Chapters 21 and 28, as well as potential vorticity from Chapter 38 and the development of continuously stratified planetary geostrophy in Chapter 41. This chapter is essential for our study of baroclinic instability in Chapter 55.

42.1	Open threads	1076
42.2	The quasi-geostrophic PV equation	1076
42.2.1	Zeroth order asymptotic equations	1077
42.2.2	First order asymptotic equations	1078
42.3	Reintroducing physical dimensions	1079
42.3.1	Hydrostatic balance	1080
42.3.2	Geostrophic balance	1080
42.3.3	Material time derivative	1080
42.3.4	Buoyancy equation	1081
42.3.5	Vorticity equation	1081
42.3.6	Velocity equation	1082
42.3.7	Potential vorticity	1082
42.3.8	Comments about doubly-periodic QG models	1083

42.4 Connecting quasi-geostrophic PV to Ertel PV	1084
42.4.1 Non-dimensionalizing the Ertel potential vorticity	1084
42.4.2 Material conservation of Ertel PV to order Ro^1	1085
42.5 Mathematical expressions of the theory	1086
42.5.1 The Jacobian form of geostropic advection	1086
42.5.2 Constant background buoyancy frequency	1086
42.5.3 Vertical boundary conditions for ψ	1087
42.5.4 Potential vorticity induction and impermeability	1089
42.6 Energetics for quasi-geostrophic flow	1090
42.6.1 Kinetic energy	1090
42.6.2 Available potential energy	1091
42.6.3 Exchange of mechanical energy	1092
42.6.4 Scaling APE and KE	1092
42.7 Exercises	1093

42.1 Open threads

- Solution needed for Exercise 42.6.

42.2 The quasi-geostrophic PV equation

In deriving the quasi-geostrophic PV equation, we proceed much like for the single layer of shallow water fluid in Section 40.5. In particular, quasi-geostrophic scaling from Section 40.5.1 is relevant for both the shallow water and for the continuously stratified fluid. We employ an asymptotic expansion in the Rossby number and stop at the first nontrivial order, which is Ro^1 . For this purpose, recall the non-dimensional momentum and continuity equations from Section 41.2.8

$$\text{Ro} \left[\frac{\partial \hat{\mathbf{u}}}{\partial \hat{t}} + (\hat{\mathbf{u}} \cdot \hat{\nabla}_{\hat{z}}) \hat{\mathbf{u}} + \hat{w} \frac{\partial \hat{\mathbf{u}}}{\partial \hat{z}} \right] + \hat{\mathbf{f}} \times \hat{\mathbf{u}} = -\hat{\nabla}_{\hat{z}} \hat{\varphi} \quad (42.1a)$$

$$\frac{\partial \hat{\varphi}}{\partial \hat{z}} = \hat{b} \quad (42.1b)$$

$$\hat{\nabla} \cdot \hat{\mathbf{v}} = 0 \quad (42.1c)$$

$$\frac{\text{Ro}}{\text{Bu}} \frac{\text{D}\hat{b}}{\text{D}\hat{t}} + \hat{w} = 0. \quad (42.1d)$$

We expand all fields in an asymptotic series in Rossby number

$$\hat{\mathbf{u}} = \hat{\mathbf{u}}_0 + \text{Ro} \hat{\mathbf{u}}_1 + \text{Ro}^2 \hat{\mathbf{u}}_2 + \dots \quad (42.2a)$$

$$\hat{\mathbf{v}} = \hat{\mathbf{v}}_0 + \text{Ro} \hat{\mathbf{v}}_1 + \text{Ro}^2 \hat{\mathbf{v}}_2 + \dots \quad (42.2b)$$

$$\hat{w} = \hat{w}_0 + \text{Ro} \hat{w}_1 + \text{Ro}^2 \hat{w}_2 + \dots \quad (42.2c)$$

$$\hat{b} = \hat{b}_0 + \text{Ro} \hat{b}_1 + \text{Ro}^2 \hat{b}_2 + \dots \quad (42.2d)$$

$$\hat{\varphi} = \hat{\varphi}_0 + \text{Ro} \hat{\varphi}_1 + \text{Ro}^2 \hat{\varphi}_2 + \dots \quad (42.2e)$$

along with the expansion (40.55) for the Coriolis parameter

$$\hat{\mathbf{f}} = \hat{\mathbf{f}}_0 + \text{Ro} \hat{\beta} \hat{\mathbf{y}}, \quad (42.3)$$

and where (equation (40.56))

$$\widehat{\beta} \widehat{y} = \frac{\beta y}{\text{Ro} f_0} = T \beta y. \quad (42.4)$$

As noted in Section 40.5.2, the velocity field is non-divergent at each order of Rossby number, so that

$$\nabla \cdot \widehat{\mathbf{v}}_n = 0 \quad \forall n. \quad (42.5)$$

The Burger number is order unity since the horizontal length scales for the quasi-geostrophic flows of concern here are on the order of the deformation radius

$$\text{Bu} \sim 1 \implies L \sim L_d, \quad (42.6)$$

where we introduced the *internal deformation radius* from Section 41.2.6

$$L_d(z) = H(N(z)/f_0). \quad (42.7)$$

It is important to retain the depth dependence of the Burger number through its dependence on the background stratification $N^2(z)$

$$\text{Bu}(z) = \left[\frac{L_d}{L} \right]^2 = N(z)^2 \left[\frac{H}{L f_0} \right]^2, \quad (42.8)$$

which motivates the name *Burger function* for continuously stratified quasi-geostrophy. Importantly, the Burger function does not commute with the vertical derivative operator.

42.2.1 Zeroth order asymptotic equations

The zeroth order asymptotic equations are

$$\widehat{\mathbf{f}}_0 \times \widehat{\mathbf{u}}_0 = -\widehat{\nabla}_z \widehat{\varphi}_0 \quad (42.9a)$$

$$\frac{\partial \widehat{\varphi}_0}{\partial \widehat{z}} = \widehat{b}_0 \quad (42.9b)$$

$$\widehat{\nabla}_z \cdot \widehat{\mathbf{u}}_0 + \frac{\partial \widehat{w}_0}{\partial \widehat{z}} = 0 \quad (42.9c)$$

$$\widehat{w}_0 = 0. \quad (42.9d)$$

The first equation represents *f*-plane geostrophy, which means that the horizontal velocity has zero divergence

$$\widehat{\nabla}_z \cdot \widehat{\mathbf{u}}_0 = 0. \quad (42.10)$$

Equation (42.9b) means the zeroth order buoyancy determines the zeroth order hydrostatic pressure. Since the horizontal velocity has zero divergence, the continuity equation (42.9c) means that the vertical velocity is depth independent

$$\frac{\partial \widehat{w}_0}{\partial \widehat{z}} = 0. \quad (42.11)$$

If it vanishes somewhere, such as a solid horizontal bottom boundary, then it vanishes everywhere. This is a manifestation of the Taylor-Proudman theorem (see Section 28.5.3). Indeed, a vanishing \widehat{w}_0 is required by the zeroth-order buoyancy equation (42.9d) even if the bottom is not flat. Hence,

the non-dimensional velocity has a nonzero contribution only at order Ro^1

$$\hat{w} = \text{Ro} \hat{w}_1 + \text{Ro}^2 \hat{w}_2 + \dots, \quad (42.12)$$

thus manifesting the vertical stiffening of fluid columns found in rotating fluids. Correspondingly, the dimensionful vertical velocity has the asymptotic expansion

$$w = W \hat{w} = W \text{Ro} (\hat{w}_1 + \text{Ro} \hat{w}_2 + \dots), \quad (42.13)$$

so that to leading to order Ro^1

$$\hat{w}_1 = \frac{w}{W \text{Ro}}. \quad (42.14)$$

Since the zeroth-order horizontal velocity is non-divergent, we can introduce a geostrophic streamfunction

$$\hat{u}_0 = -\partial \hat{\psi}_0 / \partial \hat{y} \quad \text{and} \quad \hat{v}_0 = \partial \hat{\psi}_0 / \partial \hat{x} \quad \text{and} \quad \hat{\zeta}_0 = \hat{\nabla}^2 \hat{\psi}_0, \quad (42.15)$$

where the zeroth-order streamfunction is the ratio of the zeroth order pressure to zeroth order Coriolis parameter

$$\hat{\psi}_0 = \hat{\varphi}_0 / \hat{f}_0. \quad (42.16)$$

Note also that the zeroth-order system satisfies the thermal wind balance

$$\hat{f}_0 \times \frac{\partial \hat{u}_0}{\partial \hat{z}} = -\hat{\nabla}_z \hat{b}_0. \quad (42.17)$$

Finally, note that the zeroth order buoyancy is determined by the streamfunction through the hydrostatic balance

$$\hat{b}_0 = \frac{\partial \hat{\varphi}_0}{\partial \hat{z}} = \hat{f}_0 \frac{\partial \hat{\psi}_0}{\partial \hat{z}}. \quad (42.18)$$

42.2.2 First order asymptotic equations

The zeroth order equations do not render a prognostic equation, for which we need to consider equations at order Ro^1

$$\frac{D_0 \hat{u}_0}{Dt} + \hat{f}_0 \times \hat{u}_1 + \hat{\beta} \hat{y} \hat{z} \times \hat{u}_0 = -\hat{\nabla}_z \hat{\varphi}_1 \quad (42.19a)$$

$$\frac{\partial \hat{\varphi}_1}{\partial \hat{z}} = \hat{b}_1 \quad (42.19b)$$

$$\hat{\nabla}_z \cdot \hat{u}_1 + \frac{\partial \hat{w}_1}{\partial \hat{z}} = 0 \quad (42.19c)$$

$$\frac{1}{Bu} \frac{D_0 \hat{b}_0}{Dt} + \hat{w}_1 = 0. \quad (42.19d)$$

The first order terms are often referred to as the *ageostrophic* components, though note that all contributions higher than zeroth order constitute ageostrophic contributions.

At order Ro^1 , the material time derivative makes use *only* of the zeroth order horizontal geostrophic velocity

$$\frac{D_0}{Dt} = \frac{\partial}{\partial t} + \hat{u}_0 \cdot \hat{\nabla}. \quad (42.20)$$

To close this set of equations, we produce the vorticity equation from the momentum equation, and then combine the vorticity equation and buoyancy equation to produce the quasi-geostrophic

potential vorticity equation. In Section 40.5, we performed the same procedure for deriving the shallow water quasi-geostrophic equations.

Taking the curl of the momentum equation (42.19a) eliminates the pressure gradient, $\hat{\nabla}\hat{\varphi}_1$, thus producing the vorticity equation

$$\frac{\partial \hat{\zeta}_0}{\partial \hat{t}} + (\hat{\mathbf{u}}_0 \cdot \hat{\nabla}) (\hat{\zeta}_0 + \hat{\beta} \hat{y}) = -\hat{f}_0 \hat{\nabla}_z \cdot \mathbf{u}_1. \quad (42.21)$$

We make use of the continuity equation (42.19c) to eliminate the horizontal convergence

$$\frac{\partial \hat{\zeta}_0}{\partial \hat{t}} + (\hat{\mathbf{u}}_0 \cdot \hat{\nabla}) (\hat{\zeta}_0 + \hat{\beta} \hat{y}) = \hat{f}_0 \frac{\partial \hat{w}_1}{\partial \hat{z}}. \quad (42.22)$$

The right hand side represents the contribution to vorticity evolution from stretching by the ageostrophic vertical velocity acting in a rotating reference frame. We can eliminate the ageostrophic vertical velocity through use of the buoyancy equation (42.19d). When doing so, it is important to keep the depth dependence of the Burger function, $Bu(z)$, according to equation (42.8), with this depth dependence arising from the prescribed background stratification, $N^2(z)$. The resulting vorticity equation is

$$\frac{\partial \hat{\zeta}_0}{\partial \hat{t}} + (\hat{\mathbf{u}}_0 \cdot \hat{\nabla}) (\hat{\zeta}_0 + \hat{\beta} \hat{y}) = -\hat{f}_0 \frac{\partial}{\partial \hat{z}} \left[\frac{1}{Bu} \frac{D_0 \hat{b}_0}{Dt} \right]. \quad (42.23)$$

We now use the identity

$$\frac{\partial}{\partial \hat{z}} \left[\frac{1}{Bu} \frac{D_0 \hat{b}_0}{Dt} \right] = \frac{\partial}{\partial \hat{z}} \left[\frac{1}{Bu} \left(\frac{\partial}{\partial \hat{t}} + \hat{\mathbf{u}}_0 \cdot \hat{\nabla} \right) \hat{b}_0 \right] \quad (42.24a)$$

$$= \frac{D_0}{Dt} \left[\frac{\partial}{\partial \hat{z}} \left(\frac{\hat{b}_0}{Bu} \right) \right] + \frac{1}{Bu} \frac{\partial \hat{\mathbf{u}}_0}{\partial \hat{z}} \cdot \hat{\nabla}_z \hat{b}_0 \quad (42.24b)$$

$$= \frac{D_0}{Dt} \left[\frac{\partial}{\partial \hat{z}} \left(\frac{\hat{b}_0}{Bu} \right) \right], \quad (42.24c)$$

where we set

$$\frac{\partial \hat{\mathbf{u}}_0}{\partial \hat{z}} \cdot \hat{\nabla}_z \hat{b}_0 = 0 \quad (42.25)$$

since the zeroth-order velocity maintains thermal wind balance (42.17). Bringing terms together then leads to the material conservation equation for quasi-geostrophic potential vorticity

$$\frac{D_0}{Dt} \left[\hat{\zeta}_0 + \hat{\beta} \hat{y} + \hat{f}_0 \frac{\partial}{\partial \hat{z}} \left(\frac{\hat{b}_0}{Bu} \right) \right] = 0. \quad (42.26)$$

42.3 Reintroducing physical dimensions

To expose the physical elements to the quasi-geostrophic theory, we find it useful, if not essential, to reintroduce physical dimensions much like we did for the shallow water in Section 40.6. For

that purpose, we write

$$\mathbf{u} \equiv \mathbf{u}_g + \mathbf{u}_{ag} = U (\hat{\mathbf{u}}_0 + \text{Ro} \hat{\mathbf{u}}_1) \quad (42.27a)$$

$$w \equiv w_{ag} = \text{Ro} W \hat{w}_1 \quad (42.27b)$$

$$b \equiv b_g + b_{ag} = B (\hat{b}_0 + \text{Ro} \hat{b}_1) \quad (42.27c)$$

$$\varphi \equiv \varphi_g + \varphi_{ag} = f_0 U L (\hat{\varphi}_0 + \text{Ro} \hat{\varphi}_1). \quad (42.27d)$$

The details of reintroducing dimensions are straightforward but can be tedious. We provide full details to help develop experience and confidence working with the theory.

42.3.1 Hydrostatic balance

Hydrostatic balance is maintained for terms at each Rossby number order, so that we have the dimensional equations

$$\frac{\partial \varphi_g}{\partial z} = b_g \quad \text{and} \quad \frac{\partial \varphi_{ag}}{\partial z} = b_{ag}. \quad (42.28)$$

42.3.2 Geostrophic balance

The non-dimensional geostrophic balance for the zeroth order fields

$$\hat{\mathbf{f}}_0 \times \hat{\mathbf{u}}_0 = -\hat{\nabla}_z \hat{\varphi}_0 \quad (42.29)$$

takes on the dimensional form

$$\hat{\mathbf{z}} \times \mathbf{u}_g / U = -L \nabla_z \varphi_g / (f_0 U L). \quad (42.30)$$

Cancelling factors leads to the expected form of f -plane geostrophy

$$f_0 \hat{\mathbf{z}} \times \mathbf{u}_g = -\nabla_z \varphi_g. \quad (42.31)$$

42.3.3 Material time derivative

For the material time derivative operator we write

$$D/Dt = \partial_t + \mathbf{u} \cdot \nabla + w \partial_z \quad (42.32a)$$

$$= (1/T) \partial_{\hat{t}} + (U/L) \hat{\mathbf{u}} \cdot \hat{\nabla} + (W/H) \hat{w} \partial_{\hat{z}} \quad (42.32b)$$

$$= (1/T) (\partial_{\hat{t}} + \hat{\mathbf{u}} \cdot \hat{\nabla} + \hat{w} \partial_{\hat{z}}) \quad (42.32c)$$

$$= (1/T) (\partial_{\hat{t}} + \hat{\mathbf{u}}_0 \cdot \hat{\nabla}_z) + (\text{Ro}/T) (\hat{\mathbf{u}}_0 \cdot \hat{\nabla}_z + \hat{w}_1 \partial_{\hat{z}}) \quad (42.32d)$$

$$= \partial_t + \mathbf{u}_g \cdot \nabla_z + \mathbf{u}_{ag} \cdot \nabla_z + w_{ag} \partial_z \quad (42.32e)$$

$$\equiv D_g/Dt + \mathbf{u}_{ag} \cdot \nabla_z + w_{ag} \partial_z, \quad (42.32f)$$

where time scales according to advection, $T = L/U$, vertical velocity scales according to continuity, $W = H U / L$, and we introduced the geostrophic material time derivative operator

$$D_g/Dt \equiv \partial_t + \mathbf{u}_g \cdot \nabla_z. \quad (42.33)$$

42.3.4 Buoyancy equation

The buoyancy equation requires a bit more work. For that purpose, we split buoyancy into a depth dependent static background and a deviation from the background

$$b = \tilde{b}(z) + b'(x, y, z, t), \quad (42.34)$$

with its vertical derivative

$$\partial_z b = d\tilde{b}/dz + \partial_z b' = N^2 + \partial_z b', \quad (42.35)$$

where $N^2(z)$ is the squared buoyancy frequency for the prescribed background buoyancy field. In this manner, we can write the buoyancy equation for an adiabatic fluid as

$$\frac{\partial b'}{\partial t} + \mathbf{u} \cdot \nabla b' + w(N^2 + \partial_z b') = 0. \quad (42.36)$$

We non-dimensionalize this equation by making use of the following relations between the scales

$$B = f_0 U L / H \quad W = H(U/L) \quad \text{Ro} = U/(f_0 L) \quad \text{Bu} = (N H)^2 / (f_0 L)^2, \quad (42.37)$$

in which case the buoyancy equation takes the form

$$\frac{\partial b'}{\partial t} + \mathbf{u} \cdot \nabla b' + w(N^2 + \partial_z b') = \frac{B}{T} \frac{\partial \hat{b}}{\partial \hat{t}} + \frac{U B}{L} \hat{\mathbf{u}} \cdot \hat{\nabla}_z \hat{b} + W \hat{w} N^2 + \frac{W B}{H} \hat{w} \partial_{\hat{z}} \hat{b} = 0. \quad (42.38)$$

We find it useful to divide by $f_0 N^2$, so that

$$\frac{1}{f_0 N^2} \left[\frac{\partial b'}{\partial t} + \mathbf{u} \cdot \nabla b' + w(N^2 + \partial_z b') \right] = \frac{H \text{Ro}^2}{\text{Bu}} \left[\frac{\partial \hat{b}}{\partial \hat{t}} + \hat{\mathbf{u}} \cdot \hat{\nabla} \hat{b} + \hat{w} \partial_{\hat{z}} \hat{b} \right] + \text{Ro} \hat{w} = 0. \quad (42.39)$$

The vertical velocity component, \hat{w} , is nonzero only at order Ro^1 , so the term $\text{Ro} \hat{w}$ is order Ro^2 (recall equation (42.27b)). To the same order, we drop the term, $\hat{w} \partial_{\hat{z}} \hat{b}$, that appears within the bracket and retain only the zeroth order buoyancy contribution, \hat{b}_0 . Reintroducing physical dimensions then leads to the dimensional form of the quasi-geostrophic buoyancy equation

$$\partial_t b_g + \mathbf{u}_g \cdot \nabla_z b_g + w_{ag} N^2 = D_g b_g / Dt + w_{ag} N^2 = 0. \quad (42.40)$$

This equation means that the geostrophic transport of the geostrophic buoyancy is affected by a source due to the ageostrophic vertical advection of background buoyancy

$$D_g b_g / Dt = -w_{ag} N^2 \quad \text{with} \quad b_g = f_0 \partial_z \psi. \quad (42.41)$$

42.3.5 Vorticity equation

Reintroducing dimensions to the vorticity equation (42.22) yields¹

$$\frac{\partial \hat{\zeta}_0}{\partial \hat{t}} + (\hat{\mathbf{u}}_0 \cdot \hat{\nabla}_z) (\hat{\zeta}_0 + \hat{\beta} \hat{y}) - \hat{f}_0 \frac{\partial \hat{w}_1}{\partial \hat{z}} = T^2 \left[\frac{\partial \zeta}{\partial t} + \mathbf{u}_g \cdot \nabla_z (\zeta + \beta y) \right] - \frac{H}{W \text{Ro}} \frac{\partial w_{ag}}{\partial z}. \quad (42.42)$$

¹Recall from equation (42.27b) that $W \hat{w} = \text{Ro} W \hat{w}_1 = w_{ag}$.

The identity $H/(W \text{Ro}) = f_0 T^2$ leads to the order Ro^1 vorticity equation

$$\frac{\partial \zeta_a}{\partial t} + J(\psi, \zeta_a) = f_0 \frac{\partial w_{ag}}{\partial z}, \quad (42.43)$$

with the absolute geostrophic vorticity given by

$$\zeta_a = \zeta_g + \beta y. \quad (42.44)$$

Hence, the geostrophic absolute vorticity is advected by the geostrophic flow, and it has a source (right hand side of equation (42.43)) due to vertical stretching by the ageostrophic flow. Expanding the Jacobian and introducing the geostrophic velocity, $\mathbf{u}_g = \hat{\mathbf{z}} \times \nabla \psi$, leads to the geostrophic relative vorticity equation

$$\frac{\partial \zeta_g}{\partial t} + \mathbf{u}_g \cdot \nabla_z \zeta_g = -\beta v_g + f_0 \frac{\partial w_{ag}}{\partial z}. \quad (42.45)$$

We thus see that the beta effect from the geostrophic flow, plus vertical stretching by the ageostrophic flow, provide local sources for geostrophic relative vorticity.

42.3.6 Velocity equation

The prognostic velocity equation arises from the first order asymptotic equation (42.19a)

$$\frac{D_0 \hat{\mathbf{u}}_0}{Dt} + \hat{\mathbf{f}}_0 \times \hat{\mathbf{u}}_1 + \hat{\beta} \hat{\mathbf{y}} \hat{\mathbf{z}} \times \hat{\mathbf{u}}_0 = -\hat{\nabla}_z \hat{\varphi}_1. \quad (42.46)$$

Our skills with reintroducing dimensional quantities should be sufficient to write down the dimensional velocity equation by inspection²

$$(\partial_t + \mathbf{u}_g \cdot \nabla) \mathbf{u}_g + \beta y \hat{\mathbf{z}} \times \mathbf{u}_g + f_0 \hat{\mathbf{z}} \times \mathbf{u}_{ag} = -\nabla_z \varphi_{ag}. \quad (42.47)$$

We can also choose to add the geostrophic balanced flow that holds at order Ro^0 , $f_0 \hat{\mathbf{z}} \times \mathbf{u}_g = -\nabla_z \varphi_g$, so to have the equivalent equation

$$(\partial_t + \mathbf{u}_g \cdot \nabla) \mathbf{u}_g + \beta y \hat{\mathbf{z}} \times \mathbf{u}_g + f_0 \hat{\mathbf{z}} \times (\mathbf{u}_g + \mathbf{u}_{ag}) = -\nabla_z (\varphi_g + \varphi_{ag}). \quad (42.48)$$

42.3.7 Potential vorticity

From equation (42.26), we identify the non-dimensional quasi-geostrophic potential vorticity

$$\hat{q} = \hat{\zeta}_0 + \hat{\beta} \hat{\mathbf{y}} + \hat{f}_0 \frac{\partial (\hat{b}_0 / Bu)}{\partial \hat{z}}. \quad (42.49)$$

Introducing dimensional quantities to the right hand side yields³

$$\hat{q} = \frac{L}{U} [\zeta_g + \beta y] + \frac{\partial}{\partial z} \left[\frac{H b_g}{B Bu} \right] \quad (42.50a)$$

$$= (1/(f_0 \text{Ro}) (\zeta_g + \beta y) + \frac{H}{B} \frac{\partial}{\partial z} \left[\frac{b_g}{Bu} \right]). \quad (42.50b)$$

²Recall from equation (42.27d) that $\varphi_{ag} = f_0 U L \text{Ro} \hat{\varphi}_1 = U^2 \hat{\varphi}_1$.

³Recall $\hat{f}_0 = 1$ and $\hat{\beta} \hat{\mathbf{y}} = T \beta y = (L/U) \beta y$.

The scale for the fluctuating buoyancy is given by equation (41.22), $B = f_0 U L / H$, and the inverse Burger function is given by equation (42.8), $\text{Bu}^{-1} = [(L f_0) / (H N)]^2$, so that

$$\hat{q} = (1/(f_0 \text{Ro}) (\zeta_g + \beta y) + \frac{H^2}{f_0 U L} \frac{L^2 f_0^2}{H^2} \frac{\partial}{\partial z} \left[\frac{b_g}{N^2} \right]) \quad (42.51a)$$

$$= (1/(f_0 \text{Ro}) (\zeta_g + \beta y) + \frac{1}{\text{Ro}} \left[\frac{\partial}{\partial z} \left(\frac{b_g}{N^2} \right) \right]). \quad (42.51b)$$

Introducing the geostrophic streamfunction,

$$\mathbf{u}_g = \hat{\mathbf{z}} \times \nabla_z \psi \quad \text{and} \quad \zeta = \hat{\mathbf{z}} \cdot (\nabla \times \mathbf{u}_g) = \nabla_z^2 \psi \quad \text{and} \quad b_g = f_0 \partial_z \psi, \quad (42.52)$$

leads to

$$q \equiv f_0 \text{Ro} \hat{q} = \beta y + \zeta_g + \frac{\partial}{\partial z} \left[\frac{f_0^2}{N^2} \frac{\partial \psi}{\partial z} \right]. \quad (42.53)$$

Just as for the shallow water case in Section 40.6.1, the potential vorticity (42.53) scales as $f_0 \text{Ro}$. We sometimes choose to add the constant f_0 to q , which has no effect on the dynamics but reveals the beta plane planetary vorticity

$$q = \underbrace{f_0 + \beta y}_{\text{planetary vorticity}} + \underbrace{\nabla_z^2 \psi}_{\text{relative vorticity}} + \underbrace{\frac{\partial}{\partial z} \left[\frac{f_0^2}{N^2} \frac{\partial \psi}{\partial z} \right]}_{\text{stretching by } f}. \quad (42.54)$$

Evidently, there are three contributions to the quasi-geostrophic potential vorticity.

- **PLANETARY VORTICITY:** The planetary vorticity contribution, $f_0 + \beta y$, arises from rotation of the reference frame. As noted above, the βy term is the only dynamically relevant contribution, so that we can equally well drop the f_0 contribution.
- **GEOSTROPHIC RELATIVE VORTICITY:** The vertical component of the geostrophic relative vorticity, $\zeta = \hat{\mathbf{z}} \cdot (\nabla \times \mathbf{u}) = \nabla_z^2 \psi$, acts to bring out the smaller scale features in the streamfunction.
- **VERTICAL STRETCHING:** The final contribution arises from the vertical stretching in the presence of a rotating planet. Equation (42.22) helps to remind us why this term arises from vortex stretching.

The material evolution of the quasi-geostrophic PV follows the horizontal geostrophic flow

$$(\partial_t + \mathbf{u}_g \cdot \nabla_z) q = 0. \quad (42.55)$$

The material constancy of q represents a balance, following the geostrophic flow, of time changes for the planetary vorticity, relative vorticity, and vertical stretching. This is a remarkable property of quasi-geostrophic flows.

42.3.8 Comments about doubly-periodic QG models

It is notable that we can consider a doubly periodic quasi-geostrophic β -plane model whereby there is periodicity in flow properties in both the zonal and meridional directions. The basic reason is that the value of the Coriolis parameter does not appear in the potential vorticity equation (42.55). Rather, it is only $\partial_y f = \beta$ that appears. So even though the Coriolis parameter is not meridionally periodic, its actual value has no relevance to the quasi-geostrophic flow.

Furthermore, we can study quasi-geostrophic flows in doubly periodic domains in the presence of certain idealized background flows. Namely, for a prescribed depth-independent thermal wind flow, the corresponding buoyancy that supports this flow plays no role in the quasi-geostrophic potential vorticity. For example, if the buoyancy has the form

$$b = \underbrace{M^2 y + N^2 z}_{\text{prescribed background}} + b'(x, y, z, t), \quad (42.56)$$

with M and N constant frequencies, then the corresponding quasi-geostrophic potential vorticity is independent of M . In this manner, the background buoyancy, though not meridionally periodic, prescribes a background thermal wind shear that is constant and so is trivially periodic.

42.4 Connecting quasi-geostrophic PV to Ertel PV

Following our treatment for the shallow water system in Section 40.6.5, we here determine how quasi-geostrophic potential vorticity relates to the Ertel potential vorticity from Chapter 38. For this purpose, consider the continuously stratified hydrostatic Boussinesq fluid and make use of the Ertel potential vorticity derived in Exercise 38.1

$$Q = (\boldsymbol{\omega} + \hat{\mathbf{z}} f) \cdot \nabla b = \frac{\partial u}{\partial z} \frac{\partial b}{\partial y} - \frac{\partial v}{\partial z} \frac{\partial b}{\partial x} + (\zeta + f) \frac{\partial b}{\partial z}. \quad (42.57)$$

In a perfect fluid we have the material conservation

$$(\partial_t + \mathbf{u} \cdot \nabla_z + w \partial_z) Q = 0. \quad (42.58)$$

Our strategy in this section is to non-dimensionalize both Q and the material time operator, and then to stratify terms in equation (42.58) according to the Rossby number. We will show that material conservation of Ertel potential vorticity, when expanded asymptotically to order Ro^1 , leads to the geostrophic material conservation of quasi-geostrophic potential vorticity. The continuous stratification makes the derivation more involved than for the shallow water model, prompting us to expose the details for practical experience with the formalism.

42.4.1 Non-dimensionalizing the Ertel potential vorticity

As above for the buoyancy, we are led to write the Ertel potential vorticity in the form

$$\frac{Q - f_0 N^2}{f_0 N^2} = \frac{1}{f_0 N^2} \left[\frac{\partial u}{\partial z} \frac{\partial b'}{\partial y} - \frac{\partial v}{\partial z} \frac{\partial b'}{\partial x} \right] + \frac{1}{N^2} \frac{\partial b'}{\partial z} + \frac{\beta y + \zeta}{f_0} \left[1 + \frac{1}{N^2} \frac{\partial b'}{\partial z} \right]. \quad (42.59)$$

with non-dimensionalization leading to

$$\frac{1}{f_0 N^2} \left[\frac{\partial u}{\partial z} \frac{\partial b'}{\partial y} - \frac{\partial v}{\partial z} \frac{\partial b'}{\partial x} \right] = \frac{B U}{f_0 N^2 H L} \left[\frac{\partial \hat{u}}{\partial \hat{z}} \frac{\partial \hat{b}}{\partial \hat{y}} - \frac{\partial \hat{v}}{\partial \hat{z}} \frac{\partial \hat{b}}{\partial \hat{x}} \right] = \frac{\text{Ro}^2}{\text{Bu}} \left[\frac{\partial \hat{u}}{\partial \hat{z}} \frac{\partial \hat{b}}{\partial \hat{y}} - \frac{\partial \hat{v}}{\partial \hat{z}} \frac{\partial \hat{b}}{\partial \hat{x}} \right] \quad (42.60a)$$

$$\frac{1}{N^2} \frac{\partial b'}{\partial z} = \frac{B}{H N^2} \frac{\partial \hat{b}}{\partial \hat{z}} = \frac{\text{Ro}}{\text{Bu}} \frac{\partial \hat{b}}{\partial \hat{z}} \quad (42.60b)$$

$$\frac{\beta y + \zeta}{f_0} = \text{Ro} (\hat{\beta} \hat{y} + \hat{\zeta}). \quad (42.60c)$$

The order Ro^2 terms appearing in equation (42.60a) are dropped since they do not contribute to the quasi-geostrophic potential vorticity, which involve terms only up to order Ro^1 . For the order

Ro^1 term, we only retain the zeroth order buoyancy, $\hat{b}_0 = b_g/B$, and likewise we just retain the zeroth order vorticity, $\hat{\zeta}_0 = (L/U) \zeta_g$. Hence, the Ertel potential vorticity is given by

$$Q = N^2 (f_0 + q_*) + \mathcal{O}(\text{Ro}^2) \quad (42.61)$$

where q_* is the order Ro^1 term

$$q_* = \text{Ro} f_0 \left[\frac{1}{\text{Bu}} \frac{\partial \hat{b}_0}{\partial z} + \hat{\beta} \hat{y} + \hat{\zeta}_0 \right] = \frac{f_0}{N^2} \frac{\partial b_g}{\partial z} + \beta y + \zeta_g. \quad (42.62)$$

42.4.2 Material conservation of Ertel PV to order Ro^1

The material conservation of Ertel PV now takes the form

$$(\partial_t + \mathbf{u}_g \cdot \nabla_z + w_{ag} \partial_z) (f_0 N^2 + q_* N^2) = f_0 w_{ag} \partial_z N^2 + N^2 D_g q_*/Dt = 0. \quad (42.63a)$$

We dropped the $w_{ag} \partial_z$ contribution to the advection of q_* since ageostrophic vertical advection of q_* is an order Ro^2 term. To eliminate the vertical ageostrophic velocity we make use of the buoyancy equation (42.40) so that

$$\frac{D_g q_*}{Dt} + \frac{w_{ag}}{N^2} \frac{\partial N^2}{\partial z} = \frac{D_g q_*}{Dt} - \frac{f_0}{N^4} \frac{D_g b_g}{Dt} \frac{\partial N^2}{\partial z} = 0. \quad (42.64)$$

Writing

$$\frac{\partial}{\partial z} \left[\frac{1}{N^2} \right] = - \frac{1}{N^4} \frac{\partial N^2}{\partial z} \quad (42.65)$$

leads to

$$\frac{D_g q_*}{Dt} + f_0 \left[\frac{\partial N^{-2}}{\partial z} \right] \frac{D_g b_g}{Dt} = 0. \quad (42.66)$$

Since the geostrophic material time derivative operator only involves horizontal advection, we can merge these two terms to render

$$\frac{D_g q_*}{Dt} + f_0 \left[\frac{\partial N^{-2}}{\partial z} \right] \frac{D_g b_g}{Dt} = \frac{D_g}{Dt} \left[q_* + f_0 b_g \left(\frac{\partial N^{-2}}{\partial z} \right) \right] \quad (42.67a)$$

$$= \frac{D_g}{Dt} \left[\beta y + \zeta + \frac{f_0}{N^2} \left(\frac{\partial b_g}{\partial z} \right) + f_0 b_g \left(\frac{\partial N^{-2}}{\partial z} \right) \right] \quad (42.67b)$$

$$= \frac{D_g}{Dt} \left[\beta y + \zeta + f_0 \frac{\partial}{\partial z} \left(\frac{b_g}{N^2} \right) \right] \quad (42.67c)$$

$$= \frac{D_g q}{Dt} \quad (42.67d)$$

$$= 0. \quad (42.67e)$$

In the penultimate step we introduced the quasi-geostrophic potential vorticity given by equation (42.54)

$$q = \beta y + \zeta + f_0 \frac{\partial}{\partial z} \left[\frac{b_g}{N^2} \right] = q_* + f_0 b_g \frac{\partial N^{-2}}{\partial z}. \quad (42.68)$$

We have thus established how material conservation of Ertel potential vorticity, when expanded asymptotically to order Ro^1 , leads to the geostrophic material conservation of quasi-geostrophic potential vorticity.

42.5 Mathematical expressions of the theory

In this section we sample various mathematical expressions of quasi-geostrophic theory as well as boundary conditions at the top and bottom of the domain.

42.5.1 The Jacobian form of geostropic advection

The geostrophic velocity, as a horizontally non-divergent field, can be written in terms of the quasi-geostrophic streamfunction

$$\mathbf{u}_g = \hat{\mathbf{z}} \times \nabla \psi. \quad (42.69)$$

We can thus write the following equivalent forms for the material time derivative of quasi-geostrophic PV

$$\frac{Dq}{Dt} = \frac{\partial q}{\partial t} + \mathbf{u}_g \cdot \nabla q \quad (42.70a)$$

$$= \frac{\partial q}{\partial t} + (\hat{\mathbf{z}} \times \nabla \psi) \cdot \nabla q \quad (42.70b)$$

$$= \frac{\partial q}{\partial t} + (\nabla \psi \times \nabla q) \cdot \hat{\mathbf{z}} \quad (42.70c)$$

$$= \frac{\partial q}{\partial t} + J(\psi, q). \quad (42.70d)$$

The final equality introduced the Jacobian operator $J(\psi, q) = (\nabla \psi \times \nabla q) \cdot \hat{\mathbf{z}}$, which is a notation commonly used in the geophysical fluids literature.⁴

For a perfect fluid, in which $Dq/Dt = 0$, a steady state (zero Eulerian time derivative) is realized when

$$\mathbf{u}_g \cdot \nabla q = (\nabla \psi \times \nabla q) \cdot \hat{\mathbf{z}} = J(\psi, q) = 0. \quad (42.71)$$

Hence, the velocity is parallel to surfaces of constant q . We are ensured that these equalities hold if the streamfunction is a function only of the potential vorticity

$$\psi = \psi(q) \implies (\nabla \psi \times \nabla q) \cdot \hat{\mathbf{z}} = J(\psi, q) = 0. \quad (42.72)$$

As the steady state is of physical interest, this functional relation between streamfunction and potential vorticity commonly arises in applications.

42.5.2 Constant background buoyancy frequency

Consider the quasi-geostrophic potential vorticity for the special case of a constant background buoyancy frequency, $N^2 = \text{constant}$, in which the relative potential vorticity (42.53) takes on the form

$$q - \beta y = \nabla_z^2 \psi + \frac{\partial}{\partial z} \left[\frac{f_0^2}{N^2} \frac{\partial \psi}{\partial z} \right] \quad (42.73a)$$

$$= \frac{\partial^2 \psi}{\partial x^2} + \frac{\partial^2 \psi}{\partial y^2} + \frac{f_0^2}{N^2} \frac{\partial^2 \psi}{\partial z^2} \quad (42.73b)$$

$$= [\partial_{xx} + \partial_{yy} + \partial_{zz}] \psi. \quad (42.73c)$$

⁴Recall that we also encountered the Jacobian form for horizontally non-divergent two-dimensional advection in Section 35.3.3 when studying the non-divergent barotropic flows.

For the final equality we introduced the vertical coordinate

$$\tilde{z} = (N/f) z. \quad (42.74)$$

Since $|N/f| \gg 1$ the stably stratified flows considered in QG, \tilde{z} is a *stretched* vertical coordinate so that the Laplacian operator acting on ψ is anisotropic. The linear operator acting on ψ remains elliptic even in the more general case of a depth dependent stratification, thus warranting the use of elliptical solvers when performing the inversion numerically.

42.5.3 Vertical boundary conditions for ψ

We need boundary conditions on the geostrophic streamfunction, ψ , to invert the elliptic quasi-geostrophic PV equation (42.54). For lateral boundaries, one may choose periodicity, whereby the boundaries are absent. Alternatively, we may choose to set the normal component of the flow to zero for the inviscid case, in which case ψ is a constant along material boundaries as discussed in Section 18.3.2. The top and bottom boundaries require extra considerations as discussed here.

Buoyancy equation at the boundaries

To develop the vertical boundary conditions on the streamfunction, consider the quasi-geostrophic buoyancy equation (42.40)

$$D_g b_g / Dt + w_{ag} N^2 = 0. \quad (42.75)$$

Inserting the geostrophic streamfunction, $b_g = f_0 \partial_z \psi$, leads to

$$f_0 (\partial_t + \mathbf{u}_g \cdot \nabla_z) \partial_z \psi + w_{ag} N^2 = 0. \quad (42.76)$$

We now consider how this boundary condition appears at the top and bottom.

Top boundary condition

Assuming the top boundary is a material surface, we are led to the kinematic boundary condition (16.51)

$$w = (\partial_t + \mathbf{u}_g \cdot \nabla_z) \eta. \quad (42.77)$$

How does this vertical velocity compare to that associated with motion in the fluid interior? To answer that question we assume an advective scaling for time derivatives so that the vertical velocity at the free surface scales as

$$w_{\text{surf}} \sim U \eta / L \sim U p / (\rho_0 g L) \sim U^2 f_0 / g, \quad (42.78)$$

where L is the horizontal length scale, and we scaled the surface pressure gradient according to the free surface gradient. A point in the fluid interior has a vertical velocity that scales according to the buoyancy equation (42.75)

$$w_{\text{interior}} \sim U b / (N^2 L) \sim f_0 U^2 / (H N^2) \quad (42.79)$$

where H is the vertical scale over which the thermal wind shear is sizable, and which scales the buoyancy frequency according to

$$N^2 \sim (g/\rho_0) \Delta \rho / H, \quad (42.80)$$

where $\Delta\rho \ll \rho_0$ is the scale for the density difference setting the size of the buoyancy frequency. The ratio of the two vertical velocities is thus given by

$$w_{\text{surf}}/w_{\text{interior}} = H N^2/g = \Delta\rho/\rho_0 \ll 1. \quad (42.81)$$

Evidently, we can set the surface boundary condition to that of a rigid lid, in which $w_{\text{ag}} = 0$. In this case, the top boundary condition reduces to geostrophic advection of boundary buoyancy

$$(\partial_t + \mathbf{u}_g \cdot \nabla_z) \partial_z \psi = 0 \quad \text{at top boundary where } w_{\text{ag}} = 0. \quad (42.82)$$

That is, the geostrophic buoyancy at the surface is conservatively advected by the surface geostrophic flow.

Bottom boundary condition

With a nonzero slope in the bottom topography, $\nabla\eta_b \neq 0$, the bottom kinematic boundary condition (Section 16.4.1) says that velocity is constrained so that

$$\mathbf{v} \cdot \hat{\mathbf{n}} = 0 \implies w = \mathbf{u} \cdot \nabla\eta_b, \quad (42.83)$$

where $\hat{\mathbf{n}} = -\nabla(z - \eta_b)/|\nabla(z - \eta_b)|$ is the boundary's outward normal. Expanding this kinematic boundary condition leads to

$$w_{\text{ag}} = (\mathbf{u}_g + \mathbf{u}_{\text{ag}}) \cdot \nabla\eta_b, \quad (42.84)$$

which means there is vertical motion so long as the horizontal motion is not aligned with isobaths. To be clear on the implications of this boundary condition, it is useful to examine the asymptotics by non-dimensionalizing⁵

$$\mathbf{u}_g = U \hat{\mathbf{u}}_0 \quad (42.85a)$$

$$w_{\text{ag}} = W \text{Ro} \hat{w}_1 \quad (42.85b)$$

$$\mathbf{u}_{\text{ag}} = U \text{Ro} \hat{\mathbf{u}}_1 \quad (42.85c)$$

$$\nabla\eta_b = (\mathcal{B}/L) \hat{\nabla}\hat{\eta}_b = (H \text{Ro}/L) \hat{\nabla}\hat{\eta}_b, \quad (42.85d)$$

which brings the kinematic boundary condition (42.84) to

$$f_0 H \text{Ro}^2 (\hat{\mathbf{u}}_0 + \text{Ro} \hat{\mathbf{u}}_1) \cdot \hat{\nabla}\hat{\eta}_b = W \text{Ro} \hat{w}_1 \implies (\hat{\mathbf{u}}_0 + \text{Ro} \hat{\mathbf{u}}_1) \cdot \hat{\nabla}\hat{\eta}_b = \hat{w}_1. \quad (42.86)$$

Asymptotic consistency implies that

$$\hat{\mathbf{u}}_0 \cdot \hat{\nabla}\hat{\eta}_b = \hat{w}_1 \implies \mathbf{u}_g \cdot \nabla\eta_b = w_{\text{ag}}. \quad (42.87)$$

Hence, for quasi-geostrophic flow, any projection of the horizontal geostrophic velocity in a direction not aligned with isobaths leads to an ageostrophic vertical velocity component.

Use of the bottom kinematic boundary condition in the buoyancy equation (42.76) leads to the bottom boundary evolution of buoyancy

$$f_0 \partial_t (\partial_z \psi) + \mathbf{u}_g \cdot \nabla_z [f_0 \partial_z \psi + N^2 \eta_b] = 0 \quad \text{at } z = \bar{\eta}_b. \quad (42.88)$$

The boundary condition is evaluated at $z = \bar{\eta}_b$ since the more precise boundary location, $z =$

⁵The bottom topography slope is non-dimensionalized according to the shallow water discussion in Section 40.3.4.

$\eta_b(x, y)$, is higher order in Rossby number.

42.5.4 Potential vorticity induction and impermeability

The potential vorticity equation is the sole prognostic equation required to evolve the quasi-geostrophic flow. Consequently, one often discards the the quasi-geostrophic velocity and buoyancy equations. Even so, we found it useful to use the buoyancy equation in Section 42.3.4 as part of connecting quasi-geostrophic and Ertel potential vorticities. Likewise, there are occasions when it is useful to examine the velocity equation, with a similar discussion provided in Section 40.6.4. In this section we directly connect the velocity and buoyancy equations and then reveal their connection to the potential vorticity equation.

Combining the velocity and buoyancy equations

Consider the quasi-geostrophic velocity and buoyancy equations derived in Section 42.3

$$(\partial_t + \mathbf{u}_g \cdot \nabla) \mathbf{u}_g + \hat{\mathbf{z}} \times (\beta y \mathbf{u}_g + f_0 \mathbf{u}_{ag}) = -\nabla_z \varphi_{ag} + \mathbf{F} \quad (42.89a)$$

$$(\partial_t + \mathbf{u}_g \cdot \nabla_z) b_g + w_{ag} N^2 = \dot{b} \quad (42.89b)$$

$$f_0 \hat{\mathbf{z}} \times \mathbf{u}_g + \nabla_z \varphi_g = 0 \quad (42.89c)$$

$$\nabla \cdot \mathbf{u}_g = \partial_x u_g + \partial_y v_g = 0 \quad (42.89d)$$

$$\nabla \cdot \mathbf{v}_{ag} = \nabla \cdot \mathbf{u}_{ag} + \partial_z w_{ag} = 0, \quad (42.89e)$$

where we added a non-conservative force per mass, \mathbf{F} (e.g., friction, wind stress), and irreversible buoyancy source, \dot{b} (e.g., diffusion, boundary fluxes). Taking $-\hat{\mathbf{z}} \times$ on the velocity equation and multiplying the buoyancy equation by f_0/N^2 leads to

$$(\partial_t + \mathbf{u}_g \cdot \nabla)(-\hat{\mathbf{z}} \times \mathbf{u}_g) + \beta y \mathbf{u}_g + f_0 \mathbf{u}_{ag} = \hat{\mathbf{z}} \times \nabla_z \varphi_{ag} - \hat{\mathbf{z}} \times \mathbf{F} \quad (42.90a)$$

$$(\partial_t + \mathbf{u}_g \cdot \nabla_z)(f_0 b_g / N^2) + f_0 w_{ag} = f_0 \dot{b} / N^2. \quad (42.90b)$$

Introduce the following vector fields

$$\mathbf{D} \equiv -\hat{\mathbf{z}} \times \mathbf{u}_g + (f_0 / N^2) b_g \hat{\mathbf{z}} = \nabla_z \psi + (f_0 / N)^2 \partial_z \psi \hat{\mathbf{z}} \quad (42.91a)$$

$$\mathbf{R} \equiv -\hat{\mathbf{z}} \times \mathbf{F} + (f_0 / N^2) \dot{b} \hat{\mathbf{z}}, \quad (42.91b)$$

with \mathbf{D} built from both the velocity and buoyancy fields and \mathbf{R} built from the corresponding non-conservative tendencies. These vectors allow us to combine the velocity and buoyancy equations into a single vector equation

$$(\partial_t + \mathbf{u}_g \cdot \nabla) \mathbf{D} + \beta y \mathbf{u}_g + f_0 \mathbf{v}_{ag} = \hat{\mathbf{z}} \times \nabla_z \varphi_{ag} + \mathbf{R}. \quad (42.92)$$

Potential vorticity induction

The divergence of \mathbf{D} yields the relative quasi-geostrophic potential vorticity

$$\nabla \cdot \mathbf{D} = q - (f_0 + \beta y), \quad (42.93)$$

where we made use of the expression (42.54) for the potential vorticity. In analogy to Gauss's law of electromagnetism, we refer to \mathbf{D} as the quasi-geostrophic potential vorticity *induction vector*.⁶

⁶This connection between potential vorticity dynamics and electromagnetism was pointed out by Schneider et al. (2003) and further examined by Maddison and Marshall (2013).

Additionally, the potential vorticity equation can be written (see Exercise 42.5)

$$(\partial_t + \mathbf{u}_g \cdot \nabla) q = \nabla \cdot \mathbf{R}, \quad (42.94)$$

so that the quasi-geostrophic potential vorticity flux vector

$$\mathbf{J}_q = \mathbf{u}_g q - \mathbf{R} \quad (42.95)$$

allows us to write the potential vorticity equation in the Eulerian flux-form

$$\partial_t q = -\nabla \cdot \mathbf{J}_q. \quad (42.96)$$

Kinematic PV flux and impermeability

Taking the Eulerian time derivative of the potential vorticity induction equation (42.93) renders

$$\partial_t q = \partial_t (\nabla \cdot \mathbf{D}) = \nabla \cdot (\partial_t \mathbf{D}) \equiv -\nabla \cdot \mathbf{J}_q^{\text{kin}}, \quad (42.97)$$

where we introduced the kinematic form of the potential vorticity flux

$$\mathbf{J}_q^{\text{kin}} \equiv -\partial_t \mathbf{D} = \mathbf{J}_q + \nabla \times \mathbf{A}, \quad (42.98)$$

with \mathbf{A} a gauge function. This equation is analogous to the kinematic Ertel PV flux discussed in Section 39.2.2. We determine the explicit expression for the gauge function in Exercise 42.6.

42.6 Energetics for quasi-geostrophic flow

Consider a quasi-geostrophic fluid configured with flat upper (rigid lid) and lower boundaries, and assume the lateral boundaries are periodic or material solid boundaries. These restrictive assumptions allow us to more readily study energetics within the fluid, sans the impacts from nontrivial boundary effects. To study energetics we make use of the quasi-geostrophic buoyancy equation (42.40) and relative vorticity equation (42.45)

$$\frac{\partial b}{\partial t} + \mathbf{u} \cdot \nabla b = -w N^2 \quad (42.99a)$$

$$\frac{\partial \zeta}{\partial t} + \mathbf{u} \cdot \nabla \zeta = -\beta v + f_0 \frac{\partial w}{\partial z}, \quad (42.99b)$$

where all labels are dropped from the variables to reduce clutter, and where

$$\frac{D}{Dt} = \frac{\partial}{\partial t} + \mathbf{u} \cdot \nabla \quad b = f_0 \frac{\partial \psi}{\partial z} \quad u = -\frac{\partial \psi}{\partial y} \quad v = \frac{\partial \psi}{\partial x} \quad \zeta = \nabla_z^2 \psi. \quad (42.100)$$

42.6.1 Kinetic energy

The kinetic energy per mass for the total fluid domain is given by the integral

$$\mathcal{K} = \frac{1}{2} \int \mathbf{u} \cdot \mathbf{u} dV = \frac{1}{2} \int \nabla_z \psi \cdot \nabla_z \psi dV, \quad (42.101)$$

and its time derivative is

$$\frac{d\mathcal{K}}{dt} = \int \nabla_z \psi \cdot \nabla_z (\partial \psi / \partial t) dV. \quad (42.102)$$

For the kinetic energy time derivative we noted that the fluid domain has a constant volume to allow the time derivative to move inside the integral without introducing boundary terms. Manipulation renders

$$\frac{d\mathcal{K}}{dt} = \int \nabla_z \psi \cdot \nabla_z (\partial \psi / \partial t) dV \quad (42.103a)$$

$$= \int [\nabla_z \cdot [\psi \nabla_z (\partial \psi / \partial t)] - \psi \partial (\nabla_z^2 \psi) / \partial t] dV \quad (42.103b)$$

$$= - \int \psi (\partial \zeta / \partial t) dV, \quad (42.103c)$$

where we dropped the lateral boundary term and introduced relative vorticity. Use of the vorticity equation (42.99b) yields

$$\frac{d\mathcal{R}}{dt} = - \int \psi (\partial \zeta / \partial t) dV = \int \psi [\mathbf{u} \cdot \nabla_z \zeta + \beta v - f_0 \partial_z w] dV. \quad (42.104)$$

The first and second terms vanish since

$$\int \psi (\mathbf{u} \cdot \nabla_z \zeta + \beta v) dV = \int \psi \mathbf{u} \cdot \nabla_z (\zeta + f) dV \quad (42.105a)$$

$$= \int \psi \nabla_z \cdot (\mathbf{u} \zeta_a) dV \quad (42.105b)$$

$$= \int [\nabla_z \cdot (\psi \mathbf{u} \zeta_a) - \nabla_z \psi \cdot \mathbf{u} \zeta_a] dV = 0, \quad (42.105c)$$

where the boundary term vanishes and $\mathbf{u} \cdot \nabla_z \psi = 0$ since ψ is the streamfunction for the horizontal geostrophic flow. We are thus left with the expression for the kinetic energy evolution

$$\frac{d\mathcal{K}}{dt} = -f_0 \int \psi \frac{\partial w}{\partial z} dV. \quad (42.106)$$

Since the top and bottom are assumed flat and rigid, the vertical velocity vanishes on these boundaries so that

$$\frac{d\mathcal{K}}{dt} = - \int \psi f_0 \frac{\partial w}{\partial z} dV = -f_0 \int \left[\frac{\partial(w \psi)}{\partial z} - w \frac{\partial \psi}{\partial z} \right] dV = f_0 \int w \frac{\partial \psi}{\partial z} dV. \quad (42.107)$$

Introducing the quasi-geostrophic buoyancy through $b = f_0 \partial \psi / \partial z$ leads to

$$\frac{d\mathcal{K}}{dt} = \int w b dV. \quad (42.108)$$

Kinetic energy thus increases when vertical motion is positively correlated with buoyancy. For example, upward motion ($w > 0$) of a positive buoyancy anomaly (relatively light water has $b > 0$) increases kinetic energy, as does downward motion of a negative buoyancy anomaly. This behavior is also reflected in the full fluid system discussed in Section 23.3.

42.6.2 Available potential energy

Available potential energy was introduced in Section 26.9 within the context of the Boussinesq ocean. An approximate form of the APE is given by equation (26.190), which we here write in

the form

$$\mathcal{A}_{\text{bouss}} \approx \frac{1}{2} \int \left[\frac{b}{N} \right]^2 dV = \frac{1}{2} \int \left[\frac{f_0}{N} \frac{\partial \psi}{\partial z} \right]^2 dV, \quad (42.109)$$

where we set $b = f_0 \partial \psi / \partial z$ for the second equality. Taking a time derivative leads to

$$\frac{d\mathcal{A}}{dt} = \int \left[\frac{f_0}{N} \right]^2 \frac{\partial \psi}{\partial z} \frac{\partial}{\partial t} \frac{\partial \psi}{\partial z} dV = \int \frac{f_0}{N^2} \frac{\partial \psi}{\partial z} [-w N^2 - \nabla_z \cdot (\mathbf{u} b)] dV, \quad (42.110)$$

where we used the buoyancy equation (42.99a) for the second equality. The second term vanishes since

$$\int \frac{f_0}{N^2} \frac{\partial \psi}{\partial z} [\nabla_z \cdot (\mathbf{u} b)] dV = \int \left[\frac{f_0^2}{N^2} \frac{\partial \psi}{\partial z} \right] \mathbf{u} \cdot \nabla_z \left[\frac{\partial \psi}{\partial z} \right] dV \quad (42.111a)$$

$$= \frac{1}{2} \int \nabla_z \cdot \left[\mathbf{u} \left(\frac{f_0}{N} \frac{\partial \psi}{\partial z} \right)^2 \right] dV \quad (42.111b)$$

$$= 0. \quad (42.111c)$$

Consequently, the quasi-geostrophic APE has a time derivative given by

$$\frac{d\mathcal{A}}{dt} = - \int w f_0 \frac{\partial \psi}{\partial z} dV = - \int w b dV, \quad (42.112)$$

so that the APE evolves oppositely to the kinetic energy.

42.6.3 Exchange of mechanical energy

We refer to the term

$$\text{buoyancy work} = \int w f_0 \frac{\partial \psi}{\partial z} dV = \int w b dV, \quad (42.113)$$

as the buoyancy work conversion term. It has the same form as that encountered for the conversion between potential and kinetic energy in the unapproximated equations studied in Section 23.3.

The evolution of kinetic energy involves the relative vorticity equation, whereas evolution of the APE involves the buoyancy equation. However, their sum remains constant in time since as the kinetic energy increases through buoyancy work, the available potential energy decreases

$$\frac{d(\mathcal{K} + \mathcal{A})}{dt} = 0. \quad (42.114)$$

This is a relatively simple mechanical energy budget equation reminiscent of a classical point particle discussed in Section 12.8. In particular, note the absence of a pressure work term that appears in the mechanical energy budget for other fluids such as for the Euler equations (Section 23.3) and Boussinesq ocean (Sections 26.7 and 26.8). We anticipate the absence of pressure work since knowledge of potential vorticity is sufficient to know all quasi-geostrophic dynamical fields, and yet pressure plays no explicit role in potential vorticity evolution.

42.6.4 Scaling APE and KE

The scale for the kinetic energy is given by

$$\mathcal{K} = \frac{1}{2} \int (\nabla_z \psi \cdot \nabla_z \psi) dV \sim L^{-2} \Psi^2 V \quad (42.115)$$

and the scale for the APE is

$$\mathcal{A} = \frac{1}{2} \int \left[\frac{f_0}{N} \frac{\partial \psi}{\partial z} \right]^2 dV \sim H^{-2} (f_0/N)^2 \Psi^2 V = L_d^{-2} \Psi^2 V, \quad (42.116)$$

where we wrote Ψ for the streamfunction scale, V for the domain volume, and $L_d = H(N/f_0)$ is the deformation radius (see equation (42.7)). Taking the ratio yields

$$\frac{\mathcal{K}}{\mathcal{A}} \sim \left[\frac{L_d}{L} \right]^2 = \left[\frac{H}{L} \right]^2 \left[\frac{N}{f_0} \right]^2 = Bu. \quad (42.117)$$

Hence, the Burger number is the ratio of the quasi-geostrophic kinetic energy scale to the quasi-geostrophic available potential energy scale. A large Burger number means that the horizontal scales of the flow are smaller than the deformation radius, in which case the QG dynamics is dominated by its kinetic energy. In contrast, for scales larger than the deformation radius (not much larger, as then the flow would not satisfy QG scaling), the Burger number is less than unity, in which case the QG dynamics is dominated by available potential energy.



42.7 Exercises

EXERCISE 42.1: A VARIETY OF POTENTIAL VORTICITIES

Give the mathematical expressions for dimensionful potential vorticity in the following fluid models. Define all terms in the respective expressions. Give the physical dimensions and/or SI units for the potential vorticity. Hint: the answers can be found somewhere in this book.

- (a) Ertel PV for compressible fluid in a rotating reference frame using potential temperature as the tracer.
- (b) Ertel PV for an incompressible (Boussinesq) fluid in a rotating reference frame using buoyancy as the tracer.
- (c) Single shallow water layer on a beta plane
- (d) Continuously stratified planetary geostrophic flow
- (e) Continuously stratified quasi-geostrophic flow on a beta plane

EXERCISE 42.2: QUASI-GEOSTROPHIC PV EVOLUTION WITH VERTICAL FRICTION

The first part of this exercise involves elements of the asymptotic method used for deriving the QG equations, only now with the advent of a non-zero friction. Use is made to incorporate the non-dimensionalization detailed in Section 30.1, which provides a detailed discussion of the Ekman number and Ekman layers. The second part of this exercise makes use of the thermal wind balance to connect horizontal buoyancy transfer to the vertical viscous transfer of horizontal momentum.

- (a) Derive the material evolution equation for quasi-geostrophic PV in a continuously stratified Boussinesq fluid in the presence of friction, \mathbf{F} . Assume the Ekman number is on the order of the Rossby number, so that the zeroth order asymptotic solution satisfies the usual inviscid f -plane geostrophic balance. Friction only appears in the first order equations.

- (b) Assume friction arises just from vertical shears in the horizontal velocity, so that

$$\mathbf{F} = \frac{\partial}{\partial z} \left[\nu \frac{\partial \mathbf{u}}{\partial z} \right], \quad (42.118)$$

where $\nu = \nu(z)$ is a vertical eddy viscosity that is a function of depth (dimensions of squared length per time). Also assume an approximate form of quasi-geostrophic PV in which we drop relative vorticity (i.e., quasi-geostrophic PV is dominated by planetary vorticity and stretching). Determine the form for the vertical eddy viscosity so that the approximate form of quasi-geostrophic PV is laterally diffused via

$$\frac{Dq^{\text{approx}}}{Dt} = A \nabla_z^2 q^{\text{approx}}, \quad (42.119)$$

where A is a constant eddy diffusivity for the potential vorticity.

Hint: to leading order, the friction operator is a function just of the geostrophic velocity.

EXERCISE 42.3: QUASI-GEOSTROPHIC ω -EQUATION

As we discovered in this chapter, for quasi-geostrophy the vertical component to the velocity is non-zero only at first order in Rossby number, whereas the zeroth order flow is horizontal and geostrophic. To time step the horizontal geostrophic flow it is not necessary to explicitly compute the ageostrophic vertical velocity. However, there are cases where it is of interest. In this exercise we derive the ω -equation for quasi-geostrophic flow, thus providing a diagnostic expression for the ageostrophic vertical velocity. The name for this equation originates from the atmospheric community where ω is the common symbol for transport across pressure surfaces. Here, we make use of the Boussinesq system so that the vertical velocity component is across depth surfaces.

An outline for the derivation of the traditional form for the ω -equation is given in Section 5.4 of [Vallis \(2017\)](#) for the anelastic version of quasi-geostrophy and for the f -plane. Here we work with the Boussinesq system and consider a β -plane. Nonetheless, the solution is nearly the same as in [Vallis \(2017\)](#). Hence, the aim for this exercise is to fully explain the derivation and show each of the relevant steps.

- (a) Cross-multiply the dimensional buoyancy and vorticity equations from Section 42.3 to eliminate the time derivative, thus deriving a diagnostic equation for the ageostrophic vertical velocity that is valid to order Ro^1 .
- (b) The diagnostic equation you should have derived takes the form

$$\mathcal{L}w = \sigma, \quad (42.120)$$

where

$$\mathcal{L} = N^2 \nabla_z^2 + f_0^2 \frac{\partial^2}{\partial z^2} \quad (42.121)$$

is a linear partial differential operator and

$$\sigma = f_0 \partial_z [J(\psi, \zeta + \beta y)] - \nabla_z^2 J(\psi, b) \quad (42.122)$$

is a source term. The source is a function of the geostrophic flow and the buoyancy field. For vertically stable stratification, $N^2 > 0$, characterize the differential operator, \mathcal{L} , according to the elliptic, hyperbolic, or parabolic classes discussed in Section 3.4. What about when $N^2 < 0$? What new physical phenomena do you expect when $N^2 < 0$?

EXERCISE 42.4: HOSKINS' FORM OF THE QUASI-GEOSTROPHIC ω -EQUATION

We here rederive the ω -equation from Exercise 42.3 using methods introduced by [Hoskins et al. \(1978\)](#). It is not necessary to have solved Exercise 42.3 to solve the present exercise.

Hoskins' approach reveals an insightful form for the source function contributing to vertical motion. As in Exercise 42.3, we work with the adiabatic and hydrostatic Boussinesq system (see Section 41.2)

$$\frac{Du}{Dt} - fv = -\frac{\partial \varphi}{\partial x} \quad (42.123a)$$

$$\frac{Dv}{Dt} + fu = -\frac{\partial \varphi}{\partial y} \quad (42.123b)$$

$$\frac{\partial \varphi}{\partial z} = b \quad (42.123c)$$

$$\frac{Db}{Dt} = 0 \quad (42.123d)$$

$$\nabla \cdot \mathbf{v} = \nabla_z \cdot \mathbf{u} + \frac{\partial w}{\partial z} = 0 \quad (42.123e)$$

$$\frac{D}{Dt} = \frac{\partial}{\partial t} + \mathbf{v} \cdot \nabla. \quad (42.123f)$$

In Exercise 42.3, we derived the ω -equation making use of the buoyancy equation and vorticity equation. [Hoskins et al. \(1978\)](#) worked with the momentum equation rather than the vorticity equation. For this purpose, rather than consider an asymptotic expansion, Hoskins exactly decomposed the horizontal velocity into its geostrophic and ageostrophic components

$$\mathbf{u} = \mathbf{u}_g + \mathbf{u}_{ag}, \quad (42.124)$$

with the geostrophic velocity balancing the horizontal gradient of the full pressure field

$$f\mathbf{u}_g = \hat{\mathbf{z}} \times \nabla \varphi. \quad (42.125)$$

This definition for \mathbf{u}_g is distinct from that arising from an asymptotic expansion, whereby the geostrophic velocity is the zeroth order term balancing the zeroth order pressure gradient (see Section 42.2.1 or Exercise 42.3). We are generally able to access the full hydrostatic pressure field through knowledge of the buoyancy field, in which case there is no need to make an asymptotic expansion of pressure.

Hoskins' definition for the geostrophic velocity brings the horizontal momentum equations into the rather elegant form

$$\frac{D\mathbf{u}}{Dt} + f\hat{\mathbf{z}} \times \mathbf{u}_{ag} = 0, \quad (42.126)$$

with the pressure gradient annihilated since it exactly balances the geostrophic velocity. In this manner, the material evolution of horizontal velocity is determined solely by the ageostrophic Coriolis acceleration. Again, there has been no approximation made thus far. Rather, we have only introduced a strategic decomposition of the velocity field as per Hoskins.

At this point we make the quasi-geostrophic approximation by setting the momentum equation equal to

$$\frac{\partial \mathbf{u}_g}{\partial t} + (\mathbf{u}_g \cdot \nabla_z) \mathbf{u}_g + f\hat{\mathbf{z}} \times \mathbf{u}_{ag} = 0 \quad (42.127)$$

and the buoyancy equation equal to

$$\frac{\partial b}{\partial t} + \mathbf{u}_g \cdot \nabla_z b + N^2 w = 0, \quad (42.128)$$

where $N^2(z)$ is a prescribed static background stratification. That is, both the horizontal geostrophic velocity and the buoyancy are advected just by the geostrophic velocity. The buoyancy equation is the same as derived to order Ro^1 using asymptotic methods (Section 42.2.2). However, Hoskins' momentum equation (42.127) has no pressure gradient on the right hand side, whereas an asymptotic approach has contributions from higher order pressure gradients (Section 42.2.2). Hoskins' approach dispenses with such pressure terms by defining the geostrophic velocity using the full pressure field.

- (a) Show that the evolution of horizontal buoyancy gradients by the horizontal geostrophic currents can be written

$$\left[\frac{\partial}{\partial t} + \mathbf{u}_g \cdot \nabla_z \right] |\nabla_z b|^2 = \mathbf{Q} \cdot \nabla_z b. \quad (42.129)$$

Hence, horizontal buoyancy gradients grow in magnitude in regions where the horizontal buoyancy gradient projects positively onto the \mathbf{Q} -vector. Write the expression for the vector \mathbf{Q} . Hint: A general version of this result was derived in Exercise 14.2.

- (b) Show that the quasi-geostrophic ω -equation on an f -plane can be written

$$N^2 \nabla_z^2 w + f_0^2 \frac{\partial^2 w}{\partial z^2} = 2 \nabla_z \cdot \mathbf{Q}. \quad (42.130)$$

We see that the source for vertical motion is the divergence of the \mathbf{Q} -vector. This formula offers useful insight into the origin of vertical motion, with [Hoskins et al. \(1978\)](#) offering examples. For this part of the exercise, you are to fully explain the derivation of equation (42.130) and show each of the relevant steps.

- (c) The equation (42.130) for the vertical velocity takes the form

$$\mathcal{L}w = \sigma, \quad (42.131)$$

where

$$\mathcal{L} = N^2 \nabla_z^2 + f_0^2 \frac{\partial^2}{\partial z^2} \quad (42.132)$$

is a linear partial differential operator and

$$\sigma = 2 \nabla_z \cdot \mathbf{Q} \quad (42.133)$$

is a source term. The source term is a function of the geostrophic flow and the buoyancy field. For vertically stable stratification, $N^2 > 0$, characterize the differential operator \mathcal{L} according to the elliptic, hyperbolic, or parabolic classes discussed in Section 3.4. What about when $N^2 < 0$? What new physical phenomena do you expect when $N^2 < 0$?

EXERCISE 42.5: QGPV FLUX-FORM EQUATION WITH NON-CONSERVATIVE PROCESSES

Derive the quasi-geostrophic potential vorticity equation (42.94). Show all the relevant steps. Hint: the key step requires showing that

$$\nabla \cdot [(\mathbf{u}_g \cdot) \mathbf{D}] = (\mathbf{u}_g \cdot) \nabla \cdot \mathbf{D}. \quad (42.134)$$

To do so, it is useful to express \mathbf{u}_g and b_g in terms of the geostrophic streamfunction.

EXERCISE 42.6: QGPV GAUGE FUNCTION

Derive the gauge function, \mathbf{A} , that connects the two forms of the quasi-geostrophic flux vector as per equation (42.98).



Part IX

Wave mechanics

Waves and the central role of a dispersion relation

Waves are fluctuations in fluid particles and associated fluid properties with the fluctuations possessing coherency in both space and time. Dynamically, waves exist when there is a restoring force that provides the means for fluid particles to undergo simple harmonic oscillations. Kinematically, waves arise when a symmetry is broken whereby coherent small amplitude fluctuations are a response to the symmetry breaking.

Linear waves, which form the bulk of our concern, have spatial and temporal properties that are closely linked. This linkage relates the angular frequency, ω , which measures the temporal structure of a wave, to the wavevector, \mathbf{k} , which measures the spatial structure of a wave. The *dispersion relation* is the mathematical equation that quantifies this linkage. Details of the dispersion relation are determined by the physical forces that give rise to the wave, such as compressibility for acoustic waves (Chapter 44), gravitational acceleration for gravity waves (Chapters 45, 48, and 49), the Coriolis acceleration for inertial waves (Chapters 46 and 48) and differential rotation (beta effect) for planetary Rossby waves (Chapters 47 and 48).

Linear waves satisfy the *superposition principle* that holds for linear physical phenomena. As a result, interactions between linear waves are reversible, and consist of constructive and destructive *interferences*.⁷ The superposition principle allows for the solution of a linear wave equation to be constructed from constituent elementary pieces. Linear superposition is the fundamental reason we can expose the key properties of waves by examining the behavior of a single traveling plane wave (Chapter 43). Correspondingly, linear superposition forms the basis for the mathematics of *Fourier analysis* (Chapter 5) used throughout the study of wave mechanics.

Linearization to derive the wave equations

A derivation of the governing wave equation(s) requires us to linearize the nonlinear equations of fluid motion. We approach the linearization process in a mostly heuristic manner, though do expose assumptions about what terms are small for the purpose of reducing ambiguity. After deriving the linearized equations, we study their salient properties to help understand the kinematics and dynamics of the corresponding wave solutions and dispersion relations. Each wave system offers unique facets depending on the underlying dynamical forces. Even so, the kinematical features of wave mechanics typically transcends details of the dynamics.

Wave energy transport versus matter transport

The movement of fluid particles within a fluid velocity field constitutes the movement of matter, along with properties carried by matter such as tracers, enthalpy, entropy, etc. Although waves can lead to a net transfer of matter, through a process known as *Stokes drift*, the transfer of energy by waves generally occurs without any net movement of fluid particles, where “net movement” refers to a time average over a wave period (i.e., the *phase average* from Section 5.2.2). As such, wave energy propagates at speeds that are unconstrained by fluid particle speeds. Indeed, wave energy in linear waves is generally transmitted many times faster than fluid matter. We thus conceive of waves as organized disturbances on a background fluid state (sometimes called the base state or equilibrium state) that transmit energy from one part of the media to another. The speed and direction of wave energy is determined by the dispersion relation, thus making the dispersion relation a central feature of wave dynamics.

⁷Some authors prefer to consider reversible interactions as a non-interaction, since one can exactly distinguish individual linear waves through Fourier decomposing a wave field consisting of multiple waves.

Scope for our study of wave mechanics

The study of wave phenomena forms a central part of physics, engineering, and applied mathematics. Indeed, waves can be studied by a variety of observational and mathematical means, from the insights of a poet to the analysis of a mathematician. We target the interested student aiming to learn wave mechanics for the first time, while also providing selected fruits for the experienced physicist interested in geophysical wave mechanics. For these purposes, we survey a suite of geophysical waves and dive deep into particular special topics that support understanding and develop mathematical methods. To help simplify the maths, we restrict attention to Cartesian waves (i.e., plane waves), leaving the geophysically relevant topic of spherical waves for more specialized treatments.

Our presentation is not comprehensive. Instead, we aim to offer an intellectual platform for further study and research. Insights and skills working with waves requires practice, and we get plenty from the wide variety of geophysical fluid waves. It is notable that we generally leave for other books the important, and difficult, topic of providing a wave interpretation for observed phenomena in the atmosphere and ocean. Here, we instead focus on the core of wave mechanics and the associated mathematical methods.

Chapter 43

WAVE KINEMATICS

For linear waves, physical processes determine a *dispersion relation* that connects the wave angular frequency, ω , to the *wavevector*, \mathbf{k}

$$\omega = \varpi(\mathbf{k}) \geq 0, \quad (43.1)$$

where ϖ is a function (generally nonlinear) of the wavevector. The dispersion relation couples the space and time structure of a wave, so that once a wavevector is chosen, then the angular frequency is specified. In this chapter, we are concerned with *wave kinematics*, which focuses on wave properties arising from the existence of a dispersion relation yet not concerned with the physics of how the relation arises. We are thus unconcerned with how waves are formed, but instead focus on characterizing properties of waves that exist.

A fundamental part of our description of waves concerns the *wave function*, which is a function that encapsulates the physical properties of linear waves. Example wave functions include the velocity potential (acoustic and surface waves), the streamfunction (Rossby waves), and free surface height (shallow water waves). All other dynamical fields can be generated from the wave function, thus allowing us to focus on characterizing how the wave appears through study of the wave function. The wave function has both an \mathbf{x} -space (geographic space) representation as well as a \mathbf{k} -space (wavevector space) representation. These two representations offer complementary characterizations of wave properties, with the transformation between these representations provided by Fourier's integral theorem from Section 5.4.1. One of the more remarkable aspects of this complementarity arises through the *uncertainty relation*, which states that it is not possible to simultaneously specify the position of a wave packet with arbitrary precision in both \mathbf{x} -space and \mathbf{k} -space. That is, precision in one space corresponds to imprecision in the other. We derive this uncertainty relation through the study of Gaussian wave packets.

READER'S GUIDE TO THIS CHAPTER

We assume familiarity with the use of complex variables as well as Fourier transforms, both reviewed in Chapter 5. We make use of the wave kinematics from this chapter for all the subsequent wave chapters in this part of the book. Our presentation shares much with books covering topics in wave mechanics, such as chapter 7 of [Thorne and Blandford \(2017\)](#) and chapter 6 of [Vallis \(2017\)](#). However, be mindful of the conventions followed here as summarized in Section 43.2.

43.1 Loose threads	1104
43.2 Some nomenclature and conventions	1104
43.2.1 Types of waves	1104
43.2.2 Types of dispersion relations	1105
43.2.3 Conventions for our space-time description of waves	1106

43.3	Two classes of linear waves	1106
43.3.1	Non-dispersive waves	1106
43.3.2	Dispersive waves	1107
43.3.3	Comments about time derivatives	1108
43.4	Monochromatic patterns	1108
43.5	Free plane waves	1108
43.5.1	Traveling plane wave	1109
43.5.2	Characterizing the wave	1109
43.5.3	Wavenumber and factors of 2π	1112
43.5.4	Superposition of plane waves	1112
43.5.5	Wave ansatz	1113
43.5.6	Summary of wave properties	1113
43.6	Wave packets	1114
43.6.1	Comments on the dispersion relation	1114
43.6.2	A continuum of traveling plane waves	1115
43.6.3	Basic properties of wave packets	1116
43.6.4	Wave packets in one-dimension	1116
43.6.5	The uncertainty relation for a Gaussian wave packet	1118
43.6.6	Evolution of non-dispersive Gaussian wave packets	1121
43.6.7	Evolution of a dispersive Gaussian wave packet	1122
43.6.8	Comments and further study	1125
43.7	General phase functions	1126
43.7.1	Phase velocity and phase speed	1126
43.7.2	Angular frequency and wavelength	1127
43.8	Geometric optics or ray theory	1127
43.8.1	Integral curves of the group velocity	1127
43.8.2	Eikonal equation	1127
43.8.3	Evolution of \mathbf{k} and ω along a ray	1128
43.8.4	Change in the phase along a ray	1129
43.8.5	Comments about rays	1129
43.8.6	Further study	1129
43.9	Exercises	1129

43.1 Loose threads

- Figures
- Waves on a string as an introduction to wave physics and kinematics. See Section 25 of *Fetter and Walecka (2003)*.
- Example of dispersive waves in springs from David Marion's book draft chapter 6.

43.2 Some nomenclature and conventions

Many readers have encountered wave kinematics in prior studies. Yet some of the choices for wave kinematics are not universal across all books and papers. For that purpose we summarize salient points to expose the choices made in this book. Details and motivations for these choices are further discussed in this chapter.

43.2.1 Types of waves

Table 43.1 summarizes the various types of waves considered in this book. We mostly encounter plane traveling waves, though also make use of standing waves (as for waves within a bounded

domain) and stationary waves (when a wave feature has only spatial periodicity). The wave patterns in Table 43.1 can arise from any conceivable context, physical or otherwise. The specifics of a physical system arises when enforcing that a wave function satisfies a linear partial differential equation of the form

$$\mathcal{L}\psi = 0, \quad (43.2)$$

where \mathcal{L} is a linear differential operator. Satisfying this equation is what gives rise to the dispersion relation.

We wish to emphasize the above points in a bit more mundane manner. Namely, there are many mathematical functions that give rise to oscillating patterns. However, these patterns correspond to particular solutions to a physical system only when they satisfy a partial differential equation such as (43.2). That is, there are more mathematical wave-like patterns than there are physical waves. For example, consider the function

$$\psi(x, y, t) = A \cos(k_x x - \omega t) \cos(\omega t) = (A/2) [\cos(k_x x - 2\omega t) + \cos(k_x x)], \quad (43.3)$$

where A is a constant amplitude. The second expression reveals the sum of a traveling wave plus a stationary wave. It is notable that this function is *not* in the form of a Fourier component that constitutes the wave patterns in Table 43.1. Rather, it is simply the sum of two trigonometric functions having a particular space and time structure. Is this function a particular solution to the classic wave equation with $\mathcal{L} = \partial_{tt} - c^2 \partial_{xx}$? A quick calculation reveals that it is indeed *not* a suitable solution since

$$\partial_{tt}\psi = -2A\omega^2 \cos(k_x x - 2\omega t) \quad (43.4a)$$

$$\partial_{xx}\psi = -k_x^2 \psi = -(k_x^2 A/2)[\cos(k_x x - 2\omega t) + \cos(k_x x)], \quad (43.4b)$$

revealing that there is no way to relate $\partial_{tt}\psi$ and $c^2 \partial_{xx}\psi$ at arbitrary space and time points. In turn, this function is *not* a suitable wave function ansatz for deriving a dispersion relation. We conclude that the mere presence of oscillating and/or traveling patterns is insufficient for a function to be a particular solution to a physical wave equation.

NAME	SPACE-TIME STRUCTURE
monochromatic	$\text{Re}[\Phi_0 e^{-i\omega t}]$
traveling	$\text{Re}[\mathcal{A}(\mathbf{k}) e^{i(\mathbf{k} \cdot \mathbf{x} - \omega t)}]$
standing	$\text{Re}[\mathcal{A}(\mathbf{k}) e^{i\mathbf{k} \cdot \mathbf{x}}] \cos(\omega t)$
stationary	$\text{Re}[\mathcal{A}(\mathbf{k}) e^{i\mathbf{k} \cdot \mathbf{x}}]$

TABLE 43.1: Summarizing the variety of waves encountered in this book, with distinctions based on their space-time structure. The operator, Re , extracts the real part of its argument, so that, for example, $\text{Re}[e^{i(\mathbf{k} \cdot \mathbf{x} - \omega t)}] = \cos(\mathbf{k} \cdot \mathbf{x} - \omega t)$. The first three patterns are monochromatic, which means they oscillate coherently with a single period, $2\pi/\omega$, where $\omega \geq 0$ is the angular frequency. However, note that $\text{Re}[\Phi_0 e^{-i\omega t}]$ is monochromatic and yet we cannot conclude whether it is a wave without further information about its spatial structure. Spatial dependence is introduced in the form $e^{i\mathbf{k} \cdot \mathbf{x}}$, where \mathbf{k} is the wavevector that determines the direction of the wave and its wavelength. For a plane wave in three-dimensional space, $\mathbf{k} \cdot \mathbf{x} = k_x x + k_y y + k_z z$, whereas a plane wave in two dimensions has wavevector $\mathbf{k} \cdot \mathbf{x} = k_x x + k_y y$. Standing waves do not travel in space but oscillate in place. The final three waves are *harmonic* since they have a regular spatial pattern.

43.2.2 Types of dispersion relations

The dispersion relation (43.1) is the root of all wave properties since it links the space and time structure of the wave. Yet some waves encountered in this book have a dispersion relation of the

form

$$\omega = \varpi(|\mathbf{k}|) \geq 0, \quad (43.5)$$

where $|\mathbf{k}|$ is the *wavenumber*. Hence, these waves have their angular frequency independent of the wave direction. Examples include acoustic waves (Chapter 44) and surface waves (Chapter 45). Inertial waves from Chapter 46 and internal gravity waves from Chapter 49 are the complement, with their dispersion relation independent of the wavenumber yet dependent on the wave direction,

$$\omega = \varpi(\hat{\mathbf{k}}) \geq 0 \quad \text{with} \quad \hat{\mathbf{k}} = \mathbf{k}/|\mathbf{k}|. \quad (43.6)$$

Finally, the Rossby waves introduced in Chapters 47 and 48 have a dispersion relation that depends on both the wavenumber and wave direction; i.e., on \mathbf{k} . Hence, the dispersion relation for Rossby waves is of the general form given in equation (43.1).

43.2.3 Conventions for our space-time description of waves

The suite of dispersion relations encountered in geophysical fluids motivates the following conventions that form the basis for our space-time description of waves.

- **ANGULAR FREQUENCY:** The angular frequency resulting from the dispersion relation, $\omega = \varpi(\mathbf{k})$, is a non-negative real number, $\omega \geq 0$, so that the wave period, $2\pi/\omega$, is also a non-negative number.¹
- **WAVE DIRECTION:** The direction of a wave is specified by the wavevector, \mathbf{k} (Section 43.5), and its wavelength is $2\pi/|\mathbf{k}|$, where $|\mathbf{k}| > 0$ is the wavenumber. We never consider negative wavenumbers. Some authors allow the angular frequency to be negative for waves traveling in directions opposite to those with positive angular frequency. That approach is not used in this book, since we always determine the wave direction via the wavevector.
- **PHASE SPEED:** The phase speed is a non-negative number. It is not a vector so that we do not consider components to the phase speed. Rather, we consider components to the phase vector, which is a vector whose direction is given by the wavevector and whose non-negative magnitude is the phase speed (Section 43.5.2).

43.3 Two classes of linear waves

We distinguish two types of linear wave phenomena: non-dispersive waves and dispersive waves. In this section we present a mathematical overview of these waves, offering examples of each type of wave along with hints at the physics and maths to come later.²

43.3.1 Non-dispersive waves

The canonical non-dispersive wave phenomena is described by “the” wave equation

$$(\partial_{tt} - c^2 \nabla^2) \Phi = 0, \quad (43.7)$$

¹One can use negative angular frequency when conducting time-frequency Fourier analysis as in Section 5.5. But in that context, the negative frequency is used solely for mathematical expediency in order to work with a complex Fourier transform. One could just equivalently work with real Fourier sine and cosine transforms, in which case the angular frequency is non-negative.

²Chapter 1 of [Whitham \(1974\)](#) provides a more thorough mathematical introduction to the variety of linear and nonlinear waves.

where Φ is a wave field (e.g., velocity potential, streamfunction, surface height), and $c^2 > 0$ is the squared wave speed. As discussed in Section 3.7, this wave equation is hyperbolic and its wave solutions all transmit signals with speed, c , without distortion. That is, waves of all wavelengths travel at the same speed so that there is no mixing across the spectrum of wavevectors. We find that for non-dispersive waves the angular frequency divided by the wavenumber equals to a constant phase speed shared by all waves. The acoustic waves of Chapter 44 and the shallow water gravity waves of Chapter 48 are example non-dispersive waves considered in this book.

To expose some of the mathematical details, consider the wave equation (43.7) in one space dimension and written in the factored form

$$(\partial_t - c \partial_x)(\partial_t + c \partial_x)\Phi = 0. \quad (43.8)$$

As discussed in Section 3.7, the solution to this hyperbolic partial differential equation takes the form of two signals moving in opposite directions

$$\Phi(x, t) = F(x - ct) + G(x + ct), \quad (43.9)$$

where the functions F and G are specified by boundary and initial conditions. Their respective functional dependencies, $x \pm ct$, determine the propagation direction of the signal, with $F(x - ct)$ a signal propagating in the $+\hat{x}$ direction whereas $G(x + ct)$ is a signal propagating in the $-\hat{x}$ direction. A key point is that the signals all move with the same speed, with F and G arbitrary functions that may be built from a single linear wave or an infinity of waves. Also note that the wave equation (43.8) has been factored into the product of two linear operators, so that a simpler hyperbolic wave equation is either of the two first order equations

$$(\partial_t \pm c \partial_x)\Phi = 0. \quad (43.10)$$

In other parts of this book this equation is referred to as the advection equation for a one-dimensional signal with constant advection velocity (e.g., see Sections 61.5 and 61.6).

We are generally introduced to wave physics through solutions to the hyperbolic wave equations (43.7) or (43.10). Correspondingly, much of our experience with waves is based on the non-dispersive nature of these waves. For example, when listening to a symphony, we hear the sounds from various instruments “in concert”. That is, the speed that the acoustic waves propagate are independent of the wavelength. Indeed, imagine how difficult it would be for an audience spread throughout a concert hall to equally appreciate a symphonic performance if acoustic waves were dispersive!

43.3.2 Dispersive waves

Upon studying geophysical waves, we soon realize that non-dispersive waves are the exception rather than the norm. That is, most waves in geophysical fluids are dispersive, with their governing wave equations sometimes mathematically classified as hyperbolic though many are not. A dispersive wave is one that admits solutions of the form

$$\Phi(\mathbf{x}, t) = A e^{i(\mathbf{k} \cdot \mathbf{x} - \varpi t)}, \quad (43.11)$$

where the speed of a constant phase surface, $C_p = \varpi(\mathbf{k})/|\mathbf{k}|$, is a function of the wavevector. As such, the movement of the wave signal (i.e., the *phase velocity*) depends on the wavelength of the wave. For example, if we prepare a packet of dispersive waves with a particular shape in space, the evolution of the packet is characterized by the dispersion of packet. Waves visible by eye on the surface of a pond or ocean offer a canonical example of dispersive waves, whereby long surface

gravity waves travel faster than short surface waves (as explored in Section 45.5.3). Indeed, it is this dispersion of surface gravity waves that surfers appreciate when assessing the suitability of coastal surf conditions following an offshore storm.³

43.3.3 Comments about time derivatives

As noted when discussing the non-dispersive wave equation (43.8), the presence of two time derivatives provides the means for two wave signals to result and move in opposite directions. This case occurs for acoustic waves, gravity waves, and inertial waves. It manifests as a dispersion relation written for the squared angular frequency. In contrast, when there is only one time derivative in the wave equation, then the dispersion relation is written for the angular frequency rather than its square. Furthermore, the system chooses a preferred direction for the wave signal, with the Rossby wave offering the canonical example of a dynamically anisotropic wave.

43.4 Monochromatic patterns

A *monochromatic pattern* is a feature characterized by having all points maintain the same time periodic motion with single angular frequency, ω . We are only concerned here with wave patterns, and thus focus on *monochromatic waves*. The trigonometric functions, $\cos(\omega t)$ and $\sin(\omega t)$, both exhibit time periodic behavior, which explains the factors of 2π appearing throughout wave physics. We choose the convention in which the angular frequency is a non-negative number, $\omega \geq 0$, so that the period of the oscillation is $2\pi/\omega$. The exception occurs when performing complex Fourier analysis of time signals, with the use of negative angular frequency a mathematical expedient (see Section 5.5.1).

It is often convenient to make use of the *Euler identity*

$$e^{-i\omega t} = \cos(\omega t) - i \sin(\omega t), \quad (43.12)$$

to thus write a time periodic *wave function* as⁴

$$\Phi = \text{Re}[\Phi_0 e^{-i\omega t}], \quad (43.13)$$

where Φ_0 is a complex function further specified below, and $\text{Re}[\cdot]$ is an operator that returns the real part of its argument (see Section 5.2). For linear calculations we can safely omit the Re operation until the end of the calculations. However, for products of wave fields, such as when performing energetic analyses, more care is needed, with details given in Section 5.2.⁵

43.5 Free plane waves

Plane waves are characterized by a single wavevector and single angular frequency, with the wave exhibiting symmetry in directions perpendicular to the propagation direction (hence the “plane” in its name). Any linear wave, be it acoustic, gravity, Rossby, etc., can be decomposed into a sum or integral of plane waves with a suite of frequencies and wavevectors, and with modulation by an amplitude function.

³See [Butt et al. \(2004\)](#) for a scientific view on surface ocean waves geared towards surfing.

⁴The minus sign is motivated by convenience for when we consider a traveling wave and the phase velocity in Section 43.5.2. See in particular Figure 43.1.

⁵As noted when developing the basics of Fourier analysis in Chapter 5, we use complex variables solely for mathematical convenience, with all physical fields producing real numbers in classical physics.

The general form of a plane wave function is given by

$$\Phi_0 = \mathcal{A}(\mathbf{k}) e^{i\mathbf{k}\cdot\mathbf{x}}, \quad (43.14)$$

where $\mathcal{A}(\mathbf{k})$ is a complex wave amplitude and \mathbf{k} is the *wavevector* or *wavenumber vector*. The wavevector has dimensions of inverse length and it characterizes the spatial direction of the wave propagation as well as the wavelength. The magnitude of the wavevector, $|\mathbf{k}|$, is referred to as the *wavenumber* as it measures 2π times the number of waves per unit length (we further discuss this notion in Section 43.5.2). We allow the wave amplitude, $\mathcal{A}(\mathbf{k})$, to be a function of wavevector so that different plane waves can have distinct amplitudes. We also allow for $\mathcal{A}(\mathbf{k})$ to be complex so that different plane waves can have their phases shifted relative to one another (we discuss phases in Section 43.5.1).

Given that the plane wave possesses symmetry in planes perpendicular to \mathbf{k} , it is spatially dependent only on the direction parallel to the wavevector,⁶

$$\mathbf{k} = |\mathbf{k}| \hat{\mathbf{k}}. \quad (43.15)$$

We say that the plane wave function (43.14) is *free* since it exists throughout all of space and is unaffected by boundaries. In this sense the free plane wave is not physically realizable. Even so, the mathematical simplicity of the plane wave, along with the superposition principle, affords it a central role in the study of wave mechanics.

43.5.1 Traveling plane wave

Allowing for time to evolve renders the traveling monochromatic plane wave function

$$\Phi = \text{Re}[\Phi_0 e^{-i\omega t}] = \text{Re}[\mathcal{A}(\mathbf{k}) e^{i(\mathbf{k}\cdot\mathbf{x}-\omega t)}] = |\mathcal{A}(\mathbf{k})| \text{Re}[e^{i(\mathbf{k}\cdot\mathbf{x}-\omega t+\alpha)}]. \quad (43.16)$$

We here wrote complex wave amplitude according to a real amplitude and a phase shift

$$\mathcal{A}(\mathbf{k}) = |\mathcal{A}(\mathbf{k})| e^{i\alpha} \quad \text{with} \quad \tan \alpha = \text{Im}[\mathcal{A}(\mathbf{k})]/\text{Re}[\mathcal{A}(\mathbf{k})]. \quad (43.17)$$

The traveling plane wave *phase* function is given by

$$\mathcal{P} = \mathbf{k} \cdot \mathbf{x} - \omega t + \alpha, \quad (43.18)$$

so that

$$\Phi = |\mathcal{A}(\mathbf{k})| \text{Re}[e^{i\mathcal{P}}] = |\mathcal{A}(\mathbf{k})| \cos \mathcal{P}. \quad (43.19)$$

The traveling plane wave function, Φ , depends on the wavevector as well as the space and time point. It is also a function of the angular frequency, ω . However, recall that for the study of waves realized by a physical system, once the wavevector is known then the angular frequency is specified through the dispersion relation (43.1).

The phase factor on the wave amplitude in equation (43.17) is generally a function of wavevector, $\alpha = \alpha(\mathbf{k})$. However, for most applications it is taken as a constant, in which case it is referred to as the *standard phase*.

43.5.2 Characterizing the wave

⁶Caution: many authors write $\hat{\mathbf{k}}$ for the unit vertical direction, whereas in this book we write $\hat{\mathbf{z}}$ for the unit vertical direction whereas $\hat{\mathbf{k}}$ is the direction of a wave.

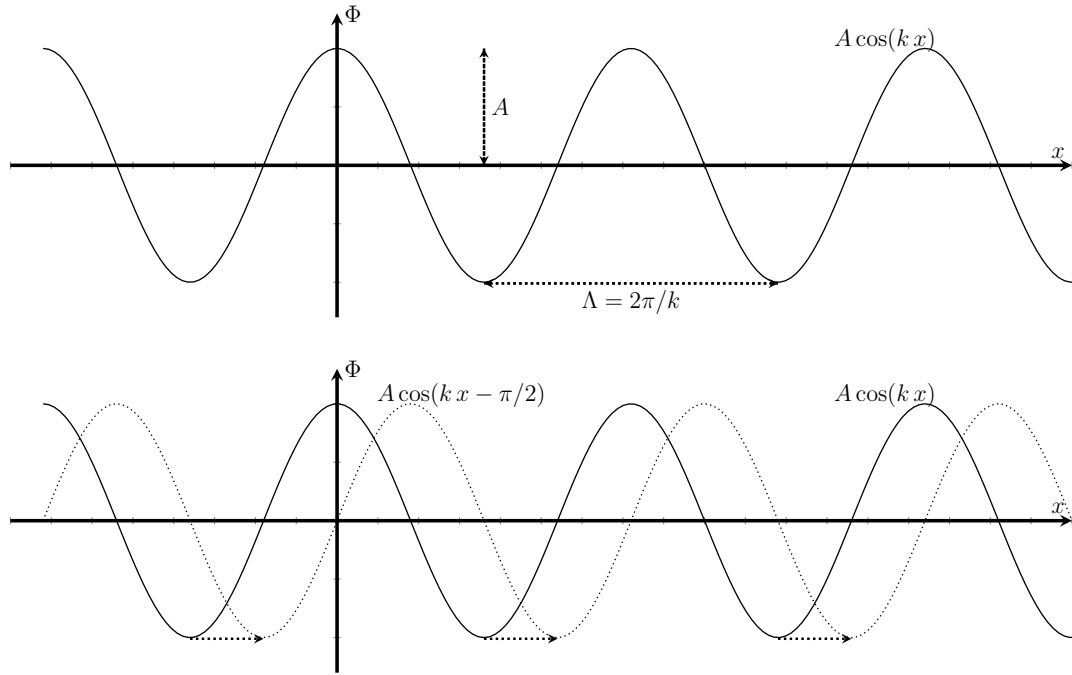


FIGURE 43.1: Top panel: a cosine wave, $\Phi = A \cos(kx - \omega t)$, along the x -axis at $t = 0$, with wavelength $\Lambda = 2\pi/|k|$, wavevector $\mathbf{k} = k \hat{x}$, and real amplitude, A . The wave is moving in the $+\hat{x}$ direction so that $k > 0$. Lower panel: two snapshots of a traveling cosine wave, one shown at $t = 0$ as in the top panel, and another shown a quarter period later, at $\omega t = \pi/2$. With $k > 0$ and $\omega t > 0$, as shown in this figure, a point with constant phase moves in the $+\hat{x}$ direction, whereas if $k < 0$ then the phase propagates in the $-\hat{x}$ direction.

Wave period

The wave function (43.16) for the traveling plane wave takes on the same value for all space and time points with a phase, \mathcal{P} , that is shifted by any integer multiple of 2π . By fixing a point in space, the plane wave is identical for all times, t_n , satisfying

$$\omega t_n = \omega t + 2\pi n = \omega(t + 2\pi n/\omega). \quad (43.20)$$

Hence, the wave period is given by

$$\text{wave period} = 2\pi/\omega. \quad (43.21)$$

Wavelength

By fixing time, we see that the plane wave is identical for all space points, \mathbf{x}_n , satisfying

$$\mathbf{k} \cdot \mathbf{x}_n = \mathbf{k} \cdot \mathbf{x} + 2\pi n = |\mathbf{k}|(\mathbf{x} \cdot \hat{\mathbf{k}} + 2\pi n/|\mathbf{k}|), \quad (43.22)$$

which allows us to identify $2\pi/|\mathbf{k}|$ as the *wavelength*, which we write as⁷

$$\Lambda = 2\pi/|\mathbf{k}| \implies \mathbf{k} = 2\pi \hat{\mathbf{k}}/\Lambda. \quad (43.23)$$

⁷We choose the uppercase, Λ , to denote wavelength rather than the more commonly used λ . We do so in order to distinguish the wavelength, Λ , from λ , which refers to longitude in this book.

Figure 43.1 provides an example cosine wave in one-dimension, illustrating the wavelength and traveling nature of the wave.

Phase velocity and phase speed

When observing a traveling plane wave from a fixed point in space, one wavelength passes by the point within a single wave period. We refer to the *phase velocity*, \mathbf{c}_p , as the velocity of a point fixed on a phase line and traveling in the direction of the wavevector. Its magnitude is the *phase speed*, C_p , which is the speed that the phase moves in the direction of the wavevector,

$$\mathbf{c}_p = C_p \hat{\mathbf{k}} = (\omega/|\mathbf{k}|) \hat{\mathbf{k}} \implies C_p = (2\pi/|\mathbf{k}|)/(2\pi/\omega) = \omega/|\mathbf{k}| \geq 0. \quad (43.24)$$

Figure 43.2 provides an illustration of the phase velocity and phase speed.

Phase distance

We can define the phase speed in another manner by introducing the projection of the position vector along the direction of the wavevector

$$S_{\hat{\mathbf{k}}} \equiv \hat{\mathbf{k}} \cdot \mathbf{x}, \quad (43.25)$$

which we refer to as the *phase distance*. Note that $S_{\hat{\mathbf{k}}}$ can be positive or negative, depending on the direction of the wavevector. The wavelength as defined by equation (43.22) takes on the form

$$\mathbf{k} \cdot \mathbf{x}_n = \mathbf{k} \cdot \mathbf{x} + 2\pi n = |\mathbf{k}|(S_{\hat{\mathbf{k}}} + 2\pi n/|\mathbf{k}|). \quad (43.26)$$

As such, the phase speed is the change in the position of the constant phase lines in the direction of the wavevector, so that

$$C_p = \left[\frac{\partial S_{\hat{\mathbf{k}}}}{\partial t} \right]_p = -\frac{\partial \mathcal{P}/\partial t}{\partial \mathcal{P}/\partial S_{\hat{\mathbf{k}}}} = \omega/|\mathbf{k}|. \quad (43.27)$$

For this equation we made use of some basic mathematics of generalized surfaces as detailed in Section 56.12.2. Finally, this notation allows us to write the phase function as

$$\mathcal{P} = \mathbf{k} \cdot \mathbf{x} - \omega t + \alpha = |\mathbf{k}|(S_{\hat{\mathbf{k}}} - C_p t) + \alpha. \quad (43.28)$$

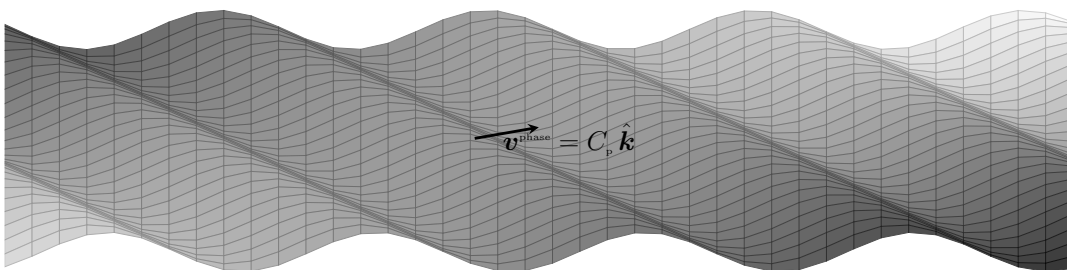


FIGURE 43.2: A mesh plot of a plane wave with phase velocity, $\mathbf{c}_p = C_p \hat{\mathbf{k}} = (\omega/|\mathbf{k}|) \hat{\mathbf{k}}$, pointing perpendicular to surfaces of constant phase.

43.5.3 Wavenumber and factors of 2π

The magnitude of the wavevector, $|\mathbf{k}|$, appears in many places in wave kinematics, such as in the definition (43.23) of the wavelength. As a shorthand terminology, we refer to $|\mathbf{k}|$ as the *wavenumber*, with the wavenumber related to the wavelength via

$$|\mathbf{k}| = 2\pi/\Lambda. \quad (43.29)$$

The wavenumber measures 2π times the number of waves per unit length, so that the wavenumber measures the *spatial angular frequency* of a wave. In some contexts it is useful to introduce the *reduced wavelength*

$$\lambda = \Lambda/2\pi, \quad (43.30)$$

so that the wavenumber is given by the inverse reduced wavelength

$$|\mathbf{k}| = \lambda^{-1}. \quad (43.31)$$

Alternatively, it is sometimes convenient to work with the *reduced wavenumber* as introduced in Section 5.4.6 when discussing Fourier transforms

$$\tilde{k} = |\mathbf{k}|/2\pi. \quad (43.32)$$

Hence, the reduced wavenumber is the inverse wavelength

$$\tilde{k} = 1/\Lambda \quad (43.33)$$

so that \tilde{k} measures the number of waves per unit length.

In Section 5.4.6 we raised some issues about various conventions for placing 2π factors in Fourier analysis. We further those concerns by noting that the 2π factor associated with wavenumbers can be unclear in the literature. The ambiguity occurs when a particular length scale, L , is considered, yet it is not specified whether the length scale refers to a wavelength, in which case the corresponding wavenumber is $|\mathbf{k}| = 2\pi/L$, or to a reduced wavelength, in which case the corresponding wavenumber is $|\mathbf{k}| = 1/L$. The bottomline is that care is necessary to ensure the proper usage.

43.5.4 Superposition of plane waves

Through the principle of superposition respected by linear waves, realistic linear waves can be decomposed into the sum or integral of modulated plane waves. Indeed, this decomposition forms the mathematical basis for *Fourier analysis* detailed in Chapter 5. We here offer an illustration of this decomposition by illustrating how two and three plane waves combine.

Consider the sum of two plane waves of the same real amplitude of unity in arbitrary units, and with very close wavevectors and frequencies

$$\mathbf{k}_{\pm} = \mathbf{k} \pm \Delta\mathbf{k} \quad \text{and} \quad \omega_{\pm} = \omega \pm \Delta\omega, \quad (43.34)$$

where $|\Delta\mathbf{k}|/|\mathbf{k}| \ll 1$, and $|\Delta\omega/\omega| \ll 1$. The resulting superposition of the two waves is given by

$$\text{Re}[e^{i(\mathbf{x} \cdot \mathbf{k}_+ - t\omega_+)} + e^{i(\mathbf{x} \cdot \mathbf{k}_- - t\omega_-)}] = 2 \cos(\Delta\mathbf{k} \cdot \mathbf{x} - \Delta\omega t) \cos(\mathbf{k} \cdot \mathbf{x} - \omega t). \quad (43.35)$$

The $\cos(\Delta\mathbf{k} \cdot \mathbf{x} - \Delta\omega t)$ factor acts as a low wavenumber and low frequency modulation of the second factor, $\cos(\mathbf{k} \cdot \mathbf{x} - \omega t)$, which is much more rapidly varying in space and time. We illustrate this superposition of two plane waves in Figure 43.3 for time $t = 0$. Adding a third wave, also

with unit amplitude, $\exp[i(\mathbf{k} \cdot \mathbf{x} - \omega t)]$, renders the superposition

$$\operatorname{Re}[e^{i(\mathbf{x} \cdot \mathbf{k}_+ - t\omega_+)} + e^{i(\mathbf{x} \cdot \mathbf{k} - t\omega)} + e^{i(\mathbf{x} \cdot \mathbf{k}_- - t\omega_-)}] = 4 \cos^2[(\Delta \mathbf{k} \cdot \mathbf{x} - \Delta\omega t)/2] \cos(\mathbf{k} \cdot \mathbf{x} - \omega t). \quad (43.36)$$

The third wave serves to double the amplitude through constructive interference, while also broadening the width of the low amplitude destructive interference region. Additionally, the modulation function, $\cos^2[(\Delta \mathbf{k} \cdot \mathbf{x} - \Delta\omega t)/2]$, is rendered non-negative when adding the third wave. We also illustrate this superposition in Figure 43.3.

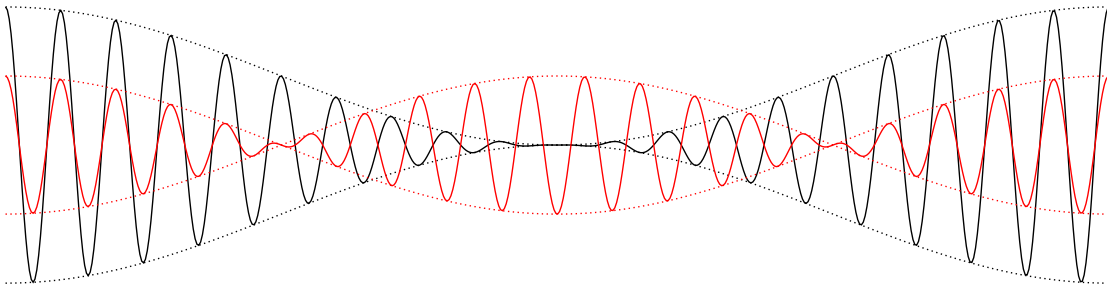


FIGURE 43.3: Superposition of two plane waves (red lines; equation (43.35)) and three plane waves (black lines; equation (43.36)), with all plane waves having equal amplitude and realized at time $t = 0$. Notice how in both cases, a high wavenumber wave (short wave) is modulated by a low wavenumber wave (long wave). The units in this figure are arbitrary.

43.5.5 Wave ansatz

The principle of superposition allows us to study properties of a linear wave equation, in particular the dispersion relation, by inserting a plane wave solution into the wave equation. In this manner we refer to the plane wave as an *ansatz*, which is a German word meaning “educated guess”.

43.5.6 Summary of wave properties

In Table 43.2, we summarize the variety of kinematic properties of waves. In this book we work mostly with the angular frequency, ω , the wavevector, \mathbf{k} , and the wavenumber, $|\mathbf{k}|$. Yet it is useful to be versed in the alternatives.

NAME	MATH SYMBOL	DIMENSIONS	MATH RELATION
period	τ_{period}	T	$\tau_{\text{period}} = 2\pi/\omega$
angular frequency	ω	T^{-1}	$\omega = 2\pi/\tau_{\text{period}}$
frequency	f	T^{-1}	$f = \omega/2\pi$
wavenumber	$ \mathbf{k} $	L^{-1}	$ \mathbf{k} = 2\pi/\Lambda$
wavevector	\mathbf{k}	L^{-1}	$\mathbf{k} = \mathbf{k} \hat{\mathbf{k}}$
reduced wavevector	$\tilde{\mathbf{k}}$	L^{-1}	$\tilde{\mathbf{k}} = \mathbf{k}/2\pi$
wavelength	Λ	L	$\Lambda = 2\pi/ \mathbf{k} = 1/ \mathbf{k} $
reduced wavelength	λ	L	$\lambda = \Lambda/2\pi = 1/ \mathbf{k} $

TABLE 43.2: Summarizing the variety of terms used to kinematically describe waves. In this book we mostly use the angular frequency, $\omega \geq 0$, the wavevector, \mathbf{k} , and the wavenumber, $|\mathbf{k}|$.

43.6 Wave packets

The modulation functions for both examples in Figure 43.3 organize the higher wavenumber/frequency oscillations into \mathbf{x} -space regions known as *wave packets*. Wave packets are physically realizable groups of waves that are localized in \mathbf{x} -space, with localization enabled by a modulation function. Examination of Figure 43.3 suggest that the velocity of a wave packet's center is not directly related to the phase velocity of the constituent plane waves. Rather, it is determined by motion of the modulation function. For the one-dimensional examples of Figure 43.3, the packet motion is determined by $\Delta\omega/\Delta k$. In this section we generalize this result to the three dimensional *group velocity*⁸

$$\mathbf{c}_g = \nabla_{\mathbf{k}}\varpi(\mathbf{k}). \quad (43.37)$$

In this equation, we introduced the wave dispersion relation (43.1) that specifies how the angular frequency is functionally connected to the wavevector. We see that the group velocity is determined by the gradient of the dispersion relation in wavevector space. Note that for non-homogeneous fluids (Section 43.7), the dispersion relation is a function of space, time, and wavevector, $\varpi(\mathbf{k}, \mathbf{x}, t)$, so it is important to expose the wavevector label on the gradient operator in expression (43.37).

Our goal in this section is to introduce the physics and maths of wave packets. Wave packets are described by complementary wave functions in \mathbf{k} -space and \mathbf{x} -space. The \mathbf{k} -space representation, $\mathcal{A}(\mathbf{k}, t)$, is also called the amplitude function for the \mathbf{x} -space wave function, $\Phi(\mathbf{x}, t)$. We prepare wave packets with a specified \mathbf{k} -space initial condition, $\mathcal{A}(\mathbf{k}, t=0)$, that has a corresponding \mathbf{x} -space initial condition, $\Phi(\mathbf{x}, t=0)$, determined by the inverse Fourier transform. Upon initializing the packets we study their evolution. Since the packets are constructed by linear plane waves, their evolution is determined by superposing evolution of the constituent plane waves. That is, we do not solve an equation of motion to determine the packet evolution. Instead, we just let them “fly” according to the evolution of the plane waves comprising the packet. Details for how the waves evolve are determined by the dispersion relation, with the dispersion relation specific to the particular physics describing the waves.

43.6.1 Comments on the dispersion relation

Details for how a wave packet evolves are fundamentally connected to details of the dispersion relation, $\omega = \varpi(\mathbf{k})$. We understand the central role fo the dispersion relation since it specifies how the spatial structure of the wave is tied to its temporal structure.

The dispersion relation for non-dispersive waves results in phase speeds that are independent of the wavenumber so that

$$\varpi = C_p |\mathbf{k}| > 0, \quad (43.38)$$

where $C_p > 0$ is the constant phase speed. Evidently, the angular frequency is identical for all waves having the same wavenumber. That is, the angular frequency only cares about the wavelength of the non-dispersive wave and not about its direction. Furthermore, we see that the continuum of wavenumbers results in a continuum of angular frequencies, with higher wavenumbers rendering higher angular frequencies. This behavior is familiar for both electromagnetic and acoustic waves, which are both non-dispersive, in which waves of smaller wavelength (higher wavenumber) have higher frequencies.

Dispersive waves are characterized by a dispersion relation with the phase speed a function of

⁸Many dispersion relations are naturally written as ω^2 , in which case it is simpler to compute the group velocity according to $\nabla_{\mathbf{k}}\omega^2 = 2\omega \mathbf{c}_g$.

the wavevector

$$\varpi = C_p(\mathbf{k}) |\mathbf{k}| > 0. \quad (43.39)$$

Again, the phase speed and angular frequency are positive, but now we find the phase speed depends on the wavenumber and possibly the wave direction. We encounter such waves in our studies.

43.6.2 A continuum of traveling plane waves

Consider the superposition of a continuum of traveling plane waves given by the integral

$$\Phi(\mathbf{x}, t) = \frac{1}{(2\pi)^3} \int \mathcal{A}(\mathbf{k}) e^{i[\mathbf{k} \cdot \mathbf{x} - \varpi t]} d\mathbf{k}, \quad (43.40)$$

where we dropped the $\text{Re}[\cdot]$ operator for brevity. Equation (43.40) builds the wave packet or wave function, $\Phi(\mathbf{x}, t)$, from a continuum of traveling plane waves. The integral computed over all of the three-dimensional wavevector space (\mathbf{k} -space), with the wavevector volume element written⁹

$$d\mathbf{k} = dk_x dk_y dk_z. \quad (43.41)$$

The angular frequency in the superposition is determined through the dispersion relation,

$$\omega = \varpi(\mathbf{k}) > 0, \quad (43.42)$$

so that the wave function (43.40) is built from a continuum of wavevectors with corresponding angular frequencies. The amplitude function, $\mathcal{A}(\mathbf{k})$, acts to modulate which wave vectors contribute to the packet. Typically, that modulation is designed to carry only a small band of wavevectors, such as realized by the Gaussian packets studied later in this section.

Duality between \mathbf{k} -space and \mathbf{x} -space representations

Recalling our discussion of Fourier transforms in Section 5.4, we identify a *Fourier transform* pair between the \mathbf{x} -space and \mathbf{k} -space wave functions

$$\Phi(\mathbf{x}, t) = \frac{1}{(2\pi)^3} \int \mathcal{A}(\mathbf{k}, t) e^{i\mathbf{k} \cdot \mathbf{x}} d\mathbf{k} \iff \mathcal{A}(\mathbf{k}, t) = \int \Phi(\mathbf{x}, t) e^{-i\mathbf{k} \cdot \mathbf{x}} dx, \quad (43.43)$$

where we defined the time dependent \mathbf{k} -space wave function

$$\mathcal{A}(\mathbf{k}, t) = \mathcal{A}(\mathbf{k}) e^{-i\varpi t}. \quad (43.44)$$

Correspondingly, we identify the Fourier transform pair for the wave packet initial conditions

$$\Phi_0(\mathbf{x}) = \frac{1}{(2\pi)^3} \int \mathcal{A}(\mathbf{k}) e^{i\mathbf{k} \cdot \mathbf{x}} d\mathbf{k} \iff \mathcal{A}(\mathbf{k}) = \int \Phi_0(\mathbf{x}) e^{-i\mathbf{k} \cdot \mathbf{x}} dx, \quad (43.45)$$

where $\Phi(\mathbf{x}, t=0) = \Phi_0(\mathbf{x})$. The duality relations (43.43) and (43.45) between the \mathbf{x} -space and \mathbf{k} -space wave functions proves fundamental to our description of wave packets.

⁹If we represent wavevector space using Cartesian components of the wavevector as in equation (43.41), then the integration limits are $k_x, k_y, k_z \in (-\infty, \infty)$, corresponding to waves traveling in all directions.

Evolution of the \mathbf{k} -space wave function

Equation (43.45) seems simple enough, as it is merely a repackaging of the wave packet definition given in equation (43.40). Even so, it does provide the full evolution for the \mathbf{k} -space representation of the wave packet, and that is an important conceptual and practical point. Namely, the evolution is simply given by the initial condition multiplied by $e^{-i\varpi t}$. It follows that the modulus of the \mathbf{k} -space wave function remains static,

$$|\mathcal{A}(\mathbf{k}, t)| = |\mathcal{A}(\mathbf{k})|. \quad (43.46)$$

This result means that the \mathbf{k} -space wave function does not spread in \mathbf{k} -space. Instead, it only oscillates with an angular frequency determined by the dispersion relation, $\varpi(\mathbf{k})$.

43.6.3 Basic properties of wave packets

The wave packet (43.40) can be written in the form

$$\Phi^{(+)}(\mathbf{x}, t) = \frac{1}{(2\pi)^3} \int \mathcal{A}(\mathbf{k}) e^{i[\mathbf{k} \cdot \mathbf{x} - \varpi(\mathbf{k})t]} d\mathbf{k} = \frac{1}{(2\pi)^3} \int \mathcal{A}(\mathbf{k}) e^{i|\mathbf{k}|[S_{\hat{\mathbf{k}}} - C_p t]} d\mathbf{k}, \quad (43.47)$$

where $S_{\hat{\mathbf{k}}} = \hat{\mathbf{k}} \cdot \mathbf{x}$ is the phase distance from equation (43.25), and $C_p = \varpi(\mathbf{k})/|\mathbf{k}| > 0$ is the phase speed. For non-dispersive waves, the phase speed is a constant, whereas for dispersive waves it is a function of the wavevector, $C_p = C_p(\mathbf{k})$. We introduce the + notation on this packet to distinguish from the oppositely traveling packet, $\Phi^{(-)}$, defined according to

$$\Phi^{(-)}(\mathbf{x}, t) = \frac{1}{(2\pi)^3} \int \mathcal{A}(-\mathbf{k}) e^{-i[\mathbf{k} \cdot \mathbf{x} + \varpi(\mathbf{k})t]} d\mathbf{k}. \quad (43.48)$$

If the amplitude function satisfies $\mathcal{A}(-\mathbf{k}) = \mathcal{A}(\mathbf{k})$, then $\Phi^{(-)}(\mathbf{x}, t) = \Phi^{(+)}(-\mathbf{x}, t)$. It follows that the sum of these two traveling packets takes the form

$$\Phi^{(-)}(\mathbf{x}, t) + \Phi^{(+)}(\mathbf{x}, t) = \frac{2}{(2\pi)^3} \int \mathcal{A}(\mathbf{k}) e^{-i\varpi(\mathbf{k})t} \cos(\mathbf{k} \cdot \mathbf{x}) d\mathbf{k} \quad \text{if } \mathcal{A}(-\mathbf{k}) = \mathcal{A}(\mathbf{k}), \quad (43.49)$$

and the initial condition is the inverse cosine transform of $\mathcal{A}(\mathbf{k})$

$$\Phi^{(-)}(\mathbf{x}, t=0) + \Phi^{(+)}(\mathbf{x}, t=0) = \frac{2}{(2\pi)^3} \int \mathcal{A}(\mathbf{k}) \cos(\mathbf{k} \cdot \mathbf{x}) d\mathbf{k} \quad \text{if } \mathcal{A}(-\mathbf{k}) = \mathcal{A}(\mathbf{k}). \quad (43.50)$$

Furthermore, note that if $\mathcal{A}(\mathbf{k})$ is a real function of even parity, then $\Phi^{(-)}(\mathbf{x}, t=0) + \Phi^{(+)}(\mathbf{x}, t=0)$ is a real function.¹⁰ As we see in Section 43.6.5, Gaussian packets that include modulated waves make use of amplitude functions with $\mathcal{A}(-\mathbf{k}) \neq \mathcal{A}(\mathbf{k})$.

43.6.4 Wave packets in one-dimension

We make use of a variety of packets moving in one space dimension due to their simpler technical features.¹¹

¹⁰This point was emphasized in our discussion of Fourier transforms in Section 5.4.4.

¹¹Note that as a wave packet in one-dimension, the wave function Φ has dimensions of its amplitude function, \mathcal{A} , times inverse length, which contrasts to the \mathcal{A} times inverse volume dimension for the three-dimensional wave packet (43.40).

The positive wave packet

For a packet built from plane waves traveling in the $+\hat{x}$ direction, we write the wavevector as $\mathbf{k} = k \hat{x}$ with $k \geq 0$ so that a positive-traveling packet takes the form

$$\Phi^{(+)}(x, t) = \frac{1}{2\pi} \int_0^\infty \mathcal{A}(k) e^{i[kx - \varpi t]} dk. \quad (43.51)$$

The negative wave packet

A packet moving in the negative \hat{x} direction is built from plane waves with $\mathbf{k} = -k \hat{x}$, again with $k \geq 0$, so that

$$\Phi^{(-)}(x, t) = \frac{1}{2\pi} \int_0^\infty \mathcal{A}(-k) e^{-i[kx + \varpi t]} dk. \quad (43.52)$$

Observe that $\Phi^{(-)}(x, t)$ can be written in the equivalent form

$$\Phi^{(-)}(x, t) = \frac{1}{2\pi} \int_0^\infty \mathcal{A}(-k) e^{-i[kx + \varpi t]} dk = \frac{1}{2\pi} \int_{-\infty}^0 \mathcal{A}(k) e^{i[kx - \varpi t]} dk, \quad (43.53a)$$

where we assumed that the dispersion relation has even parity

$$\varpi(k) = \varpi(-k) > 0. \quad (43.54)$$

This assumption means that a wave traveling to the right with wavenumber k has the same angular frequency as a wave traveling to the left with the same wavenumber. The equality (43.53a) allows us to interpret integration over negative wavenumbers to represent a wave packet traveling in a direction opposite to the sense suggested by the phase relation. That is, the phase $kx - \varpi t$ suggests a positive traveling packet, but the packet is actually a negative packet since the integration extends over negative wavenumbers.

The positive-negative wave packet

The sum of the positive packet (43.51) and negative packet (43.53a) leads us to define the positive-negative packet

$$\Phi^{(+-)}(x, t) = \Phi^{(+)}(x, t) + \Phi^{(-)}(x, t) = \frac{1}{2\pi} \int_{-\infty}^\infty \mathcal{A}(k) e^{i[kx - \varpi t]} dk. \quad (43.55)$$

The positive-positive wave packet

This final wave packet is designed to travel in a single direction, which defines the positive-positive packet

$$\Phi^{(++)}(x, t) = \frac{1}{2\pi} \int_{-\infty}^\infty \mathcal{A}(k) e^{ik(x - C_p t)} dk, \quad (43.56)$$

where $C_p = \varpi/|k| > 0$ is the phase speed. It is revealing to decompose this packet as¹²

$$\Phi^{(++)}(x, t) = \frac{1}{2\pi} \int_{-\infty}^0 \mathcal{A}(k) e^{ik(x - \varpi t/|k|)} dk + \frac{1}{2\pi} \int_0^\infty \mathcal{A}(k) e^{ik(x - \varpi t/|k|)} dk \quad (43.57a)$$

$$= \frac{1}{2\pi} \int_{-\infty}^0 \mathcal{A}(k) e^{i(kx + \varpi t)} dk + \frac{1}{2\pi} \int_0^\infty \mathcal{A}(k) e^{i(kx - \varpi t)} dk. \quad (43.57b)$$

The second integral equals to $\Phi^{(+)}(x, t)$, whereas the first is new. Again, both contributions to $\Phi^{(++)}(x, t)$ move in the $+\hat{x}$ direction.

43.6.5 The uncertainty relation for a Gaussian wave packet

The initial condition for both $\Phi^{(+-)}$ and $\Phi^{(++)}$ are the same, which we write as

$$\Phi_0(x) = \Phi^{(+-)}(x, 0) = \Phi^{(++)}(x, 0) = \frac{1}{2\pi} \int_{-\infty}^\infty \mathcal{A}(k) e^{ikx} dk. \quad (43.58)$$

The specific case of a Gaussian wave packet offers insight into the physics while allowing for analytically tractable expressions. Specifically, consider the \mathbf{k} -space representation of a wave packet with a Gaussian spread around a central wavevector, $\mathbf{k}_0 = k_0 \hat{x}$. We choose the wave amplitude as

$$\mathcal{A}(k) = A e^{-\sigma(k-k_0)^2}, \quad (43.59)$$

where $A > 0$ is a real constant and $\sigma > 0$ has dimensions of squared length. If we choose the central wavenumber to be positive, $k_0 > 0$, then the wave packet is dominated by plane waves moving in the $+\hat{x}$ direction. Referring to the discussion in Section 43.6.3, note that $\mathcal{A}(k) \neq \mathcal{A}(-k)$ when $k_0 \neq 0$. As we will see, if $k_0 = 0$ then we have a Gaussian packet without any modulated plane waves.

Width of the initial wave packet in \mathbf{k} -space

The squared modulus of the \mathbf{k} -space wave packet (43.59) provides a measure of the packet's intensity

$$|\mathcal{A}(k)|^2 = A^2 e^{-2\sigma(k-k_0)^2}, \quad (43.60)$$

with the intensity peaked at the wavenumber $k = k_0$ and declining to e^{-1} times the maximum for

$$k = k_0 \pm (2\sigma)^{-1/2} \implies \Delta k^{\text{e-fold}} \equiv 2(2\sigma)^{-1/2}, \quad (43.61)$$

where $\Delta k^{\text{e-fold}}$ measures the \mathbf{k} -space width of the wave packet. We say that the \mathbf{k} -space width of the packet is *narrow band* for σ large, in which the packet is concentrated around $k = k_0$ since $\Delta k^{\text{e-fold}} \rightarrow 0$.

The initial wave packet in \mathbf{x} -space

The inverse Fourier transform of the \mathbf{k} -space wave function (43.59) leads to the initial condition for the \mathbf{x} -space wave function (43.58)

$$\Phi_0(x) = \frac{A}{2\pi} \int_{-\infty}^\infty e^{-\sigma(k-k_0)^2} e^{ikx} dk = \frac{A e^{ik_0 x}}{2\pi} \int_{-\infty}^\infty e^{-\sigma q^2} e^{iqx} dq, \quad (43.62)$$

¹²In deriving equation (43.57b), remember that $\varpi > 0$ for all wavenumbers.

with the corresponding initial conditions for the positive and negative wave packets

$$\Phi^{(+)}(x, 0) = \frac{A}{2\pi} \int_0^\infty e^{-\sigma(k-k_0)^2} e^{ikx} dk = \frac{A e^{ik_0 x}}{2\pi} \int_{-k_0}^\infty e^{-\sigma q^2} e^{iqx} dq \quad (43.63a)$$

$$\Phi^{(-)}(x, 0) = \frac{A}{2\pi} \int_{-\infty}^0 e^{-\sigma(k-k_0)^2} e^{ikx} dk = \frac{A e^{ik_0 x}}{2\pi} \int_{-\infty}^{-k_0} e^{-\sigma q^2} e^{iqx} dq. \quad (43.63b)$$

With the central wavenumber assumed positive, $k_0 > 0$, observe that the initial negative wave packet, $\Phi^{(-)}(x, 0)$, has an exponentially small amplitude since the integral in equation (43.63b) never samples $q = k - k_0 = 0$. In contrast, $\Phi^{(+)}(x, 0)$ samples $q = 0$ so that

$$\Phi_0(x) = \Phi^{(+)}(x, 0) + \Phi^{(-)}(x, 0) \approx \Phi^{(+)}(x, 0). \quad (43.64)$$

Although there is no exact closed form expression for the initial conditions $\Phi^{(+)}(x, 0)$ and $\Phi^{(-)}(x, 0)$, we can evaluate the integral for $\Phi_0(x)$ in equation (43.62). First we observe that

$$\int_{-\infty}^\infty e^{-\sigma q^2} \sin(qx) dq = 0, \quad (43.65)$$

since the Gaussian is symmetric under $q \rightarrow -q$, whereas $\sin(qx)$ switches sign. Hence, expanding the imaginary exponential in equation (43.62) according to Euler's identity leaves only the cosine contribution, so that

$$\Phi_0(x) = \frac{A e^{ik_0 x}}{2\pi} \int_{-\infty}^\infty e^{-\sigma q^2} \cos(qx) dq = \frac{A e^{ik_0 x}}{2\pi} \sqrt{\frac{\pi}{\sigma}} e^{-x^2/(4\sigma)}, \quad (43.66)$$

where we made use of an integral tables for the final equality (e.g., integral 679 of [Beyer \(1973\)](#)).¹³

Evidently, the initial wave packet, $\Phi_0(x)$, in equation (43.66) consists of a single plane wave, $e^{ik_0 x}$, modulated by the Gaussian, $e^{-x^2/(4\sigma)}$. In this manner the plane wave, which is defined for all space, has been localized in space by the Gaussian modulation function. In some contexts, such as electrical engineering, the plane wave is referred to as the *carrier wave*. In Figure 43.4 we illustrate a Gaussian wave packet of the form (43.66).

If we choose the central wavenumber to be zero, $k_0 = 0$, then the wavenumber amplitude function has even parity, $\mathcal{A}(k) = \mathcal{A}(-k)$. The wave function, $\Phi_0(x)$, in equation (43.66) reduces to just the Gaussian modulation function without a carrier wave, so that Figure 43.4 reduces to just the positive Gaussian modulation function. Hence, the $k_0 = 0$ limit results in a Gaussian signal, constructed with a continuum of plane waves, yet without any modulated carrier wave.

The uncertainty relation

The squared modulus of the x -space wave function (43.66) is proportional to $\exp[-x^2/(2\sigma)]$, which has an e-folding width

$$\Delta x^{\text{e-fold}} = 2(2\sigma)^{1/2}. \quad (43.67)$$

This x -space wave function spread exactly complements its k -space spread (43.61), so that their product is a constant

$$\Delta x^{\text{e-fold}} \Delta k^{\text{e-fold}} = 4. \quad (43.68)$$

The precise value of the constant is not important since it depends on the somewhat arbitrary choices made for defining Δx and Δk . What is important is that if we narrow the wavenumber

¹³The integral in equation (43.66) is also encountered in Section 5.6.2 when studying Fourier transforms.

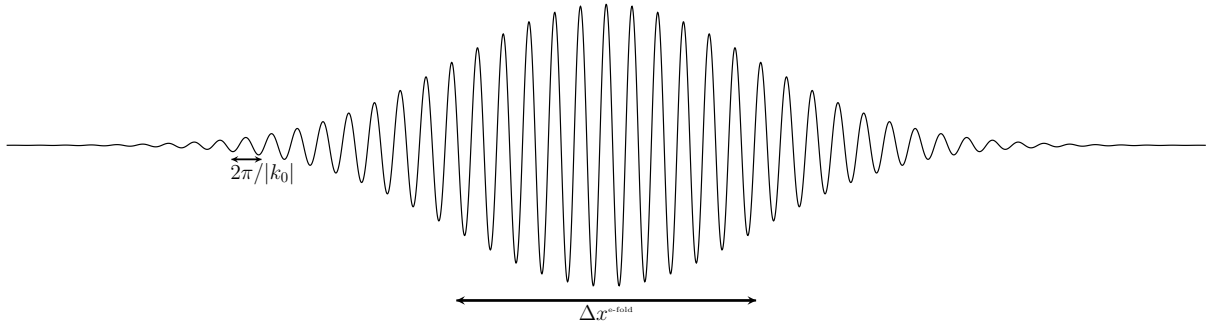


FIGURE 43.4: Example of a Gaussian wave packet (units are arbitrary), $\Phi_0(x)$, of the form given by the real part of equation (43.66), with $2\pi/|k_0|$ wavelength for the modulated waves. From equation (43.67) we also show $\Delta x^{\text{e-fold}} = 2(2\sigma)^{1/2} \gg 2\pi/|k_0|$, which determines the e-folding width of the squared modulus of the packet. In some contexts (e.g., electrical engineering), the plane wave, $e^{ik_0 x}$, is referred to as the *carrier wave*.

band by increasing σ and thus making $\mathcal{A}(\mathbf{k})$ more sharply peaked, then we broaden the \mathbf{x} -space width of the wave function. That is, a narrow Gaussian wave packet in \mathbf{k} -space leads to a broad wave packet in \mathbf{x} -space. The complement holds, whereby a narrow packet in \mathbf{x} -space leads to a broad packet in \mathbf{k} -space. This tradeoff holds for general wave packets, whereby it is not possible to have a narrow packet in both \mathbf{x} -space and \mathbf{k} -space. We refer to equation (43.68) as an *uncertainty relation*. It is a fundamental feature of quantum wave mechanics, where it is known as the *Heisenberg uncertainty principle* (e.g., Chapter 3 of [Bohm \(1951\)](#) or Chapter 2 of [Gasiorowicz \(1974\)](#)).

Extreme examples of the uncertainty relation

The uncertainty relation is a bit odd on first encounter. Why is it impossible to know arbitrarily precise information about both the \mathbf{k} -space location and \mathbf{x} -space location of a wave packet? The answer fundamentally boils down to the dual relation between these two spaces. As a means to further exemplify this relation, and thus to build understanding, we consider the most extreme example of the uncertainty relation.

First assume we know that the \mathbf{k} -space wave function is a single plane wave with just one wavevector, $\mathbf{k} = k_0 \hat{\mathbf{x}}$. In this case the \mathbf{k} -space amplitude function is

$$\mathcal{A}(k) = a_0 \delta(k - k_0), \quad (43.69)$$

where a_0 is a constant and δ is the Dirac delta discussed in Section 4.3. Note that $\delta(k - k_0)$ has physical dimensions of length and is normalized so that

$$\int_{-\infty}^{\infty} \delta(k - k_0) dk = 1. \quad (43.70)$$

The sifting property of the Dirac delta (Section 4.3.2) yields the \mathbf{x} -space wave function

$$\Phi_0(x) = \frac{a_0}{2\pi} \int_{-\infty}^{\infty} \delta(k - k_0) e^{ikx} dk = \frac{a_0 e^{ik_0 x}}{2\pi}. \quad (43.71)$$

So although we know the precise \mathbf{k} -space position, $k = k_0$, we have zero information about the wave function's \mathbf{x} -space position. That is, the wave function is a pure carrier wave without any

modulation function.

We turn the table by assuming precise \mathbf{x} -space information, in which case the modulation function is a Dirac delta

$$\Phi_0(x) = \phi_0 \delta(x - x_0), \quad (43.72)$$

where ϕ_0 is a constant and $\delta(x - x_0)$ is normalized so that

$$\int_{-\infty}^{\infty} \delta(x - x_0) dx = 1. \quad (43.73)$$

We say that the modulation function has exactly specified the spatial position of this packet. Yet the price to pay for this information is that there is zero information concerning the \mathbf{k} -space location since

$$\mathcal{A}(k) = \phi_0 \int_{-\infty}^{\infty} \delta(x - x_0) e^{-ikx} dx = \phi_0 e^{-ikx_0}. \quad (43.74)$$

That is, the carrier wave can be any plane wave with arbitrary wavenumber, k . So although we know the precise \mathbf{x} -space position, $x = x_0$, we have zero information about the wave function's \mathbf{k} -space position. Hence, this wave function carries precise \mathbf{x} -space information (delta modulated) yet zero \mathbf{k} -space information.

43.6.6 Evolution of non-dispersive Gaussian wave packets

Evolution of the \mathbf{k} -space wave function, $\mathcal{A}(k, t)$, is given by equation (43.45). We now study the evolution of the \mathbf{x} -space wave functions $\Phi^{(+)}(x, t)$ and $\Phi^{(+)}$ (x, t). Starting with the positive-negative wave function, recall that it evolves according to equation (43.55)

$$\Phi^{(+)}(x, t) = \frac{1}{2\pi} \int_{-\infty}^{\infty} \mathcal{A}(k) e^{i[kx - \varpi t]} dk = \frac{A}{2\pi} \int_{-\infty}^{\infty} e^{-\sigma(k - k_0)^2} e^{i[kx - \varpi(k)t]} dk. \quad (43.75)$$

This integral offers a complete space and time specification of $\Phi^{(+)}(x, t)$. Even so, it is useful to massage the integral to garner insight into the physics of $\Phi^{(+)}(x, t)$. We do so in this section for the case of non-dispersive waves, where we show that the \mathbf{x} -space wave packet propagates the initial wave packet without alteration. This result is expected since non-dispersive waves are described by hyperbolic equations that translate any initial pattern without alteration (Section 43.3.1). Showing this result through the mathematical formalism offers insights into certain features of wave packets, and provides practice for the technically more complex dispersive case in Section 43.6.7.

Evolution of a Gaussian $\Phi^{(+)}(x, t)$ packet of non-dispersive waves

A non-dispersive wave is characterized by a dispersion relation with a constant phase speed

$$\omega = \varpi = C_p |k|. \quad (43.76)$$

Such waves are said to be non-dispersive since waves with arbitrary wavenumber travel at the same phase speed.¹⁴ We encounter two non-dispersive waves in this book: the acoustic waves studied in Chapter 44 and the shallow water gravity waves from Section 48.5. The absolute value sign in the dispersion relation (43.76) means that the relation has a continuous derivative only when

¹⁴Electromagnetic radiation in a vacuum also has a linear dispersion relation. Since many students' initial exposure to waves is in the context of either acoustic waves or light waves, features of geophysical waves with a nonlinear dispersion relation can appear rather exotic.

$k \neq 0$. In that manner, it is a linear dispersion relation only when $k \neq 0$. Care must be exercised to account for the sign swap when moving across $k = 0$, with this movement corresponding to waves moving in opposite directions. We see how to handle this situation in the following.

The \mathbf{x} -space wave packet (43.75) propagates according to

$$\Phi^{(+)}(x, t) = \frac{A}{2\pi} \int_{-\infty}^{\infty} e^{-\sigma(k-k_0)^2} e^{ik(x-|k|C_p t)} dk \quad (43.77a)$$

$$= \frac{A}{2\pi} \int_0^{\infty} e^{-\sigma(k-k_0)^2} e^{ik(x-C_p t)} dk + \frac{A}{2\pi} \int_{-\infty}^0 e^{-\sigma(k-k_0)^2} e^{ik(x+C_p t)} dk \quad (43.77b)$$

$$= \frac{A}{2\pi} \int_0^{\infty} e^{-\sigma(k-k_0)^2} e^{ik(x-C_p t)} dk + \frac{A}{2\pi} \int_0^{\infty} e^{-\sigma(k+k_0)^2} e^{-ik(x+C_p t)} dk \quad (43.77c)$$

$$= \Phi^{(+)}(x - C_p t, 0) + \Phi^{(-)}(x + C_p t, 0), \quad (43.77d)$$

where we made use of equations (43.63a) and (43.63b) for the $\Phi^{(+)}$ and $\Phi^{(-)}$ initial conditions. Evidently, the x -space wave packet splits from its initial condition into positive and negative propagating wave packets, and the packets move without altering their respective initial conditions. However, as already discussed for the initial conditions leading up to equation (43.64), the wave packets are *not* symmetric reflections of each other if $k_0 \neq 0$. In fact, $\Phi^{(-)}$ is exponentially smaller than $\Phi^{(+)}$ if $k_0 > 0$.

Evolution of a Gaussian $\Phi^{(++)}(x, t)$ packet of non-dispersive waves

Now study the evolution of the $\Phi^{(++)}$ packet (43.56) built from non-dispersive waves. In this case we can perform the integral to produce

$$\Phi^{(++)}(x, t) = \frac{A}{2\pi} \int_{-\infty}^{\infty} e^{-\sigma(k-k_0)^2} e^{ik(x-C_p t)} dk \quad (43.78a)$$

$$= \frac{A}{2\pi} e^{ik_0(x-C_p t)} e^{-(x-C_p t)^2/(4\sigma)} \int_{-\infty}^{\infty} e^{-\sigma[q-i(x-C_p t)/(2\sigma)]^2} dq \quad (43.78b)$$

$$= \frac{A e^{ik_0(x-C_p t)}}{2\pi} \sqrt{\frac{\pi}{\sigma}} e^{-(x-C_p t)^2/(4\sigma)}. \quad (43.78c)$$

The second equality resulted from completing the square in the exponential, and the final equality evaluated the integral using methods from complex analysis.¹⁵ Comparing the expression in equation (43.78c) to the initial wave packet in equation (43.66) reveals that

$$\Phi^{(++)}(x, t) = \Phi^{(++)}(x - C_p t, 0) = \Phi_0(x - C_p t). \quad (43.79)$$

As noted when introducing $\Phi^{(++)}(x, t)$ in Section 43.6.4, the initial condition is propagated in the positive direction as a single coherent packet, which contrasts to the splitting found for the packet $\Phi^{(+)}(x, t)$ in equation (43.77d).

43.6.7 Evolution of a dispersive Gaussian wave packet

Most geophysical waves are *dispersive*. As we see in the following, dispersive waves render a spreading of the \mathbf{x} -space wave packet as it evolves, along with a decay in its amplitude. Furthermore, the packet moves at the *group velocity*, which, for dispersive waves, is distinct from

¹⁵More precisely, it makes use of the calculus of residues, with Section G_I in [Cohen-Tannoudji et al. \(1977\)](#) providing a discussion and Appendix A9 of [Fetter and Walecka \(2003\)](#) providing a tutorial for physicists.

the phase velocity. To reveal these properties analytically, we here characterize evolution of the $\Phi^{(+-)}$ wave packet when constructed with dispersive waves. Though straightforward, the maths is more tedious than for the non-dispersive packets from Section 43.6.6.

Taylor expanding the phase function

To examine the propagation of a dispersive wave packet, we Taylor expand the dispersion relation around the central wavenumber, $k = k_0$, and assume the packet is relatively narrow band in wavevector space. With these assumptions we truncate the Taylor series at second order

$$\varpi(k) \approx \varpi(k_0) + (k - k_0) \left[\frac{d\varpi}{dk} \right]_{k=k_0} + \frac{(k - k_0)^2}{2} \left[\frac{d^2\varpi}{dk^2} \right]_{k=k_0} \quad (43.80a)$$

$$\equiv \omega_0 + (k - k_0) c_g + (k - k_0)^2 \mu. \quad (43.80b)$$

We here introduced the one-dimensional group velocity evaluated at $k = k_0$

$$c_g = \hat{\mathbf{x}} c_g = \hat{\mathbf{x}} \left[\frac{d\varpi}{dk} \right]_{k=k_0}. \quad (43.81)$$

Recall the phase speed is positive by definition, $C_p > 0$ (i.e., it is a speed!). In contrast, c_g can be positive or negative, or even zero, depending on the slope of the dispersion relation at $k = k_0$. In equation (43.80b) we also introduced one-half the second derivative of the dispersion relation (dimensions of L^2/T)

$$\mu = \frac{1}{2} \left[\frac{d^2\varpi}{dk^2} \right]_{k=k_0}. \quad (43.82)$$

As shown below, a nonzero μ spreads the \mathbf{x} -space wave packet and reduces its amplitude.

Performing the integral

Making use of the Taylor expansion (43.80b) yields the approximate form of the phase function appearing in the \mathbf{x} -space wave packet (43.75)

$$k x - \varpi(k) t = (k - k_0) x + k_0 x - t [\omega_0 + c_g (k - k_0) + \mu (k - k_0)^2] \quad (43.83a)$$

$$= (k_0 x - \omega_0 t) + (x - c_g t) (k - k_0) - t \mu (k - k_0)^2. \quad (43.83b)$$

As a result, the \mathbf{x} -space wave packet takes on the approximate form

$$\Phi^{(+-)}(x, t) \approx \frac{A e^{i(k_0 x - \omega_0 t)}}{2\pi} \int_{-\infty}^{\infty} e^{-(\sigma + i\mu t)(k - k_0)^2 + i(k - k_0)(x - c_g t)} dk \quad (43.84a)$$

$$= \frac{A e^{i(k_0 x - \omega_0 t)}}{2\pi} \int_{-\infty}^{\infty} e^{-(\sigma + i\mu t)q^2 + iq(x - c_g t)} dq, \quad (43.84b)$$

where the second equality made use of the same substitution, $q = k - k_0$, used when evaluating the integral for the initial value wave packet in Section 43.6.5. Introducing the shorthand

$$\alpha = x - c_g t \quad \text{and} \quad \beta = \sigma + i\mu t, \quad (43.85)$$

proves useful for completing the square in the integral exponential

$$-(\sigma + i\mu t)q^2 + iq(x - c_g t) = -\beta [q - i\alpha/(2\beta)]^2 - \alpha^2/(4\beta), \quad (43.86)$$

which brings the \mathbf{x} -space wave packet (43.84b) to the form¹⁶

$$\Phi^{(+)}(x, t) = \frac{A e^{i(k_0 x - \omega_0 t)} e^{-\alpha^2/(4\beta)}}{2\pi} \int_{-\infty}^{\infty} e^{-\beta[q - i\alpha/(2\beta)]^2} dq \quad (43.87a)$$

$$= \frac{A e^{i(k_0 x - \omega_0 t)}}{2\pi} \sqrt{\frac{\pi}{\beta}} e^{-\alpha^2/(4\beta)}. \quad (43.87b)$$

We next expose a complex exponential multiplied by a real exponential

$$\Phi^{(+)}(x, t) = \frac{A e^{i(k_0 x - \omega_0 t)} e^{-[(x - c_g t)^2/(4(\sigma + i\mu t))]} }{2\sqrt{\pi}} \frac{1}{\sqrt{\sigma + i\mu t}} \quad (43.88a)$$

$$= \frac{A e^{i[(k_0 x - \omega_0 t) + \frac{(x - c_g t)^2 \mu t}{4(\sigma^2 + (\mu t)^2)}]} e^{-\frac{(x - c_g t)^2 \sigma}{4(\sigma^2 + (\mu t)^2)}}}{2\sqrt{\pi}} \frac{1}{\sqrt{\sigma + i\mu t}} \quad (43.88b)$$

$$= \frac{A e^{i[(k_0 x - \omega_0 t) + \frac{(x - c_g t)^2 \mu t}{4(\sigma^2 + (\mu t)^2)} + \varphi/2]} e^{-\frac{(x - c_g t)^2 \sigma}{4(\sigma^2 + (\mu t)^2)}}}{2\sqrt{\pi} [\sigma^2 + (\mu t)^2]^{1/4}} \quad (43.88c)$$

where $\tan \varphi = -\mu t / \sigma$.

Interpreting the wave packet

The phase factor in the \mathbf{x} -space wave packet (43.88c)

$$\mathcal{P} = (k_0 x - \omega_0 t) + \frac{(x - c_g t)^2 \mu t}{4(\sigma^2 + (\mu t)^2)} + \varphi/2, \quad (43.89)$$

equals to that for a non-dispersive wave, $k_0 x - \omega_0 t$, plus a space and time dependent phase shift that is nonzero for dispersive waves ($\mu \neq 0$). The phase shift simplifies for points following the group velocity, $x = c_g t$, and it is here that the Gaussian exponential is maximized

$$\Phi^{(+)}(x = c_g t, t) = \frac{A e^{i(k_0 x - \omega_0 t + \varphi/2)}}{2\sqrt{\pi} [\sigma^2 + (\mu t)^2]^{1/4}}. \quad (43.90)$$

Hence, as the \mathbf{x} -space wave packet moves with the group velocity (which can be either signed), its amplitude declines according to $(\mu t)^{-1/2}$.

Time dependent uncertainty relation

As for the \mathbf{k} -space packet in Section (43.6.5), we consider the squared modulus of the \mathbf{x} -space packet (43.88c) as a measure of its intensity

$$|\Phi^{(+)}(x, t)|^2 = \frac{A^2 e^{-\frac{(x - c_g t)^2 \sigma}{2(\sigma^2 + (\mu t)^2)}}}{4\pi [\sigma^2 + (\mu t)^2]^{1/2}}. \quad (43.91)$$

The e-folding width of $|\Phi(x, t)|^2$ is revealed by setting the decaying exponential to unity, which leads to

$$x = c_g t \pm (2\sigma)^{1/2} [1 + (\mu t/\sigma)^2]^{1/2} \implies \Delta x^{\text{e-fold}} = 2(2\sigma)^{1/2} [1 + (\mu t/\sigma)^2]^{1/2}. \quad (43.92)$$

¹⁶The integral in equation (43.87b) is evaluated using complex analysis as discussed in Section G_I of [Cohen-Tannoudji et al. \(1977\)](#), Section 54 and Appendix A9 of [Fetter and Walecka \(2003\)](#).

Multiplying by the time-independent \mathbf{k} -space packet width (43.61) leads to the time dependent uncertainty relation

$$\Delta x^{\text{e-fold}} \Delta k^{\text{e-fold}} = 2(2\sigma)^{1/2} [1 + (\mu t/\sigma)^2]^{1/2} 2(2\sigma)^{-1/2} = 4 [1 + (\mu t/\sigma)^2]^{1/2}. \quad (43.93)$$

The time dependent uncertainty relation starts from its initial condition (43.68) at $t = 0$, and then grows as $t^{1/2}$. For non-dispersive waves ($\mu = 0$), the uncertainty relation is time-independent, which is expected since non-dispersive waves translate the initial packet without changing the properties of the packet.

The non-dispersive wave limit

We set the spreading parameter $\mu = 0$ for non-dispersive waves, in which case $\varphi = 0$ as well. In this limit the wave packet (43.88c) takes on the form

$$\Phi^{(+)}(x, t) = \frac{A e^{i k_0 (x - c_g t)}}{2\pi} \sqrt{\frac{\pi}{\sigma}} e^{-(x - c_g t)^2/(4\sigma)}. \quad (43.94)$$

If we set $c_g = C_p$ then this result corresponds to equation (43.78c), which is the non-dispersive form of the packet $\Phi^{(++)}(x, t)$.

So why did the non-dispersive limit not reduce to equation (43.77d), which is the non-dispersive form of $\Phi^{(+)}(x, t)$? The reason is that when performing the Taylor series expansion for the dispersive packet, we only picked out the group velocity at the single wavenumber, $k = k_0$. Hence, we can only get one of the two packets comprising $\Phi^{(+)}(x, t)$ in equation (43.77d). Namely, we ignore the exponentially small packet using the Taylor series approach. Furthermore, note that c_g can be positive or negative for dispersive waves (indeed, it can even be zero). In contrast, C_p is the phase speed and that is always positive. So in the case of $c_g = -C_p < 0$ then equation (43.94) is a negative moving wave packet.

So in summary, the non-dispersive limit of a dispersive packet does correspond to the purely non-dispersive packet, but there are a few subtleties. In particular, if one cares about the exponentially small packet exposed with the non-dispersive analysis in Section 43.6.6, then it is necessary to follow the approach taken in that section rather than taking the non-dispersive limit of dispersive waves.

43.6.8 Comments and further study

The study of wave packets in this section revealed properties that appear throughout the study of waves. First, there is the uncertainty relation, whereby a packet that is narrow banded in wavevector space is broad banded in position space, and conversely. Second, dispersive wave packets both broaden and decay with time, thus producing a time dependent uncertainty relation. Third, the center of the packet moves with the group velocity rather than phase velocity, with the two velocities distinct for dispersive waves.

The study of wave packets and their evolution is a central concern of quantum mechanics. Most books on the subject have a discussion of quantum wave packets at the level discussed here. In particular, we made use in this section of Chapter 3 of [Bohm \(1951\)](#), Chapter 2 of [Gasiorowicz \(1974\)](#), and Section G_I of [Cohen-Tannoudji et al. \(1977\)](#). We also followed Section 54 of [Fetter and Walecka \(2003\)](#), who considered wave packets built from surface gravity waves. However, it is notable that the distinctions we made here between positive and negative moving packets in Section 43.6.6 is often obscured in the quantum mechanics literature.

43.7 General phase functions

We now consider a wave phase function, $\mathcal{P}(\mathbf{k}, \mathbf{x}, t)$, that generally differs from the plane wave form (43.18). This generalization often arises for waves moving through inhomogeneous media (e.g., stratification, currents, other wave fields, etc.), whereby the wave properties become a local function of space and time. If the fluid properties are changing slowly in space and time relative to those of the waves, then we can generalize much of the homogeneous wave properties to the inhomogeneous case. The generalization is referred to as the *eikonal approximation*, which we develop for acoustic waves in Section 44.9. Additionally, by characterizing the kinematic properties of waves using a general phase, we deepen our understanding of the notions introduced for the plane wave in Section 43.5. We further pursue these notions in Section 43.8 to develop the equations describing how the wavevector and angular frequency are modified when waves move through an inhomogeneous background state.

43.7.1 Phase velocity and phase speed

Consider an observer moving on a smooth trajectory through space and time defined by a fixed point on a constant phase surface, such as when the observer remains fixed on the crest of a traveling wave.¹⁷ As such, we assume that the trajectory is aligned in the direction of $\nabla_{\mathbf{x}}\mathcal{P}$, which we define at the local direction of the wave¹⁸

$$\hat{\mathbf{k}} \equiv \nabla_{\mathbf{x}}\mathcal{P}/|\nabla_{\mathbf{x}}\mathcal{P}| \equiv \mathbf{k}/|\mathbf{k}|, \quad (43.95)$$

with the local wavevector

$$\mathbf{k} \equiv \nabla_{\mathbf{x}}\mathcal{P}. \quad (43.96)$$

With the plane wave phase function (43.18), then $\nabla_{\mathbf{x}}(\mathbf{k} \cdot \mathbf{x} - \omega t + \alpha) = \mathbf{k}$, which is independent of space. However, more general phases functions lead to a local wavevector, $\mathbf{k}(\mathbf{x}, t)$, and corresponding wave direction, $\hat{\mathbf{k}}(\mathbf{x}, t)$.

To determine the velocity of the fixed-phase observer, consider a small spatial increment, $\delta\mathbf{x}^{\text{phase}}$, that occurs over a small time increment, δt . Assuming this space increment follows the fixed-phase observer leads to the identity

$$\mathcal{P}(\mathbf{x} + \delta\mathbf{x}^{\text{phase}}, t + \delta t) = \mathcal{P}(\mathbf{x}, t). \quad (43.97)$$

Truncating a Taylor series expansion of this identity leads to the differential equation

$$\frac{\partial \mathcal{P}}{\partial t} + \mathbf{c}_p \cdot \nabla_{\mathbf{x}}\mathcal{P} = 0, \quad (43.98)$$

where we defined the *phase velocity*

$$\mathbf{c}_p = \delta\mathbf{x}^{\text{phase}}/\delta t. \quad (43.99)$$

The partial differential equation (43.98) specifies $\mathbf{c}_p \cdot \mathbf{k}$ in terms of the time derivative of the phase

$$\mathbf{c}_p \cdot \mathbf{k} = -\partial_t \mathcal{P}. \quad (43.100)$$

Indeed, since the observer is assumed to move along the direction of the wavevector, $\hat{\mathbf{k}}$, then $\mathbf{c}_p \cdot \hat{\mathbf{k}}$

¹⁷Our formulation in this section emulates that used in Section 14.6 for the Lagrangian time derivative, which is concerned with measuring fluid properties following a fluid particle. Here, we are following a wave as defined by a surface of constant phase.

¹⁸We place an \mathbf{x} label on $\nabla_{\mathbf{x}}$ to distinguish a gradient taken in wavevector space used to compute the group velocity in equation (43.37).

is the only component of the phase velocity. We thus write the phase velocity as in our discussion of plane waves in Section 43.5.2

$$\mathbf{c}_p = (\mathbf{c}_p \cdot \hat{\mathbf{k}}) \hat{\mathbf{k}} \equiv C_p \hat{\mathbf{k}}, \quad (43.101)$$

where $C_p > 0$ is the *phase speed*, which is the magnitude of the phase velocity. Again, Figure 43.2 provides an illustration.

43.7.2 Angular frequency and wavelength

The time derivative, $\partial_t \mathcal{P}$, measures the time change of the phase at a fixed point in space, which is the angular frequency of the phase

$$\omega = -\partial_t \mathcal{P}. \quad (43.102)$$

The differential equation (43.98) for the phase can thus be written in the equivalent manners

$$\partial_t \mathcal{P} + \mathbf{c}_p \cdot \nabla_{\mathbf{x}} \mathcal{P} = 0 \iff \omega = \mathbf{c}_p \cdot \mathbf{k}, \quad (43.103)$$

which also leads to the relations

$$\mathbf{c}_p = C_p \hat{\mathbf{k}} = (\omega / |\mathbf{k}|) \hat{\mathbf{k}}, \quad (43.104)$$

as appeared for plane waves in equation (43.24). We likewise identify the wavelength

$$\Lambda = 2\pi / |\mathbf{k}| \implies C_p = \Lambda \omega / 2\pi. \quad (43.105)$$

43.8 Geometric optics or ray theory

In this section we develop the basic equations for *ray theory*, which provides a mathematical formalism for the rules of *geometric optics* commonly found in introductory physics courses. As we will see, they allow us to determine how the wavevector and angular frequency evolve through an inhomogeneous base state. There is a fundamental connection between the group velocity and changes to the wavevector and angular frequency while following a ray. As we show in this section, the connection is provided by the dispersion relation.

43.8.1 Integral curves of the group velocity

A ray is an integral curve of the group velocity. Hence, the trajectory, $\mathbf{X}(t)$, following a ray is given by a solution to the equation

$$\frac{D_g \mathbf{X}}{Dt} = \mathbf{c}_g. \quad (43.106)$$

This equation is directly analogous to that defining the trajectory of a fluid particle, which is defined in equation equation (14.71a) as the integral curve of the fluid velocity.

43.8.2 Eikonal equation

Recall from Section 43.7 that there is a relation between the wave phase, \mathcal{P} , the local angular frequency, $\omega = -\partial_t \mathcal{P}$, and the local wavevector, $\mathbf{k} = \nabla \mathcal{P}$. Inserting these identities into the local dispersion relation, $\omega = \varpi(\mathbf{x}, t, \mathbf{k})$, leads to the *eikonal equation*

$$\partial_t \mathcal{P} + \varpi(\mathbf{x}, t, \nabla \mathcal{P}) = 0. \quad (43.107)$$

This is equation is formally the same as the *Hamilton-Jacobi* equation of classical mechanics, yet with ϖ playing the role of the Hamiltonian (e.g., [Marion and Thornton \(1988\)](#) or [Goldstein](#)

(1980)). That analogy offers suggestions for how to make use of this equation.

43.8.3 Evolution of \mathbf{k} and ω along a ray

The formalism of Hamiltonian mechanics motivates us to compute the spatial derivative of the eikonal equation (43.107). For the gradient of the time tendency we can swap time and space derivatives to yield

$$\nabla(\partial_t \mathcal{P}) = \partial_t \mathbf{k}. \quad (43.108)$$

When taking the gradient of the dispersion relation we must note that ϖ has an explicit dependence on \mathbf{x} as well as an implicit dependence through $\mathbf{k} = \nabla \mathcal{P}(\mathbf{x}, t)$. For this reason we find

$$\frac{d\varpi}{dx_i} = \left[\frac{\partial \varpi}{\partial x_i} \right]_{t,\mathbf{k}} + \left[\frac{\partial \varpi}{\partial k_j} \right]_{t,\mathbf{x}} \frac{\partial k_j}{\partial x_i}. \quad (43.109)$$

We can massage the final term by commuting partial derivatives

$$\frac{\partial k_j}{\partial x_i} = \frac{\partial^2 \mathcal{P}}{\partial x_j \partial x_i} = \frac{\partial k_i}{\partial x_j}, \quad (43.110)$$

thus yielding

$$\frac{d\varpi}{dx_i} = \left[\frac{\partial \varpi}{\partial x_i} \right]_{t,\mathbf{k}} + (\mathbf{c}_g \cdot \nabla) \mathbf{k}. \quad (43.111)$$

Gathering these results leads to the evolution equation for the wavevector

$$(\partial_t + \mathbf{c}_g \cdot \nabla) \mathbf{k} = \frac{D_g \mathbf{k}}{Dt} = - \left[\frac{\partial \varpi}{\partial \mathbf{x}} \right]_{t,\mathbf{k}}. \quad (43.112)$$

This equation says that the wavevector, while following along with the group velocity, has a time change determined by minus the spatial derivative of the dispersion relation. Integral lines for the group velocity define *rays*, so that this equation determines how the wavevector evolves following a ray. Furthermore, if the dispersion relation has no explicit dependence on space, then the wavevector is a constant following a ray

$$\frac{D_g \mathbf{k}}{Dt} = 0 \quad \text{if} \quad \left[\frac{\partial \varpi}{\partial \mathbf{x}} \right]_{t,\mathbf{k}} = 0. \quad (43.113)$$

Analogous manipulations lead to the change in the angular frequency following a ray

$$\frac{D_g \omega}{Dt} = \left[\frac{\partial \varpi}{\partial t} \right]_{x,\mathbf{k}}. \quad (43.114)$$

Evidently, if the dispersion relation has no explicit dependence on time, then the wave angular frequency is a constant following a ray

$$\frac{D_g \omega}{Dt} = 0 \quad \text{if} \quad \left[\frac{\partial \varpi}{\partial t} \right]_{x,\mathbf{k}} = 0. \quad (43.115)$$

For example, this is the situation when gravity waves approach a beach, assuming the slope of the beach is static. Hence, in this case the angular frequency remains constant following a ray, whereas the wavevector changes according to equation (43.112).

43.8.4 Change in the phase along a ray

The phase function, $\mathcal{P}(\mathbf{x}, t)$, is a function of space and time. Computing the time derivative of the phase while following a ray leads to

$$D_g \mathcal{P} / Dt = -\omega + \mathbf{c}_g \cdot \mathbf{k}. \quad (43.116)$$

If the waves are non-dispersive, $\mathbf{c}_g = \mathbf{c}_p$, then this equation says that the phase remains unchanged when following a ray. But for dispersive waves, the phase does change when following a ray.

43.8.5 Comments about rays

Equations (43.106), (43.107), (43.112) and (43.114) are referred to as *Hamilton's equations for rays*, or simply the *ray equations*. Given the dispersion relation is sufficient to solve these equations (typically using numerical methods) to map out the rays and to determine the wavevector, angular frequency, and phase following a ray. This procedure works quite well, when it works. Failure can occur when rays intersect, which indicates a failure of one of the basic assumptions. In many fluid applications, ray intersection signals a nonlinear process that kicks in, such as a fluid instability and corresponding turbulent mixing. Chapters 3 and 4 of [Böhler \(2014a\)](#) provides far more details and insights into the various facets of the eikonal approximation.

43.8.6 Further study

Our treatment in this section followed that given in Section 7.3 of [Thorne and Blandford \(2017\)](#). We further pursue these ideas in Section 44.9 when developing the equation describing the amplitude of acoustic waves moving through an inhomogeneous media.



43.9 Exercises

EXERCISE 43.1: SQUARE WAVE PACKET (EXERCISE 2.1 OF [Gasiorowicz \(1974\)](#))

Consider a wave packet in one space dimension with real k -space amplitude function

$$A(k) = \begin{cases} 0 & k < -K \\ N & -K < k < K \\ 0 & k > K, \end{cases} \quad (43.117)$$

where $K > 0$.

- (a) Find the wave function (43.45), which in one space dimension takes the form

$$\Phi_0(x) = \frac{1}{2\pi} \int_{-\infty}^{\infty} A(k) e^{ikx} dk. \quad (43.118)$$

Hint: $\Phi_0(x)$ is the inverse Fourier transform of $A(k)$. The integral is simple to do.

- (b) Find the value of N for which

$$\int_{-\infty}^{\infty} |\Phi_0(x)|^2 dx = 1. \quad (43.119)$$

Hint: massage the integral until it looks like one found in a standard integral table.

- (c) Relate the above choice for N to one that makes

$$\int_{-\infty}^{\infty} |A(k)|^2 dk = 1. \quad (43.120)$$

- (d) Show that a reasonable definition for Δx in part (a) yields the uncertainty relation

$$\Delta x \Delta k > 1. \quad (43.121)$$

Hint: this uncertainty relation holds independently of K .

EXERCISE 43.2: INVERSE SQUARED WAVE PACKET (EXERCISE 2.2 OF *Gasiorowicz (1974)*)

Consider a wave packet in one space dimension with real k -space amplitude function

$$A(k) = \frac{N}{k^2 + \alpha^2} \quad (43.122)$$

with $\alpha > 0$.

- (a) Find the wave function (43.45), which in one space dimension takes the form

$$\Phi_0(x) = \frac{1}{2\pi} \int_{-\infty}^{\infty} A(k) e^{ikx} dk \quad (43.123)$$

Hint: $\Phi_0(x)$ is the inverse Fourier transform of $A(k)$. Massage the integral until it looks like one found in a standard integral table.

- (b) Show that a reasonable definition for Δx in part (a) yields the uncertainty relation

$$\Delta x \Delta k > 1. \quad (43.124)$$

Hint: this relation holds independently of α .



Chapter 44

ACOUSTIC WAVES

In this chapter we study the physics of *acoustic waves* in fluids. When reaching the human ear we interpret acoustic waves as sound, hence the synonymous term *sound waves*. The pressure fluctuations associated with standard acoustic waves (those not damaging to the human ear) are a tiny fraction of those arising from, say, a weather disturbance or a gravity wave (see Section 44.6.3 for details). Hence, acoustic waves play a negligible role in the geophysical fluid flows forming the focus of this book. Nonetheless, the relative simplicity of acoustic waves, and their ubiquitous presence in the natural environment, make them an ideal pedagogical introduction to the somewhat more complex geophysical waves considered in later chapters. We thus study acoustic waves both as an interesting topic in physics and as a platform to nurture our skills with wave physics.

We study acoustic waves in a perfect compressible fluid where the only force arises from pressure, thus ignoring gravity, rotation, and viscous friction. Even before considering this fluid, we develop an understanding of oscillatory physics by studying the motion of simple harmonic oscillators. In particular, we show that a system of coupled harmonic oscillators has a continuum limit that offers a conceptual starting point for the acoustic waves supported by a continuous fluid. We then derive the acoustic wave equation using both Lagrangian and Eulerian viewpoints, and thereafter study various properties of acoustic waves, including their energetics.

READER'S GUIDE TO THIS CHAPTER

Development of the linear equations for acoustic waves relies on the momentum dynamics from Chapter 21, and the acoustic energetics makes use of thermodynamics from Chapters 19, 20, and 23. Furthermore, we assume an understanding of wave kinematics from Chapter 43. There are many treatments of acoustic waves in the literature, and we made use of Chapter 9 in [Fetter and Walecka \(2003\)](#), Chapter VIII in [Landau and Lifshitz \(1987\)](#), Section 15.2 of [Kundu et al. \(2016\)](#), and Section 16.5 in [Thorne and Blandford \(2017\)](#). Finally, note that [the second half of this video](#) offers a pedagogical introduction to acoustic waves.

44.1 Loose threads	1132
44.2 Conceptual introduction to acoustic waves	1132
44.3 Harmonic oscillators	1133
44.3.1 Physical picture	1133
44.3.2 Oscillations from a Hooke's law restoring force	1134
44.3.3 Mechanical energy	1135
44.3.4 Coupled harmonic oscillators	1136
44.3.5 Mechanical energy for coupled oscillators	1137
44.3.6 Continuum limit of coupled oscillators	1138
44.3.7 Longitudinal waves	1139

44.3.8	Further study	1139
44.4	Lagrangian perspective	1139
44.4.1	Mass conservation	1139
44.4.2	Momentum conservation	1140
44.4.3	Equation of state and acoustic wave equation	1141
44.4.4	Sound speed	1141
44.4.5	Further study	1142
44.5	Eulerian perspective	1142
44.5.1	Generalized wave-like equation	1142
44.5.2	Inhomogeneous equilibrium state	1144
44.5.3	Acoustic wave equation	1144
44.5.4	The velocity potential and acoustic wave properties	1145
44.6	Dispersion relation and flow properties	1147
44.6.1	Dispersion relation	1147
44.6.2	Flow properties for acoustic plane waves	1147
44.6.3	Example acoustic pressure perturbations	1148
44.7	Energetics	1149
44.7.1	Expressions for the wave energies	1150
44.7.2	Equipartition of energy	1151
44.7.3	Energy budget equation	1153
44.8	Wave momentum	1153
44.9	The eikonal approximation for acoustic waves	1154
44.9.1	Scalar potential for density-weighted velocity	1155
44.9.2	Energetics in brief	1155
44.9.3	Notation used to develop the formalism	1156
44.9.4	Slowly varying amplitude and rapidly varying phase	1156
44.9.5	The eikonal equations	1157
44.9.6	Further study	1158
44.10	Exercises	1159

44.1 Loose threads

- Figures
- Fourier analysis and Green's functions from Section 50 of *Fetter and Walecka* (2003). Just do the screened Poisson equation. Or perhaps not, since also need to do the next subsection...quite extensive for now.
- Example use of the amplitude equation in Section 44.9. Need to extend the study to the energetics as in Salmon's notes for gravity waves.

44.2 Conceptual introduction to acoustic waves

Key physical processes giving rise to acoustic waves

Acoustic waves involve four physical processes: (i) the density in a compressible fluid changes according to flow divergences and convergences; (ii) density changes lead to pressure fluctuations; (iii) pressure fluctuations lead to fluid particle motion; (iv) for small fluctuations relative to an equilibrium state, fluid particle displacements can exhibit oscillatory motion that manifest as linear acoustic waves. Small fluctuations correspond to a fluid particle speed that is much smaller than the acoustic wave speed, with the ratio known as the *Mach number* (we see this relation in Section 44.6.2). Hence, we are concerned only with small Mach number flow in this chapter. As

such, acoustic wave properties such as the wave momentum and wave energy are transmitted at a much greater speed than the transport of properties arising from fluid particle motion (e.g., heat and mass transport). Furthermore, we find that fluid particles feeling the passage of an acoustic wave oscillate in the direction of the wave, with the alignment of the fluid velocity and wave direction characterizing *longitudinal waves*.

The alternating compression and rarefaction of fluid elements within an acoustic wave give rise to alternating pressure work that affects the internal energy. For small Mach number flow, acoustic waves can be assumed to be isentropic, so that the pressure work is reversible. We make use of perfect fluid mechanics throughout this chapter, thus ignoring mixing and heating so that fluid elements maintain constant specific entropy. Indeed, we generally assume the fluid has uniform specific entropy to further isolate the essential physical features. The constant entropy assumption must be dropped for the study of acoustic waves in stratified fluids.

Comments on compressible, incompressible, and the Boussinesq ocean

All real fluids are compressible and thus support acoustic waves. When compressibility is reduced towards zero, so that the continuous media becomes more rigid, the acoustic wave speed increases. Hence, we generally find acoustic waves travel faster through solids than liquids, and faster through liquids than gases. Taking the mathematical limit of a fully incompressible fluid (where the fluid density is uniform and constant) results in an infinite acoustic wave speed, in which case acoustic waves are absent from incompressible fluid dynamics.

There are occasions where we study incompressible fluids in this book. For example, the shallow water models in Part VI of this book are comprised of incompressible fluid layers with three-dimensional motion, whereas the two-dimensional non-divergent barotropic model in Chapter 35 considers just a two-dimensional velocity (zero vertical motion). The Boussinesq ocean in Chapter 26 offers an important step towards a more realistic fluid. Namely, the Boussinesq ocean is quasi-compressible since the Boussinesq velocity is non-divergent even though the fluid density varies in space and time. The varying density in the Boussinesq ocean gives rise to a divergent velocity that supports acoustic waves. Even so, we commonly ignore the divergent velocity when working with the Boussinesq ocean since this velocity, and the associated acoustic waves, never couple to the Boussinesq ocean dynamics that are the concern of the theory.

44.3 Harmonic oscillators

We here study the mechanics of a *simple harmonic oscillator* as a means to introduce aspects of longitudinal waves in a continuum. We start with the case of a single harmonic oscillator, and then consider a line of coupled oscillators, and finally take the continuum limit of the coupled oscillators. This exercise serves to introduce basic physical concepts arising in oscillatory physical processes, with applications to waves in a fluid.

44.3.1 Physical picture

Consider a tiny piece of matter (idealized as a point) with constant mass, M . Assume this mass is constrained to move along one direction on a frictionless table. Equivalently, assume the mass moves in one direction a vacuum without any gravity field. Let the coordinate position, x , of the mass be measured by the trajectory, $x = X(t)$, and apply a horizontal force to the mass that is a function just of the position, $F(x)$. Newton's equation of motion for the point mass is given by

$$M \ddot{X} = F(x), \quad (44.1)$$

where $F(x)$ is evaluated at the horizontal position of the mass, $x = X(t)$. Now assume the point mass only moves a small distance from its equilibrium position, $x = \Delta$, which is defined by the position where the force vanishes, $F(\Delta) = 0$. We thus approximate the horizontal force by its leading order Taylor expansion

$$F(x) \approx F(\Delta) + (x - \Delta) \left[\frac{dF(x)}{dx} \right]_{x=\Delta} = (x - \Delta) \left[\frac{dF(x)}{dx} \right]_{x=\Delta}, \quad (44.2)$$

where higher order terms are dropped, and we set $F(\Delta) = 0$.

44.3.2 Oscillations from a Hooke's law restoring force

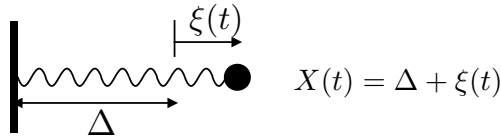


FIGURE 44.1: A simple harmonic oscillator as realized by an object of fixed mass M (approximated as a point mass) attached to a massless spring with motion in just one direction. The only force acting on the mass arises from the spring, whose spring constant, Γ , is constant. The trajectory of the point mass, $X(t) = \Delta + \xi(t)$, measures the position relative to the wall on the left, with Δ the equilibrium position (where the spring force vanishes), and $\xi(t)$ the displacement from the equilibrium position. We here depict the system where the spring is extended to the right so that $\xi(t) > 0$. In this case, the restoring force from the spring accelerates the mass to the left.

Now specialize the force to be restorative so that

$$F(x) = -\Gamma(x - \Delta) \quad \text{with} \quad \Gamma = \left[\frac{dF(x)}{dx} \right]_{x=\Delta} > 0. \quad (44.3)$$

This linear force provides the canonical *Hooke's law* force, such as realized by an idealized massless spring as depicted in Figure 44.1.¹ Introducing the displacement relative to an equilibrium position (see Figure 44.1)

$$\xi(t) = X(t) - \Delta, \quad (44.4)$$

along with the Hooke's law restoring force (44.3), we find Newton's law for the particle trajectory takes the form of the linear *oscillator equation*

$$M \ddot{X} + \Gamma(X - \Delta) = M \ddot{\xi} + \Gamma \xi = 0 \implies \ddot{\xi} + \omega_0^2 \xi = 0 \quad \text{with} \quad \omega_0^2 = \Gamma/M. \quad (44.5)$$

A solution to the oscillator equation can be written

$$X(t) - \Delta = \xi(t) = A \cos(\omega_0 t + \alpha), \quad (44.6)$$

where A is the oscillation amplitude and α a phase shift, with both A and α time independent and specified by initial conditions. We thus find that the Hooke's law restoring force leads to an oscillatory trajectory (44.6) centered on the equilibrium position, $x = \Delta$. The angular frequency, ω_0 , determines the period of oscillation according to

$$T^{\text{per}} = 2\pi/\omega_0 = 2\pi(M/\Gamma)^{1/2}. \quad (44.7)$$

¹We encountered a more complex example of Hooke's law in Section 22.8 when studying the relation between stress and rate of strain for viscous fluids.

The period increases with the square root of the mass (longer period for larger mass) and decreases with the square root of the Hooke's law restoring constant (shorter period for larger Hooke's law constant).

44.3.3 Mechanical energy

The Hooke's law force has no explicit dependence on time, $\partial F/\partial t = 0$, so that the oscillating point mass has no concern for the time origin. From Noether's theorem (Section 12.2.1) we know that dynamical systems possessing time symmetry have constant mechanical energy. We here decompose the mechanical energy into its kinetic energy plus potential energy. A constancy of mechanical energy via Noether's theorem then means that the oscillator exchanges mechanical energy between its kinetic energy and potential energy while holding their sum constant.

Potential energy and kinetic energy of the oscillator

During its motion, the point mass experiences work done by the spring and this work is given by

$$W = - \int_{\Delta}^{\Delta+\xi} F dx = \Gamma \int_{\Delta}^{\Delta+\xi} (x - \Delta) dx = \Gamma \xi^2 / 2. \quad (44.8)$$

This work to displace the mass renders a potential energy for the point mass relative to the zero potential energy it possesses when located at its equilibrium position with $\xi = 0$. Through the work-energy theorem from Section 10.1.5, we find that temporal changes in the potential energy are associated with temporal changes in kinetic energy

$$W = -M \int_{\Delta}^{\Delta+\xi} \ddot{X} dx = -M \int_{t_0}^t \ddot{X} \dot{X} dt = -\frac{M}{2} \int_{t_0}^t \frac{d\dot{X}^2}{dt} dt = -M [\mathcal{K}(t) - \mathcal{K}(t_0)], \quad (44.9)$$

where

$$\mathcal{K} = \dot{X}^2 / 2 \quad (44.10)$$

is the kinetic energy per mass for the particle. Hence, as the point mass oscillates, its potential energy changes are exactly compensated by an equal and opposite change to its kinetic energy, thus reflecting the constant mechanical energy for the harmonic oscillator. Another way to see that the mechanical energy remains constant is to note that the sum of the potential plus kinetic energies has a zero time derivative

$$(d/dt) [M \dot{\xi}^2 + \Gamma \xi^2] / 2 = \dot{\xi} [M \ddot{\xi} + \Gamma \xi] = 0, \quad (44.11)$$

where the final equality made use of the equation of motion (44.5). Indeed, making use of the trajectory (44.6) we readily see that the mechanical energy is given by the constant

$$[M \dot{\xi}^2 + \Gamma \xi^2] / 2 = (A^2 / 2) [M \omega_0^2 \sin^2(\omega_0 t + \alpha) + \Gamma \cos^2(\omega_0 t + \alpha)] = \Gamma A^2 / 2, \quad (44.12)$$

where we set $\omega_0^2 = \Gamma/M$ as per equation (44.5). The total energy is thus proportional to the square of the amplitude and linearly proportional to the Hooke's law constant.

Equipartition between time averaged kinetic and potential energies

When time averaged over a single oscillation period of length $2\pi/\omega_0$, the averaged kinetic energy and potential energy are identical

$$\frac{\omega_0}{2\pi} \int_0^{2\pi/\omega_0} (M \dot{\xi}^2/2) dt = \Gamma A^2/4 \quad (44.13a)$$

$$\frac{\omega_0}{2\pi} \int_0^{2\pi/\omega_0} (\Gamma \xi^2/2) dt = \Gamma A^2/4. \quad (44.13b)$$

This result is known as *energy equipartition*. It arises since within a single oscillation period, there is an exact exchange between kinetic energy and potential energy, so that their time averages are identical. Energy equipartition is a rather generic property of linear oscillating systems, and we encounter it again for linear waves, such as the acoustic waves in Section 44.7.2.

44.3.4 Coupled harmonic oscillators

We next consider a line of N identical frictionless point mass particles connected by massless linear Hooke's law springs with identical spring constant, Γ . Let

$$X_n(t) = n\Delta + \xi_n(t) \quad (44.14)$$

be the position of particle n relative to the left-most rigid wall, with $x = n\Delta$ the equilibrium position for particle n and $\xi_n(t)$ the displacement of the particle at time t from its equilibrium.

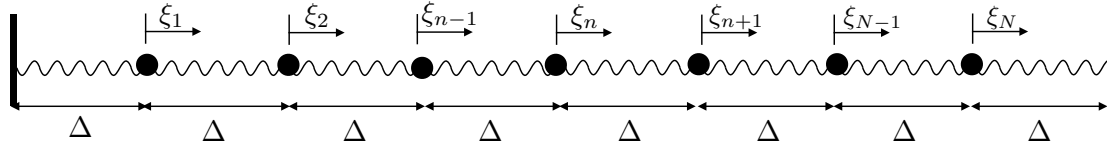


FIGURE 44.2: A line of $N = 7$ coupled simple harmonic oscillators as realized by identical point objects with fixed mass, M , each attached to two massless springs and moving in one direction. The only horizontal force acting on the masses arises from the springs, each with identical spring constants, Γ , and equilibrium length, Δ . The trajectory of any particular mass, $X_n(t)$, measures the position relative to the equilibrium at $X_n(t) = 0$, where the force from the springs vanishes. The system is here shown in its equilibrium where the distance between each mass is Δ , and the displacements all vanish, $\xi_n = 0$. Each point mass is attached to two springs, with the end springs attached to a rigid wall.

To develop the equation of motion, observe that the force acting on a particle is comprised of two terms associated with the two springs, one on the left and one on the right. Consider first the end particles where one of its springs is attached to a rigid wall. For convenience, we label a point at the left wall as $n = 0$ and $n = N + 1$ for a point on the right wall. For the $n = 1$ mass we have the force from the left spring given by

$$F_{n=0 \rightarrow n=1} = -\Gamma \xi_1, \quad (44.15)$$

just as for a single harmonic oscillator considered in Section 44.3.2. The force from the right spring is given by

$$F_{n=2 \rightarrow n=1} = -\Gamma (\xi_1 - \xi_2). \quad (44.16)$$

We understand the nature of this force by noting that if $\xi_1 > 0$ then the spring is compressed to the right, so that the restoring force is to the left as the spring expands. Conversely, if $\xi_2 > 0$

then the spring is expanded to the right, in which case the particle is itself accelerated to the right. Hence, the equation of motion for this mass is given by

$$M \ddot{\xi}_1 = -\Gamma \xi_1 - \Gamma (\xi_1 - \xi_2). \quad (44.17)$$

Anticipating the force balance that acts on the interior masses, we introduce two dummy deviations, each with fixed value of zero,

$$\xi_0 \equiv 0 \quad \text{and} \quad \xi_{N+1} \equiv 0. \quad (44.18)$$

We thus have the equation of motion for the $n = 1$ point mass given by

$$M \ddot{\xi}_1 = -\Gamma (\xi_1 - \xi_0) - \Gamma (\xi_1 - \xi_2), \quad (44.19)$$

and analogous considerations hold for the $n = N$ point mass

$$M \ddot{\xi}_N = -\Gamma (\xi_N - \xi_{N-1}) - \Gamma (\xi_N - \xi_{N+1}). \quad (44.20)$$

The interior masses have analogous equations so that the generic equation of motion for $n = 1, N$ is given by

$$M \ddot{\xi}_n = -\Gamma (\xi_n - \xi_{n-1}) - \Gamma (\xi_n - \xi_{n+1}) \implies \ddot{\xi}_n = \omega_0^2 (\xi_{n+1} - 2\xi_n + \xi_{n-1}). \quad (44.21)$$

44.3.5 Mechanical energy for coupled oscillators

Following our discussion of mechanical energy for a single oscillator in Section 44.3.3, we multiply the equation of motion (44.21) by $\dot{\xi}_n$ and sum over the $n = 1, N$ oscillators. The acceleration term leads to the time change for the total kinetic energy of the full coupled oscillator system

$$M \sum_{n=1}^N \dot{\xi}_n \ddot{\xi}_n = \frac{M}{2} \sum_{n=1}^N \frac{d\dot{\xi}_n^2}{dt}. \quad (44.22)$$

Summation over the left portion of the force in equation (44.21) can be written

$$\sum_{n=1}^N \dot{\xi}_n (\xi_n - \xi_{n-1}) = \sum_{n=1}^{N+1} \dot{\xi}_n (\xi_n - \xi_{n-1}), \quad (44.23)$$

which follows since $\xi_{N+1} \equiv 0$ so that the extra term in the summation vanishes. The summation over the right portion of the force in equation (44.21) can be written

$$\sum_{n=1}^N \dot{\xi}_n (\xi_n - \xi_{n+1}) = \sum_{n=2}^{N+1} \dot{\xi}_{n-1} (\xi_{n-1} - \xi_n) = \sum_{n=1}^{N+1} \dot{\xi}_{n-1} (\xi_{n-1} - \xi_n). \quad (44.24)$$

To reach the first equality we changed indices on the terms in the summation, and modified the summation limits accordingly. For the second equality we expanded the summation range by noting that $\xi_0 \equiv 0$, thus allowing us to bring the lower summation limit from $n = 2$ to $n = 1$. Bringing the left and right terms together leads to

$$\Gamma \sum_{n=1}^N \dot{\xi}_n (\xi_n - \xi_{n-1}) + \Gamma \sum_{n=1}^N \dot{\xi}_n (\xi_n - \xi_{n+1}) = \frac{\Gamma}{2} \frac{d}{dt} \sum_{n=1}^{N+1} (\xi_n - \xi_{n-1})^2, \quad (44.25)$$

which is the potential energy arising from the expansion and contraction of the Hooke's law springs.

Bringing the kinetic energy and potential energy together leads to the conservation of mechanical energy for the coupled oscillator system

$$\frac{d}{dt} \sum_{n=1}^{N+1} \left[\frac{M}{2} \dot{\xi}_n^2 + \frac{\Gamma}{2} (\xi_n - \xi_{n-1})^2 \right] = 0. \quad (44.26)$$

Just as for the single oscillator, we see that the coupled oscillator system maintains a fixed mechanical energy in which energy is exchanged between kinetic and potential energy reservoirs.

44.3.6 Continuum limit of coupled oscillators

Further study of the discrete coupled oscillator system involves the introduction of discrete normal modes and the associated transit of energy through discrete waves (e.g., see Section 24 of [Fetter and Walecka \(2003\)](#)). That analysis takes us somewhat outside the main topic of this chapter, which concerns waves in a continuous media. We are thus motivated to take the following continuum limit

$$\Delta \rightarrow 0 \quad \text{equilibrium distance between particles goes to zero} \quad (44.27a)$$

$$N \rightarrow \infty \quad \text{infinite number of particles} \quad (44.27b)$$

$$(N+1)\Delta = L \quad \text{equilibrium length remains constant} \quad (44.27c)$$

$$M/\Delta = \sigma \quad \text{constant mass per length} \quad (44.27d)$$

$$\Gamma\Delta = \tau \quad \text{constant compressive/expansive force} \quad (44.27e)$$

$$n\Delta = x \quad \text{continuous coordinate for equilibrium position} \quad (44.27f)$$

$$\xi_n(t) \rightarrow \xi(x, t) \quad \text{displacement becomes function of space and time.} \quad (44.27g)$$

The displacement function, $\xi(x, t)$, measures the displacement of an infinitesimal piece of matter whose equilibrium position is x . As such, the coordinate x acts as a parameter that labels an infinitesimal piece of matter whose equilibrium position is x and whose instantaneous position is $x + \xi(x, t)$. As an aside, we note that the displacement field, $\xi(x, t)$, is a one-dimensional version of the vector field, $\xi(\mathbf{x}, t)$, used for the *generalized Lagrangian mean* of Section 62.3.

Introducing the above notation, yet without taking the continuum limit, brings the coupled oscillator equation (44.21) into the form

$$\ddot{\xi}_n = \frac{\Gamma}{M} (\xi_{n+1} - 2\xi_n + \xi_{n-1}) \quad (44.28a)$$

$$= \frac{\Gamma\Delta}{M/\Delta} \frac{\xi_{n+1} - 2\xi_n + \xi_{n-1}}{\Delta^2} \quad (44.28b)$$

$$= \frac{\tau}{\sigma} \left[\frac{\xi_{n+1} - 2\xi_n + \xi_{n-1}}{\Delta^2} \right]. \quad (44.28c)$$

To take the continuum limit, note that the finite difference on the right hand side approximates the second order derivative operator, so that in the continuum limit we recover the one dimensional *wave equation*

$$(\partial_{tt} - c^2 \partial_{xx}) \xi = 0, \quad (44.29)$$

with the wave speed given by

$$c = (\tau/\sigma)^{1/2}. \quad (44.30)$$

We introduced the mathematics of the wave equation (44.29) in Section 3.7 in the context of hyperbolic partial differential equations. A general solution is given by

$$\xi(x, t) = A(x - ct) + B(x + ct), \quad (44.31)$$

where A and B are arbitrary smooth functions determined by the initial conditions and boundary conditions. The solution $A(x - ct)$ is a signal moving in the $+\hat{x}$ direction, whereas $B(x - ct)$ is a signal moving in the $-\hat{x}$ direction, both moving at speed c .

44.3.7 Longitudinal waves

We have restricted attention to motion constrained to a line whereby the harmonic oscillators render a series of alternating rarefactions and compressions that lead to wave-like motions along that line. Upon taking the continuum limit, we found that each piece of the continuum oscillates about its equilibrium position, again with the oscillations in a direction aligned with the waves. Such motions are the defining characteristic of *longitudinal waves*. The longitudinal waves resulting from the continuum limit of coupled harmonic oscillators offers a prototype for the acoustic waves studied in the remainder of this chapter.

44.3.8 Further study

The study of harmonic oscillators can be found in most classical mechanics texts, with our treatment following Sections 3.1 and 3.2 of [Marion and Thornton \(1988\)](#). Our presentation of coupled harmonic oscillators was inspired by Section 24 of [Fetter and Walecka \(2003\)](#), though we made use of a kinematic treatment following the generalized Lagrangian mean from Section 62.3.

44.4 Lagrangian perspective

Consider a continuum fluid system whose motion is constrained to one space dimension, \hat{x} . Assume that all fluid properties and flow properties are independent of the y and z directions. We assume the only forces acting on fluid elements arise from pressure, so that gravity, electromagnetism, and friction are ignored. Furthermore, all fluid motion remains close to an equilibrium base state, where the base state density and pressure are everywhere uniform with values ρ_e and p_e .

We examine small perturbations to this base state, and interpret the perturbations as acoustic waves. Our derivation of the equation for the acoustic waves proceeds in three steps. The first concerns the equation for mass conservation; the second arises from momentum conservation; and the third concerns the equation of state relating pressure, density, and specific entropy. Throughout the derivation we make use of the Lagrangian displacement field, $\xi(x, t)$, used in Section 44.3.6 when taking the continuum limit of coupled harmonic oscillators. Recall that this function measures the displacement, at time t , of a fluid element whose equilibrium position is x . We here also introduce the density, $\rho(x, t)$, as the density of a fluid element whose equilibrium position is x , and we maintain the same interpretation for the pressure field, $p(x, t)$.

44.4.1 Mass conservation

In Figure 44.3 we consider two configurations for a fluid element, in which the first assumes the fluid is in mechanical equilibrium with density ρ_e and mass per unit area

$$M/A = \rho_e \delta x, \quad (44.32)$$

where A is the horizontal cross sectional area. The second configuration has been displaced by $\xi(x, t)$ a small amount so that the fluid element is out of mechanical equilibrium. In this case its density, $\rho(x, t)$, is found through mass conservation. Namely, the mass in the original rectangle equals to that in the displaced rectangle

$$M/A = \rho_e \delta x \quad (44.33a)$$

$$= \rho [x + \delta x + \xi(x + \delta x, t + \delta t) - x - \xi(x, t + \delta t)] \quad (44.33b)$$

$$= \rho [\delta x + \xi(x + \delta x, t + \delta t) - \xi(x, t + \delta t)] \quad (44.33c)$$

$$= \rho \delta x \left[1 + \frac{\partial \xi(x^*, t)}{\partial x} \right] \quad (44.33d)$$

$$\approx \rho \delta x \left[1 + \frac{\partial \xi(x, t)}{\partial x} \right]. \quad (44.33e)$$

The penultimate equality made use of the mean value theorem from differential calculus, where x^* is a point between x and $x + \delta x$, whereas the final step involves the approximation that arises when taking the infinitesimal limit allowing us to evaluate $\partial \xi / \partial x$ at the position x . We are thus led to the relation

$$\rho(x, t) = \rho_e (1 + \partial \xi / \partial x)^{-1} \approx \rho_e (1 - \partial \xi / \partial x). \quad (44.34)$$

This equation says that the density of a fluid element, $\rho(x, t)$, whose equilibrium position is x , differs from its equilibrium density, ρ_e , according to whether the fluid element is expanded ($\partial \xi / \partial x > 0$) or contracted ($\partial \xi / \partial x < 0$).²

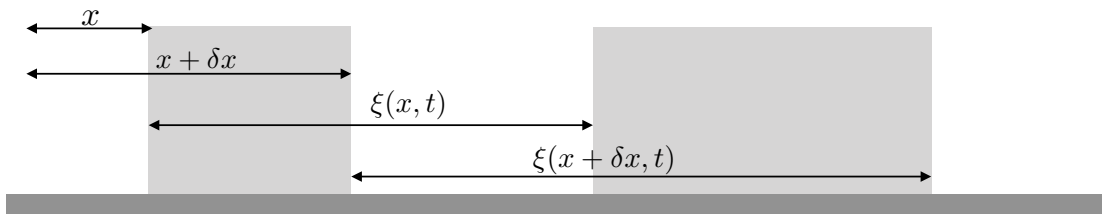


FIGURE 44.3: Schematic of a fluid constrained to move just in the \hat{x} direction with uniform properties in the \hat{y} and \hat{z} directions. We consider a tiny fluid element of constant mass, M , and with density uniform within the element. The equilibrium configuration in the left rectangle has a mass per unit area $M/A = \rho_e \delta x$, where A is the fixed cross sectional area, and ρ_e is the equilibrium density. The right rectangle shows the fluid element at a displaced non-equilibrium configuration where the density deviates from its equilibrium value. This density, $\rho(x, t)$, is the density of the displaced fluid element (specified by the displacement field $\xi(x, t)$) whose equilibrium position is x . The mass of the fluid element is identical for both the equilibrium and non-equilibrium configurations, which leads to $\rho(x, t) = \rho_e (1 + \partial \xi / \partial x)^{-1}$. This relation means, for example, if $\partial \xi / \partial x > 0$ (fluid element expands relative to equilibrium), then $\rho(x) < \rho_e$.

44.4.2 Momentum conservation

At equilibrium the fluid element experiences a pressure, p_e , that is assumed to be spatially uniform. If fluid elements are displaced in a manner that produces nonzero density perturbations, then the pressure field is likewise modified, in which case fluid moves. Recall that we interpret $p(x, t)$ as the pressure acting on a fluid element whose equilibrium position is x . Hence, the net pressure

²By assuming small perturbations relative to equilibrium, we disallow the extreme case where $\partial \xi / \partial x = -1$, in which the fluid becomes so rarefied (vanishing mass density) that we can no longer make use of the continuum description (see Chapter 13 for more on the continuum approximation).

force per area acting on the displaced fluid element is given by the gradient

$$\mathbf{F}^{\text{press}} = [-p(x + \delta x, t) + p(x, t)] \hat{\mathbf{x}} \approx -(\partial p(x, t)/\partial x) \delta x \hat{\mathbf{x}}. \quad (44.35)$$

The position of the fluid element is fully specified by the deviation function, $\xi(x, t)$, so that the acceleration is its second time derivative, $\partial_{tt}\xi(x, t)$, in which case Newton's equation of motion is given by

$$\frac{\partial}{\partial t} \left[\rho \frac{\partial \xi}{\partial t} \right] = -\frac{\partial p}{\partial x}. \quad (44.36)$$

44.4.3 Equation of state and acoustic wave equation

We now assume an equation of state whereby density is a function of pressure and specific entropy³

$$\rho = \rho(p, \mathcal{S}). \quad (44.37)$$

Assuming the fluctuations occur with constant specific entropy, \mathcal{S} , the equation of motion (44.36) takes the form

$$\frac{\partial}{\partial t} \left[\rho \frac{\partial \xi}{\partial t} \right] = - \left[\frac{\partial p}{\partial \rho} \right]_{\mathcal{S}} \frac{\partial \rho}{\partial x}. \quad (44.38)$$

Use of the continuity equation (44.34) allows us to eliminate density in favor of the displacement field

$$\frac{\partial}{\partial t} \left[\rho \frac{\partial \xi}{\partial t} \right] = \frac{\rho_e c_s^2}{(1 + \partial \xi / \partial x)^2} \frac{\partial^2 \xi}{\partial x^2}, \quad (44.39)$$

where we introduced the inverse squared speed

$$c_s^{-2} = \left[\frac{\partial \rho}{\partial p} \right]_{\mathcal{S}}, \quad (44.40)$$

where c_s is interpreted as the sound speed. We can linearize the acoustic equation (44.39) by dropping all terms with the products of the displacement field and assuming density is approximated by its equilibrium value, ρ_e , in which case we recover the acoustic wave equation

$$(\partial_{tt} - c_s^2 \partial_{xx}) \xi = 0. \quad (44.41)$$

This equation says that the displacements of the fluid elements relative to their equilibrium position satisfy the linear wave equation, and the displacements travel with the sound speed.

44.4.4 Sound speed

It is important to observe that the pressure derivative in the sound speed equation (44.40) is computed with a fixed entropy,⁴ \mathcal{S} . We are thus treating acoustic waves as reversible adiabatic waves, which accords with our use of a perfect fluid throughout this chapter. This approach is suitable for those cases where the speed of acoustic waves is much larger than the speed of fluid particles, so that an acoustic wave moves through a fluid far faster than the time for heat to be transferred by fluid particles. In this case, acoustic waves are accurately treated as reversible adiabatic waves.

³We study equations of state, including the ideal gas equation, in Chapters 20 and 27.

⁴Matter concentration is also held fixed when considering sound speeds in a fluid with multiple matter constituents.

In Section 20.4.8 we consider the sound speed in an ideal gas, in which we find

$$c_s^2 = (p/\rho) (c_p/c_v) = T R^M (c_p/c_v), \quad (44.42)$$

where R^M is the specific gas constant given by equation (20.49), c_v is the specific heat capacity holding specific volume fixed (equation (20.59)), and $c_p = c_v + R^M$ is the specific heat capacity holding pressure fixed. For air we have $c_s \approx 350 \text{ m s}^{-1}$ for $T = 300 \text{ K}$. We identify these waves as acoustic (sound) waves due to the agreement of the wave speed (44.42) with the speed of sound measured in the laboratory. Note that LaPlace discovered the relevance of the specific heats ratio, c_p/c_v , in the expression (44.42) for the sound speed. This ratio arises when recognizing acoustic waves to be constant entropy waves, whereas Newton incorrectly assumed they were isothermal, in which case the specific heat ratio does not appear.⁵

A more compressible media, such as the atmosphere, has a smaller sound speed ($c_s \approx 350 \text{ m s}^{-1}$) than a less compressible media such as the ocean ($c_s \approx 1500 \text{ m s}^{-1}$). Indeed, the sound speed is infinite when the media is fully incompressible, with the infinite speed a signature that the hyperbolic wave system has converted to an elliptic system (see Chapter 3). We offer further discussion of the sound speed in Sections 19.7.4 and 20.4.8 as part of our study of thermodynamics.

The *Mach number* is the ratio of the fluid particle speed to the sound speed. If a fluid is moving with Mach number greater than unity (supersonic), then there can be discontinuities (shocks) that break the continuum approximation (Chapter 13). In this case, the continuous fluid equations must be supplemented by other physical conditions such as those afforded by molecular dynamics. We have no occasion to study supersonic flow in this book.

44.4.5 Further study

Elements of this section were taken from Sections 2.1 and 2.2 of [Towne \(1967\)](#) and Section 47-3 in Volume I of [Feynman et al. \(1963\)](#).

44.5 Eulerian perspective

We here derive the acoustic wave equation using an Eulerian approach, thus offering a complement to the Lagrangian treatment in Section 44.4. Furthermore, we no longer restrict motion to one dimension, so that here the resulting acoustic waves travel in three space dimensions. We also generalize the background equilibrium state, here allowing for the background density and specific entropy to be static functions of space.

44.5.1 Generalized wave-like equation

We consider a single component perfect fluid that does not feel gravity, rotation, or friction, so that the only acceleration acting on a fluid element arises from pressure gradients

$$\frac{D\mathbf{v}}{Dt} = -\rho^{-1} \nabla p. \quad (44.43)$$

⁵One may consider the sound speed as the density derivative holding temperature fixed rather than entropy, thus leading to the incorrect speed of sound. This mistake was made by Newton in his studies of sound, whereas LaPlace later corrected this mistake by noting that acoustic waves more closely maintain adiabatic conditions, which means they preserve specific entropy. See Section 47-3 in Volume I of [Feynman et al. \(1963\)](#), Section 2.3 of [Towne \(1967\)](#), or Section 1.2 of [Lighthill \(1978\)](#) for more details.

This expression of the *Euler equation* is coupled to the mass continuity equation (16.16)

$$\frac{D\rho}{Dt} = -\rho \nabla \cdot \mathbf{v}, \quad (44.44)$$

that reflects the material constancy of mass following a fluid element. Furthermore, density and pressure are coupled through the equation of state (44.37), so that the density and pressure material time derivatives are related by

$$\frac{D\rho}{Dt} = \left[\frac{\partial \rho}{\partial p} \right]_s \frac{Dp}{Dt} + \left[\frac{\partial \rho}{\partial S} \right]_p \frac{DS}{Dt} = c_s^{-2} \frac{Dp}{Dt}, \quad (44.45)$$

where we set $DS/Dt = 0$ due to the isentropic nature of the perfect fluid, and introduced the squared sound speed

$$c_s^{-2} = \left[\frac{\partial \rho}{\partial p} \right]_s. \quad (44.46)$$

Combining the continuity equation (44.44) and the material time derivative of the equation of state (44.45) renders

$$\frac{1}{\rho c_s^2} \frac{Dp}{Dt} + \nabla \cdot \mathbf{v} = 0. \quad (44.47)$$

We can relate the velocity divergence to pressure by taking D/Dt of this equation and then using the Euler equation (44.43)

$$-\frac{D(\nabla \cdot \mathbf{v})}{Dt} = -(\partial_t + v_n \partial_n)(\partial_m v_m) \quad (44.48a)$$

$$= -\nabla \cdot \frac{D\mathbf{v}}{Dt} + \partial_m v_n \partial_n v_m \quad (44.48b)$$

$$= \nabla \cdot (\rho^{-1} \nabla p) + \mathbb{S}_{mn} \mathbb{S}_{mn} - \mathbb{R}_{mn} \mathbb{R}_{mn}. \quad (44.48c)$$

In the final equality we introduced components to the rate of strain tensor, \mathbb{S} , and the rotation tensor, \mathbb{R} , both of which were introduced in Section 15.3.5 when studying the velocity gradient tensor. Furthermore, note that the combination, $\mathbb{S} \cdot \mathbb{S} - \mathbb{R} \cdot \mathbb{R}$, also appears in the elliptic pressure equation for the Boussinesq ocean in Section 26.3.3. Use of equation (44.48c) along with D/Dt of equation (44.47) leads to the pressure equation

$$\frac{D}{Dt} \left[\frac{1}{\rho c_s^2} \frac{Dp}{Dt} \right] - \nabla \cdot (\rho^{-1} \nabla p) = \mathbb{S} \cdot \mathbb{S} - \mathbb{R} \cdot \mathbb{R}. \quad (44.49)$$

The left hand side is a Lagrangian form of the Eulerian acoustic wave equation to be described below. This equation describes pressure fluctuations relative to the moving flow, with the non-linear source on the right hand side arising from strain and rotation within the fluid flow. In Exercise 44.2 we consider the special case of pressure fluctuations when the background flow is a uniform constant.

The pressure equation (44.49) is nonlinear since pressure, density, and velocity are coupled. We garner insight into certain of the physical processes captured by this equation by linearizing around an equilibrium state and examining small amplitude fluctuations, to which we now turn our attention.

44.5.2 Inhomogeneous equilibrium state

In Section 44.4 we assumed the background equilibrium state has zero velocity, uniform density, uniform specific entropy, uniform pressure, and uniform sound speed. This trivial state is itself an exact solution to the perfect fluid equations of motion, thus serving as a suitable state from which to study linear fluctuations. Here we introduce a slightly less trivial background state that is also an exact solution to the equations of motion.

We continue to assume a trivial solution of the Euler equation with vanishing velocity and spatially uniform pressure. In this case, the continuity equation (44.44) can be satisfied by an equilibrium density field that is static yet spatially inhomogeneous, $\rho_e = \rho_e(\mathbf{x})$. This inhomogeneous density is consistent with the equation of state (44.37) if the specific entropy is itself inhomogeneous, $S_e = S_e(\mathbf{x})$, in which case

$$\rho_e(\mathbf{x}) = \rho[p = p_{\text{const}}, S = S_e(\mathbf{x})]. \quad (44.50)$$

By allowing ρ_e and S_e to be spatially dependent functions, we extend the applicability of the resulting wave equation to the study of acoustic waves propagating in a static inhomogeneous media. A geophysically relevant example concerns an ocean or atmosphere in exact hydrostatic balance (Section 21.4), with vanishing flow yet density and specific entropy that are functions of geopotential coordinate, z . [Pierce \(1990\)](#) considers the even more realistic case with a space and time dependent background flow, and a correspondingly nonuniform pressure field.

44.5.3 Acoustic wave equation

We now linearize the Euler equation (44.43), along with the mass continuity equation in the form of equation (44.47), and perform the linearization relative to an equilibrium state of zero motion yet inhomogeneous density. We thus write pressure, density, and velocity as

$$p = p_e + p' \quad \text{and} \quad \rho = \rho_e(\mathbf{x}) + \rho' \quad \text{and} \quad \mathbf{v} = 0 + \mathbf{v}', \quad (44.51)$$

where the pressure and density perturbations are small relative to their equilibrium values $|p'| \ll p_e$ and $|\rho'| \ll \rho_e(\mathbf{x})$, and where the equilibrium density is generally a function of space. A positive p' arises from a local *compression* in the fluid, whereas a negative p' is a local expansion or *rarefaction*.

Inserting the perturbations (44.51) into the Euler equation (44.43) leads to

$$(\rho_e + \rho') \partial_t \mathbf{v}' + (\mathbf{v}' \cdot \nabla) \mathbf{v}' = -\nabla p', \quad (44.52)$$

and dropping all products of perturbation fields leads to the linearized Euler equation

$$\rho_e \partial_t \mathbf{v}' = -\nabla p'. \quad (44.53)$$

Likewise, the linearized continuity equation (44.47) takes the form

$$\partial_t p' + \rho_e c_s^2 \nabla \cdot \mathbf{v}' = 0, \quad (44.54)$$

where the squared sound speed is here determined by compressibility of the equilibrium state

$$c_s^{-2} = \left[\left(\frac{\partial \rho}{\partial p} \right)_{S=p_e} \right]_{p=p_e}. \quad (44.55)$$

Taking the divergence of the velocity equation (44.53) and making use of the continuity equation (44.54) renders the acoustic wave equation for the anomalous pressure

$$\frac{1}{\rho_e c_s^2} \frac{\partial^2 p'}{\partial t^2} - \nabla \cdot (\rho_e^{-1} \nabla p') = 0. \quad (44.56)$$

This linear wave equation compares to its fully nonlinear analog in equation (44.49). We can perform analogous manipulations to determine the following wave equation satisfied by the velocity divergence

$$\partial_{tt} \mathcal{D}' - \nabla \cdot [\rho_e^{-1} \nabla (\rho_e c_s^2 \mathcal{D}')] = 0 \quad \text{with } \mathcal{D}' = \nabla \cdot \mathbf{v}'. \quad (44.57)$$

Finally, we note that from the linearized Euler equation (44.53) that the density weighted velocity fluctuation has a static curl

$$\partial_t [\nabla \times (\rho_e \mathbf{v}')] = 0. \quad (44.58)$$

Equation (44.56) for the pressure, equation (44.57) for the velocity divergence, and equation (44.58) for the curl of the density weighted velocity constitute the suite of equations for acoustic waves in a static yet inhomogeneous background state. In the remainder of this section we study the properties of the wave solutions to these equations, yet restricted to the homogeneous equilibrium state with ρ_e a uniform constant and with the sound speed also uniform, in which case we have the linear acoustic wave equations

$$(\partial_{tt} - c_s^2 \nabla^2) p' = 0 \quad \text{and} \quad (\partial_{tt} - c_s^2 \nabla^2) \mathcal{D}' = 0 \quad \text{and} \quad \partial_t (\nabla \times \mathbf{v}') = 0 \quad \text{with} \quad \mathcal{D}' = \nabla \cdot \mathbf{v}'. \quad (44.59)$$

The more realistic, yet complex, case of waves propagating through an inhomogeneous equilibrium background state requires extra mathematical technology that we develop in Section 44.9.

44.5.4 The velocity potential and acoustic wave properties

With the static curl, as per equation (44.59), we know that if the linear system is initialized with zero vorticity then it stays that way. That is, acoustic waves do not alter vorticity.

Velocity potential for acoustic waves

Assuming zero initial vorticity, as appropriate when considering fluctuations around a state of rest, allows us to introduce a velocity potential (dimensions squared length per time), ψ , so that

$$\mathbf{v}' = -\nabla \psi. \quad (44.60)$$

The velocity equation (44.53) thus implies

$$\nabla(p' - \rho_e \partial_t \psi) = 0 \implies p' = \rho_e (\partial_t \psi + K), \quad (44.61)$$

where $K(t)$ is an arbitrary function of time that is independent of space. The velocity potential is itself arbitrary up to a function of time. Hence, we can choose to work with a modified velocity potential, Ψ , that absorbs the function K

$$\Psi = \psi + \int^t K(t') dt', \quad (44.62)$$

so that pressure is determined by the time derivative of Ψ and velocity is determined by the gradient

$$p' = \rho_e \partial_t \Psi \quad \text{and} \quad \mathbf{v}' = -\nabla \Psi. \quad (44.63)$$

Note that the process of transforming from ψ to Ψ is referred to as a *gauge transformation*. We consider the same approach in Section 45.2.2 when studying surface waves.

Making use of the relation (44.63) in the linearized continuity equation (44.54) renders the wave equation for the velocity potential

$$(\partial_{tt} - c_s^2 \nabla^2) \Psi = 0. \quad (44.64)$$

Furthermore, we can take the gradient of this equation to find that each of the three velocity components satisfies the acoustic wave equation

$$-(\partial_{tt} - c_s^2 \nabla^2) \nabla \Psi = (\partial_{tt} - c_s^2 \nabla^2) \mathbf{v}' = 0. \quad (44.65)$$

Density fluctuations in an acoustic wave

We determine the density perturbation within an acoustic wave by linearizing the equation of state (44.37) around the equilibrium state

$$\rho = \rho(p, S) \approx \rho_e + c_s^{-2} (p - p_e), \quad (44.66)$$

so that

$$\rho' = (\rho - \rho_e) = c_s^{-2} p' = \rho_e c_s^{-2} \partial_t \Psi. \quad (44.67)$$

Taking the time derivative and using the wave equation (44.64) reveals the self-consistency of this result with the linearized mass continuity equation (44.54)

$$\partial_t \rho' = \rho_e c_s^{-2} \partial_{tt} \Psi = \rho_e \nabla^2 \Psi = -\rho_e \nabla \cdot \mathbf{v}'. \quad (44.68)$$

Temperature fluctuations in an acoustic wave

For an acoustic wave, a differential temperature increment arises just from changes to the pressure while holding entropy fixed

$$dT = \left[\frac{\partial T}{\partial p} \right]_S dp. \quad (44.69)$$

In Section 20.2 we referred to this temperature partial derivative as the *adiabatic lapse rate*. Equation (20.26) provides a practical form of the lapse rate

$$\left[\frac{\partial T}{\partial p} \right]_S = \frac{T_e \alpha_T}{\rho_e c_p}, \quad (44.70)$$

with T_e the equilibrium temperature, c_p the specific heat capacity (19.102), and α_T the thermal expansion coefficient (19.105) defined in terms of the *in situ* temperature (α_T and c_p are computed for the equilibrium state). We thus have a fluctuation of temperature given by

$$T - T_e = T' = \frac{T_e \alpha_T p'}{\rho_e c_p} = (T_e \alpha_T / c_p) \partial_t \Psi. \quad (44.71)$$

Hence, as an acoustic wave propagates it has an associated oscillation of the temperature field due to oscillations in pressure.

44.6 Dispersion relation and flow properties

We now characterize physical properties of acoustic waves, focusing on the properties as realized by a traveling acoustic plane wave in a homogeneous media (i.e., ρ_e is a uniform constant). These properties are determined largely through the acoustic wave *dispersion relation*, which provides a functional relation between the wave frequency and the wavevector. After determining the dispersion relation, we derive the pressure, density, and velocity fluctuations in an acoustic wave.

44.6.1 Dispersion relation

Not every traveling plane wave is a solution to the acoustic wave equation (44.64). Rather, the wavevector and angular frequency must be related in a specific manner that is dependent on physics of the particular wave. This relation is known as the *dispersion relation*. Plugging in the traveling plane wave (43.16) into the acoustic wave equation (44.64) renders the acoustic wave dispersion relation

$$(\omega^2 - c_s^2 \mathbf{k}^2) \Psi = 0 \implies \omega = c_s |\mathbf{k}| \implies C_p = \omega / |\mathbf{k}| = c_s. \quad (44.72)$$

Note that we only consider the positive sign for the angular frequency since $\omega \geq 0$ corresponds to our convention for wave frequencies (Section 43.4). Traveling acoustic plane waves of a given wavevector have their angular frequency specified by the dispersion relation (44.72). Evidently, the phase speed for all acoustic waves (i.e., acoustic waves of arbitrary wavevector), is given by the sound speed, $C_p = c_s$. A constant phase speed means that acoustic waves are non-dispersive.

The dispersion relation (44.72) reveals that the phase speed for the acoustic waves, C_p , equals to the sound speed, c_s . Now the sound speed is a function of the equilibrium fluid state; it is not a function of wave properties such as the wavelength or wave frequency. Hence, all acoustic waves, regardless their wavelength, travel at the same phase speed, $C_p = c_s$. Correspondingly, we say that acoustic waves are *non-dispersive*. This property accords with common experience, whereby the variety of sound waves with different frequencies from, say, an orchestra are heard together since all sounds frequencies travel with the same speed. Furthermore, it is certainly possible for any particular point in space to be comprised of multiple acoustic waves. Since each wave satisfies the wave equation (44.64), and since the wave equation is linear, acoustic waves satisfy the *principle of superposition*. That is, the sum of multiple traveling acoustic waves is also an acoustic wave that satisfies the same wave equation with same speed, c_s .

44.6.2 Flow properties for acoustic plane waves

We here establish expressions for flow fields, such as velocity, pressure, and density, in the presence of an acoustic plane wave. We start with equation (44.63), which relates pressure and velocity to derivatives of the velocity potential. Following our discussion of traveling plane wave kinematics in Section 43.5.1, we write the velocity potential for an acoustic plane wave as

$$\Psi(\mathbf{x}, t) = A \operatorname{Re}[e^{i(\mathbf{k} \cdot \mathbf{x} - \omega t + \alpha)}] = A \cos(\mathbf{k} \cdot \mathbf{x} - \omega t + \alpha), \quad (44.73)$$

which leads to the corresponding pressure fluctuation

$$p' = \rho_e \partial_t \Psi = \rho_e \operatorname{Re}[-i\omega \Psi] = \rho_e \omega A \sin(\mathbf{k} \cdot \mathbf{x} - \omega t + \alpha). \quad (44.74)$$

Hence, higher frequency acoustic plane waves have higher magnitude for their fluctuating pressure. Likewise, the fluctuating velocity of fluid particles takes on the form

$$\mathbf{v}' = -\nabla\Psi = -\operatorname{Re}[i\mathbf{k}\Psi] = A\mathbf{k}\sin(\mathbf{k}\cdot\mathbf{x} - \omega t + \alpha). \quad (44.75)$$

This relation means that fluid particles moving in an acoustic plane wave have their velocity aligned with the wave direction

$$\mathbf{v}' \times \mathbf{k} = 0. \quad (44.76)$$

Furthermore, this relation follows since the vorticity of the linear fluctuations vanish (Section 44.5.4). The alignment of particle velocity and wave vector is a defining feature of *longitudinal waves*.⁶ It also means that the squared magnitude of the particle velocity equals to the squared projection of this velocity onto the wave direction

$$|\mathbf{v}'|^2 = (\mathbf{v}' \cdot \hat{\mathbf{k}})^2 = [A|\mathbf{k}|\sin(\mathbf{k}\cdot\mathbf{x} - \omega t + \alpha)]^2. \quad (44.77)$$

Finally, the fluctuating density within an acoustic wave is given by the linearized equation of state (44.67), which takes the following form for an acoustic plane wave

$$\rho' = c_s^{-2} p' = c_s^{-2} \rho_e \omega A \sin(\mathbf{k}\cdot\mathbf{x} - \omega t + \alpha). \quad (44.78)$$

Equations (44.74), (44.75), and (44.78) imply the following relations between the fluctuating pressure, velocity, and density in an acoustic plane wave

$$\rho_e \omega \mathbf{v}' = p' \mathbf{k} \implies p' = \rho_e c_s \mathbf{v}' \cdot \hat{\mathbf{k}} \implies \rho' = \rho_e \mathbf{v}' \cdot \hat{\mathbf{k}} / c_s. \quad (44.79)$$

where we used the dispersion relation (44.72). These relations reveal that pressure, velocity, and density fluctuations are in-phase; i.e., they have the precisely the same phase. The density fluctuation in equation (44.79) reveals that its ratio with the equilibrium density equals to the ratio of the fluid particle speed to the sound speed. This ratio is the Mach number, so that for an acoustic plane wave we have

$$|p'|/(\rho_e c_s^2) = |\rho'|/\rho_e = |\mathbf{v}' \cdot \hat{\mathbf{k}}|/c_s = \text{Ma} \ll 1. \quad (44.80)$$

Hence, small Mach number corresponds to small density fluctuation relative to the equilibrium density. We made use of this relation when introducing the Boussinesq ocean at the start of Chapter 26.

44.6.3 Example acoustic pressure perturbations

We noted in the introduction to this chapter that acoustic waves, and their associated pressure perturbations, play a negligible role in large-scale geophysical fluid flows, such as those associated with atmospheric weather patterns. To support that contention, let us consider some common sounds and examine their pressure perturbations. For that purpose, consider the decibel scale (dB) for the sound pressure level (SPL)

$$\text{SPL} = 20 \log_{10}(|p'|/p_{\text{ref}}) \implies |p'| = p_{\text{ref}} 10^{\text{SPL}/20}. \quad (44.81)$$

⁶We later encounter waves in non-divergent flows, $\nabla \cdot \mathbf{v} = 0$, which are *transverse waves* whereby $\mathbf{k} \cdot \mathbf{v} = 0$. That is, for transverse waves the fluid particle motion is perpendicular to the wave direction.

It is conventional to choose the reference pressure, p_{ref} , so that 0 dB is a quiet sound at the threshold of human hearing, with

$$p_{\text{ref}} = 20 \times 10^{-6} \text{ Pa} = 20 \mu\text{Pa} \quad (44.82)$$

serving as the international convention. Following equation (44.80), we can determine the Mach number associated with a particular sound pressure level (assuming acoustic plane waves) according to

$$\text{Ma} = |p'|/(\rho_e c_s^2) = |p'|/[p(c_p/c_v)], \quad (44.83)$$

where we made use of the ideal gas relation (20.70) for the sound speed

$$\rho_e c_s^2 = p c_p / c_v. \quad (44.84)$$

We evaluate the sound speed at the standard sea level atmospheric pressure, $p = p_{\text{stand}} = 101.325 \times 10^3 \text{ Pa}$, and assume the specific heat capacity ratio, $c_p/c_v = 7/5$, which holds for an ideal diatomic gas, in which case

$$\rho_e c_s^2 = p_{\text{stand}} (c_p/c_v) = 140 \times 10^3 \text{ Pa}. \quad (44.85)$$

Table 44.1 tabulates the SPL, pressure perturbation, and Mach number for some common sounds. We see that even extremely loud sounds, relative to human hearing, have very small Mach numbers, thus justifying the use of linear acoustic wave dynamics for their description.

To gauge the size of these acoustic pressure fluctuations relative to typical atmospheric pressure fluctuations, consider a middle latitude geostrophic wind, in which case equation (28.15) gives

$$\rho f \hat{\mathbf{z}} \times \mathbf{u}_{\text{geostrophic}} = -\nabla p_{\text{geostrophic}} \implies |p'_{\text{geostrophic}}| \sim \rho f U L, \quad (44.86)$$

where U is the scale of the geostrophic wind speed, and L is the horizontal length scale over which the winds vary. Taking $f = 10^{-4} \text{ s}^{-1}$, $U = 10 \text{ m s}^{-1}$, $\rho = 1 \text{ kg m}^{-3}$, and $L = 10^6 \text{ m}$ we find a typical pressure fluctuation

$$|p'_{\text{geostrophic}}| \approx 10^3 \text{ Pa}. \quad (44.87)$$

This pressure fluctuation is on the order of that found inside of an automobile exhaust system (see Table 44.1). However, the atmospheric fluctuation associated with this geostrophic wind extends over thousands of kilometers, whereas the sound waves inside of an exhaust system extend over a fraction of a meter. Hence, the energy contained in the atmospheric weather pattern is many orders larger than that for even the loudest sounds. This example further emphasizes the irrelevance of acoustic waves for large-scale geophysical fluid flows.

44.7 Energetics

We here specialize the energetic analysis from Section 23.5 and 23.7 to study the energetics of an acoustic wave in a homogeneous media (i.e., ρ_e is a uniform constant). For an acoustic wave, the total energy is the sum of the kinetic energy of the oscillating fluid particles, plus the changes to internal energy of the fluid that arise from pressure work (recall we are ignoring gravity). We thus write the total energy per mass, \mathcal{E} , as the sum of the internal per mass, \mathcal{I} , plus kinetic energy per mass, \mathcal{K} ,

$$\mathcal{E} = \mathcal{I} + \mathcal{K}. \quad (44.88)$$

SOUND	SPL (dB)	$ p' $ (Pa)	$ p' / p'_{\text{geostrophic}} $	Ma
soft whisper	30	6.3×10^{-4}	6.3×10^{-7}	4.5×10^{-9}
normal conversation	60	2×10^{-2}	2×10^{-5}	1.4×10^{-7}
noisy factory	90	0.63	6.3×10^{-4}	4.5×10^{-6}
rock concert	115	11	1.1×10^{-2}	8×10^{-5}
aircraft engine	130	63	6.3×10^{-2}	4.5×10^{-4}
automobile exhaust system	160	2×10^3	2	1.4×10^{-2}

TABLE 44.1: Acoustic properties of common sounds, following Example 15.2 from [Kundu et al. \(2016\)](#). The first column lists the sound, the second column the sound pressure level in dB, the third column the corresponding pressure fluctuation in Pa, the fourth column the ratio of the pressure fluctuation to a pressure fluctuation associated with a geostrophic atmospheric fluctuation, $|p'_{\text{geostrophic}}| \approx 10^3$ Pa (equation (44.87)), and the fifth column the Mach number assuming standard atmospheric sea level pressure, $p_{\text{stand}} = 1.01 \times 10^5$ Pa. Since the Mach number is far smaller than unity even for the loudest sound, we are justified in using linear acoustic wave theory to describe the propagation of these sounds.

The Eulerian form of the total energy equation is given by equation (23.95), which here takes the rather simple form

$$\frac{\partial(\rho \mathcal{E})}{\partial t} + \nabla \cdot [\rho \mathbf{v} (\mathcal{I} + \mathcal{K} + p/\rho)] = 0, \quad (44.89)$$

where $\mathcal{I} + p/\rho$ is the enthalpy per mass (Section 19.6.4)

$$\mathcal{H} = \mathcal{I} + p/\rho, \quad (44.90)$$

and we set the thermal and chemical fluxes to zero as per a perfect fluid. In the remainder of this section we specialize this energy equation to the case of linear acoustic wave fluctuations.

44.7.1 Expressions for the wave energies

To linearize terms in the energy equation (44.89) requires us to drop third order products of fluctuating quantities while keeping second, first, and zeroth order terms. This procedure is further supported by our ability to develop a self-consistent and closed energy budget for acoustic waves.

Kinetic energy of an acoustic wave

Since velocity is a first order quantity, the kinetic energy per volume is given by

$$2\rho \mathcal{K} = (\rho_e + \rho') \mathbf{v}' \cdot \mathbf{v}' \approx \rho_e \mathbf{v}' \cdot \mathbf{v}'. \quad (44.91)$$

The internal energy requires a bit more work.

Internal (potential) energy of an acoustic wave

For the internal energy, recall from Section 19.6.2 that its natural functional dependence for a single-component fluid is $\mathcal{I}(\mathcal{S}, \rho)$. Since entropy is held fixed in an acoustic wave, we consider the following Taylor series approximation for the internal energy per volume as computed around the equilibrium state

$$\rho \mathcal{I} \approx \rho_e \mathcal{I}_e + (\rho - \rho_e) \left[\frac{\partial(\rho \mathcal{I})}{\partial \rho} \right]_{\rho=\rho_e} + \frac{(\rho - \rho_e)^2}{2} \left[\frac{\partial^2(\rho \mathcal{I})}{\partial \rho^2} \right]_{\rho=\rho_e}. \quad (44.92)$$

The first partial derivative is given by

$$\frac{\partial(\rho \mathcal{I})}{\partial \rho} = \mathcal{I} + \rho \frac{\partial \mathcal{I}}{\partial \rho} = \mathcal{I} + p/\rho = \mathcal{H}, \quad (44.93)$$

where we used identity (19.67) in the penultimate step. The second partial derivative is thus given by

$$\frac{\partial^2(\rho \mathcal{I})}{\partial \rho^2} = \frac{\partial \mathcal{H}}{\partial \rho} = \frac{\partial \mathcal{H}}{\partial p} \frac{\partial p}{\partial \rho} = c_s^2/\rho, \quad (44.94)$$

where we used the identity (19.79) for the final step. We also used the equation of state (44.37) to convert the density derivative to a pressure derivative in the penultimate step.

Bringing these results together leads to the approximate internal energy per volume

$$\rho \mathcal{I} \approx \rho_e \mathcal{I}_e + \rho' \mathcal{H}_e + (c_s \rho')^2/(2 \rho_e). \quad (44.95)$$

The first term on the right hand side is a constant measuring the internal energy per volume of the equilibrium state, and it has no relation to the acoustic wave. The second term is the equilibrium enthalpy per mass times the fluctuating density. When integrating over the full domain, the fluctuating density vanishes due to mass conservation. That is, we assume the mass in the domain is the same in equilibrium as well as when there are acoustic waves, so that

$$\int_{\mathcal{R}} \rho dV = \int_{\mathcal{R}} \rho_e dV \implies \int_{\mathcal{R}} \rho' dV = 0. \quad (44.96)$$

Since the $\rho' \mathcal{H}_e$ term drops out from a domain volume integral, it is common to consider the energy density for an acoustic wave as just the two quadratic terms. However, we choose not to drop this term here. Rather, we find in Section 44.7.3 that this term naturally cancels from the flux-form acoustic energy budget equation, at which point we conclude that it has no significance to the wave energetics. The third term in equation (44.95) contributing to the internal energy per volume, $(c_s \rho')^2/(2 \rho_e)$, can be interpreted as a potential energy per volume associated with the fluid compressibility.

Total energy of an acoustic wave

We conclude that the total energy per volume, accurate to second order in fluctuating acoustic wave fields, is given by

$$\rho \mathcal{E} = \rho' \mathcal{H}_e + (\rho_e/2) [(c_s \rho'/\rho_e)^2 + \mathbf{v}' \cdot \mathbf{v}']. \quad (44.97)$$

As a final step, we make use of equations (44.63) and (44.67) to write the wave energy per volume in terms of the velocity potential

$$\rho \mathcal{E} = \rho' \mathcal{H}_e + (\rho_e/2) [(c_s \rho'/\rho_e)^2 + \mathbf{v}' \cdot \mathbf{v}'] = \frac{\rho_e}{2 c_s^2} [2 \mathcal{H}_e \partial_t \Psi + (\partial_t \Psi)^2 + c_s^2 \nabla \Psi \cdot \nabla \Psi]. \quad (44.98)$$

44.7.2 Equipartition of energy

Following our study of energy for an oscillator in Section 44.3.3, we here study how energy in an acoustic wave is partitioned between kinetic energy and potential energy. Recall that oscillator equally partitions energy when time averaging over an oscillation period; i.e., performing a phase average (Section 5.2.2). As for the oscillator, we expect to realize some form of equipartition for acoustic waves, reflecting the alternating exchange of energy between kinetic and potential. Here, we show that energy equipartition holds instantaneously for a monochromatic traveling acoustic

wave. However, for a general linear fluctuation, equipartition holds only when averaging over a wave period plus integrating over the closed spatial domain.

Equipartition for a monochromatic traveling acoustic wave

For an acoustic plane wave, the energy density simplifies through use of equation (44.79) to render

$$(c_s \rho' / \rho_e)^2 = (\mathbf{v}' \cdot \hat{\mathbf{k}})^2 = \mathbf{v}' \cdot \mathbf{v}', \quad (44.99)$$

where the second equality holds since the fluid particle velocity within the plane wave is aligned with the plane wave phase velocity. We thus find that the potential energy per volume and kinetic energy per volume contribute an equal amount to the acoustic plane wave's energy per volume

$$\rho \mathcal{E} = \rho' \mathcal{H}_e + (\rho_e/2) [(c_s \rho' / \rho_e)^2 + \mathbf{v}' \cdot \mathbf{v}'] = \rho' \mathcal{H}_e + 2 \rho_e \mathcal{K}. \quad (44.100)$$

Equipartition for an arbitrary periodic linear fluctuation

The general expression (44.98) for the energy in a linear fluctuation does not render energy equipartition at each point in space and time. Rather, being inspired by the oscillator in Section 44.3.3, we here show that a phase and space averaged energy does possess equipartition. For the phase average we integrate the energy density over a single period, and doing so eliminates the equilibrium enthalpy term, $2 \mathcal{H}_e \partial_t \Psi$, thus leaving

$$\int_0^{2\pi/\omega} \rho \mathcal{E} dt = \frac{\rho_e}{2 c_s^2} \int_0^{2\pi/\omega} [(\partial_t \Psi)^2 + c_s^2 \nabla \Psi \cdot \nabla \Psi] dt. \quad (44.101)$$

Now integrate by parts and make use of the wave equation (44.64) to find

$$\int_0^{2\pi/\omega} \rho \mathcal{E} dt = \frac{\rho_e}{2 c_s^2} \int_0^{2\pi/\omega} [-\Psi \partial_{tt} \Psi + c_s^2 \nabla \Psi \cdot \nabla \Psi] dt \quad (44.102a)$$

$$= \frac{\rho_e}{2} \int_0^{2\pi/\omega} [-\Psi \nabla^2 \Psi + \nabla \Psi \cdot \nabla \Psi] dt \quad (44.102b)$$

$$= \frac{\rho_e}{2} \int_0^{2\pi/\omega} [-\nabla \cdot (\Psi \nabla \Psi) + 2 \nabla \Psi \cdot \nabla \Psi] dt. \quad (44.102c)$$

We see that for an arbitrary linear and periodic fluctuation, energy equipartition is realized by time integrating over a wave period and then integrating over a spatially closed or spatially periodic domain

$$\int_{\mathcal{R}} \left[\int_0^{2\pi/\omega} \rho \mathcal{E} dt \right] dV = \rho_e \int_{\mathcal{R}} \left[\int_0^{2\pi/\omega} \nabla \Psi \cdot \nabla \Psi dt \right] dV = 2 \rho_e \int_{\mathcal{R}} \left[\int_0^{2\pi/\omega} \mathcal{K} dt \right] dV. \quad (44.103)$$

This equation says that the phase and domain averaged flow contains an equal amount of kinetic energy as internal energy. This result holds for any periodic fluctuation, and is not specific to plane waves.

44.7.3 Energy budget equation

Taking the partial time derivative of the energy per volume, (44.98), leads to

$$\partial_t(\rho \mathcal{E}) = \frac{\rho_e}{c_s^2} [\partial_{tt}\Psi (\mathcal{H}_e + \partial_t\Psi) + c_s^2 \nabla\Psi \cdot \nabla\partial_t\Psi] \quad (44.104a)$$

$$= \rho_e [\nabla^2\Psi (\mathcal{H}_e + \partial_t\Psi) + \nabla\Psi \cdot \nabla\partial_t\Psi] \quad (44.104b)$$

$$= \rho_e \nabla \cdot [(\mathcal{H}_e + \partial_t\Psi) \nabla\Psi] \quad (44.104c)$$

$$= -\rho_e \nabla \cdot [\mathbf{v}' (\mathcal{H}_e + p'/\rho_e)]. \quad (44.104d)$$

We can thus write the acoustic energy equation in terms of the velocity potential

$$\partial_t [2\mathcal{H}_e \partial_t\Psi + (\partial_t\Psi)^2 + c_s^2 \nabla\Psi \cdot \nabla\Psi] = 2c_s^2 \nabla \cdot [(\mathcal{H}_e + \partial_t\Psi) \nabla\Psi]. \quad (44.105)$$

The two \mathcal{H}_e terms cancel identically through use of the wave equation (44.64), thus leaving the acoustic energy equation, here written in two equivalent forms

$$(1/2) \partial_t [(\partial_t\Psi)^2 + c_s^2 \nabla\Psi \cdot \nabla\Psi] = c_s^2 \nabla \cdot (\partial_t\Psi \nabla\Psi) \quad (44.106a)$$

$$(\rho_e/2) \partial_t [(c_s \rho'/\rho_e)^2 + \mathbf{v}' \cdot \mathbf{v}'] = -\nabla \cdot (\mathbf{v}' p'). \quad (44.106b)$$

The energy equation (44.106b) identifies $\mathbf{v}' p'$ as the energy flux for acoustic waves, whose convergence affects a local time change to the wave energy per volume. In this manner we have established the budget equations for acoustic energy, as summarized by⁷

$$\partial_t(\rho_e \mathcal{E}) = -\nabla \cdot \mathbf{J}_{\mathcal{E}} \quad (44.107a)$$

$$\mathcal{E} = [(c_s \rho'/\rho_e)^2 + \mathbf{v}' \cdot \mathbf{v}']/2 = [c_s^{-2} (\partial_t\Psi)^2 + \nabla\Psi \cdot \nabla\Psi]/2 \quad (44.107b)$$

$$\mathbf{J}_{\mathcal{E}} = \mathbf{v}' p' = -\rho_e \partial_t\Psi \nabla\Psi. \quad (44.107c)$$

Finally, for an acoustic plane wave, use of the relations (44.79) allows us to write the wave energy flux in terms of the wave energy density

$$\mathbf{J}_{\mathcal{E}} = \mathbf{v}' p' = \mathbf{v}' (\rho_e c_s \mathbf{v}' \cdot \hat{\mathbf{k}}) = c_s \rho_e (\mathbf{v}' \cdot \hat{\mathbf{k}})^2 \hat{\mathbf{k}} = c_s \rho_e \mathcal{E} \hat{\mathbf{k}} = \rho_e \mathcal{E} \mathbf{c}_p \iff \text{plane wave.} \quad (44.108)$$

That is, for the acoustic plane wave, the flux of energy moves with the plane wave phase velocity. For dispersive waves, we will find that the energy flux moves with the group velocity rather than the phase velocity.

44.8 Wave momentum

The linear momentum in a fluid region, \mathcal{R} , is given by (see Section 21.2.3)

$$\mathbf{P} = \int_{\mathcal{R}} \rho \mathbf{v} dV, \quad (44.109)$$

⁷As shown following equation (44.105), the term $\rho' \mathcal{H}_e$ plays no role in energy transformations. Hence, we drop it from \mathcal{E} in equation (44.107b).

so that the linear momentum of acoustic waves is given by

$$\mathbf{P} = \int_{\mathcal{R}} (\rho_e + \rho') \mathbf{v}' dV \quad (44.110a)$$

$$= -\rho_e \int_{\mathcal{R}} \nabla \Psi dV + \int_{\mathcal{R}} \rho' \mathbf{v}' dV \quad (44.110b)$$

$$= -\rho_e \oint_{\partial\mathcal{R}} \Psi \hat{\mathbf{n}} dV + c_s^{-2} \int_{\mathcal{R}} \mathbf{J}_{\mathcal{E}} dV. \quad (44.110c)$$

If the waves are localized to a finite region, such as in a wave packet rather than a plane wave, then we can drop the boundary integral so long as the boundary of the domain extends outside the region where the packet is located. In this case, the integrated energy flux equals to the squared wave speed times the linear momentum

$$c_s^2 \mathbf{P} = \int_{\mathcal{R}} p' \mathbf{v}' dV = \int_{\mathcal{R}} \mathbf{J}_{\mathcal{E}} dV. \quad (44.111)$$

44.9 The eikonal approximation for acoustic waves

In Section 44.5.3 we developed the acoustic wave equations for linear waves propagating through a static yet inhomogeneous equilibrium state with both ρ_e and c_s functions of space. However, further analysis of acoustic waves was restricted to homogeneous equilibrium whereby ρ_e and c_s are spatially constant. In this section we introduce a mathematical formalism that provides a means to compute the amplitude of the wave function when acoustic waves are moving through an equilibrium state that is spatially inhomogeneous; i.e., waves moving through an inhomogeneous media. This formalism, when combined with ray theory from Section 43.8, allows for the study of waves moving through inhomogeneous backgrounds, which is the more common case in geophysical fluids.

To make use of the formalism we assume that the spatial variations of the inhomogeneous media are much smaller than those of the waves. To be more precise, let \mathcal{L} be the spatial scale over which the equilibrium state changes, as defined by

$$\mathcal{L}^{-1} \sim |\nabla \rho_e| / \rho_e \quad \text{spatial scale for background state changes.} \quad (44.112)$$

The formalism holds for waves whose wavelengths are much smaller than \mathcal{L}

$$\mathcal{L} \gg \Lambda / 2\pi = 1/|\mathbf{k}|. \quad (44.113)$$

Correspondingly, we assume the wavelength varies only over the large length scale, \mathcal{L} , so that

$$|\nabla \Lambda| = \Lambda / \mathcal{L} \ll 1 \quad \text{or equivalently} \quad |\nabla |\mathbf{k}|^{-1}| \ll 1. \quad (44.114)$$

In these equations, Λ is the local wavelength and \mathbf{k} is a local wavevector. We introduce these local wave properties following the discussion in Section 43.7, where we introduce the local wavevector, local angular frequency, and local phase velocity according to space and time derivatives of the phase

$$\mathbf{k}(\mathbf{x}, t) = \nabla \mathcal{P} \quad \text{and} \quad \omega(\mathbf{x}, t) = -\partial_t \mathcal{P} \quad \text{and} \quad \mathbf{c}_p = (\omega / |\mathbf{k}|) \hat{\mathbf{k}}. \quad (44.115)$$

The formalism we develop is commonly referred to as *geometric optics*, *geometric acoustics*, or more generically the *eikonal approximation*. The eikonal approximation is a particular realization of *WKB theory*, which is a powerful means to approximate solutions to differential equations

(e.g., see chapter 10 of *Bender and Orszag (1978)*). As we show, the eikonal approximation determines equations for wave propagation in a form whereby the wave amplitude follows *rays* that are integral lines of the group velocity. In Section 43.8 we developed a formalism for how the wavevector and angular frequency evolve when following a ray. Here we further that formalism by considering the wave amplitude, with a particular focus on acoustic waves.

44.9.1 Scalar potential for density-weighted velocity

Before developing the eikonal approximation for acoustic waves, we return to the derivation of the acoustic wave equation in Sections 44.5.3 and 44.5.4 to generalize the velocity potential, here taking into account the nonconstant equilibrium density. Again, the linearized Euler equation (44.53), its curl, and the linearized continuity equation (44.54) are given by

$$\partial_t(\rho_e \mathbf{v}') = -\nabla p' \quad \text{and} \quad \partial_t[\nabla \times (\rho_e \mathbf{v}')] = 0 \quad \text{and} \quad \partial_t p' + \rho_e c_s^2 \nabla \cdot \mathbf{v}' = 0. \quad (44.116)$$

Assuming a vanishing initial curl, $\nabla \times (\rho_e \mathbf{v}') = 0$, as appropriate for a static initial condition, allows us to focus on fluctuations that satisfy $\nabla \times (\rho_e \mathbf{v}') = 0$ for all time. We are thus led to introduce a scalar potential for the density-weighted velocity

$$\rho_e \mathbf{v}' = -\nabla \chi, \quad (44.117)$$

with χ having dimensions of density times squared length per time (compare to the velocity potential ψ in equation (44.60)). Use of χ in the linearized Euler equation (first of equation (44.116)) leads to

$$\nabla(\partial_t \chi - p') = 0. \quad (44.118)$$

Following the procedure from Section 44.5.4, we choose a gauge so that

$$p' = \partial_t \chi. \quad (44.119)$$

Using this expression for the pressure in the linearized continuity equation (third of equation (44.116)) renders the wave equation for the velocity potential

$$\frac{1}{\rho_e c_s^2} \frac{\partial^2 \chi}{\partial t^2} - \nabla \cdot (\rho_e^{-1} \nabla \chi) = 0. \quad (44.120)$$

Once we have determined χ using the eikonal approximation, the pressure field is determined by taking the time derivative in equation (44.119), and the velocity is determined by taking the gradient according to equation (44.117).

44.9.2 Energetics in brief

We studied the energetics of acoustic waves in Section 44.7. Here we provide a terse version of that discussion starting from the wave equation (44.120) and deriving the corresponding energy equation. Multiplying equation (44.120) by $\partial_t \chi$, and recalling that ρ_e and c_s are static brings the first term to

$$[\rho_e c_s^2]^{-1} \partial_t \chi \partial_{tt} \chi = [2 \rho_e c_s^2]^{-1} \partial_t (\partial_t \chi \partial_t \chi), \quad (44.121)$$

whereas the second term in equation (44.120) gives

$$-\partial_t \chi \nabla \cdot (\rho_e^{-1} \nabla \chi) = -\nabla \cdot (\rho_e^{-1} \partial_t \chi \nabla \chi) + \partial_t (\rho_e^{-1} \nabla \chi \cdot \nabla \chi)/2. \quad (44.122)$$

We are thus led to the energy conservation law

$$(1/2) \partial_t [(\rho_e c_s^2)^{-1} (\partial_t \chi)^2 + \rho_e^{-1} (\nabla \chi)^2] = \nabla \cdot (\rho_e^{-1} \partial_t \chi \nabla \chi), \quad (44.123)$$

which compares directly to the energy equation (44.106a) derived for fluctuations around a homogeneous equilibrium state.

44.9.3 Notation used to develop the formalism

We find it useful to introduce the following notation

$$W = (\rho_e c_s^2)^{-1} \quad \text{and} \quad C = c_s, \quad (44.124)$$

so that the wave equation (44.120) is written

$$W \frac{\partial^2 \chi}{\partial t^2} - \nabla \cdot (W C^2 \nabla \chi) = 0. \quad (44.125)$$

Likewise, the energy equation (44.123) takes on the form

$$(1/2) \partial_t [W (\partial_t \chi)^2 + W C^2 (\nabla \chi)^2] = \nabla \cdot (W C^2 \partial_t \chi \nabla \chi). \quad (44.126)$$

As we will see, the local dispersion relation is independent of the weighting function, W , thus motivating the chosen definition. As one final piece of notation, we write the energy equation using the shorthand

$$\partial_t \mathcal{U} + \nabla \cdot \mathbf{F} = 0 \quad (44.127)$$

where the energy density and energy flux are

$$\mathcal{U} = W [(\partial_t \chi)^2 + C^2 (\nabla \chi)^2]/2 \quad \text{and} \quad \mathbf{F} = -W C^2 \partial_t \chi \nabla \chi. \quad (44.128)$$

44.9.4 Slowly varying amplitude and rapidly varying phase

The eikonal approximation is based on the hypothesis that waves moving through gently varying inhomogeneous media are locally close to the plane wave form realized for homogeneous media. Rather than the traveling plane wave ansatz (43.16) used for homogeneous media, we consider the more general wave function

$$\chi(\mathbf{x}, t) = \operatorname{Re}[A(\mathbf{x}, t) e^{i \mathcal{P}(\mathbf{x}, t)}] = A(\mathbf{x}, t) \cos[\mathcal{P}(\mathbf{x}, t)], \quad (44.129)$$

where A is a real amplitude and \mathcal{P} is the phase. We assume that spatial variations of the wave amplitude scale according to the length scale, \mathcal{L} , defined in equation (44.113)

$$|\nabla A|/A \sim \mathcal{L}^{-1} \sim |\nabla \rho_e|/\rho_e. \quad (44.130)$$

The complement assumption is that the phase function varies over a length scale that is much smaller than \mathcal{L} , so that the local wave number satisfies equation (44.113), here written as

$$|\nabla \mathcal{P}| \gg \mathcal{L}^{-1} \implies \frac{1/|\nabla \mathcal{P}|}{\mathcal{L}} \ll 1. \quad (44.131)$$

Combined with the definition (44.130), the eikonal approximation considers a wave amplitude and wave phase that satisfy

$$|\nabla A|/A \ll |\nabla \mathcal{P}|. \quad (44.132)$$

In developing the asymptotic equations for the eikonal approximation, it can be useful to scale the phase by a small non-dimensional parameter, ϵ , in which case

$$\mathcal{P} = \varphi/\epsilon \quad \text{where} \quad |\nabla A|/A \sim |\nabla \varphi|, \quad (44.133)$$

and equation (44.132) then takes on the form

$$|\nabla A|/A \ll |\nabla \varphi|/\epsilon. \quad (44.134)$$

An equivalent means to organize similarly scaled terms is to write the wave function (44.129) in the form

$$\chi = A e^{i\mathcal{P}/\sigma}, \quad (44.135)$$

where $\sigma = 1$ is a bookkeeping parameter. We make use of the bookkeeping approach in the following.

44.9.5 The eikonal equations

We now plug in the ansatz (44.135) to the wave equation (44.125) to develop the eikonal equations that determine how the amplitude and phase evolve. The manipulations are straightforward but somewhat tedious. We expose sufficient details to facilitate checking the maths.

The derivatives

The derivatives are given by the following expressions, organized according to powers of σ :

$$e^{-i\mathcal{P}/\sigma} \nabla \chi = (i/\sigma) A \nabla \mathcal{P} + \nabla A \quad (44.136a)$$

$$e^{-i\mathcal{P}/\sigma} \nabla^2 \chi = -\sigma^{-2} A (\nabla \mathcal{P})^2 + (i/\sigma) (2 \nabla A \cdot \nabla \mathcal{P} + A \nabla^2 \mathcal{P}) + \nabla^2 A \quad (44.136b)$$

$$e^{-i\mathcal{P}/\sigma} \partial_{tt} \chi = -\sigma^{-2} A (\partial_t \mathcal{P})^2 + (i/\sigma) (2 \partial_t A \partial_t \mathcal{P} + A \partial_{tt} \mathcal{P}) + \partial_{tt} A. \quad (44.136c)$$

$\mathcal{O}(\sigma^{-2})$ terms

We balance terms according to powers of σ , with the $\mathcal{O}(\sigma^{-2})$ terms rendering

$$(\partial_t \mathcal{P})^2 = C^2 \nabla \mathcal{P} \cdot \mathcal{P} \implies \omega^2 = C^2 |\mathbf{k}|^2. \quad (44.137)$$

This local dispersion relation is the same as the dispersion relation (44.72) holding for acoustic waves moving in a homogeneous media. Now, however, the angular frequency, wave speed, and wavenumber are each functions of the spatial position. This result accords with our original hypothesis that waves move through the inhomogeneous media with a local plane wave behavior.

$\mathcal{O}(\sigma^{-1})$ terms

The $\mathcal{O}(\sigma^{-1})$ balance to yields

$$W (2 \partial_t A \partial_t \mathcal{P} + A \partial_{tt} \mathcal{P}) = W C^2 (2 \nabla A \cdot \nabla \mathcal{P} + A \nabla^2 \mathcal{P}) + A \nabla \mathcal{P} \cdot \nabla (W C^2), \quad (44.138)$$

which can be rearranged to the form

$$(\partial_t + \mathbf{c}_p \cdot \nabla) A = -\frac{A}{2 W \omega} [\partial_t (W \omega) + \nabla \cdot (\mathbf{k} W C^2)]. \quad (44.139)$$

The left hand side is the time derivative of the amplitude computed by following the phase velocity,

$$\mathbf{c}_p = C \hat{\mathbf{k}} = (\omega/|\mathbf{k}|) \hat{\mathbf{k}}. \quad (44.140)$$

The right hand side is a source term that contributes to the amplitude change following the phase velocity.

Time derivative following a ray

For dispersive waves, it is the group velocity that appears in the amplitude time derivative in equation (44.139), with the group and phase velocities identical for the acoustic waves considered here, $\mathbf{c}_g = \mathbf{c}_p$. Inspired by our treatment of material time derivative following a fluid particle (see Section 14.6), we introduce a time derivative following the group velocity

$$\frac{D_g}{Dt} = \frac{\partial}{\partial t} + \mathbf{c}_g \cdot \nabla, \quad (44.141)$$

and we refer to D_g/Dt as the *group time derivative*. We already encountered this time derivative in Section 43.8 when developing the ray equations, with rays defined by trajectories following the group velocity. In this manner, the amplitude equation (44.139) takes on the form

$$\frac{1}{A} \frac{D_g A}{Dt} = -\frac{1}{2W\omega} [\partial_t(W\omega) + \nabla \cdot (W\mathbf{k}C^2)]. \quad (44.142)$$

Sources acting to alter the wave amplitude

In Section 43.8.3 we determined that the local angular frequency is time independent when waves are moving through a static base state (equation (43.115)). Hence, for a time independent base state, the amplitude source term is static, $\partial_t(W\omega) = 0$. Furthermore, use of the definitions (44.124) and the local dispersion relation (44.137) leads to the amplitude source term

$$-1/(2W\omega) \nabla \cdot (\mathbf{k}W C^2) = -(\rho_e/(2|\mathbf{k}|)) \nabla \cdot (\mathbf{k}/\rho_e), \quad (44.143a)$$

thus bringing the amplitude equation (44.139) to the form

$$\frac{1}{A} \frac{D_g A}{Dt} = -\frac{\rho_e c_s}{2|\mathbf{k}|} \nabla \cdot (\mathbf{k}/\rho_e) = \frac{c_s}{2} \left[\hat{\mathbf{k}} \cdot \frac{\nabla \rho_e}{\rho_e} - \frac{\nabla \cdot \mathbf{k}}{|\mathbf{k}|} \right]. \quad (44.144)$$

The term $\hat{\mathbf{k}} \cdot \nabla \rho_e$ is the gradient of the density computed along the wavevector direction, whereas $\nabla \cdot \mathbf{k}$ is the divergence of the wavevector. Each of these terms contribute to changes in the acoustic wave amplitude following a ray.

44.9.6 Further study

Our treatment in this section followed that given in Section 7.3 of [Thorne and Blandford \(2017\)](#). However, we limited attention to the case of a static equilibrium state since we only developed the physics for acoustic waves moving in a static inhomogenous equilibrium media (Section 44.5.2). [Pierce \(1990\)](#) considers the more general case with a space and time dependent equilibrium, in which the acoustic wave equation contains further terms. A thorough and mathematically complete presentation of WKB theory is given by chapter 10 of [Bender and Orszag \(1978\)](#).

We consider an example in Section 45.5.8 of a shallow water gravity wave moving into a region with decreasing depth. That example illustrates how the angular frequency remains constant and

yet the wavenumber increases towards the shore.



44.10 Exercises

EXERCISE 44.1: ACOUSTIC MODES IN RECTANGULAR CAVITY (PROBLEM 9.1 OF *Fetter and Walecka (2003)*)

A rectangular cavity with dimensions $x \in [0, L_x]$, $y \in [0, L_y]$, and $z \in [0, L_z]$ is bounded by rigid material walls on all sides. The fluid is homogeneous within the cavity. Determine the eigenfrequencies and eigenfunctions for the acoustic normal modes in this cavity.

Hint: this exercise requires solving the acoustic wave equation in a closed domain with associated kinematic boundary conditions. The resulting acoustic modes are standing waves rather than traveling waves, and the wavenumbers are quantized rather than continuous.

EXERCISE 44.2: PRESSURE FLUCTUATIONS RELATIVE TO A UNIFORM FLOW (PROBLEM 9.4 OF *Fetter and Walecka (2003)*)

Consider a homogeneous and compressible fluid with uniform flow, \mathbf{v} . Show that the pressure fluctuations relative to this fluid flow state satisfy

$$(\partial_t + \mathbf{v} \cdot \nabla)^2 p - c_s^2 \nabla^2 p = 0. \quad (44.145)$$

Hint: this solution is a one-liner that results from linearizing equation (44.49) with a nonzero background flow.

EXERCISE 44.3: DERIVING THE AMPLITUDE EQUATION

Fill in the details for deriving equation (44.144) for the wave amplitude for an acoustic wave moving through an inhomogeneous media. Start from equation (44.138) and make use of any relevant identities presented in earlier equations.



Chapter 45

SURFACE WAVES

In this chapter we consider a homogeneous (constant density) ocean with an upper surface that is a material interface separating the liquid ocean from the gaseous atmosphere. The study of moving constant density fluids is often referred to as *hydrodynamics*. Although geophysical fluids generally have density variations, we develop physical insights into waves on the upper surface interface by focusing on the constant density fluid.

There are two restoring forces studied here that affect motion: one arising from gravitation and another from surface tension. For small amplitude motions around a steady state, the waves associated with these forces are known as *surface gravity waves* and *capillary waves*, respectively. By ignoring planetary rotation we tacitly focus on ocean surface waves whose lateral extent is too short to be affected by the planetary Coriolis acceleration. That is, we are concerned with surface ocean waves that can be visually observed from a boat or the shore. Furthermore, the surface waves we study do not carry vorticity and so we make use of irrotational fluid mechanics. In this case, the fluid velocity can be written as the gradient of a scalar potential, thus leading to the term *potential flow*.

Surface gravity waves are transverse in the horizontal and yet have a vertical velocity that goes to zero with depth. This structure to the wave leads to a general class of fluid particle motion known as *Stokes drift*. So although the surface gravity waves are linear, the depth decay in their amplitude leads to a net drift of fluid particles and hence to the transport of matter. Stokes drift provides an example of how averaging at a fixed point in space (Eulerian average) yields distinct behaviors from averaging on a fixed fluid particle (Lagrangian average).¹

READER'S GUIDE TO THIS CHAPTER

We make use of dynamical ideas from Chapter 21, elements of the filtered equations from Chapter 24, and salient features of wave kinematics from Chapter 43. The study of capillary waves requires an understanding of surface tension in Section 22.11. We also make use of ideas from partial differential equations introduced in Chapter 3. The mathematical description of Stokes drift requires an understanding of Eulerian and Lagrangian kinematic descriptions from Chapter 14. Generalizations of Stokes drift appear in Chapter 62 in our study of wave-mean flow interactions, isopycnal averaging, and the corresponding eddy-induced tracer transport.

45.1 Loose threads	1162
45.2 Irrotational and non-divergent flow	1163

¹Certain treatments of linear waves suggests that they affect a zero drift of matter. That notion is incorrect, with Stokes drift of material a fundamental feature of many linear waves. As noted in Section 45.8.5, although the waves considered in this chapter are linear, the Lagrangian kinematics of particle trajectories introduces nonlinearities that lead to Stokes drift.

45.2.1	Motivating the irrotational assumption	1163
45.2.2	Harmonic scalar potential	1164
45.2.3	Equation of motion and Bernoulli's principle	1165
45.2.4	Concerning the pressure field	1166
45.2.5	Bernoulli equation of motion and boundary conditions	1167
45.2.6	Energetic balances	1168
45.2.7	Special features of the kinetic energy	1169
45.2.8	Comments	1170
45.3	Linearized dynamics	1170
45.3.1	Linear relations between the velocity potential and pressure	1170
45.3.2	Dynamic boundary condition at the free surface	1170
45.3.3	Kinematic boundary conditions	1171
45.3.4	Summary of the linear equations	1171
45.4	Energetics for the linearized equations	1172
45.4.1	Kinetic energy	1173
45.4.2	Gravitational potential and available potential energies	1173
45.4.3	Energetics for the depth integrated linear flow	1174
45.4.4	Equipartition for the phase averaged energies	1175
45.5	Traveling gravity waves in a flat domain	1175
45.5.1	Horizontally traveling plane wave	1175
45.5.2	Domain integrated mechanical energy of a traveling wave	1177
45.5.3	Dispersion relation	1177
45.5.4	Alternative forms for velocity potential and velocity	1178
45.5.5	Phase speed, group velocity, and angular frequency	1178
45.5.6	Depth integrated mechanical energy of a traveling plane wave	1179
45.5.7	Qualitative features of deep water waves	1181
45.5.8	Qualitative features of shallow water waves	1182
45.5.9	Further study	1182
45.6	Standing gravity waves in a closed basin	1182
45.6.1	Solution for the standing waves	1183
45.6.2	Comments	1184
45.6.3	Further study	1184
45.7	Capillary-gravity waves	1184
45.7.1	Pressure jump across the air-sea surface	1184
45.7.2	Dynamic boundary condition with surface tension	1185
45.7.3	Dispersion relation for capillary-gravity waves	1185
45.7.4	Deep Water capillary-gravity waves	1185
45.7.5	Comments and further study	1187
45.8	Particle trajectories and Stokes drift	1187
45.8.1	General formulation of Stokes drift	1187
45.8.2	Particle trajectories in a homogeneous wave	1189
45.8.3	Stokes drift from an inhomogeneous wave	1190
45.8.4	Stokes drift for surface gravity waves	1192
45.8.5	Comments and further study	1194
45.9	Exercises	1195

45.1 Loose threads

- Double check the derivation of the Stokes drift for gravity waves given by equation (45.166).
- Figures, including seiches from Chapter 10 of *Neumann and Pierson (1966)*
- Wave action equations for surface wave models

- Section 55 of [Fetter and Walecka \(2003\)](#) on the initial value problem and method of stationary phase.
- Problems 10.8, 10.10, 10.14 of [Fetter and Walecka \(2003\)](#).
- Wave action and geometric wave mechanics for a better treatment of waves with a sloping bottom. Follow Section 7.3.3 of [Thorne and Blandford \(2017\)](#) and Salmon's notes.
- Solitons as in Section 56 of [Fetter and Walecka \(2003\)](#).

45.2 Irrotational and non-divergent flow

Throughout this chapter we assume the fluid is inviscid with constant density and with a flow that has zero vorticity.² These assumptions greatly simplify the expression for the velocity field, which is both non-divergent and irrotational. They also mean the energy to just that associated with mechanical energy. In this section we establish some general results for a perfect homogeneous fluid with a velocity that is non-divergent and irrotational. These results hold for the full nonlinear equation set and are of use later when linearizing the equations to study surface gravity waves and capillary waves.

We place no restrictions on the domain in this section, whereas when later studying linear wave motions we assume the bottom is flat with either doubly periodic or with vertical walls for the lateral boundaries. We depict the flat bottom case in Figure 45.1, showing the material free upper ocean surface at $z = \eta(x, y, t)$ separating a homogeneous ocean from a homogeneous atmosphere. The mass of the atmosphere is assumed to be horizontally uniform and static so that atmospheric pressure does not contribute to oceanic motion. The ocean boundaries are material so that the mass of the ocean (equal to the ocean volume times the constant density, ρ) is fixed. Consequently, the domain integral of the free surface is constant,

$$\int \eta \, dx \, dy = \int \eta \, dA = \text{constant}. \quad (45.1)$$

45.2.1 Motivating the irrotational assumption

We are familiar with the non-divergent flow assumption, which is part of the Boussinesq ocean studied in Chapter 26. However, we find it necessary to justify the assumption of irrotational flow, which is not commonly made when studying geophysical fluid flows. For this purpose, consider the equation of motion for a perfect non-rotating homogeneous fluid in a gravity field

$$\rho D\mathbf{v}/Dt = -\nabla p - \rho \nabla \Phi, \quad (45.2)$$

where we assume the simple form of the geopotential (Section 11.11.4),

$$\Phi = g z, \quad (45.3)$$

with g the constant and uniform gravitational acceleration. As in our discussion of the Boussinesq ocean in Section 26.1.1, we remove the static background pressure by writing

$$p = -g \rho z + p_d = -\rho \Phi + p_d, \quad (45.4)$$

²A more general approach can be considered in which the flow is decomposed into a potential flow (irrotational) and a vortical flow. However, for linear fluctuations these two flows are uncoupled. As we are unconcerned with vortical flow in this chapter, we set the vorticity to zero and thus focus on the potential flow.

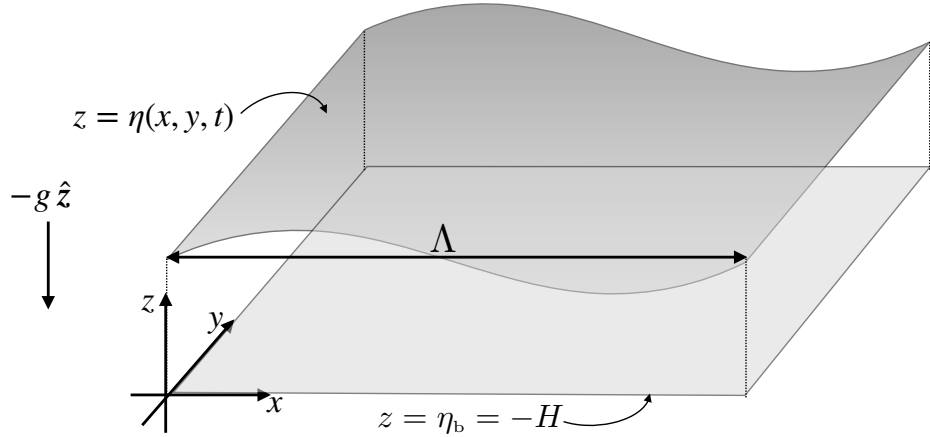


FIGURE 45.1: A depiction of the ocean as a homogeneous (i.e., constant density) fluid with an upper free surface that is a moving material interface. The atmosphere applies a pressure to the ocean due to its mass; however, that mass is assumed to be uniform and static so that it does not affect surface motion. Linear fluctuations of the free surface exhibit gravity wave motion due to the restoring effects from a uniform gravitational field, $\mathbf{g} = -g\hat{\mathbf{z}}$, as well as capillary waves due to surface tension. We here depict a single wave with wavelength, Λ , with the wavevector parallel to the $\hat{\mathbf{x}}$ direction. Our formulation of surface waves makes no restrictions on the depth of the fluid relative to the wavelength of the waves, so long as the depth is a uniform constant. We assume the ocean retains a fixed volume so that the domain integral of the free surface is constant, $\int \eta dx dy = \text{constant}$. This property follows from the assumption that the free surface is material.

in which case the velocity equation (45.2) becomes

$$\rho D\mathbf{v}/Dt = -\nabla p_d. \quad (45.5)$$

When studying linear waves later in this chapter, this equation is linearized by dropping self-advection so that

$$\rho \partial_t \mathbf{v} = -\nabla p_d. \quad (45.6)$$

The pressure gradient cannot impart any vorticity to the velocity time tendency since $\nabla \times \nabla p_d = 0$. Evidently, if the velocity is initialized with zero vorticity, then the linearized equations of motion retain that zero vorticity. We thus examine linear fluctuations around a zero vorticity rest state.

This result offers motivation for studying properties of fluid flow with an irrotational velocity. In the remainder of this section we establish some general results for a perfect, non-rotating, homogeneous fluid in a gravity field with an irrotational velocity. These results hold for the full nonlinear equations of motion and will later be specialized to the linear equations.

45.2.2 Harmonic scalar potential

A velocity field that has zero vorticity

$$\boldsymbol{\omega} = \nabla \times \mathbf{v} = 0, \quad (45.7)$$

can be written as the gradient of a scalar potential (see Section 2.3.2)³

$$\mathbf{v} = -\nabla \psi. \quad (45.8)$$

The scalar potential is unspecified up to an arbitrary function of time. The reason for this arbitrariness is that ψ and $\psi + F(t)$ yield the same velocity field, where $F(t)$ is any spatially

³The minus sign in equation (45.8) is conventional.

constant function of time. We make use of this *gauge* degree of freedom in Section 45.2.3, just like we did for acoustic waves in Section 44.5.4.

Since the fluid is assumed to have uniform density, mass conservation in the form of the continuity equation (16.16) implies that the velocity field is non-divergent. Consequently, the scalar potential satisfies Laplace's equation (Section 2.3.3)

$$\nabla \cdot \mathbf{v} = -\nabla \cdot \nabla \psi = -\nabla^2 \psi = 0, \quad (45.9)$$

in which we say that ψ is a *harmonic function*. We develop salient mathematical properties for harmonic functions in Section 3.5.

Harmonic functions do not support spatial oscillations in all three directions since the sum of the curvature in each direction (i.e., second partial derivatives) must vanish. Correspondingly, we will find that the velocity potential supports traveling waves in the horizontal and exponentially decaying in the vertical, with decay when moving away from the surface boundary. It is remarkable that the wavenumber of the horizontally traveling waves also determines the vertical decay scale. That is, the structure of the horizontal waves directly determines the vertical structure.

45.2.3 Equation of motion and Bernoulli's principle

To fully specify the scalar potential requires boundary conditions, which enter the development via the equation of motion. The vector-invariant equation of motion (21.32) for a non-rotating, irrotational, inviscid, uniform density fluid is given by

$$\partial_t \mathbf{v} = -\nabla(\Phi + \mathcal{K} + p/\rho), \quad (45.10)$$

with

$$\mathcal{K} = \mathbf{v} \cdot \mathbf{v}/2 \quad (45.11)$$

the kinetic energy per mass of a fluid element. Inserting the scalar potential, $\mathbf{v} = -\nabla\psi$, brings the equation of motion (45.10) to the form

$$\nabla(\Phi + \mathcal{K} + p/\rho - \partial_t \psi) = 0. \quad (45.12)$$

This equation means that everywhere in the fluid the dynamical fields satisfy

$$\Phi + \mathcal{K} + p/\rho - \partial_t \psi = C(t), \quad (45.13)$$

for some arbitrary time dependent function, $C(t)$. This equation is a particular expression of Bernoulli's theorem studied in Section 23.7.3.

We ascribe no physical significance to the arbitrary function, $C(t)$, appearing in equation (45.13). In fact, it can be completely removed by exploiting the gauge degree of freedom in the scalar potential as noted following equation (45.8). We do so by introducing a modified scalar potential

$$\Psi(\mathbf{x}, t) = \psi(\mathbf{x}, t) + \int_0^t C(t') dt'. \quad (45.14)$$

Both ψ and Ψ lead to the same velocity vector

$$\mathbf{v} = -\nabla\psi = -\nabla\Psi, \quad (45.15)$$

and as such the two scalar potentials are physically indistinguishable. However, Ψ is more convenient for our use since it absorbs the arbitrary time dependent function, $C(t)$, thus rendering the

simpler expression for the equation of motion

$$\partial_t \Psi = \Phi + \mathcal{K} + p/\rho. \quad (45.16)$$

In this manner we have dispensed with the need to compute $C(t)$ since it is sufficient to work with Ψ . In the following, we refer to equation (45.16) as the *Bernoulli equation of motion*.

45.2.4 Concerning the pressure field

We here explore facets of the pressure field as decomposed into either its hydrostatic and non-hydrostatic components, or its dynamically active and inactive components.

Two methods for decomposing pressure

In Section 45.2.1 we decomposed the pressure into its dynamically inactive component, $-\rho g z$, and dynamically active component, p_d . We can consider the alternative decomposition into hydrostatic and non-hydrostatic pressure components. As we will see, the dynamically active pressure is partly hydrostatic, due to motion of the free surface, and partly non-hydrostatic. We also considered these two decompositions of pressure when discussing effective buoyancy in Section 27.7, yet the discussion here is far simpler since the fluid has constant density.

Hydrostatic and non-hydrostatic pressures

The Bernoulli equation of motion (45.16) yields the vertical derivative of pressure

$$\partial_z p = -\rho \partial_z \Phi + \rho \partial_z (\partial_t \Psi - \mathcal{K}) = \partial_z p_h + \partial_z p_{nh}. \quad (45.17)$$

We here identified two contributions to the pressure. The hydrostatic pressure that satisfies

$$\partial_z p_h = -\rho \partial_z \Phi = -\rho g \implies p_h = -\rho g (z - \eta) = -\rho \Phi + \rho g \eta. \quad (45.18)$$

This expression reveals that part of the hydrostatic pressure is the dynamically inactive pressure, $-\rho \Phi = -\rho g z$, as discussed in Section 45.2.1, plus a dynamically active portion due to undulations of the free surface. The non-hydrostatic pressure has a vertical derivative given by

$$\partial_z p_{nh} = \rho \partial_z (\partial_t \Psi - \mathcal{K}). \quad (45.19)$$

Note that plugging in the hydrostatic pressure (45.18) into the Bernoulli equation of motion (45.16) leads to

$$\partial_t \Psi = \mathcal{K} + g \eta + p_{nh}/\rho, \quad (45.20)$$

whose vertical derivative yields equation (45.19) (recall $\eta = \eta(x, y, t)$ is depth independent).

Equation (45.19) indicates that depth variations in the kinetic energy and depth-time variations in the velocity potential lead the pressure to deviate from locally hydrostatic. We do not generally expect the flow to be hydrostatically balanced for two reasons: (i) the fluid layer has a uniform density so there is no stratification to suppress vertical accelerations that contribute to non-hydrostatic pressures; (ii) the fluid is nonrotating and so there is no vertical stiffening via the Taylor-Proudman result (Section 28.5.3), with vertical stiffening acting to suppress vertical accelerations that cause deviations from hydrostatic balance. Casual observations the surface ocean waves also supports the nontrivial vertical accelerations present in surface gravity waves, thus suggesting a key role for the non-hydrostatic pressure.

Comments on a hydrostatic shallow water layer

For the shallow water model we also consider a homogenous density layer. However, as emphasized in Chapter 32, the hydrostatic balance is fundamental to shallow water dynamics. Indeed, in Section 32.2 we see that the hydrostatic balance over a single homogeneous layer leads to horizontal motion that is depth independent throughout the layer. Hence, $\partial_z(\partial_t \Psi) = 0$ and the kinetic energy contained in the horizontal flow is depth independent, $\partial_z(u^2 + v^2) = 0$. Furthermore, the vertical motion has a linear depth dependence across the shallow water layer (Section 32.2.8) and its magnitude is far smaller than horizontal motions. Therefore, we can drop all contributions to $\partial_z \mathcal{K}$ for the shallow water layer, in which case equation (45.17) reduces to the hydrostatic limit

$$\partial_z p = -\rho \partial_z \Phi = -\rho g \quad \text{hydrostatic (shallow water) limit.} \quad (45.21)$$

This limit is relevant when the horizontal scales of motion are far larger than the vertical: $L \gg H$, in which case the flow is well approximated as hydrostatic.

So in summary, a homogeneous layer of fluid can have a depth dependence to its horizontal flow, and that depth dependence is driven through non-hydrostatic pressure forces. In contrast, hydrostatic pressure has a depth-independent horizontal gradient within a homogeneous layer

$$\partial_z (\nabla_z p_h) = -g \nabla_z \rho = 0 \quad \text{homogeneous density layer.} \quad (45.22)$$

Consequently, a hydrostatic pressure cannot drive depth dependence to the horizontal velocity field in a homogeneous fluid.

45.2.5 Bernoulli equation of motion and boundary conditions

Decompositions of the pressure discussed in Sections 45.2.1 and 45.2.4 render the following equivalent expressions for the Bernoulli equation of motion

$$\partial_t \Psi = \mathcal{K} + g z + p/\rho \quad \text{full pressure form} \quad (45.23a)$$

$$\partial_t \Psi = \mathcal{K} + p_d/\rho \quad \text{dynamically active/inactive pressure split} \quad (45.23b)$$

$$\partial_t \Psi = \mathcal{K} + g \eta + p_{nh}/\rho \quad \text{hydrostatic/non-hydrostatic pressure split,} \quad (45.23c)$$

and the corresponding velocity equations

$$\partial_t \mathbf{v} = -\nabla(\mathcal{K} + g z + p/\rho) \quad \text{full pressure form} \quad (45.24a)$$

$$\partial_t \mathbf{v} = -\nabla(\mathcal{K} + p_d/\rho) \quad \text{dynamically active/inactive pressure split} \quad (45.24b)$$

$$\partial_t \mathbf{v} = -\nabla(\mathcal{K} + g \eta + p_{nh}/\rho) \quad \text{hydrostatic/non-hydrostatic pressure split.} \quad (45.24c)$$

At the ocean surface we assume zero atmospheric pressure,⁴ in which case the ocean pressure must also vanish there. We are thus led to the following pressure boundary conditions

$$p = 0 \quad \text{and} \quad p_d = g \eta \rho \quad \text{and} \quad p_{nh} = 0 \quad \text{at } z = \eta, \quad (45.25)$$

each of which leads to the surface boundary condition for the velocity potential

$$\partial_t \Psi = \mathcal{K} + g \eta \quad \text{at } z = \eta. \quad (45.26)$$

We only consider the flat bottom for the bottom boundary condition. For that case $w = 0$ at the

⁴In Section 45.3.2 we show that a constant nonzero atmospheric pressure plays no role in the physics of concern here, where the fluid density is constant.

bottom so that

$$\partial_z \Psi = 0 \quad \text{at } z = \eta_b = -H. \quad (45.27)$$

The bottom boundary condition for pressure is less simple for the general case, yet for the linearized equations we have

$$\partial_z p = -g \rho \quad \text{and} \quad \partial_z p_d = 0 \quad \text{and} \quad \partial_z p_{nh} = 0 \quad \text{at } z = \eta_b = -H. \quad (45.28)$$

45.2.6 Energetic balances

Since the fluid has a constant density, the only energy arises from mechanical energy due to motion (kinetic energy) plus the gravity field (gravitational potential energy)

$$\mathcal{E} = \mathcal{K} + \Phi = \mathbf{v} \cdot \mathbf{v}/2 + g z. \quad (45.29)$$

The internal energy is a constant and so plays no role in the energetic analysis. Also, we ignore dissipation and heat transfer so that energy is modified only through reversible processes. The energetic equations are readily computed by taking the scalar product of the velocity with the velocity tendency. We consider here the three forms of the velocity equation (45.24a)-(45.23c) and their corresponding energy equations.

Velocity equation with unsplit pressure

With $\partial_t \mathbf{v}$ written in the form of equation (45.24a) we have

$$\partial_t \mathcal{K} = -\mathbf{v} \cdot \nabla(\mathcal{K} + \Phi + p/\rho) = -\nabla \cdot [\mathbf{v} (\mathcal{K} + \Phi + p/\rho)], \quad (45.30)$$

where we used $\nabla \cdot \mathbf{v} = 0$ for the second equality. Since the geopotential has a zero Eulerian time derivative, the kinetic energy equation readily leads to the total mechanical energy equation

$$\partial_t \mathcal{E} = -\nabla \cdot [\mathbf{v} (\mathcal{E} + p/\rho)] \implies \rho D\mathcal{E}/Dt = -\nabla \cdot (\mathbf{v} p). \quad (45.31)$$

Evidently, convergence of the pressure flux, $\mathbf{v} p$, leads to a material time change in the total energy.

Dynamically active/inactive pressure split

An equivalent form of the energy equation can be found by making use of the pressure split into dynamically active and inactive components according to the velocity equation (45.24b), which yields

$$\partial_t \mathcal{K} = -\nabla[\mathbf{v} \cdot (\mathcal{K} + p_d/\rho)] \implies \rho D\mathcal{K}/Dt = -\nabla \cdot (\mathbf{v} p_d). \quad (45.32)$$

We here find that convergence of the dynamic pressure flux, $\mathbf{v} p_d$, leads to a material time change in the kinetic energy.

Hydrostatic/non-hydrostatic pressure split

We now develop the energetics with the hydrostatic/non-hydrostatic pressure decomposition (45.23c) to render

$$\partial_t \mathcal{K} = -\nabla[\mathbf{v} \cdot (\mathcal{K} + g \eta + p_{nh}/\rho)]. \quad (45.33)$$

This form only lends itself to a total energy budget written in the form

$$\partial_t \mathcal{E} = -\nabla[\mathbf{v} \cdot (\mathcal{E} + p/\rho)] \implies \rho D\mathcal{E}/Dt = -\nabla \cdot [\mathbf{v} (p_h + p_{nh})]. \quad (45.34)$$

45.2.7 Special features of the kinetic energy

The kinetic energy per mass can be written in terms of the scalar potential

$$2\mathcal{K} = \mathbf{v} \cdot \mathbf{v} = \nabla\Psi \cdot \nabla\Psi = \nabla \cdot (\Psi \nabla\Psi), \quad (45.35)$$

where we used $\nabla^2\Psi = 0$ for the final equality. This total divergence form of the kinetic energy provides its global integral with some rather special properties.

Domain integrated kinetic energy is just due to surface properties

Integration of the kinetic energy in the form of equation (45.35) over the full ocean domain, \mathcal{R} , leads to the total kinetic energy

$$E_{\text{KE}} = \int_{\mathcal{R}} \rho \mathcal{K} dV = \frac{\rho}{2} \int_{\mathcal{R}} \nabla \cdot (\Psi \nabla\Psi) dV = \frac{\rho}{2} \int_{\partial\mathcal{R}} \Psi \nabla\Psi \cdot \hat{\mathbf{n}} dS, \quad (45.36)$$

where we made use of the divergence theorem. The ocean bottom is material so that the flow satisfies the no-normal flow condition (Section 16.4.1)

$$\mathbf{v} \cdot \hat{\mathbf{n}} = -\nabla\Psi \cdot \hat{\mathbf{n}} = 0, \quad (45.37)$$

where $\hat{\mathbf{n}}$ is the outward normal on the rigid material boundaries. Lateral boundaries are either periodic or rigid material walls. We thus find the remarkable result that the domain integrated kinetic energy arises solely from properties integrated over the free surface

$$E_{\text{KE}} = \frac{\rho}{2} \int_{z=\eta} \Psi \nabla\Psi \cdot \hat{\mathbf{n}} dS = -\frac{\rho}{2} \int_{z=\eta} \Psi \mathbf{v} \cdot \hat{\mathbf{n}} dS. \quad (45.38)$$

That is, contributions from interior motion play no role in the domain integrated kinetic energy. This property is fundamentally related to the harmonic nature of the velocity potential that allows the kinetic energy to be written as the total divergence in equation (45.35). We encountered a similar feature of harmonic functions in Section 3.5.2 when studying their mean-value property.

Gauge invariance of the domain integrated kinetic energy

The kinetic energy per mass, $\mathcal{K} = \nabla\Psi \cdot \nabla\Psi/2$, is manifestly gauge invariant since it remains unchanged if Ψ is shifted by a spatial constant. This property also holds for the domain integrated kinetic energy, (45.38), as follows from use of the divergence theorem and then the non-divergence of the velocity field

$$\int_{z=\eta} \mathbf{v} \cdot \hat{\mathbf{n}} dS = \int_{\partial\mathcal{R}} \mathbf{v} \cdot \hat{\mathbf{n}} dS = \int_{\mathcal{R}} \nabla \cdot \mathbf{v} dV = 0. \quad (45.39)$$

Evidently, if the scalar potential is shifted by a spatially independent function of time, then the globally integrated kinetic energy (45.38) remains unchanged and so is gauge invariant.

A more long-winded means to derive the same result is to make use of the surface kinematic boundary condition (16.51) holding for a non-divergent flow

$$\partial_t \eta + \mathbf{u} \cdot \nabla \eta = w \quad \text{material b.c. at } z = \eta(x, y, t), \quad (45.40)$$

which can be written in the equivalent form

$$\mathbf{v} \cdot \hat{\mathbf{n}} = \frac{\partial_t \eta}{|\nabla(z - \eta)|}, \quad (45.41)$$

where the outward normal is

$$\hat{\mathbf{n}} = \frac{\nabla(z - \eta)}{|\nabla(z - \eta)|} = \frac{\hat{\mathbf{z}} - \nabla\eta}{\sqrt{1 + \nabla\eta \cdot \nabla\eta}}. \quad (45.42)$$

We also make use of the relation between the area elements on the free surface given by equation (16.76)

$$d\mathcal{S} = |\nabla(z - \eta)| dA = |\nabla(z - \eta)| dA, \quad (45.43)$$

where $dA = dx dy$ is the horizontal area element. These results then lead to the identity

$$\int \mathbf{v} \cdot \hat{\mathbf{n}} d\mathcal{S} = \int \partial_t \eta dA = - \int \nabla \cdot \mathbf{U} dA = 0, \quad (45.44)$$

where we set $\partial_t \eta = -\nabla \cdot \mathbf{U}$ as per the free surface equation (18.78) holding for a volume conserving fluid, with $\mathbf{U} = \int_{-H}^{\eta} \mathbf{u} dz$ the depth integrated horizontal velocity.⁵

45.2.8 Comments

We focus on the velocity potential in our analysis of linear surface gravity waves. A directly analogous approach focuses on the dynamic pressure, p_d , which is a harmonic function for the linearized system (take the divergence of the linearized velocity equation (45.6)). Section 7.1 of [Vallis \(2017\)](#) takes the pressure approach. The two methods are equivalent, with the velocity potential and pressure closely connected.

45.3 Linearized dynamics

We develop the boundary value problem describing linear surface gravity wave motions of the free surface, and characterize physical aspects of the waves. Surface tension is ignored here, so that pressure is continuous across the free surface.⁶

45.3.1 Linear relations between the velocity potential and pressure

The Bernoulli equations of motion (45.23a)-(45.23c) provide an expression for the time tendency of the velocity potential. When linearizing the equations we drop the contribution from the kinetic energy since it is second order in the velocity field. We are thus led to the linear relations

$$\partial_t \Psi = g z + p/\rho = p_d/\rho = g \eta + p_{nh}/\rho. \quad (45.45)$$

This equation provides the linearized relation between the velocity potential and the pressure.

45.3.2 Dynamic boundary condition at the free surface

The equation of motion (45.16) applies to any point within the fluid and at any time. In particular, it applies at the free surface, $z = \eta(x, y, t)$, where pressure equals to the atmospheric pressure. As stated earlier, we assume that the atmospheric pressure is constant in space and time so that

$$g \eta + \mathcal{K} - \partial_t \Psi = -p_a/\rho = \text{constant}. \quad (45.46)$$

⁵See also Exercise 18.8.

⁶In Section 45.7 we consider the pressure jump at the ocean surface due to surface tension. This pressure jump leads to capillary waves.

Without loss of generality we can set this constant to zero,⁷ thus leaving the boundary condition

$$g\eta + \mathcal{K} - \partial_t\Psi = 0 \quad \text{at } z = \eta. \quad (45.47)$$

We now linearize relative to a state of rest with $\eta = 0$, $\mathbf{v} = 0$, and $\partial_t\Psi = 0$. Linear fluctuations about this rest state have small velocities and as such the kinetic energy, which is second order in velocity, can be dropped to leave the linearized dynamic boundary condition

$$g\eta = \partial_t\Psi \quad \text{linearized dynamic b.c. at } z = \eta. \quad (45.48)$$

This boundary condition directly connects the free surface to time tendencies of the velocity potential. The free surface fluctuates upward when the velocity potential has a positive tendency, and vice versa. Also note that we arrive at this boundary condition by making use of the pressure boundary conditions (45.25) within equation (45.45).

45.3.3 Kinematic boundary conditions

The free surface is assumed to be a material interface, meaning that we ignore effects from matter transport across this surface. Consequently, following the discussion of kinematic boundary conditions in Section 16.4.2, we have

$$\partial_t\eta + \mathbf{u} \cdot \nabla\eta = w \quad \text{at } z = \eta. \quad (45.49)$$

Linearizing this boundary condition about the state of rest, and introducing the scalar potential, leads to

$$\partial_t\eta = w = -\partial_z\Psi \quad \text{linearized kinematic b.c. at } z = \eta. \quad (45.50)$$

This is yet another constraint that links the free surface to the velocity potential.

45.3.4 Summary of the linear equations

The boundary value problem for the velocity potential and free surface is given by

$$\mathbf{v} = -\nabla\Psi \quad \text{velocity potential} \quad (45.51a)$$

$$\nabla^2\Psi = 0 \quad \text{irrotational and non-divergent velocity for } \mathbf{x} \in \text{ocean} \quad (45.51b)$$

$$\partial_t\Psi = g\eta \quad \text{linearized dynamic b.c. at } z = \eta \quad (45.51c)$$

$$\partial_z\Psi = -\partial_t\eta \quad \text{linearized kinematic b.c. at } z = \eta \quad (45.51d)$$

$$\hat{\mathbf{n}} \cdot \nabla\Psi = 0 \quad \text{no-normal flow kinematic b.c. on rigid boundaries.} \quad (45.51e)$$

Equations (45.51a) and (45.51b) hold throughout the fluid whereas the remaining equations hold only at the boundaries.

Although the equations (45.51b)-(45.51e) were derived through linearization, there is one remaining nonlinearity needs to be removed to afford an analytical treatment. Namely, when combining the boundary conditions into a single equation we compute the time derivative of equation (45.51c) according to

$$g \frac{\partial\eta}{\partial t} = \left[\frac{\partial}{\partial t} + \frac{\partial\eta}{\partial t} \frac{\partial}{\partial z} \right] \frac{\partial\Psi}{\partial t} \quad (45.52)$$

⁷Alternatively, can use a gauge transformation $\Psi' = \Psi - t(p_a/\rho)$ to eliminate the constant.

and then combine with equation (45.51d) to render

$$\left[\frac{\partial}{\partial t} + \frac{\partial \eta}{\partial t} \frac{\partial}{\partial z} \right] \frac{\partial \Psi}{\partial t} = -g \frac{\partial \Psi}{\partial z}. \quad (45.53)$$

With $w \approx \partial \eta / \partial t$ at the free surface, we identify $(\partial \eta / \partial t) \partial_z$ as a vertical advection operator. The corresponding term $(\partial \eta / \partial t) \partial_{zt} \Psi$ is nonlinear and second order in fluctuating fields. Hence, we drop this term as part of the linearization process. An equivalent means to realize this linearization is to evaluate the free surface boundary condition at $z = 0$ rather than at $z = \eta(x, y, t)$. For this approximation to be self-consistent requires the amplitude of free surface undulations to be much smaller than the typical wavelengths of the fluctuations, in which case

$$|\eta|/\Lambda \ll 1, \quad (45.54)$$

with this condition holding for the waves considered here. In summary, the fully linearized equation set takes the form

$$\mathbf{v} = -\nabla \Psi \quad \text{velocity potential} \quad (45.55a)$$

$$\nabla^2 \Psi = 0 \quad \text{irrotational and non-divergent velocity for } \mathbf{x} \in \text{ocean} \quad (45.55b)$$

$$\partial_t \Psi = g \eta \quad \text{linearized dynamic b.c. at } z = 0 \quad (45.55c)$$

$$\partial_z \Psi = -\partial_t \eta \quad \text{linearized kinematic b.c. at } z = 0 \quad (45.55d)$$

$$\hat{\mathbf{n}} \cdot \nabla \Psi = 0 \quad \text{no-normal flow kinematic b.c. on rigid boundaries.} \quad (45.55e)$$

Observe that the surface gravity wave equation set (45.55a)-(45.55e) involves a harmonic scalar potential, Ψ , defined throughout the full fluid domain (equation (45.55b)), whereas the time tendencies are determined by the kinematic boundary condition (equation (45.55d)) and dynamic boundary condition (equation (45.55c)). Mathematically, the free surface, η , lives on a two-dimensional manifold of the surface interface, whereas the velocity potential, Ψ , lives on a three-dimensional manifold defined by the ocean domain. The velocity potential and free surface are coupled by the kinematic and dynamic boundary conditions, thus requiring the velocity potential to be determined throughout the three-dimensional ocean domain even if we might only care about fluctuations of the free surface. These features of surface gravity waves make them inherently more complex, and rich, than surface fluctuations of a membrane⁸, or the volume fluctuations of a compressible fluid (Chapter 44). The surface gravity wave system provides a canonical example of a surface boundary dynamical system, with another important example being surface quasi-geostrophy.⁹

45.4 Energetics for the linearized equations

We here specialize the energetic analysis from Section 45.2.6 to study the energetics of the linearized equations in a manner analogous to the acoustic wave energetics considered in Section 44.7.

⁸A drumhead provides the canonical example of a vibrating membrane. For determining waves moving on a drumhead, we focus exclusively on the drumhead without also considering dynamics of the surrounding fluid. See Chapter 8 of [Fetter and Walecka \(2003\)](#) for details.

⁹See [Held et al. \(1995\)](#) for a classic treatment of surface quasi-geostrophy. [Yassim \(2021\)](#) and [Yassim and Griffies \(2022\)](#) provide an further study of surface quasi-geostrophy in the context of normal mode theory.

45.4.1 Kinetic energy

For linear waves, the surface integral (45.38) for the kinetic energy is approximated as an integral over $z = 0$ with $\hat{\mathbf{n}} = \hat{z}$ and $d\mathcal{S} = dx dy = dA$, in which case the domain integrated kinetic energy is

$$E_{KE} = \frac{\rho}{2} \int_{z=0} \Psi \partial_z \Psi dA = -\frac{\rho}{2} \int_{z=0} \Psi \partial_t \eta dA = -\frac{\rho}{2} \int_{z=0} \Psi w dA, \quad (45.56)$$

where we made use of the kinematic boundary condition (45.55d). Evidently, the kinetic energy is proportional to the time tendency of the free surface. Furthermore, the integrand, $\Psi w = \Psi \partial_t \eta$, is not sign-definite, and yet its area integral is non-negative.

45.4.2 Gravitational potential and available potential energies

Measuring the zero of gravitational potential energy at $z = -H$ (see Figure 45.1), yields the domain integrated gravitational potential energy

$$g \rho \int_{z=0} \left[\int_{-H}^{\eta} z dz \right] dA = \frac{g \rho}{2} \int (\eta^2 - H^2) dA. \quad (45.57)$$

The available potential energy (see Sections 26.9 and 33.5.6) is the difference between the gravitational potential energy and that contained in an ocean at rest with $\eta = 0$, so that

$$E_{APE} = g \rho \int \left[\int_{-H}^{\eta} z dz \right] dA - g \rho \int \left[\int_{-H}^0 z dz \right] dA = \frac{g \rho}{2} \int \eta^2 dA = \frac{\rho}{2g} \int (\partial_t \Psi)^2 dA, \quad (45.58)$$

where the final step made use of the dynamic boundary condition (45.55c). Hence, a non-negative available potential energy is associated with any undulation of the free surface, whether the undulation is positive or negative.

In Section 33.5.6 we computed the available potential energy for a single layer of shallow water fluid. In that discussion we chose to set $z = 0$ at the resting free surface (Figure 32.1), whereas in the current discussion we chose $z = 0$ at the flat bottom (Figure 45.1). Even so, the available potential energy (45.58) is identical to the shallow water case, which we see by noting that the area average of η vanishes for the current choice in Figure 45.1 (due to volume conservation)

$$\bar{\eta} = \frac{1}{A_{ocn}} \int \eta dA = 0, \quad (45.59)$$

where

$$A_{ocn} = \int dA \quad (45.60)$$

is the surface area of the ocean. We thus find

$$E_{APE} = \frac{g \rho}{2} \int \eta^2 dA = \frac{g \rho}{2} \int (\eta - \bar{\eta})^2 dA = \frac{g \rho}{2} \int (\eta')^2 dA, \quad (45.61)$$

which agrees with equation (33.132) derived for the shallow water layer. We expect the two energies to agree since the gravitational energy depends only on the density and the position within the gravity field; it has no concern for dynamical assumptions such as whether the fluid motion is approximately hydrostatic (as for the shallow water model) or general (as considered here).

45.4.3 Energetics for the depth integrated linear flow

We here study the mechanical energy contained in the fluid layer within the linear theory. Notably, when computing the kinetic energy in the depth integrated flow, we only integrate to $z = 0$ since going to $z = \eta$ involves third order terms which are neglected in the linear theory. Hence, we have the time derivative of the depth integrated kinetic energy per mass

$$\frac{d}{dt} \int_{-H}^0 \mathcal{K} dz = \frac{1}{2} \frac{d}{dt} \int_{-H}^0 \nabla \Psi \cdot \nabla \Psi dz = \int_{-H}^0 \nabla(\partial_t \Psi) \cdot \nabla \Psi dz, \quad (45.62)$$

which follows since the integral bounds are static so that the time derivative commutes with the integral. We next make use of the harmonic nature of the velocity potential to write

$$\frac{d}{dt} \int_{-H}^0 \mathcal{K} dz = \int_{-H}^0 \nabla \cdot (\partial_t \Psi \nabla \Psi) dz = [\partial_t \Psi \partial_z \Psi]_{z=0} + \nabla_z \cdot \int_{-H}^0 \partial_t \Psi \nabla_z \Psi dz, \quad (45.63)$$

where we used the bottom kinematic boundary condition, $\partial_z \Psi = 0$ at $z = -H$, and noted that H is a constant so that the horizontal derivative commutes with the integral. For the boundary term we use the linearized dynamic boundary condition (45.55c) and linearized kinematic boundary condition (45.55d) to yield

$$\frac{d}{dt} \int_{-H}^0 \mathcal{K} dz = -g \eta \partial_t \eta + \nabla_z \cdot \int_{-H}^0 \partial_t \Psi \nabla_z \Psi dz. \quad (45.64)$$

We observe that the boundary term is the time tendency of the depth integrated potential energy per mass

$$\int_{-H}^{\eta} g z dz = (g/2)(\eta^2 - H^2) \Rightarrow \frac{d}{dt} \int_{-H}^{\eta} g z dz = g \eta \partial_t \eta. \quad (45.65)$$

Note how the potential energy in the column is computed by integrating all the way to the free surface, even for the linear theory. That integration limit is needed since changes in the potential energy over a column of constant density fluid arise solely through changes in the free surface. Bringing the pieces together allows us to write the time derivative of the depth integrated mechanical energy per mass in the linear theory

$$\frac{d}{dt} \left[\frac{1}{2} \int_{-H}^0 \mathbf{v} \cdot \mathbf{v} dz + \int_{-H}^{\eta} g z dz \right] = \nabla_z \cdot \int_{-H}^0 \partial_t \Psi \nabla_z \Psi dz. \quad (45.66)$$

Finally, we make use of the linear theory identity, $\partial_t \Psi = p_d / \rho$ from equation (45.45) to write

$$\frac{d}{dt} \left[\rho \int_{-H}^0 (\mathcal{K} + \Phi) dz \right] = -\nabla_z \cdot \int_{-H}^0 p_d \mathbf{u} dz. \quad (45.67)$$

Evidently, it is the horizontal convergence of the layer integrated flux of dynamical pressure, $p_d \mathbf{u}$, that affects a time change to the layer integrated mechanical energy for the linear theory. That is, we find that the layer integrated mechanical energy changes due to the work done by the dynamical pressure.

45.4.4 Equipartition for the phase averaged energies

The expression (45.58) for the available potential energy can be written

$$E_{\text{APE}} = \frac{\rho}{2} \int \eta \partial_t \Psi \, dA = \frac{\rho}{2} \int [-\Psi \partial_t \eta + \partial_t(\eta \Psi)] \, dA = E_{\text{KE}} + \frac{\rho}{2} \int \partial_t(\eta \Psi) \, dA, \quad (45.68)$$

where we made use of equation (45.56) for the total kinetic energy. If the fields exhibit periodicity in time, such as for a wave field, then integration over an integer multiple of the wave period results in an equipartition between the phase averaged available potential energy and phase averaged kinetic energy

$$\langle E_{\text{APE}} \rangle = \langle E_{\text{KE}} \rangle \quad \text{with} \quad \langle E_{\text{APE}} \rangle = \frac{\omega}{2\pi} \int_0^{2\pi/\omega} E_{\text{APE}} \, dt, \quad (45.69)$$

where $2\pi/\omega$ is the wave period. We found a similar equipartition of energy in Section 44.7.2 for acoustic waves.

45.5 Traveling gravity waves in a flat domain

We now study a traveling plane wave solution to the equations (45.55b)-(45.55e) as posed in a flat bottom domain such as illustrated in Figure 45.1. The waves are assumed to travel horizontally, with the example in Figure 45.1 showing waves in the $\pm \hat{x}$ direction. There are no lateral boundaries. The waves also contain a vertical profile that, as we shall see, exponentially decays from the surface into the interior.

Besides providing an explicit realization of surface gravity waves, our analysis offers experience with the *separation of variables* method for solving certain partial differential equations. In our analysis, we are not interested in the most general wave solution. Instead, we aim to determine a particular solution of sufficient generality to expose the underlying physics of the linear wave fluctuations, and in particular to expose the exponential decay of the wave amplitude with depth. Furthermore, given linearity, the *superposition principle* holds whereby the sum or integral of particular solutions are also solutions.

45.5.1 Horizontally traveling plane wave

We seek a traveling plane wave solution with angular frequency, $\omega > 0$, and horizontal wavevector and wave direction

$$\mathbf{k} = k_x \hat{x} + k_y \hat{y} \quad \text{and} \quad \hat{\mathbf{k}} = \mathbf{k}/|\mathbf{k}|. \quad (45.70)$$

For this purpose we assume the waves appear in the velocity potential in the shape of a cosine modulated by a vertical structure function¹⁰

$$\Psi(x, y, z, t) = \Psi_0 \Gamma(z) \cos(\mathbf{k} \cdot \mathbf{x} - \omega t). \quad (45.71)$$

Plugging this ansatz into Laplace's equation $\nabla^2 \Psi = 0$ leads to the ordinary differential equation satisfied by the non-dimensional vertical structure function

$$\frac{d^2 \Gamma}{dz^2} = |\mathbf{k}|^2 \Gamma \quad -H \leq z \leq 0 \quad (45.72a)$$

$$\frac{d\Gamma}{dz} = 0 \quad \text{at } z = -H, \quad (45.72b)$$

¹⁰We could use complex exponentials for the traveling wave, as discussed in Chapter 43. We here work with the real trigonometric functions to exemplify their use.

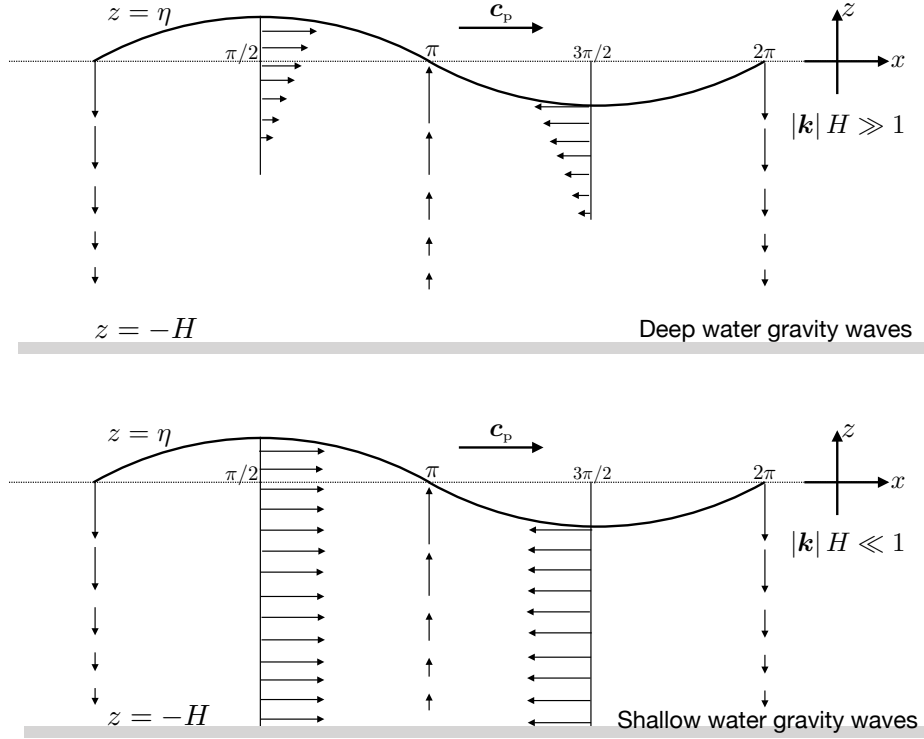


FIGURE 45.2: Snapshot of surface gravity waves over deep water (\$|k| H \gg 1\$, top panel) and shallow water (\$|k| H \ll 1\$, lower panel), with velocities computed according to equations (45.75a) and (45.75b). Shown here are the horizontal and vertical components to the velocity at a particular time instance, with the horizontal velocity in phase with the free surface undulations, and the vertical velocity \$\pi/2\$ out of phase. The horizontal axis along the top designates values for \$\mathbf{k} \cdot \mathbf{x}\$, with values of \$0, \pi/2, \pi, 3\pi/2, 2\pi\$ providing samples along the wave.

where the bottom boundary condition is required to satisfy the no-normal flow condition (45.55e). We write the solution in the form

$$\Psi = \Psi_0 \cosh[|k| (z + H)] \cos(\mathbf{k} \cdot \mathbf{x} - \omega t) \quad (45.73a)$$

$$\Psi_0 = \frac{g \eta_0 / \omega}{\cosh(|k| H)}, \quad (45.73b)$$

so that the dynamic boundary condition (45.55c) renders the free surface height

$$\eta(x, t) = \eta_0 \sin(\mathbf{k} \cdot \mathbf{x} - \omega t). \quad (45.74)$$

The corresponding fluid velocity field, \$\mathbf{v} = -\nabla\Psi\$, is given by

$$\mathbf{u} = \frac{g \eta_0 \hat{\mathbf{k}}}{C_p} \frac{\cosh[|k| (z + H)] \sin(\mathbf{k} \cdot \mathbf{x} - \omega t)}{\cosh(|k| H)} \quad (45.75a)$$

$$w = -\frac{g \eta_0}{C_p} \frac{\sinh[|k| (z + H)] \cos(\mathbf{k} \cdot \mathbf{x} - \omega t)}{\cosh(|k| H)}, \quad (45.75b)$$

where the wave phase speed is given by

$$C_p = \omega / |k| > 0. \quad (45.76)$$

Figure 45.2 depicts the horizontal and vertical velocity in a snapshot of a deep water wave

($|\mathbf{k}|H \gg 1$) and shallow water wave ($|\mathbf{k}|H \ll 1$). We emphasize the following properties of these waves.

- The horizontal fluid particle velocity, \mathbf{u} , is parallel to the horizontal wavevector, \mathbf{k} . Hence, the gravity waves are horizontally longitudinal.
- The horizontal velocity is in phase with the free surface, η , whereas they are both $\pi/2$ out of phase with the vertical velocity.
- The vertical velocity vanishes at the bottom, $z = -H$, as needed to satisfy the no-normal flow boundary condition.
- The horizontal wave number, $|\mathbf{k}|$, both determines the horizontal wavelength, $2\pi/|\mathbf{k}|$, as well as the vertical decay scale, $|\mathbf{k}|$. This coupling of the horizontal to the vertical is a notable property of surface gravity waves.
- Letting time progress at a fixed space position reveals a clockwise progression of a fluid particle, as can be imagined by letting Figure 45.2 evolve in time. Further details of fluid particle trajectories are developed in Section 45.8.
- In the shallow water limit, $|\mathbf{k}|H \ll 1$, the horizontal velocity is depth independent. The vertical velocity is a linear function of depth and it is a factor of $|\mathbf{k}|H$ times smaller in magnitude than the horizontal velocity. We provide a focused study of shallow water gravity waves in Section 48.5.

45.5.2 Domain integrated mechanical energy of a traveling wave

The domain integrated kinetic energy (45.56) contained in a traveling surface gravity wave is

$$E_{\text{KE}} = -\frac{\rho}{2} \int_{z=0} \Psi \partial_t \eta \, dA \quad (45.77\text{a})$$

$$= (\rho/2) \Psi_0 \eta_0 \omega \cosh(|\mathbf{k}|H) \int \cos^2(\mathbf{k} \cdot \mathbf{x} - \omega t) \, dA \quad (45.77\text{b})$$

$$= (\rho/2) g \eta_0^2 \int \cos^2(\mathbf{k} \cdot \mathbf{x} - \omega t) \, dA, \quad (45.77\text{c})$$

and likewise the domain integrated available potential energy (45.58) is

$$E_{\text{APE}} = (\rho/2) g \eta_0^2 \int \sin^2(\mathbf{k} \cdot \mathbf{x} - \omega t) \, dA, \quad (45.78)$$

so that their sum is a space and time constant

$$E_{\text{KE}} + E_{\text{APE}} = A_{\text{oce}} \rho g \eta_0^2 / 2, \quad (45.79)$$

where A_{oce} is the total ocean area. We also see that the phase average of the domain integrated kinetic energy and available potential energy manifest the equipartition property (45.69)

$$\langle E_{\text{APE}} \rangle = \langle E_{\text{KE}} \rangle = A_{\text{oce}} \rho g \eta_0^2 / 4. \quad (45.80)$$

45.5.3 Dispersion relation

Combining the two $z = 0$ boundary conditions (45.55c) and (45.55d) yields

$$(\partial_{tt} + g \partial_z) \Psi = 0 \quad \text{at } z = 0. \quad (45.81)$$

Substituting the traveling plane wave (45.73a) into this relation leads to the *dispersion relation*

$$\omega^2 = g |\mathbf{k}| \tanh(|\mathbf{k}| H) \implies \omega = \sqrt{g |\mathbf{k}| \tanh(|\mathbf{k}| H)}. \quad (45.82)$$

The dispersion relation constrains those values available for the radial frequency, ω , and wavenumber, $|\mathbf{k}|$. That is, the surface gravity waves only exist if their frequency and wavenumber are related according to the dispersion relation (45.82).

45.5.4 Alternative forms for velocity potential and velocity

The dispersion relation (45.82) allows for a slight rewrite of the velocity potential (45.73a) and velocity field (45.75a) and (45.75b)

$$\Psi_0 = \frac{g \eta_0}{\omega \cosh(|\mathbf{k}| H)} = \frac{\eta_0 C_p}{\sinh(|\mathbf{k}| H)} \quad (45.83a)$$

$$\Psi = \frac{g \eta_0 \cosh[|\mathbf{k}|(z + H)] \cos(\mathbf{k} \cdot \mathbf{x} - \omega t)}{\omega \cosh(|\mathbf{k}| H)} = \frac{\eta_0 C_p \cosh[|\mathbf{k}|(z + H)] \cos(\mathbf{k} \cdot \mathbf{x} - \omega t)}{\sinh(|\mathbf{k}| H)} \quad (45.83b)$$

$$\mathbf{u} = \frac{g \eta_0 \hat{\mathbf{k}}}{C_p} \frac{\cosh[|\mathbf{k}|(z + H)] \sin(\mathbf{k} \cdot \mathbf{x} - \omega t)}{\cosh(|\mathbf{k}| H)} = \frac{\eta_0 \omega \hat{\mathbf{k}} \cosh[|\mathbf{k}|(z + H)] \sin(\mathbf{k} \cdot \mathbf{x} - \omega t)}{\sinh(|\mathbf{k}| H)} \quad (45.83c)$$

$$w = -\frac{g \eta_0}{C_p} \frac{\sinh[|\mathbf{k}|(z + H)] \cos(\mathbf{k} \cdot \mathbf{x} - \omega t)}{\cosh(|\mathbf{k}| H)} = -\frac{\eta_0 \omega \sinh[|\mathbf{k}|(z + H)] \cos(\mathbf{k} \cdot \mathbf{x} - \omega t)}{\sinh(|\mathbf{k}| H)}. \quad (45.83d)$$

These alternative expressions are sometimes found in the literature.

45.5.5 Phase speed, group velocity, and angular frequency

We here characterize the phase speed, group velocity, and angular frequency for the surface gravity waves, and introduce the limits for deep water and shallow water waves.

Phase speed

The phase speed for the surface gravity wave is given by

$$C_p = \omega / |\mathbf{k}| = \sqrt{(g / |\mathbf{k}|) \tanh(|\mathbf{k}| H)}. \quad (45.84)$$

We consider the two limits: $|\mathbf{k}| H \gg 1$ are known as shortwaves or deep water waves, and $|\mathbf{k}| H \ll 1$ are known as longwaves or shallow water waves. In these two limits the phase speed is given by

$$\omega \approx \sqrt{g |\mathbf{k}|} \quad C_p \approx \sqrt{g / |\mathbf{k}|} \quad |\mathbf{k}| H \gg 1 \quad \text{shortwave/deep water} \quad (45.85a)$$

$$\omega \approx |\mathbf{k}| \sqrt{g H} \quad C_p \approx \sqrt{g H} \quad |\mathbf{k}| H \ll 1 \quad \text{longwave/shallow water.} \quad (45.85b)$$

Note that the shallow water waves are non-dispersive since the phase speed is the same for all wave numbers, $C_p \approx \sqrt{g H}$. In contrast, the deep water waves are dispersive, with the shorter waves having a smaller phase speed than longer waves.

Group velocity

The group velocity, $\mathbf{c}_g = \nabla_{\mathbf{k}}\omega$, is given by

$$\mathbf{c}_g = \frac{g \hat{\mathbf{k}}}{2\omega} \left[\frac{|\mathbf{k}|H + \cosh(|\mathbf{k}|H) \sinh(|\mathbf{k}|H)}{\cosh^2(|\mathbf{k}|H)} \right]. \quad (45.86)$$

The ratio of the group speed to the phase speed is given by

$$\frac{\hat{\mathbf{k}} \cdot \mathbf{c}_g}{C_p} = \frac{g |\mathbf{k}|^2 [|\mathbf{k}|H + \cosh(|\mathbf{k}|H) \sinh(|\mathbf{k}|H)]}{2\omega^2 \cosh^2(|\mathbf{k}|H)} = \frac{1}{2} \left[1 + \frac{2|\mathbf{k}|H}{\sinh(2|\mathbf{k}|H)} \right]. \quad (45.87)$$

The shallow water limit, with $|\mathbf{k}|H \ll 1$, has phase speed and group speed equal, whereas the deep water waves have group speed one-half the phase speed. More precisely, we find the following limiting behaviors.

$$\omega \approx \sqrt{g|\mathbf{k}|} \quad C_p \approx \sqrt{g/|\mathbf{k}|} \quad \mathbf{c}_g \approx \mathbf{c}_p/2 \quad |\mathbf{k}|H \gg 1 \quad \text{shortwave/deep water} \quad (45.88a)$$

$$\omega \approx |\mathbf{k}| \sqrt{gH} \quad C_p \approx \sqrt{gH} \quad \mathbf{c}_g \approx \mathbf{c}_p \quad |\mathbf{k}|H \ll 1 \quad \text{longwave/shallow water}. \quad (45.88b)$$

For shallow water gravity waves, the group velocity equals to the phase velocity. In contrast, for deep water gravity waves, the group velocity magnitude is one-half the phase speed. When watching a packet of deep water gravity waves, we see the phase of the carrier waves appear at the back of the packet and move forward at twice the speed of the packet, only to then disappear at the front.

Angular frequency

The deep water limit ($|\mathbf{k}|H \gg 1$) and shallow water limit $|\mathbf{k}|H \ll 1$) are set according to the wavenumber. These limits lead to a distinct frequency for the two wave. To compute the ratio of the corresponding angular frequencies, introduce two non-dimensional numbers according to

$$D_{\text{sww}} \equiv H |\mathbf{k}|_{\text{sww}} \ll 1 \quad \text{and} \quad D_{\text{dww}} \equiv H |\mathbf{k}|_{\text{dww}} \gg 1, \quad (45.89)$$

in which case we have

$$\frac{\omega_{\text{dww}}^2}{\omega_{\text{sww}}^2} = \frac{g |\mathbf{k}|_{\text{dww}}}{|\mathbf{k}|_{\text{sww}}^2 c_{\text{grav}}^2} = \frac{g H^{-1} D_{\text{dww}}}{D_{\text{sww}}^2 H^{-2} g H} = \frac{D_{\text{dww}}}{D_{\text{sww}}^2} \gg 1. \quad (45.90)$$

We conclude that motion of those short gravity waves whose extent is largely confined to the upper ocean (deep water waves) is much faster than motion of the long gravity waves that extend throughout the water column (shallow water waves). So although the shallow water waves and deep water waves feel the same gravitation acceleration, the huge scale for the shallow water waves leads to far slower wave motion than the deep water gravity waves.

45.5.6 Depth integrated mechanical energy of a traveling plane wave

In Section 45.4.3 we derived general expressions for the layer integrated mechanical energy budget. Here we specialize those results to the case of traveling plane surface gravity waves, and limit our focus to the phase averaged quantities.

Available potential energy

The layer integrated potential energy is given by

$$g \rho \int_{-H}^{\eta} z \, dz = (\rho g \eta_0^2 / 2) \sin^2(\mathbf{k} \cdot \mathbf{x} - \omega t) - \rho g H^2 / 2. \quad (45.91)$$

We are concerned with the potential energy relative to the constant term, $-\rho g H^2 / 2$. That is, we focus on the available potential energy of the waves rather than the potential energy (see Section 45.5.2), in which we compute

$$g \rho \int_{-H}^{\eta} z \, dz - g \rho \int_{-H}^0 z \, dz = g \rho \int_0^{\eta} z \, dz = (\rho g \eta_0^2 / 2) \sin^2(\mathbf{k} \cdot \mathbf{x} - \omega t). \quad (45.92)$$

The phase average of the available potential energy is thus given by

$$\left\langle g \rho \int_0^{\eta} z \, dz \right\rangle = \rho g \eta_0^2 / 4. \quad (45.93)$$

Evidently, the phase averaged and layer integrated available potential energy is proportional to the square of the amplitude of the free surface undulations, η_0^2 .

Kinetic energy

Making use of the expression (45.75a) for the horizontal wave velocity leads to the layer integrated kinetic in the horizontal flow

$$\frac{\rho}{2} \int_{-H}^0 \mathbf{u}^2 \, dz = \frac{\rho \Psi_0^2 |\mathbf{k}|^2}{2} \int_{-H}^0 \cosh^2[|\mathbf{k}|(z + H)] \sin^2(\mathbf{k} \cdot \mathbf{x} - \omega t) \, dz, \quad (45.94)$$

which has the phase average

$$\left\langle \frac{\rho}{2} \int_{-H}^0 \mathbf{u}^2 \, dz \right\rangle = \frac{\rho \Psi_0^2 |\mathbf{k}|^2}{4} \int_{-H}^0 \cosh^2[|\mathbf{k}|(z + H)] \, dz. \quad (45.95)$$

Likewise, the phase averaged kinetic energy of the layer integrated vertical wave motion (45.75b) is given by

$$\left\langle \frac{\rho}{2} \int_{-H}^0 w^2 \, dz \right\rangle = \frac{\rho \Psi_0^2 |\mathbf{k}|^2}{4} \int_{-H}^0 \sinh^2[|\mathbf{k}|(z + H)] \, dz. \quad (45.96)$$

Hence, the phase average of the layer integrated wave motion is

$$\left\langle \frac{\rho}{2} \int_{-H}^0 \mathbf{v}^2 \, dz \right\rangle = \frac{\rho \Psi_0^2 |\mathbf{k}|^2}{4} \int_{-H}^0 \cosh[2|\mathbf{k}|(z + H)] \, dz = (\Psi_0^2 |\mathbf{k}| / 8) \sinh(2|\mathbf{k}|H). \quad (45.97)$$

Making use of the expression (45.73b) for Ψ_0 , as well as the dispersion relation (45.82) yields

$$\left\langle \frac{\rho}{2} \int_{-H}^0 \mathbf{v}^2 \, dz \right\rangle = \frac{\rho g^2 \eta_0^2 |\mathbf{k}|}{8 \omega^2} \frac{\sinh(2|\mathbf{k}|H)}{\cosh^2(|\mathbf{k}|H)} = \rho g \eta_0^2 / 4, \quad (45.98)$$

which is identical to the phase averaged layer integrated available potential energy (45.93). We thus find, again, the equipartition of the phase averaged kinetic and available potential energies.

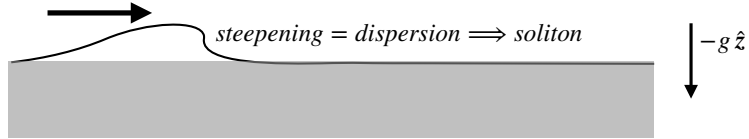


FIGURE 45.3: A soliton in the deep water limit results when the wave dispersion (long waves travel faster than short waves) balances the nonlinear steepening. The result is a soliton, which has an exact analytic expression following from the KdV equation (see [Drazin and Johnson \(1989\)](#)).

Energy flux vector

Now we determine the phase averaged horizontal flux of layer integrated mechanical energy. The general expression is given by equations (45.66) and (45.67), and is here specialized to the plane wave

$$\int_{-H}^0 p_d \mathbf{u} dz = -\rho \int_{-H}^0 \partial_t \Psi \nabla_z \Psi dz \quad (45.99a)$$

$$= (\rho \Psi_0^2 \mathbf{k} \omega) \sin^2(\mathbf{k} \cdot \mathbf{x} - \omega t) \int_{-H}^0 \cosh^2[|\mathbf{k}|(z + H)] dz, \quad (45.99b)$$

which has a phase average

$$\left\langle \int_{-H}^0 p_d \mathbf{u} dz \right\rangle = \frac{\rho \Psi_0^2 \mathbf{k} \omega}{2} \int_{-H}^0 \cosh^2[k(z + H)] dz \quad (45.100a)$$

$$= \frac{\rho \Psi_0^2 \omega \hat{\mathbf{k}}}{4} [|\mathbf{k}| H + \sinh(|\mathbf{k}| H) \cosh(|\mathbf{k}| H)] \quad (45.100b)$$

$$= (\rho g \eta_0^2 / 2) \mathbf{c}_g, \quad (45.100c)$$

where we used equation (45.86) for the group velocity and equation (45.73b) for Ψ_0 . We thus see that the mechanical energy fluxed by the waves is, in the phase average and depth integral, equal to the mechanical energy times the group velocity

$$\left\langle \int_{-H}^0 p_d \mathbf{u} dz \right\rangle = \rho \mathbf{c}_g \left\langle \int_{-H}^0 \mathcal{K} dz + \int_0^\eta \Phi dz \right\rangle. \quad (45.101)$$

This connection between wave energy flux and the group velocity provides yet another reason why the group velocity is more relevant to wave mechanics than the phase velocity.

45.5.7 Qualitative features of deep water waves

The shortwave/deep water waves are notable for having shorter waves travel slower than longer waves. In the event of a perturbation to the fluid, such as from a stone dropped into a pond or a storm on a lake or the ocean, deep water waves are energized. The dispersion relation (45.85a) means that longer waves spread away from the source faster than the shorter waves, leading to a self-organization of the wavelengths and corresponding wave packets.

Now imagine a deep water wave packet that somehow steepens and takes on a nonlinear form. Fourier decomposing this nonlinear wave into linear deep water modes requires more shortwave modes in the steep region, whereas the less steep portion of the wave requires longer deep water modes, which travel faster. If the nonlinear steepening on the wave face is exactly balanced by the faster dispersion of the long waves near the wave base and backside, then the wave pattern remains stable; it does not break. This balance of steepening and dispersion describes the fundamental

features of a *soliton* as depicted in Figure 45.3, with a soliton a *nonlinear wave*.

45.5.8 Qualitative features of shallow water waves

The shallow water limit is notable for the absence of wave dispersion; i.e., shallow water gravity waves of all wavelengths travel at speed \sqrt{gH} . Tsunamis are the prototypical shallow water waves. The shallow water dispersion relation also means that shallow water gravity waves slow down when the ocean depth shallows, as when approaching a beach. Consequently, as waves reach the shoreline there is a tendency to accumulate wave energy as the deeper waves pile up behind the shallower waves. Furthermore, the steeper part of the wave, being part of a thicker region of the fluid and thus a larger effective H , travels slightly faster than the wave trough. As such, the steeper part of the wave overtakes the trough and, at some point, the assumptions of linearity breakdown and the shallow water waves break on the shore as depicted in Figure 45.4.

We can provide quantitative support for the above qualitative considerations by making use of the ray equations from Section 43.8. For simplicity, assume a one-dimensional shallow water gravity wave approaching a beach with $\mathbf{k} = k\hat{\mathbf{x}}$ where $k > 0$. Let the resting depth be a function, $H(x)$, that decreases in the $+\hat{\mathbf{x}}$ direction, $\partial_x H < 0$. Since the background state is time-independent, the angular frequency remains fixed while following along with the group velocity.¹¹ However, the wavevector increases when moving shoreward according to the wavevector equation (43.112), here written for one-dimension

$$\frac{D_g k}{Dt} = - \left[\frac{\partial \varpi}{\partial x} \right]_{t,k}. \quad (45.102)$$

With the local shallow water dispersion relation given by

$$\varpi = k(x) \sqrt{g H(x)} \quad (45.103)$$

we have

$$-\left[\frac{\partial \varpi}{\partial x} \right]_{t,k} = -\frac{\sqrt{gH}}{2H} \partial_x H. \quad (45.104)$$

With $\partial_x H < 0$ we see that the wavenumber increases in magnitude moving along a ray toward the shallower shore. An increasing wavenumber means that the wavelength is decreasing toward the shore.

45.5.9 Further study

Further discussions of surface gravity waves, following that provided here, can be found in Section 54 of [Fetter and Walecka \(2003\)](#), Lectures 3 and 4 of [Pedlosky \(2003\)](#), and Section 7.1 of [Vallis \(2017\)](#). This video from [Prof. A. Hogg](#) provides a pedagogical introduction to shallow water wave breaking as well as deep water solitons realized in a laboratory.

45.6 Standing gravity waves in a closed basin

We now consider the surface gravity wave equations (45.55a)-(45.55e) for a closed rectangular basin of constant depth and with horizontal dimensions $x \in [0, L_x]$ and $y \in [0, L_y]$.

¹¹Standing on a pier looking at a periodic wave field approaching the beach should reveal that the angular frequency is a constant even as the waves move into shallower water.

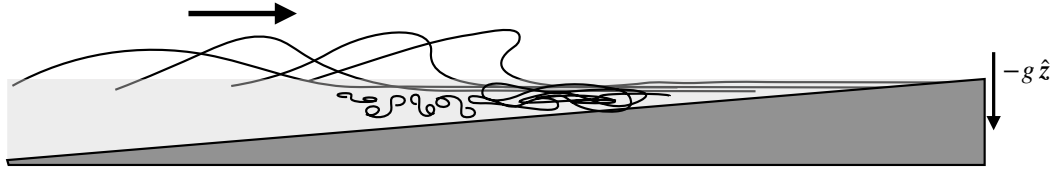


FIGURE 45.4: Shallow water waves approaching a shoreline steepen and eventually break. We can infer this behavior from the phase speed, $C_p = \sqrt{gH}$, whereby waves in deeper water move slightly faster than those in shallower water, so that the wave energy accumulates near the shore. Furthermore, water on the steeper part of the wave moves slightly faster than water in the trough, due to the difference in thickness of the water. This process causes water on the steeper portion of the wave to travel slightly faster than in the trough, leading to steepening of the waves. Nonlinearities eventually invalidate the assumptions made in deriving the linear waves. Even so, the qualitative characterization based on the linear analysis allows for a useful heuristic understanding of shallow water wave breaking on the beach. [This video](#) offers a pedagogical introduction to shallow water waves, with the 12-minute mark describing “compression” waves, in which waves steepen due to differences in the layer thickness, much like shallow water waves approaching a beach

45.6.1 Solution for the standing waves

To satisfy the no-normal flow conditions at the four walls (equation (45.55e)) requires the horizontal wave numbers to be quantized. Correspondingly, the waves are not traveling plane waves since the flow is confined in a box. Rather, the solution is in the form of spatially standing wave that oscillates in time

$$\Psi(x, y, z, t) = \Psi_0 \Gamma(z) \cos(k_m x) \cos(l_n y) \cos(\omega t), \quad (45.105)$$

where the quantized wave numbers are

$$k_m = m \pi / L_x \quad \text{and} \quad l_n = n \pi / L_y \quad \text{with } m, n \text{ integers.} \quad (45.106)$$

The vertical structure function satisfies same differential equation as for the traveling waves in a channel from Section 45.5,

$$\frac{d^2 \Gamma}{dz^2} = (k_m^2 + l_n^2) \Gamma \quad -H \leq z \leq 0 \quad (45.107a)$$

$$\frac{d\Gamma}{dz} = 0 \quad \text{at } z = -H, \quad (45.107b)$$

thus leading to the standing gravity wave solution

$$\Psi = \Psi_0 \cosh[K_{m,n}(z + H)] \cos(k_m x) \cos(l_n y) \sin(\omega t) \quad (45.108a)$$

$$\Psi_0 = \frac{g \eta_0 / \omega_{m,n}}{\cosh(K_{m,n} H)} \quad (45.108b)$$

$$\eta = \eta_0 \cos(k_m x) \cos(l_n y) \cos(\omega_{m,n} t) \quad (45.108c)$$

$$u = \frac{g \eta_0 k_m}{\omega_{m,n}} \frac{\cosh[K_{m,n}(z + H)]}{\cosh(K_{m,n} H)} \sin(k_m x) \cos(l_n y) \sin(\omega t) \quad (45.108d)$$

$$v = \frac{g \eta_0 l_n}{\omega} \frac{\cosh[K_{m,n}(z + H)]}{\cosh(K_{m,n} H)} \cos(k_m x) \sin(l_n y) \sin(\omega_{m,n} t) \quad (45.108e)$$

$$w = -\frac{g \eta_0 K_{m,n}}{\omega} \frac{\sinh[K_{m,n}(z + H)]}{\cosh(K_{m,n} H)} \cos(k_m x) \cos(l_n y) \sin(\omega_{m,n} t) \quad (45.108f)$$

$$K_{m,n}^2 = k_n^2 + l_m^2. \quad (45.108g)$$

As for the channel, we find the dispersion relation by substituting the standing wave solution into the boundary condition equation (45.81), thus leading to the quantized angular frequencies

$$\omega_{m,n}^2 = g K_{m,n} \tanh(K_{m,n} H). \quad (45.109)$$

45.6.2 Comments

These standing wave solutions are commonly referred to as *seiches*, and they can be found in enclosed lakes and ocean basins after strong and persistent winds. Winds, generally with large scale variations, tend to force the lowest or *gravest* seiche mode. For example, assume the wind blows in the zonal direction so that it excites the lowest zonal standing wave with frequency

$$\omega_{1,0}^2 = g K_{1,0} \tanh(K_{1,0} H) = (g \pi / L_x) \tanh(\pi H / L_x), \quad (45.110)$$

which has the shallow water limit ($H/L_x \rightarrow 0$)

$$\omega_{1,0}^2 \approx g H (\pi / L_x)^2. \quad (45.111)$$

As the winds relax, the seiche mode oscillates according to this angular frequency.

45.6.3 Further study

More discussion of seiche modes can be found in Section 12.5 of [Cushman-Roisin and Beckers \(2011\)](#), Section 1.6.4 of [Brown \(1999\)](#), and Chapter 10 of [Neumann and Pierson \(1966\)](#).

45.7 Capillary-gravity waves

As studied in Section 22.11, surface tension exists at the interface between two media, such as a liquid and solid or liquid and gas. In this section we add the effects from surface tension, with its presence providing the means to realize *capillary waves*.

45.7.1 Pressure jump across the air-sea surface

As studied in Section 22.11, surface tension on an interface between two fluids leads to a pressure jump across the interface. That is, the pressure on one side of the interface is different from the pressure on the other side. The pressure jump is given by the Young-Laplace formula (22.138), which when applied to the ocean free surface renders

$$p_a - p_{ocn} = \gamma \nabla^2 \eta \implies p_{ocn} = p_a - \gamma \nabla^2 \eta. \quad (45.112)$$

In this equation, $\gamma > 0$ is the surface tension (dimensions of force per length = M T⁻²), p_a is the pressure on the atmospheric side of the free surface, and p_{ocn} is the pressure on the ocean side of the free surface. To help remember signs for the pressure jump, note that the Young-Laplace formula (45.112) says that pressure on the concave side of the interface is higher than on the convex side. For example, if the free surface extends upward then $p_{ocn} - p_a > 0$ since the ocean is on the concave side and so it has the higher pressure. This result also follows since $\nabla^2 \eta < 0$ for an upward extension, which leads to a local free surface maximum.¹²

¹²The discussion in Section 22.11.4 considered bubbles, where the Young-Laplace formula shows that surface tension causes pressure inside of a bubble to be larger than outside the bubble.

45.7.2 Dynamic boundary condition with surface tension

We can continue to apply Bernoulli's theorem even in the presence of surface tension to determine the dynamic boundary condition. Hence, we proceed as in Section 45.3.2 to evaluate the Bernoulli potential at the free surface. Now, however, it is important to specify which side of the free surface we evaluate the Bernoulli potential. Since we are interested in ocean waves, we evaluate the Bernoulli potential on the ocean side, in which case equation (45.46) takes on the form

$$g \eta + \mathcal{K} - \partial_t \Psi = -p_{\text{ocn}}/\rho = -(p_a - \gamma \nabla^2 \eta)/\rho, \quad (45.113)$$

where the second equality follows from the Young-Laplace formula (45.112). We again assume the atmospheric pressure is a given constant that can be trivially absorbed by a gauge transformation. We thus have the equation of motion

$$\partial_t \Psi = \rho^{-1} [g \rho - \gamma \nabla^2] \eta + \mathcal{K}. \quad (45.114)$$

The surface tension term, $-(\gamma/\rho) \nabla^2 \eta$, is new relative to equation (45.46) holding for gravity waves.

45.7.3 Dispersion relation for capillary-gravity waves

In Section 45.3.4 we detailed the steps needed to derive the linear equations (45.55b)-(45.55e) for surface gravity waves. Those steps also hold for capillary-gravity waves, with the only difference being a modification to the dynamic boundary condition arising from surface tension

$$\nabla^2 \Psi = 0 \quad \text{irrotational and non-divergent velocity} \quad (45.115a)$$

$$\partial_t \Psi = \rho^{-1} [g \rho - \gamma \nabla^2] \eta \quad \text{linearized dynamic b.c. at } z = 0 \quad (45.115b)$$

$$\partial_z \Psi = -\partial_t \eta \quad \text{linearized kinematic b.c. at } z = 0 \quad (45.115c)$$

$$\hat{\mathbf{n}} \cdot \nabla \Psi = 0 \quad \text{no-normal flow kinematic b.c.} \quad (45.115d)$$

The analysis in Section 45.5.1 concerns the interior harmonic scalar potential as well as the kinematic boundary condition. Both of these properties hold equivalently for surface gravity waves and for capillary-gravity waves. Hence, we can write the scalar potential for capillary-gravity waves as in equations (45.73a) and (45.73b), and the corresponding free surface as (45.74). The dispersion relation is derived by using these expressions for Ψ and η in the dynamic boundary condition (45.115b), with a few lines of algebra rendering

$$\omega^2 = g |\mathbf{k}| (1 + \Upsilon) \tanh(|\mathbf{k}| H) \quad \text{capillary-gravity waves,} \quad (45.116)$$

where we introduced the non-dimensional parameter

$$\Upsilon = |\mathbf{k}|^2 \gamma / (g \rho). \quad (45.117)$$

The capillary-gravity wave dispersion relation (45.116) generalizes the gravity wave dispersion (45.82). The Υ parameter provides a regime boundary where capillary waves dominate ($\Upsilon \gg 1$) versus where gravity waves dominate ($\Upsilon \ll 1$).

45.7.4 Deep Water capillary-gravity waves

The hydrostatic limit is not relevant for capillary waves since capillary waves are generally very small (as seen below) and thus do not satisfy hydrostatic scaling. Hence, we find it physically most

interesting to examine the limit of deep water capillary-gravity waves, in which case $|\mathbf{k}| H \rightarrow \infty$ so that the dispersion relation (45.116) simplifies to

$$\omega^2 = g |\mathbf{k}| (1 + \Upsilon) \quad \text{deep water capillary-gravity waves.} \quad (45.118)$$

Phase speed

The phase speed for deep water capillary-gravity waves is given by

$$C_p = \omega / |\mathbf{k}| = \sqrt{(g / |\mathbf{k}|) (1 + \Upsilon)} = \sqrt{g / |\mathbf{k}| + \gamma |\mathbf{k}| / \rho}, \quad (45.119)$$

which has the longwave and shortwave limits

$$C_p \approx C_p^{\text{dwg}} \quad \text{for } \Upsilon \ll 1 \quad \text{and} \quad C_p \approx \sqrt{\gamma |\mathbf{k}| / \rho} \quad \text{for } \Upsilon \gg 1, \quad (45.120)$$

where we introduced the deep water gravity wave phase speed from equation (45.85a)

$$C_p^{\text{dwg}} = \sqrt{g / |\mathbf{k}|}. \quad (45.121)$$

At both extremes the phase speed is unbounded, with gravity waves dominant for longwaves and capillary waves dominant for shortwaves.

Group velocity

The transport of energy within a packet of capillary-gravity waves is determined by the group velocity, $\mathbf{c}_g = \nabla_{\mathbf{k}} \omega$, which takes the form

$$\mathbf{c}_g = \frac{\hat{\mathbf{k}} C_p^{\text{dwg}}}{2} \frac{1 + 3 \Upsilon}{(1 + \Upsilon)^{1/2}} = \frac{\hat{\mathbf{k}}}{2} \left[\frac{g \gamma}{\rho} \right]^{1/4} \frac{1 + 3 \Upsilon}{\sqrt{\Upsilon^{1/2} + \Upsilon^{3/2}}}. \quad (45.122)$$

The group velocity has the following shortwave and longwave limits

$$\mathbf{c}_g \approx \hat{\mathbf{k}} C_p^{\text{dwg}} / 2 \quad \text{for } \Upsilon \ll 1 \quad \text{and} \quad \mathbf{c}_g \approx \frac{3}{2} \hat{\mathbf{k}} \left[\frac{|\mathbf{k}| \gamma}{\rho} \right]^{1/2} \quad \text{for } \Upsilon \gg 1. \quad (45.123)$$

As for the phase speed, we find that the group velocity is unbounded at both extremes, with gravity waves dominant for longwaves and capillary waves dominant at shortwaves.

Wavelength of the minimum group velocity

As seen above, there is a continuum of wavelengths for capillary-gravity waves, with gravity waves dominating for longwaves and capillary waves dominating for shortwaves. To delineate between shortwaves and longwaves, we seek the wavenumber where the group velocity is a minimum. To simplify the algebra, assume $\mathbf{k} = k \hat{\mathbf{x}}$ so that we reach an extrema of the group velocity when

$$\frac{dc_g}{dk} = 0 \implies 3 \Upsilon_{\min}^2 + 6 \Upsilon_{\min} - 1 = 0, \quad (45.124)$$

in which case

$$\Upsilon_{\min} = 2/\sqrt{3} - 1 \approx 0.1547 \quad (45.125a)$$

$$k_{\min} = (\Upsilon_{\min} g \rho / \gamma)^{1/2} \approx 0.393 (g \rho / \gamma)^{1/2} \quad (45.125b)$$

$$(c_g)_{\min} \approx 1.086 (g \gamma / \rho)^{1/4}. \quad (45.125c)$$

For an air-water interface we take $\gamma = 0.072 \text{ N m}^{-1} = 0.072 \text{ kg s}^{-2}$, along with the water density of $\rho = 10^3 \text{ kg m}^{-3}$ and gravitational acceleration $g = 9.8 \text{ m s}^{-2}$, thus leading to

$$k_{\min} \approx 145 \text{ m}^{-1} \quad (45.126a)$$

$$\Lambda_{\min} \approx 4.3 \times 10^{-2} \text{ m} \quad (45.126b)$$

$$(c_g)_{\min} \approx 1.7 \times 10^{-1} \text{ m s}^{-1}. \quad (45.126c)$$

Evidently, for wavelengths smaller than roughly 4 cm the surface tension effects are important in their support of capillary waves. In contrast, larger wavelengths are dominated by gravity waves.

45.7.5 Comments and further study

As noted in Section 22.11.5, we can ignore the pressure jump induced by surface tension across the air-sea interface if the radius of curvature of the air-sea interface is larger than a few centimeters. Here, we also see that the boundary between gravity waves and capillary waves occurs for wavelengths of a few centimeters. It is for these reasons that capillary waves, and surface tension more generally, can be ignored when considering geophysical fluid motions with scales larger than a few centimeters. Even so, we highlight the importance of surface tension and capillary waves for the study of fundamental processes affecting air-sea exchanges of matter, energy, and momentum.

Much of the discussion in this section follows that in Section 54 of [Fetter and Walecka \(2003\)](#). We again encounter surface tension effects in Section 51.3 when studying the Rayleigh-Taylor instability in the presence of gravity and surface tension.

45.8 Particle trajectories and Stokes drift

We here consider the trajectories of fluid particles moving as part of a wave field. In homogenous linear wave fields, a fluid particle periodically returns to its original position. However, in the presence of wave inhomogeneities, such as the surface gravity waves considered in Sections 45.3 and 45.5, fluid particles generally oscillate between regions where the undulation in one direction does not match that in the other direction. In this case there is a net particle transport known as *Stokes drift*. Stokes drift occurs even though the phase average of the wave at a fixed spatial point vanishes. Formulating the mathematics of Stokes drift offers a means to explore the differences between averages formed at a fixed space point (Eulerian mean) versus averages following fluid particles (Lagrangian mean). We here introduce these notions, which form part of the rudiments for wave-mean flow interaction theory further pursued in Chapter 62. It also forms the basis for the wave-induced drift of debris on the ocean surface.

45.8.1 General formulation of Stokes drift

Consider a three-dimensional particle trajectory written in Cartesian coordinates,

$$\mathbf{X}(\mathbf{a}, t) = X(\mathbf{a}, t) \hat{\mathbf{x}} + Y(\mathbf{a}, t) \hat{\mathbf{y}} + Z(\mathbf{a}, t) \hat{\mathbf{z}}. \quad (45.127)$$

In the analysis of waves, it is common to assume the material coordinate, \mathbf{a} , is the initial position of a fluid particle, which we here assume. As discussed in Section 14.9.1, the particle trajectory is determined by time integrating the particle velocity (also known as the “flow map”)

$$\frac{\partial \mathbf{X}(\mathbf{a}, t)}{\partial t} = \mathbf{v}[\mathbf{X}(\mathbf{a}, t), t] \quad (45.128)$$

so that

$$\mathbf{X}(\mathbf{a}, t) = \mathbf{X}(\mathbf{a}, 0) + \int_0^t \mathbf{v}[\mathbf{X}(\mathbf{a}, t'), t'] dt'. \quad (45.129)$$

This equation is a trivial result of time integrating the flow map. Nonetheless, it is useful to express the content of this equation in words. It says that the position at time t of a fluid particle labelled by the material coordinate \mathbf{a} is given by the initial position of the particle, $\mathbf{X}(\mathbf{a}, 0)$, plus the time integrated movement of the particle following the fluid flow.

Equation (45.129) provides the trajectory, but only by knowing the velocity following the trajectory. To produce a result that is more readily computed analytically, we develop a Taylor series computed relative to the initial position of the fluid particle. In this manner we make use of the approximate expression for the particle velocity at time t

$$v^n[\mathbf{X}(\mathbf{a}, t), t] \approx v^n[\mathbf{X}(\mathbf{a}, 0), t] + \nabla v^n[\mathbf{X}(\mathbf{a}, 0), t] \cdot [\mathbf{X}(\mathbf{a}, t) - \mathbf{X}(\mathbf{a}, 0)] \quad (45.130a)$$

$$= v^n[\mathbf{X}(\mathbf{a}, 0), t] + \nabla v^n[\mathbf{X}(\mathbf{a}, 0), t] \cdot \int_0^t \frac{d\mathbf{X}(\mathbf{a}, t')}{dt'} dt' \quad (45.130b)$$

$$= v^n[\mathbf{X}(\mathbf{a}, 0), t] + \nabla v^n[\mathbf{X}(\mathbf{a}, 0), t] \cdot \int_0^t \mathbf{v}[\mathbf{X}(\mathbf{a}, t'), t'] dt', \quad (45.130c)$$

where the Taylor series was truncated after terms linear in the particle displacement $\mathbf{X}(\mathbf{a}, t) - \mathbf{X}(\mathbf{a}, 0)$. We emphasize two points regarding equation (45.130c).

- The velocity $v^n[\mathbf{X}(\mathbf{a}, 0), t]$ is the n 'th component of the fluid velocity field evaluated at the initial point of the fluid particle trajectory, $\mathbf{X}(\mathbf{a}, 0)$, and at the time t . That is, $v^n[\mathbf{X}(\mathbf{a}, 0), t]$ is the Eulerian velocity evaluated at the fixed Eulerian point $\mathbf{X}(\mathbf{a}, 0)$.
- What determines the accuracy of the Taylor series? A suitable non-dimensional expansion coefficient for the Taylor expansion is the ratio of the particle displacement to the scale, L , of inhomogeneities in flow properties

$$\epsilon = \frac{|\mathbf{X}(\mathbf{a}, t) - \mathbf{X}(\mathbf{a}, 0)|}{L}. \quad (45.131)$$

This ratio is small for the small amplitude waves considered here, whereby the particle displacements are far smaller than inhomogeneities in flow properties.

The integrand on the right hand side of equation (45.130c) is the Lagrangian velocity integrated over the time interval. To within the same order of accuracy as maintained thus far, we can use the Eulerian velocity evaluated at the initial position, thus rendering

$$v^n[\mathbf{X}(\mathbf{a}, t), t] \approx v^n[\mathbf{X}(\mathbf{a}, 0), t] + \nabla v^n[\mathbf{X}(\mathbf{a}, 0), t] \cdot \int_0^t \mathbf{v}[\mathbf{X}(\mathbf{a}, 0), t'] dt', \quad (45.132)$$

with rearrangement leading to

$$v^n[\mathbf{X}(\mathbf{a}, t), t] - v^n[\mathbf{X}(\mathbf{a}, 0), t] \approx \nabla v^n[\mathbf{X}(\mathbf{a}, 0), t] \cdot \int_0^t \mathbf{v}[\mathbf{X}(\mathbf{a}, 0), t'] dt'. \quad (45.133)$$

The left hand side is the difference between the velocity following a fluid particle (the Lagrangian velocity for the moving fluid particle) from the velocity at the initial particle point (the Eulerian velocity at the initial point of the trajectory). The right hand side terms are all evaluated at the initial position, $\mathbf{X}(\mathbf{a}, 0)$. Furthermore, the right hand side is non-zero where the velocity at the initial position has a nonzero gradient (i.e., it is spatially inhomogeneous), with its inhomogeneity projecting onto the time integrated velocity at that point. Equation (45.133) says that the velocity following a fluid particle is modified from the velocity at its initial position if the particle moves through an inhomogeneous velocity field.

The Stokes drift is defined as the difference of the velocities in equation (45.133) when time averaged over a wave period, which we write as

$$v_{(s)}^n[\mathbf{X}(\mathbf{a}, 0), t] = \overline{v^n[\mathbf{X}(\mathbf{a}, t), t] - v^n[\mathbf{X}(\mathbf{a}, 0), t]} \quad (45.134a)$$

$$\approx \nabla v^n[\mathbf{X}(\mathbf{a}, 0), t] \cdot \int_0^t \mathbf{v}[\mathbf{X}(\mathbf{a}, 0), t'] dt'. \quad (45.134b)$$

This expression holds for any arbitrary initial point in the fluid, so that we can write it in a concise Eulerian form that dispenses with trajectories

$$v_{(s)}^n(\mathbf{x}, t) \approx \overline{\nabla v^n(\mathbf{x}, t) \cdot \int_0^t \mathbf{v}(\mathbf{x}, t') dt'}. \quad (45.135)$$

We can draw an analogy between Stokes drift and surfing. Namely, the more a fluid particle samples larger amplitude variations in the velocity field (the gradient term), the further it drifts (the integral term).

45.8.2 Particle trajectories in a homogeneous wave

The expression (45.135) for the Stokes drift is general and will be specialized in Section 45.8.4 for the case of surface gravity waves. Before doing so, in this section and in Section 45.8.3 we determine particle trajectories for the traveling plane wave

$$\frac{dX}{dt} = U \sin(kx - \omega t) \quad (45.136a)$$

$$\frac{dZ}{dt} = -U \cos(kx - \omega t). \quad (45.136b)$$

We here set the wavevector to $\mathbf{k} = k \hat{\mathbf{x}}$, so that it is purely zonal, let $U > 0$ be the speed of the particle motion, and wrote X and Z for the Cartesian components of the particle trajectory. To simplify the mathematics we perform the analysis in a frame moving with the waves so that the phase $kx - \omega t$ can be replaced by $-\omega t$, so that we consider trajectories that satisfy

$$\frac{dX}{dt} = -U \sin(\omega t) \quad (45.137a)$$

$$\frac{dZ}{dt} = -U \cos(\omega t). \quad (45.137b)$$

Figure 45.5 shows a schematic of the particle trajectories as derived in the following.

We start by examining particle motion in the case with a constant wave amplitude, $U = U_0$.



FIGURE 45.5: Sketch of Stokes drift with the wave vector in the horizontal direction and clockwise time integrated fluid particle motion induced by the traveling wave. For the case of a wave amplitude that decreases with depth, lateral motion of the particle is larger when the particle is closer to the surface thus leading to a Stokes drift in the direction of the wave. Note that there is zero Stokes drift for the case of a homogeneous wave, in which the wave amplitude is independent of depth. Additionally, and even more trivially, if the particle motion is purely transverse to the wave vector, in this case purely vertical, then the particle merely retraces its motion along a vertical line and does not undergo any lateral Stokes drift.

Particle trajectories in this case are clockwise in the x - z plane around a circle with radius U_0/ω

$$X(t) - X_0 = (U_0/\omega) [\cos(\omega t) - 1] \quad (45.138a)$$

$$Z(t) - Z_0 = -(U_0/\omega) \sin(\omega t), \quad (45.138b)$$

where the initial position at time $t = 0$ is

$$\mathbf{X}(t = t_0) = \hat{\mathbf{x}} X_0 + \hat{\mathbf{z}} Z_0, \quad (45.139)$$

and the center of the circle is

$$\mathbf{X}_{\text{center}} = [X_0 - U_0/\omega] \hat{\mathbf{x}} + Z_0 \hat{\mathbf{z}}. \quad (45.140)$$

There is no Stokes drift since the particles return to their initial position each wave period.

45.8.3 Stokes drift from an inhomogeneous wave

Now consider the case of a vertically dependent wave amplitude, $U = U(z)$. The canonical example is where the wave amplitude decreases with depth, as for the surface gravity waves from Section 45.5. In turn, we expect there to be a fluid particle drift in the zonal direction introduced by the vertical wave inhomogeneity. This drift is a particular realization of Stokes drift.

To compute the leading order expression for the Stokes drift, expand U in a Taylor series about the initial position

$$U \approx U_0 + \sigma (Z - Z_0) \quad (45.141)$$

where the vertical shear, σ , has units of inverse time and is given by

$$\sigma = \left[\frac{dU}{dZ} \right]_{Z=Z_0}. \quad (45.142)$$

The Taylor series (45.141) is valid so long as the vertical trajectories maintain the inequality

$$|\sigma| |Z - Z_0| \ll U_0, \quad (45.143)$$

which says that the vertical shear is small

$$|\sigma| \ll \frac{U_0}{|Z - Z_0|}. \quad (45.144)$$

We use the Taylor series expansion (45.141) to solve for the vertical trajectory as determined by

$$\frac{d(Z - Z_o)}{dt} = -[U_0 + \sigma(Z - Z_o)] \cos(\omega t). \quad (45.145)$$

Rearrangement leads to

$$\int_{Z_0}^Z \frac{d(Z - Z_0)}{U_0 + \sigma(Z - Z_0)} = - \int_0^t \cos(\omega t) dt. \quad (45.146)$$

The left hand side integral can be computed by changing variables

$$\Sigma = U_0 + \sigma(Z - Z_0) \implies d\Sigma = \sigma d(Z - Z_0), \quad (45.147)$$

so that equation (45.146) becomes

$$\int_{U_0}^{\Sigma} \frac{d\Sigma}{\Sigma} = -\sigma \int_0^t \cos(\omega t) dt. \quad (45.148)$$

Performing the integrals and evaluating the end points renders

$$\ln \left[1 + \frac{\sigma}{U_0}(Z - Z_0) \right] = -\frac{\sigma \sin(\omega t)}{\omega}, \quad (45.149)$$

which yields the exponential solution

$$1 + \frac{\sigma}{U_0}(Z - Z_0) = e^{-(\sigma/\omega) \sin(\omega t)} \implies Z - Z_0 = \frac{U_0}{\sigma} \left[-1 + e^{-(\sigma/\omega) \sin(\omega t)} \right]. \quad (45.150)$$

The vertical particle position is seen to oscillate around its initial position Z_0 .

We next consider the zonal particle position, in which case

$$\frac{d(X - X_o)}{dt} = -U_0 \left[1 + \frac{\sigma}{U_0}(Z - Z_0) \right] \sin(\omega t) = -U_0 e^{-(\sigma/\omega) \sin(\omega t)} \sin(\omega t), \quad (45.151)$$

where we used equation (45.150) for the vertical trajectory. To make progress, we expand the exponential assuming the ratio of inverse time scales, σ/ω , is small

$$|\sigma/\omega| \ll 1. \quad (45.152)$$

In this limit, the vertical trajectory retains its unperturbed form (45.138b), and the zonal trajectory satisfies

$$\frac{d(X - X_o)}{dt} \approx -U_0 \sin(\omega t) \left[1 - \frac{\sigma}{\omega} \sin(\omega t) \right], \quad (45.153)$$

where we dropped terms of order $(\sigma/\omega)^2$. We can understand the scaling in equation (45.152) by noting that the period for the circular motion is given by

$$\tau_{\text{circle}} = 2\pi/\omega. \quad (45.154)$$

The inverse time, σ , introduces a time scale for the drift, defined according to

$$\tau_{\text{drift}} = 2\pi/|\sigma|. \quad (45.155)$$

A small ratio $|\sigma/\omega|$ thus implies

$$|\sigma/\omega| = \tau_{\text{circle}}/\tau_{\text{drift}} \ll 1. \quad (45.156)$$

Hence, we are solving for the zonal trajectory in the limit where the time scale for the circular motion is small (i.e., fast oscillations around the circle) relative to the time scale for the drift (i.e., slow drift).

Returning now to the approximate zonal trajectory equation (45.153) yields

$$\frac{d(X - X_o)}{dt} = -U_0 \sin(\omega t) \left[1 - \frac{\sigma}{\omega} \sin(\omega t) \right] \quad (45.157a)$$

$$= -U_0 \sin(\omega t) + \frac{U_0 \sigma}{2\omega} [1 - \cos(2\omega t)], \quad (45.157b)$$

which integrates to

$$X - X_o = \left(\frac{U_0}{\omega} \right) \left[\cos(\omega t) - 1 - \frac{\sigma \sin(2\omega t)}{4\omega} + \frac{\sigma t}{2} \right] \quad (45.158a)$$

$$= \underbrace{\left(\frac{U_0}{\omega} \right) [\cos(\omega t) - 1]}_{\text{homogeneous}} + \underbrace{\frac{U_0 \sigma t}{2\omega}}_{\text{Stokes drift}} - \underbrace{\frac{U_0 \sigma \sin(2\omega t)}{4\omega^2}}_{\text{higher harmonic}} + \mathcal{O}(\sigma/\omega)^2. \quad (45.158b)$$

The leading order term is the homogeneous motion given by equation (45.138a). The next term is the Stokes drift, followed by a higher order harmonic and then further terms on the order of $(\sigma/\omega)^2$. There is no vertical Stokes drift to this order in (σ/ω) , so that the Stokes drift velocity is given by

$$\left[\frac{\mathbf{X} - \mathbf{X}_o}{t} \right]^{\text{drift}} = \frac{\sigma U_0}{2\omega} \hat{\mathbf{x}}. \quad (45.159)$$

The circular motion of the parcels is therefore deformed by the zonal Stokes drift. The drift increases with larger wave amplitude (U_0 large); with larger vertical shear (σ large); and with longer period waves (ω small). See Figure 45.6 for an illustration based on a particular choice for the dimensional parameters.

45.8.4 Stokes drift for surface gravity waves

The velocity field for surface gravity waves, given by equations (45.75a) and (45.75b), is far more complicated than the prototypical wave considered in Sections 45.8.2 and 45.8.3. For that reason we make use of the general expression (45.135) to determine the Stokes drift velocity for surface gravity waves in a flat channel, rather than directly integrate to determine the trajectories. Hence,

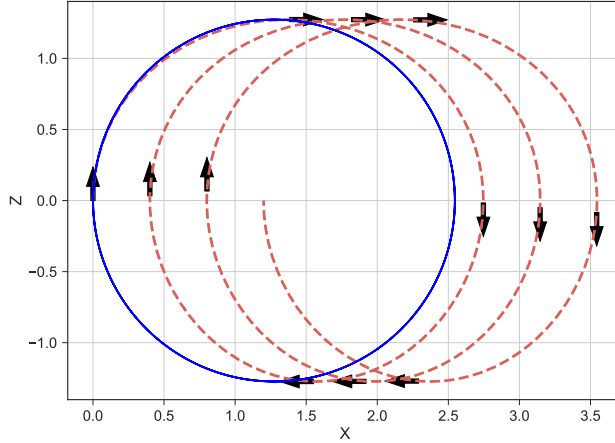


FIGURE 45.6: Example trajectories of fluid particles undergoing Stokes drift. Particle motion is clockwise in the x-z plane. For homogeneous waves, there is zero Stokes drift with circular trajectories given by equations (45.138a) and (45.138b), as depicted here by the blue trajectory. There is a Stokes drift in the presence of vertical shear in the wave amplitude and thus in the particle velocity, with the trajectories for this example given by equation (45.150) for the vertical component and equation (45.158b) for the horizontal component. We set the parameters as follows: $T = 2\pi/\omega = 60$ s, $U_0 = 0.1$ m s⁻¹, and $\sigma = \omega/10$ and exhibit trajectories over four minutes.

we need to compute terms in the following equations for surface gravity waves

$$\overline{u_{(S)}(\mathbf{x})} \approx \nabla u(\mathbf{x}, t) \cdot \int_0^t \mathbf{v}(\mathbf{x}, t') dt' \quad (45.160a)$$

$$\overline{v_{(S)}(\mathbf{x})} \approx \nabla v(\mathbf{x}, t) \cdot \int_0^t \mathbf{v}(\mathbf{x}, t') dt' \quad (45.160b)$$

$$\overline{w_{(S)}(\mathbf{x})} \approx \nabla w(\mathbf{x}, t) \cdot \int_0^t \mathbf{v}(\mathbf{x}, t') dt'. \quad (45.160c)$$

The components to the velocity field for surface gravity waves are given by equations (45.75a) and (45.75b), repeated here to be self-contained

$$\mathbf{u} = \frac{g \eta_0 \hat{\mathbf{k}}}{C_p} \frac{\cosh[|\mathbf{k}|(z + H)] \sin(\mathcal{P})}{\cosh(|\mathbf{k}|H)} \quad (45.161a)$$

$$w = -\frac{g \eta_0}{C_p} \frac{\sinh[|\mathbf{k}|(z + H)] \cos(\mathcal{P})}{\cosh(|\mathbf{k}|H)}, \quad (45.161b)$$

and their spatial gradients are given by

$$\nabla u = \frac{g \eta_0 k_x [\hat{\mathbf{k}} \cos(\mathcal{P}) \cosh[|\mathbf{k}|(z + H)] + \hat{\mathbf{z}} \sin(\mathcal{P}) \sinh[|\mathbf{k}|(z + H)]]}{C_p \cosh(|\mathbf{k}|H)} \quad (45.162a)$$

$$\nabla v = \frac{g \eta_0 k_y [\hat{\mathbf{k}} \cos(\mathcal{P}) \cosh[|\mathbf{k}|(z + H)] + \hat{\mathbf{z}} \sin(\mathcal{P}) \sinh[|\mathbf{k}|(z + H)]]}{C_p \cosh(|\mathbf{k}|H)} \quad (45.162b)$$

$$\nabla w = \frac{g \eta_0 |\mathbf{k}| [\hat{\mathbf{k}} \sin(\mathcal{P}) \sinh[|\mathbf{k}|(z + H)] - \hat{\mathbf{z}} \cos(\mathcal{P}) \cosh[|\mathbf{k}|(z + H)]]}{C_p \cosh(|\mathbf{k}|H)}, \quad (45.162c)$$

where we introduced the phase

$$\mathcal{P} = \mathbf{k} \cdot \mathbf{x} - \omega t \quad (45.163)$$

to produce more tidy expressions, and recall that

$$\hat{\mathbf{k}} = \mathbf{k}/|\mathbf{k}| = (\hat{x} k_x + \hat{y} k_y)/|\mathbf{k}| \quad (45.164)$$

is the wave direction. We also require the following time integrals

$$\int_0^t \sin(\mathbf{k} \cdot \mathbf{x} - \omega t') dt' = \omega^{-1} [\cos(\mathbf{k} \cdot \mathbf{x} - \omega t) - \cos(\mathbf{k} \cdot \mathbf{x})] \quad (45.165a)$$

$$\int_0^t \cos(\mathbf{k} \cdot \mathbf{x} - \omega t') dt' = -\omega^{-1} [\sin(\mathbf{k} \cdot \mathbf{x} - \omega t) - \sin(\mathbf{k} \cdot \mathbf{x})]. \quad (45.165b)$$

Use of these results in equations (45.160a)-(45.160c) leads to the horizontal Stokes drift velocity for surface gravity waves in a flat bottom domain

$$\mathbf{v}_{(s)} = \frac{\mathbf{k} (g \eta_0)^2}{2 \omega C_p^2} \frac{\cosh[2|\mathbf{k}|(z+H)]}{\cosh^2(|\mathbf{k}|H)} = \frac{\mathbf{k} \omega \eta_0^2 \cosh[2|\mathbf{k}|(z+H)]}{2 \sinh^2(|\mathbf{k}|H)}. \quad (45.166)$$

The purely horizontal nature of the Stokes drift agrees with that found for the prototypical wave in Section 45.8.3.

The ratio of the Stokes speed at $z = 0$ to that at $z = -H$ is given by

$$\frac{\hat{\mathbf{k}} \cdot \mathbf{v}_{(s)}(z=0)}{\hat{\mathbf{k}} \cdot \mathbf{v}_{(s)}(z=-H)} = \cosh(2|\mathbf{k}|H). \quad (45.167)$$

In the deep water limit, $kH \gg 1$, this ratio is much greater than unity, indicating a nontrivial vertical shear in the zonal Stokes velocity. In contrast, the ratio becomes unity in the shallow water limit, $kH \ll 1$, so that there is no vertical shear to the Stokes velocity, with the Stokes speed taking the shallow water form

$$\mathbf{v}_{(s)} \cdot \hat{\mathbf{k}} \approx (C_p/2)(\eta_0/H)^2 \quad \text{for } |\mathbf{k}|H \ll 1. \quad (45.168)$$

Recall our study of the shallow water fluid in Chapters 32 and 33, where we found that the fluid moves in a vertically coherent column. We thus expect no shear in the Stokes velocity for shallow water motion.

45.8.5 Comments and further study

Is Stokes drift a nonlinear wave phenomena? In answering this question we note that Stokes drift occurs with particle motion in linear waves, but the waves must be inhomogeneous such as the surface gravity waves studied in this chapter. However, nonlinearity appears in the form of the particle-following average operation, as can be seen by the expression of Stokes drift given by equation (45.135)

$$\overline{\mathbf{v}_{(s)}^n(\mathbf{x}, t)} \approx \nabla v^n(\mathbf{x}, t) \cdot \int_0^t \mathbf{v}(\mathbf{x}, t') dt'. \quad (45.169)$$

The dot product of the velocity gradient with the time integrated velocity (to give the time integrated position) is nonlinear. So although the waves are linear, the Lagrangian kinematics of particle trajectories introduces nonlinearities.

Stokes drift occurs in many guises when studying the motion of fluid particles within wave fields. We revisit elements of Stokes drift in Chapter 62 when studying the rudiments of eddy-induced tracer transport. This video from [Prof. Hogg at Australian National University](#) provides

an overview of the discussion in this section along with some laboratory experiments to illustrate Stokes drift.



45.9 Exercises

EXERCISE 45.1: SURFACE GRAVITY WAVES ON THE VIDEO CHANNEL *Veritasium*

Veritasium is a science channel that has the following [educational video on surface ocean waves](#). However, the host makes a basic error in this video. Discuss the error.

EXERCISE 45.2: SURFACE KINEMATIC BOUNDARY CONDITION

Show that for an irrotational and non-divergent flow, the surface kinematic boundary condition (45.40) can be written

$$\partial_t \eta = -\nabla \cdot [(z - \eta) \nabla \Psi] \quad \text{at } z = \eta. \quad (45.170)$$

Hint: read Section 18.2.

EXERCISE 45.3: GAUGE INVARIANCE OF KINETIC ENERGY

In Section 45.2.6 we argued that the gauge invariance of the globally integrated kinetic energy follows from equation (45.44): $\int \mathbf{v} \cdot \hat{\mathbf{n}} dS = 0$, which follows for the case where the free surface is a material interface so that $\partial_t \eta = -\nabla \cdot \mathbf{U}$. Discuss whether the kinetic energy remains gauge invariant if the upper free surface is not material, so that $\partial_t \eta = -\nabla \cdot \mathbf{U} + Q_m/\rho$, where $Q_m \neq 0$ is a mass flux crossing the free surface and with this mass flux having density equal to the constant layer density, ρ .

Hint: to write $\mathbf{v} = -\nabla \Psi$ requires $\nabla \times \mathbf{v} = 0$. Do we expect the flow to remain irrotational in the presence of nonzero Q_m when the density of Q_m equals to that of the homogeneous domain?

EXERCISE 45.4: ENERGETICS OF DEPTH INTEGRATED FLOW IN FULL NONLINEAR THEORY

In Section 45.4.3 we computed the energy budget for the depth integrated flow within the linearized theory. Derive the mechanical energy equation for the full nonlinear theory integrated over $-H \leq z \leq \eta$, thus providing the nonlinear analog to the energy equation (45.67) derived for the linear theory. Do not assume the bottom is flat for the nonlinear theory. Confirm that all terms missing from the energy budget (45.67) are third order or higher. Hint: Make use of results from Section 45.2.6.

EXERCISE 45.5: ENERGETICS OF CAPILLARY-GRAVITY WAVES

In Section 45.4 we studied the energetics for surface gravity waves. Extend that discussion to the capillary-gravity waves from Section 45.7.

- (a) What is the globally integrated kinetic energy?
- (b) What is the globally integrated available potential energy?
- (c) Determine whether there is equipartition for the phase averaged kinetic and available potential energies of capillary-gravity waves, following the approach in Section 45.4.4 for surface gravity waves.

EXERCISE 45.6: STOKES DRIFT FOR ONE-DIMENSIONAL MONOCHROMATIC WAVE

Consider a one-dimensional monochromatic longitudinal wave with velocity

$$u = u_0 \sin(k x - \omega t), \quad (45.171)$$

where u_0 is the wave amplitude, $k = 2\pi/\Lambda > 0$ the wave number, Λ the wavelength, $\omega = 2\pi/T$ the radial frequency, T the wave period, and $C_p = \omega/k = \Lambda/T$ the phase speed. A longitudinal wave is one whose particle motions are parallel to the wave vector, which in this exercise are both in the \hat{x} direction. Determine the wave period averaged Stokes velocity to first order accuracy in the small parameter

$$\epsilon = u_0/C_p = u_0 k/\omega = u_0 T/\Lambda, \quad (45.172)$$

with this parameter the ratio of the wave amplitude to wave speed, or equivalently the ratio of the length scale of particle displacements to the wavelength. Hint: make use of the general result given by equation (45.135).



Chapter 46

INERTIAL WAVES

In this chapter we study basic features of *inertial waves*, which are dispersive waves that occur in rotating fluids. Inertial waves arise from the Coriolis acceleration, and we study them in a homogeneous inviscid fluid on an unbounded f -plane. They are referred to as “inertial” since their energy is entirely kinetic. These waves are related to the anti-cyclonic *inertial oscillations* we studied in Section 12.5.

READER’S GUIDE TO THIS CHAPTER

For our study of inertial waves, we assume a working knowledge of rotational fluid mechanics from Chapter 28.

46.1	Loose threads	1197
46.2	Inertial waves in a homogeneous fluid	1198
46.2.1	Inertial oscillations of a fluid ring	1198
46.2.2	Linear theory for a rotating homogeneous fluid	1198
46.2.3	Formulating the inertial wave equation	1201
46.2.4	Dispersion relation for inertial waves	1202
46.2.5	Interpreting the dispersion relation	1203
46.2.6	Group velocity	1204
46.2.7	Relating the velocity components	1205
46.2.8	Inertial waves with $\omega \approx f $	1205
46.2.9	Inertial waves with $\omega \approx 0$	1206
46.2.10	Connecting to Taylor-Proudman	1207
46.2.11	Further study	1208
46.3	Exercises	1208

46.1 Loose threads

- Energetics of inertial waves
- Bring the inertial waves material into a new chapter “Inertial and inertia-gravity waves”, taking some of that material from the now quite large gravity waves chapter.
- More on structure of inertial waves including details of the polarization relations.
- Change the angle used for inertial waves to correspond to that used for inertia gravity waves in Section 49.10.
- Stokes drift

- Resolve the notational ambiguity between ϖ and ω .

46.2 Inertial waves in a homogeneous fluid

The vertical stiffness exhibited by the *Taylor-Proudman effect* (Section 28.5.3) has a somewhat magical appearance. As with any apparent action at a distance in classical physics, the causal mechanism for this effect arises through waves. Here, we study the *inertial waves* that provide the mechanism for mediating vertical stiffening. We expose the basics of inertial waves in a homogeneous and constantly rotating fluid without boundaries. Note that we do *not* make the hydrostatic approximation.

46.2.1 Inertial oscillations of a fluid ring

We start by considering a thought experiment consisting of a coherent and axially symmetric fluid ring within the horizontal plane. Let the plane be rotating about the vertical axis, $\Omega = \Omega \hat{z}$, that extends through the center of the ring (Figure 46.1). Now perturb the ring by expanding its radius outward, say by imposing a radial pressure gradient. This perturbation gives the ring a larger moment of inertia computed relative to the rotational axis. In Section 21.5, we studied a fluid ring looped around the planet. As in that case, the constraint imposed by angular momentum conservation (computed relative to the rotational axis) requires the ring to rotate anti-cyclonically (clockwise if $\Omega > 0$) in response to a perturbation that increases its radius.¹ Equivalently, radially outward motion induces a Coriolis acceleration that causes the ring to rotate clockwise (anti-cyclonic). In turn, as the ring rotates anti-cyclonically, each fluid particle within the ring experiences a radial Coriolis acceleration pointing towards the center of the ring (to the right of the particle motion). This Coriolis acceleration halts the outward perturbation and returns the ring towards a smaller radius, with the inward motion leading to a further Coriolis acceleration that causes the ring to rotate cyclonically (again, to the right of the inward particle motion). The whole process oscillates between radially outward and anti-cyclonic rotation, and radially inward and cyclonic rotation. These oscillations of a fluid ring exhibit the basic mechanism of inertial waves.

46.2.2 Linear theory for a rotating homogeneous fluid

We here formulate the basic linearized velocity and vorticity equations for a rotating homogeneous fluid.

Nonlinear velocity equation

Consider a homogeneous inviscid fluid on a rotating reference frame governed by the momentum equation

$$[\partial_t + (\mathbf{v} \cdot \nabla)] \mathbf{v} + 2\boldsymbol{\Omega} \times \mathbf{v} = -\nabla p/\rho - g \hat{z}, \quad (46.1)$$

where g is the effective gravitational acceleration that arises from central gravity and planetary centrifugal (Section 11.11.4). For the most part, we have in mind the *f*-plane case with $\boldsymbol{\Omega} = \Omega \hat{z} = (f/2) \hat{z}$. However, allowing for an arbitrary orientation of $\boldsymbol{\Omega}$ assists in exposing certain of the geometric features of the waves.

¹In Figure 21.3 we studied the angular momentum of an axially symmetric ring of fluid around the planet. Axial symmetry means there are no zonal pressure gradients so that axial angular momentum is materially constant for the earth spanning fluid ring. Here we are making use of the same angular momentum constraint for an axially symmetric ring of fluid in a rotating plane.

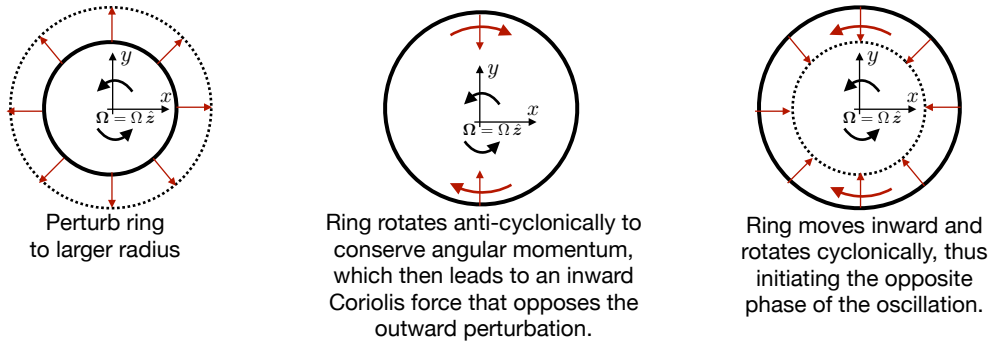


FIGURE 46.1: Schematic of inertial oscillations of an axially symmetric ring of fluid in the horizontal plane in the presence of rotation, $\Omega = \Omega \hat{z}$ with $\Omega > 0$, where the rotation axis extends through the ring center. The left panel shows the ring perturbed outward, with this perturbation increasing the ring's moment of inertia about the vertical axis running through the center of the ring. To conserve angular momentum the ring must turn opposite to the sense of the rotating reference frame; that is, it rotates anti-cyclonically, as shown in the middle panel. As it turns anti-cyclonically the ring generates a Coriolis acceleration that points inward (to the right of the motion), thus causing the ring to oscillate back to a smaller radius (right panel), where the oscillation turns around. The physics depicted in this figure, representing a three-way balance between linear acceleration, Coriolis acceleration, and pressure gradient acceleration, is summarized by the linear velocity equation (46.8).

As when formulating the Boussinesq approximation in Section 26.1.1, we find it useful to decompose pressure according to a static background hydrostatic pressure, plus a dynamical pressure

$$p = p_0 + \rho \varphi \quad \text{where} \quad dp_0/dz = -\rho g, \quad (46.2)$$

with ρ the constant density and $p_0(z)$ the static background hydrostatic pressure that exactly balances the fluid weight. This decomposition brings the momentum equation 46.1 to the form

$$[\partial_t + (\mathbf{v} \cdot \nabla)] \mathbf{v} + 2\boldsymbol{\Omega} \times \mathbf{v} = -\nabla \varphi \quad (46.3)$$

There is no buoyancy since density is uniform (Chapter 27). Hence, the only forces contributing to motion arise from Coriolis and pressure.

Nonlinear vorticity equation

In addition to the velocity equation, we make use of the vorticity equation, whose nonlinear form is derived from the vector invariant velocity equation (see Section 37.3.1)

$$\partial_t \mathbf{v} + (2\boldsymbol{\Omega} + \boldsymbol{\omega}) \times \mathbf{v} = -\nabla(\varphi + \mathcal{K}), \quad (46.4)$$

where we introduced the kinetic energy per mass and the relative vorticity

$$\mathcal{K} = \mathbf{v} \cdot \mathbf{v}/2 \quad \text{and} \quad \boldsymbol{\omega} = \nabla \times \mathbf{v}. \quad (46.5)$$

The vorticity equation (37.41) takes on the following form with a constant density inviscid fluid

$$[\partial_t + (\mathbf{v} \cdot \nabla)] \boldsymbol{\omega}_a = (\boldsymbol{\omega}_a \cdot \nabla) \mathbf{v} \quad \text{with} \quad \boldsymbol{\omega}_a = 2\boldsymbol{\Omega} + \boldsymbol{\omega}. \quad (46.6)$$

Noting that $\boldsymbol{\Omega}$ is independent of space and time allows us to write an equation for the relative vorticity

$$\partial_t \boldsymbol{\omega} = [(2\boldsymbol{\Omega} + \boldsymbol{\omega}) \cdot \nabla] \mathbf{v}. \quad (46.7)$$

Linear velocity equation

We are interested in small amplitude fluctuations relative to a state of zero motion. Linearization of the velocity equation (46.3) occurs by dropping the self-advection term, $(\mathbf{v} \cdot \nabla) \mathbf{v}$, thus leading to

$$\partial_t \mathbf{v} + 2 \boldsymbol{\Omega} \times \mathbf{v} = -\nabla \varphi. \quad (46.8)$$

With $\boldsymbol{\Omega}$ independent of time, we see that the velocity projected onto $\boldsymbol{\Omega}$ satisfies

$$\partial_t (\mathbf{v} \cdot \boldsymbol{\Omega}) = -\boldsymbol{\Omega} \cdot \nabla \varphi. \quad (46.9)$$

Hence, if there is no pressure gradient along the direction of the rotation axis, then the velocity of the linear flow in that direction remains constant in time. For example, if the rotation is around the vertical axis, $\boldsymbol{\Omega} = \Omega \hat{\mathbf{z}}$, and there is no vertical dynamic pressure gradient, $\partial_z \varphi = 0$, then the vertical velocity is static, $\partial_t w = 0$.

Specializing to the case of Figure 46.1

The linear velocity equation (46.8) contains the essential physics of Figure 46.1. In this particular example, the pressure is vertically and axially symmetric and the rotation vector is vertical, so that

$$\partial_t \mathbf{v} + 2 \Omega \hat{\mathbf{z}} \times \mathbf{v} = -\hat{\mathbf{r}} \partial_r \varphi, \quad (46.10)$$

where $\hat{\mathbf{r}}$ is the horizontal radial vector from cylindrical coordinates (see Section 9.3.2). We observe that $\partial_t w = 0$, which follows from equation (46.9) since we are assuming no pressure gradient along the rotation axis. Equation (46.10) presents a three-way balance between linear acceleration, Coriolis acceleration, and radial pressure gradient acceleration. As discussed in the context of Figure 46.1, radial motion induces an angular Coriolis acceleration that then leads to angular motion, which in turn leads to radial Coriolis acceleration. Oscillations between the three-way balance are deduced through the following analysis.

Forced oscillator equation for velocity

Taking a time derivative on the velocity equation (46.8) and back-substituting the velocity equation leads to

$$\partial_{tt} \mathbf{v} + 4 \Omega^2 \mathbf{v} - 4 \boldsymbol{\Omega} (\mathbf{v} \cdot \boldsymbol{\Omega}) = 2 \boldsymbol{\Omega} \times \nabla \varphi - \partial_t \nabla \varphi. \quad (46.11)$$

Now decompose the velocity according to the orientation of the rotation vector

$$\hat{\boldsymbol{\Omega}} = \boldsymbol{\Omega} / |\boldsymbol{\Omega}| \quad (46.12a)$$

$$\mathbf{v} = \mathbf{v}_\perp + \mathbf{v}_\parallel \quad (46.12b)$$

$$\mathbf{v}_\perp = \mathbf{v} - \hat{\boldsymbol{\Omega}} (\hat{\boldsymbol{\Omega}} \cdot \mathbf{v}) \quad (46.12c)$$

$$\mathbf{v}_\parallel = \mathbf{v} - \mathbf{v}_\perp = \hat{\boldsymbol{\Omega}} (\hat{\boldsymbol{\Omega}} \cdot \mathbf{v}), \quad (46.12d)$$

which allows us to decompose equation (46.11) into an equation for the parallel velocity and one for the perpendicular velocity

$$\partial_t [\hat{\boldsymbol{\Omega}} \cdot (\partial_t \mathbf{v} + \nabla \varphi)] = 0 \quad (46.13a)$$

$$(\partial_{tt} + 4 \Omega^2) \mathbf{v}_\perp = 2 \hat{\boldsymbol{\Omega}} \times \nabla \varphi - \partial_t [\nabla \varphi - \hat{\boldsymbol{\Omega}} (\hat{\boldsymbol{\Omega}} \cdot \nabla \varphi)] \quad (46.13b)$$

Equation (46.13a) says that the projection of $\partial_t \mathbf{v} + \nabla \varphi$ onto the rotation axis remains constant in time. For example, if $\widehat{\boldsymbol{\Omega}} = \hat{\mathbf{z}}$ then

$$\partial_t(\partial_t w + \partial_z \varphi) = 0. \quad (46.14)$$

Equation (46.13b) is a forced simple harmonic oscillator equation for motion in the plane perpendicular to the rotation axis. The natural angular frequency is 2Ω and the forcing arises from pressure gradients in the perpendicular plane. Again, for the case with $\widehat{\boldsymbol{\Omega}} = \hat{\mathbf{z}}$, equation (46.13b) takes the form

$$(\partial_{tt} + 4\Omega^2) \mathbf{u} = 2\Omega \hat{\mathbf{z}} \times \nabla \varphi - \partial_t \nabla_z \varphi. \quad (46.15)$$

The appearance of an oscillator equation anticipates the simple harmonic oscillations of fluid particles within a linear wave.

Linear vorticity equation

Taking the curl of the linear velocity equation (46.8) eliminates the pressure gradient and yields the linear vorticity equation

$$\partial_t \boldsymbol{\omega} = 2(\boldsymbol{\Omega} \cdot \nabla) \mathbf{v}. \quad (46.16)$$

To reach this result requires the identity (2.36h) for the curl of a cross product. We also assumed $\boldsymbol{\Omega}$ has no spatial dependence so that all of its derivatives vanish.

The linear vorticity equation (46.16) can also be derived by linearizing the nonlinear vorticity equation (46.7) by dropping the contributions from nonlinear stretching and tilting, which are processes we studied in Section 37.5. So the only source for vorticity in the linear theory arises from stretching and tilting along the rotational axis. That is, from the derivative of velocity in a direction aligned with the rotational axis. For example, if $\boldsymbol{\Omega} = \Omega \hat{\mathbf{z}}$, then the vorticity evolves according to

$$\partial_t \boldsymbol{\omega} = 2\Omega \partial_z \mathbf{v}, \quad (46.17)$$

in which case the horizontal vorticity components evolve according to vertical tilting whereas the vertical component evolves according to vertical stretching²

$$\partial_t(\hat{\mathbf{x}} \cdot \boldsymbol{\omega}) = 2\Omega \partial_z u \quad \text{and} \quad \partial_t(\hat{\mathbf{y}} \cdot \boldsymbol{\omega}) = 2\Omega \partial_z v \quad \text{and} \quad \partial_t(\hat{\mathbf{z}} \cdot \boldsymbol{\omega}) = 2\Omega \partial_z w. \quad (46.18)$$

Evidently, inertial waves carry a non-zero vorticity, and that vorticity is directly generated by the rotation vector, $\boldsymbol{\Omega}$, in the presence of velocity gradients.

46.2.3 Formulating the inertial wave equation

To develop a wave equation, we take a time derivative of the linear vorticity equation (46.16), and make use of the linearized momentum equation (46.8), thus leading to

$$\partial_{tt} \boldsymbol{\omega} = -2(\boldsymbol{\Omega} \cdot \nabla)(2\boldsymbol{\Omega} \times \mathbf{v} + \nabla \varphi). \quad (46.19)$$

To eliminate the pressure gradient we take another curl and again make use of the identity (2.36h) to write

$$\nabla \times \boldsymbol{\omega} = \nabla \times (\nabla \times \mathbf{v}) = \nabla(\nabla \cdot \mathbf{v}) - \nabla^2 \mathbf{v} = -\nabla^2 \mathbf{v}, \quad (46.20)$$

²We study vortex stretching and tilting in Section 37.5.3.

where $\nabla \cdot \mathbf{v} = 0$ since the fluid density is constant. We also make use of Cartesian tensor calculus from Chapter 2 to derive the identity

$$(\nabla \times [(\boldsymbol{\Omega} \cdot \nabla) (\boldsymbol{\Omega} \times \mathbf{v})])_m = \epsilon_{mnp} \partial_n [\Omega_s \partial_s (\boldsymbol{\Omega} \times \mathbf{v})_p] \quad (46.21a)$$

$$= \epsilon_{mnp} \partial_n [\Omega_s \partial_s \epsilon_{pqr} \Omega_q v_r] \quad (46.21b)$$

$$= \epsilon_{mnp} \epsilon_{qrp} \Omega_s \Omega_q \partial_n \partial_s v_r \quad (46.21c)$$

$$= (\delta_{mq} \delta_{nr} - \delta_{mr} \delta_{nq}) \Omega_s \Omega_q \partial_n \partial_s v_r \quad (46.21d)$$

$$= \Omega_s (\Omega_m \partial_r \partial_s v_r - \Omega_n \partial_n \partial_s v_m) \quad (46.21e)$$

$$= -(\boldsymbol{\Omega} \cdot \nabla)^2 v_m, \quad (46.21f)$$

where we made use of the ϵ -tensor identity (1.38) as well as $\nabla \cdot \mathbf{v} = 0$. We are thus led to the wave equation for inertial waves, which is satisfied separately for each of the Cartesian components of the velocity field

$$[\partial_{tt} \nabla^2 + (2 \boldsymbol{\Omega} \cdot \nabla)^2] \mathbf{v} = 0 \iff \partial_{tt} (\nabla \times \boldsymbol{\omega}) = (2 \boldsymbol{\Omega} \cdot \nabla)^2 \mathbf{v}. \quad (46.22)$$

The second expression makes use of equation (46.20) that relates the curl of the vorticity to the Laplacian of the velocity.

46.2.4 Dispersion relation for inertial waves

The inertial wave equation (46.22) provides the starting point for developing mechanical properties of inertial waves. To develop the dispersion relation we consider a traveling plane wave solution of the form

$$\mathbf{v} = \tilde{\mathbf{v}} e^{i(\mathbf{k} \cdot \mathbf{x} - \omega t)} \quad \text{and} \quad \varphi = \tilde{\varphi} e^{i(\mathbf{k} \cdot \mathbf{x} - \omega t)}, \quad (46.23)$$

with three-dimensional wavevector and wave direction unit vector

$$\mathbf{k} = \hat{\mathbf{x}} k_x + \hat{\mathbf{y}} k_y + \hat{\mathbf{z}} k_z \quad \text{and} \quad \hat{\mathbf{k}} = (\hat{\mathbf{x}} k_x + \hat{\mathbf{y}} k_y + \hat{\mathbf{z}} k_z) / |\mathbf{k}|. \quad (46.24)$$

We introduced complex amplitudes, $\tilde{\mathbf{v}}$ and $\tilde{\varphi}$, for the velocity and pressure. The angular frequency, $\omega \geq 0$, is determined as a function of the wavevector according to the dispersion relation (46.26) derived below.³ As we are considering free space waves (no boundaries), there is no preferred length scale for inertial waves. Furthermore, since the flow is non-divergent and the waves have a three dimensional wavevector, the constraint $\nabla \cdot \mathbf{v} = 0$ means that the velocity of fluid particles is perpendicular to the wavevector

$$\mathbf{v} \cdot \mathbf{k} = 0. \quad (46.25)$$

This orientation of wavevector and fluid velocity characterizes *transverse waves*, in which lines of constant wave phase (e.g., wave crests and troughs) are everywhere perpendicular to \mathbf{k} . We illustrate this property of transverse waves in Figure 46.2.

Plugging the wave ansatz (46.23) into the inertial wave equation (46.22) leads to the *dispersion relation*

$$\omega^2 = \varpi^2(\mathbf{k}) = (2 \boldsymbol{\Omega} \cdot \mathbf{k})^2 / |\mathbf{k}|^2 = (2 \boldsymbol{\Omega} \cdot \hat{\mathbf{k}})^2. \quad (46.26)$$

As per our previous encounter with waves, we recognize that the dispersion relation specifies the inertial wave's angular frequency, ω , once the wavevector is chosen. We write $\omega = \varpi(\mathbf{k})$ when wishing to distinguish the angular frequency, ω , from the function, ϖ , determining the angular frequency. We illustrate the basics of inertial waves in Figure 46.3.

³Be careful to distinguish the angular frequency, ω , from the vorticity vector, $\boldsymbol{\omega}$.

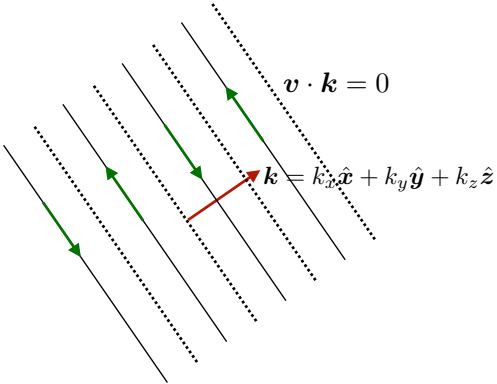


FIGURE 46.2: Illustrating the transverse nature of plane waves appearing in a homogeneous fluid with constant density, whereby $\mathbf{v} \cdot \mathbf{k} = 0$. The alternating solid-dotted lines depict lines of constant phase that differ by $\pi/2$ radians so that the velocity field switches sign between every π radians.

The dispersion relation (46.26) means that the angular frequency of inertial waves is directly proportional to the orientation of the wavevector relative to the rotation vector. Furthermore, it is independent of the magnitude of the wave vector. One way to display these geometric properties is to write

$$\Omega \cdot \hat{\mathbf{k}} = |\Omega| \cos \gamma \quad \text{with} \quad -\pi \leq \gamma \leq \pi, \quad (46.27)$$

where γ is the angle between $\boldsymbol{\Omega}$ and \mathbf{k} . The dispersion relation (46.26) thus takes on the particularly compact form

$$\omega^2 = (2\Omega \cos \gamma)^2. \quad (46.28)$$

Sweeping through the possible orientation angles, γ , reveals that the angular frequency (which is a non-negative number) for free space inertial waves spans the continuum range

$$0 \leq \omega \leq 2|\Omega|. \quad (46.29)$$

Since the magnitude of the angular frequency is bounded above by $2|\Omega| = |f|$, such waves are referred to as *sub-inertial*.⁴

46.2.5 Interpreting the dispersion relation

The dispersion relation (46.28) is quite striking. To help understand its origin, recall that inertial waves are transverse: $\mathbf{v} \cdot \mathbf{k} = 0$ (Figure 46.3). Hence, fluid particle motion associated with inertial waves occurs in directions that are parallel to the constant phase surfaces.⁵ Now all dynamical fields have the same geometric structure within a plane wave, so that all fields are spatially constant along a phase surface. It follows that there is no spatial pressure gradient along a constant phase surface at any particular time instance. Hence, fluid particles moving parallel to the phase surfaces only feel the Coriolis acceleration.⁶

⁴In Section 48.7.5 we find that shallow water waves in the presence of gravity and rotation have their angular frequency bounded below by $|f|$, in which case these shallow water *inertia-gravity* waves are *super-inertial*.

⁵We emphasize the distinction between fluid particle motion and wave motion. Namely, a fluid particle moves in the direction of a phase surface but it does not remain on a fixed phase surface. It is the oscillatory motion of the fluid particles in the transverse direction that constitutes the plane wave.

⁶The argument here holds either in an Eulerian reference frame, in which case we ignore the nonlinear self-advection contribution as per the linearized velocity equation (46.8), or in a Lagrangian reference frame, in which we are following a material fluid particle. In either case, motion of a fluid particle in an inertial wave, moving in a direction that parallels the constant phase surfaces, feels only the Coriolis acceleration; pressure forces are zero.

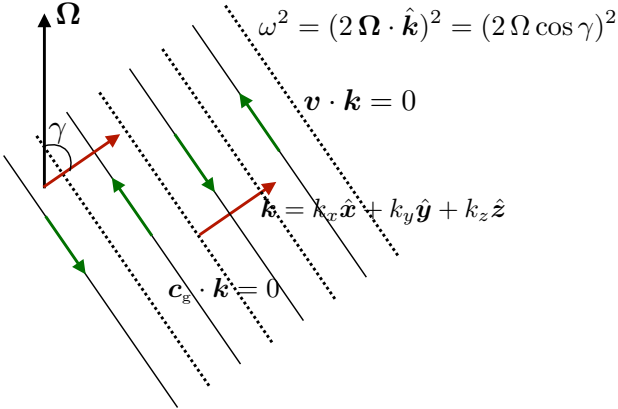


FIGURE 46.3: Illustrating the transverse nature of inertial waves, with their dispersion relation given by equation (46.26), whereby $\omega^2 = (2\Omega \cdot \hat{\mathbf{k}})^2 = (2\Omega \cos \gamma)^2$. We show lines of constant phase separated by $\pi/2$ radians so that for the velocity switches sign ever other line. Evidently, the frequency of inertial waves is maximized when the wavevector, \mathbf{k} , is aligned with the rotation vector, $\boldsymbol{\Omega}$, so that the angle $\gamma = 0$. In contrast, the angular frequency vanishes when the wavevector is orthogonal to $\boldsymbol{\Omega}$. The waves are transverse, $\mathbf{v} \cdot \mathbf{k} = 0$, so that fluid particle motion occurs within surfaces of constant phase. Furthermore, the group velocity is parallel to the fluid particle velocity since, according to equation (46.34), it satisfies $\mathbf{c}_g \cdot \mathbf{k} = 0$. Note that the angle γ in this image corresponds to the co-latitude if we let $\boldsymbol{\Omega}$ correspond to the planetary rotation. To connect to the planetary Coriolis parameter we set $\phi = \pi/2 - \gamma$, where ϕ is the latitude.

Recall that a particle moving in a rotating reference frame exhibits inertial oscillations (Section 12.5) when the particle does not feel any pressure forces. If the wavevector is aligned parallel to the rotation vector, then a fluid particle feels the Coriolis acceleration due to the full extent of the rotation. In this case the inertial oscillations have a squared angular frequency $(2\Omega \cdot \hat{\mathbf{k}})^2$. This situation corresponds to a particle at either of the poles, where it feels the full planetary rotation.⁷ When the wavevector is mis-aligned from the rotation vector, then only that portion of the rotation vector projected onto $\hat{\mathbf{k}}$ acts to produce inertial oscillations. Finally, if the wavevector is perpendicular to the rotation vector, then the particle feels no Coriolis acceleration, just like a particle on the equator feels no planetary Coriolis acceleration.

46.2.6 Group velocity

As seen from our discussion of wave packets in Section 43.6, the group velocity determines the speed and direction of wave energy propagation, with the group velocity given by the wavevector gradient of the dispersion relation

$$\mathbf{c}_g = \nabla_{\mathbf{k}} \varpi = \hat{\mathbf{x}} \frac{\partial \varpi}{\partial k_x} + \hat{\mathbf{y}} \frac{\partial \varpi}{\partial k_y} + \hat{\mathbf{z}} \frac{\partial \varpi}{\partial k_z}. \quad (46.30)$$

Making use of the dispersion relation (46.26) renders

$$\mathbf{c}_g = \frac{4(\boldsymbol{\Omega} \cdot \hat{\mathbf{k}})[\boldsymbol{\Omega} - \hat{\mathbf{k}}(\boldsymbol{\Omega} \cdot \hat{\mathbf{k}})]}{\omega |\mathbf{k}|} = \frac{(\boldsymbol{\Omega} \cdot \hat{\mathbf{k}})}{|\boldsymbol{\Omega} \cdot \hat{\mathbf{k}}|} \frac{\hat{\mathbf{k}} \times (2\boldsymbol{\Omega} \times \hat{\mathbf{k}})}{|\mathbf{k}|} \quad (46.31)$$

where we made use of the vector identity (1.40b). Since

$$\boldsymbol{\Omega} \cdot \hat{\mathbf{k}} = \pm |\boldsymbol{\Omega} \cdot \hat{\mathbf{k}}| \quad (46.32)$$

⁷From Figure 46.3 we note that the angle γ is the co-latitude, so to connect to the planetary Coriolis parameter we set $\phi = \pi/2 - \gamma$ where ϕ is the latitude.

we can write the group velocity as

$$\mathbf{c}_g = \pm \frac{\hat{\mathbf{k}} \times (2\boldsymbol{\Omega} \times \hat{\mathbf{k}})}{|\mathbf{k}|}. \quad (46.33)$$

This expression leads to a particularly remarkable property of the group velocity for inertial waves

$$\mathbf{k} \cdot \mathbf{c}_g = 0. \quad (46.34)$$

Since $\mathbf{k} \cdot \mathbf{v} = 0$, we see that the group velocity is aligned with the fluid particle velocity. The Coriolis acceleration acts perpendicular to the direction of a moving fluid particle. That orientation manifests for inertial waves via $\mathbf{k} \cdot \mathbf{c}_g = 0$, so that inertial waves carry energy (via the group velocity) in a direction parallel to wave crests (perpendicular to \mathbf{k}), which is aligned with fluid particle motion. A second property of the group velocity is found by projecting it onto the direction of the rotational axis

$$\mathbf{c}_g \cdot \boldsymbol{\Omega} = \pm 2 [\Omega^2 \mathbf{k} \cdot \mathbf{k} - (\boldsymbol{\Omega} \cdot \mathbf{k})^2] / |\mathbf{k}|^3 = \pm 2 [\Omega^2 - (\omega/2)^2] / |\mathbf{k}| = \pm 2 (\Omega^2 / |\mathbf{k}|) \sin^2 \gamma, \quad (46.35)$$

where we made use of the expressions (46.26) and (46.28) for the dispersion relation.

46.2.7 Relating the velocity components

The velocity amplitude, $\tilde{\mathbf{v}}$, is generally a complex number, which allows for there to be a variety of phase shifts between the velocity components. We here determine some general relations between these amplitudes by returning to the linear velocity equation (46.8) and inserting the wave ansatz (46.23) to render

$$-\mathrm{i}\omega \tilde{u} - f \tilde{v} = -\mathrm{i}k_x \tilde{\varphi} \quad (46.36a)$$

$$-\mathrm{i}\omega \tilde{v} + f \tilde{u} = -\mathrm{i}k_y \tilde{\varphi} \quad (46.36b)$$

$$-\mathrm{i}\omega \tilde{w} = -\mathrm{i}k_z \tilde{\varphi}. \quad (46.36c)$$

For simplicity we assumed the rotation vector is aligned with the vertical direction so that $2\boldsymbol{\Omega} = f\hat{\mathbf{z}}$. Manipulations with the horizontal velocity equations lead to the relations between the horizontal velocity amplitudes

$$\tilde{u} (f^2 - \omega^2) = -\tilde{\varphi} (k_x \omega + \mathrm{i}k_y f) \quad (46.37a)$$

$$\tilde{v} (f^2 - \omega^2) = \tilde{\varphi} (-k_y \omega + \mathrm{i}k_x f) \quad (46.37b)$$

$$\frac{\tilde{u}}{\tilde{v}} = \frac{-k_x k_y (f^2 - \omega^2) + \mathrm{i}\omega f (k_x^2 + k_y^2)}{(k_y \omega)^2 + (k_x f)^2} \quad (46.37c)$$

$$\frac{\tilde{w}}{\tilde{v}} = \frac{k_z}{k_x} \left[\frac{\tilde{u}}{\tilde{v}} - \mathrm{i} \frac{f}{\omega} \right]. \quad (46.37d)$$

We make use of these relations in the following.

46.2.8 Inertial waves with $\omega \approx |f|$

The dispersion relation (46.28) leads to a maximum angular frequency magnitude for a wavevector aligned parallel or anti-parallel to the rotation axis,

$$\mathbf{k} \times \boldsymbol{\Omega} = 0 \implies \omega = 2|\boldsymbol{\Omega}| = |f|. \quad (46.38)$$

Recall that inertial waves are transverse so that $\mathbf{v} \cdot \mathbf{k} = 0$. This property, in combination with $\mathbf{k} \times \boldsymbol{\Omega} = 0$, means that high frequency inertial waves have fluid particle motion in a plane perpendicular to the rotation axis: $\mathbf{v} \cdot \boldsymbol{\Omega} = 0$. For example, if the rotation vector is vertical, then the wavevector only has a vertical component, $\mathbf{k} = k_z \hat{\mathbf{z}}$; i.e., the plane waves are propagating vertically.

For inertial waves with $\omega = |f| > 0$ and $\mathbf{k} = k_z \hat{\mathbf{z}}$, the fluid velocity amplitude relation (46.37d) indicates that $\tilde{u}/\tilde{v} = i$ so that the horizontal velocity of the wave is given by

$$\mathbf{u}/\tilde{u} = \hat{\mathbf{x}} e^{i(k_z z - |f| t)} + \hat{\mathbf{y}} e^{i(k_z z - |f| t - \pi/2)}, \quad (46.39)$$

which is a vertically propagating plane wave. Taking the real part renders

$$\mathbf{u}/\tilde{u} = \hat{\mathbf{x}} \cos(k_z z - |f| t) + \hat{\mathbf{y}} \sin(k_z z - |f| t). \quad (46.40)$$

With $k_x = k_y = 0$ in the velocity equations (46.36a) and (46.36b), we see that there is no coupling between the horizontal velocity components and pressure. Hence, the motion of fluid particles reduces to inertial oscillations in the horizontal plane just as we studied for point particle motion in Section 12.5. As a check, we see that for a fixed vertical position, say $z = 0$, the velocity relation (46.40) for inertial waves is identical the velocity relation (12.15b) for particles undergoing inertial oscillations in a circle with a constant radius

$$\mathbf{u}/\tilde{u} = \hat{\mathbf{x}} \cos(|f| t) - \hat{\mathbf{y}} \sin(|f| t) \quad \text{for } z = 0 \text{ and } \omega = |f|. \quad (46.41)$$

In oceanography, inertial waves with $\omega \approx |f|$ are referred to as *near inertial waves*, which refers to their angular frequency being close to the Coriolis frequency. Since near inertial waves have their wavevector oriented close to the rotation axis, equation (46.33) indicates that they also have a vanishingly small group velocity.

46.2.9 Inertial waves with $\omega \approx 0$

Low frequency inertial waves occur when the wavevector is nearly perpendicular to the rotation axis

$$\boldsymbol{\Omega} \cdot \mathbf{k} \approx 0 \implies \omega/\Omega \approx 0. \quad (46.42)$$

Hence, the wave number parallel to the rotation axis is vanishingly small. For example, if the rotation axis is vertical, then low frequency inertial waves have a vanishingly small vertical wave number,

$$k_z^2 \ll k_x^2 + k_y^2. \quad (46.43)$$

Correspondingly, for the velocity vector in the form given by equation (46.23), $\boldsymbol{\Omega} \cdot \mathbf{k} \approx 0$ means that

$$(\boldsymbol{\Omega} \cdot \nabla) \mathbf{v} = i(\boldsymbol{\Omega} \cdot \mathbf{k}) \mathbf{v} \approx 0. \quad (46.44)$$

That is, the velocity vector for low frequency inertial waves is coherent in the direction aligned with the rotation axis. Furthermore, when $\boldsymbol{\Omega} \cdot \mathbf{k} \approx 0$, the group velocity (46.35) has a magnitude

$$|\mathbf{c}_g| \approx 2 |\Omega| / |\mathbf{k}|. \quad (46.45)$$

Evidently, low frequency inertial waves with long wavelength (small wavenumber $|\mathbf{k}|$) quickly transmit their energy along the direction of the rotation axis.

46.2.10 Connecting to Taylor-Proudman

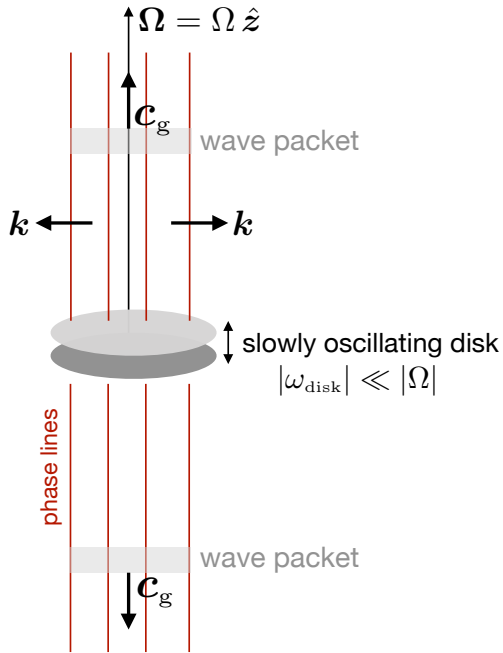


FIGURE 46.4: Schematic of inertial waves generated by a slowly oscillating disk in a rotating homogeneous fluid. The disk moves along the rotation axis (vertical axis) in small amplitude oscillations whose angular frequency is much smaller than the rotational angular frequency, $\omega_{\text{disk}} \ll |\Omega|$. The oscillating disk preferentially generates inertial waves whose frequency is close to ω_{disk} ; i.e., low frequency inertial waves as discussed in Section 46.2.9. The phase lines and group velocity for these waves are parallel to the rotation axis, and the wavevector is perpendicular to the rotation axis. We depict two wave packets that send energy vertically away from the disk, with the long wave and low frequency waves having the highest magnitude for the group velocity. Since $\boldsymbol{\Omega} \cdot \mathbf{k} = 0$, the fluid particle velocity associated with the inertial waves is constant in the direction along the rotation axis: $(\boldsymbol{\Omega} \cdot \nabla) \mathbf{v} = 0$.

We bring the previous notions together by heuristically describing a realization of low frequency inertial waves transmitting information about vertical stiffening, with reference to Figure 46.4. For this purpose, imagine a slowly oscillating disk and that moves in a direction aligned with the rotation axis. If the oscillation frequency is much slower than the rotation frequency, $\omega_{\text{disk}} \ll |\Omega|$, then the disk generates low frequency inertial waves at the frequency of the oscillating disk, $\omega = \omega_{\text{disk}}$. Following from our discussion in Section 46.2.9, we know that the low frequency inertial waves have a wavevector oriented perpendicular to the rotation axis, $\boldsymbol{\Omega} \cdot \mathbf{k} = 0$, as depicted in Figure 46.4. Since inertial waves have a group velocity that is itself perpendicular to the wavevector, the low frequency inertial waves have a group velocity parallel to the rotation axis: $\boldsymbol{\Omega} \times \mathbf{c}_g = 0$.

As seen by the equation (46.45) for the group velocity magnitude, information (i.e., energy) concerning the oscillating disk is most rapidly transmitted by long wavelength low frequency inertial waves. Such low frequency and long wavelength inertial waves generate fluid particle motion that is independent of the position along the rotational axis since $(\boldsymbol{\Omega} \cdot \nabla) \mathbf{v} = 0$. Hence, the particle motion occurs in the plane perpendicular to the rotational axis, and this motion is coherent in the direction along the rotation axis. We conclude that inertial waves transmit information about stiffening along the rotation axis, thus providing a mechanism for the Taylor-Proudman effect from Section 28.5.3.

46.2.11 Further study

Our discussion of inertial waves was inspired by Section 9.2 of [Davidson \(2015\)](#), who emphasizes the role of inertial waves in forming vertically stiff structures in rapidly rotating turbulent flows. A further pedagogical analysis of inertial waves is provided by [Mory \(1992\)](#) as well as the Epilogue of [Lighthill \(1978\)](#). For a visualization of inertial waves, refer to the 18 minute mark from the [rotating tank experiments of Prof. Fultz](#). He illustrates inertial oscillations within a bounded rotating homogeneous fluid, where the presence of boundaries quantizes the frequency of the excited inertial waves much like the gravity wave seiche modes discussed in Section 45.6.



46.3 Exercises



Chapter 47

BAROTROPIC VORTICITY WAVES

In this chapter we study basic features of waves reliant on vorticity of the base state. These *Rossby waves* arise in the presence of a gradient in the background potential vorticity field, and as such they are sometimes called *vorticity waves* or *vortical modes*. We study Rossby waves in the inviscid two-dimensional non-divergent barotropic model as posed on an unbounded β -plane. This model supports two kinds of Rossby waves: one arising from the gradient of planetary vorticity (i.e., β -effect), which gives rise to *planetary Rossby waves*, and a second arising from gradients in the vorticity of a base flow. We also study *edge waves*, which are waves that arise from a jump in the background vorticity field.

READER'S GUIDE TO THIS CHAPTER

We make extensive use of the horizontally non-divergent barotropic model from Chapter 35.

47.1	Loose threads	1210
47.2	Plane waves in a non-divergent barotropic fluid	1210
47.2.1	Transverse plane waves	1210
47.2.2	Absence of inertial waves and gravity waves	1211
47.2.3	Zero advection for a single plane wave	1211
47.2.4	Pressure equation for a single plane wave	1212
47.2.5	Velocity equation for a single plane wave	1212
47.2.6	Structure of a plane wave	1213
47.3	Barotropic and non-divergent Rossby waves	1214
47.3.1	The vorticity mechanism for planetary Rossby waves	1214
47.3.2	Flow relative to a static base state	1215
47.3.3	Rossby wave dispersion relation	1217
47.3.4	Concerning the westward phase velocity	1218
47.3.5	Stationary Rossby waves	1220
47.3.6	Group velocity	1220
47.4	Geometry of planetary Rossby waves	1221
47.4.1	Group and phase velocities for planetary Rossby waves	1221
47.4.2	Geometry of the group velocity for planetary waves	1221
47.4.3	Reflection of planetary Rossby waves	1223
47.5	Edge waves	1225
47.5.1	Replacing planetary vorticity by base state vorticity	1225
47.5.2	Point jet	1226
47.5.3	Vorticity equation and the absence of plane waves	1226
47.5.4	Rayleigh-Kuo equation	1227
47.5.5	Kinematic boundary condition at the interface	1228
47.5.6	Dynamic boundary condition at the interface	1228

47.5.7 Edge wave dispersion relation	1229
47.5.8 Comments and further study	1230
47.6 Exercises	1230

47.1 Loose threads

- Rossby waves on a sphere
- Put the Rossby wave material into a new chapter “Barotropic vorticity waves”, to also have edge waves as part of that new chapter.
- Rossby wave particle velocity and trajectories
- Rectification by Rossby waves that are radiated by a source; Section 5.4 of [McWilliams \(2006\)](#).
- Work through the Green’s function problem as in [Haidvogel and Rhines \(1983\)](#) as well as Bill Young’s Les Houches lectures.
- Need to assume base state has constant velocity so that $\zeta_b = 0$. Otherwise, the angular frequency is a function of space, and that is not consistent with the plane wave ansatz. This point needs to be cleaned up in this chapter.
- Stokes drift
- Energetics of Rossby waves
- Resolve the notational ambiguity between ϖ and ω .
- Are we really able to find plane wave solutions with a general ζ_b in Section 47.3? Seems I need to take a WKB approach? See Section 6.4.2 of [Vallis \(2017\)](#) where he assume the background zonal flow has a constant meridional shear. I might be fooling myself, or perhaps it is valid so long as equation (47.22) is maintained?

47.2 Plane waves in a non-divergent barotropic fluid

In this section we study properties of plane waves in an inviscid barotropic and horizontally non-divergent fluid on an unbounded beta plane. We then follow in Section 47.3 with a study of Rossby waves in this model. Recall that barotropic and horizontally non-divergent model was studied in Chapter 35, and the flow is fully described by the vorticity equation

$$\frac{D(\zeta + f)}{Dt} = (\partial_t + \mathbf{u} \cdot \nabla)(\zeta + f) = 0, \quad (47.1)$$

where the horizontal velocity is non-divergent and so can be written in terms of a streamfunction

$$\nabla \cdot \mathbf{u} = 0 \implies \mathbf{u} = \hat{\mathbf{z}} \times \nabla \psi \quad \text{and} \quad \zeta = \hat{\mathbf{z}} \cdot (\nabla \times \mathbf{u}) = \nabla^2 \psi. \quad (47.2)$$

47.2.1 Transverse plane waves

Consider a plane wave ansatz for the streamfunction

$$\psi(\mathbf{x}, t) = A \cos(\mathbf{k} \cdot \mathbf{x} - \omega t) \quad \text{with} \quad \mathbf{k} = k_x \hat{\mathbf{x}} + k_y \hat{\mathbf{y}}. \quad (47.3)$$

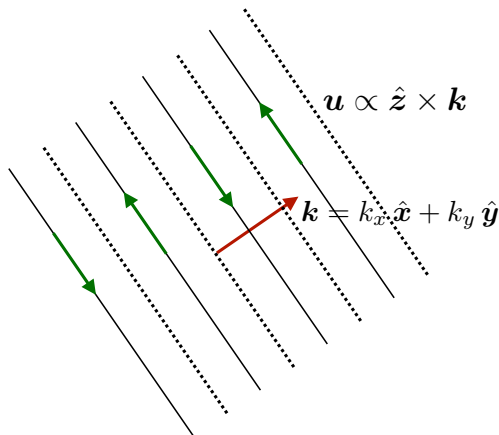


FIGURE 47.1: Illustrating the transverse nature of plane waves appearing in a horizontally non-divergent barotropic model, whereby $\mathbf{u} \cdot \mathbf{k} = 0$. The alternating solid-dotted lines depict lines of constant phase that differ by $\pi/2$ radians so that the velocity field switches sign between every π radians. Compare this figure to Figure 46.2, which illustrates transverse plane waves in three dimensions.

The velocity of fluid particles in the plane wave is thus given by

$$\mathbf{u} = -A(\hat{z} \times \mathbf{k}) \sin(\mathbf{k} \cdot \mathbf{x} - \omega t), \quad (47.4)$$

which then leads to

$$\mathbf{k} \cdot \mathbf{u} = 0. \quad (47.5)$$

Evidently, the horizontally propagating plane waves are transverse, as illustrated in Figure 47.1. This property compares to the three dimensional transverse inertial plane waves discussed in Section 46.2.4 and depicted in Figure 46.2.

47.2.2 Absence of inertial waves and gravity waves

Since there is no vertical motion in the two-dimensional non-divergent barotropic model, any wavevector must be horizontal and thus perpendicular to the vertically oriented rotation vector. Hence, the inertial wave dispersion relation (46.26) only admits a zero frequency mode, which is geostrophic balance. Furthermore, gravity waves are absent from this model since gravity waves vanish with a flow that has zero horizontal divergence (see discussion of shallow water gravity waves in Section 48.5). We thus conclude that the two-dimensional non-divergent barotropic model has neither inertial waves nor gravity waves.

As we will see, the only wave supported by this model occurs in the presence of a background or base state vorticity gradient, such as from planetary vorticity or the vorticity of a mean flow. In the absence of vorticity gradients, there are no linear waves in the two-dimensional non-divergent barotropic model. Such is the case, for example, in non-rotating and homogeneous two-dimensional flows, which are commonly used to study two-dimensional turbulence.

47.2.3 Zero advection for a single plane wave

Linearizing the equations of motion is a basic step in the development of a dispersion relation. For the vorticity equation appropriate for Rossby waves, linearization means neglecting the advection of relative vorticity. However, quite remarkably, there is no advection of relative vorticity for a plane wave in the horizontally non-divergent barotropic model. That is, the advection operator, $\mathbf{u} \cdot \nabla \zeta$, vanishes identically when \mathbf{u} and ζ are built from a plane wave. To see this property,

consider a traveling plane wave streamfunction

$$\psi(x, y, t) = A \cos(\mathbf{k} \cdot \mathbf{x} - \omega t) \implies \zeta = -|\mathbf{k}|^2 \psi \quad \text{and} \quad \nabla \zeta = -|\mathbf{k}|^2 \nabla \psi, \quad (47.6)$$

in which case we readily find

$$\mathbf{u} \cdot \nabla \zeta = (\hat{\mathbf{z}} \times \nabla \psi) \cdot (-|\mathbf{k}|^2 \nabla \psi) = 0. \quad (47.7)$$

Evidently, for this model the velocity of fluid particles in a plane wave are aligned parallel to surfaces of constant relative vorticity of the wave. Equivalently, one says that there are no nonlinear self-interactions for plane waves in this model.¹

47.2.4 Pressure equation for a single plane wave

Recall the discussion in Section 35.5 where we showed that pressure in the horizontally non-divergent barotropic model satisfies the Poisson equation (35.68)

$$-\nabla \cdot (\nabla \varphi - f \nabla \psi) = 2 [(\partial_{xy}\psi)^2 - \partial_{xx}\psi \partial_{yy}\psi]. \quad (47.8)$$

Making use of the traveling plane wave (47.6) readily reveals that the nonlinear source term vanishes identically

$$(\partial_{xy}\psi)^2 - \partial_{xx}\psi \partial_{yy}\psi = 0. \quad (47.9)$$

Although the plane wave supports a nonzero rate of strain tensor and a nonzero rotation tensor, their respective squares cancel identically. As a result, the pressure source from a plane wave is due only to the Coriolis acceleration

$$-\nabla \cdot (\nabla \varphi - f \nabla \psi) = -\nabla \cdot (\nabla \varphi + f \hat{\mathbf{z}} \times \mathbf{u}) = 0. \quad (47.10)$$

Evidently, to within an arbitrary gauge function, a plane wave is in exact geostrophic balance for the inviscid horizontally non-divergent barotropic model

$$\nabla \varphi + f \hat{\mathbf{z}} \times \mathbf{u} = -\hat{\mathbf{z}} \times \nabla \lambda, \quad (47.11)$$

where $\lambda(x, y, t)$ is a gauge function. In Section (47.2.5) we show that $\nabla \lambda = \partial_t \nabla \psi$

47.2.5 Velocity equation for a single plane wave

So what velocity equation does a single plane wave satisfy for the inviscid horizontally non-divergent barotropic model? To answer that question we make use of the vector-invariant velocity equation (35.5) written in the form

$$\partial_t \mathbf{u} + f \hat{\mathbf{z}} \times \mathbf{u} + \nabla \varphi = -(\nabla \mathcal{K} + \hat{\mathbf{z}} \times \zeta \mathbf{u}) \quad \text{with} \quad \mathcal{K} = \mathbf{u} \cdot \mathbf{u}/2. \quad (47.12)$$

Introducing the streamfunction brings the right hand side terms into the form

$$\nabla \mathcal{K} + \hat{\mathbf{z}} \times \zeta \mathbf{u} = \hat{\mathbf{x}} (\partial_y \psi \partial_{xy} \psi - \partial_x \psi \partial_{yy} \psi) + \hat{\mathbf{y}} (\partial_x \psi \partial_{xy} \psi - \partial_y \psi \partial_{xx} \psi) \quad (47.13a)$$

$$= \hat{\mathbf{x}} [\hat{\mathbf{z}} \cdot (\partial_y \nabla \psi \times \nabla \psi)] + \hat{\mathbf{y}} [\hat{\mathbf{z}} \cdot (\partial_x \nabla \psi \times \nabla \psi)]. \quad (47.13b)$$

¹The advection is distinctly nonzero when the flow has more than a single plane wave, which is the usual case for general flows. It is the nonlinear interactions between such distinct wave modes that provide the mechanism for the inverse turbulent cascade in this model (see Chapter 11 of [Vallis \(2017\)](#)).

We readily find that each of these terms vanishes when the streamfunction is given by the plane wave function (47.3)

$$\partial_y \nabla \psi \times \nabla \psi = A^2 k_y (\mathbf{k} \times \mathbf{k}) \sin(\mathbf{k} \cdot \mathbf{x} - \omega t) \cos(\mathbf{k} \cdot \mathbf{x} - \omega t) = 0 \quad (47.14a)$$

$$\partial_x \nabla \psi \times \nabla \psi = A^2 k_x (\mathbf{k} \times \mathbf{k}) \sin(\mathbf{k} \cdot \mathbf{x} - \omega t) \cos(\mathbf{k} \cdot \mathbf{x} - \omega t) = 0. \quad (47.14b)$$

Evidently, a plane wave in the horizontally non-divergent barotropic model exactly satisfies the linear velocity equation

$$\partial_t \mathbf{u} + f \hat{\mathbf{z}} \times \mathbf{u} = -\nabla \varphi. \quad (47.15)$$

Comparing to the result from the pressure equation (47.11) reveals that $\nabla \lambda = \nabla(\partial_t \psi)$. Furthermore, recall that we made no assumptions about f in arriving at equation (47.15), so that f can be a function of latitude as per the β -plane. Indeed, f can be an arbitrary function of space, $f(x, y)$.

NAME	GENERAL RELATION	PLANE WAVE
streamfunction	ψ	$\psi = A \cos \mathcal{P}$
velocity	$\mathbf{u} = \hat{\mathbf{z}} \times \nabla \psi$	$\mathbf{u} = -(\hat{\mathbf{z}} \times \mathbf{k}) A \sin \mathcal{P}$
velocity tendency	$\partial_t \mathbf{u} = \hat{\mathbf{z}} \times \nabla \partial_t \psi$	$\partial_t \mathbf{u} = \omega (\hat{\mathbf{z}} \times \mathbf{k}) A \cos \mathcal{P}$
non-divergence	$\nabla \cdot \mathbf{u} = 0$	$\mathbf{k} \cdot \mathbf{u} = 0$
relative vorticity	$\zeta = \nabla^2 \psi$	$\zeta = - \mathbf{k} ^2 \psi$
β -plane vorticity equation	$(\partial_t + \mathbf{u} \cdot \nabla) \zeta = -v \beta$	$\partial_t \zeta = -v \beta$
pressure equation	$-\nabla \cdot (\nabla \varphi - f \nabla \psi) = \mathbb{S}^2 - \mathbb{R}^2$	$-\nabla \cdot (\nabla \varphi - f \nabla \psi) = 0$
Coriolis acceleration	$-f \hat{\mathbf{z}} \times \mathbf{u} = f \nabla \psi$	$-f A \mathbf{k} \sin \mathcal{P}$
velocity equation	$\partial_t \mathbf{u} + (f + \zeta) \hat{\mathbf{z}} \times \mathbf{u} = -\nabla(\varphi + \mathcal{K})$	$\partial_t \mathbf{u} + f \hat{\mathbf{z}} \times \mathbf{u} = -\nabla \varphi$

TABLE 47.1: Properties of the inviscid horizontally non-divergent barotropic model, with $\mathcal{P} = (\mathbf{k} \cdot \mathbf{x} - \omega t)$ the phase function for a linear plane wave. Note the remarkable properties of the plane wave whereby the nonlinear terms vanish in the vorticity equation, pressure equation, and velocity equation.

47.2.6 Structure of a plane wave

TERM	$\mathcal{P} = 0$	$\mathcal{P} = \pi/2$	$\mathcal{P} = \pi$	$\mathcal{P} = 3\pi/2$	$\mathcal{P} = 2\pi$
\mathbf{u}	0	$-A (\hat{\mathbf{z}} \times \mathbf{k})$	0	$A (\hat{\mathbf{z}} \times \mathbf{k})$	0
$-f \hat{\mathbf{z}} \times \mathbf{u}$	0	$-A f \mathbf{k}$	0	$A f \mathbf{k}$	0
$-\nabla \varphi$	$A \omega (\hat{\mathbf{z}} \times \mathbf{k})$	$A f \mathbf{k}$	$-A \omega (\hat{\mathbf{z}} \times \mathbf{k})$	$-A f \mathbf{k}$	$A \omega (\hat{\mathbf{z}} \times \mathbf{k})$
$\partial_t \mathbf{u}$	$A \omega (\hat{\mathbf{z}} \times \mathbf{k})$	0	$-A \omega (\hat{\mathbf{z}} \times \mathbf{k})$	0	$A \omega (\hat{\mathbf{z}} \times \mathbf{k})$

TABLE 47.2: Values for plane wave terms in the velocity equation as the phase, $\mathcal{P} = (\mathbf{k} \cdot \mathbf{x} - \omega t)$, moves through a full range from 0 to 2π . The time tendency, $\partial_t \mathbf{u}$, is always perpendicular to the wavevector, which accords with the transverse nature of the wave. Also note that the time tendency is $\pi/2$ out of phase with the velocity itself. When the time tendency vanishes, then the pressure gradient and Coriolis accelerations are in geostrophic balance, with this balance occurring every π radians.

In Table 47.1 we summarize the properties satisfied by a plane wave in the horizontally non-divergent barotropic model. In particular, note that expression for the pressure gradient

$$-\nabla \varphi = A [\omega (\hat{\mathbf{z}} \times \mathbf{k}) \cos \mathcal{P} + f \mathbf{k} \sin \mathcal{P}], \quad (47.16)$$

which is decomposed into the linearly independent directions parallel to the wave, $\hat{\mathbf{k}}$, and perpen-

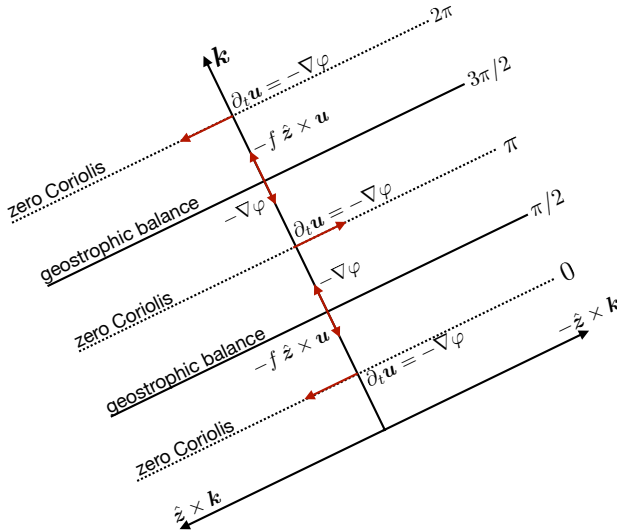


FIGURE 47.2: Schematic of the terms appearing in a plane wave in a horizontally non-divergent barotropic model as a function of the phase, $\mathcal{P} = (\mathbf{k} \cdot \mathbf{x} - \omega t)$, whose value is shown for $\mathcal{P} = 0, \pi/2, \pi, 3\pi/2, 2\pi$. The terms correspond to those given in Table 47.2. Note the oscillation between geostrophic balance, with zero time tendency, and downgradient acceleration (i.e. ageostrophic motion). Also note that the pressure gradient rotates in a clockwise direction when the phase increases.

dicular to the wave, $\hat{z} \times \hat{\mathbf{k}}$, and where

$$\mathcal{P} = (\mathbf{k} \cdot \mathbf{x} - \omega t) \quad (47.17)$$

is the plane wave phase function. Table 47.2 considers the values for each term in the velocity equation as the phase moves around the unit circle, and Figure 47.2 provides a schematic. Evidently, the transverse plane waves oscillate between geostrophic balance, with $\partial_t \mathbf{u} = 0$, and pressure driven tendency, where $\partial_t \mathbf{u} = -\nabla \varphi$.

47.3 Barotropic and non-divergent Rossby waves

In this section we build on the general properties of plane waves in the horizontally non-divergent barotropic model developed in Section 47.2. The key new ingredient considered here is the dispersion relation that couples the wavevector to the wave angular frequency. The fluctuations are organized into *Rossby waves*, which are waves that carry a nonzero vorticity and are reliant on gradients in the background potential vorticity field. In particular, those Rossby waves reliant on differential rotation (i.e., the beta effect) are referred to as *planetary Rossby waves*.

47.3.1 The vorticity mechanism for planetary Rossby waves

Before developing the detailed properties of Rossby waves, we discuss the underlying mechanism for planetary Rossby waves. This discussion serves as both a motivation and guide for the mathematics to follow. The foundational principle is that fluctuations constrained by material conservation of potential vorticity organize into Rossby waves when they are presented with a background potential vorticity gradient. The background potential vorticity gradient can arise from the meridional gradient of the planetary vorticity (as for planetary waves), gradients in the vorticity of the base flow, and, in more general models, buoyancy gradients and topography gradients. Note that the seeds for these arguments were planted in Section 35.6 when studying vorticity constraints on the flow for the non-divergent barotropic model.

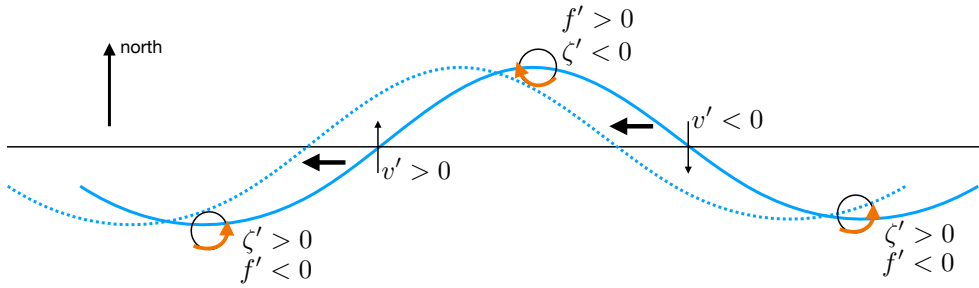


FIGURE 47.3: The westward phase propagation of a planetary Rossby wave arises from the presence of $\beta > 0$ and the constraint that absolute vorticity ($\zeta_a = f + \zeta$) is materially constant for a two-dimensional non-divergent and inviscid barotropic flow. In this figure we consider a material curve within the fluid in either the northern or southern hemispheres, with the solid curve the initial position and the dotted curve the position later in time. For a northward perturbation relative to the initial latitude, a fluid parcel moves to a latitude with Coriolis parameter more positive than its original value. Absolute vorticity conservation requires the parcel to pick up a negative relative vorticity perturbation, $\zeta' < 0$. The opposite occurs for a southward perturbation. The counter-rotating secondary flow induced by the relative vorticity anomaly acts to move the fluctuation westward. Along the nodal points, we depict the meridional motion induced by the wave. In the absence of β , the meridional movement of parcels does not render a change in the planetary vorticity since in this case f is a constant. So for the f -plane there is no induced relative vorticity anomaly so there is no coherent movement of the wave fluctuation. We thus see the central role of $\beta \neq 0$ for planetary Rossby waves. We also see that the sign of the Coriolis parameter is not relevant; it is only $\beta > 0$ that determines the westward wave motion in both northern and southern hemispheres. A generic way to orient the phase is to note that when looking in the phase direction, higher planetary vorticity is to the right.

Westward phase propagation

In Figure 47.3 we display the essential physics of planetary Rossby waves for the horizontally non-divergent barotropic model. As detailed in the figure caption, the constraint of absolute vorticity conservation for fluctuating fluid parcels, in the presence of $\beta > 0$, gives rise to the westward phase propagation of the planetary Rossby wave. As we see in Section 47.5.7, a pseudo-westward propagation arises for edge waves generated by vorticity jumps. This preferred direction for propagation is a canonical property of vorticity waves, and it distinguishes these waves from other waves whose propagation has no directional preference.

Vorticity and momentum arguments

The argument offered in Figure 47.3 does not consider forces. Rather, we make use of the constraint imposed by material conservation of absolute vorticity and infer the motion of fluid parcels by noting how the relative vorticity anomaly induces flow of a particular orientation. Rossby waves carry vorticity, so vorticity arguments offer the natural means to understand their mechanism. Even so, a complementary approach to understanding Rossby waves considers the forces acting in the wave, and as such is referred to as a *momentum argument*. This argument is concerned with the nature of pressure fluctuations within the wave. We note in Section 47.2.5 that plane waves in an inviscid horizontally non-divergent barotropic model oscillate between a state with exact geostrophic balance and a state with zero Coriolis acceleration so that acceleration is down the pressure gradient.

47.3.2 Flow relative to a static base state

In this section we examine wave fluctuations relative to a static base flow. The common example is zonal flow that is either constant or meridionally dependent. We consider a somewhat more

general static flow that is aligned along contours of the base state absolute vorticity

$$\mathbf{u}_b \cdot \nabla(f + \zeta_b) = 0. \quad (47.18)$$

This base flow maintains a materially constant absolute vorticity, so that it is an exact static solution to the equations of motion for the inviscid two-dimensional non-divergent barotropic model.² We make use of a corresponding velocity potential so that

$$\mathbf{u}_b = \hat{\mathbf{z}} \times \nabla \psi_b \quad \text{and} \quad \zeta_b = \nabla^2 \psi_b. \quad (47.19)$$

One example is a static zonal flow with meridional dependence, thus aligned with lines of constant planetary vorticity³

$$\mathbf{u}_b = \hat{\mathbf{x}} U(y) \quad \text{with} \quad \psi_b = - \int^y U(y') dy' \quad \text{and} \quad \zeta_b = -\partial_y U = \partial_{yy} \psi_b. \quad (47.20)$$

We make use of this example when providing context for some of the general results to follow.

Equations for the fluctuating vorticity and streamfunction

In the presence of a base state flow, we write the full vorticity, velocity, and streamfunction in the form

$$\zeta_{\text{full}} = \zeta + \zeta_b \quad \text{and} \quad \mathbf{u}_{\text{full}} = \mathbf{u} + \mathbf{u}_b \quad \text{and} \quad \psi_{\text{full}} = \psi + \psi_b, \quad (47.21)$$

where the static base state flow and the full flow satisfy their respective versions of the inviscid vorticity equation (47.1)

$$\mathbf{u}_b \cdot \nabla(f + \zeta_b) = 0 \quad \text{and} \quad (\partial_t + \mathbf{u}_{\text{full}} \cdot \nabla) \zeta_{\text{full}} = 0. \quad (47.22)$$

Taking the difference of these two equations leads to the vorticity equation for the fluctuating field

$$\partial_t \zeta + (\mathbf{u} + \mathbf{u}_b) \cdot \nabla \zeta + \mathbf{u} \cdot \nabla(f + \zeta_b) = 0. \quad (47.23)$$

This equation takes on the following equivalent form when exposing the streamfunction

$$\partial_t(\nabla^2 \psi) + \hat{\mathbf{z}} \cdot [\nabla \psi \times \nabla(\nabla^2 \psi + f + \nabla^2 \psi_b)] + \hat{\mathbf{z}} \cdot [\nabla \psi_b \times \nabla(\nabla^2 \psi)] = 0. \quad (47.24)$$

It is notable that this equation has only one time derivative, which contrasts to all the other wave equations we have encountered in this book (e.g., equation (44.64) for acoustic waves, equation (45.81) for surface gravity waves, and equation (46.22) for inertial waves). As seen in the following, this property reflects the preferred westward phase velocity direction for Rossby waves.

Requirements for plane waves

To develop a dispersion relation we substitute the plane wave ansatz (47.3) into the streamfunction equation (47.24). For this ansatz to lead to a dispersion relation requires us to assume the background flow is rather simple. Namely, the background velocity and background vorticity

²Although we cannot generally determine an analytic expression for the base flow, we know that a pressure can be found that accords with the flow configuration and the non-divergent nature of the flow (see Section 35.5).

³Recall that the streamfunction is arbitrary up to a constant (Section 18.3). It is for this reason that we have no concern for the lower integration limit in equation (47.20).

gradient must both be independent of space

$$\nabla f = \text{constant} \quad \text{and} \quad \mathbf{u}_b = \text{constant} \implies \zeta_b = 0, \quad (47.25)$$

with the first assumption holding for the β plane. In general, these assumptions ensure that the angular frequency for the plane wave is independent of the space position. There are waves live on the gradient of the background vorticity, but these are not plane waves. The canonical example is the *edge wave* that lives at the interface between two constant, but distinct, vorticities. We study edge waves in Section 47.5.

47.3.3 Rossby wave dispersion relation

We now assume a domain without boundaries and consider a horizontal traveling plane wave ansatz in the form of equation (47.6). Plugging this ansatz into the vorticity equation (47.24), and recalling that $\mathbf{u} \cdot \nabla \zeta = 0$ for a plane wave as discussed in Section 47.2.3, leads to

$$A \sin(\mathbf{k} \cdot \mathbf{x} - \omega t) [-\omega |\mathbf{k}|^2 + (\mathbf{k} \cdot \mathbf{u}_b) |\mathbf{k}|^2 - (\hat{\mathbf{z}} \times \mathbf{k}) \cdot \nabla f] = 0. \quad (47.26)$$

This equation is satisfied in general only when the bracketed term vanishes, which gives the dispersion relation that expresses the angular frequency as a function of the wavevector, the base flow, and geophysical parameters

$$\varpi = \underbrace{\mathbf{k} \cdot \mathbf{u}_b}_{\text{Doppler}} + \underbrace{(\mathbf{k} \times \hat{\mathbf{z}}) \cdot \nabla f / |\mathbf{k}|^2}_{\text{planetary vorticity gradient}} = \underbrace{\mathbf{k} \cdot \mathbf{u}_b}_{\text{Doppler}} - \underbrace{k_x \beta / |\mathbf{k}|^2}_{\text{planetary } \beta}. \quad (47.27)$$

As noted at the end of Section 47.3.2, the Rossby wave dispersion relation (47.27) results from a wave equation with only a single time derivative. We commented in Section 43.3.3 on such wave equations as being notable for possessing a preferred direction for wave propagation, which we see in Section 47.3.4 results in Rossby waves having a phase that moves westward.

Doppler shift from the base flow

The term

$$\varpi_{\text{Doppler}} \equiv \mathbf{k} \cdot \mathbf{u}_b \quad (47.28)$$

provides a shift in the angular frequency relative to the case with zero base flow. For example, if the wave direction is aligned with the base flow, so that $\varpi_{\text{Doppler}} > 0$, then the angular frequency is increased, whereas if the wave is directed oppositely to the base flow, so that $\varpi_{\text{Doppler}} < 0$, then the angular frequency is decreased. Finally, if the wave is directed perpendicular to the base flow, $\varpi_{\text{Doppler}} = 0$, then there is no frequency shift. This frequency shift is referred to as a *Doppler shift*. A Doppler shift is familiar from acoustic waves when, for example, the frequency of a train whistle received by a stationary listener is higher when the train approaches and lower when it is moving away.

Rossby waves supported by a gradient in the planetary vorticity

The planetary beta effect leads to the term

$$\varpi_\beta \equiv -\beta k_x / |\mathbf{k}|^2 = -(\hat{\mathbf{z}} \times \hat{\mathbf{k}}) \cdot \nabla f / |\mathbf{k}|, \quad (47.29)$$

which gives rise to the *planetary wave* or *planetary Rossby wave*. Recall that $\beta \neq 0$ arises from curvature of the spherical planet, so that planetary Rossby waves rely on planetary curvature.

Equivalently, planetary Rossby waves rely on a nonzero gradient in the planetary vorticity, $\nabla f = \beta \hat{\mathbf{y}}$. We thus see that planetary Rossby waves do not exist on an f -plane.

The dispersion relation reveals that long planetary waves (small wavenumber) have higher angular frequency than short planetary waves. The maximum angular frequency is given by the Rossby wave with zero meridional wavenumber

$$\omega_{\beta\text{-max}} = \beta / |k_x|. \quad (47.30)$$

This frequency corresponds to a purely zonal Rossby wave with no meridional structure.

We compute the ratio of the maximum angular frequency for a Rossby wave to the central value of the Coriolis parameter, f_0 , used for the beta-plane approximation (Section 21.3.4)

$$\omega_{\beta\text{-max}} / f_0 = \beta / |k_x f_0| = \beta L_x / |f_0| \ll 1. \quad (47.31)$$

In this equation we set the zonal wavenumber equal to the inverse of a zonal length scale of the flow, $k_x = 1/L_x$. The ratio $\beta L_x / |f_0|$ is much less than unity so long as the beta-plane approximation is accurate. We thus see that the maximum angular frequency of the Rossby waves is much smaller than the Coriolis frequency, thus making planetary Rossby waves vary much a sub-inertial wave.

47.3.4 Concerning the westward phase velocity

The phase velocity, $\mathbf{c}_p = (\omega / |\mathbf{k}|) \hat{\mathbf{k}}$ (see equation (43.24)), takes on the following form for a barotropic Rossby wave⁴

$$\mathbf{c}_p = \hat{\mathbf{k}} [\hat{\mathbf{k}} \cdot \mathbf{u}_b - (\hat{\mathbf{z}} \times \hat{\mathbf{k}}) \cdot \nabla f / |\mathbf{k}|^2] = \hat{\mathbf{k}} [\hat{\mathbf{k}} \cdot \mathbf{u}_b + \hat{\mathbf{k}} \cdot (\hat{\mathbf{z}} \times \nabla f) / |\mathbf{k}|^2] = \hat{\mathbf{k}} [\hat{\mathbf{k}} \cdot \mathbf{u}_b - \beta \hat{\mathbf{k}} \cdot \hat{\mathbf{x}} / |\mathbf{k}|^2]. \quad (47.32)$$

The phase velocity arising from planetary beta

$$[\mathbf{c}_p]_\beta = -\beta \hat{\mathbf{k}} (\hat{\mathbf{x}} \cdot \hat{\mathbf{k}}) / |\mathbf{k}|^2 \quad (47.33)$$

has a sign-definite zonal component

$$[\mathbf{c}_p \cdot \hat{\mathbf{x}}]_\beta = -(\hat{\mathbf{x}} \cdot \hat{\mathbf{k}})^2 / |\mathbf{k}|^2 = -k_x^2 \beta / |\mathbf{k}|^4 < 0. \quad (47.34)$$

We depict this property of the Rossby wave phase velocity in Figure 47.4. This westward phase propagation holds for both hemispheres since $\beta \geq 0$ over the globe. Furthermore, the westward propagation is larger in magnitude at lower latitudes where β is larger, with a ratio given by

$$\frac{[\mathbf{c}_p(\phi_1) \cdot \hat{\mathbf{x}}]_\beta}{[\mathbf{c}_p(\phi_2) \cdot \hat{\mathbf{x}}]_\beta} = \frac{\cos \phi_1}{\cos \phi_2}. \quad (47.35)$$

For example, $\mathbf{c}_p(\phi_1) \cdot \hat{\mathbf{x}}$ at 60° latitude is one-half that at the equator. Both the westward phase propagation and the faster phase speed at lower latitudes are canonical features of planetary Rossby waves. These properties are readily seen in large-scale flow patterns in both the atmosphere and ocean.

⁴In this book, we eschew the notion of components to the phase speed since the phase speed is not a vector and so it has no components. Rather, as discussed in Section 43.5.2, the phase speed is the magnitude of the phase velocity, $C_p = \mathbf{c}_p \cdot \hat{\mathbf{k}} = \omega / |\mathbf{k}| \geq 0$, so that the phase velocity is $\mathbf{c}_p = C_p \hat{\mathbf{k}}$.

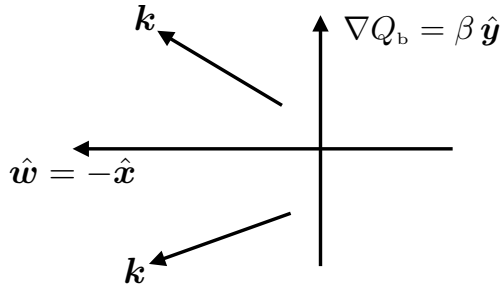


FIGURE 47.4: Illustrating the westward phase propagation of a planetary Rossby waves. In this case the westward unit vector is $\hat{w} = -\hat{x}$, and the phase velocity is projected in the westward direction, $[\mathbf{c}_p \cdot \hat{w}]_\beta > 0$. We show two possible wavevectors, $\mathbf{k} = k_x \hat{x} + k_y \hat{y}$, with $k_x < 0$ so the wavevector has a westward component, but the meridional component can be either positive or negative.

Westward phase velocity implied by positive angular frequency

Another indication that Rossby waves have a westward phase propagation is to recall that the angular frequency of a wave is positive (Section 43.2.3). This convention is maintained by noting that the direction of the phase propagation is carried by the wavevector

$$\mathbf{k} = \hat{x} k_x + \hat{y} k_y, \quad (47.36)$$

rather than allowing the angular frequency to be negative.⁵ Planetary Rossby waves have the dispersion relation (47.29)

$$\varpi_\beta = -\beta k_x / |\mathbf{k}|^2. \quad (47.37)$$

The resulting angular frequency is positive if $k_x < 0$, meaning that propagating planetary waves have a westward component to the phase velocity.

The result (47.37) generalizes by considering the dispersion relation arising from a more general background potential vorticity⁶

$$\varpi_{\text{base}+\beta} \equiv -(\hat{z} \times \hat{\mathbf{k}}) \cdot \nabla Q_b / |\mathbf{k}|, \quad (47.38)$$

with non-negative values assured only for wavevectors oriented in the pseudo-westward direction so that

$$(\hat{z} \times \hat{\mathbf{k}}) \cdot \nabla Q_b = -(\hat{z} \times \nabla Q_b) \cdot \hat{\mathbf{k}} = -(\hat{\mathbf{k}} \cdot \hat{w}) |\hat{z} \times \nabla Q_b| < 0, \quad (47.39)$$

where we introduced the *pseudo-westward* unit vector

$$\hat{w} \equiv \frac{\hat{z} \times \nabla Q_b}{|\hat{z} \times \nabla Q_b|}. \quad (47.40)$$

Emphasizing the special nature of the westward phase velocity

The westward phase velocity is a very distinct feature of Rossby waves. As seen in Section 47.3.1, it results from the constraint of material conservation of potential vorticity in the presence of a background potential vorticity gradient. Other waves that we have studied, such as inertial waves (Section 46.2), acoustic waves (Chapter 44), and surface waves (Chapter 45), support an arbitrary

⁵Our use of a positive angular frequency is not universally maintained in the literature. For example, [Pedlosky \(2003\)](#) considers $\omega < 0$ for Rossby waves.

⁶The angular frequency to be independent of spatial position (assumed for plane waves) requires ∇Q_b to be spatially independent. See discussion in Section 47.3.2 for more on the restrictions of the background flow enabling plane waves.

orientation for their phase velocity. As a result, a source for these sorts of waves will generate waves whose phases are oriented in directions constrained by details of the source rather than by any intrinsic property of the waves. In contrast, an arbitrary source for Rossby waves can only produce Rossby waves with a westward oriented phase. There are no Rossby waves moving in an eastward direction. In this manner, Rossby waves are *anisotropic waves*.

47.3.5 Stationary Rossby waves

Stationary Rossby waves have zero phase velocity, which occurs if the base flow satisfies

$$\mathbf{c}_p = 0 \implies \hat{\mathbf{k}} \cdot (\mathbf{u}_b - \beta \hat{\mathbf{x}} / |\mathbf{k}|^2) = 0. \quad (47.41)$$

That is, the zonal portion of the Doppler shift exactly cancels the westward phase propagation from planetary β

$$\mathbf{u}_b \cdot \hat{\mathbf{x}} = \beta / |\mathbf{k}|^2. \quad (47.42)$$

The corresponding wavelength, $\Lambda = 2\pi / |\mathbf{k}|$, is given by

$$\Lambda_{\text{stationary}} = 2\pi \sqrt{\mathbf{u}_b \cdot \hat{\mathbf{x}} / \beta}. \quad (47.43)$$

For example, assuming an eastward base flow speed of $\mathbf{u}_b \cdot \hat{\mathbf{x}} = 1 \text{ m s}^{-1}$ (as in portions of the Antarctic Circumpolar Current) at $\phi = 60^\circ\text{S}$, where $\beta = (2\Omega/R) \cos\phi \approx 1.14 \times 10^{-11} \text{ m}^{-1} \text{ s}^{-1}$, renders a stationary barotropic Rossby wavelength of $\Lambda_{\text{stationary}} \approx 1860 \text{ km}$, whereas for the atmosphere with $\mathbf{u}_b \cdot \hat{\mathbf{x}} = 25 \text{ m s}^{-1}$ we find $\Lambda_{\text{stationary}} \approx 9300 \text{ km}$. Evidently, at these large scales the Rossby waves feel the Coriolis acceleration and thus properly earn the name *planetary wave*.

47.3.6 Group velocity

If Rossby waves were non-dispersive, then the westward phase velocity would introduce a puzzle: how can all the wave energy propagate only in the westward direction? Since wave energy follows the group velocity (Section 43.6), would there be an unbounded accumulation of Rossby wave energy in the western side of a domain? In fact, this puzzle does not arise since Rossby waves are dispersive, with their group velocity not constrained to be westward. We here introduce the group velocity and then follow up in Sections 47.4.1 and 47.4.2 by focusing on the group and phase velocities for planetary Rossby waves.

The Rossby wave group velocity, $\mathbf{c}_g = \nabla_{\mathbf{k}}\varpi$, is given by

$$\mathbf{c}_g = \mathbf{u}_b + \frac{\hat{\mathbf{z}} \times \nabla f - 2\hat{\mathbf{k}} [\hat{\mathbf{k}} \cdot (\hat{\mathbf{z}} \times \nabla f)]}{|\mathbf{k}|^2} = \mathbf{u}_b - \frac{\beta [\hat{\mathbf{x}} - 2\hat{\mathbf{k}} (\hat{\mathbf{k}} \cdot \hat{\mathbf{x}})]}{|\mathbf{k}|^2} \quad (47.44)$$

The presence of \mathbf{u}_b signals the bulk transport of a wave packet by the base flow. The remaining terms can be related to the phase velocity (47.32) by projecting onto the wavevector direction

$$(\mathbf{c}_g - \mathbf{c}_p) \cdot \hat{\mathbf{k}} = 2\beta \hat{\mathbf{x}} \cdot \hat{\mathbf{k}} / |\mathbf{k}|^2. \quad (47.45)$$

Since wave dispersion is signaled by a difference between the phase velocity and group velocity, equation (47.45) indicates that Rossby wave dispersion arises from a nonzero gradient in the planetary vorticity, $\nabla Q_b = \nabla f = \beta \hat{\mathbf{y}}$, along with a nonzero projection of the wavevector onto the westward direction.

47.4 Geometry of planetary Rossby waves

We here focus on some special properties of planetary Rossby waves revealed by studying the geometry of the group velocity using a diagrammatic method developed by [Longuet-Higgins \(1964\)](#).

47.4.1 Group and phase velocities for planetary Rossby waves

We start by focusing on the relation between group and phase velocities for planetary Rossby waves. The β contribution to the group velocity (47.44) is given by

$$[\mathbf{c}_g]_\beta = \frac{\beta [(k_x^2 - k_y^2) \hat{x} + 2 k_x k_y \hat{y}]}{|\mathbf{k}|^4} \implies [\mathbf{c}_g \cdot \mathbf{c}_g]_\beta = \beta^2 / |\mathbf{k}|^4. \quad (47.46)$$

Recall the westward component of the phase velocity arising from planetary beta as discussed in Section 47.3.4. In contrast, the group velocity

$$[\mathbf{c}_g \cdot \hat{x}]_\beta = \frac{\beta (k_x^2 - k_y^2)}{|\mathbf{k}|^4} = -[\mathbf{c}_p \cdot \hat{x}]_\beta - \frac{\beta k_y^2}{|\mathbf{k}|^4}, \quad (47.47)$$

can be directed in any direction. Note that to reach this equality we used equation (47.34) for $[\mathbf{c}_p \cdot \hat{x}]_\beta$.

Evidently, the group velocity for planetary Rossby waves depends on the shape of the wave as characterized by $(k_x^2 - k_y^2) \hat{x} + 2 k_x k_y \hat{y}$. Consequently, the group velocity has the following properties

$$[\mathbf{c}_g \cdot \hat{x}]_\beta > 0 \quad \text{if } k_x^2 > k_y^2 \text{ eastward } \mathbf{c}_g \text{ for short zonal planetary waves} \quad (47.48a)$$

$$[\mathbf{c}_g \cdot \hat{x}]_\beta < 0 \quad \text{if } k_x^2 < k_y^2 \text{ westward } \mathbf{c}_g \text{ for long zonal planetary waves} \quad (47.48b)$$

$$[(\mathbf{c}_g + \mathbf{c}_p) \cdot \hat{x}]_\beta = 0 \quad \text{if } k_y = 0 \text{ eastward } \mathbf{c}_g \text{ for } k_y = 0 \text{ planetary waves.} \quad (47.48c)$$

We see that the wave energy moves eastward in packets of zonally short ($k_x^2 > k_y^2$) planetary Rossby waves, whereas wave energy in zonally long ($k_x^2 < k_y^2$) planetary Rossby waves moves westward. That is, zonally elongated Rossby waves have westward group velocity whereas zonally compressed Rossby waves have eastward group velocity, where elongated and compressed are relative to the meridional structure. Indeed, if $k_y = 0$, so there is no meridional structure, then Rossby of any zonal wavenumber have eastward group velocity, even while the phase velocity is westward

$$[\mathbf{c}_g \cdot \hat{x}]_\beta = -[\mathbf{c}_p \cdot \hat{x}]_\beta > 0 \quad \text{if } k_y = 0. \quad (47.49)$$

This property is consistent with the ratio

$$\frac{[\mathbf{c}_p \cdot \mathbf{c}_p]_\beta}{[\mathbf{c}_g \cdot \mathbf{c}_g]_\beta} = \frac{k_x^2}{|\mathbf{k}|^2} = (\hat{\mathbf{k}} \cdot \hat{x})^2, \quad (47.50)$$

which then allows us to write the dispersion relation in the form

$$[\omega^2]_\beta = |\mathbf{k}|^2 [\mathbf{c}_p \cdot \mathbf{c}_p]_\beta = k_x^2 [\mathbf{c}_g \cdot \mathbf{c}_g]_\beta. \quad (47.51)$$

47.4.2 Geometry of the group velocity for planetary waves

Figure 47.5 illustrates the geometry of the group velocity as realized for planetary Rossby waves. It helps to organize our understanding of the phase and group velocities for the waves. This

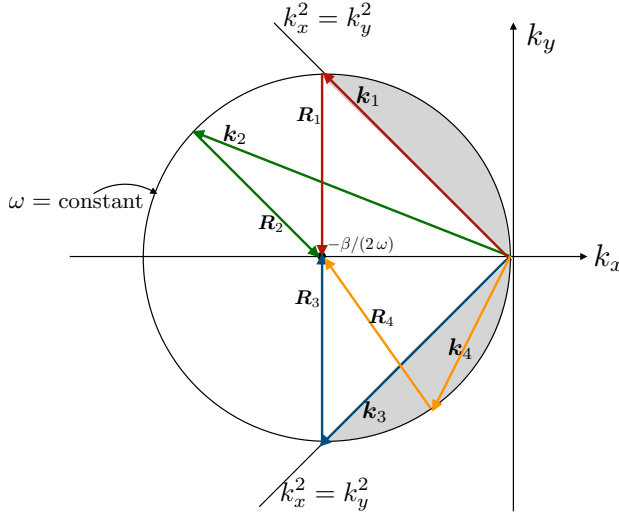


FIGURE 47.5: Orientation of the group velocity for Rossby waves as depicted by a dispersion circle in wavevector space, (k_x, k_y) , with constant angular frequency, ω . We depict four sample wavevectors, $\mathbf{k} = k_x \hat{\mathbf{x}} + k_y \hat{\mathbf{y}}$, that orient the phase velocity, $\mathbf{c}_p = \hat{\mathbf{k}} \omega / |\mathbf{k}|$. Each wavevector extends from the origin to a point on the circle, $[k_x + \beta/(2\omega)]^2 + k_y^2 = [\beta/(2\omega)]^2$, with this circle having center at $\mathbf{k}_{\text{center}} = -\beta/(2\omega) \hat{\mathbf{x}}$ and radius $\beta/(2\omega)$. Each wavevector has an associated group velocity orientation vector, $\mathbf{R} = -\mathbf{k} - \beta/(2\omega) \hat{\mathbf{x}}$, that points from the circle perimeter to the circle center. The group velocity is westward for those wavevectors that intersect the circle perimeter within the gray-shaded region, which generally includes Rossby waves with low zonal wavenumbers. The group velocity is eastward for wavevectors outside the gray region, with the lines $k_x^2 = k_y^2$ separating these regions where the group velocity is eastward or westward. In particular, the group velocity for wavevector \mathbf{k}_1 is southward; for \mathbf{k}_2 it is eastward; for \mathbf{k}_3 it is northward, and for \mathbf{k}_4 it is westward. This figure is after [Longuet-Higgins \(1964\)](#).

diagram arises from noting that the dispersion relation $\omega = -\beta k_x / |\mathbf{k}|^2$, can be written as an equation for a circle in the (k_x, k_y) plane

$$[k_x + \beta/(2\omega)]^2 + k_y^2 = [\beta/(2\omega)]^2, \quad (47.52)$$

with center at the wavevector

$$\mathbf{k}_{\text{center}} = -\beta/(2\omega) \hat{\mathbf{x}} \quad (47.53)$$

and with a radius equal to $\beta/(2\omega)$. The circle has angular frequency, ω , acting as a parameter, with lower frequency Rossby waves yielding larger circles. We further reveal the geometry of the group velocity (47.46) by writing it in the form

$$[\mathbf{c}_g]_\beta = \frac{\beta [(k_x^2 - k_y^2) \hat{\mathbf{x}} + 2 k_x k_y \hat{\mathbf{y}}]}{|\mathbf{k}|^4} = -\frac{2\omega [[k_x + \beta/(2\omega)] \hat{\mathbf{x}} + k_y \hat{\mathbf{y}}]}{|\mathbf{k}|^2}. \quad (47.54)$$

Furthermore, we introduce the group velocity orientation vector

$$\mathbf{R} = -\mathbf{k} - \beta/(2\omega) \hat{\mathbf{x}} = -[k_x + \beta/(2\omega)] \hat{\mathbf{x}} - k_y \hat{\mathbf{y}} \quad \text{with} \quad |\mathbf{R}| = \beta/(2\omega), \quad (47.55)$$

so that the group velocity can be written in the rather tidy form

$$[\mathbf{c}_g]_\beta = 2\omega \mathbf{R} / |\mathbf{k}|^2. \quad (47.56)$$

Notice that \mathbf{R} has magnitude equal to the radius of the circle, and it points from the circle perimeter to the circle center.

The geometry depicted in Figure 47.5 partitions the group velocity according to the wavevector. Again, the phase velocity always has a westward component, yet the group velocity can be

westward or eastward. Additionally, for each angular frequency there is one wave whose group velocity is northward and another that is southward. The squared magnitude of the group velocity is given by equation (47.46)

$$[\mathbf{c}_g \cdot \mathbf{c}_g]_\beta = \beta^2 / |\mathbf{k}|^4, \quad (47.57)$$

so that longer waves (smaller wavenumber) have larger group velocity.

47.4.3 Reflection of planetary Rossby waves

The geometric method developed in Section 47.4.2 provides a useful basis to characterize the reflection of Rossby wave packets from a solid boundary. In the left panel of Figure 47.6 we depict a straight wall sloped with angle γ in the counter-clockwise direction from the positive x -axis. An incident southwestward group velocity carries a wave packet to the wall at an angle θ_i relative to the wall's normal direction, $\hat{\mathbf{n}}$. We assume the group velocity represents a packet whose central carrier Rossby wave has a wavevector \mathbf{k}_i , and we seek information about the reflected wave packet. The remainder of this section describes a diagrammatic approach to garnering this information, with details summarized in the right panel of Figure 47.6.

Kinematic boundary condition at the wall

The kinematic boundary condition along the wall requires the streamfunction to be constant

$$\mathbf{u} \cdot \hat{\mathbf{n}} = (\hat{\mathbf{z}} \times \nabla \psi) \cdot \hat{\mathbf{n}} = (\hat{\mathbf{n}} \times \hat{\mathbf{z}}) \cdot \nabla \psi = -\hat{\mathbf{t}} \cdot \nabla \psi = 0, \quad (47.58)$$

where we introduced the unit tangent vector along the wall

$$\hat{\mathbf{t}} = \hat{\mathbf{z}} \times \hat{\mathbf{n}} = \hat{\mathbf{x}} \cos \gamma + \hat{\mathbf{y}} \sin \gamma. \quad (47.59)$$

The streamfunction can be any constant on the wall, which we take to be zero without loss of generality

$$\psi(\mathbf{x} = \mathbf{x}_{\text{wall}}, t) = 0 \quad \text{with } \mathbf{x}_{\text{wall}} \text{ on the wall.} \quad (47.60)$$

Relating incident and reflected wave properties

We write the velocity streamfunctions for the incident and reflected carrier waves as

$$\psi_i = A_i \cos(\mathbf{k}_i \cdot \mathbf{x} - \omega_i t) \quad \text{and} \quad \psi_r = A_r \cos(\mathbf{k}_r \cdot \mathbf{x} - \omega_r t), \quad (47.61)$$

where A_i and A_r are the real wave amplitudes, \mathbf{k}_i and \mathbf{k}_r are the wavevectors, and ω_i and ω_r are the angular frequencies. At any point in the fluid we write the streamfunction as the sum of the streamfunctions for the incident and reflected waves

$$\psi(\mathbf{x}, t) = \psi_i(\mathbf{x}, t) + \psi_r(\mathbf{x}, t). \quad (47.62)$$

Satisfaction of the boundary condition (47.60) requires

$$A_i \cos(\mathbf{k}_i \cdot \mathbf{x}_{\text{wall}} - \omega_i t) + A_r \cos(\mathbf{k}_r \cdot \mathbf{x}_{\text{wall}} - \omega_r t) = 0. \quad (47.63)$$

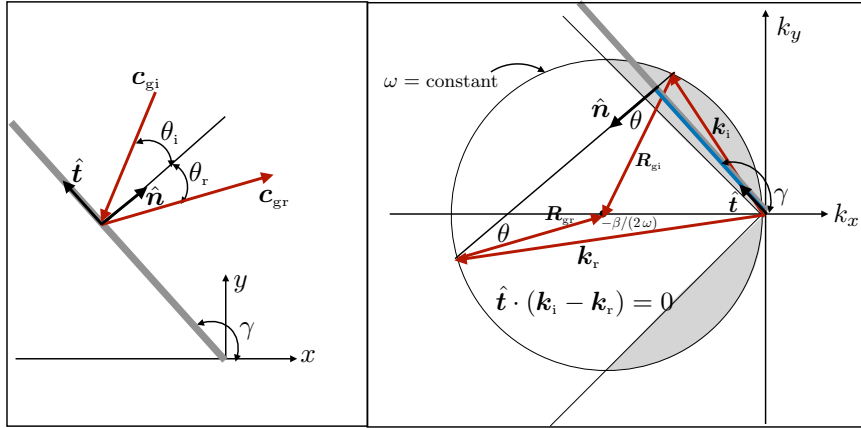


FIGURE 47.6: Depicting the reflection of a Rossby wave packet from a solid wall. The left panel shows the wall sloped at an angle, γ , relative to the positive x -axis. We orient the wall using both its tangential unit vector, $\hat{t} = \hat{z} \times \hat{n} = \hat{x} \cos \gamma + \hat{y} \sin \gamma$, as well as its unit normal $\hat{n} = \hat{x} \sin \gamma - \hat{y} \cos \gamma$. The incident wave packet has group velocity \mathbf{c}_{gi} directed to the southwest and reflected group velocity \mathbf{c}_{gr} directed to the northeast. The angle of incidence equals to the angle of reflectance, $\theta_i = \theta_r = \theta$, as required by the kinematic boundary condition. The right panel shows the wave packet reflection using the dispersion diagram from Figure 47.5. Since the incident and reflected wave have the same angular frequency, we can use the same circle for deriving the wavevectors. The incident and reflected group velocities are oriented by the vectors \mathbf{R}_{gi} (southwest) and \mathbf{R}_{gr} (northeast) that point from the perimeter to the center of the ω circle. They both make an angle of θ with respect to the normal direction, \hat{n} , of the wall. The incident and reflected wavevectors satisfy equation (47.65), which says $(\mathbf{k}_i - \mathbf{k}_r) \cdot \hat{t} = 0$. This relation provides the means to determine the reflected wavevector, \mathbf{k}_r using the diagrammatic method illustrated here. Note that the right panel depicts the western wall orientation relative to the wavevectors and group velocities in wavevector space. One should not interpret it as somehow now becoming an eastern wall.

For this equality to hold at each point along the wall and for all time requires

$$\omega_i = \omega_r \quad \text{equal incident and reflected angular frequency} \quad (47.64a)$$

$$A_i = -A_r \quad \text{equal wave amplitudes but opposite sign} \quad (47.64b)$$

$$(\mathbf{k}_i - \mathbf{k}_r) \cdot \hat{t} = 0 \quad \text{equal projection of wavevectors onto } \hat{t}. \quad (47.64c)$$

The final equality means that there is an equal projection of the incident and reflected wavevectors onto the wall's tangential direction. It arises by writing a point on the wall as

$$\mathbf{x}_{\text{wall}} = |\mathbf{x}_{\text{wall}}| \hat{t} \implies \mathbf{k}_i \cdot \hat{t} = \mathbf{k}_r \cdot \hat{t}. \quad (47.65)$$

Considering the wall to be an extreme case of a static inhomogeneous media, we can connect these relations to the ray equations in Section 43.8.3. In that discussion we found that a wave packet moving through a static but inhomogeneous media maintains a constant angular frequency along a ray, whereas the wavevector changes.

Geometry of the reflection in wavevector space

Our considerations thus far have been generic, holding for any wave packet described by a wave function such as the velocity streamfunction. To determine further details of the reflected Rossby wavevector, we return to the Rossby wave dispersion diagram in Figure 47.5, depicting the reflection process in wavevector space. We only need one dispersion circle since both the incident and reflected waves have the same angular frequency, as required by the kinematic boundary condition (47.63).

To construct the dispersion diagram we start with the known incident group velocity, \mathbf{c}_{gi} ,

which is assumed to be directed towards the southwest. We draw the corresponding group velocity orientation vector, \mathbf{R}_{gi} , from the circle perimeter to the center, also oriented in the same southwesterly direction. From knowledge of \mathbf{R}_{gi} we can draw the incident carrier wavector, \mathbf{k}_i , extending from the origin to where \mathbf{R}_{gi} meets the perimeter. Next we make use of the kinematic condition (47.65) that allows us to compute the unique reflected carrier wavevector, \mathbf{k}_r , constructed by setting $\mathbf{k}_r \cdot \hat{\mathbf{t}} = \mathbf{k}_i \cdot \hat{\mathbf{t}}$. Finally, we can now compute the reflected group velocity orientation vector, \mathbf{R}_{gr} , which points to the center of the circle from the point where \mathbf{k}_r hits the circle perimeter. It is through this construction that we find the incident and reflected group velocities make the same angle with the wall normal:

$$\theta_i = \theta_r = \theta. \quad (47.66)$$

Reflections that satisfy this property are known as *specular*.

Features of the incident and reflected waves

Both the incident and reflected carrier wavevectors have a westward component, as required for Rossby waves. However, the southwestward orientation of the incident group velocity is reflected at the wall into a northeastward group velocity. The reflected wave packet, moving eastward, has a larger zonal wavenumber than the incident wave packet:

$$|\mathbf{k}_r| > |\mathbf{k}_i|. \quad (47.67)$$

This increase in wavenumber arises from an increase in zonal wavevector component, so that the zonal wavelength of the waves within the reflected eastward wave packet are shorter than those in the incident wave packet. The larger wavenumber decreases the group velocity, so that the northeastward reflected packet is slower than the southwestward incident packet. In a fluid with dissipation, such as through viscosity (see Section 22.8), we expect smaller scale features to be dissipated more readily than larger scale features. Hence, the northeastward reflected wave packet is expected to be dissipated more readily than the southwestward incident packet.

The reflection of westerly moving Rossby wave packets off a western boundary hold in their converse for the reflection at easterly packets hitting an eastern wall. Namely, a slowly moving easterly wave packet, which is comprised of short wavelength Rossby waves, is reflected off the eastern wall as a faster moving westerly packet of longer wavelength Rossby waves. These results have particular relevance to the ocean, such as through middle latitude western boundary current intensification and the El Niño / Southern Oscillation phenomena in the tropics (see [Vallis \(2017\)](#) for further discussion).

47.5 Edge waves

Edge waves live on the interface separating two regions of different vorticity, and they share many key features with Rossby waves. Additionally, they share features with surface waves studied in Chapter 45, in that they exponentially decay in the direction away from the interface while traveling in the orthogonal direction.

47.5.1 Replacing planetary vorticity by base state vorticity

Throughout this section we set $\beta = 0$ to focus on the edge waves rather than also considering planetary Rossby waves. Hence, the equation governing the inviscid horizontally non-divergent

flow is the conservation of relative vorticity

$$D\zeta/Dt = 0. \quad (47.68)$$

For a fluid moving within the background vorticity of a base state, ζ_b , we write the relative vorticity as

$$\zeta = \zeta_b + \zeta'. \quad (47.69)$$

That is, the relative vorticity is the sum of the base state relative vorticity, ζ_b , plus the relative vorticity from motion compared to the base state, ζ' . Material conservation of relative vorticity (47.68) thus takes the form

$$D(\zeta' + \zeta_b)/Dt = 0. \quad (47.70)$$

This equation has the same form as the conservation of absolute vorticity in a rotating reference frame, $D(\zeta + f)/Dt = 0$. Here, the background vorticity from the base state fills the role of the planetary vorticity. This analog allows us to transfer many key concepts of planetary Rossby waves directly over to edge waves. Consequently, much of this section will be familiar from our study of Rossby waves.

47.5.2 Point jet

Figure 47.7 illustrates the *point jet*, which has linear velocity on both sides of a jet maxima

$$\mathbf{u}_b = u_b(y) \hat{\mathbf{x}} = U \hat{\mathbf{x}} + \begin{cases} \zeta_1 (y_0 - y) & \text{for } y > y_0 \\ \zeta_2 (y_0 - y) & \text{for } y < y_0, \end{cases} \quad (47.71)$$

where ζ_1 and ζ_2 are constants that measure the vorticity in the two half-planes

$$\zeta_b = -\partial_y u_b = \begin{cases} \zeta_1 & \text{for } y > y_0 \\ \zeta_2 & \text{for } y < y_0. \end{cases} \quad (47.72)$$

Because of the finite jump in the vorticity at $y = y_0$, the meridional derivative of the vorticity is proportional to the Dirac delta⁷

$$\partial_y \zeta_b(y = y_0) = \lim_{\epsilon \rightarrow 0} \frac{\zeta_b(y = y_0 + \epsilon/2) - \zeta_b(y = y_0 - \epsilon/2)}{\epsilon} = (\zeta_1 - \zeta_2) \delta(y - y_0). \quad (47.73)$$

As a check on this expression, we take an integral across the interface to find

$$\int_{y_0 - \epsilon/2}^{y_0 + \epsilon/2} \partial_y \zeta_b dy = \zeta_b(y_0 + \epsilon/2) - \zeta_b(y_0 - \epsilon/2) = (\zeta_1 - \zeta_2) \int_{y_0 - \epsilon/2}^{y_0 + \epsilon/2} \delta(y - y_0) dy. \quad (47.74)$$

47.5.3 Vorticity equation and the absence of plane waves

The vorticity equation (47.23) describing fluctuations relative to the point jet is given by

$$\partial_t \zeta + (\mathbf{u} + \hat{\mathbf{x}} u_b) \cdot \nabla \zeta + v [\beta + (\zeta_1 - \zeta_2) \delta(y - y_0)] = 0, \quad (47.75)$$

⁷See Section 4.3 for more on the Dirac delta. In particular, note that the Dirac delta, $\delta(y)$, has dimensions of inverse length.

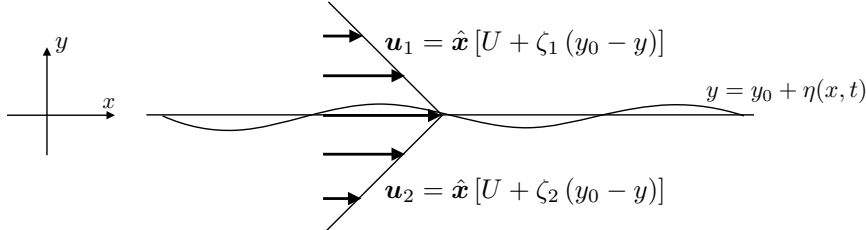


FIGURE 47.7: A zonal point jet in the horizontal x - y plane with the jet maxima at $y = y_0$. The velocity is linear on both sides of the maxima and there is a finite jump in the vorticity at the maxima. Vorticity in the upper region is given by $\zeta_1 = -\partial_y u_1$ and in the lower region $\zeta_2 = -\partial_y u_2$, with $\zeta_1 > 0$ and $\zeta_2 < 0$ depicted in this figure. Oscillations of the material interface, $y = y_0 + \eta(x, t)$, are known as *edge waves*, which exist due to the jump in the vorticity. The top half-plane is referred to as region 1 and the lower half-plane is region 2. Any surface with a finite vorticity jump support edge waves, with the symmetric point jet shown in this figure a prototypical case.

which takes on the form in terms of the streamfunction

$$\partial_t(\nabla^2\psi) + \hat{z} \cdot [\nabla\psi \times \nabla(\nabla^2\psi)] + u_b \partial_x(\nabla^2\psi) + \partial_x\psi [\beta + (\zeta_1 - \zeta_2)\delta(y - y_0)] = 0. \quad (47.76)$$

Because the base state has a nonzero vorticity, we know that there is no plane wave solution (see discussion in Section 47.3.2). That is, if we naively substitute a plane wave ansatz (47.3) into the streamfunction equation (47.76), assuming the angular frequency and wavevector are spatially independent, then we are led to the dispersion relation

$$\omega = k_x u_b - \frac{k_x [\beta + (\zeta_1 - \zeta_2)\delta(y - y_0)]}{|\mathbf{k}|^2}. \quad (47.77)$$

The meridional dependence, through the Dirac delta, is not consistent with our original assumption of spatial independence of the angular frequency. We thus need a different wave ansatz.

47.5.4 Rayleigh-Kuo equation

Meridional dependence of the background flow means that a plane wave in the meridional direction is not a suitable ansatz. Instead, we are led to consider a zonal traveling wave modulated by a meridionally dependant amplitude function

$$\psi(x, y, t) = \tilde{\psi}(y) \cos(kx - \omega t). \quad (47.78)$$

To make use of this ansatz for deriving a dispersion relation requires us to linearize the streamfunction equation (47.24)

$$\partial_t(\nabla^2\psi) + \hat{z} \cdot [\nabla\psi \times \nabla(f + \zeta_b)] + \mathbf{u}_b \cdot \nabla(\nabla^2\psi) = 0. \quad (47.79)$$

Substituting the ansatz (47.78) into this linearized streamfunction equation leads to the *Rayleigh-Kuo* equation for the meridional wave amplitude function⁸

$$(u_b - c)(\partial_{yy} - k^2)\tilde{\psi} + (\beta - \partial_{yy}u_b)\tilde{\psi} = 0 \quad \text{with} \quad c = \omega/k, \quad (47.80)$$

which can also be written in the form

$$\partial_y[(u_b - c)\partial_y\tilde{\psi} - \tilde{\psi}\partial_yu_b] + [\beta - k^2(u_b - c)]\tilde{\psi} = 0. \quad (47.81)$$

⁸Kuo extended the original Rayleigh equation to account for the β effect. In the absence of β we refer to just the *Rayleigh equation*.

The Rayleigh-Kuo equation is fundamental to our study of barotropic shear instability in Chapter 52. For current purposes we use it to derive the dispersion relation for edge waves.

47.5.5 Kinematic boundary condition at the interface

To develop properties of the edge waves requires the kinematic and dynamic boundary conditions at the material interface $y = y_0 + \eta(x, t)$, which supports the traveling edge waves

$$\eta(x, t) = \tilde{\eta} \cos(k x - \omega t). \quad (47.82)$$

The amplitude, $\tilde{\eta}$, is assumed to be much smaller than the wavelength, thus allowing us to linearize the boundary conditions and to evaluate them at $y = y_0$.

The material nature of the interface means that the meridional velocity of a fluid particle at the interface is given by⁹

$$v = D\eta/Dt = (\partial_t + u \partial_x)\eta \approx (\partial_t + u_b \partial_x)\eta, \quad (47.83)$$

where the approximation follows from linearization. This kinematic boundary condition holds on both sides of the interface so that

$$(\partial_t + u_1 \partial_x)\eta = \partial_x \psi_1 \quad \text{and} \quad (\partial_t + u_2 \partial_x)\eta = \partial_x \psi_2. \quad (47.84)$$

Applying this relation to the wave ansatz (47.82) for the interface, and the wave ansatz (47.78) for the streamfunction as evaluated at $y = y_0$, leads to

$$(u_1 - c)\tilde{\eta} = \tilde{\psi}_1 \quad \text{and} \quad (u_2 - c)\tilde{\eta} = \tilde{\psi}_2. \quad (47.85)$$

Since $u_1(y_0) = u_2(y_0) = U$, the kinematic boundary condition says that the streamfunctions match at the interface

$$\tilde{\psi}_1 = \tilde{\psi}_2 \quad \text{at } y = y_0. \quad (47.86)$$

47.5.6 Dynamic boundary condition at the interface

For the dynamic boundary condition we assume there is no surface tension on the interface, in which case pressure matches across

$$\varphi_1 = \varphi_2 \quad \text{at } y = 0. \quad (47.87)$$

To make use of this boundary condition, we introduce the linearized zonal velocity equation for the wave perturbation¹⁰

$$(\partial_t + u_b \partial_x)u' + v' \partial_y u_b = -\partial_x \varphi' \implies (\partial_t + u_b \partial_x)\partial_y \psi - \partial_x \psi \partial_y u_b = \partial_x \varphi'. \quad (47.88)$$

We consider an ansatz for the pressure in the same form as for the streamfunction

$$\varphi'(x, y, t) = \tilde{\varphi}(y) \cos(k x - \omega t), \quad (47.89)$$

⁹Equation (47.83) is the direct analog of the kinematic boundary condition developed in Section 16.4.2 for vertical position of a material surface, $z = \eta(x, y, t)$.

¹⁰The base flow is in geostrophic balance with a base state pressure, $f \hat{z} \times \mathbf{u}_b = -\nabla \varphi_b$.

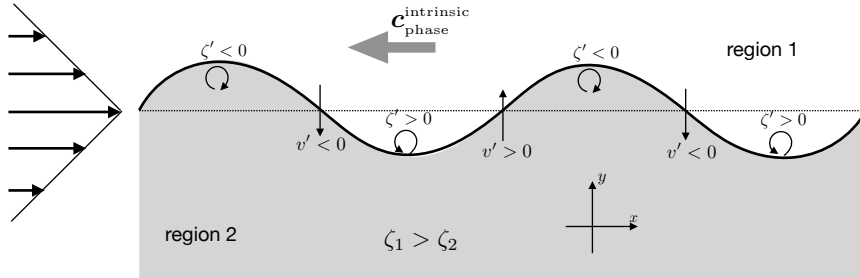


FIGURE 47.8: Depicting the pseudo-westward intrinsic phase propagation of an edge wave along a material surface separating two regions of vorticity. Here the larger relative vorticity is oriented to the north, $\zeta_1 > \zeta_2$, so that the intrinsic phase for the edge wave propagates to the west. We also show the point jet velocity profile, whose relative vorticity jump supports the westward edge wave. The vorticity mechanism for the phase propagation is identical to that for planetary Rossby waves depicted in Figure 47.3, where the background vorticity from the point jet takes the place of the background planetary vorticity. Consider a material line initially along $y = y_0$ and whose relative vorticity equals to that of the background point jet. A southward extension of this line leads to a local positive relative vorticity anomaly, $\zeta' > 0$, since the particle moves into a region with lower background relative vorticity. This anomaly is depicted by the counterclockwise induced secondary flow. Conversely, a northward extension leads to a local negative vorticity anomaly and associated clockwise secondary flow. The anomalous meridional motion is depicted every π radians, with maximal anomalies at wave nodes. The action of the coherent counter-rotating secondary vortices leads to westward propagation of the phase. In general, the phase moves with the higher vorticity to the right, which means that it moves from the convex towards the concave side of the velocity profile.

and then evaluate the velocity equation at $y = 0$ to render

$$[(u_b - c) \partial_y - \partial_y u_b] \tilde{\psi} = \tilde{\varphi} \quad \text{at } y = y_0. \quad (47.90)$$

Invoking continuity of pressure at the interface yields

$$[(U - c) \partial_y - \partial_y u_b] \tilde{\psi}_1 = [(U - c) \partial_y - \partial_y u_b] \tilde{\psi}_2 \quad \text{at } y = y_0. \quad (47.91)$$

This boundary condition also follows from integrating the Rayleigh-Kuo equation (47.81) across the interface and noting that $[\beta - k^2(u_b - c)] \tilde{\psi}$ is continuous at the interface. We can further simplify the dynamic boundary condition (47.92) by making use of the kinematic boundary condition (47.86) so that

$$(U - c) (\partial_y \tilde{\psi}_1 - \partial_y \tilde{\psi}_2) = [\partial_y u_1 - \partial_y u_2] \tilde{\psi} \quad \text{at } y = y_0. \quad (47.92)$$

47.5.7 Edge wave dispersion relation

We set $\beta = 0$ to focus on wave solutions arising just from the point jet, in which the Rayleigh-Kuo equation (47.80) simplifies to

$$(u_b - c) (\partial_{yy} - k^2) \tilde{\psi} - \partial_{yy} u_b \tilde{\psi} = 0. \quad (47.93)$$

Evaluating this equation on the two sides of the interface, and assuming the base flow is distinct from the phase velocity so that $u_b \neq c$, leads to

$$\tilde{\psi} = \psi_0 \begin{cases} e^{-|k|(y-y_0)} & \text{for } y > y_0 \\ e^{+|k|(y-y_0)} & \text{for } y < y_0. \end{cases} \quad (47.94)$$

As anticipated, the edge wave exponentially decays away from the interface. Just like the surface waves in Chapter 45, the horizontal wave number, $|k|$, determines the exponential decay scale.



FIGURE 47.9: Edge waves moving along a jump in the background vorticity field. The phase velocity is oriented with the higher relative vorticity to the right when facing downstream.

Using equation (47.94) in the boundary condition (47.92) yields the phase velocity¹¹

$$c = \omega/k = U + \frac{\partial_y u_1 - \partial_y u_2}{2|k|} = \underbrace{U}_{\text{Doppler}} - \underbrace{\frac{\zeta_1 - \zeta_2}{2|k|}}_{\text{intrinsic}}. \quad (47.95)$$

The background zonal flow, U , provides a Doppler shift to the phase velocity. The second piece arises from the vorticity jump across the interface, and we refer to it as the *intrinsic* portion to the phase velocity. If the vorticity increases northward, so that $\zeta_1 - \zeta_2 > 0$, then $c - U < 0$, thus signaling a westward phase velocity relative to the background flow. This behavior is precisely that found for planetary Rossby waves, thus prompting some to refer to edge waves as prototypical Rossby waves. In Figure 47.8, we summarize the vorticity mechanism for the *pseudo-westward* phase velocity, with the mechanism identical to the planetary Rossby wave in Figure 47.3. In general, the phase velocity for edge waves is directed so that the region of higher vorticity is to the right when facing downstream, with Figure 47.9 providing a schematic for a curved vorticity jump line.

47.5.8 Comments and further study

Edge waves are reminiscent of the planetary Rossby waves studied in earlier sections of this chapter, where the planetary Rossby waves are supported by the planetary vorticity gradient rather than jumps in the base state relative vorticity. As studied in Chapter 52, interactions between vorticity waves can lead to shear instabilities, with such instabilities forming a fundamental feature of unstable and turbulent geophysical flows.

A similar treatment of edge waves can be found in Section 3.12 of [Smythe and Carpenter \(2019\)](#) and Section 9.2.3 of [Vallis \(2017\)](#).



47.6 Exercises

EXERCISE 47.1: ROSSBY WAVES IN A ZONAL CHANNEL

In Section 47.3 we examined the physics of Rossby waves on an unbounded β -plane. Here we consider a zonal channel on a β -plane, with the channel unbounded in the zonal direction but bounded meridionally. The meridional domain is given by $y_s \leq y \leq y_n$ where $y_n - y_s = L$, and with rigid material walls at the meridional boundaries. Everything else is just as in Section 47.3. However, for simplicity assume that the base flow is purely zonal with $\mathbf{u}_b = U(y)\hat{x}$.

- (a) Write a single plane wave mode that travels in the zonal direction but is standing in the meridional direction. Hint: the plane wave ansatz (47.6) should be modified so that $\hat{n} \cdot (\hat{z} \times$

¹¹The phase of the edge wave only moves in the zonal direction, with $c > 0$ for a phase velocity in the $+\hat{x}$ direction and $c < 0$ for a phase velocity in the $-\hat{x}$ direction.

$\nabla\psi) = 0$ at the northern and southern walls. The boundary condition imposes a constraint on the meridional wavenumber. What is the constraint?

- (b) What is the dispersion relation for the Rossby waves in this channel?

EXERCISE 47.2: VORTEX MECHANISM FOR EDGE WAVES

Provide a sketch like Figure 47.8 but for edge waves in the case with $\zeta_1 < \zeta_2$.



Chapter 48

SHALLOW WATER WAVES

In this chapter we study a variety of waves appearing in shallow water fluid. In the literature these waves are sometimes referred to as *long waves* since the shallow water approximation applies when the horizontal length scale is much larger than the vertical, in which case the horizontal wavelength is larger than the fluid depth. Our presentation focuses on the case of a single shallow water layer, but we do offer brief discussions of two-layer cases to illustrate the generalizations to multiple layers. Notably, the algebraic tedium increases greatly when adding layers. Hence, from a theoretical perspective it is typically more fruitful to move to the continuous vertical stratification in Chapter 49, rather than study more than two stacked shallow water layers.

For the analysis of waves, we first consider general features of both the nonlinear and then the linear shallow water equations. For the linearized system, we develop a unified wave equation for the free surface. The derivation of this equation is rather detailed and the resulting equation somewhat complex. Even so, it serves to unify across the full suite of linear shallow water waves on a rotating β -plane, and offers insights into both the methods used to derive wave equations and the scalings used to extract their core physical features. In unpacking this wave equation we pursue a focused study of gravity waves, inertia-gravity waves, Kelvin waves, and Rossby waves. We also consider two applications of the inertia-gravity waves: geostrophic adjustment and waves generated by topography.

READER'S GUIDE TO THIS CHAPTER

This chapter builds from the shallow water studies in Chapters 32 and 33, as well as other waves chapters in this part of the book. [The first half of this video](#) offers a pedagogical introduction to non-rotating shallow water waves.

48.1	Loose threads	1234
48.2	Shallow water equations	1235
48.2.1	Generalized wave equation	1235
48.2.2	Another form of the generalized wave equation	1236
48.2.3	Comments	1236
48.3	Linearized shallow water equations	1237
48.3.1	Linearized thickness and velocity equations	1237
48.3.2	Energetics	1238
48.3.3	Potential vorticity	1239
48.3.4	Traveling plane wave ansatz and $\nabla \cdot \mathbf{v} = 0$	1239
48.4	Unified shallow water wave equation	1240
48.4.1	Use of the divergence equation	1240
48.4.2	Use of the vorticity equation	1241
48.4.3	The unified wave equation just with η'	1242

48.4.4	Scaling the wave equation	1243
48.4.5	Super-inertial wave equation	1243
48.4.6	Sub-inertial wave equation	1244
48.4.7	Further study	1247
48.5	Gravity waves	1247
48.5.1	Flat bottom gravity waves	1247
48.5.2	Relating the wave amplitudes	1248
48.5.3	Dispersion relation	1248
48.6	Gravity waves in two layers	1249
48.6.1	Linearized two-layer equations	1249
48.6.2	Gravity wave equations	1249
48.6.3	Dispersion relation	1250
48.6.4	Structure of the barotropic wave mode	1251
48.6.5	Structure of the baroclinic wave mode	1251
48.6.6	The depth averaged velocity and the velocity difference	1252
48.6.7	Comments	1253
48.7	Inertia-gravity waves over a flat bottom	1253
48.7.1	Forced oscillator equation for horizontal velocity	1253
48.7.2	Free wave equation and potential vorticity	1253
48.7.3	Dispersion relation	1254
48.7.4	Zero frequency geostrophic mode	1254
48.7.5	Inertia-gravity wave modes	1255
48.7.6	Group velocity	1255
48.7.7	Shortwave limit for inertia-gravity waves	1256
48.7.8	Longwave limit for inertia-gravity waves	1257
48.7.9	Structure of a plane inertia-gravity wave	1257
48.7.10	Energetics	1258
48.8	Kelvin waves	1260
48.9	Geostrophic adjustment	1261
48.9.1	Potential vorticity inversion	1261
48.9.2	Posing the initial value problem	1262
48.9.3	Adjustment in the absence of rotation	1263
48.9.4	Adjustment with rotation	1263
48.9.5	Comments	1264
48.10	Stationary waves generated by topography	1265
48.10.1	Linearized equations	1265
48.10.2	Galilean transformation to a moving frame	1266
48.10.3	Deriving the amplitude relation	1266
48.10.4	Comments on the amplitude relation	1269
48.11	Rossby waves	1269
48.11.1	Dispersion relation	1270
48.11.2	Connecting to quasi-geostrophic potential vorticity	1270
48.11.3	Vorticity mechanism	1270
48.11.4	Dispersion geometry for planetary Rossby waves	1271
48.11.5	Comments	1272
48.12	Exercises	1272

48.1 Loose threads

- Figures!
- Need to assume base state has constant velocity so that $\zeta_b = 0$. Otherwise, the angular frequency is a function of space, and that is not consistent with the plane wave ansatz. This point needs to be cleaned up in this chapter.

- Likewise, when writing ∇Q_r , need to be sure that this is a constant when taking a plane wave ansatz. Otherwise, need to do WKB.
- Reflection of shallow water gravity waves from a straight side boundary.
- Particle trajectories and Stokes. See Section 48.5.2 for shallow water gravity waves.
- Eikonal approximation for shallow water gravity waves so to compute the change in the amplitude of the wave. Need to reinterpret the acoustic amplitude equation 44.144 for shallow water.
- More on Kelvin waves in Section 48.8.
- What else to say about stationary waves and topography in Section 48.10?
- Salmon class notes Chapter 9 on shallow water waves induced by an earthquake: solving the initial value problem.
- Energetics of Rossby waves as per Section 6.6 of *Vallis (2017)*.

48.2 Shallow water equations

The shallow water equations of motion are given by the velocity equation (32.12) and thickness equation (32.19), written here in their Eulerian form and with zero atmospheric pressure

$$\partial_t \mathbf{u} + (\mathbf{u} \cdot \nabla) \mathbf{u} + f \hat{\mathbf{z}} \times \mathbf{u} = -g \nabla \eta \quad (48.1a)$$

$$\partial_t h + \nabla \cdot (h \mathbf{u}) = 0. \quad (48.1b)$$

In Section 48.3 we linearize these shallow water equations and study their properties in anticipation of later study of their wave fluctuations. Before doing so, however, we formulate a wave-like equation that holds for the nonlinear shallow water model.¹ Doing so provides a preface of certain features of the linear equations while offering yet another view of the shallow water system beyond that provided in Chapters 32 and 33.

48.2.1 Generalized wave equation

Consider the shallow water equations written using the material time derivative

$$D\mathbf{u}/Dt + f \hat{\mathbf{z}} \times \mathbf{u} = -g \nabla \eta \quad \text{and} \quad Dh/Dt = -h \nabla \cdot \mathbf{u}. \quad (48.2)$$

Taking the material time derivative of the thickness equation, and then using the velocity equation, yields

$$\frac{D}{Dt} \left[\frac{1}{h} \frac{Dh}{Dt} \right] = -\frac{D(\nabla \cdot \mathbf{u})}{Dt} \quad (48.3a)$$

$$= -\nabla \cdot \frac{D\mathbf{u}}{Dt} + \partial_m u_n \partial_n u_m \quad (48.3b)$$

$$= -\nabla \cdot (-f \hat{\mathbf{z}} \times \mathbf{u} - g \nabla \eta) + S \cdot S - R \cdot R, \quad (48.3c)$$

¹We pursued the analogous manipulations for acoustic waves in Section 44.5.1.

where \mathbb{S} is the rate of strain tensor and \mathbb{R} is the rotation tensor (both are discussed in Section 15.3.5), and

$$\mathbb{S} \cdot \mathbb{S} - \mathbb{R} \cdot \mathbb{R} = \mathbb{S}_{mn} \mathbb{S}_{mn} - \mathbb{R}_{mn} \mathbb{R}_{mn}. \quad (48.4)$$

Rearrangement then leads to

$$\frac{D}{Dt} \left[\frac{1}{h} \frac{Dh}{Dt} \right] - g \nabla^2 \eta = \nabla \cdot (f \hat{\mathbf{z}} \times \mathbf{u}) + \mathbb{S} \cdot \mathbb{S} - \mathbb{R} \cdot \mathbb{R}, \quad (48.5)$$

which corresponds to equation (44.49) holding for the compressible fluid. We interpret this equation as a generalized wave equation holding for movement following a shallow water fluid column. The second order material time operator acts on the thickness to propagate signals relative to the moving fluid. The linear terms, $g \nabla^2 \eta$ and $\nabla \cdot (f \hat{\mathbf{z}} \times \mathbf{u})$, also appear in the linearized equations and will be discussed later, whereas $\mathbb{S} \cdot \mathbb{S} - \mathbb{R} \cdot \mathbb{R}$ is a nonlinear source arising from gradients in the fluid velocity. We drop the nonlinear source when working with the linearized equations, and likewise the material time derivative becomes a local time derivative.

48.2.2 Another form of the generalized wave equation

To align more closely with the linear wave equation derived in Section (48.3), we consider again the velocity and thickness equations in the form of equation (48.2) yet first determine the evolution equation for the divergence of the thickness flux. For this purpose, multiply the thickness equation by the velocity and the velocity equation by the thickness, and then add to find

$$D(h \mathbf{u})/Dt = -f h \hat{\mathbf{z}} \times \mathbf{u} - g h \nabla \eta - (h \mathbf{u}) \nabla \cdot \mathbf{u}. \quad (48.6)$$

Divergence of the left hand side of this equation is given by

$$\nabla \cdot [D(h \mathbf{u})/Dt] = D[\nabla \cdot (h \mathbf{u})]/Dt + (\partial_m \mathbf{u}) \cdot \nabla (h u_m) = -D(\partial_t h)/Dt + (\partial_m \mathbf{u}) \cdot \nabla (h u_m), \quad (48.7)$$

where we used the thickness equation for the final equality. Combining with the divergence of the right hand side of equation (48.6) yields

$$-D(\partial_t h)/Dt + \partial_m \mathbf{u} \cdot \nabla (h u_m) = -\nabla \cdot (f h \hat{\mathbf{z}} \times \mathbf{u}) - \nabla \cdot (g h \nabla \eta) - \nabla \cdot (h \mathbf{u} \nabla \cdot \mathbf{u}), \quad (48.8)$$

with rearrangement leading to the nonlinear wave equation

$$\frac{D}{Dt} \frac{\partial \eta}{\partial t} - \nabla \cdot (g h \nabla \eta) = \nabla \cdot (f h \hat{\mathbf{z}} \times \mathbf{u}) + \partial_m \mathbf{u} \cdot \nabla (h u_m) + \nabla \cdot (h \mathbf{u} \nabla \cdot \mathbf{u}), \quad (48.9)$$

where we noted that $\partial_t h = \partial_t \eta$. This nonlinear equation corresponds directly to the linear wave equation (48.31) derived below. It is this alternative form that readily offers a direct decomposition of the various waves appearing in the shallow water fluid. Namely, in the linear equations we drop the nonlinear sources on the the right hand side, and convert the material time derivative to the local Eulerian time derivative.

48.2.3 Comments

This section stopped short of pursuing an analysis of nonlinear wave solutions. However, as in the analogous discussion of the compressible fluid in Section 44.5.1, these manipulations signal that wave-like equations are not restricted to linearized equations. Rather, they are basic to the nonlinear equations, though with a more complex mathematical structure that generally requires numerical or asymptotic methods to penetrate.

For the remainder of this chapter we focus on the linearized set of equations, thus enabling the use of linear analysis methods. Even though much simpler than the nonlinear equations, we uncover a rich and complex variety of linear wave phenomena within the shallow water model.

48.3 Linearized shallow water equations

In this section we linearize the shallow water velocity equation (48.1a) and thickness equation (48.1b) in a manner that supports subsequent analysis of small amplitude fluctuations. In the process we derive a linear wave equation for free surface undulations, with a number of source terms that support the variety of waves studied in later sections. This wave equation is the linearized version of equation (48.9) holding for the fully nonlinear shallow water system.

48.3.1 Linearized thickness and velocity equations

We linearize the equations around a base state that is at rest and thus with a flat free surface. Referring to Figure 32.1 leads to the expressions for the layer thickness

$$h(x, y, t) = [\bar{\eta} + \eta'(x, y, t)] - [\bar{\eta}_b + \eta'_b(x, y)] = H + \eta'(x, y, t) - \eta'_b(x, y), \quad (48.10)$$

along with the corresponding velocity

$$\mathbf{u}(x, y, t) = 0 + \mathbf{u}'(x, y, t). \quad (48.11)$$

The terms $\bar{\eta}$ and $\bar{\eta}_b$ are area means for the free surface and bottom topography, whereas η' and η'_b are deviations from these means. We assume there are no boundary sources of volume so that $\bar{\eta}$ is constant in time. The prime on the velocity in equation (48.11) acts as a reminder that it is driven by gradients in the fluctuating free surface, η' .

We make the following assumptions about the terms comprising the layer thickness.

- The layer thickness is everywhere positive, $h > 0$, thus ensuring there is water at each point in the layer at each time. We make this assumption since vanishing a layer thickness represents a nontrivial change in the domain that requires the full nonlinear equations to handle.
- A nonzero η'_b allows for local variations in the bottom topography. We assume these variations are bounded by the mean thickness,

$$H_r \equiv H - \eta'_b > 0, \quad (48.12)$$

thus ensuring the resting thickness, H_r , is nonzero everywhere. This assumption does not place strong constraints on η'_b . In particular, we do not generally assume η'_b is small other than to assume $H_r > 0$. However, we do assume that η'_b is small when studying the quasi-geostrophic motion associated with Rossby waves in Sections 48.11.

- We assume the free surface undulations are much smaller than the resting thickness

$$|\eta'| \ll H_r. \quad (48.13)$$

This is the key assumption in the linearization process. It follows from our interest in studying linear wave fluctuations of the free surface.

The above assumptions lead to the linearized version of the thickness equation (48.1b)

$$\partial_t \eta' + \nabla \cdot (H_r \mathbf{u}') = 0. \quad (48.14)$$

This equation says that a time tendency of the free surface is driven by the convergence of a thickness flux, where the thickness is approximated by its resting value

$$h = H + \eta' - \eta'_b \approx H - \eta'_b = H_r. \quad (48.15)$$

We conclude from equation (48.14) that free surface transients (i.e., waves) require a nonzero horizontal convergence, $-\nabla \cdot (H_r \mathbf{u}') \neq 0$. It follows that waves in a flat bottom domain arise only when there is a nonzero convergence in the horizontal flow, $-\nabla \cdot \mathbf{u}' \neq 0$. Such horizontal convergences are fundamental to the shallow water fluid, and provide the key distinction from waves appearing in the horizontally non-divergent barotropic fluid from Sections 47.2, 47.3, and 47.4.

The linearized shallow water velocity equation (48.1a) is

$$\partial_t \mathbf{u}' + f \hat{\mathbf{z}} \times \mathbf{u}' = -g \nabla \eta', \quad (48.16)$$

which is reached by dropping the nonlinear advection, $(\mathbf{u}' \cdot \nabla) \mathbf{u}'$. Advection is indeed smaller than the other terms since velocity tendencies are driven by the assumed small amplitude fluctuations in the free surface, thus making $(\mathbf{u}' \cdot \nabla) \mathbf{u}'$ second order in small terms.

48.3.2 Energetics

We studied energetics of a single layer of shallow water fluid in Section 33.5. We here summarize how the energetics appear for the linearized thickness equation (48.14) and velocity equation (48.16). As per the norm with energetics of linearized systems (e.g., see the study of acoustic energy in Section 44.7 and surface waves in Section 45.4), we work to second order accuracy in fluctuating fields.

The gravitational potential energy per horizontal area is given by

$$\mathcal{P}^{\text{sw}} = g \rho \int_{\eta_b}^{\eta} z \, dz = (g \rho / 2) (\eta^2 - \eta_b^2), \quad (48.17)$$

and its time tendency is

$$\partial_t \mathcal{P}^{\text{sw}} = g \rho (\bar{\eta} + \eta') \partial_t \eta' \approx -g \rho (\bar{\eta} + \eta') \nabla \cdot (H_r \mathbf{u}'). \quad (48.18)$$

Likewise, the kinetic energy per area is

$$\mathcal{K}^{\text{sw}} = \frac{\rho}{2} \int_{\eta_b}^{\eta} \mathbf{u} \cdot \mathbf{u} \, dz = (\rho / 2) h \mathbf{u}' \cdot \mathbf{u}' \approx (\rho / 2) H_r \mathbf{u}' \cdot \mathbf{u}', \quad (48.19)$$

and its time tendency is

$$\partial_t \mathcal{K}^{\text{sw}} = \rho H_r \mathbf{u}' \cdot \partial_t \mathbf{u}' = -g \rho H_r \mathbf{u}' \cdot \nabla \eta' = -g \rho H_r \mathbf{u}' \cdot \nabla (\bar{\eta} + \eta'). \quad (48.20)$$

The time tendency for the mechanical energy is thus given by

$$\partial_t (\mathcal{K}^{\text{sw}} + \mathcal{P}^{\text{sw}}) = -g \rho \nabla \cdot [H_r (\bar{\eta} + \eta') \mathbf{u}']. \quad (48.21)$$

This equation is a linearized version of the mechanical energy equation (33.120). Here, we only

have the transfer of energy due to the advection of pressure, whereas the nonlinear equations also have the advection of kinetic and potential energy.

48.3.3 Potential vorticity

The shallow water potential vorticity (Section 36.3) is given by

$$Q = \frac{f + \zeta}{h} = \frac{f + \zeta}{H + \eta' - \eta_b} \approx Q' \quad \text{where} \quad Q' = \frac{f + \zeta'}{H_r} - \frac{f \eta'}{H_r^2}, \quad (48.22)$$

where the approximation follows from assuming $|\eta'| \ll H_r$. Use of the linearized thickness equation (48.14) and linearized velocity equation (48.16) yields the time tendency for the linearized potential vorticity (see Exercise 48.1)

$$\partial_t Q' + \mathbf{u}' \cdot \nabla(f/H_r) = 0. \quad (48.23)$$

For a flat bottom f -plane domain, the linearized potential vorticity remains static at each point in the fluid, $\partial_t Q' = 0$. In contrast, nonzero gradients in f and/or H_r cause the linearized potential vorticity to be modified through advection of f/H_r , with f/H_r the potential vorticity of the background state of rest. Hence, if f and/or H_r are spatially varying, solutions to the linear equations, including waves, carry nonzero potential vorticity.

48.3.4 Traveling plane wave ansatz and $\nabla \cdot \mathbf{v} = 0$

To derive the dispersion relation for the various shallow water waves, we consider the traveling plane wave ansatz from Section 43.5, here written in the form

$$(u', v', \eta') = (\tilde{u}, \tilde{v}, \tilde{\eta}) e^{i(\mathbf{k} \cdot \mathbf{x} - \omega t)}, \quad (48.24)$$

where the real part of the right hand side is assumed. The amplitudes $(\tilde{u}, \tilde{v}, \tilde{\eta})$ are generally complex numbers that are independent of space and time. Recall from Section 32.2 that the horizontal velocity has no depth dependence in the shallow water layer, which follows from the hydrostatic approximation. Hence, a plane wave solution to the shallow water wave equations must have a zero vertical component to the wavevector, $k_z = 0$, so that

$$\mathbf{k} = \hat{\mathbf{x}} k_x + \hat{\mathbf{y}} k_y. \quad (48.25)$$

Evidently, the phase of shallow water plane waves (48.24) travels horizontally within a layer.

As a homogeneous layer, the shallow water fluid is incompressible so that $\nabla \cdot \mathbf{v} = 0$. For plane waves moving in three-dimensions, this non-divergence constraint means that the velocity of the plane waves satisfies $\mathbf{k} \cdot \mathbf{u} + k_z w = 0$ (e.g., see our study of inertial waves in Section 46.2). However, for the shallow water system we saw above that $k_z = 0$, which would then seem to imply that $\mathbf{k} \cdot \mathbf{u} = 0$. Yet shallow water waves do *not* satisfy $\mathbf{k} \cdot \mathbf{u} = 0$ since they are horizontally divergent.

The resolution of this quandary concerns the vertical velocity in a shallow water layer. Namely, the vertical velocity component is diagnosed via the horizontal convergence, $\partial_z w = -\nabla \cdot \mathbf{u}$. The depth independence of the horizontal velocity leads to a linear depth-dependence of the vertical velocity component (equation (32.38))

$$\nabla \cdot \mathbf{u} + \partial_z w = 0 \implies w(z) = w(\eta_b) - (z - \eta_b) \nabla \cdot \mathbf{u}, \quad (48.26)$$

which for the plane wave (48.24) leads to

$$w(z) = w(\eta_b) - i(z - \eta_b) \mathbf{k} \cdot \tilde{\mathbf{u}} e^{i(\mathbf{k} \cdot \mathbf{x} - \omega t)}. \quad (48.27)$$

The factor of $i = \sqrt{-1}$ out front means that the vertical velocity component is $\pi/2$ out of phase with the horizontal velocity. Also note that $|z - \eta_b| |\mathbf{k}| \leq H |\mathbf{k}|$. Since $H |\mathbf{k}| \ll 1$ for shallow water flow, we see that the vertical velocity component has a much smaller magnitude than the horizontal velocity.

48.4 Unified shallow water wave equation

In this section we combine the linearized thickness equation (48.14) and linearized velocity equation (48.16) to render a unified wave equation for the free surface. We start by closely following the steps taken for the nonlinear wave equation in Section 48.2.2. Yet we go much further for the purpose of obtaining a linear equation with the free surface as the only prognostic field. Although a rather tedious equation, it unifies the variety of waves supported by the rotating shallow water system. Once deriving the unified wave equation (equation (48.42)), we study its scaling for high frequency ($\omega^2 > f^2$; super-inertial) and low frequency ($\omega^2 < f^2$; sub-inertial) wave motion. That discussion anticipates analysis pursued in more depth in the following sections.

48.4.1 Use of the divergence equation

We start by forming an equation for the evolution of the divergence of $H_r \mathbf{u}'$, which is found by multiplying the linearized velocity equation by H_r and then taking the divergence

$$\partial_t [\nabla \cdot (H_r \mathbf{u}')] + \nabla \cdot (\hat{\mathbf{z}} \times f H_r \mathbf{u}') = -\nabla \cdot (g H_r \nabla \eta'), \quad (48.28)$$

where the divergence and time derivative commute. The thickness equation (48.14) can be used to eliminate the divergence, in which case we are led to

$$\partial_{tt} \eta' - \nabla \cdot (g H_r \nabla \eta') = -\hat{\mathbf{z}} \cdot [\nabla \times (f H_r \mathbf{u}')]. \quad (48.29)$$

where we made use of the identity

$$\nabla \cdot (\hat{\mathbf{z}} \times f H_r \mathbf{u}') = -\hat{\mathbf{z}} \cdot [\nabla \times (f H_r \mathbf{u}')]. \quad (48.30)$$

The wave equation (48.29) is the linear analog of the nonlinear equation (48.9). We can expand the cross product on the right hand side to identify the variety of physical processes supporting shallow water waves

$$\partial_{tt} \eta' = \underbrace{\nabla \cdot (g H_r \nabla \eta')}_{\text{gravity waves}} - \underbrace{\hat{\mathbf{z}} \cdot (f H_r \nabla \times \mathbf{u}')}_{\text{inertial waves}} - \underbrace{\hat{\mathbf{z}} \cdot (H_r \nabla f \times \mathbf{u}')}_{\text{planetary Rossby waves}} - \underbrace{\hat{\mathbf{z}} \cdot (f \nabla H_r \times \mathbf{u}')}_{\text{topographic Rossby waves}}. \quad (48.31)$$

Although suggestive, this equation must be further manipulated to render a wave equation just with the free surface. In so doing we unify the discussion of the dispersion relation for the various shallow water waves, and allow for a more seamless decomposition in terms of time scales. We pursue the (somewhat tedious) manipulations in Section 48.4.2. Yet before doing so we offer a heuristic discussion of the physical processes in equation (48.31).

Non-rotating gravity waves

Without rotation ($f = 0$) yet with gravity ($g \neq 0$), equation (48.31) reduces to the shallow water gravity wave equation

$$\partial_{tt}\eta' - \nabla \cdot (g H_r \nabla \eta') = 0. \quad (48.32)$$

With a flat bottom, these waves are non-dispersive plane gravity waves, whereas the case with a sloping bottom requires the eikonal approximation developed in Section 44.9. These waves are sometimes referred to as *long gravity waves*, in contrast to the shorter waves that occur in deep water (see Section 45.5.7). We study shallow water gravity waves in Section 48.5.

Inertia-gravity waves

The wave equation

$$\partial_{tt}\eta' - \nabla \cdot (g H_r \nabla \eta') = -f H_r \zeta' \quad (48.33)$$

describes dispersive inertia-gravity waves in a shallow water layer. The inertial portion of the waves rely on both rotation ($f \neq 0$) and vorticity ($\zeta' \neq 0$). In Section 46.2 we studied inertial waves in a homogeneous fluid. The key difference here is that the shallow water fluid is hydrostatic, which, as we will see, alters the dispersion relation relative to that derived for the generally non-hydrostatic homogeneous fluid. It furthermore motivates us to examine inertial waves along with gravity waves since a hydrostatic fluid only arises in a gravity field. Such *inertia-gravity* or *Poincaré waves* are the topic of Section 48.7

Planetary and topographic Rossby waves

The remaining two terms on the right hand side of equation (48.31) lead to waves supported by a background vorticity gradient. The *planetary Rossby waves* rely on a nonzero planetary vorticity gradient (i.e., the β effect), whereas *topographic Rossby waves* rely on a nonzero gradient in the bottom topography. Both of these waves are dispersive, and both have frequencies lower than inertia-gravity waves. As shown in Section 48.4.6, and as already detailed for the horizontally non-divergent barotropic model in Section 47.3, the wave equation for Rossby waves has just a single time derivative acting on the free surface. This situation contrasts to the two time derivatives found for inertia-gravity waves and currently appearing in equation (48.31). Although shallow water Rossby waves rely on a nonzero $\nabla(H_r f) \times \mathbf{u}'$, we postpone writing their wave equation until working through some more technical details.

In Chapter 47 we study many properties of Rossby waves in the horizontally non-divergent barotropic fluid. Rossby waves rely on a gradient in the background (potential) vorticity, such as the planetary vorticity (β effect) or gradient in bottom topography. Shallow water Rossby waves share key physical properties with Rossby waves in the non-divergent barotropic flow. Yet we require more technical steps to extract the physics within the shallow water model. Note also that the shallow water model supports topographic Rossby waves. In contrast, no such waves appear in the horizontally non-divergent barotropic model since the flow is restricted to move along constant depth contours.

48.4.2 Use of the vorticity equation

We now return to the wave equation (48.31) and perform some further manipulations in the quest to derive an equation that only has the free surface along with geophysical parameters. Start by writing the divergence equation (48.29) in its form that extracts the β term

$$\partial_{tt}\eta' - \nabla \cdot (g H_r \nabla \eta') = -f \hat{\mathbf{z}} \cdot [\nabla \times (H_r \mathbf{u}')] + \beta H_r u. \quad (48.34)$$

Next we work with $\hat{\mathbf{z}} \cdot [\nabla \times (H_r \mathbf{u}')]$, which is the vorticity of the thickness (resting thickness) weighted velocity. To compute its time evolution, multiply the velocity equation (48.16) by H_r and take the curl

$$\nabla \times \partial_t(H_r \mathbf{u}') = -\nabla \times (\hat{\mathbf{z}} \times f H_r \mathbf{u}') - g \nabla H_r \times \nabla \eta' \quad (48.35a)$$

$$= -\hat{\mathbf{z}} [\nabla \cdot (f H_r \mathbf{u})] - g \nabla H_r \times \nabla \eta', \quad (48.35b)$$

where the second equality made use of the identity

$$\nabla \times (\hat{\mathbf{z}} \times f H_r \mathbf{u}') = \hat{\mathbf{z}} [\nabla \cdot (f H_r \mathbf{u})]. \quad (48.36)$$

Now take the time derivative of the divergence equation (48.34) and use the vorticity equation (48.35b) to find

$$\partial_t [\partial_{tt}\eta' - \nabla \cdot (g H_r \nabla \eta')] = -f \hat{\mathbf{z}} \cdot [\nabla \times \partial_t(H_r \mathbf{u}')] + \beta H_r \partial_t u' \quad (48.37a)$$

$$= f \nabla \cdot (f H_r \mathbf{u}) + f g \hat{\mathbf{z}} \cdot (\nabla H_r \times \nabla \eta') + \beta H_r \partial_t u' \quad (48.37b)$$

$$= -f^2 \partial_t \eta' + f g \hat{\mathbf{z}} \cdot (\nabla H_r \times \nabla \eta') + \beta H_r (f v' + \partial_t u'). \quad (48.37c)$$

Rearrangement leads to

$$\partial_t [\mathcal{L}(\eta') - \nabla \cdot (g H_r \nabla \eta')] = f g \hat{\mathbf{z}} \cdot (\nabla H_r \times \nabla \eta') + \beta H_r (f v' + \partial_t u'), \quad (48.38)$$

where we introduced the linear time operator as a shorthand

$$\mathcal{L} = \partial_{tt} + f^2. \quad (48.39)$$

This operator commutes with time derivatives but commutes with space derivatives only for the f -plane. For the case of $\beta = 0$, equation (48.38) only has the free surface height as a prognostic field. Hence, this equation is suited to developing the dispersion relation for gravity waves and inertial waves. Yet, as we show in the following, we need more work for sub-inertial Rossby waves.²

48.4.3 The unified wave equation just with η'

The final step is to eliminate the term $f v' + \partial_t u'$ from equation (48.38) in favor of terms proportional to the free surface. The key step is to make use of the following identities derived in Exercise 48.2

$$\mathcal{L}(u') = -g (\partial_{xt}\eta' + f \partial_y \eta') \quad \text{and} \quad \mathcal{L}(v') = -g (\partial_{yt}\eta' - f \partial_x \eta'). \quad (48.40)$$

Acting with \mathcal{L} on equation (48.38), and using the identities (48.40), yield

$$\partial_t [\mathcal{L}[\mathcal{L}(\eta') - \nabla \cdot (g H_r \nabla \eta')]] = f g \hat{\mathbf{z}} \cdot [\nabla H_r \times \nabla \mathcal{L}(\eta')] + \beta H_r f \mathcal{L}(v') + \beta H_r \partial_t \mathcal{L}(u'). \quad (48.41)$$

Expanding the linear operator and rearranging leads to the desired unified equation

$$\partial_t [\mathcal{L}[\mathcal{L}(\eta') - \nabla \cdot (g H_r \nabla \eta')]] = f g \hat{\mathbf{z}} \cdot [\nabla H_r \times \nabla \mathcal{L}(\eta')] + g \beta H_r (f^2 \partial_x \eta' - 2 f \partial_{yt} \eta' - \partial_{xtt} \eta'). \quad (48.42)$$

This wave equation encapsulates the full suite of linear wave processes active in a shallow water layer. However, it is not so simple to parse, which motivates us to examine limiting forms of

²SMG: What about super-inertial topographic waves from equation (48.39)?

this equation for super-inertial waves ($\omega^2 > f^2$) versus sub-inertial waves ($\omega^2 < f^2$). Doing so provides the means to unpack the basic wave motions that are contained in equation (48.42).

48.4.4 Scaling the wave equation

To help analyze the super-inertial and sub-intertial wave motions contained in equation (48.42), we introduce the following length and time scales of the motions

$$L = \text{horizontal scale} \quad \text{and} \quad \omega = \text{angular frequency}. \quad (48.43)$$

We work under the assumptions of a β -plane approximation (see equation (21.46)) so that the horizontal scales of motion satisfy

$$\beta L \ll |f_0|, \quad (48.44)$$

where we wrote the Coriolis parameter as $f = f_0 + \beta y$. We also assume the topography undulation, η'_b , is much smaller than the mean layer thickness,

$$\eta'_b \ll H. \quad (48.45)$$

Both approximations (48.44) and (48.45) are familiar from our development of quasi-geostrophy theory in Section 40.5.1. Finally, we assume $f > 0$ as per the northern hemisphere, with occurrences of f merely changed to $|f|$ for southern hemisphere results.

Introducing the above scales into the wave equation (48.42) leads to

$$\partial_t \mathcal{L}^2(\eta') \sim \omega (\omega^2 + f^2)^2 \eta' \quad (48.46a)$$

$$\partial_t \mathcal{L}[\nabla \cdot (g H_r \nabla \eta')] \sim \omega (\omega^2 + f^2) (g H_r / L^2) \eta' \quad (48.46b)$$

$$f g \nabla H_r \times \nabla \mathcal{L}(\eta') \sim (f g \eta'_b / L^2) (\omega^2 + f^2) \eta' \quad (48.46c)$$

$$g \beta H_r f^2 \partial_x \eta' \sim (g \beta H_r f^2 / L) \eta' \quad (48.46d)$$

$$-2 \beta g H_r f \partial_y \eta' \sim (\beta g H_r f \omega / L) \eta' \quad (48.46e)$$

$$\beta g H_r \partial_{xxtt} \eta' \sim \beta g H_r (\omega^2 / L) \eta'. \quad (48.46f)$$

We next separately examine the super-inertial regime, $\omega^2 > f^2$, and sub-inertial regime, $\omega^2 < f^2$.

48.4.5 Super-inertial wave equation

In this subsection we derive an approximate wave equation relevant for super-inertial motions ($\omega^2 > f^2$).

Super-inertial scaling for the LHS of equation (48.42)

From equations (48.46a) and (48.46b), the two terms on the left hand side of the wave equation (48.42) scale as

$$\text{LHS} = \partial_t \mathcal{L}^2(\eta') - \partial_t \mathcal{L}[\nabla \cdot (g H_r \nabla \eta')] \sim \omega^3 [\omega^2 + g H_r / L^2] \eta'. \quad (48.47)$$

Assuming the horizontal length scale is given by the inverse wavenumber, $L = |\mathbf{k}|^{-1}$, yields

$$g H_r / L^2 \approx c_{\text{grav}}^2 |\mathbf{k}|^2 \approx \omega^2 \implies L^2 \sim g H_r / \omega^2. \quad (48.48)$$

The first approximation follows from assuming $\eta'_b \ll H$ so that $g H_r \approx g H = c_{\text{grav}}^2$, and the second approximation follows from assuming a non-rotating gravity wave dispersion relation.³ In essence, we are assuming the two terms in equation (48.47) scale the same, which holds so long as the length scale of the super-inertial waves satisfies $L^2 \sim g H_r / \omega^2$.

Ratio of RHS terms to the LHS

Now consider the magnitude for each term on the right hand side of the wave equation (48.42) relative to the left hand side terms just found in equation (48.47). The ratio for terms in equation (48.46c) satisfy

$$\frac{f g \nabla H_r \times \nabla \mathcal{L}(\eta')}{\text{LHS}} \sim \frac{\omega^2 f g \eta'_b / L^2}{\omega^3 g H_r / L^2} = \frac{f \eta'_b}{\omega H_r} \ll 1, \quad (48.49)$$

where the inequality follows from assuming that the bottom topography undulation is small as per equation (48.45). The ratio for the remaining three terms (equations (48.46d), (48.46e), and (48.46f)) are also much less than unity, with these inequalities following from the β -plane approximation (48.44)

$$\frac{g \beta H_r f^2 \partial_x \eta'}{\text{LHS}} \sim \frac{g \beta H_r f^2 / L}{\omega^3 g H_r / L^2} = (\beta L / \omega) (f / \omega)^2 < (\beta L / f) (f / \omega)^2 \ll 1 \quad (48.50a)$$

$$\frac{-2 f \partial_{yt} \eta'}{\text{LHS}} \sim \frac{\beta g H_r f \omega / L}{\omega^3 g H_r / L^2} = (\beta L / \omega) (f / \omega) < (\beta L / f) (f / \omega) \ll 1 \quad (48.50b)$$

$$\frac{\beta g H_r \partial_{xtt} \eta'}{\text{LHS}} \sim \frac{\beta g H_r (\omega^2 / L)}{\omega^3 g H_r / L^2} = (\beta L / \omega) < (\beta L / f) \ll 1. \quad (48.50c)$$

Inertia-gravity wave equation for super-inertial waves

We thus conclude that for super-inertial waves on a β -plane and with small amplitude topography, then the two terms on the left hand side of equation (48.42) balance so that

$$\partial_t \mathcal{L}[\mathcal{L}(\eta') - \nabla \cdot (g H_r \nabla \eta')] \approx 0. \quad (48.51)$$

This relation can be maintained by setting

$$(\partial_{tt} + f_0^2) \eta' - \nabla \cdot (g H_r \nabla \eta') = 0, \quad (48.52)$$

which is the equation for inertia-gravity waves on an f -plane with small amplitude topography. Note that we put $f = f_0$ in equation (48.52) since the β effect is most crucial for sub-inertial wave motions as discussed in Section 48.4.6, rather than super-inertial motions. We study non-rotating gravity waves in Section 48.5 and inertia-gravity waves in Section 48.7.

48.4.6 Sub-inertial wave equation

We here derive an equation relevant for sub-inertial wave motions ($\omega^2 < f^2$). In fact, we further restrict the motion to those that are very low frequency so that

$$\omega / f \sim \beta L / f_0 \sim \eta'_b / H \ll 1. \quad (48.53)$$

³We derive the shallow water gravity wave dispersion relation in equation (48.76). Also, see the discussion of long surface gravity waves in Section 45.5.3.

We also assume that the horizontal length scales are on the order of

$$L \sim L_d = c_{\text{grav}}/f = \sqrt{g H}/f, \quad (48.54)$$

which is known as the *deformation radius* for the shallow water layer. This length scale appears throughout our discussion of rotating shallow water waves.

The assumed scalings (48.53) along with (48.54) are precisely those assumed for the shallow water quasi-geostrophy theory detailed in Section 40.5. The corresponding sub-inertial waves are referred to as *planetary Rossby waves* and *topographic Rossby waves*. We here derive the wave equation for these waves, with further details of their dispersion relation provided in Section 48.11.

Sub-inertial scaling for the LHS of equation (48.42)

For the sub-inertial scalings (48.53), the linear operator is order $\mathcal{L} \sim \mathcal{O}(f^2)$, so that the left hand side of the wave equation (48.42) scales as

$$\text{LHS} = \partial_t \mathcal{L}^2(\eta') + \partial_t \mathcal{L}[\nabla \cdot (g H_r \nabla \eta')] \sim \omega f^2 [f^2 + g H_r/L^2] \eta'. \quad (48.55)$$

As for the super-inertial waves in Section 48.4.5, we assume these two terms scale the same. To ensure that scaling requires us to focus on horizontal length scales satisfying

$$L^2 \sim g H_r/f^2 \sim g H/f^2 = c_{\text{grav}}^2/f^2 = L_d^2. \quad (48.56)$$

This assumption of deformation scale motions for sub-inertial waves can be compared to the super-inertial length scale in equation (48.48). We find that super-inertial motions are generally smaller than the deformation radius whereas sub-inertial motions are on the order or larger than the deformation radius.

With the above scaling (48.56) for the horizontal length, the left hand side of the wave equation (48.42) scales as

$$\text{LHS} \sim (\omega f g H_r/L^2) \eta'. \quad (48.57)$$

We will later replace f with f_0 in equation (48.57), with that replacement warranted by the β -plane approximation, $\beta L \ll f_0$. For now, we reduce clutter by just writing f .

Ratio of RHS terms to the LHS

Now consider the magnitude for each term on the right hand side of the wave equation (48.42) relative to the left hand side terms just found in equation (48.57). The ratio for terms in equation (48.46c) is given by

$$\frac{f g \nabla H_r \times \nabla \mathcal{L}(\eta')}{\text{LHS}} \sim \frac{f^3 g \eta'_b/L^2}{\omega f^2 g H_r/L^2} = \frac{f \eta'_b}{\omega H_r} = \mathcal{O}(1), \quad (48.58)$$

with the final equality following from the assumed scales in equation (48.53). We also find that the ratio for terms in equation (48.46d) is given by

$$\frac{g \beta H_r f^2 \partial_x \eta'}{\text{LHS}} \sim \frac{g \beta H_r f^2/L}{\omega f^2 g H_r/L^2} = (\beta L/\omega) = \mathcal{O}(1), \quad (48.59)$$

where we again made use of equation (48.53) for the final equality. In contrast to these order unity ratios, the ratios involving terms in equations (48.46e) and (48.46f) are much less than unity

$$\frac{-2f\partial_{yt}\eta'}{\text{LHS}} \sim \frac{\beta g H_r f \omega/L}{\omega f^2 g H_r / L^2} = \beta L/f \ll 1 \quad (48.60\text{a})$$

$$\frac{\beta g H_r \partial_{xtt}\eta'}{\text{LHS}} \sim \frac{\beta g H_r (\omega^2/L)}{\omega f^2 g H_r / L^2} = (\beta L/f) (\omega/f) \ll 1. \quad (48.60\text{b})$$

The first inequality follows from the β -plane approximation (48.44), and the second follows also from the β -plane approximation as well as the low frequency assumption, $\omega^2 \ll f^2$.

Shallow water planetary and topographic Rossby wave equation

The above scalings lead to the approximate wave equation for sub-inertial waves moving on a β -plane with small amplitude bottom topography

$$\partial_t [f^2 \eta' - \nabla \cdot (g H \nabla \eta')] = f g \hat{z} \cdot (\nabla H_r \times \nabla \eta') + g H \beta \partial_x \eta'. \quad (48.61)$$

Note that we set $H_r = H$ everywhere except where it is differentiated, with this replacement consistent with the assumed $\eta'_r \ll H$ (equation (48.53)). A slightly more tidy version arises by introducing the squared gravity wave speed $c_{\text{grav}}^2 = g H$ and the deformation radius, $L_d = c_{\text{grav}}/f$, so that

$$\partial_t [(L_d^{-2} - \nabla^2) \eta'] = (f/H) \hat{z} \cdot (\nabla H_r \times \nabla \eta') + \beta \partial_x \eta'. \quad (48.62)$$

The first term on the right hand side gives rise to topographic Rossby waves, whereas the second term gives rise to planetary Rossby waves. It is notable that this equation has only a single time derivative, which contrasts with the super-inertial wave equation (48.52).

Rossby waves are supported by potential vorticity gradients

We can write the right hand side of equation (48.62) in the following equivalent form

$$\partial_t [(L_d^{-2} - \nabla^2) \eta'] = H \hat{z} \cdot (\nabla \eta' \times \nabla Q_r). \quad (48.63)$$

In this manner we see that both planetary Rossby waves and topographic Rossby waves are supported by gradients in the resting fluid's potential vorticity⁴

$$Q_r = f/H_r. \quad (48.64)$$

Equation (48.63) reveals that shallow water Rossby waves arise from a mis-alignment between contours of constant resting state potential vorticity and contours of constant surface height.

The effective β vector

We offer one further expression for the Rossby wave equation

$$\partial_t [(L_d^{-2} - \nabla^2) \eta'] = \hat{z} \cdot (\nabla \eta' \times \boldsymbol{\beta}_{\text{eff}}), \quad (48.65)$$

where we introduced the effective beta vector that combines the planetary vorticity gradient with the topographic gradient

$$\boldsymbol{\beta}_{\text{eff}} = \nabla f - Q_r \nabla H_r = \beta \hat{y} - Q_r \nabla H_r. \quad (48.66)$$

⁴When studying waves in the horizontally non-divergent barotropic fluid (Section 47.3), we also noted the need for a background potential vorticity gradient to support Rossby wave modes.

Again, this form exhibits the parallel role of both planetary beta and topographic slopes in supporting Rossby waves. Equation (48.65) says that shallow water Rossby waves arise from a mis-alignment between the effective beta vector and free surface height gradients.

48.4.7 Further study

Many of the manipulations in this section follow Lecture 14 of *Pedlosky* (2003).

48.5 Gravity waves

In this section we study shallow water gravity waves in the absence of rotation. We already encountered features of these waves in Chapter 45 when studying surface gravity waves. Even so, it is useful to start from the shallow water equations to directly derive the properties of the non-dispersive gravity waves. Additionally, we here do not introduce a velocity potential as done for the surface gravity waves, even though the non-rotating shallow water gravity waves are irrotational. We do not introduce the velocity potential since the other waves studied in this chapter carry vorticity, thus making the velocity potential an incomplete description for those cases.

48.5.1 Flat bottom gravity waves

Setting $\eta'_b = 0$ in equation (48.32) yields the shallow water gravity wave equation holding for a flat bottom domain

$$(\partial_{tt} - c_{\text{grav}}^2 \nabla^2) \eta' = 0, \quad (48.67)$$

where the gravity wave speed is determined by the two geophysical properties of the system

$$c_{\text{grav}} = \sqrt{g H}. \quad (48.68)$$

To help emphasize a few key properties, we return to the linear thickness equation (48.14) and linear velocity equation (48.16), now written with $f = 0$ and $\eta'_b = 0$

$$\partial_t \eta' = -H \nabla \cdot \mathbf{u}' \quad \text{and} \quad \partial_t \mathbf{u}' = -g \nabla \eta'. \quad (48.69)$$

Taking the time derivative of the thickness equation and then using the velocity equation readily yields the wave equation (48.67). Conversely, taking the horizontal divergence of the velocity equation yields

$$\partial_t (\nabla \cdot \mathbf{u}') = -g \nabla^2 \eta', \quad (48.70)$$

so that time changes in the horizontal divergence are driven by curvature in the free surface. Taking time derivative of this equation and using the thickness equation reveals that the horizontal divergence also satisfies the wave equation

$$(\partial_{tt} - c_{\text{grav}}^2 \nabla^2) (\nabla \cdot \mathbf{u}') = 0. \quad (48.71)$$

Hence, both the free surface and the horizontal divergence travel as non-dispersive gravity waves in the flat bottom non-rotating shallow water layer.

Finally, we note that the linearized potential vorticity equation (48.23), in the presence of $f = 0$ and $\eta'_b = 0$, means that the relative vorticity is static at each point in the fluid

$$\partial_t \zeta' = 0. \quad (48.72)$$

Hence, the linear fluctuations do not alter the flow vorticity. In particular, if the flow starts with zero vorticity then gravity wave fluctuations retain the zero vorticity.

48.5.2 Relating the wave amplitudes

Substituting the plane wave ansatz (48.24) into the linearized thickness and velocity equations (48.69) allows us to connect the wave amplitudes for the free surface and velocity

$$\omega \tilde{\mathbf{u}} = g \mathbf{k} \tilde{\eta} \implies \mathbf{k} \times \tilde{\mathbf{u}} = 0 \quad \text{and} \quad \omega \tilde{\eta} = H \mathbf{k} \cdot \tilde{\mathbf{u}}. \quad (48.73)$$

The identity $\mathbf{k} \times \tilde{\mathbf{u}} = 0$ means that the horizontal velocity of a fluid particle within the plane wave is oriented parallel to the horizontal wave vector, so that

$$\tilde{\mathbf{u}} = \hat{\mathbf{k}} (\hat{\mathbf{k}} \cdot \tilde{\mathbf{u}}) \quad \text{with} \quad \hat{\mathbf{k}} = \mathbf{k}/|\mathbf{k}|. \quad (48.74)$$

This alignment of the horizontal velocity with the wavevector is a direct result of the irrotational nature of the gravity waves, which was already noted when discussing the linearized vorticity equation (48.72). Additionally, with a real wavevector and real angular frequency, the amplitude relation $\omega \tilde{\mathbf{u}} = g \mathbf{k} \tilde{\eta}$ also holds for the traveling plane wave velocity and free surface

$$\omega \mathbf{u} = g \mathbf{k} \eta. \quad (48.75)$$

The alignment of the horizontal fluid particle velocity with the wavevector (equation (48.75)) indicates that the horizontal motion in the shallow water gravity wave is longitudinal. However, as emphasized in Section 48.3.4, a shallow water fluid has a nonzero vertical velocity component that is the linear function of depth (equation (48.26)). The presence of vertical motion within the wave means that the waves are not longitudinal in three dimensions. Rather, a fluid particle moves horizontally in the direction of the wavevector but the particle also moves vertically, thus tracing out an elliptical path in the vertical-horizontal plane.

Since the horizontal motion in a shallow water layer is depth-independent, the elliptical particle trajectories within a wave have the same major axis throughout the layer depth. This behavior contrasts to the deepwater gravity waves studied in Chapter 45, whose amplitude in all directions decreases with depth.

48.5.3 Dispersion relation

Substitution of the plane wave ansatz (48.24) into the wave equation (48.67) leads to

$$\omega^2 = g H |\mathbf{k}|^2 = c_{\text{grav}}^2 |\mathbf{k}|^2. \quad (48.76)$$

Taking the square root then leads to the shallow water gravity wave dispersion relation⁵

$$\omega = |\mathbf{k}| c_{\text{grav}} \implies C_p = \omega/|\mathbf{k}| = c_{\text{grav}}, \quad (48.77)$$

where we identified the phase speed as the gravity wave speed

$$C_p = c_{\text{grav}} = \sqrt{g H}. \quad (48.78)$$

Each wavevector propagates at the same speed since the phase speed is only dependent on geophysical parameters (gravitational acceleration and the resting layer thickness). Equivalently,

⁵Recall that we always consider the angular frequency of waves to be non-negative (Section 43.2), hence we only take the positive root for the dispersion relation (48.77).

higher wavenumber waves have correspondingly higher frequency, and the relation between the two is linear. We conclude that non-rotating shallow water gravity waves are *non-dispersive*.

48.6 Gravity waves in two layers

When adding more shallow water layers, how much can we use from the single layer results? To answer that question we here consider the linearized equations for two shallow water layers. The equations can be generalized to multiple layers, though with increased algebraic complexity. Indeed, even the two-layer case with rotation proves to be algebraically tedious, thus motivating us to examine just the case of gravity waves without rotation.

48.6.1 Linearized two-layer equations

We derived the equations for a stacked shallow water model in Section 32.4, and focused on two layers in Section 32.4.1. With reference to Figure 32.6 for notation, we write the layer thicknesses in the form

$$h_1 = H_1 + h'_1 = \eta_{1/2} - \eta_{3/2} = (\bar{\eta}_{1/2} - \bar{\eta}_{3/2}) + (\eta'_{1/2} - \eta'_{3/2}) \quad (48.79a)$$

$$h_2 = H_2 + h'_2 = \eta_{3/2} - \eta_b = (\bar{\eta}_{3/2} - \bar{\eta}_b) + (\eta'_{3/2} - \eta'_b), \quad (48.79b)$$

where we introduced the resting layer thicknesses

$$H_1 = \bar{\eta}_{1/2} - \bar{\eta}_{3/2} \quad \text{and} \quad H_2 = \bar{\eta}_{3/2} - \bar{\eta}_b \quad \text{and} \quad H = H_1 + H_2, \quad (48.80)$$

with the overbar representing the area mean, and with the half-integer labels representing interface fields. With this notation we are led to the linearized version of the thickness equations (32.61a) and (32.61b)

$$\partial_t h'_1 + H_1 \nabla \cdot \mathbf{u}'_1 = 0 \quad (48.81a)$$

$$\partial_t h'_2 + H_2 \nabla \cdot \mathbf{u}'_2 = 0, \quad (48.81b)$$

where \mathbf{u}'_1 and \mathbf{u}'_2 are the horizontal velocities in the two layers. Likewise, assuming a zero atmospheric pressure leads us to write the linearized version of velocity equations (32.76a) and (32.76b)

$$\partial_t \mathbf{u}'_1 + f \hat{\mathbf{z}} \times \mathbf{u}'_1 = -g \nabla \eta'_{1/2} \quad (48.82a)$$

$$\partial_t \mathbf{u}'_2 + f \hat{\mathbf{z}} \times \mathbf{u}'_2 = -g \nabla \eta'_{1/2} - g^r_{3/2} \nabla \eta'_{3/2}, \quad (48.82b)$$

For the linearized system, the only coupling occurs through undulations of the free surface impacting on the pressure felt in the lower layer.

48.6.2 Gravity wave equations

We restrict the analysis to the non-rotating case so that the layer equations take the form

$$\partial_t (\eta'_{1/2} - \eta'_{3/2}) + H_1 \nabla \cdot \mathbf{u}'_1 = 0 \quad \text{and} \quad \partial_t \mathbf{u}'_1 = -g \nabla \eta'_{1/2} \quad (48.83a)$$

$$\partial_t \eta'_{3/2} + H_2 \nabla \cdot \mathbf{u}'_2 = 0 \quad \text{and} \quad \partial_t \mathbf{u}'_2 = -g \nabla \eta'_{1/2} - g^r \nabla \eta'_{3/2}, \quad (48.83b)$$

where we introduced the reduced gravity for the interior layer interface

$$g^r = g_{3/2}^r = g(\rho_2 - \rho_1)/\rho_1. \quad (48.84)$$

Taking time derivatives of the thickness equations and substituting the divergence of the velocity equations leads to the matrix-vector equation

$$\begin{bmatrix} (\partial_{tt} - g H_1 \nabla^2) & -\partial_{tt} \\ -g H_2 \nabla^2 & (\partial_{tt} - g^r H_2 \nabla^2) \end{bmatrix} \begin{bmatrix} \eta'_{1/2} \\ \eta'_{3/2} \end{bmatrix} = \begin{bmatrix} 0 \\ 0 \end{bmatrix}. \quad (48.85)$$

This equation has non-trivial solutions if the determinant of the matrix vanishes, and we use that property to derive the dispersion relation in the following.

48.6.3 Dispersion relation

To derive the dispersion relation we consider the plane wave ansatz for the free surface undulation in each layer

$$\eta'_{1/2} = \tilde{\eta}_{1/2} e^{i(\mathbf{k} \cdot \mathbf{x} - \omega t)} \quad \text{and} \quad \eta'_{3/2} = \tilde{\eta}_{3/2} e^{i(\mathbf{k} \cdot \mathbf{x} - \omega t)}. \quad (48.86)$$

Note that we assume each layer has the same wavevector and same angular frequency. However, the amplitudes, $\tilde{\eta}_{1/2}$ and $\tilde{\eta}_{3/2}$, are generally complex so that the phase of the layers can differ. Plugging the wave ansatz (48.86) into equation (48.85) converts the differential operators to algebraic expressions

$$\begin{bmatrix} (-\omega^2 + g H_1 |\mathbf{k}|^2) & \omega^2 \\ g H_2 |\mathbf{k}|^2 & (-\omega^2 + g^r H_2 |\mathbf{k}|^2) \end{bmatrix} \begin{bmatrix} \tilde{\eta}_{1/2} \\ \tilde{\eta}_{3/2} \end{bmatrix} = \begin{bmatrix} 0 \\ 0 \end{bmatrix}. \quad (48.87)$$

Setting the determinant to zero leads to the quadratic equation in ω^2

$$(\omega^2 - g H_1 |\mathbf{k}|^2)(\omega^2 - g^r H_2 |\mathbf{k}|^2) - g H_2 |\mathbf{k}|^2 \omega^2 = 0. \quad (48.88)$$

Solving for the squared phase speed ($C_p^2 = \omega^2/|\mathbf{k}|^2$) leads to

$$2\omega^2/|\mathbf{k}|^2 = (g H + g^r H_2) \pm \sqrt{(g H + g^r H_2)^2 - 4 g g^r H_1 H_2}. \quad (48.89)$$

Introducing the small non-dimensional parameter,

$$\epsilon = g^r H_2 / (g H) = g^r H_2 / c_{\text{grav}}^2 \ll 1, \quad (48.90)$$

and expanding the dispersion relation (48.89) to expose the leading order behavior yields the squared phase speeds

$$C_p^2 \approx c_{\text{grav}}^2 \quad \text{barotropic phase speed squared} \quad (48.91a)$$

$$C_p^2 \approx c_{\text{grav}}^2 g^r H_1 H_2 / (g H^2) = g^r H_1 H_2 / H \quad \text{baroclinic phase speed squared.} \quad (48.91b)$$

We motivate the names *barotropic mode* and *baroclinic mode* in the following, as motivated by our study of vorticity in Section 37.7.2 for a Boussinesq fluid. Note that the phase speed for the barotropic mode is roughly given by the gravity wave speed for a single layer of fluid with resting thickness H . This speed is much greater than that for the baroclinic mode since $g^r \ll g$.

48.6.4 Structure of the barotropic wave mode

For the barotropic mode, setting $\omega^2 \approx g H |\mathbf{k}|^2$ within equation (48.87) leads to the amplitude ratio

$$\tilde{\eta}_{1/2}/\tilde{\eta}_{3/2} \approx H/H_2 > 1. \quad (48.92)$$

Hence, the two interfaces undulate in-phase and with the surface interface fluctuating more than the interior interface. For the velocity amplitude, we return to the linearized velocity equations (48.83a) and (48.83b) for plane waves, in which

$$\omega \tilde{\mathbf{u}}_1 = \mathbf{k} g \tilde{\eta}_{1/2} \quad \text{and} \quad \omega \tilde{\mathbf{u}}_2 = \mathbf{k} (g^r \tilde{\eta}_{1/2} + g \tilde{\eta}_{3/2}). \quad (48.93)$$

Now use the interface height amplitude ratio (48.92), along with the scalar product with the wavevector, to find

$$\omega \tilde{\mathbf{u}}_1 \cdot \mathbf{k} = |\mathbf{k}|^2 g \tilde{\eta}_{1/2} \quad \text{and} \quad \omega \tilde{\mathbf{u}}_2 \cdot \mathbf{k} = |\mathbf{k}|^2 (g^r + g H_2/H) \tilde{\eta}_{1/2}. \quad (48.94)$$

We thus see that the layer velocities are in-phase and their ratio is

$$\frac{\omega \tilde{\mathbf{u}}_1 \cdot \mathbf{k}}{\omega \tilde{\mathbf{u}}_2 \cdot \mathbf{k}} \approx \frac{H}{H_2} > 1, \quad (48.95)$$

which equals to the ratio of the free surface heights in equation (48.92). We thus conclude that the barotropic mode consists of velocities in the two layers that oscillate in-phase with the upper layer having larger velocity than the lower, and with the upper free surface undulation larger than the interior. This behavior is consistent with our understanding of barotropic flow from the discussion of vorticity and baroclinicity for a Boussinesq fluid in Section 37.7.2.

48.6.5 Structure of the baroclinic wave mode

For the baroclinic mode, setting $\omega^2 \approx g^r H_1 H_2 |\mathbf{k}|^2/H$ within equation (48.87) leads to the amplitude ratio

$$\tilde{\eta}_{1/2}/\tilde{\eta}_{3/2} \approx -g^r H_2/(g H). \quad (48.96)$$

Hence, the two interfaces undulate oppositely (i.e., π radians out of phase) and with the amplitude of the upper interface far less than the interior interface

$$|\tilde{\eta}_{1/2}/\tilde{\eta}_{3/2}| \ll 1. \quad (48.97)$$

That is, the free surface is nearly rigid relative to the interior interface. For the velocity amplitude, we make use of equation (48.93), the interface height amplitude ratio (48.96), and take the scalar product with the wavevector to render

$$\omega \tilde{\mathbf{u}}_1 \cdot \mathbf{k} = |\mathbf{k}|^2 g \tilde{\eta}_{1/2} \quad \text{and} \quad \omega \tilde{\mathbf{u}}_2 \cdot \mathbf{k} = |\mathbf{k}|^2 g^r - g/\epsilon) \tilde{\eta}_{1/2}. \quad (48.98)$$

We thus see that the layer velocities have the ratio

$$\frac{\omega \tilde{\mathbf{u}}_1 \cdot \mathbf{k}}{\omega \tilde{\mathbf{u}}_2 \cdot \mathbf{k}} \approx -\epsilon = -\frac{g^r H_2}{g H}, \quad (48.99)$$

so that they are π radians out of phase and their ratio is just like that for the interface heights. We thus conclude that the baroclinic mode consists of velocities in the two layers that oscillate oppositely, with the velocity and surface height in the upper layer undulating much less than in the interior. Indeed, to leading order the upper interface is rigid and the corresponding flow

stagnant. In contrast, the lower interface fluctuates as gravity wave with the squared phase speed $g^r H_1 H_2 / H$, which is far less than the barotropic gravity that is reflected by motion of the free surface. The behavior of the baroclinic mode gravity wave approximates that for a reduced gravity model (Section 32.3), yet with the upper layer nearly stagnant and the lower layer dynamic. We considered this *inverted reduced gravity* model in Exercise (32.5)).

48.6.6 The depth averaged velocity and the velocity difference

There are occasions in which it is useful to combine the layer velocity equations in a manner that directly approximates the barotropic and baroclinic motions. For this purpose we introduce the depth averaged velocity⁶

$$H \bar{\mathbf{u}} = H_1 \mathbf{u}'_1 + H_2 \mathbf{u}'_2, \quad (48.100)$$

with $H = H_1 + H_2$, along with the layer deviations from the depth average

$$\mathbf{u}_{1b} = \mathbf{u}'_1 - \bar{\mathbf{u}} \quad \text{and} \quad \mathbf{u}_{2b} = \mathbf{u}'_2 - \bar{\mathbf{u}}. \quad (48.101)$$

Making use of the linearized equations (48.82a) and (48.82b) (here returning to the case with rotation) leads to the equations of motion (see Exercise 48.3)

$$\partial_t \bar{\mathbf{u}} + f \hat{\mathbf{z}} \times \bar{\mathbf{u}} = -g \nabla \eta'_{1/2} - (H_2 g^r / H) \nabla \eta'_{3/2} \quad (48.102a)$$

$$\partial_t \mathbf{u}_{1b} + f \hat{\mathbf{z}} \times \mathbf{u}_{1b} = (g^r H_2 / H) \nabla \eta'_{3/2} \quad (48.102b)$$

$$\partial_t \mathbf{u}_{2b} + f \hat{\mathbf{z}} \times \mathbf{u}_{2b} = -(g^r H_1 / H) \nabla \eta'_{3/2}. \quad (48.102c)$$

Notice that the two deviation velocities, \mathbf{u}_{1b} and \mathbf{u}_{2b} , are independent of the free surface fluctuations. Furthermore, a layer integration of these two velocities vanishes

$$H_1 \mathbf{u}_{1b} + H_2 \mathbf{u}_{2b} = 0, \quad (48.103)$$

which is consistent with a vanishing integral for the equations of motion

$$H_1 (\partial_t \mathbf{u}_{1b} + f \hat{\mathbf{z}} \times \mathbf{u}_{1b}) + H_2 (\partial_t \mathbf{u}_{2b} + f \hat{\mathbf{z}} \times \mathbf{u}_{2b}) = 0. \quad (48.104)$$

Finally, we introduce the vertical shear velocity

$$\mathbf{u}_s = \mathbf{u}_1 - \mathbf{u}_2 = \mathbf{u}_{1b} - \mathbf{u}_{2b} \quad (48.105)$$

whose equation of motion is

$$\partial_t \mathbf{u}_s + f \hat{\mathbf{z}} \times \mathbf{u}_s = g^r \nabla \eta'_{3/2}. \quad (48.106)$$

For the barotropic wave from Section 48.6.4, whereby both layer interfaces undulate in phase and with a relatively small amplitude, then the shear velocity is nearly zero since the pressure gradient driving \mathbf{u}_s is small. In contrast, the depth averaged velocity is dominated by the pressure gradient due to undulations in the free surface height. For the baroclinic wave in Section 48.6.5, the depth averaged velocity is far smaller than for the barotropic wave. The depth average velocity, as well as the shear velocity, are dominated by the pressure from interior interface undulations. These behaviors each motivate the oceanographic colloquial terminology whereby the depth averaged velocity is referred to as the *barotropic velocity* and the shear velocity is referred to as the *baroclinic velocity*.

⁶We considered the vorticity of the depth averaged velocity for a continuous fluid in Section 37.9.7.

48.6.7 Comments

As noted at the start of this section, the addition of further layers greatly increases the algebraic complexity of the analysis, thus motivating the use of numerical models for studies with $N > 2$ layers. One generally finds that each layer adds another wave mode, with N layers realizing N modes (one barotropic mode and $N - 1$ baroclinic modes). We further the study of gravity waves in Chapter 49 by studying internal gravity waves, with such waves corresponding here to a continuum of baroclinic modes.

48.7 Inertia-gravity waves over a flat bottom

In this section we set the Coriolis parameter, f , to a nonzero constant while retaining a flat bottom. We also retain a nonzero gravity, which is consistent with the shallow water being in hydrostatic balance. The linearized thickness equation (48.14), velocity equation (48.16), and potential vorticity equation (48.23) take the form

$$\partial_t \eta' = -H \nabla \cdot \mathbf{u}' \quad (48.107a)$$

$$\partial_t \mathbf{u}' + f \hat{\mathbf{z}} \times \mathbf{u}' = -g \nabla \eta' \quad (48.107b)$$

$$\partial_t Q' = 0, \quad (48.107c)$$

where the linear flat bottom f -plane shallow water potential vorticity is given from equation (48.22)

$$H Q' = \zeta' - f \eta'/H, \quad (48.108)$$

where we dropped the constant f since it plays no dynamical role.

48.7.1 Forced oscillator equation for horizontal velocity

Taking a time derivative on the horizontal velocity equation (48.107b) and then back-substituting the velocity equation leads to the equation

$$(\partial_{tt} + f^2) \mathbf{u}' = -g (\partial_t \nabla \eta' - f \hat{\mathbf{z}} \times \nabla \eta'). \quad (48.109)$$

This equation for the horizontal velocity is in the form of a forced oscillator, with forcing from gradients in the free surface. We make use of this equation when developing the polarization relations for plane inertia-gravity waves in Section 48.7.9.

48.7.2 Free wave equation and potential vorticity

We can write the wave equation (48.31) as

$$(\partial_{tt} - c_{\text{grav}}^2 \nabla^2) \eta' = -H f \zeta'. \quad (48.110)$$

This equation describes a forced shallow water gravity wave with forcing from relative vorticity coupled to the Coriolis parameter. Recall that this coupling between Coriolis and relative vorticity is fundamental to the inertial waves studied in Section 46.2. We can now use the vorticity equation as in Section 48.4.2 to eliminate ζ' to reveal a free wave equation. Equivalently, in equation (48.38) we set f to a constant and the bottom to be flat, thus leading to

$$\partial_t [\partial_{tt} \eta' + f^2 \eta' - c_{\text{grav}}^2 \nabla^2 \eta'] = 0. \quad (48.111)$$

The linear fluctuations described by this equation are known as shallow water *inertia-gravity* or *Poincaré waves*. The name “inertia-gravity” is due to the presence of both the Coriolis frequency, f , and gravitational acceleration, g , with both playing a role as restoring forces to support the waves.

The wave equation (48.111) is in the form of a local conservation law where the term in square brackets is static. We already know about another static field, namely the potential vorticity, Q' , given by equation (48.108). We here show that the wave equation (48.111) is indeed identical to the potential vorticity equation (48.107c). For this purpose, substitute the expression (48.108) for the potential vorticity into the forced wave equation (48.110), which readily yields

$$f H^2 Q' = -(\partial_{tt} + f^2 - c_{\text{grav}}^2 \nabla^2) \eta'. \quad (48.112)$$

We thus find that

$$\partial_t Q' = 0 \implies \partial_t [\partial_{tt} \eta' + f^2 \eta' - c_{\text{grav}}^2 \nabla^2 \eta'] = 0, \quad (48.113)$$

so that the wave equation (48.111) for inertia-gravity waves is identical to the conservation equation for linear shallow water potential vorticity. We saw a similar connection between potential vorticity conservation and waves in our study of Rossby waves in Section 47.3 for the horizontally non-divergent barotropic fluid, and will see the connection yet again for shallow water Rossby waves in Section 48.11.

48.7.3 Dispersion relation

Substituting the wave ansatz (48.24) into equations (48.107a)-(48.107b) renders the homogeneous matrix-vector equation

$$\begin{bmatrix} -i\omega & -f & igk_x \\ f & -i\omega & igk_y \\ iHk_x & iHk_y & -i\omega \end{bmatrix} \begin{bmatrix} \tilde{u} \\ \tilde{v} \\ \tilde{\eta} \end{bmatrix} = \begin{bmatrix} 0 \\ 0 \\ 0 \end{bmatrix}. \quad (48.114)$$

This equation has a nontrivial solution only when the determinant of the matrix vanishes. The real part of the determinant cancels exactly, thus leaving just the imaginary part. Setting the imaginary part to zero yields the dispersion relation

$$\omega [\omega^2 - f^2 - g H |\mathbf{k}|^2] = 0. \quad (48.115)$$

We can derive the same dispersion relation by substituting the wave ansatz into the wave equation (48.113). There are three solutions to this cubic equation described in the following subsections.

48.7.4 Zero frequency geostrophic mode

The zero frequency solution to the dispersion relation (48.115) corresponds to f -plane geostrophic motion. Such motion is static so that the linearized continuity equation (48.107a) means that the flow is horizontally non-divergent, $\nabla \cdot \mathbf{u}' = 0$. Furthermore, the geostrophic solution corresponds to a static yet non-zero potential vorticity

$$f \hat{z} \times \mathbf{u}' = -g \nabla \eta' \implies (f/g) Q' = (\nabla^2 - L_d^{-2}) \eta' \neq 0, \quad (48.116)$$

where we introduced the deformation radius,

$$L_d = c_{\text{grav}}/f, \quad (48.117)$$

from equation (48.54). Turning equation (48.116) around, we see that if the potential vorticity is known, then the free surface can be found by inverting the elliptic operator, $\nabla^2 - L_d^{-2}$.

The static geostrophic mode with nonzero potential vorticity is decoupled, in the linear theory, from the ageostrophic inertia-gravity wave whose potential vorticity is identically zero and yet whose relative vorticity and free surface are time dependent. For this reason we can separately study the two linear modes without concern for interactions.

48.7.5 Inertia-gravity wave modes

The $\omega \neq 0$ solution to the dispersion relation (48.115) satisfies the quadratic dispersion relation

$$\omega^2 = f^2 (1 + L_d^2 |\mathbf{k}|^2). \quad (48.118)$$

Recall from Section 43.2 that we consider the angular frequency of waves to be non-negative. Hence, we only take the positive root for the dispersion relation (48.118)

$$\omega = |f| \sqrt{1 + L_d^2 |\mathbf{k}|^2}. \quad (48.119)$$

So rather than considering the construct of a negative angular frequency, we always consider $\omega \geq 0$ so that the wave direction is determined by the wavevector, \mathbf{k} .

The non-zero $\omega > 0$ modes satisfying the dispersion relation (48.118) are inertia-gravity waves and Figure 48.1 depicts this relation. These waves have an angular frequency greater than the inertial frequency

$$\omega \geq |f|, \quad (48.120)$$

and are thus said to be *super-inertial waves*.⁷ Furthermore, they carry zero potential vorticity (equation (48.112))

$$f H^2 Q' = -(\partial_{tt} + f^2 - c_{\text{grav}}^2 \nabla^2) \eta' = 0, \quad (48.121)$$

where we verify this property holds for plane inertia-gravity waves in Exercise 48.4.

48.7.6 Group velocity

The shallow water inertia-gravity waves have a longitudinal group velocity

$$\mathbf{c}_g = \frac{c_{\text{grav}}^2 \mathbf{k}}{\omega} = \frac{\mathbf{c}_p c_{\text{grav}}^2}{|\mathbf{c}_p|^2} = \frac{\mathbf{c}_p}{1 + (L_d |\mathbf{k}|)^{-2}}, \quad (48.122)$$

where the phase velocity is $\mathbf{c}_p = (\omega/|\mathbf{k}|) \hat{\mathbf{k}}$. Evidently, the ratio of their magnitudes is given by

$$\frac{|\mathbf{c}_g|}{|\mathbf{c}_p|} = \frac{c_{\text{grav}}^2}{|\mathbf{c}_p|^2} = \frac{1}{1 + (L_d |\mathbf{k}|)^{-2}}. \quad (48.123)$$

In the non-rotating case, where $f = 0$ so that $L_d^{-2} = (c_{\text{grav}}/f)^{-2} = 0$, the group and phase velocities are equal, which we expect since the non-rotating shallow water gravity waves from Section 48.5 are non-dispersive. The waves also approach the non-dispersive limit for wavelengths much smaller than the deformation radius, in which the waves are too small to feel the effects from rotation (we further discuss the shortwave limit in Section 48.7.7). But for the general case with dispersion, we see that rotation causes the group velocity to be smaller in magnitude than

⁷The inertial waves considered in Section 46.2, which we studied in a homogeneous fluid, have their angular frequency bounded by $\omega^2 < f^2$. These are *sub-inertial* waves. They are again encountered in Section 49.10.1 as a special case of a rotating internal gravity wave in the limit where the reference fluid state is homogeneous.

the phase velocity. Hence, the wave energy, which is carried by the group velocity (see Section 48.7.10 on energetics), is more slowly transmitted than the phase speed.

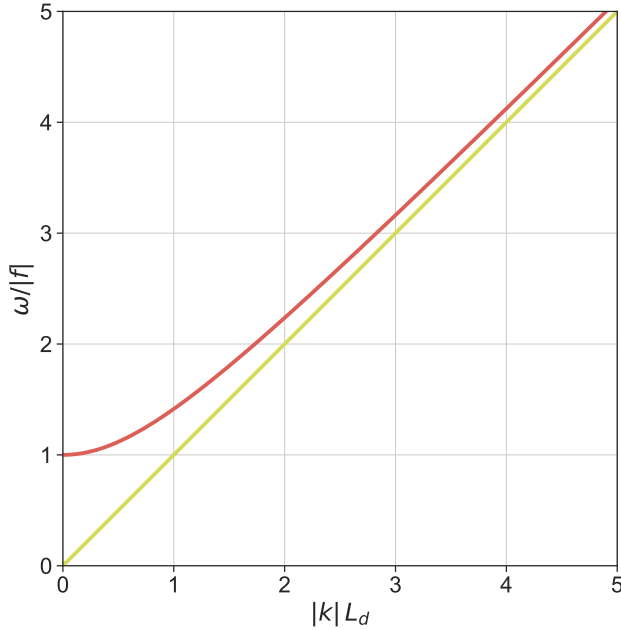


FIGURE 48.1: Illustrating the dispersion relation for shallow water inertia-gravity waves. The red hyperbolic curve is the dispersion relation (48.118), which asymptotes at high wavenumber (small wavelength) to the straight line for the non-rotating case. The angular frequency, ω , is scaled by the magnitude of the Coriolis frequency, $|f|$, and the horizontal wavenumber, $|\mathbf{k}|$, is multiplied by the deformation radius $L_d = \sqrt{gH}/f$. For small wave numbers ($|\mathbf{k}| L_d \ll 1$ or $\Lambda \gg 2\pi L_d$), the inertial-gravity wave frequency approaches the inertia frequency, f , with this behavior seen at the minimum of the dispersion curve. We expect this result since waves large relative to the deformation radius feel the Coriolis acceleration. At the opposite extreme of high wave numbers ($\Lambda \ll 2\pi L_d$), the wave frequency approaches the non-rotating gravity wave frequency, shown here by the linear dispersion relation $\omega = |\mathbf{k}| \sqrt{gH} = |\mathbf{k}| c_{\text{grav}}$. Waves small relative to the deformation radius do not feel the Coriolis acceleration and thus converge to non-rotating gravity waves. Since all inertia-gravity waves satisfy $\omega^2 \geq f^2$, they are said to be *super-inertial* waves; i.e., waves whose frequency is larger in magnitude than the inertial frequency.

48.7.7 Shortwave limit for inertia-gravity waves

The shortwave limit is in the regime where

$$|\mathbf{k}|^2 L_d^2 \gg 1, \quad (48.124)$$

so that the shortwave limit occurs when the wavelength is much shorter than the deformation radius, in which case the waves do not feel the effects from rotation. For example, consider a middle latitude shallow water gravity wave in a layer with $H = 10^3$ m and $f = 10^{-4}$ s⁻¹, in which case the shallow water deformation radius is $L_d = \sqrt{gH}/f = 10^3$ km. Maintaining the constraint (48.124) means that the wavelength of the gravity wave, $\Lambda = 2\pi/|\mathbf{k}|$, must satisfy

$$\Lambda \ll 2\pi L_d. \quad (48.125)$$

Within the shortwave limit, however, the wavelength cannot be too small since the flow must retain the hydrostatic balance as per a shallow water model. As discussed in Section 24.2, maintaining the hydrostatic balance means that the flow retains a small vertical to horizontal aspect

ratio. In terms of the wavenumber for gravity waves, the hydrostatic balance implies

$$|\mathbf{k}| H \ll 1 \iff \text{hydrostatic balance.} \quad (48.126)$$

We conclude that the shortwave limit for shallow water gravity waves is given by the regime

$$L_d^{-1} \ll |\mathbf{k}| \ll H^{-1} \iff 2\pi H \ll \Lambda \ll 2\pi L_d. \quad (48.127)$$

Although considered short from the perspective of the shallow water model, these waves are hydrostatic and thus considered long gravity waves from the perspective of the surface gravity waves studied in Chapter 45.

Finally, for the shortwave limit, the dispersion relation (48.118) reduces to the non-rotating dispersion relation (48.77)

$$\omega \approx |\mathbf{k}| c_{\text{grav}}. \quad (48.128)$$

We see that such waves are only weakly affected by the Coriolis acceleration so that their dispersion relation reduces to linear non-rotating gravity waves of Section 48.5.

48.7.8 Longwave limit for inertia-gravity waves

The longwave limit occurs when

$$|\mathbf{k}|^2 L_d^2 \ll 1, \quad (48.129)$$

so the waves are much longer than the deformation radius. In this limit the wave is strongly affected by the Coriolis acceleration. Indeed, the wave dispersion relation becomes

$$\omega^2 = f^2, \quad (48.130)$$

in which fluid particles exhibit inertial oscillations (Sections 48.7.9 and 12.5).

48.7.9 Structure of a plane inertia-gravity wave

As for the non-rotating gravity waves in Section 48.5, we study the behavior of the traveling plane wave ansatz (48.24). In contrast to the case with $f = 0$, here we require the complex nature of the wave amplitudes $(\tilde{u}, \tilde{v}, \tilde{\eta})$ in order to realize nontrivial inertia-gravity wave solutions. Such complex amplitudes mean there are differences in phase between the velocity and free surface that arise from the Coriolis parameter.

Polarization relations for the wave

Substituting the traveling plane wave ansatz (48.24) into the forced oscillator equation (48.109) leads to the amplitude relation

$$(-\omega^2 + f^2) \tilde{\mathbf{u}} = -g (\omega \mathbf{k} - i f \hat{\mathbf{z}} \times \mathbf{k}) \tilde{\eta}. \quad (48.131)$$

Without loss of generality, we assume the free surface amplitude, $\tilde{\eta}$, is real, which then leads to the free surface height

$$\eta' = \tilde{\eta} \cos(\mathbf{k} \cdot \mathbf{x} - \omega t), \quad (48.132)$$

and the fluid velocity within a plane wave

$$\mathbf{u}' = \frac{g |\mathbf{k}| \tilde{\eta}}{\omega^2 - f^2} \left[\underbrace{\omega \hat{\mathbf{k}} \cos(\mathbf{k} \cdot \mathbf{x} - \omega t)}_{\text{horizontally longitudinal}} + \underbrace{f (\hat{\mathbf{z}} \times \hat{\mathbf{k}}) \sin(\mathbf{k} \cdot \mathbf{x} - \omega t)}_{\text{horizontally transverse}} \right] \quad (48.133a)$$

$$= \frac{\tilde{\eta}}{|\mathbf{k}| H} \left[\underbrace{\omega \hat{\mathbf{k}} \cos(\mathbf{k} \cdot \mathbf{x} - \omega t)}_{\text{horizontally longitudinal}} + \underbrace{f (\hat{\mathbf{z}} \times \hat{\mathbf{k}}) \sin(\mathbf{k} \cdot \mathbf{x} - \omega t)}_{\text{horizontally transverse}} \right], \quad (48.133b)$$

where the unit vector

$$\hat{\mathbf{k}} = \mathbf{k}/|\mathbf{k}| \quad (48.134)$$

points in the direction of the wave, and equation (48.133b) follows from use of the dispersion relation (48.118) in equation (48.133a). These equations for the free surface and the velocity are sometimes referred to as *polarization relations*, which is a term taken from optics. Observe that the horizontally transverse component of the velocity vector is $\pi/2$ out of phase from the horizontally longitudinal component. Furthermore, the transverse component corresponds to fluid particle motion that is perpendicular to the wavevector, in which case we say that the transverse component is *polarized* perpendicular to the wavevector.

Drawing the polarization relations

To draw the free surface (48.132) and velocity (48.133b) we assume that $f > 0$ for the northern hemisphere, and recall that $\omega^2 \geq f^2$ since shallow water inertia-gravity waves are super-inertial. We also find it convenient to write the velocity as

$$\frac{\mathbf{u}' |\mathbf{k}| H}{\tilde{\eta} f} = (\omega/f) \hat{\mathbf{k}} \cos(\mathbf{k} \cdot \mathbf{x} - \omega t) + (\hat{\mathbf{z}} \times \hat{\mathbf{k}}) \sin(\mathbf{k} \cdot \mathbf{x} - \omega t). \quad (48.135)$$

Consider a point fixed in space and let time progress in the positive direction so that the phase, $\mathbf{k} \cdot \mathbf{x} - \omega t$, decreases. Consequently, the velocity vector rotates in a clockwise direction, forming an ellipse with the major axis along the longitudinal direction, $\hat{\mathbf{k}}$, and minor axis along the transverse direction, $(\hat{\mathbf{z}} \times \hat{\mathbf{k}})$. This motion corresponds to the inertial oscillations studied in Section 12.5 (where $\omega^2 = f^2$). Now consider a fixed time and sample the velocity field in the direction of the wave. In this case the phase increases as we move in the wave direction, so that the sampled velocity progresses counter-clockwise around the ellipse. Figure 48.2 offers three depictions of the wave field.

48.7.10 Energetics

In Section 48.3.2 we considered the general form of energy balances for the linearized shallow water equations integrated over the shallow water layer. For the special case of a flat bottom domain (with $\eta_b = 0$ for simplicity), these equations take the form

$$\partial_t (\mathcal{K}^{\text{sw}} + \mathcal{P}^{\text{sw}}) = -g \rho H \nabla \cdot [(\bar{\eta} + \eta') \mathbf{u}'] \quad (48.136a)$$

$$\mathcal{P}^{\text{sw}} = (\rho/2) g \eta^2 \quad (48.136b)$$

$$\mathcal{K}^{\text{sw}} = (\rho/2) H \mathbf{u}' \cdot \mathbf{u}'. \quad (48.136c)$$

Here we consider the energy carried by a plane inertia-gravity wave, and focus on the phase averaged energetics.

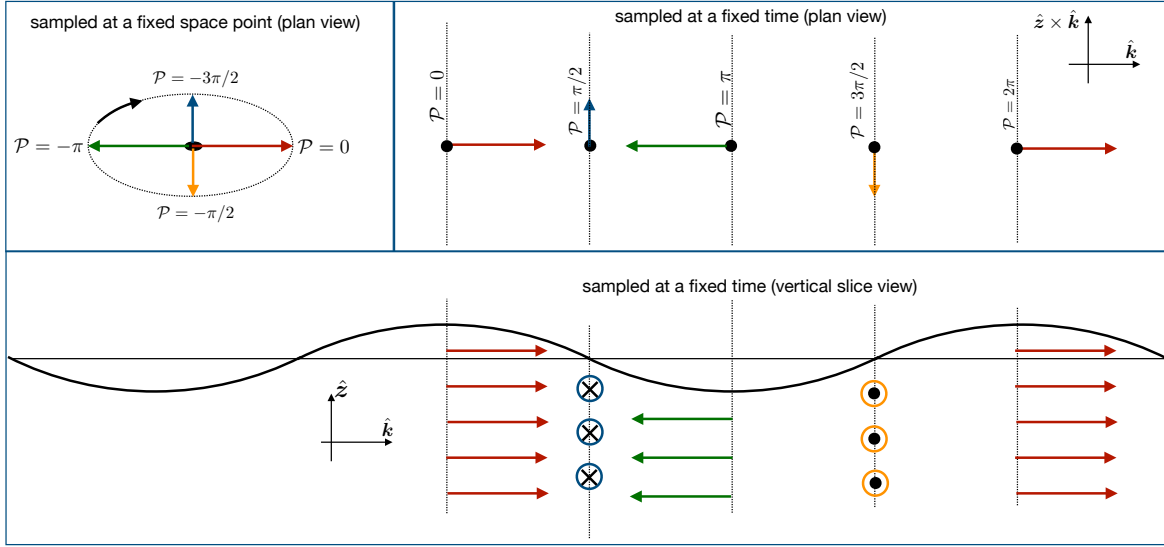


FIGURE 48.2: Illustrating the shallow water inertia gravity wave from three perspectives, with $\mathcal{P} = \mathbf{k} \cdot \mathbf{x} - \omega t$ the phase and $f > 0$. The upper left panel shows the horizontal velocity vector at a fixed point in space as time increases and so the phase decreases. The resulting velocity vector rotates clockwise and exhibits inertial oscillations. The upper right panel shows the horizontal velocity vector sampled along the wave direction, $\hat{\mathbf{k}}$, at a fixed time from a plan (horizontal) view, in which case the phase increases moving in the $\hat{\mathbf{k}}$ direction. The lower panel shows the horizontal velocity and free surface as viewed from a vertical slice aligned with the wavevector direction.

Kinetic and potential energies contained in a plane wave

Writing the free surface as in equation (48.132) and the horizontal velocity as in equations (48.133a) and (48.133b) leads to the potential energy and kinetic energy carried by the wave field

$$\mathcal{P}^{\text{sw}} = \frac{\rho g \tilde{\eta}^2}{2} \cos^2(\mathbf{k} \cdot \mathbf{x} - \omega t) \quad (48.137a)$$

$$\mathcal{K}^{\text{sw}} = \frac{\rho \tilde{\eta}^2}{|\mathbf{k}|^2 H^2} [\omega^2 \cos^2(\mathbf{k} \cdot \mathbf{x} - \omega t) + f^2 \sin^2(\mathbf{k} \cdot \mathbf{x} - \omega t)], \quad (48.137b)$$

with a corresponding phase average given by

$$\langle \mathcal{P}^{\text{sw}} \rangle = \frac{\rho g \tilde{\eta}^2}{4} \quad (48.138a)$$

$$\langle \mathcal{K}^{\text{sw}} \rangle = \frac{\rho \tilde{\eta}^2 (\omega^2 + f^2)}{2 |\mathbf{k}|^2 H^2} = \frac{\rho g \tilde{\eta}^2}{4} \frac{\omega^2 + f^2}{\omega^2 - f^2}. \quad (48.138b)$$

Evidently, for non-rotating shallow water gravity waves, $f = 0$, there is an equipartition between phase averaged potential and kinetic energy. However, for the general case with rotation, the phase averaged kinetic energy is larger than the potential energy

$$\frac{\langle \mathcal{K}^{\text{sw}} \rangle}{\langle \mathcal{P}^{\text{sw}} \rangle} = \frac{\omega^2 + f^2}{\omega^2 - f^2} = 1 + 2(L_d |\mathbf{k}|)^{-2}, \quad (48.139)$$

with equipartition approached only for wavenumbers larger than the deformation radius.

Mechanical energy and energy flux contained in a plane wave

The phase averaged mechanical energy contained in a plane wave is given by

$$\langle \mathcal{P}^{\text{sw}} \rangle + \langle \mathcal{K}^{\text{sw}} \rangle = \langle \mathcal{P}^{\text{sw}} \rangle \left[1 + \frac{\omega^2}{\omega^2 - f^2} \right] = 2 \langle \mathcal{P}^{\text{sw}} \rangle \frac{|\mathbf{c}_p|^2}{c_{\text{grav}}^2} = \frac{\rho g \tilde{\eta}^2}{2} \frac{|\mathbf{c}_p|}{|\mathbf{c}_g|}, \quad (48.140)$$

where we made use of equation (48.123) for the ratio of the group velocity magnitude to the phase velocity magnitude. For the flux of energy contained in the wave, we return to the energy equation (48.136a) and only consider the phase averaged flux, which takes the form

$$g \rho H \langle \eta' \mathbf{u}' \rangle = \frac{g \rho \tilde{\eta}^2 \omega \mathbf{k}}{2 |\mathbf{k}|^2} = \frac{g \rho \tilde{\eta}^2 \mathbf{c}_p}{2} = \frac{g \rho \tilde{\eta}^2 \mathbf{c}_g}{2} \frac{|\mathbf{c}_p|}{|\mathbf{c}_g|} = \mathbf{c}_g (\langle \mathcal{P}^{\text{sw}} \rangle + \langle \mathcal{K}^{\text{sw}} \rangle). \quad (48.141)$$

Hence, the phase averaged mechanical energy flux contained in the plane wave is given by the group velocity times the phase averaged mechanical energy. This is a standard result that we have seen before in the study of other linear waves.

48.8 Kelvin waves

The Kelvin wave is a non-dispersive inertia-gravity wave that arises from the presence of a boundary and rotation. The boundary considered here is a solid vertical wall. However, Kelvin waves also occur at the equator, with the equator acting as a boundary due to the change in sign of the Coriolis parameter, f .

To expose the key points about the shallow water Kelvin wave, it is sufficient to orient the f -plane with a boundary at $y = 0$. The meridional velocity component must vanish at $y = 0$ to satisfy the no-normal flow condition. We are thus motivated to seek nontrivial solutions with $v' = 0$ everywhere. In this case the linearized equations of motion are given by

$$\partial_t \eta' = -H \partial_x u' \quad (48.142a)$$

$$\partial_t u' = -g \partial_x \eta' \quad (48.142b)$$

$$f u' = -g \partial_y \eta'. \quad (48.142c)$$

Equations (48.142a) and (48.142c) lead to the one-dimensional wave equation for the zonal velocity fluctuation

$$(\partial_{tt} - c_{\text{grav}}^2 \partial_{xx}) u' = 0. \quad (48.143)$$

In Section 3.7 we studied how to solve this wave equation, in which we write a general solution in the form

$$u'(x, y, t) = F_1(x + c_{\text{grav}} t, y) + F_2(x - c_{\text{grav}} t, y), \quad (48.144)$$

with corresponding surface height displacement

$$\eta'(x, y, t) = \sqrt{H/g} [-F_1(x + c_{\text{grav}} t, y) + F_2(x - c_{\text{grav}} t, y)]. \quad (48.145)$$

We now substitute this form of the solution into equation (48.142c) to determine the y -dependence

$$\partial_y F_1 = f F_1 / c_{\text{grav}} \quad \text{and} \quad \partial_y F_2 = -f F_2 / c_{\text{grav}} \quad (48.146)$$

with solutions

$$F_1 = F(x + c_{\text{grav}} t) e^{y/L_d} \quad \text{and} \quad F_2 = G(x - c_{\text{grav}} t) e^{-y/L_d} \quad (48.147)$$

where $L_d = c_{\text{grav}}/f$ is the shallow water deformation radius defined earlier in equation (40.31). To ensure boundedness in the region $y > 0$ where the fluid is assumed to exist, we drop the F_1 solution, thus leaving

$$u' = e^{-y/L_d} G(x - c_{\text{grav}} t) \quad \text{and} \quad v' = 0 \quad \text{and} \quad \eta' = (H/g)^{1/2} e^{-y/L_d} G(x - c_{\text{grav}} t). \quad (48.148)$$

These wave signals are propagating in the positive \hat{x} direction, in which case the boundary $y = 0$ is on the right. This orientation holds for any boundary orientation in the northern hemisphere, whereby Kelvin waves propagate with the solid boundary on the right when looking in the direction of wave movement. For the southern hemisphere Kelvin waves propagate with the boundary to the left of the wave motion. Hence, Kelvin waves propagate in a cyclonic direction.

48.9 Geostrophic adjustment

The geostrophic balance presented in Sections 28.4 and 33.2 is very well maintained by the observed large-scale atmosphere and ocean. Hence, geostrophy (and the associated thermal wind) is a powerful diagnostic. In this section, we examine how a flow state that is initially not in geostrophic balance evolves towards geostrophy. We thus study the dynamical processes associated with the *geostrophic adjustment* problem. As we see, the adjustment occurs through the propagation of linear inertia-gravity waves. Hence, geostrophic adjustment offers an important example of the wave mechanics discussed thus far in this chapter.

A single shallow water layer on a flat f -plane is sufficient to introduce the main physical ideas. Furthermore, we focus on linear perturbations so that the governing equations are those derived in Section 48.7 when studying inertia-gravity waves. The adjustment consists of linear inertia-gravity waves that maintain a locally static potential vorticity (equation (48.23)). For brevity in notation, we here drop all primes on the linear fluctuating terms.

48.9.1 Potential vorticity inversion

Before studying the geostrophic adjustment problem, we offer a few comments about *potential vorticity inversion*, which generally refers to the process of determining the flow field given information about the potential vorticity. In a shallow water layer, the potential vorticity is given by

$$Q = h^{-1} (f + \zeta) = h^{-1} [f + \partial_x v - \partial_y u]. \quad (48.149)$$

If we further assume the flow to be in geostrophic balance (Section 33.2), then

$$Q = \frac{f}{h} + \frac{1}{h} \left[\frac{\partial}{\partial x} \left(\frac{g \partial \eta}{f \partial x} \right) + \frac{\partial}{\partial y} \left(\frac{g \partial \eta}{f \partial y} \right) \right]. \quad (48.150)$$

Assuming we know Q throughout the domain; assuming f and Q are uniformly of the same sign within the domain; and assuming we know boundary conditions for η , then equation (48.150) is a nonlinear elliptic boundary value problem (Section 3.5) for η . Nonlinearities come from the $h^{-1} = (\eta - \eta_b)^{-1}$ pre-factor, as well as the boundary conditions discussed below. Linearizing by setting $h^{-1} \approx H^{-1}$ and simplifying the boundary conditions (see below) allows equation (48.150) to be solved for η . This solution process is referred to as *inverting* the elliptic operator, so that this particular inversion process is referred to as *potential vorticity inversion*.

General boundary conditions for η can be rather complex to handle mathematically. Namely, in a domain with a sloping bottom, such as in Figure 32.1, the free surface deviation equals to the bottom deviation, $\eta = \eta_b$, along the domain boundaries since the layer thickness vanishes there.

Furthermore, the horizontal position of the domain boundary is a function of time since the layer moves up and down the sloping bottom. Vanishing layers and the associated moving boundaries are intrinsically nonlinear; i.e., there is no way to linearize this process. Instead, to facilitate the use of linear physics requires us to assume the layer thickness remains nonzero throughout the domain. Furthermore, we assume the layer thickness deviates only a small amount from the layer averaged thickness: $\eta/H \approx 1$. These assumptions are made in the following discussion of geostrophic adjustment.

48.9.2 Posing the initial value problem

We solve for the $t > 0$ evolution of surface height and velocity by making use of the linearized equations from Section 48.3

$$\partial_t \mathbf{u} + f \hat{\mathbf{z}} \times \mathbf{u} = -g \nabla \eta \quad (48.151a)$$

$$\partial_t \eta + H \nabla \cdot \mathbf{u} = 0 \quad (48.151b)$$

$$\zeta - f \eta/H = H Q(x, y). \quad (48.151c)$$

$Q(x, y)$ is the linearized potential vorticity and it is static for the flat bottom f -plane case and so it is determined by the initial conditions (Section 48.3.3). To illustrate the geostrophic adjustment in an analytically tractable manner, consider the following step initial conditions for the surface height

$$\eta(x, t = 0) = \begin{cases} +\eta_0 & x < 0 \\ -\eta_0 & x > 0, \end{cases} \quad (48.152)$$

which can be written

$$\eta(x, t = 0) = \eta_0 [1 - 2 \mathcal{H}(x)] = -\eta_0 \operatorname{sgn}(x), \quad (48.153)$$

where the sign-function is given by

$$\operatorname{sgn}(x) = \begin{cases} -1 & \text{if } x < 0 \\ 0 & \text{if } x = 0 \\ 1 & \text{if } x > 0, \end{cases} \quad (48.154)$$

which can also be written in terms of the Heaviside step function

$$\operatorname{sgn}(x) = 2 \mathcal{H}(x) - 1, \quad (48.155)$$

where

$$\mathcal{H}(x) = \begin{cases} 0 & \text{if } x < 0 \\ 1/2 & \text{if } x = 0 \\ 1 & \text{if } x > 0. \end{cases} \quad (48.156)$$

The velocity is assumed to be zero initially

$$\mathbf{u}(x, y, t = 0) = 0. \quad (48.157)$$

Correspondingly, the initial relative vorticity vanishes so that the linearized potential vorticity (equation (48.151c)) is

$$Q(x, y) = \frac{f \eta_0}{H^2} \operatorname{sgn}(x). \quad (48.158)$$

Since $\partial Q / \partial t = 0$ (equation (48.23)), this value of the potential vorticity is maintained at each point throughout the adjustment process. The velocity and surface height adjustment is thus

constrained to keep potential vorticity static. This rather basic point is key to determining evolution of the velocity and surface height, and thus in determining the final (equilibrium) state for these fields.

48.9.3 Adjustment in the absence of rotation

In the absence of rotation ($f = 0$), relative vorticity is constant at each grid point. With a zero initial velocity, relative vorticity remains zero throughout the adjustment. The adjustment is thus quite simple. Namely, it consists of linear gravity waves, which carry zero relative vorticity (equation (48.72)). These gravity waves propagate away from the initial step, converting the potential energy of the step into kinetic energy of waves that propagate to infinity. As the linear gravity waves are non-dispersive, they carry the initial pulse out to infinity without distortion in the wave form

$$\eta(x, t) = -\frac{\eta_0}{2} [\operatorname{sgn}(x + c_{\text{grav}} t) + \operatorname{sgn}(x - c_{\text{grav}} t)]. \quad (48.159)$$

The meridional velocity remains zero, whereas the zonal velocity

$$\frac{\partial u}{\partial t} = -g \frac{\partial \eta}{\partial x} \quad (48.160)$$

is given by

$$u(x, t) = \frac{g \eta_0}{2 c_{\text{grav}}} [\operatorname{sgn}(x + c_{\text{grav}} t) - \operatorname{sgn}(x - c_{\text{grav}} t)]. \quad (48.161)$$

After the transient waves have passed, the steady solution is a flat surface height with zero velocity. This steady solution is familiar from the case of a rock dropped into a still pond. After dropping the rock into the pond, the surface gravity waves radiate outward from the rock and are eventually damped upon reaching the shore. In equilibrium, the pond returns to a state of rest with a flat surface height.⁸

48.9.4 Adjustment with rotation

With rotation, the transient solution consists of inertia-gravity waves (Section 48.7) that transmit information about the initial surface height perturbation out to infinity. After the transient waves have passed, the steady solution is either the trivial solution with flat surface height (as for the non-rotating case), or a nontrivial solution that is in geostrophic balance

$$f \hat{z} \times \mathbf{u} = -g \nabla \eta \quad \text{and} \quad \nabla \cdot \mathbf{u} = 0 \quad \text{and} \quad Q = H^{-2} f \eta_0 \operatorname{sgn}(x). \quad (48.162)$$

Conservation of potential vorticity constrains the solution so that the steady state surface height is sloped according to a geostrophically balanced state. That is, an equilibrium state of no-motion is not allowed by potential vorticity conservation. This is a profound distinction from the non-rotating case.

Computing the equilibrium state

As the equilibrated flow is geostrophic on an f -plane, we make use of the geostrophic streamfunction

$$\psi = g \eta / f. \quad (48.163)$$

⁸For most purposes, a pond is better studied using deep water equations rather than shallow water equations; see Section 45.3. Even so, the key physical points in this example are maintained in either case.

The equilibrium state is written in terms of the streamfunction according to

$$u = -\partial_y \psi \quad \text{and} \quad v = \partial_x \psi \quad \text{and} \quad \zeta = \nabla^2 \psi. \quad (48.164)$$

Making use of these expressions for the linearized potential vorticity (48.151c) leads to the elliptic partial differential equation for the streamfunction

$$[\nabla^2 - L_d^{-2}] \psi = H Q(x, y), \quad (48.165)$$

where we introduced the shallow water deformation radius, L_d , from equation (48.54).

The initial condition (48.153) has no y -dependence. Furthermore, there is nothing in the adjustment process that will break this meridional symmetry. Hence, the equilibrium state is a function only of x , in which case the streamfunction satisfies the ordinary differential equation

$$\frac{d^2 \psi}{dx^2} - L_d^{-2} \psi = \frac{f \eta_0}{H} \operatorname{sgn}(x). \quad (48.166)$$

We solve this equation separately for $x > 0$ and $x < 0$ and then match the function and its first derivative at $x = 0$. Furthermore, we constrain the streamfunction to vanish at $\pm\infty$. The $x > 0$ streamfunction satisfies

$$\frac{d^2 \psi}{dx^2} - L_d^{-2} \psi = \frac{f \eta_0}{H}. \quad (48.167)$$

The particular solution is

$$\psi_p = -L_d^2 H Q = -L_d^2 f \eta_0 / H = -g \eta_0 / f \quad (48.168)$$

and the homogeneous solution is

$$\psi_h = (g \eta_0 / f) e^{-x/L_d} \quad (48.169)$$

so that

$$\psi = -\frac{g \eta_0}{f} \left[1 - e^{-x/L_d} \right]. \quad (48.170)$$

The $x < 0$ solution is found similarly, so that

$$\psi = \frac{g \eta_0}{f} \begin{cases} -\left(1 - e^{-x/L_d}\right) & x > 0 \\ \left(1 - e^{x/L_d}\right) & x < 0, \end{cases} \quad (48.171)$$

which means that the equilibrium surface height is

$$\eta = \eta_0 \begin{cases} -\left(1 - e^{-x/L_d}\right) & x > 0 \\ \left(1 - e^{x/L_d}\right) & x < 0. \end{cases} \quad (48.172)$$

Note that the streamfunction vanishes at $x = 0$ and has a first derivative of $-\eta_0 \sqrt{gH}/H$. Since the streamfunction only has a zonal dependence, the equilibrium velocity is purely meridional

$$u = 0 \quad \text{and} \quad v = -\frac{g \eta_0}{f L_d} e^{-|x|/L_d}. \quad (48.173)$$

The equilibrium velocity thus consists of a jet that is perpendicular to the surface height front.

48.9.5 Comments

As illustrated in Figure 48.3, the equilibrium profiles for the surface height and velocity both have an exponential decay, with decay length scale given by the deformation radius. It is this length

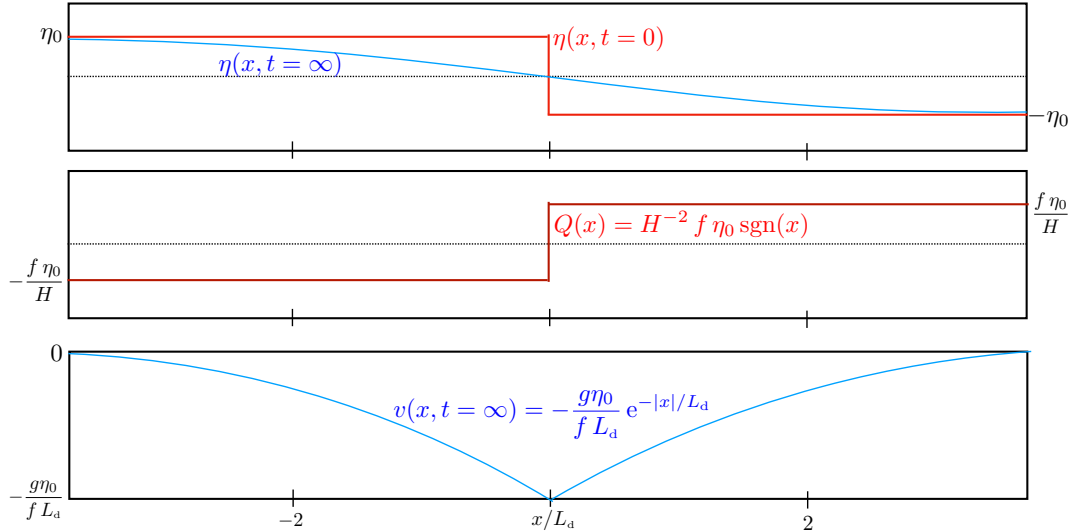


FIGURE 48.3: Depicting solutions to the linear geostrophic adjustment of a rotating shallow water layer on an f -plane. The top panel shows the initial (step-function) surface height (48.153) and the equilibrium (exponential) surface height (48.172). The second panel shows the static (step-function) potential vorticity (48.162). The third panel shows the equilibrium (exponential) meridional velocity (48.173) comprised of a jet centered at $x = 0$. The horizontal axis is scaled according to the shallow water deformation radius, $L_d = f^{-1} \sqrt{g H}$. This figure is adapted from figure 3.10 of [Vallis \(2017\)](#).

scale over which the solution is affected or “deformed” by rotation, thus motivating the name “deformation radius”.

A key feature of the rotating case is that some of the potential energy contained within the initial perturbed surface height remains in the equilibrium geostrophic flow. The conservation of potential vorticity constrains the flow so that all of the initial potential energy cannot be converted to kinetic energy. Rather, the adjustment occurs only within a deformation radius distance from the initial perturbation.

Chapter 3 of [Pratt and Whitehead \(2008\)](#) provide a thorough discussion of the geostrophic adjustment problem, for both the linear and nonlinear cases.

48.10 Stationary waves generated by topography

In this section we consider a geophysically relevant means to force inertia-gravity waves via the flow of fluid over topography. We consider a single shallow water layer on an f -plane. Rather than inviscid, we here introduce friction in the form of Rayleigh drag (Section 22.8.5). As we show, Rayleigh drag renders a phase shift that allows for pressure form stress (Section 33.42), thus illustrating a coupling between friction and form stress.

48.10.1 Linearized equations

The physical system consists of flow in a zonally reentrant f -plane channel with small amplitude topography

$$\eta_b = \bar{\eta}_b + \eta'_b = \eta'_b. \quad (48.174)$$

We also introduce a constant zonal mean flow, $U \hat{x}$. Linear inertia-gravity wave fluctuations (Section 48.7) are generated as the flow moves over the topography. Our goal is to examine

properties of these waves. We closely follow the linearization process detailed in Section 48.3, though here focused on the specifics of a reentrant channel.

The thickness and velocity take on the assumed forms

$$h = H + \eta' - \eta'_b \quad \text{and} \quad u = U + u' \quad \text{and} \quad v = 0 + v', \quad (48.175)$$

where primed variables are small so that the product of any two primed variables is neglected. We are unconcerned with how the zonal mean flow is generated, instead focusing on the small amplitude perturbations, (u', v', η') , relative to that flow. Substituting the expressions (48.175) into the shallow water equations (48.1a) and (48.1b) leads to the linearized equations

$$\partial_t \mathbf{u}' + U \partial_x \mathbf{u}' + f \hat{\mathbf{z}} \times \mathbf{u}' = -g \nabla \eta' - \gamma \mathbf{u}' \quad (48.176a)$$

$$\partial_t (\eta' - \eta'_b) + U \partial_x (\eta' - \eta'_b) = -H \nabla \cdot \mathbf{u}', \quad (48.176b)$$

with $\gamma \geq 0$ the inverse time scale for the Rayleigh friction. Note that we chose to retain η'_b as part of the time derivative even though the topography is time-independent.

48.10.2 Galilean transformation to a moving frame

The background zonal flow is constant in time and zonally symmetric. In this situation it is convenient to introduce a Galilean transformation according to

$$\bar{t} = t \quad \text{and} \quad \bar{x} = x - U t \quad \text{and} \quad \bar{y} = y. \quad (48.177)$$

Following our discussion of Galilean transformations in Section 14.7, we know that the derivative operators transform according to⁹

$$\partial_{\bar{t}} = \partial_t + U \partial_x \quad \text{and} \quad \partial_{\bar{x}} = \partial_x \quad \text{and} \quad \partial_{\bar{y}} = \partial_y. \quad (48.178)$$

With this coordinate transformation the linear equations (48.176a)-(48.176b) take the form

$$\partial_{\bar{t}} \mathbf{u}' + f \hat{\mathbf{z}} \times \mathbf{u}' = -g \nabla \eta' - \gamma \mathbf{u}' \quad (48.179a)$$

$$\partial_{\bar{t}} (\eta' - \eta'_b) = -H \nabla \cdot \mathbf{u}'. \quad (48.179b)$$

Note how the $U \partial_x$ operator has been absorbed into the time derivative, $\partial_{\bar{t}}$. However, the topography that is independent of the time, t , is now a function of the time, \bar{t} . That is, in a reference frame that moves with the mean flow with velocity $U \hat{\mathbf{x}}$, the topography moves in the opposite direction

$$\eta'_b(x, y) = \eta'_b(\bar{x} + U \bar{t}, \bar{y}). \quad (48.180)$$

This is a key feature of the following analysis.

48.10.3 Deriving the amplitude relation

We are interested in determining the relationship between the surface height perturbation, η' , and the bottom topography undulations, η'_b . For this purpose we derive a wave equation satisfied by the small amplitude perturbations, and then take plane wave ansatz allowing us to focus on individual linear wave modes. We then assume the perturbations are steady in the frame where

⁹Note that the Galilean transformation considered in Section 14.7 uses the opposite sign for the flow relative to that considered here. There is nothing fundamental about the sign; one merely needs to be careful when translating the earlier results to the current case.

the topography is steady, so that when acting on steady fields we have the operator relations

$$\partial_t = \partial_{\bar{t}} - U \partial_{\bar{x}} = 0. \quad (48.181)$$

Wave equation derivation

To derive a wave equation, take $\partial_{\bar{t}}$ of the continuity equation (48.179b) to render

$$\partial_{\bar{t}\bar{t}}(\eta' - \eta'_b) = -H \nabla \cdot \partial_{\bar{t}} \mathbf{u}'. \quad (48.182)$$

Replacing $\partial_{\bar{t}} \mathbf{u}'$ using the linearized velocity equation (48.179a) leads to the forced wave equation

$$\partial_{\bar{t}}[(\partial_{\bar{t}} + \gamma)\eta'] - g H \nabla^2 \eta' + f H \zeta' = \partial_{\bar{t}}[(\partial_{\bar{t}} + \gamma)\eta'_b], \quad (48.183)$$

where $\zeta' = \partial_x v' - \partial_y u'$ is the relative vorticity of the perturbation.

Assumptions

We now make the following assumptions.

- The topography is a function only of the zonal position so that

$$\eta'_b = \eta'_b(x) = \eta'_b(\bar{x} + U \bar{t}). \quad (48.184)$$

- We are interested only in a steady solution whereby $\partial_t = 0$ so that $\partial_{\bar{t}} = U \partial_x$.
- Assume zero meridional dependence so that $\partial_y = 0$. This assumption means that we are working on a domain that is either periodic in y or infinite in y ; i.e., there are no northern or southern walls to the zonal channel.
- Assume the topography has the structure of a single mode

$$\eta'_b(x) = \tilde{\eta}_b e^{ik_b x} = \tilde{\eta}_b e^{ik_b (\bar{x} + U \bar{t})} = \tilde{\eta}_b e^{i(k_b \bar{x} - \omega_b \bar{t})}, \quad (48.185)$$

where $\tilde{\eta}_b$ is the specified amplitude of the topography, k_b is the specified wave number of the topography, and

$$\omega_b = -U k_b \quad (48.186)$$

is the intrinsic frequency of the topography as viewed in the moving reference frame. This assumption is a strong idealization since realistic topography has many Fourier components. Nonetheless, once we obtain the solution for a single wave we can use the principle of superposition to develop a more general solution.

Wave ansatz

What sort of waves do we expect the topography to excite? To simplify the analysis we seek wave solutions with the same wave number, k_b , as the topography. We also assume the angular frequency of the waves is the same as the intrinsic frequency of the topography

$$\omega = \omega_b = -U k_b, \quad (48.187)$$

which ensures that the waves are stationary in the frame where the topography is at rest. These considerations lead us to study the wave ansatz

$$(u', v', \eta') = (\tilde{u}, \tilde{v}, \tilde{\eta}) e^{i(k_b \bar{x} - \omega_b \bar{t})}. \quad (48.188)$$

Note that the wave amplitudes, $(\tilde{u}, \tilde{v}, \tilde{\eta})$, are generally complex numbers. For this ansatz we are not in search of a dispersion relation, since the wave number and angular frequency are assumed to be specified according to the topography. Instead, our task is to determine the relation between the wave amplitudes.

Relating the amplitudes

Use of the wave ansatz (48.188), along with the assumed single Fourier mode (48.185) for the topography, brings the wave equation (48.183) to the form

$$(\omega_b^2 + i\omega_b \gamma - g H k_b^2) \tilde{\eta} - i f H k_b \tilde{v} = (\omega_b^2 + i\omega_b \gamma) \tilde{\eta}_b. \quad (48.189)$$

We can eliminate \tilde{v} by making use of the velocity equation (48.179a) and continuity equation (48.179b) written in their Fourier mode form. The modal form of the velocity equation is given by

$$(\gamma - i\omega_b) \tilde{\mathbf{u}} + f \hat{\mathbf{z}} \times \tilde{\mathbf{u}} = -i g \mathbf{k}_b \tilde{\eta}. \quad (48.190)$$

Operating with $\times \mathbf{k}_b$ eliminates the term $i g \mathbf{k}_b \tilde{\eta}$, then using the vector product identity (1.40b) and projecting onto $\hat{\mathbf{z}}$ leads to

$$(\omega_b + i\gamma) (\mathbf{k}_b \times \tilde{\mathbf{u}}) \cdot \hat{\mathbf{z}} = -i f \mathbf{k}_b \cdot \tilde{\mathbf{u}} \quad \text{modal form of velocity equation (48.179a)} \quad (48.191a)$$

$$H \mathbf{k}_b \cdot \tilde{\mathbf{u}} = \omega_b (\tilde{\eta} - \tilde{\eta}_b) \quad \text{modal form of continuity equation (48.179b), (48.191b)}$$

where the modal form of the continuity equation (48.191b) is straightforward to derive. Eliminating $\mathbf{k}_b \cdot \tilde{\mathbf{u}}$ leads to

$$H (\omega_b + i\gamma) (\mathbf{k}_b \times \tilde{\mathbf{u}}) \cdot \hat{\mathbf{z}} = i f \omega_b (\tilde{\eta}_b - \tilde{\eta}), \quad (48.192)$$

and specializing to the zonal topography wavevector, $\mathbf{k}_b = \hat{\mathbf{x}} k_b$, renders

$$H k_b (\omega_b + i\gamma) \tilde{v} = i f \omega_b (\tilde{\eta}_b - \tilde{\eta}), \quad (48.193)$$

so that

$$H k_b \tilde{v} = \frac{i f \omega_b (\tilde{\eta}_b - \tilde{\eta})}{\omega_b + i\gamma} = \frac{f \omega_b (\tilde{\eta}_b - \tilde{\eta})(\gamma + i\omega_b)}{\omega_b^2 + \gamma^2}. \quad (48.194)$$

Substitution of equation (48.194) into the dispersion relation (48.189) provides our desired relation between the amplitudes

$$\frac{\tilde{\eta}}{\tilde{\eta}_b} = \frac{A + i\gamma C}{A - B + i\gamma C}, \quad (48.195)$$

where we introduced the shorthand

$$A = \omega_b (\omega_b^2 + \gamma^2 - f^2) \quad \text{and} \quad B = \omega_b (\omega_b^2 + \gamma^2)/\text{Fr}^2 \quad \text{and} \quad C = \omega_b^2 + \gamma^2 + f^2, \quad (48.196a)$$

where introduced the shallow water Froude number,

$$\text{Fr} = U/c_{\text{grav}} \quad (48.197)$$

which is the non-dimensional ratio of the background fluid flow speed to the shallow water gravity

wave speed. If the flow is linear, as assumed here, then the Froude number is smaller than unity.¹⁰

48.10.4 Comments on the amplitude relation

We here comment on the amplitude relation (48.195), first considering the case with zero Rayleigh friction.

Zero Rayleigh friction

With zero Rayleigh friction the amplitude relation (48.195) takes on the form

$$\frac{\tilde{\eta}}{\tilde{\eta}_b} = \frac{A}{A - B} = \frac{f^2 - \omega_b^2}{f^2 + \omega_b^2 (\text{Fr}^{-2} - 1)}. \quad (48.198)$$

As we assume the Froude number is smaller than unity, the denominator is positive. Indeed, for typical linear shallow water flows we have $gH \gg U^2$, in which case the amplitude of the free surface undulations are much smaller than the topography undulations

$$|\tilde{\eta}| \ll |\tilde{\eta}_b|. \quad (48.199)$$

Furthermore, if the magnitude of the Coriolis frequency is larger than the intrinsic frequency of the bottom topography

$$f^2 > \omega_b^2 = U^2 k_b^2, \quad (48.200)$$

then the numerator in equation (48.198) is positive, in which case the bottom topography and sea surface height are in phase.

Topographic form stress with Rayleigh friction

From the discussion of topographic form stress in Section 33.7, we know that a nonzero topographic form stress requires a nonzero phase shift between the topography and the free surface height. Given the absence of a phase shift with $\gamma = 0$, we conclude that inviscid stationary gravity waves in a single shallow water layer do not generate a net topographic form stress.

However, the amplitude relation (48.195) in the presence of Rayleigh friction makes $\tilde{\eta}$ a complex number.¹¹ Hence, in this case there is a phase shift between the gravity wave amplitude and the topography amplitude. We conclude that Rayleigh friction provides a mechanism for the stationary gravity waves to impart a form stress on the shallow water layer.

48.11 Rossby waves

We now focus on the sub-inertial wave equation (48.62) derived in Section (48.4.6)

$$\partial_t [(L_d^{-2} - \nabla^2) \eta'] = H \hat{z} \cdot (\nabla \eta' \times \nabla Q_r), \quad (48.201)$$

where

$$Q_r = f/H_r \quad (48.202)$$

¹⁰When the gravity wave speed is less than the fluid particle speed, $gH \leq U^2$, then the Froude number is greater than unity and the flow can be subject to hydraulic jumps (see Exercise 32.3). Such jumps are outside the linear regime considered here.

¹¹We assume $\tilde{\eta}_b$ to be real since this is the amplitude of the bottom topography.

is the potential vorticity in the resting fluid. Equation (48.201) describes shallow water *Rossby waves*.

48.11.1 Dispersion relation

Making use of the plane wave ansatz (48.24) in the wave equation (48.201) readily leads to the shallow water Rossby wave dispersion relation

$$\omega = \frac{H(\mathbf{k} \times \hat{\mathbf{z}}) \cdot \nabla Q_r}{k_d^2 + |\mathbf{k}|^2} \quad (48.203)$$

This dispersion relation compares directly to equation (47.27) for Rossby waves in the horizontally non-divergent barotropic model. The sole difference concerns the presence of the deformation radius, L_d from equation (48.54), and its associated wavenumber

$$k_d = L_d^{-1} = f/c_{\text{grav}}, \quad (48.204)$$

which is present in the shallow water dispersion relation yet missing from the non-divergent barotropic model. It is missing from the non-divergent barotropic model since c_{grav} is formally infinite (there are no gravity waves in that model), in which case $L_d^{-2} = k_d^2 = 0$.

48.11.2 Connecting to quasi-geostrophic potential vorticity

When deriving the sub-inertial equations in Section 48.4.6, we noted that the assumptions made in that derivation are identical to the assumptions made when deriving shallow water quasi-geostrophy in Section 40.5. Indeed, the Rossby wave equation (48.201) is the linearized equation for the material evolution of shallow water quasi-geostrophic potential vorticity. We see this equality by recalling the discussion in Section (40.6.3), where we derived equation (40.87)

$$(f_0/g) Dq/Dt = \partial_t [(L_d^{-2} - \nabla^2) \eta'] - H \hat{\mathbf{z}} \cdot (\nabla \eta' \times \nabla Q_r) - (g/f_0) \hat{\mathbf{z}} \cdot [\nabla \eta' \times \nabla (\nabla^2 \eta')], \quad (48.205)$$

where q is the quasi-geostrophic potential vorticity. For an inviscid fluid, $Dq/Dt = 0$, and for small amplitude fluctuations the nonlinear term in equation (48.205) is neglected. In this case we see that the linearized equation for material evolution of quasi-geostrophic potential vorticity is identical to the Rossby wave equation (48.201).

The nonlinear term in equation (48.205) arises from the geostrophic advection of geostrophic relative vorticity. Although it is small for small amplitude fluctuations, and thus commonly dropped when deriving the dispersion relation, we note that it vanishes identically for a plane wave. It does so in precisely the same way as it vanishes for the non-divergent barotropic vorticity equation in Section 47.2.3. Namely, this result follows since for a plane wave, $\nabla(\nabla^2 \psi) = -\mathbf{k}^2 \nabla \psi$, so that it follows immediately that $\nabla \psi \times \nabla(\nabla^2 \psi) = 0$. Hence, a plane Rossby wave is an exact solution to the quasi-geostrophic potential vorticity equation in an inviscid fluid.

48.11.3 Vorticity mechanism

In Section 47.3 we studied Rossby waves in the horizontally non-divergent barotropic model, with a vorticity mechanism for the waves presented in Figure 47.3. This mechanism follows from the material evolution of absolute vorticity in the horizontally non-divergent barotropic model. The identical mechanism holds for the shallow water fluid yet with quasi-geostrophic potential vorticity replacing absolute vorticity. Hence, all conceptual points from Figure 47.3 also hold for the shallow water fluid.

48.11.4 Dispersion geometry for planetary Rossby waves

In Section 47.4.2 we described a geometric method to help interpret the dispersion relation for planetary waves in the horizontally non-divergent model. That method also proved useful in Section 47.4.3 for describing the reflection of Rossby waves from a wall. Here we extend the geometric method to shallow water planetary waves, in which the dispersion relation is given by the β portion of the general dispersion relation (48.203)

$$\varpi_\beta = -\frac{\beta k_x}{k_d^2 + |\mathbf{k}|^2}. \quad (48.206)$$

This equation compares to the β portion of the dispersion relation (47.27) holding for the non-divergent barotropic model. Again, for the shallow water we have a nonzero deformation wavenumber, $k_d \neq 0$.

Dispersion circle

Following the geometric approach from Section 47.4, we write the dispersion relation (48.206) as the equation of a circle in wavevector space

$$(k_x + \beta/2\omega)^2 + k_y^2 = (\beta/2\omega)^2 - k_d^2. \quad (48.207)$$

As written, the angular frequency, ω , is a parameter for the circle whose center is $\mathbf{k}_{\text{center}} = -(\beta/2\omega)\hat{\mathbf{x}}$ and squared radius is $(\beta/2\omega)^2 - k_d^2$. The deformation wavenumber appearing on the right hand side of the circle equation (48.207) (48.207) places an upper bound on the angular frequency allowed for propagating Rossby waves

$$\omega \leq \omega_{\max} = \beta/(2k_d) = \beta L_d/2. \quad (48.208)$$

The shallow water model supports gravity waves that render $k_d \neq 0$, thus imposing an upper bound on the shallow water Rossby wave angular frequency. In contrast, for the horizontally non-divergent barotropic model, $k_d = 0$ since there are no gravity waves, in which case there is no maximum frequency for Rossby waves. Note that for the β -plane scaling used to derive the Rossby waves,

$$\omega_{\max}/f_0 = \beta L_d/(2 f_0) \ll 1, \quad (48.209)$$

thus confirming that the shallow water Rossby waves are strictly sub-inertial.

Group velocity

The group velocity, $\mathbf{c}_g = \nabla_{\mathbf{k}}\varpi$, is given by

$$\mathbf{c}_g = \frac{\beta [(k_x^2 - k_y^2 - k_d^2) \hat{\mathbf{x}} + 2 k_x k_y \hat{\mathbf{y}}]}{(|\mathbf{k}|^2 + k_d^2)^2} = -\frac{2\omega \mathbf{R}}{|\mathbf{k}|^2 + k_d^2}, \quad (48.210)$$

where we introduced the group velocity orientation vector

$$\mathbf{R} = -\mathbf{k} - \beta/(2\omega) \hat{\mathbf{x}} = -[k_x + \beta/(2\omega)] \hat{\mathbf{x}} - k_y \hat{\mathbf{y}} \quad \text{with} \quad |\mathbf{R}|^2 = (\beta/2\omega)^2 - k_d^2. \quad (48.211)$$

As for the orientation vector (47.55) in the horizontally non-divergent barotropic model, the vector \mathbf{R} points from the perimeter of the dispersion circle to the center (its magnitude equals to the radius of the circle). We thus conclude that the dispersion geometry for shallow water planetary waves directly carries over from the horizontally non-divergent barotropic model detailed

in Section 47.4.2. We illustrate the dispersion geometry for shallow water Rossby waves in Figure 48.4, with many details provided in the figure and its caption.

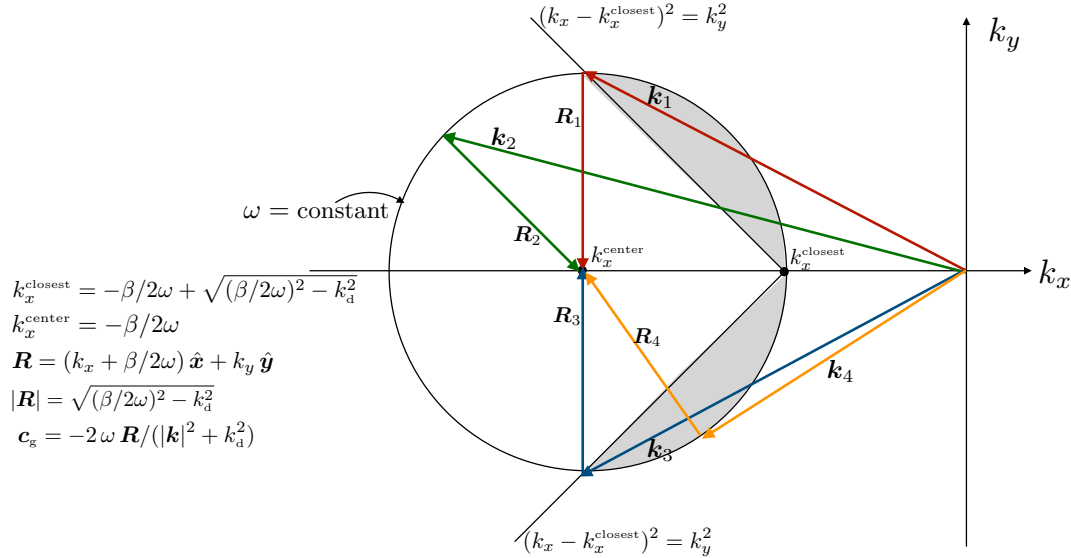


FIGURE 48.4: Dispersion diagram for shallow water planetary Rossby waves as depicted by a circle in wavevector space, (k_x, k_y) , parameterized by the angular frequency, ω . The center of the circle is at $\mathbf{k}_{\text{center}} = -(\beta/2\omega)\hat{x}$ and the squared radius is $(\beta/2\omega)^2 - k_d^2$. A positive radius requires the angular frequency to be less than the maximum, $\omega_{\max} = \beta/(2k_d)$. We depict four sample wavevectors, $\mathbf{k} = k_x\hat{x} + k_y\hat{y}$, that orient the phase velocity, $\mathbf{c}_p = \hat{\mathbf{k}}\omega/|\mathbf{k}|$. Each wavevector extends from the origin to a point on the circle. Each wavevector has an associated group velocity orientation vector, $\mathbf{R} = -\mathbf{k} - \beta/(2\omega)\hat{x}$, that points from the circle perimeter to the circle center. The group velocity is westward for those wavevectors that intersect the circle perimeter within the gray-shaded region, which generally includes Rossby waves with low zonal wavenumbers. The group velocity is eastward for wavevectors outside the gray region, with the lines $(k_x - k_x^{\text{closest}})^2 = k_y^2$ separating these regions where the group velocity is westward or eastward. In particular, the group velocity for wavevector \mathbf{k}_1 is southward; for \mathbf{k}_2 it is eastward; for \mathbf{k}_3 it is northward, and for \mathbf{k}_4 it is westward. This dispersion diagram directly compares to Figure 47.5 constructed for the horizontally non-divergent barotropic model, with the key difference being $k_d \neq 0$ for the shallow water so that the dispersion circle does not touch the origin at $\mathbf{k} = 0$.

48.11.5 Comments

A more streamlined approach to deriving the Rossby wave dispersion relation starts directly from the quasi-geostrophic potential vorticity equation. This approach is indeed motivated since we already put great effort into deriving quasi-geostrophic theory in Section 40.5. Even so, the somewhat long-winded approach taken in this chapter benefits by exposing the direct connection to other shallow water waves through the unified shallow water equation (48.42).



48.12 Exercises

EXERCISE 48.1: STEPS IN DERIVING THE LINEAR PV EQUATION

Fill in the mathematical details needed to derive the linearized potential vorticity equation (48.23).

EXERCISE 48.2: STEPS IN DERIVING EQUATION (48.40)

Derive equation (48.40) from the linearized velocity equation (48.16).

EXERCISE 48.3: EQUATIONS FOR BAROTROPIC AND BAROCLINIC VELOCITIES

Fill in the details for deriving the equations (48.102a)-(48.102c) for the depth averaged and depth-deviation velocities.

EXERCISE 48.4: VANISHING POTENTIAL VORTICITY FOR INERTIA-GRAVITY WAVES

Verify that the linearized potential vorticity, $H Q' = \zeta' - f \eta'/H$, vanishes for the plane shallow water inertia-gravity waves given by the polarization relations in Section 48.7.9.

EXERCISE 48.5: DEFORMATION RADIUS

The deformation radius appears in many contexts within rotating fluid dynamics. Here, we compute this length scale for selective geophysical flow regimes at $30^\circ N$ latitude, where $f = 7.3 \times 10^{-5} \text{ s}^{-1}$.

- Compute the shallow water deformation radius for an ocean continental shelf of depth 500 m.
- Compute the shallow water deformation radius for the deep ocean with depth 5000 m.
- The deformation radius defined in this chapter is sometimes called the *external deformation radius* as it makes use of the full depth of the fluid and the gravitational acceleration. In contrast, the deformation radius defined in terms of internal layer thickness and reduced gravity, g^r , leads to the internal deformation radius. The internal deformation radius, $L_d^{\text{int}} = \sqrt{g^r h}/f$ is the appropriate rotational length scale for density layers in the interior of the ocean or isentropic layers in the interior of the atmosphere. Compute the deformation radius for a density layer of thickness $h = 200$ m and reduced gravity of $g^r = g/1000$.

EXERCISE 48.6: GEOSTROPHIC ADJUSTMENT (BASED ON EXERCISE 4.6 OF [Vallis \(2019\)](#))

Consider the linear geostrophic adjustment problem on an f -plane with a single layer of shallow water fluid over a flat bottom. Rather than assume an initial free surface profile, as we did in Section 48.9, here we assume an initial meridional velocity profile given by

$$v(x, t=0) = v_0 \operatorname{sgn}(x) = v_0 (2 \mathcal{H}(x) - 1), \quad (48.212)$$

where v_0 is a constant, sgn is the sign-function (equation (48.154)), and \mathcal{H} is the Heaviside step function (equation (48.156)). The free surface is assumed to be initially flat.

- Show that the linearized potential vorticity, $H Q' = \zeta' - f \eta'/H$, is given by

$$H Q'(x) = 2 v_0 \delta(x), \quad (48.213)$$

where $\delta(x)$ is the Dirac delta with dimensions L^{-1} .

- As we did in Section 48.9, solve for the geostrophic streamfunction $\psi = g \eta/f$.
- Discuss this solution and draw a sketch of ψ and v .

Here are some hints.

- We discuss properties of the Dirac delta in Section 4.3. However, to answer the first part of this question it is sufficient to know that the derivative of the Heaviside step function (a dimensionless step function) is the Dirac delta

$$\delta(x) = \frac{d\mathcal{H}(x)}{dx}, \quad (48.214)$$

so that the Dirac delta has dimensions of inverse length.

- For the second part, note that the streamfunction is exponentially decaying on either side of the $x = 0$ according to $\psi = \psi_0 e^{-|x|/L_d}$, which then leads to a jump in the derivative approaching the origin from each side. Carefully use equations (48.214) and (48.165) to determine ψ_0 .



Chapter 49

INTERNAL GRAVITY WAVES

In this chapter we continue our study of how gravity affects wave motion in geophysical fluids, here focusing on gravity waves in a continuously stratified fluid. As part of anticipating this discussion, recall Section 48.6 where we studied gravity waves in two shallow water layers and decomposed the motion into two modes: the *barotropic mode* and *baroclinic mode*. When moving to a continuously stratified fluid we encounter an infinity of baroclinic modes. These modes are associated with motion of interior stratification surfaces, and have very little projection onto motion of the upper free surface. Consequently, these waves are generally referred to as *internal gravity waves*.

Although the shallow water system anticipated some features of gravity waves in a continuous system, there are many properties that are revealed only when moving to continuous stratification. In particular, the dispersion relation for internal gravity waves presents the peculiar feature of a group velocity perpendicular to the phase velocity. In fact, this property was already encountered in Section 46.2 when studying inertial waves in a homogeneous fluid. We focus most of our attention on the case of non-rotating internal gravity waves, with the case of a rotating inertia-gravity wave a straightforward extension that builds on the material from Section 46.2 as well as the shallow water inertia-gravity waves studied in Section 48.7.

READER'S GUIDE TO THIS CHAPTER

We build on the prior chapters in this wave part of the book. Throughout this chapter we make use of the equations for a Boussinesq ocean from Chapter 26 and assume familiarity with buoyancy as studied in Chapter 27. In preparing this chapter we found inspiration from [Lighthill \(1978\)](#), [Pedlosky \(2003\)](#), [Sutherland \(2010\)](#), [Cushman-Roisin and Beckers \(2011\)](#), [Kundu et al. \(2016\)](#), and [Vallis \(2017\)](#). This video from Prof. Long offers some pedagogical visualizations of stratified flow phenomena.

49.1	Loose threads	1276
49.2	Boussinesq ocean and its linearization	1277
49.2.1	Boussinesq ocean equations	1277
49.2.2	The prescribed reference state	1277
49.2.3	Buoyancy frequency compared to surface gravity waves	1278
49.2.4	Linearization around the reference state	1279
49.2.5	Energetics	1279
49.3	Buoyancy oscillations	1280
49.3.1	Unforced buoyancy oscillations	1281
49.3.2	The lack of oscillations with horizontal homogeneity	1281
49.4	The non-rotating linear Boussinesq ocean	1282
49.4.1	Relative vorticity	1282

49.4.2	Wave equation for the vertical velocity	1283
49.4.3	Linearized boundary conditions	1283
49.5	Free gravity waves with constant stratification	1285
49.5.1	Plane wave ansatz for internal gravity waves	1285
49.5.2	Transverse waves	1286
49.5.3	Pressure equation	1286
49.5.4	Relative vorticity	1286
49.5.5	Dispersion relation	1286
49.5.6	Unpacking the dispersion relation	1288
49.5.7	Group velocity	1289
49.5.8	Polarization relations and structure of a plane wave	1290
49.5.9	Force balance within an internal gravity wave	1292
49.5.10	Energetics of a plane internal gravity wave	1295
49.6	Reflection of gravity waves	1296
49.6.1	General reflection conditions	1296
49.6.2	Specializing to internal gravity waves	1297
49.6.3	Comments and further reading	1298
49.7	Gravity waves with vertically varying stratification	1299
49.7.1	The two length scale assumption	1299
49.7.2	The wave equation and the WKB ansatz	1299
49.7.3	The wave equation with the WKB ansatz	1300
49.7.4	WKB solution for the vertical velocity	1300
49.7.5	Structure of an internal gravity wave	1301
49.7.6	Wave packets within a wave guide	1302
49.7.7	Comments and further study	1303
49.8	Vertical normal modes	1303
49.9	Rotating linear Boussinesq ocean	1304
49.9.1	Forced oscillator equation for horizontal velocity	1304
49.9.2	Vertical component to the relative vorticity	1304
49.9.3	Forced oscillator equation and free wave equation for vertical velocity	1304
49.9.4	Forced oscillator equation for buoyancy	1305
49.9.5	An equation for pressure	1306
49.9.6	Potential vorticity	1306
49.10	Free inertia-gravity waves	1308
49.10.1	Dispersion relation	1308
49.10.2	Force balance in an inertia-gravity wave	1309
49.10.3	Group velocity	1310
49.10.4	Polarization relations for a plane wave	1311
49.10.5	Energetics of a plane inertia-gravity wave	1312
49.10.6	Comments	1314
49.11	Exercises	1314

49.1 Loose threads

- Figures!
- More general treatment of the group velocity property as per Section 6.7 of [Vallis \(2017\)](#) or Chapter 11 of [Whitham \(1974\)](#).
- energetic balances for reflected waves
- Section 49.7.5 is incomplete. Need to derive structure of a WKB internal wave.
- Vertical normal modes in Section 49.8 as per Lecture 9 of [Pedlosky \(2003\)](#).

- Topographic generation of waves as in Section 7.7 of [Vallis \(2017\)](#).

49.2 Boussinesq ocean and its linearization

Throughout this chapter we work with the Boussinesq ocean equations in their adiabatic and inviscid limit. We linearize these equations around an exact hydrostatic balanced rest state. In this section we review the governing equations from Chapter 26 and perform the linearization.

49.2.1 Boussinesq ocean equations

We make use of the governing equations for an adiabatic and inviscid Boussinesq ocean written in the form from (see Section 26.1.7)

$$\rho_0 (\partial_t \mathbf{v} + (\mathbf{v} \cdot \nabla) \mathbf{v} + 2\boldsymbol{\Omega} \times \mathbf{v}) = -\nabla p - \rho g \hat{\mathbf{z}} \quad \text{inviscid velocity equation} \quad (49.1a)$$

$$\nabla \cdot \mathbf{v} = 0 \quad \text{continuity equation} \quad (49.1b)$$

$$(\partial_t + \mathbf{v} \cdot \nabla) \rho = 0 \quad \text{adiabatic density equation} \quad (49.1c)$$

$$\rho = -\rho_0 \alpha_\Theta \Theta \quad \text{linear equation of state.} \quad (49.1d)$$

The density field contains a nontrivial spatial structure

$$\rho = \rho(\mathbf{x}, t), \quad (49.2)$$

with the Boussinesq reference density, ρ_0 , a constant, and we furthermore assume the thermal expansion coefficient, α_Θ , is a constant. Hence, the density and Conservative Temperature, Θ , are linearly proportional, with the adiabatic density equation (49.1c) meaning that Conservative Temperature is materially constant. The velocity field resolved by the Boussinesq ocean is non-divergent so that it does not support acoustic waves.¹ The inhomogeneous density field couples to the gravity field to render a nonzero buoyancy that appears in the velocity equation (49.1a). Buoyancy is the essential ingredient for the internal gravity waves studied in this chapter.

49.2.2 The prescribed reference state

We decompose density into a constant Boussinesq reference density, $\rho_0 > 0$, plus a prescribed static reference density, $\rho_R(z) > 0$, and a perturbation, $\rho'(\mathbf{x}, t)$,

$$\rho(\mathbf{x}, t) = \rho_0 + \rho_R(z) + \rho'(\mathbf{x}, t). \quad (49.3)$$

We assume the following inequalities hold

$$\rho_R \ll \rho_0 \quad \text{and} \quad |\rho'| \ll \rho_R, \quad (49.4)$$

with the first inequality following from the Boussinesq ocean approximation, and the second inequality supporting linearization in Section 49.2.4. The buoyancy is decomposed according to the density decomposition (49.3), so that

$$b = -g(\rho - \rho_0)/\rho_0 = -g(\rho_R + \rho')/\rho_0 = b_R + b'. \quad (49.5)$$

¹See Section 44.2 for more on how we interpret the quasi-compressible properties of the Boussinesq ocean.

Likewise, we decompose pressure so that

$$p = p_0(z) + p_R(z) + p'(\mathbf{x}, t), \quad (49.6)$$

where

$$dp_0(z)/dz = -\rho_0 g \quad \text{and} \quad dp_R(z)/dz = -\rho_R(z) g, \quad (49.7)$$

so that

$$p_0(z) = -\rho_0 g z \quad \text{and} \quad p_R(z) = g \int_z^0 \rho_R(z') dz'. \quad (49.8)$$

The corresponding pressure and gravity contributions to the velocity equation (49.1a) take the form

$$-\nabla p - \rho g \hat{\mathbf{z}} = -\rho_0 \nabla \varphi' - \rho' g \hat{\mathbf{z}} = -\rho_0 (\nabla \varphi' - b' \hat{\mathbf{z}}), \quad (49.9)$$

where we introduced the normalized dynamic pressure

$$\varphi' = p'/\rho_0. \quad (49.10)$$

Introducing the reference state into the velocity equation (49.1a) and density equation (49.1c) leads to

$$\partial_t \mathbf{v} + (\mathbf{v} \cdot \nabla) \mathbf{v} + 2\boldsymbol{\Omega} \times \mathbf{v} = -\nabla \varphi' + b' \hat{\mathbf{z}} \quad \text{decomposed velocity equation} \quad (49.11a)$$

$$(\partial_t + \mathbf{v} \cdot \nabla) b' = -w N_R^2 \quad \text{decomposed buoyancy equation.} \quad (49.11b)$$

In the buoyancy equation we introduced the squared reference state buoyancy frequency

$$N_R^2 = -\frac{g}{\rho_0} \frac{d\rho_R}{dz}. \quad (49.12)$$

It is notable that the velocity equation (49.11a) is mathematically identical to the original velocity equation (49.1a). However, the fluctuating buoyancy equation (49.11b) is distinct from the original buoyancy equation (49.1c). Namely, the reference state squared buoyancy frequency couples to the vertical velocity to provide a source, $-w N_R^2$, for the material evolution of the perturbation buoyancy.

49.2.3 Buoyancy frequency compared to surface gravity waves

The buoyancy frequency of the background state, N_R , sets the time scale for the internal gravity wave motions. To garner a sense for its scale, we compare this frequency to that found for surface gravity waves in Section 45.5.5. Making use of equation (45.85a) for deep water gravity waves leads to the ratio

$$\frac{N_R^2}{\omega_{dww}^2} = \frac{N_R^2}{g |\mathbf{k}|_{dww}} = -\frac{g}{\rho_0} \frac{\partial \rho}{\partial z} \frac{\Lambda_{dww}}{2\pi g} = -\frac{\Delta \rho}{2\pi \rho_0}. \quad (49.13)$$

In the final step we took the deep water wave length, Λ_{dww} , as the vertical scale over which to measure the vertical density difference, $\Delta \rho$. Now the deep water wavelength is just a few meters, which means that $|\Delta \rho| \ll \rho_0$. We conclude that the buoyancy frequency is much less than the frequency of deep water gravity waves. We can understand this result by noting that the gravitational restoring force acting on deep water waves is far stronger than the reduced gravity acting on internal waves, so we expect the deep water waves to oscillate faster.

The same calculation for shallow water gravity waves in equation (45.85b) yields the ratio

$$\frac{N_R^2}{\omega_{\text{sww}}^2} = \frac{N_R^2}{|\mathbf{k}|_{\text{sww}}^2 c_{\text{grav}}^2} = -\frac{g}{\rho_0} \frac{\partial \rho}{\partial z} \frac{\Lambda_{\text{sww}}}{2\pi |\mathbf{k}|_{\text{sww}} g H} = -\frac{\Delta \rho}{\rho_0} \frac{1}{2\pi |\mathbf{k}|_{\text{sww}} H}. \quad (49.14)$$

In this case the density difference, $\Delta \rho$, is computed over a vertical scale equal to the wavelength, Λ_{sww} . But since $|\mathbf{k}|_{\text{sww}} H \ll 1$ for shallow water gravity waves, we take $\Delta \rho$ over the full depth of the ocean. Even so, the density ratio remains small, $\Delta \rho / \rho_0 \ll 1$. Yet now this ratio is divided by the small number $2\pi |\mathbf{k}|_{\text{sww}} H = (2\pi)^2 H / \Lambda_{\text{sww}} \ll 1$. We thus find that the internal gravity wave frequency can be on the order of the shallow water gravity wave frequency. So although the shallow water waves feel the full gravitational acceleration, just like deep water gravity waves, the huge scale for shallow water waves leads to far slower wave motion than the deep water gravity waves. As a result, the frequency for shallow water waves is on the order of that for internal waves.

49.2.4 Linearization around the reference state

The second of the density inequalities (49.4) implies the buoyancy inequality

$$|b'| \ll b_R. \quad (49.15)$$

That is, fluctuations in the buoyancy field, which can be positive or negative, are far smaller in magnitude than the reference state buoyancy. These small fluctuations in buoyancy lead to correspondingly small fluctuations in dynamic pressure, φ' , and small fluctuations in the velocity, \mathbf{v}' . The linearized velocity equation (49.11a) and buoyancy equation (49.11b) are obtained by dropping nonlinear product of fluctuating fields

$$\partial_t \mathbf{v}' + 2\boldsymbol{\Omega} \times \mathbf{v}' = -\nabla \varphi' + b' \hat{\mathbf{z}} \quad \text{linearized velocity equation} \quad (49.16a)$$

$$\partial_t b' = -w' N_R^2 \quad \text{linearized buoyancy equation} \quad (49.16b)$$

$$\nabla \cdot \mathbf{v}' = 0 \quad \text{continuity for velocity fluctuations.} \quad (49.16c)$$

The final equation expresses the non-divergent nature of the fluctuating velocity field. These three linear equations form the basis for the remainder of this chapter.

49.2.5 Energetics

We studied the energetics of the nonlinear equation set (49.1a)-(49.1d) in Section 26.7. We here revisit that discussion and then derive energetics for the linearized equations (49.16a)-(49.16c).

Adiabatic inviscid Boussinesq ocean

The kinetic energy per volume and potential energy per volume in a Boussinesq ocean are given by

$$\rho_0 \mathcal{K} = \rho_0 \mathbf{v} \cdot \mathbf{v} / 2 \quad \text{and} \quad \rho \Phi = \rho g z, \quad (49.17)$$

where we introduced the kinetic energy per mass and potential energy per mass (i.e., the geopotential)

$$\mathcal{K} = \mathbf{v} \cdot \mathbf{v} / 2 \quad \text{and} \quad \Phi = g z. \quad (49.18)$$

Material evolution of the kinetic energy is derived by making use of the velocity equation (49.1a), in which

$$\rho_0 D\mathcal{K}/Dt = -\nabla \cdot (\mathbf{v} p) - \rho g w. \quad (49.19)$$

Material evolution of the potential energy per volume for an adiabatic Boussinesq ocean is given by

$$D(\rho\Phi)/Dt = g\rho w. \quad (49.20)$$

We are thus led to the mechanical energy equation for the adiabatic and inviscid Boussinesq ocean

$$\rho_0 D\mathcal{K}/Dt + \rho D\Phi/Dt = -\nabla \cdot (\mathbf{v} p), \quad (49.21)$$

so that mechanical energy following a fluid element is modified by convergence of the pressure flux. That is, we identify $\mathbf{v} p$ as the flux of mechanical energy in the Boussinesq ocean.

Linearized adiabatic inviscid Boussinesq ocean

It is not *a priori* clear that a sensible energetic balance exists for the linearized equation set (49.16a)-(49.16c). Indeed, in the process of linearization we gave no attention to the energetic balances. Even so, we are able to derive an energy balance that is physically relevant. For the kinetic energy per mass, $\mathcal{K}' = \mathbf{v}' \cdot \mathbf{v}'/2$, use of the velocity equation (49.16a) readily yields

$$\partial_t \mathcal{K}' = -\nabla \cdot (\mathbf{v}' \varphi') + w' b'. \quad (49.22)$$

The potential energy is a bit less straightforward. Namely, multiplying the linear buoyancy equation (49.16b) by b' readily finds

$$\partial_t \mathcal{A}' = -w' b' \quad \text{with} \quad \mathcal{A}' = (b'/N_R)^2/2. \quad (49.23)$$

Recall the discussion in Section 26.9.4, where \mathcal{A} is identified as a measure of the available potential energy contained in small amplitude fluctuations of buoyancy surfaces.² Evidently, the linear Boussinesq ocean equation set has a mechanical energy budget given by

$$\partial_t (\mathcal{K}' + \mathcal{A}') = -\nabla \cdot (\mathbf{v}' \varphi'). \quad (49.24)$$

Hence, a time tendency for the sum of the kinetic energy plus the available potential energy is driven by convergences in the dynamic pressure flux, $\mathbf{v}' \varphi'$.

49.3 Buoyancy oscillations

To start our examination of flow features emerging from the linearized Boussinesq ocean equations (49.16a)-(49.16c), consider the non-rotating case in which the buoyancy equation and vertical velocity equation are given by

$$\partial_t b' + w' N_R^2 = 0 \quad \text{and} \quad \partial_t w' = -\partial_z \varphi' + b'. \quad (49.25)$$

The time derivative of the velocity equation and use of the buoyancy equation, along with the complement operations, yield

$$(\partial_{tt} + N_R^2) w' = -\partial_{tz} \varphi' \quad \text{and} \quad (\partial_{tt} + N_R^2) b' = N_R^2 \partial_z \varphi'. \quad (49.26)$$

Each of these equations describes a forced oscillator with angular frequency given by the buoyancy frequency, N_R . We determine the forcing by determining the pressure, which satisfies the Poisson

²In Section 49.5.10 we offer a further interpretation of the available potential energy as it appears for an internal gravity wave.

equation

$$-\nabla^2 \varphi' = -\partial_z b', \quad (49.27)$$

along with boundary conditions specific to the domain. This pressure equation results from taking the divergence of the velocity equation (49.16a) (without rotation) and using the continuity equation, $\nabla \cdot \mathbf{v}' = 0$. In the absence of any vertical structure to the buoyancy, the pressure satisfies Laplace's equation, $\nabla^2 \varphi' = 0$, which renders a zero pressure fluctuation in the absence of boundaries.

49.3.1 Unforced buoyancy oscillations

Ignoring the pressure forcing in the forced oscillator equations (49.26) leads to free oscillations for the buoyancy and vertical velocity

$$(\partial_{tt} + N_R^2) w'_{\text{free}} = 0 \quad \text{and} \quad (\partial_{tt} + N_R^2) b'_{\text{free}} = 0. \quad (49.28)$$

Evidently, both the vertical velocity and the buoyancy exhibit simple harmonic oscillations with angular frequency N_R . Note that such free oscillations occur when the pressure field has zero vertical gradient, $\partial_z \varphi' = 0$, in which case there is no resistance to free oscillations in the vertical.

By ignoring the pressure fluctuations, we are in effect ignoring the impact of the buoyancy fluctuation on pressure. This approach is not dynamically self-consistent. However, it is a common approach, sometimes referred to as the *parcel method*, whereby we consider the motion of a test fluid element that is assumed to have no impact on the surrounding fluid.³ We considered the pros and cons of this approach when studying Archimedean buoyancy in Section 27.4 and effective buoyancy in Section 27.7.

As seen in Section 49.5.9, fluid particles exhibit free oscillations when they move in directions that parallel the surfaces of constant phase for internal gravity waves *if* the phase surfaces are not horizontal. On constant phase surfaces the pressure is spatially constant so that the only force acting on the fluid particle arises from gravity in a vertically stratified fluid; i.e., buoyancy. We return to this conceptual picture in Section 49.5.9 as it is fundamental to the forces acting within an internal gravity wave.

49.3.2 The lack of oscillations with horizontal homogeneity

When discussing buoyancy oscillations one sometimes finds it convenient to consider a horizontally homogenous fluid and conceive of the oscillations moving horizontal stratification surfaces up and down. However, there are caveats to this conceptual picture that offer further hints at the physics of gravity waves.

Horizontal homogeneity means that the horizontal pressure gradient vanishes, and thus the horizontal velocity vanishes (remember we are assuming non-rotating physics). To maintain continuity for the Boussinesq ocean requires $\partial_z w' = 0$, which means, with zero horizontal motion, that $w' = 0$ throughout the domain. It follows that for a Boussinesq ocean there can be no buoyancy fluctuation with $\mathbf{v}' = 0$. Although this conclusion might be clear enough, we step through the details to further support it.

A vanishing vertical velocity in the forced oscillator equation (49.26) means that the vertical pressure gradient is time independent, $\partial_t(\partial_z \varphi') = 0$. Furthermore, horizontal homogeneity for the pressure equation (49.27) means that

$$\partial_z(\partial_z \varphi' - b') = 0, \quad (49.29)$$

³See Sections 14.3.5 and 27.4 for more on test fluid elements.

so that $\partial_z \varphi' - b' = B(t)$, where B is an arbitrary function of time. Taking a time derivative, and using $\partial_t(\partial_z \varphi') = 0$, leads to $\partial_t b' = -\partial_t B$, which means that the buoyancy fluctuation is vertically independent. A vertically independent buoyancy in the forced buoyancy oscillator equation (49.26) means that $N_R^2 \partial_z \varphi'$ is also vertically independent, which can be satisfied if $\partial_z \varphi' = 0$. But then $w' = 0$ and $\partial_z \varphi' = 0$ in the vertical velocity equation (49.28) then means that $b' = 0$. We are thus led to the conclude that the horizontally homogeneous linear Boussinesq system is dynamically consistent only with the trivial solution: $\mathbf{v}' = b' = 0$. That is, horizontal homogeneity means exact hydrostatic balance in which, for a Boussinesq fluid, there is zero motion and zero buoyancy oscillations.⁴

As we see in the following sections, the study of internal gravity waves leads to fluctuations that have both horizontal and vertical spatial variations, thus allowing for nontrivial wave motions. Now a surface of constant phase for a plane wave has homogeneous flow properties, in which case fluid particles exhibit free buoyant oscillations along these surfaces.⁵ Yet as seen in the following, such buoyancy oscillations exist only if the phase surfaces are sloped relative to the horizontal plane, thus allowing the background buoyancy to produce buoyant motion along the phase surfaces. No internal gravity waves occur if the phase surface is strictly horizontal, with this result consistent with the above arguments. We further detail this physical picture in Section 49.5.9.

49.4 The non-rotating linear Boussinesq ocean

We here study properties of the linearized Boussinesq equations (49.16a)-(49.16c) in the absence of rotation

$$\partial_t \mathbf{v}' = -\nabla \varphi' + b' \hat{\mathbf{z}} \quad \text{linearized non-rotating velocity equation} \quad (49.30a)$$

$$\partial_t b' = -w' N_R^2 \quad \text{linearized buoyancy equation} \quad (49.30b)$$

$$\nabla \cdot \mathbf{v}' = 0 \quad \text{continuity for velocity fluctuations.} \quad (49.30c)$$

49.4.1 Relative vorticity

Taking the curl of the velocity equation (49.30a) leads to the evolution equation for the relative vorticity⁶

$$\partial_t (\nabla \times \mathbf{v}') = \nabla \times b' \hat{\mathbf{z}} \implies \partial_t \boldsymbol{\omega}' = -\hat{\mathbf{z}} \times \nabla b'. \quad (49.31)$$

The right hand side is the baroclinicity vector (37.140) for a Boussinesq fluid. Hence, in the linearized Boussinesq equations for a non-rotating fluid, relative vorticity has a local time tendency driven by baroclinicity. In the absence of buoyancy, the vorticity vector in the linear theory is static and will remain zero if initialized to zero.

In general, the vertical component to the vorticity is unaffected by baroclinicity since the baroclinicity vector is horizontal (see also Section 37.7.2). Consequently, in the linear theory the

⁴A non-Boussinesq fluid can exhibit vertical motion if the fluid has its density modified in a manner that does not introduce horizontal density gradients. For example, a horizontally homogeneous heating in an ocean with constant salinity will reduce the density and expand the water column, without introducing any horizontal inhomogeneities. This expansion results from the divergent nature of the flow field in a non-Boussinesq fluid. However, this expansion is not represented by a Boussinesq ocean. Namely, the Boussinesq ocean has a prognostic flow field that is non-divergent, and as a result uniform heating is not directly felt by the flow. In Section 64.7.6 we discuss the implications for global mean sea level of this limitation of the Boussinesq ocean.

⁵This conclusion follows since internal gravity waves in a Boussinesq ocean are transverse waves, so that fluid particles move along constant phase surfaces.

⁶Be careful to distinguish the relative vorticity vector, $\boldsymbol{\omega}' = \nabla \times \mathbf{v}'$, from the angular frequency, ω , of a plane wave, and from the vertical component of the velocity vector, $\mathbf{v} = \hat{\mathbf{x}} u + \hat{\mathbf{y}} v + \hat{\mathbf{z}} w$.

vertical vorticity is static

$$\partial_t \zeta' = 0 \quad \text{with} \quad \zeta' = \hat{\mathbf{z}} \cdot (\nabla \times \mathbf{v}'). \quad (49.32)$$

So if the flow starts with a zero vertical vorticity, then linear gravity waves will keep $\zeta' = 0$. In Section 48.5.1 we also found a static vertical component of relative vorticity holds for non-rotating shallow water gravity waves (equation (48.72)).

49.4.2 Wave equation for the vertical velocity

In Section 49.3 we derived the forced harmonic oscillator equation (49.26) for the vertical velocity

$$(\partial_{tt} + N_R^2) w' = -\partial_{tz} \varphi'. \quad (49.33)$$

To eliminate the pressure we first take the horizontal divergence of the horizontal velocity equation

$$\partial_t (\nabla_z \cdot \mathbf{u}') = -\nabla_z^2 \varphi', \quad (49.34)$$

where

$$\nabla_z = \hat{\mathbf{x}} \partial_x + \hat{\mathbf{y}} \partial_y \quad \text{and} \quad \nabla_z^2 = \nabla_z \cdot \nabla_z = \partial_{xx} + \partial_{yy}. \quad (49.35)$$

Equation (49.34) says that the time evolution of the horizontal velocity divergence is driven by the negative horizontal Laplacian acting on the dynamic pressure. Use of the non-divergence condition on the velocity, $\nabla_z \cdot \mathbf{u}' + \partial_z w' = 0$, brings equation (49.34) to

$$\partial_{tz} w' = \nabla_z^2 \varphi'. \quad (49.36)$$

Taking the horizontal Laplacian of the forced oscillator equation (49.33) (recall $N_R = N_R(z)$) yields

$$(\partial_{tt} + N_R^2) \nabla_z^2 w' = -\partial_{tz} \nabla_z^2 \varphi', \quad (49.37)$$

and then using equation (49.36) leads to the wave equation for the vertical velocity

$$(\partial_{tt} \nabla^2 + N_R^2 \nabla_z^2) w' = 0. \quad (49.38)$$

There is anisotropy in this equation due to the gravity that distinguishes the vertical from horizontal. The anisotropy manifests by the fully three dimensional Laplacian, ∇^2 , in the first term whereas just the horizontal Laplacian, ∇_z^2 , appears in the second. We furthermore observe that the wave equation (49.38) shares features with the wave equation (46.22) satisfied by the inertial waves in a homogeneous fluid experiencing constant rotation. Gravity, coupled to nonzero density gradients, breaks symmetry in the non-rotating Boussinesq ocean, thus resulting in internal gravity waves. Similarly, rotation breaks symmetry in the homogeneous fluid, thus resulting in inertial waves.

49.4.3 Linearized boundary conditions

Kinematic boundary conditions

The kinematic no-normal flow boundary condition for the velocity holds for both the nonlinear and linear velocity

$$\mathbf{v}' \cdot \hat{\mathbf{n}} = 0 \quad \text{at solid boundaries.} \quad (49.39)$$

At a moving material boundary (Section 16.4.2), such as the ocean free surface at $z = \eta(x, y, t)$, we linearize the kinematic boundary condition (16.51)

$$(\partial_t + \mathbf{u} \cdot \nabla) \eta = w \quad \text{at } z = \eta \quad (49.40)$$

to the linear form

$$\partial_t \eta = w \quad \text{at } z = \eta. \quad (49.41)$$

In fact, we must go one step further to fully linearize since $w(\eta)$ is nonlinear, thus prompting a Taylor expansion

$$w(z = \eta) \approx w(z = 0) + \eta \partial_z w. \quad (49.42)$$

The term $\eta \partial_z w$ is nonlinear and so is dropped for the linear theory, in which we have the linearized surface kinematic boundary condition

$$\partial_t \eta = w \quad \text{at } z = 0. \quad (49.43)$$

Note that we made the same conclusion in Section 45.3.4 when deriving the linearized boundary conditions for surface waves, in which there we also evaluate terms at $z = 0$ rather than $z = \eta$.

Pressure boundary condition

We will also find it useful to determine a boundary condition for the pressure written as the decomposition (49.6)

$$p(\mathbf{x}, t) = p_0(z) + p_R(z) + p'(\mathbf{x}, t) = -\rho_0 g z + g \int_z^0 \rho_R(z') dz' + p'(\mathbf{x}, t). \quad (49.44)$$

Assuming the pressure at the free surface is a constant, which we take to be zero without loss of generality, we have

$$0 = -\rho_0 g \eta + g \int_\eta^0 \rho_R(z') dz' + p'(x, y, z = \eta, t). \quad (49.45)$$

Since the free surface height is small for linear waves, we Taylor expand the reference density around $z' = 0$ according to

$$\int_\eta^0 \rho_R(z') dz' \approx \int_\eta^0 \left[\rho_R(0) + \frac{d\rho_R}{dz} z' \right] dz' = -\eta \rho_R(0) - (\eta^2/2) (d\rho_R/dz)_{z=0}. \quad (49.46)$$

Dropping the η^2 term since it is nonlinear leads to the boundary condition for the dynamic pressure evaluated at the free surface

$$\varphi' = g \eta [\rho_0 + \rho_R] \quad \text{at } z = \eta, \quad (49.47)$$

which linearizes by evaluating it at $z = 0$ and noting that $\rho_R \ll \rho_0$

$$\varphi' = g \eta \quad \text{at } z = 0. \quad (49.48)$$

Evidently, the dynamic pressure at the ocean surface is determined by the free surface height. This boundary condition is identical to that used for the surface gravity waves as derived in Sections 45.3.2 and 45.3.3. Note, however, that here we needed to work a bit harder than for the surface wave case. The reason is that here the fluid is stratified whereas we studied surface waves over a homogeneous ocean that resulted in irrotational motion and a simple expression of

Bernoulli's theorem (Section 45.3).

Vertical velocity boundary condition

We further combine the boundary condition (49.48) with the linearized surface kinematic boundary condition (49.43) to eliminate the free surface in favor of the vertical velocity

$$\partial_t \varphi' = g w \quad \text{at } z = 0. \quad (49.49)$$

When studying vertical normal modes in an ocean domain in Section 49.8, we find it more convenient to have a boundary condition just for the vertical velocity. To eliminate the pressure we take the divergence of the horizontal velocity equation, $\partial_t \mathbf{u}' = -\nabla_z \varphi'$, and use the non-divergence condition on the velocity to yield

$$\partial_{tz} w' = \nabla_z^2 \varphi'. \quad (49.50)$$

Taking another time derivative and evaluating the expression at $z = 0$ yields

$$\partial_{ttz} w' = \nabla_z^2 \partial_t \varphi' \implies \partial_{ttz} w' = g \nabla_z^2 w \quad \text{at } z = 0, \quad (49.51)$$

where we used the boundary condition (49.49) to eliminate pressure in favor of the vertical velocity.

49.5 Free gravity waves with constant stratification

Thus far we have assumed that the reference state buoyancy frequency is a function just of the vertical direction. We now specialize to the case of a constant frequency, N_R , in which case we can study free plane internal gravity waves. We return in Section 49.7 to the more realistic case of vertically varying buoyancy frequency, $N_R(z)$.

49.5.1 Plane wave ansatz for internal gravity waves

To examine the physics of internal gravity waves, we introduce the following plane wave ansatz for the velocity, dynamic pressure, and buoyancy

$$\mathbf{v}' = \tilde{\mathbf{v}} e^{i(\mathbf{k} \cdot \mathbf{x} - \omega t)} \quad \text{and} \quad \varphi' = \tilde{\varphi} e^{i(\mathbf{k} \cdot \mathbf{x} - \omega t)}, \quad \text{and} \quad b' = \tilde{b} e^{i(\mathbf{k} \cdot \mathbf{x} - \omega t)}, \quad (49.52)$$

where the amplitudes are generally complex, and where we write the three dimensional and horizontal wavevectors as

$$\mathbf{k} = k_x \hat{\mathbf{x}} + k_y \hat{\mathbf{y}} + k_z \hat{\mathbf{z}} \quad \text{and} \quad \mathbf{k}_h = k_x \hat{\mathbf{x}} + k_y \hat{\mathbf{y}}. \quad (49.53)$$

Substitution of the ansatz (49.52) into the linearized Boussinesq equations (49.30a)-(49.30c) allows us to determine relations between the velocity, pressure, and buoyancy for a plane wave. These relations are referred to as *polarization* relations. To help organize these relations we choose to relate the pressure and velocity amplitudes to the buoyancy amplitude. Furthermore, as part of developing polarization relations we derive the dispersion relation that relates the wavevector, \mathbf{k} , to the wave angular frequency, ω .

49.5.2 Transverse waves

The non-divergence condition holding for the Boussinesq ocean flow, $\nabla \cdot \mathbf{v}' = 0$, means that the waves are transverse, so that the velocity amplitude satisfies

$$\mathbf{k} \cdot \tilde{\mathbf{v}} = \mathbf{k}_h \cdot \tilde{\mathbf{u}} + k_z \tilde{w} = 0. \quad (49.54)$$

Consequently, fluid particles within a plane wave move within planes of constant phase, with these planes perpendicular to the wavevector. Recall that such transverse wave motion in three dimensional space also holds for plane inertial waves in a constant density fluid (Section 46.2).

49.5.3 Pressure equation

Substitution of the plane wave ansatz into the pressure equation (49.27) renders

$$\tilde{\varphi}/\tilde{b} = -i k_z / |\mathbf{k}|^2. \quad (49.55)$$

Hence, the pressure and buoyancy in the plane wave are $\pi/2$ radians out of phase. Observe that the pressure amplitude vanishes for a horizontal wavevector, in which $k_z = 0$. We expect this result for a free wave since vertical structure in the fluctuating buoyancy provides the source for pressure fluctuations as per the pressure Poisson equation (49.27).

49.5.4 Relative vorticity

The relative vorticity vector satisfies equation (49.31), which for a plane wave takes on the form

$$\omega \mathbf{k} \times \tilde{\mathbf{v}} = -i \tilde{b} (\hat{\mathbf{z}} \times \mathbf{k}) \implies \mathbf{k} \times (\omega \tilde{\mathbf{v}} + i \hat{\mathbf{z}} \tilde{b}) = 0. \quad (49.56)$$

Evidently, the vector $\omega \tilde{\mathbf{v}} + i \hat{\mathbf{z}} \tilde{b}$ is parallel to the wavevector. Taking the dot product of the relative vorticity equation (49.56) with $\hat{\mathbf{z}}$ leads to

$$\hat{\mathbf{z}} \cdot (\mathbf{k} \times \tilde{\mathbf{v}}) = 0, \quad (49.57)$$

which is the plane wave expression for a zero vertical component to the relative vorticity, $\zeta' = 0$. This constraint means that the plane waves maintain $\zeta' = 0$ so long as the horizontal velocity amplitudes are related by

$$k_x \tilde{v} = k_y \tilde{u}. \quad (49.58)$$

49.5.5 Dispersion relation

Horizontal velocity

The horizontal portion of the velocity equation (49.30a) leads to the relation satisfied for the plane wave

$$\omega \mathbf{k}_h \cdot \tilde{\mathbf{u}} = \tilde{\varphi} |\mathbf{k}_h|^2 = -i \tilde{b} k_z |\mathbf{k}_h|^2 / |\mathbf{k}|^2, \quad (49.59)$$

where we used the pressure equation (49.55) for the second equality. Equivalently, we can use the transverse nature of the wave as per equation (49.54) to write

$$\omega \mathbf{k}_h \cdot \tilde{\mathbf{u}} = -k_z \omega \tilde{w} = -\frac{i k_z^3 \omega^2 \tilde{b}}{|\mathbf{k}|^2 (N_R^2 - \omega^2)}, \quad (49.60)$$

where we used the relation (49.75) for the vertical velocity.

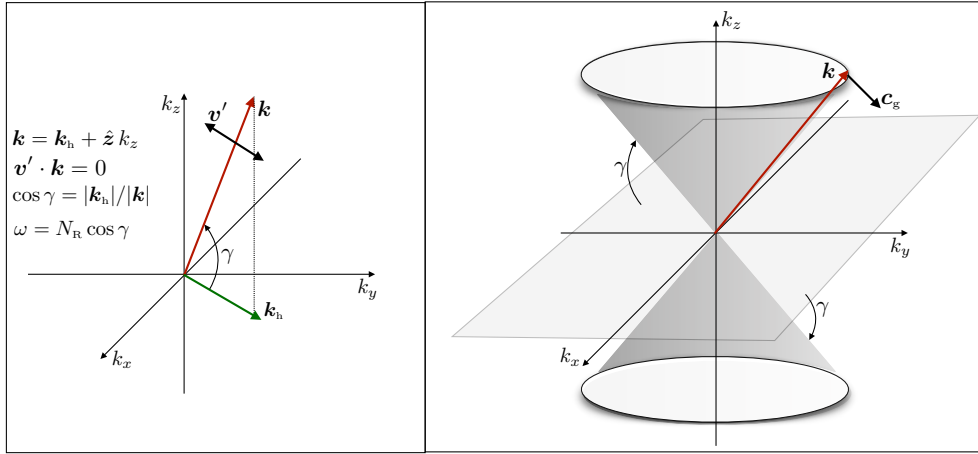


FIGURE 49.1: Left panel: A sample wavevector, $\mathbf{k} = \mathbf{k}_h + \hat{z} k_z$, for a plane internal gravity wave. The wave is transverse so that the velocity of fluid particles is orthogonal to the wavevector, $\mathbf{k} \cdot \mathbf{v}' = 0$. The dispersion relation, $\omega = N_R \cos \gamma$, is independent of the wavenumber, $|\mathbf{k}|$, but instead only depends on the cosine of the angle made with the horizontal plane, $\cos \gamma = |\mathbf{k}_h|/|\mathbf{k}|$. Right panel: a more global depiction of the dispersion relation. Again, the angular frequency of an internal gravity wave depends only on the angle, γ , the wavevector makes with the horizontal plane. Hence, the angular frequency is the same for all wavevectors on the surface of a cone extending from the origin along the \hat{z} axis and with arbitrary magnitude. Cones with $k_z > 0$ correspond to internal gravity waves with an upward phase velocity, and those with $k_z < 0$ are downward. As shown in Section 49.5.7, the group velocity, \mathbf{c}_g , is orthogonal to the wavevector, and it points in the direction of increasing frequency, which is toward the horizontal plane. Hence, upward phase velocity waves have a downward group velocity.

Dispersion relation for internal gravity waves

Equating equations (49.59) and (49.60) yields the dispersion relation for internal gravity waves

$$\omega^2 = |\mathbf{k}_h|^2 N_R^2 / |\mathbf{k}|^2 = N_R^2 \cos^2 \gamma \implies 0 \leq \omega \leq N_R. \quad (49.61)$$

In the second equality we introduced the angle between the wavevector and the horizontal plane

$$\cos \gamma = |\mathbf{k}_h|/|\mathbf{k}|, \quad (49.62)$$

with the geometry illustrated in Figure 49.1.

Another useful means to write the dispersion relation (49.61) is given by

$$\frac{N_R^2 - \omega^2}{\omega^2} = \frac{k_z^2}{|\mathbf{k}_h|^2} = \tan^2 \gamma. \quad (49.63)$$

This expression makes it clear that internal gravity waves with maximum frequency, $\omega = N_R$, correspond to a horizontal phase velocity, $k_z = 0$ and $\gamma = 0$. Conversely, the angular frequency goes to zero when the waves have a purely vertical phase velocity, $\mathbf{k}_h = 0$. We make use of equation (49.63) in Section 49.5.8 to develop polarization relations involving the vertical velocity within a plane wave.

Directly deriving the dispersion relation from the w' wave equation

The dispersion relation (49.61) can be directly derived from the wave equation (49.38) satisfied by the vertical velocity

$$(\partial_{tt}\nabla^2 + N_R^2\nabla_z^2)w' = 0 \implies \omega^2|\mathbf{k}|^2 - N_R^2|\mathbf{k}_h|^2 = 0. \quad (49.64)$$

Furthermore, note that if we only extract the horizontal and time harmonic portion of w' , so that

$$w' = W(z)e^{i(\mathbf{k}_h \cdot \mathbf{x} - \omega t)}, \quad (49.65)$$

then the vertical structure function, $W(z)$, satisfies the ordinary differential equation

$$\left[\frac{d^2}{dz^2} + \frac{|\mathbf{k}_h|^2(N_R^2 - \omega^2)}{\omega^2} \right] W = 0 \implies \left[\frac{d^2}{dz^2} + k_z^2 \right] W = 0. \quad (49.66)$$

This equation is satisfied if $W = e^{ik_z z}$, which is what we use for the constant N_R case now being studied. However, in Section 49.7 we find that equation (49.66) is generalized for the case when the background buoyancy frequency is a function of the vertical, $N_R = N_R(z)$, in which case the plane wave solution is modified.

49.5.6 Unpacking the dispersion relation

The angular frequency for an internal gravity wave only depends on the buoyancy frequency and the cosine of the angle the wavevector makes with the horizontal plane, whereas it is independent of the wavenumber, $|\mathbf{k}|$, and thus of the wavelength, $2\pi/|\mathbf{k}|$. Furthermore, the angular frequency possesses rotational (azimuthal) symmetry around the vertical direction. As such, the angular frequency is the same along the surface of a cone in wavevector space extending out from the origin along the \hat{z} axis in either direction. Figure 49.1 provides an illustration for the two cones associated with a particular γ . The upper cone has $k_z > 0$ and so corresponds to internal gravity waves with the same frequency and with upward propagating phase velocities, whereas the lower cone has $k_z < 0$ so has with downward phase velocities.

Cross-like patterns from forced internal gravity wave packets

A further remark about the relation (49.63) concerns the case where we know the frequency of the wave and the buoyancy frequency, in which case the angle γ is specified. For example, consider a local source (say an oscillating disk) with angular frequency, ω_{source} , moving with a small amplitude in a stratified fluid with $\omega_{\text{source}} < N_R$. This source preferentially forces internal waves of angular frequency $\omega = \omega_{\text{source}}$. Consequently, the left hand side of equation (49.63) is specified, in which case can determine the angle, γ , of the phase velocity. Now wave packets extend outward from the source and thus define the group velocity direction (not the phase velocity direction), and so extend outward from the source at an angle $\pi/2 - \gamma$ from the horizontal. The phase velocity is directed perpendicular to the group velocity and it makes an angle γ with the horizontal. Hence, as the source angular frequency approaches the buoyancy frequency, γ approaches zero so that the group velocity “cross” pattern steepens toward the vertical axis. Figure 49.2 provides a schematic of the experiment.

Comparing the internal gravity wave dispersion and inertial wave dispersion

The internal gravity wave dispersion relation (49.61) shares features with that for inertial waves, whose dispersion relation is given by equation (46.26). Namely, both relations are independent of

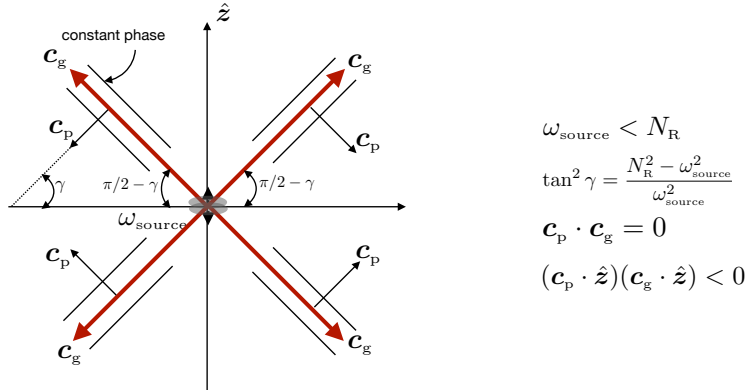


FIGURE 49.2: A small amplitude oscillating source in a stratified fluid with angular frequency, $\omega_{\text{source}} < N_R$. If the source has small amplitude then it generates linear internal gravity waves with $\omega = \omega_{\text{source}}$. These waves radiate wave packets with group velocity, \mathbf{c}_g , away from the source and with an angle, $\pi/2 - \gamma$, from the horizontal. The angle, γ , is determined by the dispersion relation through $\tan^2 \gamma = (N_R^2 - \omega_{\text{source}}^2)/\omega_{\text{source}}^2$. The group velocity is parallel to lines of constant phase and perpendicular to the phase velocity so that $\mathbf{c}_p \cdot \mathbf{c}_g = 0$. Furthermore, the phase and group velocity are oriented so that $(\mathbf{c}_g \cdot \hat{z})(\mathbf{c}_p \cdot \hat{z}) < 0$, so that if the group velocity is directed upward then the phase velocity is directed downward. As the source angular frequency approaches the buoyancy frequency, γ approaches zero so that the group velocity “cross” pattern steepens toward the vertical axis; i.e., the angle $\pi/2 - \gamma$ approaches $\pi/2$. The pattern is sometimes referred to as *St. Andrew’s cross*. [This video from Prof. Rhines’](#) illustrates the phenomena in a laboratory setting, whereas [this animation from Prof. Durran’s website](#) illustrates the phenomena in a numerical simulation.

the wavenumber and instead only depend on the orientation of the wave. For the gravity wave, the orientation is relative to the horizontal plane, with the vertical a special direction as determined by gravity. For the inertial wave the orientation is relative to the rotation vector. Furthermore, both angular frequencies have an upper bound, with inertial waves having frequencies no larger than twice the angular frequency of the rotating frame, $|2\Omega|$, and internal gravity waves having frequencies no larger than the buoyancy frequency, N_R .

Comments about forcing with higher frequency than N_R

Internal gravity waves have an angular frequency that is bounded above by the buoyancy frequency: $0 \leq \omega \leq N_R$. There are no internal gravity waves with frequency larger than the buoyancy frequency of the background reference state. This limit exists since internal gravity waves are coherent patterns of buoyancy oscillations, with the angular frequency of that oscillation taken from the background stratification (see Section 49.5.9 for more on this perspective). In Exercise 49.1 we speculate on what happens if a stratified fluid is agitated by a source with angular frequency greater than N_R .

49.5.7 Group velocity

The dispersion relation (49.61) leads to the group velocity, $\mathbf{c}_g = \nabla_{\mathbf{k}}\omega$, which for internal gravity waves is given by

$$\mathbf{c}_g = \frac{N_R k_z}{|\mathbf{k}|^3 |\mathbf{k}_h|} (k_z \mathbf{k}_h - |\mathbf{k}_h|^2 \hat{z}). \quad (49.67)$$

In this section we identify a number of properties satisfied by the group velocity.

Group velocity is orthogonal to the phase velocity

Evidently, the internal wave group velocity is orthogonal to the phase velocity

$$\mathbf{c}_g \cdot \mathbf{c}_p = 0, \quad (49.68)$$

where the phase velocity is

$$\mathbf{c}_p = (\omega/|\mathbf{k}|) \hat{\mathbf{k}}. \quad (49.69)$$

Hence, the group velocity is aligned parallel to constant phase surfaces, just like the fluid particle motion.⁷

The phase velocity and group velocity have opposing vertical components

The vertical component of the group velocity has the opposite sign of the vertical component of the phase velocity, which is seen by

$$(\mathbf{c}_p \cdot \hat{\mathbf{z}})(\mathbf{c}_g \cdot \hat{\mathbf{z}}) = -\frac{\omega k_z}{|\mathbf{k}|^2} \frac{N_R k_z |\mathbf{k}_h|}{|\mathbf{k}|^3} = -\frac{\omega^2 \sin^2 \gamma}{|\mathbf{k}|^2} < 0. \quad (49.70)$$

If the phase velocity is directed away from the horizontal plane, then the group velocity is directed toward the horizontal plane, and vice versa. This property is depicted in Figures 49.1 and 49.2.

The group velocity magnitude

The squared magnitude of the group velocity is given by

$$\mathbf{c}_g \cdot \mathbf{c}_g = \frac{N_R^2 k_z^2}{|\mathbf{k}|^4} = \frac{N_R^2 \sin^2 \gamma}{|\mathbf{k}|^2} \quad \text{where} \quad \sin \gamma = k_z/|\mathbf{k}|. \quad (49.71)$$

To help understand this expression it is useful to consider two extreme cases.

First, the group velocity vanishes when the wavevector is horizontal ($k_z = 0$ and $\gamma = 0$). As a result, no wave energy is propagated when the wavevector is horizontal.⁸ When the wavevector is horizontal, all particle motion in the wave is vertical. Evidently, even though the wave has energy when it has a horizontal phase velocity, the wave energy is not propagated.

At the opposite extreme, when the phase velocity is vertical, so that $\mathbf{k}_h = 0$, the fluid particles move along a horizontal plane in an arbitrary horizontal direction. The group velocity is also horizontal and takes the form

$$\mathbf{c}_g = (N_R/|k_z|) \hat{\mathbf{k}}_h \quad \text{with} \quad \mathbf{k}_h = 0, \quad (49.72)$$

where $\hat{\mathbf{k}}_h$ is any horizontal direction. Finally, the angular frequency vanishes so that the wave is stationary; phase does not move.

49.5.8 Polarization relations and structure of a plane wave

We now piece together the polarization relations to provide expressions for the velocity, pressure, and buoyancy within a wave. We first express all fields in terms of the buoyancy amplitude, \tilde{b} , and then in terms of the pressure amplitude, $\tilde{\varphi}$. These amplitudes are related via the pressure

⁷Recall that these properties also hold for inertial waves discussed in Section 46.2.6.

⁸In Section 49.5.10 we show how the mechanical energy flux of an internal gravity wave is proportional to the group velocity.

equation from Section 49.5.3, whereby

$$\tilde{\varphi}/\tilde{b} = -i k_z / |\mathbf{k}|^2 = -i \sin \gamma / |\mathbf{k}|. \quad (49.73)$$

Neither is more fundamental, and yet one amplitude might be more readily available than the other so it is useful to provide both expressions.

Vertical velocity component

For the vertical velocity component we make use of the forced oscillator equation (49.33) to render a relation between the vertical velocity amplitude and the amplitude of the dynamic pressure

$$\tilde{w}/\tilde{\varphi} = -\frac{k_z \omega}{N_R^2 - \omega^2}. \quad (49.74)$$

We can also relate the vertical velocity amplitude to the buoyancy amplitude through use of the pressure equation (49.55)

$$\tilde{w}/\tilde{b} = \frac{i k_z^2 \omega}{|\mathbf{k}|^2 (N_R^2 - \omega^2)}. \quad (49.75)$$

Evidently, the vertical velocity is either in phase or π radians out of phase with the pressure (depending on the sign of k_z), and it is $\pi/2$ out of phase with buoyancy. We now make use of the dispersion relation in the form of equation (49.63) to bring the vertical velocity expressions (49.74) and (49.75) into the more tidy forms

$$\tilde{w}/\tilde{\varphi} = -\frac{k_z \omega}{N_R^2 - \omega^2} = -\frac{|\mathbf{k}_h|^2}{\omega k_z} \quad (49.76a)$$

$$\tilde{w}/\tilde{b} = \frac{i k_z^2 \omega}{|\mathbf{k}|^2 (N_R^2 - \omega^2)} = \frac{i |\mathbf{k}_h|^2}{\omega |\mathbf{k}|^2} = \frac{i \cos \gamma}{N_R}. \quad (49.76b)$$

Horizontal velocity

For the horizontal velocity we use the transverse nature of the wave (Section 49.5.2) to relate the horizontal components to the vertical

$$\mathbf{k}_h \cdot \tilde{\mathbf{u}} = -k_z \tilde{w}, \quad (49.77)$$

as well as the zero vertical component of the relative vorticity (Section 49.5.4) so that

$$k_x \tilde{v} = k_y \tilde{u}. \quad (49.78)$$

These two relations, along with the vertical velocity amplitude equations (49.76a) and (49.76b), lead to

$$\tilde{\mathbf{u}} = -\frac{i \tilde{b} \mathbf{k}_h \sin \gamma}{N_R |\mathbf{k}_h|} \quad (49.79)$$

Wave solutions

Bringing the previous results together allows us to express the solutions for the velocity, pressure, and buoyancy within a freely propagating internal gravity wave. The solutions in terms of a real

buoyancy amplitude, \tilde{b} , are given by

$$b' = \tilde{b} \cos(\mathbf{k} \cdot \mathbf{x} - \omega t) \quad (49.80a)$$

$$\varphi' = \frac{\tilde{b} \sin \gamma}{|\mathbf{k}|} \sin(\mathbf{k} \cdot \mathbf{x} - \omega t) \quad (49.80b)$$

$$\mathbf{u}' = \frac{\tilde{b} \mathbf{k}_h \sin \gamma}{N_R |\mathbf{k}_h|} \sin(\mathbf{k} \cdot \mathbf{x} - \omega t) \quad (49.80c)$$

$$\tilde{w} = -\frac{\tilde{b} \cos \gamma}{N_R} \sin(\mathbf{k} \cdot \mathbf{x} - \omega t) \quad (49.80d)$$

$$\mathbf{v}' = \frac{\mathbf{c}_g \tilde{b} |\mathbf{k}|^2}{N_R^2 k_z} \sin(\mathbf{k} \cdot \mathbf{x} - \omega t). \quad (49.80e)$$

Equation (49.80e) for \mathbf{v}' made use of equation (49.67) for the group velocity, thus exposing the parallel nature of the particle velocity and group velocity for plane internal gravity waves. An alternative suite of wave solutions arises when assuming a real pressure amplitude, $\tilde{\varphi}$, which leads to

$$\varphi' = \tilde{\varphi} \cos(\mathbf{k} \cdot \mathbf{x} - \omega t) \quad (49.81a)$$

$$b' = -\frac{\tilde{\varphi} |\mathbf{k}|^2}{k_z} \sin(\mathbf{k} \cdot \mathbf{x} - \omega t) \quad (49.81b)$$

$$\mathbf{u}' = \frac{\tilde{\varphi} \mathbf{k}_h}{\omega} \cos(\mathbf{k} \cdot \mathbf{x} - \omega t) \quad (49.81c)$$

$$w' = -\frac{\tilde{\varphi} |\mathbf{k}_h|^2}{\omega k_z} \cos(\mathbf{k} \cdot \mathbf{x} - \omega t) \quad (49.81d)$$

$$\mathbf{v}' = \frac{\mathbf{c}_g \tilde{\varphi} |\mathbf{k}|^4}{N_R^2 k_z^2} \cos(\mathbf{k} \cdot \mathbf{x} - \omega t). \quad (49.81e)$$

49.5.9 Force balance within an internal gravity wave

To help understand the internal gravity wave dispersion relation (49.61), consider a test fluid element that moves with the wave in the transverse direction; i.e., parallel to surfaces of constant phase. As discussed in Section 14.3.5, a test fluid element is assumed to have zero impact on the surrounding fluid, in particular it has no impact on the pressure. This assumption is broken when considering real fluid elements, since all fluid elements affect the surrounding fluid. However, the pressure is spatially constant along a constant phase direction. Hence, for a particle displaced in this direction it only feels the change in buoyancy. So our critique of the test fluid elements in Section 49.3.1 is tempered when considering fluid particle motion along directions that parallel phase surfaces. In the following, we refer to the test fluid element as a fluid particle both for brevity and to accord with the literature.

Fluid particle displacement vector

We measure a fluid particle's position relative to its equilibrium position through the use of a displacement field,

$$\boldsymbol{\xi}(\mathbf{x}, t) = \delta x \hat{\mathbf{x}} + \delta y \hat{\mathbf{y}} + \delta z \hat{\mathbf{z}}. \quad (49.82)$$

The displacement field vanishes when the fluid particle is at its equilibrium position, and it has a time tendency that equals to the velocity of a fluid particle⁹

$$\partial_t \boldsymbol{\xi}(\mathbf{x}, t) = \mathbf{v}'(\mathbf{x}, t). \quad (49.83)$$

Evidently, since the plane wave is transverse,

$$\mathbf{v}' \cdot \mathbf{k} = \partial_t \mathbf{x} \cdot \mathbf{k} = 0. \quad (49.84)$$

If the fluid particle moves in the vertical, it moves through the background reference density field, $\rho_R(z)$. Assume the fluid particle starts at point *A* with local buoyancy equal to the reference buoyancy. As it rises an infinitesimal amount to point *B*, its buoyancy referenced to the local environment is negative since it started from a denser level. As such, the fluid particle wants to return to its deeper level. We can express the locally referenced buoyancy anomaly felt at point *B* in terms of the particle displacement

$$b' = -\boldsymbol{\xi} \cdot \nabla b_R = -\delta z \frac{db_R}{dz} = -\delta z N_R^2. \quad (49.85)$$

As a check on this expression, we find that if $\delta z > 0$, so that the fluid particle rises, then the buoyancy anomaly is negative, $b' < 0$, since it started from a deeper level where the density is larger. Hence, there is a buoyant acceleration back to the deeper level. Also observe that the time derivative of equation (49.85) leads to

$$\partial_t b' = -w' N_R^2, \quad (49.86)$$

which is the linearized buoyancy equation (49.16b).

Equation of motion

We now make use of the result (49.85) in the equation of motion (49.30a). More precisely, we project that equation onto the transverse direction, $\hat{\mathbf{t}}$. This direction is fixed in time for a plane wave so that we have

$$\partial_t (\hat{\mathbf{t}} \cdot \mathbf{v}') = \hat{\mathbf{t}} \cdot (-\nabla \varphi' + b' \hat{\mathbf{z}}). \quad (49.87)$$

As noted above, there is no spatial gradient of flow properties along a constant phase surface, so that

$$\hat{\mathbf{t}} \cdot \nabla \varphi' = 0. \quad (49.88)$$

We write δl for the displacement along the phase surface, so that

$$\hat{\mathbf{t}} \cdot \mathbf{v}' = \partial_t (\delta l), \quad (49.89)$$

which brings the equation of motion (49.87) to the form

$$\partial_{tt}(\delta l) - \hat{\mathbf{z}} \cdot \hat{\mathbf{t}} b' = 0. \quad (49.90)$$

⁹We made use of a one dimensional displacement field in Section 44.4 when considering acoustic waves using a Lagrangian perspective. We also make use of fluid particle displacement vectors when studying the generalized Lagrangian mean in Section 62.3, as well as for tracer kinematics in Section 62.4. The present discussion is heuristic and skims over details explored in these other sections. We can afford some degree of informality since all perturbations here are small.

Noting that $\hat{z} \cdot \hat{t} = \cos \gamma$ and making use of equation (49.85) for the buoyancy anomaly leads to

$$\partial_{tt}(\delta l) + \cos \gamma N_R^2 \delta z = 0. \quad (49.91)$$

Finally, we set $\delta z = \delta l \cos \gamma$ to render the simple harmonic oscillator equation for displacements along the constant phase line

$$(\partial_{tt} + N_R^2 \cos^2 \gamma) \delta l = 0. \quad (49.92)$$

The angular frequency of the oscillations, $N_R \cos \gamma$, is precisely that arising from the internal gravity wave dispersion relation (49.61).

Summary of the physical picture for internal gravity waves

The above analysis suggests the following physical picture for internal gravity waves. Namely, the waves consist of fluid particle motion in directions that parallel the constant phase surfaces, which accords with the property of all transverse waves. As the particles move along the transverse direction, \hat{t} , they sample the background buoyancy field and thus experience buoyancy accelerations that act to return the particle to its neutral buoyancy position. Oscillatory motion arises from over-shooting the neutral buoyancy position, with the oscillations having an angular frequency $N_R \cos \gamma$. The oscillations are at their maximum frequency when $\gamma = 0$, which arises since the particles are moving vertically and thus fully sampling the background buoyancy field. In contrast, there are no oscillations when the particles move along a horizontal phase surface ($\gamma = \pi/2$ so that $\hat{k} = \hat{z}$) since horizontal surfaces sample the same background buoyancy. The vanishing of oscillations with $\gamma = \pi/2$ accords with our discussion in Section 49.3.2.

We emphasize that although the fluid particles are moving in a direction that parallels the constant phase surfaces, they are *not* moving with those surfaces. Rather, the fluid particles are oscillating in the transverse direction, and it is their oscillation that gives rise to the wave itself and thus to the movement of the phase surfaces through the fluid.

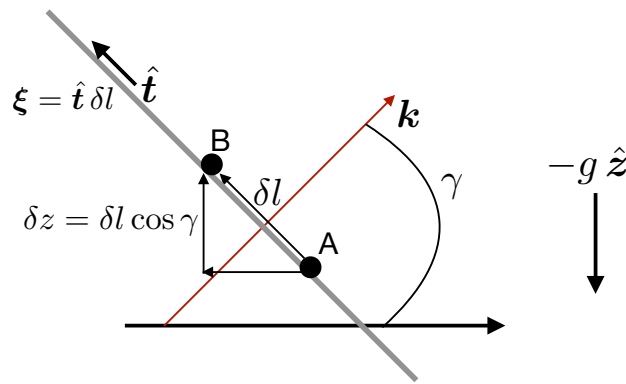


FIGURE 49.3: Depicting the displacement of a fluid particle along a direction transverse to a constant phase for a plane internal gravity wave whose wavevector makes an angle γ with the horizontal. We write the displacement vector as $\xi(\mathbf{x}, t) = \delta l \hat{t}$, with the local tangent vector, \hat{t} , pointing in a transverse direction orthogonal to the wavevector, \mathbf{k} . The displacement of the fluid particle from point A and point B occurs over a distance, δl , with a corresponding change in vertical position given by $\delta z = \delta l \cos \gamma$.

49.5.10 Energetics of a plane internal gravity wave

In Section 49.2.5 we derived the energetics for the linearized Boussinesq ocean equations and we led to the energy equation (49.24)

$$\partial_t(\mathcal{K}' + \mathcal{A}') = -\nabla \cdot (\mathbf{v}' \varphi') \quad \text{with} \quad \mathcal{K}' = \mathbf{v}' \cdot \mathbf{v}'/2 \quad \text{and} \quad \mathcal{A}' = (b'/N_R)^2/2. \quad (49.93)$$

We now consider energetics of an internal gravity wave whose small amplitude fluctuations are given by the wave equations (49.81a)-(49.81d)

Interpreting the available potential energy

We saw in Section 49.2.5 that $\mathcal{A}' = (b'/N_R)^2/2$ measures the available potential energy per mass arising from the small amplitude buoyancy fluctuation. When those fluctuations are part of a plane wave we can introduce the fluid particle displacement as in equation (49.85), in which

$$\mathcal{A}' = (b'/N_R)^2/2 = (\delta z N_R)^2/2. \quad (49.94)$$

This expression is identical to the potential energy (44.8) that we encountered for a point mass connected to a spring, where here the spring constant per mass equals by N_R^2 .

Mechanical energy in the wave field

Assuming the small amplitude fluctuations are given by the wave relations (49.81a)-(49.81d) leads to

$$\mathcal{K}' = \frac{\tilde{\varphi}^2 |\mathbf{k}|^4}{2 N_R^2 k_z^2} \cos^2(\mathbf{k} \cdot \mathbf{x} - \omega t) \quad (49.95a)$$

$$\mathcal{A}' = \frac{\tilde{\varphi}^2 |\mathbf{k}|^4}{2 N_R^2 k_z^2} \sin^2(\mathbf{k} \cdot \mathbf{x} - \omega t), \quad (49.95b)$$

so that

$$\mathcal{K}' + \mathcal{A}' = \frac{\tilde{\varphi}^2 |\mathbf{k}|^4}{2 N_R^2 k_z^2} = \frac{\tilde{\varphi}^2 |\mathbf{k}_h|^2 |\mathbf{k}|^2}{2 \omega^2 k_z^2}. \quad (49.96)$$

It is notable that the sum of the kinetic and available potential energy for the wave is time independent. Furthermore, their separate phase averages are equal

$$\langle \mathcal{K}' \rangle = \langle \mathcal{A}' \rangle, \quad (49.97)$$

which manifests equipartition for the phase averaged kinetic energy and available potential energy. We can relate the total mechanical energy to the phase average of the squared vertical velocity through use of equation (49.81d), which yields

$$\mathcal{K}' + \mathcal{A}' = \langle (w')^2 \rangle / \cos^2 \gamma. \quad (49.98)$$

Note that the first expression in equation (49.96) indicates that for vertical waves, where $\gamma = \pi/2$, the sum $\mathcal{K}' + \mathcal{A}'$ is non-singular since $(w')^2$ vanishes. More precisely, we set $\mathbf{k}_h = 0$ in equation (49.96) and find that vertical waves have mechanical energy

$$\mathcal{K}' + \mathcal{A}' = \frac{\tilde{\varphi}^2 k_z^2}{2 N_R^2} \quad \text{if } \mathbf{k}_h = 0. \quad (49.99)$$

Energy flux and group velocity

The flux of mechanical energy can be written as

$$\mathbf{v}' \cdot \varphi' = \frac{\tilde{\varphi}^2 \cos^2(\mathbf{k} \cdot \mathbf{x} - \omega t)}{k_z \omega} (k_z \mathbf{k}_h - \hat{\mathbf{z}} |\mathbf{k}_h|^2) = \frac{\mathbf{c}_g \tilde{\varphi}^2 |\mathbf{k}|^4 \cos^2(\mathbf{k} \cdot \mathbf{x} - \omega t)}{N_R^2 k_z^2}, \quad (49.100)$$

where we used equation (49.67) for the group velocity. Taking the phase average then leads to

$$\langle \mathbf{v}' \cdot \varphi' \rangle = \frac{\mathbf{c}_g \tilde{\varphi}^2 |\mathbf{k}|^4}{2 N_R^2 k_z^2} = \mathbf{c}_g (\mathcal{K}' + \mathcal{A}'). \quad (49.101)$$

We thus confirm that the phase averaged flux of mechanical energy contained in an internal gravity wave equals to the group velocity times the total mechanical energy. This result accords with both the group velocity and the particle velocity being parallel to lines of constant phase and hence perpendicular to the wavevector

$$\mathbf{c}_g \cdot \mathbf{k} = \mathbf{v}' \cdot \mathbf{k} = 0. \quad (49.102)$$

49.6 Reflection of gravity waves

In Section 47.4.3 we studied the reflection of planetary Rossby wave packets from a solid surface. That approach made use of some generic methods from geometric optics, in which we assume the waves reflect from the boundary without dissipation. Consequently, we only need to invoke the kinematic boundary condition to derive relations between incident and reflected waves. Here we pursue a similar study for internal gravity waves. One essential difference appears here. Namely, Rossby waves (and many other waves such as acoustic and electromagnetic waves) exhibit *specular* reflection, whereby the angle the incident wave packet makes with the surface is preserved upon reflection. In contrast, the dispersion relation for internal gravity waves leads to a distinctly *non-specular* property. Furthermore, we encounter a particularly striking ability for the internal gravity wave, hitting the boundary at a critical angle, to have an unbounded wavenumber upon reflection.

49.6.1 General reflection conditions

Consider a packet of internal gravity waves with group velocity, \mathbf{c}_{gi} , that is incident on a plane solid boundary, with the boundary making an angle, β , with the horizontal (see Figure 49.4). Let the carrier wave in the wave packet have an angular frequency, ω_i , and wavevector, \mathbf{k}_i , with $\mathbf{c}_{gi} \cdot \mathbf{k}_i = 0$. We can write the velocity of fluid particles in the carrier wave in the form

$$\mathbf{v}'_i = \mathbf{c}_{gi} A_i \cos(\mathbf{k}_i \cdot \mathbf{x} - \omega_i t). \quad (49.103)$$

If we assume knowledge of the pressure amplitude of the wave, $\tilde{\varphi}$, then the amplitude function, A_i , is a shorthand for the amplitude given in equation (49.81e). Otherwise, A_i is a prescribed magnitude for the incoming wave amplitude. The same considerations hold for the velocity of fluid particles in the reflected wave, so that

$$\mathbf{v}'_r = \mathbf{c}_{gr} A_r \cos(\mathbf{k}_r \cdot \mathbf{x} - \omega_r t), \quad (49.104)$$

Now consider fluid motion in which there are both incident and reflected waves, so that the

fluid velocity is given by the sum

$$\mathbf{v}' = \mathbf{v}'_i + \mathbf{v}'_r. \quad (49.105)$$

The no-normal flow boundary condition at solid boundary couples the incident and reflected wave properties, in which case

$$\mathbf{v}' \cdot \hat{\mathbf{n}} = (\mathbf{v}'_i + \mathbf{v}'_r) \cdot \hat{\mathbf{n}} = 0 \quad \text{at } \mathbf{x} = \mathbf{x}_w. \quad (49.106)$$

In these equations, $\hat{\mathbf{n}}$ is the outward normal on the boundary and $\mathbf{x}_w = |\mathbf{x}_w| \hat{\mathbf{t}}$ is a point on the solid boundary, with $\hat{\mathbf{t}}$ the unit vector pointing tangent to the boundary so that $\hat{\mathbf{n}} \cdot \hat{\mathbf{t}} = 0$. As for Rossby wave reflection considered in Section 47.4.3, the boundary condition (49.106) leads to the reflection conditions for the angular frequency and wavevectors

$$\omega_i = \omega_r \quad \text{and} \quad (\mathbf{k}_i - \mathbf{k}_r) \cdot \hat{\mathbf{t}} = 0. \quad (49.107)$$

The wavevector condition in equation (49.107) means that there is an equal projection onto the tangent direction of the incident and reflected wavevectors. This same condition holds for other waves, such as we found when studying Rossby wave reflection in Section 47.4.3 and as found for inertial waves in Exercise 49.3. The angular frequency condition, $\omega_i = \omega_r$, when coupled to the internal gravity wave dispersion relation (49.61), leads to a *non-specular* reflection of the waves. That is, the angle that a reflected internal gravity wave makes with the solid boundary is generally different from the angle made by the incident wave. To prove this result requires just a bit of trigonometry based on the boundary conditions (49.107).

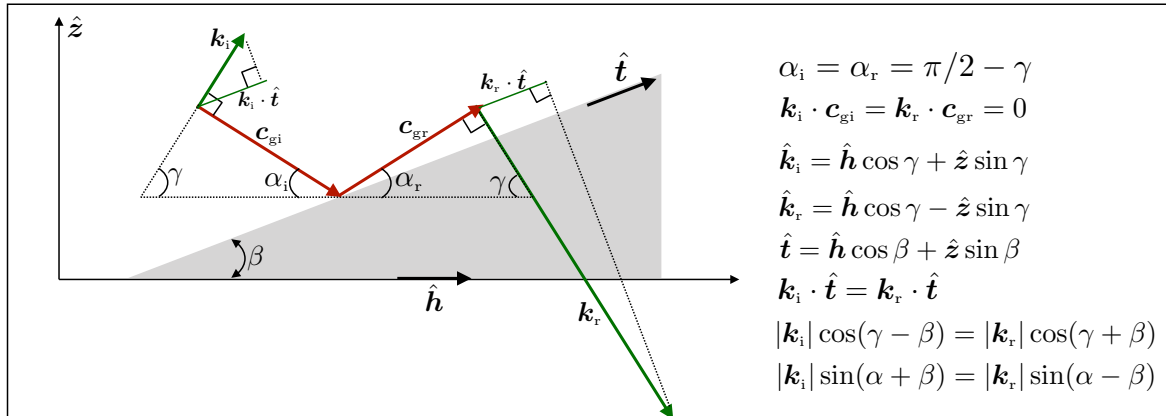


FIGURE 49.4: Depicting the reflection of an internal gravity wave packet from a planar inclined solid boundary that makes an angle, β , with the horizontal direction, $\hat{\mathbf{h}}$. The downward incident wave packet has a group velocity, \mathbf{c}_{gi} , and an upward carrier wavevector, \mathbf{k}_i with $\mathbf{c}_{gi} \cdot \mathbf{k}_i = 0$. The incident group velocity makes an angle, $\alpha_i = \pi/2 - \gamma$, with the horizontal, whereas \mathbf{k}_i makes an angle, γ , with the horizontal. The upward reflected wave packet has group velocity, \mathbf{c}_{gr} , and a downward carrier wavevector, \mathbf{k}_r , with $\mathbf{c}_{gr} \cdot \mathbf{k}_r = 0$. The angular frequency of the incident carrier wave is the same as the reflected wave, $\omega = N_R \cos \gamma$, which then means that \mathbf{k}_r makes an angle, γ , with the horizontal. Consequently, the reflected group velocity makes an angle $\alpha_r = \pi/2 - \gamma$, which is the same as the incident wave, $\alpha_r = \alpha_i$. The projection of the incident wavevector onto the surface tangent direction equals to that of the reflected wavevector, $\mathbf{k}_i \cdot \hat{\mathbf{t}} = \mathbf{k}_r \cdot \hat{\mathbf{t}}$, which means that $|\mathbf{k}_i| \cos(\gamma - \beta) = |\mathbf{k}_r| \cos(\gamma + \beta)$, or equivalently, $|\mathbf{k}_i| \sin(\alpha + \beta) = |\mathbf{k}_r| \sin(\alpha - \beta)$. For this example, the reflected wave has a larger wavenumber, $|\mathbf{k}_r|$, than the incident wave, $|\mathbf{k}_i|$, since $\alpha - \beta$ is smaller than $\alpha + \beta$. Indeed, for a packet with incident group velocity angle equal to the boundary angle, $\alpha = \beta$, then the reflected wave has an infinite wavenumber, which is a signal that the linear theory breaks down. To the right of the schematic we list the basic relations between the incident and reflected waves.

49.6.2 Specializing to internal gravity waves

Non-specular nature of internal gravity wave reflection

For internal gravity waves, the frequency condition in equation (49.107) means that the angle the wavevector makes with the horizontal, γ , remains unchanged upon reflection

$$\omega_i = \omega_r = N_R \cos \gamma. \quad (49.108)$$

This relation holds no matter what angle, β , the solid wall makes with the horizontal. This identity is depicted in Figure 49.4, where the angle α_i , which is the angle the incident packet makes with the horizontal, equals to the reflected angle, α_r . It follows that the angle that the wave packet makes relative to the solid surface is different for the incident and reflected waves. This property is referred to as *non-specular*. For the example of Figure 49.4, the reflected wave is more nearly parallel to the solid boundary than the incident wave. Reversing the sense for the wave packet provides an example of a reflected packet that is less aligned with the boundary than the incident packet.

Basic identities for internal gravity wave reflection

The frequency identity (49.108), the wavevector relation (49.107), along with some basic vector and trigonometric analysis, lead to the following identities

$$\hat{\mathbf{t}} = \hat{\mathbf{h}} \cos \beta + \hat{\mathbf{z}} \sin \beta \quad (49.109a)$$

$$\hat{\mathbf{k}}_i = \hat{\mathbf{h}} \cos \gamma + \hat{\mathbf{z}} \sin \gamma \quad (49.109b)$$

$$\hat{\mathbf{k}}_r = \hat{\mathbf{h}} \cos \gamma - \hat{\mathbf{z}} \sin \gamma \quad (49.109c)$$

$$\hat{\mathbf{k}}_i \cdot \hat{\mathbf{t}} = \cos \gamma \cos \beta + \sin \gamma \sin \beta = \cos(\gamma - \beta) = \sin(\alpha + \beta) \quad (49.109d)$$

$$\hat{\mathbf{k}}_r \cdot \hat{\mathbf{t}} = \cos \gamma \cos \beta - \sin \gamma \sin \beta = \cos(\gamma + \beta) = \sin(\alpha - \beta), \quad (49.109e)$$

where $\hat{\mathbf{h}}$ is a unit vector in the horizontal. With these results we find that the wavevector boundary condition, $\mathbf{k}_i \cdot \hat{\mathbf{t}} = \mathbf{k}_r \cdot \hat{\mathbf{t}}$, (equation (49.107)) leads to the equivalent relations

$$|\mathbf{k}_i| \cos(\gamma - \beta) = |\mathbf{k}_r| \cos(\gamma + \beta) \quad (49.110a)$$

$$|\mathbf{k}_i| \sin(\alpha + \beta) = |\mathbf{k}_r| \sin(\alpha - \beta). \quad (49.110b)$$

Critical reflection of internal gravity waves

The identity (49.110b) makes it clear that a most remarkable result holds when the incident packet hits the boundary at an angle that equals to the solid wall angle, $\alpha = \beta$. In this case the reflected wavenumber, $|\mathbf{k}_r|$, is unbounded, which means that the reflected waves have arbitrarily small wavelength. In a real fluid such small wavelength waves will eventually feel the impacts from viscous dissipation (e.g., Section 22.8), or they will break. In either case, such *critical reflection* of internal gravity waves provide a mechanism for much dissipative mixing in the ocean bottom.

49.6.3 Comments and further reading

Figure 49.4 provides an example where the reflected wave has a higher wavenumber than the incident wave. We can reverse all vectors to provide an example where an reflected wave has a smaller wavenumber than the incident wave. However, in a real fluid the reflections are not generally reversible since higher wavenumber waves are more subject to irreversible mixing, either through viscous dissipation or breaking. These, and other, wave-induced mixing processes for the ocean are reviewed in [MacKinnon et al. \(2013\)](#) and [MacKinnon et al. \(2017\)](#).

49.7 Gravity waves with vertically varying stratification

In Section 49.5 and 49.6 we assumed a constant background buoyancy frequency, N_R , thus enabling us to study plane internal gravity waves. However, for geophysical fluids it is more common for reference state stratification to be a function of vertical, $N_R(z)$. Indeed, such vertical dependence was considered in Sections 49.2, 49.3, and 49.4 when studying properties of the linear Boussinesq equations before specializing to plane waves. In this section we make use of the eikonal approximation, also known as the WKB approximation, to study internal gravity waves in the presence of $N_R(z)$. Our fundamental assumption is that the background reference density spatially varies over a vertical scale that is much larger than that of the waves.

49.7.1 The two length scale assumption

We introduced the WKB formalism in Section 44.9 for acoustic waves moving in a fluid with a spatially dependent equilibrium density. For internal gravity waves we consider the somewhat simpler case with vertical variations in the background density, rather than the fully three dimensional variations considered for acoustic waves. We thus introduce the length scale for vertical variations in the stably stratified background density field

$$\mathcal{L} \equiv |\partial_z \rho_R / \rho_R|^{-1} = (\rho_0 N_R^2 / (g \rho_R))^{-1}. \quad (49.111)$$

We assume that the internal gravity waves have a phase that has a vertical wavevector component that is a function of vertical position, $k_z = k_z(z)$, and that satisfies the following scaling

$$\mathcal{L} \gg |k_z|^{-1} \implies |k_z| \gg \rho_0 N_R^2 / (g \rho_R). \quad (49.112)$$

This assumption means that we are concerned with a vertical length scale of the waves, as measured by $|k_z(z)|^{-1}$, that is much smaller than the length scale, \mathcal{L} . Furthermore, we assume that the vertical variations of k_z^{-1} occur over the length scale \mathcal{L} , so that

$$|dk_z^{-1}/dz| = |k_z \mathcal{L}|^{-1} \ll 1. \quad (49.113)$$

In addition to having k_z now a function of vertical, we allow the wave amplitude to slowly vary with z . Writing $A(z)$ for that amplitude we assume, as for $k_z(z)$, that

$$|dA/dz| = |A/\mathcal{L}|, \quad (49.114)$$

which implies that

$$|A^{-1} d^2 A / dz^2| = \mathcal{L}^{-2} \ll k_z^2. \quad (49.115)$$

49.7.2 The wave equation and the WKB ansatz

The wave equation (49.38) for the vertical velocity holds for $N_R(z)$, so we focus our WKB attention on that equation, rewritten here in the form

$$(\partial_{tt} \nabla^2 + N_R^2 \nabla_z^2) w' = \partial_{tt} \partial_{zz} w' + (\partial_{tt} + N_R^2) \nabla_z^2 w' = 0. \quad (49.116)$$

Recall the plane wave ansatz (49.52) assumed for constant background density, which for the vertical velocity is given by

$$w'(\mathbf{x}, t) = \tilde{w} e^{i(\mathbf{k} \cdot \mathbf{x} - \omega t)} = (\tilde{w} e^{i k_z z}) e^{i(k_x x + k_y y - \omega t)} \quad \text{for constant } N_R. \quad (49.117)$$

For the case with $N_R(z)$ we generalize this ansatz to the form

$$w'(\mathbf{x}, t) = A(z) e^{i(k_x x + k_y y + \sigma(z) - \omega t)} \quad \text{for vertically varying } N_R(z), \quad (49.118)$$

with the real amplitude, $A(z)$, and real phase, $\sigma(z)$, each of which are to be determined. For the ansatz (49.118), we took a horizontal wavevector, $\mathbf{k}_h = k_x \hat{\mathbf{x}} + k_y \hat{\mathbf{y}}$, and angular frequency, ω , just as for the constant N_R waves. This form is motivated by the geometric optics results in Section 43.8. Namely, when following a ray, a wavevector component is constant if the background structure is constant in its corresponding direction, and the angular frequency is constant if the background state is time independent.

49.7.3 The wave equation with the WKB ansatz

Making use of the WKB wave ansatz (49.118) in the wave equation (49.116) leads to the following expressions

$$\partial_{zz} w'/w' = A^{-1} \partial_{zz} A - (\mathrm{d}\sigma/\mathrm{d}z)^2 + i [\mathrm{d}^2\sigma/\mathrm{d}z^2 + 2 A^{-1} (\mathrm{d}\sigma/\mathrm{d}z) (\mathrm{d}A/\mathrm{d}z)] \quad (49.119a)$$

$$\nabla_z^2 w'/w' = -|\mathbf{k}_h|^2 \quad (49.119b)$$

$$\partial_{tt} w'/w' = -\omega^2, \quad (49.119c)$$

which brings the wave equation (49.116) to the form

$$[\partial_{zz} + k_z^2(z)] w' = 0, \quad (49.120)$$

where we defined

$$k_z^2(z) = \frac{|\mathbf{k}_h|^2 (N_R^2(z) - \omega^2)}{\omega^2}. \quad (49.121)$$

This expression for $k_z(z)$ is identical to the case with a constant N_R (see equation (49.63)), only now it holds with $N_R(z)$ a function of vertical position. Equation (49.120) generalizes equation (49.66) that holds when N_R is a spatial constant.

49.7.4 WKB solution for the vertical velocity

Making use of equation (49.119a) for $\partial_{zz} w'$ in equation (49.121), and setting the real and imaginary parts to zero, leads to

$$k_z^2 - (\mathrm{d}\sigma/\mathrm{d}z)^2 = A^{-1} \mathrm{d}^2 A/\mathrm{d}z^2 \quad (49.122a)$$

$$\mathrm{d}^2\sigma/\mathrm{d}z^2 + 2 A^{-1} (\mathrm{d}\sigma/\mathrm{d}z) (\mathrm{d}A/\mathrm{d}z) = 0. \quad (49.122b)$$

Recall the amplitude scaling (49.115), which says that $A^{-1} \mathrm{d}^2 A/\mathrm{d}z^2 \ll k_z^2$. Equation (49.122a) thus leads to the vertical phase function

$$\mathrm{d}\sigma/\mathrm{d}z = k_z \implies \sigma(z) = \int_{z_0}^z k_z(z') \mathrm{d}z'. \quad (49.123)$$

The vertical position, z_0 , is generally ignored since it results only in an overall shift in the phase. Equation (49.122b) can be written in the form of a total derivative

$$\frac{\mathrm{d}}{\mathrm{d}z} \left[A \left(\frac{\mathrm{d}\sigma}{\mathrm{d}z} \right)^{1/2} \right] = 0, \quad (49.124)$$

which means that the wave amplitude is related to the vertical wavenumber via

$$A \propto (d\sigma/dz)^{-1/2} = |k_z|^{-1/2}. \quad (49.125)$$

Bringing the pieces together leads to the WKB solution for the vertical velocity component

$$w'(\mathbf{x}, t) = C |k_z|^{-1/2} e^{i(k_x x + k_y y + \sigma(z) - \omega t)}. \quad (49.126)$$

Assuming the constant C is real leads to

$$w'(\mathbf{x}, t) = C |k_z|^{-1/2} \cos(k_x x + k_y y + \sigma(z) - \omega t) \quad (49.127a)$$

$$k_z(z) = (|\mathbf{k}_h|/\omega) \sqrt{N_R^2(z) - \omega^2} \quad (49.127b)$$

$$\sigma(z) = \int^z k_z(z') dz' \quad (49.127c)$$

$$\omega = N_R(z) \cos \gamma(z) \quad (49.127d)$$

$$C [=] L^{1/2}/T. \quad (49.127e)$$

In equation (49.127b) for the vertical component to the wavevector, we exposed its z dependence along with that for the buoyancy frequency, $N_R(z)$. However, recall that the angular frequency, ω , and the horizontal wavevector, \mathbf{k}_h , are both spatially independent. Furthermore note that k_z becomes imaginary in regions where $\omega^2 > N_R^2(z)$. If a propagating wave enters such a region it becomes *evanescent*, which means that it exponentially decays. This behavior is exemplified by the wave guide discussed in Section 49.7.6.

49.7.5 Structure of an internal gravity wave

The WKB expressions (49.127a)-(49.127e) are sufficient to construct the full structure of an internal gravity wave moving through a region with non-constant background stratification. To do so requires making use of the linear relations from Section 49.4 in a manner similar to what we did in Section 49.5 for plane waves with N_R constant. We start with equation (49.16b) that relates buoyancy and vertical velocity via

$$\partial_t b' = -w' N_R^2. \quad (49.128)$$

Time integrating the vertical velocity in equation (49.127a) leads to the buoyancy field

$$b' = i C N_R^2 / (\omega |k_z|^{1/2}) e^{i(\mathbf{k}_h \cdot \mathbf{x} + \sigma(z) - \omega t)}, \quad (49.129)$$

where

$$\mathbf{k}_h \cdot \mathbf{x} = k_x x + k_y y. \quad (49.130)$$

For the horizontal velocity we use the non-divergence condition, $\nabla \cdot \mathbf{v}' = 0$ (Section 49.5.2), as well as the vanishing vertical component to the relative vorticity, $\partial_x v' = \partial_y u'$ (Section 49.5.4), to find

$$\mathbf{u}' = -\frac{C \mathbf{k}_h}{|2 k_z|^{1/2} |\mathbf{k}_h|^2} [(\partial_z \ln k_z) \sin(\mathbf{k}_h \cdot \mathbf{x} + \sigma(z) - \omega t) + 2 k_z \cos(\mathbf{k}_h \cdot \mathbf{x} + \sigma(z) - \omega t)]. \quad (49.131)$$

49.7.6 Wave packets within a wave guide

We here highlight a particularly special feature of internal gravity waves moving in a region with vertically varying stratification. These results follow from having the angular frequency remain constant within the dispersion relation, (49.127d). Again, the constancy of the angular frequency follows from our discussion of geometric optics in Section 43.8, with the angular frequency of a wave a space-time constant so long as the reference state is static. For the angular frequency to remain constant within a varying $N_R(z)$ requires the phase angle, γ , to change compensate. For example, if a wave packet moves from a region of large vertical stratification to a region with small stratification, then γ must get smaller in magnitude so to keep ω constant. At some point if N_R continues to get smaller then γ will vanish, $\gamma = 0$, which means that the waves only have a vertical wavenumber. So what happens beyond that point?

To answer this question recall equation (49.67) for the group velocity, which can be written in the form

$$\mathbf{c}_g = \frac{N_R k_z}{|\mathbf{k}|^3 |\mathbf{k}_h|} (k_z \mathbf{k}_h - |\mathbf{k}_h|^2 \hat{\mathbf{z}}) = \frac{N_R k_z}{|\mathbf{k}|^2} (\hat{\mathbf{k}}_h \sin \gamma - \hat{\mathbf{z}} \cos \gamma), \quad (49.132)$$

where $\hat{\mathbf{k}}_h = \mathbf{k}_h / |\mathbf{k}_h|$ is the unit vector pointing in the direction of the horizontal wavevector. As the wave becomes horizontal to compensate for the reduced $N_R(z)$, the group velocity vanishes, which we already noted by equation (49.71) for the group velocity magnitude. Yet the second form of equation (49.132) reveals that the horizontal component to the group velocity vanishes before the vertical component. Hence, as the wave packet approaches the region of weak stratification its trajectory forms a vertical cusp as the packet stalls. Since the packet cannot propagate into a region with $\omega^2 > N_R^2$, which is a region of evanescence, then the wave reflects back into the region where $\omega^2 < N_R^2$. If the propagation region with $\omega^2 < N_R^2$ sits between two regions with weak stratification with $\omega^2 > N_R^2$, then the bounded relatively high stratification region forms a *wave guide* for the internal gravity waves. We depict an idealized example of a wave guide in Figure 49.5.

We can compute an analytic expression for the wave packet trajectory (i.e., a ray) as it rises to a *turning level*, at $z = z_t$, defined as the level where $N_R(z = z_t) = \omega$. We do so by taking a Taylor series for the squared buoyancy frequency for points close to the turning level

$$N_R^2(z) \approx N_R^2(z_t) + (dN_R/dz)(z - z_t) = \omega^2 - |dN_R/dz|(z - z_t) = \omega^2 + |dN_R/dz|(z_t - z), \quad (49.133)$$

where we note that N_R^2 is a decreasing function as z increases towards z_t , which means that $dN_R^2/dz = -|dN_R^2/dz|$. Assuming the packet is moving in the x - z plane, we obtain the ray equation from the group velocity (49.132) and the dispersion relation (49.127b)

$$\frac{dz}{dx} = -\frac{|\mathbf{k}_h|}{k_z} = -\frac{\omega}{\sqrt{N_R^2 - \omega^2}} = -\frac{\omega}{\sqrt{|dN_R^2/dz|(z_t - z)}}. \quad (49.134)$$

We integrate along the ray as the packet moves from a point (x, z) to the turning level at (x_t, z_t) (see Figure 49.5), which yields the expression for the ray trajectory

$$(z_t - z)^{3/2} = \frac{(3\omega/2)(x_t - x)}{\sqrt{|dN_R^2/dz|}} \implies z_t - z = \left[\frac{(3\omega/2)(x_t - x)}{\sqrt{|dN_R^2/dz|}} \right]^{2/3}. \quad (49.135)$$

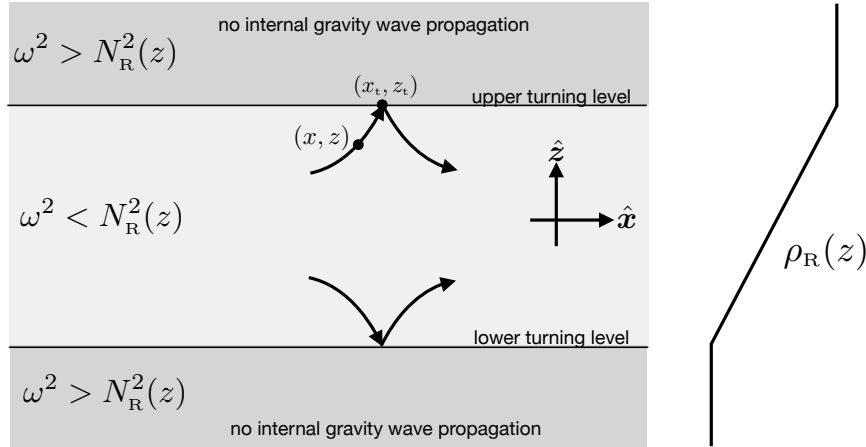


FIGURE 49.5: A waveguide for internal gravity waves, here depicted by two low stratification regions bounding a higher stratification region. The density profile on the right provides an idealized realization of such a guide. The levels where $N_R = \omega$ are referred to as *turning levels*. We depict sample rays approaching and leaving the turning levels, with the rays computed from the group velocity and dispersion relation. For example, a ray approaching the upper turning is computed from (x, t) to (x_t, z_t) , with the cusp-like trajectory given by equation (49.135).

49.7.7 Comments and further study

There remains ongoing research to understand details of what happens to internal gravity waves when they reach a turning level. For an ocean application, concerning how gravity waves interact with the upper ocean boundary layer, see [Shakespeare et al. \(2021\)](#).

49.8 Vertical normal modes

We here look for gravity waves in an ocean domain that is bounded below by a flat bottom at $z = -H$ and free surface at $z = \eta$. Since the bottom is flat we assume the waves are traveling only in the horizontal, in which we consider an ansatz of the form

$$w' = W(z) e^{i(k_x x + k_y y - \omega t)}. \quad (49.136)$$

Plugging this ansatz into the wave equation (49.38) for the vertical velocity leads to the eigenvalue problem for the vertical structure function

$$\left[\frac{d^2}{dz^2} + \frac{|\mathbf{k}_h|^2 (N_R^2 - \omega^2)}{\omega^2} \right] W = 0 \quad (49.137a)$$

$$W = 0 \quad \text{at } z = -H \quad (49.137b)$$

$$\omega^2 dW/dz = g |\mathbf{k}_h|^2 W \quad \text{at } z = 0, \quad (49.137c)$$

where we used the flat bottom kinematic boundary condition at $z = -H$, and the upper ocean boundary condition (49.51) for equation (49.137c).

INCOMPLETE.

49.9 Rotating linear Boussinesq ocean

We here establish some general properties of the rotating linear Boussinesq ocean described by equations (49.16a)-(49.16c) posed on an f -plane

$$\partial_t \mathbf{u}' + f \hat{\mathbf{z}} \times \mathbf{u}' = -\nabla_z \varphi' \quad \text{horizontal velocity equation} \quad (49.138a)$$

$$\partial_t w' = -\partial_z \varphi' + b' \quad \text{vertical velocity equation} \quad (49.138b)$$

$$\partial_t b' = -w' N_R^2 \quad \text{buoyancy equation} \quad (49.138c)$$

$$\nabla \cdot \mathbf{v}' = 0 \quad \text{continuity equation.} \quad (49.138d)$$

Since we are only concerned with f -plane motion, Rossby waves are not included in the physical system. As we see, the discussion reveals many forced oscillator equations satisfied by the linear fields, thus providing insight into the workings of the inertia-gravity waves discussed in Section 49.10. These oscillator equations also prove of use when developing the polarization relations for the plane wave in Section 49.10.4.

49.9.1 Forced oscillator equation for horizontal velocity

Taking the time derivative of the horizontal velocity equation (49.138a) and back-substituting in the horizontal velocity tendency leads to

$$(\partial_{tt} + f^2) \mathbf{u}' = f \hat{\mathbf{z}} \times \nabla_z \varphi' - \partial_t \nabla_z \varphi'. \quad (49.139)$$

This equation takes the form of a forced harmonic oscillator with natural angular frequency, f , and with forcing from the horizontal pressure gradient. Evidently, if we know the horizontal pressure gradient then that is sufficient to determine the horizontal velocity. Note that this is the same forced oscillator equation as (46.15) found for inertial oscillations in a homogeneous fluid.

49.9.2 Vertical component to the relative vorticity

Evolution of the vertical component to the relative vorticity is derived by taking the curl of the horizontal velocity equation (49.138a) and projecting onto the vertical, in which we find

$$\partial_t \zeta' = f \partial_z w'. \quad (49.140)$$

Hence, relative vorticity evolves when there is vertical stretching in the presence of planetary rotation. This property accords with our more general understanding of vortex mechanics studied in Section 37.7.3. It also reduces to the non-rotating case, in which ζ' is static since $f = 0$ (Section 49.4.1). Finally, we can derive a forced oscillator equation for relative vorticity by taking the curl of the velocity equation (49.139) to find

$$(\partial_{tt} + f^2) \zeta' = f \nabla_z^2 \varphi'. \quad (49.141)$$

49.9.3 Forced oscillator equation and free wave equation for vertical velocity

Taking the divergence of the horizontal velocity equation (49.138a), and then using the continuity equation (49.138d), leads to

$$\partial_t (\nabla_z \cdot \mathbf{u}') - f \zeta' = -\nabla_z^2 \varphi' \implies \partial_{tz} w' + f \zeta' = \nabla_z^2 \varphi'. \quad (49.142)$$

Now taking a time derivative and using the relative vorticity stretching equation (49.140) leads to the forced inertial oscillator equation for the vertical derivative of the vertical velocity

$$(\partial_{tt} + f^2)\partial_z w' = \partial_t \nabla_z^2 \varphi'. \quad (49.143)$$

This equation says that when the horizontal flow has a nonzero divergence in the presence of rotation, then it experiences a forced inertial oscillation. Notice that if the pressure is constant in the horizontal direction, then the oscillations are unforced inertial oscillations.

We can derive another forced oscillator equation, this one for w' . To do so, take the time derivative of the vertical velocity equation (49.138b) and then use the linearized buoyancy equation (49.138c), which yields the forced buoyancy oscillator equation

$$\partial_{tt} w' = -\partial_{tz} \varphi' + \partial_t b' \implies (\partial_{tt} + N_R^2) w' = -\partial_{tz} \varphi'. \quad (49.144)$$

We already encountered this equation in Section (49.3) when studying buoyancy oscillations. It says that vertical motion in the presence of a buoyancy field leads to forced buoyancy oscillations. Furthermore, if the pressure is constant in the vertical then the buoyancy oscillations are unforced.

Just like in the non-rotating case in Section 49.4.2, we can derive a free wave equation for w' by taking the vertical derivative of equation (49.143), the horizontal Laplacian of equation (49.144), and then adding to cancel the pressure contribution

$$(\partial_{tt} \nabla^2 + N_R^2 \nabla_z^2 + f^2 \partial_{zz}) w' = 0. \quad (49.145)$$

This is the fundamental wave equation for inertia-gravity waves. The build-up to this equation offers signatures of the forces acting within these waves. Namely, $\partial_z w'$ exhibits forced inertial oscillations with natural angular frequency f (equation (49.143)). Such oscillations are associated, through continuity, with horizontally diverging flow that feels the Coriolis acceleration. Likewise, w' exhibits forced buoyancy oscillations with natural angular frequency N_R (equation (49.144)). These oscillations are associated with vertical motion that feels the effects from the background vertical stratification and associated buoyancy. By eliminating the pressure forcing the two complementary modes of oscillation, we reveal a free wave equation for w' . The free wave equation exposes the roles for Coriolis and buoyancy accelerations, yet hides the intermediate role of pressure accelerations that force the oscillations.

49.9.4 Forced oscillator equation for buoyancy

Since the flow is non-divergent at each time instant, we know that

$$\nabla \cdot \partial_t \mathbf{v}' = \partial_t \nabla \cdot \mathbf{v}' = 0. \quad (49.146)$$

Hence, taking the divergence of the horizontal velocity equation (49.138a) and adding to the vertical derivative of the vertical velocity equation (49.138b) leads to the pressure equation

$$-\nabla^2 \varphi' = -(f \zeta' + \partial_z b'). \quad (49.147)$$

Evidently, a source for the dynamic pressure arises from vertical buoyancy gradients along with relative vorticity. We characterized the physics of these sources in Section 26.3.3 when studying the pressure equation in a Boussinesq ocean.

Taking the time derivative of the pressure equation (49.147) and using the stretching relative

vorticity equation (49.140) leads to

$$f^2 \partial_z w' = \partial_t \nabla^2 \varphi' - \partial_{zt} b'. \quad (49.148)$$

One more time derivative and use of the vertical velocity equation (49.138b) yields the forced inertial oscillator equation for the vertical derivative of buoyancy

$$(\partial_{tt} + f^2) \partial_z b' = (\partial_{tt} \nabla^2 + f^2 \partial_{zz}) \varphi'. \quad (49.149)$$

49.9.5 An equation for pressure

We now consider an equation for pressure that is based on taking the time derivative of the forced inertial oscillator equation (49.149) for $\partial_z b'$. Focusing on the left hand side we find

$$\partial_t [(\partial_{tt} + f^2) \partial_z b'] = \partial_z [(\partial_{tt} + f^2) \partial_t b'] \quad \text{swap } \partial_z \text{ and } \partial_t \quad (49.150a)$$

$$= -\partial_z [(\partial_{tt} + f^2) w' N_R^2] \quad \text{equation (49.138c)} \quad (49.150b)$$

$$= -\partial_z N_R^2 (\partial_{tt} + f^2) w' - N_R^2 (\partial_{tt} + f^2) \partial_z w' \quad \text{product rule} \quad (49.150c)$$

$$= -\partial_z N_R^2 (\partial_{tt} + f^2) w' - N_R^2 \partial_t \nabla_z^2 \varphi' \quad \text{equation (49.143)} \quad (49.150d)$$

Combining with the time derivative on the right hand side of equation (49.149) leads to the pressure equation

$$\partial_t [(\partial_{tt} \nabla^2 + f^2 \partial_{zz} + N_R^2 \nabla_z^2) \varphi'] = -\partial_z N_R^2 (\partial_{tt} + f^2) w'. \quad (49.151)$$

In the special case of a constant background stratification we find

$$\partial_t [(\partial_{tt} \nabla^2 + f^2 \partial_{zz} + N_R^2 \nabla_z^2) \varphi'] = 0 \quad \text{if } \partial_z N_R = 0, \quad (49.152)$$

which is nearly the same as the free wave equation (49.145) for w' .¹⁰

49.9.6 Potential vorticity

Although inertia-gravity waves modify relative vorticity, we here show they retain the linearized potential vorticity unchanged. For this purpose, use the relative vorticity equation (49.140) and the buoyancy equation (49.138c) to find¹¹

$$\partial_t [\zeta' + f \partial_z (b'/N_R^2)] = 0 \implies \partial_t Q' = 0 \quad \text{with } Q' = \zeta' + f \partial_z (b'/N_R^2). \quad (49.153)$$

Hence, an inertia-gravity wave does not alter the potential vorticity, at least to linear order. This means that any vortical portion of the flow, such as a background static geostrophic flow, can exist without either the waves or the background flow affecting one another. Furthermore, we observe that the linearized potential vorticity (49.153) concurs with the relative vorticity and buoyancy contribution to the quasi-geostrophic potential vorticity (42.54). In the present case, however, we are concerned with the f -plane rather than the β -plane considered for quasi-geostrophy. Another difference is that the potential vorticity (49.153) is locally static, $\partial_t Q' = 0$, whereas the quasi-geostrophic potential vorticity remains constant when following the geostrophic flow.

¹⁰See Lecture 11 in [Pedlosky \(2003\)](#) for connection between the pressure equation (49.152) to the potential vorticity equation in the case of constant N_R .

¹¹Note that in this chapter we define potential vorticity with dimensions of inverse time, T^{-1} , as for the continuously stratified quasi-geostrophic potential vorticity in Section 42.3.7. In contrast, in our study of shallow water waves in Chapter 48, we defined Q' in Section 48.3.3 to have dimensions of $L^{-1} T^{-1}$.

Potential vorticity and layer thickness

For yet another way to interpret the linear potential vorticity (49.153), write the buoyancy fluctuation in terms of the particle displacement as in equation (49.85)

$$\delta z = -b'/N_R^2, \quad (49.154)$$

which brings the linearized potential vorticity to the form

$$Q' = \zeta' + f \partial_z(b'/N_R^2) = \zeta' - f \partial_z(\delta z). \quad (49.155)$$

Since Q' is a static field, the presence of $\partial_z(\delta z)$ leads in a rotating reference frame to a compensating relative vorticity. In an internal gravity wave, δz measures the periodic compression and expansion of the vertical distance between constant buoyancy surfaces. This layer interpretation of potential vorticity accords with our understanding of potential vorticity from shallow water theory in Section 36.3, as well as potential vorticity in isopycnal/buoyancy coordinate models in Section 59.3.

Connection to pressure and buoyancy

The various harmonic oscillator equations established thus far in this section are not satisfied by Q' since it is a static field. However, we can derive an expression for Q' in terms of pressure and buoyancy through the following manipulations

$$(\partial_{tt} + f^2) Q' = f^2 Q' \quad (49.156a)$$

$$= (\partial_{tt} + f^2)[\zeta' + f \partial_z(b'/N_R^2)] \quad (49.156b)$$

$$= f \nabla_z^2 \varphi' + N_R^{-2} (\partial_{tt} \nabla^2 + f^2 \partial_{zz}) \varphi' + \partial_z(N_R^{-2}) (\partial_{tt} + f^2) b', \quad (49.156c)$$

where equation (49.156a) follows since $\partial_t Q' = 0$, equation (49.156b) used the definition of Q' from equation (49.153), and equation (49.156c) used the forced harmonic oscillator equations (49.141) and (49.143). Multiplying by N_R^2 leads to

$$f N_R^2 Q' = (\partial_{tt} \nabla^2 + N_R^2 \nabla_z^2 + f^2 \partial_{zz}) \varphi' + N_R^2 \partial_z(N_R^{-2}) (\partial_{tt} + f^2) b'. \quad (49.157)$$

Decomposing vortical and divergent motions for constant vertical stratification

In the special case of a constant N_R , we see that the potential vorticity can be written entirely in terms of the pressure

$$f N_R^2 Q' = (\partial_{tt} \nabla^2 + N_R^2 \nabla_z^2 + f^2 \partial_{zz}) \varphi' \quad \text{if } \partial_z N_R = 0. \quad (49.158)$$

Evidently, for constant background stratification the static nature of the potential vorticity is equivalent to the wave equation (49.152)

$$\partial_t Q' = 0 \implies \partial_t[(\partial_{tt} \nabla^2 + N_R^2 \nabla_z^2 + f^2 \partial_{zz}) \varphi'] = 0 \quad \text{if } \partial_z N_R = 0. \quad (49.159)$$

We found the same connection between the potential vorticity equation and the wave equation in Section 48.7.2 when studying shallow water inertia-gravity waves (see equation (48.113)). As for the shallow water, we conclude that for the case of constant stratification the vortical motions associated with f -plane geostrophy (hence with zero vertical velocity) are decoupled from the divergent motions associated with inertia-gravity waves. Hence, we can describe the fluid motion by a static potential vorticity whose non-zero value is set by f -plane geostrophic (vortical) flow,

plus a zero potential vorticity flow arising from inertia-gravity waves. In the linear theory, and for constant vertical stratification, there is no exchange of potential vorticity between the vortical flow and divergent waves. As a practical matter, one often has knowledge of the static potential vorticity arising from the geostrophic motion. We can obtain the associated geostrophic pressure field from inverting the elliptic operator in equation (49.158).

49.10 Free inertia-gravity waves

In this section we study the free *inertia-gravity* waves that arise under small amplitude fluctuations in a continuously stratified fluid on an *f*-plane. To enable plane wave solutions we assume the stratification is constant.

49.10.1 Dispersion relation

Returning to the wave equation (49.145) for w'

$$(\partial_{tt} \nabla^2 + N_R^2 \nabla_z^2 + f^2 \partial_{zz}) w' = 0, \quad (49.160)$$

we take the plane wave ansatz

$$w' = \tilde{w} e^{i(\mathbf{k} \cdot \mathbf{x} - \omega t)} \quad (49.161)$$

which readily leads to the dispersion relation

$$\omega^2 = \frac{N_R^2 |\mathbf{k}_h|^2 + f^2 k_z^2}{|\mathbf{k}|^2}. \quad (49.162)$$

Just like the case of non-rotating internal gravity waves studied in Section 49.5, the dispersion relation is only a function of the wave direction and is independent of its length. To manifest this property we introduce the angle, γ , between the wavevector and the horizontal plane

$$\omega^2 = N_R^2 \cos^2 \gamma + f^2 \sin^2 \gamma = (N_R^2 - f^2) \cos^2 \gamma + f^2 = N_R^2 - (N_R^2 - f^2) \sin^2 \gamma. \quad (49.163)$$

Clearly the dispersion relation reduces to that for non-rotating gravity waves when $f = 0$ given by equation (49.61).

In stratified geophysical fluids we typically find the squared buoyancy frequency is larger than the squared Coriolis frequency, $N_R^2 > f^2$. In this case the plane inertia-gravity wave angular frequency is bounded by

$$f^2 \leq \omega^2 \leq N_R^2 \quad \text{when } N_R^2 > f^2. \quad (49.164)$$

Indeed, in many cases we have $f^2 \ll N_R^2$. Even so, there are weakly stratified regions with $N_R^2 < f^2$, in which case the opposite frequency range holds whereby $N_R^2 \leq \omega^2 \leq f^2$. Indeed, when $N_R = 0$ then the inertia-gravity waves reduce to the *inertial waves* studied in Section 46.2, which are waves appearing in a rotating fluid that has homogeneous density.

Inertia-gravity waves typically have horizontal scales much larger than vertical, in which case $|\mathbf{k}_h|^2 \ll k_z^2$. The reason for this anisotropy is related to the processes forcing the waves. In particular, for the ocean the forcing by winds occurs with large horizontal patterns characteristic of the atmosphere. With $|\mathbf{k}_h|^2 \ll k_z^2$, the phase velocity for the waves is nearly vertical so that $\gamma \approx \pi/2$. We thus find that the dominant forcing frequency for inertia-gravity waves is near that of the Coriolis frequency

$$\omega^2 = f^2 + (N_R^2 - f^2) \cos^2 \gamma \approx f^2. \quad (49.165)$$

Such waves are referred to as *near inertial waves*.

49.10.2 Force balance in an inertia-gravity wave

In Section 49.5.9 we studied the buoyancy forces acting on a fluid particle that moves transverse to the constant phase surfaces in a non-rotating gravity wave. We pursue the same analysis here with the added feature of rotation. This analysis offers a force balance interpretation of the dispersion relation (49.163).

For a phase surface that has a nonzero slope in the vertical, the displaced fluid particle moving parallel to the phase surface feels the effects from buoyancy forces. Likewise, when including the Coriolis acceleration on an f -plane, a horizontal displacement of a fluid particle induces a Coriolis acceleration. Given the nature of the Coriolis acceleration, the particle turns in the horizontal. Hence, a fluid particle moving in the direction of constant phase surfaces feels the effects of the buoyant acceleration when it moves vertically plus the Coriolis acceleration when it moves horizontally. For small amplitude motion, these forces give rise to simple harmonic oscillator motion, and they represent the essential features of an an inertia-gravity wave. We here detail the mechanics of this motion.

Particle displacements and Coriolis acceleration

Following the approach in Section 49.5.9, we make use of the fluid particle displacement field, $\xi(\mathbf{x}, t)$, whose time derivative yields the velocity of the fluid particle in a small amplitude wave

$$\partial_t \xi(\mathbf{x}, t) = \mathbf{v}'(\mathbf{x}, t). \quad (49.166)$$

As discussed above, the Coriolis and buoyancy effects act in a complementary manner. To understand the role of the Coriolis acceleration, consider an inertial particle that satisfies the equation of motion

$$\partial_t \mathbf{v}' + f \hat{\mathbf{z}} \times \mathbf{v}' = 0 \implies \partial_t (\partial_t \xi + f \hat{\mathbf{z}} \times \xi) = 0. \quad (49.167)$$

Hence, in terms of particle displacements, the inertial particle satisfies

$$\partial_t \xi + f \hat{\mathbf{z}} \times \xi = \text{constant}, \quad (49.168)$$

with the constant determined by initial conditions, which can be set to zero without loss of generality. Evidently, an inertial particle in a rotating reference frame, displaced in a direction perpendicular to the rotation axis (horizontal direction here), induces a time tendency for motion in the orthogonal horizontal direction

$$\partial_t \xi = -f \hat{\mathbf{z}} \times \xi. \quad (49.169)$$

Particle displacements with buoyancy and Coriolis

The linearized equation of motion that includes the effects from pressure, Coriolis, and buoyancy, is given by

$$\partial_t \mathbf{v}' + f \hat{\mathbf{z}} \times \mathbf{v}' = -\nabla \varphi' + b' \hat{\mathbf{z}}. \quad (49.170)$$

Focusing on a fluid particle in the presence of a transverse wave, we project the equation of motion onto the transverse direction, $\hat{\mathbf{t}}$, with this direction static for a plane wave. Doing so eliminates the pressure gradient since it is constant along a surface of constant phase, so that fluid particle motion in the transverse direction satisfies

$$\partial_t (\hat{\mathbf{t}} \cdot \mathbf{v}') + f \hat{\mathbf{t}} \cdot (\hat{\mathbf{z}} \times \mathbf{v}') = b' \hat{\mathbf{t}} \cdot \hat{\mathbf{z}}. \quad (49.171)$$

Introducing the particle displacement yields

$$\hat{\mathbf{t}} \cdot \mathbf{v}' = \partial_t(\hat{\mathbf{t}} \cdot \boldsymbol{\xi}) = \partial_t \delta l \quad (49.172a)$$

$$b' \hat{\mathbf{t}} \cdot \hat{\mathbf{z}} = -N_{\text{R}}^2 \delta z \cos \gamma = -N_{\text{R}}^2 \delta l \cos^2 \gamma, \quad (49.172b)$$

with the buoyancy expression in equation (49.172b) following from equation (49.85) derived when studying internal gravity waves without rotation. For the Coriolis acceleration we make use of equation (49.169) to write

$$f \hat{\mathbf{t}} \cdot (\hat{\mathbf{z}} \times \mathbf{v}') = f \mathbf{v}' \cdot (\hat{\mathbf{t}} \times \hat{\mathbf{z}}) \quad (49.173a)$$

$$= f \partial_t \boldsymbol{\xi} \cdot (\hat{\mathbf{t}} \times \hat{\mathbf{z}}) \quad (49.173b)$$

$$= -f^2 (\hat{\mathbf{z}} \times \boldsymbol{\xi}) \cdot (\hat{\mathbf{t}} \times \hat{\mathbf{z}}) \quad (49.173c)$$

$$= f^2 \delta l \sin^2 \gamma, \quad (49.173d)$$

where we use the vector identity (1.41d) and set $\hat{\mathbf{z}} \cdot \hat{\mathbf{t}} = \sin \gamma$.

Bringing the above results together leads to the equation of motion for particle displacements

$$(\partial_{tt} + N_{\text{R}}^2 \cos^2 \gamma + f^2 \sin^2 \gamma) \delta l = 0. \quad (49.174)$$

This is an equation for a simple harmonic oscillator with angular frequency

$$\omega^2 = N_{\text{R}}^2 \cos^2 \gamma + f^2 \sin^2 \gamma, \quad (49.175)$$

which is the dispersion relation derived in Section 49.10.1 through use of the plane wave ansatz.

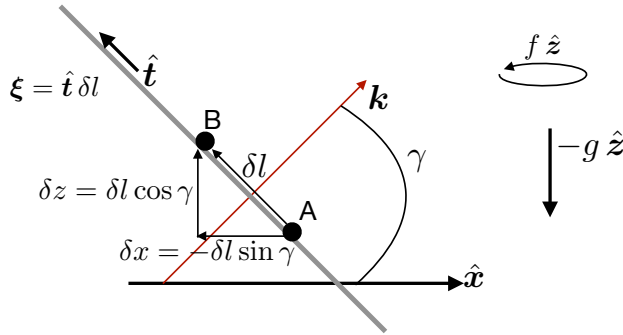


FIGURE 49.6: An extension of Figure 49.3 to now allow for a fluid particle to feel both buoyancy and rotation as it moves in the direction transverse to the plane waves. The wavevector makes an angle γ with the horizontal. We show a view in the x - z plane with the particle displacement vector $\boldsymbol{\xi}(\mathbf{x}, t) = \delta l \hat{\mathbf{t}}$. The local transverse unit vector, $\hat{\mathbf{t}}$, points in a direction that is orthogonal to the wavevector, \mathbf{k} . The displacement of the fluid particle from point A and point B occurs over a distance, δl , with a corresponding change in vertical position given by $\delta z = \delta l \cos \gamma$ and horizontal position changes by $\delta x = -\delta l \sin \gamma$. This displacement causes the fluid particle to experience accelerations from both buoyancy and Coriolis.

49.10.3 Group velocity

The wavevector gradient of the dispersion relation (49.175) yields the group velocity for inertia-gravity waves

$$c_g = \frac{(N_{\text{R}}^2 - f^2) k_z}{|k|^4 \omega} (k_z \mathbf{k}_h - |\mathbf{k}_h|^2 \hat{\mathbf{z}}). \quad (49.176)$$

As for non-rotating internal gravity waves in equation (49.67), we find that the group velocity is perpendicular to the phase velocity ($\mathbf{c}_p = \hat{\mathbf{k}}\omega/|\mathbf{k}|$)

$$\mathbf{c}_g \cdot \mathbf{c}_p = 0. \quad (49.177)$$

We also find that

$$(\mathbf{c}_g \cdot \hat{\mathbf{z}})(\mathbf{c}_p \cdot \hat{\mathbf{z}}) = -\frac{(N_R^2 - f^2)k_z^2 |\mathbf{k}_h|^2}{|\mathbf{k}|^4 \omega}, \quad (49.178)$$

so that

$$(\mathbf{c}_g \cdot \hat{\mathbf{z}})(\mathbf{c}_p \cdot \hat{\mathbf{z}}) < 0 \quad \text{if } f^2 < N_R^2 \quad (49.179a)$$

$$(\mathbf{c}_g \cdot \hat{\mathbf{z}})(\mathbf{c}_p \cdot \hat{\mathbf{z}}) > 0 \quad \text{if } f^2 > N_R^2. \quad (49.179b)$$

The usual case for the atmosphere and ocean finds $f^2 < N_R^2$, so that if the group velocity is upward then the phase velocity is downward, and vice versa. However, if $f^2 > N_R^2$, as for inertial waves where $N_R = 0$ (Section 46.2, Exercise 49.3), or more generally for inertia-gravity waves in very weak vertical stratification, then the group and phase velocities have the same orientation with respect to the vertical.

49.10.4 Polarization relations for a plane wave

We now make use of the plane wave ansatz (49.52) to derive the polarization relations that determine the structure of a plane wave. For this purpose we make use of the various forced harmonic oscillator equations from Section 49.9 to express the velocity and buoyancy in terms of a real pressure amplitude, $\tilde{\varphi}$, where pressure is assumed to take the form

$$\varphi' = \tilde{\varphi} \cos(\mathbf{k} \cdot \mathbf{x} - \omega t). \quad (49.180)$$

We also make use of the dispersion relation (49.163) to write the polarization relations in a variety of forms. Each of the expressions below reduce to the non-rotating gravity wave polarization relations (49.76a)-(49.76b) derived in Section 49.5.8.

Buoyancy

Buoyancy satisfies the forced oscillator equation (49.149), which for a plane wave takes the form

$$(-\omega^2 + f^2) i k_z \tilde{b} = (\omega^2 |\mathbf{k}|^2 - f^2 k_z^2) \tilde{\varphi}. \quad (49.181)$$

Various forms of the dispersion relation given in Section 49.10.1 lead to the identities

$$\omega^2 |\mathbf{k}|^2 - f^2 k_z^2 = N_R^2 |\mathbf{k}_h|^2 \quad (49.182a)$$

$$\omega^2 - f^2 = (N_R^2 - f^2) |\mathbf{k}_h|^2 / |\mathbf{k}|^2 = (N_R^2 - \omega^2) |\mathbf{k}_h|^2 / k_z^2 \quad (49.182b)$$

so that the ratio of amplitudes can be written in the equivalent manners

$$\tilde{b}/\tilde{\varphi} = \frac{i(\omega^2 |\mathbf{k}|^2 - f^2 k_z^2)}{k_z (\omega^2 - f^2)} = \frac{i N_R^2 |\mathbf{k}_h|^2}{k_z (\omega^2 - f^2)} = \frac{i N_R^2 |\mathbf{k}|^2}{k_z (N_R^2 - f^2)} = \frac{i N_R^2 k_z}{N_R^2 - \omega^2}, \quad (49.183)$$

which means that the real buoyancy wave is given by

$$b'/\tilde{\varphi} = -\frac{N_R^2 |\mathbf{k}_h|^2 \sin(\mathbf{k} \cdot \mathbf{x} - \omega t)}{k_z (\omega^2 - f^2)} = -\frac{N_R^2 k_z \sin(\mathbf{k} \cdot \mathbf{x} - \omega t)}{N_R^2 - \omega^2}. \quad (49.184)$$

Vertical velocity component

From Section 49.9.3 we know that the vertical velocity satisfies the two forced oscillator equations (49.143) and (49.144)

$$(\partial_{tt} + f^2)\partial_z w' = \partial_t \nabla_z^2 \varphi' \quad \text{and} \quad (\partial_{tt} + N_R^2)w' = -\partial_{tz}\varphi'. \quad (49.185)$$

For a plane wave these equations lead to

$$\tilde{w}/\tilde{\varphi} = -\frac{\omega |\mathbf{k}_h|^2}{k_z(\omega^2 - f^2)} = -\frac{\omega k_z}{N_R^2 - \omega^2} = -\frac{\omega |\mathbf{k}|^2}{k_z(N_R^2 - f^2)}, \quad (49.186)$$

so that the real wave takes on the form

$$w'/\tilde{\varphi} = -\frac{\omega |\mathbf{k}_h|^2 \cos(\mathbf{k} \cdot \mathbf{x} - \omega t)}{k_z(\omega^2 - f^2)} = -\frac{\omega k_z \cos(\mathbf{k} \cdot \mathbf{x} - \omega t)}{N_R^2 - \omega^2} = -\frac{\omega |\mathbf{k}|^2 \cos(\mathbf{k} \cdot \mathbf{x} - \omega t)}{k_z(N_R^2 - f^2)}. \quad (49.187)$$

Horizontal velocity

Equation (49.139) for the horizontal velocity leads to the relation for the plane wave amplitude

$$\tilde{\mathbf{u}}/\tilde{\varphi} = \frac{\omega \mathbf{k}_h - i f (\hat{\mathbf{z}} \times \mathbf{k}_h)}{\omega^2 - f^2}, \quad (49.188)$$

so that the real plane wave polarization relation is given by

$$\mathbf{u}/\tilde{\varphi} = \frac{\omega \mathbf{k}_h \cos(\mathbf{k} \cdot \mathbf{x} - \omega t) + f (\hat{\mathbf{z}} \times \mathbf{k}_h) \sin(\mathbf{k} \cdot \mathbf{x} - \omega t)}{\omega^2 - f^2}, \quad (49.189)$$

which compares directly to the shallow water polarization relation (48.133a).

49.10.5 Energetics of a plane inertia-gravity wave

We here extend the energetic analysis of plane internal gravity waves in Section 49.5.10 to the case of plane inertia-gravity waves, making use of the polarization relations from Section 49.10.4. Each of the expressions found here reduce to the non-rotating internal gravity waves when taking $f = 0$.

Instantaneous energetics

The plane inertia-gravity wave has squared velocity components

$$\mathbf{u}' \cdot \mathbf{u}'/\tilde{\varphi}^2 = \frac{\omega^2 |\mathbf{k}_h|^2 \cos^2(\mathbf{k} \cdot \mathbf{x} - \omega t) + f^2 |\mathbf{k}_h|^2 \sin^2(\mathbf{k} \cdot \mathbf{x} - \omega t)}{(\omega^2 - f^2)^2} \quad (49.190a)$$

$$(w')^2/\tilde{\varphi}^2 = \frac{\omega^2 |\mathbf{k}_h|^4 \cos^2(\mathbf{k} \cdot \mathbf{x} - \omega t)}{k_z^2 (\omega^2 - f^2)^2}, \quad (49.190b)$$

so that the wave's kinetic energy is

$$\mathcal{K}' = \frac{\tilde{\varphi}^2 |\mathbf{k}_h|^2}{2(\omega^2 - f^2)^2} [\omega^2 (1 + |\mathbf{k}_h|^2/k_z^2) \cos^2(\mathbf{k} \cdot \mathbf{x} - \omega t) + f^2 \sin^2(\mathbf{k} \cdot \mathbf{x} - \omega t)], \quad (49.191)$$

which can be written in the more tidy form through use of the dispersion relation

$$\mathcal{K}' = \frac{\tilde{\varphi}^2 |\mathbf{k}_h|^2 [f^2 + N_R^2 \cot^2 \gamma \cos^2(\mathbf{k} \cdot \mathbf{x} - \omega t)]}{2 (\omega^2 - f^2)^2}, \quad (49.192)$$

with $\cot \gamma = |\mathbf{k}_h|/k_z$. Likewise, the available potential energy is given by

$$\mathcal{A}' = \frac{\tilde{\varphi}^2 N_R^2 |\mathbf{k}_h|^2 \cot^2 \gamma \sin^2(\mathbf{k} \cdot \mathbf{x} - \omega t)}{2 (\omega^2 - f^2)^2}. \quad (49.193)$$

Taking the sum leads to the total mechanical energy in a plane inertia-gravity wave

$$\mathcal{K}' + \mathcal{A}' = \frac{\tilde{\varphi}^2 |\mathbf{k}_h|^2 (f^2 k_z^2 + N_R^2 |\mathbf{k}_h|^2)}{2 k_z^2 (\omega^2 - f^2)^2} \quad (49.194)$$

Time independence of mechanical energy for the plane inertia-gravity wave accords with the result (49.96) for the plane internal gravity wave.

Phase averaged energetics

Taking the phase averages on the kinetic energy and available potential energy leads to

$$\langle \mathcal{K}' \rangle = \frac{\tilde{\varphi}^2 |\mathbf{k}_h|^2 (\omega^2 |\mathbf{k}|^2 + f^2 k_z^2)}{4 k_z^2 (\omega^2 - f^2)^2} \quad \text{and} \quad \langle \mathcal{A}' \rangle = \frac{\tilde{\varphi}^2 N_R^2 |\mathbf{k}_h|^4}{4 k_z^2 (\omega^2 - f^2)^2}, \quad (49.195)$$

whose sum is

$$\langle \mathcal{K}' + \mathcal{A}' \rangle = \frac{\tilde{\varphi}^2 |\mathbf{k}_h|^2 (\omega^2 |\mathbf{k}|^2 + f^2 k_z^2 + N_R^2 |\mathbf{k}_h|^2)}{4 k_z^2 (\omega^2 - f^2)^2} = \frac{\tilde{\varphi}^2 |\mathbf{k}_h|^2 (f^2 k_z^2 + N_R^2 |\mathbf{k}_h|^2)}{2 k_z^2 (\omega^2 - f^2)^2} \quad (49.196)$$

and ratio is

$$\frac{\langle \mathcal{K}' \rangle}{\langle \mathcal{A}' \rangle} = 1 + 2 (f/N_R)^2 \tan^2 \gamma = \frac{\omega^2 |\mathbf{k}|^2 + f^2 k_z^2}{N_R^2 |\mathbf{k}_h|^2}. \quad (49.197)$$

It is notable that the ratio is bounded below by unity, so that the kinetic energy is never less than the available potential energy. The ratio is unity when the phase velocity is horizontal ($\gamma = 0$), in which fluid particles have vertical trajectories and thus exhibit purely vertical buoyancy oscillations. This equipartition of kinetic and available potential energies was found for the internal gravity wave in Section 49.5.10. When the phase velocity is vertical, so that $\gamma = \pi/2$, the plane waves have no available potential energy since the fluid particles are exhibiting horizontal inertial oscillations.

Phase averaged mechanical energy flux

The phase averaged mechanical energy flux is given by

$$\frac{\langle \mathbf{v}' \varphi' \rangle}{\tilde{\varphi}^2} = \frac{\omega (k_z \mathbf{k}_h - \hat{z} |\mathbf{k}_h|^2)}{2 k_z (\omega^2 - f^2)} \quad (49.198a)$$

$$= \frac{\omega^2 |\mathbf{k}|^4 \mathbf{c}_g}{2 k_z^2 (N_R^2 - f^2) (\omega^2 - f^2)} \quad (49.198b)$$

$$= \frac{\mathbf{c}_g |\mathbf{k}_h|^2 (f^2 k_z^2 + N_R^2 |\mathbf{k}_h|^2)}{2 k_z^2 (\omega^2 - f^2)^2}, \quad (49.198c)$$

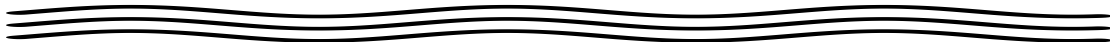
where we made use of the inertia-gravity wave group velocity (49.176). Now the phase averaged mechanical energy is given by equation (49.196), so that the plane inertia-gravity waves exhibit the group velocity property also found for internal gravity waves in equation (49.101)

$$\langle \mathbf{v}' \cdot \boldsymbol{\varphi}' \rangle = c_g (\mathcal{K}' + \mathcal{A}'). \quad (49.199)$$

That is, a plane inertia-gravity wave has a phase averaged mechanical energy flux equal to the group velocity times the phase averaged mechanical energy.

49.10.6 Comments

The inertial waves studied in Section 46.2 are the $N_R = 0$ limit of inertia-gravity waves studied in the present section. It is notable that in the presence of any nonzero vertical stratification, the squared angular frequency of propagating inertia-waves is super-inertial, $\omega^2 \geq f^2$, whereas when $N_R = 0$ the waves are sub-inertial, $\omega^2 \leq f^2$. If an inertial wave from an unstratified region, with $\omega^2 \leq f^2$, encounters stratification, then this low frequency wave cannot propagate into the stratified region. Instead, it will be reflected.



49.11 Exercises

EXERCISE 49.1: AGITATING A STRATIFIED FLUID

The internal gravity wave dispersion relation (49.61) says that no internal gravity waves exist with angular frequency greater than the buoyancy frequency of the background reference state, $\omega \leq N_R$. Speculate on what might happen if a stratified fluid is agitated at a frequency $\omega_{\text{source}} > N_R$.

EXERCISE 49.2: ENERGETICS OF INERTIA-GRAVITY WAVES

In this exercise we develop the energetics of plane inertia-gravity waves, emulating the treatment for plane internal gravity waves in Section 49.5.10.

- (a) For free inertia-gravity waves from Section 49.10, show that the ratio of the phase averaged kinetic energy to phase averaged available potential energy is given by

$$\frac{\langle \mathcal{K}' \rangle}{\langle \mathcal{A}' \rangle} = 1 + 2(f/N)^2 \tan^2 \gamma. \quad (49.200)$$

- (b) Using the dispersion relation, express this ratio in terms of $\omega, \mathbf{k}_h, k_z$.

EXERCISE 49.3: REFLECTION CONDITIONS FOR INERTIAL WAVES

Inertial waves studied in Section 46.2 are the $N^2 = 0$ limit of inertia-gravity waves from Section 49.10. Emulating the analysis in Section 49.6.2 for internal gravity waves, determine the reflection conditions for packets of plane inertial waves. Figure 49.4 is drawn for internal gravity waves. Redraw this figure for inertial waves.



Part X

Mechanics of unstable flows

For the waves studied in Part IX of this book, we assumed the waves existed on the background of an equilibrium base state. For example, in studying acoustic waves in Chapter 44, the background state is static and uniform, whereas when studying internal gravity waves in Chapter 49, the background is stratified. In each of the cases where linear waves exist, the background state is stable to the perturbations. That is, the wave perturbations do not lead a situation where the wave amplitudes grow by feeding off the base state.

In this part of the book we examine what requirements are needed to ensure such stability of base states. As we find, there are numerous mechanisms for base flows to go unstable. Our goal here is to study a suite of such unstable fluid flows and develop methods for understanding such instabilities. Rather than the exception, it turns out that instabilities are the norm in geophysical fluids.

[This video from Prof. Mollo-Christensen](#) provides a wonderful introduction to the topic of fluid mechanical instabilities.

Chapter 50

STABILITY OF SYMMETRIC FLOWS

In this chapter we study the stability of fluid flows exhibiting either axial symmetry (rotating fluid column) or spatial symmetry in one horizontal direction (geostrophic fronts). This analysis supports the study of frontal features in geophysical fluids, where a front is a region of strong buoyancy gradients that leads to a jet-like flow. We make use of three methods for stability analysis. One consists of an energetic approach due to Rayleigh (*energetic stability analysis*); one is Lagrangian and considers force balances acting on a test fluid parcel (*parcel stability analysis*); and one is Eulerian and considers wave perturbations (*modal stability analysis*). Each method leads to the same stability condition, which is here measured by local properties of the flow thus motivating the term *local stability* analysis. As part of the stability analysis we make use of material invariants, such as angular momentum, potential momentum, buoyancy, and potential vorticity. We restrict attention to the f -plane since that allows us to make use of potential momentum as a material invariant. It is notable that these flows generally exhibit secondary overturning circulations, with such circulations introduced here using the rudiments of *semi-geostrophy*.

The energetic and parcel methods probe the base state flow by perturbing test fluid parcels. A test parcel is assumed to have no impact on the flow state itself, meaning that the pressure field remains unchanged even as the parcel is moved. In effect, the test fluid parcel stability analysis makes the tacit assumption that pressure responses to a perturbation can be neglected for the purpose of detecting an unstable flow state. Ignoring the impacts on pressure is consistent with the notion of a test fluid element introduced in Section 14.3.5.¹ However, we questioned that approach when studying buoyancy in Section 27.7, where we computed the pressure response to the perturbation and found that the response has an important effect on the effective buoyancy felt by a finite fluid region. Acknowledging this limitation motivates us to complement the parcel approach with an Eulerian linear stability analysis using plane waves. This approach is dynamically consistent, and yet it works within the limitations of the linearized equations.

READER'S GUIDE FOR THIS CHAPTER

We make use of the shallow water system from Chapters 32 and 33, in particular the study of angular momentum in Section 33.8 (see also Section 24.3). We also assume an understanding of geostrophic flow as studied in Chapter 28, as well as the continuously stratified Boussinesq ocean from Chapter 26.

50.1 Loose threads	1318
------------------------------	------

¹Since the concern here is with perfect fluids, the test fluid element from Section 14.3.5 is the same as a test fluid parcel.

50.2 Instabilities in this chapter	1319
50.2.1 Summary of the instabilities studied in this chapter	1319
50.2.2 Nature of the base state and the perturbations	1320
50.2.3 Comments	1320
50.3 Centrifugal instability of cyclostrophically balanced flow	1320
50.3.1 Equations of motion	1321
50.3.2 Elements of angular momentum	1322
50.3.3 Energetic stability analysis	1323
50.3.4 Instability condition in terms of absolute vorticity	1324
50.3.5 Parcel stability analysis	1325
50.3.6 Stability condition in terms of the surface height	1327
50.3.7 Comments	1328
50.4 Potential momentum	1328
50.4.1 Linear momentum and potential momentum	1329
50.4.2 Zonal potential momentum on a β -plane	1330
50.4.3 Further reading	1330
50.5 Horizontal inertial instability of a geostrophically balanced front	1331
50.5.1 Equations of motion and equilibrium state	1331
50.5.2 Stability analysis based on energetic arguments	1332
50.5.3 Stability analysis based on parcel arguments	1334
50.5.4 Comments	1335
50.6 Symmetric instability of a baroclinic front: parcel method	1336
50.6.1 Equations of motion and equilibrium state	1336
50.6.2 Stability analysis	1337
50.6.3 Concerning the instability condition	1338
50.7 Symmetric instability of a baroclinic front: modal method	1340
50.7.1 Geostrophic base state and the perturbation equations	1340
50.7.2 Inertial-vorticity oscillator equations	1341
50.7.3 Ageostrophic overturning circulation streamfunction	1342
50.7.4 Dispersion relation for meridional-vertical plane waves	1343
50.7.5 Stability conditions	1343
50.7.6 Ertel potential vorticity and local stability	1344
50.7.7 Comments and further study	1345
50.8 Semi-geostrophy and the frontal overturning circulation	1345
50.8.1 Hydrostatic and Boussinesq fluid on an f -plane	1346
50.8.2 Geostrophic momentum approximation	1346
50.8.3 Secondary ageostrophic circulation	1347
50.8.4 Ageostrophic overturning circulation for a symmetric front	1348
50.8.5 Connection to potential vorticity and symmetric instability	1349
50.9 Exercises	1350

50.1 Loose threads

- Figures needed throughout
- Energy analysis for each instability as per Chapter 8 of *Smythe and Carpenter (2019)*, who use a modal approach and linearize the equations.
- Maximum growth rate for symmetric instability in chapter 8 of *Smythe and Carpenter (2019)*.
- Lagrangian analysis from Section 17.2 of *Cushman-Roisin and Beckers (2011)* is quite nice for inertial instability.

- Section 50.8 is a dog's breakfast that needs more order and pedagogy.
- What is the potential vorticity for the linearized perturbations in Section 50.7?

50.2 Instabilities in this chapter

The instabilities studied in this chapter are termed *local* since they are detected through a local condition that yields a necessary and sufficient condition for instability. The physical features of the flow instabilities considered here are quite similar, thus making it convenient to study them together. For centrifugal and horizontal inertial instabilities, we develop the stability conditions using both energetic and parcel analysis methods. For symmetric instability we use the parcel and modal methods.

50.2.1 Summary of the instabilities studied in this chapter

Before diving into the details, we here offer a summary of the instabilities studied in this chapter.

Centrifugal instability of cyclostrophic balanced flow

Consider an equilibrium flow state under inviscid cyclostrophic balance. As studied in Section 29.5, cyclostrophic balance arises when pressure and centrifugal accelerations are balanced, with centrifugal accelerations arising from curvature in the fluid particle trajectory. The angular momentum is materially invariant when the equilibrium state is rotationally symmetric, as in an ideal circular vortex or a rotating circular tank (Section 33.8). Flow stability can be probed by horizontally displacing a rotationally symmetric circular ring of fluid parcels, with each parcel retaining its original angular momentum. If the parcels are displaced to a position where pressure and centrifugal accelerations further support the displacement, then the base state is unstable to centrifugal instability.

Horizontal inertial instability of f -plane geostrophic flow

Consider an equilibrium flow state in a barotropic fluid under inviscid geostrophic balance on an f -plane, whereby pressure and Coriolis accelerations are balanced (Chapter 28). The potential momentum is materially invariant when the equilibrium state is symmetric in a horizontal direction, as in a zonally or meridionally symmetric f -plane front. Flow stability is probed by horizontally displacing a symmetric line of fluid parcels, with each parcel retaining its original potential momentum. If the parcels are displaced to a position where pressure and Coriolis accelerations further support the displacement, then the base state is unstable to horizontal inertial instability.

Isentropic inertial instability (symmetric instability) for f -plane flow

Consider an equilibrium flow state under inviscid geostrophic balance in a baroclinic fluid. Both potential momentum and buoyancy are materially invariant when the equilibrium state is symmetric in a horizontal direction. Flow stability is probed by isentropically displacing a symmetric line of fluid parcels, with each parcel retaining its original potential momentum and buoyancy. If the parcels are displaced to a position where pressure and Coriolis accelerations further support the displacement, then the base state is unstable to isentropic inertial instability (also called *symmetric* instability).

50.2.2 Nature of the base state and the perturbations

For the study of centrifugal instability, we make use of the shallow water model from Chapters 32 and 33, whereas we consider the continuously stratified Boussinesq ocean (Chapter 26) for the horizontal and isentropic inertial instabilities. When the fluid is continuously stratified and inviscid, all motion occurs along isentropes. However, when probing for centrifugal or horizontal inertial instabilities using parcel arguments, we examine stability to perturbations along geopotential surfaces. Such horizontal displacements generally cross isentropic surfaces in a baroclinic fluid. The isentropic inertial instability analysis in Section 50.6 maintains the adiabatic nature of displacements when probing for instabilities. Even so, these perturbations do not maintain a materially invariant potential vorticity. So what is it about these perturbations that makes them relevant to stability analysis?

The stability thought experiment using test fluid parcels assumes the parcels maintain their materially invariant property (e.g., buoyancy, angular momentum, potential momentum) as they probe stability of the surrounding fluid flow. That is the nature of the test parcels, as they do not directly interact with nor alter the surrounding fluid environment. Local flow stability is examined by having test parcels cross surfaces of constant materially invariant properties. For example, gravitational stability is probed by test parcels moving across buoyancy surfaces (Section 27.5.4). Likewise, entering the wedge of instability for symmetrically unstable flow requires a test parcel to leave its constant buoyancy and constant potential momentum surfaces (Section 50.6).

50.2.3 Comments

Holton (1992) distinguishes between *parcel* and *wave* instabilities, whereas *Cushman-Roisin and Beckers* (2011) use the terms *local* and *global*. Canonical examples of global instabilities are Kelvin-Helmholtz and baroclinic. We are not concerned with those instabilities in this chapter. Rather, the three instabilities considered here are examples of local instabilities.

Because of the rather close similarities between centrifugal and inertial instability, the oceanographic literature often uses the term centrifugal instability when referring to the inertial instability considered here (e.g., see *Thomas et al.* (2013) and *McWilliams* (2016)). However, we do not follow that usage since the inertial instability in this chapter is *not* associated with centrifugal accelerations. Rather, inertial instability is associated with Coriolis accelerations. We choose to follow the terminology of the atmospheric literature as detailed in the texts by *Holton* (1992) and *Markowski and Richardson* (2010), which also follows the fluid mechanics terminology used by *Drazin and Reid* (1981). So in brief, we use the term *centrifugal instability* for an axisymmetric base state in cyclostrophic balance, and *inertial instability* for a two-dimensional base state in geostrophic balance.

50.3 Centrifugal instability of cyclostrophically balanced flow

Consider flow of a single shallow water fluid layer in a rotating cylindrical tank with rotation about its vertical axis.² Throughout this analysis we assume all flow features maintain rotational symmetry (Figure 50.1). Hence, all dynamical fields are a spatial function only of the radial distance from the rotational axis (*axisymmetric*). We are interested in questions concerning flow stability as a function of the radial distribution of the angular momentum per mass, $l^z(r)$. In particular, we examine stability of *cyclostrophically balanced* flow, defined by flow whose radial

²The same ideas can be formulated for rotating Couette flow, in which fluid is placed between two rotating cylinders. We prefer the shallow water tank since it is familiar to geophysicists as a laboratory model for rotating fluid mechanics.

acceleration vanishes so that the radial pressure gradient balances the centrifugal acceleration (Section 29.5). Furthermore, we examine stability under perturbations that also maintain axial symmetry. We find that such cyclostrophic flow is stable to rotationally symmetric perturbations so long as the squared angular momentum increases radially outward. This system provides a pedagogical introduction to the stability of rotating vortices in the ocean and atmosphere, and it establishes analysis methods we later use for inertial and symmetric instabilities arising in two-dimensional frontal regions. The stability condition for angular momentum is reflected in observed stable vortices in both the atmosphere and ocean.

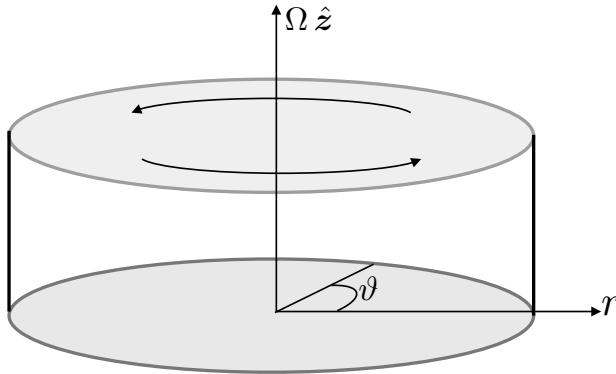


FIGURE 50.1: Rotating tank of shallow water fluid used to discuss centrifugal instability. We make use of cylindrical-polar coordinates from Section 9.3 to describe the flow. All flow features are assumed to be rotationally symmetric, including both the cyclostrophic balanced state and perturbations relative to the balanced state.

The centrifugal instability described here does *not* rely on baroclinic structure. Rather, it arises from the imbalances between centrifugal and pressure forces along a geopotential surface.³ By using the shallow water fluid to study this instability, we directly connect to Section 33.8, where we studied angular momentum in a rotating tank of shallow water fluid.

50.3.1 Equations of motion

We studied the angular momentum of this rotating shallow water system in Section 33.8, where we made use of a rotating reference frame and polar coordinates (r, ϑ) (Section 9.3) measured in the rotating frame. Here, r is the radial position from the rotational axis and ϑ is the azimuthal angle measured counter-clockwise from the rotating x -axis. We furthermore derived the acceleration in cylindrical-polar coordinates in Exercise 11.3. Making use of those results allows us to write down the horizontal components to the inviscid velocity equation as well as the thickness equation

$$Dv^r/Dt = -g \partial_r \eta + r^{-3} (l^z)^2 \quad (50.1a)$$

$$Dl^z/Dt = -g \partial_\vartheta \eta \quad (50.1b)$$

$$r \partial_t \eta = -\partial_r(h r v^r) - \partial_\vartheta(h v^\vartheta). \quad (50.1c)$$

In these equations, h is the layer thickness and η is the free surface height for the shallow water layer (see Figure 32.1). The radial and azimuthal velocity components are given by

$$v^r = Dr/Dt \quad \text{and} \quad v^\vartheta = r D\vartheta/Dt, \quad (50.2)$$

³One may conceive of centrifugal instability in a baroclinic flow where parcel displacements maintain their angular momentum and buoyancy. That analysis would lead to isentropic centrifugal instability, which is directly analogous to the isentropic inertial instability discussed in Section 50.6. See [Buckingham et al. \(2021\)](#) for a discussion of this system.

and the angular momentum per mass computed about the rotation axis (the z -axis) is

$$l^z = \hat{z} \cdot [\mathbf{r} \times (\mathbf{u} + \mathbf{U}_{\text{solid}})] = r(v^\vartheta + r\Omega). \quad (50.3)$$

Material evolution of the radial velocity (equation (50.1a)) is affected by the radial pressure gradient plus centrifugal acceleration, whereas the material evolution of angular momentum is affected by angular gradients in the pressure field.

We consider equilibrium states where the radial acceleration vanishes. Such states are said to be in *cyclostrophic balance*, whereby the radial pressure gradient balances the centrifugal acceleration

$$Dv^r/Dt = 0 \implies g \partial_r \eta = (v^\vartheta + r\Omega)^2/r = r^{-3}(l^z)^2 \quad \text{cyclostrophic balance.} \quad (50.4)$$

How stable is cyclostrophically balanced flow? To answer this question we examine the more restricted problem of stability of rotational symmetric flow, and with perturbations also assumed to be rotationally symmetric. Rotational symmetry also means that all flow fields are a function only of the radial direction. As such, angular momentum is materially constant

$$\partial_\vartheta \eta = 0 \implies Dl^z/Dt = 0. \quad (50.5)$$

This constraint on the flow plays a fundamental role in the stability analysis.

50.3.2 Elements of angular momentum

Consider a spinning top in a gravitational field, in which conservation of angular momentum (holding in the absence of friction) keeps the top upright. Yet in the presence of friction, the angular momentum is dissipated so that the top eventually falls. There is an analog with a rotating fluid. Namely, we find that a state of zero angular momentum leads to centrifugal instability. To develop this result we study basic properties for angular momentum in the rotating tank.

Solid-body motion

A fluid in solid-body motion has $v^\vartheta = 0$ and angular momentum per mass

$$l_{\text{solid-body}}^z = r^2\Omega. \quad (50.6)$$

Evidently, the magnitude of the angular momentum increases as the square of the radial distance. In the following we find it more convenient to use the square of the angular momentum (as it appears in the radial velocity equation (50.1a)), which also increases radially for the solid-body motion

$$\frac{d[l^z(r)]^2}{dr} = 4r^3\Omega^2 > 0. \quad (50.7)$$

We will find that flow is centrifugally unstable if the square of its angular momentum is a decreasing function of its radial distance. Such configurations adjust through *centrifugal instability* towards a state where its squared angular momentum increases radially. The instability is termed “centrifugal” since it is the centrifugal acceleration that “throws outward” the fluid if its squared angular momentum decreases radially, thus bringing the fluid back into a stable state. More precisely, a flow where the angular momentum decreases outward has pressure gradients that cannot balance the centrifugal acceleration from the outward movement of angular momentum conserving fluid parcels.

Zero angular momentum flow

Consider a non-rotating tank with zero flow, so that the angular momentum is zero. In a perfect fluid the angular momentum of each fluid parcel remains zero, even if we start the tank rotating. That is, for a perfect fluid with zero angular momentum, the tank simply rotates but the fluid remains at rest in the inertial reference frame. To generate non-zero angular momentum for the fluid requires friction between the rotating tank and fluid. After sufficient time, friction transfers angular momentum from the tank walls throughout the fluid, thus leading to a steady state flow in solid-body motion. Upon reaching the steady solid-body flow, there are no strains in the fluid and thus no viscous stresses to impart friction (Section 22.8).

In a flow with zero angular momentum, the relative angular velocity is given by

$$l^z = 0 \implies v^\theta = -r\Omega, \quad (50.8)$$

so that the flow is anti-cyclonic (i.e., directed counter to the tank's rotation). Furthermore, the zero angular momentum flow has the relative vorticity

$$l^z = 0 \implies \zeta = \frac{1}{r} \frac{d(rv^\theta)}{dr} = -2\Omega. \quad (50.9)$$

That is, the relative vorticity is anti-cyclonic with a Rossby number

$$l^z = 0 \implies \text{Ro} = \zeta/(2\Omega) = -1. \quad (50.10)$$

As we show in the following, the $l^z = 0$ flow is the onset point for centrifugal instability. Again, we conceive of this flow as analogous to a rotating top whose angular momentum vanishes, in which case the top falls.

Establishing zero angular momentum flow

It is relatively simple to establish solid-body motion of a fluid in a tank; all it takes is sufficient time for transients to relax and friction to fully transfer momentum from the tank walls throughout the fluid. For the complement task, consider a solid-body flow that is subjected to an irreversible force that brings the fluid to zero angular momentum. The question we ask in our stability analysis is not concerned with details of how such forces arise. Instead, we are interested in what happens to the flow when it reaches zero angular momentum.

50.3.3 Energetic stability analysis

As first introduced by Rayleigh, we consider a thought experiment in which two adjacent equal mass circular fluid rings are swapped, one originating from radial position $r = r_1$ and the other at $r = r_2 = r_1 + \Delta r$ (see Figure 50.2). Furthermore, assume that the radial velocity vanishes so that the kinetic energy of the rings is due only to their rotational motion. If swapping the rings decreases the kinetic energy in the base state, then the released kinetic energy can be used to fuel an instability.⁴ In this case we say that the flow is *centrifugally unstable*, with this name used since it is the centrifugal acceleration from the circular parcel trajectory that promotes the instability. In general, any curved flow will be exposed to centrifugal instability if swapping parcels reduces the kinetic energy of the base state while maintaining constant angular momentum.

With no radial flow, kinetic energy only arises from angular motion so that a ring of mass

⁴Gravitational potential energy plays no role here, as we are swapping fluid rings at the same vertical position.

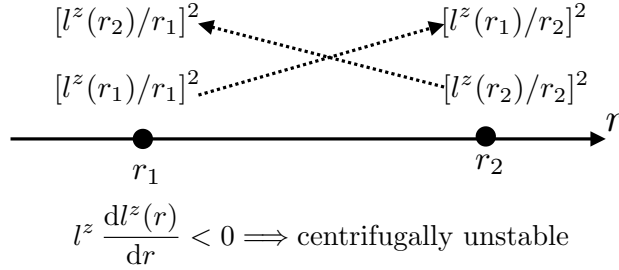


FIGURE 50.2: Illustrating Rayleigh’s energetic method for centrifugal instability. The initial configuration consists of two rings of fluid at radii r_1 and $r_2 = r_1 + \Delta r$, with kinetic energy per mass $2 E_{\text{init}} = [l^z(r_1)/r_1]^2 + [l^z(r_2)/r_2]^2$. Swapping the two rings while maintaining a constant angular momentum leads to the swapped kinetic energy per mass $2 E_{\text{swap}} = [l^z(r_1)/r_2]^2 + [l^z(r_2)/r_1]^2$. If $E_{\text{swap}} - E_{\text{init}} < 0$ then energy is released upon the swap and the rotationally symmetric flow is centrifugally unstable.

$\delta m = \rho \delta V$ and radius r_1 has kinetic energy

$$E(r_1) = (\delta m/2) [v^\theta(r_1) + r_1 \Omega]^2 = (\delta m/2) [l^z(r_1)/r_1]^2. \quad (50.11)$$

The initial kinetic energy for the two rings is thus given by the sum

$$E_{\text{init}} = (\delta m/2) ([l^z(r_1)/r_1]^2 + [l^z(r_2)/r_2]^2). \quad (50.12)$$

The equilibrium state and the perturbation each maintain rotational symmetry. Hence, when swapping their radial positions, the rings each maintain their respective angular momentum. But by changing radial positions their kinetic energy changes, thus leading to the kinetic energy of the swapped state

$$E_{\text{swap}} = (\delta m/2) ([l^z(r_1)/r_2]^2 + [l^z(r_2)/r_1]^2). \quad (50.13)$$

The difference in energy is given by

$$E_{\text{swap}} - E_{\text{init}} = (\delta m/2) ([l^z(r_2)]^2 - [l^z(r_1)]^2)(r_1^{-2} - r_2^{-2}). \quad (50.14)$$

Since $r_2 = r_1 + \Delta r > r_1$, we have a release of kinetic energy ($E_{\text{swap}} - E_{\text{init}} < 0$) if the squared angular momentum decreases upon moving outward

$$\frac{d[l^z(r)]^2}{dr} = 2 l^z \frac{dl^z(r)}{dr} < 0 \implies \text{centrifugally unstable cyclostrophic flow.} \quad (50.15)$$

Recall from equation (50.7) that the angular momentum of solid-body flow is an increasing function of radius. Hence, the instability condition (50.15) signals a rather unusual configuration of angular momentum. It is unusual since if realized, then the flow quickly goes unstable centrifugally and returns the flow to a stable state with radially increasing angular momentum.

50.3.4 Instability condition in terms of absolute vorticity

The angular momentum condition (50.15) is the traditional way to write the necessary and sufficient condition for centrifugal instability. However, to anticipate the role of vorticity found in the case of inertial and symmetric instability, we rewrite the stability condition (50.15) in the following alternate form. For this purpose, introduce the relative vorticity

$$\zeta = \frac{1}{r} \frac{d(r v^\theta)}{dr} \quad (50.16)$$

and thus write the angular velocity as the radial integral of the radius weighted vorticity

$$v^\vartheta = \frac{1}{r} \int_0^r r' \zeta(r') dr'. \quad (50.17)$$

This result allows us to write the angular momentum (50.3) in terms of the absolute vorticity

$$l^z = \Omega r^2 + \int_0^r r' \zeta(r') dr' = \int_0^r r' \zeta_a(r') dr'. \quad (50.18)$$

This equation allows us to write the stability condition (50.15) in the form

$$\frac{d[l^z(r)]^2}{dr} = 2 l^z \frac{dl^z(r)}{dr} = 2 r \zeta_a(r) \int_0^r r' \zeta_a(r') dr' < 0 \implies \text{centrifugally unstable}. \quad (50.19)$$

For this derivative to be negative at a particular radius, r , and thus for the cyclostrophic flow to be unstable, requires the absolute vorticity at that radius to have the opposite sign to the integral of the radius weighted absolute vorticity from the origin to r . Since $r \geq 0$, a necessary condition for the instability is for the absolute vorticity to have a sign change somewhere within the region from $0 \leq r$.

50.3.5 Parcel stability analysis

As a complement to the energetic stability analysis of Section 50.3.3, we here study the force balance in the radial momentum equation. This analysis shows that an unstable angular momentum profile leads to radial forces acting on a parcel that supports the parcel's movement away from its initial position. We again assume rotational symmetry so that the angular momentum is a material invariant, and assume the base state is in cyclostrophic balance. As such, the radial momentum equation (50.1a) leads to

$$0 = -g \partial_r \bar{\eta} + r^{-3} (\bar{l}^z)^2. \quad (50.20)$$

Subtracting this equilibrium flow from the full momentum equation (50.1a) leads to an equation for radial acceleration of perturbations about the equilibrium state

$$\frac{Dv^r}{Dt} = -g \frac{\partial \eta'}{\partial r} + r^{-3} [(l^z)^2 - (\bar{l}^z)^2], \quad (50.21)$$

where $\eta' = \eta - \bar{\eta}$ is the perturbation surface height. Consistent with the parcel method, we pay no attention to the perturbation pressure gradient, $-g \partial \eta'/\partial r$, and instead focus on the difference in squared angular momentum.

Probing stability by perturbing the radius of a circular fluid ring

Consider a perturbation realized by moving a constant mass circular fluid ring outward from its initial equilibrium state at radius r to a radius $r + \Delta r$. During the expansion of the ring, its angular momentum remains constant due to the rotational symmetry, so that

$$(l^z)^2(r + \Delta r) = (l^z)^2(r) = (\bar{l}^z)^2(r), \quad (50.22)$$

where the second equality holds since we are starting the ring from its cyclostrophic initial condition. To determine the radial acceleration at $r + \Delta r$ appearing on the right hand side of equation

(50.21), we compute

$$(l^z)^2(r + \Delta r) - (\bar{l}^z)^2(r + \Delta r) = (\bar{l}^z)^2(r) - (\bar{l}^z)^2(r + \Delta r) \approx -\Delta r \frac{d(\bar{l}^z)^2(r)}{dr}, \quad (50.23)$$

so that the radial momentum equation at $r + \Delta r$ takes on the form

$$\frac{Dv^r}{Dt} = -g \frac{\partial \eta'}{\partial r} - \frac{\Delta r}{(r + \Delta r)^3} \frac{d(\bar{l}^z)^2(r)}{dr}. \quad (50.24)$$

We thus see that if the squared angular momentum decreases upon moving the ring to a larger radius, then the second term in equation (50.24) provides a positive radial acceleration, thus supporting the initial outward perturbation. Ignoring the possibility for the perturbation pressure gradient, $-g\partial\eta'/\partial r$, to counter-act the acceleration, we are left with the same instability condition (50.15) derived using energetic arguments.

Describing the instability mechanism

When the fluid is in cyclostrophic balance, the radial pressure gradient acceleration balances the centrifugal acceleration as per equation (50.20). When a constant mass fluid ring is perturbed outward, from r to $r + \Delta r$, it carries its angular momentum, $\bar{l}^z(r)$, to the new location. This displaced ring is generally not in cyclostrophic balance with the pressure gradient at the new position. That is, the centrifugal acceleration of the displaced ring does not equal the pressure gradient of the new position

$$\underbrace{(r + \Delta r)^{-3} [\bar{l}^z(r)]^2}_{\text{centrifugal of displaced ring}} \neq \underbrace{g \frac{\partial \bar{\eta}(r + \Delta r)}{\partial r}}_{\text{pressure gradient at } r + \Delta r} \quad (50.25)$$

If the centrifugal acceleration of the displaced ring is greater than the local pressure gradient, then the ring will continue to move outward, which reflects a centrifugally unstable state. This is the situation when the squared angular momentum decreases when moving radially outward. Conversely, if the local pressure gradient is greater than the centrifugal acceleration of the displaced ring, then the ring returns to its original radius and exhibits centrifugal oscillations.

Centrifugal oscillations

Ignoring the perturbation pressure gradient, and introducing a centrifugal frequency

$$\sigma^2(r) \equiv \frac{1}{(r + \Delta r)^3} \frac{d(\bar{l}^z)^2(r)}{dr} \quad (50.26)$$

leads to the free oscillator equation for the fluctuation of a fluid ring from its equilibrium radial position

$$\frac{D^2 \Delta r}{Dt^2} + \sigma^2 \Delta r = 0, \quad (50.27)$$

where $u^r = D\Delta r/Dt$. For stable cases with $\sigma^2 > 0$, the ring exhibits simple harmonic centrifugal oscillations around the equilibrium radius with period $2\pi/\sigma$. In contrast, for the unstable case with $\sigma^2 < 0$, then Δr grows exponentially.

50.3.6 Stability condition in terms of the surface height

The equilibrium angular momentum and free surface height are related by the cyclostrophic balance (50.20). So rather than focusing on the angular momentum, we can develop an equivalent stability condition in terms of the radial derivatives of the free surface height. For that purpose we write the difference in angular momentum⁵

$$(\bar{l}^z)^2(r) - (\bar{l}^z)^2(r + \Delta r) = g [r^3 d_r \bar{\eta}(r) - (r + \Delta r)^3 d_r \bar{\eta}(r + \Delta r)], \quad (50.28)$$

and then perform a Taylor series

$$F(r + \Delta r) \equiv (r + \Delta r)^3 d_r \bar{\eta}(r + \Delta r) \quad (50.29a)$$

$$\approx r^3 d_r \bar{\eta}(r) + d_r F(r) \quad (50.29b)$$

$$= r^3 d_r \bar{\eta}(r) + \Delta r d_r (r^3 d_r \bar{\eta}), \quad (50.29c)$$

which renders

$$(\bar{l}^z)^2(r) - (\bar{l}^z)^2(r + \Delta r) \approx -g \Delta r \frac{d}{dr} \left[r^3 \frac{d\bar{\eta}}{dr} \right]. \quad (50.30)$$

The radial momentum equation (50.24) thus takes the form

$$\frac{Dv^r}{Dt} = -g \frac{\partial \eta'}{\partial r} - \frac{g \Delta r}{(r + \Delta r)^3} \frac{d}{dr} \left[r^3 \frac{d\bar{\eta}}{dr} \right]. \quad (50.31)$$

We are thus led to the stability condition written in terms of the surface height in the cyclostrophically balanced base state

$$\frac{d}{dr} \left[r^3 \frac{d\bar{\eta}}{dr} \right] < 0 \implies \text{centrifugally unstable}. \quad (50.32)$$

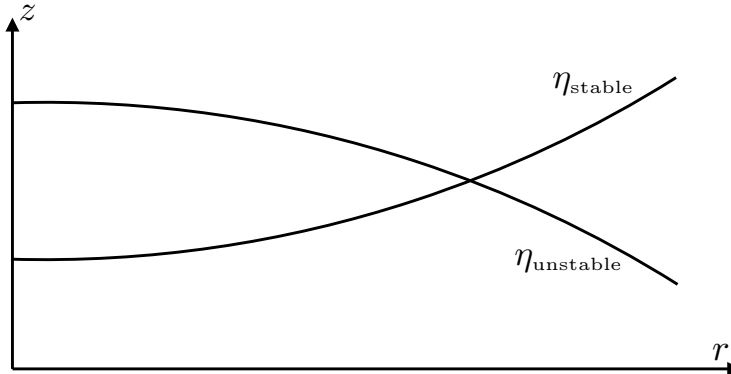


FIGURE 50.3: Example free surface heights that are stable and unstable to centrifugal instability, as determined by the condition (50.32). The stable configuration approximates the quadratic solid-body profile (50.34). The unstable profile has the layer thickness decrease with increasing radius, so that the radial pressure gradient acceleration does not balance the centrifugal acceleration.

A particularly simple example of a centrifugally unstable free surface configuration is the decreasing function

$$\bar{\eta} = \eta_0 - \alpha r^\beta \implies \left[r^3 \frac{d\bar{\eta}}{dr} \right] = -\alpha \beta (2 + \beta) r^{\beta+1}, \quad (50.33)$$

⁵As a shorthand we write $d/dr = d_r$.

with η_0 the free surface height at the origin, β a dimensionless constant, and α having dimensions so that αr^β has dimensions of length. Furthermore, we require with $\alpha \beta > 0$, and $\beta > -2$. Recall that the free surface is parabolic when the fluid is in solid-body motion, as given by equation (24.77)

$$\bar{\eta} = \eta_0 + \Omega^2 r^2 / (2 g_e) \implies \left[r^3 \frac{d\bar{\eta}}{dr} \right] = 4 \Omega^2 r^3 / g_e > 0, \quad (50.34)$$

which is stable.

50.3.7 Comments

Chapter 3 of [Drazin and Reid \(1981\)](#) is the canonical reference for centrifugal instability, where they provide a thorough stability analysis including both axisymmetric and non-axisymmetric perturbations. In our treatment, we also made use of the parcel arguments from Section 3.2 of [Markowski and Richardson \(2010\)](#). Furthermore, [Markowski and Richardson \(2010\)](#) comment on the perturbation pressure gradient in equation (50.24), emphasizing that parcel stability arguments generally ignore changes to the pressure gradient. Stated otherwise, a parcel analysis concerns the equilibrium angular momentum profile and its contribution to movement away from equilibrium. It is not concerned with back reaction from pressure perturbations associated with movement of parcels or fluid rings. A fuller treatment generally requires analysis beyond the parcel framework.

50.4 Potential momentum

A front is a region of enhanced lateral gradients in the buoyancy field (baroclinic front) or sea level (shallow water front). These fronts generally have corresponding currents (jets) arising from geostrophic balance (when off-equator). Figure 50.4 illustrates a baroclinic front that is symmetric in the zonal direction so that the buoyancy field is only a function of latitude, depth, and time, $b = b(y, z, t)$. We likewise assume that all other fields possess zonal symmetry, including pressure and velocity. Fronts can generally be oriented in any direction. Furthermore, on an f -plane there is rotational symmetry in the horizontal plane so that we can orient the coordinate system as desired.

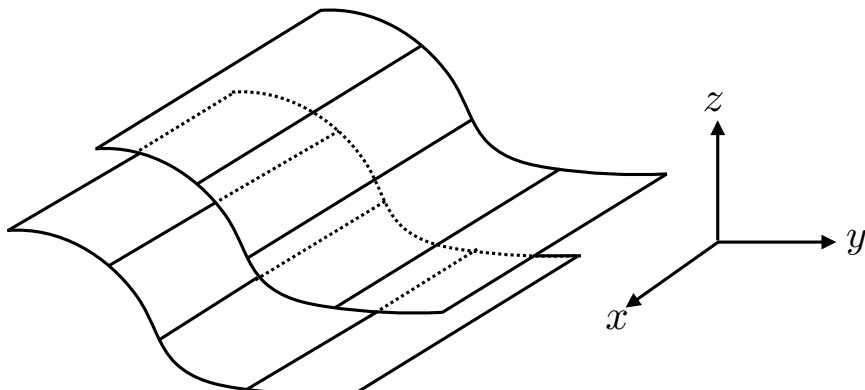


FIGURE 50.4: Example of a zonally symmetric baroclinic frontal region, showing two iso-buoyancy surfaces with $b = b(y, z, t)$. With $\partial b / \partial y > 0$ as drawn, the corresponding zonal thermal wind shear, $f \partial u / \partial z = -\partial b / \partial y < 0$, is westward for a northern hemisphere front; i.e., stronger westward flow with increasing height. The thermal wind shear is eastward for a southern hemisphere front with $\partial b / \partial y > 0$.

50.4.1 Linear momentum and potential momentum

The horizontal linear momentum per mass in a Boussinesq perfect fluid on an f -plane evolves according to (see Section 26.1.6)

$$\frac{D\mathbf{u}}{Dt} + f \hat{\mathbf{z}} \times \mathbf{u} = -\nabla_z \varphi. \quad (50.35)$$

Since f is a constant, this equation can be written

$$\frac{D\mathbf{M}}{Dt} = -\nabla_z \varphi, \quad (50.36)$$

where we introduced the *potential momentum* per mass

$$\mathbf{M} \equiv \mathbf{u} + f \hat{\mathbf{z}} \times \mathbf{x} = (u - f y) \hat{\mathbf{x}} + (v + f x) \hat{\mathbf{y}}, \quad (50.37)$$

and noted that $\mathbf{v} = D\mathbf{x}/Dt$. Notably, the potential momentum remains materially invariant in directions where the horizontal pressure gradient vanishes. We described the potential momentum for a point particle in Section 12.4, and here make use of it to study the stability of certain f -plane flow configurations.

Materially constant zonal potential momentum

For the zonally aligned buoyancy front illustrated in Figure 50.4, we assume that all fields are independent of the zonal direction so that

$$\partial_x \varphi = 0. \quad (50.38)$$

A vanishing zonal pressure gradient means that the zonal potential momentum per mass is a Lagrangian invariant

$$DM^x/Dt = 0 \quad \text{where } M^x \equiv u - f y. \quad (50.39)$$

This Lagrangian invariance greatly constrains the flow. For example, consider a fluid parcel at an initial latitude y_0 with zonal velocity u_0 . Movement of the parcel to a new latitude leads to the equality

$$u_0 - f y_0 = y_1 - f y_1, \quad (50.40)$$

so that the zonal velocity at the new latitude is given by

$$u_1 = u_0 - f(y_0 - y_1). \quad (50.41)$$

Motivating the name potential momentum

Although *absolute momentum* or *geostrophic momentum* are more commonly used in the literature, we prefer the term *potential momentum* as motivated by the same reasoning used for potential temperature (Section 20.3), potential density (Section 27.3.4), and potential vorticity (Section 36.3.2). Namely, the zonal potential momentum identifies that amount of zonal linear momentum per mass (i.e., the velocity) that a parcel would acquire if moved from an arbitrary latitude y_1 , to a reference latitude, y_0 . More specifically, inverting equation (50.41) we see that

$$u_0 = M^x(y_1) + f y_0. \quad (50.42)$$

Hence, the quantity $M^x(y_1)$ is the extra zonal momentum per mass available at the reference latitude, y_0 , upon moving a parcel from y_1 to y_0 . We thus see that the potential momentum is a material invariant in the way that potential temperature is for a perfect fluid. Furthermore, as seen in Section 50.5, meridional gradients of M^x measure the *inertial* stability of a flow configuration in a manner directly analogous to how vertical gradients of potential temperature (or buoyancy) measure gravitational stability.

Meridional potential momentum

There are occasions when a front exhibits meridional symmetry, in which case the perfect Boussinesq equations take the form

$$\mathrm{D}u/\mathrm{D}t = fv - \partial_x \varphi \quad (50.43\text{a})$$

$$\mathrm{D}v/\mathrm{D}t = -fu. \quad (50.43\text{b})$$

In this case the meridional potential momentum is materially invariant

$$\mathrm{D}M^y/\mathrm{D}t = 0 \quad \text{where} \quad M^y \equiv v + fx. \quad (50.44)$$

50.4.2 Zonal potential momentum on a β -plane

The f -plane is rotationally invariant about the rotational axis. Correspondingly, we can write the momentum equation in the form (50.36), thus exposing the potential momentum. Material invariance for potential momentum holds along the symmetry direction of an arbitrarily oriented symmetric front.

The β -plane is not rotationally invariant. Rather, it only maintains symmetry along lines of constant latitude (zonal directions). Consequently, only zonally oriented symmetric fronts maintain material invariance of zonal potential momentum. To see this property, write the zonal momentum equation in the form

$$\partial_t u + v \partial_y u + w \partial_z u - f v = 0, \quad (50.45)$$

where we assumed zonal symmetry ($\partial_x = 0$). Now write the Coriolis parameter in the form

$$\Gamma = f_0 y + \beta y^2/2 \implies f = \mathrm{d}\Gamma/\mathrm{d}y, \quad (50.46)$$

so that the zonal momentum equation takes the form

$$\partial_t(u - \Gamma) + v \partial_y(u - \Gamma) + w \partial_z(u - \Gamma) = 0. \quad (50.47)$$

Evidently, $M = u - \Gamma$ is materially invariant for this zonally symmetric front.

50.4.3 Further reading

See Section 12.5 for more discussion of potential momentum as it concerns a point particle. The term *absolute momentum* follows the arguments given on page 51 of [Markowski and Richardson \(2010\)](#).

50.5 Horizontal inertial instability of a geostrophically balanced front

We now examine stability of a geostrophically balanced front in an inviscid Boussinesq fluid. The analysis of centrifugal instability in Section 50.3 is closely followed, with rotational symmetry replaced by along-front symmetry and angular momentum replaced by potential momentum. We consider both the Rayleigh energetic stability analysis and the parcel analysis. Furthermore, the perturbations maintain symmetry in the along-front direction, so perturbations consist of a displaced row of parcels oriented along the front. Stability to more general perturbations, such as those that are not symmetric along the front, is not addressed here.

The results of our analysis are rotationally invariant since the f -plane is rotationally invariant. Hence, we choose to orient the coordinate system based on convenience whereby the x -axis is the along front axis and the y -axis is across the front. Furthermore, their relative orientation is chosen so that $\hat{x} \times \hat{y} = \hat{z}$, where \hat{z} is anti-parallel to gravity.

Although we make use of a continuously stratified Boussinesq fluid, the instability is not associated with baroclinicity. Rather, as for the centrifugal case in Section 50.3, it is associated with stability of an equilibrium state to horizontal displacements along geopotential surfaces. In a continuously stratified adiabatic fluid, such horizontal displacements generally cross isentropic surfaces and so comprise irreversible perturbations. So long as the associated mixing of momentum is negligible, we can still make use of material invariance of potential momentum. We return to this point when studying isentropic inertial (symmetric) instability in Section 50.6, in which baroclinicity plays a fundamental role in the instability mechanism.

50.5.1 Equations of motion and equilibrium state

The horizontal momentum equation for an inviscid Boussinesq fluid on an f -plane is given by (see Section 26.1)

$$D\mathbf{u}/Dt + f \hat{z} \times \mathbf{u} = -\nabla_z \varphi. \quad (50.48)$$

In the presence of along-front symmetry, an exact solution to the horizontal momentum equation is given by along-front geostrophic flow and zero flow across the front

$$u_g = -f^{-1} \partial_y \varphi \quad (50.49a)$$

$$v = 0. \quad (50.49b)$$

We examine the stability of this exact equilibrium base state to perturbations aligned with the front. To study evolution of the perturbations relative to the base state, we subtract the base state solution from the full momentum equation (50.48) to render

$$Du/Dt = f v \quad (50.50a)$$

$$Dv/Dt = f (u_g - u). \quad (50.50b)$$

We continue to assume along-front symmetry in the perturbation so that there is no along-front pressure gradient ($\partial_x \varphi = 0$) in equation (50.50a). Equation (50.50b) says that across-front accelerations are determined by deviations from geostrophy of the along-front velocity, and equation (50.50a) says that along-front accelerations are determined by the Coriolis acceleration arising from a non-zero across-front velocity.

Following the treatment of potential momentum in Section 12.4, we write the along-front momentum equation (50.50a) as the material time derivative of the along-front potential momentum

per mass⁶

$$m = u - fy, \quad (50.51)$$

bringing the suite of perturbation equations to

$$Dm/Dt = 0 \quad (50.52a)$$

$$Dv/Dt = f(u_g - u). \quad (50.52b)$$

Material invariance of the along-front potential momentum plays a fundamental role in the stability analysis.

50.5.2 Stability analysis based on energetic arguments

We follow the energetic arguments given in Section 50.3.3 for centrifugal instability of cyclostrophic flow. Here, we ask whether the along-front geostrophic flow is stable to a swap of two along-front oriented rows. If the swap releases kinetic energy from the base state, then the base state flow is *inertially unstable* to an along-front symmetric perturbation. In that case, perturbations spontaneously initiate inertial instability to affect a return to an inertially stable state.

Instability condition

The kinetic energy per mass for the along-front geostrophic flow is given by

$$E = (1/2) u_g^2 = (1/2) (m_g + fy)^2, \quad (50.53)$$

where we replaced the geostrophic velocity with the geostrophic potential momentum through equation (50.51). The kinetic energy per mass contained in two equal mass parcels at distinct cross-front positions y_1 and

$$y_2 = y_1 + (y_2 - y_1) = y_1 + \Delta y \quad (50.54)$$

is given by

$$E_{\text{init}} = (1/2) (m_g(y_1) + fy_1)^2 + (1/2) (m_g(y_2) + fy_2)^2. \quad (50.55)$$

Swapping the parcels and making use of the invariance of potential momentum leads to the kinetic energy in the swapped state

$$E_{\text{swap}} = (1/2) (m_g(y_1) + fy_2)^2 + (1/2) (m_g(y_2) + fy_1)^2. \quad (50.56)$$

A bit of algebra leads to the difference in kinetic energy between the two states

$$E_{\text{swap}} - E_{\text{init}} = -f (y_2 - y_1) [m_g(y_2) - m_g(y_1)] = -f \Delta y \Delta m_g. \quad (50.57)$$

Now compute a Taylor series of the potential momentum, $m_g(y_2)$, relative to the across-front position, $y = y_1$,

$$m_g(y_2) \approx m_g(y_1) + (y_2 - y_1) \left. \frac{dm_g}{dy} \right|_{y=y_1}, \quad (50.58)$$

⁶To reduce notational clutter, we write m for the along-front potential momentum rather than M^x . Additionally, we use m rather than M since we reserve M for the Montgomery potential in Section 50.6.

which then leads to the energy difference

$$E_{\text{swap}} - E_{\text{init}} = -f (\Delta y)^2 \frac{dM_g}{dy} \quad (50.59a)$$

$$= -f (\Delta y)^2 (\partial_y u_g - f) \quad (50.59b)$$

$$= f (\Delta y)^2 (\zeta_g + f), \quad (50.59c)$$

where

$$\zeta_g = -\partial_y u_g \quad (50.60)$$

is the vertical component to the geostrophic relative vorticity for the symmetric base state. Evidently, kinetic energy is released upon swapping the two rows if the following condition is satisfied

$$-f \partial_y M_g = f (\zeta_g + f) < 0 \implies \text{inertial instability}. \quad (50.61)$$

The second instability condition says that the base state is unstable if the absolute geostrophic vorticity, $\zeta_g + f$, has an opposite sign to the planetary rotation.

Interpreting the instability condition

The first instability condition in equation (50.61) arises if the cross-front gradient of the geostrophic potential momentum has the same sign as the Coriolis parameter. To help understand this condition we examine the inertial stability of a base state with zero flow. Zero flow in a rotating system corresponds to solid-body motion with potential momentum $M = -fy$. For this base state, the inertial stability condition (50.61) is given by

$$-f (\partial M / \partial y) = f^2 > 0, \quad (50.62)$$

thus signaling the solid-body flow is inertially stable. By contrast, we infer that an inertially unstable base state is rendered unstable by having an along-front flow that overcomes the stabilizing contribution to potential momentum from planetary rotation. This situation is directly analogous to the centrifugal instability studied in Section 50.3.

Summarizing the conditions for inertial instability

The instability condition (50.61) takes the following form for the northern and southern hemispheres. Again, the x -axis is oriented along the front and y -axis is across the front with $\hat{x} \times \hat{y} = \hat{z}$.

$$\text{northern hemisphere } (f > 0): \quad \partial_y M_g > 0 \quad \zeta_g < -|f| \quad \partial_y u_g > +|f| \quad (50.63a)$$

$$\text{southern hemisphere } (f < 0): \quad \partial_y M_g < 0 \quad \zeta_g > +|f| \quad \partial_y u_g < -|f|. \quad (50.63b)$$

In both hemispheres, instability arises when the relative geostrophic vorticity is anti-cyclonic and larger in magnitude than the cyclonic vorticity from planetary rotation. Under such conditions, inertial instability allows the flow to readjust toward a state of less extreme relative vorticity, thus returning the flow to a state with absolute vorticity dominated by planetary vorticity. Equivalently, inertial instability arises for flows where $\partial M_g / \partial y > 0$ in the northern hemisphere and $\partial M_g / \partial y < 0$ in the southern hemisphere, so that potential momentum of the geostrophic base state increases poleward.

50.5.3 Stability analysis based on parcel arguments

We now complement the energetic stability analysis by considering a parcel stability analysis. For this purpose, return to the perturbation equations (50.52a) and (50.52b), again with the equilibrium base state of along-front geostrophic balance with zero motion in the across-front direction

$$f u_g = -\partial_y \varphi. \quad (50.64)$$

We examine the stability of this geostrophic base state with respect to along-front perturbations of fluid parcels. For this purpose, imagine moving a row of fluid parcels from position y to a new position, $y + \Delta y$, and recall that this move is assumed to have no impact on the surrounding fluid environment.⁷ In general, the displaced row of fluid parcels will not be in geostrophic balance at the new position, thus providing for a non-zero acceleration in the across-front direction. If the acceleration is directed back to the original position, then the base state is stable and displaced parcels exhibit inertial oscillations. In contrast, the base state is inertially unstable if the acceleration is directed towards further displacement. We illustrate the stable and unstable situations in Figure 50.5.

Mathematical formulation

Equation (50.52b) for the across-front motion is given by

$$Dv/Dt = f(u_g - u). \quad (50.65)$$

This equation holds everywhere, in particular at the displaced cross-front position, $y + \Delta y$. At this position, the right hand side has $u(y + \Delta y)$, which is the along-front velocity of the displaced parcel at the new position. Likewise, $u_g(y + \Delta y)$ is the geostrophic velocity at $y + \Delta y$ for the background state. According to equation (50.64), the geostrophic velocity, $u_g(y + \Delta y)$, determines a Coriolis acceleration at the displaced position, $y + \Delta y$, with this Coriolis acceleration balanced by the cross-front pressure gradient, also at $y + \Delta y$.

To determine the sign of the cross-front acceleration in equation (50.65) acting on the displaced parcel at $y + \Delta y$, we make use of the material invariance of along-front potential momentum. This invariance means that each fluid parcel carries its potential momentum from the original position.⁸ For example, the potential momentum of a fluid parcel initially at position y has the value given by the geostrophic base state at that latitude

$$m(y) = m_g(y) = u_g(y) - f y. \quad (50.66)$$

Material invariance means that the parcel retains this potential momentum as it moves to the new position, $y + \Delta y$. In turn, invariance of along-front potential momentum allows us to determine the along-front velocity of the parcel at the displaced position in terms of $u_g(y)$ (recall the procedure leading to equation (50.41))

$$m(y + \Delta y) = u(y + \Delta y) - f(y + \Delta y) \quad (50.67a)$$

$$= m(y) \quad (50.67b)$$

$$= u_g(y) - f y, \quad (50.67c)$$

⁷In particular, the move is assumed to have zero effect on the pressure field. Hence, the pressure field remains in geostrophic balance with the unperturbed background geostrophic flow.

⁸We offer a cautionary remark about notation. Namely, f is a constant so that $f y$ is f times the latitude position y , and likewise for $f(y + \Delta y)$. In contrast, the zonal velocity, u , is a function of y , so that $u(y)$ and $u(y + \Delta y)$ represent the zonal velocity evaluated at the latitude positions y and $y + \Delta y$, respectively.

which leads to

$$u(y + \Delta y) = u_g(y) + f \Delta y. \quad (50.68)$$

The cross-front acceleration (50.65) at the new latitude position thus takes the form

$$\frac{Dv(y + \Delta y)}{Dt} = f [u_g(y + \Delta y) - u(y + \Delta y)] \quad (50.69a)$$

$$= f[u_g(y + \Delta y) - u_g(y) - f \Delta y] \quad (50.69b)$$

$$\approx f \Delta y \left[\frac{\partial u_g}{\partial y} - f \right] \quad (50.69c)$$

$$= -f \Delta y (\zeta_g + f). \quad (50.69d)$$

As with the energetic arguments in Section 50.5.2, we are left with the instability condition

$$f(\zeta_g + f) < 0 \implies \text{inertially unstable}. \quad (50.70)$$

A quick derivation of the instability condition

The displaced parcel at $y + \Delta y$ has zonal velocity $u(y + \Delta y) = u_g(y) + f \Delta y$ according to equation (50.68), which follows from conserving potential momentum. The velocity of the background geostrophic flow at $y + \Delta y$ is given by the Taylor series approximation relative to the flow at y :

$$u_g(y + \Delta y) \approx u_g(y) + \Delta y \partial_y u_g(y) = u_g(y) - \Delta y \zeta_g(g). \quad (50.71)$$

The difference between these two zonal velocities is

$$u_g(y + \Delta y) - u(y + \Delta y) = -(f + \zeta_g) \Delta y, \quad (50.72)$$

which recovers the inertial stability condition derived above.

Summary of the parcel argument

As summarized in Figure 50.5, at the initial location in the base state, a parcel under geostrophic balance has its Coriolis acceleration balanced by its pressure acceleration. However, the displaced parcel generally will not be in geostrophic balance at the new location, in which case its Coriolis acceleration does not balance the local pressure gradient. The parcel approach determines a stability condition based on whether the imbalance leads to an acceleration back towards its initial position (stable harmonic inertial oscillations) or further away (inertial instability). Along-front symmetry of both the base state and the perturbation ensures material invariance of along-front potential momentum. This invariance provides an explicit expression for the acceleration felt by the displaced parcel, thus determining a condition on stability of the base state to symmetric perturbations. The method of analysis is directly analogous to that applied to the rotating tank of fluid in Section 50.3 for centrifugal instability, as well as for a vertical column of fluid in Section 27.4 for gravitational stability.

50.5.4 Comments

As stated in Section 50.2.3, the rather close similarities between centrifugal and inertial instability have prompted the oceanographic literature to often use the term centrifugal instability when referring to the inertial instability considered here (e.g., [McWilliams, 2016](#)). We instead prefer the terminology of the atmospheric literature, such as detailed in the texts by [Holton \(1992\)](#) and

Markowski and Richardson (2010), which also follows the classical fluid mechanics terminology used in the text by *Drazin and Reid* (1981). In this manner, we reserve the term *centrifugal instability* for an axisymmetric base state in cyclostrophic balance, and *inertial instability* for a two-dimensional base state in geostrophic balance.

50.6 Symmetric instability of a baroclinic front: parcel method

In this section we examine the stability of a geostrophically balanced baroclinic front on an f -plane. As before, the front exhibits along-front symmetry so that the along-front potential momentum is a material invariant. Additionally, we assume the fluid to be adiabatic, so that buoyancy is also materially invariant. In this section we investigate the stability of a geostrophically balanced along-front flow using the parcel method, and follow with an Eulerian modal analysis in Section 50.7.

For the parcel approach, we consider symmetric displacements of parcels along a constant buoyancy surface. By construction, this displacement is neutral to gravitational instability since it occurs along a constant buoyancy surface. However, a displaced parcel could still find itself in an unstable position depending on the potential momentum of the environment. The analysis proceeds analogously to the horizontally inertial instability case of Section 50.5.3, with the displacements here isentropic (constant buoyancy) rather than horizontal. We are thus motivated to refer to the ensuing instability as *isentropic inertial instability*. However, this terminology is not common, with *symmetric instability* far more common.

50.6.1 Equations of motion and equilibrium state

Given the adiabatic nature of the fluid, and the role of baroclinicity, we make use of the buoyancy coordinates for a Boussinesq fluid as detailed in Section 59.2. The horizontal momentum equation is thus given by

$$D\mathbf{u}/Dt + f \hat{\mathbf{z}} \times \mathbf{u} = -\nabla_b M \quad (50.73)$$

where ∇_b is a horizontal gradient computed along constant buoyancy surfaces. Furthermore,

$$M = \varphi - b z \quad (50.74)$$

is the Montgomery potential that contributes the acceleration via

$$-\nabla_b M = -\nabla_b \varphi + b \nabla_b z. \quad (50.75)$$

The first term arises from pressure gradients and the second from geopotential gradients, both computed along constant buoyancy surfaces.⁹ In the presence of along-front symmetry, an exact solution to the horizontal momentum equation is given by along-front geostrophic flow and zero cross-front flow

$$u_g = -\frac{1}{f \rho_0} \left[\frac{\partial M}{\partial y} \right]_b \quad (50.76a)$$

$$v = 0. \quad (50.76b)$$

⁹Mathematical and physical details for the use of generalized vertical coordinates, such as buoyancy or isopycnal coordinates, are developed in Part XI of this book. In particular, the essential features of the ∇_b gradient operator are provided in Figure 56.4.

We examine the stability of this base state to perturbations symmetric in the along-front direction. Subtracting the exact equilibrium solution from the full momentum equation (50.48) leads to

$$\mathrm{D}u/\mathrm{D}t = fv \quad (50.77\text{a})$$

$$\mathrm{D}v/\mathrm{D}t = f(u_g - u), \quad (50.77\text{b})$$

where we continue to assume along-front symmetry thus allowing us to drop the along-front gradient of the Montgomery potential. Following the treatment in Sections 12.4 and 50.5.1, we write the along-front momentum equation as the material time derivative of the along-front potential momentum per mass $m = u - fy$ (equation (50.51)), thus bringing the perturbation equations to

$$\mathrm{D}m/\mathrm{D}t = 0 \quad (50.78\text{a})$$

$$\mathrm{D}v/\mathrm{D}t = f(u_g - u). \quad (50.78\text{b})$$

50.6.2 Stability analysis

We follow the parcel analysis for inertial instability in Section 50.5.3, starting with an equilibrium base state of along-front geostrophic balance with zero meridional motion. We examine the stability of this state with respect to symmetric perturbations of fluid parcels along a constant buoyancy surface. For this purpose, imagine moving a row of fluid parcels from cross-front position y to position $y + \Delta y$ while maintaining a fixed buoyancy. In general, the displaced row of parcels will not be in geostrophic balance at the new position, thus providing for a non-zero cross-front acceleration at that displaced position. What is the sign of that acceleration?

Mathematical formulation

At the new cross-front position the cross-front acceleration is given by

$$\frac{\mathrm{D}v(y + \Delta y)}{\mathrm{D}t} = f[u_g(y + \Delta y) - u(y + \Delta y)], \quad (50.79)$$

where $u(y + \Delta y)$ is the along-front velocity of the displaced parcel at the new position, and $u_g(y + \Delta y)$ is the geostrophic velocity at that position. To determine the sign of the acceleration acting on the displaced parcel, we make use of the invariance of along-front potential momentum, whereby each parcel carries its potential momentum from the original position

$$m(y) = m_g(y) = u_g(y) - fy \quad (50.80)$$

to the new position. In turn, invariance of along-front potential momentum allows us to determine the parcel's along-front velocity at the new position in terms of $u_g(y)$

$$m(y + \Delta y) = u(y + \Delta y) - f(y + \Delta y) \quad (50.81\text{a})$$

$$= m(y) \quad (50.81\text{b})$$

$$= u_g(y) - fy, \quad (50.81\text{c})$$

which leads to

$$u(y + \Delta y) = u_g(y) + f\Delta y. \quad (50.82)$$

The cross-front acceleration (50.79) thus takes the form

$$\frac{Dv(y + \Delta y)}{Dt} = f [u_g(y + \Delta y) - u(y + \Delta y)] \quad (50.83a)$$

$$= f[u_g(y + \Delta y) - u_g(y) - f\Delta y] \quad (50.83b)$$

$$\approx f\Delta y \left[\left(\frac{\partial u_g}{\partial y} \right)_b - f \right] \quad (50.83c)$$

$$= -\Delta y f (\tilde{\zeta}_g + f). \quad (50.83d)$$

In the final equality we introduced the relative geostrophic vorticity as written in buoyancy coordinates (see Section 59.2)

$$\tilde{\zeta}_g = \left[\frac{\partial v_g}{\partial x} \right]_b - \left[\frac{\partial u_g}{\partial y} \right]_b = - \left[\frac{\partial u_g}{\partial y} \right]_b. \quad (50.84)$$

Furthermore, we can introduce the Boussinesq Ertel potential vorticity in the form¹⁰

$$Q = (\boldsymbol{\omega} + f \hat{\boldsymbol{z}}) \cdot \nabla b = (\tilde{\zeta} + f) N^2, \quad (50.85)$$

with

$$N^2 = \frac{\partial b}{\partial z} \quad (50.86)$$

the squared buoyancy frequency. We assume $N^2 > 0$ since we are interested in gravitationally stable flow. Bringing these results together leads to the equivalent expressions for the symmetric instability condition

$$f(\tilde{\zeta}_g + f) < 0 \implies \text{symmetrically unstable}. \quad (50.87a)$$

$$f Q_g < 0 \implies \text{symmetrically unstable}. \quad (50.87b)$$

The instability condition (50.87a) is a direct translation of the inertial instability condition (50.70), translating from horizontal displacements to isopycnal displacements.

50.6.3 Concerning the instability condition

We here consider various ways to understand the instability condition as written by equations (50.87a) and (50.87b).

Relative slope of buoyancy and potential momentum surfaces: Part I

The instability condition (50.87a) can be written as a geometric statement about the relative slopes of buoyancy and potential momentum surfaces. For this purpose we make use of the identity for an along-front symmetric geostrophic flow

$$\left[\frac{\partial m}{\partial y} \right]_b = \left[\frac{\partial u}{\partial y} \right]_b - f = -(\tilde{\zeta} + f). \quad (50.88)$$

Consequently, the instability condition (50.87a) is equivalent to

$$f \left[\frac{\partial m_g}{\partial y} \right]_b > 0 \implies \text{symmetrically unstable}. \quad (50.89)$$

¹⁰We derive equation (50.85) when studying potential vorticity in the Boussinesq ocean using buoyancy coordinates; see equation (59.38).

This condition is directly analogous to the inertial instability condition (50.61), only here with displacement along an isopycnal rather than a geopotential. In the northern hemisphere, if one moves in the $+\hat{y}$ direction on a constant buoyancy surface and encounters increasing values for the potential momentum, then the flow is symmetrically unstable. Conversely in the southern hemisphere, if one moves in $-\hat{y}$ direction on a constant buoyancy surface and encounters increasing values for the potential momentum, then the flow is symmetrically unstable. We illustrate this situation in Figure 50.6.

Relative slope of buoyancy and potential momentum surfaces: Part II

As another way to write the instability condition (50.89), we make use of the expression (56.76b) to transform the derivative on buoyancy surfaces back to geopotential coordinates, and then introduce the cross-front derivative of the buoyancy on a potential momentum surface

$$\left[\frac{\partial m_g}{\partial y} \right]_b = \left[\frac{\partial m_g}{\partial y} \right]_z - \frac{\partial b/\partial y}{\partial b/\partial z} \frac{\partial m_g}{\partial z} \quad (50.90a)$$

$$= N^{-2} \hat{x} \cdot (\nabla m_g \times \nabla b) \quad (50.90b)$$

$$= -N^{-2} \hat{x} \cdot (\nabla b \times \nabla m_g) \quad (50.90c)$$

$$= - \left[\frac{\partial b}{\partial y} \right]_{m_g}. \quad (50.90d)$$

We are thus led to the additional expression for a symmetrically unstable base state

$$f \left[\frac{\partial b}{\partial y} \right]_{m_g} < 0 \implies \text{symmetrically unstable.} \quad (50.91)$$

Hence, a northern hemisphere symmetrically unstable configuration sees a reduction in buoyancy when moving in the $+\hat{y}$ direction along a constant potential momentum surface. This situation is illustrated in Figure 50.6.

Relative slope of buoyancy and potential momentum surfaces: Part III

We offer one final identity for writing the instability condition, pulling us back to the PV version. Here, use the geopotential coordinates to write the following relation between the absolute vorticity and gradient of the potential momentum for the front

$$\omega + f\hat{z} = \hat{x} \times \nabla m, \quad (50.92)$$

so that

$$Q = (\omega + f\hat{z}) \cdot \nabla b \quad (50.93a)$$

$$= (\nabla b \times \nabla m) \cdot \hat{x} \quad (50.93b)$$

$$= N^2 (\tilde{\zeta} + f). \quad (50.93c)$$

The condition for symmetric instability thus can be written

$$f Q_g = -N^2 f \left[\frac{\partial m_g}{\partial y} \right]_b = N^2 f \left[\frac{\partial b}{\partial y} \right]_{m_g} < 0. \quad (50.94)$$

50.7 Symmetric instability of a baroclinic front: modal method

We now consider symmetric instability following the linear stability analysis of [Hoskins \(1974\)](#). We recover the same stability condition as for the parcel method in Section 50.6. However, linear stability analysis offers added insights concerning the central role of Ertel potential vorticity and provides further details of the instability.

50.7.1 Geostrophic base state and the perturbation equations

Our goal is to examine the stability of a zonally symmetric geostrophic front to zonally symmetric perturbations. Whereas the base state for the study of gravity waves has zero baroclinicity, here we consider a geostrophic front with meridional (across-front) baroclinicity. Rather than the buoyancy coordinates used for the parcel stability analysis in Section 50.6, we here make use of geopotential vertical coordinates and linearize the Boussinesq ocean equations. The starting point for this development is the *f*-plane version of the perfect Boussinesq ocean equations from Section 26.1.6

$$\partial_t \mathbf{v} + (\mathbf{v} \cdot \nabla) \mathbf{v} + f \hat{\mathbf{z}} \times \mathbf{v} = -\nabla \varphi + b \hat{\mathbf{z}} \quad (50.95a)$$

$$\partial_t b + \mathbf{v} \cdot \nabla b = 0. \quad (50.95b)$$

Equations for the geostrophic base state

The equations describing the zonal geostrophic and hydrostatic base state are given by

$$f u_g = -\partial_y \varphi_g \quad \text{zonal flow in geostrophic balance} \quad (50.96a)$$

$$\partial_z \varphi_g = b_g \quad \text{hydrostatic balance} \quad (50.96b)$$

$$f \partial_z u_g = -\partial_y b_g \quad \text{thermal wind of zonal flow} \quad (50.96c)$$

$$\zeta_g = -\partial_y u_g \quad \text{relative vorticity.} \quad (50.96d)$$

The pressure field, $\varphi_g(y, z)$, has a meridional derivative that supports the zonal geostrophic flow, $u_g(y, z)$, and which is in hydrostatic balance with the base state buoyancy, $b_g(y, z)$. Combining geostrophy with the hydrostatic balance leads to the thermal wind shear in equation (50.96c). Due to zonal symmetry, the only contribution to the relative vorticity comes from the meridional shear of the zonal geostrophic flow, $\zeta_g = -\partial_y u_g$. Ertel potential vorticity (Chapter 38) of the base state proves to be central to the stability conditions

$$Q_g = (\boldsymbol{\omega}_b + f \hat{\mathbf{z}}) \cdot \nabla b_g = N^2 (f + \zeta_g) - f (\partial_z u_g)^2, \quad (50.97)$$

where we made use of the thermal wind equation (50.96c) as well as the relative vorticity for the zonal geostrophic flow

$$\boldsymbol{\omega}_b = \nabla \times \hat{\mathbf{x}} u_g = \hat{\mathbf{y}} \partial_z u_g - \hat{\mathbf{z}} \partial_y u_g = -\hat{\mathbf{y}} f^{-1} \partial_y b_g + \hat{\mathbf{z}} \zeta_g. \quad (50.98)$$

Linearized perturbation equations

To develop perturbation equations, we decompose the flow into the geostrophic base state plus a perturbation. The perturbation is time dependent and ageostrophic, and, importantly, is assumed

to retain the zonal symmetry of the base state¹¹

$$\mathbf{v}(y, z, t) = \mathbf{v}'(y, z, t) + \hat{\mathbf{x}} u_g(y, z) \quad (50.99a)$$

$$\varphi(y, z, t) = \varphi'(y, z, t) + \varphi_g(y, z) \quad (50.99b)$$

$$b(y, z, t) = b'(y, z, t) + b_g(y, z). \quad (50.99c)$$

The linearized version of the velocity equation (50.95a) and buoyancy equation (50.95b) take the form

$$\partial_t u' = v' (f - \partial_y u_g) - w' \partial_z u_g \quad \text{zonal velocity} \quad (50.100a)$$

$$\partial_t v' = -f u' - \partial_y \varphi' \quad \text{meridional velocity} \quad (50.100b)$$

$$\partial_t w' = -\partial_z \varphi' + b' \quad \text{vertical velocity} \quad (50.100c)$$

$$\partial_t b' = -(v' \partial_y b_g + w' \partial_z b_g) \quad \text{buoyancy} \quad (50.100d)$$

$$\partial_y v' + \partial_z w' = 0 \quad \text{continuity.} \quad (50.100e)$$

We observe that the zonal velocity evolves according to the Coriolis acceleration plus the convergence of the advective flux of the base state geostrophic velocity

$$-v' \partial_y u_g - w' \partial_z u_g = -\nabla \cdot (\mathbf{v}' u_g). \quad (50.101)$$

Likewise, the buoyancy evolves according to the convergence of the advective flux of the base state buoyancy

$$-(v' \partial_y b_g + w' \partial_z b_g) = -\nabla \cdot (\mathbf{v}' b_g). \quad (50.102)$$

In both cases, the advection velocity arises from the non-divergent anomalous flow, \mathbf{v}' , with zonal symmetry meaning there is no contribution to the flux convergences from the anomalous zonal velocity, u' .

50.7.2 Inertial-vorticity oscillator equations

As in our study of buoyancy oscillations in Section 49.3 and inertia-gravity oscillations in Section 49.9, we here develop forced oscillator equations for the zonal and meridional velocity components. To do so, take a time derivative of the zonal velocity equation (50.100a) and then substitute the meridional velocity equation (50.100b) to find the zonal velocity oscillator equation

$$[\partial_{tt} + f(f + \zeta_g)] u' = -(f + \zeta_g) \partial_y \varphi' + \partial_z u_g (\partial_z \varphi' - b'). \quad (50.103)$$

Similar manipulations lead to the forced oscillator equation for the meridional velocity

$$[\partial_{tt} + f(f + \zeta_g)] v' = f w' \partial_z u_g - \partial_{ty} \varphi'. \quad (50.104)$$

The forcing functions on the right hand side of both equations (50.103) and (50.104) are generally nonzero. However, in their absence both the zonal and meridional velocity components satisfy a free oscillator equation with squared natural angular frequency, $f(f + \zeta_g)$. We refer to these as *inertial-vorticity* oscillations given the dual role of the Coriolis and vorticity for determining the oscillations. The oscillations are simple harmonic when $f(f + \zeta_g) > 0$, whereas they are exponentially growing when $f(f + \zeta_g) < 0$. This stability condition for the oscillators is consistent with that found for the parcel stability analysis leading to equation (50.87a). To develop more insight into the nature of the instability for $f(f + \zeta_g) < 0$ we next develop an equation for the

¹¹It is this symmetry of the perturbation that gives rise to the name *symmetric instability*.

overturning streamfunction in the meridional-vertical plane.

50.7.3 Ageostrophic overturning circulation streamfunction

The continuity equation (50.100e) means that the meridional-vertical circulation is non-divergent so that we can introduce a streamfunction for the perturbation flow

$$\mathbf{v}' = -\hat{\mathbf{x}} \times \nabla \psi \implies v' = \partial_z \psi \quad \text{and} \quad w' = -\partial_y \psi. \quad (50.105)$$

The perturbed fields are ageostrophic and are sometimes referred to as the *ageostrophic secondary circulation*, with this circulation described by the ageostrophic overturning circulation streamfunction, ψ . Based on the oscillator equations (50.103) and (50.104), we anticipate that the overturning circulation is unstable for $f(f + \zeta_g) < 0$.

Zonal vorticity equation

Taking the z derivative of the meridional velocity equation (50.100b) and the y derivative of the vertical velocity equation (50.100c), and then subtracting, leads to the equation for the zonal component of the vorticity¹²

$$\partial_t(\partial_y w' - \partial_z v') - f \partial_z u' = \partial_y b', \quad (50.106)$$

which takes on the form using the overturning streamfunction

$$\partial_t(\partial_{yy} + \partial_{zz})\psi = -f \partial_z u' - \partial_y b'. \quad (50.107)$$

Further assumptions for the base state flow

To enable the next steps of the derivation, we make use of the following assumptions about the base state:

$$\zeta_g = -\partial_y u_g \quad \text{constant relative vorticity} \quad (50.108a)$$

$$f \partial_z u_g = -\partial_y b_g \quad \text{constant thermal wind shear} \quad (50.108b)$$

$$N^2 = \partial_z b_g \quad \text{constant buoyancy frequency.} \quad (50.108c)$$

These assumptions are restrictive, and yet the resulting instability calculation provides great insights into base state flow configurations that are more general.

Eliminating the zonal velocity and the buoyancy

We can eliminate the perturbation zonal velocity, u' , and the perturbation buoyancy, b' , from the vorticity equation (50.107) by taking another time derivative. Upon doing so we make use of the zonal velocity equation (50.100a) and the buoyancy equation (50.100d), and make use of the assumptions (50.108a)-(50.108c) for the base state:

$$-\partial_{tt}(\partial_{yy} + \partial_{zz})\psi = f \partial_{zt} u' + \partial_{yt} b' \quad (50.109a)$$

$$= f \partial_z[v'(f + \zeta_g) - w' \partial_z u_g] - \partial_y(v' \partial_y b_g + w' \partial_z b_g) \quad (50.109b)$$

$$= f \partial_{zz}\psi(f + \zeta_g) - 2 \partial_{yz}\psi \partial_y b_g + \partial_{yy}\psi \partial_z b_g \quad (50.109c)$$

$$= f(f + \zeta_g) \partial_{zz}\psi + 2f \partial_z u_g \partial_{yz}\psi + N^2 \partial_{yy}\psi. \quad (50.109d)$$

¹²The zonal component of the perturbation vorticity is given by $\hat{\mathbf{x}} \cdot (\nabla \times \mathbf{v}') = \partial_y w' - \partial_x v' = -(\partial_{yy} + \partial_{zz})\psi$.

Rearrangement leads to the equation for the ageostrophic overturning circulation streamfunction

$$[\partial_{tt}(\partial_{yy} + \partial_{zz}) + f(f + \zeta_g)\partial_{zz} + 2f\partial_z u_g \partial_{yz} + N^2 \partial_{yy}] \psi = 0. \quad (50.110)$$

50.7.4 Dispersion relation for meridional-vertical plane waves

Equation (50.110) is a constant coefficient partial differential equation for the overturning streamfunction. We examine its properties by considering a plane wave ansatz just as for our study of linear waves in Part IX of this book. Since the flow is non-divergent, the plane waves are transverse. Furthermore, we continue to assume zonal symmetry with the perturbations, so that the waves have no x dependence. We thus consider waves propagating in the meridional-vertical plane, in which case we take the plane wave ansatz

$$\psi(y, z, t) = \tilde{\psi} e^{i(k_y y + k_z z - \omega t)}, \quad (50.111)$$

with Figure 50.7 depicting the wave geometry. Plugging this ansatz into the streamfunction equation (50.110) leads to the dispersion relation

$$\omega^2 = \frac{f(f + \zeta_g)k_z^2 + 2f\partial_z u_g k_y k_z + N^2 k_y^2}{k_y^2 + k_z^2} \quad (50.112a)$$

$$= f(f + \zeta_g) \cos^2 \alpha + 2f\partial_z u_g \sin \alpha \cos \alpha + N^2 \sin^2 \alpha \quad (50.112b)$$

$$= \cos^2 \alpha [f(f + \zeta_g) + 2f\partial_z u_g \tan \alpha + N^2 \tan^2 \alpha]. \quad (50.112c)$$

Note that the convention for symmetric instability is to use the angle, α , that the particle trajectories make with the vertical, whereas for our study of internal gravity waves (Section 49.5) and inertia-gravity waves (Section 49.10), we used the angle $\gamma = \pi/2 - \alpha$ that the phase velocity makes with the horizontal. Either way, we see that the dispersion relation (50.112c) depends only on the wave direction along with the prescribed rotation and properties of the background flow. This “orientation-only” character of the dispersion relation is also shared by the dispersion relation for internal gravity waves (equation (49.61)) and inertia-gravity waves (equation (49.163)). Indeed, for the case with zero baroclinicity, in which $u_g = 0$, then the dispersion relation (50.112c) reduces to that for inertia-gravity waves.

50.7.5 Stability conditions

The dispersion relation (50.112c) determines the squared angular frequency, ω^2 , for a plane wave ansatz. If $\omega^2 > 0$ then there are propagating waves. However, if $\omega^2 < 0$ then the waves can be exponentially growing, in which case we say the flow is unstable. To determine the condition for stability, write the dispersion relation in the form

$$\omega^2 = F(\tan \phi) \cos^2 \alpha, \quad (50.113)$$

where we introduced the quadratic stability function

$$F(\tau) = f(f + \zeta_g) + 2f\partial_z u_g \tau + N^2 \tau^2. \quad (50.114)$$

The question of stability has been reduced to the question of whether there are wave perturbations that realize $F(\tan \phi) < 0$, in which case $\omega^2 < 0$. To answer this question we write

$$F(\tau) = (\tau - R_+) (\tau - R_-), \quad (50.115)$$

with the two roots given by the quadratic formula

$$N^2 R_{\pm} = -f \partial_z u_g \pm \sqrt{(f \partial_z u_g)^2 - N^2 f (f + \zeta_g)} = -f \partial_z u_g \pm \sqrt{-f Q_g}, \quad (50.116)$$

where the final equality introduced the base state potential vorticity, Q_g , from equation (50.97). Remarkably, local stability has boiled down to the sign of $f Q_g$ at any point within the fluid.

Stable case

If $f Q_b > 0$, then the two roots, R_{\pm} , are complex conjugates. Yet $\tan \phi$ is real for all waves with real wavevectors. Hence, if $f Q_g > 0$ then there are no waves for which $F(\tan \phi)$ vanishes, meaning that the stability function has one sign for all waves. To establish the sign, note that for very weak fronts in stably stratified fluids,

$$F(\tau) \approx f^2 + N^2 \tau^2 > 0, \quad (50.117)$$

which is the case for linear, and stable, inertia-gravity waves. Ramping up the strength of the geostrophic front, while maintaining $f Q_g > 0$, ensures that such geostrophic fronts are locally stable.

For the typical case in stratified geophysical fluids, we have $N^2 > f^2$, so that the maximum angular frequency (50.112c) occurs with horizontally propagating waves where $\alpha = \pi/2$ so that

$$\omega_{\max}^2 = N^2, \quad (50.118)$$

in which case fluid particles exhibit buoyancy oscillations in the vertical. At the other end of the spectrum, the minimum angular frequency occurs when $\alpha = 0$ so that the wavevector is vertical and

$$\omega_{\min}^2 = f(f + \zeta_g), \quad (50.119)$$

which are inertial oscillations in the presence of a nonzero relative vorticity.

Unstable case

If $f Q_g < 0$ then the two roots, R_{\pm} , are real

$$R_{\pm} = \frac{-f \partial_z u_g \pm \sqrt{|f Q_g|}}{N^2}, \quad (50.120)$$

thus ensuring that there are waves that render $F(\tan \phi) = 0$. Hence, the stability function changes sign so that waves are unstable if $\omega^2 < 0$. In the unstable case, ω is not an angular frequency but instead it measures the exponential *growth rate* for the unstable wave.

50.7.6 Ertel potential vorticity and local stability

In developing the stability conditions in Section 50.7.5, appearance of the Ertel potential vorticity might not have seemed so remarkable. Namely, it seemingly just provided a useful shorthand for the discriminant of the square root appearing the quadratic formula. In fact, potential vorticity is central to the power of the stability analysis since it provides a direct connection to physical processes required to initiate symmetric instability. Namely, potential vorticity is materially invariant in a perfect fluid (Chapters 38 and 39). Hence, if a fluid starts in a stable state with $f Q > 0$, say it starts with zero baroclinicity and with stably stratification so that $f Q = f^2 N^2 > 0$, then it has very restrictive means to evolve into an unstable state with $f Q < 0$. One means for

inducing $f Q < 0$ is to introduce friction, diffusion, boundary processes, and/or other irreversible processes that materially alter Q in such a manner that brings $f Q < 0$. Another means is for a perfect fluid parcel to cross the equator so that f changes sign. If the parcel starts from a side of the equator with $f Q > 0$, then on the other side it has $f Q < 0$ and so it is symmetrically unstable.

As noted by [Thomas et al. \(2013\)](#), the instability criteria, $f Q < 0$, embodies three instabilities. Namely, for a barotropic fluid, whereby $\nabla_z b = 0$, then the potential vorticity is given by

$$f Q = f(f + \zeta) N^2. \quad (50.121)$$

The $f Q > 0$ stability criteria is satisfied with $N^2 > 0$ (gravitational stability; Section 27.5.4) and $f(f + \zeta) > 0$ (horizontal inertial stability; Section 50.5). In the presence of baroclinicity with a symmetric front, the $f Q > 0$ stability criteria then reflects symmetric stability of the present section. [Buckingham et al. \(2021\)](#) offer a generalization of the stability criteria by allowing for curvature of the front, thus providing a criteria to determine stability with regard to gravitational, centrifugal, horizontal inertial, and symmetric instabilities.

50.7.7 Comments and further study

The bulk of this section is an elaboration of [Hoskins \(1974\)](#), which exposed the connection between symmetric instability and Ertel potential vorticity. The study from [Thomas et al. \(2013\)](#) provides an example of these ideas for the ocean, offering practical details to map out stability regimes across the spectrum of gravitational, inertial, and symmetric instabilities. [Buckingham et al. \(2021\)](#) generalized [Hoskins \(1974\)](#) to the allow for a curved front.

50.8 Semi-geostrophy and the frontal overturning circulation

We here further our understanding of the overturning circulation that arises in symmetric fronts, with the overturning occurring in the cross-front and vertical plane. This *secondary* circulation is ageostrophic, and thus sometimes referred to as the *ageostrophic secondary circulation*. We make use of elements from the symmetric stability analysis in Section 50.6. However, the focus here is not on the stability per se, but instead on deriving an expression for the overturning circulation.

[Hoskins \(1975\)](#) provided a major advance in our ability to study secondary overturning circulations along fronts by introducing the *semi-geostrophic* (SG) equations. The semi-geostrophic system is balanced (i.e., gravity waves are filtered), just like in the quasi-geostrophic theory of Chapter 42. But the semi-geostrophic system is more general than quasi-geostrophy, in particular by allowing for the study of flow with Rossby numbers of order unity, with such large Rossby numbers occurring in regions of ocean submesoscale fronts and atmospheric mesoscale fronts. Large magnitude vertical velocities are signatures of order unity Rossby number flow. We here develop elements of the semi-geostrophic frontal equations to study ageostrophic motions (including vertical motion) occurring along fronts in the ocean and atmosphere. We use the language of oceanography since much of the presentation follows the ocean submesoscale discussion in the review article by [Thomas et al. \(2008\)](#).

50.8.1 Hydrostatic and Boussinesq fluid on an f -plane

We frame our analysis within the adiabatic and hydrostatic Boussinesq equations (see Section 41.2) on an f -plane

$$\frac{Du}{Dt} - fv = -\frac{\partial \phi}{\partial x} \quad (50.122a)$$

$$\frac{Dv}{Dt} + fu = -\frac{\partial \phi}{\partial y} \quad (50.122b)$$

$$\frac{\partial \phi}{\partial z} = b \quad (50.122c)$$

$$\frac{Db}{Dt} = 0 \quad (50.122d)$$

$$\nabla \cdot \mathbf{v} = \nabla_z \cdot \mathbf{u} + \frac{\partial w}{\partial z} = 0. \quad (50.122e)$$

The geostrophic velocity is given in terms of the pressure field by

$$\mathbf{u}_g = f^{-1} \hat{\mathbf{z}} \times \nabla_z \phi \implies u_g = -\frac{1}{f} \frac{\partial \phi}{\partial y} \quad v_g = \frac{1}{f} \frac{\partial \phi}{\partial x}. \quad (50.123)$$

The horizontal momentum equations (50.122a)-(50.122b) can thus be written

$$\mathbf{u} = \mathbf{u}_g + \hat{\mathbf{z}} \times \mathcal{D}\mathbf{u} \implies u = u_g - \mathcal{D}v \quad v = v_g + \mathcal{D}u, \quad (50.124)$$

where we introduced the dimensionless material time operator

$$\mathcal{D} = \frac{1}{f} \frac{D}{Dt}. \quad (50.125)$$

One step of iteration then leads to

$$u = u_g - \mathcal{D}(v_g + \mathcal{D}u) \quad (50.126a)$$

$$v = v_g + \mathcal{D}(u_g - \mathcal{D}v). \quad (50.126b)$$

Recall that on an f -plane, the geostrophic velocity \mathbf{u}_g is horizontally non-divergent.

50.8.2 Geostrophic momentum approximation

The *geostrophic momentum approximation* assumes the horizontal velocity takes the form

$$\mathbf{u} \approx \mathbf{u}_{gm} = \mathbf{u}_g + \hat{\mathbf{z}} \times \mathcal{D}\mathbf{u}_g. \quad (50.127)$$

For simplicity in notation, we drop the “gm” subscripts in the following. The geostrophic momentum approximation holds so long as

$$|u| \gg |\mathcal{D}^2 u| \quad (50.128a)$$

$$|v| \gg |\mathcal{D}^2 v|. \quad (50.128b)$$

Rearranging the geostrophic momentum approximation (50.127) leads to

$$\mathcal{D}\mathbf{u}_g + \hat{\mathbf{z}} \times (\mathbf{u} - \mathbf{u}_g) = 0. \quad (50.129)$$

Reintroducing the material time derivative yields

$$\frac{D\mathbf{u}_g}{Dt} + f\hat{\mathbf{z}} \times \mathbf{u}_{ag} = 0 \quad (50.130)$$

where \mathbf{u}_{ag} is the ageostrophic velocity based on the geostrophic momentum velocity

$$\mathbf{u}_{ag} = \mathbf{u} - \mathbf{u}_g = \hat{\mathbf{z}} \times \mathcal{D}\mathbf{u}_g. \quad (50.131)$$

Hence, for the geostrophic momentum approximation, the material time evolution of the geostrophic velocity is forced by the Coriolis acceleration due to the ageostrophic velocity. Furthermore, the material time derivative for the semi-geostrophic system is given by

$$\frac{D}{Dt} = \frac{\partial}{\partial t} + \mathbf{v} \cdot \nabla = \frac{\partial}{\partial t} + (\mathbf{u}_g + \mathbf{u}_{ag}) \cdot \nabla_z + w \frac{\partial}{\partial z} \quad (50.132)$$

with

$$\mathbf{v} = (\mathbf{u}_g + \mathbf{u}_{ag}) + \hat{\mathbf{z}} w. \quad (50.133)$$

50.8.3 Secondary ageostrophic circulation

In Sections 50.5 and 50.6 we focused on the stability of a geostrophically balanced equilibrium with flow along a symmetric front. In addition to the geostrophic flow along the front, there is generally an ageostrophic circulation that circulates in the plane orthogonal to the front; i.e., the cross-front / vertical plane. We here derive a general equation describing this overturning circulation, and then specialize that equation in Section 50.8.4. For that purpose, start from the zonal momentum equation, buoyancy equation, and continuity equation within the semi-geostrophic system

$$\frac{\partial \mathbf{u}_g}{\partial t} + (\mathbf{u}_g \cdot \nabla_z) \mathbf{u}_g + (\mathbf{u}_{ag} \cdot \nabla_z) \mathbf{u}_g + w \frac{\partial \mathbf{u}_g}{\partial z} - f v_{ag} = 0 \quad (50.134a)$$

$$\frac{\partial b}{\partial t} + \mathbf{u}_g \cdot \nabla_z b + \mathbf{u}_{ag} \cdot \nabla_z b + w N^2(z) = 0 \quad (50.134b)$$

$$\frac{\partial \mathbf{u}_{ag}}{\partial x} + \frac{\partial \mathbf{v}_{ag}}{\partial y} + \frac{\partial w}{\partial z} = 0. \quad (50.134c)$$

Note that any vertical flow is ageostrophic, so that it is not necessary to place the “ag” subscript on w .

The vertical derivative of the zonal momentum equation and the meridional derivative of the buoyancy equation lead to

$$\frac{\partial}{\partial t} \frac{\partial \mathbf{u}_g}{\partial z} + \left(\frac{\partial \mathbf{u}_g}{\partial z} \cdot \nabla_z \right) \mathbf{u}_g + (\mathbf{u}_g \cdot \nabla_z) \frac{\partial \mathbf{u}_g}{\partial z} + \left(\frac{\partial \mathbf{u}_{ag}}{\partial z} \cdot \nabla_z \right) \mathbf{u}_g + (\mathbf{u}_{ag} \cdot \nabla_z) \frac{\partial \mathbf{u}_g}{\partial z} + \frac{\partial}{\partial z} \left(w \frac{\partial \mathbf{u}_g}{\partial z} \right) - f \frac{\partial v_{ag}}{\partial z} = 0 \quad (50.135a)$$

$$\frac{\partial}{\partial t} \frac{\partial b}{\partial y} + \left(\frac{\partial \mathbf{u}_g}{\partial y} \cdot \nabla_z \right) b + (\mathbf{u}_g \cdot \nabla_z) \frac{\partial b}{\partial y} + \left(\frac{\partial \mathbf{u}_{ag}}{\partial y} \cdot \nabla_z \right) b + (\mathbf{u}_{ag} \cdot \nabla_z) \frac{\partial b}{\partial y} + \frac{\partial w}{\partial y} N^2 = 0. \quad (50.135b)$$

We now make use of thermal wind for the geostrophic velocity

$$f \frac{\partial \mathbf{u}_g}{\partial z} = \hat{\mathbf{z}} \times \nabla_z b \implies \frac{\partial \mathbf{u}_g}{\partial z} = -\frac{1}{f} \frac{\partial b}{\partial y} \quad \frac{\partial v_g}{\partial z} = \frac{1}{f} \frac{\partial b}{\partial x} \quad (50.136)$$

thus rendering

$$\frac{\partial}{\partial t} \frac{\partial b}{\partial y} - f \left(\frac{\partial \mathbf{u}_g}{\partial z} \cdot \nabla_z \right) \mathbf{u}_g + (\mathbf{u}_g \cdot \nabla_z) \frac{\partial b}{\partial y} - f \left(\frac{\partial \mathbf{u}_{ag}}{\partial z} \cdot \nabla_z \right) \mathbf{u}_g + (\mathbf{u}_{ag} \cdot \nabla_z) \frac{\partial b}{\partial y} + \frac{\partial}{\partial z} \left(w \frac{\partial b}{\partial y} \right) + f^2 \frac{\partial v_{ag}}{\partial z} = 0 \quad (50.137a)$$

$$\frac{\partial}{\partial t} \frac{\partial b}{\partial y} + \left(\frac{\partial \mathbf{u}_g}{\partial y} \cdot \nabla_z \right) b + (\mathbf{u}_g \cdot \nabla_z) \frac{\partial b}{\partial y} + \left(\frac{\partial \mathbf{u}_{ag}}{\partial y} \cdot \nabla_z \right) b + (\mathbf{u}_{ag} \cdot \nabla_z) \frac{\partial b}{\partial y} + \frac{\partial w}{\partial y} N^2 = 0. \quad (50.137b)$$

Subtracting equation (50.137b) from equation (50.137a) eliminates the time derivative thus revealing the diagnostic relation

$$-f\left(\frac{\partial \mathbf{u}_g}{\partial z} \cdot \nabla_z\right)u_g - f\left(\frac{\partial \mathbf{u}_{ag}}{\partial z} \cdot \nabla_z\right)u_g + \frac{\partial}{\partial z}\left(w \frac{\partial b}{\partial y}\right) + f^2 \frac{\partial v_{ag}}{\partial z} - \left(\frac{\partial \mathbf{u}_g}{\partial y} \cdot \nabla_z\right)b - \left(\frac{\partial \mathbf{u}_{ag}}{\partial y} \cdot \nabla_z\right)b - \frac{\partial w}{\partial y}N^2 = 0. \quad (50.138)$$

We now make use of thermal wind and horizontal non-divergence for the geostrophic velocity to write (as in the solution to Exercise 42.4)

$$f \frac{\partial \mathbf{u}_g}{\partial z} \cdot \nabla_z u_g = \frac{\partial \mathbf{u}_g}{\partial y} \cdot \nabla_z b = -Q^{(y)}, \quad (50.139)$$

where $Q^{(y)}$ is the meridional component of the geostrophic \mathbf{Q} -vector (see Exercise 42.4)

$$\mathbf{Q} = -\left(\frac{\partial \mathbf{u}_g}{\partial x} \cdot \nabla_z b\right) \hat{x} - \left(\frac{\partial \mathbf{u}_g}{\partial y} \cdot \nabla_z b\right) \hat{y}. \quad (50.140)$$

Introduction of $Q^{(y)}$ into equation (50.138) yields

$$-f\left(\frac{\partial \mathbf{u}_{ag}}{\partial z} \cdot \nabla_z\right)u_g + \frac{\partial w}{\partial z} \frac{\partial b}{\partial y} + w \frac{\partial^2 b}{\partial z \partial y} + f^2 \frac{\partial v_{ag}}{\partial z} - \left(\frac{\partial \mathbf{u}_{ag}}{\partial y} \cdot \nabla_z\right)b - \frac{\partial w}{\partial y}N^2 = -2Q^{(y)}. \quad (50.141)$$

Again making use of thermal wind and $\nabla_z \cdot \mathbf{u}_g = 0$ allows us to write

$$-f\left(\frac{\partial \mathbf{u}_{ag}}{\partial z} \cdot \nabla_z\right)u_g - \left(\frac{\partial \mathbf{u}_{ag}}{\partial y} \cdot \nabla_z\right)b = f \frac{\partial u_{ag}}{\partial z} \frac{\partial v_g}{\partial y} - f \frac{\partial v_{ag}}{\partial z} \frac{\partial u_g}{\partial y} + f \frac{\partial u_{ag}}{\partial y} \frac{\partial v_g}{\partial z} + f \frac{\partial v_{ag}}{\partial y} \frac{\partial u_g}{\partial z}. \quad (50.142)$$

The mixed partial derivative of the buoyancy vanishes

$$\frac{\partial^2 b}{\partial z \partial y} = \frac{\partial}{\partial y} \frac{\partial b}{\partial z} = \frac{\partial N^2(z)}{\partial y} = 0, \quad (50.143)$$

which follows since we are assuming a background vertical stratification that is independent of horizontal direction. Bringing these results together into equation (50.141) leads to

$$f \frac{\partial u_{ag}}{\partial z} \frac{\partial v_g}{\partial y} + f \frac{\partial u_{ag}}{\partial y} \frac{\partial v_g}{\partial z} + f \frac{\partial v_{ag}}{\partial y} \frac{\partial u_g}{\partial z} + \frac{\partial w}{\partial z} \frac{\partial b}{\partial y} + f \frac{\partial v_{ag}}{\partial z} \left(f - \frac{\partial u_g}{\partial y}\right) - \frac{\partial w}{\partial y}N^2 = -2Q^{(y)}. \quad (50.144)$$

Another use of thermal wind brings this result to the form

$$f \frac{\partial u_{ag}}{\partial z} \frac{\partial v_g}{\partial y} + f \frac{\partial u_{ag}}{\partial y} \frac{\partial v_g}{\partial z} + f \frac{\partial u_g}{\partial z} \left(\frac{\partial v_{ag}}{\partial y} - \frac{\partial w}{\partial z}\right) + f \frac{\partial v_{ag}}{\partial z} \left(f - \frac{\partial u_g}{\partial y}\right) - \frac{\partial w}{\partial y}N^2 = -2Q^{(y)}. \quad (50.145)$$

This equation provides a relation for the ageostrophic cross-flow and vertical circulation, (v_{ag}, w) , written in terms of the buoyancy field and the geostrophic flow. We next consider flow surrounding a symmetric front, in which case equation (50.145) becomes a diagnostic equation for the ageostrophic overturning streamfunction.

50.8.4 Ageostrophic overturning circulation for a symmetric front

The general result (50.145) is now specialized by assuming the zonal velocity is purely geostrophic (as in a zonal geostrophic front) so that

$$u_{ag} = 0. \quad (50.146)$$

For this flow, the ageostrophic flow in the cross-flow/depth plane is non-divergent

$$\frac{\partial v_{ag}}{\partial y} + \frac{\partial w}{\partial z} = 0. \quad (50.147)$$

The diagnostic equation (50.145) now takes on the specialized form for a symmetric front

$$-2f \frac{\partial u_g}{\partial z} \frac{\partial w}{\partial z} + f(f + \zeta_g) \frac{\partial v_{ag}}{\partial z} - \frac{\partial w}{\partial y} N^2 = -2Q^{(y)}, \quad (50.148)$$

where

$$\zeta_g = -\frac{\partial u_g}{\partial y} \quad (50.149)$$

is the vertical component of the geostrophic relative vorticity. Introducing an overturning stream-function for the cross-flow/vertical ageostrophic circulation

$$v_{ag} = \frac{\partial \psi}{\partial z} \quad w = -\frac{\partial \psi}{\partial y}, \quad (50.150)$$

and using thermal wind brings equation (50.148) into the form

$$(N^2 \partial_{yy} - 2 \partial_y b \partial_{yz} + f(f + \zeta_g) \partial_{zz}) \psi = -2Q^{(y)}. \quad (50.151)$$

Equation (50.151) is useful for the study of ageostrophic ($Ro \sim 1$) dynamics along a front in which there is an ageostrophic overturning circulation in response to geostrophic forcing from $Q^{(y)}$.

50.8.5 Connection to potential vorticity and symmetric instability

The partial differential equation (50.151) can be written

$$\mathcal{K}\psi = -2Q^{(y)}, \quad (50.152)$$

where

$$\mathcal{K} = N^2 \partial_{yy} - 2 \partial_y b \partial_{yz} + f(f + \zeta_g) \partial_{zz} \quad (50.153)$$

is a linear partial differential operator that is a function of the geostrophic flow and the buoyancy. Following the considerations in Section 3.5, we know that this operator is elliptic if the following inequality holds

$$\left(\frac{\partial b}{\partial y}\right)^2 - N^2 f(f + \zeta_g) < 0. \quad (50.154)$$

We can relate the ellipticity condition (50.154) to the Ertel potential vorticity for the Boussinesq geostrophic flow. For this purpose, write the geostrophic vorticity as

$$\omega_g = \nabla \times \mathbf{u}_g \quad (50.155a)$$

$$= -\hat{x} \frac{\partial v_g}{\partial z} + \hat{y} \frac{\partial u_g}{\partial z} + \hat{z} \left(\frac{\partial v_g}{\partial x} - \frac{\partial u_g}{\partial y} \right) \quad (50.155b)$$

$$= -\frac{1}{f} \left(\hat{x} \frac{\partial b}{\partial x} + \hat{y} \frac{\partial b}{\partial y} \right) + \hat{z} \left(\frac{\partial v_g}{\partial x} - \frac{\partial u_g}{\partial y} \right). \quad (50.155c)$$

If we assume the front is zonally symmetric, then the geostrophic vorticity takes the form

$$\omega_g^{2d} = -\frac{1}{f} \frac{\partial b}{\partial y} \hat{y} - \hat{z} \frac{\partial u_g}{\partial y}, \quad (50.156)$$

in which case the Ertel potential vorticity (for the geostrophic and Boussinesq flow) takes the form

$$q_g^{2d} = \nabla b \cdot (\boldsymbol{\omega}_g + f\hat{z}) \quad (50.157a)$$

$$= -\frac{1}{f} \left(\frac{\partial b}{\partial y} \right)^2 + N^2 \left(f - \frac{\partial u_g}{\partial y} \right). \quad (50.157b)$$

$$= -\frac{1}{f} \left(\frac{\partial b}{\partial y} \right)^2 + N^2 (f + \zeta_g). \quad (50.157c)$$

Ellipticity of the PDE (50.151) is thus assured so long as

$$fq_g^{2d} = - \left(\frac{\partial b}{\partial y} \right)^2 + N^2 f (f + \zeta_g) > 0. \quad (50.158)$$

The PDE (50.6) transitions to a hyperbolic system when $fq_g^{2d} < 0$, which is the condition for symmetric instability detailed in Section 50.6.



50.9 Exercises

EXERCISE 50.1: INERTIAL INSTABILITY IN A SHALLOW WATER LAYER

In Section 50.5 we developed the physics of horizontal inertial instability within the continuous Boussinesq equations. Consider the analysis instead within the context of a single layer of shallow water fluid. What are the conditions for inertial instability within the shallow water layer? Are they the same as for the continuous Boussinesq equations? Why?

EXERCISE 50.2: STABILITY CRITERIA IN TERMS OF BALANCED RICHARDSON NUMBER

Consider the balanced Richardson number, defined for the geostrophic and hydrostatic balanced flow, along with a corresponding angle

$$Ri_b = \frac{N^2}{(\partial_z u_g)^2} \quad \text{and} \quad \phi_{Ri_b} \equiv \tan^{-1}(-1/Ri_b). \quad (50.159)$$

Show that the instability criteria, $f Q < 0$, from Section 50.7 can be written in the equivalent form

$$\phi_{Ri_b} < \phi_c \equiv \tan^{-1}(-(f + \zeta_g)/f). \quad (50.160)$$

As shown by [Thomas et al. \(2013\)](#), this alternative form of the instability criteria allows for a very effective means to characterize flow regimes conducive to the suite of local instabilities: gravitational, inertial, and symmetric.

EXERCISE 50.3: GROUP VELOCITY FOR SYMMETRIC MERIDIONAL-VERTICAL WAVES

In this exercise we derive some properties for the group velocity of the stable meridional-vertical plane waves discussed in Section 50.7.4.

- (a) Derive the group velocity, \mathbf{c}_g , for the stable meridional-vertical waves whose dispersion relation is given by equation (50.112c).
- (b) Compute $\mathbf{c}_g \cdot \mathbf{k}$, where the wavevector is $\mathbf{k} = k_y \hat{y} + k_z \hat{z}$.



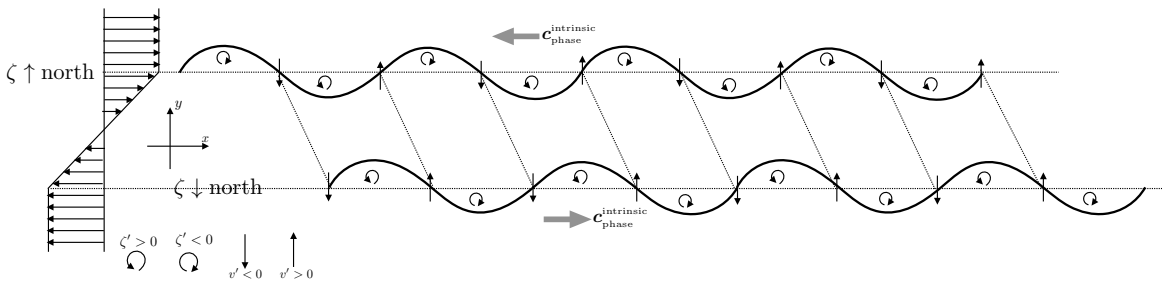


FIGURE 50.5: Schematic of an inertially stable (left panel) and inertially unstable (right panel) flow in the northern hemisphere. In both panels we display two red vectors, one for the geostrophic velocity, $u_g(y)$, and the second for the velocity at a displaced position $y + \Delta y$, with the displaced velocity determined by conservation of zonal potential momentum, $u_{\text{disp}}(y + \Delta y) = u_g(y) + f \Delta y$ (equation (50.68)). In the unperturbed flow, the eastward geostrophic velocity is generated by a northward pressure gradient acceleration that balances a southward Coriolis acceleration. The base state pressure gradient remains unchanged even as the fluid parcels are perturbed, with this assumption basic to the parcel method of stability analysis. At the displaced position we also show the base state velocity at the displaced position, $u(y + \Delta y) = u_g(y) + \partial_y u(y) \Delta y = u_g(y) - \zeta_g(y) \Delta y$. The difference between the displaced velocity and the base state velocity is $u_{\text{disp}}(y + \Delta y) - u(y + \Delta y) = (f + \zeta_g) \Delta y$. For the left panel, the flow has positive relative vorticity so that $\zeta_g + f > 0$ and the flow is inertially stable. In this case, the displaced parcel has a southward Coriolis acceleration larger than the local Coriolis, thus returning the parcel back towards its initial latitude. For the right panel, the flow has negative relative vorticity strong enough so that $\zeta_g + f < 0$, in which case the flow is inertially unstable. In this case, the displaced parcel has a southward Coriolis acceleration smaller than the local Coriolis, so that the northward pressure gradient is strong enough to keep the parcel moving northward, away from its initial position.

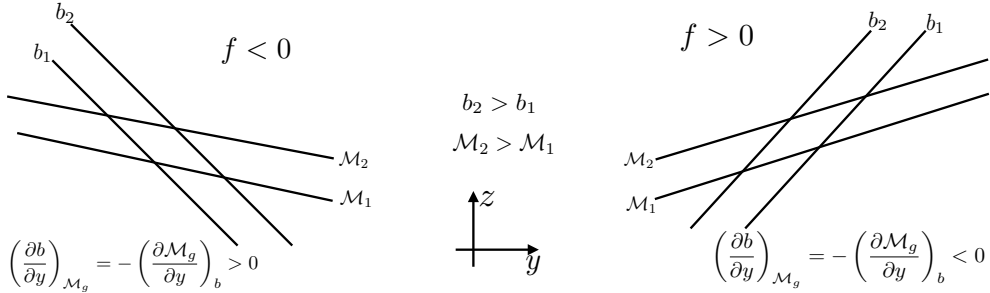


FIGURE 50.6: Example flow configurations that are symmetrically unstable; i.e., inertially unstable to a symmetric perturbation along a constant buoyancy surface. We show example buoyancy surfaces and potential momentum surfaces for the southern hemisphere (left) and northern hemisphere (right). The instability conditions (50.89) and (50.91) are indicated on the respective panels. In both cases, surfaces of constant buoyancy are more steeply sloped than constant potential momentum surfaces. The x coordinate measures distance in the along-front direction and y measures distance in the cross-front direction, oriented so that $\hat{x} \times \hat{y} = \hat{z}$ where \hat{z} is anti-parallel to gravity (\hat{x} is out of the page). A means to quickly judge whether a flow is symmetrically unstable is to note that the wedge region between buoyancy and potential momentum surfaces provides a source of available potential energy. Symmetric instability can feed off the potential energy only when buoyancy surfaces are more steeply sloped than potential momentum surfaces.

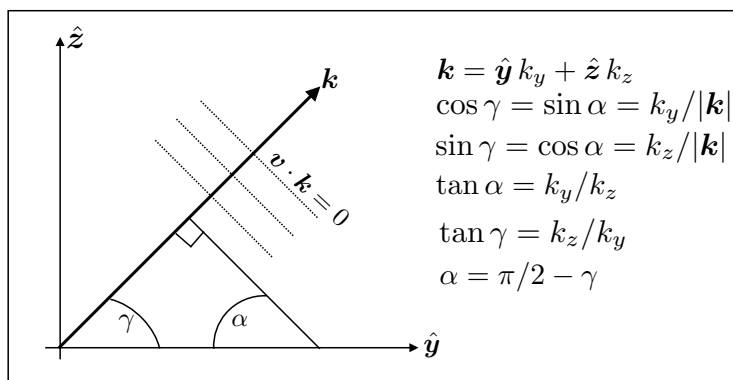


FIGURE 50.7: Transverse plane wave used to probe the stability of a baroclinic front. The phase vector, \mathbf{k} , makes an angle γ with the horizontal and α with the vertical.

Chapter 51

STABILITY OF FLUID INTERFACES

In this chapter we study the *Rayleigh-Taylor* and *Kelvin-Helmholtz* instabilities as realized along a material fluid interface that separates two homogeneous (constant density) fluid layers of differing densities, and with the two fluids immiscible and inviscid. Forces acting at the interface include gravity and surface tension, with surface tension relevant only for very small scales. We do not consider rotation in this chapter, and the relative vorticity vanishes in both layers. We make use of Fourier modal analysis method to develop necessary and sufficient conditions for instability.

Rayleigh-Taylor instability occurs when a lighter fluid layer sits below a heavier layer, and with a base state that is at rest. Instability occurs when the destabilizing effects from gravity overcome the stabilizing effects from surface tension. In the absence of surface tension, there is always a Rayleigh-Taylor instability when heavy fluid sits above light fluid.

The Kelvin-Helmholtz instability occurs when the heavy fluid sits below the light fluid (stably stratified) and with a base state velocity that differs between the two layers (i.e., there is a velocity shear). Instability occurs when the destabilizing effects from velocity shear overcome the stabilizing effects from gravity and surface tension. In the absence of gravity or surface tension, any velocity shear leads to an instability.

The system under consideration is idealized by assuming the interface between the fluid layers is infinitesimal, and that the fluids are inviscid and immiscible. Even so, the methods used to develop the instability conditions are quite useful in more realistic cases. Furthermore, experimental results support the relevance of the instability conditions found in this chapter. Finally, and most importantly for our purposes, the study offers insights into the nature of fluid instabilities.

READER'S GUIDE FOR THIS CHAPTER

This chapter is an extension of the material in Chapter 45, which is concerned with surface waves on an interface arising from gravity and/or surface tension. We here assume familiarity with that chapter.

51.1	Loose threads	1356
51.2	Governing equations for the layer interface	1356
51.2.1	Equations from potential theory	1356
51.2.2	Kinematic boundary condition at the interface	1357
51.2.3	Dynamic boundary condition at the interface	1358
51.2.4	Pressures in the two layers	1358
51.2.5	Linearized equations	1359
51.3	Rayleigh-Taylor instability	1359
51.3.1	Boundary value problem and dispersion relation	1360
51.3.2	Stable traveling plane waves	1361
51.3.3	Unstable exponentially growing plane waves	1361

51.3.4	Further study	1363
51.4	Kelvin-Helmholtz instability	1363
51.4.1	Velocity potential	1363
51.4.2	Dispersion relation from the interface conditions	1363
51.4.3	Analysis of the stability condition	1364
51.4.4	Further study	1365

51.1 Loose threads

- Figures needed throughout
- energetic analysis of the instabilities

51.2 Governing equations for the layer interface

In this section we develop the equations describing motion of an interface separating two homogeneous, immiscible, non-rotating, and inviscid fluids with densities, ρ_1 and ρ_2 and constant zonal velocities, $\hat{\mathbf{x}} u_1^0$ and $\hat{\mathbf{x}} u_2^0$. (Figure 51.1). We ignore side boundaries by assuming the domain is horizontally infinite. This is the physical system that is used to study the Rayleigh-Taylor and the Kelvin-Helmholtz instabilities.

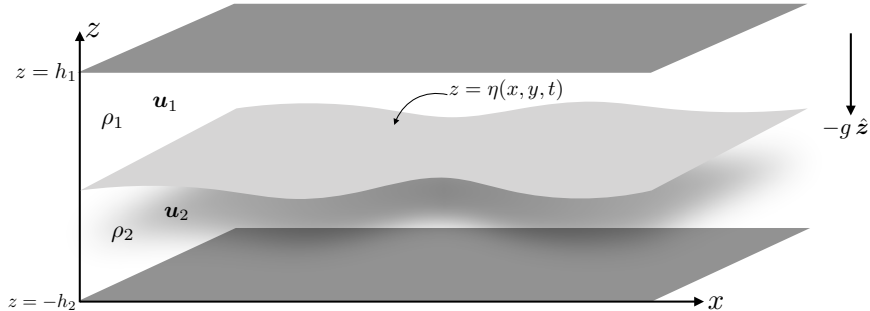


FIGURE 51.1: A non-rotating box filled with two homogeneous and immiscible fluids with densities ρ_1 and ρ_2 , and horizontal velocities \mathbf{u}_1^0 and \mathbf{u}_2^0 . The material interface between the layers is located at $z = \eta(x, y, t)$, with $\eta = 0$ when the interface is flat. The fluid region is denoted \mathcal{R} , which is infinite in the horizontal directions. For study of the Rayleigh-Taylor instability we assume rigid and flat plates located at $z = -h_2$ and $z = h_1$, whereas for Kelvin-Helmholtz instability we let h_1 and h_2 go to infinity.

51.2.1 Equations from potential theory

Since the fluid in each layer has a constant density (incompressible), the velocity in each layer is non-divergent, $\nabla \cdot \mathbf{v} = 0$. Furthermore, we assume the flow is irrotational ($\nabla \times \mathbf{v} = 0$). We can thus make use of the potential theory detailed in Section 45.2. In particular, the velocity potential has a time tendency given by Bernoulli's equation of motion (45.16)

$$\partial_t \Psi = \Phi + \mathcal{K} + p/\rho = \mathcal{K} + p_d/\rho, \quad (51.1)$$

where

$$\mathbf{v} = -\nabla\Psi \quad \text{velocity potential} \quad (51.2a)$$

$$\Phi = g z \quad \text{geopotential} \quad (51.2b)$$

$$\mathcal{K} = \mathbf{v} \cdot \mathbf{v}/2 \quad \text{kinetic energy per mass} \quad (51.2c)$$

$$p = -\rho\Phi + p_d \quad p = \text{pressure and } p_d = \text{dynamic pressure.} \quad (51.2d)$$

The velocity potential satisfies Laplace's equation in the fluid interior and the no-normal flow kinematic boundary condition (Neumann boundary condition) at the rigid top and rigid bottom

$$\nabla^2\Psi = 0 \quad \mathbf{x} \in \mathcal{R} \quad (51.3a)$$

$$\hat{\mathbf{n}} \cdot \nabla\Psi = 0 \quad \mathbf{x} \in \partial\mathcal{R}. \quad (51.3b)$$

When considering a background velocity, we extract the velocity potential for the static background potential, $\Psi_n^0 = -u_n^0 x$, with the remaining portion of the velocity potential capturing the perturbation relative to the background. Note that the background velocity potential trivially satisfies Laplace's equation and the no-normal flow boundary condition.

51.2.2 Kinematic boundary condition at the interface

Motion of the interface, $z = \eta(x, y, t)$, is determined by boundary conditions evaluated at the interface. The interface is material since the fluid layers are assumed to be immiscible. Focusing first on the lower side, in region 2, the kinematic boundary condition from Section 16.4.2 states that

$$(\mathbf{v}_2 - \mathbf{v}_\eta) \cdot \hat{\mathbf{n}}_2 = 0 \quad \text{at } z = \eta, \quad (51.4)$$

where \mathbf{v}_2 is the fluid velocity in the lower region, and

$$\hat{\mathbf{n}}_2 = \hat{\mathbf{n}} = \frac{\nabla(z - \eta)}{|\nabla(z - \eta)|} \quad \text{at } z = \eta, \quad (51.5)$$

is the outward normal direction pointing into the upper layer. The analysis for layer-2 holds equivalantly for layer-1, only with the normal direction pointing from layer-1 down to layer-2. We thus have

$$(\mathbf{v}_2 - \mathbf{v}_\eta) \cdot \hat{\mathbf{n}} = 0 \quad \text{and} \quad (\mathbf{v}_\eta - \mathbf{v}_1) \cdot \hat{\mathbf{n}} = 0 \implies (\mathbf{v}_2 - \mathbf{v}_1) \cdot \hat{\mathbf{n}} = 0. \quad (51.6)$$

That is, the normal components to the layer velocities match at the interface. Consequently, the normal derivative of the velocity potential also matches at the interface

$$\hat{\mathbf{n}} \cdot (\nabla\Psi_2 - \nabla\Psi_1) = 0 \quad \text{at } z = \eta. \quad (51.7)$$

The velocity of the interface, \mathbf{v}_η , has a normal component given by

$$|\nabla(z - \eta)| \mathbf{v}_\eta \cdot \hat{\mathbf{n}} = \partial_t \eta \quad \text{at } z = \eta, \quad (51.8)$$

so that the kinematic boundary condition (51.4) can be written in the equivalent form

$$(\partial_t + \mathbf{u}_1 \cdot \nabla) \eta = w_1 \quad \text{and} \quad (\partial_t + \mathbf{u}_2 \cdot \nabla) \eta = w_2 \quad \text{at } z = \eta. \quad (51.9)$$

Inserting the background velocity and the velocity potential leads to the kinematic boundary conditions

$$(\partial_t + u_1^0 \partial_x - \nabla \Psi_1 \cdot \nabla) \eta = -\partial_z \Psi_1 \quad \text{and} \quad (\partial_t + u_2^0 \partial_x - \nabla \Psi_2 \cdot \nabla) \eta = -\partial_z \Psi_2 \quad \text{at } z = \eta. \quad (51.10)$$

51.2.3 Dynamic boundary condition at the interface

The dynamic boundary condition from Section 22.10 says that the pressure is continuous across the interface so long as we ignore surface tension. For the case with surface tension, the discussion in Section 22.11 reveals a pressure jump across the interface, which here takes the form given by the Young-Laplace formula (22.138),¹

$$p_2 - p_1 = -\gamma \nabla_z^2 \eta \quad \text{at } z = \eta. \quad (51.11)$$

In this equation, $\gamma > 0$ is the surface tension (dimensions of force per length = M T⁻²). Evidently, pressure on the concave side of the interface is higher than on the convex side. For example, if the interface extends upward then $p_2 - p_1 > 0$ since the layer-2 fluid is on the concave side and so it has the higher interface pressure. This result also follows since $\nabla_z^2 \eta < 0$ for an upward extension of the interface, which leads to a local free surface maximum. The treatment here follows our approach for surface capillary-gravity waves in Section 45.7.1.

51.2.4 Pressures in the two layers

If the fluid is at rest in both layers, with $\eta = 0$, then the layer interface is flat. Consequently, there is no surface tension induced pressure jump across the interface, in which case the rest state pressure is hydrostatic. Pressure at a vertical position, z , in the upper layer is given by

$$p_1^0(z) = g \rho_1 (h_1 - z) \quad \text{for } \eta \leq z \leq h_1, \quad (51.12)$$

where we assumed pressure at $z = h_1$ is zero. Similarly, pressure at a vertical position within the lower layer is

$$p_2^0(z) = p_1^0(\eta) + g \rho_2 (\eta - z) = g \rho_1 (h_1 - \eta) + g \rho_2 (\eta - z) \quad \text{for } -h_2 \leq z \leq \eta. \quad (51.13)$$

If there is fluid motion within the layers, then the layer interface is no longer flat and the pressure is no longer equal to its resting pressure. In this case we write the pressure as

$$p_1(x, y, t) = p_1^0(z) + \delta p_1(x, y, t) \quad (51.14a)$$

$$p_2(x, y, t) = p_2^0(z) + \delta p_2(x, y, t) - \gamma \nabla_z^2 \eta(x, y, t), \quad (51.14b)$$

where δp_1 and δp_2 are pressures associated with the fluid motion and that vanish when the fluid is at rest. Furthermore, these pressures are continuous at the interface just like the hydrostatic pressures

$$\delta p_1 = \delta p_2 \quad \text{at } z = \eta, \quad (51.15)$$

¹We write $\nabla_z^2 \eta$ to emphasize that the Laplacian is only acting in the horizontal directions. This notation is not needed when the Laplacian acts on the interface, η , since this field is just a spatial function of the horizontal positions, x, y . However, in equation (51.23) we replace $\partial_t \eta(x, y, t)$ with $-\partial_z \Psi(x, y, z = 0, t)$ as per the linearized kinematic boundary condition (51.19c) with $u_1 = u_2 = 0$. It is this replacement that makes it important to note that the Laplacian is acting just in the horizontal.

so that the pressure jump (51.11) remains

$$p_2 - p_1 = -\gamma \nabla_z^2 \eta. \quad (51.16)$$

51.2.5 Linearized equations

Following Section 45.3 we find the linearized version of the Bernoulli equation of motion (51.1), along with the linearized kinematic boundary condition (51.9) and dynamic boundary condition (51.16). A new feature here concerns the background flow, in which case the kinetic energy contributes at linear order. In particular, for the Bernoulli equation in layer-1 we have

$$\rho_1 \partial_t \Psi_1 = g z \rho_1 + p_1 + \rho_1 [u_1^0 u_1 + (u_1^0)^2 / 2]. \quad (51.17)$$

The constant, $(u_1^0)^2 / 2$, can be eliminated by taking a gauge transformation, as detailed in Section 45.2.3 when studying surface waves. Hence, we drop this term in the following. Writing $u_1 = -\partial_x \Psi_1$ then brings the linearized Bernoulli equation to the form

$$\rho_1 (\partial_t + u_1^0 \partial_x) \Psi_1 = g z \rho_1 + p_1, \quad (51.18)$$

so that the background zonal flow provides a constant advection of the velocity potential. We are thus led to the following linearized layer equations

$$\rho_1 (\partial_t + u_1^0 \partial_x) \Psi_1 = g z \rho_1 + p_1 \quad \text{linearized Bernoulli equation} \quad (51.19a)$$

$$\rho_2 (\partial_t + u_2^0 \partial_x) \Psi_2 = g z \rho_2 + p_2 \quad \text{linearized Bernoulli equation} \quad (51.19b)$$

$$(\partial_t + u_1^0 \partial_x) \eta = -\partial_z \Psi_1 \quad \text{linearized kinematic b.c. at } z = 0 \quad (51.19c)$$

$$(\partial_t + u_2^0 \partial_x) \eta = -\partial_z \Psi_2 \quad \text{linearized kinematic b.c. at } z = 0 \quad (51.19d)$$

$$\delta p_2 - \delta p_1 = 0 \quad \text{dynamic b.c. at } z = 0. \quad (51.19e)$$

$$p_2 - p_1 = -\gamma \nabla_z^2 \eta \quad \text{dynamic jump b.c. at } z = 0. \quad (51.19f)$$

Taking the difference between the Bernoulli equations in the two layers gives

$$\rho_2 (\partial_t + u_2^0 \partial_x) \Psi_2 - \rho_1 (\partial_t + u_1^0 \partial_x) \Psi_1 = g (\rho_2 z_2 - \rho_1 z_1) + p_2 - p_1, \quad (51.20)$$

and then evaluating this difference on the interface leads to

$$\rho_2 (\partial_t + u_2^0 \partial_x) \Psi_2 - \rho_1 (\partial_t + u_1^0 \partial_x) \Psi_1 = (g \delta \rho - \gamma \nabla_z^2) \eta \quad (51.21)$$

where the density difference is written

$$\delta \rho = \rho_2 - \rho_1. \quad (51.22)$$

Note that when multiplied by gravity, we evaluate the interface position at $z = \eta$, whereas other terms in the linear theory are evaluated at $z = 0$.²

51.3 Rayleigh-Taylor instability

For the Rayleigh-Taylor instability analysis, we assume the background flow is at rest so that $u_1^0 = u_2^0 = 0$. Hence, we are here examining stability of the rest state to small perturbations of

²We detailed this treatment of the boundary position when deriving the linear equations for surface waves in Section 45.3.4.

the layer interface.

51.3.1 Boundary value problem and dispersion relation

With zero background flow it is a simple matter to eliminate the free surface from the interface condition (51.21). We do so by taking a time derivative and using the linearized kinematic boundary condition (51.19c) (or equivalently equation (51.19d))

$$\partial_{tt}(\rho_2 \Psi_2 - \rho_1 \Psi_1) = -[g \delta\rho - \gamma \nabla_z^2] \partial_z \Psi \quad \text{at } z = 0, \quad (51.23)$$

where $w_1 = w_2 = -\partial_z \Psi$ at $z = 0$. We are thus led to the boundary value problem

$$\partial_z \Psi_1 = 0 \quad z = h_1 \quad (51.24a)$$

$$\nabla^2 \Psi_1 = 0 \quad 0 < z < h_1 \quad (51.24b)$$

$$\nabla^2 \Psi_2 = 0 \quad -h_2 < z < 0 \quad (51.24c)$$

$$\partial_z \Psi_2 = 0 \quad z = -h_2 \quad (51.24d)$$

$$\partial_{tt}(\rho_2 \Psi_2 - \rho_1 \Psi_1) = -[g \delta\rho - \gamma \nabla_z^2] \partial_z \Psi \quad z = 0. \quad (51.24e)$$

Following the approach for surface waves in Section 45.5, we seek a traveling plane wave solution with horizontal wavevector

$$\mathbf{k} = k_x \hat{\mathbf{x}} + k_y \hat{\mathbf{y}} \quad \text{and} \quad \hat{\mathbf{k}} = \mathbf{k}/|\mathbf{k}|, \quad (51.25)$$

and a wave ansatz in the form of a cosine modulated by a vertical structure function

$$\Psi(x, y, z, t) = A \Gamma(z) \cos(\mathbf{k} \cdot \mathbf{x} - \omega t). \quad (51.26)$$

The solution to Laplace's equation with Neumann boundary conditions in the two half-domains is given by³

$$\Psi_1 = A \frac{\cosh[|\mathbf{k}|(z - h_1)]}{\sinh[-|\mathbf{k}|h_1]} \cos(\mathbf{k} \cdot \mathbf{x} - \omega t) \quad 0 \leq z \leq h_1 \quad (51.27a)$$

$$\Psi_2 = A \frac{\cosh[|\mathbf{k}|(z + h_2)]}{\sinh[|\mathbf{k}|h_2]} \cos(\mathbf{k} \cdot \mathbf{x} - \omega t), \quad -h_2 \leq z \leq 0, \quad (51.27b)$$

where A is a real amplitude. The dispersion relation is obtained by plugging equations (51.27a)-(51.27b) into the interface condition (51.24e), with the following pieces needed (recall each term is evaluated at $z = 0$)

$$\partial_{tt}(\rho_2 \Psi_2 - \rho_1 \Psi_1) = -\omega^2 A [\rho_2 \coth(|\mathbf{k}|h_2) - \rho_1 \coth(-|\mathbf{k}|h_1)] \cos(\mathbf{k} \cdot \mathbf{x} - \omega t) \quad (51.28a)$$

$$\partial_z \Psi_1 = \partial_z \Psi_2 = A |\mathbf{k}| \cos(\mathbf{k} \cdot \mathbf{x} - \omega t) \quad (51.28b)$$

$$(\partial_{xx} + \partial_{yy})\Psi = -|\mathbf{k}|^2 \Psi, \quad (51.28c)$$

thus leading to the dispersion relation

$$\omega^2 = \frac{|\mathbf{k}|(g \delta\rho + \gamma |\mathbf{k}|^2)}{\rho_2 \coth(|\mathbf{k}|h_2) + \rho_1 \coth(|\mathbf{k}|h_1)}. \quad (51.29)$$

³As noted in Section 45.2.2, solutions to Laplace's equation do not support spatial oscillations in all three directions since the sum of the curvature in each direction (i.e., second partial derivatives) must vanish. Correspondingly, the velocity potential supports traveling waves in the horizontal and exponential behavior in the vertical.

As for the surface waves in Chapter 45, the horizontal wavenumber, $|\mathbf{k}|$, determines the vertical scale of the wave. We now examine various cases for stable and unstable waves.

51.3.2 Stable traveling plane waves

When the squared angular frequency (51.29) is positive, $\omega^2 > 0$, then the waves are surface waves related to those studied in Chapter 45.⁴ For example, when the waves are so short that they do not feel the rigid boundaries at $z = h_1$ and $z = -h_2$, then we can set $\coth(|\mathbf{k}| h_2) \approx 1$ and $\coth(|\mathbf{k}| h_1) \approx 1$, in which case the dispersion relation takes on the approximate form

$$\omega^2 \approx \frac{|\mathbf{k}|(g\delta\rho + \gamma|\mathbf{k}|^2)}{\rho_2 + \rho_1} \quad \text{shortwave limit with } |\mathbf{k}|h_1 \gg 1 \text{ and } |\mathbf{k}|h_2 \gg 1. \quad (51.30)$$

This limit (when surface tension is set to zero) corresponds to the deep water waves from Section 45.5.5. For the longwave limit, in which case the waves feel the top and bottom boundaries, we set $\coth(|\mathbf{k}| h_1) \approx 1/(|\mathbf{k}| h_1)$ and $\coth(|\mathbf{k}| h_2) \approx 1/(|\mathbf{k}| h_2)$ so that

$$\omega^2 \approx \frac{|\mathbf{k}|^2 g \delta\rho}{\rho_2/h_2 + \rho_1/h_1} \quad \text{longwave limit with } |\mathbf{k}|h_1 \ll 1 \text{ and } |\mathbf{k}|h_2 \ll 1. \quad (51.31)$$

Note that we dropped the surface tension term since $|\mathbf{k}|$ is very small in the longwave limit. Evidently, since $\omega^2/|\mathbf{k}|^2$ is independent of \mathbf{k} , the longwaves are non-dispersive surface gravity waves and are thus the analog of non-dispersive shallow water gravity waves (Section 48.5).

51.3.3 Unstable exponentially growing plane waves

The case with $\omega^2 < 0$ leads to unstable wave growth. This case is rendered by $\delta\rho = \rho_2 - \rho_1 < 0$. That is, if there is heavy fluid above light fluid then the system can be unstable, depending on whether the gravitational instability can overcome the stabilizing effects from surface tension. We now example various cases to explore this unstable case, known as the *Rayleigh-Taylor instability*.

The growth rate

To express the temporal structure of the unstable wave, introduce the growth rate

$$\omega^2 = -\sigma^2 \implies \omega = \pm i\sigma, \quad (51.32)$$

where $\sigma > 0$ is given by

$$\sigma = \left[\frac{|\mathbf{k}|(g|\delta\rho| - \gamma|\mathbf{k}|^2)}{\rho_2 \coth(|\mathbf{k}|h_2) + \rho_1 \coth(|\mathbf{k}|h_1)} \right]^{1/2} > 0. \quad (51.33)$$

We furthermore express the velocity potential (51.27a) and (51.27b) as the real part of complex exponentials. In particular, for the top layer we write

$$\Psi_1 = A\Gamma(z) \operatorname{Re}[e^{i(\mathbf{k}\cdot\mathbf{x}-\omega t)}] = A\Gamma(z) e^{\pm\sigma t} \operatorname{Re}[e^{i\mathbf{k}\cdot\mathbf{x}}] = A\Gamma(z) e^{\pm\sigma t} \cos(\mathbf{k}\cdot\mathbf{x}). \quad (51.34)$$

The solution with the time behavior, $e^{\sigma t}$, is exponentially growing and this is the unstable wave.

⁴More precisely, if we set $\rho_1 = 0$ as for a vacuum, then the waves are identical to the surface waves from Chapter 45.

All waves are unstable in the absence of surface tension

In the absence of surface tension, the growth rate is given by

$$\sigma = \left[\frac{g |\mathbf{k}| |\delta\rho|}{\rho_2 \coth(|\mathbf{k}| h_2) + \rho_1 \coth(|\mathbf{k}| h_1)} \right]^{1/2} \quad \text{if } \gamma = 0. \quad (51.35)$$

Evidently, all waves are unstable, with the smallest waves having the largest growth rate given approximately by

$$\sigma \approx \sqrt{g |\mathbf{k}| |\delta\rho| / (\rho_1 + \rho_2)} \quad \text{with } |\mathbf{k}| h_2 \gg 1 \text{ and } |\mathbf{k}| h_1 \gg 1. \quad (51.36)$$

We thus expect to find the smallest scales rapidly going unstable, with the instability halted only after all of the denser fluid occupies the lower layer.

The stabilizing role of surface tension

The growth rate (51.33) vanishes at the critical wavenumber

$$|\mathbf{k}|_c^2 = g |\delta\rho| / \gamma. \quad (51.37)$$

All waves with wavenumbers larger than $|\mathbf{k}|_c$ are stabilized by surface tension, in which case the stable linear waves are capillary-gravity waves. We studied the physics of surface tension in Section 22.11, where we noted that it can counteract the effects from gravity when the radius of curvature is sufficiently small. To get a sense for the size of these stable waves, recall our discussion of capillary-gravity waves in Section 45.7. For an air-water interface the surface tension is approximately $\gamma = 0.072 \text{ N m}^{-1} = 0.072 \text{ kg s}^{-2}$, along with the water density of $\rho_1 = 10^3 \text{ kg m}^{-3}$ and air density $\rho_2 = 1 \text{ kg m}^{-3}$. With these physical constants the critical wavenumber is given by

$$|\mathbf{k}|_c \approx 372 \text{ m}^{-1} \implies \Lambda_c = 2\pi / |\mathbf{k}|_c \approx 1.7 \text{ cm}. \quad (51.38)$$

Again, waves of wavelength smaller than Λ_c are stable.

Maximum growth rate with both surface tension and gravity

We saw above that all waves are unstable without surface tension, with the growth rate increasing as $|\mathbf{k}|^{1/2}$ as per equation (51.36). However, surface tension introduces a high wavenumber cutoff so that all waves with $|\mathbf{k}| > |\mathbf{k}|_c^2$ are stable. Again, such waves are stabilized since surface tension dominates over gravity when the radius of curvature is small enough. What is the most unstable wave when there is both surface tension and gravity? One might expect that in the presence of random forcing, this wavenumber will be the one most visibly growing in any particular situation.

To simplify the algebra for computing the most unstable wave, we consider the growth rate (51.33) in the limit that the two rigid boundaries separate to infinity. This limit is not overly constraining since the waves exponentially decay away from the interface, and we expect that the most unstable wavenumber is within an order of magnitude of $|\mathbf{k}|_c$. With h_1, h_2 set to infinity the dispersion relation is given by

$$\sigma^2 = \frac{g |\delta\rho| |\mathbf{k}| - \gamma |\mathbf{k}|^3}{\rho_2 + \rho_1}. \quad (51.39)$$

The wavenumber leading to the maximum growth rate is found by setting $\partial\sigma^2/\partial|\mathbf{k}| = 0$, in which case we find

$$|\mathbf{k}|_{\max}^2 = g |\delta\rho| / (3\gamma) = |\mathbf{k}|_c^2 / 3. \quad (51.40)$$

Using the numbers above for an air-water interface, we see that the wavelength for the most unstable wave is roughly $1.7 \text{ cm} * \sqrt{3} \approx 3 \text{ cm}$.

51.3.4 Further study

The current section follows the approach from Section 2 from [Fetter and Walecka \(2003\)](#), and Chapter X of [Chandrasekhar \(1961\)](#) offers a far more detailed presentation. [The 18 minute mark of this video from Prof. Mollo-Christensen](#) provides a laboratory example of Rayleigh-Taylor instability.

51.4 Kelvin-Helmholtz instability

Kelvin-Helmholtz instability arises when the two fluid layers in Figure 51.1 are moving horizontally relative to each other. In the following we assume the velocities are zonal and written $\hat{x} u_1^0$ and $\hat{x} u_2^0$. Furthermore, we assume the fluids are stably stratified so that $\delta\rho > 0$. Finally, to simplify the analysis, assume the rigid boundaries are moved to infinity so that the only boundary of concern is at the fluid interface.

51.4.1 Velocity potential

The velocity potential satisfying Laplace's equation in the two half spaces is given by

$$\Psi_1 = -u_1^0 x + A_1 e^{-|\mathbf{k}|z} e^{i(\mathbf{k} \cdot \mathbf{x} - \omega t)} \quad 0 \leq z < \infty \quad (51.41a)$$

$$\Psi_2 = -u_2^0 x + A_2 e^{|\mathbf{k}|z} e^{i(\mathbf{k} \cdot \mathbf{x} - \omega t)} \quad -\infty < z \leq 0. \quad (51.41b)$$

In contrast to the Rayleigh-Taylor instability, as given by equations (51.27a) and (51.27b), we here use complex exponentials, with the real part of each expression assumed. We also introduced two real amplitudes, A_1 and A_2 . Both of these features prove of use in the following analysis. Furthermore, the nonzero background flow makes it less convenient to eliminate the interface height, so that we explicitly consider its wave ansatz in the form

$$\eta = \eta_0 e^{i(\mathbf{k} \cdot \mathbf{x} - \omega t)}. \quad (51.42)$$

To develop a dispersion relation, we make use of the difference in the Bernoulli equation of motion when evaluated at the interface (equation (51.21)), as well as the kinematic and dynamic boundary conditions (51.19c)-(51.19f).

51.4.2 Dispersion relation from the interface conditions

Evaluating equation (51.21) at $z = 0$ for the waves (51.41a), (51.41b), and (51.42), leads to the following relation between the wave amplitudes

$$i [\rho_2 (-\omega + k_x u_2^0) A_2 - \rho_1 (-\omega + k_x u_1^0) A_1] = (g \delta\rho + \gamma |\mathbf{k}|^2) \eta_0 \quad (51.43)$$

Likewise, the linearized kinematic boundary conditions (51.19c) and (51.19d) render the relations

$$i (-\omega + k_x u_1^0) \eta_0 = |\mathbf{k}| A_1 \quad (51.44a)$$

$$i (-\omega + k_x u_2^0) \eta_0 = -|\mathbf{k}| A_2. \quad (51.44b)$$

Use of equations (51.44a) and (51.44b) in equation (51.43) leads to the dispersion relation

$$\rho_1 (\omega - k_x u_1^0)^2 + \rho_2 (\omega - k_x u_2^0)^2 = |\mathbf{k}| (g \delta \rho + \gamma |\mathbf{k}|^2). \quad (51.45)$$

We can readily check that this result agrees with that found for the Rayleigh-Taylor instability in equation (51.29). Expanding equation (51.45) and solving the quadratic expression leads to the more conventional form of the dispersion relation

$$\omega = \frac{k_x (u_1^0 \rho_1 + u_2^0 \rho_2)}{\rho_1 + \rho_2} \pm \sqrt{\frac{|\mathbf{k}| (g \delta \rho + \gamma |\mathbf{k}|^2)}{\rho_1 + \rho_2} - \frac{k_x^2 \rho_1 \rho_2 (u_1^0 - u_2^0)^2}{(\rho_1 + \rho_2)^2}}. \quad (51.46)$$

We consider facets of this relation in the following.

51.4.3 Analysis of the stability condition

The angular frequency is a real number so long as the discriminant in equation (51.46) is positive,

$$\frac{\rho_1 \rho_2 (u_1^0 - u_2^0)^2}{(\rho_1 + \rho_2)} < \frac{|\mathbf{k}| (g \delta \rho + \gamma |\mathbf{k}|^2)}{k_x^2} \implies \text{stable}, \quad (51.47)$$

with the perturbations organizing into stable linear surface waves modified by the background velocity. To help understand this stability condition, we find it useful to consider a few special cases. To reduce algebra it is useful to assume the wavevector is aligned in the \hat{x} direction so that $|\mathbf{k}|^2 = k_x^2$. Now write the stability condition (51.47) as a condition on the squared velocity difference, in which case

$$(u_1^0 - u_2^0)^2 < \frac{(\rho_1 + \rho_2) (g \delta \rho + \gamma |\mathbf{k}|^2)}{|\mathbf{k}| \rho_1 \rho_2}. \quad (51.48)$$

This equation says that the waves are stable so long as the velocity difference is unable to counteract the stabilizing effects from surface tension and gravity.

Most easily growing wavenumber

Stability is satisfied if the wavenumber is large enough or small enough. Setting to zero the derivative, $\partial/\partial|\mathbf{k}|$, of the right hand of equation (51.48) renders the value of the wavenumber for which the right hand side is minimized

$$|\mathbf{k}|_c^2 = g \delta \rho / \gamma. \quad (51.49)$$

That is, when the wavenumber equals to $|\mathbf{k}|_c$, then the stability condition is most easily violated by the velocity difference, thus leading to exponential growth for this wave. Plugging in $|\mathbf{k}|_c$ to the stability condition (51.48) leads to

$$(u_1^0 - u_2^0)^4 < \frac{4 \gamma g (\rho_1 + \rho_2)^2 (\rho_2 - \rho_1)}{\rho_1^2 \rho_2^2}. \quad (51.50)$$

This expression shows how surface tension and gravity act together to maintain stability in the face of a velocity difference. Yet if the velocity difference grows, eventually the flow becomes unstable with the wavenumber $|\mathbf{k}|_c$ being the first wave to exponentially grow.

There are always unstable waves when surface tension vanishes

If the surface tension vanishes then equation (51.50) says that there are always unstable waves for an arbitrarily small velocity difference. More precisely, we return to the general condition (51.48) with $\gamma = 0$ to find

$$(u_1^0 - u_2^0)^2 < \frac{g(\rho_1 + \rho_2)\delta\rho}{|\mathbf{k}|\rho_1\rho_2}. \quad (51.51)$$

Evidently, no matter how small the velocity difference, there are small enough waves (with large enough wavenumber) that violate this inequality and thus lead to exponential growth.

Stability is enhanced when $\rho_1/\rho_2 \ll 1$

If the upper layer has a vanishingly small density relative to the lower layer, then the right hand side of the stability condition (51.48) becomes large. We say that this case is strongly stable since it takes a large velocity difference to produce an instability. A geophysically relevant example is air blowing over water with $\gamma = 0.072 \text{ N m}^{-1} = 0.072 \text{ kg s}^{-2}$, $\rho_2 = 10^3 \text{ kg m}^{-3}$ and air density $\rho_1 = 1 \text{ kg m}^{-3}$. Equation (51.50) says that the most unstable wave is stimulated with an air-sea velocity difference of⁵

$$u_1^0 - u_2^0 = 7.3 \text{ m s}^{-1}. \quad (51.52)$$

There are always unstable waves when the layers are horizontally aligned

If we align the layers horizontally rather than vertically, then gravity is no longer able to enhance stability in the face of the velocity difference. Just like in the case with zero surface tension, there are always waves that go unstable in this case.

51.4.4 Further study

Chapter XI of [Chandrasekhar \(1961\)](#) provides a detailed study of Kelvin-Helmholz instability, whereas Section 2 of [Fetter and Walecka \(2003\)](#) is more succinct. [The first half of this video from Prof. Mollo-Christensen](#) provides laboratory examples of Kelvin-Helmholz instabilities.



⁵Page 486 of [Chandrasekhar \(1961\)](#) and page 18 of [Fetter and Walecka \(2003\)](#) both compute a velocity difference $u_1^0 - u_2^0 = 0.65 \text{ m s}^{-1}$. We are unable to find an error in equation (51.52).

Chapter 52

STABILITY OF SHEARED BAROTROPIC FLOW

In this chapter we study the stability of sheared flows in a horizontally non-divergent barotropic fluid on a β -plane. This study of *shear instability* makes use of normal mode stability analysis. Analytical results are presented where the shear displays a jump in the vorticity, thus supporting the *edge waves* of Section 47.5. We then offer a mechanistic interpretation of shear instability as a *wave resonance* between two interacting edge waves. That is, shear instability involves the coherent motion of waves that constructively interfere to support mutual growth of the instability.

The wave interpretation of shear instability constrasts to the variety of symmetric instabilities studied in Chapter 50. In particular, symmetric stability can be deduced by the local necessary and sufficient condition, $f Q < 0$, with Q the Ertel potential vorticity. A corresponding mechanistic interpretation follows from parcel arguments. As emphasized by *Cushman-Roisin and Beckers (2011)* (see their Chapter 17), wave instabilities, such as shear instability of this chapter, cannot be deduced by a local flow property. The key reason is that a wave instability arises from the constructive interaction between coherent wave motion, with a quantitative understanding requiring the solution of an eigenvalue problem to determine properties of the interacting waves.

READER'S GUIDE FOR THIS CHAPTER

We assume familiarity with the horizontally non-divergent barotropic model from Chapter 35 and the associated wave mechanics in Sections 47.2 and 47.3. We make particular use of edge waves studied in Section 47.5. This chapter offers an important step towards the study of baroclinic instability in Chapter??

52.1	Loose threads	1367
52.2	Interacting edge waves	1368
52.2.1	Solving for the interacting edge waves	1368
52.2.2	Interpreting the dispersion relation	1371
52.2.3	Explicit expression for the streamfunction	1372
52.2.4	Further study	1372
52.3	Integral conditions necessary for instability	1372
52.3.1	Rayleigh-Kuo theorem	1372
52.3.2	Fjørtoft's theorem	1373
52.3.3	A sinh profile	1374
52.4	Exercises	1374

52.1 Loose threads

- Explicit expression for the streamfunction in Section 52.2.3

- More examples of stability profiles as in Figure 11.21 of *Kundu et al. (2016)*.
- Energetics as in Section 3.10 of *Smythe and Carpenter (2019)*
- Discuss the neutral wave case with $u_b = c$ and further explore Footnote 10 in Chapter 9 of *Vallis (2017)*.

52.2 Interacting edge waves

In Section 47.5 we developed the theory for edge waves riding on a single jump in the base state vorticity. Salient features of these waves are given by the following.

- Edge waves propagate along the surface where vorticity experiences a jump, and they are trapped to this surface due to their exponential decay when moving orthogonal to the surface.
- The edge wave phase velocity, c_p , is built from two contributions: one due to a Doppler shift from the background flow, and another from the vorticity jump. The vorticity jump contribution is referred to as the intrinsic phase velocity, $c_{\text{phase}}^{\text{intrinsic}}$.
- The intrinsic phase velocity is directed so that the higher relative vorticity is to the right when facing in the direction of the phase velocity. Equivalently, the phase velocity is directed towards the concave portion of the velocity profile. One can understand this orientation via the conservation of relative vorticity (holding for an inviscid non-rotating flow), just like the conservation of potential vorticity explains the phase velocity for a Rossby wave.

In this section we study the interaction between two edge waves. Our goal is to determine those circumstances in which the interactions can lead to a runaway positive feedback for wave growth, thus signaling an instability. Prior to diving into the mathematical details, consider Figure 52.1, which illustrates the *wave resonance* mechanism for shear instability. The figure caption is quite long since it provides the ingredients for the mechanism. The key point is that the two edge waves are phase locked in an orientation that mutually reinforces each other's amplitude, thus leading to a positive feedback and instability. The bulk of this chapter aims to fill in the quantitative details associated with this wave mechanism for shear instability.

52.2.1 Solving for the interacting edge waves

We here derive mathematical expressions for interacting edge waves supported by the kinks at $y = \pm L$ in the velocity profile of Figure 52.1. We are only concerned with the non-rotating case so that $\beta = 0$. Additionally, we let $H \rightarrow \infty$ so that there are no solid boundaries. That is, we focus on the stability of a free shear layer.

The ingredients for this analysis were developed in Section 47.5 in our study of a single edge wave. Namely, we solve the Rayleigh equation (i.e., the vorticity equation) in the fluid region between the interfaces, and then use the kinematic and dynamic boundary conditions to match the Rayleigh solution across the jump surfaces. In the process of matching, we derive the dispersion relation that determines the zonal phase velocity for the interacting wave system. If the phase velocity is a complex number, then that signals the appearance of an unstable wave mode.

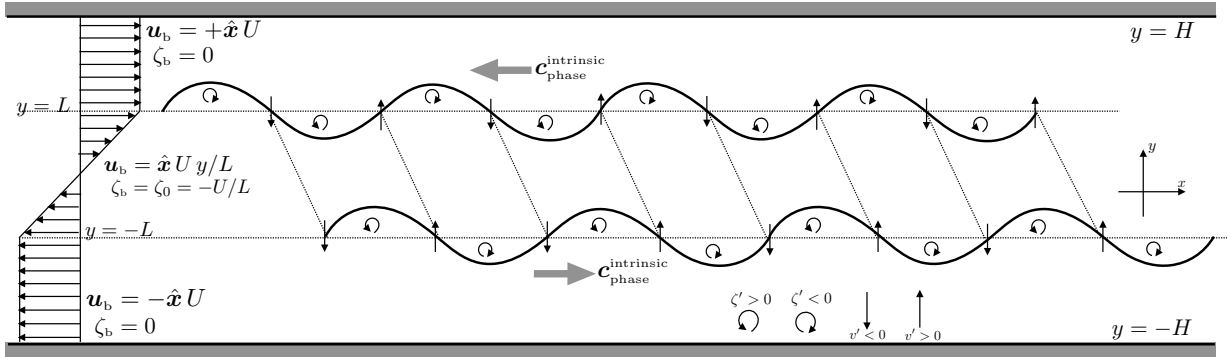


FIGURE 52.1: Depicting the interaction between two edge waves generated by a base flow that is unstable to shear instability. The left portion shows the base state zonal velocity, with two jumps in the vorticity occurring at the two kinks in the velocity at $y = \pm L$. For the southern kink the vorticity jumps from zero to negative vorticity, so that the higher vorticity is to the south. This orientation in the vorticity jump induces an edge wave with eastward intrinsic phase velocity, $c_{\text{phase}}^{\text{intrinsic}}$, that is contrary to the westward mean flow. For the northern kink, the vorticity jumps from negative to zero, so that the higher vorticity is to the north. This orientation of the vorticity jump induces an edge wave with westward intrinsic phase velocity that is contrary to the eastward mean flow. The oriented circles denote the anomalous vorticity associated with a particular fluctuation of the interface. For example, on the southern edge wave, a northward fluctuation brings fluid with higher relative vorticity northward, thus denoted by $\zeta' > 0$ and a counter-clockwise oriented circle. The secondary circulations induced by the anomalous vorticity induce anomalous meridional flows, depicted by the vertical arrows, and these flows have maximum amplitudes at the wave nodes. Interactions between the waves are optimized with a phase shift whereby the southern wave is shifted roughly $\pi/2$ to the east of the northern wave. With this phase shift, a northward anomalous flow from the southern wave will act at the peak of the northern wave, thus supporting its further growth. The opposite occurs for a wave trough. The result is an amplification of each wave's amplitude. To optimize the growth requires the waves to be *phase locked*, whereby they stay stationary relative to one another, thus allowing for a positive feedback to create the exponential wave growth that constitutes shear instability.

Modulated wave ansatz

Following our development in Section 47.5, write the streamfunction in the form of a zonally traveling wave that is modulated by a meridional amplitude function

$$\psi(x, y, t) = \tilde{\psi}(y) e^{i(kx - \omega t)} = \tilde{\psi}(y) e^{i k(x - ct)} \quad \text{with } c = \omega/k. \quad (52.1)$$

The phase moves only in the zonal direction so that the phase velocity is given by

$$\mathbf{c}_p = (\omega/|k|) \hat{k} = c \hat{x}. \quad (52.2)$$

For nomenclature, in this case of a wave traveling in one dimension, we refer to c as the phase velocity.

A real and positive wave velocity, c , indicates a stable edge wave with phase moving in the positive \hat{x} direction, and conversely for a negative c . For shear stability we are interested in whether c can also have an imaginary part, in which case

$$c = c_r + i c_i = c_r + i \sigma/k. \quad (52.3)$$

Here, the real part, c_r , yields a phase velocity, whereas c_i leads to a decay rate or growth rate for the wave

$$\psi(x, y, t) = \tilde{\psi}(y) e^{i k(x - c_r t)} e^{k c_i t} = \tilde{\psi}(y) e^{i k(x - c_r t)} e^{\sigma t}. \quad (52.4)$$

If $k c_i > 0$ then the wave is exponentially unstable with growth rate $\sigma = k c_i$, whereas if $\sigma < 0$ then the wave exponentially decays.

Rayleigh equation

Inserting the ansatz (52.1) into the vorticity equation leads to the Rayleigh equation (47.80)

$$(u_b - c)(\partial_{yy} - k^2)\tilde{\psi} + \partial_y \zeta_b \tilde{\psi} = 0. \quad (52.5)$$

The unknowns in this equation are the phase velocity, c , and the streamfunction, $\tilde{\psi}$. All other terms are real, so that the complex conjugate of the Rayleigh equation is given by

$$(u_b - c^*)(\partial_{yy} - k^2)\tilde{\psi}^* + \partial_y \zeta_b \tilde{\psi}^* = 0, \quad (52.6)$$

where the $*$ indicates complex conjugate. Hence, if c satisfies the Rayleigh equation with streamfunction $\tilde{\psi}$, then c^* satisfies the equation with streamfunction $\tilde{\psi}^*$. That is, the phase velocities come in complex conjugate pairs.

With the vorticity profile in Figure 52.1, the meridional derivative, $\partial_y \zeta_b$, has a Dirac delta at each of the vorticity jumps so that the Rayleigh equation takes the form

$$(u_b - c)(\partial_{yy} - k^2)\tilde{\psi} + \zeta_0 [\delta(y+L) - \delta(y-L)]\tilde{\psi} = 0 \quad \text{with } \zeta_0 = -U/L. \quad (52.7)$$

The solution to this equation outside of the singular vorticity layers is given by

$$\tilde{\psi}(y) = \begin{cases} A_1 e^{-|k|(y-L)} & y > L \\ A_2 e^{|k|(y-L)} + A_3 e^{-|k|(y+L)} & -L < y < L \\ A_4 e^{|k|(y+L)} & y < -L, \end{cases} \quad (52.8)$$

where $A_{1,2,3,4}$ are constants determined by the kinematic and dynamic boundary conditions.

Kinematic boundary condition at $y = \pm L$

We derived the kinematic boundary condition in Section 47.5.5, which is a statement about the material constancy of the interface. The velocity is continuous at $y = \pm L$, so that the kinematic boundary condition means that the streamfunction is also continuous. Evaluating equation (52.8) at $y = \pm L$ leads to the relations

$$A_1 = A_2 + A_3 e^{-2|k|L} \quad \text{and} \quad A_4 = A_3 + A_2 e^{-2|k|L}, \quad (52.9)$$

so that

$$\tilde{\psi}(y) = \begin{cases} A_2 e^{-|k|(y-L)} + A_3 e^{-|k|(y+L)} & y > L \\ A_2 e^{|k|(y-L)} + A_3 e^{-|k|(y+L)} & -L < y < L \\ A_2 e^{|k|(y-L)} + A_3 e^{|k|(y+L)} & y < -L, \end{cases} \quad (52.10)$$

which can be written in the more succinct form

$$\tilde{\psi}(y) = A_2 e^{-|k||y-L|} + A_3 e^{-|k||y+L|}. \quad (52.11)$$

For the dynamic boundary condition we will need the derivative, which is given by

$$\partial_y \tilde{\psi} = |k| \begin{cases} -A_2 e^{-|k|(y-L)} - A_3 e^{-|k|(y+L)} & y > L \\ A_2 e^{|k|(y-L)} - A_3 e^{-|k|(y+L)} & -L < y < L \\ A_2 e^{|k|(y-L)} + A_3 e^{|k|(y+L)} & y < -L. \end{cases} \quad (52.12)$$

Dynamic boundary condition at $y = \pm L$

As detailed in Section 47.5.6, the dynamic boundary condition is based on continuity of pressure across an interface (we are ignoring surface tension). Equivalently, it arises from integrating the Rayleigh equation (52.7) across each interface, thus allowing the Dirac delta to fire and render a jump condition. For this purpose, it is convenient to write the Rayleigh equation in the form of equation (47.81)

$$\partial_y[(u_b - c) \partial_y \tilde{\psi} - \tilde{\psi} \partial_y u_b] + [\beta - k^2 (u_b - c)] \tilde{\psi} = 0. \quad (52.13)$$

Since u_b and $\tilde{\psi}$ are everywhere continuous, integration across the top interface yields

$$\lim_{\epsilon \rightarrow 0} \int_{L-\epsilon}^{L+\epsilon} \partial_y[(u_b - c) \partial_y \tilde{\psi} - \tilde{\psi} \partial_y u_b] dy = 0, \quad (52.14)$$

which leads to the jump condition

$$[(U - c) \partial_y \tilde{\psi} + \tilde{\psi} \zeta_0]_{y=L-\epsilon} = [(U - c) \partial_y \tilde{\psi}]_{y=L+\epsilon}, \quad (52.15)$$

where we noted that there is zero vorticity for $y > L$, and the zonal velocity equals to $+U$ at $y = L$. Note that ϵ is set to zero once evaluating the expressions. Making use of the streamfunction (52.10) and the derivative (52.12) brings the $y = L$ jump boundary condition to

$$A_2 [2(U - c)|k| + \zeta_0] + A_3 \zeta_0 e^{-2L|k|} = 0. \quad (52.16)$$

Likewise, the bottom interface has the jump condition

$$[(-U - c) \partial_y \tilde{\psi}]_{y=-L-\epsilon} = [(-U - c) \partial_y \tilde{\psi} + \tilde{\psi} \zeta_0]_{y=-L+\epsilon}, \quad (52.17)$$

where the vorticity is zero for $y < -L$ and the zonal velocity is $-U$. Making use of the streamfunction (52.10) and the derivative (52.12) brings the $y = -L$ jump boundary condition to

$$A_2 \zeta_0 e^{-2L|k|} + A_3 [2(U + c)|k| + \zeta_0] = 0. \quad (52.18)$$

Dispersion relation

Writing the two jump conditions (52.16) and (52.18) in the form of a matrix-vector equation yields

$$\begin{bmatrix} [2(U - c)|k| + \zeta_0] & \zeta_0 e^{-2L|k|} \\ \zeta_0 e^{-2L|k|} & [2(U + c)|k| + \zeta_0] \end{bmatrix} \begin{bmatrix} A_2 \\ A_3 \end{bmatrix} = \begin{bmatrix} 0 \\ 0 \end{bmatrix}. \quad (52.19)$$

Nontrivial solutions exist if the determinant of the 2×2 matrix vanishes, which then leads to the dispersion relation for the phase velocity

$$(c/U)^2 = \frac{1}{4k^2 L^2} [(1 - 2|k|L)^2 - e^{-4|k|L}] = \left[1 - \frac{1}{2|k|L}\right]^2 - \frac{e^{-4|k|L}}{4|k|^2 L^2}. \quad (52.20)$$

52.2.2 Interpreting the dispersion relation

The dispersion relation (52.20) leads to two roots for the phase velocity, both of which are real or both imaginary. The case of two real roots corresponds to edge waves moving in either direction. For example, in the high wavenumber limit the roots are real and they have the approximate

value

$$c \approx \pm U \left[1 - \frac{1}{2|k|L} \right]. \quad (52.21)$$

In this limit, the two edge waves correspond to the single edge waves studied in Section 47.5, so that there are two non-interacting edge waves. As $|k|L$ gets smaller, so that the wavelength gets longer, then the two waves interact, with the interaction modifying the phase speed through the exponential term.

The real part of the phase velocity vanishes when

$$(1 - 2|k|L)^2 = e^{-4|k|L} \implies |k|_{\text{crit}} L < 0.6329. \quad (52.22)$$

For smaller wavenumbers, the squared phase speed (52.20) becomes negative

$$(c/U)^2 < 0 \implies c = i c_i. \quad (52.23)$$

Hence, the two roots lead to both an exponentially decaying mode and exponentially growing mode. Since the real part of the phase velocity vanishes, the modes are stationary relative to the shear layer, and thus they are either decaying or growing in place.

52.2.3 Explicit expression for the streamfunction

52.2.4 Further study

The linear sheared velocity profile in an unbounded domain was first analyzed by [Rayleigh \(1894\)](#) (volume II, page 393), and it forms the basis for most subsequent pedagogical treatments, such as [Chandrasekhar \(1961\)](#), [Drazin and Reid \(1981\)](#), [Vallis \(2017\)](#), and [Smythe and Carpenter \(2019\)](#).

52.3 Integral conditions necessary for instability

In this section we establish two necessary conditions for shear instability.

52.3.1 Rayleigh-Kuo theorem

The analysis in Section 52.2 is explicit but cumbersome, and inadequate to determine the stability of an arbitrary velocity profile. Here we establish the *Rayleigh instability criteria*, also known as the *Rayleigh inflection-point criteria*. In the presence of β , it is known as the *Rayleigh-Kuo condition*. The Rayleigh criteria provides a necessary condition for an instability. Notably, this criteria is not a sufficient condition for instability. Indeed, there are examples where the Rayleigh criteria is met and yet the flow is stable.

To proceed, return to the Rayleigh-Kuo equation (47.80) and write it as¹

$$(\partial_{yy} - k^2) \tilde{\psi} + \frac{(\beta - \partial_{yy} u_b) \tilde{\psi}}{u_b - c} = 0. \quad (52.24)$$

Multiplying by $\tilde{\psi}^*$ (complex conjugate of $\tilde{\psi}$) and integrating over the domain \mathcal{R} s leads to

$$\int_{\mathcal{R}} [\partial_y (\tilde{\psi}^* \partial_y \tilde{\psi}) - |\partial_y \tilde{\psi}|^2 - k^2 |\tilde{\psi}|^2] dy = - \int_{\mathcal{R}} \frac{(\beta - \partial_{yy} u_b) |\tilde{\psi}|^2}{u_b - c} dy. \quad (52.25)$$

¹Recall that the Kuo portion of Rayleigh-Kuo arises from the addition of β .

If the streamfunction or its derivatives vanish on the boundaries, then the left hand side is a negative real number. Now all terms on the right hand side are real except, possibly, the phase velocity, c . Hence, this equation is self-consistent only if the imaginary part of the right hand side vanishes

$$c_i \int_{\mathcal{R}} \frac{(\beta - \partial_{yy} u_b) |\tilde{\psi}|^2}{|u_b - c|^2} dy = 0. \quad (52.26)$$

This condition can be satisfied in two ways. The first way is if the phase velocity is real, so that $c_i = 0$ and hence all waves are stable.² The second way is if the integral vanishes. For the integral to vanish we need $\beta - \partial_{yy} u_b$ change sign somewhere in the domain, since all the other terms in the integral are positive. That is, there must be an extrema of the absolute vorticity somewhere in the domain.

There are many qualifiers to this result. In particular, for $\beta - \partial_{yy} u_b$ to change sign in the domain represents a necessary, but not sufficient, condition for a shear instability. Indeed, there are flow profiles that satisfy the inflection point criteria and yet there are still no growing wave modes.³ Turning the condition around we find that a sufficient condition for stability is that there are no sign changes for $\beta - \partial_{yy} u_b$. We summarize the result by stating the following theorem.

RAYLEIGH-KUO INFLECTION POINT THEOREM

Consider an inviscid, homogeneous (constant density), and non-rotating fluid with a base state of parallel sheared flow. A necessary condition for shear instability is that there exists an inflection point somewhere in the flow; i.e., where $\partial_{yy} u_b = 0$ and so where the relative vorticity has an extrema, $\partial_y \zeta_b = 0$. For flow on the β -plane, this criteria is generalized to $\beta - \partial_{yy} u_b = 0$, in which case the absolute vorticity must have an extrema in the domain. If there is no inflection point, then that is a sufficient condition to conclude that the flow is stable.

52.3.2 Fjørtoft's theorem

Roughly 70 years after [Rayleigh \(1880\)](#) introduced the inflection point theorem, and a year after [Kuo \(1949\)](#) extended the inflection point theorem to the β -plane, [Fjørtoft \(1950\)](#) established another necessary condition for instability that is somewhat more constraining than the Rayleigh-Kuo theorem from Section 52.3.1.

To derive Fjørtoft's theorem, return to equation (52.25). Rather than focus on the imaginary part as done for the Rayleigh criteria, consider the real part

$$\int_{\mathcal{R}} \frac{(u_b - c_r)(\beta - \partial_{yy} u_b) |\tilde{\psi}|^2}{|u_b - c|^2} dy = \int_{\mathcal{R}} [|\partial_y \tilde{\psi}|^2 + k^2 |\tilde{\psi}|^2] dy > 0. \quad (52.27)$$

We are interested in profiles that satisfy the Rayleigh criteria for instability, so that the integral (52.26) vanishes, in which case we have

$$\int_{\mathcal{R}} \frac{c_r (\beta - \partial_{yy} u_b) |\tilde{\psi}|^2}{|u_b - c|^2} dy = 0, \quad (52.28)$$

since c_r is a constant. Hence, equation (52.27) is trivially satisfied with any constant, U_s , inserted

²Recall from Section 52.2.1 that if c solves the Rayleigh equation with streamfunction $\tilde{\psi}$, then c^* also satisfies the equation with streamfunction $\tilde{\psi}^*$. Hence, for each decaying mode there is a growing mode. So a sufficient condition for instability is to find a wave in which $c_i \neq 0$.

³Discuss Couette flow.

into the integral

$$\int_{\mathcal{R}} \frac{(u_b - U_s)(\beta - \partial_{yy}u_b) |\tilde{\psi}|^2}{|u_b - c|^2} dy > 0. \quad (52.29)$$

A very useful constant is the value of the zonal velocity at the point where $\beta - \partial_{yy}u_b = 0$, which leads to the following theorem.

FJØRTOFT'S THEOREM

Under the same assumptions as the Rayleigh-Kuo theorem, a necessary condition for shear instability is that $(u_b - U_s)(\beta - \partial_{yy}u_b) > 0$ occurs somewhere in the domain. Here, the inflection point is determined by $\beta - \partial_{yy}u_b(y_s) = 0$, and $U_s = u_b(y_s)$ is the velocity at the inflection point. This theorem means that an instability can occur only if the absolute vorticity has an extrema in the domain interior rather than at the boundaries.

52.3.3 A sinh profile

Consider the zonal velocity given by

$$u_b = U [1 + \sinh(y/L)] \quad (52.30a)$$

$$\zeta_b = -\partial_y u_b = -(U/L) \cosh(y/L) \quad (52.30b)$$

$$\partial_y \zeta_b = -\partial_{yy} u_b = -(U/L^2) \sinh(y/L), \quad (52.30c)$$

and assume $\beta = 0$. This velocity has an inflection point at $y = 0$, where the relative vorticity is maximum. Consequently, the velocity satisfies Rayleigh's necessary condition for instability. However, for Fjørtoft's theorem we note that the velocity equals U at the inflection point so that

$$(u_b - U_s)(0 - \partial_{yy}u_b) = -(U/L)^2 \sinh^2(y/L) < 0. \quad (52.31)$$

Since $(u_b - U_s)(0 - \partial_{yy}u_b)$ is never positive in the domain, the flow is stable via the Fjørtoft theorem. In particular, the vorticity becomes ever more negative as y increases. So the vorticity extrema is at the boundary of the domain rather than in the interior. In Exercise 52.1 we consider $\beta > 0$, where we show that the sinh profile remains stable according to Fjørtoft.



52.4 Exercises

EXERCISE 52.1: FJØRTOFT'S THEOREM WITH SINH PROFILE AND $\beta \neq 0$

Consider the sinh velocity profile from Section 52.3.3. Show that with $\beta \neq 0$ the flow remains stable according to Fjørtoft's theorem.



Chapter 53

STABILITY OF STRATIFIED SHEAR FLOW

In this chapter we study the stability of vertically sheared flows in a vertically stratified fluid in the absence of rotation. The base state flow is statically stable to gravitational instability, so that the squared buoyancy frequency is positive, $N^2 > 0$. The presence of vertical stratification creates a potential energy barrier that stabilizes the vertically sheared flow relative to the case without gravity. If the kinetic energy of the vertical sheared flow is large enough, then the potential energy barrier can be overcome to produce a shear instability. Our study of *stratified shear instability* makes use of normal mode stability analysis just like for the barotropic shear flow in Chapter 52. The *gradient Richardson number* provides a non-dimensional measure of the potential energy to kinetic energy, with a normal mode instability occurring if the Richardson number is small enough. We offer a detailed argument following [Miles \(1961\)](#) showing that the critical Richardson number is 1/4.

READER'S GUIDE FOR THIS CHAPTER

We make use of the perfect stratified Boussinesq fluid from Chapter 26. In linearizing the equations we follow many of the same steps used for the study of internal gravity waves in Chapter 49. The linear partial differential equation appearing in the stability analysis is known as the *Taylor-Goldstein* equation, and it is very similar to the *Rayleigh* equation encountered in the barotropic shear instability of Chapter 52.

53.1 Loose threads	1375
------------------------------	------

53.1 Loose threads

- Miles calculation from Section 11.7 of [Kundu et al. \(2016\)](#).
- Howard semi-circle theorem from Section 11.7 of [Kundu et al. \(2016\)](#).
- Energetic argument from Section 14.1 of [Cushman-Roisin and Beckers \(2011\)](#). This is much clearer than that given by [Chandrasekhar \(1961\)](#).



Chapter 54

INSTABILITIES LEADING TO CONVECTION

In this chapter we study convection, double diffusion, and Rayleigh-Bernard convection.

READER'S GUIDE FOR THIS CHAPTER

54.1 Loose threads	1377
------------------------------	------

54.1 Loose threads

- Section 3 of *Fetter and Walecka* (2006)
- Chapter 18 of *Thorne and Blandford* (2017)



Chapter 55

STABILITY OF QUASI-GEOSTROPHIC FLOWS

Quasi-geostrophy is the study of flow that evolves in the presence of a prescribed and gravitationally stable base state that is in hydrostatic and geostrophic balance. The evolving flow is itself in hydrostatic balance and nearly geostrophic balance. All of the time dependent flow, including the horizontal geostrophic velocity, \mathbf{u} , and buoyancy, b are fully determined by knowledge of the quasi-geostrophic potential vorticity, q .

In this chapter we examine the stability of a thermal wind base state flow within quasi-geostrophic theory. In addition to planetary and topographic Rossby waves, a thermal wind base state supports *Eady waves* ([Eady, 1949](#)), which are edge waves that propagate along the top and bottom boundaries. The *Eady model* considers the constructive interaction of edge waves, thus leading to *wave resonance* that drives baroclinic instability. Baroclinic instability dominates the fluctuations of the middle latitude atmosphere and mesoscale ocean, thus representing a central flow instability of large-scale geophysical fluid mechanics.

READER'S GUIDE FOR THIS CHAPTER

We assume familiarity with continuously stratified perfect fluid quasi-geostrophy from Chapter 42. The wave resonance interpretation of baroclinic instability closely follows that given for shear instability in Chapter 52.

55.1 Loose threads	1380
55.2 Equations of quasi-geostrophy	1380
55.2.1 Governing equations	1381
55.2.2 Boundary conditions	1381
55.2.3 Evolution of the quasi-geostrophic fields	1382
55.3 Rossby waves in continuous stratification	1382
55.3.1 Planetary Rossby waves	1382
55.3.2 Topographic Rossby waves	1383
55.4 A zonal geostrophic base flow	1385
55.4.1 Zonal geostrophic base flow	1385
55.4.2 Fluctuating streamfunction and potential vorticity	1386
55.4.3 Linearized upper surface boundary condition	1386
55.4.4 Linearized bottom boundary condition	1386
55.5 Eady edge waves	1387
55.5.1 Assumptions for Eady waves	1387
55.5.2 Streamfunction equation	1388
55.5.3 Bottom trapped Eady waves	1388
55.5.4 Upper surface trapped Eady waves	1389
55.5.5 Further study	1389
55.6 Eady model of baroclinic instability	1389

55.6.1	Streamfunction solution	1390
55.6.2	Dispersion relation	1390
55.6.3	Growth rate	1391
55.6.4	Further study	1392
55.7	Necessary conditions for instability	1392
55.7.1	Summary of the governing linear equations	1393
55.7.2	Deriving the necessary condition for instability	1393
55.7.3	Special cases	1394

55.1 Loose threads

- Synoptic development
- Show some vertical baroclinic modes in Section 55.3.1 for constant N^2 and for an exponential thermocline.
- Polarization relations for the waves introduced in this chapter, including Eady waves.
- Is there an analog of Fjortoft for baroclinic instability?
- Discuss wedge of instability as per [Heifetz et al. \(1998\)](#) and [Pedlosky \(2003\)](#).
- More on topographic waves
- Connection to surface QG
- Wave-mean flow interactions
- Integral necessary conditions
- Energetics
- Discuss the neutral wave case with $U_g = c$ and further explore Footnote 10 in Chapter 9 of [Vallis \(2017\)](#).
- Move the stable waves material into a new chapter “Quasi-geostrophic waves” in the waves part of the book.
- Follow Chapters 18 and 19 of [Pedlosky \(2003\)](#).
- Offer further elaborations from [Vallis \(2017\)](#) and [Cushman-Roisin and Beckers \(2011\)](#).

55.2 Equations of quasi-geostrophy

We here summarize salient features of continuously stratified quasi-geostrophic theory, with conceptual and technical details provided in Chapter 42.

55.2.1 Governing equations

The quasi-geostrophic buoyancy equation (42.40), relative vorticity equation (42.45), and potential vorticity equation (42.55), are given by

$$(\partial_t + \mathbf{u} \cdot \nabla) b = -w N^2 \quad \text{buoyancy equation} \quad (55.1a)$$

$$(\partial_t + \mathbf{u} \cdot \nabla) \zeta = -\beta v + f_0 \partial_z w \quad \text{relative vorticity equation} \quad (55.1b)$$

$$(\partial_t + \mathbf{u} \cdot \nabla) q = 0, \quad \text{quasi-geostrophic potential vorticity equation,} \quad (55.1c)$$

in which

$$\psi = p/(\rho_0 f_0) \quad \text{quasi-geostrophic streamfunction (}p=\text{pressure)} \quad (55.2a)$$

$$\mathbf{u} = \hat{\mathbf{z}} \times \nabla \psi \quad \text{non-divergent geostrophic velocity} \quad (55.2b)$$

$$b = f_0 \partial_z \psi \quad \text{buoyancy} \quad (55.2c)$$

$$\zeta = \hat{\mathbf{z}} \cdot (\nabla \times \mathbf{u}) = \nabla_z^2 \psi \quad \text{geostrophic relative vorticity} \quad (55.2d)$$

$$q = f_0 + \beta y + \zeta + f_0 \partial_z (b/N^2) \quad \text{quasi-geostrophic potential vorticity} \quad (55.2e)$$

$$q = f_0 + \beta y + \nabla_z^2 \psi + f_0^2 \partial_z (\partial_z \psi / N^2) \quad \text{potential vorticity with streamfunction.} \quad (55.2f)$$

The prescribed time-independent parameters are given by

$$N^2(z) > 0 \quad \text{background stratification} \quad (55.3a)$$

$$f(y) = f_0 + \beta y \quad \beta\text{-plane Coriolis frequency.} \quad (55.3b)$$

Quasi-geostrophy is derived assuming the following scaling

$$U/f_0 L \ll 1 \quad \text{small Rossby number, so rotationally dominant} \quad (55.4a)$$

$$\beta L/f_0 \ll 1 \quad \text{horizontal length as per } \beta\text{-plane approximation.} \quad (55.4b)$$

Note that for the potential vorticity, f_0 can be dropped since it is a constant and so plays no role in the potential vorticity equation.

55.2.2 Boundary conditions

For the lateral boundaries, we assume either infinite horizontal domain or periodic boundaries, and they play no fundamental role in the dynamics of concern in this chapter. In contrast, the top and bottom boundaries are central to our study of waves and instabilities. To establish the corresponding boundary conditions, we make use of the buoyancy equation (55.1a), given the presence of the vertical velocity. Furthermore, we are concerned with perfect fluid quasi-geostrophy, so need to consider just the kinematic boundary conditions from Section 42.5.3. Dynamic boundary conditions involve frictional stresses and they are not considered here.

Along a sloping bottom, at $z = \eta_b(x, y)$, we have the boundary condition

$$(\partial_t + \mathbf{u} \cdot \nabla_z) b + \mathbf{u} \cdot \nabla_z (N^2 \eta_b) = 0 \quad \text{at } z = \bar{\eta}_b, \quad (55.5)$$

which takes on the following form with the streamfunction

$$f_0 \partial_t (\partial_z \psi) + \mathbf{u} \cdot \nabla_z [f_0 \partial_z \psi + N^2 \eta_b] = 0 \quad \text{at } z = \bar{\eta}_b. \quad (55.6)$$

The bottom boundary condition is evaluated at the horizontally averaged position, $z = \bar{\eta}_b$, since the more precise boundary location, $z = \eta_b(x, y)$, is one order higher in Rossby number and so

is dropped from quasi-geostrophic theory. Correspondingly, quasi-geostrophic theory is formally valid only for very gently sloping bottom boundaries. Note that when η_b is a constant, then $\nabla_z(N^2 \eta_b) = 0$ so that the boundary condition reduces to the material invariance of the boundary buoyancy.

For the upper surface (top) boundary, the vertical velocity is vanishingly small relative to interior vertical motion. Hence, the boundary buoyancy is materially invariant

$$(\partial_t + \mathbf{u} \cdot \nabla_z) b = 0 \implies (\partial_t + \mathbf{u} \cdot \nabla_z) \partial_z \psi = 0 \quad \text{at } z = \bar{\eta}. \quad (55.7)$$

To within the accuracy of quasi-geostrophy, this boundary condition is evaluated at the resting position of the top boundary, $z = \bar{\eta}$.

55.2.3 Evolution of the quasi-geostrophic fields

The evolution of buoyancy (equation (55.1a)) and relative vorticity (equation (55.1b)) are both affected by the ageostrophic vertical velocity, w . However, we do not need to explicitly compute w to evolve the flow. The reason is that we can instead evolve the quasi-geostrophic potential vorticity through equation (55.1c) and associated boundary conditions. Thereafter, we solve the Poisson equation (with boundary conditions) for the geostrophic streamfunction

$$\nabla_z^2 \psi + f_0^2 \partial_z (\partial_z \psi / N^2) = q - (f_0 + \beta y). \quad (55.8)$$

Upon updating the streamfunction we can then update the velocity, buoyancy, and relative vorticity.

55.3 Rossby waves in continuous stratification

We here introduce two stable linear waves that appear in continuously stratified quasi-geostrophy: planetary Rossby waves and topographic Rossby waves. We already encountered planetary Rossby waves in Section 47.3 for the horizontally non-divergent barotropic model, and in Section 48.11 for the shallow water model. We also encountered topographic waves for the shallow water layer in Section 48.4.6.

We here extend those earlier discussions of Rossby waves to the case of continuous stratification. We here assume the base state flow is static, in which case the geostrophic streamfunction is a constant and the base state potential vorticity equals to the planetary vorticity

$$Q_g = f_0 + \beta y \implies \nabla Q_g = \beta \hat{\mathbf{y}}. \quad (55.9)$$

We relax this assumption in Section 55.4, where the base state is geostrophically balanced zonal flow.

55.3.1 Planetary Rossby waves

Assume the bottom is flat so that the linearized streamfunction equation and boundary conditions take on the form

$$\partial_t q + \beta v = 0 \implies \partial_t [\nabla_z^2 \psi + f_0^2 \partial_z (\partial_z \psi / N^2)] + \beta \partial_x \psi = 0 \quad (55.10a)$$

$$\partial_{tz} \psi = 0 \quad \text{at } z = \bar{\eta} \text{ and } z = \bar{\eta}_b. \quad (55.10b)$$

In the presence of a horizontally homogeneous vertical stratification, $N^2(z)$, we assume a horizontally traveling free plane waves modulated by a vertical amplitude function

$$\psi(x, y, z, t) = \tilde{\psi}(z) e^{i(k_x x + k_y y - \omega t)}. \quad (55.11)$$

Plugging this ansatz into the streamfunction equation (55.10a) and boundary condition equation (55.10b) leads to the Sturm-Liouville eigenvalue problem

$$\frac{d}{dz} \left[\frac{f_0^2}{N^2} \frac{d\tilde{\psi}}{dz} \right] = (|\mathbf{k}|^2 + \beta k_x/\omega) \tilde{\psi} \quad (55.12a)$$

$$\frac{d\tilde{\psi}}{dz} = 0 \quad \text{at } z = \bar{\eta}, \bar{\eta}_b. \quad (55.12b)$$

An analytic solution can be readily found for the case of constant N^2 , whereby the streamfunction amplitude is

$$\tilde{\psi} = \tilde{\psi}_0 \cos[n \pi (z - \bar{\eta}_b)/H] \quad \text{with } H = \bar{\eta} - \bar{\eta}_b, \quad (55.13)$$

and the angular frequency is

$$\omega = -\frac{\beta k_x}{(n \pi / L_d)^2 + k_x^2 + k_y^2} \quad \text{with } L_d = N H / f_0 \text{ the deformation radius.} \quad (55.14)$$

The Rossby wave dispersion relation (55.14) has zero contribution from the deformation radius when $n = 0$. This *barotropic mode* has a dispersion relation equal to that for the horizontally non-divergent Rossby wave studied in Section 47.3 and given by equation (47.27). Likewise, the streamfunction has no depth dependence when $n = 0$. In contrast, the higher *baroclinic modes*, with $n > 0$, are depth dependent, with increasing vertical structure and reduced frequency as n increases. Also note that the depth integral of the horizontal velocity vanishes when $n > 0$, so that the baroclinic modes have zero depth average. Each baroclinic mode corresponds directly to the shallow water Rossby waves in the shallow water layer studied in Section 48.11. The only difference concerns the deformation radius, whereby the Rossby wave in a single layer of shallow water fluid has a deformation radius given by equation (48.204)

$$L_d = c_{\text{grav}}/f_0 = \sqrt{g H}/f_0 \quad \text{single shallow water layer.} \quad (55.15)$$

55.3.2 Topographic Rossby waves

Here we set $\beta = 0$, but regain a background potential vorticity gradient by allowing the bottom to have a gentle slope. The resulting linearized potential vorticity equation and boundary conditions are

$$\partial_t q = 0 \implies \partial_t [\nabla_z^2 \psi + f_0^2 \partial_z (\partial_z \psi / N^2)] = 0 \quad (55.16a)$$

$$\partial_{tz} \psi = 0 \quad \text{at } z = \bar{\eta}. \quad (55.16b)$$

$$f_0 \partial_{tz} \psi + N^2 \hat{\mathbf{z}} \cdot (\nabla \psi \times \nabla \eta_b) = 0 \quad \text{at } z = \bar{\eta}_b. \quad (55.16c)$$

To study plane waves in the horizontal, we assume the special case of a linear slope in the meridional direction,

$$\eta_b = \eta_{\text{const}} + \alpha_b y \quad \text{with } \alpha_b \ll 1, \quad (55.17)$$

so that the bottom boundary condition becomes

$$f_0 \partial_{tz} \psi + N^2 \alpha_b \partial_x \psi = 0 \quad \text{at } z = \bar{\eta}_b. \quad (55.18)$$

Eigenvalue problem for $\tilde{\psi}$

Assuming again that the buoyancy frequency is constant, and with the linear bottom slope (55.17), we can take the same wave ansatz (55.11) as used for planetary Rossby waves in Section 55.3.1. Doing so leads to the eigenvalue problem for the topographic Rossby waves

$$\frac{d^2 \tilde{\psi}}{dz^2} = \mu^2 \tilde{\psi} \quad \bar{\eta}_b < z < \bar{\eta} \quad (55.19a)$$

$$f_0 \omega \frac{d\tilde{\psi}}{dz} = N^2 \alpha_b k_x \tilde{\psi} \quad \text{at } z = \bar{\eta}_b \quad (55.19b)$$

$$\omega \frac{d\tilde{\psi}}{dz} = 0 \quad \text{at } z = \bar{\eta}, \quad (55.19c)$$

where we introduced the scaled wave number

$$\mu = |\mathbf{k}| N / f_0 = |\mathbf{k}| L_d / H \quad \text{with } L_d = N H / f_0. \quad (55.20)$$

This wavenumber appears frequently throughout the analysis. Note that the bottom boundary condition (55.19b) cannot be satisfied with the zero frequency wave due to the nonzero bottom slope, thus indicating the fundamental role for the bottom slope in sourcing the waves.

Bottom trapped streamfunction

To further simplify the analysis, assume the upper boundary, at $z = \bar{\eta}$, is far enough away that it can be ignored. In this case the streamfunction takes on the bottom trapped form

$$\tilde{\psi} = \tilde{\psi}_0 e^{-\mu(z-\bar{\eta}_b)}. \quad (55.21)$$

To determine what is “far enough away”, we evaluate the streamfunction at $z = \bar{\eta}$, whereby

$$\tilde{\psi}(z = \bar{\eta}) = \tilde{\psi}_0 e^{-\mu H} = \tilde{\psi}_0 e^{-|\mathbf{k}| L_d}. \quad (55.22)$$

This streamfunction is exponentially small for wavenumbers satisfying

$$|\mathbf{k}| \gg L_d^{-1} \quad \text{with } L_d = N H / f_0. \quad (55.23)$$

That is, these *topographic Rossby waves* do not feel the upper boundary if their wavelength is small compared to the deformation radius

$$\Lambda \ll 2\pi L_d. \quad (55.24)$$

Dispersion relation

Inserting the streamfunction (55.21) into the bottom boundary condition (55.19b) leads to the dispersion relation

$$\omega = -N \alpha_b k_x / |\mathbf{k}|. \quad (55.25)$$

Since the angular frequency is positive, the wave vector is constrained so that k_x is pseudo-westward. That is, the phase velocity of topographic Rossby waves is directed with the bottom

rising to the right of the wave. For example, if $\alpha_b > 0$, so that the bottom rises to the north, then $k_x < 0$ so that the wave travels to the west. In this manner the topographic slope acts as a background potential vorticity gradient in a manner analogous to the planetary beta. To further this correspondence, we introduce a topographic beta (which can be either sign),

$$\beta_{\text{topo}} = f_0 \partial_y \eta_b / H, \quad (55.26)$$

so that the dispersion relation (55.25) takes on the form

$$\omega = -\frac{\beta_{\text{topo}} k_x}{|\mathbf{k}| L_d^{-1}}, \quad (55.27)$$

which shares features with the planetary Rossby wave from Section 55.3.1.

55.4 A zonal geostrophic base flow

We here formulate the equations for the zonal base flow and fluctuations relative to that flow. In Sections 55.5 and 55.6 we make use of this formulation to study stable and unstable *Eady edge waves*.

55.4.1 Zonal geostrophic base flow

Consider a geostrophic base state described by a streamfunction $\Psi_g(y, z)$ with a corresponding zonal flow and thermal wind shear

$$U_g(y, z) = -\partial_y \Psi_g \quad \text{and} \quad \partial_z U_g = -\partial_{yz} \Psi_g = -f_0^{-1} \partial_y B_g, \quad (55.28)$$

where $B_g(y, z)$ is the buoyancy field supporting the geostrophic flow. A particular example of buoyancy supporting a geostrophic flow with a constant thermal shear is given by

$$B_g = N^2 z + (\partial_y B_g) y = N^2 z - f_0 (\partial_z U_g) y, \quad \text{with } N^2, \partial_y B_g, \text{ and } \partial_z U_g \text{ constants.} \quad (55.29)$$

We now show that the geostrophic flow (55.28) identically satisfies the quasi-geostrophic equations, and so is an exact solution to quasi-geostrophy. For this purpose, introduce the quasi-geostrophic potential vorticity

$$Q_g = f_0 + \beta y - \partial_y U_g + f_0^2 \partial_z (N^{-2} \partial_z \Psi_g). \quad (55.30)$$

Since Q_g is a function just of (y, z) , it trivially satisfies the potential vorticity equation

$$(\partial_t + U_g \hat{\mathbf{x}} \cdot \nabla_z) Q_g = U_g \partial_x Q_g = 0. \quad (55.31)$$

Likewise, the buoyancy field $B_g(y, z)$ trivially satisfies the top boundary condition (55.7) since

$$(\partial_t + U_g \hat{\mathbf{x}} \cdot \nabla_z) B_g = U_g \partial_x B_g = 0. \quad (55.32)$$

For the bottom boundary condition (55.6) we have

$$(\partial_t + U_g \partial_x) B_g + U_g \partial_x (N^2 \eta_b) = 0 \quad \text{at } z = \bar{\eta}_b, \quad (55.33)$$

which is satisfied if the topography is a function only of latitude, $\eta_b = \eta_b(y)$. Hence, the thermal wind flow $U_g(y, z)$ and buoyancy $B_g(y, z)$ are exact solutions to quasi-geostrophy when the bottom

is either constant or has a meridional slope.

55.4.2 Fluctuating streamfunction and potential vorticity

Now consider fluctuations relative to the zonal geostrophic flow, with streamfunction and buoyancy decomposed as

$$\psi(x, y, z, t) = \Psi_g(y, z) + \psi'(x, y, z, t) \quad \text{and} \quad b(x, y, z, t) = B_g(y, z) + b'(x, y, z, t). \quad (55.34)$$

The corresponding quasi-geostrophic potential vorticity is decomposed according to

$$q(x, y, z, t) = Q_g(y, z) + q'(x, y, z, t), \quad (55.35)$$

with Q_g given by equation (55.30) and the fluctuating potential vorticity due to relative vorticity and stretching

$$q' = \nabla_z^2 \psi' + f_0^2 \partial_z(N^{-2} \partial_z \psi'). \quad (55.36)$$

The quasi-geostrophic potential vorticity equation (55.1c) takes the form

$$(\partial_t + \mathbf{u} \cdot \nabla_z) q = (\partial_t + \mathbf{u}' \cdot \nabla_z) q' + v' \partial_y Q_g + U_g \partial_x q' = 0, \quad (55.37)$$

which linearizes to

$$(\partial_t + U_g \partial_x) q' = -v' \partial_y Q_g \implies (\partial_t + U_g \partial_x) [\nabla_z^2 \psi' + f_0^2 \partial_z(N^{-2} \partial_z \psi')] = -\partial_x \psi' \partial_y Q_g. \quad (55.38)$$

Evidently, q' is advected by the zonal mean flow, U_g , and it has a source determined by the anomalous meridional advection of the geostrophic potential vorticity, Q_g .

55.4.3 Linearized upper surface boundary condition

For the upper surface boundary condition we have

$$\partial_t b' + (U_g \partial_x + \mathbf{u}' \cdot \nabla_z)(B_g + b') = 0, \quad (55.39)$$

which linearizes to

$$(\partial_t + U_g \partial_x) b' = -v' \partial_y B_g \implies (\partial_t + U_g \partial_x) \partial_z \psi' = \partial_x \psi' \partial_z U_g. \quad (55.40)$$

As we see in Section 55.5, advection by the zonal geostrophic flow provides a frequency shift to the linear waves, whereas the source, $\partial_x \psi' \partial_z U_g$, supports the propagation of surface trapped edge waves relative to the flow.

55.4.4 Linearized bottom boundary condition

Likewise, the bottom boundary condition (55.6), with $\eta_b(y)$, is given by

$$f_0 (\partial_t + U_g \partial_x + \mathbf{u}' \cdot \nabla_z) \partial_z \psi' = v' (f_0 \partial_z U_g - N^2 \partial_y \eta_b), \quad (55.41)$$

which linearizes to

$$f_0 (\partial_t + U_g \partial_x) \partial_z \psi' = \partial_x \psi' (f_0 \partial_z U_g - N^2 \partial_y \eta_b). \quad (55.42)$$

The right hand side can be written in a geometric manner through the identities

$$\partial_y B_g / N^2 = \partial_y B_g / \partial_z B_g = -(\partial z / \partial y)_{B_g}, \quad (55.43)$$

where we introduced the meridional slope of the background buoyancy field¹

$$(\partial z / \partial y)_{B_g} = -\partial_y B_g / \partial_z B_g = f_0 \partial_z U_g / \partial_z B_g. \quad (55.44)$$

The bottom boundary condition (55.42) can thus be written as

$$f_0 (\partial_t + U_g \partial_x) \partial_z \psi' = \partial_x \psi' N^2 [(\partial z / \partial y)_{B_g} - \partial_y \eta_b], \quad (55.45)$$

in which the forcing on the right hand side is determined by the difference between the buoyancy slope and bottom topography slope.

55.5 Eady edge waves

The geometric expression for the bottom boundary condition (55.45) suggests that sloping buoyancy surfaces support waves play in a manner similar to that of sloping bottom. Whereas a sloping bottom in the presence of flat buoyancy surfaces supports topographic Rossby waves, a sloping buoyancy surface in the presence of a flat bottom supports *Eady waves*.

55.5.1 Assumptions for Eady waves

We make the following assumptions to support an analytic derivation of the dispersion relation for Eady waves.

- $\beta = 0$ so that there are no planetary Rossby waves;
- $\nabla \eta_b = 0$ so that there are no topographic Rossby waves;
- Linear thermal wind front supported by the buoyancy in equation (55.29), in which N^2 , $\partial_y B_g$, and $\partial_z U_g$ are constants, thus implying that the buoyancy slope, $(\partial z / \partial y)_{B_g}$, is also a constant;
- Zonal geostrophic flow that is a linear function of vertical position

$$U_g = U_g(z) = U_0 + \partial_z U_g (z - \bar{\eta}_b), \quad (55.46)$$

which means that the corresponding geostrophic streamfunction is

$$\Psi_g = -y [U_0 + \partial_z U_g (z - \bar{\eta}_b)]. \quad (55.47)$$

- With these assumptions the background potential vorticity (55.30) is a constant throughout the fluid interior

$$Q_g = 2 f_0 \implies \nabla Q_g = 0, \quad (55.48)$$

and thus it plays no dynamical role.

Each of the above assumptions is rather restrictive. However, they offer a streamlined means to analytically reveal the core physics of Eady waves.

¹See Section 56.12.2 for mathematical details on the treatment of generalized vertical coordinates.

55.5.2 Streamfunction equation

The linearized potential vorticity equation (55.38) and corresponding boundary conditions (55.40) and (55.45) take on the form

$$[\partial_t + U_g(z) \partial_x] q' = 0 \quad \bar{\eta}_b < z < \bar{\eta} \quad (55.49a)$$

$$[\partial_t + U_g(\bar{\eta}) \partial_x] \partial_z \psi' = \partial_x \psi' \partial_z U_g \quad z = \bar{\eta} \quad (55.49b)$$

$$(\partial_t + U_g(\bar{\eta}_b) \partial_x) \partial_z \psi' = \partial_x \psi' \partial_z U_g \quad z = \bar{\eta}_b, \quad (55.49c)$$

with the bottom boundary condition resulting from

$$N^2 (\partial z / \partial y)_{B_g} = -\partial_y B_g = f_0 \partial_z U_g. \quad (55.50)$$

The assumptions from Section 55.5.1 have led to a boundary value problem in which the only spatial dependence concerns the vertical. Hence, we can consider the familiar wave ansatz (55.11) for the streamfunction, in which fluctuations are organized into horizontally propagating free plane waves that are modulated by a vertical dependent amplitude function

$$\psi'(x, y, z, t) = \tilde{\psi}(z) e^{i(k_x x + k_y y - \omega t)}, \quad (55.51)$$

in which case the fluctuating potential vorticity (55.36) is given by

$$q' = (f_0/N)^2 (\partial_{zz} - \mu^2) \psi', \quad (55.52)$$

and the linear potential vorticity equation (55.49a) is

$$(-\omega + U_g k_x) (\partial_{zz} - \mu^2) \tilde{\psi} = 0, \quad (55.53)$$

where $\mu = |\mathbf{k}| N/f_0$ is the scaled wavenumber (55.20).

Throughout the analysis we assume the angular frequency satisfies

$$\omega \neq U_g k_x. \quad (55.54)$$

In this case, the streamfunction equation (55.53) reduces to

$$\frac{d^2 \tilde{\psi}}{dz^2} = \mu^2 \tilde{\psi}, \quad (55.55)$$

which is the same equation as satisfied by the topographic Rossby wave (55.19a). As seen below, the angular frequency assumption (55.54) holds for Eady waves.

55.5.3 Bottom trapped Eady waves

As in our discussion of topographic Rossby waves in Section 55.3.2, we assume the upper boundary is far from the lower boundary, as determined by the wavenumber satisfying equation (55.23),

$$|\mathbf{k}| \gg L_d^{-1}. \quad (55.56)$$

In this case, the bottom trapped streamfunction solution to equation (55.55) is given by

$$\tilde{\psi} = \tilde{\psi}_0 e^{-\mu(z - \bar{\eta}_b)}, \quad (55.57)$$

which is, as expected, the same as for the topographic Rossby wave (55.21). Even though they have the same form of their streamfunctions, the Eady wave dispersion relation differs from that of the topographic Rossby wave. Here, we derive the dispersion relation through use of the bottom boundary condition (55.49c), which takes the form

$$(-\omega + U_g(\bar{\eta}_b) k_x)(-|\mathbf{k}| N/f_0) = k_x \partial_z U_g, \quad (55.58)$$

thus leading to the dispersion relation

$$\omega_{\text{bot}} - k_x U_g(\bar{\eta}_b) = \frac{f_0 k_x \partial_z U_g}{N |\mathbf{k}|} = \frac{H k_x \partial_z U_g}{L_d |\mathbf{k}|}. \quad (55.59)$$

The $k_x U_g(\bar{\eta}_b)$ term provides a frequency shift from the coupling between the zonal component of the phase velocity and the zonal flow next to the bottom boundary. The right hand side arises from the thermal wind shear in the presence of rotation and stratification, with the zonal wind shear reliant on the sloping buoyancy surfaces that intersect the bottom boundary. To realize $\omega - k_x U_g(\bar{\eta}_b) > 0$ requires $f_0 k_x \partial_z U_g > 0$. For example, with $f_0 \partial_z U_g > 0$, as for the northern hemisphere atmospheric jet stream, then the bottom Eady wave has an eastward phase velocity, $k_x > 0$, relative to the base state flow.

55.5.4 Upper surface trapped Eady waves

Proceeding just like for the bottom, we now focus on the surface (top) boundary and assume the bottom boundary is far away. In this case the upper surface trapped streamfunction is given by

$$\tilde{\psi} = \psi_{\text{top}} e^{\mu(z-\bar{\eta})}, \quad (55.60)$$

which, when used in the upper boundary condition (55.40), leads to the dispersion relation

$$\omega_{\text{top}} - k_x U_g(\bar{\eta}) = -\frac{k_x f_0 \partial_z U_g}{N |\mathbf{k}|} = -\frac{H k_x \partial_z U_g}{L_d |\mathbf{k}|}. \quad (55.61)$$

As for the bottom boundary trapped Eady waves, the term $k_x U_g(\bar{\eta})$ is a frequency shift arising from the zonal velocity at the upper boundary that couples to the zonal component of the phase velocity. The right hand side arises from the thermal wind shear coupled to rotation and stratification, which itself relies on the slope of the buoyancy surfaces that intersect the upper boundary. We see that $\omega_{\text{top}} - k_x U_g(\bar{\eta}) > 0$ if $f_0 k_x \partial_z U_g < 0$, which is oppositely directed from the bottom trapped Eady waves. That is, the upper and lower bottom trapped Eady waves have opposite zonal components to their phase velocities.

55.5.5 Further study

The treatment in this section is compatible with Chapter 19 of [Pedlosky \(2003\)](#) and Section 8.7 of [Smythe and Carpenter \(2019\)](#).

55.6 Eady model of baroclinic instability

The analysis from Section 55.5 revealed the presence of Eady edge waves that are exponentially trapped next to the top and bottom boundaries, and the zonal component to their phase velocities are oppositely directed. The waves rely on the thermal wind shear intersecting a boundary. Evidently, the angular frequencies for the two waves (equations (55.59) and (55.61)) are equal for

wavenumbers satisfying

$$\omega_{\text{top}} = \omega_{\text{bot}} \implies |\mathbf{k}| = 2 L_{\text{d}}^{-1}. \quad (55.62)$$

For this wave, and for longer waves (smaller wavenumbers), we cannot ignore interactions between the edge waves. We here extend the analysis to allow for interactions between the edge waves. Under specific circumstances, the waves constructively interact to support exponential growth, thus signaling *baroclinic instability*. The treatment is directly analogous to our treatment in Section 52.2 of interacting vortex edge waves in a horizontally sheared fluid.

55.6.1 Streamfunction solution

As before, we take the streamfunction ansatz (55.51), which leads to the differential equation (55.55) and boundary conditions (55.49c) and (55.58) and for the streamfunction

$$d^2\tilde{\psi}/dz^2 = \mu^2 \tilde{\psi} \quad 0 < z < H \quad (55.63a)$$

$$(-\omega + U_{\text{g}}(H) k_x) \partial_z \tilde{\psi} = k_x \partial_z U_{\text{g}} \tilde{\psi} \quad z = H \quad (55.63b)$$

$$(-\omega + U_{\text{g}}(0) k_x) \partial_z \tilde{\psi} = k_x \partial_z U_{\text{g}} \tilde{\psi} \quad z = 0, \quad (55.63c)$$

where we made use of the scaled wavenumber (55.20)

$$\mu = |\mathbf{k}| N/f_0 = |\mathbf{k}| L_{\text{d}}/H \quad \text{with } L_{\text{d}} = N H/f_0. \quad (55.64)$$

Additionally, we set

$$\bar{\eta} = H \quad \text{and} \quad \bar{\eta}_{\text{b}} = 0, \quad (55.65)$$

to help reduce notational clutter.

Solution to the boundary value problem

The solution to the differential equation (55.63a) is given by the hyperbolic functions

$$\tilde{\psi} = A \cosh(\mu z) + B \sinh(\mu z), \quad (55.66)$$

where the coefficients A and B , are to be determined via the boundary conditions. Making use of the upper surface boundary condition (55.63b) and bottom boundary condition (55.63c) leads to the coupled linear equations

$$(-\tilde{c} + H \partial_z U_{\text{g}}) \mu [A \sinh(\mu H) + B \cosh(\mu H)] = \partial_z U_{\text{g}} [A \cosh(\mu H) + B \sinh(\mu H)] \quad (55.67a)$$

$$-\tilde{c} \mu B = A \partial_z U_{\text{g}}, \quad (55.67b)$$

where we introduced the shorthand

$$\tilde{c} \equiv \omega/k_x - U_{\text{g}}(0). \quad (55.68)$$

55.6.2 Dispersion relation

Equations (55.67a) and (55.67b) are two homogeneous linear equations for the two unknowns, A and B . A nontrivial solution exists if the determinant of the 2×2 coefficient matrix of vanishes. This condition leads to the quadratic equation for \tilde{c}

$$\tilde{c}^2 - \tilde{c} H \partial_z U_{\text{g}} + (\partial_z U_{\text{g}}/\mu)^2 (H \mu \coth(\mu H) - 1) = 0, \quad (55.69)$$

which has two roots given by the quadratic formula

$$\tilde{c} = \frac{H \partial_z U_g}{2} \pm \frac{\partial_z U_g}{\mu} \left[\frac{(\mu H)^2}{4} - \mu H \coth(\mu H) + 1 \right]^{1/2}. \quad (55.70)$$

A further simplification arises from use of the identity

$$2 \coth x = \tanh(x/2) + \coth(x/2), \quad (55.71)$$

in which case we have the roots

$$\omega/k_x = U(0) + \frac{H \partial_z U_g}{2} \pm \frac{\partial_z U_g}{\mu} \left[\left(\frac{\mu H}{2} - \coth(\mu H/2) \right) \left(\frac{\mu H}{2} - \tanh(\mu H/2) \right) \right]^{1/2}. \quad (55.72)$$

Since

$$x \geq \tanh x, \quad (55.73)$$

the only way to realize a negative discriminant is for

$$\mu H \leq 2 \coth(\mu H/2). \quad (55.74)$$

A graphical solution to the equality finds

$$\mu H = |\mathbf{k}| L_d \approx 2.399. \quad (55.75)$$

Note how this value is rather close to the $|\mathbf{k}| L_d = 2$ value from equation (55.62), computed by setting the frequencies equal for two non-interacting Eady edge waves.

55.6.3 Growth rate

For unstable waves, the growth rate is given by the imaginary part of the angular frequency

$$\sigma = \frac{|k_x \partial_z U_g|}{\mu} \left[\left| \frac{\mu H}{2} - \coth(\mu H/2) \right| \left| \frac{\mu H}{2} - \tanh(\mu H/2) \right| \right]^{1/2}. \quad (55.76)$$

For a given wavenumber, $|\mathbf{k}| = \sqrt{k_x^2 + k_y^2}$, the growth rate is maximized for waves with a zonal phase velocity so that $|\mathbf{k}| = |k_x|$. That is, the waves directed parallel to the background flow are most unstable

$$\sigma(\mathbf{k} = \hat{x} k_x) = \frac{H |\partial_z U_g|}{L_d} \left[\left| \frac{|\mathbf{k}| L_d}{2} - \coth(|\mathbf{k}| L_d/2) \right| \left(\frac{|\mathbf{k}| L_d}{2} - \tanh(|\mathbf{k}| L_d/2) \right) \right]^{1/2}. \quad (55.77)$$

Since the horizontal flow is non-divergent, Eady waves are transverse so that fluid particles movement is perpendicular to the phase velocity. With a zonal phase velocity, fluid particles move in the meridional direction.

Maximum growth rate

To compute the maximum growth rate we compute the $|\mathbf{k}| = |k_x|$ that satisfies

$$\frac{d\sigma^2}{dk_x} = 0, \quad (55.78)$$

which yields

$$|\mathbf{k}|_{\max} = |k_x|_{\max} \approx 1.6/L_d \implies \Lambda_{\max} \approx (2\pi/1.6) L_d \approx 3.9 L_d. \quad (55.79)$$

Evidently, the fastest growing Eady waves are purely zonal and have wavelength about four times the deformation radius. It is this connection to the deformation radius that directly connects these unstable Eady waves to synoptic eddies in the atmosphere and mesoscale eddies in the ocean.

Eady growth rate

The growth rate (55.77) is the product of an inverse time scale, T_{Eady}^{-1} , and a non-dimensional function, where the Eady time scale is given by

$$T_{\text{Eady}} = \frac{L_d}{H \partial_z U_g} = \frac{1}{f_0} \frac{N}{\partial_z U_g} = \frac{\sqrt{\text{Ri}}}{f_0}. \quad (55.80)$$

In the final equality we introduced the *balanced Richardson number* from Section 41.2.5

$$\text{Ri} = N^2 / (\partial_z U_g)^2. \quad (55.81)$$

For quasi-geostrophic flows, the balanced Richardson number is normally quite large. Evaluating the growth rate expression (55.77) with the fastest growing wave (55.79) renders

$$\sigma_{\max} = 0.31 T_{\text{Eady}}^{-1} = 0.31 \partial_z U_g (f_0/N) = 0.31 \frac{f_0}{\sqrt{\text{Ri}}}. \quad (55.82)$$

This maximum growth rate is sometimes generically called *the Eady growth rate*.

55.6.4 Further study

Our presentation of the Eady model is consistent with that found in [Pedlosky \(2003\)](#) and [Vallis \(2017\)](#). Although maths and pictures are revealing, it is also useful to observe laboratory rotating tank experiments to further ones understanding of the Eady model and baroclinic instability.

55.7 Necessary conditions for instability

In Section 52.3 we established the Rayleigh-Kuo inflection point theorem as well as Fjørtoft's theorem, each establishing necessary conditions for shear instability. We here pursue a similar approach for the baroclinic instability of a zonal base state flow. The assumption of zonal flow is somewhat restrictive. But to consider more general flows greatly adds to the technical overhead. We do, however, here consider a zonal flow that is a function of both latitude and depth

$$U_g = U_g(y, z) \quad (55.83)$$

and reintroduce planetary β .

55.7.1 Summary of the governing linear equations

From Section 55.4.2, we have the governing linear equation (55.38) for the geostrophic streamfunction and the boundary conditions (55.40) and (55.45)

$$(\partial_t + U_g \partial_x) [\nabla_z^2 \psi' + f_0^2 \partial_z (N^{-2} \partial_z \psi')] = -\partial_x \psi' \partial_y Q_g \quad \bar{\eta}_b < z < \bar{\eta} \quad (55.84a)$$

$$(\partial_t + U_g \partial_x) \partial_z \psi' = \partial_x \psi' \partial_z U_g \quad z = \bar{\eta} \quad (55.84b)$$

$$f_0 (\partial_t + U_g \partial_x) \partial_z \psi' = \partial_x \psi' N^2 [(\partial z / \partial y)_{B_g} - \partial_y \eta_b] \quad z = \bar{\eta}_b, \quad (55.84c)$$

where the meridional derivative of the base state potential vorticity is given by equation (55.30)

$$\partial_y Q_g = \partial_y [f_0 + \beta y - \partial_y U_g + f_0^2 \partial_z (N^{-2} \partial_z \Psi_g)] = \beta - \partial_{yy} U_g + f_0^2 \partial_{yz} (N^{-2} \partial_z \Psi_g). \quad (55.85)$$

The base flow is a function of both latitude and vertical, which means it does only supports freely propagating plane waves in the zonal direction. We thus consider the following wave ansatz for the streamfunction

$$\psi'(x, y, z, t) = \tilde{\psi}(y, z) e^{i(k_x x - \omega t)}. \quad (55.86)$$

Use of this ansatz in the boundary value problem (55.84a)-(55.84c) yields

$$(U_g - c) [(\partial_{yy} - k_x^2) \tilde{\psi} + f_0^2 \partial_z (N^{-2} \partial_z \tilde{\psi})] = -\tilde{\psi} \partial_y Q_g \quad \bar{\eta}_b < z < \bar{\eta} \quad (55.87a)$$

$$(U_g - c) \partial_z \tilde{\psi} = \tilde{\psi} \partial_z U_g \quad z = \bar{\eta} \quad (55.87b)$$

$$f_0 (U_g - c) \partial_z \tilde{\psi} = N^2 \tilde{\psi} [(\partial z / \partial y)_{B_g} - \partial_y \eta_b] \quad z = \bar{\eta}_b, \quad (55.87c)$$

where the zonal phase velocity is written

$$\mathbf{c}_p = (\omega / |\mathbf{k}|) \hat{\mathbf{k}} = (\omega / k_x) \hat{\mathbf{x}} = c \hat{\mathbf{x}}. \quad (55.88)$$

Note that the phase velocity, c , is generally complex, which means that the streamfunction, $\tilde{\psi}$, is also complex. Just like for the horizontal shear case in Section 52.2, if c and $\tilde{\psi}$ satisfy the boundary value problem (55.87a)-(55.87c), then so do their complex conjugates, c^* and $\tilde{\psi}^*$.

55.7.2 Deriving the necessary condition for instability

To develop a necessary condition for instability, multiply the differential equation (55.87a) by $\tilde{\psi}^*$ and integrate over the full domain

$$\int \left[\tilde{\psi}^* (\partial_{yy} - k_x^2) \tilde{\psi} + \tilde{\psi}^* f_0^2 \partial_z (N^{-2} \partial_z \tilde{\psi}) + \frac{|\tilde{\psi}|^2 \partial_y Q_g}{U - c} \right] dy dz = 0. \quad (55.89)$$

Meridional derivative term

Consider the meridional derivative term, in which we have

$$\int \tilde{\psi}^* \partial_{yy} \tilde{\psi} dy = \int [\partial_y (\tilde{\psi}^* \partial_y \tilde{\psi}) - |\partial_y \tilde{\psi}|^2] dy. \quad (55.90)$$

Assuming either meridionally periodic conditions, or fields that decay at infinity, allows us to drop the total derivative term to have

$$\int \tilde{\psi}^* \partial_{yy} \tilde{\psi} dy = - \int |\partial_y \tilde{\psi}|^2 dy. \quad (55.91)$$

Vertical derivative term

For the vertical derivative term we

$$\int \tilde{\psi}^* \partial_z (N^{-2} \partial_z \tilde{\psi}) dz = \int [\partial_z (\tilde{\psi}^* N^{-2} \partial_z \tilde{\psi}) - N^{-2} |\partial_z \tilde{\psi}|^2] dz. \quad (55.92)$$

The boundary conditions (55.87b) and (55.87c) lead to

$$\tilde{\psi}^* N^{-2} \partial_z \tilde{\psi} = \left[\frac{|\tilde{\psi}|^2 \partial_z U_g}{N^2 (U_g - c)} \right]_{z=\bar{\eta}} \quad (55.93a)$$

$$\tilde{\psi}^* N^{-2} \partial_z \tilde{\psi} = \left[\frac{|\tilde{\psi}|^2 [(\partial z / \partial y)_{B_g} - \partial_y \eta_b]}{f_0 (U_g - c)} \right]_{z=\bar{\eta}_b} \quad (55.93b)$$

Bringing all terms together

Bringing the pieces together brings the integral (55.89) into the form

$$\begin{aligned} & - \int [k_x^2 |\tilde{\psi}|^2 + |\partial_y \tilde{\psi}|^2 + (f_0/N)^2 |\partial_z \tilde{\psi}|^2] dy dz \\ &= \int \frac{|\tilde{\psi}|^2 \partial_y Q_g}{U_g - c} dy dz + \int_{z=\bar{\eta}} \frac{f_0^2 |\tilde{\psi}|^2 \partial_z U_g}{N^2 (U_g - c)} dy - \int_{z=\bar{\eta}_b} \frac{f_0 |\tilde{\psi}|^2 [(\partial z / \partial y)_{B_g} - \partial_y \eta_b]}{(U_g - c)} dy. \end{aligned} \quad (55.94)$$

The left hand side is a real and negative number. For consistency, the imaginary part of the right hand side must vanish. Making use of the identity

$$\frac{1}{U_g - c} = \frac{U_g - c_r - i c_i}{|U_g - c|^2} \quad (55.95)$$

leads to the constraint

$$c_i \left[\int \frac{|\tilde{\psi}|^2 \partial_y Q_g}{|U_g - c|^2} dy dz + \int_{z=\bar{\eta}} \frac{f_0^2 |\tilde{\psi}|^2 \partial_y U_g}{N^2 |U_g - c|^2} dy - \int_{z=\bar{\eta}_b} \frac{f_0 |\tilde{\psi}|^2 [(\partial z / \partial y)_{B_g} - \partial_y \eta_b]}{|U_g - c|^2} dy \right] = 0. \quad (55.96)$$

An instability exists only if $c_i \neq 0$. We thus see that if the sum of the integrals does not vanish, then there can be no instability. That is, a sufficient condition for baroclinic stability of a zonal geostrophic flow, $U_g(y, z)$, is that the sum of the integrals is nonzero. Conversely, a necessary condition for baroclinic instability of the zonal flow is that the sum of the three integrals in equation (55.96) vanishes. This necessary condition is known as the *Charney-Stern-Pedlosky* condition ([Charney and Stern, 1962](#); [Pedlosky, 1964](#)).

55.7.3 Special cases

To help understand features of the necessary condition (55.96), we here consider some special cases.

Necessary condition for instability of the Eady model

The Eady model has a constant interior potential vorticity of the base state, so that $\partial_y Q_g = 0$. Hence, the necessary condition for instability (55.96) reduces to a condition on the boundary

integrals

$$\int_{z=\bar{\eta}} \frac{|\tilde{\psi}|^2 \partial_y U_g}{N^2 |U_g - c|^2} dy = \int_{z=\bar{\eta}_b} \frac{|\tilde{\psi}|^2 \partial_y U_g}{N^2 |U_g - c|^2} dy, \quad (55.97)$$

where we set $\partial_y \eta_b = 0$ and

$$(\partial z / \partial y)_{B_g} = -\partial_y B_g / \partial_z B_g = f_0 \partial_z U_g / N^2. \quad (55.98)$$

Furthermore, N^2 and $\partial_z U_g$ are constants, and the zonal flow is a function only of vertical, $U_g(z)$, so that the necessary condition for instability (55.97) reduces to

$$\left[\frac{|\tilde{\psi}|^2}{|U_g - c|^2} \right]_{z=\bar{\eta}} = \left[\frac{|\tilde{\psi}|^2}{|U_g - c|^2} \right]_{z=\bar{\eta}_b}. \quad (55.99)$$

For this condition to hold requires the streamfunction to be nonzero at both boundaries, which arises from interacting edge waves with small enough wavenumber that the waves can overlap.

Effects from a bottom slope in the Eady model

Consider the Eady model but with a sloping bottom, in which case the necessary condition (55.96) becomes

$$\int_{z=\bar{\eta}} \frac{|\tilde{\psi}|^2 (\partial z / \partial y)_{B_g}}{|U_g - c|^2} dy = \int_{z=\bar{\eta}_b} \frac{|\tilde{\psi}|^2 [(\partial z / \partial y)_{B_g} - \partial_y \eta_b]}{|U_g - c|^2} dy. \quad (55.100)$$

For the Eady model the isopycnal slope is constant. We thus see that if the bottom slope has the same sign as the buoyancy slope, but is larger in magnitude, then this necessary condition cannot be satisfied. That is, if the bottom slope is steeper than the buoyancy slope, then the flow is baroclinically stable.

Flat bottom with constant buoyancy along the two boundaries

The Eady model has horizontally varying boundary buoyancy. But what is there is a constant buoyancy along the two boundaries, with the bottom boundary flat? In this case both boundary integrals vanish since $(\partial z / \partial y)_{B_g} = 0$ at both boundaries, and $\partial_y \eta_b = 0$. The necessary condition for instability (55.96) thus becomes

$$\int \frac{|\tilde{\psi}|^2 \partial_y Q_g}{|U_g - c|^2} dy dz = 0. \quad (55.101)$$

The only way to ensure this condition holds is for the meridional derivative of the background potential vorticity to change sign somewhere in the domain. This condition is reminiscent of the Rayleigh-Kuo inflection point theorem for horizontal shear instability (Section 52.3).



Part XI

Mechanics with generalized vertical coordinates

Generalized vertical coordinates (GVCs) offer a mathematical framework for describing stratified fluid mechanics. Hence, they appear in many guises throughout geophysical fluid mechanics theory and numerical modeling. GVCs were introduced by [Starr \(1945\)](#) for atmospheric modeling and [Bleck \(1978\)](#) for ocean modeling. There is a growing use of GVC-based numerical ocean (e.g., [Griffies et al. \(2020\)](#)) and atmospheric models. This usage prompts the need to master their use for analysis, model formulation, and theory, thus providing motivation for this part of the book.

GVCs are both time dependent and non-orthogonal coordinates, which represents both their strength and their complexity. Both features require extra mathematical care beyond that needed with the more familiar static and orthogonal coordinates considered in Chapter 9. The key reason to favor the use of non-orthogonal GVCs, rather than a locally orthogonal coordinate set, is that gravity plays a dominant role in orienting geophysical fluid motion. Hence, it is strategically useful to decompose the equations of motion so that lateral motions are perpendicular to gravity, just like with familiar Cartesian geopotential vertical coordinates. That is, we orient horizontal motions the same regardless whether we use Cartesian coordinates or GVCs, since doing so removes the vertical pressure force from the horizontal equations of motion.

If we were to locally rotate the components of the velocity vector to be parallel and perpendicular to the surface of constant generalized vertical coordinate, as per a locally orthogonal coordinate description, then that representation would introduce a portion of the vertical pressure gradient into the equations for lateral motion. Having the vertical pressure gradient appear in each of the three components to the equations of motion makes it very difficult to isolate the hydrostatic pressure force. In turn, it makes it difficult to describe nearly all of the basic features of geophysical flows, such as the geostrophic and hydrostatic balances. We thus consider locally orthogonal generalized vertical coordinates to be of minimal use for the dynamical equations of geophysical fluid mechanics. Even so, they are useful for orienting the tracer diffusion operator within the ocean interior, as discussed in Section 63.4.

In this part of the book we develop the mathematics of generalized vertical coordinates, and then build up the kinematics and dynamics of stratified fluid mechanics using these coordinates and then encounter some example applications. These chapters are written in the style of a monograph, with equations derived in detail and concepts explored. Here is a brief summary of these chapters.

- MATHEMATICAL FOUNDATIONS: Chapter 56 initiates our study of the mathematics of generalized vertical coordinates. As noted already, their time dependence and their non-orthogonality present some complexity in both concept and detail. Even so, with some experience, generalized vertical coordinates can become a versatile member of our theoretical and numerical toolkit.
- Chapters 57 and 58 describes elements of fluid kinematics and dynamics using generalized vertical coordinates.
- Chapter 59 formulates the hydrostatic Boussinesq equations using buoyancy as the vertical coordinate. This chapter specializes elements from the previous chapters, and in so doing provides a mathematical and physical basis for *isopycnal* models of the ocean and isentropic models of the atmosphere.
- Chapter 60 provides further insights into eddy and mean flow decomposition, this time making use of thickness weighted averaging (TWA) for the shallow water model. We position this chapter in this part of this book since it makes use of the layered perspective of generalized vertical coordinates, particularly isopycnal coordinates. Indeed, the adiabatic stacked shallow water model is a discrete realization of the perfect fluid isopycnal equations. The

TWA formalism of this chapter offers a technically less difficult rendition of the formalism when applied to the continuously stratified isopycnal coordinates.

Chapter 56

MATHEMATICAL BASICS

In this chapter we present the mathematics of generalized vertical coordinates (GVC), with Figure 56.1 offering a schematic of how these coordinates monotonically partition the vertical direction. Such coordinates are of particular use for stratified fluid mechanics, where it is often convenient to make use of a vertical coordinate distinct from, but uniquely related to, the geopotential vertical coordinate, z .

CHAPTER GUIDE

We make use of the general tensor analysis detailed in Chapter 8. We mostly consider just the spatial tensors in this chapter, consistent with the Newtonian perspective whereby time is universal. However, since the vertical coordinate is a function of time, we follow the space-time perspective from Section 8.9 for transforming the partial derivative operator. Chapters directly relying on the material from this chapter include the fluid kinematics discussed in Chapter 57, the general vertical coordinate dynamics discussed in Chapter 58, and the tracer equation diffusion and stirring operators discussed in Chapter 63,

56.1 Relating Cartesian and GVCs	1402
56.2 Example generalized vertical coordinates	1404
56.2.1 Pressure coordinates	1404
56.2.2 Terrain following coordinates	1404
56.2.3 Bottom slope oriented coordinates	1404
56.2.4 Isopycnal or buoyancy coordinates	1404
56.3 Spatial basis vectors	1405
56.3.1 More on the transformation matrix	1405
56.3.2 Expressions for the basis vectors	1405
56.4 Basis one-forms	1406
56.4.1 More on the inverse transformation matrix	1406
56.4.2 GVC basis one-forms	1407
56.4.3 Verifying the bi-orthogonality relation	1407
56.5 Triple product identities	1407
56.6 Position vector	1408
56.7 Transforming components of a vector	1410
56.8 Velocity	1411
56.8.1 Contravariant components	1411
56.8.2 Covariant components	1411
56.8.3 Introducing the material time derivative	1411
56.8.4 Equivalence to the Cartesian velocity representation	1412
56.9 Metric tensor	1412
56.9.1 Jacobian of transformation	1412

56.9.2 Covariant and contravariant representations	1413
56.10 Volume element and the Levi-Civita tensor	1413
56.11 Vector cross product of basis vectors	1413
56.12 Partial derivative operators	1414
56.12.1 Analytical derivation	1414
56.12.2 Geometrical derivation	1414
56.13 Material time derivative	1416
56.14 Divergence of a vector and the divergence theorem	1416
56.15 The diffusion operator	1416
56.15.1 Continuous expression	1417
56.15.2 Layer thickness weighted diffusion operator	1417
56.16 Vorticity	1418
56.16.1 The components	1419
56.16.2 Transforming from Cartesian coordinates	1419
56.17 Velocity circulation	1419

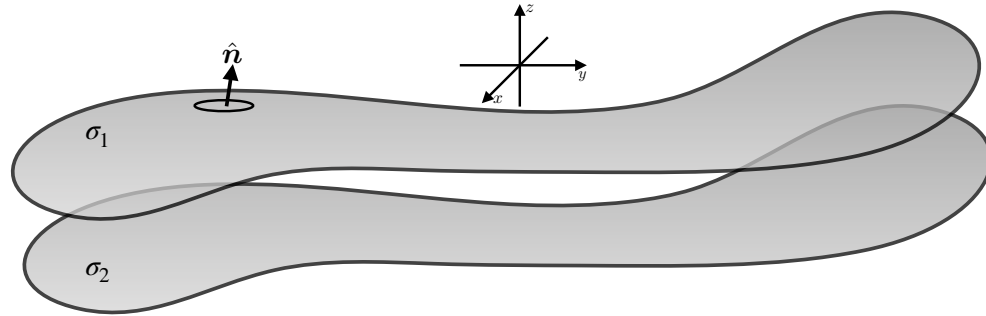


FIGURE 56.1: This stylized schematic illustrates the geometry of two surfaces of constant generalized vertical coordinate $\sigma(x, y, z, t) = \sigma_1$ and $\sigma(x, y, z, t) = \sigma_2$, here showing patches on two such surfaces. The surfaces are generally undulating in space and time yet are assumed to monotonically layer the fluid. Monotonic layering means that the surface normal, \hat{n} , always has a non-zero projection onto the vertical: $\hat{n} \cdot \hat{z} \neq 0$. That is, the surfaces never become vertical nor do they overturn. It also means that there is a 1-to-1 invertible relation between σ and geopotential, so that specifying $(x, y, \sigma(x, y, z, t))$ is sufficient to yield a unique z .

56.1 Relating Cartesian and GVCs

We make use of the symbol σ for a generalized vertical coordinate. This coordinate is *not* orthogonal to the horizontal spatial coordinates x, y . This is a central property of GVCs that influences nearly all aspects of their calculus. To help develop the mathematics for transforming between Cartesian coordinates and GVCs, it is important to distinguish the two coordinate systems. For that purpose we write the time coordinate and spatial Cartesian coordinates according to

$$\xi^\alpha = (\xi^0, \xi^a) = (\xi^0, \xi^1, \xi^2, \xi^3) = (t, x, y, z) \quad \text{with } \alpha = 0, 1, 2, 3, \text{ and } a = 1, 2, 3. \quad (56.1)$$

As defined, the tensor label a runs over the spatial coordinates 1, 2, 3 whereas α also includes the time coordinate with $\alpha = 0$. The corresponding generalized vertical coordinates are denoted with an overbar

$$\xi^{\bar{\alpha}} = (\xi^{\bar{0}}, \xi^{\bar{1}}, \xi^{\bar{2}}, \xi^{\bar{3}}) = (\bar{t}, \bar{x}, \bar{y}, \sigma). \quad (56.2)$$

The 1-to-1 coordinate transformation between Cartesian and GVC coordinates is written

$$\xi^{\bar{0}} = \xi^0 \iff \bar{t} = t \quad (56.3a)$$

$$\xi^{\bar{1}} = \xi^1 \iff \bar{x} = x \quad (56.3b)$$

$$\xi^{\bar{2}} = \xi^2 \iff \bar{y} = y \quad (56.3c)$$

$$\xi^{\bar{3}} = \sigma(x, y, z, t), \quad (56.3d)$$

with the final relation expressing the generalized vertical coordinate as a function of space and time. We ordered the appearance of independent variables in σ with time in the last position, which is the conventional ordering in this book for functions of space and time even though the zeroth coordinate is time.

The coordinate transformation is invertible so that we can write

$$\xi^0 = \xi^{\bar{0}} \quad (56.4a)$$

$$\xi^1 = \xi^{\bar{1}} \quad (56.4b)$$

$$\xi^2 = \xi^{\bar{2}} \quad (56.4c)$$

$$\xi^3 = \xi^3(\bar{x}, \bar{y}, \sigma, \bar{t}) = \xi^3(x, y, \sigma, t). \quad (56.4d)$$

The relation

$$\xi^3 = \xi^3(\xi^{\bar{a}}) = \xi^3(x, t, \sigma, t) \quad (56.5)$$

provides the vertical position of a given σ surface. Since $\xi^3 = z$ one commonly writes

$$z = z(x, y, \sigma, t). \quad (56.6)$$

However, this expression is prone to confusion since the meaning of z is overloaded.¹ Namely, one meaning ascribes z to a particular value of the vertical position; i.e., $z = -100$ m. The other meaning, as on the right hand side, is for z as the vertical coordinate function of a particular σ surface, with this value a function of space, time, and σ . Learning to distinguish when z refers to a particular vertical position or as a coordinate function takes some practice, and those who routinely work with generalized vertical coordinates typically find no problem with the overloaded meanings. Indeed, after reading this chapter we should be able to hold the two meanings in our mind without confusion. As a reminder, we commonly write the vertical coordinate function as

$$z = \eta(x, y, \sigma, t), \quad (56.7)$$

where η is used throughout this book to represent the vertical position of a surface, such as the ocean free surface, solid-earth topography, or a generalized vertical coordinate surface. Hence, for example, the vertical position of a pressure surface of chosen value p is given by the functional relation

$$\xi^3 = z = \eta(\bar{x}, \bar{y}, p, \bar{t}) = \eta(x, y, p, t). \quad (56.8)$$

We make use of the η nomenclature where it seems useful but gradually sprinkle in more use of the $z(x, y, \sigma, t)$ notation since it is proves to be natural for many of the formulations.

¹We use the term *overloaded* as in computer science where a symbol has more than one meaning or usage.

56.2 Example generalized vertical coordinates

Before further diving into the mathematics, we here offer some examples of generalized vertical coordinates commonly used to study geophysical fluid flows.

56.2.1 Pressure coordinates

Hydrostatic compressible fluids, such as the large-scale atmosphere, pressure is a convenient choice as vertical since it absorbs the appearance of density in many formula such as mass continuity as discussed in Section 57.10.2 and the geostrophic balance given by equation (28.1a). Hence, a natural expression of the compressible hydrostatic equations of motion make use of pressure rather than geopotential for the vertical coordinate, in which case $\sigma = p(x, y, z, t)$.

56.2.2 Terrain following coordinates

When allowing for a time dependent ocean free surface, the terrain following coordinate in oceanography is given by

$$\sigma = \frac{z - \eta_{\text{surf}}}{-\eta_b + \eta_{\text{surf}}} \quad \text{terrain following ocean coordinate,} \quad (56.9)$$

where $z = \eta_{\text{surf}}(x, y, t)$ is the vertical position of the ocean surface. The terrain following coordinate is non-dimensional and extends from $\sigma = 0$ at the ocean surface and $\sigma = -1$ at the ocean bottom (where $z = \eta_b(x, y)$). For rigid lid ocean models with $\eta_{\text{surf}} = 0$, the terrain following coordinate becomes time independent

$$\sigma = -\frac{z}{\eta_b} \quad \text{terrain following rigid lid ocean.} \quad (56.10)$$

Finally, for a compressible ocean, it is more convenient to use pressure to define the terrain following coordinate so that

$$\sigma = \frac{p - p_a}{p_b - p_a} \quad \text{terrain following atmosphere coordinate.} \quad (56.11)$$

In this equation, p_a is the pressure applied at the ocean surface and p_b is the pressure at the ocean bottom. For an atmosphere model we might set p_a as the top of the atmosphere pressure, which is typically assumed to be zero as in [Phillips \(1957\)](#).

56.2.3 Bottom slope oriented coordinates

[Peterson and Callies \(2022\)](#) consider an alternative to the traditional terrain following coordinates from Section 56.2.2, here defining a bottom slope oriented coordinate

$$\sigma = z - \mathbf{x} \cdot \nabla \eta_b = z - x \partial \eta_b / \partial x - y \partial \eta_b / \partial y, \quad (56.12)$$

with $\nabla \eta_b$ the slope of the bottom topography.

56.2.4 Isopycnal or buoyancy coordinates

Buoyancy surfaces are material when there is no mixing. Hence, for the study of perfect fluid mechanics it is quite convenient to use the Archimedean buoyancy, b , as the vertical coordinate, $\sigma = b(x, y, z, t)$. Equivalently, one may choose the potential density as the vertical coordinate. We

have more to say about such vertical coordinates in Chapter 59 when developing the equations for isopycnal ocean models.

56.3 Spatial basis vectors

Making use of the tensor formalism from Chapter 8, consider the transformation of the Cartesian basis vectors into their corresponding GVC representation. This transformation takes is given by

$$\vec{e}_{\bar{a}} = \Lambda_{\bar{a}}^a \vec{e}_a, \quad (56.13)$$

where the transformation matrix is

$$\Lambda_{\bar{a}}^a = \begin{bmatrix} \partial x / \partial \bar{x} & \partial x / \partial \bar{y} & \partial x / \partial \sigma \\ \partial y / \partial \bar{x} & \partial y / \partial \bar{y} & \partial y / \partial \sigma \\ \partial z / \partial \bar{x} & \partial z / \partial \bar{y} & \partial z / \partial \sigma \end{bmatrix} = \begin{bmatrix} 1 & 0 & 0 \\ 0 & 1 & 0 \\ \partial \eta / \partial \bar{x} & \partial \eta / \partial \bar{y} & \partial \eta / \partial \sigma \end{bmatrix}, \quad (56.14)$$

where the second equality used our preferred notation $z = \eta(x, y, \sigma, t)$ for the vertical position of a σ surface. The diagonal unit values for the space-space components arise since a horizontal position in Cartesian and GVCs is the same and the horizontal directions are orthogonal. Likewise, the time coordinate does not change when changing \bar{x} , \bar{y} , or σ . Additionally, $\partial x / \partial \sigma = \partial y / \partial \sigma = 0$ since the horizontal position remains unchanged when moving across a GVC surface. In contrast, a non-zero value for $\partial \eta / \partial \bar{x}$ and $\partial \eta / \partial \bar{y}$ arise since we generally change vertical position when moving horizontally along a sloped σ surface. Finally, the element $\partial \eta / \partial \sigma$ is nonzero due to vertical stratification of the fluid when represented using general vertical coordinates.

56.3.1 More on the transformation matrix

To further detail how to produce elements of the transformation matrix (56.14), it is crucial to ensure that the proper variables are held fixed when performing the partial derivatives. For example, consider the top row where we compute

$$\Lambda_{\bar{a}}^1 = [[\partial x / \partial \bar{x}]_{\bar{y}, \sigma} \quad [\partial x / \partial \bar{y}]_{\bar{x}, \sigma} \quad [\partial x / \partial \sigma]_{\bar{x}, \bar{y}}] \quad (56.15)$$

Since $x = \bar{x}$, all elements vanish except for the first. Namely, $[\partial x / \partial \bar{y}]_{\bar{x}, \sigma} = 0$ since x cannot change when \bar{x} is fixed. The same idea leads to the results for y derivatives.

56.3.2 Expressions for the basis vectors

Use of the transformation matrix (56.14) renders the spatial components of the GVC basis vectors

$$\vec{e}_{\bar{1}} = \hat{\mathbf{x}} + \hat{\mathbf{z}} (\partial \eta / \partial \bar{x}) \quad (56.16a)$$

$$\vec{e}_{\bar{2}} = \hat{\mathbf{y}} + \hat{\mathbf{z}} (\partial \eta / \partial \bar{y}) \quad (56.16b)$$

$$\vec{e}_{\bar{3}} = \hat{\mathbf{z}} (\partial \eta / \partial \sigma). \quad (56.16c)$$

The basis vectors $\vec{e}_{\bar{1}}$ and $\vec{e}_{\bar{2}}$ have a vertical component due to sloping GVC surfaces. These basis vectors lie within the tangent plane of the GVC surface. The basis vector $\vec{e}_{\bar{3}}$ is purely vertical and has a non-unit magnitude due to the inverse vertical stratification, $\partial \eta / \partial \sigma$. The left panel of Figure 56.2 illustrates the basis vectors.

As an example, consider the rigid lid terrain following vertical coordinate (56.10), where $\sigma = -z / \eta_b$. In this case, the vertical position of a generalized vertical surface is given by $\eta = -\sigma \eta_b$

so that the basis vectors are

$$\vec{e}_{\bar{1}} = \hat{x} - \hat{z} \sigma (\partial \eta_b / \partial \bar{x}) \quad \text{and} \quad \vec{e}_{\bar{2}} = \hat{y} - \hat{z} \sigma (\partial \eta_b / \partial \bar{y}) \quad \text{and} \quad \vec{e}_{\bar{3}} = -\hat{z} \eta_b. \quad (56.17)$$

Similarly, the bottom slope oriented coordinate (56.12), with $\sigma = z - \mathbf{x} \cdot \nabla \eta_b$ so that $\eta = \sigma + \mathbf{x} \cdot \nabla \eta_b$, has the corresponding basis vectors

$$\vec{e}_1 = \hat{x} + \hat{z} (\partial \eta_b / \partial \bar{x}) \quad \text{and} \quad \vec{e}_2 = \hat{y} + \hat{z} (\partial \eta_b / \partial \bar{y}) \quad \text{and} \quad \vec{e}_3 = \hat{z}. \quad (56.18)$$

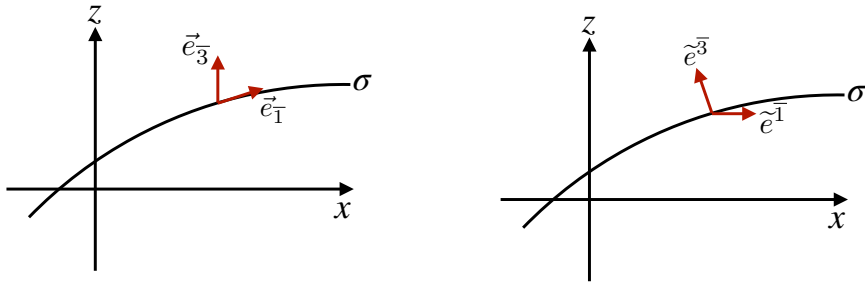


FIGURE 56.2: Illustrating the basis vectors (left panel) and basis one-forms (right panel) for generalized vertical coordinates. The $\vec{e}_{\bar{3}}$ basis vector is vertical whereas $\vec{e}_{\bar{1}}$ and $\vec{e}_{\bar{2}}$ lie within the tangent plane to the σ surface. As a complement, the basis one-form $\tilde{e}^{\bar{3}}$ is normal to the σ surface whereas the basis one-forms $\tilde{e}^{\bar{1}}$ and $\tilde{e}^{\bar{2}}$ are horizontal.

56.4 Basis one-forms

The basis one-forms are obtained by transforming from Cartesian into GVCs through use of the inverse transformation

$$\tilde{e}^{\bar{a}} = \Lambda_{\bar{a}}^{\bar{a}} \tilde{e}^a, \quad (56.19)$$

where the inverse transformation matrix takes the form

$$\Lambda_{\bar{a}}^{\bar{a}} = \begin{bmatrix} \partial \bar{x} / \partial x & \partial \bar{x} / \partial y & \partial \bar{x} / \partial z \\ \partial \bar{y} / \partial x & \partial \bar{y} / \partial y & \partial \bar{y} / \partial z \\ \partial \bar{z} / \partial x & \partial \bar{z} / \partial y & \partial \bar{z} / \partial z \end{bmatrix} = \begin{bmatrix} 1 & 0 & 0 \\ 0 & 1 & 0 \\ \partial \sigma / \partial x & \partial \sigma / \partial y & \partial \sigma / \partial z \end{bmatrix}. \quad (56.20)$$

As for the transformation matrix (56.14), the unit diagonal values arise since a horizontal position in Cartesian and GVCs is the same and the horizontal directions are orthogonal. Likewise, $\partial \bar{x} / \partial z = \partial \bar{y} / \partial z = 0$ since the horizontal position on a GVC surface remains unchanged when moving across a depth surface. The nonzero values for $\partial \sigma / \partial x$, $\partial \sigma / \partial y$, and $\partial \sigma / \partial z$, arise in the presence of horizontal and vertical stratification of the generalized vertical coordinate.

56.4.1 More on the inverse transformation matrix

When computing elements of the inverse transformation matrix (56.20), it is crucial to ensure that the proper variables are held fixed. For example, consider the top row where we compute

$$\Lambda_{\bar{a}}^{\bar{1}} = [[\partial \bar{x} / \partial x]_{y,z} \quad [\partial \bar{x} / \partial y]_{x,z} \quad [\partial \bar{x} / \partial z]_{x,y}]. \quad (56.21)$$

Just as for the transformation matrix (56.15), since $x = \bar{x}$, all but the first element vanish in equation (56.21). Namely, $[\partial \bar{x} / \partial y]_{x,z} = 0$ since the \bar{x} cannot change when x is fixed. The same idea holds for the \bar{y} row.

56.4.2 GVC basis one-forms

Use of the inverse transformation matrix (56.20) renders the spatial components of the GVC basis one-forms

$$\tilde{e}^{\bar{1}} = \hat{x} \quad (56.22a)$$

$$\tilde{e}^{\bar{2}} = \hat{y} \quad (56.22b)$$

$$\tilde{e}^{\bar{3}} = \tilde{e}^a \partial_a \sigma = \hat{x} (\partial \sigma / \partial x) + \hat{y} (\partial \sigma / \partial y) + \hat{z} (\partial \sigma / \partial z) = \nabla \sigma. \quad (56.22c)$$

The left panel of Figure 56.2 illustrates the basis one-forms.

As an example, consider again the rigid lid terrain following coordinate (56.10), $\sigma = -z/\eta_b$, in which case

$$\tilde{e}^{\bar{3}} = -(1/\eta_b) (\nabla \eta_b + \hat{z}). \quad (56.23)$$

Similarly, the bottom slope oriented coordinate (56.12), with $\sigma = z - \mathbf{x} \cdot \nabla \eta_b$, has

$$\tilde{e}^{\bar{3}} = \hat{z} - \nabla \eta_b - \hat{x} (\mathbf{x} \cdot \partial_x \nabla \eta_b) - \hat{y} (\mathbf{x} \cdot \partial_y \nabla \eta_b). \quad (56.24)$$

In the case where the bottom slope is constant in both directions then this result simplifies to

$$\tilde{e}^{\bar{3}} = \hat{z} - \nabla \eta_b. \quad (56.25)$$

56.4.3 Verifying the bi-orthogonality relation

The basis one-forms satisfy the bi-orthogonality relation (8.25) with the basis vectors

$$\tilde{e}^{\bar{a}} \cdot \tilde{e}_{\bar{b}} = \delta_{\bar{a}}^{\bar{b}}. \quad (56.26)$$

This identity is trivial to verify for all $\bar{a} = 1, 2, 3$.

56.5 Triple product identities

We find various occasions to make use of a suite of triple product identities that hold for GVCs. For this purpose we write σ as a composite function as in Section 8.9.3

$$\sigma = \sigma(x, y, z, t) = \sigma[x, y, z(\bar{t}, \bar{x}, \bar{y}, \sigma), t], \quad (56.27)$$

with $\eta(\bar{x}, \bar{y}, \sigma, \bar{t})$ written as $z(\bar{x}, \bar{y}, \sigma, \bar{t})$ as it here eases the manipulations. Use of the chain rule leads to the space-time differential increment

$$d\sigma = dt \left[\frac{\partial \sigma}{\partial t} \right]_{x,y,z} + dx \left[\frac{\partial \sigma}{\partial x} \right]_{t,y,z} + dy \left[\frac{\partial \sigma}{\partial y} \right]_{t,x,z} + dz \left[\frac{\partial \sigma}{\partial z} \right]_{t,x,y}. \quad (56.28)$$

Likewise, writing $z = z[\bar{t}, \bar{x}, \bar{y}, \sigma]$ leads to the space-time differential increment dz

$$dz = d\bar{t} \left[\frac{\partial z}{\partial \bar{t}} \right]_{\bar{x}, \bar{y}, \sigma} + d\bar{x} \left[\frac{\partial z}{\partial \bar{x}} \right]_{\bar{t}, \bar{y}, \sigma} + d\bar{y} \left[\frac{\partial z}{\partial \bar{y}} \right]_{\bar{t}, \bar{x}, \sigma} + d\sigma \left[\frac{\partial z}{\partial \sigma} \right]_{\bar{t}, \bar{x}, \bar{y}}. \quad (56.29)$$

We note the identities

$$\left[\frac{\partial \sigma}{\partial z} \right]_{t,x,y} \left[\frac{\partial z}{\partial \sigma} \right]_{\bar{t}, \bar{x}, \bar{y}} = 1 \quad d\bar{t} = dt \quad d\bar{x} = dx \quad d\bar{y} = dy, \quad (56.30)$$

which follow since $t = \bar{t}$, $x = \bar{x}$, and $y = \bar{y}$. Substituting equation (56.29) into equation (56.28) and making use of the identities (56.30) yields

$$0 = dt \left[\left[\frac{\partial \sigma}{\partial t} \right]_{x,y,z} + \left[\frac{\partial \sigma}{\partial z} \right]_{t,x,y} \left[\frac{\partial z}{\partial \bar{t}} \right]_{\bar{x},\bar{y},\sigma} \right] \\ + dx \left[\left[\frac{\partial \sigma}{\partial x} \right]_{t,y,z} + \left[\frac{\partial \sigma}{\partial z} \right]_{t,x,y} \left[\frac{\partial z}{\partial \bar{x}} \right]_{\bar{t},\bar{y},\sigma} \right] + dy \left[\left[\frac{\partial \sigma}{\partial y} \right]_{t,x,z} + \left[\frac{\partial \sigma}{\partial z} \right]_{t,x,y} \left[\frac{\partial z}{\partial \bar{y}} \right]_{\bar{t},\bar{x},\sigma} \right]. \quad (56.31)$$

For this equation to hold with general increments dt , dx , and dy requires that each bracketed term vanish, which in turn leads to the following set of triple product identities²

$$\left[\frac{\partial \sigma}{\partial z} \right]_{t,x,y} \left[\frac{\partial z}{\partial \bar{t}} \right]_{\bar{x},\bar{y},\sigma} = - \left[\frac{\partial \sigma}{\partial t} \right]_{x,y,z} \quad (56.32a)$$

$$\left[\frac{\partial \sigma}{\partial z} \right]_{t,x,y} \left[\frac{\partial z}{\partial \bar{x}} \right]_{\bar{t},\bar{y},\sigma} = - \left[\frac{\partial \sigma}{\partial x} \right]_{t,y,z} \quad (56.32b)$$

$$\left[\frac{\partial \sigma}{\partial z} \right]_{t,x,y} \left[\frac{\partial z}{\partial \bar{y}} \right]_{\bar{t},\bar{x},\sigma} = - \left[\frac{\partial \sigma}{\partial y} \right]_{t,x,z}. \quad (56.32c)$$

If the vertical stratification, $\partial \sigma / \partial z$, is non-zero, the triple product identities are equivalent to

$$\left[\frac{\partial z}{\partial \bar{t}} \right]_{\bar{x},\bar{y},\sigma} = - \frac{[\partial \sigma / \partial t]_{x,y,z}}{[\partial \sigma / \partial z]_{t,x,y}} = - \left[\frac{\partial \sigma}{\partial t} \right]_{x,y,z} \left[\frac{\partial z}{\partial \sigma} \right]_{t,x,y} \quad (56.33a)$$

$$\left[\frac{\partial z}{\partial \bar{x}} \right]_{\bar{t},\bar{y},\sigma} = - \frac{[\partial \sigma / \partial x]_{t,y,z}}{[\partial \sigma / \partial z]_{t,x,y}} = - \left[\frac{\partial \sigma}{\partial x} \right]_{t,y,z} \left[\frac{\partial z}{\partial \sigma} \right]_{t,x,y} \quad (56.33b)$$

$$\left[\frac{\partial z}{\partial \bar{y}} \right]_{\bar{t},\bar{x},\sigma} = - \frac{[\partial \sigma / \partial y]_{t,x,z}}{[\partial \sigma / \partial z]_{t,x,y}} = - \left[\frac{\partial \sigma}{\partial y} \right]_{t,x,z} \left[\frac{\partial z}{\partial \sigma} \right]_{t,x,y}. \quad (56.33c)$$

Since $t = \bar{t}$, $x = \bar{x}$, and $y = \bar{y}$ we can write these identities in the more succinct form

$$\left[\frac{\partial z}{\partial \bar{t}} \right]_\sigma = \left[\frac{\partial \eta}{\partial \bar{t}} \right]_\sigma = - \frac{[\partial \sigma / \partial t]_z}{[\partial \sigma / \partial z]} \quad (56.34a)$$

$$\left[\frac{\partial z}{\partial \bar{x}} \right]_\sigma = \left[\frac{\partial \eta}{\partial \bar{x}} \right]_\sigma = - \frac{[\partial \sigma / \partial x]_z}{[\partial \sigma / \partial z]} \quad (56.34b)$$

$$\left[\frac{\partial z}{\partial \bar{y}} \right]_\sigma = \left[\frac{\partial \eta}{\partial \bar{y}} \right]_\sigma = - \frac{[\partial \sigma / \partial y]_z}{[\partial \sigma / \partial z]}, \quad (56.34c)$$

where we reintroduced the notation $\eta(x, y, \sigma, t) = z(x, y, \sigma, t)$. These identities are quite useful for manipulating equations involving GVCs. In particular, equations (56.34b) and (56.34c) provide alternate expressions for the slope of σ isosurfaces relative to the horizontal plane (see Section 56.12).

56.6 Position vector

We are familiar with locating a point in space using Cartesian coordinates as in Figure 1.1. What about specifying the position using GVCs? We can do so by making use of the basis vectors

²These identities are directly analogous to the Maxwell relations from thermodynamics, with an introduction in Section 19.8 and full details in the book by [Callen \(1985\)](#).

(56.16a)-(56.16c) so that the position of an arbitrary point in space is given by

$$\mathcal{P} = \xi^{\bar{a}} \vec{e}_{\bar{a}} \quad (56.35a)$$

$$= \bar{x} [\hat{x} + (\partial\eta/\partial\bar{x}) \hat{z}] + \bar{y} [\hat{y} + (\partial\eta/\partial\bar{y}) \hat{z}] + \sigma (\partial\eta/\partial\sigma) \hat{z} \quad (56.35b)$$

$$= \hat{x} \bar{x} + \hat{y} \bar{y} + \hat{z} [\bar{x} (\partial\eta/\partial\bar{x}) + \bar{y} (\partial\eta/\partial\bar{y}) + \sigma (\partial\eta/\partial\sigma)] \quad (56.35c)$$

$$= \hat{x} \bar{x} + \hat{y} \bar{y} + \hat{z} \xi^{\bar{a}} \partial_{\bar{a}}\eta. \quad (56.35d)$$

We identify the following properties as a means to help understand these expressions, with Figure 56.3 offering a schematic.

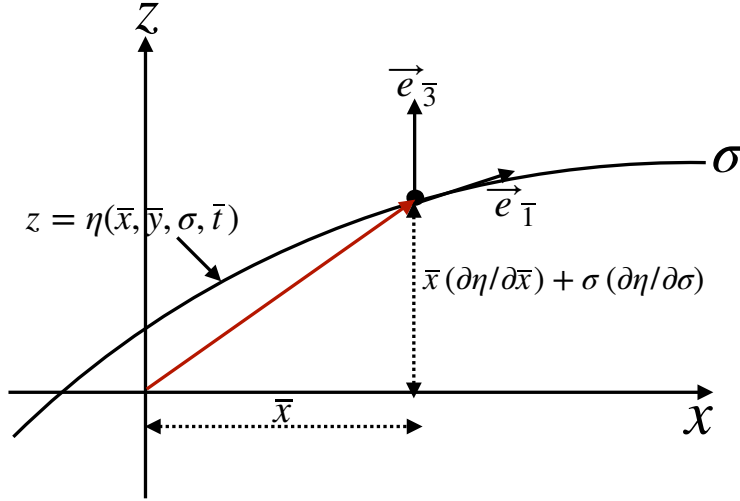


FIGURE 56.3: The position of a point in space as represented using GVCs following equation (56.36a). For this example, $\bar{y} = 0$ so that the horizontal position is determined by the coordinate $\bar{x} = x$, whereas the vertical position is determined by $\bar{x} (\partial z / \partial \bar{x}) + \sigma (\partial z / \partial \sigma) = \bar{x} (\partial \eta / \partial \bar{x}) + \sigma (\partial \eta / \partial \sigma)$.

- The expression (56.35b) has horizontal positions \bar{x} and \bar{y} multiplying the basis vectors $\vec{e}_{\bar{x}}$ and $\vec{e}_{\bar{y}}$, with these vectors oriented parallel to a surface of constant GVC as in Figure 56.3. Likewise, the third term, $\sigma (\partial\eta/\partial\sigma) \hat{z}$, positions the point vertically according to the value of the GVC and its inverse stratification.
- Consider the case of $\bar{y} = 0$ so that

$$\mathcal{P} = \bar{x} \hat{x} + \hat{z} [\bar{x} (\partial\eta/\partial\bar{x}) + \sigma (\partial\eta/\partial\sigma)] \quad (56.36a)$$

$$= \bar{x} \hat{x} + \hat{z} (\partial\eta/\partial\sigma) [\bar{x} (\partial\sigma/\partial z)_x (\partial\eta/\partial\bar{x})_\sigma + \sigma] \quad (56.36b)$$

$$= \bar{x} \hat{x} + \hat{z} (\partial\eta/\partial\sigma) [-\bar{x} (\partial\sigma/\partial x)_z + \sigma], \quad (56.36c)$$

where we used the triple product identity (56.34b) for the final equality. Consequently, a horizontal position vector is realized using GVC coordinates with $\sigma = \bar{x} (\partial\sigma/\partial x)$. That is, a horizontal position vector crosses surfaces of constant GVC when the GVC surface has a nonzero horizontal slope.

- The projection of the position vector onto the basis one-forms leads to

$$\mathcal{P} \cdot \tilde{e}^{\bar{b}} = \xi^{\bar{a}} \vec{e}_{\bar{a}} \cdot \tilde{e}^{\bar{b}} = \xi^{\bar{b}}. \quad (56.37)$$

This result follows from the orthogonality relation (8.25). So the projection of the position vector onto a basis one-form picks out the corresponding coordinate value.

- Equation (56.7) provides the spatial dependence for the vertical position of the surface of constant GVC

$$z = z(\xi^{\bar{a}}) = \eta(\xi^{\bar{a}}). \quad (56.38)$$

At any particular time instance we can perform a Taylor series about a reference geopotential $\zeta_0 = \eta_0$, so that

$$\eta(\xi^{\bar{a}}) \approx \eta_0 + \xi^{\bar{a}} \partial_{\bar{a}} \eta. \quad (56.39)$$

We can thus write the position (56.35d) in the form

$$\mathcal{P} = \hat{x} \bar{x} + \hat{y} \bar{y} + \hat{z} [\eta - \eta_0]. \quad (56.40)$$

Taking the reference geopotential as $\eta_0 = 0$ recovers the Cartesian expression. Since the position vector is a geometric object, it is reassuring that the GVC representation is the same as the Cartesian representation; it is merely a reorganization of the basis vectors and corresponding coordinates.

56.7 Transforming components of a vector

Consider a vector field \vec{F} with Cartesian representation

$$\vec{F} = \mathbf{F} = F^a \vec{e}_a = F^x \hat{x} + F^y \hat{y} + F^z \hat{z}. \quad (56.41)$$

The corresponding GVC components are related through the transformation matrix

$$F^{\bar{a}} = \Lambda_a^{\bar{a}} F^a. \quad (56.42)$$

Making use of the transformation matrix (56.20) yields the relations between GVC components and Cartesian components

$$F^{\bar{1}} = F^1 \quad \text{and} \quad F^{\bar{2}} = F^2 \quad \text{and} \quad F^{\bar{3}} = \nabla \sigma \cdot \mathbf{F}, \quad (56.43)$$

where we wrote

$$\nabla \sigma \cdot \mathbf{F} = (\partial \sigma / \partial x) F^1 + (\partial \sigma / \partial y) F^2 + (\partial \sigma / \partial z) F^3. \quad (56.44)$$

The vector field thus can be represented in GVC coordinates as

$$\vec{F} = F^{\bar{a}} \vec{e}_{\bar{a}} = F^1 \vec{e}_{\bar{1}} + F^2 \vec{e}_{\bar{2}} + (\nabla \sigma \cdot \mathbf{F}) \vec{e}_{\bar{3}}. \quad (56.45)$$

Similarly, the covariant components transform as $F_{\bar{a}} = \Lambda_a^{\bar{a}} F_a$, where use of the inverse transformation matrix (56.20) renders

$$F_{\bar{1}} = F_1 + (\partial z / \partial \bar{x}) F_3 = F_1 + (\partial \eta / \partial \bar{x}) F_3 \quad (56.46a)$$

$$F_{\bar{2}} = F_2 + (\partial z / \partial \bar{y}) F_3 = F_2 + (\partial \eta / \partial \bar{y}) F_3 \quad (56.46b)$$

$$F_{\bar{3}} = (\partial z / \partial \sigma) F_3 = (\partial \eta / \partial \sigma) F_3, \quad (56.46c)$$

and the expression for the vector field

$$\vec{F} = F_{\bar{a}} \tilde{e}^{\bar{a}} = [F_1 + (\partial \eta / \partial \bar{x}) F_3] \tilde{e}^{\bar{1}} + [F_2 + (\partial \eta / \partial \bar{y}) F_3] \tilde{e}^{\bar{2}} + (\partial \eta / \partial \sigma) F_3 \tilde{e}^{\bar{3}}. \quad (56.47)$$

Recall also that for Cartesian coordinates the contravariant and covariant components to a vector are identical: $F^a = F_a$.

56.8 Velocity

As an example of the results from Section 56.7, we here represent the velocity vector, considering both covariant and contravariant representations. As for the position vector detailed in Section 56.6, we are assured that both representations lead to the same velocity vector since the velocity is an objective geometric object (i.e., an arrow with a magnitude). In Section 56.8.4 we verify that the transformation formalism indeed respects this equivalence, with the GVC representations equivalent to the Cartesian representation

$$\vec{v} = u \hat{\mathbf{x}} + v \hat{\mathbf{y}} + w \hat{\mathbf{z}}. \quad (56.48)$$

56.8.1 Contravariant components

Following Section 56.7, we have the contravariant velocity components

$$v^{\bar{1}} = u \quad \text{and} \quad v^{\bar{2}} = v \quad \text{and} \quad v^{\bar{3}} = \mathbf{v} \cdot \nabla \sigma. \quad (56.49)$$

Use of the basis vectors (56.16a)-(56.16c) then leads to

$$\vec{v} = v^{\bar{a}} \vec{e}_{\bar{a}} \quad (56.50a)$$

$$= u \vec{e}_{\bar{x}} + v \vec{e}_{\bar{y}} + (\mathbf{v} \cdot \nabla \sigma) \vec{e}_{\sigma} \quad (56.50b)$$

$$= u [\hat{\mathbf{x}} + (\partial \eta / \partial \bar{x}) \hat{\mathbf{z}}] + v [\hat{\mathbf{y}} + (\partial \eta / \partial \bar{y}) \hat{\mathbf{z}}] + (\mathbf{v} \cdot \nabla \sigma) (\partial \eta / \partial \sigma) \hat{\mathbf{z}}. \quad (56.50c)$$

56.8.2 Covariant components

The covariant velocity components are given by

$$v_{\bar{1}} = u + (\partial \eta / \partial \bar{x}) w \quad \text{and} \quad v_{\bar{2}} = v + (\partial \eta / \partial \bar{y}) w \quad \text{and} \quad v_{\bar{3}} = (\partial \eta / \partial \sigma) w. \quad (56.51)$$

The one-form basis (56.22a)–(56.22c) thus leads to the velocity vector

$$\vec{v} = v_{\bar{a}} \tilde{e}^{\bar{a}} = [u + (\partial \eta / \partial \bar{x}) w] \hat{\mathbf{x}} + [v + (\partial \eta / \partial \bar{y}) w] \hat{\mathbf{y}} + w (\partial \eta / \partial \sigma) \nabla \sigma. \quad (56.52)$$

56.8.3 Introducing the material time derivative

The material evolution for the generalized vertical coordinate can be written

$$\frac{D\sigma}{Dt} = \frac{\partial \sigma}{\partial t} + \mathbf{v} \cdot \nabla \sigma = \dot{\sigma}, \quad (56.53)$$

with $\dot{\sigma}$ symbolizing any process contributing to motion across σ isosurfaces (as fully explained in Section 57.4). Using the expression (56.53) in the velocity vector expression (56.50c) leads to

$$\vec{v} = u [\hat{\mathbf{x}} + (\partial \eta / \partial \bar{x}) \hat{\mathbf{z}}] + v [\hat{\mathbf{y}} + (\partial \eta / \partial \bar{y}) \hat{\mathbf{z}}] + (\mathbf{v} \cdot \nabla \sigma) (\partial \eta / \partial \sigma) \hat{\mathbf{z}}. \quad (56.54a)$$

$$= u [\hat{\mathbf{x}} + (\partial \eta / \partial \bar{x}) \hat{\mathbf{z}}] + v [\hat{\mathbf{y}} + (\partial \eta / \partial \bar{y}) \hat{\mathbf{z}}] + (\dot{\sigma} - \partial \sigma / \partial t) (\partial \eta / \partial \sigma) \hat{\mathbf{z}} \quad (56.54b)$$

$$= u \hat{\mathbf{x}} + v \hat{\mathbf{y}} + [\partial \eta / \partial \bar{t} + \mathbf{u} \cdot \nabla_{\sigma} z + (\partial \eta / \partial \sigma) \dot{\sigma}] \hat{\mathbf{z}}, \quad (56.54c)$$

where the final equality made use of the triple product (56.33a): $(\partial \sigma / \partial t) (\partial \eta / \partial \sigma) = -\partial \eta / \partial \bar{t}$. In the steady state and in the absence of material changes to σ , the three dimensional flow lies within a surface of constant σ , whereby $\mathbf{v} \cdot \nabla \sigma = 0$ and

$$\vec{v} = u [\hat{\mathbf{x}} + (\partial \eta / \partial \bar{x}) \hat{\mathbf{z}}] + v [\hat{\mathbf{y}} + (\partial \eta / \partial \bar{y}) \hat{\mathbf{z}}] \quad \text{if } \partial_t \sigma = 0 \text{ and } \dot{\sigma} = 0. \quad (56.55)$$

However, in general there are transient fluctuations and material changes to σ so that $\mathbf{v} \cdot \nabla \sigma \neq 0$.

56.8.4 Equivalence to the Cartesian velocity representation

Use of the triple product identities (56.34b)-(56.34c) allows us to manipulate both expressions (56.50c) and (56.52) to recover the Cartesian expression

$$\vec{v} = u \hat{\mathbf{x}} + v \hat{\mathbf{y}} + w \hat{\mathbf{z}}. \quad (56.56)$$

Another way to see this identity is to note that in equation (56.54c), the vertical component is an expression for the material time derivative of the vertical position

$$w = \frac{Dz}{Dt} = \frac{\partial \eta}{\partial t} + \mathbf{u} \cdot \nabla_\sigma \eta + \frac{\partial \eta}{\partial \sigma} \dot{\sigma}. \quad (56.57)$$

We derive this identity in Section 57.5 where we discuss further kinematic results using GVCs.

56.9 Metric tensor

Recall from Section 8.1 that we make use of a metric tensor to measure the distance between two points in space. The GVC representation of the metric tensor is given by

$$g_{\bar{a}\bar{b}} = \vec{e}_{\bar{a}} \cdot \vec{e}_{\bar{b}} = \begin{bmatrix} 1 + (\partial \eta / \partial \bar{x})^2 & (\partial \eta / \partial \bar{x})(\partial \eta / \partial \bar{y}) & (\partial \eta / \partial \bar{x})(\partial \eta / \partial \sigma) \\ (\partial \eta / \partial \bar{x})(\partial \eta / \partial \bar{y}) & 1 + (\partial \eta / \partial \bar{y})^2 & (\partial \eta / \partial \bar{y})(\partial \eta / \partial \sigma) \\ (\partial \eta / \partial \bar{x})(\partial \eta / \partial \sigma) & (\partial \eta / \partial \bar{y})(\partial \eta / \partial \sigma) & (\partial \eta / \partial \sigma)^2 \end{bmatrix}, \quad (56.58)$$

and the GVC representation of the inverse metric tensor is given by the somewhat simpler form

$$g^{\bar{a}\bar{b}} = \vec{e}^{\bar{a}} \cdot \vec{e}^{\bar{b}} = \begin{bmatrix} 1 & 0 & \partial \sigma / \partial x \\ 0 & 1 & \partial \sigma / \partial y \\ \partial \sigma / \partial x & \partial \sigma / \partial y & |\nabla \sigma|^2 \end{bmatrix}. \quad (56.59)$$

Proof that $g^{\bar{a}\bar{b}} g_{\bar{b}\bar{c}} = \delta_{\bar{c}}^{\bar{a}}$ requires use of the triple product identities (56.34b) and (56.34c).

56.9.1 Jacobian of transformation

The determinant of the GVC representation of the metric tensor (56.58) is

$$\det(g_{\bar{a}\bar{b}}) = (\partial z / \partial \sigma)^2 = (\partial \eta / \partial \sigma)^2 \quad (56.60)$$

so that the Jacobian of transformation (Section 8.5) is the specific thickness

$$\frac{\partial(x, y, z)}{\partial(\bar{x}, \bar{y}, \sigma)} = \frac{\partial z}{\partial \sigma} = \frac{\partial \eta}{\partial \sigma}. \quad (56.61)$$

The coordinate transformation from Cartesian to generalized vertical is invertible only so long as the Jacobian remains nonzero and single-signed, meaning the fluid retains a monotonic vertical stratification of GVC surfaces. The invertible relation between z and σ means that each point in the vertical can be uniquely specified by either of the two vertical coordinates, z or σ . For example, the Jacobian for pressure as the generalized vertical coordinate in a hydrostatic fluid is

given by³

$$\frac{\partial z}{\partial \sigma} = \frac{\partial z}{\partial p} = -\frac{1}{\rho g}, \quad (56.62)$$

which is indeed single-signed since the mass density is always positive.

56.9.2 Covariant and contravariant representations

The metric tensor allows us to convert between the covariant and contravariant representations of a vector via the identity (Section 8.2.3)

$$F_{\bar{a}} = g_{\bar{a}\bar{b}} F^{\bar{b}}. \quad (56.63)$$

We use triple product identities (56.34b)-(56.34c) to verify that this relation agrees with the transformation matrix approach detailed in Section 56.7. For example,

$$F_{\bar{1}} = g_{\bar{1}\bar{b}} F^{\bar{b}} \quad (56.64a)$$

$$= [1 + (\partial\eta/\partial\bar{x})^2] F^{\bar{1}} + (\partial\eta/\partial\bar{x})(\partial\eta/\partial\bar{y}) F^{\bar{2}} + (\partial\eta/\partial\bar{x})(\partial\eta/\partial\sigma) F^{\sigma} \quad (56.64b)$$

$$= [1 + (\partial\eta/\partial\bar{x})^2] F^1 + (\partial\eta/\partial\bar{x})(\partial\eta/\partial\bar{y}) F^2 + (\partial\eta/\partial\bar{x})(\partial\eta/\partial\sigma) \nabla\sigma \cdot \mathbf{F} \quad (56.64c)$$

$$= F^1 + (\partial\eta/\partial\bar{x}) F^3 \quad (56.64d)$$

$$= F_1 + (\partial\eta/\partial\bar{x}) F_3, \quad (56.64e)$$

where the final equality holds since $F^1 = F_1$ and $F^3 = F_3$ for Cartesian tensor components.

56.10 Volume element and the Levi-Civita tensor

The square root of the determinant of the metric tensor (56.58) is

$$\sqrt{\det(g_{\bar{a}\bar{b}})} = \partial z / \partial \sigma = \partial \eta / \partial \sigma \quad (56.65)$$

so that the volume element (Section 8.5) is

$$dV = (\partial z / \partial \sigma) dx dy d\sigma. \quad (56.66)$$

The covariant Levi-Civita tensor (Section 8.7) has the GVC representations

$$\varepsilon_{\bar{a}\bar{b}\bar{c}} = (\partial z / \partial \sigma) \epsilon_{\bar{a}\bar{b}\bar{c}} \quad \varepsilon^{\bar{a}\bar{b}\bar{c}} = (\partial z / \partial \sigma)^{-1} \epsilon^{\bar{a}\bar{b}\bar{c}} \quad (56.67)$$

where ϵ is the permutation symbol introduced in Section 1.4.1 with its components independent of coordinate representation.

56.11 Vector cross product of basis vectors

We now verify the relation (8.79) for the cross product of two basis vectors using GVCs

$$\vec{e}_{\bar{a}} \times \vec{e}_{\bar{b}} = \varepsilon_{\bar{a}\bar{b}\bar{c}} \vec{e}^{\bar{c}} \implies \vec{e}_{\bar{a}} \times \vec{e}_{\bar{b}} = (\partial z / \partial \sigma) \epsilon_{\bar{a}\bar{b}\bar{c}} \vec{e}^{\bar{c}}. \quad (56.68)$$

³We derive the hydrostatic balance in Section 24.2.

Making use of the basis vectors from Section 56.3 and the basis one-forms from Section 56.4 renders

$$\vec{e}_{\bar{x}} \times \vec{e}_{\bar{y}} = \hat{z} - \hat{x} (\partial\eta/\partial\bar{x}) - \hat{y} (\partial\eta/\partial\bar{y}) = (\partial z/\partial\sigma) \nabla\sigma = \varepsilon_{\bar{x}\bar{y}\sigma} \tilde{e}^\sigma \quad (56.69a)$$

$$\vec{e}_{\bar{y}} \times \vec{e}_\sigma = \hat{x} (\partial z/\partial\sigma) = \varepsilon_{\bar{y}\sigma\bar{x}} \tilde{e}^{\bar{x}} \quad (56.69b)$$

$$\vec{e}_\sigma \times \vec{e}_{\bar{x}} = \hat{y} (\partial z/\partial\sigma) = \varepsilon_{\sigma\bar{x}\bar{y}} \tilde{e}^{\bar{y}}. \quad (56.69c)$$

56.12 Partial derivative operators

We here consider the partial derivative operators and their transformation between coordinate systems. These identities are used throughout GVC calculus. Given the importance of these expressions, we offer two derivations. Notably, the geometric derivation in Section 56.12.2 requires minimal use of the previous tensor formalism.

56.12.1 Analytical derivation

The partial derivative operators in GVCs are computed via $\partial_{\bar{a}} = \Lambda_{\bar{a}}^a \partial_a$. Including also the time component leads to the relations

$$\partial_{\bar{t}} = \partial_t + (\partial z/\partial\bar{t}) \partial_z = \partial_t + (\partial\eta/\partial\bar{t}) \partial_z \quad (56.70a)$$

$$\partial_{\bar{x}} = \partial_x + (\partial z/\partial\bar{x}) \partial_z = \partial_x + (\partial\eta/\partial\bar{x}) \partial_z \quad (56.70b)$$

$$\partial_{\bar{y}} = \partial_y + (\partial z/\partial\bar{y}) \partial_z = \partial_y + (\partial\eta/\partial\bar{y}) \partial_z \quad (56.70c)$$

$$\partial_\sigma = (\partial z/\partial\sigma) \partial_z = (\partial\eta/\partial\sigma) \partial_z. \quad (56.70d)$$

We can make use of the triple product identities (56.34b) and (56.34c) to express the slope of a constant GVC surface in the equivalent manners

$$\mathbf{S} = \nabla_\sigma \eta = \nabla_\sigma z = -(\partial\sigma/\partial z)^{-1} \nabla_z \sigma \quad (56.71)$$

where we introduced the standard shorthand notation

$$\nabla_\sigma = \hat{x} \partial/\partial\bar{x} + \hat{y} \partial/\partial\bar{y} \quad \text{and} \quad \nabla_z = \hat{x} \partial/\partial x + \hat{y} \partial/\partial y. \quad (56.72)$$

It is common to transform between the horizontal gradient operators, in which case we write

$$\nabla_\sigma = \nabla_z + (\nabla_\sigma z) \partial_z \equiv \nabla_z + \mathbf{S} \partial_z. \quad (56.73)$$

We emphasize that ∇_σ is merely a shorthand for the two partial derivative operators and that it only has components in the horizontal directions.

56.12.2 Geometrical derivation

We provide a geometric derivation for the lateral derivative operator that complements the previous analytical derivation. This operator is computed by taking the difference of a function along surfaces of constant generalized vertical coordinate, but with the lateral distance computed in the horizontal direction as shown in Figure 56.4. This feature of the horizontal derivative operator is a key aspect of the GVCs' non-orthogonality.

Consider the geometry shown in Figure 56.4, which shows a generalized vertical coordinate

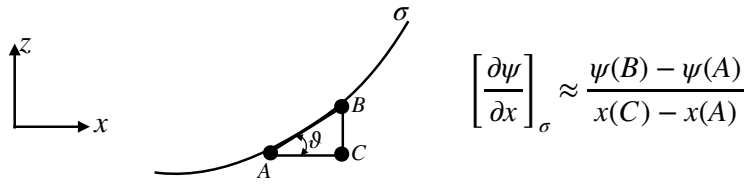


FIGURE 56.4: A surface of constant generalized vertical coordinate, σ , along with a local tangent plane with a slope $\tan \vartheta$ with respect to the horizontal plane. This figure illustrates the identities (56.75a)-(56.75d), with these identities relating a lateral derivative taken along the GVC surface to horizontal and vertical derivatives taken along orthogonal Cartesian axes.

surface (constant σ surface) along with a sample tangent plane with a slope

$$S^x = \frac{\text{rise}}{\text{run}} = \tan \vartheta = \frac{z(B) - z(C)}{x(C) - x(A)} \approx \left[\frac{\partial z}{\partial x} \right]_{\sigma} = - \frac{(\partial \sigma / \partial x)_z}{(\partial \sigma / \partial z)} \quad (56.74)$$

relative to the horizontal. We readily verify the following identities based on finite difference operations for an arbitrary function

$$\left[\frac{\partial \psi}{\partial x} \right]_{\sigma} \approx \frac{\psi(B) - \psi(A)}{x(C) - x(A)} \quad (56.75a)$$

$$= \frac{\psi(C) - \psi(A)}{x(C) - x(A)} + \frac{\psi(B) - \psi(C)}{x(C) - x(A)} \quad (56.75b)$$

$$= \frac{\psi(C) - \psi(A)}{x(C) - x(A)} + \left[\frac{z(B) - z(C)}{x(C) - x(A)} \right] \frac{\psi(B) - \psi(C)}{z(B) - z(C)} \quad (56.75c)$$

$$= \left[\frac{\partial \psi}{\partial x} \right]_z + S^x \left[\frac{\partial \psi}{\partial z} \right]_x. \quad (56.75d)$$

Taking the continuum limit then leads to the relations between horizontal derivatives computed on constant σ surfaces to those computed on constant z surfaces

$$\left[\frac{\partial}{\partial x} \right]_{\sigma} = \left[\frac{\partial}{\partial x} \right]_z + \left[\frac{\partial z}{\partial x} \right]_{\sigma} \frac{\partial}{\partial z} = \left[\frac{\partial}{\partial x} \right]_z + \left[\frac{\partial \eta}{\partial x} \right]_{\sigma} \frac{\partial}{\partial z} \quad (56.76a)$$

$$\left[\frac{\partial}{\partial y} \right]_{\sigma} = \left[\frac{\partial}{\partial y} \right]_z + \left[\frac{\partial z}{\partial y} \right]_{\sigma} \frac{\partial}{\partial z} = \left[\frac{\partial}{\partial y} \right]_z + \left[\frac{\partial \eta}{\partial y} \right]_{\sigma} \frac{\partial}{\partial z}, \quad (56.76b)$$

which can be written in the shorthand vector notation

$$\nabla_{\sigma} = \hat{x} \left[\frac{\partial}{\partial x} \right]_{\sigma} + \hat{y} \left[\frac{\partial}{\partial y} \right]_{\sigma} = \nabla_z + (\nabla_{\sigma} z) \partial_z = \nabla_z + (\nabla_{\sigma} \eta) \partial_z. \quad (56.77)$$

56.13 Material time derivative

Making use of the relations for the partial derivative operators in Section 56.12 allows us to write the material time derivative in the following equivalent forms

$$\frac{D}{Dt} = \left[\frac{\partial}{\partial t} \right]_z + \mathbf{u} \cdot \nabla_z + w \frac{\partial}{\partial z} \quad (56.78a)$$

$$= \left[\frac{\partial}{\partial t} \right]_\sigma - (\partial \eta / \partial \bar{t}) \partial_z + \mathbf{u} \cdot [\nabla_\sigma - (\nabla_\sigma \eta) \partial_z] + w \partial / \partial z \quad (56.78b)$$

$$= \left[\frac{\partial}{\partial t} \right]_\sigma + \mathbf{u} \cdot \nabla_\sigma + [w - \mathbf{u} \cdot \nabla_\sigma \eta - \partial \eta / \partial \bar{t}] (\partial \sigma / \partial z) \partial / \partial \sigma \quad (56.78c)$$

$$= \left[\frac{\partial}{\partial t} \right]_\sigma + \mathbf{u} \cdot \nabla_\sigma + \frac{D\sigma}{Dt} \frac{\partial}{\partial \sigma} \quad (56.78d)$$

$$= \left[\frac{\partial}{\partial t} \right]_\sigma + \mathbf{u} \cdot \nabla_\sigma + \frac{\partial z}{\partial \sigma} \frac{D\sigma}{Dt} \frac{\partial}{\partial z}. \quad (56.78e)$$

The equality (56.78d) made use of the identity (56.57), which is itself derived in Section 57.5 where we discuss further kinematic results using GVCs. Besides differences in the spatial operators, it is important to note that the time derivative operators are computed on constant geopotential and constant GVC surfaces, respectively. However, the horizontal velocity component is the *same* for both forms of the material time derivative

$$(u, v) = \frac{D(x, y)}{Dt}. \quad (56.79)$$

56.14 Divergence of a vector and the divergence theorem

Making use of the general expression (8.15) for the covariant divergence of a vector renders the GVC expression

$$\nabla_{\bar{a}} F^{\bar{a}} = [\det(g_{\bar{a}\bar{b}})]^{-1/2} \partial_{\bar{a}} \left[[\det(g_{\bar{a}\bar{b}})]^{1/2} F^{\bar{a}} \right] = (\partial z / \partial \sigma)^{-1} \partial_{\bar{a}} [(\partial z / \partial \sigma) F^{\bar{a}}]. \quad (56.80)$$

Recall that the GVC vector components, $F^{\bar{a}}$, are related to the Cartesian components in equation (56.43), and the GVC components of the partial derivative operator, $\partial_{\bar{a}}$, are related to the Cartesian operator in equation (56.72).

When making use of the divergence theorem (Section 8.18), we require the product of the volume element and the covariant divergence. For GVCs this product takes on the form

$$(\nabla_{\bar{a}} F^{\bar{a}}) dV = \partial_{\bar{a}} [(\partial z / \partial \sigma) F^{\bar{a}}] d\bar{x} d\bar{y} d\sigma, \quad (56.81)$$

which reduces to a boundary integral when integrating over a volume.

56.15 The diffusion operator

As an explicit example of the covariant divergence operator (56.80), we here consider the diffusion operator discussed in Chapter 61. The derivation here recovers much of what we just discussed in Section 56.14, yet we make use of a bit less tensor formalism though at the cost of more algebra.

56.15.1 Continuous expression

The diffusion operator is the divergence of the diffusive flux

$$\mathcal{R} = -\nabla \cdot \mathbf{J}, \quad (56.82)$$

where \mathbf{J} is a vector field. Let us convert the pieces of this operator from Cartesian coordinates into GVC coordinates, making use of the transformation of partial derivative operators given in Section 56.12. Also, we make use of the shorthand $z(x, y, \sigma, t)$ rather than $\eta(x, y, \sigma, t)$

$$-\mathcal{R} = \nabla \cdot \mathbf{J} \quad (56.83a)$$

$$= \nabla_z \cdot \mathbf{J}^h + \partial_z J^z \quad (56.83b)$$

$$= (\nabla_\sigma - \nabla_\sigma z \partial_z) \cdot \mathbf{J}^h + (\sigma_z) \partial_\sigma J^z \quad (56.83c)$$

$$= \sigma_z \left[z_\sigma \nabla_\sigma \cdot \mathbf{J}^h + (\hat{\mathbf{z}} \partial_\sigma - \nabla_\sigma z \partial_\sigma) \cdot \mathbf{J} \right] \quad (56.83d)$$

$$= \sigma_z \left[\nabla_\sigma \cdot (z_\sigma \mathbf{J}^h) - \mathbf{J}^h \cdot \nabla_\sigma (z_\sigma) + \partial_\sigma J^z - \partial_\sigma (\nabla_\sigma z \cdot \mathbf{J}) + \mathbf{J} \cdot \partial_\sigma (\nabla_\sigma z) \right] \quad (56.83e)$$

$$= \sigma_z \left[\nabla_\sigma \cdot (z_\sigma \mathbf{J}^h) + \partial_\sigma J^z - \partial_\sigma (\nabla_\sigma z \cdot \mathbf{J}^h) \right] \quad (56.83f)$$

$$= \sigma_z \left(\nabla_\sigma \cdot (\partial_\sigma z \mathbf{J}^h) + \partial_\sigma [(\hat{\mathbf{z}} - \nabla_\sigma z) \cdot \mathbf{J}] \right) \quad (56.83g)$$

$$= \sigma_z \left[\nabla_\sigma \cdot (z_\sigma \mathbf{J}^h) + \partial_\sigma (z_\sigma \nabla_\sigma \cdot \mathbf{J}) \right], \quad (56.83h)$$

where we used

$$z_\sigma \nabla_\sigma = \hat{\mathbf{z}} - \nabla_\sigma z \quad (56.84)$$

to reach the final equality, and made use of the shorthand

$$z_\sigma = \partial z / \partial \sigma \quad \text{and} \quad \sigma_z = \partial \sigma / \partial z = (z_\sigma)^{-1}. \quad (56.85)$$

The coordinate transformations in Section 56.7 for vector components reveal that the expression (56.83h) is identical to equation (56.80) derived using formal tensor methods. Likewise, multiplying by the volume element

$$dV = dx dy dz = dx dy z_\sigma d\sigma, \quad (56.86)$$

leads to

$$-\mathcal{R} dV = \left[\nabla_\sigma \cdot (z_\sigma \mathbf{J}^h) + \partial_\sigma (z_\sigma \nabla_\sigma \cdot \mathbf{J}) \right] dx dy d\sigma, \quad (56.87)$$

which is identical to the expression (56.81).

56.15.2 Layer thickness weighted diffusion operator

Consider a prescribed increment, $\delta\sigma$, separating two σ isosurfaces. This increment commutes with the horizontal operator ∇_σ , acting within the layer. We can thus formally consider the following

layer-integrated or thickness weighted form of the diffusion operator

$$-\mathcal{R} \delta V = \left[\nabla_\sigma \cdot (\delta\sigma z_\sigma \mathbf{J}^h) + \delta\sigma \partial_\sigma (z_\sigma \nabla\sigma \cdot \mathbf{J}) \right] \delta x \delta y \quad (56.88a)$$

$$= \frac{1}{\delta z} \left[\nabla_\sigma \cdot (\delta\sigma z_\sigma \mathbf{J}^h) + \delta\sigma \partial_\sigma (z_\sigma \nabla\sigma \cdot \mathbf{J}) \right] \delta x \delta y \delta z \quad (56.88b)$$

$$= \frac{1}{h} \left[\nabla_\sigma \cdot (h \mathbf{J}^h) + \Delta_\sigma (z_\sigma \nabla\sigma \cdot \mathbf{J}) \right] \delta x \delta y h, \quad (56.88c)$$

where we introduced the infinitesimal layer thickness

$$h = z_\sigma \delta\sigma \quad (56.89)$$

and the non-dimensional differential operator

$$\Delta_\sigma \equiv \delta\sigma \frac{\partial}{\partial\sigma}. \quad (56.90)$$

Cancelling the volume element on both sides leads to the diffusion operator

$$\mathcal{R} = -\frac{1}{h} \left[\nabla_\sigma \cdot (h \mathbf{J}^h) + \Delta_\sigma (z_\sigma \nabla\sigma \cdot \mathbf{J}) \right]. \quad (56.91)$$

This form is commonly found in the numerical modeling literature when considering generalized vertical coordinate models.

We make the following comments concerning the diffusion operator in equation (56.91).

- Our introduction of the layer thickness $h = z_\sigma \delta\sigma$ is treated a bit more formally in Sections 57.10 and 57.11 by considering a vertical integral over a coordinate layer. Even so, the resulting diffusion operator is the same as that derived here.
- The thickness weighted flux, $h \mathbf{J}^h$, is oriented within the horizontal plane. However, its contribution to the diffusion operator is computed by taking its convergence using the operator ∇_σ rather than the horizontal operator ∇_z . This distinction is fundamental to how operators, such as advection and diffusion, appear using generalized vertical coordinates.
- The flux $z_\sigma \nabla\sigma \cdot \mathbf{J}$ is commonly referred to as the dia-surface subgrid scale flux.
- For the special case of a diffusive flux with zero component parallel to $\nabla\sigma$, the diffusion operator reduces to

$$\mathcal{R} = -\frac{1}{h} \left[\nabla_\sigma \cdot (h \mathbf{J}^h) \right] \quad \text{if } \nabla\sigma \cdot \mathbf{J} = 0. \quad (56.92)$$

The neutral diffusion operator of Section 63.4.4 is an example of such an operator, with σ in that case given by the locally referenced potential density.

56.16 Vorticity

As detailed in Chapter 37, vorticity is the curl of the velocity

$$\vec{\omega} = \text{curl}(\vec{v}), \quad (56.93)$$

where the curl has components (Section 8.17)

$$\text{curl}(\vec{v}) = \tilde{e}_a \varepsilon^{abc} \partial_b v_c = \tilde{e}_{\bar{a}} \varepsilon^{\bar{a}\bar{b}\bar{c}} \partial_{\bar{b}} v_{\bar{c}}. \quad (56.94)$$

56.16.1 The components

We identify the contravariant components of the vorticity via

$$\omega^{\bar{a}} = \varepsilon^{\bar{a}\bar{b}\bar{c}} \partial_{\bar{b}} v_{\bar{c}} = (\partial z / \partial \sigma)^{-1} \epsilon^{\bar{a}\bar{b}\bar{c}} \partial_{\bar{b}} v_{\bar{c}} \quad (56.95)$$

where we made use of equation (56.67) to introduce the permutation symbol. Expanding the components leads to

$$\omega^{\bar{1}} = (\partial \sigma / \partial z) (\partial_{\bar{2}} v_{\bar{3}} - \partial_{\bar{3}} v_{\bar{2}}) \quad (56.96a)$$

$$\omega^{\bar{2}} = (\partial \sigma / \partial z) (\partial_{\bar{3}} v_{\bar{1}} - \partial_{\bar{1}} v_{\bar{3}}) \quad (56.96b)$$

$$\omega^{\bar{3}} = \omega^{\sigma} = (\partial \sigma / \partial z) (\partial_{\bar{1}} v_{\bar{2}} - \partial_{\bar{2}} v_{\bar{1}}). \quad (56.96c)$$

56.16.2 Transforming from Cartesian coordinates

The above approach works solely with the GVC coordinates. An alternative approach connects the GVC vorticity components and the Cartesian vorticity components. For that purpose we use the transformation matrix via

$$\omega^{\bar{a}} = \Lambda_a^{\bar{a}} \omega^a, \quad (56.97)$$

where ω^a are the Cartesian components

$$\boldsymbol{\omega} = \hat{x} \left(\frac{\partial w}{\partial y} - \frac{\partial v}{\partial z} \right) + \hat{y} \left(\frac{\partial u}{\partial z} - \frac{\partial w}{\partial x} \right) + \hat{z} \left(\frac{\partial v}{\partial x} - \frac{\partial u}{\partial y} \right). \quad (56.98)$$

Making use of the transformation matrix $\Lambda_a^{\bar{a}}$ from equation (56.20) yields (as in Section 56.7)

$$\omega^{\bar{x}} = \omega^x = \frac{\partial w}{\partial y} - \frac{\partial v}{\partial z} \quad \text{and} \quad \omega^{\bar{y}} = \omega^y = \frac{\partial u}{\partial z} - \frac{\partial w}{\partial x} \quad \text{and} \quad \omega^{\sigma} = \boldsymbol{\omega} \cdot \nabla \sigma. \quad (56.99)$$

Note that for isopycnal coordinates in a Boussinesq fluid, ω^{σ} equals to the potential vorticity when the vorticity is the absolute vorticity (Section 59.3). That is, the potential vorticity is the isopycnal component of the absolute vorticity.

56.17 Velocity circulation

The velocity circulation (Section 34.3) is given by the closed oriented path integral of the velocity projected into the direction of the path

$$\mathcal{C} \equiv \oint_{\partial\mathcal{S}} \mathbf{v} \cdot d\mathbf{x} \quad (56.100)$$

where $d\mathbf{x}$ is the vector line element along the path and $\partial\mathcal{S}$ is the closed path defining the boundary to a two-dimensional surface \mathcal{S} . Stokes' Theorem from Section 2.6 leads to the identity

$$\mathcal{C} = \oint_{\partial\mathcal{S}} \mathbf{v} \cdot d\mathbf{x} = \int_{\mathcal{S}} (\nabla \times \mathbf{v}) \cdot \hat{\mathbf{n}} d\mathcal{S} = \int_{\mathcal{S}} \boldsymbol{\omega} \cdot \hat{\mathbf{n}} d\mathcal{S}, \quad (56.101)$$

where $\hat{\mathbf{n}}$ is the outward normal vector orienting the area element $d\mathcal{S}$ according to the right-hand rule applied to the bounding circuit. These results are all written in a generally covariant manner (Section 7.1) so that they hold for an arbitrary coordinate representation.

As a particular case, consider the circulation around a closed path on a constant σ surface, in which

$$\hat{\mathbf{n}} = \frac{\nabla\sigma}{|\nabla\sigma|} \quad (56.102)$$

is the outward normal and

$$\boldsymbol{\omega} \cdot \hat{\mathbf{n}} = \frac{\omega^\sigma}{|\nabla\sigma|} \quad (56.103)$$

where $\omega^\sigma = \boldsymbol{\omega} \cdot \nabla\sigma$ (equation (56.99)). So long as the vertical stratification remains non-zero ($\partial\sigma/\partial z \neq 0$) we can write the area factor in the form

$$\frac{d\mathcal{S}}{|\nabla\sigma|} = \frac{d\mathcal{S}}{\sqrt{(\partial\sigma/\partial x)^2 + (\partial\sigma/\partial y)^2 + (\partial\sigma/\partial z)^2}} \quad (56.104a)$$

$$= \frac{d\mathcal{S}}{|\partial\sigma/\partial z| \sqrt{[(\partial\sigma/\partial x)/(\partial\sigma/\partial z)]^2 + [(\partial\sigma/\partial y)/(\partial\sigma/\partial z)]^2 + 1}} \quad (56.104b)$$

$$= \frac{d\mathcal{S}}{|\partial\sigma/\partial z| \sqrt{1 + \tan^2 \vartheta}} \quad (56.104c)$$

$$= \left| \frac{\partial z}{\partial \sigma} \right| |\cos \vartheta| d\mathcal{S} \quad (56.104d)$$

$$= \left| \frac{\partial z}{\partial \sigma} \right| dA. \quad (56.104e)$$

The equality (56.104c) introduces the angle, ϑ , between the boundary surface and the horizontal plane as in Figure 56.4. The squared slope of this surface given by

$$\tan^2 \vartheta = \frac{\nabla_z \sigma \cdot \nabla_z \sigma}{(\partial\sigma/\partial z)^2} = \nabla_\sigma z \cdot \nabla_\sigma z. \quad (56.105)$$

The equality (56.104d) made use of a trigonometric identity, and the equality (56.104e) introduced the horizontal projection of the area,

$$dA = |\cos \vartheta| d\mathcal{S}. \quad (56.106)$$

Bringing these results together leads to the expression for circulation around a closed loop on a constant σ surface

$$C_{\sigma-\text{surface}} = \int_{\mathcal{S}} (\boldsymbol{\omega} \cdot \nabla\sigma) |\partial z/\partial\sigma| dA. \quad (56.107)$$



Chapter 57

KINEMATIC EQUATIONS

In providing a mechanistic description of budgets within the ocean or atmosphere, it is often useful to measure the material or momentum transfer through a surface. This transport is termed the *dia-surface transport*. Our discussion in this chapter unifies ideas developed for kinematic boundary conditions in Section 16.4 with transport across an arbitrary surface in the fluid interior. We do so by making use of the generalized vertical coordinates (GVCs) first introduced in Chapter 56. We make use of the dia-surface transport formulation to express the material time derivative operator using GVCs. This form for the material time derivative allows us to decompose the vertical velocity into motion relative to a moving GVC surface. In turn, we are afforded a means to reinterpret the velocity vector and corresponding particle trajectories. GVC kinematics also provides a means to express the subduction of fluid into the ocean interior beneath the mixed layer base. We close the chapter with derivations of the GVC version of mass continuity and the tracer equation. We also introduce the layer integrated version of the continuity and tracer equations, with the layer integrated equations appropriate for discrete numerical fluid models.

CHAPTER GUIDE

We introduced mathematical properties of generalized vertical coordinates (GVCs) in Chapter 56, including the calculus using these non-orthogonal coordinates. It is essential to have a working knowledge of that material to understand the present chapter. Later in Chapter 58 we detail the dynamical equations using GVCs, with material in that chapter relying on the kinematics presented here. Following the treatment in Chapter 56, we here use the symbol σ to denote a generalized vertical coordinate.

57.1	Loose threads	1422
57.2	Example generalized vertical coordinates	1422
57.2.1	Ocean free surface	1423
57.2.2	Solid earth boundary	1423
57.2.3	Ocean mixed layer base	1423
57.2.4	Interior generalized vertical coordinate surfaces	1423
57.3	Specific thickness	1424
57.4	The dia-surface transport	1425
57.4.1	Flow normal to the GVC surface	1425
57.4.2	Accounting for movement of the surface	1426
57.4.3	We only care about divergent surface motion	1427
57.4.4	Cross GVC transport in terms of GVC material evolution	1427
57.4.5	Defining the dia-surface transport	1427
57.4.6	Expressions for the dia-surface velocity component	1429
57.4.7	An alternative definition of dia-surface velocity component	1430

57.4.8	Area integrated dia-surface transport for incompressible flows	1430
57.5	Material time derivative	1432
57.6	Vertical velocity and dia-surface velocity	1432
57.6.1	Decomposing the vertical velocity	1433
57.6.2	Another form of the vertical velocity decomposition	1433
57.7	The velocity vector and fluid particle trajectories	1435
57.8	Subduction across the mixed layer base	1436
57.9	Mass continuity	1437
57.9.1	Cartesian coordinates	1437
57.9.2	Generalized vertical coordinates	1438
57.10	Layer integrated mass continuity	1438
57.10.1	Compressible fluids	1439
57.10.2	Mass continuity using pressure coordinates	1440
57.10.3	Incompressible flow	1442
57.10.4	Rescaled geopotential coordinates	1442
57.11	Layer integrated tracer equation	1443

57.1 Loose threads

- Develop the notion of overturning streamfunctions as per Sections 32.2 to 32.4 of the MOM5 elements guide. Work through the issues for both Boussinesq and non-Boussinesq.
- Develop the notion of depth integrated transport as per Sections 32.2 to 32.4 of the MOM5 elements guide. Work through the issues for both Boussinesq and non-Boussinesq.

57.2 Example generalized vertical coordinates

We here consider some generalized vertical coordinates that will prove of use for our discussion in this chapter, with Figure 57.1 illustrating the examples.

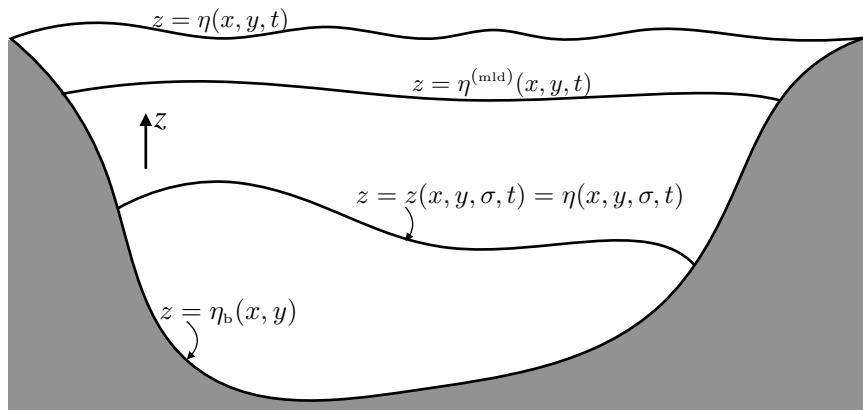


FIGURE 57.1: Example generalized vertical coordinates, $\sigma(x, y, z, t)$. The ocean free surface can be represented mathematically by $\sigma(x, y, z, t) = z - \eta(x, y, t) = 0$; the ocean mixed layer base by $\sigma(x, y, z, t) = z - \eta^{(mld)}(x, y, t) = 0$; the position of an interior GVC coordinate σ with depth $z = z(x, y, \sigma, t) = \eta(x, y, \sigma, t)$; and the solid earth bottom $\sigma(x, y, z) = z - \eta_b(x, y) = 0$.

57.2.1 Ocean free surface

The first surface is the ocean free surface, whose kinematic boundary conditions were derived in Section 16.4.3. Here, water and tracer penetrate this surface through precipitation, evaporation, river runoff (when applied as an upper ocean boundary condition), and sea ice melt. Momentum exchange arises from stresses between the ocean and atmosphere or ice. The ocean free surface can be represented mathematically by the identity

$$\sigma(x, y, z, t) = z - \eta(x, y, t) = 0 \quad \text{ocean free surface.} \quad (57.1)$$

This identity holds so long as we assume the surface height η is smooth and contains no over-turns at the scales of interest. That is, we assume breaking surface waves are filtered from the description.

57.2.2 Solid earth boundary

We may describe the solid Earth lower boundary mathematically by using the time independent expression

$$\sigma(x, y, z) = z + H(x, y) = z - \eta_b(x, y) = 0 \quad \text{ocean bottom,} \quad (57.2)$$

where we introduce the two common symbols used for the bottom, $\eta_b = -H$. We generally prefer η_b since H is used elsewhere in this book for vertical scale. As detailed in Section 16.4.1, we typically assume that there is no fluid mass transport through the solid Earth. However, in the case of geothermal heating, we may consider an exchange of heat between the ocean and the solid Earth. Momentum exchange through the action of stresses occur between the solid Earth and ocean fluid.

57.2.3 Ocean mixed layer base

Let

$$\sigma = z - \eta^{(\text{mld})}(x, y, t) = 0 \quad (57.3)$$

represent the vertical position of the ocean mixed layer base. The corresponding normal vector is given by

$$\hat{\mathbf{n}}^{(\text{mld})} = \frac{\nabla(z - \eta^{(\text{mld})})}{|\nabla(z - \eta^{(\text{mld})})|} = \frac{\nabla(\hat{z} - \nabla\eta^{(\text{mld})})}{\sqrt{1 + |\nabla\eta^{(\text{mld})}|^2}}. \quad (57.4)$$

This example is relevant for the study of ocean ventilation, whereby we are interested in measuring the transport of fluid that enters the ocean interior across the mixed layer base (see Section 57.8).

57.2.4 Interior generalized vertical coordinate surfaces

Within the ocean interior, transport across surfaces of constant generalized vertical coordinate $\sigma = \sigma(x, y, z, t)$ constitutes the dia-surface transport affecting budgets of mass, tracer, and momentum within layers bounded by two generalized vertical coordinate surfaces. A canonical example is provided by isopycnal layers formed by surfaces of constant potential density (or equivalently constant buoyancy surfaces) as used in isopycnal ocean models as well as theoretical descriptions of adiabatic ocean dynamics. The vertical position of this surface is written in one of two equivalent manners

$$z = z(x, y, \sigma, t) = \eta(x, y, \sigma, t). \quad (57.5)$$

The first expression exposes the functional dependence of the vertical position of the σ surface at a horizontal position and time. In Section 56.1 we discussed the potential for confusion between

writing z as a particular vertical position versus a function, thus motivating $z = \eta(x, y, \sigma, t)$. However, by now we should have sufficient experience with generalized vertical coordinates so that we can well distinguish when z refers to a particular vertical position versus $z(x, y, \sigma, t)$ as a coordinate function. For this reason we only infrequently use $z = \eta(x, y, \sigma, t)$ in this chapter.

57.3 Specific thickness

As mentioned in Section 56.9.1, a surface of constant generalized vertical coordinate can be successfully used to partition the vertical so long as the transformation between the generalized vertical coordinate and the geopotential coordinate is invertible. The Jacobian of transformation is given by

$$\frac{\partial z}{\partial \sigma} = z_\sigma, \quad (57.6)$$

which must be single signed for suitable generalized vertical coordinates. This constraint means that we do not allow the surfaces to overturn, which is the same assumption made about the ocean surface, $z = \eta(x, y, t)$, and solid earth bottom, $z = \eta_b(x, y)$. This restriction places a limitation on the ability of certain GVC models (e.g., isopycnal models) to describe non-hydrostatic processes, such as the overturning common in Kelvin-Helmholtz billows and gravitational convection. Note that for both the solid earth bottom and ocean free surface

$$\frac{\partial z}{\partial \sigma} = 1 \quad \text{ocean free surface and fluid/solid interface.} \quad (57.7)$$

Furthermore, this relation also holds, trivially, for geopotential coordinates in which $\sigma = z$.

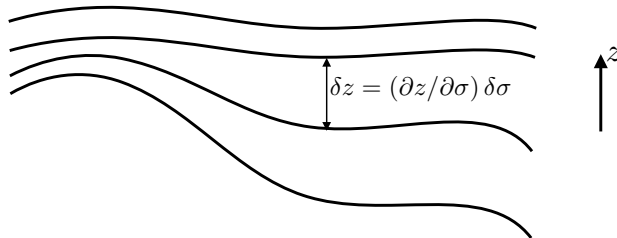


FIGURE 57.2: Illustrating the thickness between surfaces of constant generalized vertical coordinates, $\delta z = (\partial z / \partial \sigma) \delta \sigma$. In regions with larger magnitude for the specific thickness, $\partial z / \partial \sigma$, or equivalently smaller vertical stratification of the σ surfaces, $\partial \sigma / \partial z$, the layer thicknesses are further apart. The converse holds where $\partial z / \partial \sigma$ is small (equivalently $\partial \sigma / \partial z$ is large).

We refer to the Jacobian z_σ as the *specific thickness* and sometimes find it useful to write it as

$$h = z_\sigma = \frac{\partial z}{\partial \sigma}. \quad (57.8)$$

This name is motivated by noting that the vertical thickness of an infinitesimal layer of coordinate thickness $\delta \sigma$ is given by

$$\delta z = \frac{\partial z}{\partial \sigma} \delta \sigma = h \delta \sigma, \quad (57.9)$$

with Figure 57.2 providing an example with finitely thick layers. For example, if $\sigma = b(x, y, z, t)$ (buoyancy or potential density as in isopycnal models), then the thickness of a buoyancy layer is given by

$$\delta z = \frac{\partial z}{\partial \sigma} \delta b = N^{-2} \delta b, \quad (57.10)$$

with

$$N^2 = \frac{\partial b}{\partial z} \quad (57.11)$$

the squared buoyancy frequency (Section 27.5.4) in a Boussinesq fluid (Chapter 26). For a hydrostatic fluid using pressure as the vertical coordinate, the thickness of a pressure layer is

$$\delta z = \frac{\partial z}{\partial p} \delta p = -\frac{1}{\rho g} \delta p \quad (57.12)$$

where we used the hydrostatic relation (Section 24.2)

$$\frac{\partial p}{\partial z} = -\rho g \quad (57.13)$$

with g the constant acceleration due to effective gravity. Note that we assume the layer thickness is positive, $\delta z > 0$. For this purpose, with hydrostatic pressure we might choose to consider negative pressure increments, $\delta p < 0$, as this corresponds to vertically upward movement in a fluid column.

57.4 The dia-surface transport

In this section we develop the concept of dia-surface transport and derive its expression in terms of the material time derivative of the GVC surface.

57.4.1 Flow normal to the GVC surface

At an arbitrary point on a surface of constant generalized vertical coordinate (see Figure 57.3), the rate at which fluid moves in the direction normal to the surface is given by

$$\text{RATE OF FLUID FLOW IN DIRECTION } \hat{\mathbf{n}} = \mathbf{v} \cdot \hat{\mathbf{n}}, \quad (57.14)$$

where

$$\hat{\mathbf{n}} = \frac{\nabla \sigma}{|\nabla \sigma|}, \quad (57.15)$$

is the surface unit normal. Two examples are useful to ground this expression in common experience. For the ocean free surface, $\sigma = z - \eta(x, y, t) = 0$, the unit normal takes the form

$$\hat{\mathbf{n}} = \frac{\nabla(z - \eta)}{|\nabla(z - \eta)|} = \frac{\hat{\mathbf{z}} - \nabla \eta}{\sqrt{1 + |\nabla \eta|^2}}, \quad (57.16)$$

whereas at the solid Earth bottom, $\sigma = z - \eta_b(x, y) = 0$,

$$\hat{\mathbf{n}} = -\frac{\nabla(z - \eta_b)}{|\nabla(z - \eta_b)|} = -\frac{\hat{\mathbf{z}} - \nabla \eta_b}{\sqrt{1 + |\nabla \eta_b|^2}}. \quad (57.17)$$

Introducing the material time derivative

$$\frac{D\sigma}{Dt} = \frac{\partial \sigma}{\partial t} + \mathbf{v} \cdot \nabla \sigma \quad (57.18)$$

to equation (57.14) leads to the identity

$$\mathbf{v} \cdot \hat{\mathbf{n}} = \frac{1}{|\nabla\sigma|} \left[\frac{D\sigma}{Dt} - \frac{\partial\sigma}{\partial t} \right]. \quad (57.19)$$

Hence, the component to the velocity of a fluid particle that is normal to a GVC surface is proportional to the difference between the material time derivative of the surface coordinate and its partial time derivative.

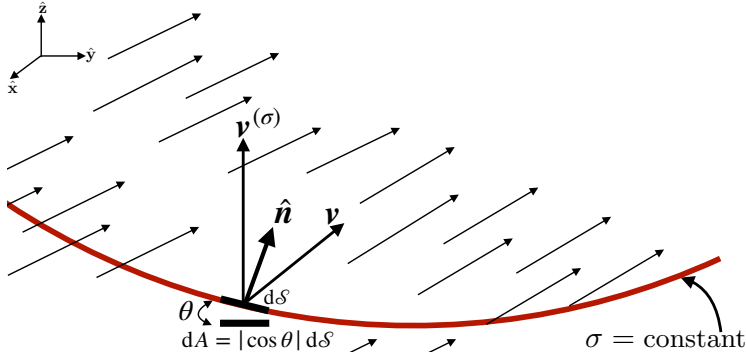


FIGURE 57.3: A surface of constant generalized vertical coordinate, $\sigma = \text{constant}$, within a fluid. The normal direction, $\hat{\mathbf{n}} = \nabla\sigma/|\nabla\sigma|$, points in the direction of increasing σ . We show an example velocity vector for a fluid particle, \mathbf{v} , at a point on the surface as well as the velocity, $\mathbf{v}^{(\sigma)}$, of a point that lives on the surface. Note that kinematics is only concerned with the normal component to the surface velocity, $\mathbf{v}^{(\sigma)} \cdot \hat{\mathbf{n}}$, as per equation (57.25). We require dynamical information to obtain information about the tangential component of $\mathbf{v}^{(\sigma)}$, but such information is not required for this chapter. Following equation (57.30), the horizontal projection of the surface area element is given by $dA = |\cos\vartheta| d\mathcal{S}$, where ϑ is the angle between the surface and the horizontal and $dA = dx dy$.

57.4.2 Accounting for movement of the surface

A generalized vertical coordinate surface is generally moving. So to diagnose the net transport of fluid penetrating the surface requires us to subtract the velocity of the surface, $\mathbf{v}^{(\sigma)}$, from the velocity of a fluid particle. We are thus led to

$$\text{RATE THAT FLUID CROSSES A MOVING GVC SURFACE} = \hat{\mathbf{n}} \cdot (\mathbf{v} - \mathbf{v}^{(\sigma)}). \quad (57.20)$$

We next develop a kinematic property of the surface velocity, or more precisely the normal component to that velocity. For that purpose, consider an infinitesimal increment in both space and time under which σ undergoes an infinitesimal change

$$\delta\sigma = \delta\mathbf{x} \cdot \nabla\sigma + \delta t \partial_t\sigma. \quad (57.21)$$

Now restrict attention to a point fixed on a constant σ surface, in which

$$\delta\sigma = \delta\mathbf{x}^{(\sigma)} \cdot \nabla\sigma + \delta t \partial_t\sigma = 0, \quad (57.22)$$

where $\delta\mathbf{x}^{(\sigma)}$ is a differential increment following the moving surface. We define the velocity of that point as

$$\mathbf{v}^{(\sigma)} = \frac{\delta\mathbf{x}^{(\sigma)}}{\delta t}, \quad (57.23)$$

in which case equation (57.22) implies that at each point within the fluid,

$$\frac{\partial \sigma}{\partial t} + \mathbf{v}^{(\sigma)} \cdot \nabla \sigma = 0. \quad (57.24)$$

We can likewise write this equation as one for the normal component of the surface velocity

$$\mathbf{v}^{(\sigma)} \cdot \hat{\mathbf{n}} = -\frac{1}{|\nabla \sigma|} \frac{\partial \sigma}{\partial t}. \quad (57.25)$$

Hence, we reach the sensible result that the normal component to the velocity of the surface vanishes when the surface is static.

57.4.3 We only care about divergent surface motion

For the kinematics of fluid motion relative to a surface of constant generalized vertical coordinates, we are only concerned with the normal component to the surface velocity, $\mathbf{v}^{(\sigma)} \cdot \hat{\mathbf{n}}$. That is, we are only concerned with divergent motion of the surface, defined as motion parallel to the surface normal direction, $\hat{\mathbf{n}}$. We have no concern for rotational or tangential motion, which is motion perpendicular to $\hat{\mathbf{n}}$. Even so, some authors, by fiat, choose to set to zero the tangential component of the surface motion. In fact, specification of the tangential surface velocity component is generally not available without extra information about the surface motion, nor is its specification necessary for developing kinematic properties of fluid motion relative to arbitrary generalized vertical coordinate surfaces. Hence, we make no statement about tangential motion of the surface.

57.4.4 Cross GVC transport in terms of GVC material evolution

Using expression (57.25) in equation (57.20) leads to the net flux of fluid crossing the GVC surface

$$\hat{\mathbf{n}} \cdot (\mathbf{v} - \mathbf{v}^{(\sigma)}) = \frac{1}{|\nabla \sigma|} \frac{D\sigma}{Dt}. \quad (57.26)$$

The material time derivative of the GVC surface thus vanishes if no fluid crosses the surface. Notably, this result holds for motion of the fluid as defined by the barycentric velocity, \mathbf{v} , of Section 17.1.2. For multi-component fluids, $\dot{\sigma} = 0$ can still, in principle, be associated with trace matter exchange across the surface via diffusion so long as the net matter crossing the surface is zero. But this situation is rather fine tuned and thus unlikely. Additionally, matter diffusion also occurs with heat diffusion, in which case $\dot{\sigma} = 0$ only occurs in the absence of both matter and heat diffusion, which then means that σ is a material surface.

57.4.5 Defining the dia-surface transport

The area normalizing the volume flux in equation (57.26) is the area $d\delta$ of an infinitesimal patch on the surface of constant generalized vertical coordinate with outward unit normal $\hat{\mathbf{n}}$. We now follow the trigonometry discussed in Section 56.17 to introduce the horizontal projection of this area, dA , which is more convenient to work with for many purposes. So long as the vertical

stratification remains non-zero ($\partial\sigma/\partial z \neq 0$) we can write the area factor in the form

$$\frac{d\mathcal{S}}{|\nabla\sigma|} = \frac{d\mathcal{S}}{\sqrt{(\partial\sigma/\partial x)^2 + (\partial\sigma/\partial y)^2 + (\partial\sigma/\partial z)^2}} \quad (57.27a)$$

$$= \frac{d\mathcal{S}}{|\partial\sigma/\partial z| \sqrt{[(\partial\sigma/\partial x)/(\partial\sigma/\partial z)]^2 + [(\partial\sigma/\partial y)/(\partial\sigma/\partial z)]^2 + 1}} \quad (57.27b)$$

$$= \frac{d\mathcal{S}}{|\partial\sigma/\partial z| \sqrt{1 + \tan^2 \vartheta}} \quad (57.27c)$$

$$= \left| \frac{\partial z}{\partial\sigma} \right| |\cos \vartheta| d\mathcal{S} \quad (57.27d)$$

$$= \left| \frac{\partial z}{\partial\sigma} \right| dA. \quad (57.27e)$$

The equality (57.27c) introduced the angle, ϑ , between the boundary surface and the horizontal plane. The squared slope of this surface given by (see Section 56.12)

$$\tan^2 \vartheta = \frac{\nabla_z \sigma \cdot \nabla_z \sigma}{(\partial\sigma/\partial z)^2} = \nabla_\sigma z \cdot \nabla_\sigma z. \quad (57.28)$$

The equality (57.27d) made use of a trigonometric identity so that

$$|\cos \vartheta|^{-1} = |z_\sigma \nabla\sigma|. \quad (57.29)$$

Furthermore, the equality (57.27e) introduced the horizontal projection of the area,

$$dA = |\cos \vartheta| d\mathcal{S}. \quad (57.30)$$

We now introduce the *dia-surface velocity component* for the GVC coordinate

$$w^{(\dot{\sigma})} = \frac{\partial z}{\partial\sigma} \frac{D\sigma}{Dt} = z_\sigma \dot{\sigma}, \quad (57.31)$$

which measures the volume of fluid passing through the surface, per unit horizontal area, per unit time

$$w^{(\dot{\sigma})} \equiv \hat{n} \cdot (\mathbf{v} - \mathbf{v}^{(\sigma)}) \frac{d\mathcal{S}}{dA} \quad (57.32)$$

$$= \frac{(\text{VOLUME/TIME}) \text{ FLUID THROUGH SURFACE}}{\text{HORIZONTAL AREA OF SURFACE}}, \quad (57.33)$$

so that

$$w^{(\dot{\sigma})} dA \equiv \hat{n} \cdot (\mathbf{v} - \mathbf{v}^{(\sigma)}) d\mathcal{S}. \quad (57.34)$$

The velocity component $w^{(\dot{\sigma})}$ is referred to as the dia-surface velocity component since it measures flow rate of fluid through the surface. We can think of $w^{(\dot{\sigma})}$ as the “vertical” velocity which, when multiplied by the horizontal area element, measures the transport of fluid that crosses the surface in the normal direction.

57.4.6 Expressions for the dia-surface velocity component

Making use of various identities derived above, as well as the transformation of partial derivative operators in Section 56.12, allows us to write the dia-surface velocity component in the following equivalent forms

$$w^{(\dot{\sigma})} = \frac{\partial z}{\partial \sigma} \frac{D\sigma}{Dt} \quad (57.35a)$$

$$= \frac{\partial z}{\partial \sigma} |\nabla \sigma| \hat{n} \cdot (\mathbf{v} - \mathbf{v}^{(\sigma)}) \quad (57.35b)$$

$$= \frac{\partial z}{\partial \sigma} \nabla \sigma \cdot \mathbf{v} - \frac{\partial z}{\partial \sigma} |\nabla \sigma| \hat{n} \cdot (\mathbf{v} - \mathbf{v}^{(\sigma)}) \quad (57.35c)$$

$$= (\hat{z} - \nabla_\sigma z) \cdot \mathbf{v} + \frac{\partial z}{\partial \sigma} \frac{\partial \sigma}{\partial t} \quad (57.35d)$$

$$= (\hat{z} - \nabla_\sigma z) \cdot \mathbf{v} - \frac{\partial z}{\partial t} \quad (57.35e)$$

$$= w - (\partial_t + \mathbf{u} \cdot \nabla_\sigma) z, \quad (57.35f)$$

where $\partial z / \partial t = (\partial z / \partial t)_\sigma$ is the time derivative for the depth of the σ surface. We also made use of the identity (see equations (56.34b) and (56.34c))

$$\nabla_\sigma z = -z_\sigma \nabla_z \sigma \quad (57.36)$$

to express the slope of the σ surface as projected onto the horizontal direction plane, as well as the corresponding identity (56.34a) for the time derivative

$$\left[\frac{\partial z}{\partial t} \right]_\sigma = -\frac{[\partial \sigma / \partial t]_z}{[\partial \sigma / \partial z]}. \quad (57.37)$$

The form given by equation (57.35f) directly relates the vertical component to the fluid particle velocity to the dia-surface velocity component

$$w = \frac{Dz}{Dt} \longleftrightarrow w^{(\dot{\sigma})} = \frac{\partial z}{\partial \sigma} \frac{D\sigma}{Dt} = w - (\partial_t + \mathbf{u} \cdot \nabla_\sigma) z. \quad (57.38)$$

When the GVC surface is static, so that it occupies a constant vertical position $\partial z / \partial t = 0$, then the dia-surface velocity component reduces to

$$w^{(\dot{\sigma})} = w - \mathbf{u} \cdot \nabla_\sigma z \quad \text{static surface,} \quad (57.39)$$

whereas if the GVC surface is flat, then the dia-surface velocity component measures the flux of fluid moving vertically relative to the motion of the GVC surface. Finally, if the surface is flat and static, the dia-surface velocity component becomes the vertical velocity component

$$w^{(\dot{\sigma})} = w = \frac{Dz}{Dt} \quad \text{GVC surface static and flat,} \quad (57.40)$$

which is the case for the geopotential vertical coordinate. This relation reveals the kinematic distinction between w and $w^{(\dot{\sigma})}$, with the two differing in the presence of GVC transients and horizontal velocities that project onto a non-horizontal GVC surface. Equation (57.35f) thus offers a useful means to distinguish w from $w^{(\dot{\sigma})}$.

57.4.7 An alternative definition of dia-surface velocity component

In some literature presentations, the dia-surface velocity component is taken to be

$$w^{\text{dia}} = \hat{\mathbf{n}} \cdot (\mathbf{v} - \mathbf{v}^{(\sigma)}) = \frac{1}{|\nabla\sigma|} \frac{D\sigma}{Dt}. \quad (57.41)$$

For example, [Groeskamp et al. \(2019\)](#) prefer this definition for watermass analysis. As seen in Chapter 65, the reason to prefer expression (57.41) for watermass analysis is that we do not wish to assume vertically stable stratification for surfaces of constant σ . Dropping that assumption allows us to consider transformation between arbitrarily oriented elements of seawater, even those that are gravitationally unstable.

57.4.8 Area integrated dia-surface transport for incompressible flows

We close this section by further emphasizing the distinction in time dependent flows between dia-surface transport and flow normal to a surface. For this purpose consider an incompressible flow whereby $\nabla \cdot \mathbf{v} = 0$. Incompressibility means that for any closed surface within the fluid interior, the following identity holds via the divergence theorem

$$0 = \int_{\mathcal{R}} \nabla \cdot \mathbf{v} dV = \oint_{\partial\mathcal{R}} \hat{\mathbf{n}} \cdot \mathbf{v} d\mathcal{S}. \quad (57.42)$$

Notably, only in the case of a static surface do we conclude there is no net flow across the surface (see Exercise 18.4). For surfaces that move, there is generally a nonzero net dia-surface transport. We clarify this rather puzzling statement in the following.

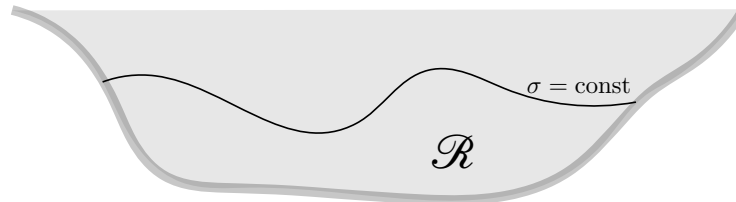


FIGURE 57.4: A constant GVC surface, $\sigma = \text{constant}$, within an ocean basin that intersects the bottom. The region \mathcal{R} is bounded above by the σ surface and below by the solid-earth. Along the constant σ surface an incompressible flow satisfies $\int_{\sigma=\text{const}} \hat{\mathbf{n}} \cdot \mathbf{v} d\mathcal{S} = 0$.

As a specific example, consider a fluid region such as shown in Figure 57.4, which is bounded by the solid-earth bottom and a constant GVC surface. Since the solid-earth bottom is static and there is no-normal flow through the bottom, the identity (57.42) means that the area integrated flow normal to the GVC vanishes

$$\int_{\sigma=\text{const}} \hat{\mathbf{n}} \cdot \mathbf{v} d\mathcal{S} = 0. \quad (57.43)$$

But what does this identity imply about the area integrated dia-surface velocity? For the case of a geopotential vertical coordinate, $\sigma = z$, it means that the area integrated vertical velocity vanishes across any geopotential surface below the ocean free surface, $\int_{z=\text{const}} w dA = 0$ (see Exercise 18.4). What about other GVCs?

To address this question consider the general result

$$\int_{\sigma=\text{const}} \hat{\mathbf{n}} \cdot (\mathbf{v} - \mathbf{v}^{(\sigma)}) d\mathcal{S} = \int_{\sigma=\text{const}} w^{\text{dia}} d\mathcal{S} = \int_{\sigma=\text{const}} w^{(\dot{\sigma})} dA, \quad (57.44)$$

where again $dA = dx dy$. Now make use of the property (57.43) for incompressible flows as well as the identity (57.25) to render

$$\int_{\sigma=\text{const}} w^{(\dot{\sigma})} dA = 0 - \int_{\sigma=\text{const}} \hat{\mathbf{n}} \cdot \mathbf{v}^{(\sigma)} d\mathcal{S} \quad (57.45a)$$

$$= \int_{\sigma=\text{const}} \frac{\partial \sigma / \partial t}{|\nabla \sigma|} d\mathcal{S} \quad (57.45b)$$

$$= \int_{\sigma=\text{const}} \frac{\partial \sigma}{\partial t} \left| \frac{\partial z}{\partial \sigma} \right| dA \quad (57.45c)$$

$$= - \int_{\sigma=\text{const}} \left[\frac{\partial z}{\partial t} \right]_\sigma dA. \quad (57.45d)$$

The final equality holds if $\partial z / \partial \sigma > 0$, whereas we swap signs when the vertical stratification is $\partial z / \partial \sigma < 0$. We can go one further step by noting that the time derivative is computed with σ constant, as is the horizontal area integral. Hence, we can pull the time derivative outside the integral to render

$$\int_{\sigma=\text{const}} w^{(\dot{\sigma})} dA = - \left[\frac{\partial}{\partial t} \right]_\sigma \int_{\sigma=\text{const}} z dA. \quad (57.46)$$

This identity means that for an incompressible flow, the integrated dia-surface transport across the GVC surface equals to minus the time tendency for the area integrated vertical position of that surface. Hence, there is an area integrated dia-surface transport across the GVC surface so long as there is a volume change for the region beneath the surface.

For the case of an isopycnal surface in an adiabatic fluid, there is no change in the volume beneath any interior isopycnal since no flow crosses the isopycnal, in which case we recover the expected result $\int_{\sigma=\text{const}} w^{(\dot{\sigma})} dA = 0$. However, this result does not hold for other coordinates, such as the rescaled vertical coordinate, $\sigma = z^*$ defined by equation (57.112). In this case

$$z^* = H \frac{z - \eta}{H + \eta} \quad (57.47a)$$

$$\frac{\partial z}{\partial z^*} = 1 + H/\eta > 0 \quad (57.47b)$$

$$\left[\frac{\partial z}{\partial t} \right]_{z^*} = \frac{\partial \eta}{\partial t} (1 + z^*/H), \quad (57.47c)$$

so that

$$\int_{z^*=\text{const}} w^{(z^*)} dA = \int_{z^*=\text{const}} (\partial \eta / \partial t) (1 + z^*/H) dA, \quad (57.48)$$

which is generally nonzero. For example, consider a flat bottom so that

$$\int_{z^*=\text{const}} w^{(z^*)} dA = (1 + z^*/H) \int_{z^*=\text{const}} (\partial \eta / \partial t) dA = (1 + z^*/H) \int_{z^*=\text{const}} (Q_m / \rho_0) dA, \quad (57.49)$$

where Q_m is the surface mass flux and we made use of the incompressible free surface equation (18.78). In this case the area integrated dia-surface transport across a z^* surface is proportional to the area integrated surface mass flux.

57.5 Material time derivative

The expression (57.31) for $w^{(\dot{\sigma})}$ brings the material time derivative operator into the following equivalent forms

$$\frac{D}{Dt} = \left[\frac{\partial}{\partial t} \right]_z + \mathbf{u} \cdot \nabla_z + w \frac{\partial}{\partial z} \quad (57.50a)$$

$$= \left[\frac{\partial}{\partial t} \right]_\sigma + \mathbf{u} \cdot \nabla_\sigma + \frac{D\sigma}{Dt} \frac{\partial}{\partial \sigma} \quad (57.50b)$$

$$= \left[\frac{\partial}{\partial t} \right]_\sigma + \mathbf{u} \cdot \nabla_\sigma + w^{(\dot{\sigma})} \frac{\partial}{\partial z}. \quad (57.50c)$$

Note that the chain-rule means that

$$\frac{\partial}{\partial \sigma} = \frac{\partial z}{\partial \sigma} \frac{\partial}{\partial z}, \quad (57.51)$$

thus providing a relationship between the two vertical coordinate partial derivatives. Furthermore, recall that subscripts in the above derivative operators denote variables held fixed when taking the partial derivatives.

We highlight the special case of no fluid particles crossing the generalized coordinate surface. This situation occurs in the case of adiabatic flows with σ equal to the buoyancy or isopycnal coordinate. For adiabatic flow, the material time derivative in equation (57.50c) only has a horizontal two-dimensional advective component, $\mathbf{u} \cdot \nabla_\sigma$. This result should not be interpreted to mean that the fluid particle velocity in an adiabatic flow is strictly horizontal. Indeed, it generally is not, as the form given by equation (57.50a) makes clear. Rather, it means that the advective transport of fluid properties occurs along surfaces of constant buoyancy, and such transport is measured by the convergence of horizontal advective fluxes as measured along these constant buoyancy surfaces.

57.6 Vertical velocity and dia-surface velocity

Making use of the material time derivative operator (57.50c) affords us an opportunity to emphasize both the differences and similarities between the vertical velocity component and the dia-surface velocity component. Namely, the vertical velocity component takes on the equivalent forms

$$w = \frac{Dz}{Dt} = \left[\frac{\partial z}{\partial t} \right]_\sigma + \mathbf{u} \cdot \nabla_\sigma z + w^{(\dot{\sigma})} = \frac{\partial z}{\partial \sigma} \left[-\frac{\partial \sigma}{\partial t} - \mathbf{u} \cdot \nabla_z \sigma + \frac{D\sigma}{Dt} \right], \quad (57.52)$$

and the corresponding expressions for the dia-surface velocity component are given by

$$w^{(\dot{\sigma})} = \frac{\partial z}{\partial \sigma} \frac{D\sigma}{Dt} = \frac{\partial z}{\partial \sigma} \left[\frac{\partial \sigma}{\partial t} + \mathbf{u} \cdot \nabla_z \sigma + w \frac{\partial \sigma}{\partial t} \right] = - \left[\frac{\partial z}{\partial t} \right]_\sigma - \mathbf{u} \cdot \nabla_\sigma z + w. \quad (57.53)$$

Whereas the vertical velocity component, w , measures the transport crossing z surfaces, which are static and horizontal, the dia-surface velocity component, $w^{(\dot{\sigma})}$, measures the transport crossing σ surfaces, which are generally moving and sloped. It is notable that the area normalization used in equation (57.33) for the dia-surface velocity component means that it appears only in the expression for the vertical velocity. However, as we will see in the following, the appearance of $w^{(\dot{\sigma})}$ in the w equation does not necessarily mean that $w^{(\dot{\sigma})}$ corresponds to vertical particle motion. Instead, when it arises from mixing, $w^{(\dot{\sigma})}$ can lead to vertical motion of the σ surface while maintaining a fixed position for the fluid particle.

57.6.1 Decomposing the vertical velocity

The expression

$$w = \left[\frac{\partial z}{\partial t} \right]_{\sigma} + \mathbf{u} \cdot \nabla_{\sigma} z + w^{(\dot{\sigma})} \quad (57.54)$$

decomposes the vertical velocity of a fluid particle into (i) changes to the vertical position of the σ -surface at a particular horizontal point, (ii) lateral particle motion projected onto a sloped σ -surface, (iii) motion that crosses a σ -surface. Importantly, the three terms are coupled. For example, consider the case of σ defined by isopycnals, in which case irreversible mixing ($w^{(\dot{\sigma})} \neq 0$) changes the configuration of σ surfaces by changing both their height, $(\partial z / \partial t)_{\sigma}$, and slope $\nabla_{\sigma} z$.

57.6.2 Another form of the vertical velocity decomposition

Consider the velocity for a point on the surface, $\mathbf{v}^{(\sigma)}$, which satisfies (Section 57.4.2)

$$\frac{\partial \sigma}{\partial t} + \mathbf{v}^{(\sigma)} \cdot \nabla \sigma = 0. \quad (57.55)$$

Making use of the triple product identities from Section 56.5

$$\frac{\partial z}{\partial \sigma} \nabla \sigma = -\nabla_{\sigma} z + \hat{\mathbf{z}} \quad \text{and} \quad \frac{\partial z}{\partial \sigma} \left[\frac{\partial \sigma}{\partial t} \right]_z = - \left[\frac{\partial z}{\partial t} \right]_{\sigma} \quad (57.56)$$

brings equation (57.55) into the form

$$\left[\frac{\partial z}{\partial t} \right]_{\sigma} = (\hat{\mathbf{z}} - \nabla_{\sigma} z) \cdot \mathbf{v}^{(\sigma)} \implies \hat{\mathbf{z}} \cdot \mathbf{v}^{(\sigma)} = \left[\frac{\partial z}{\partial t} \right]_{\sigma} + \mathbf{u}^{(\sigma)} \cdot \nabla_{\sigma} z, \quad (57.57)$$

where $\mathbf{u}^{(\sigma)}$ is the horizontal component to the surface velocity $\mathbf{v}^{(\sigma)}$. This equation shows that the vertical component to the σ -surface velocity is given by the sum of the changes to the vertical position of the surface plus the projection of the horizontal motion of the surface onto the slope of the surface. Additionally, even if the σ -surface has no component of velocity in the vertical, the depth of the σ -surface measured at a horizontal point generally changes if the surface is sloped and moves horizontally pass that point

$$\left[\frac{\partial z}{\partial t} \right]_{\sigma} = -\mathbf{u}^{(\sigma)} \cdot \nabla_{\sigma} z \quad \text{if } \hat{\mathbf{z}} \cdot \mathbf{v}^{(\sigma)} = 0. \quad (57.58)$$

Returning to the general result (57.57) allows us to write

$$\left[\frac{\partial z}{\partial t} \right]_{\sigma} + \mathbf{u} \cdot \nabla_{\sigma} z = \hat{\mathbf{z}} \cdot \mathbf{v}^{(\sigma)} + (\mathbf{u} - \mathbf{u}^{(\sigma)}) \cdot \nabla_{\sigma} z. \quad (57.59)$$

Furthermore, return to the fundamental definition of the dia-surface velocity component detailed in Section 57.4, in which we showed that

$$w^{(\dot{\sigma})} = \frac{\partial z}{\partial \sigma} \frac{D\sigma}{Dt} = \frac{\partial z}{\partial \sigma} \nabla \sigma \cdot (\mathbf{v} - \mathbf{v}^{(\sigma)}) = (-\nabla_{\sigma} z + \hat{\mathbf{z}}) \cdot (\mathbf{v} - \mathbf{v}^{(\sigma)}). \quad (57.60)$$

This expression, along with equation (57.59), leads to the rather elaborate decomposition of the

vertical velocity component according to motion of a generalized vertical coordinate surface

$$w = \underbrace{\left[\hat{z} \cdot \mathbf{v}^{(\sigma)} + (\mathbf{u} - \mathbf{u}^{(\sigma)}) \cdot \nabla_{\sigma} z \right]}_{(\partial_t + \mathbf{u} \cdot \nabla_{\sigma})z} + \underbrace{\left[\hat{z} \cdot \mathbf{v} - \hat{z} \cdot \mathbf{v}^{(\sigma)} - (\mathbf{u} - \mathbf{u}^{(\sigma)}) \cdot \nabla_{\sigma} z \right]}_{w^{(\dot{\sigma})}}. \quad (57.61)$$

Terms in the first bracket compute vertical particle motion relative to the σ -surface. The dia-surface contribution from the second bracket removes the contribution from σ -surface motion to leave just the vertical motion of the particle. All terms on the right hand side cancel, except for $\hat{z} \cdot \mathbf{v} = w$, thus trivially revealing $w = w$. The decomposition of w is rather pedantic when viewed in the unpacked form of equation (57.61). Even so, let us consider some special cases to offer further interpretation.

- NO HORIZONTAL CONTRIBUTION: Consider the case where the horizontal velocity of a fluid particle matches that of the σ -surface: $\mathbf{u} = \mathbf{u}^{(\sigma)}$. Alternatively, consider the case with flat σ -surfaces so that $\nabla_{\sigma} z = 0$. In either case the vertical velocity is given by

$$w = \underbrace{\left[\hat{z} \cdot \mathbf{v}^{(\sigma)} \right]}_{(\partial_t + \mathbf{u} \cdot \nabla_{\sigma})z} + \underbrace{\left[\hat{z} \cdot (\mathbf{v} - \mathbf{v}^{(\sigma)}) \right]}_{w^{(\dot{\sigma})}}. \quad (57.62)$$

The first contribution is from vertical motion of the σ -surface. The second contribution adjusts for the vertical motion of the particle relative to the σ -surface, leaving behind just the vertical motion of the particle. This rather trivial case exemplifies the contributions from the two pieces of the vertical velocity.

- ZERO VERTICAL PARTICLE MOTION: Consider the case where $w = 0$ so that

$$w = 0 \quad (57.63a)$$

$$= \left[\frac{\partial z}{\partial t} \right]_{\sigma} + \mathbf{u} \cdot \nabla_{\sigma} z + w^{(\dot{\sigma})} \quad (57.63b)$$

$$= \underbrace{\left[\hat{z} \cdot \mathbf{v}^{(\sigma)} + (\mathbf{u} - \mathbf{u}^{(\sigma)}) \cdot \nabla_{\sigma} z \right]}_{(\partial_t + \mathbf{u} \cdot \nabla_{\sigma})z} + \underbrace{\left[-\hat{z} \cdot \mathbf{v}^{(\sigma)} - (\mathbf{u} - \mathbf{u}^{(\sigma)}) \cdot \nabla_{\sigma} z \right]}_{w^{(\dot{\sigma})}}. \quad (57.63c)$$

The final expression is trivial since each term in one bracket identically cancels terms in the other bracket. The penultimate expression reveals the balance between dia-surface transport and motion relative to the σ surface

$$-\mathbf{w}^{(\dot{\sigma})} = \left[\frac{\partial z}{\partial t} \right]_{\sigma} + \mathbf{u} \cdot \nabla_{\sigma} z \quad \text{if } w = 0. \quad (57.64)$$

A particularly simple realization of this balance holds for σ given by isopycnals and where the isosurfaces are horizontal. In the presence of uniform mixing, the flat isopycnals stay flat and there is correspondingly no vertical motion of fluid particles even as the vertical stratification is modified. In contrast, the vertical position of an isopycnal surface changes according to the dia-surface velocity component $(\partial z / \partial t)_{\sigma} = -w^{(\dot{\sigma})} \neq 0$. This case illustrates that $w^{(\dot{\sigma})} \neq 0$ can still occur even when there is zero fluid particle motion since $w^{(\dot{\sigma})} \neq 0$ can arise from motion of a σ -surface alone.

57.7 The velocity vector and fluid particle trajectories

Recall from Section 57.6 the alternative forms for the vertical velocity component given by equation (57.52). We focus on the form

$$w = \left[\frac{\partial z}{\partial t} \right]_{\sigma} + \mathbf{u} \cdot \nabla_{\sigma} z + w^{(\dot{\sigma})} \quad (57.65)$$

so that the velocity vector is written¹

$$\mathbf{v} = u \hat{x} + v \hat{y} + w \hat{z} \quad (57.66a)$$

$$= u \hat{x} + v \hat{y} + \left[(\partial z / \partial t)_{\sigma} + \mathbf{u} \cdot \nabla_{\sigma} z + w^{(\dot{\sigma})} \right] \hat{z} \quad (57.66b)$$

$$= u [\hat{x} + \hat{z} (\partial z / \partial x)_{\sigma}] + v [\hat{y} + \hat{z} (\partial z / \partial y)_{\sigma}] + \left[(\partial z / \partial t)_{\sigma} + w^{(\dot{\sigma})} \right] \hat{z}. \quad (57.66c)$$

To help further understand these velocity expressions we consider the following three cases, each of which are illustrated in Figure 57.5.

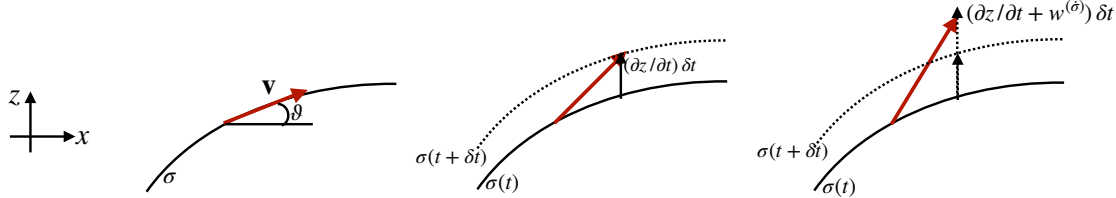


FIGURE 57.5: This schematic shows the various contributions to the fluid particle velocity (red vector) when written relative to motion of a particular generalized vertical coordinate surface. The fluid particle sits at the tail of the velocity vector at time t and at the head at time $t + \delta t$. The left panel is for the case of a static and material σ -surface so that the particle remains on the σ -surface and has a velocity vector given by equation (57.68). The slope of the σ -surface in the \hat{x} -direction is given by $\tan \vartheta = (\partial z / \partial x)_{\sigma}$. The middle panel is for a non-steady material σ -surface whereby the velocity of a particle takes on the form (57.69), with the particle remaining on the moving σ -surface. The right panel shows the case of a non-steady and non-material σ -surface with velocity (57.70). In this final case the particle position departs from the original σ -surface due to the nonzero dia-surface velocity component, $w^{(\dot{\sigma})} \neq 0$. However, it is not known *a priori* whether this departure is due to particle motion or motion of the surface. Notably, the horizontal position of the particle remains identical for each of the three cases. It is only the vertical position that is modified according to the slope of the σ -surface (left panel), motion of the σ -surface (middle panel), and motion crossing the σ -surface (right panel).

- STEADY AND MATERIAL σ -SURFACE: The velocity vector is aligned with the instantaneous σ -surface ($\mathbf{v} \cdot \nabla \sigma = 0$) when the σ -surface is steady ($\partial \sigma / \partial t = 0$) and material ($D\sigma / Dt = 0$). Hence, we can diagnose the vertical velocity component in terms of the horizontal via

$$w \partial \sigma / \partial z = -\mathbf{u} \cdot \nabla_z \sigma \implies w = \mathbf{u} \cdot \nabla_{\sigma} z, \quad (57.67)$$

where we used the triple product identities (56.34b) and (56.34c) for the final equality. The velocity vector thus takes on the form

$$\mathbf{v} = u [\hat{x} + \hat{z} (\partial z / \partial x)_{\sigma}] + v [\hat{y} + \hat{z} (\partial z / \partial y)_{\sigma}] \quad \text{if } \partial \sigma / \partial t = 0 \text{ and } D\sigma / Dt = 0. \quad (57.68)$$

¹As discussed in Section 56.7, we can connect these expressions to the contravariant representation of the velocity vector using GVCs.

In this case, the velocity vector is determined only by the horizontal velocity plus the slope of the σ surface.

- NON-STEADY AND MATERIAL σ -SURFACE: Next consider material σ surfaces ($D\sigma/Dt = 0$) that move ($\partial_t \sigma \neq 0$), in which case the velocity vector is

$$\mathbf{v} = u [\hat{\mathbf{x}} + \hat{\mathbf{z}} (\partial z / \partial x)_\sigma] + v [\hat{\mathbf{y}} + \hat{\mathbf{z}} (\partial z / \partial y)_\sigma] + (\partial z / \partial t)_\sigma \hat{\mathbf{z}} \quad D\sigma/Dt = 0. \quad (57.69)$$

To remain on the moving surface, the fluid particle must move vertically by the extra amount $(\partial z / \partial t)_\sigma \delta t \hat{\mathbf{z}}$ relative to the case of a static σ -surface.

- NON-STEADY AND NON-MATERIAL σ -SURFACE: The general case with a non-material and non-steady σ also requires the dia-surface velocity component, $w^{(\dot{\sigma})}$, which is diagnosed based on the material time derivative of σ and the inverse stratification, $w^{(\dot{\sigma})} = (\partial z / \partial \sigma) D\sigma/Dt$:

$$\mathbf{v} = u [\hat{\mathbf{x}} + \hat{\mathbf{z}} (\partial z / \partial x)_\sigma] + v [\hat{\mathbf{y}} + \hat{\mathbf{z}} (\partial z / \partial y)_\sigma] + [(\partial z / \partial t)_\sigma + w^{(\dot{\sigma})}] \hat{\mathbf{z}}. \quad (57.70)$$

The contribution $w^{(\dot{\sigma})}$ measures the vertical motion of the particle relative to the moving σ -surface. Hence, the sum, $(\partial z / \partial t)_\sigma + w^{(\dot{\sigma})}$, measures the vertical motion of the particle relative to a fixed origin. As emphasized in Section 57.6, a non-zero $w^{(\dot{\sigma})}$ arises from motion of the fluid particle relative to the σ -surface, and this relative motion does not necessarily mean that the particle moves; e.g., recall the example discussed in Section 57.6.2 with a static particle and moving σ -surface.

57.8 Subduction across the mixed layer base

Consider the generalized vertical coordinate defined according to the mixed layer base as in equation (57.3). The dia-surface mass transport across this surface leads us to define the subduction

$$-\mathcal{S}^{(\text{subduction})} \equiv \rho dA \left[\frac{D(z - \eta^{(\text{mld})})}{Dt} \right] \quad \text{at } z = \eta^{(\text{mld})}(x, y, t), \quad (57.71)$$

where the mass transport $\mathcal{S}^{(\text{subduction})}$ (dimensions of mass per time) is positive for fluid moving downward beneath the mixed layer base into the pycnocline (subduction) and negative for water moving into the mixed layer (obduction). The area element dA is the horizontal projection of the area on the mixed layer base. Expanding the material time derivative leads to

$$-\left[\frac{\mathcal{S}^{(\text{subduction})}}{\rho dA} \right] = w - [\partial_t + \mathbf{u} \cdot \nabla] \eta^{(\text{mld})} \quad \text{at } z = \eta^{(\text{mld})}(x, y, t), \quad (57.72)$$

where again we define

$$\mathcal{S}^{(\text{subduction})} > 0 \quad \text{subduction} \quad (57.73)$$

$$\mathcal{S}^{(\text{subduction})} < 0 \quad \text{obduction}. \quad (57.74)$$

We illustrate this definition in Figure 57.6, and note that this definition is consistent with that introduced by [Cushman-Roisin \(1987\)](#).

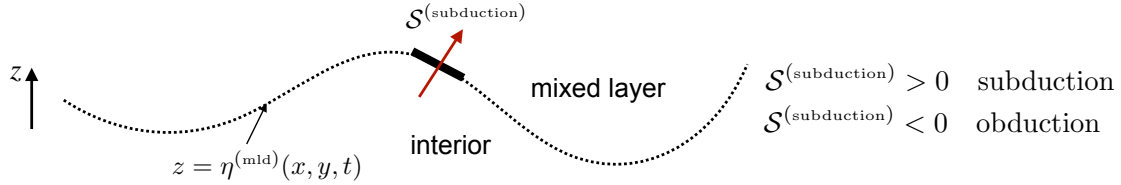


FIGURE 57.6: Illustrating the subduction rate as defined by equation (57.72), which measures the mass transport across the base of the ocean mixed layer. When water enters the ocean interior, $S^{(\text{subduction})} > 0$, and we say that water subducts from the mixed layer to the ocean interior. Conversely, when water enters the mixed layer from below, $S^{(\text{subduction})} < 0$ and we say that water is obducted from the interior to the mixed layer.

57.9 Mass continuity

We here derive the Eulerian expression for mass continuity (16.6) using generalized vertical coordinates. We then specialize to incompressible flows, in which mass conservation is converted to volume conservation. To start, recall that mass conservation for a fluid element states that

$$\rho \delta V = \rho \delta x \delta y \delta z = \rho \delta x \delta y z_\sigma \delta \sigma \quad (57.75)$$

is constant following a fluid element.² To develop the Eulerian expressions we first consider the case of Cartesian coordinates.

57.9.1 Cartesian coordinates

Consider the expression

$$\frac{1}{\rho \delta V} \frac{D(\rho \delta V)}{Dt} = \frac{1}{\rho} \frac{D\rho}{Dt} + \frac{1}{\delta V} \frac{D(\delta V)}{Dt}. \quad (57.76)$$

Now make use of Cartesian coordinates to write the volume

$$\frac{1}{\delta V} \frac{D(\delta V)}{Dt} = \frac{1}{\delta x \delta y \delta z} \frac{D(\delta x \delta y \delta z)}{Dt} \quad (57.77a)$$

$$= \frac{1}{\delta x} \frac{D(\delta x)}{Dt} + \frac{1}{\delta y} \frac{D(\delta y)}{Dt} + \frac{1}{\delta z} \frac{D(\delta z)}{Dt} \quad (57.77b)$$

$$= \frac{\delta u}{\delta x} + \frac{\delta v}{\delta y} + \frac{\delta w}{\delta z} \quad (57.77c)$$

$$= \nabla \cdot \mathbf{v}. \quad (57.77d)$$

Setting $D(\rho \delta V)/Dt = 0$ leads to the familiar expression for the continuity equation

$$\frac{D\rho}{Dt} = -\rho \nabla \cdot \mathbf{v}. \quad (57.78)$$

²Recall that we write δ as an infinitesimal increment following a fluid element.

57.9.2 Generalized vertical coordinates

We follow the above procedure but now with generalized vertical coordinates so that

$$\frac{1}{\delta V} \frac{D(\delta V)}{Dt} = \frac{1}{\delta x \delta y z_\sigma \delta \sigma} \frac{D(\delta x \delta y z_\sigma \delta \sigma)}{Dt} \quad (57.79a)$$

$$= \frac{1}{\delta x} \frac{D(\delta x)}{Dt} + \frac{1}{\delta y} \frac{D(\delta y)}{Dt} + \frac{1}{z_\sigma} \frac{D(z_\sigma)}{Dt} + \frac{1}{\delta \sigma} \frac{D(\delta \sigma)}{Dt} \quad (57.79b)$$

$$= \frac{\delta u}{\delta x} + \frac{\delta v}{\delta y} + \frac{1}{z_\sigma} \frac{D(z_\sigma)}{Dt} + \frac{\delta(\dot{\sigma})}{\delta \sigma} \quad (57.79c)$$

$$= \nabla_\sigma \cdot \mathbf{u} + \frac{1}{z_\sigma} \frac{D(z_\sigma)}{Dt} + \frac{\partial \dot{\sigma}}{\partial \sigma} \quad (57.79d)$$

where we introduced the shorthand $\dot{\sigma} = D\sigma/Dt$. Note that we set

$$\frac{\delta u}{\delta x} + \frac{\delta v}{\delta y} = \nabla_\sigma \cdot \mathbf{u} \quad (57.80)$$

since we are working with generalized vertical coordinates so that we consider infinitesimal displacements occurring on constant σ surfaces. We are thus led to

$$\frac{1}{\rho \delta V} \frac{D(\rho \delta V)}{Dt} = \nabla_\sigma \cdot \mathbf{u} + \frac{1}{z_\sigma} \frac{Dz_\sigma}{Dt} + \frac{\partial \dot{\sigma}}{\partial \sigma} + \frac{1}{\rho} \frac{D\rho}{Dt} = 0. \quad (57.81)$$

Now use the material time derivative in the form (57.50b) to derive the Eulerian expression of mass conservation

$$\frac{\partial(\rho z_\sigma)}{\partial t} + \nabla_\sigma \cdot (\rho z_\sigma \mathbf{u}) + \frac{\partial(\rho z_\sigma \dot{\sigma})}{\partial \sigma} = 0, \quad (57.82)$$

where the time derivative is computed holding σ fixed. We can furthermore introduce the dia-surface velocity component

$$w^{(\dot{\sigma})} = z_\sigma \dot{\sigma} \quad (57.83)$$

so that mass continuity takes the form

$$\frac{\partial(\rho z_\sigma)}{\partial t} + \nabla_\sigma \cdot (\rho z_\sigma \mathbf{u}) + \frac{\partial(\rho w^{(\dot{\sigma})})}{\partial \sigma} = 0. \quad (57.84)$$

Alternatively, we can reintroduce the material time derivative operator to write the mass continuity equation (57.82) in the form

$$\frac{1}{\rho z_\sigma} \frac{D(\rho z_\sigma)}{Dt} = -(\nabla_\sigma \cdot \mathbf{u} + \partial \dot{\sigma} / \partial \sigma), \quad (57.85)$$

where we used equation (57.50b) to write

$$\frac{D}{Dt} = \left[\frac{\partial}{\partial t} \right]_\sigma + \mathbf{u} \cdot \nabla_\sigma + \dot{\sigma} \frac{\partial}{\partial \sigma}. \quad (57.86)$$

57.10 Layer integrated mass continuity

The formulation thus far has been continuous, with the only assumption made that the specific thickness, $h = \partial z / \partial \sigma$, is single signed. We here consider a discrete increment in the generalized

vertical coordinate,

$$\sigma - \delta\sigma/2 \leq \sigma' \leq \sigma + \delta\sigma/2, \quad (57.87)$$

and formulate the mass budget over this layer whose thickness is given by

$$h \equiv \int_{z(\sigma-\delta\sigma/2)}^{z(\sigma+\delta\sigma/2)} dz = \int_{\sigma-\delta\sigma/2}^{\sigma+\delta\sigma/2} \frac{\partial z}{\partial \sigma} d\sigma, \quad (57.88)$$

and whose mass per horizontal area is

$$\delta m = \int_{z(\sigma-\delta\sigma/2)}^{z(\sigma+\delta\sigma/2)} \rho dz = \int_{\sigma-\delta\sigma/2}^{\sigma+\delta\sigma/2} \rho z_\sigma d\sigma = \bar{\rho} h, \quad (57.89)$$

where $\bar{\rho}$ is the layer averaged density. Note that for Boussinesq fluids the mass per area equals to the layer thickness times the reference density

$$\delta m = \rho_0 h \quad \text{Boussinesq.} \quad (57.90)$$

As defined by equation (57.88) and illustrated in Figure 57.2, the thickness of a layer is relatively large in regions where $\partial\sigma/\partial z$ is small; i.e., in regions where σ is weakly stratified in the vertical. Conversely, the layer thickness is relatively small where the vertical stratification is large. Furthermore, if the specific thickness is negative, then the layer thickness remains positive by choosing $\delta\sigma < 0$. For example, in a stably stratified fluid with σ given by potential density, $\partial\sigma/\partial z = -(g/\rho_0) N^2 < 0$ so that we take $\delta\sigma < 0$ to move vertically upward in the water column to regions of lower potential density. The same situation holds when σ is the hydrostatic pressure in which $\partial p/\partial z = -\rho g$ (Section 57.10.2).

The formulation in this section, and its companion for tracers in Section 57.11, holds across all generalized vertical coordinates, even incorporating the trivial case of geopotential coordinates ($\sigma = z$) whereby the specific thickness is unity. Application of the resulting layer integrated kinematics include the development of discrete equations for numerical layered models (see [Griffies et al. \(2020\)](#) for a review), as well as the shallow water models discussed in Part VI of this book.

57.10.1 Compressible fluids

Performing a layer integral of the specific thickness equation (57.84) renders

$$\int_{\sigma-\delta\sigma/2}^{\sigma+\delta\sigma/2} \left[\frac{\partial(\rho z_\sigma)}{\partial t} + \nabla_\sigma \cdot (\rho z_\sigma \mathbf{u}) + \frac{\partial(\rho w^{(\dot{\sigma})})}{\partial \sigma} \right] d\sigma = 0. \quad (57.91)$$

The dia-surface term integrates to a finite difference across the layer

$$\int_{\sigma-\delta\sigma/2}^{\sigma+\delta\sigma/2} \left[\frac{\partial(\rho z_\sigma)}{\partial t} + \nabla_\sigma \cdot (\rho z_\sigma \mathbf{u}) \right] = -\Delta_\sigma(\rho w^{(\dot{\sigma})}), \quad (57.92)$$

where we introduced the dimensionless finite difference operator for properties defined at the layer interface

$$\Delta_\sigma(A) = A(\sigma + \delta\sigma/2) - A(\sigma - \delta\sigma/2). \quad (57.93)$$

The time derivative and horizontal space derivative commute with the layer integral, since the limits are specified fixed values for the layer increment, $\delta\sigma$, and the derivatives are computed with

σ fixed. Hence, layer mass continuity takes the form

$$\left[\frac{\partial}{\partial t} \right]_{\sigma} \int_{\sigma-\delta\sigma/2}^{\sigma+\delta\sigma/2} \rho z_{\sigma} d\sigma + \nabla_{\sigma} \cdot \int_{\sigma-\delta\sigma/2}^{\sigma+\delta\sigma/2} \rho \mathbf{u} z_{\sigma} d\sigma = -\Delta_{\sigma}(\rho w^{(\dot{\sigma})}). \quad (57.94)$$

The first term involves the layer averaged density times the layer thickness as per equation (57.89). The second term involves the layer averaged density-weighted velocity, which is the layer averaged horizontal mass flux

$$\int_{\sigma-\delta\sigma/2}^{\sigma+\delta\sigma/2} \rho \mathbf{u} z_{\sigma} d\sigma = h \bar{\rho} \bar{\mathbf{u}}. \quad (57.95)$$

We are thus led to the layer integrated continuity equation

$$\left[\frac{\partial(h \bar{\rho})}{\partial t} \right]_{\sigma} + \nabla_{\sigma} \cdot (h \bar{\rho} \bar{\mathbf{u}}) + \Delta_{\sigma}(\rho w^{(\dot{\sigma})}) = 0. \quad (57.96)$$

When evolving the fields in a discrete numerical model, we have information only about layer averaged fields. So how do we estimate the depth average of the horizontal advective flux, $\bar{\rho} \bar{\mathbf{u}}$, appearing in equation (57.96)? One method interprets all fields as their layer averaged values so that $\bar{\rho} \bar{\mathbf{u}} = \bar{\rho} \bar{\mathbf{u}}$, thus considering uncomputed sub-layer correlations $\bar{\rho}' \bar{\mathbf{u}'}$ as part of the truncation error. Alternately, we note that compressible hydrostatic flows can be described by a pressure-based vertical coordinate in which case the layer mass per horizontal area is proportional to a prescribed increment in pressure

$$\delta m = \int_{\sigma-\delta\sigma/2}^{\sigma+\delta\sigma/2} \rho z_{\sigma} d\sigma = \bar{\rho} h = -g^{-1} \delta p. \quad (57.97)$$

Correspondingly, the layer integrated horizontal mass flux equals to the mass increment times the pressure-layer averaged velocity

$$\int_{\sigma-\delta\sigma/2}^{\sigma+\delta\sigma/2} \rho \mathbf{u} z_{\sigma} d\sigma = -g^{-1} \int_{p-\delta p/2}^{p+\delta p/2} \mathbf{u} dp = -g^{-1} \bar{\mathbf{u}} \delta p = h \bar{\rho} \bar{\mathbf{u}}. \quad (57.98)$$

With either of the above two methods, we are led to the same layer integrated continuity equation, which we write in the generic form that drops overbars

$$\left[\frac{\partial(h \rho)}{\partial t} \right]_{\sigma} + \nabla_{\sigma} \cdot (h \rho \mathbf{u}) + \Delta_{\sigma}(\rho w^{(\dot{\sigma})}) = 0. \quad (57.99)$$

We illustrate contributions to this layer mass budget in Figure 57.7.

57.10.2 Mass continuity using pressure coordinates

Let us here consider in some detail the special case of pressure coordinates in a hydrostatic fluid, and thus derive mass continuity using these coordinates.

Method I

The thickness of a hydrostatic pressure layer (equation (57.88)) takes on the following form

$$h = \int_{p-\delta p/2}^{p+\delta p/2} \frac{\partial z}{\partial p} dp = - \int_{p-\delta p/2}^{p+\delta p/2} \frac{dp}{\rho g}, \quad (57.100)$$

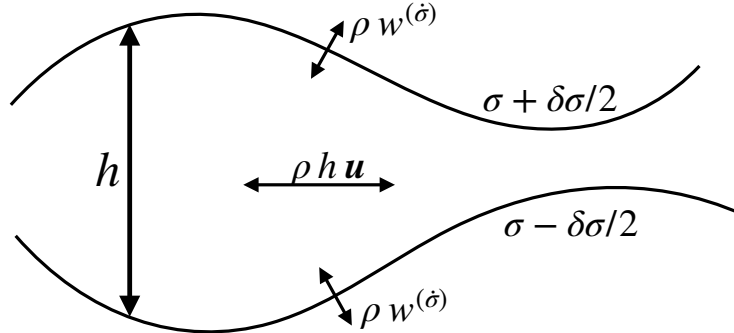


FIGURE 57.7: Illustrating the terms contributing to changes in layer mass according to the layer integrated continuity equation (57.99). The discrete layer is shown here with bounding interfaces at $\sigma - \delta\sigma/2$ and $\sigma + \delta\sigma/2$. Within a layer there is a horizontal redistribution due to horizontal advective transport. Additionally, matter can cross the layer due to dia-surface transport via $w^{(\delta)}$.

so that its mass per unit area is

$$\int_{p-\delta p/2}^{p+\delta p/2} \rho \frac{\partial z}{\partial p} dp = -\delta p/g. \quad (57.101)$$

The mass continuity equation (57.99) thus becomes

$$\frac{\partial(\delta p)}{\partial t} + \nabla_p \cdot (\mathbf{u} \delta p) + \Delta_p (\dot{p}) = 0. \quad (57.102)$$

The partial time derivative vanishes since it is computed by holding pressure fixed so that the pressure increment has a zero time tendency

$$\left[\frac{\partial(\delta p)}{\partial t} \right]_p = 0. \quad (57.103)$$

Likewise, $\nabla_p(\delta p) = 0$. Thus, we can divide by δp to render the continuity equation

$$\nabla_p \cdot \mathbf{u} + \frac{\partial \dot{p}}{\partial p} = 0 \quad \text{compressible hydrostatic.} \quad (57.104)$$

This equation is isomorphic to the incompressible continuity equation (for both hydrostatic and non-hydrostatic fluids) written using geopotential coordinates

$$\nabla_z \cdot \mathbf{u} + \frac{\partial \dot{z}}{\partial z} = \nabla_z \cdot \mathbf{u} + \frac{\partial w}{\partial z} 0 \quad \text{incompressible,} \quad (57.105)$$

where $w = \dot{z}$ is the vertical component to the velocity vector. For both compressible pressure coordinates and incompressible depth coordinates, the continuity equation is a diagnostic relation (i.e., no time derivatives) rather than prognostic (i.e., containing time derivatives).

Method II

For the second method we make use of the approach detailed in Section 57.9.2, which starts from

$$\frac{D(\rho \delta V)}{Dt} = 0. \quad (57.106)$$

In pressure coordinates the volume of the fluid element takes the form

$$\delta V = \delta x \delta y \delta z = \delta x \delta y \left[\frac{\partial z}{\partial p} \right] \delta p = -(\rho g)^{-1} \delta x \delta y \delta p. \quad (57.107)$$

Consequently,

$$0 = \frac{D(\rho \delta V)}{Dt} = g^{-1} \left(\frac{D(\delta x \delta y \delta p)}{Dt} \right), \quad (57.108)$$

so that

$$0 = \frac{1}{\delta x \delta y \delta p} \left(\frac{D(\delta x \delta y \delta p)}{Dt} \right) = \nabla_p \cdot \mathbf{u} + \frac{\partial p}{\partial p}. \quad (57.109)$$

The second step made use of the isomorphism between this result and that for equation (15.74) that holds for a geopotential vertical coordinate.

57.10.3 Incompressible flow

Specializing to an incompressible volume conserving flow (see Chapters 18 and 26) yields the incompressible layer thickness equation

$$\frac{\partial h}{\partial t} + \nabla_\sigma \cdot (h \mathbf{u}) + \Delta_\sigma w^{(\dot{\sigma})} = 0. \quad (57.110)$$

Further specializing to the case of zero dia-surface transport leads to

$$\frac{\partial h}{\partial t} + \nabla_\sigma \cdot (h \mathbf{u}) = 0 \quad \text{no dia-surface transport.} \quad (57.111)$$

This case is commonly studied for adiabatic fluids using isopycnal coordinates, in which isopycnal surfaces are material (Section 59.2).

57.10.4 Rescaled geopotential coordinates

The rescaled geopotential coordinate

$$z^* = \frac{H(z - \eta)}{H + \eta} = \frac{\eta_b(z - \eta)}{\eta_b - \eta} \quad \text{and} \quad \eta_b(x, y) \leq z^* \leq 0, \quad (57.112)$$

is commonly used in Boussinesq ocean models, where $z = \eta(x, y, t)$ is the ocean free surface and $z = \eta_b(x, y) = -H(x, y)$ is the ocean bottom. The thickness of a coordinate layer is given by

$$h = dz = \frac{\partial z}{\partial z^*} dz^* = (1 + \eta/H) dz^* = (1 - \eta/\eta_b) dz^*. \quad (57.113)$$

The depth integrated column thickness and depth integrated coordinate thickness are given by

$$\int_{\eta_b}^{\eta} dz = \eta - \eta_b = \eta + H \quad \text{and} \quad \int_{z^*(\eta_b)}^{z^*(\eta)} dz^* = -\eta_b = H. \quad (57.114)$$

Correspondingly, the depth integrated thickness equation is given by the depth integrated volume budget derived in Section 18.7

$$\frac{\partial \eta}{\partial t} + \nabla \cdot \mathbf{U} + [w_{z^*=0}^{(\dot{\sigma})} - w_{z^*=\eta_b}^{(\dot{\sigma})}] = 0. \quad (57.115)$$

We assume no volume flow through the ocean bottom so that $w_{z^*=\eta_b}^{(\dot{\sigma})} = 0$, whereas

$$-\rho_0 w_{z^*=0}^{(\dot{\sigma})} = Q_m \quad (57.116)$$

is the mass flux crossing the ocean free surface (Section 16.4.3).

57.11 Layer integrated tracer equation

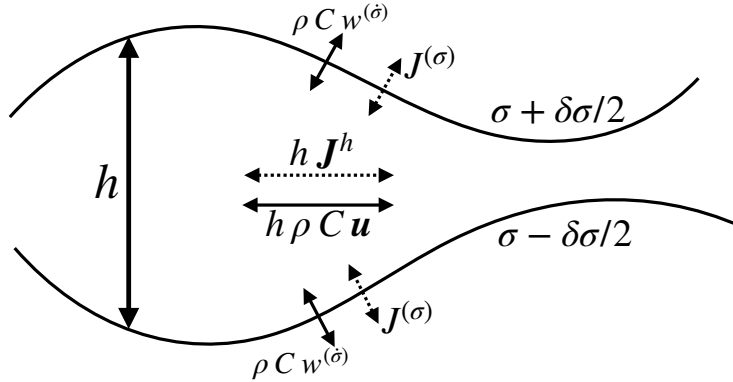


FIGURE 57.8: Illustrating the terms contributing to changes in layer tracer content according to the layer integrated tracer equation (57.121). The layer is shown here with bounding interfaces at $\sigma - \delta\sigma/2$ and $\sigma + \delta\sigma/2$. Within a layer there is a redistribution of tracer due to horizontal advective and subgrid scale tracer fluxes. Additionally, matter can cross the layer due to dia-surface transport via $\rho C w^{(\dot{\sigma})}$ and subgrid tracer transport $J^{(\sigma)}$.

The tracer equation from Section 17.1.3 is given by

$$\rho \frac{DC}{Dt} = -\nabla \cdot \mathbf{J}, \quad (57.117)$$

where \mathbf{J} is a subgrid scale flux. Now introduce the material time derivative operator in the form (57.50b) to have

$$\rho \left[\frac{\partial C}{\partial t} + \mathbf{u} \cdot \nabla_\sigma C + \dot{\sigma} \partial_\sigma C \right] = -\nabla \cdot \mathbf{J}, \quad (57.118)$$

Multiplying by the specific thickness and making use of the mass conservation equation (57.84) renders the flux-form Eulerian equation

$$\frac{\partial(z_\sigma \rho C)}{\partial t} + \nabla_\sigma \cdot (z_\sigma \rho C \mathbf{u}) + \frac{\partial(\rho C w^{(\dot{\sigma})})}{\partial \sigma} = - \left[\nabla_\sigma \cdot (z_\sigma \mathbf{J}^h) + \frac{\partial(z_\sigma \nabla_\sigma \cdot \mathbf{J})}{\partial \sigma} \right], \quad (57.119)$$

where we made use of expression (56.91) for the subgrid scale operator. Now perform a layer integral as detailed in Section 57.10 and use the layer mass continuity equation (57.99) to yield the layer integrated tracer equation

$$\frac{\partial(h \rho C)}{\partial t} + \nabla_\sigma \cdot (h \rho C \mathbf{u}) + \Delta_\sigma(\rho C w^{(\dot{\sigma})}) = - \left[\nabla_\sigma \cdot (h \mathbf{J}^h) + \Delta_\sigma(z_\sigma \nabla_\sigma \cdot \mathbf{J}) \right]. \quad (57.120)$$

Alternatively, we can bring all terms to the left hand side to yield

$$\frac{\partial(h \rho C)}{\partial t} + \nabla_\sigma \cdot (h \rho C \mathbf{u} + h \mathbf{J}^h) + \Delta_\sigma(\rho C w^{(\dot{\sigma})} + J^{(\sigma)}) = 0 \quad (57.121)$$

where we wrote

$$J^{(\sigma)} = z_\sigma \nabla \sigma \cdot \mathbf{J}. \quad (57.122)$$

We illustrate contributions to the layer tracer budget (57.121) in Figure 57.8. Note that we interpret these layer integrated fields and fluxes as per the discussion in Section 57.10.1.



Chapter 58

DYNAMICAL EQUATIONS

In this chapter we derive the dynamical equations for momentum, vorticity, and potential vorticity using generalized vertical coordinates. These equations provide the foundations for many numerical models of the atmosphere and ocean. Besides being essential for developing methods for numerical simulations, understanding the physical and mathematical basis of these equations supports the analysis of simulations.

READER'S GUIDE TO THIS CHAPTER

We assume a working knowledge of the mathematics of generalized vertical coordinates as detailed in Chapter 56 and the corresponding kinematics in Chapter 57. We make particular use of the layer integrated notions introduced for mass continuity and the tracer equations in Sections 57.10 and 57.11. We also make use of the dynamical equations derived in Chapter 21. For most purposes in this chapter we find Cartesian horizontal coordinates sufficient. However, we note some places where spherical coordinates warrant special consideration.

58.1 Equations of motion	1445
58.1.1 Notation	1446
58.1.2 Mass and tracer equations	1446
58.1.3 Momentum equation	1446
58.1.4 Eulerian flux-form horizontal momentum equation	1447
58.1.5 Vector-invariant horizontal momentum equation	1447
58.1.6 Hydrostatic balance with constant gravitational acceleration	1448
58.2 Concerning the pressure force	1449
58.2.1 Computing the horizontal pressure gradient	1449
58.2.2 Integrated pressure force on the cell faces	1450
58.2.3 Net vertical pressure force	1451
58.2.4 Net horizontal pressure force	1451
58.2.5 Comments	1451
58.3 Hydrostatic vorticity and potential vorticity	1452
58.3.1 Basic manipulations	1452
58.3.2 Vorticity and potential vorticity equation	1453
58.3.3 Boussinesq ocean	1454
58.4 Exercise	1454

58.1 Equations of motion

We here derive the equations of motion based on generalized vertical coordinates. The scalar equations were already discussed in Sections 57.9, 57.10, and 57.11, so our main focus concerns

the momentum equation.

58.1.1 Notation

For much of this chapter we focus on the continuous formulation of the generalized vertical coordinates. Following the discussion in Section 57.3, we encounter the specific thickness throughout the equations

$$\hbar = \frac{\partial z}{\partial \sigma} = z_\sigma. \quad (58.1)$$

Using this notation we write the dia-surface transport velocity as

$$w^{(\dot{\sigma})} = \frac{\partial z}{\partial \sigma} \dot{\sigma} = \hbar \dot{\sigma}, \quad (58.2)$$

and the dia-surface advection operator is

$$w^{(\dot{\sigma})} \partial_z = \dot{\sigma} \partial_\sigma. \quad (58.3)$$

58.1.2 Mass and tracer equations

The mass and tracer equations were derived in Sections 57.9, 57.10, and 57.11, with their continuous vertical coordinate formulation given by

$$\frac{\partial(\rho \hbar)}{\partial t} + \nabla_\sigma \cdot (\rho \hbar \mathbf{u}) + \partial_\sigma(\rho \hbar \dot{\sigma}) = 0 \quad (58.4a)$$

$$\frac{\partial(\hbar \rho C)}{\partial t} + \nabla_\sigma \cdot (\hbar \rho C \mathbf{u} + \hbar \mathbf{J}^h) + \partial_\sigma(\rho \hbar \dot{\sigma} C + \hbar \nabla_\sigma \cdot \mathbf{J}) = 0. \quad (58.4b)$$

Compatibility is maintained between the mass continuity equation (58.4a) and the tracer equation (58.4b) so long as the tracer equation reduces to the mass equation upon setting the tracer concentration to a spatial constant. Hence, for compatibility we must have the subgrid fluxes, \mathbf{J} , vanish when the tracer is a spatial constant. For example, diffusive fluxes, which are proportional to the tracer gradient, respect this constraint. These properties originate from our discussion of mass budgets and the barycentric velocity in Section 17.1.

58.1.3 Momentum equation

From Section 23.11, the horizontal and vertical components to the momentum equation are

$$\rho \frac{D\mathbf{u}}{Dt} + 2\rho \boldsymbol{\Omega} \times \mathbf{u} = -\rho \nabla_z \Phi - \nabla_z p + \rho \mathbf{F}^h \quad (58.5a)$$

$$\rho \frac{Dw}{Dt} = -\rho \frac{\partial \Phi}{\partial z} - \frac{\partial p}{\partial z} + \rho F^z. \quad (58.5b)$$

For the simple form of the geopotential, $\Phi = g z$ (Section 11.11), so that the horizontal gradient of the geopotential vanishes

$$\Phi = g z \implies \nabla_z \Phi = 0. \quad (58.6)$$

This gradient is nonzero in the presence of astronomical tide forcing (Chapter 31).

Horizontal momentum equation

We transform the horizontal derivatives from geopotential coordinates to generalized vertical coordinates according to (see equation (56.73))

$$\nabla_z = \nabla_\sigma - (\nabla_\sigma z) \partial_z \quad (58.7)$$

thus leading to the horizontal momentum equation

$$\rho \frac{D\mathbf{u}}{Dt} + 2\rho \boldsymbol{\Omega} \times \mathbf{u} = -\rho [\nabla_\sigma - (\nabla_\sigma z) \partial_z] \Phi - [\nabla_\sigma - (\nabla_\sigma z) \partial_z] p + \rho \mathbf{F}^h. \quad (58.8)$$

In Section 58.1.6 we present some special cases for this equation that simplify the pressure and geopotential terms.

Vertical momentum equation

The vertical momentum equation is transformed into

$$\rho \frac{Dw}{Dt} = -\frac{\partial \sigma}{\partial z} \left[\rho \frac{\partial \Phi}{\partial \sigma} + \frac{\partial p}{\partial \sigma} \right] + \rho F^z, \quad (58.9)$$

with the hydrostatic form given by

$$\frac{\partial p}{\partial \sigma} = -\rho \frac{\partial \Phi}{\partial \sigma}. \quad (58.10)$$

58.1.4 Eulerian flux-form horizontal momentum equation

Using Cartesian horizontal coordinates and generalized vertical coordinates, the horizontal momentum equation includes a contribution from the acceleration that has a form similar to that for a tracer (Section 57.11)

$$\hbar \rho \frac{Du}{Dt} = \left[\frac{\partial(\hbar \rho u)}{\partial t} \right]_\sigma + \nabla_\sigma \cdot (\hbar \rho u \mathbf{u}) + \partial_\sigma(\hbar \rho u \dot{\sigma}) \quad (58.11a)$$

$$\hbar \rho \frac{Dv}{Dt} = \left[\frac{\partial(\hbar \rho v)}{\partial t} \right]_\sigma + \nabla_\sigma \cdot (\hbar \rho v \mathbf{u}) + \partial_\sigma(\hbar \rho v \dot{\sigma}). \quad (58.11b)$$

We provide a σ subscript on the time derivative operator to signal that this derivative is taken with σ held fixed. With spherical coordinates there are additional metric terms appearing on the right hand side, as detailed in Section 21.3.1. In particular, there is a metric term that contains the vertical velocity component, $w = Dz/Dt$. The appearance of w is awkward since the vertical velocity is not naturally computed using generalized vertical coordinates. This limitation is overcome through use of the vector-invariant velocity equation derived in Section 58.1.5.

58.1.5 Vector-invariant horizontal momentum equation

As noted in Section 21.3.2, the *vector-invariant* form of the velocity equation eliminates the metric terms that appear in the non-Cartesian flux-form equations. The vector-invariant form is also suited for deriving the vorticity equation (see Section 58.3). Here, we start with the material time derivative in the form (57.50c) appropriate for generalized vertical coordinates, in which case the

horizontal acceleration is given by

$$\frac{D\mathbf{u}}{Dt} = \left[\frac{\partial \mathbf{u}}{\partial t} \right]_\sigma + (\mathbf{u} \cdot \nabla_\sigma) \mathbf{u} + (\dot{\sigma} \partial_\sigma) \mathbf{u}. \quad (58.12)$$

Now make use of the vector identity (see Section 2.3.4)

$$(\mathbf{u} \cdot \nabla_\sigma) \mathbf{u} = \nabla_\sigma K + (\nabla_\sigma \times \mathbf{u}) \times \mathbf{u}, \quad (58.13)$$

where

$$K = \mathbf{u} \cdot \mathbf{u} / 2 \quad (58.14)$$

is the kinetic energy per mass of the horizontal flow. Introducing the GVC version of the relative vorticity (see Section 59.3.1)

$$\tilde{\zeta} \equiv \hat{\mathbf{z}} \cdot (\nabla_\sigma \times \mathbf{u}) = \left[\frac{\partial v}{\partial x} \right]_\sigma - \left[\frac{\partial u}{\partial y} \right]_\sigma \quad (58.15)$$

renders

$$\frac{D\mathbf{u}}{Dt} = \left[\frac{\partial \mathbf{u}}{\partial t} \right]_\sigma + \nabla_\sigma K + \tilde{\zeta} \hat{\mathbf{z}} \times \mathbf{u} + \dot{\sigma} \partial_\sigma \mathbf{u}, \quad (58.16)$$

so that the horizontal momentum equation takes the form

$$\left[\frac{\partial \mathbf{u}}{\partial t} \right]_\sigma + \dot{\sigma} \frac{\partial \mathbf{u}}{\partial \sigma} + (2 \boldsymbol{\Omega} + \hat{\mathbf{z}} \tilde{\zeta}) \times \mathbf{u} = -\nabla_\sigma K - \nabla_z \Phi - (1/\rho) \nabla_z p + \mathbf{F}^h, \quad (58.17)$$

where again $\nabla_z = \nabla_\sigma - (\nabla_\sigma z) \partial_z$ as per equation (58.7). This equation is form-invariant regardless the horizontal coordinates, thus motivating the name *vector-invariant*.¹

58.1.6 Hydrostatic balance with constant gravitational acceleration

There are many special cases that simplify various terms in the momentum equation. For example, when considering a geopotential in the form $\Phi = g z$ (Section 11.11) with g assumed to be a constant effective gravitational acceleration, then the horizontal momentum equation (58.8) becomes

$$\rho \frac{D\mathbf{u}}{Dt} + 2\rho \boldsymbol{\Omega} \times \mathbf{u} = -[\nabla_\sigma - (\nabla_\sigma z) \partial_z] p + \rho \mathbf{F}^h. \quad (58.18)$$

Furthermore, assuming an approximate hydrostatic balance (and corresponding simplification of the Coriolis acceleration as per Section 24.1.3) allows us to write $\partial p / \partial z = -g \rho$ so that

$$\rho \frac{D\mathbf{u}}{Dt} + \rho f \hat{\mathbf{z}} \times \mathbf{u} = -[\nabla_\sigma p + \rho \nabla_\sigma \Phi] + \rho \mathbf{F}^h, \quad (58.19)$$

which also takes on the vector-invariant form

$$\left[\frac{\partial \mathbf{u}}{\partial t} \right]_\sigma + \dot{\sigma} \frac{\partial \mathbf{u}}{\partial \sigma} + (f + \tilde{\zeta}) \hat{\mathbf{z}} \times \mathbf{u} = -\nabla_\sigma(K + \Phi) - (1/\rho) \nabla_\sigma p + \mathbf{F}^h. \quad (58.20)$$

This form is commonly used for hydrostatic models of the ocean and atmosphere, such as discussed in [Griffies et al. \(2020\)](#).

¹See Section 4.4.4 of [Griffies \(2004\)](#) for a detailed derivation using arbitrary horizontal coordinates.

58.2 Concerning the pressure force

As seen in Section 22.2.3, the pressure force acting on a fluid region is given by the integral

$$\mathbf{F}^{\text{pressure}} = - \oint_{\partial\mathcal{R}} p \hat{\mathbf{n}} d\mathcal{S} = - \int_{\mathcal{R}} \nabla p dV, \quad (58.21)$$

where the second equality follows from Gauss's divergence theorem applied to a scalar field (Section 2.7.2). We refer to the right-most expression as the pressure gradient body force, and this expression is the basis for the discussion in Sections 58.1.6 and 58.2.1. In this formulation, the pressure force at a point is oriented down the pressure gradient, so that the net pressure force acting on a region is the volume integral of pressure gradient.

The middle expression in equation (58.21) formulates the pressure force as the area integrated pressure contact force acting on the region boundaries. In this form, the pressure acting on a region is computed as the integral of pressure over the area bounding the region, with the orientation determined by the inward normal at each point on the boundary. Much of this section is concerned with the contact force expression as a basis for computing the pressure force acting on a finite region as shown in Figure 58.2. The contact force perspective was taken by [Lin \(1997\)](#) and [Adcroft et al. \(2008\)](#) in their finite volume approach to computing the pressure force acting on a numerical model grid cell.

58.2.1 Computing the horizontal pressure gradient

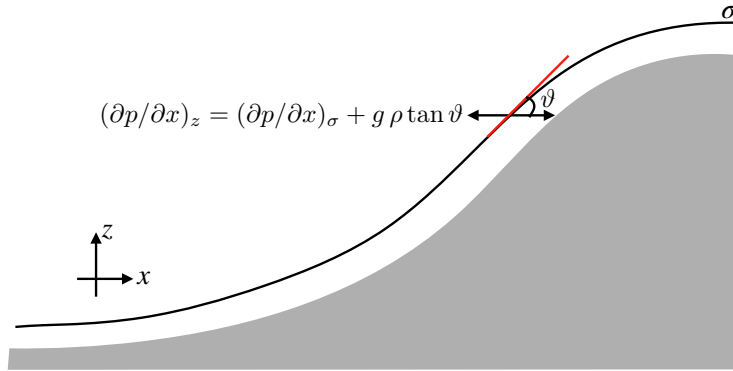


FIGURE 58.1: Illustrating how the horizontal pressure gradient is decomposed into two terms, one aligned with the surface of constant σ , and another associated with the slope of the σ -surface relative to the horizontal, $\tan \vartheta = (\partial z / \partial x)_{\sigma}$. We here consider the decomposition using terrain following vertical coordinates, where the vertical coordinate is aligned according to the solid-earth bottom (shaded region). Specifically, for terrain following ocean models we have $\sigma = (z - \eta) / (-\eta_b + \eta)$, where $z = \eta(x, y, t)$ is the ocean free surface and $z = \eta_b(x, y)$ is the ocean bottom. Terrain-following atmospheric have a similar definition, often using pressure rather than geopotential so that $\sigma = (p - p_a) / (p_b - p_a)$, where p is the pressure, $p_a = p_a(x, y, t)$ is the pressure applied at the top of the atmosphere (often assumed to be zero), and $p_b = p_b(x, y, t)$ is the pressure at the bottom of the atmosphere.

The horizontal pressure gradient is aligned perpendicular to the local gravitational direction. It is generally among the dominant horizontal forces acting on a fluid element. Hence, its accurate representation in numerical models is crucial for the physical integrity of a simulation. Unfortunately, decomposition of the horizontal pressure gradient into two terms according to the transformation (58.7) can lead to numerical difficulties. For example, with a simple geopotential and a hydrostatic fluid, equation (58.19) shows that the horizontal pressure gradient takes the

form

$$\nabla_z p = \nabla_\sigma p + \rho \nabla_\sigma \Phi = \nabla_\sigma p + g \rho \nabla_\sigma z, \quad (58.22)$$

with this decomposition illustrated in Figure 58.1 for the case of terrain following vertical coordinates. Numerical difficulties occur when the two terms on the right hand side have comparable magnitude but distinct signs. We are thus confronted with computing the small difference between two large numbers, and that situation generally exposes a numerical simulation to nontrivial truncation errors. Unfortunately, these errors can corrupt the integrity of the computed pressure forces and in turn contribute to spurious flow. An overview of this issue for ocean models is given by [Haney \(1991\)](#), [Mellor et al. \(1998\)](#), [Griffies et al. \(2000\)](#), with advances offered by [Lin \(1997\)](#), [Shchepetkin and McWilliams \(2002\)](#), and [Adcroft et al. \(2008\)](#). In the remainder of this section, we outline a finite volume method for computing the pressure force as proposed by [Lin \(1997\)](#) for atmospheric models and [Adcroft et al. \(2008\)](#) for ocean models. This approach starts from the middle expression in equation (58.21) for the pressure force; i.e., it formulates the pressure force as the area integral of the pressure contact force rather than the volume integral of the pressure gradient force.

58.2.2 Integrated pressure force on the cell faces

The inward normal on the grid cell vertical side boundaries points in the horizontal direction. For example, on the left side of Figure 58.2 the pressure force acts in the positive \hat{y} direction

$$\mathbf{F}_{\text{left}}^{\text{press}} = \hat{y} \int_{\text{left}} p dx dz \quad (58.23)$$

whereas pressure on the right wall acts in the opposite direction

$$\mathbf{F}_{\text{right}}^{\text{press}} = -\hat{y} \int_{\text{right}} p dx dz. \quad (58.24)$$

Similar expressions appear for the front and back vertical boundaries acting in the \hat{x} direction.

Since the top and bottom boundaries of the grid cell are sloped, there is a pressure force acting on this surface directed in both the horizontal and vertical directions. To unpack the form of this force, write the vertical position of a point on the top interface as $z = \eta(x, y, t)$ so that the outward normal is given by

$$\hat{\mathbf{n}} = \frac{\nabla(z - \eta)}{|\nabla(z - \eta)|} = \frac{\hat{z} - \nabla\eta}{\sqrt{1 + |\nabla\eta|^2}}. \quad (58.25)$$

Following our discussion of dia-surface transport in Section 57.4.5, we know that the product of the normal direction and the area element can be written

$$\hat{\mathbf{n}} d\mathcal{S} = (\hat{z} - \nabla\eta) dA, \quad (58.26)$$

where $dA = dx dy$ is the horizontal projection of the area element (see Figure 57.3). Hence, the net pressure force acting on the top face is given by

$$\mathbf{F}_{\text{top}}^{\text{press}} = -\hat{z} \int_{\text{top}} p dx dy + \hat{x} \int_{\text{top}} p (\partial z / \partial x)_\sigma dx dy + \hat{y} \int_{\text{top}} p (\partial z / \partial y)_\sigma dx dy, \quad (58.27)$$

where we set $z = \eta$ in the second and third terms and placed a σ subscript to emphasize that the horizontal derivative is taken with σ held constant. Notice that the pressure acts in the positive horizontal direction if the top surface slopes upward (surface shoaling) when moving in either of the two horizontal directions. Pressure acting on the bottom face has the same appearance yet

with opposite signs

$$\mathbf{F}_{\text{bott}}^{\text{press}} = \hat{\mathbf{z}} \int_{\text{bott}} p \, dx \, dy - \hat{\mathbf{x}} \int_{\text{bott}} p (\partial z / \partial x)_{\sigma} \, dx \, dy - \hat{\mathbf{y}} \int_{\text{bott}} p (\partial z / \partial y)_{\sigma} \, dx \, dy. \quad (58.28)$$

The pressure acts in the positive horizontal direction if the bottom surface slopes downward (surface deepens) when moving in either of the two horizontal directions. As discussed in Section 22.2.3, the horizontal pressure acting on a sloped surface is known as *form stress*. Here the sloped surface is defined by a constant generalized vertical coordinate.

58.2.3 Net vertical pressure force

Bringing the pieces together leads to the net vertical pressure force acting on the grid cell

$$\mathbf{F}_{\text{vertical}}^{\text{press}} = -\hat{\mathbf{z}} \left[\int_{\text{top}} p \, dx \, dy - \int_{\text{bott}} p \, dx \, dy \right]. \quad (58.29)$$

If the fluid is in hydrostatic balance, then this vertical force is given by the weight of fluid within the cell

$$\mathbf{F}_{\text{vertical}}^{\text{press}} = \hat{\mathbf{z}} M g, \quad (58.30)$$

where M is the mass of fluid in the grid cell. The net vertical hydrostatic pressure force acts vertically upward since hydrostatic pressure at the cell bottom is greater than at the cell top.

58.2.4 Net horizontal pressure force

The net meridional pressure force is given by the forces acting on the sides as well as those acting on the sloped top and bottom boundaries

$$\mathbf{F}_{\text{merid}}^{\text{press}} = \left[\int_{\text{left}} p \, dx \, dz - \int_{\text{right}} p \, dx \, dz \right] + \left[\int_{\text{top}} p (\partial z / \partial y)_{\sigma} \, dx \, dy - \int_{\text{bott}} p (\partial z / \partial y)_{\sigma} \, dx \, dy \right]. \quad (58.31)$$

We can write this expression in a more compact form by orienting our integration in a counter-clockwise manner around the cell boundaries, and making use of the identity $(\partial z / \partial y)_{\sigma} dy = dz$ on the top and bottom faces, so that

$$\mathbf{F}_{\text{merid}}^{\text{press}} = -\oint p \, dx \, dz. \quad (58.32)$$

For some purposes it is more convenient to work with the geopotential, $\Phi = g z$, than the pressure. In this case we can write the meridional pressure force as

$$\mathbf{F}_{\text{merid}}^{\text{press}} = -\oint p \, dx \, dz = -\oint dx [d(p z) - z dp] = g^{-1} \oint \Phi \, dx \, dp, \quad (58.33)$$

where $\oint dx d(p z) = 0$. This form is useful with compressible / non-Boussinesq models, in which pressure is a natural vertical coordinate (e.g., see the caption to Figure 58.1).

58.2.5 Comments

A numerical realization of the integrated contact pressure force requires a representation of pressure along the boundaries of the grid cell. A variety of methods are available with differing accuracies. [Adcroft et al. \(2008\)](#) are notable in proposing an analytic form that allows for an exact integration along the cell faces in special cases, and a highly accurate numerical integration in

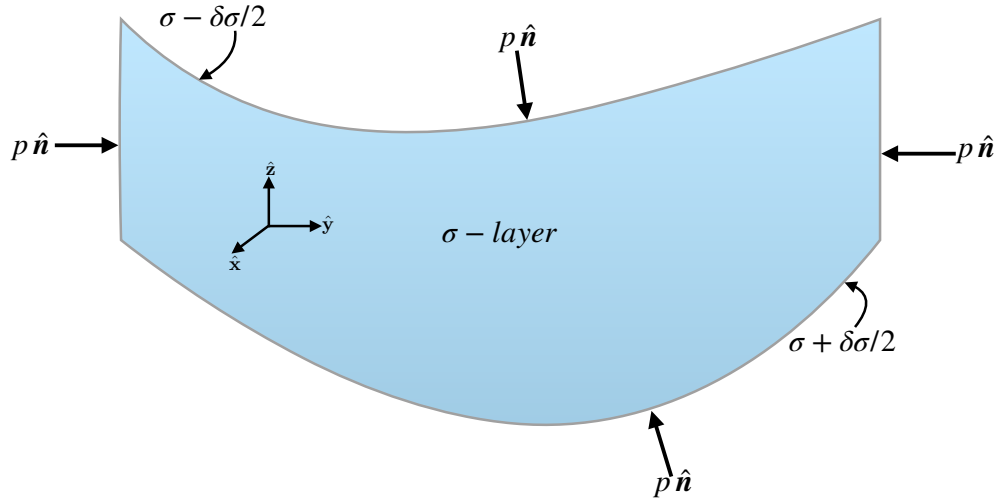


FIGURE 58.2: Schematic of pressure forces acting on the boundaries of a finite region such as a discrete model grid cell. In generalized vertical coordinate models, the side faces are vertical, so that pressure acts only in the horizontal directions. The top and bottom faces are defined by surfaces of constant generalized vertical coordinates with depth $\sigma(x, y, z, t) = \text{constant}$. We assume that these surfaces have an outward normal that has a nonzero projection into the vertical so that we can write the depth of a point on these surfaces as $z = \eta(x, y, t)$. Because of the slope of the top and bottom surfaces, pressure has both a horizontal and vertical component when acting on these surfaces. The net pressure acting on the grid cell is given by the area integral of the pressures around the grid cell boundary.

other cases. In general, this method for computing pressure forces is highly suited to generalized vertical coordinate grid cells, which was the motivation offered by [Lin \(1997\)](#) in the context of terrain following atmospheric models.

58.3 Hydrostatic vorticity and potential vorticity

Generalized vertical coordinates are most commonly used to study hydrostatic fluids. We are thus motivated to develop the equation for the vertical component of vorticity, $\tilde{\zeta}$, in a hydrostatic fluid as written using generalized vertical coordinates.

58.3.1 Basic manipulations

Our starting point is the vector-invariant velocity equation given by equation (58.20)

$$\left[\frac{\partial \mathbf{u}}{\partial t} \right]_\sigma + \dot{\sigma} \frac{\partial \mathbf{u}}{\partial \sigma} + \tilde{\zeta}_a \hat{z} \times \mathbf{u} = -\nabla_\sigma (K + \Phi) - (1/\rho) \nabla_\sigma p + \mathbf{F}^h, \quad (58.34)$$

where $\tilde{\zeta}_a = \tilde{\zeta} + f$ is the absolute vorticity. Taking the curl of this equation and projecting onto the vertical direction leads to

$$\frac{D\tilde{\zeta}_a}{Dt} = -\tilde{\zeta}_a \nabla_\sigma \cdot \mathbf{u} + \frac{\hat{z} \cdot (\nabla_\sigma \rho \times \nabla_\sigma p)}{\rho^2} + \hat{z} \cdot \left[\frac{\partial \mathbf{u}}{\partial \sigma} \times \nabla_\sigma \dot{\sigma} + \nabla_\sigma \times \mathbf{F}^h \right] \quad (58.35)$$

where we noted that the planetary vorticity, f , is independent of time and vertical position.

Making use of the mass conservation equation

Mass conservation in the form of equation (57.85)

$$\frac{1}{\rho h} \frac{D(\rho h)}{Dt} = -(\nabla_\sigma \cdot \mathbf{u} + \partial \dot{\sigma} / \partial \sigma), \quad (58.36)$$

renders

$$\rho h \frac{D}{Dt} \left[\frac{\tilde{\zeta}_a}{\rho h} \right] = \frac{\hat{\mathbf{z}} \cdot (\nabla_\sigma \rho \times \nabla_\sigma p)}{\rho^2} + \tilde{\zeta}_a \frac{\partial \dot{\sigma}}{\partial \sigma} + \hat{\mathbf{z}} \cdot \left[\frac{\partial \mathbf{u}}{\partial \sigma} \times \nabla_\sigma \dot{\sigma} + \nabla_\sigma \times \mathbf{F}^h \right]. \quad (58.37)$$

Massaging the $\dot{\sigma}$ terms

The terms containing $\dot{\sigma}$ can be written in the form

$$\tilde{\zeta}_a \partial_\sigma \dot{\sigma} + \hat{\mathbf{z}} \cdot (\partial_\sigma \mathbf{u} \times \nabla_\sigma \dot{\sigma}) = \tilde{\zeta}_a \partial_\sigma \dot{\sigma} + \hat{\mathbf{z}} \cdot [-\nabla_\sigma \times (\dot{\sigma} \partial_\sigma \mathbf{u}) + \dot{\sigma} \nabla_\sigma \times \partial_\sigma \mathbf{u}] \quad (58.38a)$$

$$= \tilde{\zeta}_a \partial_\sigma \dot{\sigma} + \dot{\sigma} \partial_\sigma \tilde{\zeta}_a - \hat{\mathbf{z}} \cdot [\nabla_\sigma \times (\dot{\sigma} \partial_\sigma \mathbf{u})] \quad (58.38b)$$

$$= \partial_\sigma (\dot{\sigma} \tilde{\zeta}_a) - \hat{\mathbf{z}} \cdot [\nabla_\sigma \times (\dot{\sigma} \partial_\sigma \mathbf{u})]. \quad (58.38c)$$

58.3.2 Vorticity and potential vorticity equation

The above results allow us to write equation (58.37) in the form

$$\rho h \frac{DQ}{Dt} = \frac{\hat{\mathbf{z}} \cdot (\nabla_\sigma \rho \times \nabla_\sigma p)}{\rho^2} + \partial_\sigma (\dot{\sigma} \tilde{\zeta}_a) + \nabla_\sigma \cdot [\hat{\mathbf{z}} \times \dot{\sigma} \partial_\sigma \mathbf{u} - \hat{\mathbf{z}} \times \mathbf{F}^h], \quad (58.39)$$

where we introduced the potential vorticity defined according to the generalized vertical coordinates

$$Q = \frac{\tilde{\zeta}_a}{h \rho}. \quad (58.40)$$

The potential vorticity equation (58.39) has a generally nonzero baroclinicity contribution (see Section 37.4 for more on baroclinicity)

$$\frac{\hat{\mathbf{z}} \cdot (\nabla_\sigma \rho \times \nabla_\sigma p)}{\rho^2} \quad (58.41)$$

so that the potential vorticity (58.40) is generally not materially invariant even for a perfect fluid.

Pressure coordinates

The baroclinicity (58.41) vanishes when choosing $\sigma = p$. We already noted this property in our general discussion of baroclinicity in Section 37.4. This choice, however, does not offer us a materially invariant potential vorticity since $\dot{\sigma} = \dot{p}$ does not generally vanish for a perfect fluid. Namely, a nonzero \dot{p} merely signals vertical motion, so that $\dot{p} \neq 0$ for both real and perfect fluids. Hence, even though the baroclinicity vanishes by choosing $\sigma = p$, the $\partial_\sigma (\dot{\sigma} \tilde{\zeta}_a)$ term does not.

Eulerian flux-form equation

Expanding the material time derivative in equation (58.39) allows us to cancel the $\partial_\sigma (\dot{\sigma} \tilde{\zeta}_a)$ term since it appears on both sides of the equation. We are thus led to the Eulerian flux-form potential

vorticity equation written using generalized vertical coordinates

$$\left[\frac{\partial(\rho h Q)}{\partial t} \right]_\sigma = \frac{\hat{z} \cdot (\nabla_\sigma \rho \times \nabla_\sigma p)}{\rho^2} - \nabla_\sigma \cdot [\rho h \mathbf{u} Q + \hat{z} \times \dot{\sigma} \partial_\sigma \mathbf{u} + \hat{z} \times \mathbf{F}^h], \quad (58.42)$$

which, since $\tilde{\zeta}_a = h \rho Q$, is equivalent to the absolute vorticity equation

$$\left[\frac{\partial \tilde{\zeta}_a}{\partial t} \right]_\sigma = \frac{\hat{z} \cdot (\nabla_\sigma \rho \times \nabla_\sigma p)}{\rho^2} - \nabla_\sigma \cdot [\mathbf{u} \tilde{\zeta}_a + \hat{z} \times \dot{\sigma} \partial_\sigma \mathbf{u} + \hat{z} \times \mathbf{F}^h]. \quad (58.43)$$

As a check, note that setting $\sigma = z$ so that $h = 1$ reduces the vorticity equation (58.43) to the vertical component of the vorticity equation (37.41) (see Exercise 58.1).

58.3.3 Boussinesq ocean

Recall our discussion of vorticity for the Boussinesq ocean in Section 37.7, where we noted that the vertical component to the absolute vorticity is not affected by baroclinicity. We see this property in the present context by returning to the vector-invariant velocity equation (58.34) and setting the factor $1/\rho$ multiplying the pressure gradient to $1/\rho_0$ as part of the Boussinesq ocean

$$(1/\rho) \nabla_\sigma p \longrightarrow (1/\rho_0) \nabla_\sigma p, \quad (58.44)$$

in which ρ_0 is a constant. In this case the $\nabla_\sigma \times$ operation annihilates pressure and we are left with no vertical component to the baroclinicity. We are thus led to define the Boussinesq potential vorticity

$$Q = \frac{\tilde{\zeta}_a}{h} \quad (58.45)$$

which satisfies the material and Eulerian evolution equations

$$h \frac{DQ}{Dt} = \partial_\sigma(\dot{\sigma} \tilde{\zeta}_a) + \nabla_\sigma \cdot [\hat{z} \times \dot{\sigma} \partial_\sigma \mathbf{u} - \hat{z} \times \mathbf{F}^h] \quad (58.46)$$

$$\left[\frac{\partial(h Q)}{\partial t} \right]_\sigma = -\nabla_\sigma \cdot [h \mathbf{u} Q + \hat{z} \times \dot{\sigma} \partial_\sigma \mathbf{u} + \hat{z} \times \mathbf{F}^h]. \quad (58.47)$$

If we choose a vertical coordinate that vanishes when there is no mixing, then this potential vorticity is materially invariant for a perfect fluid. The most common choice for this vertical coordinate is buoyancy or potential density, with the corresponding potential vorticity developed in Sections 59.3 and 59.4.

58.4 Exercise

EXERCISE 58.1: CHECKING THE VORTICITY EQUATION

Verify that for $2\Omega = f\hat{z}$ the choice $\sigma = z$ reduces the vorticity equation (58.43) to the vertical component of the vorticity equation (37.41).



Chapter 59

ISOPYCNAL PRIMITIVE EQUATIONS

For stably stratified fluids, buoyancy is a particularly useful generalized vertical coordinate. Most notably, physical processes away from turbulent boundary layers are oriented according to buoyancy surfaces, and horizontal buoyancy gradients give rise to thermal wind shears in a geostrophically balanced flow. For this reason buoyancy (or entropy) plays a key role in theoretical and numerical models of ocean and atmospheric circulation.

In this chapter we study the hydrostatic Boussinesq equations using buoyancy as the vertical coordinate. The resulting primitive equation set forms the basis for *isopycnal* models of the ocean or isentropic models of the atmosphere. We pay particular attention to the needs of vertically integrating the equations over discrete layers, as required to develop discrete numerical models. In the adiabatic limit, the isopycnal equations reduce to the stacked shallow water equations. After deriving the primitive equations using isopycnal coordinates, we derive the corresponding vorticity and potential vorticity equations. Throughout this chapter we expose details for the practitioner interested in the mathematical formalism for the purpose of analyzing ocean momentum, vorticity and potential vorticity budgets using isopycnal models.

READER'S GUIDE FOR THIS CHAPTER

We assume an understanding of the generalized vertical coordinate mathematics in Chapter 56, kinematics in Chapter 57, and dynamics in Chapter 58. Furthermore, we are concerned with details of vorticity and PV budgets in isopycnal coordinates, with the presentation building from our study of vorticity and potential vorticity in generalized vertical coordinates from Chapter 58.

59.1	Loose threads	1456
59.2	Layered isopycnal primitive equations	1456
59.2.1	Montgomery potential and the pressure force	1457
59.2.2	Material time derivative	1458
59.2.3	Layer thickness and specific thickness	1458
59.2.4	Ocean equations	1460
59.2.5	Thickness weighted velocity equation	1460
59.2.6	Vector-invariant horizontal momentum equation	1460
59.2.7	Connection to the stacked shallow water equations	1461
59.2.8	Diapycnal transfer	1461
59.2.9	Momentum transfer	1462
59.2.10	Allowing for layers to vanish and reappear	1462
59.3	Perfect fluid PV using isopycnal coordinates	1462
59.3.1	Derivation of the vorticity equation	1462
59.3.2	Derivation of the potential vorticity equation	1463

59.3.3	Coordinate transforming vorticity and potential vorticity	1463
59.4	Isopycnal coordinate PV with irreversible processes	1464
59.4.1	Derivation method I	1464
59.4.2	Derivation method II	1466
59.4.3	Comments	1467

59.1 Loose threads

When defining PV using h versus \hbar , it is best to use different symbols to avoid confusion.

59.2 Layered isopycnal primitive equations

Rather than specializing the generalized vertical coordinate equations provided in Section 58.1, we find it pedagogical to start from the equations written using the geopotential vertical coordinate (see Section 26.1.6)

$$\frac{D\mathbf{u}}{Dt} + f \hat{z} \times \mathbf{u} = -\nabla_z \varphi + \mathbf{F} \quad \text{horizontal momentum} \quad (59.1a)$$

$$\frac{\partial \varphi}{\partial z} = b \quad \text{hydrostatic} \quad (59.1b)$$

$$\nabla_z \cdot \mathbf{u} + \frac{\partial w}{\partial z} = 0 \quad \text{continuity} \quad (59.1c)$$

$$\frac{Db}{Dt} = \dot{b} \quad \text{thermodynamics} \quad (59.1d)$$

$$\frac{DC}{Dt} = \dot{C} \quad \text{tracers,} \quad (59.1e)$$

where $\mathbf{v} = (\mathbf{u}, w)$ is the velocity field, \mathbf{u} is its horizontal component, φ is the dynamic pressure, b is the buoyancy, and C is an arbitrary tracer concentration. A discrete realization of the isopycnal layer-integrated form of these equations is depicted in Figure 59.1, with the remainder of this section detailing the formulation using isopycnal coordinates for the vertical.

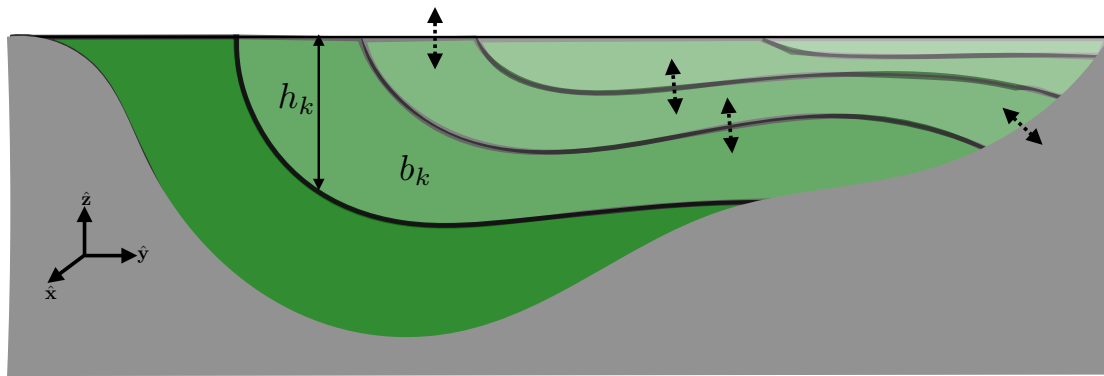


FIGURE 59.1: Schematic of an isopycnal model, formulated as stacked shallow water layers (green layers) that generally allow for the transfer of matter and energy across the layer interfaces as well as across the ocean surface and ocean bottom (as depicted by the double-headed dashed arrows). The dark gray region is land. Discrete layer thicknesses are denoted h_k with corresponding layer buoyancy, b_k .

59.2.1 Montgomery potential and the pressure force

We here consider the horizontal pressure force appearing in isopycnal models, in which we uncover the importance of the Montgomery potential.

Horizontal pressure gradient force

Throughout this chapter we make use of the horizontal derivatives on constant buoyancy surfaces (derived in Section 56.12), written here in the form

$$\nabla_b = \hat{\mathbf{x}} \left[\frac{\partial}{\partial x} \right]_b + \hat{\mathbf{y}} \left[\frac{\partial}{\partial y} \right]_b. \quad (59.2)$$

Following the discussion in Section 58.1.3, the horizontal pressure thus gradient transforms as

$$\nabla_z \varphi = \nabla_b \varphi - \frac{\partial \varphi}{\partial z} \nabla_b z \quad (59.3a)$$

$$= \nabla_b \varphi - b \nabla_b z \quad (59.3b)$$

$$= \nabla_b (\varphi - b z) \quad (59.3c)$$

$$= \nabla_b M, \quad (59.3d)$$

where

$$M = \varphi - b z \quad (59.4)$$

defines the Montgomery potential. As the contribution to the horizontal pressure force, the Montgomery potential is the geostrophic streamfunction in buoyancy coordinates (see Section 59.2.4).

The horizontal pressure gradient force for numerical models

It is notable that the horizontal pressure gradient force is determined by the horizontal isopycnal gradient of a single term, the Montgomery potential. Furthermore, as shown below, the Montgomery potential satisfies the buoyancy coordinate form of the hydrostatic balance. Hence, numerical isopycnal models do not suffer from problems with computing the horizontal pressure gradient that can occur with other generalized vertical coordinate models, such as terrain-following models (see Figure 58.1).

Equation (59.3c) is the key step in the formulation, whereby we made use of $\nabla_b b = 0$. This step is available only under certain cases that utilize an idealized equation of state for seawater. In more realistic cases, the buoyancy determining the hydrostatic pressure (i.e., the *mass buoyancy*) is defined locally whereas the generalized vertical coordinate must be defined globally. As a result, there are two terms contributing to the pressure gradient in a manner similar to terrain-following models. [Sun et al. \(1999\)](#) and [Hallberg \(2005\)](#) discuss this issue in the context of numerical ocean modeling. For present purposes we ignore this detail and continue to assume a simplified equation of state so that $\nabla_b b = 0$.

Hydrostatic balance

Supporting our use of the Montgomery potential as a pressure field, the hydrostatic balance takes the form

$$\frac{\partial M}{\partial b} = \frac{\partial \varphi}{\partial b} - b \frac{\partial z}{\partial b} - z = \frac{\partial \varphi}{\partial z} \frac{\partial z}{\partial b} - b \frac{\partial z}{\partial b} - z = -z, \quad (59.5)$$

where we made use of the hydrostatic balance $\partial\varphi/\partial z = b$ (equation (59.1b)). This result means that M is the buoyancy coordinate version of pressure.

59.2.2 Material time derivative

As seen in Section 57.5, there are two equivalent forms for the material time derivative

$$\frac{D}{Dt} = \left[\frac{\partial}{\partial t} \right]_z + \mathbf{u} \cdot \nabla_z + w \frac{\partial}{\partial z} \quad \text{geopotential form} \quad (59.6a)$$

$$= \left[\frac{\partial}{\partial t} \right]_b + \mathbf{u} \cdot \nabla_b + w^{(b)} \frac{\partial}{\partial z} \quad \text{isopycnal form,} \quad (59.6b)$$

where

$$w^{(b)} = \frac{\partial z}{\partial b} \frac{Db}{Dt} \quad (59.7)$$

is the diapycnal velocity component that measures the rate of flow crossing buoyancy surfaces (Section 57.4). Besides differences in the spatial operators, it is important to note that the time derivative operators in equations (59.6a) and (59.6b) are computed on constant geopotential and constant buoyancy surfaces, respectively. However, the horizontal velocity component is the *same* for both forms of the material time derivative

$$\mathbf{u} = \hat{\mathbf{x}} u + \hat{\mathbf{y}} v = (D/Dt)(\hat{\mathbf{x}} x + \hat{\mathbf{y}} y). \quad (59.8)$$

59.2.3 Layer thickness and specific thickness

The continuity equation, $\nabla_z \cdot \mathbf{u} + \partial_z w = 0$, is an expression of volume conservation. We already derived the generalized vertical coordinate version of this equation in Section 57.10.3, and thus quote the isopycnal layer thickness result here

$$\left[\frac{\partial h}{\partial t} \right]_b + \nabla_b \cdot (h \mathbf{u}) + \Delta_b w^{(b)} = 0. \quad (59.9)$$

The field h measures the isopycnal layer thickness (dimensions of length) and is given by the vertical integral over a layer

$$h = \int_{z(b-\delta b/2)}^{z(b+\delta b/2)} dz = \int_{b-\delta b/2}^{b+\delta b/2} \frac{\partial z}{\partial b} db = \int_{b-\delta b/2}^{b+\delta b/2} \hbar db = \int_{b-\delta b/2}^{b+\delta b/2} N^{-2} db = \bar{\hbar} db. \quad (59.10)$$

The specific thickness, \hbar , equals to the inverse squared buoyancy frequency

$$\hbar = \frac{\partial z}{\partial b} = N^{-2}, \quad (59.11)$$

and its layer averaged value is

$$\bar{\hbar} = h/\delta b. \quad (59.12)$$

Furthermore, the dia-surface transport velocity is given by

$$w^{(b)} = \hbar \dot{b}. \quad (59.13)$$

Its difference across layer interfaces

$$\Delta_b w^{(b)} = \int_{b-\delta b/2}^{b+\delta b/2} \frac{\partial w^{(b)}}{\partial b} db = w^{(b)}(b + \delta b/2) - w^{(b)}(b - \delta b/2) \quad (59.14)$$

measures the amount of fluid that diverges from the layer through cross-layer transport.

In the limit that $\delta b \rightarrow 0$, we find that the non-dimensional vertical difference operator can be written in one of the following equivalent manners

$$\lim_{\delta b \rightarrow 0} \Delta_b = \delta b \frac{\partial}{\partial b} = \delta b \frac{\partial z}{\partial b} \frac{\partial}{\partial z} = \delta z \frac{\partial}{\partial z} = h \frac{\partial}{\partial z}. \quad (59.15)$$

The relations are useful in moving between discrete and continuous formulations of the isopycnal equations.

Specific thickness equation

Inserting $h = \bar{h} \delta b$ into the thickness equation (59.9) leads to

$$\left[\frac{\partial \bar{h}}{\partial t} \right]_b + \nabla_b \cdot (\bar{h} \mathbf{u}) + \partial_b w^{(b)} = 0, \quad (59.16)$$

where we pulled the buoyancy increment, δb , outside of the time and horizontal derivative operators since δb is a fixed number for a chosen layer. We also used the identity (59.15) relating the difference operator to a differential operator

$$\delta b \partial_b = \Delta_b. \quad (59.17)$$

For a vertically continuous treatment, equation (59.16) can be written with h rather than the discrete layer averaged value

$$\left[\frac{\partial h}{\partial t} \right]_b + \nabla_b \cdot (h \mathbf{u}) + \partial_b w^{(b)} = 0. \quad (59.18)$$

It is generally more convenient to use the specific thickness when working with the vertically continuous equations, whereas the finite layer thickness, h , is more suitable for the layer integrated equations.

Adiabatic limit

When $w^{(b)} \neq 0$, the three terms in the thickness equation (59.9) or the specific thickness equation (59.16) are coupled. We discussed this coupling in Section 57.6 as part of our broader study of the vertical velocity and the dia-surface velocity. When considering perfect fluids, we can set $w^{(b)} = h \dot{b} = 0$ since the fluid has no mixing. In this case the layer thickness is altered only through horizontal rearrangements of volume within a layer according to the adiabatic thickness equation

$$\left[\frac{\partial h}{\partial t} \right]_b + \nabla_b \cdot (h \mathbf{u}) = 0. \quad (59.19)$$

As further discussed in Section 59.2.7, the adiabatic limit brings the discrete isopycnal model into accord with the immiscible stacked shallow water models discussed in Part VI of this book.

59.2.4 Ocean equations

Bringing the pieces together leads to the isopycnal version of the hydrostatic Boussinesq equations, which are the basis for numerical isopycnal ocean models

$$\left[\frac{\partial \mathbf{u}}{\partial t} \right]_b + (\mathbf{u} \cdot \nabla_b) \mathbf{u} + (w^{(b)} \partial_z) \mathbf{u} + f \hat{\mathbf{z}} \times \mathbf{u} = -\nabla_b M + \mathbf{F}^h \quad (59.20a)$$

$$\frac{\partial M}{\partial b} = -z \quad (59.20b)$$

$$\left[\frac{\partial h}{\partial t} \right]_b + \nabla_b \cdot (h \mathbf{u}) + \Delta_b w^{(b)} = 0 \quad (59.20c)$$

$$\left[\frac{\partial (h C)}{\partial t} \right]_b + \nabla_b \cdot (h C \mathbf{u} + h \mathbf{J}^h) + \Delta_b (C w^{(b)} + J^{(b)}) = 0, \quad (59.20d)$$

where the tracer equation includes possible subgrid scale flux contributions as well as advective transport. Notice how the advective transport is two-dimensional in the adiabatic case with $\dot{b} = 0$, in which case layer-integrated scalar properties, such as volume and tracer content, are constant within buoyancy layers. Also note that geostrophic balance in the horizontal momentum equation (59.20a) gives

$$f \hat{\mathbf{z}} \times \mathbf{u}_g = -\nabla_b M \implies f u_g = - \left[\frac{\partial M}{\partial y} \right]_b \quad \text{and} \quad f v_g = \left[\frac{\partial M}{\partial x} \right]_b. \quad (59.21)$$

Hence, the Montgomery potential is the streamfunction for geostrophic flow as represented using buoyancy coordinates.

59.2.5 Thickness weighted velocity equation

As in our discussion of the stacked shallow water system in Section 33.3, we can write the velocity equation (59.20a) in its thickness weighted form, with this form suited to studying momentum balances and pressure form stresses. The manipulations are directly analogous to the shallow water case in Section 33.3, whereby we multiply equation (59.20a) by the thickness, h , and multiply the thickness equation (59.20c) by the horizontal velocity, \mathbf{u} , and then summing to find

$$\left[\frac{\partial (h \mathbf{u})}{\partial t} \right]_b + \nabla_b \cdot (h \mathbf{u} \otimes \mathbf{u}) + \Delta_b (w^{(b)} \mathbf{u}) + f \hat{\mathbf{z}} \times (h \mathbf{u}) = -h \nabla_b M + h \mathbf{F}^h. \quad (59.22)$$

For the diapycnal transfer term, we made use of the identity

$$\lim_{\delta b \rightarrow 0} \Delta_b = h \partial_z \quad (59.23)$$

from equation (59.15).

59.2.6 Vector-invariant horizontal momentum equation

It is common for isopycnal models to make use of the vector-invariant form of the momentum equation derived in Section 58.1.5. Introducing the isopycnal version of the relative vorticity

$$\hat{\mathbf{z}} \tilde{\zeta} \equiv \nabla_b \times \mathbf{u} = \left[\frac{\partial v}{\partial x} \right]_b - \left[\frac{\partial u}{\partial y} \right]_b \quad (59.24)$$

renders the vector-invariant horizontal momentum equation

$$\left[\frac{\partial \mathbf{u}}{\partial t} \right]_b + w^{(b)} \partial_z \mathbf{u} + \tilde{\zeta}_a \hat{z} \times \mathbf{u} = -\nabla_b \mathcal{B} + \mathbf{F}^h, \quad (59.25)$$

where

$$\mathcal{B} = M + \mathbf{u} \cdot \mathbf{u}/2 = \varphi - b z + \mathbf{u} \cdot \mathbf{u}/2 \quad (59.26)$$

is the Bernoulli potential for a hydrostatic Boussinesq fluid (see Section 23.7.3), and

$$\tilde{\zeta}_a = \tilde{\zeta} + f \quad (59.27)$$

is the vertical component to the absolute vorticity using isopycnal coordinates. Note that we can further introduce the isopycnal potential vorticity (Section 59.3.2)

$$h Q = \tilde{\zeta}_a \quad (59.28)$$

to bring the momentum equation to the form

$$\left[\frac{\partial \mathbf{u}}{\partial t} \right]_b + w^{(b)} \partial_z \mathbf{u} + Q \hat{z} \times (h \mathbf{u}) = -\nabla_b \mathcal{B} + \mathbf{F}^h. \quad (59.29)$$

This form is commonly used as the starting point for certain theoretical analyses, particularly when considering the adiabatic limit in which $w^{(b)} = 0$.

59.2.7 Connection to the stacked shallow water equations

We can make use of the material time derivative operator (59.6b) to write the material form of the adiabatic and inviscid equations (59.20a)-(59.20c)

$$\frac{D\mathbf{u}}{Dt} + f \hat{z} \times \mathbf{u} = -\nabla_b M \quad (59.30a)$$

$$\frac{\partial M}{\partial b} = -z \quad (59.30b)$$

$$\frac{Dh}{Dt} + h \nabla_b \cdot \mathbf{u} = 0. \quad (59.30c)$$

These isopycnal momentum and thickness equations are isomorphic to those for a single layer of adiabatic shallow water fluid (see Section 32.2). This isomorphism allows us to derive the vorticity and potential vorticity equations in Section 59.3, making use of the shallow water manipulations from Section 36.3.

59.2.8 Diapycnal transfer

At ocean boundaries, the diapycnal term, $w^{(b)}$, accounts for the transfer of matter across the ocean boundaries via precipitation, evaporation, ice melt/form, and river runoff. Notably, this matter transfer also generally gives rise to a transfer of trace matter (tracers), heat (evaporation and precipitation carry a heat content), and momentum (precipitation generally has nonzero momentum). In the ocean interior, $w^{(b)}$ affects the transfer of volume, tracer, and momentum between layers as induced by irreversible processes such as mixing.

59.2.9 Momentum transfer

Pressure form stress mechanically couples isopycnal layers even in the absence of diapycnal matter transfer. We discussed the physics of form stress for the shallow water system in Section 33.4 and more generally in Section 25.1. Furthermore, there are a suite of unresolved processes giving rise to lateral and vertical stresses. Typical ocean model treatments incorporate a turbulent friction in the ocean interior, with lateral stresses acting within a layer and diapycnal stresses acting across isopycnal layer interfaces. A bottom drag is typically applied at the ocean bottom and a turbulent stress applied at the ocean surface. Details for the boundary stresses involve the physics of boundary layer turbulence, which is a topic outside of our scope.

59.2.10 Allowing for layers to vanish and reappear

Isopycnal layers have a transient existence at any particular horizontal position since a layer can incrop at the ocean bottom and outcrop at the ocean surface (see Figure 59.1). The seasonal cycle of warming and cooling is a canonical example of layer outcropping at the surface ocean. A formulational expedient to handle vanishing layers is to assume that all layers exist everywhere horizontally across the ocean domain, but to allow for zero layer thickness where a layer has zero volume. We made use of this approach when discussing available potential energy in Section 26.9. To admit this feature in a discrete model requires a careful realization of L'Hôpital's rule of differential calculus, thus ensuring the discrete model conserves properties in the presence of layers that can appear and disappear at any particular point in the domain.

59.3 Perfect fluid PV using isopycnal coordinates

In Section 38.5, we showed that the absolute vorticity in a Boussinesq hydrostatic fluid with a simplified seawater equation of state (Section 39.3), when projected into the direction normal to constant buoyancy surface, $\omega_a \cdot \nabla b$, is not affected by baroclinicity; i.e., that projection annihilates the baroclinicity vector. From that property we conclude that $\omega_a \cdot \nabla b$ is the potential vorticity for the Boussinesq hydrostatic fluid.

For a Boussinesq hydrostatic fluid, isopycnal coordinates build in the above feature of buoyancy surfaces. Indeed, as shown in Section 58.3.3, the vertical component to baroclinicity vanishes for any generalized vertical coordinate representation of a Boussinesq fluid. Hence, buoyancy coordinates are not special from this perspective. Instead, they are special since in the case of a perfect fluid, the buoyancy based potential vorticity is materially invariant. Deriving this result is one purpose of this section. Note that in Section 58.3, we derived the potential vorticity equation for a hydrostatic fluid represented with generalized vertical coordinates. We could merely specialize that result to the current case. However, we prefer to here work through the maths to help further our experience performing certain of the key manipulations arising with vorticity in rotating and stratified fluids. Hence, consider this section, as well as Section 59.4, to be extended worked exercises.

59.3.1 Derivation of the vorticity equation

Acting with the vertical projection of the curl, $\hat{z} \cdot (\nabla_b \times)$, onto the adiabatic and inviscid form of the vector-invariant velocity equation (59.25) leads to the isopycnal vorticity equation

$$\left[\frac{\partial \tilde{\zeta}_a}{\partial t} \right]_b + (\mathbf{u} \cdot \nabla_b) \tilde{\zeta}_a = -\tilde{\zeta}_a \nabla_b \cdot \mathbf{u} \quad (59.31)$$

where

$$\tilde{\zeta}_a = f + \hat{z} \cdot (\nabla_b \times \mathbf{u}) = f + \tilde{\zeta} \quad (59.32)$$

is the absolute vorticity, written as the planetary vorticity plus the isopycnal relative vorticity. The left hand side of equation (59.31) is the material time derivative of absolute vorticity (see equation (59.6b)), so that we can write

$$\frac{D\tilde{\zeta}_a}{Dt} = -\tilde{\zeta}_a \nabla_b \cdot \mathbf{u}. \quad (59.33)$$

As advertised above, there is no baroclinicity vector on the right hand side of this vorticity equation. Again, that property results from our choice to use isopycnal coordinates.

59.3.2 Derivation of the potential vorticity equation

We now make use of the thickness equation derived in Section 59.2.3, here realized in its material form to eliminate the convergence $\nabla_b \cdot \mathbf{u}$ on the right hand side of equation (59.33), thus leading to

$$\frac{D\tilde{\zeta}_a}{Dt} - \frac{\tilde{\zeta}_a}{h} \frac{Dh}{Dt} = 0. \quad (59.34)$$

Introducing the isopycnal potential vorticity

$$Q = \frac{\tilde{\zeta}_a}{h} = \frac{f + \tilde{\zeta}}{h} \quad (59.35)$$

leads to

$$\frac{DQ}{Dt} = 0. \quad (59.36)$$

Expanding the material time derivative into its components according to equation (59.6b), and making use of the adiabatic form of the thickness equation leads to the Eulerian flux-form equation

$$\left[\frac{\partial(hQ)}{\partial t} \right]_b + \nabla_b \cdot (hQ \mathbf{u}) = 0. \quad (59.37)$$

As noted in Section 59.2.3, when formulating the vertically continuous equations rather than finite thickness layered equations, it is more convenient to make use of the specific thickness, h , rather than the layer thickness, h . In this case we are motivated to define the potential vorticity as

$$Q = \frac{\tilde{\zeta}_a}{h} = \frac{f + \tilde{\zeta}}{h} = (f + \tilde{\zeta}) N^2. \quad (59.38)$$

The corresponding PV equation is identical to equation (59.37), only now with h replaced by h .

59.3.3 Coordinate transforming vorticity and potential vorticity

As just shown, PV for a hydrostatic Boussinesq fluid can be written in the relatively simple form of a shallow water PV when choosing isopycnal coordinates. Here is a direct transformation from

Cartesian to isopycnal coordinates that also reveals this form

$$(\boldsymbol{\omega}^{\text{hy}} + f \hat{\mathbf{z}}) \cdot \nabla b = -\frac{\partial v}{\partial z} \frac{\partial b}{\partial x} + \frac{\partial u}{\partial z} \frac{\partial b}{\partial y} + \left(\frac{\partial v}{\partial x} - \frac{\partial u}{\partial y} + f \right) \frac{\partial b}{\partial z} \quad (59.39a)$$

$$= \frac{\partial b}{\partial z} \left[f + \left(\frac{\partial v}{\partial x} - \frac{\partial v}{\partial z} \frac{\partial b/\partial x}{\partial b/\partial z} \right) - \left(\frac{\partial u}{\partial y} - \frac{\partial u}{\partial z} \frac{\partial b/\partial y}{\partial b/\partial z} \right) \right] \quad (59.39b)$$

$$= \frac{\partial b}{\partial z} \left[f + \left(\frac{\partial v}{\partial x} \right)_b - \left(\frac{\partial u}{\partial y} \right)_b \right] \quad (59.39c)$$

$$= \frac{f + (\partial v/\partial x)_b - (\partial u/\partial y)_b}{\partial z/\partial b} \quad (59.39d)$$

$$= \frac{f + \tilde{\zeta}}{h} \quad (59.39e)$$

$$= Q. \quad (59.39f)$$

59.4 Isopycnal coordinate PV with irreversible processes

In Section 59.3, we considered the PV equation for an adiabatic, inviscid, hydrostatic, Boussinesq fluid using isopycnal vertical coordinates. We here extend to the case of friction in the momentum equation and diabatic heating in the buoyancy equation. We consider two ways to derive the governing equations. One is to convert the non-hydrostatic PV equation in Exercise 38.2 to isopycnal coordinates, after making the hydrostatic approximation. The second is to start from the equations of motion in isopycnal coordinates and derive the vorticity equation and then the PV equation. We make use of the vertically continuous equations, thus warranting our use of specific thickness, h , rather than layer thickness, δz (see Section 59.2.3).

Note that much of this section is a specialization of the more general considerations of Section 58.3. Nonetheless, we here revisit some of the earlier derivations as a means to bolster our mathematical manipulation muscle.

59.4.1 Derivation method I

As derived earlier in this chapter, the equations of motion with diabatic heating and friction, written using isopycnal (or buoyancy) vertical coordinates, take the form

$$\left[\frac{\partial \mathbf{u}}{\partial t} \right]_b + (\mathbf{u} \cdot \nabla_b) \mathbf{u} + b \frac{\partial \mathbf{u}}{\partial b} + \mathbf{f} \times \mathbf{u} = -\nabla_b M + \mathbf{F} \quad (59.40a)$$

$$\frac{\partial M}{\partial b} = -z \quad (59.40b)$$

$$\left[\frac{\partial h}{\partial t} \right]_b + \nabla_b \cdot (h \mathbf{u}) = -\frac{\partial (h \dot{b})}{\partial b} \quad (59.40c)$$

$$\frac{D b}{D t} = \dot{b}. \quad (59.40d)$$

Note that in this section choose to write the dia-surface transport operator in the form

$$w^{(\dot{b})} \partial_z = \dot{b} \partial_b. \quad (59.41)$$

We can make use of the material time derivative operator (59.6b) to write the material form of the equations

$$\frac{D\mathbf{u}}{Dt} + \mathbf{f} \times \mathbf{u} = -\nabla_b M + \mathbf{F} \quad (59.42a)$$

$$\frac{\partial M}{\partial b} = -z \quad (59.42b)$$

$$\frac{Dh}{Dt} + h \nabla_b \cdot \mathbf{u} = -h \frac{\partial \dot{b}}{\partial b}. \quad (59.42c)$$

Curl of the velocity equation

We start taking the curl, $\nabla_b \times$, of the velocity equation (59.40a), thus leading to the isopycnal vorticity equation

$$\left[\frac{\partial \tilde{\zeta}_a}{\partial t} \right]_b + (\mathbf{u} \cdot \nabla_b) \tilde{\zeta}_a + \dot{b} \left[\frac{\partial \tilde{\zeta}_a}{\partial b} \right] = -\tilde{\zeta}_a \nabla_b \cdot \mathbf{u} + \hat{z} \cdot \left[\frac{\partial \mathbf{u}}{\partial b} \times \nabla_b \dot{b} + \nabla_b \times \mathbf{F} \right]. \quad (59.43)$$

The left hand side of equation (59.43) is the material time derivative of absolute vorticity (see equation (59.6b)), so that

$$\frac{D\tilde{\zeta}_a}{Dt} = -\tilde{\zeta}_a \nabla_b \cdot \mathbf{u} + \hat{z} \cdot \left[\frac{\partial \mathbf{u}}{\partial b} \times \nabla_b \dot{b} + \nabla_b \times \mathbf{F} \right]. \quad (59.44)$$

Now make use of the thickness equation in the material form (59.42c) to eliminate the convergence $\nabla_b \cdot \mathbf{u}$ on the right hand side, thus leading to

$$\frac{D\tilde{\zeta}_a}{Dt} - \frac{\tilde{\zeta}_a}{h} \left[\frac{Dh}{Dt} - h \frac{\partial \dot{b}}{\partial b} \right] = \hat{z} \cdot \left[\frac{\partial \mathbf{u}}{\partial b} \times \nabla_b \dot{b} + \nabla_b \times \mathbf{F} \right]. \quad (59.45)$$

Introducing the isopycnal potential vorticity

$$Q = \frac{\tilde{\zeta}_a}{h} = \frac{\tilde{\zeta} + f}{h} \quad (59.46)$$

leads to

$$h \frac{DQ}{Dt} = \zeta_a \frac{\partial \dot{b}}{\partial b} + \hat{z} \cdot \left[\frac{\partial \mathbf{u}}{\partial b} \times \nabla_b \dot{b} + \nabla_b \times \mathbf{F} \right]. \quad (59.47)$$

Massaging the diabatic terms

The diabatic terms can be written

$$\zeta_a \frac{\partial \dot{b}}{\partial b} + \hat{z} \cdot \left[\frac{\partial \mathbf{u}}{\partial b} \times \nabla_b \dot{b} \right] = \zeta_a \frac{\partial \dot{b}}{\partial b} + \dot{b} \frac{\partial \tilde{\zeta}}{\partial b} - \hat{z} \cdot \left[\nabla_b \times \dot{b} \frac{\partial \mathbf{u}}{\partial b} \right] \quad (59.48a)$$

$$= \zeta_a \frac{\partial \dot{b}}{\partial b} + \dot{b} \frac{\partial \tilde{\zeta}_a}{\partial b} - \hat{z} \cdot \left[\nabla_b \times \dot{b} \frac{\partial \mathbf{u}}{\partial b} \right] \quad (59.48b)$$

$$= \frac{\partial(\tilde{\zeta}_a \dot{b})}{\partial b} - \hat{z} \cdot \left[\nabla_b \times \dot{b} \frac{\partial \mathbf{u}}{\partial b} \right] \quad (59.48c)$$

$$= \frac{\partial(\tilde{\zeta}_a \dot{b})}{\partial b} + \nabla_b \cdot \left[\hat{z} \times \dot{b} \frac{\partial \mathbf{u}}{\partial b} \right], \quad (59.48d)$$

where the second equality follows since the Coriolis parameter is independent of the buoyancy.

The PV equation

The PV equation takes the material form

$$\hbar \left[\frac{DQ}{Dt} \right] = \frac{\partial(\tilde{\zeta}_a \dot{b})}{\partial b} + \nabla_b \cdot \left[\hat{z} \times \dot{b} \frac{\partial \mathbf{u}}{\partial b} - \hat{z} \times \mathbf{F} \right]. \quad (59.49)$$

Expanding the material time derivative into its components (59.6b), and making use of the thickness equation (59.40c), leads to the Eulerian flux-form equation

$$\left[\frac{\partial(\hbar Q)}{\partial t} \right]_b + \nabla_b \cdot (\hbar Q \mathbf{u}) + \frac{\partial(\hbar Q \dot{b})}{\partial b} = \frac{\partial(\tilde{\zeta}_a \dot{b})}{\partial b} + \nabla_b \cdot \left[\hat{z} \times \dot{b} \frac{\partial \mathbf{u}}{\partial b} - \hat{z} \times \mathbf{F} \right]. \quad (59.50)$$

Since $\hbar Q = \tilde{\zeta}_a$, the ∂_b terms cancel, thus leaving the flux-form PV equation

$$\left[\frac{\partial(\hbar Q)}{\partial t} \right]_b = -\nabla_b \cdot \left[\hbar Q \mathbf{u} - \hat{z} \times \dot{b} \frac{\partial \mathbf{u}}{\partial b} + \hat{z} \times \mathbf{F} \right]. \quad (59.51)$$

59.4.2 Derivation method II

The alternative method to derive the PV equation in isopycnal coordinates is to start from the hydrostatic Boussinesq PV equation in geopotential vertical coordinates, and directly transform to isopycnal coordinates. For this purpose we start from the discussion in Section 38.5.2 to write the material evolution of PV for a hydrostatic and Boussinesq fluid

$$\frac{DQ}{Dt} = \nabla \cdot \left[(f \hat{z} + \boldsymbol{\omega}_{hy}) \dot{b} + b \nabla \times \mathbf{F} \right], \quad (59.52)$$

where

$$Q = \boldsymbol{\omega}_a^{\text{hy}} \cdot \nabla b = \boldsymbol{\omega}^{\text{hy}} \cdot \nabla b + f \frac{\partial b}{\partial z} \quad \text{and} \quad \boldsymbol{\omega}_{hy} = -\hat{x} \frac{\partial v}{\partial z} + \hat{y} \frac{\partial u}{\partial z} + \hat{z} \left[\frac{\partial v}{\partial x} - \frac{\partial u}{\partial y} \right]. \quad (59.53)$$

The simplest term in equation (59.52) to transform to isopycnal coordinates is the curl of the horizontal friction vector

$$\hat{z} \cdot (\nabla \times \mathbf{F}) = \hat{z} \cdot \nabla \times (F^x, F^y, 0), \quad (59.54)$$

which takes the form

$$\hat{z} \cdot (\nabla \times \mathbf{F}) = h^{-1} \hat{z} \cdot (\nabla_b \times \mathbf{F}) = -h^{-1} \nabla_b \cdot (\hat{z} \times \mathbf{F}). \quad (59.55)$$

The diabatic term requires some more work. Since the vorticity has zero divergence, the diabatic term can be written as

$$\nabla \cdot [(f \hat{z} + \boldsymbol{\omega}_{hy}) \dot{b}] = (f \hat{z} + \boldsymbol{\omega}_{hy}) \cdot \nabla \dot{b} \quad (59.56a)$$

$$= f \frac{\partial \dot{b}}{\partial z} - \frac{\partial v}{\partial z} \frac{\partial \dot{b}}{\partial x} + \frac{\partial u}{\partial z} \frac{\partial \dot{b}}{\partial y} + \left[\frac{\partial v}{\partial x} - \frac{\partial u}{\partial y} \right] \frac{\partial \dot{b}}{\partial z}. \quad (59.56b)$$

We now introduce horizontal derivatives on isopycnal surfaces according to the following relation (see Section 56.12.2)

$$\nabla_z = \nabla_b + \nabla_z b \left[\frac{\partial z}{\partial b} \right] \frac{\partial}{\partial z} \quad (59.57)$$

Doing so leads to

$$\begin{aligned} \nabla \cdot [(f \hat{z} + \boldsymbol{\omega}_{hy}) \dot{b}] &= f \frac{\partial \dot{b}}{\partial z} - \frac{\partial v}{\partial z} \frac{\partial \dot{b}}{\partial x} + \frac{\partial u}{\partial z} \frac{\partial \dot{b}}{\partial y} + \left[\frac{\partial v}{\partial x} - \frac{\partial u}{\partial y} \right] \frac{\partial \dot{b}}{\partial z} \\ &= f \frac{\partial \dot{b}}{\partial z} - \frac{\partial v}{\partial z} \left(\left[\frac{\partial \dot{b}}{\partial x} \right]_b + \left[\frac{\partial b}{\partial x} \right]_z \frac{\partial z}{\partial b} \frac{\partial \dot{b}}{\partial z} \right) + \frac{\partial u}{\partial z} \left(\left[\frac{\partial \dot{b}}{\partial y} \right]_b + \left[\frac{\partial b}{\partial y} \right]_z \frac{\partial z}{\partial b} \frac{\partial \dot{b}}{\partial z} \right) \\ &\quad + \frac{\partial \dot{b}}{\partial z} \left(\left[\frac{\partial v}{\partial x} \right]_b + \left[\frac{\partial b}{\partial x} \right]_z \frac{\partial z}{\partial b} \frac{\partial v}{\partial z} \right) - \frac{\partial \dot{b}}{\partial z} \left(\left[\frac{\partial u}{\partial y} \right]_b + \left[\frac{\partial b}{\partial y} \right]_z \frac{\partial z}{\partial b} \frac{\partial u}{\partial z} \right) \\ &= f \frac{\partial \dot{b}}{\partial z} - \frac{\partial v}{\partial z} \left[\frac{\partial \dot{b}}{\partial x} \right]_b + \frac{\partial u}{\partial z} \left[\frac{\partial \dot{b}}{\partial y} \right]_b + \tilde{\zeta} \left[\frac{\partial \dot{b}}{\partial z} \right] \\ &= \frac{\partial b}{\partial z} \left(\tilde{\zeta}_a \left[\frac{\partial \dot{b}}{\partial b} \right] - \frac{\partial v}{\partial b} \left[\frac{\partial \dot{b}}{\partial x} \right]_b + \frac{\partial u}{\partial b} \left[\frac{\partial \dot{b}}{\partial y} \right]_b \right) \\ &= h^{-1} \left(\tilde{\zeta}_a \left[\frac{\partial \dot{b}}{\partial b} \right] + \hat{z} \cdot \left[\frac{\partial \mathbf{u}}{\partial b} \times \nabla_b \dot{b} \right] \right) \\ &= h^{-1} \left(\tilde{\zeta}_a \left[\frac{\partial \dot{b}}{\partial b} \right] + \dot{b} \left[\frac{\partial \tilde{\zeta}_a}{\partial b} \right] + \nabla_b \cdot \left[\hat{z} \times \dot{b} \frac{\partial \mathbf{u}}{\partial b} \right] \right) \\ &= h^{-1} \left(\frac{\partial(\dot{b} \tilde{\zeta}_a)}{\partial b} + \nabla_b \cdot \left[\hat{z} \times \dot{b} \frac{\partial \mathbf{u}}{\partial b} \right] \right). \end{aligned} \quad (59.58)$$

To reach the penultimate step we noted that $\partial f / \partial b = 0$ so that we could form the derivative of the absolute vorticity. Bringing the pieces together leads to the PV equation (59.49) derived starting from the isopycnal version of the equations of motion.

59.4.3 Comments

The flux-form PV equation (59.51) manifests the impermeability theorem of Chapter 39 since the right hand side is the isopycnal convergence of a flux.



Chapter 60

SHALLOW WATER THICKNESS WEIGHTED AVERAGING

There are a variety of mathematical formalisms used to frame the study of how linear waves, nonlinear waves, eddies, and fully developed turbulence interact with a mean flow. A distinctly geophysical element enters these studies through the primary role of vertical stratification arising from gravitation, with stratification particularly important for large scales flows where motions are approximately hydrostatic. A further specialization to the oceanographic context arises since there are few regions where zonal averages apply, which contrasts to the atmospheric case.¹ The *thickness weighted averaging* (TWA) method has emerged as a useful formalism for stratified flows, with particular use for studies of geostrophic eddies and their parameterization. In this chapter, we develop the TWA equations for the adiabatic stacked shallow water model. Our focus concerns the derivation of the TWA equations as well as their physical interpretation.

As noted in the introduction to Part VI of this book, the adiabatic stacked shallow water model exposes key facets of stratified geophysical flows without requiring the mathematics of generalized vertical coordinates developed in Chapters 56, 57, 58, and 59. The core simplification arises by assuming that horizontal motion has no vertical dependence within each shallow water layer, which then means that vertical motion as well as the hydrostatic pressure are linear functions of vertical position within each layer. That is, the shallow water fluid moves as extensible vertical columns (Section 32.2.8). It follows that horizontal pressure gradients do not need to be projected along the slope of the layer since they are vertically constant within a layer. In contrast, this projection is needed for a continuously stratified fluid described by generalized vertical coordinates, as illustrated in Figure 56.4. Hence, the shallow water equations for momentum, thickness, and tracers retain their use of Cartesian coordinates even though the layer interfaces undulate and are thus not generally horizontal. This mathematical feature of shallow water fluids aids in our pedagogical development of the TWA method.

[Young \(2012\)](#) offers an elegant application of the TWA to the continuously stratified Boussinesq hydrostatic fluid, with this paper the culmination of many years of prior work (see [Young \(2012\)](#) for citations). Penetrating the TWA approach for continuously stratified fluids requires an understanding of generalized vertical coordinates and the attendant tensor analysis such as that developed in Chapters 56, 57, 58, and 59. In the present chapter, we focus on the TWA equations for the adiabatic shallow water model. Doing so minimizes the mathematical requirements while exposing the key physical concepts. It also offers a useful baseline for those using stacked shallow water models for studies of adiabatic waves and geostrophic turbulence. Digesting the material in this chapter, and then coupling to skills in generalized vertical coordinate tensor analysis, prepares one for penetrating [Young \(2012\)](#). Afterward, the mathematically inclined reader may study the work of [Maddison and Marshall \(2013\)](#), who provide a somewhat more general mathematical framework for thickness weighted averaging.

¹The Southern Ocean is a notable ocean exception, as discussed in Sections 25.5 and 33.7.

READER'S GUIDE FOR THIS CHAPTER

In this chapter we assume a working knowledge of the shallow water model presented in Chapters 32, 33, and 36, with particular attention given to the pressure force as realized both as a contact force and a body force (see Chapter 25 and Section 33.4). The TWA equations offer a useful framework for eddy parameterizations, with parameterizations for the tracer equation discussed in Chapters 62 and 63. Parameterizations for both the tracer equation and the momentum equation remain a topic of ongoing research, particularly in the oceanography literature.

60.1	Loose threads	1470
60.2	The unaveraged thickness weighted equations	1471
60.3	Thickness transport by the bolus velocity	1472
60.3.1	Rectified effects	1472
60.3.2	An undulating fluid layer	1472
60.3.3	Stokes drift	1473
60.3.4	Linearized thickness perturbations	1474
60.3.5	Correlation between thickness and velocity	1474
60.3.6	Do we need the bolus velocity?	1475
60.4	Averaging operators	1475
60.4.1	Reynolds average	1475
60.4.2	Ensemble average	1476
60.4.3	Thickness weighted average	1476
60.4.4	Comments	1477
60.5	Thickness equation and tracer equation	1477
60.5.1	TWA thickness equation	1477
60.5.2	Tracer equation	1478
60.5.3	Vertical velocity	1479
60.6	Horizontal momentum equation	1479
60.6.1	Kinetic stress and Reynolds stress	1479
60.6.2	Thickness and pressure gradient correlation	1480
60.6.3	Unpacking the thickness and pressure gradient correlation	1480
60.6.4	Zonal and meridional Eliassen-Palm fluxes: Version I	1483
60.6.5	Zonal and meridional Eliassen-Palm fluxes: Version II	1484
60.6.6	Interfacial stresses from geostrophic eddies	1485
60.6.7	Comments	1486
60.7	Vorticity and potential vorticity	1486
60.7.1	Derivation	1486
60.7.2	Concerning the mean field potential vorticity	1487
60.7.3	Comments	1487
60.8	Vorticity fluxes for non-divergent barotropic flow	1488

60.1 Loose threads

- Build more into the bolus discussion in Section 60.3 as per Section 4.5 of *McWilliams* (2006).
- More discussion of Taylor-Bretherton relation (60.92).
- Write the EP fluxes for quasi-geostrophic shallow water Rossby waves.
- Write the EP fluxes for 2d non-divergent Rossby waves.

- Formulate the TWA energy equations as in Loose et al.
- Is there a gauge that offers good options for parameterization?

60.2 The unaveraged thickness weighted equations

The thickness weighted averaging formalism starts from flux-form evolution equations rather than advective form equations. Applying this approach to the shallow water model means that we focus on the thickness equation (32.78a), the thickness weighted tracer equation (32.78b), and the thickness weighted velocity equation (33.45) (also called the momentum equation)

$$\frac{\partial h_k}{\partial t} + \nabla \cdot (h_k \mathbf{u}_k) = 0 \quad (60.1a)$$

$$\frac{\partial(h_k C)}{\partial t} + \nabla \cdot (h_k \mathbf{u}_k C) = 0 \quad (60.1b)$$

$$\frac{\partial(h_k \mathbf{u}_k)}{\partial t} + \nabla \cdot [h_k \mathbf{u}_k \otimes \mathbf{u}_k] + f \hat{z} \times (h_k \mathbf{u}_k) = -(h_k / \rho_{\text{ref}}) \nabla p_k. \quad (60.1c)$$

The density, ρ_{ref} , appearing in the momentum equation (60.1c) is the Boussinesq reference density, often chosen as the density of the uppermost layer,

$$\rho_{\text{ref}} = \rho_1. \quad (60.2)$$

The thickness and tracer equations do not couple to other layers, and as such we can drop the layer index, $k = 1, N$, when analyzing these equations. For the momentum equation, we expose the interface indices, $k \pm 1/2$, when considering pressure form stresses.

For this chapter, it proves useful to move seamlessly between the thickness weighted pressure gradient body force and its equivalent contact force version studied in Section 33.4. The contact force version of the momentum equation reveals the pressure form stresses acting on the upper and lower interfaces of a shallow water layer. It also brings stresses (kinetic stresses and pressure stresses) together into the divergence of a momentum flux. As such, this formulation follows that of Cauchy as discussed in Section 21.2.3. The eddy correlation portion of the momentum flux is known as the *Eliassen-Palm* flux.²

When the dust settles, the TWA equations are isomorphic to the unaveraged equations (60.1a)-(60.1c), yet with the addition of momentum flux convergences to the right hand sides that arise from subgrid correlations (i.e., convergence of the Eliassen-Palm flux). The momentum eddy fluxes are connected to the potential vorticity fluxes, with the connection known as the *Taylor-Bretherton identity*. The isomorphism provides some motivation to favor the TWA approach since properties of the unaveraged equations are directly reflected in the TWA equations. It also provides a suitable framework for parameterizing the subgrid correlations within the context of flux-form conservation laws. Even so, any formalism for an eddy and mean decomposition is subjective since the mean flow and eddying fluctuations are defined by the analyst not by the physics. Hence, arguments concerning what is a preferable framework are subject to the needs of the analyst and have no physically objective foundation.

²See [Bühler \(2014b\)](#) for a historical perspective on the Eliassen-Palm flux, which was introduced by [Eliassen and Palm \(1960\)](#) in their study of stationary mountain waves.

60.3 Thickness transport by the bolus velocity

Prior to diving into the formalism of thickness weighted averaging, we study the eddy-induced volume transport (more precisely, thickness transport) realized by linear waves within a layer of shallow water fluid. This discussion provides a specific example of the thickness transport by the *bolus velocity*, with further discussion offered in Sections 60.5.1 and 62.5.5. Much of our intuition for bolus transport is based on the following relatively simple example of Stokes drift.³

Part of the motivation for TWA is that we do not need to compute the bolus velocity. Even so, understanding the basic physics of the bolus velocity renders useful insights into how eddies, even eddies as simple as linear waves, can provide a rectified transport of properties. We also comment on this point in Section 33.4.

60.3.1 Rectified effects

Rectification is the conversion of a fluctuating motion into motion in a particular direction. For example, the transformation of an alternating electrical current into a direct electrical current occurs through a rectifier. More generally, rectification arises from the breaking of a symmetry typically through a nonlinear mechanism. The primary example in fluid mechanics is the Stokes drift discussed in Section 45.8 as well as the current section. Stokes drift arises when linear waves have an amplitude that is a function of space, with this spatial dependence giving rise to net particle transport (the Stokes drift) in a preferred direction. Another example concerns the turbulent Stokes drift arising from nonlinear geostrophic waves and eddies in the ocean and atmosphere that lead to a net transport of buoyancy. In Section 33.7 we discuss the meridional transport of buoyancy by eddies in a channel, which is the canonical geophysical example of eddy induced transport.

60.3.2 An undulating fluid layer

Figure 60.1 shows a layer of constant density shallow water fluid within an adiabatic stacked shallow water model. Since the layers are immiscible, the total volume of fluid within this layer remains constant. In its unperturbed state with flat layer interfaces, the meridional velocity in the fluid layer is zero and the thickness is a constant, h_o . When perturbed, the thickness is written

$$h(y, t) = h_o + h'(y, t), \quad (60.3)$$

where we assume the perturbation only depends on (y, t) for simplicity. The layer thickness changes in time according to the convergence of the advective transport of thickness as found by the thickness equation (60.1a)

$$\frac{\partial h}{\partial t} = -\nabla \cdot (h \mathbf{u}), \quad (60.4)$$

where the convergence is computed within the layer and we drop the k layer index for brevity. As seen by Figure 60.1, undulations of the layer thickness at a point arise from the convergence of thickness advected to that point. Further assuming that there is no zonal dependence ($\partial_x = 0$) leads to the one-dimensional thickness equation

$$\frac{\partial h}{\partial t} = -\frac{\partial (h v)}{\partial y}. \quad (60.5)$$

³This example is based Section 2 of [Lee et al. \(1997\)](#).

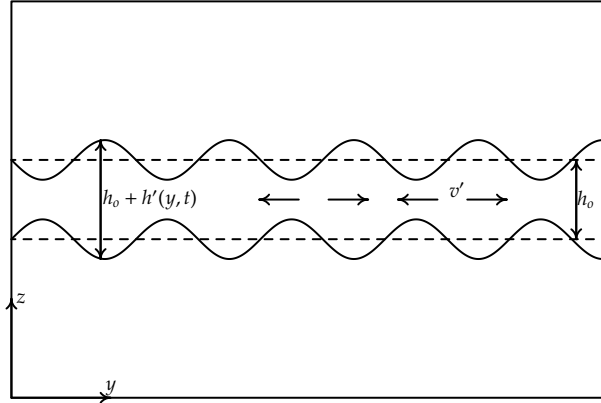


FIGURE 60.1: Shown here is a single layer of constant density fluid, with resting thickness $h = h_o$ and instantaneous thickness $h = h_o + h'(y, t)$. Associated with the undulations in thickness are fluctuations in the meridional velocity $v' = v_o \sin(k y - \omega t)$, depicted here by the alternating vectors within the layer. Vertical-meridional axes are shown in the lower left corner for orientation. We are not concerned with boundaries in the meridional direction.

60.3.3 Stokes drift

Consider a linear wave perturbation in the meridional velocity that propagates in the meridional direction

$$v'(y, t) = v_o \sin(\kappa y - \omega t), \quad (60.6)$$

where κ is a constant wave number and ω is a constant frequency. This longitudinal wave is depicted in Figure 60.1. We now follow the general formalism developed in Section 45.8 (or equivalently in Section 62.3.4) to determine the Stokes drift associated with this wave.

We are only concerned with the meridional component of the velocity, so the fluid particle trajectory equation is given by

$$\frac{dY}{dt} = v_o \sin(\kappa Y - \omega t), \quad (60.7)$$

where $Y = Y(Y_o, t)$ is the meridional trajectory with initial position Y_o . Following equation (45.133) we can write the difference between the velocity following a fluid particle (the Lagrangian velocity for the moving fluid particle) from the velocity at the initial particle point (the Eulerian velocity at the initial point of the trajectory)

$$\frac{dY}{dt} - v(y, t) = v_o^2 \kappa \cos(\kappa y - \omega t) \int_0^t \sin(\kappa y - \omega t') dt' \quad (60.8a)$$

$$= \frac{v_o^2 \kappa}{\omega} [\cos^2(\kappa y - \omega t) - \cos(\kappa y - \omega t) \cos(\kappa y)]. \quad (60.8b)$$

Time averaging over a single wave period,

$$T = 2\pi/\omega \quad (60.9)$$

leads to the Stokes drift as per the general expression in equation (45.135)

$$V_{\text{Stokes}} = \frac{v_o^2 \kappa}{2\omega}. \quad (60.10)$$

Introducing the phase speed for the monochromatic wave,

$$c = \omega/\kappa \quad (60.11)$$

allows us to write the Stokes drift as

$$V_{\text{Stokes}} = \frac{v_o^2}{2c}. \quad (60.12)$$

Notice how the Stokes drift becomes small when the phase speed is large. The reason is that for this case, the fluid particles have only a short time to feel each wave, and thus can only experience a relatively small amount of drift. Correspondingly, there is only a small difference between the Eulerian and Lagrangian velocities. The converse holds for slow phase speeds, where Eulerian and Lagrangian velocities have a relatively large difference.⁴

60.3.4 Linearized thickness perturbations

The velocity and thickness are written in terms of their rest state plus a perturbation due to the wave

$$h = h_o + h' \quad \text{and} \quad v = v', \quad (60.13)$$

where the velocity vanishes when the wave is absent. The thickness equation (60.5) thus takes the form

$$\frac{\partial h'}{\partial t} + h_o \frac{\partial v'}{\partial y} + v' \frac{\partial h'}{\partial y} = 0. \quad (60.14)$$

Linearizing this equation, and using the wave perturbation (60.6), leads to

$$\frac{\partial h'}{\partial t} + h_o v_o \kappa \cos(\kappa y - \omega t) = 0. \quad (60.15)$$

Time integrating this equation, and making use of the velocity perturbation in the form of equation (60.6), renders the thickness perturbation

$$h' = h_o v'/c. \quad (60.16)$$

Hence, to leading order, the thickness perturbation is directly proportional to and in phase with the velocity perturbation.

60.3.5 Correlation between thickness and velocity

Over a single wave period, $T = 2\pi/\omega$, the temporal correlation between the linear thickness perturbation and velocity perturbation is given by

$$\overline{h' v'} = \frac{1}{T} \int_0^T h' v' dt \quad (60.17a)$$

$$= \frac{h_o}{c T} \int_0^T v' v' dt \quad (60.17b)$$

$$= \frac{v_o^2 h_o}{c T} \int_0^T \sin^2(\kappa y - \omega t) dt \quad (60.17c)$$

$$= \frac{v_o^2 h_o}{2c} \quad (60.17d)$$

$$= h_o V_{\text{Stokes}}, \quad (60.17e)$$

where we introduced the Stokes drift (60.12) to reach the final equality. A nonzero correlation $\overline{h' v'}$ means that the thickness has a nonzero tendency when averaged over a wave period.

⁴If we were to consider a formal asymptotic expansion, then the case of relatively slow phase speeds would require us to keep more terms in the expansion than those carried here.

The nonzero correlation in equation (60.17e) induces a thickness transport from the one-dimensional linear longitudinal waves. This transport arises from the Stokes drift induced by the waves; without Stokes drift there is no eddy thickness transport. This behavior exemplifies the case for more general waves and nonlinear eddies moving through fluid layers. For the general case, a nonzero bolus velocity (Section 60.5.1), as determined by velocity-thickness correlations, induces an eddy thickness transport. We see that for the one-dimensional linear longitudinal wave example, the bolus velocity is the Stokes velocity, thus prompting certain authors to make the equality in general.

60.3.6 Do we need the bolus velocity?

The bolus transport is of fundamental importance for how we think about eddy induced Stokes transport from shallow water waves. More general fluctuations, such as those from turbulent geostrophic eddies, require a parameterization to determine the thickness transport. We consider such in Section 28.6 when studying geostrophic eddies in a zonally reentrant channel. As we see in the remainder of the current chapter, the allure of the thickness weighted averaging formalism is that it dispenses with the need to parameterize the bolus velocity. Instead, the TWA equations absorb the bolus transport into the residual mean advection operator. Operationally, the TWA exposes the eddy correlation terms only in the momentum equation, leaving the TWA thickness and TWA tracer equations in a form directly parallel to the unaveraged equations.

60.4 Averaging operators

There are many averaging operators used in fluid mechanics, such as the wave average from Section 60.3, which is useful when the flow is dominantly linear waves; a long time average (formally an infinitely long time average), which is commonly used for climate studies; a space average, which is appropriate when the spatial sampling is coarse; general space filters or kernels, which are commonly used in large eddy simulations; and ensemble averages, which are generally assumed in traditional studies of turbulence. In the following, we denote the averaging or mean operator by an overbar

$$\text{average}(\Phi) = \overline{\Phi}, \quad (60.18)$$

where Φ is any field such as velocity, thickness, or tracer concentration. Deviations (also called fluctuations) from the mean are denoted by a prime so that the full field is decomposed into a mean and eddy term according to

$$\Phi = \overline{\Phi} + \Phi'. \quad (60.19)$$

Since the equations of fluid mechanics are nonlinear, this decomposition into eddy and mean leads to nonlinear eddy correlation terms, which are the source of both the richness and complexity of eddying fluid flows.

60.4.1 Reynolds average

A *Reynolds average* is an operator that annihilates its corresponding fluctuating quantity, which then means that the average of an average is the identity operator

$$\overline{\Phi'} = 0 \iff \overline{\overline{\Phi}} = \overline{\Phi}, \quad (60.20)$$

which in turn means that

$$\overline{\Phi \Psi} = \overline{(\overline{\Phi} + \Phi') \Psi} = \overline{\Phi} \overline{\Psi}. \quad (60.21)$$

Reynolds averages are commonly used when deriving mean field equations. Even so, the assumptions of Reynolds averaging operators are not satisfied by many operators in practice. Extra technical issues arise when averaging operators do not satisfy the properties of a Reynolds average, with these issues beyond our aims in the present chapter. Hence, in this chapter we retain the Reynolds average assumption (60.20) for the averaging operator.

60.4.2 Ensemble average

A further assumption we make is that the average operator commutes with space and time derivatives as well as integrals. This assumption does not strictly hold if the operator is a space and/or time average operator, at least not without a bit of work. However, this assumption holds for ensemble averages. An *ensemble average* is computed over an infinite number of realizations of the fluid flow, with approximations to this average afforded by finite sized ensembles.

Ensemble averages are typically assumed in traditional fluid turbulence studies. However, they are not always very practical nor are they the obvious choice when targeting a framework for parameterization. Even so, we prefer ensemble averages for this chapter in order to dispense with concerns about commutation of the averaging operator with derivative and integral operators. We also make use of ensemble averaging for our discussion of tracer kinematics in Chapter 62.

60.4.3 Thickness weighted average

The thickness weighted average of a field is defined as the ensemble average of the thickness weighted field, and then divided by the averaged thickness:

$$\widehat{\Phi} \equiv \frac{\overline{h\Phi}}{\overline{h}} \iff \overline{h}\widehat{\Phi} = \overline{h\Phi}, \quad (60.22)$$

with widehats adorning a thickness weighted average. Deviations from the thickness weighted average are denoted with two primes so that the unaveraged field is decomposed into its average plus fluctuation

$$\Phi = \widehat{\Phi} + \Phi''. \quad (60.23)$$

Since the overline average from Section 60.4.1 satisfies the Reynolds averaging assumption, so too does the thickness weighted average

$$\Phi = \widehat{\Phi} + \Phi'' \implies \widehat{\Phi''} = \frac{\overline{h\Phi''}}{\overline{h}} = 0. \quad (60.24)$$

We are thus able to derive the following related identities

$$\Phi\Psi = (\widehat{\Phi} + \Phi'') (\widehat{\Phi} + \Phi'') \implies \widehat{\Phi\Psi} = \widehat{\Phi}\widehat{\Psi} + \widehat{\Phi''}\widehat{\Psi''} \implies \overline{h\Phi\Psi} = \overline{h}\widehat{\Phi\Psi}. \quad (60.25)$$

We sometimes need to consider mixed averages and primes, such as for

$$\overline{\overline{h}\widehat{\Phi}} = \overline{h\Phi} = \overline{h}\widehat{\Phi}, \quad (60.26)$$

in which case⁵

$$\overline{h\Phi''} = \overline{h}(\overline{\Phi} - \widehat{\Phi}) = \overline{h\Phi} - \overline{h'\Phi'} \neq 0. \quad (60.27)$$

Hence, the ensemble average of a fluctuation, Φ'' (which is computed relative to the thickness weighted mean), is generally nonzero. Furthermore, we sometimes find it useful to write the

⁵Footnote #4 in [Young \(2012\)](#) is missing the $\overline{h\Phi}$ term appearing in equation (60.27).

ensemble mean correlation between thickness and a field according to

$$\bar{h} \hat{\Phi}' = \bar{h} \bar{\Phi}' = \bar{h}' \bar{\Phi}', \quad (60.28)$$

with the second equality following since

$$\bar{\bar{h}} \bar{\Phi}' = \bar{h} \bar{\Phi}' = 0. \quad (60.29)$$

The identity (60.28) allows us to write equation (60.27) as

$$\bar{h} \bar{\Phi}'' = \bar{h} (\bar{\Phi} - \hat{\Phi}'). \quad (60.30)$$

A similar identity holds according to the following manipulations

$$\bar{h}' \bar{\Phi}' = \bar{h} \bar{\Phi}' = \bar{h} (\bar{\Phi} - \bar{\Phi}) = \bar{h} \bar{\Phi} - \bar{h} \bar{\Phi} = \bar{h} (\hat{\Phi} - \bar{\Phi}), \quad (60.31)$$

so that

$$\hat{\Phi}' = \hat{\Phi} - \bar{\Phi} = \frac{\bar{h}' \bar{\Phi}'}{\bar{h}}. \quad (60.32)$$

Derivative operators *do not* commute with the thickness weighted average, so that, for example,

$$\partial_x \hat{u} \neq \widehat{\partial_x u}. \quad (60.33)$$

Hence, when deriving differential equations for thickness weighted fields, we first derive equations for the unaveraged thickness weighted quantities, and only thereafter do we apply the ensemble mean operator.

60.4.4 Comments

For the most part, we follow the notation of [Young \(2012\)](#). Nonetheless, we caution that notational clutter and variations on conventions can present a nontrivial barrier to penetrating the TWA literature. Indeed, for our purposes with the stacked shallow water model, there is one additional piece of notation concerning the discrete layer indices. Fortunately, much of the discrete layer notation can be streamlined by exposing just the half-integer indices for fields situated at layer interfaces, along with the layer density.

60.5 Thickness equation and tracer equation

In this section we derive the TWA versions of the thickness equation (60.1a) and the tracer equation (60.1b). The derivations involve straightforward applications of the TWA averaging properties (60.24) and (60.25).

60.5.1 TWA thickness equation

Taking the ensemble average of the thickness equation (60.1a) renders

$$\partial_t \bar{h} + \nabla \cdot \bar{h} \bar{u} = 0, \quad (60.34)$$

where we dropped the layer index, k , to reduce notation. Introducing the thickness weighted average according to equation (60.22) brings the thickness equation to the form

$$\partial_t \bar{h} + \nabla \cdot (\bar{h} \hat{\mathbf{u}}) = 0. \quad (60.35)$$

Consequently, the mean layer thickness, \bar{h} , evolves at a point in space according to the convergence of the thickness flux, $-\nabla \cdot (\bar{h} \hat{\mathbf{u}})$, with the flux determined by the thickness weighted velocity, $\hat{\mathbf{u}}$.

We find it useful to introduce the material time derivative operator defined with the thickness weighted velocity

$$\frac{D^\sharp}{Dt} = \frac{\partial}{\partial t} + \hat{\mathbf{u}} \cdot \nabla = \frac{\partial}{\partial t} + \hat{u} \partial_x + \hat{v} \partial_y, \quad (60.36)$$

so that the Eulerian flux-form thickness equation (60.35) can be written in the material time derivative or advective form

$$\frac{D^\sharp \bar{h}}{Dt} = -\bar{h} \nabla \cdot \hat{\mathbf{u}}. \quad (60.37)$$

The D^\sharp/Dt notation is based on that used by [Young \(2012\)](#). The alternative \widehat{D}/Dt is less suitable since $\bar{h}(D/Dt) \neq (D/Dt)\bar{h}$. In brief, an object adorned with a sharp symbol is consistent with thickness weighted averaging but is itself not the direct result of a thickness weighted average. In the following, we find it useful to also introduce the vertical velocity, w^\sharp , in equation (60.43), and the potential vorticity, Π^\sharp , in equation (60.91).

The isomorphism between the TWA thickness equation (60.35) with the unaveraged thickness equation (60.1a) illustrates a distinct advantage of using the thickness weighted velocity, $\hat{\mathbf{u}}$. Even so, for some purposes it is useful to unpack the thickness weighted velocity into its two components

$$\hat{\mathbf{u}} = \bar{u} + \frac{\bar{h}' \mathbf{u}'}{\bar{h}} \equiv \bar{u} + \mathbf{u}^{\text{bolus}}, \quad (60.38)$$

where we defined the bolus velocity via

$$\bar{h} \mathbf{u}^{\text{bolus}} = \bar{h}' \mathbf{u}' = \bar{h} \hat{\mathbf{u}}', \quad (60.39)$$

where the second equality follows from the identity (60.28).

We discussed the bolus velocity in Section 60.3 and see it again in Section 62.5.5 when developing the ensemble mean tracer equation in isopycnal coordinates. However, as per our discussion in Section 60.3.6, we do not need to know the bolus velocity if we write the averaged tracer and momentum equations in terms of the thickness weighted velocity, $\hat{\mathbf{u}}$.

60.5.2 Tracer equation

Taking the ensemble average of the tracer concentration equation (60.1b) for a shallow water fluid layer renders

$$\partial_t (\bar{h} \bar{C}) + \nabla \cdot (\bar{h} \bar{C} \mathbf{u}) = 0. \quad (60.40)$$

Making use of the thickness weighted averages from Section 60.4.3 allows us to write

$$\bar{h} \bar{C} = \bar{h} \hat{C} \quad \text{and} \quad \bar{h} \bar{C} \mathbf{u} = \bar{h} (\hat{C} \hat{\mathbf{u}} + \widehat{\bar{C}'' \mathbf{u}''}), \quad (60.41)$$

thus yielding the TWA tracer equation

$$\partial_t (\bar{h} \hat{C}) + \nabla \cdot (\bar{h} \hat{C} \hat{\mathbf{u}}) = -\nabla \cdot (\widehat{\bar{h} \bar{C}'' \mathbf{u}''}). \quad (60.42)$$

The right hand side is the convergence of the thickness weighted eddy tracer flux. As seen in Section 62.6, the isopycnal form of the tracer equation is identical to that given here for a shallow water layer. In that discussion we present methods commonly used to parameterize the eddy flux convergence.

60.5.3 Vertical velocity

We generally have no need for the vertical velocity when working with the adiabatic stacked shallow water model. Nonetheless, it is interesting to define a vertical velocity component, w^\sharp , satisfying the continuity equation

$$\nabla_z \cdot \hat{\mathbf{u}} + \partial_z w^\sharp = 0. \quad (60.43)$$

As for the unaveraged vertical velocity component discussed in Section 32.2.8, w^\sharp is a linear function of z within the ensemble mean shallow water layers (see equation (32.38)). Note that w^\sharp is not a thickness weighted velocity. Rather, it is the vertical velocity that is compatible, through the continuity equation, with the thickness weighted horizontal velocity. A vertical velocity is needed for the continuously stratified Boussinesq fluid, and it is defined as done here for the shallow water.⁶

60.6 Horizontal momentum equation

Taking the ensemble mean of the horizontal momentum equation (60.1c) renders

$$\partial_t(\bar{h}\mathbf{u}) + \nabla \cdot [\bar{h}\mathbf{u} \otimes \mathbf{u}] + f\hat{\mathbf{z}} \times (\bar{h}\mathbf{u}) = -\bar{h}\nabla p/\rho_{\text{ref}}, \quad (60.44)$$

where we dropped the layer interface label, k , for brevity. Again, we make use of the thickness weighted averages from Section 60.4.3 to write

$$\bar{h}\mathbf{u} = \bar{h}\hat{\mathbf{u}} \quad (60.45a)$$

$$\bar{h}\mathbf{u} \otimes \mathbf{u} = \bar{h}(\hat{\mathbf{u}} \otimes \hat{\mathbf{u}} + \widehat{\mathbf{u}'' \otimes \mathbf{u}''}), \quad (60.45b)$$

so that equation (60.44) becomes

$$\partial_t(\bar{h}\hat{\mathbf{u}}) + \nabla \cdot [\bar{h}\hat{\mathbf{u}} \otimes \hat{\mathbf{u}}] + f\hat{\mathbf{z}} \times (\bar{h}\hat{\mathbf{u}}) = -\nabla \cdot [\bar{h}\widehat{\mathbf{u}'' \otimes \mathbf{u}''}] - \bar{h}\nabla p/\rho_{\text{ref}}. \quad (60.46)$$

The first term on the right hand side is similar to the eddy tracer flux convergence appearing in the TWA tracer equation (60.42). In contrast, the thickness weighted pressure gradient is fundamentally distinct from anything appearing in the tracer equation. Much in the remainder of this section is devoted to developing a physical and mathematical understanding of $\bar{h}\nabla p$.

60.6.1 Kinetic stress and Reynolds stress

Following our discussion in Section 22.6, we introduce the shallow water kinetic stress tensor

$$\mathbb{T}^{\text{sw kinetic}} = -\rho_{\text{ref}}\mathbf{u} \otimes \mathbf{u}. \quad (60.47)$$

The kinetic stress arises from motion of the fluid, with its divergence, $\nabla \cdot (h\mathbb{T}^{\text{kinetic}})$, contributing to changes in the momentum of a shallow water fluid column. Decomposing the velocity into the

⁶See equation (73) in [Young \(2012\)](#).

TWA velocity and fluctuation leads to the ensemble mean of the thickness weighted kinetic stress

$$\overline{h \mathbb{T}^{\text{kinetic}}(\mathbf{u})} = -\rho_{\text{ref}} \overline{h \mathbf{u} \otimes \mathbf{u}} \quad (60.48a)$$

$$= -\rho_{\text{ref}} \overline{h} [\widehat{\mathbf{u}} \otimes \widehat{\mathbf{u}} + \widehat{\mathbf{u}'' \otimes \mathbf{u}''}] \quad (60.48b)$$

$$= \overline{h} \mathbb{T}^{\text{kinetic}}(\widehat{\mathbf{u}}) + \overline{h} \mathbb{T}^{\text{Reynolds}}, \quad (60.48c)$$

where the eddy correlation is known as the *Reynolds stress*. The divergence of the thickness weighted Reynolds stress provides a rectified effect onto the mean flow due to nonzero eddy correlations.

60.6.2 Thickness and pressure gradient correlation

The ensemble mean of the thickness weighted pressure gradient can be written

$$\overline{h_k \nabla p_k} = \overline{h}_k \widehat{\nabla p_k} \quad \text{equation (60.22) defining the TWA} \quad (60.49a)$$

$$= \overline{h}_k \nabla \overline{p}_k + \overline{h'_k \nabla p'_k} \quad \text{expanding the ensemble mean} \quad (60.49b)$$

$$= \overline{h}_k (\nabla \overline{p}_k + \widehat{\nabla p'_k}) \quad \text{equation (60.28).} \quad (60.49c)$$

The eddy term is the correlation between layer thickness fluctuations and horizontal pressure gradient fluctuations

$$\overline{h}_k \widehat{\nabla p'_k} = \overline{h'_k \nabla p'_k}, \quad (60.50)$$

which can be written in terms of the eddy geostrophic velocity

$$\overline{h}_k \widehat{\nabla p'_k} = -\rho_{\text{ref}} f \hat{\mathbf{z}} \times \overline{h'_k \mathbf{u}'_{k,g}} = -\rho_{\text{ref}} f \hat{\mathbf{z}} \times \overline{h}_k \widehat{\mathbf{u}'_{k,g}}. \quad (60.51)$$

For geostrophic flows, the bolus velocity (60.39) equals to $\widehat{\mathbf{u}'_{k,g}}$, in which case we write

$$\overline{h}_k \widehat{\nabla p'_k} = -\rho_{\text{ref}} f \hat{\mathbf{z}} \times \overline{h}_k \mathbf{u}^{\text{bolus}}_k. \quad (60.52)$$

60.6.3 Unpacking the thickness and pressure gradient correlation

We here unpack the correlation between eddy thickness and eddy pressure gradient as given by $\overline{h}_k \widehat{\nabla p'_k} = \overline{h'_k \nabla p'_k}$ in equation (60.50). We do so by writing the pressure as a contact force rather than a body force. Doing so exposes the eddy interfacial form stresses that provide a vertical transfer of horizontal momentum. In addition, there is a term arising from the gradient in the layer depth integrated pressure or, alternatively, the layer potential energy. To proceed we rely on the development given in Section 33.4.9, in which we exposed two equivalent expressions for the contact pressure.

As part of the following derivation we make use of relations for pressure within a layer and at an interface

$$p_k(z) = p_{k-1/2} + g \rho_k (\eta_{k-1/2} - z) \quad (60.53a)$$

$$p_{k+1/2} - p_{k-1/2} = g \rho_k h_k = -g \rho_k (\eta_{k+1/2} - \eta_{k-1/2}) \quad (60.53b)$$

$$p_{1/2} = p_a, \quad (60.53c)$$

with p_a the applied (or atmospheric) pressure at the ocean surface. We emphasize that the layer pressure, $p_k(z)$, is a linear function of vertical position within the layer so that its horizontal

gradient, $\nabla_z p_k$, is depth independent.

Interfacial form stress plus gradient of layer depth integrated pressure

The first expression for thickness weighted pressure gradient is given by

$$-h_k \nabla p_k = -\nabla P_k + \mathbf{F}_k^{\text{form}}. \quad (60.54)$$

In this equation we introduced the pressure vertically integrated over layer-k

$$P_k = \int_{\eta_{k+1/2}}^{\eta_{k-1/2}} p_k(z) dz = h_k (g \rho_k h_k / 2 + p_{k-1/2}), \quad (60.55)$$

with its negative gradient

$$-\nabla P_k = -\nabla [h_k (p_{k-1/2} + g \rho_k h_k / 2)] \quad (60.56a)$$

$$= -\nabla [h_k (p_{k+1/2} - g \rho_k h_k / 2)] \quad (60.56b)$$

$$= -[h_k \nabla p_{k+1/2} + p_{k-1/2} \nabla h_k] \quad (60.56c)$$

leading to a horizontal acceleration from imbalances in the contact pressure acting along the vertical sides of a shallow water column. The second stress in equation (60.54) is the pressure form stress acting on the upper and lower layer interfaces

$$\mathbf{F}_k^{\text{form}} = p_{k-1/2} \nabla \eta_{k-1/2} - p_{k+1/2} \nabla \eta_{k+1/2} \equiv \delta_k (p_{k-1/2} \nabla \eta_{k-1/2}), \quad (60.57)$$

where

$$\delta_k \Phi_{k-1/2} = \Phi_{k-1/2} - \Phi_{k+1/2} = -(\Phi_{k+1/2} - \Phi_{k-1/2}) \quad (60.58)$$

is a difference operator acting on interface properties. The use of a backward difference operator is motivated since k increases down whereas \hat{z} points up. Additionally, we define the difference operator to only act on fields defined at the layer interface, with layer fields commuting with this operator so that, for example,

$$\delta_k (h_k \eta_{k-1/2}) = h_k \delta_k (\eta_{k-1/2}). \quad (60.59)$$

This convention helps produce a tidy form of the Eliassen-Palm flux in Sections 60.6.4 and 60.6.5.

Making use of the depth integrated pressure and form stress as given by equation (60.54) allows us to write the ensemble mean thickness weighted pressure gradient as

$$-\overline{h_k \nabla p_k} = -\nabla \overline{P_k} + \delta_k [\overline{p_{k-1/2} \nabla \eta_{k-1/2}}]. \quad (60.60)$$

Following equation (60.56a), we write the ensemble mean for the layer integrated pressure as

$$-\nabla \overline{P_k} = -\nabla [\overline{h_k} (p_{k-1/2} + g \rho_k \overline{h_k} / 2)] - \nabla [\overline{h'_k} (p'_{k-1/2} + g \rho_k \overline{h'_k} / 2)] \quad (60.61)$$

and the vertical divergence of the form stress is

$$\overline{\mathbf{F}_k^{\text{form}}} = \delta_k [\overline{p_{k-1/2} \nabla \eta_{k-1/2}}] = \delta_k [\overline{p_{k-1/2} \nabla \eta_{k-1/2}} + \overline{p'_{k-1/2} \nabla \eta'_{k-1/2}}]. \quad (60.62)$$

We are thus led to the following decomposition of the eddy contribution to the thickness weighted

pressure gradient

$$-\overline{h'_k \nabla p'_k} = -\nabla[\overline{h'_k (p'_{k-1/2} + g \rho_k h'_k / 2)}] + \delta_k [\overline{p'_{k-1/2} \nabla \eta'_{k-1/2}}]. \quad (60.63)$$

For orientation, in Figure 60.2 we illustrate the deviations of the interface positions relative to the ensemble mean.

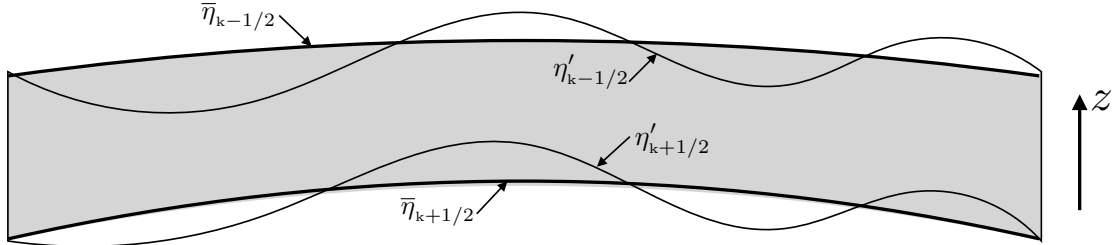


FIGURE 60.2: Schematic of the interface positions for a shallow water layer. The ensemble mean layer interfaces have vertical positions given by $z = \bar{\eta}_{k\pm 1/2}$, whereas the fluctuating interfaces are located at $z = \bar{\eta}_{k\pm 1/2} + \eta'_{k\pm 1/2}$. As depicted here, the ensemble mean interface positions are not generally horizontal.

Dual interfacial pressure form stress plus gradient of layer potential energy

An alternative formulation uses the dual form stress and potential energy, in which case we write the thickness weighted horizontal pressure gradient as

$$-h_k \nabla p_k = -\nabla \mathcal{P}_k + \mathbf{F}_k^{\text{dual}}. \quad (60.64)$$

In this equation we introduced the layer gravitational potential energy per area

$$\mathcal{P}_k = g \rho_k \int_{\eta_{k+1/2}}^{\eta_{k-1/2}} z dz = (g \rho_k / 2) (\eta_{k-1/2}^2 - \eta_{k+1/2}^2) = (g \rho_k / 2) \delta_k (\eta_{k-1/2}^2), \quad (60.65)$$

and the *dual pressure form stress* (see Section 33.4.8),

$$\mathbf{F}_k^{\text{dual}} = -\delta_k (\eta_{k-1/2} \nabla p_{k-1/2}) = \mathbf{F}_k^{\text{form}} - \nabla [\delta_k (\eta_{k-1/2} p_{k-1/2})]. \quad (60.66)$$

Since they differ by a gradient, the form stress and dual form stress have identical curls and so they contribute the same interfacial pressure torque as part of the layer vorticity evolution

$$-\nabla \times (h_k \nabla p_k) = \nabla \times \mathbf{F}_k^{\text{dual}} = \nabla \times \mathbf{F}_k^{\text{form}}. \quad (60.67)$$

Making use of the potential energy and dual form stress as given by equation (60.64) allows us to write the ensemble mean thickness weighted pressure gradient as

$$-\overline{h_k \nabla p_k} = -\nabla \overline{\mathcal{P}_k} - \delta_k [\overline{\eta_{k-1/2} \nabla p_{k-1/2}}] \quad (60.68)$$

where minus the potential energy gradient is decomposed as

$$-\nabla \overline{\mathcal{P}_k} = -(g \rho_k / 2) \delta_k [\nabla (\overline{\eta_{k-1/2}})^2 + \nabla (\overline{\eta'_{k-1/2}})^2] \quad (60.69)$$

and the vertical convergence of the dual form stress is

$$-\delta_k [\overline{\eta_{k-1/2} \nabla p_{k-1/2}}] = -\delta_k [\overline{\eta_{k-1/2} \nabla p_{k-1/2}} + \overline{\eta'_{k-1/2} \nabla p'_{k-1/2}}]. \quad (60.70)$$

We are thus led to decompose the thickness weighted pressure gradient correlation as

$$-\overline{h'_k \nabla p'_k} = -(g \rho_k / 2) \nabla [\delta_k \overline{(\eta'_{k-1/2})^2}] - \delta_k \overline{[\eta'_{k-1/2} \nabla p'_{k-1/2}]}.$$
 (60.71)

Again, the first term on the right hand side arises from the eddy potential energy and the second term from the dual eddy form stress.

60.6.4 Zonal and meridional Eliassen-Palm fluxes: Version I

Making use of the thickness and pressure gradient correlation in the form of equation (60.63) (the version with the form stress) leads to the thickness weighted momentum equation

$$\begin{aligned} \partial_t (\bar{h} \hat{\mathbf{u}}) + \nabla \cdot (\bar{h} \hat{\mathbf{u}} \otimes \hat{\mathbf{u}}) + f \hat{z} \times \bar{h} \hat{\mathbf{u}} + \bar{h} \nabla \bar{p} / \rho_{\text{ref}} \\ = -\nabla \cdot (\bar{h} \widehat{\mathbf{u}'' \otimes \mathbf{u}''}) - \rho_{\text{ref}}^{-1} \nabla [\bar{h}'_k (p'_{k-1/2} + g \rho_k h'_k / 2)] + \rho_{\text{ref}}^{-1} \delta_k \overline{(p' \nabla \eta')_{k-1/2}}, \end{aligned}$$
 (60.72)

where we only exposed the interface indices to reduce notational clutter, and where we introduced the shorthand for the eddy form stress at the $k - 1/2$ interface

$$(p' \nabla \eta')_{k-1/2} = p'_{k-1/2} \nabla \eta'_{k-1/2}.$$
 (60.73)

The subgrid scale correlations on the right hand side of equation (60.72) can be organized into the divergence of two tensors

$$\begin{aligned} & \nabla \cdot (\bar{h} \widehat{\mathbf{u}'' \otimes \mathbf{u}''}) + \rho_{\text{ref}}^{-1} \nabla [\bar{h}'_k (p'_{k-1/2} + g \rho_k h'_k / 2)] - (\bar{h} \rho_{\text{ref}})^{-1} \delta_k \left[\bar{h} \overline{(p' \nabla \eta')_{k-1/2}} \right] \\ &= [\partial_x \quad \partial_y \quad (1/\bar{h}) \delta_k] \begin{bmatrix} \bar{h} \widehat{u'' u''} & \bar{h} \widehat{u'' v''} & 0 \\ \bar{h} \widehat{u'' v''} & \bar{h} \widehat{v'' v''} & 0 \\ 0 & 0 & 0 \end{bmatrix} \\ &+ \rho_{\text{ref}}^{-1} [\partial_x \quad \partial_y \quad (1/\bar{h}) \delta_k] \begin{bmatrix} \bar{h}'_k (p'_{k-1/2} + g \rho_k h'_k / 2) & 0 & 0 \\ 0 & \bar{h}'_k (p'_{k-1/2} + g \rho_k h'_k / 2) & 0 \\ -\bar{h} \overline{(p' \partial_x \eta')_{k-1/2}} & -\bar{h} \overline{(p' \partial_y \eta')_{k-1/2}} & 0 \end{bmatrix}, \end{aligned}$$
 (60.74)

where we recall from equation (60.59) that the vertical difference operator, δ_k , only acts on layer interface fields so that \bar{h}_k commutes with δ_k . The first tensor in equation (60.74) arises from Reynolds stresses and the second tensor arises from eddy pressures, including the eddy form stress in the third row.

When combined, the columns of the tensors appearing in equation (60.74) are the thickness weighted shallow water *Eliassen-Palm fluxes* for the zonal (column 1) and meridional (column 2) momentum equation

$$\mathbf{E}^{(\text{uEP})} = \left[\bar{h} \widehat{u'' u''} + \rho_{\text{ref}}^{-1} \bar{h}'_k (p'_{k-1/2} + g \rho_k h'_k / 2) \right] \hat{\mathbf{x}} + \bar{h} \widehat{u'' v''} \hat{\mathbf{y}} - (\bar{h} / \rho_{\text{ref}}) \overline{(p' \partial_x \eta')_{k-1/2}} \hat{\mathbf{z}} \quad (60.75a)$$

$$\mathbf{E}^{(\text{vEP})} = \bar{h} \widehat{u'' v''} \hat{\mathbf{x}} + \left[\bar{h} \widehat{v'' v''} + \rho_{\text{ref}}^{-1} \bar{h}'_k (p'_{k-1/2} + g \rho_k h'_k / 2) \right] \hat{\mathbf{y}} - (\bar{h} / \rho_{\text{ref}}) \overline{(p' \partial_y \eta')_{k-1/2}} \hat{\mathbf{z}}.$$
 (60.75b)

The Eliassen-Palm flux has physical dimensions of thickness times squared velocity. We encountered the unaveraged version of the Eliassen-Palm flux in Sections 33.3.3 and 33.4.9 when studying the shallow water momentum equation. [Maddison and Marshall \(2013\)](#) included the third column of zeros in equation (60.74) to emphasize that the Eliassen-Palm fluxes are the first and second columns to the *Eliassen-Palm flux tensor*. They illustrated the utility of this perspective

by considering gauge transformations that result in non-zero elements in the third column.

The Eliassen-Palm fluxes are second order in eddy amplitude; i.e., they are quadratic in eddy fluctuations. Furthermore, they bring together the Reynolds stress and eddy pressure terms, including the eddy form stress. The convergence of the Eliassen-Palm fluxes provides an eddy rectified acceleration on the thickness weighted velocity. To explicitly see this forcing, write the components to the mean field momentum equation (60.72) as⁷

$$\partial_t(\bar{h}\hat{u}) + \nabla \cdot (\bar{h}\hat{u}\hat{u}) - f\bar{h}\hat{v} + \bar{h}\partial_x\bar{p}/\rho = -(\nabla_z + \hat{z}\bar{h}^{-1}\delta_k) \cdot \mathbf{E}^{(uEP)} \quad (60.76a)$$

$$\partial_t(\bar{h}\hat{v}) + \nabla \cdot (\bar{h}\hat{u}\hat{v}) + f\bar{h}\hat{u} + \bar{h}\partial_y\bar{p}/\rho = -(\nabla_z + \hat{z}\bar{h}^{-1}\delta_k) \cdot \mathbf{E}^{(vEP)}. \quad (60.76b)$$

Equations (60.76a) and (60.76b) are isomorphic to the unaveraged horizontal momentum equation (60.1c), yet with the addition of the convergence of the Eliassen-Palm flux on the right hand side that encapsulates rectified effects from eddies. They can be written using the material time derivative (60.36)

$$\frac{D^\sharp \hat{u}}{Dt} - f\hat{v} + \partial_x\bar{p}/\rho = -\bar{h}^{-1}(\nabla_z + \hat{z}\bar{h}^{-1}\delta_k) \cdot \mathbf{E}^{(uEP)} \quad (60.77a)$$

$$\frac{D^\sharp \hat{v}}{Dt} + f\hat{u} + \partial_y\bar{p}/\rho = -\bar{h}^{-1}(\nabla_z + \hat{z}\bar{h}^{-1}\delta_k) \cdot \mathbf{E}^{(vEP)}. \quad (60.77b)$$

We emphasize that these equations only make use of the thickness weighted velocity, $\hat{\mathbf{u}}$, as do the averaged thickness equation (60.35) and averaged tracer equation (60.42). We advertised this point near the start of this chapter, noting that it facilitates the practical use of the TWA equations for numerical simulations. We further this correspondence in Section 60.7 by showing that the vorticity and potential vorticity equations also make use of $\hat{\mathbf{u}}$.

60.6.5 Zonal and meridional Eliassen-Palm fluxes: Version II

We here follow the development in Section 60.6.4, only now making use of the thickness and pressure gradient correlation in the form of equation (60.71) (the version with the dual form stress). Our presentation is terse since there are few differences from Section 60.6.4. We start from the thickness weighted momentum equation

$$\begin{aligned} \partial_t(\bar{h}\hat{\mathbf{u}}) + \nabla \cdot (\bar{h}\hat{\mathbf{u}} \otimes \hat{\mathbf{u}}) + f\hat{z} \times \bar{h}\hat{\mathbf{u}} + \bar{h}\nabla\bar{p}/\rho \\ = -\nabla \cdot (\widehat{\bar{h}\mathbf{u}'' \otimes \mathbf{u}''}) - (g\rho_k/2\rho_{ref})\nabla[\delta_k\overline{(\eta'_{k-1/2})^2}] - \delta_k\overline{[(\eta'\nabla p')_{k-1/2}/\rho_{ref}]} \end{aligned} \quad (60.78)$$

⁷Recall from equation (60.59) that the operator δ_k only acts on interface fields, so that $\bar{h}^{-1}\delta_k(\bar{h}) = \delta_k$. This convention allows us to combine the horizontal components to the Eliassen-Palm flux with the vertical component, as written in equations (60.80a) and (60.80b).

The subgrid scale correlations on the right hand side can be organized into the divergence of two tensors

$$\begin{aligned} & \nabla \cdot (\bar{h} \widehat{\mathbf{u}'' \otimes \mathbf{u}''}) + (g \rho_k / 2\rho_{\text{ref}}) \nabla [\delta_k \overline{(\eta'_{k-1/2})^2}] + \delta_k [\overline{(\eta' \nabla p')_{k-1/2}} / \rho_{\text{ref}}] \\ &= \begin{bmatrix} \partial_x & \partial_y & \bar{h}^{-1} \delta_k \end{bmatrix} \begin{bmatrix} \bar{h} \widehat{u'' u''} & \bar{h} \widehat{u'' v''} & 0 \\ \bar{h} \widehat{u'' v''} & \bar{h} \widehat{v'' v''} & 0 \\ 0 & 0 & 0 \end{bmatrix} \\ &+ \begin{bmatrix} \partial_x & \partial_y & \bar{h}^{-1} \delta_k \end{bmatrix} \begin{bmatrix} (g \rho_k / 2 \rho_{\text{ref}}) [\delta_k \overline{(\eta'_{k-1/2})^2}] & 0 & 0 \\ 0 & (g \rho_k / 2 \rho_{\text{ref}}) [\delta_k \overline{(\eta'_{k-1/2})^2}] & 0 \\ (\bar{h} / \rho_{\text{ref}}) \overline{(\eta' \partial_x p')_{k-1/2}} & (\bar{h} / \rho_{\text{ref}}) \overline{(\eta' \partial_y p')_{k-1/2}} & 0 \end{bmatrix}. \quad (60.79) \end{aligned}$$

The first tensor arises from Reynolds stresses and the second arises from eddy potential energy and dual eddy form stresses. When combined, the columns are the thickness weighted *Eliassen-Palm fluxes* for the zonal (column 1) and meridional (column 2), here making use of the dual form stress

$$\mathbf{E}_{\text{dual}}^{(\text{uEP})} = \left[\bar{h} \widehat{u'' u''} + (g \rho_k / 2 \rho_{\text{ref}}) [\delta_k \overline{(\eta'_{k-1/2})^2}] \right] \hat{x} + \bar{h} \widehat{u'' v''} \hat{y} + \bar{h} \overline{(\eta' \partial_x p')_{k-1/2}} / \rho_{\text{ref}} \hat{z} \quad (60.80a)$$

$$\mathbf{E}_{\text{dual}}^{(\text{vEP})} = \bar{h} \widehat{u'' v''} \hat{x} + \left[\bar{h} \widehat{v'' v''} + (g \rho_k / 2 \rho_{\text{ref}}) [\delta_k \overline{(\eta'_{k-1/2})^2}] \right] \hat{y} + \bar{h} \overline{(\eta' \partial_y p')_{k-1/2}} / \rho_{\text{ref}} \hat{z}. \quad (60.80b)$$

The convergence of the Eliassen-Palm fluxes provides an eddy rectified acceleration on the thickness weighted velocity

$$\partial_t (\bar{h} \hat{u}) + \nabla \cdot (\bar{h} \hat{\mathbf{u}} \hat{u}) - f \bar{h} \hat{v} + \bar{h} \partial_x \bar{p} / \rho = -(\nabla_z + \hat{z} \bar{h}^{-1} \delta_k) \cdot \mathbf{E}_{\text{dual}}^{(\text{uEP})} \quad (60.81a)$$

$$\partial_t (\bar{h} \hat{v}) + \nabla \cdot (\bar{h} \hat{\mathbf{u}} \hat{v}) + f \bar{h} \hat{u} + \bar{h} \partial_y \bar{p} / \rho = -(\nabla_z + \hat{z} \bar{h}^{-1} \delta_k) \cdot \mathbf{E}_{\text{dual}}^{(\text{vEP})}. \quad (60.81b)$$

60.6.6 Interfacial stresses from geostrophic eddies

In Section 28.6 we studied the rectified effects from geostrophic eddies in a zonally re-entrant channel for a continuously stratified fluid. In that analysis we found that the zonal mean of isopycnal eddy form stresses are equivalent to the meridional eddy flux of buoyancy. We here consider similar questions within the context of the TWA shallow water fluid, here focusing on the interfacial transfer of momentum due to eddy dual form stresses as given by the vertical vectors

$$\rho_{\text{ref}} \left[\mathbf{E}_{\text{dual}}^{(\text{uEP})} \right]_{\text{interface}} = \hat{z} \bar{h} \overline{(\eta' \partial_x p')_{k-1/2}} \quad (60.82a)$$

$$\rho_{\text{ref}} \left[\mathbf{E}_{\text{dual}}^{(\text{vEP})} \right]_{\text{interface}} = \hat{z} \bar{h} \overline{(\eta' \partial_y p')_{k-1/2}}. \quad (60.82b)$$

Let us now write the interface pressure gradient fluctuation as

$$\nabla p_{k-1/2} = \nabla p_k - g \rho_k \nabla \eta_{k-1/2} \quad (60.83)$$

so that

$$\overline{(\eta' \nabla p')_{k-1/2}} = \overline{\eta'_{k-1/2} \nabla p'_k} + g \rho_k \overline{(\eta' \nabla \eta')_{k-1/2}}. \quad (60.84)$$

As for the analysis in Section 28.6, we assume the fluctuations are geostrophic so that we can introduce the layer geostrophic velocity corresponding to the gradient of the layer pressure fluctuations

$$\partial_x p'_k = f \rho_{\text{ref}} v'_k \quad \text{and} \quad \partial_y p'_k = -f \rho_{\text{ref}} u'_k, \quad (60.85)$$

in which case the dual form stress portion of the Eliassen-Palm fluxes take the form

$$\rho_{\text{ref}} \left[\mathbf{E}_{\text{dual}}^{(\text{uEP})} \right]_{\text{interface}} = \hat{\mathbf{z}} \bar{h} \left[f \rho_{\text{ref}} \overline{\eta'_{k-1/2} v'_k} + g \rho_k \overline{(\eta' \partial_x \eta')_{k-1/2}} \right] \quad (60.86\text{a})$$

$$\rho_{\text{ref}} \left[\mathbf{E}_{\text{dual}}^{(\text{vEP})} \right]_{\text{interface}} = \hat{\mathbf{z}} \bar{h} \left[-f \rho_{\text{ref}} \overline{\eta'_{k-1/2} u'_k} + g \rho_k \overline{(\eta' \partial_y \eta')_{k-1/2}} \right]. \quad (60.86\text{b})$$

The $\overline{\eta'_{k-1/2} u'_k}$ term is an eddy transport of the area between $z = \bar{\eta}_{k-1/2}$ and $z = \eta'_{k-1/2}$ (see Figure 60.2). We studied the same transport for the continuously stratified fluid in Section 28.6. In that discussion, we found that the interface fluctuations, η' , can be related to the buoyancy fluctuations, b' , in which case $\overline{\eta'_{k-1/2} u'_k}$ is proportional to the eddy buoyancy flux for the layer.

60.6.7 Comments

Greatbatch and Lamb (1990) and *Greatbatch* (1998) pursue a similar analysis for the purpose of framing the mesoscale eddy parameterization problem. They focus on the interfacial form stress contribution since, for geostrophic eddies, it dominates over the other terms in the Eliassen-Palm fluxes (60.80a) and (60.80b).

60.7 Vorticity and potential vorticity

We follow the procedure from Chapter 36 to derive the vorticity and potential vorticity for the thickness weighted shallow water equations. In the process, we connect the eddy flux of potential vorticity to the Eliassen-Palm fluxes (60.75a) and (60.75b). Note that the same manipulations also hold for the dual Eliassen-Palm fluxes (60.80a) and (60.80b).

60.7.1 Derivation

Use the vector identities from Sections 32.5 and 36.1 to bring the material evolution equations (60.77a) and (60.77b) into their equivalent vector invariant forms⁸

$$\partial_t \hat{\mathbf{u}} - (f + \hat{\zeta}) \hat{\mathbf{v}} = -\partial_x (\bar{p}/\rho + \hat{\mathbf{u}} \cdot \hat{\mathbf{u}}/2) - \bar{h}^{-1} (\nabla_z + \hat{\mathbf{z}} \bar{h}^{-1} \delta_k) \cdot \mathbf{E}^{(\text{uEP})} \quad (60.87\text{a})$$

$$\partial_t \hat{\mathbf{v}} + (f + \hat{\zeta}) \hat{\mathbf{u}} = -\partial_y (\bar{p}/\rho + \hat{\mathbf{u}} \cdot \hat{\mathbf{u}}/2) - \bar{h}^{-1} (\nabla_z + \hat{\mathbf{z}} \bar{h}^{-1} \delta_k) \cdot \mathbf{E}^{(\text{vEP})}, \quad (60.87\text{b})$$

where we introduced the relative vorticity of the thickness weighted horizontal velocity

$$\hat{\zeta} = \partial_x \hat{\mathbf{v}} - \partial_y \hat{\mathbf{u}}. \quad (60.88)$$

Taking ∂_x of the meridional equation (60.87b) and subtracting ∂_y of the zonal equation (60.87a) renders the evolution equation for absolute vorticity, $\hat{\zeta}_a = \hat{\zeta} + f$,

$$\frac{D^\# \hat{\zeta}_a}{Dt} + \hat{\zeta}_a \nabla \cdot \hat{\mathbf{u}} = \partial_y [\bar{h}^{-1} (\nabla_z + \hat{\mathbf{z}} \bar{h}^{-1} \delta_k) \cdot \mathbf{E}^{(\text{uEP})}] - \partial_x [\bar{h}^{-1} (\nabla_z + \hat{\mathbf{z}} \bar{h}^{-1} \delta_k) \cdot \mathbf{E}^{(\text{vEP})}]. \quad (60.89)$$

Making use of the thickness equation (60.37) to replace $\nabla \cdot \hat{\mathbf{u}}$ leads to the potential vorticity equation

$$\bar{h} \frac{D^\# \Pi^\#}{Dt} = -\nabla \cdot \mathbf{F}^\# \quad (60.90)$$

⁸In Section D.6 of *Griffies et al.* (2020), the authors state “In contrast to the flux-form momentum equation, the vector-invariant velocity equation does not admit a finite volume formulation.” That statement is incorrect, with equations (60.87a) and (60.87b) the finite volume vector-invariant velocity equation.

where

$$\Pi^\sharp = \frac{f + \partial_x \hat{v} - \partial_y \hat{u}}{\bar{h}} = \frac{f + \zeta}{\bar{h}} \quad (60.91)$$

is the potential vorticity defined with the thickness weighted velocity and ensemble mean thickness. The corresponding eddy potential vorticity flux is a horizontal vector and given in terms of the divergence of the Eliassen-Palm fluxes

$$\mathbf{F}^\sharp = \hat{x} [\bar{h}^{-1} (\nabla_z + \hat{z} \bar{h}^{-1} \delta_k) \cdot \mathbf{E}^{(vEP)}] - \hat{y} [\bar{h}^{-1} (\nabla_z + \hat{z} \bar{h}^{-1} \delta_k) \cdot \mathbf{E}^{(uEP)}] + \hat{z} \times \nabla \Upsilon, \quad (60.92)$$

where Υ is an arbitrary gauge function.⁹ This equation connects the potential vorticity flux to the Eliassen-Palm fluxes and it is known as the *Taylor-Bretherton identity*. Remarkably, the potential vorticity flux also provides the eddy forcing to the thickness weighted velocity equation

$$\partial_t \hat{\mathbf{u}} + (f + \zeta) \hat{z} \times \hat{\mathbf{u}} + \nabla(\bar{p}/\rho + \hat{\mathbf{u}} \cdot \hat{\mathbf{u}}/2) = -\hat{z} \times (\mathbf{F}^\sharp - \hat{z} \times \nabla \Upsilon), \quad (60.93)$$

which can also be written

$$\partial_t \hat{\mathbf{u}} + \hat{z} \times (\bar{h} \hat{\mathbf{u}} \Pi^\sharp + \mathbf{F}^\sharp - \hat{z} \times \nabla \Upsilon) + \nabla(\bar{p}/\rho + \hat{\mathbf{u}} \cdot \hat{\mathbf{u}}/2) = 0, \quad (60.94)$$

where $\bar{h} \hat{\mathbf{u}} \Pi^\sharp + \mathbf{F}^\sharp - \hat{z} \times \nabla \Upsilon$ is the net (mean plus eddy plus gauge) potential vorticity flux.

60.7.2 Concerning the mean field potential vorticity

We emphasize that the mean field potential vorticity arising from our development is Π^\sharp , which is defined by equation (60.91) using the thickness weighted velocity, $\hat{\mathbf{u}}$ for the relative vorticity. This potential vorticity is distinct from the thickness weighted average potential vorticity

$$\hat{\Pi} = \frac{\bar{\Pi} \bar{h}}{\bar{h}} = \frac{f + \bar{\zeta}}{\bar{h}} = \frac{f + \partial_x \bar{v} - \partial_y \bar{u}}{\bar{h}}, \quad (60.95)$$

which is the mean field potential vorticity considered by [Greatbatch \(1998\)](#) and [Peterson and Greatbatch \(2001\)](#). The two forms of potential vorticity differ by the potential vorticity of the bolus velocity

$$\Pi^\sharp - \hat{\Pi} = \frac{(f + \zeta) - (f + \bar{\zeta})}{\bar{h}} = \frac{\hat{z} \cdot [\nabla \times (\hat{\mathbf{u}} - \bar{\mathbf{u}})]}{\bar{h}} = \frac{\hat{z} \cdot (\nabla \times \hat{\mathbf{u}'})}{\bar{h}} = \frac{\hat{z} \cdot (\nabla \times \mathbf{u}^{\text{bolus}})}{\bar{h}}, \quad (60.96)$$

where the penultimate equality made use of equation (60.32) for $\hat{\mathbf{u}'}$, and the final equality introduced the bolus velocity according to equation (60.39). Use of Π^\sharp allows us to develop a potential vorticity conservation statement solely in terms of $\hat{\mathbf{u}}$, whereas the use of $\hat{\Pi}$ by [Greatbatch \(1998\)](#) and [Peterson and Greatbatch \(2001\)](#) requires both $\bar{\mathbf{u}}$ and $\hat{\mathbf{u}}$.

60.7.3 Comments

As in [Young \(2012\)](#), and as advertised at the start of this chapter, we have developed the equations for the thickness weighted averaged shallow water solely in terms of the thickness weighted velocity, $\hat{\mathbf{u}}$. This development includes the thickness equation (60.35), the tracer equation (60.42), the velocity equation (60.46) and the potential vorticity equation (60.90). There is no need for the ensemble mean velocity, $\bar{\mathbf{u}}$, and thus no need to parameterize the bolus velocity.

⁹Equation (129) in [Young \(2012\)](#) should have a gauge function on its right hand side, which follows from his footnote #3. We provide an example of the need for a gauge function in Section 60.8.

60.8 Vorticity fluxes for non-divergent barotropic flow

In Chapter 35 we studied the mechanics of a two dimensional fluid whose horizontal flow is non-divergent. As for the shallow water, the fluid moves as columns. However, since the horizontal flow is non-divergent, each column is rigid and so there is no stretching or squashing of columns. Correspondingly, there are no form stresses acting on these columns. We specialize the shallow water analysis in this section to rigid columnar motion as a means to verify that the Reynolds stresses appearing in the Eliassen-Palm flux formulation correspond to that arising in the non-divergent barotropic model.

For rigid fluid columns, the thickness weighted average reduces to just the ensemble mean since all layer thicknesses are fixed. Correspondingly, there are no form stresses acting at the layer interfaces since interfaces are horizontal. Hence, the Eliassen-Palm fluxes (60.75a) and (60.75b) reduce to just their Reynold stress contributions

$$h^{-1} \mathbf{E}^{(uEP)} = \overline{u' u'} \hat{\mathbf{x}} + \overline{u' v'} \hat{\mathbf{y}} \quad (60.97a)$$

$$h^{-1} \mathbf{E}^{(vEP)} = \overline{u' v'} \hat{\mathbf{x}} + \overline{v' v'} \hat{\mathbf{y}}. \quad (60.97b)$$

The corresponding eddy potential vorticity flux (60.92), absent the gauge term, is

$$\mathbf{F}^\sharp = \hat{\mathbf{x}} \nabla \cdot [\overline{u' v'} \hat{\mathbf{x}} + \overline{v' v'} \hat{\mathbf{y}}] - \hat{\mathbf{y}} \nabla \cdot [\overline{u' u'} \hat{\mathbf{x}} + \overline{u' v'} \hat{\mathbf{y}}] \quad (60.98a)$$

$$= \hat{\mathbf{x}} [\partial_x(\overline{u' v'}) + \partial_y(\overline{v' v'})] - \hat{\mathbf{y}} [\partial_x(\overline{u' u'}) + \partial_y(\overline{u' v'})]. \quad (60.98b)$$

Does the eddy potential vorticity flux (60.98b) agree, to within a gauge function, with the eddy flux resulting from a direct decomposition into eddy and mean within a two dimensional non-divergent model? To address this question, recall that the advective flux of potential vorticity for the two dimensional non-divergent flow is given by equation (35.47)

$$\mathbf{u} q = \mathbf{u} f + \nabla \cdot (\hat{\mathbf{z}} \times \mathcal{E}), \quad (60.99)$$

where \mathcal{E} is the trace-free anisotropic portion of the kinetic stress tensor

$$\mathcal{E} = \begin{bmatrix} -(u^2 - v^2)/2 & -uv \\ -uv & (u^2 - v^2)/2 \end{bmatrix}. \quad (60.100)$$

The mean of the potential vorticity flux is (60.99) is given by

$$\overline{\mathbf{u} q} = \overline{\mathbf{u} q} + \overline{\mathbf{u}' q'}, \quad (60.101)$$

where the flux computed from the mean fields is

$$\overline{\mathbf{u} q} = \overline{\mathbf{u}} (f + \bar{\zeta}), \quad (60.102)$$

whereas the eddy potential vorticity flux is

$$\overline{\mathbf{u}' q'} = \nabla \cdot [\hat{\mathbf{z}} \times \overline{\mathcal{E}(\mathbf{u}')}] \quad (60.103a)$$

$$= \hat{\mathbf{x}} [\partial_x(\overline{u' v'}) + \partial_y(\overline{v' v'} - \overline{u' u'})/2] + \hat{\mathbf{y}} [\partial_x(\overline{v' v'} - \overline{u' u'})/2 - \partial_y(\overline{u' v'})] \quad (60.103b)$$

$$= \hat{\mathbf{x}} [\partial_x(\overline{u' v'}) + \partial_y(\overline{v' v'})] - \hat{\mathbf{y}} [\partial_x(\overline{u' u'}) + \partial_y(\overline{u' v'})] + (\hat{\mathbf{x}} \partial_y - \hat{\mathbf{y}} \partial_x) \overline{\mathbf{u}' \cdot \mathbf{u}'}/2 \quad (60.103c)$$

$$= \mathbf{F}^\sharp - \hat{\mathbf{z}} \times \nabla(\overline{\mathbf{u}' \cdot \mathbf{u}'})/2. \quad (60.103d)$$

Hence, $\overline{\mathbf{u}' q'}$ agrees with \mathbf{F}^\sharp in equation (60.98b) to within a gauge function given by the rotated

gradient of the eddy kinetic energy, so that their divergences are equal

$$\nabla \cdot \mathbf{F}^\sharp = \nabla \cdot \overline{\mathbf{u}' q'}. \quad (60.104)$$

That is, when diagnosing contributions to the potential vorticity flux, the gauge term, $-\hat{\mathbf{z}} \times \nabla(\overline{\mathbf{u}' \cdot \mathbf{u}'})/2$, plays no role in forcing potential vorticity.



Part XII

Mechanics of scalar fields

A scalar field provides a number (e.g., temperature, humidity, density) at every point in the fluid. This property contrasts to a vector field, such as velocity, which provides a vector valued function at each point. In this part of the book, we focus on tracers, density, and Archimedean buoyancy, which are scalar fields that offer fundamental information about the mechanics of fluid motion. Much of the material is relevant to both the atmosphere and ocean, though we also present specialized topics motivated from ocean applications. Our study of *scalar mechanics* complements the mechanics of momentum, vorticity, and energy considered earlier in this book.

Here is a synopsis of the chapters in this part of the book.

- In Chapter 61 we develop the basic maths and physics of advection and diffusion, which are the two processes that affect the evolution of *conservative tracers*.
- In Chapter 62 we introduce the notions of wave-mean flow interactions that give rise to eddy-induced advection (or skew diffusion) as well as diffusion. This chapter makes use of both geopotential coordinates as well as isopycnal coordinate equations from Chapter 59, thus providing an example of the dual roles these coordinates make in describing turbulent geophysical flows.
- Chapter 63 presents elements of standard tracer parameterizations used for coarse resolution models of the ocean circulation. We here study the mathematics of the parameterizations and connect to the basic physics.
- Chapter 64 focuses on ocean density and the study of global sea level. This topic is of growing concern for climate science given the role of the ocean as the dominant sink of anthropogenically induced enthalpy.
- Chapter 65 considers a theoretical study of water mass transformation analysis.

Chapter 61

TRACER ADVECTION AND DIFFUSION

In this chapter we study physical and mathematical aspects of advection and diffusion. These two processes affect matter concentrations through stirring and mixing, and as such we frame the presentation in terms of the tracer equation. Advection and diffusion also affect momentum and vorticity, though both are also affected by other processes such as pressure and Coriolis (for momentum; see Chapter 21) and stretching, twisting, and baroclinicity (for vorticity; see Chapter 37).

In the absence of diffusion, advection imparts a reversible stirring of fluid elements that increases the magnitude of tracer gradients. In contrast, diffusion provides an irreversible mixing of fluid elements that reduces the magnitude of tracer gradients. When acting together, advection is no longer a pure stirring and diffusion is no longer a pure mixing. [Eckart \(1948\)](#) articulated what has become the standard conceptual paradigm for stirring and mixing in geophysical fluids, with elements of that paradigm reflected in this chapter.

CHAPTER GUIDE

We make use of the tracer equation derived in Section 17.1, with results relevant for matter transport in both the atmosphere and ocean. Notably, results for the oceanic Boussinesq fluid of Chapter 26 are found merely by setting the density factor, ρ , to a constant where it appears in the non-Boussinesq equations. The discussion of Green's functions in Section 61.10 supplements the [Haine et al. \(2022\)](#) review paper that summarizes many applications of Green's functions for passive ocean tracers. We assume familiarity with the Green's function material presented in Chapter 4.

61.1	Loose threads	1494
61.2	Introduction	1494
61.3	Diffusion physics	1495
61.3.1	Diffusion of matter by random molecular motions	1495
61.3.2	Diffusion of matter by random turbulent motions	1496
61.3.3	Fick's law for matter diffusion	1496
61.3.4	Fourier's law for heat diffusion	1497
61.3.5	Newtonian frictional stress and momentum diffusion	1498
61.3.6	Further study	1498
61.4	Diffusion maths	1498
61.4.1	Sample diffusion tensors	1499
61.4.2	Diffusion of tracer concentration powers	1500
61.4.3	Moments of tracer concentration	1500
61.4.4	Connecting tracer variance to the diffusion operator	1501
61.5	Advection physics	1504

61.5.1	The advection equation	1504
61.5.2	Eulerian time tendencies from advection	1505
61.5.3	Impermeability property of tracer isosurfaces	1505
61.6	Advection maths	1505
61.6.1	Material constancy of C^Γ	1506
61.6.2	Mass transport	1506
61.6.3	Advective tracer fluxes and skew tracer fluxes	1507
61.6.4	Skew diffusion	1508
61.6.5	A comment about skew fluxes and Lagrangian kinematics	1509
61.6.6	Further reading	1509
61.7	Advection and skewson	1509
61.7.1	Choosing a gauge	1509
61.7.2	Vertical gauge	1510
61.7.3	Boundary conditions	1511
61.8	Finite volume budgets with eddy velocities	1512
61.8.1	Advective formulation	1512
61.8.2	Skew flux formulation	1513
61.8.3	Domain with a tracer boundary	1514
61.8.4	Budget for a region with interior sides	1516
61.8.5	Budget for a stirred fluid in a region with interior sides	1518
61.9	Active tracers and dia-surface flow	1521
61.9.1	Adiabatic flow	1521
61.9.2	Diabatic processes generating dia-surface transport	1521
61.10	Green's function method for passive tracers	1523
61.10.1	Concerning time dependent domain boundaries	1523
61.10.2	Passive tracer boundary conditions	1523
61.10.3	Advection-diffusion initial-boundary value problem	1525
61.10.4	The Green's function and its adjoint	1525
61.10.5	Reciprocity relation	1526
61.10.6	Composition property	1529
61.10.7	Integral expression for the tracer concentration	1530
61.10.8	Properties of the solution	1532
61.10.9	Boundary propagator	1533
61.11	Exercises	1535

61.1 Loose threads

- Schematic for the boundary propagator.
- Schematic of the effects from diffusion on different length scales. Emulate figure 14.8 of *Cushman-Roisin and Beckers* (2011).
- Section 12.2 of *Smythe and Carpenter* (2019) have a diffusion example that would form the basis of a nice exercise.

61.2 Introduction

As derived in Section 17.1, the tracer equation takes on the general form

$$\rho \frac{DC}{Dt} = -\nabla \cdot \mathbf{J}(C), \quad (61.1)$$

where \mathbf{J} is a flux that embodies molecular diffusion as well as subgrid scale advection and subgrid scale diffusion (Chapter 63). Advective transport appears when transforming to an Eulerian or

laboratory reference frame, in which case

$$\rho \frac{DC}{Dt} = \frac{\partial(\rho C)}{\partial t} + \nabla \cdot (\mathbf{v} \rho C), \quad (61.2)$$

with $\mathbf{v} \rho C$ the advective flux. In the absence of diffusion, advection renders a reversible stirring and stretching of fluid elements that generally increases the magnitude of concentration gradients. Advection does so while maintaining, for each fluid element, a fixed mass for all matter constituents and fixed specific entropy.¹ In contrast, diffusion affects an irreversible exchange, or mixing, of matter, thermodynamic, and mechanical properties between fluid elements. Correspondingly, diffusion reduces the magnitude of property gradients as it irreversibly exchanges properties between fluid elements.

61.3 Diffusion physics

The continuum approximation from Chapter 13 proposes that a macroscopic description of fluid motion does not require direct information about the motion of individual molecules. Nonetheless, random molecular motion and properties of the constituent molecules impact on fluid motion through the process of *molecular diffusion* of matter. Analogously, the random motion of fluid elements within a turbulent fluid give rise to *turbulent diffusive transport*.² In this section, we explore the basic physical nature of molecular and turbulent diffusion.

61.3.1 Diffusion of matter by random molecular motions

Consider a fluid comprised of a single matter constituent, such as a lake of pure H_2O . As discussed in Section 14.3, for a macroscopic description of this single-component fluid, a constant mass fluid element is identical to a constant mass material fluid parcel. That is, there is no mixing of matter since there is just a single matter component. Now place a dye tracer (Section 17.2) into a corner of the lake so that the lake is comprised of two material components (H_2O and dye). Even in the absence of ambient macroscopic fluid motion, the random motion of water and dye molecules produces an exchange of matter constituents between fluid elements. Consequently, the dye spreads outward from its initial position; i.e., it *diffuses* into the surrounding water.

We introduced the notion of matter exchange between fluid elements when discussing the tracer equation in Section 17.1. In the present context, matter exchange occurs through the random motion of molecules acting in the presence of a matter concentration gradient. Even though the continuum approximation has removed all explicit concern for details of molecular motion, we confront the underlying molecular nature of matter since molecular motions have a measurable impact on macroscopic fluid properties. This transport of matter by random molecular motions is known as *molecular diffusion*. A statistical description of molecular diffusion was first given by Einstein through his investigations of Brownian Motion ([Einstein, 1905](#)).

Diffusion of matter is a familiar process. For example, the odor from an open perfume bottle will spread throughout a room, even in the absence of macroscopic motion of air in the room. When the ambient macroscopic motion is zero, the spread of the perfume arises from random molecular motions whose properties depend on details of the molecules (e.g., their size, speed, inter-molecular forces). The time scale for molecular diffusion is generally much longer than the analogous *turbulent diffusion* that results if there is random motion in the macroscopic fluid, such as occurs by placing a fan next to the perfume bottle.

¹Recall from Chapter 19 that specific entropy remains materially constant on fluid elements in the absence of mixing.

²For our purposes, turbulence is characterized by a quasi-random motion of fluid elements.

61.3.2 Diffusion of matter by random turbulent motions

It is common for geophysical fluid systems to exhibit some form of turbulent motion. In these systems, the spread of matter by macroscopic turbulent motion is many times more efficient than the spread of matter from molecular motion. In such cases, we are justified in ignoring molecular diffusion since the efficiency of the turbulent diffusive transport is far greater than that from molecular diffusion.

[Taylor \(1921\)](#) described the statistical properties of turbulent diffusion, with many of his insights forming the basis for theories of how turbulent motion impacts on matter concentrations. In Taylor's theory, turbulent diffusion is not concerned with details of the molecular properties of the fluid. Rather, the properties of turbulent diffusion (e.g., the efficiency of the turbulent diffusion) depend just on the nature of the turbulent motion of fluid elements. In this way, turbulent diffusion as described by Taylor is a phenomena that sits fully in the realm of continuum mechanics, whereas molecular diffusion in a gas is a subject for kinetic theory and statistical mechanics. Correspondingly, each type of turbulent motion gives rise to a distinct form of turbulent diffusion. For example, in a geophysical context, turbulent diffusion associated with the breaking of internal gravity waves is distinct from turbulent diffusion by geostrophic eddies.

61.3.3 Fick's law for matter diffusion

Consider a fluid with a non-uniform matter concentration such as that drawn for a one-dimensional case in Figure 61.1. Random motion, due either to molecular motion or turbulent fluctuations, will transfer matter across an arbitrary point, line, or plane. Random motion preferentially moves matter from regions of high concentration to regions of low concentration, thus smoothing gradients. To a good approximation, the mass flux (mass per time per cross-sectional area) of matter is linearly proportional to the concentration gradient, and thus can be written in the form

$$\mathbf{J} = -\kappa_c \rho \nabla C. \quad (61.3)$$

In this equation, we introduced the positive proportionality factor, $\kappa_c > 0$, known as the *kinematic diffusivity*, whereas the product $\kappa_c \rho$ is known as the *dynamic diffusivity*:

$$\kappa_c \quad \text{kinematic diffusivity with SI units m s}^{-2} \quad (61.4)$$

$$\rho \kappa_c \quad \text{dynamic diffusivity with SI units kg m}^{-2} \text{ s}^{-2}. \quad (61.5)$$

The kinematic diffusivity has dimensions of squared length per time and it sets the efficiency or strength of the diffusion. The diffusive flux (61.3) is known as *Fick's law* of matter diffusion. It is the most common mathematical form used to represent the mixing of matter through diffusion. The minus sign in the diffusive flux arises since the flux is directed down the concentration gradient. When considering molecular diffusion, we distinguish diffusivities according to their respective tracers since they generally differ, whereas turbulent diffusivities are generally independent of tracer, in which case we write the generic, κ .

The kinematic diffusivity has physical dimensions equal to the product of a length and a speed. For molecular diffusion, the kinematic diffusivity is proportional to the mean free path, L_{mfp} (see Section 13.3.3), and the root-mean-square molecular speed, v_{rms} (see Section 13.3.4). Each of these properties is a function of the molecules comprising the matter. For air, the mean free path is roughly 2×10^{-7} m and the root-mean-square speed is 500 m s^{-1} , so that $L_{\text{mfp}} v_{\text{rms}} \approx 10^{-4} \text{ m}^2 \text{ s}^{-1}$. The precise value for the molecular diffusivity depends on the molecular properties of the matter diffusing through air. For turbulent diffusion, Prandtl suggested that we consider a characteristic length and velocity scale determined by properties of the turbulent flow. The turbulent length

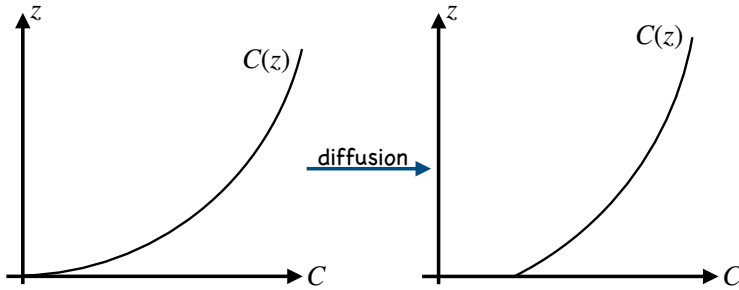


FIGURE 61.1: Shown here is a line graph illustrating the concentration, C , of a tracer drawn as a function of the space coordinate z , with the left panel showing the concentration at an earlier time than the right panel. Across any arbitrary point, transport of matter through random motions generally reduces the magnitude of the concentration gradient; i.e., the diffusive transport is down the concentration gradient. For example, where the concentration is relatively high, random motion mixes this high concentration with adjacent lower concentration, acting to lower the concentration in the originally high concentration region and raise the concentration in the originally low concentration region. In this particular example, $\partial C / \partial z > 0$, so that random fluid motions (either molecular or turbulent) lead to a diffusive flux directed in the $-\hat{z}$ direction; i.e., downward. This downward flux brings high concentration fluid into the lower/deeper regions and low concentration fluid into higher/shallower regions. The concentration is vertically uniform if allowed to equilibrate under the action of diffusion, thus leading to a vertical concentration profile.

scale (also called the *mixing length*) is generally much larger than the molecular mean free path, whereas the turbulent velocity scale is much smaller than molecular speeds. Determination of these turbulent length and velocity scales is subject to large uncertainties and is the topic of much research.

In regions where the diffusive flux is not a constant, there will be a net transport of matter that leads to the reduction of the tracer concentration gradient. At a particular point in space, the concentration changes in time according to the convergence of the diffusive flux

$$\rho \frac{DC}{\partial t} = -\nabla \cdot \mathbf{J} = \nabla \cdot (\kappa_c \rho \nabla C). \quad (61.6)$$

That is, the concentration increases in regions where the diffusive flux, \mathbf{J} , converges, and decreases where the flux diverges. Expanding the divergence operator leads to

$$\rho \frac{DC}{\partial t} = \nabla(\kappa_c \rho) \cdot \nabla C + \rho \kappa_c \nabla^2 C. \quad (61.7)$$

The first term is nonzero in regions where the dynamic diffusivity, $\kappa_c \rho$, spatially varies. The second term is nonzero in regions where the curvature of the concentration is nonzero. Correspondingly, when the tracer concentration is uniform in space then both terms vanish, whereas the Laplacian term also vanishes when the concentration is linear in space.

61.3.4 Fourier's law for heat diffusion

In the same way that matter concentration gradients lead to diffusion by random motions, temperature gradients lead to diffusion of heat. The corresponding phenomenological relation is known as *Fourier's law*, with the diffusive flux given by

$$\mathbf{J} = -\kappa_T \rho \nabla T, \quad (61.8)$$

where $\kappa_T > 0$ is the temperature diffusivity. As for the matter diffusivity, the molecular thermal diffusivity can be expressed in terms of fundamental properties of the fluid, and it is different from the matter diffusivity. In general, matter diffuses by molecular processes slower than heat, so that

the matter molecular diffusivity is smaller than the heat molecular diffusivity. The reason for the difference is that matter diffusion requires the movement of matter (molecules), whereas heat diffusion occurs through the exchange of thermal energy between molecules, and that exchange does not require the motion of matter. In contrast, the turbulent thermal diffusivity is roughly the same as the matter diffusivity. The reason is that the turbulent diffusion of matter and heat are both mediated by the same turbulent fluctuations of fluid elements.

61.3.5 Newtonian frictional stress and momentum diffusion

In the same way that matter concentration and temperature gradients lead to diffusion by random motions, the momentum of fluid elements is exchanged through diffusion in the presence of viscosity. The corresponding phenomenological relation is known as *Newton's law* of viscous friction. As momentum is a vector, a general treatment of momentum transport through irreversible viscous processes involves a second order stress tensor and a fourth order viscosity tensor. For the specific case shown in Figure 61.2, with shear (i.e., nonzero velocity gradient) in a single direction, Newtonian frictional stress takes the form

$$\tau = \rho \mu \frac{\partial u}{\partial z}, \quad (61.9)$$

where $\mu > 0$ is the kinematic viscosity. Note the absence of a minus sign, in contrast to diffusive fluxes of scalars. The sign difference arises since it is the divergence of the stress tensor that leads to contact forces on the fluid, whereas it is the convergence of diffusive fluxes that leads to diffusion of matter and heat. We consider these general properties of the stress tensor when exploring the fluid dynamical equations in Chapter 21 and the nature of stress in Chapter 22.

For geophysical fluid mechanics, we are most generally interested in the molecular viscosity of water and air. Quite generally, the dynamic viscosity of water ($\rho \mu$) is about 10^2 times larger than that for air. But since the density of water is about 10^3 times larger than air, the kinematic viscosity of air is roughly 10 times greater than that of water.

The molecular kinematic viscosity can be expressed in terms of fundamental properties of the fluid, and it is different from the molecular matter diffusivity and molecular thermal diffusivity. For some turbulent processes, the turbulent viscosity, μ , is proportional to the turbulent diffusivity, κ , of scalar fields (e.g., temperature, salinity, humidity). In general, the non-dimensional ratio of the viscosity to the diffusivity is known as the *Prandtl number*

$$\text{Pr} = \mu/\kappa. \quad (61.10)$$

Theories for the turbulent Prandtl number are largely empirical, with first principles arguments elusive.

61.3.6 Further study

More thorough treatments of molecular diffusion for ideal gases can be found in books that describe the kinetic theory of gases, such as [Reif \(1965\)](#) and [Huang \(1987\)](#). The more terse treatment given in this section largely follows that from Section 1.5 of [Kundu et al. \(2016\)](#). A lucid treatment of Brownian motion in the context of turbulent diffusion is given by [Vallis \(2017\)](#).

61.4 Diffusion maths

We now explore various mathematical properties of the diffusion equation, here generalized to allow for distinct behavior in the different directions. Such distinctions are relevant especially

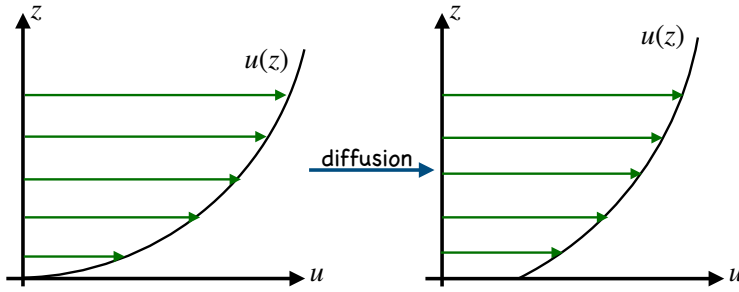


FIGURE 61.2: Shown here is a line graph illustrating the zonal velocity, u , as a function of the space coordinate z , with the left panel showing the velocity at an earlier time than the right panel. Across any arbitrary point, transport of momentum through random motions generally reduces the magnitude of the velocity gradient; i.e., the diffusive transport leads to a viscous stress that acts to reduce the velocity shear.

in stratified fluids, where turbulent mixing across stratification surfaces is suppressed relative to turbulent mixing parallel to these surfaces (see Section 27.4). For this purpose, introduce the second order symmetric and positive definite *diffusion tensor* $\mathbb{K}_{mn} = \mathbb{K}_{nm}$. The resulting diffusive tracer flux takes the form

$$J_m = -\rho \mathbb{K}_{mn} \frac{\partial C}{\partial x^n}, \quad (61.11)$$

and the corresponding material diffusion equation is

$$\rho \frac{DC}{dt} = -\nabla \cdot \mathbf{J} = \frac{\partial(\rho \mathbb{K}_{mn} \partial_n C)}{\partial x_m}. \quad (61.12)$$

61.4.1 Sample diffusion tensors

For the isotropic case of molecular diffusion considered in equation (61.3), the diffusion tensor takes on the form

$$\mathbb{K}_{mn} = \kappa \delta_{mn} \quad \text{isotropic diffusion.} \quad (61.13)$$

If we rotate the diffusive fluxes to be along surfaces of constant a constant scalar field, $\gamma(\mathbf{x}, t)$, then

$$\mathbb{K}_{mn} = \kappa (\delta_{mn} - \hat{\gamma}_m \hat{\gamma}_n) \quad \text{rotated diffusion,} \quad (61.14)$$

where

$$\hat{\gamma} = \frac{\nabla \gamma}{|\nabla \gamma|} \quad (61.15)$$

is the normal to the surface. The most common case in geophysical fluids, especially in oceanography, to set γ equal to a measure of the buoyancy, in which case we have *neutral diffusion* (see Section 63.4).

61.4.2 Diffusion of tracer concentration powers

For certain applications it is of interest to determine how diffusion acts on powers of the tracer concentration. For this purpose consider the material evolution of C^Γ , where $\Gamma \geq 1$

$$\rho \frac{DC^\Gamma}{Dt} = \Gamma C^{\Gamma-1} \rho \frac{DC}{Dt} \quad (61.16a)$$

$$= -\Gamma C^{\Gamma-1} \nabla \cdot \mathbf{J} \quad (61.16b)$$

$$= -\Gamma \nabla \cdot (C^{\Gamma-1} \mathbf{J}) + \Gamma (\Gamma - 1) C^{\Gamma-2} \nabla C \cdot \mathbf{J} \quad (61.16c)$$

$$= \partial_m \left[\rho \mathbb{K}_{mn} \frac{\partial C^\Gamma}{\partial x^n} \right] - \rho \Gamma (\Gamma - 1) C^{\Gamma-2} \frac{\partial C}{\partial x^m} \mathbb{K}_{mn} \frac{\partial C}{\partial x^m} \quad (61.16d)$$

$$= -\nabla \cdot \mathbf{J}(C^\Gamma) + \Gamma (\Gamma - 1) C^{\Gamma-2} \mathbf{J} \cdot \nabla C. \quad (61.16e)$$

The first term in equation (61.16e) is the convergence of the diffusive flux defined in terms of C^Γ , and it acts to diffuse C^Γ just like diffusion acts on C . The second term in equation (61.16e) is negative since the diffusion tensor is symmetric and positive-definite

$$\mathbf{J} \cdot \nabla C = -\rho \mathbb{K}_{mn} \frac{\partial C}{\partial x^m} \frac{\partial C}{\partial x^n} < 0. \quad (61.17)$$

That is, the diffusive flux, by construction, is oriented down the tracer concentration gradient. Consequently, the second term in equation (61.16e) always acts to reduce the magnitude of C^Γ towards zero.

61.4.3 Moments of tracer concentration

Consider the evolution of domain integrated tracer concentration and its powers, and focus on impacts just from diffusion. For that purpose, assume the boundaries are insulating so that $\mathbf{J} \cdot \hat{\mathbf{n}} = 0$ with $\hat{\mathbf{n}}$ the outward normal at the boundary. Also assume the total fluid mass in the domain remains fixed

$$m = \int \rho dV \iff \frac{dm}{dt} = 0. \quad (61.18)$$

We can thus treat the domain as material given that there is no exchange of mass or tracer across the boundaries.

Domain average tracer concentration

The domain averaged tracer concentration is given by

$$\bar{C} = \frac{\int C \rho dV}{m}, \quad (61.19)$$

and it follows that its time derivative vanishes since

$$m \frac{d\bar{C}}{dt} = \frac{d}{dt} \int C \rho dV = \int \frac{DC}{Dt} \rho dV = - \int \nabla \cdot \mathbf{J} dV = - \oint \mathbf{J} \cdot \hat{\mathbf{n}} d\mathcal{S} = 0, \quad (61.20)$$

where we set $\mathbf{J} \cdot \hat{\mathbf{n}} = 0$ to reach the last equality. Also note that we brought the time derivative inside the integral as a material derivative since the region is itself material, thus allowing us to make use of Reynold's transport theorem from Section 17.3.6. The result (61.20) follows since there is no change in the total mass of fluid nor is there any exchange of tracer across the boundaries. Hence, the domain averaged tracer concentration remains fixed in time.

Tracer variance within the domain

The variance of the tracer concentration is defined by

$$\text{var}(C) \equiv \frac{\int (C - \bar{C})^2 \rho dV}{m} = \bar{C^2} - \bar{C}^2 \geq 0. \quad (61.21)$$

The tracer variance measures the deviation of the tracer concentration relative to the domain averaged concentration. Since the domain average remains fixed in time, the time change of the variance is given by

$$\frac{d[\text{var}(C)]}{dt} = \frac{d\bar{C^2}}{dt}. \quad (61.22)$$

Thus, it is common to refer to $\bar{C^2}$ as the tracer variance, though strictly speaking only time derivatives of $\bar{C^2}$ and $\text{var}(C)$ are equal as per equation (61.22). Performing the time derivative, and again noting that the domain is material thus allowing us to use Reynolds transport theorem, renders

$$m \frac{d\bar{C^2}}{dt} = \frac{d}{dt} \int C^2 \rho dV = 2 \int C \frac{DC}{Dt} \rho dV = -2 \int C \nabla \cdot \mathbf{J} dV = 2 \int \nabla C \cdot \mathbf{J} dV. \quad (61.23)$$

The final equality again made use of the assumed boundary condition $\mathbf{J} \cdot \hat{\mathbf{n}} = 0$. The time change in the tracer variance is thus determined by the integral of the projection of the tracer flux onto the tracer gradient. We already saw from equation (61.17) that diffusive fluxes are oriented down the tracer gradient. Consequently, diffusion of the tracer concentration results in a reduction in tracer variance

$$\frac{d[\text{var}(C)]}{dt} = \frac{d\bar{C^2}}{dt} \leq 0. \quad (61.24)$$

This result further supports our common experience where diffusion removes differences (i.e., gradients) within the tracer field.

Diffusion of arbitrary tracer moments

Proceeding as before, and dropping boundary contributions since the domain is material and insulating, it is straightforward to show that the time derivative of an arbitrary tracer moment is given by

$$\frac{d\bar{C^\Gamma}}{dt} = \Gamma(\Gamma - 1) \int C^{\Gamma-2} \nabla C \cdot \mathbf{J} dV \leq 0. \quad (61.25)$$

For $\Gamma = 0$ we have an expression of mass conservation for the domain, whereas $\Gamma = 1$ is an expression of tracer conservation. The case of $\Gamma = 2$ yields the tracer variance result (61.24). The result for higher powers also holds. Hence, we conclude that the downgradient orientation of diffusive tracer fluxes acts to dissipate all powers of tracer concentration when integrated globally; i.e., all tracer moments are dissipated by diffusion.

61.4.4 Connecting tracer variance to the diffusion operator

We take a brief and very informal excursion into linear operator theory, in which we note that with natural boundary conditions (defined below) on the diffusive tracer flux, the diffusion operator is a linear *self-adjoint operator*.³ Consequently, the diffusion operator is related to a negative semi-

³We discussed the self-adjoint nature of the diffusion operator in Section 4.6.4 in our study of the Green's function for the diffusion equation.

definite functional (e.g., *Courant and Hilbert*, 1953, 1962). In the simplest case, the Laplacian operator $\nabla^2 C$ is equal to the functional derivative $\nabla^2 C = \delta\mathcal{F}/\delta C$, where

$$\mathcal{F} \equiv -\frac{1}{2} \int |\nabla C|^2 \rho \, d\mathbf{x} \quad (61.26)$$

is the associated functional. In this subsection we prove this result for a general diffusion tensor \mathbb{K}_{mn} acting on an arbitrary tracer concentration, C , so long as the diffusion tensor is not a function of the tracer concentration. As detailed by *Griffies et al.* (1998) and Chapter 16 of *Griffies* (2004), the connection between the diffusion operator and the functional derivative of the diffusion dissipation provides a useful framework for deriving numerical discretizations of the diffusion operator.

For this subsection it is useful to write the volume element for integration using the notation

$$d\mathbf{x} = dV. \quad (61.27)$$

The reason will become apparent when reaching equation (61.35).

Derivative of the diffusion dissipation functional

We introduce the *diffusion dissipation functional*

$$\mathcal{F} = \int \mathcal{L} \, d\mathbf{x} \quad (61.28)$$

where the integrand is the negative semi-definite quadratic form

$$2\mathcal{L} = \mathbf{J} \cdot \nabla C = -\rho \partial_m C \mathbb{K}_{mn} \partial_n C \leq 0. \quad (61.29)$$

Our goal is to relate the diffusion operator, given by the convergence of the diffusion flux, $\mathcal{R} = -\nabla \cdot \mathbf{J}$, to the functional derivative of \mathcal{F} . To compute the functional derivative requires us to insert functional variations to the tracer field, written as δC , into the dissipation functional

$$\delta\mathcal{F} = \int \left[\delta C \frac{\delta\mathcal{L}}{\delta C} + \delta(\partial_m C) \frac{\delta\mathcal{L}}{\delta(\partial_m C)} \right] d\mathbf{x}. \quad (61.30)$$

Functional variations are small perturbations to the form of the function, in which case

$$C \rightarrow C + \delta C \quad \text{with} \quad |\delta C| \ll |C|. \quad (61.31)$$

Notably, δC is itself a function of space and time, $\delta C(\mathbf{x}, t)$, but it is assumed to have much smaller magnitude than the concentration, $C(\mathbf{x}, t)$. Integration by parts on the second term leads to

$$\delta\mathcal{F} = \int \left[\delta C \frac{\delta\mathcal{L}}{\delta C} + \partial_m \left(\delta C \frac{\delta\mathcal{L}}{\delta(\partial_m C)} \right) - \delta C \partial_m \left(\frac{\delta\mathcal{L}}{\delta(\partial_m C)} \right) \right] d\mathbf{x}. \quad (61.32)$$

The middle term is a total derivative that integrates to a boundary contribution and the associated *natural boundary condition*

$$\hat{\mathbf{n}} \cdot \frac{\delta\mathcal{L}}{\delta \nabla C} = \hat{\mathbf{n}} \cdot \mathbf{J} = \text{boundary flux}, \quad (61.33)$$

with $\hat{\mathbf{n}}$ the boundary outward normal. This natural boundary condition is the familiar *Neumann boundary condition* from Chapter 4.

To focus on the connection between the diffusion operator and the diffusion dissipation functional, we ignore boundary fluxes so that the functional variation is given by

$$\delta\mathcal{F} = \int \delta C \left[\frac{\delta\mathcal{L}}{\delta C} - \partial_m \left(\frac{\delta\mathcal{L}}{\delta(\partial_m C)} \right) \right] d\mathbf{x}. \quad (61.34)$$

Consequently, the functional derivative is given by

$$(d\mathbf{y})^{-1} \frac{\delta\mathcal{F}}{\delta C(\mathbf{y})} = \frac{\delta\mathcal{L}}{\delta C} - \partial_m \left[\frac{\delta\mathcal{L}}{\delta(\partial_m C)} \right], \quad (61.35)$$

where $d\mathbf{y}$ is the volume element at the field point, \mathbf{y} . To reach the last step required the identity

$$\frac{\delta C(\mathbf{x})}{\delta C(\mathbf{y})} = d\mathbf{y} \delta(\mathbf{x} - \mathbf{y}), \quad (61.36)$$

where $\delta(\mathbf{x} - \mathbf{y})$ is the *Dirac delta*⁴ satisfying

$$\int \delta(\mathbf{x} - \mathbf{y}) d\mathbf{y} = 1, \quad (61.37)$$

so long as the integration range includes the singular point $\mathbf{x} = \mathbf{y}$. Note that the Dirac delta has dimensions of inverse volume, which necessitates the appearance of the volume factor, $d\mathbf{y}$, on the right hand side of equation (61.36).⁵

Connection to the diffusion operator

Reintroducing the specific form of the diffusion integrand $2\mathcal{L} = -\rho \partial_m C \mathbb{K}_{mn} \partial_n C$ leads to

$$\frac{\delta\mathcal{F}}{\delta C(\mathbf{y})} = -\partial_m \left[\frac{\delta\mathcal{L}}{\delta(\partial_m C)} \right] d\mathbf{y} = \partial_m (\rho \mathbb{K}_{mn} \partial_n C) d\mathbf{y}. \quad (61.38)$$

The second equality identifies the diffusion operator, thus revealing the connection between the dissipation functional, the diffusion fluxes, and the diffusion operator

$$\frac{\delta\mathcal{F}}{\delta C(\mathbf{y})} = -(\nabla \cdot \mathbf{J}) d\mathbf{y} = \mathcal{R} d\mathbf{y}. \quad (61.39)$$

Why did we assume \mathbb{K}_{mn} is independent of C ?

There are many geophysical applications in which the diffusion tensor is a function of the tracer concentration, in which case the diffusion equation is no longer a linear differential equation. For example, the neutral diffusion of Section 63.4 makes use of a diffusion tensor that is a function of temperature and salinity gradients. In this case the functional derivative in terms of temperature or salinity appearing in equation (61.38) becomes

$$2 \frac{\delta\mathcal{L}}{\delta(\partial_m C)} = -2\rho \mathbb{K}_{mn} \partial_n C - \rho \partial_m C \partial_n C \frac{\delta \mathbb{K}_{mn}}{\delta(\partial_m C)}. \quad (61.40)$$

⁴We provide a thorough discussion of the Dirac delta in Section 4.3.

⁵Many treatments of functional derivatives in mathematics texts ignore the volume factor in equation (61.36). For physical applications it is important to maintain dimensional consistency, thus requiring us to retain the volume factor.

The specific form of the term $\delta K_{mn}/\delta(\partial_m C)$ depends on details of the diffusion tensor. Hence, the general results derived above for the linear diffusion equation no longer hold for this nonlinear diffusion equation. We have more to say about nonlinear advection-diffusion in Section 61.9.

61.5 Advection physics

A *perfect* fluid is comprised of material fluid elements whose matter content and thermodynamic properties remain fixed. From the discussion of molecular diffusion in Section 61.3, we know that a perfect fluid can at most consist of a single matter constituent and uniform thermodynamic properties. The reason is that in the presence of multiple constituents with non-uniform concentrations, molecular motions irreversibly exchange matter and thermodynamic properties (e.g., temperature, specific entropy) among fluid elements. This exchange, or mixing, breaks the assumption of a perfect fluid. Nonetheless, we find many occasions to ignore molecular diffusion when focusing on macroscopic motions of the continuum fluid. Such is the case when considering the advection equation in the absence of any mixing.

61.5.1 The advection equation

In the absence of mixing or other irreversible processes, the matter content of a fluid element remains fixed as the element moves with the fluid. Since the total mass of the element is also constant, then the tracer concentration remains constant and thus satisfies the reversible (source-free) *advection equation*

$$\frac{DC}{Dt} = \frac{\partial C}{\partial t} + \mathbf{v} \cdot \nabla C = 0. \quad (61.41)$$

The first equality relates the material time derivative to the Eulerian time derivative plus advective transport (see Section 14.6), with \mathbf{v} the velocity of a fluid element. We can convert the *material* form of the advection equation (61.41) into its flux-form by combining with the mass continuity equation (16.6)

$$\frac{\partial \rho}{\partial t} + \nabla \cdot (\rho \mathbf{v}) = 0, \quad (61.42)$$

which yields

$$\frac{\partial(\rho C)}{\partial t} + \nabla \cdot (\rho C \mathbf{v}) = 0. \quad (61.43)$$

Again, the material form of the advection equation is the trivial statement that tracer concentration remains constant on a fluid element in the absence of sources or mixing. Hence, a general solution to the advection equation is given by

$$C(\mathbf{x}, t) = C[\mathbf{X}(0)], \quad (61.44)$$

where $\mathbf{X}(0)$ is the initial position of a fluid element that is at the position \mathbf{x} at time t . If we know the trajectories for all fluid elements and their initial tracer concentration, we know the tracer concentration for all space and time. For those cases where trajectories are unknown, it is useful to make use of the Eulerian form of the advection equation in order to deduce the evolution of tracer.

61.5.2 Eulerian time tendencies from advection

At a point in the fluid, the advection equation (61.41) leads to the Eulerian time tendency for tracer concentration

$$\frac{\partial C}{\partial t} = -\mathbf{v} \cdot \nabla C. \quad (61.45)$$

Geometrically, the tendency arises from the projection of the fluid velocity onto the normal to concentration iso-surfaces. The concentration remains fixed in time (steady) at points where the velocity is parallel to concentration iso-surfaces. From the flux-form advection equation (61.43), the density-weighted tracer concentration (the tracer mass per volume) has an Eulerian time tendency given by the convergence of the advective flux

$$\frac{\partial(\rho C)}{\partial t} = -\nabla \cdot (\rho C \mathbf{v}). \quad (61.46)$$

The tendency vanishes at a point if there is no convergence of tracer mass towards the point.

61.5.3 Impermeability property of tracer isosurfaces

We now offer a geometric interpretation of the advection equation

$$\frac{\partial C}{\partial t} + \mathbf{v} \cdot \nabla C = 0, \quad (61.47)$$

following the discussion of dia-surface transport in Section 57.4. For this purpose, introduce the unit normal on a tracer isosurface

$$\hat{\mathbf{n}} = \frac{\nabla C}{|\nabla C|} \quad (61.48)$$

and the normal projection for the velocity of a point on that surface

$$\mathbf{v}^{(b)} \cdot \hat{\mathbf{n}} = -\frac{\partial_t C}{|\nabla C|}. \quad (61.49)$$

The advection equation (61.47) thus can be written as an impermeability condition for a tracer isosurface

$$\rho(\mathbf{v} - \mathbf{v}^{(b)}) \cdot \hat{\mathbf{n}} = 0 \quad \text{on } C \text{ isosurfaces.} \quad (61.50)$$

We encountered this condition in Section 16.4.2 when studying the kinematics of a moving material surface. Hence, in the absence of mixing, tracer isosurfaces are indeed material surfaces since they allow no fluid elements, moving with the fluid velocity \mathbf{v} , to cross them. This is an important kinematic result that will be extended in Section 61.8.5 to include effects from an eddy induced velocity.

61.6 Advection maths

We now explore various mathematical properties of the advection equation. For that purpose, recall the mass continuity equation (61.42) and flux-form tracer advection equation (61.46)

$$\frac{\partial \rho}{\partial t} + \nabla \cdot (\rho \mathbf{v}) = 0 \quad (61.51a)$$

$$\frac{\partial(\rho C)}{\partial t} + \nabla \cdot (\rho C \mathbf{v}) = 0. \quad (61.51b)$$

These equations are manifestly compatible in that the tracer equation (61.51b) reduces to the continuity equation (61.51a) if the tracer concentration is spatially uniform (see Section 17.1.4 for more discussion of compatibility).

61.6.1 Material constancy of C^Γ

A trivial consequence of the material constancy of tracer concentration is that C^Γ is also materially constant, for Γ an arbitrary number. We show this property mathematically by noting that the chain rule holds for a material time derivative, so that

$$\frac{DC^\Gamma}{Dt} = \Gamma C^{\Gamma-1} \frac{DC}{Dt} = 0. \quad (61.52)$$

Likewise, making use of the Eulerian form yields

$$\frac{\partial C^\Gamma}{\partial t} + \mathbf{v} \cdot \nabla C^\Gamma = \Gamma C^{\Gamma-1} \left[\frac{\partial C}{\partial t} + \mathbf{v} \cdot \nabla C \right] = 0. \quad (61.53)$$

We conclude that advection, in the absence of diffusion, serves to reversibly transport the tracer concentration without altering any of its powers. Correspondingly, all tracer moments are untouched by advection, which contrasts to the case of diffusion considered in Section 61.4.3.

61.6.2 Mass transport

The mass density time tendency

$$\frac{\partial \rho}{\partial t} = -\nabla \cdot (\mathbf{v} \rho) \quad (61.54)$$

remains unchanged if the advective mass flux, $\rho \mathbf{v}$ (dimensions of mass per time per area), is modified by the addition of a total curl

$$\rho \mathbf{v} \rightarrow \rho \mathbf{v}^\dagger = \rho \mathbf{v} + \nabla \times (\rho \Psi^*). \quad (61.55)$$

As in Section 18.4.1, the arbitrariness manifest in equation (61.55) is known as a *gauge symmetry*. The additional mass flux, $\nabla \times (\rho \Psi^*)$, leads to no accumulation of mass at a point since it has zero divergence. In the Boussinesq case with ρ set to a constant ρ_0 , the divergent-free velocity $\nabla \times \Psi^*$ leads to zero accumulation of volume at a point.

The non-divergent mass flux

$$\rho \mathbf{v}^* \equiv \nabla \times (\rho \Psi^*) \quad (61.56)$$

often arises when we decompose the mass flux into a mean and non-divergent eddy fluctuations. In that context, we make use of the following terminology:

$$\mathbf{v} = \text{Eulerian mean velocity} \quad (61.57a)$$

$$\rho \mathbf{v} = \text{Eulerian mean mass flux} \quad (61.57b)$$

$$\mathbf{v}^* = \text{eddy-induced velocity} \quad (61.57c)$$

$$\rho \Psi^* = \text{eddy-induced mass streamfunction} \quad (61.57d)$$

$$\rho \mathbf{v}^* = \nabla \times (\rho \Psi^*) = \text{eddy-induced mass flux} \quad (61.57e)$$

$$\mathbf{v}^\dagger = \mathbf{v} + \mathbf{v}^* = \text{residual mean velocity} \quad (61.57f)$$

$$\rho \mathbf{v}^\dagger = \rho (\mathbf{v} + \mathbf{v}^*) = \text{residual mean mass flux}. \quad (61.57g)$$

The name “residual mean” is motivated since the sum $\mathbf{v} + \mathbf{v}^*$ is often smaller than either term individually. That is, the eddy contribution often compensates for the mean, with sum of the mean and eddy representing a residual. We study particular forms of the eddy induced velocity in Chapter 63.

61.6.3 Advection tracer fluxes and skew tracer fluxes

Following from the previous discussion, we consider the advection equation with the advective tracer transport determined by the residual mean velocity

$$\frac{\partial(\rho C)}{\partial t} + \nabla \cdot (\rho C \mathbf{v}^\dagger) = 0. \quad (61.58)$$

Given the form (61.56) for the eddy mass flux $\rho \mathbf{v}^*$, we can write the *advective tracer flux* as

$$\rho C \mathbf{v}^\dagger = C(\rho \mathbf{v} + \rho \mathbf{v}^*) \quad (61.59a)$$

$$= C \rho \mathbf{v} + C \nabla \times (\rho \Psi^*) \quad (61.59b)$$

$$= C \rho \mathbf{v} + \nabla \times (C \rho \Psi^*) - \nabla C \times \rho \Psi^*. \quad (61.59c)$$

It is the divergence of the tracer flux that determines the time tendency, in which case the total curl plays no role

$$\nabla \cdot (\rho C \mathbf{v}^\dagger) = \nabla \cdot (\rho C \mathbf{v} + \rho C \mathbf{v}^*) \quad (61.60a)$$

$$= \nabla \cdot (\rho C \mathbf{v} - \nabla C \times \rho \Psi^*). \quad (61.60b)$$

That is, the divergence of the advective mass flux equals to the divergence of the *skew tracer flux*

$$\underbrace{\nabla \cdot (\rho C \mathbf{v}^*)}_{\text{advective flux divergence}} = \underbrace{\nabla \cdot (-\nabla C \times \rho \Psi^*)}_{\text{skew flux divergence}} \quad (61.61)$$

since the advective flux and skew flux differ by a rotational flux

$$\mathbf{J}^{\text{adv}} = \mathbf{J}^{\text{skew}} + \mathbf{J}^{\text{rot}} \quad (61.62)$$

where

$$\mathbf{J}^{\text{adv}} = C \rho \mathbf{v}^* \quad \text{and} \quad \mathbf{J}^{\text{skew}} = -\nabla C \times \rho \Psi^* \quad \text{and} \quad \mathbf{J}^{\text{rot}} = \nabla \times (\rho C \Psi^*). \quad (61.63)$$

Notably, the skew tracer flux is neither upgradient nor downgradient. Rather, it is oriented parallel to iso-surfaces of tracer concentration

$$\nabla C \cdot \mathbf{J}^{\text{skew}} = \nabla C \cdot (-\nabla C \times \rho \Psi^*) = 0. \quad (61.64)$$

This orientation serves as motivation for the name “skew.” Figure 61.3 provides a schematic of the skew tracer fluxes.

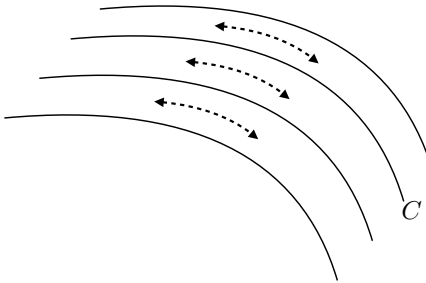


FIGURE 61.3: Skew fluxes (dashed lines with arrows) for a tracer C are oriented parallel to lines of constant tracer concentration (tracer isolines are the solid lines).

61.6.4 Skew diffusion

Introducing tensor labels brings the skew tracer flux into the form

$$J_m^{\text{skew}} = -(\nabla C \times \rho \Psi^*)_m \quad (61.65\text{a})$$

$$= -\epsilon_{mnp} \frac{\partial C}{\partial x^n} \rho \Psi_p^* \quad (61.65\text{b})$$

$$= -\rho \mathbb{A}_{mn} \frac{\partial C}{\partial x^n}, \quad (61.65\text{c})$$

where we defined the anti-symmetric *skew diffusion* tensor

$$\mathbb{A}_{mn} = \epsilon_{mnp} \Psi_p^* \implies \mathbb{A} = \begin{bmatrix} 0 & \Psi_3^* & -\Psi_2^* \\ -\Psi_3^* & 0 & \Psi_1^* \\ \Psi_2^* & -\Psi_1^* & 0 \end{bmatrix}. \quad (61.66)$$

We thus conclude that advection by a non-divergent mass flux is equivalent to skew-diffusion through the action of an anti-symmetric tensor.

Although leading to the same stirring operator, skew and advective fluxes possess rather complementary properties as listed here.

- **DERIVATIVE OPERATOR:** The skew flux is proportional to the vector streamfunction and the gradient of the tracer, whereas the advective flux is related to the curl of the streamfunction and the value of the tracer concentration. That is, the fluxes in effect swap the placement of the derivative operator. Correspondingly, the advective flux vanishes only if the velocity vanishes, whereas the skew flux vanishes when the tracer gradient vanishes (as for a diffusive flux).
- **FLUX ORIENTATION:** The orientation of the advective flux is determined by the velocity field, which is oriented according to trajectories of fluid particles. This orientation is the same regardless of the tracer. In contrast, a skew tracer flux is directed along lines of constant tracer; i.e., it is neither upgradient nor downgradient. Hence, orientation of the skew flux is directly tied to the tracer field, with each tracer yielding a generally distinct flux orientation. The very distinct orientations of the advective and skew fluxes is the origin of much confusion in regards to these fluxes. We explore many features of these geometric distinctions in Section 62.4 when studying eddy induced tracer fluxes.
- **MATERIAL FLUX:** Fluid elements carry a particular amount of trace matter so that an advective flux of a material tracer measures the passage of matter across an area per unit time (dimensions of mass per area per time), whereas a skew flux is not interpreted as the

passage of matter across an area per time. This distinction is particularly important when interpreting boundary conditions discussed in Section 61.7.3.

In Section 61.7 we pursue the above points to further detail the dual relation between advection and skewson.

61.6.5 A comment about skew fluxes and Lagrangian kinematics

The advective tracer flux and skew tracer flux are very distinct vectors and we further explore the distinction in Sections 61.7 and 62.4. As detailed in each of those sections, it is a matter of convenience how one chooses to formulate the Eulerian tracer equation since the advective flux and skew flux lead to the same tracer evolution. Furthermore, the choice to formulate the tracer equation in terms of a skew flux in no way eliminates the Lagrangian perspective. That is, fluid particles, or fluid elements, still move through the fluid and transport tracer as part of this motion. The Lagrangian formulation of tracer evolution is naturally connected, via a transformation of reference frames, to the Eulerian advection equation. Even so, we do not somehow eliminate fluid particle motion when choosing to work with skew tracer fluxes. Instead, we merely choose to formulate the tracer equation in terms of the vector streamfunction rather than the velocity.

61.6.6 Further reading

The uses of residual-mean transport are many and varied in the ocean and atmospheric literature. *Vallis (2017)* offers a thorough and pedagogical treatment. Skew diffusion is treated in *Moffatt (1983)*, in which he raises the connection to fluids with rotation and/or magnetic fields. *Middleton and Loder (1989)* applied these ideas to ocean gravity waves, tides, and Rossby waves. *Griffies (1998)* applied these ideas to the methods used for parameterizing tracer transport from ocean mesoscale eddies.

61.7 Advection and skewson

We introduced skew diffusion in Section 61.6.4 and will again encounter it in Chapterd 62 and 63. Following the terminology of Section 9.2 of *Griffies (2004)*, we refer to *skewson* as any process that leads to tracer transport via skew fluxes, with skew diffusion a particular example. There are occasions where it is conceptually and operationally more convenient to use advective fluxes, such as when considering the transport of tracers by the flow field explicitly resolved by a numerical simulation. In contrast, skew fluxes are sometimes more convenient for certain subgrid scale eddy parameterizations, such as the one discussed in Section 63.1. We here consider facets of advection and skewson for those interested in diving deeper into the details.

61.7.1 Choosing a gauge

Consider an arbitrary divergent-free mass transport

$$\nabla \cdot (\rho \mathbf{v}^*) = 0, \quad (61.67)$$

where the divergent-free constraint is satisfied by introducing a vector streamfunction

$$\rho \mathbf{v}^* = \nabla \times (\rho \Psi^*). \quad (61.68)$$

The streamfunction is arbitrary up to a gauge transformation

$$\rho \Psi' = \rho \Psi^* + \nabla(\rho \Lambda), \quad (61.69)$$

where Λ is a gauge function.

Changes to the skew flux under a gauge transformation

Although the velocity is invariant up to an arbitrary gauge function, the skew flux, $\mathbf{J}^{\text{skew}} = -\nabla C \times \rho \Psi^*$, changes. Nonetheless, the divergence of the skew flux is invariant, as we see by noting that

$$\nabla C \times [\rho \Psi^* + \nabla(\rho \Lambda)] = \nabla C \times (\rho \Psi^*) + \nabla \times [C \nabla(\rho \Lambda)]. \quad (61.70)$$

and since $\nabla \cdot \nabla \times [C \nabla(\rho \Lambda)] = 0$, the flux divergence, $\nabla \cdot \mathbf{J}^{\text{skew}}$, remains unchanged.

Coulomb gauge

We have some freedom in specifying the gauge function. One choice is to set $\Lambda = 0$. However, there are occasions in which it is useful to set the gauge function in a manner to cancel unwanted terms. A gauge commonly used in electrodynamics (e.g., Jackson (1975)) is the *Coulomb gauge*, in which

$$\nabla \cdot (\rho \Psi^*) = 0 \quad \text{Coulomb gauge.} \quad (61.71)$$

Making use of the curl identity (2.37c) leads to the Poisson equation for the vector potential

$$\nabla^2(\rho \Psi^*) = -\nabla \times (\rho \mathbf{v}^*). \quad (61.72)$$

This equation has a free-space Green's function given by the Coulomb-Ampere expression

$$\rho(\mathbf{x}, t) \Psi^*(\mathbf{x}, t) = \nabla \times \int \frac{\rho(\mathbf{x}', t) \mathbf{v}^*(\mathbf{x}', t)}{4\pi |\mathbf{x} - \mathbf{x}'|} dV', \quad (61.73)$$

where dV' is the volume element for integration over the test points, \mathbf{x}' . Although common in electrodynamics, we know of no geophysical fluid application making use of the Coulomb gauge.

61.7.2 Vertical gauge

As introduced in Section 18.4.2, a gauge commonly used for eddy parameterizations (Section 63.1) sets to zero one of the three components of the vector streamfunction. This gauge choice is available since there are only two independent functional degrees of freedom available from a divergence-free mass transport field. A common choice is the *vertical gauge* in which

$$\Psi_3^* = 0 \quad \text{vertical gauge.} \quad (61.74)$$

Let us see how we can generally make this gauge choice. Consider a vector streamfunction Φ that has all three components nonzero. Now consider the alternative streamfunction $\rho \Psi^* = \rho \Phi + \nabla(\rho \Lambda)$, with $\nabla(\rho \Lambda) = -\hat{\mathbf{z}} \rho \Phi_3$. This choice in turn means that the third component of Ψ^* is zero.

To further specify the vertical gauge we invert the relations

$$\rho u^* = -\partial_z(\rho \Psi_2^*) \quad \text{and} \quad \rho v^* = \partial_z(\rho \Psi_1^*) \quad \text{and} \quad \rho w^* = \partial_x(\rho \Psi_2^*) - \partial_y(\rho \Psi_1^*) \quad (61.75)$$

to render the vector streamfunction

$$\rho \Psi^* = \hat{z} \times \int_{-H}^z \rho \mathbf{u}^* dz' = \hat{z} \times \underline{\mathbf{U}}^{(*\rho)} \quad (61.76)$$

where

$$\underline{\mathbf{U}}^{(*\rho)}(z) = \int_{-H}^z \rho \mathbf{u}^* dz' \quad (61.77)$$

is the horizontal mass transport associated with \mathbf{u}^* passing between the bottom and a depth $z \geq -H$. The anti-symmetric stirring tensor for the vertical gauge is given by

$$\rho \mathbb{A}_{mn} = \begin{pmatrix} 0 & 0 & \underline{U}^{(*\rho)} \\ 0 & 0 & \underline{V}^{(*\rho)} \\ -\underline{U}^{(*\rho)} & -\underline{V}^{(*\rho)} & 0 \end{pmatrix}, \quad (61.78)$$

and the corresponding skew, rotational, and advective fluxes are

$$\mathbf{J}^{\text{skew}} = -\underline{\mathbf{U}}^{(*\rho)} \partial_z C + \hat{z} \underline{\mathbf{U}}^{(*\rho)} \cdot \nabla_z C \quad (61.79a)$$

$$\mathbf{J}^{\text{rot}} = \partial_z(C \underline{\mathbf{U}}^{(*\rho)}) - \hat{z} \nabla_z \cdot (C \underline{\mathbf{U}}^{(*\rho)}) \quad (61.79b)$$

$$\mathbf{J}^{\text{adv}} = C(\partial_z \underline{\mathbf{U}}^{(*\rho)}) - \hat{z} C \nabla_z \cdot \underline{\mathbf{U}}^{(*\rho)}. \quad (61.79c)$$

Note that the identity $\mathbf{J}^{\text{adv}} = \mathbf{J}^{\text{skew}} + \mathbf{J}^{\text{rot}}$ is maintained by these expressions. The horizontal components to the skew flux vanish when the tracer is uniform in the vertical, and the vertical skew flux vanishes with a horizontally uniform tracer field. These properties manifest the skewed nature of the fluxes.

61.7.3 Boundary conditions

We assume that all external domain boundaries are material in regards to the velocity \mathbf{v}^* . Furthermore, even for moving domain boundaries, we assume that the suite of kinematic boundary conditions is based on the barycentric velocity \mathbf{v} (see Section 16.4), so that \mathbf{v}^* satisfies the no-normal flow condition even on moving boundaries

$$\hat{\mathbf{n}} \cdot \mathbf{v}^* = 0 \quad \text{external domain boundaries.} \quad (61.80)$$

As we discuss in Section 61.8.1, this boundary condition is required for the eddy-induced velocity to have zero impact on the total mass of an arbitrary tracer within the full fluid domain.

Correspondingly, the advective tracer flux also satisfies a no-normal boundary condition on all external boundaries

$$\hat{\mathbf{n}} \cdot \mathbf{J}^{\text{adv}} = \hat{\mathbf{n}} \cdot \mathbf{v}^* \rho C = 0. \quad (61.81)$$

The corresponding boundary condition for the skew flux is found by inserting the relation (61.62) into the advective flux boundary condition (61.81) to render

$$\hat{\mathbf{n}} \cdot \mathbf{J}^{\text{adv}} = \hat{\mathbf{n}} \cdot [\mathbf{J}^{\text{skew}} + \mathbf{J}^{\text{rot}}] = 0. \quad (61.82)$$

Hence, the skew flux generally has a non-zero normal component at the solid boundaries as determined by the rotational flux

$$\hat{\mathbf{n}} \cdot \mathbf{J}^{\text{skew}} = -\hat{\mathbf{n}} \cdot \mathbf{J}^{\text{rot}}. \quad (61.83)$$

Even so, there might be occasions in which $\hat{\mathbf{n}} \cdot \mathbf{J}^{\text{skew}} = 0$, which is ensured so long as

$$(-\nabla C \times \rho \Psi^*) \cdot \hat{\mathbf{n}} = -(\rho \Psi^* \times \hat{\mathbf{n}}) \cdot \nabla C = 0. \quad (61.84)$$

A sufficient condition is to have $\Psi^* \times \hat{\mathbf{n}} = 0$, in which case the vector streamfunction is parallel to the boundary normal. An alternative sufficient condition is to have the streamfunction vanish at the boundary. Further details for boundary conditions depend on physical properties of the velocity \mathbf{v}^* . We discuss one example in Section 63.1 as prescribed by the [Gent et al. \(1995\)](#) mesoscale eddy parameterization.

61.8 Finite volume budgets with eddy velocities

In this section we examine how an eddy induced velocity modifies the budgets for fluid mass and tracer mass in finite domains. For this purpose, write the local/differential mass and tracer budgets in the form

$$\frac{\partial \rho}{\partial t} + \nabla \cdot (\rho \mathbf{v}^\dagger) = 0 \quad (61.85a)$$

$$\frac{\partial(\rho C)}{\partial t} + \nabla \cdot (\rho \mathbf{v}^\dagger C + \mathbf{J}^{\text{diff}}) = 0, \quad (61.85b)$$

where (see Section 61.7)

$$\mathbf{v}^\dagger = \mathbf{v} + \mathbf{v}^* \quad \text{and} \quad \nabla \cdot (\rho \mathbf{v}^*) = 0, \quad (61.86)$$

and where \mathbf{J}^{diff} is a subgrid scale flux encompassing all processes, such as diffusion and boundary conditions, that are not represented by an eddy-induced advection. Given that $\nabla \cdot (\rho \mathbf{v}^*) = 0$, the mass budget (61.85a) can be written in the equivalent manners

$$\frac{\partial \rho}{\partial t} + \nabla \cdot (\rho \mathbf{v}^\dagger) = \frac{\partial \rho}{\partial t} + \nabla \cdot (\rho \mathbf{v}) = 0. \quad (61.87)$$

That is, the eddy-induced velocity does not lead to any local sources of fluid mass. This property will prove to be very important in the budget analyses of this section.

As shown in the following, the finite volume budgets for fluid mass and tracer mass also make use of the residual mean velocity, \mathbf{v}^\dagger . That result is not surprising, since the finite volume budgets are consistent with the differential budgets (61.85a) and (61.85b). Nonetheless, it is useful to expose the details as they appear in many budget analysis applications, such as the water mass and tracer mass analysis of Chapter 65. We furthermore explore how the budgets for tracer mass appear when formulated using advective fluxes versus skew fluxes. As we will see, the finite volume budgets are consistent across the variety of formulations only if the eddy velocity and eddy vector streamfunction satisfy specific boundary conditions as discussed in Section 61.7.3.

61.8.1 Advection formulation

Making use of the tracer equation (61.85b) in the Leibniz-Reynolds transport theorem (17.46) renders the finite volume tracer mass budget for an arbitrary domain, \mathcal{R}

$$\frac{d}{dt} \left[\int_{\mathcal{R}} \rho C dV \right] = - \oint_{\partial \mathcal{R}} \left[\rho C (\mathbf{v}^\dagger - \mathbf{v}^{(b)}) + \mathbf{J}^{\text{diff}} \right] \cdot \hat{\mathbf{n}} d\mathcal{S}, \quad (61.88)$$

where $\mathbf{v}^{(b)}$ is the velocity of a point on the domain boundary. Appearance of the residual mean velocity, \mathbf{v}^\dagger , in the finite volume budget (61.88) follows from its appearance in the local tracer

budget (61.85b). We thus see that the eddy-induced velocity impacts on the tracer mass budget for an arbitrary domain. However, its impacts disappear when integrating over a closed or periodic fluid domain so long as

$$\mathbf{v}^* \cdot \hat{\mathbf{n}} = 0 \quad \text{on external fluid boundaries.} \quad (61.89)$$

We already encountered this boundary condition in Section 61.7.3. It holds on all boundaries, including those such as the ocean free surface that are time dependent and/or permeable. It is required if we assume the eddy-induced velocity does not modify the mass of any tracer in the full fluid domain. That assumption is generally made for eddy-induced velocities such as those associated with mesoscale and submesoscale eddies in the ocean (see Section 63.3).

Setting the tracer concentration to a constant in equation (61.88) leads to the fluid mass budget

$$\frac{d}{dt} \left[\int_{\mathcal{R}} \rho dV \right] = - \oint_{\partial\mathcal{R}} \rho (\mathbf{v}^\dagger - \mathbf{v}^{(b)}) \cdot \hat{\mathbf{n}} d\mathcal{S}, \quad (61.90)$$

where we set the diffusive tracer flux, \mathbf{J}^{diff} , to zero since there is no diffusion of fluid mass between fluid elements (Section 17.1). As for the differential form (61.85a), the mass budget for any domain is not changed by the eddy-induced velocity since

$$\nabla \cdot (\rho \mathbf{v}^*) = 0 \implies \oint_{\partial\mathcal{R}} \rho \mathbf{v}^* \cdot \hat{\mathbf{n}} d\mathcal{S} = 0, \quad (61.91)$$

so that the mass budget is given by

$$\frac{d}{dt} \left[\int_{\mathcal{R}} \rho dV \right] = - \oint_{\partial\mathcal{R}} [\rho (\mathbf{v}^\dagger - \mathbf{v}^{(b)})] \cdot \hat{\mathbf{n}} d\mathcal{S} = - \oint_{\partial\mathcal{R}} [\rho (\mathbf{v} - \mathbf{v}^{(b)})] \cdot \hat{\mathbf{n}} d\mathcal{S} \quad (61.92)$$

Hence, the eddy velocity contribution to the mass budget for any finite region vanishes, which is expected since it provides no net mass source to a region. Furthermore, one may choose to diagnose the right hand side of the mass budget in either the residual mean or Eulerian mean form. The choice is based on convenience, such as whether one has easier access to the residual mean velocity or the Eulerian mean velocity. Although the patterns of the fluxes across any particular boundary differs if $\mathbf{v}^* \neq 0$, the accumulation of mass within the region are identical for the two formulations.

61.8.2 Skew flux formulation

Now consider the complement perspective afforded by the skew flux formulation from Section 61.7. Here we decompose the advective tracer flux according to

$$C \rho \mathbf{v}^\dagger = C \rho \mathbf{v} - \nabla C \times \rho \Psi^* + \nabla \times (C \rho \Psi^*) = C \rho \mathbf{v} + \mathbf{J}^{\text{skew}} + \nabla \times (C \rho \Psi^*), \quad (61.93)$$

where we introduced the skew tracer flux arising from the eddy-induced streamfunction

$$\mathbf{J}^{\text{skew}} = -\nabla C \times (\rho \Psi^*). \quad (61.94)$$

The differential budget for tracer is thus given by

$$\frac{\partial(\rho C)}{\partial t} + \nabla \cdot [\rho C \mathbf{v} + \mathbf{J}^{\text{skew}} + \mathbf{J}^{\text{diff}}] = 0, \quad (61.95)$$

where the rotational term, $\nabla \times (C \rho \Psi^*)$, has zero divergence and thus does not affect the tracer budget. The corresponding finite volume tracer mass budget is

$$\frac{d}{dt} \left[\int_{\mathcal{R}} \rho C dV \right] = - \oint_{\partial\mathcal{R}} [\rho C (\mathbf{v} - \mathbf{v}^{(b)}) - \nabla C \times (\rho \Psi^*) + \mathbf{J}^{\text{diff}}] \cdot \hat{\mathbf{n}} d\mathcal{S}. \quad (61.96)$$

In this form, the contribution from the eddies is inside the skew flux rather than in the residual mean advective flux. Setting C to a constant reveals the mass budget as in the second form of equation (61.92).

61.8.3 Domain with a tracer boundary

We now apply the previous general budget discussion to a specific domain that anticipates the more complete budget analysis provided in Section 65.10. Here, we consider the fluid mass and tracer mass within an ocean region with at least one of its bounds determined by an isosurface of constant tracer concentration, as in Figure 61.4.

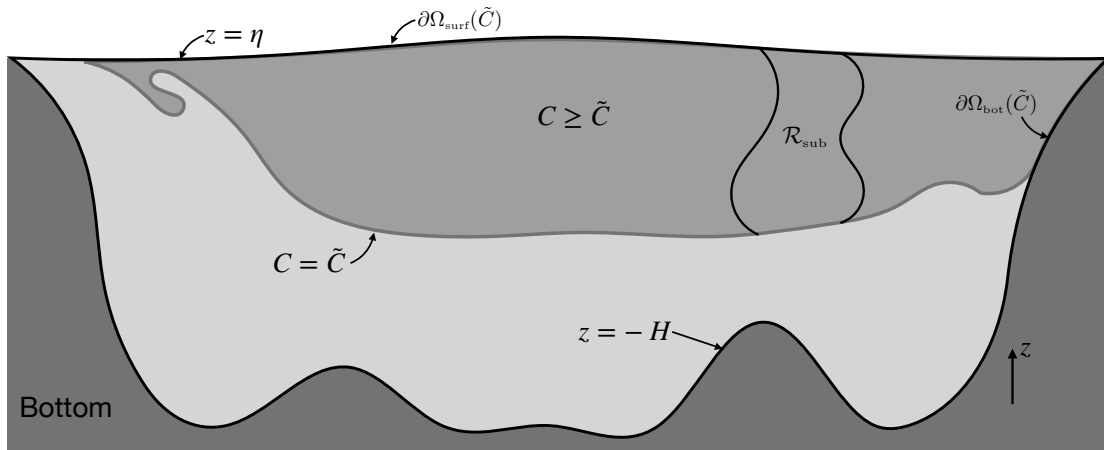


FIGURE 61.4: An ocean region with one of its boundaries set by a surface of constant tracer, $C = \tilde{C}$. Note that the region need not be monotonically stratified in the tracer concentration, nor does it need to be simply connected. The region is bounded at the top by $\partial\Omega_{\text{surf}}(\tilde{C})$; at the bottom by the $C = \tilde{C}$ isosurface as well as the solid-earth bottom $\partial\Omega_{\text{bot}}(\tilde{C})$. The region can generally be multiply connected. A subregion, \mathcal{R}_{sub} , is also considered where its sides extend from the free surface to the tracer isosurface, and they are assumed to be fully within the fluid domain. We develop the tracer and fluid mass budgets for region \mathcal{R}_{sub} in Section 61.8.4, whereas the budget in the full region $C \geq \tilde{C}$ is considered in Section 61.8.3.

Advection formulation

The tracer mass budget written using the advective formulation (61.88) takes the form

$$\frac{d}{dt} \left[\int_{\mathcal{R}} \rho C dV \right] = \int_{\partial\Omega_{\text{surf}}(\tilde{C})} Q_m C dA - \tilde{C} \int_{C=\tilde{C}} \rho (\mathbf{v}^\dagger - \mathbf{v}^{(b)}) \cdot \hat{\mathbf{n}} d\mathcal{S} - \oint_{\partial\mathcal{R}} \mathbf{J}^{\text{diff}} \cdot \hat{\mathbf{n}} d\mathcal{S}. \quad (61.97)$$

For the first right hand side term we made use of the surface kinematic boundary condition (16.73c), with $Q_m dA$ the mass per time crossing the surface interface and where dA is the horizontal projection of the interface area element $d\mathcal{S}$. We also made use of the exterior boundary condition (61.89) for the eddy-induced velocity. For the second term we pulled the tracer concentration outside of the boundary integral over the $C = \tilde{C}$ interface since the concentration is fixed at \tilde{C} on this interface.

The mass budget for this region, also formulated using advective fluxes, is given by

$$\frac{d}{dt} \left[\int_{\mathcal{R}} \rho dV \right] = \int_{\partial\Omega_{\text{surf}}(\tilde{C})} Q_m dA - \int_{C=\tilde{C}} \rho (\mathbf{v}^\dagger - \mathbf{v}^{(b)}) \cdot \hat{\mathbf{n}} d\mathcal{S}. \quad (61.98)$$

Combining this budget with the tracer mass budget allows us to write

$$\frac{d}{dt} \left[M_C - \tilde{C} M \right] = \int_{\partial\Omega_{\text{surf}}(\tilde{C})} Q_m (C - \tilde{C}) dA - \oint_{\partial\mathcal{R}} \mathbf{J}^{\text{diff}} \cdot \hat{\mathbf{n}} d\mathcal{S}, \quad (61.99)$$

where we introduced the shorthand for the tracer mass and fluid mass in the region

$$M_C = \int_{\mathcal{R}} C \rho dV \quad \text{and} \quad M = \int_{\mathcal{R}} \rho dV. \quad (61.100)$$

In Section 65.10.2 we motivate the name *internal tracer mass* for the quantity $M_C - \tilde{C} M$.

Skew flux formulation

The tracer mass budget formulated using skew tracer fluxes is generally given by equation (61.96). It takes on the following form for the domain in Figure 61.4

$$\frac{d}{dt} \left[\int_{\mathcal{R}} \rho C dV \right] = \int_{\partial\Omega_{\text{surf}}(\tilde{C})} Q_m C dA - \tilde{C} \int_{C=\tilde{C}} \rho (\mathbf{v} - \mathbf{v}^{(b)}) \cdot \hat{\mathbf{n}} d\mathcal{S} - \oint_{\partial\mathcal{R}} [-\nabla C \times (\rho \Psi^*) + \mathbf{J}^{\text{diff}}] \cdot \hat{\mathbf{n}} d\mathcal{S}, \quad (61.101)$$

and the corresponding budget for the fluid mass is

$$\frac{d}{dt} \left[\int_{\mathcal{R}} \rho dV \right] = \int_{\partial\Omega_{\text{surf}}(\tilde{C})} Q_m dA - \int_{C=\tilde{C}} \rho (\mathbf{v} - \mathbf{v}^{(b)}) \cdot \hat{\mathbf{n}} d\mathcal{S}. \quad (61.102)$$

As for the advective formulation, we combine the fluid mass budget equation (61.102) with the tracer mass equation (61.101) to render a budget equation for the internal mass content

$$\frac{d}{dt} \left[M_C - \tilde{C} M \right] = \int_{\partial\Omega_{\text{surf}}(\tilde{C})} Q_m (C - \tilde{C}) dA - \oint_{\partial\mathcal{R}} \mathbf{J}^{\text{diff}} \cdot \hat{\mathbf{n}} d\mathcal{S}, \quad (61.103)$$

which is the same as for the advective formulation given by equation (61.99).

Proving the budgets based on the two formulations are equivalent

The two tracer budgets, (61.97) and (61.101), must be the same since they measure changes to the tracer mass within the same region. Likewise, the two mass budgets, (61.98) and (61.102), must be the same, as are the two internal tracer mass budgets (61.99) and (61.103). We here expose the manipulations required to verify these equalities.

To prove the $C = \tilde{C}$ terms in the tracer budget equations (61.97) and (61.101) are the same, consider the identity (61.91) applied to the region under consideration

$$0 = \oint_{\partial\mathcal{R}} \rho \mathbf{v}^* \cdot \hat{\mathbf{n}} d\mathcal{S} = \int_{\partial\Omega_{\text{surf}}(\tilde{C})} \rho \mathbf{v}^* \cdot \hat{\mathbf{n}} d\mathcal{S} + \int_{\partial\Omega_{\text{bot}}(\tilde{C})} \rho \mathbf{v}^* \cdot \hat{\mathbf{n}} d\mathcal{S} + \int_{C=\tilde{C}} \rho \mathbf{v}^* \cdot \hat{\mathbf{n}} d\mathcal{S}. \quad (61.104)$$

The surface and bottom boundary terms vanish due to the external boundary condition (61.89); namely, $\mathbf{v}^* \cdot \hat{\mathbf{n}} = 0$ for each point along an external fluid boundary. We are thus led to conclude

that

$$\int_{C=\tilde{C}} \rho \mathbf{v}^* \cdot \hat{\mathbf{n}} d\mathcal{S} = 0. \quad (61.105)$$

This boundary integral means that there is no net accumulation of mass in the region due to action of the eddy velocity. Notably, we generally have $\mathbf{v}^* \cdot \hat{\mathbf{n}} \neq 0$ at any particular point on the $C = \tilde{C}$ surface. Given the boundary integral (61.105) we are thus led to conclude

$$\int_{C=\tilde{C}} \rho (\mathbf{v}^\dagger - \mathbf{v}^{(b)}) \cdot \hat{\mathbf{n}} d\mathcal{S} = \int_{C=\tilde{C}} \rho (\mathbf{v} - \mathbf{v}^{(b)}) \cdot \hat{\mathbf{n}} d\mathcal{S}. \quad (61.106)$$

This identity proves that the two mass budgets (61.98) and (61.102) are indeed measuring changes to the same fluid mass, even though one computes the domain boundary fluxes based on the residual mean velocity, \mathbf{v}^\dagger , whereas the other uses the Eulerian mean, \mathbf{v} .

Next we need to show that the skew flux term vanishes when integrated around the domain boundary. For the $C = \tilde{C}$ boundary we have

$$\int_{C=\tilde{C}} [\nabla C \times (\rho \Psi^*)] \cdot \hat{\mathbf{n}} d\mathcal{S} = 0, \quad (61.107)$$

which follows since $\hat{\mathbf{n}}$ is parallel to ∇C along this boundary. For the external boundaries, equality of the tracer mass budgets (61.97) and (61.101) is satisfied for an arbitrary tracer concentration if one of the boundary conditions discussed in Section (61.7.3) is maintained; i.e., if Ψ^* vanishes on an external boundary or if it is parallel to the boundary normal direction ($\hat{\mathbf{n}} \times \Psi^* = 0$). Maintenance of either of these two boundary conditions allows us to conclude that the two budgets (61.97) and (61.101) are indeed identical.

61.8.4 Budget for a region with interior sides

Consider the subregion \mathcal{R}_{sub} shown in Figure 61.4. This region is bounded above by the free surface and below by the tracer isosurface, $C = \tilde{C}$, just like the region \mathcal{R} encountered in Section 61.8.3. Additionally, region \mathcal{R}_{sub} is bounded along its sides by surfaces assumed to be within the fluid interior. For much of this discussion we allow the sides to have an arbitrary shape and to move. Towards the end of this section we specialize to the case of static sides, such as might be relevant for a vertical section through the fluid and/or a numerical model grid cell.

Fluid mass budget

The fluid mass budget for the region \mathcal{R}_{sub} can be formulated using either the residual mean velocity or the Eulerian mean velocity

$$\frac{d}{dt} \left[\int_{\mathcal{R}_{\text{sub}}} \rho dV \right] = \int_{\partial\Omega_{\text{surf}}(\tilde{C})} Q_m dA - \int_{C=\tilde{C}} \rho (\mathbf{v}^\dagger - \mathbf{v}^{(b)}) \cdot \hat{\mathbf{n}} d\mathcal{S} - \int_{\text{sides}} \rho (\mathbf{v}^\dagger - \mathbf{v}^{(b)}) \cdot \hat{\mathbf{n}} d\mathcal{S} \quad (61.108a)$$

$$\frac{d}{dt} \left[\int_{\mathcal{R}_{\text{sub}}} \rho dV \right] = \int_{\partial\Omega_{\text{surf}}(\tilde{C})} Q_m dA - \int_{C=\tilde{C}} \rho (\mathbf{v} - \mathbf{v}^{(b)}) \cdot \hat{\mathbf{n}} d\mathcal{S} - \int_{\text{sides}} \rho (\mathbf{v} - \mathbf{v}^{(b)}) \cdot \hat{\mathbf{n}} d\mathcal{S}. \quad (61.108b)$$

The two budgets are identical since the eddy velocity satisfies $\oint \rho \mathbf{v}^* \cdot \hat{\mathbf{n}} d\mathcal{S} = 0$ for any domain, as well as $\mathbf{v}^* \cdot \hat{\mathbf{n}} = 0$ along any external domain boundary. Hence, as already noted in Section 61.8.1, the eddy velocity contribution to the right hand side of equation (61.108a) vanishes; it

provides no net mass source to any region. We next show the same equality holds for the tracer mass budgets, with that equality shown with a bit more effort.

Tracer mass budget

The advective flux formulation of the tracer mass budget is given by

$$\frac{d}{dt} \left[\int_{\mathcal{R}_{\text{sub}}} \rho C dV \right] = \int_{\partial \Omega_{\text{surf}}(\tilde{C})} Q_m C dA - \tilde{C} \int_{C=\tilde{C}} \rho (\mathbf{v}^\dagger - \mathbf{v}^{(b)}) \cdot \hat{\mathbf{n}} d\mathcal{S} - \oint_{\partial \mathcal{R}_{\text{sub}}} \mathbf{J}^{\text{diff}} \cdot \hat{\mathbf{n}} d\mathcal{S} - \int_{\text{sides}} C \rho (\mathbf{v}^\dagger - \mathbf{v}^{(b)}) \cdot \hat{\mathbf{n}} d\mathcal{S}, \quad (61.109)$$

and the corresponding skew flux formulation is

$$\frac{d}{dt} \left[\int_{\mathcal{R}_{\text{sub}}} \rho C dV \right] = \int_{\partial \Omega_{\text{surf}}(\tilde{C})} Q_m C dA - \tilde{C} \int_{C=\tilde{C}} \rho (\mathbf{v} - \mathbf{v}^{(b)}) \cdot \hat{\mathbf{n}} d\mathcal{S} - \oint_{\partial \mathcal{R}_{\text{sub}}} \mathbf{J}^{\text{diff}} \cdot \hat{\mathbf{n}} d\mathcal{S} - \int_{\text{sides}} C \rho (\mathbf{v} - \mathbf{v}^{(b)}) \cdot \hat{\mathbf{n}} d\mathcal{S} - \int_{\text{sides}} [-\nabla C \times (\rho \Psi^*)] \cdot \hat{\mathbf{n}} d\mathcal{S}. \quad (61.110)$$

As for the discussion in Section 61.8.3, we introduce the internal tracer mass and make use of the fluid mass budgets (61.108a) and (61.108b) to write the advective form of the internal mass budget

$$\frac{d}{dt} [M_C - \tilde{C} M] = \int_{\partial \Omega_{\text{surf}}(\tilde{C})} Q_m (C - \tilde{C}) dA - \oint_{\partial \mathcal{R}} \mathbf{J}^{\text{diff}} \cdot \hat{\mathbf{n}} d\mathcal{S} - \int_{\text{sides}} (C - \tilde{C}) \rho (\mathbf{v}^\dagger - \mathbf{v}^{(b)}) \cdot \hat{\mathbf{n}} d\mathcal{S}, \quad (61.111)$$

and the corresponding skew flux form of the same budget

$$\frac{d}{dt} [M_C - \tilde{C} M] = \int_{\partial \Omega_{\text{surf}}(\tilde{C})} Q_m (C - \tilde{C}) dA - \oint_{\partial \mathcal{R}} \mathbf{J}^{\text{diff}} \cdot \hat{\mathbf{n}} d\mathcal{S} - \int_{\text{sides}} (C - \tilde{C}) \rho (\mathbf{v} - \mathbf{v}^{(b)}) \cdot \hat{\mathbf{n}} d\mathcal{S} - \int_{\text{sides}} [-\nabla C \times (\rho \Psi^*)] \cdot \hat{\mathbf{n}} d\mathcal{S}. \quad (61.112)$$

We now examine the right hand side of the budgets (61.111) and (61.112) to show they are indeed measuring the same tracer mass budget. For that purpose, consider the skew flux integral in equation (61.112) and note that the integrand vanishes on both the top of the domain, at $z = \eta$, and bottom at $C = \tilde{C}$, thus allowing us to write

$$-\int_{\text{sides}} [-\nabla C \times (\rho \Psi^*)] \cdot \hat{\mathbf{n}} d\mathcal{S} = -\oint_{\partial \mathcal{R}_{\text{sub}}} [-\nabla C \times (\rho \Psi^*)] \cdot \hat{\mathbf{n}} d\mathcal{S}, \quad (61.113)$$

where the right hand side is an integral around the full domain boundaries. Now reintroduce the eddy induced velocity and rotational flux to have

$$-\oint_{\partial \mathcal{R}_{\text{sub}}} [-\nabla C \times (\rho \Psi^*)] \cdot \hat{\mathbf{n}} d\mathcal{S} = -\oint_{\partial \mathcal{R}_{\text{sub}}} [C \rho \mathbf{v}^* - \nabla \times (C \rho \Psi^*)] \cdot \hat{\mathbf{n}} d\mathcal{S}. \quad (61.114)$$

The rotational flux has zero divergence, so that Gauss's divergence theorem means that the rotational flux vanishes when integrated along the domain boundaries

$$\oint_{\partial \mathcal{R}_{\text{sub}}} \nabla \times (C \rho \Psi^*) \cdot \hat{\mathbf{n}} d\mathcal{S} = 0. \quad (61.115)$$

The eddy advection term in equation (61.114) vanishes on the top boundary at $z = \eta$ due to the boundary condition $\mathbf{v}^* \cdot \hat{\mathbf{n}} = 0$, thus yielding

$$\oint_{\partial\mathcal{R}_{\text{sub}}} C \rho \mathbf{v}^* \cdot \hat{\mathbf{n}} d\mathcal{S} = \int_{\text{sides}} C \rho \mathbf{v}^* \cdot \hat{\mathbf{n}} d\mathcal{S} + \int_{C=\tilde{C}} C \rho \mathbf{v}^* \cdot \hat{\mathbf{n}} d\mathcal{S} \quad (61.116a)$$

$$= \int_{\text{sides}} C \rho \mathbf{v}^* \cdot \hat{\mathbf{n}} d\mathcal{S} + \tilde{C} \int_{C=\tilde{C}} \rho \mathbf{v}^* \cdot \hat{\mathbf{n}} d\mathcal{S}. \quad (61.116b)$$

Again make use of the property $\nabla \cdot (\rho \mathbf{v}^*) = 0$ and $\hat{\mathbf{n}} \cdot \mathbf{v}^* = 0$ at $z = \eta$ to write

$$0 = \oint_{\partial\mathcal{R}_{\text{sub}}} \rho \mathbf{v}^* \cdot \hat{\mathbf{n}} d\mathcal{S} = \oint_{\text{sides}} \rho \mathbf{v}^* \cdot \hat{\mathbf{n}} d\mathcal{S} + \oint_{C=\tilde{C}} \rho \mathbf{v}^* \cdot \hat{\mathbf{n}} d\mathcal{S}, \quad (61.117)$$

which gives us

$$-\int_{\text{sides}} [-\nabla C \times (\rho \Psi^*)] \cdot \hat{\mathbf{n}} d\mathcal{S} = -\oint_{\partial\mathcal{R}_{\text{sub}}} C \rho \mathbf{v}^* \cdot \hat{\mathbf{n}} d\mathcal{S} = -\int_{\text{sides}} (C - \tilde{C}) \rho \mathbf{v}^* \cdot \hat{\mathbf{n}} d\mathcal{S}. \quad (61.118)$$

Making use of this result in the skew flux formulated budget equation (61.112) brings it to the advective flux form found in equation (61.111).

We are thus led to conclude that the right hand side to equation (61.112) does indeed equal to the right hand side of equation (61.111). So although the formulation of the boundary flux contributions is rather distinct between the advective flux and skew flux formulations, the resulting tracer mass budget is the same. The choice for how to formulate the budget is thus a matter of convenience.

61.8.5 Budget for a stirred fluid in a region with interior sides

Although contained within the formalism developed in Section 61.8.4, it is revealing to specialize those budgets to the case of zero mixing, in which $\mathbf{J}^{\text{diff}} = 0$ and there is zero boundary mass flux, $Q_m = 0$. In this case the fluid is reversibly stirred. Examining the finite region budgets for this pure stirring case allows us to further reveal the complementary treatments available from advection versus skewusion.

Summary of the differential stirring formalism

As explored in this chapter, an Eulerian description of tracer stirring can arise from either advection or skewusion. In the presence of an eddy induced velocity we here consider two representations of tracer stirring, with the first being advection by the residual mean velocity, \mathbf{v}^\dagger

$$\rho \frac{D^\dagger C}{Dt} = \frac{\partial(\rho C)}{\partial t} + \nabla \cdot (\rho \mathbf{v}^\dagger C) = 0. \quad (61.119)$$

This formulation makes it clear that surfaces of constant C are material as defined by the residual mean velocity rather than by the Eulerian mean, \mathbf{v} . That is, tracer isosurfaces satisfy the residual mean impermeability condition

$$\rho (\mathbf{v}^\dagger - \mathbf{v}^{(b)}) \cdot \hat{\mathbf{n}} = 0 \quad \text{on } C \text{ isosurfaces,} \quad (61.120)$$

with

$$\hat{\mathbf{n}} = \frac{\nabla C}{|\nabla C|} \quad \text{and} \quad \mathbf{v}^{(b)} \cdot \hat{\mathbf{n}} = -\frac{\partial_t C}{|\nabla C|}. \quad (61.121)$$

The impermeability condition (61.120) offers a geometric interpretation of the tracer equation (61.119) following from the discussion of dia-surface transport in Section 57.4. Correspondingly, Lagrangian fluid particles moving with the residual mean velocity do not cross tracer isosurfaces even if those isosurfaces move. Furthermore, we observe that the eddy induced velocity has a nonzero projection across tracer isosurfaces

$$(\mathbf{v}^\dagger - \mathbf{v}^{(b)}) \cdot \hat{\mathbf{n}} = 0 \implies (\mathbf{v} - \mathbf{v}^{(b)}) \cdot \hat{\mathbf{n}} = -\mathbf{v}^* \cdot \hat{\mathbf{n}} \quad \text{on } C \text{ isosurfaces.} \quad (61.122)$$

This property of the eddy induced velocity was emphasized by [McDougall and McIntosh \(2001\)](#). It reveals that in the absence of mixing, eddy motion crossing tracer isosurfaces is exactly balanced by Eulerian plus boundary motion, thus leaving a net zero residual mean transfer of matter across the surface. Equation (61.122) is a key kinematic property used for interpreting features of the finite volume budgets detailed below.

Our second means to represent tracer stirring makes use of advection by the Eulerian mean velocity plus skewson by the eddy induced streamfunction

$$\rho \frac{DC}{Dt} + \nabla \cdot [-\nabla C \times (\rho \Psi^*)] = \frac{\partial(\rho C)}{\partial t} + \nabla \cdot [\rho \mathbf{v} C - \nabla C \times (\rho \Psi^*)] = 0. \quad (61.123)$$

In terms of the eddy streamfunction, $\rho \Psi^*$, the impermeability condition (61.120) takes on the form

$$[\rho \mathbf{v} + \nabla \times (\rho \Psi^*) - \rho \mathbf{v}^{(b)}] \cdot \hat{\mathbf{n}} = 0 \quad \text{on } C \text{ isosurfaces.} \quad (61.124)$$

Budgets via residual mean advection

The mass budget formulated in terms of residual mean advection, and the corresponding residual mean advective flux formulation of the tracer mass budget, are given by

$$\frac{d}{dt} \left[\int_{\mathcal{R}_{\text{sub}}} \rho dV \right] = - \int_{C=\tilde{C}} \rho (\mathbf{v}^\dagger - \mathbf{v}^{(b)}) \cdot \hat{\mathbf{n}} d\mathcal{S} - \int_{\text{sides}} \rho (\mathbf{v}^\dagger - \mathbf{v}^{(b)}) \cdot \hat{\mathbf{n}} d\mathcal{S} \quad (61.125a)$$

$$\frac{d}{dt} \left[\int_{\mathcal{R}_{\text{sub}}} \rho C dV \right] = - \tilde{C} \int_{C=\tilde{C}} \rho (\mathbf{v}^\dagger - \mathbf{v}^{(b)}) \cdot \hat{\mathbf{n}} d\mathcal{S} - \int_{\text{sides}} C \rho (\mathbf{v}^\dagger - \mathbf{v}^{(b)}) \cdot \hat{\mathbf{n}} d\mathcal{S}. \quad (61.125b)$$

The residual mean impermeability condition (61.120) for the $C = \tilde{C}$ surface renders a simplification to the fluid mass and tracer mass budgets

$$\frac{d}{dt} \left[\int_{\mathcal{R}_{\text{sub}}} \rho dV \right] = - \int_{\text{sides}} \rho (\mathbf{v}^\dagger - \mathbf{v}^{(b)}) \cdot \hat{\mathbf{n}} d\mathcal{S} \quad (61.126a)$$

$$\frac{d}{dt} \left[\int_{\mathcal{R}_{\text{sub}}} \rho C dV \right] = - \int_{\text{sides}} C \rho (\mathbf{v}^\dagger - \mathbf{v}^{(b)}) \cdot \hat{\mathbf{n}} d\mathcal{S}. \quad (61.126b)$$

Hence, in the residual mean formulation, the only fluxes that affect changes to the mass budgets are those that cross the side faces of the region.

Budgets via Eulerian mean advection plus eddy skewusion

The mass budget formulated in terms of Eulerian mean advection, and the corresponding tracer mass budget using eddy skewusion, are given by

$$\frac{d}{dt} \left[\int_{\mathcal{R}_{\text{sub}}} \rho dV \right] = - \int_{C=\tilde{C}} \rho (\mathbf{v} - \mathbf{v}^{(b)}) \cdot \hat{\mathbf{n}} d\mathcal{S} - \int_{\text{sides}} \rho (\mathbf{v} - \mathbf{v}^{(b)}) \cdot \hat{\mathbf{n}} d\mathcal{S} \quad (61.127a)$$

$$\begin{aligned} \frac{d}{dt} \left[\int_{\mathcal{R}_{\text{sub}}} \rho C dV \right] &= -\tilde{C} \int_{C=\tilde{C}} \rho (\mathbf{v} - \mathbf{v}^{(b)}) \cdot \hat{\mathbf{n}} d\mathcal{S} - \int_{\text{sides}} C \rho (\mathbf{v} - \mathbf{v}^{(b)}) \cdot \hat{\mathbf{n}} d\mathcal{S} \\ &\quad - \int_{\text{sides}} [-\nabla C \times (\rho \Psi^*)] \cdot \hat{\mathbf{n}} d\mathcal{S}. \end{aligned} \quad (61.127b)$$

We already saw in Section 61.8.4 how to bring the right hand side terms into the form realized by the residual mean advective approach. So there is no question concerning the equivalence of the advective and skew flux formulations for the tracer mass budget. Nonetheless, what is here clearly emphasized is that the skew flux approach requires us to account for Eulerian advective transport across the $C = \tilde{C}$ isosurface, whereas for the advective flux approach the only flux in equation (61.126b) is that crossing the region side boundaries. Even so, as stated earlier, an Eulerian mean transport of tracer across the $C = \tilde{C}$ isosurface *does not* correspond to material transport across this surface. The reason is that material transport is determined by the residual mean velocity, \mathbf{v}^\dagger , as per the residual mean impermeability conditions 61.122 and 61.124. So even though there is a contribution to the skew flux formulated budget from Eulerian transport across the $C = \tilde{C}$ material surface, there remains zero net material crossing that surface.

Zero Eulerian mean advection and static side walls

One further specialization serves to clearly emphasize the complementary nature of the advective and skew flux approaches. Here, we assume the sides of the region are static and the Eulerian mean velocity vanishes. With a zero Eulerian velocity, the residual mean impermeability condition (61.122) means that on the $C = \tilde{C}$ isosurface, the normal component of the eddy velocity is balanced by the boundary velocity as per the impermeability condition (61.128):

$$(\mathbf{v}^* - \mathbf{v}^{(b)}) \cdot \hat{\mathbf{n}} = 0 \quad \text{on } C \text{ isosurfaces and with } \mathbf{v} = 0. \quad (61.128)$$

When formulated using the residual mean advection, the fluid mass budget (61.126a) and tracer mass budget (61.126b) reduce in this case to

$$\frac{d}{dt} \left[\int_{\mathcal{R}_{\text{sub}}} \rho dV \right] = - \int_{\text{sides}} \rho \mathbf{v}^* \cdot \hat{\mathbf{n}} d\mathcal{S} \quad (61.129a)$$

$$\frac{d}{dt} \left[\int_{\mathcal{R}_{\text{sub}}} \rho C dV \right] = - \int_{\text{sides}} C \rho \mathbf{v}^* \cdot \hat{\mathbf{n}} d\mathcal{S}, \quad (61.129b)$$

so that these budgets are only affected by eddy advection across the side boundaries. The corresponding mass budget written in terms of Eulerian mean advection, (61.127a), and tracer mass budget written in terms of skew fluxes, (61.127b), are given by

$$\frac{d}{dt} \left[\int_{\mathcal{R}_{\text{sub}}} \rho dV \right] = + \int_{C=\tilde{C}} \rho \mathbf{v}^{(b)} \cdot \hat{\mathbf{n}} d\mathcal{S} \quad (61.130a)$$

$$\frac{d}{dt} \left[\int_{\mathcal{R}_{\text{sub}}} \rho C dV \right] = +\tilde{C} \int_{C=\tilde{C}} \rho \mathbf{v}^{(b)} \cdot \hat{\mathbf{n}} d\mathcal{S} - \int_{\text{sides}} [-\nabla C \times (\rho \Psi^*)] \cdot \hat{\mathbf{n}} d\mathcal{S}. \quad (61.130b)$$

For the mass budget, (61.130a), there are no contributions to the side walls since they are static and the Eulerian advection is assumed to vanish. The only contribution comes from the eddy term acting on the $C = \tilde{C}$ isosurface where $\mathbf{v}^{(b)} \cdot \hat{\mathbf{n}} = \mathbf{v}^* \cdot \hat{\mathbf{n}}$. For the tracer mass budget, (61.130b), we also have the eddy contribution on the $C = \tilde{C}$ isosurface, plus skew fluxes that penetrate the side walls.

The right hand sides to the fluid mass budgets (61.129a) and (61.130a), and tracer mass budgets (61.129b) and (61.130b), are remarkably distinct. Even so, they both measure the same budgets. Furthermore, in both cases the $C = \tilde{C}$ boundary is a material boundary as defined by the residual mean velocity.

61.9 Active tracers and dia-surface flow

An *active tracer* is a tracer that impacts the dynamics, with potential temperature and salinity the canonical examples. Active tracers directly impact the buoyancy, which in turn affects pressure and velocity. Hence, the advection-diffusion equation for active tracers is nonlinear since the velocity field is dependent on active tracers. We here write the advection-diffusion equation in terms of the residual mean velocity using potential temperature as an example active tracer

$$\rho \frac{D^\dagger \theta}{Dt} = \rho \left[\frac{\partial}{\partial t} + \mathbf{v}^\dagger \cdot \nabla \right] \theta = -\nabla \cdot \mathbf{J}^{\text{diff}}(\theta). \quad (61.131)$$

Further nonlinearities arise when the subgrid scale diffusion tensor is itself a function of the buoyancy, as discussed at the end of Section 61.4.4, and/or when the parameterized eddy-induced velocity is a function of the buoyancy, as discussed in Section 63.3.

61.9.1 Adiabatic flow

In an adiabatic fluid, potential temperature is materially invariant. When advected by the residual mean velocity this material invariance takes on the form

$$\frac{D^\dagger \theta}{Dt} = \frac{\partial \theta}{\partial t} + \mathbf{v}^\dagger \cdot \nabla \theta = 0 \quad \text{adiabatic.} \quad (61.132)$$

Furthermore, following the kinematics of Section 16.4.2, the adiabatic residual mean flow field does not penetrate surfaces of constant potential temperature (θ -isosurfaces are impermeable) since

$$\mathbf{v}^\dagger \cdot \nabla \theta = -\frac{\partial \theta}{\partial t}. \quad (61.133)$$

In this case we say that residual mean advection reversibly stirs the potential temperature field. This property of the residual mean velocity was also considered in the discussion of pure stirring in Section 61.8.4.

61.9.2 Diabatic processes generating dia-surface transport

Potential temperature is no longer materially invariant in the presence of diabatic processes such as mixing typically parameterized by diffusion. Correspondingly, the residual mean velocity picks up a component, w^{dia} , that crosses the moving potential temperature surface thus making it permeable. Hence, advective transport in the presence of mixing is no longer reversible. We follow the kinematics from Section 57.4 to render the expression (57.26) for w^{dia} , which we here

write as

$$w^{\text{dia}} \equiv \hat{\mathbf{n}} \cdot (\mathbf{v}^\dagger - \mathbf{v}^{(\theta)}) = \frac{1}{|\nabla\theta|} \frac{D^\dagger\theta}{Dt} \quad (61.134)$$

where

$$\hat{\mathbf{n}} = \frac{\nabla\theta}{|\nabla\theta|} \quad \text{and} \quad \mathbf{v}^{(\theta)} \cdot \nabla\theta = -\frac{\partial\theta}{\partial t}. \quad (61.135)$$

Rearrangement of equation (61.134) renders the kinematic identity

$$\frac{D^\dagger\theta}{Dt} = \frac{\partial\theta}{\partial t} + \mathbf{v}^\dagger \cdot \nabla\theta = w^{\text{dia}} |\nabla\theta|. \quad (61.136)$$

With nonzero w^{dia} , we no longer have residual mean advection preserving properties along fluid element trajectories. We offer examples to illustrate the physics underlying this identity.

Diffusion with no fluid motion

Diffusion is the canonical example of a diabatic process (Section 61.3)

$$\rho \frac{D^\dagger\theta}{Dt} = \nabla \cdot (\kappa \rho \nabla\theta), \quad (61.137)$$

with $\kappa > 0$ the scalar kinematic diffusivity. Diffusion in turn drives a diabatic transport velocity

$$\rho w^{\text{dia}} = \frac{\nabla \cdot (\kappa \rho \nabla\theta)}{|\nabla\theta|}. \quad (61.138)$$

Consider a horizontally homogeneous potential temperature field. If buoyancy is alone determined by potential temperature then there is no fluid motion since buoyancy surfaces are flat (and we assume the eddy-induced motion is also zero). Yet in the presence of vertical diffusion and vertical stratification there is a diabatic transport since

$$\rho w^{\text{dia}} = \frac{\partial_z(\kappa \rho \partial_z\theta)}{|\partial_z\theta|} \neq 0. \quad (61.139)$$

In the absence of fluid flow, the dia-surface transport is determined solely by movement of the potential temperature surfaces. Correspondingly, potential temperature evolution is determined only by vertical diffusion since with $\mathbf{v}^\dagger = 0$ we have

$$\frac{\partial\theta}{\partial t} = \rho^{-1} \frac{\partial}{\partial z} \left[\kappa \rho \frac{\partial\theta}{\partial z} \right] = w^{\text{dia}} \left| \frac{\partial\theta}{\partial z} \right|. \quad (61.140)$$

Steady state advective-diabatic balance

A steady state potential temperature field in the presence of diabatic processes is realized when there is an exact balance between advective transport and dia-surface transport enabled by diffusion

$$\rho \mathbf{v}^\dagger \cdot \nabla\theta = \rho w^{\text{dia}} |\nabla\theta| = \nabla \cdot (\kappa \rho \nabla\theta). \quad \text{steady state.} \quad (61.141)$$

That is, maintaining static θ -surfaces ($\partial_t\theta = 0$) requires the residual mean advective transport to cross θ surfaces (left hand side) by an amount that exactly balances diabatic processes such as diffusion (right hand side). This example illustrates that in the presence of mixing, advection is no longer an adiabatic stirring process. Namely, in the steady state, advection equals diffusion.

61.10 Green's function method for passive tracers

Passive tracers (Section 17.2) have no impact on the flow field (and so do not impact the seawater density or diffusion tensor). Hence, passive tracer patterns serve to “trace” the effects from advective and diffusive transport without affecting the transport velocity or diffusion tensor. Correspondingly, the passive tracer advection-diffusion equation is a linear partial differential equation. With some qualifications identified below, we are able to make use of the Green’s function methods from Chapter 4 when studying solutions to the passive tracer equation.

In this section we develop the Green’s function method for use with the advection-diffusion equation. This section offers a supplement to the review paper from [Haine et al. \(2022\)](#) who synthesize the variety of Green’s function methods of use for studying geophysical fluids. Although our formulation is largely based on ocean applications, the Green’s function method for the advection-diffusion equation is also applicable to the atmosphere.

61.10.1 Concerning time dependent domain boundaries

The ocean free surface is time dependent, so that the domain, \mathcal{R} , is itself time dependent. Mathematically, this time dependence means that time and space integrations do not commute. In particular, space integration is generally written in the form

$$\int_{\mathcal{R}} dV = \iint \left[\int_{\eta_b}^{\eta} dz \right] dx dy, \quad (61.142)$$

where $z = \eta_b(x, y)$ is the static bottom and $z = \eta(x, y, t)$ is the time dependent free surface. We must, in turn, first compute the space integration over the full domain and then do the time time integration when deriving the reciprocity relation and the Green’s function solution.

The free surface undulations make the vertical extent of the domain time dependent. Additionally, in an ocean with sloping sidewalls, the horizontal domain boundaries are also time dependent as the ocean moves up and down the sloping sides. However, allowing for the horizontal domain extent to fluctuate does not introduce any fundamentally new kinematics in our analysis. The reason is that when integrating to the lateral domain boundaries, all terms vanish since the water depth vanishes at the edge of the sloping beaches. We saw this kinematic result when integrating the angular momentum budget in a channel with sloping sidewalls in Section 25.5.

Therefore, we assume the horizontal extent of the domain to be static in order to slightly ease the analysis. We do so by imagining a few meter high vertical seawall placed around the ocean domain edges, and by assuming a minimum depth so that there is nonzero water everywhere in the domain. These assumptions are common in ocean modeling, except in models allowing for wetting and drying of land/ocean cells. So in conclusion, we limit our analysis to time dependence of the vertical extent of the domain, with the horizontal extent static. Such limitation can be removed without much difficulty but doing so adds nothing new fundamentally.

61.10.2 Passive tracer boundary conditions

In this section, we are concerned with the evolution of a smooth passive tracer concentration, C , which is the dimensionless ratio of the tracer mass to seawater mass. Boundary conditions play a key role in the evolution. We here discuss the boundary conditions placed on the passive tracer along the ocean bottom, at $z = \eta_b(x, y)$, and the free surface, at $z = \eta(x, y, t)$.

Ocean bottom

At the static ocean bottom we generically consider a no-flux condition for the diffusive flux

$$\mathbf{J} \cdot \hat{\mathbf{n}} = -\rho \mathbb{K} \cdot \nabla C \cdot \hat{\mathbf{n}} = 0 \quad \text{at } z = \eta_b. \quad (61.143)$$

Along with the kinematic no-normal flow condition, $\mathbf{v} \cdot \hat{\mathbf{n}} = 0$, the no-flux condition means that there is zero tracer flux through the bottom.

Ocean free surface

At the ocean free surface we use results from Section 16.4.3, which developed the boundary conditions for mass flux \mathcal{Q}_m (mass per time per area) across a permeable free surface, as well as Section 17.6, which developed the analogous boundary conditions for tracers. In particular, equation (17.85) provides an expression for the net mass flux of tracer crossing the free surface, \mathcal{Q}_C , written as the sum of an advective flux plus a non-advective flux

$$\mathcal{Q}_C = C \mathcal{Q}_m - \mathbf{J} \cdot \hat{\mathbf{n}} = \underbrace{C \mathcal{Q}_m}_{\text{advective}} + \underbrace{\rho \mathbb{K} \cdot \nabla C \cdot \hat{\mathbf{n}}}_{\text{diffusive}} \quad \text{for } \mathbf{x} \in \partial \mathcal{R}_{\text{surface}}, \quad (61.144)$$

where C is the concentration at $z = \eta$, and we assumed the non-advective flux is given by a diffusive flux. We consider the following prescribed boundary conditions.

- ROBIN CONDITIONS: Prescribing the boundary tracer mass flux, \mathcal{Q}_C , leads to a Robin or mixed boundary condition

$$\mathcal{Q}_C = \text{prescribed} = C \mathcal{Q}_m + \rho \mathbb{K} \cdot \nabla C \cdot \hat{\mathbf{n}} \quad \text{for } \mathbf{x} \in \partial \mathcal{R}_{\text{surface}}. \quad (61.145)$$

This boundary condition is relevant for enthalpy and salt, with full discussion given in Section 64.5. However, the Robin condition is rarely used for passive tracers along the ocean surface and so it will not be considered further.

- NEUMANN CONDITIONS: Prescribing the diffusive flux leads to the Neumann boundary condition

$$\rho \mathbb{K} \cdot \nabla C \cdot \hat{\mathbf{n}} = \text{prescribed} \equiv \Sigma(\mathbf{x}, t) \quad \text{for } \mathbf{x} \in \partial \mathcal{R}_{\text{surface}}. \quad (61.146)$$

This surface ocean boundary condition is also rarely used for passive tracers, though we will examine it within the following.

- DIRICHLET CONDITIONS: Prescribing the value of the tracer concentration at the boundary leads to the Dirichlet boundary condition

$$C = \text{prescribed} \equiv \sigma(\mathbf{x}, t) \quad \text{for } \mathbf{x} \in \partial \mathcal{R}_{\text{surface}}. \quad (61.147)$$

This boundary condition is the most commonly used condition for passive tracers, and thus will be our favored choice in the following. Note that both the Neumann and Dirichlet conditions generally involve a net transport of tracer, $\mathcal{Q}_C \neq 0$, across the ocean boundary.

As we will see in Section 61.10.5, the Neumann boundary condition in the presence of a surface mass flux is problematic due to the associated non-closed reciprocity relation satisfied by the Green's function and its adjoint. The absence of a suitable reciprocity relation makes it difficult to use the Green's function method, since one would need to solve for both the Green's function and its adjoint. In contrast, the Dirichlet condition allows for a simple reciprocity

relation, identical to that for the diffusion equation (Section 4.8.4), thus making the Green's function method for the advection-diffusion equation with a Dirichlet condition suitable even in the presence of a surface mass flux (see page 2450 of [Larson \(1999\)](#) for a similar point).

61.10.3 Advection-diffusion initial-boundary value problem

We study the initial-boundary value problem for a smooth passive tracer concentration, C , which is the dimensionless ratio of the tracer mass to seawater mass. The tracer is affected by advection and diffusion on a spatial domain, \mathcal{R} , in the presence of a tracer source, $\rho \Lambda$ (with dimensions of tracer mass per volume per time), with initial data available for the density and tracer concentration at time $t = t_{\text{init}}$. The initial-boundary value problem in the presence of Neumann or Dirichlet boundary conditions is given by

$$\frac{\partial(\rho C)}{\partial t} + \nabla \cdot (\rho \mathbf{v}^\dagger C - \rho \mathbb{K} \cdot \nabla C) = \rho \Lambda \quad \mathbf{x} \in \mathcal{R}, t \geq t_{\text{init}} \quad (61.148a)$$

$$\rho C = \rho I \quad \mathbf{x} \in \mathcal{R}, t = t_{\text{init}} \quad (61.148b)$$

$$\hat{\mathbf{n}} \cdot \rho \mathbb{K} \cdot \nabla C = \rho \Sigma \quad \text{or} \quad \rho C = \rho \sigma \quad \mathbf{x} \in \partial \mathcal{R}, t \geq t_{\text{init}}. \quad (61.148c)$$

The prescribed initial condition data for the tracer concentration at time $t = t_{\text{init}}$ is given by $I(\mathbf{x})$, and the initial density is also prescribed at this time, $\rho(\mathbf{x}, t_{\text{init}})$. We consider two options for the boundary condition at $\mathbf{x} \in \partial \mathcal{R}$: (i) the Neumann boundary condition with a prescribed flux, $\hat{\mathbf{n}} \cdot \rho \mathbb{K} \cdot \nabla C = \rho \Sigma$, or the (ii) Dirichlet boundary condition with a prescribed value, $\rho C = \rho \sigma$. Furthermore, we assume the flow field, $\mathbf{v}(\mathbf{x}, t)$, the eddy-induced velocity, $\mathbf{v}^*(\mathbf{x}, t)$, the seawater density, $\rho(\mathbf{x}, t)$, and the diffusivity tensor, $\mathbb{K}(\mathbf{x}, t)$, are known functions of space-time that are determined by solving for the dynamics, kinematics, thermodynamics, and active tracers. Finally, we assume the tracer concentration source, $\Lambda(\mathbf{x}, t)$, does not itself depend on the tracer concentration, C , thus ensuring linearity of the partial differential equation (61.148a).

61.10.4 The Green's function and its adjoint

Green's function problem

The Green's function corresponding to the passive tracer advection-diffusion equations (61.148a)-(61.148c) satisfies the following causal boundary value problem

$$\frac{\partial[\rho G(\mathbf{x}, t | \mathbf{x}_0, t_0)]}{\partial t} + \nabla_{\mathbf{x}} \cdot [\rho \mathbf{v}^\dagger G(\mathbf{x}, t | \mathbf{x}_0, t_0) - \rho \mathbb{K} \cdot \nabla_{\mathbf{x}} G(\mathbf{x}, t | \mathbf{x}_0, t_0)] = \delta(\mathbf{x} - \mathbf{x}_0) \delta(t - t_0) \quad (61.149a)$$

$$G(\mathbf{x}, t < t_0 | \mathbf{x}_0, t_0) = 0 \quad (61.149b)$$

$$\hat{\mathbf{n}}_{\mathbf{x}} \cdot \mathbb{K} \cdot \nabla_{\mathbf{x}} G(\mathbf{x} \in \partial \mathcal{R}, t | \mathbf{x}_0, t_0) = 0 \quad \text{or} \quad G(\mathbf{x} \in \partial \mathcal{R}, t | \mathbf{x}_0, t_0) = 0. \quad (61.149c)$$

The space-time point (\mathbf{x}_0, t_0) is where the Dirac delta source is located, which is located within the spatial domain, \mathcal{R} , and occurs after the initial time

$$\mathbf{x}_0 \in \mathcal{R} \quad \text{and} \quad t_0 \geq t_{\text{init}}. \quad (61.150)$$

The Green's function satisfies homogeneous boundary conditions corresponding to those satisfied by the passive tracer concentration in equation (61.148c). Finally, since the Dirac delta source, $\delta(\mathbf{x} - \mathbf{x}_0) \delta(t - t_0)$, has dimensions of inverse volume times inverse time, the Green's function has dimensions of inverse mass. We physically interpret the Green's function as the tracer concentration resulting from an impulsive tracer concentration source, divided by the mass of tracer injected by the source.

Adjoint Green's function problem

The adjoint Green's function, \tilde{G} , satisfies the adjoint problem

$$-\frac{\partial[\rho \tilde{G}(\mathbf{x}, t|\mathbf{x}_0, t_0)]}{\partial t} + \nabla_{\mathbf{x}} \cdot [-\rho \mathbf{v}^\dagger \tilde{G}(\mathbf{x}, t|\mathbf{x}_0, t_0) - \rho \mathbb{K} \cdot \nabla_{\mathbf{x}} \tilde{G}(\mathbf{x}, t|\mathbf{x}_0, t_0)] = \delta(\mathbf{x} - \mathbf{x}_0) \delta(t - t_0) \quad (61.151a)$$

$$\tilde{G}(\mathbf{x}, t > t_0|\mathbf{x}_0, t_0) = 0 \quad (61.151b)$$

$$\hat{\mathbf{n}}_{\mathbf{x}} \cdot \mathbb{K} \cdot \nabla_{\mathbf{x}} \tilde{G}(\mathbf{x} \in \partial\mathcal{R}, t|\mathbf{x}_0, t_0) = 0 \text{ or } \tilde{G}(\mathbf{x} \in \partial\mathcal{R}, t|\mathbf{x}_0, t_0) = 0. \quad (61.151c)$$

Note the sign change on both the time derivative, as for the diffusion equation in Section 4.8.3, as well as the advection term. The sign change on advection is expected since with time running backwards, so too does the velocity of a fluid particle. Hence, the adjoint advection-diffusion equation is a backwards in time advection-diffusion equation.

61.10.5 Reciprocity relation

We here derive the reciprocity relation satisfied by the Green's function, G , and its adjoint, \tilde{G} . The derivation follows that in Section 4.6.4 for the Poisson equation and Section 4.8.4 for the diffusion equation. A new feature here arises from the advection operator, and another arises from allowing the domain boundary to be time dependent as occurs at the ocean free surface. We will see that the reciprocity relation for Neumann boundary conditions (61.149c) and (61.151c) does not “close” when there is mass transport across the ocean free surface (see equation (61.166) below). In contrast, the reciprocity relation closes with Dirichlet boundary conditions, taking the same form as for the diffusion equation in equation (4.129). We have more to say on this distinct behavior after its derivation.

Notation and setup

We consider the Green's function partial differential equation (61.149a) with a Dirac delta source $\delta(\mathbf{x} - \mathbf{x}_1) \delta(t - t_1)$, along with the adjoint Green's function equation (61.151a) with a Dirac delta source, $\delta(\mathbf{x} - \mathbf{x}_2) \delta(t - t_2)$, where both sources are within the spatial domain and both occur later than the initial time:

$$\mathbf{x}_1, \mathbf{x}_2 \in \mathcal{R} \quad \text{and} \quad t_{\text{init}} < t_1, t_2. \quad (61.152)$$

We also follow the approach in Section 4.8.4 for the diffusion equation by introducing the arbitrarily large time, T , such that $-T < t_1, t_2 < T$. As for the diffusion problem, causality conditions will ensure that T drops out from the final expression for the tracer concentration. Additionally, to help ease notational clutter, we make use of the following shorthand where convenient

$$G(\mathbf{x}, t|\mathbf{x}_1, t_1) = G(1) \quad \text{and} \quad \tilde{G}(\mathbf{x}, t|\mathbf{x}_2, t_2) = \tilde{G}(2). \quad (61.153)$$

Cross-multiplication

Multiply the Green's function equation by $\tilde{G}(2)$ and the adjoint equation by $G(1)$ to find

$$\tilde{G}(2) \left(\partial_t[\rho G(1)] + \nabla_{\mathbf{x}} \cdot [\rho \mathbf{v}^\dagger G(1) - \rho \mathbb{K} \cdot \nabla_{\mathbf{x}} G(1)] \right) = \tilde{G}(2) \delta(\mathbf{x} - \mathbf{x}_1) \delta(t - t_1) \quad (61.154a)$$

$$G(1) \left(-\partial_t[\rho \tilde{G}(2)] + \nabla_{\mathbf{x}} \cdot [-\rho \mathbf{v}^\dagger \tilde{G}(2) - \rho \mathbb{K} \cdot \nabla_{\mathbf{x}} \tilde{G}(2)] \right) = G(1) \delta(\mathbf{x} - \mathbf{x}_2) \delta(t - t_2). \quad (61.154b)$$

In the following, we work from the left hand side of equation (61.154a) and bring the differential operators from $G(1)$ onto $\tilde{G}(2)$. The result of this movement will be equation (61.154b) plus some

extra terms whose form depends on the causality condition and boundary conditions. Integration over space and time will then render the reciprocity relation.

Self-adjointness of the generalized Laplacian operator

The generalized Laplacian operator term on the left hand side of equation (61.154a) can be written

$$\begin{aligned} & -\tilde{G}(2) \nabla_{\mathbf{x}} \cdot [\rho \mathbb{K} \cdot \nabla_{\mathbf{x}} G(1)] \\ & = \nabla_{\mathbf{x}} \cdot [-\tilde{G}(2) \rho \mathbb{K} \cdot \nabla_{\mathbf{x}} G(1) + G(1) \rho \mathbb{K} \cdot \nabla_{\mathbf{x}} \tilde{G}(2)] - G(1) \nabla_{\mathbf{x}} \cdot [\rho \mathbb{K} \cdot \nabla_{\mathbf{x}} \tilde{G}(2)]. \end{aligned} \quad (61.155)$$

A spatial integration of this equation over the region \mathcal{R} , and use of the homogeneous boundary conditions in equations (61.148c) or (61.151c) eliminates the divergence term to reveal

$$\begin{aligned} & \int_{\mathcal{R}} \tilde{G}(\mathbf{x}, t | \mathbf{x}_2, t_2) \nabla_{\mathbf{x}} \cdot [\rho \mathbb{K} \cdot \nabla_{\mathbf{x}} G(\mathbf{x}, t | \mathbf{x}_1, t_1)] dV \\ & = \int_{\mathcal{R}} G(\mathbf{x}, t | \mathbf{x}_1, t_1) \nabla_{\mathbf{x}} \cdot [\rho \mathbb{K} \cdot \nabla_{\mathbf{x}} \tilde{G}(\mathbf{x}, t | \mathbf{x}_2, t_2)] dV. \end{aligned} \quad (61.156)$$

This equality proves that the generalized Laplacian operator with a symmetric diffusion tensor is self-adjoint, which is a result already encountered in Section 4.8.4 when discussing the diffusion equation. This result holds for either Neumann or Dirichlet boundary conditions.

Time derivative plus advection

Next write the time derivative and advection portion of equation (61.154a) as

$$\begin{aligned} & \tilde{G}(2) \left(\partial_t [\rho G(1)] + \nabla_{\mathbf{x}} \cdot [\rho \mathbf{v}^\dagger G(1)] \right) \\ & = \partial_t [\tilde{G}(2) \rho G(1)] + \nabla_{\mathbf{x}} \cdot [\tilde{G}(2) \rho \mathbf{v}^\dagger G(1)] - G(1) \rho \left[\partial_t \tilde{G}(2) + \mathbf{v}^\dagger \cdot \nabla_{\mathbf{x}} \tilde{G}(2) \right] \\ & = \partial_t [\tilde{G}(2) \rho G(1)] + \nabla_{\mathbf{x}} \cdot [\tilde{G}(2) \rho \mathbf{v}^\dagger G(1)] - G(1) \left(\partial_t (\rho \tilde{G}(2)) + \nabla \cdot [\rho \mathbf{v}^\dagger \tilde{G}(2)] \right), \end{aligned} \quad (61.157)$$

where we used the mass continuity equation (16.6) for the final equality. Rearrangement thus leads to

$$\begin{aligned} & \tilde{G}(2) \left(\partial_t [\rho G(1)] + \nabla_{\mathbf{x}} \cdot [\rho \mathbf{v}^\dagger G(1)] \right) - G(1) \left(-\partial_t [\rho \tilde{G}(2)] - \nabla \cdot [\rho \mathbf{v}^\dagger \tilde{G}(2)] \right) \\ & = \partial_t [\tilde{G}(2) \rho G(1)] + \nabla_{\mathbf{x}} \cdot [\tilde{G}(2) \rho \mathbf{v}^\dagger G(1)]. \end{aligned} \quad (61.158)$$

Space integration

Now integrate equations (61.154a) and (61.154b) over the spatial domain, \mathcal{R} , subtract these two equations, and make use of the results (61.156) and (61.158) to reveal

$$\begin{aligned} & \tilde{G}(\mathbf{x}_1, t | \mathbf{x}_2, t_2) \delta(t - t_1) - G(\mathbf{x}_2, t | \mathbf{x}_1, t_1) \delta(t - t_2) \\ & = \int_{\mathcal{R}} \left[\partial_t [\tilde{G}(2) \rho G(1)] + \nabla_{\mathbf{x}} \cdot [\tilde{G}(2) \rho \mathbf{v}^\dagger G(1)] \right] dV. \end{aligned} \quad (61.159)$$

The divergence term on the right hand side takes the form

$$\int_{\mathcal{R}} \nabla_{\mathbf{x}} \cdot [\tilde{G}(2) \rho \mathbf{v}^\dagger G(1)] dV = \oint_{\partial\mathcal{R}} \tilde{G}(2) G(1) \rho \mathbf{v}^\dagger \cdot \hat{\mathbf{n}}_{\mathbf{x}} dS \quad \text{divergence theorem} \quad (61.160a)$$

$$= \oint_{\partial\mathcal{R}} \tilde{G}(2) G(1) \rho \mathbf{v} \cdot \hat{\mathbf{n}}_{\mathbf{x}} dS \quad \hat{\mathbf{n}} \cdot \mathbf{v}^* = 0 \quad (61.160b)$$

$$= \int_{z=\eta} \tilde{G}(2) G(1) \rho \mathbf{v} \cdot \hat{\mathbf{n}}_{\mathbf{x}} dS \quad \mathbf{v} \cdot \hat{\mathbf{n}} = 0 \text{ for } z = \eta_b \quad (61.160c)$$

$$= \int_{z=\eta} \tilde{G}(2) G(1) \rho \mathbf{v} \cdot \nabla(z - \eta) dA \quad \text{equation (16.76)} \quad (61.160d)$$

$$= \int_{z=\eta} \tilde{G}(2) G(1) \rho (w - \mathbf{u} \cdot \nabla \eta) dA. \quad (61.160e)$$

The time derivative term takes the form

$$\int_{\mathcal{R}} \partial_t [\tilde{G}(2) G(1) \rho] dV = \frac{\partial}{\partial t} \left[\int_{\mathcal{R}} \tilde{G}(2) G(1) \rho dV \right] - \int_{z=\eta} [\tilde{G}(2) G(1) \rho \partial_t \eta] dA, \quad (61.161)$$

where we made use of Leibniz's rule to bring the time derivative across the integral sign and made note of the time dependent free surface, $z = \eta(x, y, t)$. Combining equations (61.161) and (61.160e) leads to

$$\tilde{G}(\mathbf{x}_1, t | \mathbf{x}_2, t_2) \delta(t - t_1) - G(\mathbf{x}_2, t | \mathbf{x}_1, t_1) \delta(t - t_2) \quad (61.162a)$$

$$= \frac{\partial}{\partial t} \left[\int_{\mathcal{R}} \tilde{G}(2) G(1) \rho dV \right] + \int_{z=\eta} \tilde{G}(2) G(1) [\rho (w - \mathbf{u} \cdot \nabla \eta - \partial_t \eta)] dA \quad (61.162b)$$

$$= \frac{\partial}{\partial t} \left[\int_{\mathcal{R}} \tilde{G}(2) G(1) \rho dV \right] - \int_{z=\eta} \tilde{G}(2) G(1) Q_m dA, \quad (61.162c)$$

where the final equality follows from the surface ocean kinematic boundary condition (16.79), with Q_m the mass per time per horizontal area crossing the ocean surface.

Time integration

We are now ready to integrate equation (61.162c) over time, with its left hand side leading to

$$\begin{aligned} \int_{-T}^T & \left[\tilde{G}(\mathbf{x}_1, t | \mathbf{x}_2, t_2) \delta(t - t_1) - G(\mathbf{x}_2, t | \mathbf{x}_1, t_1) \delta(t - t_2) \right] dt \\ &= \tilde{G}(\mathbf{x}_1, t_1 | \mathbf{x}_2, t_2) - G(\mathbf{x}_2, t_2 | \mathbf{x}_1, t_1), \end{aligned} \quad (61.163)$$

which used the sifting property (4.28). There are two terms that appear when time integrating the time derivative from equation (61.162c), with each term vanishing due to the causality conditions (61.149b) and (61.151b)

$$\int_{\mathcal{R}} \tilde{G}(\mathbf{x}, t = T | \mathbf{x}_2, t_2) G(\mathbf{x}, t = T | \mathbf{x}_1, t_1) \rho dV = 0 \iff \tilde{G}(\mathbf{x}, t = T | \mathbf{x}_2, t_2) = 0 \quad (61.164)$$

$$\int_{\mathcal{R}} \tilde{G}(\mathbf{x}, t = t_{\text{init}} | \mathbf{x}_2, t_2) G(\mathbf{x}, t = t_{\text{init}} | \mathbf{x}_1, t_1) \rho dV = 0 \iff G(\mathbf{x}, t = t_{\text{init}} | \mathbf{x}_1, t_1) = 0. \quad (61.165)$$

We are thus left with

$$\tilde{G}(\mathbf{x}_1, t_1 | \mathbf{x}_2, t_2) - G(\mathbf{x}_2, t_2 | \mathbf{x}_1, t_1) = - \int_{t_{\text{init}}}^{t_1} \left[\int_{z=\eta} \tilde{G}(\mathbf{x}, t | \mathbf{x}_2, t_2) G(\mathbf{x}_1, t_1 | \mathbf{x}, t) Q_m dA \right] dt, \quad (61.166)$$

which we refer to as a *non-closed reciprocity relation* between G and \tilde{G} . Note that the time limits on the integral follow from causality on the Green's function and its adjoint.

Closed form reciprocity in special cases

There are two cases in which the relation (61.166) leads to a closed reciprocity relation:

- Zero mass flux across surface: $Q_m = 0$.
- Homogeneous Dirichlet boundary conditions: $\tilde{G}(\mathbf{x} \in \partial\mathcal{R}, t | \mathbf{x}_0, t_0) = G(\mathbf{x} \in \partial\mathcal{R}, t | \mathbf{x}_0, t_0) = 0$.

In either case we are led to

$$\tilde{G}(\mathbf{x}_1, t_1 | \mathbf{x}_2, t_2) = G(\mathbf{x}_2, t_2 | \mathbf{x}_1, t_1), \quad (61.167)$$

which is the same reciprocity (4.129) satisfied for the diffusion equation Green's functions.

The more nuanced reciprocity for the advection-diffusion equation arises from the advective mass flux at the ocean free surface boundary. The mass flux couples the ocean with its surrounding media (e.g., the atmosphere, rivers, or cryosphere), and in so doing precludes a general closed reciprocity relation. However, the Dirichlet boundary condition closes the surface boundary through the homogeneous Green's function boundary conditions. Most applications of Green's function methods for passive ocean tracers make use of Dirichlet boundary conditions, in which case we are afforded a closed reciprocity relation even with a free surface open to mass transport.

61.10.6 Composition property

We here follow the analysis of Section 4.8.5 to derive the composition property of the Green's function for the advection-diffusion equation. For this purpose, return to the cross-multiplication equations (61.154a) and (61.154b) used to derive reciprocity, here written as

$$\tilde{G}(2) \left(\partial_t [\rho G(1)] + \nabla_{\mathbf{x}} \cdot [\rho \mathbf{v}^\dagger G(1) - \rho \mathbb{K} \cdot \nabla_{\mathbf{x}} G(1)] \right) = \tilde{G}(2) \delta(\mathbf{x} - \mathbf{x}_1) \delta(t - t_1) \quad (61.168a)$$

$$G(1) \left(\partial_t [\rho \tilde{G}(2)] + \nabla_{\mathbf{x}} \cdot [\rho \mathbf{v}^\dagger \tilde{G}(2) + \rho \mathbb{K} \cdot \nabla_{\mathbf{x}} \tilde{G}(2)] \right) = -G(1) \delta(\mathbf{x} - \mathbf{x}_2) \delta(t - t_2). \quad (61.168b)$$

Adding these two equations and use of mass continuity (16.6) brings the left hand side to

$$\text{LHS} = \partial_t [\rho G(1) \tilde{G}(2)] + \nabla_{\mathbf{x}} \cdot [\rho \mathbf{v}^\dagger G(1) \tilde{G}(2) + \rho G(1) \mathbb{K} \cdot \nabla_{\mathbf{x}} \tilde{G}(2) - \rho \tilde{G}(2) \mathbb{K} \cdot \nabla_{\mathbf{x}} G(1)]. \quad (61.169)$$

Integration over the domain \mathcal{R} eliminates the diffusion terms for both the Dirichlet and Neumann boundary conditions. For the time derivative term we use Leibniz's rule to write

$$\int_{\mathcal{R}} \partial_t [\rho G(1) \tilde{G}(2)] dV = \frac{d}{dt} \int_{\mathcal{R}} \rho G(1) \tilde{G}(2) dV - \int_{z=\eta} \rho G(1) \tilde{G}(2) \partial_t \eta dA. \quad (61.170a)$$

For the advection term we follow the manipulations used for equation (61.160e) to derive

$$\int_{\mathcal{R}} \nabla_{\mathbf{x}} \cdot [\rho \mathbf{v}^\dagger G(1) \tilde{G}(2)] dV = \int_{z=\eta} \rho G(1) \tilde{G}(2) \mathbf{v}^\dagger \cdot \hat{\mathbf{n}} dS \quad (61.171a)$$

$$= \int_{z=\eta} \rho G(1) \tilde{G}(2) (w - \mathbf{u} \cdot \nabla \eta) dA \quad (61.171b)$$

$$= \int_{z=\eta} G(1) \tilde{G}(2) (\rho \partial_t \eta - Q_m) dA. \quad (61.171c)$$

Bringing the pieces together and expanding the arguments leads to

$$\begin{aligned} \frac{d}{dt} \int_{\mathcal{R}} \rho(\mathbf{x}, t) G(\mathbf{x}, t | \mathbf{x}_1, t_1) \tilde{G}(\mathbf{x}, t | \mathbf{x}_2, t_2) dV &= \tilde{G}(\mathbf{x}_1, t | \mathbf{x}_2, t_2) \delta(t - t_1) \\ &\quad - G(\mathbf{x}_2, t | \mathbf{x}_1, t_1) \delta(t - t_2) - \int_{z=\eta} G(\mathbf{x}, t | \mathbf{x}_1, t_1) \tilde{G}(\mathbf{x}, t | \mathbf{x}_2, t_2) Q_m(\mathbf{x}, t) dA. \end{aligned} \quad (61.172)$$

As for the derivation of reciprocity in Section 61.10.5, we here assume either $Q_m = 0$ or a homogeneous Dirichlet boundary condition so that

$$\begin{aligned} \frac{d}{dt} \int_{\mathcal{R}} \rho(\mathbf{x}, t) G(\mathbf{x}, t | \mathbf{x}_1, t_1) \tilde{G}(\mathbf{x}, t | \mathbf{x}_2, t_2) dV &= \tilde{G}(\mathbf{x}_1, t | \mathbf{x}_2, t_2) \delta(t - t_1) \\ &\quad - G(\mathbf{x}_2, t | \mathbf{x}_1, t_1) \delta(t - t_2). \end{aligned} \quad (61.173)$$

This equation is directly analogous to equation (4.138) satisfied by the diffusion equation Green's function. Following from that analysis, and making use of reciprocity (61.167), we find the composition property for the advection-diffusion equation in a non-Boussinesq fluid

$$G(\mathbf{x}_2, t_2 | \mathbf{x}_1, t_1) = \int_{\mathcal{R}} \rho(\mathbf{x}, \tau) G(\mathbf{x}_2, t_2 | \mathbf{x}, \tau) G(\mathbf{x}, \tau | \mathbf{x}_1, t_1) dV \quad \text{if } t_1 < \tau < t_2. \quad (61.174)$$

The left hand side of this equation is the response from a Dirac source that is advected-diffused from (\mathbf{x}_1, t_1) and measured at the space-time point (\mathbf{x}_2, t_2) . The right hand side is the composition of a Green's function feeling the source at (\mathbf{x}_1, t_1) but now sampled at an intermediate space-time position, (\mathbf{x}, τ) , and then further advective-diffused to (\mathbf{x}_2, t_2) , with integration over all possible intermediate positions \mathbf{x} . The intermediate sampling can occur at an arbitrary intermediate time τ , so long as $t_1 < \tau < t_2$. The composition property (61.174) allows us to conceive of a long-time interval Green's function as the composition of an arbitrary number of shorter time interval Green's functions.

61.10.7 Integral expression for the tracer concentration

We are now ready to express the passive tracer concentration, C , as a suite of integrals involving the Green's function and the known boundary and initial conditions as well as the known source function. The process for deriving this expression is identical to that used in Section 61.10.5 for reciprocity, with the following steps offered for completeness.

Derivation setup

The initial-boundary value problem for the passive tracer is given by

$$\frac{\partial(\rho C)}{\partial t} + \nabla \cdot (\rho \mathbf{v}^\dagger C - \rho \mathbb{K} \cdot \nabla C) = \rho \Lambda \quad \mathbf{x} \in \mathcal{R}, t \geq t_{\text{init}} \quad (61.175a)$$

$$\rho C = \rho I \quad \mathbf{x} \in \mathcal{R}, t = t_{\text{init}} \quad (61.175b)$$

$$\rho C = \rho \sigma \quad \mathbf{x} \in \partial \mathcal{R}, t \geq t_{\text{init}} \quad (61.175c)$$

where we only consider the Dirichlet boundary condition to ensure a closed reciprocity relation in the presence of surface mass fluxes (Section 61.10.5). The corresponding adjoint Green's function satisfies

$$-\frac{\partial[\rho \tilde{G}(\mathbf{x}, t|\mathbf{x}_0, t_0)]}{\partial t} + \nabla_{\mathbf{x}} \cdot [-\rho \mathbf{v}^\dagger \tilde{G}(\mathbf{x}, t|\mathbf{x}_0, t_0) - \rho \mathbb{K} \cdot \nabla_{\mathbf{x}} \tilde{G}(\mathbf{x}, t|\mathbf{x}_0, t_0)] = \delta(\mathbf{x} - \mathbf{x}_0) \delta(t - t_0) \quad (61.176a)$$

$$\tilde{G}(\mathbf{x}, t > t_0|\mathbf{x}_0, t_0) = 0 \quad (61.176b)$$

$$\tilde{G}(\mathbf{x} \in \partial \mathcal{R}, t|\mathbf{x}_0, t_0) = 0, \quad (61.176c)$$

with the reciprocity condition (61.167) holding since we chose Dirichlet boundary conditions. Multiplying the adjoint Green's function equation (61.176a) by $C(\mathbf{x}, t)$ and performing manipulations just like those for reciprocity leads to

$$\begin{aligned} -\partial_t(\rho C \tilde{G}) + \nabla_{\mathbf{x}} \cdot [\tilde{G} \rho \mathbb{K} \cdot \nabla C - C \rho \mathbb{K}(\mathbf{x}, t) \cdot \nabla_{\mathbf{x}} \tilde{G} - C \rho \mathbf{v}^\dagger \tilde{G}] + \tilde{G} \rho \Lambda \\ = C(\mathbf{x}, t) \delta(\mathbf{x} - \mathbf{x}_0) \delta(t - t_0). \end{aligned} \quad (61.177)$$

With the homogeneous Dirichlet conditions satisfied by \tilde{G} on the spatial boundaries, a space and time integration over (\mathbf{x}, t) leads to

$$\begin{aligned} C(\mathbf{x}_0, t_0) &= \int_{\mathcal{R}} \tilde{G}(\mathbf{x}, t_{\text{init}}|\mathbf{x}_0, t_0) \rho(\mathbf{x}, t_{\text{init}}) I(\mathbf{x}) dV + \int_{t_{\text{init}}}^{t_0} \left[\int_{\mathcal{R}} \tilde{G}(\mathbf{x}, t|\mathbf{x}_0, t_0) \rho(\mathbf{x}, t) \Lambda(\mathbf{x}, t) dV \right] dt \\ &\quad - \int_{t_{\text{init}}}^{t_0} \left[\oint_{\partial \mathcal{R}} \sigma(\mathbf{x}, t) \rho(\mathbf{x}, t) \mathbb{K}(\mathbf{x}, t) \cdot \nabla_{\mathbf{x}} \tilde{G}(\mathbf{x}, t|\mathbf{x}_0, t_0) \cdot \hat{\mathbf{n}}_{\mathbf{x}} d\mathcal{S} \right] dt. \end{aligned} \quad (61.178)$$

Use of the reciprocity relation (61.167) allows us to write this equation in terms of the Green's function rather than the adjoint Green's function

$$\begin{aligned} C(\mathbf{x}_0, t_0) &= \int_{\mathcal{R}} G(\mathbf{x}_0, t_0|\mathbf{x}, t_{\text{init}}) \rho(\mathbf{x}, t_{\text{init}}) I(\mathbf{x}) dV + \int_{t_{\text{init}}}^{t_0} \left[\int_{\mathcal{R}} G(\mathbf{x}_0, t_0|\mathbf{x}, t) \rho(\mathbf{x}, t) \Lambda(\mathbf{x}, t) dV \right] dt \\ &\quad - \int_{t_{\text{init}}}^{t_0} \left[\oint_{\partial \mathcal{R}} \sigma(\mathbf{x}, t) \rho(\mathbf{x}, t) \mathbb{K}(\mathbf{x}, t) \cdot \nabla_{\mathbf{x}} G(\mathbf{x}_0, t_0|\mathbf{x}, t) \cdot \hat{\mathbf{n}}_{\mathbf{x}} d\mathcal{S} \right] dt. \end{aligned} \quad (61.179)$$

Finally, swapping labels $(\mathbf{x}_0, t_0) \leftrightarrow (\mathbf{x}, t)$ renders

$$\begin{aligned} C(\mathbf{x}, t) &= \int_{\mathcal{R}} G(\mathbf{x}, t|\mathbf{x}_0, t_{\text{init}}) \rho(\mathbf{x}_0, t_{\text{init}}) I(\mathbf{x}_0) dV_0 + \int_{t_{\text{init}}}^t \left[\int_{\mathcal{R}} G(\mathbf{x}, t|\mathbf{x}_0, t_0) \rho(\mathbf{x}_0, t_0) \Lambda(\mathbf{x}_0, t_0) dV_0 \right] dt_0 \\ &\quad - \int_{t_{\text{init}}}^t \left[\oint_{\partial \mathcal{R}} \sigma(\mathbf{x}_0, t_0) \rho(\mathbf{x}_0, t_0) \mathbb{K}(\mathbf{x}_0, t_0) \cdot \nabla_{\mathbf{x}_0} G(\mathbf{x}, t|\mathbf{x}_0, t_0) \cdot \hat{\mathbf{n}}_{\mathbf{x}_0} d\mathcal{S}_0 \right] dt_0. \end{aligned} \quad (61.180)$$

This solution manifests causality since the concentration at time t is a function only of processes occurring from t_{init} up to time t .

61.10.8 Properties of the solution

The integral solution (61.180) is of the same form as equation (4.150) for the diffusion equation. Properties of this solution, and corresponding properties of the Green's function, follow from those satisfied by the diffusion equation as detailed in Section 4.8.7. We here summarize these properties for completeness.

The role of advection and diffusion at boundaries

Explicit contributions from the advective flux are absent from the solution (61.180). Namely, there are no advective flux contributions at the surface boundary due to the homogeneous Dirichlet boundary conditions imposed on the Green's function. For the ocean bottom, material and rigid no-flux conditions mean that $\mathbf{v} \cdot \hat{\mathbf{n}} = 0$ at the bottom. The presence of advection arises only through its effect on the Green's function, which is affected by both advection and diffusion.

Furthermore, notice how in the absence of diffusion (i.e., $K = 0$) the Dirichlet boundary data is unable to penetrate into the ocean interior since the surface boundary integral vanishes from equation (61.180). In effect, the surface boundary becomes a material surface when there is no diffusion. That is, diffusive mixing is needed for boundary data to move into the interior. This role for diffusion was also identified when studying the surface flux condition for salt and freshwater in Section 64.5 (see also [Nurser and Griffies \(2019\)](#)).

Initial conditions

When sampling the tracer concentration at the initial time, $t \rightarrow t_{\text{init}}$, all the time integrals vanish from the solution (61.180), thus leaving

$$\lim_{t \rightarrow t_{\text{init}}} C(\mathbf{x}, t) = \lim_{t \rightarrow t_{\text{init}}} \int_{\mathcal{R}} G(\mathbf{x}, t | \mathbf{x}_0, t_{\text{init}}) \rho(\mathbf{x}_0, t_{\text{init}}) I(\mathbf{x}_0) dV_0. \quad (61.181)$$

Self-consistency implies that the Green's function satisfies

$$\lim_{t \rightarrow t_{\text{init}}} G(\mathbf{x}, t | \mathbf{x}_0, t_{\text{init}}) \rho(\mathbf{x}_0, t_{\text{init}}) = \delta(\mathbf{x} - \mathbf{x}_0) \quad \text{with } \mathbf{x}, \mathbf{x}_0 \in \mathcal{R}, \quad (61.182)$$

so that

$$\lim_{t \rightarrow t_{\text{init}}} \int_{\mathcal{R}} \rho(\mathbf{x}, t_{\text{init}}) G(\mathbf{x}, t | \mathbf{x}_0, t_{\text{init}}) I(\mathbf{x}_0) dV_0 = \int_{\mathcal{R}} \delta(\mathbf{x} - \mathbf{x}_0) I(\mathbf{x}_0) dV_0 = I(\mathbf{x}). \quad (61.183)$$

Dirichlet boundary conditions

Evaluating the Dirichlet solution (61.180) on a spatial boundary, $\mathbf{x} \in \partial\mathcal{R}$, eliminates both the volume integrals given that the Green's function satisfies homogeneous Dirichlet boundary conditions. The tracer concentration (61.180) thus takes the form

$$C(\mathbf{x}, t) = - \int_{t_{\text{init}}}^t \left[\oint_{\partial\mathcal{R}} \sigma(\mathbf{x}_0, t_0) \rho(\mathbf{x}_0, t_0) K(\mathbf{x}_0, t_0) \cdot \nabla_{\mathbf{x}_0} G(\mathbf{x}, t | \mathbf{x}_0, t_0) \cdot \hat{\mathbf{n}}_{\mathbf{x}_0} d\mathcal{S}_0 \right] dt_0 \\ \text{with } \mathbf{x} \in \partial\mathcal{R}. \quad (61.184)$$

Self-consistency with the Dirichlet boundary condition (61.148c) implies that the Green's function, when both spatial points are evaluated on the boundary, satisfies

$$\rho(\mathbf{x}_0, t_0) \mathbb{K}(\mathbf{x}_0, t_0) \cdot \nabla_{\mathbf{x}_0} G(\mathbf{x}, t | \mathbf{x}_0, t_0) \cdot \hat{\mathbf{n}}_{\mathbf{x}_0} = -\delta(t - t_0) \delta^{(2)}(\mathbf{x} - \mathbf{x}_0) \quad \text{with } \mathbf{x}, \mathbf{x}_0 \in \partial\mathcal{R}, \quad (61.185)$$

so that

$$C(\mathbf{x}, t) = \int_{t_{\text{init}}}^t \left[\oint_{\partial\mathcal{R}} \sigma(\mathbf{x}_0, t_0) \delta(t - t_0) \delta^{(2)}(\mathbf{x} - \mathbf{x}_0) d\mathcal{S}_0 \right] dt_0 = \sigma(\mathbf{x}, t) \quad \text{with } \mathbf{x} \in \partial\mathcal{R}. \quad (61.186)$$

61.10.9 Boundary propagator

Defining the boundary propagator

As for the diffusion equation in Section 4.8.8, we here introduce the boundary propagator for the advection-diffusion equation with Dirichlet boundary conditions. For this purpose, consider the special case of a passive tracer with zero interior source and with zero initial condition, thus satisfying the initial-boundary value problem

$$\frac{\partial(\rho C)}{\partial t} + \nabla \cdot (\rho \mathbf{v}^\dagger C - \rho \mathbb{K} \cdot \nabla C) = 0 \quad \mathbf{x} \in \mathcal{R}, t \geq t_{\text{init}} \quad (61.187a)$$

$$\rho C = 0 \quad \mathbf{x} \in \mathcal{R}, t = t_{\text{init}} \quad (61.187b)$$

$$\rho C = \rho \sigma \quad \mathbf{x} \in \partial\mathcal{R}, t \geq t_{\text{init}}, \quad (61.187c)$$

which leads to the simplification of the Green's function solution (61.180)

$$C(\mathbf{x}, t) = - \int_{t_{\text{init}}}^t \left[\oint_{\partial\mathcal{R}} \sigma(\mathbf{x}_0, t_0) \rho(\mathbf{x}_0, t_0) \mathbb{K}(\mathbf{x}_0, t_0) \cdot \nabla_{\mathbf{x}_0} G(\mathbf{x}, t | \mathbf{x}_0, t_0) \cdot \hat{\mathbf{n}}_{\mathbf{x}_0} d\mathcal{S}_0 \right] dt_0. \quad (61.188)$$

The tracer concentration at a point in space-time is determined by the history of the advection and diffusion that transfers boundary information to this point. To manifest this cause-effect relation, it is useful to define the boundary propagator just as for the diffusion equation

$$G^{\text{bp}}(\mathbf{x}, t | \mathbf{x}_0, t_0) \equiv -\rho(\mathbf{x}_0, t_0) \mathbb{K}(\mathbf{x}_0, t_0) \cdot \nabla_{\mathbf{x}_0} G(\mathbf{x}, t | \mathbf{x}_0, t_0) \cdot \hat{\mathbf{n}}_{\mathbf{x}_0} \quad \text{with } \mathbf{x}_0 \in \partial\mathcal{R}, \quad (61.189)$$

with G^{bp} having dimensions $\text{L}^{-2} \text{T}^{-1}$. The boundary propagator thus brings the tracer concentration (61.188) into the rather tidy form

$$C(\mathbf{x}, t) = \int_{t_{\text{init}}}^t \left[\oint_{\partial\mathcal{R}} \sigma(\mathbf{x}_0, t_0) G^{\text{bp}}(\mathbf{x}, t | \mathbf{x}_0, t_0) d\mathcal{S}_0 \right] dt_0. \quad (61.190)$$

Inhomogeneous Dirichlet at the surface and homogeneous Neumann at the bottom

In applications of passive tracers to study ocean circulation, it is common to apply inhomogeneous Dirichlet boundary conditions just at the ocean surface, and homogeneous Neumann boundary

conditions (no-flux) at the ocean bottom

$$\frac{\partial(\rho C)}{\partial t} + \nabla \cdot (\rho \mathbf{v}^\dagger C - \rho \mathbb{K} \cdot \nabla C) = 0 \quad \mathbf{x} \in \mathcal{R}, t \geq t_{\text{init}} \quad (61.191a)$$

$$C = 0 \quad \mathbf{x} \in \mathcal{R}, t = t_{\text{init}} \quad (61.191b)$$

$$\rho C = \rho \sigma \quad \mathbf{x} \in \partial \mathcal{R}_{\text{surface}}, t \geq t_{\text{init}} \quad (61.191c)$$

$$\hat{\mathbf{n}}_\mathbf{x} \cdot \mathbb{K} \cdot \nabla_\mathbf{x} C = 0 \quad \mathbf{x} \in \partial \mathcal{R}_{\text{bottom}}, t \geq t_{\text{init}}. \quad (61.191d)$$

Note that since $\hat{\mathbf{n}} \cdot \mathbf{v} = 0$ at the solid earth ocean bottom, kinematics imposes no advective flux through the bottom, $\hat{\mathbf{n}} \cdot \mathbf{v} C = 0$. Since the bottom boundary conditions are homogeneous, the solution (61.188) also holds for the initial-boundary value problem (61.191a)-(61.191d). The key distinction, however, is that the Green's function now satisfies the following boundary value problem

$$\frac{\partial[\rho G(\mathbf{x}, t | \mathbf{x}_0, t_0)]}{\partial t} + \nabla_\mathbf{x} \cdot [\rho \mathbf{v}^\dagger G(\mathbf{x}, t | \mathbf{x}_0, t_0) - \rho \mathbb{K} \cdot \nabla_\mathbf{x} G(\mathbf{x}, t | \mathbf{x}_0, t_0)] = \delta(\mathbf{x} - \mathbf{x}_0) \delta(t - t_0) \quad (61.192a)$$

$$G(\mathbf{x}, t < t_0 | \mathbf{x}_0, t_0) = 0 \quad (61.192b)$$

$$G(\mathbf{x}, t | \mathbf{x}_0, t_0) = 0 \quad \mathbf{x} \in \partial \mathcal{R}_{\text{surface}} \quad (61.192c)$$

$$\hat{\mathbf{n}}_\mathbf{x} \cdot \mathbb{K} \cdot \nabla_\mathbf{x} G(\mathbf{x}, t | \mathbf{x}_0, t_0) = 0 \quad \mathbf{x} \in \partial \mathcal{R}_{\text{bottom}}. \quad (61.192d)$$

Boundary value problem for the boundary propagator

Following the more detailed presentation in Section 4.8.8 for the diffusion equation, we are led to the following boundary value problem satisfied by the boundary propagator

$$\frac{\partial[\rho G^{\text{bp}}(\mathbf{x}, t | \mathbf{x}_0, t_0)]}{\partial t} + \nabla_\mathbf{x} \cdot [\rho \mathbf{v}^\dagger G^{\text{bp}}(\mathbf{x}, t | \mathbf{x}_0, t_0) - \rho \mathbb{K} \cdot \nabla_\mathbf{x} G^{\text{bp}}(\mathbf{x}, t | \mathbf{x}_0, t_0)] = 0, \quad \mathbf{x} \in \mathcal{R} \quad (61.193a)$$

$$G^{\text{bp}}(\mathbf{x}, t | \mathbf{x}_0, t_0) = 0, \quad \mathbf{x} \notin \partial \mathcal{R}, t \leq t_0 \quad (61.193b)$$

$$G^{\text{bp}}(\mathbf{x}, t | \mathbf{x}_0, t_0) = \delta(t - t_0) \delta^{(2)}(\mathbf{x} - \mathbf{x}_0), \quad \mathbf{x}, \mathbf{x}_0 \in \partial \mathcal{R}. \quad (61.193c)$$

The boundary propagator acts as the mediator between boundary data, σ , and interior points, with the transfer of information realized through both advection and diffusion. A focus on the boundary propagator rather than the Green's function allows us to dispense with the need to compute the normal gradient of the Green's function at the boundary, with that calculation rather awkward in practice. Also recall our discussion in Section 4.9.5, where we argued that the boundary propagator can be considered the impulse response function for spatially distributed sources. Here, the mediation of the Dirac boundary sources is performed by advection plus diffusion, whereas in Section 4.9 we only considered linear damping and diffusion.

Normalization of the boundary propagator

As seen in Sections 61.3 and 61.4, diffusion acts to smooth all structure in the tracer field. Hence, if the boundary data is a uniform constant, $\sigma = \sigma_{\text{const}}$, then given sufficient time the tracer concentration will equal to this constant, $C = \sigma_{\text{const}}$. This steady state result is independent of details for the velocity field and for the diffusivity tensor, with details of advection and the diffusivity acting only to modify the time scale for the equilibration. Assuming we wait long enough, or equivalently that the initial condition occurs infinitely far in the past, then the tracer

concentration solution (61.190) leads to the normalization of the boundary propagator

$$\lim_{t_{\text{init}} \rightarrow -\infty} \int_{t_{\text{init}}}^t \left[\oint_{\partial\mathcal{R}} G^{\text{bp}}(\mathbf{x}, t | \mathbf{x}_0, t_0) d\mathcal{S}_0 \right] dt_0 = 1 \quad \text{for } \mathbf{x} \in \mathcal{R}. \quad (61.194)$$

This normalization holds for all field points, \mathbf{x} , within the region. Even though this condition was derived by assuming the special case of constant boundary data, it holds in general since the Green's function, and by extension the boundary propagator, are independent of the boundary data prescribed for the tracer concentration.



61.11 Exercises

EXERCISE 61.1: VERTICAL DIFFUSION OF TEMPERATURE IN THE OCEAN ([Vallis, 2017](#))

There is a natural time scale associated with diffusive transport. This time scale can be found from scaling the diffusion equation, which reveals that it takes the form

$$\tau_{\text{diffusion}} = \Delta^2 / \kappa, \quad (61.195)$$

where Δ is the length scale and κ is the kinematic diffusivity (dimensions of squared length per time). We now make use of this time scale to consider the diffusion of temperature in the ocean, with diffusion due solely to molecular processes.

Using the observed value of molecular diffusivity of temperature in water (look it up), estimate the time for a temperature anomaly to mix from the top of the ocean to the bottom, assuming vertical diffusion through the molecular diffusivity is the only means for mixing. This time scale follows from the one-dimensional diffusion equation and is determined by the diffusivity and the depth of the ocean. Comment on whether you think the real ocean has reached equilibrium after the last ice age (which ended about 12Kyr ago).

EXERCISE 61.2: ANALYTICAL SOLUTION TO ONE-DIMENSIONAL DIFFUSION EQUATION

Consider a one-dimensional diffusion equation

$$\frac{\partial C}{\partial t} = \kappa \frac{\partial^2 C}{\partial z^2}, \quad (61.196)$$

where C is a tracer concentration (e.g., temperature or salinity), κ is a constant kinematic diffusivity, and z is the vertical coordinate. Assume the domain has fixed boundaries at $z = 0$ and $z = H$.

- (a) Assume there is a zero flux of tracer at the two boundaries. Mathematically express this no-flux boundary condition.
- (b) Assume that the initial tracer concentration is confined to an area near the center of the domain. Use dimensional analysis to estimate the time scale for the concentration to homogenize throughout the domain.

- (c) Consider the initial-boundary value problem

$$\frac{\partial C}{\partial t} = \kappa \frac{\partial^2 C}{\partial z^2}, \quad (61.197a)$$

no-flux boundary condition from part (b) (61.197b)

$$C(z, t = 0) = C_0 \cos(Kz), \quad (61.197c)$$

where C_0 is a constant. What values for the wave-number, K , satisfy the no-flux boundary condition?

- (d) Solve the diffusion equation analytically for the given initial condition. Hint: consult your favorite partial differential equation book to learn how to solve this linear 1+1 dimensional diffusion equation.
- (e) Explain how the analytical answer you obtained is consistent with the dimensional analysis answer from part (b).

EXERCISE 61.3: DISSIPATIVE PROPERTIES OF DIFFUSION

This exercise explores the dissipative property of diffusion when acting on a tracer extrema.

- (a) ONE-DIMENSIONAL DIFFUSION

Consider the diffusion equation in one spatial dimension, and assume a Boussinesq fluid in which case the density factors are all constant and so can be dropped

$$\frac{\partial C}{\partial t} = \frac{\partial}{\partial z} \left[\kappa \frac{\partial C}{\partial z} \right] \quad (61.198a)$$

$$= \frac{\partial \kappa}{\partial z} \frac{\partial C}{\partial z} + \kappa \frac{\partial^2 C}{\partial z^2}, \quad (61.198b)$$

where $\kappa(z, t)$ is an *eddy diffusivity* (also *turbulent diffusivity*). The eddy diffusivity is assumed to be a function of (z, t) , with the spatial dependence determined by the flow. Show that a tracer extrema, C^* , evolves under diffusion according to

$$\frac{\partial C^*}{\partial t} = \kappa \frac{\partial^2 C^*}{\partial z^2}. \quad (61.199)$$

So what does diffusion do to a local maxima (e.g., a local hot region) in the tracer field? What about a minima (e.g., a local cold region)?

- (b) THREE-DIMENSIONAL DIFFUSION

Generalize the above one dimensional result to three dimensions, whereby the diffusivity κ becomes a symmetric positive-definite diffusion *tensor*, in which case

$$\frac{\partial C}{\partial t} = \frac{\partial}{\partial x^m} \left[\mathbb{K}^{mn} \frac{\partial C}{\partial x^n} \right]. \quad (61.200)$$

Now consider an extrema in the tracer field, which is defined by

$$\frac{\partial C^*}{\partial x^n} = 0 \quad \forall n = 1, 2, 3. \quad (61.201)$$

Prove that three dimensional diffusion acts to *dissipate* an extrema. Hint: recall some linear algebra properties of a symmetric positive-definite matrix. In particular, note that a symmetric positive-definite matrix has positive eigenvalues.

EXERCISE 61.4: DIFFUSION INCREASES INFORMATION ENTROPY OF A TRACER CONCENTRATION
 Diffusion is an irreversible process. Here we illustrate this property by considering the *information entropy* associated with a non-negative tracer concentration⁶

$$\mathcal{S}_C \equiv - \int (C \ln C) \rho dV. \quad (61.202)$$

Show that

$$\frac{d\mathcal{S}_C}{dt} \geq 0 \quad (61.203)$$

over a material region with $C > 0$ and diffusion downgradient, $\mathbf{J} \cdot \nabla C < 0$. That is, diffusion always increases the information entropy. Hint: follow the discussion of tracer moments in Section 61.4.3.

EXERCISE 61.5: ONE-DIMENSIONAL ADVECTION

Consider the advection equation in one space dimension without boundaries

$$\frac{\partial C}{\partial t} + u \frac{\partial C}{\partial x} = 0 \quad (61.204a)$$

$$C(x, z, t=0) = C_0 \cos(kx) \quad (61.204b)$$

$$u(z, t) = \alpha z \cos(\omega t). \quad (61.204c)$$

The specified zonal velocity is non-divergent, oscillatory in time, and vertically sheared

$$\frac{\partial u}{\partial z} = \alpha \cos(\omega t), \quad (61.205)$$

with ω the radial frequency of the temporal oscillations. What is the tracer concentration at times $t > 0$? Hint: make use of the exact solution given by equation (61.44).

EXERCISE 61.6: SKEW FLUX FOR OCEAN MESOSCALE EDDIES

Consider a middle-latitude mesoscale ocean eddy respecting geostrophic balance (see Section 28.4) on an f -plane (constant Coriolis parameter) and incompressibility. In this case, the horizontal eddy-induced velocity at the ocean surface is non-divergent

$$\mathbf{u}^* = \nabla \times \hat{\mathbf{z}} \psi. \quad (61.206)$$

In this equation, the geostrophic streamfunction is given by

$$\psi = -\hat{\mathbf{z}} \frac{g \eta}{f}, \quad (61.207)$$

with f the Coriolis parameter, g the gravitational acceleration, and η the sea level undulation associated with the eddy. Since the fluid is incompressible, the mass transport equals to the volume transport times a constant reference density, ρ_0 .

- (a) Determine the skew diffusion tensor (61.66).
- (b) Determine the skew tracer flux (61.79a).

EXERCISE 61.7: INTEGRATION BETWEEN TWO CLOSED TRACER CONTOURS

This exercise introduces some ideas of use for determining processes affecting the transport of

⁶Information entropy is used in statistical physics as a measure of the order/disorder of a probability distribution. We here apply these notions to measure the information entropy of a tracer concentration.

matter across a tracer contour. Note that in general, the tracer concentration is a function of time. However, the present suite of questions concerns the instantaneous geometry of the tracer field, so that time dependence is not considered.

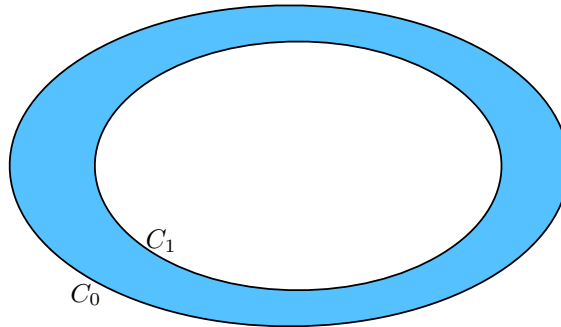


FIGURE 61.5: Illustrating the area contained between two closed tracer contours, $C_0 \leq C(x, y, t) \leq C_1$. Exercise 61.7 develops some mathematical expressions for integration within this area, with the resulting expressions of use for the analyses of tracer transport.

- (a) Consider a closed two-dimensional region bounded by two contours of tracer concentration, $C_0 \leq C(x, y, t) \leq C_1$, such as shown in Figure 61.5. Derive the following expression for the area enclosed by the two contours

$$\mathcal{A} = \int_{C_0}^{C_1} dC \oint \frac{dl}{|\nabla C|}. \quad (61.208)$$

In this expression, dl is the line element for a path taken in a counter-clockwise direction along a contour of constant C . We also assume the tracer concentration is not uniform in the region of interest so that $\nabla C \neq 0$.

- (b) As a corollary, show that for

$$\mathcal{A}(C) = \int_{C_0}^C dC' \oint \frac{dl}{|\nabla C'|} \quad (61.209)$$

we have the identity

$$\frac{\partial \mathcal{A}(C)}{\partial C} = \oint \frac{dl}{|\nabla C|}. \quad (61.210)$$

In words, this result means that the area between two tracer contours has a partial derivative, with respect to the tracer contour, equal to the line integral on the right hand side. The area per C is smaller in regions where the tracer gradient is larger; i.e., there is less area “concentration” in regions of strong tracer gradient.

- (c) Use the above two results to prove the following form of the Fundamental Theorem of Calculus

$$\frac{\partial}{\partial C} \left[\int \Phi(\mathbf{x}) d\mathcal{A} \right] = \frac{\partial}{\partial C} \left[\int_{C_0}^C dC' \oint \frac{\Phi dl}{|\nabla C'|} \right] \quad (61.211a)$$

$$= \oint \frac{\Phi dl}{|\nabla C|}, \quad (61.211b)$$

with Φ an arbitrary function. This is a remarkable identity with many useful applications such as those in [Marshall et al. \(2006\)](#).

EXERCISE 61.8: EVOLUTION OF TRACER CENTER OF MASS IN A STATIC DOMAIN

The exercise introduces us to how the tracer center of mass evolves within a Boussinesq fluid. We define the tracer center of mass as

$$\langle \mathbf{x} \rangle^C = \frac{\int \mathbf{x} C dV}{\int C dV}, \quad (61.212)$$

with C the tracer concentration, \mathbf{x} the coordinate of a point in the fluid, and integration is over the full fluid domain. For example, with a spherically symmetric tracer cloud, the center of mass position is at the sphere's center. The center of mass position is not necessarily where the largest tracer concentration sits, in the same way that the center of mass of a massive object is not necessarily where the object is most dense. For example, a hollow spherical shell has its center of mass at the center of the sphere, even though there is no mass there.

For this exercise, assume the fluid is within a domain whose static boundaries are either material (no normal component to the boundary flux) or periodic. Hence, the total fluid volume and total tracer content remain constant

$$\mathcal{V} = \int dV \quad \text{and} \quad \mathcal{C} = \int C dV. \quad (61.213)$$

Furthermore, when computing the time derivative acting on the integral, make use of the kinematic results from Section 17.3.3, in which for any integrand φ

$$\frac{d}{dt} \int \varphi dV = \int \frac{\partial \varphi}{\partial t} dV, \quad (61.214)$$

which follows since the region boundaries are assumed to be static. Equivalently, since the region under consideration is material (no matter crosses the boundaries), we can make use of Reynold's transport theorem from Section 17.3.4 to write

$$\frac{d}{dt} \int \varphi dV = \int \frac{D\varphi}{Dt} dV. \quad (61.215)$$

- (a) Consider a tracer concentration whose tendency at a point in space is affected only by advection

$$\frac{DC}{Dt} = 0 \implies \frac{\partial C}{\partial t} + \nabla \cdot (\mathbf{v} C) = 0, \quad (61.216)$$

with \mathbf{v} a non-divergent velocity, $\nabla \cdot \mathbf{v} = 0$. Show that the tracer center of mass position evolves according to the tracer center of mass velocity

$$\frac{d\langle \mathbf{x} \rangle^C}{dt} = \langle \mathbf{v} \rangle^C, \quad (61.217)$$

where the tracer center of mass velocity is given by

$$\langle \mathbf{v} \rangle^C = \frac{\int \mathbf{v} C dV}{\int C dV} = \frac{1}{\mathcal{C}} \int \mathbf{v} C dV. \quad (61.218)$$

- (b) Consider a tracer concentration whose tendency at a point in space affected only by diffusion

$$\frac{\partial C}{\partial t} = \nabla \cdot (K \cdot \nabla C), \quad (61.219)$$

where $K = K(\mathbf{x}, t) > 0$ is a kinematic diffusivity (physical dimensions of squared length per time), and which is assumed to vanish at the domain boundaries. Show that the tracer center of mass drifts up the diffusivity gradient

$$\frac{d\langle \mathbf{x} \rangle^C}{dt} = \langle \nabla K \rangle^C. \quad (61.220)$$

Hint: use the product rule and drop boundary terms.

- (c) Consider an initial tracer concentration that is a function only of latitude,

$$C(x, y, z, t = 0) = C_0(y), \quad (61.221)$$

and assume a smooth spherical domain. Assume the diffusivity, K , is a turbulent diffusivity proportional to the eddy kinetic energy of the flow, so that large diffusivity occurs in regions with large eddy activity; i.e., there is a lot of turbulent mixing where turbulence is active. Introduce an stirring from the eddies that breaks the zonal symmetry. Qualitatively discuss the process whereby this turbulent diffusive mixing causes the tracer center of mass to drift towards the turbulent region.

- (d) Generalize the result from part (b) to the case of the diffusion equation

$$\frac{\partial C}{\partial t} = \nabla \cdot (\mathbb{K} \cdot \nabla C) = \partial_p (\mathbb{K}^{pq} \partial_q C), \quad (61.222)$$

where \mathbb{K} is a second order symmetric diffusion tensor.

EXERCISE 61.9: EVOLUTION OF TRACER CENTER OF MASS IN MOVING REGION

Consider a finite region of fluid with fixed mass that is moving with the fluid velocity field, $\mathcal{R}(\mathbf{v})$. The fluid is assumed to have a tracer whose concentration is affected by an irreversible process so that

$$\frac{DC}{Dt} = \dot{C} \neq 0. \quad (61.223)$$

For example, \dot{C} may represent a diffusive process, in which case the tracer content within the region changes due to diffusion of tracer across the region boundary.

Determine the evolution equation for the tracer center of mass position

$$\langle \mathbf{x} \rangle^C = \frac{\int_{\mathcal{R}(\mathbf{v})} \mathbf{x} C \rho dV}{\int_{\mathcal{R}(\mathbf{v})} C \rho dV}. \quad (61.224)$$

Hint: the region under consideration is moving with the fluid and has constant mass. Although the region boundaries are not material, we can make use of Reynold's transport theorem from Section 17.3.6 since the region has a constant mass. Consequently, we can set

$$\frac{d}{dt} \int_{\mathcal{R}(\mathbf{v})} \psi \rho dV = \int_{\mathcal{R}(\mathbf{v})} \frac{D\psi}{Dt} \rho dV. \quad (61.225)$$

EXERCISE 61.10: DIFFUSIVE HOMOGENIZATION OF SCALARS INSIDE CLOSED CONTOURS

The advection-diffusion equation for a tracer concentration is given by

$$\frac{\partial(\rho C)}{\partial t} + \nabla \cdot (\rho \mathbf{v} C) = -\nabla \cdot \mathbf{J} \quad (61.226)$$

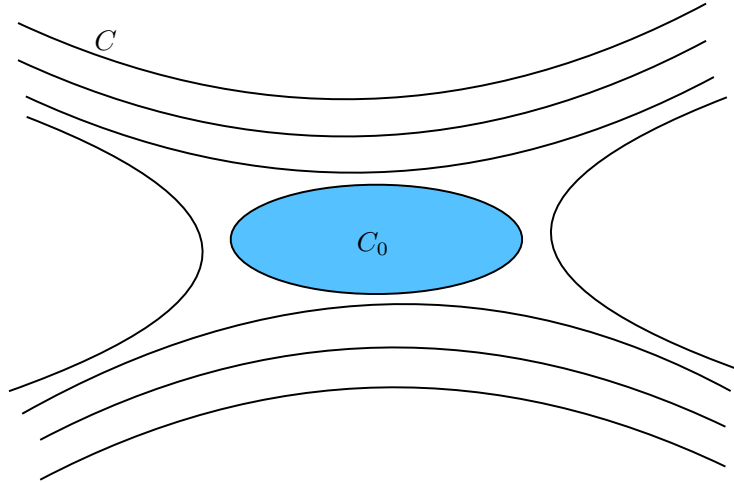


FIGURE 61.6: In a steady state flow, the tracer concentration within a constant C contour is constant. Diffusion has thus acted to remove all variations in tracer concentration within the region. In this figure, the concentration within the closed region has constant value $C = C_0$, whereas the region with open tracer contours remains non-homogeneous.

where

$$\mathbf{J} = -\rho \mathbb{K} \cdot \nabla C \quad (61.227)$$

is a downgradient diffusive flux with \mathbb{K} a symmetric positive-definite diffusion tensor. In the steady state, the divergence of the advective tracer flux balances the convergence of the diffusive flux

$$\nabla \cdot (\rho \mathbf{v} C) = -\nabla \cdot \mathbf{J}. \quad (61.228)$$

Consider a two-dimensional steady state flow and consider a region enclosed by a constant tracer contour. Prove that the tracer concentration is homogeneous (i.e., a spatially constant) within the contour of constant C , as shown in Figure 61.6. Hence, in the steady state, diffusion removes all tracer variations within closed tracer contours; i.e., there are no tracer extrema within a closed tracer contour.

Hint: make use of a *reductio ad absurdum* argument and study the material in Section 65.10.

EXERCISE 61.11: STEADY TWO DIMENSIONAL ADVECTION-DIFFUSION

Consider the steady state advection-diffusion equation for a scalar field, Q , in a two dimensional non-divergent flow

$$\nabla \cdot (\mathbf{u} Q) = \nabla \cdot (\mathbb{K} \cdot \nabla Q) \quad \text{with } \mathbf{u} = \hat{\mathbf{z}} \times \nabla \psi, \quad (61.229)$$

and \mathbb{K} a diffusion tensor. Show that when evaluated along a contour of constant Q we can write

$$-(\hat{\mathbf{n}} \cdot \nabla Q)(\hat{\mathbf{t}} \cdot \nabla \psi) = \nabla \cdot (\mathbb{K} \cdot \nabla Q) \quad (61.230)$$

where $\hat{\mathbf{t}}$ is the unit tangent along the contour and $\hat{\mathbf{n}}$ is a unit vector pointing to the left of the tangent (e.g., see Figure 6.6). Assuming $\hat{\mathbf{n}} \cdot \nabla Q \neq 0$, this equation takes on the form

$$\hat{\mathbf{t}} \cdot \nabla \psi = -\frac{\nabla \cdot (\mathbb{K} \cdot \nabla Q)}{(\hat{\mathbf{n}} \cdot \nabla Q)}, \quad (61.231)$$

which provides a means to integrate the streamfunction, ψ , along contours of constant Q .

If Q is the quasi-geostrophic potential vorticity (Chapter 42), then contours of constant Q are known as *geostrophic contours*. Within this context, [Rhines and Holland \(1979\)](#) made use of the

identity (61.231) in their study of ocean circulation in the presence of eddy diffusion of potential vorticity.

Hint: write the advection operator as a Jacobian and make use of Exercise 6.1.

EXERCISE 61.12: DISTRIBUTION OF ONE TRACER WITH RESPECT TO ANOTHER

Consider two tracers, ψ and B , that satisfy the advection-diffusion equation with the same diffusion tensor

$$\rho \frac{D\psi}{Dt} = \nabla \cdot (\rho \mathbb{K} \cdot \nabla \psi) \quad (61.232a)$$

$$\rho \frac{DB}{Dt} = \nabla \cdot (\rho \mathbb{K} \cdot \nabla B). \quad (61.232b)$$

Having access to two tracers allows us to diagnose certain properties of the flow, both in geographical/depth space as well as in the space defined by the tracers. We here study how the tracer B is distributed within layers defined by ψ , and how that distribution evolves in time. These considerations are partly motivated by the work of [Ruan and Ferrari \(2021\)](#), who assumed B to be buoyancy (with a linear equation of state). Whereas [Ruan and Ferrari \(2021\)](#) assumed a Boussinesq fluid with a constant scalar diffusivity, here we generalize to a non-Boussinesq fluid with a flow-dependent diffusion tensor, \mathbb{K} , which is a symmetric and positive-definite second order tensor.

- (a) Derive the following identity

$$\rho \frac{D(\psi B^n)}{Dt} = \nabla \cdot (B^n \rho \mathbb{K} \cdot \nabla \psi - \psi \rho \mathbb{K} \cdot \nabla B^n) + n \psi \nabla B^{n-1} \cdot \rho \mathbb{K} \cdot \nabla B + 2n \psi B^{n-1} \rho \dot{B}, \quad (61.233)$$

where B^n is B raised to the power n , and where we made use of the shorthand

$$\dot{B} = \frac{DB}{Dt}. \quad (61.234)$$

For reference, recall from Chapter 1 that the scalar product leads to the following index expressions using Cartesian tensors

$$\nabla \cdot (\rho \mathbb{K} \cdot \nabla B) = \partial_a (\rho \mathbb{K}_{ab} \partial_b B) \quad \text{and} \quad \nabla B \cdot \mathbb{K} \cdot \nabla B = \partial_a B \mathbb{K}_{ab} \partial_b B. \quad (61.235)$$

Show all relevant steps in the derivation of equation (61.233). Hint: as an optional warm-up, derive the special case with $n = 1$

$$\rho \frac{D(\psi B)}{Dt} = \nabla \cdot (B \rho \mathbb{K} \cdot \nabla \psi - \psi \rho \mathbb{K} \cdot \nabla B) + 2 \psi \rho \dot{B} \quad (61.236)$$

and then the case with $n = 2$

$$\rho \frac{D(\psi B^2)}{Dt} = \nabla \cdot (B^2 \rho \mathbb{K} \cdot \nabla \psi - \psi \rho \mathbb{K} \cdot \nabla B^2) + 2 \psi \nabla B \cdot \rho \mathbb{K} \cdot \nabla B + 4 \psi B \rho \dot{B}. \quad (61.237)$$

- (b) Introduce the ψ -weighted mean of an arbitrary field, Γ , according to

$$\bar{\Gamma} \equiv \frac{\int_V \Gamma \psi \rho dV}{\int_V \psi \rho dV}. \quad (61.238)$$

Furthermore, assume all boundaries to the domain are material, which means that the

domain matter content is fixed in time

$$\frac{d}{dt} \int_V \rho dV = 0 \quad \text{and} \quad \frac{d}{dt} \int_V \psi \rho dV = 0 \quad \text{and} \quad \frac{d}{dt} \int_V B \rho dV = 0. \quad (61.239)$$

Make use of equation (61.236) to derive the following identity

$$\frac{d\bar{B}}{dt} = 2 \bar{\dot{B}}, \quad (61.240)$$

and offer some discussion.



Chapter 62

EDDY AND MEAN TRACER KINEMATICS

Geophysical fluid flows exhibit multiple scales in both space and time. In the analysis of these flows, it is useful to seek a description that decomposes fluid properties into a mean component and a fluctuation relative to the mean. We perform an eddy-mean decomposition when interest concerns the mean field and impacts on the mean by the fluctuating instantaneous flow, with such impacts often termed *rectified* effects. The mean field can be defined in many fashions with subjective choices based on particulars of the flow and the analysis goals. The definition for the mean in turn affects what we refer to as the fluctuation. Quite generally, fluctuations take the form of transient linear waves, nonlinear and/or breaking waves, coherent structures, and/or a chaotic/turbulent soup of eddying features. In this chapter we develop a kinematic framework originally motivated by the analysis of scalar transport induced by small amplitude wave-like eddying features, but is also of use for turbulent processes and their parameterizations (e.g., Chapter 63).

We consider two kinematic methods to decompose the flow into a mean and eddy. The first is the *generalized Lagrangian mean (GLM)*, which is a hybrid Eulerian/Lagrangian method that introduces an Eulerian disturbance field to measure the position of a fluid particle relative to its mean position ([Andrews and McIntyre, 1978a,b](#); [Bühler, 2014a](#)). For our purposes it is sufficient to use only a small piece of the GLM framework to help unpack the kinematics of eddy tracer fluxes. The second kinematic method makes use of isopycnal vertical coordinates. We connect an isopycnal description to the GLM by applying the GLM just in the vertical direction. In this sense the isopycnal approach is quasi-Lagrangian since it fixes the horizontal position (Eulerian) yet allows the vertical to follow an adiabatic fluid parcel (Lagrangian). The isopycnal approach is frequently used to help understand how ocean mesoscale eddies affect stratification and tracer transport in stably stratified flows. Our presentation follows the methods developed by [McDougall and McIntosh \(2001\)](#) and summarized in Chapter 9 of [Griffies \(2004\)](#).

CHAPTER GUIDE

Material in this chapter relies on an understanding of the tracer equation as derived in Section 17.1 and the maths and physics of the advection-diffusion equation explored in Chapter 61. We focus most discussion on incompressible flows discussed in Chapter 18 and applicable to the Boussinesq fluid commonly assumed for the ocean (Chapter 26). Generalizations to compressible fluids are straightforward, with examples provided by [Griffies and Greatbatch \(2012\)](#). The kinematics of isopycnal fluid layers in a perfect fluid (Sections 62.5 and 62.6) are posed using the isopycnal vertical coordinates detailed in Chapter 56 and further pursued in Chapter 58.

62.1	Loose threads	1546
62.2	Reynolds decomposition	1546
62.3	Basic kinematics of the GLM	1547
62.3.1	Motivation	1547
62.3.2	Length scales and the small parameter	1549
62.3.3	Decomposing the particle trajectory	1549
62.3.4	GLM and the Stokes mean	1550
62.3.5	An example linear wave	1551
62.3.6	GLM with a materially constant scalar	1553
62.3.7	Further study	1554
62.4	Kinematics of eddy tracer fluxes	1554
62.4.1	Particle displacements and eddy tracer fluxes	1554
62.4.2	Symmetric and skew symmetric tracer fluxes	1555
62.4.3	Massaging the mean field tracer equation	1557
62.4.4	Connection to Stokes drift	1558
62.4.5	A linear rotating periodic wave example	1559
62.4.6	Further study	1560
62.5	Kinematics of volume transport in isopycnal layers	1560
62.5.1	Isopycnal mean	1561
62.5.2	Modified mean	1561
62.5.3	Transformed residual mean (TRM)	1563
62.5.4	Volume conservation and the thickness equation	1565
62.5.5	Ensemble mean kinematics in isopycnal coordinates	1565
62.5.6	Ensemble mean kinematics in geopotential coordinates	1566
62.5.7	Approximate ensemble mean kinematics in geopotential coordinates	1567
62.5.8	Further study	1569
62.6	Mean tracer equation	1569
62.6.1	Thickness weighted average or mean	1569
62.6.2	Isopycnal mean thickness weighted tracer equation	1569
62.6.3	Subgrid scale tracer transport tensor	1570
62.6.4	Mean tracer transport beneath a density surface	1570
62.6.5	Summary of the tracer parameterization problem	1571
62.6.6	Comments	1571

62.1 Loose threads

- Redo Figure 62.4.

62.2 Reynolds decomposition

At any point in space and time, we can decompose a field into a mean, $\bar{\Phi}(\mathbf{x}, t)$, and a departure from the mean, $\Phi'(\mathbf{x}, t)$

$$\Phi(\mathbf{x}, t) = \bar{\Phi}(\mathbf{x}, t) + \Phi'(\mathbf{x}, t). \quad (62.1)$$

The departure from the mean is generally termed the “eddy” or the “fluctuation”. The following offers a non-exhaustive list of mean operators.

- TIME MEAN: If the mean operator is based on a long time mean, then the mean fields are assumed to be time independent: $\bar{\Phi}(\mathbf{x}, t) = \bar{\Phi}(\mathbf{x})$. This is a common operator when interest is focused on the long term mean fluid properties.
- PHASE AVERAGE: Rather than a time mean, we may choose to average over the phase (or period) of a wave. This choice is particularly relevant when the fluctuating field involves

quasi-linear waves.

- **ZONAL MEAN:** If the mean operator is based on an average along a particular coordinate direction (e.g., zonal average), then the mean tracer concentration is independent of the “averaged out” direction.
- **COARSE GRAINING:** If the mean operator is based on an average over a spatial and temporal region, such as the mesoscale, then such coarse-graining averages out smaller scales.
- **ENSEMBLE AVERAGE:** Rather than a space or time mean operation, we may consider the mean or average computed over an ensemble of many flow realizations. For many purposes this is the most analytically convenient operator.

If a mean operator satisfies the following properties then it is said to provide a “Reynolds decomposition”

$$\overline{\Phi'} = 0 \quad (62.2a)$$

$$\overline{\Phi} = \Phi \quad (62.2b)$$

$$\overline{\gamma \Phi} = \gamma \overline{\Phi} \quad \text{for } \gamma \text{ a constant.} \quad (62.2c)$$

Equation (62.2a) says that the mean of an eddy fluctuation vanishes. The equality (62.2b) says that the mean of a mean field returns the mean field. The final equality, (62.2c), says that a constant commutes with the mean operator. Notably, some or all of these properties are not satisfied by certain operators used for eddy-mean decompositions. However, in the following we assume they are satisfied.

62.3 Basic kinematics of the GLM

We here consider basic elements of generalized Lagrangian mean (GLM) theory. GLM is distinct from both the Eulerian mean and the Lagrangian mean. Rather, GLM is a hybrid between Lagrangian and Eulerian descriptions of fluid motions, so that it might be more appropriate to refer to it as the “hybrid Lagrangian-Eulerian mean theory”.

The GLM and the Eulerian mean for a fluid property are generally distinct, with their difference referred to as the *Stokes mean*

$$\text{Lagrangian mean} = \text{Eulerian mean} + \text{Stokes mean.} \quad (62.3)$$

This name is motivated from the *Stokes drift* introduced in Section 45.8, which we again encounter in Section 62.3.4. Note that the literature typically refers to the Stokes mean as the “Stokes correction”. We avoid that terminology in order to avoid the spurious notion that one type of mean operator is more correct than the other. We instead propose that a mean operator is subjectively chosen based on its suitability to a particular scientific question. Furthermore, no mean operator is suitable for all questions.

62.3.1 Motivation

Consider a materially constant scalar field

$$\frac{D\Phi}{Dt} = \frac{\partial \Phi}{\partial t} + \mathbf{v} \cdot \nabla \Phi = 0. \quad (62.4)$$

The scalar Φ is constant following fluid particles whose trajectories are integral curves of the fluid velocity \mathbf{v} . The question arises how to develop a mean operator that averages over fluctuations in the trajectories while preserving the material constancy nature of the instantaneous equation $D\Phi/Dt = 0$. This aspiration is not trivial.

Eulerian mean

An Eulerian mean operator considered in Section 62.2 leads to the mean field equation

$$\frac{\partial \bar{\Phi}}{\partial t} + \bar{\mathbf{v}} \cdot \nabla \bar{\Phi} = -\overline{\mathbf{v}' \cdot \nabla \Phi'}. \quad (62.5)$$

Whereas Φ is materially constant when following the instantaneous flow field \mathbf{v} , the Eulerian mean $\bar{\Phi}$ is not materially constant when following $\bar{\mathbf{v}}$ due to the source term $-\overline{\mathbf{v}' \cdot \nabla \Phi'}$ provided by the eddy correlation. Furthermore, when given information only about the mean fields, then we must develop a closure for the unresolved correlation. Such closures are the topic of extensive research typical of eddy-mean decompositions. Nonetheless, we ask whether there are methods that offer insights into mean field behaviour even without making a closure assumption. GLM is one such method.

Lagrangian mean

An alternative approach is to remain in the Lagrangian frame, where material constancy of Φ takes on the linear form

$$\frac{\partial \Phi(\mathbf{a}, t)}{\partial t} = 0. \quad (62.6)$$

Consider a mean operator computed as an average over a region of material space coordinate \mathbf{a} . For example, if \mathbf{a} is the initial fluid particle position, then an average coordinate, $\bar{\mathbf{a}}$, and corresponding averaged field, $\bar{\Phi}$, render a coarse-graining over the initial positions. Since each member of the Lagrangian average satisfies the linear equation (62.6), so too does the Lagrangian mean

$$\frac{\partial \bar{\Phi}(\bar{\mathbf{a}}, t)}{\partial t} = 0. \quad (62.7)$$

Although this equation retains the simplicity of the unaveraged version, it still requires information about trajectories. Trajectories are computed based on the flow map (i.e., the velocity field), with trajectories an impractical means for describing chaotic or turbulent fluids. GLM offers an alternative that aims to meld elements of the Eulerian (e.g., computability) to the Lagrangian (e.g., material constancy).

Generalized Lagrangian mean

The GLM approach produces a GLM field that remains constant following the GLM velocity

$$\frac{\partial \bar{\Phi}^{(L)}}{\partial t} + \bar{\mathbf{v}}^{(L)} \cdot \nabla \bar{\Phi}^{(L)} = 0. \quad (62.8)$$

Hence, GLM maintains the desirable properties of the Lagrangian mean. However, it does so using Eulerian methods which can prove to be more practical for many cases. Notably, even if the Eulerian velocity is non-divergent, as for a Boussinesq fluid, the GLM velocity is generally divergent. Although we will not prove the GLM result (62.8), we will motivate the GLM average from the analysis of small amplitude eddying motions.

62.3.2 Length scales and the small parameter

There are two length scales associated with an eddy or wave fluctuation. One characterizes the size of the eddy whose length scale we write as λ . If the eddy is a monochromatic wave, then λ is its wave length. The other length scale characterizes the size of particle displacements, $|\xi|$. In the following, we assume the particle displacements are small relative to λ

$$|\xi| \ll \lambda \quad \text{small amplitude waves.} \quad (62.9)$$

We thus introduce the small non-dimensional ratio of length scales for the following analysis

$$\alpha = \frac{|\xi|}{\lambda} \ll 1. \quad (62.10)$$

62.3.3 Decomposing the particle trajectory

Recall the discussion of fluid particle trajectories given in Chapter 14. In this description, the trajectory of a particle is determined by integrating the relation between the particle trajectory and the particle velocity

$$\left[\frac{\partial \mathbf{X}(\mathbf{a}, t)}{\partial t} \right]_{\mathbf{a}} = \mathbf{v}[\mathbf{X}(\mathbf{a}, t)] \implies \mathbf{X}(\mathbf{a}, t) = \mathbf{X}(\mathbf{a}, 0) + \int_0^t \mathbf{v}[\mathbf{X}(\mathbf{a}, t')] dt', \quad (62.11)$$

so that the trajectory measures the position of a particle relative to a chosen origin. The material coordinate, \mathbf{a} , distinguishes the continuum of fluid particles, thus making the trajectory a field in material space-time.

The GLM develops a hybrid Eulerian-Lagrangian method and it is motivated by linear or quasi-linear disturbances. Keeping this motivation in mind, we consider each point in space, \mathbf{x} , to be the mean position of a unique fluid particle. In turn, we introduce an Eulerian field, $\xi(\mathbf{x}, t)$, that measures the position of a fluid particle relative to its mean position. Correspondingly, the Eulerian mean of the disturbance field vanishes

$$\overline{\xi(\mathbf{x}, t)} = 0. \quad (62.12)$$

Note that the Eulerian mean operator can be any of the operators (or others) satisfying the Reynold's decomposition property discussed in Section 62.2

Specification of $\xi(\mathbf{x}, t)$ for large amplitude disturbances (i.e., nonlinear waves) requires the full machinery of GLM, which is beyond our scope. Instead, to expose the rudiments we assume linear waves such as shown in Figure 62.1, for which the particle displacement amplitude is much smaller than the wavelength of the disturbance

$$\alpha = \frac{|\xi|}{\lambda} \ll 1. \quad (62.13)$$

In this case the disturbance field is constructed by time integration of the eddy velocity field

$$\left[\frac{\partial \xi(\mathbf{x}, t)}{\partial t} \right]_{\mathbf{x}} = \mathbf{v}'(\mathbf{x}, t) \implies \xi(\mathbf{x}, t) = \int_0^t \mathbf{v}'(\mathbf{x}, t') dt'. \quad (62.14)$$

With this specification for the disturbance field, we see that if the eddy velocity is non-divergent then so is the disturbance particle position field

$$\nabla \cdot \mathbf{v}' = 0 \implies \nabla \cdot \xi = 0. \quad (62.15)$$

The definition (62.14) for the disturbance field, $\xi(\mathbf{x}, t)$, is directly analogous to the particle trajectory position, $\mathbf{X}(\mathbf{a}, t)$, given by equation (62.11). However, there are important distinctions. Namely, the disturbance, $\xi(\mathbf{x}, t)$, is an Eulerian field that measures the position of a fluid particle relative to its mean position, with each Eulerian position \mathbf{x} corresponding to the mean position for a distinct fluid particle. In contrast, the particle position, $\mathbf{X}(\mathbf{a}, t)$, is a Lagrangian field that is attached to each fluid particle and measures the position of that particle relative to a unique origin.

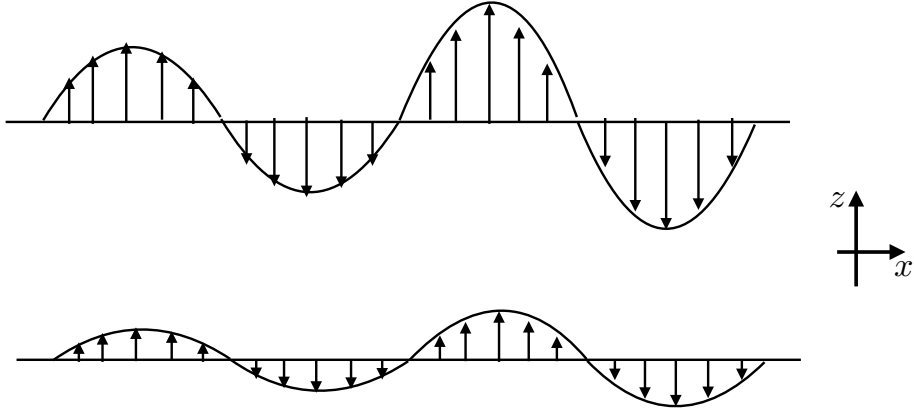


FIGURE 62.1: Illustrating the displacement of fluid particles at two selective vertical positions due to a linear transverse wave disturbance. The particle positions, $\mathbf{x}^{(\xi)} = \mathbf{x} + \xi(\mathbf{x}, t)$, have a disturbance field of the form $\xi(\mathbf{x}, t) = \hat{\mathbf{z}} \xi_0(x, z) \sin(kx - \omega t)$, with $\xi_0(x, z)$ a spatially dependent wave amplitude, $\lambda = 2\pi/k$ the wavelength, $\mathbf{k} = \hat{\mathbf{x}} k$ the wavevector, $\omega = ck$ the angular frequency, and c the wavespeed. Small amplitude waves satisfy $|\xi_0| \ll \lambda$. Note that this wave does not produce a Stokes drift since particle displacements are perpendicular to the wavevector: $\xi \cdot \mathbf{k} = 0$ (see Section 62.3.5), whereas Stokes drift requires particle motion to have a nonzero component in the wave direction (see Figures 45.5 and 45.6). Even so, it does generally produce a Stokes mean for an arbitrary field Φ (Section 62.3.4).

62.3.4 GLM and the Stokes mean

The mean of a fluid property, Φ , is generally a function of how the property is sampled to compute the mean. For example, the mean of Φ sampled on a fluctuating fluid particle differs from the mean sampled at the particle's mean position. Mathematically, this distinction means that

$$\underbrace{\overline{\Phi(\mathbf{x} + \xi(\mathbf{x}, t))}}_{\text{GLM}} \neq \underbrace{\overline{\Phi(\mathbf{x}, t)}}_{\text{Eulerian}}, \quad (62.16)$$

where it is common to make use of the shorthand¹

$$\mathbf{x}^{(\xi)}(\mathbf{x}, t) \equiv \mathbf{x} + \xi(\mathbf{x}, t) \quad (62.17)$$

for the instantaneous position of the fluid particle. The average

$$\overline{\Phi}^{(L)}(\mathbf{x}, t) \equiv \overline{\Phi(\mathbf{x} + \xi(\mathbf{x}, t), t)} = \overline{\Phi(\mathbf{x}^{(\xi)}, t)} \quad (62.18)$$

defines the generalized Lagrangian mean. As defined, the GLM is computed by evaluating the property Φ at the position of a fluid particle, $\mathbf{x}^{(\xi)}(\mathbf{x}, t) = \mathbf{x} + \xi(\mathbf{x}, t)$, where \mathbf{x} is both an arbitrary Eulerian field point and the mean position of a fluid particle, $\mathbf{x}^{(\xi)} = \mathbf{x}$. In contrast, the Eulerian

¹We place superscripts ξ, S, L, E inside parentheses to distinguish from tensor labels.

mean is determined by evaluating Φ at the fixed Eulerian point in space

$$\overline{\Phi}^{(E)}(\mathbf{x}, t) \equiv \overline{\Phi(\mathbf{x}, t)}. \quad (62.19)$$

Following our discussion at the start of Section 62.3, we define the difference between the GLM and Eulerian mean as the Stokes mean

$$\overline{\Phi}^{(S)}(\mathbf{x}, t) = \overline{\Phi}^{(L)}(\mathbf{x}, t) - \overline{\Phi}^{(E)}(\mathbf{x}, t). \quad (62.20)$$

The Stokes mean arises from inhomogeneities in Φ , which in turn lead to differences in its mean depending on how that field is sampled, whether sampled on a fluid particle, $\mathbf{x}^{(\xi)}(\mathbf{x}, t)$, or sampled at the mean position of the fluid particle, \mathbf{x} .

We mathematically expose the origin of the Stokes mean by performing a Taylor series expansion around the mean particle position

$$\Phi(\mathbf{x} + \boldsymbol{\xi}, t) = \Phi(\mathbf{x}, t) + \boldsymbol{\xi} \cdot \nabla \Phi(\mathbf{x}, t) + \frac{1}{2} \xi_m \xi_n \partial_m \partial_n \Phi(\mathbf{x}, t) + \mathcal{O}(\alpha^3). \quad (62.21)$$

The non-dimensional ratio $\alpha = |\boldsymbol{\xi}|/\lambda \ll 1$ was introduced in equation (62.13), which measures the ratio of the amplitude for particle displacements to the wavelength, λ , of fluctuations in the field Φ . Taking the mean of equation (62.21) then leads to an expression for the Stokes mean

$$\overline{\Phi}^{(S)}(\mathbf{x}, t) = \overline{\Phi}^{(L)}(\mathbf{x}, t) - \overline{\Phi}^{(E)}(\mathbf{x}, t) \quad (62.22a)$$

$$= \overline{\boldsymbol{\xi} \cdot \nabla \Phi} + \frac{1}{2} \overline{\xi_m \xi_n \partial_m \partial_n \Phi} + \mathcal{O}(\alpha^3). \quad (62.22b)$$

$$= \overline{\boldsymbol{\xi} \cdot \nabla \Phi'} + \frac{1}{2} \overline{\xi_m \xi_n \partial_m \partial_n \overline{\Phi}^{(E)}} + \mathcal{O}(\alpha^3), \quad (62.22c)$$

where we introduced the Eulerian fluctuation

$$\Phi'(\mathbf{x}, t) = \Phi(\mathbf{x}, t) - \overline{\Phi}^{(E)}(\mathbf{x}, t) \quad (62.23)$$

and all terms on the right hand side of equation (62.22c) are evaluated at (\mathbf{x}, t) . The Stokes drift (Section 45.8) associated with the GLM arises from setting Φ equal to one of the velocity components

$$\bar{v}_p^{(S)} = \overline{\boldsymbol{\xi} \cdot \nabla v_p'} + \frac{1}{2} \overline{\xi_m \xi_n \partial_m \partial_n \bar{v}_p^{(E)}} + \mathcal{O}(\alpha^3). \quad (62.24)$$

62.3.5 An example linear wave

We exemplify the previous discussion by considering the small amplitude linear wave

$$\boldsymbol{\xi} = -\frac{\mathbf{U}(\mathbf{x})}{\omega} \sin(\mathbf{k} \cdot \mathbf{x} - \omega t) \quad (62.25a)$$

$$\mathbf{v}' = \partial_t \boldsymbol{\xi} = \mathbf{U}(\mathbf{x}) \cos(\mathbf{k} \cdot \mathbf{x} - \omega t) \quad (62.25b)$$

$$\nabla v_p' = \nabla U_p \cos(\mathbf{k} \cdot \mathbf{x} - \omega t) - \mathbf{k} U_p \sin(\mathbf{k} \cdot \mathbf{x} - \omega t) \quad (62.25c)$$

$$\nabla \cdot \mathbf{v}' = (\nabla \cdot \mathbf{U}) \cos(\mathbf{k} \cdot \mathbf{x} - \omega t) - \mathbf{k} \cdot \mathbf{U} \sin(\mathbf{k} \cdot \mathbf{x} - \omega t) \quad (62.25d)$$

where \mathbf{U} is the velocity amplitude that is generally a function of space, \mathbf{k} is the wavevector, and

$$T = 2\pi/\omega \quad (62.26)$$

is the wave period. The wave renders an oscillatory motion to fluid particles, with the disturbance field specifying the instantaneous position of fluid particles whose mean position is \mathbf{x} . The disturbance field and velocity field both have a zero mean when time integrated over a wave period

$$\bar{\boldsymbol{\xi}}(\mathbf{x}) = \frac{1}{T} \int_0^T \boldsymbol{\xi}(\mathbf{x}, t') dt' = 0 \quad (62.27a)$$

$$\bar{\mathbf{v}}'(\mathbf{x}) = \frac{1}{T} \int_0^T \mathbf{v}'(\mathbf{x}, t') dt' = 0. \quad (62.27b)$$

To maintain a non-divergent eddy velocity at arbitrary times requires

$$\nabla \cdot \mathbf{v}' = 0 \implies \nabla \cdot \mathbf{U} = \mathbf{U} \cdot \mathbf{k} = 0. \quad (62.28)$$

The second condition means that the wave is transverse, so that particle displacements are orthogonal to the wavevector (e.g., Figure 62.1)

Stokes drift

Specializing to the velocity field (62.25b), substituting into the Stokes drift expression (62.24), and making use of an average over a wave period yields

$$\bar{\boldsymbol{\xi}} \cdot \nabla v'_p = \frac{U_p \mathbf{U} \cdot \mathbf{k}}{2\omega} \quad (62.29a)$$

$$\bar{v}_p^{(E)} = 0. \quad (62.29b)$$

The second equality holds since the velocity at a point arises just from the wave field, which has a zero Eulerian mean. Hence, to $\mathcal{O}(\alpha^2)$, the Stokes drift velocity associated with the GLM is given by

$$\bar{\mathbf{v}}^{(S)} = \frac{\mathbf{U} (\mathbf{U} \cdot \mathbf{k})}{2\omega} + \mathcal{O}(\alpha^2). \quad (62.30)$$

The Stokes drift vanishes at this order of accuracy for transverse waves in which $\mathbf{U} \cdot \mathbf{k} = 0$.

As a check on our formalism we consider a one-dimensional longitudinal wave, in which the Stokes drift is given by

$$\bar{v}^{(S)} = \frac{U^2}{2c} + \mathcal{O}(\alpha^2). \quad (62.31)$$

This result agrees with that derived using Lagrangian trajectories in Section 45.8 (see Exercise 45.6). Use of the GLM displacement field offers a somewhat more streamlined method for computing Stokes drift.

Stokes mean for an arbitrary field

The Stokes mean for an arbitrary field is given by

$$\bar{\Phi}^{(S)}(\mathbf{x}, t) = -\omega^{-1} \mathbf{U} \cdot \nabla \bar{\Phi}' \sin(\mathbf{k} \cdot \mathbf{x} - \omega t) + \mathcal{O}(\alpha^2) \quad (62.32a)$$

$$= -\omega^{-1} \nabla \cdot (\mathbf{U} \bar{\Phi}') \sin(\mathbf{k} \cdot \mathbf{x} - \omega t) + \mathcal{O}(\alpha^2), \quad (62.32b)$$

where the second equality made use of the non-divergent nature of the wave field (62.28). To second order in wave amplitude, the Stokes mean is determined by the projection of the gradient of the Eulerian fluctuation, $\nabla \Phi'$, onto the wave amplitude, \mathbf{U} . For example, consider a transverse wave such as that shown in Figure 62.1. Even though the Stokes drift vanishes to order $\mathcal{O}(\alpha^2)$,

the Stokes mean, $\bar{\Phi}^{(S)}(\mathbf{x}, t)$, can be nonzero so long as there is a nonzero vertical gradient in the Eulerian fluctuation.

62.3.6 GLM with a materially constant scalar

Consider a materially constant scalar field, such as a tracer concentration in the absence of mixing and sources

$$\frac{DC}{Dt} = 0. \quad (62.33)$$

How the GLM for C is related to the instantaneous C

The GLM for C equals to the value of C on a fluid particle

$$\bar{C}^{(L)}(\mathbf{x}, t) = C(\mathbf{x} + \boldsymbol{\xi}, t). \quad (62.34)$$

This is a very important identity that packs in a lot of information. In words, it says that when evaluated at the mean fluid particle position, \mathbf{x} , the GLM field $\bar{C}^{(L)}(\mathbf{x}, t)$ equals to the concentration, C , evaluated on a fluid particle at $\mathbf{x} + \boldsymbol{\xi}$. One means to understand this identity is to assume the GLM is an ensemble mean following fluid particles. Since C is constant on fluid particles, each ensemble member has the same value for C , in which case the GLM for C clearly equals the value of C for each ensemble member. We make particular use of the identity (62.34) when considering isopycnal kinematics in Sections 62.5 and 62.6.

Relating the particle disturbance field to Eulerian properties of C

There is a frequently used consequence of the identity (62.34) involving the disturbance field, the Eulerian fluctuation

$$C'(\mathbf{x}, t) = C(\mathbf{x}, t) - \bar{C}(\mathbf{x}, t) \quad (62.35)$$

and the Eulerian mean

$$C^{(E)}(\mathbf{x}, t) = \bar{C}(\mathbf{x}, t). \quad (62.36)$$

To derive it, recall the Taylor series expansion (62.21) truncated here to first order accuracy

$$C(\mathbf{x} + \boldsymbol{\xi}, t) = C(\mathbf{x}, t) + \boldsymbol{\xi} \cdot \nabla \bar{C}(\mathbf{x}, t) + \mathcal{O}(\alpha^2). \quad (62.37)$$

Taking the Eulerian mean of both sides renders

$$\overline{C(\mathbf{x} + \boldsymbol{\xi}, t)} = \bar{C}(\mathbf{x}, t) + \mathcal{O}(\alpha^2). \quad (62.38)$$

This identity means that the GLM equals to the Eulerian mean to order $\mathcal{O}(\alpha^2)$, which is a result consistent with the Stokes mean being an order $\mathcal{O}(\alpha^2)$ quantity as seen by equation (62.22c). From equation (62.34) we know that $C(\mathbf{x} + \boldsymbol{\xi}, t) = \bar{C}(\mathbf{x} + \boldsymbol{\xi}, t)$, so that we can subtract equations (62.37) and (62.38) to find

$$C'(\mathbf{x}, t) = -\boldsymbol{\xi} \cdot \nabla \bar{C}(\mathbf{x}, t) + \mathcal{O}(\alpha^2). \quad (62.39)$$

Hence, to first order accuracy, the Eulerian fluctuation equals to minus the disturbance field projected onto the gradient of the mean field; i.e., the Eulerian fluctuation in the tracer is first order in the disturbance. We make use of this result when discussing the kinematics of eddy tracer fluxes in Section 62.4. Furthermore, for the isopycnal kinematics in Sections 62.5 and 62.6, we focus on vertical particle displacements, $\boldsymbol{\xi} = \xi \hat{z}$, in which case the Eulerian fluctuation is given

by

$$C'(z, t) = -\xi \partial_z \bar{C}(z, t) + \mathcal{O}(\alpha^2). \quad (62.40)$$

62.3.7 Further study

GLM was introduced in the seminal papers by [Andrews and McIntyre \(1978a,b\)](#). These papers offer a wealth of intellectual rewards after much study. GLM is also detailed in the monograph on waves and mean flows by [Bühler \(2014a\)](#).

62.4 Kinematics of eddy tracer fluxes

Consider the Eulerian eddy-mean decomposition for a materially constant tracer in an incompressible fluid. The advection equation for this tracer is given by

$$\frac{\partial C}{\partial t} + \nabla \cdot (\mathbf{v} C) = 0, \quad (62.41)$$

and its Eulerian mean is

$$\frac{\partial \bar{C}}{\partial t} + \nabla \cdot (\bar{\mathbf{v}} \bar{C}) = -\nabla \cdot \bar{\mathbf{v}}' \bar{C}'. \quad (62.42)$$

The eddy advective flux, $\mathbf{v}' C'$, is the product of the eddy velocity and eddy tracer concentration. Its mean provides the correlation or mean eddy flux, $\bar{\mathbf{v}}' \bar{C}'$. The convergence of this mean eddy flux provides a source to the advection equation for the Eulerian mean tracer concentration.

In this section we make use of the particle disturbance field of Section 62.3 to unpack the kinematics of eddy tracer fluxes induced by small amplitude waves. Although not offering new dynamical information, the particle disturbance field is a very useful means to frame the kinematics of tracer eddy fluxes.

62.4.1 Particle displacements and eddy tracer fluxes

Following Section 62.3, we here introduce a particle disturbance vector corresponding to small amplitude eddy fluctuations

$$\partial_t \boldsymbol{\xi}(\mathbf{x}, t) = \mathbf{v}'(\mathbf{x}, t) + \mathcal{O}(\alpha^2) \quad (62.43a)$$

$$\bar{\boldsymbol{\xi}} = 0. \quad (62.43b)$$

Correspondingly, each spatial point, \mathbf{x} , is the mean position of a fluid particle whose instantaneous position is $\mathbf{x} + \boldsymbol{\xi}(\mathbf{x}, t)$. Following the results from Section 62.3.6, to leading order we can write the Eulerian fluctuation in terms of the particle displacement (equation (62.39))

$$C'(\mathbf{x}, t) = -\boldsymbol{\xi} \cdot \nabla \bar{C}(\mathbf{x}, t) + \mathcal{O}(\alpha^2) \quad (62.44)$$

Notice that if the particle displacement is oriented along a mean tracer iso-surface, then $\boldsymbol{\xi} \cdot \nabla \bar{C}(\mathbf{x}, t) = 0$ and there is no tracer fluctuation, $C' = 0$, to order $\mathcal{O}(\alpha^2)$. More general eddy motions lead to a nonzero tracer fluctuation with the eddy tracer flux taking on the form

$$\mathbf{v}' C' = -\partial_t \boldsymbol{\xi} (\boldsymbol{\xi} \cdot \nabla) \bar{C} + \mathcal{O}(\alpha^2). \quad (62.45)$$

We unpack this expression for the purpose of characterizing kinematic properties of the eddy tracer flux

62.4.2 Symmetric and skew symmetric tracer fluxes

From equation (62.45), the m'th component of the eddy tracer flux is given by

$$v'_m C' = -[(\partial_t \xi_m) \xi_n] \partial_n \bar{C}. \quad (62.46)$$

We here decompose this flux in order to characterize its kinematic properties.

Decomposing the tracer flux

Let us decompose the second order tensor $(\partial_t \xi_m) \xi_n$ into its symmetric and anti-symmetric components²

$$2(\partial_t \xi_m) \xi_n = [(\partial_t \xi_m) \xi_n + (\partial_t \xi_n) \xi_m] + [(\partial_t \xi_m) \xi_n - (\partial_t \xi_n) \xi_m] \quad (62.47a)$$

$$= \partial_t(\xi_m \xi_n) + [(\partial_t \xi_m) \xi_n - (\partial_t \xi_n) \xi_m]. \quad (62.47b)$$

Introducing the symmetric and anti-symmetric correlation tensors

$$2\mathbb{K}_{mn} \equiv \overline{\partial_t(\xi_m \xi_n)} \quad (62.48a)$$

$$2\mathbb{A}_{mn} \equiv \overline{(\partial_t \xi_m) \xi_n} - \overline{(\partial_t \xi_n) \xi_m} \quad (62.48b)$$

allows us to write the mean eddy tracer flux

$$\overline{v'_m C'} = -(\mathbb{K}_{mn} + \mathbb{A}_{mn}) \partial_n \bar{C} \quad (62.49)$$

and the mean field tracer equation (62.42)

$$\frac{\partial \bar{C}}{\partial t} + \nabla \cdot (\bar{v} \bar{C}) = \nabla \cdot [(\mathbb{K} + \mathbb{A}) \cdot \nabla \bar{C}]. \quad (62.50)$$

The right hand side of this equation equals to the convergence of the symmetric and skew-symmetric tracer fluxes³

$$\nabla \cdot [(\mathbb{K} + \mathbb{A}) \cdot \nabla \bar{C}] = -\nabla \cdot (\mathbf{F}^{(\text{sym})} + \mathbf{F}^{(\text{skew})}), \quad (62.51)$$

where

$$\mathbf{F}^{(\text{sym})} = -\mathbb{K} \cdot \nabla \bar{C} \quad (62.52a)$$

$$\mathbf{F}^{(\text{skew})} = -\mathbb{A} \cdot \nabla \bar{C} \quad (62.52b)$$

$$\overline{v' C'} = \mathbf{F}^{(\text{sym})} + \mathbf{F}^{(\text{skew})}. \quad (62.52c)$$

The symmetric flux

In terms of particle displacements, the symmetric flux (62.52a) is given by

$$F_m^{(\text{sym})} = -\mathbb{K}_{mn} \partial_n \bar{C} = -\frac{1}{2} \overline{\partial_t(\xi_m \xi_n)} \partial_n \bar{C}. \quad (62.53)$$

The symmetric tensor \mathbb{K} vanishes when the average is over the period of a periodic wave, in which the particle displacements undergo reversible periodic excursions (see Section 62.4.5). For waves

²See Section 15.3.5 for a similar decomposition of the velocity gradient tensor.

³We place parentheses around “skew” and “sym” to distinguish the name for these vectors from what may otherwise appear to be tensor labels.

that decay in amplitude over the averaging period, particle displacements decrease in magnitude thus leading to an upgradient symmetric flux. In contrast, particle displacements increase in magnitude for waves that grow over the averaging period, in which case the flux is downgradient just as for diffusion. Furthermore, growing nonlinear waves generally break and then develop into turbulence, with turbulence leading to further particle separation and dispersive tracer mixing. Dispersive mixing is well parameterized by diffusion, and we have more to say about diffusive parameterizations of lateral dispersion in Section 63.4.

The skew, advective, and rotational fluxes

Following our discussion in Section 61.7, we write the skew flux as

$$F_m^{(\text{skew})} = -\mathbb{A}_{mn} \partial_n \bar{C} = -\epsilon_{mnp} \Psi_p \partial_n \bar{C} = -(\nabla \bar{C} \times \Psi)_m, \quad (62.54)$$

where we introduced the vector streamfunction (dimensions squared length per time)⁴

$$\Psi = \frac{1}{2} \overline{\partial_t \boldsymbol{\xi} \times \boldsymbol{\xi}} = \frac{1}{2} \overline{\boldsymbol{v}' \times \boldsymbol{\xi}}. \quad (62.55)$$

The vector streamfunction is half the angular momentum per mass of a fluid particle undergoing eddying motion, with the angular momentum computed relative to the mean particle position. The vector streamfunction is nonzero only if the eddy has a preferred sense of rotation, in which case the wave field is said to be *polarized*.

The skew flux can be written

$$\mathbf{F}^{(\text{skew})} = -\nabla \bar{C} \times \Psi \quad (62.56a)$$

$$= (\nabla \times \Psi) \bar{C} - \nabla \times (\bar{C} \Psi) \quad (62.56b)$$

$$= \mathcal{U}^{(\Psi)} \bar{C} - \nabla \times (\bar{C} \Psi) \quad (62.56c)$$

$$= \mathbf{F}^{(\text{adv})} - \mathbf{F}^{(\text{rot})}, \quad (62.56d)$$

so that the skew flux equals to an advective flux minus a rotational flux. We here introduced the non-divergent velocity

$$\mathcal{U}^{(\Psi)} = \nabla \times \Psi \quad (62.57)$$

and the non-divergent rotational flux

$$\mathbf{F}^{(\text{rot})} = \nabla \times (\bar{C} \Psi). \quad (62.58)$$

The divergence of the skew flux equals to the divergence of the advective flux

$$\nabla \cdot \mathbf{F}^{(\text{skew})} = \nabla \cdot (\mathbf{F}^{(\text{adv})} - \mathbf{F}^{(\text{rot})}) = \nabla \cdot \mathbf{F}^{(\text{adv})}, \quad (62.59)$$

so that the rotational flux has no impact on evolution of the mean tracer field.

What does a point measurement estimate?

From equation (62.52c), we see that a point measurement of the correlation $\overline{\boldsymbol{v}' \bar{C}'}$ provides an estimate of the diffusive and skew diffusive tracer fluxes

$$\overline{\boldsymbol{v}' \bar{C}'} = \mathbf{F}^{(\text{sym})} + \mathbf{F}^{(\text{skew})} = -(\mathbb{K} + \mathbb{A}) \cdot \nabla \bar{C}. \quad (62.60)$$

⁴ Middleton and Loder (1989) and Garrett (2006) introduce a skew-diffusivity, \mathbf{D} , which is opposite in sign to the vector streamfunction: $\Psi = -\mathbf{D}$.

Furthermore, for a periodic wave field, where the symmetric tensor vanishes, the correlation, $\overline{\mathbf{v}' C'}$, provides a direct estimate of the skew flux, $-\nabla \overline{C} \times \Psi$. One might instead presume that the point measurement offers a direct estimate of the advective flux, $\overline{C} \mathcal{U}^{(\Psi)}$, rather than the skew flux. But that presumption is wrong. Instead, since the skew flux equals to a rotational flux plus the advective flux, we have

$$\overline{\mathbf{v}' C'} = -\mathbb{K} \cdot \nabla \overline{C} - \nabla \overline{C} \times \Psi \quad (62.61a)$$

$$= -\mathbb{K} \cdot \nabla \overline{C} - \nabla \times (\overline{C} \Psi) + \overline{C} \nabla \times \Psi \quad (62.61b)$$

$$= -\mathbb{K} \cdot \nabla \overline{C} - \nabla \times (\overline{C} \Psi) + \overline{C} \mathcal{U}^{(\Psi)}. \quad (62.61c)$$

The rotational flux is generally nontrivial for polarized waves and so cannot be ignored. As detailed by [Fox-Kemper et al. \(2003\)](#), there is no general method for removing the rotational flux. We therefore find it more convenient to work directly with the skew flux than the advective flux.

Area integrated tracer flux

We now offer an interpretation for the rotational contribution by considering the mean of the tracer flux integrated over a static area \mathcal{S}

$$\mathcal{T} = \overline{\int_{\mathcal{S}} \mathbf{v} C \cdot \hat{\mathbf{n}} dS} = \int_{\mathcal{S}} \overline{\mathbf{v} C} \cdot \hat{\mathbf{n}} dS = \int_{\mathcal{S}} [\overline{\mathbf{v} C} + \overline{\mathbf{v}' C'}] \cdot \hat{\mathbf{n}} dS. \quad (62.62)$$

In terms of particle displacements, the eddy correlation, $\overline{\mathbf{v}' C'}$, equals to the sum of the symmetric flux and the skew flux as in equation (62.60). Introducing the diffusive, advective, and rotational flux then renders

$$\mathcal{T} = \int_{\mathcal{S}} [\overline{\mathbf{v} C} + \mathcal{U}^{(\Psi)} \overline{C} - \nabla \times (\overline{C} \Psi) - \mathbb{K} \cdot \nabla \overline{C}] \cdot \hat{\mathbf{n}} dS. \quad (62.63)$$

Use of Stokes' Theorem transforms the rotational term to a line integral around the boundary of the area

$$\mathcal{T} = \int_{\mathcal{S}} [\overline{\mathbf{v} C} + \mathcal{U}^{(\Psi)} \overline{C} - \mathbb{K} \cdot \nabla \overline{C}] \cdot \hat{\mathbf{n}} dS - \oint_{\partial \mathcal{S}} \overline{C} \Psi \cdot dl. \quad (62.64)$$

Following Section 2b of [Middleton and Loder \(1989\)](#), we interpret the boundary term as a Stokes contribution associated with the correlation of particle motion and perturbation velocity along the boundary

$$\oint_{\partial \mathcal{S}} \overline{C} \Psi \cdot dl = (1/2) \oint_{\partial \mathcal{S}} \overline{C} (\overline{\mathbf{v}' \times \xi}) \cdot dl. \quad (62.65)$$

We further this interpretation when considering the transport beneath a fluctuating isopycnal surface in Section 62.6.4.

62.4.3 Massaging the mean field tracer equation

We here write the mean tracer equation (62.50) in various forms that can be found throughout the literature. For this purpose, write the right hand side of equation (62.50) in the form

$$\nabla \cdot [(\mathbb{K} + \mathbb{A}) \cdot \nabla \overline{C}] = \partial_m [(\mathbb{K}_{mn} + \mathbb{A}_{mn}) \partial_n \overline{C}] \quad (62.66a)$$

$$= \partial_m (\mathbb{K}_{mn} + \mathbb{A}_{mn}) \partial_n \overline{C} + (\mathbb{K}_{mn} + \mathbb{A}_{mn}) \partial_m \partial_n \overline{C} \quad (62.66b)$$

$$= \partial_m (\mathbb{K}_{mn} + \mathbb{A}_{mn}) \partial_n \overline{C} + \mathbb{K}_{mn} \partial_m \partial_n \overline{C}. \quad (62.66c)$$

The final equality follows from the identity

$$\mathbb{A}_{mn} \partial_m \partial_n \bar{C} = 0, \quad (62.67)$$

which results from the contraction of the anti-symmetric, \mathbb{A}_{mn} , to the symmetric operator $\partial_m \partial_n$. The second term, $\mathbb{K}_{mn} \partial_m \partial_n \bar{C}$, is a diffusion operator if symmetric tensor \mathbb{K} is also positive-definite. The first term in equation (62.66c) can be interpreted as an advection operator through the action of a non-divergent plus a divergent advection velocity

$$\partial_m (\mathbb{K}_{mn} + \mathbb{A}_{mn}) \partial_n \bar{C} = [\mathcal{U}^{(K)} + \mathcal{U}^{(\Psi)}] \cdot \nabla \bar{C}, \quad (62.68)$$

where⁵

$$\mathcal{U}_n^{(K)} \equiv -\partial_m \mathbb{K}_{mn} \implies \nabla \cdot \mathcal{U}^{(K)} = -\partial_n \partial_m \mathbb{K}_{mn} \neq 0 \quad (62.69a)$$

$$\mathcal{U}_n^{(\Psi)} \equiv -\partial_m \mathbb{A}_{mn} \implies \nabla \cdot \mathcal{U}^{(\Psi)} = \partial_n \partial_m \mathbb{A}_{mn} = 0. \quad (62.69b)$$

Bringing the above results together allows us to write the mean field tracer equation (62.50) in the following equivalent forms

$$\frac{\partial \bar{C}}{\partial t} + [\bar{v} + \mathcal{U}^{(\Psi)} + \mathcal{U}^{(K)}] \cdot \nabla \bar{C} = \mathbb{K}_{mn} \partial_m \partial_n \bar{C} \quad \text{advective form} \quad (62.70a)$$

$$\frac{\partial \bar{C}}{\partial t} + \nabla \cdot (\bar{v} + \mathcal{U}^{(\Psi)}) \bar{C} = \nabla \cdot (\mathbb{K} \cdot \nabla \bar{C}) \quad \text{flux form,} \quad (62.70b)$$

where we made use of the identities

$$\nabla \cdot \bar{v} = 0 \quad \nabla \cdot \mathcal{U}^{(\Psi)} = 0 \quad \nabla \cdot \mathcal{U}^{(K)} \neq 0. \quad (62.71)$$

62.4.4 Connection to Stokes drift

From equation (62.24) we have the leading order expression for the Stokes drift

$$\bar{v}_p^{(S)} = \overline{\xi_n \partial_n \partial_t \xi_p} + \mathcal{O}(\alpha^2). \quad (62.72)$$

As noted in equation (62.15), with $\partial_t \boldsymbol{\xi} = \mathbf{v}'$ and with $\nabla \cdot \mathbf{v}' = 0$, the corresponding particle displacements are non-divergent, $\nabla \cdot \mathbf{v}' = 0 \Rightarrow \nabla \cdot \boldsymbol{\xi} = 0$. Consequently, to second order accuracy, the Stokes drift velocity can be written

$$\bar{v}_p^{(S)} = \overline{\xi_n \partial_n \partial_t \xi_p} \quad (62.73a)$$

$$= \partial_n [\overline{(\partial_t \xi_p) \xi_n}] \quad (62.73b)$$

$$= \partial_n (\mathbb{K}_{pn} + \mathbb{A}_{pn}) \quad (62.73c)$$

$$= \partial_n (\mathbb{K}_{np} - \mathbb{A}_{np}) \quad (62.73d)$$

$$= -\mathcal{U}_p^{(K)} + \mathcal{U}_p^{(\Psi)}. \quad (62.73e)$$

For the case of periodic waves, the Stokes drift velocity equals to the non-divergent skew velocity

$$\bar{v}^{(S)} = \mathcal{U}^{(\Psi)} \Rightarrow \nabla \cdot \bar{v}^{(S)} = 0 \quad \text{periodic waves.} \quad (62.74)$$

⁵Note that [Middleton and Loder \(1989\)](#) define $\mathcal{U}_n^{(K)} \equiv +\partial_m \mathbb{K}_{mn}$, which is the opposite sign to that used here in equation (62.69a), whereas they define $\mathcal{U}_n^{(\Psi)} = -\partial_m \mathbb{A}_{mn}$ as in equation (62.69b).

More generally, for non-periodic waves the divergent velocity is non-zero so that the Stokes velocity is also divergent

$$\bar{\mathbf{v}}^{(S)} = \mathcal{U}^{(\Psi)} - \mathcal{U}^{(K)} \Rightarrow \nabla \cdot \bar{\mathbf{v}}^{(S)} = -\nabla \cdot \mathcal{U}^{(K)} \neq 0 \quad \text{non-periodic waves.} \quad (62.75)$$

62.4.5 A linear rotating periodic wave example

We illustrate some of the previous analysis by considering Consider a displacement vector comprised of a linear periodic wave in two-dimensions

$$\xi(\mathbf{x}, t) = \Gamma [\hat{\mathbf{x}} \cos(kx - \omega t) + \hat{\mathbf{y}} \sin(kx - \omega t)] \quad (62.76a)$$

$$\partial_t \xi(\mathbf{x}, t) = \omega \Gamma [\hat{\mathbf{x}} \sin(kx - \omega t) - \hat{\mathbf{y}} \cos(kx - \omega t)], \quad (62.76b)$$

where Γ the time-independent wave amplitude, $T = 2\pi/\omega$ is the wave period, and $\lambda = 2\pi/k$ is the wavelength. The fluid particles exhibit counter-clockwise circular motion in the horizontal plane with squared radius

$$\xi \cdot \xi = \Gamma^2. \quad (62.77)$$

We are motivated to let the mean operator be a phase average

$$\bar{\phi} = \frac{1}{T} \int_0^T \phi(t) dt, \quad (62.78)$$

which is the traditional operator used when examining the impacts of linear waves on mean fields. For spatially constant wave amplitude, we will see the the mean tracer concentration, \bar{C} , remains unchanged by these waves. The absence of a rectified change to \bar{C} reflects the linear periodic nature of the wave field.

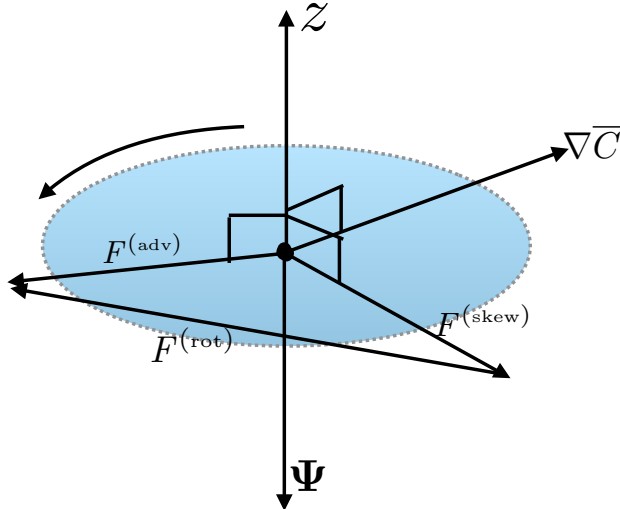


FIGURE 62.2: Sketch of the various tracer fluxes associated with the polarized displacement vector (62.76a). The particles are moving on the horizontal plane in a circle with time-independent radius Γ . The vector streamfunction (62.81) points in the negative $\hat{\mathbf{z}}$ direction. The mean concentration gradient, $\nabla \bar{C}$, generally points outside of the horizontal plane. However, it is only the horizontal components that contribute since the displacement vector is in the horizontal plane, thus resulting in horizontal skew, advective, and rotational fluxes.

Symmetric mixing tensor

The symmetric mixing tensor

$$\mathbb{K}_{mn} = \frac{\Gamma^2}{2T} \int_0^T dt \frac{\partial}{\partial t} \begin{bmatrix} \cos^2(kx - \omega t) & \cos(kx - \omega t) \sin(kx - \omega t) \\ \cos(kx - \omega t) \sin(kx - \omega t) & \sin^2(kx - \omega t) \end{bmatrix} \quad (62.79)$$

vanishes identically since the wave field is periodic so that the particle motion has an amplitude whose growing phase is exactly matched by its decaying phase.

Skew symmetric stirring tensor

In contrast, the skew-symmetric tensor has non-zero components

$$\mathbb{A}_{12} = -\mathbb{A}_{21} = \frac{\Gamma^2 \omega}{2} [\sin^2(kx - \omega t) + \cos^2(kx - \omega t)] = \frac{\Gamma^2 \omega}{2}, \quad (62.80)$$

which reflects the counter-clockwise polarization. The corresponding vector streamfunction is vertical

$$\Psi = \frac{\Gamma^2 \omega}{2} \hat{z}, \quad (62.81)$$

and the skew flux is horizontal

$$\mathbf{F}^{(\text{skew})} = \frac{\Gamma^2 \omega}{2} (\hat{z} \times \nabla \bar{C}). \quad (62.82)$$

Finally, the advective velocity is given by

$$\nabla \times \Psi = \omega \Gamma \nabla \Gamma \times \hat{z}, \quad (62.83)$$

with the advective velocity vanishing when the wave amplitude, Γ , is a constant. In this case, the advective tracer flux is zero, although the skew flux is non-zero. With a constant Γ , the skew flux has a zero divergence (it is a purely rotational flux when Γ is constant). Hence, for a constant wave amplitude, neither the skew flux nor the advective flux affect the evolution of \bar{C} . Figure 62.2 offers a schematic of the skew, advective, and rotational fluxes induced by a linear rotating particle wave in the horizontal plane.

62.4.6 Further study

Much of this section follows [Plumb \(1979\)](#), [Middleton and Loder \(1989\)](#), and [Garrett \(2006\)](#), each of whom considered elements of tracer dispersion by waves and nonlinear eddies. Additional treatments can be found in the review article of [Moffatt \(1983\)](#), who considers rotating fluids and magnetic fluids.

62.5 Kinematics of volume transport in isopycnal layers

In this section we consider the reversible stirring of fluid parcels by turbulent flow in a perfect (i.e., no mixing or sources) stratified Boussinesq fluid. As the fluid parcels are stirred, they preserve their volume while changing their shape and stretching into finer scale filaments. Stirring by ocean mesoscale/baroclinic eddies offers the canonical example of such stirring. Eventually, small-scale processes, such as those summarized in Section 63.1.1 mix properties irreversibly. We are here focused just on the stirring part of this scenario.

Over space and time scales larger than the mesoscale, the stirring by ocean mesoscale eddies can be considered chaotic, which in turn motivates a stochastic perspective in which an ensemble of eddies is considered. The goal is to describe the ensemble mean properties of the perfect fluid, with a focus in this section on the kinematics of parcel rearrangement. Hence, eddy correlations in the present section appear between the thickness of a fluid layer and the velocity. We introduce trace matter in Section 62.6, at which point we also consider eddy correlations between velocity and tracer as in Section 62.4.

The material in this section is rather detailed. However, its mastery comes readily by keeping in mind the more general (and somewhat simpler) presentation of GLM offered in Section 62.3. We are motivated to provide full details in this section since the kinematics of isopycnal ensembles appears throughout the study of wave-mean flow interactions in adiabatic geophysical fluid mechanics, such as in the study of ocean mesoscale eddies.

62.5.1 Isopycnal mean

Each fluid parcel in a stably stratified perfect Boussinesq fluid preserves its potential density. We are interested in following the vertical motion of potential density layer interfaces as waves and turbulent processes transport layer thickness from one region to another. In contrast, we are not concerned with following the lateral position of a fluid parcel within a layer. Here we introduce the isopycnal mean, which is based on describing ensembles of perfect fluid parcels using isopycnal coordinates. In Section 62.5.3, we relate this isopycnal approach to the vertical/isopycnal GLM.

Defining the isopycnal ensemble

An overbar with a potential density label, $\overline{(\cdot)}^{(\varrho)}$, denotes a mean over an ensemble of fluid parcels, each having the same potential density, ϱ , the same horizontal position, (x, y) , and the same time, t . Isopycnals undulate in space and time, which means that each ensemble member has a vertical position that is generally distinct from the ensemble mean depth, z . Furthermore, when the context is clear, it is useful to drop the dependence on (x, y, t) to highlight the dependence on potential density and/or the vertical position.

Isopycnal ensemble mean

The isopycnal ensemble mean makes use of potential density as a vertical coordinate (Chapters 56 and 58), with the mean field denoted by

$$\overline{\Phi}^{(\varrho)}(x, y, \varrho, t) \equiv \text{ensemble mean using isopycnal vertical coordinates.} \quad (62.84)$$

This average is straightforward to compute when using isopycnal coordinates, thus producing an isopycnal mean that is a function of the potential density, ϱ .

62.5.2 Modified mean

As a complement to the isopycnal approach in Section 62.5.1, we here introduce the vertical/isopycnal GLM, also known as the modified mean.

FIGURE 62.3: Schematic of the ensemble mean depth $\bar{z}^\rho(x, y, \rho, t)$ of a particular potential density surface ρ . In general, different members of an isentropic ensemble live at different depths. Therefore, when considering ensemble members with the same potential density, the ensemble mean depth is the average over the different members. For the case of a two-member ensemble, as shown here, $2\bar{z}^\rho(\rho) = z(1, \rho) + z(2, \rho)$, where the depth $z(1, \rho)$ is generally different from $z(2, \rho)$.

Vertical/isopycnal GLM

The discussion in Section 62.3 considered a three-vector particle displacement vector $\xi(x, t)$. In contrast, we are here interested just in the vertical displacement of an isopycnal layer interface

$$\xi(x, y, \varrho, t) = \hat{z}\xi(x, y, \varrho, t). \quad (62.85)$$

The displacement field $\xi(x, y, \varrho, t)$ measures the vertical position of a potential density interface, ϱ , relative to its ensemble mean depth. For any particular ensemble member with potential density ϱ , we write its vertical position as (dropping x, y, t dependence for brevity)

$$z(\varrho) = \bar{z}^{(\varrho)} + \xi(\varrho), \quad (62.86)$$

where

$$\bar{z}^{(\varrho)} = \overline{z(\varrho)}^{(\varrho)} \quad (62.87)$$

is the isopycnal ensemble mean depth, and the displacement field has a zero ensemble mean

$$\overline{\xi(\varrho)}^{(\varrho)} = 0. \quad (62.88)$$

Given the above definitions for the vertical position, we define the *vertical/isopycnal GLM* for an arbitrary function

$$\tilde{\Phi}(x, y, \bar{z}^{(\varrho)}, t) \equiv \overline{\Phi(x, y, \bar{z}^{(\varrho)} + \xi(x, y, \varrho, t), t)}^{(\varrho)}. \quad (62.89)$$

As defined, the vertical/isopycnal GLM, $\tilde{\Phi}$, is a function of the ensemble mean vertical position, $\bar{z}^{(\varrho)}$ (left hand side), and is determined by an ensemble mean of Φ sampled at the depth of each ensemble member, $\bar{z}^{(\varrho)} + \xi(\varrho)$. [McDougall and McIntosh \(2001\)](#) refer to the vertical/isopycnal GLM (62.89) as the *modified mean*.

Relating the modified mean to the isopycnal mean

Following the general result (62.34), we know that the modified mean potential density, $\tilde{\varrho}(x, y, \bar{z}^{(\varrho)}, t)$, equals to the potential density of each ensemble member so that

$$\tilde{\varrho}(x, y, \bar{z}^{(\varrho)}, t) = \varrho(x, y, \bar{z}^{(\varrho)} + \xi(x, y, \varrho, t), t). \quad (62.90)$$

This relation means that the modified mean potential density is the functional inverse of the isopycnal ensemble mean vertical position. Consequently, the isopycnal ensemble mean of a function, $\overline{\Phi}^{(\varrho)}$ (equation (62.84)), when evaluated at the modified mean potential density, $\tilde{\varrho}$, equals to the modified mean $\tilde{\Phi}$ when evaluated at the vertical position of the mean density

$$\overline{\Phi}^{(\varrho)}(x, y, \tilde{\varrho}, t) = \tilde{\Phi}(x, y, \bar{z}^{(\varrho)}, t). \quad (62.91)$$

This is a very important identity that will be used in the following.

62.5.3 Transformed residual mean (TRM)

When working with isopycnal layers, it is very useful to use specific thickness weighting to account for the net amount of material within a layer, or to measure the net transport in the layer. For this purpose we make use of the *specific thickness* from Section 57.3 as given by⁶

$$\hbar = \partial z / \partial \varrho = 1 / (\partial \varrho / \partial z) \quad (62.92)$$

and thus make use of thickness weighted fields, $\hbar \Phi$, and the corresponding thickness weighted isopycnal ensemble mean

$$\hat{\Phi}(\varrho) = \frac{\hbar \overline{\Phi}^{(\varrho)}}{\hbar^{(\varrho)}}. \quad (62.93)$$

The identity (62.90) then renders

$$\overline{\Phi}^{\#}(x, y, \bar{z}^{(\varrho)}, t) \equiv \hat{\Phi}(x, y, \tilde{\varrho}, t), \quad (62.94)$$

where $\overline{\Phi}^{\#}$ is the *transformed residual mean* (TRM) evaluated at the isopycnal ensemble mean vertical position. This is yet another important identity that will be used in the following.

Depth integrated TRM transport

A particularly key TRM field is the TRM horizontal velocity

$$\hat{\mathbf{u}}(x, y, \tilde{\varrho}, t) = \overline{\mathbf{u}}^{\#}(x, y, \bar{z}^{(\varrho)}, t). \quad (62.95)$$

Following the discussion of the vertical gauge in Section 61.7.1 (see in particular equation (61.77)), we are led to define the depth integrated TRM transport

$$\overline{\mathbf{U}}^{\#}(\bar{z}^{(\varrho)}) = \int_{-H}^{\bar{z}^{(\varrho)}} \overline{\mathbf{u}}^{\#}(z) dz = \int_{\varrho(-H)}^{\tilde{\varrho}(\bar{z}^{(\varrho)})} \hat{\mathbf{u}}(\gamma) \hbar^{(\gamma)} d\gamma, \quad (62.96)$$

with the second equality following from a change of coordinates from geopotential to isopycnal. We can go further with this expression by writing

$$\overline{\mathbf{U}}^{\#}(\bar{z}^{(\varrho)}) = \int_{\varrho(-H)}^{\tilde{\varrho}(\bar{z}^{(\varrho)})} \hat{\mathbf{u}}(\gamma) \hbar^{(\gamma)} d\gamma \quad \text{from equation (62.96)} \quad (62.97a)$$

$$= \int_{\varrho(-H)}^{\tilde{\varrho}(\bar{z}^{(\varrho)})} \overline{\mathbf{u}} \hbar^{(\gamma)} d\gamma \quad \text{from equation (62.93)} \quad (62.97b)$$

$$= \int_{\varrho(-H)}^{\varrho(\bar{z}^{(\varrho)} + \xi)} \overline{\mathbf{u}} \hbar^{(\gamma)} d\gamma \quad \text{from equation (62.90).} \quad (62.97c)$$

The final equality makes it clear that the TRM transport, $\overline{\mathbf{U}}^{\#}(\bar{z}^{(\varrho)})$, is the ensemble mean volume transport for fluid denser than $\varrho(\bar{z}^{(\varrho)} + \xi) = \tilde{\varrho}(\bar{z}^{(\varrho)})$. This transport can also be written using

⁶As discussed in Section 56.9.1, specific thickness is the Jacobian of transformation between geopotential coordinates, (x, y, z, t) , and isopycnal coordinates, (x, y, ϱ, t) . For stably stratified ideal fluids, \hbar is one-signed, hence making the coordinate transformation well defined. It is also related to the buoyancy frequency through (Section 27.5.5) $N^2 = -(g/\rho_0) (\partial \varrho / \partial z) = -g/(\rho_0 \hbar)$.

geopotential coordinates

$$\bar{\mathbf{U}}^\#(\bar{z}^{(\varrho)}) = \overline{\int_{-H}^{\bar{z}^{(\varrho)} + \xi} \mathbf{u} dz}. \quad (62.98)$$

The transport from each ensemble member is determined by integrating from the bottom to the depth, $\bar{z}^{(\varrho)} + \xi$, and then the TRM transport is determined by computing the ensemble mean for this transport.

Quasi-Stokes transport

The TRM transport (62.98) can be decomposed into an Eulerian mean plus the correlation of a fluctuation

$$\bar{\mathbf{U}}^\#(\bar{z}^{(\varrho)}) \equiv \bar{\mathbf{U}}(\bar{z}^{(\varrho)}) + \bar{\mathbf{U}}^{\text{qs}}(\bar{z}^{(\varrho)}). \quad (62.99)$$

The first term,

$$\bar{\mathbf{U}}(\bar{z}^{(\varrho)}) = \int_{-H}^{\bar{z}^{(\varrho)}} \mathbf{u} dz \quad (62.100)$$

is the ensemble mean transport between the bottom and the ensemble mean depth, $\bar{z}^{(\varrho)}$. We interpret this transport as an Eulerian mean since the depth ranges are fixed. In contrast, the *quasi-Stokes* transport

$$\bar{\mathbf{U}}^{\text{qs}}(\bar{z}^{(\varrho)}) \equiv \overline{\int_{\bar{z}^{(\varrho)}}^{\bar{z}^{(\varrho)} + \xi} \mathbf{u} dz} \quad (62.101)$$

measures the ensemble mean transport between the mean vertical position of an isopycnal, $\bar{z}^{(\varrho)}$, and that of each ensemble member, $\bar{z}^{(\varrho)} + \xi(\varrho)$. We refer to transport as “quasi-Stokes” given that is the difference between an isopycnal (i.e., quasi-Lagrangian) mean and an Eulerian mean (see Section 62.3)

$$\bar{\mathbf{U}}^{\text{qs}} = \bar{\mathbf{U}}^\# - \bar{\mathbf{U}}. \quad (62.102)$$

As for the traditional Stokes drift discussed in Sections 45.8, and 62.3.5, which arises from a correlation between larger velocity when a wave crest is present, so too does the quasi-Stokes transport arise from a correlation between a larger velocity and a larger undulation in isopycnal thickness.

Three-component TRM velocity

Following from the vertical gauge expression (61.76), we introduce the TRM vector streamfunction

$$\bar{\Psi}^\# = \bar{\mathbf{U}}^\# \times \hat{\mathbf{z}}, \quad (62.103)$$

and the corresponding three-dimensional non-divergent TRM velocity

$$\bar{\mathbf{v}}^\# = \nabla \times \bar{\Psi}^\#. \quad (62.104)$$

The vertical component,

$$\bar{w}^\# = \hat{\mathbf{z}} \cdot (\nabla \times \bar{\Psi}^\#), \quad (62.105)$$

has no corresponding component in an isopycnal description, which only requires the horizontal thickness weighted transport, $\hat{\mathbf{u}}$. However, the TRM vector streamfunction only requires the horizontal TRM transport, $\bar{\mathbf{U}}^\#$, so the two descriptions in effect make use of the same number of degrees of freedom.

62.5.4 Volume conservation and the thickness equation

Consider two perspectives on volume conservation: one based on isopycnal coordinates and the other based on geopotential coordinates.

Isopycnal coordinates

In isopycnal vertical coordinates, the volume of a fluid element is written

$$\delta V = \delta x \delta y \delta z = \delta x \delta y \delta \varrho h, \quad (62.106)$$

where we introduced the specific thickness, h , from equation (62.92). Geometrically, the product $|h \delta \varrho|$ represents the vertical distance, or *thickness*, between the two infinitesimally close density classes ϱ and $\varrho + \delta \varrho$ (see Figure 57.2). Material conservation of both volume and potential density implies conservation of the product of specific thickness and horizontal area $\delta x \delta y h$, which leads to the thickness equation (Section 59.2.3)

$$\frac{\partial h}{\partial t} + \nabla_\varrho \cdot (h \mathbf{u}) = 0, \quad (62.107)$$

with \mathbf{u} the horizontal velocity field, the time derivative is computed with ϱ held fixed, and

$$\nabla_\varrho = \nabla_z + \mathbf{S} \frac{\partial}{\partial z} \quad (62.108)$$

is the horizontal derivative operator with ϱ held fixed and

$$\mathbf{S} = \nabla_\varrho z \quad (62.109)$$

is the horizontal slope of the potential density surface.

Geopotential coordinates

An Eulerian z -coordinate description of volume stirring within isopycnal layers is rendered via a combination of volume conservation, $\nabla \cdot \mathbf{v} = 0$, and material conservation of potential density, $D\varrho/Dt = 0$. When written as skewson rather than advection, the natural gauge is the vertical gauge introduced in Section 61.7.1 (equation (61.74)), since this gauge only requires the same horizontal velocity field \mathbf{u} used with the isopycnal coordinate description. This gauge has an associated skew flux of potential density $\mathbf{F}^{\text{skew}} = -\nabla \varrho \times \Psi$, which leads to the evolution

$$\frac{\partial \varrho}{\partial t} = \nabla \cdot (\nabla \varrho \times \Psi), \quad (62.110)$$

where all derivatives are here taken with fixed Eulerian (geopotential) coordinates, (x, y, z) , and the divergence operator is three-dimensional.

62.5.5 Ensemble mean kinematics in isopycnal coordinates

Consider an ensemble of stably stratified (so that the layer specific thickness h is single-signed and nonvanishing) perfect Boussinesq fluid parcels with the same infinitesimal volume, $\delta V = \delta x \delta y \delta z = \delta x \delta y h \delta \varrho$, and same potential density, ϱ . Lacking any other marker, such as a tracer concentration, the ensemble members are distinguished from one another by values of their horizontal area, $\delta A = \delta x \delta y$, and their specific thickness, h , that is, their geometric attributes. The ensemble members are assumed to be stirred by different stochastic realizations of the fluid flow.

FIGURE 62.4: Schematic of the ensemble averaged potential density as measured by an observer at a fixed point (x, y, z, t) in space-time. In general, different members of the ensemble have potential density surfaces that live at different depths. That is, a fixed Eulerian space-time observer measures an ensemble mean potential density as the average over different potential density surfaces. For the case of a two-member ensemble as shown here, $2\bar{\rho}^z(z) = \rho(1, z) + \rho(2, z)$, where $\rho(1, z)$ is generally different from $\rho(2, z)$.

Since each flow realization alters the geometric properties of the parcels, a mean field description focuses on the mean of these geometric properties.

In isopycnal coordinates, (x, y, ϱ, t) , the thickness equation (62.107) is satisfied by each ensemble member

$$\frac{\partial h}{\partial t} + \nabla_\varrho \cdot (h \mathbf{u}) = 0. \quad (62.111)$$

The ensemble mean computed over these fluid parcels with potential density ϱ satisfies

$$\partial_t \bar{h}^{(\varrho)} + \nabla_\varrho \cdot (\bar{h}^{(\varrho)} \bar{\mathbf{u}}^{(\varrho)} + \bar{h}' \bar{\mathbf{u}}'^{(\varrho)}) = 0, \quad (62.112)$$

where primed variables represent deviations from the isopycnal mean. The mean specific thickness $\bar{h}^{(\varrho)}$ of parcels with potential density ϱ therefore satisfies the conservation equation

$$\partial_t \bar{h}^{(\varrho)} + \nabla_\varrho \cdot (\bar{h}^{(\varrho)} \hat{\mathbf{u}}) = 0. \quad (62.113)$$

In this equation we introduced the thickness weighted isopycnal ensemble mean horizontal velocity

$$\hat{\mathbf{u}} = \frac{\bar{h} \mathbf{u}^{(\varrho)}}{\bar{h}^{(\varrho)}} = \bar{\mathbf{u}}^{(\varrho)} + \frac{\bar{h}' \bar{\mathbf{u}}'^{(\varrho)}}{\bar{h}^{(\varrho)}} \equiv \bar{\mathbf{u}}^{(\varrho)} + \mathbf{u}^{\text{bolus}}, \quad (62.114)$$

along with the isopycnal ensemble mean horizontal velocity, $\bar{\mathbf{u}}^{(\varrho)}$, and the horizontal *bolus velocity*, $\mathbf{u}^{\text{bolus}}$ originally introduced by [Rhines \(1982\)](#). The bolus velocity for an isopycnal layer corresponds to the transport

$$\bar{h}^{(\varrho)} \mathbf{u}^{\text{bolus}} = \bar{h}^{(\varrho)} (\hat{\mathbf{u}} - \bar{\mathbf{u}}^{(\varrho)}) = \bar{h}' \bar{\mathbf{u}}'^{(\varrho)} \quad (62.115)$$

arises from the along-isopycnal correlations between specific thickness and horizontal velocity.

Quite conveniently, the mean conservation equation (62.113) takes the *same* mathematical form as the conservation equation (62.111) satisfied by each ensemble member. The key difference is that the isopycnal ensemble mean thickness $\bar{h}^{(\varrho)}$ is stirred by the thickness weighted isopycnal ensemble mean horizontal velocity $\hat{\mathbf{u}}$, whereas the thickness of each ensemble member is stirred by a randomly different realization of the horizontal velocity \mathbf{u} . The simplicity of the mean field description (62.113) is afforded by use of the Lagrangian vertical coordinate ϱ .

62.5.6 Ensemble mean kinematics in geopotential coordinates

We now consider a geopotential coordinate description of the isopycnal ensemble. For this purpose, we interpret a vertical position, z , as the ensemble mean vertical position, $\bar{z}^{(\varrho)}$. Consequently, mean fields defined at the fixed vertical position correspond to either modified mean fields when not thickness weighted (equation (62.89)), or TRM fields when thickness weighted (equation (62.94)).

Evolution of modified mean density

Following the skewson formulation from Section 61.7, at the ensemble mean depth $z = \bar{z}^\rho$, the streamfunction $\bar{\Psi}^\#$ defines an effective skew flux of the modified mean potential density given by

$$\bar{\mathbf{F}}^\# = -\nabla \tilde{\varrho} \times \bar{\Psi}^\#. \quad (62.116)$$

Using the identity $\bar{\Psi}^\# = \bar{\mathbf{U}}^\# \times \hat{\mathbf{z}}$, we can write this expression in one of the forms

$$\bar{\mathbf{F}}^\# = -\bar{\mathbf{U}}^\# \partial_z \tilde{\varrho} + \hat{\mathbf{z}} \bar{\mathbf{U}}^\# \cdot \nabla_z \tilde{\varrho} \quad (62.117a)$$

$$= -(\bar{\mathbf{U}}^\# + \hat{\mathbf{z}} \mathbf{S} \cdot \bar{\mathbf{U}}^\#) \partial_z \tilde{\varrho}, \quad (62.117b)$$

where

$$\mathbf{S} = -\frac{\nabla_z \tilde{\varrho}}{\partial_z \tilde{\varrho}} \quad (62.118)$$

is the slope of the modified mean density field and $\nabla_z = (\partial_x, \partial_y, 0)$ is the horizontal gradient operator taken with constant depth $z = \bar{z}^{(\varrho)}$. The convergence of the effective skew flux leads to a stirring of the modified mean density $\tilde{\varrho}$ at the mean depth $z = \bar{z}^{(\varrho)}$,

$$\frac{\partial \tilde{\varrho}}{\partial t} = \nabla \cdot (\nabla \tilde{\varrho} \times \bar{\Psi}^\#). \quad (62.119)$$

This equation represents an geopotential coordinate specification of the evolution of the modified mean density due to stirring by the mean eddies. It corresponds directly to the evolution equation (62.110) satisfied at depth z by a single member of the ensemble.

62.5.7 Approximate ensemble mean kinematics in geopotential coordinates

Equation (62.119) represents an exact z -coordinate description of the stirring of modified mean potential density. However, when working in geopotential coordinates, all that is available is Eulerian information. Hence, the Lagrangian information used to realize this exact description must be approximated.

Estimating the quasi-Stokes transport

The approximation requires us to estimate the quasi-Stokes transport $\bar{\mathbf{U}}^{\text{qs}}$ defined by equation (62.101). We addressed a similar estimation in Section 62.3.4 when discussing the Stokes mean. Here, we expand the TRM transport in a Taylor series about the geopotential $z = \bar{z}^{(\varrho)}$

$$\bar{\mathbf{U}}^\#(z) = \overline{\int_{-H}^{z+\xi} \mathbf{u}(s) \, ds} \quad (62.120a)$$

$$= \bar{\mathbf{U}}(z) + \bar{\mathbf{u}} \xi^{(z)} + \frac{1}{2} \overline{\partial_z \mathbf{u} \xi \xi^{(z)}} + \mathcal{O}(\alpha^3), \quad (62.120b)$$

where neglected terms are third order in deviation quantities. Note that all ensemble means are taken at fixed vertical position, which accords with taking a Taylor series about the ensemble mean depth $z = \bar{z}^{(\varrho)}$.

The ensemble means in equation (62.120b) are interpreted as follows. The first term is the Eulerian mean horizontal transport passing beneath the ensemble mean depth, $z = \bar{z}^{(\varrho)}$. The second term, $\bar{\mathbf{u}} \xi$ is the horizontal velocity evaluated at the ensemble mean depth and multiplied by the deviation, ξ , of the potential density surface from its mean depth, all averaged at fixed

depth. An Eulerian split of the horizontal velocity \mathbf{u} into its Eulerian mean $\bar{\mathbf{u}}^{(z)}$ and deviation \mathbf{u}' leads to the correlation

$$\bar{\mathbf{u}}\xi^{(z)} = \bar{\mathbf{u}}'\xi^{(z)}. \quad (62.121)$$

For the second order term, similar considerations lead to

$$\overline{\partial_z \mathbf{u} \xi \xi^{(z)}} \approx \partial_z \bar{\mathbf{u}}^z \bar{\xi} \xi^{(z)}, \quad (62.122)$$

where neglected terms are third order and higher. Combining these relations leads to the second order accurate expression

$$\bar{\mathbf{U}}^\# \approx \bar{\mathbf{U}} + \bar{\mathbf{u}}'\xi^{(z)} + \frac{1}{2} \bar{\xi} \xi^z \partial_z \bar{\mathbf{u}}^{(z)}. \quad (62.123)$$

The disturbance field

Following the discussion in Section 62.3.6, we here determine the disturbance field, ξ , in terms of fields at constant depth. For this purpose, use the identity (62.90) to give

$$\tilde{\varrho}(z) = \varrho(z + \xi) \quad (62.124a)$$

$$= \varrho(z) + \partial_z \varrho(z) \xi + \frac{1}{2} \partial_{zz} \varrho(z) \xi^2 + \mathcal{O}(\alpha^3). \quad (62.124b)$$

Subtracting the Eulerian mean of equation (62.124b) from the unaveraged equation (62.124b), and noting that $\tilde{\varrho}$ is already a mean field, leads to the second order accurate expression for the deviation

$$\xi = -\varrho'(z)/\partial_z \bar{\varrho}^{(z)} + \mathcal{O}(\alpha^2), \quad (62.125)$$

where

$$\varrho(z) = \bar{\varrho}^{(z)} + \varrho'(z). \quad (62.126)$$

To within the same order, the deviation can be written

$$\xi = -\varrho'(z)/\partial_z \tilde{\varrho}(z) + \mathcal{O}(\alpha^2). \quad (62.127)$$

Approximate quasi-Stokes transport

Substituting the deviation (62.127) into the approximate expression (62.120b) for the TRM transport yields an approximate expression for the Stokes transport

$$\mathbf{U}^{\text{qs}} = -\frac{\bar{\mathbf{u}}' \varrho'(z)}{\partial_z \tilde{\varrho}} + \frac{\bar{\phi}^{(z)} \partial_z \bar{\mathbf{u}}^{(z)}}{(\partial_z \tilde{\varrho})^2} + \mathcal{O}(\alpha^3), \quad (62.128)$$

where

$$\bar{\phi}^{(z)} = \frac{1}{2} \bar{\varrho}' \bar{\varrho}'^{(z)} \quad (62.129)$$

is the mean potential density variance. [McDougall and McIntosh \(2001\)](#) noted that the [Gent et al. \(1995\)](#) scheme offers a parameterization of the two correlations on the right hand side of equation (62.128). We have more to say regarding this parameterization in Section 63.1.

Substituting the deviation (62.127) into the approximate expression (62.124b) yields, to within terms of third order, the relation

$$\tilde{\varrho} = \bar{\varrho}^{(z)} - \partial_z \left[\frac{\bar{\phi}^{(z)}}{\partial_z \bar{\varrho}^{(z)}} \right] + \mathcal{O}(\alpha^3). \quad (62.130)$$

As for the Stokes transport, the modified mean density and Eulerian mean density, when evaluated at the same depth, differ by terms that are second order in eddy amplitude.

62.5.8 Further study

This section is largely based on approaches used by [DeSzeke and Bennett \(1993\)](#), [McIntosh and McDougall \(1996\)](#), [Kushner and Held \(1999\)](#), and [McDougall and McIntosh \(2001\)](#) as summarized in Section 9.3 of [Griffies \(2004\)](#). Many other papers have applied this formalism to a variety of analyses, with examples including [Nurser and Lee \(2004a\)](#), [Nurser and Lee \(2004b\)](#), [Wolfe \(2014\)](#).

62.6 Mean tracer equation

We now include a tracer field to the ideal Boussinesq parcel and determine a mean field description for the tracer. The transport of tracer by eddies has both a reversible stirring component and an irreversible mixing component. The stirring arises from both the thickness correlation to velocity as well as the velocity correlated with tracer.

62.6.1 Thickness weighted average or mean

Equation (62.114) introduced a specific thickness weighted average (or mean) operator, which will prove to be quite useful when considering the mean tracer equation. In general, for any field Φ associated with a potential density layer ϱ , we define the decomposition into thickness weighted average and deviation

$$\Phi(\varrho) = \widehat{\Phi}(\varrho) + \Phi''(\varrho) \quad (62.131a)$$

$$= \frac{\overline{h \Phi}^{(\varrho)}}{\overline{h}^{(\varrho)}} + \Phi''. \quad (62.131b)$$

It follows by definition that

$$\overline{h \Phi''}^{(\varrho)} = 0. \quad (62.132)$$

62.6.2 Isopycnal mean thickness weighted tracer equation

When attaching a tracer to fluid parcels, each member of the ensemble satisfies the isopycnal tracer equation

$$\frac{\partial C}{\partial t} + \mathbf{u} \cdot \nabla_{\varrho} C = 0. \quad (62.133)$$

Combining the tracer and thickness equations leads to the thickness weighted tracer equation

$$\frac{\partial(h C)}{\partial t} + \nabla_{\varrho} \cdot (h \mathbf{u} C) = 0. \quad (62.134)$$

Hence, in isopycnal coordinates and in the absence of irreversible processes, the evolution of thickness weighted tracer occurs via the isopycnally oriented convergence of the two-dimensional thickness weighted horizontal advective flux, $h \mathbf{u} C$.

To address the problem of describing the ensemble mean tracer equation in isopycnal coordinates, decompose the tracer and velocity field into their thickness weighted average and deviation to give

$$\partial_t[h(\widehat{C} + C'')] + \nabla_{\varrho} \cdot [h(\widehat{\mathbf{u}} + \mathbf{u}'')](\widehat{C} + C'') = 0. \quad (62.135)$$

Taking an ensemble average over fluid elements with the same potential density, and using equation (62.132), yield the mean thickness weighted tracer equation

$$\partial_t (\bar{h}^{(\varrho)} \hat{C}) + \nabla_\varrho \cdot (\bar{h}^{(\varrho)} \hat{C} \hat{\mathbf{u}}) = -\nabla_\varrho \cdot (\bar{h} C'' \bar{\mathbf{u}}''). \quad (62.136)$$

Now introduce the correlation

$$\bar{h} C'' \bar{\mathbf{u}}'' = \bar{h}^{(\varrho)} \widehat{C'' \mathbf{u}''} \quad (62.137)$$

(see equation (62.131b)), and recall that the mean thickness $\bar{h}^{(\varrho)}$ satisfies the mean thickness equation (62.113). These two points lead to the evolution equation for the mean thickness weighted tracer concentration

$$(\partial_t + \hat{\mathbf{u}} \cdot \nabla_\varrho) \hat{C} = -\frac{1}{\bar{h}^{(\varrho)}} \nabla_\varrho \cdot (\bar{h}^{(\varrho)} \widehat{C'' \mathbf{u}''}). \quad (62.138)$$

62.6.3 Subgrid scale tracer transport tensor

The correlation between tracer and velocity found on the right-hand side of the mean thickness weighted tracer equation (62.138) is typically written in terms of a subgrid scale tracer transport tensor

$$\widehat{C'' \mathbf{u}''} = -\mathbb{J} \cdot \nabla_\varrho \hat{C}. \quad (62.139)$$

This definition leads to the evolution equation

$$(\partial_t + \hat{\mathbf{u}} \cdot \nabla_\varrho) \hat{C} = \frac{1}{\bar{h}^{(\varrho)}} \nabla_\varrho \cdot (\bar{h}^{(\varrho)} \mathbb{J} \cdot \nabla_\varrho \hat{C}). \quad (62.140)$$

The subgrid scale operator on the right hand side has the same general form as the diffusion operator written in isopycnal coordinates as derived in Section 56.15. However, in addition to symmetric diffusion processes, this operator includes skewed fluxes that lead to skew diffusion as discussed in Section 62.4.2. Whereas the diffusive aspect is commonly parameterized as dianeutral diffusion and neutral diffusion (Section 63.1), there is no parameterization for the skewed correlations for use in ocean models. We comment further on this situation in Section 63.3.9.

62.6.4 Mean tracer transport beneath a density surface

It is useful to further elucidate the relevance of mean thickness weighted fields. For this purpose, consider the mean horizontal tracer transport occurring beneath a particular potential density surface $\varrho = \tilde{\varrho}$,

$$\bar{\mathbf{C}}^\#(\bar{z}^{(\varrho)}) = \overline{\int_{-H}^{\bar{z}^{(\varrho)} + \xi} C \mathbf{u} dz}. \quad (62.141)$$

Setting tracer concentration to unity recovers the expression (62.98) for the TRM transport. Changing coordinates and making use of the tracer correlation tensor renders

$$\bar{\mathbf{C}}^\#(\bar{z}^{(\varrho)}) = \int_{\varrho(-H)}^{\tilde{\varrho}(\bar{z}^{(\varrho)})} \bar{\mathbf{C}} \bar{\mathbf{u}} \bar{h}^{(\varrho)} d\varrho \quad (62.142a)$$

$$= \int_{\varrho(-H)}^{\tilde{\varrho}(\bar{z}^{(\varrho)})} \bar{h}^{(\varrho)} d\varrho (\hat{\mathcal{C}} \hat{\mathbf{u}} + \widehat{\mathcal{C}'' \mathbf{u}''}) \quad (62.142b)$$

$$= \int_{\varrho(-H)}^{\tilde{\varrho}(\bar{z}^{(\varrho)})} \bar{h}^{(\varrho)} d\varrho (\hat{\mathcal{C}} \hat{\mathbf{u}} - \mathbb{J} \cdot \nabla_\varrho \hat{\mathcal{C}}) \quad (62.142c)$$

$$= \int_{-H}^{\bar{z}^{(\varrho)}} dz (\hat{\mathcal{C}} \hat{\mathbf{u}} - \mathbb{J} \cdot \nabla_\varrho \hat{\mathcal{C}}). \quad (62.142d)$$

Hence, the mean thickness weighted fields naturally appear when considering such physically interesting quantities as the mean horizontal transport of a tracer beneath the modified mean potential density surface.

62.6.5 Summary of the tracer parameterization problem

Traditionally, the isopycnal parameterization problem for the evolution of the mean thickness weighted tracer requires a parameterization of the bolus velocity $\mathbf{u}^{\text{bolus}}$, which again is related to the thickness weighted horizontal velocity via

$$\hat{\mathbf{u}}((\varrho)) = \frac{\bar{h} \mathbf{u}^{(\varrho)}}{\bar{h}^{(\varrho)}} = \bar{\mathbf{u}}^{(\varrho)} + \frac{\bar{h}' \mathbf{u}'^{(\varrho)}}{\bar{h}^{(\varrho)}} = \bar{\mathbf{u}}^{(\varrho)} + \mathbf{u}^{\text{bolus}}. \quad (62.143)$$

In addition to the bolus velocity, it is necessary to parameterize the subgrid scale tracer transport tensor

$$\widehat{\mathcal{C}'' \mathbf{u}''} = -\mathbb{J} \cdot \nabla_\varrho \hat{\mathcal{C}}, \quad (62.144)$$

which generally has symmetric (diffusive) and antisymmetric (stirring) components (Section 62.4).

For a geopotential coordinate description, equation (62.94) is used to relate thickness weighted mean fields, defined as a function of ϱ , and TRM fields, defined as a function of the mean vertical position of ϱ , to write for the tracer field

$$\hat{\mathcal{C}}(x, y, \tilde{\varrho}, t) = \bar{\mathcal{C}}^\#(x, y, \bar{z}^{(\varrho)}, t). \quad (62.145)$$

Equation (62.145), and the developed formalism, leads to the mean field tracer equation in geopotential coordinates

$$\partial_t \bar{\mathcal{C}}^\# = \nabla \cdot (\nabla \bar{\mathcal{C}}^\# \times \bar{\Psi}^\#) + R(\bar{\mathcal{C}}^\#), \quad (62.146)$$

where $R(\bar{\mathcal{C}}^\#)$ is the geopotential coordinate form of the mixing/stirring operator on the right-hand side of equation (62.140). Details for the transformation of the mixing/stirring operator from isopycnal to geopotential coordinates are provided in Section 56.15.

62.6.6 Comments

Much in this section follows from [Smith \(1999\)](#), [McDougall and McIntosh \(2001\)](#), and [Young \(2012\)](#), each of which focused on the hydrostatic primitive equations assuming a vertically stable buoyancy stratification. The paper by [Young \(2012\)](#) is a milestone in the literature as he succeeded in formulating the ensemble mean primitive equations in a form where only the thickness weighted

(residual mean) velocity appears. Prior attempts failed due to their insufficient mathematical framework. Hence, the formulation of [Young \(2012\)](#) eliminates the need to parameterize the bolus velocity or the quasi-Stokes transport since neither appear as separately identified terms.

Even so, realistic ocean general circulation models are not formulated as “residual mean” models. The key reason is that outside of the stably stratified interior, as in boundary layers, thickness weighted averaging is inappropriate. Instead, we need Eulerian averaged fields when formulating boundary layer closures (e.g., [Large et al., 1994](#)). [Young \(2012\)](#) thus provides a compelling method to decompose the flow into eddies and mean within the stably stratified interior. However, it is not sufficient to capture the full suite of flow regimes represented or parameterized by realistic ocean circulation models.



Chapter 63

MATHEMATICS OF PARAMETERIZED TRACER TRANSPORT

In the presence of turbulent flow processes, tracer variance directly cascades to the small scales. This *downscale cascade* is facilitated by reversible stirring from balanced and unbalanced fluctuations (e.g., mesoscale eddies, submesoscale eddies, breaking gravity and lee waves, turbulent boundary layer processes). The cascade to progressively smaller scales eventually reaches the *Batchelor scale* (order millimetres; e.g., Section 11.5.1 of [Vallis \(2017\)](#)). At this scale, tracer gradients are sufficiently large in magnitude that molecular diffusion can readily act to dissipate tracer variance through irreversible diffusive mixing. Tracer transport at scales larger than the Batchelor scale is dominated by reversible stirring, whereas transport at and below the Batchelor scale is dominated by irreversible mixing from molecular diffusion. This phenomenology provides a constraint on the form of the tracer equation to be used for coarse grained numerical models, where the model grid scale, Δ , is generally much larger than the Batchelor scale.

In this chapter, we study certain of the mathematical and physical properties of parameterized advective and diffusive tracer transport. In general, such parameterizations aim to encapsulate key aspects of physical processes too small to observe and/or simulate. This *subgrid scale parameterization problem* is far broader and deeper than available from a single chapter. We focus mostly on subgrid scale advection and diffusion operators arising from mesoscale eddy motions, yet even this limited focus involves far more than can be covered here. In particular, we do not discuss theories for how the eddy diffusivities are computed. Furthermore, we only consider parameterizations of the subgrid scale tracer flux, whose convergence provides a subgrid tendency for the coarse-grained tracer equation. Focusing on fluxes supports locality and conservation for the coarse-grained tracer equation, with these properties also shared by the uncoarsened tracer equation.

CHAPTER GUIDE

Tracers evolve according to the advection-diffusion equation discussed in Chapter 61 and further unpacked in the tracer kinematics Chapter 62. We here build on material in these two chapters in summarizing the basics of advective-diffusive parameterizations of tracer transport. We also make use of neutral directions as detailed in Section 27.5. Mathematically we rely on Cartesian tensor analysis from Chapters 1 and 2.

63.1 Summarizing tracer transport parameterizations	1574
63.1.1 A synopsis of ocean mixing processes	1574
63.1.2 A rough comparison	1575
63.1.3 Diffusive parameterization of fine scale mixing	1576
63.1.4 Advection-diffusive parameterization of eddy-induced transport	1576
63.1.5 Mathematical elements of eddy-induced stirring	1577

63.1.6	Dianeutral unit vector and the neutral slope	1578
63.2	Various forms for small scale diffusion	1578
63.2.1	Isotropic diffusion	1579
63.2.2	Vertical diffusion	1579
63.2.3	Dianeutral diffusion	1579
63.3	Gent-McWilliams stirring	1580
63.3.1	Details of the parameterization	1581
63.3.2	Effects on buoyancy	1581
63.3.3	Local adiabatic dissipation of available potential energy	1582
63.3.4	Meridional overturning mass transport	1584
63.3.5	Connection to form stress	1585
63.3.6	Connection to isopycnal thickness diffusion	1586
63.3.7	Connection to Gent-McWilliams parameterization	1587
63.3.8	A parameterization based on a boundary value problem	1588
63.3.9	Comments	1589
63.4	Neutral diffusion	1589
63.4.1	Motivation for neutral diffusion	1589
63.4.2	Redi neutral diffusion	1590
63.4.3	Small slope neutral diffusion	1590
63.4.4	Neutral tangent plane neutral diffusion	1591
63.4.5	Neutrality condition	1592
63.4.6	Symmetry condition	1593
63.4.7	GM skewson plus small slope neutral diffusion	1593
63.4.8	Generalized vertical coordinates	1594
63.5	Anisotropic neutral diffusion	1595
63.5.1	Orthonormal triad of basis vectors	1595
63.5.2	Anisotropic neutral diffusion tensor	1596
63.5.3	Properties of the anisotropic neutral diffusive fluxes	1597
63.5.4	Small slope anisotropic neutral diffusion	1598
63.6	Anisotropic Gent-McWilliams stirring	1599
63.6.1	Streamfunction and anti-symmetric tensor	1599
63.6.2	Anisotropic Gent-McWilliams skew tracer flux	1600
63.6.3	Anisotropic GM skewson plus small slope neutral diffusion	1600
63.6.4	A parameterization based on a boundary value problem	1600

63.1 Summarizing tracer transport parameterizations

In this section we offer an outline of the tracer transport parameterizations, starting from the small scales and moving to the mesoscale.

63.1.1 A synopsis of ocean mixing processes

Irreversible mixing in the ocean takes place at the millimeter scale through the process of molecular or *Brownian motion* acting to dissipate property gradients. This mixing is generally represented by downgradient molecular diffusion ([Einstein, 1905](#)). The molecular diffusivity of matter (e.g., salt) in seawater is roughly $10^{-9} \text{ m}^2 \text{ s}^{-1}$, whereas the molecular thermal diffusivity is roughly 100 times larger (it is easier to diffuse enthalpy (heat) than matter, [Gill, 1982](#)). Reversible stirring by turbulent eddies greatly increases the magnitude of property gradients upon which *molecular diffusion* acts ([Eckart, 1948](#); [Nakamura, 2001](#); [Müller and Garrett, 2002](#)), thereby increasing the total amount of irreversible mixing. Motivated by molecular diffusion, and following the pioneering work of [Taylor \(1921\)](#), it is common to parameterize mixing induced by eddy stirring as a diffusive closure with an eddy diffusivity that is far larger than molecular values. Furthermore, the eddy

diffusivities are generally the same for all tracers since eddies generally act the same regardless the tracer. Double diffusive processes is the notable counter-example to this equivalence [Schmitt \(1994\)](#).

Mixing induced by eddies of length scale $\mathcal{O}(\text{centimeters} - \text{metres})$ is associated with, among other *fine scale mixing* processes such as gravitational instability, shear instability and breaking internal gravity waves ([MacKinnon et al., 2013](#)), as well as a suite of boundary layer processes ([Large et al., 1994](#)). This mixing is commonly parameterized by a flow dependent isotropic eddy diffusivity. The magnitude of the eddy diffusivity is typically $\mathcal{O}(10^{-3} - 10^{-2} \text{ m}^2 \text{ s}^{-1})$ in boundary layers, and $\mathcal{O}(10^{-5} \text{ m}^2 \text{ s}^{-1})$ in the quiescent ocean interior ([Polzin et al., 1997; Whalen et al., 2012; Waterhouse et al., 2014](#)).

Mesoscale eddies, with size $\mathcal{O}(10 - 100) \text{ km}$, preferentially stir tracers along neutral directions ([McDougall, 1987a,b; McDougall et al., 2014](#)). The mesoscale eddy stirring in turn induces a mixing that is parametrized by downgradient diffusion along neutral directions (Section 63.4). When feeling the geometric constraints of the surface boundary, mesoscale stirring leads to horizontal oriented mixing across outcropped density surfaces ([Treguier et al., 1997; Ferrari et al., 2008; Danabasoglu et al., 2008](#)). This mixing is parameterized by downgradient horizontal diffusion. The neutral and horizontal eddy diffusivities associated with mesoscale processes are typically $\mathcal{O}(10^2 - 10^3 \text{ m}^2 \text{ s}^{-1})$ in the ocean interior and can rise to $\mathcal{O}(10^4 \text{ m}^2 \text{ s}^{-1})$ in the ocean surface layer ([Abernathay et al., 2013; Klocker and Abernathay, 2014; Cole et al., 2015](#)).

63.1.2 A rough comparison

What process is more important for setting tracer distributions: neutral diffusion induced by mesoscale eddies or small scale isotropic diffusion induced by breaking gravity waves? Since the neutral diffusivity arises from mesoscale eddy stirring, it is many orders of magnitude larger than the isotropic diffusivity arising from fine scale mixing. However, these two eddy diffusivities act on very different tracer gradients, in which case the net effects on tracer distributions could be more comparable.

To help answer the question, consider a scaling with a constant neutral diffusivity and a constant isotropic diffusivity. Furthermore, assume Cartesian orientation of the diffusion operators (i.e., zero neutral slope) and assume the isotropic diffusion is dominated by vertical diffusion (see Section 63.2). We are thus comparing the following two diffusion processes

$$\text{horizontal diffusion} = \kappa_{\text{horz}} \nabla_z^2 C \quad \text{and} \quad \text{vertical diffusion} = \kappa_{\text{vert}} \partial_{zz} C. \quad (63.1)$$

Now introduce a vertical scale H and horizontal scale L over which the tracer concentration changes by an amount δC . Doing so leads to the scaled diffusion operators

$$\text{horizontal diffusion} \sim (\kappa_{\text{horz}}/L^2) \delta C \quad \text{and} \quad \text{vertical diffusion} \sim (\kappa_{\text{vert}}/H^2) \delta C. \quad (63.2)$$

These operators have the same scale when

$$\kappa_{\text{vert}} = (H/L)^2 \kappa_{\text{horz}}. \quad (63.3)$$

Choosing $L = 10^5 \text{ m}$ and $H = 10^1 \text{ m}$ leads to

$$\kappa_{\text{vert}} = 10^{-8} \kappa_{\text{horz}}. \quad (63.4)$$

Furthermore, if $\kappa_{\text{horz}} = 10^3 \text{ m}^2 \text{ s}^{-1}$, then the two operators provide a similar contribution to tracer evolution if $\kappa_{\text{vert}} = 10^{-5} \text{ m}^2 \text{ s}^{-1}$. This is a rather small diffusivity that is generally thought to be on the order of that afforded by the background of breaking gravity waves in the ocean interior

(*MacKinnon et al.*, 2013). This scaling is crude since the length scales are dependent on details of the flow regime as are the eddy diffusivities. Even so, it suggests that the two diffusive processes can indeed contribute to tracer distributions by a similar amount.

63.1.3 Diffusive parameterization of fine scale mixing

Ignoring the cross-diffusion processes introduced in Section 23.8 (see also *IOC et al.* (2010), Section 2.5 of *Olbers et al.* (2012), and *Graham and McDougall* (2013)), the molecular diffusion of Θ and S lead to the material evolution equations

$$\rho \frac{D\Theta}{Dt} = \nabla \cdot (\rho \kappa_\Theta \nabla \Theta) \quad (63.5a)$$

$$\rho \frac{DS}{Dt} = \nabla \cdot (\rho \kappa_S \nabla S), \quad (63.5b)$$

where $\kappa_\Theta > 0$ and $\kappa_S > 0$ are the molecular kinematic diffusivities for Θ and S , respectively. For a measured scale, Δ , larger than the scale where gravity waves break and dissipate kinetic energy (i.e., tens to hundreds of metres), diffusion is commonly used to parameterize the associated irreversible tracer mixing (e.g., *MacKinnon et al.*, 2013). Diffusion is also used to parameterize mixing from other small scale processes, such as turbulent boundary layer processes, double-diffusion, breaking leewaves, and other processes. As discussed in Section 4 of *McDougall et al.* (2014), small scale mixing generally takes place in an isotropic manner. Its parameterization thus appears just as for isotropic molecular diffusion given by equation (63.5b), yet with a far larger eddy diffusivity $\kappa_{\text{fine}} \gg \kappa_\Theta, \kappa_S$ that is a function of the flow

$$\rho \frac{D\Theta}{Dt} = \nabla \cdot (\rho \kappa_{\text{fine}} \nabla \Theta) \quad (63.6a)$$

$$\rho \frac{DS}{Dt} = \nabla \cdot (\rho \kappa_{\text{fine}} \nabla S). \quad (63.6b)$$

The same eddy diffusivity is used for both Θ and S . This assumption follows the general approach for turbulent transport parameterizations (e.g, *Vallis*, 2017), whereby eddies are assumed to act in the same manner on any conserved scalar tracer.

63.1.4 Advection-diffusive parameterization of eddy-induced transport

Stirring from turbulent scales smaller than the grid scale is commonly parameterized by an eddy-induced stirring velocity, \mathbf{v}^* . For ocean mesoscale eddies, such parameterized stirring generally follows a variant of *Gent and McWilliams* (1990) and *Gent et al.* (1995), with this stirring quite important for setting large-scale ocean tracer distributions. In addition, mixing is promoted by the direct cascade from stirring. This mixing is parameterized by a diffusion operator distinct from that used for the small scale mixing discussed in Section 63.1.3.

Consider a second order subgrid scale transport tensor, \mathbb{M} , meant to parameterize both subgrid scale eddy stirring and eddy mixing. With this tensor, the evolution of salinity and Conservative Temperature takes the form

$$\rho \frac{DS}{Dt} = \nabla \cdot (\rho \mathbb{M} \cdot \nabla S) \quad (63.7a)$$

$$\rho \frac{D\Theta}{Dt} = \nabla \cdot (\rho \mathbb{M} \cdot \nabla \Theta). \quad (63.7b)$$

As for the fine scale diffusion equations (63.6a) and (63.6b), we here use the same transport tensor

for both S and Θ as eddies are assumed to act in the same manner on any conserved scalar tracer. As presented in Chapter 61, we decompose the second order transport tensor into the sum of its symmetric and anti-symmetric components

$$\mathbb{M} = \mathbb{K} + \mathbb{A}. \quad (63.8)$$

When the symmetric tensor, \mathbb{K} , is positive-definite, it gives rise to downgradient diffusion. In contrast, the anti-symmetric tensor, \mathbb{A} , gives rise to skew-diffusion or eddy-induced advection.

63.1.5 Mathematical elements of eddy-induced stirring

As detailed in Sections 61.5, 61.6, and 62.4, the anti-symmetric tensor, \mathbb{A} , contributes to the parameterized transport according to

$$\nabla \cdot (\rho \mathbb{A} \cdot \nabla S) = \partial_m(\rho \mathbb{A}^{mn} \partial_n S) \quad (63.9a)$$

$$= \partial_m(\rho \mathbb{A}^{mn}) \partial_n S + \rho \mathbb{A}^{mn} \partial_m \partial_n S \quad (63.9b)$$

$$= -\rho v^{*n} \partial_n S, \quad (63.9c)$$

where we made use of the Einstein index notation with repeated indices summed over their range $m, n = 1, 2, 3$, and where \mathbb{A}^{mn} are the components to the anti-symmetric transport tensor \mathbb{A} . Additionally, we noted that

$$\rho \mathbb{A}^{mn} \partial_m \partial_n S = 0 \quad (63.10)$$

since \mathbb{A}^{mn} is anti-symmetric whereas $\partial_m \partial_n S$ is symmetric (see Exercise 1.2). Finally, we introduced a density-weighted *eddy-induced velocity*

$$\rho v^{*n} = -\partial_m(\rho \mathbb{A}^{mn}). \quad (63.11)$$

Importantly, $\rho \mathbf{v}^*$ has a zero divergence, again due to anti-symmetry of \mathbb{A}^{mn}

$$\nabla \cdot (\rho \mathbf{v}^*) = \partial_n(\rho v^{*n}) = -\partial_n \partial_m(\rho \mathbb{A}^{mn}) = 0. \quad (63.12)$$

A zero-divergence for $\rho \mathbf{v}^*$ means that it contributes no mass sources or sinks to the fluid.¹

Transport from the anti-symmetric tensor thus provides a means to stir tracers due to unresolved eddy processes. The mathematical form of the stirring can be either through skew-diffusion or through advection (see Section 61.6). Choosing to make use of the advection form allows us to combine the contribution from the anti-symmetric transport tensor with the resolved advection operator, thus resulting in a *residual mean material transport equation*

$$\rho \frac{D^\dagger S}{Dt} = \nabla \cdot (\rho \mathbb{K} \cdot \nabla S) \quad (63.13a)$$

$$\rho \frac{D^\dagger \Theta}{Dt} = \nabla \cdot (\rho \mathbb{K} \cdot \nabla \Theta), \quad (63.13b)$$

where the residual mean material time derivative is given by

$$\frac{D^\dagger}{Dt} = \frac{\partial}{\partial t} + \mathbf{v}^\dagger \cdot \nabla \quad (63.14)$$

¹For a Boussinesq fluid, the density factor is replaced by the constant reference density, ρ_0 , so that $\nabla \cdot \mathbf{v}^* = 0$ in the Boussinesq fluid. See section 7 of [Griffies and Greatbatch \(2012\)](#) for more details of the Boussinesq and non-Boussinesq forms for the parameterized eddy-induced transport.

and the *residual mean velocity* is

$$\mathbf{v}^\dagger = \mathbf{v} + \mathbf{v}^*. \quad (63.15)$$

63.1.6 Dianeutral unit vector and the neutral slope

When considering closures for subgrid mixing and stirring arising from mesoscale motions, we orient the parameterized processes according to buoyancy as that reflects the physics of mesoscale motions.² We thus follow the discussion in Section 27.5 by working with locally referenced Archimedean buoyancy to determine neutral directions. In particular, at each point in the fluid we orient stirring and mixing through use of the dianeutral unit vector (Section 27.5.3)

$$\hat{\gamma} = \frac{-\alpha \nabla \Theta + \beta \nabla S}{|-\alpha \nabla \Theta + \beta \nabla S|} \quad \text{and} \quad \hat{\gamma} = \hat{x} \hat{\gamma}_x + \hat{y} \hat{\gamma}_y + \hat{z} \hat{\gamma}_z \quad \text{and} \quad \hat{\gamma} \cdot \hat{\gamma} = \hat{\gamma}_x^2 + \hat{\gamma}_y^2 + \hat{\gamma}_z^2 = 1, \quad (63.16)$$

with $\hat{\gamma}$ pointing perpendicular to the neutral tangent plane in a direction towards larger density.³ Furthermore, when the fluid is stably stratified in the vertical, which is common for the mesoscale and larger, then the squared buoyancy frequency is positive (Section 27.4)

$$N^2 = -g (-\alpha \partial_z \Theta + \beta \partial_z S) > 0. \quad (63.17)$$

We can thus introduce the slope of the neutral tangent plane relative to the (x, y) horizontal plane

$$\mathbf{S} = - \begin{bmatrix} -\alpha \nabla_z \Theta + \beta \nabla_z S \\ -\alpha \partial_z \Theta + \beta \partial_z S \end{bmatrix} = \frac{g (-\alpha \nabla_z \Theta + \beta \nabla_z S)}{N^2} = \hat{x} S_x + \hat{y} S_y. \quad (63.18)$$

For such stably stratified fluids, the dianeutral direction can be written in terms of the neutral slope

$$\hat{\gamma} = \frac{\mathbf{S} - \hat{z}}{(1 + \mathbf{S}^2)^{1/2}}. \quad (63.19)$$

In this form we see that the dianeutral direction is vertically downward when the slopes vanish, which accords with this direction generally pointing toward increasing density.

63.2 Various forms for small scale diffusion

We here follow Section 4 from [McDougall et al. \(2014\)](#) to highlight distinctions between isotropic diffusion, dianeutral diffusion,⁴ and vertical diffusion. Although commonly considered interchangeable in the literature as parameterizations of small scale mixing, there are conceptual distinctions that we identify here. Note that the distinctions between these three diffusions are quantitatively small when neutral slopes are modest and when $\kappa_{\text{ntr}} \gg \kappa_{\text{fine}}$.

²We offer further discussion of this point at the start of Section 63.4.

³Equation (4) in [McDougall et al. \(2014\)](#) makes use of the opposite convention so that their dianeutral direction points towards decreasing density. We instead follow the water mass transformation convention as in equation (65.38), so that $\hat{\gamma}$ points in the direction of increasing density.

⁴Dianeutral diffusion is commonly also referred to as *diapycnal diffusion*, with diapycnal diffusion referring to diffusion across constant potential density surfaces. We distinguish dianeutral from diapycnal in this chapter since neutral directions are defined by locally referenced potential density, and as such neutral directions generally differ from isopycnals. Further discussion is provided in Section 27.5 as well as [McDougall \(1987a\)](#).

63.2.1 Isotropic diffusion

As discussed in Section 63.1.3, we generally parameterize fine scale mixing processes via an isotropic diffusion process using a diffusivity $\kappa_{\text{fine}} > 0$, diffusion tensor

$$\mathbb{K}_{\text{iso}} = \kappa_{\text{fine}} \begin{bmatrix} 1 & 0 & 0 \\ 0 & 1 & 0 \\ 0 & 0 & 1 \end{bmatrix}, \quad (63.20)$$

and corresponding diffusion flux

$$\mathbf{J}_{\text{iso}} = -\rho \mathbb{K}_{\text{iso}} \cdot \nabla C. \quad (63.21)$$

As illustrated in Figure 63.1, under the effects from isotropic diffusion, a region of tracer is diffused the same in all three directions so that, for example, a spherical tracer distribution remains spherical.

63.2.2 Vertical diffusion

Because vertical density gradients are generally much larger than lateral gradients, it is common to approximate the small scale isotropic diffusion tensor with a vertical diffusion tensor

$$\mathbb{K}_{\text{vert}} = \kappa_{\text{fine}} \begin{bmatrix} 0 & 0 & 0 \\ 0 & 0 & 0 \\ 0 & 0 & 1 \end{bmatrix}, \quad (63.22)$$

with a corresponding vertical diffusive flux

$$\mathbf{J}_{\text{vert}} = -\rho \kappa_{\text{fine}} (\nabla C \cdot \hat{\mathbf{z}}) \hat{\mathbf{z}} = -\rho \mathbb{K}_{\text{iso}} \cdot \nabla C = -\rho \kappa_{\text{fine}} \partial_z C \hat{\mathbf{z}}. \quad (63.23)$$

In this manner, vertical mixing of a tracer patch occurs only in the vertical direction (see Figure 63.1).

63.2.3 Dianeutral diffusion

Dianeutral diffusion orients tracer fluxes according to the dianeutral direction (63.16)

$$\mathbf{J}_{\text{dia}} = -\rho \kappa_{\text{fine}} (\nabla C \cdot \hat{\gamma}) \hat{\gamma} = -\rho \mathbb{K}_{\text{dia}} \cdot \nabla C, \quad (63.24)$$

where the dianeutral diffusion tensor is given by

$$\mathbb{K}_{\text{dia}} = \kappa_{\text{fine}} \begin{bmatrix} \hat{\gamma}_x^2 & \hat{\gamma}_x \hat{\gamma}_y & \hat{\gamma}_x \hat{\gamma}_z \\ \hat{\gamma}_x \hat{\gamma}_y & \hat{\gamma}_y^2 & \hat{\gamma}_y \hat{\gamma}_z \\ \hat{\gamma}_x \hat{\gamma}_z & \hat{\gamma}_y \hat{\gamma}_z & \hat{\gamma}_z^2 \end{bmatrix}. \quad (63.25)$$

Assuming a vertically stable stratification, we can make use of the relation (63.19) to write $\hat{\gamma}$ in terms of the slope, \mathbf{S} , thus rendering

$$(\nabla C \cdot \hat{\gamma}) \hat{\gamma} = \frac{(\mathbf{S} - \hat{\mathbf{z}}) \cdot \nabla C}{1 + \mathbf{S}^2} (\mathbf{S} - \hat{\mathbf{z}}) = \frac{1}{1 + \mathbf{S}^2} \begin{bmatrix} S_x^2 & S_x S_y & -S_x \\ S_x S_y & S_y^2 & -S_y \\ -S_x & -S_y & 1 \end{bmatrix} \begin{bmatrix} \partial_x C \\ \partial_y C \\ \partial_z C \end{bmatrix}, \quad (63.26)$$

so that the dianeutral diffusion tensor now takes on the form

$$\mathbb{K}_{\text{dia}} = \frac{\kappa_{\text{fine}}}{1 + S^2} \begin{bmatrix} S_x^2 & S_x S_y & -S_x \\ S_x S_y & S_y^2 & -S_y \\ -S_x & -S_y & 1 \end{bmatrix}. \quad (63.27)$$

As illustrated in Figure 63.1, dianeutral diffusion elongates a tracer patch in the direction normal to the neutral tangent plane.

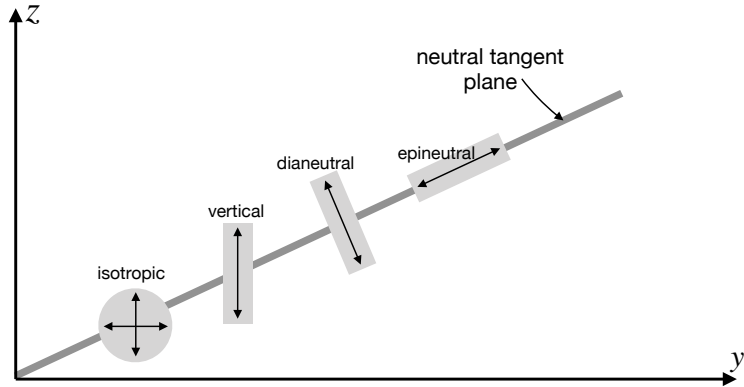


FIGURE 63.1: Illustrating the effects from various forms of diffusion on a tracer patch. When diffused with an isotropic diffusion tensor (equation (63.20)), a spherical patch remains spherical. When diffused with a vertical diffusion tensor (equation (63.22)), a tracer patch elongates in the vertical direction. When diffused with a dianeutral diffusion tensor (equation (63.27)), a tracer patch elongates in the direction normal to the slanted neutral tangent plane. Finally, when diffused with a neutral diffusion tensor, such as the Redi tensor (63.74) or the small slope tensor (63.75), a tracer patch elongates along the neutral tangent plane; i.e., in the *epineutral* direction. This figure is adapted from Figure 4 of [McDougall et al. \(2014\)](#).

63.3 Gent-McWilliams stirring

As mentioned in Section 62.6.3, there are two processes that contribute to eddy-induced stirring. One involves the correlations between eddy fluctuations in the velocity and tracer fields. In Section 62.4, we considered the kinematics of correlations induced by small amplitude eddying motions, where we found that the eddy-induced motion of fluid particles leads to both a symmetric (mixing) and anti-symmetric (stirring) dispersion of tracer concentrations. There is currently no method proposed for parameterizing this form of eddy-induced stirring when it arises from subgrid scale processes, thus leaving unanswered its importance to large-scale tracer distributions.

The second process leading to eddy-induced stirring arises from correlations between fluctuations in isopycnal layer thickness and horizontal velocity. As detailed in Section 62.5, this second effect leads to a movement of volume between isopycnal layers, or equivalently we can conceive of it as the quasi-Stokes transport of volume arising from transient eddy motion. This eddy-induced volume stirring in turn affects an eddy-induced tracer stirring within isopycnal layers. Transient mesoscale eddies are the canonical dynamical process leading to this form of stirring. For simulations that do not resolve transient mesoscale eddies, we commonly parameterize the subgrid scale stirring through variants of the [Gent et al. \(1995\)](#) scheme. Various elements of this scheme are detailed in this section.

Most presentations of the [Gent et al. \(1995\)](#) scheme assume a Boussinesq fluid, though with Section 7 of [Griffies and Greatbatch \(2012\)](#) an exception. We here present the non-Boussinesq form, though in places make the Boussinesq approximation since doing so simplifies the presen-

tation without losing anything fundamental.⁵

63.3.1 Details of the parameterization

Gent et al. (1995) parameterize the three-dimensional non-divergent eddy-induced mass flux (recall Section 61.6.2) according to

$$\rho \mathbf{v}^* = \nabla \times (\rho \Psi^*) \quad \text{with} \quad \Psi^* = \hat{\mathbf{z}} \times \kappa_{\text{gm}} \mathbf{S}, \quad (63.28)$$

where \mathbf{S} is the neutral slope given by equation (63.18), and $\kappa_{\text{gm}} > 0$ is a kinematic diffusivity with dimensions of velocity times a length. Performing the curl on the streamfunction leads to the horizontal and vertical components to the eddy-induced mass flux

$$\rho \mathbf{u}^* = -\partial_z (\kappa_{\text{gm}} \rho \mathbf{S}) \quad \text{and} \quad \rho w^* = \nabla_z \cdot (\kappa_{\text{gm}} \rho \mathbf{S}), \quad (63.29)$$

along with the antisymmetric stirring tensor (*Griffies*, 1998)

$$\mathbb{A}_{\text{gm}} = \kappa_{\text{gm}} \begin{bmatrix} 0 & 0 & -S_x \\ 0 & 0 & -S_y \\ S_x & S_y & 0 \end{bmatrix}. \quad (63.30)$$

Following the discussion in Section 61.6.3, we can identify the advective tracer flux, skew tracer flux, and rotational tracer flux corresponding to the Gent-McWilliams parameterization

$$\mathbf{J}^{\text{adv}} = \mathbf{J}^{\text{skew}} + \mathbf{J}^{\text{rot}} \quad (63.31)$$

where

$$\mathbf{J}^{\text{adv}} = C \rho \mathbf{v}^* = C \rho [-\partial_z (\kappa_{\text{gm}} \rho \mathbf{S}) + \hat{\mathbf{z}} \nabla_z \cdot (\kappa_{\text{gm}} \rho \mathbf{S})] \quad (63.32a)$$

$$\mathbf{J}^{\text{skew}} = -\nabla C \times \rho \Psi^* = \rho \kappa_{\text{gm}} [\mathbf{S} \partial_z C - \hat{\mathbf{z}} (\mathbf{S} \cdot \nabla C)] \quad (63.32b)$$

$$\mathbf{J}^{\text{rot}} = \nabla \times (\rho C \Psi^*). \quad (63.32c)$$

63.3.2 Effects on buoyancy

We now consider a Boussinesq fluid with a linear equation of state in order to focus on the impact of the Gent-McWilliams parameterization on buoyancy, which we measure with potential density, ϱ . In this case the parameterized skew flux of potential density due to the quasi-Stokes transport is given by

$$\rho_0^{-1} \mathbf{J}^{\text{skew}} = -\kappa_{\text{gm}} [\nabla_z \varrho - \hat{\mathbf{z}} \mathbf{S}^2 \partial_z \varrho] = -\kappa_{\text{gm}} [\nabla_z \varrho + \hat{\mathbf{z}} (\rho_0/g) (\mathbf{S} N)^2], \quad (63.33)$$

with the squared neutral slope and squared buoyancy frequency written

$$\mathbf{S}^2 = \mathbf{S} \cdot \mathbf{S} \quad \text{and} \quad N^2 = -\frac{g}{\rho_0} \frac{\partial \varrho}{\partial z}. \quad (63.34)$$

The parameterization yields a horizontal downgradient diffusive flux of potential density along with a vertical upgradient diffusive flux. As illustrated by Figure 63.2, so long as the stratification is stable ($N^2 > 0$), which is assumed by the parameterization, the vertical component to the potential density skew flux is vertically downward, which corresponds to a vertically upward

⁵In brief, for a Boussinesq fluid, the *in situ* density factor found throughout this section is set to the constant Boussinesq reference density, ρ_0 .

buoyancy skew flux. As we see in Section 63.3.3, this orientation ensures that the parameterization reduces available potential energy. Additionally, [Gent et al. \(1995\)](#) prescribe a diffusivity that vanishes on all boundaries, including the ocean surface. [McIntosh and McDougall \(1996\)](#) and [McDougall and McIntosh \(2001\)](#) present more discussion of vertical boundary conditions, which can be understood by considering the exact form of the quasi-Stokes transport defined by equation (62.101). Finally, we introduce a boundary value problem approach in Section 63.3.8 that also pays particular attention to the boundary conditions.

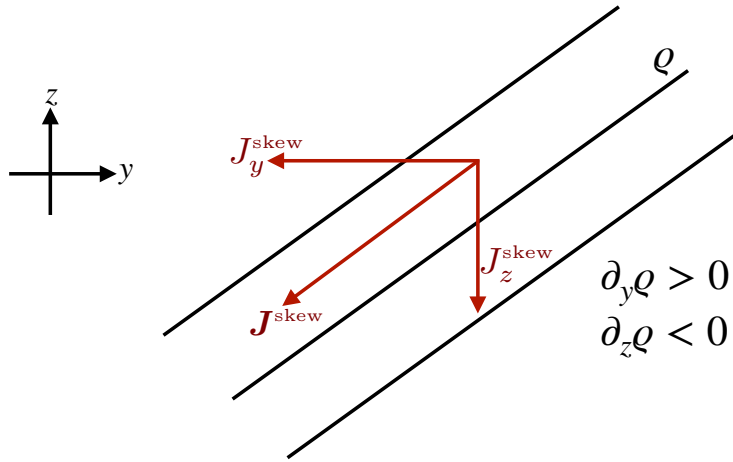


FIGURE 63.2: Orientation of the skew flux of potential density, ϱ , arising from the [Gent et al. \(1995\)](#) parameterization and as described by [Griffies \(1998\)](#). The sloped black lines are constant ϱ isosurfaces; i.e., isopycnals. The horizontal skew flux of potential density is downgradient (directed from high density to low density), whereas the vertical skew flux component is upgradient (directed from low density to high density). The net effect is a skew flux that is oriented parallel to isopycnals.

Figure 63.3 brings the elements of the parameterization together by illustrating the *Gent-McWilliams effect* for a meridional potential density front in the southern hemisphere. The mean geostrophic thermal wind flow is eastward, as in the Antarctic Circumpolar Current, whereas a parameterized *secondary circulation* acts to weaken the front. That is, the parameterization assumes that the mean effects from geostrophic eddies, whose kinetic energy is supported by the potential energy in the front, lead to a weakening of the potential density slope so that the front relaxes to the horizontal.

63.3.3 Local adiabatic dissipation of available potential energy

We here consider the effects from the [Gent et al. \(1995\)](#) scheme on the available potential energy, continuing to assume a Boussinesq fluid with a linear equation of state. We express the behavior using both skew fluxes and advective fluxes. Since we are assuming the parameterization is adiabatic, the change in potential energy is identical to the change in available potential energy.

Skew flux approach

Let us approach the parameterization problem from the perspective of satisfying two general properties: (I) the subgrid scale operator adiabatically stirs while maintaining the same amount of fluid within isopycnal layers, (II) the subgrid operator locally dissipates potential energy through an adiabatic rearrangement of the potential density surfaces, with the dissipation vanishing when there is zero baroclinicity. That is, the scheme dissipates available potential energy. What is the form of the stirring operator implied by these two assumptions?

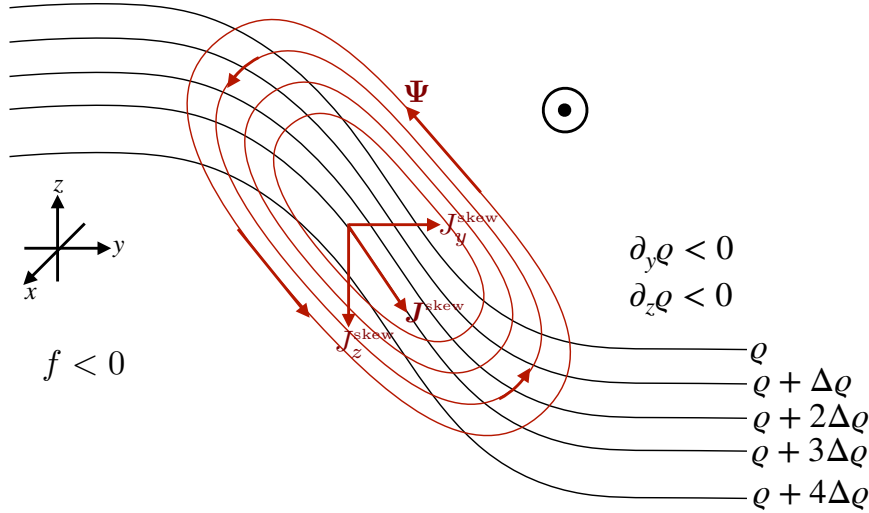


FIGURE 63.3: The Gent-McWilliams effect for a meridional potential density front in the Southern Hemisphere. Dense water rises to the south so that $\partial_y \varrho < 0$. The mean geostrophic thermal wind flow is eastward (out of the page), as in the Antarctic Circumpolar Current. With a stable stratification whereby $\partial_z \varrho < 0$ the Gent-McWilliams streamfunction, equation (63.28), circulates counter-clockwise (red isolines), whereas the Gent-McWilliams skew flux for potential density, given by equation (63.33), has a northward (downgradient) meridional component and downward (upgradient) vertical component (red vectors). The result is a potential density tendency that relaxes the front towards the horizontal thus rendering a zero slope.

Adiabatic stirring of potential density can be realized via the convergence of a skew flux oriented parallel to potential density surfaces

$$\rho_0^{-1} \mathbf{J}^{\text{skew}} = -\nabla \varrho \times \Psi^*, \quad (63.35)$$

where at this point we have yet to specify Ψ^* . To see what the local dissipation of available potential energy imposes, consider the gravitational potential energy of the adiabatic Boussinesq system

$$P = g \int \varrho z \, dV, \quad (63.36)$$

where, again, we assume the *in situ* density equals to the potential density as per a linear equation of state (Section 27.3.5). Assuming all boundaries are material and static allows us to focus on the time tendency of potential energy associated with the unknown flux

$$\frac{dP}{dt} = g \int z \frac{\partial \varrho}{\partial t} \, dV = -\frac{g}{\rho_0} \int (z \nabla \cdot \mathbf{J}^{\text{skew}}) \, dV = -\frac{g}{\rho_0} \int (z \partial_z J^z) \, dV = \frac{g}{\rho_0} \int J^z \, dV, \quad (63.37)$$

where J^z is the vertical flux component. We drop boundary effects by assuming the subgrid scale flux vanishes on all boundaries. To provide a *local* available potential energy sink requires

$$J^z \leq 0, \quad (63.38)$$

where zero occurs when the isopycnals are flat. It is sufficient to construct the vertical flux component using only the potential density field itself. For a stably stratified fluid in which $\partial_z \varrho < 0$, the following form provides a local available potential energy sink

$$\rho_0^{-1} J^z = \kappa_{\text{gm}} S^2 \frac{\partial \varrho}{\partial z} = -(\kappa_{\text{gm}} \rho_0 / g) (S N)^2 \leq 0. \quad (63.39)$$

The corresponding horizontal flux is given by a downgradient diffusive flux

$$\mathbf{J}^h = -\rho_0 \kappa_{\text{gm}} \nabla_z \varrho. \quad (63.40)$$

We have thus recovered the skew flux (63.33) as proposed by [Gent et al. \(1995\)](#). Note that [Aiki et al. \(2004\)](#) proceed in a similar manner yet do not assume locality of the available potential energy sink, thus deriving a more general subgrid scale operator.

Advection flux approach

The impacts on potential energy should be the same when representing the parameterization as an advective flux. To verify this result, return to equation (63.37) and make use of the vertical component of the advective flux rather than the skew flux

$$\frac{dP}{dt} = g \int \varrho w^* dV \quad (63.41a)$$

$$= g \int \varrho \nabla_z \cdot (\kappa_{\text{gm}} \mathbf{S}) dV \quad (63.41b)$$

$$= g \int \nabla_z \cdot (\varrho \kappa_{\text{gm}} \mathbf{S}) dV - g \int \nabla_z \varrho \cdot \kappa_{\text{gm}} \mathbf{S} dV \quad (63.41c)$$

$$= -\rho_0 \int \kappa_{\text{gm}} (\mathbf{S} N)^2 dV, \quad (63.41d)$$

which is the same result as for the skew flux.

63.3.4 Meridional overturning mass transport

It is often of interest to compute the mass transport across a portion of the ocean. In particular, meridional-depth or meridional-potential density streamfunctions allow one to visualize and quantify the zonally integrated transport occurring in a closed basin or over the full globe. The quasi-Stokes transport provides a transport in addition to that from the resolved scale Eulerian mean transport, and the parameterization of [Gent et al. \(1995\)](#) leads to a straightforward computation of the quasi-Stokes contribution. For this purpose, write the net meridional mass transport of fluid across a basin and passing beneath a particular depth in the form (the minus sign is conventional)

$$\mathcal{T}(y, z, t) = - \int dx \int_{-H}^z \rho (v + v^*) dz \quad (63.42a)$$

$$= - \int dx \int_{-H}^z \rho v dz + \int dx \int_{-H}^z \partial_z (\kappa_{\text{gm}} \rho S_y) dz \quad (63.42b)$$

$$= - \int dx \int_{-H}^z \rho v dz + \int \kappa_{\text{gm}} \rho S_y dx \quad (63.42c)$$

$$\equiv \mathcal{T}^{\text{eulerian}}(y, z, t) + \mathcal{T}^{\text{gm}}(y, z, t). \quad (63.42d)$$

For the penultimate step we set the parameterized quasi-Stokes transport to zero at the ocean bottom. We thus see that the parameterized quasi-Stokes transport adds a contribution that scales linearly with basin size, isopycnal slope, and diffusivity,

$$\mathcal{T}^{\text{qs}} \sim \rho_0 L |\mathbf{S}| \kappa_{\text{gm}}. \quad (63.43)$$

As an example, let $\rho = 1035 \text{ kg m}^{-3}$, $\kappa_{\text{gm}} = 10^3 \text{ m}^2 \text{ s}^{-1}$, $|\mathbf{S}| = 10^{-3}$, and $L = 10^7 \text{ m}$, which yields $\mathcal{T}^{\text{qs}} \approx 10 \times 10^9 \text{ kg s}^{-1}$, which represents a nontrivial addition to that from the resolved scale velocity field.

63.3.5 Connection to form stress

We now connect the [Gent et al. \(1995\)](#) closure, normally implemented in the tracer equation, to vertical transfer of momentum through form stress. For this purpose we anticipate our general discussion of form stress in Section 25.1 and more detailed discussions in Sections 28.6 and 33.4. In those discussions, we identify form stress as the horizontal pressure force acting on a sloped surface, with our present concern with surfaces of constant isopycnals as discussed in Sections 28.6 and 33.4.

[Young \(2012\)](#) provides a general means for making the connection between [Gent et al. \(1995\)](#) and form stress for a continuously stratified fluid. For our more schematic purposes, we follow the treatment in [Greatbatch and Lamb \(1990\)](#), [Gent et al. \(1995\)](#) (their Section 4), [Ferreira and Marshall \(2006\)](#) (their Section 2), and [Zhao and Vallis \(2008\)](#) (their Section 2.2). For this purpose, assume the fluid is in Boussinesq planetary geostrophic balance (detailed in Section 28.5) whereby the horizontal momentum satisfies

$$\rho_0 f (\hat{\mathbf{z}} \times \mathbf{u}) = -\nabla_z p + \partial_z \boldsymbol{\tau}. \quad (63.44)$$

The Coriolis acceleration balances the acceleration from horizontal pressure gradients plus a vertical transfer of horizontal stress. The horizontal stress term is generally quite small in the ocean interior, where the flow is in geostrophic balance, whereas it is large at the ocean surface where it arises from turbulent air-sea interactions; i.e., wind stress. Furthermore, it can be large at the bottom through turbulent bottom stresses.

To make the connection between [Gent et al. \(1995\)](#) and the vertical transfer of horizontal form stress, add $\rho_0 f (\hat{\mathbf{z}} \times \mathbf{u}^*)$ to both sides of equation (63.44) to obtain

$$\rho_0 f (\hat{\mathbf{z}} \times \mathbf{u}^\dagger) = -\nabla_z p + \partial_z \boldsymbol{\tau} + \rho_0 f (\hat{\mathbf{z}} \times \mathbf{u}^*), \quad (63.45)$$

where $\mathbf{u}^\dagger = \mathbf{u} + \mathbf{u}^*$ is the horizontal residual mean velocity. This equation says that the Coriolis acceleration from the horizontal residual mean velocity balances pressure gradients, vertical frictional stresses, plus the Coriolis acceleration from the eddy-induced velocity. We further unpack the eddy Coriolis acceleration by noting that the planetary geostrophic velocity satisfies the thermal wind relation in the ocean interior (Section 28.5.6), whereby

$$f \partial_z \mathbf{u} = -(g/\rho_0) \hat{\mathbf{z}} \times \nabla \rho = -\hat{\mathbf{z}} \times N^2 \mathbf{S}. \quad (63.46)$$

We can thus write the Coriolis acceleration from the eddy-induced velocity in the form

$$f (\hat{\mathbf{z}} \times \mathbf{u}^*) = -f [\hat{\mathbf{z}} \times \partial_z (\kappa_{\text{gm}} \mathbf{S})] \quad (63.47a)$$

$$= -\partial_z [\hat{\mathbf{z}} \times (f \kappa_{\text{gm}} \mathbf{S})] \quad (63.47b)$$

$$= \frac{\partial}{\partial z} \left[\frac{\kappa_{\text{gm}} f^2}{N^2} \frac{\partial \mathbf{u}}{\partial z} \right] \quad (63.47c)$$

$$= \frac{\partial}{\partial z} \left[\nu_e \frac{\partial \mathbf{u}}{\partial z} \right], \quad (63.47d)$$

where the final equality introduced an eddy-induced vertical viscosity

$$\nu_e \equiv \kappa_{\text{gm}} (f^2/N^2). \quad (63.48)$$

Making use of this result in the planetary geostrophic equation (63.45) thus leads to

$$\rho_0 f (\hat{\mathbf{z}} \times \mathbf{u}^\dagger) = -\nabla_z p + \partial_z (\boldsymbol{\tau} + \boldsymbol{\tau}_e), \quad (63.49)$$

where

$$\rho_0^{-1} \boldsymbol{\tau}_e = \nu_e \partial_z \mathbf{u} \quad (63.50)$$

defines a horizontal mesoscale eddy stress arising from the thermal wind shears. Equation (63.49) says that the Coriolis acceleration from the horizontal residual mean velocity is in balance with the horizontal pressure gradient plus the vertical transfer of horizontal shears arising from both friction/wind/bottom drag *plus* a contribution from parameterized mesoscale eddies.

We conclude that the [Gent et al. \(1995\)](#) parameterization appears in the planetary geostrophic residual mean momentum equation as a vertical transport of horizontal stress determined by a viscosity $\nu_e = \kappa_{\text{gm}} (f/N)^2$. Notably, this vertical eddy transfer occurs in the absence of irreversible mixing. We thus interpret it as a parameterization of the vertical transfer of pressure form stress via mesoscale eddies that act between isopycnal layers. That is, the [Gent et al. \(1995\)](#) scheme offers a means to parameterize vertical transfer of horizontal form stress arising from undulating mesoscale eddies in the ocean interior. This interpretation is more thoroughly discussed in Section 28.6.

63.3.6 Connection to isopycnal thickness diffusion

Recall the ensemble mean thickness equation (62.113) for a Boussinesq fluid was derived in Section 62.5.5

$$\partial_t h + \nabla_\varrho \cdot (h \hat{\mathbf{u}}) = 0, \quad (63.51)$$

where

$$\hat{\mathbf{u}} = \mathbf{u} + \mathbf{u}^{\text{bolus}} \quad (63.52)$$

is the thickness weighted transport velocity affecting evolution of the ensemble mean thickness h . Note that for brevity we here drop the nomenclature $()^{(\varrho)}$ used in Section 62.5.5.

Isopycnal correlations of horizontal velocity and layer thickness define the bolus velocity via

$$h \mathbf{u}^{\text{bolus}} = \overline{h' \mathbf{u}'^T} \quad (63.53)$$

Now consider a downgradient diffusive closure for this correlation

$$h \mathbf{u}^{\text{bolus}} = \overline{h' \mathbf{u}'^T}^{(\varrho)} = -\mathbb{K}_{\text{thick}} \cdot \nabla_\varrho h, \quad (63.54)$$

with $\mathbb{K}_{\text{thick}}$ a symmetric and positive-definite 2×2 diffusion tensor. The mean thickness equation thus takes the form of an advection-diffusion equation in isopycnal coordinates

$$\partial_t h + \nabla_\varrho \cdot (h \mathbf{u}) = \nabla_\varrho \cdot (\mathbb{K}_{\text{thick}} \cdot \nabla_\varrho h). \quad (63.55)$$

We note one special property of the closure (63.54) that follows when the thickness diffusion tensor is depth independent. Considering the layers to be discrete, we vertically sum the eddy

transport from the ocean bottom up to a particular layer

$$\sum_{n=k_b}^{n=k} \overline{h'_n u'_n}^{(\varrho)} = - \sum_{n=k_b}^{n=k} \mathbb{K}_{\text{thick}} \cdot \nabla_\varrho h_n = - \mathbb{K}_{\text{thick}} \cdot \sum_{n=k_b}^{n=k} \nabla_\varrho h_n = - \mathbb{K}_{\text{thick}} \cdot \nabla_\varrho \eta_{k-1/2}, \quad (63.56)$$

where $\eta_{k-1/2}$ is the upper interface of layer k (see Figure 32.6), and where k_b is the index for the layer at the ocean bottom. In this case we see that the eddy transport below an isopycnal interface is directly proportional to the slope of that interface.

63.3.7 Connection to Gent-McWilliams parameterization

To make a direct connection between the thickness diffusion closure (63.54) and the [Gent et al. \(1995\)](#) closure discussed in Section 63.3.1, note that the specific thickness is the inverse of the vertical derivative of the potential density

$$h = 1/\partial_z \varrho. \quad (63.57)$$

Correspondingly, using the relation between derivative operators, $\nabla_\varrho = \nabla_z + \mathbf{S} \partial_z$, gives

$$h^{-1} \nabla_\varrho h = -h \nabla_\varrho (1/h) \quad \text{product rule identity} \quad (63.58a)$$

$$= -(\partial_z \varrho)^{-1} (\nabla_z + \mathbf{S} \partial_z) \partial_z \varrho \quad h = \partial z / \partial \varrho \text{ and } \nabla_\varrho = \nabla_z + \mathbf{S} \partial_z \quad (63.58b)$$

$$= -\frac{\partial_z (\nabla_z \varrho)}{\partial_z \varrho} + \frac{\partial_{zz} \varrho \nabla_z \varrho}{(\partial_z \varrho)^2} \quad \text{rearrangement} \quad (63.58c)$$

$$= -\partial_z [\nabla_z \varrho / (\partial_z \varrho)] \quad \text{product rule identity} \quad (63.58d)$$

$$= \partial_z \mathbf{S} \quad \text{isopycnal slope } \mathbf{S} = -\nabla_z \varrho / (\partial_z \varrho). \quad (63.58e)$$

Consequently, the bolus velocity takes the form

$$\mathbf{u}^{\text{bolus}} = -h^{-1} \mathbb{K}_{\text{thick}} \cdot \nabla_\varrho h = -\mathbb{K}_{\text{thick}} \cdot \partial_z \mathbf{S}. \quad (63.59)$$

The special case of depth independent diffusivity

For the special case where $\mathbb{K}_{\text{thick}}$ is independent of depth and proportional to the 2×2 identity matrix, then

$$\mathbf{u}^{\text{bolus}} = -\partial_z (\kappa_{\text{gm}} \mathbf{S}) = \mathbf{u}^*, \quad (63.60)$$

where the horizontal component of the [Gent et al. \(1995\)](#) velocity, \mathbf{u}^* , was identified from equation (63.29). Again, this identity holds only for the special case of a vertically independent diffusivity tensor proportional to the identity.

Further caveats

The relevance of a depth-independent diffusivity has been questioned by many authors, such as [Killworth \(1997\)](#), [Treguier et al. \(1997\)](#), [Smith and Vallis \(2002\)](#), [Smith and Marshall \(2009\)](#), and [Abernathy et al. \(2013\)](#). We conclude from these studies that a depth independent diffusivity is not the best choice for the [Gent et al. \(1995\)](#) parameterization, in which case where one places the vertical derivative is crucial.

The relation between thickness diffusion with the [Gent et al. \(1995\)](#) parameterization further breaks down near boundaries. The reason is that the eddy diffusivity vanishes next to boundaries and thus has a depth-dependence. Additionally, as noted by [Holloway \(1997\)](#) and [Griffies et al.](#)

(2000), thickness diffusion next to solid earth boundaries leads to an increase in potential energy, with isopycnals creeping up the topographic slope. Such unphysical behavior motivates isopycnal modelers instead to use *interfacial height* diffusion to dissipate noise in the thickness field.

63.3.8 A parameterization based on a boundary value problem

There have been variants of the [Gent et al. \(1995\)](#) scheme proposed in the literature, such as those of [Aiki et al. \(2004\)](#) and [Ferrari et al. \(2010\)](#). As for the [Gent et al. \(1995\)](#) scheme, these alternatives dissipate available potential energy without mixing between isopycnal classes. We here briefly discuss the scheme of [Ferrari et al. \(2010\)](#), which is used by a variety of ocean climate models largely since it contains a natural means to numerically regularize the eddy-induced streamfunction in regions of weak vertical stratification. These considerations are relevant especially in ocean climate models, where weak or zero vertical stratification is inevitable and so it is necessary to handle such regimes.

For the [Ferrari et al. \(2010\)](#) scheme we write the parameterized eddy streamfunction as

$$\Psi^* = \hat{z} \times \boldsymbol{\Upsilon} \implies \mathbf{u}^* = -\partial_z \boldsymbol{\Upsilon} \quad \text{and} \quad w^* = \nabla_z \cdot \boldsymbol{\Upsilon}, \quad (63.61)$$

with $\boldsymbol{\Upsilon}$ determined by solving the following vertical boundary value problem at each horizontal position⁶

$$c^2 \frac{d^2 \boldsymbol{\Upsilon}}{dz^2} - N^2 \boldsymbol{\Upsilon} = -N^2 \boldsymbol{\Upsilon}^{\text{gm}} \quad \text{and} \quad \boldsymbol{\Upsilon}(\eta_b) = \boldsymbol{\Upsilon}(\eta) = 0, \quad (63.62)$$

where (see equation (63.28))

$$\boldsymbol{\Upsilon}^{\text{gm}} = \kappa_{\text{gm}} \mathbf{S} \quad \text{and} \quad N^2 \mathbf{S} = (g/\rho_0) \nabla_z \varrho. \quad (63.63)$$

We recover the [Gent et al. \(1995\)](#) scheme when setting the squared speed to zero, $c^2 = 0$, in which case $\boldsymbol{\Upsilon} = \boldsymbol{\Upsilon}^{\text{gm}}$. For $c^2 > 0$, the second order differential operator ensures that $\boldsymbol{\Upsilon}$ smoothly and continuously transitions through regions where the vertical stratification is weak (N^2 is small), and hence where $|\mathbf{S}|$ is large. In contrast, the standard regularization approaches, with $c^2 = 0$, are somewhat more *ad hoc* (e.g., see Chapter 15 of [Griffies \(2004\)](#)) or rather tedious (e.g., [Ferrari et al. \(2008\)](#)).

Following the discussion in Section 63.3.3, we deduce the impacts on potential energy (assuming a linear equation of state) via equation (63.37), where we make use of the vertical component of the potential density skew flux

$$\frac{1}{g} \frac{dP}{dt} = \frac{1}{\rho_0} \int J^z dV = - \int \hat{z} \cdot (\nabla \varrho \times \boldsymbol{\Psi}^*) dV = - \int \nabla_z \varrho \cdot \boldsymbol{\Upsilon} dV = - \frac{\rho_0}{g} \int N^2 \mathbf{S} \cdot \boldsymbol{\Upsilon} dV. \quad (63.64)$$

The governing differential equation (63.62) leads to

$$\boldsymbol{\Upsilon} \cdot \left[c^2 \frac{d^2 \boldsymbol{\Upsilon}}{dz^2} - N^2 \boldsymbol{\Upsilon} \right] = -(g/\rho_0) \kappa_{\text{gm}} \boldsymbol{\Upsilon} \cdot \nabla_z \varrho, \quad (63.65)$$

which rearranges to

$$(g/\rho_0) \kappa_{\text{gm}} \boldsymbol{\Upsilon} \cdot \nabla_z \varrho = -c^2 \frac{d(\boldsymbol{\Upsilon} \cdot \boldsymbol{\Upsilon}')}{dz} + c^2 \boldsymbol{\Upsilon}' \cdot \boldsymbol{\Upsilon}' + N^2 \boldsymbol{\Upsilon} \cdot \boldsymbol{\Upsilon}, \quad (63.66)$$

where $\boldsymbol{\Upsilon}' = d\boldsymbol{\Upsilon}/dz$. Integrating over a vertical column and making use of the homogeneous

⁶Note that [Ferrari et al. \(2010\)](#) used the opposite sign convention on $\boldsymbol{\Upsilon}$ from that used here.

Dirichlet boundary conditions from equation (63.62) leads to

$$\frac{g}{\rho_0} \int \kappa_{gm} \boldsymbol{\Upsilon} \cdot \nabla_z \varrho dz = \int [c^2 \boldsymbol{\Upsilon}' \cdot \boldsymbol{\Upsilon}' + N^2 \boldsymbol{\Upsilon} \cdot \boldsymbol{\Upsilon}] dz \geq 0. \quad (63.67)$$

This inequality means that the potential energy of a vertical column is dissipated. However, locally at any point in the column the potential energy might increase due to the sign-indefinite term $-c^2 d(\boldsymbol{\Upsilon} \cdot \boldsymbol{\Upsilon}')/dz$. Notably, there is no *a priori* reason that mesoscale eddies dissipate potential energy at every point in space. Furthermore, numerical experiments documented in [Ferrari et al. \(2010\)](#) suggest that local potential energy dissipation is not necessary for a numerically stable operator. We conclude that this approach offers a suitable method for ocean climate simulations.

63.3.9 Comments

As noted in Section 62.6.3, there is presently no parameterization of subgrid scale stirring along neutral directions arising from the correlations between tracer and velocity fluctuations. Rather, the only parameterized subgrid scale stirring is associated with quasi-Stokes transport, with [Gent et al. \(1995\)](#) providing the canonical approach as summarized in this section. To parameterize the skew fluxes arising from tracer-velocity correlations requires one to study the polarization of the eddies giving rise to these skew fluxes, as per the discussion in Section 62.4.2 and [Middleton and Loder \(1989\)](#).

63.4 Neutral diffusion

Neutral diffusion, also referred to as *epineutral diffusion*, parameterizes the mixing induced by mesoscale eddy stirring. The parameterization assumes that the neutral diffusive flux of a tracer is oriented along a neutral direction or a *neutral tangent plane*. The neutral diffusive tracer flux for an arbitrary tracer, C , is perpendicular to the dianeutral unit vector

$$\mathbf{J} \cdot \hat{\gamma} = 0 \implies \mathbf{J} \cdot (-\alpha \nabla \Theta + \beta \nabla S) = 0, \quad (63.68)$$

where $\hat{\gamma}$ is defined by equation (63.16).

63.4.1 Motivation for neutral diffusion

Pioneering models of the ocean circulation, such as that [Cox and Bryan \(1984\)](#), were formulated with the tracer mixing tensor oriented according to the horizontal and vertical directions. These simulations exhibited problems near strong density fronts, such as those found in western boundary currents, where temperature spuriously mixed across isopyncnals, thus degrading the strength of the front and leading to, among other problems, unphysically weak meridional heat transport ([Böning et al., 1995](#)). In earlier work based on tracer measurements, [Montgomery \(1938\)](#), [Veronis \(1975\)](#), and [Rooth \(1982\)](#) suggested that ocean properties were preferentially homogenized along local potential density surfaces rather than geopotential surfaces. Such measurements motivated [Solomon \(1971\)](#) and [Redi \(1982\)](#) to propose rotating the tracer mixing tensor according to neutral directions.

We offer further indirect evidence that mesoscale eddy induced diffusion is preferentially aligned along neutral directions. For that purpose, consider a diffusive flux is not aligned with neutral directions. In this case, diffusive mixing can cause tracer distributions to cross neutral directions, thus adding to that already parameterized from small scale mixing processes. As discussed in Section 14.1.5 of [Griffies \(2004\)](#) as well as Section 1 of [McDougall et al. \(2014\)](#), the

extra mixing induced by this non-neutral orientation of the mesoscale induced diffusive fluxes is proportional to the squared slope between the proposed new direction and the neutral tangent plane. Estimates based on field measurements for interior ocean mixing constrain the magnitude of the tangent to be less than 10^{-4} . This number is very small, indeed it is zero within error bars of field measurements. Although the measurements are sparse, they do support the use of a neutral diffusion operator oriented so to respect the constraint (64.24). We thus make use of this constraint in designing the diffusion tensor in the remainder of this section.

63.4.2 Redi neutral diffusion

One diffusive flux satisfying the property (63.68) is given by

$$\mathbf{J}_{\text{redi}} = -\rho \kappa_{\text{ntr}} [\nabla C - \hat{\gamma} (\hat{\gamma} \cdot \nabla C)], \quad (63.69)$$

where $\kappa_{\text{ntr}} > 0$ is the neutral diffusivity (dimensions of squared length per time). We confirm that \mathbf{J}_{redi} is oriented down the tracer gradient by noting that

$$\mathbf{J}_{\text{redi}} \cdot \nabla C = -\rho \kappa_{\text{ntr}} [|\nabla C|^2 - (\hat{\gamma} \cdot \nabla C)^2] \leq 0. \quad (63.70)$$

We can write the neutral diffusive flux (63.69) in the downgradient flux-gradient relation

$$\mathbf{J}_{\text{redi}} = -\rho \mathbb{K}_{\text{redi}} \cdot \nabla C, \quad (63.71)$$

with the neutral diffusion tensor, \mathbb{K}_{redi} , given by

$$\mathbb{K}_{\text{redi}} = \kappa_{\text{ntr}} \begin{bmatrix} 1 - \hat{\gamma}_x^2 & -\hat{\gamma}_x \hat{\gamma}_y & -\hat{\gamma}_x \hat{\gamma}_z \\ -\hat{\gamma}_x \hat{\gamma}_y & 1 - \hat{\gamma}_y^2 & -\hat{\gamma}_y \hat{\gamma}_z \\ -\hat{\gamma}_x \hat{\gamma}_z & -\hat{\gamma}_y \hat{\gamma}_z & 1 - \hat{\gamma}_z^2 \end{bmatrix} \implies \mathbb{K}_{\text{redi}}^{mn} = \kappa_{\text{ntr}} (\delta^{mn} - \hat{\gamma}^m \hat{\gamma}^n). \quad (63.72)$$

The corresponding neutral diffusion operator is given by the three-dimensional flux convergence

$$\mathcal{R}_{\text{redi}} = -\nabla \cdot \mathbf{J}_{\text{redi}} = \partial_m (\rho \mathbb{K}_{\text{redi}}^{mn} \partial_n C). \quad (63.73)$$

When the neutral surfaces are stably stratified in the vertical, so that their slopes are bounded, then the diffusion tensor takes the following form originally suggested by *Redi* (1982), which is written in terms of the neutral slope

$$\mathbb{K}_{\text{redi}} = \frac{\kappa_{\text{ntr}}}{1 + \mathbf{S}^2} \begin{bmatrix} 1 + S_y^2 & -S_x S_y & S_x \\ -S_x S_y & 1 + S_x^2 & S_y \\ S_x & S_y & \mathbf{S}^2 \end{bmatrix}. \quad (63.74)$$

63.4.3 Small slope neutral diffusion

Another form of the neutral diffusion flux is based on assuming a small magnitude for the slope of the neutral tangent plane relative to the horizontal, which is the case for most of the ocean interior even in frontal regions. With this approximation, the small slope neutral diffusion tensor takes the form

$$\mathbb{K}_{\text{small}} = \kappa_{\text{ntr}} \begin{bmatrix} 1 & 0 & S_x \\ 0 & 1 & S_y \\ S_x & S_y & \mathbf{S}^2 \end{bmatrix}. \quad (63.75)$$

The corresponding small slope neutral diffusive flux is

$$\mathbf{J}_{\text{small}} = -\rho \kappa_{\text{ntr}} [\nabla_\gamma + \hat{\mathbf{z}} (\mathbf{S} \cdot \nabla_\gamma)] C \quad (63.76)$$

where

$$\nabla_\gamma = \nabla_z + \mathbf{S} \partial_z \quad (63.77)$$

is the horizontal derivative operator computed on the neutral tangent plane (see equation (56.73)). To show that $\mathbf{J}_{\text{small}} \cdot \hat{\gamma} = 0$, we make use of the identity (63.19) so that

$$\mathbf{J}_{\text{small}} \cdot \hat{\gamma} = \frac{\mathbf{J}_{\text{small}} \cdot \mathbf{S} - \mathbf{J}_{\text{small}} \cdot \mathbf{S}}{(1 + \mathbf{S}^2)^{1/2}} = 0. \quad (63.78)$$

Furthermore, we confirm that $\mathbf{J}_{\text{small}}$ is oriented down the tracer gradient by noting that

$$\mathbf{J}_{\text{small}} \cdot \nabla C = -\rho \kappa_{\text{ntr}} [\nabla_\gamma C \cdot \nabla_z C + (\mathbf{S} \cdot \nabla_\gamma C) \partial_z C] \quad (63.79a)$$

$$= -\rho \kappa_{\text{ntr}} [|\nabla_z C|^2 + 2(\mathbf{S} \cdot \nabla_z C) \partial_z C + |\mathbf{S} \partial_z C|^2] \quad (63.79b)$$

$$= -\rho \kappa_{\text{ntr}} |\nabla_z C + \mathbf{S} \partial_z C|^2 \quad (63.79c)$$

$$= -\rho \kappa_{\text{ntr}} |\nabla_\gamma C|^2 \quad (63.79d)$$

$$\leq 0. \quad (63.79e)$$

The small slope approximation was proposed by [Cox \(1987\)](#). However, his form for the small slope neutral diffusion flux was incorrect as it did not satisfy $\mathbf{J}_{\text{small}} \cdot \hat{\gamma} = 0$. The corrected form given by equation (63.76) was first written by [Gent and McWilliams \(1990\)](#). The resulting small slope neutral diffusion operator is commonly used in ocean climate models ([Griffies et al., 1998](#); [Lemarié et al., 2012](#)), which results from computing the three-dimensional convergence

$$\mathcal{R}_{\text{small}} = -\nabla \cdot \mathbf{J}_{\text{small}} = \nabla_z \cdot (\rho \kappa_{\text{ntr}} \nabla_\gamma C) + \partial_z (\rho \kappa_{\text{ntr}} \mathbf{S} \cdot \nabla_\gamma C). \quad (63.80)$$

63.4.4 Neutral tangent plane neutral diffusion

A third method to compute neutral diffusion is motivated by the form of isopycnal diffusion in isopycnal layered models. Rather than isopycnal layers, we work with layers determined locally by neutral tangent planes. The neutral tangent frame makes use of projected non-orthogonal generalized vertical coordinates detailed in Chapter 56.

Following the derivations given in Section 56.15, the neutral diffusive flux in the neutral tangent frame is given by the horizontal flux

$$\mathbf{J}_{\text{ntp}} = -\rho \kappa_{\text{ntr}} \nabla_\gamma C. \quad (63.81)$$

This flux is oriented down the tracer gradient as oriented along neutral directions

$$\mathbf{J}_{\text{ntp}} \cdot \nabla_\gamma C = -\rho \kappa_{\text{ntr}} |\nabla_\gamma C|^2, \quad (63.82)$$

which is the same as equation (63.79d) for the small slope fluxes. However, as a purely horizontal flux, \mathbf{J}_{ntp} is not oriented along neutral directions

$$\mathbf{J}_{\text{ntp}} \cdot \hat{\gamma} \neq 0. \quad (63.83)$$

Nevertheless, rather than computing the neutral diffusion operator as a horizontal convergence of this flux, the neutral tangent plane diffusion operator is computed by taking the convergence of

\mathbf{J}_{ntp} along the neutral tangent plane as per equation (56.92)

$$\mathcal{R}_{\text{ntp}} = -\frac{1}{h^\gamma} [\nabla_\gamma \cdot (h^\gamma \mathbf{J}_{\text{ntp}})] = \frac{1}{h^\gamma} [\nabla_\gamma \cdot (h^\gamma \rho \kappa_{\text{nt}} \nabla_\gamma C)], \quad (63.84)$$

where

$$h^\gamma = \frac{\partial z}{\partial \gamma} d\gamma = - \left[\frac{g}{\rho_0 N^2} \right] d\gamma \quad (63.85)$$

measures the thickness of a layer defined by two neutral tangent planes (see equation (56.89)).

As detailed in Section 56.15, \mathcal{R}_{ntp} is identical to the small slope neutral diffusion operator (63.80)

$$\mathcal{R}_{\text{ntp}} = \mathcal{R}_{\text{small}}. \quad (63.86)$$

In principle, it is a matter of convenience which form of the operator one uses. However, there are certain issues to consider when implementing these operators in a numerical model. Notably, a discrete realization of \mathcal{R}_{ntp} allows for a diagonal downgradient implementation of neutral diffusion, just as isopycnal diffusion in an isopycnal ocean model. In contrast, a discrete realization of either $\mathcal{R}_{\text{redi}}$ or $\mathcal{R}_{\text{small}}$ cannot guarantee downgradient fluxes due to the off-diagonal nature of its neutral diffusive flux components ([Griffies et al. \(1998\)](#), [Beckers et al. \(1998\)](#), [Gnanadesikan \(1999\)](#), [Beckers et al. \(2000\)](#) [Lemarié et al. \(2012\)](#), [Shao et al. \(2020\)](#)). As a result, discrete realizations of $\mathcal{R}_{\text{redi}}$ or $\mathcal{R}_{\text{small}}$ can produce extrema, which are distinctly not properties of diffusion in the continuum (see Exercise 61.3). Hence, even though the continuum identity holds $\mathcal{R}_{\text{ntp}} = \mathcal{R}_{\text{small}}$, there are important differences that arise upon realizing these operators on a discrete lattice. [Shao et al. \(2020\)](#) provide further discussion of these points as part of their numerical realization of neutral diffusion.

63.4.5 Neutrality condition

Given the expression (63.16) for the dianeutral unit vector, $\hat{\gamma}$, it is straightforward to show that the neutral diffusive flux for Conservative Temperature and salinity satisfy the constraints

$$\nabla \Theta \cdot [-\alpha \mathbf{J}(\Theta) + \beta \mathbf{J}(S)] = 0 \quad \text{and} \quad \nabla S \cdot [-\alpha \mathbf{J}(\Theta) + \beta \mathbf{J}(S)] = 0. \quad (63.87)$$

These constraints are generally satisfied if the diffusive fluxes satisfy the balance

$$\alpha \mathbf{J}(\Theta) = \beta \mathbf{J}(S) \implies \mathbb{K} \cdot \hat{\gamma} = 0. \quad (63.88)$$

We refer to this balance as the *neutrality condition*. It reflects the vanishing of the neutral diffusive flux of locally referenced potential density. It is maintained by the diffusive flux (63.69) of [Redi \(1982\)](#), the small slope flux (63.76) of [Gent and McWilliams \(1990\)](#), and the neutral tangent frame neutral diffusive flux (63.81). However, it is not maintained by the small slope fluxes from [Cox \(1987\)](#). Furthermore, [Griffies et al. \(1998\)](#) argued for the importance of maintaining this balance to avoid a nonlinear instability plaguing certain numerical realizations of neutral diffusion such as that from [Cox \(1987\)](#).

63.4.6 Symmetry condition

Since the neutral diffusion tensor is symmetric (as are all diffusion tensors as discussed in Section 61.4), we have

$$\mathbf{J}(\Theta) \cdot \nabla S = -\kappa_{\text{ntr}} \rho \mathbb{K}^{mn} \partial_n \Theta \partial_m S \quad (63.89a)$$

$$= -\kappa_{\text{ntr}} \rho \mathbb{K}^{nm} \partial_n S \partial_m \Theta \quad (63.89b)$$

$$= -\kappa_{\text{ntr}} \rho \mathbb{K}^{nm} \partial_n S \partial_m \Theta \quad (63.89c)$$

$$= \mathbf{J}(S) \cdot \nabla \Theta. \quad (63.89d)$$

This symmetry condition holds for both the Redi neutral diffusion tensor and its small slope limit, and it is particularly useful in our discussion of cabbeling and thermobaricity in Section 64.3.

63.4.7 GM skewusion plus small slope neutral diffusion

A parameterization of mesoscale eddy stirring and mixing often appears in geopotential coordinate ocean models in the form of GM skewusion (Section 63.3.1) and small slope neutral diffusion (Section 63.4.3). The combined tracer flux takes the form

$$\rho^{-1} \mathbf{J} = -\kappa_{\text{ntr}} \nabla_z C - (\kappa_{\text{ntr}} - \kappa_{\text{gm}}) \mathbf{S} \partial_z C - \hat{\mathbf{z}} [(\kappa_{\text{ntr}} + \kappa_{\text{gm}}) \mathbf{S} \cdot \nabla_z C + \kappa_{\text{ntr}} \mathbf{S}^2 \partial_z C], \quad (63.90)$$

which can be written in terms of a subgrid scale transport tensor ([Griffies, 1998](#))

$$\rho^{-1} \begin{bmatrix} J^x \\ J^y \\ J^z \end{bmatrix} = - \begin{bmatrix} \kappa_{\text{ntr}} & 0 & (\kappa_{\text{ntr}} - \kappa_{\text{gm}}) S_x \\ 0 & \kappa_{\text{ntr}} & (\kappa_{\text{ntr}} - \kappa_{\text{gm}}) S_y \\ (\kappa_{\text{ntr}} + \kappa_{\text{gm}}) S_x & (\kappa_{\text{ntr}} + \kappa_{\text{gm}}) S_y & \kappa_{\text{ntr}} \mathbf{S}^2 \end{bmatrix} \begin{bmatrix} \partial_x C \\ \partial_y C \\ \partial_z C \end{bmatrix}. \quad (63.91)$$

In the 1990s and throughout much of the 2000s, it was common to assume that $\kappa_{\text{ntr}} = \kappa_{\text{gm}}$, in which case the combined mixing tensor is

$$\mathbb{K}_{\text{small}} + \mathbb{A}_{\text{gm}} = \kappa_{\text{ntr}} \begin{bmatrix} 1 & 0 & 0 \\ 0 & 1 & 0 \\ 2 S_x & 2 S_y & \mathbf{S}^2 \end{bmatrix} \quad \text{if } \kappa_{\text{ntr}} = \kappa_{\text{gm}}, \quad (63.92)$$

so that the subgrid scale flux simplifies to

$$\rho^{-1} \mathbf{J} = -\kappa_{\text{ntr}} \nabla_z C - \hat{\mathbf{z}} \kappa_{\text{ntr}} (2 \mathbf{S} \cdot \nabla_z C + \mathbf{S}^2 \partial_z C) \quad \text{if } \kappa_{\text{ntr}} = \kappa_{\text{gm}}. \quad (63.93)$$

Notably, the 2×2 horizontal mixing tensor is diagonal. Hence, the horizontal tracer flux is the same as that which arises from downgradient horizontal tracer diffusion. The simplicity of the horizontal flux component was alluring to modelers. It was furthermore argued by [Dukowicz and Smith \(1997\)](#) to be a fundamental property of mesoscale turbulence. However, as emphasized through the works of [Treguier et al. \(1997\)](#), [Ferrari et al. \(2008\)](#), [Danabasoglu et al. \(2008\)](#), and [Ferrari et al. \(2010\)](#), the boundary conditions for neutral diffusion and GM skewusion are distinct, thus breaking their symmetry. Furthermore, studies such as [Smith and Marshall \(2009\)](#) and [Abernathy et al. \(2013\)](#) clearly point to the distinct vertical structure for the two diffusivities. Such distinctions are expected since the skew diffusivity and neutral diffusivity parameterize physically distinct processes: one parameterizes the quasi-Stokes transport and the other parameterizes downgradient diffusion along neutral directions.

63.4.8 Generalized vertical coordinates

Thus far we have considered neutral diffusion as realized in geopotential coordinates or using neutral tangent plane coordinates. Here, we detail the steps needed to realize neutral diffusion using the generalized vertical coordinates (GVCs) detailed in Chapters 56 and 57. This formulation is relevant for the now common use of generalized vertical coordinates for ocean modeling as reviewed by [Griffies et al. \(2020\)](#).

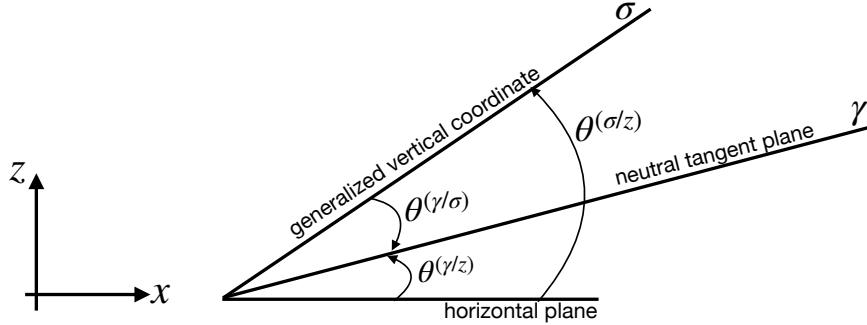


FIGURE 63.4: Slopes of a neutral tangent plane (denoted by γ) relative to both the horizontal plane, $\tan \theta^{(\gamma/z)}$, and relative to a generalized vertical coordinate isoline, $\tan \theta^{(\gamma/\sigma)}$, where σ is a generalized vertical coordinate. We assume positive angles as measure counter-clockwise relative to the horizontal and relative to the σ -isoline, respectively. Hence, for this example, $\theta^{(\gamma/z)} > 0$ yet $\theta^{(\gamma/\sigma)} < 0$. When extending to the two horizontal directions, the slopes generally satisfy $\mathbf{S}^{(\sigma/z)} = \mathbf{S}^{(\gamma/z)} - \mathbf{S}^{(\gamma/\sigma)}$, where $|\mathbf{S}^{(\gamma/z)}| = |\tan \theta^{(\gamma/z)}|$ and $|\mathbf{S}^{(\gamma/\sigma)}| = |\tan \theta^{(\gamma/\sigma)}|$. Note that this relation between slope vectors also holds for arbitrary orientations of the σ isolines and neutral tangent planes.

We start by recalling the expression (56.91) for a general diffusion operator written in terms of the generalized vertical coordinate, $\sigma = \sigma(x, y, z, t)$

$$\mathcal{R} = -\frac{1}{h^\sigma} \left[\nabla_\sigma \cdot (h^\sigma \mathbf{J}^h) + \delta_\sigma(z_\sigma \nabla_\sigma \cdot \mathbf{J}) \right], \quad (63.94)$$

where $\delta_\sigma \equiv d\sigma / \partial_\sigma$ is the dimensionless derivative operator, and the thickness of a σ -layer is

$$h^\sigma = dz = z_\sigma d\sigma = \frac{\partial z}{\partial \sigma} d\sigma. \quad (63.95)$$

Now assume the flux, \mathbf{J} , is given by equation (63.76) for small slope neutral diffusion. Transforming to GVCs leads to the horizontal flux component

$$\mathbf{J}_{\text{small}}^h = -\rho \kappa_{\text{ntr}} \nabla_\gamma C \quad (63.96a)$$

$$= -\rho \kappa_{\text{ntr}} [\nabla_z + (\nabla_\gamma z) \partial_z] C \quad (63.96b)$$

$$= -\rho \kappa_{\text{ntr}} [\nabla_\sigma + (-\nabla_\sigma z + \nabla_\gamma z) \partial_z] C \quad (63.96c)$$

$$= -\rho \kappa_{\text{ntr}} [\nabla_\sigma + (-\mathbf{S}^{(\sigma/z)} + \mathbf{S}^{(\gamma/z)}) \partial_z] C \quad (63.96d)$$

$$= -\rho \kappa_{\text{ntr}} (\nabla_\sigma + \mathbf{S}^{(\gamma/\sigma)} \partial_z) C, \quad (63.96e)$$

where the neutral slopes as shown in Figure 63.4 satisfy the identity

$$\mathbf{S}^{(\sigma/z)} = \mathbf{S}^{(\gamma/z)} - \mathbf{S}^{(\gamma/\sigma)}. \quad (63.97)$$

Furthermore, we made use of the identity (56.73) relating the partial derivative operators

$$\nabla_\gamma = \nabla_z + (\nabla_\gamma z) \partial_z \quad \text{and} \quad \nabla_z = \nabla_\sigma - (\nabla_\sigma z) \partial_z. \quad (63.98)$$

The horizontal flux (63.96e) has the same form as when written using geopotential coordinates, only now with the derivative operator ∇_σ and the slope $\mathbf{S}^{(\gamma/\sigma)}$. Correspondingly, the vertical flux component

$$J_{\text{small}}^z = \mathbf{J}_{\text{small}}^h \cdot \mathbf{S}^{(\gamma/z)} \quad (63.99)$$

takes the form

$$z_\sigma \nabla_\sigma \cdot \mathbf{J}_{\text{small}} = -\mathbf{S}^{(\sigma/z)} \cdot \mathbf{J}_{\text{small}}^h + J_{\text{small}}^z = \mathbf{J}_{\text{small}}^h \cdot \mathbf{S}^{(\gamma/\sigma)}, \quad (63.100)$$

which in turn yields the diffusion operator (63.94)

$$\mathcal{R} = -\frac{1}{h^\sigma} \left[\nabla_\sigma \cdot (h^\sigma \mathbf{J}_{\text{small}}^h) + \delta_\sigma (\mathbf{J}_{\text{small}}^h \cdot \mathbf{S}^{(\gamma/\sigma)}) \right]. \quad (63.101)$$

In the special case when σ is parallel to the neutral direction so that $\mathbf{S}^{(\gamma/\sigma)} = 0$, the diffusion operator (63.101) reduces to the neutral tangent plane version given by equation (63.84).

63.5 Anisotropic neutral diffusion

The neutral diffusion discussed in Section 63.4 is based on isotropic diffusion in the neutral tangent plane. That assumption has been questioned by [Smith and Gent \(2004\)](#) and [Fox-Kemper et al. \(2013\)](#). We here develop some of the formalism appropriate for studying anisotropic neutral diffusion.

63.5.1 Orthonormal triad of basis vectors

We make use of the following orthonormal unit vectors⁷ as depicted in Figure 63.5

$$\hat{\mathbf{e}}_{\bar{1}} = \frac{\hat{\mathbf{d}} \times \hat{\gamma}}{|\hat{\mathbf{d}} \times \hat{\gamma}|} \quad (63.102a)$$

$$\hat{\mathbf{e}}_{\bar{2}} = \frac{\hat{\gamma} \times (\hat{\mathbf{d}} \times \hat{\gamma})}{|\hat{\mathbf{d}} \times \hat{\gamma}|} = \frac{\hat{\mathbf{d}} - (\hat{\gamma} \cdot \hat{\mathbf{d}}) \hat{\gamma}}{|\hat{\mathbf{d}} \times \hat{\gamma}|} \quad (63.102b)$$

$$\hat{\mathbf{e}}_{\bar{3}} = \hat{\gamma} \quad (63.102c)$$

where

$$\hat{\mathbf{d}} = \hat{\mathbf{x}} \hat{d}_x + \hat{\mathbf{y}} \hat{d}_y + \hat{\mathbf{z}} \hat{d}_z \quad (63.103)$$

is an arbitrary unit vector that is not parallel to $\hat{\gamma}$. The three unit vectors $(\hat{\mathbf{e}}_{\bar{1}}, \hat{\mathbf{e}}_{\bar{2}}, \hat{\mathbf{e}}_{\bar{3}})$ form an orthonormal triad at each point in the fluid so that

$$\hat{\mathbf{e}}_{\bar{1}} = \hat{\mathbf{e}}_{\bar{2}} \times \hat{\mathbf{e}}_{\bar{3}} \quad \text{and} \quad \hat{\mathbf{e}}_{\bar{2}} = \hat{\mathbf{e}}_{\bar{3}} \times \hat{\mathbf{e}}_{\bar{1}} \quad \text{and} \quad \hat{\mathbf{e}}_{\bar{3}} = \hat{\mathbf{e}}_{\bar{1}} \times \hat{\mathbf{e}}_{\bar{2}}. \quad (63.104)$$

These vectors are oriented by the arbitrary direction, $\hat{\mathbf{d}}$, and the dianeutral direction, $\hat{\gamma}$. We verify that $\hat{\mathbf{e}}_{\bar{2}}$ has unit magnitude by noting that

$$|\hat{\mathbf{d}} \times \hat{\gamma}|^2 = |\hat{\gamma} \times (\hat{\mathbf{d}} \times \hat{\gamma})|^2 = 1 - (\hat{\mathbf{d}} \cdot \hat{\gamma})^2. \quad (63.105)$$

⁷The basis vectors (63.102a)-(63.102c) are more suitable for present purposes than the analogous basis vectors defined by equations (14.4)-(14.6) in [Griffies \(2004\)](#). In particular, the basis (63.102a)-(63.102c) has a sensible limit when the neutral slopes are horizontal, in which $\hat{\gamma} = -\hat{\mathbf{z}}$.

It is also useful to verify that $\hat{\mathbf{e}}_{\bar{3}} = \hat{\mathbf{e}}_{\bar{1}} \times \hat{\mathbf{e}}_{\bar{2}}$ through the following vector identity (see equation (1.40b))

$$(\hat{\mathbf{d}} \times \hat{\gamma}) \times [\hat{\gamma} \times (\hat{\mathbf{d}} \times \hat{\gamma})] = \hat{\gamma} |\hat{\mathbf{d}} \times \hat{\gamma}|^2. \quad (63.106)$$

The unit vectors $\hat{\mathbf{e}}_{\bar{1}}$ and $\hat{\mathbf{e}}_{\bar{2}}$ are both within the neutral tangent plane since they are both orthogonal to $\hat{\gamma}$.

The unit vector $\hat{\mathbf{e}}_{\bar{1}}$ is orthogonal to $\hat{\mathbf{d}}$ whereas $\hat{\mathbf{e}}_{\bar{2}}$ is parallel to $\hat{\mathbf{d}}$ if $\hat{\mathbf{d}} \cdot \hat{\gamma} = 0$. For example, [Smith and Gent \(2004\)](#) proposed setting $\hat{\mathbf{d}}$ to be a horizontal vector set according to the local horizontal flow direction, in which case

$$\hat{\mathbf{d}} = \frac{u \hat{\mathbf{x}} + v \hat{\mathbf{y}}}{(u^2 + v^2)^{1/2}}. \quad (63.107)$$

With $\hat{\gamma}$ nearly vertical for much of the ocean interior, then $\hat{\mathbf{e}}_{\bar{2}}$ becomes nearly aligned with $\hat{\mathbf{d}}$. For these reasons we refer to $\hat{\mathbf{e}}_{\bar{1}}$ as the across- $\hat{\mathbf{d}}$ direction and $\hat{\mathbf{e}}_{\bar{2}}$ as the along- $\hat{\mathbf{d}}$ direction.

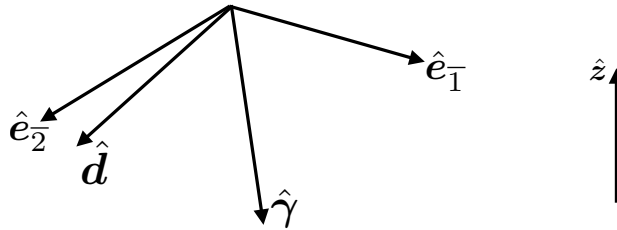


FIGURE 63.5: Depicting the orthonormal triad of basis vectors given by equations (63.102a)-(63.102c). Our convention is such that $\hat{\gamma}$ typically points downward toward increasing density. The unit vector $\hat{\mathbf{d}}$ is arbitrary so long as it is not parallel to the dianeutral unit vector, $\hat{\gamma}$. It is horizontal when making use of the [Smith and Gent \(2004\)](#) proposal whereby $\hat{\mathbf{d}} = \mathbf{u}/|\mathbf{u}|$, with $\mathbf{u} = \hat{\mathbf{x}} u + \hat{\mathbf{y}} v$ the horizontal velocity vector. Since $\hat{\mathbf{e}}_{\bar{1}}$ is orthogonal to $\hat{\mathbf{d}}$, we refer to $\hat{\mathbf{e}}_{\bar{1}}$ as the cross- $\hat{\mathbf{d}}$ basis vector. Likewise, since $\hat{\mathbf{e}}_{\bar{2}}$ is nearly parallel to $\hat{\mathbf{d}}$, especially when $\hat{\mathbf{d}}$ is close to horizontal and $\hat{\gamma}$ is close to vertical (e.g., Section 63.5.4), then $\hat{\mathbf{e}}_{\bar{2}}$ is referred to as the along- $\hat{\mathbf{d}}$ basis vector.

63.5.2 Anisotropic neutral diffusion tensor

We consider anisotropy according to the unit vectors $\hat{\mathbf{e}}_{\bar{1}}$ and $\hat{\mathbf{e}}_{\bar{2}}$. Hence, the diffusion tensor as represented using the locally orthogonal triad $(\hat{\mathbf{e}}_{\bar{1}}, \hat{\mathbf{e}}_{\bar{2}}, \hat{\mathbf{e}}_{\bar{3}})$ is given by

$$\bar{\mathbb{K}}_{\text{aniso}} = \begin{bmatrix} \kappa_{\text{cross}} & 0 & 0 \\ 0 & \kappa_{\text{along}} & 0 \\ 0 & 0 & 0 \end{bmatrix}, \quad (63.108)$$

where $\kappa_{\text{cross}} > 0$ and $\kappa_{\text{along}} > 0$ are the generally distinct neutral diffusivities. This tensor takes on the component form

$$\mathbb{K}_{\text{aniso}}^{\bar{m}\bar{n}} = \kappa_{\text{cross}} \hat{\mathbf{e}}_{\bar{1}}^{\bar{m}} \hat{\mathbf{e}}_{\bar{1}}^{\bar{n}} + \kappa_{\text{along}} \hat{\mathbf{e}}_{\bar{2}}^{\bar{m}} \hat{\mathbf{e}}_{\bar{2}}^{\bar{n}} \quad (63.109a)$$

$$= \kappa_{\text{cross}} (\delta^{\bar{m}\bar{n}} - \hat{\mathbf{e}}_{\bar{2}}^{\bar{m}} \hat{\mathbf{e}}_{\bar{2}}^{\bar{n}} - \hat{\mathbf{e}}_{\bar{3}}^{\bar{m}} \hat{\mathbf{e}}_{\bar{3}}^{\bar{n}}) + \kappa_{\text{along}} (\delta^{\bar{m}\bar{n}} - \hat{\mathbf{e}}_{\bar{1}}^{\bar{m}} \hat{\mathbf{e}}_{\bar{1}}^{\bar{n}} - \hat{\mathbf{e}}_{\bar{3}}^{\bar{m}} \hat{\mathbf{e}}_{\bar{3}}^{\bar{n}}), \quad (63.109b)$$

where the second expression made use of the following decomposition of the unit tensor in terms of the orthonormal basis vectors

$$\delta^{\bar{m}\bar{n}} = \hat{\mathbf{e}}_{\bar{1}}^{\bar{m}} \hat{\mathbf{e}}_{\bar{1}}^{\bar{n}} + \hat{\mathbf{e}}_{\bar{2}}^{\bar{m}} \hat{\mathbf{e}}_{\bar{2}}^{\bar{n}} + \hat{\mathbf{e}}_{\bar{3}}^{\bar{m}} \hat{\mathbf{e}}_{\bar{3}}^{\bar{n}}. \quad (63.110)$$

Note that $\mathbb{K}_{\text{aniso}}^{\overline{mn}}$ is invariant under $\hat{\mathbf{d}} \rightarrow -\hat{\mathbf{d}}$. Likewise, it is invariant under a change in the sign of $\hat{\boldsymbol{\gamma}}$. Furthermore, note that we recover the isotropic Redi diffusion tensor (63.72) by setting $\kappa_{\text{cross}} = \kappa_{\text{along}} = \kappa_{\text{ntr}}$ and in which case

$$\mathbb{K}_{\text{aniso}}^{\overline{mn}} = 2\kappa_{\text{ntr}}(\delta^{\overline{mn}} - \hat{e}_3^{\overline{m}}\hat{e}_3^{\overline{n}}) - \kappa_{\text{ntr}}(\hat{e}_1^{\overline{m}}\hat{e}_1^{\overline{n}} + \hat{e}_2^{\overline{m}}\hat{e}_2^{\overline{n}}) \quad (63.111\text{a})$$

$$= \kappa_{\text{ntr}}(\delta^{\overline{mn}} - \hat{e}_3^{\overline{m}}\hat{e}_3^{\overline{n}}) \quad (63.111\text{b})$$

$$= \mathbb{K}_{\text{redi}}^{\overline{mn}}. \quad (63.111\text{c})$$

To render a geopotential-Cartesian representation of the anisotropic diffusion tensor, we can make use of the transformation methods for Cartesian tensors developed in Section 1.7. We do so by transforming from the locally orthogonal neutral plane coordinate system, defined by the orthonormal triad (63.102a)-(63.102c), to the geopotential-Cartesian coordinate system, defined by the Cartesian triad

$$\hat{\mathbf{e}}_1 = \hat{\mathbf{x}} \quad \text{and} \quad \hat{\mathbf{e}}_2 = \hat{\mathbf{y}} \quad \text{and} \quad \hat{\mathbf{e}}_3 = \hat{\mathbf{z}}. \quad (63.112)$$

Since we are working with Cartesian tensors, this transformation is a local rotation matrix, \mathcal{R} , so that⁸

$$\mathbb{K}_{\text{aniso}}^{mn} = \mathcal{R}_{\overline{m}}^m \mathcal{R}_{\overline{n}}^n \mathbb{K}_{\text{aniso}}^{\overline{mn}} \implies \mathbb{K}_{\text{aniso}} = \mathcal{R} \bar{\mathbb{K}}_{\text{aniso}} \mathcal{R}^T, \quad (63.113)$$

where the second equality made use of matrix notation with \mathcal{R}^T the transpose, and where the elements to the rotation matrix are given by the direction cosines following equation (1.53)

$$\mathcal{R} = \begin{bmatrix} \hat{\mathbf{e}}^1 \cdot \hat{\mathbf{e}}_{\overline{1}} & \hat{\mathbf{e}}^1 \cdot \hat{\mathbf{e}}_{\overline{2}} & \hat{\mathbf{e}}^1 \cdot \hat{\mathbf{e}}_{\overline{3}} \\ \hat{\mathbf{e}}^2 \cdot \hat{\mathbf{e}}_{\overline{1}} & \hat{\mathbf{e}}^2 \cdot \hat{\mathbf{e}}_{\overline{2}} & \hat{\mathbf{e}}^2 \cdot \hat{\mathbf{e}}_{\overline{3}} \\ \hat{\mathbf{e}}^3 \cdot \hat{\mathbf{e}}_{\overline{1}} & \hat{\mathbf{e}}^3 \cdot \hat{\mathbf{e}}_{\overline{2}} & \hat{\mathbf{e}}^3 \cdot \hat{\mathbf{e}}_{\overline{3}} \end{bmatrix} = \begin{bmatrix} \hat{\mathbf{x}} \cdot \hat{\mathbf{e}}_{\overline{1}} & \hat{\mathbf{x}} \cdot \hat{\mathbf{e}}_{\overline{2}} & \hat{\mathbf{x}} \cdot \hat{\mathbf{e}}_{\overline{3}} \\ \hat{\mathbf{y}} \cdot \hat{\mathbf{e}}_{\overline{1}} & \hat{\mathbf{y}} \cdot \hat{\mathbf{e}}_{\overline{2}} & \hat{\mathbf{y}} \cdot \hat{\mathbf{e}}_{\overline{3}} \\ \hat{\mathbf{z}} \cdot \hat{\mathbf{e}}_{\overline{1}} & \hat{\mathbf{z}} \cdot \hat{\mathbf{e}}_{\overline{2}} & \hat{\mathbf{z}} \cdot \hat{\mathbf{e}}_{\overline{3}} \end{bmatrix}. \quad (63.114)$$

The machinery outlined here for the transformation is straightforward but tedious (i.e., two matrix multiplies). A more streamlined approach, also used for determining the Cartesian components to the Redi tensor (63.74), is to simply express $(\hat{\mathbf{e}}_{\overline{1}}, \hat{\mathbf{e}}_{\overline{2}}, \hat{\mathbf{e}}_{\overline{3}})$ using geopotential-Cartesian coordinates and then plug directly into equation (63.109b).

63.5.3 Properties of the anisotropic neutral diffusive fluxes

We here verify some standard properties for the anisotropic neutral diffusive flux for tracers

$$\mathbf{J}_{\text{aniso}} = -\rho \mathbb{K}_{\text{aniso}} \cdot \nabla C. \quad (63.115)$$

Downgradient orientation within the neutral tangent plane

By construction, the flux is downgradient along the two orthogonal directions, $\hat{\mathbf{e}}_{\overline{1}}$ and $\hat{\mathbf{e}}_{\overline{2}}$,

$$\mathbf{J}_{\text{aniso}} = -\rho \kappa_{\text{cross}} \hat{\mathbf{e}}_{\overline{1}} (\hat{\mathbf{e}}_{\overline{1}} \cdot \nabla C) - \rho \kappa_{\text{along}} \hat{\mathbf{e}}_{\overline{2}} (\hat{\mathbf{e}}_{\overline{2}} \cdot \nabla C). \quad (63.116)$$

Furthermore, the flux is within the neutral tangent plane

$$\mathbf{J}_{\text{aniso}} \cdot \hat{\boldsymbol{\gamma}} = 0 \quad (63.117)$$

⁸Since we are dealing with Cartesian tensors there is no distinction between raised or lowered tensor indices in equation (63.113). We choose to follow the convention of general tensors in Chapters 7 and 8 simply to help organize elements of the tensor.

due to orthogonality between the basis vectors

$$\hat{\mathbf{e}}_{\bar{1}} \cdot \hat{\boldsymbol{\gamma}} = \hat{\mathbf{e}}_{\bar{2}} \cdot \hat{\boldsymbol{\gamma}} = 0. \quad (63.118)$$

Neutrality condition

The neutrality condition (63.88) follows since

$$(-\alpha \nabla \Theta + \beta \nabla S) \cdot \hat{\mathbf{e}}_{\bar{1}} = (-\alpha \nabla \Theta + \beta \nabla S) \cdot \hat{\mathbf{e}}_{\bar{2}} = 0, \quad (63.119)$$

so that

$$\alpha \mathbf{J}_{\text{aniso}}(\Theta) = \beta \mathbf{J}_{\text{aniso}}(S). \quad (63.120)$$

63.5.4 Small slope anisotropic neutral diffusion

We now consider the special case in which the orientation direction, $\hat{\mathbf{d}}$, is strictly horizontal and normalized so that

$$\hat{\mathbf{d}} \cdot \hat{\mathbf{d}} = \hat{d}_x^2 + \hat{d}_y^2 = 1. \quad (63.121)$$

Additionally, we assume the neutral slope is small so that the neutral directions are nearly horizontal. In this case the basis vectors (63.102a)-(63.102c) take on the following form valid to $\mathcal{O}(|\mathbf{S}|)$

$$\hat{\mathbf{e}}_{\bar{1}\text{small}} = \hat{\mathbf{d}} \times (\mathbf{S} - \hat{\mathbf{z}}) \quad (63.122a)$$

$$\hat{\mathbf{e}}_{\bar{2}\text{small}} = \hat{\mathbf{d}} + \hat{\mathbf{z}} (\hat{\mathbf{d}} \cdot \mathbf{S}) \quad (63.122b)$$

$$\hat{\mathbf{e}}_{\bar{3}\text{small}} = \mathbf{S} - \hat{\mathbf{z}}. \quad (63.122c)$$

Note that $\hat{\mathbf{e}}_{\bar{3}\text{small}}$ is orthogonal to $\hat{\mathbf{e}}_{\bar{1}\text{small}}$ and $\hat{\mathbf{e}}_{\bar{2}\text{small}}$, however $\hat{\mathbf{e}}_{\bar{1}\text{small}} \cdot \hat{\mathbf{e}}_{\bar{2}\text{small}}$ is $\mathcal{O}(\mathbf{S} \cdot \mathbf{S})$. Likewise, each of these vectors is normalized only to $\mathcal{O}(\mathbf{S} \cdot \mathbf{S})$.

Making use of the small slope basis vectors in the anisotropic diffusion tensor (63.109a), and expressing them in geopotential-Cartesian coordinates leads to the small slope anisotropic neutral diffusion tensor⁹

$$\mathbb{K}_{\text{small aniso}} = \kappa_{\text{cross}} \begin{bmatrix} 1 & 0 & S_x \\ 0 & 1 & S_y \\ S_x & S_y & \mathbf{S} \cdot \mathbf{S} \end{bmatrix} + \Delta \kappa_{\text{ntr}} \begin{bmatrix} \hat{d}_x^2 & \hat{d}_x \hat{d}_y & (\hat{\mathbf{d}} \cdot \mathbf{S}) \hat{d}_x \\ \hat{d}_x \hat{d}_y & \hat{d}_y^2 & (\hat{\mathbf{d}} \cdot \mathbf{S}) \hat{d}_y \\ (\hat{\mathbf{d}} \cdot \mathbf{S}) \hat{d}_x & (\hat{\mathbf{d}} \cdot \mathbf{S}) \hat{d}_y & (\hat{\mathbf{d}} \cdot \mathbf{S})^2 \end{bmatrix}, \quad (63.123)$$

where

$$\Delta \kappa_{\text{ntr}} = \kappa_{\text{along}} - \kappa_{\text{cross}}. \quad (63.124)$$

As for the unapproximated anisotropic neutral diffusion tensor (63.109a), its small slope version, $\bar{\mathbb{K}}_{\text{small aniso}}$, is invariant if we swap the direction $\hat{\mathbf{d}} \rightarrow -\hat{\mathbf{d}}$. Furthermore, in the form (63.123) we trivially see that $\bar{\mathbb{K}}_{\text{small aniso}} = \bar{\mathbb{K}}_{\text{small}}$ (equation (63.75)) in the isotropic limit where $\kappa_{\text{cross}} = \kappa_{\text{along}} = \kappa_{\text{ntr}}$.

The anisotropic small slope neutral diffusive flux is given by

$$\mathbf{J}_{\text{small aniso}} = -\rho \mathbb{K}_{\text{small aniso}} \cdot \nabla C, \quad (63.125)$$

⁹Equation (63.123) agrees with equations (10) and (14) from [Smith and Gent \(2004\)](#).

with horizontal and vertical components

$$\mathbf{J}_{\text{small aniso}}^h = -\rho \kappa_{\text{cross}} \nabla_\gamma C - \rho \Delta \kappa_{\text{ntr}} \hat{\mathbf{d}} (\hat{\mathbf{d}} \cdot \nabla_\gamma) C \quad (63.126a)$$

$$J_{\text{small aniso}}^z = \mathbf{S} \cdot \mathbf{J}_{\text{small aniso}}^h, \quad (63.126b)$$

where $\nabla_\gamma = \nabla_z + \mathbf{S} \partial_z$ is the horizontal operator as per equation (63.77). By making use of the expression (63.19), $\hat{\gamma} = (\mathbf{S} - \hat{\mathbf{z}})(1 + \mathbf{S}^2)^{-1/2}$, we readily find that

$$\mathbf{J}_{\text{small aniso}} \cdot \hat{\gamma} = 0. \quad (63.127)$$

Similarly, we can verify that the neutrality condition (Section 63.4.5) is maintained

$$\mathbb{K}_{\text{small aniso}} \cdot \hat{\gamma} = 0 \implies \alpha \mathbf{J}_{\text{small aniso}}(\Theta) = \beta \mathbf{J}_{\text{small aniso}}(S). \quad (63.128)$$

Finally, as per the discussion in Section 63.4.4, we can evaluate the small slope anisotropic neutral diffusion operator by following the non-orthogonal neutral tangent approach rather than the three-dimensional Cartesian approach. It is the non-orthogonal neutral tangent approach that is appropriate for vertical Lagrangian ocean models such as detailed in [Griffies et al. \(2020\)](#) and [Shao et al. \(2020\)](#).

63.6 Anisotropic Gent-McWilliams stirring

In addition to proposing the use of a small slope anisotropic neutral diffusion tensor (equation (63.123)), [Smith and Gent \(2004\)](#) proposed a complementary anisotropic version of the Gent-McWilliams stirring. We here detail the parameterization, again assuming the orientation direction, $\hat{\mathbf{d}}$, is horizontal

$$\hat{\mathbf{d}} = \hat{\mathbf{x}} \hat{d}_x + \hat{\mathbf{y}} \hat{d}_y, \quad (63.129)$$

just as assumed when discussing the anisotropic small slope neutral diffusion operator in Section 63.5.4.

63.6.1 Streamfunction and anti-symmetric tensor

The parameterized eddy-induced streamfunction is generalized from that in equation (63.28) to read

$$\Psi^* = \hat{\mathbf{z}} \times \kappa_{\text{gm-cross}} \mathbf{S} + \hat{\mathbf{z}} \times (\kappa_{\text{gm-cross}} - \kappa_{\text{gm-along}}) (\hat{\mathbf{d}} \cdot \mathbf{S}) \hat{\mathbf{d}}, \quad (63.130)$$

and the corresponding anti-symmetric stirring tensor is

$$\mathbb{A}_{\text{gm-aniso}} = \kappa_{\text{gm-cross}} \begin{bmatrix} 0 & 0 & -S_x \\ 0 & 0 & -S_y \\ S_x & S_y & 0 \end{bmatrix} + \Delta \kappa_{\text{gm}} (\hat{\mathbf{d}} \cdot \mathbf{S}) \begin{bmatrix} 0 & 0 & -\hat{d}_x \\ 0 & 0 & -\hat{d}_y \\ \hat{d}_x & \hat{d}_y & 0 \end{bmatrix}, \quad (63.131)$$

where

$$\Delta \kappa_{\text{gm}} = \kappa_{\text{gm-along}} - \kappa_{\text{gm-cross}}. \quad (63.132)$$

As for the small slope anisotropic neutral diffusion tensor (63.123), we write the skew tensor $\mathbb{A}_{\text{gm-aniso}}$ in equation (63.131) in a form that manifestly reduces to the isotropic Gent-McWilliams stirring tensor \mathbb{A}_{gm} when $\kappa_{\text{gm-along}} = \kappa_{\text{gm-cross}} = \kappa_{\text{gm}}$.

63.6.2 Anisotropic Gent-McWilliams skew tracer flux

The anisotropic Gent-McWilliams skew tracer flux is

$$\mathbf{J}_{\text{gm-aniso}} = -\rho \mathbb{A}_{\text{gm-aniso}} \cdot \nabla C \quad (63.133a)$$

$$= \rho \kappa_{\text{gm-cross}} [\mathbf{S} \partial_z C - \hat{\mathbf{z}} (\mathbf{S} \cdot \nabla_z C)] + \rho \Delta \kappa_{\text{gm}} (\hat{\mathbf{d}} \cdot \mathbf{S}) [\hat{\mathbf{d}} \partial_z C - \hat{\mathbf{z}} (\hat{\mathbf{d}} \cdot \nabla_z C)]. \quad (63.133b)$$

When acting on locally referenced potential density, $C = \gamma$, the flux reduces to

$$\mathbf{J}_{\text{gm-aniso}} = \rho \kappa_{\text{gm-cross}} [-\nabla_z \gamma + \hat{\mathbf{z}} \mathbf{S}^2 \partial_z \gamma] + \rho \Delta \kappa_{\text{gm}} (\mathbf{d} \cdot \mathbf{S}) [\hat{\mathbf{d}} + \hat{\mathbf{z}} (\hat{\mathbf{d}} \cdot \mathbf{S})] \partial_z \gamma. \quad (63.134)$$

As discussed in Section 63.3.3, a negative vertical component to the potential density skew flux ensures that the available potential energy is dissipated,

$$\hat{\mathbf{z}} \cdot \mathbf{J}_{\text{gm-aniso}} = \rho [\kappa_{\text{gm-cross}} \mathbf{S}^2 + \Delta \kappa_{\text{gm}} (\mathbf{d} \cdot \mathbf{S})^2] \partial_z \gamma < 0 \implies \text{APE dissipated}. \quad (63.135)$$

Stably stratified water means that $\partial_z \gamma < 0$, in which case $\hat{\mathbf{z}} \cdot \mathbf{J}_{\text{gm-aniso}} < 0$ since

$$\kappa_{\text{gm-cross}} \mathbf{S}^2 + \Delta \kappa_{\text{gm}} (\mathbf{d} \cdot \mathbf{S})^2 = \kappa_{\text{gm-cross}} [\mathbf{S}^2 - (\hat{\mathbf{d}} \cdot \mathbf{S})^2] + \kappa_{\text{gm-along}} (\hat{\mathbf{d}} \cdot \mathbf{S})^2 > 0. \quad (63.136)$$

63.6.3 Anisotropic GM skewson plus small slope neutral diffusion

As noted in Section 63.4.7, there are strong reasons to keep the Gent-McWilliams skew flux parameterization distinct from the neutral diffusion parameterization. The central practical reason for the distinction concerns their different treatment of boundary conditions and generally distinct diffusivities. Even so, we here briefly comment on the special case where we ignore these distinctions and set the skew flux and neutral diffusivities the same

$$\kappa_{\text{gm-cross}} = \kappa_{\text{cross}} \quad \text{and} \quad \kappa_{\text{gm-along}} = \kappa_{\text{along}}. \quad (63.137)$$

This is the approach assumed by [Smith and Gent \(2004\)](#). With the small slope approximation to neutral diffusion, we find the combined anisotropic mixing tensor becomes

$$\begin{aligned} \mathbb{K}_{\text{small aniso}} + \mathbb{A}_{\text{gm-aniso}} = \\ \kappa_{\text{cross}} \begin{bmatrix} 1 & 0 & 0 \\ 0 & 1 & 0 \\ 2 S_x & 2 S_y & \mathbf{S} \cdot \mathbf{S} \end{bmatrix} + \Delta \kappa \begin{bmatrix} \hat{d}_x^2 & \hat{d}_x \hat{d}_y & 0 \\ \hat{d}_x \hat{d}_y & \hat{d}_y^2 & 0 \\ 2(\hat{\mathbf{d}} \cdot \mathbf{S}) \hat{d}_x & 2(\hat{\mathbf{d}} \cdot \mathbf{S}) \hat{d}_y & (\hat{\mathbf{d}} \cdot \mathbf{S})^2 \end{bmatrix}. \end{aligned} \quad (63.138)$$

The vanishing right hand column terms simplifies the horizontal tracer fluxes computed from this tensor. However, again, this formulation lacks support from theory that supports the distinct treatments of the skew flux and neutral flux.

63.6.4 A parameterization based on a boundary value problem

We now follow the approach from Section 63.3.8 to develop a boundary value problem version of the anisotropic Gent-McWilliams stirring. For this purpose we consider the vertical boundary value problem

$$c^2 \frac{d^2 \boldsymbol{\Upsilon}}{dz^2} - N^2 \boldsymbol{\Upsilon} = -N^2 \boldsymbol{\Upsilon}_{\text{gm-aniso}} \quad \text{and} \quad \boldsymbol{\Upsilon}(\eta_b) = \boldsymbol{\Upsilon}(\eta) = 0, \quad (63.139)$$

where (see equation (63.130))

$$\boldsymbol{\Upsilon}^{\text{gm-aniso}} = \kappa_{\text{gm-cross}} \mathbf{S} + \hat{\mathbf{z}} \times \Delta \kappa_{\text{gm}} (\hat{\mathbf{d}} \cdot \mathbf{S}) \hat{\mathbf{d}}. \quad (63.140)$$

As in Section 63.3.8, we deduce the impacts on potential energy (assuming a linear equation of state) via the vertical component of the potential density skew flux,

$$\frac{1}{g} \frac{dP}{dt} = \frac{1}{\rho_0} \int J^z dV = - \int \nabla_z \varrho \cdot \boldsymbol{\Upsilon} dV. \quad (63.141)$$

The governing differential equation (63.139) leads to

$$\boldsymbol{\Upsilon} \cdot \left[c^2 \frac{d^2 \boldsymbol{\Upsilon}}{dz^2} - N^2 \boldsymbol{\Upsilon} \right] = -N^2 \boldsymbol{\Upsilon} \cdot \boldsymbol{\Upsilon}^{\text{gm-aniso}} \quad (63.142)$$

which rearranges to

$$N^2 \boldsymbol{\Upsilon} \cdot \boldsymbol{\Upsilon}^{\text{gm-aniso}} = -c^2 \frac{d(\boldsymbol{\Upsilon} \cdot \boldsymbol{\Upsilon}')}{dz} + c^2 \boldsymbol{\Upsilon}' \cdot \boldsymbol{\Upsilon}' + N^2 \boldsymbol{\Upsilon} \cdot \boldsymbol{\Upsilon}. \quad (63.143)$$

Integrating over a vertical column and making use of the homogeneous Dirichlet boundary conditions in equation (63.139) leads to

$$\frac{g}{\rho_0} \int \boldsymbol{\Upsilon} \cdot \nabla_z \varrho dz = - \int N^2 \Delta \kappa_{\text{gm}} (\hat{\mathbf{d}} \cdot \mathbf{S}) (\hat{\mathbf{d}} \cdot \boldsymbol{\Upsilon}) dz + \int [c^2 \boldsymbol{\Upsilon}' \cdot \boldsymbol{\Upsilon}' + N^2 \boldsymbol{\Upsilon} \cdot \boldsymbol{\Upsilon}] dz, \quad (63.144)$$

which can be rearranged into the equivalent form

$$\begin{aligned} & \frac{g}{\rho_0} \int \boldsymbol{\Upsilon} \cdot \nabla_z \varrho dz \\ &= \underbrace{\int [c^2 \boldsymbol{\Upsilon}' \cdot \boldsymbol{\Upsilon}' + N^2 (\boldsymbol{\Upsilon} \cdot \boldsymbol{\Upsilon} - (\hat{\mathbf{d}} \cdot \boldsymbol{\Upsilon})^2)] dz}_{\text{positive semi-definite}} + \underbrace{\int N^2 (\hat{\mathbf{d}} \cdot \boldsymbol{\Upsilon}) \hat{\mathbf{d}} \cdot (\boldsymbol{\Upsilon} - \mathbf{S} \Delta \kappa_{\text{gm}}) dz}_{\text{sign indefinite}}. \end{aligned} \quad (63.145)$$

The first term on the right hand side is positive semi-indefinite whereas the second term is sign indefinite. If the second term is positive, or smaller in magnitude than the first term, then the parameterization provides a column integrated sink of potential energy. Otherwise, potential energy for the column can increase. There are no existing numerical implementations of this scheme to determine its suitability for realistic ocean climate simulations.



Chapter 64

OCEAN DENSITY AND SEA LEVEL

Conservative temperature, Θ , is the preferred means to measure the transport of enthalpy in the ocean, and salinity, S , measures the concentration of dissolved salt matter. These two scalar fields are referred to as *active* tracers as they both impact density and in turn affect pressure and ocean currents. In this chapter we study how the evolution of Θ and S affects density. Θ and S are conservative tracers so that the net changes in potential enthalpy and salt over the global ocean domain arise from net imbalances in their boundary fluxes. Likewise, ocean mass is a conserved field, with global mass changes arising from imbalances in boundary mass fluxes such as those occurring from increases in land ice melt. However, ocean volume, and hence ocean density and buoyancy, are not conserved fields. These points have direct impact on how global mean sea level is affected by ocean processes such as mixing, with rudiments presented in this chapter.

CHAPTER GUIDE

Basic notions of thermodynamics, such as Section 23.9, motivate the use of Conservative Temperature as a measure of ocean enthalpy transfer, rather than *in situ* temperature. The material in this chapter considers how we measure air-sea buoyancy fluxes and analyze changes to global mean sea level. Both of these topics are increasingly important for studies of anthropogenic climate change.

64.1 Loose threads	1604
64.2 Material evolution of <i>in situ</i> density	1604
64.2.1 Material changes to pressure	1605
64.2.2 Material changes to Θ and S	1605
64.2.3 General expression for density changes	1605
64.2.4 Unpacking the subgrid contributions	1606
64.2.5 Synthesis of the density equation	1608
64.3 Cabbeling and thermobaricity	1609
64.3.1 Basic manipulations	1609
64.3.2 A tidy form	1610
64.3.3 Cabbeling	1611
64.3.4 Thermobaricity	1611
64.3.5 Comments	1612
64.4 Salt and freshwater budgets	1612
64.4.1 Salt and freshwater	1612
64.4.2 Mass budgets	1613
64.5 Surface boundary conditions for S and Θ	1614
64.5.1 Salt and freshwater	1614
64.5.2 The non-advection salt flux boundary condition	1615
64.5.3 Conservative Temperature boundary condition	1617

64.5.4	Comments and further reading	1617
64.6	Surface boundary fluxes of buoyancy	1617
64.6.1	Outlining the boundary fluxes of enthalpy and salt	1618
64.6.2	Evolution from surface boundary fluxes	1618
64.6.3	Buoyancy tendency from surface boundary fluxes	1619
64.6.4	Comments	1620
64.7	Global mean sea level	1620
64.7.1	Definitions and assumptions	1620
64.7.2	Budget for global mean sea level	1621
64.7.3	Changes due to mass input	1622
64.7.4	Steric changes due to changes in density	1622
64.7.5	Enthalpy flux imbalances giving rise to thermosteric sea level	1623
64.7.6	Global sea level in a Boussinesq ocean	1623
64.7.7	Why global halosteric sea level changes are negligible	1624
64.7.8	Further study	1626

64.1 Loose threads

- Schematics for cabbeling and thermobaricity.

64.2 Material evolution of *in situ* density

Changes to the *in situ* density of seawater affects pressure forces in the ocean as well as the volume occupied by the ocean fluid (i.e., sea level). As discussed in Section 27.3.2, it is common to write the seawater equation of state for density as a function of potential temperature, salinity, and pressure. A somewhat more accurate approach makes use of the Conservative Temperature rather than the potential temperature, where the Conservative Temperature, Θ , is the potential enthalpy divided by a constant heat capacity ([McDougall, 2003](#); [IOC et al., 2010](#)). We thus make use of the empirical relation for the seawater density in the functional form

$$\rho = \rho(\Theta, S, p), \quad (64.1)$$

where S is the salinity rather than the salt concentration ($S = 1000 \text{ S}$).

We formulate the material evolution of density as weighted by the specific volume¹

$$\nu = \rho^{-1}, \quad (64.2)$$

so that we study

$$\frac{D \ln \rho}{Dt} = \frac{\partial \ln \rho}{\partial \Theta} \frac{D\Theta}{Dt} + \frac{\partial \ln \rho}{\partial S} \frac{DS}{Dt} + \frac{\partial \ln \rho}{\partial p} \frac{Dp}{Dt} \quad (64.3a)$$

$$= -\alpha \frac{D\Theta}{Dt} + \beta \frac{DS}{Dt} + \frac{\dot{p}}{\rho c_s^2}. \quad (64.3b)$$

In this equation we introduced the thermal expansion coefficient, the haline contraction coefficient,

¹In other chapters we write the specific volume as $\nu_s = 1/\rho$ to distinguish it from ν that is used for kinematic viscosity. However, in this chapter we write $\nu = 1/\rho$ to enable a shorthand for partial derivatives as defined by equation (64.8). We have no use kinematic viscosity in this chapter.

the squared speed of sound, and the vertical pseudo-velocity in pressure

$$\alpha = - \left[\frac{\partial \ln \rho}{\partial \Theta} \right]_{p,S} \quad \beta = \left[\frac{\partial \ln \rho}{\partial S} \right]_{p,\Theta} \quad c_s^2 = \left[\frac{\partial p}{\partial \rho} \right]_{S,\Theta} \quad \dot{p} = \frac{Dp}{Dt}. \quad (64.4)$$

For the remainder of this section we unpack the processes contributing to the density material time evolution (64.3).

64.2.1 Material changes to pressure

To garner some exposure to the physics of \dot{p} as it appears in equation (64.3), we consider the special case of a hydrostatic fluid, where the volume per time per horizontal area of fluid crossing a surface of constant hydrostatic pressure is given by (see Section 57.4.6)

$$w^{(p)} = \frac{\partial z}{\partial p} \frac{Dp}{Dt} = -(\rho g)^{-1} \dot{p}. \quad (64.5)$$

The transport measured by $w^{(p)}$ is the pressure-coordinate analog of the vertical velocity component $w = Dz/Dt$ in a geopotential coordinate representation of the vertical. That is, fluid moving into regions of increasing hydrostatic pressure ($\dot{p} > 0$) represents downward movement of fluid, with $w^{(p)} < 0$ in this case. Conversely, motion into decreasing hydrostatic pressure represents upward motion, with $w^{(p)} > 0$. This vertical movement generally occurs in the presence of waves, currents, and mixing; i.e., both reversible and irreversible processes give rise to vertical motion.

64.2.2 Material changes to Θ and S

We now focus on the salinity and temperature contributions to the evolution of *in situ* density. To do so, assume that the material evolution of Θ and S are given by the convergence of a subgrid scale flux

$$\rho \frac{D\Theta}{Dt} = -\nabla \cdot \mathbf{J}^{(\Theta)} \quad (64.6a)$$

$$\rho \frac{DS}{Dt} = -\nabla \cdot \mathbf{J}^{(S)}. \quad (64.6b)$$

The Conservative Temperature equation (64.6a) was derived in Section 23.9, whereas the Absolute Salinity equation (64.6b) follows from our derivation of the tracer equation in Section 17.1.²

64.2.3 General expression for density changes

The expressions (64.6a) and (64.6b) for material changes in Θ and S then lead to

$$-\alpha \frac{D\Theta}{Dt} + \beta \frac{DS}{Dt} = \nu_\Theta \nabla \cdot \mathbf{J}^{(\Theta)} + \nu_S \nabla \cdot \mathbf{J}^{(S)} \quad (64.7a)$$

$$= \nabla \cdot [\nu_\Theta \mathbf{J}^{(\Theta)} + \nu_S \mathbf{J}^{(S)}] - [\mathbf{J}^{(\Theta)} \cdot \nabla \nu_\Theta + \mathbf{J}^{(S)} \cdot \nabla \nu_S] \quad (64.7b)$$

where again $\nu = \rho^{-1}$ is the specific volume and its partial derivatives are

$$\nu_\Theta = \frac{\partial \nu}{\partial \Theta} = \frac{\alpha}{\rho} \quad \text{and} \quad \nu_S = \frac{\partial \nu}{\partial S} = -\frac{\beta}{\rho}. \quad (64.8)$$

²We here ignore remineralization processes that can contribute to a source term in the salinity equation (64.6b). Such source terms are discussed in [IOC et al. \(2010\)](#).

Bringing the above results together leads to the density equation

$$\frac{D \ln \rho}{Dt} - \frac{\dot{p}}{\rho c_s^2} = \nabla \cdot [\nu_\Theta \mathbf{J}^{(\Theta)} + \nu_S \mathbf{J}^{(S)}] - [\mathbf{J}^{(\Theta)} \cdot \nabla \nu_\Theta + \mathbf{J}^{(S)} \cdot \nabla \nu_S], \quad (64.9)$$

which has the equivalent form

$$\frac{D \rho}{Dt} - \frac{\dot{p}}{c_s^2} = \nabla \cdot [\alpha \mathbf{J}^{(\Theta)} - \beta \mathbf{J}^{(S)}] - [\mathbf{J}^{(\Theta)} \cdot \nabla \alpha - \mathbf{J}^{(S)} \cdot \nabla \beta]. \quad (64.10)$$

We brought the source term from motion across pressure surfaces (Section 64.2.1) onto the left hand side, as this term appears in the absence of subgrid processes. The first term on the right hand side represents the divergence of a buoyancy flux due to subgrid scale fluxes of Conservative Temperature and salinity. In turn, density increases in regions where the buoyancy flux diverges (e.g., Θ reducing and S increasing). These fluxes arise from a variety of mixing processes, some of which are surveyed in Section 63.1.1. The second term on the right hand side of equations (64.9) and (64.10) relates to properties of the locally referenced potential density surface. We study this source term arising from neutral diffusion in Section 64.3, where we encounter cabbeling and thermobaricity. Further effects arise from unresolved eddy-induced stirring, with that process contributing to the material time derivative operator to render a residual mean velocity (Section 63.1.4).

64.2.4 Unpacking the subgrid contributions

Recall from Section 63.1 that the subgrid scale fluxes are generally written in terms of a second order mixing tensor, \mathbb{M} ,

$$\mathbf{J}^{(\Theta)} = -\rho \mathbb{M} \cdot \nabla \Theta \quad \text{and} \quad \mathbf{J}^{(S)} = -\rho \mathbb{M} \cdot \nabla S. \quad (64.11)$$

Furthermore, \mathbb{M} is typically decomposed as in equation (63.8) into its symmetric diffusion tensor, \mathbb{K} , and anti-symmetric stirring tensor, \mathbb{A} ,

$$\mathbb{M} = \mathbb{K} + \mathbb{A}. \quad (64.12)$$

We decompose the contributions to density according to these subgrid stirring and diffusion processes via the following manipulations

$$\frac{D \rho}{Dt} - \frac{\dot{p}}{c_s^2} = \alpha \nabla \cdot \mathbf{J}^{(\Theta)} - \beta \nabla \cdot \mathbf{J}^{(S)} \quad (64.13a)$$

$$= -\alpha \nabla \cdot (\rho \mathbb{M} \cdot \nabla \Theta) + \beta \nabla \cdot (\rho \mathbb{M} \cdot \nabla S). \quad (64.13b)$$

Expanding the Θ term leads to

$$\alpha \nabla \cdot \mathbf{J}^{(\Theta)} = -\alpha \nabla \cdot (\rho \mathbb{M} \cdot \nabla \Theta) \quad (64.14a)$$

$$= -\alpha \nabla \cdot (\rho \mathbb{A} \cdot \nabla \Theta) - \alpha \nabla \cdot (\rho \mathbb{K} \cdot \nabla \Theta) \quad (64.14b)$$

$$= -\alpha \nabla \cdot (\rho \mathbb{A}) \cdot \nabla \Theta - \alpha \nabla \cdot (\rho \mathbb{K} \cdot \nabla \Theta), \quad (64.14c)$$

$$= -\alpha \mathbf{v}^* \cdot \nabla \Theta - \alpha \nabla \cdot (\rho \mathbb{K} \cdot \nabla \Theta). \quad (64.14d)$$

To reach this result we made use of the identities

$$\nabla \cdot (\rho \mathbb{A} \cdot \nabla \Theta) = \partial_m(\rho \mathbb{A}^{mn} \partial_n \Theta) \quad \text{expose tensor indices} \quad (64.15a)$$

$$= \partial_m(\rho \mathbb{A}^{mn}) \partial_n \Theta + \rho \mathbb{A}^{mn} \partial_m \partial_n \Theta \quad \text{product rule} \quad (64.15b)$$

$$= \partial_m(\rho \mathbb{A}^{mn}) \partial_n \Theta \quad \mathbb{A}^{mn} \partial_m \partial_n \Theta = 0 \quad (64.15c)$$

$$= -\rho \mathbf{v}^* \cdot \nabla \Theta \quad \partial_m(\rho \mathbb{A}^{mn}) = -\rho \mathbf{v}^{*n}. \quad (64.15d)$$

In the final equality we introduced the density weighted eddy-induced velocity, $\rho \mathbf{v}^*$, defined by equation (63.11). The same manipulations for the salinity term lead to

$$\frac{D\rho}{Dt} - \frac{\dot{p}}{c_s^2} + \rho \mathbf{v}^* \cdot (-\alpha \nabla \Theta + \beta \nabla S) = -\alpha \nabla \cdot (\rho \mathbb{K} \cdot \nabla \Theta) + \beta \nabla \cdot (\rho \mathbb{K} \cdot \nabla S). \quad (64.16)$$

We can write this expression in terms of the residual mean material time operator

$$\frac{D^\dagger}{Dt} = \frac{D}{Dt} + \mathbf{v}^* \cdot \nabla, \quad (64.17)$$

through adding and subtracting $c_s^{-2} \mathbf{v}^* \cdot \nabla p$

$$\rho \mathbf{v}^* \cdot (-\alpha \nabla \Theta + \beta \nabla S) = \mathbf{v}^* \cdot (-\rho \alpha \nabla \Theta + \rho \beta \nabla S + c_s^{-2} \nabla p) - c_s^{-2} \mathbf{v}^* \cdot \nabla p = \mathbf{v}^* \cdot (\nabla \rho - c_s^{-2} \nabla p), \quad (64.18)$$

which then leads to

$$\frac{D\rho}{Dt} - \frac{\dot{p}}{c_s^2} + \rho \mathbf{v}^* \cdot (-\alpha \nabla \Theta + \beta \nabla S) = \frac{D^\dagger \rho}{Dt} - \frac{1}{c_s^2} \frac{D^\dagger p}{Dt}, \quad (64.19)$$

so that

$$\frac{D^\dagger \rho}{Dt} - \frac{1}{c_s^2} \frac{D^\dagger p}{Dt} = -\alpha \nabla \cdot (\rho \mathbb{K} \cdot \nabla \Theta) + \beta \nabla \cdot (\rho \mathbb{K} \cdot \nabla S). \quad (64.20)$$

Transport from the symmetric tensor, \mathbb{K} , corresponds to diffusion so long as the tensor is positive definite. The diffusion operator in the residual mean evolution equation (64.20) can be written

$$-\alpha \nabla \cdot (\rho \mathbb{K} \cdot \nabla \Theta) + \beta \nabla \cdot (\rho \mathbb{K} \cdot \nabla S) = \nabla \cdot [\rho \mathbb{K} \cdot (-\alpha \nabla \Theta + \beta \nabla S)] + \rho \nabla \alpha \cdot \mathbb{K} \cdot \nabla \Theta - \rho \nabla \beta \cdot \mathbb{K} \cdot \nabla S, \quad (64.21)$$

so that the *in situ* density evolves according to

$$\frac{D^\dagger \rho}{Dt} - \frac{1}{c_s^2} \frac{D^\dagger p}{Dt} = -\underbrace{\nabla \cdot [\rho \mathbb{K} \cdot (\alpha \nabla \Theta - \beta \nabla S)]}_{\text{conservative processes}} + \underbrace{\rho \nabla \alpha \cdot \mathbb{K} \cdot \nabla \Theta - \rho \nabla \beta \cdot \mathbb{K} \cdot \nabla S}_{\text{sources from nonlinear EOS processes}}. \quad (64.22)$$

We now discuss the physical processes associated with the right hand side terms.

- LINEAR EQUATION OF STATE: A linear equation of state has $\nabla \alpha = \nabla \beta = 0$ and is independent of pressure, so that the evolution equation (64.22) takes the form

$$\frac{D^\dagger \rho}{Dt} = -\nabla \cdot [\rho \mathbb{K} \cdot (\alpha \nabla \Theta - \beta \nabla S)]. \quad (64.23)$$

Under the residual mean transport with a linear equation of state, density remains materially constant in the absence of any diffusion.

- NONLINEAR EQUATION OF STATE: A nonlinear equation of state is characterized by spatially

dependent thermal expansion and haline contraction coefficients. Mixing of Θ and S in the presence of a nonlinear equation of state generally gives rise to material evolution of *in situ* density through cabbeling and thermobaricity ([McDougall, 1987b](#)). We offer a summary of these processes in Section 64.3.

- NEUTRAL DIFFUSION:

Neutral diffusion from Section 63.4 maintains a density-compensated diffusive flux of Θ and S so that

$$\mathbb{K}_{\text{neutral}} \cdot (\alpha \nabla \Theta - \beta \nabla S) = 0. \quad (64.24)$$

Hence, neutral diffusion leaves *in situ* density changed only via the nonlinear equation of state processes.

- ISOTROPIC SMALL SCALE DIFFUSION:

As discussed in Section 63.1.3, it is common to parameterize fine scale mixing processes using an isotropic diffusivity so that the diffusion tensor is given by

$$\mathbb{K}_{\text{isotropic}} = \kappa \mathbb{I}, \quad (64.25)$$

where \mathbb{I} is the unit tensor and $\kappa > 0$ is the isotropic eddy diffusivity.

64.2.5 Synthesis of the density equation

In summary, the material time evolution equation for *in situ* density in the presence of subgrid scale processes takes the form

$$\frac{D\rho}{Dt} = \underbrace{\frac{1}{c_s^2} \frac{Dp}{Dt}}_{\text{compressibility}} - \underbrace{\mathbf{v}^* \cdot (-\alpha \nabla \Theta + \beta \nabla S)}_{\text{eddy-induced stirring}} - \underbrace{\nabla \cdot [\rho \kappa (-\alpha \nabla \Theta + \beta \nabla S)]}_{\text{small scale diffusive mixing}} + \underbrace{\rho \nabla \alpha \cdot \mathbb{K} \cdot \nabla \Theta - \rho \nabla \beta \cdot \mathbb{K} \cdot \nabla S}_{\text{nonlinear EOS processes from eddy mixing}}. \quad (64.26)$$

We thus have the following physical processes contributing to the evolution of *in situ* density.

- ADIABATIC COMPRESSION: Material changes to pressure in the presence of a finite sound speed lead to changes in the fluid density.
- SMALL SCALE MIXING: Small scale mixing is parameterized by an isotropic diffusivity, κ . This diffusivity is the same for all tracers, with the exception of double-diffusive processes whereby material tracers (e.g., salinity, nutrients) have a diffusivity distinct from temperature ([Schmitt, 1994](#)). Given the dominance of vertical stratification over the horizontal, it is common to approximate the isotropic diffusion operator with a vertical diffusion operator (but see Section 4 of [McDougall et al. \(2014\)](#) for caveats).
- EDDY-INDUCED STIRRING: For subgrid scale stirring, such as from mesoscale (and submesoscale) eddies, we introduce a parameterized eddy-induced advection operator. When combined with the resolved advection, we are led to a residual mean material time derivative, D^\dagger/Dt .
- EDDY-INDUCED DIFFUSION: Subgrid scale eddy-induced stirring leads to a direct cascade of Θ and S variance to the small scales. Mixing arising from this cascade is parameterized by neutral diffusion, whereby the diffusive fluxes of Θ and S are density compensated according to the constraint (64.24).

- NONLINEAR EOS PROCESSES: Mixing of Θ and S in the presence of a nonlinear equation of state means that *in situ* density evolves due to cabbeling and thermobaricity (Section 64.3). The dominant contributions to these processes arise from eddy-stirring induced mixing (i.e., neutral diffusion) (McDougall, 1987b), though small scale mixing also has a contribution.

64.3 Cabbeling and thermobaricity

We now return to the density equation (64.10)

$$\frac{D \ln \rho}{Dt} - \frac{\dot{p}}{\rho c_s^2} = \nabla \cdot [\nu_\Theta \mathbf{J}^{(\Theta)} + \nu_S \mathbf{J}^{(S)}] - (\mathbf{J}^{(\Theta)} \cdot \nabla \nu_\Theta + \mathbf{J}^{(S)} \cdot \nabla \nu_S), \quad (64.27)$$

and here focus on temperature and salinity fluxes just from the neutral diffusion process described in Section 63.4. The neutrality condition (63.88) is a fundamental property of neutral diffusion, and it takes the following form in terms of specific volume

$$\nu_\Theta \mathbf{J}^{(\Theta)} + \nu_S \mathbf{J}^{(S)} = 0. \quad (64.28)$$

Consequently, neutral diffusion affects density evolution only through the source term

$$\left[\frac{D \ln \rho}{Dt} \right]_{\text{ntral diff}} = -\mathbf{J}^{(\Theta)} \cdot \nabla \nu_\Theta - \mathbf{J}^{(S)} \cdot \nabla \nu_S. \quad (64.29)$$

In the remainder of this section we manipulate this expression in order to more clearly identify the variety of physical processes associated with neutral diffusion in the presence of a nonlinear equation of state.

64.3.1 Basic manipulations

As a first step, eliminate the salt flux by using the neutrality condition (64.28)

$$\mathbf{J}^{(\Theta)} \cdot \nabla \nu_\Theta + \mathbf{J}^{(S)} \cdot \nabla \nu_S = \mathbf{J}^{(\Theta)} \cdot [\nu_S \nabla \nu_\Theta - \nu_\Theta \nabla \nu_S]/\nu_S. \quad (64.30)$$

Next, expand the gradients of the specific volume to write

$$\nabla \nu_\Theta = \nu_{\Theta\Theta} \nabla \Theta + \nu_{\Theta S} \nabla S + \nu_{\Theta p} \nabla p \quad \text{and} \quad \nabla \nu_S = \nu_{SS} \nabla S + \nu_{\Theta S} \nabla \Theta + \nu_{Sp} \nabla p, \quad (64.31)$$

so that

$$\begin{aligned} \nu_S \nabla \nu_\Theta - \nu_\Theta \nabla \nu_S &= \nabla \Theta (\nu_S \nu_{\Theta\Theta} - \nu_\Theta \nu_{\Theta S}) \\ &\quad + \nabla S (\nu_S \nu_{\Theta S} - \nu_\Theta \nu_{SS}) + \nabla p (\nu_S \nu_{Sp} - \nu_\Theta \nu_{Sp}). \end{aligned} \quad (64.32)$$

We again make use of the neutrality condition (64.28), as well as the symmetry condition (63.89d) to write

$$\mathbf{J}^{(\Theta)} \cdot \nabla S (\nu_S \nu_{\Theta S} - \nu_\Theta \nu_{SS}) = -\mathbf{J}^{(\Theta)} \cdot \nabla \Theta \left[\nu_\Theta \nu_{\Theta S} - \nu_{SS} \frac{(\nu_\Theta)^2}{\nu_S} \right]. \quad (64.33)$$

Bringing these results together leads to

$$\begin{aligned} \mathbf{J}^{(\Theta)} \cdot \nabla \nu_{\Theta} + \mathbf{J}^{(S)} \cdot \nabla \nu_S &= \mathbf{J}^{(\Theta)} \cdot \nabla p \left[\nu_{\Theta p} - \nu_{pS} \frac{\nu_{\Theta}}{\nu_S} \right] \\ &\quad + \mathbf{J}^{(\Theta)} \cdot \nabla \Theta \left[\nu_{\Theta \Theta} - 2 \nu_{\Theta S} \frac{\nu_{\Theta}}{\nu_S} + \nu_{SS} \left(\frac{\nu_{\Theta}}{\nu_S} \right)^2 \right], \end{aligned} \quad (64.34)$$

which can be written in terms of density partial derivatives as

$$\begin{aligned} \mathbf{J}^{(\Theta)} \cdot \nabla \nu_{\Theta} + \mathbf{J}^{(S)} \cdot \nabla \nu_S &= -\rho^{-2} \mathbf{J}^{(\Theta)} \cdot \nabla p \left[\rho_{\Theta p} - \rho_{pS} \frac{\rho_{\Theta}}{\rho_S} \right] \\ &\quad - \rho^{-2} \mathbf{J}^{(\Theta)} \cdot \nabla \Theta \left[\rho_{\Theta \Theta} - 2 \rho_{\Theta S} \frac{\rho_{\Theta}}{\rho_S} + \rho_{SS} \left(\frac{\rho_{\Theta}}{\rho_S} \right)^2 \right]. \end{aligned} \quad (64.35)$$

64.3.2 A tidy form

We next write the bracket terms in forms consistent with those introduced by [McDougall \(1987b\)](#) in his classic paper discussing cabbeling and thermobaricity. For that purpose, introduce the *thermobaricity* parameter (dimensions of inverse temperature times inverse pressure) whose form is given by

$$\mathcal{T} = \beta \partial_p \left[\frac{\alpha}{\beta} \right] \quad (64.36a)$$

$$= \frac{\partial \alpha}{\partial p} - \frac{\alpha}{\beta} \frac{\partial \beta}{\partial p} \quad (64.36b)$$

$$= \rho \nu_S \partial_p \left[\frac{\nu_{\Theta}}{\nu_S} \right] \quad (64.36c)$$

$$= -\rho^{-1} \rho_S \partial_p \left[\frac{\rho_{\Theta}}{\rho_S} \right] \quad (64.36d)$$

$$= -\rho^{-1} \left[\rho_{\Theta p} - \rho_{pS} \left[\frac{\rho_{\Theta}}{\rho_S} \right] \right], \quad (64.36e)$$

and the *cabbeling* parameter (dimensions of squared inverse temperature)

$$\mathcal{C} = \frac{\partial \alpha}{\partial \Theta} + 2 \frac{\alpha}{\beta} \frac{\partial \alpha}{\partial S} - \left(\frac{\alpha}{\beta} \right)^2 \frac{\partial \beta}{\partial S} \quad (64.37a)$$

$$= -\rho^{-1} \left[\rho_{\Theta \Theta} - 2 \rho_{\Theta S} \left[\frac{\rho_{\Theta}}{\rho_S} \right] + \rho_{SS} \left[\frac{\rho_{\Theta}}{\rho_S} \right]^2 \right] \quad (64.37b)$$

$$= \rho \left[\nu_{\Theta \Theta} - 2 \nu_{\Theta S} \left[\frac{\nu_{\Theta}}{\nu_S} \right] + \nu_{SS} \left[\frac{\nu_{\Theta}}{\nu_S} \right]^2 \right] \quad (64.37c)$$

to render the very compact result

$$\mathbf{J}^{(\Theta)} \cdot \nabla \nu_{\Theta} + \mathbf{J}^{(S)} \cdot \nabla \nu_S = \rho^{-1} \mathbf{J}^{(\Theta)} \cdot (\mathcal{T} \nabla p + \mathcal{C} \nabla \Theta) \quad (64.38)$$

which in turn yields the material evolution of *in situ* density due to neutral diffusion

$$\left[\frac{D\rho}{Dt} \right]_{\text{ntral diff}} = -\mathbf{J}^{(\Theta)} \cdot (\mathcal{T} \nabla p + \mathcal{C} \nabla \Theta). \quad (64.39)$$

64.3.3 Cabbeling

Consider the mixing of two seawater elements. Let the fluid elements separately have distinct Conservative Temperature and/or salinity, but equal locally referenced potential density. For a linear equation of state, whereby density is a linear function of Θ and S , then the resulting mixed fluid element has the same density as the unmixed separate elements. However, for a nonlinear equation of state, the mixed element generally has a different density. Furthermore, a property of seawater is that the density of the mixed element is actually greater than the unmixed elements. This densification upon mixing is a physical process known as *cabbeling* ([McDougall, 1987b](#)).

The sign definite nature of cabbeling (i.e., cabbeling always results in denser fluid elements after mixing) is a direct result of the geometry of the locally referenced potential density surface when viewed in Conservative Temperature and salinity space. This property in turn manifests with the following inequality for the cabbeling parameter

$$\mathcal{C} = \frac{\partial \alpha}{\partial \Theta} + 2 \frac{\alpha}{\beta} \frac{\partial \alpha}{\partial S} - \left[\frac{\alpha}{\beta} \right]^2 \frac{\partial \beta}{\partial S} \geq 0. \quad (64.40)$$

Given the downgradient nature of the neutral diffusive fluxes, we have

$$\text{Cabbeling} \equiv -\mathcal{C} \mathbf{J}^{(\Theta)} \cdot \nabla \Theta \geq 0, \quad (64.41)$$

thus providing a mathematical expression for the cabbeling source (with dimensions of density per time). That is, cabbeling results in a positive material evolution of density; i.e., density increases due to cabbeling. An increase in the density within a column of fluid results in the reduction of the sea level due to compression of the column.

64.3.4 Thermobaricity

The thermobaricity parameter

$$\mathcal{T} = \beta \frac{\partial}{\partial p} \left[\frac{\alpha}{\beta} \right] \quad (64.42)$$

is nonzero due to pressure dependence of the ratio of the thermal expansion coefficient to the haline contraction coefficient. As both thermal and haline effects are present, the parameter \mathcal{T} is more precisely split into two terms

$$\begin{aligned} \mathcal{T} &= \frac{\partial \alpha}{\partial p} - \frac{\alpha}{\beta} \frac{\partial \beta}{\partial p} \\ &= -\frac{\rho_{\Theta p}}{\rho} + \frac{\rho_\Theta}{\rho_S} \frac{\rho_{pS}}{\rho} \end{aligned} \quad (64.43)$$

Thermobaricity is the common name for the sum, since pressure variations in the thermal expansion coefficient dominate those of the haline contraction coefficient. The thermal expansion coefficient generally increases as pressure increases, thus making the thermobaric parameter positive.

Since neutral gradient of temperature need not be oriented in a special manner relative to the neutral gradient of pressure, there is no sign-definite nature to the thermobaricity source term

(with units of density per time)

$$\text{Thermobaricity} \equiv -\mathcal{T} \mathbf{J}^{(\Theta)} \cdot \nabla p \quad (64.44)$$

appearing in equation (64.38). Thus, thermobaricity can either increase or decrease density, depending on details of the density and fluxes. However, as noted by [McDougall and You \(1990\)](#), thermobaricity typically increases density in much of the World Ocean.

64.3.5 Comments

[Griffies and Greatbatch \(2012\)](#) discuss the impacts on global mean sea level from thermobaricity and cabbeling as diagnosed from an ocean model. Given that cabbeling always densifies and thermobaricity is also dominated by densification, these processes lead to a general reduction in global mean sea level. [Klocker and McDougall \(2010a\)](#), [Groeskamp et al. \(2016\)](#), and [Groeskamp et al. \(2019\)](#) diagnose cabbeling and thermobaricity from observational based measurements, with [Groeskamp et al. \(2019\)](#) also offering a more robust numerical method for performing that diagnostic calculation.

Although cabbeling and thermobaricity lead to watermass transformation and associated transport of water across neutral directions, they are distinct from other mixing processes such as breaking gravity waves (Section 63.1). Namely, cabbeling and thermobaricity arise from the stirring by mesoscale eddies along neutral directions, which in turn leads to neutral diffusion acting on Conservative Temperature and salinity. Transient mesoscale eddies impart a downscale cascade of tracer variance that is ultimately halted by irreversible molecular mixing, or microscale processes active before reaching the molecular level. This mixing is the ultimate cause for cabbeling and thermobaricity, with the overall strength of the cabbeling and thermobaricity determined by the strength of the mesoscale stirring.

64.4 Salt and freshwater budgets

We here specialize the kinematics of material tracers given in Section 17.6 to the case of seawater, which we treat as a two component fluid comprised of salt and freshwater concentrations. We extend this discussion in Section 64.6 by studying the role of surface boundary salt, enthalpy, and water transports on changes in ocean buoyancy.³

64.4.1 Salt and freshwater

Seawater is comprised of two material tracers: freshwater along with a suite of dissolved trace “salts”. The ratio of salts is roughly constant over the World Ocean. We are thus able to make use of a single effective mass concentration known as the *salt concentration*⁴

$$S = \frac{\text{mass of salt}}{\text{mass of seawater}} = \frac{\text{mass of salt}}{\text{mass of freshwater} + \text{mass of salt}} \quad (64.45)$$

³We provide a theoretical discussion of Conservative Temperature in Section 23.9. For present purposes, we merely need to know it is the ocean tracer best suited to measuring enthalpy (heat) transport ([McDougall, 2003](#); [IOC et al., 2010](#)).

⁴We use the salt concentration, S , in this section to avoid 1/1000 factors needed if working with salinity, $S = 1000 \text{S}$.

to specify the amount of salt within an element of seawater. In practice oceanographers choose to work with the *salinity*,⁵

$$S = 1000 \text{ S}, \quad (64.46)$$

which converts from typical salt concentrations of $S = 0.035$ to a salinity of $S = 35$. The complement to salt concentration is the freshwater concentration or mass fraction for an element of seawater

$$F = \frac{\text{mass of freshwater}}{\text{mass of seawater}} = \frac{\text{mass of freshwater}}{\text{mass of freshwater} + \text{mass of salt}} = 1 - S. \quad (64.47)$$

Other trace matter occurs at very low concentrations so as to make seawater, in effect, a two-component fluid consisting of freshwater plus dissolved salt.⁶ We here derive the mass budget for salt and freshwater as well as the associated kinematic boundary conditions.

64.4.2 Mass budgets

Following our discussion of the tracer equation in Section 17.1, the mass budget equations for an element of seawater take the form

$$\frac{\partial \rho}{\partial t} + \nabla \cdot (\rho \mathbf{v}) = 0 \quad \text{seawater} \quad (64.48)$$

$$\frac{\partial(\rho S)}{\partial t} + \nabla \cdot (\rho \mathbf{v} S + \mathbf{J}^{(S)}) = 0 \quad \text{salt} \quad (64.49)$$

$$\frac{\partial(\rho F)}{\partial t} + \nabla \cdot (\rho \mathbf{v} F + \mathbf{J}^{(F)}) = 0 \quad \text{freshwater}. \quad (64.50)$$

Equation (64.48) is the mass budget for seawater and equation (64.49) is the mass budget for salt. The freshwater budget (64.50) is derived by subtracting the salt budget (64.49) from the seawater mass budget (64.48). Hence, only two of the three mass budget equations (64.48)-(64.50) are independent.

We make use of the barycentric velocity in the above conservation laws, where the barycentric velocity for the ocean is given by

$$\mathbf{v} = S \mathbf{v}^{(S)} + F \mathbf{v}^{(F)}. \quad (64.51)$$

The velocities $\mathbf{v}^{(S)}$ and $\mathbf{v}^{(F)}$ are, respectively, the molecular center of mass velocities for salt and freshwater within a fluid element, in which case

$$\frac{\partial S}{\partial t} + \mathbf{v}^{(S)} \cdot \nabla S = 0 \quad \text{and} \quad \frac{\partial F}{\partial t} + \mathbf{v}^{(F)} \cdot \nabla F = 0. \quad (64.52)$$

Furthermore, the fluxes $\mathbf{J}^{(S)}$ and $\mathbf{J}^{(F)}$ arise from the difference between the salt and freshwater velocities from the barycentric velocity

$$\mathbf{J}^{(S)} = \rho S (\mathbf{v}^{(S)} - \mathbf{v}) \quad \text{and} \quad \mathbf{J}^{(F)} = \rho F (\mathbf{v}^{(F)} - \mathbf{v}). \quad (64.53)$$

These fluxes are often parameterized by downgradient diffusive fluxes

$$\mathbf{J}^{(S)} = -\rho K \cdot \nabla S \quad \text{and} \quad \mathbf{J}^{(F)} = -\rho K \cdot \nabla F, \quad (64.54)$$

⁵More precisely, the salinity, S , as defined by equation (64.46) is the *Absolute Salinity*. Absolute Salinity is distinct from the *practical salinity* determined by conductivity measurements. IOC et al. (2010) provides a full accounting of the theory and practice of ocean salinity.

⁶See IOC et al. (2010) for more discussion of the variations of salt concentration ratios over the ocean, as well as the impacts from biogeochemical tracers.

where \mathbb{K} is the kinematic diffusivity tensor for salt in seawater, which is a positive definite symmetric tensor. We use the same diffusivity tensor for salt and freshwater since the diffusion of one is balanced by the other. When concerned with molecular processes, the diffusivity tensor is isotropic with diffusivities set by the molecular value of $10^{-9} \text{ m}^2 \text{ s}^{-1}$. However, as discussed in Section 63.1, the eddy diffusivity is far larger than the molecular diffusivity in the presence of turbulent eddy processes, which also introduces anisotropies to the diffusion tensor.

The advective flux of seawater is comprised of a salt flux plus a freshwater flux

$$\rho \mathbf{v} = \rho S \mathbf{v}^{(S)} + \rho F \mathbf{v}^{(F)}. \quad (64.55)$$

Conversely, the salt flux and freshwater flux can be represented as a *non-advection flux* plus an advective flux where advection is defined by the barycentric velocity

$$\rho S \mathbf{v}^{(S)} = \rho S (\mathbf{v}^{(S)} - \mathbf{v}) + \rho S \mathbf{v} = \mathbf{J}^{(S)} + \rho S \mathbf{v} \quad (64.56a)$$

$$\rho F \mathbf{v}^{(F)} = \rho F (\mathbf{v}^{(F)} - \mathbf{v}) + \rho F \mathbf{v} = \mathbf{J}^{(F)} + \rho F \mathbf{v}. \quad (64.56b)$$

The non-advection fluxes, $\mathbf{J}^{(S)}$ and $\mathbf{J}^{(F)}$, lead to an exchange of mass with zero net movement of mass. In contrast, the advective flux moves mass as determined by the barycentric velocity. Furthermore, note that the center of mass velocities, $\mathbf{v}^{(S)}$ and $\mathbf{v}^{(F)}$, offer a conceptual framework of use to formulate the kinematic boundary conditions. Even so, they offer no new information beyond that contained in the fluxes $\mathbf{J}^{(S)}$ and $\mathbf{J}^{(F)}$.

64.5 Surface boundary conditions for S and Θ

In this section we summarize the surface boundary conditions holding for the salinity and Conservative Temperature equations. This treatment complements that given in Section 17.6.3.

64.5.1 Salt and freshwater

In deriving the boundary condition (17.84) in Section 16.4.3, we made use of the barycentric velocity \mathbf{v} for an element of seawater. We can garner further kinematic insights into the two-component ocean system by decomposing the total mass flux into contributions from salt and freshwater

$$\mathcal{Q}_m = \mathcal{Q}_S + \mathcal{Q}_F, \quad (64.57)$$

and by introducing the center of mass velocities for salt and freshwater according to

$$-\mathcal{Q}_m = \rho (\mathbf{v} - \mathbf{v}^{(\eta)}) \cdot \hat{\mathbf{n}} \quad (64.58a)$$

$$= \rho [S \mathbf{v}^{(S)} + F \mathbf{v}^{(F)} - \mathbf{v}^{(\eta)}] \cdot \hat{\mathbf{n}} \quad (64.58b)$$

$$= \rho [S (\mathbf{v}^{(S)} - \mathbf{v}^{(\eta)}) + \mathbf{v}^{(\eta)} + F \mathbf{v}^{(F)} - \mathbf{v}^{(\eta)}] \cdot \hat{\mathbf{n}} \quad (64.58c)$$

$$= S \rho (\mathbf{v}^{(S)} - \mathbf{v}^{(\eta)}) \cdot \hat{\mathbf{n}} + (1 - S) \rho (\mathbf{v}^{(F)} - \mathbf{v}^{(\eta)}) \cdot \hat{\mathbf{n}} \quad (64.58d)$$

$$= S \rho (\mathbf{v}^{(S)} - \mathbf{v}^{(\eta)}) \cdot \hat{\mathbf{n}} + F \rho (\mathbf{v}^{(F)} - \mathbf{v}^{(\eta)}) \cdot \hat{\mathbf{n}} \quad (64.58e)$$

$$\equiv -(\mathcal{Q}_S + \mathcal{Q}_F), \quad (64.58f)$$

where we wrote

$$S \rho (\mathbf{v}^{(S)} - \mathbf{v}^{(\eta)}) \cdot \hat{\mathbf{n}} = -\mathcal{Q}_S \quad (64.59a)$$

$$F \rho (\mathbf{v}^{(F)} - \mathbf{v}^{(\eta)}) \cdot \hat{\mathbf{n}} = -\mathcal{Q}_F. \quad (64.59b)$$

In these equations, we introduced the velocity, $\mathbf{v}^{(\eta)}$, of a point fixed to the free surface. We only need the projection of this velocity in the outward normal direction, which is written by equation (16.77)

$$\mathbf{v}^{(\eta)} \cdot \hat{\mathbf{n}} = \frac{\partial \eta / \partial t}{|\nabla(z - \eta)|} = \frac{\partial \eta / \partial t}{\sqrt{1 + |\nabla \eta|^2}} \implies \mathbf{v}^{(\eta)} \cdot \hat{\mathbf{n}} dS = \partial_t \eta dA, \quad (64.60)$$

where dS is the area element on the free surface and dA is its horizontal projection. Note that in many regions, the ocean surface is impermeable to salt, in which case the ocean surface acts as a material surface in terms of the salt velocity

$$\rho (\mathbf{v}^{(S)} - \mathbf{v}^{(\eta)}) \cdot \hat{\mathbf{n}} = 0 \quad \text{zero surface salt flux.} \quad (64.61)$$

The key exception to this boundary condition concerns sea ice, whereby salt is exchanged between liquid seawater and sea ice upon the melting or freezing of ice.

For most applications, it is preferable to make use of equation (64.56a) to eliminate the salt velocity $\mathbf{v}^{(S)}$ in favor of the non-advection flux $\mathbf{J}^{(S)} = \rho S (\mathbf{v}^{(S)} - \mathbf{v})$, in which case the kinematic boundary condition (64.59a) takes the form

$$-\mathcal{Q}_S = S \rho (\mathbf{v}^{(S)} - \mathbf{v}^{(\eta)}) \cdot \hat{\mathbf{n}} = S \rho (\mathbf{v}^{(S)} - \mathbf{v} + \mathbf{v} - \mathbf{v}^{(\eta)}) \cdot \hat{\mathbf{n}} = \mathbf{J}^{(S)} \cdot \hat{\mathbf{n}} - S \mathcal{Q}_m. \quad (64.62)$$

Turning this equation around leads to the non-advection flux

$$\mathbf{J}^{(S)} \cdot \hat{\mathbf{n}} = S \mathcal{Q}_m - \mathcal{Q}_S = S \mathcal{Q}_F - F \mathcal{Q}_S, \quad (64.63)$$

which relates the mass transport crossing the ocean surface at $z = \eta$ (right hand side) to the non-advection salt transport on the ocean side of the surface boundary (left hand side). A form of this equation was also given by equation (17.86). To support intuition and to check signs, consider the case with $\mathcal{Q}_S = 0$ so that $\mathbf{J}^{(S)} \cdot \hat{\mathbf{n}} = S \mathcal{Q}_F$. This expression means there is an upward non-advection flux of salt ($\mathbf{J}^{(S)} \cdot \hat{\mathbf{n}} > 0$) on the ocean side of the $z = \eta$ boundary in the presence of an input of freshwater through the ocean surface ($S \mathcal{Q}_F > 0$). For the converse, let $\mathcal{Q}_F = 0$ so that $\mathbf{J}^{(S)} \cdot \hat{\mathbf{n}} = -F \mathcal{Q}_S$. Now, there is a downward non-advection flux of salt ($\mathbf{J}^{(S)} \cdot \hat{\mathbf{n}} < 0$) on the ocean side of the $z = \eta$ boundary in the presence of salt input through the ocean surface ($F \mathcal{Q}_S > 0$).

64.5.2 The non-advection salt flux boundary condition

The above properties of boundary mass transfer result from the kinematic property of a fluid element whose mass is constant, and so the transfer of freshwater across the boundary of a fluid element is compensated by an opposite transfer of salt. The ocean boundary interface acts as a boundary for the fluid elements adjacent to the surface. Hence, to move mass across the $z = \eta$ interface requires mass to be replenished to the surface fluid elements.

Diffusive closure for the non-advection flux

Consider an ocean without any mixing, such as for a perfect fluid. In this case, mass arriving to the ocean surface from $\mathcal{Q}_m > 0$ will not be incorporated into the ambient ocean fluid, but instead will form a separate unmixed surface lens. When mass is exchanged across the ocean surface, mixing is required to incorporate the mass into the ambient ocean fluid. To determine the level of mixing, assume that $\mathbf{J}^{(S)}$ takes the form of a diffusive flux (64.54) so that the boundary condition (64.63) becomes

$$\mathbf{J}^{(S)} \cdot \hat{\mathbf{n}} = -\rho [\mathbb{K} \cdot \nabla S] \cdot \hat{\mathbf{n}} = S \mathcal{Q}_m - \mathcal{Q}_S = S \mathcal{Q}_F - F \mathcal{Q}_S. \quad (64.64)$$

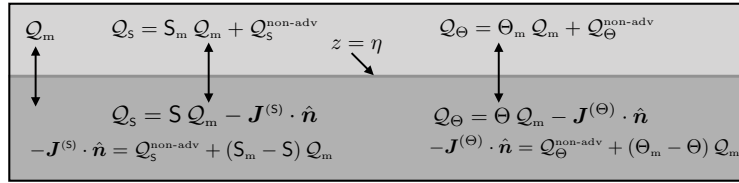


FIGURE 64.1: A schematic of an infinitesimal region of the ocean surface boundary at $z = \eta(x, y, t)$, with $z < \eta$ the ocean. $Q_m d\delta = Q_m dA$ is the mass transport (mass per time) that crosses the interface and carries a tracer concentration. We depict the case for salt concentration, S , and Conservative Temperature, Θ , and the expressions for their net boundary fluxes.

This equation sets the level of diffusion on the ocean side of the surface boundary that is needed to generate the non-advectional transport. The diffusive mixing of salt and freshwater mediate the transfer of mass across the ocean surface so to incorporate that mass into the ambient ocean fluid. For example, freshwater added to the ocean ($Q_f > 0$) diffuses downward as salt diffuses upward toward the surface.

Salt dissolved within the mass transport

In the case when salt is transported across the ocean boundary, as occurs with sea ice melting and formation, it does so largely dissolved in the water that is transported. There can also be a non-advectional transport, such as via parameterized turbulent fluxes, so that the net salt flux is given by

$$Q_S = S_m Q_m + Q_S^{\text{non-adv}}. \quad (64.65)$$

If there are more sources of this transfer then a relation such as this holds for each process. We are thus led to the net salt flux

$$Q_S = -[\rho S(\mathbf{v} - \mathbf{v}^{(\eta)}) + \mathbf{J}^{(S)}] \cdot \hat{\mathbf{n}} = S Q_m - \mathbf{J}^{(S)} \cdot \hat{\mathbf{n}} = S_m Q_m + Q_S^{\text{non-adv}}. \quad (64.66)$$

which leads to the non-advectional salt flux on the ocean side of the boundary

$$-\mathbf{J}^{(S)} \cdot \hat{\mathbf{n}} = Q_S^{\text{non-adv}} + (S_m - S) Q_m. \quad (64.67)$$

Figure 64.1 provides a schematic summary of the salt flux boundary condition. Furthermore, note that this boundary condition is consistent with that derived in Section 17.6.3 for a general tracer, in particular with equation (17.83).

Treatment in observational analyses and numerical models

In ocean climate modeling applications, the salt mass flux, Q_S , typically does not affect the kinematic boundary conditions. This approximation is reasonable given that the dominant contributor to the mass flux, Q_m , is the freshwater. Even so, there remains a net salt transported across the ocean surface in the presence of sea ice melt and formation. The above boundary conditions, in particular equations (64.66) and (64.67), remain unchanged. Furthermore, it is necessary to specify the boundary tracer concentration, $S(z = \eta)$. For salt, this value is typically set equal to that within the ocean model surface grid cell. This choice is also common for observation-based studies.

64.5.3 Conservative Temperature boundary condition

Conservative Temperature, potential temperature, potential vorticity, and passive tracers each satisfy the tracer equation (64.49), with distinct tracer flux vectors \mathbf{J} . However, they are not material tracers and so the kinematic constraints holding for salt do not hold for these other tracers. We describe the thermodynamic properties of Conservative Temperature in Section 23.9 and the processes affecting its boundary fluxes in Section 64.6. Here we begin our treatment of this tracer by outlining its surface boundary condition.

As per the general discussion in Section 17.6.3, the net surface boundary flux of Conservative Temperature is written

$$\mathcal{Q}_\Theta = \Theta_m \mathcal{Q}_m + \mathcal{Q}_\Theta^{\text{non-adv}} = [-\rho \Theta (\mathbf{v} - \mathbf{v}^{(\eta)}) + \mathbf{J}^{(\Theta)}] \cdot \hat{\mathbf{n}} = \Theta \mathcal{Q}_m - \mathbf{J}^{(\Theta)} \cdot \hat{\mathbf{n}}. \quad (64.68)$$

In this equation, $\mathcal{Q}_\Theta^{\text{non-adv}}$ arises from the non-advection enthalpy fluxes outside the ocean domain that impact on the upper ocean interface, such as from radiant and turbulent fluxes, whereas Θ_m is the Conservative Temperature of the boundary mass flux. Rearrangement leads to the net expression for the non-advection flux on the ocean side of the upper ocean boundary

$$-\mathbf{J}^{(\Theta)} \cdot \hat{\mathbf{n}} = \mathcal{Q}_\Theta^{\text{non-adv}} + (\Theta_m - \Theta) \mathcal{Q}_m, \quad (64.69)$$

where $\Theta = \Theta(z = \eta)$ is the Conservative Temperature at the surface interface. A common assumption made for models and observational studies is to set $\Theta_m - \Theta(z = \eta) = 0$, in which case

$$-\mathbf{J}^{(\Theta)} \cdot \hat{\mathbf{n}} = \mathcal{Q}_\Theta^{\text{non-adv}} \text{ if } \Theta_m - \Theta(z = \eta) = 0. \quad (64.70)$$

Figure 64.1 provides a schematic summary of the Θ flux boundary condition.

64.5.4 Comments and further reading

Nurser and Griffies (2019) offer further discussion of the kinematic boundary condition for salt and freshwater. We make use of many results from this section when discussing surface ocean buoyancy fluxes in Section 64.6 and water mass transformation in Section 65.6.

64.6 Surface boundary fluxes of buoyancy

As introduced in Chapter 27, buoyancy measures the gravitational acceleration of a fluid element relative to that of the fluid environment surrounding the element. A reduction in density for the fluid element is associated with an increase in buoyancy; that is, the fluid element becomes more *buoyant*. Changes in buoyancy arise through changes in density associated with temperature and salinity changes, with buoyancy changes computed relative to a fixed pressure level. In this way, buoyancy changes are directly related to processes that impact locally referenced potential density through changes in the temperature and salinity of a fluid element.

In this section we derive the equation describing the changes in ocean buoyancy due to enthalpy (commonly referred to as “heat”), salt, and water fluxes crossing the ocean boundaries. For this purpose, we expose certain of the issues associated with coupling numerical models of the ocean, atmosphere, and land. A detailed treatment of boundary layer physics is well outside of our scope. We thus take a phenomenological perspective, developing budget equations but not diving into details of the turbulent exchange of matter and enthalpy across the ocean surface boundary. Furthermore, we are only concerned with the upper ocean boundary, so that we ignore geothermal fluxes crossing the ocean bottom boundary.

64.6.1 Outlining the boundary fluxes of enthalpy and salt

Broadly, the boundary fluxes are associated with the following physical processes.

- Turbulent processes transfer enthalpy through latent and sensible heating.
- Longwave radiation cools the upper ocean, with this radiation affected by the upper ocean skin temperature.
- Penetrative shortwave radiation is absorbed in seawater and so increases buoyancy in regions where the thermal expansion coefficient is positive.⁷
- All of the above processes are referred to as *non-advection* transports. They are not associated with a net mass transport across the ocean surface. In contrast, advective processes transfer enthalpy and salt across the ocean surface through the transfer of mass across the interface.
- Salt is transferred between the liquid ocean and sea ice when sea ice melts and forms. This transfer is proportional to the water mass flux and the difference in salinity between the liquid ocean and sea ice. There may be additional turbulent salt fluxes as well, but there is a negligible transfer of salt associated with precipitation, evaporation, or river runoff.

64.6.2 Evolution from surface boundary fluxes

We now develop finite volume budget equations for potential enthalpy (via Conservative Temperature, Θ), salt, and seawater mass for a grid cell region next to the ocean surface, with a focus on contributions due to surface boundary fluxes. For that purpose, introduce the following quantities for a grid cell,

$$M = \int_{\text{cell}} \rho dV = \langle \rho \rangle V \quad V = \int_{\text{cell}} dV = A \bar{h} \quad A = \int_{\text{cell}} dA \quad (64.71\text{a})$$

$$\bar{h} A = \int_{\text{cell}} \left[\int_{\text{cell}} dz \right] dA \quad \langle C \rangle M = \int_{\text{cell}} C \rho dV, \quad (64.71\text{b})$$

so that $\langle \rho \rangle$ is the cell averaged density, $\langle C \rangle$ is the cell mass weighted averaged tracer concentration, \bar{h} is the cell area averaged thickness, V is the cell volume, and A is the cell horizontal area. These definitions allow us to write

$$\frac{d}{dt} \left[\int_{\text{cell}} \rho C dV \right] = \frac{d}{dt} [\langle C \rangle M] = A \frac{d}{dt} [\bar{h} \langle C \rangle \langle \rho \rangle], \quad (64.72)$$

where the horizontal area of a cell is assumed to be constant in time. The surface boundary fluxes have similar grid cell area averages.

Focusing just on contributions from surface boundary transport leads to the budget equations

$$\frac{\partial(\rho h \Theta)}{\partial t} = Q_m \Theta_m + Q_\Theta^{\text{non-adv}} \quad (64.73\text{a})$$

$$\frac{\partial(\rho h S)}{\partial t} = Q_m S_m + Q_S^{\text{non-adv}} \quad (64.73\text{b})$$

$$\frac{\partial(\rho h)}{\partial t} = Q_m, \quad (64.73\text{c})$$

⁷The Baltic Sea is an outlier in the World Ocean, whose fresh and cold waters often realize a negative thermal expansion so that heating can increase rather than reduce density.

where we used a partial time derivative since we are holding the horizontal position fixed. Furthermore, we reduced notational clutter by dropping the angle brackets for volume average and the horizontal overline for area average. For a three-dimensional budget, the right hand side to these equations is combined with fluxes crossing interior cell boundaries. Finally, we wrote the fluxes as

$$Q_m A = \mathcal{Q}_m \mathcal{S} \quad \text{and} \quad Q_\Theta^{\text{non-adv}} A = \mathcal{Q}_\Theta^{\text{non-adv}} \mathcal{S} \quad \text{and} \quad Q_S^{\text{non-adv}} A = \mathcal{Q}_S^{\text{non-adv}} \mathcal{S}, \quad (64.74)$$

where \mathcal{S} is the area on the free surface and A is the corresponding horizontal area of the grid cell.

64.6.3 Buoyancy tendency from surface boundary fluxes

For many purposes, it is of interest to quantify the impacts on ocean buoyancy arising from surface boundary fluxes. For that purpose, we here develop the budget for buoyancy in a surface model grid cell region, focusing on surface flux contributions.

Buoyancy has a time tendency given by

$$-\frac{\rho_0}{g} \frac{\partial b}{\partial t} = \rho_\Theta \frac{\partial \Theta}{\partial t} + \rho_S \frac{\partial S}{\partial t}, \quad (64.75)$$

where we introduced the shorthand

$$\rho_\Theta = \left[\frac{\partial \rho}{\partial \Theta} \right]_{S,p} \quad \text{and} \quad \rho_S = \left[\frac{\partial \rho}{\partial S} \right]_{\Theta,p} \quad (64.76)$$

for the partial derivatives of density with respect to Conservative Temperature and salinity, respectively, each with pressure held constant. We wish to form an evolution equation for buoyancy at the ocean surface grid cell just due to the effects of surface forcing. For this purpose, multiply the temperature equation (64.73a) by ρ_Θ and add to the salinity equation (64.73b) multiplied by ρ_S

$$\rho_\Theta \left[\frac{\partial(\rho h \Theta)}{\partial t} \right] + \rho_S \left[\frac{\partial(\rho h S)}{\partial t} \right] = Q_m (\rho_\Theta \Theta_m + \rho_S S_m) + \rho_\Theta Q_\Theta^{\text{non-adv}} + \rho_S Q_S^{\text{non-adv}}. \quad (64.77)$$

Now use the mass budget (64.73c) and introduce the buoyancy tendency according to equation (64.75) to render an expression for the time tendency of the surface ocean buoyancy

$$-(\rho_0/g) \rho h \left[\frac{\partial b}{\partial t} \right]^{\text{surface}} = Q_m [\rho_\Theta (\Theta_m - \Theta) + \rho_S (S_m - S)] + \rho_\Theta Q_\Theta^{\text{non-adv}} + \rho_S Q_S^{\text{non-adv}}. \quad (64.78)$$

Introducing the thermal expansion and saline contraction coefficients

$$\alpha = -\frac{1}{\rho} \left[\frac{\partial \rho}{\partial \Theta} \right]_{S,p} \quad \text{and} \quad \beta = \frac{1}{\rho} \left[\frac{\partial \rho}{\partial S} \right]_{\Theta,p} \quad (64.79)$$

yields

$$\left[\frac{\partial b}{\partial t} \right]^{\text{surface}} = \frac{g}{\rho_0 h} \left(Q_m [\alpha (\Theta_m - \Theta) - \beta (S_m - S)] + \alpha Q_\Theta^{\text{non-adv}} - \beta Q_S^{\text{non-adv}} \right) \quad (64.80a)$$

$$= \frac{g}{\rho_0 h} \left(\alpha [Q_m (\Theta_m - \Theta) + Q_\Theta^{\text{non-adv}}] - \beta [Q_m (S_m - S) + Q_S^{\text{non-adv}}] \right). \quad (64.80b)$$

In regions where the thermal expansion coefficient is positive (α_Θ), adding a boundary mass

$(Q_m > 0)$ that has $\Theta_m > \Theta$ increases the buoyancy of the surface ocean; i.e., adding relatively warm water increases surface ocean buoyancy. Likewise, where the haline contraction coefficient is positive ($\beta > 0$), adding boundary mass with $S_m < S$ increases buoyancy of the surface ocean; i.e., adding relatively freshwater increases surface ocean buoyancy. The same behavior holds for the turbulent fluxes, where $Q_\Theta^{\text{non-adv}} > 0$ (adding turbulent thermal energy to the ocean) increases surface ocean buoyancy whereas $Q_S^{\text{non-adv}} > 0$ (adding salt to the ocean) decreases buoyancy. Finally, note that in some contexts it is useful to take the limit as the thickness, h , becomes vanishingly small and to introduce a Dirac delta (see Section 4.3) and thus write⁸

$$\left[\frac{\partial b}{\partial t} \right]^{\text{surface}} = \frac{g \delta(z - \eta)}{\rho_0} \left(Q_m [\alpha(\Theta_m - \Theta) - \beta(S_m - S)] + \alpha Q_\Theta^{\text{non-adv}} - \beta Q_S^{\text{non-adv}} \right) \quad (64.81\text{a})$$

$$= \frac{g \delta(z - \eta)}{\rho_0} \left(\alpha [Q_m (\Theta_m - \Theta) + Q_\Theta^{\text{non-adv}}] - \beta [Q_m (S_m - S) + Q_S^{\text{non-adv}}] \right). \quad (64.81\text{b})$$

This form is of use when organizing processes according to interior processes and surface boundary processes, such as when considering water mass transformation analysis in Section 65.8.

64.6.4 Comments

The buoyancy flux expression (64.80b) is of use for boundary layer parameterizations, such as the KPP scheme of [Large et al. \(1994\)](#) and [Van Roekel et al. \(2018\)](#). It is furthermore used when studying water mass transformations as reviewed by [Groeskamp et al. \(2019\)](#) and summarized in Chapter 65.

64.7 Global mean sea level

In this section we consider some basic features of global mean sea level by making use of the mass budget of liquid seawater. This analysis highlights the distinction between the mass budget and the volume (sea level) budget.

64.7.1 Definitions and assumptions

Seawater mass is a conserved quantity so that the total liquid seawater mass, m , changes only via boundary mass fluxes

$$\frac{dm}{dt} = \mathcal{A} \overline{Q_m}, \quad (64.82)$$

where \mathcal{A} is the ocean surface area, $\overline{Q_m}$ is the area averaged surface mass flux, and we assume there is no mass entering through the ocean bottom. The global volume of liquid seawater

$$V = m / \langle \rho \rangle \quad (64.83)$$

changes due to mass changes *and* changes to the global mean density, $\langle \rho \rangle$. Throughout this section we assume the surface area is constant in time, thus neglecting the relatively small changes associated with volume changes along sloping beaches. We also assume a temporally constant area averaged ocean bottom depth, \bar{H} . These two assumptions mean that changes in ocean volume arise just from changes in global mean sea level, $\bar{\eta}$. Since around the year 2000, measurements

⁸From Section 4.3, we know that the Dirac delta, $\delta(z - \eta)$, has dimensions of inverse length, so that equation (64.81b) is dimensionally consistent.

estimate that global area mean sea level has increased at a rate of

$$\left[\frac{d\bar{\eta}}{dt} \right]_{\text{observed}} \approx 3 \text{ mm yr}^{-1}, \quad (64.84)$$

and that this rate is increasing (positive sea level acceleration). As part of the analysis in this section we make use of the following phenomenological numbers and make a few assumptions to facilitate calculations.

- global seawater volume $\mathcal{V} \approx 1.3 \times 10^{18} \text{ m}^3$
- global ocean surface area $\mathcal{A} \approx 3.6 \times 10^{14} \text{ m}^2$
- global ocean mean density $\langle \rho \rangle \approx 1035 \text{ kg m}^{-3}$
- specific heat capacity for seawater $c_p \approx 3992 \text{ J kg}^{-1}\text{K}^{-1}$
- Ignore mass fluxes transported through the sea floor, which are small relative to surface mass fluxes.
- Ignore salinity and pressure effects on density, so that changes in global mean density arise just from changes in global mean Conservative Temperature.
- Assume a constant thermal expansion coefficient

$$\alpha = -\frac{1}{\rho} \left[\frac{\partial \rho}{\partial \Theta} \right]_{S,p} \approx 2 \times 10^{-4} \text{ K}^{-1}. \quad (64.85)$$

This is not a great approximation, since the thermal expansion coefficient ranges over the ocean by a factor of 10. Nonetheless, for this section it is sufficient for deducing rough numbers that are consistent with errors in measurements for global boundary enthalpy and mass fluxes.

64.7.2 Budget for global mean sea level

Expression (64.83) for ocean volume leads to its time derivative

$$\frac{d\mathcal{V}}{dt} = \frac{1}{\langle \rho \rangle} \frac{dm}{dt} - \frac{m}{\langle \rho \rangle^2} \frac{d\langle \rho \rangle}{dt} \quad (64.86a)$$

$$= \frac{\mathcal{A} \overline{Q_m}}{\langle \rho \rangle} - \frac{\mathcal{V}}{\langle \rho \rangle} \frac{d\langle \rho \rangle}{dt}, \quad (64.86b)$$

where we used equation (64.82) to express mass changes in terms of the surface mass flux. Additionally, the ocean volume is given by

$$\mathcal{V} = \int dA \int_{-H}^{\eta} dz = \mathcal{A} (\bar{H} + \bar{\eta}), \quad (64.87)$$

so that its time changes arise from changes in the global mean sea level

$$\frac{d\mathcal{V}}{dt} = \mathcal{A} \frac{d\bar{\eta}}{dt}. \quad (64.88)$$

Combining the two volume equations (64.86b) and (64.88) yields the budget equation for global mean sea level

$$\frac{d\bar{\eta}}{dt} = \frac{\overline{Q_m}}{\langle \rho \rangle} - \frac{\mathcal{V}}{\mathcal{A} \langle \rho \rangle} \frac{d\langle \rho \rangle}{dt}. \quad (64.89)$$

The first term arises from changes in ocean mass whereas the second term arises from changes in global mean seawater density.

64.7.3 Changes due to mass input

To ground these formulae in phenomenology, assume that a surface mass flux gives one-half of the observed sea level rise

$$\frac{1}{2} \left[\frac{d\bar{\eta}}{dt} \right]_{\text{observed}} = \frac{\overline{Q_m}}{\langle \rho \rangle}. \quad (64.90)$$

This distribution of measured sea level is roughly correct. With $\langle \rho \rangle = 1035 \text{ kg m}^{-3}$ and $d\bar{\eta}/dt \approx 3 \text{ mm yr}^{-1}$, we need an area averaged mass flux across the ocean surface

$$\overline{Q_m} \approx 5 \times 10^{-8} \text{ kg m}^{-2} \text{ s}^{-1}. \quad (64.91)$$

Integrated over the global ocean area, this flux leads to a mass transport of

$$\mathcal{T} = \mathcal{A} \overline{Q_m} \approx 1.8 \times 10^7 \text{ kg s}^{-1} \approx 0.015 \times \mathcal{T}^{\text{river}}. \quad (64.92)$$

That is, global mean sea level rises at a rate of 1.5 mm yr^{-1} if there is a net additional mass added to the ocean equal to roughly 1.5% of the net river water entering the ocean, $\mathcal{T}^{\text{river}}$. This additional net mass is largely coming from the melting of land-ice.

64.7.4 Steric changes due to changes in density

Steric effects generally refer to properties of a substance associated with the space occupied by atoms. In the sea level context, steric effects refer to changes in sea level associated with density changes, with changes in density associated with changes in the volume occupied by seawater molecules. Changes in global mean sea level arising from changes in the global mean density are called global steric sea level changes. From the sea level budget equation (64.89) we know that steric changes are written mathematically as

$$\left[\frac{d\bar{\eta}}{dt} \right]_{\text{steric}} \equiv - \frac{\mathcal{V}}{\mathcal{A} \langle \rho \rangle} \frac{d\langle \rho \rangle}{dt}. \quad (64.93)$$

Global mean density will change primarily from changes in global mean Conservative Temperature. If we assume the ocean thermal expansion is constant, then

$$\frac{1}{\langle \rho \rangle} \frac{d\langle \rho \rangle}{dt} = -\alpha \frac{d\langle \Theta \rangle}{dt}, \quad (64.94)$$

so that steric sea level changes are primarily driven by *thermosteric* effects

$$\left[\frac{d\bar{\eta}}{dt} \right]_{\text{thermosteric}} \equiv \frac{\alpha \mathcal{V}}{\mathcal{A}} \frac{d\langle \Theta \rangle}{dt}. \quad (64.95)$$

With $\alpha \approx 2 \times 10^{-4} \text{ K}^{-1}$ and $d\bar{\eta}/dt \approx 1.5 \text{ mm yr}^{-1}$, we have

$$\frac{d\langle\Theta\rangle}{dt} \approx 0.2 \text{ K century}^{-1}. \quad (64.96)$$

That is, a global thermosteric sea level rise of 1.5 mm yr^{-1} corresponds to a rate of increase in the global volume mean ocean temperature of roughly $0.2 \text{ K century}^{-1}$.

64.7.5 Enthalpy flux imbalances giving rise to thermosteric sea level

A global mean ocean temperature change can arise from an area averaged surface ocean enthalpy flux

$$\overline{Q_H} \approx \langle \rho \rangle c_p \overline{H} \frac{d\langle\Theta\rangle}{dt}. \quad (64.97)$$

Plugging in numbers leads to the enthalpy flux

$$\overline{Q_H} \approx 1 \text{ W m}^{-2}. \quad (64.98)$$

That is, a surface ocean enthalpy flux of roughly 1 W m^{-2} (ocean area normalized) gives rise to a global mean thermosteric sea level rise of roughly 1.5 mm yr^{-1} .

An enthalpy flux of 1 W m^{-2} is small compared to, say, that crossing the surface of a typical light bulb. However, 1 W m^{-2} is comparable to that accumulating within the earth system due to increases in greenhouse gases (Otto et al., 2013). That is, 1 W m^{-2} averaged over the global ocean, or 0.7 W m^{-2} averaged over the surface area of the planet,⁹ is roughly the net heating associated with anthropogenic climate change. Such seemingly small increases in surface heating represent a nontrivial increase in the earth's energy budget that are leading to the observed sizable climate changes and sea level rise.

A specific means to gauge the magnitude of 1 W m^{-2} distributed over the ocean surface area, \mathcal{A} , is to compare to the enthalpy flux due to blasting one atomic bomb per second ($\Delta t = 1 \text{ s}$) and uniformly distributing its released energy over the ocean surface area every second. $\mathcal{E}_{\text{bomb}} \approx 6.3 \times 10^{13} \text{ J}$ distributed over the ocean area each second corresponds to a surface ocean enthalpy flux of

$$Q_{\text{bomb}} = \frac{\mathcal{E}_{\text{bomb}}}{\mathcal{A} \Delta t} \approx 0.17 \text{ W m}^{-2}. \quad (64.99)$$

Hence, an enthalpy flux of 1 W m^{-2} due to anthropogenic climate warming corresponds to $1/0.17 \approx 6$ atomic bombs per second. This way of framing the net heating of the ocean due to anthropogenic climate change dramatically illustrates the huge magnitude of the heating created by the burning of carbon based energy sources.

64.7.6 Global sea level in a Boussinesq ocean

The sea level for a Boussinesq ocean evolves according to the kinematic free surface equation (18.78)

$$\partial_t \eta^{\text{bouss}} = -\nabla \cdot \mathbf{U} + Q_m/\rho_0, \quad (64.100)$$

where

$$\mathbf{U} = \int_{-H}^{\eta} \mathbf{u} dz \quad (64.101)$$

is the depth integrated horizontal velocity and ρ_0 is the Boussinesq reference density. This equation results from ignoring all changes to density, except for those related to the buoyancy force

⁹The ocean covers roughly 70% of the earth surface.

appearing in the momentum equations. Integrating the sea surface height equation (64.100) over the surface area of the global ocean reveals that the global mean Boussinesq sea level evolves according to

$$\frac{d\bar{\eta}^{\text{bouss}}}{dt} = \frac{\overline{Q}_m}{\rho_0}. \quad (64.102)$$

Hence, $\bar{\eta}^{\text{bouss}}$ changes only so long as there are boundary mass fluxes. In contrast to the real ocean, the sea level computed from a Boussinesq ocean is unaffected by a surface enthalpy flux, $\overline{Q}_H \neq 0$. This result in turn means that we cannot use the prognostic sea surface height, η^{bouss} , level from a Boussinesq ocean model to compute changes the global mean sea level. Instead, corrections are required, as first identified by [Greatbatch \(1994\)](#) and further detailed in Appendix D of [Griffies and Greatbatch \(2012\)](#).

64.7.7 Why global halosteric sea level changes are negligible

When freshwater enters the ocean, such as from melting continental ice sheets, it adds to the ocean mass and in turn increases global mean sea level. This change is referred to as *barystatic sea level change* according to the sea level terminology paper from [Gregory et al. \(2019\)](#). Although ocean salinity changes upon changing the freshwater content, the net effect on global mean sea level is almost entirely barystatic since the global halosteric effect is negligible. We can understand why the global halosteric effect is so tiny by recognizing that freshwater entering the ocean sees its salinity increase whilst the ambient seawater is itself freshened. These compensating salinity changes (which are often mistakenly ignored) have corresponding compensating sea level changes, thus bringing the global halosteric effect to near zero.

We here summarize the two-bucket thought experiment from Appendix B of [Gregory et al. \(2019\)](#). In this experiment, one bucket holds freshwater and the other holds seawater, with the Conservative Temperature and pressures assumed to be identical for the two buckets. By working through this example we expose the rather tiny effects on global mean sea level arising from halosteric effects.

Formulating the change in volume

Consider two buckets containing seawater with mass M_n , volume V_n , density $\rho_n = M_n/V_n$, and salinity S_n , where $n = 1, 2$ labels the two buckets. Now fully mix the water in the two buckets, whereby the total mass, M , of seawater remains constant, as does the total mass of salt

$$M = M_1 + M_2 \quad \text{and} \quad M S = M_1 S_1 + M_2 S_2, \quad (64.103)$$

where S is the salinity of the homogenized fluid so that $M S$ is the total mass of salt in the combined system. Now place a mass M_1 of the homogenized fluid back in the first bucket, and a mass M_2 into the second bucket. Our goal is to compute the change in seawater volume

$$\delta V = \delta V_1 + \delta V_2. \quad (64.104)$$

In determining this volume change, we ignore pressure changes as well as changes in enthalpy associated with the heat of mixing. So the only change in volume arises from changes in the salinity.

Since the mass of each bucket remains the same before and after homogenization, then the density of seawater in each bucket changes only due to the volume changes

$$\delta\rho_n = \delta(M_n/V_n) = -(M_n/V_n^2)\delta V_n \implies \delta\rho_n/\rho_n = -\delta V_n/V_n. \quad (64.105)$$

That is, the relative change in density equals to minus the relative change in volume. Now the density changes arise just from salinity changes, in which

$$\delta\rho_n/\rho_n = \beta_n \delta S_n, \quad (64.106)$$

where β_n is the haline contraction coefficient that measures changes in density when fixing pressure and Conservative Temperature. We are thus led to the volume change

$$\delta V = -(V_1 \delta\rho_1/\rho_1 + V_2 \delta\rho_2/\rho_2) = -(V_1 \beta_1 \delta S_1 + V_2 \beta_2 \delta S_2). \quad (64.107)$$

We can simplify this expression by making use of salt conservation in equation (64.103), thus constraining salinity changes according to

$$M_1 \delta S_1 + M_2 \delta S_2 = 0 \implies \delta S_2 = -(M_1/M_2) \delta S_1, \quad (64.108)$$

in which case the volume change takes on the form

$$\delta V = -V_1 \delta S_1 (\beta_1 - \beta_2 \rho_1/\rho_2). \quad (64.109)$$

The haline contraction coefficient changes only by a few percent globally (see [Roquet et al. \(2015\)](#) or Figure 1 in [Griffies et al. \(2014\)](#)), in which case we set $\beta_1 = \beta_2 = \beta$. Furthermore, to connect to sea level changes we assume the horizontal cross-sectional area of the two buckets is the same, so that the total water column thickness between the two buckets is given by

$$\delta h = -\beta \delta S_1 (1 - \rho_1/\rho_2). \quad (64.110)$$

Oceanographic numbers

From equation (64.110) we see that $\delta h = 0$ if there is no salinity change; if $\beta = 0$; or if $\rho_1 = \rho_2$. None of these cases is of interest here, where instead we assume the first bucket is initially filled with freshwater whereas the second bucket is initially filled with ambient seawater. Homogenization of the two buckets then raises salinity in the first bucket by $\delta S_1 = S$, with $S = 35$ ppt a representative value. Furthermore, let the density ratio be $\rho_1/\rho_2 = 1000/1028$, and the haline contraction coefficient be $\beta = 0.8 \times 10^{-3}$. These ocean values yield a thickness change

$$\delta h = -7.6 \times 10^{-4} h_1. \quad (64.111)$$

Hence, for every meter of fresh water added to the ocean surface, the halosteric effect contributes a 0.76 mm decrease in water thickness. That is, the total volume of homogenized water equals to the sum of the volume initially in the two separate buckets to within better than 0.1%. We conclude that the volume change is almost entirely barystatic, so that the global halosteric effect is quite negligible when considering global sea level changes.

Comments on global thermosteric sea level changes

The above derivation for the global halosteric changes can be directly transferred to the case of mixing two buckets whose water has different Conservative Temperatures but identical pressure and salinity. Conservation of salt is here replaced by conservation of potential enthalpy; i.e., heat, so that the thickness change is given by

$$\delta h = \alpha \delta \Theta_1 (1 - \rho_1/\rho_2), \quad (64.112)$$

where α is the thermal expansion coefficient. The thermal expansion coefficient varies quite a lot over the World Ocean (e.g., see Figure 1 in [Griffies et al. \(2014\)](#)). Even so, with typical lower to middle latitude surface values on the order of $\alpha \approx 2 \times 10^{-4} \text{ K}^{-1}$, we find that δh from thermal effects are on the same order as those from haline effects given by equation (64.110). That is, the contributions to the column thickness are dominated by the barystatic (mass) effects.

However, there is a key distinction between thermal and haline contributions to sea level. Namely, thermal properties are also affected by boundary radiatant and turbulent enthalpy fluxes that can arise in the absence of boundary mass fluxes. These extra effects of boundary heating were studied in Section 64.7.5, where we identified the key role for ocean warming on global thermosteric sea level changes. Such changes are certainly not negligible, comparing to the observed global barystatic contributions.

64.7.8 Further study

The discussion of steric and thermosteric sea level changes are further explored in [Griffies and Greatbatch \(2012\)](#) and [Griffies et al. \(2014\)](#). The global halosteric discussion is based on Appendix B of the sea level terminology paper from [Gregory et al. \(2019\)](#). The [Gregory et al. \(2019\)](#) paper is also notable for providing a conceptual rationalization of the often confusing terminology used in sea level studies.



Chapter 65

WATER MASS TRANSFORMATION ANALYSIS

A *water mass* refers to a region of seawater characterized by a suite of quasi-homogeneous properties used to distinguish this water from other water masses. Water masses are typically formed through surface boundary processes. As these waters enter the ocean interior they are advected over basin scales while they are also eroded or *transformed* by irreversible mixing processes. Water masses offer a conceptual means to partition or bin the ocean into distinct classes whose origin, movement, and transformation can be measured, modeled, and studied. Scalar properties generally used to classify water masses are simpler to measure than vector properties such as velocity. Hence, a water mass perspective offers the means to infer ocean circulation within water mass space without directly measuring the velocity.

In this chapter we develop the mathematical and physical basis for *water mass analysis* and its extension to *tracer mass analysis*. This formalism considers the budgets for seawater mass and tracer mass within layers or classes defined by properties such as buoyancy, Conservative Temperature, salinity, or biogeochemical tracers. It offers a framework for understanding certain facets of geophysical fluid mechanics that is distinct from the more familiar Eulerian and Lagrangian methods used in fluid mechanics. It has thus found use throughout oceanography and atmospheric sciences.

Readers of this chapter may appreciate the following paraphrase from A. Sommerfeld's quote given at the start of the thermodynamics part of this book (Part IV).

Water mass analysis appears somewhat mysterious and puzzling on first encounter. On second encounter things start to fall into place, except perhaps for a few pesky math niceties. On third encounter, when deciding to do calculations, one returns to that unsettled feeling of the first encounter. However, by now, familiarity with the words and maths means that the mystery presents no practical bother. One simply turns the crank without thinking too much about the underlying foundations.

In hopes of partially dispelling the mystery, and maintaining an appreciation for the foundations, we here couple the many mathematical equations with schematics and conceptual descriptions. Even so, there should be no presumption that this subject can be mastered without a healthy degree of head-scratching.

CHAPTER GUIDE

The development in this chapter requires the vector calculus encountered in Chapter 2; elements of the generalized vertical coordinates from Chapters 56 and 57; kinematics from Chapter 16; tracer budgets from Chapter 17; advection and diffusion maths in Chapter 61, and features of parameterized tracer transport and mixing discussed in Chapter 63. This is a rather long chapter that works through a number of related budget analyses with the aim to ground the theory with examples motivated from the growing literature.

65.1	Conceptual framework	1629
65.1.1	Water mass configuration space	1629
65.1.2	A novel kinematic lens	1630
65.1.3	Transformation and formation	1631
65.2	Buoyancy transformation and formation	1631
65.2.1	A three-layer thought experiment	1632
65.2.2	How processes lead to transformations	1633
65.3	Mathematical framework	1634
65.3.1	Seawater mass in an infinitesimal cylinder	1635
65.3.2	Seawater mass within a finite region	1635
65.3.3	Seawater mass distribution/density function	1635
65.3.4	Example regions	1636
65.3.5	Integrals of arbitrary functions	1639
65.3.6	Moments of λ	1639
65.3.7	Internal and external λ -moments	1640
65.3.8	Further study	1641
65.4	Water mass transformation across a λ-surface	1641
65.4.1	Dia-surface flux and interior transformation	1641
65.4.2	Transformation as the derivative of an integral	1642
65.4.3	Processes and kinematics	1643
65.4.4	Some details concerning interior transformation	1645
65.5	Budget for seawater mass in a $\Delta\lambda$-layer	1647
65.5.1	Transport crossing interior open boundaries	1647
65.5.2	Mass transport crossing the ocean surface	1647
65.5.3	Mass budget	1648
65.6	Budget for λ mass in a λ_∞-region	1648
65.6.1	Processes affecting the mass of λ -stuff	1649
65.6.2	Summary of the λ budget	1651
65.6.3	Processes leading to water mass transformation	1651
65.7	Surface water mass transformation	1653
65.7.1	Circulation driven by surface transformation	1653
65.7.2	Further study	1654
65.8	Buoyancy water mass transformation	1654
65.8.1	Material time changes to S and Θ	1654
65.8.2	Interior buoyancy water mass transformation	1655
65.8.3	Surface non-advectional flux for S and Θ	1656
65.8.4	Surface buoyancy water mass transformation	1656
65.9	Tracer mass analysis	1657
65.9.1	General form of the mass budget	1658
65.9.2	Tracer processes	1659
65.9.3	Transport across an interior layer interface	1660
65.9.4	Transport across interior and surface boundaries	1660
65.9.5	The layer tracer budget	1661
65.9.6	Further study	1661

65.10 Regions bounded by a tracer contour/surface	1661
65.10.1 Closed region bounded by a tracer surface/contour	1662
65.10.2 Region with $C \geq \tilde{C}$	1663
65.10.3 Comments and further study	1665

65.1 Conceptual framework

Water mass analysis is a mathematical formalism supporting the study of budgets for seawater mass and tracer mass within layers or classes defined by properties such as Archimedean buoyancy (Chapter 27; shortened to “buoyancy” here), Conservative Temperature, salinity, or biogeochemical tracers. Water mass analysis is concerned with processes affecting the evolution of fluid within layers and in the characterization of circulation inferred from this evolution. This analysis is quite useful for oceanography since it is common to describe ocean geography in terms of characteristic water properties, with such properties often originating through extremely large buoyancy fluxes at the high latitudes that form waters such as the Antarctic Bottom Water (AABW) and North Atlantic Deep Water (NADW). Our goals here are fundamental, so that we do not delve into the phenomenology of ocean water masses. Rather, we dive into the maths and physics underlying the method.

We speak of a *water mass configuration space*, in which some or all of the coordinates of this space are determined by properties other than geographic/depth coordinates.¹ For example, Figure 65.1 provides an example configuration space described by (S, Θ, p) , whereby a fluid element has its position in water mass configuration space² determined by its Conservative Temperature, Θ , salinity, S , and pressure, p . We may also consider the water mass configuration space defined by binning the ocean according to potential density classes, or some other measure of buoyancy. We can also retain some degree of geographical information through binning according to latitude and buoyancy. Note that there is no implied constraint that the buoyancy surfaces remain stably stratified in the vertical, nor indeed that any of the water mass coordinates retain a 1-to-1 relation with geographic/depth space. We have more to say on this point in the following.

65.1.1 Water mass configuration space

We specify the position of a fluid element within water mass configuration space by specifying a list of properties and/or spatial information. That is, we can choose any number of properties or geographical coordinates to specify water mass configuration space. Consequently, water mass configuration space has an arbitrary number of dimensions. We furthermore observe that water mass configuration space generally has no metric³, particularly when none of the chosen coordinates are geographical (latitude or longitude) or depth. Hence, there is generally no notion of distance or angles between points in water mass configuration space. Indeed, what does it mean to be orthogonal and temperature-salinity space or when studying the density-binned distribution of seawater?

The absence of a metric is something we have already seen when studying thermodynamic configuration space in Chapter 19, with mention of this point given in Section 19.1.5. Mathematically, we say that both thermodynamic configuration space and water mass configuration space

¹We prefer the term “configuration space” over the alternative “phase space”, since phase space in Hamiltonian dynamics specifically refers to position and momentum coordinates. In contrast, configuration space, as used in our discussion of water masses, can be determined by most any property or geographic position.

²This water mass configuration space also serves as a thermodynamic configuration space when using the Gibbs potential discussed in Section 19.6.6.

³See Section 8.1 for a discussion of metric tensors, which are needed to measure distance on a manifold.

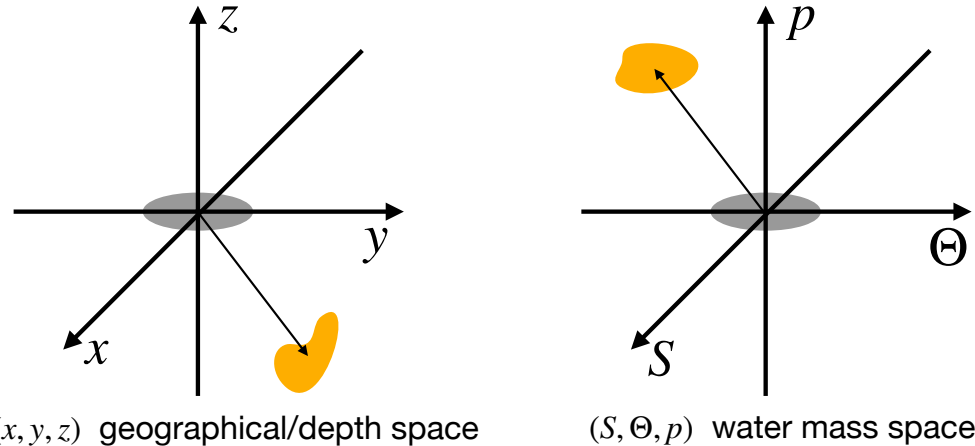


FIGURE 65.1: Left panel: a fluid element is positioned in geographical/depth space (x, y, z) according to its horizontal (x, y) (longitude, latitude) position and its vertical geopotential, z . Right panel: the same fluid element is positioned in a particular water mass configuration space, here defined by (S, Θ, p) with salinity, S , Conservative Temperature, Θ , and pressure, p . Mapping between the two spaces is generally not 1-to-1. Namely, a point in configuration space can be occupied by more than one point in geographical space since more than a single point in geographical space can have the same values for (S, Θ, p) . Although the coordinate axes are depicted as mutually orthogonal in the right panel, there is no objective means to determine angles in water mass configuration space since it contains no metric. That is, water mass configuration space, just as thermodynamic state space (Section 19.1.5), is a *differentiable manifold*.

are *differentiable manifolds*. Even so, one commonly sees a point in thermodynamic space depicted on a diagram with orthogonal axes (e.g., pressure-volume diagrams), or a position in water mass configuration space similarly depicted with orthogonal axes as in Figure 65.1. However, this depiction is arbitrary since there is no geometric structure afforded to such spaces since there is no metric tensor, which in turn means we cannot determine angles or orthogonality. Depictions with orthogonal axes merely satisfy a subjective desire for geometric structure when in fact there is none afforded to the manifold. Differential forms provide a suitable formalism for conducting calculus on a differential manifold sans a metric as detailed by [Nurser et al. \(2022\)](#).

65.1.2 A novel kinematic lens

A water mass configuration space views the ocean circulation through the lens afforded by layers or classes. This perspective contrasts to the fixed points or regions of an Eulerian perspective, or the moving fluid particles or corresponding fluid regions of a Lagrangian perspective. Hence, the kinematic perspective of water mass analysis complements that from the Eulerian and Lagrangian kinematics encountered in other parts of this book (see Chapter 14 for a reminder of Eulerian and Lagrangian kinematics).

A point in water mass configuration space can be comprised of many points in geographic/depth space. Hence, there is no presumption of a 1-to-1 mapping between geographic/depth space and water mass configuration space. This situation is familiar to descriptive oceanographers who well know that there can be more than one fluid element in the ocean that has a particular (S, Θ, p) value. Or more precisely, when classifying seawater according to binned values, $(\Theta \pm \Delta\Theta/2, S \pm \Delta S/2, p \pm \Delta p/2)$, fluid elements from any part of the ocean can fit into a particular bin so that a distribution of seawater in water mass configuration space is non-local in geographical/depth space. Even when classifying seawater according to latitude, longitude, and potential density, the possible case of a non-monotonic vertical potential density profile means that there is generally no 1-to-1 mapping between potential density and depth.

The lack of 1-to-1 mapping between water mass configuration space and geographic/depth

space is a fundamental kinematic distinction from the 1-to-1 relation that holds between the Eulerian and Lagrangian descriptions of fluid motion (see Chapter 14). The lack of a 1-to-1 relation can be frustrating since circulation viewed in water mass configuration space generally has incomplete geographic/depth information, and yet oceanographers wish to know where on the planet something is happening.⁴ Even so, abandoning the 1-to-1 relation can be liberating since water mass configuration space provides a framework to infer ocean circulation, within the water mass space, even without measuring velocity of the fluid in geographical space. Correspondingly, the view of ocean circulation through a water mass lens can offer understanding that complements traditional Eulerian or Lagrangian views.

65.1.3 Transformation and formation

Water moves through water mass configuration space as it is modified or *transformed* by boundary and interior ocean processes that cause water to cross surfaces defined by the chosen water mass property.⁵ Stated differently, a transformation process leads to material changes in the property of a fluid element, with sources of transformation arising from mixing, solar radiation, and chemical reactions. The convergence (i.e., the local imbalance) of such transformation processes leads to the *formation* and destruction of water mass classes. As water moves through water mass configuration space we are afforded a distinct view of ocean circulation that has both direct and indirect connections to circulation in geographical/depth space. Notably, and quite trivially, we measure zero motion along a coordinate axis in water mass configuration space when the property defining that axis remains materially unchanged. For example, adiabatic and isohaline processes such as linear waves can render nontrivial motion in geographical/depth space whereas they lead to no motion in (S, Θ) space.

If one is interested in processes that do not give rise to material changes in a fluid property, then the corresponding water mass configuration space generally offers a rather bland kinematic perspective. Furthermore, given the possible non-local (x, y, z) aspects of water mass configuration space, it provides an unnatural venue to study forces and stresses acting between spatially adjacent fluid elements. Hence, the study of momentum and vorticity dynamics is better handled via Eulerian or Lagrangian kinematics. Where water mass configuration space shines is by revealing the dynamics associated with processes that affect material changes to those properties defining the water mass classes. For example, a water mass perspective has found use in framing key questions of primary interest in the Anthropocene, such as ocean buoyancy and its transformation through interior and boundary mixing, ocean heat uptake and transport, the hydrological cycle, steric sea level rise, and irreversible changes to biogeochemical properties (see [Groeskamp et al. \(2019\)](#) for a review with many references).

65.2 Buoyancy transformation and formation

Archimedean buoyancy is a common property used to distribute seawater, with Archimedean buoyancy commonly approximated by potential density (Chapter 27). In this section we introduce the notions of *transformation* and *formation* when partitioning the ocean according to density (γ) classes that locally measure buoyancy.⁶ The ideas presented here extend to any scalar property used to bin the ocean fluid.

⁴Auxiliary methods such as the water tagging method of [Groeskamp et al. \(2014\)](#) can be used to recover some geographical information.

⁵In many parts of this book the word “transformation” refers to coordinate transformations. Here, “transformation” refers to a process acting to change seawater properties.

⁶Many researchers make use of the *neutral density* coordinate defined by [Jackett and McDougall \(1997\)](#).

Water mass *transformation* measures the mass per time of water that moves across an isosurface in space, or moves from one bin to another bin within a distribution. By convention, the transformation is positive if water moves to larger density (more generally to a larger value for the water mass property chosen to define the layer or class) and negative if it enters a lighter density layer (smaller value for the property). Water mass *formation* refers to the difference in transformation across the surfaces bounding a layer, so that formation measures the change in mass of the layer. That is, *formation is the layer integrated convergence of transformation in water mass configuration space*.

Both transformation and formation have dimensions of mass per time (or volume per time when considering Boussinesq fluids) and are typically measured in Sverdrup units:

$$1 \text{ Sv} = 10^6 \text{ m}^3 \text{ s}^{-1} \quad \text{volume-Sverdrup} \quad (65.1\text{a})$$

$$1 \text{ Sv} = 10^9 \text{ kg s}^{-1} \quad \text{mass-Sverdrup.} \quad (65.1\text{b})$$

The volume-Sverdrup is commonly used in Boussinesq fluids with kinematics based on volume conservation (Chapter 26), whereas the mass-Sverdrup is commonly used in non-Boussinesq fluids whose kinematics is based on mass conservation. Even so, the mass-Sverdrup can be used for Boussinesq fluids merely by multiplying the volume-Sverdrup by the constant Boussinesq reference density, ρ_0 .

65.2.1 A three-layer thought experiment

To illustrate the concepts of transformation and formation, bin the World Ocean into density classes, thus ignoring all geographic and depth information. Furthermore, assume we can partition the total ocean into just three density classes that are bounded by four density interfaces:

$$\text{light density layer} = [\gamma - \delta\gamma/2, \gamma + \delta\gamma/2] \quad (65.2\text{a})$$

$$\text{middle density layer} = [\gamma + \delta\gamma/2, \gamma + 3\delta\gamma/2] \quad (65.2\text{b})$$

$$\text{heavy density layer} = [\gamma + 3\delta\gamma/2, \gamma + 5\delta\gamma/2], \quad (65.2\text{c})$$

where $\delta\gamma > 0$ is the size for the density bins. Figure 65.2 depicts a sample mass distribution; i.e., the mass census for seawater binned into these three density layers.⁷ Now consider a physical, chemical, or biological process that results in water leaving the middle density layer and entering both the light layer and the heavy layer. Let $G(\sigma)$ measure the mass per time that water crosses the density interface $\gamma = \sigma$; i.e., $G(\sigma)$ is the transformation. This particular thought experiment has the following transformations across the various layer interfaces

$$G(\sigma) = \begin{cases} 0 & \sigma = \gamma - \delta\gamma/2 \quad \text{closed boundary} \\ < 0 & \sigma = \gamma + \delta\gamma/2 \quad \text{mass moves to light density from middle density} \\ > 0 & \sigma = \gamma + 3\delta\gamma/2 \quad \text{mass moves from middle density to heavy density} \\ 0 & \sigma = \gamma + 5\delta\gamma/2 \quad \text{closed boundary.} \end{cases} \quad (65.3)$$

The difference in the transformation across the interface boundaries of a particular layer determines the formation/destruction of water into that layer. Here, the convergence of water into the light and heavy layers means that there is a positive formation of water in these two density layers. In contrast, the divergence of water from the middle density layer means there is a negative

⁷A realistic ocean experiences boundary forcing that makes the maximum and minimum density a function of time. It is thus common to fix the lower density limit to be well below the lightest water in the ocean and the upper density limit well above the maximum density, thus ensuring that all seawater is contained by the chosen binning. We introduce such “infinity” bounds in Section 65.3.3.

formation or a destruction of some of its water. We write these layer formations mathematically as follows

$$\text{light-formation} = -[G(\gamma + \delta\gamma/2) - G(\gamma - \delta\gamma/2)] > 0 \quad (65.4a)$$

$$\text{middle-formation} = -[G(\gamma + 3\delta\gamma/2) - G(\gamma + \delta\gamma/2)] < 0 \quad (65.4b)$$

$$\text{heavy-formation} = -[G(\gamma + 5\delta\gamma/2) - G(\gamma + 3\delta\gamma/2)] > 0. \quad (65.4c)$$

The minus sign out front emphasizes that the formation is the layer integrated *convergence* of the transformation.

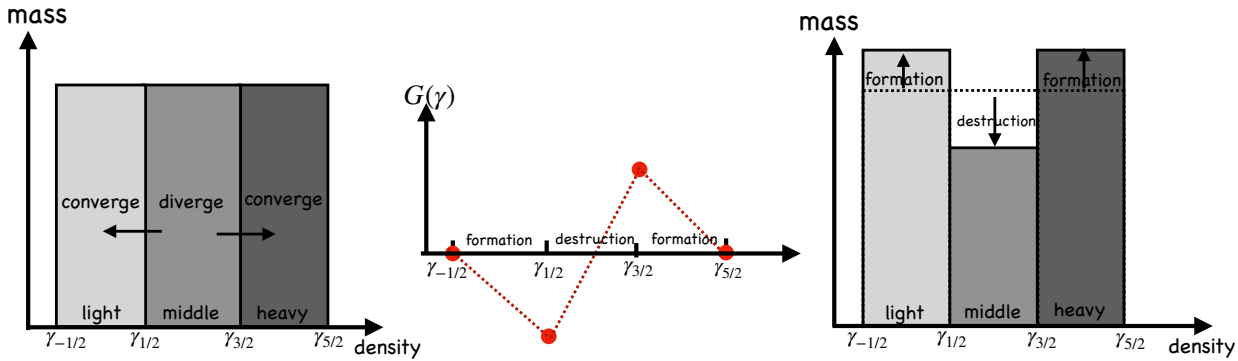


FIGURE 65.2: A sample mass distribution of the ocean binned into three density layers (light, middle, heavy) bounded by four density interfaces: $\gamma_{n/2} = \gamma + n\delta\gamma/2$ for $n = -1, 1, 3, 5$. The left panel depicts an ocean state with equal mass in each layer. Some process is then imagined to cause water to diverge from the middle layer and converge to the light and heavy layers. The right panel shows the mass distribution after the water has moved, so that the middle layer has experienced a negative *formation* (i.e., net loss of mass) whereas the light and heavy layers have experienced a positive *formation* (i.e., net mass gain). The middle panel depicts the *transformation*, G , which measures the mass per time moving across the layer boundaries. By convention, $G > 0$ for water moving into a heavier density layer and $G < 0$ for water entering a lighter density layer. The addition of more layers refines the picture (e.g., by smoothing the plot of G) but it does not modify the basic ideas illustrated in this thought experiment.

65.2.2 How processes lead to transformations

The central focus of water mass analysis is the movement of water between layers or classes, with this movement modifying the water mass distribution within the chosen water mass configuration space. Here we outline a few of the processes that affect this movement within water mass space, again focusing on buoyancy yet with an easy generalization to any other property that defines the water mass. Notably, we are not concerned with whether the fluid element moves, the boundary moves, or both, since it is only the relative motion that changes the water mass distribution. Indeed, we cannot determine motion of the fluid element in geographic space without direct information about the velocity field. We return to this notion when providing a mathematical expression for these ideas in Section 65.4.1.

Interior transformation from mixing

Mixing moves water across layer boundaries, with properties materially modified in the presence of mixing (so long as there are spatial gradients in the property). For example, recall our discussion in Chapter 17 where we saw that mixing causes tracers to move between fluid elements even as mixing does not alter the net mass of fluid elements (see the discussion of barycentric velocity in Section 17.1.2). Hence, in the presence of mixing, seawater fluid elements retain a fixed mass, and

yet the mass is redistributed among layers defined by property isosurfaces since the isosurfaces move in the presence of mixing.

Surface mass fluxes

Rain and evaporation alter the mass of the ocean. In turn, the layers where rain and evaporation occur; i.e., layers that outcrop, have their mass altered through the surface mass fluxes. Additionally, if the buoyancy of the mass flux differs from that of the ocean layer that it enters/leaves, then the buoyancy of the ocean layer is modified.

Surface and bottom boundary transformation

Buoyancy surfaces that outcrop at the ocean surface or incrop at the ocean bottom are exposed to boundary fluxes that generally modify the buoyancy of the fluid within a layer. This modification causes the layer boundaries to move so that the mass distributed within the layers can be modified if the mass moves with a velocity distinct from the buoyancy surface. A particularly striking example occurs in the upper ocean boundary layer where surface forcing leads to the seasonal migration of density outcrops. The associated lateral movement of density layers causes water to entrain and detrain from a layer since the layer boundaries generally have a velocity distinct from fluid elements. In so doing, the seasonal cycle of surface buoyancy forcing can inflate or deflate a buoyancy layer by moving the layer boundaries so that the layer entrains or detrains mass.

Penetrative shortwave radiation provides another means to modify water masses, with penetrative radiation a function of the optical properties of the fluid. This radiation provides a source of heating that can penetrate into the upper few tens of meters in the ocean, and can impact on the temperature and density structure of the ocean layers affected by radiation.

Finally, layers that intersect the ocean bottom are exposed to geothermal heating as well as enhanced mixing from bottom boundary layer mixing. Each of these processes affects a transformation of the buoyancy, thus modifying the buoyancy layer interfaces and mass distribution within the layers.

Interior sources and sinks

When studying water masses defined by biogeochemical tracers (e.g., carbon, oxygen, nutrients), there are a variety of chemical reactions and biological processes that act to modify these properties. These processes generally cannot be represented mathematically as the convergence of a flux. They are thus sometimes referred to as “non-conservative” processes (see Section 23.10) and written as a source/sink term.

65.3 Mathematical framework

In this section we develop a suite of mathematical tools of use to quantify the conceptual ideas presented in Sections 65.1 and 65.2. In particular, we develop a formalism for integrating properties within a region bounded by isosurfaces of a scalar field, $\lambda = \lambda(\mathbf{x}, t)$. The formulation is given from both a geometric perspective afforded by geographic/depth space, and a complementary distributional perspective afforded by binning seawater mass according to λ -classes. As in our study of Eulerian and Lagrangian kinematics elsewhere in this book, it is here useful to be adept at both the geographic/depth space perspective and the distributional perspective.

In Section 65.2 we assumed λ is the buoyancy field, $\lambda = \gamma$, whereas here we assume it is a generic scalar field, $\lambda(\mathbf{x}, t)$. In contrast to the case of a generalized vertical coordinate (Chapters 56 and 57), we make no assumption regarding the stratification of λ . Rather, λ -isosurfaces are free to

overtake or even to be situated in spatially disconnected regions. This freedom is motivated by the behavior of most oceanographic scalar properties, which commonly exhibit vertically unstratified or negatively stratified profiles, particularly within boundary layers.

65.3.1 Seawater mass in an infinitesimal cylinder

Consider the calculation of seawater mass within an infinitesimal λ -layer bounded by two isosurfaces, $[\lambda - \delta\lambda/2, \lambda + \delta\lambda/2]$, as in Figure 65.3. The mass within a tiny cylinder extending from one interface to the other is given by the seawater density, ρ , multiplied by the volume of the cylinder,⁸

$$\delta M = \rho \delta V = \rho \delta h \delta \mathcal{S}, \quad (65.5)$$

where $\delta \mathcal{S}$ is the cross-sectional area element and δh is the layer thickness. The geometric thickness, δh , is related to the differential λ -increment separating the two interfaces according to

$$\delta \lambda = \nabla \lambda \cdot \delta \mathbf{x} = |\nabla \lambda| \hat{\mathbf{n}} \cdot \delta \mathbf{x} = |\nabla \lambda| \delta h \quad \text{with} \quad \hat{\mathbf{n}} = \nabla \lambda |\nabla \lambda|^{-1}, \quad (65.6)$$

where $\delta \mathbf{x}$ is a position vector connecting points on the two interfaces. We thus see that the layer thickness is given by

$$\delta h = \frac{\delta \lambda}{|\nabla \lambda|}, \quad (65.7)$$

which connects a geometric property of the layer, δh , to the λ -increment, $\delta \lambda > 0$. For a given λ -increment, the layer thickness is smaller with more tightly packed λ -isosurfaces as reflected by a larger $|\nabla \lambda|$. Furthermore, the geometric thickness is oriented according to the normal direction, $\hat{\mathbf{n}}$, so that δh measures the distance between the λ -interfaces in the direction of the normal direction. It follows that the seawater mass within the cylinder is given by

$$\delta M = \rho \delta V = \rho \delta h \delta \mathcal{S} = \frac{\rho \delta \lambda \delta \mathcal{S}}{|\nabla \lambda|}. \quad (65.8)$$

65.3.2 Seawater mass within a finite region

Making use of the infinitesimal cylinder mass (65.8) allows us to write the mass of seawater within the λ -region $\lambda_1 \leq \lambda \leq \lambda_2$

$$M(\lambda_1, \lambda_2) \equiv \int_{\Omega(\lambda_1 \leq \lambda \leq \lambda_2)} dM = \int_{\lambda_1}^{\lambda_2} \left[\int_{\partial\Omega(\lambda)} \frac{\rho d\mathcal{S}}{|\nabla \lambda|} \right] d\lambda. \quad (65.9)$$

In this equation, $\Omega(\lambda_1 \leq \lambda \leq \lambda_2)$ is the region in space bounded by the λ_1 -interface and λ_2 -interface, and $\partial\Omega(\lambda)$ is the surface defined by a λ -isosurface. The $\partial\Omega(\lambda)$ integral is taken over the area of the λ -isosurface, which is then integrated over the range, $\lambda_1 \leq \lambda \leq \lambda_2$, to thus accumulate the layer mass.

65.3.3 Seawater mass distribution/density function

The region bounded by the layer interfaces can have any shape in space and can even be spatially disconnected. This complexity motivates us to introduce the *mass distribution* or *mass density*

⁸Recall our notational convention is as follows: δ refers to an infinitesimal increment of a property measured within the fluid whereas d is a differential increment used for computing integrals. We made use of the same geometric analysis in Section 38.1.2 when studying potential vorticity.

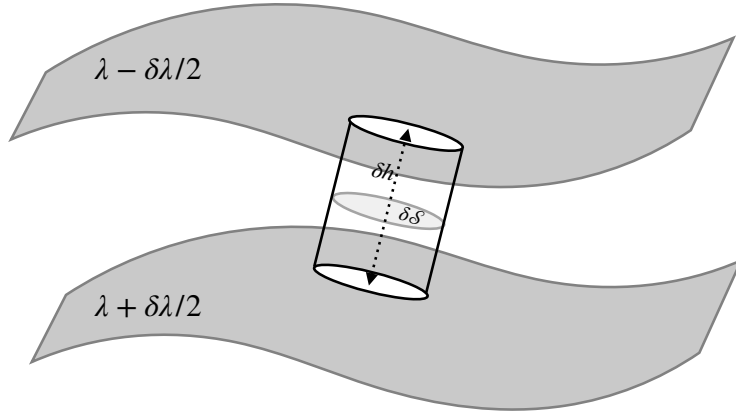


FIGURE 65.3: This schematic shows an infinitesimally thin λ -layer bounded by two interfaces $[\lambda - \delta\lambda/2, \lambda + \delta\lambda/2]$, with the λ -increment $\delta\lambda > 0$. The cylinder region extends between the two iso-surfaces and it has thickness $\delta h = \delta\lambda/|\nabla\lambda|$ and cross-sectional area δS . The cylinder is oriented according to the normal direction $\hat{n} = |\nabla\lambda|^{-1} \nabla\lambda$. We assume $|\nabla\lambda| \neq 0$, as required to define a normal direction. Indeed, if $\nabla\lambda = 0$ then we could not perform a binning according to λ classes, so the $|\nabla\lambda| \neq 0$ assumption is basic to the use of the scalar field, λ , for water mass analysis.

function by integrating the mass over the surface, $\partial\Omega(\lambda)$

$$m(\lambda) \equiv \frac{dM}{d\lambda} = \int_{\partial\Omega(\lambda)} \frac{\rho dS}{|\nabla\lambda|}. \quad (65.10)$$

A mass distribution function is quite useful when the distribution is highly non-local in geographic/depth space. It is also effective when using multiple water mass coordinates such as Θ and S as discussed in [Nurser et al. \(2022\)](#). These points motivate leaving geographic/depth perspective to simply define the mass distribution function so that

$$dM = m(\lambda) d\lambda = \text{mass within the infinitesimal } \lambda\text{-layer } [\lambda - d\lambda/2, \lambda + d\lambda/2], \quad (65.11)$$

with an illustration given by Figure 65.4. The mass distribution function is the mass density within λ space; i.e., the mass per λ . Knowledge of the mass distribution function allows us to compute the seawater mass within a finite region, as in equation (65.9), according to

$$M(\lambda_1, \lambda_2) \equiv \int_{\Omega(\lambda_1 \leq \lambda \leq \lambda_2)} dM = \int_{\lambda_1}^{\lambda_2} m(\lambda) d\lambda. \quad (65.12)$$

65.3.4 Example regions

To help ground the previous expressions for mass, we here consider some example regions that are commonly considered in water mass analysis.

Δλ-layer defined by $[\lambda_1, \lambda_2] = [\lambda - \Delta\lambda/2, \lambda + \Delta\lambda/2]$

A $\Delta\lambda$ -layer is defined with the bounding interface values

$$\lambda_1 = \lambda - \Delta\lambda/2 \text{ and } \lambda_2 = \lambda + \Delta\lambda/2, \quad (65.13)$$

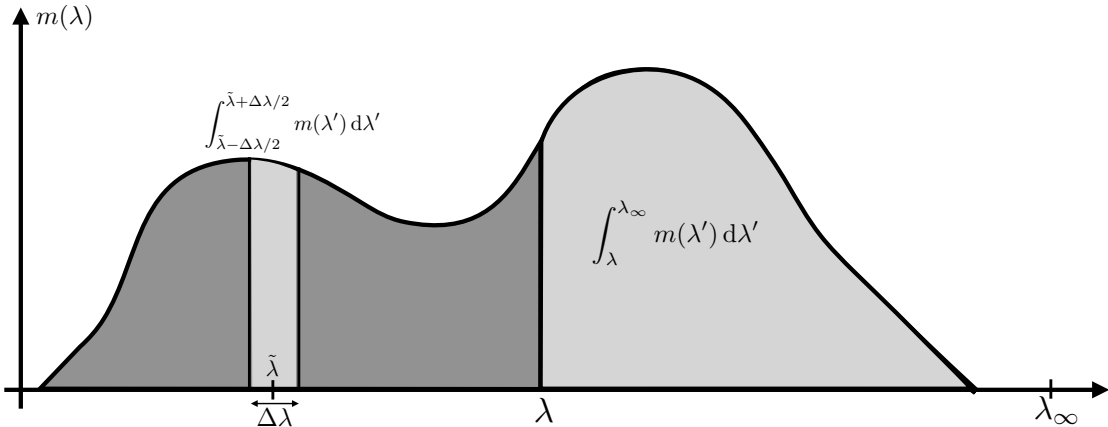


FIGURE 65.4: An example mass distribution function, $m(\lambda) = dM/d\lambda$, which measures the mass of seawater per λ -increment. Integration over a finite λ -region measures the seawater mass within that region. For example, the mass within a $\Delta\lambda$ -layer is given by $M(\tilde{\lambda} - \Delta\lambda/2, \tilde{\lambda} + \Delta\lambda/2) = \int_{\tilde{\lambda} - \Delta\lambda/2}^{\tilde{\lambda} + \Delta\lambda/2} m(\lambda') d\lambda'$ whereas the mass within the λ_∞ -region is $M(\lambda, \lambda_\infty) = \int_\lambda^{\lambda_\infty} m(\lambda') d\lambda'$, where we assume that λ_∞ is an arbitrary fixed value that is larger than any λ realized within the ocean.

for some finite difference increment $\Delta\lambda > 0$. In this case the layer mass is

$$M(\lambda - \Delta\lambda/2, \lambda + \Delta\lambda/2) = \int_{\lambda - \Delta\lambda/2}^{\lambda + \Delta\lambda/2} \left[\int_{\partial\Omega(\lambda')} \frac{\rho d\mathcal{S}}{|\nabla\lambda'|} \right] d\lambda' = \int_{\lambda - \Delta\lambda/2}^{\lambda + \Delta\lambda/2} m(\lambda') d\lambda'. \quad (65.14)$$

Characterizing ocean properties according to their value of λ is generally performed by decomposing the ocean into $\Delta\lambda$ -bins and forming histograms to estimate the continuous distribution.

λ_∞ -region defined by $[\lambda_1, \lambda_2] = [\lambda, \lambda_\infty]$

A λ_∞ -region is defined with

$$\lambda_1 = \lambda \text{ and } \lambda_2 = \lambda_\infty, \quad (65.15)$$

where λ_∞ is an arbitrary fixed constant that is larger than any value of λ realized in the ocean. The region mass is thus given by

$$M(\lambda, \lambda_\infty) = \int_{\Omega(\lambda \leq \lambda_\infty)} dM = \int_\lambda^{\lambda_\infty} \left[\int_{\partial\Omega(\lambda')} \frac{\rho d\mathcal{S}}{|\nabla\lambda'|} \right] d\lambda' = \int_\lambda^{\lambda_\infty} m(\lambda') d\lambda'. \quad (65.16)$$

An example λ_∞ -region is shown in Figure 65.5. The λ_∞ -region as so defined provides an expression for the differential mass increment

$$M(\lambda, \lambda_\infty) = \int_\lambda^{\lambda_\infty} m(\lambda') d\lambda' \implies dM(\lambda, \lambda_\infty) = -m(\lambda) d\lambda, \quad (65.17)$$

which follows since λ_∞ is a constant.

The value of the fixed constant, λ_∞ , is arbitrarily large, indeed it could be infinite. We can set it to an arbitrarily large constant value since there is no contribution to the integral from regions with λ' outside the range realized within the ocean, merely since there is no ocean mass in that region. As an example, let $\lambda = \Theta$, the Conservative Temperature, in which the region $\Theta \leq \Theta_\infty$ encompasses the ocean region where the Conservative Temperature is larger (warmer) than Θ .

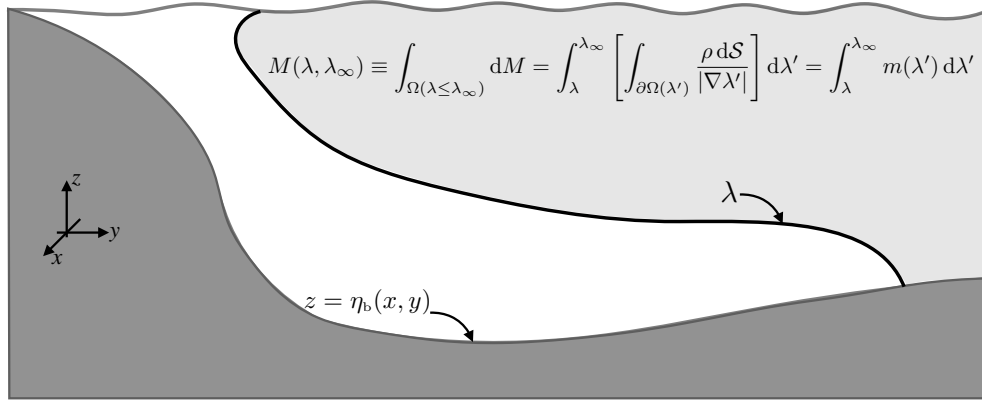


FIGURE 65.5: Depicting the mass of fluid within a λ_∞ -region, where $\lambda \leq \lambda_\infty$ with λ_∞ is an arbitrary constant that is larger than any value of λ in the ocean domain. This figure is oriented for the southern hemisphere with Antarctica on the left. An example of such a region is for $\lambda = \Theta$, whereby warmer waters are typically shallower and towards the equator.

$\lambda_{-\infty}$ -region defined by $[\lambda_1, \lambda_2] = [\lambda_{-\infty}, \lambda]$

A $\lambda_{-\infty}$ -region is defined with

$$\lambda_1 = \lambda_{-\infty} \text{ and } \lambda = \lambda, \quad (65.18)$$

where $\lambda_{-\infty}$ is an arbitrary constant that is smaller than any value of λ realized in the ocean. The region mass is thus given by

$$M(\lambda_{-\infty}, \lambda) \equiv \int_{\Omega(\lambda_{-\infty} \leq \lambda)} dM = \int_{\lambda_{-\infty}}^{\lambda} \left[\int_{\partial\Omega(\lambda')} \frac{\rho dS}{|\nabla\lambda'|} \right] d\lambda' = \int_{\lambda_{-\infty}}^{\lambda} m(\lambda') d\lambda'. \quad (65.19)$$

This mass is the complement of that contained in the λ_∞ -region. The $\lambda_{-\infty}$ -region mass implies a corresponding differential mass increment via

$$M(\lambda_{-\infty}, \lambda) = \int_{\lambda_{-\infty}}^{\lambda} m(\lambda') d\lambda' \implies dM(\lambda_{-\infty}, \lambda) = m(\lambda) d\lambda. \quad (65.20)$$

$\lambda_{\pm\infty}$ -region defined by $[\lambda_1, \lambda_2] = [\lambda_{-\infty}, \lambda_\infty]$

The full ocean is contained in the $\lambda_{\pm\infty}$ -region

$$\lambda_1 = \lambda_{-\infty} \text{ and } \lambda_2 = \lambda_\infty, \quad (65.21)$$

so that the full ocean mass is written

$$M(\lambda_{-\infty}, \lambda_\infty) = \int_{\Omega(\lambda_{-\infty} \leq \lambda \leq \lambda_\infty)} dM = \int_{\lambda_{-\infty}}^{\lambda_\infty} \left[\int_{\partial\Omega(\lambda)} \frac{\rho dS}{|\nabla\lambda|} \right] d\lambda = \int_{\lambda_{-\infty}}^{\lambda_\infty} m(\lambda') d\lambda'. \quad (65.22)$$

Difference of mass between two λ_∞ -regions

The difference in mass between two λ_∞ -regions is given by

$$M(\lambda_1, \lambda_\infty) - M(\lambda_2, \lambda_\infty) = \int_{\lambda_1}^{\lambda_\infty} \left[\int_{\partial\Omega(\lambda)} \frac{\rho dS}{|\nabla\lambda|} \right] d\lambda - \int_{\lambda_2}^{\lambda_\infty} \left[\int_{\partial\Omega(\lambda)} \frac{\rho dS}{|\nabla\lambda|} \right] d\lambda. \quad (65.23)$$

The arbitrary constant, λ_∞ , drops out when taking the difference so that we are left with the mass within the intersection of the two regions

$$M(\lambda_1, \lambda_2) = M(\lambda_1, \lambda_\infty) - M(\lambda_2, \lambda_\infty) = \int_{\lambda_1}^{\lambda_2} \left[\int_{\partial\Omega(\lambda)} \frac{\rho dS}{|\nabla \lambda|} \right] d\lambda = \int_{\lambda_1}^{\lambda_2} m(\lambda') d\lambda'. \quad (65.24)$$

65.3.5 Integrals of arbitrary functions

We can extend the above formalism to integrals of an arbitrary function, $\mathcal{F}(\mathbf{x}, t)$, over a region defined by $\lambda_{1,2}$ -interfaces

$$\mathcal{I}_{\mathcal{F}}(\lambda_1, \lambda_2) \equiv \int_{\Omega(\lambda_1 \leq \lambda \leq \lambda_2)} \mathcal{F} dM = \int_{\lambda_1}^{\lambda_2} \left[\int_{\partial\Omega(\lambda)} \frac{\mathcal{F} \rho dS}{|\nabla \lambda|} \right] d\lambda. \quad (65.25)$$

Performing the area integral amounts to binning the function according to λ -increments, in which case we define the distribution function

$$m_{\mathcal{F}}(\lambda) = \int_{\partial\Omega(\lambda)} \frac{\mathcal{F} \rho dS}{|\nabla \lambda|}, \quad (65.26)$$

so that an integral over the distribution is given by

$$\mathcal{I}_{\mathcal{F}}(\lambda_1, \lambda_2) = \int_{\lambda_1}^{\lambda_2} m_{\mathcal{F}}(\lambda) d\lambda. \quad (65.27)$$

In particular, consider the integral over a λ_∞ -region

$$\mathcal{I}_{\mathcal{F}}(\lambda, \lambda_\infty) = \int_{\lambda}^{\lambda_\infty} \left[\int_{\partial\Omega(\lambda')} \frac{\mathcal{F} \rho dS}{|\nabla \lambda'|} \right] d\lambda' = \int_{\lambda}^{\lambda_\infty} m_{\mathcal{F}}(\lambda') d\lambda', \quad (65.28)$$

which has the derivative

$$\frac{\partial \mathcal{I}_{\mathcal{F}}(\lambda, \lambda_\infty)}{\partial \lambda} = - \int_{\partial\Omega(\lambda)} \frac{\mathcal{F} \rho dS}{|\nabla \lambda|} = -m_{\mathcal{F}}(\lambda), \quad (65.29)$$

as follows from the fundamental theorem of calculus. Note how the derivative removes the reference value, λ_∞ . Analogously, the integral over a $\lambda_{-\infty}$ -region has the derivative

$$\frac{\partial \mathcal{I}_{\mathcal{F}}(\lambda_{-\infty}, \lambda)}{\partial \lambda} = \int_{\partial\Omega(\lambda)} \frac{\mathcal{F} \rho dS}{|\nabla \lambda|} = m_{\mathcal{F}}(\lambda). \quad (65.30)$$

65.3.6 Moments of λ

Setting $\mathcal{F} = \lambda$ in the integral (65.25) renders

$$\Lambda(\lambda_1, \lambda_2) \equiv \int_{\Omega(\lambda_1 \leq \lambda \leq \lambda_2)} \lambda dM = \int_{\Omega(\lambda_1 \leq \lambda \leq \lambda_2)} \lambda \rho dV = \int_{\lambda_1}^{\lambda_2} \left[\int_{\partial\Omega(\lambda)} \frac{\lambda \rho dS}{|\nabla \lambda|} \right] d\lambda. \quad (65.31)$$

If λ is a tracer concentration (tracer mass per seawater mass), then $\Lambda(\lambda_1, \lambda_2)$ is the mass of tracer within the layer. Observe that λ can be pulled outside of the surface integral in equation (65.31)

since λ is constant along $\partial\Omega(\lambda)$, thus rendering

$$\Lambda(\lambda_1, \lambda_2) = \int_{\lambda_1}^{\lambda_2} \left[\int_{\partial\Omega(\lambda)} \frac{\rho d\mathcal{S}}{|\nabla\lambda|} \right] \lambda d\lambda = \int_{\lambda_1}^{\lambda_2} m(\lambda) \lambda d\lambda. \quad (65.32)$$

We can likewise define any higher powers as

$$\Lambda^{(n)}(\lambda_1, \lambda_2) \equiv \int_{\lambda_1}^{\lambda_2} \left[\int_{\partial\Omega(\lambda)} \frac{\rho d\mathcal{S}}{|\nabla\lambda|} \right] \lambda^n d\lambda = \int_{\lambda_1}^{\lambda_2} m(\lambda) \lambda^n d\lambda = M(\lambda_1, \lambda_2) \langle \lambda^n \rangle. \quad (65.33)$$

The final equality introduced the mean value for the power

$$\langle \lambda^n \rangle = \frac{\int_{\lambda_1}^{\lambda_2} m(\lambda) \lambda^n d\lambda}{\int_{\lambda_1}^{\lambda_2} m(\lambda) d\lambda} \quad (65.34)$$

as defined over the $[\lambda_1, \lambda_2]$ region. We refer to $\langle \lambda^n \rangle$ as the n -moment of λ , with $n = 1$ yielding the mean.

65.3.7 Internal and external λ -moments

Now specify the region $[\lambda_1, \lambda_2] = [\tilde{\lambda}, \lambda_\infty]$ for the moment equation (65.33). Making use of the differential mass increment, $dM(\lambda, \lambda_\infty) = -m(\lambda) d\lambda$ as in equation (65.17) allows us to integrate the moment equation by parts

$$\Lambda^{(n)}(\tilde{\lambda}, \lambda_\infty) = \int_{\tilde{\lambda}}^{\lambda_\infty} \lambda^n m(\lambda) d\lambda \quad (65.35a)$$

$$= - \int_{\tilde{\lambda}}^{\lambda_\infty} \lambda^n dM \quad (65.35b)$$

$$= \int_{\tilde{\lambda}}^{\lambda_\infty} [-d(\lambda^n M) + n M \lambda^{n-1} d\lambda] \quad (65.35c)$$

$$= -\lambda_\infty^n M(\lambda_\infty, \lambda_\infty) + \lambda_\infty^n M(\tilde{\lambda}, \lambda_\infty) + n \int_{\tilde{\lambda}}^{\lambda_\infty} M(\lambda, \lambda_\infty) \lambda^{n-1} d\lambda \quad (65.35d)$$

$$= \lambda_\infty^n M(\tilde{\lambda}, \lambda_\infty) + n \int_{\tilde{\lambda}}^{\lambda_\infty} M(\lambda, \lambda_\infty) \lambda^{n-1} d\lambda, \quad (65.35e)$$

where the final equality follows since $M(\lambda_\infty, \lambda_\infty) = 0$. Making use of equation (65.33) thus leads to

$$M(\tilde{\lambda}, \lambda_\infty) \langle \lambda^n \rangle = \underbrace{M(\tilde{\lambda}, \lambda_\infty) \tilde{\lambda}^n}_{\text{external moment}} + \underbrace{n \int_{\tilde{\lambda}}^{\lambda_\infty} M(\lambda, \lambda_\infty) \lambda^{n-1} d\lambda}_{\text{internal moment}}. \quad (65.36)$$

We refer to the rightmost term as the *internal moment* since it is an integral over the region, whereas $M(\tilde{\lambda}, \lambda_\infty) \tilde{\lambda}^n$ is the *external moment*, which is the region mass times the boundary value, $\tilde{\lambda}^n$. We choose the moniker “external” since the external moment increases in direct proportion to the mass crossing the ocean layer boundaries, including the external boundaries. In Section 65.6 we develop a budget for the $n = 1$ moment, in which the internal moment from equation (65.36) takes the form

$$M(\tilde{\lambda}, \lambda_\infty) [\langle \lambda \rangle - \tilde{\lambda}] = \int_{\tilde{\lambda}}^{\lambda_\infty} M(\lambda, \lambda_\infty) d\lambda. \quad (65.37)$$

We return to the notion of internal and external moments in Section 65.10.2.

65.3.8 Further study

The formulation given here in terms of mass distribution functions follows that of [Waln \(1977\)](#) and [Waln \(1982\)](#). In these two papers, Waln pioneered the formalism of water mass analysis, which is sometimes referred to as *Waln analysis* in his honor. The concept of internal and external tracer moments follows the internal and external heat introduced by [Holmes et al. \(2019\)](#).

65.4 Water mass transformation across a λ -surface

We here develop the formalism to quantify transport of seawater crossing an interior λ -interface. This transport is referred to as the *water mass transformation* and is written as $G(\lambda)$. Figure 65.6 illustrates how this transformation appears in a mass budget for a $\Delta\lambda$ -layer. We assume that λ satisfies a scalar equation taking the form of a tracer equation (discussed in Section 65.4.3).

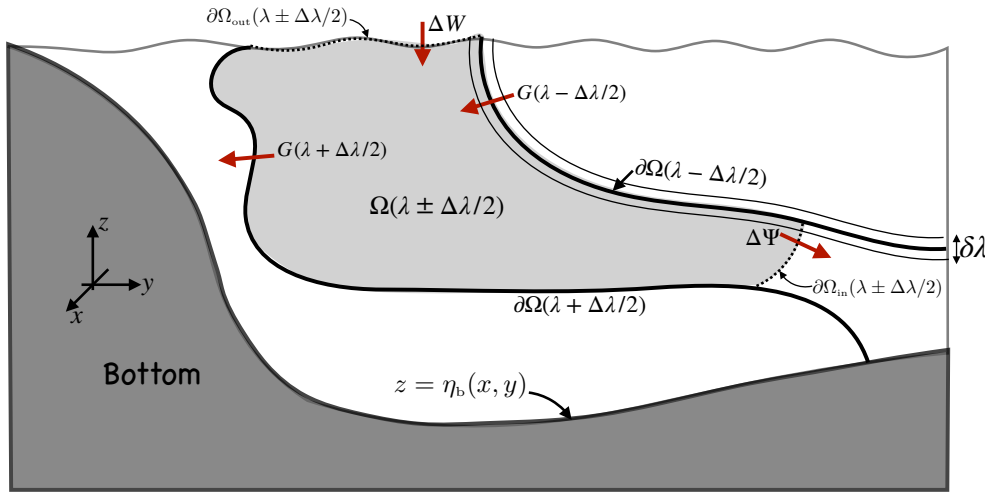


FIGURE 65.6: A layer of seawater with scalar property λ within the range $[\lambda - \Delta\lambda/2, \lambda + \Delta\lambda/2]$ and defined over a geographical domain $\Omega(\lambda \pm \Delta\lambda/2)$. In this example, λ increases to the south, towards Antarctica, with $\lambda = \gamma$ (Section 65.2) an example. The net seawater mass transport crossing the layer interfaces $\partial\Omega(\lambda \pm \Delta\lambda/2)$ is $G(\lambda \pm \Delta\lambda/2)$, with $G > 0$ for water moving to regions of larger λ . The seawater mass crossing the layer through the geographical bounds $\partial\Omega_{in}(\lambda \pm \Delta\lambda/2)$ is written $\Delta\Psi(\lambda \pm \Delta\lambda/2)$, with $\Delta\Psi(\lambda \pm \Delta\lambda/2) > 0$ for water leaving $\Omega(\lambda \pm \Delta\lambda/2)$. The boundary $\partial\Omega_{in}(\lambda \pm \Delta\lambda/2)$ is absent when the domain extends across a basin or the global ocean (e.g., see Figure 65.8). The mass crossing the sea surface, $\partial\Omega_{out}(\lambda \pm \Delta\lambda/2)$, through rain, evaporation, melt, or rivers is written $\Delta W(\lambda \pm \Delta\lambda/2)$, with $\Delta W(\lambda \pm \Delta\lambda/2) > 0$ for mass entering $\Omega(\lambda \pm \Delta\lambda/2)$. A layer interface can have an arbitrary stratification, such as the vertically non-monotonic profile depicted here for the $\lambda + \Delta\lambda/2$ interface. Additionally, the domain $\Omega(\lambda \pm \Delta\lambda/2)$ can generally be disconnected. The net domain boundaries are written $\partial\Omega_{in}(\lambda \pm \Delta\lambda/2) + \partial\Omega_{out}(\lambda \pm \Delta\lambda/2) + \partial\Omega(\lambda + \Delta\lambda/2) + \partial\Omega(\lambda - \Delta\lambda/2)$. The $\delta\lambda$ layer surrounding the $\partial\Omega(\lambda - \Delta\lambda/2)$ arises as part of the method detailed in Section 65.4.2 for computing G according to the λ -derivative of an integral over the $\delta\lambda$ layer.

65.4.1 Dia-surface flux and interior transformation

The object that measures the local water mass transformation is the dia-surface flux detailed in Section 57.4.7. This flux is given by

$$w^{\text{dia}} = \hat{\mathbf{n}} \cdot (\mathbf{v} - \mathbf{v}^{(\lambda)}) = \frac{\dot{\lambda}}{|\nabla\lambda|} \quad \text{with} \quad \hat{\mathbf{n}} = \frac{\nabla\lambda}{|\nabla\lambda|} \quad \text{and} \quad \dot{\lambda} = \frac{D\lambda}{Dt}, \quad (65.38)$$

with $w^{\text{dia}} > 0$ for water moving to regions of larger λ . It is computed as the projection of the relative velocity, $(\mathbf{v} - \mathbf{v}^{(\lambda)})$, onto the direction normal to the surface, with the relative velocity being the difference between the fluid particle velocity, \mathbf{v} , and the velocity of a point on the λ -interface, $\mathbf{v}^{(\lambda)}$. The velocity of a point on the surface, $\mathbf{v}^{(\lambda)}$, satisfies the following kinematic constraint⁹

$$(\partial_t + \mathbf{v}^{(\lambda)} \cdot \nabla) \lambda = 0. \quad (65.39)$$

This constraint is based on assuming $\mathbf{v}^{(\lambda)}$ measures the velocity of a point fixed to the λ -surface. So in brief, the dia-surface flux, w^{dia} , locally measures the flux of seawater (volume per area per time) that penetrates a λ -interface in the direction of increasing λ .

The interior water mass transformation, $G(\lambda)$, is the area integral of ρw^{dia} over the full extent of the λ -surface

$$G(\lambda) \equiv \int_{\partial\Omega(\lambda)} \rho w^{\text{dia}} dS = \int_{\partial\Omega(\lambda)} \rho \hat{\mathbf{n}} \cdot (\mathbf{v} - \mathbf{v}^{(\lambda)}) dS = \int_{\partial\Omega(\lambda)} \frac{\rho \dot{\lambda}}{|\nabla \lambda|} dS, \quad (65.40)$$

where $\partial\Omega(\lambda)$ is the surface occupied by the λ -interface (see Figure 65.6). Furthermore, the dimensions of $G(\lambda)$ are mass per time

$$G(\lambda) \quad [=] \quad \text{M T}^{-1}, \quad (65.41)$$

thus measuring the mass per time crossing the λ -interface.

Based on the definition (65.40), we see that interior water mass transformation across a λ -interface occurs when there is a material change, $\dot{\lambda} \neq 0$, in the property defining the interface. Interior material changes arise from mixing, which generally causes irreversible changes to λ , thus driving seawater across the moving λ -interfaces. Material changes can also arise from sources and sinks, as when considering buoyancy surfaces in the presence of a nonlinear equation of state (Chapter 64). Sources and sinks are also commonly encountered by biogeochemical tracers.

65.4.2 Transformation as the derivative of an integral

Following the discussion from Section 65.3.5, we set $\mathcal{F} = \dot{\lambda}$ and consider the mass integral

$$\mathcal{I}_{\dot{\lambda}}(\lambda, \lambda_{\infty}) = \int_{\Omega(\lambda \leq \lambda_{\infty})} \dot{\lambda}' dM = \int_{\lambda}^{\lambda_{\infty}} \left[\int_{\partial\Omega(\lambda')} \frac{\rho \dot{\lambda}'}{|\nabla \lambda'|} dS \right] d\lambda' = \int_{\lambda}^{\lambda_{\infty}} G(\lambda') d\lambda'. \quad (65.42)$$

The fundamental theorem of calculus leads to the expression of the water mass transformation as the derivative

$$G(\lambda) = -\frac{\partial \mathcal{I}_{\dot{\lambda}}(\lambda, \lambda_{\infty})}{\partial \lambda} \quad (65.43a)$$

$$= -\lim_{\delta\lambda \rightarrow 0} \frac{1}{\delta\lambda} \left[\int_{\lambda+\delta\lambda/2}^{\lambda_{\infty}} G(\lambda') d\lambda' - \int_{\lambda-\delta\lambda/2}^{\lambda_{\infty}} G(\lambda') d\lambda' \right] \quad (65.43b)$$

$$= \lim_{\delta\lambda \rightarrow 0} \frac{1}{\delta\lambda} \int_{\lambda-\delta\lambda/2}^{\lambda+\delta\lambda/2} G(\lambda') d\lambda' \quad (65.43c)$$

$$= \lim_{\delta\lambda \rightarrow 0} \frac{1}{\delta\lambda} \int_{\Omega(\lambda \pm \delta\lambda/2)} \rho \dot{\lambda}' dV. \quad (65.43d)$$

⁹We encountered the relation (65.39) in Section 16.4.2 when deriving the kinematic boundary condition for a moving surface.

We conclude that calculation of interior water mass transformation requires the various contributions to the material time change, $\dot{\lambda}$, a weighting of the time changes according to the mass of the fluid element, $dM = \rho dV$, and a binning of $\rho \dot{\lambda} dV$ according to λ -classes. Note that in the final equality, equation (65.43d), the limit $\delta\lambda \rightarrow 0$ might appear to lead to a singularity. However, as seen by the form in equation (65.43c), the integration region volume also gets smaller as $\delta\lambda \rightarrow 0$ so that the limit is well defined.

65.4.3 Processes and kinematics

There are two equivalent and complementary methods to view interior water mass transformation: the process method and the kinematic method.

Process method

The *process method* focuses on physical processes leading to movement of fluid across the λ -interface, thus providing information concerning *why* interior transformation occurs. It does so by binning processes contributing to the right hand side of the equation

$$\rho \dot{\lambda} = -\nabla \cdot \mathbf{J} + \rho \dot{\Upsilon}, \quad (65.44)$$

where \mathbf{J} is a flux arising from non-advection processes such as diffusion, and $\dot{\Upsilon}$ is a source/sink term (dimensions of λ per time) that cannot be written as the convergence of a flux. The tracer equation (65.44) inserted into the transformation equation (65.43d) leads to

$$G(\lambda) = \lim_{\delta\lambda \rightarrow 0} \frac{1}{\delta\lambda} \int_{\Omega(\lambda \pm \delta\lambda/2)} [-\nabla \cdot \mathbf{J} + \rho \dot{\Upsilon}] dV \quad (65.45a)$$

$$= \lim_{\delta\lambda \rightarrow 0} \frac{1}{\delta\lambda} \oint_{\partial\Omega(\lambda \pm \delta\lambda/2)} [-\mathbf{J} \cdot \hat{\mathbf{n}}] dS + \lim_{\delta\lambda \rightarrow 0} \frac{1}{\delta\lambda} \int_{\Omega(\lambda \pm \delta\lambda/2)} \rho \dot{\Upsilon} dV, \quad (65.45b)$$

The second equality made use of the divergence theorem to convert the volume integral into a surface integral. For the tracer sources, we assume they do not modify the seawater mass at a point so that there is no source in the seawater mass equation.

For many purposes it is useful to decompose the non-advection flux divergence into contributions from interior processes, such as ocean mixing, and boundary fluxes

$$\nabla \cdot \mathbf{J} = \nabla \cdot [\mathbf{J}_{\text{int}} + \mathbf{J}_{\text{out}} + \mathbf{J}_{\text{bot}}]. \quad (65.46)$$

By definition,

$$\mathbf{J}_{\text{int}} \cdot \hat{\mathbf{n}} = 0 \quad \text{on } \partial\Omega_{\text{out}}(\lambda \pm \delta\lambda/2) \text{ and } \partial\Omega_{\text{bot}}(\lambda \pm \delta\lambda/2), \quad (65.47)$$

whereas $\mathbf{J}_{\text{int}} \cdot \hat{\mathbf{n}}$ is generally nonzero on interior layer boundaries. In contrast, the boundary fluxes, $\mathbf{J}_{\text{out}} \cdot \hat{\mathbf{n}}$ and $\mathbf{J}_{\text{bot}} \cdot \hat{\mathbf{n}}$, are identically zero everywhere except on their respective boundaries. Correspondingly, it is convenient to bin the volume weighted divergence, $\nabla \cdot \mathbf{J}_{\text{int}} dV$, according to λ -classes, and to likewise bin the area weighted boundary fluxes, $\mathbf{J}_{\text{out}} \cdot \hat{\mathbf{n}} dS$ and $\mathbf{J}_{\text{bot}} \cdot \hat{\mathbf{n}} dS$. In

this way we write the non-advection contribution to water mass transformation in the form

$$\begin{aligned} G(\lambda)_{\text{non-adv}} = & \underbrace{-\lim_{\delta\lambda\rightarrow 0} \frac{1}{\delta\lambda} \int_{\Omega(\lambda\pm\delta\lambda/2)} \nabla \cdot \mathbf{J}_{\text{int}} \, dV}_{\text{interior transformation} = \text{volume integral of convergence}} \\ & -\underbrace{\lim_{\delta\lambda\rightarrow 0} \frac{1}{\delta\lambda} \int_{\partial\Omega_{\text{out}}(\lambda\pm\delta\lambda/2)} \mathbf{J}_{\text{out}} \cdot \hat{\mathbf{n}} \, d\mathcal{S}}_{\text{surface transformation} = \text{area integral of surface boundary fluxes}} \\ & -\underbrace{\lim_{\delta\lambda\rightarrow 0} \frac{1}{\delta\lambda} \int_{\partial\Omega_{\text{bot}}(\lambda\pm\delta\lambda/2)} \mathbf{J}_{\text{bot}} \cdot \hat{\mathbf{n}} \, d\mathcal{S}}_{\text{bottom transformation} = \text{area integral of bottom boundary fluxes}}. \end{aligned} \quad (65.48)$$

Again, this expression decomposes the contribution from interior processes, here represented as the volume integral of the interior flux convergence, from the surface and bottom contributions, here represented as the area integral of the boundary fluxes. This decomposition is further examined in Section 65.7 where we focus on the surface contribution to water mass transformation.

Since the boundary fluxes are, by definition, zero except on the boundaries, their divergence can be written in terms of a Dirac delta distribution¹⁰

$$\nabla \cdot [\mathbf{J}_{\text{out}} + \mathbf{J}_{\text{bot}}] = \mathbf{J}_{\text{out}} \cdot \hat{\mathbf{n}} \delta(z - \eta) + \mathbf{J}_{\text{bot}} \cdot \hat{\mathbf{n}} \delta(z - \eta_b). \quad (65.49)$$

Although this equation is more physically formal than mathematically rigorous, its use in the transformation equation (65.45a) correctly leads to the expression (65.48). Consequently, equation (65.49) proves to be a useful shorthand that is commonly used in the literature (e.g., [Groeskamp et al. \(2019\)](#)).

Kinematic method

The *kinematic method* focuses on the kinematic means for realizing dia-surface transport, thus providing information concerning *how* interior transformation occurs. It does so by binning processes contributing to the right hand side of

$$\rho \dot{\lambda} = \partial_t(\rho \lambda) + \nabla \cdot (\rho \lambda \mathbf{v}), \quad (65.50)$$

which arises from the local time tendency plus advection, so that

$$G(\lambda) = \lim_{\delta\lambda\rightarrow 0} \frac{1}{\delta\lambda} \int_{\Omega(\lambda\pm\delta\lambda/2)} [\partial_t(\rho \lambda) + \nabla \cdot (\rho \lambda \mathbf{v})] \, dV. \quad (65.51)$$

Comments

As we saw, equality of the process method and kinematic method follows simply because the two provide equivalent expressions for the material time derivative. However, in the analysis of numerical model output, it can be nontrivial to realize this equivalence due to the extreme care required to diagnose the terms appearing in the scalar budget equation.

¹⁰We detail properties of the Dirac delta distribution in Section 4.3. It has dimensions equal to the inverse the dimensions of its argument (Section 4.3.9). For example, when the argument has dimensions of length then the Dirac delta has dimensions of inverse length. We thus see that equation (65.49) is dimensionally consistent.

65.4.4 Some details concerning interior transformation

We here consider some details of the water mass transformation arising just from interior processes such as diffusion.

A global integrated constraint on $G(\lambda)_{\text{int}}$

Consider the integrated water mass transformation given by equation (65.42), only now integrate over the full ocean domain

$$\mathcal{G}_{\dot{\lambda}}(\lambda_{-\infty}, \lambda_{\infty}) = \int_{\lambda_{-\infty}}^{\lambda_{\infty}} G(\lambda') d\lambda' = \int_{\Omega(\lambda_{-\infty}, \lambda_{\infty})} \rho \dot{\lambda}' dV. \quad (65.52)$$

This integral vanishes for water mass transformations arising from conservative interior processes (i.e., those processes determined by the convergence of a flux)

$$[\mathcal{G}_{\dot{\lambda}}(\lambda_{-\infty}, \lambda_{\infty})]_{\text{int}} = \int_{\lambda_{-\infty}}^{\lambda_{\infty}} G(\lambda')_{\text{int}} d\lambda' \quad (65.53a)$$

$$= - \int_{\Omega(\lambda_{-\infty}, \lambda_{\infty})} \nabla \cdot \mathbf{J}_{\text{int}} dV \quad (65.53b)$$

$$= - \oint_{\partial\Omega(\lambda_{-\infty}, \lambda_{\infty})} \mathbf{J}_{\text{int}} \cdot \hat{\mathbf{n}} dS \quad (65.53c)$$

$$= 0, \quad (65.53d)$$

which follows since $\mathbf{J}_{\text{int}} \cdot \hat{\mathbf{n}} = 0$ on the ocean boundaries. Hence, there can be no net water mass transformation across a λ surface arising from conservative interior processes

$$\int_{\lambda_{-\infty}}^{\lambda_{\infty}} G(\lambda')_{\text{int}} d\lambda' = 0. \quad (65.54)$$

Instead, conservative interior processes only lead to rearrangement of water within the λ -bins. This result follows since these interior processes conserve the total content of λ within the global domain. Equation (65.54) provides a constraint that should be verified by any numerical realization of water mass transformation.

Interior transformation across constant λ surfaces

We now focus on the transformation occurring along surfaces of constant λ (Figure 65.7) so that

$$G(\lambda)_{\text{int}} = - \lim_{\delta\lambda \rightarrow 0} \frac{1}{\delta\lambda} \int_{\Omega(\lambda \pm \delta\lambda/2)} \nabla \cdot \mathbf{J}_{\text{int}} dV \quad (65.55a)$$

$$= - \lim_{\delta\lambda \rightarrow 0} \frac{1}{\delta\lambda} \left[\int_{\Omega(\lambda + \delta\lambda/2)} \hat{\mathbf{n}} \cdot \mathbf{J}_{\text{int}} dS - \int_{\Omega(\lambda - \delta\lambda/2)} \hat{\mathbf{n}} \cdot \mathbf{J}_{\text{int}} dS \right]. \quad (65.55b)$$

Transformation occurs if there is an imbalance between the diffusive transport across the two bounding surfaces, $\Omega(\lambda + \delta\lambda/2)$ and $\Omega(\lambda - \delta\lambda/2)$. As a special case, assume the ocean surface is a constant λ surface with $\lambda = \lambda_{\text{top}}$. Along this surface we have $\hat{\mathbf{n}} \cdot \mathbf{J}_{\text{int}} = 0$, so that the transformation at $\lambda_{\text{top}} - \delta\lambda/2$ has a contribution just from the flux crossing the $\Omega(\lambda_{\text{top}} - \delta\lambda)$ surface

$$\lim_{\delta\lambda \rightarrow 0} G(\lambda_{\text{top}} - \delta\lambda/2)_{\text{int}} = \lim_{\delta\lambda \rightarrow 0} \frac{1}{\delta\lambda} \int_{\Omega(\lambda_{\text{top}} - \delta\lambda)} \hat{\mathbf{n}} \cdot \mathbf{J}_{\text{int}} dS. \quad (65.56)$$

Likewise, along the top surface we have

$$G(\lambda_{\text{top}})_{\text{int}} = \lim_{\delta\lambda \rightarrow 0} \frac{1}{\delta\lambda} \int_{\Omega(\lambda_{\text{top}} - \delta\lambda/2)} \hat{\mathbf{n}} \cdot \mathbf{J}_{\text{int}} \, d\mathcal{S}, \quad (65.57)$$

where we set $\hat{\mathbf{n}} \cdot \mathbf{J}_{\text{int}} = 0$ for the surface $\Omega(\lambda_{\text{top}} + \delta\lambda/2)$, since this surface exists outside of the ocean.

The results (65.56) and (65.57) make it appear that $G(\lambda_{\text{top}} - \delta\lambda/2)_{\text{int}}$ and $G(\lambda_{\text{top}})_{\text{int}}$ are unbounded as $\delta\lambda \rightarrow 0$, so long as there is a nonzero diffusive transport through $\Omega(\lambda_{\text{top}} - \delta\lambda)$ or $\Omega(\lambda_{\text{top}} + \delta\lambda/2)$. However, this unbounded water mass transformation is not realized since the diffusive flux gets smaller in magnitude when approaching the ocean surface, and it does so in order to satisfy the no-flux surface boundary condition (65.47) satisfied by interior processes¹¹

$$\hat{\mathbf{n}} \cdot \mathbf{J}_{\text{int}} = 0 \quad \text{at } z = \eta. \quad (65.58)$$

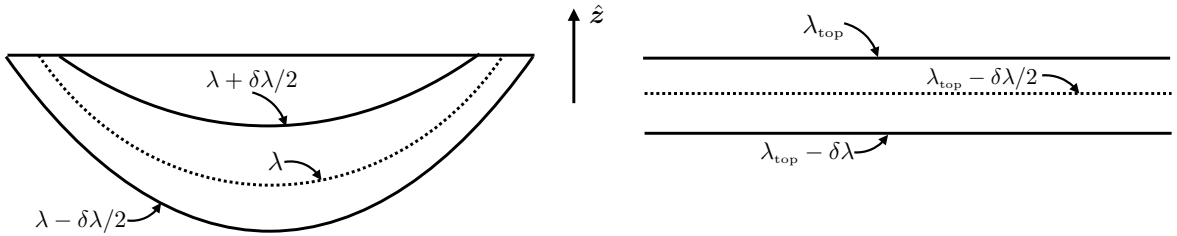


FIGURE 65.7: Example λ surfaces for studying interior transformation due to diffusion. The left panel shows λ surfaces that outcrop to the ocean surface, with the dotted surface the chosen λ surface across which we compute the water mass transformation. The right panel assumes the λ surfaces are flat and with $\lambda = \lambda_{\text{top}}$ the value along the ocean surface.

To further our understanding of the transformation in the region near the ocean surface, let the λ surfaces be flat near the ocean surface so that $\hat{\mathbf{n}} = -\hat{\mathbf{z}}$ along $\Omega(\lambda_{\text{top}} - \delta\lambda)$. Setting the diffusive flux to

$$\mathbf{J} = -\rho_0 \kappa \nabla \lambda \quad (65.59)$$

as per a Boussinesq fluid with reference density ρ_0 and diffusivity $\kappa > 0$, leads to the transformation

$$G(\lambda_{\text{top}} - \delta\lambda/2)_{\text{int}} = \frac{1}{\delta\lambda} \int_{\Omega(\lambda_{\text{top}} - \delta\lambda)} (\rho_0 \kappa \partial_z \lambda) \, d\mathcal{S}. \quad (65.60)$$

With $\kappa \partial_z \lambda > 0$, the transformation is positive, $G(\lambda_{\text{top}} - \delta\lambda/2)_{\text{int}} > 0$, so that water is entrained into the layer bounded by $\lambda_{\text{top}} - \delta\lambda$ and λ_{top} . Note that in the absence of boundary fluxes, the value of λ_{top} is reduced due to diffusive mixing with interior waters since these waters have lower values of λ . Furthermore, as the surface is approached, $\partial_z \lambda$ reduces in magnitude to satisfy the no-flux condition, $\kappa \partial_z \lambda = 0$, at the ocean surface. In this manner, the transformation remains bounded even as $\delta\lambda \rightarrow 0$.

¹¹As discussed in Sections 17.6.3, 64.5, and 65.8.3, when water is transported across the ocean surface the diffusive flux picks up a nonzero boundary contribution. That contribution is assumed to be part of the surface transformation in equation (65.48) so that the interior diffusive flux still satisfies the no-flux boundary condition (65.58). *Nurser and Griffies (2019)* discuss these points for salinity.

65.5 Budget for seawater mass in a $\Delta\lambda$ -layer

In this section we construct the seawater mass budget for a $\Delta\lambda$ -layer, making reference to Figure 65.6 for the notation. As a shorthand, we write the layer mass as

$$\Delta M(\lambda \pm \Delta\lambda/2) \equiv M(\lambda - \Delta\lambda/2, \lambda + \Delta\lambda/2), \quad (65.61)$$

along with a similar notation for other contributions to the layer mass budget.

65.5.1 Transport crossing interior open boundaries

As depicted in Figure 65.6, the layer region has an open boundary that is within the interior of the ocean. The mass transport leaving the layer through this interior open boundary is written

$$\Delta\Psi(\lambda \pm \Delta\lambda/2) = \int_{\partial\Omega_{in}(\lambda \pm \Delta\lambda/2)} \rho (\mathbf{v} - \mathbf{v}^{(b)}) \cdot \hat{\mathbf{n}} dS, \quad (65.62)$$

where $\mathbf{v}^{(b)}$ is the velocity for a point on the boundary and $\hat{\mathbf{n}}$ is the outward normal along the boundary. Introducing the mass distribution for this transport renders the equivalent expression

$$\Delta\Psi(\lambda \pm \Delta\lambda/2) = \int_{\lambda - \Delta\lambda/2}^{\lambda + \Delta\lambda/2} \dot{m}_\Psi(\lambda') d\lambda', \quad (65.63)$$

where

$$\dot{m}_\Psi(\lambda) d\lambda = \text{mass per time crossing } \partial\Omega_{in} \text{ within the increment } [\lambda - d\lambda/2, \lambda + d\lambda/2]. \quad (65.64)$$

We make particular use of \dot{m}_Ψ in Section 65.6 when studying the λ -budget in a $\Delta\lambda$ -layer. One common example for an open interior boundary is when choosing a particular latitude, in which case $\mathbf{v}^{(b)} = 0$ and $\hat{\mathbf{n}} = \hat{\mathbf{y}}$ so that

$$\Delta\Psi(\lambda \pm \Delta\lambda/2) = \int_{\partial\Omega_{in}(\lambda \pm \Delta\lambda/2)} \rho v dx dz. \quad (65.65)$$

In this case, $\partial\Omega_{in}(\lambda \pm \Delta\lambda/2)$ specifies the depth and longitude range for the layer at its intersection along the constant latitude boundary.

65.5.2 Mass transport crossing the ocean surface

The mass transport crossing the ocean free surface is written

$$\Delta W(\lambda \pm \Delta\lambda/2) = - \int_{\partial\Omega_{out}(\lambda \pm \Delta\lambda/2)} \rho (\mathbf{v} - \mathbf{v}^{(\eta)}) \cdot \hat{\mathbf{n}} dS = \int_{\partial\Omega_{out}(\lambda \pm \Delta\lambda/2)} \mathcal{Q}_m dS, \quad (65.66)$$

where we made use of the surface kinematic boundary condition (16.63) to write

$$\rho (\mathbf{v} - \mathbf{v}^{(b)}) \cdot \hat{\mathbf{n}} \equiv -\mathcal{Q}_m, \quad (65.67)$$

where $\mathcal{Q}_m dS$ is the mass transport of water crossing the free surface ($\mathcal{Q}_m > 0$ for water entering the ocean). Introducing the mass distribution leads to the equivalent expression

$$\Delta W(\lambda \pm \Delta\lambda/2) = \int_{\lambda - \Delta\lambda/2}^{\lambda + \Delta\lambda/2} \dot{m}_w(\lambda') d\lambda', \quad (65.68)$$

where

$$\dot{m}_W(\lambda) d\lambda = \text{mass per time crossing } \partial\Omega_{\text{out}} \text{ within the increment } [\lambda - d\lambda/2, \lambda + d\lambda/2]. \quad (65.69)$$

We make particular use of \dot{m}_W in Section 65.6 when studying the λ -budget in a $\Delta\lambda$ -layer.

65.5.3 Mass budget

Bringing the above pieces together leads to the layer mass budget

$$\frac{d\Delta M}{dt} = -\Delta\Psi + \Delta W - [G(\lambda + \Delta\lambda/2) - G(\lambda - \Delta\lambda/2)], \quad (65.70)$$

where for brevity we dropped $\lambda \pm \Delta\lambda/2$ arguments for ΔM , $\Delta\Psi$, and ΔW . It is common to define the layer mass *formation* as the mass accumulation within the layer

$$\underbrace{\frac{d\Delta M}{dt} + \Delta\Psi}_{\text{storage + outflow}} = \underbrace{\Delta W - [G(\lambda + \Delta\lambda/2) - G(\lambda - \Delta\lambda/2)]}_{\text{formation into layer } \Omega_{(\lambda \pm \Delta\lambda/2)}}. \quad (65.71)$$

This equality defines water mass formation as the time change for the mass within the layer (sometimes referred to as the *storage term*), plus the net mass leaving the interior open boundary. Formation into a layer occurs if there is mass converging through transformation across interior layer interfaces, plus mass entering through the surface boundary outcrop region.

We arrive at a differential equation for the mass budget (65.71) by dividing through by the layer increment, $\Delta\lambda$, and taking the limit as this increment tends to zero

$$\frac{\partial}{\partial\lambda} \left[\frac{dM}{dt} + \Psi - W + G \right] = 0. \quad (65.72)$$

Integrating from a reference value $\lambda_{-\infty}$ to λ leads to

$$\int_{\lambda_{-\infty}}^{\lambda} \frac{\partial\Psi}{\partial\lambda} d\lambda = \int_{\lambda_{-\infty}}^{\lambda} \frac{\partial}{\partial\lambda} \left[-\frac{dM}{dt} + W - G \right] d\lambda \implies \Psi = -\frac{dM}{dt} + W - G. \quad (65.73)$$

We dropped the contribution from the constant reference value, $\lambda_{-\infty}$, since it sits outside of the ocean domain. The differential water mass equation (65.73) is a continuous version of the discrete equation (65.71). We wrote this equation as an expression for Ψ given that an accumulation from the bottom up leads to a transport streamfunction in the steady limit.

65.6 Budget for λ mass in a λ_∞ -region

We build from our understanding of the seawater mass budget in Section 65.5 to develop a budget for the mass of λ within the λ_∞ -region of Section 65.3.4 and as illustrated in Figure 65.8. Part of our aim is to further develop the formalism while also offering added insights into the causes for water mass transformation, $G(\lambda)$.

We here choose to be specific by considering λ to be an intensive property such as a material tracer concentration, in which case $\lambda \rho dV$ has dimensions of tracer mass.¹² For non-material scalar fields, such as Conservative Temperature or buoyancy, the dimensions are modified accordingly.

¹²See Section 17.3.1 for more on intensive and extensive fluid properties.

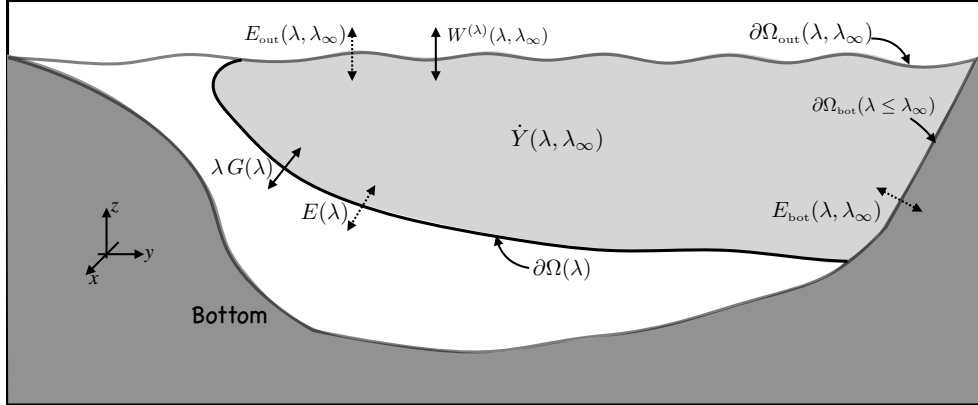


FIGURE 65.8: A λ_∞ -region for studying the λ budget, with the region bounded by the solid-earth bottom, $\partial\Omega_{\text{bot}}(\lambda \leq \lambda_\infty)$, the ocean surface boundary, $\partial\Omega_{\text{out}}(\lambda, \lambda_\infty)$, and the λ -interface, $\partial\Omega(\lambda)$. Hence, in contrast to the $\Delta\lambda$ -region shown in Figure 65.6, the λ_∞ -region has no interior open boundary. Along the surface boundary, the λ budget is affected by the non-advective transport, $E_{\text{out}}(\lambda, \lambda_\infty)$, arising from processes such as diffusion, plus advective transport, $W^{(\lambda)}(\lambda, \lambda_\infty)$, arising from mass transported across the surface that can carry a non-zero amount of λ . Along the bottom boundary, the λ budget is affected by non-advective transport, $E_{\text{bot}}(\lambda, \lambda_\infty)$, arising from processes such as geothermal heating. There is no corresponding advective transport along the bottom since we assume there is no mass crossing the ocean bottom. Along the interior boundary, $\partial\Omega(\lambda)$, the budget is affected by non-advective transport, $E(\lambda)$, arising from diffusion, as well as advective transport through $\lambda G(\lambda)$, with $G(\lambda)$ the interior water mass transformation from Section 65.4. Finally, there is the possibility for an interior volume source, $\dot{Y}(\lambda \leq \lambda_\infty)$, particularly for buoyancy in the presence of a nonlinear equation of state, and for biogeochemical tracers.

65.6.1 Processes affecting the mass of λ -stuff

Our starting point is the Leibniz-Reynolds budget for a scalar field derived in Section 17.3.4, here including the possibility of scalar sources

$$\frac{d}{dt} \left[\int_{\Omega(\lambda \leq \lambda_\infty)} \rho \lambda dV \right] = \int_{\Omega(\lambda \leq \lambda_\infty)} \rho \dot{Y} dV - \int_{\partial\Omega(\lambda \leq \lambda_\infty)} \left[\rho \lambda (\mathbf{v} - \mathbf{v}^{(b)}) + \mathbf{J} \right] \cdot \hat{\mathbf{n}} dS. \quad (65.74)$$

The right hand side of this budget equation can be decomposed into the following processes illustrated in Figure 65.8.

Non-conservative sources and sinks

As noted in Section 65.4.3, the source term $\rho \dot{Y}$ accounts for processes that cannot be represented as the convergence of a flux. We write its region integrated contribution using the shorthand

$$\dot{Y}(\lambda \leq \lambda_\infty) \equiv \int_{\Omega(\lambda \leq \lambda_\infty)} \rho \dot{Y} dV \equiv \int_\lambda^{\lambda_\infty} \dot{m}_{\dot{Y}}(\lambda') d\lambda'. \quad (65.75)$$

The final equality introduced the distribution function for the source, in which

$$\dot{m}_{\dot{Y}}(\lambda) d\lambda = \text{mass per time of } \lambda \text{ created within the region } [\lambda - d\lambda/2, \lambda + d\lambda/2]. \quad (65.76)$$

Transport from non-advection processes

The contribution from boundary area integrated non-advection fluxes appears in the term

$$-\int_{\partial\Omega(\lambda \leq \lambda_\infty)} \mathbf{J} \cdot \hat{\mathbf{n}} d\mathcal{S} = -\int_{\partial\Omega_{\text{out}}(\lambda \leq \lambda_\infty)} \mathbf{J} \cdot \hat{\mathbf{n}} d\mathcal{S} - \int_{\partial\Omega_{\text{bot}}(\lambda \leq \lambda_\infty)} \mathbf{J} \cdot \hat{\mathbf{n}} d\mathcal{S} - \int_{\partial\Omega(\lambda)} \mathbf{J} \cdot \hat{\mathbf{n}} d\mathcal{S}. \quad (65.77)$$

Recall the minus signs arise since a non-advection flux increases the λ content of the region if the flux is oriented into the region, whereas $\hat{\mathbf{n}}$ is the region outward normal. The surface $\partial\Omega_{\text{out}}(\lambda \leq \lambda_\infty)$ extends along the upper ocean boundary and supports non-advection surface boundary fluxes. Likewise, the boundary $\partial\Omega_{\text{bot}}(\lambda \leq \lambda_\infty)$ intersects the ocean bottom and generally experiences bottom boundary fluxes such as geothermal heating. Finally, the surface $\partial\Omega(\lambda)$ has non-advection fluxes that cross the λ -interface, with diffusive fluxes the canonical example. The boundary area integrated non-advection fluxes give rise to non-advection transports, with dimensions of mass of λ per time, that are written using the shorthand

$$-\int_{\partial\Omega(\lambda \leq \lambda_\infty)} \mathbf{J} \cdot \hat{\mathbf{n}} d\mathcal{S} = E_{\text{out}}(\lambda, \lambda_\infty) + E_{\text{bot}}(\lambda, \lambda_\infty) + E(\lambda), \quad (65.78)$$

with a term having a positive value if it increases the λ mass of the region. We furthermore find it useful to introduce the distribution functions according to

$$E_{\text{out}}(\lambda, \lambda_\infty) + E_{\text{bot}}(\lambda, \lambda_\infty) = \int_\lambda^{\lambda_\infty} [\dot{m}_{\text{out}}^{\text{E}}(\lambda') + \dot{m}_{\text{bot}}^{\text{E}}(\lambda')] d\lambda', \quad (65.79)$$

where

$$\dot{m}_{\text{out}}^{\text{E}}(\lambda) d\lambda = \text{mass of } \lambda \text{ per time from } \partial\Omega_{\text{out}} \text{ transport in range } [\lambda - d\lambda/2, \lambda + d\lambda/2] \quad (65.80\text{a})$$

$$\dot{m}_{\text{bot}}^{\text{E}}(\lambda) d\lambda = \text{mass of } \lambda \text{ per time from } \partial\Omega_{\text{bot}} \text{ transport in range } [\lambda - d\lambda/2, \lambda + d\lambda/2]. \quad (65.80\text{b})$$

 λ transported with interior boundary mass fluxes

We next consider the contribution to the budget equation (65.74) arising from the transport of λ with mass that crosses the interior boundary, $\partial\Omega(\lambda)$, whereby

$$-\int_{\partial\Omega(\lambda)} \rho \lambda (\mathbf{v} - \mathbf{v}^{(\lambda)}) \cdot \hat{\mathbf{n}} d\mathcal{S} = -\lambda \int_{\partial\Omega(\lambda)} \rho (\mathbf{v} - \mathbf{v}^{(\lambda)}) \cdot \hat{\mathbf{n}} d\mathcal{S} = \lambda G(\lambda), \quad (65.81)$$

To reach this result we noted that λ can be pulled outside of the $\partial\Omega(\lambda)$ integral since it is constant along this surface, thus allowing for the introduction of the water mass transformation, $G(\lambda)$, given by equation (65.40).

Surface boundary mass fluxes

The final term contributing to the right hand side of the λ budget equation (65.74) arises from the surface mass transport along the boundary $\partial\Omega_{\text{out}}(\lambda \leq \lambda_\infty)$

$$-\int_{\partial\Omega(\lambda \leq \lambda_\infty)} \rho \lambda (\mathbf{v} - \mathbf{v}^{(b)}) \cdot \hat{\mathbf{n}} d\mathcal{S} = \int_{\partial\Omega_{\text{out}}(\lambda \leq \lambda_\infty)} \lambda \mathcal{Q}_m d\mathcal{S} \equiv W^{(\lambda)}(\lambda, \lambda_\infty). \quad (65.82)$$

To reach the first equality we followed the steps in Section 65.5.2 by using the kinematic boundary condition (16.63) to introduce the surface mass transport, $\mathcal{Q}_m d\mathcal{S}$. The final equality introduced a shorthand that corresponds to the $W(\lambda, \lambda_\infty)$ from Section 65.5.2. In the following, we find it

useful to introduce the mass distribution function $\dot{m}_w(\lambda)$ from equation (65.69), thus rendering

$$W(\lambda, \lambda_\infty) = \int_\lambda^{\lambda_\infty} \dot{m}_w(\lambda') d\lambda' \quad \text{and} \quad W^{(\lambda)}(\lambda, \lambda_\infty) = \int_\lambda^{\lambda_\infty} \lambda \dot{m}_w(\lambda') d\lambda'. \quad (65.83)$$

Following the discussion in Sections 64.5.2, we have not assumed a relation between λ along the interface, $\partial\Omega_{\text{out}}(\lambda \leq \lambda_\infty)$, and the concentration, λ_m , contained in the entering mass. We prefer to keep the discussion general for now, providing a relation only when necessary.

65.6.2 Summary of the λ budget

Bringing terms together leads to the λ mass budget equation (65.74) in the form

$$\begin{aligned} \frac{d}{dt} \left[\int_{\Omega(\lambda \leq \lambda_\infty)} \rho \lambda dV \right] \\ = \dot{Y}(\lambda \leq \lambda_\infty) + E_{\text{out}}(\lambda, \lambda_\infty) + E_{\text{bot}}(\lambda, \lambda_\infty) + E(\lambda) + W^{(\lambda)}(\lambda, \lambda_\infty) + \lambda G(\lambda). \end{aligned} \quad (65.84)$$

This budget takes the equivalent form in terms of the distribution functions

$$\frac{d}{dt} \int_\lambda^{\lambda_\infty} \lambda' m(\lambda') d\lambda' = \int_\lambda^{\lambda_\infty} [\dot{m}_{\dot{Y}}(\lambda') + \dot{m}_{\text{out}}^E(\lambda') + \dot{m}_{\text{bot}}^E(\lambda') + \lambda \dot{m}_w(\lambda')] d\lambda' + E(\lambda) + \lambda G(\lambda). \quad (65.85)$$

Setting λ to a global constant and assuming there are no seawater mass sources leads to the seawater mass budget for the λ_∞ -region

$$\frac{d}{dt} \left[\int_{\Omega(\lambda \leq \lambda_\infty)} \rho dV \right] = W(\lambda, \lambda_\infty) + G(\lambda), \quad (65.86)$$

which takes on the following form in terms of distributions

$$\frac{d}{dt} \int_\lambda^{\lambda_\infty} m(\lambda') d\lambda' = \int_\lambda^{\lambda_\infty} \dot{m}_w(\lambda') d\lambda' + G(\lambda). \quad (65.87)$$

65.6.3 Processes leading to water mass transformation

We now focus on the left hand side of equation (65.86) for the purpose of identifying terms leading to water mass transformation by making use of the moment equation (65.37) to write

$$\int_{\Omega(\lambda \leq \lambda_\infty)} \rho \lambda dV = M(\lambda, \lambda_\infty) \langle \lambda \rangle = M(\lambda, \lambda_\infty) \lambda + \int_\lambda^{\lambda_\infty} M(\lambda', \lambda_\infty) d\lambda', \quad (65.88)$$

which then leads to

$$\frac{d[M(\lambda, \lambda_\infty) \langle \lambda \rangle]}{dt} = \lambda \frac{dM(\lambda, \lambda_\infty)}{dt} + \int_\lambda^{\lambda_\infty} \frac{dM(\lambda', \lambda_\infty)}{dt} d\lambda'. \quad (65.89)$$

Integrated water mass transformation over the λ_∞ -region

Use of the λ budget equation (65.86) for the left hand side of equation (65.89), and the mass budget equation (65.86) for the right hand side renders

$$\begin{aligned}\dot{Y}(\lambda \leq \lambda_\infty) + E_{\text{out}}(\lambda, \lambda_\infty) + E_{\text{bot}}(\lambda, \lambda_\infty) + E(\lambda) + W^{(\lambda)}(\lambda, \lambda_\infty) + \lambda G(\lambda) \\ = \lambda [W(\lambda, \lambda_\infty) + G(\lambda)] + \int_\lambda^{\lambda_\infty} [W(\lambda', \lambda_\infty) + G(\lambda')] d\lambda'.\end{aligned}\quad (65.90)$$

Contributions from the surface boundary mass fluxes cancel as per the following identity

$$W^{(\lambda)}(\lambda, \lambda_\infty) - \lambda W(\lambda, \lambda_\infty) = \int_\lambda^{\lambda_\infty} (\lambda' - \lambda) \dot{m}_w(\lambda') d\lambda' \quad (65.91a)$$

$$= \int_\lambda^{\lambda_\infty} \left[\int_{\lambda'}^{\lambda_\infty} \dot{m}_w(\lambda'') d\lambda'' \right] d\lambda' \quad (65.91b)$$

$$= \int_\lambda^{\lambda_\infty} W(\lambda', \lambda_\infty) d\lambda', \quad (65.91c)$$

where the second equality follows from the double integral formula (3.99). To understand the physical reason we see no water mass transformation from surface mass fluxes, recall the discussion in Section 64.5.2. Namely, mixing and internal sources provide the only means for irreversible changes to water masses and thus to water mass transformation. In contrast, boundary mass transport contributes to transformation only if the mass participates in mixing. That is, the mass associated with boundary mass transport is incorporated into the ocean (or leaves the ocean) only in the presence of mixing. It is thus reassuring that the formalism leads to this same conclusion. Furthermore, this result is consistent with the expression (65.45b), whereby the water mass transformation is, again, determined solely in terms of the non-advectional fluxes at the region boundaries plus the interior source term.

Cancelling the mass transport terms thus leads to the integrated water mass transformation

$$\int_\lambda^{\lambda_\infty} G(\lambda') d\lambda' = \dot{Y}(\lambda \leq \lambda_\infty) + E_{\text{out}}(\lambda, \lambda_\infty) + E_{\text{bot}}(\lambda, \lambda_\infty) + E(\lambda), \quad (65.92)$$

which is, again, just another way to write equation (65.45b). We thus see that the accumulated effects from sources within the interior plus non-advectional fluxes along the surface and interior boundaries lead to an integrated interior water mass transformation. Note that each term in this equation has dimensions of λ -mass per time.

Water mass transformation across the λ -interface

We can develop an expression for the water mass transformation across the λ -interface by taking $\partial/\partial\lambda$ of equation (65.92) to reveal

$$G(\lambda) = -\frac{\partial}{\partial\lambda} \left[\dot{Y}(\lambda \leq \lambda_\infty) + E_{\text{out}}(\lambda, \lambda_\infty) + E_{\text{bot}}(\lambda, \lambda_\infty) + E(\lambda) \right], \quad (65.93)$$

thus revealing that the water mass transformation across a λ -surface is the λ -convergence of the mixing processes plus the interior sources. Finally, this equation takes on the following distributional form

$$G(\lambda) = \dot{m}_{\dot{Y}}(\lambda) + \dot{m}_{\text{bot}}^E(\lambda) + \dot{m}_{\text{out}}^E(\lambda) - \frac{\partial E(\lambda)}{\partial\lambda}. \quad (65.94)$$

65.7 Surface water mass transformation

We have articulated all the terms needed to form the $\Delta\lambda$ -layer mass budget according to Figure 65.6 as well as the λ_∞ -region mass budget according to Figure 65.8. In this section we focus on contributions to transformation from surface processes in the transformation equation (65.94)

$$G_{\text{out}}(\lambda) \equiv -\frac{\partial E_{\text{out}}(\lambda, \lambda_\infty)}{\partial \lambda} = \dot{m}_{\text{out}}^E(\lambda) = -\lim_{\delta\lambda \rightarrow 0} \frac{1}{\delta\lambda} \int_{\partial\Omega_{\text{out}}(\lambda \pm \delta\lambda/2)} \mathbf{J} \cdot \hat{\mathbf{n}} \, d\mathcal{S}, \quad (65.95)$$

where the final equality made use of equation (65.45b). Such *surface transformation* forms the focus of many studies of water mass transformation because it only requires surface boundary information, which is generally more accessible than information from interior ocean mixing processes or bottom geothermal processes. Furthermore, much of the transformation of water occurs in surface regions since this region is home to large contributions from surface boundary fluxes and associated ocean mixing. The basic equation we use is the non-advection flux equation (17.86), rewritten here for our scalar field λ

$$-\mathbf{J} \cdot \hat{\mathbf{n}} = \mathcal{Q}_\lambda - \lambda \mathcal{Q}_m = \mathcal{Q}_\lambda^{\text{non-adv}} + (\lambda_m - \lambda) \mathcal{Q}_m. \quad (65.96)$$

65.7.1 Circulation driven by surface transformation

The layer mass budget (65.71) and its continuous expression (65.73) provide the basis for inferences about circulation and transformation. As an illustration, consider the continuous expression (65.73) and integrate from the reference value up to λ

$$\int_{\lambda_\infty}^\lambda \Psi \, d\lambda' = \int_{\lambda_\infty}^\lambda \left[-\frac{\partial M}{\partial t} + W - G \right] \, d\lambda'. \quad (65.97)$$

The left hand side is an expression for the circulation in λ -space at the specified interior open boundary. The right hand side means that a nonzero circulation is driven by mass through the ocean surface, convergence of mass transformed across the λ -interfaces, and/or time changes to the mass within the domain. Correspondingly, in the absence of surface boundary mass fluxes, a steady circulation is driven just by water mass transformation

$$\int_{\lambda_\infty}^\lambda \Psi \, d\lambda' = - \int_{\lambda_\infty}^\lambda G \, d\lambda'. \quad (65.98)$$

We depict an example in Figure 65.9 where the surface outcrop of the layer is exposed to air-sea interactions that lead to a meridional movement of the $\lambda - \Delta\lambda/2$ -interface. This movement laterally entrains mass into the layer. If there is a net convergence of mass into the layer, then the layer mass increases. A steady state mass budget for the layer is reached if the amount of mass entrained through surface transformation is reflected in the same mass leaving through the circulation at the open boundary $\partial\Omega_{\text{in}}(\lambda \pm \Delta\lambda/2)$. We depict another case in Figure 65.10, here focusing on how a meridional gradient in the surface buoyancy loss causes entrainment into buoyancy layers. These and other statements related to the water mass budget are rather routine mathematically. Yet since the mass budget is formulated over layers, the mass budget offers the means to make very general statements about the circulation even without a direct measurement of the flow. This is a key power of water mass analysis.

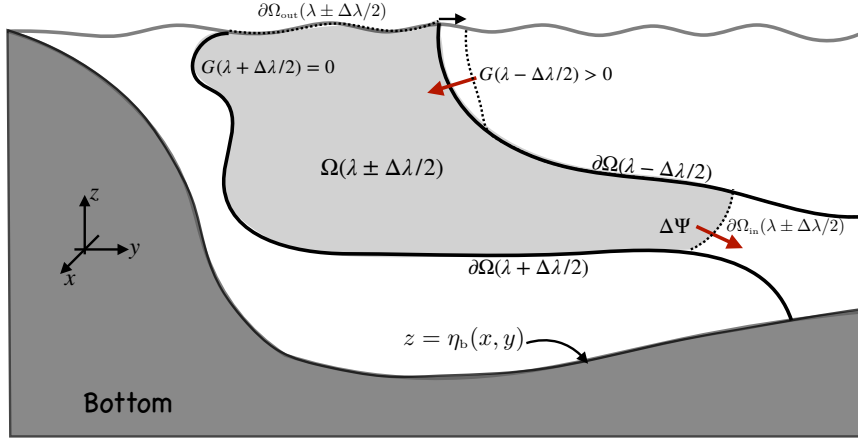


FIGURE 65.9: An example of a surface transformation driven circulation oriented according to the Southern Ocean with Antarctica to the left. Here we depict a layer that is exposed to some form of air-sea interaction that causes the $\lambda - \Delta\lambda/2$ -interface to move meridionally. For example, if $\lambda = \gamma$, then an air-sea buoyancy flux generally causes γ outcrops to move laterally. Movement of the near-surface portion of the $\partial\Omega(\lambda - \Delta\lambda/2)$ interface causes seawater to entrain into the layer and thus contribute to the surface water mass transformation $G(\lambda - \Delta\lambda/2) > 0$ (red arrow near the surface directed to the south). In turn, the boundary $\partial\Omega_{in}(\lambda \pm \Delta\lambda/2)$ expands as the near-surface portion of the interface $\partial\Omega(\lambda - \Delta\lambda/2)$ moves to the south as a result of the entrained new water (black arrow moving to the north). If there is a net convergence of water mass into the layer (e.g., by having less mass move across the other layer interface at $\partial\Omega(\lambda + \Delta\lambda/2)$), then mass accumulates within the layer $[\lambda - \Delta\lambda/2, \lambda + \Delta\lambda/2]$. There is a steady state (i.e., layer mass is constant) only if the same amount of mass that converges into the layer via surface or interior water mass transformation leaves the layer through circulation at the boundary $\partial\Omega_{in}(\lambda \pm \Delta\lambda/2)$.

65.7.2 Further study

Much of the formalism in this section follows that reviewed by [Groeskamp et al. \(2019\)](#). This paper offers specific examples of water mass transformation analysis as well as citations to numerous research papers.

65.8 Buoyancy water mass transformation

In Section 65.2 we considered the transformation of water masses as defined by buoyancy classes, with $\lambda = \gamma$ where γ is a field whose isosurfaces approximate constant buoyancy directions; i.e., the neutral directions from Section 27.5. We here fill in further details for such buoyancy water mass analysis.

65.8.1 Material time changes to S and Θ

The material time derivative of γ can be written as the sum of contributions from salinity and Conservative Temperature

$$\rho \dot{\gamma} = \frac{\partial \gamma}{\partial S} \rho \dot{S} + \frac{\partial \gamma}{\partial \Theta} \rho \dot{\Theta}. \quad (65.99)$$

Following the decomposition of the water mass transformation in Section 65.4.3, for a general tracer, we here write the material time derivatives in the form

$$\rho \dot{S} = -\nabla \cdot \mathbf{J}_{int}^{(S)} - \mathbf{J}_{out}^{(S)} \cdot \hat{\mathbf{n}} \delta(z - \eta) - \mathbf{J}_{bot}^{(S)} \cdot \hat{\mathbf{n}} \delta(z - \eta_b) \quad (65.100a)$$

$$\rho \dot{\Theta} = -\nabla \cdot \mathbf{J}_{int}^{(\Theta)} - \mathbf{J}_{out}^{(\Theta)} \cdot \hat{\mathbf{n}} \delta(z - \eta) - \mathbf{J}_{bot}^{(\Theta)} \cdot \hat{\mathbf{n}} \delta(z - \eta_b), \quad (65.100b)$$

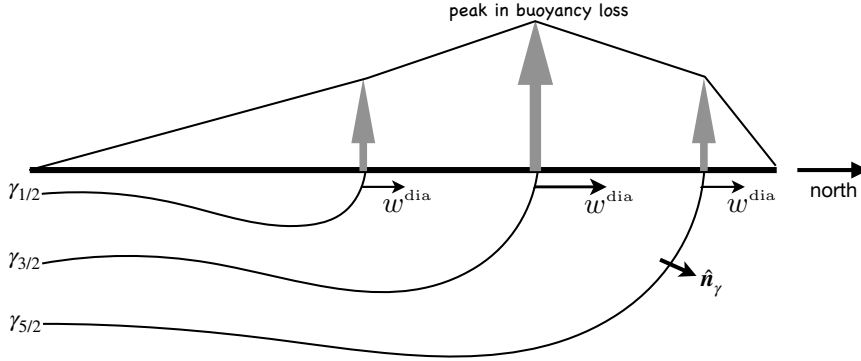


FIGURE 65.10: An example of surface water mass transformation, here illustrating the effects of transformation due to a meridional gradient in the surface buoyancy loss (we here assume that λ is buoyancy as measured by the neutral density γ). The example is oriented for the northern hemisphere with increasing latitudes to the north/right. Buoyancy loss is denoted by the blue vertical arrows indicating the removal of buoyancy from the ocean, thus causing surface water to loose buoyancy. The surface buoyancy loss causes γ interfaces to migrate to the south, which in turn causes dianeutral mass flux to move from lighter layers to denser layers (black vectors pointed to the north, w^{dia}). With a peak in the buoyancy loss at a particular latitude, more entrainment is driven into the layer to the north of the peak (water converges to the layer $\gamma_{3/2} \leq \gamma \leq \gamma_{5/2}$) and less entrainment into the layer to the south (water diverges from the layer $\gamma_{1/2} \leq \gamma \leq \gamma_{3/2}$).

where we assumed there are no interior sources of S or Θ . The surface and bottom boundary contributions are weighted by Dirac delta distributions and projected into the normal direction along the two respective boundary surfaces. Following from the decomposition of water mass transformation given by equation (65.48), we are thus led to the following form for buoyancy

$$\begin{aligned}
G(\gamma) = & - \underbrace{\lim_{\delta\gamma \rightarrow 0} \frac{1}{\delta\gamma} \int_{\Omega(\gamma \pm \delta\gamma/2)} \left(\frac{\partial\gamma}{\partial S} \nabla \cdot \mathbf{J}_{int}^{(S)} + \frac{\partial\gamma}{\partial \Theta} \nabla \cdot \mathbf{J}_{int}^{(\Theta)} \right) dV}_{\text{interior buoyancy transformation} = \text{volume integral of convergence}} \\
& - \underbrace{\lim_{\delta\gamma \rightarrow 0} \frac{1}{\delta\gamma} \int_{\partial\Omega_{out}(\gamma \pm \delta\gamma/2)} \left(\frac{\partial\gamma}{\partial S} \mathbf{J}_{out}^{(S)} + \frac{\partial\gamma}{\partial \Theta} \mathbf{J}_{out}^{(\Theta)} \right) \cdot \hat{\mathbf{n}} d\mathcal{S}}_{\text{surface buoyancy transformation} = \text{area integral of surface boundary fluxes}} \\
& - \underbrace{\lim_{\delta\gamma \rightarrow 0} \frac{1}{\delta\gamma} \int_{\partial\Omega_{bot}(\gamma \pm \delta\gamma/2)} \left(\frac{\partial\gamma}{\partial S} \mathbf{J}_{bot}^{(S)} + \frac{\partial\gamma}{\partial \Theta} \mathbf{J}_{bot}^{(\Theta)} \right) \cdot \hat{\mathbf{n}} d\mathcal{S}}_{\text{bottom buoyancy transformation} = \text{area integral of bottom boundary fluxes}}. \tag{65.101}
\end{aligned}$$

This expression is explored in the remainder of this section.

65.8.2 Interior buoyancy water mass transformation

Contributions from cabling, thermobaricity, and halobaricity (Section 64.3) arise from the interior transformation appearing in equation (65.101). Furthermore, in the special case of a linear equation of state, whereby $\partial\gamma/\partial\Theta$ and $\partial\gamma/\partial S$ are constants, then equation (65.54) means that the global integral of the interior transformation vanishes

$$\int_{\gamma_{-\infty}}^{\gamma_{\infty}} G_{int}(\gamma) d\gamma = \int_{\mathcal{R}} \left(\frac{\partial\gamma}{\partial S} \nabla \cdot \mathbf{J}_{int}^{(S)} + \frac{\partial\gamma}{\partial \Theta} \nabla \cdot \mathbf{J}_{int}^{(\Theta)} \right) dV = 0 \quad \text{if } \nabla(\partial\gamma/\partial\Theta) = 0, \nabla(\partial\gamma/\partial S) = 0, \tag{65.102}$$

where \mathcal{R} is the global ocean domain. By inference, we conclude that any nonzero result for this integral is a global measure of the effects from the nonlinear equation of state

$$\text{contribution from nonlinear equation of state} = \int_{\gamma_{-\infty}}^{\gamma_{\infty}} G_{\text{int}}(\gamma) d\gamma. \quad (65.103)$$

65.8.3 Surface non-advection flux for S and Θ

We review a few of the distinct characteristics of surface non-advection fluxes of S and Θ as detailed in Section 64.5.2, here working with salinity, S , rather than salt concentration, $S = S/1000$.

Non-advection salt flux

The non-advection surface boundary flux for salt is given by equation (64.67), here written as

$$-\mathbf{J}^{(S)} \cdot \hat{\mathbf{n}} = \mathcal{Q}_S^{\text{non-adv}} + (S_m - S) \mathcal{Q}_m, \quad (65.104)$$

where $\mathcal{Q}_S^{\text{non-adv}}$ is a non-advection salt flux, such as might arise from parameterized turbulent transfer. For the salt concentration of water crossing the ocean surface, we generally take $S_m = 0$ for precipitation, evaporation, and river runoff, whereas $S_m \neq 0$ for ice melt and formation. Furthermore, the boundary term, $S = S(z = \eta)$, is commonly approximated by the bulk salt concentration in the upper ocean.

Non-advection flux for Conservative Temperature

For Conservative Temperature we follow the discussion in Section 64.5.3, whereby the non-advection flux is given by equation

$$-\mathbf{J}^{(\Theta)} \cdot \hat{\mathbf{n}} = \mathcal{Q}_{\Theta}^{\text{non-adv}} + (\Theta_m - \Theta) \mathcal{Q}_m. \quad (65.105)$$

It is common to approximate the difference $\Theta_m - \Theta(z = \eta) = 0$, in which case the non-advection flux is just due to turbulent and radiative heat fluxes

$$-\mathbf{J}^{(\Theta)} \cdot \hat{\mathbf{n}} = \mathcal{Q}_{\Theta}^{\text{non-adv}} \text{ if } \Theta_m - \Theta(z = \eta) = 0. \quad (65.106)$$

65.8.4 Surface buoyancy water mass transformation

To touch base with the commonly employed surface buoyancy transformation, insert the surface fluxes into equation (65.101) as per Section 65.8.3 to write

$$\begin{aligned} G(\gamma)^{\text{surface}} &= \\ &\lim_{\delta\gamma \rightarrow 0} \frac{1}{\delta\gamma} \int_{\partial\Omega_{\text{out}}(\gamma \pm \delta\gamma/2)} (\gamma \beta_S [\mathcal{Q}_S^{\text{non-adv}} + (S_m - S) \mathcal{Q}_m] - \gamma \alpha_{\Theta} [\mathcal{Q}_{\Theta}^{\text{non-adv}} + (\Theta_m - \Theta) \mathcal{Q}_m]) d\mathcal{S}, \end{aligned} \quad (65.107)$$

where we introduced the thermal expansion and saline contraction coefficients, here defined according to¹³

$$\alpha_{\Theta} = -\frac{1}{\gamma} \frac{\partial \gamma}{\partial \Theta} \quad \text{and} \quad \beta_S = \frac{1}{\gamma} \frac{\partial \gamma}{\partial S}. \quad (65.108)$$

¹³In practice, it is common to replace the factor of γ^{-1} with ρ_0^{-1} on the right hand side of equation (65.108), with ρ_0 the constant Boussinesq reference density from Chapter 26.

Recall that $G(\gamma) > 0$ occurs when water is transformed into regions with larger γ . For example, net surface cooling in the presence of a positive thermal expansion coefficient ($\alpha_\Theta > 0$) leads to $\mathcal{Q}_\Theta^{\text{non-adv}} + (\Theta_m - \Theta) \mathcal{Q}_m < 0$. Such cooling then leads to a positive contribution to $G(\gamma)_{\text{surface}}$ as water is transformed from light to heavy γ -classes. Likewise, a positive net salt transport into the upper ocean, $\mathcal{Q}_S^{\text{non-adv}} + (S_m - S) \mathcal{Q}_m > 0$, leads to a positive contribution to $G(\gamma)_{\text{surface}}$.

The integrand to equation (65.107) corresponds to minus the surface buoyancy flux derived in Section 64.6.3. The only difference is that we here make use of the surface element, $d\mathcal{S}$, and the corresponding fluxes $\mathcal{Q}_\Theta^{\text{non-adv}}$, $\mathcal{Q}_S^{\text{non-adv}}$, and \mathcal{Q}_m . However, if the ocean surface has no overturns, we can write its vertical position as $z = \eta(x, y, t)$ and can also define the horizontal projection of the area element as (see equation (6.33))

$$d\mathcal{S} = \sqrt{1 + |\nabla \eta|^2} dA. \quad (65.109)$$

In this case we can introduce the fluxes $Q_\Theta^{\text{non-adv}}$, $Q_S^{\text{non-adv}}$, and Q_m used in Section 64.6.3 via

$$\mathcal{Q}_\Theta^{\text{non-adv}} d\mathcal{S} = Q_\Theta^{\text{non-adv}} dA \quad \text{and} \quad \mathcal{Q}_S^{\text{non-adv}} d\mathcal{S} = Q_S^{\text{non-adv}} dA \quad \text{and} \quad \mathcal{Q}_m d\mathcal{S} = Q_m dA, \quad (65.110)$$

to render

$$\begin{aligned} G(\gamma)^{\text{surface}} = \\ \lim_{\delta\gamma \rightarrow 0} \frac{1}{\delta\gamma} \int_{\partial\Omega_{\text{out}}(\gamma \pm \delta\gamma/2)} (\gamma \beta_s [Q_S^{\text{non-adv}} + (S_m - S) Q_m] - \gamma \alpha_\Theta [Q_\Theta^{\text{non-adv}} + (\Theta_m - \Theta) Q_m]) dA. \end{aligned} \quad (65.111)$$

Integrating the surface transformation (65.111) over all γ -classes leads to the identity¹⁴

$$\begin{aligned} \int_{\gamma=-\infty}^{\gamma=\infty} G(\gamma)^{\text{surface}} d\gamma = \\ \int_{z=\eta} (\gamma \beta_s [Q_S^{\text{non-adv}} + (S_m - S) Q_m] - \gamma \alpha_\Theta [Q_\Theta^{\text{non-adv}} + (\Theta_m - \Theta) Q_m]) dA. \end{aligned} \quad (65.112)$$

This equality means that the diagnosed surface transformation, $G(\gamma)^{\text{surface}}$, which is obtained by binning surface fluxes into γ -classes, must properly add up to the area integrated surface fluxes as weighted by the surface value of γ . This equality can be a useful check on the integrity of numerical binning code used to diagnose surface water mass transformation.

65.9 Tracer mass analysis

In Sections 65.5 and 65.6 we developed the budgets for λ within layers defined λ . Here we extend that analysis to develop budgets for a tracer concentration, C , localized in a region within a layer of buoyancy, γ , as depicted in Figure 65.11. The upper panels to this figure illustrate a tracer patch in geographic/depth space along with isolines of buoyancy, whereas the lower panels show the tracer distribution (histogram) binned within the buoyancy classes. If the tracer is mixed within a layer, such as via the neutral diffusion process of Section 63.4, then the tracer patch is spread laterally within the buoyancy layer and yet the distribution (lower panel) is unchanged. In contrast, if the tracer is mixed across layer interfaces then the tracer distribution is spread within buoyancy space.

¹⁴The density bound $\gamma_{-\infty}$ is a constant that is lower than any γ realized in the global domain, whereas γ_∞ is a constant that is larger than any realized γ .

Another means to alter the tracer distribution is to modify the buoyancy field. This situation is especially common for tracer near the surface, where boundary buoyancy forcing can act to move the layers thus causing tracer to move between layers even if the tracer patch is stationary in geographical space. That is, if the tracer moves at a velocity distinct from the buoyancy field, then its distribution within buoyancy classes will change.

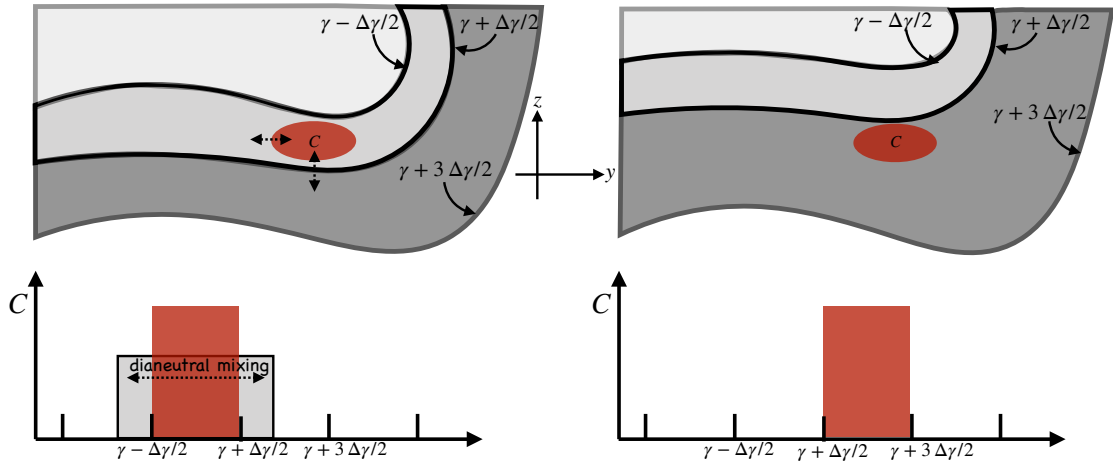


FIGURE 65.11: Depicting a tracer patch within the buoyancy layer bounded by the interface values $[\gamma - \Delta\gamma/2, \gamma + \Delta\gamma/2]$ (left panel) and $[\gamma + \Delta\gamma/2, \gamma + 3\Delta\gamma/2]$ (right panel). The upper panels show the tracer and buoyancy in geographic/depth space whereas the bottom panels show the tracer distribution (histogram) binned according to buoyancy. There are two general means to modify the distribution of tracer within the buoyancy classes. The first occurs via dianeutral mixing that spreads the tracer distribution to other buoyancy layers as depicted by the vertical arrow in the upper left panel and the horizontal arrows in the lower left panel. The lateral arrow in the upper left panel depicts neutral diffusion, which laterally spreads the tracer within a layer but does not alter the distribution across layers (see Section 63.4). The second means to alter the distribution occurs when the buoyancy surfaces move relative to the tracer. This scenario is depicted in the lower right panel whereby the tracer patch originally in buoyancy layer $[\gamma - \Delta\gamma/2, \gamma + \Delta\gamma/2]$ now finds itself in the layer $[\gamma + \Delta\gamma/2, \gamma + 3\Delta\gamma/2]$. This depiction is not realistic, since motion of interior buoyancy surfaces generally occurs along with mixing of tracer patches. Nonetheless, this example emphasizes that motion of the buoyancy surfaces need not coincide with motion of the tracer patch.

65.9.1 General form of the mass budget

As depicted in Figure 65.11 for buoyancy layers, and Figure 65.12 for generic layers, there are two general processes whereby a tracer distribution within layers can be modified: (i) the tracer can mix between layers and (ii) the layers can move relative to the tracer. These ideas transcend buoyancy and thus can be applied to any scalar field, λ , used to classify water masses. We quantify these two processes by writing the time change of tracer content within a λ -layer, which is arrived at by applying the Leibniz-Reynolds transport theorem from Section 17.3.4 to a λ -layer

$$\frac{d}{dt} \Delta M_C(\lambda \pm \Delta\lambda/2) = \int_{\Omega(\lambda \pm \Delta\lambda/2)} \rho \dot{C} dV - \oint_{\partial\Omega(\lambda \pm \Delta\lambda/2)} \rho C (\mathbf{v} - \mathbf{v}^{(b)}) \cdot \hat{\mathbf{n}} dS, \quad (65.113)$$

where

$$\Delta M_C(\lambda \pm \Delta\lambda/2) = \int_{\Omega(\lambda \pm \Delta\lambda/2)} \rho C dV \quad (65.114)$$

is the mass of tracer within the layer. The volume integral on the right hand side of equation (65.113) arises from material time changes to the tracer within the layer, whereas the surface integral arises from dia-surface transport across the layer boundary.

65.9.2 Tracer processes

We determine the material time changes for a “conservative” tracer according to the convergence of a flux

$$\rho \dot{C} = \rho \frac{DC}{Dt} = -\nabla \cdot \mathbf{J}. \quad (65.115)$$

Many biogeochemical tracers have additional “non-conservative” source terms beyond the flux convergence considered here. These effects can be readily incorporated into the following by adding a source term that acts throughout a layer and not just at the layer boundaries.

Gauss’ divergence theorem converts the convergence, $-\nabla \cdot \mathbf{J}$, into the area integral of fluxes over the layer boundaries, including interior layer interfaces as well as intersections with the surface and bottom boundaries. For the interior interfaces it is typically simpler diagnostically to bin the volume integrated material time changes within the λ -classes. In contrast, the surface and bottom boundary contributions are fed into the budget via Neumann boundary conditions applied to the flux \mathbf{J}

$$\mathbf{J} \cdot \hat{\mathbf{n}} d\mathcal{S} = \text{boundary tracer transport}. \quad (65.116)$$

Note that when there is an advective/skew diffusive component to the subgrid scale flux (Chapters 62 and 63), then it adds to the resolved advective component to render a residual mean material time operator

$$\rho \frac{D^\dagger C}{Dt} = -\nabla \cdot \mathbf{J}_{\text{non-advect}}, \quad (65.117)$$

where

$$\frac{D^\dagger}{Dt} = \frac{\partial}{\partial t} + (\mathbf{v} + \mathbf{v}^*) \cdot \nabla, \quad (65.118)$$

with \mathbf{v}^* an eddy-induced velocity (see Section 63.1). For the purposes of water mass transformation analysis, we write

$$\dot{C} = \frac{D^\dagger C}{Dt}, \quad (65.119)$$

thus incorporating the eddy-induced stirring into the kinematic expression for the material time derivative.

There are many interior and boundary processes that contribute to \dot{C} within a layer. As a general expression for these contributions to the layer budget we write

$$\Delta E_C(\lambda \pm \Delta\lambda/2) = \int_{\Omega(\lambda \pm \Delta\lambda/2)} \rho \dot{C} dV = - \int_{\Omega(\lambda \pm \Delta\lambda/2)} \nabla \cdot \mathbf{J} dV \quad (65.120)$$

which is sometimes usefully decomposed into interior and surface boundary processes

$$\Delta E_C^{\text{int}}(\lambda \pm \Delta\lambda/2) = \int_{\Omega(\lambda \pm \Delta\lambda/2)} \rho \dot{C}^{\text{int}} dV \quad (65.121a)$$

$$\Delta E_C^{\text{out bdy}}(\lambda \pm \Delta\lambda/2) = - \int_{\partial\Omega_{\text{out}}(\lambda \pm \Delta\lambda/2)} \mathbf{J} \cdot \hat{\mathbf{n}} d\mathcal{S}. \quad (65.121b)$$

If the region boundary intersects the ocean bottom along $\partial\Omega_{\text{bot}}(\lambda \pm \Delta\lambda/2)$, then there is an additional bottom boundary contribution in the form

$$\Delta E_C^{\text{bot bdy}}(\lambda \pm \Delta\lambda/2) = - \int_{\partial\Omega_{\text{bot}}(\lambda \pm \Delta\lambda/2)} \mathbf{J} \cdot \hat{\mathbf{n}} d\mathcal{S}. \quad (65.122)$$

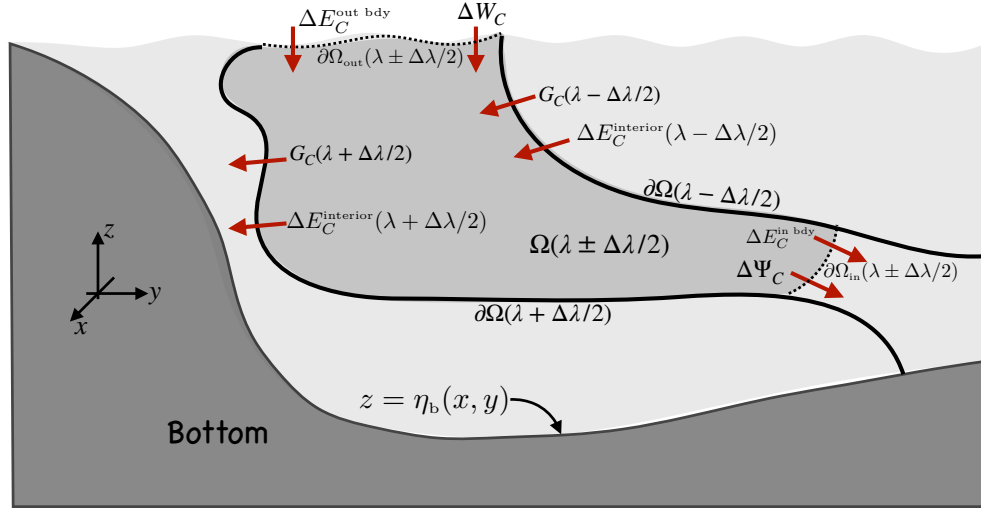


FIGURE 65.12: As for the schematic of a layer seawater mass budget depicted in Figure 65.6, we here illustrate the tracer budget within a layer of seawater with scalar property λ within the range $[\lambda - \Delta\lambda/2, \lambda + \Delta\lambda/2]$ and defined over a geographical/depth domain $\partial\Omega_{in}(\lambda \pm \Delta\lambda/2) + \partial\Omega_{out}(\lambda \pm \Delta\lambda/2) + \partial\Omega(\lambda + \Delta\lambda/2) + \partial\Omega(\lambda - \Delta\lambda/2)$. The budget for a tracer, C , over this layer is affected by the transport of tracer substance across the variety of layer boundaries. Transport processes include those determined by mixing and/or radiation across interior and surface boundaries, ΔE_C (equation (65.121b)). This term has no associated transfer of seawater mass and thus is absent from the water mass budget in Figure 65.6. Tracer budgets are also affected by processes that move seawater mass across layer boundaries: water mass transformation processes giving rise to $G_C(\lambda \pm \Delta\lambda/2)$ (equation (65.123)); transport across the surface domain boundary, ΔW_C , arising from precipitation, evaporation, runoff, and melt (equation (65.124)); and transport within the circulation crossing an interior domain boundary, $\Delta\Psi_C$ (equation (65.125)).

65.9.3 Transport across an interior layer interface

The surface integral in the budget (65.113) involves transport across the layer interfaces, with this transport requiring motion of the interface relative to a fluid particle. The same formalism introduced earlier can be used to compute this transport. That is, we can generalize the transformation equation (65.43d) to write

$$G_C(\lambda) = \int_{\partial\Omega(\lambda)} \rho C (\mathbf{v} - \mathbf{v}^{(b)}) \cdot \hat{\mathbf{n}} dS = \frac{\partial}{\partial \lambda} \int_{\Omega(\lambda_0 \leq \lambda)} \rho \dot{C} dV. \quad (65.123)$$

As a check, note that for the special case where the tracer concentration is a constant along the layer interface, then $G_C(\lambda) = C G(\lambda)$. We consider this special case in Section 65.10 when studying budgets over regions bounded by a tracer isosurface.

65.9.4 Transport across interior and surface boundaries

We now consider the impact on layer tracer mass budgets due to boundary transport. The budget contribution from mass fluxes crossing the ocean surface boundary is determined by making use of the surface kinematic boundary condition (17.85)

$$\Delta W_C = \int_{\partial\Omega_{out}(\lambda \pm \Delta\lambda/2)} \rho C (\mathbf{v} - \mathbf{v}^{(b)}) \cdot \hat{\mathbf{n}} dS = \int_{\partial\Omega_{out}(\lambda \pm \Delta\lambda/2)} Q_m C_m dA, \quad (65.124)$$

where C_m is the tracer concentration within the mass transported across the boundary.¹⁵ As a check, note that in the special case of a constant tracer concentration in the mass transported across the boundary, then $\Delta W_C = C_m \Delta W$, where ΔW is the water mass transported across the ocean free surface as given by equation (65.66).

For the interior open boundary the contribution is written in the generic manner

$$\Delta\Psi_C = \int_{\partial\Omega_{in}(\lambda \pm \Delta\lambda/2)} C \rho (\mathbf{v} - \mathbf{v}^{(b)}) \cdot \hat{\mathbf{n}} d\mathcal{S}. \quad (65.125)$$

Again, in the special case where the tracer concentration is a constant along the interior boundary, C_b , then $\Delta\Psi_C = C_b \Delta\Psi$, where $\Delta\Psi$ is the seawater mass transport given by equation (65.62).

65.9.5 The layer tracer budget

Bringing all terms together leads to the layer tracer mass budget

$$\frac{d\Delta M_C}{dt} + \Delta\Psi_C = \Delta E_C + \Delta W_C - [G_C(\lambda + \Delta\lambda/2) - G_C(\lambda - \Delta\lambda/2)], \quad (65.126)$$

which is directly analogous to the seawater layer mass budget (65.70), with the added term ΔE_C arising from material tracer changes. As for the seawater mass budget discussed in Section 65.5.3, the layer tracer budget (65.126) provides the framework for rather general inferences about tracer transport within λ -classes.

65.9.6 Further study

Much in this section follows the treatment given by [Groeskamp et al. \(2019\)](#). This paper offers specific examples of tracer mass analysis, which is an area seeing many new applications within the ocean and atmospheric communities.

65.10 Regions bounded by a tracer contour/surface

In Section 65.9 we developed equations for a layer tracer budget where the scalar field, λ , that defines the layer is generally distinct from the tracer, C , whose budget we are studying. In this section we specialize to the case where we set $\lambda = C$ so that the region boundaries are determined by the tracer whose budget is under study. These budgets were introduced in Sections 65.5 and 65.6, and here we derive some rather useful simplifications that arise as a result of setting $\lambda = C$.

As in Section 65.9, our starting point is the Leibniz-Reynolds budgets from Section 17.3.4 for seawater mass and tracer mass computed over an arbitrary region, \mathcal{R}

$$\frac{d}{dt} \left[\int_{\mathcal{R}} \rho C dV \right] = - \int_{\partial\mathcal{R}} [\rho C (\mathbf{v} - \mathbf{v}^{(b)}) + \mathbf{J}] \cdot \hat{\mathbf{n}} d\mathcal{S} \quad (65.127a)$$

$$\frac{d}{dt} \left[\int_{\mathcal{R}} \rho dV \right] = - \int_{\partial\mathcal{R}} [\rho (\mathbf{v} - \mathbf{v}^{(b)})] \cdot \hat{\mathbf{n}} d\mathcal{S}. \quad (65.127b)$$

The region \mathcal{R} is rather arbitrary, and can in general be disconnected. Throughout this section we

¹⁵Note that equation (26) in [Groeskamp et al. \(2019\)](#) incorrectly writes the integrand in equation (65.124) as $Q_m (C_m - C)$.

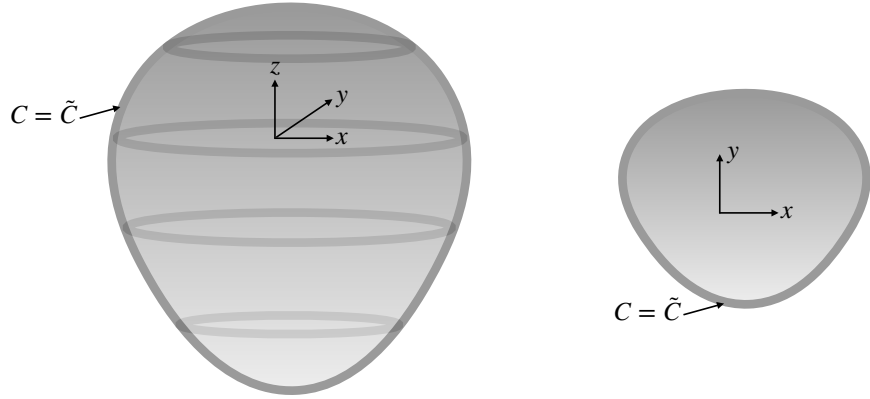


FIGURE 65.13: Left panel: a closed three-dimensional region, $\tilde{\mathcal{R}}$, with its boundary, $\partial\tilde{\mathcal{R}}$, defined by a surface of constant tracer concentration, $C = \tilde{C}$. Right panel: the analog closed two-dimensional region with its boundary defined by a contour of constant tracer concentration, $C = \tilde{C}$.

make use of the following shorthand notation for region-integrated quantities

$$M = \int_{\mathcal{R}} \rho dV \quad \text{region seawater mass} \quad (65.128a)$$

$$M_C = \int_{\mathcal{R}} C \rho dV \quad \text{region tracer mass} \quad (65.128b)$$

$$\langle C \rangle = \frac{1}{M} \int_{\mathcal{R}} C \rho dV = \frac{M_C}{M} \quad \text{region averaged tracer concentration.} \quad (65.128c)$$

65.10.1 Closed region bounded by a tracer surface/contour

Consider a closed region, $\tilde{\mathcal{R}}$, bounded by a surface of constant tracer concentration, $C = \tilde{C}$, such as depicted in Figure 65.13. The tracer budget (65.127a) for this region is given by

$$\frac{d(M \langle C \rangle)}{dt} = -\tilde{C} \int_{\partial\tilde{\mathcal{R}}} \rho (\mathbf{v} - \mathbf{v}^{(b)}) \cdot \hat{\mathbf{n}} d\mathcal{S} - \int_{\partial\tilde{\mathcal{R}}} \mathbf{J} \cdot \hat{\mathbf{n}} d\mathcal{S} \quad (65.129)$$

where we pulled the tracer concentration outside of the surface integral since, by construction, it is constant on the boundary, $\partial\tilde{\mathcal{R}}$. Use of the mass budget (65.127b) then leads to the rather tidy result

$$\frac{d[M(\langle C \rangle - \tilde{C})]}{dt} = - \int_{\partial\tilde{\mathcal{R}}} \mathbf{J} \cdot \hat{\mathbf{n}} d\mathcal{S}. \quad (65.130)$$

The left hand side is the time change of the mass-weighted difference between the region averaged tracer concentration, $\langle C \rangle$, and the value of the tracer concentration defining the region boundary, \tilde{C} . These time changes are driven by a nonzero diffusive tracer transport bringing tracer mass across the region boundary. A nonzero diffusive flux on the region boundary arises only when there is a gradient of tracer concentration across that boundary. In the special case of a zero net diffusive tracer transport across the region boundary, the budget equation (65.130) reaches a steady state whereby

$$\frac{d}{dt} [M(\langle C \rangle - \tilde{C})] = 0 \iff \int_{\partial\tilde{\mathcal{R}}} \mathbf{J} \cdot \hat{\mathbf{n}} d\mathcal{S} = 0. \quad (65.131)$$

A 3D region bounded by a constant tracer concentration is not commonly encountered in large-scale ocean and atmospheric fluids. In contrast, we often encounter quasi-2D regions as depicted in Figure 65.14, in which one may find 2D regions bounded by a closed contour of

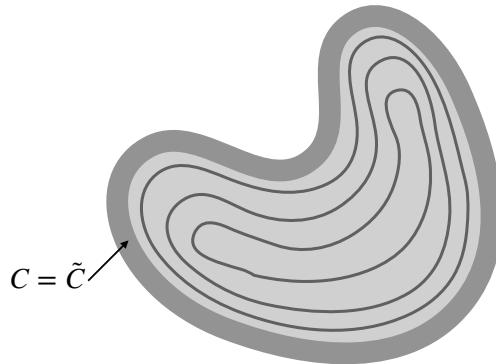


FIGURE 65.14: A two-dimensional region bounded by a finite-thick shell with constant tracer concentration, $C = \tilde{C}$. Inside the shell region the tracer concentration is not uniform.

constant tracer concentration. For example, in many parts of the ocean and atmosphere transport occurs predominantly along 2D surfaces defined by a constant buoyancy. We may thus find closed contours of tracer concentrations along constant buoyancy surfaces.

To help illustrate a necessary condition to reach a steady state, consider the particular example depicted in Figure 65.14. In this figure, the tracer contour defining the region boundary is a thick shell defined by a uniform concentration $C = \tilde{C}$. The diffusive flux vanishes at each point within the boundary shell since the tracer concentration is uniform. Hence, the steady budget (65.131) leads to

$$(\langle C \rangle - \tilde{C}) \frac{dM}{dt} + M \frac{d\langle C \rangle}{dt} = 0. \quad (65.132)$$

If the total seawater mass within the region is constant, then the averaged tracer concentration is also constant, so that both terms in this steady budget vanish individually. Even so, this configuration does not reach a steady state at each point throughout the domain interior. The reason is that diffusion in the interior causes tracer to move from regions of high concentration to low concentration. Consequently, at any particular point within the domain there is an evolving tracer concentration. The only way for each point to reach a steady state within a region bounded by a tracer contour is for the tracer concentration to be a uniform constant throughout the region interior

$$C = \tilde{C} \quad \text{steady state tracer throughout a closed tracer region.} \quad (65.133)$$

Diffusion thus expells tracer gradients from steady state regions bounded by closed tracer contours, thus leaving a homogenous interior.

65.10.2 Region with $C \geq \tilde{C}$

As a second example of the formalism, consider the tracer budget for a region where the tracer concentration is greater than or equal to a particular tracer value as depicted in Figure 65.15. In contrast to the domain in Figure 65.12, here there is no inner boundary. We introduce the

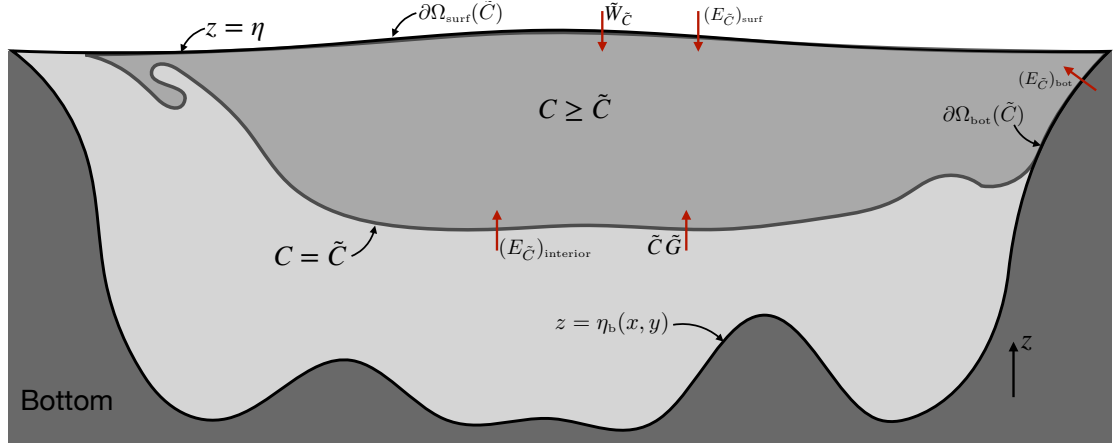


FIGURE 65.15: An ocean region where the tracer concentration is greater than a nominal value, $C \geq \tilde{C}$. A specific example is with $C = \Theta$, the Conservative Temperature, in which we are concerned with the ocean with temperature greater than $\tilde{\Theta}$. Here we depict a case where the tracer concentration generally increases upward (as with $C = \Theta$), and yet with vertical stratification not everywhere monotonic, such as for $C = \Theta$ in the high latitudes where salinity effects on density stratification become dominant. Transport processes affecting the budget of C within this region arise from mixing at the interior boundary and surface boundary, $(E_{\tilde{C}})_{int}$ and $(E_{\tilde{C}})_{surf}$, advection at the surface, $\tilde{W}_{\tilde{C}}$, and the tracer weighted water mass transformation across the interior layer boundary, $\tilde{C}\tilde{G}$.

following terms in developing both the seawater mass budget and the tracer substance budget

$$\tilde{M} = \int_{C \geq \tilde{C}} \rho dV \quad \text{seawater mass in the region } C \geq \tilde{C} \quad (65.134a)$$

$$\tilde{M}_{\tilde{C}} = \int_{C \geq \tilde{C}} C \rho dV = \tilde{M} \langle C \rangle \quad \text{tracer mass in the region } C \geq \tilde{C} \quad (65.134b)$$

$$\tilde{G} = - \int_{C = \tilde{C}} \rho (\mathbf{v} - \mathbf{v}^{(b)}) \cdot \hat{\mathbf{n}} d\mathcal{S} = - \int_{C = \tilde{C}} \rho w^{\text{dia}} d\mathcal{S} \quad \text{transformation across } \tilde{C} \quad (65.134c)$$

$$\tilde{G}_{\tilde{C}} = - \int_{C = \tilde{C}} C \rho (\mathbf{v} - \mathbf{v}^{(b)}) \cdot \hat{\mathbf{n}} d\mathcal{S} = - \int_{C = \tilde{C}} C \rho w^{\text{dia}} d\mathcal{S} \quad \text{tracer advected across } \tilde{C} \quad (65.134d)$$

$$\tilde{W} = - \int_{\partial\Omega_{\text{surf}}(\tilde{C})} \rho (\mathbf{v} - \mathbf{v}^{(b)}) \cdot \hat{\mathbf{n}} d\mathcal{S} = \int_{\partial\Omega_{\text{surf}}(\tilde{C})} Q_m dA \quad \text{surface mass transport} \quad (65.134e)$$

$$\tilde{W}_{\tilde{C}} = - \int_{\partial\Omega_{\text{surf}}(\tilde{C})} C \rho (\mathbf{v} - \mathbf{v}^{(b)}) \cdot \hat{\mathbf{n}} d\mathcal{S} = \int_{\partial\Omega_{\text{surf}}(\tilde{C})} C Q_m dA \quad \text{surface mass } C\text{-transport} \quad (65.134f)$$

$$(E_{\tilde{C}})_{int} = - \int_{C = \tilde{C}} \mathbf{J} \cdot \hat{\mathbf{n}} d\mathcal{S} \quad \text{subgrid } C\text{-transport across } \tilde{C} \quad (65.134g)$$

$$(E_{\tilde{C}})_{surf} = - \int_{\partial\Omega_{\text{surf}}(\tilde{C})} \mathbf{J} \cdot \hat{\mathbf{n}} d\mathcal{S} \quad \text{subgrid } C\text{-transport across surface} \quad (65.134h)$$

$$(E_{\tilde{C}})_{bot} = - \int_{\partial\Omega_{\text{bot}}(\tilde{C})} \mathbf{J} \cdot \hat{\mathbf{n}} d\mathcal{S} \quad \text{subgrid } C\text{-transport across bottom} \quad (65.134i)$$

Recall that $\hat{\mathbf{n}}$ is the *outward* normal on a boundary so that positive values for the above transports increase the tracer mass within the region. For equations (65.134c) and (65.134d), we introduced the dia-surface transport velocity according to equation (65.38) for flow across the $C = \tilde{C}$ layer interface. Likewise, for equations (65.134e) and (65.134f) we made use of the surface kinematic boundary condition (16.73c)

$$\rho(\mathbf{v} - \mathbf{v}^{(s)}) \cdot \hat{\mathbf{n}} d\mathcal{S} = -Q_m dA, \quad (65.135)$$

where Q_m is the mass transport across the free surface, with $Q_m > 0$ adding mass to the ocean, and dA is the horizontal projection of the surface area element. By inspection of Figure 65.15, the seawater mass and tracer mass budgets for this region are given by

$$\frac{d\widetilde{M}}{dt} = \widetilde{G} + \widetilde{W} \quad (65.136a)$$

$$\frac{d[\widetilde{M} \langle C \rangle]}{dt} = \widetilde{C} \widetilde{G} + \widetilde{W}_{\widetilde{C}} + (E_{\widetilde{C}})_{\text{surf}} + (E_{\widetilde{C}})_{\text{bot}} + (E_{\widetilde{C}})_{\text{int}}, \quad (65.136b)$$

where we assumed that no mass crosses through the solid earth. Furthermore, along the \tilde{C} -boundary we pulled the tracer concentration outside of the surface integral to write $\widetilde{G}_{\widetilde{C}} = \widetilde{C} \widetilde{G}$.

Just as we did in Section 65.10.1, the tracer budget (65.136b) can be simplified by making use of the seawater mass budget (65.136a) to eliminate the water mass transformation contribution \widetilde{G} , thus rendering

$$\frac{d\widetilde{M}_{I\widetilde{C}}}{dt} = [\widetilde{W}_{\widetilde{C}} - \widetilde{W} \widetilde{C}] + (E_{\widetilde{C}})_{\text{surf}} + (E_{\widetilde{C}})_{\text{bot}} + (E_{\widetilde{C}})_{\text{int}}. \quad (65.137)$$

In this equation we introduced the *internal tracer mass* according to

$$\widetilde{M}_{I\widetilde{C}} \equiv \widetilde{M} (\langle C \rangle - \widetilde{C}) = \int_{C \geq \widetilde{C}} (C - \widetilde{C}) \rho dV. \quad (65.138)$$

For completeness we express the internal tracer mass budget (65.137) in its integral form

$$\frac{d\widetilde{M}_{I\widetilde{C}}}{dt} = \int_{\partial\Omega_{\text{out}}} \left[Q_m (C - \widetilde{C}) dA - \mathbf{J} \cdot \hat{\mathbf{n}} d\mathcal{S} \right] - \int_{\partial\Omega_{\text{bot}}} \mathbf{J} \cdot \hat{\mathbf{n}} d\mathcal{S} - \int_{C=\widetilde{C}} \mathbf{J} \cdot \hat{\mathbf{n}} d\mathcal{S}. \quad (65.139)$$

65.10.3 Comments and further study

Elimination of the water mass transformation, \widetilde{G} , from the internal tracer mass budget equations (65.137) and (65.139) offers a practical advantage since \widetilde{G} can be rather noisy in applications. Furthermore, for some applications (e.g., see [Holmes et al. \(2019\)](#)) it is sufficient to consider the simpler budget (65.137) for internal tracer mass, rather than the budget (65.136b) for the total tracer mass.

The two-dimensional version of the result (65.133) was studied by [Rhines and Young \(1982\)](#) when studying the mechanics of isopycnal quasi-geostrophic potential vorticity in ocean gyres. We further consider their result in Exercise 61.10. It is satisfying to see their result follow from the present formalism based on Leibniz-Reynolds.



Part XIII

Bibliography and Index

BIBLIOGRAPHY

- Abernathay, R., D. Ferreira, and A. Klocker, Diagnostics of isopycnal mixing in a circumpolar channel, *Ocean Modelling*, 72(0), 1 – 16, doi:10.1016/j.ocemod.2013.07.004, 2013. 1575, 1587, 1593
- Acheson, D., *Elementary Fluid Dynamics*, Oxford Applied Mathematics and Computing Science Series, Oxford, Oxford, 1990. 31, 851
- Adcock, S., and D. P. Marshall, Interactions between geostrophic eddies and the mean circulation over large-scale bottom topography, *Journal of Physical Oceanography*, 30, 3223–3238, 2000. 923
- Adcroft, A., R. Hallberg, and M. Harrison, A finite volume discretization of the pressure gradient force using analytic integration, *Ocean Modelling*, 22, 106–113, doi:10.1016/j.ocemod.2008.02.001, 2008. 1449, 1450, 1451
- Aiki, H., T. Jacobson, and T. Yamagata, Parameterizing ocean eddy transports from surface to bottom, *Journal of Geophysical Research*, 31, L19 302, doi:10.1029/2004GL020703, 2004. 1584, 1588
- Anderson, J., Ludwig Prandtl's boundary layer, *Physics Today*, 58, 42–48, doi:10.1063/1.2169443, 2005. 507, 509
- Andresen, B., R. Berry, R. Gilmore, E. Ihrig, and P. Salamon, Thermodynamic geometry and the metrics of Weinhold and Gilmore, *Physical Review A*, 37(3), 845–848, doi:10.1103/PhysRevA.37.845, 1988. 411
- Andrews, D., and M. McIntyre, An exact theory of nonlinear waves on a Lagrangian-mean flow, *Journal of Fluid Mechanics*, 89, 609–646, 1978a. 1545, 1554
- Andrews, D. G., A finite-amplitude Eliassen-Palm theorem in isentropic coordinates, *Journal of Atmospheric Sciences*, 40, 1877–1883, doi:10.1175/1520-0469(1983)040<1877:AFAEPT>2.0.CO;2, 1983. 639
- Andrews, D. G., and M. E. McIntyre, On wave action and its relatives, *Journal of Fluid Mechanics*, 89, 647–664, 1978b. 1545, 1554
- Anstey, J., and L. Zanna, A deformation-based parametrization of ocean mesoscale eddy Reynolds stresses, *Ocean Modelling*, 112, 99–111, 2017. 503
- Apel, J. R., *Principles of Ocean Physics*, International Geophysics Series, vol. 38, Academic Press, London, 1987. 226, 723, 747

- Arakawa, A., and V. R. Lamb, The UCLA general circulation model, in *Methods in Computational Physics: General Circulation Models of the Atmosphere*, vol. 17, edited by J. Chang, pp. 174–265, Academic Press, 1977. [860](#)
- Arbic, B., S. T. Garner, R. W. Hallberg, and H. L. Simmons, The accuracy of surface elevations in forward global barotropic and baroclinic tide models, *Deep Sea Research*, 51, 3069–3101, 2004. [748](#)
- Aris, R., *Vectors, Tensors and the Basic Equations of Fluid Mechanics*, Dover Publishing, New York, 1962. [5](#), [159](#), [279](#), [305](#), [306](#), [318](#), [335](#), [361](#), [368](#), [465](#), [475](#), [486](#), [497](#), [498](#), [503](#)
- Atkins, P., and J. de Paula, *Atkin's Physical Chemistry*, 8th ed., 1053 pp., W.H. Freeman and Co., 2006. [421](#), [425](#)
- Badin, G., and F. Crisciani, *Variational formulation of fluid and geophysical fluid dynamics*, Springer International Publishing, Switzerland, 218 pages, 2018. [298](#)
- Barthel, A., A. Hogg, S. Waterman, and S. Keating, Jet-topography interactions affect energy pathways to the deep Southern Ocean, *Journal of Physical Oceanography*, 47(1799–1816), doi: 10.1175/JPO-D-16-0220.1, 2017. [808](#)
- Barton, K. N., N. Pal, S. R. Brus, M. R. Petersen, B. K. Arbic, D. Engwirda, A. F. Roberts, J. J. Westerink, D. Wirasaet, and M. Schindeleger, Global barotropic tide modeling using inline self-attraction and loading in MPAS-Ocean, *Journal of Advances in Modeling Earth Systems (JAMES)*, 14, doi:10.1029/2022MS003207, 2022. [757](#)
- Batchelor, G. K., *An Introduction to Fluid Dynamics*, Cambridge University Press, Cambridge, England, 1967. [272](#), [278](#), [309](#), [345](#), [486](#), [515](#), [534](#)
- Becker, E., Frictional heating in global climate models, *Monthly Weather Review*, 131, 508–520, doi:10.1175/1520-0493(2003)131<0508:FHIGCM>2.0.CO;2, 2003. [535](#)
- Becker, J. M., Effect of a western continental slope on the wind-driven circulation, *Journal of Physical Oceanography*, 29, 512–518, doi:10.1175/1520-0485(1999)029<0512:EOAWCS>2.0.CO;2, 1999. [916](#)
- Becker, J. M., and R. Salmon, Eddy formation on a continental slope, *Journal of Marine Research*, 55, 181–200, 1997. [914](#), [916](#)
- Beckers, J.-M., H. Burchard, J.-M. Campin, E. Deleersnijder, and P. P. Mathieu, Another reason why simple discretizations of rotated diffusion operators cause problems in ocean models: Comments on isoneutral diffusion in a z -coordinate ocean model, *Journal of Physical Oceanography*, 28, 1552–1559, 1998. [1592](#)
- Beckers, J.-M., H. Burchard, E. Deleersnijder, and P. P. Mathieu, Numerical discretization of rotated diffusion operators in ocean models, *Monthly Weather Review*, 128, 2711–2733, 2000. [1592](#)
- Bender, C., and S. Orszag, *Advanced Mathematical Methods for Scientists and Engineers*, McGraw-Hill Book Company, New York, 593 pp, 1978. [1155](#), [1158](#)
- Bennett, A., The geometry of neutral paths, *Journal of Physical Oceanography*, 49, 3037–3044, doi:10.1175/JPO-D-19-0047.1, 2019. [671](#)

BenthuySEN, J., and L. N. Thomas, Friction and diapycnal mixing at a slope: Boundary control of potential vorticity, *Journal of Physical Oceanography*, 42, 1509–1523, doi:10.1175/JPO-D-11-0130.1, 2012. [1020](#)

Beyer, W., *Standard Mathematical Tables*, 24th Edition, CRC Press, 1973. [1119](#)

Bhatia, H., G. Norgard, V. Pascucci, and P.-T. Bermer, The Helmholtz-Hodge decomposition—a survey, *IEEE Transactions on Visualization and Computer Graphics*, 19, 1386–1404, doi:10.1109/TVCG.2012.316, 2013. [327](#)

Bishop, S., R. Small, and F. Bryan, The global sink of available potential energy by mesoscale air-sea interaction, *Journal of Advances in Modeling Earth Systems, in review*, 2020. [645](#)

Bladwell, C., R. M. Holmes, J. D. Zika, and S. M. Griffies, The hat average: Improved time-averaging for budget analyses in climate models, *Journal of Advances in Modeling Earth Systems, in prep*, 2022. [67](#)

Bleck, R., Finite difference equations in generalized vertical coordinates. Part I: Total energy conservation, *Contributions to Atmospheric Physics*, 51, 360–372, 1978. [1398](#)

Bohm, D., *Quantum Theory*, Dover Publications, Inc., New York, 646 pp, 1951. [1120](#), [1125](#)

Böning, C. W., W. R. Holland, F. O. Bryan, G. Danabasoglu, and J. C. McWilliams, An overlooked problem in model simulations of the thermohaline circulation and heat transport in the Atlantic Ocean, *Journal of Physical Oceanography*, 8, 515–523, 1995. [1589](#)

Bretherton, C., and C. Schär, Flux of potential vorticity substance: a simple derivation and uniqueness property, *Journal of the Atmospheric Sciences*, 50, 1834–1836, doi:10.1175/1520-0469(1993)050<1834:FOPVSA>2.0.CO;2, 1993. [1006](#), [1009](#)

Bretherton, F. P., Critical layer instability in baroclinic flows, *Quarterly Journal of the Royal Meteorological Society*, 92, 325–334, 1966. [96](#), [640](#)

Brown, E., *Waves, tides, and shallow-water processes*, 227 pp., The Open University, Milton Keys, UK, 1999. [747](#), [1184](#)

Bryan, K., A numerical investigation of a nonlinear model of a wind-driven ocean, *Journal of Atmospheric Sciences*, 20, 594–606, doi:10.1175/1520-0469(1963)020<0594:ANIOAN>2.0.CO;2, 1963. [916](#)

Bryan, K., A numerical method for the study of the circulation of the world ocean, *Journal of Computational Physics*, 4, 347–376, 1969. [878](#), [1071](#)

Buckingham, C., J. Gula, and X. Carton, The role of curvature in modifying frontal instabilities. Part I: Review of theory and presentation of a nondimensional instability criterion, *Journal of Physical Oceanography*, 51, 299–315, doi:10.1175/JPO-D-19-0265.1, 2021. [1321](#), [1345](#)

Bühler, O., *Waves and mean flows*, 2nd ed., Cambridge University Press, Cambridge, UK, doi:10.1017/CBO9781107478701, 2014a. [45](#), [1129](#), [1545](#), [1554](#)

Bühler, O., A gentle stroll through EP flux theory, *European Journal of Mechanics B*, 47, 12–15, doi:10.1016/j.euromechflu.2014.01.010, 2014b. [1471](#)

Bühler, O., J. Callies, and R. Ferrari, Wave-vortex decomposition of one-dimensional ship-track data, *Journal of Fluid Mechanics*, 756, 1007–1026, doi:10.1017/jfm.2014.488, 2014. [646](#)

- Butt, T., P. Russell, and R. Grigg, *Surf Science - An Introduction To Waves For Surfing*, University of Hawaii Press, 2004. [1108](#)
- Caldwell, D., Thermal and Fickian diffusion of sodium chloride in a solution of oceanic concentration, *Deep-Sea Research*, *20*, 1029–1039, doi:10.1016/0011-7471(73)90073-9, 1973. [548](#)
- Caldwell, D., and S. Eide, Soret coefficient and isothermal diffusivity of aqueous solutions of five principal salt constituents of seawater, *Deep-Sea Research*, *28A*, 1605–1618, doi:10.1016/0198-0149(81)90100-X, 1981. [548](#)
- Callen, H. B., *Thermodynamics and an Introduction to Thermostatics*, John Wiley and Sons, New York, 493 + xvi pp, 1985. [407](#), [410](#), [411](#), [412](#), [536](#), [546](#), [549](#), [1408](#)
- Callies, J., and R. Ferrari, Dynamics of an abyssal circulation driven by bottom-intensified mixing on slopes, *Journal of Physical Oceanography*, *48*, 1257–1282, doi:10.1175/JPO-D-17-0125.1, 2018. [1002](#)
- Cane, M., V. Kamenkovich, and A. Krupitsky, On the utility and disutility of JEBAR, *Journal of Physical Oceanography*, *28*, 519–526, doi:10.1175/1520-0485(1998)028<0519:OTUADO>2.0.CO;2, 1998. [1074](#)
- Carnevale, G., R. Kloosterziel, and G. van Heijst, Propagation of barotropic vortices over topography in a rotating tank, *Journal of Fluid Mechanics*, *233*, 119–139, doi:10.1017/S0022112091000411, 1991. [883](#)
- Cauchy, A.-L., *Résumé des leçons données à l'école royale polytechnique sur le calcul infinitésimal*, Imprimerie royale, 1823. [68](#)
- Chaikin, P. M., and T. C. Lubensky, *Principles of Condensed Matter Physics*, Cambridge University Press, Cambridge, United Kingdom, 1995. [137](#)
- Chandrasekhar, S., *Hydrodynamic and Hydromagnetic Stability*, Dover Publications, New York, 654 pp, 1961. [614](#), [1363](#), [1365](#), [1372](#), [1375](#)
- Chang, E. K. M., and C. L. P. Wolfe, The horizontal components of the real gravity are not relevant to ocean dynamics, *Scientific Reports*, *12*, doi:10.1038/s41598-021-82882-1, 2022. [237](#)
- Charney, J., R. Fjörtoft, and J. von Neumann, Numerical integration of the barotropic vorticity equation, *Tellus*, *2*, 237–254, doi:10.3402/tellusa.v2i4.8607, 1950. [863](#), [873](#)
- Charney, J. G., and M. E. Stern, On the stability of internal baroclinic jets in a rotating atmosphere, *Journal of the Atmospheric Sciences*, *19*, 159–172, doi:10.1175/1520-0469(1962)019<0159:OTSOIB>2.0.CO;2, 1962. [1394](#)
- Chatwin, P. C., The vorticity equation as an angular momentum equation, *Mathematical Proceedings of the Cambridge Philosophical Society*, *74*, 365–367, doi:10.1017/S0305004100048131, 1973. [859](#)
- Cohen-Tannoudji, C., B. Diu, and F. Laloë, *Quantum Mechanics: Volumes One and Two*, John Wiley and Sons, New York, 1524 pp, 1977. [117](#), [1122](#), [1124](#), [1125](#)
- Cole, S. T., C. Wortham, E. Kunze, and W. B. Owens, Eddy stirring and horizontal diffusivity from argo float observations: Geographic and depth variability, *Geophysical Research Letters*, *42*(10), 3989–3997, doi:10.1002/2015GL063827, 2015GL063827, 2015. [1575](#)

BIBLIOGRAPHY

- Courant, R., and D. Hilbert, *Methods of Mathematical Physics Volume I*, Wiley-Interscience, New York, 1953. [1502](#)
- Courant, R., and D. Hilbert, *Methods of Mathematical Physics Volume II: Partial Differential Equations*, Wiley-Interscience, 1962. [1502](#)
- Cox, M., and K. Bryan, A numerical model of the ventilated thermocline, *Journal of Physical Oceanography*, 14, 674–687, 1984. [1589](#)
- Cox, M. D., Isopycnal diffusion in a z -coordinate ocean model, *Ocean Modelling*, 74, 1–5, 1987. [1591](#), [1592](#)
- Crocco, L., Eine neue stromfunktion fur die erforschung der bewegung der gas emit rotation, *Zamm-zeitschrift Fur Angewandte Mathematik Und Mechanik*, 17, 1, doi:10.1002/ZAMM. 19370170103, 1937. [560](#)
- Cushman-Roisin, B., Subduction, in *Dynamics of the oceanic surface mixed-layer*, pp. 181–196, Hawaii Institute of Geophysical Special Publications, 1987. [1436](#)
- Cushman-Roisin, B., and J.-M. Beckers, *Introduction to Geophysical Fluid Dynamics*, Academic Press, Amsterdam, 828, 2011. [xxviii](#), [xxix](#), [xxx](#), [xxxii](#), [722](#), [723](#), [773](#), [781](#), [1184](#), [1275](#), [1318](#), [1320](#), [1367](#), [1375](#), [1380](#), [1494](#)
- Dahler, J., and L. Scriven, The angular momentum of continua, *Nature*, 4797, 36–37, 1961. [487](#)
- Danabasoglu, G., R. Ferrari, and J. McWilliams, Sensitivity of an ocean general circulation model to a parameterization of near-surface eddy fluxes, *Journal of Climate*, 21, 1192–1208, doi: 10.1175/2007JCLI1508.1, 2008. [1575](#), [1593](#)
- Davidson, P., *Turbulence: an introduction for scientists and engineers*, Oxford University Press, Oxford, UK, 2015. [xxx](#), [xxxii](#), [859](#), [1208](#)
- Davies-Jones, R., Comments on "A Generalization of Bernoulli's Theorem", *Journal of the Atmospheric Sciences*, 60, 2039–2041, doi:10.1175/1520-0469(2003)060<2039:COAGOB>2.0.CO;2, 2003a. [1006](#)
- Davies-Jones, R., An expression for effective buoyancy in surroundings with horizontal density gradients, *Journal of the Atmospheric Sciences*, 60, 2922–2925, doi:10.1175/1520-0469(2003)060<2922:AEFEBI>2.0.CO;2, 2003b. [680](#)
- Davis, R. E., Diapycnal mixing in the ocean: equations for large-scale budgets, *Journal of Physical Oceanography*, 24, 777–800, doi:10.1175/1520-0485(1994)024<0777:DMITOE>2.0.CO;2, 1994. [534](#)
- DeGroot, S. R., and P. Mazur, *Non-Equilibrium Thermodynamics*, Dover Publications, New York, 510 pp, 1984. [361](#), [368](#), [517](#), [534](#), [536](#)
- Denaro, F., On the application of the Helmholtz-Hodge decomposition in projection methods for incompressible flows with general boundary conditions, *International Journal of Numerical Methods in Fluids*, 43, 43–69, doi:10.1002/fld.598, 2003. [327](#)
- DeSzeoke, R. A., and A. F. Bennett, Microstructure fluxes across density surfaces, *Journal of Physical Oceanography*, 23, 2254–2264, 1993. [1569](#)

- Doering, C., and J. Gibbon, *Applied analysis of the Navier-Stokes equations*, Cambridge University Press, Cambridge, UK, 217 pp, 1995. 481, 500
- Doswell, C., and P. Markowski, Is buoyancy a relative quantity?, *Monthly Weather Review*, 132, 853–863, doi:10.1175/1520-0493(2004)132<0853:IBARQ>2.0.CO;2, 2004. 680
- Drazin, P., and R. Johnson, *Solitons: an introduction*, Cambridge University Press, Cambridge, UK, 226 pp, 1989. 1181
- Drazin, P., and W. Reid, *Hydrodynamic stability*, Cambridge University Press, Cambridge, UK, 527 pp, 1981. 1320, 1328, 1336, 1372
- Drijfhout, S. S., D. P. Marshall, and H. A. Dijkstra, Conceptual models of the wind-driven and thermohaline circulation, in *Ocean Circulation and Climate, 2nd Edition: A 21st Century Perspective, International Geophysics Series*, vol. 103, edited by G. Siedler, S. M. Griffies, J. Gould, and J. Church, pp. 257–282, Academic Press, 2013. 1074
- Duchateau, P., and D. Zachmann, *Partial differential equations*, Schaum's Outline Series in Mathematics, McGraw-Hill, New York, 1986. 49
- Dukowicz, J. K., and R. D. Smith, Stochastic theory of compressible turbulent fluid transport, *Physics of Fluids*, 9, 3523–3529, 1997. 1593
- Durran, D. R., Is the coriolis force really responsible for the inertial oscillation?, *Bulletin of the American Meteorological Society*, 74, 2179–2184, doi:10.1175/1520-0477(1993)074<2179:ITCFRR>2.0.CO;2, 1993. 242
- Dyke, M. V., *Perturbation methods in fluid mechanics*, 1st ed., The Parabolic Press, Stanford, California, USA, 271, 1975. 509
- Eady, E., Long waves and cyclone waves, *Tellus*, 1, 33–52, doi:10.1111/j.2153-3490.1949.tb01265.x, 1949. 1379
- Early, J. J., The forces of inertial oscillations, *Quarterly Journal of the Royal Meteorological Society*, 138, 1914, doi:10.1002/qj.1917, 2012. 242
- Ebeling, W., and R. Feistel, *Physics of Self-Organization and Evolution*, John Wiley & Sons, 2011. 407, 412
- Eckart, C., An analysis of the stirring and mixing processes in incompressible fluids, *Journal of Marine Research*, 7, 265–275, 1948. 1493, 1574
- Einstein, A., Über die von der molekularkinetischen theorie der wärme geforderte bewegung von in ruhenden flüssigkeiten suspendierten teilchen, *Annalen der Physik (in German)*, 322, 549–560, 1905. 1495, 1574
- Einstein, A., *Autobiographical Notes*, Open Court, 1949. 406
- Eliassen, A., and E. Palm, On the transfer of energy in stationary mountain waves, *Geofysiske Publikasjoner*, 22(1–23), 1960. 1471
- Ertel, H., Ein neuer hydrodynamicscher Wirbelsatz, *Meteorol. Z. (Braunschweig)*, 59, 271–281, 1942. 979, 982
- Falkovich, G., *Fluid Mechanics: A short course for physicists*, Cambridge University Press, 167pp, 2011. 515

- Farrell, W., and J. Clark, On postglacial sea level, *Geophysical Journal of the Royal Astronomical Society*, 46, 646–667, 1976. 747
- Feistel, R., Equilibrium thermodynamics of seawater revisited, *Progress in Oceanography*, 31, 101–179, 1993. 431
- Ferrari, R., J. C. McWilliams, V. M. Canuto, and M. Dubovikov, Parameterization of eddy fluxes near oceanic boundaries, *Journal of Climate*, 21, 2770–2789, doi:10.1175/2007JCLI1510.1, 2008. 1575, 1588, 1593
- Ferrari, R., S. M. Griffies, A. J. G. Nurser, and G. K. Vallis, A boundary-value problem for the parameterized mesoscale eddy transport, *Ocean Modelling*, 32, 143–156, doi:10.1016/j.ocemod.2010.01.004, 2010. 1588, 1589, 1593
- Ferreira, D., and J. Marshall, Formulation and implementation of a residual-mean ocean circulation model, *Ocean Modelling*, 13, 86–107, 2006. 1585
- Fetter, A. L., and J. D. Walecka, *Theoretical Mechanics of Particles and Continua*, Dover Publications, Mineola, New York, 570 pp, 2003. 135, 197, 210, 515, 1104, 1122, 1124, 1125, 1131, 1132, 1138, 1139, 1159, 1163, 1172, 1182, 1187, 1363, 1365
- Fetter, A. L., and J. D. Walecka, *Nonlinear Mechanics*, Dover Publications, Mineola, New York, 154 pp, 2006. 1377
- Fetterer, F., K. Knowles, W. Meier, and M. Savoie, Sea ice index, *Tech. rep.*, National Snow and Ice Data Center, Boulder, USA, 2009. 211
- Feynman, R. P., R. B. Leighton, and M. L. Sands, *The Feynman lectures on physics*, Addison-Wesley Publishing Company, Reading, Mass, 1963. 536, 553, 1142
- Fjørtoft, R., An application of integral theorems in deriving criteria for laminar flows and for the baroclinic circular vortex, *Geophysics Publications*, 17, 1–52, 1950. 1373
- Fofonoff, N. P., Steady flow in a frictionless homogeneous ocean, *Journal of Marine Research*, 13, 254–262, 1954. 916
- Fox-Kemper, B., R. Ferrari, and J. Pedlosky, On the indeterminacy of rotational and divergent eddy fluxes, *Journal of Physical Oceanography*, 33, 478–483, doi:10.1175/1520-0485(2003)033<0478:OTIORA>2.0.CO;2, 2003. 1557
- Fox-Kemper, B., R. Lumpkin, and F. Bryan, Lateral transport in the ocean interior, in *Ocean Circulation and Climate, 2nd Edition: A 21st Century Perspective, International Geophysics Series*, vol. 103, edited by G. Siedler, S. M. Griffies, J. Gould, and J. Church, pp. 185–209, Academic Press, 2013. 1595
- Frankel, T., *The Geometry of Physics: An Introduction*, Cambridge University Press, 686pp, 2012. 327
- French, A. P., *Newtonian Mechanics*, 743 pp., W.W. Norton and Company, New York, 1971. 211
- Frisch, U., *Turbulence, the Legacy of A.N. Kolmogorov*, Cambridge University Press, 1995. 298
- Frisch, U., and B. Villone, Cauchy's almost forgotten Lagrangian formulation of the Euler equation for 3D incompressible flow, *European Physical Journal*, 39, 325–351, doi:10.1140/epjh/e2014-50016-6, 2014. 313

- Gardiner, C. W., *Handbook of stochastic methods for physics, chemistry and the natural sciences*, 2nd ed., 442 pp., Springer-Verlag, Berlin, Heidelberg, New York, 1985. 101
- Garrett, C., Turbulent dispersion in the ocean, *Progress in Oceanography*, 70, 113–125, 2006. 1556, 1560
- Garrett, C., P. MacCready, and P. Rhines, Boundary mixing and arrested ekman layers: Rotating stratified flow near a sloping boundary, *Annual Review of Fluid Mechanics*, 25, 291–323, doi: 10.1146/annurev.fl.25.010193.001451, 1993. 743, 744
- Gasiorowicz, S., *Quantum Physics*, Wiley International, Hoboken, NJ, USA, 1974. 117, 1120, 1125, 1129, 1130
- Gavriel, N., and Y. Kaspi, The number and location of Jupiter's circumpolar cyclones explained by vorticity dynamics, *Nature Geoscience*, 14, 559–563, doi:10.1038/s41561-021-00781-6, 2021. 884
- Gent, P. R., and J. C. McWilliams, Isopycnal mixing in ocean circulation models, *Journal of Physical Oceanography*, 20, 150–155, doi:10.1175/1520-0485(1990)020<0150:IMIOCM>2.0.CO;2, 1990. 704, 705, 1576, 1591, 1592
- Gent, P. R., J. Willebrand, T. J. McDougall, and J. C. McWilliams, Parameterizing eddy-induced tracer transports in ocean circulation models, *Journal of Physical Oceanography*, 25, 463–474, doi:10.1175/1520-0485(1995)025<0463:PEITTI>2.0.CO;2, 1995. 651, 1512, 1568, 1576, 1580, 1581, 1582, 1584, 1585, 1586, 1587, 1588, 1589
- Gill, A., *Atmosphere-Ocean Dynamics, International Geophysics Series*, vol. 30, Academic Press, London, 662 + xv pp, 1982. 234, 236, 238, 273, 426, 504, 505, 668, 700, 713, 717, 723, 748, 1574
- Gnanadesikan, A., A global model of silicon cycling: Sensitivity to eddy parameterization and dissolution, *Global Biogeochemical Cycles*, 13, 199–220, 1999. 1592
- Gnanadesikan, A., and R. Weller, Structure and instability of the ekman spiral in the presence of surface gravity waves, *Journal of Physical Oceanography*, 25, 3148–3171, doi:10.1175/1520-0485(1995)025<3148:SAIOTE>2.0.CO;2, 1995. 743
- Godfrey, J., A Sverdrup model of the depth-integrated flow for the World Ocean allowing for island circulations, *Geophysical and Astrophysical Fluid Dynamics*, 45, 89–112, doi:10.1080/03091928908208894, 1989. 922, 923
- Goldstein, H., *Classical Mechanics*, Addison-Wesley Publishing, Reading, MA, 1980. 197, 1127
- Graham, F., and T. McDougall, Quantifying the nonconservative production of Conservative Temperature, potential temperature, and entropy, *Journal of Physical Oceanography*, 43, 838–862, doi:10.1175/JPO-D-11-0188.1, 2013. 548, 551, 552, 1576
- Gray, A., and S. Riser, A global analysis of Sverdrup balance using absolute geostrophic velocities from Argo, *Journal of Physical Oceanography*, 44, 1213–1229, doi:10.1175/JPO-D-12-0206.1, 2014. 1067
- Greatbatch, R. J., A note on the representation of steric sea level in models that conserve volume rather than mass, *Journal of Geophysical Research*, 99, 12,767–12,771, doi:10.1029/94JC00847, 1994. 400, 1624

- Greatbatch, R. J., Exploring the relationship between eddy-induced transport velocity, vertical momentum transfer, and the isopycnal flux of potential vorticity, *Journal of Physical Oceanography*, 28, 422–432, doi:10.1175/1520-0485(1998)028<0422:ETRBEI>2.0.CO;2, 1998. 1486, 1487
- Greatbatch, R. J., and K. G. Lamb, On parameterizing vertical mixing of momentum in non-eddy resolving ocean models, *Journal of Physical Oceanography*, 20, 1634–1637, doi:10.1175/1520-0485(1990)020<1634:OPVMOM>2.0.CO;2, 1990. 1486, 1585
- Gregg, M. C., Entropy generation in the ocean by small-scale mixing, *Journal of Physical Oceanography*, 14, 688–711, 1984. 534
- Gregory, J., Vertical heat transports in the ocean and their effect on time-dependent climate change, *Climate Dynamics*, 15, 501–515, doi:10.1007/s003820000059, 2000. 628
- Gregory, J., S. M. Griffies, C. Hughes, J. Lowe, J. Church, I. Fukimori, N. Gomez, R. Kopp, F. Landerer, R. Ponte, D. Stammer, M. Tamisiea, and R. van den Wal, Concepts and terminology for sea level–mean, variability and change, both local and global, *Surveys in Geophysics*, 40, 1251–1289, doi:10.1007/s10712-019-09555-7, 2019. 237, 748, 1624, 1626
- Griffies, S., and R. Hallberg, Biharmonic friction with a Smagorinsky-like viscosity for use in large-scale eddy-permitting ocean models, *Monthly Weather Review*, 128, 2935–2946, doi:10.1175/1520-0493(2000)128<2935:BFWASL>2.0.CO;2, 2000. 528
- Griffies, S., A. Adcroft, and R. Hallberg, A primer on the vertical lagrangian-remap method in ocean models based on finite volume generalized vertical coordinates, *Journal of Advances in Modeling Earth Systems*, 12, doi:10.1029/2019MS001954, 2020. 281, 374, 375, 773, 958, 1398, 1439, 1448, 1486, 1594, 1599
- Griffies, S. M., The Gent-McWilliams skew-flux, *Journal of Physical Oceanography*, 28, 831–841, doi:10.1175/1520-0485(1998)028<0831:TGMWSF>2.0.CO;2, 1998. 1509, 1581, 1582, 1593
- Griffies, S. M., *Fundamentals of Ocean Climate Models*, Princeton University Press, Princeton, USA, 518+xxxiv pages, 2004. 33, 159, 194, 277, 393, 467, 498, 499, 503, 528, 878, 1448, 1502, 1509, 1545, 1569, 1588, 1589, 1595
- Griffies, S. M., and A. J. Adcroft, Formulating the equations for ocean models, in *Ocean Modeling in an Eddying Regime, Geophysical Monograph*, vol. 177, edited by M. Hecht and H. Hasumi, pp. 281–317, American Geophysical Union, 2008. 614
- Griffies, S. M., and R. J. Greatbatch, Physical processes that impact the evolution of global mean sea level in ocean climate models, *Ocean Modelling*, 51, 37–72, doi:10.1016/j.ocemod.2012.04.003, 2012. 355, 400, 765, 1545, 1577, 1580, 1612, 1624, 1626
- Griffies, S. M., A. Gnanadesikan, R. C. Pacanowski, V. Larichev, J. K. Dukowicz, and R. D. Smith, Isoneutral diffusion in a z -coordinate ocean model, *Journal of Physical Oceanography*, 28, 805–830, doi:10.1175/1520-0485(1998)028<0805:IDIAZC>2.0.CO;2, 1998. 1502, 1591, 1592
- Griffies, S. M., C. W. Böning, F. O. Bryan, E. P. Chassignet, R. Gerdes, H. Hasumi, A. Hirst, A.-M. Treguier, and D. Webb, Developments in ocean climate modelling, *Ocean Modelling*, 2, 123–192, doi:10.1016/S1463-5003(00)00014-7, 2000. 1450, 1587
- Griffies, S. M., J. Yin, P. J. Durack, P. Goddard, S. Bates, E. Behrens, M. Bentzen, D. Bi, A. Biastoch, C. W. Böning, A. Bozec, C. Cassou, E. Chassignet, G. Danabasoglu, S. Danilov, C. Domingues, H. Drange, R. Farneti, E. Fernandez, R. J. Greatbatch, D. M. Holland, M. Ilicak,

- J. Lu, S. J. Marsland, A. Mishra, W. G. Large, K. Lorbacher, A. G. Nurser, D. Salas y Mélia, J. B. Palter, B. L. Samuels, J. Schröter, F. U. Schwarzkopf, D. Sidorenko, A.-M. Treguier, Y. Tseng, H. Tsujino, P. Uotila, S. Valcke, A. Voldoire, Q. Wang, M. Winton, and Z. Zhang, An assessment of global and regional sea level for years 1993–2007 in a suite of interannual CORE-II simulations, *Ocean Modelling*, 78, 35–89, doi:10.1016/j.ocemod.2014.03.004, 2014. 575, 776, 1625, 1626
- Groeskamp, S., J. Zika, T. McDougall, B. Sloyan, and F. Laliberté, The representation of ocean circulation and variability in thermodynamic coordinates, *Journal of Physical Oceanography*, 44, 1735–1750, doi:10.1175/JPO-D-13-0213.1, 2014. 1631
- Groeskamp, S., R. P. Abernathey, and A. Klocker, Water mass transformation by cabbeling and thermobaricity, *Geophysical Research Letters*, doi:10.1002/2016GL070860, 2016. 1612
- Groeskamp, S., S. M. Griffies, D. Iudicone, R. Marsh, A. G. Nurser, and J. D. Zika, The water mass transformation framework for ocean physics and biogeochemistry, *Annual Review of Marine Science*, 11, 1–35, doi:10.1146/annurev-marine-010318-095421, 2019. 1430, 1612, 1620, 1631, 1644, 1654, 1661
- Guggenheim, E. A., *Thermodynamics: An Advanced Treatment for Chemists and Physicists*, 5th ed., North-Holland, Amsterdam, 390, 1967. 425, 437
- Gula, J., M. Molemaker, and J. McWilliams, Gulf Stream dynamics along the southeastern U.S. seaboard, *Journal of Physical Oceanography*, 45, 690–715, doi:10.1175/JPO-D-14-0154.1, 2015. 585, 968, 978
- Haidvogel, D. B., and P. B. Rhines, Waves and circulation driven by oscillatory winds in an idealized ocean basin, *Geophysical and Astrophysical Fluid Dynamics*, 25, 1–63, doi:10.1080/03091928308221747, 1983. 1210
- Haine, T. W. N., S. Griffies, E. Delhez, G. Gebbie, M. Holzer, and D. Waugh, Tracer methods in ocean modeling: a review of theory and concepts, *Journal of Advances in Modeling Earth Systems (JAMES)*, in prep, 2022. 59, 368, 1493, 1523
- Hallberg, R., A thermobaric instability in Lagrangian vertical coordinate ocean models, *Ocean Modelling*, 8, 227–300, 2005. 1457
- Hallberg, R., and P. Rhines, Buoyancy-driven circulation in a ocean basin with isopycnals intersecting the sloping boundary, *Journal of Physical Oceanography*, 26, 913–940, 1996. 964, 969, 1020
- Haller, G., Lagrangian coherent structures, *Annual Reviews of Fluid Mechanics*, 47, 137–162, doi:10.1146/annurev-fluid-010313-141322, 2015. 309
- Haltiner, G. T., and R. T. Williams, *Numerical Prediction and Dynamic Meteorology*, John Wiley and Sons, New York, USA, 1980. 873
- Haney, R. L., On the pressure gradient force over steep topography in sigma-coordinate ocean models, *Journal of Physical Oceanography*, 21, 610–619, 1991. 1450
- Hasselmann, K., Stochastic climate models. Part I: Theory, *Tellus*, 28, 473–485, 1976. 110
- Hasselmann, K., R. Sausen, E. Maier-Reimer, and R. Voss, On the cold start problem in transient simulations with coupled atmosphere-ocean models, *Climate Dynamics*, 9, 53–61, doi:10.1007/BF00210008, 1993. 114

Haynes, P. H., and M. E. McIntyre, On the evolution of vorticity and potential vorticity in the presence of diabatic heating and frictional or other forces, *Journal of Atmospheric Sciences*, 44, 828–841, 1987. [1003](#), [1004](#), [1005](#), [1006](#)

Haynes, P. H., and M. E. McIntyre, On the conservation and impermeability theorems for potential vorticity, *Journal of Atmospheric Sciences*, 47, 2021–2031, 1990. [1006](#)

Heifetz, E., P. Alpert, and A. da Silva, On the parcel method and the baroclinic wedge of instability, *Journal of Atmospheric Sciences*, 55, 788–795, doi:10.1175/1520-0469(1998)055<0788:OTPMAT>2.0.CO;2, 1998. [1380](#)

Held, I., R. Pierrehumbert, S. Garner, and K. L. Swanson, Surface quasi-geostrophic dynamics, *Journal of Fluid Mechanics*, 282, 1–20, doi:10.1017/S0022112095000012, 1995. [1172](#)

Helmholtz, H., On integrals of the hydrodynamical equations, which express vortex-motion, *The London, Edinburgh, and Dublin Philosophical Magazine and Journal of Science*, 33, 485–512, doi:10.1080/14786446708639824, 1867. [327](#)

Hildebrand, F., *Advanced Calculus for Applications*, Prentice-Hall Publishers, Englewood Cliffs, New Jersey, 1976. [49](#), [52](#), [61](#), [117](#), [122](#)

Holland, G. J., Tropical cyclone motion: environmental interaction plus a beta effect, *Journal of the Atmospheric Sciences*, 40, 328–342, doi:10.1175/1520-0469(1983)040<0328:TCMEIP>2.0.CO;2, 1983. [883](#)

Holloway, G., Eddy transport of thickness and momentum in layer and level models, *Journal of Physical Oceanography*, 27, 1153–1157, 1997. [1587](#)

Holloway, G., and P. Rhines, Angular momenta of modeled ocean gyres, *Journal of Geophysical Research*, 27, 843–846, doi:10.1029/90JC02256, 1991. [885](#)

Holmes, R. M., J. Zika, and M. H. England, Diathermal heat transport in a global ocean model, *Journal of Physical Oceanography*, 49, 141–161, doi:10.1175/JPO-D-18-0098.1, 2019. [1641](#), [1665](#)

Holton, J. R., *An Introduction to Dynamic Meteorology*, Academic Press, San Diego, USA, 507 pp, 1992. [453](#), [474](#), [475](#), [596](#), [604](#), [713](#), [716](#), [718](#), [721](#), [722](#), [880](#), [905](#), [954](#), [973](#), [1320](#), [1335](#)

Holzer, M., The path density of interhemispheric surface-to-surface transport. Part I: Development of the diagnostic and illustration with an analytic model, *Journal of Atmospheric Sciences*, 66(8), 2159–2171, doi:10.1175/2009jas2894.1, 2009. [101](#)

Hoskins, B., The role of potential vorticity in symmetric stability and instability, *Quarterly Journal of the Royal Meteorological Society*, 100, 480–482, 1974. [1340](#), [1345](#)

Hoskins, B., The geostrophic momentum approximation and the semi-geostrophic equations, *Journal of Atmospheric Sciences*, 32, 233–242, 1975. [1345](#)

Hoskins, B., Towards and $p\theta$ -view of the general circulation, *Tellus*, 43AB, 27–35, 1991. [979](#), [985](#)

Hoskins, B., I. Draghici, and H. Davies, A new look at the ω equation, *Quarterly Journal of the Royal Meteorological Society*, 104, 31–38, 1978. [1095](#), [1096](#)

- Hoskins, B., I. James, and G. White, The shape, propagation, and mean flow interaction of large-scale weather systems, *Journal of the Atmospheric Sciences*, 40, 1595–1612, doi:10.1175/1520-0469(1983)040<1595:TSPAMF>2.0.CO;2, 1983. 868
- Hoskins, B. J., and I. N. James, *Fluid Dynamics of the Midlatitude Atmosphere*, Wiley Blackwell, Chichester, UK, 2014. 325, 326
- Huang, K., *Statistical Mechanics*, John Wiley and Sons, New York, 493 pp, 1987. 269, 278, 1498
- Huang, R. X., and R. W. Schmitt, Goldsbrough-Stommel circulation of the World Oceans, *Journal of Physical Oceanography*, 23, 1277–1284, 1993. 1064
- Hughes, C. W., and B. de Cueves, Why western boundary currents in realistic oceans are inviscid: A link between form stress and bottom pressure torques, *Journal of Physical Oceanography*, 31, 2871–2885, 2001. 603, 604, 827, 914, 916, 964, 969
- Hughes, C. W., I. Fukumori, S. M. Griffies, J. M. Huthnance, S. Minobe, P. Spence, K. R. Thompson, and A. Wise, Sea level and the role of coastal trapped waves in mediating the influence of the open ocean on the coast, *Surveys in Geophysics*, 40, 1467–1492, doi:10.1007/s10712-019-09535-x, 2019. 916
- IOC, SCOR, and IAPSO, *The international thermodynamic equation of seawater-2010: calculation and use of thermodynamic properties*, Intergovernmental Oceanographic Commission, Manuals and Guides No. 56, UNESCO, doi:10.25607/OPB-1338, 196pp, 2010. 431, 444, 536, 548, 552, 555, 657, 659, 660, 1576, 1604, 1605, 1612, 1613
- Jackett, D. R., and T. J. McDougall, A neutral density variable for the world's oceans, *Journal of Physical Oceanography*, 27, 237–263, 1997. 1631
- Jackson, J. D., *Classical Electrodynamics*, John Wiley and Sons, New York, USA, 848 pp, 1975. 71, 328, 687, 1510
- Jackson, L., C. Hughes, and R. Williams, Topographic control of basin and channel flows: the role of bottom pressure torques and friction, *Journal of Physical Oceanography*, 36, 1786–1805, doi:10.1175/JPO2936.1, 2006. 914, 968
- Jeevanjee, N., and D. Romps, Effective buoyancy, inertial pressure, and the mechanical generation of boundary layer mass flux by cold pools, *Journal of Atmospheric Sciences*, 72, 3199–3213, doi:10.1175/JAS-D-14-0349.1, 2015a. 680, 878
- Jeevanjee, N., and D. Romps, Effective buoyancy at the surface and aloft, *Quarterly Journal of the Royal Meteorological Society*, 142, 811–820, doi:10.1002/qj.2683, 2015b. 671, 680
- Kamenkovich, V., *Fundamentals of Ocean Dynamics*, Elsevier Scientific Publishing Company, Amsterdam, 249 pp, 1977. 426, 437, 441, 537
- Killworth, P. D., On the parameterization of eddy transfer Part I: Theory, *Journal of Marine Research*, 55, 1171–1197, 1997. 1587
- Klinger, B., and T. Haine, *Ocean Circulation in Three Dimensions*, Cambridge University Press, 466, 2019. 543, 923
- Klocker, A., and R. Abernathey, Global patterns of mesoscale eddy properties and diffusivities, *Journal of Physical Oceanography*, 44, 1030–1046, 2014. 1575

BIBLIOGRAPHY

- Klocker, A., and T. J. McDougall, Influence of the nonlinear equation of state on global estimates of dianeutral advection and diffusion, *Journal of Physical Oceanography*, 40, 1690–1709, doi: 10.1175/2010JPO4303.1, 2010a. [671](#), [1612](#)
- Klocker, A., and T. J. McDougall, Quantifying the consequences of the ill-defined nature of neutral surfaces, *Journal of Physical Oceanography*, 40, 1866—1880, doi:10.1175/2009JPO4212.1, 2010b. [671](#)
- Kooloth, P., L. Smith, and S. Stechmann, Conservation laws for potential vorticity in a salty ocean or cloudy atmosphere, *Geophysical Research Letters*, 49, doi:10.1029/2022GL100009, 2022. [937](#), [997](#)
- Kopp, R. E., J. X. Mitrovica, S. M. Griffies, J. Yin, C. C. Hay, and R. J. Stouffer, The impact of Greenland melt on regional sea level: a preliminary comparison of dynamic and static equilibrium effects, *Climatic Change Letters*, 103, 619–625, doi:10.1007/s10584-010-9935-1, 2010. [747](#)
- Kraichnan, R. H., and D. Montgomery, Two-dimensional turbulence, *Reports on Progress in Physics*, 43, 547–619, 1980. [873](#)
- Kreuzer, H. J., *Nonequilibrium thermodynamics and its statistical foundations*, 438 pp., Oxford Science Publications, New York, 1981. [361](#), [368](#)
- Kundu, P., I. Cohen, and D. Dowling, *Fluid Mechanics*, Academic Press, 921 + xxiv pp, 2016. [xxx](#), [xxxii](#), [278](#), [295](#), [306](#), [468](#), [481](#), [496](#), [498](#), [503](#), [515](#), [1131](#), [1150](#), [1275](#), [1368](#), [1375](#), [1498](#)
- Kuo, H. L., Dynamic stability of two-dimensional nondivergent flow in a barotropic atmosphere, *Journal of the Meteorology*, 6, 105–122, doi:10.1175/1520-0469(1949)006<0105:DIOTDN>2.0.CO;2, 1949. [1373](#)
- Kushner, P. J., and I. M. Held, Potential vorticity thickness fluxes and wave-mean flow interaction, *Journal of Atmospheric Sciences*, 56, 948–958, 1999. [1569](#)
- Landau, L. D., and E. M. Lifshitz, *Mechanics*, Pergamon Press, Oxford, UK, 170 pp, 1976. [197](#), [243](#)
- Landau, L. D., and E. M. Lifshitz, *Statistical Physics: Part 1*, Pergamon Press, Oxford, UK, 544 pp, 1980. [407](#), [437](#), [441](#), [519](#), [537](#)
- Landau, L. D., and E. M. Lifshitz, *Fluid Mechanics*, Pergamon Press, Oxford, UK, 539 pp, 1987. [429](#), [515](#), [517](#), [530](#), [534](#), [536](#), [538](#), [1131](#)
- Large, W., J. McWilliams, and S. Doney, Oceanic vertical mixing: a review and a model with a nonlocal boundary layer parameterization, *Reviews of Geophysics*, 32, 363–403, doi:10.1029/94RG01872, 1994. [1572](#), [1575](#), [1620](#)
- Larson, V. E., The relationship between the transilient matrix and the Green's function for the advection-diffusion equation, *Journal of Atmospheric Sciences*, 56(14), 2447–2453, doi: 10.1175/1520-0469(1999)056<2447:trbtmm>2.0.co;2, 1999. [101](#), [1525](#)
- Lauritzen, P., N. Kevlahan, T. Toniazzo, C. Eldred, T. Dubos, A. Gassmann, V. Larson, C. Jablonowski, O. Guba, B. Shipway, B. Harrop, F. Lemarie, R. Tailleux, A. Herrington, W. Large, P. Rasch, A. Donahue, H. Wan, A. Conley, and J. Bacmeister, Reconciling and improving formulations for thermodynamics and conservation principles in Earth System Models

- (ESMs), *Journal of Advances in Modeling Earth Systems*, doi:10.1029/2022MS003117, 2022. 552
- LeCorre, M., J. Gula, and A.-M. Treguier, Barotropic vorticity balance of the North Atlantic sub-polar gyre in an eddy-resolving model, *Ocean Science*, 16, 451–468, doi:10.5194/os-16-451-2020, 2020. 968, 969
- Lee, M.-M., D. Marshall, and R. Williams, On the eddy transfer of tracers: advective or diffusive?, *Journal of Marine Research*, 55, 483–505, 1997. 1472
- Lemarié, F., L. Debreu, A. F. Shchepetkin, and J. C. McWilliams, On the stability and accuracy of the harmonic and biharmonic isoneutral mixing operators in ocean models, *Ocean Modelling*, 52-53, 9–35, 2012. 1591, 1592
- Lighthill, J., *Waves in Fluids*, Cambridge University Press, Cambridge, UK, 504 pp, 1978. 1142, 1208, 1275
- Lilly, J., Kinematics of a fluid ellipse in a linear flow, *Fluids*, 3(16), doi:10.3390/fluids3010016, 2018. 326
- Lin, S. J., A finite volume integration method for computing pressure gradient force in general vertical coordinates, *Quarterly Journal of the Royal Meteorological Society*, 123, 1749–1762, 1997. 1449, 1450, 1452
- Longuet-Higgins, H. C., Planetary waves on a rotating sphere, *Proceedings of the Royal Society of London A*, 279, 446–473, doi:10.1098/rspa.1964.0116, 1964. 1221, 1222
- Loose, N., S. Bachman, I. Grooms, and M. Jansen, Diagnosing scale-dependent energy cycles in a high-resolution isopycnal ocean model, *Journal of Physical Oceanography*, doi:10.1175/JPO-D-22-0083.1, 2022. 820
- Lorenz, E. N., Available potential energy and the maintenance of the general circulation, *Tellus*, 7, 157–167, 1955. 639
- Lovelock, D., and H. Rund, *Tensors, Differential Forms, and Variational Principles*, 366 pp., Dover Publications, New York, 1989. 5
- MacCready, P., and P. Rhines, Buoyant inhibition of ekman transport on a slope and its effect on stratified spin-up, *Journal of Fluid Mechanics*, 223, 631–661, doi:10.1017/S0022112091001581, 1991. 743, 744
- MacCready, P., and P. Rhines, Slippery bottom boundary layers on a slope, *Journal of Physical Oceanography*, 23, 5–22, doi:10.1175/1520-0485(1993)023<0005:SBBLOA>2.0.CO;2, 1993. 743, 744, 1050
- MacKinnon, J., Louis St. Laurent, and A. C. Naveira Garabato, Diapycnal mixing processes in the ocean interior, in *Ocean Circulation and Climate, 2nd Edition: A 21st century perspective, International Geophysics Series*, vol. 103, edited by G. Siedler, S. M. Griffies, J. Gould, and J. Church, pp. 159–183, Academic Press, doi:10.1016/B978-0-12-391851-2.00007-6, 2013. 528, 1298, 1575, 1576
- MacKinnon, J., Z. Zhao, C. Whalen, A. Waterhouse, D. Trossman, O. Sun, L. S. Laurent, H. Simmons, K. Polzin, R. Pinkel, A. Pickering, N. Norton, J. Nash, R. Musgrave, L. Merchant,

- A. Melet, B. Mater, S. Legg, W. Large, E. Kunze, J. Klymak, M. Jochum, S. Jayne, R. Hallberg, S. M. Griffies, P. Gent, S. Diggs, G. Danabasoglu, E. Chassignet, M. Buijsman, F. Bryan, B. Briegleb, A. Barna, B. Arbic, J. Ansong, and M. Alford, Climate process team on internal-wave driven ocean mixing, *Bulletin of the American Meteorological Society*, pp. 2429–2454, doi:10.1175/BAMS-D-16-0030.1, 2017. 1298
- Maddison, J., and D. Marshall, The Eliassen-Palm flux tensor, *Journal of Fluid Mechanics*, 729, 69–102, doi:10.1017/jfm.2013.259, 2013. 799, 808, 1089, 1469, 1483
- Marion, J. B., and S. T. Thornton, *Classical Dynamics of Particles and Systems*, Harcourt Brace Jovanovich, San Diego, USA, 602 pp, 1988. v, 197, 205, 211, 893, 1127, 1139
- Markowski, P., and Y. Richardson, *Mesoscale Meteorology in Midlatitudes*, Wiley-Blackwell Publishers, Oxford, UK, 2010. 245, 623, 680, 973, 1320, 1328, 1330, 1336
- Marshall, D., Vertical fluxes of potential vorticity and the structure of the thermocline, *Journal of Physical Oceanography*, 30, 3102–3112, 2000. 995, 1009
- Marshall, D. P., and H. R. Pillar, Momentum balance of the wind-driven and meridional overturning circulation, *Journal of Physical Oceanography*, 41, 960–978, doi:10.1175/2011JPO4528.1, 2011. 625
- Marshall, D. P., J. Maddison, and P. Berlov, A framework for parameterizing eddy potential vorticity fluxes, *Journal of Physical Oceanography*, 42, 539–557, doi:10.1175/JPO-D-11-048.1, 2012. 923
- Marshall, J., and R. A. Plumb, *Atmosphere, Ocean, and Climate Dynamics*, 1st ed., Academic Press, Amsterdam, 319pp, 2008. 474, 578, 700, 723, 729, 832
- Marshall, J., D. Jamous, and J. Nilsson, Entry, flux, and exit of potential vorticity in ocean circulation, *Journal of Physical Oceanography*, 31, 777–789, doi:10.1175/1520-0485(2001)031<0777:EFAEOP>2.0.CO;2, 2001. 995, 1006, 1008, 1009, 1020
- Marshall, J., K. Armour, J. Scott, Y. Kostov, U. Hausmann, D. Ferreira, T. Shepherd, and C. Bitz, The ocean's role in polar climate change: asymmetric Arctic and Antarctic responses to greenhouse gas and ozone forcing, *Philosophical Transactions of the Royal Society A*, A372, doi:10.1098/rsta.2013.0040, 2014. 114
- Marshall, J. C., E. Shuckburgh, H. Jones, and C. Hill, Estimates and implications of surface eddy diffusivity in the Southern Ocean derived from tracer transport, *Journal of Physical Oceanography*, 36, 1806–1821, 2006. 1539
- Maxwell, J., *Theory of Heat*, 3rd ed., Longmans, Green, and Company, London, 313, 1872. 406, 452
- McCabe, R., P. MacCready, and G. Pawlak, Form drag due to flow separation at a headland, *Journal of Physical Oceanography*, 36, 2136–2152, doi:10.1175/JPO2966.1, 2006. 588
- McDougall, T., R. Feistel, and R. Pawlowicz, Thermodynamics of seawater, in *Ocean Circulation and Climate, 2nd Edition: A 21st Century Perspective, International Geophysics Series*, vol. 103, edited by G. Siedler, S. M. Griffies, J. Gould, and J. Church, pp. 141–158, Academic Press, 2013. 660
- McDougall, T. J., Double-diffusive convection caused by coupled molecular diffusion, *Journal of Fluid Mechanics*, 126, 379–397, doi:10.1017/S0022112083000221, 1983. 548

- McDougall, T. J., Neutral surfaces, *Journal of Physical Oceanography*, 17, 1950–1967, doi:10.1175/1520-0485(1987)017<1950:NS>2.0.CO;2, 1987a. 668, 1575, 1578
- McDougall, T. J., Thermobaricity, cabbeling, and water-mass conversion, *Journal of Geophysical Research*, 92, 5448–5464, doi:10.1029/JC092iC05p05448, 1987b. 668, 1575, 1608, 1609, 1610, 1611
- McDougall, T. J., Potential enthalpy: a conservative oceanic variable for evaluating heat content and heat fluxes, *Journal of Physical Oceanography*, 33, 945–963, doi:10.1175/1520-0485(2003)033<0945:PEACOV>2.0.CO;2, 2003. 444, 551, 552, 1604, 1612
- McDougall, T. J., and R. Feistel, What causes the adiabatic lapse rate, *Deep-Sea Research*, 50, 1523–1535, 2003. 443
- McDougall, T. J., and D. R. Jackett, On the helical nature of neutral trajectories in the ocean, *Progress in Oceanography*, 20, 153–183, 1988. 668, 671
- McDougall, T. J., and P. C. McIntosh, The temporal-residual-mean velocity. Part II: isopycnal interpretation and the tracer and momentum equations, *Journal of Physical Oceanography*, 31, 1222–1246, doi:10.1175/1520-0485(2001)031<1222:TTRMVP>2.0.CO;2, 2001. 1519, 1545, 1562, 1568, 1569, 1571, 1582
- McDougall, T. J., and J. Turner, The role of cross-diffusion on finger double-diffusive convection, *Nature*, 299, 812–814, doi:10.1038/299812a0, 1982. 548
- McDougall, T. J., and Y. You, Implications of the nonlinear equation of state for upwelling in the ocean interior, *Journal of Geophysical Research*, 95, 13,263—13,276, 1990. 1612
- McDougall, T. J., S. Groeskamp, and S. M. Griffies, On geometric aspects of interior ocean mixing, *Journal of Physical Oceanography*, 44, 2164–2175, 2014. 664, 668, 1575, 1576, 1578, 1580, 1589, 1608
- McDougall, T. J., P. Barker, R. Holmes, R. Pawlowicz, S. Griffies, and P. Durack, The interpretation of temperature and salinity variables in numerical ocean model output, and the calculation of heat fluxes and heat content, *Geoscientific Model Development*, 14, 6445–6466, doi:10.5194/gmd-14-6445-2021, 2021. 444, 552
- McIntosh, P. C., and T. J. McDougall, Isopycnal averaging and the residual mean circulation., *Journal of Physical Oceanography*, 26, 1655–1660, 1996. 1569, 1582
- McWilliams, J., *Fundamentals of Geophysical Fluid Dynamics*, Cambridge University Press, Cambridge, Cambridge, UK, 2006. 863, 884, 1210, 1470
- McWilliams, J., and G. Flierl, On the evolution of isolated, nonlinear vortices, *Journal of Physical Oceanography*, 9, 1155–1182, doi:10.1175/1520-0485(1979)009<1155:OTEON>2.0.CO;2, 1979. 883
- McWilliams, J. C., Submesoscale currents in the ocean, *Proceedings of the Royal Society, A* 472, doi:10.1098/rspa.2016.0117, 2016. 1320, 1335
- Mellor, G. L., L.-Y. Oey, and T. Ezer, Sigma coordinate pressure gradient errors and the seamount problem, *Journal of Atmospheric and Oceanic Technology*, 15, 1122–1131, 1998. 1450
- Mermin, N. D., What's wrong with these equations?, *Physics Today*, 42, 9–11, doi:10.1063/1.2811173, 1989. iv

BIBLIOGRAPHY

- Mertz, G., and D. Wright, Interpretations of the JEBAR term, *Journal of Physical Oceanography*, 22, 301–305, doi:10.1175/1520-0485(1992)022<0301:IOTJT>2.0.CO;2, 1992. 1074
- Meyer, R., *Introduction to mathematical fluid dynamics*, Dover Publications, New York, 1971. 497, 501
- Middleton, J. F., and J. W. Loder, Skew fluxes in polarized wave fields, *Journal of Physical Oceanography*, 19, 68–76, doi:10.1175/1520-0485(1989)019<0068:SFIPWF>2.0.CO;2, 1989. 1509, 1556, 1557, 1558, 1560, 1589
- Miles, J. W., On the stability of heterogeneous shear flows, *Journal of Fluid Mechanics*, 10, 496–508, doi:10.1017/S0022112061000305, 1961. 1375
- Minobe, S., M. Terada, B. Qiu, and N. Schneider, Western boundary sea level: A theory, rule of thumb, and application to climate models, *Journal of Physical Oceanography*, 47, 957–977, doi:10.1175/JPO-D-16-0144.1, 2017. 916
- Mitrovica, J. X., M. E. Tamisiea, J. L. Davis, and G. A. Milne, Recent mass balance of polar ice sheets inferred from patterns of global sea-level change, *Nature*, 409, 1026–1029, 2001. 747, 748
- Moffatt, H., Transport effects associated with turbulence with particular attention to the influence of helicity, *Reports on Progress in Physics*, 46, 621–664, doi:10.1088/0034-4885/46/5/002, 1983. 1509, 1560
- Molemaker, M., J. McWilliams, and W. Dewar, Submesoscale instability and generation of mesoscale anticyclones near a separation of the California Undercurrent, *Journal of Physical Oceanography*, 45, 613–629, doi:10.1175/JPO-D-13-0225.1, 2015. 585, 978
- Montgomery, R. B., Circulation in upper layers of southern North Atlantic, *Papers in Physical Oceanography*, 6, 55, 1938. 1589
- Morel, Y., J. Gula, and A. Ponte, Potential vorticity diagnostics based on balances between volume integral and boundary conditions, *Ocean Modelling*, 138, 23–35, doi:10.1016/j.ocemod.2019.04.004, 2019. 1009, 1010, 1014
- Morse, P. M., and H. Feshbach, *Methods of Theoretical Physics Part I and II*, McGraw-Hill Book Company, New York, 1953. 72, 92, 238
- Mory, M., Inertial oscillations, in *Rotating Fluids in Geophysical and Industrial Applications*, International Centre for Mechanical Sciences (Courses and Lectures), Springer, Vienna, doi:10.1007/978-3-7091-2602-8_8, 1992. 1208
- Müller, P., Ertel's potential vorticity theorem in physical oceanography, *Reviews of Geophysics*, 33, 67–97, 1995. 984
- Müller, P., *The Equations of Oceanic Motions*, 1st ed., Cambridge University Press, Cambridge, 302pp, 2006. 536
- Müller, P., and C. Garrett, From stirring to mixing in a stratified ocean, *Oceanography*, 15, 12–19, 2002. 1574
- Munk, W., and E. Palmén, Note on the dynamics of the Antarctic Circumpolar Current, *Tellus*, 3, 53–55, 1951. 604, 824, 827

- Munk, W. H., On the wind-driven ocean circulation, *Journal of Meteorology*, 7, 79–93, 1950. 604, 915
- Nakamura, N., A new look at eddy diffusivity as a mixing diagnostic, *Journal of the Atmospheric Sciences*, 58(24), 3685–3701, doi:10.1175/1520-0469(2001)058<3685:ANLAED>2.0.CO;2, 2001. 1574
- Naveira Garabato, A., E. Frajka-Williams, C. Spingys, A. Legg, K. Polzin, A. Forryan, E. Abrahamsen, C. Buckingham, S. Griffies, S. McPhail, K. Nicholls, L. Thomas, and M. Meredith, Rapid mixing and exchange of deep-ocean waters in an abyssal boundary current, *Proceedings of the National Academy of Sciences*, doi:10.1073/pnas.1904087116, 2019. 1020
- Neumann, G., and W. Pierson, *Principles of Physical Oceanography*, Prentice-Hall, Englewood Cliffs, USA, 545 pp, 1966. 1162, 1184
- Noether, E., Invariante variationsprobleme, *Nachrichten von der Gesellschaft der Wissenschaften zu Göttingen, Math-phys. Klasse*, pp. 235–257, 1918. 243
- Noether, E., and M. Tavel, Invariant variational problems, *arXiv:physics/0503066 [physics.hist-ph]*, 2018. 243
- Nurser, A., S. Griffies, J. Zika, and G. Stanley, Mathematics of circulation in arbitrary fluid property spaces, *Earth and Space Science Open Archive (ESSOar)*, doi:10.1002/essoar.10511370.1, 2022. 9, 155, 1630, 1636
- Nurser, A. G., and S. M. Griffies, Relating diffusive surface salinity fluxes to boundary freshwater and salt fluxes, *Journal of Physical Oceanography*, 49, 2365–2376, doi:10.1175/JPO-D-19-0037. 1, 2019. 1532, 1617, 1646
- Nurser, A. G., and M.-M. Lee, Isopycnal averaging at constant height. Part I: The formulation and a case study, *Journal of Physical Oceanography*, 34, 2721–2739, 2004a. 1569
- Nurser, A. G., and M.-M. Lee, Isopycnal averaging at constant height. Part II: Relating to the residual streamfunction in Eulerian space, *Journal of Physical Oceanography*, 34, 2740–2755, 2004b. 1569
- Nurser, A. G., R. Marsh, and R. Williams, Diagnosing water mass formation from air-sea fluxes and surface mixing, *Journal of Physical Oceanography*, 29, 1468–1487, doi:10.1175/1520-0485(1999)029<1468:DWMFFA>2.0.CO;2, 1999. 640
- Olbers, D. J., J. Willebrand, and C. Eden, *Ocean Dynamics*, 1st ed., Springer, Berlin, Germany, 704 pages, 2012. 237, 278, 279, 283, 318, 426, 427, 536, 548, 552, 668, 828, 829, 1576
- Ottino, J. M., *The kinematics of mixing: stretching, chaos, and transport*, Cambridge University Press, Cambridge, UK, 396 pp, 1989. 309
- Otto, A., F. Otto, O. Boucher, J. Church, G. Hegerl, P. Forster, N. Gillett, J. Gregory, G. Johnson, R. Knutti, N. Lewis, U. Lohmann, J. Marotzke, G. Myhre, D. Shindell, B. Stevens, and M. Allen, Energy budget constraints on climate response, *Nature Geosciences*, 6, 415–416, doi:10.1038/ngeo1836, 2013. 1623
- Patmore, R., P. Holland, D. Munday, A. Naveira Garabato, D. Stevens, and M. Meredith, Topographic control of Southern Ocean gyres and the Antarctic Circumpolar Current: a barotropic perspective, *Journal of Physical Oceanography*, 49, 3221–3244, doi:10.1175/JPO-D-19-0083.1, 2019. 914, 968

Pedlosky, J., The stability of currents in the atmosphere and ocean, Part I, *Journal of the Atmospheric Sciences*, 21, 201–219, doi:10.1175/1520-0469(1964)021<0201:TSOCIT>2.0.CO;2, 1964. 1394

Pedlosky, J., *Waves in the Ocean and Atmosphere: Introduction to Wave Dynamics*, Springer-Verlag, Berlin Heidelberg New York, 206 + viii pp, 2003. xxix, 1182, 1219, 1247, 1275, 1276, 1306, 1380, 1389, 1392

Pedlosky, J., L. Pratt, M. Spall, and K. Helfrich, Circulation around islands and ridges, *Journal of Marine Research*, 55, 1199–1251, 1997. 923

Peterson, H., and J. Callies, Rapid spin up and spin down of flow along slopes, *Journal of Physical Oceanography*, doi:10.1175/JPO-D-21-0173.1, 2022. 745, 1050, 1404

Peterson, K. A., and R. J. Greatbatch, Vorticity fluxes in shallow water ocean models, *Atmosphere-Ocean*, 39, 1–14, doi:10.1080/07055900.2001.9649662, 2001. 1487

Phillips, N. A., A coordinate system having some special advantages for numerical forecasting, *Journal of Meteorology*, 14, 184–185, doi:10.1175/1520-0469(1957)014<0184:ACSHSS>2.0.CO;2, 1957. 1404

Pierce, A. D., Wave equation for sound in fluids with unsteady inhomogeneous flow, *Journal of the Acoustical Society of America*, 87, 2292–2299, doi:10.1121/1.399073, 1990. 1144, 1158

Plumb, R. A., Eddy fluxes of conserved quantities by small-amplitude waves, *Journal of Atmospheric Sciences*, 36, 1699–1704, 1979. 1560

Polton, J., and D. Marshall, Overturning cells in the Southern Ocean and subtropical gyres, *Ocean Science*, 3, 17–30, 2007. 995, 1009

Polzin, K., and T. McDougall, Mixing at the ocean's bottom boundary, in *Ocean Mixing : Drivers, Mechanisms and Impacts*, edited by M. Meredith and A. N. Garabato, pp. 145–180, Elsevier, doi:10.1016/B978-0-12-821512-8.00014-1, 2021. 1017

Polzin, K. L., J. M. Toole, J. R. Ledwell, and R. W. Schmitt, Spatial variability of turbulent mixing in the abyssal ocean, *Science*, 276, 93–96, 1997. 1575

Pratt, L. J., and J. A. Whitehead, *Rotating Hydraulics: Nonlinear Topographic Effects in the Ocean and Atmosphere*, 589 pp., Springer Science + Business Media, New York, 2008. 294, 543, 795, 1265

Pugh, D. T., *Tides, surges, and mean sea-level*, 472 pp., John Wiley and Sons, 1987. 747

Rayleigh, L., On the stability, or instability, of certain fluid motions, *Proceedings of the London Mathematical Society*, 9, 57–70, doi:10.1112/plms/s1-11.1.57, 1880. 1373

Rayleigh, L., *The Theory of Sound*, Macmillan, London, UK, 1894. 1372

Redi, M. H., Oceanic isopycnal mixing by coordinate rotation, *Journal of Physical Oceanography*, 12, 1154–1158, doi:10.1175/1520-0485(1982)012<1154:OIMBCR>2.0.CO;2, 1982. 1589, 1590, 1592

Reif, F., *Fundamentals of Statistical and Thermal Physics*, McGraw-Hill, New York, 1965. 269, 278, 407, 410, 411, 1498

- Rhines, P. B., Basic dynamics of the large-scale geostrophic circulation, in *WHOI 1982 Summer Study Program*, Woods Hole Oceanographic Institute, 1982. 1566
- Rhines, P. B., and W. R. Holland, A theoretical discussion of eddy-driven mean flows, *Dynamics Of Atmospheres And Oceans*, 3, 289–325, doi:10.1016/0377-0265(79)90015-0, 1979. 1541
- Rhines, P. B., and W. R. Young, Homogenization of potential vorticity in planetary gyres, *Journal of Fluid Mechanics*, 122, 347–367, 1982. 1665
- Ringler, T., J. Saenz, P. Wolfram, and L. Van Roekel, A thickness-weighted average perspective of force balance in an idealized Circumpolar Current, *Journal of Physical Oceanography*, 47, 285–302, doi:10.1175/JPO-D-16-0096.1, 2017. 639
- Rintoul, S. R., The global influence of localized dynamics in the Southern Ocean, *Nature*, 558, 209–218, doi:10.1038/s41586-018-0182-3, 2018. 604
- Rintoul, S. R., and A. C. Naveira Garabato, Dynamics of the Southern Ocean circulation, in *Ocean Circulation and Climate, 2nd Edition: A 21st Century Perspective, International Geophysics Series*, vol. 103, edited by G. Siedler, S. M. Griffies, J. Gould, and J. Church, pp. 471–492, Academic Press, 2013. 604
- Rintoul, S. R., C. W. Hughes, and D. Olbers, The Antarctic Circumpolar Current system, in *Ocean Circulation and Climate, 1st Edition, International Geophysics Series*, vol. 103, edited by G. Siedler, J. Gould, and J. Church, pp. 271–301, Academic Press, 2001. 604
- Rooth, C., Hydrology and the ocean circulation, *Progress in Oceanography*, 11, 131–149, 1982. 1589
- Roquet, F., G. Madec, L. Brodeau, and J. Nylander, Defining a simplified yet realistic equation of state for seawater, *Journal of Physical Oceanography*, 45, 2464–2579, doi:10.1175/JPO-D-15-0080.1, 2015. 1625
- Rossby, C.-G., Planetary flow patterns in the atmosphere, *Quarterly Journal of the Royal Meteorological Society (suppl)*, 66, 68–87, 1940. 838, 900
- Rossby, C.-G., On displacements and intensity changes of atmospheric vorticity, *Journal of Marine Research*, 7, 175–187, 1948. 476, 882
- Ruan, X., and R. Ferrari, Diagnosing diapycnal mixing from passive tracers, *Journal of Physical Oceanography*, 51, 757–767, doi:10.1175/JPO-D-20-0194.1, 2021. 1542
- Ruan, X., J. Wenegrat, and J. Gula, Slippery bottom boundary layers: The loss of energy from the general circulation by bottom drag, *Geophysical Research Letters*, 48, doi:10.1029/2021GL094434, 2021. 745
- Sadourny, R., and C. Basdevant, Parameterization of subgrid scale barotropic and baroclinic eddies in quasi-geostrophic models: anticipated potential vorticity method, *Journal of Atmospheric Sciences*, 42, 1353–1363, 1985. 887
- Salmon, R., *Lectures on Geophysical Fluid Dynamics*, Oxford University Press, Oxford, England, 378 + xiii pp., 1998. 269, 278, 279, 496, 761, 895
- Samelson, R., *The Theory of Large-Scale Ocean Circulation*, Cambridge University Press, Cambridge, UK, 193 pp., 2011. 700, 1063, 1074

Santiago, J., and M. Visser, Gravity's universality: The physics underlying Tolman temperature gradients, *International Journal of Modern Physics D*, 27, doi:10.1142/S021827181846001X, 2018. 438

Schär, C., A generalization of Bernoulli's Theorem, *Journal of the Atmospheric Sciences*, 50, 1437–1443, doi:10.1029/2003JC001823, 1993. 995, 1008, 1009

Schey, H., *Div, grad, curl and all that: an informal text on vector calculus*, W.W. Norton and Company, Inc., 176 pp, 2004. 23

Schmitt, R. W., Double diffusion in oceanography, *Annual Review of Fluid Mechanics*, 26, 255–285, 1994. 1575, 1608

Schneider, T., I. M. Held, and S. Garner, Boundary effects in potential vorticity dynamics, *Journal of Atmospheric Sciences*, 60, 1024–1040, doi:10.1175/1520-0469(2003)60<1024:BEIPVD>2.0.CO;2, 2003. 640, 1089

Schutz, B. F., *Geometrical Methods of Mathematical Physics*, Cambridge University Press, Cambridge, UK, 250 pp, 1980. 157

Schutz, B. F., *A First Course in General Relativity*, Cambridge University Press, Cambridge, UK, 392 pp, 1985. 151

Segel, L., *Mathematics Applied to Continuum Mechanics*, 590 pp., Dover Publications, 1987. 5, 23, 317, 318, 335, 498, 501

Shakespeare, C. J., B. K. Arbic, and A. M. Hogg, Dissipating and reflecting internal waves, *Journal of Physical Oceanography*, 51, 2517–2531, doi:10.1175/JPO-D-20-0261.1, 2021. 1303

Shao, A., A. Adcroft, R. Hallberg, and S. Griffies, A general-coordinate, nonlocal neutral diffusion operator, *Journal of Advances in Modeling Earth Systems*, 12, doi:10.1029/2019MS001992, 2020. 1592, 1599

Shchepetkin, A., and J. McWilliams, A method for computing horizontal pressure-gradient force in an ocean model with a non-aligned vertical coordinate, *Journal of Geophysical Research*, 108, 35.1–35.34, 2002. 1450

Smagorinsky, J., General circulation experiments with the primitive equations: I. The basic experiment, *Monthly Weather Review*, 91, 99–164, 1963. 565

Smagorinsky, J., Some historical remarks on the use of nonlinear viscosities, in *Large Eddy Simulation of Complex Engineering and Geophysical Flows*, edited by B. Galperin and S. A. Orszag, pp. 3–36, Cambridge University Press, 1993. 503

Smith, K. S., and J. Marshall, Evidence for enhanced eddy mixing at middepth in the southern ocean, *Journal of Physical Oceanography*, 39, 50–69, 2009. 1587, 1593

Smith, K. S., and G. K. Vallis, The scales and equilibration of midocean eddies: freely evolving flow, *Journal of Physical Oceanography*, 31, 554–570, doi:10.1175/1520-0485(2001)031<0554:TSAEOM>2.0.CO;2, 2001. 700, 873

Smith, K. S., and G. K. Vallis, The scales and equilibration of midocean eddies: forced-dissipative flow, *Journal of Physical Oceanography*, 32, 1699–1721, 2002. 1587

- Smith, R., A hurricane beta drift law, *Journal of Atmospheric Sciences*, 50, doi:10.1175/1520-0469(1993)050<3213:AHBDL>2.0.CO;2, 1993. 883
- Smith, R. D., The primitive equations in the stochastic theory of adiabatic stratified turbulence, *Journal of Physical Oceanography*, 29, 1865–1880, 1999. 1571
- Smith, R. D., and P. R. Gent, Anisotropic Gent-McWilliams parameterization for ocean models, *Journal of Physical Oceanography*, 34, 2541–2564, 2004. 1595, 1596, 1598, 1599, 1600
- Smythe, W. D., and J. R. Carpenter, *Instability in Geophysical Flows*, Cambridge University Press, Cambridge, UK, 327 pp, 2019. xxx, xxxi, 1230, 1318, 1368, 1372, 1389, 1494
- Solomon, H., On the representation of isentropic mixing in ocean models, *Journal of Physical Oceanography*, 1, 233–234, doi:10.1175/1520-0485(1971)001<0233:OTROIM>2.0.CO;2, 1971. 1589
- Spence, P., O. A. Saenko, W. Sijp, and M. England, The role of bottom pressure torques on the interior pathways of North Atlantic Deep Water, *Journal of Physical Oceanography*, 42, 110–125, doi:10.1175/2011JPO4584.1, 2012. 967
- Spence, P., R. M. Holmes, A. McC. Hogg, S. M. Griffies, K. D. Stewart, and M. H. England, Localized rapid warming of West Antarctic subsurface waters by remote winds, *Nature Climate Change*, doi:10.1038/NCLIMATE3335, 2017. 745
- Spiegel, M., *Theory and Problems of Vector Analysis*, Schaum's Outline Series, McGraw-Hill International Book Company, New York, 1974a. 23
- Spiegel, M., *Fourier Analysis with Applications to Boundary Value Problems*, Schaum's Outline Series, McGraw-Hill International Book Company, New York, 1974b. 117, 121, 126
- Stakgold, I., *Boundary value problems of mathematical physics, volume I*, SIAM, Philadelphia, 340 pp, 2000a. 49, 66, 72, 77, 89, 114
- Stakgold, I., *Boundary value problems of mathematical physics, volume II*, SIAM, Philadelphia, 408 pp, 2000b. 49, 66, 72, 74, 89
- Stanley, G. J., Neutral surface topology, *Ocean Modelling*, doi:10.1016/j.ocemod.2019.01.008, 2019. 671
- Stanley, G. J., T. McDougall, and P. Barker, Algorithmic improvements to finding approximately neutral surfaces, *Journal of Advances in Modeling Earth Systems*, 13, doi:10.1029/2020MS002436, 2021. 671
- Starr, V. P., A quasi-Lagrangian system of hydrodynamical equations, *Journal of Meteorology*, 2, 227–237, doi:10.1175/1520-0469(1945)002<0227:AQLSOH>2.0.CO;2, 1945. 1398
- Stewart, A., and J. McWilliams, Gravity is vertical in geophysical fluid dynamics, *Scientific Reports*, 12, doi:10.1038/s41598-022-10023-3, 2022. 237
- Stewart, A., J. McWilliams, and A. Solococh, On the role of bottom pressure torques in wind-driven gyres, *Journal of Physicao Oceanography*, 51, 1441–1464, doi:10.1175/JPO-D-20-0147.1, 2021. 914, 916
- Stewart, R., *An Introduction to Physical Oceanography*, 345 pp., Texas A& M, College Station, Texas, USA, 2008. 747

- Stommel, H., The westward intensification of wind-driven ocean currents, *Transactions of the American Geophysical Union*, 29, 202–206, 1948. 604, 915
- Straub, D. N., On the transport and angular momentum balance of channel models of the Antarctic Circumpolar Current, *Journal of Physical Oceanography*, 23, 776–782, doi:10.1175/1520-0485(1993)023<776:OTTAAM>2.0.CO;2, 1993. 604
- Straub, D. N., On thermobaric production of potential vorticity in the ocean, *Tellus*, 51A, 314–325, 1999. 988
- Stull, R., *An Introduction to Boundary Layer Meteorology*, 670 pp., Kluwer Academic Publishers, 1988. 723
- Sun, S., R. Bleck, C. Rooth, J. Dukowicz, E. Chassignet, and P. D. Killworth, Inclusion of thermobaricity in isopycnic-coordinate ocean models, *Journal of Physical Oceanography*, 29, 2719–2729, 1999. 1457
- Sutherland, B. R., *Internal Gravity Waves*, Cambridge University Press, 2010. 1275
- Symon, K., *Mechanics*, Addison-Wesley Publishing Co., Reading, MA, USA, 639 pp, 1971. v, 197
- Talley, L. D., G. L. Pickard, W. J. Emery, and J. H. Swift, *Descriptive Physical Oceanography*, 6th ed., Elsevier, 555pp, 2011. 775
- Tarshish, N., N. Jeevangee, and D. Lecoanet, Buoyant motion of a turbulent thermal, *Journal of the Atmospheric Sciences*, 75, 3233–3244, doi:10.1175/JAS-D-17-0371.1, 2018. 655, 680
- Taylor, G., Diffusion by continuous movements, *Proceedings of the London Mathematical Society*, 20, 196–212, 1921. 1496, 1574
- Tennekes, H., and J. Lumley, *A First Course in Turbulence*, 300 pp., MIT Press, Cambridge, USA, 1972. 509, 723, 843
- Thomas, L., A. Tandon, and A. Mahadevan, Submesoscale processes and dynamics, in *Eddy resolving ocean models*, edited by M. Hecht and H. Hasumi, Geophysical Monograph 177, pp. 17–38, American Geophysical Union, 2008. 993, 1020, 1345
- Thomas, L., J. R. Taylor, R. Ferrari, and T. Joyce, Symmetric instability in the Gulf Stream, *Deep Sea Research II*, 91, 96–110, doi:10.1016/j.dsr2.2013.02.025, 2013. 993, 1020, 1320, 1345, 1350
- Thorne, K., and R. Blandford, *Modern Classical Physics*, Princeton University Press, Princeton, USA, 1511 + xl pp, 2017. 2, 117, 159, 536, 538, 944, 1103, 1129, 1131, 1158, 1163, 1377
- Thorpe, S., The dynamics of the boundary layers of the deep ocean, *Science Progress*, 72, 189–206, 1988. 723
- Thorpe, S., *The Turbulent Ocean*, 439 pp., Cambridge University Press, Cambridge, UK, 2005. 723
- Tomczak, M., and J. S. Godfrey, *Regional Oceanography: An Introduction*, Pergamon Press, Oxford, England, 422 + vii pp, 1994. 575, 776, 923
- Towne, D. H., *Wave phenomena*, Dover Publications, New York, 482 pp, 1967. 1142

- Treguier, A. M., I. M. Held, and V. D. Lariehev, On the parameterization of quasi-geostrophic eddies in primitive equation ocean models, *Journal of Physical Oceanography*, 27, 567–580, 1997. 1575, 1587, 1593
- Truesdell, C., Notes on the history of the general equations of hydrodynamics, *American Mathematical Monthly*, 60, 445–458, doi:10.2307/2308407, 1953. 281
- Vallis, G., and B.-L. Hua, Eddy viscosity of the anticipated potential vorticity method, *Journal of the Atmospheric Sciences*, 45, 617–627, doi:10.1175/1520-0469(1988)045<617:EVOTAP>2.0.CO;2, 1988. 887
- Vallis, G. K., *Atmospheric and Oceanic Fluid Dynamics: Fundamentals and Large-scale Circulation*, 1st ed., Cambridge University Press, Cambridge, 745 + xxv pp, 2006. 788, 832
- Vallis, G. K., *Atmospheric and Oceanic Fluid Dynamics: Fundamentals and Large-scale Circulation*, 2nd ed., Cambridge University Press, Cambridge, 946 + xxv pp, 2017. xxviii, xxix, xxx, xxxi, 73, 188, 237, 238, 239, 278, 426, 443, 465, 505, 536, 559, 575, 604, 606, 614, 638, 646, 649, 657, 660, 668, 700, 704, 713, 723, 743, 761, 773, 776, 781, 829, 873, 881, 888, 915, 916, 951, 988, 1014, 1037, 1051, 1094, 1103, 1170, 1182, 1210, 1212, 1225, 1230, 1235, 1265, 1275, 1276, 1277, 1368, 1372, 1380, 1392, 1498, 1509, 1535, 1573, 1576
- Vallis, G. K., *Essentials of Atmospheric and Oceanic Dynamics*, 1st ed., Cambridge University Press, Cambridge, 2019. 1273
- van Heijst, G., Dynamics of vortices in rotating and stratified flows, in *Fronts, Waves, and Vortices in Geophysical Flows*, Lecture notes in Physics 805, p. 192, Springer, 2010. 712, 722
- Van Roekel, L., A. Adcroft, G. Danabasoglu, S. M. Griffies, B. Kauffman, W. Large, M. Levy, B. Reichl, T. Ringler, and M. Schmidt, The KPP boundary layer scheme for the ocean: revisiting its formulation and benchmarking one-dimensional simulations relative to LES, *Journal of Advances in Modeling Earth Systems*, doi:10.1029/2018ms001336, 2018. 1620
- van Sebille, E., S. M. Griffies, R. Abernathey, T. Adams, P. Berloff, A. Biastoch, B. Blanke, E. Chassignet, Y. Cheng, C. Cotter, E. Deleersnijder, K. Döös, H. Drake, S. Drijfhout, S. Gary, A. Heemink, J. Kjellsson, I. Koszalka, M. Lange, C. Lique, G. MacGilchrist, R. Marsh, G. M. Adame, R. McAdam, F. Nencioli, C. Paris, M. Piggott, J. Polton, S. Rühs, S. Shah, M. Thomas, J. Wang, P. Wolfram, L. Zanna, and J. Zika, Lagrangian ocean analysis: fundamentals and practices, *Ocean Modelling*, 121, 49–75, doi:10.1016/j.ocemod.2017.11.008, 2018. 284
- Venaille, A., G. K. Vallis, and S. M. Griffies, The catalytic role of beta effect in barotropization processes, *Journal of Fluid Dynamics*, doi:10.1017/jfm.2012.344, 2012. 873
- Veronis, G., Large scale ocean circulation, *Advances in Applied Mechanics*, 13, 2–92, 1973. 238
- Veronis, G., The role of models in tracer studies, in *Numerical Models of Ocean Circulation*, pp. 133–146, National Academy of Sciences, 1975. 1589
- von Arx, W. S., *An Introduction to Physical Oceanography*, Addison-Wesley Publishing Company, Reading, Massachusetts, USA, 422 pp, 1962. 718, 735, 738
- Wåhlin, A., R. Muench, L. Arneborg, G. Björk, H. Ha, S. Lee, and A. Alsén, Some implications of Ekman layer dynamics for cross-shelf exchange in the amundsen sea, *Journal of Physical Oceanography*, 42, 1461–1474, doi:10.1175/JPO-D-11-041.1, 2012. 744, 745

BIBLIOGRAPHY

- Waln, G., A theoretical framework for the description of estuaries, *Tellus*, 29(2), 128–136, doi: 10.1111/j.2153-3490.1977.tb00716.x, 1977. 1641
- Waln, G., On the relation between sea-surface heat flow and thermal circulation in the ocean, *Tellus*, 34, 187–195, doi:10.1111/j.2153-3490.1982.tb01806.x, 1982. 1641
- Wallace, J., and P. Hobbs, *Atmospheric Science: An Introductory Survey*, Academic Press, 2006. 832
- Ward, M., and A. Hogg, Establishment of momentum balance by form stress in a wind-driven channel, *Ocean Modelling*, 40(133–146), doi:10.1016/j.ocemod.2011.08.004, 2011. 808
- Waterhouse, A. F., J. A. MacKinnon, J. D. Nash, M. H. Alford, E. Kunze, H. L. Simmons, K. L. Polzin, L. C. St. Laurent, O. M. Sun, R. Pinkel, L. D. Talley, C. B. Whalen, T. N. Huussen, G. S. Carter, I. Fer, S. Waterman, A. C. Naveira Garabato, T. B. Sanford, and C. M. Lee, Global Patterns of Diapycnal Mixing from Measurements of the Turbulent Dissipation Rate., *Journal of Physical Oceanography*, 44(7), 1854–1872, doi:10.1175/JPO-D-13-0104.1, 2014. 1575
- Waterman, S., and B. J. Hoskins, Eddy shape, orientation, propagation, and mean flow feedback in western boundary current jets, *Journal of Physical Oceanography*, 43, 1666–1690, 2013. 868
- Waterman, S., and J. Lilly, Geometric decomposition of eddy feedbacks in barotropic systems, *Journal of Physical Oceanography*, 45, 1009–1024, 2015. 868
- Webb, D., R. Holmes, P. Spence, and M. England, Barotropic Kelvin wave-induced bottom boundary layer warming along the West Antarctic Peninsula, *Journal of Geophysical Research: Oceans*, 124, 1595–1615, doi:10.1029/2018JC014227, 2019. 745
- Weiss, J., The dynamics of enstrophy transfer in two-dimensional hydrodynamics, *Physica D*, 273–294, 1991. 326
- Welander, P., Wind-driven ocean circulation in one and two layer oceans of variable depth, *Tellus*, 20, 1–16, doi:10.1111/j.2153-3490.1968.tb00347.x, 1968. 915, 916
- Wenegrat, J., L. Thomas, J. Gula, and J. McWilliams, Effects of the submesoscale on the potential vorticity budget of the ocean mode waters, *Journal of Physical Oceanography*, 48, 2141–2165, doi:10.1175/JPO-D-17-0219.1, 2018. 1020
- Whalen, C. B., L. D. Talley, and J. A. MacKinnon, Spatial and temporal variability of global ocean mixing inferred from argo profiles, *Geophysical Research Letters*, 39(18), n/a–n/a, doi: 10.1029/2012GL053196, 2012. 1575
- Whitham, G. B., *Linear and nonlinear waves*, John Wiley and Sons, New York, 636 + xvi pp, 1974. 1106, 1276
- Wise, A., C. W. Hughes, and J. Polton, Bathymetric influence on the coastal sea level response to ocean gyres at western boundaries, *Journal of Physical Oceanography*, 481, 2949–2964, doi: 10.1175/JPO-D-18-0007.1, 2018. 916, 917
- Wise, A., C. W. Hughes, J. A. Polton, and J. M. Huthnance, Leaky slope waves and sea level: Unusual consequences of the beta effect along western boundaries with bottom topography and dissipation, *Journal of Physical Oceanography*, 50, 217–237, doi:10.1175/JPO-D-19-0084.1, 2020a. 916

- Wise, A., J. A. Polton, C. W. Hughes, and J. M. Huthnance, Idealised modelling of offshore-forced sea level hot spots and boundary waves along the north american east coast, *Ocean Modelling*, 155, doi:10.1016/j.ocemod.2020.101706, 2020b. 916
- Wolfe, C., Approximations to the ocean's residual circulation in arbitrary tracer coordinates, *Ocean Modelling*, 75, 20–35, doi:10.1016/j.ocemod.2013.12.004, 2014. 1569
- Yassin, H., Normal modes with boundary dynamics in geophysical fluids, *Journal of Mathematical Physics*, 62, doi:10.1063/5.0048273, 2021. 1172
- Yassin, H., and S. Griffies, On the discrete normal modes of quasigeostrophic theory, *Journal of Physical Oceanography*, 52, 243–259, doi:10.1175/JPO-D-21-0199.1, 2022. 1172
- Yeager, S., Topographic coupling of the Atlantic overturning and gyre circulations, *Journal of Physical Oceanography*, 45, 1258–1284, doi:10.1175/JPO-D-14-0100.1, 2015. 1074
- Young, W. R., Dynamic enthalpy, Conservative Temperature, and the seawater Boussinesq approximation, *Journal of Physical Oceanography*, 40, 394–400, doi:10.1175/2009JPO4294.1, 2010. 633, 634, 638
- Young, W. R., An exact thickness-weighted average formulation of the Boussinesq equations, *Journal of Physical Oceanography*, 42, 692–707, doi:10.1175/JPO-D-11-0102.1, 2012. 639, 1469, 1476, 1477, 1478, 1479, 1487, 1571, 1572, 1585
- Zanna, L., S. Khatiwala, J. Gregory, J. Ison, and P. Heimbach, Global reconstruction of historical ocean heat storage and transport, *Proceedings of the National Academy of Science*, doi:10.1073/pnas.1808838115, 2019. 114
- Zhao, R., and G. K. Vallis, Parameterizing mesoscale eddies with residual and Eulerian schemes, and a comparison with eddy-permitting models, *Ocean Modelling*, 23, 1–12, 2008. 1585

INDEX

- AABW, 1627
- absolute circulation, 952
- absolute momentum, 245, 1329
- absolute reference frame, 200
- absolute salinity, 426, 657, 1612
- absolute temperature, 274
- absolute vorticity, 891
 - impermeability, 1005
- absolute vorticity invariance, 879
- acceleration, 198
 - centrifugal, 224, 228
 - centripetal, 224
 - Coriolis, 224, 228
 - inertial, 220, 226
 - planetary Cartesian, 224
 - spherical, 227
 - spherical metric, 229
- accelertion
- centrifugal, 229
- acoustic wave
 - density, 1146
 - pressure, 1145
 - temperature, 1146
 - velocity, 1145
- acoustic waves, 55, 554, 1131, 1144
 - Boussinesq ocean, 613
 - density, 1147
 - energetics, 1149
 - Eulerian, 1142
 - Lagrangian, 1139
 - pressure, 1147
 - speed, 1141, 1144
 - velocity, 1147
- action/reaction law, 479
- active tracer, 50, 1521
- adiabatic, 409
- adiabatic flow, 1521
 - adiabatic lapse rate, 441, 1146
 - adjoint diffusion equation, 98
 - adjoint operator, 99, 101
 - advection, 1509
 - maths, 1505
 - reversible, 533
 - advection equation, 50, 771, 1504
 - geometric, 1505
 - advection of velocity vector identity, 32
 - advection operator, 292
 - advection-diffusion equation, 380, 1523
 - advective boundary transport, 1618
 - advective flux, 1614
 - advective time scale, 1027
 - advective tracer flux, 365, 1507, 1581
 - affine tensor algebra, 5
 - ageostrophic components, 1078
 - ageostrophic overturning, 1345
 - ageostrophic secondary circulation, 1342, 1345
 - ageostrophic velocity, 724, 1035
 - air-water interface, 510
 - anelastic approximation, 386, 614
 - angular frequency, 212
 - angular momentum, 200, 242, 248, 486, 855, 856, 893, 898, 942, 1322
 - and strain, 855, 858
 - and vorticity, 855, 858
 - axial, 256
 - barotropic model, 885
 - conservation, 249
 - free vortex, 845
 - shallow water, 829
 - angular velocity, 200
 - anisotropic Gent-McWilliams, 1599
 - anisotropic neutral diffusion, 1595
 - anisotropic tensor, 20

- ansatz, 64, 1113
anti-cyclonic, 246, 688
anticipated potential vorticity, 887
antiderivative, 65
arc length, 34, 140, 146, 389
Archimedean buoyancy, 608, 653, 655
Archimedes' Principle, 655
area
 evolution, 319, 322, 395
 of a surface, 144
arrested Ekman layer, 743
aspect ratio, 568, 616, 617, 1026, 1028
association versus causation, vi, 621
asymptotic methods, 1033
atmospheric form stress, 582, 585
atmospheric pressure torque, 912, 961, 966
atomic bomb, 1623
available potential energy, 638, 1280, 1295, 1582
 approximate, 644
 exact, 643
 QG fluid, 1091
averaging, 1475
 Reynolds, 1475
 thickness equation, 1477
 thickness weighted, 1476
 thickness weighted tracer, 1478
Avogadro's number, 274
axial angular momentum, 224, 472
 atmosphere, 473
 depth integrated, 598
 ocean, 596
 ring of air, 472
 steady state, 600
 zonal acceleration, 252
axial vector, 10
axisymmetric flow, 1320
- back-reaction, 653
backward diffusion equation, 98
balanced model, 1075
balances, vi
baroclinic, 573, 694, 942
baroclinic instability, 1379, 1389
 necessary condition, 1394
baroclinic mode, 1250, 1275, 1383
baroclinic velocity, 592, 807, 1252
baroclinicity, 689, 933, 942, 962, 982
 Boussinesq, 958
generalized vertical coordinates, 1453
ideal gas, 935, 973
seawater, 986
solenoid, 942
barodiffusion, 545
barometric law, 452
barotropic, 573, 942
barotropic mode, 1250, 1275, 1383
barotropic model, 863, 1210
barotropic velocity, 592, 698, 807, 935, 1252
barotropization, 693
barycenter, 364
barycentric velocity, 281, 283, 361, 363, 366, 374, 482, 933, 1613
barystatic sea level changes, 1624
basis one-forms, 164, 218
basis vectors, 156, 163, 218
 operator notation, 156
 rotation, 216
Batchelor scale, 1573
Beltrami flow, 45
Bernoulli
 equation of motion, 1165
 function, 1007
 head, 542
 potential, 537, 1165, 1460
 potential for Boussinesq hydrostatic, 995
 principle, 539
 theorem, 539
 theorem for hydraulic control, 542
 theorem for pipe flow, 540
Bernoulli theorem
 shallow water, 813
Bessel-Parseval relation, 125
beta
 effective, 1246
beta drift, 882
beta effect, 230, 868, 879, 895, 908, 911, 953, 966, 1059
 topographic, 902, 1037
 two-dimensional example, 955
beta gyre, 883
beta-plane approximation, 469, 470, 868
bi-orthogonality relation, 164
Bjerknes circulation theorem, 953
body forces, xii, 408, 409, 462, 479
 homogeneous layer, 907
boldface notation, 157
Boltzmann constant, 448

- bolus velocity, 1472, 1474, 1478, 1480
bottom
drag, 629
following coordinates, 1404
geostrophic velocity, 966
kinematic boundary condition, 768
pressure torque, 912, 944, 961, 962, 966, 1060
vertical velocity, 1061
water mass transformation, 1643
bottom drag
shallow water, 787
boundary
conditions, 55, 1523
Green's function, 90, 92
layers, 509, 723, 724, 731
propagator, 92, 107, 109, 1533
stress, 629
velocity, 373
water mass transformation, 1648
boundary condition
natural, 1502
Neumann, 1502
Boussinesq approximation, 385, 386
traditional, 614
Boussinesq ocean, 605, 607, 684, 1133
density evolution, 613
dynamic enthalpy, 633, 634
energetics, 630, 648
equations, 611
generalized, 647
mass, 614
mass continuity, 610
momentum equation, 608
non-dimensional, 1046, 1053
reference density, 387, 610
weight, 614
Brownian motion, 1574
Buckingham-II theorem, 1024
budget analysis, 369
bulk viscosity, 498
buoyancy, 570, 653, 828, 1603
boundary condition, 1617
coordinates, 154, 1404
effective, 671, 675
force, 656
frequency, 664, 778
frequency for ideal gas, 666
globally referenced, 661, 775
homogeneous fluid, 613
relation to height, 642
sorting, 645
stratification, 662
surface ocean budget, 1619
work, 631
buoyancy oscillations, 1280
buoyancy work
shallow water, 811
Burger function, 1077
Burger number, 1029, 1050, 1077, 1092
slope, 1050
cabbeling, 611, 1609, 1611
cabbeling parameter, 1610
capillary
capillary-gravity waves, 505
pressure, 511, 513
tube, 509
waves, 1161, 1184
carrier wave, 1119
Cartesian coordinates, 153, 181
summary, 182
Cartesian tensor algebra, 5
Cauchy
equation of motion, 464
fundamental lemma, 482
solution, 312, 313
stress principle, 481
theorem, 484
Cauchy problem
hyperbolic, 62
parabolic, 59
Cauchy-Green strain tensor, 313
Cauchy-Stokes decomposition, 318, 330
causal free space Green's function, 97
causal Green's function, 97, 110
causal relations, v
causality condition, 97
causation versus association, 621
center of mass motion, 356
center of mass velocity, 364, 1614
centrifugal acceleration, 235, 575, 708, 710, 875
particle motion, 246
planetary orbital, 753
planetary rotation, 753
spherical, 229
centrifugal instability, 1319, 1322

- centrifugal oscillations, 1326
centripetal acceleration, 235, 708, 710
channel, 820
channel flow, 700
Chapman-Kolmogorov relation, 101, 103
characteristic curves, 52
 advection equation, 53
 wave equation, 62
chemical energy flux, 532
chemical potential, 420, 426, 431
chemical reactions, 361
chemical work, 422
Christoffel symbols, 20, 175
 metric connection, 176
 related to metric, 177
circuit, 35, 138
 reducible, 138
circulation, 35, 43, 843
 absolute, 952
 around a streamline, 906
 free vortex, 846
 friction effects, 905
 Kelvin's theorem and work, 934
 Rayleigh drag, 907
 rotating fluids, 951
 shallow water, 905
 solid-body rotation, 847
 tornado, 850
 wind stress, 907
circulation induction, 954
circulation theorem, 906
co-tangent space, 164
coarse graining, 1547
coherent structure, 309
cold core eddy, 793
column vorticity, 919
compatibility
 total mass + tracer mass, 366
complex numbers
 absolute value, 118
 modulus, 118
 phase, 118
composition property
 Green's function, 101, 1529
compression, 326, 1144
concentration equation, 98
conservation equation
 Eulerian flux-form, 369
 material form, 369
conservation law, 369
 material, 554
 non-material, 554
conservation laws, 199, 243, 261, 266, 553
conservation of indices, 156
conservative force, 202
Conservative Temperature, 444, 549, 551, 657, 1603
conservative tracers, 1492
conservative vector field, 45
constitutive relation, 495, 496
contact forces, xii, 409, 462, 479
contact pressure force, 483, 796, 799
continuity, 386
continuity equation, 340, 361
continuum approximation, 269, 270, 280
continuum hypothesis, 269
continuum limit, 1138
contour, 138
contraction, 10
contrapositive proposition, 669
contravariant, 157
contravariant tensor index, 153, 217
convective time derivative, 292
converging flow
 PV constraints, 904
converse proposition, 669
coordinate
 buoyancy, 154
 Cartesian, 153, 181
 cylindrical, 153
 cylindrical-polar, 188
 general vertical, 286
 geopotential, 236
 invariance, 150
 isopycnal, 154
 Lagrangian, 154
 material, 154, 285–287
 non-orthogonal, 154
 oblique, 166
 planetary Cartesian, 221
 position, 285, 287
 quasi-Lagrangian, 154
 representation, 6
 spherical, 153, 183, 221
 time, 152
 tracer, 155
Coriolis acceleration, 224, 250
 large-scale motion, 230

- shallow atmosphere, 230
spherical, 230
- Coriolis parameter, 230
- Couette flow, 496, 507
- Coulomb gauge, 327, 1510
- couplet, 492
- covariant, 157
- covariant curl, 179
- covariant derivative, 151
metric tensor, 177
one-form, 176
scalar, 175
vector, 175
- covariant divergence, 177
- covariant Laplacian, 178
- covariant tensor index, 153, 217
- critical reflection, 1297
- Crocco's theorem, 559
- cross-diffusion, 368, 1576
- curl integrated over a closed surface, 40
- curl of a curl, 32
- curl of cross product, 32
- curl of vector, 29
- curl-free vector, 30
- curvature, 512
circle, 142
curve, 142
Gaussian, 145
surface, 144
- curves on a surface, 146
- cyclonic, 246, 688
- cyclonic eddy, 793
- cyclostrophic balance, 717, 1319, 1320
- cylindrical-polar coordinates, 153, 188
- D'Alembert
paradox, 497
theorem, 497
wave solution, 63
- decibel scale, 1148
- deformation gradient tensor, 287, 312
discrete algorithm, 288
- deformation radius, 1051, 1092, 1264, 1383
internal, 1077
shallow water, 1029, 1040, 1244, 1245, 1255, 1263
- deformation rate, 315, 326
- deformational flow, 325
- delta sheets of potential vorticity, 639
- density, 658
evolution, 1576, 1604
- depth of no motion, 696
- determinant, 178
- developing flow, 292
- deviator, 498
- deviatoric friction tensor, 498
- deviatoric rate of strain tensor, 498, 524
- deviatoric stress, 463, 497
- dia-surface flow, 1521
- dia-surface transport, 380, 1421, 1425
incompressible, 1430
shallow water, 785
- dia-surface velocity, 1428
compared to vertical, 1432
- diabatic process, 409, 1521
- diagnostic equation, vi, 295
- dianeutral direction, 663, 1578
- diapycnal transport velocity, 353
- diapycnal velocity component, 1458
- differentiable manifold, 411, 1629
- differential forms, 159
- diffusion, 1495, 1613
dissipation functional, 1502
Fick's law, 1496
isotropic, 1499
molecular, 1495
momentum, 1498
neutral, 1499, 1503
operator, 1501
skew, 1508
temperature, 1497
tensor, 1498
tracer moments, 1500, 1501
tracer powers, 1500
tracer variance, 1501
turbulent, 1495
- diffusion equation, 59, 97
- diffusion tensor, 1560, 1576, 1614
- diffusion tensor transformation, 1596
- diffusive tracer flux, 365, 374
- diffusive tracer fluxes, 366
- diffusively driven flow, 1056
- diffusivity, 1614
air, 1496
dynamic, 1496
eddy, 628
kinematic, 1496
molecular, 1496

- temperature, 1497
turbulent, 1496
- dilation, 318
- dimensionless numbers, 1024
- Dirac delta, 71, 74, 134, 1502, 1643, 1654
Cartesian, 75
Fourier transform, 134
sifting property, 75
spherical, 75
- Dirac delta sheet, 95, 107
- direct stress, 497
- direction cosines, 17
- Dirichlet boundary condition, 57, 58, 82, 85, 621, 1524, 1525
- dispersion relation, 1100, 1103, 1106
acoustic, 1147
inertia-gravity waves, 1254
inertial waves, 1202
interacting Eady waves, 1390
shallow water gravity wave, 1248
- displacement tensor, 312
- dissipation, 463, 525
- distance, 8
- distance to polar axis, 223
- divergence, 501
- divergence of cross product, 31
- divergence of curl, 31
- divergence operator
Cartesian, 28
- divergence theorem, 38, 339
scalar fields, 39
- diverging flow, 325
- domain of influence, 64
- Doppler shift, 1217
- dot product, 9
- double integral identity, 68
- double-diffusion, 1377
- downscale cascade, 1573
- drag coefficient, 629
- dual form stress, 585, 593, 602, 799, 804
- dual pressure form stress, 1482
- duality
Eulerian and Lagrangian, 311
one-form and vector, 163, 164
- Dufour effect, 545
- Duhamel's integral
heat equation, 60
wave equation, 65
- dynamic enthalpy, 633
- dynamic topography, 573
- dynamic viscosity, 498
- dynamical constraints, 242, 243, 261, 266
- dynamical pressure, 570, 712, 785
- dynamical pressure gradient, 467
- Eötvös correction, 230
- Eady growth rate, 1392
- Eady model, 1379
- Eady waves, 1385, 1387
- earth
angular frequency, 212
angular rotation, 212
equatorial radius, 236
geopotential, 233
gravitational acceleration, 233
gravitational potential, 233
mass, 232, 233
planetary centrifugal, 233
polar radius, 236
radius, 213, 232, 233, 748
solid body speed, 213
- eddy diffusivity, 628
- eddy tracer fluxes, 1554
- eddy viscosity, 629, 724
Ekman layer, 731
- eddy-induced
mass flux, 1506
mass streamfunction, 1506
velocity, 628, 651, 1506, 1577
- edge waves, 1209, 1216, 1225, 1367, 1379, 1385
- edge waves interactions, 1368
- effective beta, 902, 1038, 1246
- effective buoyancy, 653, 661, 671, 675, 1281
- effective free surface height, 764
- effective gravity, 469
- eikonal approximation
acoustics, 1154
gravity waves, 1299
- eikonal equation, 1127
- Einstein index convention, 7
- Einstein summation convention, 156
- Ekman
arrested, 743
balance, 724
bottom layer, 739
boundary layers, 509, 723, 724
downwelling, 737

- generalized Ekman velocity, 1018
 horizontal transport, 732
 layer thickness, 731
 mass transport, 732
 mechanics, 723
 natural coordinates, 726
 number, 730, 731
 ocean surface layer, 732
 pumping, 735, 737
 Rayleigh drag, 727
 spiral motion, 729
 suction, 735, 737
 transport, 734
 upwelling, 737
 velocity, 1061
 velocity profile, 739
- Eliassen-Palm
 flux, 805, 807, 1471, 1483, 1484
 flux tensor, 798, 1483, 1484
- elliptic PDE
 classification, 54
 geostrophic adjustment, 1263
 properties, 55
- energetic stability analysis, 1317
- energetics
 shallow water, 808
 shallow water kinetic, 810–812
 shallow water mechanical, 813
 shallow water potential, 809
- energy
 dissipation of kinetic, 524
 dissipation of mechanical, 524
 gravitational potential, 519–522
 internal, 534
 internal budget, 535
 kinetic, 523
 mechanical, 523, 526
 mechanical energy flux, 526
 total, 534
 total energy conservation, 547
- energy equipartition
 acoustic, 1151
 oscillator, 1136, 1151
- ensemble average, 1476, 1547
- ensemble averaging
 ensemble, 1476
- enthalpy, 429, 549
 budget, 532, 535, 547
 capacity, 433
- entrain, 353
 entropy, 412, 415, 417, 428
 budget, 543
 flux, 544
 maximum, 418
 perfect fluid, 533
 source, 544, 547
- epineutral diffusion, 1589
- epsilon product identity, 15, 32
- equation of motion, 464
 Cartesian, 234
 particle, 234
 rotating, 465
 spherical, 235, 466
- equation of state, 427–430, 447, 657
 Boussinesq ocean, 612
 linear, 611
- equilibrium tide, 749
- equivalent barotropic depth, 872
- equivalent barotropic flow, 872
- Ertel potential vorticity, 979, 981, 1001
- Euclidean
 isomorphism to \mathbb{R}^3 , 5
 metric, 6, 8
 norm, 6
 space, 5, 6, 149
- Euler equation, 465, 500, 1142
 reversible, 475
- Euler form, 420
- Euler identity, 118, 1108
- Euler's theorem, 419, 420
- Eulerian
 duality with Lagrangian, 311
 flux-form conservation law, 553
 mean, 1548
 reference frame, 266, 284
 region, 370
 time derivative, 152, 292
- evanescence, 1301
- evolution equation, 66
- evolving flow, 292
- exact differential, 42, 202, 203, 390, 414, 415, 422
- hiker analogy, 43
- exact geostrophic balance, 713
- exact hydrostatic balance, 470
- Exner function, 452, 454, 935
- extensive property, 361, 369, 410, 414
- exterior calculus, 159

- exterior moment of λ , 1639
external
 moment, 1640
 pressure gradient, 570
 tracer mass, 1663
 velocity, 592, 807
external forces, 479
- f-plane approximation, 245, 469
fetch, 826
Fick's law, 1496
Fick's law of diffusion, 545
field point, 73, 79
fine scale mixing, 1575, 1576
first kinematic viscosity, 498
first law of thermodynamics, 43, 412, 413, 425, 535
 moving fluid, 531
 potential temperature, 533
Fjørtoft's criteria, 1373
flat space, 149
flow lines, 301
flow versus fluid property, 385
fluid
 dynamics, xii
 element, 283, 362, 363, 366, 653
 kinematics, xii
 material region, 283
 parcel, 282, 362
 particle, 281
 particle trajectory, 285, 301
 region, 284
fluid versus flow property, 385
flux, 46
flux-form conservation law, 338, 553, 989
force couplet, 492
force potential, 202
forces
 body, 408, 409, 462
 central, 205
 contact, 462
 external, 204
 fictitious, 214
 internal, 204
 kinematic, 214
form stress, 483, 593, 602, 796, 799, 802, 803, 812, 1585
 dual, 799, 804
geostrophic eddies, 700
- isopycnal layer, 703
isopycnal surface, 701
mathematical expression, 583
formation, 1648
Fourier
 complementarity, 134
 conjugate symmetry, 124, 127
 cosine transform, 129
 Dirac delta, 134
 exponential series, 124
 Gaussian, 135
 integral theorem, 126
 integrals, 126
 inverse transform, 127
 Parseval's identity, 125, 131
 position space, 117
 reality condition series, 124
 reduced wavenumber, 131
 series, 121
 sine transform, 130
 sine/cosine series, 122
 time domain, 132
 transform, 127
 transform pairs, 127
 transforms, 126
 wavenumber, 122
 wavevector space, 117
Fourier analysis, 1100, 1112, 1175
Fourier transform, 1115
 inverse, 1115
Fourier's heat law, 381
Fourier's law, 532, 1497
Fourier's law of conduction, 545
free
 falling particle, 259
 particle, 261
 space Green's function, 79
 vortex, 844, 860
free surface patterns, 916
frequency, 132
freshwater
 boundary condition, 1614, 1615
 budget, 1612
 velocity, 1614
friction
 dissipation, 524, 535
 driven velocity, 724
 force, 500
 tensor, 496

- torque, 1065
- vertical shear, 501
- frontal equations, 1345
- Froude number, 294, 617, 788, 1025, 1027, 1029, 1268
- functional degrees of freedom, 386
- functional variations, 1502
- functions versus scalars, 165
- fundamental
 - solution for Laplace operator, 79
 - theorem of calculus, 36
 - thermodynamic relation, 415
- Galilean
 - boost, 199
 - invariance, 199, 203, 213, 296, 497, 887
 - invariance of kinetic energy, 255
 - transformation, 199, 296, 297, 369, 1266
- gauge
 - freedom, 991, 993, 1019
 - function, 535, 902, 1145, 1164
 - invariance, 327, 1509
 - symmetry, 389, 392, 463, 535
 - transformation, 1165
- gauge function, 950
- Gauss's divergence theorem, 38, 179, 1449
- Gaussian
 - Fourier transform, 135
- Gaussian curvature, 145
- general covariance, 150
- general orthogonal coordinates, 193
- general vertical coordinates, 286, 374
 - basis one-forms, 1406
 - basis vectors, 1405
 - circulation, 1419
 - common confusion, 1403
 - contravariant velocity, 1411
 - covariant velocity, 1411
 - diffusion operator, 1416
 - divergence, 1416
 - divergence theorem, 1416
 - examples, 1422
 - Jacobian, 1412
 - layer integrated diffusion, 1417
 - Levi-Civita tensor, 1413
 - material time derivative, 1416
 - metric tensor, 1412
 - partial derivatives, 1414
 - position vector, 1408
- related to Cartesian, 1402
- specific thickness, 1412
- triple product identity, 1407
- vector, 1410
 - vector cross product, 1413
- velocity, 1411
- volume element, 1413
- vorticity, 1418
- generalized Lagrangian mean, 1138, 1545, 1550
- isopycnal, 1562
- kinematics, 1547
- tracers, 1553
- generalized vertical coordinates, 1398
- Gent-McWilliams
 - anisotropic, 1599
 - available potential energy, 1582
 - boundary value problems, 1588
 - effect, 1582
 - form stress, 1585
 - parameterization, 1580
 - secondary circulation, 1582
 - thickness diffusion, 1586, 1587
- geometric acoustics, 1154
- geometric optics, 1127
- geopotential, 203, 233, 612
 - coordinates, 236
 - height, 451
 - height in ideal gas, 574
 - reference, 520
 - thickness, 451
- geostrophic
 - adjustment, 1261, 1263
 - advection, 1086
 - balance, vi, 683, 686
 - contours, 903, 1541
 - eddies, 700, 793
 - exact balance, 713
 - momentum, 927
 - number, 1049
 - streamfunction, 1035, 1037
 - Sverdrup balance, 694, 1066
 - transport, 792
- geostrophic streamfunction, 688
- geostrophy
 - isopycnal models, 1460
 - pressure coordinates, 690
 - shallow water, 790
- geothermal heating, 381

- Gibbs potential, 422, 430, 438, 530
Gibbs relation, 415
Gibbs-Duhem, 422
global conservation, 554
global conservation law, 989
global instability, 1320
global mean sea level, 1620
Godfrey's island rule, 922
gradient operator, 24
 Cartesian, 1414
 general vertical coordinate, 1414
gradient wind balance, 719
 barotropic flow, 874
 regular high, 721
gravest mode, 1184
gravest vertical mode, 693
gravitational acceleration, 231, 750
 approximate, 233
 effective, 233
gravitational force, 203
gravitational mass, 605
gravitational potential, 748
 earth-moon, 753
 general case, 748
gravitational potential energy, 233, 519
 mixing, 522
 regional, 520
 stratification, 521
gravitational stability, 664
gravitational work, 438, 540
gravity waves, 842, 1241
 non-rotating, 1263
 polarized, 1257
 speed, 1248
Green's function, 327
 advection-diffusion equation, 1525
 causal, 97
 composition, 101, 1529
 diffusion, 97
 diffusion adjoint, 98
 diffusion equation, 97
 diffusion free space, 97
 free space for Laplace, 79
 method, 73
 non-closed reciprocity, 1528
 one-dimensional Poisson, 81
 passive tracers, 1523
 reciprocity, 88, 99, 1526
Green's identities, 40
group time derivative, 1158
growth rate, 1344, 1361
 Eady waves, 1391
gyre circulation, 910
gyres and channels, 827
Hadley circulation, 473
haline, 658
 contraction coefficient, 434, 658, 659
halosteric sea level, 1624
Hamilton's operator, 24
Hamilton's equations for rays, 1127
harmonic function, 29, 31, 55, 328, 390, 842,
 1164
 mean-value property, 55
harmonic oscillator
 simple, 1133
Haynes-McIntyre PV flux, 1002
heat capacity, 433
heat equation, 59, 97
heat flow direction, 418
heat function, 429
heating, 413
Heaviside step function, 77, 97, 1262
height and buoyancy relation, 642
Heisenberg uncertainty principle, 1119
helicity, 976
Helmholtz
 decomposition, 327, 390, 623
 decomposition of Coriolis, 47
 equation, 64
 first theorem, 850
 free energy, 430
 second theorem, 851
 third theorem, 851
Helmholtz-Hodge decomposition, 327, 330
heuristics, 71
homogeneous
 fluid, 410
 function, 419, 420
 solution, 54
 tensor, 20
Hooke's Law, 497
Hooke's law, 1133
Hughes gyre model, 915
hydraulic control, 788
hydraulic jump, 542
hydrodynamics, 605, 1161
hydrostatic, 254

- approximate balance, 470, 562, 566, 612, 671, 772
approximate balance for ocean, 611
background state, 569
exact balance, 470, 489
exact versus approximate, 471
number, 1049
pressure, 566, 656, 762
pressure evolution, 566, 619
pressure forces, 489
primitive equations, 562
scaling, 568, 615
torque balance, 492
vertical motion, 562, 575
hyperbolic PDE, 61, 1106
classification, 54
domain of influence, 64
hypsometric equation, 451
- ice skater, 893
ideal fluid, 282
ideal gas, 447
adiabatic lapse rate, 450
baroclinicity, 935
buoyancy frequency, 666
compressibility, 450
enthalpy, 449
equation of state, 447
geopotential thickness, 451
heat capacity, 448
internal energy, 448
lapse rate, 666
law, 274
potential temperature, 452
sound speed, 450
thermal expansion coefficient, 449
- impermeability
compare to material invariance, 1006
impermeability theorem, 901, 1001, 1002, 1016, 1090
absolute vorticity components, 1005
confusions, 1006
kinematics, 1004
planetary geostrophy, 1057
seawater, 1006
- impulse, 78
impulse response function, 78, 83, 110, 1534
in situ density, 659
in situ temperature, 443, 549
- evolution, 549
incompressible, 385
incompressible flow, 386
incropping buoyancy, 639
induction vector, 1089
inertia-gravity waves, 1241, 1244, 1253, 1255
topographic forcing, 1265
- inertial
acceleration, 220
frequency, 685
motion, 715
near inertial waves, 1206
oscillation, 716
oscillation in ocean, 247
oscillation period, 247
oscillations, 245, 1051, 1198
reference frame, 198, 200, 266
velocity, 219, 227
waves, 1198
waves dispersion relation, 1202
waves group velocity, 1204
- inertial instability, 1319, 1331
inertial mass, 605
inertial waves, 1308
inertial-vorticity oscillations, 1341
inexact differential, 42, 413–415, 422
integrating factor, 43
influence function, 83
information entropy, 1537
initial value problem, 109, 1262
injection work, 537
inner product, 9, 332
- instability
baroclinic, 1379, 1389
barotropic, 1367
centrifugal, 1319
convection, 1377
global, 1320
inertial, 1319, 1331
interfaces, 1355
Kelvin-Helmholtz, 1355
local, 1317, 1319
Rayleigh-Taylor, 1355
stratified shear, 1375
symmetric, 1319
wave, 1320
- integral curve, 281, 302
integral surface, 52
integrating factor, 43, 415, 422

- integration in λ -space, 1635
intensive property, 361, 369, 410, 414
interfacial form stress, 582, 588, 799, 802, 1480
interior moment of λ , 1639
interior water mass transformation, 1643
intermolecular forces, 510
internal
 energy, 406, 411, 428, 534, 638
 energy budget, 535
 energy capacity, 433
 forces, 462, 479
 moment, 1640
 pressure gradient, 570
 tracer mass, 1663
 velocity, 592, 807
internal gravity waves, 1275
inverse barometer sea level, 764
inverse energy cascade, 873
inverse proposition, 669
inversion, 1261
irreversible process, iii, 417
irreversible thermodynamics, 517
irrotational, 841, 1164
 flow, 391, 842, 853
 vector, 30
island rule, 922
isobar, 470
isolated system, 409
isopycnal, 353
 coordinates, 154, 1404
 ensemble, 1561
 layer transport, 1560
 mean, 1561
 primitive equations, 1456
isotropic tensor, 20
- Jacobian
 evolution, 324
 of transformation, 162, 169
 on a curve, 147, 1541
 operator, 147, 1086, 1541
 ratio of volumes, 290
Jacobian operator, 870
JEBAR, 1071
jets, 881
Joule heating, 535
Joule unit of energy, 275
Kelvin's circulation theorem, 933, 943, 980, 984
Kelvin-Helmholtz instability, 1050, 1355
kinematic
 free surface equation, 354, 399
 two-dimensional flow, 324
 viscosity, 498
 water mass transformation, 1642
kinematic boundary condition, 346, 768, 1614
 buoyancy surface, 353
 geometric derivation, 349
 material interface, 348
 moving material, 347
 non-divergent flow, 387
 ocean free surface, 353
 permeable surface, 350
 static material, 346
 surface waves, 1171
kinetic energy, 201, 255, 523, 1135
 axial angular momentum, 256
Boussinesq, 630
cartesian coordinates, 255
dissipation, 524, 525
geopotential coordinates, 256
hydrostatic Boussinesq, 648
spherical coordinates, 256
kinetic stress, 493, 591, 795, 1479
kinetic stress tensor, 867
kinetic theory, 274
Knudsen number, 271, 455
Kronecker tensor, 8, 161, 164, 218
- L2 inner product, 332
laboratory reference frame, 200, 284
Lagrangian
 coordinates, 154
 mean, 1548
 reference frame, 266, 284, 1138
 region, 366
 time derivative, 152, 292
laminar subregion, 509
Laplace's equation, 55, 842
 properties, 55
Laplacian friction, 729
Laplacian operator, 29
law of atmospheres, 452
law of cosines, 753
layer mass continuity, 1438
 compressible, 1439

- pressure coordinates, 1440
- Legendre transformation, 427, 429, 430
- Leibniz's rule, 354, 371, 961
- Leibniz-Reynolds transport theorem, 370, 377, 1015
- length scale
 - gradient, 273
 - macroscopic, 270
 - mean free path, 270, 275
 - measurement, 273
 - molecular, 270
 - simulation, 273
- level of no motion, 573, 773
- Levi-Civita tensor, 9, 170, 875
 - general coordinates, 171
 - volume element, 172
- lid pressure, 863, 873
- linear equation of state, 660
- linear instability analysis, 1340
- linear momentum, 198, 855
 - conservation, 199
 - finite volume, 494
 - Lagrangian volume, 495
- local conservation, 553
- local instability, 1317, 1319
- local Rossby number, 711
- local thermodynamic equilibrium, 517, 528
- locally referenced potential density, 665
- long waves, 1233
- longitudinal waves, 1131, 1132, 1139, 1144, 1147, 1248
- longwave radiation, 1618
- Lorenz convention, 639
- Möbius strip, 36
- Mach number, 605, 1131, 1132, 1142, 1148
- macroscopically small, 269
- macrostate, 406
- macrostates, 408
- Magnus acceleration, 468, 712, 785
- Margules' relation, 782, 791, 794
- Marshall potential vorticity flux, 1007
- mass
 - λ -layer, 1635
 - gravitational, 605
 - inertial, 605
- mass budget, 374
 - λ -layer, 1648
 - fluid column, 355, 356
- weak formulation, 363
- mass conservation, 266, 342
 - arbitrary Eulerian region, 339, 340
 - Eulerian flux-form, 338
 - finite Eulerian region, 338
 - Jacobian derivation, 341
 - Lagrangian, 340, 1139
 - Lagrangian derivation, 343
 - multi-components, 363
- mass continuity
 - generalized vertical coordinates, 1437
 - layer integrated, 1438
- mass density, 657
- mass density function, 1635
- mass distribution function, 1635
- mass equation
 - general vertical coordinates, 1446
- mass flux, 338
- mass flux through a surface, 350
- mass-Sverdrup, 1631
- material
 - area evolution, 318
 - closed system, 409, 413
 - constant, 369
 - coordinate choices, 286
 - coordinates, 154, 285, 287
 - curve, 312
 - curve evolution, 313
 - fluid parcel, 282, 409
 - invariance, 294, 295
 - invariant, 369
 - invariant volume, 386
 - line elements, 946
 - open system, 409
 - surface, 294
 - thickness evolution, 323
 - volume evolution, 322
- material time derivative, 152, 292
 - general vertical coordinates, 1432
- invariance, 298, 299
- isopycnal models, 1458
- space-time, 301
- mathematically rigorous, 71, 74
- matrices, 19
- matter
 - concentration, 425
 - conservation, 553
 - flow direction, 425
- Maxwell relations, 422, 434

- mean free path, 270, 1496
mean tracer equation, 1569
mean value theorem, 1139
mechanical
 pressure, 495, 499
 stress, 493
 work, 201, 255, 414, 1135
 work from geopotential, 438
mechanical energy, 202, 523, 526
 Boussinesq, 630, 632, 634, 649
 conservation, 257
 dissipation, 505, 524
 finite volume, 526
 particle, 255
membranes, 509
meridional
 overturning circulation, 396
 overturning transport, 1584
 transport, 1059
mesoscale eddies, 1573, 1576
mesoscale eddy mixing, 1575
method of characteristics, 52
metric acceleration, 220, 229, 467
metric tensor, 8, 160, 313
 Cartesian coordinates, 160
 coordinate representation, 161
 coordinate transformation, 162
 determinant, 169
 general, 161
 inverse, 164, 165
 relating vectors and one-forms, 164
metricity condition, 177
microscopically large, 269
microstates, 408
mixed boundary condition, 1524
mixing, 1576
 surface boundary, 1615
 tensor, 1576
mixing length, 1496
modal stability analysis, 1317
modified mean, 1561
molar mass, 421
mole, 274
molecular
 composition of air, 274
 composition of water, 274
 diffusion, 1574, 1576
 diffusivity, 649
 viscosity, 504, 649
moment arm, 224, 472
moment of inertia, 200, 202, 893
moment-arm, 248, 254
moments of λ , 1639
momentum
 absolute, 1329
 angular, 200
 approximate axial angular, 254
 axial angular, 224, 248, 262, 472, 578
 axial angular and Coriolis, 250
 geostrophic, 1329
 linear, 261
 potential, 235, 244, 262, 1328
momentum argument, 1215
momentum equation, 795
 flux form, 493, 1447
 general vertical coordinates, 1446
 horizontal, 1447
 natural coordinates, 711
 spherical, 466
 vertical, 1447
momentum flux, 338
momentum-based, vi
Monge gauge, 137
monochromatic patterns, 1108
monochromatic waves, 1108
Montgomery potential, 703, 1457
 shallow water, 781
motional forces, 671
Munk gyre model, 915

NADW, 1627
natural boundary condition, 1502
natural coordinates, 707, 708
 isobars, 725
 vorticity, 851
Navier-Stokes equation, 465, 500, 503
 non-dimensional, 503
near inertial wave, 1308
near inertial waves, 1206
nearly horizontal motion, 254
net stress tensor, 502
Neumann boundary condition, 57, 58, 82, 93,
 381, 621, 1502, 1524, 1525
neutral
 anisotropic neutral diffusion, 1595
 density, 1631
 diffusion, 1589
 directions, 661, 662, 1589

- helicity, 668
- slope, 1578
- surface, 670
- tangent plane, 1589
- tangent plane coordinates, 1596
- neutral diffusion, 1503
- neutrality condition, 664, 1592, 1598
- neutrally buoyant, 653, 656
- Newton's
 - equation of motion, 464
 - first law, 197
 - gravitational constant, 231
 - gravitational law, 231
 - second law, 197, 198
 - third law, 197, 479, 482, 505, 582, 803
 - third law and pressure, 482
 - third law strong form, 205
 - third law weak form, 205
- Newtonian
 - fluid, 496, 497
 - gravity, 74
 - gravity field, 753
 - time, 6, 149, 152
- Newtonian friction, 1498
- no normal flow boundary condition, 346
- no-flux boundary condition, 381, 743
- no-slip boundary condition, 501, 507
- Noether's Theorem, 266
- Noether's theorem, 241, 243, 244, 1135
- non-advection
 - flux, 1614
 - transport, 1618
- non-Boussinesq steric effect, 355
- non-conservative
 - forces, 203
 - process, 553
- non-dimensionalization, 1030
 - Ekman balance, 730
 - hydrostatic approximation, 615
- non-dispersive waves, 1248
- non-divergent
 - barotropic model, 863, 864, 1210
 - velocity field, 386
- non-hydrostatic
 - pressure, 765
 - primitive equations, 565
- non-inertial reference frame, 200
- non-Newtonian constitutive relations, 503
- non-orthogonal coordinates, 154
- normal
 - derivative, 26
 - direction, 26, 138, 346
 - evolution equation, 321
 - solid-earth bottom, 347
 - stress, 497
 - vector, 389
- nuclear reactions, 361
- obduction, 1436
- oblate spheroid, 236
- oblique coordinates, 166
- observation point, 79
- ocean
 - buoyancy, 1603
 - free surface, 1423
 - gyres, 908
 - gyres and topographic form stress, 911
 - mesoscale eddy, 793
 - mixed layer base, 1423
 - mixing processes, 1574
- ocean submesoscale, 1345
- oceanic form stress, 582
- one-forms, 163
 - basis, 164
 - coordinate representation, 163
- one-way wave equation, 61
- orbital motion, 753
- orientation, 9, 10, 35, 36, 138
- orthogonal curvilinear coordinates, 193
- oscillator equation, 246, 1134
- outcropping buoyancy, 639
- outer product, 19, 493, 795
- overturning circulation, 1342
- overturning streamfunction, 396
- parabolic PDE, 59
 - classification, 54
 - smoothing property, 59
- parameterizations, 273, 1573
- parcel method, 1281
- parcel stability analysis, 1317
- parity, 122, 123
- Parseval-Plancherel formula, 131
- partial
 - entropy, 423
 - internal energy, 423
 - volumes, 423
- partial derivatives
 - transformation, 174

- particle displacement, 1554
particle mechanics, 198
particle trajectory
 fall to equatorial plane, 260
 free fall to center, 259
 freely falling, 260
 geopotential motion, 260
 spherical motion, 259
particular solution, 54
passive
 tracer, 50, 368, 1523
 tracer source, 1525
path, 138
 orientable, 138
 simple, 138
path integral
 arc length, 34
 path dependent, 413
 scalar function, 33
 vector function, 35
pathlines, 301
 analog to car flow, 302
perfect fluid, iii, 282, 409, 1504
periodic channel, 820
periodic function, 121
permutation symbol, 9, 170, 875
 product identity, 15
phase
 averaging, 1546
phase averaging, 119
phase speed, 1126
physically formal, 71, 74
physics as geometry, 150
Pitot tube, 467
planar curves, 140
plane wave, 1108, 1109
planetary
 beta effect, 693
 Cartesian coordinates, 221
 centrifugal acceleration, 224, 235
 centripetal acceleration, 224
 induction, 954
 spherical coordinates, 221
 vorticity, xiii, 693
planetary geostrophy, 690, 968, 1031
 continuously stratified, 1045
 energetics, 1055
 equations, 1054
 potential vorticity, 903, 1056
vorticity equation, 691
planetary Rossby waves, 1210, 1244, 1382
planetary waves
 dispersion relation, 1217
plumb line, 260
Poincaré waves, 1253
point, 6
 mass, 74
 transformation, 287
point jet, 1226
Poisson equation, 55, 57, 79, 231, 327, 871, 873
 Dirichlet boundaries, 90
 Green's function, 85, 93
 max-min principle, 57
 Neumann boundaries, 94
 pressure, 673
polar coordinates, 188
Pontryagin duality, 117
position coordinates, 287
position vector
 Cartesian representation, 221
 spherical representation, 221
postulate of total energy conservation, 547
potential
 enthalpy, 444, 550
 momentum, 235, 262
 property, 444, 657
 scalar properties, 555
potential density, 659
 locally referenced, 665
potential energy, 202
 Boussinesq, 631
 shallow water layer, 1482
potential enstrophy, 983
potential flow, 842, 1161
potential momentum, 1328
potential temperature, 442, 443, 452, 549, 657
 evolution, 550
 specific entropy, 446
potential vorticity, 1419
 substance, 990
 baroclinic fluid, 982
 barotropic fluid, 980
 Bernoulli potential, 996
 Boussinesq, 1454
 concentration, 1009
 cylinder, 892

- delta sheet, 639
derivation, 993
dynamical tracer, 985
Ertel, 979, 981, 1084
Eulerian flux-form budget, 989
flux, 901, 990, 993, 996, 1002, 1007
flux-form equation, 901
gauge choice, 996
generalized vertical coordinates, 1452
Haynes-McIntyre PV flux, 1002
hydrostatic Boussinesq, 992
impermeability, 1001, 1057
impermeability kinematics, 1004
induction vector, 1089
inertia-gravity waves, 1306
integrated substance, 1009
inversion, 1022, 1261
isopycnal coordinates, 1462
iterated, 983
Kelvin circulation theorem, 897
kinematic derivation, 994
layer budget, 1014
Marshall PV flux, 1007
material invariance, 1001
name, 896, 984
non-conservative processes, 900, 988
non-divergent barotropic flow, 985
ocean layer, 1013
pancake, 997
perfect fluid, 980
planetary geostrophy, 903, 1040, 1056
potential density, 986
preferred flux forms, 1019
quasi-geostrophy, 1036, 1037, 1040, 1084
Rossby, 896
seawater, 1006
seawater equation of state, 986
shallow water, 895
stuff, 901
substance, 1002
symmetric instability, 1019
thickness weighted average, 1486
two-dimensional non-divergent, 869
- potential vorticity flux
air-sea boundary, 1017
land-sea boundary, 1016
steady state constraints, 1008
- power, 255
practical salinity, 1612
- Prandtl number, 1498
Prandtl ratio, 1051
pressure
boundary conditions, 620
contact force, 796, 799, 1450
contact stress, 481, 1449
coordinates, 1404
driven velocity, 724
dynamical pressure, 607
gradient force, 1449
Lagrange multiplier, v
mechanical, 495, 499
Pascal unit, 275
Poisson equation, 619, 873
shallow water dynamic, 781
stagnation, 539
standard atmosphere, 274
thermodynamic, 495
time derivative, 1605
total, 539
transport, 554
two-dimensional flow, 875
work, 414, 540
- pressure form stress, 483, 796, 799, 812, 1268
dual, 1482
interfacial stress, 1451
shallow water, 802
- pressure gradient
bottom, 572
external, 570, 572, 828
hydrostatic, 570, 572, 618, 689
ideal gas, 574
internal, 570, 572, 618, 828
- pressure gradient work
shallow water, 810
- pressure source, 621
Coriolis, 877
friction, 878
irrotational flow, 877
rotation, 875
self-advection, 875
solid-body flow, 875
strain, 875
- pressure torque, 806, 965, 1060
atmosphere, 1064
bottom, 1064
- primitive equations, 250, 562, 684
nomenclature, 565
- process water mass transformation, 1642

- prognostic equation, 66, 295
pseudo angular momentum, 245
pseudo vector, 10, 840
pseudo-westward phase, 1219, 1229
pulling back, 33
pycnocline, 793
Pythagoras' theorem, 8
- quasi-equilibrium thermodynamics, 517
quasi-geostrophy, 1032, 1245
 potential vorticity, 1036, 1037
quasi-Lagrangian coordinates, 154
quasi-static process, 269, 276, 410, 517
quasi-Stokes transport, 1564, 1567
quotient rule, 486
- radius of curvature, 142, 144, 708, 715, 851
rarefaction, 1144
rarefied gas, 272
rate of strain tensor, 315, 316, 325, 524, 621,
 840, 858, 875, 1143
 vorticity source, 946
ray equations, 1127
ray theory, 1127
Rayleigh drag, 203, 498, 727, 907, 918, 963
Rayleigh equation, 1368, 1375
Rayleigh inflection-point criteria, 1372
Rayleigh-Bernard convection, 1377
Rayleigh-Kuo condition, 1372
Rayleigh-Kuo equation, 1227
Rayleigh-Taylor instability, 1355, 1361
re-entrant channel, 820
real fluid, iii
reciprocity, 1526
reciprocity condition
 diffusion equation, 99
 Poisson equation, 83, 88
rectification, 1472, 1545
reduced gravity, 773–775, 778, 791
 model, 573, 773, 788, 793, 1251
reference
 density, 387
 geopotential, 520
 pressure, 660
 shallow water density, 778
reference frames, 199
 absolute, 213
 inertial, 199, 213
 non-inertial, 200, 213
 rotating, 213
- reflection
 non-specular, 1296
 specular, 1296
region following the flow, 342
relative chemical potential, 426
representation, 6
rescaled geopotential coordinate, 1442
residual mean
 transport, 1577
 velocity, 1577
resonance, 1368
response function, 78, 110, 432
reversibility, 243
reversible process, 417
Reynolds
 average, 1475
 decomposition, 1546
 stress, 493, 1479
Reynolds number, 272, 503, 730, 745
 atmosphere, 504
 Gulf Stream rings, 504
 turbulence, 504
Reynolds transport theorem, 341, 344, 1500
 linear momentum, 495
 multi-component fluid, 374
Richardson number, 617, 1050, 1375
 balanced, 1392
Riemannian differential geometry, 150, 159
right hand rule, 9
rigid body rotation, 318
rigid lid, 873
 approximation, 694, 783, 1071
rigid lid ocean models, 878
Robin boundary condition, 1524
Rossby
 deformation radius, 1051
 effect, 476, 882
 potential vorticity, 900
Rossby number, 684, 745, 1027–1029, 1049
 Gulf Stream ring, 686
 kitchen sink, 686
 local, 711
Rossby waves, 470, 1210, 1241
 baroclinic, 1383
 dispersion relation, 1217
 group velocity, 1220
 stationary, 1220
 topographic, 1383
rotating tank, 575, 829, 876

- parabolic free surface, 577
solid body motion, 577
rotation matrix, 17, 1596
rotation tensor, 315, 317, 325, 621, 840, 858, 875, 946, 1143
rotational
 flow, 325
 fluxes, 1556
 tracer flux, 1507, 1581
row vector, 19
salinity, 426, 657, 1603
salt
 boundary condition, 1614, 1615
 budget, 1612
 concentration, 1612
 velocity, 1614
scalar
 field, 6
 general tensor scalar product, 166
 mechanics, 1492
 potential, 30, 1164
 potential harmonic, 1164
 product, 8, 9
 scalar product invariance, 18
 streamfunction, 393
scale analysis, 615, 1024
scale height, 451, 605
sea breeze, 973
sea level, 1620
 thermal expansion, 400
 Boussinesq ocean, 1623
 budget, 1621
 steric, 1622
 thermosteric, 1622, 1623
sea level pressure, 582
seawater
 chemical potential, 426, 431
 equation of state, 986
 mass distribution, 1635
second kinematic viscosity, 498, 499
second law of thermodynamics, 412, 415, 417
secondary circulation, 883, 1345
seiche, 1184
self-adjoint operator, 89, 99, 1501, 1527
self-advection, 875
self-attraction and loading (SAL), 757
semi-geostrophy, 1317, 1345
separation of variables, 1175
sgn function, 77
shallow fluid approximation, 251, 254, 562
shallow water
 N -layer equations, 800
 columns, 772
 gravity wave dispersion, 1255
 gravity wave speed, 1247
 hydrostatic approximation, 772
 inertia-gravity waves, 1253
 linearized equations, 1237
 model formulation, 762
 momentum, 766
 momentum equation, 795
 non-dimensional, 1030
 non-rotating gravity waves, 1247
 planetary geostrophy, 1031
 potential vorticity, 895
 potential vorticity invariance, 896
 pressure, 762
 quasi-geostrophy, 1032, 1245
 stacked model, 776
 Sverdrup balance, 908
 thickness, 766
 two-layer, 776
 vertical velocity, 770
 vorticity, 890, 949
shear
 flow, 647
 strain, 326
 stress, 497
shear instability, 1367, 1375
shortwave radiation, 1618
sign-function, 1262
simple ideal gas, 447, 448
simply connected, 327
singular limit, 731
skew
 diffusion, 1508, 1577
 diffusion tensor, 1508
 skew diffusion and skewson, 1509
 symmetric stirring tensor, 1560
 symmetric tracer fluxes, 1555
 tracer flux, 1507, 1581
slippery Ekman layer, 743
slope Burger number, 1050
slope of a surface, 352
smooth velocity field, 301
solenoid, 942
solenoidal velocity, 385

- solid-body
 rotation, 44, 215, 846, 859, 860
 spherical velocity, 223
- solid-body motion, 1322
- soliton, 1181
- Sorret effect, 545
- sorting buoyancy, 645
- sound pressure level, 1148
- sound speed, 434, 636, 658, 1141, 1144
 ideal gas, 450
 ocean, 987
- sound waves, 1131
- source point, 73, 79
- Southern Ocean, 828
 channel, 820
- space increments
 Eulerian, 310
 Lagrangian, 311
- space-time tensors, 158, 301
- specific
 entropy, 446
 gas constant for air, 447, 451
 thickness, 1424, 1563, 1565
 volume, 530
- specific volume, 425
- specular reflection, 1224
- spherical coordinates, 153, 183, 218
 basis one-forms, 185
 basis vectors, 185
 differential operators, 187
 Levi-Civita tensor, 186
 metric, 186
 position, 185
 summary, 188
 transformation from Cartesian, 183
 vector components, 187
 vector cross product, 187
 velocity, 185
 volume element, 186
- spin, 621
- splat, 621, 875
- St. Andrew's cross, 1288
- stability analysis
 energetic, 1317
 modal, 1317
 parcel, 1317
- stagnation pressure, 467
- standard
 atmosphere, 274
- pressure, 270
 temperature, 270, 274
- state function, 413
- static
 equilibrium sea level, 748, 749
 forces, 653, 671
 pressure, 569
- steady flow, 292
- steady state, 55, 292, 295, 369, 408, 827
- steepest descent, 25
- step response function, 111
- steric sea level, 573
 changes, 1622
- stirring, 1576
 reversible, 533
- Stokes
 drift, 1187, 1248, 1472, 1473, 1552, 1558
 drift and surfing, 1189
 drift for surface prototypical waves, 1190
 mean, 1547, 1550
 theorem, 36, 179, 393, 669, 843
- Stokes drift, 1100
- Stokesian fluid, 496
- Stommel gyre model, 915
- storage, 1648
- stratification, 662
- streaklines, 301, 304
- streamfunction, 390, 864
 meridional-depth overturning, 396
- quasi-geostrophy, 1037
- streamlines, 388
 transport, 388, 392, 393
 two-dimensional flow, 387
 vector, 391
 vertical gauge, 392
- streamlines, 301, 302, 346, 388
 compared to pathlines, 303
- streamtubes, 302
- stress
 boundary, 629
 contact, 462
 deviatoric, 463, 497
 direct, 497
 friction, 463
 local equilibrium, 482, 505
 normal, 497
 on an interface, 505
 pressure, 463
 shallow water, 787

- shear, 497
- stress boundary condition
Lagrangian interface, 507
permeable interface, 508
solid boundary, 506
- stress tensor, 462, 479, 484
net, 502
symmetry, 486
- stress-strain relation, 495
- stretching, 947, 1201
material lines, 316
- strong formulation, 280, 376, 489, 492
- sub-inertial waves, 1244
- subduction, 1436
- subgrid scales, 1573
- subgrid-scale parameterizations, 691
- subharmonic function, 57
- substantial time derivative, 292
- super-inertial waves, 1243
- superposition principle, 73, 1100, 1108, 1112, 1147, 1175
- superposition property, 91, 94
- surface
derivative operator, 320
gravity waves, 765, 1161, 1170
orientable, 138
velocity, 347
- surface area, 144
horizontal projection, 351, 352, 378
- surface gravity waves
dispersion relation, 1177
kinematic boundary condition, 1171
longwave limit, 1181
shortwave limit, 1181
wave breaking, 1182
- surface tension, 415, 479, 481, 505, 509, 1184, 1358
gas bubbles, 514
- surface water mass transformation, 1643, 1652, 1653
- buoyancy, 1654
- circulation, 1653
- Sverdrup, 1631
- Sverdrup balance, vi, 694, 908, 969, 1064, 1066
geostrophic, 1066
topographic, 969, 1068
- symmetric
mixing tensor, 1560
- tracer fluxes, 1555
- symmetric instability, 1319, 1340
- symmetry, 199, 241, 243, 266
condition, 1593
spatial, 261
- tangent
Cartesian for tangent plane, 221
direction, 26, 138
plane approximation, 217, 469
space, 155, 164, 176
vector, 34, 389
- Taylor
columns, 693, 772
curtains, 700
- Taylor series, 24
- Taylor-Bretherton identity, 870, 1471, 1486
- Taylor-Goldstein, 1375
- Taylor-Proudman effect, 692, 700, 1198, 1207
- temperature, 443, 657
- tensile force, 510
- tension strain, 326
- tensor analysis
algebra summarized, 217
contraction of indices, 151
contravariant, 217
covariant, 217
covariant differentiation, 151
operations, 151
outer product, 151
permissible operations, 151
quotient rule, 151
tensor fields, 6
tensor product, 151
tensors, 6
tensors and matrices, 19
uses for GFM, 2
- tensor index
contravariant, 153
convention, 7
covariant, 153
gymnastics, 15, 156
raising and lowering, 164
- terrain following coordinates, 1404
- test
charges, 281
fluid element, 283, 653, 661
paddle wheel, 840
particles, 281

- tetrahedron fluid region, 484
theorem of stress means, 475
thermal
 energy, 411
 equation of state, 448, 657
 expansion coefficient, 433, 658, 659
thermal wind balance, 683, 689, 794, 1079
 Antarctic Circumpolar Current, 695
 atmosphere, 696
 diagnostics, 696
 ocean, 694, 698
 potential density, 698
 shallow water, 782, 791
thermobaricity, 611, 1609, 1611
thermobaricity parameter, 1610
thermodynamic
 configuration space, 411, 634
 laws, 412
 moving fluid, 528
 postulates, 412
 potential, 413, 427
 pressure, 495
 pressure in non-divergent flow, 496
 specific relations, 425
 state, 408
 systems exchanges, 409
 temperature, 412
thermodynamic equilibrium, 408, 412, 418, 424, 441, 443, 536
 fluid elements, 537
 macroscopic motion, 536
 salinity, 440, 546
 with geopotential, 438
thermodynamics
 integrating factor, 43
thermohaline circulation, 607, 613
thermosteric sea level, 1625
thickness, 1565
 diffusion, 703
 equation, 1442
 isopycnal thickness equation, 1458
 specific, 1424, 1446
 specific thickness, 1458
 weighted average, 1476, 1569
 weighted velocity, 1460
 weighting, 1563
third law of thermodynamics, 412
tidal acceleration, 750
tides
- earth-moon system, 751
realistic effects, 757
semi-diurnal, 751
tilting, 947, 1201
 material lines, 316
time
 averages, 66
 coordinate, 152
 mean, 1546
 notation for derivative, 345
 parameter, 152
 reversal symmetry, 243
 scale for molecular collisions, 276
 tendency, v, 66, 292
 variety of derivatives, 376
topographic beta, 902, 1037, 1038
topographic form stress, 582, 585, 912, 1269
 components, 588
 gyres, 911
 zonal ridge, 586
topographic nonlinear balance, 968
topographic Rossby waves, 1241, 1244, 1382
topographic Sverdrup balance, 969
topographic waves, 1241
tornado, 718, 850
torque, 200, 942, 1059
 density, 488
total
 energy, 411, 534
 pressure, 467
 time derivative, 291
tracer
 budget, 374, 380
 concentration, 364, 425
 mass flux, 364
 mechanics, xiv, 266
 parameterization, 1573
 passive, 368
 transport tensor, 1570
 variance, 1501
tracer boundary condition, 380
 air-sea boundary, 382
 bottom, 380
 no-normal derivative, 381
tracer equation, 362, 364
 derived, 364
 Eulerian and Lagrangian forms, 365
 general vertical coordinates, 1446
 layer integrated, 1443

- mean, 1569
- shallow water, 771
- tracer fluxes
 - rotational, 1556
 - skew symmetric, 1555
 - symmetric, 1555
- tracer mass
 - external, 1663
 - internal, 1663
- tracer mass analysis, 1627, 1657
 - external, 1663
 - internal, 1663
 - special cases, 1661
- tracer moments, 1500
- traditional approximation, 469, 563
- trajectory, 152, 198, 285, 301
 - generalized vertical coordinates, 1435
- transformation
 - between material and position, 287
 - Cartesian, 18
 - Cartesian coordinates, 16
 - geometric, 17
 - inverse, 16
 - Jacobian, 287
 - of vectors, 218
 - orthogonal, 17
 - rotation, 17
 - tensor, 19
 - two-point, 287
- transformation matrix, 162, 287, 312
 - coordinates, 162
 - determinant, 170, 173
 - discrete algorithm, 288
 - general vertical coordinates, 1402
 - inverse, 174
 - Jacobian, 162, 169
 - space-time components, 172
- transformed residual mean, 1563
 - velocity, 1564
- transforming Cartesian to spherical, 223, 228
- transition to turbulence, 504
- translation, 318
- translation motion, 846
- transport, 46
 - streamfunction, 388, 595
 - theorem for mechanical energy, 526
 - theorem for scalar fields, 374
- transverse waves, 1144, 1202
- traveling wave, 1109
- turbulence, 500, 504
- turbulence closure, 273
- turbulent
 - cascade of energy, 505
 - turbulent cascade, 951
 - vortex stretching, 951
 - vorticity, 843
- turbulent transport, 1576, 1618
- turning level, 1302
- two-dimensional
 - flow, 863
 - flow kinematics, 324
 - non-divergent flow, 955
 - turbulence, 873
- ultraviolet catastrophe, 505
- uncertainty relation, 1103, 1118, 1119, 1124
- uniqueness
 - diffusion equation, 106
 - Dirichlet problem, 85, 86
 - Neumann problem, 94
- unit vector, 8
 - rotation, 26
- universal gas constant, 274, 447
- vanishing layers, 1462
- vector, 6
 - field, 6
 - general coordinate product, 172
 - geometry of product, 12
 - invariant velocity equation, 712, 784, 938
 - product, 9
 - rotation, 215
 - streamfunction, 391
- velocity, 198
 - basis vectors, 219
 - circulation, 843
 - coordinate, 219
 - external, 592
 - gradient tensor, 315, 858
 - harmonic potential, 395
 - internal, 592
 - molecular rms speed, 276
 - particle motion, 219
 - potential, 390, 395
 - self-advection, 875, 938
 - spherical, 227
 - surface, 347
- velocity equation, 467
- vector-invariant, 467, 970, 1447, 1460

- velocity potential, 1145
velocity vector, 155
generalized vertical coordinates, 1435
planetary Cartesian, 221
spherical, 222
vertical
Ekman transport, 734
energetics with stratification, 521
flow induced acceleration, 675
gauge, 392, 1510
shear, 316
stiffness, 692, 700, 1198
stratification, 664
vertical velocity, 1432, 1479
decomposed, 1433
shallow water, 770
two-dimensional non-divergent, 866
viscosity, 496, 1498
air, 273
dynamic, 273
eddy, 629
kinematic, 273
molecular, 1498
water, 273
viscous
dissipation, 525
flux, 525
tensor, 496
volume
 n -space, 15
between isosurfaces, 980
defined by vectors, 13
element for integration, 14
evolution, 322
volume budget
column of water, 354
material region, 342
volume element
general coordinates, 172
invariant, 169
volume evolution, 341, 374, 395
volume-Sverdrup, 1631
vortex
force, 468
line, 848, 947
lines, 316
stretching, 896, 1059
tilting, 896
tube, 848, 947
vortical flow, 390, 1022
vortical mode, 1209
vortical waves, 1215
vorticity, 43, 317, 324, 325, 501, 539, 840, 858, 868
absolute, 846, 891
acoustic waves, 1145
baroclinicity, 933
barotropic flow, 935
beta effect, 1059
bottom boundary, 962
Boussinesq, 956
curvature, 853, 879
depth averaged velocity, 1070
depth integrated, 961
depth integrated velocity, 1067
dynamics, 890, 938
filaments, 946
flux vector, 960
free vortex, 844, 853
frozen-in, 946
Gaussian jet, 854
general vertical coordinate, 1447, 1452
hydrostatic, 956
isopycnal coordinates, 1462
isopycnal models, 1460
line element rotation, 840
meridional transport, 1064
natural coordinates, 851
non-divergent, 842
of a column, 919
orbital, 853, 879
planetary, 846
planetary geostrophic, 691
quasi-geostrophy, 1036
relative, 846, 1447
rotating fluids, 951
rotating reference frame, 841
shallow water, 890, 949
shear, 853, 879
solid-body, 853
solid-body rotation, 847
stretching, 947, 1059, 1201
surface boundary, 963
thickness weighted average, 1486
tilting, 947, 1201
torques, 942
turbulent cascade, 843
two-dimensional non-divergent, 868

vertical component, 959

vorticity budget

depth integrated, 1059

flux-form, 939

normal component, 941

vorticity equation, 938

hydrostatic, 957

planetary geostrophy, 960

warm core eddy, 793

water mass, 444, 1627

water mass analysis

mathematics, 1634

tracers, 1657

water mass configuration space, 1629

water mass formation, 1631, 1648

buoyancy, 1631

water mass transformation, 1627, 1631, 1641

boundary, 1648

buoyancy, 1631, 1654

dia-surface flux, 1641

interior, 1641

kinematic, 1642

kinematic method, 1644

process, 1642

process method, 1643

processes, 1633, 1651

surface, 1652, 1653

wave

acoustic, 613, 1131, 1144

action, 1154

amplitude, 1109

angular frequency, 1108

baroclinic mode, 1250, 1275

barotropic mode, 1250, 1275

capillary, 1161, 1184

carrier, 1119

deep water waves, 1178

discrete wavenumber, 122

dispersion relation, 1100, 1103, 1106,

1114, 1147

dispersive, 66

dispersive packet, 1122

Eady, 1385, 1387

edge, 1209, 1216, 1225, 1368, 1379, 1385

equation, 1106

function, 1108

Gaussian wave packet, 1118

gravity, 1244

gravity wave critical reflection, 1297

group velocity, 1114

guide, 1302

harmonic, 1104, 1105

inertia-gravity, 1308

inertia-gravity dispersion, 1308

inertial, 1197, 1198, 1308

interference, 1100

internal gravity, 1275

internal gravity energetics, 1295

internal gravity polarization, 1285

kinematics, 1103

length, 1109

longitudinal, 1131, 1132, 1139, 1248

mathematics, 1103

monochromatic, 1104, 1105, 1108

narrow band packet, 1118

near inertial, 1308

non-dispersive, 66, 1147, 1248

non-dispersive packet, 1121

nonlinear, 1181

number, 1103, 1109

packet, 1112

packets, 1114

period, 1109

phase, 1103, 1109, 1126

phase averaging, 119

phase distance, 1111

phase speed, 1111, 1126

phase velocity, 1106, 1111, 1126

plane, 1108, 1109

planetary Rossby, 1382

polarization relation, 1257

ray time derivative, 1158

rays, 1154

reduced wavelength, 1112

reduced wavenumber, 131, 1112

resonance, 1368

Rossby, 1209, 1244

Rossby phase velocity, 1218

Rossby shallow water, 1269

seiche, 1184

shallow water gravity, 1241

shallow water inertia-gravity, 1241

shallow water Rossby, 1241

shallow water topographic, 1241

shallow water waves, 1178

sound, 1131

spatial frequency, 1112

- standard phase, 1109
standing, 1104, 1105
standing waves, 1182
stationary, 1104, 1105
sub-inertial, 1202, 1244, 1255
super-inertial, 1243, 1255
superposition, 1112
topographic Rossby, 1382
traveling, 1104, 1105, 1109, 1175
uncertainty, 1118
uncertainty relation, 1119, 1124
vector, 1103, 1109
vortical and divergent motions, 1306
vorticity, 1209
wavenumber, 1108, 1112
wavevector, 1108
wave equation, 62, 1138, 1266
 domain of influence, 64
wave instability, 1320
wave resonance, 1367, 1379
waves
 anisotropic, 1219
 edge, 1367
 evanescent, 1301
 internal gravity reflection, 1296
 pseudo-west phase, 1219, 1229
 Rossby reflection, 1223
 transverse, 1210
 turning level, 1302
weak formulation, 280, 363, 376, 489, 492
well-defined surface, 669
western boundary layer, 880
western intensification, 908, 910
wind driven circulation, 736
wind stress
 homogeneous layer, 907
 shallow water, 787
wing flow, 539
WKB approximation
 acoustics, 1154
 gravity waves, 1299
work, 255
 by gravity, 203
 on circulation, 934
work-energy theorem, 201, 540, 1135
working, 413
world line, 281
Young-Laplace formula, 511, 513, 1184, 1358
 derivation, 511
zero buoyancy layer thickness, 639
zeroth law of thermodynamics, 412
zonal
 mean, 1547
 re-entrant, 820
 ridge and topographic form stress, 586
 vorticity constraints on zonal flow, 879